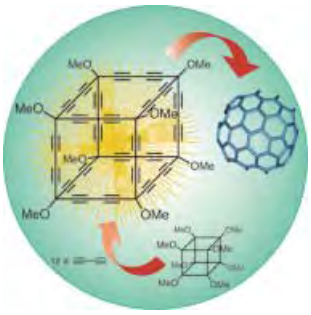
ANGEWANDTE CHEMIE
INTERNATIONAL EDITION
A Journal of the Gesellschaft Deutscher Chemiker
2002
41/22
Pages 4155 – 4354

COVER PICTURE

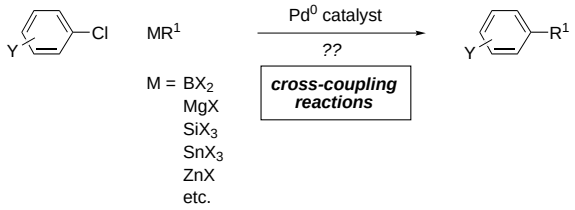
The cover picture shows the first expanded cubane with a C_{56} core. Formally derived by insertion of buta-1,3-diynediyl moieties into all 12 C–C single bonds of octamethoxycubane, its synthesis actually proceeds by the formation of corners, edges, and faces as key building blocks and intermediates. The expanded cubane is highly strained and explodes upon scraping. Under conditions of Fourier-transform ion-cyclotron-resonance mass spectrometry it rearranges into fullerenes, which, in the positive-ion mode, undergo fullerene coalescence reactions. Full details are described by Diederich et al. on p. 4339 ff.



REVIEW

Contents

Their relatively low cost and wide availability can make aryl chlorides more attractive substrates for coupling reactions than the corresponding bromides or iodides. Although scattered examples of couplings of aryl chlorides had been reported earlier, for most processes it was not until the last few years that comparatively general and mild methods were described (see scheme for a general reaction). This article furnishes an overview both of the pioneering early developments and the exciting recent discoveries in this area.



A. F. Littke, G. C. Fu* ..... 4176 – 4211

Palladium-Catalyzed Coupling Reactions of Aryl Chlorides

Angew. Chem. **2002**, *114*, 4350 – 4386

Keywords: catalysis · cross-coupling · ligand effects · palladium · synthetic methods

 © 2002 WILEY-VCH Verlag GmbH & Co. KGaA, Weinheim 1433-7851/02/4122-4157 $ 20.00+.50/0

ESSAY

Concerned skepticism about the direction "his" science had taken dominated the last 30 years of the life of the biochemist Erwin Chargaff, who died on June 20 this year at the age of almost 97. This obituary is an eloquent account of the life of this faciscinating person who never forgot his European roots in spite of spending more than two thirds of his life in America.

Angew. Chem. **2002**, *114*, 4387 – 4390

L. Jaenicke* ..... 4213 – 4216

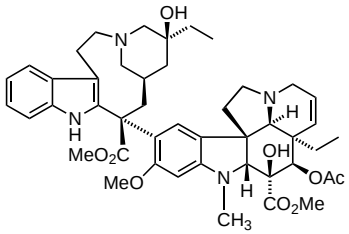
The Torch of Erwin Chargaff and the Fire of Heraklitus Devour Their Children

Keywords: Chargaff, Erwin · history of chemistry · nucleic acids

HIGHLIGHTS

More than 40 years after the isolation of vinblastine (**1**), and after considerable synthetic effort, Fukuyama et al. have now successfully completed the first de novo synthesis of this bisindole alkaloid and tumor therapeutic agent. Thus, not only should the synthesis of analogues and potentially more active compounds be possible, but the methods developed during the course of the synthesis should also expand the repertoire of the synthetic chemist.

Angew. Chem. **2002**, *114*, 4391 – 4393



1

C. Schneider* ..... 4217 – 4219

First De Novo Synthesis of the Bisindole Alkaloid Vinblastine

Keywords: alkaloids · asymmetric synthesis · radical reactions · total synthesis · vinblastine

VIPs

The following communications are "Very Important Papers" in the opinion of two referees. They will be published shortly. Short summaries of these articles can be found on the *Angewandte Chemie* homepage at the address http://www.angewandte.org

Experimental Observation and Confirmation of Icosahedral $W@Au_{12}$ and $Mo@Au_{12}$ Molecules — X. Li, B. Kiran, J. Li, H.-J. Zhai, L.-S. Wang*

Tuning the Regioselectivity in the Palladium(II)-Catalyzed Isomerization of Alkylidenecyclopropyl Ketones: A Dramatic Salt Effect — S. Ma*, J. Zhang

Porphyrazines as Molecular Scaffolds: Periphery–Core Spin Coupling Between Metal Ions of a Schiff Base Porphyrazine — M. Zhao, C. Stern, A. G. M. Barrett,* B. M. Hoffman*

Beyond the Icosahedron: The First 13-Vertex Carborane — A. Burke, D. Ellis, B. T. Giles, B. E. Hodson, S. A. Macgregor, G. M. Rosair, A. J. Welch*

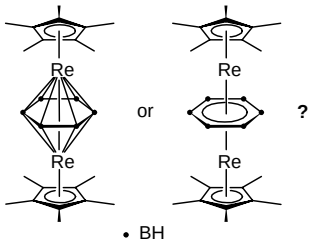
Topomerization of a Distorted-Rhomboid Tetraborane(4) and its Hydroboration to a Pentaborane(7) — C. Präsang, M. Hofmann, G. Geiseler, W. Massa, A. Berndt*

A New Diversity-Oriented Synthesis of α-Amino Acid Derivatives by a Silyltelluride-Mediated Radical Coupling Reaction of Imines and Isonitriles — S. Yamago,* H. Miyazoe, T. Nakayama, M. Miyoshi, J. Yoshida

Facile Solid-State Synthesis of Highly Conducting Poly(ethylenedioxythiophene) — H. Meng, D. F. Perepichka, F. Wudl*

 © 2002 WILEY-VCH Verlag GmbH & Co. KGaA, Weinheim 1433-7851/02/4122-4158 $ 20.00+.50/0

Cluster or triple-decker—that is the question! The recently described electron-deficient metallaboranes $[\{(C_5Me_5)Re\}_2B_nH_n]$ ($n = 6-10$; see scheme) conform neither to the Wade-Mingos' rules for clusters nor to the 18-valence-electron rule as applied to triple-decker sandwich complexes. Does this mean that these rules are no longer valid?



Angew. Chem. **2002**, *114*, 4394 – 4397

H. Wadepohl* ..... 4220 – 4223

Hypoelectronic Dimetallaboranes

Keywords: cluster compounds · electron-counting rules · isolobal relationships · metallaboranes · triple-decker sandwich complexes

COMMUNICATIONS

Chiral network: Poly(phenylacetylene) chains were derivatized with chiral side chains and bulky pentiptycene groups to give interlocking optically active aggregates (see figure; **A** forms initially and the aggregate then tightens to form **B**) in both solution and solid state. The resultant grid is a stable organization with high optical activity, high quantum yields, and superior detection limits for trinitrotoluene.



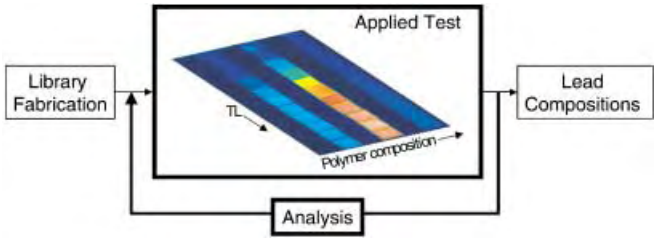
Angew. Chem. **2002**, *114*, 4399 – 4404

S. Zahn, T. M. Swager* ..... 4225 – 4230

Three-Dimensional Electronic Delocalization in Chiral Conjugated Polymers

Keywords: circular dichroism · fluorescence spectroscopy · materials science · polymers · supramolecular chemistry

A new general high-throughput screening approach is described that incorporates performance testing of materials arrays at multiple levels (see scheme; TL = test level). This approach is essential when intrinsic properties of materials do not provide knowledge about their long-term performance. The approach is illustrated by fluorescence screening of polymer compositions for their weathering, providing materials ranking up to 800 times faster than by traditional methods.



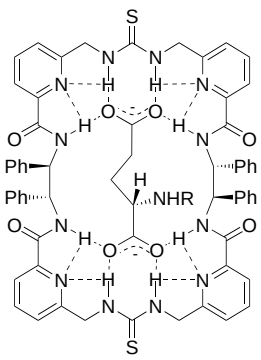
Angew. Chem. **2002**, *114*, 4404 – 4407

R. A. Potyrailo,*
J. E. Pickett ..... 4230 – 4233

High-Throughput Multilevel Performance Screening of Advanced Materials

Keywords: analytical methods · combinatorial chemistry · high-throughput screening · materials science

Solvation of the macrocycle by polar solvents leads to strong binding of an *N*-protected excitatory amino acid neurotransmitter. A 1:1 complex forms highly enantioselectively between the macrocycle and *N*-Boc-L-glutamate (as the dicarboxylate anion, see picture) in CH_3CN and DMSO (with a larger entropic driving force for binding), but no binding occurs in the less competitive solvent $CDCl_3$.



Angew. Chem. **2002**, *114*, 4407 – 4409

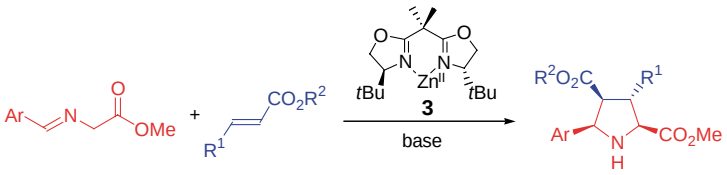
S. Rossi, G. M. Kyne, D. L. Turner, N. J. Wells, J. D. Kilburn* ... 4233 – 4236

A Highly Enantioselective Receptor for *N*-Protected Glutamate and Anomalous Solvent-Dependent Binding Properties

Keywords: amino acids · enantioselectivity · glutamate · receptors · solvent effects

 © 2002 WILEY-VCH Verlag GmbH & Co. KGaA, Weinheim 1433-7851/02/4122-4159 $ 20.00+.50/0

Highly substituted pyrrolidines 4 are formed in a highly diastereo- and enantioselective 1,3-dipolar cycloaddition reaction of azomethine ylides with electron-deficient alkenes **2**. The azomethine ylides are generated from glycinates **1** catalyzed by a chiral zinc(II) bisoxazoline catalyst **3**.



1 **2** **4**

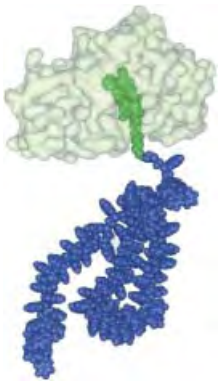
Angew. Chem. **2002**, *114*, 4410 – 4412

A. S. Gothelf, K. V. Gothelf, R. G. Hazell, K. A. Jørgensen* ..... 4236 – 4238

Catalytic Asymmetric 1,3-Dipolar Cycloaddition Reactions of Azomethine Ylides—A Simple Approach to Optically Active Highly Functionalized Proline Derivatives

Keywords: asymmetric catalysis · cycloaddition · nitrogen heterocycles · ylide · zinc

Controlled modification of horseradish peroxidase with an apolar polymer chain (see figure) by cofactor reconstitution leads to giant amphiphiles, which form vesicular aggregates in aqueous solution.



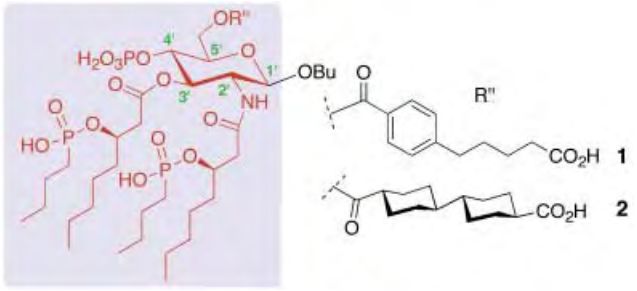
Angew. Chem. **2002**, *114*, 4413 – 4415

M. J. Boerakker, J. M. Hannink, P. H. H. Bomans, P. M. Frederik, R. J. M. Nolte,* E. M. Meijer, N. A. J. M. Sommerdijk* .... 4239 – 4241

Giant Amphiphiles by Cofactor Reconstitution

Keywords: aggregation · amphiphiles · enzyme catalysis · enzymes · polymers

Septic shock may be treated by this new immunomodulatory approach: Active immunization of mice (three strains) with synthetic lipid X bisphosphonate glycoconjugates **1** and **2** resulted in significant protection (up to 94%) against a sublethal challenge of lipid A (from *E. coli* serotype *O111:B4*).



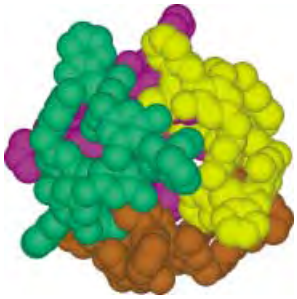
Angew. Chem. **2002**, *114*, 4415 – 4418

L. H. Jones, L. J. Altobell III, M. T. MacDonald, N. A. Boyle, P. Wentworth, Jr.,* R. A. Lerner, K. D. Janda* ..... 4241 – 4244

Active Immunization with a Glycolipid Transition State Analogue Protects against Endotoxic Shock

Keywords: endotoxicosis · glycoconjugates · immunochemistry · lipid A

Bowls to balls: Triangular bowl-shaped copper(I) circular helicates based on pyridylimine ligands are assembled by mixing readily available reagents. The bowl-shaped topography of the triangles controls the supramolecular aggregation of four of these units into a chiral tetrameric ball-shaped structure (see picture) held together by face – edge (CH···π) π interactions and CH···F interactions.



Angew. Chem. **2002**, *114*, 4418 – 4421

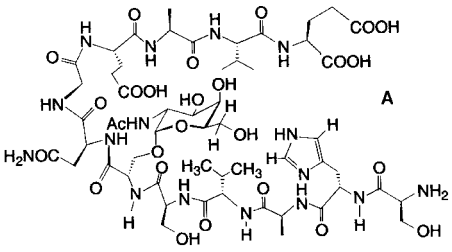
L. J. Childs, N. W. Alcock, M. J. Hannon* ..... 4244 – 4247

Assembly of a Nanoscale Chiral Ball through Supramolecular Aggregation of Bowl-Shaped Triangular Helicates

Keywords: copper · helical structures · nanostructures · self-assembly · supramolecular chemistry

 © 2002 WILEY-VCH Verlag GmbH & Co. KGaA, Weinheim 1433-7851/02/4122-4160 $ 20.00+.50/0

The conformation in water of synthetic (glyco)peptides from the recognition domain of E-cadherin determines how they interact with transformed keratinocytes. Among a peptide, a cycloglycopeptide, and a linear glycopeptide with identical sequences, only the glycopeptide with the preferred conformation **A** can induce cell differentiation.



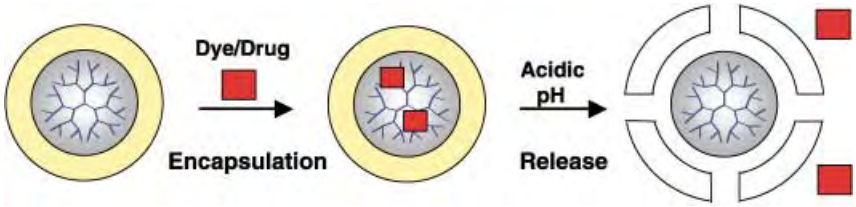
Angew. Chem. **2002**, *114*, 4423 – 4426

J. Habermann, K. Stüber, T. Skripko, T. Reipen, R. Wieser, H. Kunz* ..... 4249 – 4252

Induction of Cell Differentiation in Transformed Keratinocytes by Synthetic (Glyco)peptides from the Homophilic Recognition Domain of E-Cadherin

Keywords: cell differentiation · cycloglycopeptides · E-cadherin · glycopeptides · solid-phase synthesis

A simple and efficient concept has been developed for the synthesis of pH-responsive molecular nanocarriers based on commercially available hyperbranched polymers. These dendritic core-shell architectures can encapsulate, transport, and selectively release polar guest molecules in an acidic environment (pH 3 – 6, see scheme). The observed release properties render these molecular nanocarriers promising candidates for controlled drug and gene delivery.



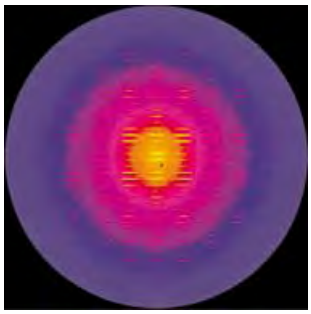
Angew. Chem. **2002**, *114*, 4426 – 4431

M. Krämer, J.-F. Stumbé, H. Türk, S. Krause, A. Komp, L. Delineau, S. Prokhorova, H. Kautz, R. Haag* ..... 4252 – 4256

pH-Responsive Molecular Nanocarriers Based on Dendritic Core-Shell Architectures

Keywords: dendrimers · drug delivery · micelles · polymers · supramolecular chemistry

Two in one: Only the combination of the analysis of diffuse X-ray scattering (see picture) and high-resolution electron microscopy reveals that the structure of $Tb_{13}Br_{18}B_3$ consists of discrete clusters as well as chains of condensed clusters.



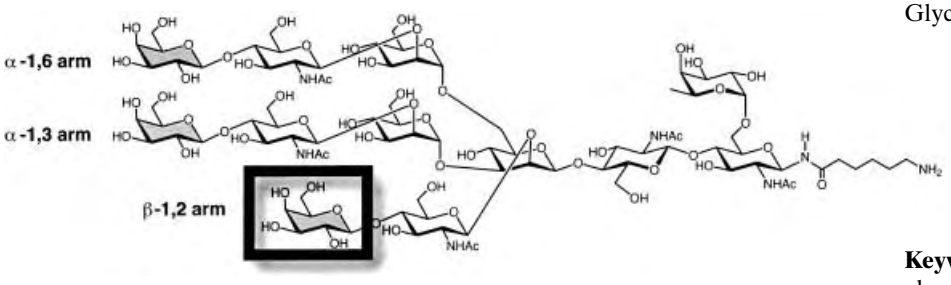
Angew. Chem. **2002**, *114*, 4431 – 4433

O. Oeckler, L. Kienle, H. Mattausch, A. Simon* ..... 4257 – 4259

$Ln_{13}Br_{18}B_3$ (Ln = Gd, Tb)—A Compound Containing a Combination of Discrete and Condensed Clusters

Keywords: boron · cluster compounds · electron microscopy · lanthanides · solid-state structures

Three arms carry more than two: By the total synthesis of the entire oligosaccharide, the proposed structure of the LEC14 antigen from a CHO cell line was confirmed. Surprisingly, enzymatic galactosylation of LEC14 gave the shown compound, which has a novel three-armed structural motif.



Angew. Chem. **2002**, *114*, 4434 – 4437

I. Prahl, C. Unverzagt* ..... 4259 – 4262

Enzymatic Elongation of the LEC14 Antigen Generates a β-1,2 Arm on *N*-Glycans

Keywords: glycans · glycosides · glycosylation · oligosaccharides · total synthesis

 © 2002 WILEY-VCH Verlag GmbH & Co. KGaA, Weinheim 1433-7851/02/4122-4161 $ 20.00+.50/0

By fusing an aptamer to a ribozyme, an aptazyme was constructed (see picture) which sensitively and specifically detects the presence of HIV-1 reverse transcriptase (RT). The fusion construct not only serves as a biosensor, but is also well suited for screening lead structures binding to the primer/template binding site of HIV-1 RT.



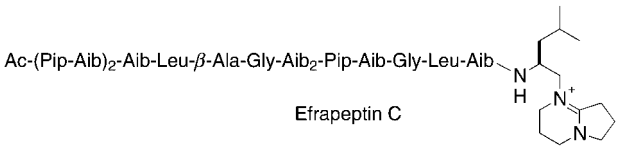
Angew. Chem. **2002**, *114*, 4440 – 4444

J. S. Hartig, M. Famulok* ... 4263 – 4266

Reporter Ribozymes for Real-Time Analysis of Domain-Specific Interactions in Biomolecules: HIV-1 Reverse Transcriptase and the Primer – Template Complex

Keywords: hammerhead ribozyme · proteins · reverse transcriptase · ribozymes · RNA · RNA – protein interactions

Synthetically challenging, the efrapeptins are a class of peptide antibiotics rich in α,α-dialkylated amino acids. Efrapeptin C (see picture) was synthesized for the first time by a combination of solution-phase and solid-phase peptide synthesis steps with segment condensations.



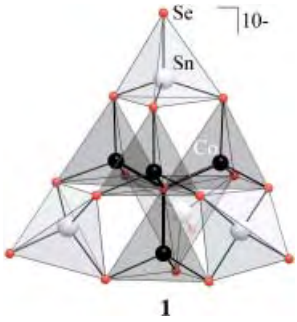
Angew. Chem. **2002**, *114*, 4438 – 4440

M. Jost, J.-C. Greie, N. Stemmer, S. D. Wilking, K. Altendorf, N. Sewald* ... 4267 – 4269

The First Total Synthesis of Efrapeptin C

Keywords: α-aminoisobutyric acid · efrapeptins · peptides · solid-phase synthesis · total synthesis

A water and methanol mixture permits the transfer of the tin – chalcogen substructure of chalcogenostannate anions into the coordination sphere of transition-metal ions without decomposition. The reaction of $K_4[SnSe_4]$ with $[Co(en)_3]Cl_3$ yields compound **1**, which contains highly charged, purely inorganic ternary anions.



1

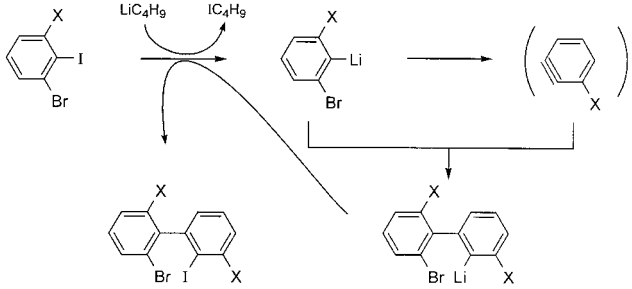
Angew. Chem. **2002**, *114*, 4444 – 4447

C. Zimmermann, M. Melullis, S. Dehnen* ... 4269 – 4272

Reactivity of Chalcogenostannate Salts: Unusual Synthesis and Structure of a Compound Containing Ternary Cluster Anions $[Co_4(\mu_4\text{-}Se)(SnSe_4)_4]^{10-}$

Keywords: chalcogens · cluster compounds · cobalt · density functional calculations · stannates · structure elucidation

1,2-Didehydroarenes ("arynes") mediate as extremely reactive, short-lived intermediates in selective aryl – aryl coupling processes to form biaryls with unprecedented substituent patterns (see scheme, X = H, F, Cl). Possible applications include the synthesis of novel ligands for asymmetric catalysis.



Angew. Chem. **2002**, *114*, 4447 – 4450

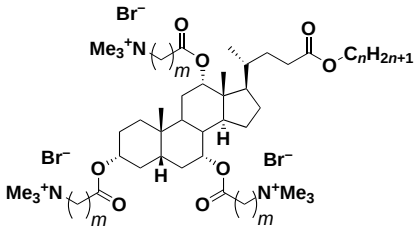
F. Leroux, M. Schlosser* .... 4272 – 4274

The "Aryne" Route to Biaryls Featuring Uncommon Substituent Patterns

Keywords: aryl – aryl coupling · arynes · atropisomerism · biaryls · lithium reagents

 © 2002 WILEY-VCH Verlag GmbH & Co. KGaA, Weinheim 1433-7851/02/4122-4162 $ 20.00+.50/0

Charged trident: A new facial amphiphile (see structure) based on cholic acid and with a permanent ionic character was prepared. The aggregation of this three-headed surfactant into small micelles and its inhibitory effect on bacterial growth are presented.



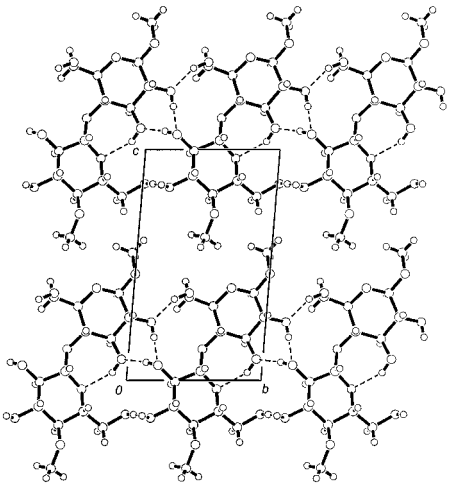
H. M. Willemen, L. C. P. M. de Smet, A. Koudijs, M. C. A. Stuart, I. G. A. M. Heikamp-de Jong, A. T. M. Marcelis,* E. J. R. Sudhölter ..... 4275 – 4277

Micelle Formation and Antimicrobial Activity of Cholic Acid Derivatives with Three Permanent Ionic Head Groups

Angew. Chem. **2002**, *114*, 4451 – 4453

Keywords: amphiphiles · antibiotics · cholic acid · micelles · self-assembly

A parallel arrangement of molecules (see figure) that can be compared to the proposed models of native cellulose I is found in crystals of triclinic methyl 4-*O*-methyl-β-D-glucopyranosyl-(1-4)-β-D-glucopyranoside. This cellobiose derivative crystallizes in the triclinic space group $P1$ and the monoclinic space group $P2_1$.



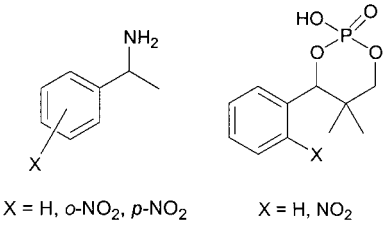
A. Rencurosi, J. Röhrling, J. Pauli, A. Potthast, C. Jäger, S. Pérez, P. Kosma, A. Imberty* ..... 4277 – 4281

Polymorphism in the Crystal Structure of the Cellulose Fragment Analogue Methyl 4-*O*-Methyl-β-D-Glucopyranosyl-(1-4)-β-D-Glucopyranoside

Angew. Chem. **2002**, *114*, 4453 – 4457

Keywords: carbohydrates · cellobiose · cellulose · polymorphism

Not double Dutch! The resolution of racemates with families of structurally related resolving agents (see examples depicted) is termed Dutch Resolution. Certain family members are regularly not incorporated; these turn out to be nucleation inhibitors. This leads to a simplified, two-component resolution procedure with a high chance of initial success.



X = H, *o*-NO_2, *p*-NO_2 X = H, NO_2

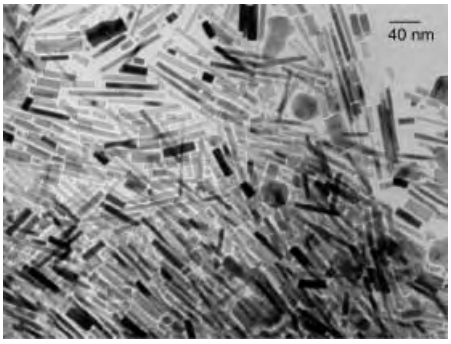
J. W. Nieuwenhuijzen, R. F. P. Grimbergen, C. Koopman, R. M. Kellogg,* T. R. Vries,* K. Pouwer, E. van Echten, B. Kaptein, L. A. Hulshof, Q. B. Broxterman* ..... 4281 – 4286

The Role of Nucleation Inhibition in Optical Resolutions with Families of Resolving Agents

Angew. Chem. **2002**, *114*, 4457 – 4462

Keywords: chiral resolution · chirality · combinatorial chemistry

The shape of things to come: Nanospheres, thermodynamically stable nanorods, and nanowires are selectively produced in solution from $[Co(\eta^3\text{-}C_8H_{13})(\eta^4\text{-}C_8H_{12})]$ in the presence of oleic acid and various amines. The aspect ratio of the nanorods is controlled by the length of the alkyl chain of the amine. Nanorods with approximate dimensions of 9×40 nm (see Figure) are ferromagnetic at room temperature.



F. Dumestre, B. Chaudret,* C. Amiens, M.-C. Fromen, M.-J. Casanove, P. Renaud, P. Zurcher ..... 4286 – 4289

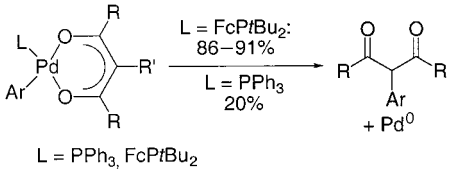
Shape Control of Thermodynamically Stable Cobalt Nanorods through Organometallic Chemistry

Angew. Chem. **2002**, *114*, 4462 – 4465

Keywords: cobalt · magnetic properties · nanostructures · organometallic synthesis · self-assembly

 © 2002 WILEY-VCH Verlag GmbH & Co. KGaA, Weinheim 1433-7851/02/4122-4163 $ 20.00+.50/0

Steric hindrance of the ancillary phosphane ligand triggers reductive elimination from aryl palladium complexes of typically unreactive ligands derived from 1,3-dicarbonyl anions [Eq. (1); $FcPtBu_2$ = di-*tert*-butylphosphanylferrocene]. This reaction is the product-forming step of the recently developed palladium-catalyzed malonate arylations.



(1)

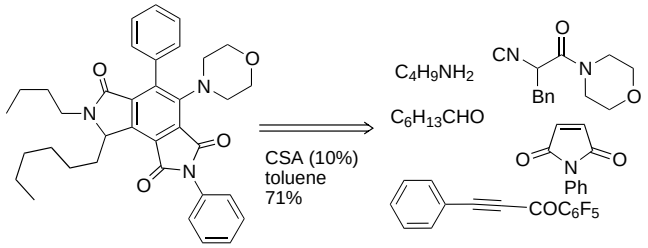
Angew. Chem. **2002**, *114*, 4465 – 4467

J. P. Wolkowski,
J. F. Hartwig* ..... 4289 – 4291

Generation of Reactivity from Typically Stable Ligands: C–C Bond-Forming Reductive Elimination from Aryl Palladium(II) Complexes of Malonate Anions

Keywords: arylation · C–C coupling · elimination · malonate · palladium

Seven functional groups are involved in a highly ordered five-component domino process, which leads to a biologically relevant polyheterocycle. In this one-pot transformation, the formation of seven chemical bonds provides a hexasubstituted benzene core (see scheme; CSA = camphorsulfonic acid).



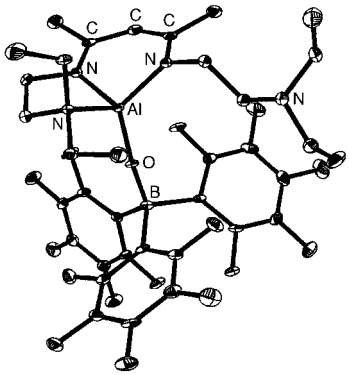
Angew. Chem. **2002**, *114*, 4467 – 4470

P. Janvier, H. Bienaymé,
J. Zhu* ..... 4291 – 4294

A Five-Component Synthesis of Hexasubstituted Benzene

Keywords: cycloaddition · domino reactions · heterocycles · multicomponent reactions · synthetic methods

Stabilization of the presumed Al–O double bond in $LAlO \cdot B(C_6F_5)_3$, the simplest member of the alumoxane series, was achieved by the strong Lewis acid $B(C_6F_5)_3$. $LAlO \cdot B(C_6F_5)_3$ was synthesized by hydrolysis of $LAlMe_2$ with $H_2O \cdot B(C_6F_5)_3$ and characterized by X-ray structure analysis (see picture) L = $Et_2NCH_2CH_2NC(Me)CHC(Me)NCH_2CH_2NEt_2$.



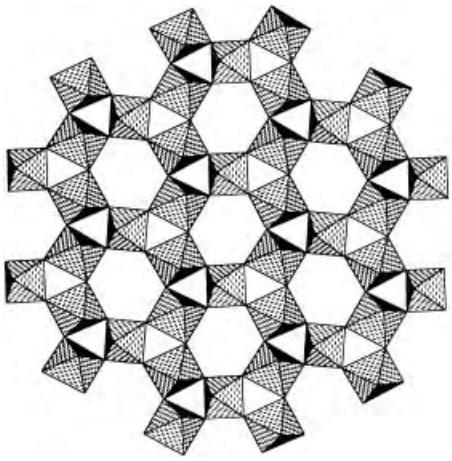
Angew. Chem. **2002**, *114*, 4470 – 4472

D. Neculai, H. W. Roesky,*
A. M. Neculai, J. Magull, B. Walfort,
D. Stalke ..... 4294 – 4296

Formation and Characterization of the First Monoalumoxane, $LAlO \cdot B(C_6F_5)_3$

Keywords: aluminum · Lewis acids · monoalumoxane · multiple bonds

A perfect Kagomé lattice is displayed by the mixed-valent layered structure of $[HN(CH_2)_6NH][Fe^{III}Fe^{II}_2F_6(SO_4)_2] \cdot [H_3O]$ (see picture), in which 100% of the iron sites are occupied. The complex exhibits unusual magnetic properties; both magnetic frustration and ferrimagnetic behavior are observed.



Angew. Chem. **2002**, *114*, 4473 – 4476

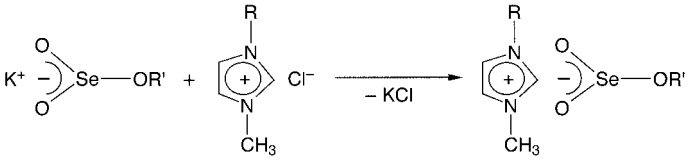
G. Paul, A. Choudhury,
E. V. Sampathkumaran,
C. N. R. Rao* ..... 4297 – 4300

Organically Templated Mixed-Valent Iron Sulfates Possessing Kagomé and Other Types of Layered Networks

Keywords: hydrothermal synthesis · iron · Kagomé lattice · layered structures · magnetic properties

 © 2002 WILEY-VCH Verlag GmbH & Co. KGaA, Weinheim 1433-7851/02/4122-4164 $ 20.00+.50/0

Highly active catalysts for the carbonylation of a variety of substrate materials have been prepared in the form of selenium-containing ionic liquids. Products from the reactions of [$KSeO_2(OCH_3)$] and 1-alkyl-3-methylimidazolium chlorides (see scheme) exhibit surprisingly high activity for the oxidative carbonylation of aniline, even at temperatures as low as 40 °C.



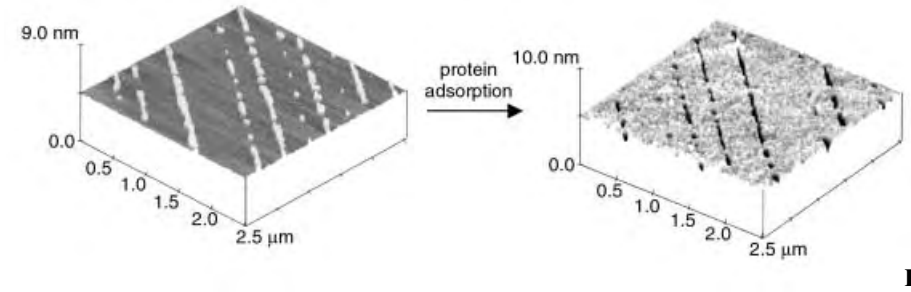
Angew. Chem. **2002**, *114*, 4476 – 4479

H. S. Kim,* Y. J. Kim, H. Lee, K. Y. Park, C. Lee, C. S. Chin ..... 4300 – 4303

Ionic Liquids Containing Anionic Selenium Species: Applications for the Oxidative Carbonylation of Aniline

Keywords: carbonylation · cyclic voltammetry · homogeneous catalysis · ionic liquids · selenium

Selective adsorption of human serum albumin and human γ globulin to the liquidlike phase of chemically homogeneous, mixed phospholipid monolayers supported on a solid surface gives rise to arrays of linear 150 – 200-nm-wide grooves (see images). The protein-covered areas could be metallized by the adsorption of Au nanoparticles.



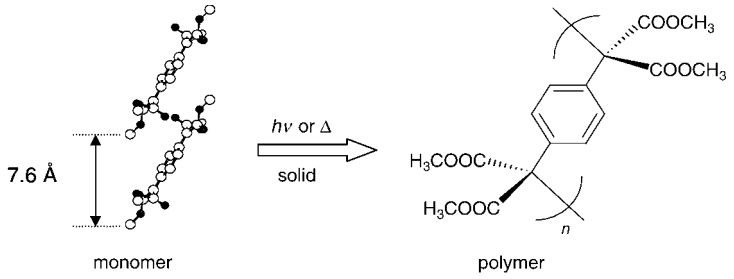
Angew. Chem. **2002**, *114*, 4479 – 4482

P. Moraille, A. Badia* ..... 4303 – 4306

Spatially Directed Protein Adsorption by Using a Novel, Nanoscale Surface Template

Keywords: adsorption · monolayers · nanostructures · phospholipids · proteins

The difference in the crystal-packing mode of a monomer can significantly affect its polymerization reactivity. Synthesis of 7,7,8,8-tetrakis(methoxycarbonyl)quinodimethane (**1**) afforded two polymorphs: prisms (**1a**), and needles (**1b**). The former, **1a**, polymerized topochemically under thermal polymerization and photopolymerization (see scheme) but **1b** did not.



Angew. Chem. **2002**, *114*, 4482 – 4485

T. Itoh,* S. Nomura, T. Uno, M. Kubo, K. Sada, M. Miyata* ..... 4306 – 4309

Topochemical Polymerization of 7,7,8,8-Tetrakis(methoxycarbonyl)quinodimethane

Keywords: polymerization · polymorphism · quinodimethanes · topochemistry

 © 2002 WILEY-VCH Verlag GmbH & Co. KGaA, Weinheim 1433-7851/02/4122-4165 $ 20.00+.50/0

The 2(N+1)^2 electron-counting rule for spherical aromaticity can also be applied to spherical homoaromatic systems: The adamantane-, cubane-, and dodecahedrane-based species containing two or eight delocalized electrons were designed by bridging the sp^2 carbon atoms of highly symmetrical (T_d, T_h) carbon polyhedrane units. Their aromatic character was demonstrated by the highly negative nucleus-independent chemical shift (NICS) values at the cage centers, for example $C_{20}H_{12}$ (see picture) has an NICS value of -36.4 ppm.



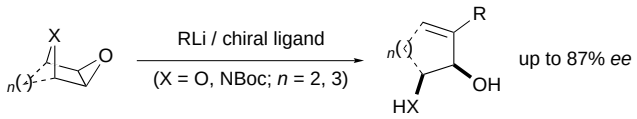
Z. Chen, H. Jiao, A. Hirsch,*
P. von Ragué Schleyer* ..... 4309 – 4312

Spherical Homoaromaticity

Angew. Chem. **2002**, *114*, 4485 – 4488

Keywords: aromaticity · cage compounds · electron-counting rules · NICS · spherical homoaromaticity

Enantioselective generation and intermolecular trapping of a lithium carbenoid occurs in the reaction of epoxides of 2,5-dihydrofuran, 2,5-dihydropyrrole, and oxa- and aza-bicyclo[*n*.2.1]alkenes ($n = 2, 3$) with organolithium compounds in the presence of external chiral ligands. This methodology leads to the synthesis of important unsaturated diol and amino alcohol functionality (see scheme; *tert*-butoxycarbonyl).



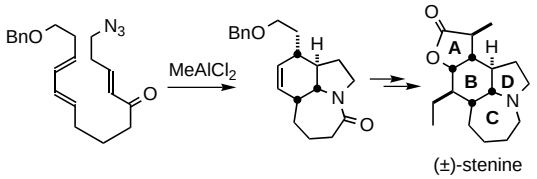
D. M. Hodgson,* C. R. Maxwell, T. J. Miles, E. Paruch, M. A. H. Stent, I. R. Matthews, F. X. Wilson, J. Witherington ..... 4313 – 4316

Enantioselective Alkylative Double Ring Opening of Epoxides: Synthesis of Enantioenriched Unsaturated Diols and Amino Alcohols

Angew. Chem. **2002**, *114*, 4489 – 4492

Keywords: alkenes · amino alcohols · diols · enantioselectivity · epoxides

Four stereocenters and three rings are established in one step in a new formal synthesis of (±)-stenine (see scheme). This key reaction cascade consists of an intramolecular Diels – Alder reaction followed by an intramolecular Schmidt reaction. The resulting tricyclic intermediate was readily transformed into a known intermediate en route to stenine, thus completing the formal synthesis.



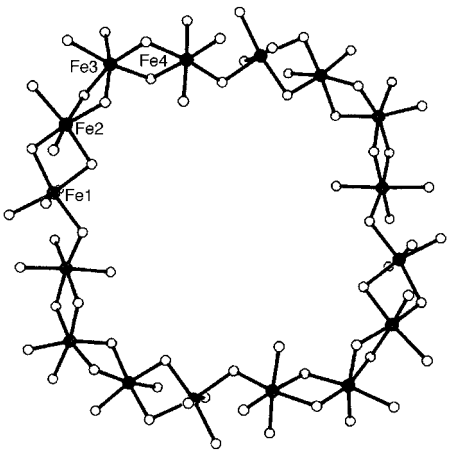
J. E. Golden, J. Aubé* ..... 4316 – 4318

A Combined Intramolecular Diels – Alder/Intramolecular Schmidt Reaction: Formal Synthesis of (±)-Stenine

Angew. Chem. **2002**, *114*, 4492 – 4494

Keywords: Diels – Alder reaction · domino reactions · lactams · natural products · ring expansion

Wheels of iron: The synthesis, structure, and initial magnetic properties of two new ferric wheels are reported; these are the first examples of unsupported octametallic and hexadecametallic (see picture) iron wheels.



L. F. Jones, A. Batsanov, E. K. Brechin,* D. Collison,* M. Helliwell, T. Mallah, E. J. L. McInnes, S. Piligkos . 4318 – 4321

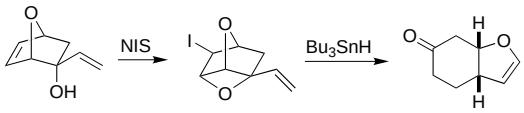
Octametallic and Hexadecametallic Ferric Wheels

Angew. Chem. **2002**, *114*, 4494 – 4497

Keywords: cluster compounds · EPR spectroscopy · iron · magnetic properties · metal – metal interactions

 © 2002 WILEY-VCH Verlag GmbH & Co. KGaA, Weinheim 1433-7851/02/4122-4166 $ 20.00+.50/0

A radical alternative to the anionic oxy-Cope rearrangement is reported (e.g., see scheme; NIS = *N*-iodosuccinimide). In contrast to the sigmatropic rearrangement, this nonconcerted fragmentation–cyclization process is independent of the stereochemistry of the starting material.



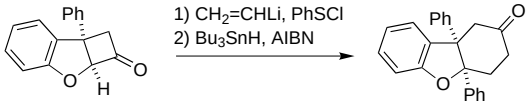
Angew. Chem. **2002**, *114*, 4497–4499

R. Chuard, A. Giraud, P. Renaud* 4321–4323

A Radical Alternative to the Anionic Oxy-Cope Rearrangement

Keywords: domino reactions · radical reactions · sigmatropic rearrangement

The two-carbon ring expansion of cycloalkanones is now possible in a two-step procedure. This procedure is based on an unusual cascade reaction that consists of a [2,3]-sigmatropic rearrangement (Mislow–Braverman–Evans rearrangement) of an allylic sulfoxide followed by a radical fragmentation–cyclization process (see scheme; AIBN = azobisisobutyronitrile).



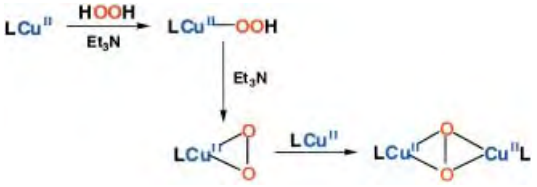
Angew. Chem. **2002**, *114*, 4499–4501

R. Chuard, A. Giraud, P. Renaud* 4323–4325

Allyl Sulfoxides as Precursors for Radical Two-Carbon Ring Expansion of Cyclobutanones

Keywords: ketones · radical reactions · ring expansion · sigmatropic rearrangement · sulfoxides

A mononuclear (η^2-peroxo)copper(II) complex is observed in the reaction of H_2O_2 and a copper(II) complex supported by a tridentate pyridylethylamine ligand (see scheme). The formation of this unprecedented intermediate species can be followed at $-90\,^{\circ}C$ by EPR and UV/Vis absorption spectroscopy.



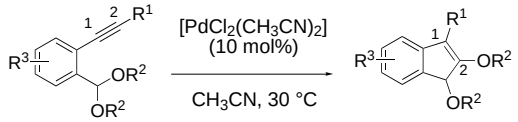
Angew. Chem. **2002**, *114*, 4501–4504

T. Osako, S. Nagatomo, Y. Tachi, T. Kitagawa, S. Itoh* 4325–4328

Low-Temperature Stopped-Flow Studies on the Reactions of Copper(II) Complexes and H_2O_2: The First Detection of a Mononuclear Copper(II)–Peroxo Intermediate

Keywords: copper · kinetics · ligand effects · peroxides · stopped-flow studies

Activated ethers: The shown reaction of the dialkylacetals **1** gave the carboalkoxylation products **2** in high to moderate yields. Mechanistic investigation revealed that the reaction proceeded through the addition of an acetal C–O bond to the C–C triple bond, followed by an unprecedented rearrangement of an alkynyl group substituent.



1 **2**

Angew. Chem. **2002**, *114*, 4504–4507

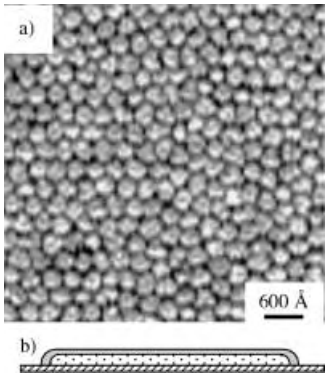
I. Nakamura, G. B. Bajracharya, Y. Mizushima, Y. Yamamoto* 4328–4331

Indenol Ether Formation from Aryl Alkynes Bearing *ortho*-Acetals: An Unprecedented Rearrangement in Palladium-Catalyzed Carboalkoxylation

Keywords: acetals · alkynes · palladium · rearrangement · synthetic methods

 © 2002 WILEY-VCH Verlag GmbH & Co. KGaA, Weinheim 1433-7851/02/4122-4167 $ 20.00+.50/0

A small nonpolar amphiphile, namely, the semifluorinated alkane $C_8F_{17}C_{16}H_{33}$, forms monodisperse surface micelles [ca. 300 Å in diameter; see AFM image (a)] in which the fluorinated segments point outwards and the hydrocarbon segments inwards. A disklike model (b) allows the micelle size to be predicted from the lengths of the fluorinated and hydrocarbon segments of such molecules.



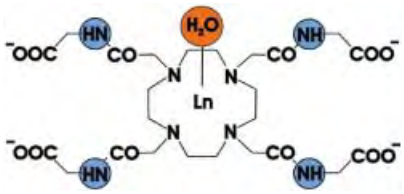
Angew. Chem. **2002**, *114*, 4507 – 4510

M. Maaloum, P. Muller, M. P. Krafft* ..... 4331 – 4334

Monodisperse Surface Micelles of Nonpolar Amphiphiles in Langmuir Monolayers

Keywords: amphiphiles · micelles · monolayers · self-assembly · semifluorinated alkanes

Attractive alternatives to conventional contrast agents for magnetic resonance imaging applications are the paramagnetic chemical exchange saturation transfer (CEST) agents based on saturation transfer (ST) to the solvent water resonance. The ratio of ST effects obtained upon irradiating Ln-coordinated water and amide protons in [Ln(dotamGly)] (dotam = 1,4,7,10-tetrakis(carbamoylmethyl)-1,4,7,10-tetrazacyclododecane; see picture) complexes is pH dependent and concentration independent.



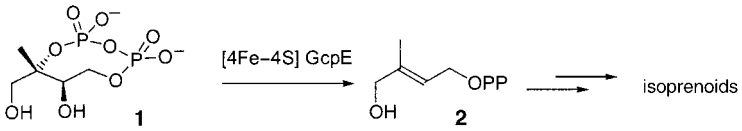
Angew. Chem. **2002**, *114*, 4510 – 4512

S. Aime,* D. Delli Castelli, E. Terreno ..... 4334 – 4336

Novel pH-Reporter MRI Contrast Agents

Keywords: imaging agents · lanthanides · NMR spectroscopy · pH sensors · saturation transfer

One of the last bottlenecks in the elucidation of the methylerythritol phosphate pathway for isoprenoid biosynthesis has been solved. A [4Fe – 4S] cluster is the prosthetic group of the GcpE protein from *E. coli*. This enzyme is involved in the conversion of **1** into **2**, through two successive one-electron transfers.



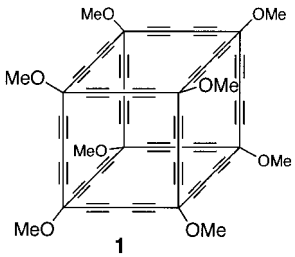
Angew. Chem. **2002**, *114*, 4513 – 4515

M. Seemann, B. T. S. Bui, M. Wolff, D. Tritsch, N. Campos, A. Boronat, A. Marquet, M. Rohmer* ... 4337 – 4339

Isoprenoid Biosynthesis through the Methylerythritol Phosphate Pathway: The (*E*)-4-Hydroxy-3-methylbut-2-enyl Diphosphate Synthase (GcpE) is a [4Fe – 4S] Protein

Keywords: biosynthesis · electron transfer · enzymes · isoprenoids

Formal insertion of buta-1,3-diynediyl moieties into all twelve C–C single bonds of octamethoxycubane gives the explosive expanded cubane **1**. Fourier-transform ion-cyclotron-resonance (FT-ICR) mass spectrometric studies show that **1** readily loses its eight MeO groups and subsequently rearranges into fullerene ions. In the positive ion mode, these ions undergo fullerene coalescence reactions.



Angew. Chem. **2002**, *114*, 4515 – 4519

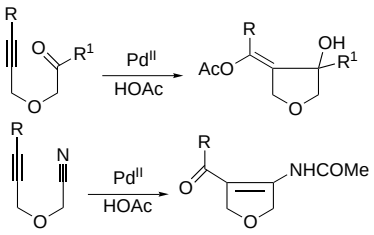
P. Manini, W. Amrein, V. Gramlich, F. Diederich* ..... 4339 – 4343

Expanded Cubane: Synthesis of a Cage Compound with a C_{56} Core by Acetylenic Scaffolding and Gas-Phase Transformations into Fullerenes

Keywords: alkynes · cage compounds · cubanes · fullerenes · mass spectrometry

 © 2002 WILEY-VCH Verlag GmbH & Co. KGaA, Weinheim 1433-7851/02/4122-4168 $ 20.00+.50/0

The insertion of carbonyl or nitrile units into a carbon–palladium bond has been achieved under mild reaction conditions (see scheme). The Pd^{II}-catalyzed system, which does not require organometallic reagents, redox systems, or additives to obtain a high yield of cyclized product, is effective with a wide variety of functionalized alkyne compounds.



L. Zhao, X. Lu* 4343–4345

Pd^{II}-Catalyzed Cyclization of Alkynes Containing Aldehyde, Ketone, or Nitrile Groups Initiated by the Acetoxypalladation of Alkynes

Angew. Chem. **2002**, *114*, 4519–4521

Keywords: carbonyl ligands · insertion · nitrile group · N ligands · palladium

Supporting information on the WWW (see article for access details).

Accelerated publications

* Author to whom correspondence should be addressed

BOOKS

Pharmacokinetics and Metabolism in Drug Design — Dennis A. Smith, Han van de Waterbeemd, Don K. Walker — *J. Maas* 4347

Near-Infrared Spectroscopy — H. W. Siesler, Y. Ozaki, S. Kawata, H. M. Heise — *R. Salzer* 4347

Chemical Properties of Material Surfaces — Marek Kosmulski — *W. von Rybinski* 4348

Encyclopedia of Electrochemistry. Vol. 6: Semiconductor Electrodes and Photoelectrochemistry — Allen J. Bard, Martin Stratmann, Stuart Licht — *H. Kisch* 4349

Optical Sensors and Switches — V. Ramamurthy, Kirk S. Schanze — *G. Orellana* 4350

WEB SITES

http://www.proweb.org/kinesin/ — Constantly on the Move — *G. Lattanzi* 4351

SERVICE

- **VIPs** 4158
- ***Angewandte's* Sister-Journals** 4171–4173
- **Keywords** 4352
- **Authors** 4353
- **Preview** 4354

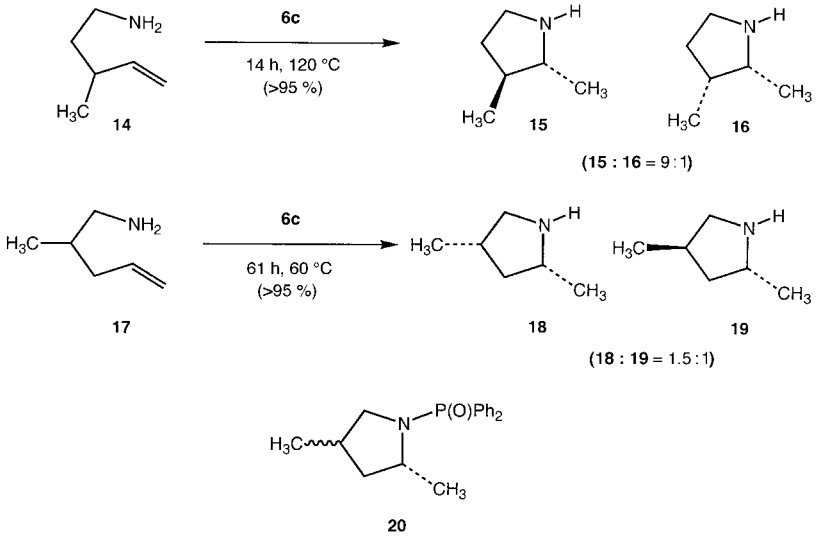
Don't forget all the Tables of Contents from 1998 onwards may be still found on the WWW under: http://www.angewandte.org

Issue 21, 2002 was published online on October 31.

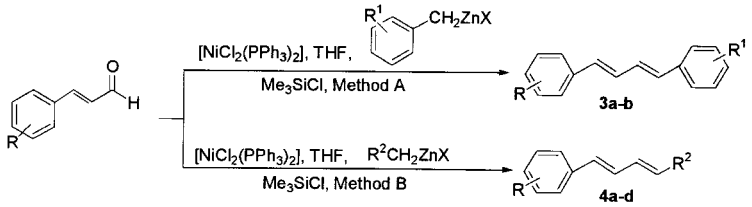
 © 2002 WILEY-VCH Verlag GmbH & Co. KGaA, Weinheim 1433-7851/02/4122-4169 $ 20.00+.50/0

In the Review by **A. Schnepf** and **H. Schnöckel** in Issue 19, **2002**, pp. 3533 – 3552, two formulas were accidentally swapped in Section 4.4.2. The cluster $[Ga_{10}R_6]^-$ (R = Si*t*Bu) should be number **23** and the cluster $[Ga_{10}R_6]$ (R = $Si(SiMe_3)_3$) should be number **22**.

In the Communication by **Y. K. Kim** and **T. Livinghouse** in Issue 19, **2002**, pp. 3645 – 3647, the incorrect complex number was printed above the reaction arrows in Scheme 4: **6 f** should be replaced by **6 c**. The editorial team apologizes for this error.



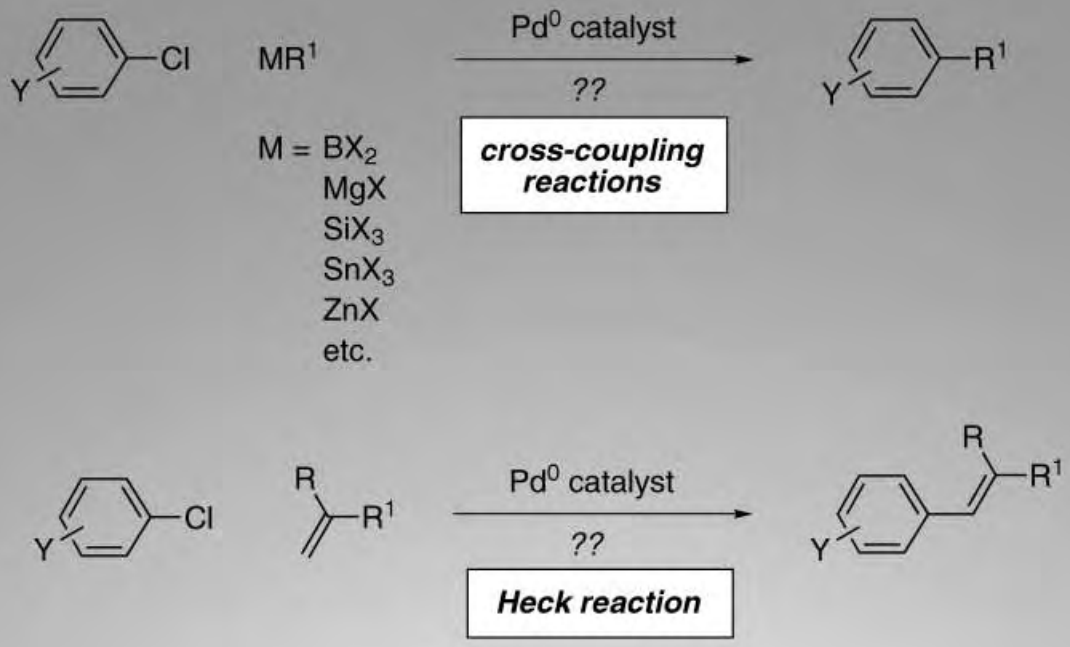
In the Communication by **J.-X. Wang et al.** in Issue 15, **2002**, pp. 2757 – 2760 the lower section of Scheme 1 should have appeared as follows:



In addition, the compounds labeled **1** – **8** in Scheme 2 are distinct from any other numbered species in either the main text, the Experimental Section, or the Supporting Information.

 © 2002 WILEY-VCH Verlag GmbH & Co. KGaA, Weinheim 1433-7851/02/4122-4170 $ 20.00+.50/0 *Angew. Chem. Int. Ed.* **2002**, *41*, No. 22

Palladium-Catalyzed Coupling Reactions of Aryl Chlorides

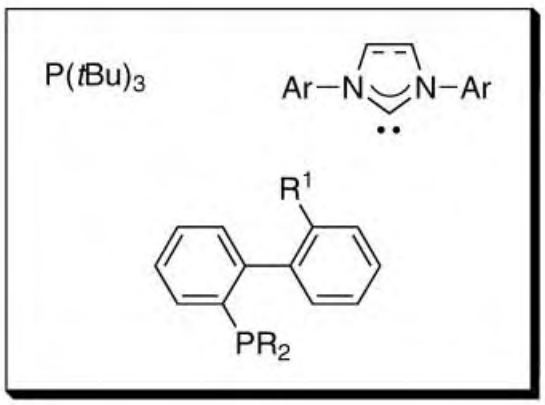


State-of-the-art

1998: *Essentially no general methods*

2002: *Mild and versatile catalysts*

Key: choice of ligand



ANGEWANDTE CHEMIE ©WILEY-VCH

Palladium-Catalyzed Coupling Reactions of Aryl Chlorides

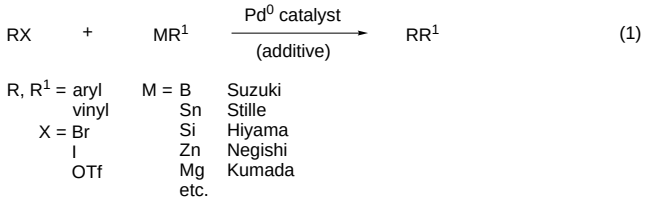
Adam F. Littke and Gregory C. Fu*

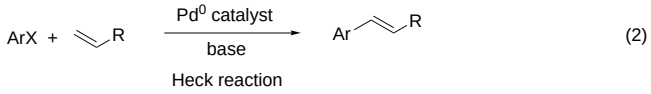
Collectively, palladium-catalyzed coupling reactions represent some of the most powerful and versatile tools available to synthetic organic chemists. Their widespread popularity stems in part from the fact that they are generally tolerant to a large number of functional groups, which allows them to be employed in a wide range of applications. However, for many years a major limitation of palladium-catalyzed coupling processes has been the poor reactivity of aryl chlorides, which from the standpoints of cost and availability are more attractive substrates than the corresponding bromides, iodides, and triflates. Traditional palladium/triarylphosphane catalysts are only effective for the coupling of certain activated aryl chlorides (for example, heteroaryl chlorides and substrates that bear electron-withdrawing groups), but not for aryl chlorides in general. Since 1998, major advances have been described by a number of research groups addressing this challenge; catalysts based on bulky, electron-rich phosphanes and carbenes have proved to be particularly mild and versatile. This review summarizes both the seminal early work and the exciting recent developments in the area of palladium-catalyzed couplings of aryl chlorides.

Keywords: catalysis · cross-coupling · ligand effects · palladium · synthetic methods

1. Introduction

During the final quarter of the twentieth century, palladium catalysts emerged as extremely powerful tools for the construction of carbon–carbon [Eq. (1) and Eq. (2)], as well





as carbon–heteroatom, bonds.[1] Numerous monographs and review articles have documented the increasing frequency with which palladium-catalyzed coupling processes are applied to a wide array of endeavors, which range from synthetic organic chemistry to materials science. Their popularity stems in part from their tolerance of many functional groups, which allows them to be employed in the synthesis of highly complex molecules.[2]

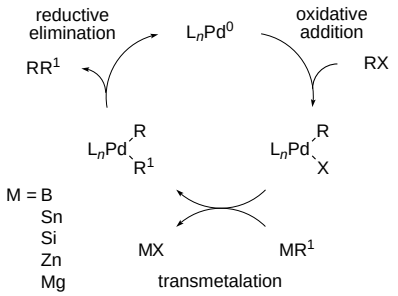
Until recently, nearly all reports of palladium-catalyzed couplings described the use of organic bromides, iodides, and triflates as substrates—organic chlorides were noticeably uncommon partners, despite the fact that, among the halides, chlorides are arguably the most useful single class of substrates, because of their lower cost and the wider diversity of available compounds.[3] Unfortunately, chlorides were generally unreactive under the conditions employed to couple bromides, iodides, and triflates.[4, 5]

The low reactivity of chlorides is usually attributed to the strength of the C–Cl bond (bond dissociation energies for Ph–X: Cl: 96 kcal mol^{-1}; Br: 81 kcal mol^{-1}; I: 65 kcal mol^{-1}),[3] which leads to reluctance by aryl chlorides to oxidatively add to Pd^0 centers, a critical initial step in palladium-catalyzed coupling reactions (Schemes 1 and 2).[6, 7]

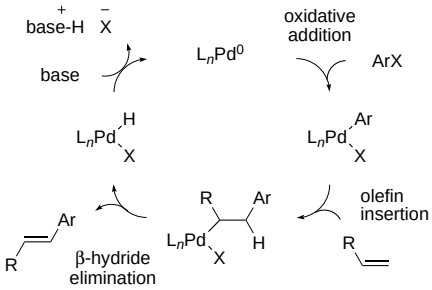
Fortunately, remarkable progress has been achieved since 1998 in the development of palladium-based catalysts that can in fact accomplish cross-couplings and Heck reactions of a wide array of chlorides. In this review, we summarize these exciting recent discoveries, as well as some of the seminal studies that laid the groundwork for these advances.[8]

[*] Prof. G. C. Fu, A. F. Littke
Massachusetts Institute of Technology
Department of Chemistry
77 Massachusetts Avenue, Room 18-411
Cambridge, MA 02139-4307 (USA)
Fax: (+1) 617-258-7500
E-mail: gcf@mit.edu

 © 2002 WILEY-VCH Verlag GmbH & Co. KGaA, Weinheim 1433-7851/02/4122-4177 $ 20.00+.50/0



Scheme 1. Generalized mechanism for palladium-catalyzed cross-coupling reactions.



Scheme 2. Mechanism of the Heck reaction.

2. Carbon–Carbon Bond-Forming Reactions

2.1. Cross-Coupling Reactions

The palladium-catalyzed cross-coupling of aryl and vinyl halides/triflates with organometallic reagents serves as a straightforward and powerful method for formation of carbon–carbon bonds (Eq. (1) and Scheme 1). The R^1 group of the organometallic reagent can be any of a variety of saturated or unsaturated groups, for example, alkyl, aryl, vinyl, and alkynyl. Most magnesium, tin, and zinc reagents are sufficiently reactive to undergo transmetalation with palladium without the need for an additive; boron and silicon reagents, on the other hand, are usually reluctant to transmetalate in the absence of an activator. As a consequence, Suzuki and Hiyama cross-couplings are typically carried out in the presence of an additive, the role of which is to form a higher valent, more reactive "ate" complex.

2.1.1. Suzuki Reactions

Among palladium-catalyzed cross-coupling processes, the Suzuki reaction of aryl and vinyl halides/triflates with boronic acids is emerging as a favorite,[9] and it has been applied industrially to the production of compounds such as losartan, a Merck antihypertensive drug.[10] This popularity is attributable to a variety of factors, such as the commercial availability of a large number of boronic acids, as well as their nontoxic nature and stability to heat, air, and moisture. Furthermore, the boron-containing by-product of the Suzuki cross-coupling can readily be separated from the desired compound.

2.1.1.1. Suzuki Reactions of Activated Aryl Chlorides

As for many other palladium-catalyzed coupling processes, certain aryl chlorides, specifically, electron-poor aryl chlorides, which are activated toward oxidative addition, have long been known to serve as suitable substrates for Suzuki reactions. Thus, Suzuki couplings of heteroaryl chlorides such as chloropyridines can often be achieved with traditional triarylphosphane-based palladium catalysts.[11] This reactivity is especially significant because of the abundance of chlorine-containing nitrogen heterocycles (as compared with bromine- or iodine-containing nitrogen heterocycles) that are commercially available.

One of the earliest examples of a Suzuki reaction of a heteroaryl chloride was provided by Gronowitz et al., who

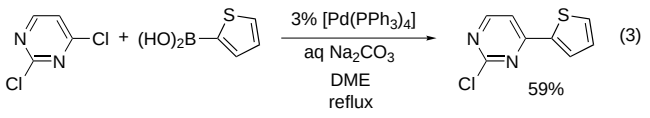
Gregory C. Fu was born in Galion, Ohio in 1963. He received an S.B. degree in 1985 from MIT, where he studied in the laboratory of Prof. K. Barry Sharpless. He earned a PhD in 1991 under the guidance of Prof. David A. Evans at Harvard, and he then spent two years as a postdoctoral fellow with Prof. Robert H. Grubbs at Caltech. In 1993, he returned to MIT as an Assistant Professor of Chemistry. He was promoted to Associate Professor in 1998 and to Professor in 1999. His research program is focused on the development of enantioselective nucleophilic catalysts, the design of chiral ligands for transition metals, and the discovery of new catalysts for palladium-catalyzed coupling reactions.


G. C. Fu


A. F. Littke

Adam F. Littke was born in Toronto, Canada in 1974. He earned his B.Sc. in 1997 from the University of Ottawa, where he worked in the laboratory of Prof. Darrin S. Richeson. In 2002, he received his PhD from the Massachusetts Institute of Technology, where he studied under the direction of Prof. Gregory C. Fu. He initiated the group's program in palladium-catalyzed coupling reactions, and focused his efforts on Suzuki, Stille, and Heck reactions of aryl chlorides. He is currently employed as a process chemist at Bristol–Myers Squibb in New Jersey.

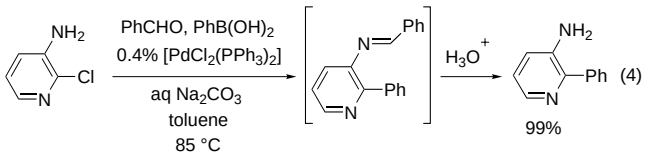
examined the coupling of 2,4-dichloropyrimidine with 2-thienylboronic acid and established that the 4-chloro group is more reactive than the 2-chloro group [Eq. (3)].[12, 13] Subsequently, other chloro-substituted nitrogen heterocycles



(3)

have been shown to undergo Suzuki coupling in the presence of traditional palladium catalysts including pyridines,[13a–c, 14] pyridine *N*-oxides,[14h] pyrazines,[12d, 13b–d, 15] pyridazines,[12d, 16] triazines,[13e, g, 17] quinolines,[13c, 18] isoquinolines,[13a, 19] quinazolines,[20] cinnolines,[20b] phthalazines,[21] β-carbolines,[22] phenanthrolines,[23] imidazo[1,2-*b*]pyridazines,[24] pyrazolo[1,5-*a*]-pyrimidines,[18b] pyrazolopyrimidines,[13e] triazolopyrimidines,[13e] pyrrolopyrimidines,[13e] and purines.[25]

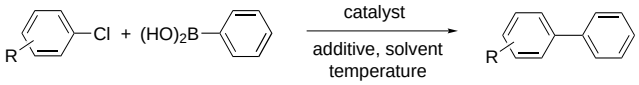
The use of a Suzuki reaction of a heteroaryl chloride to produce 2-phenyl-3-aminopyridine, a key intermediate in the synthesis of 2-phenyl-3-aminopiperidine (an important pharmacophore present in potent non-peptidic NK1 receptor antagonists) has recently been reported. Direct coupling of 2-chloro-3-aminopyridine with phenylboronic acid was unsuccessful; however, a one-pot protection/Suzuki coupling/deprotection sequence furnished the target compound in excellent yield on a greater than 100-gram scale [Eq. (4)].[26]

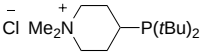
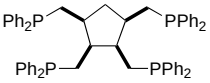
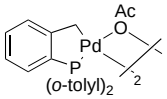
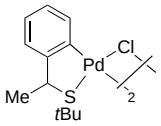
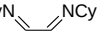
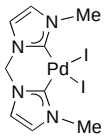


(4)

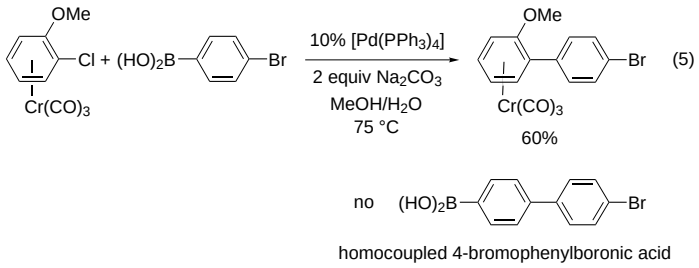
Within the last decade, a number of examples of Suzuki reactions of non-heteroaryl electron-deficient aryl chlorides have been described, and some representative couplings are depicted in Table 1. Equation (5) furnishes a particularly interesting illustration of the activation that can be provided by a powerful electron-withdrawing group. Thus, Uemura et al. have shown that aryl chlorides that are η^6-bound to $Cr(CO)_3$ are remarkably reactive coupling partners in Suzuki reactions.[27, 28] The aryl chloride couples with an aryl boronic acid even in the presence of the electron-donating, deactivating *ortho*-methoxy substituent. Furthermore, no homocou-

Table 1. Suzuki cross-couplings of activated aryl chlorides.



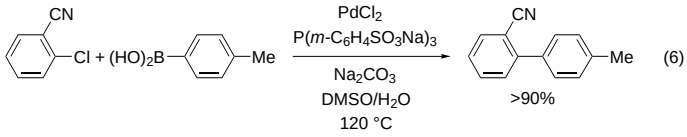
Entry	R	Catalyst	Conditions	Yield [%]
1	4-CN	$Pd(OAc)_2$/ 	Na_2CO_3, H_2O/MeCN, 80 °C	92
2	4-NO_2, CN, 2-CN, 2-Cl-, 3-Cl-pyridine	$PdCl_2$ · polymer-CH_2PPh_2	aq K_3PO_4, toluene, 80 °C	72 – 91[a]
3	4-NO_2, COMe, CF_3, CN, CHO, 2-COMe, CF_3, CN, CHO	$[PdCl(allyl)]_2$/ 	K_2CO_3, xylene, 130 °C	13 – 100
4	4-COMe		K_2CO_3, *o*-xylene, 130 °C	82
5	4-COMe, CN, NO_2		K_3PO_4, DMF, 25, 130 °C	90 – 95[b]
6	4-COMe, CN, CF_3, 3-CHO, COMe, NO_2, 2-CO_2Me, NO_2, CHO	$Pd(OAc)_2$/dppp or $[PdCl_2(PCy_3)_2]$	CsF, NMP, 100 °C	42 – 97
7	4-COMe, 3-CF_3, 2-CN	$Pd(OAc)_2$/$P(OiPr)_3$	Na_2CO_3 or NaOH, toluene, 120 °C	78 – 94
8	4-COMe, CO_2Me	$Pd(OAc)_2$/ 	Cs_2CO_3, dioxane, 100 °C	85 – 98
9	4-CN, NO_2	$Pd(OAc)_2$	K_3PO_4, DMF, 25, 130 °C	85 – 100[b]
10	4-CN, COMe, NO_2, CF_3	Pd/C	K_2CO_3, DMA/H_2O, 80 °C	79 – 95
11	4-COMe		K_2CO_3, toluene, 120 °C	60

[a] 4-Methylphenylboronic acid was used. [b] nBu_4NBr was used as a co-catalyst. Abbreviations: dppp = 1,3-bis(diphenylphosphanyl)propane; NMP = *N*-methylpyrrolidine; DMA = *N*,*N*-dimethylacetamide; DMF = dimethylformamide.

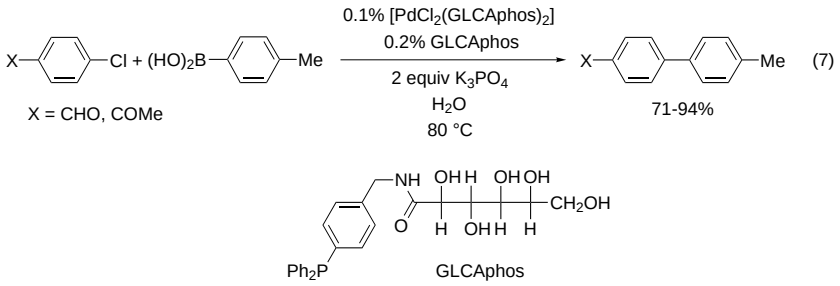


pled 4-bromophenylboronic acid is observed, thus establishing that highly selective activation of a C–Cl bond occurs in the presence of a typically more reactive C–Br bond.

Conducting reactions in aqueous media can be advantageous, particularly for large-scale industrial applications, as a result of the ease of purification as well as the environmental friendliness and low cost of water.[29] Hoechst has employed the water-soluble triphenylphosphane derivative P(*m*-$C_6H_4SO_3Na)_3$ in the Suzuki cross-coupling of an activated aryl chloride, 2-chlorobenzonitrile for the commercial production (100 tons/year) of 2-cyano-4′-methylbiphenyl,[30] a key intermediate in the synthesis of angiotension II receptor antagonists that are used for the treatment of hypertension [Eq. (6)].[31]



Another water-soluble triarylphosphane, GLCAphos, derived from D-glucono-1,5-lactone, has been introduced by Miyaura and co-workers.[32] Palladium catalysts based on GLCAphos are effective at low loadings for Suzuki couplings of activated aryl chlorides [Eq. (7)]. More recently, Shaughnessy and Booth have reported that water-soluble alkyl phosphanes are suitable ligands for such processes (Table 1, entry 1).[33]



Inada and Miyaura have established that (polystyrene-CH_2PPh_2)·$PdCl_2$ catalyzes Suzuki reactions of activated aryl chlorides, chloropyridines, and chloroquinolines (Table 1, entry 2).[34] The ligand used for the coupling of 2-chloropyridine with *p*-tolylboronic acid has been recovered and reused six times, and provided yields ranging from 86–96%. Miyaura and co-workers have also noted that [$Pd(PPh_3)_4$] can be useful for reactions of activated aryl chlorides.[35]

Santelli and co-workers have reported that high turnover numbers (TONs) can be obtained for Suzuki couplings of activated aryl chlorides by using their recently introduced tetrapodal phosphane ligand Tedicyp (Table 1, entry 3).[36] A TON of 6800000 is achieved in the case of highly activated 2-chloro-5-(trifluoromethyl)nitrobenzene; in contrast, a turnover number of just 21 is observed for electron-rich, deactivated 4-chloroanisole. Bidentate ligands such as 1,2-bis(diphenylphosphanyl)ethane (dppe) and 1,4-bis(diphenylphosphanyl)butane (dppb) are considerably less effective. The authors believe that multidentate coordination by Tedicyp imparts increased stability to the palladium catalyst.

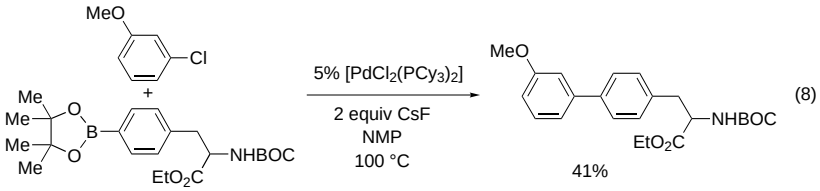
Herrmann et al. introduced phosphorus-based palladacycles[37] to catalyze Suzuki couplings of activated aryl chlorides with catalyst loadings as low as 0.1% Pd (Table 1, entry 4).[38] More recently, metalated benzylphosphane complexes of palladium were shown also to be active in these processes.[39]

Monteiro et al. have established that sulfur-containing palladacycles are effective catalysts for Suzuki reactions of activated aryl chlorides at room temperature (Table 1, entry 5).[40] DMF and K_3PO_4 were the best solvent and base, respectively, among those that were surveyed, and the addition of tetrabutylammonium bromide was found to be beneficial for the reaction rate.[41] Despite the high activity of this catalyst system toward activated aryl chlorides, only poor yields (13–46%; 130 °C) were obtained in couplings of electron-neutral and electron-rich aryl chlorides.

Bedford et al. have recently applied "PCP"-pincer complexes to Suzuki cross-couplings of highly activated 4-chloronitrobenzene with phenylboronic acid, and observed turnover numbers as high as 4300. The catalysts are ineffective for reactions of deactivated aryl chlorides.[42]

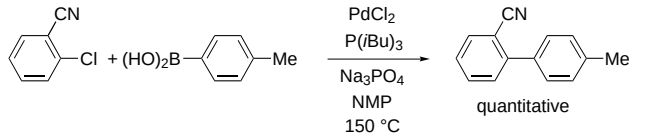
An important observation regarding Suzuki couplings of aryl chlorides was reported in 1997 by Shen, who established that palladium complexes that include a bulky, electron-rich trialkylphosphane (PCy_3, Cy = cyclohexyl) catalyze cross-couplings of activated aryl chlorides at 100 °C (Table 1, entry 6).[43] Bidentate 1,3-bis(diphenylphosphanyl)propane (dppp) is also useful in certain cases, whereas dppb, PPh_3, P(2-furyl)$_3$, and $AsPh_3$ are generally ineffective. However, [$PdCl_2(PPh_3)_2$] can be employed if the aryl chloride is highly activated (that is, it bears two electron-withdrawing groups).[44] It was speculated that the electron-richness of PCy_3 might facilitate oxidative addition of the Ar–Cl bond to Pd^0 and that the steric demand of PCy_3 might favor ligand dissociation to afford an active monophosphanepalladium catalyst.

Firooznia et al. subsequently applied Pd/PCy_3 to Suzuki cross-couplings of activated aryl chlorides with boronate esters to generate 4-substituted phenylalanines protected with a *tert*-butoxycarbonyl (Boc) group [Eq. (8)].[45] Unfortunately, attempts to extend this chemistry to the synthesis of enantiopure 4-aryl-substituted phenylalanines led to nearly racemic products.[46]



(8)

The high catalytic activity of palladium complexes of bulky, electron-rich trialkylphosphanes in Suzuki couplings of activated aryl chlorides has also been observed by Monteith during the development of a manufacturing route to 2-cyano-4′-methylbiphenyl.[47] Although PCy_3 and $P(i\text{Pr})_3$ provided the most active catalysts for this process, their cost was a drawback. Fortunately, $P(i\text{Bu})_3$, which is significantly less expensive, is also effective, thereby rendering the route economically viable [Eq. (9), NMP = *N*-methylpyrrolidine].



(9)

Although the success of Pd/trialkylphosphane-based catalysts for Suzuki reactions of activated aryl chlorides has been attributed in part to the electron-richness of the ligands, it is important to note that this feature is not absolutely essential for activity. Thus, Zapf and Beller have shown that Pd/phosphite complexes can catalyze couplings of activated aryl chlorides (Table 1, entry 7).[48] Phosphites are relatively electron-poor phosphorus ligands,[49] yet bulky tris(2,4-di-*tert*-butylphenyl)phosphite and triisopropylphosphite are effective for palladium-catalyzed couplings of activated aryl chlorides with phenylboronic acid. A modest yield (54%) is obtained with chlorobenzene, an unactivated aryl chloride. Less bulky phosphites (for example, triethyl- or triphenylphosphite) are significantly less effective, which is attributed to their greater propensity to hydrolyze under the reaction conditions. It is also possible that more bulky ligands favor the formation of highly reactive palladium complexes with only one ligand.

Until recently, palladium-catalyzed coupling chemistry relied nearly exclusively on phosphorus-based ligands. This has changed rapidly during the past few years (for example, with the development of N-heterocyclic carbenes; see Section 2.1.1.2). In 2001, Nolan and co-workers reported the use of 1,4-diazabutadienes, which are chelating nitrogen-based ligands, in palladium-catalyzed Suzuki reactions (Table 1, entry 8).[50] They determined that an *N*-alkyl substituent furnishes higher reactivity than an *N*-aryl substituent and that couplings of electron-deficient aryl chlorides with phenylboronic acid proceed in good yield at 100 °C with the cyclohexyl-substituted diazabutadiene. Under the same conditions, 4-chlorotoluene and 4-chloroanisole react in poor yield (< 35%), perhaps because the ligand is not sufficiently electron-rich to facilitate oxidative addition of more challenging C–Cl bonds.

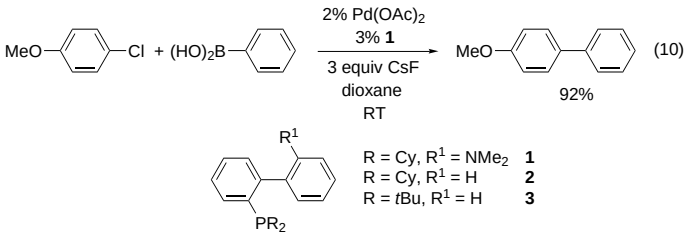
Interestingly, "ligandless" palladium catalysts can effect Suzuki couplings of certain activated aryl chlorides. Thus, Dupont and co-workers have reported that $Pd(OAc)_2$/$N(n\text{Bu})_4Br$ and $[PdCl_2(SEt_2)_2]$ catalyze the reaction of 4-chlorobenzonitrile with phenylboronic acid at 130 °C; in the case of $Pd(OAc)_2$/$N(n\text{Bu})_4Br$, the coupling can be conducted at room temperature, although long reaction times are required (Table 1, entry 9).[51] Unactivated aryl chlorides do not couple under these "ligandless" conditions.[52, 53]

LeBlond et al. have recently described the application of heterogeneous Pd/C to Suzuki reactions of activated aryl chlorides with phenylboronic acid (Table 1, entry 10).[54] Couplings of electron-neutral and electron-rich aryl chlorides proceed in only modest yields (32–54%). The choice of solvent (DMA/H_2O = 20/1) is important—more water leads to a significant amount of homocoupling, and less water results in severely retarded reaction rates. Separation of the product from the catalyst can be achieved through simple filtration, which leaves less than 1.0 ppm palladium in the product (< 0.10% loss, based on the initial amount of palladium). Coupling does not occur in the presence of an equivalent of PPh_3, an interesting contrast to the analogous Ni/C-based catalyst for Suzuki reactions of aryl chlorides, for which PPh_3 appears to be required for activity.[55]

2.1.1.2. Suzuki Reactions of Unactivated Aryl Chlorides

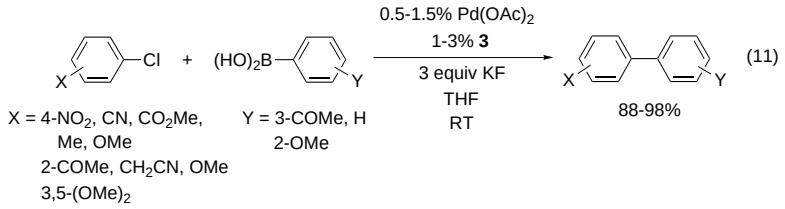
Prior to 1998, there were no reports of effective palladium-catalyzed Suzuki reactions of electron-neutral or electron-rich aryl chlorides. Clearly, this represented a serious limitation in the scope of this important process. In 1998, the groups of Buchwald and Fu developed catalyst systems that couple a wide range of aryl chlorides in good yield.

In their study in 1998, Buchwald and co-workers reported that aminophosphane **1** is a very effective ligand for palladium-catalyzed Suzuki reactions of aryl chlorides [Eq. (10)].[56] Remarkably, this catalyst system couples a broad spectrum of aryl chlorides, such as electron-neutral and electron-rich substrates, at room temperature. CsF was the base of choice, although the less expensive K_3PO_4 could be employed at 100 °C.



(10)

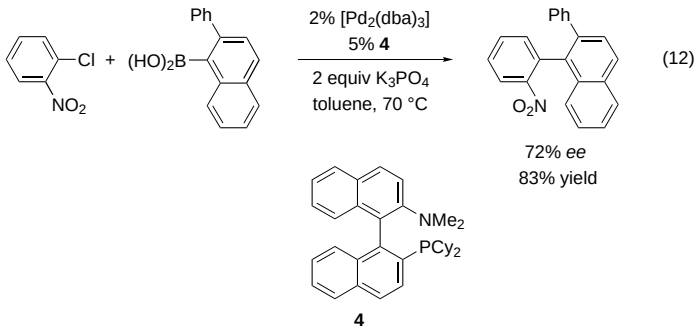
Buchwald and co-workers subsequently determined that biphenyl ligands **2** and **3** can be even more effective than **1** in palladium-catalyzed Suzuki reactions of aryl chlorides, thereby establishing that the amino group of **1** is not essential for high activity.[57] Room-temperature Suzuki couplings of a



wide array of partners can be achieved using ligand **3** with 0.5 – 1.5 % Pd and KF as the activator [Eq. (11)].

9-Alkyl-9-BBN derivatives are also suitable substrates for this catalyst system (BBN = 9-borabicyclo[3.3.1]nonane). Ligands **1** and **2** (with K_3PO_4 in toluene) are more effective than **3** for hindered reactants. The air stability and commercial availability of these biphenyl-based ligands make them particularly attractive.[58]

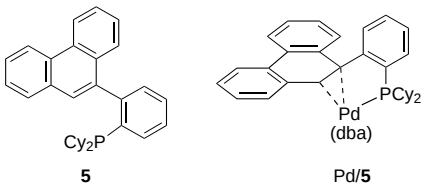
Parrish and Buchwald have developed a polymer-bound dicyclohexylphosphanylbiphenyl ligand that can be employed for Suzuki reactions of electron-neutral and hindered aryl chlorides; the coupling product can be isolated without the need for column chromatography.[59] In addition, binaphthyl derivative **4**, an enantiopure variant of biphenyl ligand **1**, can be applied to the catalytic asymmetric synthesis of axially chiral biaryls, which are present in a number of natural products [Eq. (12); dba = *trans*,*trans*-dibenzylideneacetone].[60]

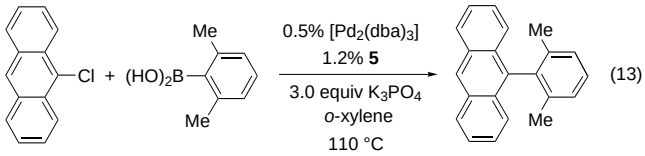


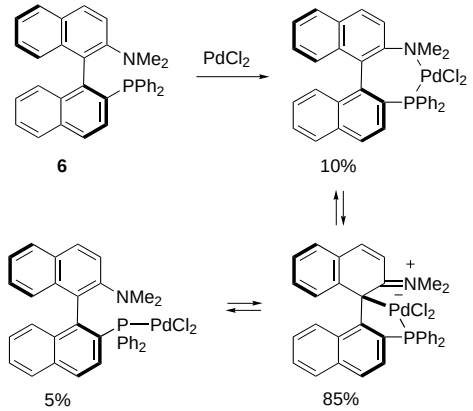
A stabilizing interaction between the *ortho*-aryl group and a palladium d orbital has been suggested as being responsible for the high activity exhibited by catalysts based on biphenyl ligands.[61] An X-ray crystal structure of a palladium complex of phenanthrene derivative **5** is consistent with this hypothesis (Pd/**5**).[62] The first efficient Suzuki couplings to generate tetra-*ortho*-substituted biaryls have been achieved in the presence of $[Pd_2(dba)_3]$/**5** [Eq. (13)].

Observations of Kocovsky et al. are consistent with the idea that an interaction between the *ortho*-aryl group and palladium may be responsible for the unusual reactivity that Buchwald described.[63] Through crystallographic and spectroscopic studies, Kocovsky et al. have established that aminophosphane **6** preferentially serves as a P,C chelate, not a P,N chelate, to palladium (Scheme 3). Interestingly, $Pd(OAc)_2$/**6** catalyzes the Suzuki coupling of 4-chlorobenzaldehyde with phenylboronic acid at room temperature, a surprising level of reactivity for a catalyst based on a triarylphosphane.

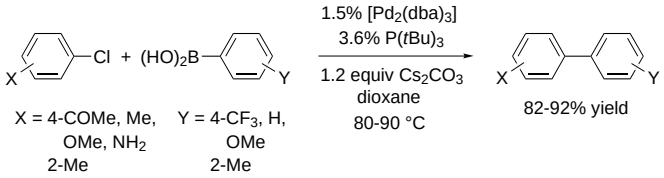
In the same year as the original report by Buchwald et al., Littke and Fu also described a versatile method for palladium-catalyzed Suzuki cross-couplings of aryl chlorides in which they used a sterically demanding and electron-rich trialkylphosphane, $P(tBu)_3$ [Eq. (14)].[64] A $P(tBu)_3$:Pd ratio between 1.0 – 1.5:1 was most effective. Deactivated and hindered aryl chlorides were suitable substrates for this catalyst system. In this initial study, $[Pd_2(dba)_3]$, Cs_2CO_3, and dioxane were employed as the palladium source, activator, and solvent, respectively. A variety of other





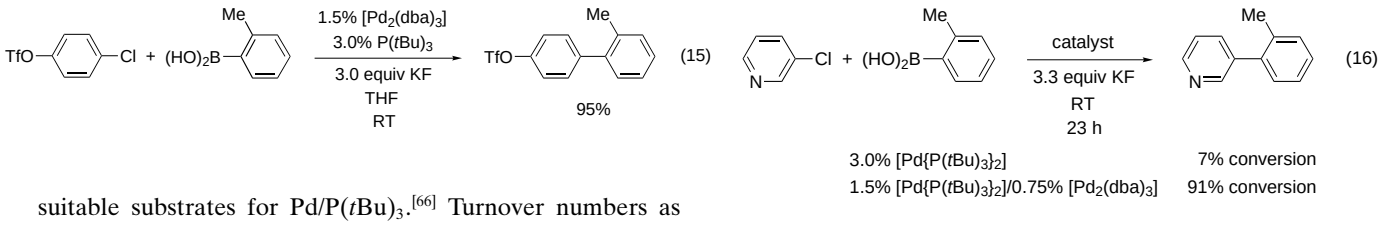


Scheme 3. Pd^{II} complexes of 2-dimethylamino-2′-diphenylphosphanyl-1,1′-binaphthyl.



commercially available phosphanes were screened, including PPh_3 and 1,1′-binaphthalene-2,2′-diylbis(diphenylphosphane) (binap); however, the only phosphane that showed useful reactivity was sterically demanding and electron-rich PCy_3.

Fu and co-workers subsequently determined that KF is a more effective additive than Cs_2CO_3, which allowed Suzuki cross-couplings of activated aryl chlorides, including heteroaryl chlorides, to proceed at room temperature ($P(tBu)_3$:Pd = 1:1).[65] This Pd/$P(tBu)_3$-based catalyst system exhibits a highly unusual reactivity profile—that is, unprecedented selectivity for the coupling of an aryl chloride in preference to an aryl triflate [Eq. (15)]. Alkyl boronic acids, which are often less reactive in Suzuki reactions than aryl boronic acids, are



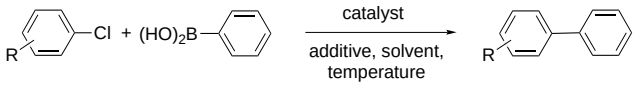
suitable substrates for Pd/P(tBu)$_3$.[66] Turnover numbers as high as 9700 can be achieved with this catalyst system. Since the original report, a number of research groups have applied Pd/P(tBu)$_3$ to Suzuki couplings of a wide range of activated and unactivated aryl and heteroaryl chlorides.[21, 46, 67]

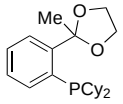
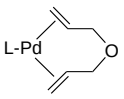
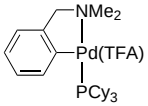
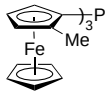
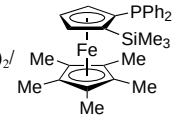
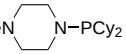
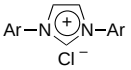
The observation that the use of a 1:1 ratio of P(tBu)$_3$:Pd is important for obtaining high reactivity in room-temperature Suzuki reactions of aryl chlorides prompted a preliminary mechanistic investigation. According to ^{31}P NMR measurements, Pd(PtBu$_3$)$_2$[68] is the only palladium–phosphane complex that is present in an appreciable quantity during the catalytic reaction. Interestingly, though, [Pd(PtBu$_3$)$_2$] is itself a rather ineffective catalyst for room-temperature Suzuki cross-couplings [Eq. (16)]; however, the addition of phosphane-free [Pd$_2$(dba)$_3$], so as to achieve a 1:1 P(tBu)$_3$:Pd ratio, results in a much more active catalyst system [Eq. (16)].

These observations suggest that a monophosphane–palladium adduct may play a key role in Pd/P(tBu)$_3$-catalyzed couplings and that phosphane-free palladium complexes that are present in the reaction mixture may serve to increase the concentration of this active species.[69, 70] Thus, P(tBu)$_3$ may be a particularly effective ligand for couplings of aryl chlorides because the steric demand of P(tBu)$_3$ facilitates dissociation to a monophosphane adduct, to which the aryl chloride rapidly oxidatively adds as a result of the electron richness of P(tBu)$_3$.[71, 72]

More recently, a number of research groups have described other ligands that can provide active catalysts for palladium-catalyzed Suzuki couplings of aryl chlorides (Table 2). Like Buchwald et al., Guram and co-workers have determined that dialkylarylphosphanes are effective (Table 2, entry 1).[73] In

Table 2. Suzuki cross-couplings of aryl chlorides.



Entry	R	Catalyst	Conditions	Yield [%]
1	4-CF$_3$, OPh, 3-OMe, 3,5-Me$_2$, 2-CN, Me, COMe	[Pd(dba)$_2$]/ 	CsF in dioxane, toluene, or o-xylene, 80–130 °C	83–97[a]
2	4-Me, OMe, 2-CN, F, Me, 2,6-Me$_2$, 3-Cl-pyridine	Pd(OAc)$_2$/nBuP(1-Ad)$_2$	K$_3$PO$_4$, toluene, 100 °C	55–100
3	4-F, Me, OMe, H, 2-CN	 L = PCy$_3$, (o-biphenyl)PCy$_2$	K$_3$PO$_4$/KF, THF, 100 °C	34–97
4	4-COMe, CHO, NO$_2$, OMe, 2-Me, OMe		Cs$_2$CO$_3$, dioxane, 100 °C	74–100[b]
5	4-NO$_2$, Me, H, 2-Me, OMe	[Pd$_2$(dba)$_3$]/ 	Cs$_2$CO$_3$, dioxane, 60 °C	36–90[c]
6	4-COMe, Me, OMe, 2-CN, Me, 2,6-Me$_2$, 2-Cl-pyridine	[Pd$_2$(dba)$_3$] or Pd(OAc)$_2$/ 	K$_3$PO$_4$·H$_2$O, toluene, RT–70 °C	82–95[d]
7	4-COMe, CF$_3$, Me, 3-CHO	[Pd$_2$(dba)$_3$]/ 	CsF, toluene, 90 °C	93–100[b]
8	4-H, OMe, 2-OMe	[Pd$_2$(dba)$_3$]/ 	CsF or Cs$_2$CO$_3$, dioxane, 100 °C	83–99[e]
9	4-CO$_2$Me, Me, OMe, 2,5-Me$_2$	[Pd$_2$(dba)$_3$]/  Ar = 2,4,6-(Me)$_3$C$_6$H$_2$	Cs$_2$CO$_3$, dioxane, 80 °C	88–99[f]

[a] 4-CF$_3$-, 4-Me-, and 2-Me-substituted phenylboronic acids were also used. [b] GC conversions. [c] o-Tolylboronic acid was also used. [d] 4-OMe- and 2-Me-substituted phenylboronic acids were also used. [e] 4-Me- and 4-OMe-substituted phenylboronic acids were also used. [f] 4-OMe-, 3-OMe-, and 2-Me-substituted phenylboronic acids were also used. Abbreviations: dba = *trans*,*trans*-dibenzylideneacetone; Ad = adamantyl.

addition, Beller and co-workers have demonstrated that the new bulky ligand di(1-adamantyl)-*n*-butylphosphane can afford excellent turnover numbers in palladium-catalyzed Suzuki reactions (Table 2, entry 2).[74] This phosphane achieves a TON of 17400 (0.005% Pd, 87% yield) for the coupling of 4-chlorotoluene, compared with a turnover number of 9200 with commercially available $P(t\mathrm{Bu})_3$ (0.01% Pd, 92% yield). High TONs (>10000) can also be obtained with challenging aryl chlorides such as 2-chloro-*m*-xylene and 4-chloroanisole.

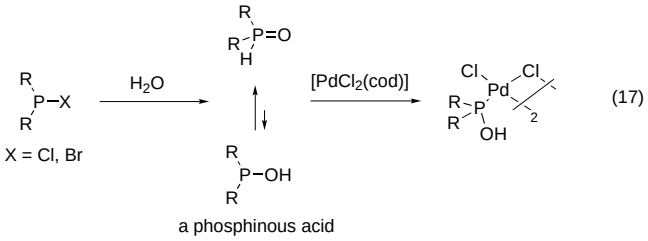
Since monophosphane–palladium adducts have been implicated as the active catalyst in many of the systems described above, Beller and co-workers have investigated the relative reactivity of several discrete $[PdL_1(\mathrm{diene})]$ complexes (Table 2, entry 3).[75, 76] As expected, a complex derived from PPh_3 does not catalyze couplings of unactivated aryl chlorides, which indicates that generation of a $[PdL_1]$ complex is not a sufficient condition for achieving this process. On the other hand, the corresponding electron-rich PCy_3-based catalyst is effective for Suzuki reactions of both electron-neutral and electron-rich aryl chlorides; furthermore, this preformed catalyst is significantly more reactive than a mixture of $[Pd_2(dba)_3]$ or $Pd(OAc)_2$ with PCy_3. The complex derived from the (*o*-biphenyl)PCy_2 ligand of Buchwald et al. was also studied, and, among the three ligands examined, it furnished the highest turnover numbers.

In related work, Bedford and Cazin demonstrated that a Pd/PCy_3 complex that bears an orthometalated nitrogen-donor ligand is effective for Suzuki cross-couplings of electron-rich aryl chlorides with loadings down to 0.01% Pd (Table 2, entry 4).[77] The active catalyst is believed to be a low-coordinate Pd^0/PCy_3 species that is generated by loss of the orthometalated nitrogen donor ligand. The cross-couplings can be conducted under air.

As described earlier, it was established in 1999 that a triarylphosphane can serve as a useful ligand for a room-temperature palladium-catalyzed Suzuki coupling of 4-chlorobenzaldehyde. Until recently, though, triarylphosphanes had not proved to be effective for reactions of unactivated aryl chlorides. However, in 2001, Pickett and Richards demonstrated that Pd/tris(2-methylferrocenyl)phosphane can achieve Suzuki cross-couplings of this family of substrates in modest to good yield (Table 2, entry 5).[78] During the same year, Fu and co-workers reported that a diphenylferrocenylphosphane ligand provides a versatile method for palladium-catalyzed Suzuki reactions of aryl chlorides: Activated substrates couple at room temperature and unactivated aryl chlorides react at 70°C (Table 2, entry 6).[79] Since PPh_3 is ineffective under these conditions, the unusual reactivity of the diphenylferrocenylphosphane ligand can be attributed to the greater electron-donating ability[80] and the increased bulk of the ferrocenyl group, relative to a phenyl substituent. With regard to the influence of the steric demand of the ligand, it was noted that removal of the trimethylsilyl group or replacement of C_5Me_5 with C_5H_5 results in a considerably less-effective ligand.

Woolins and co-workers have determined that *N*-dicyclohexylphosphanyl-*N*′-methylpiperazine is useful for the palladium-catalyzed coupling of 4-chlorotoluene with phenylboronic acid at 90°C (Table 2, entry 7).[81] The analogous *N*-diisopropylphosphanyl-substituted ligand furnishes a less-reactive catalyst.

Phosphinous acids are a promising new class of phosphorus ligands for Suzuki cross-couplings of unactivated aryl chlorides. Hydrolysis of diorganophosphorus halides generates phosphane oxides and their less-stable phosphinous acid tautomers [Eq. (17); cod = cycloocta-1,5-diene]. Binding of a



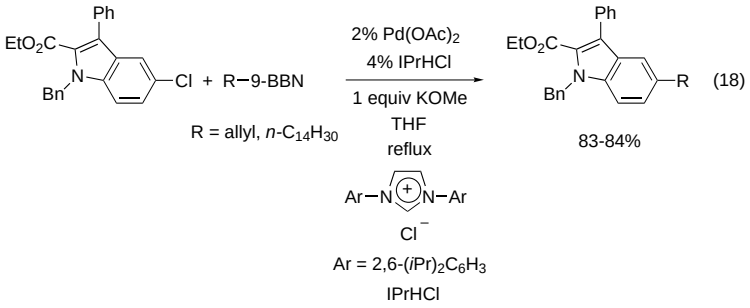
(17)

phosphinous acid to palladium can provide a P-bound adduct, which may be deprotonated to yield an electron-rich, anionic palladium–phosphane complex suitable as a catalyst for coupling processes. Li has recently demonstrated the viability of this strategy, in which he established that $[Pd_2(dba)_3]/(t\mathrm{Bu})_2P(O)H$, as well as $[Pd_2(dba)_3]/(t\mathrm{Bu})_2PCl/H_2O$, effect Suzuki reactions of hindered and electron-rich aryl chlorides (Table 2, entry 8).[82]

All of the catalysts for Suzuki couplings of unactivated aryl chlorides that have been discussed above have been based on phosphorus ligands. Carbon-based ligands, specifically, nucleophilic N-heterocyclic carbenes, are also effective for such processes.[83] Herrmann et al. were the first to apply this family of ligands to palladium-catalyzed coupling reactions, and showed that a first-generation catalyst can achieve the cross-coupling of an activated aryl chloride with phenylboronic acid (Table 1, entry 11).[84] It was subsequently determined that mixed PCy_3/carbene complexes can couple unactivated aryl chlorides at elevated temperature.[85]

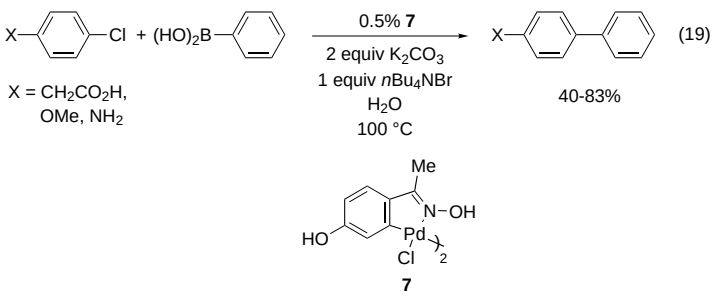
Palladium adducts of 1,3-bis(2,4,6-trimethylphenyl)imidazol-2-ylidene (IMes)[86] have been reported to be active catalysts for the Suzuki cross-couplings of a wide variety of aryl chlorides with aryl boronic acids (Table 2, entry 9).[87] Handling the air- and moisture-sensitive carbene can be avoided through the use of the easier-to-handle, commercially available, chloride salt (IMesHCl), which can be deprotonated in situ to generate the carbene ligand. Herrmann and co-workers independently explored the catalytic activity of Pd/IMes in Suzuki reactions of aryl chlorides.[88] They observed that the preformed bis(carbene) complex $[Pd(IMes)_2]$ is ineffective as a catalyst, in analogy with the observations for $[Pd(Pt\mathrm{Bu}_3)_2]$ by Fu and co-workers [Eq. (16)].[89, 90]

Furstner and Leitner have significantly expanded the scope of Pd/carbene-catalyzed Suzuki reactions of aryl chlorides by employing 9-alkyl-9-BBN derivatives as coupling partners [Eq. (18)].[91] Interestingly, the most effective ligand for these processes is not IMes, but is instead the more bulky 2,6-diisopropylphenyl-substituted carbene, IPr (from commer-



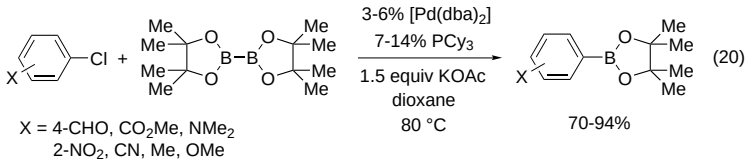
cially available IPrHCl). Use of the preformed carbene, rather than in situ generation from the chloride salt, leads to significantly worse results. Alkenyl- and alkynyl-9-BBN derivatives are also suitable partners in these cross-couplings. In the course of the synthesis of a large, highly diverse library of heterocycles, Schultz and co-workers recently employed Pd/IPr as a catalyst for Suzuki reactions of a wide array of solid-supported heteroaryl chlorides and aryl boronic acids.[92]

Air- and water-stable oxime palladacycles such as **7** represent another class of non-phosphorus-based ligands that show promise in Suzuki couplings of unactivated aryl chlorides. Thus, Botella and Nájera have reported that **7** catalyzes cross-couplings of a range of aryl and heteroaryl chlorides, including electron-rich substrates, in water in variable yield [Eq. (19)].[93]



Related to the Suzuki reaction is the cross-coupling of aryl halides and triflates with tetraalkoxydiboron reagents, an efficient and versatile method for the synthesis of aryl boronates from electrophilic arenes.[94] This process is particularly useful for substrates that contain functional groups that are not compatible with traditional routes to aryl boronic acids/esters, which involve Grignard or organolithium reagents.

Miyaura and co-workers have recently disclosed that $[Pd(dba)_2]/PCy_3$ is an effective catalyst for the borylation of aryl chlorides using 4,4,5,5-tetramethyl[1,3,2]-dioxaborolane [Eq. (20)].[95] A broad spectrum of functional groups are tolerated. Highly electron-rich chlorides (for example,



4-chlorodimethylaniline) are suitable substrates, as are heteroaryl chlorides such as 3-chloropyridine and 2-chlorobenzo[*b*]furan. PCy_3 is more efficient than $P(tBu)_3$, dialkylarylphosphanes, and triarylphosphanes. Furstner and Seidel subsequently reported that carbene ligand IPr can be employed in palladium-catalyzed couplings of electron-deficient aryl chlorides with 4,4,5,5-tetramethyl[1,3,2]-dioxaborolane.[96] However, reactions of unactivated aryl chlorides result in competitive reduction of the C–Cl bond.

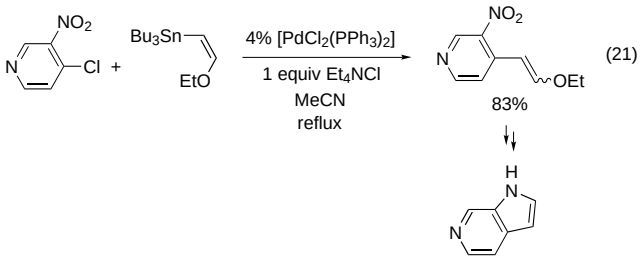
2.1.2. Stille Reactions

The palladium-catalyzed Stille cross-coupling of aryl and vinyl halides/triflates with organostannanes is a powerful and widely used method for formation of carbon–carbon bonds.[97, 98] Stille reactions have proved to be an especially popular tool in complex natural product synthesis, as a result in part of the air- and moisture-stability of organotin reagents and the excellent functional-group compatibility of the process. Thus, the Stille cross-coupling has played a pivotal role in a number of total syntheses, such as those of rapamycin[99] and dynemicin.[100, 101]

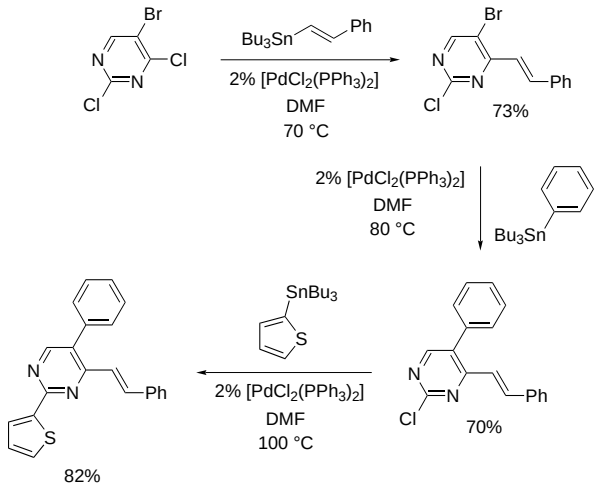
2.1.2.1. Stille Reactions of Activated Aryl Chlorides

Stille cross-couplings of heteroaryl chlorides, mainly nitrogen-containing heterocycles, have a rich history. As for Suzuki reactions of this class of substrates (Section 2.1.1.1), many of these processes have employed traditional Pd/triarylphosphane-based catalysts.

A wide array of chloropyridines participate in Stille couplings.[14b–d, f, g, i, 102] In one of the earliest examples, Yamanaka and co-workers demonstrated that 2- and 4-chloro-3-nitropyridines react with (*Z*)-1-ethoxy-2-tributylstannylethylene in good yield; the products can be converted to 1*H*-pyrrolopyridines [Eq. (21)].[103]

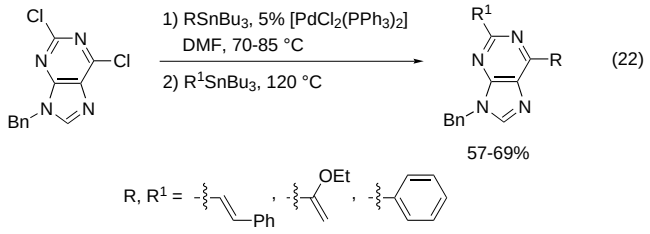


Stille cross-couplings of chloro-substituted pyridazines,[16c] pyrimidines,[104] pyrazines,[105] thiadiazoles,[106] and triazines[107] have also been reported. For halopyrimidines, the 4-position is the most activated, followed by the 2-position, and then the 5-position. Therefore, selective coupling can be achieved of the 4-position of 2,4-[108] and 4,5-dichloropyrimidines[109] as well as the 2-position of 2,5-dichloropyrimidines.[108a] Interestingly, a 4-chloro group can react in preference to a 5-bromo group, thus allowing the stepwise functionalization of 2,4-dichloro-5-bromopyrimidine (Scheme 4).[108a]



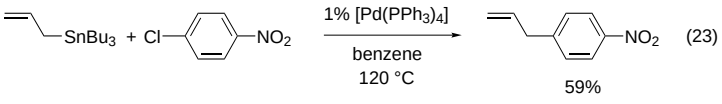
Scheme 4. Stepwise coupling of 2,4-dichloro-5-bromopyrimidine.

Fused heterocycles, such as chloro-substituted quinolines,[18, 110] isoquinolines,[19b, 110d] quinolones,[111] 1,8-naphthyridines,[112] quinazolines,[113] quinoxalines,[114] benzothiazoles,[115] purines,[25d, 116] diazaoxindoles,[117] β-carbolines,[22a, 118] phenanthrolines,[23] and benzo[*c*][2,7]naphthyridines[119] also undergo Stille cross-coupling. Good selectivity for coupling 6,8-dichlorosubstituted purines at the more activated 6-position is observed with a variety of stannanes, although small amounts of disubstituted purines (namely, reaction at both the 6- and the 8-positions) are obtained.[120] Similarly, in the presence of $[PdCl_2(PPh_3)_2]$ or $[Pd\{P(2\text{-furyl})_3\}_4]$, the 6-position of 2,6-dichlorosubstituted purines cross-couples in preference to the 2-position; in contrast to 6,8-dichloro-substituted purines, no disubstituted purines are observed if the temperature and the reaction time are carefully controlled.[121] This high selectivity allows the one-pot Stille cross-coupling of 2,6-dichloropurines with two different organostannanes [Eq. (22)].



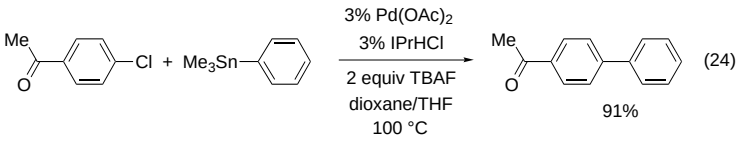
(22)

In contrast to Suzuki reactions (Section 2.1.1), there are relatively few examples of palladium-catalyzed Stille couplings of non-heteroaryl chlorides, even activated ones. The first example of such a process was provided by Migita and coworkers, who established that $[Pd(PPh_3)_4]$ catalyzes the cross-coupling of allyltributyltin with the highly activated 1-chloro-4-nitrobenzene in moderate yield [Eq. (23)].[122] As for the Suzuki reaction [Eq. (5)], tricarbonyl(η^6-chloroarene)chromium complexes are suitable substrates for palladium-catalyzed Stille couplings;[27b, 123] the reaction proceeds at room temperature with $AsPh_3$ as the ligand.[27c]



(23)

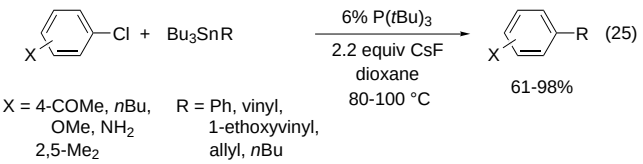
In 2001, Grasa and Nolan reported that Pd/N-heterocyclic carbene complexes, in combination with a fluoride additive, catalyze the Stille cross-coupling of electron-deficient aryl chlorides [Eq. (24); TBAF = tetrabutylammonium fluoride].[124] The fluoride ion presumably accelerates transmetalation through formation of a more reactive hypervalent tin species (see Section 2.1.2.2), as well as deprotonates the imidazolium salt to generate the free carbene ligand in situ. 2,6-Diisopropylphenyl-substituted carbene IPr and 1-adamantyl-substituted carbene IAd were found to be superior to other carbenes, including mesityl-substituted IMes. Poor to moderate yields (15–54%) were obtained for reactions of unactivated aryl chlorides.



(24)

2.1.2.2. *Stille Reactions of Unactivated Aryl Chlorides*

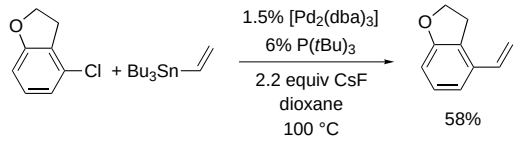
Currently, the only general method for achieving Stille cross-couplings of unactivated aryl chlorides is the Pd/$P(t\text{Bu})_3$/CsF system described by Littke and Fu.[125] This catalyst works well for electron-deficient, electron-rich, and hindered aryl chlorides [Eq. (25)]. A variety of groups



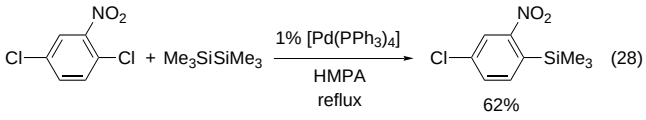
(25)

can be transferred from tin, including typically unreactive alkyl substituents. The coupling proceeds much more slowly in the absence of fluoride ions. The fluoride ions appear to play at least two useful roles in this chemistry—they activate the organotin reagent for transmetalation, and produce insoluble Bu_3SnF, which is straightforward to separate from the product (difficulty in eliminating tin impurities is commonly encountered during purifications of Stille reactions[126]). Zhu et al. have recently applied this method to the generation of 4-vinyl-2,3-dihydrobenzofuran, an intermediate in the synthesis of melatonergic agents [Eq. (26)].[127]

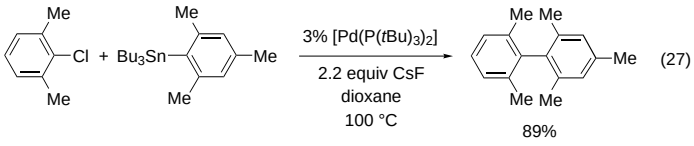
It was subsequently demonstrated that commercially available $[Pd\{P(t\text{Bu})_3\}_2]$ can be employed as a catalyst for Stille couplings of aryl chlorides.[128] This method is effective even for very hindered substrates, as evidenced by the synthesis of a tetra-*ortho*-substituted biaryl, an extremely challenging family of targets for cross-coupling methods [Eq. (27)].[129] Fu and



(26)

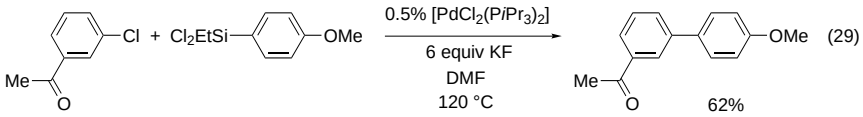


(28)



(27)

co-workers also reported that $[Pd\{P(t\mathrm{Bu})_3\}_2]$ accomplishes the selective coupling of an aryl chloride in the presence of a triflate and that reactions with certain activated aryl chlorides can be carried out at room temperature. A turnover number as high as 920 was achieved for the Stille cross-coupling of an unactivated aryl chloride.



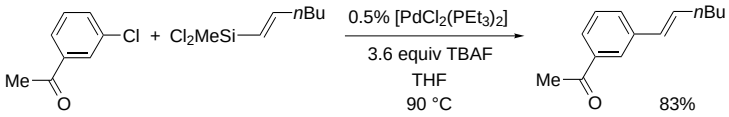
(29)

2.1.3. Hiyama Reactions

The palladium-catalyzed cross-coupling of organosilanes with aryl/vinyl halides and triflates, commonly referred to as the Hiyama reaction, is an attractive alternative to the Stille coupling, because organosilicon compounds are nontoxic.[130] The first examples of aryl chlorides participating in this type of process were provided by Matsumoto et al., who observed that $[Pd(PPh_3)_4]$ catalyzes the cross-coupling of nitro-substituted aryl chlorides with hexamethyldisilane to furnish arylsilanes;[131] a high level of selectivity for substitution at the *ortho*-position can be obtained in the case of 2,5-dichloronitrobenzene [Eq. (28); HMPA = hexamethyl phosphoramide].[132, 133]

In 1996 Hatanaka and co-workers considerably expanded the scope of this process by using $[PdCl_2(P\mathit{i}Pr_3)_2]$ as the catalyst in the presence of KF, and established that a wide variety of electron-deficient aryl chlorides cross-couple with aryl chlorosilanes [Eq. (29)].[134] The bulky, electron-rich bidentate ligand 1,2-bis(dicyclohexylphosphanyl)ethane is also effective in certain instances, whereas PPh_3-based catalysts are ineffective. Unactivated aryl chlorides do not couple in satisfactory yields under these conditions.

Hatanaka and co-workers have demonstrated that alkenylchlorosilanes also participate in Hiyama cross-couplings with activated aryl chlorides in the presence of $[PdCl_2(PEt_3)_2]$ as the catalyst and TBAF as the fluoride source [Eq. (30)]. They subsequently determined that inexpensive NaOH is a superior promotor to fluoride salts, although a large excess is required (ca. 6 equiv; Table 3, entry 1).[135]

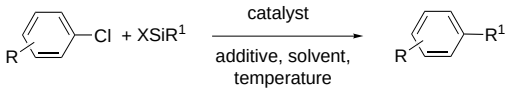


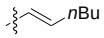
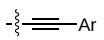
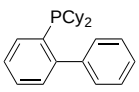
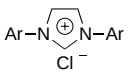
(30)

Tricarbonyl(η^6-chloroarene)chromium complexes also undergo Hiyama coupling with organofluorosilanes in the presence of TBAF. A wide variety of organic groups, such as aryl, 2-thienyl, alkenyl, and alkynyl, can be transferred.[136]

Mori and co-workers have reported that electron-poor aryl chlorides can be cross-coupled with alkynyltrimethylsilanes

Table 3. Hiyama cross-couplings of aryl chlorides.

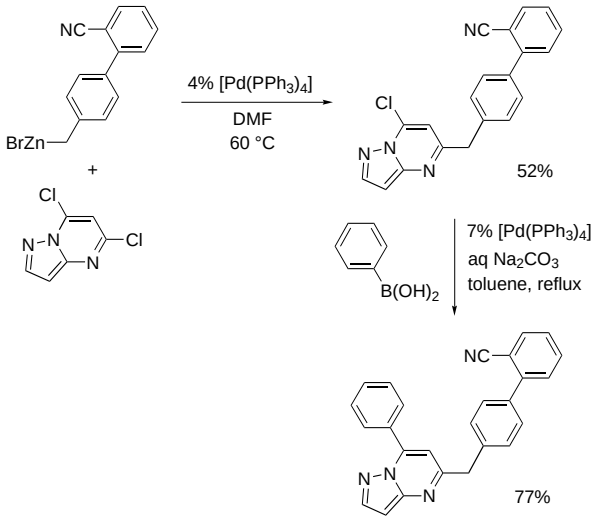


Entry	R	R^1	Catalyst	Conditions	Yield [%]
1	4-CF_3, 3-COMe, Me, 2-Cl-pyridine		$[PdCl_2(P\mathit{i}Pr_3)_2]$	NaOH, benzene, 80 °C	65 – 95[a]
2	4-COMe, H		$[PdCl_2(dppb)]$	cat. CuCl, DMF, 120 °C	42 – 86[b,c]
3	4-COMe, Me, OMe	Ph	$[Pd_2(dba)_3]$/ 	TBAF, DMF, 85 °C	47 – 71[d]
4	4-COMe, CN, 2-chloropyridine	Ph	$Pd(OAc)_2$/  Ar = 2,6-$(\mathit{i}Pr)_2C_6H_3$	TBAF, dioxane/THF, 80 °C	81 – 100[d,e]

[a] X = $MeCl_2$. [b] X = Me_3. [c] Ar = 4-$MeOC_6H_4$, 4-NCC_6H_4, C_6H_5. [d] X = $(OMe)_3$. [e] 100 % conversion when R^1 = vinyl and R = 4-COMe. Abbrevia-

using [$PdCl_2$(dppb)]/CuCl as the catalyst (Table 3, entry 2).[137] However, under these conditions, unactivated chlorobenzene couples in a modest 43% yield. In this reaction, transmetalation from silicon to copper may be occurring to generate an alkynylcopper species, which then transfers the alkynyl group to palladium. This method is noteworthy in that no fluoride or hydroxide ions are required, which may be especially beneficial for alkynylations of base-sensitive substrates (see Section 2.1.7, Sonogashira reactions).

Siloxanes serve as useful partners in Hiyama cross-couplings of aryl chlorides. Mowery and DeShong have demonstrated that palladium-catalyzed reactions of phenyltrimethylsiloxane with a range of substrates, including challenging electron-neutral and electron-rich aryl chlorides, can be achieved in the presence of 2-(dicyclohexylphosphanyl)biphenyl ligand (Table 3, entry 3).[138] In addition, Lee and Nolan have determined that the use of N-heterocyclic carbenes allows for couplings of phenyl- and vinyltrimethylsiloxane with activated aryl chlorides (Table 3, entry 4).[139]



Scheme 5. Selective Negishi cross-coupling of a heteroaryl dichloride.

2.1.4. Negishi Reactions

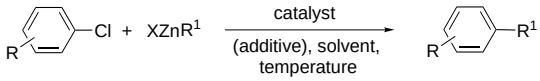
The palladium-catalyzed Negishi cross-coupling—the reaction of aryl and vinyl halides/triflates with organozinc reagents—represents a powerful tool for the formation of carbon–carbon bonds because of the ready availability and high functional-group compatibility of organozinc compounds.[140] As with Suzuki and Stille couplings, there are quite a few examples of heteroaryl chlorides, mainly nitrogen-containing species, which participate in the Negishi reaction. Thus, chloropyridines,[141] pyrazines,[15a, 142] pyrimidines,[143] and triazines[144] are suitable substrates, as are fused heterocycles such as chloroquinolines,[18b, 110d, 145] quinazolines,[113] and purines.[25d, 116b]

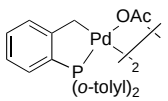
One particular example of such a cross-coupling was provided by Shiota and Yamamori during the course of a synthesis of a family of angiotension II receptor antagonists. Their strategy relied upon a regioselective Negishi coupling of 5,7-dichloropyrazolo[1,5-*a*]pyrimidine, which proceeds as desired when the reaction is performed in DMF (Scheme 5; 7% of the unwanted isomer is produced);[18b] in contrast, no selectivity is observed in THF. A second palladium-catalyzed cross-coupling (Suzuki reaction) then furnishes the target compound in good yield. Interestingly, direct nucleophilic substitution of the starting dichloride by the benzylzinc reagent in the presence of LiCl, but in the absence of a palladium catalyst, leads to preferential reaction of the other Ar–Cl bond.

Miller and Farrell have described a Pd/dppf-based catalyst for the cross-coupling of activated aryl chlorides with aryl zinc reagents (Table 4, entry 1).[146] They found that other phosphanes, such as PPh_3, P(*o*Tol)$_3$, and binap, are inferior to dppf. These cross-couplings can also be carried out with a Grignard reagent and a catalytic amount of a zinc salt such as $ZnCl_2$ (Table 4, entry 2).[147, 148]

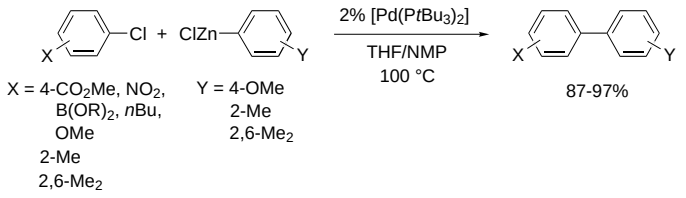
The first example of a palladium-catalyzed Negishi coupling of an unactivated aryl chloride (chlorobenzene) was reported by Herrmann et al., in which they used a palladacycle as the catalyst (Table 4, entry 3).[37a] The scope of this method for this family of substrates was not discussed. The first general protocol for accomplishing Negishi couplings of unactivated and electron-rich aryl chlorides was provided by Dai and Fu in 2001, in which commercially available [Pd{P(*t*Bu)$_3$}$_2$] was used as the catalyst [Eq. (31)].[149] Functionalities such as nitro and ester groups are tolerated, and chlorothiophenes and chloropyridines are suitable substrates. Hindered compounds can be cross-coupled effectively, thus allowing the synthesis of a tetra-*ortho*-substituted biaryl. In addition, turnover numbers as high as 3000 can be achieved. Finally, primary and secondary alkyl zinc reagents can be

Table 4. Negishi cross-couplings of aryl chlorides.

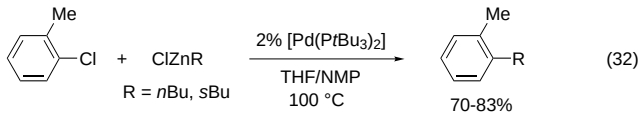


Entry	R	R^1	Catalyst	Conditions	Yield [%]
1	4-CO_2Me, CN, 2-CN	*p*Tol, Ph	[$PdCl_2$(dppf)]	THF, reflux	75–82[a]
2	4-CN	Ph[b]	[$PdCl_2$(dppf)]	cat. $ZnCl_2$, THF, 55–60 °C	88
3	4-NO_2, H	Ph		THF, 90 °C	76–88[c]

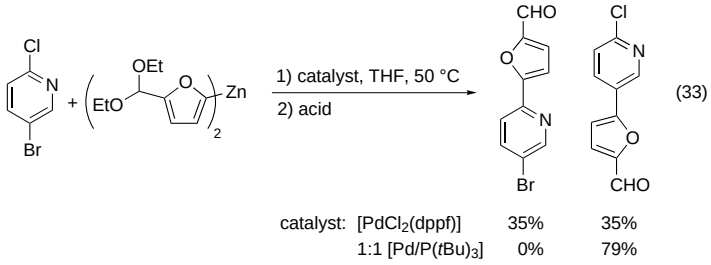
[a] X = Cl or Ph. [b] PhMgCl was used instead of $XZnR^1$. [c] X = Br. Abbreviations: dppf = bis(diphenylphosphanyl)ferrocene; *p*Tol = *para*-tolyl.



employed; the coupling of *s*BuZnCl with 2-chlorotoluene generates predominantly the desired compound 2-*s*-butyltoluene along with 8% of the isomerized product 2-*n*-butyltoluene. [Eq. (32)].



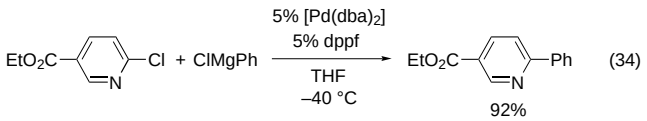
Gauthier et al. have recently applied Pd/P(*t*Bu)$_3$ to Negishi couplings of 2- and 3-chloropyridines with di(2-furyl)zinc reagents.[150] The use of a 1:1 ratio of Pd:P(*t*Bu)$_3$ furnishes significantly better results than a 1:2 ratio. [PdCl$_2$(dppf)] is an equally effective catalyst for reactions that involve 2-chloropyridine derivatives. Interestingly, the Negishi coupling of 5-bromo-2-chloropyridine by [PdCl$_2$(dppf)] affords a 1:1 mixture of products as a result of reaction of the chloride and the bromide, whereas exclusive coupling of the bromide is observed with Pd/P(*t*Bu)$_3$ [Eq. (33)].



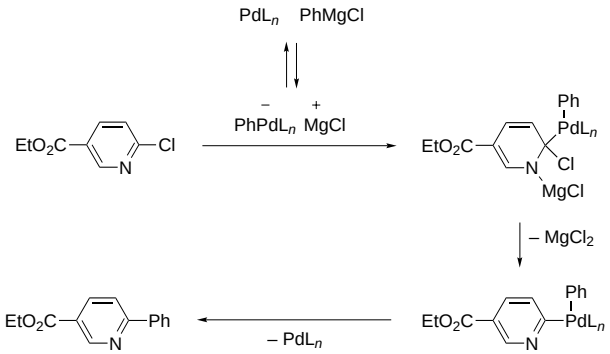
2.1.5. Kumada Reactions

The palladium-catalyzed coupling of Grignard reagents with aryl/vinyl halides and triflates is most commonly called the Kumada reaction.[151, 152] This process is of great significance among cross-couplings because of its relatively early discovery, but its utility is somewhat limited, compared to the reactions described above, as a consequence of the incompatibility of Grignard reagents with many functional groups.

A few palladium-catalyzed Kumada cross-couplings of heteroaryl chlorides have been reported.[153] Knochel and co-workers have recently determined that certain 2-chloropyridine derivatives react with functionalized aryl Grignard reagents under very mild conditions [Eq. (34)].[154] The use of



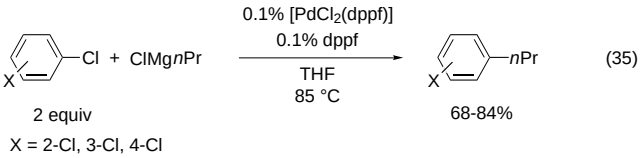
the low temperature means that the presence of normally incompatible esters is tolerated. The facility of this process at low temperature suggests that an addition–elimination mechanism is operative (Scheme 6). Nucleophilic addition of a palladium "ate" complex, formed from the reaction of PdL$_n$ and PhMgCl, to the highly electrophilic 2-chloropyridine yields a stabilized magnesium amide which, after loss



Scheme 6. Possible mechanism for the Pd^0-catalyzed Kumada coupling of a 2-chloropyridine with PhMgCl.

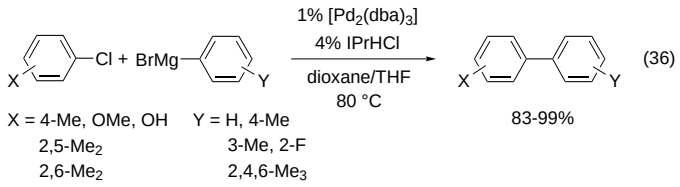
of MgCl$_2$ and reductive elimination, furnishes the coupled product. The corresponding 3-halopyridine derivatives are considerably less reactive under these conditions.

Katayama and Umeno described the first examples of palladium-catalyzed Kumada cross-couplings of (activated) non-heteroaryl chlorides. Thus, selective monocoupling of dichlorobenzenes with aryl and alkyl Grignard reagents can be achieved with [PdCl$_2$(dppf)] as the catalyst [Eq. (35)]; in



all cases, less than 5% of the dialkylated product is observed.[155] Uemura et al. have noted that tricarbonyl(η^6-chloroarene)chromium complexes participate in Kumada couplings, although dehalogenation is a significant side reaction.[27a]

The first report of a palladium-catalyzed Kumada cross-coupling of an unactivated aryl chloride was provided by Herrmann et al., who showed that palladacycles accomplish the coupling of chlorobenzene with MeMgBr and PhMgCl.[37a] Electron-rich aryl chlorides have been shown to react with aryl magnesium bromides in the presence of [Pd$_2$(dba)$_3$] and carbene salt IPrHCl; a slight excess of Grignard reagent is used to deprotonate the salt and generate the free carbene ligand in situ [Eq. (36)].[156] Hindered substrates such as 2-chloro-*m*-xylene can be coupled efficiently. However, the utility of this Kumada cross-coupling process is limited by its relatively low functional-group tolerance; for example, the



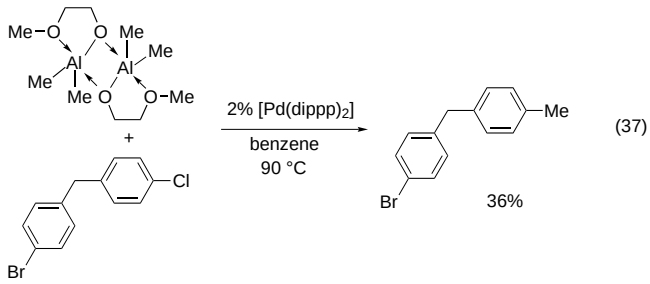
(36)

reaction of methyl 4-chlorobenzoate results in the formation of significant amounts of side products.

2.1.6. Related Cross-Coupling Reactions

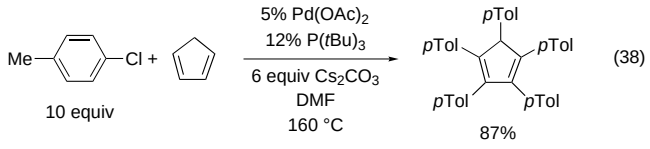
Palladium-catalyzed cross-couplings of aryl chlorides with organometallic species other than B-, Sn-, Si-, Zn-, and Mg-based compounds are relatively uncommon, with most of the reports involving heteroaryl chlorides.[157] For example, Undheim and co-workers have demonstrated that alkenylzirconocenes, readily available through hydrozirconation of terminal alkynes, selectively couple at the 4-, rather than the 2-position of 2,4-dichloropyrimidine and 2,4-dichloroquinazoline.[158] Furthermore, palladium-catalyzed methylations and ethylations with $AlMe_3$ and $AlEt_3$ have been described for chloropyrazines,[15a, 159] pyrazine *N*-oxides,[160] quinazolines,[161] purines,[25b, 162] and β-carbolines.[22b, 163, 164]

Blum et al. have recently shown that aryl chlorides can be methylated by hypervalent aluminum and gallium complexes.[165] $[Pd(PPh_3)_4]$ is an acceptable catalyst for highly activated nitro-substituted aryl chlorides, but the palladium complex of a bulky, electron-rich, chelating ligand such as 1,3-bis(diisopropylphosphanyl)propane (dippp) is required for electron-neutral substrates. Surprisingly, this catalyst is ineffective for couplings of typically more reactive aryl bromides, thereby allowing the selective reaction of a chloride in preference to a bromide, albeit in quite modest yield [Eq. (37)].



(37)

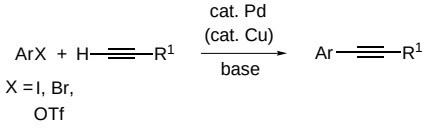
A very interesting palladium-catalyzed pentaarylation of cyclopentadienes has been reported by Dyker et al. in which they used $P(tBu)_3$ as a ligand [Eq. (38)].[166] The authors suggest that the coupling proceeds by transmetalation of the cyclopentadienyl anion with $[ArClPd\{P(tBu)_3\}_n]$, which is the product of oxidative addition of an aryl chloride to palladium.



(38)

2.1.7. Sonogashira Reactions

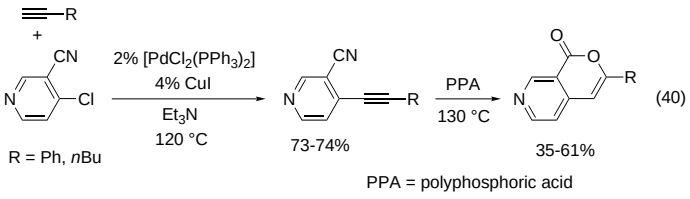
The palladium-catalyzed coupling of terminal alkynes with aryl/vinyl halides and triflates, usually in the presence of a copper co-catalyst, is commonly known as the Sonogashira reaction [Eq. (39)].[167] Despite its utility and the effort that



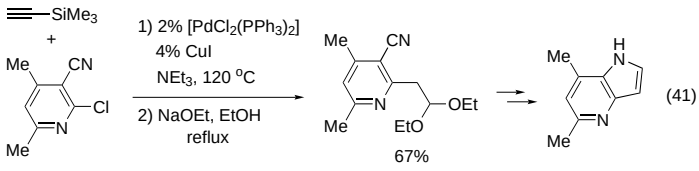
(39)

has been dedicated to expanding its scope, a general protocol for employing unactivated aryl chlorides in this process has not yet been developed. On the other hand, there have been numerous reports of couplings of activated aryl chlorides, particularly nitrogen-containing heteroaryl chlorides, which afford alkynylated N-heteroaromatic compounds that can cyclize to form a variety of interesting fused heterocycles.[168]

An array of naphthyridinones[169] and pyranopyridinones[170] can be obtained by Sonogashira coupling of cyano-substituted 2-, 3-, or 4-chloropyridines, followed by cyclization [Eq. (40)]. Indoles may be synthesized from cyano-substituted 2-chloropyridines utilizing a Hofmann rearrangement as a key step [Eq. (41)].[171, 172]

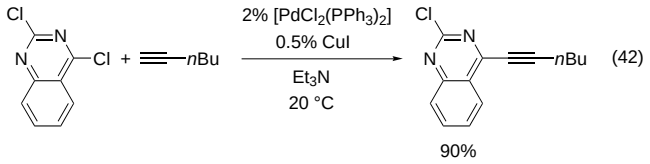


(40)

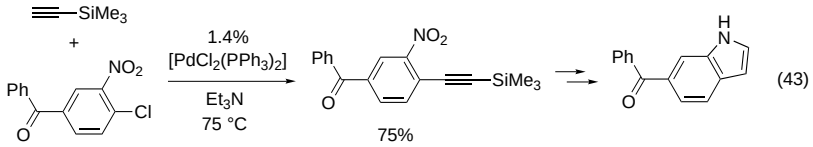


(41)

Other chloro-substituted six-membered heterocycles, such as pyridazines,[172a, 173] pyrimidines,[158, 172a, c, 174] pyrazines,[172a, b, 173d, 175] and triazines,[176] are also suitable substrates for Sonogashira couplings. Furthermore, fused heteroaromatics, for example, chloroquinolines,[18a, 172a, 173c, 175c] isoquinolines,[172a, 173c, 177] quinazolines,[178] quinoxalines,[179] pterins,[175d, 180] purines,[181] naphthyridines,[182] and phenanthrolines,[182] are useful coupling partners. In the case of 2,4-dichlorosubstituted quinazolines, selective Sonogashira coupling at the 4-position can be achieved at 20 °C; introduction of a second alkynyl group requires heating to 65 °C [Eq. (42)].[158]



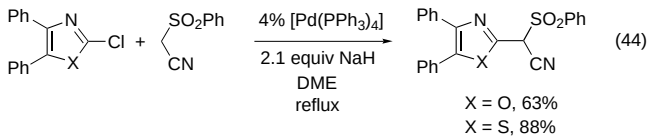
The first example of a Sonogashira reaction of an aryl chloride, activated 4-chlorobenzonitrile, was provided by Cassar, using $[Pd(PPh_3)_4]$ as the catalyst and a somewhat unusual base, NaOMe, in DMF at 80 °C (coupling with phenylacetylene; 64% yield).[183] Several additional reports of Sonogashira reactions of electron-deficient aryl chlorides have subsequently appeared.[144, 184, 185] One interesting example involves substituted *o*-nitrochlorobenzenes, which can be converted into indoles through a four-step process that begins with a Sonogashira coupling with trimethylsilylacetylene [Eq. (43)].[186] This method is noteworthy because indoles that bear an electron-withdrawing group at the 6-position can be difficult to synthesize.



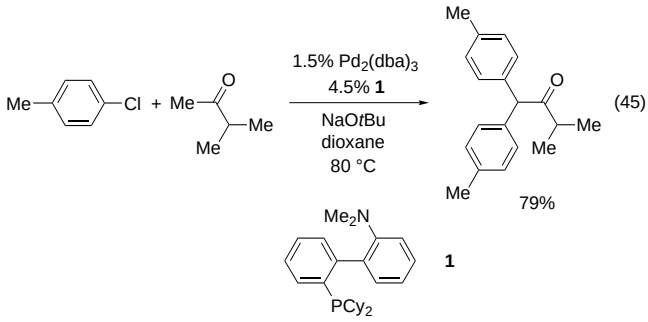
2.1.8. α-Arylation Reactions of Enolates and Other Stabilized Carbanions

The palladium-catalyzed α-arylation of enolates and other stabilized carbanions has been extensively investigated during the past several years.[187] Initial efforts focused largely on couplings of aryl bromides, but more recently a number of catalysts have been developed that permit the use of aryl chlorides as substrates.

The first example of a palladium-catalyzed arylation of a stabilized carbanion by a heteroaryl or aryl chloride was provided by Yamanaka and co-workers, who showed that diphenyl-substituted 2-chlorooxazoles and thiazoles can be coupled with phenylsulfonylacetonitrile in the presence of NaH [Eq. (44)].[188] The analogous 2-chloro-1-methylimidazole is unreactive under these conditions.

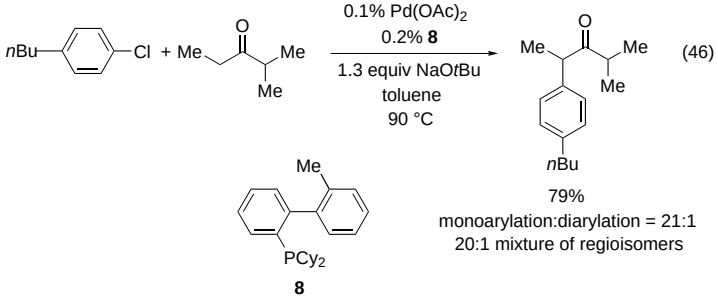


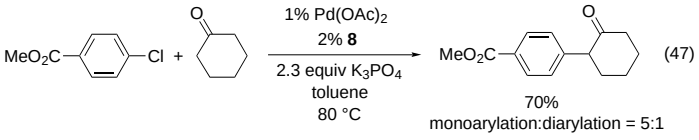
The palladium-catalyzed α-arylation of a ketone with an aryl chloride was first reported by Buchwald and co-workers in which they used biphenyl ligand **1** [Eq. (45)].[56] While Pd/binap is selective for monoarylation of methyl ketones by aryl bromides, Pd/**1** favors diarylation of methyl ketones by aryl chlorides.



In a subsequent study, Buchwald and co-workers surveyed an array of dialkylarylphosphanes, and determined that phosphane **8**, now commercially available, is unusually effective in palladium-catalyzed α-arylations of ketones. With this ligand, electron-poor, electron-neutral, electron-rich, and hindered aryl chlorides can efficiently be coupled with a wide range of ketones. Furthermore, a low catalyst loading (0.1–1.0% Pd) can be employed.[189] Ligand **8** provides high selectivity for monoarylation over diarylation and for arylation at a methylene, rather than a methine, position [Eq. (46)].

Buchwald and co-workers have also established that NaO*t*Bu can be replaced with K_3PO_4, which significantly enhances the functional-group compatibility of the α-arylation process involving substrates that contain base-sensitive functional groups [Eq. (47)]. One unsolved challenge, however, is the regioselective arylation of ketones such as 2-hexanone that require differentiation between a methyl and a methylene group.

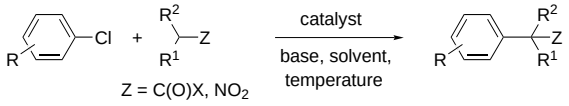


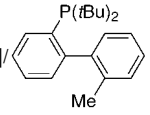
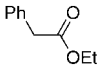
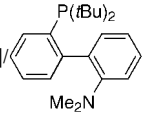
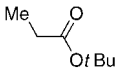
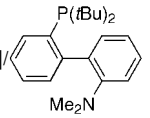
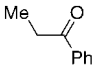
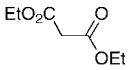
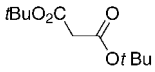
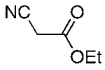
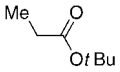
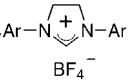
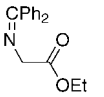
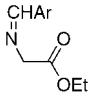


α-Arylation with aryl chlorides can be expanded to other stabilized carbanions, including the conjugate base of nitroalkanes (Table 5, entry 1)[190] and esters (entries 2 and 3).[191] When an ester is the substrate, $LiN(SiMe_3)_2$ must be used for deprotonation to selectively obtain monoarylated, rather than diarylated, product.

Kawatsura and Hartwig have investigated the palladium-catalyzed α-arylation of ketones with aryl chlorides, in which

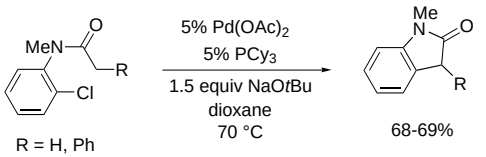
Table 5. α-Arylations of Enolates and Other Stabilized Carbanions.



Entry	R	Carbonyl or nitro compound	Catalyst	Conditions	Yield [%]
1	4-CO_2Me, 3-OMe, CO_2Me		[$Pd_2(dba)_3$]/ 	Cs_2CO_3, DME, 55–60 °C	65–86
2	4-Me, OMe		[$Pd_2(dba)_3$]/ 	$LiN(SiMe_3)_2$, toluene, 80 °C	82–87
3	4-OMe, OPh		[$Pd_2(dba)_3$]/ 	$LiN(SiMe_3)_2$, toluene, 80 °C	54–56
4	4-COPh, H, OMe, 2-Me		$Pd(OAc)_2$ or [$Pd(dba)_2$]/PCy_3, $P(tBu)_3$, or D*t*BPF	NaO*t*Bu, THF, 50–70 °C	80–95
5	4-CF_3, H, OMe, 2-OMe, 2,5-Me_2		[$Pd(dba)_2$]/$Ph_5FcP(tBu)_2$	K_3PO_4, toluene, 100 °C	81–89
6	4-CF_3, H, OMe, 2,5-Me_2		[$Pd(dba)_2$]/$P(tBu)_3$ or [$PdCl(allyl)]_2$/$P(tBu)_3$	NaO*t*Bu, dioxane, 100 °C	84–90
7	4-H, F, OMe, 2,5-Me_2		[$PdCl(allyl)]_2$/$P(tBu)_3$	Na_3PO_4, toluene, 100 °C	82–90
8	4-H		[$Pd(dba)_2$]/ 	$NaN(SiMe_3)_2$, toluene, RT	71[a]
9	4-CN, CF_3, F, H, OMe, 2-Me, 3-Cl-pyridine		[$Pd(dba)_2$]/$P(tBu)_3$	K_3PO_4, toluene, 120 °C	80–85
10	4-CF_3, H		[$Pd(dba)_2$]/$P(tBu)_3$	K_3PO_4, toluene, 120 °C	67[b]

they focused initially on a potentially bidentate ligand, 1,1′-bis(di-*tert*-butylphosphanyl)ferrocene (D*t*BPF). Since ^{31}P NMR studies of independently synthesized [ArPdL(enolate)] complexes revealed that only one phosphorus atom of D*t*BPF is bound to the palladium center, the use of monodentate $P(tBu)_3$ and PCy_3 (Cy = cyclohexyl) was also explored. In fact, all three ligands have proved to be effective for coupling a variety of aryl chlorides with ketones (Table 5, entry 4).[192] Arylations of malonates can also be achieved. Pentaphenylferrocenylphosphane $Ph_5FcP(tBu)_2$ is the ligand of choice for diethyl malonate (Table 5, entry 5), while $P(tBu)_3$ is the ligand of choice for di-*tert*-butyl malonate (entry 6).[193] A range of aryl chlorides serve as suitable coupling partners, with exceptions being chloropyridines and cyano-substituted substrates.

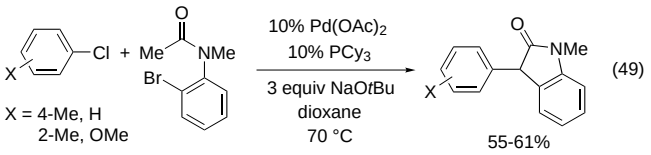
Amides also undergo palladium-catalyzed α-arylation. An intramolecular process can furnish biologically interesting oxindoles; PCy_3, as well as carbene ligands SIPr and IPr,[194] are the most effective of the ligands that have been screened [Eq. (48)].[195] A combined, one-pot intra- and intermolecular



(48)

amide arylation can provide 3-aryloxindoles from readily available 2-bromoanilides and aryl chlorides, including hindered and electron-rich compounds [Eq. (49)].

Hartwig and co-workers have also determined that palladium-catalyzed couplings of ethyl cyanoacetate with aryl



(49)

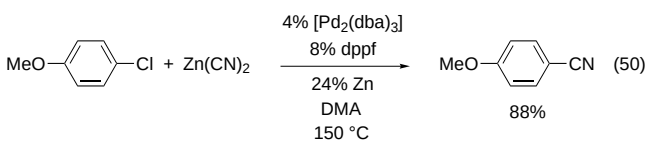
chlorides can be accomplished (Table 5, entry 7).[193, 196] Both electron-rich and hindered chlorides can be employed in the presence of Pd/P(tBu)$_3$, although the presence of certain electron-withdrawing groups, such as esters, ketones, and nitriles, is not well-tolerated. This catalyst system emerged from a high-throughput screen that was based on a fluorescence resonance energy transfer assay.[197] A wide range of ligands (>100), palladium sources, and bases was explored.

Like Buchwald and co-workers, Hartwig and co-workers have described a method for the α-arylation of esters—with a Pd/carbene catalyst, the coupling of chlorobenzene with *tert*-butyl propionate proceeds at room temperature (Table 5, entry 8).[198] In addition, alkylidene glycinates may be arylated with a wide range of chlorides, thereby providing facile access to α-aryl-α-amino acid derivatives (Table 5, entries 9–10).

2.1.9. Cyanation Reactions

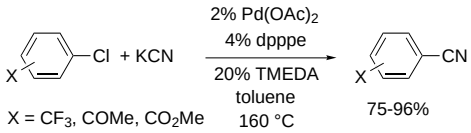
Although there are a number of methods for achieving the synthesis of aryl cyanides (for example, Rosenmund–von Braun reaction and Sandmeyer-based routes), milder and less expensive routes are nevertheless desirable.[199] Metal-catalyzed cyanation of aryl chlorides has the potential to furnish a solution to this challenge, and useful progress has been made. For example, palladium-catalyzed cyanations of activated heteroaryl chlorides, such as pyrazines[200] and 2- and 6-chloropurines,[201] have been described. Furthermore, Andersson and Langstrom reported in 1994 that the coupling of unactivated chlorobenzene can be accomplished by [Pd(PPh$_3$)$_4$] at 90 °C, albeit in modest yield (45%).[202]

In 2000, Jin and Confalone established that Pd/dppf catalyzes the cyanation of an electronically and sterically diverse array of aryl chlorides with Zn(CN)$_2$ used as the cyanide source [Eq. (50)].[203] The yields for the couplings are uniformly excellent (≥85%), although the reaction temperatures are somewhat high (120–150 °C).



(50)

More recently, Beller and co-workers reported the palladium-catalyzed cyanation of chloroquinolines and activated aryl chlorides using KCN as the source of cyanide, 1,5-bis(diphenylphosphanyl)pentane (dpppe) as the ligand, and tetramethylethylenediamine (tmeda) as an additive [Eq. (51)].[204] Among the monodentate and bidentate phosphanes that were screened, dpppe, which can form an eight-membered chelate, was found to clearly be the most effective.

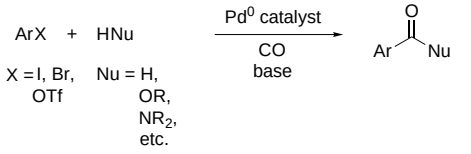


(51)

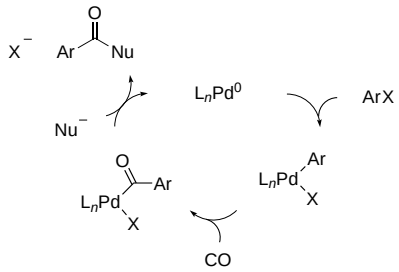
2.1.10. Related Processes

2.1.10.1. Carbonylation Reactions

The palladium-catalyzed carbonylation of aryl halides and triflates furnishes a powerful method for synthesizing an array of carbonyl compounds, such as aldehydes, esters, and amides (Eq. (52) and Scheme 7).[205] From a historical perspective, some of the earliest studies of the activation of aryl chlorides focused on carbonylation processes.

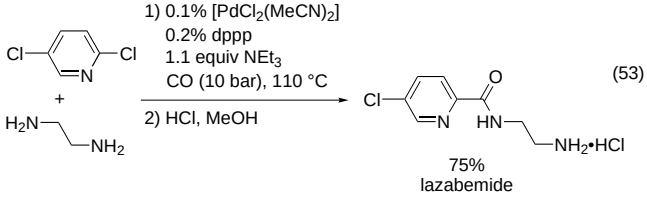


(52)



Scheme 7. Generalized mechanism for palladium-catalyzed carbonylation reactions.

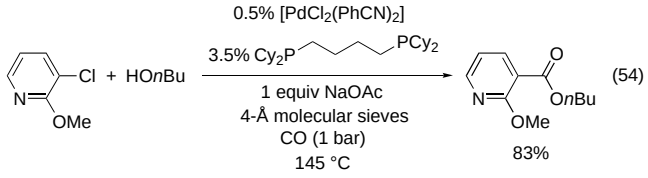
The palladium-catalyzed carbonylation of chloropyridines and other nitrogen-containing heterocycles is of particular interest to industrial chemists because the products are valuable intermediates for the production of a variety of herbicides and pharmaceuticals.[206] The Hoffmann–La Roche one-step synthesis of lazabemide, a monoamine oxidase B inhibitor, exploits a highly selective monoamidocarbonylation of 2,5-dichloropyridine [Eq. (53)]; the previous syntheses of lazabemide had required four to eight steps.[207, 208]



(53)

There are quite a few examples of carbonylations of other heteroaryl chlorides, for example, chloropyrazines,[208b, 209] pyrimidines,[210] quinolines,[18a, 208f] chlorothiophenes,[208c]

naphthyridines,[211] and phenanthrolines.[211] A thorough study by Beller et al. revealed that bidentate phosphanes, including dppf, are very effective for palladium-catalyzed alkoxycarbonylations of 2-chloropyridines, 2- and 4-chloroquinolines, pyrazines, pyrimidines, and pyridazines; a turnover number of 13 000 was achieved for a carbonylation of 2-chloropyridine using dppb as the ligand.[212] For less reactive 3-chloropyridines, more bulky and electron-rich 1,4-bis(dicyclohexylphosphanyl)butane was found to be most useful [Eq. (54)].

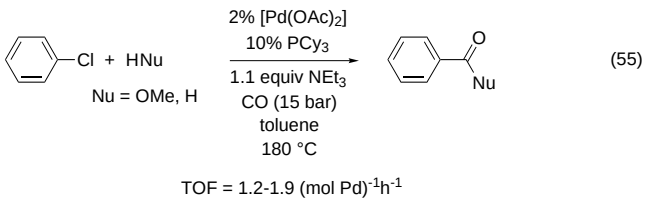


(54)

Monodentate ligands were found to be less effective for these carbonylation processes, perhaps because bidentate ligands disfavor formation of an unproductive dimer after the substrate oxidatively adds to palladium(**0**). Consistent with this hypothesis, the oxidative-addition dimer that is generated upon reaction of $[Pd(PPh_3)_4]$ with 2-chloropyridine does not undergo carbonylation when treated with CO at elevated temperature.

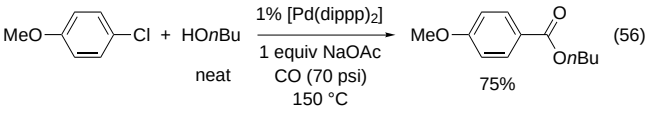
In 1989, the research groups of Milstein and Osborn independently provided the first examples of palladium-catalyzed carbonylations of unactivated aryl chlorides.[213] These landmark studies furnished early evidence that bulky, electron-rich phosphanes can be unusually effective in activating carbon–chlorine bonds.

Osborn and co-workers demonstrated that Pd/PCy_3 and $Pd/P(i\text{Pr})_3$ are active catalysts for both alkoxycarbonylation and hydrocarbonylation (formylation) of chlorobenzene [Eq. (55)].[214] Perhaps not surprisingly, less electron-rich and less bulky phosphanes such as PPh_3 are ineffective. Interestingly, the more electron-rich and more bulky $P(t\text{Bu})_3$ is also ineffective, which indicates that the electronic and steric properties of the ligand define a window of reactivity.



(55)

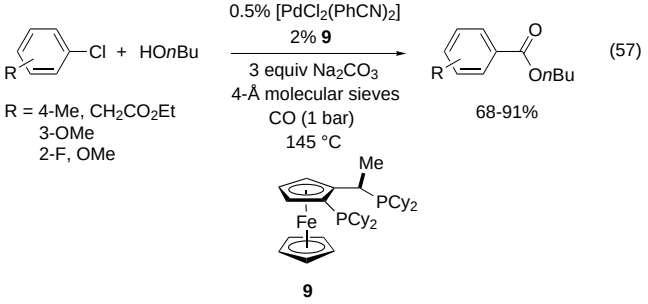
At the same time, Milstein and co-workers established that a palladium complex bearing sterically demanding, electron-rich, chelating 1,3-bis(diisopropylphosphanyl)propane (dippp) achieves the amidocarbonylation, alkoxycarbonylation,[215] and formylation[216] of aryl chlorides, including deactivated substrates [Eq. (56)]. The catalyst with a dippp ligand was much more effective than catalysts with the other monodentate and bidentate ligands screened. Milstein and co-workers believe that the distinguishing features of dippp are its capacity to chelate to form a six-membered ring, its bulk, and its basicity.



(56)

Subsequently, additional homogeneous[208c, 217] and heterogeneous[218] methods for the carbonylation of aryl chlorides have been developed. One example of an application of such processes comes from polymer chemistry, where poly(imideamides)[219] and poly(amides)[220] have been synthesized by palladium-catalyzed amidocarbonylation of aryl chlorides with aromatic amines.

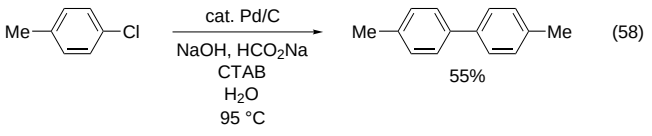
Beller and co-workers has very recently employed commercially available 1-[2-(dicyclohexylphosphanyl)ferrocenyl]-ethyldicyclohexylphosphane (**9**) in carbonylations of aryl chlorides [Eq. (57)].[221] In contrast to other catalysts, which generally require considerable CO pressure, this reaction proceeds at 1 bar.



(57)

2.1.10.2. *Homocoupling Reactions*

The palladium-catalyzed homocoupling of aryl halides can offer a mild alternative to the classical Ullmann coupling, which employs a stoichiometric amount of copper and very high temperature.[222] A very early example of this type of reaction was reported by Bamfield and Quan, who discovered that heterogeneous Pd/C catalyzes the homocoupling of unactivated aryl chlorides and of chloropyridines to produce symmetrical biaryls in moderate yield [Eq. (58)].[223] Alkaline sodium formate is employed as the reducing agent and cetyltrimethylammonium bromide (CTAB) is used as a surfactant.



(58)

Sasson and co-workers subsequently investigated Pd/C-catalyzed homocouplings of aryl chlorides in detail. They determined that not only formate salts,[224] but also hydrogen gas[225] and zinc,[226] may serve as the reductant. There have been several reports of homocouplings of aryl chlorides catalyzed by homogeneous complexes, but they are very limited in scope.[227]

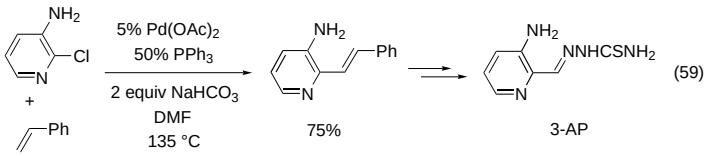
2.2. Heck Reactions

The palladium-catalyzed coupling of aryl/vinyl halides and triflates with olefins, usually referred to as the Heck reaction [Eq. (2)], is arguably one of the most important carbon–carbon bond-forming processes in synthetic organic chemistry (Scheme 2).[228, 229] It is mechanistically distinct from the cross-coupling reactions described above, although the first step, oxidative addition of the halide or triflate to Pd^0, is the same (Scheme 1).

2.2.1. Heck Reactions of Activated Aryl Chlorides

Heck couplings of 2-halopyridines are sometimes problematic as a result of the formation of an unreactive dimer from the oxidative addition adduct.[153a, 230] Nevertheless, several successful Heck reactions of 2-chloropyridines have been described,[102e, 231] as well as couplings of other heteroaryl chlorides, such as pyrazines,[175a, 232] chloroquinolines,[110d, 233] quinoxalines,[234] and pterins.[235]

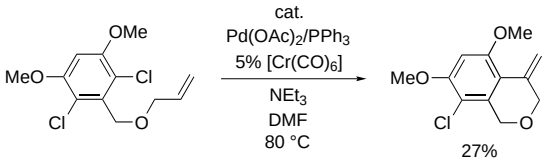
The synthesis of the antitumor agent 3-aminopyridine-2-carboxaldehyde thiosemicarbazone (3-AP) furnishes an interesting example of a Heck reaction of a 2-chloropyridine [Eq. (59)].[14g] The initial routes to 3-AP focused on Stille and



(59)

Suzuki cross-couplings of 2-chloro-3-nitropyridine with vinyltributyltin and methylboronic acid, respectively, followed by a $SnCl_2$-mediated reduction of the nitro group. Work-up and purification problems associated with the reduction step prohibited large-scale production of 3-AP, so direct Suzuki and Stille reactions of 2-chloro-3-aminopyridine were investigated; unfortunately, neither process provides the desired product in satisfactory yield. Fortunately, however, the Heck coupling of 2-chloro-3-aminopyridine with styrene can be achieved and affords the target stilbene derivative, which can be converted in several steps into 3-AP.

The earliest examples of Heck reactions of activated non-heteroaryl chlorides were described by Spencer, who established that $Pd(OAc)_2/PPh_3$ catalyzes couplings of electron-deficient aryl chlorides with electron-deficient alkenes at 150 °C in poor to modest yield (21–51%).[236] As for many of the cross-couplings that were discussed in Section 2.1, it is possible to activate the C–Cl bond for Heck reactions through η^6-complexation of the aryl chloride to tricarbonylchromium complexes.[123a, 213d, 213e] In one particularly interesting report, the Heck coupling of an aryl chloride with only a catalytic amount of chromium has been achieved, albeit in low yield [Eq. (60)].[237] During this process, the starting material presumably binds to chromium and undergoes a Heck reaction; the chromium-complexed product thus generated



(60)

then releases the tricarbonyl chromium, which can then bind to additional starting material to continue the catalytic cycle.

Herrmann et al. were the first to demonstrate that palladacycles can catalyze Heck couplings of activated aryl chlorides (Table 6, entry 1).[238] To obtain high conversions, nBu_4NBr was employed as a co-catalyst. These conditions were not effective for electron-neutral or electron-rich aryl chlorides. Subsequently, both nitrogen- (Table 6, entry 2)[239, 240] and sulfur-containing palladacycles[241] have also been shown to be reasonably efficient catalysts for Heck reactions of activated aryl chlorides.

Herrmann et al. pioneered not only the use of palladacycles, but also of palladium carbenes as catalysts for Heck couplings of activated aryl chlorides (Table 6, entry 3).[242] Recently, additional palladium–carbene adducts have been shown to be active, but, as with the original catalyst, only electron-poor chlorides are suitable substrates, and elevated temperatures are required (Table 6, entries 4–6).[243–246]

Beller and Zapf have established that Pd/phosphite mixtures catalyze Heck couplings of activated aryl chlorides; both trialkyl- and triarylphosphites are effective (Table 6, entry 7).[247] In addition, Li et al. have demonstrated that commercially available, air-stable Pd^{II} complexes that bear phosphinous acid ligands are useful for the Heck reaction of an electron-poor aryl chloride (Table 6, entry 8).[248]

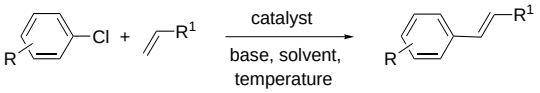
A wide-ranging study of palladium-catalyzed Heck couplings of activated aryl chlorides in the presence of a variety of phosphorus ligands has recently been described by Zapf and Beller. With nBu_4NBr as a co-catalyst, even simple phosphanes can provide turnover numbers approaching 1000 at 160 °C (Table 6, entry 9).[249] Unfortunately, electron-neutral and electron-rich aryl chlorides did not furnish appreciable amounts of product under any of the broad array of conditions that were screened.

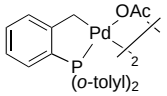
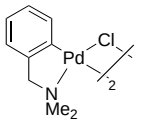
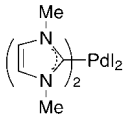
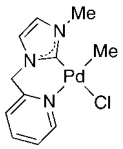
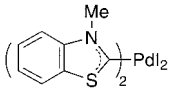
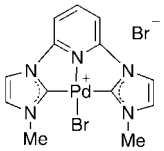
Dupont and co-workers have reported that the phosphane-free catalyst system $[PdCl_2(SEt_2)_2]/nBu_4NBr$, which was found to be effective for Suzuki reactions of activated aryl chlorides (see Section 2.1.1.1), can also be applied to Heck couplings of this family of substrates with styrene and *n*-butyl acrylate. This method can be conducted in air with little loss in efficiency.[250] An example of a Heck reaction of an activated aryl chloride by a heterogeneous catalyst has been provided by Djakovitch et al., who showed that a palladium complex entrapped in a zeolite cage can achieve the coupling of 4-chloroacetophenone with styrene.[251]

2.2.2. Heck Reactions of Unactivated Aryl Chlorides

Davison et al. were the first to describe significant success in a Heck coupling of an unactivated aryl chloride: The palladium-catalyzed Heck reaction of electron-neutral chlorobenzene with styrene proceeds in modest yield in the presence

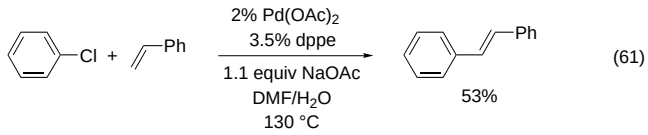
Table 6. Heck cross-couplings of activated aryl chlorides.



Entry	R	R^1	Catalyst	Conditions	Yield [%]
1	4-CHO, CN, COMe	Ph, CO_2nBu		NaOAc, DMA, 130 °C	32 – 81[a]
2	4-NO_2	Ph, CO_2Et		K_2CO_3, NMP, 150 °C	51 – 71
3	4-CHO, NO_2	CO_2nBu		NaOAc, DMA, 130 °C	99[a]
4	4-CHO	CO_2nBu		NaOAc, DMA, 120 °C	75[b,c]
5	4-NO_2	CO_2nBu		$NaHCO_3$, nBu_4NBr, 130 °C	95
6	4-CHO	Ph		NaOAc, DMA, reflux	75[a]
7	4-CF_3, 3-CF_3	Ph, $CONMe_2$	$Pd(OAc)_2/P(OR)_3$	Na_2CO_3, DMA, 160 °C	15 – 89[a,d]
8	4-COMe	CO_2tBu	$[PdCl_2\{P(t\text{Bu})_2OH\}_2]$	NaOAc, DMF, 135 °C	66[a]
9	4-COMe	Ph	$Pd(OAc)_2/P(n\text{Bu})_3$	Na_2CO_3, DMA, 160 °C	85[a]

[a] nBu$_4$NBr was used as a co-catalyst. [b] nPr$_4$NBr was used as a co-catalyst. [c] GC conversions. [d] R = 2,4-(tBu)$_2$C$_6$H$_3$ or Et.

of bidentate 1,2-bis(diphenylphosphanyl)ethane (dppe) [Eq. (61)].[252] A lower yield (45 %) is obtained if PPh_3 is employed instead of dppe.



(61)

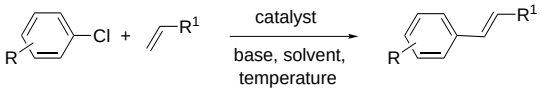
Milstein and co-workers subsequently revealed several important findings regarding Heck reactions of aryl chlorides. They determined that use of a bulky, electron-rich, chelating phosphane ligand (1,4-bis(diisopropylphosphanyl)butane; dippb) furnishes a palladium catalyst that can efficiently couple electron-poor and electron-neutral aryl chlorides (Table 7, entry 1).[253] Unfortunately, the catalyst affords low yields for reactions of electron-rich chlorides. Remarkably, other bulky, electron-rich chelating phosphanes, such as dippp and dippe, as well as monodentate phosphanes such as P(iPr)$_3$, provide essentially inactive catalysts. Milstein and co-workers attribute this difference in reactivity to:

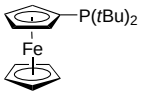
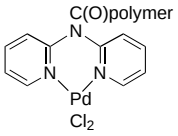
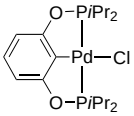
1) Easier dissociation of one of the phosphane groups in the case of dippb (versus dippp and dippe), which allows olefin coordination;
2) Faster oxidative addition of the aryl chloride to PdL_1 (L = dippb) than to L_2Pd (L = monophosphane);
3) More rapid olefin insertion (versus monodentate phosphanes), as a result of chelation by dippb.[254]

Heck reactions of unactivated aryl chlorides with styrene can be performed in the presence of Pd/dippp under reducing, nonbasic conditions to preferentially generate *cis*-stilbenes (Table 7, entry 2).[255] Coupling of electron-rich 4-chloroanisole proceeds in a respectable yield of 49 %, although dehalogenation is a significant side reaction.

Herrmann et al. used palladium complexes and simple triarylphosphanes (for example, PPh_3) and obtained modest success (up to 48 % yield) in effecting Heck reactions of 4-chloroanisole with *n*-butyl acrylate, although quite high temperatures were required (160 °C) and side products arising from P–C bond cleavage were observed.[256] Palladium-supported on MgO[257] and nanostructured palladium clusters stabilized with propylene carbonate also exhibit some activity in Heck couplings of chlorobenzene and styrene.[258]

Table 7. Heck couplings of aryl chlorides.



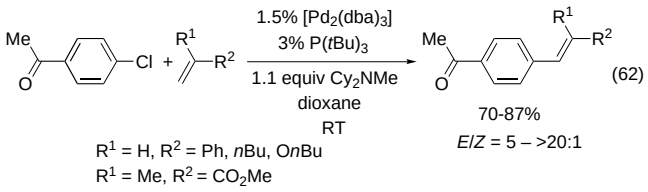
Entry	R	R^1	Catalyst	Conditions	Yield [%]
1	4-NO_2, CHO, H, CH_3	Ph	$Pd(OAc)_2$/iPr$_2$P(CH$_2$)$_4$PiPr$_2$	NaOAc, DMF, 150 °C	55 – 95
2	4-COMe, H, OMe, 3-OMe	Ph	$Pd(OAc)_2$/iPr$_2$P(CH$_2$)$_4$PiPr$_2$	Zn, DMF, 140 °C	49 – 88
3	4-CHO, H	Ph	$[PdCl_2(MeCN)_2]/PPh_4Cl$	NaOAc, NMP, 150 °C	96 – 98[a,b]
4	4-COMe, H, OMe, 2-Me	Ph, CO_2Me	$[Pd_2(dba)_3]/P(t\text{Bu})_3$	Cs_2CO_3, dioxane, 100 – 120 °C	70 – 84
5	4-CO_2Me, Me, OMe	CO_2nBu	$[Pd(dba)_2]/P(t\text{Bu})_3$ or 	NaOAc, DMF, 110 °C	48 – 97
6	4-COMe, H	Ph		Na_2CO_3/K_2CO_3, DMA, 140 °C	89 – 95[c]
7	4-CHO, COMe, H, OMe, 2-Me	Ph		CsOAc, dioxane, 120, 180 °C	81 – 99
8	4-H, Me, OMe, 2-Me	Ph, $CO_2C_8H_{17}$	$[Pd(dba)_2]/n$BuP(1-Ad)$_2$	K_3PO_4, dioxane, 120 °C	33 – 98

[a] GC conversions. [b] *N*,*N*-Dimethylglycine was used as an additive. [c] nBu$_4$NBr was used as a co-catalyst.

An important contribution in the development of Heck chemistry of unactivated aryl chlorides was described by Reetz et al. in 1998. In this study, they noted that simple Pd^{II} complexes such as $[PdCl_2(MeCN)_2]$ and $Pd(OAc)_2$ exhibit high activities in Heck couplings of electron-neutral aryl chlorides with styrene in the presence of tetraphenylphosphonium salts (Table 7, entry 3).[259] The addition of *N*,*N*-dimethylglycine improves the regioselectivity of the reaction. Turnover numbers as high as 130 and 950 can be obtained for chlorobenzene and 4-chlorobenzaldehyde, respectively.

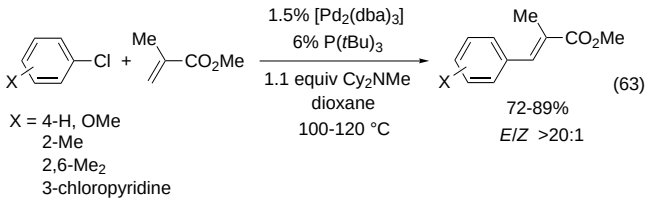
The most versatile method that has been reported to date for Heck couplings of unactivated aryl chlorides employs Pd/$P(t\text{Bu})_3$ as the catalyst. In 1999, Littke and Fu reported a first-generation system based on this combination. In the presence of Cs_2CO_3, this catalyst couples both electron-rich and hindered aryl chlorides with styrene and methyl acrylate (Table 7, entry 4).[260] Although the reaction temperature was still high (100 – 120 °C), it was lower than for other catalysts that had been described at that time. Interestingly, $P(t\text{Bu})_3$ was the only effective ligand among the commercially available phosphanes that were screened, which included PCy_3[261] and tris(2,4,6-trimethoxyphenyl)phosphane,[262] both of which are also quite bulky and electron-rich.[263]

A significant improvement in the scope and the mildness of this catalyst system was realized by replacing Cs_2CO_3 with Cy_2NMe.[264, 265] Heck couplings of activated aryl chlorides can be accomplished at room temperature with this new method [Eq. (62)]. Importantly, the scope of the reaction with respect to the olefin partner is considerably widened—a range of



(62)

monosubstituted and disubstituted olefins are arylated with high *E*/*Z* stereoselectivity; essentially all previous studies of Heck couplings of aryl chlorides had focused exclusively on styrene and acrylic acid derivatives, which are particularly reactive coupling partners. The catalyst is effective for electron-rich, hindered, and heteroaryl aryl chlorides [Eq. (63)]. In addition, a high turnover number (~300) can



(63)

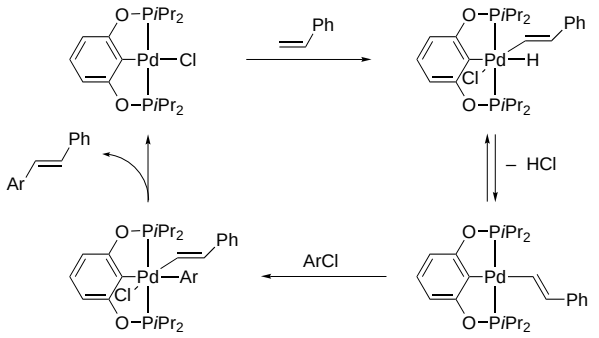
be achieved in the relatively challenging coupling of chlorobenzene with methyl methacrylate. Commercially available $[Pd\{P(t\text{Bu})_3\}_2]$, sometimes in combination with $[Pd_2(dba)_3]$, can be employed for many of these reactions.

The unusually high reactivity of Pd/P(tBu)$_3$ in Heck reactions of aryl chlorides was discovered independently by Hartwig and co-workers through a fluorescence-based assay in which over 40 phosphane ligands were screened for activity. Only two, P(tBu)$_3$ and di(*tert*-butyl)phosphanylferrocene, were effective for Heck couplings of unactivated aryl chlorides (Table 7, entry 5).[266]

In 1999, Buchmeiser and Wurst described a heterogeneous catalyst for Heck reactions of aryl chlorides based on a polymer-bound dichloropalladium(di(pyrid-2-yl)amide) that was prepared by ring-opening metathesis (Table 7, entry 6).[267] The use of this air- and moisture-stable catalyst can, with the addition of nBu$_4$NBr, enable turnover numbers as high as 23 600 to be achieved for the coupling of chlorobenzene with styrene.

Nonaqueous ionic liquids have been reported by Herrmann and Bohm to be excellent media for conducting palladacycle-catalyzed Heck reactions of unactivated aryl chlorides.[268] Phosphane- and phosphite-based palladacycles, as well as carbene-derived catalysts, show improved activity for couplings of chlorobenzene in molten nBu$_4$NBr, relative to DMF, which is a traditional solvent for the Heck reaction.[269] Even catalysts such as [Pd(PPh$_3$)$_4$] and PdCl$_2$ exhibit some reactivity under these conditions. However, only [Pd$_2$(dba)$_3$]/P(tBu)$_3$ displays high activity for Heck couplings of electron-rich aryl chlorides.

Jensen and co-workers have determined that a phosphite PCP-pincer complex, which can be prepared in two steps,[270] is an effective catalyst for Heck reactions of a range of aryl chlorides, including hindered and electron-rich substrates (Table 7, entry 7).[271] A disadvantage of this system is that a very high temperature (180 °C, 24 hours) or a prolonged reaction time (120 °C, 5 days) is required. Interestingly, under identical conditions, the more electron-rich phosphane PCP-pincer complex[272] is almost inactive. The Heck-type reactions catalyzed by the phosphite PCP-pincer complex may proceed through Pd^{II} and Pd^{IV} intermediates (Scheme 8). Thus,



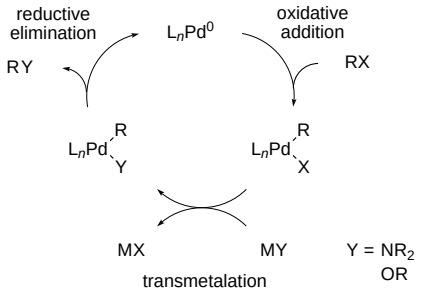
Scheme 8. Proposed mechanism for Heck-type reactions catalyzed by a phosphite PCP-pincer complex.

oxidative addition of a vinyl C–H bond is followed by reductive elimination of H–Cl, oxidative addition of Ar–Cl, and finally reductive elimination of the coupled product. The markedly lower reactivity of the more electron-rich phosphane PCP-pincer complex may be attributed to slower reductive elimination of HCl, which is believed to be the turnover-limiting step of the catalytic cycle.

Beller and co-workers have established that di(1-adamantyl)-*n*-butylphosphane is a highly effective ligand for Heck couplings of unactivated aryl chlorides, although hindered aryl chlorides furnish modest yields (Table 7, entry 8).[273] An array of bulky, electron-rich dialkylaryl- and trialkyphosphanes were screened for the palladium-catalyzed coupling of 4-chlorotoluene and styrene, and it was determined that di(1-adamantyl)-*n*-butylphosphane and P(tBu)$_3$ afford the highest yields and turnover numbers.

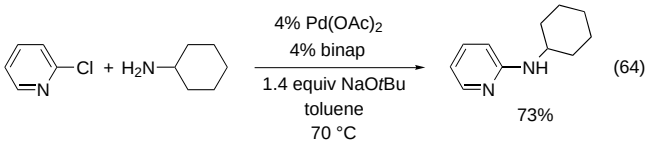
3. Carbon–Nitrogen Bond-Forming Reactions

As a result of the pioneering efforts of Buchwald and co-workers[274] and Hartwig et al.,[69b, 275] metal-catalyzed C(aryl)–N bond formation has recently emerged as an extremely powerful tool for the synthesis of aniline derivatives, which are important to a diverse array of fields, such as pharmaceuticals, agrochemicals, and photography.[276, 277] A simplified overview of the mechanism of the Buchwald–Hartwig reaction, as well as a related C–O bond-forming process (Section 4), is provided in Scheme 9. The pathway is analogous to that of the C–C bond-forming reactions described above (Scheme 1), except that the transmetalating agent is a metal amide or a metal alkoxide.



Scheme 9. Simplified mechanism for palladium-catalyzed C–N and C–O bond formation.

Although initial studies by the research groups of Buchwald and Hartwig focused on traditional coupling partners such as aryl bromides, later reports by these and other groups have described mild and general protocols for the palladium-catalyzed amination of aryl chlorides. In 1996, Wagaw and Buchwald furnished the first example of a reaction of a heteroaryl chloride, the Pd(OAc)$_2$/binap-catalyzed amination of 2-chloropyridine with cyclohexylamine [Eq. (64)].[278]

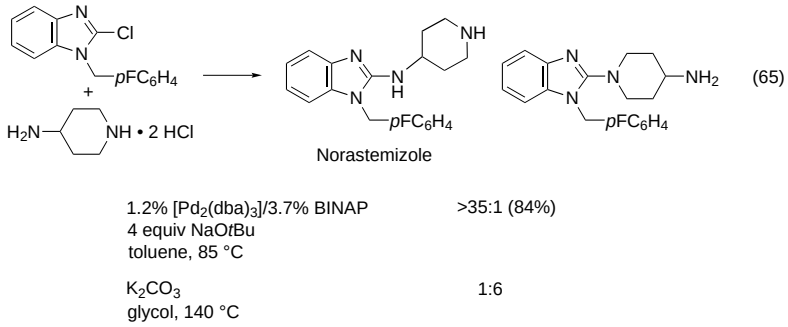


(64)

Subsequently, palladium-catalyzed aminations of chloroquinolines,[279] heteroarylimidoyl chlorides,[280] chloropur-

ines,[281] chlorothiophenes,[282] chlorobenzothiazoles,[283] chlorobenzooxazoles,[283] and other chloropyridines[279, 284] have been achieved, generally with either Pd/binap or Pd/dppf as the catalyst. For dichloro-substituted pyridines, Pd/binap/K_2CO_3 can effect highly selective aminations of the 2-chloro group, in preference to the 3-, 5-, and 6-chloro, group.[285]

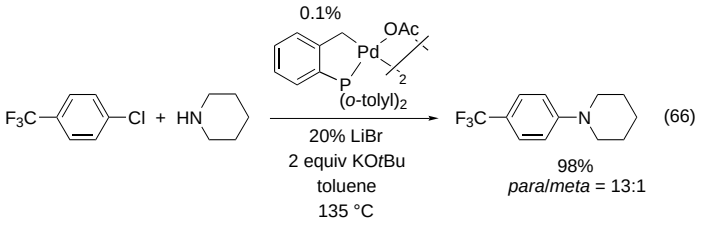
Senanayake and co-workers have devised a practical synthesis of the nonsedating antihistamine norastemizole that relies upon the amination of 4-fluorobenzyl-2-chlorobenzimidazole [Eq. (65)].[286] This work furnishes the first example of



(65)

a selective palladium-catalyzed coupling of a primary amine in the presence of a secondary amine. This selectivity is not limited to 4-aminopiperidine, but can be extended to acyclic diamines and triamines. In contrast, thermal amination leads to preferential reaction of the secondary amine with 6:1 selectivity.

The first report of a palladium-catalyzed amination of an activated, but non-heteroaryl, chloride was provided by Beller et al. in which they used a palladacycle complex [Eq. (66)].[287] A small amount of the *meta*-substituted product is obtained,



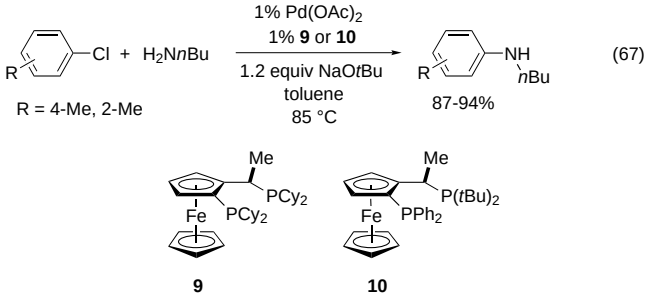
(66)

which suggests that at least some benzyne is generated under these conditions (in the absence of a catalyst, a 1:1 mixture of *para* and *meta* isomers is observed).[288] The choice of base is crucial—KO*t*Bu is far superior to NaO*t*Bu, which is more commonly used in palladium-catalyzed aminations.

In 1997, Reddy and Tanaka described the first examples of palladium-catalyzed aminations of unactivated aryl chlorides using $[PdCl_2(PCy_3)_2]$ as the catalyst (Table 8, entry 1).[289] $[PdCl_2(PiPr_3)_2]$ is also effective, but binap-,[290] dppf-, and P(*o*tol)$_3$-based catalysts provide less than 10% of the desired product. $[PdCl_2(PCy_3)_2]$-catalyzed aminations of *ortho*-substituted aryl chlorides proceed in poor yield. Reactions of cyclic secondary amines furnish the highest yields, and secondary anilines afford modest to good yields. On the other hand, acyclic secondary amines are not suitable substrates for this method, because of their propensity to undergo β-hydride elimination, which results in imine formation and hydrodehalogenation of the aryl chloride. Thus, PCy_3 appears to be effective at achieving oxidative addition of the aryl chloride to palladium, but it is not always ideal for subsequent steps in the catalytic cycle, such as promoting reductive elimination over β-hydride elimination.

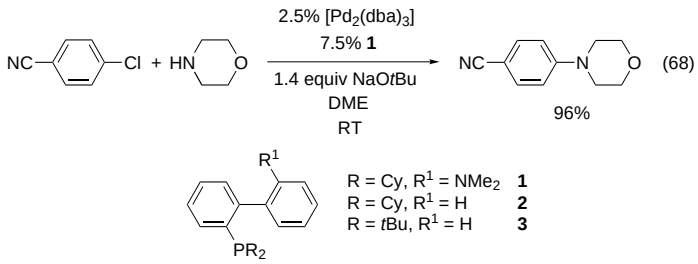
Hindered, chelating ferrocenyldialkylphosphanes, in particular 1,1′-bis(di-*tert*-butylphosphanyl)ferrocene (D*t*BPF), are useful in palladium-catalyzed aminations of aryl chlorides (Table 8, entry 2).[291] The high reactivity furnished by this ligand may be a result both of its electron-richness, which promotes the oxidative addition of unactivated aryl chlorides to Pd^0, and its steric demand and chelating nature, which favor reductive elimination over β-hydride elimination. Thus, Pd/D*t*BPF efficiently couples aniline and secondary cyclic amines with electron-neutral aryl chlorides. Ferrocenyl ligands **9** and **10** are very effective for arylations of primary alkylamines [Eq. (67)].

Buchwald and co-workers have demonstrated that the dialkylarylphosphane ligands that are so efficient for Suzuki couplings of aryl chlorides



(67)

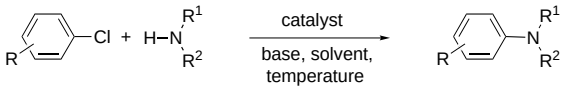
[Eqs. (10) and (11)] are also useful for aminations of this family of substrates. Thus, Pd/**1** provided the first example of a room-temperature reaction of an aryl chloride (4-chlorobenzonitrile) [Eq. (68)].[56] This catalyst couples a wide array of

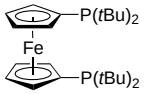
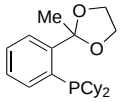
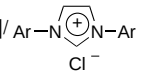
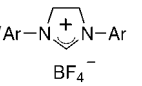
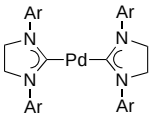


(68)

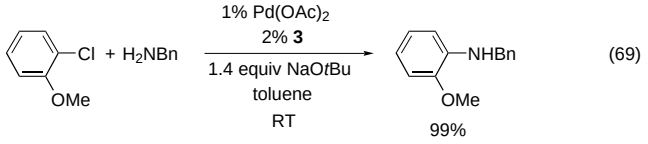
chlorides, including electron-rich ones, with secondary and primary alkyl amines and anilines. Subsequent studies revealed that di(*tert*-butyl)phosphanyl-substituted biphenyl ligand **3** is considerably more effective in achieving room-temperature aminations, and effects coupling of even hindered and electron-rich aryl chlorides [Eq. (69)].[57a]

Table 8. Carbon–nitrogen bond-forming reactions of aryl chlorides.



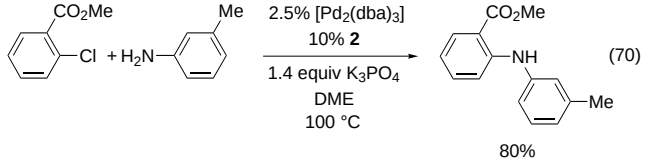
Entry	R	Amine	Catalyst	Conditions	Yield [%]
1	4-CN, H, CH_3	2° cyclic; 2° aryl	$[PdCl_2(PCy_3)_2]$	NaO*t*Bu, toluene, 120 °C	56–88
2	4-Me, 3-OMe, 2-Me	2° cyclic; 1° alkyl; 1° aryl	Pd/ 	NaO*t*Bu, toluene, 100–110 °C	57–93[a]
3	4-CN, H, Me, OMe	2° alkyl; 2° aryl; 1° aryl	$[Pd(dba)_2]/P(tBu)_3$	NaO*t*Bu, toluene, RT-70 °C	75–97
4	4-CO_2Me, H, F, Me, OMe, 2-Cl-pyridine	$LiN(SiMe_3)_2$	$[Pd(dba)_2]/P(tBu)_3$	toluene, RT-90 °C	62–99[b]
5	4-COPh, CF_3, CN, 3,5-Me_2, 2,5-Me_2, 2-OMe	2° cyclic; 2° alkyl; 1° alkyl; 1° aryl	$[Pd(dba)_2]$/ 	NaO*t*Bu, toluene, 105 °C	83–97
6	4-Me	1° aryl	$[PdCl_2(P(tBu)_2OH)_2]$	NaO*t*Bu, dioxane, 110 °C	97
7	4-Me, OMe, 2,5-Me_2	2° cyclic; 2° alkyl; 2° aryl; 1° alkyl; 1° aryl	$[Pd_2(dba)_3]$/ 	KO*t*Bu, dioxane, 100 °C	59–99 %[c]
8	4-CN, Me, OMe, 2-Me, 2-Cl-pyridine, 3-Cl-pyridine	2° cyclic; 2° alkyl; 2° aryl; 1° aryl	$[Pd(dba)_2]$/ 	NaO*t*Bu, DME, RT	82–99[c]
9	4-Me	2° cyclic; 2° alkyl; 2° aryl; 1° alkyl; 1° aryl		KO*t*Bu, dioxane, 100 °C	81–99[c,d]

[a] Both $[Pd(dba)_2]$ and $Pd(OAc)_2$ were used as the Pd sources. [b] The isolated product was the desilylated aniline. [c] Ar = 2,6-(iPr)$_2$C$_6$H$_3$. [d] The [Pd(carbene)P(oTol)$_3$] complex was also an efficient catalyst.



(69)

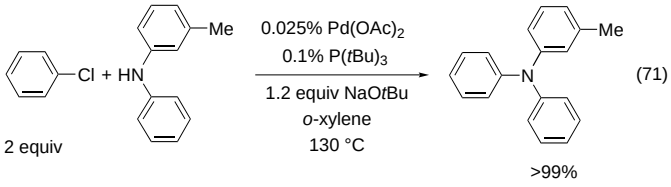
The scope of aminations catalyzed by Pd/**3** is enhanced at 80–110 °C; primary and secondary anilines, primary amines, diarylamines, benzophenone imine, and benzophenone hydrazone can all be coupled with aryl chlorides, including very hindered chlorides and chloropyridines.[292] Catalyst loadings as low as 0.05 % Pd can be employed for certain substrate combinations. Aminations of aryl chlorides that contain sensitive functional groups can be achieved by using a weaker base (K_3PO_4) and phosphanes **1** or **2** [Eq. (70)].



(70)

Since the initial work of Buchwald and co-workers, there have been numerous applications of these versatile dialkylphosphanylbiphenyl ligands to aminations of aryl chlorides, for example, to the *N*-arylation of indoles[293] and vinylogous amides,[294] as well as to the activation of halobenzyl ether protecting groups for oligosaccharide synthesis[295] and the "one-pot" synthesis of unsymmetrical triarylamines.[296, 297] Polymer-supported versions of these ligands can be used.[298] Primary anilines can be synthesized from aryl and heteroaryl chlorides by employing lithium hexamethyldisilazide (LiHMDS) or Ph_3SiNH_2 as ammonia equivalents and Pd/**2** as the catalyst; in addition, symmetrical di- and triarylamines may be obtained through Pd/**3**-catalyzed arylations of $LiNH_2$.[299]

In 1998, a group at the Tosoh Corporation reported that P(tBu)$_3$ is an effective ligand for palladium-catalyzed aminations of aryl chlorides. Chlorobenzene can be coupled with piperazine[300] and *N*-(3-methyphenyl)aniline[301] in good yield; in the latter case, just 0.025 % Pd is required [Eq. (71)]. The scope of Pd/P(tBu)$_3$-catalyzed aminations of



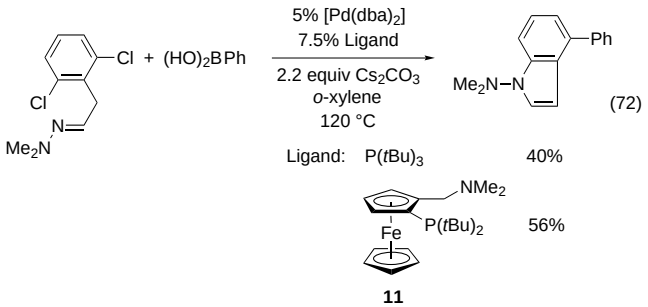
(71)

aryl chlorides is quite broad. Unactivated chlorides can be coupled with secondary amines at 70 °C, and activated aryl chlorides and even chlorobenzene can be aminated at room

temperature (Table 8, entry 3).[302] As was observed for Suzuki reactions [Eq. (16)], a low $P(tBu)_3$:Pd ratio (0.8:1) can provide an improved reaction rate. $Pd/P(tBu)_3$ catalyzes the coupling of aryl chlorides with a range of nitrogen-containing substrates, including indoles[303] and *tert*-butyl carbamate,[304] which leads to Boc-protected anilines. LiHMDS can be arylated to afford primary anilines, after treatment of the coupling products with HCl (Table 8, entry 4).[305] Aryl chlorides that bear ortho substituents are not suitable substrates.

Alcazar-Ramon and Hartwig have pursued mechanistic studies of $Pd/P(tBu)_3$-catalyzed aminations of aryl chlorides in the presence of alkoxide bases, and have proposed that two distinct pathways can be followed.[306] One mechanism involves turnover-limiting oxidative addition to the monophosphane–palladium complex that is formed upon ligand dissociation from the resting state complex $[Pd\{P(tBu)_3\}_2]$. The second mechanism involves oxidative addition to an anionic adduct of the alkoxide and palladium, namely, $[Pd(alkoxide)\{P(tBu)_3\}]^-$.[307] For aminations that employ $P(tBu)_3$:Pd (1:1) and NaO*t*Bu, the reaction rate is first-order in base, which Hartwig and co-workers cite as evidence for the predominance of the second pathway. In contrast, a zero-order dependence on base is observed when the more hindered $NaOCEt_3$ is used, which suggests that the first pathway is being followed. A zero-order dependence on base is observed for both NaO*t*Bu and $NaOCEt_3$ for Pd/binap-catalyzed aminations.[308]

Watanabe et al. have established that both $P(tBu)_3$ and P,N ligand **11**, available in one step from commercially available dimethylaminomethylferrocene, can be used to synthesize 1-aminoindole derivatives by intramolecular aminations of *N*,*N*-disubstituted *o*-chloroacetaldehyde hydrazones.[67a] Two palladium-catalyzed bond-forming reactions can be achieved in one pot to generate functionalized 1-aminoindoles by use of dichloroarylacetaldehyde hydrazones in the presence of an amine, an azole, or an arylboronic acid [Eq. (72)]. For the illustrated transformation, the Suzuki coupling proceeds more quickly than the amination/cyclization.[309]



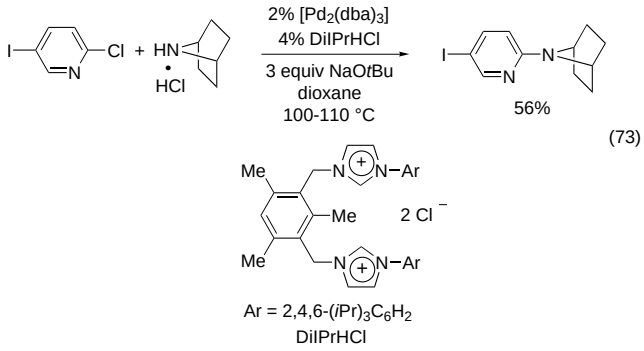
(72)

The dialkylarylphosphane prepared by Guram and co-workers is a suitable ligand for palladium-catalyzed aminations of sterically and electronically diverse aryl chlorides. Unhindered chlorides couple well with secondary amines, whereas *ortho*-substituted aryl chlorides are aminated cleanly by primary amines (Table 8, entry 5).[310] Studies of closely related ligands indicate that the oxygen atom(s) of the phosphane are important for its effectiveness.

Li has demonstrated that Pd/phosphinous acid complexes can catalyze the amination of electron-neutral aryl chlorides in moderate to excellent yield. With respect to the amine component, only $ArNH_2$ and secondary cyclic amines have been shown to be efficient coupling partners. The catalyst can be generated in situ from a phosphane oxide and $[Pd_2(dba)_3]$,[82] or commercially available Pd^{II}/phosphinous acid complexes may be used (Table 8, entry 6).[248]

The amination of aryl chlorides can also be achieved with Pd/carbene catalysts. Nolan and co-workers screened a variety of salts of N-heterocyclic carbene ligands, and found diisopropylaryl-substituted IPr, which is effective for Kumada reactions of unactivated aryl chlorides, to be the most efficient. Both primary and secondary amines can be coupled with electron-neutral and electron-rich aryl chlorides in good yield (Table 8, entry 7).[311] The scope of Pd/IPr-catalyzed aminations was subsequently expanded to include reactions of chloropyridines and of benzophenone imine.[312]

Cheng and Trudell established that related Pd/bis(carbene) complexes catalyze the amination of 2-chloro-5-iodopyridine by 7-azabicyclo[2.2.1]heptane. Interestingly, the chloride reacts preferentially [Eq. (73)]; the product arising from coupling of the iodide is isolated in just 5% yield.[313]



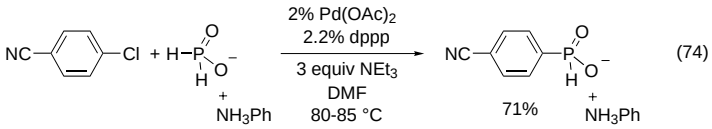
(73)

The saturated analogue of IPr, which can be generated from dihydroimidazolium salt $SIPrHBF_4$,[86b, c, 314, 315] was later reported to provide a more active catalyst than IPr itself for aminations of aryl chlorides (Table 8, entry 8).[316] It is possible to accomplish room-temperature couplings of unactivated and deactivated aryl chlorides and of chloropyridines with a variety of unhindered secondary amines by using the more electron-rich SIPr as the ligand. The catalyst is not effective, however, for reactions of primary alkyl amines, for which rates are slower and substantial amounts of hydrodehalogenated arene are formed. At elevated temperature, a high turnover number can be achieved (for example, nearly 5000 for the coupling of 4-chlorotoluene and morpholine after 7 hours at 100 °C).

Caddick and co-workers have demonstrated that discrete, two-coordinate bis(SIPr) and $SIPr/P(o\text{tol})_3$ complexes of palladium are active catalysts for couplings of electron-neutral 4-chlorotoluene with a variety of amines, including primary amines (Table 8, entry 9).[317] In contrast to the SIPr-

based catalyst system, which was generated in situ, these preformed palladium complexes of SIPr are not effective coupling catalysts at room temperature.[318]

Related to C–N bond construction are C–P bond-forming processes. Although there are quite a few examples of such reactions catalyzed by palladium,[319] the only one that involves an aryl chloride is the cross-coupling of activated 4-chlorobenzonitrile with anilinium hypophosphite in the presence of Pd/dppp [Eq. (74)].[320] [$Pd(PPh_3)_4$], the catalyst of choice for the corresponding reactions of aryl bromides, iodides, and triflates, furnishes no coupling product when 4-chlorobenzonitrile is the substrate.

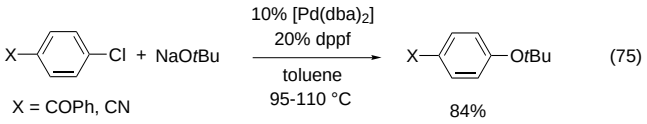


(74)

4. Carbon – Oxygen Bond-Forming Reactions

Diaryl and aryl alkyl ethers are important to a range of fields, including pharmaceutical and natural products chemistry.[277a, 321] Compared to palladium-catalyzed formation of C(aryl)–N bonds, the formation of C(aryl)–O bonds is much less well-developed. Nevertheless, during the past few years, important progress has been described, largely by the Buchwald and the Hartwig research groups, and a number of these advances have involved coupling reactions of aryl chlorides.

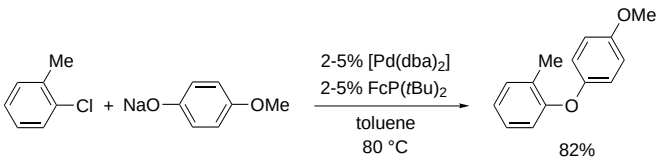
The first report of palladium-catalyzed C–O bond formation with an aryl chloride was provided by Mann and Hartwig, who determined that Pd/dppf effects coupling of electron-deficient aryl chlorides with NaO*t*Bu to generate *tert*-butyl aryl ethers, which can serve as useful protected versions of phenols [Eq. (75)].[322] Of course, the uncatalyzed reaction of



(75)

alkoxides with aryl halides by nucleophilic aromatic substitution is well-established, with highly electron-poor aryl fluorides generally being the most reactive substrates.[323] The control experiments by Mann and Hartwig revealed that, under the conditions used, C–O bond formation does not proceed in the absence of the palladium catalyst.

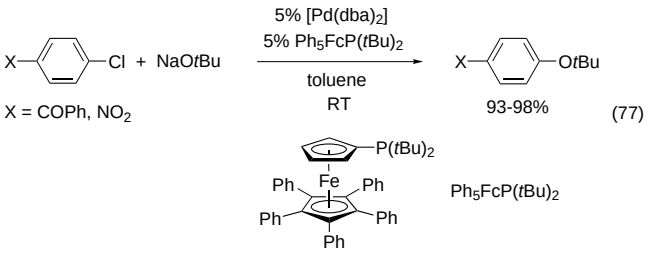
Since electron-neutral and electron-rich aryl chlorides are not suitable substrates for C–O bond formation through nucleophilic aromatic substitution, the development of a method for coupling these compounds using palladium catalysts would be a worthwhile achievement. In 1999, Hartwig and co-workers described the first system for accomplishing C–O bond formation with electron-neutral aryl chlorides by employing either $P(tBu)_3$ or di(*tert*-butyl)-phosphanylferrocene ($FcP(tBu)_2$) as the ligand [Eq. (76)];[324]



(76)

under these conditions, binap, dppf, and $P(o\text{tol})_3$ are ineffective. Both NaO*t*Bu and electron-rich sodium phenoxides are useful coupling partners, but aryl chlorides that lack an *ortho* substituent are not. The beneficial effect of an *ortho* substituent may be the result of steric acceleration of turnover-limiting reductive elimination. In 1999, Watanabe et al. also reported that $Pd/P(tBu)_3$ can catalyze the coupling of electron-neutral aryl chlorides with NaO*t*Bu.[325]

In a subsequent study, it was revealed that, under the reaction conditions described above, $FcP(tBu)_2$ undergoes pentaarylation to generate $Ph_5FcP(tBu)_2$,[166] which provides a more active palladium catalyst than that furnished by $FcP(tBu)_2$ itself.[326] The first room-temperature C–O bond-forming reactions of aryl chlorides, albeit activated ones, were achieved with $[Pd(dba)_2]/Ph_5FcP(tBu)_2$ [Eq. (77)].

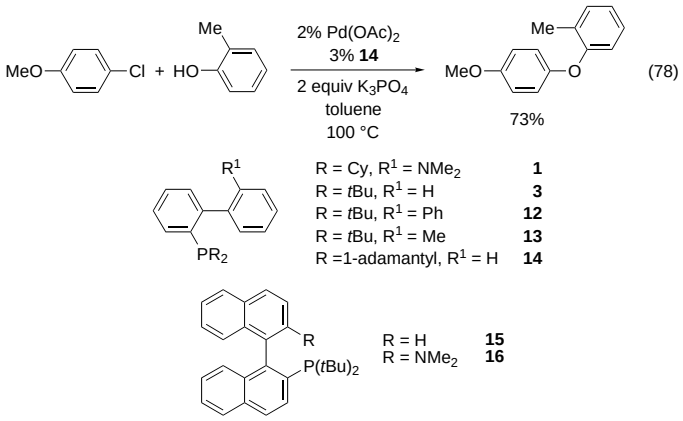


(77)

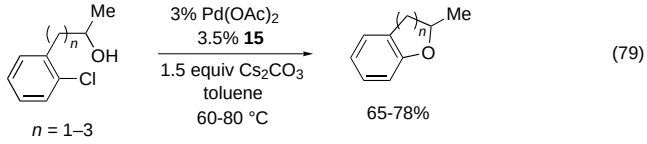
A significant expansion in the scope of palladium-catalyzed C–O bond-forming reactions of aryl chlorides was reported by Buchwald and co-workers, in which they used bulky, electron-rich dialkylarylphosphanes **3**, **12**, **14**, and **16**.[327] Electron-deficient chlorides couple smoothly with phenols using commercially available **3** as the ligand, whereas more challenging reactions of electron-neutral and electron-rich aryl chlorides require the use of **12**, **14**, and **16**. The first example of a coupling of a highly electron-rich chloride was achieved using ligand **14** [Eq. (78)]. This method has recently been applied to the solid-phase synthesis of a diverse library of heterocycles.[92]

Parrish and Buchwald determined that, with the aid of ligands **1** and **13**, it is also possible to efficiently couple NaO*t*Bu with a wide range of aryl chlorides—electron-neutral, electron-rich, and hindered—to form aryl *tert*-butyl ethers.[328] It is believed that bulky ligands are necessary for these coupling processes to destabilize the $[Pd(OAr^1)ArL_n]$ intermediate by forcing the Ar and OAr^1 groups closer together. This process facilitates reductive elimination, which is postulated to be the turnover-limiting step of the catalytic cycle.[329]

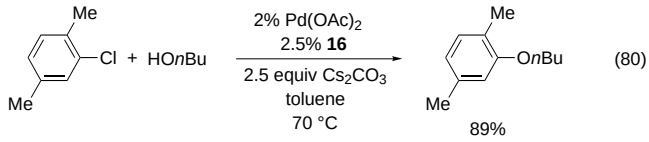
A significant limitation of most methods for palladium-catalyzed C–O bond formation is their inability to effectively couple alcohols that contain β-hydrogen atoms, that is,



primary and secondary alcohols. This limitation is attributed to the propensity of $[PdAr(OR)L_n]$ to undergo β-hydride elimination from the OR group, rather than reductive elimination to generate ArOR. However, both primary and secondary alcohols can be employed in intramolecular C–O bond-forming reactions of aryl chlorides by utilizing commercially available phosphane **15** [Eq. (79)].[330] This method achieves the synthesis of five-, six-, and seven-membered oxygen heterocycles in good yield. Enantioenriched secondary alcohols cyclize with only small losses in enantiomeric purity (1–10% *ee*).[330b]

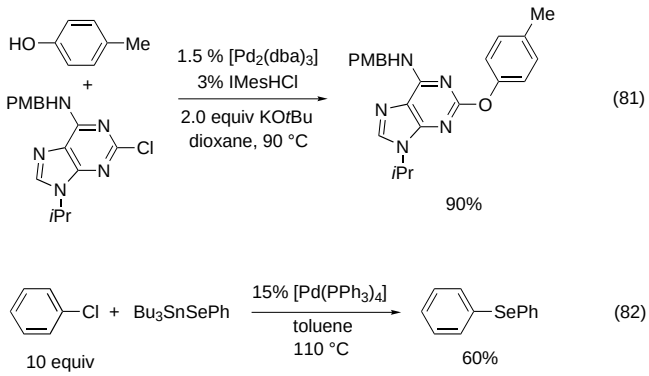


Ligand **16** (and sometimes **15**) is effective for palladium-catalyzed intermolecular C–O bond-forming reactions of primary alcohols.[331] Electron-neutral aryl chlorides with at least one *ortho* substituent, electron-deficient chlorides, and 2-chloropyridine are suitable substrates [Eq. (80)].



To date, there have been only two reports of the use of a non-phosphane-based ligand system for a C–O bond-forming reaction of an aryl chloride. Thus, Schultz and co-workers have demonstrated that couplings of 2-chloropurine derivatives with phenols proceed in high yields with Pd/IMes as the catalyst [Eq. (81); PMB = *para*-methoxybenzyl].[89, 92]

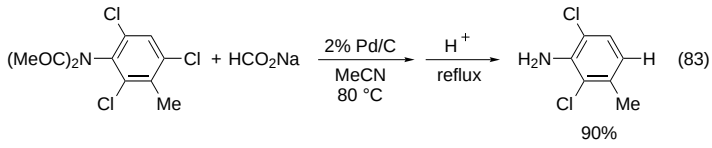
In a related reaction (C–Se bond formation), Nishiyama et al. have observed that $[Pd(PPh_3)_4]$ catalyzes the coupling of chlorobenzene with $SnBu_3SePh$ to generate diphenylselenide [Eq. (82)].[332]



5. Hydrodechlorination Reactions

The dechlorination of aryl chlorides is an important process not only for synthetic organic chemistry,[333] but also for environmental chemistry, since the dechlorination of polychlorinated biphenyls (PCBs) and related chlorinated aromatics provides a mechanism for the detoxification of these persistent pollutants.[334] The heterogeneous palladium-catalyzed dechlorination of aryl and heteroaryl chlorides has been applied extensively for many years.[335] Most commonly, palladium on carbon is employed in the presence of a reducing agent such as hydrogen,[336] triethylsilane,[337] sodium hypophosphite,[338] 1,4-cyclohexadiene,[336c] formic acid,[339] and formate salts.[340]

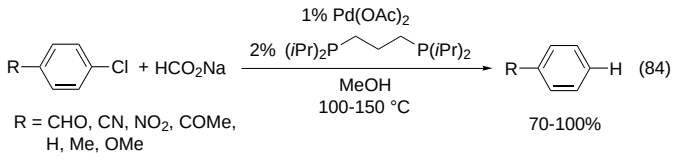
One interesting application of heterogeneous palladium-catalyzed dechlorination is the synthesis of 2,6-dichloroanilines by selective reduction of the *para* chlorine atom of a 2,4,6-trichloro precursor [Eq. (83)].[341] This can be a useful



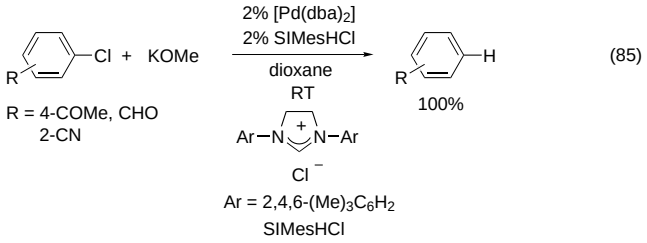
strategy, since these dichloroanilines cannot be directly accessed by electrophilic aromatic halogenation of the aniline.

In contrast to the numerous reports of dechlorination by heterogeneous palladium catalysts, there are comparatively few studies that employ homogenous complexes. Chlorobenzene can be reduced to benzene in 76% yield at 140 °C with catalytic $PdCl_2$ and indoline as the hydrogen donor; Rh-, Ru-, Re-, Fe-, Ni-, Co-, Ir-, and Pt-based complexes are less effective.[342, 343] $[Pd(PPh_3)_4]$ has also been applied as a catalyst for the reduction of aryl chlorides,[344] but most of the investigations have focused on activated substrates.[345] On the other hand, palladium complexes of the bulky, electron-rich, chelating ligand dippp may be employed for dechlorinations of an electronically diverse set of functionalized aryl chlorides [Eq. (84)].[346]

Pd/carbene-based catalysts can accomplish dechlorination under milder conditions. Saturated mesityl-substituted carbene SIMes was found to be particularly effective among a



number of carbenes and phosphanes that were screened [Eq. (85)].[347] Electron-deficient aryl chlorides are sufficiently reactive to undergo reduction at room temperature, whereas unactivated substrates and chloropyridines are dechlorinated at 100 °C.



6. Conclusions

A remarkable amount of progress has been reported during the last few years toward solving the long-standing challenge of bringing readily available and inexpensive aryl chlorides into the family of generally useful substrates for palladium-catalyzed coupling reactions. Thus, through the appropriate choice of ligand—bulky, electron-rich phosphanes and carbenes have thus far proved to be the most versatile—a number of surprisingly mild and general catalyst systems have been developed. Although the traditional view has been that oxidative addition is the problematic step in the catalytic cycle for reactions of aryl chlorides, facilitating this step is simply a necessary, not a sufficient, condition for achieving effective catalysis. Thus, the ligands that have been developed also have steric and electronic properties that are appropriate for subsequent steps in the catalytic cycle.

In view of these recent advances one can anticipate a marked increase in the use of palladium-catalyzed coupling reactions, particularly in industry, where the relatively low cost of aryl chlorides makes these new developments especially attractive. Importantly, many of the key ligands are now commercially available.

Despite the impressive progress, a number of challenges remain. Clearly, the price advantage of aryl chlorides over other coupling partners only holds if comparable turnover numbers can be attained and if the catalysts are of similar cost. In many of the pioneering studies that have been described above, relatively high catalyst loadings have been employed (>1%). For industrial applications in particular, it will be important to establish that higher turnover numbers and turnover frequencies can indeed be achieved. Furthermore, it is desirable to develop effective supported variants of these new catalysts, since this can provide a significant practical benefit in industry. Finally, there is clearly still room for improvement in terms of both scope and mildness for nearly all of the methods that have been discusssed. In view of the ever-increasing level of activity in this rapidly developing area, one can reasonably expect that solutions to these challenges will quickly emerge in the near future.

Support has been provided by the National Institutes of Health (National Institute of General Medical Sciences, R01-GM62871) and the Natural Sciences and Engineering Research Council of Canada (predoctoral fellowship to A.F.L.).

Received: March 22, 2002 [A 527]

[1] a) *Metal-Catalyzed Cross-Coupling Reactions* (Eds.: F. Diederich, P. J. Stang), Wiley-VCH, New York, **1998**; b) J. Tsuji, *Palladium Reagents and Catalysts, Innovations in Organic Synthesis*, Wiley, New York, **1995**.

[2] K. C. Nicolaou, E. J. Sorensen, *Classics in Total Synthesis*, VCH, New York, **1996**, chap. 31.

[3] For a discussion, see a) V. V. Grushin, H. Alper in *Activation of Unreactive Bonds and Organic Synthesis*, (Ed.: S. Murai), Springer, Berlin, **1999**, pp. 193–226; b) V. V. Grushin, H. Alper, *Chem. Rev.* **1994**, *94*, 1047–1062.

[4] For an example in which an aryl chloride was converted into an aryl iodide (33% yield) to enable a palladium-catalyzed Suzuki coupling to take place, see J. M. Lovell, J. A. Joule, *Synth. Commun.* **1997**, *27*, 1209–1215.

[5] Nickel-based complexes can show higher reactivity toward aryl chlorides than palladium-based complexes, and they will certainly play an important role in efforts to utilize these substrates in coupling processes. At the same time, nickel can suffer from disadvantages relative to palladium, including lower tolerance of functional groups (L. Brandsma, S. F. Vasilevsky, H. D. Verkruijsse, *Application of Transition Metal Catalysts in Organic Synthesis*, Springer, New York, **1998**, pp. 150, 228–229), lower selectivity (H. Geissler in *Transition Metals for Organic Synthesis*, *Vol. 1* (Eds.: M. Beller, C. Bolm), Wiley-VCH, New York, **1998**, p. 177), and higher toxicity (F. W. Sunderman, Jr. in *Handbook on Toxicity of Inorganic Compounds* (Eds.: H. G. Seiler, H. Sigel), Marcel Dekker, New York, **1988**, chap. 37; C. W. Bradford, B. J. Chase in *Handbook on Toxicity of Inorganic Compounds* (Eds.: H. G. Seiler, H. Sigel), Marcel Dekker, New York, **1988**, chap. 43; B. L. Carson, *Toxicology and Biological Monitoring of Metals in Humans*, Lewis Publishers, Chelsea, MI, **1986**).

[6] P. Fitton, E. A. Rick, *J. Organomet. Chem.* **1971**, *28*, 287–291.

[7] In reality, this is an oversimplification of the problem. For discussions, see a) V. V. Grushin, H. Alper in *Activation of Unreactive Bonds and Organic Synthesis* (Ed.: S. Murai), Springer, Berlin, **1999**, p. 203; b) W. A. Herrmann in *Applied Homogeneous Catalysis with Organometallic Compounds. A Comprehensive Handbook*, *Vol. 1* (Eds.: B. Cornils, W. A. Herrmann), VCH, Weinheim, **1996**, p. 722.

[8] For a brief overview of recent advances in palladium-catalyzed coupling reactions of aryl chlorides, see R. Stürmer, *Angew. Chem.* **1999**, *111*, 3509–3510; *Angew. Chem. Int. Ed.* **1999**, *38*, 3307–3308.

[9] For reviews, see a) A. Suzuki, *J. Organomet. Chem.* **1999**, *576*, 147–168; b) N. Miyaura in *Advances in Metal-Organic Chemistry*, *Vol. 6* (Ed.: L. S. Liebeskind), JAI, London, **1998**, pp. 187–243; c) A. Suzuki in *Metal-Catalyzed Cross-Coupling Reactions* (Eds.: F. Diederich, P. J. Stang), Wiley-VCH, New York, **1998**, chap. 2; d) S. P. Stanforth, *Tetrahedron* **1998**, *54*, 263–303; e) N. Miyaura, A. Suzuki, *Chem. Rev.* **1995**, *95*, 2457–2483.

[10] G. B. Smith, G. C. Dezeny, D. L. Hughes, A. O. King, T. R. Verhoeven, *J. Org. Chem.* **1994**, *59*, 8151–8156.

[11] For reviews of applications of palladium-catalyzed coupling reactions to heterocyclic chemistry, see a) J. J. Lie, G. W. Gribble, *Palladium in Heterocyclic Chemistry*, Pergamon, New York, **2000**; b) K. Undheim,

T. Benneche, *Adv. Heterocycl. Chem.* **1995**, *62*, 305 – 418; c) V. N. Kalinin, *Synthesis* **1992**, 413 – 432.

[12] S. Gronowitz, A.-B. Hornfeldt, V. Kristjansson, T. Musil, *Chem. Scr.* **1986**, *26*, 305 – 309; for more recent examples of this selectivity, see a) A. J. Cocuzza, F. W. Hobbs, C. R. Arnold, D. R. Chidester, J. A. Yarem, S. Culp, L. Fitzgerald, P. J. Gilligan, *Bioorg. Med. Chem. Lett.* **1999**, *9*, 1057 – 1062; b) B. Jiang, C.-g. Yang, *Heterocycles* **2000**, *53*, 1489 – 1498; c) J. M. Schomaker, T. J. Delia, *J. Org. Chem.* **2001**, *66*, 7125 – 7128; d) Y. Gong, H. W. Pauls, *Synlett* **2000**, 829 – 831.

[13] For other examples of Suzuki couplings of pyrimidines, see a) M. Ishikura, M. Kamada, M. Terashima, *Synthesis* **1984**, 936 – 938; b) M. B. Mitchell, P. J. Wallbank, *Tetrahedron Lett.* **1991**, *32*, 2273 – 2276; c) N. M. Ali, A. McKillop, M. B. Mitchell, R. A. Rebelo, P. J. Wallbank, *Tetrahedron* **1992**, *48*, 8117 – 8126; d) Y. Yang, A. R. Martin, *Heterocycles* **1992**, *34*, 1395 – 1398; e) A. J. Cocuzza, D. R. Chidester, S. Culp, L. Fitzgerald, P. Gilligan, *Bioorg. Med. Chem. Lett.* **1999**, *9*, 1063 – 1066; f) B. Jiang, C.-G. Yang, W.-N. Xiong, J. Wang, *Bioorg. Med. Chem.* **2001**, *9*, 1149 – 1154; g) G. Cooke, H. A. de Cremiers, V. M. Rotello, B. Tarbit, P. E. Vanderstraeten, *Tetrahedron* **2001**, *57*, 2787 – 2789.

[14] a) M. Ishikura, T. Ohta, M. Terashima, *Chem. Pharm. Bull.* **1985**, *33*, 4755 – 4763; b) P. Rocca, F. Marsais, A. Godard, G. Queguiner, *Tetrahedron* **1993**, *49*, 3325 – 3342; c) M. P. Cruskie, Jr., J. A. Zoltewicz, K. A. Abboud, *J. Org. Chem.* **1995**, *60*, 7491 – 7495; d) J. A. Zoltewicz, M. P. Cruskie, Jr., *Tetrahedron* **1995**, *51*, 11393 – 11400; e) H. Zhang, K. S. Chan, *Tetrahedron Lett.* **1996**, *37*, 1043 – 1044; f) R. W. Friesen, C. Brideau, C. C. Chan, S. Charleson, D. Deschenes, D. Dube, D. Ethier, R. Fortin, J. Y. Gauthier, Y. Girard, R. Gordon, G. M. Greig, D. Riendeau, C. Savoie, Z. Wang, E. Wong, D. Visco, L. J. Xu, R. N. Young, *Bioorg. Med. Chem. Lett.* **1998**, *8*, 2777 – 2782; g) C. Niu, J. Li, T. W. Doyle, S.-H. Chen, *Tetrahedron* **1998**, *54*, 6311 – 6318; h) O. Lohse, P. Thevenin, E. Waldvogel, *Synlett* **1999**, 45 – 48; i) R. Crous, C. Dwyer, C. W. Holzapfel, *Heterocycles* **1999**, *51*, 721 – 726; j) M. Gray, I. P. Andrews, D. F. Hook, J. Kitteringham, M. Voyle, *Tetrahedron Lett.* **2000**, *41*, 6237 – 6240; k) W.-N. Xiong, C.-G. Yang, B. Jiang, *Bioorg. Med. Chem.* **2001**, *9*, 1773 – 1780; l) G. A. Molander, M. R. Rivero, *Org. Lett.* **2002**, *4*, 107 – 109; m) G. A. Molander, C.-S. Yun, *Tetrahedron* **2002**, *58*, 1465 – 1470.

[15] a) A. Ohta, M. Ohta, Y. Igarashi, K. Saeki, K. Yuasa, T. Mori, *Heterocycles* **1987**, *26*, 2449 – 2454; b) W. J. Thompson, J. H. Jones, P. A. Lyle, J. E. Thies, *J. Org. Chem.* **1988**, 53 – 2052 – 2055.

[16] a) A. Turck, N. Ple, L. Mojovic, G. Queguiner, *Bull. Soc. Chim. Fr.* **1993**, *130*, 488 – 492; b) I. Parrot, Y. Rival, C. G. Wermuth, *Synthesis* **1999**, 1163 – 1168; c) B. U. W. Maes, G. L. F. Lemiere, R. Dommisse, K. Augustyns, A. Haemers, *Tetrahedron* **2000**, *56*, 1777 – 1781; d) S. Guery, I. Parrot, Y. Rival, C. G. Wermuth, *Tetrahedron Lett.* **2001**, *42*, 2115 – 2117.

[17] a) D. Janietz, M. Bauer, *Synthesis* **1993**, 33 – 34.

[18] a) M. A. Ciufolini, J. W. Mitchell, F. Roschangar, *Tetrahedron Lett.* **1996**, *37*, 8281 – 8284; b) T. Shiota, T. Yamamori, *J. Org. Chem.* **1999**, *64*, 453 – 457.

[19] a) N. W. Alcock, J. M. Brown, D. I. Hulmes, *Tetrahedron: Asymmetry* **1993**, *4*, 743 – 756; b) A. Ford, E. Sinn, S. Woodward, *J. Chem. Soc. Perkin Trans. 1* **1997**, 927 – 934; c) T. D. W. Claridge, J. M. Long, J. M. Brown, D. Hibbs, M. B. Hursthouse, *Tetrahedron* **1997**, *53*, 4035 – 4050.

[20] a) V. G. Chapouland, J. Audoux, N. Ple, A. Turck, G. Queguiner, *Tetrahedron Lett.* **1999**, *40*, 9005 – 9007; b) V. G. Chapouland, N. Ple, A. Turck, G. Queguiner, *Tetrahedron* **2000**, *56*, 5499 – 5507.

[21] S. Guery, I. Parrot, Y. Rival, C. G. Wermuth, *Synthesis* **2001**, 699 – 701.

[22] a) F. Bracher, D. Hildebrand, *Liebigs Ann. Chem.* **1992**, 1315 – 1319; b) F. Bracher, D. Hildebrand, *Liebigs Ann. Chem.* **1993**, 1335 – 1337.

[23] G. B. Bates, D. Parker, *Tetrahedron Lett.* **1996**, *37*, 267 – 270.

[24] C. Enguehard, M. Hervet, H. Allouchi, J.-C. Debouzy, J.-M. Leger, A. Gueiffier, *Synthesis* **2001**, 595 – 600.

[25] a) M. Havelkova, M. Hocek, M. Cesnek, D. Dvorak, *Synlett* **1999**, 1145 – 1147; b) M. Cesnek, M. Hocek, A. Holy, *Collect. Czech. Chem. Commun.* **2000**, *65*, 1357 – 1373; c) M. Hocek, A. Holy, I. Votruba, H. Dvorakova, *Collect. Czech. Chem. Commun.* **2000**, *65*, 1683 – 1697; d) M. Hocek, A. Holy, I. Votruba, H. Dvorakova, *Collect. Czech. Chem. Commun.* **2001**, *66*, 483 – 499; e) M. Havelkova, D. Dvorak, M. Hocek, *Synthesis* **2001**, 1704 – 1710.

[26] S. Caron, S. S. Massett, D. E. Bogle, M. J. Castaldi, T. F. Braish, *Org. Process Res. Dev.* **2001**, *5*, 254 – 256.

[27] a) M. Uemura, H. Nishimura, K. Kamikawa, K. Nakayama, Y. Hayashi, *Tetrahedron Lett.* **1994**, *35*, 1909 – 1912; b) M. Uemura, H. Nishimura, T. Hayashi, *J. Organomet. Chem.* **1994**, *473*, 129 – 137; c) D. Prim, J.-P. Tranchier, F. Rose-Munch, E. Rose, J. Vaissermann, *Eur. J. Inorg. Chem.* **2000**, 901 – 905.

[28] For a review of palladium-catalyzed carbon – carbon bond formation using tricarbonyl(η^6-chloroarene)chromium complexes, see J. F. Carpentier, F. Petit, A. Mortreux, V. Dufand, J.-M. Basset, J. Thivolle-Cazat, *J. Mol. Catal.* **1993**, *81*, 1 – 15.

[29] For leading references, see B. Cornils, *Org. Process Res. Dev.* **1998**, *2*, 121 – 127; and references therein.

[30] a) S. Haber, H. J. Kleinert (Hoechst AG), DE 19527118, **1997**; S. Haber, H. J. Kleinert (Hoechst AG), DE 19535528, **1997**; S. Haber, H. J. Kleinert (Hoechst AG), DE 19620023, **1997**; b) See also: S. Haber in *Aqueous-Phase Organometallic Catalysis* (Eds. B. Cornils, W. A. Herrmann), Wiley-VCH, Weinheim, **1998**, chap. 6.10.2.3.

[31] For leading references, see D. Goubet, P. Meric, J.-R. Dormoy, P. Moreau, *J. Org. Chem.* **1999**, *64*, 4516 – 4518.

[32] M. Ueda, M. Nishimura, N. Miyaura, *Synlett* **2000**, 856 – 858.

[33] K. H. Shaughnessy, R. S. Booth, *Org. Lett.* **2001**, *3*, 2757 – 2759.

[34] K. Inada, N. Miyaura, *Tetrahedron* **2000**, *56*, 8661 – 8664.

[35] S. Saito, M. Sakai, N. Miyaura, *Tetrahedron Lett.* **1996**, *37*, 2993 – 2996.

[36] M. Feuerstein, H. Doucet, M. Santelli, *Synlett* **2001**, 1458 – 1460.

[37] For reviews of applications of palladacycles in coupling reactions, see a) W. A. Herrmann, V. P. W. Bohm, C.-P. Reisinger, *J. Organomet. Chem.* **1999**, *576*, 23 – 41; b) J. Dupont, M. Pfeffer, J. Spencer, *Eur. J. Inorg. Chem.* **2001**, 1917 – 1927.

[38] M. Beller, H. Fischer, W. A. Herrmann, K. Öfele, C. Brossmer, *Angew. Chem.* **1995**, *107*, 1992 – 1993; *Angew. Chem. Int. Ed. Engl.* **1995**, *34*, 1848 – 1849.

[39] S. Gibson, D. F. Foster, G. R. Eastham, R. P. Tooze, D. J. Cole-Hamilton, *Chem. Commun.* **2001**, 779 – 780.

[40] D. Zim, A. S. Gruber, G. Ebeling, J. Dupont, A. L. Monteiro, *Org. Lett.* **2000**, *2*, 2881 – 2884.

[41] For leading references to studies of the role of anionic Pd^0 and Pd^{II} intermediates in palladium-catalyzed coupling reactions, see C. Amatore, A. Jutand, *Acc. Chem. Res.* **2000**, *33*, 314 – 321.

[42] R. B. Bedford, S. M. Draper, P. N. Scully, S. L. Welch, *New J. Chem.* **2000**, *24*, 745 – 747.

[43] W. Shen, *Tetrahedron Lett.* **1997**, *38*, 5575 – 5578.

[44] W. Shen, S. Fakhoury, G. Donner, K. Henry, J. Lee, H. Zhang, J. Cohen, R. Warner, B. Saeed, S. Cherian, S. Tahir, P. Kovar, J. Bauch, S.-C. Ng, K. Marsh, H. Sham, S. Rosenberg, *Bioorg. Med. Chem. Lett.* **1999**, *9*, 703 – 708.

[45] F. Firooznia, C. Gude, K. Chan, Y. Satoh, *Tetrahedron Lett.* **1998**, *39*, 3985 – 3988. For other applications of Pd/PCy_3 to couplings of (hetero)aryl chlorides, see a) P. A. Otten, R. E. London, L. A. Levy, *Bioconjugate Chem.* **2001**, *12*, 203 – 212; b) J. M. McKenna, J. Moliterni, Y. Qiao, *Tetrahedron Lett.* **2001**, *42*, 5797 – 5800; c) F. Minutolo, S. Bertini, C. Papi, K. E. Carlson, J. A. Katzenellenbogen, M. Macchia, *J. Med. Chem.* **2001**, *44*, 4288 – 4291.

[46] F. Firooznia, C. Gude, K. Chan, N. Marcopulos, Y. Satoh, *Tetrahedron Lett.* **1999**, *40*, 213 – 216. $Pd/P(t\mathrm{Bu})_3$ provides the desired product in high enantiomeric excess (99 % *ee*), but in modest yield (30 – 36 %).

[47] a) M. J. Monteith (Zeneca Ltd), WO 9816486, **1998**; b) M. J. Monteith, *Spec. Chem. Mag.* **1998**, *18*, 436 – 438.

[48] A. Zapf, M. Beller, *Chem. Eur. J.* **2000**, *6*, 1830 – 1833.

[49] For example, $pK_a\ P(OEt)_3 = 3.31$, $pK_a\ PEt_3 = 8.69$. For an extensive compilation of cone angles and pK_a data for phosphanes and phosphites, see M. M. Rahman, H.-Y. Liu, K. Eriks, A. Prock, W. P. Giering, *Organometallics* **1989**, *8*, 1 – 7.

[50] G. A. Grasa, A. C. Hillier, S. P. Nolan, *Org. Lett.* **2001**, *3*, 1077 – 1080.

[51] D. Zim, A. L. Monteiro, J. Dupont, *Tetrahedron Lett.* **2000**, *41*, 8199 – 8202.

[52] For ligandless Suzuki couplings of 4-chloronitrobenzene using Pd/Ni bimetallic clusters, see M. T. Reetz, R. Breinbauer, K. Wanninger, *Tetrahedron Lett.* **1996**, *37*, 4499 – 4502.

[53] For ligandless palladium-catalyzed Suzuki couplings of (hetero)aryl chlorides with sodium tetraphenylborate, see a) N. A. Bumagin, V. V. Bykov, *Tetrahedron* **1997**, *53*, 14437 – 14450; b) D. Villemin, M. J. Gomez-Escalonilla, J.-F. Saint-Clair, *Tetrahedron Lett.* **2001**, *42*, 635 – 637.
[54] C. R. LeBlond, A. T. Andrews, Y. Sun, J. R. Sowa, Jr., *Org. Lett.* **2001**, *3*, 1555 – 1557.
[55] B. H. Lipshutz, J. A. Sclafani, P. A. Blomgren, *Tetrahedron* **2000**, *56*, 2139 – 2144.
[56] D. W. Old, J. P. Wolfe, S. L. Buchwald, *J. Am. Chem. Soc.* **1998**, *120*, 9722 – 9723.
[57] a) J. P. Wolfe, S. L. Buchwald, *Angew. Chem.* **1999**, *111*, 2570 – 2573; *Angew. Chem. Int. Ed.* **1999**, *38*, 2413 – 2416; Erratum: J. P. Wolfe, S. L. Buchwald, *Angew. Chem.* **1999**, *111*, 3621; *Angew. Chem. Int. Ed.* **1999**, *38*, 3415; b) J. P. Wolfe, R. A. Singer, B. H. Yang, S. L. Buchwald, *J. Am. Chem. Soc.* **1999**, *121*, 9550 – 9561.
[58] For some recent applications of Buchwald biphenyl ligands to Suzuki couplings of aryl and heteroaryl chlorides, see a) M. A. Kothare, J. Ohkanda, J. W. Lockman, Y. Qian, M. A. Blaskovich, S. M. Sebti, A. D. Hamilton, *Tetrahedron* **2000**, *56*, 9833 – 9841; b) M. K. Lakshman, J. H. Hilmer, J. Q. Martin, J. C. Keeler, Y. Q. V. Dinh, F. N. Ngassa, L. M. Russon, *J. Am. Chem. Soc.* **2001**, *123*, 7779 – 7787; c) J.-F. Marcoux, F.-A. Marcotte, J. Wu, P. G. Dormer, I. W. Davies, D. Hughes, P. J. Reider, *J. Org. Chem.* **2001**, *66*, 4194 – 4199.
[59] C. A. Parrish, S. L. Buchwald, *J. Org. Chem.* **2001**, *66*, 3820 – 3827.
[60] J. Yin, S. L. Buchwald, *J. Am. Chem. Soc.* **2000**, *122*, 12051 – 12052.
[61] For some examples of (η^2-arene)Pd complexes, see a) H. Osser, M. Pfeffer, J. T. B. H. Jastrzebski, C. H. Stam, *Inorg. Chem.* **1987**, *26*, 1169 – 1171; b) L. R. Falvello, J. Fornies, R. Navarro, V. Sicilia, M. Tomas, *Angew. Chem.* **1990**, *102*, 952 – 953; *Angew. Chem. Int. Ed. Engl.* **1990**, *29*, 891 – 893; c) C.-S. Li, C.-H. Cheng, F.-L. Liao, S.-L. Wang, *J. Chem. Soc. Chem. Commun.* **1991**, 710 – 712; d) M. Sommovigo, M. Pasquali, P. Leoni, D. Braga, P. Sabatino, *Chem. Ber.* **1991**, *124*, 97 – 99.
[62] J. Yin, M. P. Rainka, X.-X. Zhang, S. L. Buchwald, *J. Am. Chem. Soc.* **2002**, *124*, 1162 – 1163.
[63] P. Kocovsky, S. Vyskocil, I. Cisarova, J. Sejbal, I. Tislerova, M. Smrcina, G. C. Lloyd-Jones, S. C. Stephen, C. P. Butts, M. Murray, V. Langer, *J. Am. Chem. Soc.* **1999**, *121*, 7714 – 7715.
[64] A. F. Littke, G. C. Fu, *Angew. Chem.* **1998**, *110*, 3586 – 3587; *Angew. Chem. Int. Ed.* **1998**, *37*, 3387 – 3388.
[65] A. F. Littke, C. Dai, G. C. Fu, *J. Am. Chem. Soc.* **2000**, *122*, 4020 – 4028.
[66] With [Pd(PPh_3)$_4$] as the catalyst, trimethylboroxine (the cyclic anhydride of methylboronic acid) can methylate highly activated aryl chlorides: ref. [14j].
[67] a) M. Watanabe, T. Yamamoto, M. Nishiyama, *Angew. Chem.* **2000**, *112*, 2620 – 2623; *Angew. Chem. Int. Ed.* **2000**, *39*, 2501 – 2504; b) A. E. Sutton, J. Clardy, *Tetrahedron Lett.* **2001**, *42*, 547 – 551; c) M. Allegretti, A. Arcadi, F. Marinelli, L. Nicolini, *Synlett* **2001**, 609 – 612; d) A. Sudo, S. Uchino, T. Endo, *J. Polym. Sci. Part A Polym. Chem.* **2001**, *39*, 2093 – 2102; e) W. K.-D. Brill, C. Riva-Toniola, S. Müller, *Synlett* **2001**, 1097 – 1100; f) G. Zou, J. R. Falck, *Tetrahedron Lett.* **2001**, *42*, 5817 – 5819; g) J. V. Mello, N. S. Finney, *Org. Lett.* **2001**, *3*, 4263 – 4265.
[68] a) S. Otsuka, T. Yoshida, M. Matsumoto, K. Nakatsu, *J. Am. Chem. Soc.* **1976**, *98*, 5850 – 5858; b) T. Yoshida, S. Otsuka, *J. Am. Chem. Soc.* **1977**, *99*, 2134 – 2140; c) T. Yoshida, S. Otsuka, *Inorg. Synth.* **1990**, *28*, 113 – 119.
[69] For early studies of P(*o*tol)$_3$-based monophosphane – palladium complexes, see a) J. F. Hartwig, F. Paul, *J. Am. Chem. Soc.* **1995**, *117*, 5373 – 5374; b) J. F. Hartwig, *Synlett* **1997**, 329 – 340.
[70] This contrasts with the conventional view of Pd/PPh_3-catalyzed coupling processes, wherein a bisphosphane complex is generally invoked as a key reactive intermediate. See ref. [1a].
[71] P(*t*Bu)$_3$: pK_a = 11.40, cone angle = 182°. PPh_3: pK_a = 2.73, cone angle = 145°.
[72] Monophosphane – palladium species would also be expected to undergo transmetalation and reductive elimination at higher rates than L_nPd ($n > 1$) species: J. F. Hartwig, *Pure Appl. Chem.* **1999**, *71*, 1417 – 1423.
[73] a) X. Bei, T. Crevier, A. S. Guram, B. Jandeleit, T. S. Powers, H. W. Turner, T. Uno, W. H. Weinberg, *Tetrahedron Lett.* **1999**, *40*, 3855 – 3858; b) X. Bei, H. W. Turner, W. H. Weinberg, A. S. Guram, J. L. Petersen, *J. Org. Chem.* **1999**, *64*, 6797 – 6803.
[74] A. Zapf, A. Ehrentraut, M. Beller, *Angew. Chem.* **2000**, *112*, 4315 – 4317; *Angew. Chem. Int. Ed.* **2000**, *39*, 4153 – 4155.
[75] M. G. Andreu, A. Zapf, M. Beller, *Chem. Commun.* **2001**, 2475 – 2476.
[76] The [PdL_1(diene)] complexes were synthesized by the method of Porschke and co-workers (reaction of [$PdMe_2$(tmeda)] with a phosphane in the presence of a diene): J. Krause, G. Cestaric, K.-J. Haack, K. Seevogel, W. Storm, K.-R. Porschke, *J. Am. Chem. Soc.* **1999**, *121*, 9807 – 9823.
[77] R. B. Bedford, C. S. J. Cazin, *Chem. Commun.* **2001**, 1540 – 1541.
[78] T. E. Pickett, C. J. Richards, *Tetrahedron Lett.* **2001**, *42*, 3767 – 3769.
[79] S.-Y. Liu, M. J. Choi, G. C. Fu, *Chem. Commun.* **2001**, 2408 – 2409.
[80] For example, see S. Allenmark, *Tetrahedron Lett.* **1974**, *15*, 371 – 374.
[81] M. L. Clarke, D. J. Cole-Hamilton, J. D. Woollins, *J. Chem. Soc. Dalton Trans.* **2001**, 2721 – 2723.
[82] G. Y. Li, *Angew. Chem.* **2001**, *113*, 1561 – 1564; *Angew. Chem. Int. Ed.* **2001**, *40*, 1513 – 1516.
[83] For reviews of carbene ligands and their applications in homogenous catalysis, see a) W. A. Herrmann, C. Köcher, *Angew. Chem.* **1997**, *109*, 2256 – 2282; *Angew. Chem. Int. Ed. Engl.* **1997**, *36*, 2162 – 2187; b) D. Bourissou, O. Guerret, F. P. Gabbai, G. Bertrand, *Chem. Rev.* **2000**, *100*, 39 – 91; c) L. Jafarpour, S. P. Nolan, *Adv. Organomet. Chem.* **2001**, *46*, 181 – 222.
[84] W. A. Herrmann, C.-P. Reisinger, M. Spiegler, *J. Organomet. Chem.* **1998**, *557*, 93 – 96.
[85] a) T. Weskamp, V. P. W. Bohm, W. A. Herrmann, *J. Organomet. Chem.* **1999**, *585*, 348 – 352; b) W. A. Herrmann, V. P. W. Bohm, C. W. K. Gstottmayr, M. Grosche, C.-P. Reisinger, T. Weskamp, *J. Organomet. Chem.* **2001**, *617 – 618*, 616 – 628.
[86] a) A. J. Arduengo III, H. V. R. Dias, R. L. Harlow, M. Kline, *J. Am. Chem. Soc.* **1992**, *114*, 5530 – 5534; b) A. J. Arduengo III, R. Krafczyk, R. Schmutzler, H. A. Craig, J. R. Goerlich, W. J. Marshall, M. Unverzagt, *Tetrahedron* **1999**, *55*, 14523 – 14534; c) A. J. Arduengo III, *Acc. Chem. Res.* **1999**, *32*, 913 – 921.
[87] C. Zhang, J. Huang, M. L. Trudell, S. P. Nolan, *J. Org. Chem.* **1999**, *64*, 3804 – 3805.
[88] V. P. W. Bohm, C. W. K. Gstottmayr, T. Weskamp, W. A. Herrmann, *J. Organomet. Chem.* **2000**, *595*, 186 – 190.
[89] For an application of IMes and its saturated analogue, the dihydroimidazolium tetrafluoroborate salt (SIMes) to palladium-catalyzed Suzuki couplings of 2-chloropurines, see S. Ding, N. S. Gray, Q. Ding, P. G. Schultz, *Tetrahedron Lett.* **2001**, *42*, 8751 – 8755.
[90] For the application of related bis(imidazol-2-ylidene)palladium complexes to Suzuki couplings of deactivated aryl chlorides, see C. Zhang, M. L. Trudell, *Tetrahedron Lett.* **2000**, *41*, 595 – 598.
[91] A. Furstner, A. Leitner, *Synlett* **2001**, 290 – 292.
[92] S. Ding, N. S. Gray, X. Wu, Q. Ding, P. G. Schultz, *J. Am. Chem. Soc.* **2002**, *124*, 1594 – 1596.
[93] L. Botella, C. Nájera, *Angew. Chem.* **2002**, *114*, 187 – 189; *Angew. Chem. Int. Ed.* **2002**, *41*, 179 – 181.
[94] T. Ishiyama, M. Murata, N. Miyaura, *J. Org. Chem.* **1995**, *60*, 7508 – 7510.
[95] T. Ishiyama, K. Ishida, N. Miyaura, *Tetrahedron* **2001**, *57*, 9813 – 9816.
[96] A. Furstner, G. Seidel, *Org. Lett.* **2002**, *4*, 541 – 543.
[97] a) M. Kosugi, K. Sasazawa, Y. Shimizu, T. Migita, *Chem. Lett.* **1977**, 301 – 302; b) D. Milstein, J. K. Stille, *J. Am. Chem. Soc.* **1978**, *100*, 3636 – 3638.
[98] For general reviews of the Stille cross-coupling reaction, see a) T. N. Mitchell in *Metal-Catalyzed Cross-Coupling Reactions* (Eds.: F. Diederich, P. J. Stang), Wiley-VCH, Weinheim, **1998**, chap. 4; b) V. Farina, V. Krishnamurthy, W. J. Scott, *Org. React.* **1997**, *50*, 1 – 652; c) J. K. Stille, *Angew. Chem.* **1986**, *98*, 504 – 519; *Angew. Chem. Int. Ed. Engl.* **1986**, *25*, 508 – 524.
[99] K. C. Nicolaou, T. K. Chakraborty, A. D. Piscopio, N. Minowa, P. Bertinato, *J. Am. Chem. Soc.* **1993**, *115*, 4419 – 4420.
[100] M. D. Shair, T. Y. Yoon, K. K. Mosny, T. C. Chou, S. J. Danishefsky, *J. Am. Chem. Soc.* **1996**, *118*, 9509 – 9525.

[101] For some recent examples of applications in natural products synthesis, see a) D. R. Williams, K. G. Meyer, *J. Am. Chem. Soc.* **2001**, *123*, 765 – 766; b) J. D. White, R. G. Carter, K. F. Sundermann, M. Wartmann, *J. Am. Chem. Soc.* **2001**, *123*, 5407 – 5413; c) S. Liras, C. L. Lynch, A. M. Fryer, B. T. Vu, S. F. Martin, *J. Am. Chem. Soc.* **2001**, *123*, 5918 – 5924; d) S. Hannessian, J. Ma, W. Wang, *J. Am. Chem. Soc.* **2001**, *123*, 10200 – 10206; e) A. B. Smith III, K. P. Minbiole, P. R. Verhoest, M. Schelhaas, *J. Am. Chem. Soc.* **2001**, *123*, 10942 – 10953.

[102] a) P. Rocca, F. Marsais, A. Godard, G. Queguiner, *Tetrahedron Lett.* **1993**, *34*, 2937 – 2940; b) G. V. Long, S. E. Boyd, M. M. Harding, I. E. Buys, T. W. Hambley, *J. Chem. Soc. Dalton Trans.* **1993**, 3175 – 3178; c) S. Gronowitz, P. Bjork, J. Malm, A.-B. Hornfeldt, *J. Organomet. Chem.* **1993**, *460*, 127 – 129; d) B. Zhang, R. Breslow, *J. Am. Chem. Soc.* **1997**, *119*, 1676 – 1681; e) J. Li, S. -H. Chen, X. Li, C. Niu, T. W. Doyle, *Tetrahedron* **1998**, *54*, 393 – 400; f) P. N. W. Baxter, *J. Org. Chem.* **2000**, *65*, 1257 – 1272; g) P. N. W. Baxter, *J. Org. Chem.* **2001**, *66*, 4170 – 4179.

[103] T. Sakamoto, C. Satoh, Y. Kondo, H. Yamanaka, *Heterocycles* **1992**, *34*, 2379 – 2384.

[104] a) T. Sakamoto, C. Satoh, Y. Kondo, H. Yamanaka, *Chem. Pharm. Bull.* **1993**, *41*, 81 – 86; b) J. Sandosham, K. Undheim, F. Rise, *Heterocycles* **1993**, *35*, 235 – 244; c) U. S. Schubert, C. Eschbaumer, *Org. Lett.* **1999**, *1*, 1027 – 1029.

[105] a) A. Ohta, M. Ohta, T. Watanabe, *Heterocycles* **1986**, *24*, 785 – 792; b) T. Watanabe, K. Hayashi, J. Sakurada, M. Ohki, N. Takamatsu, H. Hirohata, K. Takeuchi, K. Yuasa, A. Ohta, *Heterocycles* **1989**, *29*, 123 – 131; c) L. J. Street, R. Baker, T. Book, A. J. Reeve, J. Saunders, T. Willson, R. S. Marwood, S. Patel, S. B. Freedman, *J. Med. Chem.* **1992**, *35*, 295 – 305; d) J. A. Zoltewicz, M. P. Cruskie, Jr., *J. Org. Chem.* **1995**, *60*, 3487 – 3493; e) N. Sato, N. Narita, *Synthesis* **2001**, 1551 – 1555; f) D. Cuperly, P. Gros, Y. Fort, *J. Org. Chem.* **2002**, *67*, 238 – 241.

[106] Y. Hanasaki, *Heterocycles* **1996**, *43*, 2435 – 2441.

[107] R. Faust, B. Gobelt, *Tetrahedron Lett.* **1997**, *38*, 8017 – 8020.

[108] a) J. Solberg, K. Undheim, *Acta Chem. Scand.* **1989**, *43*, 62 – 68; b) T. Benneche, *Acta Chem. Scand.* **1990**, *44*, 927 – 931.

[109] a) Y. Kondo, R. Watanabe, T. Sakamoto, H. Yamanaka, *Chem. Pharm. Bull.* **1989**, *37*, 2814 – 2816; b) A. J. Majeed, O. Antonsen, T. Benneche, K. Undheim, *Tetrahedron* **1989**, *45*, 993 – 1006.

[110] a) A. Dondoni, G. Fantin, M. Fogagnolo, A. Medici, P. Pedrini, *Synthesis* **1987**, 693 – 696; b) A. Godard, J. M. Fourquez, R. Tamion, F. Marsais, G. Queguiner, *Synlett* **1994**, 235 – 236; c) W. E. Hume, R. Nagata, *Synlett* **1997**, 473 – 474; d) J.-Y. Legros, G. Primault, J.-C. Fiaud, *Tetrahedron* **2001**, *57*, 2507 – 2514.

[111] M. P. Wentland, R. B. Perni, P. H. Dorff, R. P. Brundage, M. J. Castaldi, T. R. Bailey, P. M. Carabateas, E. R. Bacon, D. C. Young, M. G. Woods, D. Rosi, M. L. Drozd, R. K. Kullnig, F. J. Dutko, *J. Med. Chem.* **1993**, *36*, 1580 – 1596.

[112] a) E. Laborde, L. E. Lesheski, J. S. Kiely, *Tetrahedron Lett.* **1990**, *31*, 1837 – 1840; b) E. Laborde, J. S. Kiely, L. E. Lesheski, M. C. Schroeder, *J. Heterocycl. Chem.* **1991**, *28*, 191 – 198.

[113] B. Charpiot, J. Brun, I. Donze, R. Naef, M. Stefani, T. Mueller, *Bioorg. Med. Chem. Lett.* **1998**, *8*, 2891 – 2896.

[114] K. S. Kim, L. Qian, K. E. J. Dickinson, C. L. Delaney, J. E. Bird, T. L. Waldron, S. Moreland, *Bioorg. Med. Chem. Lett.* **1993**, *3*, 2667 – 2670.

[115] M. Kosugi, M. Koshiba, A. Atoh, H. Sano, T. Migita, *Bull. Chem. Soc. Jpn.* **1986**, *59*, 677 – 679.

[116] a) L.-L. Gundersen, *Tetrahedron Lett.* **1994**, *35*, 3155 – 3158; b) L.-L. Gundersen, A. K. Bakkestuen, A. J. Aasen, H. Overas, F. Rise, *Tetrahedron* **1994**, *50*, 9743 – 9756; c) M. Hocek, M. Masojidkova, A. Holy, *Tetrahedron* **1997**, *53*, 2291 – 2302; d) A. Brathe, L.-L. Gundersen, F. Rise, A. B. Eriksen, A. V. Vollsnes, L. Wang, *Tetrahedron* **1999**, *55*, 211 – 228; e) A. K. Bakkestuen, L.-L. Gundersen, G. Langli, F. Liu, J. M. J. Nolsoe, *Bioorg. Med. Chem. Lett.* **2000**, *10*, 1207 – 1210.

[117] M. Cheung, P. A. Harris, K. E. Lackey, *Tetrahedron Lett.* **2001**, *42*, 999 – 1001.

[118] F. Bracher, D. Hildebrand, *Liebigs Ann. Chem.* **1993**, 837 – 839.

[119] a) F. Guillier, F. Nivoliers, C. Cochennec, A. Godard, F. Marsais, G. Queguiner, *Synth. Commun.* **1996**, *26*, 4421 – 4436; b) F. Guillier, F. Nivoliers, A. Godard, F. Marsais, G. Queguiner, *J. Heterocycl. Chem.* **1999**, *36*, 1157 – 1165.

[120] J. M. J. Nolsoe, L.-L. Gundersen, F. Rise, *Acta Chem. Scand.* **1999**, *53*, 366 – 372.

[121] G. Langli, L.-L. Gundersen, F. Rise, *Tetrahedron* **1996**, *52*, 5625 – 5638.

[122] M. Kosugi, K. Sasazawa, Y. Shimizu, T. Migita, *Chem. Lett.* **1977**, 301 – 302; see also: A. N. Kashin, I. G. Bumagina, N. A. Bumagin, I. P. Beletskaya, *Zh. Org. Khim.* **1981**, *17*, 21 – 28.

[123] a) W. J. Scott, *J. Chem. Soc. Chem. Commun.* **1987**, 1755 – 1756; b) J. M. Clough, I. S. Mann, D. A. Widdowson, *Tetrahedron Lett.* **1987**, *28*, 2645 – 2648; c) T. N. Mitchell, K. Kwekat, D. Rutschow, U. Schneider, *Tetrahedron* **1989**, *45*, 969 – 978; d) M. E. Wright, *Organometallics* **1989**, *8*, 407 – 411; e) M. E. Wright, *Macromolecules* **1989**, *22*, 3256 – 3259.

[124] G. A. Grasa, S. P. Nolan, *Org. Lett.* **2001**, *3*, 119 – 122.

[125] A. F. Littke, G. C. Fu, *Angew. Chem.* **1999**, *111*, 2568 – 2570; *Angew. Chem. Int. Ed.* **1999**, *38*, 2411 – 2413.

[126] a) V. Farina, G. P. Roth in *Advances in Metal-Organic Chemistry*, *Vol. 5* (Ed.: L. S. Liebeskind), JAI, London, **1996**, pp. 45 – 46; b) L. Brandsma, S. F. Vasilevsky, H. D. Verkruijsse, *Application of Transition Metal Catalysts in Organic Synthesis*, Springer, New York, **1998**, p. 246; c) V. Farina, V. Krishnamurthy, W. J. Scott, *Org. React.* **1997**, *50*, pp. 54 – 55.

[127] J. Zhu, B. A. Price, S. X. Zhao, P. M. Skonezny, *Tetrahedron Lett.* **2000**, *41*, 4011 – 4014.

[128] A. F. Littke, L. Schwarz, G. C. Fu, *J. Am. Chem. Soc.* **2002**, *124*, 6343 – 6348.

[129] For a discussion and leading references, see ref. [62].

[130] a) T. Hiyama in *Metal-Catalyzed Cross-Coupling Reactions* (Eds.: F. Diederich, P. J. Stang), Wiley-VCH, New York, **1998**, chap. 10; b) T. Hiyama, Y. Hatanaka, *Pure Appl. Chem.* **1994**, *66*, 1471 – 1478.

[131] a) H. Matsumoto, S. Nagashima, K. Yoshihiro, Y. Nagai, *J. Organomet. Chem.* **1975**, *85*, C1 – C3; b) H. Matsumoto, K. Yoshihiro, S. Nagashima, H. Watanabe, Y. Nagai, *J. Organomet. Chem.* **1977**, *128*, 409 – 413.

[132] H. Matsumoto, K. Shono, Y. Nagai, *J. Organomet. Chem.* **1981**, *208*, 145 – 152.

[133] For other examples of couplings of aryl chlorides with organodisilanes, see a) D. Azarian, S. S. Dua, C. Eaborn, D. R. M. Walton, *J. Organomet. Chem.* **1976**, *117*, C55 – C57; b) P. Babin, B. Bennetau, M. Theurig, J. Dunogues, *J. Organomet. Chem.* **1993**, *446*, 135 – 138; c) N. Lachance, M. Gallant, *Tetrahedron Lett.* **1998**, *39*, 171 – 174.

[134] K.-i. Gouda, E. Hagiwara, Y. Hatanaka, T. Hiyama, *J. Org. Chem.* **1996**, *61*, 7232 – 7233.

[135] E. Hagiwara, K.-i. Gouda, Y. Hatanaka, T. Hiyama, *Tetrahedron Lett.* **1997**, *38*, 439 – 442.

[136] S.-K. Kang, W.-Y. Kim, *Synth. Commun.* **1998**, *28*, 3743 – 3749.

[137] Y. Nishihara, K. Ikegashira, K. Hirabayashi, J.-i. Ando, A. Mori, T. Hiyama, *J. Org. Chem.* **2000**, *65*, 1780 – 1787.

[138] M. E. Mowery, P. DeShong, *Org. Lett.* **1999**, *1*, 2137 – 2140.

[139] H. M. Lee, S. P. Nolan, *Org. Lett.* **2000**, *2*, 2053 – 2055.

[140] a) E.-i. Negishi in *Metal-Catalyzed Cross-Coupling Reactions* (Eds.: F. Diederich, P. J. Stang), Wiley-VCH, Weinheim, **1998**, chap. 1; b) E. Erdik, *Tetrahedron* **1992**, *48*, 9577 – 9648.

[141] a) A. Minato, K. Tamao, T. Hayashi, K. Suzuki, M. Kumada, *Tetrahedron Lett.* **1980**, *21*, 845 – 848; b) J. H. Hall, J. Y. Chien, J. M. Kauffman, P. T. Litak, J. K. Adams, R. A. Henry, R. A. Hollins, *J. Heterocycl. Chem.* **1992**, *29*, 1245 – 1273; c) M. Amat, S. Hadida, G. Pshenichnyi, J. Bosch, *J. Org. Chem.* **1997**, *62*, 3158 – 3175.

[142] M. Amat, S. Hadida, G. Pshenichnyi, J. Bosch, *J. Org. Chem.* **1997**, *62*, 3158 – 3175.

[143] a) T. Sakamoto, S. Nishimura, Y. Kondo, H. Yamanaka, *Synthesis* **1988**, 485 – 486; b) J. Sandosham, K. Undheim, F. Rise, *Heterocycles* **1993**, *35*, 235 – 244; c) M. E. Angiolelli, A. L. Casalnuovo, T. P. Selby, *Synlett* **2000**, 905 – 907.

[144] M. Sonoda, A. Inaba, K. Itahashi, Y. Tobe, *Org. Lett.* **2001**, *3*, 2419 – 2421.

[145] a) F. Bracher, D. Hildebrand, *Tetrahedron* **1994**, *50*, 12329 – 12336; b) N. Murata, T. Sugihara, Y. Kondo, T. Sakamoto, *Synlett* **1997**, 298 – 300.

[146] J. A. Miller, R. P. Farrell, *Tetrahedron Lett.* **1998**, *39*, 6441 – 6444.

[147] J. A. Miller, R. P. Farrell, *Tetrahedron Lett.* **1998**, *39*, 7275 – 7278.

[148] For other examples of Negishi couplings of activated aryl chlorides, including (η^6-chloroarene)$Cr(CO)_3$ complexes, see refs. [27a,b], and [144].
[149] C. Dai, G. C. Fu, *J. Am. Chem. Soc.* **2001**, *123*, 2719 – 2724.
[150] D. R. Gauthier, Jr., R. H. Szumigala, Jr., P. G. Dormer, J. D. Armstrong III, R. P. Volante, P. J. Reider, *Org. Lett.* **2002**, *4*, 375 – 378.
[151] M. Yamamura, I. Moritani, S.-i. Murahashi, *J. Organomet. Chem.* **1975**, *91*, C39 – C42.
[152] For a review of the Kumada reaction, see E.-i. Negishi in *Metal-Catalyzed Cross-Coupling Reactions* (Eds.: F. Diederich, P. J. Stang), Wiley-VCH, Weinheim, **1998**, chap. 1.
[153] For example, see a) K. Isobe, S. Kawaguchi, *Heterocycles* **1981**, *16*, 1603 – 1612; b) A. Minato, K. Suzuki, K. Tamao, M. Kumada, *J. Chem. Soc. Chem. Commun.* **1984**, 511 – 513.
[154] V. Bonnet, F. Mongin, F. Trecourt, G. Queguiner, P. Knochel, *Tetrahedron Lett.* **2001**, *42*, 5717 – 5719.
[155] T. Katayama, M. Umeno, *Chem. Lett.* **1991**, 2073 – 2076.
[156] J. Huang, S. P. Nolan, *J. Am. Chem. Soc.* **1999**, *121*, 9889 – 9890.
[157] For a review of palladium-catalyzed cross-couplings with aluminum- and zirconium-based reagents, see E.-i. Negishi in *Metal-Catalyzed Cross-Coupling Reactions* (Eds.: F. Diederich, P. J. Stang), Wiley-VCH, Weinheim, **1998**, chap. 1.
[158] I. Mangalagiu, T. Benneche, K. Undheim, *Acta Chem. Scand.* **1996**, *50*, 914 – 917.
[159] A. Ohta, M. Ohta, Y. Igarashi, K. Saeki, K. Yuasa, T. Mori, *Heterocycles* **1987**, *26*, 2449 – 2454.
[160] A. Ohta, A. Inoue, K. Ohtsuka, T. Watanabe, *Heterocycles* **1985**, *23*, 133 – 137.
[161] I. Mangalagiu, T. Benneche, K. Undheim, *Tetrahedron Lett.* **1996**, *37*, 1309 – 1312.
[162] K. Hirota, Y. Kitade, Y. Kanbe, Y. Maki, *J. Org. Chem.* **1992**, *57*, 5268 – 5270.
[163] For the coupling of a heteroaryl chloride with an organoindium compound, see ref. [110d].
[164] For the coupling of organocuprates, see H. Dvorakova, D. Dvorak, A. Holy, *Tetrahedron Lett.* **1996**, *37*, 1285 – 1288.
[165] J. Blum, O. Berlin, D. Milstein, Y. Ben-David, B. C. Wassermann, S. Schutte, H. Schumann, *Synthesis* **2000**, 571 – 575.
[166] G. Dyker, J. Heiermann, M. Miura, J.-I. Inoh, S. Pivsa-Art, T. Satoh, M. Nomura, *Chem. Eur. J.* **2000**, *6*, 3426 – 3433.
[167] a) K. Sonagashira in *Metal-Catalyzed Cross-Coupling Reactions* (Eds.: F. Diederich, P. J. Stang), Wiley-VCH, Weinheim, **1998**, chap. 5; b) L. Brandsma, S. F. Vasilevsky, H. D. Verkruijsse, *Application of Transition Metal Catalysts in Organic Synthesis*, Springer, New York, **1998**, chap. 10; c) R. Rossi, A. Carpita, F. Bellina, *Org. Prep. Proced. Int.* **1995**, *27*, 127 – 160; d) K. Sonagashira in *Comprehensive Organic Synthesis*, *Vol. 3* (Ed.: B. M. Trost), Pergamon, New York, **1991**, chap. 2.4.
[168] For a general review, see T. Sakamoto, Y. Kondo, H. Yamanaka, *Heterocycles* **1988**, *27*, 2225 – 2249.
[169] T. Sakamoto, Y. Kondo, H. Yamanaka, *Chem. Pharm. Bull.* **1985**, *33*, 626 – 633.
[170] T. Sakamoto, M. An-naka, Y. Kondo, T. Araki, H. Yamanaka, *Chem. Pharm. Bull.* **1988**, *36*, 1890 – 1894.
[171] T. Sakamoto, Y. Kondo, H. Yamanaka, *Chem. Pharm. Bull.* **1986**, *34*, 2362 – 2368.
[172] For other examples of Sonogashira couplings of chloropyridines, see a) T. Sakamoto, M. Shiraiwa, Y. Kondo, H. Yamanaka, *Synthesis* **1983**, 312 – 314; b) N. Sato, A. Hayakawa, R. Takeuchi, *J. Heterocycl. Chem.* **1990**, *27*, 503 – 506; c) C.-S. Kim, K. C. Russell, *J. Org. Chem.* **1998**, *63*, 8229 – 8234; d) M. Erdelyi, A. Gogoll, *J. Org. Chem.* **2001**, *66*, 4165 – 4169.
[173] a) Y. Abe, A. Ohsawa, H. Arai, H. Igeta, *Heterocycles* **1978**, *9*, 1397 – 1401; b) A. Ohsawa, Y. Abe, H. Igeta, *Chem. Pharm. Bull.* **1980**, *28*, 3488 – 3493; c) A. Ohsawa, Y. Abe, H. Igeta, *Bull. Chem. Soc. Jpn.* **1980**, *53*, 3273 – 3275; d) H. Yamanaka, M. Mizugaki, T. Sakamoto, M. Sagi, Y. Nakagawa, H. Takayama, M. Ishibashi, H. Miyazaki, *Chem. Pharm. Bull.* **1983**, *31*, 4549 – 4553; e) W. Dostal, G. Heinisch, G. Lotsch, *Monatsh. Chem.* **1988**, *119*, 751 – 759; f) S. Konno, M. Sagi, F. Siga, H. Yamanaka, *Heterocycles* **1992**, *34*, 225 – 228.
[174] a) K.-I. Tanji, T. Sakamoto, H. Yamanaka, *Chem. Pharm. Bull.* **1982**, *30*, 1865 – 1867; b) T. Sakamoto, Y. Kondo, H. Yamanaka, *Chem. Pharm. Bull.* **1982**, *30*, 2410 – 2416.
[175] a) Y. Akita, A. Ohta, *Heterocycles* **1982**, *19*, 329 – 331; b) Y. Akita, A. Inoue, A. Ohta, *Chem. Pharm. Bull.* **1986**, *34*, 1447 – 1458; c) Y. Akita, H. Kanekawa, T. Kawasaki, I. Shiratori, A. Ohta, *J. Heterocycl. Chem.* **1988**, *25*, 975 – 977; d) E. C. Taylor, R. Dotzer, *J. Org. Chem.* **1991**, *56*, 1816 – 1822.
[176] a) S. Konno, S. Fujimura, H. Yamanaka, *Heterocycles* **1984**, *22*, 2245 – 2248; b) R. Menicagli, S. Samaritani, S. Gori, *Tetrahedron Lett.* **1999**, *40*, 8419 – 8422; c) S. Samaritani, R. Menicagli, *Tetrahedron* **2002**, *58*, 1381 – 1386.
[177] T. Sakamoto, N. Miura, Y. Kondo, H. Yamanaka, *Chem. Pharm. Bull.* **1986**, *34*, 2760 – 2765.
[178] K. Edo, T. Sakamoto, H. Yamanaka, *Chem. Pharm. Bull.* **1978**, *26*, 3843 – 3850.
[179] a) D. E. Ames, M. I. Brohi, *J. Chem. Soc. Perkin Trans. 1* **1980**, 1384 – 1389; b) D. E. Ames, D. Bull, C. Takundwa, *Synthesis* **1981**, 364 – 365; c) D. E. Ames, J. C. Mitchell, C. C. Takundwa, *J. Chem. Res. Synop.* **1985**, 144 – 145; d) A. Dinsmore, J. H. Birks, C. D. Garner, J. A. Joule, *J. Chem. Soc. Perkin Trans. 1* **1997**, 801 – 807; e) B. Bradshaw, A. Dinsmore, C. D. Garner, J. A. Joule, *Chem. Commun.* **1998**, 417 – 418; f) C. Kim, K. C. Russell, *J. Org. Chem.* **1998**, *63*, 8229 – 8234.
[180] E. C. Taylor, P. S. Roy, *J. Org. Chem.* **1987**, *52*, 3997 – 4000.
[181] S. Nishikawa, H. Mizutani, Z. Kumazawa, N. Kashimura, *Agric. Biol. Chem.* **1986**, *50*, 2377 – 2379; b) K.-I. Tanji, T. Higashino, *Chem. Pharm. Bull.* **1988**, *36*, 1935 – 1941.
[182] R. Ziessel, J. Suffert, M.-T. Youinou, *J. Org. Chem.* **1996**, *61*, 6535 – 6546.
[183] L. Cassar, *J. Organomet. Chem.* **1975**, *93*, 253 – 257.
[184] a) R. Singh, G. Just, *J. Org. Chem.* **1989**, *54*, 4453 – 4457; b) K.-W. Poon, W. Liu, P.-K. Chan, Q. Yang, T.-W. D. Chan, T. C. W. Mak, D. K. P. Ng, *J. Org. Chem.* **2001**, *66*, 1553 – 1559.
[185] For examples of Sonogashira couplings of tricarbonyl(η^6-chloroarene)chromium complexes, see a) D. Villemin, E. Schigeko, *J. Organomet. Chem.* **1985**, *293*, C10 – C12; b) T. J. J. Muller, M. Ansorge, *Tetrahedron* **1998**, *54*, 1457 – 1470; c) T. J. J. Muller, M. Ansorge, K. Polborn, *J. Organomet. Chem.* **1999**, *578*, 252 – 259; d) M. Ansorge, T. J. J. Muller, *J. Organomet. Chem.* **1999**, *585*, 174 – 178.
[186] A. N. Tischler, T. J. Lanza, *Tetrahedron Lett.* **1986**, *27*, 1653 – 1656.
[187] a) M. Palucki, S. L. Buchwald, *J. Am. Chem. Soc.* **1997**, *119*, 11108 – 11109; b) B. C. Hamann, J. F. Hartwig, *J. Am. Chem. Soc.* **1997**, *119*, 12382 – 12383; c) T. Satoh, Y. Kawamura, M. Miura, M. Nomura, *Angew. Chem.* **1997**, *109*, 1820 – 1822; *Angew. Chem. Int. Ed. Engl.* **1997**, *36*, 1740 – 1742.
[188] T. Sakamoto, Y. Kondo, T. Suginome, S. Ohba, H. Yamanaka, *Synthesis* **1992**, 552 – 554.
[189] J. M. Fox, X. Huang, A. Chieffi, S. L. Buchwald, *J. Am. Chem. Soc.* **2000**, *122*, 1360 – 1370.
[190] E. M. Vogl, S. L. Buchwald, *J. Org. Chem.* **2002**, *67*, 106 – 111.
[191] W. A. Moradi, S. L. Buchwald, *J. Am. Chem. Soc.* **2001**, *123*, 7996 – 8002.
[192] M. Kawatsura, J. F. Hartwig, *J. Am. Chem. Soc.* **1999**, *121*, 1473 – 1478.
[193] N. A. Beare, J. F. Hartwig, *J. Org. Chem.* **2002**, *67*, 541 – 555.
[194] See also: T. Y. Zhang, H. Zhang, *Tetrahedron Lett.* **2002**, *43*, 193 – 195.
[195] S. Lee, J. F. Hartwig, *J. Org. Chem.* **2001**, *66*, 3402 – 3415.
[196] S. R. Stauffer, N. A. Beare, J. P. Stambuli, J. F. Hartwig, *J. Am. Chem. Soc.* **2001**, *123*, 4641 – 4642.
[197] For another application of this method, see J. F. Stambuli, S. R. Stauffer, K. H. Shaughnessy, J. F. Hartwig, *J. Am. Chem. Soc.* **2001**, *123*, 2677 – 2678.
[198] S. Lee, N. A. Beare, J. F. Hartwig, *J. Am. Chem. Soc.* **2001**, *123*, 8410 – 8411.
[199] For a review, see a) G. P. Ellis, T. M. Romney-Alexander, *Chem. Rev.* **1987**, *87*, 779 – 794; for additional discussion, see b) M. Sundermeier, A. Zapf, M. Beller, J. Sans, *Tetrahedron Lett.* **2001**, *42*, 6707 – 6710.
[200] Y. Akita, M. Shimazaki, A. Ohta, *Synthesis* **1981**, 974 – 975.
[201] L.-L. Gundersen, *Acta Chem. Scand.* **1996**, *50*, 58 – 63.

[202] Y. Andersson, B. Langstrom, *J. Chem. Soc. Perkin Trans. 1* **1994**, 1395 – 1400.
[203] F. Jin, P. N. Confalone, *Tetrahedron Lett.* **2000**, *41*, 3271 – 3273.
[204] M. Sundermeier, A. Zapf, M. Beller, J. Sans, *Tetrahedron Lett.* **2001**, *42*, 6707 – 6710.
[205] For reviews on carbonylation, see a) M. Beller in *Applied Homogeneous Catalysis with Organometallic Compounds. A Comprehensive Handbook*, *Vol. 1* (Eds.: B. Cornils, W. A. Herrmann), VCH, Weinheim, **1996**, chap. 2.1.2.3; b) M. Beller, B. Cornils, C. D. Frohning, C. W. Kohlpaintner, *J. Mol. Catal. A* **1995**, *104*, 17 – 85.
[206] M. Beller, W. Magerlein, A. F. Indolese, C. Fischer, *Synthesis* **2001**, 1098 – 1109, and references therein.
[207] a) M. Scalone, P. Vogt (F. Hoffmann – La Roche AG), EP 385210, **1990**; b) R. Schmid, *Chimia* **1996**, *50*, 110 – 113.
[208] For other examples of carbonylations of chloropyridines, see a) R. A. Head, A. Ibbotson, *Tetrahedron Lett.* **1984**, *25*, 5939 – 5942; b) R. Takeuchi, K. Suzuki, N. Sato, *J. Mol. Catal.* **1991**, *66*, 277 – 288; c) M. Kudo, *Shokubai* **1994**, *36*, 580 – 584; d) Y. Bessard, J. P. Roduit, *Tetrahedron* **1999**, *55*, 393 – 404; e) Y. Bessard, R. Crettaz, *Heterocycles* **1999**, *51*, 2589 – 2602; f) D. Najiba, J.-F. Carpentier, Y. Castanet, C. Biot, J. Brocard, A. Mortreux, *Tetrahedron Lett.* **1999**, *40*, 3719 – 3722; g) A. Schnyder, M. Beller, G. Mehltretter, T. Nsenda, M. Studer, A. F. Indolese, *J. Org. Chem.* **2001**, *66*, 4311 – 4315.
[209] R. Takeuchi, K. Suzuki, N. Sato, *Synthesis* **1990**, 923 – 924.
[210] Y. Bessard, R. Crettaz, *Tetrahedron* **1999**, *55*, 405 – 412.
[211] A. El-ghayoury, R. Ziessel, *J. Org. Chem.* **2000**, *65*, 7757 – 7763.
[212] M. Beller, W. Magerlein, A. F. Indolese, C. Fischer, *Synthesis* **2001**, 1098 – 1109.
[213] Previously, the only examples of palladium-catalyzed carbonylations of aryl chlorides had employed activated tricarbonyl(η^6-chloroarene)chromium complexes: a) R. Mutin, C. Lucas, J. Thivolle-Cazat, V. Dufaud, F. Dany, J. M. Basset, *J. Chem. Soc. Chem. Commun.* **1988**, 896 – 898; b) F. Dany, R. Mutin, C. Lucas, V. Dufaud, J. Thivolle-Cazat, J. M. Basset, *J. Mol. Catal.* **1989**, *51*, L15 – L20; for more recent examples, see c) J.-F. Carpentier, Y. Castanet, J. Brocard, A. Mortreux, F. Petit, *Tetrahedron Lett.* **1992**, *33*, 2001 – 2004; d) B. Crousse, L.-H. Xu, G. Bernardinelli, E. P. Kundig, *Synlett* **1998**, 658 – 660; e) E. P. Kundig, H. Ratni, B. Crousse, G. Bernardinelli, *J. Org. Chem.* **2001**, *66*, 1852 – 1860.
[214] M. Huser, M.-T. Youinou, J. A. Osborn, *Angew. Chem.* **1989**, *101*, 1427 – 1430; *Angew. Chem. Int. Ed. Engl.* **1989**, *28*, 1386 – 1388.
[215] Y. Ben-David, M. Portnoy, D. Milstein, *J. Am. Chem. Soc.* **1989**, *111*, 8742 – 8744.
[216] Y. Ben-David, M. Portnoy, D. Milstein, *J. Chem. Soc. Chem. Commun.* **1989**, 1816 – 1817.
[217] a) V. V. Grushin, H. Alper, *J. Chem. Soc. Chem. Commun.* **1992**, 611 – 612; b) G. Jenner, A. B. Taleb, *J. Organomet. Chem.* **1994**, *470*, 257 – 261; c) T. Miyawaki, K. Nomura, M. Hazama, G. Suzukamo, *J. Mol. Catal. A* **1997**, *120*, L9 – L11.
[218] V. Dufaud, J. Thivolle-Cazat, J.-M. Basset, *J. Chem. Soc. Chem. Commun.* **1990**, 426 – 427.
[219] a) R. J. Perry, S. R. Turner, R. W. Blevins, *Macromolecules* **1995**, *28*, 2607 – 2609; for related work, see b) R. J. Perry, B. D. Wilson, *J. Org. Chem.* **1996**, *61*, 7482 – 7485.
[220] J. S. Kim, A. Sen, *J. Mol. Catal. A* **1999**, *143*, 197 – 201.
[221] a) W. Mägerlein, A. F. Indolese, M. Beller, *Angew. Chem.* **2001**, *113*, 2940 – 2943; *Angew. Chem. Int. Ed.* **2001**, *40*, 2856 – 2859; b) W. Mägerlein, A. F. Indolese, M. Beller, *J. Organomet. Chem.* **2002**, *641*, 30 – 40.
[222] For a review of the Ullmann coupling, see P. E. Fanta, *Synthesis* **1974**, 9 – 21.
[223] P. Bamfield, P. M. Quan, *Synthesis* **1978**, 537 – 538.
[224] a) S. Mukhopadhyay, G. Rothenberg, D. Gitis, H. Wiener, Y. Sasson, *J. Chem. Soc. Perkin Trans. 2* **1999**, 2481 – 2484; b) S. Mukhopadhyay, G. Rothenberg, N. Qafisheh, Y. Sasson, *Tetrahedron Lett.* **2001**, *42*, 6117 – 6119; see also: c) S. Munavalli, D. I. Rossman, L. L. Szafraniec, W. T. Beaudry, D. K. Rohrbaugh, C. P. Ferguson, M. Gratzel, *J. Fluorine Chem.* **1995**, *73*, 1 – 6.
[225] S. Mukhopadhyay, G. Rothenberg, H. Weiner, Y. Sasson, *Tetrahedron* **1999**, *55*, 14763 – 14768.
[226] a) S. Mukhopadhyay, G. Rothenberg, D. Gitis, Y. Sasson, *Org. Lett.* **2000**, *2*, 211 – 214; b) S. Mukhopadhyay, G. Rothenberg, D. Gitis, M. Baidossi, D. E. Ponde, Y. Sasson, *J. Chem. Soc. Perkin Trans. 2* **2000**, 1809 – 1812.
[227] a) J. Hassan, V. Penalva, L. Lavenot, C. Gozzi, M. Lemaire, *Tetrahedron* **1998**, *54*, 13793 – 13804; b) J. Hassan, L. Lavenot, C. Gozzi, M. Lemaire, *Tetrahedron Lett.* **1999**, *40*, 857 – 858; c) S. Mukhopadhyay, G. Rothenberg, D. Gitis, Y. Sasson, *J. Org. Chem.* **2000**, *65*, 3107 – 3110.
[228] a) T. Mizoroki, K. Mori, A. Ozaki, *Bull. Chem. Soc. Jpn.* **1971**, *44*, 581; b) R. F. Heck, J. P. Nolley, Jr., *J. Org. Chem.* **1972**, *37*, 2320 – 2322.
[229] For reviews of the Heck reaction, see a) N. J. Whitcombe, K. K. Hii, S. E. Gibson, *Tetrahedron* **2001**, *57*, 7449 – 7476; b) J. G. de Vries, *Can. J. Chem.* **2001**, *79*, 1086 – 1092; c) I. P. Beletskaya, A. V. Cheprakov, *Chem. Rev.* **2000**, *100*, 3009 – 3066; d) S. Bräse, A. de Meijere in *Metal-Catalyzed Cross-Coupling Reactions* (Eds.: F. Diederich, P. J. Stang), Wiley, Weinheim, **1998**, chap. 3; e) G. T. Crisp, *Chem. Soc. Rev.* **1998**, *27*, 427 – 436; f) T. Jeffery in *Advances in Metal-Organic Chemistry*, *Vol. 5* (Ed.: L. S. Liebeskind), JAI, London, **1996**, pp. 153 – 260; g) W. Cabri, I. Candiani, *Acc. Chem. Res.* **1995**, *28*, 2 – 7; h) A. de Meijere, F. E. Meyer, *Angew. Chem.* **1994**, *106*, 2473 – 2506; *Angew. Chem. Int. Ed. Engl.* **1994**, *33*, 2379 – 2411; i) R. F. Heck in *Comprehensive Organic Synthesis*, *Vol. 4* (Ed.: B. M. Trost), Pergamon, New York, **1991**, chap. 4.3; j) R. F. Heck, *Org. React.* **1982**, *27*, 345 – 390.
[230] a) B. Basu, T. Frejd, *Acta Chem. Scand.* **1996**, *50*, 316 – 322; b) K. Nakatsu, K. Kinoshita, H. Kanda, K. Isobe, Y. Nakamura, S. Kawaguchi, *Chem. Lett.* **1980**, 913 – 914.
[231] a) D. E. Ames, A. Opalko, *Tetrahedron* **1984**, *40*, 1919 – 1925; b) R. Grigg, *J. Heterocycl. Chem.* **1994**, *31*, 631 – 639; c) Y. Blache, M.-E. Sinibaldi-Troin, A. Voldoire, O. Chavignon, J.-C. Gramain, J.-C. Teulade, J.-P. Chapat, *J. Org. Chem.* **1997**, *62*, 8553 – 8556.
[232] a) Y. Akita, A. Inoue, K. Yamamoto, A. Ohta, T. Kurihara, M. Shimizu, *Heterocycles* **1985**, *23*, 2327 – 2333; b) Y. Akita, T. Noguchi, M. Sugimoto, A. Ohta, *J. Heterocycl. Chem.* **1986**, *23*, 1481 – 1485; c) Y. Akita, Y. Itagaki, S. Takizawa, A. Ohta, *Chem. Pharm. Bull.* **1989**, *37*, 1477 – 1480; d) Y. Aoyagi, A. Inoue, I. Koizumi, R. Hashimoto, K. Tokunaga, K. Gohma, J. Komatsu, K. Sekine, A. Miyafuji, J. Kunoh, R. Honma, Y. Akita, A. Ohta, *Heterocycles* **1992**, *33*, 257 – 272.
[233] a) F. G. Fang, D. D. Bankston, E. M. Huie, M. R. Johnson, M.-C. Kang, C. S. LeHoullier, G. C. Lewis, T. C. Lovelace, M. W. Lowery, D. L. McDougald, C. A. Meerholz, J. J. Partridge, M. J. Sharp, S. Xie, *Tetrahedron* **1997**, *53*, 10953 – 10970; b) D. L. Comins, J. M. Nolan, *Org. Lett.* **2001**, *3*, 4255 – 4257.
[234] J. J. Li, *J. Org. Chem.* **1999**, *64*, 8425 – 8427.
[235] E. C. Taylor, P. S. Ray, *Synth. Commun.* **1987**, *17*, 1865 – 1868.
[236] A. Spencer, *J. Organomet. Chem.* **1984**, *270*, 115 – 120.
[237] S. Bräse, *Tetrahedron Lett.* **1999**, *40*, 6757 – 6759.
[238] a) W. A. Herrmann, C. Brossmer, K. Ofele, C.-P. Reisinger, T. Priermeier, M. Beller, H. Fischer, *Angew. Chem.* **1995**, *107*, 1989 – 1992; *Angew. Chem. Int. Ed. Engl.* **1995**, *34*, 1844 – 1847; b) W. A. Herrmann, C. Brossmer, C.-P. Reisinger, T. H. Riermeier, K. Ofele, M. Beller, *Chem. Eur. J.* **1997**, *3*, 1357 – 1364.
[239] S. Iyer, C. Ramesh, *Tetrahedron Lett.* **2000**, *41*, 8981 – 8984.
[240] a) S. Iyer, A. Jayanthi, *Tetrahedron Lett.* **2001**, *42*, 7877 – 7878; b) Y. Wu, J. Hou, H. Yun, X. Cui, R. Yuan, *J. Organomet. Chem.* **2001**, *637 – 639*, 793 – 795.
[241] A. S. Gruber, D. Zim, G. Ebeling, A. L. Monteiro, J. Dupont, *Org. Lett.* **2000**, *2*, 1287 – 1290.
[242] W. A. Herrmann, M. Elison, J. Fischer, C. Kocher, G. R. J. Artus, *Angew. Chem.* **1995**, *107*, 2602 – 2605; *Angew. Chem. Int. Ed. Engl.* **1995**, *34*, 2371 – 2373.
[243] Table 6, entry 4: D. S. McGuinness, K. J. Cavell, *Organometallics* **2000**, *19*, 741 – 748.
[244] Table 6, entry 5: V. Calo, A. Nacci. L. Lopez, N. Mannarini, *Tetrahedron Lett.* **2000**, *41*, 8973 – 8976.
[245] Table 6, entry 6: E. Peris, J. A. Loch, J. Mata, R. H. Crabtree, *Chem. Commun.* **2001**, 201 – 202.
[246] a) V. Calo, A. Nacci, A. Monopoli, L. Lopez, A. di Cosmo, *Tetrahedron* **2001**, *57*, 6071 – 6077; b) A. A. D. Tulloch, A. A. Danopoulos, G. J. Tizzard, S. J. Coles, M. B. Hursthouse, R. S. Hay-Motherwell, W. B. Motherwell, *Chem. Commun.* **2001**, 1270 – 1271;

c) S. Grundemann, M. Albrecht, J. A. Loch, J. W. Faller, R. H. Crabtree, *Organometallics* **2001**, *20*, 5485 – 5488; d) J. A. Loch, M. Albrecht, E. Peris, J. Mata, J. W. Faller, R. H. Crabtree, *Organometallics* **2002**, *21*, 700 – 706.
[247] M. Beller, A. Zapf, *Synlett* **1998**, 792 – 793.
[248] G. Y. Li, G. Zheng, A. F. Noonan, *J. Org. Chem.* **2001**, *66*, 8677 – 8681.
[249] A. Zapf, M. Beller, *Chem. Eur. J.* **2001**, *7*, 2908 – 2915.
[250] A. S. Gruber, D. Pozebon, A. L. Monteiro, J. Dupont, *Tetrahedron Lett.* **2001**, *42*, 7345 – 7348.
[251] a) L. Djakovitch, H. Heise, K. Kohler, *J. Organomet. Chem.* **1999**, *584*, 16 – 26; b) L. Djakovitch, K. Koehler, *J. Am. Chem. Soc.* **2001**, *123*, 5990 – 5999.
[252] J. B. Davison, N. M. Simon, S. A. Sojka, *J. Mol. Catal.* **1984**, *22*, 349 – 352.
[253] Y. Ben-David, M. Portnoy, M. Gozin, D. Milstein, *Organometallics* **1992**, *11*, 1995 – 1996.
[254] M. Portnoy, Y. Ben-David, I. Rousso, D. Milstein, *Organometallics* **1994**, *13*, 3465 – 3479.
[255] M. Portnoy, Y. Ben-David, D. Milstein, *Organometallics* **1993**, *12*, 4734 – 4735.
[256] W. A. Herrmann, C. Brossmer, K. Ofele, M. Beller, H. Fischer, *J. Mol. Catal. A* **1995**, *103*, 133 – 146.
[257] K. Kaneda, M. Higuchi, T. Imanaka, *J. Mol. Catal.* **1990**, *63*, L33 – L36.
[258] M. T. Reetz, G. Lohmer, *Chem. Commun.* **1996**, 1921 – 1922.
[259] M. T. Reetz, G. Lohmer, R. Schwickardi, *Angew. Chem.* **1998**, *110*, 492 – 495; *Angew. Chem. Int. Ed.* **1998**, *37*, 481 – 483.
[260] A. F. Littke, G. C. Fu, *J. Org. Chem.* **1999**, *64*, 10 – 11.
[261] For an example of an intramolecular coupling of an aryl chloride with an aromatic ring using $[PdCl_2(PCy_3)_2]$ as the catalyst at elevated temperature, see L. Wang, P. B. Shevlin, *Tetrahedron Lett.* **2000**, *41*, 285 – 288.
[262] M. Wada, S. Higashizaki, *J. Chem. Soc. Chem. Commun.* **1984**, 482 – 483.
[263] $P(t\text{Bu})_3$: $pK_a = 11.4$, cone angle = 182°. PCy_3: $pK_a = 9.7$, cone angle = 170°. $P(2,4,6\text{-}(OMe)_3C_6H_2)_3$, $pK_a = 11.0$, cone angle = 184°.
[264] A. F. Littke, G. C. Fu, *J. Am. Chem. Soc.* **2001**, *123*, 6989 – 7000.
[265] Gurtler and Buchwald were the first to describe the unusual effectiveness of Cy_2NMe as a base in Heck reactions (couplings of aryl bromides with disubstituted olefins at elevated temperature): C. Gurtler, S. L. Buchwald, *Chem. Eur. J.* **1999**, *5*, 3107 – 3112.
[266] K. H. Shaughnessy, P. Kim, J. F. Hartwig, *J. Am. Chem. Soc.* **1999**, *121*, 2123 – 2132.
[267] a) M. R. Buchmeiser, K. Wurst, *J. Am. Chem. Soc.* **1999**, *121*, 11 101 – 11 107; b) J. Silberg, T. Schareina, R. Kempe, K. Wurst, M. R. Buchmeiser, *J. Organomet. Chem.* **2001**, *622*, 6 – 18.
[268] a) W. A. Herrmann, V. P. W. Bohm, *J. Organomet. Chem.* **1999**, *572*, 141 – 145; for an earlier report of an application of molten salts as a medium for the Heck reaction of an *activated* aryl chloride, see b) D. E. Kaufmann, M. Nouroozian, H. Henze, *Synlett* **1996**, 1091 – 1092.
[269] V. P. W. Bohm, W. A. Herrmann, *Chem. Eur. J.* **2000**, *6*, 1017 – 1025.
[270] D. Morales-Morales, C. Grause, K. Kasaoka, R. Redon, R. E. Cramer, C. M. Jensen, *Inorg. Chim. Acta* **2000**, *300 – 302*, 958 – 963.
[271] D. Morales-Morales, R. Redon, C. Yung, C. M. Jensen, *Chem. Commun.* **2000**, 1619 – 1620.
[272] Similar observations have been made for the TFA complex: M. Ohff, A. Ohff, M. E. van der Boom, D. Milstein, *J. Am. Chem. Soc.* **1997**, *119*, 11 687 – 11 688.
[273] A. Ehrentraut, A. Zapf, M. Beller, *Synlett* **2000**, 1589 – 1592.
[274] J. P. Wolfe, S. Wagaw, J.-F. Marcoux, S. L. Buchwald, *Acc. Chem. Res.* **1998**, *31*, 805 – 818.
[275] a) J. F. Hartwig, *Acc. Chem. Res.* **1998**, *31*, 852 – 860; b) J. F. Hartwig, *Pure Appl. Chem.* **1999**, *71*, 1417 – 1423.
[276] M. Kosugi, M. Kameyama, T. Migita, *Chem. Lett.* **1983**, 927 – 928.
[277] For some general reviews of palladium-catalyzed C–N bond formation, see a) J. F. Hartwig, *Angew. Chem.* **1998**, *110*, 2154 – 2177; *Angew. Chem. Int. Ed.* **1998**, *37*, 2046 – 2067; b) B. H. Yang, S. L. Buchwald, *J. Organomet. Chem.* **1999**, *576*, 125 – 146; c) J. F. Hartwig in *Modern Amination Methods* (Ed.: A. Ricci), Wiley, Weinheim, **2000**, chap. 7.
[278] S. Wagaw, S. L. Buchwald, *J. Org. Chem.* **1996**, *61*, 7240 – 7241.
[279] S. Jaime-Figueroa, Y. Liu, J. M. Muchowski, D. G. Putnam, *Tetrahedron Lett.* **1998**, *39*, 1313 – 1316.
[280] J. Rouden, A. Bernard, M.-C. Lasne, *Tetrahedron Lett.* **1999**, *40*, 8109 – 8112.
[281] N. Chida, T. Suzuki, S. Tanaka, I. Yamada, *Tetrahedron Lett.* **1999**, *40*, 2573 – 2576.
[282] T. J. Luker, H. G. Beaton, M. Whiting, A. Mete, D. R. Cheshire, *Tetrahedron Lett.* **2000**, *41*, 7731 – 7735.
[283] Y. Hong, G. J. Tanoury, H. S. Wilkinson, R. P. Bakale, S. A. Wald, C. H. Senanayake, *Tetrahedron Lett.* **1997**, *38*, 5607 – 5610.
[284] a) J. B. Arterburn, K. V. Rao, R. Ramdas, B. R. Dible, *Org. Lett.* **2001**, *3*, 1351 – 1354; b) L. F. Frey, K. Marcantonio, D. E. Frantz, J. A. Murry, R. D. Tillyer, E. J. J. Grabowski, P. J. Reider, *Tetrahedron Lett.* **2001**, *42*, 6815 – 6818.
[285] T. H. M. Jonckers, B. U. W. Maes, G. L. F. Lemiere, R. Dommisse, *Tetrahedron* **2001**, *57*, 7027 – 7034.
[286] Y. Hong, C. H. Senanayake, T. Xiang, C. P. Vandenbossche, G. J. Tanoury, R. P. Bakale, S. A. Wald, *Tetrahedron Lett.* **1998**, *39*, 3121 – 3124.
[287] M. Beller, T. H. Riermeier, C.-P. Reisinger, W. A. Herrmann, *Tetrahedron Lett.* **1997**, *38*, 2073 – 2074.
[288] M. Beller, C. Breindl, T. H. Riermeier, A. Tillack, *J. Org. Chem.* **2001**, *66*, 1403 – 1412.
[289] N. P. Reddy, M. Tanaka, *Tetrahedron Lett.* **1997**, *38*, 4807 – 4810.
[290] For examples of successful Pd/binap-catalyzed aminations of aryl chlorides, see a) I. P. Beletskaya, A. D. Averin, A. G. Bessmertnykh, R. Guilard, *Tetrahedron Lett.* **2001**, *42*, 4983 – 4986; b) I. P. Beletskaya, A. D. Averin, A. G. Bessmertnykh, R. Guilard, *Tetrahedron Lett.* **2001**, *42*, 4987 – 4989; c) I. P. Beletskaya, A. D. Averin, A. G. Bessmertnykh, F. Denat, R. Guilard, *Tetrahedron Lett.* **2002**, *43*, 1193 – 1196.
[291] B. C. Hamann, J. F. Hartwig, *J. Am. Chem. Soc.* **1998**, *120*, 7369 – 7370.
[292] J. P. Wolfe, H. Tomori, J. P. Sadighi, J. Yin, S. L. Buchwald, *J. Org. Chem.* **2000**, *65*, 1158 – 1174.
[293] D. W. Old, M. C. Harris, S. L. Buchwald, *Org. Lett.* **2000**, *2*, 1403 – 1406.
[294] S. D. Edmondson, A. Mastracchio, E. R. Parmee, *Org. Lett.* **2000**, *2*, 1109 – 1112.
[295] O. J. Plante, S. L. Buchwald, P. H. Seeberger, *J. Am. Chem. Soc.* **2000**, *122*, 7148 – 7149.
[296] M. C. Harris, S. L. Buchwald, *J. Org. Chem.* **2000**, *65*, 5327 – 5333.
[297] For an additional application, see ref. [285].
[298] C. A. Parrish, S. L. Buchwald, *J. Org. Chem.* **2001**, *66*, 3820 – 3827.
[299] X. Huang, S. L. Buchwald, *Org. Lett.* **2001**, *3*, 3417 – 3419.
[300] M. Nishiyama, T. Yamamoto, Y. Koie, *Tetrahedron Lett.* **1998**, *39*, 617 – 620.
[301] T. Yamamoto, M. Nishiyama, Y. Koie, *Tetrahedron Lett.* **1998**, *39*, 2367 – 2370.
[302] J. F. Hartwig, M. Kawatsura, S. I. Hauck, K. H. Shaughnessy, L. M. Alcazar-Roman, *J. Org. Chem.* **1999**, *64*, 5575 – 5580.
[303] For a related coupling of 4-chlorobenzaldehyde with carbazole using $Pd/P(t\text{Bu})_3$, see M. Watanabe, M. Nishiyama, T. Yamamoto, Y. Koie, *Tetrahedron Lett.* **2000**, *41*, 481 – 483.
[304] For a related coupling of a secondary amide with an activated aryl chloride using Xantphos as a ligand, see J. Yin, S. L. Buchwald, *Org. Lett.* **2000**, *2*, 1101 – 1104.
[305] S. Lee, M. Jorgensen, J. F. Hartwig, *Org. Lett.* **2001**, *3*, 2729 – 2732.
[306] L. M. Alcazar-Roman, J. F. Hartwig, *J. Am. Chem. Soc.* **2001**, *123*, 12 905 – 12 906.
[307] For leading references to studies of the role of anionic Pd^0 and Pd^{II} intermediates in palladium-catalyzed coupling reactions, see ref. [41].
[308] L. M. Alcazar-Roman, J. F. Hartwig, A. L. Rheingold, L. M. Liable-Sands, I. A. Guzei, *J. Am. Chem. Soc.* **2000**, *122*, 4618 – 4630.
[309] For an application of $Pd/P(t\text{Bu})_3$ to aminations of chloropurines, see ref. [67e].
[310] a) X. Bei, A. S. Guram, H. W. Turner, W. H. Weinberg, *Tetrahedron Lett.* **1999**, *40*, 1237 – 1240; b) X. Bei, T. Uno, J. Norris, H. W. Turner, W. H. Weinberg, A. S. Guram, J. L. Petersen, *Organometallics* **1999**, *18*, 1840 – 1853.
[311] J. Huang, G. Grasa, S. P. Nolan, *Org. Lett.* **1999**, *1*, 1307 – 1309.

[312] G. A. Grasa, M. S. Viciu, J. Huang, S. P. Nolan, *J. Org. Chem.* **2001**, *66*, 7729 – 7737.
[313] J. Cheng, M. L. Trudell, *Org. Lett.* **2001**, *3*, 1371 – 1374.
[314] A. J. Arduengo III, J. R. Goerlich, W. J. Marshall, *J. Am. Chem. Soc.* **1995**, *117*, 11 027 – 11 028.
[315] For a recent application of a saturated carbene ligand in ruthenium-catalyzed olefin metathesis, see M. Scholl, S. Ding, C. W. Lee, R. H. Grubbs, *Org. Lett.* **1999**, *1*, 953 – 956.
[316] S. R. Stauffer, S. Lee, J. P. Stambuli, S. I. Hauck, J. F. Hartwig, *Org. Lett.* **2000**, *2*, 1423 – 1426.
[317] L. R. Titcomb, S. Caddick, F. G. N. Cloke, D. J. Wilson, D. McKerrecher, *Chem. Commun.* **2001**, 1388 – 1389.
[318] For other examples of Pd/carbene-catalyzed aminations of aryl chlorides, see S. Caddick, F. G. N. Cloke, G. K. B. Clentsmith, P. B. Hitchcock, D. McKerrecher, L. R. Titcomb, M. R. V. Williams, *J. Organomet. Chem.* **2001**, *617 – 618*, 635 – 639; b) ref. [89]; c) ref. [92].
[319] D. Baranano, G. Mann, J. F. Hartwig, *Curr. Org. Chem.* **1997**, *1*, 287 – 305.
[320] J.-L. Montchamp, Y. R. Dumond, *J. Am. Chem. Soc.* **2001**, *123*, 510 – 511.
[321] a) F. Theil, *Angew. Chem. Int. Ed.* **1999**, *111*, 2493 – 2495; *Angew. Chem. Int. Ed.* **1999**, *38*, 2345 – 2347; b) J. S. Sawyer, *Tetrahedron* **2000**, *56*, 5045 – 5065.
[322] G. Mann, J. F. Hartwig, *J. Org. Chem.* **1997**, *62*, 5413 – 5418.
[323] T. F. Woiwode, C. Rose, T. J. Wandless, *J. Org. Chem.* **1998**, *63*, 9594 – 9596.
[324] G. Mann, C. Incarvito, A. L. Rheingold, J. F. Hartwig, *J. Am. Chem. Soc.* **1999**, *121*, 3224 – 3225.
[325] M. Watanabe, M. Nishiyama, Y. Koie, *Tetrahedron Lett.* **1999**, *40*, 8837 – 8840.
[326] Q. Shelby, N. Kataoka, G. Mann, J. F. Hartwig, *J. Am. Chem. Soc.* **2000**, *122*, 10 718 – 10 719.
[327] A. Aranyos, D. W. Old, A. Kiyomori, J. P. Wolfe, J. P. Sadighi, S. L. Buchwald, *J. Am. Chem. Soc.* **1999**, *121*, 4369 – 4378.
[328] C. A. Parrish, S. L. Buchwald, *J. Org. Chem.* **2001**, *66*, 2498 – 2500.
[329] J.-E. Backvall, E. E. Bjorkman, L. Pettersson, P. Siegbahn, *J. Am. Chem. Soc.* **1984**, *106*, 4369 – 4373.
[330] a) K. E. Torraca, S.-I. Kuwabe, S. L. Buchwald, *J. Am. Chem. Soc.* **2000**, *122*, 12 907 – 12 908; b) S.-I. Kuwabe, K. E. Torraca, S. L. Buchwald, *J. Am. Chem. Soc.* **2001**, *123*, 12 202 – 12 206.
[331] K. E. Torraca, X. Huang, C. A. Parrish, S. L. Buchwald, *J. Am. Chem. Soc.* **2001**, *123*, 10 770 – 10 771.
[332] Y. Nishiyama, K. Tokunaga, N. Sonoda, *Org. Lett.* **1999**, *1*, 1725 – 1727.
[333] For reviews, see a) P. N. Rylander, *Catalytic Hydrogenation over Platinum Metals*, Academic Press, New York, **1967**, chap. 24; b) A. R. Pinder, *Synthesis* **1980**, 425 – 452.
[334] a) *PCBs and the Environment*, *Vol. 1 – 3* (Ed.: J. S. Waid), CRC, Boca Raton, FL, **1987**; b) O. Hutzinger, S. Safe, V. Zitko, *The Chemistry of PCBs*, CRC, Cleveland, OH, **1974**.
[335] P. N. Rylander, *Catalytic Hydrogenation over Platinum Metals*, Academic Press, New York, **1967**, chap. 24, and references therein.
[336] a) C. A. Marques, M. Selva, P. Tundo, *J. Org. Chem.* **1993**, *58*, 5256 – 5260; b) C. A. Marques, M. Selva, P. Tundo, *J. Org. Chem.* **1994**, *59*, 3830 – 3837; c) D. G. Wishka, D. R. Graber, E. P. Seest, L. A. Dolak, F. Han, W. Watt, J. Morris, *J. Org. Chem.* **1998**, *63*, 7851 – 7859.
[337] J. D. Citron, J. E. Lyons, L. H. Sommer, *J. Org. Chem.* **1969**, *34*, 638 – 640.
[338] S. K. Boyer, J. Bach, J. McKenna, E. Jagdmann, Jr., *J. Org. Chem.* **1985**, *50*, 3408 – 3411.
[339] a) P. N. Pandey, M. L. Purkayastha, *Synthesis* **1982**, 876 – 878; b) J. P. Barren, S. S. Baghel, P. J. McCloskey, *Synth. Commun.* **1993**, *23*, 1601 – 1609.
[340] a) N. A. Cortese, R. F. Heck, *J. Org. Chem.* **1977**, *42*, 3491 – 3494; b) M. K. Anwer, A. F. Spatola, *Tetrahedron Lett.* **1985**, *26*, 1381 – 1384; c) H. Wiener, J. Blum, Y. Sasson, *J. Org. Chem.* **1991**, *56*, 6145 – 6148; d) S. Rajagopal, A. F. Spatola, *J. Org. Chem.* **1995**, *60*, 1347 – 1355.
[341] R. G. Pews, J. E. Hunter, R. W. Wehmeyer, *Tetrahedron* **1993**, *49*, 4809 – 4820.
[342] H. Imai, T. Nishiguchi, M. Tanaka, K. Fukuzumi, *J. Org. Chem.* **1977**, *42*, 2309 – 2313.
[343] For other examples of phosphane-free, palladium-catalyzed dechlorinations of aryl chlorides, see a) Y. Zhang, S. Liao, Y. Xu, *Tetrahedron Lett.* **1994**, *35*, 4599 – 4602; b) H. Li, S. Liao, Y. Xu, D. Yu, *Synth. Commun.* **1997**, *27*, 829 – 836.
[344] a) A. Zask, P. Helquist, *J. Org. Chem.* **1978**, *43*, 1619 – 1620; b) Y. Akita, A. Ohta, *Heterocycles* **1981**, *16*, 1325 – 1328; c) Y. Akita, A. Inoue, K. Ishida, K. Terui, A. Ohta, *Synth. Commun.* **1986**, *16*, 1067 – 1072; d) A. Angeloff, J.-J. Brunet, P. Legars, D. Neibecker, D. Souyri, *Tetrahedron Lett.* **2001**, *42*, 2301 – 2303.
[345] See also: L. Lassova, H. K. Lee, T. S. A. Hor, *J. Org. Chem.* **1998**, *63*, 3538 – 3543.
[346] Y. Ben-David, M. Gozin, M. Portnoy, D. Milstein, *J. Mol. Catal.* **1992**, *73*, 173 – 180.
[347] M. S. Viciu, G. A. Grasa, S. P. Nolan, *Organometallics* **2001**, *20*, 3607 – 3612.

The Torch of Erwin Chargaff and the Fire of Heraklitus Devour Their Children**

Lothar Jaenicke*

To forget is a risk—therefore let's remember!
Berthold Viertel (1885–1953)

A Prophet Counts for Nothing in His Father Land

Erwin Chargaff died on the 20th June, 2002. He was almost 97 years old, therefore he had experienced the 20th century almost totally in its ineffableness. However, he had much to say on the matter, for he had a clever, critical mind and was a resourceful stylist, with standards which have been more or less lost, or which are donned only on Sundays. It was this lack of character which enraged him, and his response brought him into disrepute with the closed peer-society of science as a regressive and everything else blowhards could throw at him. Even during his lifetime it was not possible to pay due tribute to Erwin Chargaff without rebuke. I did it—briefly—by congratulating this great, old pillar of biochemistry (not only of nucleic acids) on his 85th birthday in the then "Green Pages" of the German Biochemical Society (GBM). Immediately I received a rebuke from a notorious scientific philosopher: a proper person does not touch upon someone who dirties his own nest. I am not proper, and I have benefited from it, for to ignore someone of Erwin Chargaff's métier is to put on blinkers and follow only the well-trodden rut, driven merely by the opportunism of the time. Moreover, he was never a Mr. hundred percent, but someone of analytical and considered reserve who also knew that his far-reaching condemnations would return to haunt him. He had a serious desire not to resist the considerable influx of ideas and their associations and the temptation of pointed expression. He raised questions to be taken seriously, and received ignorant answers. A whole catalogue of comments on the attitude and behavior of major scientists can be compiled from the many critical utterances of insiders—who can justifyingly refute them with equanimity from the same position?

[*] Prof. Dr. L. Jaenicke
Institut für Biochemie der Universität zu Köln
Zülpicher Strasse 47, 50674 Cologne (Germany)
Fax: (+49) 470-6431

[**] *Das Feuer des Heraklit* (The Fire of Heraklitus) is the title of Erwin Chargaff's autobiography published in 1979 by Cotta, Stuttgart.

"The Time when Everyone Believed in the Dignity of Man"

Erwin Chargaff came from the eastern fringe of the former Habsburg monarchy, Bukowina, in whose capital Czernowitz situated in range of hills above a Pruth ford he was born on the 11th August, 1905. His parents were prosperous bankers who gave their two children the middle-class upbringing assimilated from Germany which Society so valued. They were first made aware that they were Jews by the "racist" anti-Semitism of the Austro-Germans. The liberal family had viewed the many synagogues in Czernowitz only from the outside. Important for them were the centrally located theater, library, and the station in Ring-Strasse architecture, painted ocher like all official buildings, which led the way into the intellectual and liberal world. Bukowina was provincial, if also ambitious. At the time of Erwin Chargaff's birth it had been "Crown Land" for only 130 years, and before and since the corridor for all movement in the Danube basin between the Balkans and the Baltic, between Istanbul and Paris. The lethargy of the old Kaiser Franz Joseph reigned over a Leyden jar bursting with violent emotions. One gets a (humorous) impression from the descriptions of Gregor von Rezzori, also a native of Czernowitz who knew his "Maghrebinians". The surrounding agricultural region of Vlachs, Ruthenians, Poles, and Huzules began to migrate into the town in which with the "Schwaben" from Austria, the Jews from nearby Galicia and Bessarabia, and the Armenian and Greeks were the civic and industrializing element. From a few thousand at the start of the 19th Century it grew in that way to 50000 by about 1900, a third of whom were Jews of differing orthodoxy, from Hasidites in dozens of prayer rooms, to agnostics who, like the Chargaffs, went past the splendid temples, a quarter were Greek-orthodox Moldavians with their cathedral, an eighth Germans in their suburb of Rosch and the archbishop's palace, and a tenth each of Poles, Russniaks, and "etcetera". One can imagine the heady mixture of life-styles, languages, and smells—a lively town, and a focus of education with the Francisco-Josephina university, founded in 1875, (without sciences and medicine, but with a notable 1000 students in the four faculties, amongst them almost two thirds of "mosaic confession", of which in turn two thirds gave German as the mother tongue) and half a dozen, solely German-language daily newspapers which reached as far as Vienna, Budapest, and Cracow.

 © 2002 WILEY-VCH Verlag GmbH & Co. KGaA, Weinheim 0044-8249/02/11422-4213 $ 20.00+.50/0

The theater, in front of which the Schiller monument endowed by the Jewish Club, was a focus of interest and discussion. There were poets en masse within the younger generation (with Karl Kraus' "Torch" as marshal's baton under the jacket); each wrote for the other; they found encouragement and sponsorship and platform in the feuilletons of the press. Most are forgotten, and those remembered were yet to be born. The time between, from the enforced Romanianization (although with retention of educational standards) to the 2nd World War, after which Bukowina was divided between Romania and the Soviet Union, is described lively by the biophysicist Henryk (Heini) Eisenberg in his "peripatetic" reminiscences.[1] Today's town is called Chernovtsy and is a large provincial city in the Ukraine.

Vienna, the Spiritual Homeland

The change began with the 1st World War as the Austrians were forced to retreat before the Russians in the direction of Vienna, and with them a part of the upper classes of the border provinces, these included the Chargaffs. They left Czernowitz for ever, but retained the homeland accent and remained true to their educational ideals, sending the boy to the Maximilian Gymnasium, where he received comprehensively the Josephinic-humanistic education of the time up to his excellent graduation, and the remainder from the Viennese ambience. Vienna was culturally a very lively center in which many modernizing currents merged, mixed, and reinforced each other, and departed again. This applied especially to the aesthetic side: decorative secessional art, produced and reproduced music, poetry, writing, and theater, but also to classical and psychoanalytical medicine, which found a well-informed and devoted clientele, and the precise scientific philosophy in the shape of the theoretical physics of E. Mach and L. Boltzmann. These were imposing thinkers, capable of a holistic viewpoint. Arts and styles were daily topics of the aesthetic flâneurs in the many, mostly liberal, newspapers. Authors and musicians were stars, the Viennese school of scientific philosophy discussed method and association to the social sciences. The social conditions screamed for change. Young people found cultural stimulus outside of school, and were prepared by the schools to absorb it, to lay claim to it as their own, and to express it. The critical, stylistic, and aesthetic feuilletonists, of whom Karl Kraus enflamed the like-minded with the red volumes of his "Torch", had a public both willing and able to debate, including the young Erwin Chargaff, who looked upon himself as a life-long pupil of this sensitive analyst of words and values. Later he dedicated his collection of scientific essays on nucleic acid coquettishly and mystifyingly to this "teacher", whom clearly no natural scientist knew.

Bread-and-Butter Studies and the Parting of the Ways

The frivolously started war was lost, Austria was reduced to German Austria that had to undertake a precarious war of survival between black and red (the church triumphed, but finally, brown) in which fortunes and culture were lost. Erwin Chargaff, who left school in 1923 with the best grades so that he was exempt from study fees, could no longer drift, as planned, into the humanities in which he was interested, but had to take up a purposeful course of study, and to complete it as quickly as possible. With dialectic linguistics for which he had an affinity, like N. Chomski, he lived illegitimately; the choice of reason was chemistry with which the daily bread was most likely to be earned. His doctoral supervisor was "Tüpfel (spot test) Fritz" Feigl, with whom topics were plentiful, but (as everywhere in Austria) means were sparse, and who therefore distinguished himself in meticulous microanalysis. Educationally it left a lasting impression. Chargaff always remained a knowledgeable chemist of the pre-electronic days. The dissertation followed a straightforward course: the identification of oxidizable sulfur compounds by the catalyzed iodine–azide reaction in polar and non-polar solvents, also amenable to spot analysis, gave useful results which 75 years later appear predictable. In 1928 he concluded his studies with the fashionable sine-qua-non of the Doctor's title, in fact of philosophy (Dr. Phil.). The question of the future was answered by a scholarship with the lipid chemist R. J. Anderson at Yale University. He became a Research Fellow on the other side of the Atlantic in a new and, for him, strange research and social environment. Here he felt comfortable and successful, although his old-world snobbishness did not adapt, but there he married his Viennese bride Vera Broilo with whom he was to celebrate gold, diamond, and iron wedding anniversaries. The work on the fatty acids of tuberculosis bacilli went well and was successful. He was offered a position, but then withdrew from this country, which was "younger than the toilets in Vienna", and returned to "old" Europe. The bacteriologist M. Hahn (of E. Buchner's fame) had offered him a position at the Charité, and Berlin was the center of attraction in the "golden twenties", which were soon to end in the brown thirties. The research on the lipid composition of the tuberculosis and diphtheria bacteria and the lipid-transport proteins of blood plasma went well, cultural life flourished—for the time being. At the beginning of 1933 he had enough publications to think of "habilitation" and a respectable existence; then the Nazis came upon the scene and branded him "a racial Jew", he who to that day had never seen a synagogue from the inside and who shared the commonly voiced prejudice on "the" Jews. But he was clever enough to recognize the signs of the time. Since he had an invitation from P. Calmette at the Pasteur Institute he took his unsubmitted habilitation thesis, his wife, and belongings and spent two years in Paris, hungry, but free from what was occurring in Germany, and later in Austria. In 1935 he emigrated for the last time, across the Atlantic, to New York, where he spent the remaining 62 years of his life. He was by nature sedentary, and even more so through his love of books. In New York he was offered a position at the newly founded Department of Biochemistry of the Columbia College of Physicians and Surgeons, whose chairman H. T. Clarke was a man of character and vision, who seized the opportunity to build up a flourishing institute through altruistic deed and, thanks to Mr. Hitler's gifts, it became the cradle of experimental biochemistry in the USA, which until then was little

 © 2002 WILEY-VCH Verlag GmbH & Co. KGaA, Weinheim 0044-8249/02/11422-4214 $ 20.00+.50/0

more than a clinical complementary bedside science. Thus within the space of a few years there came, for example, Konrad Bloch, Hermann Blaschko, Rudolf Schönheimer,—now Erwin Chargaff and later David Nachmansohn. Together with intelligent and enthusiastic graduate students of both sexes, and in the neighborhood of the Rockefeller Institute and the Chemistry Department, a free haven of material and metabolic biochemistry arose, ranging from active compounds to nucleic acids. After the lipoproteins, about which Erwin Chargaff wrote the first comprehensive presentation, the nucleic acids became the central focus of his research.

Rules Without Vision

Things began to move in the field of nucleic acids after O. T. Avery announced that protein-free nucleic acid from smooth, virulent Type III Pneumococci can transform rough, avirulent Type II strains. Today this appears to us as being the beginning of the awareness of the function of DNA, but few heard this drum beat. Amongst them was Erwin Chargaff, who commenced in his meticulous, analytical chemist's style to purify and analyze nucleic acids from different sources. It was assumed that the four constituent nucleotides were present as stoichiometric tetrads which, as a concession to macromolecular evidence, are aggregated. Similarly this occurred in the area of proteins until, at the end of the 1940s, F. Sanger provided the evidence for the polypeptide chain made up from numerous amino acids. The tetranucleotide hypothesis from Phoebes Levene may have been pleasing to chemists who thought in terms of integers and crystal structure, but biologists and biochemists knew of the diversity of nature, and their earlier data put the hard-edged procrustean bed of Phoebes Levene into question. To clarify the structure of nucleic acids, proper, quantitative analyses of pure preparations of uniform alkali-stable "thymus" and alkali-labile "yeast" nucleic acids (DNA and RNA, respectively) from different organisms and organs were needed. Erwin Chargaff took up this pioneering work. He had to miniaturize reliably the current methods and was able to adapt paper chromatographic separation coupled with spectrographic identification which had just been applied to protein analysis. That sounds simple today, but the information had to be obtained from wherever possible. It was good that the "Scientific Community" was at that time still open within itself yet at the same time a closed society; it had not yet been tempted by the wider community. On the contrary, researchers were eccentric, pitiful "egg heads". They did not even earn proper money with their art. If they were inventors, that would be a different story!

With the help of enthusiastic New Yorkers and dedicated Swiss co-workers the data in statistically parallel experiments from numerous, minute samples of nucleic acids from bacteria and animals and their organs were collected within five years (Figure 1) and, in 1950, were formulated with all due care as the "Chargaff Rules", which, in summary, state that the base composition of DNA and RNA is different, but species specific, the base relationships suggest a pairing of adenine with thymine and guanine with cytosine, and the sum of 6-amino bases is equal to that of the 6-hydroxy bases.[2]

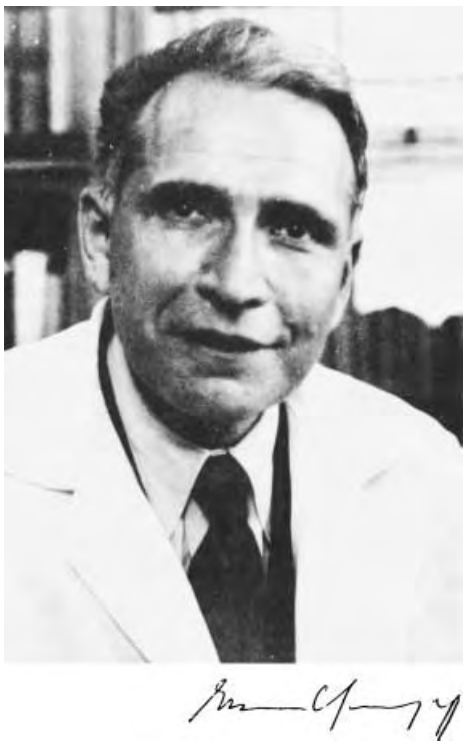


Figure 1. Chargaff at the time he formulated his rules (around 1950); reproduced with permission from *Annu. Rev. Biochem.* **1975**, *44*.

Voilà—the framework of the double helix which was also used by Watson and Crick, as were the structural data of Rosalind Franklin. The pathway to this symbolic structure was as twisted as it is itself. It outshone the leading lights and dazzled the Nobel committee. The ways of such bodies are inscrutable, but seldomly wholly challengeable. These dioscuri (Watson and Crick) were of sterner stuff than the extrapolation-shy physical and chemical-data collectors. Therefore, the hurriedly introduced work area is no longer called chemistry, but molecular biology. For Ernst Chargaff there remained other prizes (Bertner, Heinekens, etc.), medals (Pasteur, Neuberg, Mendel amongst others), and honors (Collège de France, Stazione Zoologica, the Universities of Basle and Vienna).

What Is Life?—Warning Anxieties

How far such disappointment intrudes into one's behavior in life is known only to the individual and surely not to the little man according to his own disposition: jealousy, enviousness, pessimism, tantrums.

Erwin Chargaff did not behave like this, for through Karl Kraus' precedent he was already a "critic of the system", and more so after the dropping of the atomic bomb on large civilian communities. The fanfares of victory sounded shrill and unworthy, no matter how much he had wished it, and he had made no secret that the perpetrators should have to face a deserved punishment. But, that now, after abusing the nucleus of the atom such equally frivolous and ill-prepared hands wanted to usurp the nucleus of the cell frightened him deeply. Nature does not deserve it. It has a dignity which is inviolable,

 © 2002 WILEY-VCH Verlag GmbH & Co. KGaA, Weinheim 0044-8249/02/11422-4215 $ 20.00+.50/0

just as mankind demands for itself. Mankind was ill-equipped to handle its technical progress and to leave alone that which is irreversible, such as the genetic program of an organism. Had not the pharmaceutical industry already turned the human body and mind into a tool to manipulate according to intent and desire—ostensibly at one's own will, or is it the will of others? Now the heredity material is falling into the same grasp, to be handled according to wish and reward. At this point intellect and the strands of tradition went their separate ways. On the one hand, the forward looking, enterprising manager, on the other, the caretaker, trying to reconcile the ways and means; Old World tradition against New World pioneering spirit (Figure 2).

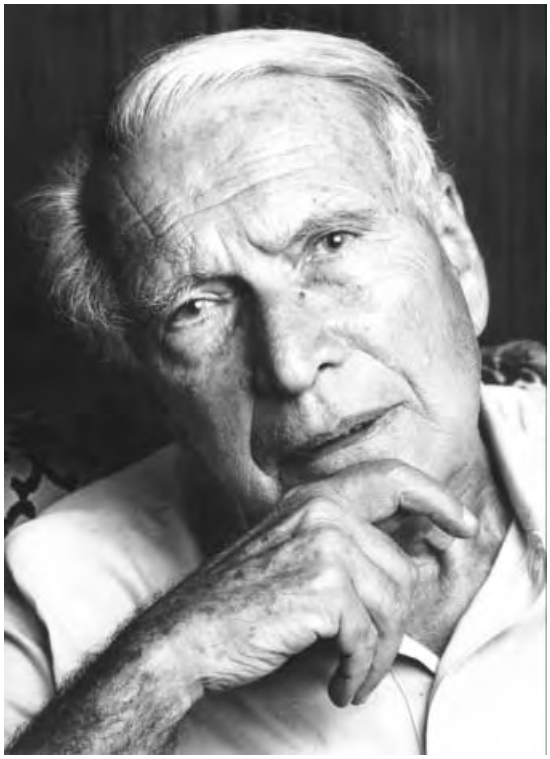


Figure 2. Chargaff, the thoughtful skeptic. Copyright© Herlinde Koelbl 1989.

Honi Soit Qui Mal y Pense (The Shame Is His Who Thinks Ill of It)

Nature is apparently easy to dupe in its naivety if its mechanisms have been recognized, in which the individual parts do not "play a role" but have an inscribed, developmentally optimized function which is governed and controlled by all other simultaneously and like-wise positioned functioning events in non-linear networks and layers "Chaos" like to unpredictable effects. Interfere here? Erwin Chargaff shuddered when he saw and heard the people who intended and endorsed it, the people who "wanted to eat, sell, and worship the cake all at the same time". During the years of this intent he viewed the future with increasing gloom. And he said it and he wrote it, always more pessimistically and often carried by his love of pointed phrasing, with caricaturistic oversubtlety. That occupied him, for whom Karl Kraus had held the torch of discrimination of truth and propaganda, for the last 30 years of his life after he retired as Director of the Biochemical Division of Columbia University (Figure 2). In ever new analyses and critiques, in aphorisms and essays he attempted to make himself understood and to make clear what moved him to become the little boy from the fairy tale, whom not only the first encounter with a fairy showed the way from the arts to science, but who also had retained the eye of the child who did not see the emperor's new clothes. He knew from the experience of history that effective change came only through criticism from inside, and he signed it with his name. He equanimously consoled himself that he had "caused himself some damage, but not very much". He battled as a scientist against the dogma of the infallibility of scientists to which they were not entitled, not against the entity of science. "What is true is not tentatively true, until revoked". For this he received literary prizes (J. H. Merck Prize of the Darmstadt Akademie; Vienna Literature Prize) and was also honored elsewhere as remonstrator; by the like-minded. But it was no use. He changed nothing. Quite the opposite, he was denigrated as an old fool, a negator of progress, and an enemy of technology, at best derided as Narcissus of the world's end and as Tolstoyan character. He demonstrated the obstinacy of the doer and the helplessness of Cassandra, which he knew well. Now his window on the 13th Floor, 350 Central Park West, New York, is dark, the warning beacon against and for prejudiced and reckless chargers through creation, and we have lost someone who was worth listening to, to reflect upon—and now to mourn (Figure 3).

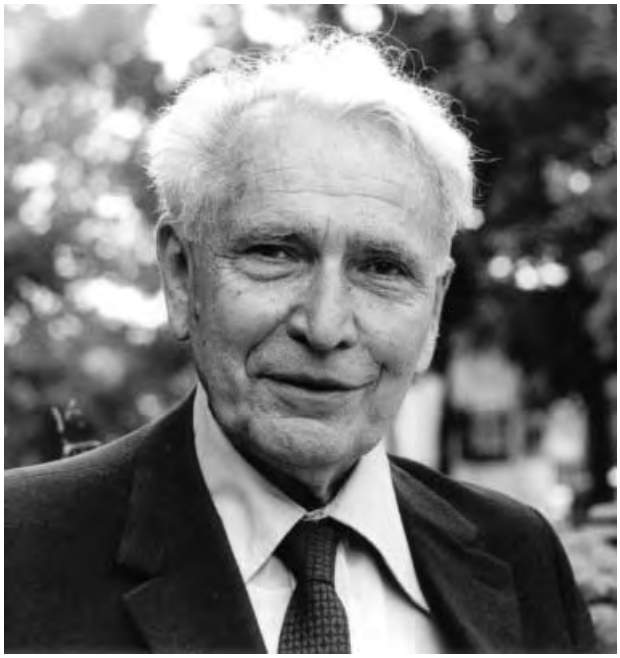


Figure 3. Chargaff a few years before his death. Copyright© Isolde Ohlbaum 2002.

[1] H. Eisenberg, *Comprehensive Biochemistry, Vol. 37*, Elsevier, Amsterdam **1990**, pp. 265 – 348.
[2] E. Chargaff, *Experientia* **1950**, *6*, 201 – 209.

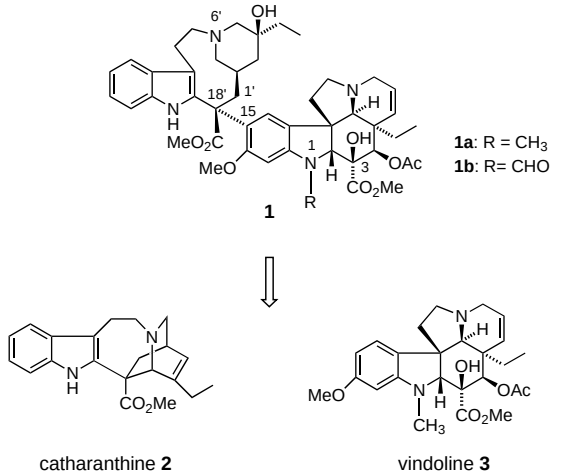
 © 2002 WILEY-VCH Verlag GmbH & Co. KGaA, Weinheim 0044-8249/02/11422-4216 $ 20.00+.50/0

First De Novo Synthesis of the Bisindole Alkaloid Vinblastine

Christoph Schneider*

As a result of their extremely potent cytotoxic activity the bisindole alkaloids vinblastine (**1a**) and vincristine (**1b**) (see Scheme 1), isolated at the end of the 1950s independently by the groups of Noble and Svoboda,[1a] have become one of the most attractive research targets in medicine, biology, and chemistry[2] and are currently used in the therapy of particularly fast growing tumor types (leukemia, lymphoma). The complete chemical structure of **1b** was completely solved relatively early by Lipscomb and Moncrief by crystal structure analysis of the methiodide[1b] and applied to **1a** because of the known relationship of the two natural products. A pentacyclic, relatively rigid vindoline alkaloid is connected to a tetracyclic, conformationally flexible velbanamine fragment through a central C–C bond buried in the interior of the molecule.

Extensive biosynthetic investigations have suggested the monomeric indole alkaloids catharanthine (**2**) and vindoline (**3**) as direct biogenetic precursors (Scheme 1),[2] which after oxidative activation of catharanthine—presumably as the 7-hydroperoxyindolenine—are coupled to anhydrovinblastine and finally converted into vinblastine. The potent cytotoxic action derives from an antimitotic activity which comprises an inhibition of tubulin polymerization and consequent prevention of cell division.[2] Problematic and in the final instance dose-limiting are the side effects on hemopoiesis (vinblastine) and the nervous system (vincristine).



Scheme 1. Vinblastine (**1a**) and vincristine (**1b**) and the biogenetic precursors of **1a**.

Whereas the monomers catharanthine (**2**) and vindoline (**3**) can be obtained in significant amounts from *Catharanthus roseus*, vinblastine and vincristine themselves are present there only in traces. It is for this reason that semi-synthetic strategies were initially followed for their construction, when usually vindoline from natural sources was used as starting material. Difficulties soon arose in constructing the correct stereochemistry at the quaternary C(18′) chiral center essential for the biological activity. The groups of Potier and Langlois,[3] Kutney,[4] Kuehne,[5] and Magnus[6] were able to solve this problem elegantly in their respective vinblastine syntheses, but they all used natural vindoline as the starting material for their syntheses.

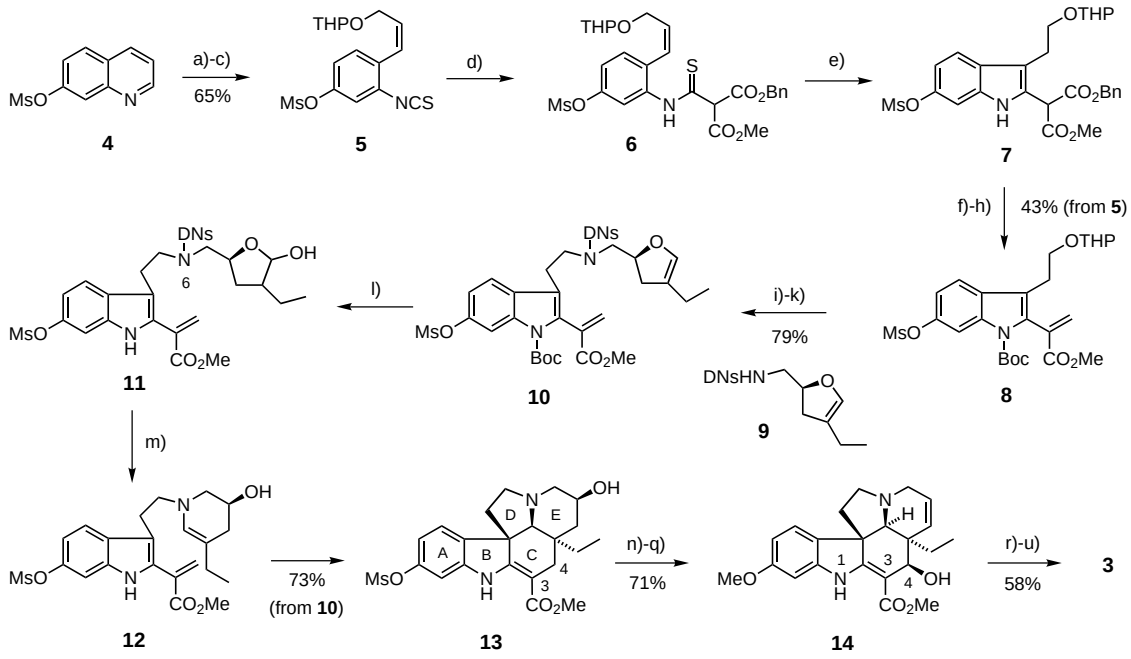
After more than 40 years of intensive vinblastine research Fukuyama et al. have now successfully achieved the first total synthesis from simple starting materials, which provides the natural product in an overall yield of 1 %[7] and thus for the first time makes it possible to carry out broadly based structure-activity studies which also include the vindoline fragment of the natural product.

Sufficient amounts of synthetic vindoline (**3**) were obtained by means of a new indole synthesis that uses quinolines as starting materials (Scheme 2).[8] The reaction of 7-(methylsulfonyloxy)quinoline (**4**) with thiophosgene/$NaBH_4$ led to a reductive ring opening of the heterocycle to give the isothiocyanate **5**, from which the thioanilide **6**, the actual substrate for the indole synthesis, was obtained by the addition of an unsymmetrical malonate ester. The known thiophilic nature of the tributyltin radical was now used to produce an N,S-substituted carbon radical from **6** under classical Bu_3SN/AIBN conditions. This radical reacted in a 5-*exo* cyclization with the neighboring double bond after which in situ elimination of BuSnSH gave the complete indole framework **7** of vindoline.

Selective cleavage of the malonate ester paved the way for a Mannich reaction with concomitant decarboxylation to form the conjugated ester **8**, which was coupled through the subsequently liberated OH function with the enantiomerically pure sulfonamide **9** (synthesis not shown here) under Mitsunobu conditions to yield **10**. The dinitrosulfonyl (DNs)

[*] Priv.-Doz. Dr. C. Schneider
Institut für Organische Chemie
Georg-August-Universität
Tammannstrasse 2, 37077 Göttingen (Germany)
Fax: (+49) 551-399660
E-mail: cschnei1@gwdg.de

 © 2002 WILEY-VCH Verlag GmbH & Co. KGaA, Weinheim 1433-7851/02/4122-4217 $ 20.00+.50/0



Scheme 2. Synthesis of vindoline (**3**) by a novel indole synthesis according to Fukuyama et al. a) $CSCl_2$, Na_2CO_3; b) $NaBH_4$, MeOH; c) dihydropyran, H^+; d) benzylmethylmalonate, NaH; e) Bu_3SnH, AIBN; f) Boc_2O, NEt_3; g) $Pd/C/H_2$; h) $Me_2NH \cdot HCl$, HCHO; i) MeOH, H^+, k) DEAD, PPh_3, **9**; l) TFA, Me_2S; m) pyrrolidine, $0 \rightarrow 50\,^{\circ}C$; n) PPh_3, CCl_4; o) KO*t*Bu, MeI; q) $(PhSeO)_2O$; r) mCPBA, MeOH; s) HCl, $Na(CNBH_3)$; t) HCHO, $Na(CNBH_3)$; u) Ac_2O, NaOAc. AIBN = azobisisobutyronitrile, DEAD = diethylazodicarboxylate, Boc = *tert*-butoxycarbonyl, TFA = trifluoroacetic acid, mCPBA = *meta*-chloroperbenzoic acid; Ms = methylsulfonyl, THP = tetrahydropyranyl, Bn = benzyl.

protecting group for N(6) was chosen for two reasons: it allowed a facile N-alkylation with the Mitsunobu reaction, and it could be readily cleaved with nucelophiles under extremely mild conditions. Its use was developed specially as part of the synthesis of this natural product.[9]

Compound **10** constitutes the complete vindoline carbon framework in a partly acyclic form. The stereochemically correct construction of the ABCDE ring system now followed in only two simple, elegant synthetic operations. Under acidic conditions the enol ether was first hydrated to the lactol **11**, followed by deprotection of the central N(6) by reaction with pyrrolidine by which the aminolactol was transformed into the cyclic hydroxyeneamine **12** (E ring). This on heating underwent a Diels–Alder reaction with inverse electron demand with the opposing diene unit and afforded the pentacyclic vindoline ring system **13** stereoselectively in 73% yield. Thus in their synthesis of the CD ring system the authors followed the biogenic pathway proposed by Wenkert and Scott[10] and the biomimetic synthesis of a whole series of indole alkaloids by Kuehne et al.[11]

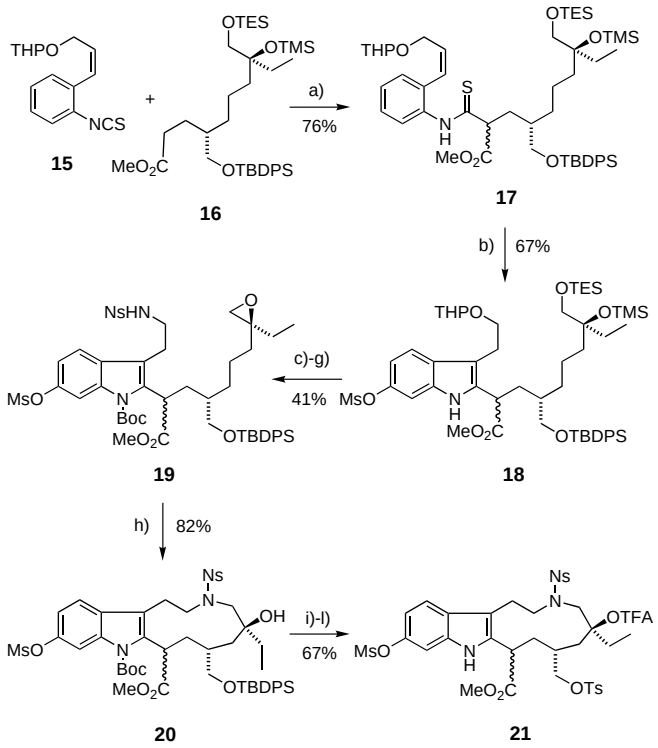
The conversion of **13** into vindoline (**3**) follows closely work by Danieli et al.[12] for the stereoselective introduction of hydroxy groups at C(3) and C(4). After regioselective elimination of the secondary hydroxy function in the E ring and protective group exchange at the phenolic hydroxy group of the A ring dehydration with benzeneseleninic anhydride gave the conjugated imine which was hydrated at C(4) and yielded **14**. By treatment with *meta*-chloroperbenzoic acid, **14** was first oxidized at C(3) and then methylated at N(1) by imine reduction and reductive amination. Remarkably, both the introduction of the hydroxy groups and the imine reduction occurred stereoselectively in each case on the β side of the vindoline framework, presumably because the neighboring ethyl group sterically shielded the α side. Vindoline (**3**) is thus very efficiently accessible in an overall yield of more than 6% (starting from **4**).

For attachment of the velbanamine fragment an 11-membered N-heterocycle **21** was envisaged in which after successful coupling with vindoline cyclization to the piperidine ring should occur by intramolecular S_N reaction at the tosylate (Scheme 3). In-depth investigations by Schill et al. on similar model compounds had shown that aromatic substitution on vindoline with such a substrate should give the correct configuration at C(18′).[13]

Again, for the synthesis of the indole fragment **21** the reliable Fukuyama method under radical conditions was used. For this purpose the required thioanilide **17** was generated from the isothiocyanate **15** by addition of ester **16** (synthesis not shown here), and radical cyclization with Bu_3SnH/Et_3B gave the indole **18** in 67% yield even at room temperature. A number of protective group manipulations and renewed Mitsunobu reaction with 4-nitrobenzenesulfonamide ultimately gave the sulfonamide **19** which underwent an intramolecular S_N2 reaction at the epoxide with K_2CO_3 in refluxing DMF to give the 11-membered N-heterocycle **20** in 82% yield. Further standard reactions led finally to the second key compound **21** (2% overall yield over the longest linear sequence).

For the critical coupling of fragments **3** and **21** to form the central C(15)–C(18′) bond in vinblastine use was made of the established *t*BuOCl indole activation introduced by the groups of Kutney and Neuss[14] which produced the chloroindolenine **22** from **21**. By reaction with trifluoroacetic acid **22** was activated to the iminium salt **23** (Scheme 4). In an

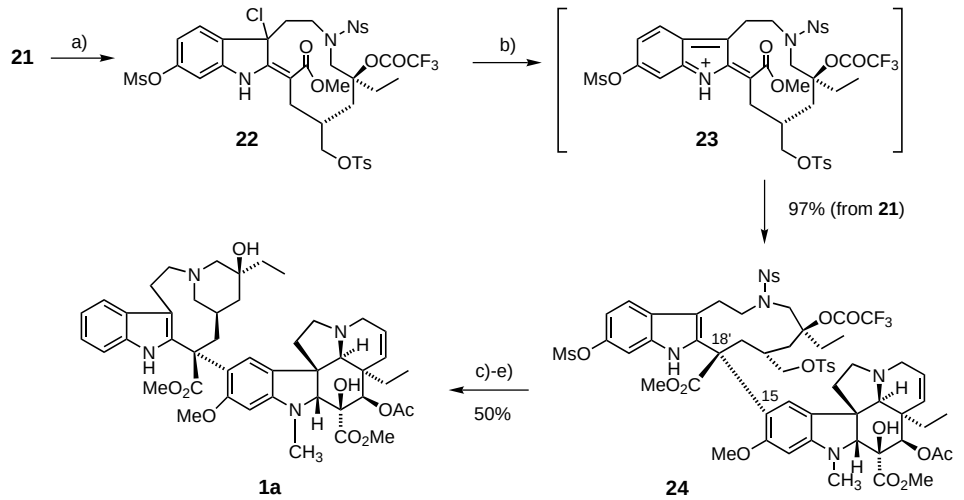
 © 2002 WILEY-VCH Verlag GmbH & Co. KGaA, Weinheim 1433-7851/02/4122-4218 $ 20.00+.50/0 *Angew. Chem. Int. Ed.* **2002**, *41*, No. 22



Scheme 3. Synthesis of the 11-membered N heterocycle **21** as velbanamine fragment. a) LDA; b) Bu_3SnH, Et_3B; c) Boc_2O, NEt_3; d) $AcOH/H_2O$; e) TsCl, Bu_2SnO, NEt_3; f) $NaHCO_3$, DMF; g) $NsNH_2$, DEAD, PPh_3; h) K_2CO_3, DMF; i) TFA; k) TsCl, $Me_2N(CH_2)_3NMe_2$; l) TFAA, pyridine. LDA = lithium diisopropylamide, Ts = tolylsufonyl, DMF = dimethylformamide, Ns = 4-nitrobenzenesulfonyl, TFAA = trifluoroacetic anhydride; TES = triethylsilyl, TMS = trimethylsilyl, TBDPS = *tert*-butyldiphenylsilyl.

electrophilic aromatic substitution reaction coupling with vindoline (**3**) occurred almost quantitatively, and the vinblastine precursor **24** was formed with correct and uniform (18′*S*) configuration. This stereochemical result is in agreement with the formation of an *E*-configured C(17′)–C(18′) double bond in **23** and the subsequent nucleophilic addition of vindoline on the front of the molecule controlled by the ring conformation of the 11-membered heterocycle.[13] Deprotection of the alcohol and amino groups in the velbanamine fragment led then directly to cyclization to the piperidine ring by which the synthesis of **1a** was completed.

The synthesis described here has not only made the biologically highly active and pharmacologically interesting bisindole alkaloid vinblastine accessible for the first time by total synthesis, thus opening the way for the syntheses of analogues and potentially "better" compounds by this route. Also it has led to the development of versatile new methods which equally will provide valuable service in the solution of other synthetic problems.



Scheme 4. Final synthesis of vinblastine (**1a**). a) *t*BuOCl; b) TFA, vindoline **3**; c) NEt_3, MeOH; d) $HSCH_2CH_2OH$, DBU; e) $NaHCO_3$, *i*PrOH. DBU = 1,6-diazabicycloundecene.

[1] a) R. L. Noble, C. T. Beer, J. H. Cutts, *Ann. N. Y. Acad. Sci.* **1958**, *76*, 882; G. H. Svoboda, N. Neuss, M. Gorman, *J. Am. Pharm. Assoc.* **1959**, *48*, 659; b) J. W. Moncrief, W. N. Lipscomb, *Acta Crystallogr.* **1966**, *21*, 311.

[2] Comprehensive review of the medicine, biology, and chemistry of the bisindole alkaloids: *The Alkaloids, Vol. 37* (Ed.: A. Brossi), Academic Press, New York, **1990**.

[3] P. Mangeney, R. Z. Andriamialisoa, N. Langlois, Y. Langlois, P. Potier, *J. Am. Chem. Soc.* **1979**, *101*, 2243.

[4] J. P. Kutney, L. S. L. Choi, J. Nakano, H. Tsukamoto, M. McHugh, C. A. Boulet, *Heterocycles* **1988**, *27*, 1845.

[5] M. E. Kuehne, P. A. Matson, W. G. Bornmann, *J. Org. Chem.* **1991**, *56*, 513.

[6] P. Magnus, J. S. Mendoza, A. Stamford, M. Ladlow, P. Willis, *J. Am. Chem. Soc.* **1992**, *114*, 10232.

[7] S. Yokoshima, T. Ueda, S. Kobayashi, A. Sato, T. Kuboyama, H. Tokuyama, T. Fukuyama, *J. Am. Chem. Soc.* **2002**, *124*, 2137.

[8] H. Tokuyama, T. Yamashita, M. T. Reding, Y. Kaburagi, T. Fukuyama, *J. Am. Chem. Soc.* **1999**, *121*, 3791.

[9] T. Fukuyama, C.-K. Jow, M. Cheung, *Tetrahedron Lett.* **1995**, *36*, 6373; T. Fukuyama, M. Cheung, C.-K. Jow, Y. Hidai, T. Kan, *Tetrahedron Lett.* **1997**, *38*, 5831.

[10] E. Wenkert, *J. Am. Chem. Soc.* **1962**, *84*, 98; A. I. Scott, *Acc. Chem. Res.* **1970**, *3*, 151.

[11] See amongst others: M. E. Kuehne, D. E. Podhorez, *J. Org. Chem.* **1985**, *50*, 924; M. E. Kuehne, D. E. Podhorez, T. Mulamba, W. G. Bornmann, *J. Org. Chem.* **1987**, *52*, 347.

[12] B. Danieli, G. Lesma, G. Palmisano, R. Riva, *J. Chem. Soc. Chem. Commun.* **1984**, 909.

[13] G. Schill, C. U. Priester, U. F. Windhövel, H. Fritz, *Tetrahedron* **1987**, *43*, 3765.

[14] N. Neuss, M. Gorman, N. J. Cone, L. L. Huckstep, *Tetrahedron Lett.* **1968**, 783; J. P. Kutney, J. Beck, F. Bylsma, W. J. Cretney, *J. Am. Chem. Soc.* **1968**, *90*, 4504.

 © 2002 WILEY-VCH Verlag GmbH & Co. KGaA, Weinheim 1433-7851/02/4122-4219 $ 20.00+.50/0

Hypoelectronic Dimetallaboranes**

Hubert Wadepohl*

Dedicated to Professor Thomas P. Fehlner on the occasion of his 65th birthday

"There are no such things as electron-deficient compounds, only theory-deficient chemists."

R. E. Rundle[1]

Polyhedral boranes and their heteroatom-substituted derivatives have inspired an entire generation of chemists.[2] The great fascination of these compounds, which have demonstrated very few applications up to the present, lay and lies in the apparent complexity of the structures and their bonding schemes, which have resisted attempts at explanation for many years. Even after the pioneering work of H. C. Longuet-Higgins and W. N. Lipscomb,[3] the boranes and their bonding received little scientific attention. This situation changed drastically in the seventies when a simple set of electron-counting rules (the Wade–Mingos' rules)[4] were suddenly not only able to explain the bonding in nearly all the boranes and carboranes known at that time, but also proved extremely useful in the emerging area of metal-cluster complexes.[5]

Following the Wade–Mingos' rules from the boranes through to the transition-metal clusters metallaboranes play an important role. The very existence of metallaboranes provided encouragement and their adherence to the rules was explained later by the simple but powerful concept of the isolobal analogy.[6]

However, metallaboranes soon appeared that did not obey the rules. The problems began with a group of electron-deficient compounds that exhibited a closed deltahedron framework but that did not take on the form of the "canonical" polyhedron. Geometrically, their most obvious violation of the rules was that certain polyhedral vertices (occupied by metals) exhibited a higher connectivity at the cost of other positions. Depending on the counting method, the number of valence electrons (VE) in the cluster can be made to agree with the *closo* rule at least (*isocloso*-structure; the electron deficiency is localized on the metal),[7] or otherwise an electron deficiency delocalized in the cluster would have to be accepted (*hypercloso*-structure; cluster lacks 2 VE).[8]

This violation of the rules reached a climax with the recent preparation of a series of extremely electron-deficient metallaboranes, by T. P. Fehlner et al.[9] These are unusually stable compounds with elements from the manganese and iron subgroups, that are directly or indirectly accessible from (pentamethylcyclopentadienyl)metal halides and monoboranes. The salient features of the unusual structures of these complexes are the high coordination number of the metal centers and a metal–metal bond extending through the borane framework.

The new structure and bonding types are illustrated here by the homologous series of dirhenaboranes $[\{(C_5Me_5)Re\}_2B_nH_n]$ ($n = 6$—10; **1**–**5**; Figure 1, top). With the exception of **1**, which to date has only been isolated as the dichloro derivative $[\{(C_5Me_5)Re\}_2B_6H_4Cl_2]$ (**1a**), all the members of the series are well characterized, both spectroscopically and structurally (Figure 1, below).[10]

"Blind" application of the Wade–Mingos' rules classifies **1**–**5** as clusters with $p = n + 2$ framework atoms and $(p - 2)$ skeletal electron pairs (SEPs), since the nBH groups are expected to provide two electrons each for bonding in the cluster framework. The two 12 VE fragments $(C_5R_5)Re$ should not contribute any electrons to the cluster bonding (see below). According to the capping rule[5] the structures of **1**–**5** should be derived from ($p - 3 = n - 1$)-vertex canonical polyhedra in which three faces are additionally capped. For example, the structure of **2** should be a tricapped octahedron. The actual structures are, however, completely different. They are noncapped closed polyhedra that, as a result of their mostly low symmetry, show little similarity to the canonical deltahedra.

Even at an early stage it was recognized that the structures of the *isocloso*- (or *hypercloso*-) metallaboranes can be generated from the canonical *closo*-structure by diamond-square-diamond (DSD) framework rearrangements.[8,11] During any DSD rearrangement the connectivity of two of the four participating atoms increases by one while that of the other two decreases by one (Scheme 1). The overall connectivity of all the vertices (total vertex connectivity, TVC) of the cluster therefore remains constant; this quantity is the lowest common denominator for structures that either conform to or contravene the rules. The retention of a constant TVC can be used to limit the number of possible structures, but does not yield a more exact structural prediction. In addition a purely topological analysis such as this cannot provide any information about the electronic structure of the rearrangement product.

A simple count of the bonding contacts (the blue and red lines in Figure 1) shows that the structures **1**–**5** have the same overall connectivity as the corresponding canonical *closo*-polyhedra with 8–12 vertices (Table 1). Therefore, it is no surprise that they can be transformed from one to the other by means of the DSD rearrangement: In a thought experiment the corresponding canonical *closo*-structure types can be

[*] Prof. Dr. H. Wadepohl
Anorganisch-Chemisches Institut der Ruprecht-Karls-Universität
Im Neuenheimer Feld 270, 69120 Heidelberg (Germany)
Fax: (+49) 6221-544197
E-mail: bu9@ix.urz.uni-heidelberg.de

[**] I would like to thank Professors Mike Mingos (Oxford) and Walter Siebert (Heidelberg) for stimulating discussions.

 © 2002 WILEY-VCH Verlag GmbH & Co. KGaA, Weinheim 1433-7851/02/4122-4220 $ 20.00+.50/0

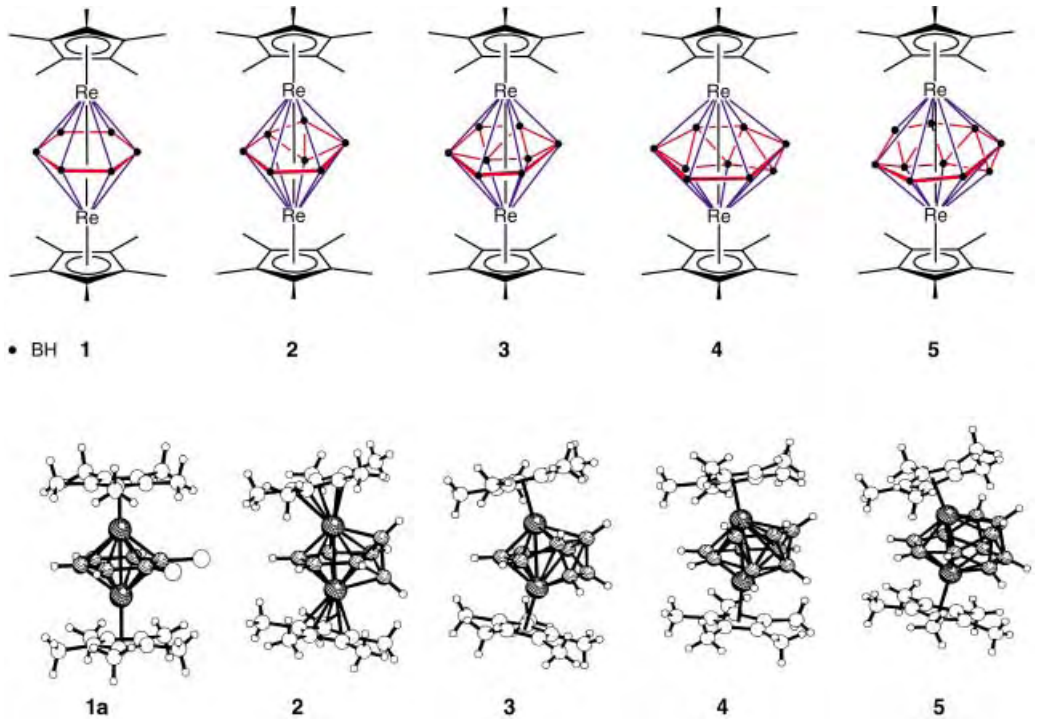
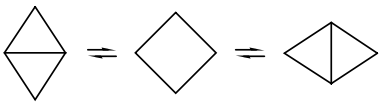


Figure 1. Formulae and molecular structures of the dirhenaboranes **1**–**5**. For $n=6$ only the dichloro derivative **1a** has been structurally characterized.



Scheme 1. Schematic representation of the diamond-square-diamond (DSD) rearrangement.

Table 1. Electron count and cluster connectivity for the dirhenaboranes **1**–**5**.

	1	**2**	**3**	**4**	**5**
d(Re-Re) [Å]	2.689	2.787	2.835	2.860	2.819
n	6	7	8	9	10
p	8	9	10	11	12
SEP (found)[a] ($p-2$)	6	7	8	9	10
SEP (canon.)[b] ($p+1$)	9	10	11	12	13
point group (canon.)[c]	D_{2d}	D_{3h}	D_{4d}	C_{2v}	I_h
TVC	36	42	48	54	60
Connectivity (found)[a,d,e]	$2^{(6)}6^{(4)}$	$2^{(6)}2^{(5)}5^{(4)}$	$2^{(6)}4^{(5)}4^{(4)}$	$1^{(7)}1^{(6)}5^{(5)}4^{(4)}$	$2^{(7)}6^{(5)}4^{(4)}$
Connectivity (canon.)[b,d]	$4^{(5)}4^{(4)}$	$6^{(5)}3^{(4)}$	$8^{(5)}2^{(4)}$	$6^{(1)}8^{(5)}4^{(2)}$	$12^{(5)}$

[a] Actual value. [b] Canonical value for a *closo*-structure derived from the Wade–Mingos' rules. [c] Symmetry of the canonical deltahedron. [d] In the form: number of vertices$^{(\text{connectivity})}$; the connectivity of a vertex is related to the cluster framework only. [e] The metals always occupy the sites of highest connectivity.

unraveled to generate the open B_nH_n "bridging ligands" that are capped by highly coordinated rhenium atoms in **1**–**5** and which have not been observed in the free state. In fact, it has been shown that, apart from for **5**, two steps are sufficient.[10] The number of SEPs are reduced by three from $p+1$ (canonical *closo*) to $p-2$ (in **1**–**5**). One electron pair is compensated by the formation of the metal–metal bond so that each DSD process in **1**–**4** apparently "costs" one electron pair (i.e. one CbMO is lost).

But why is it that the structures of the rhenaboranes **1**–**5** (and many other hypoelectronic metallaboranes) do not conform to the Wade–Mingos' rules? It is not a deficiency of the rules because they were not conceived for such a situation! They require that the framework atoms lie approximately on the surface of a sphere.[12] In polyhedral boranes, two p orbitals (π symmetry with respect to the radius vector) and one sp-hybrid orbital (σ symmetry) from each BH group participate in the bonding (the second sp-hybrid orbital forms a two-center-two electron (2c–2e) bond to the *exo*-hydrogen atom). The "magic" electron counts are determined by the number of molecular orbitals that are *not* available for occupation by electrons (or electron pairs from ligands). The classical example of the octahedral $[B_6H_6]^{2-}$ ion ($p=6$) illustrates the $(p+1)$-SEP rule for *closo*-clusters: Of the allowed 18 linear combinations of atomic orbitals, 11 have high energy so that only one σ orbital oriented to the center of the cluster and six π orbitals on the cluster surface can be occupied by $p+1=7$ electron pairs. In general the Wade–Mingos' rules only apply when each framework atom provides three valence orbitals for bonding in the cluster and when both the σ and π interactions are significant.[13]

The isolobal concept relates the CH_{4-x} fragments derived from CH_4 with metal-complex fragments that are formally generated from electronically saturated complexes $d^m[ML_n]$ by homolysis of M–L bonds.[6] This approach leads to well-known isolobal relationships such as $CH_3 \multimap\!\circ\!\rightarrow d^7ML_5$, $CH_2 \multimap\!\circ\!\rightarrow d^8ML_4$, and $CH \multimap\!\circ\!\rightarrow d^9ML_3 \multimap\!\circ\!\rightarrow d^{10}M(C_5R_5)$, in which the fragments to the left and right of the isolobal arrow have a similar number of frontier orbitals with similar symmetry characteristics and energy. The same applies to $BH \multimap\!\circ\!\rightarrow d^8ML_3 \multimap\!\circ\!\rightarrow d^9M(C_5R_5)$. These conical metal-complex fragments provide, as in BH, exactly three frontier orbitals ($1\sigma+2\pi$) and two valence electrons and are therefore able to represent BH in clusters. If the remaining requirements are

 © 2002 WILEY-VCH Verlag GmbH & Co. KGaA, Weinheim 1433-7851/02/4122-4221 $ 20.00+.50/0

fulfilled, the Wade–Mingos' rules will apply. Different "rule-breaking" electron counts are found in clusters in which σ interactions dominate (such as alkali-metal and gold clusters), or in clusters in which δ orbitals are involved (e.g. $[M_6Cl_8L_6]^{4+}$ (M = Mo) W and $[M_6Cl_{12}L_6]^{2+}$ (M = Nb, Ta)). The latter situation can be easily understood for systems lacking π-acceptor ligands.[14]

However, in the case of the *isocloso*-metallaboranes it is not really clear why the typical organometallic fragments (e.g. (C_5H_5)Fe, (arene)Ru) that are part of the framework of these clusters, should contribute a number of orbitals and electron pairs that deviate from the isolobal rule. R. B. King made a proposal that only requires three skeletal orbitals per metal:[15] Canonical *closo* clusters are characterized by a radial σ orbital over *p* centers and *p* 2c–2e bonds on the surface, but in this case only *p* 3c–2e bonds in *p* of the $(2p-4)$ triangular faces of the *isocloso*-polyhedron can be present. It is not, however, clear if such topological considerations can be used for the even less symmetrical compounds **1**–**5**.

An alternative description of the metallaboranes **1**–**5** considers these as triple-decker sandwich complexes that have increasingly complicated bridging ligands as the number of boron atoms increases (marked red in Figure 1). This viewpoint is particularly compelling for **1**. The 18 VE rule (d electrons of the metal + π electrons of the decks) for sandwich complexes can be extended to a 30 VE electron rule for triple-decker complexes.[16] Triple-decker complexes with 30 VE conform to the Wade–Mingos' rules for the central $M_2(\mu_2\text{-}\eta^n\text{:}\eta^n\text{-}cyclo\text{-}X_n)$ unit. The $(p=n+2)$-vertex *closo*-polyhedra then have $p+1=n+3$ SEPs (8 SEPs for $n=5$, 9 SEPs for $n=6$). With 24 VE $(\pi^5+d^7+\pi^0+d^7+\pi^5)$ however, the complexes **1**–**5** do not conform to the VE rule for triple-decker-sandwich complexes either. The geometrically simplest case, complex **1**, is in fact the most electron deficient of all triple-decker complexes currently known with a planar middle deck!

The apparent electron deficiency of the triple-decker complex **1** can be convincingly explained by simple arguments. All triple-decker-sandwich complexes are based on the qualitative frontier orbital scheme for the $[\{(C_5H_5)Ni\}_2(\mu\text{-}\eta^5\text{:}\eta^5\text{-}C_5H_5)]^+$ ion (Figure 2, left).[17] The HOMO of this complex (e_1') is derived from the d_{xz} and d_{yz} orbitals of the two metal atoms (or the (C_5H_5)M fragments). Since the bridging ligand has no π orbitals of suitable symmetry, these orbitals are essentially nonbonding. At larger metal–metal distances a lower-lying group of six molecular orbitals, often designated t_{2g}, (d_{xy}, $d_{x^2-y^2}$, and d_{z^2}) participate in the bonding to the bridging ligand to a lesser extent. A (30–34) VE rule can be derived from the occupancy of the e_1' orbitals. With 30 VE ($[(C_5Me_5)_3Ru_2]^+$), these orbitals are empty, with 34 VE they are fully occupied ($[(C_5H_5)_3Ni_2]^+$). Triple-decker-sandwich complexes with 31–33 VE are paramagnetic.

If the bridging ligand of a triple-decker complex has a large diameter, the metal atoms can approach each other to bonding distance without their bonds to the bridging ligand becoming too short. The short metal–metal distance causes the a_1' (d_{z^2}, M–M bonding) and a_2'' orbitals (d_{z^2}, M–M antibonding) to be strongly split; the later orbital now lies so high that it can no longer be occupied. The e_1' set (d_{xz}, d_{yz}) is also raised (interaction with σ orbitals of the bridge) and always remains unoccupied. The magic electron count is now 28 (e.g. $[\{(C_5Me_5)Mo\}_2(\mu\text{-}\eta^6\text{:}\eta^6\text{-}P_6)]$[19]).[20] The electronic structure can also be described on the basis of a 30 VE triple-decker complex in which an electron pair has been removed from the valence shell by the formation of a metal–metal σ bond.

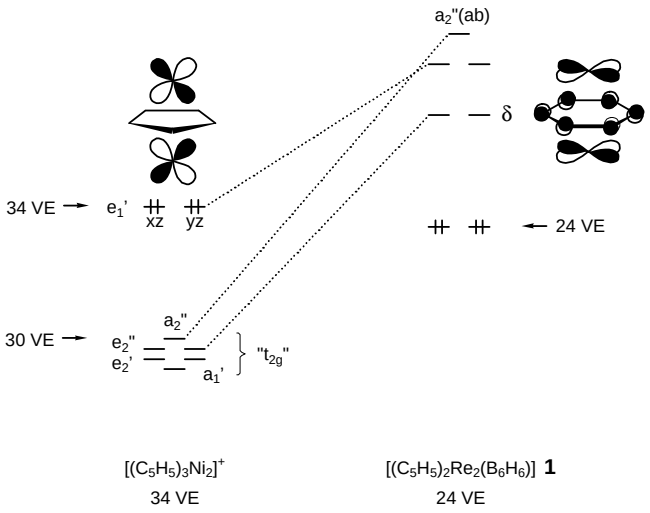


Figure 2. Qualitative MO scheme for $[\{(C_5H_5)Ni\}_2\{\mu\text{-}\eta^5\text{:}\eta^5\text{-}(C_5H_5)\}]$[17] and $[\{(C_5H_5)Re\}_2\{\mu\text{-}\eta^6\text{:}\eta^6\text{-}(B_6H_6)\}]$ **1**.[18] Only the most important frontier orbitals are shown.

Further reinforcement of the interaction between the metal center and the bridging ligand, for example, by increased proximity and/or more diffuse metal orbitals, results in even more orbitals leaving the "t_{2g}" set. This phenomenon involves the e_2' combinations ($d_{x^2-y^2}$, d_{xy}; M–M bonding with δ symmetry) that are extensively destabilized by an antibonding interaction with bonding σ orbitals in the plane of the bridging ligand.[20c] This effect is shown in Figure 2 (right) for **1**. The electron count is further reduced by four to 24 VE. Corresponding bonding combinations with δ symmetry are of course stabilized. For **1** this means that the Re–Re and Re–B bonds strengthen at the cost of the B–B bonds (an Re–Re antibonding (a_2'') and two Re–B antibonding, B–B bonding orbitals (e_2') are emptied).

So are the rule-breakers **1**–**5** dimetallaborane clusters or triple-decker-sandwich complexes? The answer to this question could be the following: What is the difference? In fact the structural principle of a triple-decker—an equatorial ring and two apical (polar) fragments—was already used for the factorization of the secular equation for boron cages a long time ago.[21] Boranes and carboranes lack, of course, energetically accessible orbitals with δ symmetry in the axial direction; the canonical structures are highly preferred. There are also no known metallaboranes structurally analogous to **1**–**5** with the later (electron rich) transition metals (e.g. with $Ni(C_5R_5)$ which is isolobal to CH). In the present case all the metal-centered δ orbitals are filled so that any interaction with (filled) δ orbitals of the borane fragment would be repulsive. The "rule-breaking" structures of complexes such as **1**–**5** are therefore only possible with the early transition metals.

 © 2002 WILEY-VCH Verlag GmbH & Co. KGaA, Weinheim 1433-7851/02/4122-4222 $ 20.00+.50/0 *Angew. Chem. Int. Ed.* **2002**, *41*, No. 22

There is the danger with successful models that their potential is overestimated. There are many cases where a simple (and within its limitations very successful) concept inhibited further development of our understanding. To cite only one example from chemistry, neither the boranes or the noble gas compounds could exist if only the 2c–2e bond model was to apply. With such "bad news for successful models"[22] we should be grateful for the "good news about rule violations".

[1] Cited in ref. [2], p. 1.

[2] K. Wade, *Electron Deficient Compounds*, Nelson, London, **1971**.

[3] a) W. H. Eberhardt, B. L. Crawford, W. N. Lipscomb, *J. Chem. Phys.* **1954**, *22*, 989; b) H. C. Longuet-Higgins, M. de Roberts, *Proc. R. Soc. London Ser. A* **1954**, *224*, 336; H. C. Longuet-Higgins, M. de Roberts, *Proc. R. Soc. London Ser. A* **1955**, *230*, 110; c) W. N. Lipscomb in *Les prix Nobel 1976* (Ed.: The Nobel Foundation), Almqvist & Wiksell, Stockholm, **1977**, p. 108; W. N. Lipscomb, *Angew. Chem.* **1977**, *89*, 685.

[4] a) K. Wade, *J. Chem. Soc. Chem. Commun.* **1971**, 792; K. Wade, *Adv. Inorg. Radiochem.* **1976**, *18*, 1; b) D. M. P. Mingos, *Nature Phys. Sci.* **1972**, *236*, 99; D. M. P. Mingos, *Nature Phys. Sci.* **1972**, *239*, 16.

[5] In a simplified form, the rules require *p*-vertex deltahedra as the basic form of the *closo*-polyhedral framework; these have $(p+1)$ cluster-bonding MOs (CbMOs). The sequential removal of m vertices ($m=1-3$) leads to *nido- arachno-*, and *hypho*-structures with $p'=p-m$ vertices and $(p'+1+m)$ CbMOs. Capping the l faces ($l=1-4$) results in $(p'+1-l)$ CbMOs ($p'=p+l$; "capping" rule). The general formula for the number x of CbMOs in any given cluster with p' framework atoms is therefore $x=p'+m-l+1$.

[6] R. Hoffmann in *Les prix Nobel 1981* (Ed.: The Nobel Foundation), Almqvist & Wiksell, Stockholm, **1982**, p. 173; R. Hoffmann, *Angew. Chem.* **1982**, *94*, 725; *Angew. Chem. Int. Ed. Engl.* **1982**, *21*, 711.

[7] J. D. Kennedy, *Prog. Inorg. Chem.* **1984**, *32*, 519; J. D. Kennedy, *Inorg. Chem.* **1986**, *25*, 111.

[8] R. T. Baker, *Inorg. Chem.* **1986**, *25*, 109.

[9] a) K. Kawamura, M. Shang, O. Wiest, T. P. Fehlner, *Inorg. Chem.* **1998**, *37*, 608; b) A. S. Weller, M. Shang, T. P. Fehlner, *Organometallics* **1999**, *18*, 853; c) T. P. Fehlner, *Organometallics* **2000**, *19*, 2643; d) S. Ghosh, X. Lei, M. Shang, T. P. Fehlner, *Inorg. Chem.* **2000**, *39*, 5373; e) S. Ghosh, A. L. Rheingold, T. P. Fehlner, *Chem. Commun.* **2001**, 895.

[10] a) S. Ghosh, M. Shang, Y. Li, T. P. Fehlner, *Angew. Chem.* **2001**, *113*, 1159; *Angew. Chem. Int. Ed.* **2001**, *40*, 1125; b) S. Ghosh, A. M. Beatty, T. P. Fehlner, *J. Am. Chem. Soc.* **2001**, *123*, 9188.

[11] W. N. Lipscomb, *Science* **1966**, *153*, 373.

[12] D. M. P. Mingos, D. J. Wales, *Introduction to Cluster Chemistry*, Prentice-Hall, Englewood Cliffs, **1990**, chap. 3.

[13] One exception is the polar deltahedra (exactly one framework atom on a C_3 axis) with p or $p+2$ SEPs (R. L. Johnston, D. M. P. Mingos, *J. Chem. Soc. Dalton Trans.* **1987**, 647).

[14] F. A. Cotton, T. E. Haas, *Inorg. Chem.* **1969**, *8*, 2041.

[15] R. B. King, *Inorg. Chem.* **1999**, *38*, 5151; R. B. King, *Inorg. Chim. Acta* **2000**, *300–302*, 537; R. B. King, *J. Organomet. Chem.* **2001**, *635*, 75.

[16] W. Siebert, *Adv. Organomet. Chem.* **1980**, *18*, 301.

[17] J. W. Lauher, M. Elian, R. H. Summerville, R. Hoffmann, *J. Am. Chem. Soc.* **1976**, *98*, 3219.

[18] Our own extended Hückel and DFT calculations; see also ref. [9a].

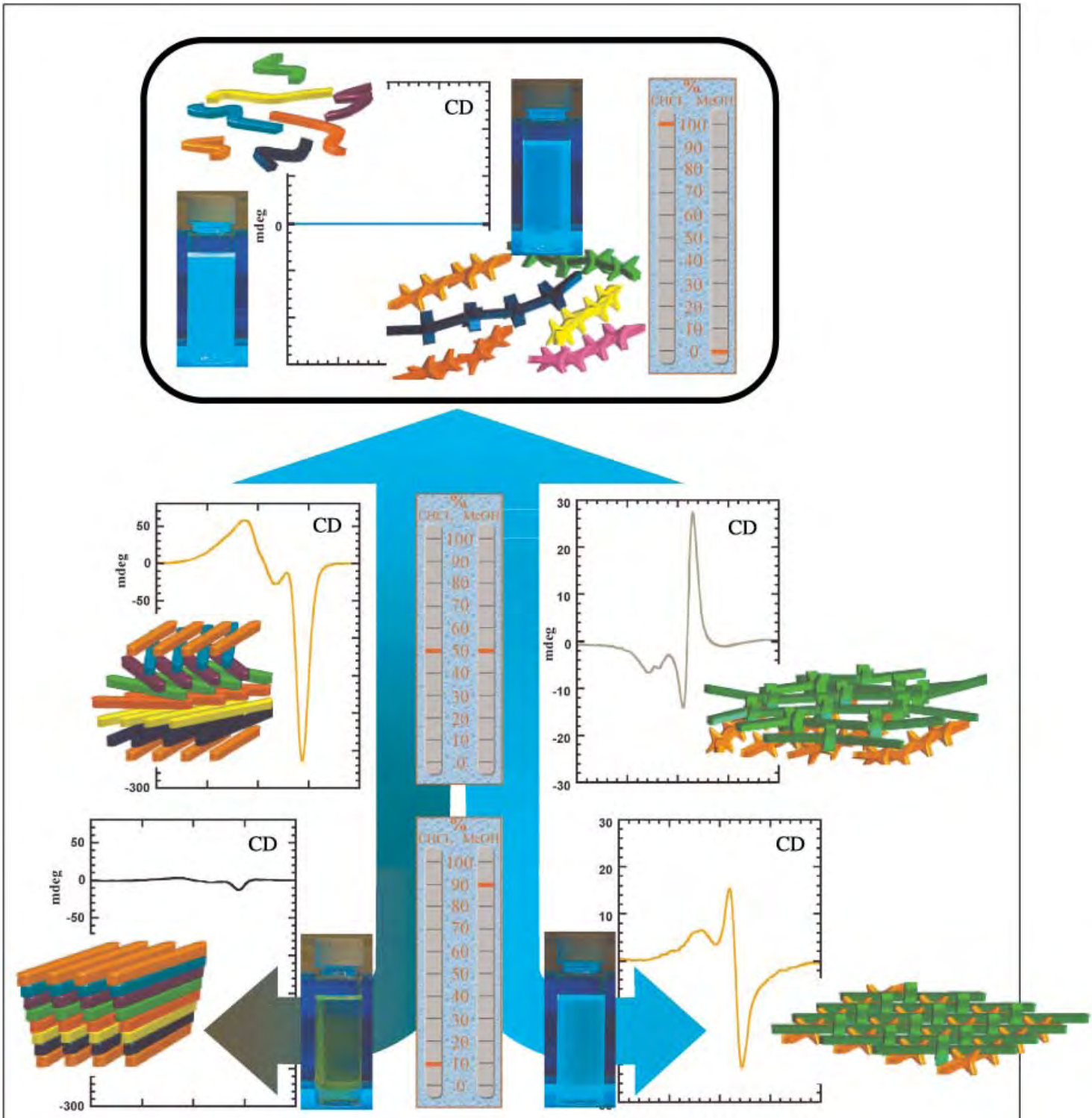
[19] O. J. Scherer, H. Sitzmann, G. Wolmershäuser, *Angew. Chem.* **1985**, *97*, 358; *Angew. Chem. Int. Ed. Engl.* **1985**, *24*, 351.

[20] a) E. D. Jemmis, A. C. Reddy, *Organometallics* **1988**, *7*, 1561; b) W. Tremel, R. Hoffmann, M. Kertesz, *J. Am. Chem. Soc.* **1989**, *111*, 2030; c) A. C. Reddy, E. D. Jemmis, O. J. Scherer, R. Winter, G. Heckmann, G. Wolmershäuser, *Organometallics* **1992**, *11*, 3894.

[21] R. Hoffmann, W. N. Lipscomb, *J. Chem. Phys.* **1962**, *36*, 2179.

[22] T. P. Fehlner, *Struct. Bonding (Berlin)* **1997**, *87*, 111; T. P. Fehlner, *J. Chem. Soc. Dalton Trans.* **1998**, 1525.

 © 2002 WILEY-VCH Verlag GmbH & Co. KGaA, Weinheim 1433-7851/02/4122-4223 $ 20.00+.50/0



Solvent-induced aggregation of optically active poly(phenylene ethynylene)s (PPEs) can follow different pathways, depending on the ability of the PPEs to stabilize the chiral macrostructure. A new approach has been developed that utilizes chirality in combination with "pillarlike" structural elements for the first time to create strong electronic coupling systematically while maintaining high quantum yields. For more information see the following publication by Swager et al.

 © 2002 WILEY-VCH Verlag GmbH & Co. KGaA, Weinheim 1433-7851/02/4122-4225 $ 20.00+.50/0

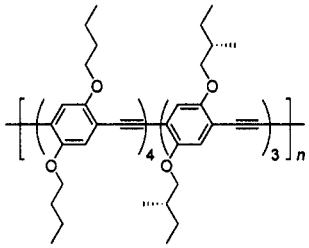
Three-Dimensional Electronic Delocalization in Chiral Conjugated Polymers**

Steffen Zahn and Timothy M. Swager*

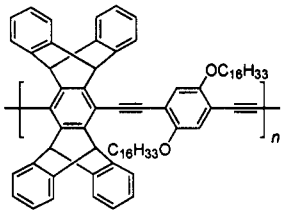
Transport properties are the central performance determinant of electronic materials in most applications. Strong, extended electronic interactions have long been understood to be critical to obtaining molecules and polymers with high charge-carrier mobility. It has been further revealed recently that strong electronic coupling is the dominant contributor to intramolecular exciton transport in solutions of some conjugated polymers.[1] As a result, the production of extended electronic interactions both within and between electronic polymers is critical to the optimization of their transport of charge and excitons, which underpins future applications in transistors,[2] electroluminescent devices,[3] sensors,[4] and photovoltaic devices.[5] However, in devices requiring luminescence and/or exciton transport, researchers have generally avoided the strong interpolymer electronic coupling that will enhance transport because of the strong self-quenching that nearly exclusively accompanies these interactions. Self-quenching lowers the light output of luminescent devices and also lowers the diffusion length of excitons, which reduces sensory responses. As a result, most researchers seeking to create highly emissive films of electronic polymers use large structures such as dendrimers[6] or smaller rigid scaffolds[7] to prevent interchain interactions. It can therefore be stated that present design principles for maintaining high emission quantum yields in conjugated polymers have been diametrically opposed to those for the optimization of charge and exciton transport. To address this limitation we present herein a general design for producing strongly interacting polymer chains with 3D electronic interactions while maintaining high luminescence efficiency. This ability to optimize charge and exciton transport simultaneously in conjugated polymers has broad implications for optoelectronic devices. Herein we describe experimental results that demonstrate that 3D electronic interactions enhance exciton transport.

With few exceptions, strong electronic interactions between chains of conjugated polymers (often accompanying aggregation) dramatically lower their quantum efficiency. Previous studies on carefully designed Langmuir films have revealed that interchain interactions in poly(phenylene ethynylene) species (PPEs) give new low energy bands in the UV/Vis absorption spectra.[8] Recently, a theoretical account by Brédas, et al.[9] and an unexpected result reported by us[10] have suggested that an oblique orientation between neighboring transition dipole moments of conjugated polymers might prevent fluorescence quenching upon aggregation. Indeed, based upon the exciton-coupling model,[11] a parallel orientation of polymer chains is expected to result in cancellation of transition dipoles to give a forbidden S_0–S_1 transition, whereas coupled chromophores with oblique organizations should exhibit an allowed S_0–S_1 transition. Considering that polymer-backbones twist, which is promoted by introducing chirality, may introduce such an oblique arrangement we embarked on a program to produce chiral PPEs that would self-assemble into stable aggregates with high quantum yields.

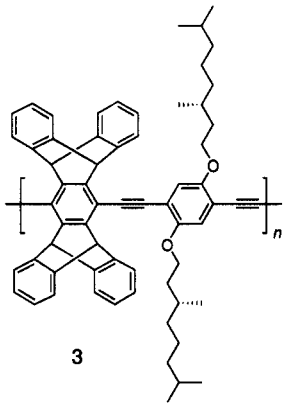
These studies build on a detailed understanding of the electronic spectra of PPEs deduced through studying ordering and phase transitions in Langmuir films, which allowed for a deconvolution of the effects of backbone planarization (conjugation length) and interpolymer interactions (aggregation).[12] To promote high degrees of aggregation, we initially investigated simple structures, such as **1**, which contains chiral alkyloxy groups. Poly(2,5-bis[2-(*S*)-methylbutoxy]-1,4-phenylene ethynylene) was previously investigated.[13] However, our results contrasted significantly from the earlier studies,[14] which prompted a detailed investigation. The addition of poor solvents to a solution of the conjugated polymer generates stable solutions of very small nonscattering particles[15] that allow quantitative studies of the optical properties by avoiding the scattering, reflection, and waveguiding of the emitted light that complicate thin-film studies. To develop a comprehensive understanding of polymers containing chiral alkyloxy side chains, we undertook the systematic investigation of the 58 different compositions shown in Scheme 1. While a detailed description of all of these materials is beyond the scope of this present contribution, we have established that molecular weight is a critical variable and that lower molecular-weight materials ($M_n < 12\,000$) gave different results from higher molecular-weight compounds.



1



2



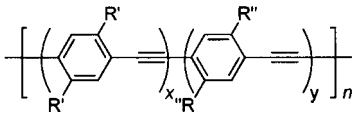
3

We chose to study the well-defined polymer **1**, because it yielded consistent results that are representative of the entire family of polymers. The addition of methanol ($\geq 40\,\%$) to

[*] Prof. T. M. Swager, Dr. S. Zahn
Department of Chemistry
Massachusetts Institute of Technology
Cambridge, Massachusetts 02139 (USA)
Fax: (+1) 617-253-7929
E-mail: tswager@mit.edu

[**] We are grateful for research funding from the Department of Energy, Army Research Office, and NASA.

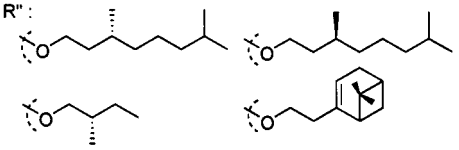
 © 2002 WILEY-VCH Verlag GmbH & Co. KGaA, Weinheim 0044-8249/02/4122-4226 $ 20.00+.50/0



For $x = y = 1$

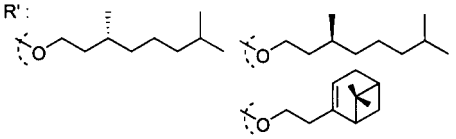
R' : 2-naphthyl; H; CH_3; iC_3H_7; OCH_3; OC_2H_5; OC_4H_9; OC_6H_{13}; $OCH_2CH(C_2H_5)C_4H_9$; OC_8H_{17}; $OC_{10}H_{21}$; $OC_{16}H_{33}$;

R'' :



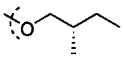
For $x = 1$; $y = 0$

R' :



For $x = 1$–4; $y = 1,3$

R' : OC_4H_9; R'' :



Scheme 1. Structures of the polymers under investigation.

chloroform solutions of **1** introduces an band at 492 nm in the UV/Vis absorption spectrum (Figure 1) caused by an aggregate. Consistent with our previous studies, the fluorescence is strongly quenched by the aggregate. Commensurate with the appearance of the band arising from the aggregate at low methanol concentrations, we see circular dichroism (CD) bands indicative of a chiral structure.[16] The large peak in the CD spectrum at low methanol concentrations is coincident with the band caused by aggregation and confirms that the new aggregate chromophore is chiral.[17] The other features in the CD spectrum indicate the presence of a second chromophore at higher energy, which has the same sign in the CD. The inflection point at 454 nm is the same as the absorption maxima of unaggregated and less-conjugated segments of the polymer, which indicates the presence of exciton-coupled CD (ECCD).[18] The small negative CD peak at 467 nm in the composite spectrum at low methanol concentrations is the result of cancellation of the strong positive second Cotton Effect (CE) from the aggregate chromophore and the negative first CE from the exciton-coupled polymers.

The most striking feature of the behavior of **1**, and indeed related structures in Scheme 1, is that above methanol concentrations of 50% the CD drops off dramatically, while the aggregate peak continues to grow (UV/Vis). This effect can be understood as shown schematically in Figure 2a–c. Initially a chiral aggregate forms with a small angle between polymer chains to give an organization reminiscent of a cholesteric liquid crystal. However, the polymer ultimately favors a stronger aggregate structure with coincident alignment of polymer chains and the helical structure is lost. We note that in previous studies this behavior was not observed.[13] The resultant organization gives a low or nonexistent dihedral angle between polymer chains and, as expected, the fluorescence quantum yield drops to only $<5\%$ ($\Phi = 0.04$) of its original value.

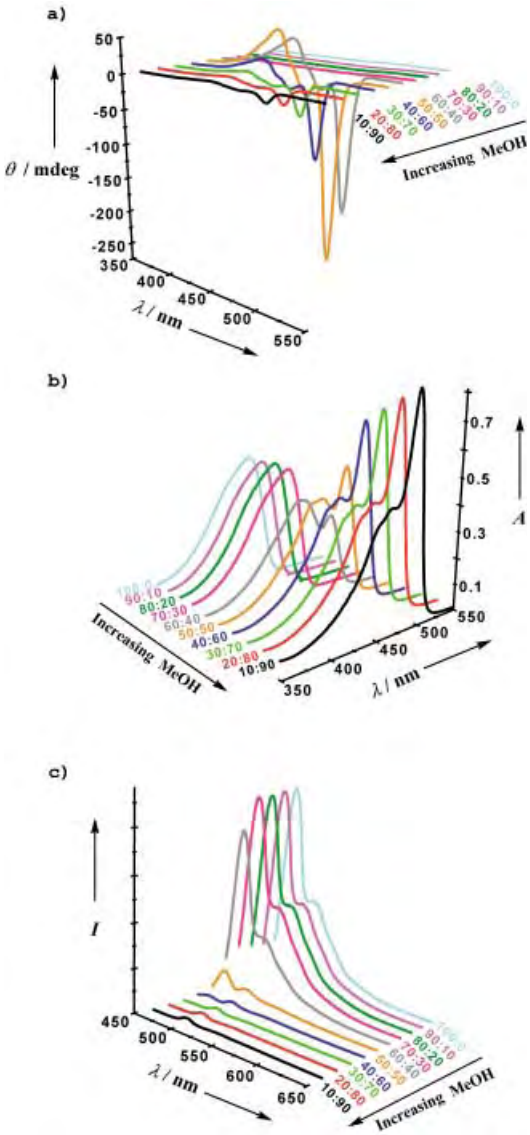


Figure 1. Circular dichroism (a), absorption (b), and fluorescence (c) spectra of (*S*)-**1** recorded in good solvent/poor solvent mixtures at 25 °C (100:0 denotes 100 v/v % of chloroform and 0 v/v % of methanol, 20:80 indicates a solvent mixture consisting of 20 v/v % chloroform and 80 v/v % methanol).

To stabilize a strongly aggregated chiral and emissive organization of polymers, we have investigated specific architectures that prevent aggregated chains from achieving a collinear structure. We had previously developed the polymers **2** containing the pentiptycene group and found that this group was excellent in preventing chain aggregation in spin-cast films.[19] We have found, however, that addition of methanol (30%) to solutions of **2** gives aggregates with significantly quenched emission ($\Phi = 0.21$). This aggregate is much slower to assemble than **1** and we hypothesized that the polymer chains assemble into an interlocking structure, in which the polymer chains are constrained in the clefts between pentiptycene groups.

We considered that an interlocking structure, such as that of **2**, would stabilize chiral aggregates by preventing a coincidence of strongly interacting polymer chains. Studies of the chiral analogue **3** confirm the restricted nature of the aggre-

 © 2002 WILEY-VCH Verlag GmbH & Co. KGaA, Weinheim 0044-8249/02/4122-4227 $ 20.00+.50/0

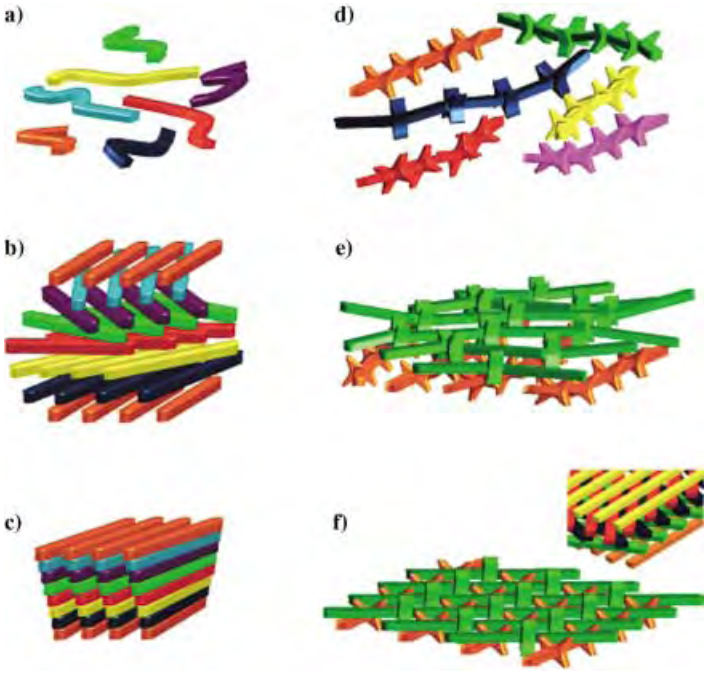


Figure 2. Illustration of three stages of aggregation of **1** (a)–(c) and **3** (d)–(f). Top: **1** (a) and **3** (d) dissolved in neat chloroform. Both polymers are highly solvated and there are no interactions between polymer chains. Middle: Aggregation of **1** occurred and the rigid-rod PPEs form a lamella structure within each plane (b). The chiral side chains guide the polymers into a chiral macrostructure as depicted. The formation of the optically active macrostructure is guided by the influence of the chiral side chains. Polymer **3** aggregates analogously to **1**, but because of the presence of the pentiptycene groups, a slightly irregular interlocked structure results (e). Macrostructure **3** is shown in a two-layer graphic for simplification and clarity. Bottom: The initial chiral macrostructure of **1** has been "untwisted" (c), which is favorable as it maximizes π–π stacking in the edge-on conformation. The dihedral angle assumes a very small value, affording a very weak dichroic signal and low fluorescence quantum yield. Polymer **3** self-assembles into a tighter structure (f) by incorporating the polymer into the clefts of the pentiptycene groups. Because the "untwisting" motion observed in **1** is hindered, polymer **3** is able to maintain its optically active structure and its high fluorescence quantum yield. The inset illustrates the anticipated chiral gridlike structure.

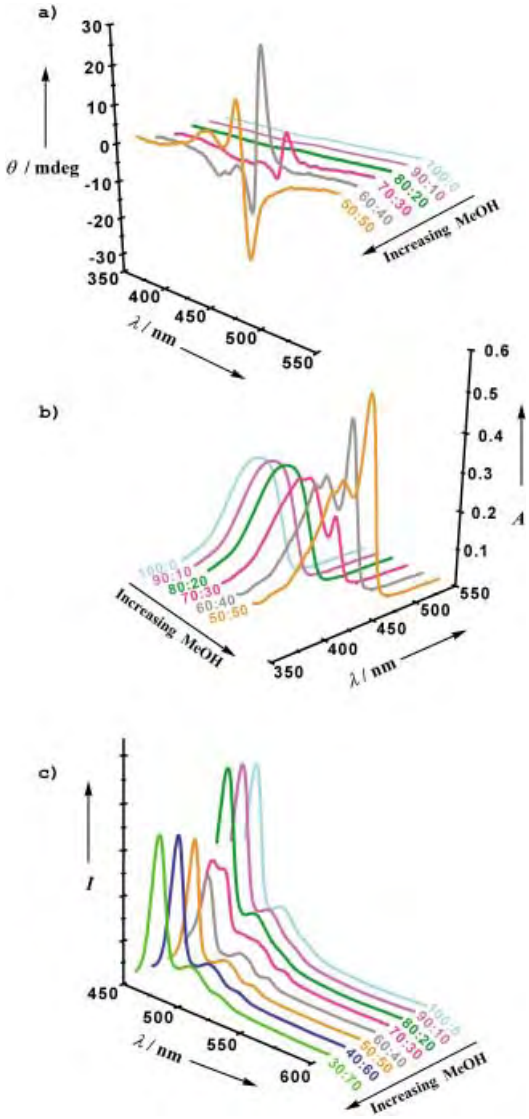


Figure 3. Circular dichroism (a), absorption (b), and fluorescence (c) spectra of (*R*)-**3** recorded in good solvent/poor solvent mixtures at 25 °C (100:0 denotes 100 v/v % of chloroform and 0 v/v % of methanol, 30:70 indicates a solvent mixture consisting of 30 v/v % chloroform and 70 v/v % methanol).[24]

gated state; the structure of the CD and absorption spectra evolve slowly over approximately five minutes. Although the absorption spectra are similar to those of **1**, with more fine structure, the CD spectra are very different (Figure 3). Like that of **1** in the aggregated state (≥ 30 % methanol), the spectrum of **3** displays two dominant contributions that are associated with the "aggregate" band at $\lambda_{max} = 460$ nm and the band arising from unaggregated species at 430 nm. However, there are key differences between **1** and **3**. Most striking is the change in shape and even sign of the CD bands upon forming the tightest aggregate structure in high methanol concentrations (≥ 50 %). We believe this complication is the result of the polymer chains being constrained in interlocked irregular structures as shown in Figure 2e. The position of the CD band and the near coincidence of the inflection point with the λ_{max} of the aggregate indicates an ECCD effect that only originates from the interpolymer interaction of the planar chromophores. Hence it appears that only well-structured (planar) polymer chains are incorporated into the grid. Portions of the material that probably have a less ordered and therefore a less conjugated electronic structure are not incorporated into the gridlike structure because of their higher steric demands that make them unsuitable to fit in the cleft of the polymer. These "solutionlike" portions of the material communicate poorly with each other electronically and therefore give rise to a broad CD band at 430 nm, which is difficult to analyze.

The CD signal and the aggregate band in the absorption spectrum are both consistent with interpolymer electronic interactions. However, as shown in Figure 3, in contrast to other polymers, **3** maintains the majority of its fluorescence intensity with aggregation ($\Phi = 0.61$).[25] The CD does not diminish at high methanol concentration and, interestingly, upon initial aggregation the intensity is slightly lower than the more highly aggregated form. Control experiments utilizing the opposing enantiomer to **3** yielded UV/Vis and fluorescence spectra of identical shape and intensity, and a CD spectrum that differs only in the signs of the Cotton effects.

 © 2002 WILEY-VCH Verlag GmbH & Co. KGaA, Weinheim 0044-8249/02/4122-4228 $ 20.00+.50/0

Furthermore, a solution containing 50% (*S*)-**3** and 50% (*R*)-**3** gave absorption spectra similar to pure solutions of (*S*)-**3** or (*R*)-**3**, but no CD signals, as expected. Consistent with chirality being a critical element to maintain a high quantum yield, this aggregate maintained a Φ of only 0.3. Achiral aggregates present in the 50:50 mixture of enantiomeric polymers are probably responsible because the long-range dipole–dipole interactions responsible for the excitonic coupling are extended beyond nearest neighbors.

To illustrate the advantages of a 3D structure for the design of optoelectronic devices, the performance of **3** as a self-amplifying sensory polymer was investigated under solution and solid-state conditions by means of Stern–Volmer quenching experiments (Figure 4). In solution, fully aggregated **3** displayed a 15-fold steeper quenching slope toward the

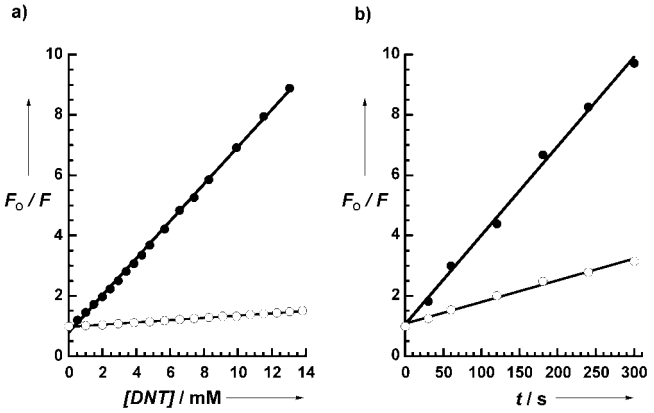


Figure 4. Stern–Volmer plots of **3** in a nonaggregated form (○) and an aggregated form (●) in solutions at OD = 0.09 (a). Stern–Volmer plot of **2** (○) and **3** (●) in films of OD = 0.03 upon exposure to TNT vapors (b).

explosives dinitrotoluene (DNT) and trinitrotoluene (TNT) than nonaggregated **3**. In solid-state experiments, **3** was compared to **2**, a material with a self-amplified sensory response arising from efficient exciton transport that is the basis of new landmine detection technology with femtogram detection limits.[7] Polymer **2** exhibits its best performance when spin-coated from nonaggregated solutions to give films of non-interacting chains. These films of **2** were compared with films that were spin-coated from aggregated solutions of **3** (55:45 chloroform:methanol). Both films were uniform and of identical optical density. Upon exposure to a static 10 ppb vapor of TNT,[20] **3** displayed a Stern–Volmer plot that is four times steeper than that of **2**. It should be noted that thin films of **3** (optical density (OD) = 0.04) exhibit a quenching response of $\approx$75% in 10 seconds that is significantly more sensitive than previously published materials.[7,21–23] We attribute this observation to the improved diffusion length of excitons in 3D-coupled chiral grids of **2**. Our recent work[1] suggested that strong electronic coupling provides the best exciton transport and hence the excitonic coupling enhances the interchain transport. Further, the highly organized aggregate probably extends the conjugation length of the polymer, which may also enhance exciton transport. We have ruled out the possibility that the sensitivity enhancement is caused by a higher partitioning of TNT to **3** than to **2** by conducting studies as a function of film thickness. Because of limited exciton transfer between polymer chains, which limits exciton diffusion, **2** displayed a dramatic 45% decrease in sensitivity in thicker films (OD = 0.3) relative to thinner films (OD = 0.04).[23] In contrast, **3** displays only a 10% decrease in quenching sensitivity in thick films (OD = 0.2) relative to thin films (OD = 0.02).

To summarize, the high quantum yield of **3** in its aggregated state results from the formation of a helical grid structure and an oblique orientation of the transition dipole moments of the neighboring polymer chains. We have discovered that rigid scaffolds prevent collinear aggregation of polymer chains. Chirality has been used for the first time to create strong electronic coupling systematically while maintaining high fluorescence efficiency. These chiral, 3D interactions produce sensitive sensory materials with excellent quantum yields. Similar approaches will probably enhance the performance of electronic polymers for many other optoelectronic-device applications.

Received: July 8, 2002 [Z19683]

[1] A. Rose, C. G. Lugmair, T. M. Swager, *J. Am. Chem. Soc.* **2001**, *123*, 11298.

[2] H. Sirringhaus, P. J. Brown, R. H. Friend, M. M. Nielsen, K. Bechgaard, B. M. W. Langeveld-Voss, A. J. H. Spiering, R. A. J. Janssen, E. W. Meijer, P. Herwig, D. M. De Leeuw, *Nature* **1999**, *401*, 685.

[3] R. H. Friend, R. W. Gymer, A. B. Holmes, J. H. Burroughes, R. N. Marks, C. Taliani, D. D. C. Bradley, D. A. dos Santos, J.-L. Brédas, M. Logdlund, W. R. Salaneck, *Nature* **1999**, *397*, 121; S. Sibley, M. E. Thompson, P. E. Burrows, S. R. Forrest, *Optoelectron. Prop. Inorg. Compd.* **1999**, 29.

[4] D. T. McQuade, A. E. Pullen, T. M. Swager, *Chem. Rev.* **2000**, *100*, 2537.

[5] C. J. Brabec, N. S. Sariciftci, J. C. Hummelen, *Adv. Funct. Mater.* **2001**, *11*, 15.

[6] T. Sato, D.-L. Jiang, T. Aida, *J. Am. Chem. Soc.* **1999**, *121*, 10658.

[7] J.-S. Yang, T. M. Swager, *J. Am. Chem. Soc.* **1998**, *120*, 5321.

[8] D. T. McQuade, J. Kim, T. M. Swager, *J. Am. Chem. Soc.* **2000**, *122*, 5885.

[9] J.-L. Brédas, J. Cornil, D. Beljonne, D. A. dos Santos, Z. Shuai, *Acc. Chem. Res.* **1999**, *32*, 267.

[10] R. Deans, J. Kim, M. Machacek, T. M. Swager, *J. Am. Chem. Soc.* **2000**, *122*, 8565.

[11] This model is most properly used to understand only very weakly interacting chromophores. However, it guided our studies. M. Kasha in *Spectroscopy of the Excited State* (Ed.: B. Di Bartollo), Plenum, New York, **1976**, pp. 337–363.

[12] J. Kim, T. M. Swager, *Nature* **2001**, *411*, 1030.

[13] R. Fiesel, U. Scherf, *Macromol. Rapid Commun.* **1998**, *19*, 427.

[14] There are a number of contrasting results. However, in this earlier report an absorption maximum of 420 nm ($\varepsilon = 12400\ \mathrm{L\,mol^{-1}\,cm^{-1}}$) is reported, which is considerably (34 nm) blue-shifted relative to the carefully characterized polymers investigated here, and to other achiral polymers having the same electronic structure. Hence we attribute the differences to the analysis in the previous studies of very low molecular-weight oligomeric samples.

[15] B. M. W. Langeveld-Voss, R. A. Janssen, M. P. T. Christiaans, S. C. J. Meskers, H. P. J. M. Dekkers, E. W. Meijer, *J. Am. Chem. Soc.* **1996**, *118*, 4908.

[16] A. F. M. Kilbinger, A. P. H. J. Schenning, F. Goldoni, W. J. Feast, E. W. Meijer, *J. Am. Chem. Soc.* **2000**, *122*, 1820.

[17] B. M. W. Langeveld-Voss, D. Beljonne, Z. Shuai, R. A. J. Janssen, S. C. J. Meskers, E. W. Meijer, J.-L. Brédas, *Adv. Mater.* **1998**, *10*, 1343; B. M. W. Langeveld-Voss, R. A. J. Janssen, E. W. Meijer, *J. Mol. Struct.* **2000**, *521*, 285.

 © 2002 WILEY-VCH Verlag GmbH & Co. KGaA, Weinheim 0044-8249/02/4122-4229 $ 20.00+.50/0

[18] N. Berova, K. Nakanishi in *Circular Dichroism: Principles and Applications* (Eds.: N. Berova, K. Nakanishi, R. W. Woody), Wiley-VCH, New York, **2000**, pp. 337 – 382.
[19] We found that thin films of these materials do not aggregate even with extended thermal annealing at 160 °C. Possibly the PPE main chains are collinear and kept apart by the presence of the pentiptycene groups.
[20] The saturation vapor pressure of TNT at 22 °C is 8.02×10^{-6} mmHg or about 10 ppb. *Handbook of Physical Properties of Organic Chemicals* (Eds.: P. H. Howard, W. M. Meylan), CRC, Boca Raton, FL, **1997**.
[21] For comparison, other electronic polymers reportedly decreased their fluorescence intensity by 8.2% after exposure to similar vapor concentrations with turbulent flow for 10 min (H. Sohn, R. M. Calhoun, M. J. Sailor, W. C. Trogler, *Angew. Chem. Int. Ed.* **2001**, *113*, 2162; *Angew. Chem. Int. Ed.* **2001**, *40*, 2104). Hence **3**, which was studied under static conditions, is at least 560 times more sensitive.
[22] Y. Liu, R. C. Mills, J. M. Boncella, K. S. Schanze, *Langmuir* **2001**, *17*, 7452; G. A. Bakken, G. W. Kauffman, P. C. Jurs, K. J. Albert, S. S. Stitzel, *Sens. Actuators B* **2001**, *79*, 1.
[23] Y.-S. Yang, T. M. Swager, *J. Am. Chem. Soc.* **1998**, *120*, 11 864.
[24] The CD and absorption spectra end at 50:50 chloroform:methanol as the rigid, gridlike aggregates precipitate readily at higher methanol content. The fluorescence spectra could be recorded up to 30:70 chloroform:methanol as the concentration of the polymer was only 1/10 of that of the absorption studies and therefore precipitation occurred at higher methanol concentrations.
[25] Similarly, **3** had a photoluminescence efficiency which was four times higher than that of **2** in films of identical optical density.

High-Throughput Multilevel Performance Screening of Advanced Materials

Radislav A. Potyrailo* and James E. Pickett

High-throughput screening and combinatorial chemistry have been successfully extended from pharmaceutical applications into other scientific disciplines.[1] Performance of rapidly fabricated compounds is typically evaluated by relating results of high-throughput analysis to the intrinsic properties of starting materials or final products.[2] We report a general scheme for screening of complex materials developed by using high-throughput and combinatorial methods, where simple screening for intrinsic properties of starting materials or final compounds does not provide information about long-term material performance.

Our general approach employs fabrication of materials arrays followed by their testing against single or several performance parameters at *multiple* levels. This testing process imitates the end-use application and alters materials properties in a detectable manner that is impossible to quantitatively predict using existing knowledge.[3] Our scheme of high-throughput evaluation of advanced materials fabricated by using high-throughput and combinatorial methods is very general and includes diverse testing methodologies such as solar radiation, mechanical stress, aggressive fluids, heat, and others. Tested arrays are further analyzed by using high-throughput screening (HTS) tools.

We demonstrated our strategy for high-throughput performance screening of polymeric materials. Weathering is a critical consideration in the development of new engineering thermoplastics for outdoor applications.[4] A determining factor in the outdoor weathering lifetime of these materials is the received UV radiation dose. It leads to material photodegradation that initially causes the loss of appearance such as surface discoloration and gloss loss.[5,6] Other environmental (humidity, temperature, frequency of light/dark cycles) and material (catalyst residues, crystallinity, molecular weight, end groups) factors do not appreciably affect the appearance of engineering thermoplastics upon weathering.[4,7] These factors, however, do have a pronounced effect on other types of polymers.[4,6] Additives and pigments (typical loadings of 0.01–5 wt%) greatly affect the stability of engineering and other types of polymers.[8] Thus, studies of polymer–additive and polymer–pigment combinations are of great importance.

Resistance toward weathering presents a particular challenge for HTS since exposure times for adequate outdoor weatherability testing are thousands of hours.[4] In principle, acceleration of this process can be achieved either by increasing the level of environmental stress or by very early detection of material degradation. In laboratory weathering methods, a dose equivalent to one year of exposure to conditions in Florida can be reduced to about 1100 h.[9] However, a further acceleration of materials weathering to the HTS level becomes problematic because of loss of correlation with traditional test methods.[4,8,10]

We use fluorescence imaging and spectroscopy to quantify photodegradation in arrays of materials at short exposure times that open up HTS capabilities in weathering studies. Our libraries combine the variables of polymer composition, pigment type, and exposure time, but are easily extendable to incorporation of stabilizers and other additives at different loadings that may affect the rate of degradation.

Unlike traditional measurements of weatherability-related appearance based on color changes and gloss loss,[4,8b,11] fluorescence analysis[12] advances the studies of polymeric materials libraries produced by using high-throughput methods to a previously unavailable level of capabilities. Fluorescence detects trace amounts of weathering degradation products and thus requires a considerably shorter testing time. Measurements are performed on both lightly and highly colored samples with a comparable level of sensitivity. Because fluorescence light is isotropic, the whole combinatorial library is imaged without the need for an integrating sphere or a goniophotometer. Different fluorescence excitation–emission conditions can be selected to analyze different fluorescent species.

To demonstrate the applicability of our screening strategy, three types of aromatic polymers (polycarbonate, PC; poly(butylene terephthalate), PBT; and their 45/55 wt% blend, PC/PBT) were made in combination with two types of pigments (rutile TiO_2 and carbon black, CB) and tested under

[*] Dr. R. A. Potyrailo, Dr. J. E. Pickett
General Electric Company
Global Research Center
Niskayuna, NY 12309 (USA)
Fax: (+1) 518-387-5604
E-mail: Potyrailo@crd.ge.com

Supporting information for this article is available on the WWW under http://www.angewandte.org or from the author.

 © 2002 WILEY-VCH Verlag GmbH & Co. KGaA, Weinheim 0044-8249/02/4122-4230 $ 20.00+.50/0

11 levels of weathering conditions. The pigments were selected to provide a wide range of potential weathering performance of materials. The mass loadings (2 and 0.6 wt % for TiO_2 and CB, respectively) were within the application range in polymers.[8] The testing scheme of these arrays of polymer compositions is shown in Figure 1 a. For comparison of fluorescence with conventional methods, the maximum exposure dose (1030 kJ m^{-2} at 340 nm) was accumulated over 417 h.

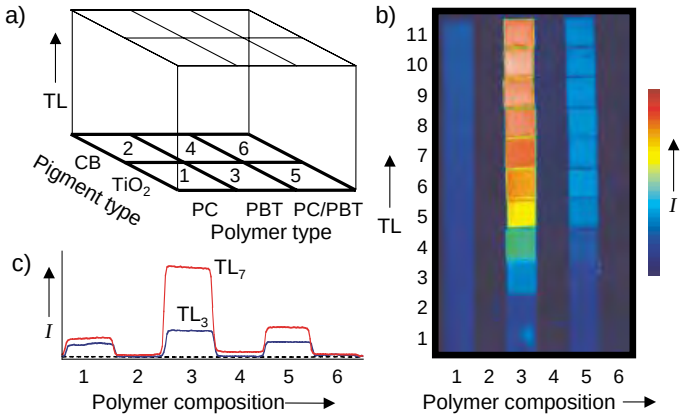


Figure 1. Screening of complex materials developed by using high-throughput methods under multilevel performance test conditions. a) Testing scheme for the arrays of polymeric materials with pigment compositions and multiple test levels (TL_x). b) Fluorescence image of 11 arrays of polymeric materials after weatherability testing at 11 levels. c) Cross sections of arrays 3 (TL_3) and 7 (TL_7) demonstrating fluorescence signals in different polymeric compositions. Dotted line, background.

We determined the amount of UV-induced degradation in the arrays of polymeric materials using fluorescence imaging and spectroscopy. A fluorescence image of 11 arrays is shown in Figure 1 b. These experiments demonstrated that fluorescence intensity increases as a function of exposure dose and depends on both the nature of the polymer and the nature of the pigment. Fluorescence imaging revealed the increase in fluorescence intensity of all dark polymer samples pigmented with CB indicating polymer degradation (see Figure 1 c, polymer compositions 2, 4, and 6), although the emission was about 20× weaker than that for the same polymers pigmented with TiO_2.

For detailed analysis of weatherable performance of arrays, we coupled a fiber-optic spectrograph to automatically operate with a X–Y translation stage. Results of these experiments are presented in Figure 2. Using multilevel performance screening, we found similar kinetic rates of weathering of polymers with quite different pigments. In contrast, traditional analysis of weathering of dark polymers involves measurements of gloss loss after the surface is heavily degraded (accumulation of 800–1000 kJ m^{-2} dose) and does not provide kinetic information at early weathering stages.

Comparison of fluorescence and color analysis of TiO_2-pigmented polymers is presented in Figure 3.[13] Color is analyzed as an increase in yellowness index (YI)[4,8b,11] which corresponds well to how the human eye perceives yellowness of lightly colored materials. In color analysis, YI is a well-established value of merit.[4,8b,11,14] However, as shown in the inset of Figure 3, fluorescence is much more sensitive than YI

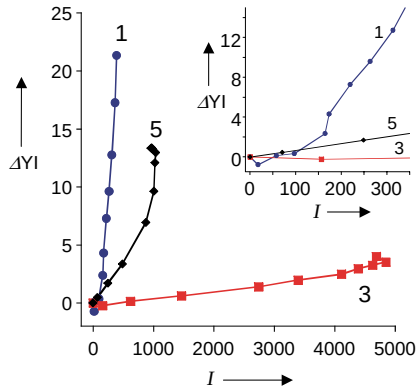


Figure 3. Correlation between fluorescence and color analysis of TiO_2-pigmented polymers 1–6 (see Figure 1 a). Inset, early stage of weatherability studies. $\Delta YI = YI - YI_o$, where YI_o is at test level TL_1.

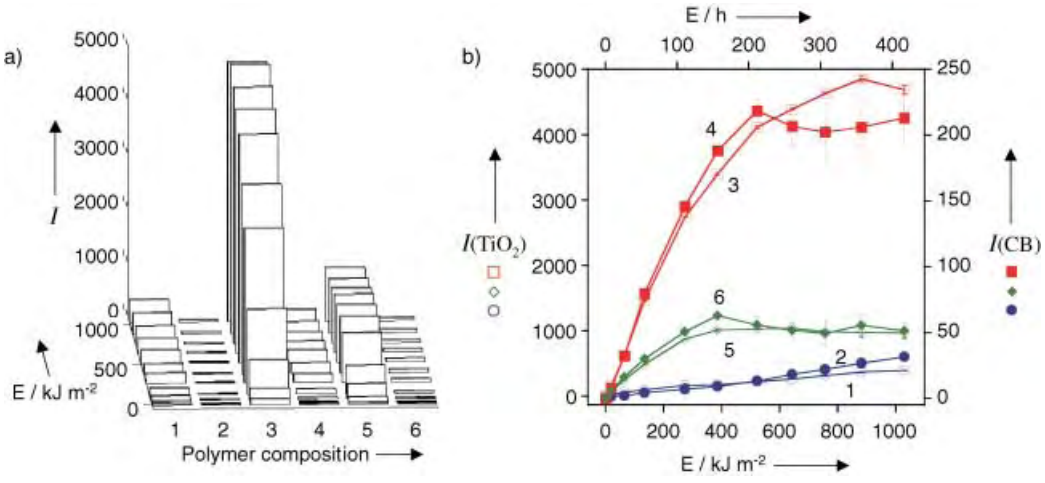


Figure 2. a) Effect of increasing exposure dose on the weatherability of arrays of polymer compositions 1–6 (see Figure 1 a). b) High-throughput determination of weatherability kinetics of arrays of polymer compositions 1–6. Open markers, TiO_2 pigment; filled markers, CB pigment.

 © 2002 WILEY-VCH Verlag GmbH & Co. KGaA, Weinheim 0044-8249/02/4122-4231 $ 20.00+.50/0

at early stages of polymer degradation. Also, the problems of bleaching and instability of colorants at early stages of weathering tests do not confound it.[15] The fluorescence intensity alone slightly decreases at prolonged exposures as shown in Figure 3 for PBT and PC/PBT. In addition to fluorescence intensity determinations, distortions and shifts of excitation and emission peaks can also serve as a polymer-lifetime prediction tool.[16]

We evaluated the capabilities of our method by determining the smallest exposure time required to detect a change in fluorescence signal.[17] For the TiO_2-pigmented polymers, the fluorescence signal change can be detectable after only 28, 19, and 26 min of irradiation for PC, PBT, and PC/PBT, respectively. Similarly, this time was 138, 30, and 72 min for the CB-pigmented PC, PBT, and PC/PBT, respectively. Using fluorescence, the throughput of screening can be increased by 200–650-fold and 150–800-fold, compared to determination of color change and gloss loss, respectively. Thus, information about the kinetics of photodegradation is available much sooner.

The multilevel screening provides robust ranking of material performance. Figure 4 shows the ranking of weatherability of polymeric materials with 18.9 and 522 kJ m^{-2} exposures

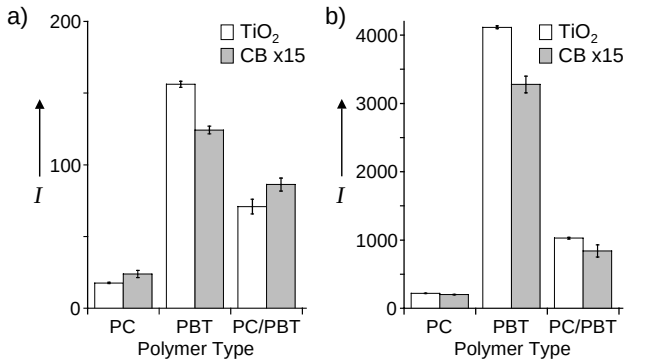


Figure 4. Applicability of fluorescence analysis for ranking of materials weatherability at a) 18.9 kJ m^{-2} and b) 522 kJ m^{-2} stages of performance testing.

for each polymer type. The ranking of the weatherability at the smallest used exposure is the same as at more advanced exposure levels when the analytical signal is 10–25 times stronger.[18] Similar to evaluation of discoloration, this method shows utility for formulation/stability development within a preselected material type, however with much higher screening throughput.[19]

In summary, we present a new approach for high-throughput screening of complex material systems when performance of materials cannot be evaluated based on simple measurements of their intrinsic properties immediately after fabrication. Multiple levels of end-use testing conditions provide more reliable ranking of performance of materials made by using high-throughput and combinatorial methods and serve as a robust predictive tool. With a combination of testing and high-sensitivity analysis steps in a single discovery cycle, it should be possible to design screening systems for just about any advanced material.

Experimental Section

Polymer/pigment combinations were injection molded by using small-scale equipment. Individual $2 \times 12.5 \times 12.5$ mm elements of all six polymer compositions were arranged in a holder in 11 replicate rows as a 6×11 array. Multilevel performance testing of polymeric arrays was done in a borosilicate-filtered Xe-arc Weatherometer (Atlas Ci4000, 0.75 W m^{-2} irradiance at 340 nm). The exposure dose ranged from 18.9 to 1030 kJ m^{-2} (at 340 nm) and was produced by unmasking certain arrays of six polymer compositions at predetermined time points.

Fluorescence imaging was done with a cooled CCD camera (Roper Scientific) through a 420 nm cutoff long-pass filter. Excitation was provided by a 450-W Xe arc lamp and a 340 nm interference filter. Fluorescence spectroscopic measurements were performed by using a custom-built automatic modular system (Xe arc lamp, monochromator, bifurcated fiber-optic reflection probe, spectrograph, X–Y translation stage). Reference measurements of color and gloss were performed on MacBeth 7000 and BYK-Gardner Micro Trigloss instruments, respectively. Minimal exposures for color and gloss measurements were 250–500 kJ m^{-2} (100–200 h) and 800–1000 kJ m^{-2} (320–400 h), respectively.

Received: April 29, 2002
Revised: September 3, 2002 [Z19189]

[1] a) B. Jandeleit, D. J. Schaefer, T. S. Powers, H. W. Turner, W. H. Weinberg, *Angew. Chem.* **1999**, *111*, 2648; *Angew. Chem. Int. Ed.* **1999**, *38*, 2494; b) "Combinatorial Approaches to Materials Development": *ACS Symp. Ser.* **2002**, *814*; c) "Combinatorial and Arficial Intelligence Methods in Materials Science": *MRS Symp. Proc.* **2002**, *700*.

[2] Examples of measured properties of reaction components and final products in combinatorial libraries: a) catalytic properties, A. Holzwarth, H.-W. Schmidt, W. Maier, *Angew. Chem.* **1998**, *110*, 2788; *Angew. Chem. Int. Ed.* **1998**, *37*, 2644; H. Su, E. S. Yeung, *J. Am. Chem. Soc.* **2000**, *122*, 7422; b) polymer molecular weight, S. Brocchini, K. James, V. Tangpasuthadol, J. Kohn, *J. Am. Chem. Soc.* **1997**, *119*, 4553; c) thin-film dewetting, J. C. Meredith, A. P. Smith, A. Karim, E. J. Amis, *Macromolecules* **2000**, *33*, 9747; d) materials resistivity, X.-D. Xiang, X. Sun, G. Briceño, Y. Lou, K.-A. Wang, H. Chang, W. G. Wallace-Freedman, S.-W. Chen, P. G. Schultz, *Science* **1995**, *268*, 1738; e) mechanical properties, J.-C. Zhao, *Adv. Eng. Mater.* **2001**, *3*, 143.

[3] Examples of high-throughput performance testing: a) R. A. Potyrailo, D. R. Olson, B. J. Chisholm, M. J. Brennan, J. P. Lemmon, J. N. Cawse, W. P. Flanagan, R. E. Shaffer, T. K. Leib, Pittcon 2001 (New Orleans, LA), **2001**, paper 992; b) C. Meredith, J.-L. Sormana, A. Tona, H. Elgendy, A. Karim, E. Amis, *Polym. Prepr. Am. Chem. Soc. Div. Polym. Chem.* **2001**, *42*, 649 – 650; c) J. W. Gilman, COMBI 2002 (San Diego, CA), **2002**.

[4] G. Wypych, *Handbook of Material Weathering*, ChemTec, Toronto, **1995**.

[5] J. E. Pickett, K. K. Webb, *Makromol.Chem.* **1997**, *252*, 217.

[6] Loss of appearance in engineering thermoplastic materials is observed much earlier than changes in physical, solution, and mechanical properties. See: A. Davis, D. Sims, *Weathering of Polymers*, Elsevier, London, **1986**.

[7] J. E. Pickett, *Polym. Prepr. Am. Chem. Soc. Div. Polym. Chem.* **2001**, *42*, 424.

[8] a) *Plastics and Coatings. Durability, Stabilization, Testing* (Ed.: R. A. Ryntz), Hanser, Cincinnati, **2001**; b) H. Zweifel, *Plastics Additives Handbook*, Hanser, Munich, **2001**.

[9] J. E. Pickett, J. E. Moore, *Makromol.Chem.* **1995**, *232*, 229.

[10] V. D. Sherbondy in *Paint and Coating Testing Manual* (Ed.: J. V. Koleske), ASTM, Philadelphia, **1995**, chap. 53.

[11] V. Shah, *Handbook of Plastics Testing Technology*, Wiley, New York, **1998**.

[12] H. Shah, I. B. Rufus, C. E. Hoyle, *Macromolecules* **1994**, *27*, 553.

[13] For exposure time and dose, see the Supporting Information.

[14] Mechanisms of color formation in engineering aromatic thermoplastics upon weathering are complex and still are poorly understood. Suggested mechanisms include oxidation of aromatic rings of polymers, side chain oxidation, and others. See: A. Factor in *Polymer*

 © 2002 WILEY-VCH Verlag GmbH & Co. KGaA, Weinheim 0044-8249/02/4122-4232 $ 20.00+.50/0

Durability. Degradation, Stabilization, and Lifetime Prediction (Eds.: R. L. Clough, N. C. Billingham, K. T. Gillen), ACS, Washington, DC, **1996**, pp. 59–76 (*Adv. Chem. 249*).

[15] N. D. Searle, N. L. Maecker, L. F. E. Crewdson, *J. Polym. Sci. A* **1989**, *27*, 1341.

[16] Excitation and emission spectra of TiO_2- and CB-PBT showed only an exposure-dependent intensity increase, while TiO_2- and CB-PC and PC-PBT showed also distortions and shifts of excitation and emission spectral bands. This suggested that upon weathering the number of different types of generated fluorescent chromophores was roughly constant in PBT and was increasing in PC. For fluorescence spectra, see the Supporting Information.

[17] Calculated for the signal-to-noise ratio of three, see: J. D. Ingle, Jr., S. R. Crouch, *Spectrochemical Analysis*, Prentice Hall, Englewood Cliffs, NJ, **1988**.

[18] For additional experiments exploring further improvement of the screening throughput, see the Supporting Information.

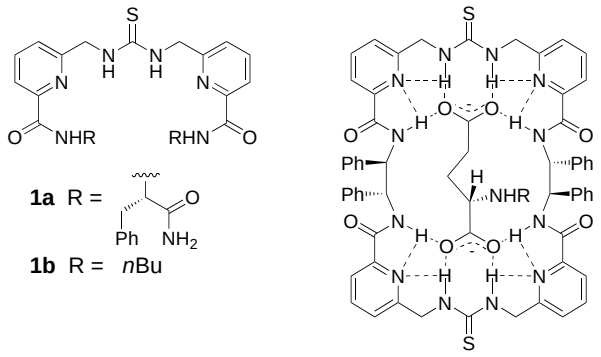
[19] Measurements of polymer fluorescence can be applicable for a variety of aromatic and other types of polymers during weathering testing. If fluorescent additives or initial impurities in polymers present a problem, molecular probes for analysis of surface oxidation products may be more applicable. See: S. R. Holmes-Farley, G. M. Whitesides, *Langmuir* **1986**, *2*, 266; V. B. Ivanov, J. Behnisch, A. Hollaender, F. Mehdorn, H. Zimmermann, *Surf. Interface Anal.* **1996**, *24*, 257.

A Highly Enantioselective Receptor for *N*-Protected Glutamate and Anomalous Solvent-Dependent Binding Properties**

Sara Rossi, Graham M. Kyne, David L. Turner, Neil J. Wells, and Jeremy D. Kilburn*

The development of enantioselective receptors continues to be a challenging endeavor for supramolecular chemists, and enantioselective recognition of biologically relevant molecules in competitive solvents is particularly demanding.[1] Although numerous receptors have been developed for dicarboxylic acids and dicarboxylates,[2] only a few enantioselective receptors for chiral dicarboxylic acids (in the neutral diprotonated form) have been described,[3] and very few examples of enantioselective receptors for chiral dicarboxylates have been reported.[4]

We recently described an acyclic monothiourea receptor **1a**, which bound a range of *N*-protected amino acid carboxylate salts with modest enantioselectivity.[5] Building on this work, we have now prepared macrocyclic receptor **2**, which features two thiourea moieties flanked by carboxypyridines and separated by a chiral diamine. The receptor was designed to produce a chiral pocket for dicarboxylates by forming up to eight hydrogen-bonding interactions with the carboxylate oxygen atoms and intramolecular hydrogen bonding with the pyridine unit to help preorganize[6] the receptor (Scheme 1). Binding measurements, by NMR titration and isothermal

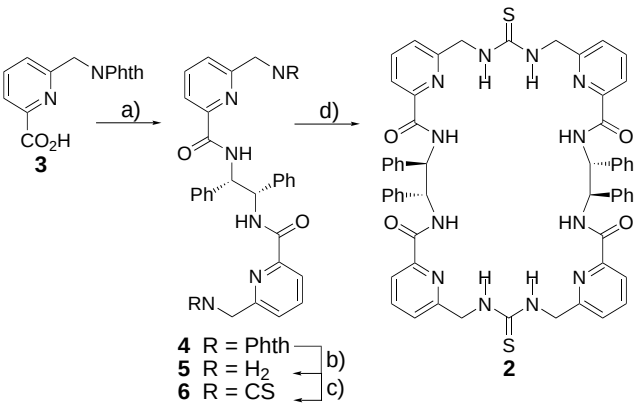


Scheme 1. Acyclic monothiourea **1** and the proposed complex of *N*-Boc-L-glutamate with macrocycle **2**. Boc = *tert*-butoxycarbonyl.

calorimetry, indicate that the macrocycle exhibits strong and highly enantioselective 1:1 binding of *N*-Boc-L-glutamate (as the dicarboxylate dianion) in relatively polar solvents (CH_3CN, DMSO) and that complexation involves a large, favorable entropic contribution. Remarkably, however, no binding of *N*-Boc-glutamate by the macrocycle is observed in a less polar solvent ($CDCl_3$).

The synthesis of receptor **2** was readily achieved by coupling acid **3**[5] with (*S*,*S*)-1,2-diphenylethylenediamine to give bisphthalimide **4** (Scheme 2). Removal of the phthalimide protecting groups and treatment of the resulting bisamine **5** with CS_2 and DCC produced the bis(isothiocyanate) **6**. A further equivalent of bisamine **5** was added to bisisothiocyanate **6**, in the presence of DMAP, by syringe pump over three hours to yield the macrocyclic bisthiourea **2** in 26% yield.

The ^1H NMR spectrum[7] of macrocycle **2** in $CDCl_3$ at room temperature is poorly resolved, with very broad signals for all protons, and resolution is not improved at higher temper-



Scheme 2. Reagents: a) $SOCl_2$; (1*S*,2*S*)-(−)-1,2-diphenylethylenediamine, DMAP, CH_2Cl_2 (68%); b) $N_2H_4 \cdot H_2O$, EtOH (84%); c) CS_2, DCC, CH_2Cl_2; d) simultaneous addition of 1 equiv of **5** and 1 equiv of **6** by syringe pumps over 3 h (26% over steps c and d). DMAP = 4-dimethylaminopyridine, DCC = *N*,*N*′-dicyclohexylcarbodiimide.

[*] Prof. J. D. Kilburn, S. Rossi, G. M. Kyne, Dr. D. L. Turner, N. J. Wells
Department of Chemistry
University of Southampton
Southampton, SO17 1BJ (UK)
Fax: (+44) 2380-596-805
E-mail: jdk1@soton.ac.uk

[**] We thank the Commission of the European Union (TMR Network grant "Enantioselective Separations" ERB FMRX-CT-98-0233) for financial support and postgraduate fellowships (S.R.) and the EPSRC for a quota studentship (G.M.K.).

Supporting information for this article is available on the WWW under http://www.angewandte.org or from the author.

 © 2002 WILEY-VCH Verlag GmbH & Co. KGaA, Weinheim 0044-8249/02/4122-4233 $ 20.00+.50/0

atures. At −40 °C, however, a well-resolved spectrum is obtained, but it is not the simple spectrum expected, given the fourfold D_2 symmetry of the macrocycle. The spectrum instead indicates twofold C_2 symmetry. In particular, the thiourea NH protons give signals at $\delta = 8.96$ and 8.08 ppm and the amide NH protons give signals at $\delta = 10.10$ and 7.88 ppm.[7] A well-resolved and simple ^{1}H NMR spectrum is obtained in [D$_6$]DMSO or CD_3CN, however, which is consistent with the expected fourfold D_2 symmetry of the macrocycle.

Binding studies[7] with macrocycle **2** were carried out with the bis(tetrabutylammonium) salts of the enantiomers of *N*-Boc-glutamate in a range of solvents, by using standard NMR titration experiments[8] and isothermal calorimetry.[9,10] The addition of the *N*-Boc-L-glutamate salt to a solution of **2** in CD_3CN led to significant downfield shifts of the thiourea NH ($\Delta\delta_{max} = 1.43$ ppm), the amide NH ($\Delta\delta_{max} = 1.06$ ppm), and the benzylic CH signals ($\Delta\delta_{max} = 0.59$), which is consistent with the formation of strong hydrogen bonds and the proposed mode of binding (Scheme 1). The binding data could be readily fitted to a 1:1 binding isotherm and gave $K_a^{1:1} > 10^4\,\text{M}^{-1}$.[11] Addition of the *N*-Boc-D-glutamate salt also led to significant downfield shifts of the NH and the benzylic CH signals. The binding data, however, could not be fitted to a 1:1 binding isotherm, but instead could be fitted to a 1:2 (host:guest) isotherm and yielded $K_a^{1:2} > 10^4\,\text{M}^{-1}$. The binding stoichiometry was confirmed by Job plots[7,12] and is further evident from the ^{1}H NMR titrations, since saturation is rapidly reached after addition of approximately one equivalent of the *N*-Boc-L-glutamate salt, whereas saturation is reached only after addition of approximately two equivalents of the *N*-Boc-D-glutamate salt (Figure 1). The relatively smooth titration curve obtained with *N*-Boc-D-glutamate, and the lack of a clear transition after addition of only one equivalent of the guest, suggests that binding of the second guest molecule is stronger than the binding of the first (positive cooperativity), such that the receptor tends to saturate both binding sites simultaneously, that is, the 1:1 complex is only present in very small amounts relative to the uncomplexed receptor or the 1:2 complex.

The calorimetric binding data[13] obtained with the *N*-Boc-L-glutamate salt as the guest confirmed the strong 1:1 binding ($K_a^{1:1} = (2.83 \pm 0.48) \times 10^4\,\text{M}^{-1}$, $\Delta G_a^{1:1} = -25.5 \pm 0.5\,\text{kJ mol}^{-1}$) which is dominated by the entropic contribution ($\Delta H_a^{1:1} = -4.5 \pm 0.2\,\text{kJ mol}^{-1}$, $T\Delta S_a^{1:1} = 21.0\,\text{kJ mol}^{-1}$). The calorimetric binding data obtained with the *N*-Boc-D-glutamate salt, using a two-site binding model, yielded a small 1:1 binding constant ($K_a^{1:1} = 38.4 \pm 1.66\,\text{M}^{-1}$, $\Delta G_a^{1:1} = -9.0 \pm 0.1\,\text{kJ mol}^{-1}$) and a large 1:2 (host:guest) binding constant ($K_a^{1:2} = (4.92 \pm 0.07) \times 10^4\,\text{M}^{-1}$, $\Delta G_a^{1:2} = -26.8 \pm 0.1\,\text{kJ mol}^{-1}$), which again is dominated by the entropic contribution ($\Delta H_a^{1:2} = -6.7 \pm 0.1\,\text{kJ mol}^{-1}$, $T\Delta S_a^{1:2} = 20.1\,\text{kJ mol}^{-1}$). This data confirms the stronger binding of the second *N*-Boc-D-glutamate guest relative to the first (positive cooperativity), as indicated by the NMR titration data, and suggests that the enantioselectivity exhibited by macrocycle **2** for the 1:1 binding of the *N*-Boc-glutamates is >700:1.

Binding studies with the *N*-Boc-L-glutamate salt in [D$_6$]DMSO give a similar picture, with significant downfield shifts of the NH signals observed on NMR titration and simple 1:1 binding, obtained by either NMR titration ($K_a^{1:1} = 3720\,\text{M}^{-1}$, $\Delta G_a^{1:1} = -20.4\,\text{kJ mol}^{-1}$) or isothermal calorimetry ($K_a^{1:1} = 2280 \pm 258\,\text{M}^{-1}$, $\Delta G_a^{1:1} = -19.2 \pm 0.3\,\text{kJ mol}^{-1}$), again with a large entropic contribution ($\Delta H_a^{1:1} = -10.7 \pm 0.3\,\text{kJ mol}^{-1}$, $T\Delta S_a^{1:1} = -8.5\,\text{kJ mol}^{-1}$). However, the binding data obtained with the *N*-Boc-D-glutamate salt in [D$_6$]DMSO deviates from the saturation curves expected for simple 1:1 or 1:2 binding, and reliable binding constants could not be obtained. Presumably several binding equilibria (1:2, 2:1, and possibly 2:2) are competing when the *N*-Boc-D-glutamate salt is the guest, although the NMR titration binding curve approaches saturation after addition of approximately two equivalents of guest, which indicates that a 1:2 (host:guest) binding stoichiometry is dominant.[7]

In the less competitive solvent, $CDCl_3$, addition of either enantiomer of the glutamate salt did not lead to any discernible change in the ^{1}H NMR spectrum of the macrocycle either at −40 °C or at room temperature. No change was observed even after warming the solution for several days. A 1:1 sample of macrocycle **2** and *N*-Boc-L-glutamate salt was also dissolved in CD_3CN (to allow formation of the 1:1

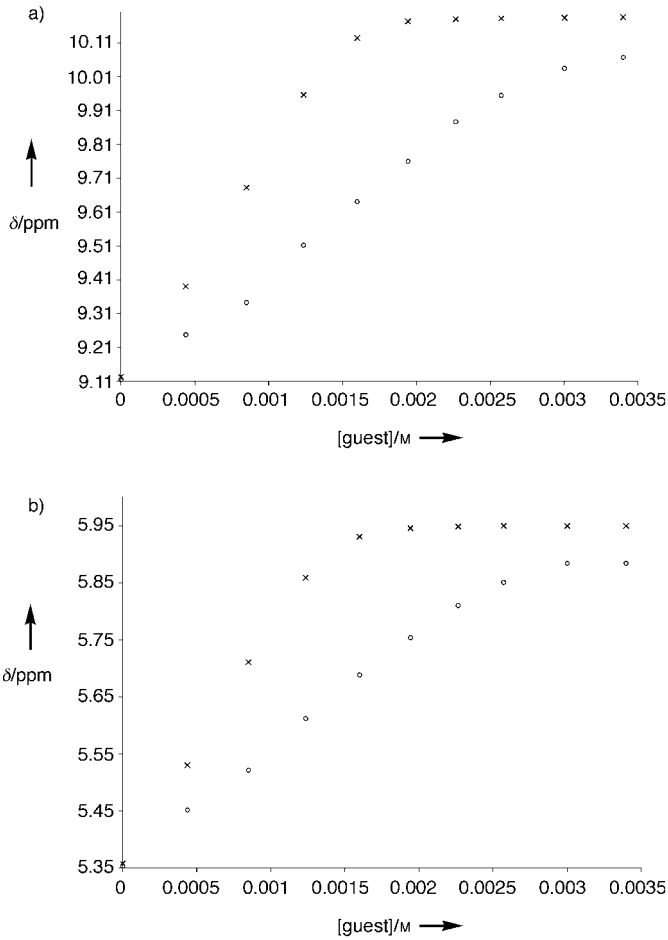


Figure 1. Binding titration curves for macrocycle **2** showing the shift of a) the amide and b) the benzylic CH protons on addition of the bis(tetrabutylammonium) salts of *N*-Boc-L-glutamate (×) and *N*-Boc-D-glutamate (○) in CD_3CN. The graphs indicate the strong 1:1 binding with the former, and 1:2 binding with the latter (the 1:1 [host]:[guest] is reached when [guest] = 1.5 mM).

 © 2002 WILEY-VCH Verlag GmbH & Co. KGaA, Weinheim 0044-8249/02/4122-4234 $ 20.00+.50/0

complex), the solvent removed, and redissolved in $CDCl_3$. The resulting ^1H NMR spectrum again showed unperturbed macrocycle. Thus, it is clear that macrocycle **2** does not bind the glutamate guests in the less polar solvent ($CDCl_3$), and it is improbable that this is because of slow binding kinetics.

It is a generally held view that binding interactions (for example, hydrogen bonds) between polar functionalities will lead to strong complexation in a nonpolar solvent (typically $CHCl_3$), but to weak (or negligible) complexation in more polar (competitive) solvents or solvent mixtures, and numerous examples of this phenomenon exist. For example, *N*-tolyl-*N*′-*n*-butylurea binds tetrabutylammonium benzoate with $K_a = 1300\,M^{-1}$ in $CDCl_3$ and $K_a = 150\,M^{-1}$ in [D_6]DMSO,[14] and thiourea **1a** binds the tetrabutylammonium salt of *N*-Ac-L-Phe with $K_a = 4800\,M^{-1}$ in $CDCl_3$ and $K_a = 680\,M^{-1}$ in 10% [D_6]DMSO/$CDCl_3$.[5]

The lack of binding exhibited by macrocycle **2** in $CDCl_3$, in contrast to the results observed in CH_3CN and DMSO, is thus remarkable. To probe the origin of this anomalous behavior the conformation of the macrocycle in $CDCl_3$ solution was established using torsion angle dynamics with NOE and scalar coupling constant constraints.[15] The NMR studies reveal that in $CDCl_3$ the macrocycle adopts a tightly wrapped conformation that is stabilized by a number of intramolecular hydrogen bonds, particularly from an amide carbonyl oxygen atom to the thiourea NH and adjacent amide NH protons (Figure 2). This hydrogen-bonding motif has been previously observed in the crystal structure of **1b** which forms a dimeric pair in the solid state.[5]

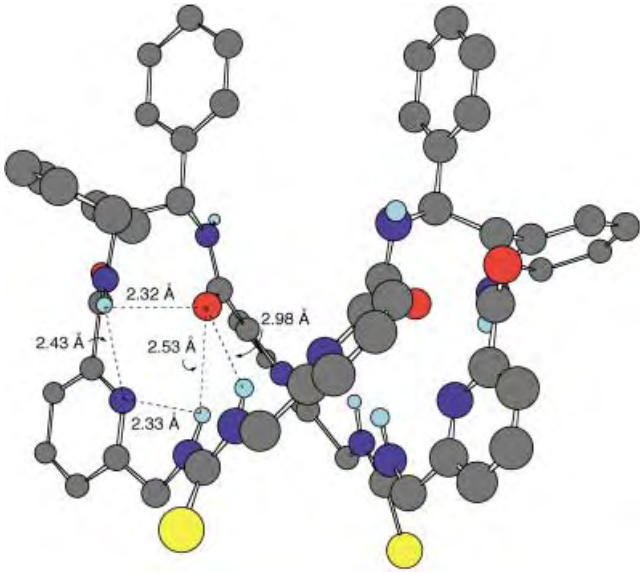


Figure 2. Conformation of macrocycle **2** in $CDCl_3$ as determined by ^1H NMR spectroscopy showing intramolecular H-bonding distances.

Clearly the energy required to reorganize the macrocycle into a suitable binding conformation (that is, to break the intramolecular hydrogen bonds) is not compensated for by binding interactions that would thereby be established. The more polar solvents, CH_3CN and DMSO, can solvate the hydrogen-bonding functionality of the macrocycle leading to a less rigidly constrained molecule and the ^1H NMR spectra which reflect the fourfold D_2 symmetry of the molecule in these solvents. Solvation of the macrocycle by the more polar solvents allows tight binding of the *N*-Boc-L-glutamate salt—albeit with some conformational reorganization of the receptor (and associated energetic cost), as evidenced by the large shifts of various CH signals in the ^1H NMR spectrum on addition of the guest. Binding, in these solvents, is driven to a large extent by entropy, presumably produced by releasing bound solvent molecules from the cavity of the macrocycle. The same cavity is unable to accommodate the enantiomeric guest (*N*-Boc-D-glutamate) in a simple 1:1 binding mode, and instead binds two *N*-Boc-D-glutamate guests with a small binding constant for the first glutamate anion and a significantly larger binding constant for the second (positive cooperativity). At first sight this may seem surprising. However, the two carboxylate guests may bind on opposite faces and at opposite ends of the macrocycle, in which case the electrostatic repulsion between the two guests should be small. Furthermore, if binding of the first *N*-Boc-D-glutamate requires considerable reorganization of the receptor, and consequent energetic cost, then, once the first carboxylate is bound, the receptor may bind the second carboxylate without significant additional energetic penalty. Conformational changes in the receptor on binding *N*-Boc-D-glutamate in acetonitrile are, again, clearly evidenced by the large shifts in many of the CH signals in the ^1H NMR spectrum of the receptor (particularly the benzylic CH signals ($\Delta\delta = 0.53$ ppm)) on addition of *N*-Boc-D-glutamate.

In summary macrocycle **2** is highly enantioselective for the 1:1 binding of the *N*-protected glutamate dianion, but the binding shows anomalous solvent-dependent behavior. We are now developing analogous receptors incorporating recognition elements for the ammonium group to produce enantioselective receptors, and hence sensors, for zwitterionic glutamate.

Received: May 16, 2002 [Z19311]

[1] For a review on enantioselective recognition, see C. S. Wilcox, *Chem. Soc. Rev.* **1993**, 383; for a recent review on synthetic receptors, see J. H. Hartley, T. D. James, C. J. Ward, *J. Chem. Soc. Perkin Trans. 1* **2000**, 3155.

[2] For a review of carboxylate/carboxylic acid recognition, see R. J. Fitzmaurice, G. M. Kyne, D. Douheret, J. D. Kilburn, *J. Chem. Soc. Perkin Trans. 1* **2002**, 841.

[3] a) F. Garcia-Tellado, J. Albert, A. D. Hamilton, *Chem. Commun.* **1991**, 1761; b) V. A. Montero, L. Tomlinson, K. N. Houk, F. Diederich, *Tetrahedron Lett.* **1991**, *32*, 5309; c) V. Alcazar, F. Diederich, *Angew. Chem.* **1992**, *104*, 1503; *Angew. Chem. Int. Ed.* **1992**, *31*, 1521; d) R. J. Pieters, F. Diederich, *Chem. Commun.* **1996**, 2255; e) R. J. Pieters, J. Cuntze, M. Bonnet, F. Diederich, *J. Chem. Soc. Perkin Trans. 2* **1997**, 1891; f) J. Cuntze, F. Diederich, *Helv. Chim. Acta.* **1997**, 897; g) P. Lustenberger, E. Martinborough, T. M. Denti, F. Diederich, *J. Chem. Soc. Perkin Trans. 1* **1998**, 747; h) J. V. Hernandez, M. Almaraz, C. Raposo, M. Martin, A. Lithgow, M. Crego, C. Caballero, J. R. Moran, *Tetrahedron Lett.* **1998**, *39*, 7401; i) S. Goswami, K. Ghosh, S. Dasgupta, *J. Org. Chem.* **2000**, *65*, 1907.

[4] a) J. L. Sessler, A. Andrievsky, V. Král, V. Lynch, *J. Am. Chem. Soc.* **1997**, *119*, 9385; b) I. Alfonso, B. Dietrich, F. Robolledo, V. Gotor, J. M. Lehn. *Helv. Chim. Acta* **2001**, *84*, 280.

[5] G. M. Kyne, M. E. Light, M. B. Hursthouse, J. de Mendoza, J. D. Kilburn, *J. Chem. Soc. Perkin Trans. 1* **2001**, 1258.

[6] C. A. Hunter, D. H. Purvis, *Angew. Chem.* **1992**, *104*, 779; *Angew. Chem. Int. Ed.* **1992**, *31*, 792. See also ref [5].

 © 2002 WILEY-VCH Verlag GmbH & Co. KGaA, Weinheim 0044-8249/02/4122-4235 $ 20.00+.50/0

[7] Copies of the NMR spectra recorded in $CDCl_3$ and $[D_6]$DMSO, all binding data from NMR titration and isothermal calorimetry experiments, and Job plots are provided in the Supporting Information.
[8] The binding constants were calculated by fitting the data using NMRTit HG software, kindly provided by Prof. C. A. Hunter, University of Sheffield. See: A. P. Bisson, C. A. Hunter, J. C. Morales, K. Young, *Chem. Eur. J.* **1998**, *4*, 845.
[9] A. Cooper, *Curr. Opin. Chem. Biol.* **1999**, *3*, 557, and references therein.
[10] For the specific application of isothermal calorimetry to dicarboxylate recognition, see a) B. R. Linton, M. S. Goodman, E. Fan, S. A. van Arman, A. D. Hamilton, *J. Org. Chem.* **2001**, *66*, 7313. See also, for example, b) F. P. Schmidtchen, *Org. Lett.* **2002**, *4*, 431; c) B. Linton, A. D. Hamilton, *Tetrahedron* **1999**, *55*, 6027.
[11] The data give binding constants at the upper limit of detectability by NMR titrations (10^4–$10^5\,M^{-1}$) and it can be concluded that $K_a > 10^4\,M^{-1}$, but more precise values cannot be reliably obtained from the NMR titration data: a) L. Fielding, *Tetrahedron* **2000**, *56*, 6151; b) C. S. Wilcox, *Frontiers in Supramolecular Organic Chemistry and Photochemistry* (Eds.: H.-J. Schneider, H. Dürr), VCH, Weinheim, **1991**, p. 123; c) G. Weber, S. R. Anderson, *Biochemistry* **1965**, *4*, 1942. See also the Supporting Information.
[12] K. A. Connors, *Binding Constants*, Wiley, New York, **1987**.
[13] The ITC data was obtained with a MicroCal VP-ITC isothermal calorimeter. Data was analyzed by nonlinear least-squares fitting using the Origin software supplied by MicroCal: T Wiseman, S. Williston, J. F. Brandts, L.-N. Lin, *Anal. Biochem.* **1989**, *179*, 131. Data was modeled using the 1:1 binding site model, or the model with two independent binding sites in cases where the data could not be fitted with the 1:1 binding site model (see ref. [10c])
[14] T. R. Kelly, M. H. Kim, *J. Am. Chem. Soc.* **1994**, *116*, 7072.
[15] a) P. Güntert, C. Mumenthaler, K. Wüthrich, *J. Mol. Biol.* **1997**, *273*, 283; L. Brennan, D. L. Turner, A. C. Messias, M. L. Teodoro, J. LeGall, H. Santos, A. V. Xavier, *J. Mol. Biol.* **2000**, *298*, 61. Full details of experimental methods are provided in the Supporting Information.

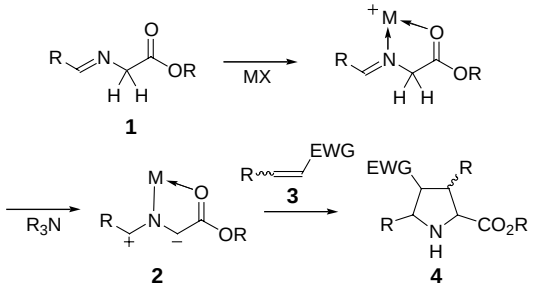
Catalytic Asymmetric 1,3-Dipolar Cycloaddition Reactions of Azomethine Ylides—A Simple Approach to Optically Active Highly Functionalized Proline Derivatives**

Aase Sejr Gothelf, Kurt V. Gothelf, Rita G. Hazell, and Karl Anker Jørgensen*

The 1,3-dipolar cycloaddition reaction constitutes one of the most fundamental reactions for the stereoselective construction of five-membered heterocyclic compounds.[1] In recent years, the development of catalytic asymmetric reactions has been one of the challenging areas within the field of 1,3-dipolar cycloaddition reactions, and especially nitrones have been the focus of attention[2,3] as a result of the importance of the formed isoxazolidines as building blocks for more complex molecules.

Azomethine ylides can react in a 1,3-dipolar cycloaddition reaction with alkenes to form pyrrolidines, and several examples of the formation of optically active pyrrolidines based on diastereoselective reactions are known.[4,5] However, investigations on the metal-catalyzed enantioselective version of the 1,3-dipolar cycloaddition of azomethine ylides with alkenes are very limited. Grigg and co-workers[6] were the first to demonstrate that applying a stoichiometric amount of chiral cobalt or manganese complexes with ephedrine derivatives as the chiral ligand could give the cycloaddition product of azomethine ylides derived from imines of glycine alkyl esters with up to 96% *ee*. It has also been mentioned that silver(I) salts in combination with chiral phosphane ligands can catalyze the 1,3-dipolar cycloaddition reaction of azomethine ylides.[6b,7]

We present herein a new highly diastereo- and enantioselective 1,3-dipolar cycloaddition reaction of azomethine ylides with alkenes catalyzed by readily available chiral Lewis acids. Although there are few stable azomethine ylides,[8] most are unstable. Azomethine ylides **2** can be generated from, for example, imines of glycine alkyl esters **1** by reaction with a base in the presence of a Lewis acid complex. The metal-stabilized azomethine ylide **2** reacts with an alkene **3** to give highly functionalized pyrrolidines **4** (Scheme 1).



Scheme 1. Formation of highly functionalized pyrrolidines **4** from azomethine ylides **2** and alkenes **3**. EWG = electron-withdrawing group.

The reactions of *N*-benzylidene- and *N*-(2-naphthylmethylidene) glycinates **1a** and **1b**, respectively, with methyl acrylate (**3a**) and Et_3N as the base in the presence of chiral ligands such as the bisoxazolines (BOX) **5a**,**b**[9] and dibenzofuranyl-2,2′-bisoxazoline (DBFOX) **5c**[10] and Lewis acids were used in the screening process (Scheme 2). Some representative results are listed in Table 1.

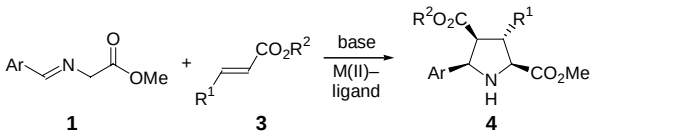
The use of copper(II) salts in combination with the chiral bisoxazoline ligands **5a**,**b** as catalysts for the reaction of *N*-benzylidene glycinate **1a** with methyl acrylate (**3a**) gave high conversion only when using the (*S*)-*t*Bu-BOX (**5a**) ligand, but unfortunately product **4a** was formed as a racemate (Table 1, entries 1 and 2). When zinc(II)[9e] was used as the Lewis acid instead, the reaction proceeded smoothly and **4a** was formed with 76% *ee* using **5a** as the chiral ligand and THF as the solvent at room temperature (Table 1, entry 3). Furthermore, the reaction is also highly diastereoselective as only one

[*] Prof. Dr. K. A. Jørgensen, A. S. Gothelf, Dr. K. V. Gothelf, Dr. R. G. Hazell
Danish National Research Foundation: Center for Catalysis
Department of Chemistry, Aarhus University
8000 Aarhus C (Denmark)
Fax: (+45) 8619–6199
E-mail: kaj@chem.au.dk

[**] We wish to expressed our gratitude to The Danish National Research Foundation for financial support.

Supporting information for this article is available on the WWW under http://www.angewandte.org or from the author.

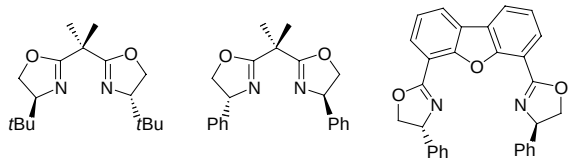
 © 2002 WILEY-VCH Verlag GmbH & Co. KGaA, Weinheim 0044-8249/02/4122-4236 $ 20.00+.50/0



1
a: Ar = Ph
b: Ar = 2-Np
c: Ar = *p*-BrC_6H_4

3
a: R^1 = H, R^2 = Me
b: R^1 = H, R^2 = Et
c: R^1 = H, R^2 = *t*Bu
d: R^1 = CO_2Me, R^2 = Me

4
a: Ar = Ph, R^1 = H, R^2 = Me
b: Ar = 2-Np, R^1 = H, R^2 = Me
c: Ar = 2-Np, R^1 = H, R^2 = Et
d: Ar = 2-Np, R^1 = H, R^2 = *t*Bu
e: Ar = *p*-BrC_6H_4, R^1 = H, R^2 = Me
f: Ar = Ph, R^1 = CO_2Me, R^2 = Me
g: Ar = 2-Np, R^1 = CO_2Me, R^2 = Me
h: Ar = *p*-BrC_6H_4, R^1 = CO_2Me, R^2 = Me



5a: (*S*)-*t*-Bu-BOX **5b**: (*R*)-Ph-BOX **5c**: (*R,R*)-Ph-DBFOX

Scheme 2. Chiral ligands **5a–c** used in the preparation of optically active pyrrolidines **4**.

Table 1. Representative results for the screening of reaction conditions for the catalytic enantioselective 1,3-dipolar cycloaddition reaction of *N*-benzylidene and *N*-(2-naphthylmethylidene) glycinate **1a**,**b** with methyl acrylate **3a**.[a]

Entry	Lewis acid	Ligand	Solvent	**1**	Conversion[b] (%)	*ee*[c] [%]
1	$Cu(OTf)_2$	**5a**	THF	**a**	**4a** (>95)	rac
2	$Cu(OTf)_2$	**5b**	THF	**a**	**4a** (<10)	n.d.[d]
3	$Zn(OTf)_2$	**5a**	THF	**a**	**4a** (>95)	78
4	$Zn(OTf)_2$	**5a**	neat	**a**	**4a** (>95)	79
5	$Zn(OTf)_2$	**5b**	THF	**a**	**4a** (<50)	n.d.[d]
6	$Zn(OTf)_2$	**5a**	THF	**b**	**4b** (>95)	78
7	$Zn(OTf)_2$	**5a**	neat	**b**	**4b** (>95)	76
8	$Zn(OTf)_2$	**5b**	neat	**b**	**4b** (>95)	17
9	$Zn(OTf)_2$	**5c**	neat	**b**	**4b** (>95)	7

[a] Lewis acid, ligand, and Et_3N (10 mol% each) were used. For experimental details, see Supporting Information. [b] Conversion determined by crude ^1H NMR spectroscopy. [c] Enantiomeric excesses were measured by chiral HPLC. [d] Not detected.

diastereomer of **4a** was observed by ^1H NMR spectroscopy. The same trends are found for *N*-(2-naphthylmethylidene) glycinate **1b** in the presence of Zn^{II}-*t*Bu-BOX (Table 1, entries 6 and 7), whereas the use of the Zn^{II}-Ph-BOX and Zn^{II}-Ph-DBFOX catalysts in the absence of solvent gave **4b** with low enantiomeric excess (Table 1, entries 8 and 9).

The reaction of *N*-(2-naphthylmethylidene) glycinate **1b** with methyl acrylate (**3a**) and Et_3N as the base catalyzed by Zn^{II}-*t*Bu-BOX was studied in different solvents. In less polar solvents such as Et_2O and toluene in which **1b** has a low solubility, the enantiomeric excess of **4b** was decreased to 23 and 25% *ee*, respectively, although complete conversion and diastereoselectivity was observed. In solvents such as CH_2Cl_2 and MeCN, the enantiomeric excess of **4b** was only slightly lower (65 and 62% *ee*) than in reactions performed in THF.

The influence of the amount of base on the enantiomeric excess of the reaction of **1b** with **3a** catalyzed by Zn^{II}-*t*Bu-BOX (10 mol%) in THF at room temperature was investigated. The addition of Et_3N (5–20 mol% relative to the azomethine ylide) showed that the enantioselectivity of **4b** was independent of the amount of base used, as *ee* values of 78–80% were found for all the reactions studied.

The potential of this new catalytic enantioselective 1,3-dipolar cycloaddition reaction of azomethine ylides with alkenes is demonstrated in the reactions of a series of imines of glycine methyl ester **1a-d** with different electron-deficient alkenes **3a–d** catalyzed by Zn^{II}-*t*Bu-BOX (Scheme 2). The results are presented in Table 2.

Table 2. Catalytic enantioselective 1,3-dipolar cycloaddition reaction of **1a–d** with various alkenes **3a–d** in the presence of Zn^{II}-*t*Bu-BOX (10 mol%) as catalyst in THF.[a]

Entry	Azomethine ylide	Dienophile	Yield[b] (%)	*ee*[c] [%]
1	**1a**	**3a**	**4a** (>95[d])	78
2[e]	**1a**	**3a**	**4a** (80)	88
3	**1b**	**3a**	**4b** (93)	78
4[e]	**1b**	**3a**	**4b** (84)	91
5[e,f]	**1b**	**3a**	**4b** (86)	87
6	**1b**	**3b**	**4c** (76)	68
7	**1b**	**3c**	**4d** (12)	<5
8	**1c**	**3a**	**4e** (89)	61
9[e]	**1c**	**3a**	**4e** (89)	94
10[e]	**1a**	**3d**	**4f** (78)	76
11	**1b**	**3d**	**4g** (84)	90
12	**1c**	**3d**	**4h** (87)	68

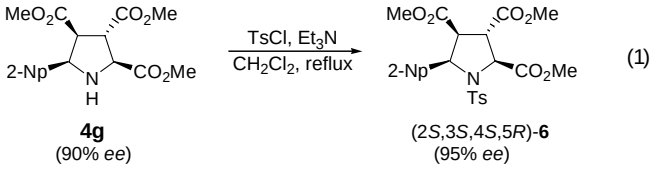
[a] $Zn(OTf)_2$-*t*Bu-BOX and Et_3N (10 mol% each) were used. For experimental details, see Supporting Information. [b] Yield of isolated product. [c] Determined by chiral HPLC. [d] Conversion based on ^1H NMR spectroscopy. [e] Reaction temperature −20°C. [f] Reaction in the absence of solvent.

The reaction of *N*-benzylidene glycinate **1a** with methyl acrylate (**3a**) proceeds in high yield and only one diastereomer of **4a** is formed at room temperature with 78% *ee* (Table 2, entry 1). Performing the reaction at −20°C leads to an improvement in the enantioselectivity of **4a** to 88% *ee* (Table 2, entry 2). *N*-(2-Naphthylmethylidene) glycinate **1b** was treated with the different acrylates **3a-c** under various reaction conditions. At room temperature, the 1,3-dipolar cycloaddition adduct **4b** was obtained in high yield and as a diastereomerically pure product with 78% *ee* and an improvement in the enantioselectivity to 91% ee was observed at −20°C (Table 2, entries 3,4). The enantiomeric excess of the 1,3-dipolar cycloadducts formed is dependent on the ester substituent of the acrylate used. Ethyl acrylate (**3b**) reacted with **1b** to give the pyrrolidine **4c** in the same high yield and diastereoselectivity as did the methyl acrylate; however, the enantiomeric excess of **4c** dropped to 68% *ee* (Table 2, entry 6). For *tert*-butyl acrylate (**3c**), pyrrolidine **4d** was obtained in only 12% yield with <5% *ee* (Table 2, entry 7). The *p*-bromo-*N*-benzylidene glycinate **1c** reacted smoothly with **3a** in a highly diastereo- and enantioselective reaction with up to 94% *ee* (Table 2, entries 8 and 9). Dimethyl fumarate (**3d**) reacted in a highly diastereo- and enantioselective 1,3-dipolar cycloaddition reaction with the different azomethine ylides **1a–c**. The reaction of **1a** with **3d** gives four new stereogenic centers in the addition step, and in this reaction pyrrolidine **4f** was obtained in high yield and as one diastereomer with 76% *ee* (Table 2, entry 10). The 1,3-dipolar cycloaddition reaction of **1b** with **3d** at −20°C provided **4g**

 © 2002 WILEY-VCH Verlag GmbH & Co. KGaA, Weinheim 0044-8249/02/4122-4237 $ 20.00+.50/0

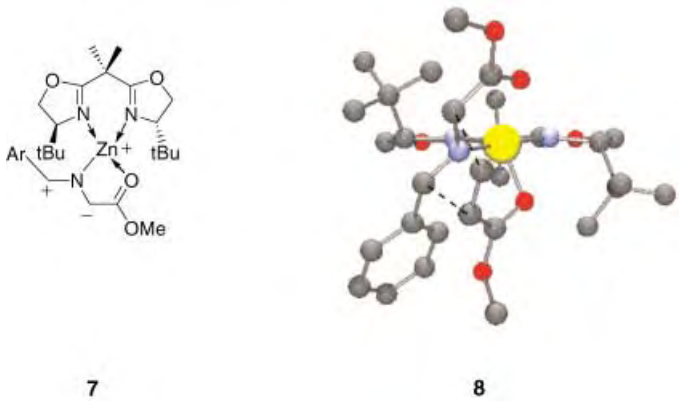
(Table 2, entry 11) in high yield and with excellent enantioselectivity (90% *ee*), whereas the reaction of **1c** gives a slightly lower enantiomeric excess, but the same high yield and diastereoselectivity (Table 2, entry 12).

To determine the absolute configuration of the product of the asymmetric Zn^{II}-*t*Bu-BOX-catalyzed 1,3-dipolar cycloaddition, compound **4g** was converted into **6** by tosylation [Eq. (1)]. An X-ray analysis of crystals of **6** revealed a 2*S*,3*S*,4*S*,5*R* configuration for **6** and therefore also for **4g** (see Supporting Information. CCDC 188992 contains the supplementary crystallographic data for this paper. These data can be obtained free of charge via www.ccdc.cam.ac.uk/conts/retrieving.html (or from the Cambridge Crystallographic Data Centre, 12, Union Road, Cambridge CB21EZ, UK; fax: (+44) 1223-336-033; or deposit@ccdc.cam.ac.uk).).



4g (90% *ee*) (2*S*,3*S*,4*S*,5*R*)-**6** (95% *ee*) (1)

Based on the absolute configuration of **6**, we propose a model for the intermediate in the Zn^{II}-*t*Bu-BOX-catalyzed 1,3-dipolar cycloaddition reactions. This intermediate **7** (Figure 1), which consists of the azomethine ylide coordinating to the Zn^{II}-*t*Bu-BOX catalyst is an 18-electron complex and should, from an electronic point of view, give a tetrahedral arrangement of the ligands around the zinc center.[9d] The tetrahedral conformation would, however, lead to the opposite enantiomer as observed in the reaction. To account for the stereochemical outcome of the reaction, we propose a bipyramidal intermediate **8**, which also involves coordination of the α,β-unsaturated ester carbonyl group to the metal center (Figure 1). This additional coordination activates the α,β-unsaturated ester for reaction with the azomethine ylide, thus leading to the experimentally observed diastereomer and enantiomer of the product. Experimentally, the additional coordination is supported by the fact that acrylonitrile does not undergo reaction with metal-stabilized azomethine ylides, whereas the acrylates **3a–c** do.



7 **8**

Figure 1. Coordination complex **7** (unspecified geometry) consisting of the Zn^{II}-*t*Bu-BOX catalyst and the azomethine ylide, and the proposed bipyramidal intermediate **8**, involving coordination of the α,β-unsaturated ester carbonyl group to the metal center.

In conclusion, we have developed a new catalytic asymmetric 1,3-dipolar cycloaddition reaction of azomethine ylides with alkenes. The reactions are catalyzed by zinc(II) bisoxazolines and proceed in high yield, thus giving diastereomerically pure products with up to 94% *ee*. This reaction provides an easy entry to optically active highly substituted pyrrolidines.

Received: July 5, 2002 [Z19669]

[1] a) *Synthetic Applications of Dipolar Cycloaddition Chemistry towards Heterocyclic and Natural Products* (Eds.: A. Padwa, W. Pearson), Wiley-VCH, Weinheim, **2002**; b) P. A. Wade in *Comprehensive Organic Synthesis, Vol 4* (Eds.: B. M. Trost, I. Fleming, M. F. Semmelhack), Pergamon Press, Oxford, **1991**, p. 1111; c) K. B. G. Torssell, *Nitrile Oxides, Nitrones and Nitronates in Organic Synthesis*, VCH, Weinheim, **1988**.

[2] For reviews, see: a) K. V. Gothelf, K. A. Jørgensen, *Chem. Rev.* **1998**, *98*, 863; b) K. V. Gothelf, K. A. Jørgensen, *Chem. Commun.* **2000**, 1449; c) M. Frederickson, *Tetrahedron* **1997**, *53*, 403; d) S. Karlsson, H.-E. Högsberg, *Org. Prep. Proced. Int.* **2001**, *33*, 103.

[3] Other types of dipoles: nitrile oxides: Y. Yoshida, Y. Ukaji, S. Fujinami, K. Inomata, *Chem. Lett.* **1998**, 1023; carbonyl ylides: D. M. Hodgson, P. A. Stubble, C. Johnstone, *Chem. Commun.* **1999**, 2185; A. Padwa, D. J. Austin, S. F. Hornbuckle, *J. Org. Chem.* **1996**, *61*, 63; S. Kitagaki, A. Anada, K. Kataoka, K. Matsuno, C. Umeda, N. Watanabe, S. Hashimoto, *J. Am. Chem. Soc.* **1999**, *121*, 1417; diazoalkanes: S. Kanemasa, T. Kanai, *J. Am. Chem. Soc.* **2000**, *122*, 10710.

[4] M. Pichon, B. Figadère, *Tetrahedron: Asymmetry* **1996**, *7*, 927.

[5] a) J. Barluenga, M. A. Fernández-Rodríguez, E. Aguilar, F. Fernández-Mari, A. Salinas, B. Olano, *Chem. Eur. J.* **2001**, *7*, 3533; b) R. Chinchilla, L. R. Falvello, N. Galindo, N. Carmen, *Eur. J. Org. Chem.* **2001**, 3133; c) S. Karlsson, H.-E. Högberg, *Tetrahedron: Asymmetry* **2001**, *12*, 1977; d) P. R. Sebahar, R. M. Williams, *J. Am. Chem. Soc.* **2000**, *122*, 5666; e) A. Viso, R. Pradilla, A. Garcia, M. Alonso, C. Guerrero-Strachan, I. Fonseca, *J. Org. Chem.* **1997**, *62*, 2316; f) M. E. Kopach, A. H. Fray, A. I. Meuers, *J. Am. Chem. Soc.* **1996**, *118*, 9876; g) H. Waldmann, E. Blaeser, M. Jansen, H.-P. Letschert, *Chem. Eur. J.* **1995**, *1*, 150; h) A. D. Reed, L. S. Hegedus, *J. Org. Chem.* **1995**, *60*, 3787; i) M. T. Rispens, E. Keller, B. de Lange, R. W. J. Zijlstra, B. L. Feringa, *Tetrahedron: Asymmetry* **1994**, *5*, 607; j) J. E. Baldwin, S. C. M. Turner, M. G. Moloney, *Synlett* **1994**, *925*; k) P. Garner, W. B. Ho, H. Shin, *J. Am. Chem. Soc.* **1993**, *115*, 10742; l) P. Deprez, J. Royer, H. P. Husson, *Tetrahedron: Asymmetry* **1991**, *2*, 1189; m) S. Kanemasa, T. Hayashi, J. Tanaka, H. Yamamoto, T. Sakurai, *J. Org. Chem.* **1991**, *56*, 4473.

[6] a) P. Allway, R. Grigg, *Tetrahedron Lett.* **1991**, *32*, 5817; b) R. Grigg, *Tetrahedron: Asymmetry* **1995**, *6*, 2475.

[7] Patent application: X. Zhang, **2002**, WO 01/58588 A1.

[8] G. Kill, J.-P. Fleury, *Bull. Soc. Chim. Fr.* **1968**, 4636.

[9] For reviews on *C*2-bisoxazoline–Lewis acid complexes as catalysts, see: a) A. K. Ghosh, P. Matahvivan, J. Capiello, *Tetrahedron: Asymmetry* **1998**, *9*, 1; b) K. A. Jørgensen, M. Johannsen, S. Yao, H. Audrian, J. Thorhauge, *J. Acc. Chem. Res.* **1999**, *32*, 605; c) J. S. Johnson, D. A. Evans, *Acc. Chem. Res.* **2000**, *32*, 325; see also: d) J. Thorhauge, M. Roberson, R. G. Hazell, K. A. Jørgensen, *Chem. Eur. J.* **2002**, *8*, 1888, and references therein; e) S. Yao, M. Johansen, K. A. Jørgensen, *J. Chem. Soc. Perkin Trans.* **1997**, 2345.

[10] S. Kanemasa, S. Oderaotoshi, S. Sakaguchi, H. Yamamoto, J. Tanaka, E. Wada, D. P. Curran, *J. Am. Chem. Soc.* **1998**, *120*, 3074.

 © 2002 WILEY-VCH Verlag GmbH & Co. KGaA, Weinheim 0044-8249/02/4122-4238 $ 20.00+.50/0

Giant Amphiphiles by Cofactor Reconstitution**

Mark J. Boerakker, Jurry M. Hannink, Paul H. H. Bomans, Peter M. Frederik, Roeland J. M. Nolte,* Emmo M. Meijer, and Nico A. J. M. Sommerdijk*

Low molecular-weight amphiphilic molecules are known to form a large variety of self-assembled structures in water, such as monolayers, micelles, vesicles, bilayers, rod- and sheetlike structures, and also helices.[1] Well-defined diblock copolymers—so-called superamphiphiles—have been shown to generate these highly ordered structures as well.[2] Recently, we reported on a new type of macromolecular surfactant, termed "giant amphiphile", in which a protein or an enzyme acts as the polar head group and a synthetic polymer as the apolar tail.[3] These biohybrid polymers differ from other protein–polymer conjugates in the sense that the protein to polymer ratio is predefined and the position of the conjugation site is precisely known. Herein we describe the construction of a giant amphiphile by direct coupling of a hydrophobic polymer chain to a redox enzyme by cofactor reconstitution. The functionalization of proteins through the reconstitution of an apoprotein with a (synthetically modified) cofactor has been demonstrated to yield a variety of proteins, many of them with interesting new properties.[4] The cofactor reconstitution method has also been applied for the controlled generation of bioactive surfaces for example, in biosensors and bio-fuel cells.[5] Here we demonstrate that the coupling of a polystyrene chain to the horseradish peroxidase (HRP) enzyme results in a giant amphiphile which forms vesicular structures in solution.

[*] Dr. N. A. J. M. Sommerdijk, M. J. Boerakker
Laboratory of Macromolecular and Organic Chemistry
Eindhoven University of Technology
P.O. Box 513, 5600 MB Eindhoven (The Netherlands)
Fax: (+31) 40-245-1036
E-mail: N.Sommerdijk@tue.nl

Prof. Dr. R. J. M. Nolte,[+] J. M. Hannink
Department of Organic Chemistry, NSR Center
University of Nijmegen
6525 ED Nijmegen (The Netherlands)
Fax: (+31) 24-365-2929
E-mail: nolte@sci.kun.nl

Prof. Dr. E. M. Meijer[+]
DSM Research
Geleen (The Netherlands)

P. H. H. Bomans, Dr. P. M. Frederik
Department of Pathology, Electron Microscopy
University of Limburg, Maastricht (The Netherlands)

[+] Laboratory of Macromolecular and Organic Chemistry
Eindhoven University of Technology
Eindhoven (The Netherlands)

[**] We thank the National Research School Combination Catalysis (NRSC-Catalysis) for support of this work, J. J. L. M. Cornelissen (University of Nijmegen) for a generous gift of monocarboxylic acid functionalized polystyrene, H. P. M. Geurts (University of Nijmegen), and J. L. J. van Dongen and J. J. J. M. Donners (Eindhoven University of Technology) for technical assistance.

Supporting information for this article is available on the WWW under http://www.angewandte.org or from the author.

We selected horseradish peroxidase (EC 1.11.1.7) as the biological component because it contains a cofactor (ferriprotoporphyrin IX) that can be easily modified with one or two hydrophobic chains on its carboxylic acid functional groups. Generally, the reconstitution of apo-HRP with cofactors bearing only one unmodified carboxylic acid unit leads to higher enzymatic activities compared to cofactors bearing substituents on both carboxylic acid moieties.[4e,6] Therefore, a single polymer chain end-capped with a carboxylic acid group ($M_n = 9458$, $M_w/M_n = 1.05$) was coupled to one of the carboxylic acid groups of ferriprotoporphyrin IX by a hydrophilic bis(aminoethoxy)ethane spacer (see Supporting Information for synthetic procedure).[7] The latter spacer was used to ascertain the compatibility of the polymer (**1**, Figure 1a) with the apoenzyme. The length of the spacer was chosen such that it can span the distance between the carboxylic acid moiety of the cofactor in the active site and the surface of the enzyme (approximately 10 Å, Figure 1b).

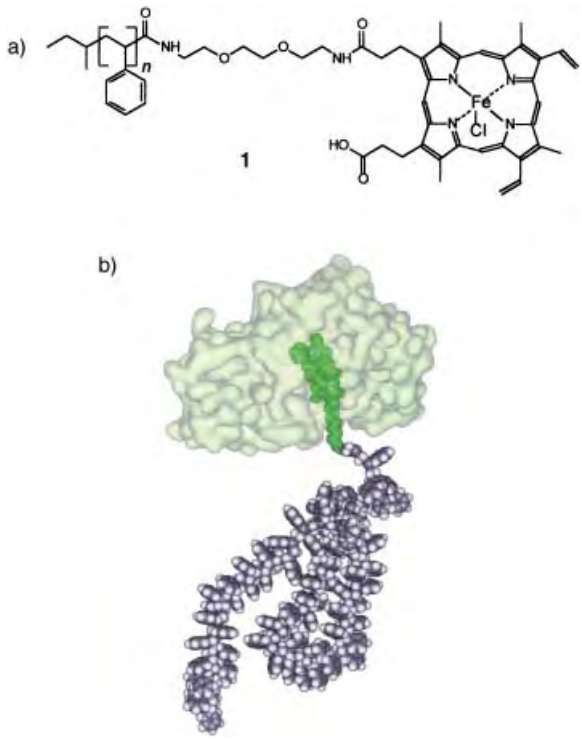


Figure 1. a) Structure of the polystyrene-modified cofactor **1**, $n = 90$; b) computer-generated model of the HRP–polystyrene-based giant amphiphile.

In a first series of experiments, cofactor reconstitution was tried by first preparing aggregates of **1**. A THF solution of the polymer (100 μL of a 0.3 mg/mL solution) was added to a phosphate buffer (1.0 mL, 20 mM potassium phosphate, pH 7.5). As expected, in the absence of the apoenzyme the resulting aggregates did not show any catalytic activity; this was determined using an 2,2'-azino-bis(3-ethylbenzthiazoline-6-sulfonic acid) diammonium salt (ABTS)/H_2O_2 assay in which apo-HRP was taken as the blank.[8,9] Both TEM (see Supporting Information) and SEM (Figure 2a) demonstrated that polymer **1** in water forms spherical aggregates with diameters of 100–1000 nm and a perforated wall structure.

 © 2002 WILEY-VCH Verlag GmbH & Co. KGaA, Weinheim 0044-8249/02/4122-4239 $ 20.00+.50/0

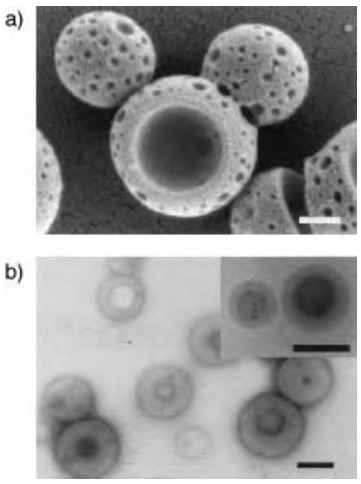


Figure 2. a) SEM micrograph of aggregates formed by **1** in aqueous solution; b) TEM and cryo-TEM (inset) images of aggregates of complexes formed between apo-HRP and **1** in aqueous solution. Scale bars represent 200 nm.

Notably, similar structures have been described for low molecular weight surfactants, but to our knowledge they are unprecedented for polymeric materials.[10,11] Attempts to construct biohybrid amphiphiles by incubating the aggregates of **1** with apo-HRP were not successful as no changes in morphology or enzymatic activity were observed.

The desired biohybrid amphiphiles could be prepared, however, by adding a THF solution of **1** to an aqueous solution containing an excess of the apoenzyme. After incubation at 4 °C for 4 days a stable homogeneous dispersion was obtained, from which the excess apoenzyme was removed by dialysis. UV/Vis spectroscopy revealed that, upon incorporation into the apoenzyme, **1** attains the spectral features of native hemin inside HRP (Figure 3). The electrophoretic migration-shift assay showed the formation of large protein-containing aggregates,[12] that were unable to penetrate the electrophoresis gel and, as expected, no apo-HRP was detected (see Supporting Information). Samples of the dialyzed solutions were transferred to carbon-coated copper grids and studied by TEM. Electron micrographs revealed that the enzyme–polymer hybrid formed vesicular aggregates with diameters of 80–400 nm (Figure 2b). In most cases these aggregates enclosed spherical objects, which were often located away from the center of the aggregates. A number of vesicles were found to contain more than one of these objects. Cryo-TEM studies showed that the aggregates in solution have a spherical nature and confirmed that the objects are only found in association with the vesicles (Figure 2b).

Although the present results are not yet conclusive, we presume that **1** in the presence of apo-HRP forms aggregates onto which the apo-HRP can be reconstituted. In this way the desired amphiphile is formed. The latter biohybrid subsequently forms vesicles, which enclose the initial aggregate. The vesicles grow from the aggregates of **1** until all apo-HRP inside the vesicles is reconstituted, leaving nonreconstituted cofactor as dark spherical objects inside or attached to the vesicles.

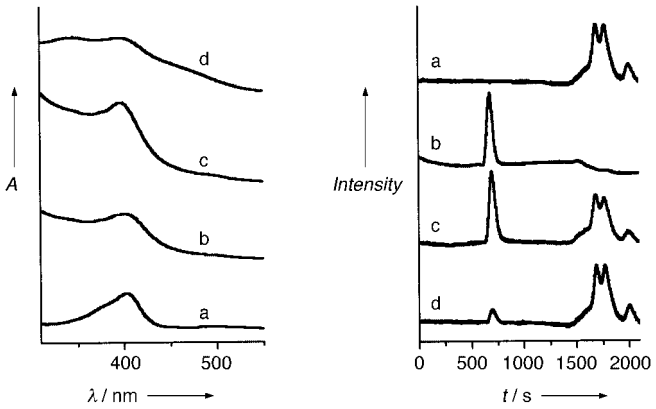


Figure 3. Left: UV/Vis spectra in the Soret-band region of a) native HRP; b) apo-HRP reconstituted at 4 °C with the modified cofactor **1**; c) apo-HRP reconstituted at 22 °C with **1**; d) cofactor **1**. Spectra were recorded in aqueous solution (pH 7.5, 20 mM potassium phosphate) at a concentration of 0.0066 mM. Right: aqueous gel permeation chromatograms of a) 4(5)-carboxyfluorescein (the commercially obtained material contains isomers, each having a different interaction with the column material); b) and c) sample of an aggregate solution prepared in the presence of 4(5)-carboxyfluorescein; d) sample of the aggregate solution after the addition of pure water to break up the aggregates. In the case of a), c), and d) the sample was excited at $\lambda_{ex} = 492$ nm and the emission of the dye was monitored at $\lambda_{em} = 516$ nm. In the case of b), for the detection of the aggregates formed by the enzyme–polymer hybrid, the UV/Vis absorption of the cofactor at 408 nm was monitored. Trace b) shows that the retention time of the water-soluble dye coincides with that of the vesicles.

Inclusion experiments were carried out to establish further the vesicular nature of the aggregates. These experiments showed that it is possible to include a water-soluble dye (4(5)-carboxyfluorescein) in the aggregates, which is released upon rupture of the aggregates through osmotic pressure induced by the addition of pure water to the buffered aggregate dispersion (Figure 3).

The enzymatic activity of the HRP–polystyrene–**1** aggregates was tested, but no enzymatic activity could be observed when the enzyme was reconstituted with **1** at 4 °C. However, when the reconstitution of apo-HRP with **1** was carried out at 22 °C the enzyme–polymer hybrid surprisingly regained activity. After 5 days the aggregates displayed a turn-over frequency (TOF) of 360 h^{-1} in 20 mM potassium phosphate buffer at pH 7.5.[13] Longer reconstitution times resulted in a decrease in activity, probably caused by thermal denaturation. Under the same conditions for HRP, a TOF of 76000 h^{-1} was found after 5 days.

In summary, we have shown for the first time that the modification of an enzyme with a macromolecular chain by the cofactor reconstitution method yields giant amphiphiles that can form aggregates in aqueous media, and which still retain some catalytic activity.

Experimental Section

Reconstitutions were carried out by adding 1.0 mL of a THF solution of the modified cofactor **1** by syringe into 10.0 mL of an aqueous phosphate-buffered solution (20 mM, pH 7.5) containing a 2.5-fold excess of the apoenzyme. After 4 days, the excess of apoenzyme was removed by dialysis using a membrane with a 300 kDa cut-off, which allows the apoenzyme

 © 2002 WILEY-VCH Verlag GmbH & Co. KGaA, Weinheim 0044-8249/02/4122-4240 $ 20.00+.50/0

(44 kDa) and the individual heme cofactors (10 kDa) to pass through, while retaining any aggregates formed by the enzyme–polymer hybrid.

Received: July 5, 2002 [Z19372]

[1] M. C. Feiters, R. J. M. Nolte, in *Advances in Supramolecular Chemistry, Vol. 6* (Ed.: G. W. Gokel), Jai, Stamford CT, **2000**, pp. 41 – 156.

[2] a) I. Gitsov, K. L. Wooley, J. M. J. Fréchet, *Angew. Chem.* **1992**, *104*, 1282 – 1285; *Angew. Chem. Int. Ed. Engl.* **1992**, *31*, 1200 – 1202; b) J. C. M. v. Hest, M. W. P. L. Baars, D. A. P. Delnoye, M. H. P. v. Genderen, E. W. Meijer, *Science* **1995**, *268*, 1592 – 1595; c) J. P. Spatz, S. Mössmer, M. Möller, *Angew. Chem.* **1996**, *108*, 1673 – 1676; *Angew. Chem. Int. Ed. Engl.* **1996**, *35*, 1510 – 1512; d) J. J. L. M. Cornelissen, M. Fischer, N. A. J. M. Sommerdijk, R. J. M. Nolte, *Science* **1998**, *280*, 1427 – 1430.

[3] a) J. M. Hannink, J. J. L. M. Cornelissen, J. A. Farrera, P. Foubert, F. C. De Schryver, N. A. J. M. Sommerdijk, R. J. M. Nolte, *Angew. Chem.* **2001**, *113*, 4868 – 4870; *Angew. Chem. Int. Ed.* **2001**, *40*, 4732 – 4734; b) K. Velonia, A. E. Rowan, R. J. M. Nolte, *J. Am. Chem. Soc.* **2002**, *124*, 4224 – 4225.

[4] a) For a review on chemical modifications of proteins by the cofactor-reconstitution method, see: I. Hamachi, S. Shinkai, *Eur. J. Org. Chem.* **1999**, 539–549. Recent reports: b) T. Hayashi, Y. Hitomi, T. Ando, T. Mizutani, Y. Hisaeda, S. Kitagawa, H. Ogoshi, *J. Am. Chem. Soc.* **1999**, *121*, 7747 – 7750; c) K. Kobayashi, T. Nagamune, T. Furuno, H. Sasabe, *Bull. Chem. Soc. Jpn.* **1999**, *72*, 691 – 696; d) I. Hamachi, H. Takashima, Y.-Z. Hu, S. Shinkai, S. Oishi, *Chem. Commun.* **2000**, 1127 – 1128; e) A. D. Ryabov, V. N. Goral, L. Gorton, E Csöregi, *Chem. Eur. J.* **1999**, *5*, 961 – 967; f) A. Riklin, E. Katz, I. Willner, A. Stocker, A. F. Bückmann, *Nature* **1995**, *376*, 672 – 675; g) R. Blonder, E. Katz, I. Willner, V. Wray, A. F. Bückmann, *J. Am. Chem. Soc.* **1997**, *119*, 11747 – 11757.

[5] a) For a review containing several examples of surface modification by the cofactor-reconstitution method, see: I. Willner, E. Katz, *Angew. Chem.* **2000**, *112*, 1230 – 1269; *Angew. Chem. Int. Ed.* **2000**, *39*, 1180 – 1218; b) H. Zimmermann, A. Lindgren, W. Schuhmann, L. Gorton, *Chem. Eur. J.* **2000**, *6*, 592 – 599; c) E. Katz, A. F. Bückmann, I. Willner, *J. Am. Chem. Soc.* **2001**, *123*, 10752 – 10753.

[6] M. Tamura, T. Asakura, T. Yonetani, *Biochim. Biophys. Acta* **1972**, *268*, 292 – 304.

[7] I. Hamachi, T. Matsugi, K. Wakigawa, S. Shinkai, *Inorg. Chem.* **1998**, *37*, 1592 – 1597.

[8] F. W. Teale, *Biochim. Biophys. Acta* **1959**, *35*, 543. Apo-HRP was prepared according to this procedure using butanone instead of acetone.

[9] N. P. Groome, *J. Clin. Chem. Clin. Biochem.* **1980**, *18*, 345 – 349.

[10] a) H. Hoffmann, C. Thunig, U. Munkert, H. Meyer, W. Richter, *Langmuir* **1992**, *8*, 2629 – 2638; b) M. Almgren, *Biochim. Biophys. Acta* **2000**, *1508*, 146 – 163, and references therein.

[11] The observed pore structure is assumed to be induced by high surface charges and is a way for the system to minimize its energy, see also M. Dubois, B. Demé, T. Gulik-Krzywicki, J.-C. Dedieu, C. Vautrin, S. Désert, E. Perez, T. Zemb, *Nature* **2001**, *411*, 672 – 675.

[12] M. Arnold, P. Ringler, A. Brisson, *Biochim. Biophys. Acta* **1995**, *1233*, 198 – 204.

[13] When **1** was incubated with glucose oxidase (GOx) or acylase, two non-heme enzymes containing several lysine and histidine residues on their periphery, no peroxidase activity was observed. This implies that the enzymatic activity of **1** incubated with apo-HRP is not caused by the interaction of **1** with amino acid residues on the apo-HRP periphery.

Active Immunization with a Glycolipid Transition State Analogue Protects against Endotoxic Shock**

Lyn H. Jones, Laurence J. Altobell III, Mary T. MacDonald, Nicholas A. Boyle, Paul Wentworth, Jr.,* Richard A. Lerner, and Kim D. Janda*

Septic shock is one of the ten leading causes of both infant and adult mortality in the United States and, according to the Centers for Disease Control and Prevention, directly resulted in over 30000 deaths in 1999 alone. Lipopolysaccharide (LPS) released from the bacterial membrane after bacteriolysis is responsible for many of the toxic effects associated with gram-negative bacterial septic shock.[1] Lipid A (**1**; the *E. coli* structural form is shown in Figure 1) is the main toxic determinant of LPS and is known to stimulate host macrophages to secrete increased amounts of various cytokines, which include tumor necrosis factor-α (TNF-α), interleukin-1β, and interleukin-6.[2] Immunomodulation of this inflammatory cascade has been suggested as a crucial but inadequately addressed element in the treatment of sepsis.[3] While passive immunization with monoclonal antibodies directed against components of the inflammatory cascade or LPS itself[4] have shown promise at the research level, these strategies have to date been ineffective in extensive clinical trials.[5]

As a primary step in a strategy that may ultimately lead to a new immunomodulatory treatment for septic shock, we report that active immunization with keyhole limpet hemocyanin (KLH) glycoconjugates of novel bisphosphonate analogues of lipid X **2a**,**b** (see Figure 1) offers significant in vivo protection against a sublethal lipid A challenge.

Raetz[6] has shown that the biological effects of the *E. coli* lipid A (**1**) require the presence of several key structural features: both phosphate groups, the glucosamine disaccharide, and all the fatty acyl chains, especially the 2′-lauroyl and 3′-myristoyl acyloxy residues (R′ and R of **1** in Figure 1).

Our designed lipid A mimics (**2a**,**b**, Figure 1) incorporate the following features: 1) a glucosamine 4′-phosphate β-*O*-butyl lipid X saccharide analogue of lipid A; 2) truncated 2′- and 3′-acyloxychains that contain both the lipid A *R* stereo-

[*] Prof. Dr. P. Wentworth, Jr., Prof. Dr. K. D. Janda, Dr. L. H. Jones, Mr. L. J. Altobell III, Dr. M. T. MacDonald, Dr. N. A. Boyle, Prof. Dr. R. A. Lerner
Department of Chemistry
The Scripps Research Institute and
The Skaggs Institute for Chemical Biology
10550 North Torrey Pines Road, La Jolla, CA 92037 (USA)
Fax: (+1) 858-784-2590 (P.W.)
Fax: (+1) 858-784-2595 (K.D.J.)
E-mail: paulw@scripps.edu
kdjanda@scripps.edu

[**] This work was supported by NIH Grant GM-43858 (K.D.J.) and The Skaggs Institute for Chemical Biology. M.T.M. is a UNCF Merck Science Initiative Research Fellow. The authors thank Dr. A. D. Wentworth for assistance with the TNF-α ELISA (ELISA = enzyme-linked immunosorbent assay).

Supporting information for this article is available on the WWW under http://www.angewandte.org or from the author.

 © 2002 WILEY-VCH Verlag GmbH & Co. KGaA, Weinheim 0044-8249/02/4122-4241 $ 20.00+.50/0

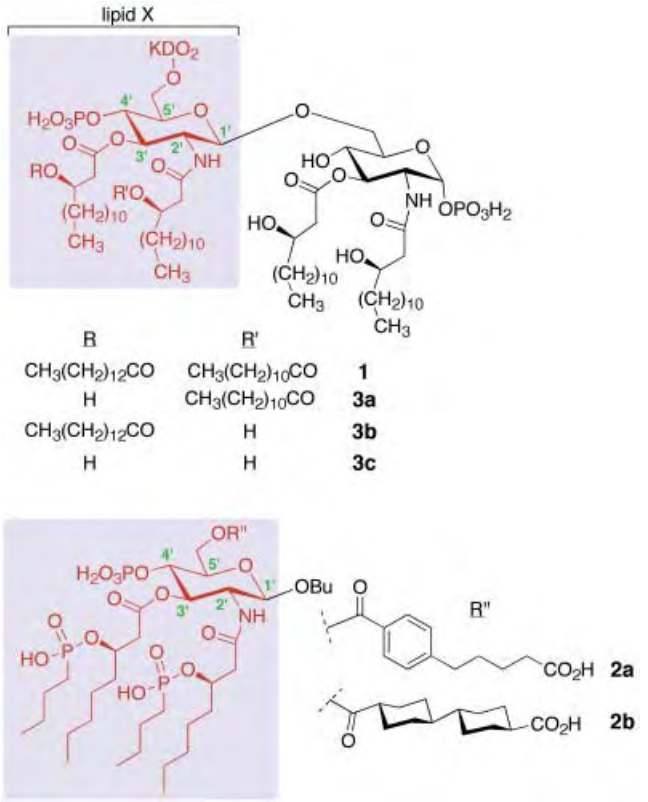


Figure 1. Bisphosphonates **2a**,**b** were synthesized as immunogens for active immunization to treat lipid A mediated endotoxicosis. The derivatives **3a–c** are less toxic derivatives of lipid A. The lipid X component of **1** and its structural mimic in haptens **2a**,**b** are shown boxed. KDO = 3-deoxy-D-*manno*-octulosonate.

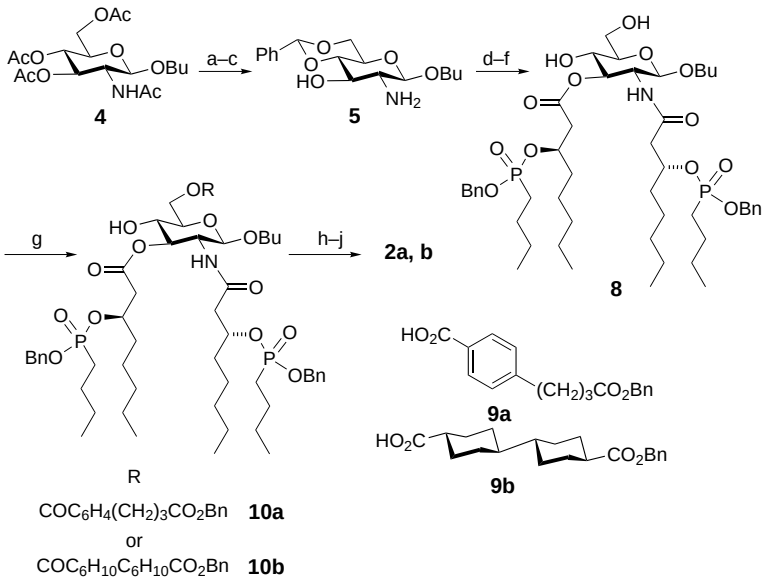
chemistry and a phosphonate group; 3) a flexible and a rigid linker moiety for attachment to a carrier protein.

It was anticipated that active immunization of mice with the KLH-**2a**,**b** glycoconjugates would produce serum antibodies that could either bind to and neutralize lipid A (as a result of the structural similarity of **2a**,**b** with **1**) or that may catalyze the hydrolysis of the key 2′- and or 3′-acyloxyacyl ester linkages of **1**, which thus generates the functionally inactive lipid A derivatives **3a–c**. For the latter reason, the phosphonate groups were incorporated into **2a**,**b** as stable mimics of the presumed tetrahedral intermediates formed during hydroxide-catalyzed ester hydrolysis (Figure 1).[7] Truncated lipid chains were used to minimize micelle formation and aid antibody recognition of the glucosamine core and phosphoryl components of the 2′- and 3′-acyloxy side chains.

Given that carbohydrates have notoriously poor immunogenicity,[8] the linker was seen as a key locus at which to incorporate an immunostimulatory chemical motif that would facilitate the immunogenicity of the associated carbohydrate core. In this regard, we have studied the immunogenicity imparted by possession of either a flexible (*para*-substituted benzoic acid, see R″ in Figure 1 **2a**) or rigid (1,1′-bis(cyclohexyl)-substituted carboxylic acid **2b**) spacer group.

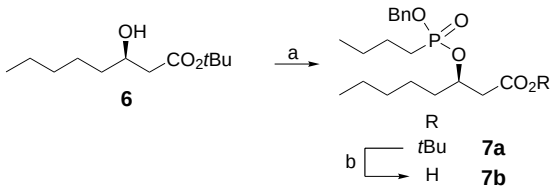
Our synthesis of the phosphonates **2a** and **2b** is highly convergent and efficient (Scheme 1 and 2).[9] Thus, transesterification of the known β-butyl glycoside **4**[10] with catalytic sodium methoxide in methanol, followed by protection of the two free hydroxy groups as a benzylidene group and deprotection of the *N*-acetate with hydrazine, at elevated temperatures, furnished the aminoalcohol **5** (Scheme 1). The side chain, which bears the quintessential phosphonate ester moiety, was prepared from the known enantiomerically pure β-hydroxy ester **6**[11] (Scheme 2). The mixed phosphonate diester **7a** was prepared as a 1:1 mixture of diastereomers[12] by an initial tetrazole-catalyzed monoaddition of the alcohol **6** to *n*-butyl phosphonic dichloride and subsequent addition of benzyl alcohol.[13] Removal of the *tert*-butyl ester from **7a** provided the key side-chain acid **7b**. Subsequent coupling of **7b** to the amino alcohol **5** (DCC, DMAP), followed by acetal deprotection, afforded the diol **8**. Selective acylation of the C6 hydroxy group of **8** using DCC with either **9a** or **9b**[14] installed the flexible or rigid linkers, respectively. Transformation of the C4 hydroxy group of **10a** or **10b** into a phosphite group with Watanabe's reagent, followed by oxidation with *m*CPBA and complete hydrogenolysis furnished the desired haptens **2a** and **2b**. Glycoprotein conjugates of KLH, for active immunization, and bovine serum albumin (BSA), for serum titer measurement, were prepared by coupling haptens **2a**,**b** to the ε-amino groups of the protein lysine residues by activation to their sulfo-*N*-hydroxysuccinimidoyl esters as previously described.[15]

The protective effect of active immunization with KLH-**2a** and KLH-**2b** against a lipid A challenge was investigated using an in vivo mouse model (three strains: Swiss-Webster



Scheme 1. Reagents and conditions: a) NaOMe cat., MeOH, 93%; b) α-dimethoxytoluene, cat. TsOH, DMF, 82%; c) N_2H_4, EtOH, 130°C, 80%; d) DCC, cat. 4-pyrrolidinopyridine, **7b**, CH_2Cl_2; e) 80% AcOH (aq); f) **9a** or **b**, DCC, cat. DMAP, 82%; g) *N*,*N*-diethyl-1,5-dihydro-3*H*-2,4,3-benzodioxaphosphepin-3-amine, cat. 1*H*-tetrazole, CH_2Cl_2; h) *m*CPBA, 64% (2 steps); i) H_2, 10% Pd-C, EtOH/MeOH/H_2O 2:2:1; j) NEt_3 (100%), 60°C, 51% (2 steps).Ts = *p*-toluenesulfonyl, DMAP = N,N-dimethyl-4-aminopyridine, *m*CPBA = *m*-chloroperbenzoic acid, DCC = dicyclohexyl carbodiimide.

 © 2002 WILEY-VCH Verlag GmbH & Co. KGaA, Weinheim 0044-8249/02/4122-4242 $ 20.00+.50/0 *Angew. Chem. Int. Ed.* **2002**, *41*, No. 22



Scheme 2. Reagents and conditions: a) *n*-butylphosphonyl dichloride, 4*H*-tetrazole, **6** followed by BnOH (excess) (95%); b) 50% TFA in CH_2Cl_2 (87%). Bn = benzyl, TFA = trifluoroacetic acid.

(SW), 129Gix$^+$, and A/J; $n = 8$). The procedure involved preimmunization with either KLH-**2a** or **2b** (equivalent to 20 μg of glycoconjugate on day 1, day 7, and day 14) with ALUM (aluminum hydroxide gel) as adjuvant. Control groups received KLH (20 μg) with ALUM. Anti-BSA-**2a** and **2b** immunoglobulin G serum titers were measured by ELISA on day 21 and ranged from 14300 ± 1600 (A/J, KLH-**2b** antigen) to 3200 ± 800 (A/J, KLH-**2a** antigen; Table 1). Significant cross-reactivity was observed between the antibodies generated to the glycoconjugates, which suggests that the major epitope on **2a** and **2b** is the lipid X analogue and not the immunogenic side chain (Table 1). Interestingly, in all three murine strains investigated, the serum titers against hapten **2b**, which contains the rigid *trans,trans*-bis(cyclohexyl) linker, were significantly higher than those achieved with the flexible linker **2a** ($n = 8$, $p < 0.05$, Table 1); this offers strong support for the use of this new linker to improve hapten immunogenicity. In fact, the immunostimulatory effect of the bis(cyclohexyl) linker, when coupled with the cross-reactivity described above, results in higher observed serum titers for BSA-**2a** in mice immunized with KLH-**2b** rather than KLH-**2a** (Table 1).[16]

It is well-documented that decreased TNF-α production during lipid A challenge correlates well with survival during murine gram-negative sepsis.[17] Therefore, the extent of protection following active immunization with KLH-**2a** and KLH-**2b** was assessed by comparative serum analysis of TNF-α concentrations in the immunized and control groups. The immunized mice (see above) were subjected to a bolus sublethal challenge of lipid A (*E. coli O111:B4*, 20 μg in sterile saline, intravenous, day 24) and their serum TNF-α levels were measured 1.5 h after treatment. The lipid A associated elevation in serum TNF-α levels in the control group (which was immunized with only KLH) was significantly abrogated in all three strains that were immunized with KLH-**2a** or **2b** (129Gix+ −100.0 ± 0.3% (KLH) versus 6.5 ± 2.0% (KLH-**2a**), 6.4 ± 2.8% (KLH-**2b**). SW −100.0 ± 5.8% (KLH) versus 16.4 ± 14.8% (KLH-**2a**), 10.3 ± 0.1% (KLH-**2b**). A/J −100.0 ± 2.9% (KLH) versus 33.0 ± 0.2% (KLH-**2a**), 27.2 ± 5.0% (KLH-**2b**; $n = 8$, $p < 0.05$); Figure 2). This profound reduction of serum TNF-α levels (ranging from 94.6–72.8%) in the KLH-**2a** or **2b** active-immunization approach protects the host in vivo against the lipid A challenge. Preliminary studies have revealed that mice immunized with KLH-**2a** and KLH-**2b** possess serum antibodies that recognize *E. coli* (*E. coli O111:B4*) lipid A (see Table 1). However, a question still remains as to whether the protection conferred during the active immunization is caused by clearance of lipid A from serum by antibody binding and/or antibody-catalyzed destruction. This issue is under investigation.[18]

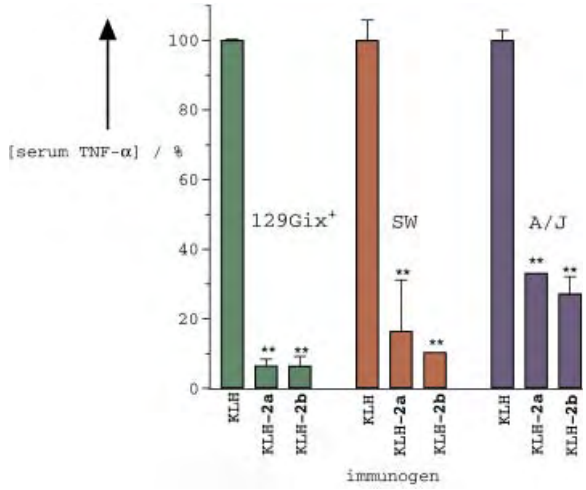


Figure 2. Serum TNF-α levels measured by ELISA 1.5 h after sublethal intravenous *E. coli O111:B4* lipid A (20 μg) challenge in mice (■ 129 GiX +, ■ SW, ■ A/J) after active immunization with either KLH (control), KLH-**2a** or KLH-**2b**. Data are reported as the mean value ± S.E.M ($n = 8$, ** denotes a p value < 0.05 relative to mice immunized with KLH alone).

This study shows for the first time that active immunization with a bisphosphonate lipid X analogue can offer significant protection against the effects of *E. coli* lipid A in a murine model. This preliminary result brings into focus a potential new immunopharmacotherapeutic approach that may ultimately offer significant help in the treatment of the serious and lethal clinical septic shock syndrome.

Received: July 3, 2002 [Z19661]

[1] R. R. Schumann, S. R. Leong, G. W. Flaggs, P. W. Gray, S. D. Wright, J. C. Mathison, P. S. Tobias, R. J. Ulevitch, *Science* **1990**, *249*, 1429; S. D. Wright, R. A. Ramos, P. S. Tobias, R. J. Ulevitch, J. C. Mathison, *Science* **1990**, *247*–250, 1431.

[2] C. R. H. Raetz, R. J. Ulevitch, S. D. Wright, C. H. Sibley, A. Ding, C. F. Nathan, *FASEB J.* **1991**, *5*, 2652; *Endotoxin Research Series: Bacterial Endotoxin: Recognition and Effector Mechanisms, Vol. 2*

Table 1. Serum titers[a] following immunization with either KLH-**2a** or KLH-**2b**.

	Titer [× 10^3]		KLH-**2a** immunogen		KLH-**2b** immunogen	
Strain	BSA-**2a**	BSA-**2b**	Lipid A[b]	BSA-**2a**	BSA-**2b**	Lipid A
129Gix+	4.8 ± 1.6	2.8 ± 0.4	1.2 ± 0.4	9.6 ± 1.2	13.9 ± 2.0[c]	1.2 ± 0.3
SW	4.8 ± 1.2	2.1 ± 0.8	0.8 ± 0.4	8.2 ± 1.2	11.6 ± 2.0[c]	2.0 ± 0.4
A/J	3.2 ± 0.8	1.2 ± 0.4	0.8 ± 0.2	4.1 ± 0.8	14.3 ± 1.6[c]	0.8 ± 0.2

[a] For experimental details of the ELISA procedures see the Supporting Information. Prevaccination control titers against KLH-**2a** or KLH-**2b** in all three strains were zero. [b] Lipid A from *E. coli (O111:B4)*. [c] These values have a significant difference in serum titer between BSA-**2b** and BSA-**2a** in the same strain after immunization with KLH-**2b** or KLH-**2a**, respectively ($n = 8$, $p < 0.05$).

 © 2002 WILEY-VCH Verlag GmbH & Co. KGaA, Weinheim 0044-8249/02/4122-4243 $ 20.00+.50/0

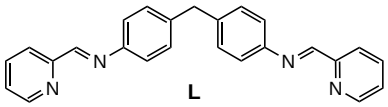
(Eds.: J. Levin, C. R. Alving, R. S. Munford, P. L. Stütz), Excerpta Medica, Amsterdam, **1993**.
[3] For a review outlining the underlying principles of sepsis therapy, see R. L. Anel, A. Kumar, *Expert Opin. Invest. Drugs* **2001**, *10*, 1471, and references therein.
[4] D. L. Dunn, W. C. Bogard, F. B. Cerra, *Arch. Surg.* **1985**, *120*, 50; N. N. Teng, H. S. Kaplan, J. M. Hebert, C. Moore, H. Douglas, A. Wunderlich, A. I. Braude, *Proc. Natl. Acad. Sci. USA* **1985**, *82*, 1790.
[5] M. Williams, J. B. Summers, *Expert Opin. Invest. Drugs* **1994**, *3*, 1051; E. J. Ziegler, C. J. Fisher, Jr., C. L. Sprung, R. C. Straube, J. C. Sadoff, G. E. Foulke, C. H. Nortel, M. P. Fink, R. P. Dellinger, N. N. Tang, *N. Engl. J. Med.* **1988**, *324*, 429; R. L. Greenman, R. M. Schein, M. A. Martin, R. P. Wenzel, N. R. MacIntyre, G. Emmanuel, H. Chmel, R. B. Kohler, M. McCarthy, J. Plauffe, *J. Am. Med. Assoc.* **1991**, *266*, 1097–1099.
[6] C. R. H. Raetz in *Escherichia coli and Salmonella: Cellular and Molecular Biology, Vol. 1* (Ed.: F. C. Neidhart), American Society of Microbiology, Washington, DC, **1996**, pp. 1035.
[7] For reviews detailing the use of phosphonic acid derivatives to produce catalytic antibody esterases, see G. M. Blackburn, A. Datta, H. Denham, P. Wentworth, Jr., *Adv. Phys. Org. Chem.* **1998**, *31*, 249; P. Wentworth, Jr., K. D. Janda, *Curr. Opin. Chem. Biol.* **1998**, *2*, 138.
[8] S. Danishefsky, J. R. Allen, *Angew. Chem.* **2000**, *112*, 882; *Angew. Chem. Int. Ed.* **2000**, *39*, 836.
[9] K. Fukase, Y. Fukase, M. Oikawa, W.-C. Liu, Y. Suda, S. Kusumoto, *Tetrahedron* **1998**, *54*, 4033; W.-C. Liu, M. Oikawa, K. Fukase, Y. Suda, S. Kusumoto, *Bull. Chem. Soc. Jpn.* **1999**, *72*, 1377.
[10] P. Boullanger, M. Jouineau, B. Bouammali, D. Lafont, G. Descontes, *Carbohydr. Res.* **1990**, *202*, 151.
[11] Prepared in six steps according to the procedure of B. Bollbuck, P. Kraft, W. Tochtermann, *Tetrahedron* **1996**, *52*, 4581.
[12] The diastereomeric phosphonates were not separable by chromatography, however, the final step in the synthesis of the hapten is hydrogenolytic removal of the benzyl esters, which destroys the chirality at the phosphorus atom.
[13] K. Zhao, D. W. Landry, *Tetrahedron* **1993**, *49*, 363.
[14] The benzyl ester **9a** was prepared in seven steps from 4-bromomethylbenzoic acid (**7**). The benzyl ester **9b** was prepared by monoesterification of *trans*,*trans*-bicyclohexyl-4,4′-dicarboxylic acid (J. G. Cannon, C.-Y. Liang, *Synth. Commun.* **1995**, *25*, 2079). See Supporting Information for synthetic procedures and product analysis.
[15] C.-H. L. Lo, P. Wentworth, Jr., K. W. Jung, J. Yoon, J. A. Ashley, K. D. Janda, *J. Am. Chem. Soc.* **1997**, *119*, 10251.
[16] For this study, the key comparison is lipid A recognition and in this regard KLH-**2a** and KLH-**2b** give similar serum titers. Therefore the benefit of the rigid linker in this biological context is not clear. We are investigating the benefits of a rigid versus flexible linker approach more fully.
[17] J. M. Mayoral, C. J. Schweich, D. L. Dunn, *Arch. Surg.* **1990**, *125*, 24.
[18] We consider that analysis of catalytic activity of polyclonal IgG, purified from serum, against lipid A is not a valid approach to assess the presence of antibody catalysts because of the risk of serum esterase contamination. However, we are generating monoclonal antibodies from mice immunized with KLH-**2a** and **2b** in the hope of isolating purified monoclonal antibodies that catalyze lipid A hydrolysis.

Assembly of a Nanoscale Chiral Ball through Supramolecular Aggregation of Bowl-Shaped Triangular Helicates**

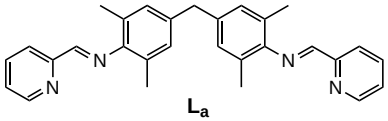
Laura J. Childs, Nathaniel W. Alcock, and Michael J. Hannon*

Biological systems provide many intricate and elegant examples of the use of self-assembly through noncovalent recognition events to generate large functional arrays. Chemists have also been attempting to mimic this approach by using supramolecular interactions to construct a wide range of arrays of defined size and architecture (albeit on a smaller size scale).[1] Metallo-supramolecular chemistry in particular has been a popular and effective tool.[2] However, in common with other supramolecular systems synthesis of building blocks (in this case of the ligands) by the formation of *covalent* bonds places restrictions on the size of the architectures that have been generated. This situation represents a potential barrier to progress in this field. One approach to address this problem is to use multiple recognition events in sequence. Thus, an initial event generates a supramolecular structure which is then aggregated into a larger array in a second supramolecular event.[3–6] As in the assembly of "simple" supramolecular structures, a challenge is to control the aggregation such that a discrete array (rather than a polymeric array) is obtained. We have been exploring the use of shape to control such aggregation and we recently reported the use of imine-based ligands to form arc-shaped double-helicates which aggregate into a discrete circular array as a result of their curved topography.[4] We have been investigating whether the same approach can be applied to form three dimensional (rather than planar) structures and herein we report the assembly of a supramolecular ball from commercially available components by this approach.

We have shown that the reaction of ligand **L** with metal ions capable of tetrahedral coordination leads to a solution equilibrium of two dimeric isomers; a helicate (*rac* isomer)



L



L$_a$

[*] Dr. M. J. Hannon, L. J. Childs, Dr. N. W. Alcock
Centre for Supramolecular and Macromolecular Chemistry
Department of Chemistry
University of Warwick
Coventry, CV4 7AL (UK)
Fax: (+44) 24-7652-4112
E-mail: m.j.hannon@warwick.ac.uk

[**] This work was supported by the University of Warwick (L.J.C.). We thank EPSRC and Siemens Analytical Instruments for grants in support of the diffractometer and the EPSRC National Mass Spectrometry Centre, Swansea for recording the mass spectra.

 © 2002 WILEY-VCH Verlag GmbH & Co. KGaA, Weinheim 0044-8249/02/4122-4244 $ 20.00+.50/0

and a metallo-cyclophane (*meso* isomer).[7] In an attempt to perturb this equilibrium, we designed ligand $\mathbf{L_a}$ in which methyl groups are introduced into the spacer with the goal of (sterically) twisting the phenyl rings out of planarity with the pyridylimine units and thus disfavoring the *meso* isomer.[8] While the methyl groups do indeed bring about this effect, their presence also has other dramatic consequences.

Ligand $\mathbf{L_a}$ was prepared in 81% yield by mixing two equivalents of 2-pyridinecarboxaldehyde and one equivalent of 4,4′-methylenebis(2,6-dimethylaniline) in methanol. Reaction of $\mathbf{L_a}$ with $[Cu(MeCN)_4][PF_6]$ in methanol yielded a red solution from which a deep red solid precipitated on cooling. The color ($\lambda = 470$ nm in MeCN) arises from a metal-to-ligand charge transfer (MLCT) and is characteristic of copper(I) in a bispyridylimine environment[7]. The same compound can be prepared in a one-pot reaction simply by mixing the aldehyde with the diamine, then adding the copper salt. The compound can also be prepared in a solvent-free reaction by grinding the three reactants together.[9] The electrospray mass spectrum shows peaks corresponding to a dimeric species and a trimer. The ^{1}H NMR spectra of the compound have been recorded in both CD_2Cl_2 and CD_3CN solution. In acetonitrile at room temperature, a single set of resonance signals is observed. However, in CD_2Cl_2 at room temperature, a second set of resonance signals is observed consistent with the presence of two solution species. The CH_2 region of the ^{1}H NMR spectrum is particularly informative (Figure 1): two singlets are observed and there is no evidence (even at low temperature) of the pair of doublets which is characteristic of the CH_2 group in the cyclophane architecture[7]. This result implies that, as envisaged, the introduction of the methyl group has sterically disfavored the formation of the *meso* isomer. The NMR spectroscopic data, coupled with the ESIMS data, leads us to conclude that the solution species must be a dimeric helix $[Cu_2(\mathbf{L_a})_2]^{2+}$ and a trinuclear circular helicate $[Cu_3(\mathbf{L_a})_3]^{3+}$.[10]

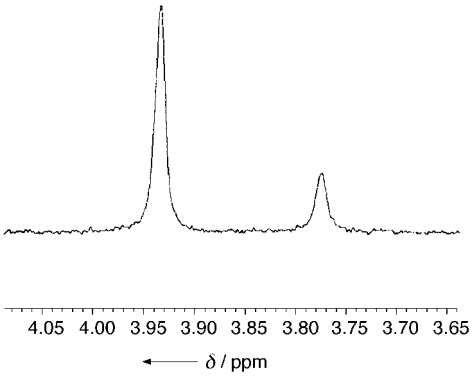


Figure 1. The CH_2 resonance signals in the ^{1}H NMR spectrum of the copper(I) complex of $\mathbf{L_a}$ in CD_2Cl_2 at 273 K.

The results of NMR diffusion experiments in CD_2Cl_2 are consistent with the presence of two species of different volumes and indicate that the major component is the smaller (i.e. dimeric) species.

Diffusion of diethyl ether into a nitromethane solution of the compound afforded X-ray quality crystals, the solid-state structure of which reveals a chiral trinuclear circular helicate $[Cu_3(\mathbf{L_a})_3]^{3+}$ (Figure 2).[11]

Each copper(I) center, as expected, is four coordinate, in a pseudo-tetrahedral coordination environment bound to two pyridylimine units from two different ligands. These metal ions prescribe the three vertices of the triangle. Each ligand wraps "over and under" the plane formed by the three metal ions leading to a trinuclear, triangular, circular helicate.[12] The structure reveals why the methyl groups have favored a trimeric species (which is not observed with ligand **L**). There are six CH–π interactions (CH–centroid 2.9–3.0 Å) within the triangle which occur between the methyl groups of one ligand and the phenyl rings of an adjacent ligand and presumably these factors contribute to the energetic stability.

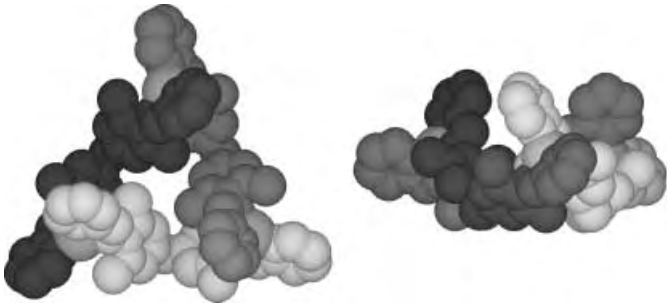


Figure 2. Molecular structure of the $[Cu_3(\mathbf{L_a})_3]^{3+}$ ion a) top view and b) side view; to emphasize the helical nature each ligand is shown in a different shading. Hydrogen atoms are omitted for clarity.

The side view of the $[Cu_3(\mathbf{L_a})_3]^{3+}$ ion (Figure 2b) reveals that the triangle is not planar, but slightly bent to give a bowl-shaped motif. This bowl-shaped distortion arises to accommodate the CH–π interactions and the constraints of the ligand connectivity. Three pyridyl rings (one from each ligand) point towards the cavity of the bowl and are arranged like the blades of a propeller. These "blades", together with the bowl-shaped topography, have dramatic consequences for the solid-state aggregation of the $[Cu_3(\mathbf{L_a})_3]^{3+}$ triangular circular helicates (Figure 3).[13,14] Four of the bowl-shaped triangular units assemble in a tetrahedral fashion through CH–π interactions to form a tetrameric ball-shaped aggre-

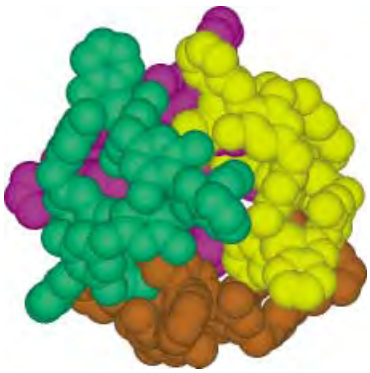


Figure 3. Molecular structure of the ball shaped array resulting from the aggregation of four $[Cu_3(\mathbf{L_a})_3]^{3+}$ circular helicates; each circular helicate is shown in a different color. Hydrogen atoms are omitted for clarity.

 © 2002 WILEY-VCH Verlag GmbH & Co. KGaA, Weinheim 0044-8249/02/4122-4245 $ 20.00+.50/0

gate. The blades of each triangle point into the cavity of the ball and a total of 12 CH–π interactions (CH–centroid 2.9 Å) are formed between the pyridyl rings of the triangles with the phenylene spacers of adjacent triangles. Each triangle in the ball is of identical chirality so that the overall ball-shaped structure is also chiral. This chiral recognition is a consequence of the propeller-type twist arrangment of the pyridyl blades of each triangle. The four sets of blades lock together and the propeller twisting of the triangles needs to be in the same direction to allow the triangles to fit together.[15] The diameter of the resulting ball is approximately 2.5 nm (C···C). Four PF_6^- counterions are located in the internal cavity and form short F···H contacts (2.35–2.88 Å).[16] Each of these anions is located above a triangular face and makes three contacts with that triangle and four additional contacts to each of the other three triangles (15 contacts per anion in total). These contacts may contribute to the stabilization of the structure.

The resulting nanoscale structure[17] is quite remarkable, it is a supramolecular assembly of 12 copper(I) ions and 12 ligands. It is striking as it can be assembled in a one-pot reaction simply by mixing inexpensive commercial reagents: 24 aldehydes, 12 diamines, and 12 copper(I) hexafluorophosphate units. While the structure described does not yet approach the complexity of assembly and level of sophistication seen in biological systems, it does indicate that with judicious (and/or fortuitous) design, large, complex architectures of nanoscale dimensions may be assembled from simple and small molecular components through controlled aggregation using multiple recognition events.

Experimental Section

L_a: 2-pyridinecarboxyaldehyde (0.829 g, 6.84 mmol) was dissolved in methanol (90 mL) and stirred under a nitrogen atmosphere. A solution of 4,4′-methylenebis(2,6-dimethylaniline) (0.678 g, 3.42 mmol) in methanol was added and the mixture stirred at room temperature for 24 h. The yellow solution was then concentrated by rotary evaporation to produce a yellow solid (1.125 g, 81 %). IR (KBr): $\tilde{\nu}$ = 2996w, 2905m, 2846w, 1638s, 1583m, 1476s, 1433s, 1385s, 1318w, 1283w, 1200s, 1141m, 1089w, 1042w, 987m, 876m, 837m, 774s, 742m, 695w, 647w, 616w cm^{-1}; MS (EI/CI): *m*/*z* 433 [*M*+H]; ^{1}H NMR ($CDCl_3$): δ = 8.72 (d, *J* = 4.6 Hz, 1H; H6), 8.35 (s, 1H; Hi), 8.28 (d, *J* = 7.7 Hz, 1H; H3), 7.84 (t, *J* = 7.7 Hz, 1H; H4/5), 7.40 (dd, *J* = 7.5, 7.7, 4.6 Hz, 1H; H4/5), 6.94 (s, 2H; Ph), 3.85 (s, 1H; CH_2), 2.15 ppm (s, 6H; CH_3).

$[Cu_3(\mathbf{L_a})_3][PF_6]_3$: Ligand **$L_a$** (0.084 g,0.019 mmol) was dissolved in methanol and treated with $[Cu(MeCN)_4][PF_6]$ (0.072 g,0.19 mmol) under nitrogen to give a dark red solution. The solution was heated at reflux overnight then cooled to room temperature affording a very deep red precipitate on standing. This solid was collected by filtration and washed with diethyl ether (0.173 g, 71 % yield). IR (KBr): $\tilde{\nu}$ = 2902w, 1586m, 1474m, 1440m, 1380m, 1303w, 1200m, 1140w, 900w, 836s, 772m, 742w, 558m cm^{-1}; MS (ESI in MeCN): *m*/*z* 1135 $\{Cu_2(\mathbf{L_a})_2(PF_6)\}^+$, 927 $\{Cu(\mathbf{L_a})_2\}^+$, 816 $\{Cu_3(\mathbf{L_a})_3(PF_6)\}^{2+}$, 495 $\{Cu_2(\mathbf{L_a})_2\}^{2+}$, $\{Cu(\mathbf{L_a})\}^+$; ^{1}H NMR: (CD_2Cl_2, 273 K): δ = 8.67 (d, *J* = 5.0 Hz, 4H; H6 helix), 8.65 (d, *J* = 4.8 Hz, 1H; H6 trimer), 8.49 (s, 4H; Hi helix), 8.39 (s, 1H; Hi trimer), 8.21 (td, *J* = 7.8, 1.6 Hz, 4H; H4/5 helix), 8.13 (td, *J* = 7.7, 1.5 Hz, 1H; H4/5 trimer), 8.00 (m, 5H; H3 helix and trimer), 7.85 (ddd, *J* = 7.5, 5.0, 1.0 Hz, 4H; H4/5 helix), 7.76 (ddd, *J* = 7.7, 5.1, 1.1 Hz, 1H; H4/5 trimer), 6.99 (s, 4H; Ph helix), 6.95 (s, 1H; Ph trimer), 6.84 (s, 1H; Ph trimer), 6.65 (s, 4H; Ph helix), 3.92 (s, 4H; CH_2 helix), 3.75 (s, 1H; CH_2 trimer), 2.16 (s, 12H; CH_3 helix); 2.02 (s, 3H ;CH_3 trimer), 1.27 ppm (s, 15H; CH_3 helix and trimer); UV/Vis (MeCN): 470 (ε = 12000), 334 (ε = 28000), 328 (ε = 75000) nm.

Received: July 22, 2002 [Z19784]

[1] J.-M. Lehn, *Supramolecular Chemistry—Concepts and Perspectives*, VCH, Weinheim, **1995**; D. Philp, J. F. Stoddart, *Angew. Chem.* **1996**, *108*, 1242 – 1286; *Angew. Chem. Int. Ed. Engl.* **1996**, *35*, 1155 – 1196.

[2] M. Fujita, *Acc. Chem. Res.* **1999**, *32*, 53 – 61; S. Leininger, B. Olenyuk, P. J. Stang, *Chem. Rev.* **2000**, *100*, 853 – 907; R. W. Saalfrank, I. Bernt, *Curr. Opin. Solid State Mater. Sci.* **1998**, *3*, 407 – 413; D. L. Calder, K. N. Raymond, *Acc. Chem. Res.* **1999**, *32*, 975 – 982; C. Piguet, *J. Inclusion Phenom. Macrocyclic Chem.* **1999**, *34*, 361 – 391; E. C. Constable, *Prog. Inorg. Chem.* **1994**, *42*, 67 – 138; A. F. Williams, *Pure Appl. Chem.* **1996**, *68*, 1285 – 1289; M. Albrecht, *J. Inclusion Phenom. Macrocyclic Chem.* **2000**, *36*, 127 – 151.

[3] R. F. Carina, G. Bernardinelli, A. F. Williams, *Angew. Chem.* **1993**, *105*, 1483 – 1485; *Angew. Chem. Int. Ed. Engl.* **1993**, *32*, 1461 – 1463.

[4] L. J. Childs, N. W. Alcock, M. J. Hannon, *Angew. Chem.* **2001**, *113*, 1113 – 1115; *Angew. Chem. Int. Ed.* **2001**, *40*, 1079 – 1081.

[5] M. J. Hannon, C. L. Painting, W. Errington, *Chem. Commun.* **1997**, 1805 – 1806; N. W. Alcock, P. R. Barker, J. M. Haider, M. J. Hannon, C. L. Painting, Z. Pikramenou, E. A. Plummer, K. Rissanen, P. Saarenketo, *J. Chem. Soc. Dalton Trans.* **2000**, 1447 – 1461.

[6] See for example: S.-Y. Yu, T. Kusukawa, K. Biradha, M. Fujita, *J. Am. Chem. Soc.* **2000**, *122*, 2665 – 2666; R. W. Saalfrank, I. Bernt, F. Hampel, *Chem. Eur. J.* **2001**, *7*, 2770 – 2774.

[7] M. J. Hannon, C. L. Painting, A. Jackson, J. Hamblin, W. Errington, *Chem. Commun.* **1997**, 1807 – 1808; M. J. Hannon, C. L. Painting, N. W. Alcock, *Chem. Commun.* **1999**, 2023 – 2024.

[8] The Ph rings are approximately coplanar with the pyridylimine units in the *meso* isomers of other compounds that we have crystallographically characterized, whereas in the *rac* isomers of similar supramolecular structures there is twisting about the interannular bonds, see ref. 7.

[9] For recent examples of solvent-free reactions see, for metal complexes A. Orita, L. Jiang, T. Nakano, N. Ma, J. Otera, *Chem. Commun.* **2002**, 1362 – 1363; for ligands G. W. V. Cave, C. L. Raston, *J. Chem. Soc. Perkin Trans. 1* **2001**, *24*, 3258 – 3264.

[10] At low temperature, the NMR spectrum in acetonitrile also shows signals arising from two species and is analogous to the room-temperature NMR spectrum in dichloromethane.

[11] a) Crystal-structure data for $C_{29.25}H_{29}N_4O_{0.25}CuPF_6$, M_r = 649.07, cubic, space group $P4_232$, *a* = 27.5381(2), *b* = 27.5381(2), *c* = 27.5381(2) Å, α = 90, β = 90, γ = 90¤, *V* = 20883.4(3) Å^3, *T* = 180(2) K, λ = 0.71073, *Z* = 24, ρ_{calcd} = 1.239 Mg m^{-3}, *F*(000) = 2232, $\mu(Mo_{K\alpha})$ = 0.729 mm^{-1}, crystal: red plates, crystal dimensions = 0.4 × 0.02 × 0.01 mm, data collected with a Siemens SMART three-circle system with CCD area detector. The crystal was held at 180(2) K with an Oxford Cryosystem Cryostream Cooler; θ_{max} = 22.48°. A total of 88425 reflections were measured, 4550 unique [R_{int} = 0.1737]. Absorption correction by Psi-scan. Weighting scheme $w = 1/[\sigma^2(F_O^2) + (0.0383P)^2]$, where $P = (F_O^2 + 2F_c^2)/3$. GOF on F^2 was 1.499, *R*1 [for 10956 reflections with $I > 2\sigma(I)$] = 0.0830, *wR*2 = 0.2037. Data/restraints/parameters 22935/0/1317. Largest difference Fourier peak and hole 0.502 and −0.459 eÅ^{-3}. Refinement used SHELXL 97 (G. M. Sheldrick, **1997**); b) CCDC-187879 contains the supplementary crystallographic data for this paper. These data can be obtained free of charge via www.ccdc.cam.ac.uk/conts/retrieving.html (or from the Cambridge Crystallographic Data Centre, 12, Union Road, Cambridge CB2 1EZ, UK; fax: (+44) 1223-336-033; or deposit@ccdc.cam.ac.uk).

[12] B. Hasenknopf, J. M. Lehn, N. Boumediene, A. DupontGervais, A. VanDorsselaer, B. O. Kneisel, D. Fenske, *J. Am. Chem. Soc.* **1997**, *119*, 10956 – 10962; B. Hasenknopf, J. M. Lehn, B. O. Kneisel, G. Baum, D. Fenske, *Angew. Chem.* **1996**, *108*, 1987 – 1990; *Angew. Chem. Int. Ed. Engl.* **1996**, *35*, 1838 – 1846; O. Mamula, A. von Zelewsky, G. Bernardinelli, *Angew. Chem.* **1998**, *110*, 301 – 305; *Angew. Chem. Int. Ed.* **1998**, *37*, 290 – 293; P. L. Jones, K. J. Byrom, J. C. Jeffery, J. A. McCleverty, M. D. Ward, *Chem. Commun.* **1997**, 1361 – 1362; G. Baum, E. C. Constable, D. Fenske, C. E. Housecroft, T. Kulke, *Chem. Commun.* **1999**, 195 – 196; C. Provent, E. Rivara-Minten, S. Hewage, G. Brunner, A. F. Williams, *Chem. Eur. J.* **1999**, *5*, 3487 – 3494.

[13] Supramolecular triangles (assembled using square-planar Pd/Pt chemistry) which stack linearly through the faces were reported and give infinite tubes or discrete dimers: R. -D, Schnebeck, E. Freisinger, B. Lippert, *Chem. Commun.* **1999**, 675 – 676; M. C. Jennings, R. J. Puddephatt, *Chem. Commun.* **2001**, 2676 – 2677, and references there-

 © 2002 WILEY-VCH Verlag GmbH & Co. KGaA, Weinheim 0044-8249/02/4122-4246 $ 20.00+.50/0

in. Metal–ligand interactions have been used to assemble planar triangular ligands into a tetrahedral array: I. M. Müller, R. Robson, F. Separovic, *Angew. Chem.* **2001**, *113*, 4519 – 4520; *Angew. Chem. Int. Ed.* **2001**, *40*, 4385 – 4386.

[14] NMR dilution studies in CD_2Cl_2 over the range 15.5–0.5 mM revealed no change in the positions of the resonance signals corresponding to either trimer or dimer implying no further aggregation of the triangle (or dimer) into a higher-order species occurs at these concentrations. The ratio of the two species varies over the concentration ratios as expected.

[15] The crystals resolve spontaneously and all the balls in the crystal are of the same chirality.

[16] For discussions of C–H···X bonds see for example: T. Steiner, *Chem. Commun.* **1997**, 727 – 734; T. Steiner, *Chem. Commun.* **1999**, 313 – 314; G. R. Desiraju, *Acc. Chem. Res.* **1991**, *24*, 290 – 296; G. R. Desiraju, *Acc. Chem. Res.* **1996**, *29*, 441 – 449; For short contacts to anions see for example: M. L. Tong, H. K. Lee, X. M. Chen, R. B. Huang, T. C. W. Mak, *J. Chem. Soc. Dalton Trans.* **1999**, 3657 – 3659; C. V. K. Sharma, S. T. Griffin, R. D. Rogers, *Chem. Commun.* **1998**, 215 – 216, and references therein; M. J. Hannon, C. L. Painting, E. A. Plummer, L. J. Childs, N. W. Alcock, *Chem. Eur. J.* **2002**, *8*, 2226 – 2238.

[17] Recent work has demonstrated that nanoscale capsules may also be assembled from poly-monodentate ligands and suitable metal ions. See for example: B. F. Abrahams, S. J. Egan, R. Robson, *J. Am. Chem. Soc.* **1999**, *121*, 3535 – 3536; N. Takeda, K. Umemoto, K. Yamaguchi, M. Fujita, *Nature* **1999**, *398*, 794 – 796; B. Olenyuk, J. A. Whiteford, A. Fechtenkötter, P. J. Stang, *Nature* **1999**, *398*, 796 – 799; Poly-didentate ligands with octahedral metal centers can also give capsules: D. L. Caulder, K. N. Raymond, *J. Chem. Soc. Dalton Trans.* **1999**, 1185 – 1200; Z. R. Bell, J. C. Jeffery, J. A. McCleverty, M. D. Ward, *Angew. Chem.* **2002**, *114*, 2625 – 2628; *Angew. Chem. Int. Ed.* **2002**, *41*, 2515 – 2518; R. W. Saalfrank, E. Uller, B. Demleitner, I. Bernt, *Struct. Bonding* **2000**, *96*, 149 – 175; R. W. Saalfrank, N. Löw, B. Demleitner, D. Stalke, M. Teichert, *Chem. Eur. J.* **1998**, *4*, 1305 – 1311.

 © 2002 WILEY-VCH Verlag GmbH & Co. KGaA, Weinheim 0044-8249/02/4122-4247 $ 20.00+.50/0

Induction of Cell Differentiation in Transformed Keratinocytes by Synthetic (Glyco)peptides from the Homophilic Recognition Domain of E-Cadherin**

Jörg Habermann, Kerstin Stüber, Tanja Skripko, Tanja Reipen, Raimund Wieser, and Horst Kunz*

Dedicated to Professor Peter Welzel on the occasion of his 65th birthday

The epithelial cell adhesion glycoprotein E-cadherin plays an essential role in the adhesion of epithelial cells.[1] E-cadherin is also involved in other important processes of cellular organization, including differentiation,[2] growth regulation, and morphogenesis.[3,4] The E-cadherin-mediated cell adhesion is decreased in carcinomas, whereas the CD44-mediated adhesion is increased.[5] The reduced expression of E-cadherin is evidently a significant indication of tumorigenesis.[5–8] E-Cadherin is linked to the actin filament network through the catenins and, therefore, integrated into key pathways of adhesion-dependent morphogenetic processes.[7] The interaction of E-cadherin on epithelial cells is both homotypic (i.e. among the same cell type) and homophilic (i.e. among the same molecules).[9,10] The homophilic recognition between molecules of E-cadherin occurs through the formation of dimers and is mediated by a recognition domain that is embedded in the furthermost (E-CAD1) of five extracellular units (Figure 1). According to NOE NMR spectroscopic analysis, a surface formed by three β sheets (βC, βF, βG) seems to be crucial for the recognition.[9] This surface includes the turn-motif Ser 83–Gly 85 and presents the recognition motif His 79-Ala 80-Val 81 located in βF in a well-defined steric arrangement (Figure 1).

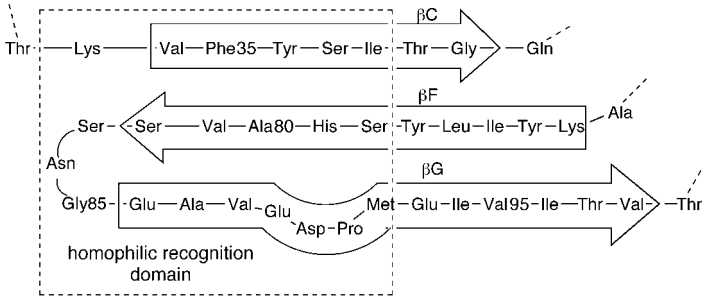


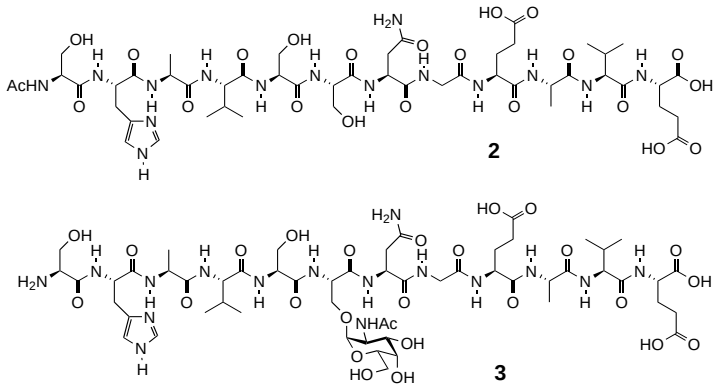
Figure 1. Schematic representation of the homophilic recognition domain of E-cadherin according to ref. [9].

As a result of the importance of E-cadherin to morphogenesis, tumor development, and self-recognizing effects[9,10] it is interesting to investigate the influence of synthetic partial structures of the recognition domain of E-cadherin on the self-recognition phenomenon.

The peptide, glycopeptide, and cycloglycopeptide structures of sequence **1** from the homophilic recognition surface were synthesized by solid-phase methodologies on Tentagel resin[11] as a solid support by using the allylic HYCRON linker.[12] These partial structures begin with Glu 89 at the C-terminus (Figure 1) and contain a portion of β-sheet βG, the turn-motif Ser 83–Gly 85 (partly glycosylated on serine), and a portion of β-sheet βF, including the His 79-Ala 80-Val 81 recognition motif.[1,9]

–Ser 78-His-Ala 80-Val-Ser-Ser-Asn-Gly 85-Glu-Ala-Val-Glu– **1**

The first synthesis of the dodecapeptide Ser 78–Glu 89 (**2**) with tetramethyl-*O*-(1-benzotriazolyl)uronium tetrafluoroborate (TBTU)[13] as coupling reagent suffered from low coupling yields from the eighth coupling step onwards (Val 81), apparently as a result of backfolding effects. Hence *N*,*N*,*N*′,*N*′-bis(tetramethylene)-*O*-pentafluorophenyluronium hexafluorophosphate (PfPyU)[14] was used as the coupling reagent in further solid-phase syntheses.



Whereas acid-labile side-chain protection could be employed in the syntheses of linear peptide **2** and glycosylated peptide **3** (*tert*-butyl group for serine and glutamic acid as well as trityl group for asparagine and histidine),[14] the synthesis of the cyclized peptides needed a more differentiating protecting-group strategy at the γ-carboxy group of the glutamic acid units. The formation of the cyclopeptide should favor a turn-type conformation that is in accordance with the secondary structure of the homophilic-binding domain of E-CAD1.

In view of the sequence it appeared to be favorable to carry out the cyclization not through the C-terminal carboxy group in solution[15,16] or on a solid-phase,[17,18] but rather through the γ-carboxy group of the C-terminal glutamic acid. The absence of lysine at the N-terminus[19] required the use of the terminal amino group of Ser 78 in the cyclization. Glycopeptide **5** was synthesized by starting from fluorenylmethoxycarbonyl (Fmoc)-glutamic acid γ-*tert*-butylester **4** loaded on a solid support.[14] Cyclization on the solid-phase to provide **6**,

[*] Prof. Dr. H. Kunz, Dr. J. Habermann, Dr. T. Skripko, Dipl.-Chem. T. Reipen
Institut für Organische Chemie, Universität Mainz
Duesbergweg 10–14, 55128 Mainz (Germany)
Fax: (+49) 6131-392-4786
E-mail: hokunz@mail.uni-mainz.de
K. Stüber, Priv.-Doz. Dr. R. Wieser[+]
Institut für Toxikologie, Universität Mainz
[+] Present address: Innotides GmbH, its 52499 Baesweiler (Germany)

[**] This work was supported by the Volkswagenstiftung and the Deutsche Forschungsgemeinschaft. JH is grateful for a postdoctoral grant from the Fonds der Chemischen Industrie.

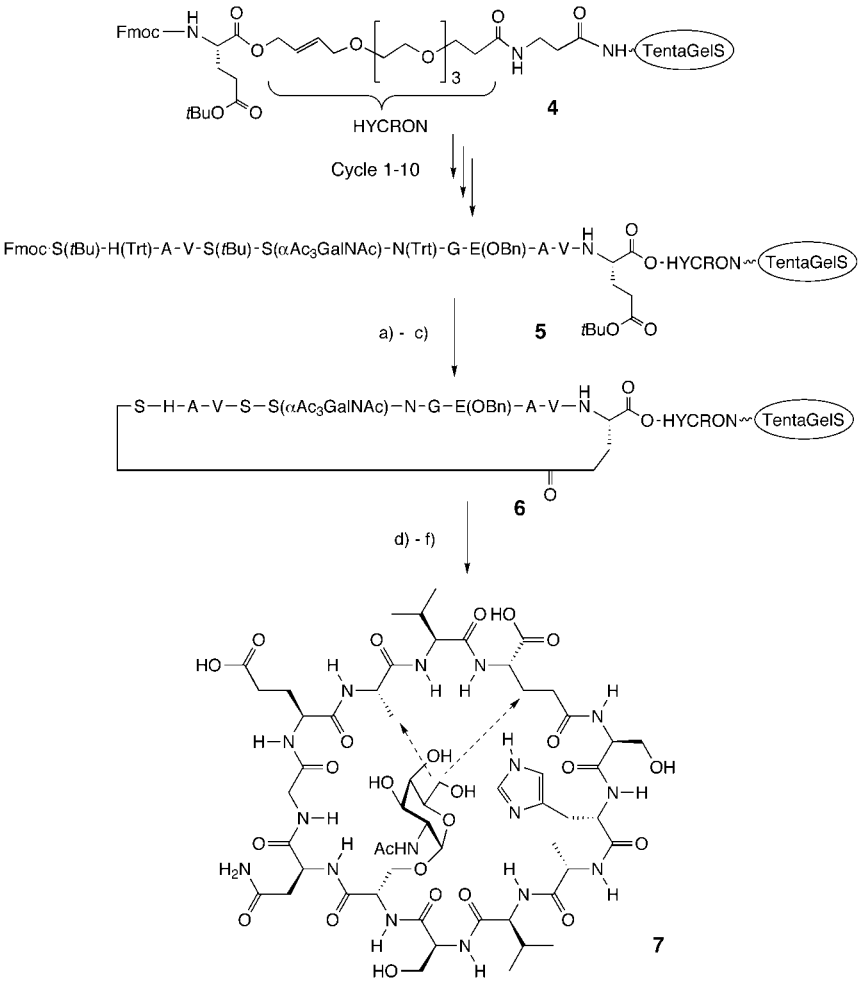
 © 2002 WILEY-VCH Verlag GmbH & Co. KGaA, Weinheim 0044-8249/02/4122-4249 $ 20.00+.50/0

removal from the solid support, and subsequent deprotection yielded cyclopeptide **7** (Scheme 1).

After cleavage of the Fmoc group of **4**, the dipeptide Fmoc-Ala-Val-OH was coupled by the use of PfPyU[14] in the presence of 1-hydroxy-7-aza-benzotriazol (HOAT).[20] The coupling of a dipeptide requires a mild but efficient carboxy activation owing to the risk of epimerization, but in the subsequent Fmoc removal the detachment of the peptide from the resin by intramolecular aminolysis is prevented. The second glutamic acid building block was utilized as γ-benzyl ester (Fmoc-Glu(OBzl)-OH) in a five- to sixfold excess, as was the case with all the carboxy building blocks. As an exception, only 2 equivalents of the α-*O*-galactosamine–serine conjugate were used.

Prior to the on-resin cyclization, the immobilized glycododecapeptide **5** was deprotected by a mixture of trifluoroacetic acid (TFA)/water/triisopropylsilane (95:5:5), and the Fmoc group was cleaved with morpholine/DMF. The allylic linker was not affected under these conditions. Activation of the γ-carboxy group of Glu 89 by PfPyU in the presence of Hünig's base and *sym*-collidine furnished the cyclized structure **6**. The cycloglycopeptide was detached from the resin by using Pd^0-catalyzed allyl transfer to morpholine.[12] Hydrogenation of the Glu-γ-benzyl ester and removal of the *O*-acetyl groups from the carbohydrate moiety by Zemplén transesterification (pH 9) yielded the pure cycloglycopeptide **7**[21] after purification by preparative HPLC in water/acetonitrile (0.1 % TFA). The analytical HPLC showed that **7** exists in several conformations,[16] which can be converted into one another by tempering at 40 °C.

The structure of **7** was confirmed by ROESY NMR spectroscopy experiments in D_2O which showed contacts between 6-H of the *N*-acetylgalactosamine and one methyl group of alanine group (presumably position 3, i.e. Ala 87) and the β-methylene group of a glutamic acid residue (presumably position 1). This orientation was surprising at first, as the nonglycosylated peptide **2** does not adopt any preferred conformation in solution (D_2O) and, in contrast, the glycosylated glycododecapeptide **3** prefers a different turn-type structure in water. In its ROESY NMR spectrum, cross peaks caused by dipolar coupling between the valine γ-methyl protons and 2-H of the imidazole ring on the one hand and 6-H of the GalNAc residue on the other hand are found. In addition, a cross peak between the α-H of Val and 2-H of the imidazole ring and a weaker coupling between the γ-H of Val and 4-H of the imidazole ring is observed (Figure 2).



Scheme 1. Solid-phase synthesis of cycloglycododecapeptide **7** on allylic HYCRON resin (experimental description in ref. [11]). Cycle 1: 1) morpholine/*N*,*N*-dimethylformamide (DMF); 2) Fmoc-Ala-Val-OH, PfPyU, HOAt, *s*-collidine, *N*-methylpyrrolidone (NMP); 3) Ac_2O, pyridine; cycles 2–10: 1) morpholine/DMF; 2) Fmoc-Xaa-OH, PfPyU, HOAt, *s*-collidine, NMP; a) Trifluoroacetic acid (TFA), triisopropylsilane, H_2O; b) morpholine, DMF; c) PfPyU, Et*i*Pr_2N, *s*-collidine, NMP; d) [$Pd(Ph_3P)_4$], morpholine, DMF, dimethyl sulfoxide; e) H_2/Pd in MeOH; f) NaOMe in MeOH, pH 9. In the scheme, the amino acids are represented with their 1-letter codes.

The dipolar coupling between the side chains of the His-Ala-Val motif and between the side chains and the GalNAc residue indicate a turn conformation **A** of structure **3** that is different from the cycloglycopeptide **7**. Further confirmation for the turn conformation **A** comes from the downfield shift of the signals for 6-H of the carbohydrate residue, presumably caused by the proximity of the aromatic imidazole ring.

It is remarkable that the different conformational properties of (glyco)peptides **2**, **3**, and **7** from the homophilic recognition domain of E-cadherin reflect the dissimilar effects of these compounds on transformed HaCat keratinocytes.

HaCat cells[22] are transformed, immortalized basal keratinocytes that express E-cadherin. However, within one week no differentiation to normal keratinocytes can be detected. These HaCat cells, confluently cultivated in a cell-culture medium (CG medium, Vitromex), supplemented with fetal calf serum (FCS; 0.5 %) were treated with the E-CAD-(glyco)peptide structures **2**, **3**, and **7** (25 μmol mL^{-1}; 18–20 μM) under an atmosphere containing 10 % CO_2 at a humidity of 85 %. They were incubated for 24 h. To investigate

 © 2002 WILEY-VCH Verlag GmbH & Co. KGaA, Weinheim 0044-8249/02/4122-4250 $ 20.00+.50/0

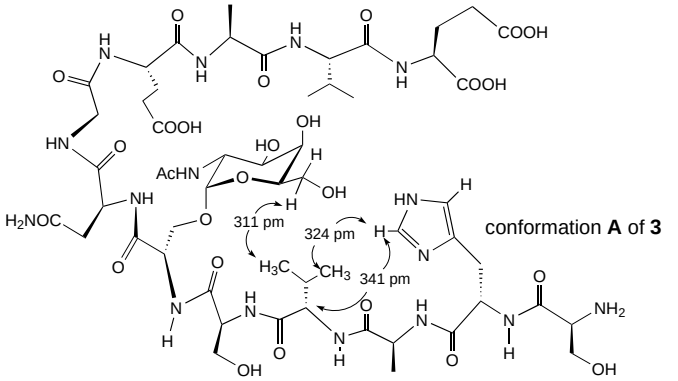


Figure 2. NOE effects (arrows) derived from the ROESY ^{1}H NMR spectrum of E-CAD-glycododecapeptide **3** in D_2O and the deduced conformation **A**.

their cell status, the cells were washed three times with buffer solution (PBS, pH 7.4, 37 °C), fixed, and permeabilized with acetone (5 min). Subsequently, the following antibody solutions containing 5% BSA (bovine serum albumin) were added to the cells: mouse-anti-involucrin (1:50), mouse-anti-CD44 (1:20), and rabbit-anti-contactinhibin receptor[23] (1:20). To visualize the binding of these antibodies in immunofluorescence assays, the second antibodies attached to the first antibodies were tagged with CY3 dye: anti-mouse-CY3 (1:300) and anti-rabbit-CY3 (1:300) in PBS buffer solution. Typical results of the immunofluorescence assay of fixed and permeabilized HaCat cells are shown in Figure 3.

Involucrin (hINV)[24] is an important marker in the keratinocyte differentiation process. Compared to the control (Figure 3a,) the amount of involucrin is clearly increased in HaCat cells after treatment with linear glycododecapeptide **3** (Figure 3b,). In contrast, this is not the case after treatment with linear peptide **2** (Figure 3c) or cyclopeptide **7**. The interaction of the contactinhibin receptor[23] with the cell-surface glycoprotein contactinhibin is decisively involved in the contact-dependent regulation and inhibition of cell growth. The expression of the contactinhibin receptor is strongly induced by the E-CAD1 glycododecapeptide **3** (Figure 3e), whereas peptide **2** (Figure 3d, control is similar) and cyclopeptide **7** (Figure 3f) do not show any influence on the contactinhibin receptor. In addition, the expression of the CD44 receptor,[25] which plays a role in the adhesion and metastasis of tumors, is distinctly decreased after treatment of the HaCat cells with synthetic glycopeptide **3** (Figure 3h) in comparison with the control (Figure 3g). The results of the immunohistochemical experiments are associated with the impressive alteration of the cellular morphology and the three-dimensional architecture of the HaCat cell culture after addition of the biologically active glycopeptide **3**: the HaCat keratinocytes grow into the suprabasal level, form supracellular structures and a differentiated cytoskeleton. Furthermore, the expression of differentiation markers such as involucrin and the contactinhibin receptor is enhanced (Figure 3b and e). The contactinhibin receptor is transferred from the cytosol into the cell membrane. Cells treated with the inactive peptides **2** and **7** show no alteration compared to the control experiments and do not undergo distinct differentiation within 10 days, even though both structures contain the identical amino acid sequence as the active structure **3**.

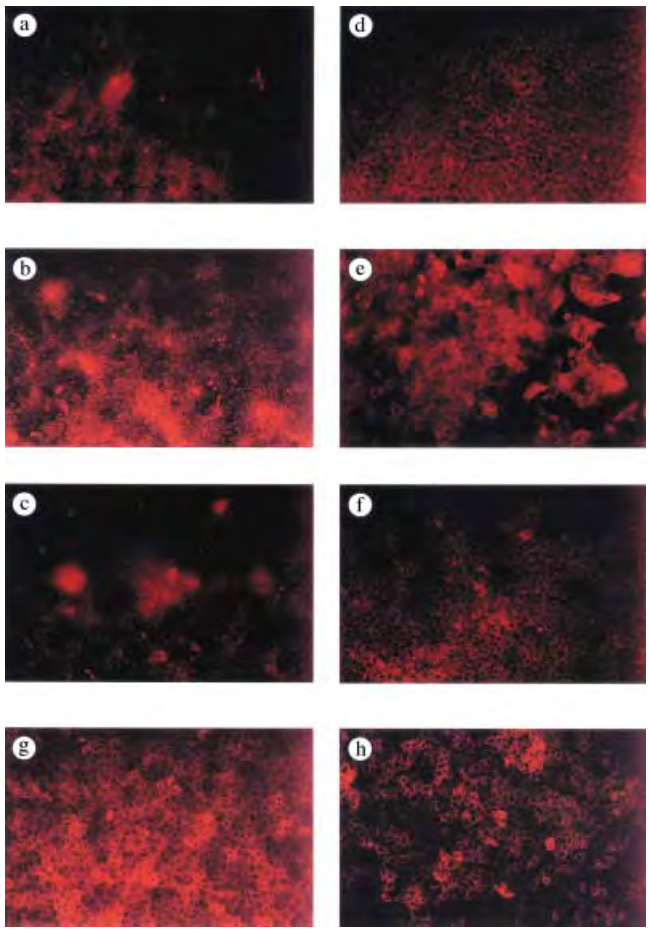


Figure 3. Biological effects of the synthetic (glyco)peptides **2**, **3**, and **7** on transformed basal keratinocytes of the HaCat cell line;[22] immunofluorescence microscopy assays: a) control, 1. mouse-anti-involucrin (Sigma, 1:50 in blocking solution), 2. anti-mouse-CY3 (Jackson, 1:1 in glycerol, 1:300 in PBS; b) E-CAD-glycododecapeptide **3**, 24 h, then immunostaining identical to (a); c) E-CAD-dodecapeptide **2**, 24 h, then immunoassay, for involucrin as in a); d) E-CAD-dodecapeptide **2**, 24 h, rabbit-anti-contactinhibin receptor (ref. [15], 1:2 in blocking solution), 2. anti-rabbit-CY3 (Jackson, 1:1 with glycerol, 1:300 in PBS); e) E-CAD-glycododecapeptide **3**, 24 h, then immunoassay for contactinhibin receptor as in (d); f) E-CAD-cycloglycododecapeptide **7**, 24 h, then immunoassay for contactinhibin receptor as in (d); g) control, 1. mouse-anti-CD44, PE conjugated (Natu-Tec, 1:20 in blocking solution), 2. anti-mouse-CY3 (Jackson, 1:1 with glycerol, 1:300 in PBS); h) E-CAD-glycododecapeptide **3**, then immunoassay identical to (g).

In conclusion, the significant induction of differentiation seems to be connected to the preferred conformation of the E-CAD-glycopeptide in water in which the recognition motif His-Ala-Val is presented in a well-defined steric arrangement. The mechanism of the induction of differentiation in HaCat cells[22] has to be investigated further, in particular whether the synthetic E-CAD-glycopeptides **3** bind to E-cadherin itself as is presumed by the homophilic recognition mechanism.[9,10] The expression and activation of E-cadherin seems to be crucial for tumor suppression.[6,7,25] Hence the conformation-dependent effects of the E-CAD-glycopeptide **3** that induce differentiation, as well as adhesion and integration

 © 2002 WILEY-VCH Verlag GmbH & Co. KGaA, Weinheim 0044-8249/02/4122-4251 $ 20.00+.50/0

abilities in transformed HaCaT keratinocytes within 24 h, is of interest to the development of tumor suppressors.

Received: May 21, 2002 [Z19348]

[1] O. Huber, C. Bierkamp, R. Kemler, *Curr. Opin. Cell Biol.* **1996**, *8*, 685 – 691.
[2] Y. Saeki, K. Hazeki, M. Matsumoto, K. Toyoshima, H. Akedo, T. Seya, *Oncol. Rep.* **2000**, *7*, 731 – 735.
[3] M. Takeichi, *Science* **1991**, *251*, 1451 – 1455.
[4] a) M. Takeichi, *Curr. Opin. Cell Biol.* **1995**, *7*, 619 – 627; b) S. K. Runswick, M. J. O'Hare, L. Jones, C. H. Streuli, D. R. Garrod, *Nat. Cell. Biol.* **2002**, *3*, 823 – 830.
[5] a) S. Jothy, S. B. Munro, L. LeDuy, D. McClure, O. W. Blaschuk, *Cancer Metastasis Rev.* **1995**, *14*, 363 – 376; b) T. Mikami, M. Saegusa, H. Mitomi, N. Yanagisawa, M. Ichinoe, I. Okayasu, *Am. J. Clin. Pathol.* **2001**, *116*, 369 – 376.
[6] A.-K. Perl, P. Wilgenbus, U. Dahl, H. Semb, G. Christofori, *Nature* **1998**, *392*, 190 – 193.
[7] W. Birchmeier, J. Behrens, *Biochim. Biophys. Acta* **1994**, *1198*, 11 – 26.
[8] I. K. Bukholm, J. M. Nesland, R. Karessen, U. Jacobsen, A. L. Borresen-Dale, *Virchows Arch.* **1997**, *431*, 317 – 321.
[9] M. Overduin, T. S. Harvey, S. Bagby, K. I. Tong, P. Yau, M. Takeichi, M. Ikura, *Science* **1995**, *267*, 386 – 389.
[10] E. Y. Jones, *Curr. Opin. Cell Biol.* **1996**, *8*, 602 – 608.
[11] W. Rapp, E. Bayer in *Innovations and Perspectives in Solid Phase Synthesis: Peptides, Polypeptides and Oligonucleotides* (Ed.: R. Epton), Intercept, Andover, **1992**, pp. 259 – 266.
[12] O. Seitz, H. Kunz, *J. Org. Chem.* **1997**, *62*, 813 – 826.
[13] R. Knorr, A. Trzeciak, W. Bannwarth, D. Gillessen, *Tetrahedron Lett.* **1989**, *30*, 1927 – 1930.
[14] a) J. Habermann, H. Kunz, *J. Prakt. Chem.* **1998**, *340*, 233 – 239; b) J. Habermann, H. Kunz, *Tetrahedron Lett.* **1998**, *39*, 265 – 268.
[15] a) H. Matter, G. Gemmecker, H. Kessler, *Int. J. Pept. Protein Res.* **1995**, *45*, 430 – 440; b) R. Haubner, D. Finsinger, H. Kessler, *Angew. Chem.* **1997**, *109*, 1440 – 1456; *Angew. Chem. Int. Ed. Engl.* **1997**, *36*, 1374 – 1389.
[16] M. Gobbo, L. Biondi, F. Filira, R. Rocchi, T. Piek, *Int. J. Pept. Protein. Res.* **1995**, *45*, 282 – 289.
[17] A. Trzeciak, W. Bannwarth, *Tetrahedron Lett.* **1992**, *33*, 4557 – 4560.
[18] H. F. Brugghe, H. A. M. Timmermans, L. M. A. van Unen, G. J. Ten Hove, G. van de Werken, J. T. Poolman, P. Hoogerhout, *Int. J. Pept. Protein. Res.* **1994**, *43*, 166 – 172.
[19] V. Wittmann, S. Seeberger, *Angew. Chem.* **2000**, *112*, 4508 – 4512; *Angew. Chem. Int. Ed.* **2000**, *39*, 4348 – 4352.
[20] L. A. Carpino, A. El-Faham, *J. Org. Chem.* **1994**, *59*, 695 – 698.
[21] **7:** $[\alpha]_D^{23} = -48.2$ ($c = 1.0$, H_2O); MALDI TOF (2,5-dihydroxybenzoic acid, positive-ion mode): m/z: 1371.9 $[M+H]^+$; 1393.8 $[M+Na]^+$; ^{1}H NMR (D_2O, 600 MHz, ^{1}H,^{1}H-ROESY): $\delta = 8.60$ (s, 1H; Im 2-H), 7.29 (s, 1H; Im 4-H), 4.88 (br s, 1H; Gal 2-H), 3.57–3.54 (m, 2H; Gal 6-H), 2.20–1.96 ppm (m, 11H; Sβ, 2 × Eβ, 2 × Vβ, CH_3CO_2).
[22] a) P. Boukamp, R. T. Petrussevska, D. Breitkreutz, J. Hornung, A. Markham, N. E. Fusenig, *J. Cell Biol.* **1988**, *106*, 761 – 771; b) V. M. Schoop, N. Mirancea, N. E. Fusenig, *J. Invest. Dermatol.* **1999**, *112*, 343 – 353.
[23] G. Gradl, D. Faust, F. Oesch, R. J. Wieser, *Curr. Biol.* **1995**, *5*, 526 – 535.
[24] N. A. Robinson, P. T. LaCelle, R. L. Eckert, *J. Invest. Dermatol.* **1996**, *107*, 101 – 107.
[25] a) A. Stöckinger, A. Eger, J. Wolf, H. Beug, R. Foisner, *J. Cell Biol.* **2001**, *154*, 1185 – 1196; b) I. El-Hariry, M. Pignatelli, N. R. Lemoine, *Int. J. Cancer* **2001**, *94*, 652 – 661; c) M. A. Perez Moreno, A. Locascio, I. Rodrigo, G. Dhondt, F. Portillo, M. A. Nieto, A. Cano, *J. Biol. Chem.* **2001**, *276*, 27424 – 27431.

pH-Responsive Molecular Nanocarriers Based on Dendritic Core-Shell Architectures**

Michael Krämer, Jean-François Stumbé, Holger Türk, Simon Krause, Ansgar Komp, Lydie Delineau, Svetlana Prokhorova, Holger Kautz, and Rainer Haag*

Physical aggregates of amphiphilic molecules, such as micellar structures, are frequently proposed as drug-delivery systems.[1] These aggregates can be unstable under shear force and other kinds of environmental effects as a result of their weak assembly. They are also not very suitable for the active release of the encapsulated species through the application of an external trigger, such as pH change. For drug delivery in biological systems, in particular, the release of the encapsulated species must occur as a result of a weak external signal, for example, a pH drop in tumor and infected tissues (pH 5–6).[2,3] Furthermore, it has been demonstrated that nanoparticles larger than 5 nm, such as liposomes and macromolecular carriers, can pass through biological membranes by different mechanisms than small molecules, and thereby enhance the specificity of drugs for certain tissues (for example, tumor).[4–6]

In contrast to physical aggregates of amphiphilic molecules, the covalent modification of dendritic macromolecules[7] with an appropriate shell results in stable micelle-type structures, which are suitable for the noncovalent encapsulation of guest molecules.[8] While the encapsulation and the transport of guest molecules into these dendritic architectures have been studied by several research groups,[9–16] relatively little is known about the active release of the encapsulated guest molecules by the pH-triggered cleavage of the shell under physiological conditions. So far, a pH-dependent release from dendritic architectures has only been reported under drastic conditions[17] or by protonation of poly(propyleneimine) dendrimers[18] and their derivatives.[19,20]

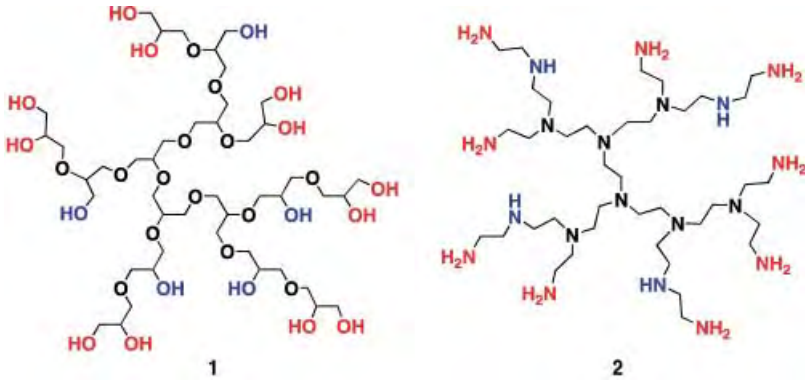
Herein we describe a simple and general synthetic concept for the generation of pH-responsive molecular nanocarriers based on the selective and reversible shell functionalization of dendritic polymers, such as polyglycerol (PG, **1**) and polyethyleneimine (PEI, **2**, Scheme 1). Polyglycerol (**1**) and polyethyleneimine (**2**) are randomly branched, but well-defined dendritic structures with a degree of branching of 60

[*] Dr. R. Haag, Dipl.-Chem. M. Krämer, Dr. J.-F. Stumbé, Dipl.-Chem. H. Türk, S. Krause, A. Komp, Dr. L. Delineau, Dr. S. Prokhorova, Dipl.-Chem. H. Kautz
Freiburger Materialforschungszentrum und
Institut für Makromolekulare Chemie
Universität Freiburg
Stefan-Meier-Strasse 21, 79104 Freiburg (Germany)
Fax: (+49) 761-203-4709
E-mail: rainer.haag@fmf.uni-freiburg.de

[**] The authors would like to thank Prof. Rolf Mülhaupt for his support, and Katrin Armbruster and Bernhard Siegel for the preparation of some intermediates. BASF AG is kindly acknowledged for the donation of chemicals. R.H. is indebted to the Deutsche Forschungsgemeinschaft Fonds der chemischen Industrie and the Dr. Otto-Röhm Gedächtnisstiftung for financial support.

Supporting information for this article is available on the WWW under http://www.angewandte.org or from the author.

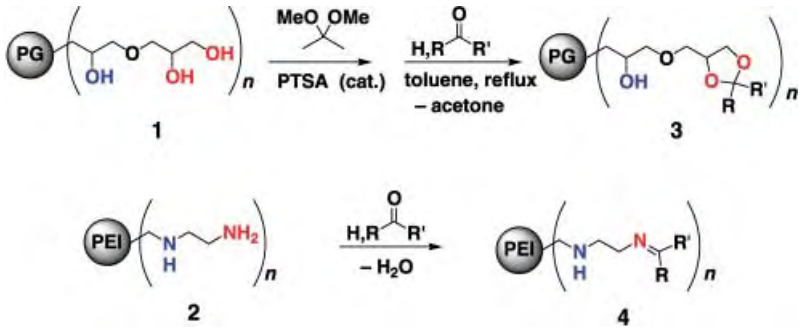
 © 2002 WILEY-VCH Verlag GmbH & Co. KGaA, Weinheim 0044-8249/02/4122-4252 $ 20.00+.50/0



Scheme 1. Polyglycerol (PG, **1**) and polyethyleneimine (PEI, **2**) were used as hydrophilic dendritic core molecules for the selective generation of pH-responsive molecular nanocarriers. The depicted structures containing 30–40 % of linear functional groups (blue) and 60–70 % terminal groups (red) are only small idealized fragments of the large polymer cores.

to 75 %. They are prepared in a one-step process and are readily available on a large scale with low polydispersities (<2).[21] The chemical differentiation and selective modification of the linear (blue) and terminal groups (red) in polyglycerol (**1**) results in core-shell-type architectures.[22] However, a pronounced polarity difference between core and shell is necessary to generate unimolecular micelle-type architectures with good transport properties,[8] but this was not possible with the previously reported core-shell-type architectures.[22] We have now developed a general synthetic concept to construct amphiphilic dendritic architectures for potential application in pH-dependent delivery of the encapsulated guest by using two types of acid-sensitive linkages for the shell: PG-acetals/ketals **3** and PEI-imines **4** (Scheme 2).

Formally, the selective functionalization of the shell of both dendritic polymers (PG (**1**) and PEI (**2**)) is a simple condensation reaction between the terminal groups (1,2-diol or NH_2, respectively) and a carbonyl compound. However, the direct conversion of polyglycerol (**1**) with unreactive or lipophilic carbonyl compounds was not possible.[23] A two-step (one-pot) protocol based on two consecutive transketalization reactions (see Supporting Information) was developed to generate pH-responsive molecular nanocarriers. In the first step PG (**1**) was treated with an excess of acetone dimethylacetal to give the corresponding PG-acetonide,[22] which can subsequently be converted with an equimolar amount of a large variety of carbonyl compounds, for example, long-chain alkyl ketones, into dendritic core-shell architectures **3**. The situation is even more straight forward in the case of PEI (**2**), since simple nonpolar carbonyl compounds, such as 6-undecanone and 1-hexadecanal, can be directly treated with PEI (**2**) to give the corresponding core-shell architectures **4**.[24] The reaction even occurs spontaneously at room temperature in the case of hexadecanal. Both types of core-shell architectures (**3** and **4**) are now accessible in high yields (70–90 %) and multigram quantities. We have investigated several dendritic core-shell architectures which differ in 1) the type of the core polymer, 2) the molecular weight of the core polymer, 3) the structure of the attached shell, and 4) the density of the attached shell (the degree of alkylation).

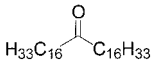
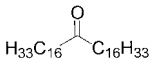
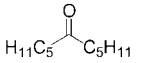


Scheme 2. General synthetic concept for the generation of amphiphilic core-shell architectures (compare Table 1). Terminal groups (red: 1,2-diols or NH_2, respectively) were selectively functionalized with aldehydes and ketones by either a twofold transketalization or imine condensation. Linear units (blue) remain unreacted. PTSA = *p*-toluene sulfonic acid.

The transport capacities (amount of encapsulated guest molecules per polymer molecule) of these molecular nanocarriers were first determined using congo red as an easily detectable polar model compound (Table 1). For this purpose the dendritic core-shell architecture was dissolved in chloroform and treated with aqueous dye solutions of different concentrations. Alternatively the guest can also be encapsulated from the solid-phase/organic-solution interface. The amount of encapsulated dye was determined in all cases by UV absorption of the organic phase (see Supporting Information). Similar to other dendritic core-shell architectures,[8] a minimum core size (ca. 3000 g mol^{-1}) and a highly branched architecture are required for successful encapsulation of the guest molecules.[14b] For efficient transport the degree of alkylation should be about 45–50 % and the alkyl chains should have a minimum length ($>C_{10}$). For example, the conversion of the terminal groups in polygylcerol **1** (21 000 g mol^{-1}) with a C_{16} aldehyde (**3a**) containing one alkyl chain per diol unit results in an effective degree of alkyl functionalization of 25 % (Table 1) and a poor transport capacity (0.15 congo red molecules). With the same PG core (21 000 g mol^{-1}), the ketal functionalized nanocarrier **3b** with two alkyl chains per diol unit and 45 % effective alkyl functionalization (Table 1) can transport up to 13 congo red molecules. A higher degree of ketal functionalization (**3c**: 55 %, Table 1) indicates an optimal shell density of 45–50 %. However, only two dye molecules were encapsulated in **3c** and the encapsulation process was very slow. Smaller core polymers, shorter alkyl chains, and lower degrees of functionalization also result in lower transport capacities. It is also noteworthy that the selective core-shell architecture **3b** (Table 1) can be up to eight times more efficient than polyglycerols of the same core size randomly functionalized with palmityl ester.[14a,25] This comparison demonstrates that the polar core environment of these nanocarriers is maximized as a result of the selective core-shell functionalization. The exact determination of the transport capacities for the amine based nanocarriers **4** (Table 1) was complicated because of the hydrolytic sensitivity of the imine-

 © 2002 WILEY-VCH Verlag GmbH & Co. KGaA, Weinheim 0044-8249/02/4122-4253 $ 20.00+.50/0

Table 1. Sizes and transport capacities of dendritic nanocarriers **3** and **4**.

Structure	Polymer core	M_n core [g mol^{-1}]	Shell	Degree of alkylation	Size[a] [nm]	Height[a] [nm]	Transport capacity[b]
1	PG	21 000	–	–	8 ± 2	2.7 ± 0.6	–[c]
3a	PG	21 000		25 %	10 ± 2	2.5 ± 0.5	0.15 ± 0.05
3b	PG	21 000		45 %	10 ± 2	2.7 ± 0.6	13 ± 4
3c	PG	21 000		55 %	10 ± 2	2.5 ± 0.5	2 ± 0.5
2	PEI	25 000	–	–	18 ± 4	3.2 ± 0.5	0.02 ± 0.005[d]
4a	PEI	25 000		33 %	20 ± 4	3.5 ± 0.5	0.6 ± 0.1[d]
4b	PEI	25 000		53 %	84 ± 16	9 ± 2[e]	0.2 ± 0.05[d,e]

[a] Corrected particle diameter and height without encapsulated guest molecules from AFM data (see Supporting Information). [b] Number of encapsulated dye molecules (congo red) per polymeric nanotransporter and transport into the chloroform phase. [c] Not soluble in chloroform. [d] Loading capacities were determined in chloroform without aqueous phase by using a UV calibration curve. [e] Partial hydrolysis and aggregate formation is possible with water.

bound shell in the PEI-based systems in some cases, for example, **4b** (see below). To avoid hydrolysis the dye was directly encapsulated from the solid/organic solution interface. Nevertheless, underestimation might occur because of partial cleavage of the shell.[26] For comparison, a chemically stable PEI-amide, for example, M_n(PEI) = 6000 g mol^{-1} with a palmitylic amide shell (50 %), can encapsulate up to 15 congo red molecules.[27]

The structure and the particle sizes of these nanocarriers in the unloaded and fully loaded states have been determined with molecular resolution by atomic force microscopy (AFM) in the tapping mode (Table 1, see also Supporting Information). The C_{33}-ketal-functionalized polyglycerol **3b** is shown as an example in Figure 1 a. The height of the nanocapsules was obtained from the cross-sectional profiles (for example, recorded along the track marked by the dotted line in Figure 1 a) to be in the range of 2–3 nm. The diameter distribution of the particles was calculated by evaluation of more than 120 particles of each sort and subsequent deconvolution with the AFM tip (Table 1). The number-average diameter of the nanocarrier **3b** appeared to be 10 ± 2 nm for the unloaded state and 13 ± 2 nm for the dye-loaded state (Figure 1 b,c). This behavior can be explained by a swelling of the polymer core upon encapsulation of the guest molecules. All the particle sizes determined by AFM studies for the PG-based systems **3** are in good agreement with those calculated by extrapolation from a core with a molecular weight of 4000 g mol^{-1}.[28] This observation indicates that these dendritic nanocarriers act as inverted unimolecular micelles in dilute solutions ($< 10^{-4}$ M). However, larger aggregates are observed at higher concentrations ($> 10^{-3}$ M).[29] The particle sizes of the PEI-based nanocarriers **4** indicate formation of partial aggregates in some cases as a result of partial hydrolysis on the mica surface (see Supporting Information).[26] For comparison, the hydrolytically stable PEI-amides, for example, M_n(PEI) = 6000 g mol^{-1} with a palmityl amide shell (d = 6 nm), show the expected particle sizes.[27]

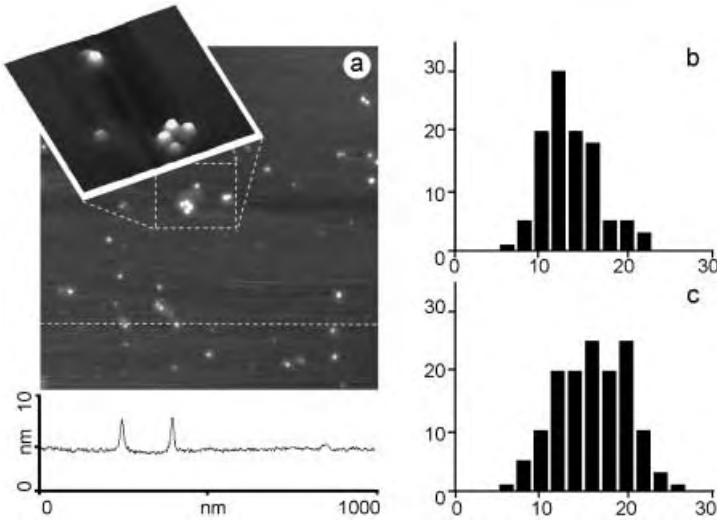


Figure 1. a) AFM images and cross-sectional height profile of individual nanocapsules **3b** prepared by spin-casting of a 10^{-5} M solution in chloroform onto a mica substrate. The z-axis scale is 10 nm. The length of the inserted 3D area is 200 nm. Histograms of the size distribution of the: b) unloaded nanocarriers and c) loaded nanocarriers. The histograms were plotted based on the evaluation of more than 120 particles in the AFM images.

The transport properties of these nanocarriers were then tested with different guest structures using the PG- and PEI-based nanocarriers **3** and **4**. Different types of dye molecules containing polar or ionic organic groups were used as model systems. Many organic dyes, such as bromophenol blue, congo red, methyl orange, methyl red, and fluorescein,[30] all of which contain polar anionic sulfonate or carboxylate groups and sodium counterions, were readily encapsulated and transported by both types of carrier systems **3** and **4** (see also Supporting Information). In contrast, cationic dyes, such as the triphenylmethane-based malachite green with an oxalate counterion, were not transported at all.

The complexation of an antitumor drug (mercaptopurine), several oligonucleotides, as well as bacteriostatic silver compounds (for example, Ag^I salts and Ag^0 nanoparticles)[27] have been studied for the potential use of these nanocarriers in drug and gene delivery. Successful encapsulation and transport were observed in all cases by the PEI-based nanocarriers **4**. No complexation, however, was observed with the PG-based nanocarriers **3** for these guest molecules.

 © 2002 WILEY-VCH Verlag GmbH & Co. KGaA, Weinheim 0044-8249/02/4122-4254 $ 20.00+.50/0 *Angew. Chem. Int. Ed.* **2002**, *41*, No. 22

The initial objective to develop a pH-sensitive carrier was now tested using several buffer solutions for both the acetal- and imine-bound shells. The encapsulated congo red dye in the nanocarrier **3b** was stable for several months at neutral and basic pH values (pH > 7). However, an immediate release of the guest molecules occurred in acidic media (pH < 3; Figure 2). Since congo red is a pH indicator dye (for pH 4–5), a change of color (red→blue) was observed concurrently with the cleavage of the shell (Figure 2). The cleavage of the PG-ketals also depends significantly on the percentage of shell functionalization: 45% (**3b**: 2 h, pH 2–3, 37°C) versus 55% (**3c**: 2 days, pH 0–1, 37°C). The imine-based nanocarriers are even more sensitive to an external drop in the pH value. In the case of nanocarrier **4a** the hydrolysis of the shell and the release of the encapsulated guest (namely, congo red) occurs over a period of four days at pH 6. However, it is stable over several weeks at neutral pH. On the other hand, the hydrolysis of the nanocarrier **4b** and the release of the encapsulated guest even occurs spontaneously at pH < 7. In the case of **4b**, a slow release can be observed after several hours (pH 8, ca. 3 h, 25°C) or days (pH 12, 2 days, 25°C) even without acidification. These PEI-based nanocarriers **4a**,**b** also show no color change of the indicator dye upon release (Figure 2).

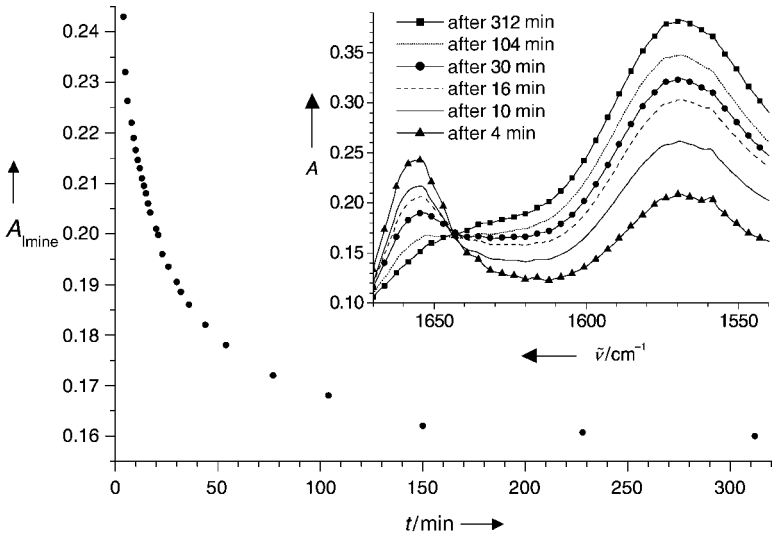


Figure 3. Time-dependence of the shell cleavage of PEI-imine **4b** on a KBr plate. Inset: The IR band of the imine peak at 1655 cm^{-1} decreases because of cleavage, while the N–H out of plane vibration at 1565 cm^{-1} increases.

In these release experiments it was demonstrated by dialysis (see Supporting Information) that no complexation of the encapsulated guest (for example, sodium picrate) occurred with either nanocarriers **3** or **4** in the aqueous phase at pH < 7.[31] For the PEI-based nanocarrier **4b**, the amount of dye release/shell cleavage was followed by IR spectroscopy through the disappearance of the imine signal (Figure 3). The kinetics of the imine hydrolysis on a KBr surface shows a rapid decay over about 3 h. This observation might also explain the formation of aggregates seen by AFM measurements as arising from partial shell cleavage on the mica surface. The analysis of different cleavage stages showed that approximately 30% shell cleavage is sufficient to destroy the ability of the dendritic macromolecules to act as molecular nanocarriers. This is also supported by the poor transport capacity of a 25% alkylated core-shell architecture **3a** (Table 1).

Although the detailed mechanism of encapsulation is currently being investigated, the higher selectivity for large anionic guest molecules can be explained by the strong interaction of such species with the polar groups in the core of these dendritic macromolecules. The hydroxy or amine groups in the dendritic core (shown in blue, Scheme 1) can replace the hydrate shell of the polar guest molecules, thus leading to a significant entropic gain by the liberated water molecules. The location of the encapsulated guest molecules (for example, methyl red) inside the dendritic architecture **3b** is also supported by a significant high-field shift (0.2 ppm) of the methyl group signal as a result of the shielding effect of the core-shell architecture, as observed in the ^{1}H NMR spectrum of the methyl red complex with **3b** (see Supporting Information). In addition, it was not possible to release the encapsulated methyl red from **3b** by either heating to reflux or ultrasonication at neutral pH. This result clearly dem-

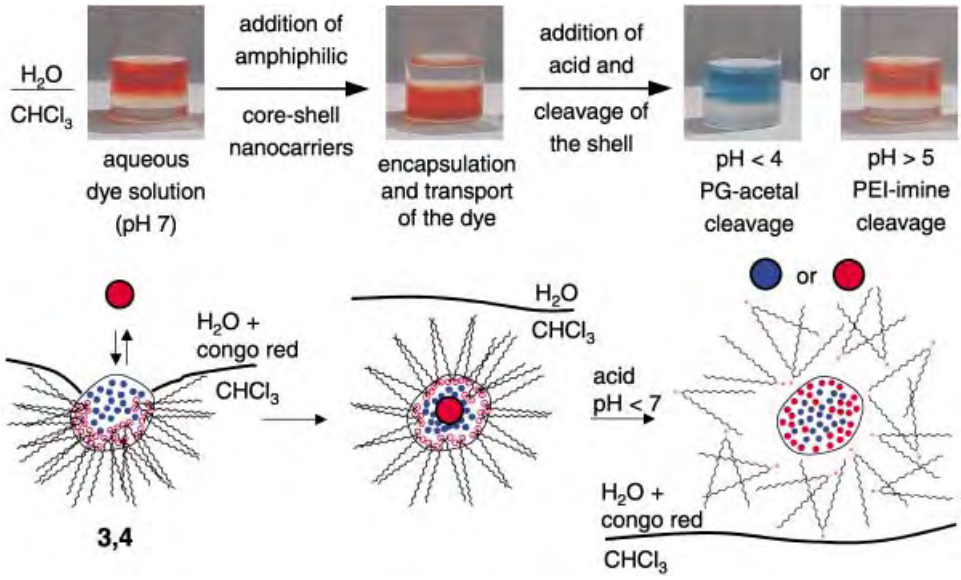


Figure 2. Encapsulation and transportation of polar guest molecules with dendritic nanocarriers **3** and **4** (blue and red dots indicate linear and terminal groups, respectively) into the organic phase. Cleavage of the shell leads to the release of the encapsulated guest back to the aqueous phase. Congo red (pH indicator: pH 4–5) was used as a model compound for the demonstration of the pH-dependent shell cleavage.

 © 2002 WILEY-VCH Verlag GmbH & Co. KGaA, Weinheim 0044-8249/02/4122-4255 $ 20.00+.50/0

onstrates the high mechanical stability of these unimolecular nanocarriers, which is not observed for physical aggregates, such as liposomes or micellar systems. Nevertheless, the release of an encapsulated guest molecule can be achieved by substitution with a molecule of higher binding affinity, as demonstrated by the titration of a bromophenol blue loaded nanocarrier **3b** with a solution of congo red (see Supporting Information). Hence, the encapsulation process is an equilibrium phenomena, which allows the guest molecules to be exchanged by competitive binding. This experiment also indicates that the binding mechanism can not be purely entropically driven and should also contain an enthalpic component.

In summary we have presented a simple general synthetic concept for the selective shell functionalization of dendritic polymers (namely, PG (**1**) and PEI (**2**)) to generate molecular nanocarriers **3** and **4** for the encapsulation and transport of polar guest molecules. The concept is highly flexible in terms of the shell and the core molecules. Dendritic polymers with a pH-responsive shell have been prepared which, for the first time, can selectively release the encapsulated guest molecules in a physiologically relevant pH range. AFM measurements with molecular resolution indicate that these nanocarriers act as inverted unimolecular micelles in concentrations below 10^{-3} M. In addition, various dyes and drugs, for example, bacteriostatic, cytostatic compounds, as well as oligonucleotides have been successfully encapsulated and transported by the amine-based nanocarriers **4**. This concept of pH-responsive molecular nanocarriers might have potential application for selective drug delivery in tissues of a lower pH value (for example, infected or tumor tissue). Further work on the pH sensitivity, biocompatibility, and water solubility of these controlled release systems is in progress.

Received: June 24, 2002 [Z19603]

[1] K. Kataoka, A. Harada, Y. Nagasaki, *Adv. Drug Delivery Rev.* **2001**, *47*, 113 – 131.

[2] D. E. Hallanan, *Semin. Radiat. Oncol.* **1996**, *6*, 243 – 244.

[3] P. Vaupel, F. Kallinowski, P. Okunieff, *Cancer Res.* **1989**, *49*, 6449 – 6465.

[4] H. Maeda, Y. Matsumura, *CRC Crit. Rev. Ther. Drug Carrier Syst.* **1989**, *6*, 193 – 210.

[5] Y. Takakura, M. Hashida, *Crit. Rev. Oncol. Hematol.* **1994**, *18*, 207 – 231.

[6] F. Yuan, M. Deilian, D. Fukumura, M. Leuning, D. A. Berk, V. P. Torchilin, R. K. Jain, *Cancer Res.* **1995**, *55*, 3752 – 3756.

[7] The general term "dendritic" (treelike) structure is used for both hyperbranched polymers as well as perfect dendrimers because of their similar properties with respect to the formation of supramolecular complexes; see also: G. R. Newkome, C. N. Moorefield, F. Vögtle, *Dendritic Molecules: Concepts, Syntheses, Perspectives*, 2nd ed., Wiley-VCH, Weinheim, **2001**.

[8] M. W. P. L. Baars, E. W. Meijer, *Top. Curr. Chem.* **2000**, *210*, 131 – 182, and references therein.

[9] G. R. Newkome, C. N. Moorefield, G. R. Baker, M. J. Saunders, S. H. Grossman, *Angew. Chem.* **1991**, *103*, 1207 – 1209; *Angew. Chem. Int. Ed. Engl.* **1991**, *30*, 1178 – 1180.

[10] J. F. G. A. Jansen, E. M. M. de Brabander-van den Berg, E. W. Meijer, *Science* **1994**, *266*, 1226 – 1229.

[11] S. Stevelmans, J. C. M. van Hest, J. F. G. A. Jansen, D. A. F. J. van-Boxtel, E. M. M. de Brabander-van den Berg, E. W. Meijer, *J. Am. Chem. Soc.* **1996**, *118*, 7398 – 7399.

[12] A. P. H. J. Schenning, C. Elissen-Román, J.-W. Weener, M. W. P. L. Baars, S. J. van der Gaast, E. W. Meijer, *J. Am. Chem. Soc* **1998**, *120*, 8199 – 8208.

[13] V. Chechik, M. Zhao, R. M. Crooks, *J. Am. Chem. Soc.* **1999**, *121*, 4910 – 4911.

[14] a) A. Sunder, M. Krämer, R. Hanselmann, R. Mülhaupt, H. Frey, *Angew. Chem.* **1999**, *111*, 3758 – 3761; *Angew. Chem. Int. Ed.* **1999**, *38*, 3552 – 3556; b) S.-E. Stiriba, H. Kautz, H. Frey, *J. Am. Chem. Soc.* **2002**, *124*, 9698 – 9699.

[15] M. Liu, K. Kono, J. M. J. Fréchet, *J. Controlled Release* **2000**, *65*, 121 – 131.

[16] C. Kojima, K. Kono, K. Maruyama, T. Takagishi, *Bioconjugate Chem.* **2000**, *11*, 910 – 917.

[17] J. F. G. A. Jansen, E. W. Meijer, *J. Am. Chem. Soc.* **1995**, *117*, 4417 – 4418.

[18] G. Pistolis, A. Malliaris, D. Tsiourvas, C. M. Paleos, *Chem. Eur. J.* **1999**, *5*, 1440 – 1444.

[19] H. Stephan, H. Spies, B. Johannsen, C. Kauffmann, F. Vögtle, *Org. Lett.* **2000**, *2*, 2343 – 2346.

[20] Z. Sideratou, D. Tsiourvas, C. M. Paleos, *Langmuir* **2000**, *16*, 1766 – 1769.

[21] For recent reviews, see a) H. Frey, R. Haag in *Encyclopedia of Materials, Science and Technology* (Eds.: K. H. J. Buschow, R. H. Cahn, M. C. Flemings, B. Ilschner, E. J. Kramer, S. Majahan), Elsevier, Oxford, **2001**, pp. 3997 – 4000; b) H. Frey, R. Haag, *Rev. Mol. Biotechnol.* **2002**, *90*, 257 – 267; c) A. Sunder, R. Mülhaupt, R. Haag, H. Frey, *Adv. Mater.* **2000**, *12*, 235 – 239.

[22] R. Haag, J.-F. Stumbé, A. Sunder, H. Frey, A. Hebel, *Macromolecules* **2000**, *33*, 8158 – 8166.

[23] R. Haag, A. Sunder, A. Hebel, S. Roller, *J. Comb. Chem.* **2002**, *4*, 112 – 119.

[24] The reaction of the symmetrical C_{33}-ketone with PEI (**2**) was not successful according to this procedure.

[25] For the direct comparison of the transport capacity a polyglycerol palmityl ester (50 % functionalized) was prepared from the same PG core (21 000 g mol^{-1}) according to the procedure published in ref. [14a]: M. Krämer, Diplomarbeit, Universität Freiburg, **2001**.

[26] A lower degree of alkylation or shorter alkyl chains in **4a**,**b**, respectively, can result in aggregate formation and hence lower transport capacities.

[27] R. Haag, M. Krämer, J.-F. Stumbé, S. Krause, A. Komp, S. Prokhorova, *Polym. Prepr. Am. Chem. Soc. Div. Polym. Chem.* **2002**, *43*, 328.

[28] The diameter (d) of a PG core with $M_n = 4000$ g mol^{-1} is about 4 nm according to force-field calculations. Following a mass–volume correlation $M = \rho 4/3\pi(d/2)^3$, the expected radius for a PG core with $M_n = 21\,000$ g mol^{-1} is approximately 8 nm. The diameter of the flexible shell can be estimated to be 1–3 nm.

[29] Preliminary light-scattering experiments in chloroform gave similar diameters, however, larger aggregates of these particles have been observed at higher concentrations: M. Soddemann, W. Richtering, M. Krämer, R. Haag, unpublished results, **2002**.

[30] The fluorescence is quenched upon fluorescein encapsulation, which indicates the encapsulated dye molecules are below the Förster distance.

[31] A salt- and pH-dependent size variation has been reported for amine dendrimers.[8] However, in the case of compound **4**, this effect should be of minor importance because the terminal amine groups are liberated at the same time as the guest molecules are released.

 © 2002 WILEY-VCH Verlag GmbH & Co. KGaA, Weinheim 0044-8249/02/4122-4256 $ 20.00+.50/0

$Ln_{13}Br_{18}B_3$ (Ln = Gd, Tb)—A Compound Containing a Combination of Discrete and Condensed Clusters**

Oliver Oeckler, Lorenz Kienle, Hansjürgen Mattausch, and Arndt Simon*

Dedicated to Professor Dieter Fenske on the occasion of his 60th birthday

Metal-rich ternary halides of rare-earth metals form a large group of compounds,[1] the diverse structures of which can be understood within the concept of condensed clusters.[2a] As a rule, the cluster units of the valence-electron-poor rare-earth metals need stabilization by interstitial (endohedral) atoms.[2b] While several types of clusters are observed, octahedral units of metal atoms condensed through edges dominate. The structural systematics range from compounds with discrete clusters to those with chains and layers to those with three-dimensional (3D) networks, as illustrated with some arbitrary examples of the particularly rich chemistry of boride and carbide halides.[3]

The structure of $Tb_7X_{12}B$ (X = halogen) contains discrete Tb_6BX_{12} clusters.[1c] The compound $Tb_{10}Br_{15}B_2$, which contains a $Tb_{10}B_2X_{18}$-type cluster built from two octahedral units fused through a common edge,[3a] represents the first condensation step towards the formation of infinite chains as in Tb_4X_5B.[3b] Four Tb_6B octahedra are linked to form discrete clusters with a $Tb_{16}B_4$ core in $Tb_{16}Br_{23}B_4$,[3c] and this cluster type is the building block of double chains as found in the carbide halide $Gd_6Br_7C_2$.[3d] Fusing an infinite number of chains results in a layer as, for example, in Gd_2X_2C.[3e] Last but not least, a 3D network is present in the structure of Gd_3X_3B.[3f,g]

Here we report on the structure of a reduced rare-earth metal halide that is the first to contain both discrete clusters and chains. This combination is found in the compounds $Ln_{13}Br_{18}B_3$ (Ln = Gd, Tb), which can be prepared from mixtures of $LnBr_3$, Ln, and B at approximately 1000 °C[4] and which form pillar-shaped, dark golden crystals.

X-ray diffraction patterns of single crystals of these compounds are characterized by sharp Bragg reflections besides pronounced diffuse scattering arranged in the form of rods along the c^* direction (Figure 1a). This indicates a disordered stacking of ordered layers. The average structure of the compound was solved on the basis of the intensities of Bragg reflections only, and the refinement converged to R values below 0.03. It is described in the orthorhombic space group *Immm*.[5] Figure 2a depicts the structure of $Ln_{13}Br_{18}B_3$ in a projection along [100]; the disorder is not obvious because it only affects the site occupation factors of some of the atoms. The structure consists of a honeycomb packing of well-ordered, single chains of *trans* edge-sharing Ln_6 octahedra, which are centered by B atoms and surrounded by Br atoms (Figure 2b). The channels between these single chains are filled by double chains (Figure 2a). In spite of the very convincing agreement between observed and calculated Bragg intensities, the average structure does not allow a reasonable chemical interpretation as some of the atomic positions are partially occupied as mentioned above and/or characterized by highly anisotropic displacement parameters.

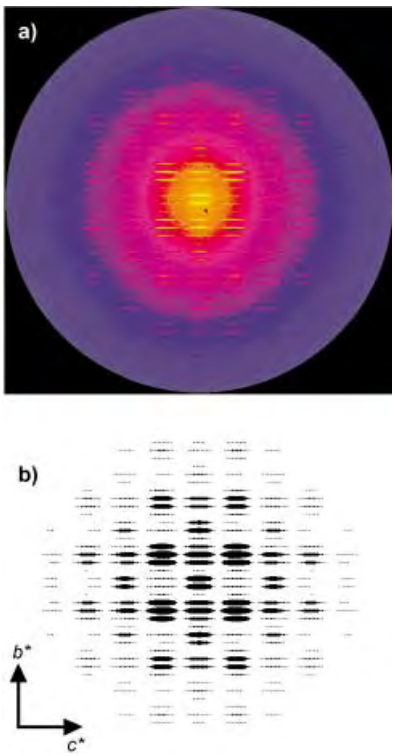


Figure 1. X-ray diffraction patterns of the 0.5*kl* section of reciprocal space: a) experiment (calculated from a series of imaging plate exposures); b) simulated on the basis of a $2 \times 2 \times 2$ supercell model, which approximates statistical disorder of the ordered layers.

The disorder problem could be solved by means of high-resolution transmission electron microscopy (HRTEM).[6] A HRTEM image taken along the [110] zone axis (Figure 3) clearly shows the nature of the disorder. First, the double chain resolves into a regular stacking of $Ln_{10}B_2$ units formed by edge-sharing Ln_6B octahedra and surrounded by Br atoms (Figure 2c). The image simulation image based on this model is in good agreement with the observed image (cf. the inset in Figure 3). Second, the stacks of well-ordered clusters are shifted relative to each other in an irregular way. This statistical arrangement is the origin of the diffuse scattering shown in Figure 1. A calculated diffraction pattern based on perfectly ordered clusters within layers parallel (001) and assuming stochastic disorder along [001] in the stacking of such layers in a suitable supercell mimics the intensity distribution of the diffuse scattering very well (Figure 1b).

The real structure of $Ln_{13}Br_{18}B_3$ (Ln = Gd, Tb) corresponds to the earlier mentioned honeycomb packing of single chains of condensed Ln_6B units surrounded by Br as in the M_6X_{12} cluster. The composition of one chain is Ln_4BBr_6. Owing to linkage through i–i contacts, that is contacts between anions of

[*] Prof. Dr. A. Simon, Dr. O. Oeckler, Dr. L. Kienle, Dr. H. Mattausch
Max-Planck-Institut für Festkörperforschung
Heisenbergstrasse 1, 70569 Stuttgart (Germany)
Fax: (+49) 711-689-1091
E-mail: a.simon@fkf.mpg.de

[**] We thank V. Duppel for recording high-resolution transmission electron microscopy images and electron diffraction patterns and R. Eger for the preparation of numerous samples.

 © 2002 WILEY-VCH Verlag GmbH & Co. KGaA, Weinheim 0044-8249/02/4122-4257 $ 20.00+.50/0

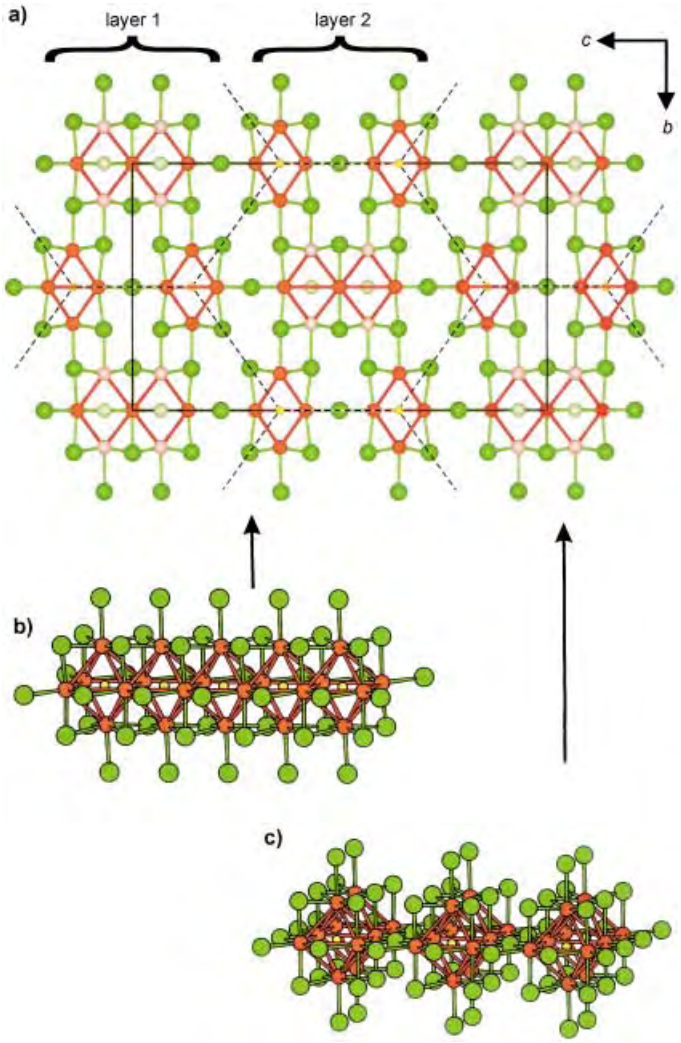


Figure 2. Crystal structure of $Ln_{13}Br_{18}B_3$ (Ln: red, Br: green, B: yellow): a) projection along [100] (the unit cell and layerlike structure are indicated, the honeycomb arrangement of single chains is highlighted by broken lines), Ln positions that are partially (50%) occupied in the average structure are depicted in pale red, pale green symbolizes a 1:1 mixture of Br and B; b) single chains of Ln_6B octahedra surrounded by Br atoms; c) regular stacking of $Ln_{10}B_2$ units along [100] within the ordered layers (appears as a double chain with partially occupied positions in the average structure).

the inner sphere, the substructure of the chains can be described as $Ln_{16}B_4Br_{18}Br^{i-i}_{6/2}$ in the notation of Schäfer and Schnering.[7] The channels are filled with $Ln_{10}B_2Br_{18}$ clusters. The Br atoms only partially belong to one cluster according to the formula $Ln_{10}B_2Br_{12}Br^{i-i}_{6/2}$. The chains and the clusters add up to the compound composition $Ln_{26}B_6Br_{36} = Ln_{13}Br_{18}B_3$. According to the Zintl–Klemm concept, the formal charge balance corresponds to the formula $Ln^{3+}{}_{13}Br^{-}{}_{18}B^{5-}{}_{3}e^{-}{}_{6}$. The excess of electrons leads to metallic properties as verified by conductivity measurements.

In addition to the i–i type bonds, in which Br atoms coordinate only edges of the Ln_6 octahedra, there are also i–a type connections that involve both an edge and a corner of neighboring octahedra. Figure 2a shows that the number of i–a type bonds is particularly large in layers parallel to (001), in fact, twice as many as i–i bonds in the orthogonal direction.

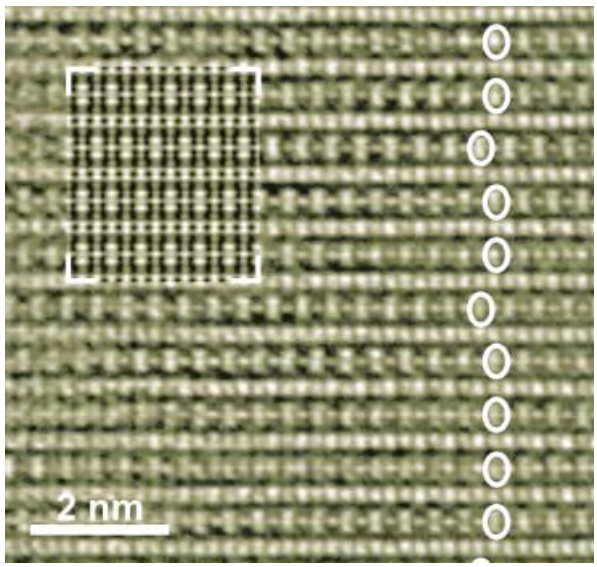


Figure 3. HRTEM image (zone axis [110]): the ellipsoidal marks highlight the positions of the disordered layers; inset: image simulation (defocus −45 nm, crystal thickness 3.5 nm) based on the $2\times2\times2$ supercell mentioned with Figure 1b.

This bond pattern yields an argument for both the perfect order in the layers and their statistical disorder.

The chain octahedra adopt positions around $x = 0, 1, 2, \ldots$ (layer 1) and $x = 1/2, 3/2, 5/2, \ldots$ (layer 2) in adjacent layers. The number of $Ln_{10}B_2$ double octahedra is half that of chain octahedra, hence the double octahedra lie either in $x = 1/2, 5/2, 9/2, \ldots$ or $x = 3/2, 7/2, 11/2, \ldots$ in layer 1 and either in $x = 0, 2, 4, \ldots$ or $x = 1, 3, 5, \ldots$ in layer 2. Electrostatic repulsion maximizes the distances between clusters and leads to a strict alternation of $x = 1/2, 5/2, 9/2, \ldots$ and $x = 3/2, 7/2, 11/2, \ldots$, respectively, for neighboring rows of double octahedra within the strongly interconnected layer 1, that is along [010]. With respect to the restriction for layer 1, there is no energetic difference between the alternatives $x = 0, 2, 4, \ldots$ and $x = 1, 3, 5, \ldots$, for the positioning of the clusters in layer 2. The origin of the resulting disorder is therefore due to a type of frustration, which is reminiscent of the fundamental phenomenon of frustrated antiferromagnetism in a triangular Ising net.[8] The interaction between disordered clusters belonging to neighboring layers is identical. The same situation would hold for the magnetic moments in a distorted orthohexagonal Ising net, in which the axial ratio is larger than $\sqrt{3}$ and where the interaction within a layer is stronger than between layers.

Received: May 31, 2002
Revised: August 15, 2002 [Z19420]

[1] a) J. D. Corbett, *J. Chem. Soc. Dalton Trans.* **1996**, 575–585; b) G. Meyer, *Chem. Rev.* **1988**, *88*, 93–107; c) A. Simon, H. Mattausch, G. J. Miller, W. Bauhofer, R. K. Kremer, *Handbook on the Physics and Chemistry of Rare Earths, Vol. 15* (Eds.: K. A. Gschneidner, Jr., L. Eyring), North Holland, Amsterdam, **1991**, pp. 191–285.
[2] a) A. Simon, *Angew. Chem.* **1981**, *93*, 23–44; *Angew. Chem. Int. Ed. Engl.* **1981**, *20*, 1–22; b) A. Simon, *Angew. Chem.* **1988**, *100*, 163–188; *Angew. Chem. Int. Ed. Engl.* **1988**, *27*, 159–183.
[3] a) H. Mattausch, E. Warkentin, O. Oeckler, A. Simon, *Z. Anorg. Allg. Chem.* **2000**, *626*, 2117–2124; b) H. Mattausch, O. Oeckler, A. Simon, *Inorg. Chim. Acta* **1999**, *289*, 174–190; c) H. Mattausch, G. V. Vajenine,

 © 2002 WILEY-VCH Verlag GmbH & Co. KGaA, Weinheim 0044-8249/02/4122-4258 $ 20.00+.50/0

O. Oeckler, R. K. Kremer, A. Simon, *Z. Anorg. Allg. Chem.* **2001**, *627*, 2542 – 2546; d) U. Schwanitz-Schüller, Ph.D. thesis, Stuttgart, **1984**; e) U. Schwanitz-Schüller, A. Simon, *Z. Naturforsch. B* **1985**, *40*, 710 – 716; f) E. Warkentin, A. Simon, *Rev. Chim. Miner.* **1983**, *20*, 488 – 495; g) C. Zheng, O. Oeckler, Hj. Mattausch, A. Simon, *Z. Anorg. Allg. Chem.* **2001**, *627*, 2151 – 2162.

[4] For the synthesis of $Tb_{13}Br_{18}B_3$ [$Gd_{13}Br_{18}B_3$], Ta capsules were filled with $TbBr_3$ (1000 mg) [$GdBr_3$ (750 mg)], Tb (433 mg) [Gd (323 mg)] and B (14.4 [10.7] mg; 5N, Aldrich) and sealed under Ar by arc-melting. These were heated for 30 days at 950 °C [6 days at 1000 °C]. Further details are analogous to the procedures described in reference [3g]. The compounds can be obtained as almost single-phase products according to X-ray powder diagrams. They are sensitive to moisture and need to be handled in a dry inert gas atmosphere.

[5] Single-crystal X-ray investigation (average structure): Stoe IPDS diffractometer, $Mo_{K\alpha}$ (0.71073 Å), $2\theta_{max} = 60.6°$; orthorhombic, space group *Immm*; $a = 3.9923(2)$, $b = 17.0462(12)$, $c = 28.3039(19)$ Å for $Gd_{13}Br_{18}B_3$ and $a = 3.9637(3)$, $b = 16.9063(13)$, $c = 28.1068(18)$ Å for $Tb_{13}Br_{18}B_3$; least-squares refinement on F^2 (G. M. Sheldrick, SHELXL 97 program for the refinement of crystal structures, University of Göttingen, Göttingen (Germany), **1997**); R_1 [$I \geq 2\sigma(I)$] = 0.025 (0.022), wR_2 [all data] = 0.057 (0.046) for 1668 (1627) reflections and 76 (76) parameters for $Gd_{13}Br_{18}B_3$ ($Tb_{13}Br_{18}B_3$). Further details on the crystal structure investigation may be obtained from the Fachinformationszentrum Karlsruhe, 76344 Eggenstein-Leopoldshafen, Germany (fax: (+49) 7247-808-666; e-mail: crysdata@fiz-karlsruhe.de), on quoting the depository numbers CSD-412541 ($Gd_{13}Br_{18}B_3$) and CSD-412540 ($Tb_{13}Br_{18}B_3$). A detailed description of the structural analysis as well as an analysis of symmetry relationships and additional real structure phenomena will be published elsewhere (O. Oeckler, L. Kienle, H. Mattausch, O. Jarchow, A. Simon, *Z. Kristallogr.*, submitted).

[6] HRTEM images were recorded with a Philips CM30 ST electron microscope (300 kV, LaB_6 cathode, Gatan multiscan CCD camera). The multislice formalism (P. A. Stadelmann, *Ultramicroscopy* **1987**, *21*, 131 – 146) was used for image simulations.

[7] H. Schäfer, H. G. Schnering, *Angew. Chem.* **1964**, *76*, 833 – 849.

[8] G. H. Wannier, *Phys. Rev.* **1950**, *79*, 357 – 364.

Enzymatic Elongation of the LEC14 Antigen Generates a β-1,2 Arm on *N*-Glycans**

Ingo Prahl and Carlo Unverzagt*

This work is dedicated to Professor Hans Paulsen on the occasion of his 80th birthday

Nearly all proteins of the blood serum and on cell surfaces in higher organisms are glycosylated.[1,2] On these glycoproteins, a multitude of asparagine-linked oligosaccharides (*N*-glycans) with similar structures are found. The structural diversity of these *N*-glycans is generated biosynthetically from a common core pentasaccharide $Man_3GlcNAc_2$. In biologically relevant complex *N*-glycans, this core pentasaccharide is extended by up to five antennae and can be modified further by the addition of single sugar residues, for example, core fucose or a bisecting GlcNAc residue. Recently, mutants of Chinese hamster ovary cells (CHO cells) termed LEC14 were found to exhibit *N*-glycans with a new glycosylation motif at the core pentasaccharide.[3] The structural analysis indicated an additional GlcNAc residue β-1,2 linked to the β-mannoside of the core trisaccharide. The relevant glycosyltransferase was characterized and termed GlcNAc-TVII.[4] To confirm the proposed structure and generate derivatives for biological evaluation, we have synthesized the LEC14 nonasaccharide, functionalized with a spacer. Analysis of the NMR spectroscopic data indicates that the proposed structure is correct. Unexpectedly, the single GlcNAc residue present in the LEC14 motif of the synthetic target compound was recognized by galactosyltransferase, which resulted in a to date unknown type of branching extension. The occurrence of this novel antenna (β-1,2 arm) generates a third branch at the central β-mannoside. This arm adds a new element to the structural motifs of *N*-glycan cores, which permits even greater variability.

A protected form of the LEC14 nonasaccharide **1** was obtained by using a modular building-block approach[5] based on regio- and stereoselective glycosylations.[6] The synthesis of the LEC14 *N*-glycan was designed to allow a comparison with the isolated natural compound and to give access to neoglycoconjugates for future investigation of the biological activity of this unusual *N*-glycan.[7] Furthermore, the synthetic LEC14 *N*-glycan should be elongated using glycosyltransferases to give full length *N*-glycans with biologically relevant termini.

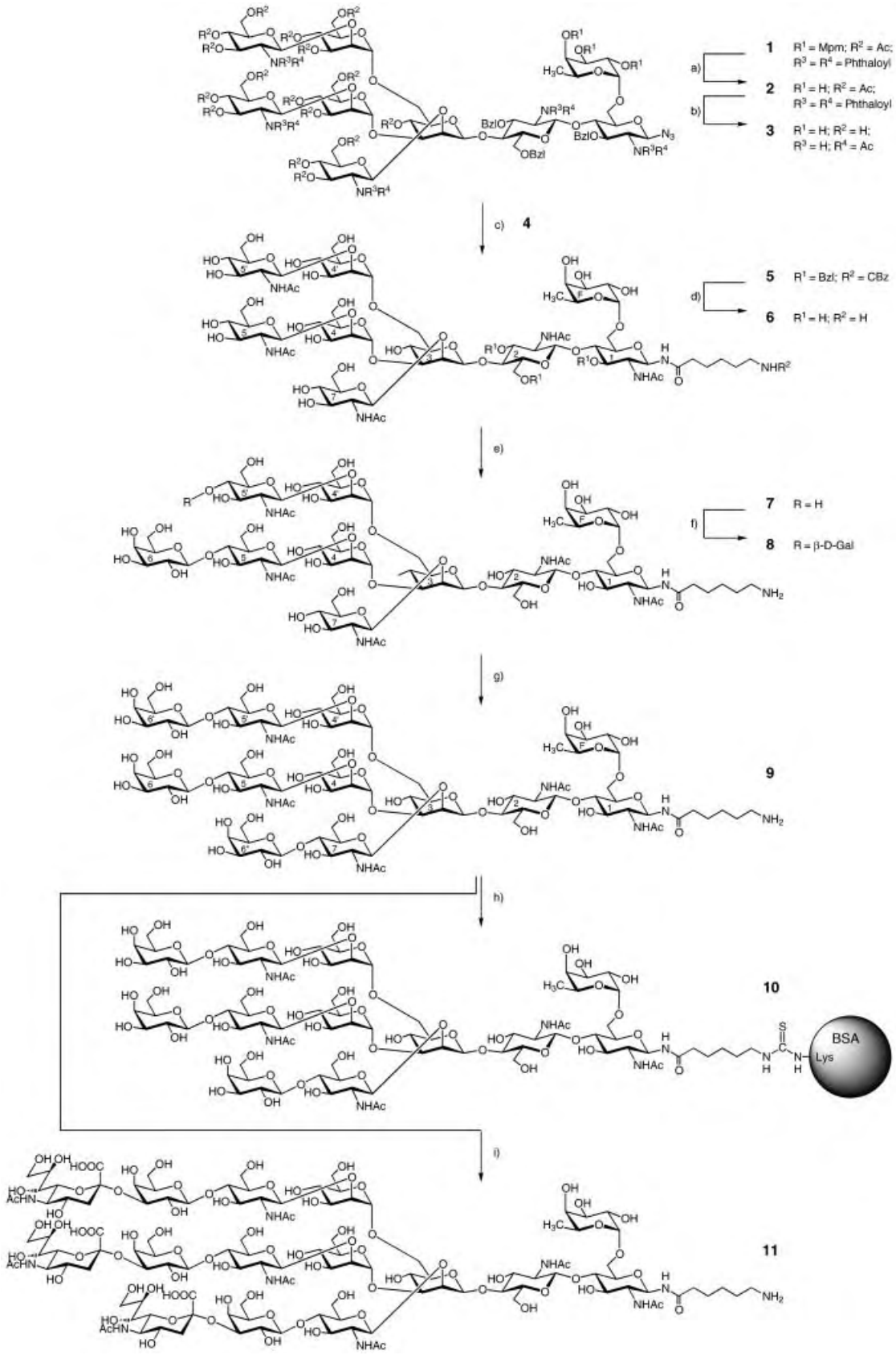
The conversion of the protected nonasaccharide **1** into neoglycoconjugates required several synthetic steps, which included the coupling of the carbohydrate moiety to a spacer that can be selectively activated for later attachment to the carrier.[8] Prior to the coupling of the spacer, all protecting groups except the three benzyl groups and the anomeric azido group were removed sequentially.

First, the three *p*-methoxybenzyl groups (Mpm) of the fucose residue in compound **1** were oxidatively removed using ceric ammonium nitrate (CAN) in acetonitrile/water. The phthaloyl groups of the nonasaccharide **2** were removed in a one-pot reaction comprising three steps, which was developed for use with *N*-glycans without affecting anomeric azido groups. Using ethylene diamine in *n*-butanol[9] at 80 °C yielded an intermediate pentaamino compound. After acetylation and *O*-deacetylation, the water-soluble nonasaccharide **3** was isolated by solid-phase extraction (SPE) in 96 % overall yield. Subsequent reduction of the azido group using excess propanedithiol in methanol/triethylamine[10] yielded the corresponding glycosylamine after removal of the volatile reagents. The amine was immediately acylated with excess *N*-benzyloxycarbonyl-6-aminohexanoic acid **4** using *O*-(benzotriazol-1-yl)-1,1,3,3-tetramethyluronium tetrafluoroborate/hydroxybenzotriazole (TBTU/HOBt) in *N*-methyl-2-pyrrolidone (NMP). Under these conditions, *O*-acylation was observed, which could be reversed by quenching the reaction mixture with aqueous methylamine prior to workup. After purification by reverse-phase (RP)-HPLC, **5** was obtained in 31 % yield. Catalytic hydrogenation over palladium hydroxide furnished the aminohexanoyl-derivatized nonasaccharide **6** in 95 % yield after size-exclusion chromatography (Scheme 1).

[*] Prof. C. Unverzagt, I. Prahl
Bioorganische Chemie, Gebäude NW1
Universität Bayreuth, 95440 Bayreuth (Germany)
Fax: (+49) 921-555365
E-mail: carlo.unverzagt@uni-bayreuth.de

[**] We thank the Deutsche Forschungsgemeinschaft and the Fonds der Deutschen Chemischen Industrie as well as Aventis Research and Technology for funding. Gratitude is expressed to Roche Diagnostics for supplying reagents.

 © 2002 WILEY-VCH Verlag GmbH & Co. KGaA, Weinheim 0044-8249/02/4122-4259 $ 20.00+.50/0



Scheme 1. Synthesis of LEC14 conjugates: a) $[(NH_4)_2Ce(NO_3)_6]$ (CAN), CH_3CN/H_2O, 80 °C (71 %); b) 1. ethylenediamine, *n*BuOH, 80 °C; 2. Ac_2O, pyridine; 3. $MeNH_2$ (41 %) in H_2O (96 % for steps 1–3); c) 1. propanedithiol, NEt_3, MeOH; 2. CBz-aminohexanoic acid **4**, TBTU, HOBt, *N*-methylpyrrolidone (31 % for steps 1 and 2 after RP-HPLC); d) $PdO/H_2O/H_2$, MeOH/AcOH (95 %); e,f,g) UDP-Gal (1 equiv), galactosyltransferase, alkaline phosphatase (80 %, 84 %, and 88 %, respectively); h) 1. thiophosgene, CH_2Cl_2/H_2O, $NaHCO_3$; 2. BSA, H_2O, $NaHCO_3$; i) CMP-*N*-acetylneuraminic acid (CMP-Neu5Ac), α-2,3-sialyltransferase, alkaline phosphatase (yield not determined). Mpm = *p*-methoxybenzyl, Ac = acetyl, Bzl = benzyl, CBz = benzyloxycarbonyl.

The structure of **6** was confirmed by electrospray ionization (ESI) MS[11] and a series of 2D NMR experiments[12] (COSY, TOCSY, HMQC, HMQC–COSY, NOESY). Compound **6**[13] and the isolated LEC14[3] nonasaccharide differ only in their aglycon part, which is aminohexanoic acid or asparagine, respectively. Despite this difference, both compounds show nearly identical proton resonances throughout the molecule (Table 1).

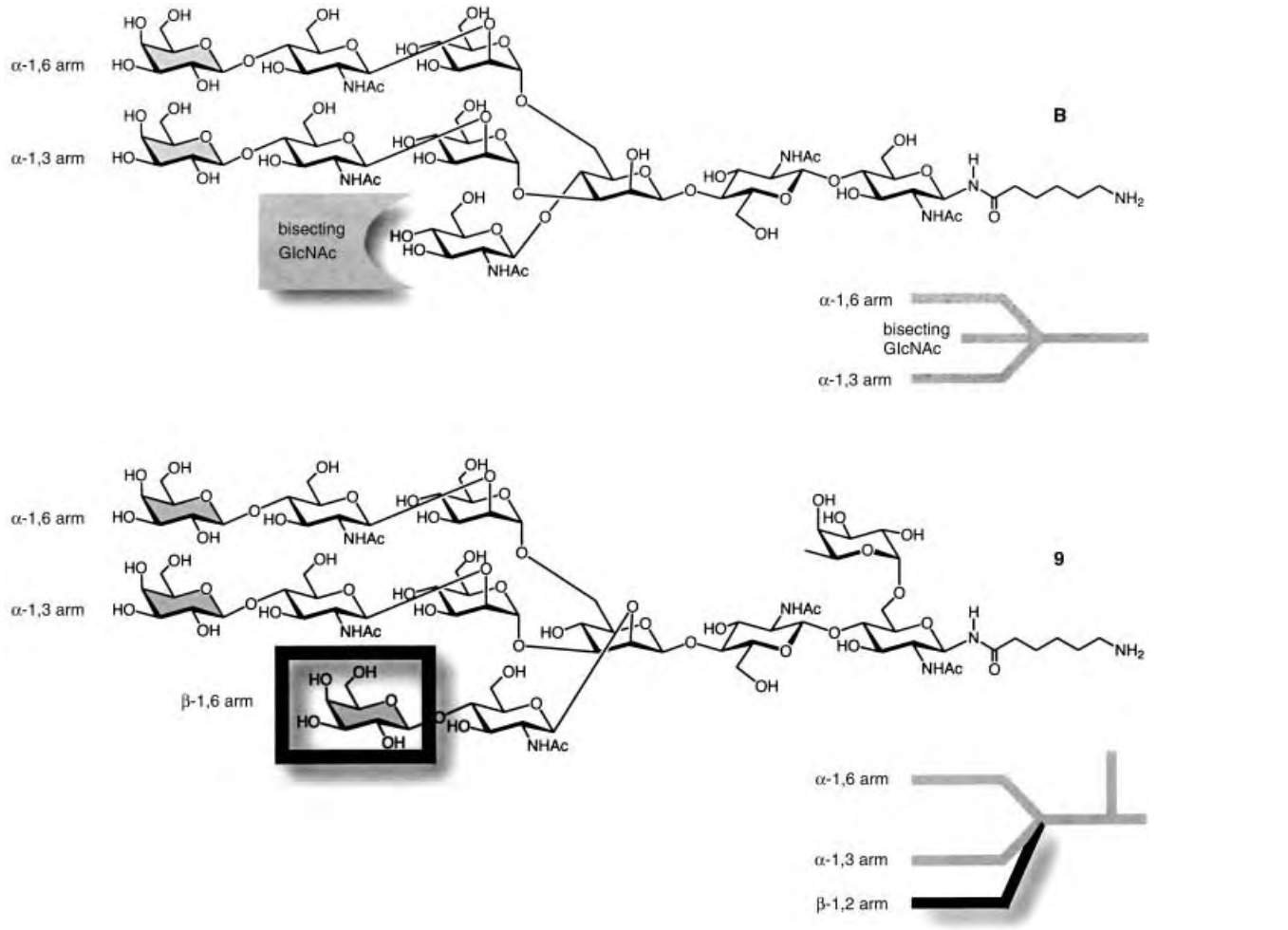
The very high level of similarity throughout the anomeric fingerprint region[14] led us to the conclusion that the structural assignments obtained from minute amounts of isolated LEC14 nonasaccharide–asparagine[3] are correct. In particular, the novel β-1,2 linkage of the GlcNAc residue attached to the central β-mannoside (LEC14 motif) was confirmed by a total synthesis of the entire *N*-glycan fragment.

Table 1. Comparison of the ^{1}H NMR spectroscopic data of **6** with that of isolated LEC14. Spectra were recorded in D_2O with DMSO (in the case of **6**) or acetone (isolated LEC14) as an internal standard. H-6^F of compound **6** has been calibrated to H-6^F of the natural LEC14 for better comparison.

Compound	δ of anomeric protons^{residue} [ppm][a]									
	1^1	1^2	1^3	1^4	$1^{4'}$	1^5	$1^{5'}$	1^7	1^F	6^F
6	5.03	4.71	4.77	5.11	4.89	4.49	4.53	4.69	4.87	1.20
LEC14[3]	5.07	4.57	(4.75)	5.11	4.88	4.54	4.54	4.68	4.86	1.20

[a] Ring description see Scheme 1.

The conversion of the spacer-bound synthetic **6** into a neoglycoprotein was then planned. A continuation of the synthesis by enzymatic methods is convenient and efficient for obtaining biologically relevant galactose termini on *N*-glycans.[15] Compound **6** carries two terminal *N*-acetylglucosamine residues (5 and 5′, see Scheme 1), which are known to be readily elongated by galactosyl transferase (EC 2.4.1.22). An initial reaction using galactosyl transferase, alkaline phosphatase,[16] and excess uridine-5′-diphospho (UDP)-galactose under conditions optimized for *N*-glycans surprisingly yielded not only the expected undecasaccharide **8**, but also the dodecasaccharide **9**. Both structures were later confirmed by ESI–MS and high-field 2D NMR spectroscopy. Compound **9** carries an additional galactose residue on the β-1,2-linked GlcNAc moiety. The occurrence of this novel enzymatic extension was highly unusual because an enzymatic galactosyl functionalization of the homologous β-1,4-linked single *N*-acetylglucosamine residue in the bisecting-type *N*-glycan (type **B**; Scheme 2) is not observed here.[17,18] On the other hand, the isolated LEC14 asparagine was obtained after a series of glycosidase



Scheme 2. Enzymatic formation of the β-1,2 arm as a novel branching motif, which extends the β-1,2-linked GlcNAc residue of the LEC14 conjugate **9**. In contrast, enzymatic extension does not occur on the bisecting GlcNAc residue of the homologous compound **B** with two antennae. BSA = bovine serum albumin.

 © 2002 WILEY-VCH Verlag GmbH & Co. KGaA, Weinheim 0044-8249/02/4122-4261 $ 20.00+.50/0

treatments, which makes it likely that the unusual extension was lost during the isolation process.

To investigate the regioselectivity of the unexpected enzymatic elongation of compound **6** in detail, only one equivalent of UDP-galactose was used in the galactosyltransferase reaction. After size-exclusion chromatography, the decasaccharide **7** was obtained in 80% yield. The selectivity of the galactosylation of the α-1,3 arm versus the α-1,6 arm was greater than 3.8:1. This is in good accordance with the known preference of glycosyltransferases for the α-1,3 arm of *N*-glycans.[19] Subsequent galactosylation of **7** with one equivalent of UDP-galactose yielded **8**. During this step, the formation of **9** (**8**:**9** approximately 4:1) was observed. Compounds **8** and **9** could not be separated by size-exclusion chromatography.

In a final reaction using excess UDP-galactose the undecasaccharide **8** was converted into the pergalactosyl dodecasaccharide **9** in 88% yield. The galactosyl derivatization of the different GlcNAc residues takes place in the following sequence, as shown by NMR spectroscopy: α-1,3 arm > α-1,6 arm > β-1,2-linked GlcNAc. The low accessibility of the unusual β-1,2-linked GlcNAc residue appears to coincide with the least reactivity towards galactosyltransferase.

As pergalactosyl derivatization could be readily achieved, enzymatic persialyl derivatization was also investigated. Sialylation was performed by incubation of **9** with α-2,3-sialyl transferase (E.C. 2.4.99.6), alkaline phosphatase,[16] and an excess of the donor substrate CMP-*N*-acetylneuraminic acid (CMP = cytidine-5′-monophospho-). Within two hours, ESI–MS revealed single, double, and a small amount of triple sialyl derivatization. After two days, the persialylated compound **11** was found to be the main product by ESI–MS.

To investigate the ligand properties of the novel galactosyl-derivatized LEC14-*N*-glycan **9** in comparison with core fucosyl-derivatized,[7] bisecting,[18] or unsubstituted *N*-glycans[7,20] the neoglycoconjugate **10** was synthesized. First, the free amino group of **9** was converted into an isothiocyanate,[21] which was then coupled to carbohydrate-free bovine serum albumin. On the purified neoglycoconjugate **10**, the ligand density averaged 3.2 *N*-glycans per carrier protein, as determined by a colorimetric assay[22] and supported by MALDI-TOF spectrometry. Neoglycoconjugate **10** can be used to probe the to date unknown biological properties of the novel galactosyl-derivatized LEC14-*N*-glycan in glycobiological studies.[20]

In summary, we have shown by total synthesis that the structure of the LEC14 motif is correct and that the single GlcNAc residue can be built up enzymatically to form a novel third branch attached to the central β-mannoside. The occurrence of this extended β-1,2 arm in vitro suggests that this additional branch is also generated in the cellular system, which thus expands the structural variability of *N*-glycans in general.

Received: May 31, 2002 [Z19414]

[1] W. Tanner, *Glyco- and Cellbiology*, Springer, Heidelberg, **1994**, pp. 81–89.
[2] B. Lowe, A. Varki, *Essent. Glycobiol.* **1999**, 253–266.
[3] T. S. Raju, P. Stanley, *J. Biol. Chem.* **1996**, *271*, 7484–7493.
[4] T. S. Raju, P. Stanley, *J. Biol. Chem.* **1998**, *273*, 14090–14098.
[5] C. Unverzagt, *Angew. Chem.* **1997**, *109*, 2078–2081; *Angew. Chem. Int. Ed. Engl.* **1997**, *36*, 1989–1992.
[6] I. Prahl, C. Unverzagt, *Tetrahedron Lett.* **2000**, *41*, 10189–10193.
[7] C. Unverzagt, S. André, J. Seifert, S. Kojima, C. Fink, G. Srikrishna, H. Freeze, K. Kayser, H. J. Gabius, *J. Med. Chem.* **2002**, *45*, 478–491.
[8] J. Seifert, C. Unverzagt, *Tetrahedron Lett.* **1997**, *38*, 7857–7860.
[9] O. Kanie, S. C. Crawley, M. M. Palcic, O. Hindsgaul, *Carbohydr. Res.* **1993**, *243*, 139–164.
[10] A. Bayley, D. N. Standring, J. R. Knowles, *Tetrahedron Lett.* **1978**, *19*, 3633–3634.
[11] ESI-MS (methanol) of **6**: $M_{calcd} = 1777.72$; $M_{found} = 1778.8$ $[M+H]^+$, 1800.8 $[M+Na]^+$.
[12] a) H. Kessler, M. Gehrke, C. Griesinger, *Angew. Chem.* **1988**, *100*, 507–554; *Angew. Chem. Int. Ed. Engl.* **1988**, *27*, 490–536; b) H. Kessler, P. Schmieder, M. Kurz, *J. Magn. Reson.* **1989**, *65*, 400–405.
[13] **6**: $[\alpha]_D^{25} = -18.6°$ (1.1, H_2O); ^{1}H-NMR (500 MHz, D_2O, [D_6]DMSO as internal standard): $\delta = 4.92$ (d, $J_{1,2} < 1.0$ Hz, 1H, H-1^4), 4.84 (d, $J_{1,2} = 9.7$ Hz, 1H, H-1^1), 4.70 (d, $J_{1,2} < 1.0$ Hz, 1H, H-1$^{4'}$), 4.68 (d, $J_{1,2} = 3.2$ Hz, 1H, H-1^F), 4.58 (d, $J_{1,2} < 1.0$ Hz, 1H, H-1^3), 4.52 (d, $J_{1,2} = 8.4$ Hz, 1H, H-1^2), 4.50 (d, $J_{1,2} = 8.4$ Hz, 1H, H-1^7), 4.34 (d, $J_{1,2} = 8.4$ Hz, 1H, H-1$^{5'}$), 4.30 (d, $J_{1,2} = 8.4$ Hz, 1H, H-1^5), 4.18 (m, 1H, H-2^3), 3.97–3.91 (m, 2H, H-2^4, H-5^F), 3.87 (m, 1H, H-2$^{4'}$), 3.79–3.19 (m, 47H, H-5^4, H-6a^4, H-6a$^{5'}$, H-6a^5, H-6a^7, H-3^4, H-6a$^{4'}$, H-6a^1, H-6a^2, H-3^F, H-3^2, H-2^1, H-3$^{4'}$, H-6a^3, H-3^3, H-6b^3, H-2^F, H-4^F, H-6b$^{5'}$, H-6b^5, H-6b^7, H-3^1, H-4^1, H-2^2, H-6b^2, H-5^1, H-6b^1, H-2$^{5'}$, H-2^7, H-2^5, H-5^2, H-4^3, H-6b$^{4'}$, H-5^3, H-6b^4, H-4^2, H-3$^{5'}$, H-3^7, H-3^5, H-5$^{4'}$, H-4^4, H-4$^{4'}$, H-4$^{5'}$, H-4^7, H-5$^{5'}$, H-4^5, H-5^5), 3.13 (m, 1H, H-5^7), 2.70 (t, $J_{\delta,\varepsilon} = 7.1$ Hz, 2H, ε-CH_2), 2.08 (t, $J_{\alpha,\beta} = 7.1$ Hz, 2H, α-CH_2), 1.89, 1.85, 1.84, 1.83, 1.80 (5s, 15H, NAc), 1.46–1.36 (m, 4H, δ-CH_2, β-CH_2), 1.14 (m, 2H, γ-CH_2), 1.01 ppm (d, $J_{5,6} = 6.5$ Hz, 3H, H-6^F); ^{13}C NMR (125 MHz, D_2O, [D_6]DMSO as internal standard; chemical shifts were determined by using an HMQC spectrum): $\delta = 178.35$, 175.70, 175.65, 175.59, 175.52, 174.91 (C=O), 102.74 (C-1^3), 102.36 (C-1^7), 102.04 (C-1^2), 101.02 (C-1^5), 100.94 (C-1$^{5'}$), 100.70 (C-1^F), 100.32 (C-1^4), 98.29 (C-1$^{4'}$), 82.72 (C-4^2), 80.23 (C-4^1), 79.63 (C-1^1), 78.61 (C-3^3), 77.86 (C-2^4, C-2$^{4'}$), 77.28 (C-5^7), 77.16 (C-5$^{5'}$, C-5^5), 76.42 (C-5^1), 76.28 (C-2^3), 75.68 (C-5^3), 75.47 (C-5^2), 74.70 (C-5^4), 74.55 (C-3$^{5'}$), 74.52 (C-3^7), 74.49 (C-3^5), 74.23 (C-5$^{4'}$), 73.86 (C-3^1), 73.19 (C-3^2), 73.09 (C-4^F), 71.20 (C-4^7), 71.18 (C-4$^{5'}$, C-4^5), 70.82 (C-3^F), 70.74 (C-3^4), 70.61 (C-3$^{4'}$), 69.45 (C-2^F), 68.64 (C-4^4), 68.55 (C-4$^{4'}$), 68.09 (C-6^3), 68.04 (C-6^1), 67.96 (C-5^F), 67.88 (C-4^3), 62.92 (C-6^4), 62.72 (C-6$^{4'}$), 61.87 (C-6$^{5'}$), 61.83 (C-6^5), 61.68 (C-6^7), 61.37 (C-6^2), 56.96 (C-2^7), 56.70 (C-2$^{5'}$), 56.64 (C-2^5), 56.34 (C-2^2), 55.12 (C-2^1), 40.69 (C-6 AH), 36.77 (C-2 AH), 28.75 (C-5 AH), 26.36 (C-4 AH), 25.85 (C-3 AH), 23.87, 23.71, 23.38 (NAc), 16.80 ppm (C-6^F).
[14] L. Dorland, H. van Halbeek, J. F. Vliegenthart, R. Schauer, H. Wiegandt, *Carbohydr. Res.* **1986**, *151*, 233–245.
[15] C. Unverzagt, *Angew. Chem.* **1996**, *108*, 2507–2510; *Angew. Chem. Int. Ed. Engl.* **1996**, *35*, 2350–2353.
[16] C. Unverzagt, H. Kunz, J. C. Paulson, *J. Am. Chem. Soc.* **1990**, *112*, 9308–9309.
[17] S. Narasimhan, J. C. Freed, H. Schachter, *Biochemistry* **1985**, *24*, 1694–1700.
[18] C. Unverzagt, J. Seifert, *Tetrahedron Lett.* **2000**, *41*(23), 4549–4553.
[19] D. H. Joziasse, W. E. Schiphorst, D. H. Van den Eijnden, J. A. Van-Kuik, H. Van Halbeek, J. F. Vliegenthart, *J. Biol. Chem.* **1987**, *262*, 2025–2033.
[20] S. André, C. Unverzagt, S. Kojima, X. Dong, C. Fink, K. Kayser, H. J. Gabius, *Bioconjugate Chem.* **1997**, *8*, 845–855.
[21] C. R. McBroom, C. H. Samanen, I. J. Goldstein, *Methods Enzymol.* **1972**, *28*, 212–219.
[22] M. Monsigny, C. Petit, A.-C. Roche, *Analyt. Biochem.* **1988**, *175*, 525–530.

 © 2002 WILEY-VCH Verlag GmbH & Co. KGaA, Weinheim 0044-8249/02/4122-4262 $ 20.00+.50/0

Reporter Ribozymes for Real-Time Analysis of Domain-Specific Interactions in Biomolecules: HIV-1 Reverse Transcriptase and the Primer–Template Complex**

Jörg S. Hartig and Michael Famulok*

The major task in the postgenome-era is to decipher the function of thousands of new proteins, their involvement in regulatory networks and to check their suitability as pharmaceutical drug targets. For this reason, novel methods are required that facilitate rapid and reliable identification of molecular interactions of complex biological systems compatible with high-throughput screening protocols. Knowledge about the interaction partners, binding affinity, and interacting domains represent the basis for identification of the biological function and discovery of novel inhibitors, modulators, and drug leads of a given protein.[1] Although there are several powerful methods available for detection and quantification of molecular interactions,[2–7] they are often not generally applicable or compatible with high-throughput screening protocols, in real time. Hence, the development of novel, broadly applicable methods, independent of target protein function, is of fundamental importance.

We are interested in using ribozymes for developing functional assays that allow the analysis of interactions of biologically relevant molecules in real-time. We have reported a novel system for rapid and reliable measurement of the catalytic activity of the hammerhead ribozyme (HHR) by using substrate oligonucleotides labeled with two fluorescent dyes.[8] The spatial proximity of the two dyes results in fluorescence quenching of the donor fluorophore by fluorescence resonance energy transfer (FRET). Ribozyme cleavage activity can be then monitored by a time-dependent increase of fluorescence in real-time. By using these reporter ribozymes we have identified novel inhibitors of the hammerhead ribozyme[9] and of the HIV-1 Rev protein,[10] which were also able to inhibit the biological function of the target molecule in vivo.

Herein, we report the rational design of a reporter ribozyme, which is specifically regulated by HIV-1 reverse transcriptase (HIV-1 RT). We demonstrate that the HIV-1 RT dependent reporter ribozyme is not only capable of selectively detecting the presence of HIV-1 RT but also of sensing the domain-specific interaction of other HIV-1 RT binders such as the primer–template complex.

For the construction of the reporter ribozyme we have chosen a strategy similar to that used for previous systems that are regulated by small organic molecules, by inserting an aptamer sequence into stem II of the HHR. Proper folding of stem III is essential for cleavage activity of the HHR.[11–14] We have chosen an aptamer which was selected by Tuerk et al. from a combinatorial RNA-library and which binds HIV-1 RT with an affinity of 25 pM.[15] The crystal structure of the RNA–protein complex shows that the *anti*-HIV-1 RT aptamer in the complex with HIV-1 RT forms a pseudoknot structure, in which the 5′- and 3′-ends of the aptamers are spatially separated.[16]

We have deliberately chosen an aptamer with a pseudoknot structure because this motif is often used as a regulatory element in nature. For example, formation of a pseudoknot induces a frameshift in some viral mRNA sequences.[17] In some eukaryotic transcripts, a pseudoknot structure in the 5′-untranslated region leads to activation of a regulatory protein, which then locally controls translation of the transcript.[18]

Owing to these known structural and regulatory features of pseudoknot motifs the *anti*-HIV-1 RT aptamer seemed to be well suited as a regulatory element of a hammerhead ribozyme. The aptamer was inserted into stem II of the HHR, as shown in Figure 1a, resulting in a fusion construct FK-1 with competing folds of the ribozyme and the pseudoknot structures. The simultaneous folding of both domains is impossible in this design, because in the absence of HIV-1 RT the inserted aptamer sequence folds into a hairpin loop structure (see Figure 1a, left). As shown in Figure 1b, the reporter ribozyme FK-1 is active in the absence of HIV-1 RT due to the folding of the hairpin loop, forming stem II in FK-1. The presence of an unpaired loop was proven by digestion with ribonucleases specific for single-stranded RNA (Figure 2). In the presence of HIV-1 RT, the catalytic activity of FK-1 is inhibited (Figure 1b) due to the induction of the pseudoknot fold by the protein. This leads to disruption of stem II and, hence, to the inhibition of cleavage activity.

To further characterize and verify the influence of the stability of stem II on the capability of structural changes of FK-1, two variants of FK-1 were generated, one with weakened and one with stabilized stem II structures. Deletion of the GC base pair highlighted in gray in Figure 1a yields construct FK-2 with a destabilized stem II (Figure 1c). The complete absence of catalytic activity of FK-2 (Figure 1d) indicates that the lack of the stabilizing GC base pair diminishes formation of the catalytically active conformation in favor of the pseudoknot fold. Indeed, nuclease digest reactions of FK-2 shown in Figure 2 resulted in cleavage patterns, which are in accordance with the kinetic data in Figure 1d, thus supporting the exclusive formation of the pseudoknot.

For further validation of this hypothesis we constructed a third version of the reporter ribozyme, which is only capable of forming the catalytically active fold, but not the pseudoknot structure. Starting from FK-1, an additional GC base pair was inserted, which leads to stabilization of stem II in the construct FK-3 (Figure 1e). Figure 1f shows, as expected, that FK-3 is catalytically active, with the cleavage activity remaining unchanged even in the presence of HIV-1 RT. Owing to the increased stability of stem II, the protein is no longer able to induce the folding of the pseudoknot. Indeed, the nuclease

[*] Prof. Dr. M. Famulok, Dipl.-Chem. J. S. Hartig
Kekulé-Institut für Organische Chemie und Biochemie
Gerhard-Domagk-Strasse 1, 53121 Bonn (Germany)
Fax: (+49) 228-735-388
E-mail: m.famulok@uni-bonn.de

[**] This work was supported by the Deutsche Forschungsgemeinschaft. We thank Dr. T. Restle (MPI Dortmund) for providing us with samples of HIV-1 and HIV-2 reverse transcriptase and Dr. Andreas Marx for helpful comments.

Supporting information for this article is available on the WWW under http://www.angewandte.org or from the author.

 © 2002 WILEY-VCH Verlag GmbH & Co. KGaA, Weinheim 0044-8249/02/4122-4263 $ 20.00+.50/0

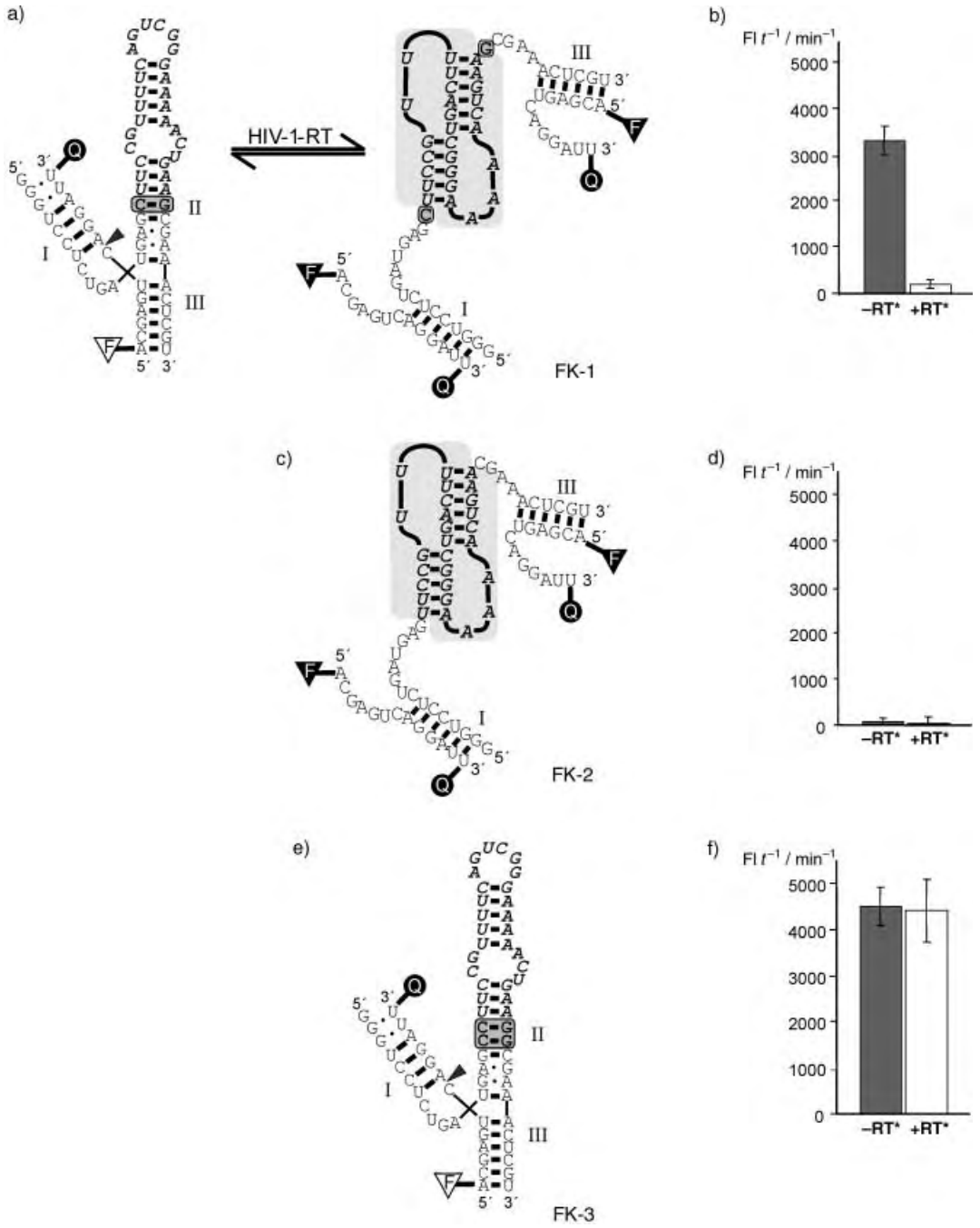


Figure 1. Structures and cleavage activities of the fusion constructs FK-1, FK-2, and FK-3. Aptamer sequences inserted into the hammerhead ribozyme are highlighted in boldface italics. Complexes with one or two FRET-labeled substrates are shown (5′-fluorophore: F, 3′-quencher: Q). a) The fusion of the HIV-1 RT aptamer with a hammerhead ribozyme forms the correct ribozyme fold with stems I, II, and III (left). The arrow indicates the cleavage site. Addition of HIV-1 RT induces the formation of the pseudoknot (highlighted in pale gray), disrupting the formation of stem II (right). b) Cleavage activity of FK-1 in absence and presence of 200 nM HIV-1 RT (RT*). The cleavage rate of a FRET-labeled substrate in the initial 5 min is shown, measured in fluorescence per time interval (Fl t^{-1}/min^{-1}).[8–10] c) Structure of FK-2. FK-2 was obtained by deletion of the GC base pair marked in gray in FK-1. d) Cleavage activity of FK-2 in absence and presence of 200 nM HIV-1 RT (RT*). e) Structure of FK-3. FK-3 was obtained by insertion of an additional GC base pair (marked in gray). f) Cleavage activity of FK-3 in absence and presence of 200 nM HIV-1 RT (RT*).

digest of FK-3 shows a cleavage pattern that is similar to that of FK-1 in its active form (Figure 2).

Thus, the fusion construct FK-1 represents a reporter ribozyme that can be regulated by HIV-1 RT. FK-1 reports the presence of HIV-1 RT with highest sensitivity; half-maximum inhibition of the aptazyme is already observed at a protein concentration of 10.4 nM (Figure 3a). This enhanced sensitivity reflects the extraordinarily high affinity of the aptamer-HIV-1 RT complex of 25 pM.[19] Compared to the few protein-regulated ribozymes described in the literature, this represents an improvement of sensitivity of more than two orders of magnitude. A ligase evolved by SELEX requires 1.5 μM lysozyme for half-maximum effect.[19] Micromolar concentrations of a fusion of HIV Rev and bacteriophage λN proteins are necessary for regulation of a Tetrahymena group I intron ribozyme.[20]

 © 2002 WILEY-VCH Verlag GmbH & Co. KGaA, Weinheim 0044-8249/02/4122-4264 $ 20.00+.50/0 *Angew. Chem. Int. Ed.* **2002**, *41*, No. 22

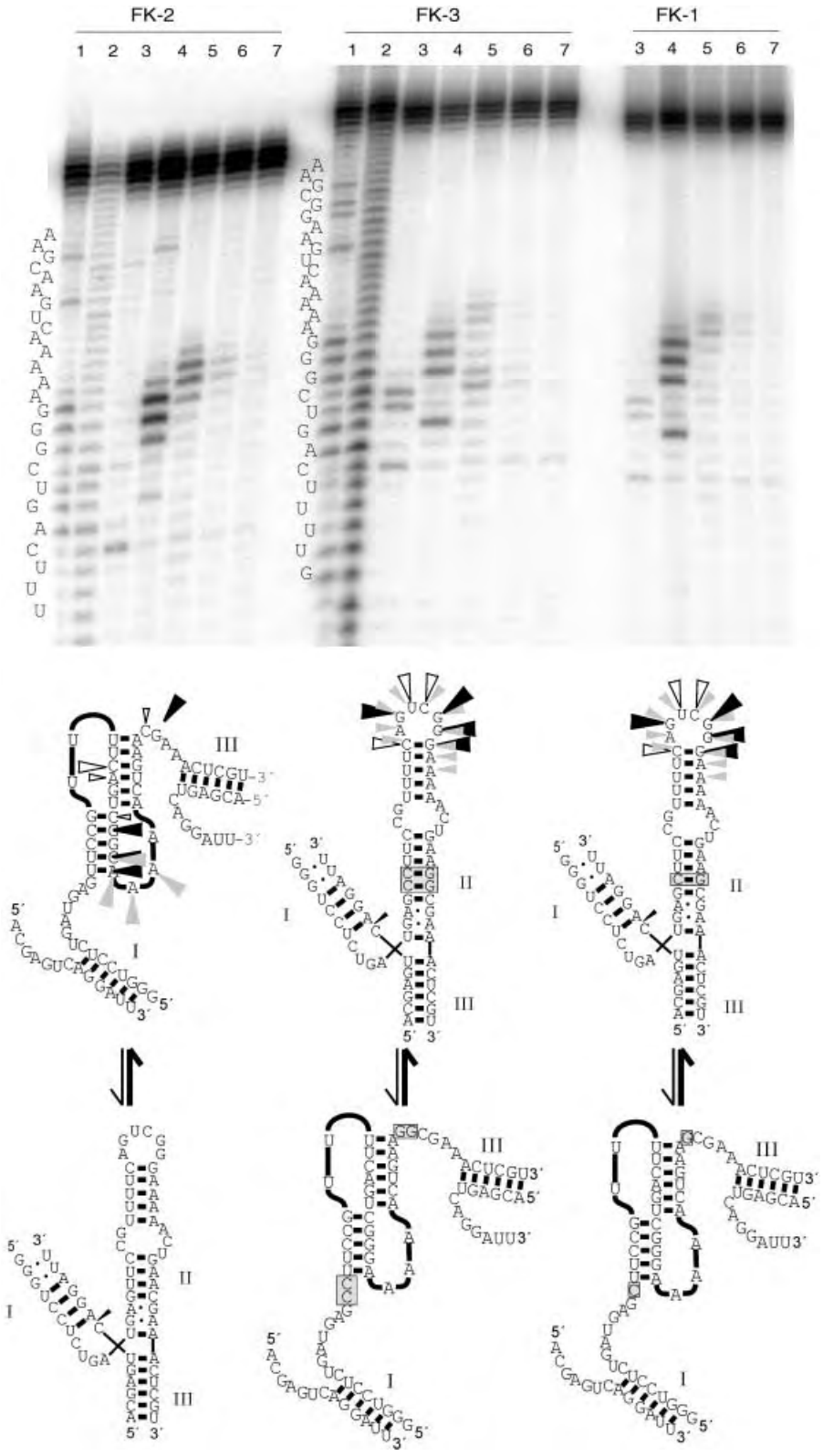


Figure 2. Nuclease-digest of fusion constructs FK-1, FK-2, and FK-3: lane 1: RNase T1 ladder under denaturing conditions; lane 2: OH ladder; lane 3: RNase A; lane 4: RNase T1; lane 5: S1 nuclease; lane 6: S1 nuclease 1/10 dilution; lane 7: S1 nuclease 1/100 dilution. RNase A cleaves single-stranded RNA at C and U (white arrows), RNase T1 single-stranded at G (black arrows), and S1 nuclease at single-stranded nucleosides (gray arrows). The size of the arrows corresponds to the intensity of the cleavage. The nuclease cleavage sites are in good accordance with the observed ribozyme activities: FK-2 forms no hammerhead structure, as for example indicated by the strong digest by S1 nuclease at the right bottom loop of the pseudoknot. FK-3 and FK-1 only show digestion at the loop of the hairpin structure of stem II, indicating the ribozyme fold.

To investigate the specificity of the reporter ribozyme, we carried out cleavage reactions in the presence of various noncognate proteins. As shown in Figure 3b, from a collection of ten proteins, only HIV-1 RT was able to significantly inhibit ribozyme activity (Figure 3a and b). Even with the homologous reverse transcriptase of HIV-2, no effect is observed. These results demonstrate that the HIV-1 RT dependent ribozyme described in this study is a highly specific reporter for HIV-1 RT. That this discrimination, which is also found for the free aptamer, is maintained in the ribozyme context demonstrates that the folded pseudoknot retains its functional properties, without the rest of the fusion construct having a disturbing influence.

To determine if the inhibition of the aptazyme FK-1 is reversible, we used the fact that the aptamer binds to the primer/template binding site of HIV-1 RT.[16] Thus the addition of a DNA primer/template complex[21] to the cleavage reaction should lead to competitive displacement of the pseudoknot-containing FK-1 from the protein, which should in turn result in a reactivation of the cleavage reaction. Figure 3c shows that this is indeed observed. The effect is even more pronounced by addition of free aptamer instead of the DNA primer/template complex (see Figure 1 in the Supporting Information). However, ribozyme activity decreases again at high concentrations due to hybridization of the free aptamer with the reporter ribozyme (see Figure 1 in the Supporting Information).

With respect to the domain-specificity of the reporter ribozyme we were interested in whether the competition effect observed with the free aptamer or the DNA primer/template complex would be specific for binders of the primer/template recognition site. This was investigated by adding nevirapine instead of the primer/template complex. Nevirapine is an inhibitor of RT binding at a region near the active site and not the primer/template recognition domain.[22] Figure 3c shows that even with higher concentrations of nevirapine no reactivation of the ribozyme is observed. This is an important result because it shows that reporter ribozymes can be used as probes in high-throughput screening formats for identification of binding molecules in a domain-specific fashion. In the example described

 © 2002 WILEY-VCH Verlag GmbH & Co. KGaA, Weinheim 0044-8249/02/4122-4265 $ 20.00+.50/0

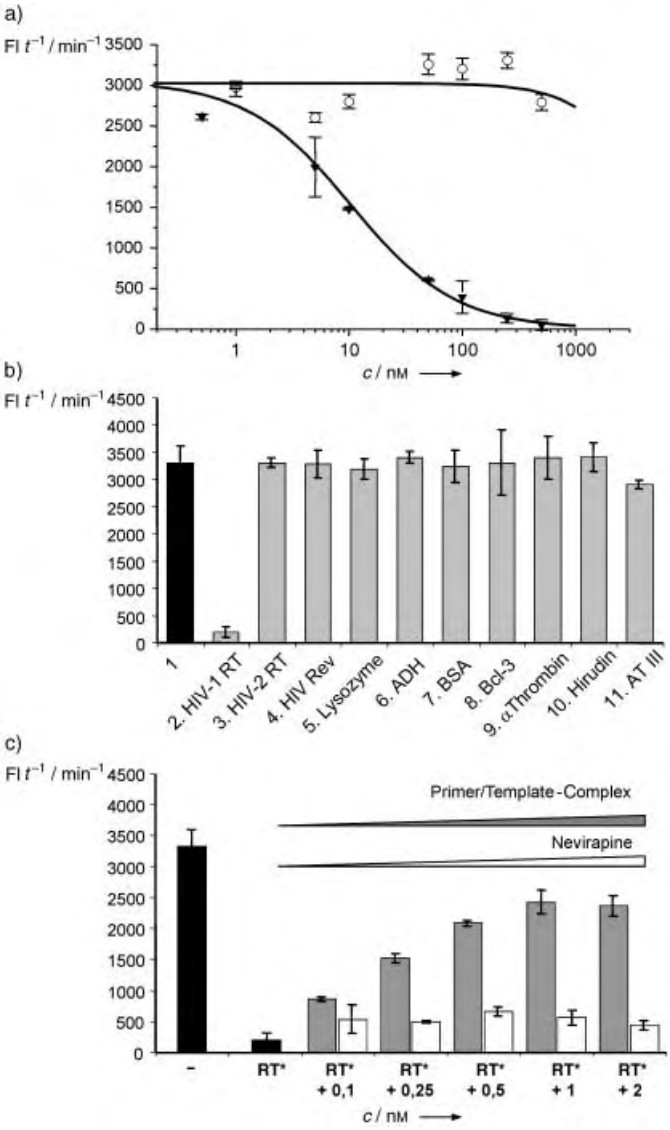


Figure 3. Concentration dependence and specificity of the inhibition of FK-1. a) Concentration dependence of the inhibition of FK-1 by HIV reverse transcriptase (filled triangles: HIV-1 RT, open circles: HIV-2 RT), half-maximum inhibition at $K_I = 10.4$ nM. b) Specificity of inhibition of FK-1. From a collection of randomly chosen control proteins, only HIV-1 RT was able to inhibit the reporter ribozyme. Protein concentration was always 200 nM. 1: without protein; 2: HIV-1 RT; 3: HIV-2 RT; 4: HIV-1 Rev; 5: Lysozym from hen egg white; 6: ADH, alcoholdehydrogenase; 7: BSA, bovine serum albumin; 8: Bcl-3, a member of the IκB-family; 9: hirudin; 10: human γ-thrombin; 11: AT III, antithrombin III. c) Competition of the aptazyme FK-1 from the HIV-1 RT by a DNA-primer/template complex. Black columns: cleavage activity of fusion construct FK-1 alone (–) and in presence of 200 nM HIV-1 RT (RT*). Gray columns: Reactivation of the FK-1-catalyzed cleavage reaction by increasing amounts of DNA–primer/template complex in presence of 200 nM HIV-1 RT (RT*). White columns: Increasing concentrations of nevirapine, a NNRTI (non-nucleoside reverse transcriptase inhibitor) that does not compete with the aptazyme for the same binding site of HIV-1 RT, is not able to reactivate the reporter ribozyme.

here, molecules are identified that bind to the primer/template binding site but not to the active site. HIV-1 RT inhibitors that interact with the primer/template binding site are not known to date.

To our knowledge, the introduced fusion construct FK-1 represents the first example of an artificially constructed switch based on a pseudoknot structure. FK-1 shows very high sensitivity and specificity. Thus, the concept of inserting pseudoknot motifs into functional RNA sequences represents a novel principle for constructing RNA switches, also applicable for natural pseudoknot/protein complexes.

Experimental Section

Synthesis of fusion constructs FK-1, 2 and 3: The corresponding DNA sequences of the fusion constructs including a 5′-T7-RNA polymerase promoter sequence were synthesized by standard phosphoramidite solid-phase technology, amplified by PCR, transcribed by T7 RNA polymerase, and purified as described in reference [23].

Ribozyme reactions: Reactions were carried out in 50 mM Tris HCl-buffer, pH 7.9, 25 mM NaCl. Reactions contained 10 nM of RNA fusion constructs FK-1, -2 or -3, 500 nM fluorescence labeled substrate,[8–10] and optional varying protein concentrations in a final volume of 50 μL. After incubation for 15 min at 37 °C, the reactions were started by adding $MgCl_2$ to a final concentration of 8 mM. The increase of fluorescence in the initial 5 min was measured as a function of catalytic activity.[8–10] Increase of fluorescence from control reactions lacking ribozyme was subtracted automatically for correction of artificial effects such as dye bleaching.

Nuclease reactions: The digestions were carried out at 37 °C in the presence of 200 μM of a noncleavable ribozyme substrate (2′-deoxycytosine at the reactive cleavage site). The reactions contained 8 μM of fusion construct and traces of 5′-^{32}P-labeled construct in 10 mM Tris buffer, pH 7.5, 100 mM KCl, 10 mM $MgCl_2$ in the case of RNase A and RNase T1. S1 Nuclease reactions were carried out in the reaction buffer supplied by the manufacturer (Promega). After precipitation with ethanol and separation by 10 % PAGE, cleavage fragments were analyzed by autoradiography.

Received: June 5, 2002 [Z19472]

[1] M. F. Engels, P. Venkatarangan, *Curr. Opin. Drug Discovery Dev.* **2001**, *4*, 275.
[2] S. Fields, R. Sternglanz, *Trends Genet.* **1994**, *10*, 286.
[3] J. Huang, S. L. Schreiber, *Proc. Natl. Acad. Sci. USA* **1997**, *94*, 13396.
[4] M. Vidal, H. Endoh, *Trends Biotechnol.* **1999**, *17*, 374.
[5] M. Mann, R. C. Hendrickson, A. Pandey, *Annu. Rev. Biochem.* **2001**, *70*, 437.
[6] C. L. Tucker, S. Fields, *Nat. Biotechnol.* **2001**, *19*, 1042.
[7] J. Rappsilber, M. Mann, *Trends Biochem. Sci.* **2002**, *27*, 74.
[8] A. Jenne, W. Gmelin, N. Raffler, M. Famulok, *Angew. Chem.* **1999**, *111*, 1383; *Angew. Chem. Int. Ed.* **1999**, *38*, 1300.
[9] A. Jenne, J. S. Hartig, N. Piganeau, A. Tauer, D. A. Samarsky, M. R. Green, J. Davies, M. Famulok, *Nat. Biotechnol.* **2001**, *19*, 56.
[10] J. S. Hartig, S. H. Najafi-Shoushtari, I. Grüne, A. Yan, A. D. Ellington, M. Famulok, *Nat. Biotechnol.* **2002**, *20*, 717.
[11] G. A. Soukup, R. R. Breaker, *Curr. Opin. Struct. Biol.* **2000**, *10*, 318.
[12] G. A. Soukup, R. R. Breaker, *Proc. Natl. Acad. Sci. USA* **1999**, *96*, 3584.
[13] N. Piganeau, A. Jenne, V. Thuiller, M. Famulok, *Angew. Chem.* **2000**, *112*, 4538; *Angew. Chem. Int. Ed.* **2000**, *39*, 4369.
[14] M. Koizumi, G. A. Soukup, J. N. Kerr, R. R. Breaker, *Nat. Struct. Biol.* **1999**, *6*, 1062.
[15] C. Tuerk, S. MacDougal, L. Gold, *Proc. Natl. Acad. Sci. USA* **1992**, *89*, 6988; O. Kensch, B. A. Connolly, H. J. Steinhoff, A. McGregor, R. S. Goody, T. Restle, *J. Biol. Chem.* **2002**, *275*, 18271.
[16] J. Jaeger, T. Restle, T. A. Steitz, *EMBO J.* **1998**, *17*, 4535.
[17] D. P. Giedroc, C. A. Theimer, P. L. Nixon, *J. Mol. Biol.* **2000**,*298*, 167.
[18] Y. Ben-Asouli, Y. Banai, Y. Pel-Or, A. Shir, R. Kaempfer, *Cell* **2002**, *108*, 221.
[19] M. P. Robertson, A. D. Ellington, *Nat. Biotechnol.* **2001**, *19*, 650.
[20] S. Atsumi, Y. Ikawa, H. Shiraishi, T. Inoue, *EMBO J.* **2001**, *20*, 5453.
[21] D. Summerer, A. Marx, *Angew. Chem.* **2001**, *113*, 3806; *Angew. Chem. Int. Ed.* **2001**, *40*, 3693.
[22] J. Ren, R. Esnouf, E. Garman, D. Somers, C. Ross, I. Kirby, J. Keeling, G. Darby, Y. Jones, D. Stuart, *Nat. Struct. Biol.* **1995**, *2*, 293.
[23] M. Famulok, *J. Am. Chem. Soc.* **1994**, *116*, 1698.

 © 2002 WILEY-VCH Verlag GmbH & Co. KGaA, Weinheim 0044-8249/02/4122-4266 $ 20.00+.50/0

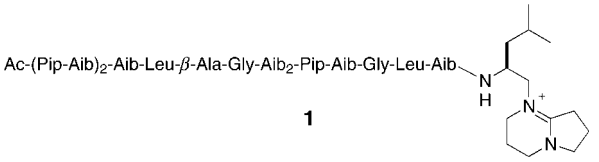
The First Total Synthesis of Efrapeptin C**

Micha Jost, Jörg-Christian Greie, Nina Stemmer, Sven David Wilking, Karlheinz Altendorf, and Norbert Sewald*

Dedicated to Professor Peter Welzel on the occasion of his 65th birthday

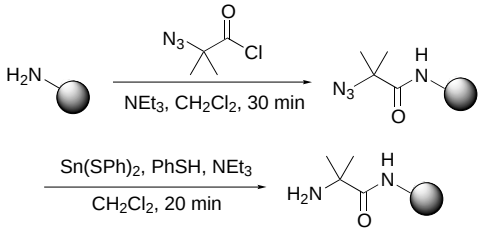
The efrapeptins are a class of peptide antibiotics produced by the fungus *Tolypocladium niveum* and other members of this species as a mixture of closely related sequence analogues (efrapeptins C–G).[1] They are inhibitors of F_1-ATPase and are active also against the malaria pathogen *Plasmodium falciparum*.[2] The efrapeptins are rich in α,α-dialkylated amino acids, and contain one β-alanine and several pipecolic acid residues. The C-terminus bears an unusual cationic head group derived from leucinol. Although the efrapeptins have been applied in numerous biological studies,[3] no chemical total synthesis has been reported so far.[4] This may be because the synthesis of peptides rich in α,α-dialkylated amino acids is hampered by incomplete coupling reactions caused by steric hindrance.[5] As we are interested in the structural and biological properties of efrapeptins we launched a project aimed towards the synthesis of efrapeptin C and analogues thereof.

We succeeded in assembling efrapeptin C (**1**) from three fragments: an N-terminal fragment (Pip 1–Gly 8), a central



1

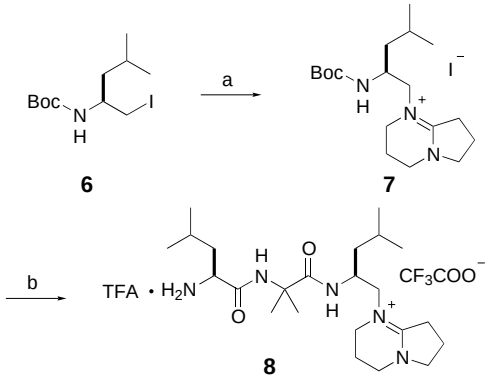
fragment (Aib 9–Gly 13), and a C-terminal fragment containing the residues Leu 14–Aib 15 as well as the head group. For the introduction of Aib residues in solid-phase syntheses we successfully modified a strategy first described by Meldal et al.,[6] in which the resin-bound amino component was acylated with the highly reactive α-azidoisobutyric acid chloride (Azib-Cl), and the azide was reduced to the primary amine. According to their original procedure reduction is achieved by treatment with 1,4-dithio-D,L-threitol (DTT) at elevated temperature and requires reaction times of up to 6 h. Use of Vilarrasa's reagent $[Et_3NH]^+[Sn(SPh)_3]^-$,[7] which is commonly applied to the reduction of alkyl and aryl azides, safeguarded the smooth conversion of the azide at room temperature within short reaction times (Scheme 1).[8] The reduction can easily be monitored by FT-IR spectroscopy and was found to be complete in all cases examined after only a few minutes.



Scheme 1. Introduction of Aib residues in solid-phase syntheses by using coupling of Azib-Cl and subsequent reduction. Aib = α-aminoisobutyric acid, Azib = α-azidoisobutyryl.

The C-terminal fragment of efrapeptin C (**1**) was synthesized starting from α-aminoisobutyric acid H-Aib-OH (**2**). Acid-catalyzed esterification of **2** with allyl alcohol to give H-Aib-OAl (**3**) and subsequent coupling of Boc-Leu-OH with **3** gave dipeptide Boc-Leu-Aib-OAl (**4**), which was deprotected at the C-terminus by allyl transfer to morpholine in the presence of $[Pd(PPh_3)_4]$ to yield Boc-Leu-Aib-OH (**5**).[9] Synthesis of the head group (Scheme 2) started from the known iodide **6**,[10] which was used to alkylate DBN in hot toluene[11] giving rise to the amidinium salt **7**. The Boc group in **7** was removed by treatment with TFA in dichloromethane and the resulting amine was subsequently coupled to **5** using N-HATU[12] as the coupling reagent. The C-terminal fragment **8** was isolated by preparative reverse-phase (RP) HPLC after cleavage of the Boc group by treatment with TFA. Compound **8** has already been described by Gupta et al.,[1] who obtained it by treatment of efrapeptin C (**1**) with HCl.

The central and N-terminal fragments of efrapeptin C (**1**) were synthesized by solid-phase methods using the highly acid-labile *o*-chlorotrityl resin.[13] Application of this type of



Scheme 2. a) DBN, toluene, reflux, 75%; b) 1. TFA/CH_2Cl_2; 2. **5** (1.2 equiv), N-HATU (1.2 equiv), DIPEA (2.2 equiv), DMF; 3. TFA/CH_2Cl_2, 27%. DBN = 1,4-diazabicyclo[4.3.0]non-5-ene, N-HATU = 1-[bis(dimethylamino)methyliumyl]-1*H*-1,2,3-triazolo[4,5-*b*]pyridine-3-oxide-hexafluorophosphate, DIPEA = diisopropylethylamine.

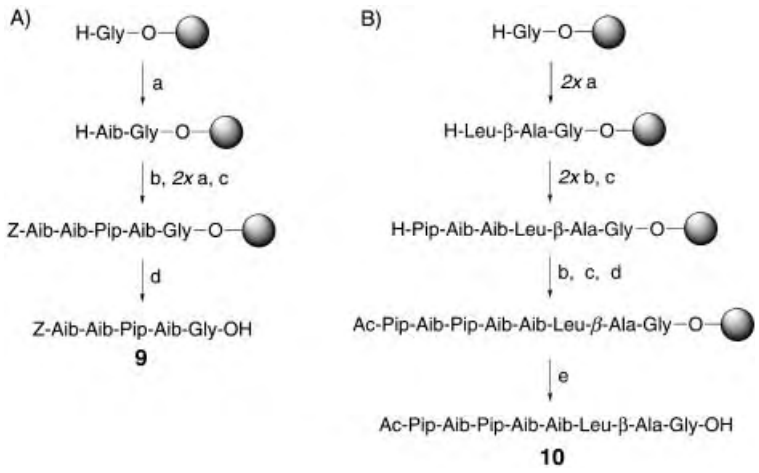
[*] Prof. Dr. N. Sewald, Dipl.-Chem. M. Jost, N. Stemmer, Dipl.-Chem. S. D. Wilking
Faculty of Chemistry
University of Bielefeld
Universitätsstrasse 25, 33615 Bielefeld (Germany)
Fax: (+49) 521-106-8094
E-mail: norbert.sewald@uni-bielefeld.de
Dr. J.-C. Greie, Prof. Dr. K. Altendorf
Fachbereich Biologie/Chemie
Universität Osnabrück
Barbarastrasse 11, 49069 Osnabrück (Germany)

[**] This work was supported by the Deutsche Forschungsgemeinschaft and the Fonds der Chemischen Industrie. We thank Dr. Holger Wenschuh for helpful discussions.

Supporting information for this article is available on the WWW under http://www.angewandte.org or from the author.

 © 2002 WILEY-VCH Verlag GmbH & Co. KGaA, Weinheim 0044-8249/02/4122-4267 $ 20.00+.50/0

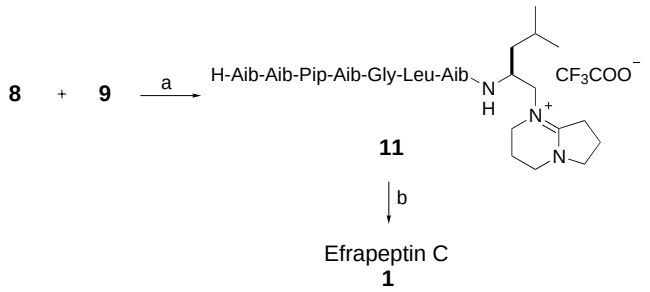
resin is crucial for the success of the synthesis because of the pronounced acid sensitivity of some -Aib-Xaa- peptide bonds.[14] Peptides **9** and **10** (Scheme 3 A and B) were synthesized according to Fmoc strategy with the exception of Aib residues, which were introduced by using Azib-Cl as described above. Proteinogenic amino acids were coupled with TBTU as the condensation reagent, and PyBOP was used for the introduction of L-pipecolic acid.



Scheme 3. A) a) 1. Azib-Cl (15 equiv), NEt_3 (22 equiv), CH_2Cl_2, 2. $Sn(SPh)_2$ (10 equiv), PhSH (30 equiv), NEt_3 (50 equiv), CH_2Cl_2; b) 1. Fmoc-Pip-OH (3 equiv), PyBOP (3 equiv), DIPEA (6 equiv), DMF; 2. DBU/piperidine, DMF; c) Z-OSu (10 equiv), NEt_3 (25 equiv), DMF/CH_2Cl_2; d) 1% TFA/CH_2Cl_2. B) a) 1. Fmoc-Xaa-OH (3 equiv), TBTU (3 equiv), DIPEA (6 equiv), DMF; 2. DBU/piperidine, DMF; b) 1. Azib-Cl (15 equiv), NEt_3 (22 equiv), CH_2Cl_2, 2. $Sn(SPh)_2$ (10 equiv), PhSH (30 equiv), NEt_3 (50 equiv), CH_2Cl_2; c) 1. Fmoc-Pip-OH (3 equiv), PyBOP (3 equiv), DIPEA (6 equiv), DMF; 2. DBU/piperidine, DMF; d) Ac_2O (30 equiv), DMAP (20 equiv), CH_2Cl_2; e) 1% TFA/CH_2Cl_2. DBU = 1,8-diazabicyclo[5.4.0]undec-7-ene, Pip = L-pipecolic acid, Z-OSu = *N*-(benzyloxycarbonyloxy)succinimide, PyBOP = benzotriazol-1-yloxytripyrrolidinophosphonium hexafluorophosphate, DMAP = 4-dimethylaminopyridine, TBTU = 1-[bis(dimethylamino)methyliumyl]-1*H*-benzotriazole-3-oxidetetrafluoroborate.

N-HATU was used as the coupling reagent for the final assembly of **1** from the three fragments (Scheme 4). Compound **11** was obtained upon reaction of **9** with **8** and removal of the Z group. Finally condensation of **10** with **11** gave efrapeptin C (**1**) as the trifluoroacetate.

The product was characterized by ^{1}H NMR spectroscopy and ESI-FT-ICR-MS.[15] Its homogeneity was proven by RP-HPLC. To demonstrate its bioactivity, we studied the inhibition of *E. coli* F_1-ATPase by synthetic **1** and found the K_i value to be in the range of 10 μM. This is in good agreement with a value of 21.5 μM reported by Wise et al.[16] for the mixture of efrapeptins as isolated from fermentation broths.



Scheme 4. a) 1. N-HATU, DIPEA, CH_2Cl_2/DMF, 2. H_2, Pd/C, MeOH/AcOH, 44%; b) **10** (1.3 equiv), N-HATU (1.3 equiv), DIPEA (2.3 equiv), CH_2Cl_2/DMF, 67%.

In summary we have synthesized for the first time a member of the efrapeptin class of peptide antibiotics by applying a convenient method for the introduction of Aib residues. The full sequence was assembled by a combination of solution-phase and solid-phase peptide synthesis steps with segment condensations. We are currently using this synthetic route for the synthesis of a number of efrapeptin analogues, which will be examined for bioactivity and conformational preferences to derive structure–activity relationships.

Received: May 27, 2002
Revised: August 7, 2002 [Z19491]

[1] a) S. Gupta, S. B. Krasnoff, D. W. Roberts, J. A. A. Renwick, L. S. Brinen, J. Clardy, *J. Am. Chem. Soc.* **1991**, *113*, 707–709; b) S. Gupta, S. B. Krasnoff, D. W. Roberts, J. A. A. Renwick, L. S. Brinen, J. Clardy, *J. Org. Chem.* **1992**, *57*, 2306–2313.

[2] a) J. P. Abrahams, S. K. Buchanan, M. J. van Raau, I. M. Fearnley, A. G. W. Leslie, J. E. Walker, *Proc. Natl. Acad. Sci. USA* **1996**, *93*, 9420–9424; b) G. Nagaraj, M. V. Uma, M. S. Shivayogi, H. Balaram, *Antimicrob. Agents Chemother.* **2001**, *45*, 145–149.

[3] Representative examples: a) A. R. Bandani, B. Amiri, T. M. Butt, R. Gordon-Weeks, *Biochim. Biophys. Acta* **2001**, *1510*, 367–377; b) M. Muroi, N. Kaneko, K. Suzuki, T. Nishio, T. Oku, T. Sato, A. Takatsuki, *Biochem. Biophys. Res. Commun.* **1996**, *227*, 800–809; c) V. N. Kasho, W. S. Allison, P. D. Boyer, *Arch. Biochem. Biophys.* **1993**, *300*, 293–301; d) G. E. Dean, P. J. Nelson, G. Rudnick, *Biochemistry* **1986**, *25*, 4918–4925; e) A. Matsuno-Yagi, Y. Hatefy, *J. Biol. Chem.* **1986**, *261*, 14031–14038.

[4] Benedetti et al. reported the synthesis of the C-terminal pentapeptide of efrapeptin C in a fully blocked form: E. Benedetti, R. Iacovino, M. Saviano, J. Kamphuis, M. Crisma, F. Formaggio, V. Moretto, C. Toniolo, *Protein Pept. Lett.* **1996**, *3*, 283–288.

[5] E. Frérot, J. Coste, A. Pantaloni, M.-N. Dufour, P. Jouin, *Tetrahedron* **1991**, *47*, 259–270.

[6] M. Meldal, M. A. Juliano, A. M. Jansson, *Tetrahedron Lett.* **1997**, *38*, 2531–2534.

[7] a) M. Bartra, F. Urpi, J. Vilarrasa, *Tetrahedron Lett.* **1987**, *28*, 5941–5944; b) M. Bartra, P. Romea, F. Urpi, J. Vilarrasa, *Tetrahedron* **1990**, *46*, 587–594.

[8] Procedure for the introduction of Aib residues in solid-phase synthesis**:** The peptidyl resin (1 equiv) was swollen in a solution of NEt_3 (22 equiv, ca. 0.7 M) in CH_2Cl_2, and Azib-Cl (15 equiv) was added. The mixture was left for 30 min and agitated occasionally. The resin was washed with CH_2Cl_2 (4×), DMF (4×), and again with CH_2Cl_2 (4×). Thiophenol (30 equiv) and NEt_3 (50 equiv) were added to a suspension of $Sn(SPh)_2$ (10 equiv; ca. 0.3 M) in CH_2Cl_2. After 5 min the resulting mixture was filtered and the yellow filtrate was added to the resin-bound azide. The mixture was left for 20 min and agitated occasionally. The resin was washed with CH_2Cl_2 (4×), DMF (4×), and again with CH_2Cl_2 (4×).

[9] a) H. Schmitt, G. Jung, *Liebigs Ann. Chem.* **1985**, 321–344; b) T. M. Balasubramanian, N. C. E. Kendrick, M. Taylor, G. R. Marshall, J. E. Hall, I. Vodyanoy, F. Reusser, *J. Am. Chem. Soc.* **1981**, *103*, 6127–6132; c) H. Kunz, H. Waldmann, C. Unverzagt, *Int. J. Pept. Protein Res.* **1985**, *26*, 493–497.

[10] R. Caputo, E. Cassano, L. Longobardo, G. Palumbo, *Tetrahedron* **1995**, *51*, 12337–12350.

[11] G. A. Reynolds, F. D. Saeva, J. J. Doney, C. H. Chen, *J. Org. Chem.* **1984**, *49*, 4843–4848.

 © 2002 WILEY-VCH Verlag GmbH & Co. KGaA, Weinheim 0044-8249/02/4122-4268 $ 20.00+.50/0

[12] L. A. Carpino, H. Imazumi, A. El-Faham, F. J. Ferrer, C. Zhang, Y. Lee, B. M. Foxman, P. Henklein, C. Hanay, C. Mügge, H. Wenschuh, J. Klose, M. Beyermann, M. Bienert, *Angew. Chem.* **2002**, *114*, 457 – 461; *Angew. Chem. Int. Ed.* **2002**, *41*, 441 – 445.
[13] K. Barlos, D. Gatos, J. Kallitsis, G. Papaphotiu, P. Sotiriu, Y. Wenqing, W. Schäfer, *Tetrahedron Lett.* **1989**, *30*, 3943 – 3946.
[14] H. Brückner, W. A. König, M. Greiner, G. Jung, *Angew. Chem.* **1979**, *91*, 508 – 509; *Angew. Chem. Int. Ed. Engl.* **1979**, *18*, 476 – 477.
[15] See Supporting Information.
[16] J. G. Wise, T. M. Duncan, L. R. Latchney, D. N. Cox, A. E. Senior, *Biochem. J.* **1983**, *215*, 343 – 350.

Reactivity of Chalcogenostannate Salts: Unusual Synthesis and Structure of a Compound Containing Ternary Cluster Anions $[Co_4(\mu_4\text{-}Se)(SnSe_4)_4]^{10-}$**

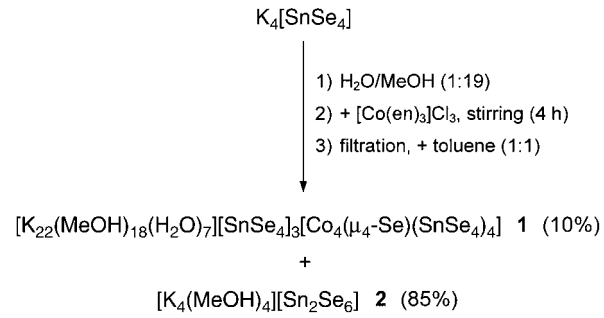
Christian Zimmermann, Maike Melullis, and Stefanie Dehnen*

Dedicated to Professor Dieter Fenske on the occasion of his 60th birthday

The stabilization of binary aggregates of main group elements $[E'_xE_y]^{q-}$ in the coordination sphere of transition-metal ions M^{n+} (E′ or E = Group 13–15 or 16 element), and thus the formation of structures that contain ternary heavy atom frameworks, is an area of increasing research activity.[1–16] Besides diverse range of molecular and crystal structures, the synthesis of some ternary M/E′/E systems that show polymeric anion substructures representing "open solid-state structures", as found in $Rb_3[AgGe_4Se_{10}]\cdot 2\,H_2O$[10] or $K_2[MnSnS_4]$,[11] have recently attracted attention. Such compounds combine both zeolite-type and semiconducting properties. If binary alloys or salts of binary anions are used for the construction of the E′/E aggregates instead of separate components, the investigations additionally serve to study the reaction behavior and stability of these systems in the presence of transition-metal compounds. However, most reports on the latter deal with binary reactants of Groups 15/16,[1,13–16] for example the synthesis of $[PPh_4]_2[Mn(CO)_3(As_3Se_3)_5]$ by using $[As_4Se_4]$.[13b] Only most recently, were some results published that considered the surfactant-templated solvothermal synthesis of mesoporous solids like $(C_{16}H_{33}NC_5H_5)_x[Pt_ySn'_4Se_{10}]$ ($x = 1.9$–2.8; $y = 0.9$–1.6).[12]

One of our current aims is to generate coordination compounds by reacting binary anions of Groups 14 and 16. However, reactions under conditions similar to those for the binary reactants from Groups 15 and 16—that is reactions with organometallic complexes in aprotic solvents—led to the reductive decomposition of the Sn–E framework under E^{2-} donation to the transition-metal ion.[17,18]

By employing protic solvents and another type of transition-metal complex, it was possible to synthesize a compound by completely transferring the binary anionic structures into the coordination sphere of the transition-metal ions. Scheme 1 depicts the reaction of $K_4[SnSe_4]$[19] and



Scheme 1. Synthesis of the compounds **1** and **2**.

$[Co(en)_3]Cl_3$ (en = 1,2-diaminoethane) in a water/methanol mixture that yielded compounds **1** and **2**.[20,21] Compounds **1** and **2** were structurally characterized by single-crystal X-ray diffraction,[22] and the formal oxidation state of the cobalt centers in **1** was additionally checked by quantum-chemical investigations. Compound **1** crystallizes as black cubes in the cubic space group $Ia\bar{3}$. It is an ionic compound that features complex, ternary anions $[Co_4(\mu_4\text{-}Se)(SnSe_4)_4]^{10-}$ that are embedded in the crystal lattice by K···Se interactions to MeOH- or H_2O-coordinated potassium cations.The composition of the C_3 symmetric anion suggests that the $[SnSe_4]^{4-}$ ions of the starting material have acted as both a ligand and—in a well-known manner—as an Se^{2-} donor. This is additionally confirmed by the formation of compound **2** which can be viewed as a dimer of $[SnSe_3]^{2-}$ ions generated by removal of Se^{2-} ions from the tetraselenostannate anions $[SnSe_4]^{4-}$. Under the assumption that the formal oxidation state of the tin atoms in **1** remains +4, the cluster anion emerges as a Co^{II} compound. Thus, in contrast to the reactions in aprotic solvents, one observed a reduction of the transition metal ions by partially released Se^{2-} ions.[23] Figure 1 gives the molecular structure of the ternary anion.

In the cluster anion, four barrelane-type $[SnCo_3Se_4]$ cages are linked by a μ_4-bridging selenium atom that centers an inner $[SeCo_4]$ fragment (barrelane = bicyclo[2,2,2]octane). In addition, the anion contains four terminal selenido ligands, which form the corners of a large tetrahedron with Se···Se edges of 1057.7(4)–1071.3(3) pm. Each of the metal atoms is almost tetrahedrally surrounded by selenido ligands. The narrow range of the observed bond lengths allows a deviation from ideal T_d symmetry by at most 1.1 pm.

Some cluster complexes are known that are topologically identical to **1**. These are chalcogenido- or pnictido-bridged clusters of the d^{10} elements, for example $[M^{II}_8(\mu_4\text{-}E)$-

[*] Dr. S. Dehnen, C. Zimmermann, M. Melullis
Institut für Anorganische Chemie
Universität Karlsruhe (TH)
Engesserstrasse, Geb. 30.45, 76128 Karlsruhe (Germany)
Fax: (+49) 721-608-7021
E-mail: dehnen@achibm6.chemie.uni-karlsruhe.de

[**] This work was supported by the state of Baden-Württemberg (Margarete-von-Wrangell habilitation fellowship for S.D., Landesgraduierten fellowship for M.M.), the Deutsche Forschungsgemeinschaft, and the Fonds der Chemischen Industrie. We thank Prof. D. Fenske for his generous support of our research activities, and Prof. R. Ahlrichs for provision of computational resources.

 © 2002 WILEY-VCH Verlag GmbH & Co. KGaA, Weinheim 0044-8249/02/4122-4269 $ 20.00+.50/0

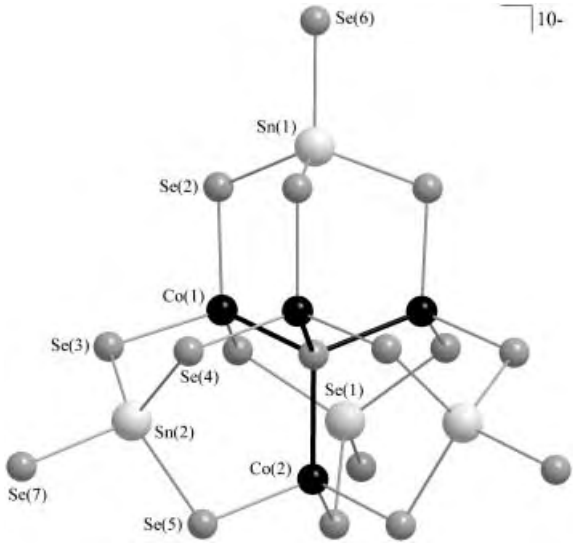


Figure 1. Structure of the cluster anion in **1**. Selected distances [pm] and angles [°]: Sn–Se_t 247.8(2)–249.0(1), Sn–(μ_2-Se) 250.9(1)–252.8(1), Co–(μ_2-Se) 242.6(2)–244.8(1), Co–(μ_4-Se) 243.5(2)–244.9(3), Co···Co 394.5(4)–402.1(5); Se_t-Sn-Se 105.29(4)–109.37(4), (μ_2-Se)-Sn-(μ_2-Se) 109.20(4)–112.59(4), (μ_4-Se)-Co-Se 109.13(5)–113.33(6), (μ_2-Se)-Co-(μ_2-Se) 105.92(5)–107.49(5), Co-(μ_4-Se)-Co 108.15(4)–110.76(4).

$(\mu_2\text{-EPh})_{12}Cl_4]^{2-}$ (M^{II} = Zn: E = Se, Te;[24] M^{II} = Cd: E = S,[25a] Se[26]) or $[Cd_8(\mu_4\text{-S})(\mu_2\text{-SPh})_{16}]^{2-}$.[25b] In contrast to all known M_8 clusters, the ternary anion in **1** contains two different sorts of metal atoms. Moreover, the cluster anions in **1** are the first ligand-free examples of this type, as they do not covalently bind to any ligand molecules at the μ_2-bridging or at the terminal selenium atoms. Finally, the twelve μ_2-bridging selenido ligands form a slightly distorted cubooctahedron rather than a Se_{12} icosahedron which has been observed for all the analogous species characterized so far.

Being a purely inorganic, discrete anion, the cluster in **1** differs from all Co/E′/E systems reported to date (E′ = Ge, Sn; E = chalcogen); for $[\{(CO)_4Co\}_4Sn_2E_2]$,[4b] or $[(Cp^*Co)_2(\mu_3\text{-}E)_2\{Sn\{CH(SiMe_3)_2\}_2\}]$ (E = S, Se),[5a] such compounds are either protected by an organic ligand shell,[4,5] or they feature polymeric anionic networks such as the phases mentioned at the outset.[10–12] To our knowledge, only one further type of complex has been reported that contains ligand-free, discrete anions of the combination transition metal/tetrel/chalcogen: $[PPh_4]_4[E'_2(WSe_4)_4]$ (E′ = Sn, Pb),[9] which was generated from $E'Cl_2$ and $[NH_4]_2[WSe_4]$.

The Sn–Se bond lengths in **1** (Sn–Se_t 247.8(2), 249.0(1) pm, Sn–(μ_2-Se) 250.9(1)–252.8(1) pm) correspond with those of the adamantane-type selenostannate(IV) anion in [2,2,2-crypt-K]$_4[Sn_4Se_{10}]$[27] (2,2,2-crypt = 4,7,13,16,21,24-hexaoxa-1,10-diazabicyclo[8.8.8]hexacosane). The Co–(μ_2-Se) and Co–(μ_4-Se) distances are very similar (Co–(μ_2-Se) 242.5(2)–244.8(1) pm; Co–(μ_4-Se) 243.6(1), 245.0(2) pm). They range within the upper values of bond lengths reported for the few known cobalt–selenide compounds with similar structural characteristics (tetrahedral coordination of Co^{III} and/or Co^{II} centers, μ_4-bridging Se^{2-} ligands),[28] which corroborates the formal oxidation state of +2 assigned to the cobalt atoms in **1**.

All investigations of re-dissolved **1** (NMR spectroscopy, cyclic voltammetry measurements, ESI mass spectrometry) were frustrated by instantaneous decomposition of the compound in solution; therefore we are currently undertaking solid-state measurements to ascertain the formal charge of the cobalt centers as well as to exclude the existence of $(OR)^-$ groups (R = H, Me). To get an impression of whether the structural parameters observed in the cluster anion in **1** might indeed be in accord with the assigned total charge, that is whether the assumed reduction by Se^{2-} ions turns out to be plausible, we performed density functional theoretical (DFT)[29] investigations on the cluster anions $[Co_4(\mu_4\text{-}Se)(SnSe_4)]^{q-}$ (q = 6–10; program system Turbomole[30]). Simulation of mirror charges[31] allowed the theoretical treatment of the highly charged molecules. The calculated Sn–Se distances in the Co/Sn/Se cluster anions tended to be larger than the experimentally observed ones; a comparable situation was found for the results of calculations on the $[Sn_4Se_{10}]^{4-}$ ion[27] (Sn–Se_t: +4 to +5 pm, Sn–(μ_2-Se): +7 to +10 pm with respect to the crystallographically determined values). In contrast, the computed Co–Se bond lengths in the ternary anions were all somewhat shorter than the experimental ones, which likewise was in accordance with the results of calculations on the adamantane-type anion $[\{Co(SPh)\}_4(\mu_2\text{-}SPh)_6]^{2-}$[32] (Co–S: −3 to −4 pm with respect to the crystallographically determined values). The best agreement between calculated and experimentally determined structural parameters—within the limits of the methods used—was observed for the ternary anion with the charge 10− (Sn–Se_t 255.0–255.2, Sn–(μ_2-Se) 259.2–259.8, Co–(μ_4-Se) 239.3–241.9, Co–(μ_2-Se) 242.1–244.3 pm), whereas deviation and divergence of the interatomic distances increased with decreasing total charge of the ternary anion (minimum 6−, corresponding to four Co^{III}).

In the crystal lattice, the high charge of the ternary anions is compensated by interactions with neighboring potassium ions. By coordinating to oxygen atoms of the solvent molecules and to selenido ligands of both the Co/Sn/Se anions and the additional $[SnSe_4]^{4-}$ units, potassium ions obtain coordination numbers of six ($[KO_nSe_{6-n}]$, n = 0–4) or seven ($[KO_nSe_{7-n}]$, n = 1, 2; K···Se 319.6(2)–376.9(3), K···(μ_1-, μ_2-O) 234.0(9)–327.4(10) pm). The terminal selenido ligands of the cluster anion show coordination numbers of five to seven by interacting with adjacent potassium ions or, through hydrogen bonds, with three adjacent oxygen atoms (Se(6)···O 325.4(4) pm). The coordination environment of the ternary anion is shown in Figure 2.

The results presented herein reveal for the first time that complete orthochalcogenostannate anions can be transferred into the coordination sphere of transition metal ions to give highly charged, purely inorganic, ternary cluster complexes. Decisive for the retention of the Sn–E bonds was the use of a Co^{III} complex with weaker coordinating en ligands instead of CO, PR_3, or Cp^R, and the presence of donor solvents H_2O and MeOH that enabled the design of a suitable aggregation of the counterions, embedding and thus stabilizing the anionic cluster molecules. Future investigations will focus on the synthesis and characterization of further M/Sn/E aggregates, containing other transition metal ions and/or other chalcogenostannate groups.

 © 2002 WILEY-VCH Verlag GmbH & Co. KGaA, Weinheim 0044-8249/02/4122-4270 $ 20.00+.50/0

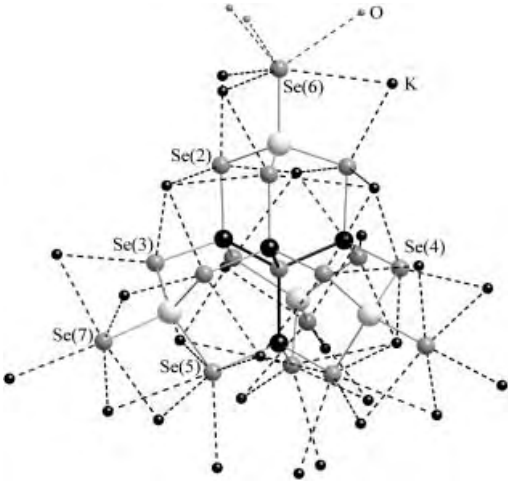


Figure 2. Embedding of the cluster anion in **1** in the coordination sphere of adjacent potassium ions and oxygen atoms (Co: black, Se: medium gray, Sn: light gray). Interatomic distances within the coordination sphere [pm]: K···Se 319.6(2)–376.9(3), Se···O 325.4(4). Structural parameters of the additional $[SnSe_4]^{4-}$ unit (not shown) [pm; °]: Sn-Se 250.8(1)–252.9(1); Se-Sn-Se: 105.56(4)–112.67(5).

Experimental Section

All synthesis steps were performed under exclusion of air and external moisture (N_2 atmosphere at a high-vacuum, double-manifold Schlenk line, or Ar atmosphere in a glove box). Methanol and toluene were dried and freshly distilled prior to use; water was degassed by applying dynamic vacuum (10^{-3} Torr) for several hours.

Synthesis of **1** and **2**: $K_4[SnSe_4]$ (0.201 g, 0.34 mmol)[19] was added to a suspension of $[Co(en)_3]Cl_3$ (0.115 g, 0.33 mmol) in H_2O/methanol (0.5/9.5 mL), whereupon the reaction mixture immediately turned dark brown. After the mixture had been stirred for 4 h, an insoluble, black precipitate was removed by filtration. The remaining solution was layered with toluene (10 mL). In the course of one week, the solution brightened under formation of black, cubic crystals of **1** and large quantities of **2**. Yields: **1**: 0.024 g (0.005 mmol, 10% with respect to $[SnSe_4]^{4-}$), **2**: 0.144 g (0.145 mmol, 85% with respect to $[SnSe_4]^{4-}$). C,H analyses (%): **1**: calcd: C 4.39, H 1.76; found: C 4.41, H 1.75; **2**: calcd: C 4.83, H 1.64; found: C 4.86, H 1.62.

Quantum-chemical investigations: Density functional (DFT) calculations[29] were performed by using the program system Turbomole[30] (RIDFT program;[33] Becke–Perdew functional (B-P-86);[34] basis sets of SV(P) quality;[35] relativistically corrected effective core potentials (ECP) for Sn atoms (ECP-46)[36]). Compensation of the negative charges of all calculated molecules was achieved by simulating mirror charges;[31] accordingly, negative values were obtained for all orbital energies and structural parameters were better than those from the computation of free anions. All geometry optimizations were performed without symmetry restrictions (C_1 symmetry), therefore convergence into local minimum structures can be assumed.

Received: June 21, 2002 [Z19577]

[1] Reviews: a) J. Wachter, *Angew. Chem.* **1998**, *110*, 782 – 800; *Angew. Chem. Int. Ed.* **1998**, *37*, 750 – 768; b) G. W. Drake, J. W. Kolis, *Coord. Chem. Rev.* **1994**, *137*, 131 – 178.

[2] P. T. Wood, J. D. Woolins, *Transition Met. Chem.* **1986**, *11*, 358 – 360.

[3] B. Schiemenz, F. Ettel, G. Huttner, L. Zsolnai, *J. Organomet. Chem.* **1993**, *458*, 159 – 166.

[4] a) H. Kraus, K. Merzweiler, *Z. Naturforsch. B* **1997**, *52*, 635 – 638, and references therein; b) K. Merzweiler, H. Kraus, L. Weisse, *Z. Naturforsch. B* **1993**, *48*, 287 – 290.

[5] a) J. J. Schneider, J. Hagen, D. Spickermann, D. Bläser, R. Boese, F. F. de Biani, F. Laschi, P. Zanello, *Chem. Eur. J.* **2000**, *6*, 237 – 246; b) J. J. Schneider, J. Hagen, D. Bläser, R. Boese, C Krüger, *Angew. Chem.* **1997**, *109*, 771 – 773; *Angew. Chem. Int. Ed. Engl.* **1997**, *36*, 378 – 741.

[6] J. Lee, T. J. Emge, J. G. Brennan, *Inorg. Chem.* **1997**, *36*, 5064 – 5068.

[7] a) Y.-J. Lu, J. A. Ibers, *Acta Crystallogr. Sect. C* **1991**, *47*, 1600 – 1602; b) A. Müller, I. Paulat-Böschen, B. Krebs, H. Dornfeld, *Angew. Chem.* **1976**, *88*, 691 – 692; *Angew. Chem. Int. Ed. Engl.* **1976**, *15*, 643 – 644.

[8] A. Eichhöfer, D. Fenske, *J. Chem. Soc. Dalton Trans.* **2000**, 941 – 944.

[9] B. Y.-J. Lu, J. A. Ibers, *Acta Crystallogr. Sect. C* **1991**, *47*, 1600 – 1602.

[10] A. Loose, W. S. Sheldrick, *Z. Naturforsch. B* **1997**, *52*, 687 – 692, and references therein.

[11] G. D. Albertelli II, J. A. Cowen, C. N. Hoff, T. A. Kaplan, S. D. Mahanti, J. H. Liao, M. G. Kanatzidis, *Phys. Rev. B* **1997**, *55*, 11056 – 11059.

[12] P. N. Trikalitis, K. K. Rangan, M. G. Kanatzidis, *J. Am. Chem. Soc.* **2002**, *124*, 2604 – 2613, and references therein.

[13] a) G. W. Drake, G. L. Schimek, J. W. Kolis, *Inorg. Chem.* **1996**, *35*, 5434 – 5435; b) T. M. Martin, P. T. Wood, G. L. Schimek, W. T. Pennington, J. W. Kolis, *Inorg. Chem.* **1995**, *34*, 4385 – 4391.

[14] a) H.-O. Stephan, M. G. Kanatzidis, *Inorg. Chem.* **1997**, *36*, 6050 – 6057; b) H.-O. Stephan, M. G. Kanatzidis, *J. Am. Chem. Soc.* **1996**, *118*, 12226 – 12227, and references therein.

[15] O. Blacque, H. Brunner, M. M. Kubicki, F. Leis, D. Lucas, Y. Mugnier, B. Nuber, J. Wachter, *Chem. Eur. J.* **2001**, *7*, 1342 – 1349.

[16] a) R. Stähler, W. Bensch, *Eur. J. Inorg. Chem.* **2001**, 3073 – 3078; b) R. Stähler, C. Näther, W. Bensch, *Eur. J. Inorg. Chem.* **2001**, 1835 – 1840.

[17] a) C. Zimmermann, S. Dehnen, *Z. Anorg. Allg. Chem.* **1999**, *625*, 1963 – 1965; b) S. Dehnen, C. Zimmermann, C. E. Anson, *Z. Anorg. Allg. Chem.* **2002**, *628*, 279 – 288.

[18] a) S. Dehnen, C. Zimmermann, *Chem. Eur. J.* **2000**, *6*, 2256 – 2261; b) C. Zimmermann, S. Dehnen, *Z. Anorg. Allg. Chem.* **2001**, *627*, 847 – 850; c) S. Dehnen, C. Zimmermann, *Eur. J. Inorg. Chem.* **2000**, 1471 – 1473.

[19] K. O. Klepp, *Z. Naturforsch. B* **1992**, *47*, 411 – 417.

[20] Two independent $[Sn_2Se_6]^{4-}$ ions are observed in the crystal structure of **2** (C_i symmetry; idealized D_{2h} symmetry, as observed for solvent-free $K_4[Sn_2Se_6]$);[21] Sn–Se_t 246.2(1)–248.3(1), Sn–(μ_2-Se) 259.0(2)–259.9(1) pm. K^+ ions show distorted octahedral coordination geometry (n O- and 6–n Se atoms; $n = 1, 2$; K···O 267.3(6)–291.7(6), K···Se 331.4(3)–365.8(3) pm). Terminal selenido ligands have coordination numbers five (Sn atom, n K^+ ions, 4–n hydrogen bonds to adjacent O atoms, $n = 2$–4; Se···O 330.0(6)–342.2(6) pm); bridging selenium atoms have coordination numbers four ($SeSn_2K_2$) or five ($SeSn_2K_3$). All O atoms are situated in a distorted tetrahedral coordination geometry by binding/coordinating to C and H atoms and two K^+ ions each.

[21] B. Eisenmann, J. Hansa, *Z. Kristallogr.* **1993**, *203*, 299 – 300.

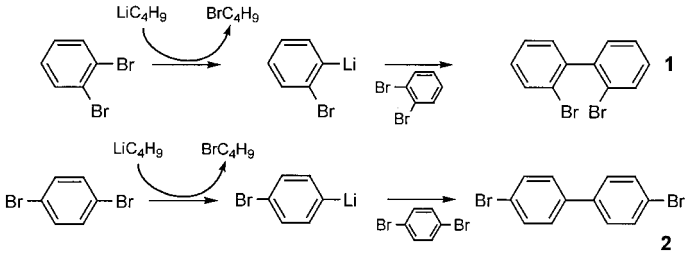
[22] Data of the X-ray structural analyses: $T = 203$ K, $Ag_{K\alpha}$ radiation ($\lambda = 0.56087$ Å), graphite monochromator, imaging plate detector STOE IPDS. Structure solution by direct methods, full-matrix least-squares refinement against F^2; used software: Shelxl-96,[37] shelxl-97.[38] $C_{18}H_{86}O_{25}Co_4K_{22}Se_{29}Sn_7$, **1:** cubic, space group $Ia\bar{3}$, $Z = 16$, $a = 3681.5(4)$ pm, $V = 49897(10) \times 10^6$ pm^3, $\rho_{calcd} = 2.619$ g cm^{-3}, $2\theta = 2$–42°, 8962 independent reflections ($R_{int} = 0.1579$), 6146 with $I > 2\sigma(I)$; $\mu(Mo_{K\alpha}) = 5.869$ mm^{-1}, 332 parameters (refinement of Sn, Se, and K atomic sites by employing anisotropic displacement parameters; one K atom threefold disordered, another K atomic site occupied to a 1/3; some of the C and O atoms twofold or threefold disordered; respective assignment of split positions; refinement of O and C atomic sites by employing isotropic displacement parameters; H atoms not calculated), residual electron density 1.541 e$^-$ $\times 10^{-6}$ pm^{-3}. R values for reflections with $I > 2\sigma(I)$: $R_1 = 0.0533$, $wR_2 = 0.1156$. $C_4H_{16}K_4O_4Se_6Sn_2$, **2**: triclinic, space group $P\bar{1}$, $Z = 2$, $a = 1022.1(2)$, $b = 1084.7(2)$, $c = 1311.5(3)$ pm, $\alpha = 104.01(3)$, $\beta = 106.83(3)$, $\gamma = 108.60(3)$°, $V = 1226.1(4) \times 10^6$ pm^3, $\rho_{calcd} = 2.697$ g cm^{-3}, $2\theta = 3$–42°, 5005 independent reflections ($R_{int} = 0.0486$), 4177 with $I > 2\sigma(I)$; $\mu(Mo_{K\alpha}) = 6.137$ mm^{-1}, 209 parameters (refinement of Sn, Se, K, O, and C atomic sites by employing anisotropic displacement parameters; some H atoms localized from the Fourier map), residual electron denisty: 1.645 e$^-$ $\times 10^{-6}$ pm^{-3}. R values for reflections with $I > 2\sigma(I)$: $R_1 = 0.0424$, $wR_2 = 0.1044$. CCDC-187775 (**1**) and CCDC-187776 (**2**) contain the supplementary crystallographic data for this paper. These data can be obtained free of charge via www.ccdc.cam.ac.uk/conts/retrieving.html (or from the Cambridge Crystallographic Data Centre,

12, Union Road, Cambridge CB2 1EZ, UK; fax: (+44) 1223-336-033; or deposit@ccdc.cam.ac.uk).
[23] The pH value of the reaction mixture is ≈11; standard redox potentials under basic conditions: a) $[Co^{III}(en)_3]^{2+} \rightarrow [Co^{II}(en)_3]^{3+}$: −0.18; J. E. Huheey, E. A. Keiter, R. L. Keiter, *Anorganische Chemie: Prinzipien von Struktur und Reaktivität*, 2nd ed., de Gruyter, Berlin, **1995**, p. 477; b) $Se^{2-} \rightarrow 1/n\,Se_n$: −0.92 V; A. F. Hollemann, N. Wiberg, *Lehrbuch der Anorganischen Chemie*, 100th ed., de Gruyter, Berlin, **1985**, p. 543.
[24] A. Eichhöfer, D. Fenske, H. Pfistner, M. Wunder, *Z. Anorg. Allg. Chem.* **1998**, *624*, 1909–1914.
[25] a) I. G. Dance, K. Fisher, *Prog. Inorg. Chem.* **1994**, *41*, 637–803; b) G. S. H. Lee, K. J. Fisher, D. C. Craig, M. L. Scudder, I. G. Dance, *J. Am. Chem. Soc.* **1990**, *112*, 6435–6437.
[26] S. Behrens, M. Bettenhausen, A. C. Deveson, A. Eichhöfer, D. Fenske, A. Lohde, U. Woggon, *Angew. Chem.* **1996**, *108*, 2360–2362; *Angew. Chem. Int. Ed. Engl.* **1996**, *35*, 2215–2218.
[27] J. Campbell, D. P. DiCiommo, H. P. A. Mercier, A. M. Pirani, G. J. Schrobilgen, M. Willuhn, *Inorg. Chem.* **1995**, *34*, 6265–6272.
[28] a) D. Fenske, J. Ohmer, K. Merzweiler, *Z. Naturforsch. B* **1987**, *42*, 802–809; b) D. Fenske, J. Ohmer, J. Hachgenei, *Angew. Chem.* **1985**, *97*, 993–995; *Angew. Chem. Int. Ed. Engl.* **1985**, *24*, 993–995.
[29] a) R. G. Parr, W. Yang, *Density Functional Theory of Atoms and Molecules*, Oxford University Press, New York, **1988**; b) T. Ziegler, *Chem. Rev.* **1991**, *91*, 651–667.
[30] a) R. Ahlrichs, M. Bär, M. Häser, H. Horn, C. Kölmel, *Chem. Phys. Lett.* **1995**, *242*, 652–657; b) O. Treutler, R. Ahlrichs, *J. Chem. Phys.* **1995**, *102*, 346–354.
[31] A. Klamt, *J. Chem. Phys.* **1995**, *103*, 9312–9320.
[32] I. G. Dance, *J. Am. Chem. Soc.* **1979**, *101*, 6264–6273.
[33] a) K. Eichkorn, O. Treutler, H. Öhm, M. Häser, R. Ahlrichs, *Chem. Phys. Lett.* **1995**, *242*, 652–660; b) K. Eichkorn, F. Weigend, O. Treutler, R. Ahlrichs, *Theor. Chim. Acta* **1997**, *97*, 119–124.
[34] a) A. D. Becke, *Phys. Rev. A* **1988**, *38*, 3098–3109; b) S. H. Vosko, L. Wilk, M. Nusair, *Can. J. Phys.* **1980**, *58*, 1200–1205; c) J. P. Perdew, *Phys. Rev. B* **1986**, *33*, 8822–8837.
[35] A. Schäfer, H. Horn, R. Ahlrichs, *J. Chem. Phys.* **1992**, *97*, 2571–2577.
[36] M. Dolg, H. Stoll, A. Savin, H. Preuss, *Theor. Chim. Acta* **1989**, *75*, 173–194.
[37] G. M. Sheldrick, shelxs-96, Program for the Solution of Crystal Structures, University of Göttingen, Göttingen (Germany), **1996**.
[38] G. M. Sheldrick, shelxl-97, Program for the Refinement of Crystal Structures, University of Göttingen, Göttingen (Germany), **1997**.

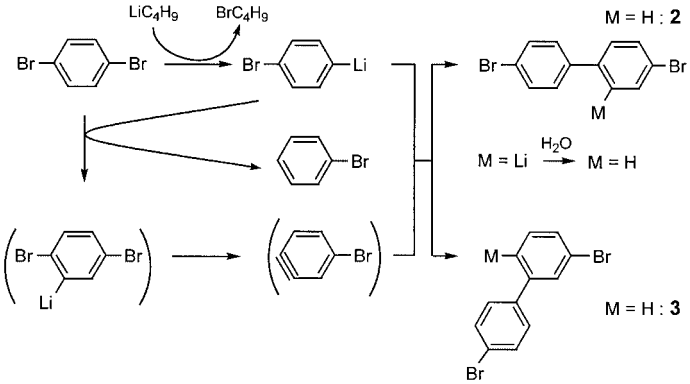
The "Aryne" Route to Biaryls Featuring Uncommon Substituent Patterns**

Frédéric Leroux and Manfred Schlosser*

In 1957, Gilman and Gaj[1] disclosed a facile preparation of 2,2′-dibromobiphenyl (**1**) in 21% yield by treatment of 1,2-dibromobenzene with half a molar equivalent of butyllithium (Scheme 1). In support of the surmised condensation process between dibromobenzene and a phenyllithium intermediate derived from it by halogen–metal permutation, they analogously converted 1,4-dibromobenzene into 4,4′-dibromobiphenyl (**2**; 18%).[1] Effective aryl–aryl coupling in general requires the participation of transition elements. When Lau and co-workers[2] succeeded in raising the yield of 2,2′-dibromobiphenyl to 81% by a careful optimization of the reaction conditions, the condensation hypothesis had to be abandoned. It was tempting to base an alternative mechanism on the intermediacy of 1,2-didehydrobenzene (1,3-cyclohexadien-5-yne, the so-called "benzyne"). However, if such a species were really involved, 1,4-dibromobenzene would have to give rise not only to **2**, as reported,[1] but also to its 3,4′-isomer **3**. As revealed by gas chromatographic analysis, the isomers **2** (M = H; 41%) and **3**[3] (M = H; 21%) were indeed formed concomitantly with bromobenzene (14%; Scheme 2). These findings are in agreement with a metalation, elimination, addition sequence featuring 4-bromophenyllithium, 2,5-dibromophenyllithium, and 4-bromo-1,2-didehydrobenzene as transient entities.



Scheme 1. Reported[1] reaction of 1,2- and 1,4-dibromobenzene with butyllithium to form **1** or **2**, respectively.



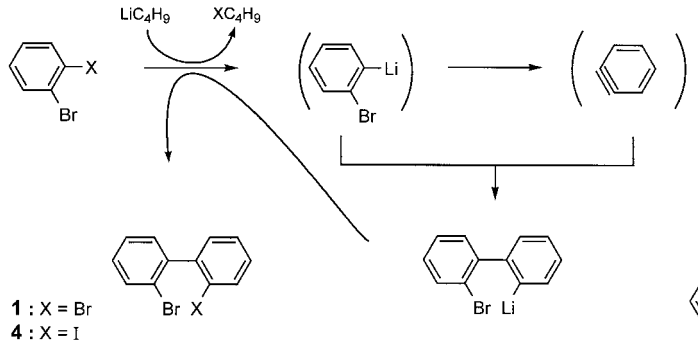
Scheme 2. Postulated mechanism of the coupling of 1,4-dibrombenzene with butyllithium to account for the formation of a mixture of **2** and **3**.

The ensuing work developed in three stages. The first objective was to provide evidence for the suspected aryne intermediate in the 1,2-dibromobenzene transformation. Once the essential details of this reaction are understood, one should be able to make use of this knowledge to construct first symmetrical and eventually unsymmetrical biaryls. According to our hypothesis, the final step in the formation of **1** should be bromine abstraction from 1,2-dibromobenzene by the 2′-bromo-2-biphenylyllithium species resulting from the combination of 2-bromophenyllithium with 1,2-didehydrobenzene (Scheme 3). If the starting material were replaced with 1-bromo-2-iodobenzene, iodine transfer would have to occur. In fact, treatment of this dihalo compound with half a

[*] Prof. Dr. M. Schlosser, Dr. F. Leroux
Institut de chimie moléculaire et biologique
Ecole Polytechnique Fédérale
1015 Lausanne (Switzerland)
Fax: (+41) 21-693-9365
E-mail: manfred.schlosser@epfl.ch

[**] This work was supported by the Swiss National Science Foundation, Bern (grant 20-63′584-00).

 © 2002 WILEY-VCH Verlag GmbH & Co. KGaA, Weinheim 0044-8249/02/4122-4272 $ 20.00+.50/0

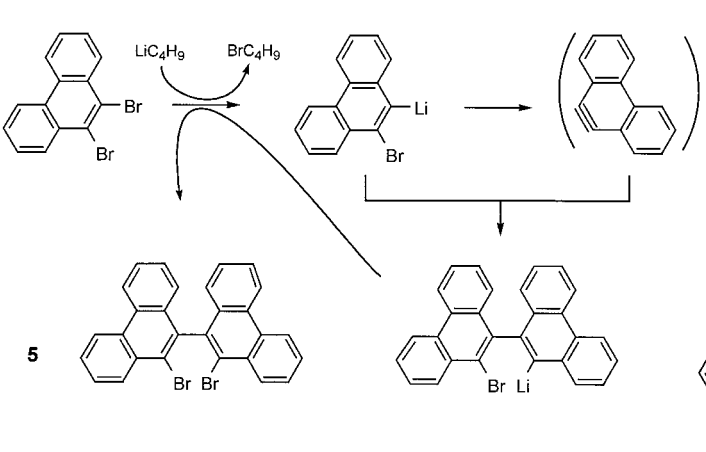


Scheme 3. Reaction of 1,2-dibrombenzene or 1-bromo-2-iodobenzene with butyllithium to form **1** or **4**, respectively.

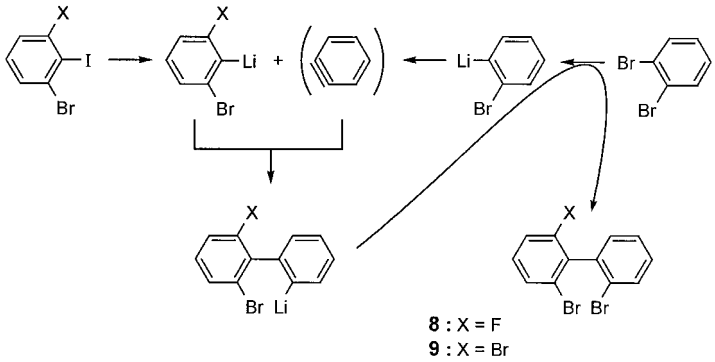
molar equivalent of butyllithium afforded 2-bromo-2′-iodobiphenyl[4] (**4**; X = I, Scheme 3) in 81 % yield.

To demonstrate the general applicability of the new aryl–aryl linking mode, 9,10-dibromophenanthrene[5] was converted into 10,10′-dibromo-9,9′-bisphenanthryl[6] (**5**; 63 %), 1-bromo-3-fluoro-2-iodobenzene[7] into 2-bromo-3′,6-difluoro-2′-iodobiphenyl[8] (**6**; 64 %), and 1-bromo-3-chloro-2-iodobenzene[9] into 2-bromo-3′,6-dichloro-2′-iodobiphenyl (**7**; 62 %; Scheme 4). The crucial steps in all these reactions were, first the nucleophilic addition of the organolithium precursor to the transient aryne species released from it by β-elimination of a lithium halide and, second, stabilization of the resulting 2-biaryl lithium intermediate by in situ transfer of bromine or iodine from the starting material.

This aryl–aryl coupling method can be modified by generating the aryne from a thermally labile 2-haloaryllithium species in the presence of a more stable aryllithium compound which will then act as the trapping reagent. For example, when a solution of 2-bromo-6-fluorophenyllithium was treated with one equivalent of 1,2-dibromobenzene at −75 °C, 2,2′-dibromo-6-fluorobiphenyl[10] (**8**; Scheme 5, X = F) was obtained in 79 % yield. The 2-bromophenyllithium



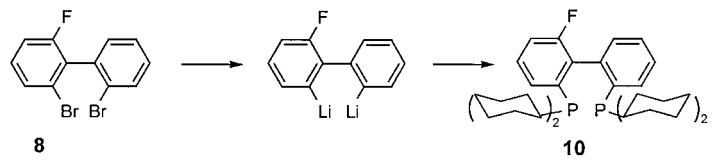
Scheme 4. Formation of the biaryls **5**, **6**, and **7**.



Scheme 5. Trapping of the labile haloaryllithium intermediates by more stable aryl lithium compounds.

species formed by halogen–metal permutation from 1,2-dibromobenzene is labile at temperatures above −125 °C, did not survive the experimental conditions but instantaneously released benzyne, which was trapped by the thermally less sensitive aryllithium component. A similar reaction between the labile 2,6-dibromophenyllithium (made from 1,3-dibromo-2-iodobenzene[7]) and 1,2-dibromobenzene gave 2,2′,6-tribromobiphenyl[11] (**9**) in 43 % yield.

Biaryl species carrying three or four *ortho*-substituents can be resolved into antipodal atropisomers. Therefore, our results provide mechanistic insight and at the same time provide an entry to axially dissymmetric bisphosphanes and other ligands for enantioselective catalysis. 6′-Fluoro-1,1′-biphenylene-2,2′-bis(dicyclohexylphosphane)[12] (**10**) was prepared in 66 % yield by consecutive treatment of 2,2′-dibromo-6-fluorobiphenyl (**8**) with butyllithium and chlorodicyclohexylphosphane (Scheme 6). Its ^{13}C NMR DEPT spectrum



Scheme 6. Formation of the biaryl atropisomeric **10**.

([D$_8$]toluene, 25 °C) showed signals arising from the cyclohexyl methine units as four different doublets ($J_{C,P} \approx 17$ Hz), thus exhibiting stereotopicity. This signal pattern did not change noticeably when the sample was heated to 125 °C. Thus, the barrier to torsional isomerization must exceed 22 kcal mol^{-1} and may well fall in the range of 25–30 kcal mol^{-1} if one bases the estimate on the findings of Jendralla et al.[13] with 6,6′-difluoro-2,2′-biphenylenebis(diphenylphosphane), the planarization of which is hampered

 © 2002 WILEY-VCH Verlag GmbH & Co. KGaA, Weinheim 0044-8249/02/4122-4273 $ 20.00+.50/0

by two P–F interactions. The bisphosphane **10** should racemize at ambient temperature only slowly, if at all.

A related approach to the synthesis of asymmetric biaryls is presently pursued by Buchwald and co-workers.[14–16] These authors isolated 2′-substituted 2-biphenylylphosphanes in 18–58% yield after having heated a solution of 1-bromo-2-chlorobenzene in tetrahydrofuran under reflux in the presence of magnesium turnings and an *ortho*-substituted Grignard reagent (such as 2-tolylmagnesium bromide, 2-anisylmagnesium bromide, or 2-(dimethylamino)phenylmagnesium chloride), before quenching the mixture with chlorodi-*tert*-butylphosphane or chlorodicyclohexylphosphane.

Received: May 24, 2002 [Z19382]

[1] H. Gilman, B. J. Gaj, *J. Org. Chem.* **1957**, *22*, 447 – 449.

[2] T. K. Dougherty, K. S. Y. Lau, F. L. Hedberg, *J. Org. Chem.* **1983**, *48*, 5273 – 5280.

[3] F. H. Case, *J. Am. Chem. Soc.* **1938**, *60*, 424 – 427.

[4] **4**: colorless needles (from ethanol); m.p. 88.5–89 °C; ^{1}H NMR ($CDCl_3$, 400 MHz): $\delta = 7.94$ (d, $J = 7.9$ Hz, 1H), 7.66 (d, $J = 8.0$ Hz, 1H), 7.39 (dt, $J = 12.8$, 7.5 Hz, 2H), 7.2 (m, 3H), 7.08 ppm (dt, $J = 7.6$, 1.4 Hz, 1H); elemental analysis (%) calcd for $C_{12}H_8BrI$ (359.00): C 40.15, H 2.25; found C 40.13, H 2.29.

[5] J. Schmid, G. Ladner, *Ber. Dtsch. Chem. Ges.* **1904**, *37*, 4402 – 4405.

[6] **5**: colorless needles (from ethanol); m.p. 344–348 °C (dec.); ^{1}H NMR ([D_6]DMSO, 400 MHz): $\delta = 9.10$ (d, $J = 8.2$ Hz, 2H), 9.05 (d, $J = 8.5$ Hz, 2H), 8.46 (d, $J = 8.0$ Hz, 2H), 7.91 (sym m, 4H), 7.77 (t, $J = 7.9$ Hz, 2H), 7.46 (t, $J = 7.6$ Hz, 2H), 7.13 ppm (d, $J = 8.1$ Hz, 2H); elemental analysis (%) calcd for $C_{28}H_{16}Br_2$ (512.24): C 65.65, H 3.15; found C 65.59, H 3.37.

[7] a) 1-Bromo-3-fluoro-2-iodobenzene: Diisopropylamine (14 mL, 10 g, 0.10 mol) and 1-bromo-3-fluorobenzene (11 mL, 18 g, 0.10 mol) were consecutively added to a solution of butyllithium (0.10 mol) in tetrahydrofuran (150 mL) and hexanes (50 mL) in a methanol/dry-ice bath. After 2 h at −75 °C iodine (25 g, 0.1 mmol) in THF (50 mL) was added, the solvents were evaporated and the residue dissolved in diethyl ether (100 mL). After washing with a 10% aqueous solution of sodium thiosulfate (2 × 50 mL), the organic layer was dried. Upon distillation, a colorless oil was collected; b.p. 108–109 °C (10 Torr); $n_D^{20} = 1.6354$; yield: 24 g (78%); elemental analysis (%) calcd for C_6H_3BrFI (300.89): C 23.95, H 1.00; found C 24.07, H 1.08. b) 1-Bromo-3-chloro-2-iodobenzene**:** Analogously to ref. [7a], the synthesis was carried out from 1-bromo-3-chlorobenzene (12 mL, 19 g, 0.10 mol); colorless needles; m.p. 75–76 °C (from ethanol); yield: 27 g (86%); elemental analysis (%) calcd for C_6H_3BrClI (317.35): C 22.71, H 0.95; found C 22.82, H 0.93. c) 1,3-Dibromo-2-iodobenzene: The synthesis was carried out analogously to ref. [7a] from 1,3-dibromobenzene (12 mL, 24 g, 0.10 mol); colorless platelets; m.p. 99–100 °C (from ethanol); yield: 33 g (91%); elemental analysis (%) calcd for $C_6H_3Br_2I$ (361.80): C 19.92, H 0.84; found C 19.97, H 0.80.

[8] **6**: colorless needles (from ethanol); m.p. 100–101 °C; ^{1}H NMR ($CDCl_3$, 400 MHz): $\delta = 7.50$ (td, $J = 8.1$, 0.9 Hz, 1H), 7.39 (dt, $J = 7.9$, 5.2 Hz, 1H), 7.28 (dt, $J = 8.2$, 5.7 Hz, 1H), 7.14 (dt, $J = 8.6$, 1.1 Hz, 1H), 7.10 (dt, $J = 8.0$, 1.5 Hz, 1H), 7.02 ppm (dd, $J = 7.5$, 1.1 Hz, 1H); elemental analysis (%) calcd $C_{12}H_6BrF_2I$ (394.98): C 36.49, H 1.53; found C 36.50, H 1.29.

[9] **7**: colorless needles (from ethanol); m.p. 136–138 °C; ^{1}H NMR ($CDCl_3$, 400 MHz): $\delta = 7.57$ (dd, $J = 8.0$, 0.7 Hz, 1H), 7.52 (dd, $J = 8.1$, 1.6 Hz, 1H), 7.48 (dd, $J = 8.0$, 0.8 Hz, 1H), 7.41 (t, $J = 7.9$ Hz, 1H), 7.25 (t, $J = 8.2$ Hz, 1H), 7.06 ppm (dd, $J = 7.5$, 1.2 Hz, 1H); elemental analysis (%) calcd for $C_{12}H_6BrCl_2I$ (427.89): C 33.68, H 1.41; found C 33.80, H 1.27.

[10] **8**: colorless needles (from ethanol); m.p. 68–70 °C; ^{1}H NMR ($CDCl_3$, 400 MHz): $\delta = 7.70$ (dd, $J = 8.0$, 1.2 Hz, 1H), 7.48 (td, $J = 7.9$, 1.0 Hz, 1H), 7.40 (dt, $J = 7.8$, 1.3 Hz, 1H), 7.3 (m, 3H), 7.13 ppm (dt, $J = 8.6$, 1.1 Hz, 1H); elemental analysis (%) calcd for $C_{12}H_7Br_2F$ (329.99): C 43.68, H 2.14; found C 44.00, H 2.10.

[11] **9**: colorless needles (from ethanol); m.p. 95–97 °C; ^{1}H NMR ($CDCl_3$, 400 MHz): $\delta = 7.69$ (d, $J = 8.1$ Hz, 1H), 7.64 (dd, $J = 8.1$, 0.7 Hz, 2H), 7.42 (tt, $J = 7.5$, 0.9 Hz, 1H), 7.29 (ddt, $J = 7.8$, 1.8, 0.7 Hz, 1H), 7.18 (dd, $J = 7.6$, 1.6 Hz, 1H), 7.12 ppm (dd, $J = 8.1$, 0.7 Hz, 1H); elemental analysis (%) calcd for $C_{12}H_7Br_3$ (390.90): C 36.87, H 1.81; found C 36.82, H 1.66.

[12] **10**: colorless needles (from ethyl acetate/hexanes (1:5)); m.p. 184–186 °C; ^{1}H NMR ($CDCl_3$, 400 MHz): $\delta = 7.5$ (m, 1H), 7.3 (m, 4H), 7.1 (m, 1H), 1.7 (m, 24H), 1.2 ppm (m, 20H); ^{13}C NMR ([D_8]toluene, 101 MHz): $\delta = 162.7$ (d, $J = 10.6$ Hz), 160.2 (d, $J = 10.4$ Hz), 143.8 (d, $J = 5.2$ Hz), 143.8 (d, $J = 5.0$ Hz), 139.6 (d, $J = 22.4$ Hz), 137.1 (d, $J = 19.6$ Hz), 133.6 (d, $J = 5.2$ Hz), 133.4 (s), 133.1 (s), 128.5 (d, $J = 22.4$ Hz), 128.2 (d, $J = 12.2$ Hz), 115.9 (d, $J = 23.6$ Hz), 37.8 (d, $J = 18.4$ Hz), 36.8 (d, $J = 17.2$ Hz), 34.6 (d, $J = 16.6$ Hz), 34.4 (d, $J = 16.8$ Hz), 31 (m), 30.9 (d, $J = 14.2$ Hz), 30.5 (d, $J = 9.3$ Hz), 30.4 (d, $J = 8.4$ Hz), 28 (m), 27.4 ppm (s); elemental analysis (%) calcd for $C_{36}H_{51}FP_2$ (564.75): C 76.56, H 9.10; found C 76.43, H 9.04.

[13] H. Jendralla, C.-h. Li, E. Paulus, *Tetrahedron: Asymmetry* **1994**, *5*, 1297 – 1320.

[14] H. Tomori, J. M. Fox, S. L. Buchwald, *J. Org. Chem.* **2000**, *65*, 5334 – 5341.

[15] C. Parrish, S. L. Buchwald, *J. Org. Chem.* **2001**, *66*, 3820 – 3827.

[16] S. Kaye, J. M. Fox, F. A. Hicks, S. L. Buchwald, *Adv. Synth. Catal.* **2001**, *343*, 789 – 794.

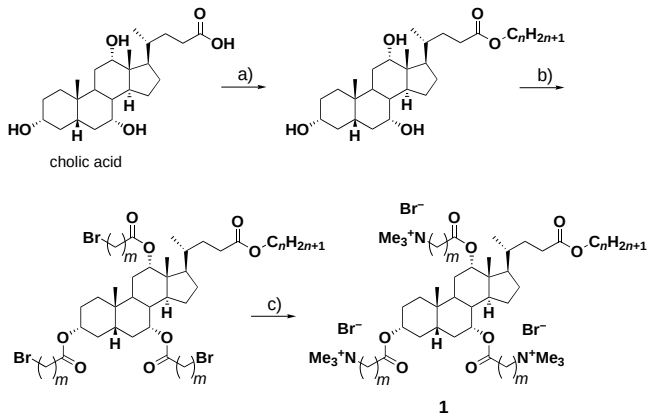
 © 2002 WILEY-VCH Verlag GmbH & Co. KGaA, Weinheim 0044-8249/02/4122-4274 $ 20.00+.50/0

Micelle Formation and Antimicrobial Activity of Cholic Acid Derivatives with Three Permanent Ionic Head Groups**

Hendra M. Willemen, Louis C. P. M. de Smet, Arie Koudijs, Marc C. A. Stuart, Ineke G. A. M. Heikamp-de Jong, Antonius T. M. Marcelis,* and Ernst J. R. Sudhölter

Cholic acid, a main bile acid, is a biosurfactant involved in the digestion of dietary lipids. With the carboxylate group as the ionic head group it resembles a "classical" surfactant. However, the steroid part with three hydroxy groups on one side is often considered to be a facial amphiphile. These hydroxy groups can have specific interactions, such as those found in inclusion compounds,[1,2] organogelators,[3–6] and receptors[7,8] based on cholic acid. Furthermore, the hydroxy groups, each with a different reactivity,[9] make cholic acid an ideal starting point for a synthetic procedure. The polarity of the hydroxy groups can be increased to emphasize the facial amphiphilicity of the steroid unit. The resulting facial amphiphiles have many applications in ion transport,[10,11] combinatorial chemistry,[12] vesicle fusion,[13] and improvement of membrane permeability.[14] Even facial amphiphiles with three ionic groups are reported.[15,16] However, the properties of these cationic (NH_3^+) or anionic (COO^-) facial amphiphiles are dependent on the pH of the solution. Herein, a series of new facial amphiphiles with a permanent ionic character is presented. Three cationic trimethylammonium groups were attached to cholic acid and the carboxylate group was esterified, to yield a new class of three-headed surfactants. We know of only one other example of a surfactant with three permanent ionic head groups and only one hydrophobic tail.[17] We report on the aggregation of this new type of surfactant into spherical micelles and on its antimicrobial activity.

Synthesis of this series of ionic facial amphiphiles was completed in three steps from cholic acid (Scheme 1). First, the carboxylate group was esterified with a long alkyl group.



Scheme 1. a) $C_nH_{2n+1}OH$, *p*-toluenesulfonic acid, benzene, 90 °C, 24 h, 75 %; b) Br-$(CH_2)_m$-COCl, DMAP, benzene, pyridine, RT, 24 h, 65 %; c) NMe_3, EtOH, 100 °C, 24 h, 90 %. Prepared compounds: **1a** ($n=8$, $m=3$), **1b** ($n=10$, $m=3$), **1c** ($n=12$, $m=3$), **1d** ($n=12$, $m=4$), **1e** ($n=12$, $m=5$), **1f** ($n=12$, $m=7$), and **1g** ($n=16$, $m=3$). DMAP = *N*,*N*-dimethylamino pyridine.

Then, a spacer was attached to all three hydroxy groups using an ω-bromoalkanoic chloride. Finally, the bromine atoms were substituted by trimethylamine to give trimethylammonium groups on **1**. Variation was made in the length of the alkyl tail ($n=8$, 10, 12, or 16) and in the length of the spacer ($m=3$, 4, 5, or 7).

These new compounds are very hygroscopic. Solutions with accurately defined concentration were therefore prepared from lyophilized solutions. Because of the long aliphatic tail, aggregation occurs at rather low concentrations, about 1 mM, depending on the length of both the alkyl tail and the spacer.

Evidence for micelle formation was obtained from cryo-TEM measurements. For several compounds, cryo-TEM images were recorded of aqueous solutions (1 wt %, about 8 mM). Two examples are shown in Figure 1. The images show

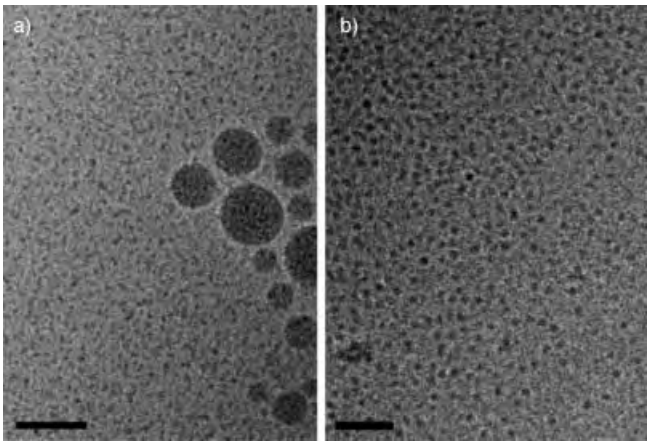


Figure 1. Cryo-TEM images of 1 wt % aqueous solutions of **1f** (a), and **1g** (b); scale bar indicates 50 nm.

small aggregates with an average diameter of 3–6 nm. The aggregates formed from **1a** ($n=8$, $m=3$) are smaller than from **1g** ($n=16$, $m=3$; 3–4 nm and 5–6 nm respectively), which demonstrates the influence of the alkyl tail length on micellar size. No elliptical or bar-shaped aggregates are

[*] Dr. A. T. M. Marcelis, H. M. Willemen, L. C. P. M. de Smet, A. Koudijs, Prof. Dr. E. J. R. Sudhölter
Laboratory of Organic Chemistry
Wageningen University
Dreijenplein 8, 6703 HB Wageningen (The Netherlands)
Fax: (+31) 317-484-914
E-mail: ton.marcelis@phys.oc.wau.nl
Dr. M. C. A. Stuart
Department of Biophysical Chemistry
University of Groningen
Nijenborgh 4, 9747 AG Groningen (The Netherlands)
I. G. A. M. Heikamp-de Jong
Laboratory of Microbiology
Wageningen University
Hesselink van Suchtelenweg 4, 6703 CT Wageningen (The Netherlands)

[**] The authors thank Remco Fokkink for help with dynamic light scattering (DLS), Dr. Elaine Vaughan for discussion about antimicrobial tests, Dr. Maarten Posthumus and Elbert van der Klift for help with MS, and Beb van Veldhuizen for help with NMR spectroscopy.

Supporting information for this article is available on the WWW under http://www.angewandte.org or from the author.

 © 2002 WILEY-VCH Verlag GmbH & Co. KGaA, Weinheim 0044-8249/02/4122-4275 $ 20.00+.50/0

visible, which indicates that the aggregates are spherical micelles. To verify this, a density histogram was created for a single aggregate; this indeed shows a Gaussian distribution. Occasionally, larger aggregates with a diameter of 15–50 nm can be seen. These aggregates have the same density variation as the small ones, so they are not vesical structures. We assume the occurrence of secondary micelles, formed by clustering of the small, primary micelles, similar to the two-step aggregation behavior of cholic acid itself.[18]

Dynamic light scattering (DLS) measurements on aqueous solutions of compounds **1b** ($n = 10$, $m = 3$) and **1g** ($n = 16$, $m = 3$) roughly show the presence of many aggregates with a diameter of about 5 nm and a few larger aggregates with a diameter of several tens of nanometers, assuming a spherical shape of the aggregates. These values correspond with those obtained from cryo-TEM images.

Several cholic acid-derived facial amphiphiles have been reported that improve the permeability of membranes such as bacterial cell walls.[14] These compounds, which make bacteria vulnerable to other antibiotics, have nitrogen-containing groups such as amine or guanidine groups, which are coupled to the hydroxy groups. The positive charges associate with the negatively charged membrane. Attaching a hydrophobic chain of about eight carbon atoms to these molecules facilitates "self-promoted" transport across the bacterial outer membrane and therefore results in strong antimicrobial activity.[19,20] Our surfactants contain the same structural elements (three nitrogen-containing, positively charged groups and a hydrophobic alkyl tail), therefore some tests were performed to investigate their antimicrobial activity. The minimum inhibition concentration (MIC) was measured using two bacterial cultures: *Escherichia coli* and *Enterococcus faecalis*. Compounds **1a** ($n = 8$, $m = 3$) and **1b** ($n = 10$, $m = 3$) inhibited growth of both bacterial cultures. The MIC was established to be 25 and 12.5 $\mu g\,mL^{-1}$ for **1a** and **1b**, respectively. This is far below the critical micelle concentration (CMC), so the inhibition mechanism does not involve aggregate structures but single molecules. The activity of **1b** is almost equal to that of the well-known antibiotic chloramphenicol. It is noteworthy that these compounds act as competent bacterial growth inhibitors against both gram-positive and gram-negative bacterial cultures. The other compounds with longer alkyl tails showed no inhibitory effect, not even in concentrations up to 200 $\mu g\,mL^{-1}$. The hydrophobic tail of 12 or 16 carbon atoms may be too long to facilitate transport through the bacterial membrane because of stronger hydrophobic interaction with the membrane.

In conclusion, we report the synthesis of a series of new facial amphiphiles, based on cholic acid, with a permanent ionic character. These compounds act as three-headed surfactants, forming small primary and larger secondary spherical micelles. Micellar size depends on the lengths of the alkyl tail. Two compounds display antimicrobial activity against gram-positive as well as gram-negative bacteria. Further research to the micelle-forming behavior of this new class of three-headed ionic surfactants as a function of their molecular structure is ongoing.

Experimental Section

General procedure for the synthesis of **1**: Alkyl cholate (3 mmol)[4] was dissolved in benzene (10 mL) and pyridine (2 mL). A catalytic amount of DMAP was added and the mixture was stirred for 45 min at room temperature. A solution of ω-bromoalkanoic acid chloride (15 mmol) in benzene (10 mL) was added and the mixture stirred overnight at room temperature. The reaction mixture was filtered, diluted with CH_2Cl_2, and washed with 3 M HCl solution. The organic phase was dried and the solvent was evaporated under vacuum. The residue was purified by column chromatography on silica, using CH_2Cl_2:MeOH (99.5:0.5) as eluent, to give a yellow oil. 1 mmol of this 24-(alkyloxy)-24-oxo-3,7,12-tris{[ω-bromoalkanoyl]oxy}cholane was dissolved in a solution of trimethylamine in ethanol (20 wt %, 15 mL) and the solution stirred for 24 h in a closed reaction vessel at 100 °C. After cooling and concentrating the mixture, chloroform was added. The precipitate was filtered and evaporation of the filtrate under vacuum gave a white solid. The overall yield of this route is about 45 %. Spectroscopic data for all compounds are listed in the Supporting Information.

Cryo-TEM: a drop of sample suspension was placed on a glow-discharged, perforated carbon film. Excess liquid was blotted away with filter paper and the grid was subsequently vitrified in liquid ethane and cooled with liquid nitrogen. The frozen, hydrated grid was mounted in a Gatan cryostage (Gatan model 626) and observed in a Philips CM120 cryotransmission electron microscope operating at 120 kV. Images were recorded on a slow-scan charge-coupled device (CCD) camera under low-dose conditions.

DLS measurements: 1 wt % aqueous solutions were placed in a Lexel 85 Argon Ion Laser beam with $\lambda = 514.5$ nm and power = 100–300 mW; scattering was recorded at an angle of 90°, using an ALV-5000 digital correlator, ALV-125 goniometer, ALV-800 transputerboard from ALV-GmbH (Langen, Germany). 30 measurements of 20 s were accumulated and analyzed with Contin-fit.

Antimicrobial tests: cultures of gram-negative *Escherichia coli* (JM109, Promega) and gram-positive *Enterococcus faecalis* (93103, kind gift from VTT Biotechnology, Finland) were grown in LB broth or M17 broth with 1 % of glucose, respectively. A fresh overnight culture of *E. coli* (16 h at 37 °C) was inoculated into LB broth containing 100 $\mu g\,mL^{-1}$ of a compound and incubated for 24 h at 37 °C. On the compounds which showed no turbidity after incubation, a more extensive test was performed.[21] The MIC (the lowest concentration of surfactant that showed no turbidity) was measured using a series of glass test-tubes containing the compound in concentrations of 200, 100, 50, 25, and 12.5 $\mu g\,mL^{-1}$. Each tube was inoculated with exponential-growth-phase organisms (*E. coli* or *E. faecalis*) to a concentration of 1 % and incubated at 37 °C for 20 h. The optical density at 660 nm was measured before and after incubation. Broth containing bacteria alone was used as a positive control and, for comparison, bacteria were also tested in broth supplemented with 15 μg of chloramphenicol mL^{-1}. Tests were performed in duplicate.

Received: May 16, 2002
Revised: July 18, 2002 [Z19310]

[1] Y. Hishikawa, R. Watanabe, K. Sada, M. Miyata, *Chirality* **1998**, *10*, 600–618.
[2] V. Bertolasi, O. Bortolini, M. Fogagnolo, G. Fantin, P. Pedrini, *Tetrahedron: Asymmetry* **2001**, *12*, 1479–1483.
[3] H. M. Willemen, T. Vermonden, A. T. M. Marcelis, E. J. R. Sudhölter, *Eur. J. Org. Chem.* **2001**, 2329–2335.
[4] H. M. Willemen, T. Vermonden, A. T. M. Marcelis, E. J. R. Sudhölter, *Langmuir* **2002**, *18*, 7102–7106.
[5] K. Nakano, Y. Hiswikawa, K. Sada, M. Miyata, K. Hanabusa, *Chem. Lett.* **2000**, 1170–1171.
[6] Y. Hishikawa, K. Sada, R. Watanabe, M. Miyata, K. Hanabusa, *Chem. Lett.* **1998**, 795–796.
[7] J. Tamminen, E. Kolehmainen, *Molecules* **2001**, *6*, 21–46, and references therein.
[8] L. Vaton-Chanvrier, H. Oulyadi, Y. Combret, G. Coquerel, J. C. Combret, *Chirality* **2001**, *13*, 668–674.
[9] H. Gao, J. R. Dias, *Org. Prep. Proced. Int.* **1999**, *31*, 145–166.
[10] Y. Kobuke, T. Nagatani, *Chem. Lett.* **2000**, 298–299.

 © 2002 WILEY-VCH Verlag GmbH & Co. KGaA, Weinheim 0044-8249/02/4122-4276 $ 20.00+.50/0

[11] P. Bandyopadhyay, V. Janout, L. Zhang, S. L. Regen, *J. Am. Chem. Soc.* **2001**, *123*, 7691 – 7696.
[12] J. F. Barry, A. P. Davis, M. N. Pérez-Payan, M. R. J. Elsegood, R. F. W. Jackson, C. Gennari, U. Piarulli, M. Gude, *Tetrahedron Lett.* **1999**, *40*, 2849 – 2852.
[13] Y. R. Vandenburg, B. D. Smith, M. N. Pérez-Payán, A. P. Davis, *J. Am. Chem. Soc.* **2000**, *122*, 3252 – 3253.
[14] C. Li, A. S. Peters, E. L. Meredith, G. W. Allman, P. B. Savage, *J. Am. Chem. Soc.* **1998**, *120*, 2961 – 2962.
[15] S. Broderick, A. P. Davis, R. P. Williams, *Tetrahedron Lett.* **1998**, *39*, 6083 – 6086.
[16] U. Taotafa, D. B. McMullin, S. C. Lee, L. D. Hansen, P. B. Savage, *Org. Lett.* **2000**, *2*, 4117 – 4120.
[17] J. Haldar, V. K. Aswal, P. S. Goyal, S. Bhattacharya, *Angew. Chem.* **2001**, *113*, 1278 – 1282; *Angew. Chem. Int. Ed.* **2001**, *40*, 1228 – 1232.
[18] D. M. Small in *The Bile Acids, Vol. 1* (Eds.: P. P. Nair, D. Kritchevsky), Plenum, New York, **1971**, pp. 249 – 356.
[19] C. Li, L. P. Budge, C. D. Driscoll, B. M. Willardson, G. W. Allman, P. B. Savage, *J. Am. Chem. Soc.* **1999**, *121*, 931 – 940.
[20] C. Li, M. R. Lewis, A. B. Gilbert, M. D. Noel, D. H. Scoville, G. W. Allman, P. B. Savage, *Antimicrob. Agents Chemother.* **1999**, *43*, 1347 – 1349.
[21] W. G. Pitt, M. O. McBride, J. K. Lunceford, R. J. Roper, R. D. Sagers, *Antimicrob. Agents Chemother.* **1994**, *38*, 2577 – 2582.

Polymorphism in the Crystal Structure of the Cellulose Fragment Analogue Methyl 4-*O*-Methyl-β-D-Glucopyranosyl-(1-4)-β-D-Glucopyranoside**

Anna Rencurosi, Jürgen Röhrling, Jutta Pauli, Antje Potthast, Christian Jäger, Serge Pérez, Paul Kosma, and Anne Imberty*

Cellulose, the most abundant polymer on earth, usually consists of a mixture of highly crystalline and amorphous regions. The crystalline parts display one chain conformation, made up of a twofold ribbon, but many possible packing arrangements, with either parallel chains (cellulose I, III_I, and IV_I) or antiparallel chains (cellulose II, III_{II}, and IV_{II}) (for a review see ref. [1]). The three-dimensional structure of native cellulose is highly complex and not yet completely resolved because two distinct crystalline forms, cellulose Iα and Iβ[2] showing triclinic and monoclinic symmetry, respectively, coexist. The crystalline phases Iα and Iβ occur in variable proportions according to the source of the cellulose; that of primitive organisms (bacteria, alga, etc.) is enriched in the Iα phase whereas that of higher plants (woody tissues, cotton, ramie, etc.) consists mainly of the Iβ phase,[3] and cellulose of the outer membrane of marine animals is uniquely composed of the Iβ phase.[4] Modeling studies have established that the two crystalline arrangements correspond to two low-energy structures arising from parallel associations of cellulose chains.[5]

Cellobiose has been crystallized in its native form and in the form of derivatives and salts.[6] In all crystals, the packing arrangement corresponds to a low-energy arrangement of small molecules and does not provide any clues to the polymorphism of the polysaccharide. Only in crystals of methyl β-cellotrioside[7] and β-cellotetraose[8,9] chain-like arrangements were found. In these two cases, the molecules are arranged in an antiparallel way, which represents the packing of lowest energy, and the resulting structures are similar to that of cellulose II. We describe here the crystal structure analysis of a cellulose fragment that displays a parallel arrangement of molecules and that can therefore be directly compared with the two polymorphs of natural cellulose I.

Crystals of methyl 4-*O*-methyl-β-D-glucopyranosyl-(1-4)-β-D-glucopyranoside were obtained in the triclinic space group *P*1 (form **I**) using conditions which decreased the crystallization rate as compared to the crystallization of the monoclinic polymorph (group $P2_1$, form **II**).[10] The crystal structure of form **II** has been described recently from data collected at low temperature (220 K).[11] We redetermined the structure at room temperature[12] and found the differences in cell dimensions, cell volumes, and geometrical details to be less than 0.8%. Therefore, the structure is not shown here, but its data will be used in the tables to allow direct comparison between form **I** and form **II** geometries.

The molecular structure of form **I** is shown in Figure 1. Geometry calculations and ORTEP illustrations of the crystal structure were obtained with PLATON.[13] Both glucose rings have the usual $^4C_1$ shape. Intra-ring bond lengths and valence angles are in the range of standard values (Table 1). The short C1′–O4 bond at the glycosidic linkage is in agreement with the anomeric effect.[14] The C5–C6 and C6–O6 linkages of the

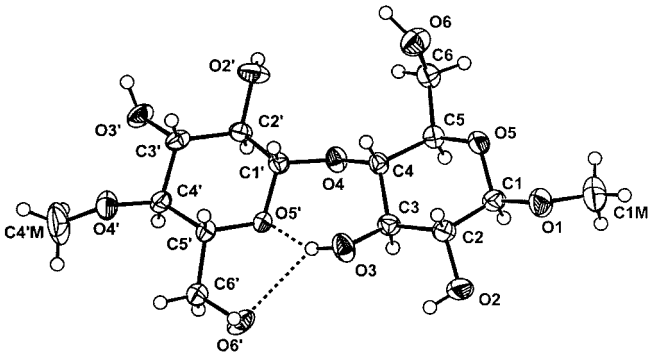


Figure 1. ORTEP representation of the molecular structure of form **I**. Thermal ellipsoids are drawn at the 50% probability level. Intramolecular hydrogen bonds are represented as dashed lines.

[*] Dr. A. Imberty, Dr. A. Rencurosi, Dr. S. Pérez
CERMAV-CNRS
601 rue de la Chimie, BP 53, 38041 Grenoble cedex 9 (France)
Fax: (+33) 476-54-7203
E-mail: imberty@cermav.cnrs.fr
Dr. J. Röhrling, Dr. A. Potthast, Prof. P. Kosma
Christian-Doppler-Labor, Institut für Chemie
Universität für Bodenkultur
Muthgasse 18, 1190 Wien (Austria)
Dr. J. Pauli, Prof. C. Jäger
Laboratorium I.31, Bundesanstalt für Materialforschung und -prüfung (BAM)
Richard-Willstätter-Strasse 11, 12489 Berlin (Germany)

[**] Anna Rencurosi is an EEC postdoctoral fellow (HPRN-CT2000-00001).

Supporting information for this article is available on the WWW under http://www.angewandte.org or from the author.

 © 2002 WILEY-VCH Verlag GmbH & Co. KGaA, Weinheim 0044-8249/02/4122-4277 $ 20.00+.50/0

Table 1. Comparison of geometrical characteristics of form **I** and form **II** cellobioside.

	Form **I**	Form **II**
glycosidic bond lengths [Å]		
C1′-O4	1.395(2)	1.386(2)
C4-O4	1.445(2)	1.437(2)
hydroxymethyl groups bond lengths [Å]		
C5-C6	1.489(2)	1.511(2)
C6-O6	1.396(2)	1.406(2)
C5′-C6′	1.502(2)	1.510(3)
C6′-O6′	1.431(2)	1.414(2)
C1M-O1	1.414(3)	1.423(3)
glycosidic valence angle [°]		
C1′-O4-C4	116.7(1)	117.3(1)
glycosidic torsion angles [°]		
O5′-C1′-O4-C4	−90.0(2)	−88.8(1)
C1′-O4-C4-C5	−159.2(1)	−151.3(1)
exocyclic torsion angles [°]		
O5-C5-C6-O6	−59.4(2)	−54.5(2)
O5-C1-O1-C1M	−83.0(2)	−67.7(2)
O5′-C5′-C6′-O6′	57.8(2)	59.0(1)
C3′-C4′-O4′-C4′M	107.5(2)	96.9(2)

hydroxymethyl group of the reducing unit are significantly shorter than standard bonds and also shorter than the bonds of the equivalent group in polymorph **II** (Table 1). In both forms, the orientations of the hydroxymethyl groups at O6 and O6′ are *gg* and *gt*, respectively, as found in most crystal structures of cellodextrins.[15]

The conformation at the glycosidic linkage of form **I** is characterized by interglycosidic torsion angles Φ(O5′-C1′-O4-C4) = −90.0° and Ψ(C1′-O4-C4-C5) = −159.2°, almost identical to those observed in methyl cellobioside crystallized as solvate complex with methanol (Φ = −88.9°, Ψ = −160.7°).[16] Form **II** has a similar conformation, with only 8° difference in Ψ (Φ = −88.8°, Ψ = −151.3°). Both forms are therefore similar in shape and can be compared with the longer cellodextrins such as methyl cellotrioside (average value of Φ = −94.4° and Ψ = −146.4°)[7] and cellotetraose (average value of Φ = −94.4° and Ψ = −146.8°).[8,9] As reported recently,[15] the structures cited above cluster in one group of cellobiose glycosidic linkage conformations that are characterized by a pseudo-2_1 axis of rotation around the long axis of the molecule: propagating such conformations leads to a flat ribbon-like molecule, similar to the conformation observed in all crystalline cellulose. This family of conformations is significantly different from the conformation of lowest energy found in the crystal structure of β-cellobiose having a more folded shape (Φ = −75° and Ψ = −130°).[17]

The "flat" disaccharide conformation observed in cellodextrins and in the two polymorphs of methyl 4′-*O*-methyl-β-cellobioside described here is also characterized by the

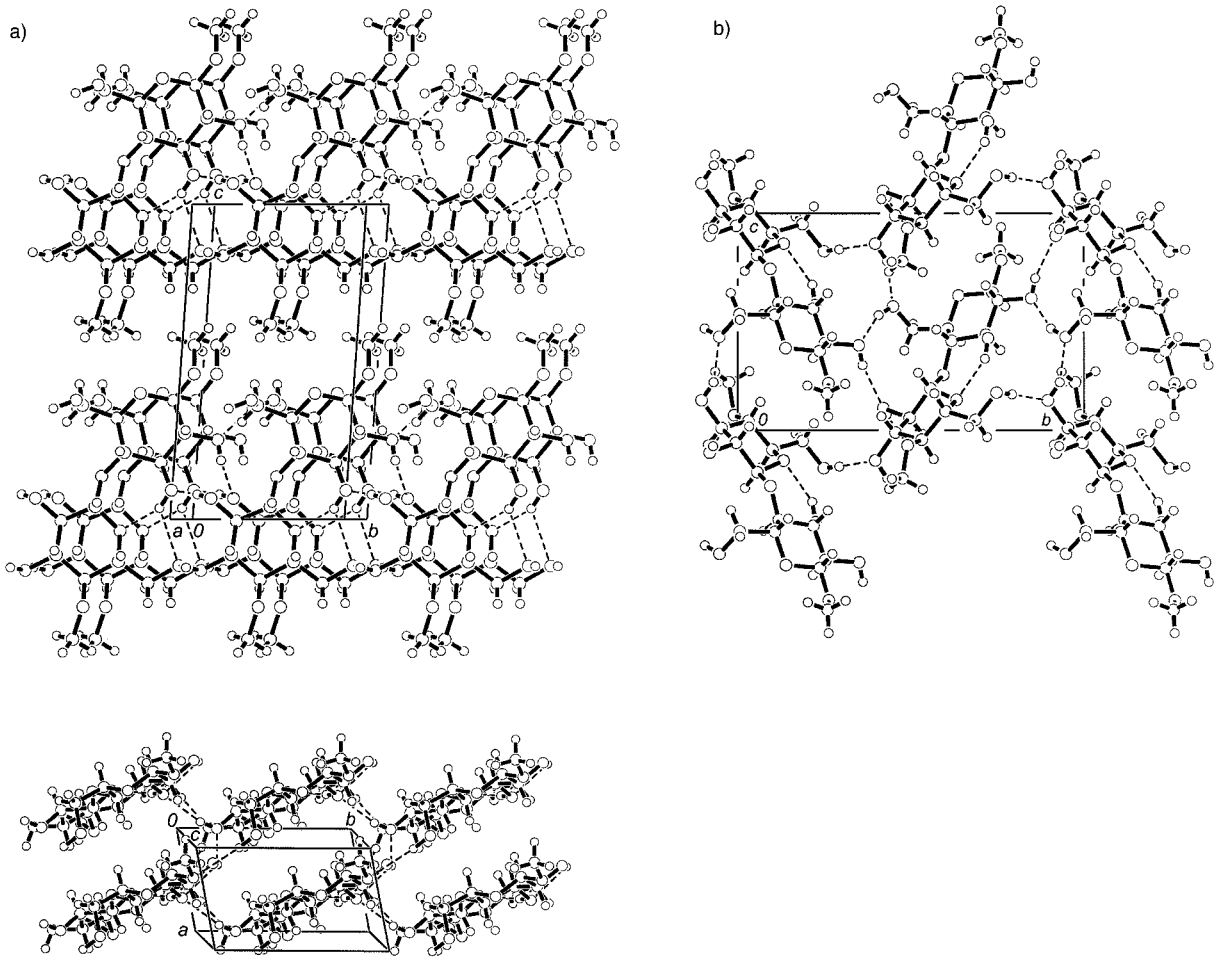


Figure 2. a) Two different views of the packing arrangement of form **I** cellobioside. b) Packing arrangement of form **II** cellobioside. Hydrogen bonds are represented as dashed lines.

 © 2002 WILEY-VCH Verlag GmbH & Co. KGaA, Weinheim 0044-8249/02/4122-4278 $ 20.00+.50/0

occurrence of two hydrogen bonds between the two rings involving O3 as donor and O5′ and O6′ as acceptors. In this three-centered hydrogen bond O3–H···O5′ is the stronger (d(O···O) > 2.8 Å) and O3–H···O6′ the weaker part (d(O···O) > 3.0 Å) (for details see the Supporting Information). This is also observed in crystals of longer cellodextrins and in cellulose chains studied by neutron diffraction.[18]

Whereas the molecular structures of the two polymorphs are very similar (rms calculated on all heavy atoms: 0.206 Å), their packing arrangements are completely different. In the triclinic form **I** (Figure 2a), the disaccharides are arranged as parallel molecules, connected by a complex network of intermolecular hydrogen bonds. Each molecule establishes ten intermolecular O–H···O hydrogen bonds (Figure 3a and Supporting Information), four with its two neighbors on each side, resulting from a single translation along the b axis, and six with the neighbors in the sheets above and below (translation along a). In addition, four intermolecular C–H···O hydrogen bonds are also observed (not shown). The translation along a is the shortest cell parameter (a = 4.6726(2) Å). It corresponds to the stacking of a cellobiose molecule with the ones above, in which numerous van der Waals contacts and hydrogen bonds are involved. Van der Waals interactions are established by the methyl groups on both sides of the disaccharide. As can be seen from Figure 2a, a hydrophobic layer of methyl groups at O1 interacts with an equivalent layer of methyl groups at O4′. The contact along the c axis is therefore mediated only by hydrophobic interactions.

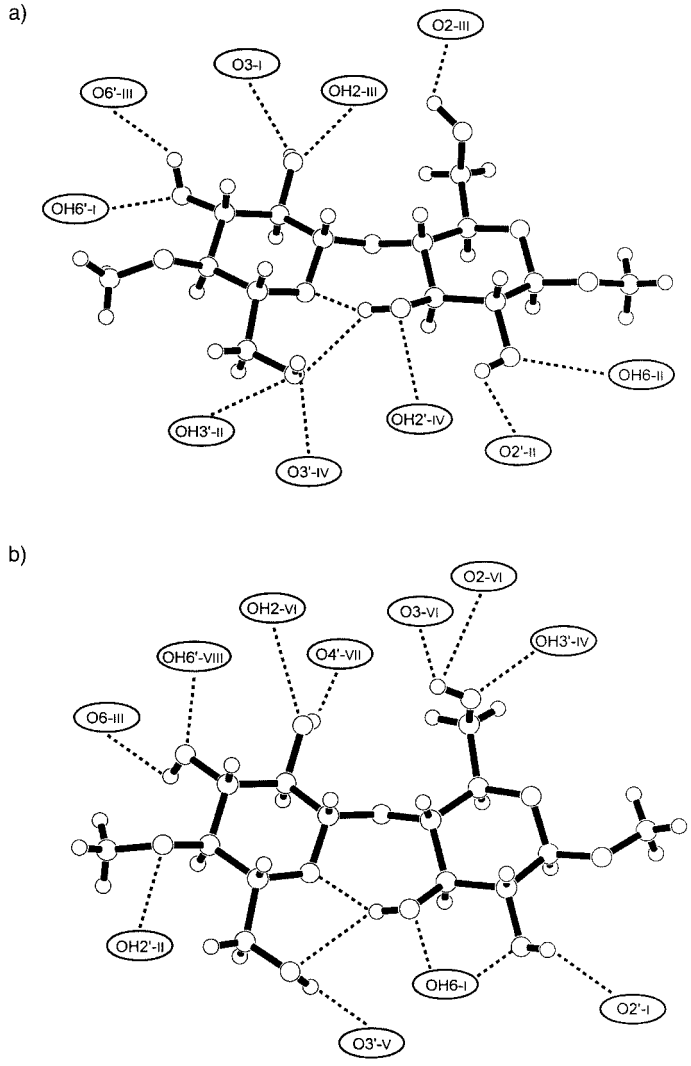


Figure 3. Network of hydrogen bonds O–H···O in the crystal structures of form **I** cellobioside (a) and form **II** cellobioside (b). The neighboring atoms have been given a code to indicate the symmetry involved (**I/II**): (I) $x,y-1,z/-x,y+1/2,-z+1$; (II) $x-1,y+1,z/x-1,y,z$; (III) $x+1,y-1,z/x,y,z+1$; (IV) $x,y+1,z/x,y,z-1$; (V) $/-x,y+1/2,-z+2$; (VI) $/-x,y-1/2,-z+1$; (VII) $/-x+1,y+1/2,-z$; (VIII) $/-x,y-1/2,-z+2$.

The packing arrangement of the monoclinic form **II** is completely different (Figure 2b). As described previously from the low-temperature data,[11] the disaccharides adopt an almost perpendicular orientation. Each molecule establishes twelve O–H···O and six C–H···O intermolecular hydrogen bonds with its neighbors (Figure 3b and Supporting Information).

We report here the first detection of crystalline polymorphism in an anhydrous oligosaccharide. A comparison of the two crystal structures may allow for rationalization of observed physicochemical data such as differences in melting points and in solid-state NMR spectra. The melting point of form **II** is 22 K higher than that of form **I** (493 K versus 471 K), suggesting that the monoclinic polymorph is thermodynamically preferred. Also, crystals of form **I** are more difficult to obtain; they have to be grown slowly. The crystal stability can be estimated by counting the number of contacts that a single molecule establishes with its neighbors and by evaluating the resulting energy of interaction or lattice energy. The mode of molecular packing was analyzed by applying the atom-pair procedure of Kitaigorodsky.[19] In this procedure, all contacts of a reference molecule with the surrounding molecules are explored. The energy of interaction was evaluated by molecular mechanics, comparing the energy of a minicrystal (11 and 15 molecules for forms **I** and **II**, respectively) with the energy of the same ensemble but with the reference molecule placed 100 Å away from the minicrystal.[20] In form **II**, each molecule makes contacts with 14 neighbors, compared to only 10 in form **I**. Both the number of contacts and the energy of interaction (Table 2) indicate that the monoclinic form **II** is thermodynamically favoured over form **I**.

In the solid-state NMR spectra of both polymorphs (Figure 4), there are clear differences, especially for the resonances of carbons C1, C1′, and C4, C4′ and in the region of

Table 2. Evaluation of the interaction between one molecule and its neighbors in both crystal forms.

	Form **I**	Form **II**
number of neighboring molecules[a]	10	14
number of intermolecular contacts[a]	84	106
number of intermolecular hydrogen bonds[b]		
O–H···O	5	6
C–H···O	2	3
energy of interaction in the minicrystal		
van der Waals contribution	−55.1 kcal mol^{-1}	−61.2 kcal mol^{-1}
electrostatic contribution	−6.9 kcal mol^{-1}	−7.1 kcal mol^{-1}
total interaction energy	−62.0 kcal mol^{-1}	−68.3 kcal mol^{-1}

[a] Evaluated as proposed by Kitaigorodski.[19] [b] Evaluated according to the criteria described by Jeffrey.[26]

 © 2002 WILEY-VCH Verlag GmbH & Co. KGaA, Weinheim 0044-8249/02/4122-4279 $ 20.00+.50/0

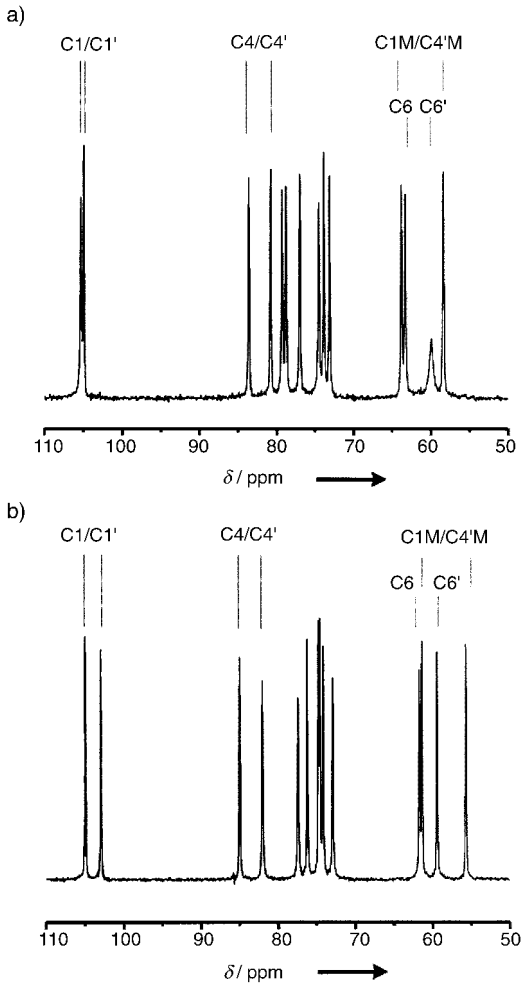


Figure 4. CP-MAS ^{13}C NMR spectra of form **I** (a) and form **II** (b) cellobioside.

carbons C6 and C6′. Since both forms have nearly identical shapes in the crystal the differences in chemical shifts cannot be attributed to differences in the conformation but suggest that the packing has a strong effect on the chemical shifts in the solid state. Another intriguing feature is the broadening of the C6 peak in the spectrum of form **I**. The assignment of C6 and C6′ to $\delta = 59.9$ and 63.3 ppm, respectively, is based on previous studies by Horii et al.,[21] and is in agreement with the *gg* and *gt* orientations of their hydroxymethyl groups. Broadening of only the peak for C6 in form **I** cannot be attributed to an increased mobility of this group since thermal parameters do not indicate any additional mobility and no disorder is observed. The only special features at this group are that O6 is involved in a C–H···O hydrogen bond with C5 of a neighboring molecule and that both C5–C6 and C6–O6 bonds are shorter than usual values (see Table 1).

The parallel arrangement of molecules in the triclinic form **I** and the proposed models for native cellulose Iα and Iβ[5] are compared in Figure 5. In the latter, the molecules have the shape of a flat ribbon with 2_1 symmetry, whereas in form **I** cellobioside, the symmetry is less perfect. The three stacking modes differ in the orientation of each ribbon compared to the sheet plane and in the translation between different planes. The main difference between the present crystal

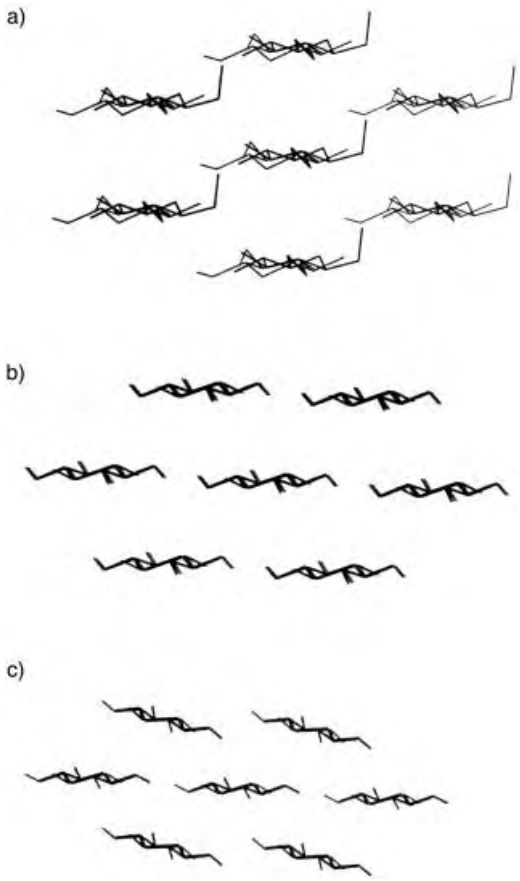


Figure 5. Parallel arrangement of molecules in triclinic form **I** cellobioside (a) compared to models for native cellulose Iα (b) and Iβ (c).

structure and the two polymer models is that the dimer does not form flat sheets. This opens up new perspectives about the occurrence of structures of parallel cellulose.

Received: June 14, 2002 [Z19532]

[1] A. C. Sullivan, *Cellulose* **1997**, *4*, 173.
[2] R. H. Atalla, D. L. VanderHart, *Science* **1984**, *223*, 283.
[3] J. Sugiyama, T. Okana, H. Yamamoto, F. Horii, *Macromolecules* **1990**, *23*, 3198.
[4] P. S. Belton, S. F. Tanner, N. Cartier, H. Chanzy, *Macromolecules* **1989**, *22*, 1615.
[5] R. J. Vietor, K. Mazeau, M. Lakin, S. Pérez, *Biopolymers* **2000**, *54*, 342.
[6] S. Pérez, C. Gautier, A. Imberty in *Oligosaccharides in Chemistry and Biology: A Comprehensive Handbook* (Eds.: B. Ernst, G. Hart, P. Sinay), Wiley-VCH, Weinheim, **2000**.
[7] S. Raymond, B. Henrissat, D. T. Qui, A. Kvick, H. Chanzy, *Carbohydr. Res.* **1995**, *277*, 209.
[8] K. Gessler, N. Krauss, T. Steiner, C. Betzel, A. Sarko, W. Saenger, *J. Am. Chem. Soc.* **1995**, *117*, 11397.
[9] S. Raymond, A. Heyraud, D. Tran Qui, A. Kvick, H. Chanzy, *Macromolecules* **1995**, *28*, 2096.
[10] Conditions for crystal growing: Form **I** crystals were obtained by the hanging-drop method using 9:1 PEG 400/water as precipitant. The stock solution had a concentration of 60 mg mL^{-1} water which was diluted to give a 3:2 ratio of stock solution and PEG. The drop volume was 20 μL. Crystals were isolated after 3 days.
[11] I. D. Mackie, J. Röhrling, R. O. Gould, J. Pauli, C. Jäger, M. Walkinshaw, A. Potthast, T. Rosenau, P. Kosma, *Carbohydr. Res.* **2002**, *337*, 161.

 © 2002 WILEY-VCH Verlag GmbH & Co. KGaA, Weinheim 0044-8249/02/4122-4280 $ 20.00+.50/0

[12] X-ray analyses: Cellobioside crystals **I** and **II** were mounted on glass fibres. Diffraction data were collected on a κ-CCD (ENRAF-NONIUS) diffractometer, $T = 298$ K, $Mo_{K\alpha}$, $\lambda = 0.71073$ Å (graphite monochromator). The structures were solved by direct methods (SIR-92).[22] Lorentz and polarization corrections were applied, but no correction was made for absorption, given the small crystal dimensions and the wavelength used. Refinement was performed using full-matrix least-squares on F^2 (TeXsan program[23]). Crystal data for form **I**: triclinic, $P1$; $a = 4.6726(2)$, $b = 7.5120(7)$, $c = 12.427(1)$ Å, $\alpha = 84.7(5)$, $\beta = 86.0(3)$, $\gamma = 79.7(4)°$, $V = 426.7(5)$ Å^3, $Z = 1$, $\rho_{calcd} = 1.44$ g cm^{-3}, $\mu = 1.25$, 10936 reflections measured, 8271 crystallographically independent ($R_{int} = 0.0345$), and 6419 with $I > 2\sigma(I)$, $2\theta_{max} = 64°$, $R = 0.055$, $Rw = 0.065$, 223 parameters, H atoms isotropic. Crystal data for form **II**: monoclinic, $P2_1$; $a = 6.617(7)$, $b = 14.117(6)$, $c = 9.344(6)$ Å, $\beta = 108.81(9)°$; $V = 826(1)$ Å^3, $Z = 2$, $\rho_{calcd} = 1.49$ g cm^{-3}, $\mu = 1.25$, 2631 reflections measured, 2500 crystallographically independent ($R_{int} = 0.0218$), and 2053 with $I > 2\sigma(I)$, $2\theta_{max} = 60°$, 226 parameters: $R = 0.0387$, $Rw = 0.0367$. CCDC-184139 (form **I**) and CCDC-184140 (form **II**) contain the supplementary crystallographic data for this paper. These data can be obtained free of charge via www.ccdc.cam.ac.uk/conts/retrieving.html (or from the Cambridge Crystallographic Data Centre, 12, Union Road, Cambridge CB2 1EZ, UK; fax: (+44) 1223-336-033; or deposit@ccdc.cam.ac.uk).
[13] A. L. Spek, *J. Appl. Crystallogr.* **1988**, *21*, 578.
[14] I. Tvaroska, T. Bleha, *Adv. Carbohydr. Chem. Biochem.* **1989**, *47*, 45.
[15] Z. Peralta-Inga, G. P. Johnson, M. K. Dowd, J. A. Rendleman, E. D. Stevens, A. D. French, *Carbohydr. Res.* **2002**, *337*, 851.
[16] J. T. Ham, D. G. Williams, *Acta Crystallogr. Sect. B* **1970**, *26*, 1373.
[17] S. S. C. Chu, G. A. Jeffrey, *Acta Crystallogr. Sect. B* **1968**, *24*, 830.
[18] P. Langan, Y. Nishiyama, H. Chanzy, *J. Am. Chem. Soc.* **1999**, *121*, 9940.
[19] A. I. Kitaigorodsky, *Molecular Crystals and Molecules*, Academic Press, New York, **1973**.
[20] To evaluate the difference in the energy of interaction in forms **I** and **II**, energy calculations were performed using the Tripos force field[24] present in Sybyl software.[25] Gasteiger–Marsili charges were assigned to the molecules, and the lengths of C–H···O and O–H···O hydrogen bonds were corrected to the theoretical lengths (1.050 and 0.950 Å, respectively). The interaction energy was defined as the difference between the energy of a minicrystal composed of a reference molecule surrounded by the nearest neighbors (i.e., by 11 molecules for form **I** and by 15 molecules for form **II**) and the energy of the same minicrystal but with the reference molecule pulled 100 Å away from its central position (i.e., noninteracting).
[21] F. Horii, A. Hirai, R. Kitamura, *Polymer Bull.* **1983**, *10*, 357.
[22] A. Altomare, M. C. Burla, G. Camalli, G. Cascarano, C. Giacovazzo, A. Guagliardi, G. Polidori, *J. Appl. Crystallogr.* **1984**, *27*, 435.
[23] TeXsan, MSC, The Woodlands, TX.
[24] M. Clark, R. D. I. Cramer, N. van den Opdenbosch, *J. Comput. Chem.* **1989**, *8*, 982.
[25] SYBYL, 1699 S. Hanley Road, Suite 303, St Louis, MO, USA.
[26] G. A. Jeffrey, *J. Mol. Struct.* **1999**, *485*–486, 293.

The Role of Nucleation Inhibition in Optical Resolutions with Families of Resolving Agents**

José W. Nieuwenhuijzen, Reinier F. P. Grimbergen, Carla Koopman, Richard M. Kellogg,* Ton R. Vries,* Kees Pouwer, Erik van Echten, Bernard Kaptein, Lumbertus A. Hulshof, and Quirinius B. Broxterman*

The separation of enantiomers by diastereomeric salt formation, essentially unchanged in technique since the original description by Pasteur,[1] remains the most widely used method in industry for obtainment of enantiomerically pure organic compounds.[2] In 1998 a significant modification of this classic technique was reported by some of us.[3] Upon simultaneous addition of structurally related resolving agents, high diastereomeric excesses (*de* values) of the first salts were obtained in a large number of resolutions. The success rate was 90–95 % compared to the usual 20–30 % estimated in one of the few studies published.[4] Structurally related resolving agents were denoted as family members and the method itself has become known as "Dutch Resolution".

In practice, three structurally related resolving agents are used in a 1:1:1 ratio. A mixture of these resolving agents was usually found in the first salt, but in nonstoichiometric ratios. In general, the families of resolving agents show solid-solution behavior. However, in the 46 examples of resolutions of single racemates reported in ref. [3], in ten cases no detectable amount of one (or more) of the three resolving agents was present in the salt. In three other cases, one of the resolving agents was present in < 10 mol %. The resolving agents that are regularly not incorporated, or which are incorporated only to a small extent, in the salt are shown in italics in Scheme 1 for the families used in the current work.[5]

Although direct comparisons are difficult owing to differences in solubilities and the almost certain involvement of

[*] Prof. Dr. R. M. Kellogg, Dr. T. R. Vries, J. W. Nieuwenhuijzen, Dr. K. Pouwer, E. van Echten
Syncom B.V.
Kadijk 3, 9747 AT Groningen (The Netherlands)
Fax: (+31) 50-575-7399
E-mail: r.m.kellogg@syncom.nl

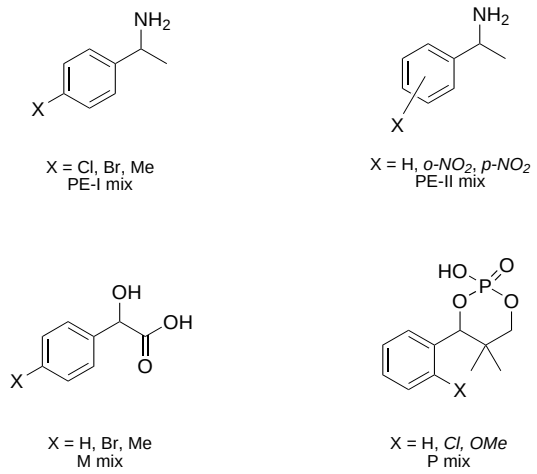
Dr. Q. B. Broxterman, Dr. B. Kaptein
DSM Research
DSM Fine Chemicals – Advanced Synthesis & Catalysis
PO Box 18, 6160 MD Geleen (The Netherlands)
Fax: (+31) 046-4767604
E-mail: rinus.broxterman@dsm.com

Dr. R. F. P. Grimbergen, Dr. Ir. C. Koopman
DSM Research
Centre for Particle Technology
PO Box 18, 6160 MD Geleen (The Netherlands)

Dr. L. A. Hulshof
DSM Fine Chemicals
PO Box 81, 5900 AB Venlo (The Netherlands)

[**] We gratefully acknowledge Prof. Lahav from the Weizmann Institute of Science in Israel for his hospitality during a three-month stay of J.W.N. in his group. We also would like to thank Dr. M. van der Sluis, Dr. P. G. H. Uiterweerd, Prof. Dr. E. Vlieg, Dr. W. van Enckevort, and Dr. J. Loh for fruitful discussions.

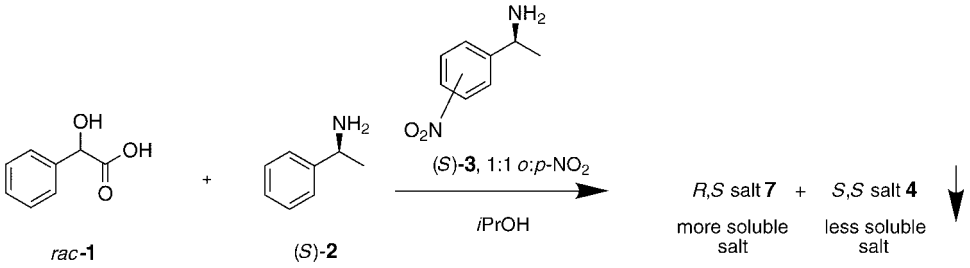
 © 2002 WILEY-VCH Verlag GmbH & Co. KGaA, Weinheim 0044-8249/02/4122-4281 $ 20.00+.50/0



Scheme 1. Families of structurally related resolving agents and the abbreviations from ref. [3].

kinetic effects, we had the strong feeling that resolutions proceeded less well in the absence of these unincorporated (or poorly incorporated) resolving agents. The suspicion arose that they might be "the dog that didn't bark".[6]

To test this idea, a model resolution was designed with two resolving agents: one the "parent" resolving agent and the other the "additive" that was poorly or not at all incorporated. The solubility differences between the pure "parent" and "parent/additive" system are assumed to be minimal. The model system chosen was the resolution of *rac*-mandelic acid (**1**) with (*S*)-phenylethylamine ((*S*)-**2**) (Scheme 2). A 1:1



Scheme 2. Resolution of (*rac*)-mandelic acid (**1**) with (*S*)-phenylethylamine (**2**), with or without 10% (*S*)-nitrophenylethylamines (**3**).

ortho:para mixture of nitro-substituted (*S*)-phenylethylamines (**3**; this material is readily available and is used commercially) was chosen as the additive; this mixture together with **2** forms the family "PE-II"[3] and shows little or no incorporation in "family" resolutions. One resolution was done with one equiv of **2** and the other with 0.9 equiv of **2** and 0.1 equiv of **3**.

In an early experiment we observed that at the non-optimum concentrations chosen, the resolution of **1** with **2** (Scheme 2) delivered the first salt with a *de* value of 14% and an S factor[7] of 0.19. In the presence of 0.1 equiv of **3** and 0.9 equiv of **2** the *de* value of the first salt increased from 14% to 55% and the S factor to 0.41.[8] No detectable amount of *ortho*- or *para*-(*S*)-**3** was incorporated into the salt.[9]

Crystallization in the presence of (*S*)-**3** as the additive to (*S*)-**2** was qualitatively observed to begin at a lower temperature than with (*S*)-**2** alone. To quantify this observation, turbidity measurements were carried out. For the less soluble diastereomer (*S*)-**2**/(*S*)-mandelic acid (**4**) the dissolution temperature is 70.2°C and the nucleation temperature is

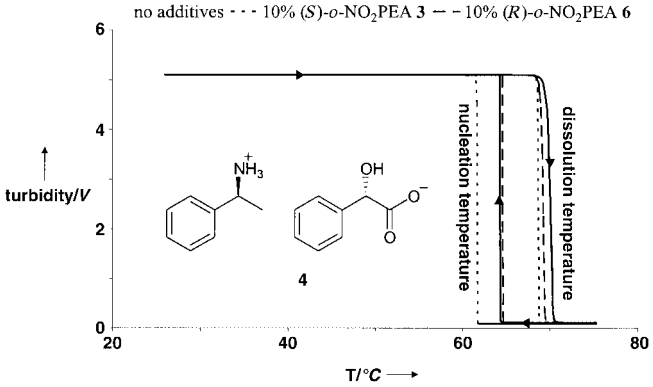


Figure 1. Turbidity measurements on the less soluble diastereomer **4**; 10 mol% (*S*)-*o*-NO_2PEA (**5**; PEA = phenylethylamine) or (*R*)-*o*-NO_2PEA (**6**) used as inhibitors.

64.2°C (Figure 1). Replacement of 10 mol% of (*S*)-**2** with (*S*)-*o*-nitrophenylethylamine (**5**)[10] led to a shift in nucleation temperature to 61.6°C. The metastable zone is enlarged from 6.0 to 7.1°C, which change is significantly beyond the experimental error.[11] For comparison, the effect of 10% (*R*)-*o*-nitrophenylethylamine (**6**) is also shown in Figure 1. The *R* additive has no statistically significant effect on nucleation or dissolution temperature.

In the case of the more soluble diastereomer (*S*)-**2**/(*R*)-mandelic acid (**7**; at a much higher concentration) a clear effect on nucleation temperature is also observed (Figure 2). The metastable zone width increases from 11.4 to 28.0°C on substitution of 0.1 equiv of (*S*)-**2** with (*S*)-**5**.[12]

For both diastereomers, nucleation inhibition is observed, whereas the dissolution temperatures remain more or less identical. These results can be better understood in terms of a qualitative ternary phase diagram (at constant temperature).[4] In Figure 3, the area that would lead to 100% *de* value in the less soluble salt, without

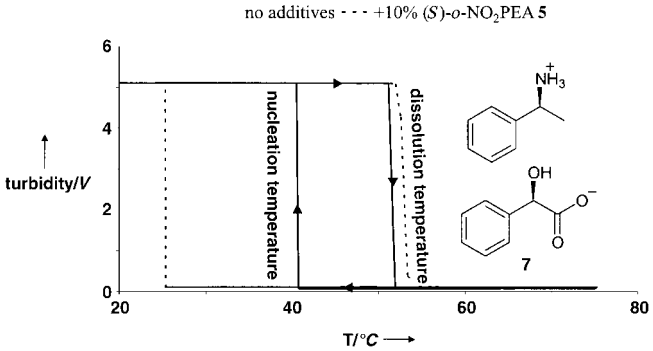


Figure 2. Turbidity measurements on the more soluble diastereomer **7**; 10 mol% (*S*)-*o*-NO_2PEA (**5**).

© 2002 WILEY-VCH Verlag GmbH & Co. KGaA, Wein-

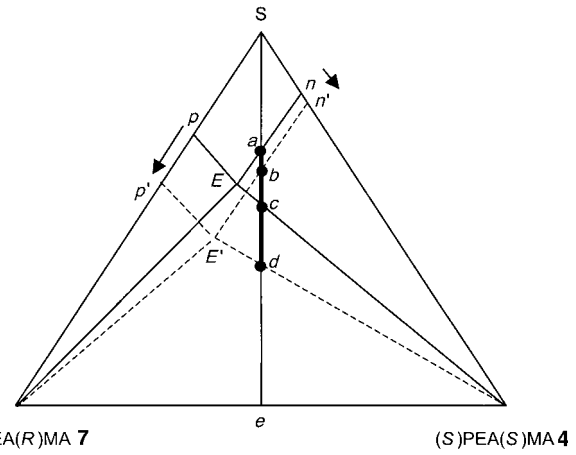


Figure 3. Ternary phase diagram with representation of the metastable zone width. MA = mandelic acid

additives, is represented by the triangle nE**4**. Starting from the 1:1 mixture (the line Se), the line ac shows the concentration range in which diastereomerically pure salt will be obtained, without the use of additives. The turbidity measurements (Figures 1 and 2) indicate that the nucleation lines without additive fall in between the solubility lines and the nucleation lines with additive. For clarity of illustration these former lines have been omitted. The dashed lines $p'E'$ and $n'E'$ represent the metastable nucleation lines that come into play on use of the additive. The intersection points of triangle $n'E'$**4** with line Se define the line bd, which is longer than the line ac, which implies that the operating window for a successful resolution is larger. Also, it can be seen that high *de* values should be obtainable at higher concentrations than in the situation without additive.

To verify this latter conclusion, the resolution of **1** with (*S*)-**2** was performed at different concentrations using in this case an even smaller amount, 5 mol%, of (*S*)-**3**. The resolution in the presence of the additive is still successful at 0.50 M in 2-propanol, whereas the resolution efficiency without additive drops dramatically to between 0.25 and 0.33 M, as shown in Figure 4.[8]

To establish generality, additional resolutions were carried out, all based on the same principle: the use of 10% of an unincorporated family member of the resolving agent as the

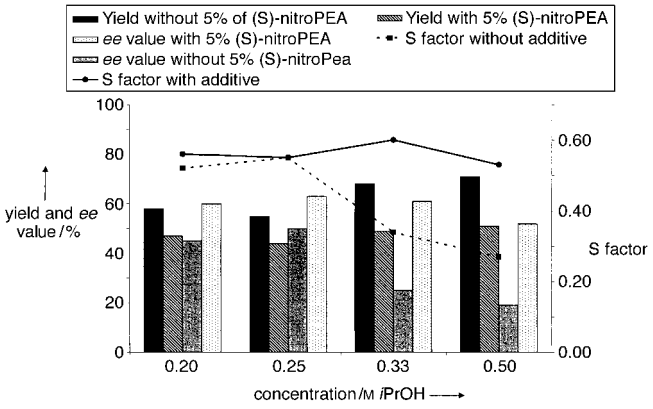


Figure 4. Concentration dependent resolutions with and without 5% additive (*S*)-**3**.

suspected nucleation inhibitor together with the resolving agent. The additives were initially chosen from the pool of known families of resolving agents.[3] The 2-nitrosubstituted phosphoric acid (entry 8b, see Table 1) was not reported in ref. [3], but was investigated on the basis of the present developments. In nine out of the ten systems given in Table 1, there were significant improvements in the *de* value of the first salt. The S factors were in the same range or in some cases even higher in the presence of an additive. Improvements were sometimes dramatic, for example, entries 8a/b. Only for the resolution of *p*-chloromandelic acid, as shown in entries 4a/b, was no significant improvement observed. The resolutions were deliberately performed in such a way that the *de* value without additive was not high because of simultaneous crystallization of both diastereomeric salts, so that improvements could be easily detected. Concentrations and conditions for the experiments with additives were analogous to those without additives. The resolutions given in entries 9 and 10 were performed in a reverse manner, that is, an enantiomerically pure family member of the racemate was added instead of a compound structurally related to the resolving agent.[13]

The salts that were obtained in the presence of additives were sometimes difficult to filter or sticky. On examination under a microscope, it was found that, in general, the crystals were smaller and/or the crystal habit less well-defined. These observations indicate the involvement of a kinetic effect of the additive as a habit modifier.

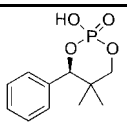
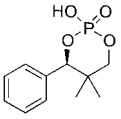
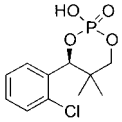
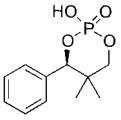
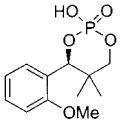
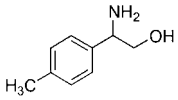
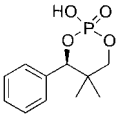
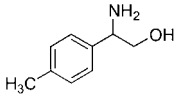
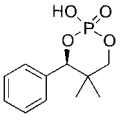
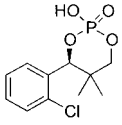
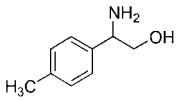
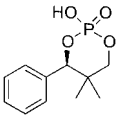
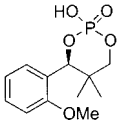
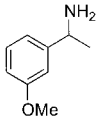
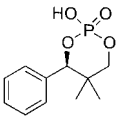
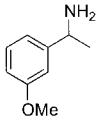
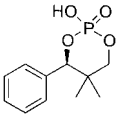
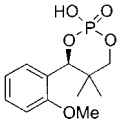
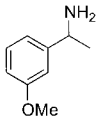
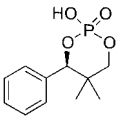
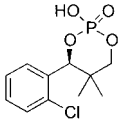
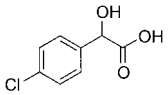
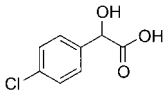
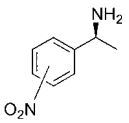
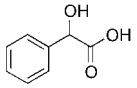
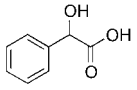
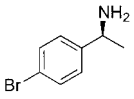
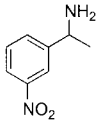
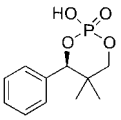
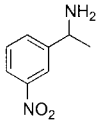
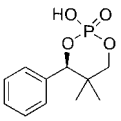
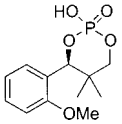
The Dutch Resolution approach, with families of resolving agents, provides a high chance of finding a successful resolution in which nucleation inhibition can be involved. Some characteristics of potential nucleation inhibitors are clear, although at this stage we obviously cannot predict with certainty all the structural aspects. Substitution in an aromatic ring can be especially effective, particularly with nitro as well as methoxy groups and sometimes haloatoms. The position of the substituent must also be a contributing factor.[14] Dutch Resolution provides a simple search procedure for discovery of potential nucleation inhibitors. If a component of a Dutch Resolution process is not, or only poorly, incorporated, one may then turn to a single resolving agent approach aided by the "missing component" as a potential nucleation inhibitor.

The use of an additive in a resolution by using crystallization is related to the work of Lahav and co-workers, who used enantiopure "tailor-made additives" in the resolution of conglomerates by preferential crystallization.[15] By addition of small amounts of certain structurally related compounds, the crystallization rate of one of the enantiomers was retarded dramatically, which thereby leads to efficient resolution. Modification of the habit of the crystals was observed, caused by the selective adsorption of the additive on a crystal face. We deal here with diastereomers rather than enantiomers that form conglomerates. To our knowledge, this approach has not been described before. Habit modification of a diastereomeric salt has been reported by Saigo and co-workers,[16] but resolutions in the presence of a habit modifier have not been reported.

We have shown here that nucleation inhibition and associated kinetic effects can play a role in Dutch Resolution.

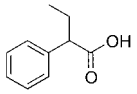
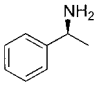
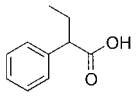
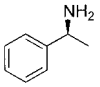
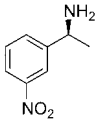
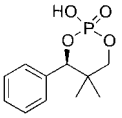
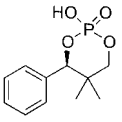
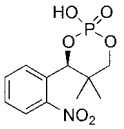
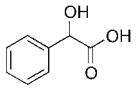
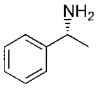
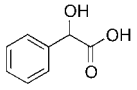
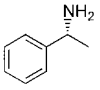
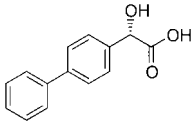
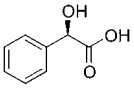
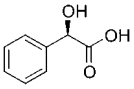
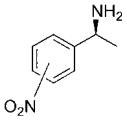
 © 2002 WILEY-VCH Verlag GmbH & Co. KGaA, Weinheim 0044-8249/02/4122-4283 $ 20.00+.50/0

Table 1. Resolutions in the presence of 10% of a family member of the resolving agent.

Entry	Substrate	Resolving agent	Additive	Concentration	Yield [%]	*ee* value [%]	S factor	HPLC[b]
1a			–	0.20 M EtOH	23	68	0.31	2
1b[a]				0.20 M EtOH	29	86	0.50	2
1c				0.20 M EtOH	30	88	0.53	2
2a			–	0.10 M *i*PrOH	40	74	0.59	2
2b[a]				0.10 M *i*PrOH	39	93	0.73	2
2c				0.10 M *i*PrOH	36	89	0.64	2
3a			–	0.25 M *i*PrOH	41	14	0.11	1
3b				0.25 M *i*PrOH	33	28	0.18	1
3c[a]				0.25 M *i*PrOH	29	53	0.31	1
4a			–	0.10 M *i*PrOH	39	73	0.57	3
4b				0.10 M *i*PrOH	34	76	0.52	3
5a			–	0.25 M *i*PrOH	58	49	0.57	1
5b[a]				0.25 M *i*PrOH	45	63	0.57	1
6a			–	0.20 M *i*PrOH/H_2O 4:1	61	12	0.15	4
6b				0.20 M *i*PrOH/H_2O 4:1	39	38	0.30	4

 © 2002 WILEY-VCH Verlag GmbH & Co. KGaA, Weinheim 0044-8249/02/4122-4284 $ 20.00+.50/0

Table 1 (Continued)

Entry	Substrate	Resolving agent	Additive	Concentration	Yield [%]	*ee* value [%]	S factor	HPLC[b]
7a			–	0.50 M *i*PrOH	56	40	0.45	1
7b				0.50 M *i*PrOH	43	55	0.47	1
8a			–	0.25 M *i*PrOH	58	22	0.26	2
8b				0.25 M *i*PrOH	36	86	0.62	2
	Reverse resolutions with a family member of the racemate as the additive.							
9a[c]			–	0.50 M *i*PrOH	61	43	0.52	1
9b				0.50 M *i*PrOH	38	65[d]	0.49	1
10a			–	0.25 M *i*PrOH	39	44	0.34	2
10b				0.25 M *i*PrOH	10	87[e]	0.17	2

[a] In this case some of the additive is incorporated in the crystal, but always less than 10 %. [b] HPLC columns: 1: Chiralpak AD; 2: Crownpak Cr; 3: Ultron ES OVM; 4: Chiralpak AS. [c] The resolution of mandelic acid (**1**) with (*S*)-phenylethylamine (**2**) in this experiment was performed at a different concentration than the one described in the text, hence the difference in results. [d] The *R*,*R* salt precipitates selectively in this case. [e] The *R*,*R* salt is presumed to precipitate selectively; however, the absolute configuration of 2-chlorophenylethylamine has not been determined unambiguously.

This leads to a second generation of Dutch Resolution, namely the use of small amounts of a certain family member of the resolving agent as an additive. This procedure seems to be reasonably general among several available families of resolving agents and may well have industrial applications. A two-component resolution system, especially one in which the minor component is not incorporated, is potentially more interesting for industrial applications than the (typically) three-component Dutch Resolution approach. In addition, the use of higher concentrations is beneficial, because more material can be resolved in one batch.

Experimental Section

General procedure for the resolutions described in Table 1: The resolving agent (2 mmol), suspended or dissolved in the appropriate solvent, was added to the substrate (2 mmol). In cases where an additive (0.2 mmol) was used, 1.8 mmol of the racemate or the resolving agent was added, so that the ratio racemate: resolving agent was always 1:1. The mixture was heated until a clear solution was obtained. The Kimble test tube (diameter 25 mm and height 150 mm) was covered and placed in a Reactivate, an apparatus that can hold ten tubes. A stirring speed of 900 rpm was chosen, using standard 1 cm magnetic stirring bars. The temperature program started at 65 °C, cooling to 20 °C at 0.1 °C min^{-1}. After reaching 20 °C, the mixture was stirred overnight at that temperature. The salt present in the Kimble test tube was collected and analyzed by ^1H NMR spectroscopy and LC–MS to check if additive was present. HPLC analysis was used to determine the *ee* value of the substrate.

Turbidity measurements were performed in a double-walled vessel, equipped with a He/Ne laser and a detector. The temperature of the solution was monitored with a Pt (100) temperature sensor. All equipment was connected to a computer that monitored the development of turbidity in the solution as a function of temperature. The vessel was connected to a water bath, the temperature of which could be programmed. The temperature program consisted of consecutive cooling and heating runs, each at 10 °C h^{-1}. Because of the limitations of the equipment used, the cooling rate in the turbidity measurements is not the same as that in the resolution experiments. When the turbidity is close to zero, the solution is clear. An (arbitrary) turbidity value close to 5 corresponds to a fully crystallized solution.

Chemicals: Phencyphos (2-hydroxy-5,5-dimethyl-2-oxo-4-phenyl-1,3,2-dioxaphosphorinane), chlocyphos (4-(2-chlorophenyl)-2-hydroxy-5,5-dimethyl-2-oxo-1,3,2-dioxaphosphorinane), and anicyphos (2-hydroxy-4-(2-methoxyphenyl)-5,5-dimethyl-2-oxo-1,3,2-dioxaphosphorinane) were prepared and resolved according to a standard procedure.[5]Compounds **1**, 2-phenylbutyric acid, and **2** were obtained from Aldrich. A standard Suzuki

 © 2002 WILEY-VCH Verlag GmbH & Co. KGaA, Weinheim 0044-8249/02/4122-4285 $ 20.00+.50/0

coupling method was used to prepare (*S*)-4-phenylmandelic acid from (*S*)-4-bromomandelic acid. The corresponding (*S*)-4-bromomandelic acid was obtained from 4-bromoacetophenone by standard procedures and was resolved with **2**. The substituted phenylethylamines were prepared from the corresponding acetophenones by a standard Leuckardt procedure. A Strecker reaction was used to prepare 4-methylphenylglycine, which was reduced to 4-methylphenylglycinol.

Received: June 5, 2002
Revised: August 15, 2002 [Z19422]

[1] L. Pasteur, *C. R. Hebd. Seances Acad. Sci.* **1848**, *26*, 535.
[2] a) R. A. Sheldon, *Chirotechnology*, Marcel Dekker, New York, **1993**, chap. 6; b) *Chirality in Industry II* (Eds.: N. A. Collins, G. N. Sheldrake, J. Crosby), Wiley, Chichester, **1997**.
[3] a) T. Vries, H. Wynberg, E. van Echten, J. Koek, W. ten Hoeve, R. M. Kellogg, Q. B. Broxterman, A. Minnaard, B. Kaptein, S. van der Sluis, L. A. Hulshof, J. Kooistra, *Angew. Chem.* **1998**, *110*, 2491; *Angew. Chem. Int. Ed.* **1998**, *37*, 2349; b) Eur. Pat. Appl. , EP 0,838,448 (to DSM).
[4] J. Jacques, A. Collet, S. H. Wilen, *Enantiomers, Racemates, and Resolutions*, Wiley, New York, **1981**.
[5] The cyclic phosphoric acids (P mix) were developed as resolving agents in our lab and have been patented: W. ten Hoeve, H. Wynberg, *J. Org. Chem.* **1985**, *50*, 4508; Eur. Pat. , 180,276; US Pat. , 4,814,477.
[6] Arthur Conan Doyle, *Silver Blaze*, Strand Magazine, **1892**.
[7] E. Fogassy, A. Lopata, F. Faigl, F. Darvas, M. Ács, L. Toke, *Tetrahedron Lett.* **1980**, *21*, 647.
[8] Reproducibilities are good; the experimentally determined error limit of the S factor is ±5%.
[9] Analogous experiments with pure (*S*)-*o*-nitrophenylethylamine (**5**) as the inhibitor led to a *de* value of 51% and an S factor of 0.55. With pure (*S*)-*p*-nitrophenylethylamine as the inhibitor the *de* value was 62% and the S factor was 0.56. We conclude that use of the more readily available mixture instead of the pure materials is entirely justified and allows direct comparison with the data given in ref. [3].
[10] In this experiment we used only *o*-nitrophenylethylamine instead of the 1:1 mixture of *o*,*p* isomers for reasons of simplicity.
[11] The experimentally determined error limit is ±0.3°C for this experiment.
[12] The dissolution temperatures differ somewhat, owing to the high concentrations in this experiment (1.6 M); the experimentally determined error limit is ±0.7°C.
[13] A manuscript covering the concept of reverse resolutions is in preparation: Dutch Resolution of Alaninol with (*R*)-Mandelic acid by addition of (*S*)-or (*R*)-2-Amino-1-butanol; the Role of Nucleation Inhibition; B. Kaptein, K. L. Pouwer, T. R. Vries, R. F. P. Grimbergen, H. M. J. Grooten, H. L. M. Elsenberg, J. W. Nieuwenhuijzen, R. M. Kellogg, Q. B. Broxterman, *Chem. Eur. J.*, unpublished work.
[14] a) K. Kinbara, K. Oishi, Y. Harada, K. Saigo, *Tetrahedron* **2000**, *56*, 6651; b) K. Kinbara, Y. Harada, K. Saigo, *Tetrahedron: Asymmetry* **1998**, *9*, 2219.
[15] a) L. Addadi, Z. Berkovitch-Yellin, N. Domb, E. Gati, M. Lahav, L. Leiserowitz, *Nature* **1982**, *296*, 21; b) Z. Berkovitch-Yellin, L. Addadi, M. Idelson, L. Leiserowitz, M. Lahav, *Nature* **1982**, *296*, 27; c) L. Addadi, S. Weinstein, E. Gati, I. Weissbuch, M. Lahav, *J. Am. Chem. Soc.* **1982**, *104*, 4610; d) D. Zbaida, M. Lahav, K. Drauz, G. Knaup, M. Kottenhahn, *Tetrahedron* **2000**, *56*, 6645.
[16] K. Sakai, Y. Maekawa, K. Saigo, M. Sukegawa, H. Murakami, H. Nohira, *Bull. Chem. Soc. Jpn.* **1992**, *65*, 1747.

Shape Control of Thermodynamically Stable Cobalt Nanorods through Organometallic Chemistry **

Frédéric Dumestre, Bruno Chaudret,* Catherine Amiens, Marie-Claire Fromen, Marie-José Casanove, Philippe Renaud, and Peter Zurcher

The synthesis of nanoparticles is of fundamental importance for the development of novel technologies based on nanomaterials. This is particularly true for magnetic nanomaterials which could be used, amongst other things, for high-density information storage.[1] These materials would ideally consist of spatially separated particles in the nanometer range that would function as a single magnetic domain that exhibits ferromagnetic behavior at room temperature, and could be electronically isolated. In addition, the organization of the particles in the solid state or in solution (self-assembly) should be controllable as desired for the intended application.

Several methods are available for the production of magnetic nanomaterials. They can be divided into physical methods, which produce essentially thin layers,[2,3] template methods, which involves the growth of nanorods or nanowires by different approaches, frequently electrochemical, within the channels of inorganic or track-etch organic matrixes,[4] and chemical methods involving synthesis in a solution of nanoparticles.[5,6] The latter may generally allow, after size selection, the formation of self-assembled superlattices. Sun and Murray[5] have, for example, recently reported a high-temperature preparation of 9 nm cobalt nanoparticles displaying a long-range self-organization. This method has been extended to the synthesis of Fe/Pt particles to increase the magnetic anisotropy of the materials, with the goal of producing high-density memories.[7] Self-organized cobalt nanoparticles have also been reported by the group of Pileni by reverse micelle synthesis.[8]

In all cases, as a result of their small dimension, the particles are superparamagnetic at room temperature and thus not usable for many applications, such as magnetic recording. One way to increase the magnetic anisotropy of the particles is to modify their shape. This problem has been addressed by Alivisatos who initially demonstrated the importance of reaction conditions, in particular the concentration of the

[*] Dr. B. Chaudret, F. Dumestre, Dr. C. Amiens
Laboratoire de Chimie de Coordination du CNRS
205, route de Narbonne, 31077 Toulouse Cédex 04 (France).
Fax: (+33) 5-61-55-30-03
E-mail: chaudret@lcc-toulouse.fr

F. Dumestre, Dr. P. Renaud
Digital DNA Labs, Semiconductor Products Sector, Motorola
le Mirail B.P. 1029, 31023 Toulouse Cédex (France)

M.-C. Fromen, Dr. M.-J. Casanove
CEMES-CNRS
29 Rue Marvig, BP 4347, F 31055 Toulouse, France.

Dr. P. Zurcher
Digital DNA Labs, Semiconductor Products Sector, Motorola
2100 E. Elliot Road, Tempe, AZ-85824 (USA)

[**] The authors thank CNRS and MOTOROLA S.P.S. for support, M. Vincent Collière, Lucien Datas, and TEMSCAN service (Université Paul Sabatier Toulouse) for transmission electron microscopy.

 © 2002 WILEY-VCH Verlag GmbH & Co. KGaA, Weinheim

precursors and the ratio of surfactants, for preparing CdSe nanocrystals of various shapes including nanorods.[9] The same methodology was employed for synthesizing cobalt nanorods, which were found to be thermodynamically unstable and to rearrange into spherical particles.[10] This result contrasts with a recent report by Hyeon and co-workers, who show that spherical iron nanoparticles may be used at 320 °C as initiators for the growth of nanorods.[11] However, no systematic study on the influence of ligand-type on the particle aspect ratio, and hence on the magnetic properties of prepared metal nanoparticles, has been reported so far.

In our group we have previously described the synthesis of magnetic nanoparticles using olefinic complexes as precursors.[12,13] These compounds rapidly decompose to give alkane by-products which do not interact with the surface of the particles under the reaction conditions. This methodology allows the synthesis of magnetic nanoparticles that display the same magnetic moment as particles of similar size in the gas phase.[14] The absence of oxidation and of strongly coordinating ligands at the surface of the particles may also favor size and shape changes in solution, as recently demonstrated for ruthenium,[15] and therefore an easier control of these parameters by the surrounding medium. In separate studies, we have emphasized the role of amines for the formation of nanorods or nanowires.[16] This technique has been used to produce nickel nanorods, the surface magnetism of which is not altered by the presence of amine ligands.[17]

In this paper we describe the synthesis and magnetic properties of novel cobalt nanoparticles. We demonstrate that by varying the synthesis parameters it is possible to selectively prepare spherical nanoparticles of uniform size, nanorods, the aspect ratio of which is controlled by the alkyl chain-length of the ligand, or even very long nanowires. Finally, we report the magnetic properties of these nanoparticle materials.

The decomposition reactions of $[Co(\eta^3\text{-}C_8H_{13})(\eta^4\text{-}C_8H_{12})]$[18] were carried out in anisole under a preesure of 3 bar H_2 (initial pressure at room temperature in the reactor) in the presence of ligands. The use of a single ligand such as hexadecylamine (1:1 Co/amine molar ratio) leads to small, agglomerated nanoparticles at room temperature. Similarly, the use of oleylamine ($CH_3(CH_2)_7CH{=}CH(CH_2)_8NH_2$) at 150 °C produces particles that display a large size distribution, whereas monodisperse particles with a mean size of 5 nm are obtained when using oleic acid under the same conditions (sample 1). These particles self-organize on a microscopy grid into 2D and 3D crystalline arrays. When both oleic acid and oleylamine are used as ligands (1 equivalent each, 150 °C, and 3 bar H_2, standard conditions), the synthesis initially produces nanoparticles with mean dimensions of approximately 3 nm, as shown by transmission electron microscopy (TEM, sample 2; Figure 1 A), which are the only species present after reacting for 3 h. However, after 48 h, regular nanorods of approximately 9×40 nm are the unique species in solution (sample 3; Figure 1 B). To determine the importance of dihydrogen, two parallel reactions were carried out. In both cases the precursor was decomposed under standard conditions. After 3 h the reactors were evacuated, and the first reactor was pressurized again to 3 bar with H_2 whereas the second reactor was placed under argon. After 48 h nanorods were found in the first reactor and 4 nm nanoparticles in the second. The nature of the precursor complex is also important since, under standard conditions, the use of $[Co_2(CO)_8]$ in place of $[Co(\eta^3\text{-}C_8H_{13})(\eta^4\text{-}C_8H_{12})]$ leads to polydisperse particles with a mean size of approximately 10 nm. The role of the ligands, with particular respect to the concentration of oleic acid and the nature of the amine, was then examined in order to understand the formation of the particles. If the oleic acid concentration was decreased (0.3 equivalents, with respect to Co), particles of regular size (approximately 3 nm) were formed, whereas if the concentration was doubled (2 equivalents), very long (micron range) nanowires of 4 nm diameter were produced (sample 4; Figure 1 C). Replacing oleylamine by octyl-, dodecyl-, hexadecyl-, and octadecylamine causes a dramatic change in the dimensions of the nanorods that are produced (Figure 2). The use of octadecylamine yields nanorods of comparable size, but with greater regularity, to those obtained with oleylamine (47×6 nm, Figure 2 C); hexadecylamine produces longer and thinner rods (120×5.5 nm, Figure 2 E) whereas octylamine yields smaller and wider ones (17×10 nm, Figure 2 F). Therefore, particles displaying aspect ratios between 1.7 and 22 can be controlled solely by the number of carbon atoms in the alkyl chain of the amine, whereas a very large aspect ratio may be obtained for the nanowires prepared in the presence of excess oleic acid. The variation of the length and diameter of the produced nanorods is summarized in Figure 2 A, 2 B.

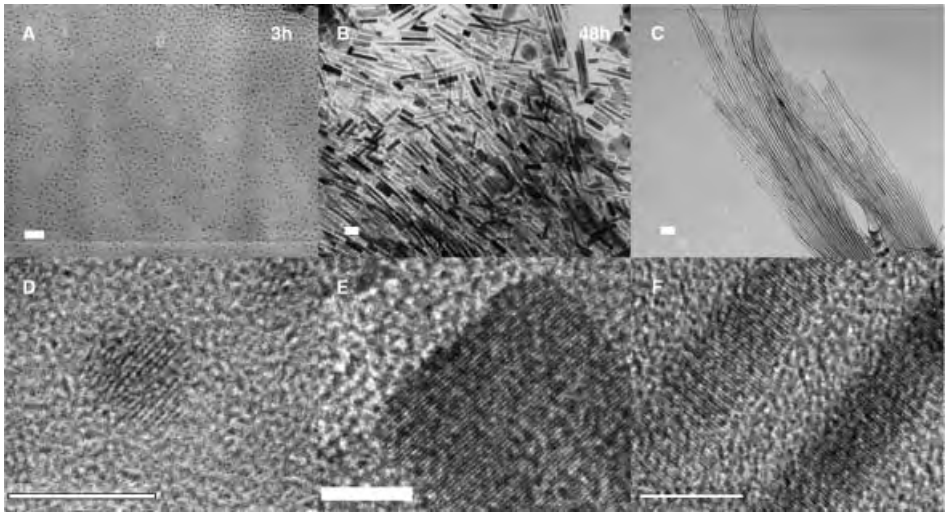


Figure 1. Variation of size and shape with reaction time and the ratio of stabilizing agents. A, B) TEM micrographs of nanoparticles and nanorods obtained with 1 mmol of oleylamine and 1 mmol of oleic acid after 3 h and 48 h, respectively: Bar = 30 nm; C) TEM micrograph of nanowires obtained with 1 mmol of oleylamine and 1 mmol of oleic acid after 48 h: Bar = 30 nm; D, E, F) High resolution (HR)TEM images of the nanoparticles, nanorods, and nanowires presented in A, B, and C, respectively: Bar = 5 nm.

 © 2002 WILEY-VCH Verlag GmbH & Co. KGaA, Weinheim 0044-8249/02/4122-4287 $ 20.00+.50/0

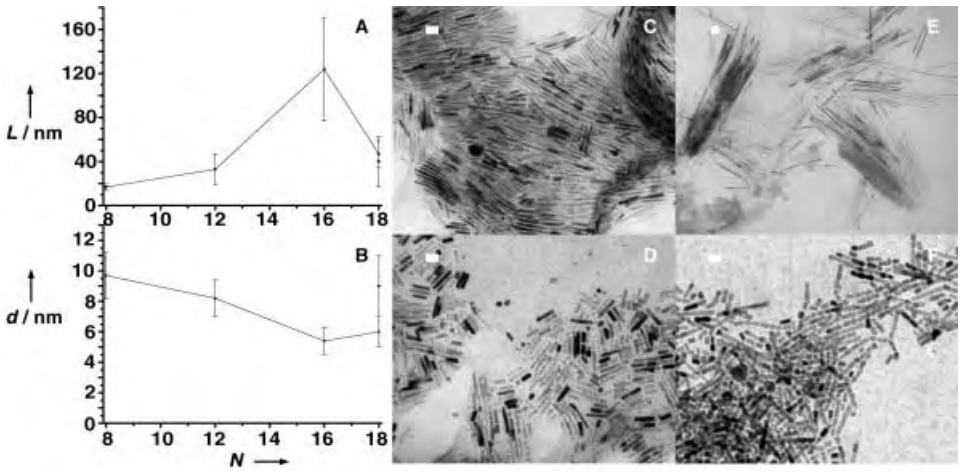


Figure 2. Variation of the aspect ratio of nanorods with respect to the change in the alkyl chain length of the amine. A) Evolution of nanorod length; B) Evolution of nanorod diameter; C–F) TEM micrographs of hcp cobalt nanorods obtained with oleic acid and octadecylamine, dodecylamine, hexadecylamine, and octylamine, respectively: Bar = 30 nm.

These results demonstrate the possibility to selectively synthesize nanorods, but raise questions concerning the exact growth mechanism and, in particular, the exact role of the ligands. It has been previously proposed that the growth mechanism of nanorods could be related to the preferred coordination of the ligand along a face of a growing crystal.[6,10,19] In the present case, the employed amine ligands display similar chemical properties, in terms of basicity and affinity for the metal, but form very different nanoobjects. This suggests that, in the present case, the nanorod synthesis is controlled by supramolecular organization and/or the dynamics of the ligands in solution; it is conceivable that longer alkyl chains could organize across longer distances. Oleylamine displays a "cis" configuration, which leads to an apparent rod length comparable to that of octylamine, with less opportunity for long-range organization; this could be a reason for the relatively low regularity of the rods obtained in this case. Oleic acid can also play an important role in this organization since its concentration relative to the amine has a strong influence on the aspect ratio of the nanoobjects produced. In addition, it presumably transforms rapidly in the medium into the oleate anion by deprotonation in the presence of amines, which may lead to a strongly associated medium and/or coordination to cobalt. The necessity of dihydrogen for the synthesis of rods from nanospheres probably arises from the necessity to remove the carboxylate groups from the surface to allow coalescence and growth to occur. This, therefore, suggests a strong coordination of oleate anions to the nanoparticles formed at the early stage of the reaction.[20]

All of the particles, rods, and wires described above consist of a pure hexagonal close-packed (hcp) cobalt structure, which displays no sign of oxidation as evidenced by wide-angle X-ray scattering (WAXS) and high-resolution electron microscopy (HREM) studies. The rods and wires are monocrystalline and adopt the *c* axis of the hcp structure as the growth axis. Magnetic measurements were carried out on all samples, in particular the 3 nm nanoparticles obtained after 3 h under standard conditions (sample 2) and nanorods produced after 48 h under the same conditions (sample 3). The former are superparamagnetic at room temperature with a blocking temperature of 20 K, whereas the latter are ferromagnetic at room temperature. Hysteresis loop measurements at 2 K record, for both samples, a saturation magnetization (M_s) of 160 A m^2 kg$_{Co}^{-1}$, which corresponds to a magnetic moment per atom of $\mu = 1.71\,\mu_B$, identical to that found in bulk cobalt. In addition, a coercive field (H_c) of respectively 1100 and 8900 Oe is found for samples 2 and 3, hence demonstrating the importance of the shape anisotropy in such systems (see Figure 3).

This work emphasizes the role of the organometallic precursor in the synthesis of the nanomaterial. The high decomposition rate of the precursor and, more importantly, the absence of by-products that could potentially interact with the surface allows the particles to grow without losing their intrinsic magnetic properties. These objects display a saturation magnetization per cobalt atom that is identical or very close to that of bulk cobalt, which is consistent with the pure σ-donor behavior of both the amine and the acid ligands.[14,17] Furthermore, their magnetic

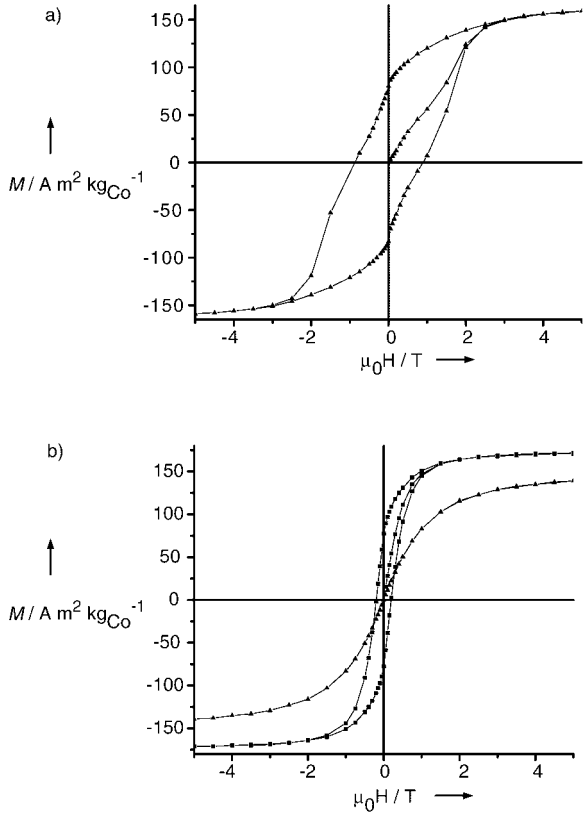


Figure 3. Plots of magnetization against applied magnetic field. a) Hysteresis loop of cobalt nanorods obtained with 1 mmol of oleylamine and 1 mmol of oleic acid: (▲) measured at 300 K. b) Hysteresis loops of cobalt nanoparticles obtained with 1 mmol of oleylamine and 1 mmol of oleic acid: (■) measured at 2 K, (▲) measured at 300 K.

 © 2002 WILEY-VCH Verlag GmbH & Co. KGaA, Weinheim 0044-8249/02/4122-4288 $ 20.00+.50/0 *Angew. Chem. Int. Ed.* **2002**, *41*, No. 22

anisotropy may be controlled by their aspect ratio, which gives rise to ferromagnetic nanomaterials at room temperature. The rods grow after the initial formation of spherical nanoparticles; the exact mechanism of this process is not known but we note that the initial formation of nanoparticles, followed by formation of nanorods or nanowires either through coalescence of the initial particles[21] or upon using the particles as nuclei for an anisotropic growth process, have been very recently reported.[22] Further work will be necessary to determine the exact mechanism that operates in our case.

In conclusion, we describe in this report a new and simple method for the preparation of cobalt nanoparticles, nanorods, and nanowires of uniform diameter that does not require a special procedure or size selection. The magnetic nanowires have no equivalent, whereas the rods differ from those previously described by their uniformity of diameter, their thermodynamic stability, and the possibility of fine tuning of their aspect ratio. We further demonstrate that, under these conditions, the nanomaterials maintain a magnetization at saturation similar to bulk cobalt. This results from the choice of ligands that do not display π-accepting behavior, which is in agreement with previous research work from our group. All of these aspects emphasize the role of an organometallic approach in the design of precursors and ligands. Finally, these objects may find use in many practical applications such as, for example, in data storage.

Received: July 10, 2002
Revised: September 3, 2002 [Z19713]

[1] D. Weller, A. Moser, *IEEE Trans. Magn.* **1999**, *35*, 4423.
[2] Y. M. Kim, D. Choi, K. H. Kim, S. H. Han, H. J. Kim, *IEEE Trans. Magn.* **2001**, *37*, 2288.
[3] M. Dumm, M. Zölfl, R. Moosbühler, M. Brockmann, T. Schmidt, G. Bayreuther, *J. Appl. Phys.* **2000**, *87*, 5457.
[4] H. Cao, Z. Xu, H. Sang, D. Sheng, C. Tie, *Adv. Mater.* **2001**, *13*, 121.
[5] S. Sun, C. B. Murray, *J. Appl. Phys.* **1999**, *85*, 4325.
[6] V. F. Puntes, K. M. Krishnan, A. P. Alivisatos, *Appl. Phys. Lett.* **2001**, *78*, 2187.
[7] S. Sun, C. B. Murray, D. Weller, L. Folks, A. Moser, *Science* **2000**, *287*, 1989.
[8] J. Legrand, A. T. Ngo, C. Petit, M. P. Pileni, *Adv. Mater.* **2001**, *13*, 58.
[9] L. S. Li, J. Hu, W. Yang, A. P. Alivisatos, *Nano Lett.* **2001**, *1*, 349.
[10] V. F. Puntes, K. M. Krishnan, A. P. Alivisatos, *Science* **2001**, *291*, 2115.
[11] J. Park-Sang, K. Seungsoo, S. Lee, Z. G. Khim, K. Char, T. Hyeon, *J. Am. Chem. Soc.* **2000**, *122*, 8581.
[12] T. Ould Ely, C. Amiens, B. Chaudret, E. Snoeck, M. Verelst, M. Respaud, J. M. Broto, *Chem. Mater.* **1999**, *11*, 526.
[13] M. Verelst, T. Ould Ely, C. Amiens, E. Snoeck, P. Lecante, A. Mosset, M. Respaud, J. M. Broto, B. Chaudret, *Chem. Mater.* **1999**, *11*, 2702.
[14] M. Respaud, J. M. Broto, H. Rakoto, A. R. Fert, L. Thomas, B. Barbara, M. Verelst, E. Snoeck, P. Lecante, A. Mosset, J. Osuna, T. Ould Ely, C. Amiens, B. Chaudret, *Phys. Rev. B* **1998**, *57*, 2925.
[15] C. Pan, K. Pelzer, K. Philippot, B. Chaudret, F. Dassenoy, P. Lecante, M. J. Casanove, *J. Am. Chem. Soc.* **2001**, *123*, 7584.
[16] K. Soulantica, A. Maisonnat, F. Senocq, M. C. Fromen, M. J. Casanove, B. Chaudret, *Angew. Chem.* **2001**, *113*, 3071; *Angew. Chem. Int. Ed.* **2001**, *40*, 2983.
[17] N. Cordente, M. Respaud, F. Senocq, M. J. Casanove, C. Amiens, B. Chaudret, *Nano Lett.* **2001**, *1*, 565.
[18] S. Otsuka, M. Rossi, *J. Chem. Soc. A* **1968**, 2630.
[19] Z. A. Peng, X. Peng, *J. Am. Chem. Soc.* **2001**, *123*, 1389.
[20] J. S. Bradley, B. Tesche, W. Busser, M. Maase, M. Reetz, *J. Am. Chem. Soc.* **2000**, *122*, 4631.
[21] Z. Tang, N. A. Kotov, M. Giersig, *Science* **2002**, *297*, 237.
[22] Z. A. Peng, X. Peng, *J. Am. Chem. Soc.* **2002**, *124*, 3343.

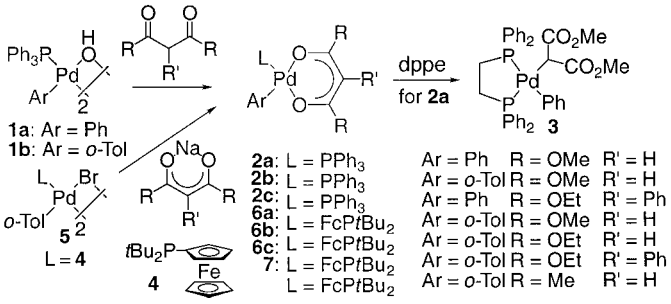
Generation of Reactivity from Typically Stable Ligands: C–C Bond-Forming Reductive Elimination from Aryl Palladium(II) Complexes of Malonate Anions**

Joanna P. Wolkowski and John F. Hartwig*

Anions of 1,3-dicarbonyl compounds are some of the most common ligands in transition-metal chemistry.[1,2] They typically bind in an η^2-O,O fashion,[3] have delocalized charge, and donate electron density more weakly to a metal center than alkyls or alkoxides. They are usually supporting ligands that are ancillary to the site of reaction. Anions of 1,3-dicarbonyl compounds are also common nucleophiles in metal-catalyzed allylic substitution,[4–6] but the facility of this chemistry relies on external attack of the anion without coordination to the metal center. If metal fragments could induce reactivity from coordinated versions of these anions, then complexes of these common ligands could serve as intermediates in catalytic processes.

Complexes of malonate anions are likely intermediates in recently developed palladium-catalyzed arylations of malonates.[7–11] Although palladium complexes of malonate anions have been isolated previously,[12–16] their reactivity has been limited.[17–20] We report here reductive elimination of arylmalonate and acetylarylacetone from isolated aryl palladium complexes of malonate and acetylacetone anions, respectively. Our results suggest that the propensity of these complexes to undergo reductive elimination depends critically on the steric properties of the ancillary phosphane ligand.

Our synthesis of aryl palladium malonates is summarized in Scheme 1. Addition of dimethyl malonate or diethyl phenylmalonate to the basic PPh_3-ligated palladium hydroxide dimers **1a**[21,22] and **1b** generated the O,O′-bound palladium dimethyl malonate complexes **2a–c**. Complexes **2a** and **2c** were characterized by X-ray diffraction (Figure 1). No unusual angles at the palladium center were found in **2a** or



Scheme 1. Synthesis of aryl palladium malonates.

[*] Prof. J. F. Hartwig, J. P. Wolkowski
Department of Chemistry
Yale University
P.O. Box 208107, New Haven, CT 06520-8107 (USA)
Fax: (+1) 203-432-3917
E-mail: john.hartwig@yale.edu

[**] We thank the National Institutes of Health for support of this work (GM-58108) and Johnson-Matthey for a gift of palladium salts.

Supporting information for this article is available on the WWW under http://www.angewandte.org or from the author.

 © 2002 WILEY-VCH Verlag GmbH & Co. KGaA, Weinheim 0044-8249/02/4122-4289 $ 20.00+.50/0

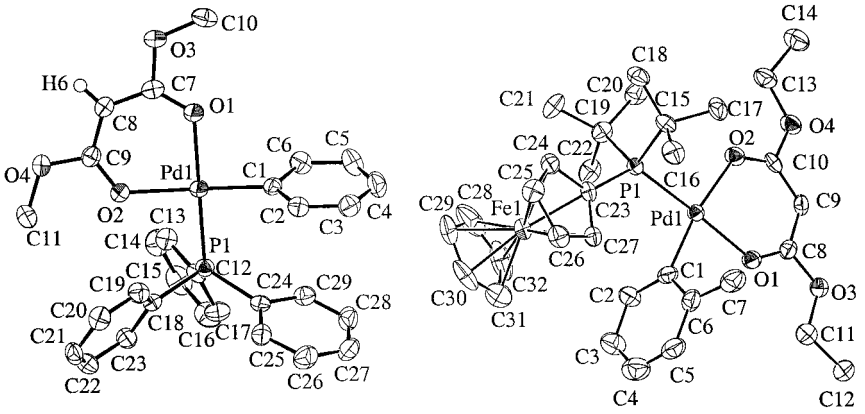
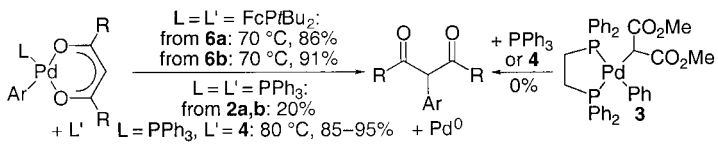


Figure 1. ORTEP plot of **2a** (left) and **6b** (right).

2c. The Pd–O bonds located *trans* to the phenyl ligand in **2a** and **2c** are longer than those *trans* to the phosphane (2.113(2) Å vs. 2.088(2) Å for **2a**; 2.097(2) Å vs. 2.070(2) Å for **2c**). The Pd–O distances in **2c** are shorter than those in **2a**, but addition of diethyl phenylmalonate to **2a** or visa versa indicated an equilibrium constant for the exchange that is close to unity and, therefore, equivalent thermodynamic stabilities for the two malonate complexes.

Coordination of two phosphorus donors generated C-bound isomers. For example, addition of 1,2-bis(diphenylphosphanyl)ethane (dppe) to **2a** generated the C-bound palladium dimethyl malonate **3** (Scheme 1). However, addition of excess PPh_3 to **2a** did not generate a stable diphosphane complex. Instead, exchange of free and coordinated phosphane occurred on the NMR timescale. A single broad ^{31}P NMR resonance was observed for the free and coordinated PPh_3, and the same ^1H NMR resonance for the central malonate proton was observed in the presence and absence of added PPh_3.

Heating of **2a** or **2b** for 48 h at 110 °C in THF or C_6D_6 in the presence of added PPh_3 to trap the Pd^0 product fully converted the starting complex into a PPh_3-ligated Pd^0 species, but arylmalonate was formed in only 20 % yield (Scheme 2) from **2a** and in <5 % yield from **2b**. Biaryls from the phosphane and palladium-bound aryl group, along with free malonate (25 %), were the major organic products formed. Heating of **3** for 15 h at 70 °C fully converted it to PPh_3- and dppe-ligated Pd^0 complex, but free dimethyl malonate, toluene, and products from self-condensation of dimethyl malonate were the major organic products. In contrast to the slow and low-yielding reductive elimination from these complexes, aryl palladium methyl complexes undergo facile reductive elimination.[21,22] Thus, the electron-withdrawing property of the two carbonyl groups dramatically increases the barrier for reductive elimination.



Scheme 2. Reductive elimination of malonates.

To generate complexes that could be induced to undergo reductive elimination because of increased steric hindrance, we prepared complexes ligated by di-*tert*-butylphosphanylferrocene ($FcPtBu_2$) (**4**)[23] (Scheme 1). Metathetical exchange between the anion of dimethyl malonate and the halide of dimeric aryl palladium bromide complexes **5** ligated by **4** occurred readily to form the desired palladium malonate complexes **6a** and **6b** in high yield. Reaction with the sodium anion of diethyl-2-phenylmalonate occurred similarly.

Complexes **6a–c** were isolated and fully characterized by spectroscopic and microanalytical methods, and the diethyl malonate complex **6b** was characterized by X-ray diffraction (Figure 1). Complex **6b** displays the same η^2-O,O-coordination mode as **2a** and **2c**, but the geometry is distorted. The Pd–O distances are much longer than those of **2a** and **2c**. For example, the Pd–O bond *trans* to the aryl group (2.189(3) Å) is nearly 0.1 Å longer than that in complex **2c**. Moreover, the P1-Pd1-O2 angle is larger (100.4(1)°), and the O1-Pd1-C1 is smaller (82.6(2)°) than the ideal 90°. These distorted angles and long metal–ligand bond distances presumably arise from the steric demands of the hindered phosphane.

Warming of malonate complexes **6a** and **6b** to 60–105 °C in the presence of **4** to trap the Pd^0 product formed dimethyl and diethyl *o*-tolylmalonate in 86 % and 91 % yield, respectively (by ^1H NMR spectroscopy with an internal standard, Scheme 2). Heating of the phenylmalonate complex **6c** formed the diarylmalonate from reductive elimination in less than 10 % yield. This difference in reactivity between **6a**,**b** and **6c** is consistent with the high selectivity for monoarylation observed from the palladium-catalyzed reaction of aryl halides with malonates.[7]

Heating of the PPh_3-ligated **2a** at 80 °C in the presence of 3–15 equivalents of the bulky ligand **4** also led to reductive elimination of arylmalonate in 75–90 % yield. This reaction was nearly complete after 45 min when conducted with 15 equivalents of added **4**. In contrast, it occurred to about 50 % conversion after this time when 3 equivalents of **4** were added. The same reaction required roughly 12 h for completion at 110 °C and formed only 65 % yield of arylmalonate when conducted in the presence of 3 equivalents of **4** and 1 equivalent of PPh_3. dppe-ligated **3** did not form arylmalonate when heated in the presence of added **4**. Thus, reductive elimination from **2a** most likely occurs after exchange of **4** for PPh_3, and the increased steric hindrance of the $FcPtBu_2$ ligand triggers the reductive elimination. Most important, this steric hindrance dominates the electronic and structural properties of the malonate anion that are unfavorable for reductive elimination.

Aryl palladium acetylacetonate complex **7** ligated by phosphane **4** was prepared by addition of the sodium salt of 2,4-pentanedione to aryl palladium halide **5**. Complex **7** was much more stable than the malonate complexes. Complete consumption of **7** in the presence of ligand **4** required 36 h at 140 °C, instead of the similar times at 110 °C for the analogous

 © 2002 WILEY-VCH Verlag GmbH & Co. KGaA, Weinheim 0044-8249/02/4122-4290 $ 20.00+.50/0

malonate complex **6b**. Complex **7** did form the corresponding 2-aryl 1,3-diketone during this thermolysis, but in only 22% yield.

One would expect that rearrangement of the η^2-O,O-bound complexes to their C-bound tautomers would precede reductive elimination. Indeed, complexes of 1,3-dicarbonyl anions that we could not observe as a C-bound isomer did not undergo reductive elimination in high yield. For example, arylmalonate anions **2c** and **6c**, and acetylacetonate **7** produced Pd^0 complexes and free malonate or acetylacetone upon addition of the chelating ligands dppe, dppbz = 1,2-bis(diphenylphospnanyl)benzene (dppbz), 2,2′-bis(diphenylphosphanyl)-1,1′-binaphthyl (binap), and 1,1′-bis(diphenylphosphanyl)ferrocene (dppf). No complex of a C-bound anion was detected.

In summary, the greater steric hindrance of $FcPtBu_2$ (**4**), relative to that of phenylphosphanes, induces reductive elimination from complexes of typically unreactive ligands derived from malonate and actylacetonate anions. This steric effect overrides the stabilizing effect of the η^2-O,O-coordination mode and the electron-withdrawing groups on the central carbon atom of the malonate anion. Studies on the mechanism of these new reductive eliminations and the synthesis of complexes with related stabilized anions are in progress.

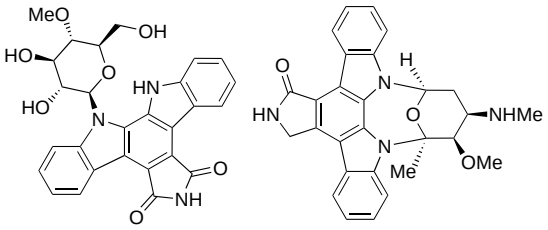
Received: July 22, 2002 [Z19785]

[1] S. Kawaguchi, *Coord. Chem. Rev.* **1986**, *70*, 51.
[2] F. A. Cotton, G. Wilkinson, *Advanced Inorganic Chemistry*, 5th ed., Wiley, New York, **1988**.
[3] D. F. Shriver, P. W. Atkins, *Inorganic Chemistry*, 3rd ed., Freeman, New York, **1999**.
[4] J. Tsuji, *Acc. Chem. Res.* **1969**, *2*, 144.
[5] B. M. Trost, *Tetrahedron* **1977**, *33*, 2615.
[6] A. Pfaltz, M. Lautens, *Allylic substitution reactions in Comprehensive Asymmetric Catalysis I–III, Vol. 2* (Eds.: E. N. Jacobsen, A. Pfaltz, H. Yamamoto), Springer, Berlin, **1999**, pp. 833–884.
[7] N. A. Beare, J. F. Hartwig, *J. Org. Chem.* **2002**, *67*, 541.
[8] M. Kawatsura, J. F. Hartwig, *J. Am. Chem. Soc.* **1999**, *121*, 1473.
[9] J. M. Fox, X. Huang, A. Chieffi, S. L. Buchwald, *J. Am. Chem. Soc.* **2000**, *122*, 1360.
[10] L. Djakovitch, K. Kohler, *J. Organomet. Chem.* **2000**, *606*, 101.
[11] M. A. Aramendia, V. Borau, C. Jimenez, J. M. Marinas, J. R. Ruiz, F. J. Urbano, *Tetrahedron Lett.* **2002**, *43*, 2847.
[12] K. Hiraki, M. Onishi, H. Matsuo, *J. Organomet. Chem.* **1980**, *185*, 111.
[13] P. J. Chung, H. Suzuki, Y. Moro-oka, T. Ikawa, *Chem. Lett.* **1980**, 63.
[14] G. R. Newkome, T. Kawato, D. K. Kohli, W. E. Puckett, B. D. Olivier, G. Chiari, F. R. Fronczek, W. A. Deutsch, *J. Am. Chem. Soc.* **1981**, *103*, 3423.
[15] B. F. Straub, F. Rominger, P. Hofmann, *Inorg. Chem. Commun.* **2000**, *3*, 358.
[16] J. Ruiz, V. Rodriguez, N. Cutillas, M. Pardo, J. Perez, G. Lopez, P. Chaloner, P. B. Hitchcock, *Organometallics* **2001**, *20*, 1973.
[17] G. R. Newkome, V. K. Gupta, *Inorg. Chim. Acta* **1982**, *65*, L165.
[18] G. R. Newkome, V. K. Gupta, H. C. R. Taylor, F. R. Fronczek, *Organometallics* **1984**, *3*, 1549.
[19] T. Kawato, T. Uechi, H. Koyama, H. Kanatomi, Y. Kawanami, *Inorg. Chem.* **1984**, *23*, 764.
[20] H. Kurosawa, K. Ishii, Y. Kawasaki, S. Murai, *Organometallics* **1989**, *8*, 1756.
[21] V. V. Grushin, H. Alper, *Organometallics* **1993**, *12*, 1890.
[22] M. S. Driver, J. F. Hartwig, *Organometallics* **1997**, *16*, 5706.
[23] G. Mann, C. Incarvito, A. L. Rheingold, J. F. Hartwig, *J. Am. Chem. Soc.* **1999**, *121*, 3224.

A Five-Component Synthesis of Hexasubstituted Benzene**

Pierre Janvier, Hugues Bienaymé, and Jieping Zhu*

Bis(indolyl)maleimides and indolo[2,3-*a*]carbazole alkaloids constitute a rapidly growing family of natural products with diverse biological activities.[1] Thus, rebeccamycin (**1**)[2] and staurosporine (**2**)[3] are potent topoisomerase I and



1 **2**

protein kinase C inhibitors, respectively. Structurally, this class of compounds is characterized by an hexasubstituted benzene ring with a fused indolo (forming an indolocarbazole entity) and a fused lactam or an imide ring with a pendant sugar moiety. The novelty of the structures combined with their interesting biological profile have stimulated numerous synthetic efforts from both academic and industrial researchers.[4]

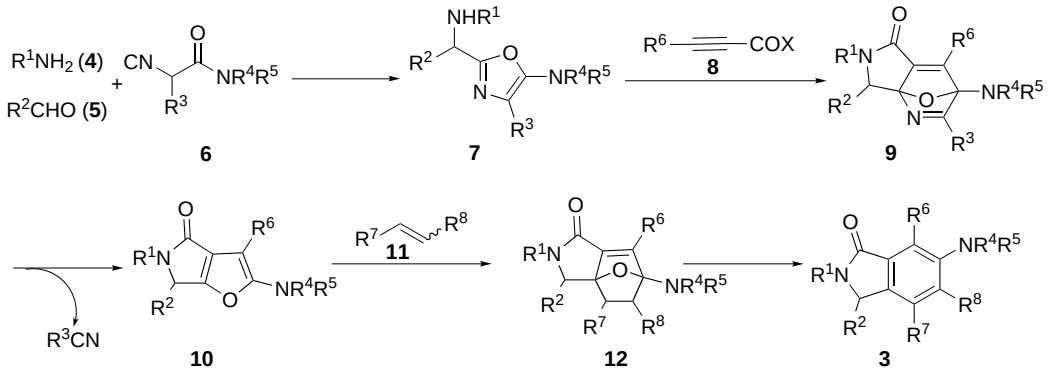
Transition-metal-mediated cyclization of appropriately functionalized enynes[5] and Diels–Alder cycloaddition of furan[6] are two main strategies used for the synthesis of hexasubstituted benzenes.[7] Although high level of structural complexity can be generated from these two key transformations, the overall efficiency is often counter-balanced by efforts associated with the synthesis of linear precursors. In connection with our continued interest in the development of highly efficient synthesis of druglike polyheterocycles,[8] we report herein a conceptually new strategy for the synthesis of hexasubstituted benzenes **3** based on a novel one-pot five-component domino process.[9,10]

The underlying principle of our synthesis is shown in Scheme 1. A recently developed three-component reaction based on Ugi chemistry pioneered by Ugi and co-workers[9] provides the 5-aminooxazole **7**.[11] Reaction of the latter with acyl chloride **8** (X = Cl) should give 5,6-dihydrofuro[2,3-*c*]-pyrrol-4-one **10** following a sequence of acylation, intramolecular Diels–Alder cycloaddition and retro-Diels–Alder cycloreversion.[12] Addition of a second dienophile **11** to the reaction mixture should initiate an intermolecular Diels–Alder reaction of furan[6,7e] to give, after directed fragmenta-

[*] Dr. J. Zhu, P. Janvier
Institut de Chimie des Substances Naturelles, CNRS, 91198 Gif-sur-Yvette (France)
Fax: (+33) 1-69077247
E-mail: zhu@icsn.cnrs-gif.fr
Dr. H. Bienaymé
Chrysalon, 11 Avenue Albert Einstein, 69100 Villeurbanne (France)

[**] Financial support from the CNRS and a doctoral fellowship from Rhodia (PJ) is gratefully acknowledged.

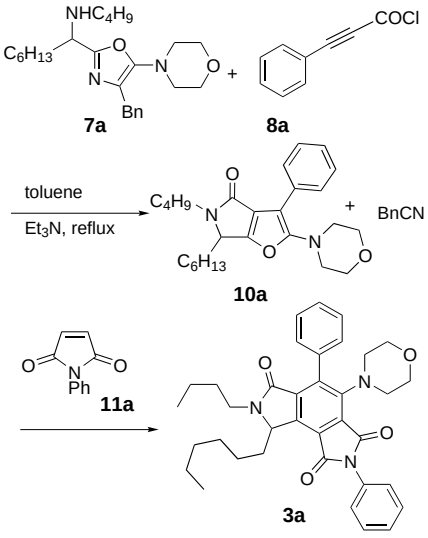
 © 2002 WILEY-VCH Verlag GmbH & Co. KGaA, Weinheim 0044-8249/02/4122-4291 $ 20.00+.50/0



Scheme 1. Five-component synthesis of hexasubstituted benzene.

tion, the hexasubstituted benzenes **3**. The development of conditions for the three-component synthesis of oxazole that are compatible with the subsequent two cycloaddition-based domino processes would enable a five-component synthesis of hexasubstituted benzene **3**. The sequence would allow rapid and efficient construction of structurally complex molecules from readily available starting materials.

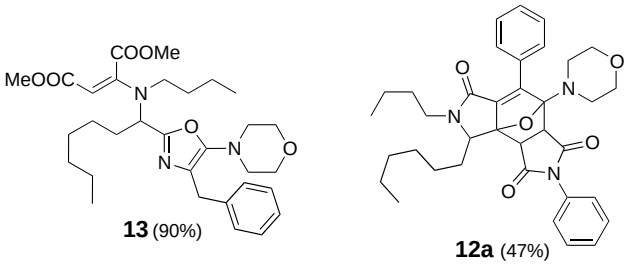
Whereas the cycloaddition of oxazole with acetylene is a well-established method for furan synthesis,[12] the corresponding reaction of 5-aminooxazole was, to the best of our knowledge, unknown. To test the feasibility of the overall process, the reaction between purified 5-aminooxazole **7a** and acyl chloride **8a**[13] was first examined (Scheme 2). The



Scheme 2. From 5-aminooxazole to hexasubstituted benzene.

reaction proceeded smoothly to provide the 5,6-dihydrofuro[2,3-*c*]pyrrol-4-one **10a** (> 95 % yield). A triple domino sequence involving acylation/intramolecular Diels–Alder cycloaddition/retro Diels–Alder cycloaddition could explain the reaction outcome. On the other hand, the reaction of **7a** with dimethylacetylenedicarboxylate (DMAD) provided the Michael adduct **13**; no Diels–Alder cycloaddition took place. Attempts to promote the cycloaddition between **13** and DMAD led only to the recovery of starting materials or to degradation under forcing conditions.

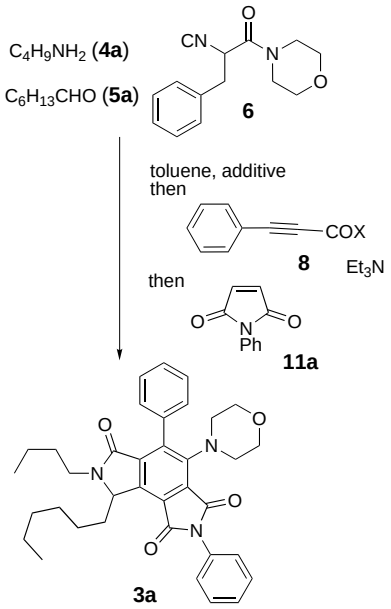
The reaction of the resulting aminofuran with *N*-phenylmaleimide (**11a**) in toluene was next examined. When this reaction was performed at 70 °C in toluene, we were able to isolate the unstable oxa-bridged intermediate **12a** as a



mixture of two diastereomers in 47 % yield. However, on heating the solution in toluene at reflux, hexasubstituted benzene was produced directly. In view of the similar reaction conditions leading to the production of **10a** and **3a**, we reasoned that it might be possible to combine these two domino processes. In the event, heating a solution of oxazole **7a** and acyl chloride **8a** in the presence of triethylamine for 12 h, followed by addition of *N*-phenylmaleimide **11a**, provided **3a** in over 90 % overall yield (Scheme 2).

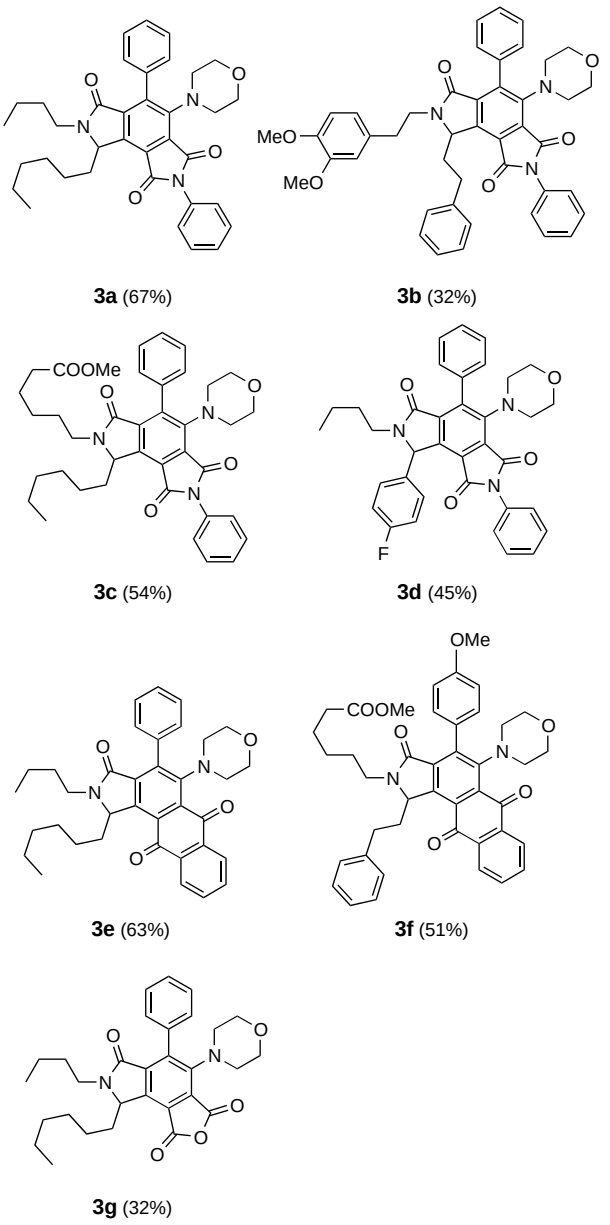
Encouraged by the efficiency of the two consecutive domino processes, we set out to explore conditions that would enable its combination with the three-component synthesis of 5-aminooxazole **7**. Initial results regarding the quest for this one-pot five-component domino process with lithium bromide gave unsatisfactory results.[14] On the other hand, a stoichiometric amount of ammonium chloride[15] and a catalytic amount of camphorsulfonic acid (CSA, 10 %) were able to promote the five-component domino process, which led to the hexasubstituted benzene **3a** in 40 and 52 % yields, respectively (Scheme 3, X = Cl). Subsequent experiments indicated that the use of pentafluorophenyl ester **8b** (X = OC_6F_5) instead of the acyl chloride **8a** (X = Cl) provided an improved yield of **3a** (67 %). Significantly, in this operationally simple five-component domino process, at least seven reactive functionalities participated in the chemical transformation that led to the concomitant creation of seven chemical bonds (two C–N and five C–C bonds) and a biologically relevant polyheterocycle.

 © 2002 WILEY-VCH Verlag GmbH & Co. KGaA, Weinheim 0044-8249/02/4122-4292 $ 20.00+.50/0 *Angew. Chem. Int. Ed.* **2002**, *41*, No. 22



Additive	Equiv.	X	Yield of **3a**
NH_4Cl	1	Cl	40%
CSA	0.1	Cl	52%
CSA	0.1	OC_6F_5	67%

Scheme 3. One-pot five-component synthesis of polyheterocycles with an hexasubstituted benzene core under various conditions.



Scheme 4. Five-component synthesis of polyheterocycles with an hexasubstituted benzene core: selected structures.

The use of three different amines, three aldehydes, one isocyanoacetamide, two pentafluorophenyl 3-arylprop-2-ynoates, and three dienophiles as starting materials allowed the synthesis of the polyheterocycles shown in Scheme 4. The potential and general applicability of this five-component domino process are readily seen from these selected examples.

In conclusion, we have developed a novel five-component domino process for the synthesis of highly functionalized polyheterocycles from simple and readily accessible starting materials. The overall process leads to the creation of seven chemical bonds and delivers five elements of diversity into the compact polyheterocycle, thus providing a large increase in molecular complexity. This constitutes a rare example in which more than four reagents were assembled together to provide a biologically relevant scaffold.[16] The operational simplicity and good chemical yield made these novel heterocycle syntheses highly attractive in diversity-oriented parallel synthesis.[17]

Experimental Section

Typical procedure: Heptanal **5a** (20.0 μL, 0.144 mmol) was added to a solution of butylamine (**4a**, 15.2 μL, 0.156 mmol) in dry toluene (1.0 mL). After the mixture was stirred at room temperature for 30 min, isocyanide **6** (29.0 mg, 0.120 mmol) and camphorsulfonic acid (3.0 mg, 0.012 mmol, 0.1 equiv) were added successively. The reaction mixture was stirred at 60 °C until the disappearance of isonitrile. The reaction mixture was cooled to 0 °C. Et_3N (83.6 μL, 0.60 mmol) was added, followed by a solution of pentafluorophenyl ester **8b** (64.0 mg, 0.2 mmol) in toluene (1.0 mL). Stirring was continued at room temperature for 30 min and at 110 °C for 12 h. *N*-Phenylmaleimide (23.0 mg, 0.132 mmol) was then added. The reaction mixture was stirred for an additional 15 min at 110 °C. After being cooled to room temperature, the reaction mixture was diluted with water and extracted with EtOAc. The combined organic extracts were washed with brine, dried (Na_2SO_4), and evaporated under reduced pressure. The crude reaction mixture was purified by preparative TLC (silica gel, eluent: AcOEt/heptane = 1:2) to give the corresponding hexasubstituted benzene **3a** (46.6 mg, 67 %) as a slight yellow oil. IR: $\tilde{\nu}$ = 3011, 2963, 2931, 2862, 1764, 1714, 1684, 1600, 1502, 1438, 1383, 1234 cm^{-1}; ^1H NMR ($CDCl_3$, 250 MHz): δ = 7.58–7.28 (m, 10 H), 5.01 (t, J = 3.5 Hz, 1 H), 3.95 (ddd, J = 6.8, 9.2, 13.8 Hz, 1 H), 3.61 (m, 4 H), 3.00 (ddd, J = 5.0, 8.9, 13.8 Hz, 1 H), 2.95 (m, 4 H), 2.63 (m, 1 H), 2.09 (m, 1 H), 1.62 (m, 2 H), 1.33 (sextet, J = 7.2 Hz, 2 H), 1.19 (m, 6 H), 1.02 (m, 1 H), 0.92 (t, J = 7.2 Hz, 3 H), 0.84 (t, J = 6.6 Hz, 3 H), 0.69 ppm (m, 1 H); ^{13}C NMR ($CDCl_3$, 75 MHz): δ = 165.9, 165.8, 165.3, 149.1, 143.6, 137.4, 137.1, 134.6, 131.5, 130.1, 129.7, 129.1, 129.0, 128.2, 128.1, 127.7, 127.6, 126.7, 126.0, 67.0, 57.0, 52.0, 39.7, 31.4, 29.9, 28.9, 28.5, 22.4, 21.8, 20.2, 13.9, 13.7 ppm; MS (ES, positive mode): m/z $[M+H]^+$: 580.0

Received: July 15, 2002 [Z19740]

 © 2002 WILEY-VCH Verlag GmbH & Co. KGaA, Weinheim 0044-8249/02/4122-4293 $ 20.00+.50/0

[1] For reviews, see: a) G. W. Gribble, S. J. Berthel in *Studies in Natural Products Chemistry, Vol. 12* (Ed.: Atta-Ur-Rahman), Elsevier, New York, **1993**, pp. 365 – 409; b) J. Bergman, T. Janosik, N. Wahlström in *Advances in Heterocyclic Chemistry, Vol. 80* (Ed.: A. R. Katritzky), Academic Press, New York, **2001**, pp. 1 – 71.
[2] P. Moreau, F. Anizon, M. Sancelme, M. Prudhomme, D. Sevère, J. F. Riou, J. F. Goossens, J. P. Hénichart, C. Bailly, E. Labourier, J. Tazzi, D. Fabbro, T. Meyer, A. M. Aubertin, *J. Med. Chem.* **1999**, *42*, 1816 – 1822.
[3] P. Schupp, C. Eder, P. Porksch, V. Wray, B. Schneider, M. Herderich, V. Paul, *J. Nat. Prod.* **1999**, *62*, 959 – 962.
[4] For a review, see: U. Pindur, Y. S. Kim, F. Mehrabani, *Curr. Med. Chem.* **1999**, *6*, 29 – 69.
[5] a) K. P. C. Vollhardt, *Angew. Chem.* **1984**, *96*, 525; *Angew. Chem. Int. Ed. Engl.* **1984**, *23*, 539 – 556; b) A. J. Fletcher, S. D. R. Christie, *J. Chem. Soc. Perkin Trans. 1* **2000**, 1657 – 1668; c) S. Saito, Y. Yamamoto, *Chem. Rev.* **2000**, *100*, 2901 – 2916.
[6] a) H. N. C. Wong, T. K. Ng, T. Y. Wong, *Heterocycles* **1983**, *20*, 1815 – 1840; b) H. N. C. Wong, T. K. Ng, T. Y. Wong, Y. D Xing, *Heterocycles* **1984**, *22*, 875 – 890; c) C. O. Kappe, S. S. Murphree, A. Padwa, *Tetrahedron* **1997**, *53*, 14179 – 14233; d) P. Vogel, J. Cossy, J. Plumet, O. Arjona, *Tetrahedron* **1999**, *55*, 13521 – 13642.
[7] Recent selected examples: metal-catalyzed: a) B. Witulski, T. Stengel, *Angew. Chem.* **1999**, *111*, 2521 – 2524; *Angew. Chem. Int. Ed.* **1999**, *38*, 2426 – 2430; b) D. Suzuki, H. Urabe, F. Sato, *J. Am. Chem. Soc.* **2001**, *123*, 7925 – 7926; c) T. Sugihara, A. Wakabayashi, Y. Nagai, H. Takao, H. Imagawa, M. Nishizawa, *Chem. Commun.* **2002**, 576 – 577; d) M. Petit, G. Chouraqui, P. Phansavath, C. Aubert, M. Malacria, *Org. Lett.* **2002**, *4*, 1027 – 1029; cycloaddition: e) A. Padwa, J. P. Snyder, E. A. Curtis, S. M. Sheehan, K. J. Worsencroft, C. O. Kappe, *J. Am. Chem. Soc.* **2000**, *122*, 8155 – 8167.
[8] a) J. Drews, *Science* **2000**, *287*, 1960 – 1964; b) W. Wess, M. Urmann, B. Sickenberger, *Angew. Chem.* **2001**, *113*, 3443 – 3453; *Angew. Chem. Int. Ed.* **2001**, *40*, 3341 – 3350.
[9] For recent reviews on multicomponent reactions, see: a) G. H. Posner, *Chem. Rev.* **1986**, *86*, 831 – 844; b) L. Weber, K. Illgen, M. Almstetter, *Synlett* **1999**, 366 – 374; c) A. Domling, I. Ugi, *Angew. Chem.* **2000**, *112*, 3300 – 3344; *Angew. Chem. Int. Ed.* **2000**, *39*, 3168 – 3210; d) H. Bienaymé, C. Hulme, G. Oddon, P. Schmitt, *Chem. Eur. J.* **2000**, *6*, 3321 – 3329.
[10] For recent reviews on domino process, see: a) L. F. Tietze, *Chem. Rev.* **1996**, *96*, 115 – 136; b) M. H. Filippini, J. Rodriguez, *Chem. Rev.* **1999**, *99*, 27 – 76; c) R. A. Bunce, *Tetrahedron* **1995**, *51*, 13103 – 13160; d) L. F. Tietze, F. Haunert in *Stimulating concepts in Chemistry* (Eds.: M. Shibasaki, J. F. Stoddart, F. Vögtle), **2000**, pp. 39 – 64.
[11] X. Sun, P. Janvier, G. Zhao, H. Bienaymé, J. Zhu, *Org. Lett.* **2001**, *3*, 877 – 880.
[12] a) For a review on the intramolecular Diels–Alder reaction of oxazole and acetylene, see: P. A. Jacobi in *Advances in Heterocyclic Natural Product Synthesis, Vol. 2* (Ed.: W. H. Pearson), **1992**, pp. 251 – 298; for a recent application in natural product synthesis, see: b) B. Liu, A. Padwa, *Tetrahedron Lett.* **1999**, *40*, 1645 – 1648; c) P. A. Jacobi, K. Lee, *J. Am. Chem. Soc.* **2000**, *122*, 4295 – 4303; d) L. A. Paquette, I. Efremov, *J. Am. Chem. Soc.* **2001**, *123*, 4492 – 4501.
[13] 3-Arylpropiolic acid was synthesized from the corresponding cinnamate according to a literature procedure: K. J. Schofield, J. C. E. Simpson, *J. Chem. Soc.* **1945**, 512 – 520.
[14] E. Gonzalez-Zamora, A. Fayol, M. Bois-Choussy, A. Chiaroni, J. Zhu, *Chem. Commun.* **2001**, 1684 – 1685.
[15] a) P. Cristau, J.-P. Vors, J. Zhu, *Org. Lett.* **2001**, *3*, 4079 – 4082; b) P. Janvier, X. Sun, H. Bienaymé, J. Zhu, *J. Am. Chem. Soc.* **2002**, *124*, 2560 – 2567.
[16] For a five-component synthesis of α-acylaminocarbonamide, see: a) I. Ugi, C. Steinbrückner, *Chem. Ber.* **1961**, *94*, 2802 – 2814; for a seven-component reaction, see: b) A. Dömling, I. Ugi, *Angew. Chem.* **1993**, *105*, 634 – 635; *Angew. Chem. Int. Ed. Engl.* **1993**, *32*, 563 – 564.
[17] a) S. L. Schreiber, *Science* **2000**, *287*, 1964 – 1969; b) P. Arya, D. T. H. Chou, M. G. Baek, *Angew. Chem.* **2001**, *113*, 351 – 358; *Angew. Chem. Int. Ed.* **2001**, *40*, 339 – 346.

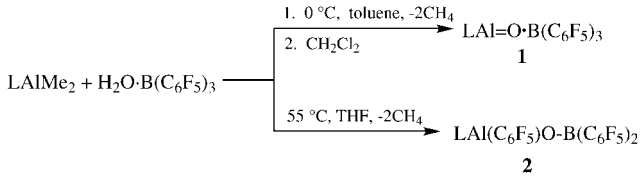
Formation and Characterization of the First Monoalumoxane, $LAlO{\cdot}B(C_6F_5)_3$**

Dante Neculai, Herbert W. Roesky,*
Ana Mirela Neculai, Jörg Magull, Bernhard Walfort, and Dietmar Stalke

Dedicated to Professor Heribert Offermanns on the occasion of his 65th birthday

It has been shown that alumoxanes of the general formula $(RAlO)_n$ for $n > 1$ can be obtained by the controlled reaction of organoaluminum compounds with either water or water contained in hydrated salts or $(Me_2SiO)_3$.[1] Although the simplest member of the series, namely (RAlO), was predicted to be obtainable based on the analogy with aluminum imides,[2] its formation and characterization has remained elusive, presumably because it implies the presence of an Al–O double bond, which is likely to be very unstable even though π interactions between Al and O atoms have been invoked by several groups.[3] However, compounds with such bonds may be either sterically (by using bulky ligands bonded to the aluminum) or electronically (by using Lewis acids) stabilized. Our approach for the stabilization was to use $H_2O{\cdot}B(C_6F_5)_3$, which has been shown to act as a strong Brønsted acid,[4] and whose ability to protonate M–R bonds has been verified.[5] Furthermore if a monoalumoxane is formed, $B(C_6F_5)_3$ may hinder the aggregation owing to its strong Lewis acid character.[6]

Indeed, the reaction of $LAlMe_2$ (where L is a monoanionic β-diketiminato ligand, Scheme 1)[7] and $H_2O{\cdot}B(C_6F_5)_3$ in toluene gave $LAlO{\cdot}B(C_6F_5)_3$ (**1**), which was filtered off at room temperature and crystallized from dichloromethane (−26 °C). In contrast, when the same reagents were allowed to react in THF at 55 °C for 2 h, after the solvent had been removed, an oily product was formed which crystallized as an isomer of **1**, formulated as $LAl(C_6F_5)OB(C_6F_5)_2$ (**2**; Scheme 1).



where L = $Et_2NCH_2CH_2NC(Me)CHC(Me)NCH_2CH_2NEt_2$

Scheme 1. Synthesis of compounds **1** and **2**.

[*] Prof. Dr. H. W. Roesky, D. Neculai, A. M. Neculai, Prof. Dr. J. Magull
Institut für Anorganische Chemie
Universität Göttingen
Tammannstrasse 4, 37077 Göttingen (Germany)
Fax: (+49) 551-393-373
E-mail: hroesky@gwdg.de
Dr. B. Walfort, Prof. Dr. D. Stalke
Institut für Anorganische Chemie
Universität Würzburg
Am Hubland, 97074 Würzburg (Germany)

[**] This work was supported by the Deutsche Forschungsgemeinschaft.

 © 2002 WILEY-VCH Verlag GmbH & Co. KGaA, Weinheim 0044-8249/02/4122-4294 $ 20.00+.50/0

Both complexes were characterized by multinuclear NMR spectroscopy, elemental analysis, and X-ray structural analysis.[8] However, contrary to the ^{1}H NMR spectra of **1** and **2** in solution, which are consistent with the equivalency of the dangling arms of the ligand, the solid-state structures of **1** and **2** reveal that only one arm of the ligand is coordinated to the Al atom (see Figure 1 and 2). One possible explanation for this equivalency is a rapid interconversion in solution.

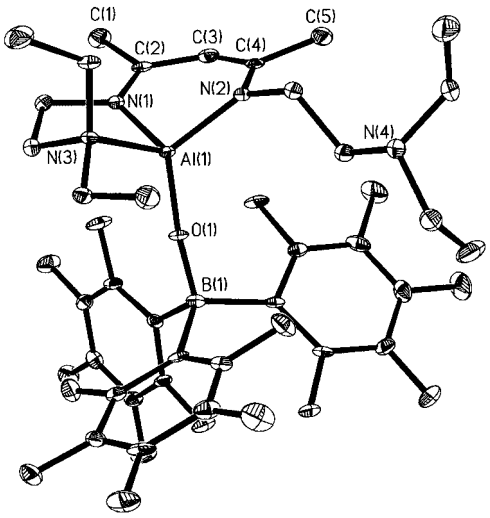
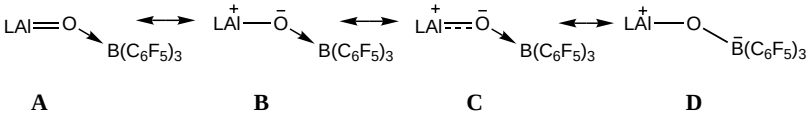


Figure 1. Structure of **1** (50% thermal ellipsoids; hydrogen atoms omitted for clarity). Selected bond lengths [Å] and angles [°]: Al(1)-N(1) 1.853(2), Al(1)-N(2) 1.857(4), Al(1)-N(3) 1.988(4), N(2)-C(4) 1.356(3), C(3)-C(2) 1.401(3), C(4)-C(3) 1.402(0), N(1)-C(2) 1.334(4), Al(1)-O(1) 1.659(3), B(1)-O(1) 1.444(3); Al(1)-O(1)-B(1) 163.76(2), N(2)-C(4)-C(3) 123.45(2), N(2)-Al(1)-N(1) 96.69(1), C(4)-C(3)-C(2) 126.79(2), N(1)-Al(1)-N(3) 86.50(1), C(3)-C(2)-N(1) 119.68(2), Al(1)-N(2)-C(4) 118.02(2), C(2)-N(1)-Al(1) 123.44(2).

The Al–O bond length in **1** is 1.659(3) Å, which is, to the best of our knowledge, the shortest Al–O bond reported for a tetracoordinate Al atom (Figure 1); an Al–O distance of 1.6877(4) Å was reported for a tricoordinate Al atom.[3] This short bond can be explained by considering the resonance structures given in Scheme 2. Resonance forms **A** and **C** can be considered with regard to the shortness of the Al–O bond, and imply a certain double-bond character. These resonance structures can also be taken into account to explain the B–O bond length (1.444(3) Å), which is intermediate between the coordinative B–O bond in $H_2O{\cdot}B(C_6F_5)_3$ (1.597(2) Å)[4d] and a B–O covalent bond (1.311(2) Å for **2**). Even so the $B(C_6F_5)_3$ group stabilizes the monoalumoxane by dispersing the negative charge from oxygen (**B**, **C**, and **D**; Scheme 2). The β-diketiminato ligand must also be taken into consideration because it reduces the positive charge on the Al center by acting as a Lewis base.[7] In addition these resonance structures support the irreversible isomerization of **1** to **2**.



Scheme 2. Proposed resonance structures for **1**.

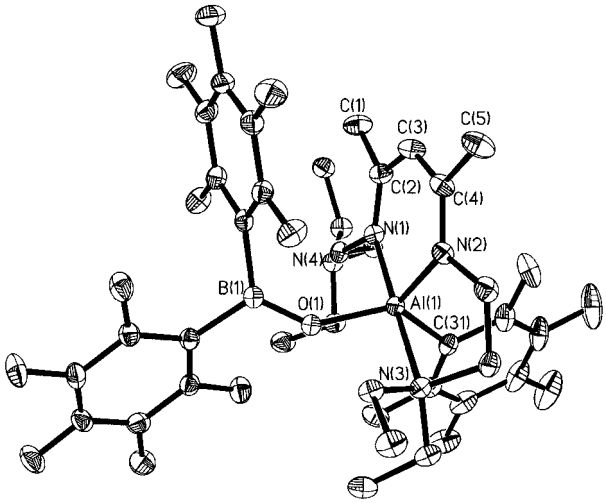


Figure 2. Structure of **2** (30% thermal ellipsoids; hydrogen atoms omitted for clarity). Selected bond lengths [Å] and angles [°]: Al(1)-O(1) 1.780(2), O(1)-B(1) 1.311(2), Al(1)-N(1) 1.964(2), Al(1)-N(2) 1.890(2), Al(1)-N(3) 2.195(2), N(1)-C(2) 1.322(2), N(2)-C(3) 1.346(3), C(2)-C(3) 1.384(3), C(3)-C(4) 1.409(3), Al(1)-C(31) 2.043(2); Al(1)-O(1)-B(1) 141.69(13), C(3)-C(2)-N(1) 122.50(17), N(2)-Al(1)-N(1) 94.11(7), Al(1)-N(1)-C(2) 125.19(13), Al(1)-N(2)-C(4) 125.62(13), N(2)-Al(1)-N(3) 82.48(6), N(2)-C(4)-C(3) 123.68(17), C(31)-Al(1)-O 123.43(7), C(2)-C(3)-C(4) 127.43(18).

For complex **2**, the Al–O and B–O bond lengths of 1.780(2) and 1.311(2) Å (Figure 2), respectively, are in the range of those in previously reported compounds.[1,6c]

In both complexes the Al atom is a member of two nonplanar, five- and six-membered heterocycles. The Al–N bond lengths for **1** (av 1.855 Å) are somewhat shorter than those previously reported for similar compounds (av 1.90 Å).[9] In **2** the Al–N distances have normal values (av 1.925 Å).[9,10] A similar trend is observed for the coordinative Al–N bond lengths; the Al–N(3) bond length in **1** (1.988(4)) is shorter than the Al–N(3) bond length in **2** (2.195(29), however they are in the range found for previously reported similar compounds.[11] The β-diketiminato C–N and C–C ring distances of both compounds have values (av 1.34 and 1.40 Å) corresponding to a delocalized π-electron system.[9] In the light of the different Al–O bond order for the complexes **1** and **2** (seen from the different bond lengths), deviation of the Al-O-B angles from 163.76(2) (**1**) to 141.69(13) (**2**) is expected.

In conclusion, we have provided evidence for the existence of the monomeric member of the $(RAlO)_n$ series. Nevertheless it has to be stated that the nature of the Al–O bond in complex **1** is still under debate; additional insights from future calculations may make things clearer. $H_2O{\cdot}B(C_6F_5)_3$ has been shown to be an excellent reagent for the synthesis of the first monoalumoxane, and its further application towards the synthesis and stabilization of other unusual compounds with multiple M–O bonds is in progress.

Experimental Section

All operations involving air- and moisture-sensitive compounds were performed by using standard Schlenk line and dry box techniques under a purified nitrogen atmosphere. $H_2O{\cdot}B(C_6F_5)_3$ was prepared according to the procedure

 © 2002 WILEY-VCH Verlag GmbH & Co. KGaA, Weinheim 0044-8249/02/4122-4295 $ 20.00+.50/0

described in reference [4a]. Toluene, THF, hexane, and CH_2Cl_2 were dried from appropriate drying agents, Na/K alloy (toluene, THF, hexane), CaH_2 (CH_2Cl_2), and distilled under nitrogen prior to use. C_6D_6 and [D_8]THF were dried over Na/K alloy and degassed. ^{1}H, ^{13}C, ^{19}F, ^{11}B, and ^{27}Al NMR spectra were recorded at ambient temperature on a Bruker AM 200. Chemical shifts are reported in δ units downfield from TMS (^{1}H, ^{13}C), C_6F_6 (^{19}F), $Et_2O{\cdot}BF_3$ (^{11}B), $AlCl_3$ (^{27}Al), with the solvent as the reference signal. Elemental analyses were carried out at the Analytical Laboratory of the Institute of Inorganic Chemistry of the University of Göttingen. Melting points were determined in sealed capillary tubes under nitrogen and are uncorrected.

$LAlMe_2$: Dry hexane (50 mL) was added to LH (1.553 g, 5.24 mmol; for L see Scheme 1) in a 100 mL Schlenk flask. The mixture was cooled to −78 °C and a solution of $AlMe_3$ (7.38 mL, 5.3 mmol of a 1.42 M solution in hexane) was added dropwise. The mixture was stirred for 2 h at −78 °C, and then stirred overnight at room temperature until the methane evolution had ceased. The solvent was removed and the yellowish oil obtained (1.832 g; 99 %) was used without any further purification. Elemental analysis (%) calcd for $C_{17}H_{41}AlN_4$: C 64.73, H 11.72, N 15.89; found: C 64.50, H 11.80, N 16.30; ^{1}H NMR (200 MHz, TMS; C_6D_6): $\delta = 4.45$ (s, 1H; CH), 3.26 (m, 4H; $NCH_2CH_2NEt_2$), 2.41 (m, 12H; $CH_2N(CH_2CH_3)_2$), 1.72 (s, 6H; $CHCCH_3$), 0.91 (t, $J = 7.07$ Hz, 12H; CH_2CH_3), −0.47 ppm (s, 6H; $Al(CH_3)_2$); ^{13}C NMR (125.75 MHz, TMS, C_6D_6): $\delta = 167.91$ (*C*CH*C*), 96.938 (CH), 54.20 ($CNCH_2$), 47.90 (NCH_2CH_2), 46.69 (NCH_2CH_3), 20.84 ($CHCCH_3$), 12.58 (NCH_2CH_3), −8.73 ppm ($AlCH_3$); ^{27}Al NMR (65 MHz, $AlCl_3$ in D_2O, C_6D_6): $\delta = 150.36$ ppm.

$LAlO{\cdot}B(C_6F_5)_3$ (**1**): A solution of $LAlMe_2$ (0.217 g, 0.61 mmol) in toluene (15 mL) was allowed to react with $H_2O{\cdot}B(C_6F_5)_3$ (0.326 g, 0.61 mmol) in toluene (10 mL) at 0 °C. The mixture was stirred for 1 h at 0 °C, and then stirred overnight at room temperature until the methane evolution had ceased. The suspension was filtered and the precipitate was redissolved in CH_2Cl_2 (10 mL). Colorless crystals were obtained by cooling the CH_2Cl_2 solution at −26 °C. Then the crystals were filtered off. Yield 0.317 g (60 %); m.p. 156 °C; elemental analysis (%) calcd for **1**, $C_{35}H_{35}AlBF_{15}N_4O$: C 49.43, H 4.15, N 6.59; found: C 49.81, H 4.33, N 6.63; ^{1}H NMR (200 MHz, TMS; C_6D_6/[D_8]THF): $\delta = 4.82$ (s, 1H; CH), 3.11 (t, $J = 6.85$ Hz, 4H; $NCH_2CH_2NEt_2$), 2.41 (m, $J = 7.19$ Hz, 12H; $CH_2N(CH_2CH_3)_2$), 1.76 (s, 6H; $CHCCH_3$), 0.78 ppm (t, $J = 7.1$ Hz, 12H; CH_2CH_3); ^{13}C NMR (125.75 MHz, TMS, C_6D_6): $\delta = 171.82$ (*C*CH*C*), 98.32 (*C*H),54.31 ($CNCH_2$), 51.78 (NCH_2CH_2), 45.58 (NCH_2CH_3), 20.95 ($CHCCH_3$), 10.17 ppm (NCH_2CH_3); ^{19}F NMR (188 MHz, ext. C_6F_6, C_6D_6/[D_8]THF) $\delta = -134.5$ (m, 6F; *ortho*), −163.7 (t, 3F; *para*), −166.5 ppm (m, 6F; *meta*); ^{11}B NMR (80 MHz, ext. $Et_2O{\cdot}BF_3$, C_6D_6/[D_8]THF): $\delta = -4.83$ ppm.

$LAl(C_6F_5)OB(C_6F_5)_2$ (**2**): A solution of $LAlMe_2$ (0.25 g, 0.71 mmol) in THF (15 mL) was allowed to react in a solution of $H_2O{\cdot}B(C_6F_5)_3$ (0.375 g, 0.71 mmol) in THF (10 mL) at 55 °C for 2 h. The solvent was removed and the oily product was left to crystallize at room temperature. The crystals formed were washed with cold hexane. Yield 0.44 g (73 %); m.p. 85–87 °C; elemental analysis (%) calcd for **2**, $C_{35}H_{35}AlBF_{15}N_4O$: C 49.43, H 4.15, N 6.59; found: C 49.75, H 4.27, N 6.46; ^{1}H NMR (200 MHz, TMS; C_6D_6): $\delta =$ 4.28 (s, 1H; C*H*), 3.22 (m, 2H, $NCH_2CH_2N(CH_2)_2$), 2.95 (m, 2H, $NCH_2CH_2NEt_2$), 2.19 (q, $J = 7.53$ Hz, 8H; CH_2CH_3), 1.85 (m, 2H; $NCH_2CH_2NEt_2$), 1.51 (s, 6H; $CHCCH_3$), 0.70 ppm (t, 12H; CH_2CH_3); ^{13}C NMR (125.75 MHz, TMS, C_6D_6): $\delta = 168.61$ (*C*CH*C*), 97.29 (*C*H), 50.51 ($CNCH_2$), 45.48 (NCH_2CH_2), 45.28 (NCH_2CH_3), 21.57 ($CHCCH_3$), 9.62 ppm (NCH_2CH_3); ^{19}F NMR (188 MHz, ext. C_6F_6, C_6D_6): $\delta = -118.09$ (m 2F; AlC_6F_5 *ortho*), −133.2 (m, 4F; BC_6F_5 *ortho*), −152.5 (t, 2F; BC_6F_5 *para*), −155.3 (t, 1F; AlC_6F_5 *para*), −159.7 (m, 2F; AlC_6F_5 *meta*), −161.5 ppm (m, 4F; AlC_6F_5 *meta*); ^{11}B NMR (80 MHz, ext. $Et_2O{\cdot}BF_3$, C_6D_6): $\delta = 36.83$ ppm.

Received: June 21, 2002 [Z19578]

[1] a) S. Pasynkiewicz, *Polyhedron* **1990**, *9*, 429; b) J. L. Atwood in *Coordination Chemistry of Aluminium* (Ed.: G. H. Robinson), VCH, New York, **1993**, p. 219; c) M. K. Mason, J. M. Smith, S. G. Bott, A. R. Barron, *J. Am. Chem. Soc.* **1993**, *115*, 4971; d) C. J. Harlan, M. R. Mason, A. R. Barron, *Organometallics* **1994**, *13*, 2957; e) J. Storre, C. Schnitter, H. W. Roesky, H.-G. Schmidt, M. Noltemeyer, R. Fleischer, D. Stalke, *J. Am. Chem. Soc.* **1997**, *119*, 7505; f) M. Watanabi, C. N. McMahon, C. J. Harlan, A. R. Barron, *Organometallics* **2001**, *20*, 460; g) R. J. Wehmschulte, P. P. Power, *J. Am. Chem. Soc.* **1997**, *119*, 8387.

[2] a) S. Schulz, L. Häming, R. Herbst-Irmer, H. W. Roesky, G. M. Sheldrick, *Angew. Chem.* **1994**, *106*, 1052; *Angew. Chem. Int. Ed. Engl.* **1994**, *33*, 969; b) J. D. Fisher, P. J. Shapiro, G. P. A. Yap, A. L. Rheingold, *Inorg. Chem.* **1996**, *35*, 271; c) N. J. Hardman, C. Cui, H. W. Roesky, W. H. Fink, P. P. Power, *Angew. Chem.* **2001**, *113*, 2230; *Angew. Chem. Int. Ed.* **2001**, *40*, 2172.

[3] a) W. Uhl, M. Koch, W. Hiller, M. Heckel, *Angew. Chem.* **1995**, *107*, 1123; *Angew. Chem. Int. Ed. Engl.* **1995**, *34*, 989; b) M. A. Petrie, M. M. Olmstead, P. P. Power, *J. Am. Chem. Soc.* **1991**, *113*, 8705.

[4] a) D. C. Bradley, I. S. Harding, A. D. Keefe, M. Motevalli, D. H. Zheng, *J. Chem. Soc. Dalton Trans.* **1996**, 3931; b) C. Bergquist, B. M. Bridgewater, C. J. Harlan, K. R. Norton, R. A. Friesner, G. Parkin, *J. Am. Chem. Soc.* **2000**, *122*, 10581; c) T. Beringhelli, D. Maggioni, G. D'Alfonso, *Organometallics* **2001**, *20*, 4927; d) L. D. Doerrer, M. L. H. Green, *J. Chem. Soc. Dalton Trans.* **1999**, 4325.

[5] a) G. S. Hill, L. Manojlovic-Muir, K. W. Muir, R. J. Puddephatt, *Organometallics* **1997**, *16*, 525; b) M. Stender, A. D. Philips, P. P. Power, *Inorg. Chem.* **2001**, *40*, 5314.

[6] a) A. K. Dash, R. F. Jordan, *Organometallics* **2002**, *21*, 777; b) J. M. Blackwell, W. E. Piers, M. Parvez, R. McDonald, *Organometallics* **2002**, *21*, 1400; c) D. Vagedes, R. Fröhlich, G. Erker, *Angew. Chem.* **1999**, *111*, 3561; *Angew. Chem. Int. Ed.* **1999**, *38*, 3362.

[7] D. Neculai, H. W. Roesky, A. M. Neculai, J. Magull, H.-G. Schmidt, M. Noltemeyer, *J. Organomet. Chem.* **2002**, *643*, 47.

[8] Unfortunately, ^{27}Al NMR spectra for **1** and **2** could not be recorded. The ^{13}C resonances of the C atoms from C_6F_5 groups from both complexes could not be assigned. a) Crystal data for **1**, $C_{35}H_{35}AlBF_{15}N_4O$, $M_r = 850.46$, $T = 130(2)$ K, monoclinic, space group $P2(1)/n$; $a = 10.618(3)$, $b = 17.108(4)$, $c = 20.457(6)$ Å, $\beta = 100.402(6)°$, $V = 3655.0(18)$ Å^3, $Z = 4$, $\rho_{cald} = 1.546$ g cm^{-3}, $\mu = 0.169$ mm^{-1}, $R = 0.0614$ for 8646 independent reflections ($R_1 = 0.0823$ for all 28476 data), GOF = 0.977. The data were collected from shock-cooled crystals on a Bruker Smart-Apex diffractometer (graphite-monochromated $Mo_{K\alpha}$ radiation, $\lambda = 0.71073$ Å) equipped with a low-temperature device at 130(2) K. a) D. Stalke, *Chem. Soc. Rev.* **1998**, *27*, 171; b) T. Kottke, R. J. Lagow, D. Stalke, *J. Appl. Crystallogr.* **1996**, *29*, 465; c) T. Kottke, D. Stalke, *J. Appl. Crystallogr.* **1993**, *26*, 615. For the refinement of the data of compound **1**, which crystallized as a non meroedric twin, two separate matrices of the two domains were determined. Every domain was integrated on its own. The structure solution was performed by direct methods by using the data of the first domain. A new hklf5 file with the reflections of both domains was then written. The reflections are divided into five overlapping ranges, and the data was refined well with 10 scaling factors (one for each range and domain). b) Crystal data for **2**, $C_{35}H_{35}AlBF_{15}N_4O$, $M_r = 850.46$, $T = 133(2)$ K, monoclinic, space group $P2(1)/n$; $a = 9.8994(6)$, $b = 21.4678(17)$, $c = 18.1143(12)$ Å, $\beta = 104.315(5)°$, $V = 3730.09(4)$ Å^3, $Z = 4$, $\rho_{cald} = 1.514$ g cm^{-3}, $\mu = 0.166$ mm^{-1} $R = 0.0388$ for 5121 reflections with $I > 2\sigma(I)$ ($R_1 = 0.0492$ for all 28476 data), GOF = 1.021. Data for crystal structure of **2** were collected on a Stoe Image Plate IPDS II-System. Both structures were solved by direct methods (SHELXS-97) (G. M. Sheldrick, *Acta Crystallogr. Sect. A* **1990**, *46*, 467) and refined by full-matrix least-squares methods against F^2 (SHELXL-97), (G. M. Sheldrick, SHELXL-97, Program for Crystal Structure Refinement, University of Göttingen, Göttingen (Germany), **1997**). CCDC-187737 (**1**) and 187738 (**2**) contain the supplementary crystallographic data for this paper. These data can be obtained free of charge via www.ccdc.cam.ac.uk/conts/retrieving.html (or from the Cambridge Crystallographic Data Centre, 12, Union Road, Cambridge CB2 1EZ, UK; fax: (+44) 1223-336-033; or deposit@ccdc.cam.ac.uk).

[9] C. Cui, S. Köpke, R. Herbst-Irmer, H. W. Roesky, M. Noltemeyer, H.-G. Schmidt, B. Wrackmeyer, *J. Am. Chem. Soc.* **2001**, *123*, 9091.

[10] B. Qian, D. L. Ward, M. R. Smith III, *Organometallics* **1998**, *17*, 3070.

[11] C. N. McMahon, A. R. Barron, *J. Chem. Soc. Dalton Trans.* **1998**, 3693.

 © 2002 WILEY-VCH Verlag GmbH & Co. KGaA, Weinheim 0044-8249/02/4122-4296 $ 20.00+.50/0

Organically Templated Mixed-Valent Iron Sulfates Possessing Kagomé and Other Types of Layered Networks

Geo Paul, Amitava Choudhury,
E. V. Sampathkumaran, and C. N. R. Rao*

We have been interested in developing strategies for designing new open-framework architectures. One such strategy is the case of the sulfate tetrahedron and its utilization as a primary building unit, in place of the silicate or the phosphate tetrahedron commonly employed for the purpose.[1,2] Our efforts in this direction have enabled us to obtain organically templated open-framework metal sulfates under hydrothermal conditions with one-dimensional chain structures as well as two-dimensional layered structures.[3] In the case of iron sulfates, Fe is present generally in the $+2$ or the $+3$ oxidation state; they all show the presence of antiferromagnetic interactions. In this communication, we report the successful synthesis of organically templated mixed-valent iron sulfates of the compositions, $[H_2N(CH_2)_4NH_2]_2[Fe^{III}_2Fe^{II}_3F_{12}(SO_4)_2(H_2O)_2]$ (**1**) and $[HN(CH_2)_6NH][Fe^{III}Fe^{II}_2F_6(SO_4)_2]\cdot[H_3O]$ (**2**), with novel structural features and magnetic properties. In particular, **2** is an unusual example of an iron compound with a perfect Kagomé structure. The discovery of such an unusual Kagomé lattice is significant considering the current interest in these compounds[4] and the fact that iron compounds possessing the Kagomé lattice generally contain Fe in a single oxidation state.

The asymmetric unit of **1** contains four crystallographically distinct iron atoms and one sulfur atom. The fluorine and oxygen neighbors are coordinated octahedrally to the Fe atoms ($Fe(1)F_5O$, $Fe(2)F_4O_2$, $Fe(3)F_2O_2(H_2O)_2$ and $Fe(4)F_4O_2$). The structure of **1** is constructed from the anionic framework layers of $[Fe^{III}_2Fe^{II}_3F_{12}(SO_4)_2(H_2O)_2]^{4-}$. The $Fe(2)F_4O_2$ and $Fe(4)F_4O_2$ octahedra are vertex-shared through *trans*-Fe-F-Fe linkages to form an infinite chain along the *a* axis. Such chains are connected by an edge-shared trimer of two $Fe(1)F_5O$ and one $Fe(3)F_2O_4$ octahedra to yield a layered network in the *ac* plane. In the trimer, the $Fe(3)F_2O_4$ octahedra are flanked by two $Fe(1)F_5O$ octahedra. Such connectivity creates a triangular lattice formed by $Fe(1)F_5O$, $Fe(2)F_4O_2$, and $Fe(4)F_4O_2$ octahedra. The SO_4 tetrahedron caps the triangular lattice, creating a 10-membered aperture within the layer, as shown in Figure 1a. The layers are stacked one over the other along the *b* axis in *AAAA* fashion and are held together by hydrogen bonding interactions with the diprotonated piperazine (PIP) molecules residing in the interlamellar space (see Figure 1b). The bond lengths and

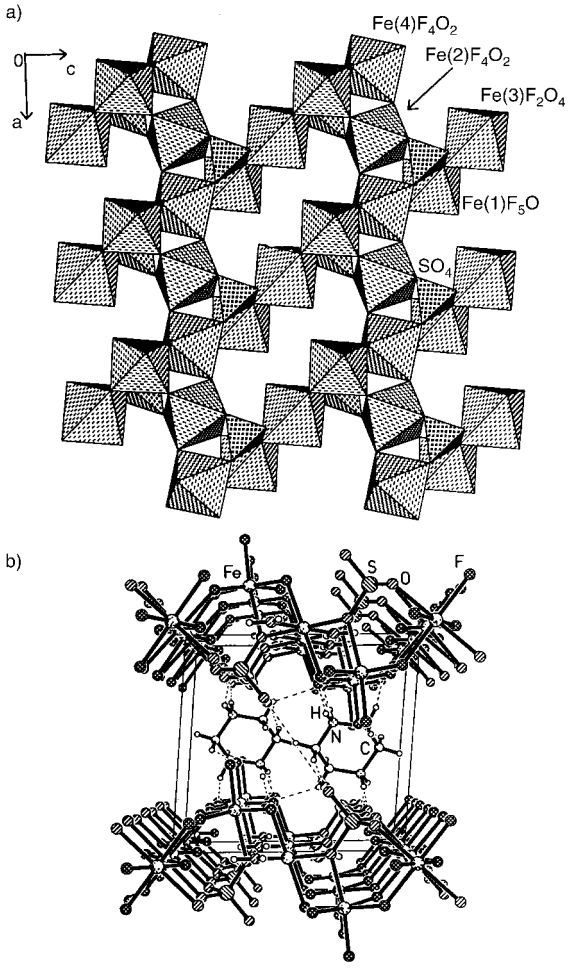


Figure 1. a) Polyhedral view of the $[Fe^{III}_2Fe^{II}_3F_{12}(SO_4)_2(H_2O)_2]^{4-}$ layer in **1**, viewed perpendicular to the *ac* plane. Here, Fe(1) is in the $+3$ oxidation state and the remaining iron atoms are in the $+2$ state. Note the symmetrical capping of the sulfate tetrahedra in the triangular lattice and the 10-membered aperture within the layer; b) Structure of **1** showing the presence of the amine group located in the interlayer space.

angles indicate perfect octahedral geometry around Fe^{II}-centers and a slightly distorted geometry for the Fe^{III} centers. Bond-valence sum (BVS) calculations[5] ($Fe(1) = 3.03$, $Fe(2) = 2.02$, $Fe(3) = 1.98$, and $Fe(4) = 2.05$) and the average Fe–O/F bond lengths indicate the oxidation state of Fe(1) to be $+3$, and the remaining Fe centers to be $+2$. The positions of the fluorine atoms find indirect support from BVS calculations ($F(1) = 0.616$, $F(2) = 0.563$, $F(3) = 0.896$, $F(4) = 0.804$, $F(5) = 0.786$ and $F(6) = 0.74$). The mixed-valent nature of **1** was also confirmed by Mössbauer spectroscopy. DC magnetic susceptibility data (at 100 Oe) show a sharp magnetic transition around 15 K and what appears to be a ferrimagnetic transition at around 3 K, the field-cooled (FC) and the zero-field-cooled (ZFC) data being identical (Figure 2a). The inverse susceptibility data recorded at 5 kOe (Figure 2b) show a linear

[*] Prof. Dr. C. N. R. Rao, G. Paul, A. Choudhury
Chemistry and Physics of Materials Unit and
CSIR Center of Excellence in Chemistry
Jawaharlal Nehru Center for Advanced Scientific Research
Jakkur, P.O., Bangalore 560 064 (India)
Fax: (+91) 80-846-2766
E-mail: cnrrao@jncasr.ac.in
Prof. Dr. C. N. R. Rao, A. Choudhury
Solid State and Structural Chemistry Unit
Indian Institute of Science
Bangalore 560 012 (India)
Prof. Dr. E. V. Sampathkumaran
Department of Condensed Matter Physics and Materials Science
Tata Institute of Fundamental Research
Mumbai 400005 (India)

 © 2002 WILEY-VCH Verlag GmbH & Co. KGaA, Weinheim 0044-8249/02/4122-4297 $ 20.00+.50/0

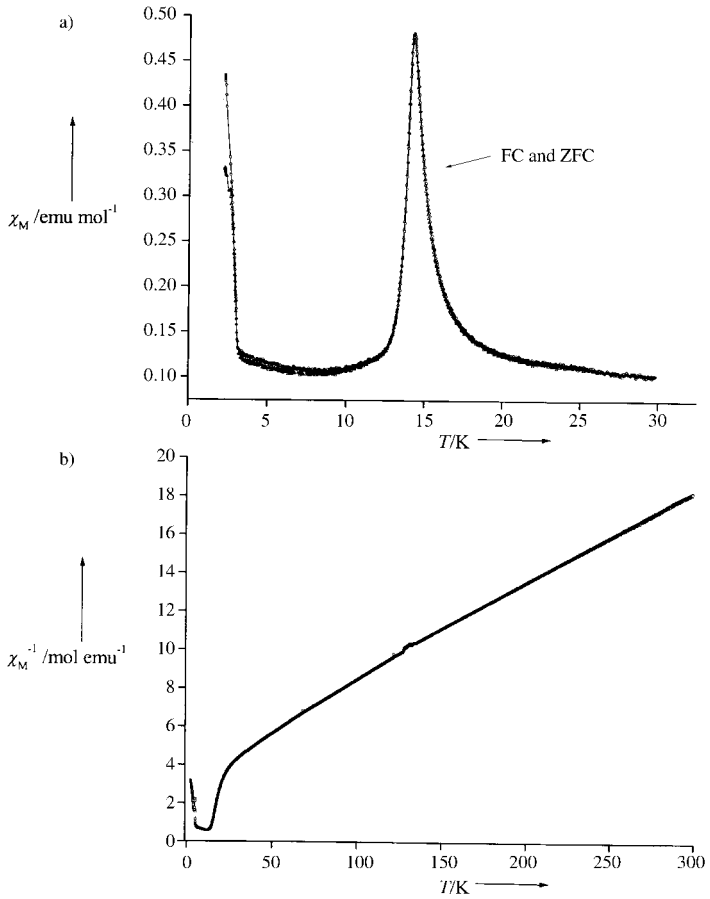


Figure 2. a) Temperature dependence of the DC magnetic susceptibility of **1** measured at 100 Oe under field-cooled (FC) and zero-field-cooled (ZFC) conditions; b) Temperature variation of the inverse DC susceptibility measured at 5 kOe.

behavior at high temperatures, which yields a negative Curie temperature ($T_c = -86$ K). These data also reveal a transition to a canted antiferromagnetic state at low temperatures.

The asymmetric unit of **2** contains 28 non-hydrogen atoms, of which 21 belong to the inorganic framework and seven belong to the extra-framework guest molecules; one extra-framework oxygen atom belongs to the hydronium ion. The structure of **2** consists of anionic layers of vertex-sharing $Fe^{III}F_4O_2$ and $Fe^{II}F_4O_2$ octahedra and tetrahedral SO_4 units, which are fused together by $Fe^{III/II}$-F-$Fe^{III/II}$ and $Fe^{III/II}$-O-S moieties. Each $Fe^{III/II}F_4O_2$ unit shares four of its $Fe^{III/II}$–F vertices with similar neighbors, with the $Fe^{III/II}$-F-$Fe^{III/II}$ bonds roughly aligned in the *ab* plane. The $Fe^{III/II}$–O bond is canted from the *ab* plane and this $Fe^{III/II}$–O vertex effectively forces a three-ring trio of apical $Fe^{III/II}$–O bonds closer together to allow them to be capped by the SO_4 tetrahedra. The three- and six-rings of octahedra result from the in-plane connectivity, as shown in Figure 3a. The layers in **2** are typical of a Kagomé lattice with hexagonal tungsten bronze-type sheets [6] of vertex-sharing $Fe^{III/II}F_4O_2$ octahedra, as shown in Figure 3b. The amine molecules are present between the layers just as in **1**. The structure of **2** is akin to that of the mineral jarosite[7] where all of the Fe atoms are in the +3 oxidation state. The Fe–O bond lengths in **2** are in the range 2.003(3)–2.149(3) Å ($(Fe(1)–O)_{av}$ 2.140(3), $(Fe(2)–O)_{av}$ 2.146(3), and $(Fe(3)–O)_{av}$ 2.011(3) Å), and the Fe–F bond lengths are in the range 1.906(2)–2.157(2) Å ($(Fe(1)–F)_{av}$ 2.081(2), $(Fe(2)–F)_{av}$ 2.080(2), and $(Fe(3)–F)_{av}$ 1.936(2) Å). BVS calculations (Fe(1) = 1.93, Fe(2) = 1.92, and Fe(3) = 3.01) as well as the average bond distances indicate that the oxidation state of Fe(1) and Fe(2) is +2 and that of Fe(3) is +3. The positions of the six F atoms are also supported by the bond valence calculations (F(1) = 0.734, F(2) = 0.669, F(3) = 0.797, F(4) = 0.70, F(5) = 0.76, and F(6) = 0.71). Thus, the framework stoichiometry of the $[Fe^{III}Fe^{II}_2F_6(SO_4)_2]$ unit with a −3 charge requires the amine to be doubly protonated, in addition to the presence of the hydronium ion. Mössbauer spectra also confirm the presence of the Fe^{II} and Fe^{III} states in the ratio 2:1.

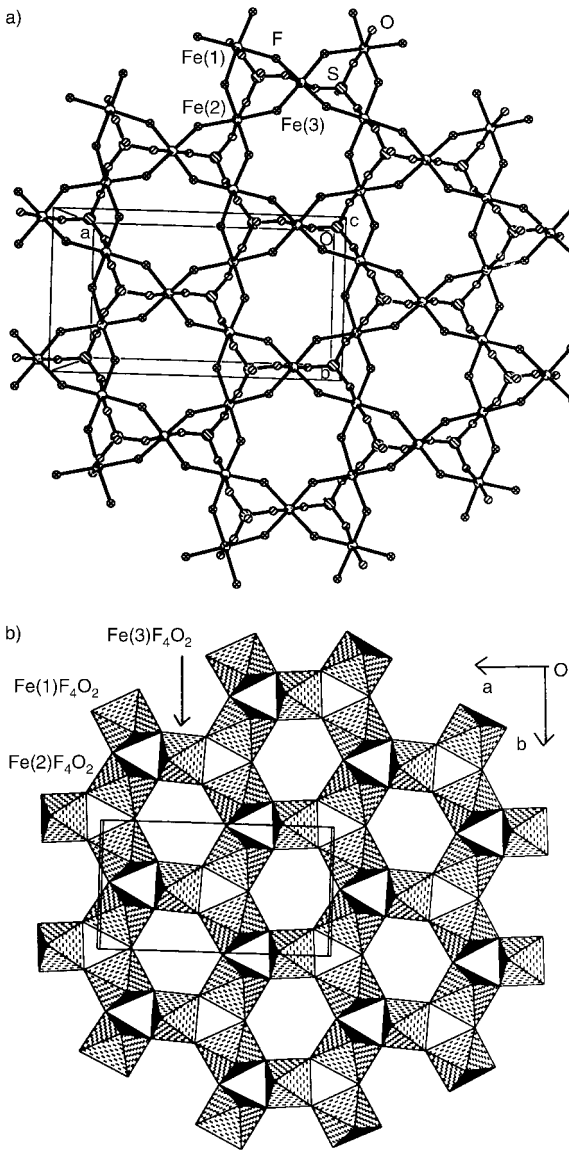


Figure 3. a) Ball-and-stick representation of a section of $[Fe^{III}Fe^{II}_2F_6(SO_4)_2]^{3-}$ in **2**, which shows the presence of the 3- and 6-rings; the 3-rings are capped by the sulfate tetrahedra; b) Polyhedral view of the 2D network of corner-sharing iron octahedra in **2**, viewed perpendicular to the *ab* plane. Here, Fe(1) and Fe(2) are in the +2 oxidation state and Fe(3) is in the +3 state.

The Kagomé lattice in **2** is unusual in several respects. There is 100% occupation of the iron sites[8] and this is the first

 © 2002 WILEY-VCH Verlag GmbH & Co. KGaA, Weinheim 0044-8249/02/4122-4298 $ 20.00+.50/0

example of a Kagomé lattice where the Fe centers are found in two oxidation states. Extensive protonation of the OH sites in jarosite results in vacancies in the Fe lattice, but we seem to be able to overcome this problem by replacing OH groups with fluorine atoms. The magnetic behavior of **2** is quite different from that of **1** and is even more complex. Compound **2** shows magnetic frustration, as typified by the divergence in the FC and ZFC magnetization data shown in Figure 4a. The spin-freezing temperature (T_f) is around 12 K.[9] AC susceptibility measurements confirm a typical spin-glass transition behavior. The inverse magnetic susceptibility data recorded at 5 kOe are linear at high temperatures giving a negative Curie temperature ($T_c = -180$ K). The data show a ferrimagnetic-type transition, as can be seen from Figure 4b. This unusual behavior of **2** requires further study. It may be noted that most of the Fe compounds with the Kagomé lattice show either spin-glass behavior or long-range antiferromagnetic ordering.[4,10,11] The only other Kagomé-type structures exhibiting ferromagnetic features are the vanadium compound reported by Grohol et al.[12] and the dimeric copper compound reported by Zaworotko and co-workers[13] The magnetic moment obtained by extrapolating the high-field [12 T] portion of M versus H to $H = 0$ is 2.95 μ_B mol^{-1} at 10 K for **2** (calcd 9 μ_B mol^{-1}), compared to 4.8 μ_B mol^{-1} for **1** (calcd 16 μ_B mol^{-1}). It should be noted that other mixed-valent iron compounds comparable to **2** exhibit entirely different magnetic properties. Thus $[Fe_3F_8(H_2O)_2]$, with hexagonal bronze-type layers, is antiferromagnetic (Néel temperature, $T_N = 157$ K) and shows weak ferromagnetism at low temperatures.[14] $[Fe_2F_5(H_2O)_2]$, with an inverse weberite structure, is ferrimagnetic ($T_C = 48$ K).[15] Na_2NiFeF_7, with the weberite structure, is also ferrimagnetic ($T_C = 88$ K)[16] while in $BaMnFeF_7$, ferromagnetic sublattices of Mn and Fe are coupled antiferromagnetically giving a T_N value of 85 K.[17] In contrast, compound **2** exhibits a clear spin-glass behavior, as well as ferrimagnetism.

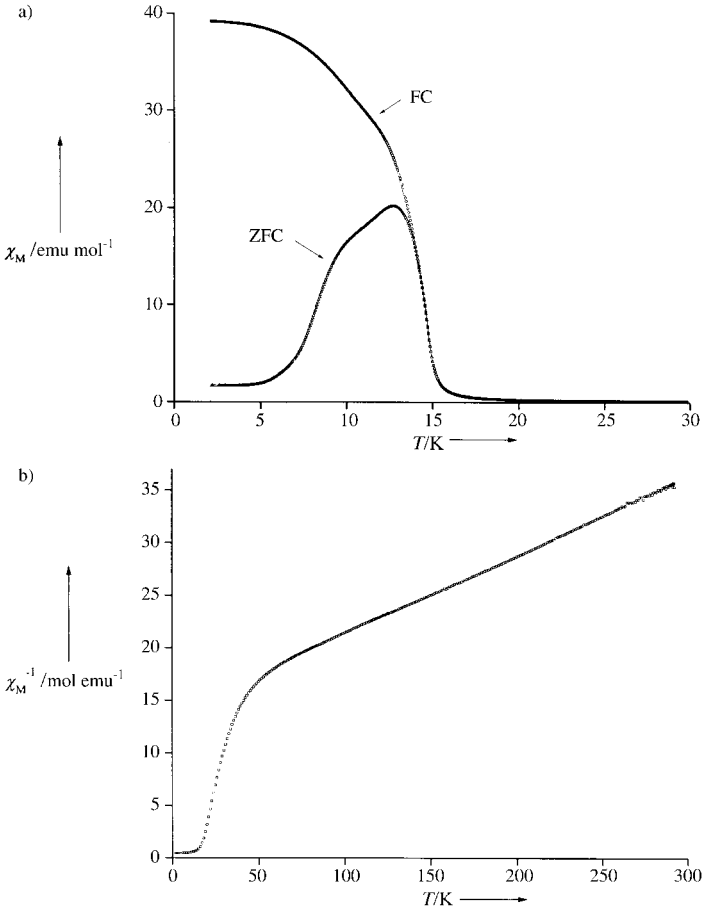


Figure 4. a) DC susceptibility data of **2** measured at 100 Oe which displays the divergence between the ZFC and FC measurements; b) Temperature variation of the inverse DC susceptibility measured at 5 kOe.

Besides demonstrating that the sulfate tetrahedron can be conveniently employed to generate novel organically templated transition metal sulfates, the present study reveals that layered mixed-valent iron sulfates have unusual magnetic properties. The mixed-valent iron Kagomé compound deserves to be further explored both experimentally and theoretically.

Experimental Section

The synthesis of **1** and **2** was carried out in teflon-lined acid digestion bombs with an internal volume of 23 cm^3 under constant pressure by heating the starting mixture at 180 °C for 2 days. Compound **1** was prepared from the following reagents: ferric citrate (1 mmol), piperazine sulfate[18] (4 mmol), HF (48%, 8 mmol), H_2O (50 mmol), and ethylene glycol (50 mmol). The product (yield 50%), which consisted of red rod-shaped crystals, was monophasic. Compound **2** was prepared from the following reagents: ferric citrate (1 mmol), H_2SO_4 (98%, 4 mmol), 1,4-diazabicyclo[222]octane (DABCO, 6 mmol), HF (48%, 4 mmol), H_2O (50 mmol), and *n*-butanol (30 mmol). The product (yield = 40%), consisting of red hexagonal plate-shaped crystals was monophasic. The identities of **1** and **2** were established by various techniques, which included X-ray crystallography. X-ray powder diffraction patterns of **1** and **2** were in good agreement with the simulated patterns based on single-crystal data, indicative of their phase purity. The Fe:S ratios in **1** and **2** were determined by energy-dispersive X-ray analysis (EDAX) to be 5:2 and 3:2, respectively, which is commensurate with their molecular formulas. Furthermore, thermogravimetric analysis gave the exact mass losses expected for the removal of water, amine, and SO_3 in both **1** and **2**. The final product of the decomposition of **1** was Fe_2O_3, which was also verified from its powder XRD pattern. Complex **2** gave FeO as the final product. The fluorine analysis was also satisfactory, which indicated that the OH groups are, generally, replaced by fluorine atoms.

Structure determination: Single-crystal data were collected on a Siemens SMART-CCD diffractometer (graphite-monochromated $Mo_{K\alpha}$ radiation, $\lambda = 0.71073$ Å, $T = 298$ K). An absorption correction based on symmetry-equivalent reflections was applied using SADABS.[19] The structures were solved by direct methods using SHELXS-86[20] and difference Fourier synthesis. Full-matrix least-squares structure refinement against $|F^2|$ was carried out using the SHELXTL-PLUS[21] package of programs. Hydrogen positions for the bonded water molecule (O(3) in **1**) as well as the extra-framework hydronium ion (O(100) in **2**) were located from the difference Fourier map and placed in the observed position and refined isotropically. All the remaining hydrogen positions for **1** and **2** were initially located in the difference Fourier maps, and for the final refinement, the hydrogen atoms were placed geometrically and held in the riding mode. The non-hydrogen atoms were refined anisotropically.

Crystal data. **1**: $M_r = 911.72$, triclinic, space group = $P\bar{1}$ (no. 2), $a = 7.222(2)$, $b = 9.043(2)$, $c = 9.463(4)$ Å, $\alpha = 94.58(3)$, $\beta = 91.71(2)$, $\gamma = 95.08(2)$°, $V = 613.2(3)$ Å^3, $Z = 2$, $\mu = 3.204$ mm^{-1}, $\rho_{calcd} = 2.469$ mg m^{-3}, 1724 unique reflections ($R_{int} = 0.0208$), final $R = 0.0359$, $R_W = 0.0905$, GOF = 1.043. **2**: $M_r = 606.89$, orthorhombic, space group = $Pna2_1$ (no. 33), $a = 12.9269(6)$, $b = 7.4091(3)$, $c = 17.5970(8)$ Å, $\alpha = \beta = \gamma = 90$°, $V = 1685.38(13)$ Å^3, $Z = 4$, $\mu = 2.908$ mm^{-1}, $\rho_{calcd} = 2.392$ mg m^{-3}, 2362 unique reflections ($R_{int} = 0.0333$), final $R = 0.0243$, $R_w = 0.0562$, GOF = 1.000.

 © 2002 WILEY-VCH Verlag GmbH & Co. KGaA, Weinheim 0044-8249/02/4122-4299 $ 20.00+.50/0

CCDC-185168 (**1**) and CCDC-185167 (**2**) contains the supplementary crystallographic data for this paper. These data can be obtained free of charge via www.ccdc.cam.ac.uk/conts/retrieving.html (or from the Cambridge Crystallographic Data Centre, 12, Union Road, Cambridge CB21EZ, UK; fax: (+44) 1223-336-033; or deposit@ccdc.cam.ac.uk).

Received: May 14, 2002
Revised: August 26, 2002 [Z19300]

[1] a) D. W. Breck, *Zeolite Molecular Sieves*, Wiley, New York, **1974**; b) W. M. Meier, D. H. Oslen, C. Baerlocher, *Atlas of Zeolite Structure Types*, Elsevier, London, **1996**.
[2] A. K. Cheetham, G. Férey, T. Loiseau, *Angew. Chem.* **1999**, *111*, 3466 – 3492; *Angew. Chem. Int. Ed.* **1999**, *38*, 3268 – 3292.
[3] a) A. Choudhury, J. Krishnamoorthy, C. N. R. Rao, *Chem. Commun.* **2001**, 2610 – 2611; b) G. Paul, A. Choudhury, C. N. R. Rao, *Chem. Commun.* **2002**, 1904 – 1905.
[4] a) A. P. Ramirez, *Annu. Rev. Mater. Sci.* **1994**, *24*, 453 – 480; b) J. E. Greedan, *J. Mater. Chem.* **2001**, *11*, 37 – 53; c) A. S. Wills, A. Harrison, *J. Chem. Soc. Faraday Trans.* **1996**, *92*, 2161 – 2166; d) T. Inami, M. Nishiyama, S. Maegawa, Y. Oka, *Phys. Rev. B* **2000**, *61*, 12181 – 12186; e) J. N. Reimers, A. J. Berlinsky, *Phys. Rev. B* **1993**, *48*, 9539 – 9554; f) J. Frunzke, T. Hansen, A. Harrison, J. S. Lord, G. S. Oakley, D. Visser, A. S. Wills, *J. Mater. Chem.* **2001**, *11*, 179 – 185.
[5] a) N. E. Brese, M. O'Keeffe, *Acta Crystallogr. Sect. B* **1991**, *47*, 192 – 197; b) I. D. Brown, D. Altermatt, *Acta Crystallogr. Sect. B* **1985**, *41*, 244 – 247.
[6] A. Magneli, *Acta Chem. Scand.* **1953**, *7*, 315.
[7] a) J. E. Dutrizac, S. Kaiman, *Can. Mineral.* **1976**, *14*, 151 – 158; b) F. C. Hawthrone, S. V. Krivovichev, P. C. Burns, *Rev. Mineral. Geochem.* **2000**, *40*, 1 – 101.
[8] A. S. Wills, A. Harrison, S. A. M. Mentink, T. E. Mason, Z. Tun, *Europhys. Lett.* **1998**, *42*, 325 – 330.
[9] a) G. S. Oakley, D. Visser, J. Frunzke, K. H. Andersen, A. S. Wills, A. Harrison, *Phys. B* **1999**, *267–268*, 142 – 144; b) A. Harrison, A. S. Wills, C. Ritter, *Phys. B* **1998**, *241–243*, 722 – 723.
[10] H. Serrano-Gonzalez, S. T. Bramwell, K. D. M. Harris, B. M. Kariuki, L. Nixon, I. P. Parkin, C. Ritter, *Phys. Rev. B* **1999**, *59*, 14451 – 14460.
[11] a) G. S. Oakley, S. Pouget, A. Harrison, J. Frunzke, D. Visser, *Phys. B* **1999**, *267–268*, 145 – 148; b) A. S. Wills, A. Harrison, C. Ritter, R. I. Smith, *Phys. Rev. B* **2000**, *61*, 6156 – 6169; c) E. A. Earle, A. P. Ramirez, R. J. Cava, *Phys. B* **1999**, *262*, 199 – 204; d) S.-H. Lee, C. Broholm, M. F. Collins, L. Heller, A. P. Ramirez, Ch. Kloc, E. Bucher, R. W. Erwin, N. Lacevic, *Phys. Rev. B* **1997**, *56*, 8091 – 8097.
[12] a) D. Grohol, D. Papoutsakis, D. G. Nocera, *Angew. Chem.* **2001**, *113*, 1567 – 1569; *Angew. Chem. Int. Ed.* **2001**, *40*, 1519 – 1521; b) D. Papoutsakis, D. Grohol, D. G. Nocera, *J. Am. Chem. Soc.* **2002**, *124*, 2647 – 2656; c) D. Grohol, D. G. Nocera, *J. Am. Chem. Soc.* **2002**, *124*, 2640 – 2646.
[13] B. Moulton, J. Lu, R. Hajndl, S. Hariharan, M. J. Zaworotko, *Angew. Chem.* **2002**, *114*, 2945 – 2948; *Angew. Chem. Int. Ed.* **2002**, *41*, 2821 – 2824.
[14] a) M. Leblanc, G. Férey, Y. Calage, R. De Pape, *J. Solid State Chem.* **1984**, *53*, 360 – 368; b) M. Leblanc, G. Férey, P. Lacone, J. Punnetier, *J. Magn. Magn. Mater.* **1991**, *92*, 359 – 365.
[15] Y. Laligant, M. Leblanc, J. Pannetier, G. Férey, *J. Phys. C* **1986**, *19*, 1081 – 1095.
[16] Y. Laligant, Y. Calage, G. Heger, J. Pannetier, G. Férey, *J. Solid State Chem.* **1989**, *78*, 66 – 77.
[17] P. Lacorre, J. Pannetier, J. Pebler, S. Nagel, D. Babel, A. De Kozak, M. Samouel, G. Férey, *J. Solid State Chem.* **1992**, *101*, 296 – 308.
[18] K. Jayaraman, A. Choudhury, C. N. R. Rao, *Solid State Sci.* **2002**, *4*, 413 – 422.
[19] G. M. Sheldrick, SADABS Siemens Area Detector Absorption Correction Program, University of Göttingen, Göttingen (Germany), **1994**.
[20] a) G. M. Sheldrick, SHELXS-86 Program for crystal structure determination, University of Göttingen, **1986**; b) G. M. Sheldrick, *Acta Crystallogr. Sect. A* **1990**, *35*, 467.
[21] G. M. Sheldrick, SHELXTL-PLUS Program for Crystal Structure Solution and Refinement, University of Göttingen, Göttingen (Germany).

Ionic Liquids Containing Anionic Selenium Species: Applications for the Oxidative Carbonylation of Aniline**

Hoon Sik Kim,* Yong Jin Kim, Hyunjoo Lee, Kun You Park, Chongmok Lee, and Chong Shik Chin

Non-phosgene processes for the synthesis of carbamates and/or substituted ureas have attracted increasing interest in recent years, particularly in the area of green chemistry because of the environmental concern regarding the use of highly toxic phosgene.[1] Of the various non-phosgene processes, one approach involves the catalytic oxidative carbonylation of an amine in the presence of an appropriate catalyst or catalytic system.[2]

In previous reports, we have demonstrated that alkali metal-containing selenium compounds, obtained from the reaction of SeO_2 and M_2CO_3 (M = alkali metal) in methanol, are effective catalysts for the oxidative carbonylation of aniline to produce phenyl carbamate and diphenylurea.[3] The major disadvantage of using these selenium compounds is the difficulty in separating the product and the catalyst from the reaction mixture, which arises from the coproduction of insoluble diphenylurea and soluble alkyl phenyl carbamate, with high conversion of aniline. A further disadvantage is the formation of small quantities of unknown, highly volatile, malodorous, and possibly toxic selenium species at relatively high reaction temperatures.

Recently, there have been a considerable number of papers regarding ionic liquids and their use in immobilizing volatile, precious, and/or toxic homogeneous catalysts, thereby improving the stability and facilitating the recovery of the catalyst.[4]

In this context, the alkali metal-containing selenium compound $[KSeO_2(OCH_3)]$ can be reacted with 1-alkyl-3-methylimidazolium chlorides to prepare new imidazolium-based ionic liquids containing anionic selenium species. The ionic liquids are found to show surprisingly high activity for the

[*] Dr. H. S. Kim
CFC Alternatives Research Center
KIST
39-1, Hawolgokdong, Seongbukgu, Seoul 136-791 (Korea)
Fax: (+82) 2-958-5859
E-mail: khs@kist.re.kr
H. Lee, K. Y. Park
Korea Institute of Science and Technology
Seoul (Korea)
Prof. C. Lee
Department of Chemistry
Ewha Womans University
Seoul (Korea)
Y. J. Kim, Prof. C. S. Chin
Department of Chemistry
Sogang University
Seoul (Korea)

[**] This work was supported by the Ministry of Science and Technology. We thank to Prof. Myoung Soo Lah for the X-ray crystallographic analysis at Hanyang University.

Supporting information for this article is available on the WWW under http://www.angewandte.org or from the author.

 © 2002 WILEY-VCH Verlag GmbH & Co. KGaA, Weinheim

carbonylation of aniline, even at temperatures as low as 40 °C. Furthermore, malodorous selenium species are not formed when the immobilized selenium compound is used as a catalyst for carbonylation.

We now report, for the first time, the synthesis and reactivity of a series of new, room-temperature ionic liquids consisting of imidazolium cations (1-R-3-methylimidazolium, $R = CH_3$, C_2H_5, n-C_4H_9) and selenium-containing anions $[SeO_2(OR')]^-$ ($R' = CH_3$, CH_2CH_3, CH_2CF_3, C_6H_5), which are highly active, easily recyclable, and air and moisture stable.

The reaction of SeO_2 with 0.5 equiv of K_2CO_3 in methanol for 1 h at room temperature, followed by the addition of THF into the resulting solution produced $[KSeO_2(OCH_3)]$ (**1**) as an extremely hygroscopic white precipitate [Eq. (1)], which was characterized by elemental analysis and ^{1}H NMR spectroscopy.

$$2\,SeO_2 + K_2CO_3 + 2\,CH_3OH \rightarrow 2\,KSeO_2(OCH_3) + H_2O + CO_2 \quad (1)$$

The ambiguous spectroscopic data of **1** led us to carry out a single-crystal X-ray diffraction study to elucidate its structure, which revealed that **1** was, indeed, potassium methyl selenite, $[KSeO_2(OCH_3)]$, in which the methoxy group is bonded to the selenium center (Figure 1).[5]

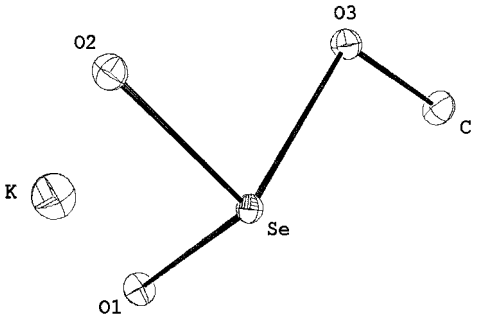
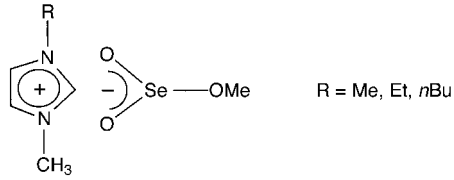


Figure 1. Single-crystal X-ray structure of **1**. Selected bond lengths [Å] and angles [°]: Se···K 3.7364(9), Se-O1 1.6590(19), Se-O2 1.6579(19), Se-O3 1.8460(19), O3-C 1.438(4); O2-Se-O1 106.27(10), O2-Se-O3 95.31(9), O1-Se-O3 101.44(10), C-O3-Se 112.74(16).

To immobilize the selenite anion within an imidazolium-based ionic liquid, (bmim)Cl (bmim = 1-n-butyl-3-methylimidazolium) and **1** were reacted in methanol at room temperature for 6 h. Filtration of KCl and subsequent removal of methanol under reduced pressure afforded an air-stable yellow liquid, which was characterized as $[bmim][SeO_2(OCH_3)]$ (**2a**) by ^{1}H NMR spectroscopy, elemental analysis, and mass spectrometry. Similarly, $[emim][SeO_2(OCH_3)]$ (**3a**) and $[dmim][SeO_2(OCH_3)]$ (**4a**) were prepared by reacting **1** with (emim)Cl (emim = 1-ethyl-3-methylimidazolium) and (dmim)Cl (dmim = 1,3-dimethylimidazolium), respectively. Although the melting points of **2a**, **3a**, and **4a** were not precisely established, they were all liquids at -10 °C.



Interestingly, reactions of **3a** with various alcohols produced a series of new selenium-containing ionic liquids, as shown in Equation (2).

$$[emim][SeO_2(OCH_3)] + ROH \rightarrow [emim][SeO_2(OR)] + CH_3OH \quad (2)$$
(**3b**: R = CH_3CH_2, **3c**: R = CF_3CH_2, **3d**: R = Ph)

The viscosity and conductivity of **2a**, $[bmim][SeO_2(OCH_2CF_3)]$ (**2c**), and $(bmim)BF_4$ were measured. Ionic liquid **2c** surprisingly exhibits lower viscosity (15 cP) and higher conductivity (4.33 mS cm^{-1}) than both **2a** (viscosity: 6055 cP, conductivity: 0.14 mS cm^{-1}) and $(bmim)BF_4$ (viscosity: 233 cP, conductivity: 1.73 mS cm^{-1}).[6] These results demonstrate that the physical properties of the ionic liquids could be significantly altered by replacing the alkoxide group in the anionic moiety.

The activities of various ionic liquids consisting of imidazolium cations and selenium-based anions were evaluated as catalysts for the oxidative carbonylation of aniline, and compared with the activities of **1** and 5% Pd/C–KI (a catalyst for the Asahi process).[7]

The results in Table 1 show that the activities of the ionic-liquid catalysts **2a**, **3a–c**, and **4** are significantly higher than those of **1** and 5% Pd/C–KI at 40 °C. The reason for the enhanced activities of ionic liquid-immobilized selenium catalysts cannot be fully explained at the moment, but it is likely that the imidazolium cation plays an important role in the catalytic process by electronically communicating with the anionic selenium species. This is partially supported by

Table 1. Activities of various catalysts for the oxidative carbonylation reactions of aromatic amines.[a]

Amine	Catalyst	T [°C]	Conversion [%]	Selectivity [%][b]	TOF [h^{-1}][c]
$PhNH_2$	**1**	40	5.1	100	18
$PhNH_2$	**2a**	40	51.3	100	93
$PhNH_2$	**3a**	40	53.6	100	97
$PhNH_2$	**4a**	40	52.6	100	96
$PhNH_2$	**3b**	40	52.4	100	95
$PhNH_2$	**3c**	40	54.5	100	99
$PhNH_2$	Pd/C–KI[d]	40	7.2	100	26
$PhNH_2$	**3a**	60	97.4	98.9	177
$PhNH_2$	**3a**[e]	120	36.8	99.3	3680
o-Tolu[f]	**3a**	60	28.0	100	51
p-Tolu	**3a**	60	95.2	100	173
MDA[g]	**3a**	60	81.8	100	149
$PhCH_2NH_2$	**3a**	60	92.4	100	168

[a] amine (40 mmol), catalyst (0.11 mmol), methanol (25 mL), $P = 1.36$ MPa (O_2/CO, 20:80 v/v), $t = 2$ h. [b] *N*,*N*′-diphenylurea for aniline; $(CH_3C_6H_4NH)_2CO$ for toluidine, $(NH_2C_6H_4CH_2C_6H_4NH)_2CO$ for MDA; $(C_6H_5CH_2NH)_2CO$ for $PhCH_2NH_2$. [c] TOF = (moles of aniline consumed/moles of catalyst) h^{-1}. [d] 5% Pd/C (234 mg, 0.11 mmol Pd), KI (90 mg, 0.55 mmol). [e] $t = 1$ h, aniline (160 mmol), **3a** (0.016 mmol). [f] Tolu = toluidine. [g] MDA = 4,4′-methylenedianiline.

 © 2002 WILEY-VCH Verlag GmbH & Co. KGaA, Weinheim 0044-8249/02/4122-4301 $ 20.00+.50/0

comparing the cyclic voltammograms (CVs) of [dmim][$SeO_2(OCH_3)$], (dmim)Cl, and [$KSeO_2(OCH_3)$] (Figure 2), where the reversibility of the oxidation wave of [dmim][$SeO_2(OCH_3)$] at $+0.3$ V (versus Ag/AgCl) is pronounced, while such a reversible wave is not observed in the CVs of **1** and (dmim)Cl.

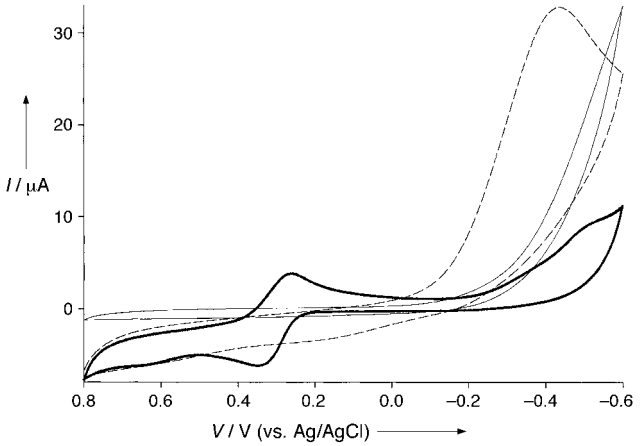


Figure 2. Cyclic voltammograms of 0.12 M solutions of **4a** (——), (dmim)Cl (——), and **1** (– – –) in CH_3OH at a platinum disk with a Ag/AgCl reference electrode at a scan rate of 0.05 $V s^{-1}$.

Compound **3a** was also found to be a highly active catalyst for the carbonylation of other substrates including toluidines (both *ortho* and *para*), benzylamine, and 4,4-methylenedianiline. Interestingly, *p*-toluidine shows much higher conversion than *o*-toluidine, possibly as a result of the steric hindrance of the methyl group next to the $-NH_2$ group. Only one amino group in 1,4-methylenedianiline is carbonylated to give $(NH_2C_6H_4CH_2C_6H_4NH)_2CO$ under the reaction conditions.

The catalytic activity of **3a** for the carbonylation of aniline increases with increasing temperature, resulting in a high turnover frequency (TOF) of 3680 h^{-1} at 120 °C. It should be mentioned that TOFs for the selenium-based catalyst systems reported by other groups are usually lower than 100 h^{-1}.[8]

During the oxidative carbonylation of aniline, **3a** is likely to react with aniline to form an intermediate species, [emim][$SeO_2(NHC_6H_5)$], which in turn reacts with CO to give [emim][$SeO_2(CONHC_6H_5)$]. The in situ ^{1}H NMR spectrum of the reaction mixture in [d_4]methanol clearly demonstrates the transformation of **3a** into two other selenium species that contain the imidazolium cation (see Figure 3); there is no evidence that selenium species without imidazolium cations are present.

To investigate the possibility of recycling these novel catalyst systems, experiments have been conducted with aniline and **3a** at 60 ° and 1.4 MPa of O_2/CO (20:80 v/v) for 2 h, at which time the reaction mixture was filtered off to remove diphenylurea and the solution containing the ionic liquid was reused for further carbonylation reactions with a fresh charge of consumed aniline and methanol. As can be seen in Table 2, **3a** retains most of its original activity even after five cycles, which indicates that **3a** is, indeed, a recyclable catalyst.

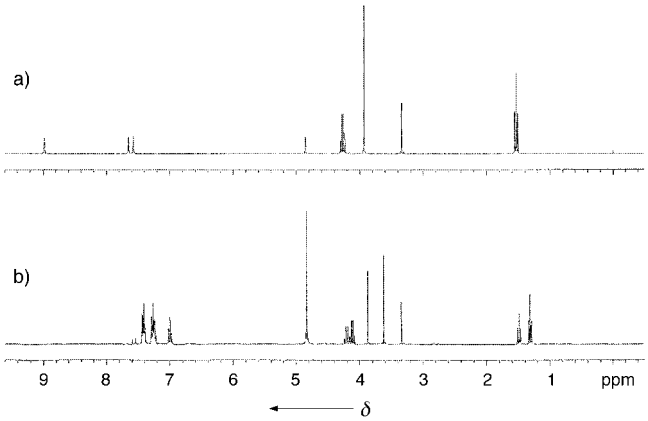


Figure 3. ^{1}H NMR spectra: a) **3a** in [d_4]methanol; b) after the carbonylation reaction with 2 equiv of $PhNH_2$ at 100 °C and 1.0 MPa of O_2/CO (20:80 v/v) for 2 h.

Table 2. Catalyst recycling studies with **3a**.[a]

Cycle	Conversion [%]	Selectivity [%][b]	TOF [h^{-1}]
1	97.0	99.1	176
2	96.8	99.4	176
3	95.3	99.0	173
4	94.2	98.9	171
5	93.9	99.3	170

[a] aniline (40 mmol), **3a** (0.11 mmol), methanol (25 mL), $P = 1.36$ MPa (O_2/CO 20:80 v/v), $t = 2$ h. [b] *N*,*N*′-diphenylurea.

As a consequence of the possible toxicity of the selenium-based ionic liquids, the level of selenium contamination in the isolated urea was measured using induced coupled plasma (ICP) analysis. When **3a** was used as the catalyst for the carbonylation of aniline, the isolated diphenylurea was found to contain 45.4 ppm of selenium, which was significantly reduced to 2.5 ppm after additional washing with methanol (2×10 mL). After this treatment, the isolated diphenylurea was found not to have an unpleasant odor. This was in contrast to similar experiments using **1** as the catalyst, in which the isolated urea did exhibit a strong, unpleasant odor even after additional washing with methanol (2×10 mL), and showed higher levels of selenium contamination (54.3 ppm after filtration and 13.2 ppm after additional washing).

There are many advantages to selenium-containing ionic-liquid catalyst systems. In addition to the improved catalytic performance and the absence of species responsible for potentially foul odors, they are recyclable without losing their initial activity. Furthermore, they are air stable and highly soluble in various organic solvents including CH_2Cl_2, $CHCl_3$, and CH_3CN. Spectroscopic and electrochemical investigations to elucidate the mechanism for the oxidative carbonylation of amines are now in progress.

Experimental Section

The imidazolium salts (bmim)Cl, (emim)Cl, and (dmim)Cl were prepared according to the literature procedure.[9] Aniline, *o*-toluidine, *p*-toluidine, benzylamine, and 4,4′-methylenedianiline were purchased from Aldrich Chemical Co. and used as received.

1: A solution of SeO_2 (3.3 g, 30 mmol) in methanol (30 mL) was treated with K_2CO_3 (2.0 g, 15 mmol) in a 100-mL 2-neck flask at room temperature

 © 2002 WILEY-VCH Verlag GmbH & Co. KGaA, Weinheim 0044-8249/02/4122-4302 $ 20.00+.50/0

for 1 h. As soon as K_2CO_3 was added, CO_2 started to evolve. Addition of THF into the resulting colorless solution produced a white solid (yield 92%). Elemental analysis calcd (%) for CH_3KSe: C 6.6, H 1.7, K 21.5, Se 43.6; found: C 6.8, H 1.8, K 21.4, Se 42.7; ^{1}H NMR (300 MHz, [D$_4$]methanol, 25°C): $\delta = 3.35$ (s).

Single crystals of **1** suitable for X-ray diffraction studies were grown inside a dry-box (under argon). Compound **1** (0.5 g) was dissolved in methanol (3 mL) in a vial which was contained within a larger vial charged with approximately 2 mL of diethyl ether. The diethyl ether was allowed to slowly diffuse into the methanol solution by maintaining the vials at room temperature for several days.

2a: A solution of (bmim)Cl (3.1 g, 18 mmol) in methanol (30 mL) was treated with 1.1 equiv of **1** (3.6 g, 19.8 mmol) in methanol (30 mL) at room temperature. After stirring for 6 h, the solution was filtered to remove KCl and the solvent was evaporated under reduced pressure to give a yellow liquid. The resulting liquid was further purified by adding CH_2Cl_2 and filtering to remove excess **1** and KCl, followed by drying under high vacuum for 12 h (yield 85%). Elemental analysis calcd (%) for $C_9H_{18}N_2Se$: C 38.45, H 6.41, N 9.97, Se 28.09; found: C 38.18, H 6.30, N 9.60, Se 28.10; ^{1}H NMR (300 MHz, $CDCl_3$, 25°C): $\delta = 0.91$ (t, ^3J(H,H) = 7.5 Hz, 3H; CH_3), 1.34 (m, 2H; CH_2), 1.83 (m, 2H; CH_2), 3.45 (s, 3H; OCH_3), 4.06 (s, 3H; NCH_3), 4.27 (t, ^3J(H,H) = 7.2 Hz, 2H; NCH_2), 7.23 (d, ^3J(H,H) = 1.5 Hz, 1H; $C_3H_3N_2$), 7.33 (d, ^3J(H,H) = 1.5 Hz, 1H; $C_3H_3N_2$), 10.58 ppm (s, 1H; $C_3H_3N_2$); LC-MS (CH_3OH): positive ion: 139 $[bmim]^+$; negative ion: 143 $[SeO_2(OCH_3)]^-$.

3a and **4a** were prepared in a similar manner to that of **2a**, by replacing (bmim)Cl with (emim)Cl and (dmim)Cl, respectively.

3a: Yield 86%; elemental analysis calcd (%) for $C_7H_{14}N_2Se$: C 33.21, H 5.54, N 11.07, Se 31.20; found: C 32.90, H 5.50, N 11.50, Se 29.70; ^{1}H NMR (300 MHz, $CDCl_3$, 25°C): $\delta = 1.51$ (t, ^3J(H,H) = 7.8 Hz, 3H; CH_3), 3.47 (s, 3H; OCH_3), 4.04 (s, 3H; NCH_3), 4.35 (q, ^3J(H,H) = 7.5 Hz, 2H; NCH_2), 7.28 (s, 1H; $C_3H_3N_2$), 7.30 (s, 1H; $C_3H_3N_2$), 10.88 ppm (s, 1H; $C_3H_3N_2$). LC-MS (CH_3OH): Positive ion: 111 $[emim]^+$; Negative ion: 143 $[SeO_2(OCH_3)]^-$.

4a: Yield 87%; elemental analysis calcd (%) for $C_6H_{12}N_2Se$: C 30.14, H 5.02, N 11.72, Se 33.03; found: C 30.00, H 5.00, N 11.90, Se 32.10; ^{1}H NMR (300 MHz, $CDCl_3$, 25°C): $\delta = 3.45$ (s, 3H; OCH_3), 3.98 (s, 6H; $2(NCH_3)$), 7.31 (s, 2H; $C_3H_3N_2$), 10.83 ppm (s, 1H; $C_3H_3N_2$). LC-MS (CH_3OH): Positive ion: 97 $[dmim]^+$; Negative ion: 143 $[SeO_2(OCH_3)]^-$.

Transformation reactions of **3a** to give **3b** and **3c:**[10] A solution of **3a** (0.1 g, 0.4 mmol) in CH_3CH_2OH (3 mL) or CF_3CH_2OH (3 mL) was stirred at room temperature for 6 h, followed by removal of the solvent under high vacuum for 12 h to give a yellow liquid (yield 99%).

Transformation of **3a** to give **3d:**[10] A solution of **3a** (0.1 g, 0.4 mmol) in CH_2Cl_2 (3 mL) was treated with 1.3 equiv of PhOH (0.05 g, 0.52 mmol) at room temperature for 6 h. The subsequent removal of the solvent and excess PhOH under high vacuum for 12 h gave a yellow liquid (yield 99%).

Catalysis reaction: All of the carbonylation reactions were conducted in a 100-mL Parr reactor with a magnetic drive stirrer and an electrical heater. The reactor was charged with an aromatic amine, methanol, an appropriate catalyst and toluene (1 mL) as an internal standard. The reactor was pressurized with a gaseous mixture of O_2 and CO (20:80 v/v), and then heated to a specified temperature. The pressure was maintained at 1.4 MPa throughout the reaction using a reservoir tank equipped with a high-pressure regulator and a pressure transducer. After the reaction was completed, the reactor was cooled to room temperature and the reaction mixture was filtered off to remove the solid diaryl urea. The resulting solution and the isolated urea were analyzed by GC, HPLC, and GC-MS.

Recycling experiment: The 100-mL reactor was charged with aniline (40 mmol), methanol (25 mL), **3a**, and toluene (1 mL) as the internal standard, and then reacted at 60°C for 2 h under pressure of 1.4 MPa of O_2/CO (20:80 v/v). When the reaction was completed, diphenylurea was removed by filtration and the solution that contained the ionic liquid was reused for further carbonylation reactions with a fresh charge of consumed aniline.

Received: June 20, 2002
Revised: August 1, 2002 [Z19573]

[1] a) A. M. Tafesh, J. Weiguny, *Chem. Rev.* **1996**, *96*, 2035 – 2052; b) J. D. Gargulak, W. L. Gladfelter, *Organometallics* **1994**, *13*, 698 – 705; c) I. Vauthey, F. Valot, C. Gozzi, F. Fache, M. Lemaire, *Tetrahedron Lett.* **2000**, *41*, 6347 – 6350.

[2] a) T. W. Leung, B. D. Dombek, *J. Chem. Soc. Chem. Commun.* **1992**, 205 – 206; b) K. V. Prasad, R. V. Chaudhari, *J. Catal.* **1994**, *145*, 204 – 215.

[3] a) H. S. Kim, Y. J. Kim, H. Lee, K. Y. Park, C. S. Chin, *J. Catal.* **1998**, *176*, 264 – 266; b) H. S. Kim, Y. J. Kim, H. Lee, S. D. Lee, C. S. Chin, *J. Catal.* **1999**, *184*, 526 – 534.

[4] a) R. Sheldon, *Chem. Commun.* **2001**, 2399 – 2407; b) C. M. Gordon, *Appl. Catal. A* **2001**, *222*, 101 – 117; c) R. J. C. Brown, P. J. Dyson, D. J. Ellis, T. Welton, *Chem. Commun.* **2001**, 1862 – 1863; d) J. E. L. Dullius, P. A. Z. Suarez, S. Einloft, R. F. de Souza, J. Dupont, *Organometallics* **1998**, *17*, 815 – 819; e) C. J. Adams, M. J. Earle, K. R. Seddon, *Chem. Commun.* **1999**, 1043 – 1044.

[5] X-ray single-crystal diffraction data for **1** was collected on a Siemens SMART CCD diffractometer. Crystal data for **1**: monoclinic, space group $P2_1/c$, $a = 10.2502(16)$, $b = 7.3115(12)$, $c = 6.4330(10)$ Å, $\beta = 103.012(2)°$, $V = 469.74(13)$ Å^3, $Z = 2$, $\rho_{calcd} = 2.561$ g cm^{-1}, $\mu(Mo_{K\alpha}) = 8.746$ mm^{-1}, $R1 = 0.0332$, $wR2 = 0.0886$, ($I > 2\sigma I$); $R1 = 0.0340$, $wR2 = 0.0893$ (all data). CCDC-185119 contains the supplementary crystallographic data for this paper. These data can be obtained free of charge via www.ccdc.cam.ac.uk/conts/retrieving.html (or from the Cambridge Crystallographic Data Centre, 12, Union Road, Cambridge CB2 1EZ, UK; fax: (+44) 1223-336-033; or deposit@ccdc.cam.ac.uk).

[6] R. Hagiwara, Y. Ito, *J. Fluorine Chem.* **2000**, *105*, 221 – 227.

[7] S. Fukuoka, M. Chono, M. Kohno, *J. Chem. Soc. Chem. Commun.* **1984**, 399 – 400.

[8] a) S. A. Akyüz, A. B. Dempster, R. L. Morehouse, N. Zengin, *J. Chem. Soc. Chem. Commun.* **1972**, 307 – 308; b) N. Sonoda, T. Yasuhara, K. Kondo, T. Ikeda, S. Tsutsumi, *J. Am. Chem. Soc.* **1971**, *93*, 6344; c) K. Kondo, N. Sonoda, K. Yoshida, M. Koishi, S. Tsutsumi, *Chem. Lett.* **1972**, 401 – 404; d) J. G. Zajacek, J. J. McCoy, K. E. Fuger, USP 3956360 **1976**.

[9] a) M. Hasan, I. V. Kozhevnikov, M. R. H. Siddiqui, A. Steiner, N. Winterton, *Inorg. Chem.* **1999**, *38*, 5637 – 5641; b) J. S. Wilkes, J. A. Levisky, R. A. Wilson, C. L. Hussey, *Inorg. Chem.* **1982**, *21*, 1263 – 1264.

[10] See the Supporting Information for the ^{1}H NMR data of the transformation reactions of **3a** into **3b**, **3c**, and **3d**.

Spatially Directed Protein Adsorption by Using a Novel, Nanoscale Surface Template**

Patricia Moraille and Antonella Badia*

Phase-separated, ultrathin organic films can serve as surface templates for the selective and patterned deposition of macromolecules on the submicron scale.[1–6] Deposition is generally directed by chemical differences in the domains or domain edges generated by phase separation. We demonstrate herein that a chemically *homogeneous* surface exhibiting solid/fluid-phase coexistence can also be used as an

[*] Prof. A. Badia, P. Moraille
Department of Chemistry, Université de Montréal
C.P. 6128, succursale Centre-ville, Montréal, QC H3C 3J7 (Canada)
Fax: (+1) 514-343-7586
E-mail: antonella.badia@umontreal.ca

[**] This work was supported by the NSERC (Canada), the FCAR (Québec), the CFI (Canada), and the Université de Montréal. A.B. is a Cottrell Scholar of the Research Corporation. P.M. gratefully acknowledges salary support from VRQ-NanoQuébec.

Supporting information for this article is available on the WWW under http://www.angewandte.org or from the author.

 © 2002 WILEY-VCH Verlag GmbH & Co. KGaA, Weinheim 0044-8249/02/4122-4303 $ 20.00+.50/0

adsorption template. This greatly expands the repertoire of template composition and pattern form usable.

The adsorption template used in this study consists of nanoscale, parallel stripes generated by the Langmuir–Blodgett (LB) transfer of a mixed phospholipid monolayer from the air–water (A/W) interface onto a solid substrate.[7] This regular stripe pattern is composed of two saturated dialkylphosphatidylcholines, L-α-dipalmitoylphosphatidylcholine (DPPC) and L-α-dilauroylphosphatidylcholine (DLPC), in different phases.

The adsorption of human serum albumin (HSA) and human γ globulin (HGG) to the DPPC/DLPC monolayers was investigated. These blood-plasma proteins bind to alkylated surfaces either through specific interactions with alkyl-chain binding pockets (HSA) or through hydrophobic interactions (HSA and HGG).[8–11] This study was motivated by the possibility of spatially directing protein adsorption through differences in the alkyl-chain packing density and/or surface energies of the condensed versus fluid phases of mixed phospholipid monolayers.[12,13] We report herein the generation of novel protein and Au nanoparticle/protein patterns based on the selective adsorption of HSA and HGG to the liquidlike phase of the stripe pattern.

Monolayers, formed by the compression of binary mixtures of DPPC and DLPC at the A/W interface, were deposited onto mica by the LB technique. Films were transferred at surface pressures of 15 mN m^{-1} and 32 or 35 mN m^{-1}, which correspond to the liquid-condensed (LC) and solid-condensed (SC) phase of DPPC, respectively.[14] DLPC is in a liquid-expanded (LE) or fluid state at these surface pressures.[15] In the resulting LB films, the phosphocholine headgroups are adsorbed onto the mica and the lipid alkyl chains extend vertically from the surface. The protein solution thus "sees" a surface of alkyl chains terminated with CH_3 groups.

Typical atomic force microscopy (AFM) images of 0.25/0.75 and 0.50/0.50 (mol mol^{-1}) DPPC/DLPC monolayers transferred at 35 mN m^{-1} and 15 mN m^{-1}, respectively, are presented in Figure 1. Parallel stripes (continuous and broken) protrude from the background matrix by ~0.9 nm. The stripes are 160 ± 60 nm wide for 0.25/0.75 DPPC/DLPC and 210 ± 40 nm wide for 0.50/0.50 DPPC/DLPC. Circular domains also coexist with the stripes in the case of 0.25/0.75 DPPC/DLPC deposited at higher surface pressure (Figure 1 A). The stripe formation mechanism has already been reported.[7] The area fraction covered by the stripes and circular domains, the measured step-height differences, and the mechanical responses of the domains observed by AFM phase imaging are consistent with phase separation into condensed DPPC-rich stripes and circles and a liquidlike, DLPC-rich background matrix.[15]

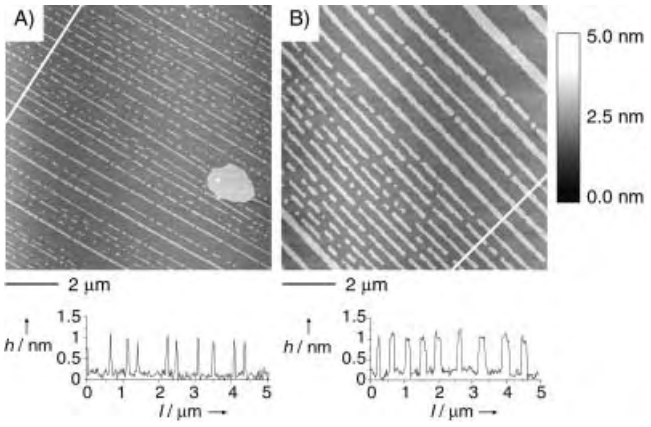


Figure 1. Top: AFM images of monolayers deposited on mica at 20 °C: A) 0.25/0.75 (mol mol^{-1}) DPPC/DLPC, 35 mN m^{-1}; B) 0.50/0.50 (mol mol^{-1}) DPPC/DLPC, 15 mN m^{-1}; right: height scale. Bottom: Height–length profiles (step-heights: A) 0.89 ± 0.10 nm; B) 0.85 ± 0.07 nm).

Figure 2 A shows the 0.25/0.75 DPPC/DLPC monolayer after the adsorption of delipidated HSA. A periodic array of grooves is observed in place of the protruding stripes. This is a result of preferential HSA adsorption to the fluid background matrix. From the higher magnification image shown in Figure 2 B, it can be clearly seen that the adsorbed protein molecules avoid the surface of the solidlike DPPC stripes. HSA adsorption was limited to the LE phase of DLPC by the choice of protein concentration and adsorption time. The mean depth of the grooves (1.7 ± 0.3 nm) and the step-height difference of the 0.25/0.75 DPPC/DLPC stripe pattern (0.89 nm) give a protein-layer thickness of ~2.6 nm. This is consistent with a monolayer of protein adsorbed on the DLPC matrix, given that HSA has the shape of an equilateral triangle with ~8-nm sides and ~3-nm height.[6,16]

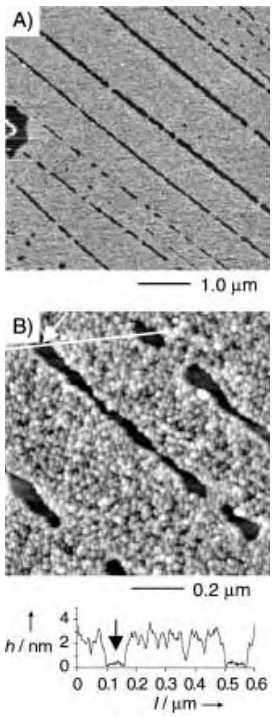


Figure 2. AFM images of HSA adsorbed on a DPPC/DLPC (0.25/0.75) monolayer (35 mN m^{-1}): A) lower and B) higher magnification. Bottom: height–length profile for B). The arrow in B) indicates a "groove". Grooves or depressions are not observed for mixed monolayers exposed to H_2O.[15]

HGG adsorbs primarily to the DLPC matrix of the 0.25/0.75 DPPC/DLPC monolayer (Figure 3 A). In this case, the depth of the grooves is 3.3 ± 0.6 nm. HGG is a Y-shaped protein, 14 nm in width, 10 nm in height, and 4.5 nm in thickness.[17–19] The adsorbed protein-layer thickness (~4.2 nm) deduced from the groove depth therefore suggests that the HGG molecules lie as a flat monolayer on the DLPC matrix.[18,20] The selective adsorption of HGG and its ability to aggregate Au nanoparticles in solution was exploited to direct the surface adsorption of the nanoparticles (Figure 3 B).[21] After nanoparticle (11 ± 3 nm diameter) adsorption to the HGG-covered DLPC matrix, the grooves are visibly narrower. A comparison of the cross-section analyses of Figure 3 A and B reveals an increase in the average groove depth from 3.3 ± 0.6 nm to 12.8 ± 1.5 nm. By comparison, exposure of the DPPC/DLPC monolayer surface to the Au colloid solution resulted in unselective adsorption.[15]

 © 2002 WILEY-VCH Verlag GmbH & Co. KGaA, Weinheim 0044-8249/02/4122-4304 $ 20.00+.50/0 *Angew. Chem. Int. Ed.* **2002**, *41*, No. 22

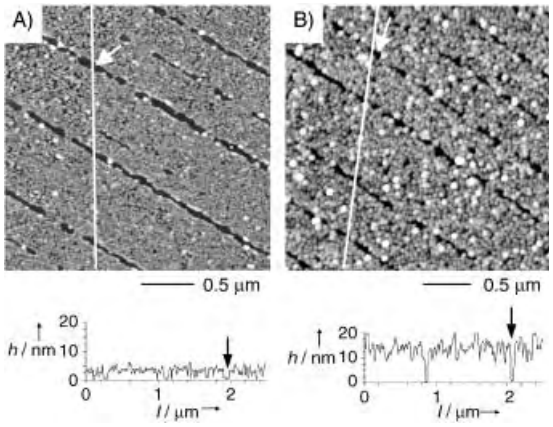


Figure 3. AFM images and height–length profiles of A) HGG adsorbed on a DPPC/DLPC (0.25/0.75) monolayer (35 mN m^{-1}) and B) Au nanoparticles ($d = 11$ nm) adsorbed on the HGG protein pattern (not the same area shown in A)).

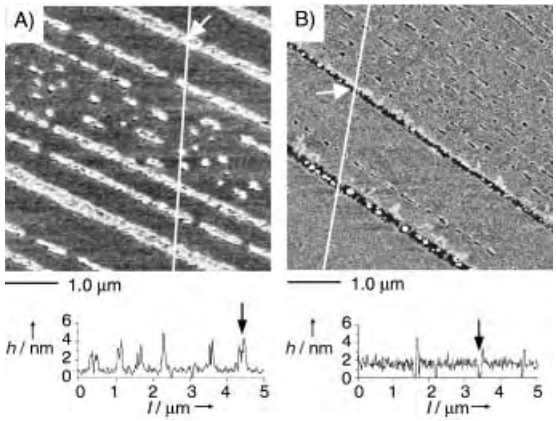


Figure 5. AFM images and height–length profiles of HSA adsorbed on a DPPC/DLPC (0.50/0.50) monolayer deposited at: A) 15 mN m^{-1} and B) 32 mN m^{-1}. The arrows indicate a protrusion in A) and a groove in B).

The adsorption of HSA is sensitive to the phase state of the DPPC stripe domains, but that of HGG is not. This was established in the following way. HSA and HGG adsorption to a 0.50/0.50 DPPC/DLPC monolayer transferred at 15 mN m^{-1} was investigated. Film transfer at this lower surface pressure produces DPPC stripes that are in the more disordered LC state.[12,14,22] Figure 4 shows the monolayer surface after HGG adsorption. HGG is primarily adsorbed to the DLPC matrix. The depth of the grooves is 3.4 ± 0.6 nm, which gives an adsorbed HGG layer thickness of ~4.3 nm. Au nanoparticles also adsorb selectively to the HGG-covered areas.[15] By contrast, HSA adsorbs to the surface of the DPPC stripes (Figure 5A), thus resulting in a step-height difference of 2.8 ± 0.7 nm. If HSA adsorbs to the DPPC stripes and the DLPC background to the same extent, a step-height difference of ~0.9 nm would be expected. The AFM results instead suggest that HSA adsorbs to a greater extent to the LC phase of DPPC.

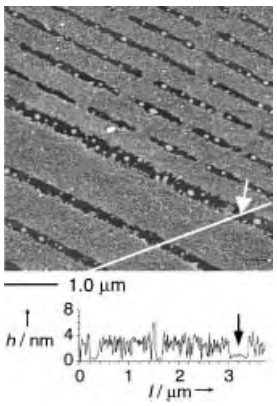


Figure 4. AFM image and height–length profile of HGG adsorbed on a DPPC/DLPC (0.50/0.50) monolayer transferred at 15 mN m^{-1}. The spherical structures present on the DPPC stripes are probably desorbed phospholipid, as these are also observed for the mixed monolayer exposed to H_2O.

For comparison, HSA adsorption to a 0.50/0.50 DPPC/DLPC monolayer deposited at 32 mN m^{-1} was also investigated. In this case, the DPPC domains are in the SC phase. Grooves (2.2 ± 0.3 nm deep) are observed on the monolayer surface after exposure to HSA (Figure 5B). A preferential adsorption of HSA to the LE matrix of DLPC is thus evident.

Overall, these results indicate that the surface adsorption of HSA is determined by the phase state of the template. This behavior can be explained by HSA interacting with the mixed monolayer surface through its alkyl-chain binding pockets. Previous studies report that the affinity and kinetics of HSA adsorption to alkylsilane monolayers are affected by the alkyl-chain packing density; HSA binds more strongly to loosely packed films.[9] This is consistent with the fact that the alkyl-chain packing density of DPPC (~23.2–23.5 Å^2 chain^{-1}) in the SC stripes formed at 32–35 mN m^{-1} prevents HSA from binding to the alkyl chains. HSA does bind to the more disordered LC phase of DPPC (15 mN m^{-1}) because the lower alkyl-chain density (~25 Å^2 chain^{-1}) allows HSA to interact directly with the alkyl chains, and not just with a surface of CH_3 groups.[9] The preferential adsorption of HSA to the LE matrix of DLPC in monolayers transferred at 32 or 35 mN m^{-1} (~29 Å^2 chain^{-1}) is consistent with this direct chain interaction.[20] HSA does not, however, effectively attach itself to the LE phase of DLPC (i.e. submonolayer coverage) when the alkyl chains are too loosely packed (~35 Å^2 chain^{-1} in the 0.50/0.50 DPPC/DLPC film deposited at 15 mN m^{-1}).

On the other hand, HGG adsorbs primarily to the LE phase of DLPC in the range of surface pressures and mixed monolayer compositions investigated in this study. A likely source of this selectivity is the inherent contrast in surface energies between the disordered LE phase of DLPC (~31 mJ m^{-2}) and the ordered LC or SC phases of DPPC (~23 mJ m^{-2}).[13] The preferential adsorption of HGG to the LE matrix of DLPC can be rationalized in terms of binding to the highest-energy sites available.[5,6,19]

In conclusion, we have used the selective adsorption of HSA and HGG to the LC or LE phase of a nanostructured LB monolayer of DPPC and DLPC to generate well-defined protein and Au nanoparticle/protein patterns. Whereas the usual approach to producing patterns and arrays of biomolecules involves chemically differentiated templates, we have shown in a proof-of-concept that patterning can be effected by using the solid/fluid-phase properties of coexisting domains on an organic film surface.

Experimental Section

L-α-DPPC and L-α-DLPC were obtained from Avanti Polar Lipids (>99%). Mixed DPPC/DLPC monolayers were deposited onto freshly cleaved mica by the LB technique, as previously described.[7]

 © 2002 WILEY-VCH Verlag GmbH & Co. KGaA, Weinheim 0044-8249/02/4122-4305 $ 20.00+.50/0

Delipidated HSA (~99%) and HGG (99%) were obtained from Sigma. Aqueous HSA and HGG solutions (0.1 mg mL^{-1}) were adsorbed to the DPPC/DLPC films at 23°C by placing a sufficiently large drop of the protein solution to cover a surface of approximately 1 cm^2. After 15 min, the drop was blown off of the surface by using $N_{2(g)}$.

Au nanoparticles were prepared by the citrate reduction of $HAuCl_4$ (Aldrich).[23] A drop of the 10 nM Au-colloid solution was deposited on the protein-covered monolayer surface. After 5 min, the drop was blown off of the substrate surface. The surface was rinsed with a drop of H_2O and blown dry.

AFM images were acquired in air (relative humidity = 25–30%, T = 21–24°C) by using the tapping mode of a Nanoscope IIIa-MultiMode AFM (Digital Instruments) and etched Si cantilevers (resonance frequency = ~300 kHz, spring constant ~42 N m^{-1}). A cantilever-oscillation amplitude of 60–65 mV and an oscillation damping of 15–25% were used.

Received: June 4, 2002 [Z19447]

[1] M. Goren, R. B. Lennox, *Nano Lett.* **2001**, *1*, 735.
[2] W. A. Hayes, C. Shannon, *Langmuir* **1998**, *14*, 1099.
[3] T. Lee, N. Yao, I. A. Aksay, *Langmuir* **1997**, *13*, 3866.
[4] R. W. Zehner, W. A. Lopes, T. L. Morkved, H. Jaegar, L. R. Sita, *Langmuir* **1998**, *14*, 241.
[5] J. Frommer, R. Lüthl, E. Meyer, D. Anselmetti, M. Dreler, R. Overney, H.-J. Güntherodt, M. Fujihira, *Nature* **1993**, *364*, 198.
[6] J. Fang, C. M. Knobler, *Langmuir* **1996**, *12*, 1368.
[7] P. Moraille, A. Badia, *Langmuir* **2002**, *18*, 4414.
[8] R. H. McMenamy, in *Albumin Structure, Function and Uses* (Eds.: V. M. Rosenoer, O. Murray, M. A. Rothschild), Pergamon, New York, **1977**.
[9] a) S. Petrash, N. B. Sheller, W. Dando, M. D. Foster, *Langmuir* **1997**, *13*, 1881; b) S. Petrash, T. Cregger, B. Zhao, E. Pokidysheva, M. D. Foster, W. J. Brittain, V. Sevastianov, C. F. Majkrzak, *Langmuir* **2001**, *17*, 7645.
[10] V. Silin, H. Weetall, D. J. Vanderah, *J. Colloid Interface Sci.* **1997**, *185*, 94.
[11] S. Kidoaki, T. Matsuda, *Langmuir* **1999**, *15*, 7639.
[12] K. S. Birdi, *Lipid and Biopolymer Monolayers at Liquid Interfaces*, Plenum, New York, **1989**.
[13] C. E. H. Berger, K. O. van der Werf, R. P. H. Kooyman, B. G. de Grooth, J. Greve, *Langmuir* **1995**, *11*, 4188.
[14] J. Hwang, L. K. Tamm, C. Böhm, T. S. Ramalingam, E. Betzig, M. Edidin, *Science* **1995**, *270*, 610.
[15] See Supporting Information.
[16] M. X. He, D. C. Carter, *Nature* **1992**, *358*, 209.
[17] E. D. Day, *Advanced Immunochemistry*, 2nd ed., Wiley-Liss, New York, **1990**.
[18] E. S. Grabbe, *Langmuir* **1993**, *9*, 1574.
[19] A. Baszkin, D. J. Lyman, *J. Biomed. Mater. Res.* **1980**, *14*, 393.
[20] As a result of AFM tip effects and changes in the protein conformation that occur upon adsorption and air drying, other HGG orientations are possible. For these same reasons, it was impossible to estimate the depth of HSA penetration into the lipid domains.
[21] HGG can bind to Au through the asparagine subunits of its antigen-binding fragments or through the many S–S bonds that link its polypeptide chains.[17]
[22] The 0.25/0.75 DPPC/DLPC monolayer is not phase-separated at 15 mN m^{-1}.
[23] K. C. Grabar, R. G. Freeman, M. B. Hommer, M. J. Natan, *Anal. Chem.* **1995**, *67*, 735.

Topochemical Polymerization of 7,7,8,8-Tetrakis(methoxycarbonyl)quinodimethane

Takahito Itoh,* Shinji Nomura, Takahiro Uno, Masataka Kubo, Kazuki Sada, and Mikiji Miyata*

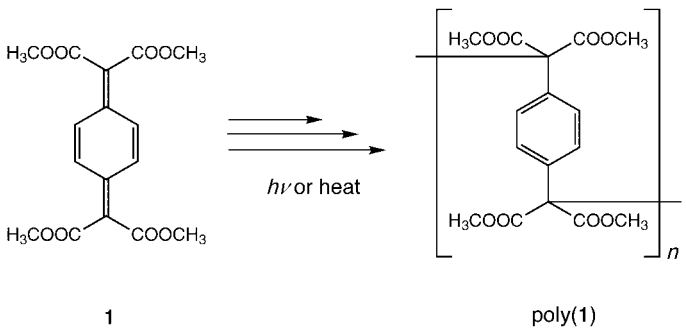
Topochemical polymerization, where the symmetry of the crystal lattice of the monomer is retained after polymerization, leads to a polymer with a highly controlled chemical structure because of the structural restraint imposed by the crystal lattice. This method is promising from the viewpoint of polymer structure control. However, monomers that can be polymerized topochemically are still limited because of the difficulties involved in controlling and predicting their crystal structures. Hasegawa reported topochemical polymerization reactions of 2,5-distyrylpyradine derivatives and related compounds and named them "four-centered photopolymerizations".[1] Topochemical polymerizations of diacetylene derivatives were first reported by Wegner[2] and afterwards a large number of diacetylene derivatives[3] and triacetylene derivatives[4] were prepared and their corresponding polymers were investigated and found to have interesting optical and electronic properties.[5] More recently, Matsumoto et al. found that polymerization reactions of derivatives of muconic acid and derivatives of sorbic acid proceed topochemically.[6] They determined several parameters for the molecular stacking of the diene moieties, and explained the relationship between the topochemical polymerization and monomer packing in crystals for diene monomers.[6] Herein we report that the conjugated monomer 7,7,8,8-tetrakis(methoxycarbonyl)quinodimethane (**1**) can be polymerized topochemically.

The monomer **1** was originally synthesized by Acker and Hertler.[7] They briefly described its properties and noted that it oligomerized on heating or on leaving it to stand at room temperature in diffuse light to give pink materials which were insoluble in common organic solvents. Later, Iwatsuki and Itoh,[8] and Hall and Bentley[9] independently reported the polymerization behavior of **1** in solution. However, the polymer products of **1** were not given much attention and not well characterized because of their insolubility. These factors gave us an indication that **1** may undergo topochemical polymerization (Scheme 1).

The monomer **1** was prepared by a new synthetic route. Knoevenagel condensation of 1,4-cyclohexanedione with methyl malonate using titanium tetrachloride and pyridine as a dehydrating system afforded 1,4-[bis(methoxycarbonyl)-

[*] Prof. Dr. T. Itoh, S. Nomura, Dr. T. Uno, Dr. M. Kubo
Department of Chemistry for Materials
Faculty of Engineering
Mie University
1515 Kamihama-cho, Tsu-shi, Mie 514-8507 (Japan)
Fax: (+81) 59-231-9410
E-mail: itoh@chem.mie-u.ac.jp
Prof. Dr. M. Miyata, Dr. K. Sada
Department of Material and Life Science
Graduate School of Engineering
Osaka University and Handai FRC
2-1 Yamadaoka, Suita, Osaka 565-0871 (Japan)
Fax: (+81) 6-6879-7406
E-mail: miyata@mls.eng.osaka-u.ac.jp

 © 2002 WILEY-VCH Verlag GmbH & Co. KGaA, Weinheim 0044-8249/02/4122-4306 $ 20.00+.50/0



1 poly(1)

Scheme 1. Polymerization of **1**

methylene]cyclohexane (**2**) (59% yield).[10] Oxidation of **2** with activated manganese dioxide in refluxing benzene gave **1** (16% yield). Recrystallization of **1** from *n*-hexane afforded a mixture of two crystal forms, yellow prisms and yellow needles, which indicates that the organic crystals are polymorphic. After many trials to prepare each crystal form separately, we found that recrystallization from chloroform/*n*-hexane (1/3 v/v) yields yellow prisms (**1a**) exclusively and recrystallization from methanol gives yellow needles (**1b**). The two forms of **1** were each subjected to polymerization by irradiation by using a high-pressure Hg lamp at room temperature, or by heating in the dark. When the crystals of **1a** were exposed to UV light at 34°C, or heated at 60°C for 3 h in vacuo, insoluble polymers (poly(**1a**)) formed as off-white crystal-like solids in quantitative and 47% yields, respectively. In contrast, **1b** did not polymerize under either polymerization conditions and **1b** was recovered quantitatively (Table 1) after 6 hours.

Table 1. Thermal polymerization and photopolymerization of **1a** and **1b** in the solid state under vacuum, and thermal polymerization of **1** in benzene.

Entry	Compound	Amount [mg]	Light source	T [°C]	t [h]	Conv. [%]
1	**1a**	52.7	Hg lamp	34	3	100
2	**1a**	54.3	dark,	60	3	47
3	**1b**	23.5	Hg lamp	34	6	0
4	**1b**	22.2	dark	60	6	0
5	**1**[a]	418.9	dark	60	50	13.3

[a] Solution polymerization in benzene, 10 mL; AIBN, 13.5 mg.

The resulting polymers from **1a** were only characterized by IR spectroscopy, elemental analysis, and powder XRD, because of their insolubility in common organic solvents.

A characteristic absorption band at 1540 cm^{-1} assigned to the exocyclic conjugated carbon–carbon double bond of **1a** was absent in the IR spectrum of poly(**1a**), signals arising from carbon-carbon double bonds of the ring were observed at 1492 and 1411 cm^{-1} and a signal arising from out-of-plane deformation of the *para* disubstituted benzene, characteristic of a two-adjacent-hydrogen system, was observed at 811 cm^{-1}.[11] Moreover, the spectrum was identical to that obtained in the solution polymerization of **1** in benzene initiated by 2,2′-azobis[(2-methyl)propanenitrile] (AIBN, Table 1, entry 5). It is well established that polymerization reactions of substituted quinodimethane molecules occur at the disubstituted *exo* methylene carbon atoms with the formation of the corresponding stable aromatic structure.[12] Therefore, the spectrum change observed in the solid-state polymerization of **1a** strongly supports the theory that the reaction of **1a** proceeds with a conventional polymerization mode as observed for substituted quinodimethane molecules.[12] The powder XRD patterns of monomer **1a**, the reaction mixture at 36% conversion, poly(**1a**) obtained by solid state polymerization, and poly(**1**) obtained by solution polymerization are shown in Figure 1.

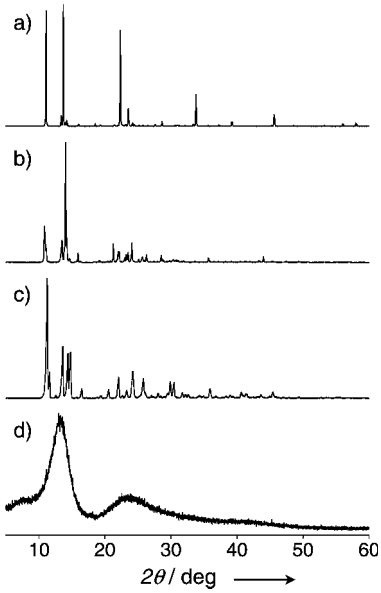


Figure 1. Powder X-ray diffraction patterns of a) monomer **1a**, b) reaction mixture at 36% conversion, c) poly(**1a**) obtained by solid-state polymerization (100% conversion), and d) poly(**1**) obtained by solution polymerization.

The very sharp diffraction patterns of the reaction mixture at 36% conversion, and of poly(**1a**) obtained from the solid-state reaction indicate that **1a** shows no loss of crystallinity during and after completion of the polymerization. Furthermore, signal positions arising from monomer **1a** are in fairly good agreement with those of poly(**1a**). The powder XRD pattern of poly(**1a**) obtained from the solid-state polymerization product is significantly different from that obtained from the solution polymerization product. These points indicate that the polymerization of **1a** proceeds topochemically. To clarify the steric requirement of the topochemical polymerization of the quinodimethane group and the drastic differences between the abilities of **1a** and **1b** to undergo polymerization, we investigated the crystal structures of both forms by X-ray crystallography (Figure 2).[13]

In the crystal structures of **1a** and **1b**, both polymorphs construct a similar one-dimensional columnar structure by the stacking of the quinodimethane rings along the crystallographic *b* axis for **1a** and *c* axis for **1b**, (Figure 3). As the stacking axes are not perpendicular to the molecular plane of the quinodimethane rings, we examined the tilt angles, defined as the angle formed between the stacking axis and longer axis of the monomer molecule (θ_1), and the shorter axis of the monomer molecule (θ_2). In the case of **1a**, θ_1 and θ_2 are

 © 2002 WILEY-VCH Verlag GmbH & Co. KGaA, Weinheim 0044-8249/02/4122-4307 $ 20.00+.50/0

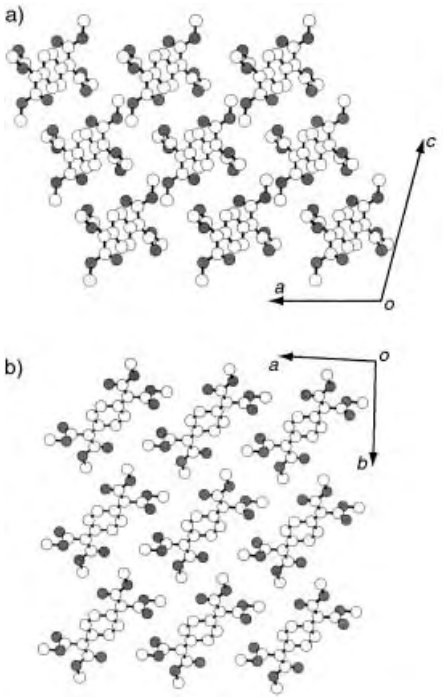


Figure 2. Crystal structures of a) **1a** viewed from the crystallographic *b* axis and b) **1b** viewed from the crystallographic *c* axis. Hydrogen atoms are omitted for clarity. Open and filled circles represent carbon and oxygen atoms, respectively.

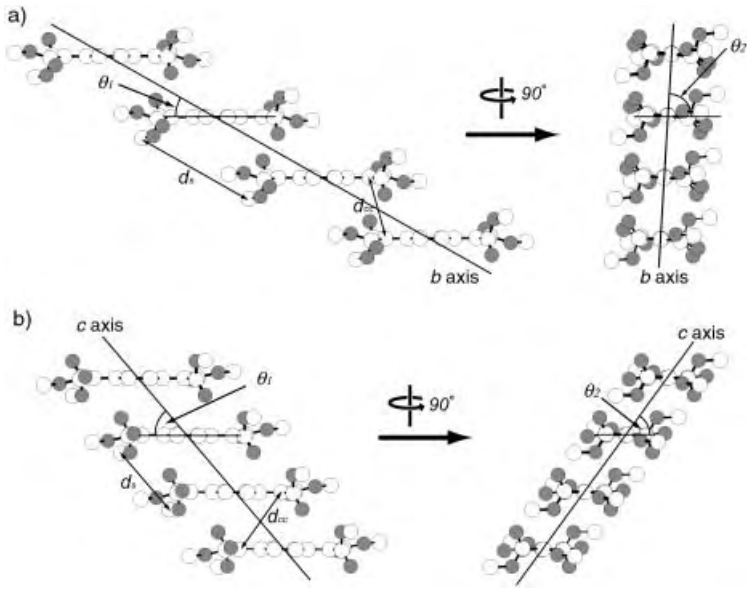


Figure 3. Geometries of **1** in the columns of a) **1a** and b) **1b** viewed from the direction parallel to the quinodimethane plane. Open and filled circles represent carbon and oxygen atoms, respectively.

30° and 89°, respectively. As a consequence of the larger θ_1 value in **1a**, the distance between equivalent atoms in the stacked monomers ($d_s = 7.6$ Å, Figure 3), and the distances between the reacting exomethylene carbon atoms ($d_{cc} =$ 3.9 Å) are elongated. The latter value is similar to those found in the topochemical polymerizations of diacetylene and diene derivatives.[3] The former value can be compared to the translational distance for topochemical 1,6-polymerization of triacetylene derivatives (7.4 Å).[4] From the above points, we conclude that the polymerization reaction occurs along the columnar axis.

The **1b** form has offset stacking of the quinodimethane rings giving values of θ_1 and θ_2 as 55° and 62°, respectively. This gives a shorter stacking distance (d_s) between the quinodimethane moieties ($d_s = 5.3$ Å), and a longer intermolecular distance between the exomethylene carbon atoms ($d_{cc} = 5.0$ Å) than in **1a**. The difference in the polymerization reactivity between **1a** and **1b** indicates that the packing mode of molecules in the crystals significantly affects the polymerization reactivity in the solid state.

In conclusion, we describe the first example of the topochemical polymerization of the quinodimethane-type monomer, and compare the crystal structures of the reactive **1a** polymorph and the non-reactive **1b** polymorph. Detailed studies on the crystal structures and polymerization reactivities of other substituted quinodimethanes are now in progress.

Experimental Section

2: Titanium tetrachloride (20 mL, 183 mmol) in carbon tetrachloride (33 mL) was added dropwise under nitrogen to dry stirred THF (220 mL) cooled in an ice bath. 1,4-Cyclohexanedione (2.28 g, 20.3 mmol) and dimethyl malonate (6.69 g, 50.6 mmol) were added to the yellow mixture. Pyridine (24 mL) in THF (26 mL) was added dropwise to the resulting brown suspension over 1 h, and the reaction mixture was stirred at room temperature for 3 days. Water (150 mL) and chloroform (100 mL) were added to the reaction mixture, then the organic layer was extracted with chloroform (5 × 100 mL). The combined organic fractions were successively washed with saturated aqueous sodium chloride solution (3 × 100 mL), saturated aqueous sodium bicarbonate solution (3 × 100 mL), and dried over anhydrous magnesium sulfate, filtered, and the solvent of the filtrate was evaporated under reduced pressure. The crude product was purified by column chromatography (SiO_2, chloroform/ethyl acetate (20/1 v/v)) followed by recrystallization from a mixture of benzene and hexane to give **2** as white needles (4.11 g, 59.4 %): m.p. 133–134 °C; IR (KBr): $\tilde{\nu} = 2960$ (CH), 1695 (C=O), 1603 (C=C), 1230 (C–O) cm^{-1}; ^1H NMR (270 MHz, $CDCl_3$, TMS): $\delta = 3.78$ (s, 12 H, CH_3), 2.75 ppm (s, 8 H, CH_2); ^{13}C NMR (67.5 MHz, $CDCl_3$, TMS): $\delta = 165.5$ (C=O), 158.4 (=C<), 122.9 (=C<), 52.2 (CH_3), 29.4 ppm (CH_2); elemental analysis calcd (%) for $C_{16}H_{20}O_8$: H 5.92, C 56.47, O 37.61; found: H 5.87, C 55.87, O 38.26.

1: Compound **2** (344 mg, 1.01 mmol) was dissolved in benzene (50 mL) and this solution was added as one portion to activated manganese dioxide (4.09 g, 47.0 mmol) in benzene (300 mL) at reflux. After stirring for 1 min at reflux, the activated manganese dioxide was removed by filtration and the solvent of the filtrate was evaporated under reduced pressure. The crude yellow product was purified by column chromatography (SiO_2, chloroform) followed by recrystallization from hexane to give **1** (52.9 mg, 16 %) as a mixture of yellow prisms (**1a**) and yellow needles (**1b**). **1a**: m.p. ≈110 °C (it was difficult to determine the melting point clearly because of facile polymerization of **1a** at 110 °C), **1b**: m.p. 141.5–143 °C; IR (KBr): $\tilde{\nu} = 2912$ (CH), 1680 (C=O), 1543 (C=C), 1197 (C–O) cm^{-1}; ^1H NMR (270 MHz, $CDCl_3$, TMS): $\delta = 7.45$ ppm (s, 4 H, CH), 3.86 ppm (s, 12 H, CH_3); ^{13}C NMR (67.5 MHz, $CDCl_3$, TMS): $\delta = 165.1$ (C=O), 139.2 (=C<), 130.1 (CH), 125.6 (=C<), 52.7 ppm (CH_3); elemental analysis calcd (%) for $C_{16}H_{16}O_8$: H 4.80, C 57.14, O 38.06; found: H 4.78, C 56.93, O 38.29.

Polymerization: A given amount of **1a** and **1b** (see Table 1) was put in a Pyrex ampoule, which was degassed under reduced pressure and then sealed. Thermal polymerization was carried out by setting the ampoule in an oil bath at 60 °C for a given time. The polymer yield was determined by

 © 2002 WILEY-VCH Verlag GmbH & Co. KGaA, Weinheim 0044-8249/02/4122-4308 $ 20.00+.50/0

gravimetrical analysis after removing the residual **1a** and **1b** with chloroform. Photopolymerization was carried out at 34 °C in vacuo under UV irradiation by using a high-pressure mercury lamp (Fuji Glass Work Type BH-400, 400 W) at a distance of 12 cm. Poly(**1a**): IR (KBr): $\tilde{\nu}$ = 2914 (CH), 1706 (C=O), 1492 (C=C), 1411 (C=C), 1218 (C–O), 811 (CH) cm^{-1}; powder XRD ($Cu_{K\alpha_1}$/40 kV/150 mV, 2θ (relative intensity %): 11.24 (100), 11.62 (23), 13.60 (44), 14.38 (38), 14.78 (39), 16.46 (8), 20.56 (8), 22.06 (18), 23.30 (7), 24.18 (23), 25.80 (17), 29.90 (14), 30.44 (14), 35.94 (8), 40.66 (5), 45.42 (5); elemental analysis calcd (%) for $C_{16}H_{16}O_8$: H 4.80, C 57.14, O 38.06, found: H 4.76, C 56.99, O 38.25.

Received: April 2, 2002
Revised: August 26, 2002 [Z19021]

[1] a) M. Hasegawa, *Chem. Rev.* **1983**, *83*, 507–518; b) M. Hasegawa, *Adv. Phys. Org. Chem.* **1995**, *30*, 117–171.
[2] G. Wegner, *Z. Naturforsch. B* **1969**, *24*, 824–832.
[3] a) G. Wegner, *Pure Appl. Chem.* **1977**, *49*, 443–454; b) V. Enkelmann, *Adv. Polym. Sci.* **1984**, *63*, 91–131; c) T. Ogawa, *Prog. Polym. Sci.* **1995**, *20*, 943–985; d) W. D. Huntsman in *The Chemistry of Functional Groups. Supplement C: The Chemistry of Triple-bonded Functional Groups* (Eds.: S. Patai, Z. Rappoport), Wiley, New York, **1983**, Chap. 22.
[4] a) J. Kiji, J. Kaiser, J. G. Wegner, R. C. Schulz, *Polymer* **1973**, *14*, 433–439; b) V. Enkelmann, *Chem. Mater.* **1994**, *6*, 1337–1340; c) J. Xiao, M. Yang, J. W. Lauher, F. W. Fowler, *Angew. Chem.* **2000**, *112*, 2216–2219; *Angew. Chem. Int. Ed.* **2000**, *39*, 2132–2135.
[5] a) S. Okada, H. Matsuda, H. Nakanishi, in *Polymeric Materials Encyclopedia* (Ed.: J. C. Salamone), CRC, Boca Raton, **1996**, pp. 8393–8398; b) "Polydiacetylenes": D. Bloor, R. R. Chance, *NATO ASI Ser. Ser. E* **1985**, *102*; c) *Nonlinear Optical Properties of Organic Molecules and Crystals* (Eds.: D. S. Chemla, J. Zyss), Academic Press, New York, **1987**.
[6] a) A. Matsumoto, T. Matsumura, S. Aoki, *Macromolecules* **1996**, *29*, 423–432; b) A. Matsumoto, K. Yokoi, S. Aoki, K. Tashiro, T. Kamae, M. Kobayashi, *Macromolecules* **1998**, *31*, 2129–2136; c) A. Matsumoto, T. Odani, M. Chikada, K. Sada, M. Miyata, *J. Am. Chem. Soc.* **1999**, *121*, 11122–11129; d) S. Nagahara, A. Matsumoto, *J. Am. Chem. Soc.* **2001**, *123*, 12176–12181; e) A. Matsumoto, K. Katayama, T. Odani, K. Oka, K. Tashiro, S. Saragami, S. Nakamoto, *Macromolecules* **2000**, *33*, 7786–7792; f) A. Matsumoto, T. Odani, *Macromol. Rapid Commun.* **2001**, *22*, 1195–1215; g) A. Matsumoto, K. Sada, K. Tashiro, M. Miyata, T. Tsubouchi, T. Tanaka, T. Odani, S. Nagahama, T. Tanaka, K. Inoue, S. Saragai, S. Nakamoto, *Angew. Chem.* **2002**, *114*, 2612–2615; *Angew. Chem. Int. Ed.* **2002**, *41*, 2502–2505.
[7] D. S. Acker, W. R. Hertler, *J. Am. Chem. Soc.* **1962**, *84*, 3370–3374.
[8] S. Iwatsuki, T. Itoh, *Macromolecules* **1980**, *13*, 983–989.
[9] H. K. Hall, Jr., J. H. Bentley, *Polym. Bull.* **1980**, *3*, 203–210.
[10] W. Lehnert, *Tetrahedron* **1973**, *29*, 635–638.
[11] D. J. Pasto, C. R. Johnson, *Organic Structure Determinatio*n, Prentice-Hall, Englewood Cliffs, NJ, **1969**.
[12] T. Itoh, *Prog. Polym. Sci.* **2001**, *26*, 1019–1059.
[13] Crystal structure data for **1a** (single crystal from chloroform/hexane): formula $C_8H_8O_4$, M_r = 168.15, crystal dimensions 0.50 × 0.30 × 0.30 mm, monoclinic, space group $P2_1/n$ (no. 14), a = 8.6787(7), b = 7.5719(7), c = 12.761(1) Å, β = 105.193(2)°, V = 809.2(1) Å^3, Z = 4, ρ_{calcd} = 1.380 g cm^{-3}, $2\theta_{max}$ = 55.0°, Rigaku RAXIS-RAPID Imaging Plate diffractometer ($Mo_{K\alpha}$, λ = 0.71069 Å, graphite monochromator), ω scans, T = 303 K, 1828 measured reflections, all 1477 independent reflections used in the refinement, Lorenz and polarization factors were applied, μ = 1.12 cm^{-1}. Structure solution and refinement: direct methods (SIR92), full-matrix least-squares refinement of F^2, 109 parameters, all non-hydrogen atoms were refined anisotropically, and hydrogen atoms were located in the ideal positions without further refinement, R_1 = 0.046, R = 0.106, Rw = 0.133, GOF = 1.273, $\Delta\rho_{max}$ = 0.19 e Å^{-3}, $\Delta\rho_{min}$ = −0.25 e Å^{-3}. Crystal structure data for **1b** (single crystal from methanol): formula $C_8H_8O_4$, M = 168.15, crystal dimensions 2.00 × 0.40 × 0.10 mm, triclinic, space group $P\bar{1}$ (no. 2), a = 8.6023(4), b = 8.889(2), c = 5.2870(6) Å, α = 96.305(4), β = 105.636(5), γ = 87.323(8)°, V = 386.87(9) Å^3, Z = 2, ρ_{calcd} = 1.443 g cm^{-3}, $2\theta_{max}$ = 54.9°, Rigaku RAXIS-RAPID Imaging Plate diffractometer ($Mo_{K\alpha}$, λ = 0.71069 Å, graphite monochromator), ω scans, T = 303 K, 1711 measured reflections, all 1360 independent reflections used in the refinement, Lorenz and polarization factors were applied, μ = 1.12 cm^{-1}. Structure solution and refinement: direct methods (SIR92), full-matrix least-squares refinement of F^2, 109 parameters, all non-hydrogen atoms were refined anisotropically, and hydrogen atoms were located in the ideal positions without further refinement, R_1 = 0.062, R = 0.131, Rw = 0.183, GOF = 1.822, $\Delta\rho_{max}$ = 0.30 e Å^{-3}, $\Delta\rho_{min}$ = −0.33 e Å^{-3}. CCDC-182493 (**1a**) and CCDC-182492 (**1b**) contains the supplementary crystallographic data for this paper. These data can be obtained free of charge via www.ccdc.cam.ac.uk/conts/retrieving.html (or from the Cambridge Crystallographic Data Centre, 12, Union Road, Cambridge CB2 1EZ, UK; fax: (+44) 1223-336-033; or deposit@ccdc.cam.ac.uk).

Spherical Homoaromaticity**

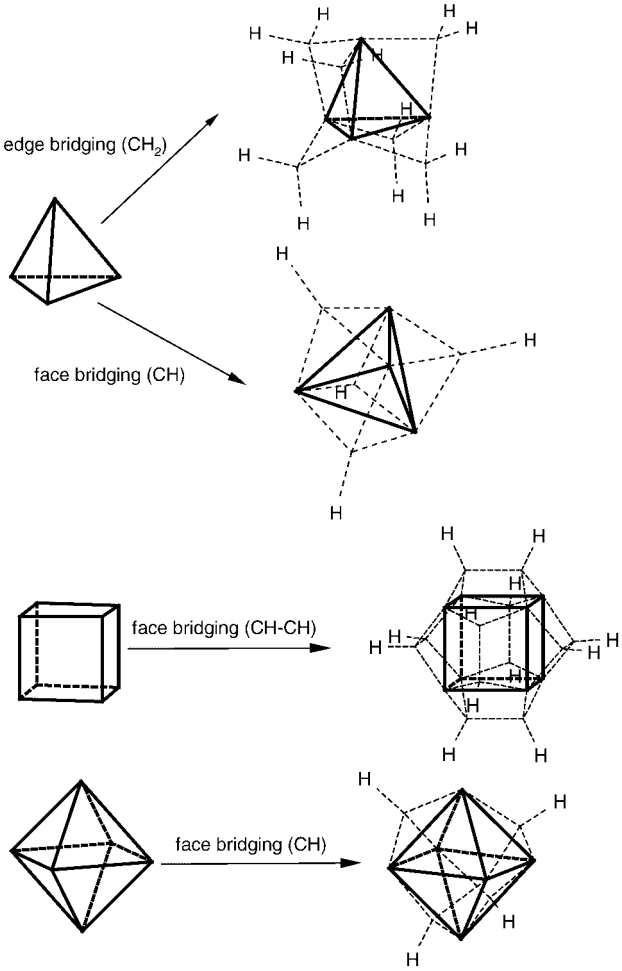
Zhongfang Chen, Haijun Jiao, Andreas Hirsch,* and Paul von Ragué Schleyer*

Since aromaticity[1] is not confined only to planar rings but also exists in three-dimensional systems,[2] the same should be true of homoaromaticity.[3–5] Although the $4N+2$ Hückel electron-counting rule is defined for planar systems it has been applied to rationalize the properties of three-dimensional homoaromatic systems.[5] Recently, the $2(N+1)^2$ counterpart of the Hückel rule[6] has been extended successfully[2e,7,8] to the aromaticity of three-dimensional delocalized systems with near spherical geometries: fullerenes, hydrogen and lithium clusters, as well as some well-known *closo*-boranes and Zintl ions. It was found that the highest degree of aromaticity can only be achieved in systems with fully filled valence shells. We now present new conceptual applications of this electron-counting rule to three-dimensional homoaromatic systems with cubane, dodecahedrane, and adamantane frameworks. Families of spherical homoaromatics with both two and eight mobile electrons (including several neutral

[*] Prof. Dr. A. Hirsch, Prof. Dr. P. von Ragué Schleyer, Dr. Z. Chen
Institut für Organische Chemie
Universität Erlangen-Nürnberg
Henkestrasse 42, 91054 Erlangen (Germany)
Fax: (+49) 9131-85-26864
E-mail: hirsch@organik.uni-erlangen.de
schleyer@chem.uga.edu
Prof. Dr. P. von Ragué Schleyer
Computational Chemistry Annex
The University of Georgia
Athens, GA 30602-2525 (USA)
Fax: (+1) 706-542-7514
Dr. H. Jiao
Department of Chemistry
Shanxi Normal University
Linfen, 041004 (P. R. China)
and
Institut für Organische Katalyseforschung
Universität Rostock e.V.
Buchbinderstrasse 5–6, 18055 Rostock (Germany)

[**] This work was supported by the Alexander von Humboldt Stiftung (Z.C.), the Fonds der Chemischen Industrie, the University of Georgia, and the National Science Foundation (Grant CHE-0209857).

homoaromatic compounds) have been designed and characterized computationally. Each set has complete spherical homoaromaticity, that is, all the sp^2 carbon atoms in the highly symmetrical frameworks are separated by one or two sp^3-hybridized atoms. As shown in Scheme 1, these systems can be constructed by alkyl-bridging of smaller, highly symmetrical carbon cages.



Scheme 1. Construction principles for spherical homoaromatic compounds.

Four-center two-electron systems: Adding six edge-bridging methylene groups to a C_4 tetrahedron gives the adamantane framework. Removal of two electrons leads to the 1,3-dehydro-5,7-adamantanediyl dication ($C_{10}H_{12}^{2+}$, **1**; Figure 1) reported by Schleyer et al.[4] This system represents the three-dimensional four-center two-electron (4c-2e) homoaromatic prototype. A series of isoelectronic charged and neutral 4c-2e species based on this framework also are homoaromatic.[5] Coincidently, both the Hückel rule defined for planar molecules and the $2(N+1)^2$ rule predict the aromaticity of three-dimensional systems with only two π electrons. In addition to the ease of preparation of **1**, its aromaticity was evidenced by magnetic criteria,[4,5] in particular the calculated nucleus-independent chemical shift (NICS)[9] at the cage center: $\delta = -49.5$ ppm in the present work and $\delta = -43.0$ ppm in ref. [5b] determined at a lower level of calculation.

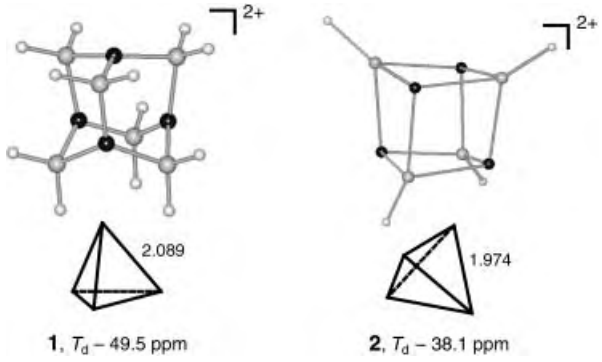


Figure 1. MP2/6-31G* optimized structures and NICS values of **1** and **2** and schematic representation of the inherent sp^2 framework together with the conjugative distance in Å.

Grafting four face-bridging CH groups onto a C_4 tetrahedron results in a cubane framework with isolated sp^2 C atoms at opposite corners (Scheme 1). Removal of two electrons leads to **2** (Figure 1), which is also highly aromatic: the NICS value is $\delta = -38.1$ ppm at the cage center. The homoconjugative C–C bond lengths of 1.974 Å in **2**, which are shorter than those (2.089 Å) in **1**, facilitate the four-center, two-electron (4c-2e) bonding interactions (Figure 1). Replacing tertiary cations in **2** by boron atoms and adding or removing electrons gives the isoelectronic analogues **3**–**6**, which are also characterized as aromatic by their highly negative NICS values (Figure 2).

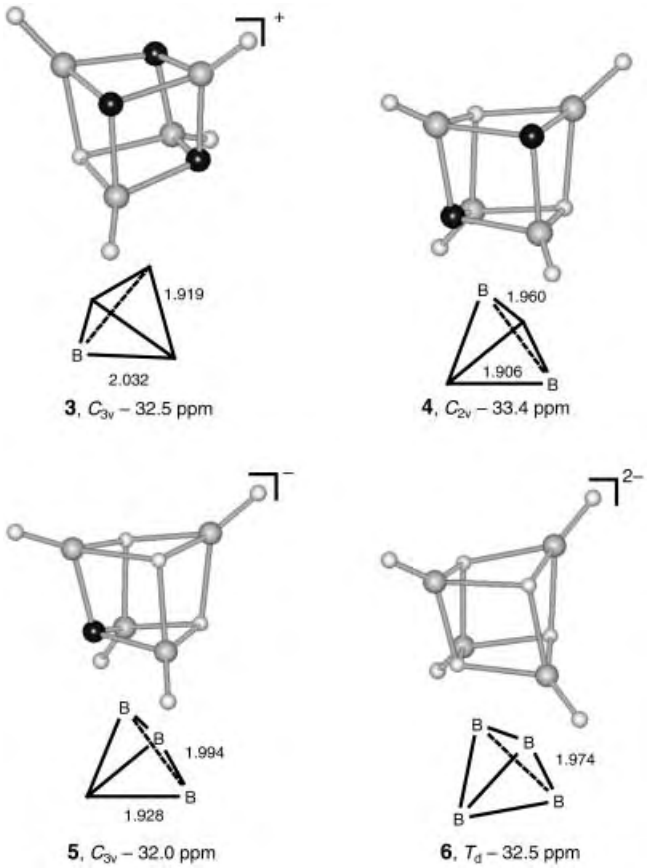


Figure 2. MP2/6-31G* optimized structures and NICS values of **3**–**6** and schematic representation of the inherent sp^2 framework together with the conjugative distance in Å.

 © 2002 WILEY-VCH Verlag GmbH & Co. KGaA, Weinheim 0044-8249/02/4122-4310 $ 20.00+.50/0

Eight-center eight-electron systems: The $4N+2$ Hückel and the $2(N+1)^2$ rules differ when the next level of electron occupancy in spherical systems is considered. The Hückel rule is based upon only double degeneracy being possible in the planar ring. The second set of interacting orbitals is triply degenerate in spherical systems, and a total of eight, rather than six, electrons must be accommodated in closed-shell species. More than four interacting orbitals are required for possible delocalization. We consider here eight-electron systems with both six and eight centers.

Complete face bridging a C_8 cube with six $>CH-CH<$ units (Scheme 1) leads to $C_{20}H_{12}$ (T_h) **7**, which has a dodecahedrane framework. Dodecahedrane ($C_{20}H_{20}$)[10] fascinates both theoretical and experimental chemists because of the aesthetic appeal of its unusually high symmetry (I_h). Symmetrical removal of eight noncontiguous hydrogen atoms also gives **7**, in which the eight sp^2 carbon atoms describe a cube (Figure 3). This neutral eight-center, eight-π-electron

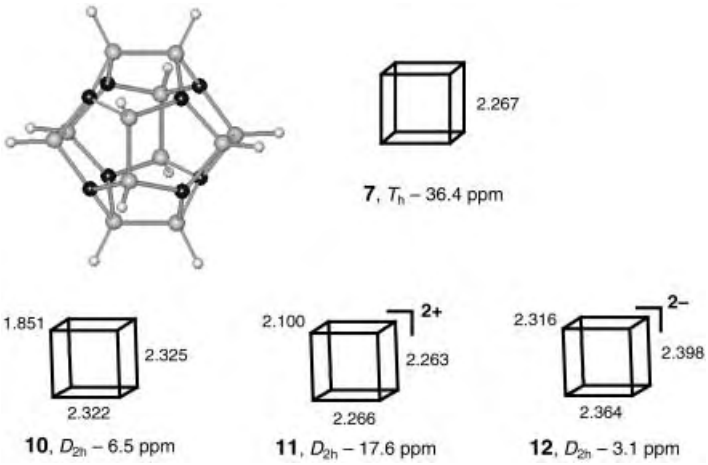


Figure 3. MP2/6-31G* optimized structures and NICS values of $C_{20}H_{12}$ (**7**) and its charged singlet analogues (**9**–**10**) and schematic representation of the inherent sp^2 framework together with the conjugative distance in Å. (For simplicity, only cuboid frameworks of **10**–**12** are given).

(8c-8e) species is highly aromatic as indicated by the NICS value of $\delta = -36.4$ ppm. The homoconjugative distance (2.267 Å) is similar to the partial bond distances computed in typical electrocyclic transition states.[11]

The stabilization energy (SE) of **7** is very large, and can be estimated in various ways. The simplest (and perhaps the best when the number of centers equal the number of mobile electrons) is to compare the energy of the singlet with its much less stable (84.9 kcal mol^{-1}) high-spin nonet state. As expected, **7** is much higher in energy than the classical $C_{20}H_{12}$ dodecahedratetraenes (131.9 and 131.0 kcal mol^{-1} for the two isomers **8** (D_{2h}) and **9** (C_2), respectively;[12] Figure 4), as a result of the bond energy of the four C=C bonds. However, taking 65–70 kcal mol^{-1} to be the π-bond energy range of ethene,[13] the total π-bond energy of **7** would be in the 260–280 kcal mol^{-1} energy range. The energy difference between **7** and **8** or **9** (without the π-bond energy) would be about 128–149 kcal mol^{-1}, thus providing a very rough, but confirming, SE estimate for **7**. This estimate is consistent with its large

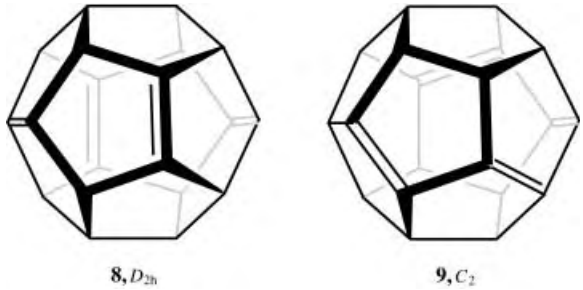


Figure 4. Structures of classical $C_{20}H_{12}$ dodecahedratetraenes **8** and **9**.

NICS value (the NICS(π) value at the center of benzene is −20.7 ppm).[14]

An important point is that direct overlap may not be required for such spherical homoaromaticity. The symmetry of the wavefunction is the key and this does not depend on the separation among the component orbitals. Hoffmann anticipated this long ago with his "through bond coupling."[15]

As a demonstration, the NICS value was computed on $C_{20}H_{12}$ (T_h) using the B3LYP-6-31G* optimized $C_{20}H_{20}$ (I_h) geometry (by just removing the eight hydrogen atoms). The GIAO NICS in the center is −30.1 ppm (not much different from the value of −36.4 ppm found with the optimized geometry) despite the larger C···C separations (2.518 Å), which are too large for effective overlap. Thus, the symmetry is more important than the separations.

Isomer **7** is also 32.3 kcal mol^{-1} more stable than its nonhomoconjugative analogue **10** with a distorted sp^2 carbon framework (D_{2h} symmetry). Thus, **7** is a beautiful example of a neutral spherical homoaromatic system. Removing or adding two electrons to **7** leads to the Jahn–Teller-distorted six- or ten-electron systems, **11** ($C_{20}H_{12}^{2+}$) and **12** ($C_{20}H_{12}^{2-}$), respectively, that conform formally to the $4N+2$ rule. However, according to the NICS criterion **11** and especially **12** are less aromatic than their 8c-8e analogue **7**.

Six-center eight-electron systems: Bridging four non-adjacent delta faces of a carbon octahedron by CH groups (Scheme 1) and removing four electrons leads to the 6c-8e system **13** ($C_{10}H_4^{4+}$; Figure 5). This electron count may not be obvious, but can be understood easily by considering this system in another way. Removal of all twelve methylene hydrogen atoms from adamantane ($C_{10}H_{16}$) leaves six carbene

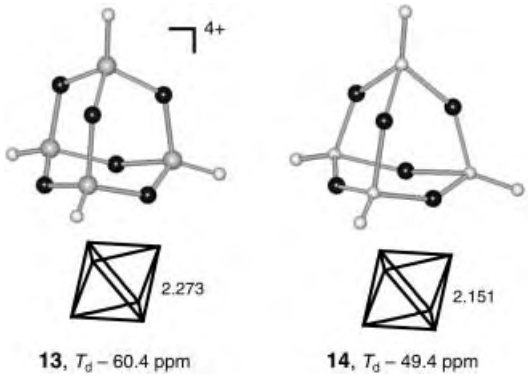


Figure 5. MP2/6-31G* optimized structures and NICS values of **13** and **14** and schematic representation of the inherent sp^2 framework together with the conjugative distance in Å.

 © 2002 WILEY-VCH Verlag GmbH & Co. KGaA, Weinheim 0044-8249/02/4122-4311 $ 20.00+.50/0

centers with twelve electrons; further removal of four electrons leads to tetracation **13** ($C_{10}H_4^{4+}$), which is a 6c-8e system. The eight electrons are delocalized over six centers in overall T_d symmetry. The separation among the six homoconjugating carbon atoms is 2.273 Å, nearly the same as in **7**. The NICS value of −60.4 ppm for **13** is very large, which indicates there is a high degree of electron delocalization (spherical aromaticity). The neutral isoelectronic T_d analogue ($C_6H_4B_4$, **14**) is a more realistic synthetic target than the tetracation **13**. The homoconjugative separation is only 2.151 Å in **14** and the NICS value of $\delta = -49.4$ ppm (Figure 5) illustrates its strong aromaticity.

The homoaromatic character of three-dimensional species arises from their closed π-electron-shell structures. As an example, the closed π shell of **7** is shown in the molecular orbital scheme in Figure 6. Incomplete filling of the shells reduces the aromatic character as in the doubly charged analogues, **11** and **12** (with 6 and 10 electrons, respectively).

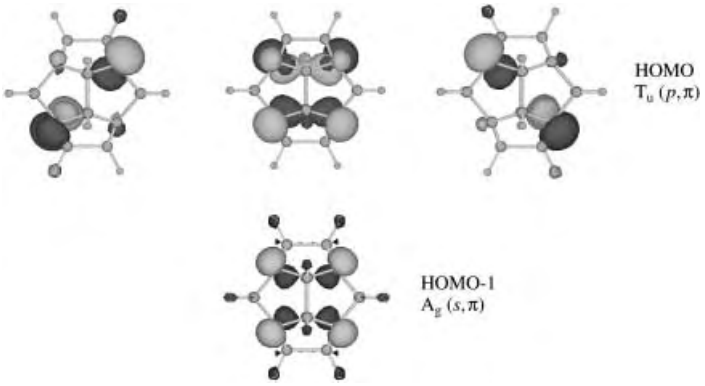


Figure 6. Representation of cluster s and π and p and π orbitals of of $C_{20}H_{12}$ (T_h).

In summary, guided by the $2(N+1)^2$ rule for spherical aromaticity, three-dimensional homoaromatics were designed by bridging sp^2 carbon atoms in highly symmetrical carbon polyhedrane units. After adjusting the number of electrons to two or to eight, the aromaticity is manifested by their highly negative NICS values and reasonable separations among the homoconjugative centers. In particular, the neutral, **4**, **7,** and **14** homoaromatic compounds challenge the synthetic ingenuity of experimental chemists.

Calculations

The geometries reported were optimized at the MP2/6-31G* and B3LYP/6-31G* levels. Vibrational frequencies, computed at the B3LYP/6-31G* level, were all real, and characterized all the stationary points as minima. Nucleus independent chemical shifts (NICS, in ppm),[9] calculated at the centers of the cages by using the GIAO-SCF/6-31G* method on the optimized geometries, were employed to evaluate the mobility of electrons on the cage surfaces. NICS is a well-evaluated criterion of aromaticity.[9] All the calculations were carried out with the Gaussian 98 program.[16]

Received: July 1, 2002 [Z19637]

[1] See the following reviews: a) *Aromaticity and Antiaromaticity. Electronic and Structural Aspects* (Eds.: V. I. Minkin, M. N. Glukhovtsev, B. Y. Simkin), Wiley, New York, **1994**; b) P. von R. Schleyer, H. Jiao, *Pure Appl. Chem.* **1996**, *68*, 209–218; c) special issue on aromaticity *Chem. Rev.* **2001** (guest editor: P. von R. Schleyer).

[2] See the following reviews: a) R. B. King, *Chem. Rev.* **2001**, *101*, 1119–1152; b) P. von R. Schleyer, K. Najafian, *Inorg. Chem.* **1998**, *37*, 3454–3470; c) M. Bühl, A. Hirsch, *Chem. Rev.* **2001**, *101*, 1153–1184; d) H. Jiao, P. von R. Schleyer, M. N. Glukhovtsev, *J. Phys. Chem.* **1996**, *100*, 12299–12304; e) Z. Chen, H. Jiao, A. Hirsch, spherical aromaticity—an overview, in *Fullerenes: From Synthesis to Optoelectronic Applications* (Eds.: D. M. Guldi, N. Martin), Kluwer Academic, in press.

[3] The latest review on homoaromaticity, R. V. Williams, *Chem. Rev.* **2001**, *101*, 1185–1204; for a further reference on neutral trihomoaromaticity, see F. Stahl, P. von R. Schleyer, H. Jiao, H. F Schaefer III, K.-S. Chen, N. L. Allinger, *J. Org. Chem.* **2002**, *67*, 6599–6611.

[4] M. Bremer, P. von R. Schleyer, K. Schoetz, M. Kausch, M. Schindler, *Angew. Chem.* **1987**, *99*, 795–797; *Angew. Chem. Int. Ed. Engl.* **1987**, *26*, 761–763.

[5] a) M. S. W. Chan, D. R. Arnold, *Can. J. Chem.* **1997**, *75*, 192–201; b) A. A. Fokin, B. Kiran, M. Bremer, X. Yang, H. Jiao, P. von R. Schleyer, P. R. Schreiner, *Chem. Eur. J.* **2000**, *6*, 1615–1628; c) G. A. Olah, G. Rasul, G. K. S. Prakash, *J. Org. Chem.* **2000**, *65*, 5956–5959.

[6] A. Hirsch, Z. Chen, H. Jiao, *Angew. Chem.* **2000**, *112*, 4079–4081; *Angew. Chem. Int. Ed.* **2000**, *39*, 3915–3917.

[7] Z. Chen, H. Jiao, A. Hirsch, W. Thiel, *J. Mol. Model.* **2001**, *7*, 161–163.

[8] A. Hirsch, Z. Chen, H. Jiao, *Angew. Chem.* **2001**, *113*, 2916–2920; *Angew. Chem. Int. Ed.* **2001**, *40*, 2834–2838.

[9] a) P. von R. Schleyer, C. Maerker, A. Dransfeld, H. Jiao, N. J. R. van Eikema Hommes, *J. Am. Chem. Soc.* **1996**, *118*, 6317–6318; b) L. Nyulaszi, P. von R. Schleyer, *J. Am. Chem. Soc.* **1999**, *121*, 6872–6875; c) M. K. Cyrañski, T. M. Krygowski, A. R. Katritzky, P. von R. Schleyer, *J. Org. Chem.* **2002**, *67*, 1333–1338; d) S. Patchkovskii, W. Thiel, *J. Mol. Model.* **2000**, *6*, 67–75.

[10] See the following reviews: a) L. A. Paquette, *Chem. Rev.* **1989**, *89*, 1051–1065; b) P. E. Eaton, *Tetrahedron* **1979**, *35*, 2189–2223; c) P. E. Eaton, *Top. Curr. Chem.* **1979**, *79*, 41–165.

[11] See, for example, K. N. Houk, Y. Li, J. D. Evanseck, *Angew. Chem.* **1992**, *104*, 711–739; *Angew. Chem. Int. Ed. Engl.* **1992**, *31*, 682–708.

[12] J. Reinbold, E. Sackers, T. Osswald, K. Weber, A. Weiler, T. Voss, D. Hunkler, J. Worth, L. Knothe, F. Sommer, N. Morgner, B. Von Issendorff, H. Prinzbach, *Chem. Eur. J.* **2002**, *8*, 509–524.

[13] P. von R. Schleyer, D. Kost, *J. Am. Chem. Soc.* **1988**, *110*, 2105–2109.

[14] P. von R. Schleyer, M. Manoharan, Z. X. Wang, B. Kiran, H. Jiao, R. Puchta, N. J. R. van Eikema Hommes, *Org. Lett.* **2001**, *3*, 2465–2468.

[15] a) R. Hoffmann, A. Imamura, W. J. Hehre, *J. Am. Chem. Soc.* **1968**, *90*, 1499–1509; b) W. D. Stohrer, R. Hoffmann, *J. Am. Chem. Soc.* **1972**, *94*, 779–786; c) C. C. Levin, R. Hoffmann, W. J. Hehre, J. Hudec, *J. Chem. Soc. Perkin Trans. 2* **1973**, 210–220.

[16] Gaussian 98, Revision A.11, M. J. Frisch, G. W. Trucks, H. B. Schlegel, G. E. Scuseria, M. A. Obb, J. R. Cheeseman, V. G. Zakrzewski, J. A. Montgomery, Jr., R. E. Stratmann, J. C. Burant, S. Dapprich, J. M. Millam, A. D. Daniels, K. N. Kudin, M. C. Strain, O. Farkas, J. Tomasi, V. Barone, M. Cossi, R. Cammi, B. Mennucci, C. Pomelli, C. Adamo, S. Clifford, J. Ochterski, G. A. Petersson, P. Y. Ayala, Q. Cui, K. Morokuma, D. K. Malick, A. D. Rabuck, K. Raghavachari, J. B. Foresman, J. Cioslowski, J. V. Ortiz, A. G. Baboul, B. B. Stefanov, G. Liu, A. Liashenko, P. Piskorz, I. Komaromi, R. Gomperts, R. L. Martin, D. J. Fox, T. Keith, M. A. Al-Laham, C. Y. Peng, A. Nanayakkara, M. Challacombe, P. M. W. Gill, B. Johnson, W. Chen, M. W. Wong, J. L. Andres, C. Gonzalez, M. Head-Gordon, E. S. Replogle, J. A. Pople, Gaussian, Inc., Pittsburgh, PA, **2001**.

 © 2002 WILEY-VCH Verlag GmbH & Co. KGaA, Weinheim 0044-8249/02/4122-4312 $ 20.00+.50/0

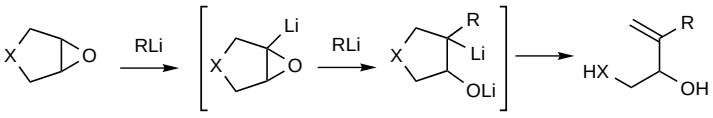
Enantioselective Alkylative Double Ring Opening of Epoxides: Synthesis of Enantioenriched Unsaturated Diols and Amino Alcohols**

David M. Hodgson,* Christopher R. Maxwell, Timothy J. Miles, Edyta Paruch, Matthew A. H. Stent, Ian R. Matthews, Francis X. Wilson, and Jason Witherington

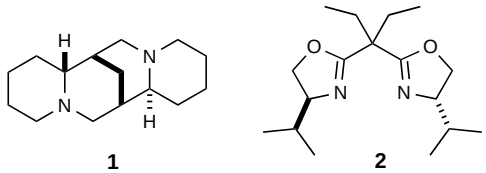
Enantioselective desymmetrization of achiral materials is an attractive and powerful concept in asymmetric synthesis.[1] *meso*-Epoxides represent an important class of substrates for new desymmetrization methodologies,[1,2] and base-induced enantioselective transformations of such epoxides are a focus of current interest.[3,4]

Recently, we showed that epoxides derived from dihydrofuran and dihydropyrrole undergo organolithium-induced alkylative double ring opening, to give acyclic alkenediols and amino alcohols (Scheme 1, X = O or NBus (Bus = *tert*-butylsulfonyl)).[5] Here we report the first example of enantioselective alkylative double ring opening of epoxides, especially the epoxides of oxa- and aza-bicyclic alkenes which lead to enantioenriched cyclic unsaturated diols and amino alcohols.

A preliminary screen of ligands known to mediate asymmetric deprotonations with (or additions of) organolithium compounds[6] was carried out for the reaction of 3,4-epoxytetrahydrofuran with *n*BuLi.[7] This study revealed that (−)-sparteine (**1**) and bisoxazoline **2** (Scheme 2) gave the more encouraging levels of enantioenrichment in the current process (Table 1, entries 1 and 2), an observation which is in line with our previous results on enantioselective epoxide deprotonation/rearrangements.[3,8]



Scheme 1. Alkylative double ring opening of epoxides.



Scheme 2. External chiral ligands used.

When this process was investigated with epoxides derived from oxabicyclo[*n*.2.1]alkenes (*n* = 2, 3),[9] we were pleased to observe the formation of cycloalkenediols. The best results, with *n*BuLi and *i*PrLi (up to 85 % *ee*), were generally obtained when the reaction was conducted with **1** as the external ligand (entries 3–13). The method provides a new access to substituted cyclohexenediols (entries 3–7), arenediols (entries 8–10), and cycloheptenediols (entries 11–13), and in an enantioenriched form.

The product distribution arising from the alkylative double ring opening of 3,4-epoxytetrahydropyrroles (Scheme 1) was previously found to be dependant on the nitrogen protecting group.[5b] In the current study, the use of the Bus protecting group[10] was again found to result in superior yields of the amino alcohol (in comparison to using Boc (Boc = *tert*-butyloxycarbonyl) protection) in the ligand-mediated process (Table 2, entries 1–4). However, significantly better results were observed through the use of Boc protection for epoxides derived from 7-azabicyclo[2.2.1]hept-2-ene (Table 2, entries 5–7).

The reaction of further Boc-protected azabicyclo[*n*.2.1]alkene-derived epoxides (*n* = 2, 3) with *n*BuLi or *i*PrLi in the presence of either **1** or **2** gave the corresponding amino cycloalkenols in generally good yields and *ee* values (Table 2, entries 7–17).[11] Noteworthy is the introduction of the versatile allylsilane functionality (Table 2, entries 18–19), which is best effected using a mixed organolithium system.

Enantioselective nucleophilic ring opening of unsaturated oxa- and (to a lesser extent) aza-bicyclic compounds, which is principally being developed by Lautens et al.,[12] results in cycloalkenes bearing the nucleophile in an allylic position. The results described herein represent, to the best of our knowledge, the first enantioselective generation–intermolecular nucleophilic trapping of a lithium carbenoid[13] (see Scheme 1). The reaction proceeds by double ring opening and comprises an intermolecular C–C bond-forming reaction with cogeneration of unsaturation and two functional group reorganizations, which leads to nucleophile incorporation at a vinylic position as well as synthetically valuable 1,2-diol and 1,2-amino alcohol functionality. The method provides a new and enantioselective access to sought-after cyclic unsaturated diols and amino alcohols[14] in a regio-, stereo-, and enantiocontrolled fashion, and thus has the potential to be a powerful method for organic synthesis.

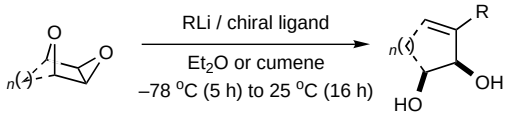
[*] Dr. D. M. Hodgson, C. R. Maxwell, T. J. Miles, Dr. E. Paruch, M. A. H. Stent
Dyson Perrins Laboratory
Department of Chemistry, University of Oxford
South Parks Road, Oxford, OX1 3QY (UK)
Fax: (+44) 1865–275–674
E-mail: david.hodgson@chem.ox.ac.uk
Dr. I. R. Matthews
Syngenta
Jealott's Hill International Research Centre
Berkshire, RG42 6EY (UK)
Dr. F. X. Wilson
Roche Discovery (Welwyn)
40 Broadwater Road, Welwyn Garden City, Herts, AL7 3AY (UK)
Dr. J. Witherington
GlaxoSmithKline
New Frontiers Science Park
Third Avenue, Harlow, Essex, CM19 5AW (UK)

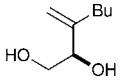
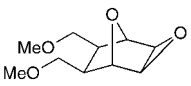
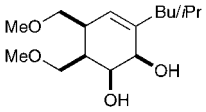
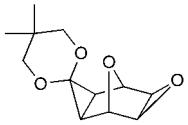
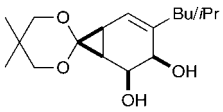
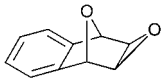
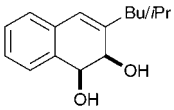
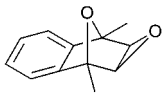
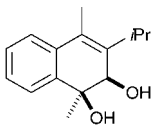
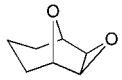
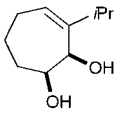
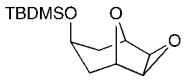
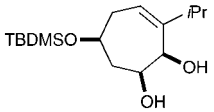
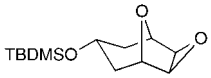
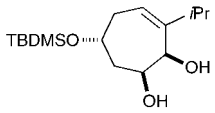
[**] We thank the EPSRC for a Research Grant (GR/M72340), Syngenta (C.R.M.), GlaxoSmithKline (T.J.M.), and Roche (M.A.H.S.) for CASE awards, the European Community for a Marie Curie Fellowship (E.P.; program TMR under contract number HPMF-CT-2000–00560), and the EPSRC National Mass Spectrometry Service Centre for providing mass spectra.

Supporting information for this article is available on the WWW under http://www.angewandte.org or from the author.

 © 2002 WILEY-VCH Verlag GmbH & Co. KGaA, Weinheim 0044-8249/02/4122-4313 $ 20.00+.50/0

Table 1. Formation of enantioenriched diols.



Entry[a]	Epoxide	RLi/ligand	Product[b]	Yield [%][c]	*ee* [%][d]
1		*n*BuLi/**1**		16	43
2		*n*BuLi/**2**		44	−42
3		*n*BuLi/**1**		46	34
4		*n*BuLi/**2**		34	−40
5		*i*PrLi/**1**		34	63
6		*n*BuLi/**2**		57	27
7		*i*PrLi/**1**		49	59
8		*n*BuLi/**2**		50	51
9		*i*PrLi/**1**		44	74
10		*i*PrLi/**2**		42	56
11		*i*PrLi/**1**		44	85
12		*i*PrLi/**1**		46	69
13		*i*PrLi/**1**		54	84

[a] Entries 1–10 carried out in Et_2O; entries 11–13 carried out in cumene. [b] Absolute configuration of predominant enantiomer obtained with (−)-sparteine (**1**) is shown (assigned by analogy with the sense of asymmetric induction in deprotonations of other *meso*-epoxides).[3] Bisoxazoline **2** preferentially produced the opposite configuration. [c] Yield of isolated product. [d] Determined by HPLC on a chiral stationary phase. TBDMS = *tert*-butyldimethylsilyl.

Experimental Section

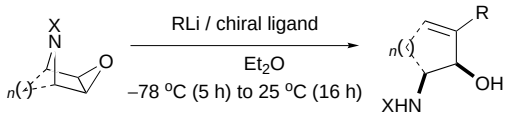
Typical procedure for enantioselective alkylative double ring-opening reaction (Table 2, entry 7): *i*PrLi (1.4 M in petroleum ether, 3.0 mL, 4.1 mmol) was added dropwise to a solution of (−)-sparteine (**1**; 0.95 mL, 4.1 mmol) in Et_2O (4 mL) at −78 °C. After stirring the mixture at −78 °C for 1 h, a solution of *N*-*tert*-butyloxycarbonyl-3-oxa-8-azatricyclo[3.2.1.0^{2,4}]octane[11] (0.25 g, 1.2 mmol) in Et_2O (10 mL) was added dropwise. The mixture was stirred at −78 °C for 5 h and then allowed to warm to 25 °C over 16 h. 1.0 M HCl (10 mL) was added and the aqueous layer extracted with Et_2O (3 × 20 mL). The combined organic layers were dried ($MgSO_4$), filtered, and concentrated under reduced pressure. Purification of the residue by column chromatography (SiO_2, Et_2O/petroleum ether (1/1)) gave *N*-*tert*-butyloxycarbonyl-6-amino-2-isopropylcyclohex-2-enol as a white solid (0.24 g, 78%); R_f: 0.22 (Et_2O/petroleum ether (1/1)); m.p. 77.5–80.5 °C (Et_2O/petroleum ether). Elemental analysis calcd (%) for $C_{14}H_{25}NO_3$: C 65.85, H 9.9, N 5.5; found: C 65.8, H 9.8, N 5.5. $[\alpha]_D^{24}$ −65 (c = 1.00 in $CHCl_3$) IR (KBr): 3437, 2960, 1691, 1501, 1367 cm^{-1}; ^{1}H NMR($CDCl_3$, 500 MHz): δ = 5.56 (t, J = 3.5 Hz, 1H), 5.15 (d, J = 8.0 Hz, 1H), 4.03 (d, J = 2.5 Hz, 1H), 3.62–3.58 (m, 1H), 2.38 (sept., J = 6.5 Hz, 1H), 2.19–2.08 (m, 2H), 1.81–1.69 (m, 1H), 1.60–1.51 (m, 1H), 1.45 (s, 9H), 1.06 (d, J = 7.0 Hz, 3H), 1.03 (d, J = 7.0 Hz, 3H); ^{13}C NMR($CDCl_3$, 125 MHz): δ = 155.5, 144.1, 122.9, 79.2, 67.0, 50.8, 32.1, 28.4, 24.7, 22.9, 22.6, 21.6; *m/z* (CI) 256 [M^++H^+], 5%), 156 (5), 138 (100); The *ee* value was determined to be 87% by HPLC on a chiral stationary phase (Chiralpak AD column, EtOH/hexane (1:1), flow rate 1.0 mL min^{-1}, retention times 4.0 min (major) and 10.0 min (minor)) following derivatization as the 2,4-dinitrobenzoate.

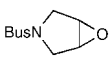
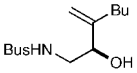
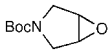
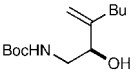
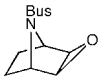
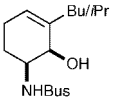
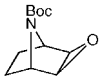
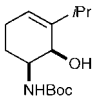
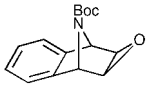
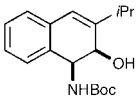
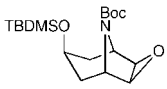
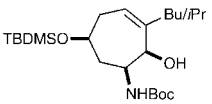
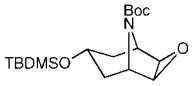
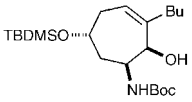
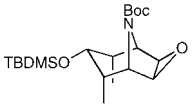
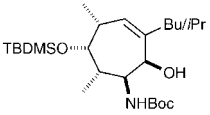
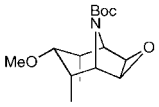
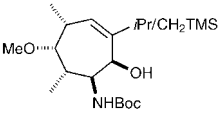
Received: July 15, 2002 [Z19728]

[1] M. C. Willis, *J. Chem. Soc. Perkin Trans. 1* **1999**, 1765 – 1784.
[2] a) E. Schoffers, A. Golebiowski, C. R. Johnson, *Tetrahedron* **1996**, *52*, 3769 – 3826; b) E. N. Jacobsen, *Acc. Chem. Res.* **2000**, *33*, 421 – 431.
[3] a) D. M. Hodgson, A. R. Gibbs, G. P. Lee, *Tetrahedron* **1996**, *52*, 14361 – 14384; b) D. M. Hodgson, I. D. Cameron, M. Christlieb, R. Green, G. P. Lee, L. A. Robinson, *J. Chem. Soc. Perkin Trans. 1* **2001**,

 © 2002 WILEY-VCH Verlag GmbH & Co. KGaA, Weinheim 0044-8249/02/4122-4314 $ 20.00+.50/0

Table 2. Formation of enantioenriched amino alcohols.



Entry[a]	Epoxide	RLi/ligand	Product[b]	Yield [%][c]	*ee* [%][d]
1		*n*BuLi/**1**		69	24
2		*n*BuLi/**2**		79	–45
3		*n*BuLi/**1**		25	45
4		*n*BuLi/**2**		0	–
5		*n*BuLi/**1**		52	40
6		*i*PrLi/**1**		42	64
7		*i*PrLi/**1**		78	87
8		*i*PrLi/**1**		44	71
9		*n*BuLi/**1**		83	41
10		*n*BuLi/**2**		60	–67
11		*i*PrLi/**1**		59	65
12		*n*BuLi/**1**		68	79
13		*n*BuLi/**1**		84	66
14		*n*BuLi/**2**		71	–67
15		*i*PrLi/**1**		85	71
16		*i*PrLi/**2**		72	–75
17		*i*PrLi/**1**		69	82
18		$TMSCH_2Li$/**1**		61	57
19		mixed[e]/**1**		66[f]	64

[a] Quenched at 25 °C, apart from entries 9–11 and 18, 19 (–5 °C), entry 12 (–78 °C), entries 13–16 (–30 °C), and entry 17 (–50 °C). [b] See Table 1 footnote [b]. [c] Yield of isolated product. [d] Determined by HPLC or GC on a chiral stationary phase. [e] *i*PrLi (1.1 equiv) and $TMSCH_2Li$ (2.5 equiv). [f] Allylsilane major product, 7 % of *i*Pr incorporation additionally observed. TMS = trimethylsilyl.

2161 – 2174; c) for a recent review, see D. M. Hodgson, E. Gras, *Synthesis*, **2002**, 1625 – 1642.

[4] D. M. Hodgson, E. Gras, *Angew. Chem.* **2002**, *114*, 2482 – 2484; *Angew. Chem. Int. Ed.* **2002**, *41*, 2376 – 2378.

[5] a) D. M. Hodgson, M. A. H. Stent, F. X. Wilson, *Org. Lett.* **2001**, *3*, 3401 – 3403; b) D. M. Hodgson, T. J. Miles, J. Witherington, *Synlett* **2002**, 310 – 312; c) D. M. Hodgson, M. A. H. Stent, F. X. Wilson, *Synthesis* **2002**, 1445 – 1453.

[6] For reviews, see a) K. Tomioka, *Synthesis* **1990**, 541 – 549; b) D. Hoppe, T. Hense, *Angew. Chem.* **1997**, *109*, 2376 – 2410; *Angew. Chem. Int. Ed. Engl.* **1997**, *36*, 2282 – 2316; c) A. Basu, S. Thayumanavan, *Angew. Chem.* **2002**, *114*, 740 – 763; *Angew. Chem. Int. Ed.* **2002**, *41*, 716 – 738.

[7] Full details will be reported in due course.

[8] D. M. Hodgson, C. R. Maxwell, I. R. Matthews, *Tetrahedron: Asymmetry* **1999**, *10*, 1847 – 1850.

[9] The epoxides in Table 1 are known (entries 1 and 2: P. L. Barili, G. Berti, E. Mastrorilli, *Tetrahedron* **1993**, *49*, 6263 – 6276; entries 8 and 9: L. G. French, T. P. Charlton, *Heterocycles* **1993**, *35*, 305 – 313; entry 10: L. G. French, E. E. Fenlon, T. P. Charlton, *Tetrahedron Lett.* **1991**, *32*, 851 – 854), prepared from the known alkenes (entries 4–7: M. Nakamura, A. Hirai, E. Nakamura, *J. Am. Chem. Soc.* **2000**, *122*, 978 – 979), or derived from 8-oxabicyclo[3.2.1]oct-6-en-3-one (entries 11–13: H. Kim, H. M. R. Hoffmann, *Eur. J. Org. Chem.* **2000**, 2195 – 2201).

[10] P. Sun, S. M. Weinreb, M. Y. Shang, *J. Org. Chem.* **1997**, *62*, 8604 – 8608.

[11] The epoxides in Table 2 are known (entries 1–4,[5b] 7: D. M. Hodgson, C. R. Maxwell, R. M. Wisedale, I. R. Matthews, K. J. Carpenter, A. H. Dickenson, S. Wonnacott, *J. Chem. Soc. Perkin Trans. 1* **2001**, 3150 – 3158), prepared by analogy (entries 5–6 similar to entry 7), derived from the known alkene (entry 8: L. A. Carpino, R. E. Padykula, D. E.

 © 2002 WILEY-VCH Verlag GmbH & Co. KGaA, Weinheim 0044-8249/02/4122-4315 $ 20.00+.50/0

Barr, F. H. Hall, J. G. Krause, R. F. Dufresne, C. Thomas, *J. Org. Chem.* **1988**, *53*, 2565 – 2572), or derived from the corresponding alkenylketones (entries 10–19: J.-L. Paparin, C. Crevisy, L. Toupet, R. Grée, *Eur. J. Org. Chem.* **2000**, 3909 – 3918).

[12] a) M. Lautens, C. Gajda, P. Chiu, *J. Chem. Soc. Chem. Commun.* **1993**, 1193 – 1194; b) P. Chiu, M. Lautens, *Top. Curr. Chem.* **1997**, *190*, 1 – 85; c) M. Lautens, C. Dockendorff, K. Fagnou, A. Malicki, *Org. Lett.* **2002**, *4*, 1311 – 1314.

[13] G. Boche, J. C. W. Lohrenz, *Chem. Rev.* **2001**, *101*, 697 – 756.

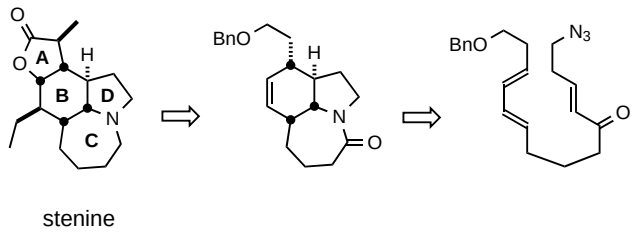
[14] S. C. Bergmeier, *Tetrahedron* **2000**, *56*, 2561 – 2575.

A Combined Intramolecular Diels–Alder/ Intramolecular Schmidt Reaction: Formal Synthesis of (±)-Stenine**

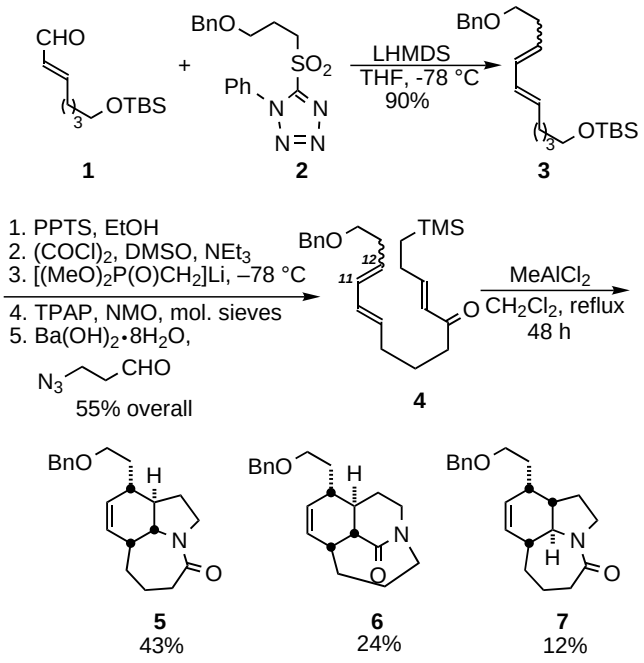
Jennifer E. Golden and Jeffrey Aubé*

One hallmark of an attractive synthetic strategy is the efficient assembly of advanced intermediates. One way of achieving this goal has been the development of cascade reactions.[1] An objective of this laboratory has been to advance the utility of the intramolecular Schmidt reaction of azides and ketones in total synthesis.[2] Herein, we describe the combination of an intramolecular Schmidt reaction with an intramolecular Diels–Alder process—two efficient reactions that benefit from Lewis-acid promotion. The specific context of this work is the formal total synthesis of stenine, shown retrosynthetically in Scheme 1.

Stenine and related alkaloids[3–11] have drawn considerable attention from synthetic chemists, partly because of the historical use of root extracts of stemonaceous plants in Japanese and Chinese folk medicine.[6] Efforts in this area have already culminated in four total syntheses of stenine by teams led by Hart,[7] Wipf,[8] Morimoto,[9] and, most recently, Padwa.[10] The first three of these syntheses feature the stepwise construction of the ABD ring substructure followed by final formation of the C ring. Additionally, routes developed by Hart and Morimoto utilize a Diels–Alder reaction as the key step, and both subsequently implement a Curtius rearrangement to install a nitrogen atom adjacent to the carbonyl group. While the present work was in progress, Jung and co-workers[11] published a partial synthesis, in which a Diels–Alder reaction similar to that shown in Scheme 1 was used, followed by a four-step Beckmann rearrangement/N-alkylation sequence to form the BCD ring skeleton. We now report an approach in which all three rings of a key intermediate and four of the stereocenters were formed in a single chemical step beginning with the acyclic precursor **4** (Scheme 2).



Scheme 1. Retrosynthesis of (±)-stenine.



Scheme 2. Construction of the ABD-ring framework of stenine. TBS = *tert*-butyldimethylsilyl, LHMDS = lithium bis(trimethylsilyl)amide, PPTS = pyridinium 4-toluenesulfonate, TPAP = tetrapropylammonium perruthenate, NMO = 4-methylmorpholine *N*-oxide.

The cascade reaction substrate **4** was prepared by using standard methodology (Scheme 2). Diene **3** was generated in 90% yield from a modified Julia coupling[12] between aldehyde **1** and sulfone **2** to afford an inseparable 85:15-mixture of isomers at the new double bond.[13] Removal of the silyl group of **3**, followed by Swern oxidation, gave an aldehyde that was treated with the lithium anion of dimethyl methylphosphonate. This provided a β-hydroxyphosphonate that was subsequently oxidized with TPAP/NMO. The resulting β-oxophosphonate was subjected to a Horner–Wadsworth–Emmons reaction[14] with 3-azidopropanal[15] to afford triene **4** in 55% yield from **3**.

Treatment of **4** with $MeAlCl_2$ in refluxing dichloromethane afforded tricyclic lactams **5**, **6**, and **7** in 79% overall yield and

[*] Prof. Dr. J. Aubé
University of Kansas, Department of Medicinal Chemistry
Malott Hall, 1251 Wescoe Hall Drive, Room 4070
Lawrence, KS 66045-2506 (USA)
Fax: (+1) 785-864-5326
E-mail: jaube@ku.edu

Dr. J. E. Golden
Stanford University, Department of Chemistry
Stanford, CA 94305 (USA)

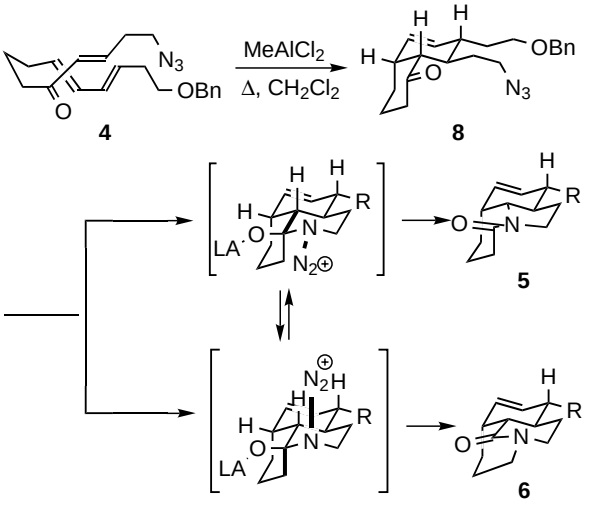
[**] Financial support was provided by the National Institutes of Health (grant GM-49093). J.E.G. gratefully acknowledges the Madison A. and Lila Self Fellowship Program for its support. The authors also thank Dr. David Vander Velde for NMR assistance and Dr. Doug Powell for crystallographic data.

Supporting information for this article is available on the WWW under http://www.angewandte.org or from the author.

 © 2002 WILEY-VCH Verlag GmbH & Co. KGaA, Weinheim 0044-8249/02/4122-4316 $ 20.00+.50/0

a ratio of 3.6:2:1, respectively. As expected (see below), the major diastereomer, **5**, has the stereochemistry required for the stenine synthesis. The structures of lactams **5** and **7** were confirmed by X-ray crystallographic analysis of the corresponding debenzylated derivatives. We assign the unusual bridged lactam structure to compound **6** based on ^{13}C NMR chemical shifts (the signal of the carbonyl group of **6** appears at $\delta = 188$ ppm vs. $\delta = 171$–175 ppm for compounds **5** and **7**) and a $\tilde{\nu}_{C=O}$ value of 1690 cm^{-1} (cf. $\tilde{\nu} = 1625$–1600 cm^{-1} for **5** and **7**). These data are consistent with considerable loss of conjugation between the nitrogen lone pair and the carbonyl group in the twisted amide linkage and are in agreement with data of similar bridged lactams.[16] Additionally, this structure is consistent with the 2D NMR spectrum of **6**.

Both **5** and **6** are proposed to result from a single Diels–Alder adduct **8** via an *endo* transition state (Scheme 3).[17] The azide can then add to the Lewis acid coordinated ketone.

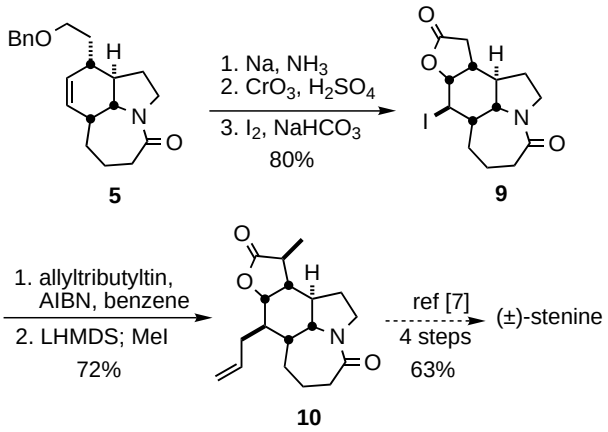


Scheme 3. Domino reaction of **4** consisting of a Diels–Alder reaction and an intramolecular Schmidt reaction to give **6**. LA = Lewis acid.

Assuming *anti*-periplanar C→N bond migration,[18] an intermediate containing an equatorial N_2^+ group en route to lactam would afford lactam **5**, whereas an axially oriented leaving group would give the bridged compound **6**. Formation of bridged lactams has not been observed previously in an intramolecular Schmidt reaction, although an analogous case was recently observed in a ketal-mediated reaction.[2d] Lactam **7** results from an *exo* transition state in the Diels–Alder cyclization, followed by the D-ring-forming/C-ring-expansion process.

We could affect modest changes in product distribution by modifying the Lewis acid and the reaction conditions, but the overall yield of 43% for **5** is reproducible and the most favorable result to date. In the context of the inseparable 85:15 mixture of 11,12-double bond stereoisomers of **4**, this yield corresponds to an overall conversion of the reactive *trans-trans* triene isomer to **5** of 51%.

The formal synthesis was finished as shown in Scheme 4. Removal of the benzyl ether from **5**, oxidation of the resulting hydroxy group, and iodolactonization gave butyrolactone **9** in



Scheme 4. Elaboration of **5** to give compound **10**, an intermediate in the synthesis of (±)-stenine by Hart and Chen.[7] AIBN = 2,2′-azobisisobutyronitrile.

80% yield from **5**. Keck allylation[19] followed by methylation[20] of the lactone proceeded stereoselectively to provide Hart intermediate **10** in 72% yield over two steps. All spectroscopic and physical data of compound **10** were in agreement with the published data.[7]

In summary, we have completed a formal synthesis of (±)-stenine by using a domino Diels–Alder/Schmidt reaction strategy. Our route affords advanced intermediate **10** in 12 steps and in 12% overall yield from **1**. We are currently streamlining this overall approach and applying it to the synthesis of other *stemona* alkaloids.[21]

Received: May 29, 2002 [Z19405]

[1] For reviews of domino processes in organic synthesis, see: a) L. F. Tietze, U. Beifuss, *Angew. Chem.* **1993**, *105*, 137–170; *Angew. Chem. Int. Ed. Engl.* **1993**, *32*, 131–163; b) R. A. Bunce, *Tetrahedron* **1995**, *51*, 13103–13159; c) K. Neuschuetz, J. Velker, R. Neier, *Synthesis* **1998**, 227–255; d) P. J. Parsons, C. S. Penkett, A. Shell, *Chem. Rev.* **1996**, *96*, 195–206; e) H. Waldmann, *Organic Synthesis Highlights II*, Wiley-VCH, Weinheim, **1995**, pp. 193–202; f) L. F. Tietze, *Chem. Rev.* **1996**, *96*, 115–136; g) L. F. Tietze, A. Modi, *Med. Res. Rev.* **2000**, *20*, 304–322.

[2] a) J. Aubé, G. L. Milligan, *J. Am. Chem. Soc.* **1991**, *113*, 8965–8966; b) J. Aubé, P. S. Rafferty, G. L. Milligan, *Heterocycles* **1993**, *35*, 1141–1147; c) G. L. Milligan, C. J. Mossman, J. Aubé, *J. Am. Chem. Soc.* **1995**, *117*, 10449–10459; d) R. Iyengar, K. Schildknegt, J. Aubé, *Org. Lett.* **2000**, *2*, 1625–1627.

[3] For approaches to croomine, see: a) S. F. Martin, K. J. Barr, *J. Am. Chem. Soc.* **1996**, *118*, 3299–3300; b) S. F. Martin, K. J. Barr, D. W. Smith, S. K. Bur, *J. Am. Chem. Soc.* **1999**, *121*, 6990–6997; c) D. R. Williams, D. L. Brown, J. W. Benbow, *J. Am. Chem. Soc.* **1989**, *111*, 1923–1925.

[4] For approaches to stemoamide, see: a) P. A. Jacobi, K. Lee, *J. Am. Chem. Soc.* **1997**, *119*, 3409–3410; b) P. A. Jacobi, K. Lee, *J. Am. Chem. Soc.* **2000**, *122*, 4295–4303; c) A. S. Kende, J. I. Martin Hernando, J. B. J. Milbank, *Org. Lett.* **2001**, *3*, 2505–2508; d) A. Kinoshita, M. Mori, *J. Org. Chem.* **1996**, *61*, 8356–8357; e) A. Kinoshita, M. Mori, *Heterocycles* **1997**, *46*, 287–299; f) Y. Kohno, K. Narasaka, *Bull. Chem. Soc. Jpn.* **1996**, *69*, 2063–2070; g) D. R. Williams, J. P. Reddy, G. S. Amato, *Tetrahedron Lett.* **1994**, *35*, 6417–6420.

[5] For approaches to other stemona alkaloids, see: a) D. R. Williams, M. G. Fromhold, J. D. Earley, *Org. Lett.* **2001**, *3*, 2721–2724; b) J. H. Rigby, S. Laurent, A. Cavezza, M. J. Heeg, *J. Org. Chem.* **1998**, *63*, 5587–5591; c) C. H. Heathcock, M. M. Hinman, *J. Org. Chem.* **2001**, *66*, 7751–7756; d) L. Xiang, A. P. Kozikowski, *Synlett* **1990**, 279–281.

 © 2002 WILEY-VCH Verlag GmbH & Co. KGaA, Weinheim 0044-8249/02/4122-4317 $ 20.00+.50/0

[6] a) M. Gotz, O. E. Edwards in *Alkaloids, Vol. IX* (Ed.: R. H. F. Manske), Academic Press, New York, **1967**, pp. 545 – 551; b) M. Gotz, O. E. Edwards in *Alkaloids, Vol. IX* (Ed.: K. Weisner), Academic Press, London, **1973**, pp. 143 – 160; c) For a review of stemona alkaloids, see: R. A. Pilli, M. d. C. Ferreira De Oliveira, *Nat. Prod. Rep.* **2000**, *17*, 117 – 127.
[7] a) C. Y. Chen, D. J. Hart, *J. Org. Chem.* **1990**, *55*, 6236 – 6240; b) D. J. Hart, C. Y. Chen, *J. Org. Chem.* **1993**, *58*, 3840 – 3849.
[8] a) P. Wipf, Y. Kim, D. M. Goldstein, *J. Am. Chem. Soc.* **1995**, *117*, 11 106 – 11 112; b) P. Wipf, Y. Kim, *Tetrahedron Lett.* **1992**, *33*, 5477 – 5480; c) P. Wipf, D. M. Goldstein, *Tetrahedron Lett.* **1996**, *37*, 739 – 742.
[9] a) Y. Morimoto, M. Iwahashi, K. Nishida, Y. Hayashi, H. Shirahama, *Angew. Chem.* **1996**, *108*, 968 – 970; *Angew. Chem. Int. Ed. Engl.* **1996**, *35*, 904 – 906; b) Y. Morimoto, M. Iwahashi, *Synlett* **1995**, 1221 – 1222; c) Y. Morimoto, M. Iwahashi, T. Kinoshita, K. Nishida, *Chem. Euro. J.* **2001**, *7*, 4107 – 4116.
[10] J. D. Ginn, A. Padwa, *Org. Lett.* **2002**, *4*, 1515 – 1517.
[11] S. H. Jung, J. E. Lee, H. J. Joo, S. H. Kim, H. Y. Koh, *Bull. Korean Chem. Soc.* **2000**, *21*, 159 – 160.
[12] a) P. R. Blakemore, W. J. Cole, P. J. Kocienski, A. Morley, *Synlett* **1998**, 26 – 28; b) P. J. Kocienski, A. Bell, P. R. Blakemore, *Synlett* **2000**, 365 – 366.
[13] Aldehyde **1** was prepared in 94% overall yield from 1,5-pentanediol by the following route: a) NaH, TBSCl, THF; b) oxalyl chloride, DMSO, NEt_3; c) Ph_3PCHCO_2Et, CH_2Cl_2, reflux 16 h; d) DIBAL-H, Et_2O, 2 h; e) oxalyl chloride, DMSO, NEt_3. Sulfone **2** was synthesized from 1,3-propanediol in 84% overall yield by the following sequence: a) NaH, BnBr, DMF, 24 h; b) CBr_4, PPh_3, CH_2Cl_2; c) 1-phenyl-1*H*-tetrazole-5-thiol, NaH, DMF; d) *m*-chloroperbenzoic acid, $NaHCO_3$, CH_2Cl_2.
[14] I. Paterson, K. S. Yeung, J. B. Smaill, *Synlett* **1993**, 774 – 776.
[15] J. H. Boyer, *J. Am. Chem. Soc.* **1951**, *73*, 5248 – 5252.
[16] a) A. Greenberg in *Structure and Reactivity* (Eds.: J. F. Liebman, A. Greenberg), VCH, New York, **1988**, pp. 139 – 178; b) A. Greenberg, D. T. Moore, T. D. DuBois, *J. Am. Chem. Soc.* **1996**, *118*, 8658 – 8668; c) A. Greenberg, C. A. Venanzi, *J. Am. Chem. Soc.* **1993**, *115*, 6951 – 6957; d) K. J. Shea, T. G. Lease, J. W. Ziller, *J. Am. Chem. Soc.* **1990**, *112*, 8627 – 8629.
[17] For a discussion of preferential boatlike transition states in this type of Diels–Alder reaction, see: J. W. Coe, W. R. Roush, *J. Org. Chem.* **1989**, *54*, 915 – 930.
[18] Y. Kishi, R. M. Goodman, *J. Am. Chem. Soc.* **1998**, *120*, 9392 – 9393, and references therein.
[19] J. B. Yates, G. E. Keck, *J. Am. Chem. Soc.* **1982**, *104*, 5829 – 5830.
[20] M. W. Rathke, *J. Am. Chem. Soc.* **1970**, *92*, 3222 – 3223.
[21] CCDC 185839 and 185840 contain the supplementary crystallographic data for this paper. These data can be obtained free of charge via www.ccdc.cam.ac.uk/conts/retrieving.html (or from the Cambridge Crystallographic Data Centre, 12, Union Road, Cambridge CB2 1EZ, UK; fax: (+44) 1223-336-033; or deposit@ccdc.cam.ac.uk).

Octametallic and Hexadecametallic Ferric Wheels**

Leigh F. Jones, Andrei Batsanov, Euan K. Brechin,* David Collison,* Madeleine Helliwell, Talal Mallah, Eric J. L. McInnes, and Stergios Piligkos

The synthesis of paramagnetic molecular clusters has become an area of intense research since the discovery that such molecules can act as nanoscale magnets below a critical temperature.[1,2] Such single-molecule magnets (SMMs) are promising new materials for data storage and quantum computing, which exhibit not only magnetization hysteresis but also display quantum tunneling of magnetization and quantum phase interference.[3,4] In order to function as a SMM a molecule must possess the combination of a large spin and large, easy-axis-type anisotropy. The first SMM was $[Mn_{12}O_{12}(O_2CMe)_{16}(H_2O)_4]$ ("Mn12"), and since its preparation a number of molecules have been reported as new members of this family.[5–9] An intriguing class of cluster in this respect is the "molecular wheel". Most even-membered wheels are antiferromagnetic and characterized by $S=0$ ground states, however, this is not the case for the reported "Ni12" and "Cr10" wheels.[10,11] Indeed "Ni12" was recently reported as the first example of a Ni SMM.[10] Although compounds with $S=0$ ground states cannot function as SMMs, they represent ideal model systems for the study of 1D magnetic materials, quantum effects, and magnetic anisotropy. To this end, molecular wheels and metallocycles with 6, 8, 10, 12, 18, and 24 metal ions have been reported.[12] We have chosen to investigate the use of the pro-ligand 1,1,1-tris(hydroxymethyl)ethane (H_3thme) in the synthesis of novel transition metal clusters, and herein report the synthesis and initial magnetic properties of two new Fe^{III} clusters, the first unsupported octametallic and hexadecametallic ferric wheels (unsupported in the sense that there are no central metal ions present). The H_3thme ligand has been successfully used in vanadium chemistry[13] but has been sparingly employed for other transition metal complexes.[14]

[*] Dr. E. K. Brechin, Dr. D. Collison, L. F. Jones, Dr. M. Helliwell, Dr. E. J. L. McInnes, S. Piligkos
Department of Chemistry
The University of Manchester
Oxford Road, Manchester, M13 9PL (UK)
Fax: (+44) 161-275-4616
E-mail: euan.k.brechin@man.ac.uk
david.collison@man.ac.uk

Dr. A. Batsanov
Department of Chemistry
University Science Laboratories
South Road, Durham DH1 3LE (UK)

Prof. T. Mallah
Université Paris-Sud, Bat. 420
Laboratoire de Chimie Inorganique, UMR CNRS 8613
91405 Orsay (France)

[**] This work was supported by the EPSRC (UK), Lloyd's of London Tercentenary Foundation, and the European Community (contract HPRN-CT-1999-00012/TMR network "MolNanoMag").

Supporting information for this article is available on the WWW under http://www.angewandte.org or from the author.

 © 2002 WILEY-VCH Verlag GmbH & Co. KGaA, Weinheim 0044-8249/02/4122-4318 $ 20.00+.50/0

Treatment of the triangular iron complex $[Fe_3O(PhCOO)_6(H_2O)_3](NO_3)$ with H_3thme in acetonitrile yields a precipitate that can be recrystallized from CH_2Cl_2/Et_2O to give the octametallic complex $[Fe_8(PhCOO)_{12}(thme)_4]\cdot 2\,Et_2O$ (**1**, see Experimental Section). Complex **1** crystallizes in the monoclinic $P2_1$ space group.[15] The structure (Figure 1) can be described as a wheel of eight Fe^{III} ions bridged by a

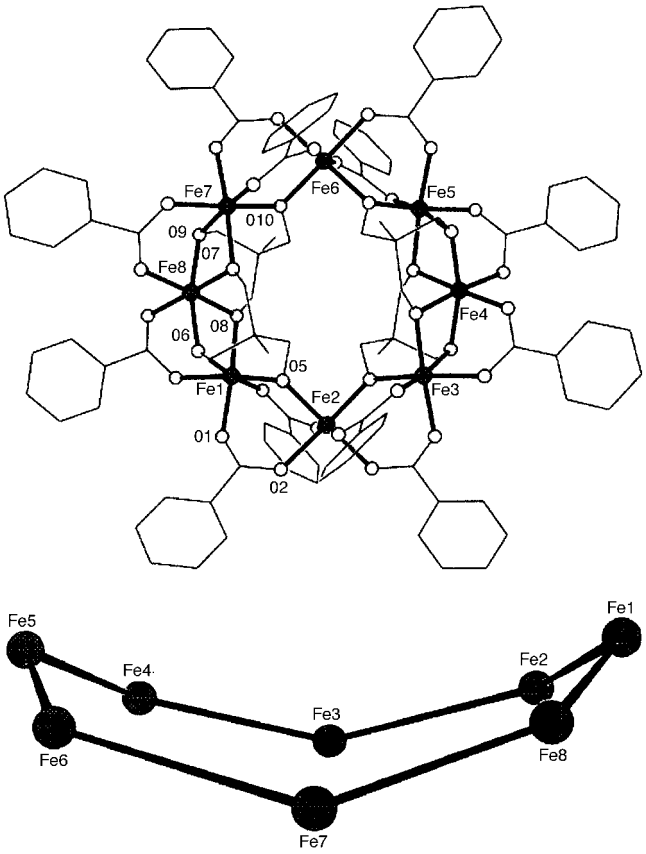


Figure 1. The molecular structure (top) and the arrangement of metal centers (bottom) of **1**. Selected interatomic distances [Å]: Fe-O 1.847(19)–2.054(12), Fe3···Fe7 7.997(7), Fe1···Fe5 7.971(7).

combination of $PhCOO^-$ and $thme^{3-}$ ligands. The $PhCOO^-$ groups bridge neighboring Fe^{III} ions in the usual μ_2-manner, while the triply deprotonated $thme^{3-}$ ligands show much greater flexibility in each bridging four iron centers, with each arm providing a μ_2-oxygen atom for adjacent iron centers. The Fe ions all lie in distorted octahedral geometries, and are of three distinct types: Fe1, Fe3, Fe5, and Fe7 are bridged to three $PhCOO^-$ and two $thme^{3-}$ ligands (Figure 1) and have single and double 2-bond bridges through an oxygen atom to neighboring iron ions (that is, that each of these metal centers is coordinated to one oxygen atom from one $thme^{3-}$ ligand, and two oxygen atoms from the other); Fe2 and Fe6 are bound to four $PhCOO^-$ and two $thme^{3-}$ ligands with 2 single 2-bond bridged oxygen atoms; Fe4 and Fe8 are bound to two $PhCOO^-$ and two $thme^{3-}$ ligands with 2 double 2-bond bridges fulfilling the coordination at these centers. The single and double 2-bond bridges are characterized by Fe-O-Fe angles of 118.3(7)–121.3(7) and 98.0(7)–103.0(7)°, respectively. The "Fe8" wheel is nonplanar and is perhaps best described as ladle-shaped. The plane defined by the rectangular array {Fe2, Fe4, Fe6, Fe8} lies between, and effectively coparallel to the approximately mutually perpendicular vectors defined by Fe1–Fe5 and Fe3–Fe7, which are themselves nearly parallel to the sides of the rectangle. The ring is approximately 8 Å in diameter.

The size of the wheel is doubled by the addition of a coordinating alcohol group in the crystallization step. A similar procedure to that for **1**, but using $EtOH/CH_2Cl_2$ for recrystallization, produces the hexadecametallic wheel $[Fe_{16}(EtO)_4(PhCOO)_{16}(Hthme)_{12}](NO_3)_4\cdot 4\,CH_2Cl_2\cdot 10\,H_2O$ (**2,** see Experimental Section). Complex **2** (Figure 2) crystallizes in the tetragonal $P4_2/n$ space group [15] and is isolated in good

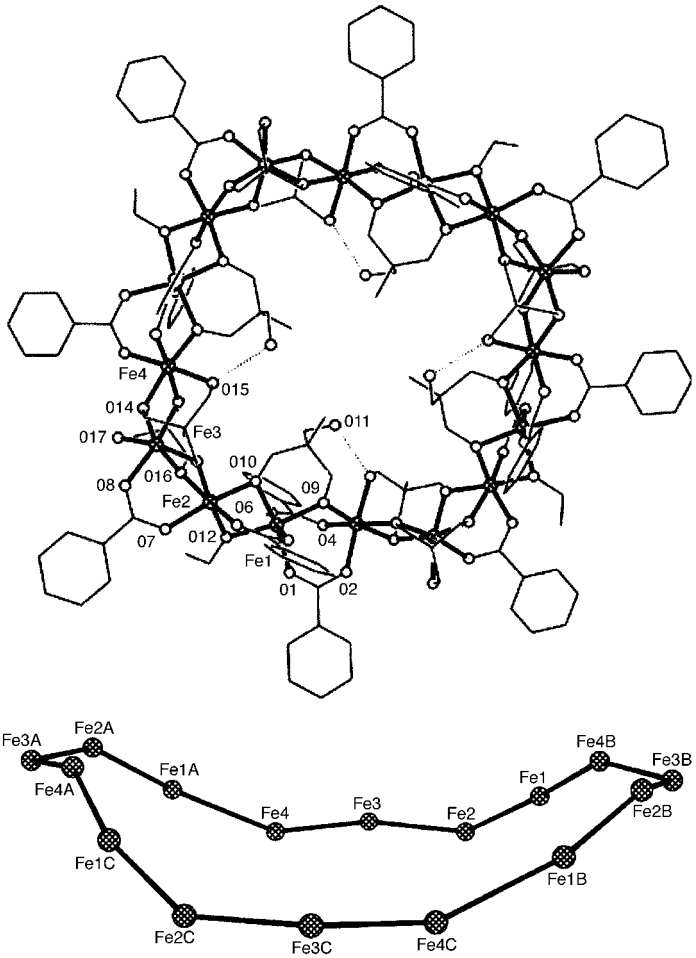


Figure 2. The cation (top) and the arrangement of metal centers (bottom) of **2**. Selected interatomic distances [Å]: Fe-O, 1.962(6)–2.072(6); Fe3A···Fe3B 15.999(6).

yield after 2 days. It can be described as a wheel of sixteen Fe^{III} ions bridged by $PhCOO^-$, $Hthme^{2-}$ and EtO^- ligands. The $PhCOO^-$ ligands again bridge in their familiar μ_2-mode, and are located above, below and in the "plane" of the wheel. The $Hthme^{2-}$ ligands are of two types. Eight ligands use their two deprotonated arms as μ_2-bridges to form a near-linear chain of three metal centers, with the third protonated arm bonded only to the middle ion these three. Four $Hthme^{2-}$ ligands occupy the central cavity of the wheel, with the

 © 2002 WILEY-VCH Verlag GmbH & Co. KGaA, Weinheim 0044-8249/02/4122-4319 $ 20.00+.50/0

deprotonated arms again acting as μ_2-bridges and the protonated arm hydrogen bonding to the monodentate arm of an adjacent $Hthme^{2-}$ ligand (for example, O11–O15B 2.591(6) Å) and to a water molecule above the central cavity of the wheel (O11-O1S 2.804(6) Å). The four EtO^- ligands each bridge two iron centers on the outside edge of the wheel. The iron centers are all bound to six oxygen atoms in a distorted octahedral geometry; for Fe1, the coordination is derived from one EtO^-, three $PhCOO^-$, and two $Hthme^{2-}$ ligands, whereas Fe2 is coordinated to one EtO^-, two $PhCOO^-$, and three $Hthme^{2-}$ ligands. The Fe3 center is coordinated to one $PhCOO^-$ and five $Hthme^{2-}$ ligands, and Fe4 is bonded to two $PhCOO^-$ and four $Hthme^{2-}$ ligands. As for complex **1**, the wheel is nonplanar (Figure 2) and is best described as bowl-shaped, with an approximate diameter of 16 Å. Fe2, Fe3, Fe4, Fe2C, Fe3C, and Fe4C form the basal "plane"; the four symmetry equivalent Fe1 ions form the next plane up, with Fe2A, Fe3A, Fe4A Fe2B, Fe3B, and Fe4B constituting the upper plane. The arrangement of 2-bond oxygen-atom bridges between iron centers in this complex is different from that in **1**. Connections between Fe1 and Fe2, Fe2 and Fe3, and Fe3 and Fe4 are made by two 2-bond oxygen-atom bridges (Fe-O-Fe, 97.9(3)–100.7(3)°), whereas the connections between Fe4 and Fe1′, and Fe1 and Fe4′ are from only one 2-bond oxygen-atom bridge (Fe-O-Fe, 117.8(3)°).

Initial magnetic studies of both **1** and **2** indicate that antiferromagnetic exchange exists between the metal centers. For both complexes the value of $\chi_M T$ declines rapidly from room temperature (approximately 19 and 28 emu K mol^{-1}, respectively) to a value approaching 0 emu K mol^{-1} at 1.8 K, indicative of $S = 0$ ground states for both complexes. The values of $\chi_M T$ at room temperature are approximately half of the expected values for eight or sixteen noninteracting iron centers (approximately 35 and 70 emu K mol^{-1}, respectively), which indicates the existence of strong antiferromagnetic interactions, even at room temperature. This behavior is commonly found for iron–oxo clusters with Fe-O-Fe angles between 100–120°.[12] The EPR spectrum of a polycrystalline powder of **1**, measured at the Q-band frequency, increases in intensity between 5 and 50 K and comprises a series of very broad resonances separated by approximately 2500 G, which start at 2000 G and exhibits a more intense derivative-shaped broad resonance centered around 12 000 G. This spectrum has maximum intensity and resolution at 20 K. These data are consistent with the observation of an $S = 2$ excited state with a zero-field splitting ($|D_2|$) of approximately 0.23 cm^{-1}. Further measurements will be required to confirm this tentative assignment. Note that the population of an $S = 2$ state at these temperatures is consistent with the preliminary modeling of the magnetic susceptibility behavior for both **1** and **2**. In contrast, under the same recording conditions, **2** has a relatively well-resolved EPR spectrum at 5 K (see Figure 3) dominated by resonances in the "$g = 2$" region and with much weaker features to lower field. By raising the temperature, the signals broaden and at 30 K a much broader feature starts to grow at around 0 G. A plausible interpretation of the low-temperature spectrum is an $S = 2$ state with a $|D_2|$ value of around 0.1 cm^{-1}, although the profile of the signal implies a somewhat rhombic character.[16] In common with the situation for **1**, further measurements will be required to produce more definitive values of the spin-Hamiltonian parameters. For comparison, estimated values of $|D_2|$ have been reported for other ferric wheels from cantilever torque measurements, such as $[LiFe_6(OMe)_{12}(dbm)_6][PF_6]$ (0.295 cm^{-1}, dbm = 1,3-diphenyl-1,3-propanedionato),[12] $[Fe_{10}(OMe)_{20}(O_2CCH_2Cl)_{10}]$ (0.540 cm^{-1}),[17] and $[CsFe_8\{N(CH_2CH_2O)_3\}_8]Cl$ (0.315 cm^{-1}).[12] However, there is a clear distinction between the zero-field splitting parameters of **1** and **2**. Furthermore, we have now demonstrated that minor modifications to the coordination sphere in ferric wheels of different iron content, whilst using the same type of ligand donor function, can produce different values of $|D_2|$ within the same excited state spin multiplicity, which has presumably derived from a substantially different magnetic coupling composition. Interestingly, this observed change in $|D_2|$ is in agreement with our observations concerning monomeric, high-spin tris-malonato complexes of Fe^{III}, $[Fe(O_2CCR_2CO_2)_3]^{3-}$, in which $|D_2|$ ranged from 0.04 to 0.2 cm^{-1} for the same coordination sphere as R was varied between H, Me, and Et.[18]

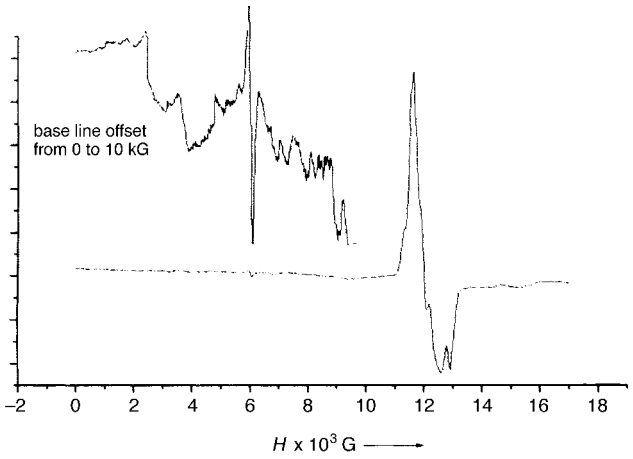


Figure 3. Q-band EPR spectrum of a polycrystalline sample of **2** at 5 K.

In summary, the use of the pro-ligand H_3thme has led to two new structural types: unsupported octametallic[19] and hexadecametallic iron wheels. Previously reported cyclic Fe_8-compounds have contained alkali-metal ions within the central cavity of the wheel, and the Fe_{16} complex is unprecedented. The effect of the coordinating alcoholate groups is remarkable and prompts further investigation.

Experimental Section

1: $[Fe_3O(PhCOO)_6(H_2O)_3](NO_3)$ (0.5 mmol) and H_3thme (0.5 mmol) were stirred in MeCN (30 mL) for 4 h. The resulting precipitate was filtered, air-dried, and redissolved in CH_2Cl_2. Crystals were formed in 2 days after diffusion of diethyl ether into the solution, in approximately 30% yield. Elemental analysis calcd (%) for $Fe_8C_{92}H_{104}O_{36}$: C 52.74, H 4.09; found: C 52.68, H 4.01; selected IR data (KBr pellet): $\tilde{\nu} = 1601$ (s), 1561 (s), 1519 (s), 1493 (m), 1409 (s), 1307 (w), 1176 (m), 1158 (w), 1117 (w), 1069 (m), 1045 (m), 1025 (m), 877 (w), 717 cm^{-1} (s).

2: $[Fe_3O(PhCOO)_6(H_2O)_3](NO_3)$(0.5 mmol) and H_3thme (0.5 mmol) were stirred in MeCN (30 mL) for 4 h. The resulting precipitate was filtered, air-dried, and redissolved in a 1:1 mixture of CH_2Cl_2 and EtOH. Crystals formed after 2 days in approximately 40% yield. Elemental analysis calcd

 © 2002 WILEY-VCH Verlag GmbH & Co. KGaA, Weinheim 0044-8249/02/4122-4320 $ 20.00+.50/0

(%) for $Fe_{16}C_{180}H_{216}O_{84}N_4$: C 46.22, H 4.74, N 1.20; found: C 46.08, H 4.41, N 1.14; selected IR data (KBr pellet): $\tilde{\nu}$ = 1554 (s), 1528 (s) 1493 (m), 1409 (s), 1307 (w), 1176 (m), 1158 (w), 1069 (w), 1045 (m), 1025 (m), 877 (w), 717 cm^{-1} (s).

Received: July 17, 2002 [Z19756]

[1] R. Sessoli, D. Gatteschi, A. Caneschi, M. A. Novak, *Nature* **1993**, *365*, 141.

[2] R. Sessoli, H.-L. Tsai, A. R. Schake, S. Wang, J. B. Vincent, K. Folting, D. Gatteschi, G. Christou, D. N. Hendrickson, *J. Am. Chem. Soc.* **1993**, *115*, 1804.

[3] J. R. Friedman, M. P. Sarachik, J. Tejada, R. Ziolo, *Phys. Rev. Lett.* **1996**, *76*, 3830.

[4] W. Wernsdorfer, R. Sessoli, *Science* **1999**, *284*, 133.

[5] J. Yoo, E. K. Brechin, A. Yamaguchi, M. Nakano, J. C. Huffman, A. L. Maniero, L.-C. Brunel, K. Awaga, H. Ishimoto, G. Christou, D. N. Hendrickson, *Inorg. Chem.* **2000**, *39*, 3615.

[6] C. Boskovic, E. K. Brechin, W. E. Streib, K. Folting, J. C. Bollinger, D. N. Hendrickson, G. Christou, *J. Am. Chem. Soc.* **2002**, *124*, 3725.

[7] S. L. Castro, Z. Sun, C. M. Grant, J. C. Bollinger, D. N. Hendrickson, G. Christou, *J. Am. Chem. Soc.* **1998**, *120*, 2365.

[8] A.-L. Barra, A. Caneschi, A. Cornia, F. Fabrizi de Biani, D. Gatteschi, C. Sangregorio, R. Sessoli, L. Sorace, *J. Am. Chem. Soc.* **1999**, *121*, 5302.

[9] A.-L. Barra, P. Debrunner, D. Gatteschi, C. E. Schulz, R. Sessoli, *Europhys. Lett.* **1996**, *35*, 133.

[10] C. Cadiou, M. Murrie, C. Paulsen, V. Villar, W. Wernsdorfer, R. E. P. Winpenny, *Chem. Commun.* **2001**, 2666.

[11] E. J. L. McInnnes, C. Anson, A. K. Powell, A. J. Thomson, S. Poussereau, R. Sessoli, *Chem. Commun.* **2001**, 89.

[12] See for example: a) K. L. Taft, S. J. Lippard, *J. Am. Chem. Soc.* **1990**, 112, 9629; b) J. van Slageren, R. Sessoli, D. Gatteschi, A. A. Smith, M. Helliwell, R. E. P. Winpenny, A. Cornia, A.-L. Barra, A. G. M. Jansen, E. Rentscheler, G. A. Timco, *Chem. Eur. J.* **2002**, *8*, 277; c) O. Waldmann, R. Kock, S. Schromm, J. Schülein, P. Müller, I. Bernt, R. W. Saalfrank, F. Hampel, E. Balthes. *Inorg. Chem.* **2001**, *40*, 2986; d) A. Cornia, M. Affronte, A. G. M. Jansen, G. L. Abbati, D. Gatteschi, *Angew. Chem.* **1999**, *111*, 2409; *Angew. Chem. Int. Ed.* **1999**, *38*, 2264.

[13] M. I. Khan, J. Zubieta, *J. Prog. Inorg. Chem.* **1995**, *43*, 1.

[14] A. Cornia, D. Gatteschi, K. Hegetschweiler, L. Hausherr-Primo, V. Gramlich, *Inorg. Chem.* **1996**, 35, 4414.

[15] Crystal structure data for **1**: $C_{117}H_{96}Fe_8O_{38}$, M_r = 2556.74, monoclinic, space group $P2_1$, a = 16.490(15), b = 22.51(2), c = 18.531(7) Å, β = 115.563(1)°, V = 6204(10) Å^3, T = 100(2) K, Z = 2, 44455 reflections collected, 21439 unique (R_{int} = 0.1373), $R(F)$ = 0.0970 and $wR2$ = 0.2369 using 14358 reflections with $I > 2\sigma(I)$. Crystal structure data for **2**: $C_{196}H_{204}Cl_8Fe_{16}O_{82}$, M_r = 5048.81, tetragonal, space group $P4_2/n$, a = 24.7413(16), c = 20.6068(19) Å, V = 12614.1(16) Å^3, T = 100(2) K, Z = 2, 64051 reflections collected, 11123 unique (R_{int} = 0.1432), $R(F)$ = 0.0952 and $wR2$ = 0.2717 using 8547 reflections with $I > 2\sigma(I)$. CCDC-189565 and -189566 contains the supplementary crystallographic data for this paper. These data can be obtained free of charge via www.ccdc.cam.ac.uk/conts/retrieving.html (or from the Cambridge Crystallographic Data Centre, 12, Union Road, Cambridge CB2 1EZ, UK; fax: (+44) 1223-336-033; or deposit@ccdc.cam.ac.uk).

[16] F. E. Mabbs, D. Collison, *Electron Paramagnetic Resonance of d transition metal compounds*, Elsevier, Amsterdam, **1992**.

[17] A. Cornia, A. G. M. Jansen, M. Affronte, *Phys. Rev. B* **1999**, 60, 12177.

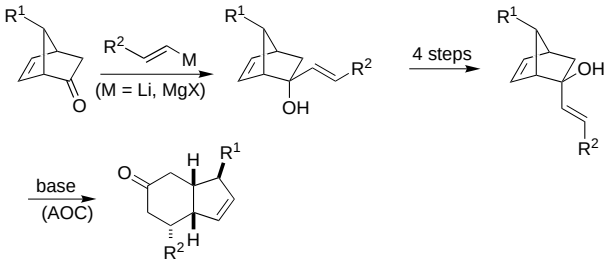
[18] D. Collison, A. K. Powell, *Inorg. Chem.* **1990**, *29*, 4735.

[19] The same molecular product may also be obtained using the mixed-valent triangular complex $[Fe_3O(PhCOO)_6(H_2O)_2(MeCN)]$. This has been confirmed by determination of the complete crystal and molecular structure: orthorhombic, space group Fddd, a = 20.9903, b = 25.4990, c = 46.6602 Å.

A Radical Alternative to the Anionic Oxy-Cope Rearrangement**

Rachel Chuard, Anne Giraud, and Philippe Renaud*

The anionic oxy-Cope rearrangement has emerged as a highly useful tool for organic synthesis.[1,2] Various 1,5-dien-3-ols readily undergo this electronic reorganization, and the usually easy preparation of the precursors contributes to the popularity of this reaction. However, a limitation of this sigmatropic rearrangement is the requirement of proximal double bonds. Indeed, the distance and the angular relationship between the two double bonds should be close to optimal values in order to achieve the rearrangement.[2,3] For example, with 1,5-dien-3-ols that result from the addition of alkenyl anions to 2-norbornenones, the double bonds are not proximal and therefore anionic sigmatropy is not possible. Two protocols that allow the inversion of the configuration of the quaternary center have been developed to remedy this problem. However, both are lengthy (four steps) and not high-yielding (Scheme 1).[4,5]



Scheme 1. Inversion of the stereogenic center of the alcohol is required prior to anionic oxy-Cope rearrangements (AOC) of norbornenone derivatives.[4,5]

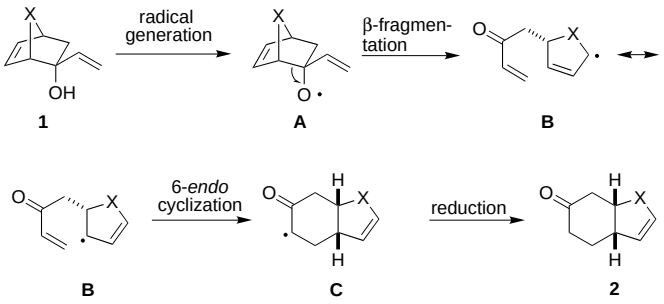
We report herein a mechanistically different approach to solve this problem: a radical alternative to the oxy-Cope rearrangement. A cascade reaction that involves the fragmentation of an alkoxyl radical followed by a 6-*endo*-cyclization process leads to the oxy-Cope product (Scheme 2). According to this mechanism, the relative configuration of the alcohol has no influence on the efficacy of the rearrangement. Related anionic stepwise mechanisms have been observed for anionic amino-Cope rearrangements[6] as well as for oxy-Cope rearrangements of 4-phenylthio-1,5-dien-3-alkoxides.[7,8]

We investigated several methods to generate the desired alkoxyl radical **A**, starting from 2-norbornenone. Treatment

[*] Prof. P. Renaud, R. Chuard
Department of Chemistry and Biochemistry, University of Bern
Freiestrasse 3, 3000 Bern 9 (Switzerland)
Fax: (+41) 31-631-4359
E-mail: philippe.renaud@ioc.unibe.ch
A. Giraud
Department of Chemistry, University of Fribourg
Pérolles, 1700 Fribourg (Switzerland)

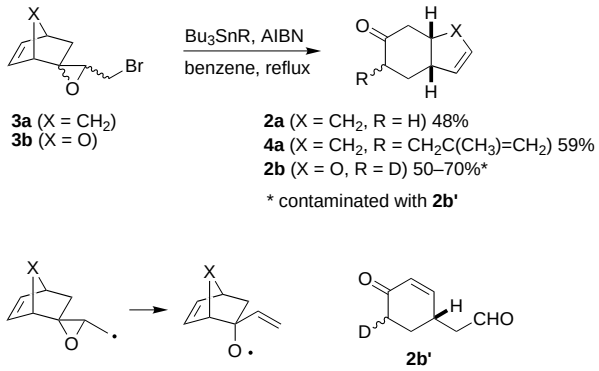
[**] This work was supported by the *Swiss National Science Foundation* and by the *Federal Office for Science and Education* (*OFES/BBW*). We are also very grateful to the *Stiftung zur Förderung der Wissenschaftlichen Forschung* and the *University of Bern* for financial support.

 © 2002 WILEY-VCH Verlag GmbH & Co. KGaA, Weinheim 0044-8249/02/4122-4321 $ 20.00+.50/0



Scheme 2. Radical alternative to the oxy-Cope rearrangement.

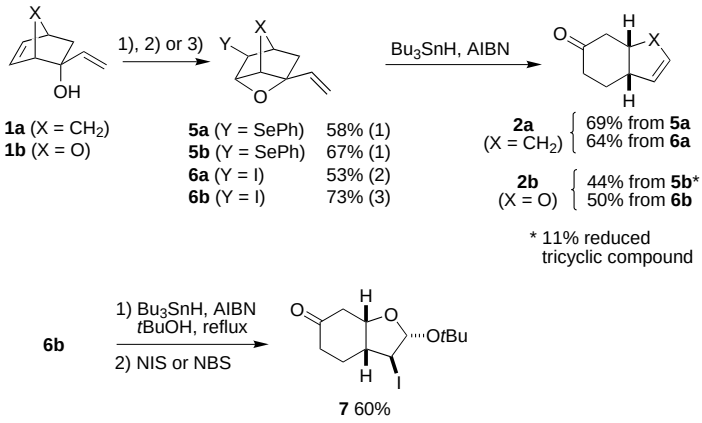
of the alcohol **1** with different oxidants and under various reaction conditions failed to give the desired rearranged compound. Instead, products of the oxidation of the allylic alcohol were observed. A milder route to the alkoxyl radical **A** from bromomethyloxiranes was then examined.[9–15] The desired radical precursors were prepared as a mixture of the four possible diastereomers from the corresponding ketones over four steps and in modest overall yields (not optimized). The radical reactions are shown in Scheme 3.



Scheme 3. Radical oxy-Cope rearrangement starting from bromomethyloxiranes.

Upon treatment of **3a** with tributyltin hydride and azobisisobutyronitrile (AIBN), the desired rearranged product **2a** was obtained in 48% yield. When the reaction was repeated with 2-methallyltributylstannane, the allylated product **4a** was isolated in 59% yield. Reaction of **3b** with Bu_3SnD afforded the rearranged product **2b** in variable yields. Apparently, this enol ether decomposes already during the radical reaction, presumably through a Lewis acid (Bu_3SnBr) catalyzed reaction, to afford **2b′**. Reactions of the bromomethyloxiranes give only moderate yields but proved the feasibility of the radical oxy-Cope rearrangement. No effort to optimize yields was attempted because the preparation of the radical precursors (four steps) from 2-norborneneone and 7-oxanorbornenone is clearly unsatisfactory.

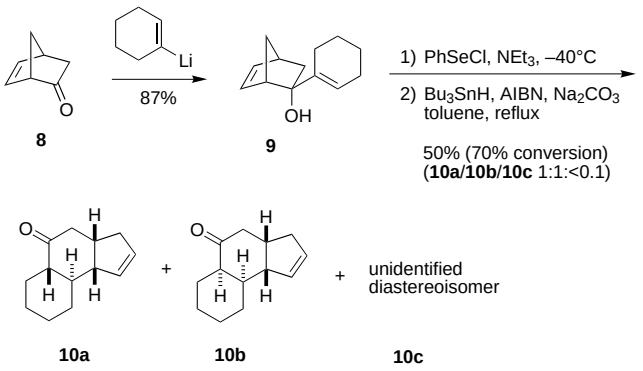
We next turned our attention towards a more efficient alkoxyl radical precursor that can be obtained directly from the *endo* alcohols **1a** and **1b**. Treatment of **1a** and **1b** with phenylselenyl chloride and triethylamine afforded the tricyclic oxetanes **5a** and **5b** in 60% and 67% yield, respectively (Scheme 4).[16] Similarly the iodides **6a** and **6b** were prepared



Scheme 4. The tricyclic oxetane approach. 1) $PhSeCl$, NEt_3; 2) NIS, NaH; 3) NIS, DBU.

by treatment with *N*-iodosuccinimide (NIS) in the presence of a base. Treatment of **5a** and **6a** with Bu_3SnH in refluxing toluene afforded the rearranged product **2a** in 69% and 64% yields (Scheme 4). The same treatment of oxygenated analogues **5b** and **6b** in refluxing *tert*-butanol gave lower yields. A better result was obtained when the reaction was immediately followed by iodoacetalization upon treatment with NIS or NBS (*N*-bromosuccinimide). In this case, the stable iodide **7** was isolated in 60% yield.[17]

Finally, the radical oxy-Cope rearrangement was tested for the preparation of a tricyclic framework (Scheme 5). Reaction of 2-norbornenone **8** with cyclohexenyllithium afforded the



Scheme 5. Preparation of a tricyclic system.

endo alcohol **9** in good yield. Reaction of **9** with $PhSeCl/Et_3N$ gave an unstable tricylic selenide that was used without purification for the next step. Treatment of this crude selenide with Bu_3SnH/AIBN in refluxing toluene in the presence of sodium carbonate (to minimize acid catalyzed degradation) afforded the rearranged compound **10** in 50% yield (70% conversion) as a mixture of three isomers **10a/b/c** (1:1:$<$0.1). After separation by HPLC, the relative configuration of **10a** and **10b** was established by ^1H NMR and NOE differential experiments.

In conclusion, we have developed a radical alternative to the anionic oxy-Cope rearrangement that is independent of the stereochemistry of the starting material. A nonconcerted fragmentation–cyclization mechanism is involved. Further

 © 2002 WILEY-VCH Verlag GmbH & Co. KGaA, Weinheim 0044-8249/02/4122-4322 $ 20.00+.50/0 *Angew. Chem. Int. Ed.* **2002**, *41*, No. 22

extension of this chemistry to more complex substrates is currently under investigation, along with the development of alternative methods to generate the starting tertiary alkoxyl radicals.[18]

Experimental Section

6b: 1,8-Diazabicyclo[5.4.0]undec-7-ene (DBU; 1.08 mL, 7.24 mmol) was added to a solution of allylic alcohol **1b** (1.00 g, 7.24 mmol) in dry CH_2Cl_2 (123 mL) at room temperature. NIS (5.32 g, 21.7 mmol) was added in portions over 3 h at −40 °C. The reaction was stirred overnight at room temperature and then water was added. After extraction with CH_2Cl_2, the organic phases were washed with aqueous $Na_2S_2O_3$ and brine, dried over $MgSO_4$, and concentrated. Flash column chromatography (Et_2O/hexane 1:12) of the crude product afforded **6b** (1.4 g, 73 %) as a white solid. M.p.: 74–76 °C; IR (KBr): $\tilde{\nu}$ = 3009, 2930, 2361, 1633, 1408, 1147, 1049, 964, 927 cm^{-1}; ^1H NMR (360 MHz, $CDCl_3$): δ = 5.87 (dd, J = 17.7, 10.9 Hz, 1H; C*H*=CH_2), 5.31 (dd, J = 17.2, 0.9 Hz, 1H; CH=C*H*H), 5.23 (m, CH=CH*H*, 2H; 1-H), 5.06 (d, J = 5.0 Hz, 1H; 6-H), 4.90 (dd, J = 3.2, 1.4 Hz, 1H; 3-H), 4.29 (s, 1H; I-CH), 2.26 (d, J = 12.7 Hz, 1H; *endo* 8-H), 1.93 ppm (dd, J = 12.9, 4.5 Hz, 1H; *exo* 8-H); ^{13}C NMR (90.5 MHz, $CDCl_3$): δ = 135.1 (d), 116.4 (t), 92.7 (s), 85.9 (d), 83.8 (d), 82.1 (d), 43.4 (d), 28.2 ppm (t). MS (CI): m/z (%): 265 (26) $[M^+ + 1]$, 137 (72) $[M\text{-}I]^+$, 109 (100), 95 (95), 83 (50), 55 (51); elemental analysis: calcd for $C_8H_9IO_2$ (264.06): C 36.39, H 3.44; found: C 36.44, H 3.39.

7: A solution of Bu_3SnH (0.3 mL, 1.14 mmol) and AIBN (6 mg, 0.04 mmol) in benzene (3 mL) was added over 15 h (syringe pump) to the iodide **6b** (200 mg, 0.76 mmol) in refluxing *t*BuOH (74 mL). Heating was stopped at the end of the addition process and CH_2Cl_2 (30 mL) was added. The mixture was cooled at −20 °C and NBS[17] (137 mg, 0.77 mmol) was added in portions over 15 min. After 2 h at −20 °C, the organic layer was washed with water, dried over Na_2SO_4, and concentrated. Flash column chromatography of the residue (EtOAc/hexane 1:9) gave the stable iodoacetal **7** (143 mg, 60 %) as a colorless oil. IR (film): $\tilde{\nu}$ = 2974, 2936, 1722, 1368, 1003 cm^{-1}; ^1H NMR (360 MHz, $CDCl_3$): δ = 5.51 (d, J = 3.2 Hz, 1H; OCHO), 4.57 (td, J = 6.4, 6.4 Hz, 1H; 7a-H), 3.88 (dd, J = 3.9, 4.1 Hz, 1H; ICH), 2.6–2.82 (m, 3H, 2 × 7-H, 3a-H), 2.43–2.54 (m, 1H; 5-H), 1.95–2.26 (m, 3H; 2 × 4-H, 5-H), 1.23 ppm (s, 9H; *t*Bu); ^{13}C NMR (125.8 MHz, $CDCl_3$): δ = 209.6 (s), 106.5 (d), 75.7 (d), 75.6 (s), 47.2 (d), 44.3 (t), 36.8 (t), 31.0 (d), 28.6 (q), 24.5 ppm (t); MS (CI): m/z (%):339 (1) $[M^+]$, 265 (100) $[M^+ - O$*t*$Bu]$, 137 (29); HRMS (CI, isobutane) for $C_{12}H_{19}O_3I$ ($[M^+$-O*t*Bu]): calcd 264.97199; found 264.97194.

Received: July 17, 2002 [Z19749]

[1] R. K. Hill in *Comprehensive Organic Synthesis, Vol. 5* (Eds.: B. M. Trost, I. Fleming, L. A. Paquette), Pergamon Press, Oxford, **1991**, p. 785.
[2] L. A. Paquette, *Tetrahedron* **1997**, *53*, 13971.
[3] L. A. Paquette, *Angew. Chem.* **1990**, *102*, 642; *Angew. Chem. Int. Ed. Engl.* **1990**, *29*, 609.
[4] I. Fleming, N. K. Terrett, *Tetrahedron Lett.* **1984**, *25*, 5103.
[5] W. L. Brown, A. G. Fallis, *Tetrahedron Lett.* **1985**, *26*, 607.
[6] T. J. Sprules, J. D. Galpin, D. Macdonald, *Tetrahedron Lett.* **1993**, *34*, 247.
[7] D. A. Evans, D. J. Baillargeon, J. V. Nelson, *J. Am. Chem. Soc.* **1978**, *100*, 2242.
[8] F. Haeffner, K. N. Houk, Y. R. Reddy, L. A. Paquette, *J. Am. Chem. Soc.* **1999**, *121*, 11880.
[9] E. S. Huyser, L. R. Munson, *J. Org. Chem.* **1965**, *30*, 1436.
[10] E. L. Stogryn, E. L. Gianni, *Tetrahedron Lett.* **1970**, 3025.
[11] A. Suzuki, N. Miyaura, M. Itoh, H. C. Brown, G. W. Holland, E. Negishi, *J. Am. Chem. Soc.* **1971**, *93*, 2792.
[12] A. Johns, J. Murphy, *Tetrahedron Lett.* **1988**, *29*, 837.
[13] R. C. Gash, F. MacCorquodale, J. Walton, *Tetrahedron* **1989**, *45*, 5531.
[14] S. Kim, S. Lee, *Tetrahedron Lett.* **1991**, *32*, 6575.
[15] V. Rawal, S. Iwasa, *Tetrahedron Lett.* **1992**, *33*, 4687.
[16] For a related reaction with PhSCl, see W. L. Brown, A. G. Fallis, *Tetrahedron Lett.* **1985**, *26*, 607; W. L. Brown, A. G. Fallis, *Can. J. Chem.* **1987**, *65*, 1828; S. M. Tuladhar, A. G. Fallis, *Can. J. Chem.* **1987**, *65*, 1933; O. Arjona, R. Fernandez de la Pradilla, J. Plumet, A. Viso, *J. Org. Chem.* **1992**, *57*, 772.
[17] Both NIS and NBS furnished iodide **7b**; we assume that NBS reacts rapidly with Bu_3SnI to give Bu_3SnBr and NIS.
[18] For a first attempt, see the following communication: R. Chuard, A. Giraud, P. Renaud, *Angew. Chem.* **2002**, *114*, 4499; *Angew. Chem. Int. Ed.* **2002**, *41*, 4323

Allyl Sulfoxides as Precursors for Radical Two-Carbon Ring Expansion of Cyclobutanones**

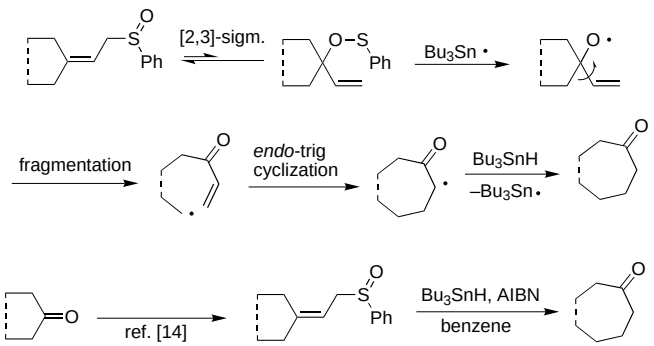
Rachel Chuard, Anne Giraud, and Philippe Renaud*

Ring-expansion reactions are extremely useful processes that take advantage of existing ring structures for the construction of larger cyclic systems. Various ion-based methods have been developed for selective ring-expansion reactions.[1] More recently, following the tremendous development of preparative radical chemistry, ring expansion of ketones by using alkoxyl radicals (Dowd–Beckwith reaction) has been reported.[2–5] This approach proved to be quite efficient for one-, three-, and four-carbon ring expansions. However, enlargement by two carbon atoms is not possible.[3] For this purpose, Galatsis et al. developed a three-step method based on the rearrangement of 1-vinylcycloalkoxyl radicals.[6–8] The low yields and lack of regioselectivity make this procedure unsatisfactory for preparative purposes.[6] Therefore, an efficient two-step procedure for the ring expansion of cycloalkanones would be useful.[9,10] The strategy that we developed is based on an unusual cascade reaction, which consists of a [2,3]-sigmatropic rearrangement (Mislow–Braverman–Evans rearrangement)[11–13] of an allylic sulfoxide followed by a radical fragmentation–cyclization process (Scheme 1). The experimental reaction sequence involves the one-pot preparation of an allylic sulfoxide from the ketone according to the procedure of Evans et al.,[14] followed by treatment of the sulfoxide with tributyltin hydride in refluxing benzene. The challenge of this approach is to develop a chain process with a radical precursor that is available from an equilibrium reaction. The efficacy of the reaction will depend on the ability of the intermediate sulfenate, present only in small amounts, to sustain a chain reaction.

[*] Prof. P. Renaud, R. Chuard
Department of Chemistry and Biochemistry, University of Bern
Freiestrasse 3, 3000 Berne 9 (Switzerland)
Fax: (+41) 31-631-4359
E-mail: philippe.renaud@ioc.unibe.ch
A. Giraud
Department of Chemistry, University of Fribourg
Pérolles, 1700 Fribourg (Switzerland)

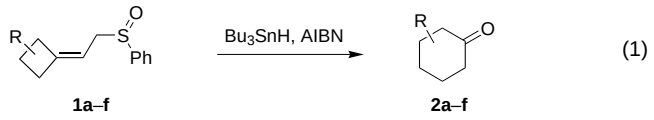
[**] This work was supported by the *Swiss National Science Foundation* and by the *Federal Office for Science and Education* (*OFES/BBW*). We are also very grateful to the *Stiftung zur Förderung der Wissenschaftlichen Forschung* and the *Universität Bern* for financial support.

 © 2002 WILEY-VCH Verlag GmbH & Co. KGaA, Weinheim 0044-8249/02/4122-4323 $ 20.00+.50/0



Scheme 1. General strategy for the two-carbon ring expansion.

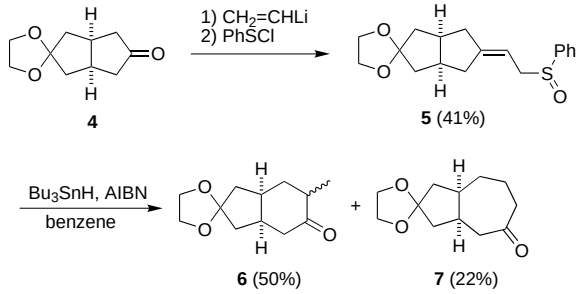
Allylic sulfoxides are easily prepared from cyclobutanones by treatment with vinyllithium followed by phenylsulfenyl chloride.[14] Yields for this transformation lie between 40 and 75%, depending on the freshness of phenylsulfenyl chloride (see Experimental Section for a typical example). The radical rearrangement [Eq. (1)] was examined and optimized with



(1)

the sulfoxide **1a**, which was prepared from 3-phenylcyclobutanone. The best results are obtained by adding 1.5 equivalents of Bu_3SnH over 12 hours to a 0.01M solution of the sulfoxide in refluxing benzene. Under these conditions, the expected product of the two-carbon ring expansion, **2a**, was isolated in 66% yield (Table 1, entry 1). As a side product, 2-methyl-4-phenylcyclopentanone **3a**, which results from a final 5-*exo* cyclization, was isolated in 19% yield.[15] Bicyclic sulfoxides were also investigated. Sulfoxides **1b** and **1c** give the desired products of ring expansion **2b** and **2c** in 43% and 67% yield, respectively (Table 1, entries 2 and 3). In these two examples, the final product results from the regioselective ring opening of the cyclobutyloxyl radical followed by a 6-*endo* cyclization. Sulfoxide **1d** gives **2d** and **2d′** in 64% and 10% yields, respectively (Table 1, entry 4). In this case, the ring opening of the cyclobutane is not completely regioselective, and the major product results from the fragmentation, which leads to a secondary alkyl radical followed by a 6-*endo* cyclization. The precursor **1e** affords the fused cyclohexanone **2e** in 66% yield (Table 1, entry 5). The regioselectivity is explained by the formation of the more stable 1-oxysubstituted radical. The limitation of the regioselectivity control of the ring-opening process is demonstrated by the reaction of sulfoxide **1f** (Table 1, entry 6). In this case, a 1:1 mixture of two secondary alkyl radicals is generated and their cyclization furnishes **2f** (36%) and **2f′** (36%).

The ring expansion of a cyclopentanone derivative was examined next (Scheme 2). Galatsis et al.[6] and Walton and co-workers[7] have shown that the ring expansion of cyclopentanones provides mainly 2-methylcyclohexanone through a 6-*exo* cyclization. Our result confirms this observation, as

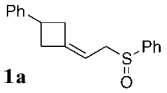
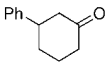
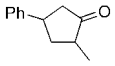
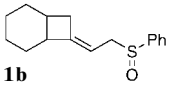
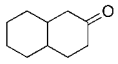
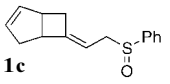
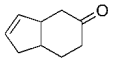
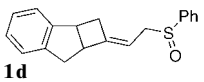
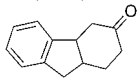
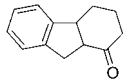
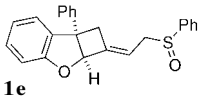
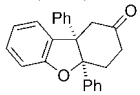
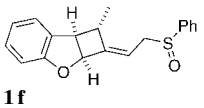
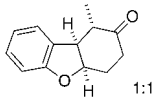
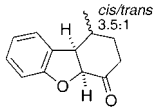


Scheme 2. Ring expansion of cyclopentanone.

sulfoxide **5** obtained from the ketone **4** gives the bicyclo[4.3.0] ketone **6** as the major product (50% yield) together with the bicyclo[5.3.0] ketone **7** (22% yield). Interestingly, the yield of this transformation (72%) is much higher than that obtained by the procedure of Galatsis et al. (29% yield).[16]

Finally, we have tested our novel method for the generation of the allyloxyl radical in a different reaction cascade, that is,

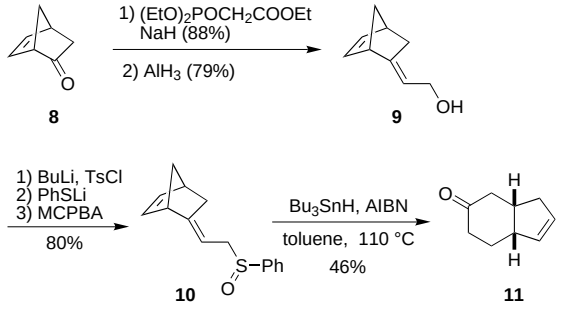
Table 1. Ring expansion of cyclobutanones according to Equation (1).

Entry	Substrate	Ring-expansion products[a]	
1	 **1a**	 **2a** (66%)	 **3a** (19%)
2	 **1b**	 **2b** (43%)	
3	 **1c**	 **2c** (67%)	
4	 **1d**	 **2d** (64%)	 **2d′** (10%)
5	 **1e**	 **2e** (66%)	
6	 **1f**	 1:1 **2f** (36%)	 cis/trans 3.5:1 **2f′** (36%) 1:1

[a] Bu_3SnH (1.5 equiv) was added over 12 h to a solution of the sulfoxide **1** (0.01M) in refluxing benzene.

 © 2002 WILEY-VCH Verlag

the radical oxy-Cope rearrangement.[17] For this purpose, the sulfoxide **10** was prepared from norbornenone **8** via the allylic alcohol **9** (the direct synthesis with the procedure of Evans et al. does not work in this particular case). By treating the sulfoxide **10** with Bu_3SnH and azobisisobutyronitrile (AIBN) in refluxing toluene, the desired rearranged compound **11** is obtained in an unoptimized 46% yield (Scheme 3). This reaction consists of a sequence of a [2,3]-sigmatropic rearrangement followed by generation of an allyloxyl radical, regioselective fragmentation to an allyl radical, and finally a 6-*endo* cyclization.[17]



Scheme 3. Radical oxy-Cope rearrangement.[17] MCPBA = *meta*-chloroperbenzoic acid.

In conclusion, we have demonstrated that allylsulfoxides, which are easily available from ketones, are suitable precursors for allyloxyl radicals. An unique method for the two-carbon ring expansion of cyclobutanones has been developed based on a sequential radical-chain reaction. To the best of our knowledge, this is the first cascade process in which the radical precursor is continuously generated in an equilibrium reaction as a minor component of the reaction mixture. The stability of the sulfoxide radical precursors and the mild reaction conditions of the ring expansion renders this reaction attractive for preparative purposes. The control of the regioselectivity of the process requires a proper design of the system. Extension of this reaction to other ring sizes and more complexed systems is currently under investigation.

Experimental Section

General procedure for the radical ring expansion: A solution of Bu_3SnH (0.49 mL, 1.84 mmol) and AIBN (10 mg, 0.06 mmol) in C_6H_6 (3 mL) was added over 12 h with a syringe pump to a refluxing solution of the allylic sulfoxide (1.23 mmol) in C_6H_6 (123 mL, 0.01M). (For sulfoxide **1e**, better results were obtained when irradiation with a 300-W sunlamp was performed during the reaction.) The solvent was removed under reduced pressure and the crude product was purified by flash chromatography.

2c: From **1c** (300 mg, 1.23 mmol), flash-column chromatography (EtOAc/hexane) afforded **2c** (112 mg, 67%) as a colorless oil. IR (film): $\tilde{\nu} = 3050$, 2930, 2360, 1720, 1450, 1410, 1230 cm^{-1}, ^1H NMR (360 MHz, $CDCl_3$): $\delta =$ 5.72 (m, 1H; C*H* = CH), 5.54 (m, 1H; CH = C*H*), 3.15 (m, 1H; 3a-H), 2.66–2.79 (m, 1H; 1-H), 2.49–2.65 (m, 2H; 7a-H, 4-H), 2.1–2.36 (m, 4H; 2 × 6-H, 1-H, 4-H), 1.93–2.03 (m, 1H; 7-H), 1.65–1.76 ppm (m, 1H; 7-H); ^{13}C NMR (90.5 MHz, $CDCl_3$): $\delta = 213.7$ (s), 133.3 (d), 130.2 (d), 43.2 (d), 42.4 (t), 39.6 (t), 37.5 (t), 33.6 (d), 27.1 (t). MS (EI): *m/z* (%): 136 (53) [M^+], 79 (100); HRMS (EI-MS) for $C_9H_{12}O$ ([M^+]): calcd 136.08826; found 136.08836.

Received: July 17, 2002 [Z19750]

[1] M. Hesse, *Ring Enlargement in Organic Chemistry*, **1990**.
[2] P. Dowd, W. Zhang, *Chem. Rev.* **1993**, *93*, 2091.
[3] P. Dowd, S.-C. Choi, *Tetrahedron* **1989**, *45*, 77.
[4] A. L. J. Beckwith, D. M. O'Shea, S. W. Westwood, *J. Am. Chem. Soc.* **1988**, *110*, 2565.
[5] W. Zhang in *Radicals in Organic Synthesis, Vol. 2* (Eds.: P. Renaud, M. P. Sibi), Wiley-VCH, **2001**, pp. 234.
[6] P. Galatsis, S. D. Millan, T. Faber, *J. Org. Chem.* **1993**, *58*, 1215.
[7] For a mechanistical study of this reaction, see: M. Afzal, J. C. Walton, *J. Chem. Soc. Perkin Trans. 2* **1999**, 937.
[8] S. Kim, S. Lee, *Tetrahedron Lett.* **1991**, *32*, 6575.
[9] M. Nagel, H.-J. Hansen, G. Frater, *Synlett* **2002**, 275.
[10] M. Nagel, H.-J. Hansen, G. Frater, *Synlett* **2002**, 280.
[11] E. G. Miller, D. R. Rayner, K. Mislow, *J. Am. Chem. Soc.* **1966**, *88*, 3139.
[12] S. Braverman, Y. Stabinsky, *Chem. Commun.* **1967**, 270.
[13] D. A. Evans, G. C. Andrews, C. L. Sims, *J. Am. Chem. Soc.* **1971**, *93*, 4956.
[14] D. A. Evans, C. L. Sims, G. C. Andrews, *J. Am. Chem. Soc.* **1977**, *99*, 5453.
[15] Experiments with tributyltin deuteride have demonstrated that the cyclohexanone **2a** results mainly from a 6-*endo* cyclization (deuteration at C2) and that a 5-*exo*-cyclization process followed by a Beckwith–Dowd-type rearrangement (deuteration at C3) only contributes marginally to the formation of **2a**.
[16] A deuterium-labeling experiment with Bu_3SnD proved that the cycloheptanone derivative **7** results from a 7-*endo* cyclization and not from a 6-*exo* cyclization followed by ring expansion.
[17] R. Chuard, A. Giraud, P. Renaud, *Angew. Chem.* **2002**, *114*, 4497; *Angew. Chem. Int. Ed.* **2002**, *41*, 4321.

Low-Temperature Stopped-Flow Studies on the Reactions of Copper(II) Complexes and H_2O_2: The First Detection of a Mononuclear Copper(II)–Peroxo Intermediate**

Takao Osako, Shigenori Nagatomo, Yoshimitsu Tachi, Teizo Kitagawa, and Shinobu Itoh*

Mononuclear copper-active oxygen complexes are key reactive intermediates in many biological and catalytic oxidation processes.[1–4] Aliphatic hydroxylation by O_2 is accomplished at the mononuclear copper-active sites in dopamine β-hydroxylase (DβH) and peptidylglycine α-amidating monooxygenase (PAM), and the oxidative modifications of tyrosine to 2,4,5-trihydroxyphenylalanine quinone (TPQ) and lysine tyrosylquinone (LTQ) cofactors are per-

[*] Prof. S. Itoh, T. Osako, Dr. Y. Tachi
Department of Chemistry
Graduate School of Science, Osaka City University
3-3-138 Sugimoto, Sumiyoshi-ku, Osaka 558-8585 (Japan)
Fax: (+81) 6-6605-2564
E-mail: shinobu@sci.osaka-cu.ac.jp
S. Nagatomo, Prof. T. Kitagawa
Institute for Molecular Science
Myodaiji, Okazaki 444-8585 (Japan)

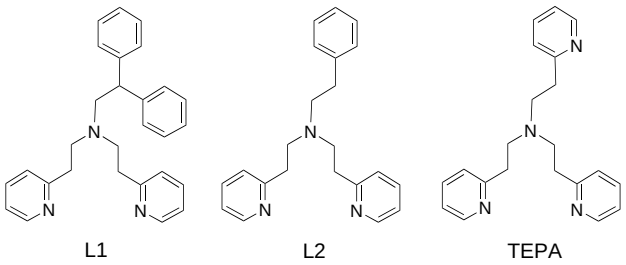
[**] This work was financially supported in part by Grants-in-Aid for Scientific Research on Priority Area (No. 11228206) and Grants-in-Aid for Scientific Research (No. 13480189) from the Ministry of Education, Culture, Sports, Science, and Technology, Japan.

Supporting information for this article is available on the WWW under http://www.angewandte.org or from the author.

 © 2002 WILEY-VCH Verlag GmbH & Co. KGaA, Weinheim 0044-8249/02/4122-4325 $ 20.00+.50/0

formed with the aid of cupric ions in the active sites of copper-containing amine oxidases and lysyl oxidase, respectively.[4,5] In these reactions, mononuclear Cu^{II}–hydroperoxo and/or Cu^{II}–peroxo species have been invoked as the active oxygen intermediates that participate in aliphatic and aromatic hydroxylation reactions.[4,5] To assess such intermediates, much effort has been made to develop metastable mononuclear copper model compounds. Thus, Cu^{II}–hydroperoxo complexes have been prepared by the reactions of copper(II) precursors and H_2O_2,[6–9] and mononuclear Cu^{II}–superoxo exhibiting either end-on (η^1-superoxo) or side-on (η^2-superoxo) binding mode have been prepared from the reactions of copper(I) complexes and O_2.[10–13] Although these studies have provided profound insights into the structure and spectroscopic features of the hydroperoxo and superoxo complexes, no information is presently available about mononuclear Cu^{II}–peroxo species.

Herein, low-temperature stopped-flow studies are described for the reactions of copper(II) complexes supported by tridentate ligands (L1 and L2) with H_2O_2 to demonstrate that a mononuclear Cu^{II}–peroxo complex is generated from an initially formed Cu^{II}–hydroperoxo intermediate [Eqs. (2) and (3)].[14] The results represent the first example of the direct detection of a mononuclear Cu^{II}–peroxo complex, which provides important information about the reactive intermediates involved in biological and industrial oxidation processes.



The reactions of copper(II) complexes with H_2O_2 were studied using a multi-scan double mixing stopped-flow spectrophotometer at −90 °C in methanol. Figure 1 shows a UV/Vis absorption spectral change for the first rapid process ($t = 0$–60 ms) of the reaction of $[Cu^{II}(L1)(ClO_4)_2]$ (0.2 mM), which contains the tridentate L1 ligand, and H_2O_2 (2.0 mM) in the presence of triethylamine (2.0 mM), where an absorption band at 360 nm ($\varepsilon = 2280\,M^{-1}\,cm^{-1}$) quickly appeared (spectrum (a)). The reaction obeys first-order kinetics, as shown in the inset of Figure 1, and a plot of the first-order rate constant $k_{obs(1)}$ against the concentration of H_2O_2 (2–10 mM) at a fixed concentration of triethylamine (2.0 mM) gave a Michaelis–Menten type saturation curve (as shown in Figure S1 in the Supporting Information). A similar saturation curve was obtained when the triethylamine concentration was increased from 2 to 10 mM at a fixed concentration of H_2O_2 (2.0 mM, Figure S2 in the Supporting Information). These kinetic results can be explained by the reaction sequences shown in Equations (1) and (2), where the counter anions (ClO_4^-) are omitted for simplicity.

Under the reaction conditions described above, the kinetic equation can be given as $k_{obs(1)} = (k_1 K_1[H_2O_2][Et_3N])/(K_1[H_2O_2] + 1)$ in the presence of excess H_2O_2 (for Figure S1 in the Supporting Information) and as $k_{obs(1)} = (k_1 K_1[H_2O_2][Et_3N])/(K_1[Et_3N] + 1)$ in the presence of excess Et_3N (for Figure S2 in the Supporting Information). Double reciprocal plots in both cases gave straight lines as shown in the insets of the respective figures from which the acid/base equilibrium constant K_1 and the rate constant k_1 have been determined as $7.2 \pm 0.5 \times 10^2\,M^{-1}$ and $4.1 \pm 0.3 \times 10^4\,M^{-1}\,s^{-1}$ from Figure S1, and $7.7 \pm 0.4 \times 10^2\,M^{-1}$ and $4.0 \pm 0.3 \times 10^4\,M^{-1}\,s^{-1}$ from Figure S2, respectively. The good agreement in the K_1 and k_1 values, determined independently from the rate dependence on $[H_2O_2]$ and $[Et_3N]$, strongly support the accuracy of the proposed mechanism shown in Equations (1) and (2).

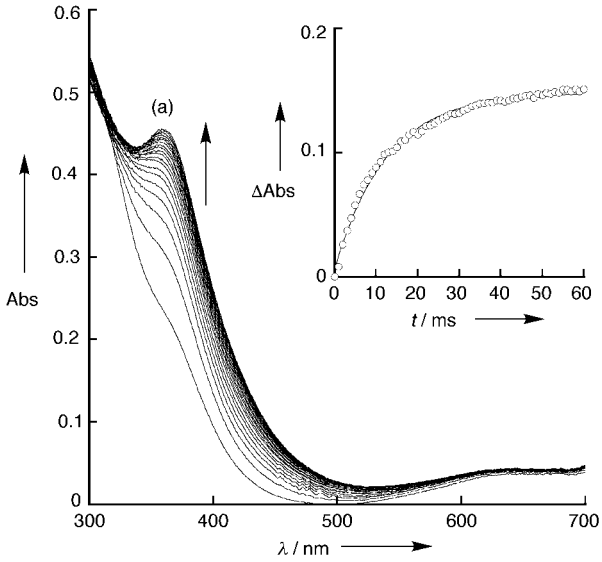


Figure 1. UV/Vis absorption spectra illustrating the first 60 ms of the reaction of $[Cu^{II}(L1)(ClO_4)_2]$ (0.2 mM) with H_2O_2 (2.0 mM) in the presence of triethylamine (2.0 mM) in CH_3OH at −90 °C. Inset: The change in absorption at 360 nm from $t = 0$–60 ms and its fit to a first-order model.

$$H_2O_2 + Et_3N \underset{}{\overset{K_1}{\rightleftharpoons}} HO_2^- Et_3NH^+ \quad (1)$$

$$[LCu^{II}]^{2+} + HO_2^- Et_3NH^+ \xrightarrow{k_1} [LCu^{II}\text{–}OOH]^+ + Et_3NH^+ \quad (2)$$

(A)

The reaction of $[Cu^{II}(TEPA)(ClO_4)](ClO_4)$, which contains the tetradentate tris[2-(2-pyridyl)ethyl]amine (TEPA) ligand, and H_2O_2 under the same experimental conditions also gave an intermediate that exhibited a similar absorption spectrum ($\lambda_{max} = 332$ nm, $\varepsilon = 4240\,M^{-1}\,cm^{-1}$, Figure S3 in the Supporting Information), and also similar kinetic behavior ($K_1 = 7.6 \pm 0.4 \times 10^2\,M^{-1}$ and $k_1 = 8.2 \pm 0.4 \times 10^2\,M^{-1}\,s^{-1}$, and $K_1 = 8.3 \pm 0.4 \times 10^2\,M^{-1}$ and $k_1 = 7.9 \pm 0.4 \times 10^2\,M^{-1}\,s^{-1}$ from Figures S4 and S5, respectively, in the Supporting Information) as the reactions described above for the complex with the L1 ligand. Moreover, the λ_{max} and ε values in the UV/Vis spectra, as well as the resonance Raman band at 851 cm^{-1} (Figure S6 in the Supporting Information)[15] of the intermediate are fairly close to those for the reported mononuclear Cu^{II}–hydroperoxo complexes supported by other tetradentate pyridine ligands.[7–9] All of the spectroscopic features, as well as the

 © 2002 WILEY-VCH Verlag GmbH & Co. KGaA, Weinheim 0044-8249/02/4122-4326 $ 20.00+.50/0 *Angew. Chem. Int. Ed.* **2002**, *41*, No. 22

good agreement in the K_1 values between the TEPA and L1 ligand systems ($K_1 = 7.2–7.9 \times 10^2\,M^{-1}$) indicate that the initially formed intermediates for both the tridentate and tetradentate ligand systems involve an η^1-OOH group, as shown in Equation (2).

Notably, the product resulting from the Cu^{II}–hydroperoxo intermediate of L1 was totally different from that resulting from the TEPA complex. The hydroperoxo intermediate (**A**) supported by TEPA was converted into the corresponding copper(I) complex, $[Cu^{I}(TEPA)]^+$ ($k_{obs(2)} = 0.19 \pm 0.1\ s^{-1}$),[16] whereas the hydroperoxo species supported by L1 readily gave a mononuclear Cu^{II}–peroxo intermediate (**B**) as demonstrated below.

The Cu^{II}–OOH intermediate **A** further reacted in the next timeframe ($t = 100$ ms–1.5 s) to give the spectral change shown in Figure 2, where the absorption band of intermediate **A** (spectrum (a)) further increased to give spectrum (b) with $\lambda_{max} = 366$ nm ($\varepsilon = 3110\,M^{-1}cm^{-1}$). The observed first-order rate constant ($k_{obs(2)} = 1.6 \pm 0.1\ s^{-1}$) of this process was independent of both $[H_2O_2]$ and $[Et_3N]$ (Figures S7 and S8), which indicates that an intramolecular reaction of the mononuclear hydroperoxo intermediate **A** is involved. The position of the peak maximum in spectrum (b) of Figure 2 is consistent with that of the reported (μ-η^2:η^2-peroxo)dicopper(II) complexes, but the absorption intensity (ε) is significantly smaller than that of the reported dinuclear copper(II) peroxo complexes.[17,18] Furthermore, an ESR spectrum of a copper(II) complex with a $d_{x^2-y^2}$ ground state (spectrum (b) in Figure S9 in the Supporting Information) was recorded in the early stage of the reaction. This spectrum differed from that of the starting material (spectrum (a) in Figure S9). In addition, a similar absorption spectrum was obtained in the reaction of $[Cu^{II}(L2)(ClO_4)_2]$ with H_2O_2 under the same experimental conditions ($\lambda_{max} = 362$ nm, $\varepsilon = 4880\,M^{-1}cm^{-1}$), although the Cu^{II}–OOH intermediate of L2 was too reactive to be detected. Based on these results, together with the totally different reaction patterns of intermediate **A** in the tridentate and tetradentate ligand systems, we tentatively assigned the second intermediate observed in Figure 2 as a mononuclear Cu^{II}–peroxo complex (**B**), presumably having a side-on binding mode, as indicated in Equation (3).

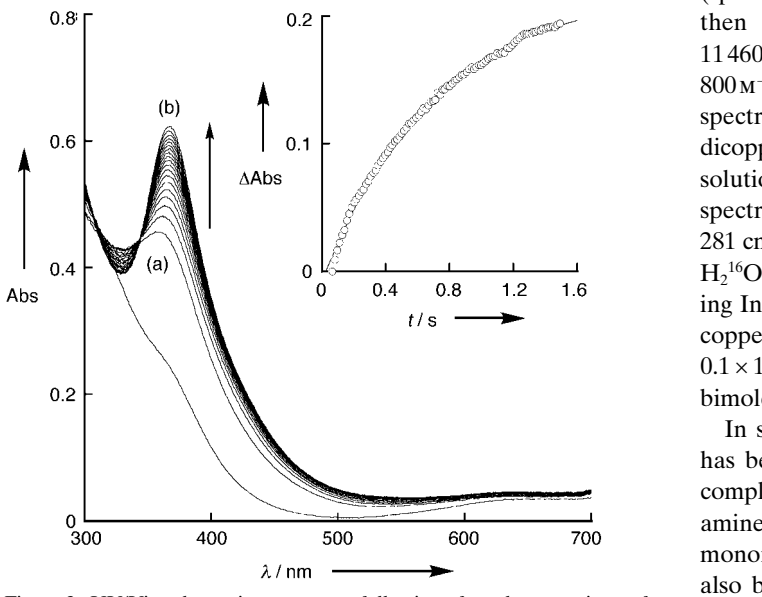


Figure 2. UV/Vis absorption spectra following for the reaction of $[Cu^{II}(L1)(ClO_4)_2]$ (0.2 mM) with H_2O_2 (2.0 mM) in the presence of triethylamine (2.0 mM) in CH_3OH at −90 °C from $t = 0.1$–1.5 s. Inset: The change in absorption at 366 nm from $t = 0.1$–1.5 s and its fit to a first-order model.

$$\underset{\textbf{(A)}}{LCu^{II}\text{-}OOH} \xrightarrow{k_2} \underset{\textbf{(B)}}{LCu^{II}(O_2)} \xrightarrow{k_3[Cu^{II}(L)]} \underset{\textbf{(C)}}{LCu^{II}(O_2)Cu^{II}L} \qquad (3)$$

The lack of rate-dependence on $[Et_3N]$ in the $k_{obs(2)}$ process (Figure S8) may suggest that internal rearrangement of the ligand framework from the η^1-hydroperoxo motif (**A**) to an η^2-hydroperoxo form (**A′**, a side-on hydroperoxo binding mode, not shown in Equation (3)) is rate-determining, while the following deprotonation from **A′** to give **B** is much faster. The higher reactivity of intermediate **A** for ligand L2, as compared to that of L1, can be attributed to the relative steric bulk of the *N*-alkyl substituents (-CH_2CHPh_2 in L1 versus -CH_2CH_2Ph in L2). The larger *N*-alkyl group in L1 may retard the rearrangement of the monodentate η^1-hydroperoxo ligand in **A** to the bidentate η^2-hydroperoxo ligand in **A′**, which stabilizes intermediate **A** in the L1 complex more strongly than in the L2 system. Furthermore, this process is completely prohibited in the case of the tetradentate TEPA ligand system, since there is no extra coordination site available for formation of side-on (hydro)peroxo intermediate(s). Thus the kinetic results, as well as the ligand effects of L2 and TEPA, are all consistent with formation of the proposed side-on peroxo intermediate **B**.

Intermediate **B** was further converted into a (μ-η^2:η^2-peroxo)dicopper(II) complex (**C**) at higher concentrations of the copper complex. Thus, the reaction of $[Cu^{II}(L1)(ClO_4)_2]$ (2.0 mM) with H_2O_2 (2.0 mM) in the presence of triethylamine (2.0 mM) in methanol at −90 °C gave absorption spectra where the peak for intermediate **B** immediately appeared (spectrum b in Figure S10 in the Supporting Information), and then the characteristic absorption band at 366 nm ($\varepsilon = 11\,460\,M^{-1}cm^{-1}$) together with a small band at 540 nm ($\varepsilon = 800\,M^{-1}cm^{-1}$) gradually developed (spectrum (c)). The final spectrum is nearly the same as that of the (μ-η^2:η^2-peroxo)-dicopper(II) complex supported by L2,[18] and the resulting solution was ESR-silent. Furthermore, the resonance Raman spectrum of the product exhibits Raman bands at 741 and 281 cm^{-1}, the former of which is shifted to 700 cm^{-1} when $H_2{}^{16}O_2$ is substituted with $H_2{}^{18}O_2$ (Figure S11 in the Supporting Information).[19] The formation of the (μ-η^2:η^2-peroxo)dicopper(II) complex obeys second-order kinetics ($k_3 = 2.6 \pm 0.1 \times 10^2\,M^{-1}s^{-1}$), which demonstrates that this reaction is a bimolecular process, with respect to the copper(II) complex.

In summary, the low-temperature stopped-flow technique has been applied to study the reactions between copper(II) complexes of the tridentate and tetradentate pyridylethylamine ligands and H_2O_2, which has enabled us to detect a mononuclear Cu^{II}–peroxo complex for the first time. It has also been found that the ligand denticity (tridentate versus tetradentate) and the steric effects of the *N*-alkyl substituents in the pyridylethylamine derivatives drastically alter the reactivity of the initially formed Cu^{II}–hydroperoxo intermedi-

 © 2002 WILEY-VCH Verlag GmbH & Co. KGaA, Weinheim 0044-8249/02/4122-4327 $ 20.00+.50/0

ates. These results provide significantly important information about the dioxygen-activation mechanism in biological and industrial systems.

Experimental Section

Synthetic procedures of ligands L2 and TEPA, as well as the copper(II) complex of L2 have been reported elsewhere.[18,20]

L1: 2,2-Diphenylethylamine (1.97 g, 10 mmol) and 2-vinylpyridine (5.25 g, 50 mmol) were heated to reflux in CH_3OH (20 mL) containing acetic acid (3.01 g, 50 mmol) for 10 days. The solvent was removed by evaporation, and the resulting viscous material was dissolved in H_2O (200 mL) and extracted with $CHCl_3$ (3×200 mL). After drying over anhydrous K_2CO_3, evaporation of the organic solvent gave yellow oily material, from which L1 was isolated by SiO_2 column chromatography ($CHCl_3$/AcOEt as eluent) in 54% yield (2.21 g); ^{1}H NMR (300 MHz, $CDCl_3$): $\delta = 2.76$–2.96 (m, 8H; -CH_2-CH_2-Py), 3.16 (d, $J = 7.5$ Hz, 2H; -CH_2-CH-Ph_2), 4.09 (t, $J = 7.5$ Hz, 1H; -CH-Ph_2), 6.76 (d, $J = 7.8$ Hz, 2H; $H_{py\text{-}5}$), 7.03–7.26 (m, 12H; C_6H_4 and $H_{py\text{-}3}$), 7.43 (td, $J = 1.8$ and 7.8 Hz, 2H; $H_{py\text{-}4}$), 8.50 ppm (ddd, $J = 0.9$, 1.8, and 4.8 Hz, 2H; $H_{py\text{-}6}$); FAB-HRMS (positive ion): calcd for $C_{28}H_{29}N_3$: m/z 406.2283; found: m/z 406.2289 [M^+].

$[Cu^{II}(L1)(ClO_4)_2]\cdot H_2O$: Ligand L1 (122.3 mg, 0.3 mmol) was treated with $Cu^{II}(ClO_4)_2\cdot 6H_2O$ (111.2 mg, 0.3 mmol) in CH_3OH (10 mL) for 30 min at room temperature. Addition of Et_2O (200 mL) to the mixture gave blue solids that were isolated by decantation, washed three times with Et_2O, and dried (83% yield). Single crystals were obtained by vapor diffusion of Et_2O into a solution of the complex in CH_3OH. FTIR (KBr): $\tilde{\nu} = 1130$, 1043, 621 cm^{-1} (ClO_4^-); FAB-MS (positive ion): m/z 569.2 [M^+]; elemental analysis for $[Cu^{II}(L1)(ClO_4)_2]\cdot H_2O$, calcd (%) for $C_{28}H_{31}O_9N_3CuCl_2$: C 48.88, H 4.54, N 6.11; found: C 48.72, H 4.48, N 6.06.

$[Cu^{II}(TEPA)(ClO_4)]ClO_4$: The TEPA ligand (332.5 mg, 1.0 mmol) was treated with $Cu^{II}(ClO_4)_2\cdot 6H_2O$ (370.5 mg, 1.0 mmol) in CH_3CN (10 mL) for 30 min at room temperature. Addition of Et_2O (200 mL) to the mixture gave a blue oily material that was isolated by decantation and redissolved into CH_3OH (10 mL). Addition of the CH_3OH solution into Et_2O (200 mL) gave blue solids that were isolated by decantation, washed with Et_2O three times, and dried (95% yield). Single crystals were obtained by vapor diffusion of Et_2O into a solution of the complex in CH_3OH. FTIR (KBr): $\tilde{\nu} = 1143$, 1081, 625 cm^{-1} (ClO_4^-); FAB-MS (positive ion): m/z 494.07 [M^+]; elemental analysis for $[Cu^{II}(TEPA)(ClO_4)](ClO_4)$, calcd (%) for $C_{21}H_{28}O_8N_4CuCl_2$: C 39.98, H 4.47, N 8.88; found: C 40.18, H 4.16, N 8.87.

Caution! The perchlorate salts in this study are all potentially explosive and should be handled with care.

Kinetic measurements for the reaction of copper(II) complexes (0.2 mM) and H_2O_2 were performed by using a multi-scan double mixing stopped-flow spectrophotometer designed for low-temperature measurements (RSP-1000, Unisoku Co., Ltd.) in CH_3OH at $-90\,^\circ$C. The reaction of $[Cu^{II}(L1)(ClO_4)_2]$ and H_2O_2 at the higher concentration (Figure S10 in the Supporting Information) was followed using the previously reported[18] Hewlett Packard HP8453 diode array spectrophotometer with a Unisoku thermostated cell holder designed for low-temperature measurements.

Received: June 26, 2002
Revised: August 28, 2002 [Z19616]

[1] A. G. Blackman, W. B. Tolman in *Metal-Oxo and Metal-Peroxo Species in Catalytic Oxidations* (Ed.: B. Meunier), Springer, Berlin, **2000**, pp. 179–211.
[2] S. Schindler, *Eur. J. Inorg. Chem.* **2000**, 2311–2326.
[3] E. I. Solomon, U. M. Sundaram, T. E. Machonkin, *Chem. Rev.* **1996**, *96*, 2563–2605.
[4] J. P. Klinman, *Chem. Rev.* **1996**, *96*, 2541–2561.
[5] N. M. Okeley, W. A. van der Donk, *Chem. Biol.* **2000**, *7*, R159-R171.
[6] P. Chen, K. Fujisawa, E. I. Solomon, *J. Am. Chem. Soc.* **2000**, 122, 10177–10193.
[7] A. Wada, M. Harata, K. Hasegawa, K. Jitsukawa, H. Masuda, M. Mukai, T. Kitagawa, H. Einaga, *Angew. Chem.* **1998**, *110*, 874–875; *Angew. Chem. Int. Ed.* **1998**, *37*, 798–799.
[8] M. Kodera, T. Kita, I. Miura, N. Nakayama, T. Kawata, K. Kano, S. Hirota, *J. Am. Chem. Soc.* **2001**, *123*, 7715–7716.
[9] H. Ohtsu, S. Itoh, S. Nagatomo, T. Kitagawa, S. Ogo, Y. Watanabe, S. Fukuzumi, *Inorg. Chem.* **2001**, *40*, 3200–3207.
[10] K. Fujisawa, M. Tanaka, Y. Moro-oka, N. Kitajima, *J. Am. Chem. Soc.* **1994**, *116*, 12079–12080.
[11] D. J. E. Spencer, N. W. Aboelella, A. M. Reynolds, P. L. Holland, W. B. Tolman, *J. Am. Chem. Soc.* **2002**, *124*, 2108–2109.
[12] K. D. Karlin, N. Wei, B. Jung, S. Kaderli, P. Niklaus, A. D. Zuberbühler, *J. Am. Chem. Soc.* **1993**, *115*, 9506–9514.
[13] D.-H. Lee, N. Wei, N. N. Murthy, Z. Tyeklár, K. D. Karlin, S. Kaderli, B. Jung, A. D. Zuberbühler, *J. Am. Chem. Soc.* **1995**, *117*, 12498–12513.
[14] The low-temperature stopped-flow technique has been well documented as a useful tool for the detection of unstable copper–dioxygen intermediates; a) J. A. Halfen, S. Mahapatra, E. C. Wilkinson, S. Kaderli, V. G. Young, Jr., L. Que, Jr., A. D. Zuberbühler, W. B. Tolman, *Science* **1996**, *271*, 1397–1400; b) K. D. Karlin, S. Kaderli, A. D. Zuberbühler, *Acc. Chem. Res.* **1997**, *30*, 139–147; c) M. Weitzer, M. Schatz, F. Hampel, F. W. Heinemann, S. Schindler, *J. Chem. Soc. Dalton Trans.* **2002**, 686–694.
[15] Because of the low intensity of the Raman band of the ^{18}O-derivative, the size of the isotope shift could not be determined accurately. Although the evidence for the (η^1-hydroperoxo)copper(II) species from Raman spectroscopy is not as strong as in earlier instances,[6–9] the structural similarity of this molecule to others in the series[9] and great similarities of the UV/Vis and the ^{16}O-Raman data to those of the other (η^1-hydropeeroxo)copper(II) complexes[6–9] are strong enough arguments for the presence of the hydroperoxo intermediate.
[16] UV/Vis spectroscopy and ESI-MS analysis of the final solution were identical to those of an authentic sample of $[Cu^I(TEPA)](ClO_4)$.
[17] N. Kitajima, K. Fujisawa, Y. Moro-oka, *J. Am. Chem. Soc.* **1989**, *111*, 8975–8976.
[18] S. Itoh, H. Nakao, L. M. Berreau, T. Kondo, M. Komatsu, S. Fukuzumi, *J. Am. Chem. Soc.* **1998**, *120*, 2890–2899.
[19] The isotope-insensitive Raman band at 281 cm^{-1} has recently been assigned to an A_g "accordion" mode of the Cu_2O_2 peroxo core, predominantly involving Cu–Cu motion; M. J. Henson, V. Mahadevan, T. D. P. Stack, E. I. Solomon, *Inorg. Chem.* **2001**, *40*, 5068–5069.
[20] K. D. Karlin, S. E. Sherman, *Inorg. Chim. Acta* **1982**, *65*, L39-L40.

Indenol Ether Formation from Aryl Alkynes Bearing *ortho*-Acetals: An Unprecedented Rearrangement in Palladium-Catalyzed Carboalkoxylation

Itaru Nakamura, Gan B. Bajracharya, Yuya Mizushima, and Yoshinori Yamamoto*

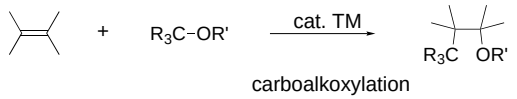
The catalytic addition reaction to a C–C multiple bond is one of the most important processes for organic synthesis, because this process can construct new chemical bonds in an efficient and atom-economic manner. A wide variety of transition-metal-catalyzed (TM-catalyzed) addition reactions of pronucleophiles (H–CR_3,[1] H–NR_2,[2] H–OR,[3] H–OC(O)R,[4] H–SR,[5] H–PR_2,[6] etc.) and hydrides (H–B,[7]

[*] Prof. Dr. Y. Yamamoto, Dr. I. Nakamura, G. B. Bajracharya, Y. Mizushima
Department of Chemistry
Graduate School of Science
Tohoku University, Sendai 980-8578 (Japan)
Fax: (+81) 22-217-6784
E-mail: yoshi@yamamoto1.chem.tohoku.ac.jp

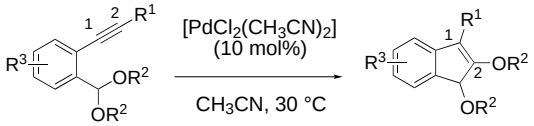
Supporting information for this article is available on the WWW under http://www.angewandte.org or from the author.

 © 2002 WILEY-VCH Verlag GmbH & Co. KGaA, Weinheim 0044-8249/02/4122-4328 $ 20.00+.50/0

H–Si,[8] H–Sn,[9] etc.) have been developed and become a powerful method to construct various kinds of carbon–carbon and carbon–heteroatom bonds. More recently, transition-metal-catalyzed addition of other types of bonds, such as B–B,[10] B–Si,[11,12] Si–Si,[8a,11,13] Si–Sn,[11,14] Sn–Sn,[15] etc., have been reported. However, catalytic addition of a carbon–oxygen bond to carbon–carbon multiple bonds, so-called carboalkoxylation, has rarely been investigated, perhaps because of the lower reactivity of ether C–O bonds,[16] although this process is useful to construct both carbon–-carbon and carbon–oxygen bonds simultaneously [Eq. (1)]. It occurred to us that an acetal C–O bond would be more reactive than that in ethers. We now report that the palladium-catalyzed reaction of the aryl alkynes bearing *ortho*-acetals **1** gives the indenol ether **2** in high to moderate yields [Eq. (2)]. The mechanistic investigation of this unprecedented rearrangement[17] reveals that R^1 migrates from the C-2 atom to the C-1 atom under the palladium-catalysis conditions.



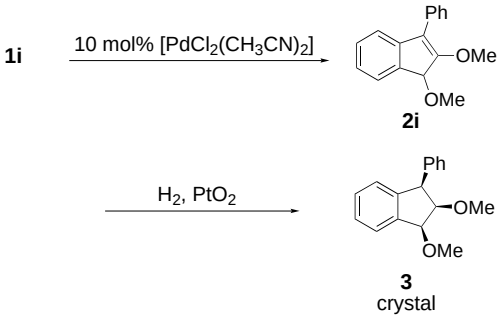
(1)



(2)

The results of our study are summarized in Table 1. In the presence of 10 mol% of $[PdCl_2(CH_3CN)_2]$, the reaction of 2-(1-pentynyl)benzaldehyde dimethyl acetal (**1a**) proceeded smoothly at 30°C, and the corresponding 1,2-dimethoxyindene derivative **2a** was obtained in 75% yield (entry 1). Other transition-metal compounds, such as $[Pd(PPh_3)_4]$, $Pd(OAc)_2$, $NiCl_2$, and $[RhCl(cod)]_2$ (cod = 1,5-cyclooctadiene), didn't promote the reaction at all. The reaction of **1a** proceeded even at room temperature and produced **2a** in 63% yield, although the reaction took slightly longer. The reaction of the corresponding diethylacetal **1b** and dibutylacetal **1c** gave **2b** and **2c** in 87% and 80% yield, respectively (entries 2 and 3). The reaction of the dimethylacetal **1d** and diethylacetal **1e** of 2-(1-octynyl)benzaldehyde also proceeded very smoothly (entries 4 and 5). Chloro, bromo, and ester substituents were tolerated in this reaction (entries 6 and 7). The steric bulk of R^1 exerted significant influence on the speed of the reaction. The reaction of 2-(cyclohexylethynyl)-benzaldehyde dimethylacetal **1h** proceeded at 60°C, producing **2h** in 52% yield after 15 h (entry 8). The presence of the *tert*-butyl group ($R^1 = t$Bu) totally halted the reaction and the starting material was recovered under the reaction conditions described above. The reaction of 2-(2-phenylethynyl)benzaldehyde dimethylacetal **1i** gave the corresponding 3-aryl indenol ether **2i** in a moderate yield (entry 9). The reaction of **1j**, **1k**, and **1l** with substituents on the initial aromatic ring, proceeded in a similar manner (entries 10–12). On the contrary, the reaction of **1m** and **1n**, which had a methoxy group at the 4 and 5-positions, respectively, did not proceed at all.

The structure of **2** was confirmed by spectroscopic methods (especially by NOE analysis, see Supporting Information). Furthermore, the structure of **2i** was determined unambiguously by an X-ray crystallographic analysis of **3**, which was obtained through the hydrogenation of the double bond of **2i** [Eq. (3)]. The ORTEP structure of **3** is shown in Figure 1. It is



(3)

clear that the phenyl group of **1i** is at the benzylic position (C-1) of **2i** and the two methoxy groups at the C-2 and C-3 positions.

Plausible mechanisms of this reaction are illustrated in Scheme 1. The acetal group of **1** coordinates to an electron deficient Pd^{II} center as shown in **4** (route **A**). A carbon–oxygen bond would be cleaved to generate the oxonium cation **5** and the palladium alkoxide species. Nucleophilic attack of the oxonium cation by the alkynyl group would produce the five-membered ring species **6**. Alkoxypalladation of the C–C double bond of **6** would form the palladium–carbene complex **7**.[18] Migration of R^1 followed by elimination of $PdCl_2$ would produce the carboalkoxylation product **2**. Alternatively, it is conceivable that coordination of the alkynyl moiety of **1** to Pd^{II} (as shown in **8**) occurs at the beginning of catalytic cycle (route **B**). Nucleophil-

Table 1. Palladium-catalyzed carboalkoxylation of the *o*-alkynylbenzaldehyde dialkylacetals **1**.[a]

Entry	**1**	R^1	R^2	R^3	**2**	Yield [%][b]
1	**1a**	*n*Pr	Me	H	**2a**	75
2	**1b**	*n*Pr	Et	H	**2b**	87
3	**1c**	*n*Pr	Bu	H	**2c**	80
4	**1d**	*n*Hex	Me	H	**2d**	65
5	**1e**	*n*Hex	Et	H	**2e**	54
6	**1f**	$(CH_2)_4Cl$	Me	H	**2f**	45
7	**1g**	$(CH_2)_4OCO(p\text{-}BrC_6H_4)$	Me	H	**2g**	45
8[c]	**1h**	cyclohexyl	Me	H	**2h**	52
9	**1i**	Ph	Me	H	**2i**	40
10	**1j**	*n*Pr	Me	4-CF_3	**2j**	57
11	**1k**	*n*Pr	Me	5-CF_3	**2k**	52
12	**1l**	*n*Pr	Me	4-Me	**2l**	51

[a] The reaction of **1** was carried out in the presence of 10 mol% of $[PdCl_2(CH_3CN)_2]$ in CH_3CN at 30°C for 15 h. [b] Yield of product isolated. [c] The reaction was carried out at 60°C.

 © 2002 WILEY-VCH Verlag GmbH & Co. KGaA, Weinheim 0044-8249/02/4122-4329 $ 20.00+.50/0

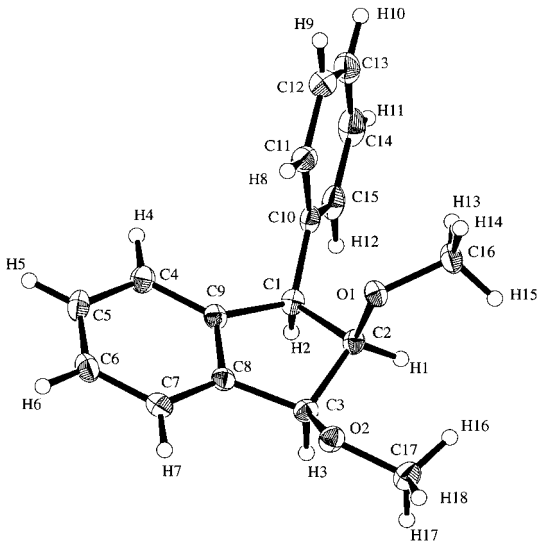
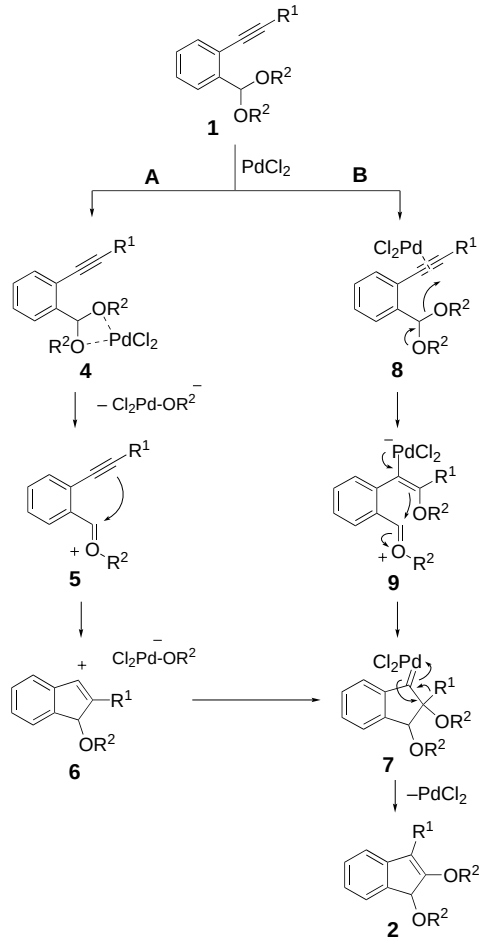


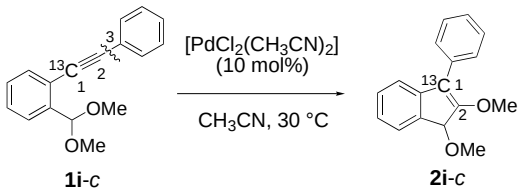
Figure 1. ORTEP drawing of **3** (thermal ellipsoids set at 50% probability).



Scheme 1. Plausible mechanisms which lead to the formation of **2**.

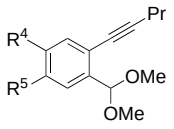
ic attack of the electron-deficient carbon–carbon triple bond by an alkoxide would give the vinylpalladium species **9**, which subsequently undergoes the ring-closing C–C bond formation to produce the palladium carbene species **7**.

To confirm the proposed step from **7** to **2** in Scheme 1, we carried out a ^{13}C labeling experiment [Eq. (4)]. In the



(4)

presence of catalytic amounts of $[PdCl_2(CH_3CN)_2]$, the reaction of **1i**-*c*, which has a ^{13}C carbon atom at the C-1 position, gave **2i**-*c* in 40% yield along with a trace amount of unknown byproducts. This result clearly indicates that the bond cleavage occurred between the C-2 and C-3 positions of **1i**-*c*.



1j ($R^4 = CF_3$, $R^5 = H$)
1k ($R^4 = H$, $R^5 = CF_3$)
1l ($R^4 = Me$, $R^5 = H$)
1m ($R^4 = MeO$, $R^5 = H$)
1n ($R^4 = H$, $R^5 = MeO$)

The palladium-catalyzed hydrolysis of acetals and ketals, which lead to the corresponding carbonyl compounds, was reported by Lipshutz et al.,[19] and the rhodium-catalyzed substitution reaction of acetals with TMSCN (TMS = trimethylsilyl) to produce α-alkoxycyanides was reported by Mukaiyama and co-workers.[20] To our knowledge, however, catalytic addition of an acetal carbon–oxygen bond to carbon–carbon multiple bonds is not known. The structural framework of indenol derivatives is often found in naturally occurring compounds,[21] and the alkenyl ether functionality may be synthetically elaborated by reaction with a variety of electrophiles.

Experimental Section

Synthesis of **2a**: **1a** (109.2 mg, 0.5 mmol) in acetonitrile (1 mL) was added to $[PdCl_2(CH_3CN)_2]$ (12.9 mg, 0.05 mmol) in acetonitrile (1 mL) under an Ar atmosphere, in a pressure vial. After heating at 30 °C for 15 h, the reaction mixture was filtered through a short silica-gel column using ethyl acetate as an eluent. Separation by silica-gel column chromatography using hexane/EtOAc as an eluent afforded the product **2a**. IR (neat): $\tilde{\nu} = 3067$–2823, 1648, 1607, 1469, 1350, 1332, 1249, 1164, 1099, 1060, 1035, 933, 758, 731 cm^{-1}; ^1H NMR (500 MHz, $CDCl_3$): $\delta = 0.95$ (t, $J = 7.3$ Hz, 3H), 1.58 (m, 2H), 2.39 (m, 2H), 3.10 (s, 3H), 3.96 (s, 3H), 5.18 (s, 1H), 7.06–7.03 (m, 2H), 7.31–7.21 ppm (m, 2H); ^{13}C NMR (125 MHz, $CDCl_3$): $\delta = 14.07$, 21.22, 25.11, 51.44, 57.85, 78.33, 117.68, 119.70, 123.23, 123.55, 128.64, 136.19, 144.53, 156.89 ppm; elemental analysis (%) calcd for $C_{14}H_{18}O_2$ (218.30): C 77.03, H 8.31; found: C 76.78, H 8.37; HRMS (EI) calcd for $C_{14}H_{18}O_2$: *m*/*z* 218.1306, found: *m*/*z* 218.1307.

Received: July 11, 2002 [Z19716]

[1] Review: a) S. Murai, *Activation of Unreactive Bonds and Organic Synthesis: Topics in Organometallic Chemistry, Vol. 3*, Springer, New York, **1999**, pp. 47–79; b) Y. Yamamoto, U. Radhakrishnan, *Chem. Soc. Rev.* **1999**, *28*, 199; c) G. Dyker, *Angew. Chem.* **1999**, *111*, 1808; *Angew. Chem. Int. Ed.* **1999**, *38*, 1698.

[2] Review: a) M. B. Gasc, A. Lattes, J. J. Perie, *Tetrahedron* **1983**, *39*, 703; b) D. Savoia, *Methoden Org. Chem. (Houben-Weyl) 4th ed. 1952–, Vol. E21e*, **1995**, p. 5356; c) T. E. Müller, M. Beller, *Chem. Rev.* **1998**, *98*, 675.

[3] a) E. J. Smutny, *J. Am. Chem. Soc.* **1967**, *89*, 6793; b) H. Yagi, E. Tanaka, H. Ishiwatari, M. Hidai, Y. Uchida, *Synthesis* **1977**, 334; c) Y. Inoue, Y. Ohtsuka, H. Hashimoto, *Bull. Chem. Soc. Jpn.* **1984**, *57*, 3345; d) D. R. Coulson, *J. Org. Chem.* **1973**, *38*, 1483; e) D. H. Camacho, I. Nakamura, S. Saito, Y. Yamamoto, *Angew. Chem.* **1999**,

 © 2002 WILEY-VCH Verlag GmbH & Co. KGaA, Weinheim 0044-8249/02/4122-4330 $ 20.00+.50/0

111, 3576; *Angew. Chem. Int. Ed.* **1999**, *38*, 3365; f) D. H. Camacho, I. Nakamura, S. Saito, Y. Yamamoto, *J. Org. Chem.* **2001**, *66*, 270.
[4] a) T. Mitsudo, Y. Hori, Y. Yamakawa, Y. Watanabe, *J. Org. Chem.* **1987**, *52*, 2230; b) D. M. T. Chan, T. B. Marder, D. Milstein, N. J, Taylor, *J. Am. Chem. Soc.* **1987**, *109*, 6385; c) B. M. Trost, W. Brieden, K. H. Baringhaus, *Angew. Chem.* **1992**, *104*, 1392; *Angew. Chem. Int. Ed. Engl.* **1992**, *31*, 1335; d) H. Doucet, B. Martin-Vaca, C. Bruneau, P. H. Dixneuf, *J. Org. Chem.* **1995**, *60*, 7247; e) M. Al-Masum, Y. Yamamoto, *J. Am. Chem. Soc.* **1998**, *120*, 3809.
[5] Review: a) T. Kondo, T. Mitsudo, *Chem. Rev.* **2000**, *100*, 3205; for hydrothiolation of alkynes, b) A. Ogawa, T. Ikeda, K. Kimura, T. Hirao, *J. Am. Chem. Soc.* **1999**, *121*, 5108.
[6] Addition of P–H bonds to alkynes: a) L.-B. Han, R. Hua, M. Tanaka, *Angew. Chem.* **1998**, *110*, 98; *Angew. Chem. Int. Ed.* **1998**, *37*, 94; b) M. A. Kazankova, I. V. Efimova, A. N. Kochetkov, V. V. Afanas′ev, I. P. Beletskaya, P. H. Dixneuf, *Synlett* **2001**, 497.
[7] Review: a) I. Beletskaya, A. Pelter, *Tetrahedron* **1997**, *53*, 4957; b) "Metal-catalyzed Hydroboration Reactions": G. C. Fu in *Transition Metals for Organic Synthesis* (Eds.: M. Beller, C. Bolm), Wiley-VCH, Weinheim, **1998**, pp. 141 – 146.
[8] Review: a) K. A. Horn, *Chem. Rev.* **1995**, *95*, 1317; b) "Hydrosilylation of Olefins": K. Yamamoto, T. Hayashi in *Transition Metals for Organic Synthesis* (Eds.: M. Beller, C. Bolm), Wiley-VCH, Weinheim, **1998**, pp. 120 – 129.
[9] Review: N. D. Smith, J. Mancuso, M. Lautens, *Chem. Rev.* **2000**, *100*, 3257.
[10] Diboration of alkynes: a) T. Ishiyama, N. Matsuda, N. Miyaura, A. Suzuki, *J. Am. Chem. Soc.* **1993**, *115*, 11018; b) T. Ishiyama, N. Matsuda, M. Murata, F. Ozawa, A. Suzuki, N. Miyaura, *Organometallics* **1996**, *15*, 713; c) G. Lesley, P. Nguyen, N. J. Taylor, T. B. Marder, A. J. Scott, W. Clegg, N. C. Norman, *Organometallics* **1996**, *15*, 5137; d) C. N. Iverson, M. R. Smith III, *Organometallics* **1996**, *15*, 5155.
[11] Review: M. Suginome, Y. Ito, *Chem. Rev.* **2000**, *100*, 3221.
[12] Silaboration of alkynes, a) M. Suginome, H. Nakamura, Y. Ito, *Chem. Commun.* **1996**, 2777; b) M. Suginome, T. Matsuda, H. Nakamura, Y. Ito, *Tetrahedron* **1999**, *55*, 8787.
[13] Disilylation of alkynes: a) H. Sakurai, Y. Kamiyama, Y. Nakadaira, *J. Am. Chem. Soc.* **1975**, *97*, 931; b) F. Ozawa, M. Sugawara, T. Hayashi, *Organometallics* **1994**, *13*, 3237.
[14] Silastannylation of alkynes: M. Hada, Y. Tanaka, M. Ito, M. Murakami, H. Amii, Y. Ito, H. Nakatsuji, *J. Am. Chem. Soc.* **1994**, *116*, 8754.
[15] E. Piers, R. T. Skerlj, *J. Chem. Soc. Chem. Commun.* **1986**, 626.
[16] a) H. Nakamura, M. Sekido, M. Ito, Y. Yamamoto, *J. Am. Chem. Soc.* **1998**, *120*, 6838; b) N. Moneiro, G. Balme, *Synlett* **1998**, 746; c) A. Fürstner, H. Szillat, F. Stelzer, *J. Am. Chem. Soc.* **2000**, *122*, 6785.
[17] Catalytic skeletal rearrangement: a) T. J. Katz, T. M. Sivavec, *J. Am. Chem. Soc.* **1985**, *107*, 737; b) A. Kinoshita, M. Mori, *Synlett* **1994**, 1020; c) B. M. Trost, G. J. Tanoury, *J. Am. Chem. Soc.* **1988**, *110*, 1636; d) B. M. Trost, M. K. Trost, *J. Am. Chem. Soc.* **1991**, *113*, 1850; e) B. M. Trost, A. S. K. Hashmi, *Angew. Chem.* **1993**, *105*, 1130; Angew. *Chem. Int. Ed.* **1993**, *32*, 1085; f) N. Chatani, T. Morimoto, T. Muto, S. Murai, *J. Am. Chem. Soc.* **1994**, *116*, 6049; g) N. Chatani, N. Furukawa, H. Sakurai, S. Murai, *Organometallics* **1996**, *15*, 901; h) N. Chatani, K. Kataoka, S. Murai, N. Furukawa, Y. Seki, *J. Am. Chem. Soc.* **1998**, *120*, 9104; i) ref. [16c].
[18] a) W. A. Herrmann, C.-P. Reisinger, M. Spiegler, *J. Organomet. Chem.* **1998**, *557*, 93; b) K. L. Greenman, D. S. Carter, D. L. Van Vranken, *Tetrahedron* **2001**, *57*, 5219; c) K. Miki, F. Nishino, K. Ohe, U. Sakae, *J. Am. Chem. Soc.* **2002**, *124*, 5260.
[19] B. H. Lipshutz, D. Pollart, J. Monforte, H. Kotsuki, *Tetrahedron Lett.* **1985**, *26*, 705.
[20] T. Soga, H. Takenoshita, M. Yamada, T. Mukaiyama, *Bull. Chem. Soc. Jpn.* **1990**, *63*, 3122.
[21] a) T. Kumamoto, N. Tabe, K. Yamaguchi, H. Yagishita, H. Iwasa, T. Ishikawa, *Tetrahedron* **2001**, *57*, 2717; b) V. M. Marathias, P. H. Bolton, *Biochemistry* **1999**, *38*, 4355; c) W. M. Clark, A. M. Ticker-Eldridge, G. Kris Huang, L. N. Pridgen, M. A. Olsen, R. J. Mills, I. Lantos, N. H. Baine, *J. Am. Chem. Soc.* **1998**, *120*, 4550.

Monodisperse Surface Micelles of Nonpolar Amphiphiles in Langmuir Monolayers**

Mounir Maaloum, Pierre Muller, and Marie Pierre Krafft*

There are several examples of surface micelles (hemimicelles) formed by self-assembly of small molecules and macromolecules that are adsorbed on solid surfaces and in equilibrium with aqueous solutions.[1] On the other hand, reports on surface micelles in Langmuir monolayers are essentially limited to copolymers.[2] Although their existence has long been predicted,[3,4] so far only one example of surface micelles made from small amphiphilic molecules exists.[5] These surface micelles were made from *strongly polar* surfactants. Furthermore no rule for predicting the size of the hemimicelles has been found. We report here on novel surface micelles made of a nonpolar amphiphile, namely, the semifluorinated alkane $C_8F_{17}C_{16}H_{33}$ (F8H16), their structure, and a model that accounts for their size.

Since the pioneering work of Gaines demonstrated that semifluorinated alkanes $C_nF_{n+1}C_mH_{2m+1}$ (F*n*H*m* diblocks) form Langmuir monolayers,[6] their structure has remained controversial. A primary issue was the orientation of the F*n*H*m* molecules at the air–water interface. Grazing-incidence X-ray diffraction (GIXD) and X-ray reflectivity (GIXR) studies on F12H18 concluded that the most probable arrangement was a monolayer in which the H*m* segments are in contact with water and the F*n* segments extend upwards from the surface.[7] However, a bilayer structure in which the diblocks are antiparallel, with tilted F8 segments outside and interleaved H18 segments inside, was recently proposed on the basis of X-ray reflectivity measurements.[8] In the bulk, F*n*H*m* molecules crystallize in a large number of different stable smectic phases, depending on temperature and on *n* and *m* block lengths.[9–11] F*n*H*m* were instrumental in allowing reversible vertical phase separation from phospholipids upon compression of Langmuir monolayers.[12] They allowed substantial stabilization of fluorocarbon-in-water emulsions and control over particle size.[13,14]

F8H16[15] was thoroughly purified by column chromatography, and its purity (> 99 %) determined by GC, TLC, NMR spectroscopy, and elemental analysis. Monolayers were spread from a 1 mM solution of F8H16 in chloroform onto pure water from a milli-Q system. Surface pressure P_s (Wilhelmy plate method) versus molecular area isotherms were recorded at 22.0 ± 0.5 °C on a Langmuir trough (Riegler & Kirstein, Germany) equipped with two movable barriers.

F8H16 formed a monolayer that remained stable up to about 8 mN m^{-1} (Figure 1) with a limiting area of about 30 Å^2 that corresponds to the cross section of a perfluorinated chain, which is larger than that of a typical hydrocarbon chain (ca.

[*] Dr. M. P. Krafft, Dr. M. Maaloum, Dr. P. Muller
Institut Charles Sadron (CNRS)
6, rue Boussingault, 67083 Strasbourg Cedex (France)
Fax: (+ 33) 3-88-41-4099
E-mail: krafft@ics.u-strasbg.fr

[**] This work was supported by the CNRS. We thank AtoFina (Pierre-Bénite, France) for the gift of fluorinated precursors.

 © 2002 WILEY-VCH Verlag GmbH & Co. KGaA, Weinheim 0044-8249/02/4122-4331 $ 20.00+.50/0

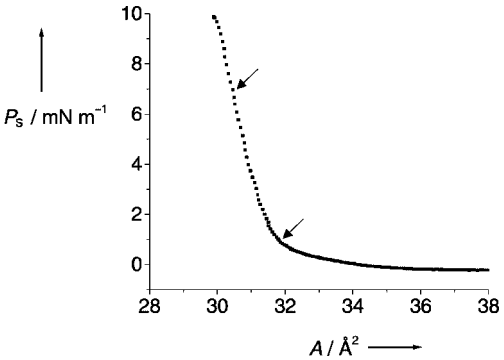


Figure 1. Isotherm of surface pressure P_s versus molecular area A, obtained by compressing F8H16 at an air–water interface at 22 °C. The two arrows indicate the surface pressures of transfer for AFM imaging (Figure 2).

20 Å^2).[16] Because the van der Waals radius of fluorine is larger than half the C–C bond length, steric hindrance causes the chain to adopt a (15/7) helical conformation, which renders the carbon backbone rigid.[17] The isotherm was reversible, without hysteresis, in compression/expansion cycles. The monolayers were transferred onto a silicon wafer, previously treated with a "piranha solution" (conc. H_2SO_4/30% H_2O_2 3/1) by using the Langmuir–Blodgett technique. The transferred films were analyzed with an atomic force microscope (AFM, NanoScope III) in tapping mode with a nitride cantilever. All scans were performed in the repulsive regime.

Figure 2a shows an AFM image of the F8H16 monolayer transferred at 7 mN m^{-1} onto a silicon wafer. It shows the presence of two-dimensional micelles that form a nanoscale structure on the surface. The AFM images of these surface micelles were analyzed quantitatively by two-dimensional Fourier analysis (Figure 2b). Diffusion rings were observed that originate from hard-core repulsions. For both pressures (0.5 and 7 mN m^{-1}) investigated, the surface micelles have a characteristic diameter of 300 Å. The size distribution of the micelles was highly monodisperse. The average height H of a micelle was assessed by a series of AFM line scans to be 23 ± 5 Å. At 7 mN m^{-1}, the surface micelles pack in an hexagonal arrangement, as assessed by the position of the Bragg peaks (see the two rings in Figure 2b).

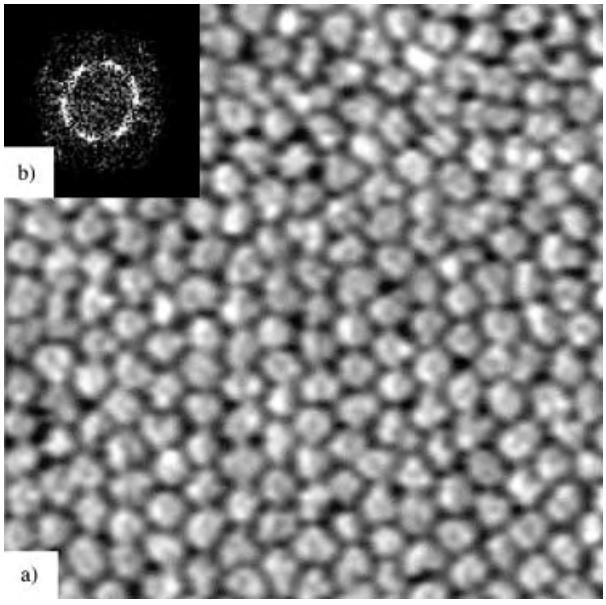


Figure 2. a) AFM image (0.5 × 0.5 μm) of surface micelles in a F8H16 monolayer transferred to a silicon wafer at 7 mN m^{-1}. b) Two-dimensional Fourier transform of (a), showing two rings.

When surface pressure was increased from 0 to 7 mN m^{-1}, the density of the micelles increased progressively. However, the size of the micelles was independent of surface density. When the pressure was further increased to 9 mN m^{-1}, the micelle arrangement became even more compact, but no coalescence between domains was observed.

The F8H16 monolayers were also analyzed by X-ray specular reflectivity. Figure 3 shows X-ray data obtained from a monolayer compressed and transferred at 7 mN m^{-1}. The

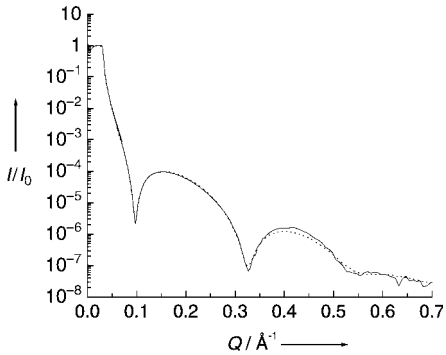


Figure 3. Experimental curve of X-ray reflectivity obtained from the monolayer of F8H16 transferred to a silicon wafer at 7 mN m^{-1}. The dotted curve is the fit obtained with the model in Figure 4a.

experimental curve was fitted to single- and two-layer models with Parratt 32 software. The single-layer model gave poor results, because the corresponding fit always had its second minimum at three times the first minimum, which is clearly not the case in the experimental curve. A two-layer model provided good agreement with the experimental data.

The electron density distribution of the two-layer model (fitted curve in Figure 3) is given in Figure 4a. It consists of an upper layer (in contact with air) with a thickness of 10.0 Å and an electron density of 487 e nm^{-3}, and a lower layer with a thickness of 19.3 Å and an electron density of 290 e nm^{-3}. The total thickness is 29.3 Å. It is noteworthy that the height of the micelle, as measured by X-ray reflectivity, is in close agreement with the length l_C of a fully extended F8H16 molecule, as calculated[18,19] from $l_C = 1.3n + 1.265m + 2.58 = 33.2$ Å for $n = 8$ and $m = 16$). Integration over the whole layer gives a total electron density of $D = 1050$ e nm^{-2}. F8H16 consists of an F8 segment bearing 201 electrons and an H16 segment with 129 electrons. The mean area per molecule is obtained by dividing the total number of electrons of a molecule by D, which gives a molecular area of 31.5 Å^2, which is the value expected if the density is preserved during transfer onto the wafer. However, note that the proportion of electrons in the upper layer is only 46%, while a simple model in which the fluorinated segments of all molecules point towards air would give an upper layer representing 61% of the total. Likewise,

 © 2002 WILEY-VCH Verlag GmbH & Co. KGaA, Weinheim 0044-8249/02/4122-4332 $ 20.00+.50/0

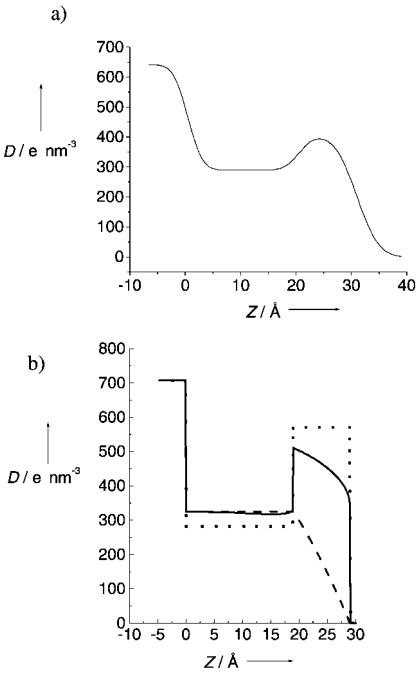


Figure 4. a) Variation of the electron density D as a function of height Z corresponding to the fit of the experimental reflectivity curve (Figure 3). This clearly shows that the first layer is less dense than the second. b) Theoretical electron density profiles (D) for the disklike model (full line) and ellipsoidal model (dashed line) depicted in Figure 5. The density of a homogeneous layer is represented by a dotted line.

the density of the lower layer is larger than that expected for a alkane hydrocarbon layer.

Given the AFM and X-ray data, we tested two models for the shape of the micelles. As the domains are roughly circular, we assumed a circular shape. The X-ray data suggest that the micelle height is close to the length of an extended molecule, but a homogeneous layer of extended molecules whose fluorinated parts point towards air would lead to an unrealistically low density for the hydrocarbon part. Bending the molecules towards the surface at the edge of the domain can substantially reduce this mismatch. The two models that we considered are a disklike shape with quarter circles at the borders and an ellipsoidal shape (Figure 5).

The fluorinated external layer is considered to be composed of rigid F8 rods with a thickness of 11.5 Å and and an area per chain of 30 Å^2. The density of the hydrocarbon part can then be deduced from the molecular constraint by simply calculating the volumes of the two layers. If we set the thickness of the hydrocarbon layer to the measured X-ray value, the mean electron density of the internal hydrocarbon layer becomes a function of the radius R of the micelle. An estimation of the density of the hydrocarbon part can be obtained by using the van der Waals volumes of CH_3 and CH_2 [Eq. (1)] which leads to an electron density of 282 e nm^{-3}. For the disklike model we find $R = 13.0$ nm, while the ellipsoid model gives $R = 15.5$ nm. Varying the density by $\pm 5\,\%$ leads to variation of R from 11.5 to 14.8 nm and from 13.5 to 17.8 nm, respectively. This shows that closing of the domains to reduce the density mismatch provides a reasonable explanation for the observed micelle size.

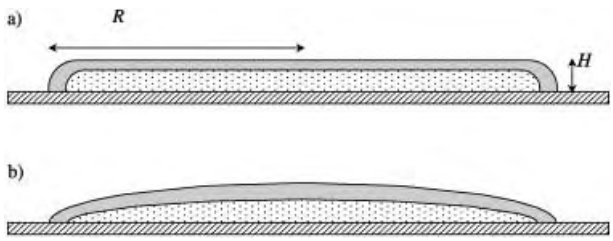


Figure 5. Schematic representation of the cross section of a surface micelle of F8H16 after transfer of the monolayer onto a silicon wafer: a) disklike model; b) ellipsoidal model. The gray area represents the region of fluorinated segments F8, and the dotted area the region of hydrocarbon segments H16.

$$V = V_{CH_3} + 15\,V_{CH_2} = 54.3 + 15 \times 26.9 = 457.8\,\text{Å}^3 \quad (1)$$

We then calculated the theoretical electron density profiles for the two models (Figure 4b). Only the disklike model shows an upper region of higher electron density. Moreover, we can also understand the apparent electron deficiency of the upper layer by comparing the density profile of the disklike model to that of a homogeneous layer. The hydrocarbon volume fraction ϕ_H of the disklike surface micelle can be calculated by using Equation (2) where V_H is the hydrocarbon volume of the surface micelle, $V_F + V_H$ is the total volume, H_H and H_F are the lengths of the fluorinated and hydrocarbon segments of the semifluorinated alkane molecule, and R is the radius of the surface micelle.

$$\phi_H = \frac{V_H}{V_H + V_F} = \frac{\left((R-(H_F+H_H))^2 H_h + \frac{\pi}{2}(R-(H_F+H_H))H_H^2 + \frac{2}{3}H_H^3\right)}{\left((R-(H_F+H_H))^2(H_F+H_H) + \frac{\pi}{2}(R-(H_F+H_H))(H_F+H_H)^2 + \frac{2}{3}(H_F+H_H)^3\right)} \quad (2)$$

Since ϕ_H must be equal to the hydrocarbon volume fraction of the semifluorinated alkane molecule and V_H, V_F, H_H, and H_F depend on m and n, it appears that R is a simple function of n and m. This means that we can predict the size of the surface micelles for a given semifluorinated alkane molecule.

In conclusion, we have found that the nonpolar semifluorinated alkane F8H16 self-assembles into Langmuir monolayers which, transferred to silicon wafers, consist of highly monodisperse stable surface micelles. The hydrocarbon segments of the F8H16 molecules are directed toward the substrate, while the fluorinated segments point outwards toward the air. We demonstrated that the size of these micelles is controlled by the density mismatch between the fluorinated and hydrogenated segments. The radius of the surface micelle is a function of the lengths of the hydrocarbon and fluorinated segments of the FnHm molecules. These results demonstrate the possibility of decorating surfaces with molecular clusters of predetermined size in the nanometer range.

Received: June 21, 2002 [Z19585]

[1] G. G. Warr, *Curr. Opin. Colloid Interface Sci.* **2000**, *5*, 80 – 94.
[2] J. Zhu, A. Eisenberg, R. B. Lennox, *J. Am. Chem. Soc.* **1991**, *113*, 5583 – 5588.

 © 2002 WILEY-VCH Verlag GmbH & Co. KGaA, Weinheim 0044-8249/02/4122-4333 $ 20.00+.50/0

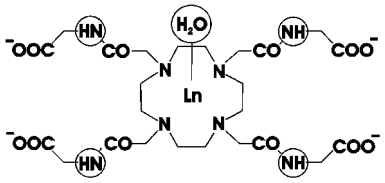
[3] O. Albrecht, H. Gruler, E. Sackmann, *J. Phys. (Paris)* **1978**, *39*, 301 – 313.
[4] M. Flörsheimer, H. Möhwald, *Colloids Surf.* **1991**, *55*, 173 – 189.
[5] T. Kato, M. Kameyama, M. Ehara, K. Iimura, *Langmuir* **1998**, *14*, 1786 – 1786.
[6] G. L. Gaines, Jr., *Langmuir* **1991**, *7*, 3054 – 3056.
[7] Z. Huang, A. A. Acero, N. Lei, S. A. Rice, Z. Zhang, M. L. Schlossmann, *J. Chem. Soc. Faraday Trans.* **1996**, *92*, 545 – 552.
[8] A. El Abed, E. Pouzet, M.-C. Fauré, M. Sanière, O. Abillon, *Phys. Rev. E* **2000**, *62*, R5895 – R5898.
[9] J. F. Rabolt, T. P Russell, R. Twieg, *Macromolecules* **1984**, *17*, 2786 – 2794.
[10] T. P. Russell, J. F. Rabolt, R. Twieg, R. L. Siemens, B. L. Farmer, *Macromolecules* **1986**, *19*, 1135 – 1143.
[11] P. Marczuk, P. Lang, M. Möller, *Colloids Surf. A* **2000**, *163*, 103 – 113.
[12] M. P. Krafft, F. Giulieri, P. Fontaine, M. Goldmann, *Langmuir* **2001**, *17*, 6577 – 6584.
[13] J. G. Riess, *Chem. Rev.* **2001**, *101*, 2797 – 2919.
[14] J. G. Riess, *Tetrahedron* **2002**, *58*, 4113 – 4131.
[15] N. O. Brace, *J. Org. Chem.* **1973**, *38*, 3167 – 3172.
[16] A. A. Acero, M. Li, B. Lin, S. A. Rice, M. Goldmann, I. Z. Azouz, A. Goudot, F. Rondelez, *J. Chem. Phys.* **1993**, *99*, 7214 – 7220.
[17] C. W. Bunn, E. R. Howell, *Nature* **1954**, 174, 549 – 541.
[18] C. Tanford, *The Hydrophobic Effect: Formation of Micelles and Biological Membranes*, Wiley, New York, **1973**.
[19] P. Lo Nostro, S. H. Chen, *J. Phys. Chem.* **1993**, *97*, 6535 – 6540.

Novel pH-Reporter MRI Contrast Agents**

Silvio Aime,* Daniela Delli Castelli, and Enzo Terreno

The contrast obtained in magnetic resonance imaging (MRI) relies essentially on differences in the intensity of the ^{1}H water signal. Therefore, the contrast can be augmented by the use of chemicals (contrast agents, CAs) able to enhance the relaxation properties of water protons.[1] Recently, a novel class of paramagnetic CAs has been proposed for MRI applications.[2,3] Such chemicals contain paramagnetically shifted mobile protons whose exchange with the bulk water is slow on the NMR timescale ($|k_{ex}| < |\Delta\omega|$). Thus, irradiation of the mobile protons of the agent determines a decrease of the ^{1}H water signal through the so-called chemical exchange saturation transfer (CEST) effect.[4,5]

One of the major advantages of the CEST agents relies on the possibility of designing responsive agents in which the effectiveness of the CA is not dependent on its concentration. This goal can be pursued when the CEST properties of two independent exchanging pools are monitored in the same experiment (ratiometric method).[6] This possibility has been demonstrated using a mixture of two compounds.[3] An improvement in such ratiometric methods would be obtained if the two proton-exchanging pools were parts of the same molecule (single-molecule CEST procedure). Paramagnetic [Ln(dotamGly)]$^-$ complexes (dotam = 1,4,7,10-tetrakis(carbamoylmethyl)-1,4,7,10-tetrazacyclododecane) would be appropriate for this purpose since they are characterized by the presence of two kinds of mobile protons, namely, the four equivalent amide protons and the two protons of the water molecule coordinated to the Ln^{III} ion. It has been previously shown that the use of a cocktail formed by [Yb(dotamGly)]$^-$ and [Eu(dotamGly)]$^-$ allows the set-up of a ratiometric method for pH measurements by making use of the two exchanging pools provided by the amide protons of the Yb derivative and by the metal-coordinated water protons of the Eu complex, respectively. Herein we demonstrate that the paramagnetic dotamGly complexes of the lighter Ln^{III} ions (Pr, Nd, and Eu) behave as pH-responsive "single-molecule CEST" agents. The efficiency of saturation transfer (ST), once the irradiation time is sufficiently long to reach a steady-state ST value,[3] is directly related to the exchange rate of the irradiated protons (k_{ex}), their molar concentration (defined by the product $n[C]$, where n is the number of irradiated protons and $[C]$ is the molar concentration of the agent), and inversely related to the longitudinal relaxation rate of the bulk water protons during the irradiation $R_{1,irr}$ [Eq. (1)].



$$\mathrm{ST}\,\% = \left(1-\frac{I_S}{I_0}\right)100 = \frac{k_{ex}\,n[C]}{111.2\,R_{1,irr} + k_{ex}\,n[C]}\,100 \qquad (1)$$

The latter parameter, in the presence of a paramagnetic Ln^{III} complex, is mainly determined by the relaxation rate of the metal-coordinated water protons, and this is directly dependent on the intrinsic paramagnetism of the metal ion (μ_{eff}).[7]

I_S and I_0 refer to the intensity of the bulk water signal when the irradiation pulse is set on-resonance (frequency ν^{on}, signal intensity I_S) and off-resonance with respect to the frequency of the bulk water protons ($\nu^{off} = -\nu^{on}$, I_0). The off-resonance measurement is necessary to take into account the direct saturation effect on the bulk water signal which is determined by the irradiation pulse.

The data reported in Figure 1 clearly show that all the three complexes ($[C] = 30$ mM) yield significant ST effects (at 312 K and pH 7.4) upon selective irradiation of their pools of mobile protons. In the case of [Eu(dotamGly)]$^-$, the ST effect from the coordinated water is so efficient that a 10% effect is still detectable when the concentration of the complex is as low as 1 mM. This result makes this system the most efficient CEST agent so far reported if the ST effect is normalized to the number of irradiated spins.[2,4,8] The ST effect from the amide protons $(ST)_{NH}$ follows a reverse order with respect to the

[*] Prof. S. Aime, Dr. D. Delli Castelli, Dr. E. Terreno
Dipartimento di Chimica I.F.M.
Via P. Giuria 7, 10125 Torino (Italy)
Fax: (+39) 011-670-7855
E-mail: silvio.aime@unito.it

[**] Financial support from Bracco Imaging S.p.A., MIUR (PRIN), and CNR (PF Oncology, L. 95/95) are gratefully acknowledged. This work has been carried out under the framework of the EU-COST D 18 action.

 © 2002 WILEY-VCH Verlag GmbH & Co. KGaA, Weinheim 0044-8249/02/4122-4334 $ 20.00+.50/0

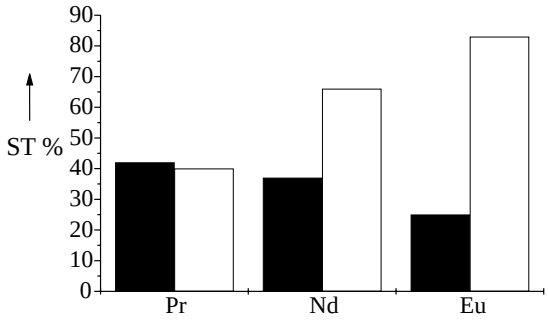


Figure 1. ST effects on the solvent water resonance upon irradiating the amide protons (black bars) and the coordinated water protons (white bars) in 30 mM solutions of [Ln(dotamGly)]$^-$ chelates (312 K, pH 7.4, irradiation time: 4 s).

irradiation of Ln-$\underline{H_2}$O signal, that is, it is higher for the Pr^{III} complex and smaller for the Eu^{III} complex.

The pH dependence of the ST efficiency (at 312 K) in a separate irradiation of the two pools of protons in the Pr, Nd, and Eu complexes is reported in Figure 2. $(ST)_{H_2O}$ is not pH-dependent in the interval investigated because the prototropic

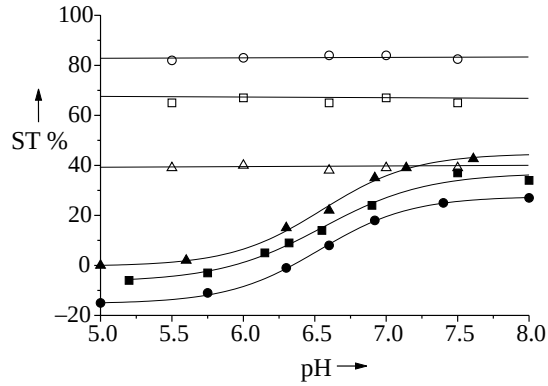


Figure 2. pH-dependence of the ST efficiency measured at 312 K upon irradiation (4 s) of the amide protons (filled symbols) and of the metal-coordinated water protons (open symbols) for 30 mM solutions of [Ln(dotamGly)]$^-$. Pr: triangle, Nd: square, Eu: circle.

exchange rate is still slower than the exchange rate of the whole water molecule. Conversely, $(ST)_{NH}$ is pH dependent in the 6–8 range. At pH < 6, the value of k_{NH} is too small to transfer saturation (Table 1), whereas at pH > 8, the value of k_{NH} becomes too high, thus approaching the coalescence condition where ST can no longer be detected. The ratiometric method is based on the assessment of a ST ratio through Equation (2).

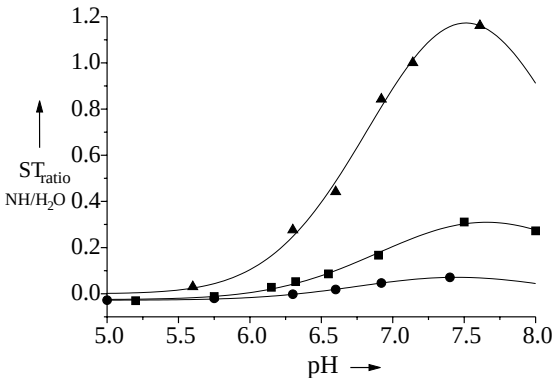


Figure 3. Ratiometric plot for [Ln(dotamGly)]$^-$ complexes (312 K, irradiation time: 4 s, selective e-burp pulse, [Ln(dotamGly)] = 30 mM). Pr^{III}: triangle, Nd^{III}: square, and Eu^{III}: circle.

$$\frac{\left(\frac{I_0-I_S}{I_0}\right)_{NH}}{\left(\frac{I_0-I_S}{I_0}\right)_{H_2O}} = \frac{n^{NH}\,k_{NH}\,R_{1,irr}^{H_2O}}{n^{H_2O}\,k_{H_2O}\,R_{1,irr}^{NH}} \qquad (2)$$

In Figure 3 the ST ratio calculated according to the above equation are reported for [Ln(dotamGly)]$^-$ (Ln = Eu, Pr, Nd) at 312 K. Although the three complexes are characterized by similar shaped ratiometric plots, the ST ratio and consequently the accuracy and the sensitivity of the pH responsiveness is, at 7.05 T, considerably higher for the Pr^{III} complex. The ratiometric method based on a "single-molecule CEST" agent overcomes the main limitations associated to the procedure based on the use of a cocktail of two paramagnetic complexes, for which the same biodistribution pattern has to be assumed. Furthermore, the total concentration of metal-containing agent administered may be lower in the case of a single agent. Conversely, the use of the cocktail could be advantageous to enhance the sensitivity of the response, because the ST ratio can be made dependent on the concentration ratio between the two CEST agents.[3]

In conclusion, the data reported in this work illustrate that paramagnetic CEST agents may be considered as attractive alternatives to the conventional Gd^{III}- or Fe^{III}-based CAs for MRI applications. In fact, ratiometric procedures such as that described here provide a route to overcome the major conceptual problem usually encountered with Gd-based responsive systems, for which it is difficult, if not impossible, to differentiate a change in the concentration of the paramagnetic agent from the variation in relaxivity eventually occurring in response to a change of a given parameter of interest.

Table 1. Exchange rates and chemical shift separation for the amide protons and the metal-coordinated water protons (312 K, pH 6, 7.05 T) in the [Ln(dotamGly)]$^-$ series.

Complex	$^{312}k_{H_2O}$ [s^{-1}]	$^{312}\Delta\omega_{H_2O}$ [rad s^{-1}]	$^{312}k_{NH}$ [s^{-1}]	$^{312}\Delta\omega_{NH}$ [rad s^{-1}]
[Pr(dotamGly)]$^-$	1.06×10^5	-1.32×10^5	128.5	2.5×10^4
[Nd(dotamGly)]$^-$	3.92×10^4	-9.4×10^4	125.0	2.02×10^4
[Eu(dotamGly)]$^-$	4.20×10^4	9.4×10^4	127.0	-7.85×10^3

 © 2002 WILEY-VCH Verlag GmbH & Co. KGaA, Weinheim 0044-8249/02/4122-4335 $ 20.00+.50/0

Experimental Section

The $[Ln(dotamGly)]^-$ complexes were synthesized accordingly to the procedure reported in the literature.[3]

All the measurements were carried out on a Bruker Avance 300 spectrometer at 312 K. The concentration of the metal complexes in the samples were determined by means of the Evans' method by using *tert*-butyl alchool as a reference.[9] The exchange rates of the two proton pools, k_{H_2O} and k_{NH}, were evaluated at pH 6.1 by analyzing the temperature dependence of the transverse relaxation rate of the bulk water signal and of the amide protons, respectively, in aqueous solutions of $[Ln(dotamGly)]^-$.[10]

The ST measurements were performed by using a saturation pulse (4 s) which constituted a train of selective e-burp pulses, whose duration and power were optimized according to the signal to be irradiated (20 ms and 1.35 μT for the amide protons and 1 ms and 17.1 μT for the metal-coordinated water protons).

Received: May 14, 2002 [Z19701]

[1] R. N. Müller in *Methods in Biomedical Magnetic Resonance Imaging and Spectroscopy, Vol. 1* (Ed.: I. R. Young), Wiley, Chichester, **2000**, pp. 698 – 705.

[2] a) S. Zhang, P. Winter, K. Wu, A. D. Sherry, *J. Am. Chem. Soc.* **2001**, *123*, 1517 – 1518; b) S. R. Zhang, L. Michaudet, S. Burgess, A. D. Sherry, *Angew. Chem.* **2002**, *114*, 1999 – 2001; *Angew. Chem. Int. Ed.* **2002**, *41*, 1919 – 1921; c) S. Zhang, A. D. Sherry, *Proc. Int. Soc. Magn. Reson. Med.* **2002**, *10*, 2590.

[3] a) S. Aime, A. Barge, D. Delli Castelli, F. Fedeli, A. Mortillaro, F. U. Nielsen, E. Terreno, *Magn. Reson. Med.* **2002**, *47*, 639 – 648; b) S. Aime, D. Delli Castelli, F. Fedeli, E. Terreno, *J. Am. Chem. Soc.* **2002**, *124*, 9364 – 9365.

[4] K. M. Ward, A. H. Aletras, R. S. Balaban, *J. Magn. Reson.* **2000**, *143*, 79 – 87.

[5] A. P. Dagher, A. Aletras, P. Choyke, R. S. Balaban, *JMRI* **2000**, *12*, 745 – 748.

[6] K. M. Ward, R. S. Balaban, *Magn. Reson. Med.* **2000**, *44*, 799 – 802.

[7] J. A. Peters, J. Huskens, D. J. Raber, *Prog. Nucl. Magn. Reson. Spectrosc.* **1996**, *28*, 283 – 350.

[8] N. Goffeney, J. V. M. Bulte, J. Duyn, L. H. Bryant, Jr., P. C. M. Van Zijl, *J. Am. Chem. Soc.* **2001**, *123*, 8628 – 8629.

[9] D. M. Corsi, C. Platas-Iglesias, H. Van Bekkum, J. A. Peters, *Magn. Reson. Chem.* **2001**, *39*, 723 – 726.

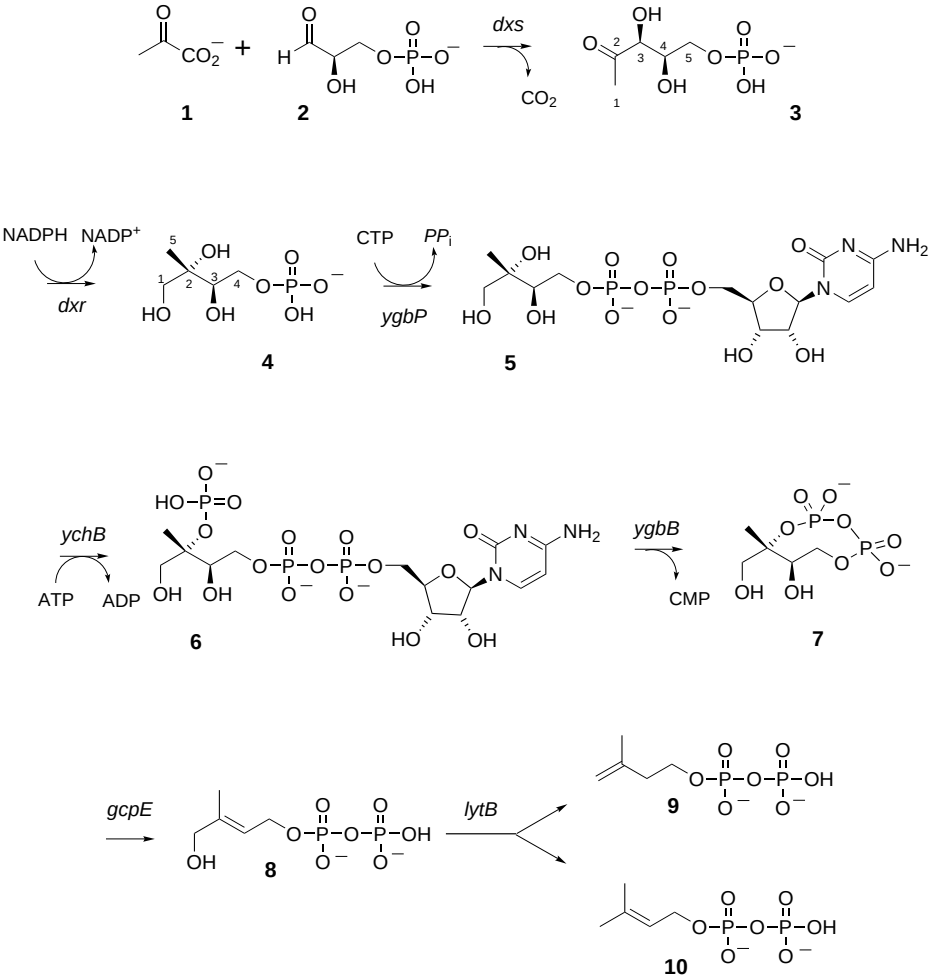
[10] J.-J. Delpuech in *Dynamics of Solutions and Fluid Mixtures by NMR* (Ed.: J.-J. Delpuech), Wiley, Chichester, **1995**, pp. 109 – 120.

 © 2002 WILEY-VCH Verlag GmbH & Co. KGaA, Weinheim 0044-8249/02/4122-4336 $ 20.00+.50/0

Isoprenoid Biosynthesis through the Methylerythritol Phosphate Pathway: The (*E*)-4-Hydroxy-3-methylbut-2-enyl Diphosphate Synthase (GcpE) is a [4Fe–4S] Protein**

Myriam Seemann, Bernadette Tse Sum Bui, Murielle Wolff, Denis Tritsch, Narciso Campos, Albert Boronat, Andrée Marquet, and Michel Rohmer*

Isopentenyl diphosphate (IPP, **9**), the fundamental unit in terpenoid biosynthesis, was widely accepted to be solely formed through the mevalonate pathway.[1] An alternative metabolic route, the methylerythritol phosphate (MEP) pathway (Scheme 1), was later discovered for the formation of isoprenoids in many bacteria, green algae, and plant chloroplasts.[2] Whereas the first steps leading from pyruvate (**1**) and glyceraldehyde 3-phosphate (**2**) to 2-methylerythritol (ME) 2,4-cyclodiphosphate (**7**) are well-known,[2] the last steps leading to IPP (**9**) and dimethylallyl diphosphate (DMAPP, **10**) and involving the *gcpE*[3] and *lytB*[4] genes are still a matter of investigation. Cyclodiphosphate **7** is the substrate of the GcpE protein.[5] A crude cell-free system of an *Escherichia coli* strain that overexpresses the *gcpE* gene converts **7** into (*E*)-4-hydroxy-3-methylbut-2-enyl diphosphate (HMBPP, **8**).[6] *In vivo* studies were in accord with these results. Cyclodiphosphate **7** was accumulated from ^{13}C-labeled 1-deoxy-D-xylulose (DX) by an *E. coli* strain that overexpresses xylulose kinase (which is capable of phosphorylating DX to yield deoxyxylulose phosphate **3**) and the four genes of the MEP pathway (*dxr*, *ygbP*, *ychB*, and *ygbB*). Additional overexpression of the *gcpE* gene (or *ispG*) was followed by the formation of HMBPP (**8**).[7] The reaction catalyzed by the GcpE protein formally involves elimination and reduction steps. The reducing cofactor was, however, not identified, as no assay with the purified enzyme was available. In a bioinformatic search on the *gcpE* gene,[6b] we found strong homologies between the GcpE protein and enzymes



Scheme 1. Methylerythritol 4-phosphate pathway for isoprenoid biosynthesis in *E. coli*.

that possess a [4Fe–4S] cluster. Herein we describe a purified His_6-tagged GcpE protein (His-GcpE), which is active after reconstitution of its Fe/S cluster.

A crude cell-free system obtained from *E. coli* strain XL1-blue [pBAD-HisGcpE], which overexpresses His-GcpE, was capable of catalyzing the formation of HMBPP (**8**) from [^{14}C2]**7** under the conditions described for the nontagged protein.[6] The His-GcpE (30 mg from a 500-mL transformed cell culture) was purified on a Ni^{2+} nitrilotriacetic acid agarose column. The enzyme was found to be 95% pure by SDS-PAGE (sodium dodecyl sulfate polyacrylamide gel electrophoresis) and presented an apparent molecular mass of 43 kDa. The purified protein was inactive, even in the presence of the reducing systems detailed below. Such a lack of catalytic activity was probably a result of the predominant

[*] Prof. Dr. M. Rohmer, Dr. M. Seemann, M. Wolff, Dr. D. Tritsch
Université Louis Pasteur, UMR 7123 CNRS, Institut Le Bel
4 rue Blaise Pascal, 67070 Strasbourg Cedex (France)
Fax: (+33) 3-9024-1345
E-mail: mirohmer@chimie.u-strasbg.fr
Dr. B. T. S. Bui, Prof. Dr. A. Marquet
Laboratoire de Chimie Organique Biologique
Université Paris VI, UMR 7613 CNRS
4 place Jussieu, 75252 Paris Cedex 05 (France)
Dr. N. Campos, Prof. Dr. A. Boronat
Departament de Bioquímica i Biologia Molecular
Facultat de Química, Universitat de Barcelona
Martí i Franquès 1, 09028 Barcelona (Spain)

[**] We thank Professor P. Reichard for providing the *E. coli* strains that overexpress flavodoxin and flavodoxin reductase. M.R. was supported by a grant from the "Institut Universitaire de France".

Supporting information for this article is available on the WWW under http://www.angewandte.org or from the author.

production of the apoenzyme without the Fe/S cluster. The Fe/S cluster was therefore restored using $FeCl_3$ and Na_2S in the presence of dithiothreitol as reductant.[8] As such prosthetic groups are often oxygen-sensitive, all operations were performed under an inert argon atmosphere. The UV/Vis spectrum of the khaki solution of the reconstituted enzyme displayed an absorption band at 410 nm, which is characteristic for proteins that possess a $[4Fe–4S]^{2+}$ cluster (Figure 1).[9] Exposure of the reconstituted enzyme solution to air led to bleaching, corresponding to the fast degradation of the $[4Fe–4S]^{2+}$ cluster to yield again the spectrum of the apoenzyme. The determination of the iron content revealed 4.4 iron ions per reconstituted GcpE molecule, affording additional evidence for the presence of a [4Fe–4S] cluster.

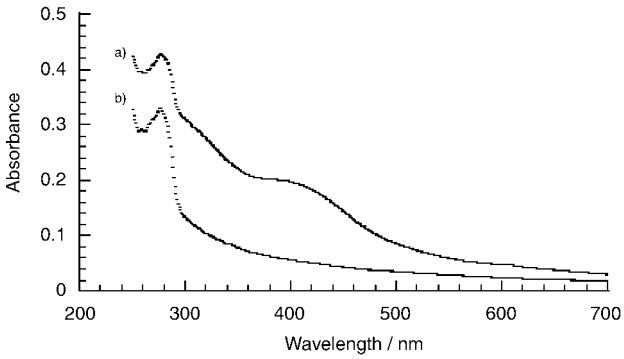
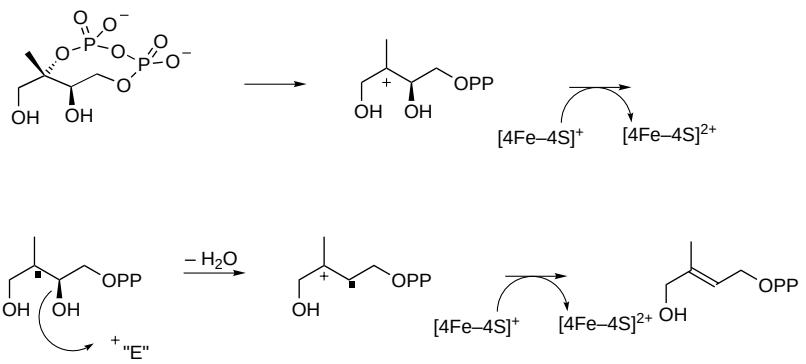


Figure 1. UV/Vis absorption spectra of His-GcpE: a) reconstituted His-GcpE, b) apoenzyme (protein concentration: 1.3 mg mL^{-1}, 50 mM Tris HCl, pH 8).

According to the assay conditions described for other enzymes with Fe/S clusters,[8,10,11] the test with the purified His-GcpE was performed in the presence of flavodoxin, flavodoxin reductase, and NADPH as regeneration systems. In the presence of this reducing system, the purified enzyme quantitatively converted **7** into HMBPP (**8**) after 4 h. The formerly utilized crude cell-free system allowed only a 4–50% conversion under the same conditions, depending on the method used to break the cells.[6] The former reducing system was efficiently replaced by the 5-deazaflavin (DAF) semiquinone radical obtained by photoreduction of DAF in the presence of Tris–HCl and used in excess with respect to the substrate.[8] Under these conditions, **7** was quantitatively converted into **8** after 15 min.

The presence of a [4Fe–4S] cluster as a prosthetic group in GcpE suggested a radical reaction involving a reduction through two one-electron transfers (Scheme 2). This was efficiently performed in our assays in two different ways: either by an endogenous reducing system, already present in *E. coli* (starting from the reduced $FMNH_2$ of flavodoxin and leading to the oxidized FMN via the semiquinone radical FMNH·, and recycling of the oxidized flavodoxin cofactor by the flavodoxin reductase and NADPH), or by the partially reduced DAF semiquinone radical. Such a successive double



Scheme 2. Hypothetical biogenetic pathway for the GcpE-catalyzed reaction in the presence of flavodoxin, flavodoxin reductase, and NADPH (intermediates are not free species but enzyme-bound stabilized entities).

one-electron transfer has been proposed in a $[2Fe\text{-}2S]^+$ cluster in the biosynthesis of the 3,6-dideoxyhexose ascarylose.[12] Cyclodiphosphate **7** is accumulated in some bacteria in the presence of benzylviologen, an inhibitor of one-electron transfer reactions.[13] This feature may be explained by an interference of the inhibitor with the electron-transfer process catalyzed by GcpE. The two previously proposed mechanisms for the GcpE-catalyzed reaction now appear rather unlikely. The fact that GcpE is functional in the presence of the semiquinone form of DAF alone (in the absence of any other reducing cofactor such as NADPH) is in contradiction with a mechanism resembling that of the reaction catalyzed by the vitamin K epoxyquinone reductase.[7] In contrast to other enzymes that have a $[4Fe–4S]^{2+}$ prosthetic group (e.g. biotin synthase, ribonucleotide reductase, pyruvate formate lyase, and lysine 2,3-aminomutase),[11] an initiator of radical reactions such as *S*-adenosylmethionine is not required for the activity of GcpE, a feature that is not in favor of a mechanism resembling that of the reaction catalyzed by the ribonucleotide reductase.[6b,7] Opening of the cyclodiphosphate ring and elimination of the C3 hydroxy group remain to be solved. The Lewis acid character of a Fe/S cluster, which may coordinate to a hydroxy group and facilitate its elimination, has been reported for a dehydratase,[14] but it is not known whether the Fe/S cluster and/or other acidic groups are involved. Finally, the proposed mechanism (Scheme 2) is in accord with the fate of the hydrogen atoms in the MEP pathway. From incorporations performed with deuterium-labeled isotopomers of DX or ME into the prenyl chain of ubiquinone from *E. coli*, no deuterium loss from C1, C4, and C5 of MEP (**4**) was observed in its conversion into IPP (**9**) and DMAPP (**10**).[15] It is also in accord with the retention of the C3 hydrogen atom of MEP (**4**) or cyclodiphosphate **7** in the isoprene units derived from DMAPP in *E. coli*[16] or in those derived from DMAPP and from IPP in the tobacco BY-2 cell culture.[17] The GcpE-catalyzed reaction does not lead to a premature loss of this hydrogen atom, which is still retained in HMBPP (**8**), the intermediate located at the branching towards IPP or DMAPP.[18] It is the successive action of the *lytB*-encoded enzyme, the IPP isomerase, and the prenyl transferase that is responsible for its retention or elimination.[17]

One of the last bottlenecks in the elucidation of the MEP pathway has been solved. A [4Fe–4S] cluster is the prosthetic

 © 2002 WILEY-VCH Verlag GmbH & Co. KGaA, Weinheim 0044-8249/02/4122-4338 $ 20.00+.50/0

group of the GcpE protein in *E. coli*. This enzyme efficiently converts cyclodiphosphate **7** into HMBPP (**8**) in the presence of flavodoxin, flavodoxin reductase, and NADPH. Whether the latter system is the effective regeneration system in *E. coli* still has to be determined. The oxygen sensitivity of the GcpE Fe/S cluster is one of the major reasons for the failure of crude cell-free systems to convert intermediates of this pathway into IPP (**9**), DMAPP (**10**), or further metabolites, and for the late discovery of the MEP pathway.

Experimental Section

Supporting information for this article (expression, purification, and characterization of the GcpE protein) is available on the WWW under http://www.angewandte.org.

Reconstitution of the FeS centers in the apoenzyme: The apo-GcpE solution (250 μL, 197 μM), a 20 mM Na_2S solution in argon-saturated buffer (50 mM Tris–HCl, pH 8), a 20 mM $FeCl_3$ and a 100 mM DTT solution in water were deoxygenated separately in Eppendorf tubes for 1 h under a stream of moist argon. All tubes were transferred to a glovebox (Jacomex BS531 NMT) equipped with an oxymeter (ARELCO ARC) and filled with argon containing less than 2 ppm O_2, where they were left to stand overnight at 15 °C before beginning the reconstitution procedure. DTT (to a final concentration of 5 mM) as well as $FeCl_3$ and Na_2S (in a fivefold molar excess with respect to the apoenzyme) were added successively to the enzyme solution. After 5 h, the reaction mixture was desalted on a PD 10 column (Pharmacia) equilibrated with 50 mM Tris–HCl buffer (pH 8). For recording the UV/Vis absorption spectrum, a fraction of the reconstituted protein was directly transferred into a cuvette, which was closed with a septum before being removed from the glove box.

GcpE assay with flavodoxin and flavodoxin reductase: Flavodoxin and flavodoxin reductase from *E. coli* were obtained as previously described.[8] A mixture (70 μL final volume) containing [^{14}C2]**7** (39 μM, 0.04 μCi), DTT (5 mM), NADPH (1 mM), flavodoxin (1 μM), flavodoxin reductase (0.5 μM) in Tris–HCl (50 mM, pH 8) was degassed for 45 min at room temperature under a stream of moist argon before adding the previously reconstructed GcpE with a gas-tight syringe to a final concentration of 2 μM. The incubation was performed in anaerobic conditions at 37 °C for 4 h.

GcpE assay with 5-deazaflavin: A mixture (70 μL final volume) containing [^{14}C2]**7** (39 μM, 0.04 μCi), DTT (5 mM) in Tris–HCl (50 mM, pH 8) was degassed for 45 min at room temperature under a stream of wet argon before adding successively, through a gas-tight syringe, the GcpE solution (final concentration: 2 μM) and a degassed 5-deazaflavin solution (final concentration: 50 μM) in the above-mentioned buffer. After generation of the reducing semiquinone radical from 5-deazaflavin and Tris–HCl by irradiation with a white fluorescent tube (30 °C, 1 h), the assay was incubated at 37 °C for 15 min or up to 3 h.

Received: September 6, 2002 [Z50115]

[1] K. Bloch, *Steroids* **1992**, *57*, 378 – 383.

[2] a) M. Rohmer, *Nat. Prod. Rep.* **1999**, *16*, 565 – 573; b) W. Eisenreich, F. Rohdich, A. Bacher, *Trends Plant Sci.* **2001**, *6*, 78 – 84, and references therein.

[3] a) N. Campos, M. Rodríguez-Concepción, M. Seemann, M. Rohmer, A. Boronat, *FEBS Lett.* **2001**, *488*, 170 – 173; b) B. Altincicek, A. K. Kollas, S. Sanderbrand, J. Wiesner, M. Hintz, E. Beck, H. Jomaa, *J. Bacteriol.* **2001**, *183*, 2411 – 2416.

[4] a) F. Cunningham, Jr., T. P. Lafond, E. Gantt, *J. Bacteriol.* **2000**, *182*, 5841 – 5848; b) B. Altincicek, A. K. Kollas, M. Eberl, J. Wiesner, S. Sanderbrand, M. Hintz, E. Beck, H. Jomaa, *FEBS Lett.* **2001**, *499*, 37 – 40; c) S. McAteer, A. Coulson, N. McLennann, M. Masters, *J. Bacteriol.* **2001**, *183*, 7403 – 7407.

[5] M. Seemann, N. Campos, M. Rodríguez-Concepción, J. F. Hoeffler, C. Grosdemange-Billiard, A. Boronat, M. Rohmer, *Tetrahedron Lett.* **2002**, *43*, 775 – 778.

[6] a) M. Seemann, N. Campos, M. Rodríguez-Concepción, E. Ibañez, T. Duvold, D. Tritsch, A. Boronat, M. Rohmer, *Tetrahedron Lett.* **2002**, *43*, 1413 – 1415; b) M. Wolff, M. Seemann, C. Grosdemange-Billiard, D. Tritsch, N. Campos, M. Rodríguez-Concepción, A. Boronat, M. Rohmer, *Tetrahedron Lett.* **2002**, *43*, 2555 – 2559.

[7] S. Hecht, W. Eisenreich, P. Adam, S. Amslinger, K. Kis, A. Bacher, D. Arigoni, F. Rohdich, *Proc. Natl. Acad. Sci. USA* **2001**, *98*, 14837 – 14842.

[8] B. Tse Sum Bui, D. Florentin, F. Fournier, O. Ploux, A. Méjean, A. Marquet, *FEBS Lett.* **1998**, *440*, 226 – 230.

[9] N. B. Ugalava, R. B. Gibney, J. T. Jarrett, *Biochemistry* **2000**, *39*, 5206 – 5214.

[10] S. Ollagnier, E. Mulliez, P. P. Schmidt, R. Eliasson, J. Gaillard, C. Deronzier, T. Bergman, A. Gräslund, P. Reichard, M. Fontecave, *J. Biol. Chem.* **1997**, *272*, 24216 – 24223.

[11] J. Cheek, J. B. Broderick, *J. Biol. Inorg. Chem.* **2001**, *6*, 209 – 226, and references therein.

[12] C. W. T. Chang, D. A. Johnson, V. Bandarian, H. Q. Zhou, R. LoBrutto, G. H. Reed, H. W. Liu, *J. Am. Chem. Soc.* **2000**, *122*, 4239 – 4240.

[13] a) D. Ostrovsky, E. Kharatian, I. Malarova, I. Shipanova, L. Sibeldina, A. Shashkov, G. Tantsirev, *BioFactors* **1992**, *3*, 261 – 264; b) D. Ostrovsky, G. Diomina, E. Lysak, E. Matveeva, O. Ogrel, S. Trutko, *Arch. Microbiol.* **1998**, *171*, 69 – 72.

[14] W. Buckel, *FEBS Lett.* **1996**, *389*, 20 – 24.

[15] a) J. L. Giner, B. Jaun, *Tetrahedron Lett.* **1998**, *39*, 8021 – 8022; b) L. Charon, J. F. Hoeffler, C. Pale-Grosdemange, L. M. Lois, N. Campos, A. Boronat, M. Rohmer, *Biochem. J.* **2000**, *346*, 737 – 742.

[16] J. L. Giner, B. Jaun, D. Arigoni, *Chem. Commun.* **1998**, 1857 – 1858.

[17] J. F. Hoeffler, A. Hemmerlin, C. Grosdemange-Billiard, T. J. Bach, M. Rohmer, *Biochem. J.* **2002**, *366*, 573 – 583.

[18] F. Rohdich, S. Hecht, K. Gärtner, P. Adam, C. Krieger, S. Amslinger, D. Arigoni, A. Bacher, W. Eisenreich, *Proc. Natl. Acad. Sci. USA* **2002**, *99*, 1158 – 1163.

Expanded Cubane: Synthesis of a Cage Compound with a C_{56} Core by Acetylenic Scaffolding and Gas-Phase Transformations into Fullerenes**

Peter Manini, Walter Amrein, Volker Gramlich, and François Diederich*

We have been interested since the early 1990s in the geometrically defined expansion of molecules by the introduction of buta-1,3-diynediyl fragments between all C–C single bonds, thereby enhancing both the carbon atom content and the optoelectronic properties of the resulting chromophores.[1] Application of this general concept to linear systems led from poly(acetylenes) to poly(triacetylenes)[2] and from dendralenes to expanded dendralenes.[3] Novel macrocyclic systems prepared following this strategy were dehydro[*n*]annulenes[4] and expanded radialenes.[1,5] We now report the first

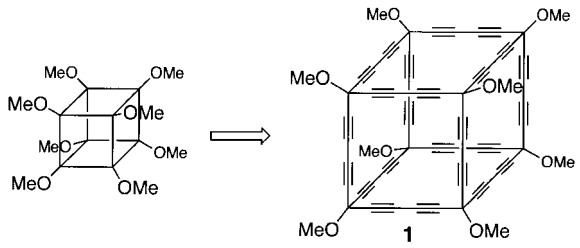
[*] Prof. Dr. F. Diederich, P. Manini, Dr. W. Amrein
Laboratorium für Organische Chemie
ETH-Hönggerberg, HCI
8093 Zürich (Switzerland)
Fax: (+41) 1-632-1109
E-mail: diederich@org.chem.ethz.ch
Prof. Dr. V. Gramlich
Institut für Kristallographie und Petrographie
ETH-Zentrum, Sonnenggstrasse 5, 8092 Zürich (Switzerland)

[**] We thank Oliver Scheidegger and Rolf Häfliger for the mass spectrometric analysis. This research was supported by the ETH Research Council and the German Fonds der Chemischen Industrie.

 © 2002 WILEY-VCH Verlag GmbH & Co. KGaA, Weinheim 0044-8249/02/4122-4339 $ 20.00+.50/0

application of this concept[6] to form three-dimensional structures.

In 1964, Eaton and Cole, Jr., achieved the first synthesis of cubane.[7] This "platonic hydrocarbon" possesses remarkable kinetic stability despite its highly strained structure.[7,8] The expanded platonic molecule **1** with a C_{56} core is obtained by formal insertion of buta-1,3-diynediyl moeties into all twelve C–C single bonds of octamethoxycubane (Scheme 1). Here,

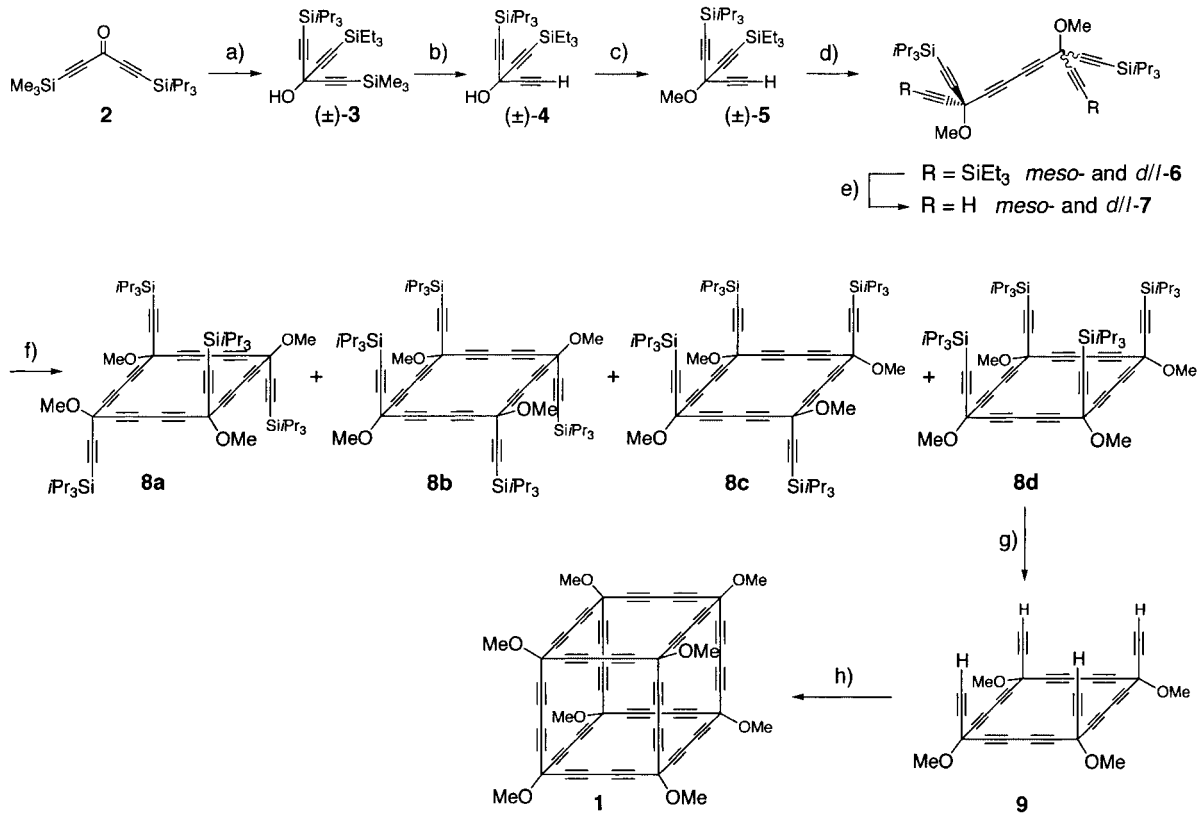


Scheme 1. From cubane to expanded cubane by formal insertion of twelve buta-1,3-diynediyl moieties.

we describe the first synthesis of **1** as well as investigations of its gas-phase ion chemistry which leads to the formation of fullerenes[9,10] and subsequent fullerene coalescence reactions.[11]

The synthesis of expanded cubane **1** was planned to proceed through the formation of corners, edges, and faces as key building blocks and intermediates (Scheme 2). Addition of lithium triethylsilylacetylide to bispropargylic ketone **2**[12] afforded the racemic corner module (±)-**3** with three differentially protected alkyne moieties[1] in 95% yield.[13] The $SiMe_3$ protecting group was selectively removed by stirring (±)-**3** for 1 h in MeOH/THF (1/1) containing a few drops of 1N NaOH and yielded (±)-**4** in 86% yield. Traces of bisdeprotected compound were readily separated by column chromatography (SiO_2; hexane/CH_2Cl_2 (2/1)). Subsequent methylation using BuLi at −78°C followed by addition of MeI provided (±)-**5** in 98% yield. Oxidative Hay coupling[14] of (±)-**5** was carried out in CH_2Cl_2 to afford edge **6** as an unseparable mixture of stereoisomers (*meso* and *d*/*l* forms) in 97% yield. Subsequent cleavage of the $SiEt_3$ protecting groups with K_2CO_3 in MeOH/THF (1/1) gave *meso*- and *d*/*l*-**7** (93% yield), which was subjected to oxidative coupling under high dilution conditions. The macrocyclic product **8** was obtained in a remarkable 72% yield as a powder consisting of four diastereoisomers. Separation of the mixture by column chromatography (SiO_2; hexane/CH_2Cl_2 (3/1→1/3)) provided, in the order of elution, **8a** (8%), **8b** (18%), **8c** (36%), and the desired diastereoisomer **8d** (10%). The four compounds are stable in the solid state at room temperature, but decompose in CH_2Cl_2 solution within a few days.

The structural assignments for the four macrocycles were unambiguously made based on ^{13}C NMR spectroscopic analysis ($CDCl_3$), X-ray analysis, and chemical reactivity studies. The C_{2h}-symmetrical structure of **8b** was proven by X-ray analysis and ^{13}C NMR spectroscopy (10 out of 10 resonances



Scheme 2. Synthesis of the expanded cubane **1**. Reagents and conditions: a) $Et_3SiC{\equiv}CH$, BuLi, THF, 0°C, 3 h, 95%; b) 1N NaOH, MeOH/THF (1/1), RT, 1 h, 86%; c) BuLi, THF, −78°C, 10 min, then MeI, −78°C→RT, 16 h, 98%; d) CuCl, TMEDA, air, CH_2Cl_2, RT, 5 h, 97%; e) K_2CO_3, MeOH/THF (1/1), RT, 2.5 h, 93%; f) CuCl, TMEDA, air, CH_2Cl_2, RT, 18 h, 8% (**8a**), 18% (**8b**), 36% (**8c**), 10% (**8d**); g) Bu_4NF, wet THF, −15°C, 2.5 h, 87%; h) CuCl, TMEDA, air, CH_2Cl_2, RT, 3 h, 16%. TMEDA = *N*,*N*,*N*′,*N*′-tetramethyl-1,2-ethanediamine.

 © 2002 WILEY-VCH Verlag GmbH & Co. KGaA, Weinheim 0044-8249/02/4122-4340 $ 20.00+.50/0 *Angew. Chem. Int. Ed.* **2002**, *41*, No. 22

observed). Diastereoisomer **8c** possesses the lowest symmetry (C_s), which is reflected by a much larger number of resonances in the ^{13}C NMR spectrum (15 out of 26 observed). Both D_{2d}-symmetrical **8a** and C_{4v}-symmetrical **8d** show the expected eight resonances in their ^{13}C NMR spectra; differentiation between the two diastereoisomers is based on the fact that only **8d** continued to react to give expanded cubane **1**.

The X-ray crystal structure of **8b** (Figure 1) revealed that the symmetry in the crystal (C_i) is reduced from the ideal C_{2h} symmetry, as a result of crystal packing effects.[15] The

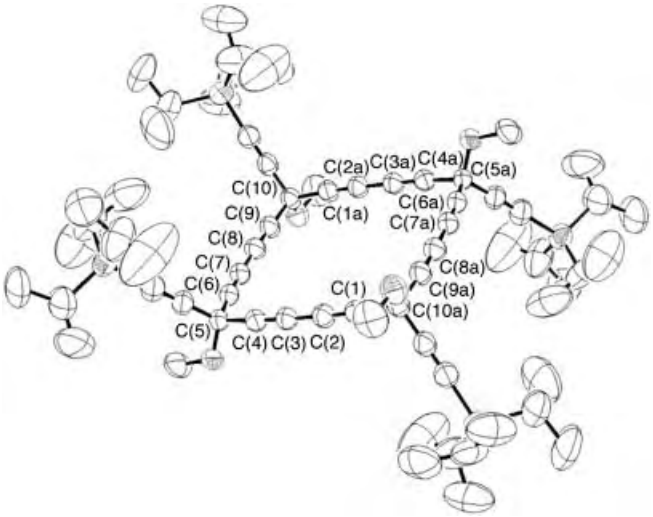


Figure 1. ORTEP plot of **8b** with arbitrary numbering. H atoms are omitted for clarity. Atomic displacement parameters at 293 K are drawn at the 50% probability level. Selected bond lengths [Å] and bond angles [°]: C(1)-C(2) 1.190(5), C(2)-C(3) 1.373(6), C(3)-C(4) 1.188(5), C(4)-C(5) 1.476(5), C(5)-C(6) 1.485(5), C(6)-C(7) 1.193(5), C(7)-C(8) 1.378(6), C(8)-C(9) 1.186(5), C(9)-C(10) 1.481(5), C(10)-C(1a) 1.481(5); C(10a)-C(1)-C(2) 175.5(4), C(1)-C(2)-C(3) 178.3(4), C(2)-C(3)-C(4) 179.0(4), C(3)-C(4)-C(5) 175.9(4), C(4)-C(5)-C(6) 107.3(3), C(5)-C(6)-C(7) 172.7(3), C(6)-C(7)-C(8) 175.2(4), C(7)-C(8)-C(9) 174.7(4), C(8)-C(9)-C(10) 172.4(4), C(9)-C(10)-C(1a) 106.8(3).

cyclic framework is planar with a mean out-of-plane deviation of 0.041 Å and a maximum deviation of 0.09 Å (C(5)).[16] The distances between neighboring C(sp^3) atoms are 6.64 Å (C(5)–C(10)) and 6.69 Å (C(5)–C(10a)). Strain in the 20-membered ring is mainly expressed by weak bends in the four butadiynediyl moieties. The C≡C–C(sp^3) angles are as low as 172.4°, and the maximal reduction of the C≡C-C(sp) angles from the ideal 180° is approximately 5°. In contrast, the angles at the corner C(sp^3) atoms ((C(9)-C(10)-C(1a): 106.8°; C(4)-C(5)-C(6): 107.3°) are close to the ideal tetrahedral angle of 109.5°.

For the completion of the synthesis of **1**, **8d** was deprotected with Bu_4NF in wet THF at −15 °C to give powdery **9** in 87% yield after column chromatography (SiO_2; hexane/EtOAc (2/1)). Deprotection at room temperature failed because of complete decomposition. Although **9** is explosive, and detonates upon scratching, it was fully characterized, with the ^{13}C NMR spectrum ($CDCl_3$) depicting the expected six resonances at 77.42, 75.97, 74.50, 69.03, 61.09, and 53.61 ppm. Oxidative cyclization of **9** under Hay conditions in CH_2Cl_2 afforded **1** in low yield (up to 16%). Purification and characterization were severely hampered by the instability of the target compound, which, similar to **9**, explodes upon scraping.[16d,17] Nevertheless, the substantial amounts of side products could mostly be removed by tedious column chromatography (SiO_2; hexane/CH_2Cl_2 (1/2)) to leave a brownish powder of sufficient purity for complete spectral characterization.

The ^1H and ^{13}C NMR spectra of **1** in $CDCl_3$ demonstrate its O_h symmetry. The proton resonances of the MeO groups appear as a singlet at $\delta = 3.44$ ppm, whereas the ^{13}C NMR spectrum depicts the expected four resonances at $\delta = 54.38$ (MeO), 61.98 (C(sp^3)), 70.82 (C(sp)), and 79.39 ppm (C(sp); Figure 2). The C(sp)-H stretching band at 3302 cm^{-1}, typical of **9**, is completely absent in the IR spectrum ($CHCl_3$).

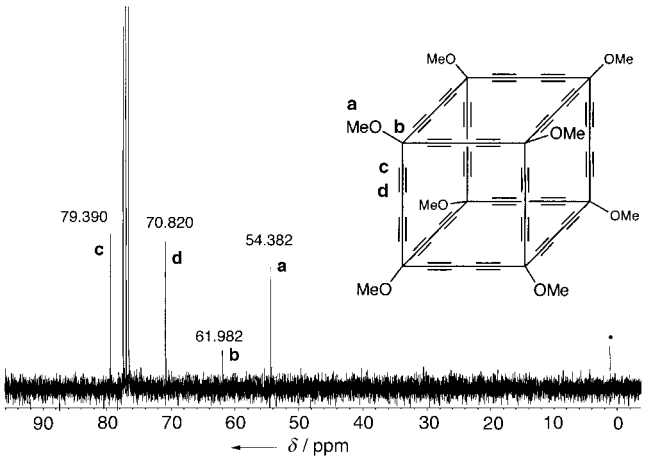


Figure 2. ^{13}C NMR (75 MHz, $CDCl_3$) spectrum of expanded cubane **1** at 298 K; ●: impurity.

In matrix-assisted laser-desorption-ionization time-of-flight (MALDI-TOF) experiments in the negative ion mode, expanded cubane **1** readily undergoes a loss of a methoxy group. The peak for the $[M^- - OMe]$ ion at m/z: 889 is actually the only major one in the entire spectrum (Figure 3). None of the numerous spectra recorded from crude or purified product gave any evidence for oxidative trimerization or higher cyclo-oligomerizations of **9** to give larger carbon cages.

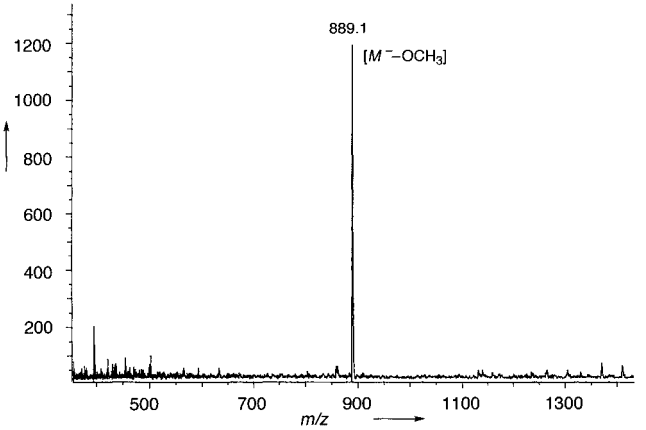


Figure 3. MALDI-TOF mass spectra of **1** in the negative ion mode; N_2 laser (337 nm, 7 ns duration), matrix: 2-[(2*E*)-3-(4-*tert*-butylphenyl)-2-methylprop-2-enylidene] malononitrile (DCTB).

 © 2002 WILEY-VCH Verlag GmbH & Co. KGaA, Weinheim 0044-8249/02/4122-4341 $ 20.00+.50/0

Very promising results were obtained by high-resolution Fourier-transform ion-cyclotron-resonance (HR-FT-ICR) MALDI mass spectrometry. The stepwise loss of up to six MeO fragments is observed in the negative ion mode (Figure 4a). The C_{56}^- ion, which results from the loss of all eight MeO groups, is weakly visible at lower mass (m/z: 672). However, it is rather improbable that this ion has the structure of the expanded cubane. Rather, we prefer to assign this weak peak to a fullerene ion resulting from rapid isomerization of the initially formed anionic C_{56} cluster. This hypothesis is supported by the subsequent facile C_2 fragmentations, which are highly characteristic of fullerenes.[18] Thus, C_2 fragmentations of C_{56}^- generate intense peaks which we assign to the fullerene ions C_{54}^- (m/z: 648), C_{52}^- (m/z: 624), and C_{50}^- (m/z: 600).

The loss of all methoxy groups and subsequent rearrangement to fullerene ions seems even more favorable in the positive ion mode (Figure 4b). Neither the fragment ions $[M^+ - n\,OCH_3]$ ($n = 1$–7) nor the C_{56}^+ ion can be detected. The spectrum is instead dominated by the fullerene ions C_{54}^+, C_{52}^+, and C_{50}^+, which result from C_2 fragmentations. Furthermore, these ions undergo remarkable ion–molecule coalescence reactions[11] with formation of higher fullerene ions from C_{100}^+ (m/z: 1201) to C_{106}^+ (m/z: 1273), which, upon C_2 fragmentation, generate the fullerene ions C_{94}^+, C_{96}^+, and C_{98}^+.

We are now continuing the gas-phase ion studies with **1** in greater detail, by using collaboration methods to possibly isolate some of the fullerenes after mass selection and neutralization. Also, we are working on further improving the synthesis of **1** and target differently substituted derivatives. The results of the gas-phase investigations actually suggest that the loss of a tris-propargylic MeO group leading to a highly unstable nonplanar carbocation might be at the origin of the highly exothermic decomposition of **1**. Therefore, we plan adding other substituents such as alkyl or aryl groups to the eight corner C(sp^3) atoms to generate more stable expanded cubanes that are amenable to X-ray crystallography.

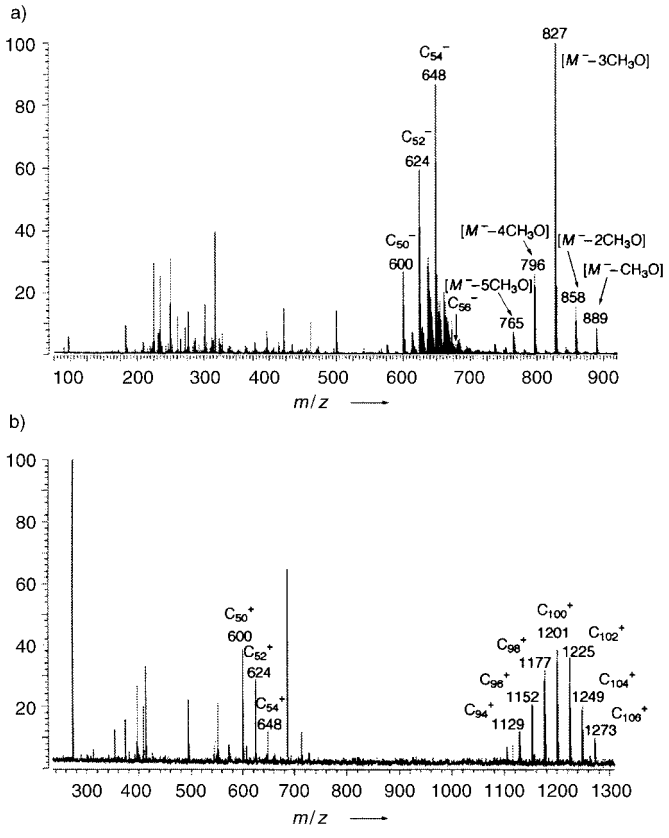


Figure 4. HR-FT-ICR-MALDI mass spectra of **1** a) in the negative (matrix: DCTB) and b) in the positive ion mode (matrix 2,5-dihydroxybenzoic acid). A N_2 laser (337 nm) was employed. All observed m/z values were accurate to within 2 ppm of the postulated elemental compositions.

Received: August 29, 2002 [Z50070]

[1] A. M. Boldi, F. Diederich, *Angew. Chem.* **1994**, *106*, 482–485; *Angew. Chem. Int. Ed. Engl.* **1994**, *33*, 468–471.

[2] M. Schreiber, J. Anthony, F. Diederich, M. E. Spahr, R. Nesper, M. Hubrich, F. Bommeli, L. DeGiorgi, C. Bosshard, P. Günter, M. Colussi, U. W. Suter, C. Boudon, J.-P. Gisselbrecht, M. Gross, *Adv. Mater.* **1994**, *6*, 786–790.

[3] a) E. Burri, F. Diederich, M. Bronsted-Nielsen, *Helv. Chim. Acta* **2002**, *85*, 2169–2182; b) Y. Zhao, R. McDonald, R. R. Tykwinski, *J. Org. Chem.* **2002**, *67*, 2805.

[4] J. Anthony, C. B. Knobler, F. Diederich, *Angew. Chem.* **1993**, *105*, 437–440; *Angew. Chem. Int. Ed. Engl.* **1993**, *32*, 406.

[5] M. Nielsen, M. Schreiber, Y. G. Baek, P. Seiler, S. Lecomte, C. Boudon, R. Tykwinski, J.-P. Gisselbrecht, V. Gramlich, P. Skinner, C. Bosshard, P. Günter, M. Gross, F. Diederich, *Chem. Eur. J.* **2001**, *7*, 3263–3280.

[6] For a review, see F. Diederich, *Chem. Commun.* **2001**, 219–227.

[7] a) P. E. Eaton, T. W. Cole, Jr., *J. Am. Chem. Soc.* **1964**, *86*, 962–964, 3157–3158; b) P. E. Eaton, *Angew. Chem.* **1992**, *104*, 1447–1462; *Angew. Chem. Int. Ed. Engl.* **1992**, *31*, 1421–1436, and references therein.

[8] H. Hopf, *Classics in Hydrocarbon Chemistry*, Wiley-VCH, Weinheim, **2000**.

[9] a) S. W. McElvany, M. M. Ross, N. S. Goroff, F. Diederich, *Science* **1993**, *259*, 1594–1596; b) Y. Rubin, T. C. Parker, S. J. Pastor, S. Jalisatgi, C. Boulle, C. L. Wilkins, *Angew. Chem.* **1998**, *110*, 1226–1229; *Angew. Chem. Int. Ed.* **1998**, *37*, 1353–1356; c) Y. Tobe, N. Nakagawa, K. Naemura, T. Wakabayashi, T. Shida, Y. Achiba, *J. Am. Chem. Soc.* **1998**, *120*, 4544–4545; d) M. M. Boorum, Y. V. Vasil'ev, T. Drewello, L. T. Scott, *Science* **2001**, *294*, 828–831.

[10] For a total gas-phase synthesis yielding macroscopic quantities of C_{60}, see L. T. Scott, M. M. Boorum, B. J. McMahon, S. Hagen, J. Mack, J. Blank, H. Wegner, A. de Meijere, *Science* **2002**, *295*, 1500–1503.

[11] a) C. Yeretzian, K. Hansen, F. Diederich, R. C. Whetten, *Nature* **1992**, *359*, 44–47; b) R. D. Beck, P. Weis, G. Bräuchle, M. M. Kappes, *J. Chem. Phys.* **1994**, *100*, 262–270; c) Z. X. Xie, Z. Y. Liu, C. R. Wang, R. B. Huang, F. C. Lin, L. S. Zheng, *J. Chem. Soc. Faraday Trans.* **1995**, *91*, 987–990.

[12] J. Anthony, A. M. Boldi, Y. Rubin, M. Hobi, V. Gramlich, C. B. Knobler, P. Seiler, F. Diederich, *Helv. Chim. Acta* **1995**, *78*, 13–43.

[13] All new compounds were fully characterized by ^1H and ^{13}C NMR spectroscopy, FTIR spectroscopy, EI- or MALDI-MS, and elemental analysis or high-resolution MS.

[14] A. S. Hay, *J. Org. Chem.* **1962**, *27*, 3320–3321.

[15] X-ray crystal data for **8b** at 293 K ($C_{68}H_{96}O_4Si_4$, $M_r = 1089.81$): monoclinic, space group $P2_1/n$ (no. 14), $\rho_{calcd} = 0.981\ g\,cm^{-3}$, $Z = 2$, $a = 10.789(10)$, $b = 14.865(13)$, $c = 23.07(2)$ Å, $\beta = 94.23(8)°$, $V = 3690(6)$ Å^3. Picker–Stoe diffractometer, $Cu_{K\alpha}$ radiation, $\lambda = 1.5418$ Å. A single crystal with linear dimensions of about $0.1 \times 0.04 \times 0.03$ mm, grown by vapor-phase diffusion of hexane into a CH_2Cl_2 solution at RT, was used. The structure was solved by direct methods and refined by full-matrix least-squares analysis (SHELXTL). All heavy atoms were refined anisotropically and H-atoms fixed isotropically with atomic positions based on stereochemical considerations. Final $R(F) = 0.061$, $wR(F^2) = 0.157$ for 343 parameters and 3074 reflections with $I > 2\sigma(I)$ and $3.54 < \theta < 50.0°$ (corresponding R values based on all 3795 reflections are 0.075 and

 © 2002 WILEY-VCH Verlag GmbH & Co. KGaA, Weinheim 0044-8249/02/4122-4342 $ 20.00+.50/0

0.169, respectively). CCDC-192482 contains the supplementary crystallographic data for this paper. These data can be obtained free of charge via www.ccdc.cam.ac.uk/conts/retrieving.html (or from the Cambridge Crystallographic Data Centre, 12 Union Road, Cambridge CB2 1EZ, UK; fax: (+44) 1223-336-033; or deposit@ccdc.cam.ac.uk).

[16] a) For the X-ray crystal structure of a planar molecular square with the same 20-membered perimeter as in **8** but lacking the four additional ethynyl groups, see A. Boldi, Ph.D. thesis, University of California at Los Angeles, **1994**; for related macrocycles, see b) A. de Meijere, S. I. Kozhushkov, *Top. Curr. Chem.* **1999**, *201*, 1–42; c) L. T. Scott, M. J. Cooney in *Modern Acetylene Chemistry* (Eds.: P. J. Stang, F. Diederich), VCH, Weinheim, **1995**, pp. 321–351; d) A. de Meijere, S. Kozhushkov, T. Haumann, R. Boese, C. Puls, M. J. Cooney, L. T. Scott, *Chem. Eur. J.* **1995**, *1*, 124–131; e) M. Brake, V. Enkelmann, U. H. F. Bunz, *J. Org. Chem.* **1996**, *61*, 1190–1191.

[17] AM1 and PM3 calculations within Spartan (SGI Version 5.1.3, Wavefunction, Inc. 18401 Von Karman Ave., Irvine, CA 82715, **1998**) confirmed that **1** is an exceptionally strained molecule. The calculated heats of formation ΔH_f^0 of 1084 kcal mol^{-1} (AM1) and 1023 kcal mol^{-1} (PM3) are much higher than those calculated by AM1 for fullerenes such as C_{60} (973 kcal mol^{-1}). However, it should be pointed out that the heat of formation for C_{60} calculated by AM1 is much higher than the experimentally determined one (ca. 610 kcal mol^{-1}; see H. D. Beckhaus, C. Rüchardt, M. Kao, F. Diederich, C. S. Foote, *Angew. Chem.* **1992**, *104*, 69–70; *Angew. Chem. Int. Ed. Engl.* **1992**, *31*, 63–64; b) H. D. Beckhaus, S. Verevkin, C. Rüchardt, F. Diederich, C. Thilgen, H. U. ter Meer, H. Mohn, W. Müller, *Angew. Chem.* **1994**, *106*, 1033–1035; *Angew. Chem. Int. Ed. Engl.* **1994**, *33*, 996–998).

[18] a) S. C. O'Brien, J. R. Heath, R. F. Curl, R. E. Smalley, *J. Chem. Phys.* **1988**, *88*, 220–230; b) P. P. Radi, T. L. Bunn, P. R. Kemper, M. E. Molchan, M. T. Bowers, *J. Chem. Phys.* **1988**, *88*, 2809–2814; c) M. M. Ross, J. H. Callahan, *J. Chem. Phys.* **1991**, *95*, 5720–5723; d) T. Weiske, D. K. Böhme, J. Hrusák, W. Krätschmer, H. Schwarz, *Angew. Chem.* **1991**, *103*, 898–900; *Angew. Chem. Int. Ed. Engl.* **1991**, *30*, 884–886; e) Z. Wan, J. F. Christian, S. L. Anderson, *J. Chem. Phys.* **1992**, *96*, 3344–3347.

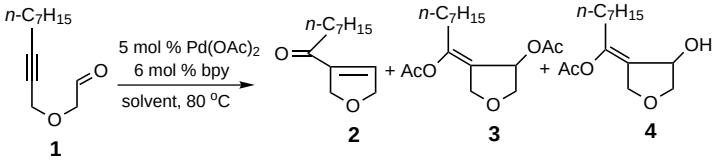
Pd^{II}-Catalyzed Cyclization of Alkynes Containing Aldehyde, Ketone, or Nitrile Groups Initiated by the Acetoxypalladation of Alkynes**

Ligang Zhao and Xiyan Lu*

The insertion of carbon–carbon multiple bonds into carbon–transition-metal bonds as a facile method of carbon–carbon bond formation is a very important fundamental reaction in transition-metal organometallic chemistry.[1] However, in contrast to the numerous reports regarding the insertion of carbon–carbon multiple bonds into carbon–transition-metal bonds, direct insertion of carbon–heteroatom multiple bonds, such as carbonyl and nitrile groups, without using stoichiometric organometallic reagents, has received scant attention.[1] The disadvantages of such insertion processes are that the carbon–heteroatom π bond is stronger than the carbon–carbon π bond,[2] and that electrophilic metals tend to form σ complexes with the heteroatom of carbon–heteroatom multiple bonds, instead of π complexes,[3] which makes the insertion unfavorable. Such obstacles make this area of research particularly challenging. Recently, some examples of the insertion of carbonyl groups into late-transition-metal–carbon bonds, for example with Rh[4] and Ni,[5] have been reported, although most of these require the use of stoichiometric organometallic reagents or additives. In palladium chemistry, a limited number of examples catalyzed by Pd^0 have been reported by Vicente,[6] Yamamoto,[7a–d] Yang,[8a–c] and Larock.[8d,e] To the best of our knowledge, there are no examples of the direct insertion of a carbonyl or nitrile group into a carbon–palladium bond by reactions catalyzed by a palladium(II) species through the acetoxypalladation of alkynes.

The fact that a Pd^{II} species is formed after quenching an oxygen–palladium bond through protonolysis, even in Pd^0-catalyzed reactions, suggests that a redox system must be involved in the reported Pd^0-catalyzed carbonyl insertion reactions. It occurs to us that a Pd^{II}-catalyzed reaction may be advantageous for such insertion reactions. Recently, we reported a Pd^{II}-catalyzed cyclization reaction of enyne esters initiated by the acetoxypalladation of alkynes which utilized bipyridine as a ligand.[9] This novel catalytic system encouraged us to develop new reactions using carbon–heteroatom multiple bonds as insertion species, instead of carbon–carbon double bonds. Herein, we wish to exhibit another mechanism involving the cyclization of alkynes with carbonyl or nitrile groups through the acetoxypalladation of alkynes, followed by the insertion of carbon–heteroatom multiple bonds into the carbon–palladium bond and subsequent protonolysis.

Our investigation of the reaction conditions began by using dec-2-ynyloxyacetaldehyde (**1**, 0.5 mmol), $Pd(OAc)_2$ (5 mol%) as the catalyst, and 2,2′-bipyridine (bpy, 6 mol%) as the ligand in acetic acid (5 mL) at 80°C (Scheme 1). The



Scheme 1. Pd^{II}-catalyzed cyclization of an aldehyde-containing alkyne.

reaction afforded products **2**–**4** (**2**:**3**:**4** 20:40:40) in 78% total yield. Control experiments confirmed that **4** can partially transform into either **3** (by acetylation) or **2** (by transformation) in this system. Reactions with ketones gave the corresponding tertiary alcohols as a single product in good yield using acetic acid/dioxane as the solvent, while the reactions of aldehydes proceeded smoothly to afford the sole product **3** in moderate yield (50%) using acetic acid/1,4-

[*] Prof. X. Lu, L. Zhao
State Key Laboratory of Organometallic Chemistry
Shanghai Institute of Organic Chemistry
Chinese Academy of Sciences
354 Fenglin Lu, Shanghai 200032 (China)
Fax: (+86) 21-6416-6128
E-mail: xylu@pub.sioc.ac.cn

[**] Major State Basic Research Program (Grant G20000077502-A). We also thank the National Natural Science Foundation of China and the Chinese Academy of Sciences for financial support.

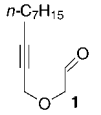
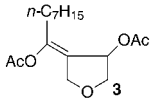
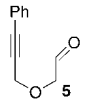
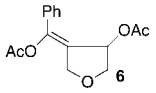
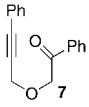
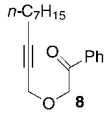
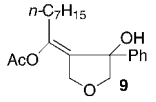
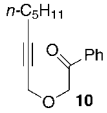
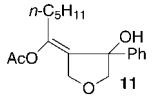
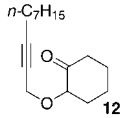
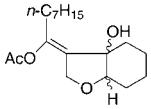
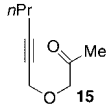
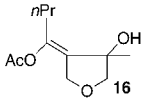
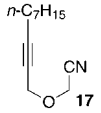
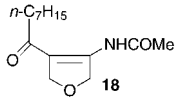
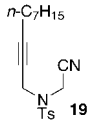
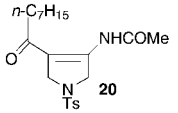
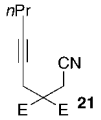
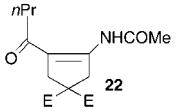
Supporting information for this article is available on the WWW under http://www.angewandte.org or from the author.

 © 2002 WILEY-VCH Verlag GmbH & Co. KGaA, Weinheim 0044-8249/02/4122-4343 $ 20.00+.50/0

dioxane/acetic anhydride (1:1:1) as the solvent system. When the reaction of **1** was performed in the absence of $Pd(OAc)_2$ or bpy, no cyclization products were obtained. These experiments indicate that both the catalyst and ligand are necessary in these reactions. Employment of 1,10-phenanthroline as the ligand gave similar results to those obtained using bpy. Other ligands such as halide ions, PPh_3, or PBu_3 have no effect in this system. The *Z* configuration of the exocylic double bond, which was assigned by ^{1}H NMR spectroscopy and confirmed by the NOESY spectra of compound **4** and crystal data of compound **9,** indicated a *trans*-acetoxypalladation process in the reaction.[10,11]

The scope and generality of the present reaction is shown in Table 1. Aliphatic aldehydes, ketones, and nitriles are all effective in this catalytic system. The reaction of carbon, oxygen, and nitrogen-tethered alkynyl nitriles proceeded smoothly and five-membered carbocyclic and heterocyclic compounds were obtained in good yields (entries 8–10).[10] The structure of compound **22** was confirmed by X-ray analysis,[11] which indicates that the rearrangement occurred as described in Scheme 2. We believe this represents a rare example of the insertion of a nitrile group into a carbon–palladium bond, catalyzed by a Pd^{II} species without the use of a redox system.

Table 1. Pd^{II}-catalyzed cyclization of alkynes containing aldehyde, ketone, or nitrile groups.[a]

Entry	Substrate	Temperature [°C]	Duration [h]	Product	Yield [%][b]
1	 **1**	80	10	 **3**	50
2	 **5**	80	24	 **6**	22
3[c]	 **7**	100	24	—	—
4	 **8**	80	14	 **9**	71
5	 **10**	80	11	 **11**	80
6[d]	 **12**	80	8	 *cis* **13**: *trans* **14** = 2.2:1	65
7	 **15**	80	11	 **16**	66
8	 **17**	80	16	 **18**	72
9[e]	 **19**	80	16	 **20**	79
10[f]	 **21**	100	16	 **22**	95

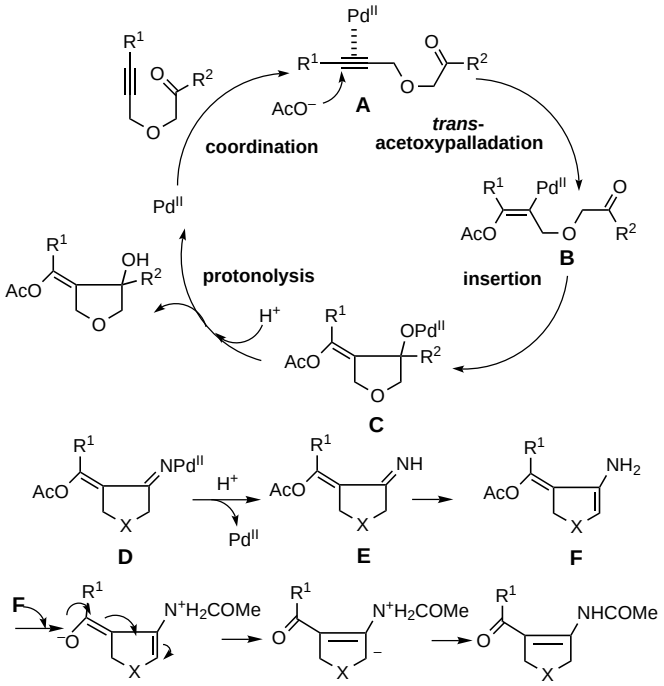
[a] Reaction conditions: substrate (0.5 mmol), $Pd(OAc)_2$ (0.025 mmol), and bpy (0.03 mmol) in solvent (5 mL). Entries 1 and 2 using acetic acid/1,4-dioxane/acetic anhydride (1:1:1) as solvent, entries 3–9 using acetic acid/1,4-dioxane (1:4) as solvent, entry 10 using acetic acid as solvent. [b] Yield of isolated product. [c] Compound **7** was recovered in 80% yield; the reaction did not lead to the isolation of the expected product. [d] *cis*:*trans* = 2.2:1. The assignment of the relative configurations of **13** and **14** was based on their NMR spectra and NOE experiments (entry 6). [e] 0.25 mmol of substrate. [f] E = CO_2Me.

The mechanism shown in Scheme 2 is proposed for this reaction. First, the *trans*-acetoxypalladation of the carbon–carbon triple bond affords vinylpalladium species **B**, followed by insertion of the carbonyl or nitrile group into the carbon–palladium bond of **B** to give oxypalladium species **C** or iminopalladium species **D**, respectively; protonolysis of the intermediate **C** or **D** then gives the corresponding products and imines **E** in the presence of an acid medium, with regeneration of the original palladium species. The unstable intermediate imine **E** may isomerize to the amine products **F**, followed by an intermolecular aminolysis of the acetoxy group to give further products. It is noteworthy that bidentate nitrogen-containing ligands are important in this reaction, possibly for their ability in stabilizing vinylpalladium intermediates that allow the catalytic reaction to proceed.[9]

Vicente et al. provided straightforward evidence for the above possible mechanism through stoichiometric reactions.[6] Moreover, similar species to intermediate **C** have been isolated by treating a cyclopalladated phenyl 2-pyridyl ketone complex with alkynes, which was a direct observation of carbonyl group insertion into a carbon–palladium bond.[12] It should be noted that Hartwig recently reported the direct insertion of an aldehyde into the rhodium–carbon bond,[4i] which provides strong evidence for this mechanism.

In conclusion, we have developed a Pd^{II}-catalyzed cyclization reaction of alkynes with carbon–heteroatom multiple

 © 2002 WILEY-VCH Verlag GmbH & Co. KGaA, Weinheim 0044-8249/02/4122-4344 $ 20.00+.50/0



Scheme 2. Proposed mechanism of the reaction.

bonds under mild conditions, where the insertion of carbon–heteroatom multiple bonds into the carbon–palladium bond is the key step. This is a reaction with high atom economy, which does not require the use of organometallic reagents, additives, or redox systems. This acetoxypalladation/carbon–heteroatom multiple-bond-insertion/protonolysis catalytic system may extend the scope of transition-metal-catalyzed reactions pertaining to the insertion of carbon–heteroatom multiple bonds into metal–carbon bonds, and provide a new methodology in organic synthesis.

Experimental Section

Typical procedure for the cyclization of substrate **8** (Table 1, entry 4): Under nitrogen atmosphere, substrate **8** (136 mg, 0.5 mmol) was added to a mixture of $Pd(OAc)_2$ (5.6 mg, 0.025 mmol), bpy (4.5 mg, 0.030 mmol), acetic acid (1 mL), and 1,4-dioxane (4 mL). The solution was stirred at 80 °C for 14 h until the reaction was complete, which was confirmed by thin-layer chromatography. On cooling, the reaction mixture was neutralized with saturated $NaHCO_3$ and extracted with Et_2O. The combined Et_2O solutions were washed with saturated NaCl, dried (Na_2SO_4) and concentrated. The residue was purified by flash chromatography (ethyl acetate/petroleum ether 1:4) to give the product **9** as a white solid in 71 % yield, mp. 73–74 °C.

Received: August 23, 2002 [Z50028]

[1] a) J. Tsuji, *Palladium Reagents and Catalysis: Innovation in Organic Synthesis*, Wiley, Chichester, **1995**; b) L. S. Hegedus in *Comprehensive Organic Synthesis, Vol. 4* (Eds. B. M. Trost, L. Fleming, M. F. Semmelhack), Pergamon, Oxford, **1990**, p. 571.

[2] T. H. Lowry, K. S. Richardson, *Mechanism and Theory in Organic Chemistry*, Harper and Row, New York, **1987**, p. 162.

[3] a) S. Shambayati, S. L. Schreiber in *Comprehensive Organic Synthesis, Vol. 1* (Eds.: B. M. Trost, I. Fleming, S. L. Schreiber), Pergamon, Oxford, **1991**, pp. 283–324; b) R. Noyori, M. Yamakawa, S. Hashiguchi, *J. Org. Chem.* **2001**, *66*, 8364.

[4] For recent rhodium-catalyzed reactions using stoichiometric organometallic reagents, see: a) T. Huang, Y. Meng, S. Venkatraman, D. Wang, C. J. Li, *J. Am. Chem. Soc.* **2001**, *123*, 7451; b) C. J. Li, Y. Meng, *J. Am. Chem. Soc.* **2000**, *122*, 9538; c) S. Oi, M. Moro, Y. Inoue, *Organometallics* **2001**, *20*, 1036; d) M. Sakai, M. Ueda, N. Miyaura, *Angew. Chem.* **1998**, *110*, 3475; *Angew. Chem. Int. Ed.* **1998**, *37*, 3279; e) T. Fujii, T. Koike, A. Mori, K. Osakada, *Synlett* **2002**, 298; f) T. Hayashi, M. Ishigedani, *J. Am. Chem. Soc.* **2000**, *122*, 976; g) R. A. Batey, A. N. Thadani, D. V. Smil, *Org. Lett.* **1999**, *1*, 1683; h) T. Ishiyama, J. F. Hartwig, *J. Am. Chem. Soc.* **2000**, *122*, 12043; i) C. Krug, J. F. Hartwig, *J. Am. Chem. Soc.* **2002**, *124*, 1674.

[5] For nickel-catalyzed reactions, see: a) Y. Sato, N. Saito, M. Mori, *J. Am. Chem. Soc.* **2000**, *122*, 2371; b) Y. Sato, M. Takimoto, K. Hayashi, T. Katsuhara, K. Takagi, M. Mori, *J. Am. Chem. Soc.* **1994**, *116*, 9771; c) K. Shibata, M. Kimura, M. Shimizu, Y. Tamaru, *Org. Lett.* **2001**, *3*, 2181; d) K. K. Majumdar, C.-H. Cheng, *Org. Lett.* **2000**, *2*, 2295; e) Y.-C. Huang, K. K. Majumdar, C.-H. Cheng, *J. Org. Chem.* **2002**, *67*, 1682; f) E. Oblinger, J. Montgomery, *J. Am. Chem. Soc.* **1997**, *119*, 9065; g) M. V. Chevliakov, J. Montgomery, *J. Am. Chem. Soc.* **1999**, *121*, 11139; h) K. K. D. Amarasinghe, J. Montgomery, *J. Am. Chem. Soc.* **2002**, *124*, 9366.

[6] a) J. Vicente, J. A. Abad, B. López-Peláez, E. Martínez-Viviente, *Organometallics* **2002**, *21*, 58; b) J. Vicente, J. A. Abad, J. Gil-Rubio, *Organometallics* **1996**, *15*, 3509; c) J. Vicente, J. A. Abad, J. Gil-Rubio, *J. Organomet. Chem.* **1992**, *436*, C9.

[7] For Pd^0-catalyzed reactions of carbonyl group, see: a) V. Gevorgyan, L. G. Quan, Y. Yamamoto, *Tetrahedron Lett.* **1999**, *40*, 4089; b) L. G. Quan, M. Lamrani, Y. Yamamoto, *J. Am. Chem. Soc.* **2000**, *122*, 4827; c) L. G. Quan, V. Gevorgyan, Y. Yamamoto, *J. Am. Chem. Soc.* **1999**, *121*, 3545; d) X. Gai, R. Grigg, S. Collard, J. E. Muir, *Chem. Commun.* **2000**, 1765; for reactions using stoichiometric organostannanes, see: e) Y.-H. Ha, S.-K. Kang, *Org. Lett.* **2002**, *4*, 1143, and references therein.

[8] For Pd^0-catalyzed reactions of nitriles, see: a) C.-C. Yang, P.-J. Sun, J.-M. Fang, *J. Chem. Soc. Chem. Commun.* **1994**, 2629; b) C.-C. Yang, H.-M. Tai, P.-J. Sun, *Synlett* **1997**, 812; c) C.-C. Yang, H.-M. Tai, P.-J. Sun, *J. Chem. Soc. Perkin Trans. 1* **1997**, 2843; d) R. C. Larock, Q. Tian, A. A. Pletnev, *J. Am. Chem. Soc.* **1999**, *121*, 3238; e) A. A. Pletnev, R. C. Larock, *Tetrahedron Lett.* **2002**, *43*, 2133.

[9] a) Q. Zhang, X. Lu, *J. Am. Chem. Soc.* **2000**, *122*, 7604; b) Q. Zhang, X. Lu, X. Han, *J. Org. Chem.* **2001**, *66*, 7676.

[10] Spectroscopic and analytical data for all new compounds, NOESY spectra of **4**, ^1H NMR and ^{13}C NMR spectra of compounds **1**, **2**, **4**–**6**, **13**–**18**, **21**, and **23** are available in the Supporting Information.

[11] CCDC-188743 (**9**) and CCDC-188742 (**22**) contains the supplementary crystallographic data for this paper. These data can be obtained free of charge via www.ccdc.cam.ac.uk/conts/retrieving.html (or from the Cambridge Crystallographic Data Centre, 12, Union Road, Cambridge CB2 1EZ, UK; fax: (+44) 1223-336-033; or deposit @ccdc.cam.ac.uk).

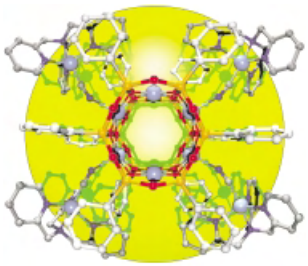
[12] F. Maassarani, M. Pfeffer, J. Spencer, E. Wehman, *J. Organomet. Chem.* **1994**, *466*, 265.

 © 2002 WILEY-VCH Verlag GmbH & Co. KGaA, Weinheim 0044-8249/02/4122-4345 $ 20.00+.50/0

ANGEWANDTE CHEMIE
INTERNATIONAL EDITION
A Journal of the Gesellschaft Deutscher Chemiker
2002
41/23
Pages 4355 – 4594

COVER PICTURE

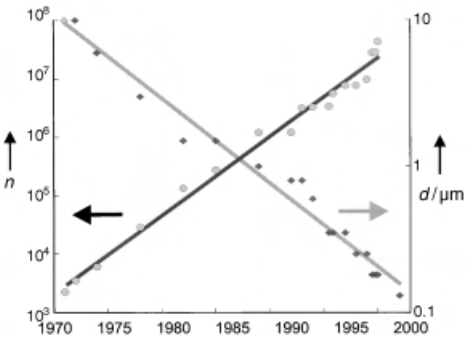
The cover picture shows a magnetic cluster, which was rationally designed by following a two-step synthetic approach (color code: light blue = Cu, orange = Si, gray and white = C, dark blue = N, red = O). The compound, which features ten copper(II) ions in three different coordination environments (trigonal-bipyramidal, square-pyramidal and square-planar), was obtained in crystalline form by self-assembly of four monodentate $[Cu(tmpa)(CN)]^+$ units (tmpa = tris(2-pyridylmethyl)amine) around a preformed hexacopper(II)-siloxanolate cage, $[Cu_6\{(PhSiO_2)_6\}_2]$. Further details on the synthesis, structure, and magnetic properties are reported by G. L. Abbati, A. Cornia et al. on p. 4517 ff.



REVIEWS

Contents

The current state of molecular electronics: Following Moore's law the ultimate miniaturization of electronic devices is molecular-scale electronics (see picture; n = number of transistors per cm^2, d = the pitch size). Although several critical challenges remain unmet, a lot has been learned about how molecules behave in device architectures. This review summarizes what is only the beginning of molecular electronics.



R. L. Carroll,
C. B. Gorman* ..... 4378 – 4400

The Genesis of Molecular Electronics

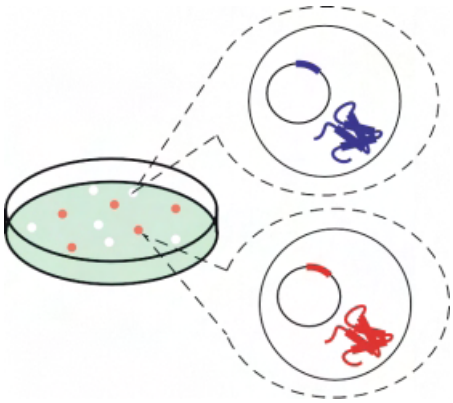
Angew. Chem. **2002**, *114*, 4556 – 4579

Keywords: molecular electronics · molecular switches · monolayers · scanning-probe techniques

 © 2002 WILEY-VCH Verlag GmbH & Co. KGaA, Weinheim 1433-7851/02/4123-4357 $ 20.00+.50/0

The identification of proteins based on function from large protein libraries is the key to protein engineering and proteomics. What has been done in this field and what remains? In this Review, existing methods for analyzing protein function on a large scale are overviewed, for example, the yeast three-hybrid system (see picture), and the challenges and opportunities that lie ahead are identified.

Angew. Chem. **2002**, *114*, 4580 – 4606



H. Lin, V. W. Cornish* ..... 4402 – 4425

Screening and Selection Methods for Large-Scale Analysis of Protein Function

Keywords: directed evolution · high-throughput screening · protein engineering · proteomics · selection

MINIREVIEW

Chemical dark horses: With the advent of antibody catalysis, chemists asked for the first time whether one could use this sophisticated system of molecular diversity to create new chemical functions, that is, efficient, selective chemical catalysts. From these experiments have come a host of antibody catalysts, new insights into the evolution of binding and catalytic function, as well as the discovery of a previously unrecognized role for the antibody molecule in the immune response. The picture shows the detection of H_2O_2 in the crystal of an antibody Fab (Fab = antigen-binding fragment of the antibody) after UV irradiation.

Angew. Chem. **2002**, *114*, 4607 – 4618



P. G. Schultz,* J. Yin, R. A. Lerner* ..... 4427 – 4437

The Chemistry of the Antibody Molecule

Keywords: catalytic antibodies · diversity · evolution

VIPs

The following communications are "Very Important Papers" in the opinion of two referees. They will be published shortly (those marked with a diamond will be published in the next issue). Short summaries of these articles can be found on the *Angewandte Chemie* homepage at the address http://www.angewandte.org

Experimental Observation and Confirmation of Icosahedral $W@Au_{12}$ and $Mo@Au_{12}$ Molecules — X. Li, B. Kiran, J. Li, H.-J. Zhai, ◆ L.-S. Wang*

Tuning the Regioselectivity in the Palladium(II)-Catalyzed Isomerization of Alkylidenecyclopropyl Ketones: A Dramatic Salt Effect — S. Ma*, J. Zhang

Porphyrazines as Molecular Scaffolds: Periphery–Core Spin Coupling Between Metal Ions of a Schiff Base Porphyrazine — M. Zhao, C. Stern, A. G. M. Barrett,* B. M. Hoffman*

Beyond the Icosahedron: The First 13-Vertex Carborane — A. Burke, D. Ellis, B. T. Giles, B. E. Hodson, S. A. Macgregor, G. M. Rosair, A. J. Welch*

Topomerization of a Distorted-Rhomboid Tetraborane(4) and its Hydroboration to a Pentaborane(7) — C. Präsang, M. Hofmann, G. Geiseler, W. Massa, A. Berndt*

A New Diversity-Oriented Synthesis of α-Amino Acid Derivatives by a Silyltelluride-Mediated Radical Coupling Reaction of Imines and Isonitriles — S. Yamago,* H. Miyazoe, T. Nakayama, M. Miyoshi, J. Yoshida*

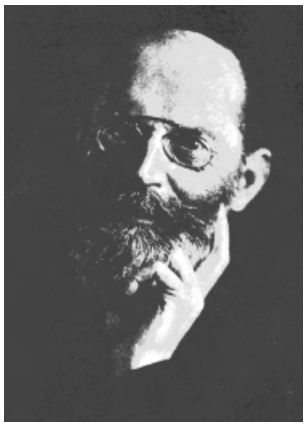
Facile Solid-State Synthesis of Highly Conducting Poly(ethylenedioxythiophene) — H. Meng, D. F. Perepichka, F. Wudl*

[3+2]/[4+1] Cycloaddition Reactions of Fischer Alkoxy(alkenyl)carbene Complexes with Electronically Neutral 1,3-Dienes — J. Barluenga,* S. López, J. Flórez

 © 2002 WILEY-VCH Verlag GmbH & Co. KGaA, Weinheim 1433-7851/02/4123-4358 $ 20.00+.50/0

ESSAY

The founder of the chemistry of primary natural products (carbohydrates, purines and nucleosides, and peptides and proteins) was Emil Fischer (see picture). He elucidated the stereochemistry of carbohydrates, introduced the assignment of configuration, developed asymmetric syntheses and protecting-group chemistry, and was the first to obtain synthetic peptides by targeted chain extension. He uncovered the substrate selectivity and stereoselectivity of enzyme reactions, formulated the lock-and-key principle of biological recognition, and became the father of biochemistry. He was born 150 years ago, and 100 years ago he received the Nobel Prize for Chemistry.



Angew. Chem. **2002**, *114*, 4619 – 4632

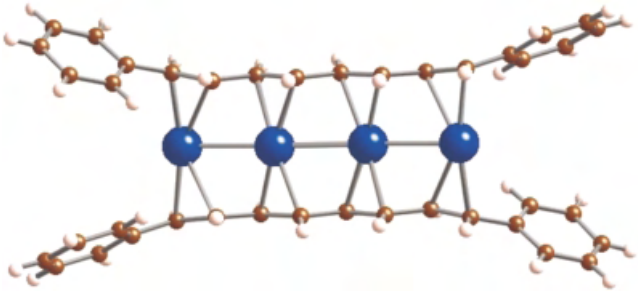
H. Kunz* ..... 4439 – 4451

Emil Fischer—Unequalled Classicist, Master of Organic Chemistry Research, and Inspired Trailblazer of Biological Chemistry

Keywords: asymmetric synthesis · carbohydrates · Fischer, Emil · history of chemistry

HIGHLIGHT

A new link in the chain: After a long period of inactivity, research into one-dimensional compounds based on linear arrays of transition metals is experiencing a renaissance. Recently, oligomeric and polymeric chains have been reported for a variety of transition metals. One such compound of a particularly exotic variety is depicted here, in which a $\{Pd_4\}^{2+}$ unit is surrounded by a "π-electron sheath" of conjugated polyene ligands.



Angew. Chem. **2002**, *114*, 4633 – 4637

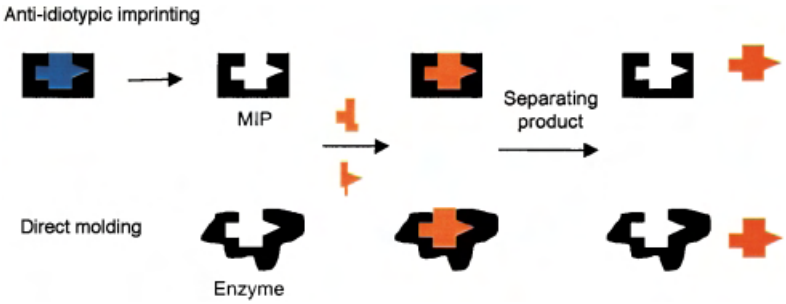
J. K. Bera, K. R. Dunbar* .. 4453 – 4457

Chain Compounds Based on Transition Metal Backbones: New Life for an Old Topic

Keywords: chain structures · conducting materials · metal – metal interactions · nanotechnology · transition metals

COMMUNICATIONS

Two mutually complementary, target-directed synthetic approaches have been used to generate a class of bio-effective molecules (inhibitors). In the first, condensation reactions were performed within the cavities of a molecularly imprinted polymer (MIP) prepared against a known kallikrein inhibitor. In the second approach, the enzyme itself directed the assembly of small building blocks within the biologically active site (see scheme).



Angew. Chem. **2002**, *114*, 4640 – 4643

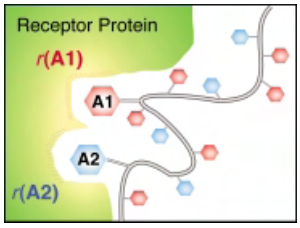
Y. Yu, L. Ye,* K. Haupt, K. Mosbach* ..... 4459 – 4463

Formation of a Class of Enzyme Inhibitors (Drugs), Including a Chiral Compound, by Using Imprinted Polymers or Biomolecules as Molecular-Scale Reaction Vessels

Keywords: biomimetic synthesis · drug research · imprinting · inhibitors

 © 2002 WILEY-VCH Verlag GmbH & Co. KGaA, Weinheim 1433-7851/02/4123-4359 $ 20.00+.50/0

A highly practical strategy for mimicking the synthesis of cell-surface oligosaccharides involves the segmentation of a given oligosaccharide into polymerizable carbohydrate modules containing two glycoside residues (A1 and A2) that provide key binding interactions with the receptor protein at the *r*(A1) and *r*(A2) binding sites. The bioactive structures are then regenerated by radical copolymerization.



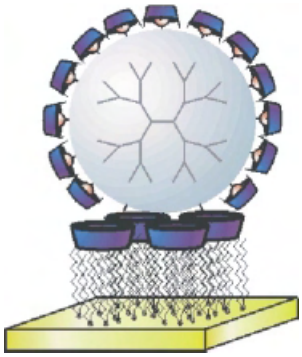
Angew. Chem. **2002**, *114*, 4643 – 4647

K. Sasaki, Y. Nishida,* T. Tsurumi, H. Uzawa, H. Kondo, K. Kobayashi* ..... 4463 – 4467

Facile Assembly of Cell Surface Oligosaccharide Mimics by Copolymerization of Carbohydrate Modules

Keywords: biomimetic synthesis · carbohydrates · oligosaccharides · polymers · sialic acids

Monolayers of cyclodextrin host molecules on gold substrates are used as "molecular printboards" for the stable attachment of functionalized molecules through multiple supramolecular interactions. Adsorption is achieved through delivery as a supramolecular complex (see picture), whereas the desorption kinetics can be tuned by varying the cyclodextrin concentration in solution.



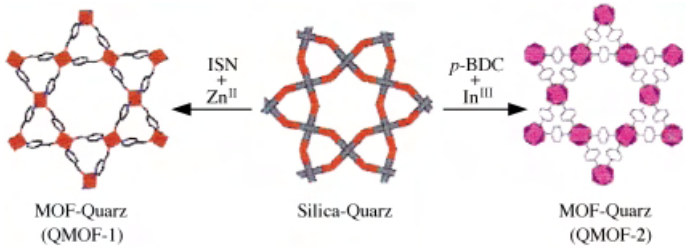
Angew. Chem. **2002**, *114*, 4647 – 4651

J. Huskens,* M. A. Deij, D. N. Reinhoudt* ..... 4467 – 4471

Attachment of Molecules at a Molecular Printboard by Multiple Host – Guest Interactions

Keywords: cyclodextrins · host – guest systems · monolayers · self-assembly · surface plasmon resonance

Man-made minerals: The synthesis of two α- and β-quartz structures with open metal – organic frameworks (QMOF-1 and QMOF-2) is reported. QMOF-1 is assigned to $Zn(ISN)_2 \cdot 2H_2O$ (ISN = isonicotinic acid) with the low symmetry of α-quartz, while QMOF-2 to $InH(BDC)_2$ (BDC = terephthalate) with the high symmetry of β-quartz.



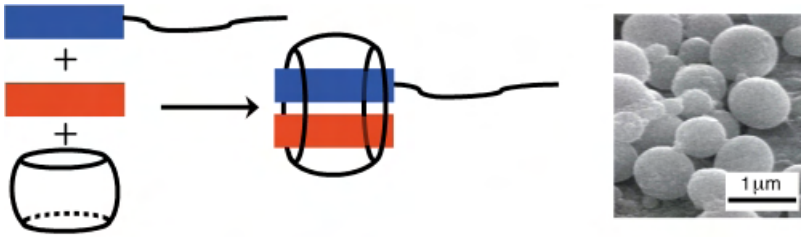
Angew. Chem. **2002**, *114*, 4651 – 4653

J. Sun, L. Weng, Y. Zhou, J. Chen, Z. Chen, Z. Liu, D. Zhao* .. 4471 – 4473

QMOF-1 and QMOF-2: Three-Dimensional Metal – Organic Open Frameworks with a Quartzlike Topology

Keywords: carboxylate ligands · chirality · coordination polymers · microporus materials · supramolecular chemistry · zeolite analogues

A stable ternary inclusion complex comprising a host, an electron donor, and an electron acceptor with a long alkyl tail (see schematic representation) triggers the spontaneous formation of giant vesicles (see TEM image). The ternary complex behaves as a supramolecular amphiphile with a large polar head group and a single hydrophobic tail. Treatment of the complex with an oxidizing agent results in disruption of the vesicles.



Angew. Chem. **2002**, *114*, 4654 – 4656

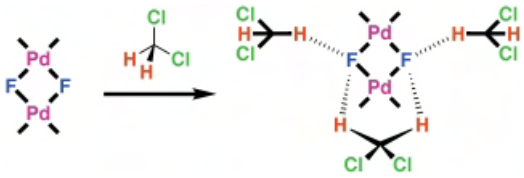
Y. J. Jeon, P. K. Bharadwaj, S. Choi, J. W. Lee, K. Kim* ..... 4474 – 4476

Supramolecular Amphiphiles: Spontaneous Formation of Vesicles Triggered by Formation of a Charge-Transfer Complex in a Host

Keywords: charge transfer · cucurbituril · host – guest systems · supramolecular chemistry · vesicles

 © 2002 WILEY-VCH Verlag GmbH & Co. KGaA, Weinheim 1433-7851/02/4123-4360 $ 20.00+.50/0

The unexpectedly high basicity of bridging fluoride ions in novel dinuclear Pd complexes is manifested by intramolecular CH···F interactions and the unprecedented hydrogen bonding of three CH_2Cl_2 molecules to the Pd_2F_2 framework (see scheme). Novel deprotonation of a coordinated $(alkyl)_3P$ ligand to produce a bifluoride is reported.



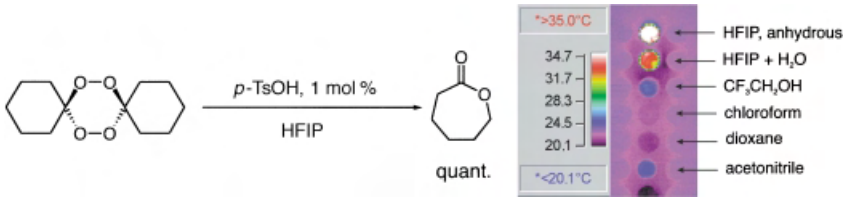
Angew. Chem. **2002**, *114*, 4656 – 4659

V. V. Grushin,*
W. J. Marshall ..... 4476 – 4479

Is Fluoride Bonded to Two Pd Acceptors Still Basic? Three CH_2Cl_2 Molecules Encapsulating a $Pd_2(\mu\text{-}F)_2$ Square and New Implications for Catalysis

Keywords: fluorides · hydrogen bonds · palladium · X-ray diffraction

What a difference the solvent makes! Unlike in conventional solvents, non-strained ketones such as cyclohexanone react smoothly with hydrogen peroxide in 1,1,1,3,3,3-hexafluoro-2-propanol (HFIP) to give lactones. The reaction proceeds via an isolatable spiro-bisperoxide, which undergoes a highly exothermic acid-catalyzed rearrangement to two equivalents of lactone (see Equation and IR thermogram).



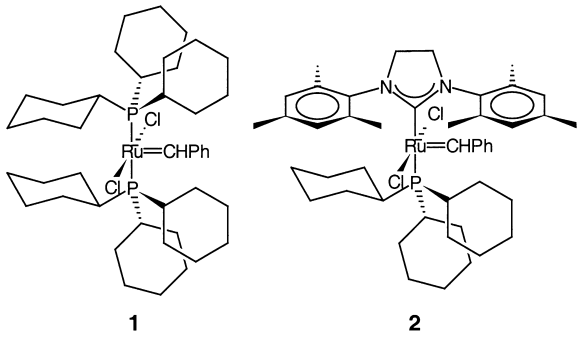
Angew. Chem. **2002**, *114*, 4661 – 4664

A. Berkessel,* M. R. M. Andreae, H. Schmickler, J. Lex ..... 4481 – 4484

Baeyer – Villiger Oxidations with Hydrogen Peroxide in Fluorinated Alcohols: Lactone Formation by a Nonclassical Mechanism

Keywords: Baeyer – Villiger oxidation · fluorinated solvents · IR thermography · peroxides · rearrangement

QM/MM provides a new twist: In olefin metathesis with first-generation Ru catalyst **1**, the rotation of the phosphane ligand with threefold symmetry is the rate-determining step. Second-generation catalyst **2** is more active: the rotation step is not required as the carbene ligand has twofold symmetry. Combined QM/MM calculations confirm the results of earlier experimental investigations.



1 **2**

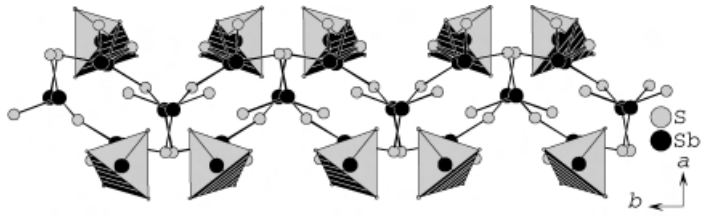
Angew. Chem. **2002**, *114*, 4668 – 4671

C. Adlhart, P. Chen* ..... 4484 – 4487

Ligand Rotation Distinguishes First- and Second-Generation Ruthenium Metathesis Catalysts

Keywords: density-functional calculations · force-field calculations · homogeneous catalysis · metathesis · theoretical chemistry

Antimony in two oxidation states: The mixed-valent thioantimonate anion $[Sb_4S_9]^{4-}$ in the compound $[Ni(dien)_2]_2Sb_4S_9$ contains Sb^VS_4 tetrahedra, which are bound by one terminal S atom to the Sb_3S_7 backbone of the anion (see figure). dien = diethylenetriamine.



Angew. Chem. **2002**, *114*, 4671 – 4673

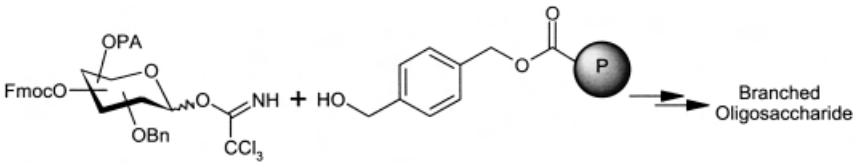
R. Stähler, B.-D. Mosel, H. Eckert, W. Bensch* ..... 4487 – 4489

Solvothermal Synthesis, Crystal Structure, Thermal Stability, and Mössbauer Spectroscopic Investigation of the Mixed-Valent Thioantimonate(III,V) $[Ni(dien)_2]_2Sb_4S_9$

Keywords: antimony · mixed-valent compounds · Moessbauer spectroscopy · solvothermal synthesis · structure elucidation

 © 2002 WILEY-VCH Verlag GmbH & Co. KGaA, Weinheim 1433-7851/02/4123-4361 $ 20.00+.50/0

A solid basis for sugar synthesis: A simple, yet efficient method for the regio- and stereocontrolled synthesis of linear and branched oligosaccharides on a solid support should be an important step forward for the development of generally applicable automated oligosaccharide syntheses. The combination of different esters (9-fluorenylmethyloxycarbonyl (Fmoc), phenoxyacetate (PA), benzoyl) for temporary, or *O*-benzyl groups for permanent protection as well as binding to the solid phase and *O*-glycosyl trichloroacetimidates as donors offers this possibility, as shown in the synthesis of an *N*-glycan hexasaccharide (see scheme).



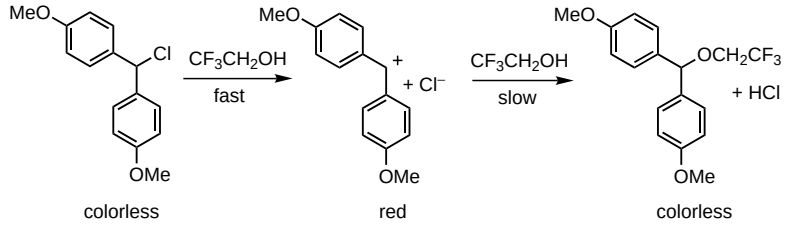
Angew. Chem. **2002**, *114*, 4664 – 4668

X. Wu, M. Grathwohl, R. R. Schmidt* ..... 4489 – 4493

Efficient Solid-Phase Synthesis of a Complex, Branched *N*-Glycan Hexasaccharide: Use of a Novel Linker and Temporary-Protecting-Group Pattern

Keywords: glycosidation · *N*-glycans · oligosaccharides · protecting groups · solid-phase synthesis

Which step is faster? Carbocations are not necessarily short-lived intermediates in solvolytic displacement reactions. In many cases, ionization of the carbocation's precursor is faster than the subsequent reaction with the solvent (see scheme), which allows one to directly observe the intermediate carbocation.



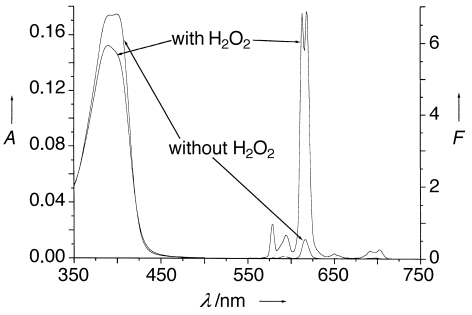
Angew. Chem. **2002**, *114*, 4674 – 4676

H. Mayr,* S. Minegishi ..... 4493 – 4495

First Direct Observation of the Two Distinct Steps in an S_N1 Reaction

Keywords: carbocations · nucleophilic substitution · reaction kinetics · reactive intermediates · solvent effects · solvolysis

A bright idea: A 15-fold increase in fluorescence intensity occurs when the complex formed between Eu^{3+} and the antibiotic tetracycline binds to hydrogen peroxide at neutral pH. The complex can be used in the determination of the concentration of H_2O_2, the activity of oxidases, the concentration of glucose, and also in an optical sensor for H_2O_2.



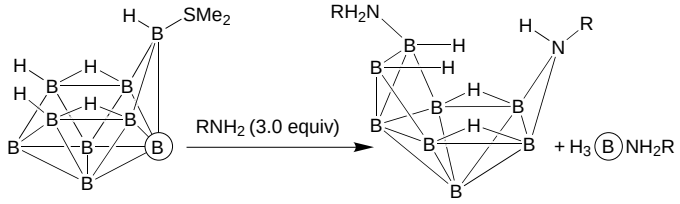
Angew. Chem. **2002**, *114*, 4681 – 4684

O. S. Wolfbeis,* A. Dürkop, M. Wu, Z. Lin ..... 4495 – 4498

A Europium-Ion-Based Luminescent Sensing Probe for Hydrogen Peroxide

Keywords: fluorescent probes · hydrogen peroxide · lanthanides · oxidases · sensors

The great escape! In the transition of $(Me_2S)B_9H_{13}$ into $(RH_2N)B_8H_{11}NHR$, one boron atom is lost. Boron-substituted derivatives of $(Me_2S)B_9H_{13}$ were used to identify this boron atom, which turned out to be firmly integrated in the starting cluster (see scheme). A pathway for the conversion is proposed.



Angew. Chem. **2002**, *114*, 4676 – 4678

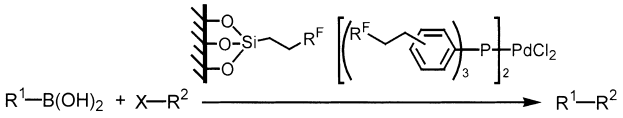
M. E. El-Zaria,* U. Dörfler, M. Hofmann, D. Gabel ..... 4498 – 4500

Conversion of *arachno*-Nonaborane into Azanonaborane: Unexpected Loss of a Firmly Integrated Boron Atom

Keywords: boranes · boron · cluster compounds · NMR spectroscopy · rearrangements

 © 2002 WILEY-VCH Verlag GmbH & Co. KGaA, Weinheim 1433-7851/02/4123-4362 $ 20.00+.50/0

With and now without: Perfluoro-tagged catalysts immobilized on fluorous reversed-phase silica gel can be used for Suzuki and Sonogashira C–C coupling reactions (see scheme; R^1 = e.g., phenyl, 4-$MeOC_6H_4$, R^2 = e.g., 4-$NO_2C_6H_4$, 4-$MeCOC_6H_4$, X = Br, I) without the need for perfluorinated solvents. After the reaction the products were isolated by decantation and the Pd catalysts were recovered and reused.



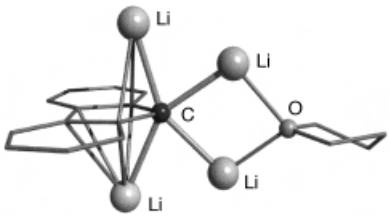
Angew. Chem. **2002**, *114*, 4678 – 4681

C. C. Tzschucke, C. Markert, H. Glatz, W. Bannwarth* ..... 4500 – 4503

Fluorous Biphasic Catalysis without Perfluorinated Solvents: Application to Pd-Mediated Suzuki and Sonogashira Couplings

Keywords: biaryls · C – C coupling · fluorous biphasic catalysis · supported catalysts

Six-coordinate carbon: 9,9-Dilithiofluorene – thf complex (see picture) crystallizes as chains of lithium atoms which are alternately bridged by fluorenylidene and THF units. These polymer chains are held together by Li – C π and σ interactions; the tetrametallated carbon atom is six-coordinated. This means, structural elements are found here, which are known from lithioalkanes, on the one hand, and from the lithocene anion, on the other hand.



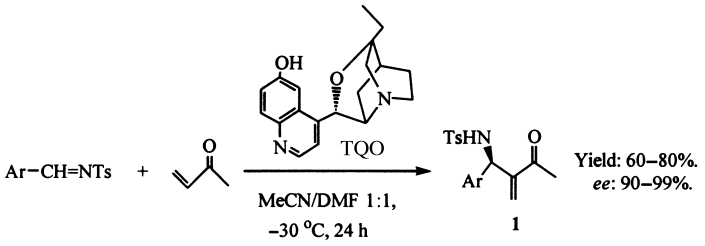
Angew. Chem. **2002**, *114*, 4685 – 4687

G. Linti,* A. Rodig, H. Pritzkow ..... 4503 – 4506

9,9-Dilithiofluorene: The First Crystal-Structure Analysis of an α,α-Dilithiated Hydrocarbon

Keywords: carbanions · density functional calculations · lithiation · lithium · structure determination

The chiral Lewis base catalyst TQO, a cinchona alkaloid derivative, facilitates the Baylis – Hillman reaction of various *N*-arylidene-4-methylbenzenesulfonamides with methyl vinyl ketone (MVK) or methyl acrylate to give the Baylis – Hillman adducts **1** in good yields with high enantioselectivity (90 – 99 % *ee*).



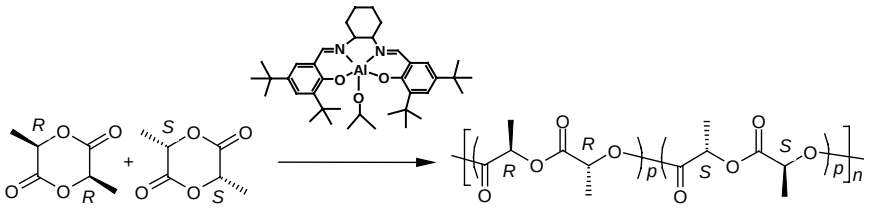
Angew. Chem. **2002**, *114*, 4689 – 4692

M. Shi,* Y.-M. Xu ..... 4507 – 4510

Catalytic, Asymmetric Baylis – Hillman Reaction of Imines with Methyl Vinyl Ketone and Methyl Acrylate

Keywords: asymmetric catalysis · asymmetric synthesis · Baylis – Hillman reactions · C–C coupling · Lewis bases

Easily accessible [(salen)(*i*PrO)Al] exerts excellent molecular-weight and stereochemical control in lactide polymerization either in solution or in the absence of solvent. The *R,R* initiator shows a marked preference for L-lactide over D-lactide. Stereoblock copolylactides (see scheme) with high melting points can be prepared directly from D,L-lactides by using a racemic initiator.



rac-D,L-LA isotactic stereoblock copolylactide

Angew. Chem. **2002**, *114*, 4692 – 4695

Z. Zhong, P. J. Dijkstra, J. Feijen* ..... 4510 – 4513

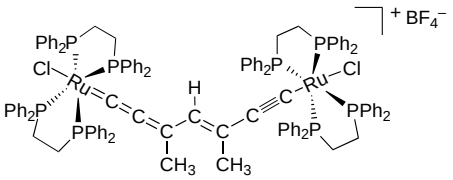
[(salen)Al]-Mediated, Controlled and Stereoselective Ring-Opening Polymerization of Lactide in Solution and without Solvent: Synthesis of Highly Isotactic Polylactide Stereocopolymers from Racemic D,L-Lactide

Keywords: aluminum · polymers · ring-opening polymerization · stereoselectivity

 © 2002 WILEY-VCH Verlag GmbH & Co. KGaA, Weinheim 1433-7851/02/4123-4363 $ 20.00+.50/0

A planar "W"-shaped π-conjugated C_7 bridge occurs in the bimetallic complexes, such as **1**, that are formed by addition of cationic ruthenium allenylidenes to the $C_\gamma \equiv C_\delta$ bond of a ruthenium diyne. These complexes possess attractive redox and optical properties that can be tuned by varying the pendant groups.

Angew. Chem. **2002**, *114*, 4695 – 4699



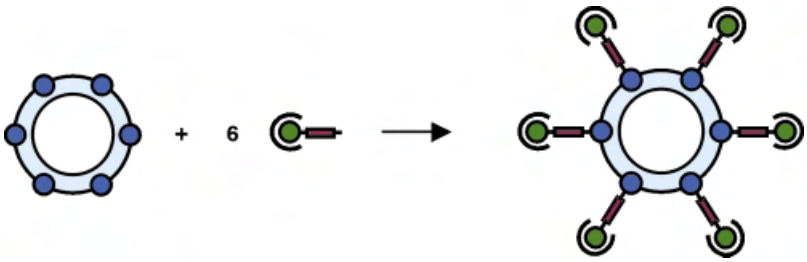
1

S. Rigaut, J. Massue, D. Touchard,* J.-L. Fillaut, S. Golhen, P. H. Dixneuf ..... 4513 – 4517

Unprecedented Coupling of Allenylidene and Diynyl Metal Complexes: A Bimetallic Ruthenium System with a C_7 Conjugated Bridge

Keywords: allenylidenes · bimetallic complexes · bridging ligands · cumulenes · ruthenium

A decacopper(II) cluster. Clusters (shown in blue) can be expanded and their magnetic properties tuned by the addition of suitable metal-complex ligands (shown in green). By using this method, $[Cu_6\{(PhSiO_2)_6\}_2\{(NC)Cu(tmpa)\}_4](PF_6)_4$ was rationally designed by self-assembly of four $\{(NC)Cu(tmpa)\}^+$ units around a robust hexacopper(II)-siloxanolate cage (tmpa = tris(2-pyridylmethyl)amine).



Angew. Chem. **2002**, *114*, 4699 – 4702

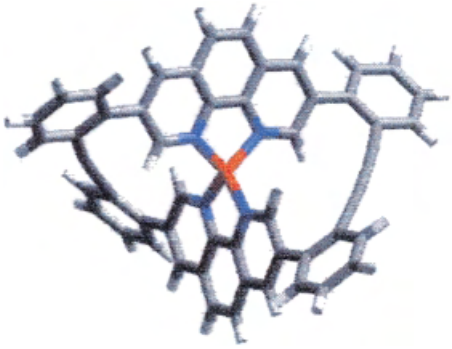
G. L. Abbati,* A. Caneschi, A. Cornia,* A. C. Fabretti, Y. A. Pozdniakova, O. I. Shchegolikhina ..... 4517 – 4520

Towards Stepwise Cluster Assembly: A Decacopper(II) Complex Obtained by Controlled Expansion of a Metallasiloxane Cage

Keywords: cluster compounds · copper · cyanides · magnetic properties · synthesis design

A helical home for copper: A sequential, in situ desilylation/dimerization/decomplexation protocol has been used to generate helical enyne-bridged heterocycles in a copper(I) templated synthesis. Variable temperature ^{13}C NMR analysis of the copper complex (see calculated structure) indicated the barrier to helical isomerization was 13.6 kcal mol^{-1}, an increase of about 4 kcal mol^{-1} relative to the uncomplexed cyclophane.

Angew. Chem. **2002**, *114*, 4702 – 4705



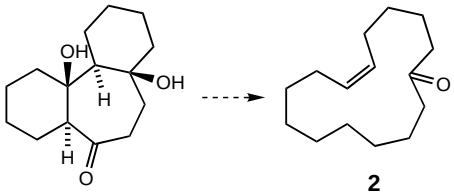
M. A. Heuft, A. G. Fallis* .. 4520 – 4523

Template-Directed Synthesis of Helical Phenanthroline Cyclophanes

Keywords: copper · cyclophanes · helical structures · N ligands · template synthesis

The scent of success! New highly valued unsaturated C-15-macrocyclic musks were synthesized in a stereocontrolled manner by two consecutive fragmentations, starting from tricyclic dihydroxy ketone **1**.

Angew. Chem. **2002**, *114*, 4705 – 4708



1 **2**

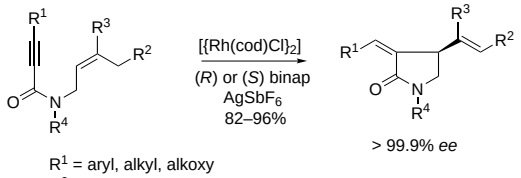
C. Fehr,* J. Galindo, O. Etter, W. Thommen ..... 4523 – 4526

Access to C-15 Macrocyclic Ketones by Iterative Fragmentations of a Tricyclic System

Keywords: fragmentation · fragrances · ketones · macrocycles · reduction

 © 2002 WILEY-VCH Verlag GmbH & Co. KGaA, Weinheim 1433-7851/02/4123-4364 $ 20.00+.50/0

Values of over 99 % *ee* were obtained for all the tested substrates in the Rh^{I}-catalyzed Alder-ene reaction, as applied to the highly enantioselective formation of functionalized lactams. In most cases, α-substituted γ-butyrolactams were obtained in high yields by simply mixing commercially available $[\{Rh(cod)Cl\}_2]$ and binap with the substrates (see scheme).



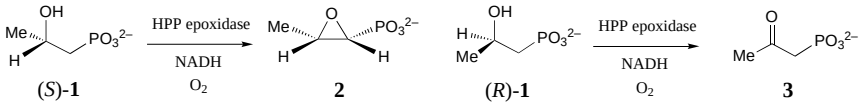
A. Lei, J. P. Waldkirch, M. He, X. Zhang* ..... 4526 – 4529

Highly Enantioselective Cycloisomerization of Enynes Catalyzed by Rhodium for the Preparation of Functionalized Lactams

Angew. Chem. **2002**, *114*, 4708 – 4711

Keywords: enantioselectivity · heterocycles · homogeneous catalysis · rhodium · synthetic methods

The regiospecificity of the initial H-atom abstraction may explain the fact that HPP epoxidase, a non-heme iron-containing enzyme, catalyzes not only the conversion of (*S*)-HPP ((*S*)-**1**) to fosfomycin (**2**), but also the oxidation of the 1*R* enantiomer, which leads exclusively to **3** with nearly equal efficiency.



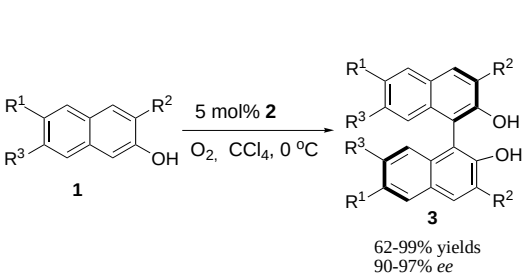
Z. Zhao, P. Liu, K. Murakami, T. Kuzuyama, H. Seto, H.-w. Liu* ..... 4529 – 4532

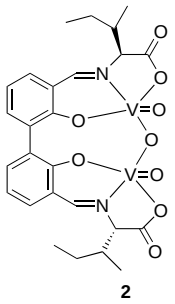
Mechanistic Studies of HPP Epoxidase: Configuration of the Substrate Governs Its Enzymatic Fate

Angew. Chem. **2002**, *114*, 4711 – 4714

Keywords: biosynthesis · enzymes · fosfomycin · radicals · reaction mechanisms

Chiral binaphthols 3 were obtained by oxidative coupling of 2-naphthols in the presence of achiral biphenol-derived diastereomeric V^{IV} oxo complexes. Despite its conformationally flexible biphenyl moiety, the best catalyst **2** (90 – 97 % *ee*, 62 – 99 % yield) exhibits comparable or even higher enantioselectvities than an analogue with an optically pure 1,1′-binaphthyl group.





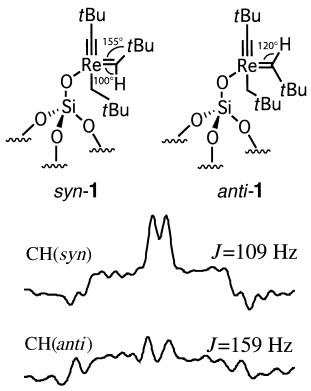
Z. Luo, Q. Liu, L. Gong,* X. Cui, A. Mi, Y. Jiang ..... 4532 – 4535

Novel Achiral Biphenol-Derived Diastereomeric Oxovanadium(IV) Complexes for Highly Enantioselective Oxidative Coupling of 2-Naphthols

Angew. Chem. **2002**, *114*, 4714 – 4717

Keywords: asymmetric catalysis · binaphthols · C–C coupling · N,O ligands · vanadium

Carbenic $J_{C,H}$ coupling as an indicator of agostic interactions in surface species: In the highly active heterogeneous catalyst for olefin metathesis **1**, this coupling constant is 109 Hz for the *syn* and 159 Hz for the *anti* rotamer. From this, a H-agostic interaction in the *syn* rotamer can be deduced and the high electrophilicity of the Re center can be rationalized.



A. Lesage, L. Emsley,* M. Chabanas, C. Copéret,* J.-M. Basset* .. 4535 – 4538

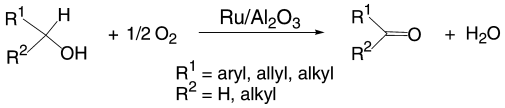
Observation of a H-Agostic Bond in a Highly Active Rhenium – Alkylidene Olefin Metathesis Heterogeneous Catalyst by Two-Dimensional Solid-State NMR Spectroscopy

Angew. Chem. **2002**, *114*, 4717 – 4720

Keywords: agostic interactions · heterogeneous catalysis · NMR spectroscopy · rhenium

 © 2002 WILEY-VCH Verlag GmbH & Co. KGaA, Weinheim 1433-7851/02/4123-4365 $ 20.00+.50/0

Round and round it goes! A supported ruthenium catalyst, easily prepared by treatment of $RuCl_3$ with γ-Al_2O_3, is an efficient heterogeneous catalyst for the oxidations of alcohols with 1 atm of molecular oxygen or air without any additives (see scheme). The spent catalyst was recyclable without an appreciable loss of the catalytic activity and selectivity for the oxidation.



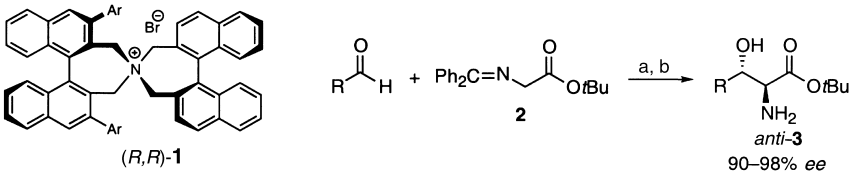
Angew. Chem. **2002**, *114*, 4720 – 4724

K. Yamaguchi, N. Mizuno * 4538 – 4542

Supported Ruthenium Catalyst for the Heterogeneous Oxidation of Alcohols with Molecular Oxygen

Keywords: alcohols · heterogeneous catalysis · oxidation · ruthenium · supported catalysts

A practical and environmentally benign chemical process for the synthesis of optically active β-hydroxy-α-amino acids involves the reaction of an aldehyde, glycine Schiff base **2**, in the presence of catalytic *N*-spiro chiral quaternary ammonium bromide **1**. The cross-aldol product **3** is obtained with excellent stereochemical control (see scheme; a) (*R*,*R*)-**1** (2 mol %), toluene/aqueous NaOH (1 %), 0 °C, 2 h; b) HCl (1 N)/THF).



Angew. Chem. **2002**, *114*, 4724 – 4726

T. Ooi, M. Taniguchi, M. Kameda, K. Maruoka * 4542 – 4544

Direct Asymmetric Aldol Reactions of Glycine Schiff Base with Aldehydes Catalyzed by Chiral Quaternary Ammonium Salts

Keywords: aldol reactions · amino acids · asymmetric synthesis · phase-transfer catalysis · Schiff bases

Stereochemistry revisited: Density functional theoretical predictions of specific rotation values for (*S*)-bromochlorofluoromethane were obtained using three large basis sets at different wavelengths and compared to the corresponding experimental values. Density functional theoretical predictions of Raman optical activity (ROA) parameters for (*S*)-bromochlorofluoromethane were also obtained and compared to the corresponding experimental values. These data suggest that the absolute configuration of bromochlorofluoromethane is (*S*)-(+).

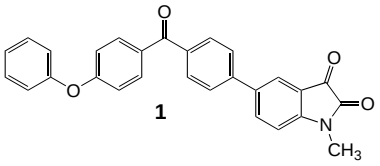
Angew. Chem. **2002**, *114*, 4726 – 4728

P. L. Polavarapu * 4544 – 4546

The Absolute Configuration of Bromochlorofluoromethane

Keywords: alkyl halogenides · chirality · density functional calculations · Raman spectroscopy · specific rotation

Excellent thermal stability and a relatively high glass-transition temperature are exhibited by the hyperbranched poly(arylene oxindoles), which were prepared by an acid-catalyzed polycondensation of the substituted isatine **1**. The polymers thus obtained can also be readily functionalized further.



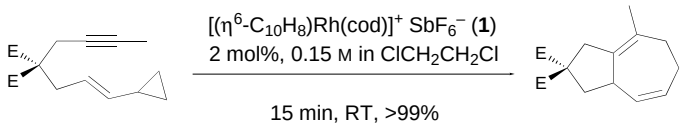
Angew. Chem. **2002**, *114*, 4729 – 4732

M. Smet,* E. Schacht, W. Dehaen 4547 – 4550

Synthesis, Characterization, and Modification of Hyperbranched Poly(arylene oxindoles) with a Degree of Branching of 100 %

Keywords: dendrimers · isatin · polymerization · polymers · spiro compounds

Within a few minutes at room temperature, intramolecular [5+2] cycloaddition reactions of vinylcyclopropanes and tethered alkenes or alkynes reach completion when arene-ligated rhodium(I) complexes are used as catalysts (see scheme). In particular, naphthalene complex **1** was found to be an exceptionally effective and, in cases where comparisons have been made, preferred catalyst.



Angew. Chem. **2002**, *114*, 4732 – 4735

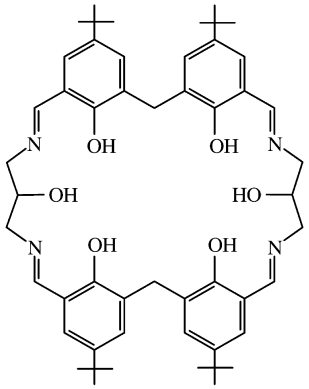
P. A. Wender,* T. J. Williams 4550 – 4553

[(arene)Rh(cod)]+ Complexes as Catalysts for [5+2] Cycloaddition Reactions

Keywords: arene ligands · cycloaddition · homogeneous catalysis · medium-sized rings · rhodium

 © 2002 WILEY-VCH Verlag GmbH & Co. KGaA, Weinheim 1433-7851/02/4123-4366 $ 20.00+.50/0

The wide range of nuclearity, geometry, and protonation levels possible with the hybrid Schiff base/calixarene ligand H_6L3 are illustrated in the formation and characterization of three different copper(II) complexes. The X-ray structures show the complexes to have clearly defined clefts where exogenous ligands are bound.



H_6L3

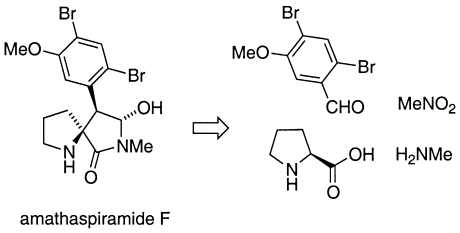
J. Barreira Fontecha, S. Goetz, V. McKee* . . . . . 4553 – 4556

Di-, Tri-, and Tetracopper(II) Complexes of a Pseudocalixarene Macrocycle

Angew. Chem. **2002**, *114*, 4735 – 4738

Keywords: coordination modes · copper · macrocyclic ligands · O ligands · structure elucidation

Breaking the *cis* rule: L-Proline and not as expected D-proline led to (−)-amathaspiramide F with the correct configuration in a short sequence of steps (see retrosynthetic scheme). This synthesis features an exception to the principle of self-regeneration of chirality and a strategy for circumventing a problematic Nef reaction in the presence of densely spaced polar functionality.



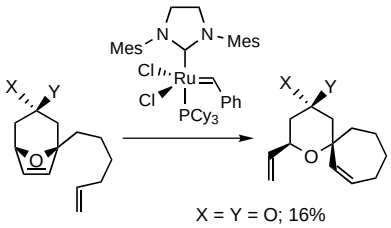
C. C. Hughes, D. Trauner* . . 4556 – 4559

The Total Synthesis of (−)-Amathaspiramide F

Angew. Chem. **2002**, *114*, 4738 – 4741

Keywords: alkaloids · amathaspiramides · Nef reaction · proline · total synthesis

Consecutive ring-opening/ring-closing metathesis reactions of oxabicyclo[3.2.1]octene systems that bear an olefinic tether at the bridgehead lead to highly functionalized, spiro-annulated pyrans (see scheme). The facility of the reaction is greatly influenced by remote substituents.



X = Y = O; 16%
X = OH, Y = H; 48%
X = OTBS, Y = H; 80%

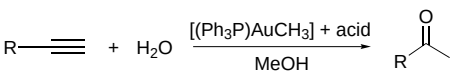
L. C. Usher, M. Estrella-Jimenez, I. Ghiviriga, D. L. Wright* . . 4560 – 4562

Synthesis of Functionalized Pyrans by Domino Metathesis Reaction of Oxabicyclo Derivatives: Dramatic Effect of Remote Substituents on Reactivity and Selectivity

Angew. Chem. **2002**, *114*, 4742 – 4744

Keywords: cyclization · heterocycles · metathesis · pyrans · ruthenium

As good as gold: Hydration of alkynes by using gold – acid catalyst systems with high turnover frequencies provides a greener synthetic route to carbonyl compounds in high yields, as shown.



E. Mizushima, K. Sato, T. Hayashi,* M. Tanaka* . . . . . 4563 – 4565

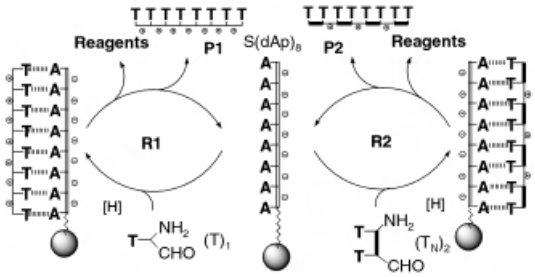
Highly Efficient Au^I-Catalyzed Hydration of Alkynes

Angew. Chem. **2002**, *114*, 4745 – 4747

Keywords: alkynes · gold · homogeneous catalysis · hydration

 © 2002 WILEY-VCH Verlag GmbH & Co. KGaA, Weinheim 1433-7851/02/4123-4367 $ 20.00+.50/0

A powerful strategy to translate DNA directly into synthetic polymers: A solid-phase synthetic strategy is applied to DNA-templated synthesis by using immobilized native DNA octamer $S(dA_p)_8$ as a template to direct the specific polymerization of synthetic DNA analogues $(T)_1$ and $(T_N)_2$ (see figure). The solid-supported template provides advantages in chemical amplification and purification.



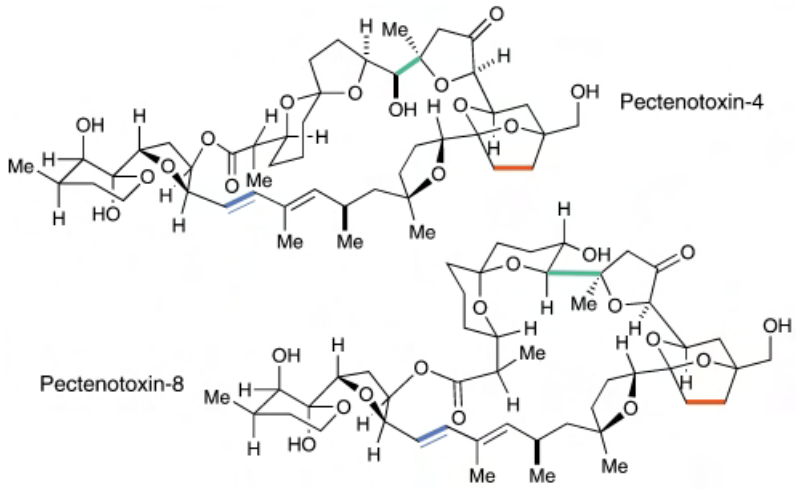
Angew. Chem. **2002**, *114*, 4749 – 4751

X. Li, D. G. Lynn* ..... 4567 – 4569

Polymerization on Solid Supports

Keywords: DNA replication · polymerization · reduction · solid-phase synthesis · template synthesis

The total syntheses of the marine macrolides pectenotoxins-4 and -8 have been realized. The pectenotoxins are a new class of marine macrolides that exhibit a high level of biological activity. Key fragment couplings include a Felkin-selective Grignard addition reaction (green), a metalated dimethylhydrazone alkylation (red), and a late-stage olefination reaction with a β-alkoxy sulfone (blue). The utility of the *N*-phenylamide as a carboxy surrogate and the use of the base labile *tert*-butoxydiphenylsilyl ether is also described.



Angew. Chem. **2002**, *114*, 4751 – 4755

D. A. Evans,* H. A. Rajapakse, D. Stenkamp ..... 4569 – 4573

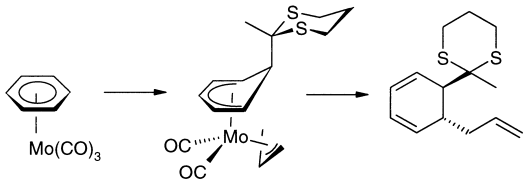
Asymmetric Syntheses of Pectenotoxins-4 and -8, Part I: Synthesis of the C1 – C19 Subunit

D. A. Evans,* H. A. Rajapakse, A. Chiu, D. Stenkamp ..... 4573 – 4576

Asymmetric Syntheses of Pectenotoxins-4 and -8, Part II: Synthesis of the C20 – C30 and C31 – C40 Subunits and Fragment Assembly

Keywords: aldol reactions · natural products · pectenotoxin · total synthesis

No CO insertion occurs in the first $Mo(CO)_3$-mediated dearomatization reaction sequence (shown). In contrast to the analogous $Cr(CO)_3$ reaction, the intermediate allyl complex can be isolated.



Angew. Chem. **2002**, *114*, 4759 – 4761

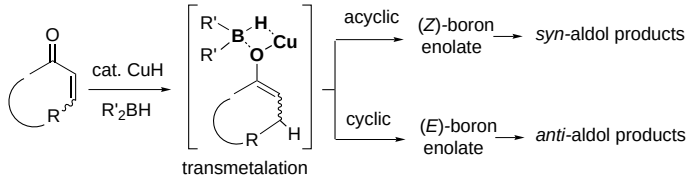
E. P. Kündig,* C.-H. Fabritius, G. Grossheimann, F. Robvieux, P. Romanens, G. Bernardinelli ..... 4577 – 4579

trans-Addition of Two Carbon Substituents across a Benzene Double Bond in $[(\eta^6\text{-Benzene})Mo(CO)_3]$

Keywords: allylation · arene ligands · molybdenum · nucleophilic addition

 © 2002 WILEY-VCH Verlag GmbH & Co. KGaA, Weinheim 1433-7851/02/4123-4368 $ 20.00+.50/0

Looking for an alternative to prepare your regio- and stereodefined boron enolates? Concerned about using expensive and moisture-sensitive Bu_2BOTf? Consider this new procedure for regiospecific enolization based on a catalytic CuH-initiated 1,4-reduction followed by in situ transmetalation with a simple borane (R'_2BH; see scheme).



B. H. Lipshutz,* P. Papa ..... 4580 – 4582

Copper-Catalyzed Reductive Alkylations of Enones: A Novel Transmetalation Protocol

Angew. Chem. **2002**, *114*, 4762 – 4764

Keywords: boron · copper · hydrides · reduction · transmetalation

Supporting information on the WWW (see article for access details).

Accelerated publications

* Author to whom correspondence should be addressed

BOOKS

Voyage Through Time: Walks of Life to the Nobel Prize	Ahmed H. Zewail	*M. Chergui* 4583
Name Reactions	Jie Jack Li	*K. Banert* 4584
Directed Molecular Evolution of Proteins	Susanne Brakmann, Kai Johnsson	*J.-L. Jestin* 4585
Applied Homogeneous Catalysis with Organometallic Compounds	Boy Cornils, Wolfgang A. Herrmann	*I. Tkatchenko* 4586
Host-Guest Chemistry	Soledad Penadés	*J. A. Peters, L. Frullano* 4587
Encyclopedia of Chemical Physics and Physical Chemistry	John H. Moore, Nicholas D. Spencer	*R. Ludwig* 4588
Handbook of Chemical Health and Safety	Robert J. Alaimo	*H. Greim* 4589

WEB SITES

http://www.cermav.cnrs.fr/lectines/	The Gallery of Sweet Rendezvous	*H.-J. Gabius, H. Rüdiger* 4591

SERVICE

- **VIPs** 4358
- ***Angewandte's* Sister-Journals** 4371 – 4373
- **Sources** A107
- **Keywords** 4592
- **Authors** 4593
- **Preview** 4594

Don't forget all the Tables of Contents from 1998 onwards may be still found on the WWW under: http://www.angewandte.org

Issue 22, 2002 was published online on November 12.

 © 2002 WILEY-VCH Verlag GmbH & Co. KGaA, Weinheim 1433-7851/02/4123-4369 $ 20.00+.50/0

In the Communication by **C. Ortiz Mellet**, **J. M. García Fernández et al.** in Issue 19, **2002**, 3674 – 3676, the addresses of the authors were inadvertently swapped. The new fax number for Dr. Ortiz Mellet is (+34) 95-462-49-60. On page 3675, the sentence starting on line 9 of the first column should read: "Preliminary modeling studies suggested that the inner wall in these macrocycles (cyclotrehalins, CTs)[6] would expose the H-1, H-2, and H-4 protons for contacts with an included guest, …" On page 3676, line 8 of the second paragraph (first column), "more stable than that with AC" should read "more stable than that with benzoate". In the literature section, references [6] and [8] should be swapped.

In the Communication by **B. Hedman**, **K. O. Hodgson**, **A. Llobet**, **T. D. P. Stack et al.** in Issue 16, **2002**, 2991 – 2994, Figure 2 and its legendare not correct. The corrected Figure and legend are shown below.

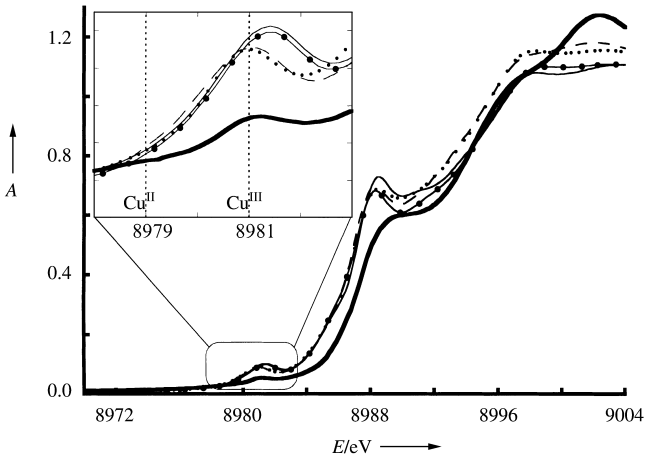
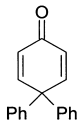


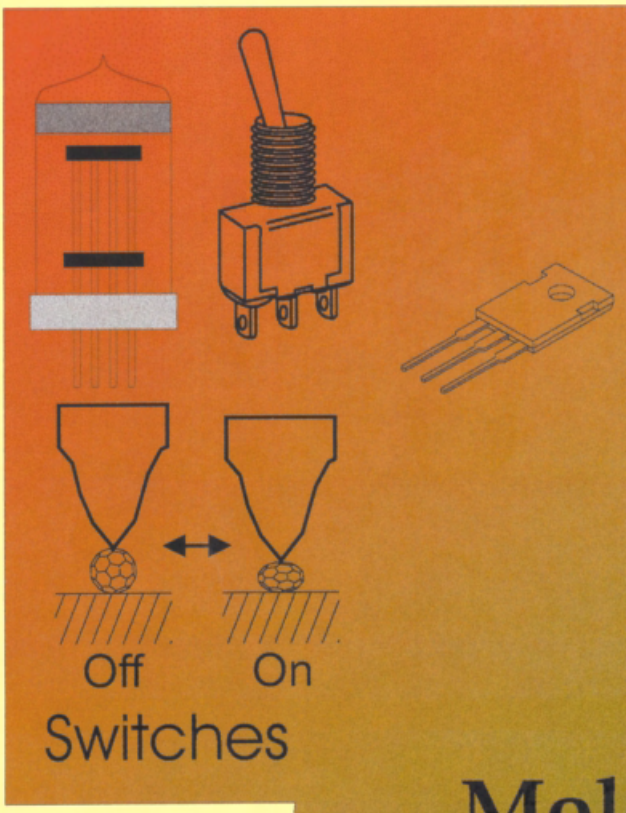
Figure 2. Cu K-edges for Cu^{III} complexes **1**-$(CF_3SO_3)_2$ (——), **1**-$(ClO_4)_2$ (•–•–), **2**-$(ClO_4)_2$ (– – –), **3**-$(ClO_4)_2$ (••••), and $[Cu^{III}(H_{-3}Aib_3)]$[14] (▬▬). The amplified inset shows the pre-edge region ($1s \rightarrow 3d_{x^2-y^2}$ transition, 8978–8983 eV). A = normalized absorption, E = energy.

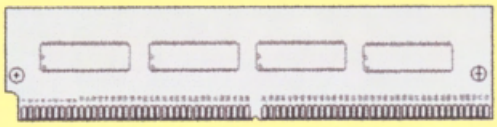
In the Communication by **A. Nangia**, **W. T. Robinson**, **J. A. K. Howard**, **F. H. Allen et al**. in Issue 20, **2002**, 3848 – 3851, the structural formula of diphenylcyclohexadienone **1** on page 3848 was inadvertently cut off on the right-hand side. The correct formula is shown below.

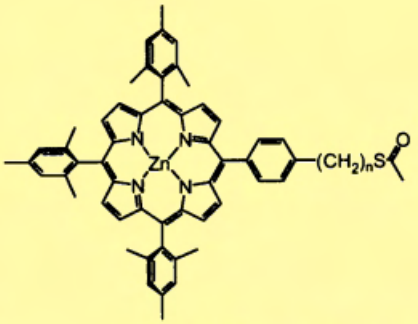


1

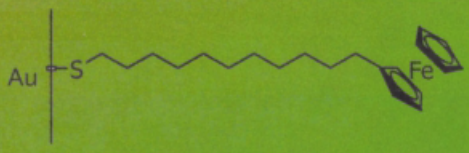
 © 2002 WILEY-VCH Verlag GmbH & Co. KGaA, Weinheim 1433-7851/02/4123-4370 $ 20.00+.50/0

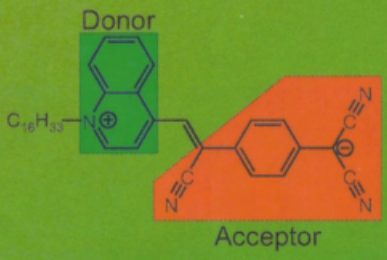


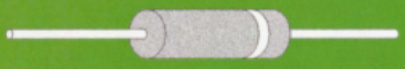




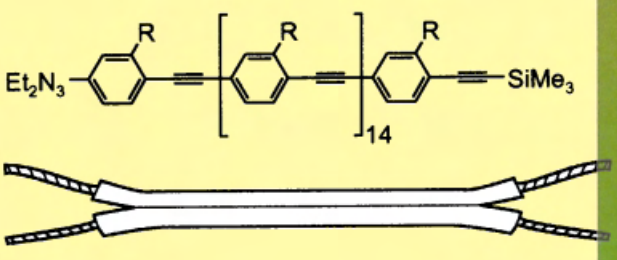
Molecular Electronics







Diodes/Rectifiers



Wire

ANGEWANDTE CHEMIE
© WILEY-VCH

The Genesis of Molecular Electronics

R. Lloyd Carroll and Christopher B. Gorman*

Molecular electronics is, relatively speaking, a young field. Even so, there have been many significant advances and a much greater understanding of the types of materials that will be useful in molecular electronics, and their properties. The purpose of this review is to provide a broad basis for understanding the areas where new advances might arise, and to provide introduction to the subdisciplines of molecular electronics. This review is divided into two major parts; an historical examination of the development of conventional electronics, which should provide some understanding of the push towards molecular electronics. The problems associated with continuing to shrink conventional systems are presented, along with references to some of the efforts to solve them. This section is followed by an in-depth look at the most important research into the types of behaviors that molecular systems have been found to display.

Keywords: · molecular electronics · molecular switches · monolayers · scanning-probe techniques

1. Conventional Electronics and Its Boundaries

1.1. Transistor Development and Moore's Law

In the first half of the 20th century, both the study of electronics and the electronics industry grew at a rapid pace. This growth was, in large part, a result of the proliferation of communication devices such as the radio and telephone, and the wartime development of radar. The foremost problem associated with these devices was that of signal amplification. Early efforts used semiconductor crystals as rectifiers to convert an AC signal into DC. However, these systems did not respond well to rapid changes in the signal and were prone to burn-out.

AT&T opened their transcontinental telephone system in 1915. For a telephone signal to travel from one coast to the other, the signal required amplification at several points along the trip. After World War II, it was felt that the system in place, based on vacuum-tube amplifiers called "audions", could be improved by using solid-state devices. In August of 1945, AT&T Bell Labs set up the Solid State Physics group and set them to work to develop a solid-state amplifier.

The first transistor was invented in 1947 by John Bardeen and Walter Brattain at Bell Labs. The point-contact transistor consisted of a slab of germanium in contact with three gold wires (Figure 1). William Shockley followed in 1948 with the invention of the bipolar junction transistor, which controlled current flow through alternating layers of p-type and n-type germanium (Figure 2). Easier to fabricate than the point contact devices, the junction devices were manufactured for many years, with reductions in size and improvements in semiconductor quality. In 1954, germanium was replaced with the development of the silicon transistor at Texas Instruments.

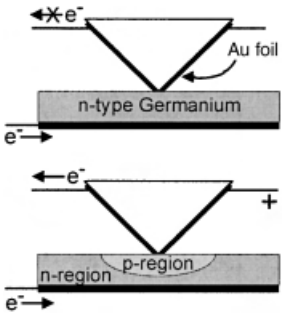


Figure 1. Schematic of a point contact transistor without applied bias (above) and with applied bias (below).

Junction transistors were used in the development of the first integrated circuit in 1958 by Jack Kilby at Texas Instruments (2000 Nobel Prize in Physics),[1] and their use continued until 1961 when they began to be replaced by

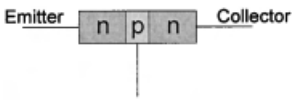


Figure 2. Schematic of bipolar junction transistor.

[*] Prof. C. B. Gorman, Dr. R. L. Carroll
Department of Chemistry
North Carolina State University
Box 8204, Raleigh, NC 27695-8204 (USA)
Fax: (+1) 919-515-8920
E-mail: chris_gorman@ncsu.edu

 © 2002 WILEY-VCH Verlag GmbH & Co. KGaA, Weinheim 1433-7851/02/4123-4379 $ 20.00+.50/0

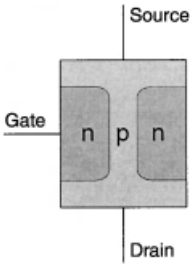


Figure 3. Schematic of field effect transistor.

field-effect transistors (FETs; Figure 3). A FET functions by controlling the migration of electrons or holes into a conduction channel between a source and drain electrode. The amount of migration controls the current through the conduction channel; a large migration (caused by a large signal) can be turned into an even larger current flow between source and drain, thus amplifying the signal.

The integration of complete circuits (including wires, resistors, capacitors, and transistors) on a single piece of silicon was the stimulus for the increase of computational power in the late Fifties. By developing new techniques to fabricate smaller and smaller components, and thus fit more and more components into each cm^2 of silicon, engineers have driven the speed and capabilities of computing at a predictably fast pace. In 1965, Intel co-founder Gordon Moore observed that the number of transistors per cm^2 of silicon doubled every year, and predicted that it would do so for the next 10 years.[2] This statement, or "Moore's Law" as it became known, was revised by Moore in 1975 to state that chip densities would double every 2 years.[3] Looking back, it is now accepted that computational power (which is a convolution of the number of transistors, clock speed, pitch size, and other factors) doubles every 18 months. The predictive power of this statement can be observed on the plot in Figure 4.

Obviously, this reduction in size of components, and thus increase in speed, can only continue for some finite time. Given the current rate of technological advancement, Moore's Law will be accurate for, at most, 20 more years before the components will be reduced to the molecular scale. At this point, and in fact, well before it, current techniques for integrated-circuit fabrication will have been surpassed. New processes will have to be developed, and in fact are in development, in an effort to extend the useful functionality of silicon integrated circuits.

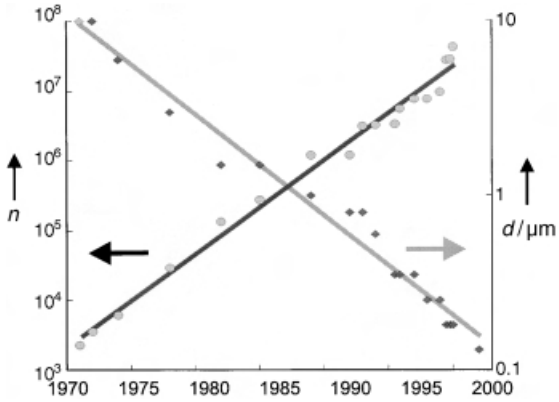


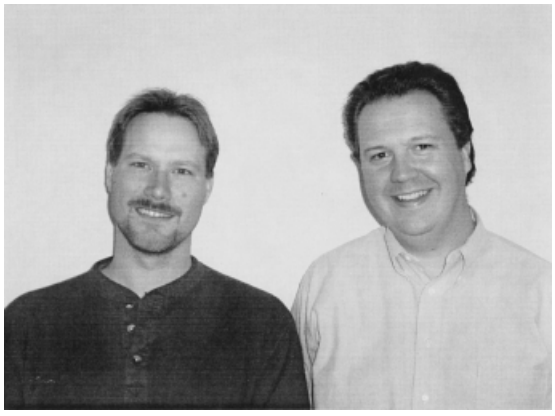
Figure 4. "Moore's Law"—the development of the number of transistors per square centimeter (n) and the pitch size (d) over time.

1.2. Conventional Techniques—Limitations and Outlook

Currently, integrated circuits are made by a photolithographic process, with multiple steps including metal deposition and deposition and doping of silicon to form p-type and n-type silicon. The steps necessary to construct a Junction FET are outlined in Figure 5. There exist several significant challenges in the miniaturization of conventional techniques to prepare integrated circuits. One important limitation in the fabrication process lies in the photolithography step. The wafer, with a layer of photoresist, is exposed through a patterned mask, or reticle. In development, the exposed regions are washed away, leaving the unexposed regions (in positive photoresists), or the exposed regions remain while

Lloyd Carroll received his Ph.D. in chemistry from North Carolina State University in 2001. Prior to that, he taught high school for three years after receiving his BS in secondary education at North Carolina State University. He currently is a postdoctoral research associate in Richard Superfine's laboratory in the Department of Physics at University of North Carolina, Chapel Hill.

Christopher Gorman was born in Summit, New Jersey in 1965. He received his BA in chemistry and computer science from Drew University in 1987 and a Ph.D. in chemistry from the California Institute of Technology in 1991 (with R. H. Grubbs). He then did postdoctoral work with Dr. Seth Marder at the NASA Jet Propulsion Laboratory and with Professor George Whitesides at Harvard University. In 1994, he joined the faculty of North Carolina State University where he is now an associate Professor of chemistry. His present research interests include the design and synthesis of new, polymeric materials with interesting and useful electronic properties at nanometer length scales and the use of scanned probe microscopies in nanoscience to establish molecular structure–property relationships for single-molecule electronic behavior.



R. L. Carroll C. B. Gorman

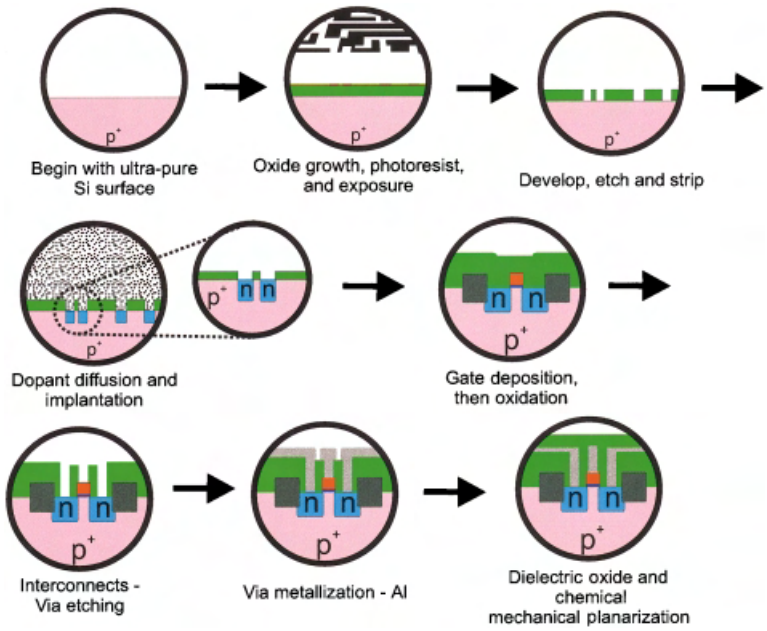


Figure 5. The basic steps to fabricate a Junction FET: an ultra-pure silicon wafer is oxidized, then the oxide patterned by photolithography. The resulting pattern is developed, etched, then any remaining photoresist is stripped. The patterned oxide protects part of the surface during the implantation step, when dopants are added to certain regions of the surface. Using photolithography and chemical vapor deposition, a polysilicon gate is deposited on top of a thin gate oxide. Further layers of oxide are added to separate components and to protect others. Vias are etched through the oxides to allow contact to active regions. Interconnects are deposited—aluminum is evaporated, copper is electrolytically deposited. Further oxides protect one layer from the layer of interconnections above. Finally, the surface is polished by chemical–mechanical polishing to prepare it for the next layer of interconnects and components.

the unexposed regions are washed away (in negative photoresists). The achievable resolution is somewhat dependent on system requirements (both the line resolution d and depth-of-focus D_f requirements), and these obey Equations (1) and (2) where k_1 and k_2 are experimentally determined parameters dependent on the desired critical dimensions, λ the wave length, and NA is numerical aperture.

$$d = \frac{k_1\lambda}{NA} \quad (1)$$

$$D_f = \frac{\pm k_2\lambda}{(NA)^2} \quad (2)$$

It is thus apparent that there are a few ways to improve the resolution of integrated-circuits features. Notably, shorter wavelengths, and larger NAs provide better resolution. There are a number of resolution-enhancing techniques being researched (and already in use) that use longer wavelengths to produce smaller resolution lines than would be immediately attainable, but many of these techniques require greater fabrication time, and thus sacrifice throughput. The most direct means of improving resolution is to move to shorter wavelengths.

Currently, fabrication of state-of-the-art integrated circuits uses 248-nm radiation from a mercury arc lamp (the "I-line") to produce 0.18 and 0.25 μm features, but other fabrication facilities are switching to the use of 248-nm KrF Excimer lasers. Further plans (based on the 2000 International Technology Roadmap for Semiconductors (ITRS)[4]) call for the implementation of 193 nm (ArF Excimer laser) and 157 nm (KrCl Excimer laser) by 2002 and 2005, respectively, to reach the Roadmap goals of 0.13 μm and 0.10 μm pitch. Below 100 nm, there are several options being researched, which include X-Ray lithography ($\lambda < 1$ nm), to attain critical dimensions of down to 70 nm,[5] and extreme UV lithography ($\lambda \approx 13-4.5$ nm), to attain critical dimensions of 70–30 nm.[6] At these wavelengths, there are a number of problems, which include difficulties in focusing the exposing radiation and designing appropriate mask materials and photoresists.

Not only must the pitch of chip features (that is, the distance between parallel features) be minimized, but the depth, or thickness of the features must also scale with width. This requirement is most problematic in the FET-polysilicon-gate region, where in current integrated circuits the gate is insulated by approximately 3 nm of thermally grown oxide from the current channel. To maintain the development path, the oxide layer must continue to shrink. However, it has been shown that once the oxide layer reaches a thickness of <1.2 nm, it no longer insulates effectively.[7] According to the ITRS, this thickness should be reached by around 2012, and further development of integrated circuits will require the development of new dielectric materials. Current research is focused on metal oxides (notably: Al_2O_3, Ta_2O_5, ZrO_2, and HfO_2) as high-k dielectric gate materials.[8]

As the dimensions of components are reduced, the wiring connecting them must also decrease in size. Such interconnects are currently composed of an Al/Cu alloy, and are insulated from each other by an SiO_2 dielectric. One of the primary problems with such systems is that of electromigration. As current passes through a wire (or interconnect), it has a tendency to transfer some of its momentum to the atoms in the lattice of the metal, particularly at grain boundaries or other defect sites in the lattice. At high current densities (such as those found in the very narrow interconnects), this can, over time, open voids in the interconnect or crack the surrounding dielectric and extrude the metal of the interconnect.[9] In either case, the connection eventually fails. There are many factors that affect electromigration, but the most important is that of temperature. High resistivity in the interconnect (as a result of grain boundaries, defects or poorly oriented grains) can increase resistive heating, which increases the rate of electromigration. Similarly, some of the dielectrics in use to insulate interconnects have very low thermal-conduction properties, and heat generated in the interconnect is not easily removed. Copper is much less susceptible to electromigration,[10] and thus, the use of copper instead of aluminum interconnects should solve several of these problems. However, copper is not as easily processed (at least by current methods) during fabrication. Other effects

that the use of copper introduces are the poor adhesion between copper and the substrate, and the tendency of copper to diffuse into the semiconductor, poisoning it. To solve these new problems, the pre-deposition of a layer, such as titanium or palladium that acts as both a diffusion barrier and adhesion promoter is used.[11] One further limitation that will manifest itself as conventional semiconductor structures grow smaller is that of tunneling. As the distance between device components shrinks, it becomes more likely that current will tunnel between components, rather than conduct along them, introducing errors into computation. The development of low-*k*-value dielectric insulators, such as SiLK,[12] will extend the functional life of conventional integrated circuits. In addition, high-quality lithographic techniques that minimize edge and feature roughness should also minimize unwanted tunneling between closely spaced components.

Even considering further advancements in the science of making integrated circuits, the fact remains that the materials and processes currently in use will reach their fundamental limits sometime in the near future. That eventuality forces us to consider other options. Instead of continuing to make the existing components smaller and smaller, much research is focused towards going directly to the smallest components that are likely to be functional—single molecules and small groups of molecules.

1.3. Definition of Molecular Electronics[13, 14]

Since the size of components in integrated circuits are shrinking in accordance with Moore's law, it is a simple matter to suggest that the ultimate integrated circuits will be constructed at the molecular or atomic level. Such a scenario was suggested in a 1959 lecture by the eminent physicist and visionary, Richard Feynman:

> "I don't know how to do this on a small scale in a practical way, but I do know that computing machines are very large; they fill rooms. Why can't we make them very small, make them of little wires, little elements—and by little, I mean little. For instance, the wires should be 10 or 100 atoms in diameter, and the circuits should be a few thousand angstroms across…there is plenty of room to make them smaller. There is nothing that I can see in the physical laws that says the computer elements cannot be made enormously smaller than they are now. In fact, there may be certain advantages."[15]

At this time, it is impossible to position atom by atom—the capability simply has not been realized. However, what about molecules? Can we control the position of individual molecules or particular groups of molecules such that we can make them do useful tasks? Can we use the electronic properties intrinsic in these molecules to replace larger scale devices? The search for answers to these questions is the field of molecular electronics.

Molecular electronics can be defined as technology utilizing single molecules, small groups of molecules, carbon nanotubes, or nanoscale metallic or semiconductor wires to perform electronic functions.[16] Some have defined it as technologies utilizing only single molecules, but this definition is far too limiting. From the broader definition, it can be suggested that any device utilizing molecular properties is a molecular electronic device. However, in order for a molecular system to be considered a device, there are several requirements that it must meet.

The simplest device that is easily conceived is a switch. The defining characteristic of a switch is that of bistability—it has an "ON" and "OFF" position. Thus, any molecular switch must perform in a similar manner. In its "ON" position, the switch must either perform some function or allow another device to perform its function. In the "OFF" position, it must totally impede the function. Similarly, the switch must not spontaneously change states—it must remain in the position that it is placed until its position is changed. *The development of a molecular switch is perhaps the single most important element in developing molecular replacements for conventional integrated circuits.*

For a molecular switch to be useful, it must be addressable—that is, it must remain in the physical location in space where it is placed, and it must maintain a separate identity from other switches around it. There are two important concerns in this regard. First, it is presently somewhat difficult to position molecules exactly where they are desired. Certainly there are examples of both atomic and single molecular[17] positioning, however, these examples have not been focused at limiting the long-term propensity of the molecule to diffuse. In addition, these previous experiments examined the movement and positioning of mobile molecules on a surface—in a molecule-based system, the molecules must be bound in place (and that they should be in some sort of array) to facilitate addressibility. A primary consideration of any molecular electronic candidate must be that of chemical stability. It is important to understand the long-term stability of any molecular electronics component under a wide variety of conditions. If a molecule tends to decompose when exposed to elevated temperatures, then it is not a good candidate for use in a molecular electronic device. Similarly, the species must be inert with regards to other molecules of the same type, a requirement that is particularly important in devices involving charge-storage or redox-active molecules. Species that show poor "insulation" from each other would tend to exchange stored electrons, scrambling any data represented by the storage of those electrons. Conversely, a molecule which shows an irreversible electron transfer would not be a good candidate for any sort of molecular electronic device as the point of electronics is to utilize reversible charge transfer from one element to the next.

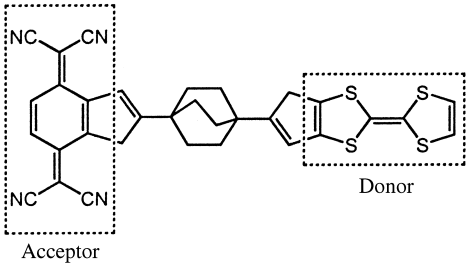
Finally, describing a molecule doing some useful function does not automatically make it a molecular electronic device—there must be a way to interact with the component, both on a microscopic level and through input from the macroscopic world. Thus it is important to consider how a molecular electronic device can be "wired up". It must be able to exchange information, or transfer states to other molecular electronic devices, or it must be able to interface with the components in the system that are not nanoscopic. These requirements present challenges which, as of the date of this review, are just beginning to be addressed.

2. Towards Molecular Devices

2.1. Historical Beginnings—Molecular Rectifiers

The first theoretical and experimental efforts in the molecular electronics arena began in the 1970s with the work of Aviram and Ratner, and their preparation and characterization of donor–acceptor (D–A) species. As is detailed below, some of these results eventually had to be retracted. However, from a historical perspective, they represent an important first attempt to predict and characterize a molecular-scale electronic phenomenon.

By studying an organic analogue of a p–n junction, Aviram and Ratner surmised[18] that such a molecule would act as a molecular rectifier. The computational results from a study of one such D–A molecule **1**, composed of a donor moiety



1

tetrathiafulvalene connected by a methylene bridge to an acceptor moiety, tetracyanoquinodimethane, showed a rectification of current should be possible (Figure 6). The rectification behavior can be explained by examining energy-level diagrams for the system (Figure 7). At positive bias (Figure 7b), upon alignment of the metal energy levels with the acceptor LUMO (II), the passage of current begins with the

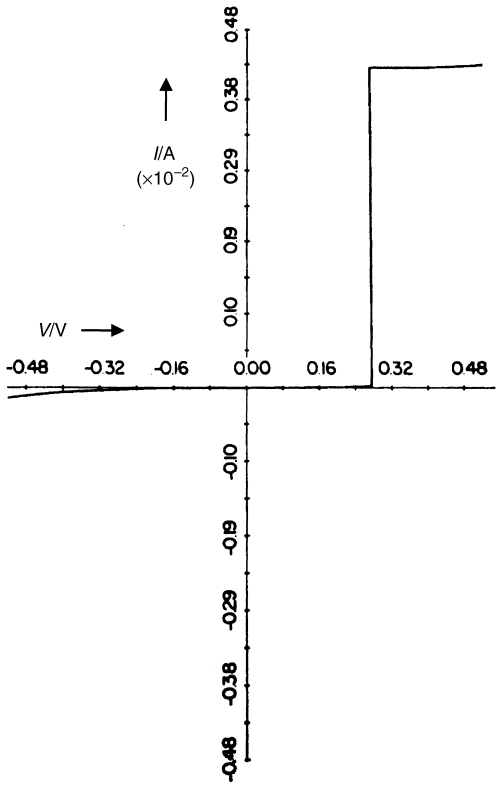


Figure 6. Calculated *I*/*V* Curve for Molecule **1**. Reproduced with permission from ref. [18].

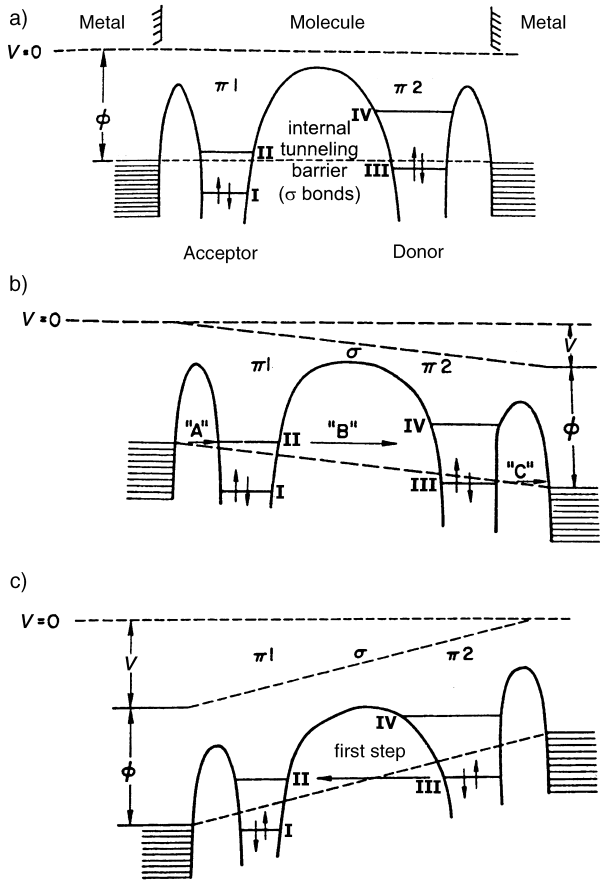


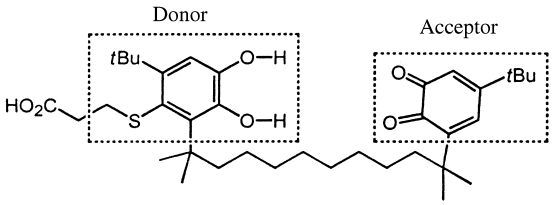
Figure 7. a) Energy-level diagrams of **1**, the donor–acceptor system, between two metal electrodes, b) under positive applied bias c) under reverse applied bias. ϕ = Fermi energy, V = applied bias; modified with permission from ref. [18].

transfer of charge from the cathode to the acceptor (this transfer is represented by "A" in Figure 7b). Charge cannot flow between acceptor and donor, however, until the energy levels of the metal anode are lowered enough to allow charge transfer from the donor HOMO (III) to the metal (this transfer is represented by "C" in Figure 7b). The tunneling process from the acceptor LUMO (II) to the donor HOMO (III) occurs irreversibly ("B" in Figure 7b). Overall, this process has a fairly low threshold voltage, since the molecular energy levels and the metal Fermi energies (E_F) are initially close in energy, and in the proper configuration.

In the reverse bias direction (Figure 7c), there are two mechanisms that must be considered. In one mechanism, similar to that occurring at positive bias, the E_F of the electrode adjacent to the acceptor must be lowered below the acceptor HOMO (I), allowing charge transfer from I to the metal. This allows an electron to tunnel from III to I. The vacancy in III can then be filled by charge transfer from the electrode adjacent to the donor. Another mechanism must also be considered, however, in which the first step is an internal process of tunneling from III to II. Then, charge

transfer can occur from II to the metal, and from the metal to III. Each of these mechanisms requires a substantially larger threshold voltage than at positive bias, and it is this difference in threshold voltage that should give rise to rectifying behavior in such a molecule.

An early effort by Aviram et al. to demonstrate rectifying behavior in a molecule experimentally used a hemiquinone monolayer **2**, the *I*/*V* characteristics of which were probed by

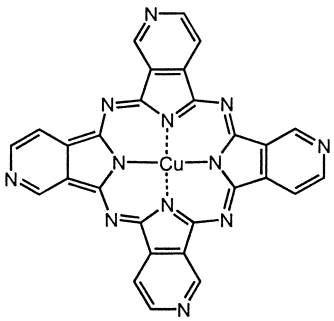


2

an STM tip.[19] In this study, the molecules were immobilized in a self-assembled monolayer on a flat Au surface, the STM-tip motion was stopped and the voltage was varied while monitoring the current. The results seemed to indicate a rectifying behavior in that current flowed very effectively at negative (tip) bias but not at positive bias. It was noted that the catechol moiety in the hemiquinone **2** acts as a donor, while the quinone component is an acceptor. Under negative tip bias (that is, tip negative, surface positive), an electron can flow from the tip to the quinone unit and from the catechol unit to the surface. Proton transfer from the catechol to the quinone unit would very rapidly cancel the dipole, producing semiquinones, which are free-radicals. Since many organic conductors have a partially unfilled HOMO, it was suggested that a semiquinone unit would be a conductor, and thus give enhanced current flow through the molecule. At positive tip bias, the molecular energy levels are unfavorably disposed to carry out this process. Thus, no appreciable current flowed.

As reasonable as the proposed explanation seems, the results were called into question, and eventually retracted[20] when Aviram observed similar behavior in systems lacking these D–A molecules. In addition, there was some evidence that the STM tip was in contact with the surface. These results indicate the experimental difficulties, at least early on, in carrying out these types of studies.

In another attempt to demonstrate rectifying behavior in a molecule, Pomerantz et al.[21] acidified a highly oriented pyrolytic graphite (HOPG) surface, and bound base-substituted copper–phthalocyanine **3** to the modified HOPG.



3

Angle-dependent X-ray photoelectron spectroscopy (XPS) indicated that the molecules were bound to the surface at an angle, apparently through one or two of the peripheral amines. The tip was scanned over the surface, and the substrate bias was swept from $+1.2$ V to -1.2 V in less than 100 ms. On clean HOPG, or on HOPG that had been acidified but not exposed to **3**, a relatively symmetric *I*/*V* curve was observed, with a maximum asymmetry ratio $R \leq 2$ as given by Equation (3).

$$R = \frac{|I(-V)|}{|I(+V)|} \tag{3}$$

On HOPG to which **3** had been bound, a large current response was observed at a substrate bias voltage of -1.2 V, with an asymmetry ratio ranging from 10 (over $\approx 60\%$ of the surface) to 40 or more (over $\approx 10\%$ of the surface). These data indicated a strong rectifying effect, presumably because of the presence of **3**. In control experiments, other molecules, specifically, an amine-terminated *n*-alkyl thiol ($HS\text{-}(CH_2)_2\text{-}NH_2$) and a bisquinone-containing amine thiol, were bound to the acidified HOPG and showed *I*/*V* responses identical to the pristine HOPG.

It is apparent that the proposed mechanism for previous systems, based on a donor–acceptor arrangement, is not at work in the HOPG–**3** system. This molecular system has no obvious donor and acceptor. In addition compound **3** is symmetrical, unlike the donor–acceptor systems used in other studies, which have inherent asymmetry in their structure, which gives rise to asymmetry in their *I*/*V* curves.

In an effort to understand the origin of the rectification of current by the bound molecules, UV photoelectron spectroscopy (UPS) was used to determine the density of states (DOS) of the graphite surface both before and after the binding of molecules of **3**. UPS spectra for acidified graphite with and without **3**, and their differences are presented in Figure 8. The difference curve gives the occupied energy

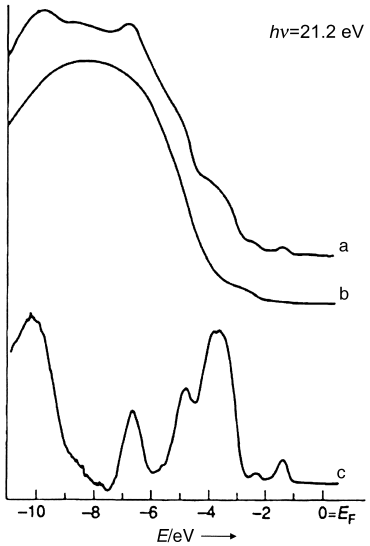


Figure 8. UPS spectra for a) acidified HOPG with bound **3**, b) acidified HOPG (without **3**), c) difference spectrum (a – b). Reproduced with permission from ref. [21].

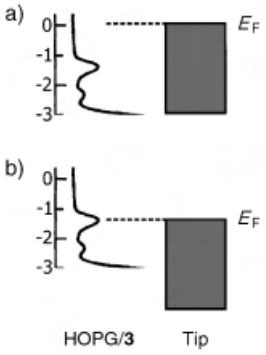
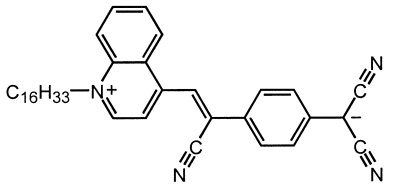


Figure 9. DOS of **3** and HOPG compared to the Fermi energy of the STM tip, at substrate bias of a) 0 V, and b) approximately −1.3 V.

levels/DOS of **3** below the E_F of the HOPG and shows a maximum at about −1.3 V. The UPS spectra for the control molecules show no features within several eVs of the E_F. The difference spectrum Figure 9 illustrates that a negative substrate bias of approximately −1.3 V would bring the Fermi level of the STM-tip into resonance with the feature in the DOS, a requirement for the enhanced tunneling process. Thus, the molecule was responsible for the rectifying behavior present in the system.

Following the work of Martin et al.,[22] Metzger and co-workers[23] have studied Langmuir–Blodgett (LB) films of γ-(*n*-hexadecyl)quinolinium tricyanoquinodimethanide (**4**) between metal electrodes and observed strong rectification behavior. Although compound **4** is a donor–acceptor system,



4

it is slightly different from the systems studied by Aviram and Ratner. The major difference is that in **4**, the donor is the quinolinium moiety, connected to the acceptor, tricyanoquinodimethanide by a π bridge. The hexadecyl tail facilitates the formation of LB films (Figure 10). The head-to-tail arrangement was found to be the most stable structure of the LB film. The systems that Aviram and Ratner examined were composed of neutral ground-state donor–acceptor species that became selectively zwitterionic [Eq. (4)].

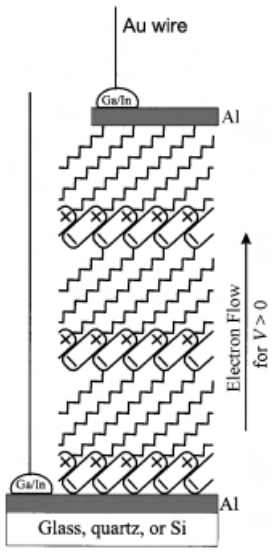


Figure 10. Representation of the LB-film structure of **4** on aluminum. The one and four monolayer films have the same orientation of the molecule.

$$D^+-\sigma-A^- \xleftarrow{1-2\,eV} D-\sigma-A \xrightarrow{9\,eV} D^--\sigma-A^+ \quad (4)$$

The nature of **4**, however, until the work of Metzger et al., was unclear. It was proposed that the ground state was a mixture of zwitterionic and neutral molecules, and that intramolecular electron transfer gave rise to the rectification. Metzger et al. made LB films of **4** on aluminum coated quartz, then with the film at 77 K added a second Al layer on top by evaporation (Figure 10). Connections to the metal pads were made with Ga/In eutectic or an Ag paste. Electrical measurements showed strong rectification. Figure 11 shows the *I*/*V* curves from two different experiments using **4**. In one, a single monolayer of **4** was sandwiched between two Al electrodes. The rectification ratio (RR—identical to the "asymmetric ratio" of Aviram and Ratner) for this sample was about 40. In an analogous experiment, a four-layer-thick LB film was measured with Al electrodes and gave an RR value of more than 10 (Figure 11b).

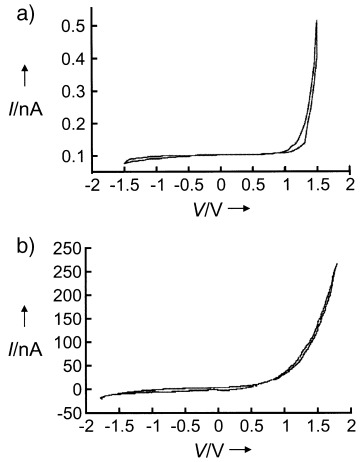


Figure 11. *I*/*V* curves from two different LB-film configurations. a) Ga/In eutectic | Al(100nm) | 1 LB monolayer | Al(100nm) | Ga/In eutectic. b) Ga/In eutectic | Al(100nm) | 4 LB monolayers | Al(100nm) | Ga/In eutectic. Reproduced with permission from ref. [23].

Upon consideration of the LB film structure (Figure 10), a mechanism for the rectifying behavior can be proposed. In the Aviram–Ratner model, electron transfer to/from metal electrodes to a neutral ground-state molecule (Figure 12a, forward bias) creates a zwitterionic form that by intervalence transfer (IVT) can regenerate the neutral form. The overall electron transfer is from acceptor towards donor. If the

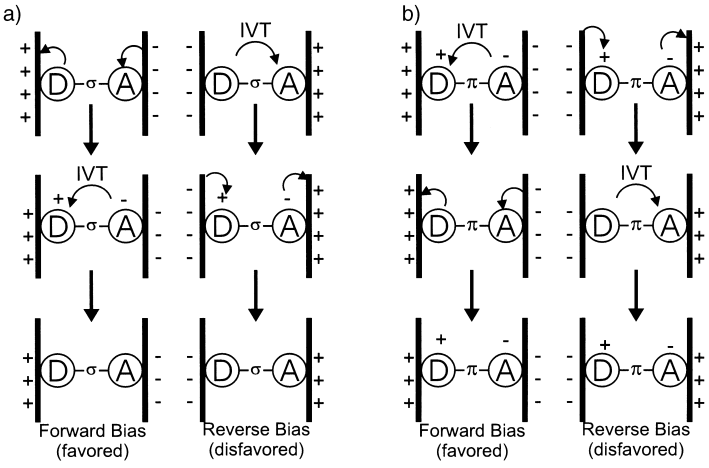


Figure 12. a) Aviram-Ratner model for neutral D-σ-A species, and b) modified model for zwitterionic D^+-π-A^- species.

process is initiated in a zwitterionic molecule (such as **4**), under forward bias the IVT occurs first, creating a neutral molecule (Figure 12b, forward bias), followed by electron transfer to and from the metal to recover the zwitterionic form. As before, this process results in overall electron transfer from acceptor towards donor. The difference in the magnitude of the I/V responses between one and four LB layers (Figure 11a, b) is not entirely clear, but it has been suggested that the larger current flow in the thicker layer results from conduction through defects.[24]

2.2. Wiring Up—Molecular Wires

One of the requirements to using any molecular electronic component is the ability to wire it into a device architecture. To connect molecules to one another, or to the macroscopic world, molecular-scale wires are necessary. In an effort to understand the important characteristics of such a molecular wire, most research in this area has concentrated on linear, conjugated oligomers.

Conjugated oligomers are proconductors.[25, 26] A conductor can be derived from this type of proconductor by either an oxidation or a reduction. In the bulk, polythiophene is a poor conductor, upon oxidation it becomes polythiophenium, a cation, and a much better conductor by virtue of the unfilled HOMO and a change in geometry to create mid-gap states (Figure 13). One can rationalize the relative conductance of

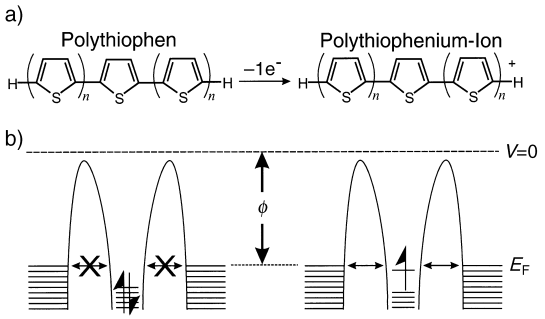
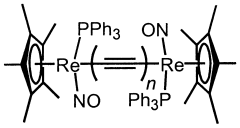


Figure 13. a) Conversion of proconductor (polythiophene) into conductor (polythiophenium) by oxidation, b) simplified energy-level diagrams for the proconductor (left) and conductor (right) between two metal electrodes.

thiophene oligomers in an analogous fashion. Conductor and proconductor pairs may find usefulness in molecular electronics, however, the need to oxidize or reduce them, or introduce a dopant into the bulk makes them less than ideal. Recent work into metal-containing carbon chains and porphyrinic arrays has provided a possible route around these potential limitations.

Gladysz and co-workers[27] have synthesized metal-terminated carbon chains similar to **5**, with up to ten alkynyl units ($Re(C{\equiv}C)_nRe$, $n \leq 10$). Cyclic voltammograms (CV) of three of these molecules are shown in Figure 14a. For the shorter $Re(C{\equiv}C)_2Re$, two single-electron oxidations are observed. For the longer chains ($Re(C{\equiv}C)_3Re$ and $Re(C{\equiv}C)_4Re$), the oxidation becomes increasingly irreversible. The solution cyclic-voltammetry results for the entire family of complexes from $n = 2$ through 10 are shown in Figure 14b. The presence of only a single, presumably two-electron oxidation wave in $Re(C{\equiv}C)_{10}Re$ indicates that once the chain reaches this length, the metals are effectively isolated from one another and do not communicate by the conjugated bridge. These molecules have not been studied under electrode-bound device conditions. However, these results indicate that such a molecule will not be expected to function as an ideal molecular wire.



5

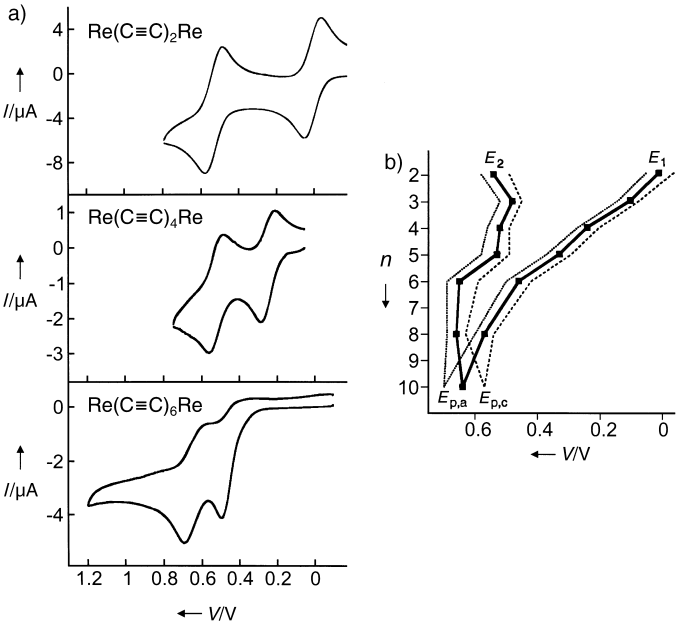
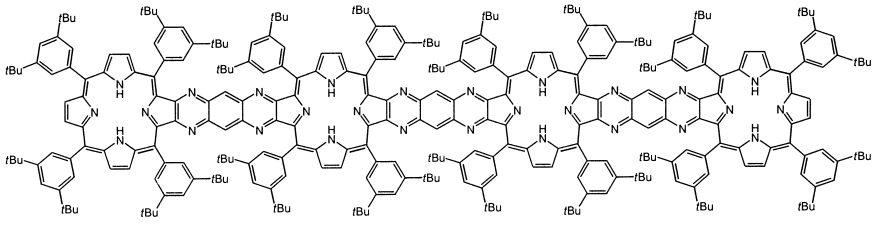
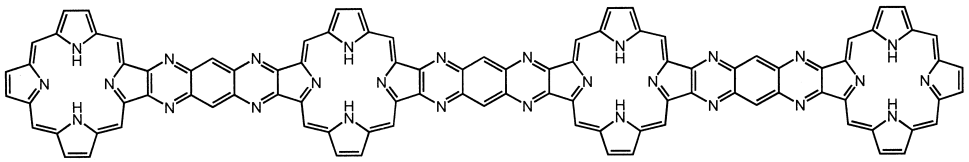


Figure 14. a) Cyclic voltamograms of **5** (10^{-5} M in 0.1M Bu_4N^+ BF_4^-/CH_2Cl_2, Pt working and counter electrodes, potential versus Ag-wire pseudoreference, scan rate = 100 mV s^{-1}, ferrocene = 0.46 V). b) Plot of cyclic voltammetry results for series from $Re(C{\equiv}C)_2Re$ to $Re(C{\equiv}C)_{10}Re$, E_1 is first oxidation, E_2 is second oxidation, $E_{p,c}$ and $E_{p,a}$ are cathodic and anodic peak potentials, respectively. Reproduced with permission from ref. [27].

Potential molecular wires composed of fused porphyrin rings have also been constructed, for example, Crossley and Burn synthesized oligomeric linear porphyrin arrays, such as **6**.[28, 29] Over 100 such systems (e.g., **7**) have been studied



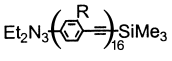
6



7

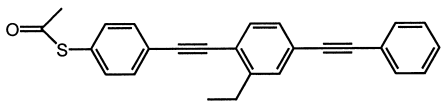
computationally[30] in an effort to gauge their potential as molecular wires. These results suggest that the molecular-wire characteristics of these fused ring porphyrins are highly tunable, depending on the substitution of the porphyrin ring, the nature of the bridging unit (1,4,5,8-tetra-azaanthracene in **6** and **7**), and the metal (or lack thereof) in the system. They suggest that the electronic properties of these systems (and presumably others) are dominated by the degree of π delocalization. In π systems of discrete single and double bonds the electrons are more locked in place (localized) than those in which the formal single and double bonds are similar in length. Concomitantly, in nonconjugated systems there is less electronic communication from one end of the molecule to the other. Highly delocalized systems, however, support long-distance communication between parts of the molecule, and thus are desirable in molecular wires. This computational work has laid significant groundwork for understanding the experimental behavior of such molecules.

A large body of experimental work has emerged regarding the electronic behavior of oligo(phenylene ethynylene)s. Tour and co-workers have synthesized many of these types of molecules, the longest is **8** with a length of 128 Å.[31, 32] While the conductivity of this particular molecule has not been determined, a number of significant experiments have been performed on similar shorter molecules to measure their effectiveness as molecular wires.



8

Bumm et al.[33, 34] used the tip of an STM to measure the conductivity of single molecular-wire molecules of **9** embedded in a self-assembled monolayer (SAM) support composed



9

of dodecanethiolate (DT). When the thioacetate group on **9** was deprotected to the thiol (**9′**—Figure 15a) in the presence of the crystalline SAM, single molecules, or at most a few molecules, were bound to the underlying Au(111) surface at disordered defects in the SAM. STM imaging revealed bright, stable, isolated spots at domain boundaries and defect sites in the DT SAM (Figure 15b). These bright spots were consistent in size, shape, and orientation, which indicates that they were features sharper than the tip used to image them. In addition, Bumm et al. measured the apparent tunneling-barrier height (ATBH) over DT–**9′**. The ATBH, a measurement of the relative conductivity of the underlying film, may be determined by modulating the position of the STM tip (z) and observing the change in the current (I) with respect to the position (dI/dz). There are many convoluting factors, such as mechanical distortion of the film or tip, in determining a quantitative measure of ATBH.

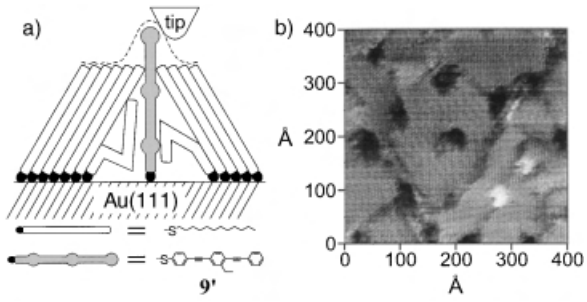
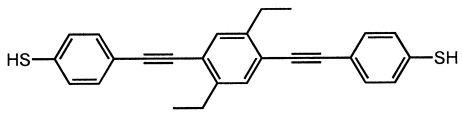


Figure 15. a) Schematic illustration of the insertion of **9′** into a disordered domain boundary of a DT SAM. The dashed line represents the feature as imaged by the STM tip, b) STM image of the arrangement illustrated in (a); the bright spots of similar shape and size are the molecules of **9′**. Figure 15b modified with permission from ref. [33].

By comparing the ATBH over DT with that over **9′**, these factors could be ignored to obtain a relative measure of conductivity. The ATBH over **9′** was observed to be at least two times higher than over DT. The bright spots in Figure 15b indicate the tip withdrawing from the surface, and thus increasing the tip-substrate separation. Considering that the tip is farther away from the substrate, and the ATBH is larger, it was inferred that molecules of **9′** have a greater conductivity than molecules of DT.

These results suggest that oligo(phenylene ethynylene)-type molecules might make good molecular wires. However, some of the results of experiments performed by Myrick's group[35] suggest that this may not be the case. SAMs of **10** (a dithiol similar to **9′**) on Au electrodes were found to passivate



10

the Au electrode in a manner similar to DT-SAMs (Figure 16). Anodic stripping voltammetry (ASV) showed that deposition of Cu occurred at high negative potentials on both DT and **10**. This process happens on bare Au surfaces at about −0.1 V. Copper ions required a significant overpotential to be reduced at defect sites in a DT SAM,[36] and the same effect was observed in SAMs of **10**. Although the relative ease of nucleation of copper metal islands on the SAM of **10** can not be ignored when ascribing reasons for the observed overpotential, the significant shift in potential still suggests that SAMs of **10** are poor electrical conductors.

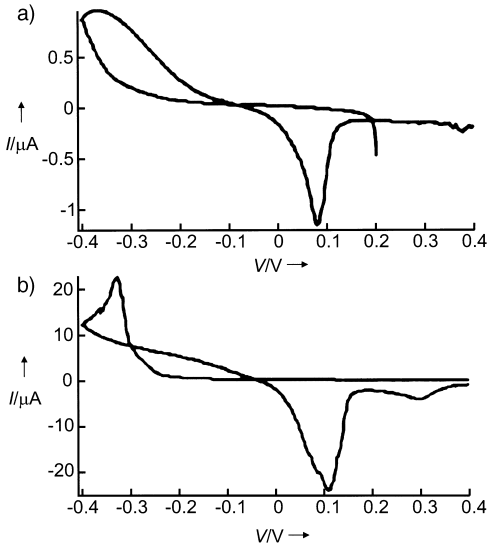


Figure 16. Anodic stripping voltammetry (ASV) of copper on a) Au electrode with a DT SAM b) Au electrode with a SAM of **10**. Reproduced with permission from ref. [35].

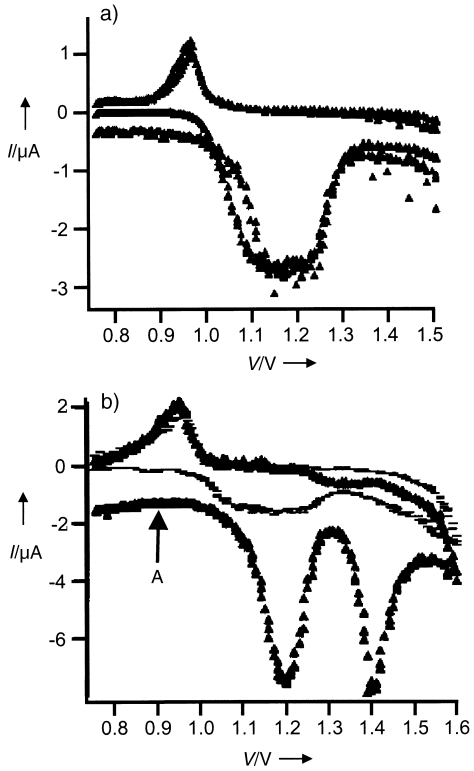


Figure 17. ASV of vapor-deposited Cu on a) a DT SAM, and b) a SAM of **10**. ▲ first scan, – second scan. "A" indicates the position at which potential sweep was stopped and the sample imaged by SEM. Reproduced with permission from ref. [35].

The poor relative conductivity of SAMs of **10** was further suggested in the following experiment. Copper was vapor deposited onto the SAM in an attempt to ensure that a layer of Cu was present atop the defect-free portions of the SAM. Stripping voltammetry on SAMs of both DT and **10** revealed the characteristic stripping peak for copper at +0.1 V. In the DT system also showed a broad peak at +1.2 V indicative of gold oxidation, and the corresponding stripping peak for the oxide at +0.9 V (Figure 17a). A SAM composed of **10** also showed a peak at +1.2 V, but the peak was much sharper than that observed for the DT SAM (Figure 17b). A second sweep on the SAM of **10** revealed the Au oxidation peak that was hidden beneath this sharper peak. The SAM of **10** also showed a peak at +1.4 V that was assigned as the oxidation (and subsequent desorption) of the **10** molecule. The nature of the sharper peak at +1.2 V was made clear when the surface was examined by SEM. When the Cu-covered SAM of **10** was swept to +0.9 V (point A in Figure 17b) then removed from the electrochemical cell, SEM images revealed the presence of Cu islands on top of the SAM of **10**. SEM images of the SAM after sweeping past the +1.2 V sharp peak showed that the islands were gone. Thus the initial sharp peak at +1.2 V on the **10** SAM arises from the stripping of the Cu islands that were on defect-free, ordered domains of the **10** SAM.

The large overpotential (1.1 V) across the molecule (25.2 Å) indicates an electric field strength of about 450 MV m^{-1}, which suggests a tunneling mechanism and therefore, a tunneling barrier. Charge tunneling through a SAM of **10** can occur with holes or electrons as charge carriers. Holes must tunnel through a barrier the height of which is determined by the difference between the Au Fermi energy and the HOMO of the SAM of **10**. The barrier height for electron tunneling is the difference between the Cu Fermi energy and the LUMO of the SAM of **10**. Whichever barrier height is lower will dictate the dominant charge carrier in the molecule. The barrier height can be estimated from the overpotential. Thus, an overpotential of 1.1 V is a crude measure of a barrier height of 1.1 V. The formal oxidation of **10** occurred at +1.4 V, very near to the copper stripping peak at +1.2 V, which suggests that the dominant charge carriers are holes injected from the gold electrode into the HOMO of **10**. Further estimates of the barrier height by independent methods corroborated the value of 1.1 V. The authors concluded that a barrier height of 1.1 V is unsuitable for a molecule intended as a conductor. While at odds with predictions that such a molecule should be a good conductor, the authors concede that there are likely to be differences in the electrical environment of the molecule when probed by a sharp STM tip than with a planar Cu contact.

In any effort to describe a molecular wire, perhaps the most important characteristic is the conductivity of the wire. In other words, how effectively, both in time and distance, is charge transferred from one end of the molecule to the other? An ideal molecular wire would transfer charge over long distances at very fast rates. These are issues that are dealt with at great length in the field of electron transfer.[37] Most molecular entities appear to transfer charge through a tunneling mechanism where the rate of electron transfer shows an exponential dependence on distance. Determining the distance dependence of electron transfer allows comparison of the conductivity of different molecules, regardless of their length. This distance dependence may be represented by an experimentally determined value β, determined from the slope of a plot of $\ln(k_0)$ against distance. Several conjugated oligomer systems have been studied as potential molecular-wire systems, and their β values are presented in Table 1.

Particularly for *n*-alkane chains, β values (for single-electron transfers) have been correlated with the relative conductivity of single-molecule-thick junctions (Majda et al.[38, 39] and by Rampi and Whitesides et al.[40–42] by using metal | molecule | mercury-drop junctions and by Frisbie and Wold[43] using

Table 1. Exponential decay constants β for various molecular repeat units.

Repeat unit	β_{calcd} [Å^{-1}]	β_{exp} [Å^{-1}]	Ref.
oligophenylenevinylene[a]		0.06	[46]
oligophenylethynyl		0.36	[110]
oligoporphyrin **6**	0.045		[111]
polyene	0.078		[112]
alkyl		0.85	[113]

[a] One to four repeat units.

conducting atomic force microscopy). These efforts do not overcome all of the device-related challenges of attaching molecular wires between molecular components, but they do indicate relevant behaviors of different molecular wires.

Using β values to assess the behavior of molecular wires has several important limitations. The exponential distance dependence of electron transfer indicates a single, non-adiabatic transfer using a superexchange (tunneling) mechanism. Recently, systems that show little rate dependence with distance have been illustrated. Davis et al. showed that there is only a weak distance dependence when the energy of donors and acceptors are matched to that of an oligo-phenylene vinylene bridge.[44] While this type of behavior has yet to be observed in a molecular device, the importance of binding between molecule and electrode has been appreciated.[45] Transition from a non-adiabatic to an adiabatic mechanism, which would have consequences for the distance dependence of electron-transfer rates,[47] may have recently been observed in ferrocene-terminated oligophenylene vinylene SAMs on gold.[46] Conformational changes can stimulate a transition from superexchange-mediated electron transfer to thermally activated (hopping) transport.[48, 49] This latter mode has a weak distance dependence and has been proposed to explain the electron-transfer behavior of DNA.[50–54] Arguably, systems with a small or non-existent distance dependence on rate are much better candidates for molecular-wires.

Carbon nanotubes represent another emerging area of interest for molecular scale wires. In recent years, synthesis of single-wall nanotubes (SWNT) has improved dramatically,[55, 56] increasing the amounts of material available and aiding efforts to investigate their properties. It was predicted that the electrical properties of SWNTs should vary depending on their specific chirality and diameter,[57, 58] and scanning probe techniques have been successfully used to verify this by correlating structure with density-of-states.[59, 60]

Generally it has been observed that the largest resistance in a nanotube wire arises from the contact resistance between an electrode and the nanotube. Bachtold et al.[61] studied multi-walled nanotubes in a four-probe configuration and found the contact resistance to be as high as 1 GΩ, while the resistivity of the tube could be as low as 0.3 $\Omega\,\mu m^{-1}$. They modified the contact resistance to around 60 kΩ by scanning the nanotube–electrode junction with the SEM beam, apparently "soldering" the tube to the electrode with the ubiquitous amorphous carbon contaminant.

de Pablo and co-workers[62, 63] used scanning force microscopy to characterize single-wall nanotubes onto which electrodes had been lithographically patterned. They found a contact resistance of 44 kΩ and a tube resistivity of 0.15$\Omega\,\mu m^{-1}$. These results suggest that carbon nanotubes will make very efficient wires in nanoscale systems, if they can be connected well.

There are additionally several significant challenges remaining for the use on carbon nanotubes in molecular electronics. First, there is, as yet, no technique to produce only one type of tube, either metallic or semiconducting. This may not matter given the nature of the examples above. In neither case is the chirality of the tube controllable. Further, there is not yet a reasonable method of separating the different types of tubes produced by current synthetic techniques. Avouris and co-workers have selectively oxidized metallic single-wall nanotubes in bundles with semiconducting nanotubes, so that only semiconducting nanotubes are left. This method may provide a potential route to utilization of only one type of tube in an electrical circuit.[114] Finally, the nanotubes must be explicitly positioned and connected, which is limited currently to serial techniques (electron-beam lithography, scanned probe manipulation). Other techniques are under development (fluid alignment, dielectrophoretic alignment, self-assembly) which will probably improve the outlook for nanotube wires.

Semiconductor nanowires have also emerged as a set of materials with potentially very high utility in molecular electronics. As of the date of this review, this field is moving rapidly—several-hundred papers describing their synthesis and properties have appeared in just the last two years. Some significant efforts are highlighted here—this discussion is far from comprehensive. Advances have been reported for the efficient synthesis of semiconductor nanowires including materials containing segments of different materials along their length.[64–66] This latter type of material builds the equivalent of semiconductor junctions into the nanowire, a potential route into junction-based devices. Polarized luminescence and lasing action has been illustrated in single nanowires.[67–70] Well defined laser sources of nanometer size open up the possibility of photonic information processing at the nanometer scale. The binding of molecules to nanowires influences their electronic properties—this behavior can be the basis of novel, nanoscale sensors (perhaps even for single-molecule detection).[71, 72] By crossing nanowires, multi-terminal junction devices have been fabricated that are capable of logic operations.[73–75] Large-scale integration of crossed nanowires has not yet been achieved. However, several examples have been illustrated in which superlattice structures[76–78] have been prepared using flow techniques.

2.3. Static Elements: Data Storage

In contrast to the dynamic nature of a molecular wire, with its ability to transfer charge from one location to another, a memory device represents a static component. In the current

computational architecture, data is stored in a bit-wise manner—the smallest part of data is either 0 or 1. In a molecular system, there are a number of ways this might be realized, which include charge storage, conformational or positional shifting, and physical transformation.

Nanotubes and their cousins, the fullerenes, have been exploited in the design of prototype nanoscale memories. Lieber's group[79] has proposed a nonvolatile random access memory (RAM) based on a suspended crossbar array of nanotubes (Figure 18). The authors presented calculations

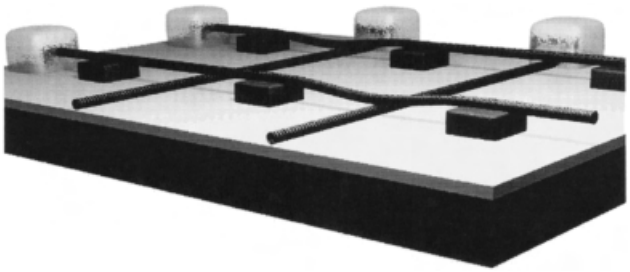


Figure 18. Suspended crossbar configuration of the nonvolatile RAM proposed by Lieber et al. The Figure shows a 3D view of four junctions in the proposed architecture, with two crossbar devices in the ON state (in contact) and two in the OFF state (separated). The upper nanotubes are supported on organic or inorganic supports (black blocks), while the lower nanotubes are directly in contact with insulating substrate (SiO_2, white) on conducting layer (highly doped Si, black). The light gray blocks represent the electrodes used to address each nanotube. Reproduced with permission from ref. [79].

that suggest that, for nanotubes in relatively close proximity to one another, there are two energy minima corresponding to the nanotubes remaining either suspended (OFF) or in contact (ON). The ON state persists as a result of van der Waals interactions between the two nanotubes, and may be initiated in a separated pair by applying voltage pulses of *opposite* polarity to the two crossed nanotubes. The ON state may be switched to the OFF state by applying a larger voltage pulse of *identical* polarity to each of the nanotubes. The device elements may be as small as 5 nm, giving a density of 10^{12} devices per cm^2. The switching time was calculated to be on the order of 10^{-11} s, which gives an operating frequency of approximately 100 GHz.

The theoretical work was supported by experimental measurement of a suspended nanotube junction. The junction was fabricated by mechanical manipulation of the nanotubes and the evaporation of contact electrodes onto them. The device could be switched ON and OFF with applied voltage pulses. The state of the device could be read by measuring the resistance of the junction—the resistance in the OFF state was greater by up to five orders of magnitude than the ON state. The reading of the device should be non-destructive, and thus the junction represents a nonvolatile memory element. Lieber et al. proposed the fabrication of large arrays of such junctions by either patterned growth of the nanotubes in an array, or directed self-assembly, both of which have been demonstrated in different systems.

Kwon and co-workers[80] have proposed the use of so-called "bucky-shuttles" as nonvolatile memory elements. A bucky-shuttle consists of a fullerene (a "buckyball") with a diameter close to that of C_{60} encapsulated inside a short nanotube. These objects were made in abundance from the treatment of nanodiamond powder at 1800 °C. The buckyball was observed to stay at one end or the other of the nanotube, presumably because of van der Waals interactions and weak covalent forces, as has been observed in crystalline C_{60} and nanotube bundles.[55] Calculations of the potential energy of a C_{60} as it shuttles inside a C_{240} shell show a 0.24 eV stabilization at the ends of the shell, compared to anywhere along the length. Reading and writing such a structure necessitates that the fullerene is charged. It was proposed to accomplish this with $K@C_{60}^+$, one of a family of known fullerenes with a caged metal ion. The metal ion within the C_{60} imparts a net positive charge that is evenly distributed over the whole fullerene. Writing of data would occur when a field is applied along the axis of the shell through integrated electrodes in the ends of the shell. A bias of about 1.5 V was calculated to be enough to destabilize one of the energy minima, causing the $K@C_{60}^+$ to migrate to the other end of the tube in around 4 ps. The state of the device can be read nondestructively by measuring the polarity of the capsule, or destructively by applying a probe voltage and measuring the resulting current pulse.

Kwon et al. envisioned arrays of these capsules packed side by side, with crossing electrodes connected to their ends (Figure 19). Individual element addressing is carried out by

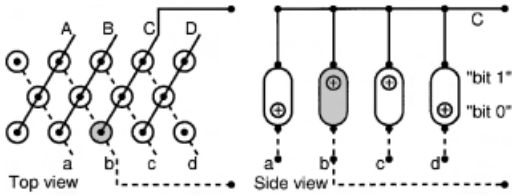


Figure 19. Configuration of "bucky-shuttle" memory elements. left: Top view showing an array of bucky-shuttles and the crossed electrodes used to address them. Right: side view showing the elements addressed by electrode C. By applying a reading or writing pulse between electrodes C and b, a specific element may be queried or written. Reproduced with permission from ref. [80].

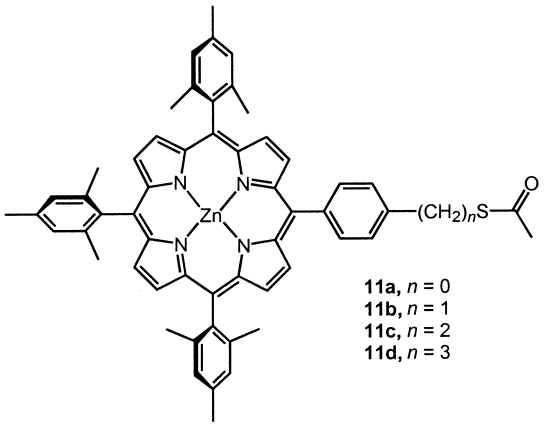
applying read or write pulses to crossed electrodes, thereby reading from or writing to the element between them. Under ideal conditions, such an element may be switched at a rate of 100 GHz. The authors did not suggest any method by which an array of closely packed, vertically oriented nanotube-based memory elements might be produced, and thus did not present any predictions on element density.

Other examples of data-storage proposals involve the modification of polymeric materials. While such examples of data storage are not truly molecular electronics, they bear consideration in the context of discussing the current state of the field. Binnig et al.[81] studied the use of thermomechanical techniques to write data into soft polymers. This was accomplished by using a modified cantilever in which the tip was heated by applying a voltage across the legs of the cantilever. Placing this heated cantilever in contact with a polymer layer melted a small region of the surface, forming a pit. Each pit represents a bit of data. It was observed in

previous efforts that using a thick polymer layer led to larger pit sizes and reduced lifetime for the reading/writing tip. This technique has been refined through many iterations to employ multilayer polymer surfaces. The described work of Binning et al. uses a dual-layer substrate composed of 40 nm of polymethylmethacrylate (PMMA) on 70 nm of photoresist baked onto Si. The PMMA is the actual medium of data storage, while the photoresist serves as a physical buffer between the tip and the underlying Si surface.

The actual writing of data into the PMMA layer was accomplished by applying short (2 μs) voltage pulses to the thermomechanical cantilever. This heated the cantilever tip to approximately 400 °C, melting the PMMA and forming a pit. The reading of data employed the writing tip in a constantly heated (≈350 °C) mode. The resistance across the legs of the cantilever shifted linearly with changes in temperature. The temperature of the tip depended on how effectively heat was transferred through the air between tip and substrate or through the legs of the cantilever. When the tip was outside of a pit, the heat transfer was dominated by the cantilever legs, and the tip reached a stable temperature. When the tip moved into a pit, the heat transfer through air became more efficient than through the cantilever legs, and the tip temperature (and resistance) fell. By monitoring the resistance as the tip was scanned over the surface, the presence of pits in the substrate was detected. Erasure of data was accomplished in a similar manner—heating the entire substrate above 150 °C for a moment erased the presence of pits. Multiple writing and erasing cycles were carried out with no degradation of the substrate. Recently, Lutwyche et al.[82] furthered this technique by utilizing an array of 32 × 32 thermomechanical tips to working in a parallel fashion to write data in bit densities as high as 100–200 Gbit per square inch. Improvements in the read and write rates of the parallel array have moved the device closer to production, with a prototype device called "Millipede".[83]

Roth et al.[84] suggested that data may be stored in the oxidation states of molecules, specifically, metalloporphyrins such as **11**. The family of molecules all exhibit reversible one- and two-electron oxidation to the mono- or dication radical. It was suggested that the neutral molecule might represent a bit state of "00", while the monocation represents state "01", and the dication, state "10". To demonstrate the effectiveness of charge storage in the molecule, a SAM of **11a** was prepared on a microelectrode and studied by open-circuit potential (OCP) amperometry. In this electrochemical technique, the molecules in the SAM were oxidized (and data "stored") by a potential step to +800 mV for the monocation ("01"



state) or +1100 mV for the dication ("10" state). The counter-electrode (CE) was then disconnected for some time to allow for the dissipation of charge from the electrochemical double-layer. To "read" the data, the CE was then reconnected at the open-circuit potential, which is normally negative enough to reduce the oxidized porphyrin. The current measured is proportional to the oxidation state of the molecules (or their bit state) and the number of molecules in that state (Figure 20). The response time of the measurement was limited by the RC (where R is the total effective resistance of the cell and C is the capacitance of the cell) time constant of the cell. Thus, shrinking the active area of the electrode increased the instantaneous current from the SAM (Figure 20c). In addition, the length of the methylene spacer between the

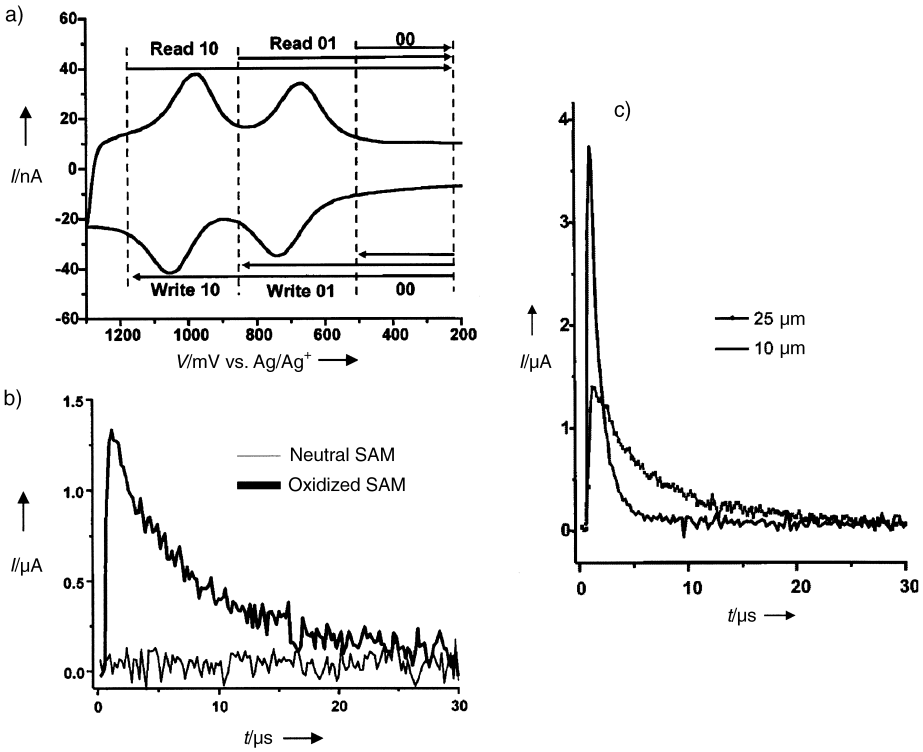


Figure 20. a) CV of **11a** (25 μm diameter Au electrode, in electrolyte solution of 0.1 M $Bu_4N^+PF_6^-$ in dried, distilled CH_2Cl_2 with Ag-wire counter electrode), b) current trace for reconnection of the counter electrode at OCP for neutral and oxidized **11b** SAMs, c) current trace for two Au electrodes (diameter: 25 and 10 μm) with **11b** SAMs, oxidized at +800 mV (versus Ag/Ag^+), disconnected for several seconds, then reconnected at the OCP (+125 mV versus Ag/Ag^+). Reproduced with permission from ref. [84].

porphyrin and the thioacetate was found to have a direct effect on the retention time of the charge storage, based on a determination of decay half life ($t_{1/2} = 116$, 167, 656, and 885 s for **11a–d**, respectively).

2.4. Transistorized: Molecular Switches

The switch is the basic element of control in any electronic architecture—by its very function it either allows current to flow or not. There are many examples of proposed molecular and atomic switches, which use a myriad of different mechanisms and motifs for operation.[85] Aside from "simple" switches there have also been several significant suggestions of more complex switching behaviors, which include the use of arrays of switches to implement logic operations and the use of two-terminal resonant tunneling devices to do the job of switching. A number of examples of molecular switching have been proposed based on quantum effects; single molecules, carbon nanotubes, and quantum dots or nanoparticles have all been found, under the right circumstances, to display some of these quantum effects.

Dekker and co-workers[86] fabricated a field-effect transistor based on a carbon nanotube, and demonstrated weak gain under room temperature conditions. The device consisted of a semiconducting tube positioned across two Pt electrodes, on a SiO_2 substrate, with doped Si as the back gate (Figure 21). The electronic characteristics of the device were measured by sweeping the bias between the two electrodes at various applied gate biases (V_{gate}). The resulting I/V curves are shown in Figure 21c. At $V_{gate} = 0$, the I/V curve showed deviation from linearity, which indicates that this is a semiconducting nanotube. At positive values of V_{gate}, the device displayed a widening gap as V_{gate} was increased. At negative values of V_{gate}, the I/V curve showed ohmic behavior corresponding to a resistance of approximately 1 MΩ. This behavior is similar to that observed in metallic nanotubes in a similar configuration, and thus is likely to be a result of contact resistance between the nanotube and the electrodes. The inset in Figure 21c shows the change in conductance G of the device at $V_{bias} = 0$ as the V_{gate} was varied. The value of G decreased by six orders of magnitude (from 10^{-6} to $10^{-12}\,\Omega^{-1}$) as V_{gate} was made more positive. The energy diagram in Figure 21b offers an explanation for this behavior. The work function for the carbon nanotube (4.5 eV) is lower than that of the Pt electrodes (5.7 eV), but the contact between the two Pt electrodes pins the potential at the ends of the nanotube to the Fermi-level of the electrode. Thus, the valence band in the central portion of the nanotube (in contact with the SiO_2 layer, Figure 21a section B) is predicted to bend to meet the Fermi level of the electrodes. The reduced conductance at $V_{bias} = 0$ and $V_{gate} > 0$ (Figure 21b, section B) is thus a result of hole depletion, which leads to a more insulating state. At $V_{gate} < 0$, hole accumulation in section B of Figure 21b gives rise to enhanced conductance, and an ohmic (i.e., metallic) I/V curve.

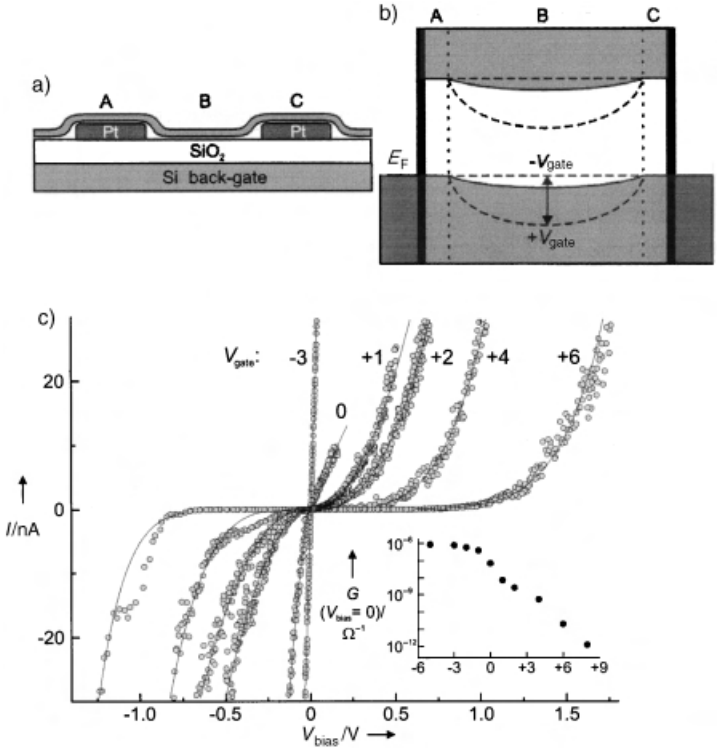


Figure 21. Nanotube field-effect transistor (TUBEFET). a) Schematic of device configuration, b) band diagram for device; the nanotube Fermi energy (E_F) is pinned at the E_F of the metal electrodes, c) I/V curves at varying V_{gate} for the device ($T = 300$ K). Inset: dependence of conductance G at $V_{bias} = 0$ with V_{gate}. Reproduced with permission from ref. [86].

The gain of the TUBEFET was low. A shift in V_{gate} from $+4$ V to $+6$ V resulted in V_{bias} shift of only around 0.7 V (Figure 21c), with a gain of approximately 0.35. Also, the frequency of operation was only about 100 GHz. A number of ways were suggested to improve these characteristics. By reducing the thickness of the SiO_2 layer from 300 nm to 5 nm and by decreasing the contact resistance to the nanotube, a theoretical operating frequency of 10 THz and a gain of approximately 3.5 were predicted.

Transistor devices based on nanosized junctions have been fabricated and display staircase I/V profiles because of a blockage of additional current flow until some threshold voltage is reached (Coulomb blockade). The threshold voltage depends on the size and nature of the particle in the semiconductor junction and varies with the junction resistance and capacitance. A Coulomb staircase profile is a special case of Coulomb blockade. When a nanostructure is small enough, the transfer of one electron onto it blocks the flow of further electrons by electrostatic repulsion. To overcome the repulsion, the voltage must be increased, until two electrons at a time can tunnel onto and off of the nanostructure. This cycle is repeated for greater numbers of electrons, and results in a step shaped I/V curve. These behaviors are useful for controlling switching behavior in very small devices, with very small currents, in very specific ways.

Sato and co-workers[87] measured the I/V properties of a single-electron transistor (SET) fabricated from a chain of colloidal gold particles with nominally 10 nm diameters. A schematic of the experimental setup is shown in Figure 22. Source, drain, and gate electrodes composed of 20 nm of Au on 5 nm of Cr were patterned on a SiO_2 surface by using electron-beam lithography. Citrate-modified Au particles, were deposited onto the surface, whereupon the citrate

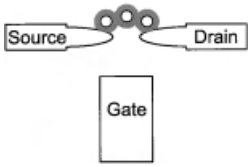


Figure 22. Schematic of an in-plane single-electron transistor. Approximately 30 nm separates the source, drain, and gate electrodes.

capping was exchanged for 1,6-hexanedithiol. A second deposition of Au particles led to the formation of short, isolated chains of Au particles on the surface. *I*/*V* measurements were carried out on samples in which the source and drain electrodes were found to be bridged by one of these chains.

I/*V* curves collected at 300, 77, and 4.2 K are shown in Figure 23 a. At 300 K, any electrons in the system have enough thermal energy to overcome any electrostatic repulsion from the particles, and tunneling onto and off of the particles is

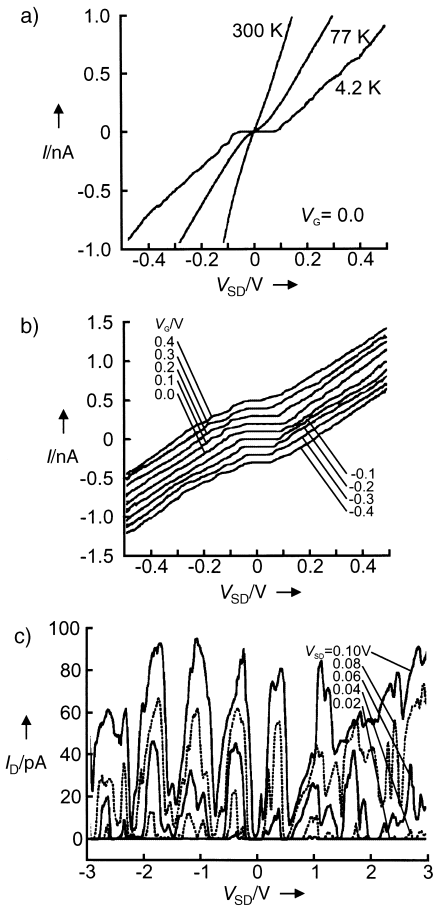


Figure 23. a) Plot of *I*/*V* curves collected between a source and drain electrode (shown in Figure 22) connected by a chain of three Au colloidal particles. V_{SD} = source – drain current. The curves were collected at the temperatures indicated, with $V_{gate} = 0$. b) Plot of *I*/*V* curves for various V_{gate} values against V_{SD}. The curves are offset from each other for clarity. c) Plot of conductance (I/V_{gate}) at various V_{SD} values. Reproduced with permission from ref. [87].

unhindered, which gives a linear *I*/*V* curve. At 4.2 K, the thermal energy of electrons in the system is much lower, and electrostatic repulsion has an effect, which gives rise to the Coulomb staircase. Figure 23 b, measured at 4.2 K, shows the variation in the *I*/*V* curve as V_{gate} is varied. The most obvious feature here is the narrowing of the Coulomb blockade as the magnitude of V_{gate} increases. Figure 23 c shows that periodic oscillations in the conductance (conductance = I/V_{gate}) become more pronounced at higher source – drain bias. Based on comparison with computational results for the system, single-electron tunneling across a four-junction system was proposed.

Andres et al. have shown Coulomb-staircase behavior at room temperature in a system composed of an Au nanoparticle (ca. 1.3 nm) bound to an Au substrate by α,ω-xylyldithiol (Figure 24).[88, 89] Previously, this behavior, characteristic of single-electron transfer events, had only been

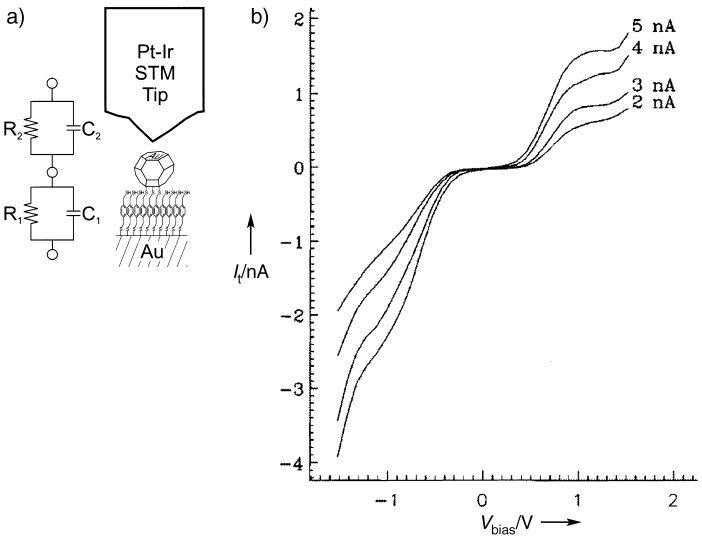
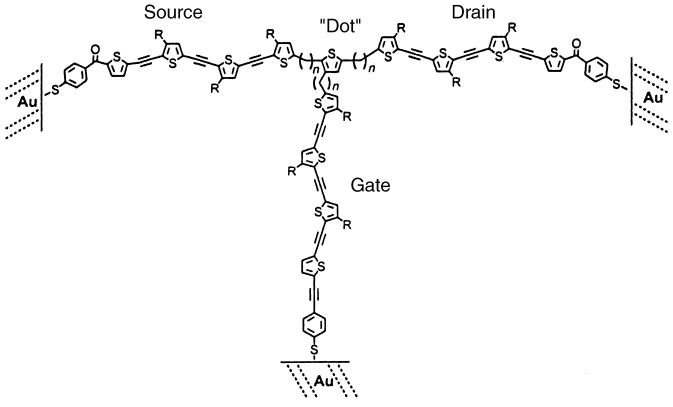


Figure 24. a) Schematic of self-assembled nanostructure, composed of xylyldithiol on an Au(111) substrate, and the circuit diagram that describes the system. b) Plot of *I*/*V* curves collected at varied setpoint currents; I_t = tunnel current. Reproduced with permission from ref. [89].

observed at very low temperatures. Fitting these *I*/*V* curves to the classical Coulomb-blockade model (each junction has a capacitance and a resistance associated with it, see Figure 24 a) verified that these curves were consistent with those of a double-tunnel junction. Further, these data allowed estimation of the resistance of a single xylyldithiol molecule ($\sim 18 \pm 12$ MΩ).

Wada has proposed using three-terminal molecular systems, such as **12**, to function as molecular single-electron switches



12

(MOSES).[90, 91] The source, drain, and gate are polythiophene chains or other molecular wires, and the "dot" is isolated from them by a methylene-based spacer. There still exists the very real problem of making reproducible low-resistance contacts to the "electrodes". Theoretical studies of these systems have suggested that switching speeds approaching 1 THz may be possible.

Other types of switching devices depend on the close relationship in the molecular realm between physical form and electronic structure. By changing a molecular conformation or deforming the structure of a molecule, experiments have shown that the electronic properties of the system may be modified. One of the clearest examples of this phenomenon has been the demonstration by Joachim and Gimzewski of a single-molecule electromechanical amplifier, consisting of a single C_{60} molecule between a substrate and an STM tip (Figure 25a).[92] In this experiment, a signal (V_{in}) was applied

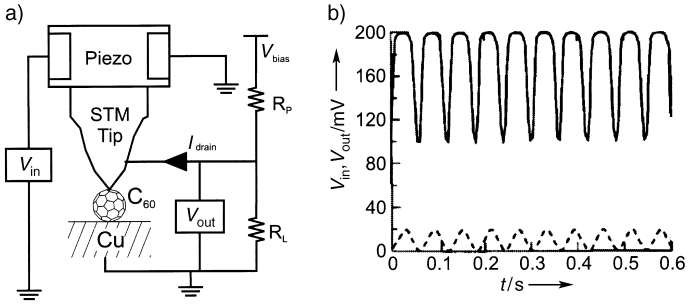
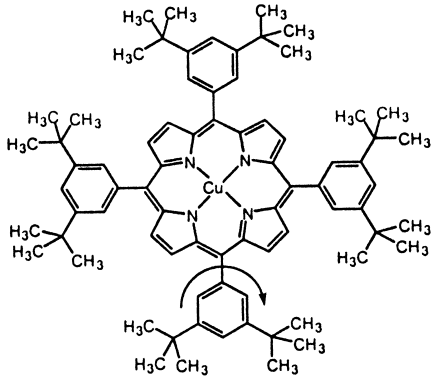


Figure 25. a) Circuit diagram of a single-molecule electromechanical amplifier based on the interaction of an STM tip with a C_{60} molecule. b) Plot of V_{in} (----) applied to piezoelectric tube and resulting V_{out} (——). Permission from ref. [92].

to the piezoelectric tube that controls the z positioning of the STM tip. This induced a distortion in the piezoelectric material, causing the STM tip to press down on the C_{60} molecule and distort it. Theoretical studies of C_{60} indicate that as it is distorted, the HOMO and LUMO are shifted and broadened,[93] which leads to a greater conductance through the molecule. The conductance of the junction was shown to increase by two orders of magnitude upon distortion. This effect is the source of the amplification in the system. In Figure 25b, the dashed sinusoidal line is V_{in}, and has a magnitude of 20 mV. The solid line is the measured output voltage (V_{out}), which shows a magnitude of 100 mV, and thus shows a gain of 5. It was suggested that the inherent limit of operational speed in this system is the first vibrational mode of C_{60} of approximately 14.7 THz. Since reporting these results, Joachim and Gimzewski have also proposed a memory device using four nano-electromechanical transistors.[14] While such a device is not terribly useful in such a configuration, the fact that a single molecule can provide a substantial gain is important for future developments in this field.

Further work showing the close relationship of conformation and electronic structure in molecules has been undertaken by Moresco et al.[94] Low-temperature STM (LT-STM) was utilized to study a substituted metalloporphyrin **13** on a Cu(211) surface. At 15 K, **13** was found to lie on the Cu(211)



13

surface with the metalloporphyrin plane parallel to the surface. The molecule could be moved on the surface in a controllable way with the STM tip. In addition, the phenyl-*t*-butyl arms of the molecule could be oriented in two conformations (assigned from a combination of experimentation and computation)—one in which the plane of the phenyl group is about 10° from being parallel to the surface, the other in which the plane of the phenyl group is rotated at about 55° to the surface. The two conformations could be differentiated by STM (Figure 26a, b). It was also observed

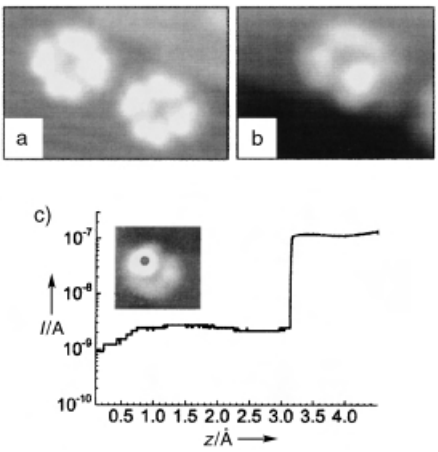


Figure 26. Low-temperature STM images of **13** on Cu(211) showing a) all *t*Bu-phenyl arms in the OFF position (nearly flat on surface), b) one arm (brighter point) in ON position (oriented 55° out of the plane of the porphyrin), and c) Plot of current on turning the ON arm OFF—the tip is moved from $z = 7.5$ Å towards surface. The dot on the inset picture indicates the tip position over the ON arm. Reproduced with permission from ref. [94].

that a lateral or vertical motion of the STM tip could induce the arm to change orientation. Further, $I(z)$ measurements (that is, variation in current as the tip was raised or lowered, with STM feedback disabled) indicated that the two different configurations have different conductances. When the STM tip was moved towards an arm in the ON position, initially the conductance was higher (indicated by current of $\approx$100 nA), until at approximately 3.0 Å, the arm had been tilted into the OFF position and current dropped by two orders of magnitude (Figure 26c).

Perhaps the smallest switching device possible would consist of an atomic relay—a single atom that can controllably be positioned in a gap and provide a clear indication of whether the switch is OFF or ON. This device would most easily operate by measuring a difference in conductance or measuring a current flow. Wada and co-workers proposed such a device with dimensions of less than 10 nm and theoretical switching speeds of 1 THz.[95] The proposal is ambitious, but out of reach with current technologies. Even so, within very strict limits based on material, a wire composed of single atoms should be able to conduct a charge from one end to the other. With this in mind, a simple atomic relay transistor can be imagined (Figure 27). In the ON state, the atom wire would carry charge through the switching atom. To turn the switch OFF, a voltage would be applied to the switching gate, and the switching atom would be shifted out of place, leaving a gap. This effectively would break the wire and stop charge transfer. To return to the ON state, a reset gate is necessary.

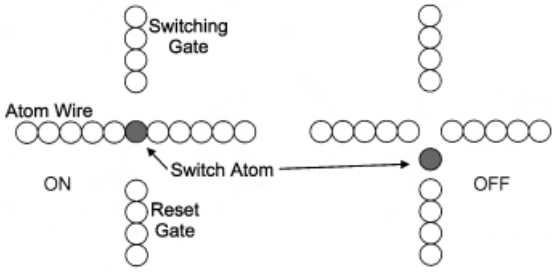


Figure 27. Proposal for an atomic relay transistor.

Clearly, such a system is not trivial to build, nor is it even obvious that the materials exist to make the device. After all, the atom wire must remain stuck to the substrate while transferring charge and must not short out to the substrate. The atom switch has to be able to shift reversibly into and out of the wire, rather than finding an energetically favorable position in the wire. The switching and reset gates must also be insulated from the atom wire, and the switching atom. Other considerations exist as well, and suggest that this is not a device that is likely to be implemented in the near future.

Even so, single-atom switching behavior has been observed. Eigler et al.[96] used the STM to reproducibly pick up and deposit a single Xe atom on a surface. At 4 K, the STM tip (composed of polycrystalline W) was used to slide a Xe atom to a kink in the Ni(110) surface. The Xe atom could be reproducibly imaged there. By applying a +800 mV pulse to the tip, the Xe atom could be made to jump onto the tip. Application of a −800 mV pulse to the tip caused the Xe atom to reattach itself to the kink. At −20 mV, with the Xe atom on the tip, a tip current of 90 nA was observed. When the Xe atom was on the surface, the current in the naked tip reduced to 15 nA. The Xe atom could be switched back and forth reproducibly by the application of the appropriate voltage pulses. To date several examples have been presented in which a probe microscope tip was used to initiate and probe switching behaviors. It is not clear if such feedback-based junctions could be viable devices (certainly there is doubt as to whether they could form viable, integrated devices). However, the probe microscope has opened up these opportunities to explicate molecular properties directly relevant to switching.

Other properties have also been used to control switching behaviors. Stoddart, Kaifer, and co-workers[97] constructed a molecular shuttle that could be switched electrostatically from one state to another. The rotaxane (Figure 28) consisted of a

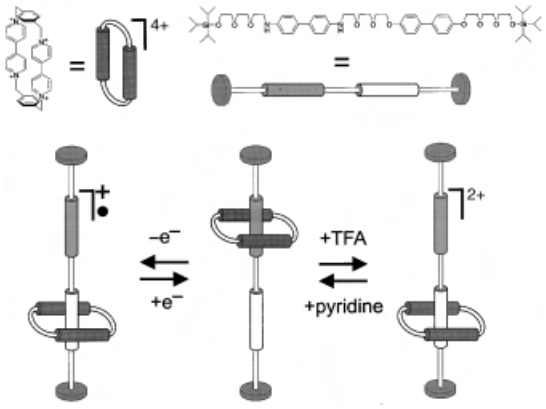


Figure 28. Representation of the construction and function of a molecular shuttle.

molecular "rod" with two "docking stations" (benzidine and benzophenol, gray and white rod segments in Figure 28, respectively), onto which was threaded a "bead" (tetracationic cyclophane). The bead was unable to dissociate from the rod because of the presence of two bulky stopper groups (tri-isopropanylsilanyl) at the ends of the rod. At room temperature, the bead traversed the length of the rod at very high rates (frequencies near 100 MHz), and there was no apparent selectivity of position on one station or the other. However, at 229 K, it was determined (by 2D NMR) that the bead exhibited 84 % occupancy at the benzidine station.

Upon addition of trifluoroacetic acid (TFA—a proton source), the bead shifted, nearly quantitatively, to the biphenol station. Neutralizing the TFA with pyridine shifted the bead back to the benzidine station. Presumably, the positive charge on the protonated benzidine repelled the cationic bead. Similarly, oxidation of the benzidine station to the radical cation shifted the bead to the benzophenol, and reduction returned it back to the benzidine. Again, this behavior is likely to be a result of electrostatic repulsion between the bead and the charged benzidine. This example, while admittedly unlikely to serve as a switch as-is, illustrates further the possibilities for controlling switching behavior in molecular devices.

The family of molecules known as rotaxanes has also been indicated as having possible utility as logical devices. A good example of this is the work by Balzani, Stoddart and co-workers[98] in which a molecular system exhibits behavior consistent with an XOR gate (Figure 29). The two starting molecules, **14** (π-electron accepting 2,7-dibenzyldiazapyrenium dication) and **15** (a crown ether containing two π-electron-

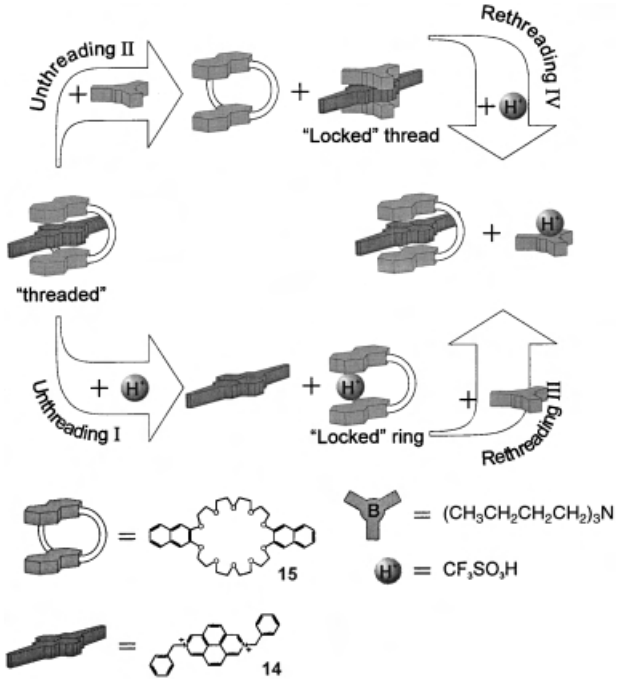


Figure 29. Schematic representation of pseudorotaxane-based logic operation.

donating 2,3-dioxynaphthalenes) form a charge-transfer complex. Separately, each of the molecules were observed to fluoresce strongly ($\lambda_{max} = 432$ and 343 nm for **14** and **15**, respectively), but upon forming the CT-complex, the fluorescence was extinguished. Adding trifluoromethanesulfonic acid ("H^+" in Figure 29) in stoichiometric amounts protonated the crown ether, largely dissociating the CT-complex ("unthreading I", in Figure 29). This action recovered the emission from **15** $\cdot H^+$ (nearly the same as the unprotonated crown ether), as well as the emission from **14**. Adding tributylamine ("B" in Figure 29) in equivalent amount to H^+ from previous step ("rethreading III") released **15** and allowed the CT complex between **14** and **15** to reform, quenching their emission bands. In a similar fashion, adding B to the CT-complex of **14** and **15** broke up the complex ("unthreading II"), to form a **14** $\cdot B_2$ complex. This action recovered the strong emission from **15**. In addition to a new broad emission from the **14** $\cdot B_2$ at 670 nm was observed. Adding H^+ to this adduct released **14**, which rethreaded with **15** ("rethreading IV"), once again quenching the fluorescence of the separate components.

Examination of this sequence reveals a pattern: Whenever the two components **14** and **15** are in the presence of either B or H^+, there was a strong fluorescence at 343 nm. If both B or H^+, were present, there was no fluorescence. If neither was present, there was no fluorescence. If the fluorescence is taken as an indicator of truth, and B and H^+ are taken as inputs, then the system has the same behavior as an XOR gate (see Table 2).

Drawing comparisons between chemical systems and logic operations or switching behavior must be undertaken carefully. The purpose here is to illustrate the very great flexibility of purpose to be found when dealing with molecular systems,

Table 2. XOR Truth Table.

Input X	Input Y	Output
false	false	false
false	true	true
true	false	true
true	true	false

not to suggest that either of these systems might somehow be integrated into a "wet" computer.

Using another, catenane-based system, anchored with amphiphilic phospholipid counterions, and sandwiched between an n-type polycrystalline Si electrode and a Ti/Al top electrode, a device exhibiting hysteretic (bistable) current/voltage characteristics was demonstrated (Figure 30).[99] This switch could be opened at $+2$ V, closed at -2 V, and read between 0.1 and 0.3 V. Using this hysteretic behavior, many read–write cycles were demonstrated. The demonstration of hysteretic behavior here is particularly notable—this basic illustration convincingly establishes that the device can retain its state after the application of the read voltage.

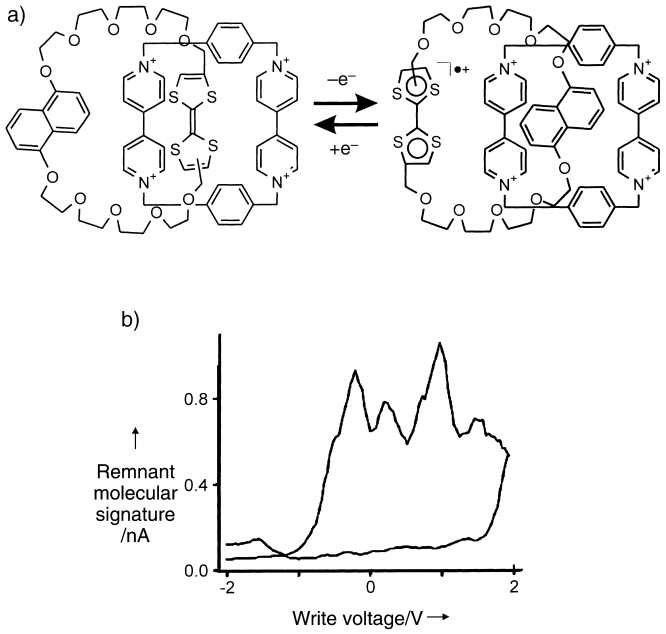


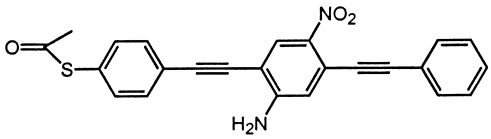
Figure 30. a) Two conformers of an electroactive, bistable molecule. b) The remnant molecular signature of a catenane-based device, measured by varying the write voltage in 40-mV steps and by reading the device at -0.2 V. Reproduced with permission from ref. [99].

2.5. Nonlinear Behaviors—Negative Differential Resistance

A negative differential resistance (NDR) is characterized by a discontinuity in the monotonic increase of current as the voltage is increased. That is, as voltage goes up, current plateaus, or in the most interesting cases, decreases before eventually rising again. This behavior is found in Esaki[100] and resonant tunneling diodes[101] for which several applications have been proposed. Several of these devices can be combined to give *I*/*V* curves with multiple peaks—this

behavior has been proposed to lead to multi-state memory and logic devices. From the standpoint of molecular-device construction, wiring a molecule to two-terminals appears technically more feasible than wiring to three-terminals (transistors are three terminal electronic devices). Thus, this avenue of molecular electronics has been pursued extensively. However, it is not clear that such devices can be integrated as they do not, by themselves, offer the opportunity to introduce gain into a circuit. Thus, two-terminal devices represent a tradeoff between what is currently feasible and potential real utility in circuit construction. At this time, the "jury is still out" with respect to two-terminal, molecular-based electronics.

Reed and Tour et al. reported the clearest example of molecule-based NDR to date.[102] Molecule **16** was sandwiched between two metal contacts. At 60 K, this assembly was found to display a very strong NDR with a peak-to-valley ratio (PVR) of 1030:1 and this value decreased as temperature increased (Figure 31). Control molecules (having no nitro or amine moieties) showed no NDR. The NDR was proposed to arise as a consequence of a two-step reduction: an initial one-electron reduction of the molecule provides charge carriers, and allows current flow. Current flow continues until the second reduction potential is reached, and the molecule is reduced to the dianion. Recently, Reed and Tour et al. have examined another molecule, similar to **16**, but without the amine functionality, which shows weak NDR at room temperature.[103] The proposed mechanism has been investigated computationally, and the results have proven somewhat contentious. Seminario and co-workers[104] tested the proposed mechanism with ab initio techniques, and found that, as observed, the current flow should be able to travel through the molecule only when it was reduced, as the LUMO at this point extended across the whole length of the molecule. Birge et al., however, have suggested that an oxidation occurs, and conduction occurs resonantly through the HOMO.[105]



16

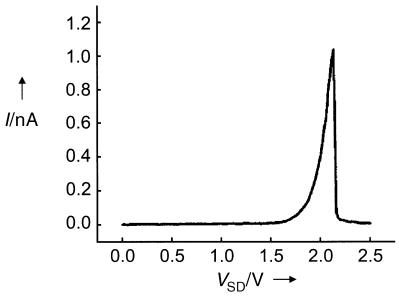
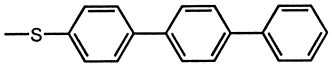


Figure 31. Graph of an *I*/*V* curve of **16** collected at 60 K. Reproduced with permission from ref. [102].

In another notable example of molecular NDR,[106] the *I*/*V* properties of **17** were studied with tunneling spectroscopy.



17

Figure 32 shows the observed *I*/*V* curve, with NDR at both negative and positive potentials. To explain this result a different mechanism was proposed. In this instance, the NDR was thought to arise not from any sort of oxidation or reduction, but rather a resonance between the tip and the molecule–substrate complex. In the case of a very sharp STM tip, it was suggested that the tip presents narrow features in the density-of-states (DOS) profile. The molecule, with discrete molecular levels, also presents narrow features in its DOS profile. Since the molecule is bound to a substrate through a relatively strong thiol–gold bond, the molecular DOS tends to float with the E_F of the substrate. As a bias is applied between the substrate and the tip, the molecular levels shift in one direction, while the tip DOS shifts the other. If the narrow features in the two DOS should cross one another, NDR should occur. Very recently, Brèdas et al. have presented some computational data to further illustrate the necessity of a reduced density of states in the contact for NDR behavior to be displayed in a molecular system.[107]

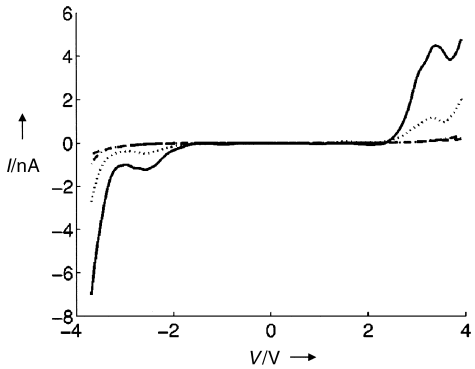
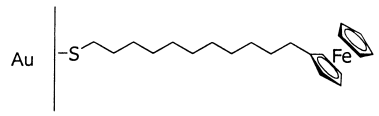


Figure 32. The *I*/*V* curve collected by STM over a monolayer of **17**. Setpoint bias was −5.0 V, and the tunneling current was varied from 3.05 to 30.5 nA. Reproduced with permission from ref. [106].

We recently observed NDR in *I*/*V* curves collected with an STM tip over a ferrocene-terminated SAM composed of **18**.[108] Figure 33a shows representative *I*/*V* curves collected over a region composed of **18** and dodecanethiol SAM. Those



18

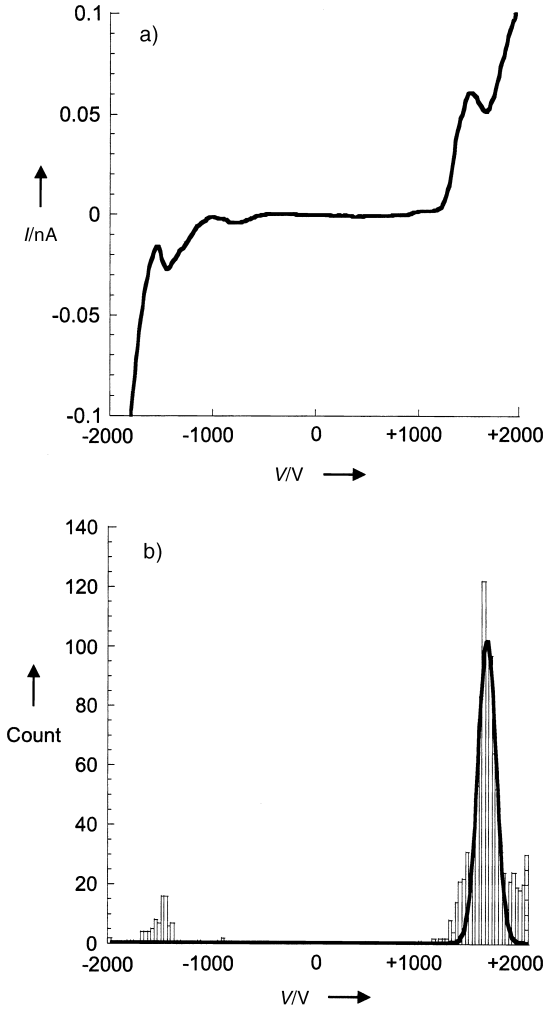


Figure 33. a) A typical *I/V* curve collected from a SAM of **18** under dodecane. b) Histogram representing the position of the NDR in a SAM of **18** under dodecane. Reproduced with permission from ref. [108].

curves from the **18** region show a nonlinearity characteristic of NDR. A histogram of the peak position from many different measurements is shown in Figure 33 b. It was suggested that the accessible redox states in the ferrocene headgroup of **18** allow resonant tunneling through the molecule, giving rise to the NDR. This observation is significant in that it suggests that the position of NDR should be related to redox potential, and may offer a route to tunable NDR. Further work to characterize the generality of the behavior in other systems is underway.

Berg et al.[109] examined the published reports of molecular and III-V semiconductor resonant tunneling devices (RTDs), to determine if they met the requirements set forth by the International Technology Roadmap for Semiconductors. The roadmap goals for 2008 regarding RTD usage as a Dynamic-RAM-refresh were used for the criteria. The published *I/V* curves for a number of systems, which included **16**, were used to determine the operating parameters for each RTD. The results are presented in Figure 34 where "Mol60 K" represents the results based on **16**. The area occupied on the plot determines the effectiveness of an RTD. The larger the plotted area, then the larger the acceptable range of supply

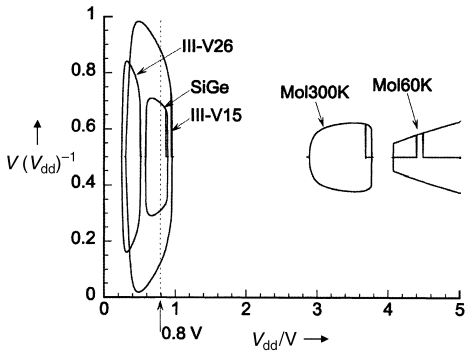


Figure 34. Plot of stable voltages for recently published RTDs as a function of supply voltage; V_{dd} = supply voltage. Reproduced with permission from ref. [109].

voltages for the device and the larger the difference in it's ON and OFF states. Berg and co-workers concluded that the currently available molecular and semiconductor species do not meet the requirements for a useful RTD, and suggest a number of goals. They suggest that while good PVRs are important, it is more important to have a low valley current, and that the "simplest" way to achieve this is to use fewer, or even single, molecules as operative devices. In addition, future molecules will have to be designed to show a much lower "turn-on" voltage.

3. Closing Thoughts

There is great promise to molecular electronics—electronics that are smaller, faster, more efficient, and potentially more flexible (in multiple ways) than conventional electronics. Clearly, some viable, fundamental demonstrations have been made of molecular-scale electronic-device behaviors. This review is entitled a "genesis", however, as the fundamental understanding of these behaviors is still lacking. More extensive characterization to deduce the molecular origin of these behaviors is in order. All of this must happen in a highly collaborative, interdisciplinary arena and a broad view will be required from all involved. Chemists, physicists, materials scientists, and electrical and chemical engineers must work together to understand the many facets of the research problems that are being uncovered as the field grows. The excitement of new demonstration coupled with the simpler, more elegant quest to understand makes molecular electronics an exciting and potentially very lucrative field.[115]

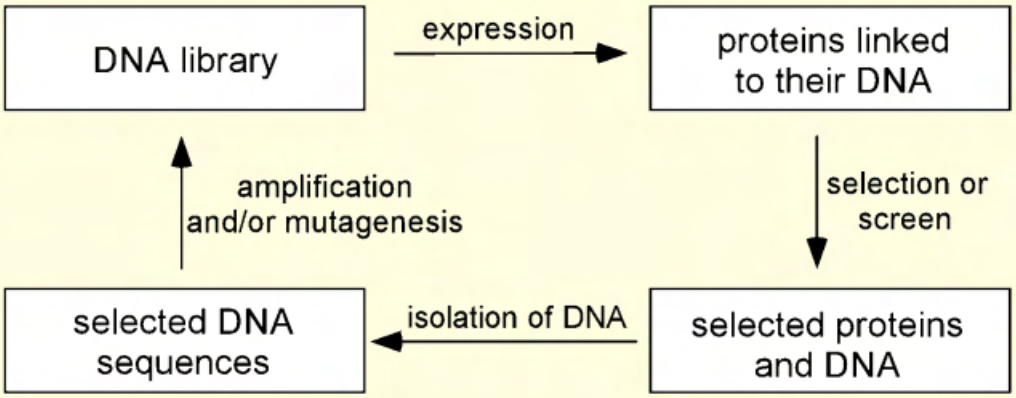
We thank the National Science Foundation (Grants CHE-9900072 and DMR-9600138) and the Office of Naval Research for support of this work. We also thank Stefan Kraemer and Ryan Fuier for critical reading of this work.

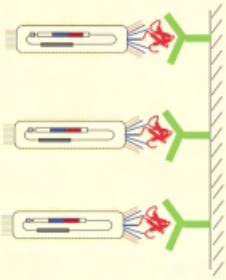
Received: December 18, 2001 [A 507]

[1] J. S. C. Kilby, *ChemPhysChem* **2001**, *2*, 482.
[2] G. E. Moore, *Electronics* **1965**, *38*, 114.
[3] G. E. Moore in *Digest of the 1975 International Electron Devices Meeting*, IEEE, New York, **1975**, p. 1113.

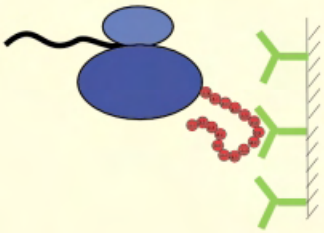
[4] *The International Technology Roadmap for Semiconductors—2000 Update* (http://public.itrs.net/).
[5] K. Deguchi, T. Haga, *C. R. Acad. Sci. Ser. IV:Phys. Astrophys.* **2000**, *1*, 829.
[6] G. F. Cardinale, C. C. Henderson, J. E. M. Goldsmith, P. J. S. Mangat, J. Cobb, S. D. Hector, *J. Vac. Sci. Technol. B* **1999**, *17*, 2970.
[7] D. A. Muller, T. Sorsch, S. Moccio, F. H. Baumann, K. Evans-Lutterodt, G. Timp, *Nature* **1999**, *399*, 758.
[8] G. Ghibaudo, R. Clerc, E. Vincent, S. Bruyere, J. L. Autran, *C. R. Acad. Sci. Ser. IV*: *Phys. Astrophys.* **2000**, *1*, 911.
[9] S. Chiras, D. R. Clarke, *J. Appl. Phys.* **2000**, *88*, 6302.
[10] D. Edelstein, J. Heidenreich, R. Goldblatt, W. Cote, C. Uzoh, N. Lustig, P. Roper, T. McDevitt, W. Motsiff, A. Simon, J. Dukovic, R. Wachnik, H. Rathore, R. Schulz, L. Su, S. Luce, J. Slattery, *Tech. Dig. Int. Electron Devices Meet.* **1997**, 773.
[11] D. J. Kim, Y. B. Jung, M. B. Lee, Y. H. Lee, J. H. Lee, *Thin Solid Films* **2000**, *372*, 276.
[12] S. J. Martin, J. P. Godschalx, M. E. Mills, E. O. Shaffer, P. H. Townsend, *Adv. Mater.* **2000**, *12*, 1769.
[13] Review: D. GoldhaberGordon, M. S. Montemerlo, J. C. Love, G. J. Opiteck, *Proc. IEEE* **1997**, *85*, 521.
[14] Review: C. Joachim, J. K. Gimzewski, A. Aviram, *Nature* **2000**, *408*, 541.
[15] Richard Feynman gave this talk entitled "There's Plenty of Room at the Bottom" on December 29th, 1959, at the annual meeting of the American Physical Society at the California Institute of Technology.
[16] A similar definition was used recently, see: http://www.darpa.mil/DSO/solicitations/00/Baa00–39/cbd.htm and http://www.darpa.mil/MTO/mole/.
[17] T. A. Jung, R. R. Schlittler, J. K. Gimzewski, H. Tang, C. Joachim, *Science* **1996**, *271*, 181.
[18] A. Aviram, M. A. Ratner, *Chem. Phys. Lett.* **1974**, *29*, 277.
[19] A. Aviram, C. Joachim, M. Pomerantz, *Chem. Phys. Lett.* **1988**, *146*, 490.
[20] A. Aviram, *Chem. Phys. Lett.* **1989**, *162*, 416.
[21] M. Pomerantz, A. Aviram, R. A. McCorkle, L. Li, A. G. Schrott, *Science* **1992**, *255*, 1115.
[22] A. S. Martin, J. R. Sambles, G. J. Ashwell, *Phys. Rev. Lett.* **1993**, *70*, 218.
[23] R. M. Metzger, B. Chen, U. Höpfner, M. V. Lakshmikantham, D. Vuillaume, T. Kawai, X. L. Wu, H. Tachibana, T. V. Hughes, H. Sakurai, J. W. Baldwin, C. Hosch, M. P. Cava, L. Brehmer, G. J. Ashwell, *J. Am. Chem. Soc.* **1997**, *119*, 10455.
[24] A. Broo, M. C. Zerner, *Chem. Phys.* **1995**, *196*, 423.
[25] A. Aviram, *J. Am. Chem. Soc.* **1988**, *110*, 5687.
[26] K. Müllen, G. Wegner, *Electronic Materials: The Oligomer Approach*, Wiley-VCH, Weinheim, **1998**.
[27] R. Dembinski, T. Bartik, B. Bartik, M. Jaeger, J. A. Gladysz, *J. Am. Chem. Soc.* **2000**, *122*, 810.
[28] M. J. Crossley, P. L. Burn, *J. Chem. Soc. Chem. Commun.* **1991**, 1569.
[29] M. J. Crossley, P. L. Burn, *J. Chem. Soc. Chem. Commun.* **1987**, 39.
[30] J. R. Reimers, L. E. Hall, M. J. Crossley, N. S. Hush, *J. Phys. Chem. A* **1999**, *103*, 4385.
[31] D. L. Pearson, J. M. Tour, *J. Org. Chem.* **1997**, *62*, 1376.
[32] L. Jones, J. S. Schumm, J. M. Tour, *J. Org. Chem.* **1997**, *62*, 1388.
[33] M. T. Cygan, T. D. Dunbar, J. J. Arnold, L. A. Bumm, N. F. Shedlock, T. P. Burgin, L. Jones II, D. L. Allara, J. M. Tour, P. S. Weiss, *J. Am. Chem. Soc.* **1998**, *120*, 2721.
[34] L. A. Bumm, J. J. Arnold, M. T. Cygan, T. D. Dunbar, T. P. Burgin, L. Jones, D. L. Allara, J. M. Tour, P. S. Weiss, *Science* **1996**, *271*, 1705.
[35] M. S. Doescher, J. M. Tour, A. M. Rawlett, M. L. Myrick, *J. Phys. Chem. B* **2001**, *105*, 105.
[36] A. Ulman, *An Introduction to Ultrathin Organic Films from Langmuir-Blodgett to Self-Assembly*, Academic Press, New York, **1991**, p. 278.
[37] V. Balzani, *Electron Transfer in Chemistry*, Wiley-VCH, Weinheim, **2001**.
[38] K. Slowinski, H. K. Y. Fong, M. Majda, *J. Am. Chem. Soc.* **1999**, *121*, 7257.
[39] K. Slowinski, R. V. Chamberlain, C. J. Miller, M. Majda, *J. Am. Chem. Soc.* **1997**, *119*, 11910.
[40] R. E. Holmlin, R. Haag, M. L. Chabinyc, R. F. Ismagilov, A. E. Cohen, A. Terfort, M. A. Rampi, G. M. Whitesides, *J. Am. Chem. Soc.* **2001**, *123*, 5075.
[41] M. A. Rampi, O. J. A. Schueller, G. M. Whitesides, *Appl. Phys. Lett.* **1998**, *72*, 1781.
[42] R. E. Holmlin, R. F. Ismagilov, R. Haag, V. Mujica, M. A. Ratner, M. A. Rampi, G. M. Whitesides, *Angew. Chem.* **2001**, *113*, 2378; *Angew. Chem. Int. Ed.* **2001**, *40*, 2316.
[43] D. J. Wold, C. D. Frisbie, *J. Am. Chem. Soc.* **2000**, *122*, 2970.
[44] W. B. Davis, W. A. Svec, M. A. Ratner, M. R. Wasielewski, *Nature* **1998**, *396*, 60.
[45] S. N. Yaliraki, M. Kemp, M. A. Ratner, *J. Am. Chem. Soc.* **1999**, *121*, 3428.
[46] H. D. Sikes, J. F. Smalley, S. P. Dudek, A. R. Cook, M. D. Newton, C. E. D. Chidsey, S. W. Feldberg, *Science* **2001**, *291*, 1519.
[47] D. E. Khoshtariya, T. D. Dolidze, L. D. Zusman, D. H. Waldeck, *J. Phys. Chem. A* **2001**, *105*, 1818.
[48] W. B. Davis, M. A. Ratner, M. R. Wasielewski, *J. Am. Chem. Soc.* **2001**, *123*, 7877.
[49] D. Segal, A. Nitzan, W. B. Davis, M. R. Wasielewski, M. A. Ratner, *J. Phys. Chem. B* **2000**, *104*, 3817.
[50] B. Giese, *Acc. Chem. Res.* **2000**, *33*, 631.
[51] M. W. Grinstaff, *Angew. Chem.* **1999**, *111*, 3845; *Angew. Chem. Int. Ed.* **1999**, *38*, 3629.
[52] Y. A. Berlin, A. L. Burin, M. A. Ratner, *J. Am. Chem. Soc.* **2001**, *123*, 260.
[53] Y. A. Berlin, A. L. Burin, M. A. Ratner, *J. Phys. Chem. A* **2000**, *104*, 443.
[54] F. D. Lewis, X. Y. Liu, J. Q. Liu, S. E. Miller, R. T. Hayes, M. R. Wasielewski, *Nature* **2000**, *406*, 51.
[55] A. Thess, R. Lee, P. Nikolaev, H. J. Dai, P. Petit, J. Robert, C. H. Xu, Y. H. Lee, S. G. Kim, A. G. Rinzler, D. T. Colbert, G. E. Scuseria, D. Tomanek, J. E. Fischer, R. E. Smalley, *Science* **1996**, *273*, 483.
[56] C. Journet, W. K. Maser, P. Bernier, A. Loiseau, M. L. de la Chapelle, S. Lefrant, P. Deniard, R. Lee, J. E. Fischer, *Nature* **1997**, *388*, 756.
[57] M. S. Dresselhaus, G. Dresselhaus, P. C. Eklund, *Science of Fullerenes and Carbon Nanotubes*, Academic Press, San Diego, **1996**.
[58] M. S. Dresselhaus, G. Dresselhaus, P. Avouris, *Carbon Nanotubes: Synthesis, Structure, Properties, and Applications*, Springer, Berlin, **2001**.
[59] J. W. G. Wildoer, L. C. Venema, A. G. Rinzler, R. E. Smalley, C. Dekker, *Nature* **1998**, *391*, 59.
[60] T. W. Odom, J. L. Huang, P. Kim, C. M. Lieber, *Nature* **1998**, *391*, 62.
[61] A. Bachtold, M. Henny, C. Tarrier, C. Strunk, C. Schonenberger, J. P. Salvetat, J. M. Bonard, L. Forro, *Appl. Phys. Lett.* **1998**, *73*, 274.
[62] P. J. de Pablo, C. Gómez-Navarro, A. Gil, J. Colchero, M. T. Martinez, A. M. Benito, W. K. Maser, J. Gómez-Herrero, A. M. Baró, *Appl. Phys. Lett.* **2001**, *79*, 2979.
[63] P. J. de Pablo, M. T. Martinez, J. Colchero, J. Gómez-Herrero, W. K. Maser, A. M. de Benito, E. Munoz, A. M. Baró, *Mater. Sci. Eng. C* **2001**, *15*, 149.
[64] T. Hanrath, B. A. Korgel, *J. Am. Chem. Soc.* **2002**, *124*, 1424.
[65] Y. Y. Wu, R. Fan, P. D. Yang, *Nano Lett.* **2002**, *2*, 83.
[66] Z. W. Pan, Z. R. Dai, C. Ma, Z. L. Wang, *J. Am. Chem. Soc.* **2002**, *124*, 1817.
[67] J. C. Johnson, H. Q. Yan, R. D. Schaller, L. H. Haber, R. J. Saykally, P. D. Yang, *J. Phys. Chem. B* **2001**, *105*, 11387.
[68] H. Kind, H. Q. Yan, B. Messer, M. Law, P. D. Yang, *Adv. Mater.* **2002**, *14*, 158.
[69] J. F. Wang, M. S. Gudiksen, X. F. Duan, Y. Cui, C. M. Lieber, *Science* **2001**, *293*, 1455.
[70] M. H. Huang, S. Mao, H. Feick, H. Q. Yan, Y. Y. Wu, H. Kind, E. Weber, R. Russo, P. D. Yang, *Science* **2001**, *292*, 1897.
[71] F. Favier, E. C. Walter, M. P. Zach, T. Benter, R. M. Penner, *Science* **2001**, *293*, 2227.
[72] Y. Cui, Q. Q. Wei, H. K. Park, C. M. Lieber, *Science* **2001**, *293*, 1289.
[73] Y. Cui, C. M. Lieber, *Science* **2001**, *291*, 851.
[74] X. F. Duan, Y. Huang, Y. Cui, J. F. Wang, C. M. Lieber, *Nature* **2001**, *409*, 66.
[75] Y. Huang, X. F. Duan, Y. Cui, L. J. Lauhon, K. H. Kim, C. M. Lieber, *Science* **2001**, *294*, 1313.
[76] B. Messer, J. H. Song, P. D. Yang, *J. Am. Chem. Soc.* **2000**, *122*, 10232.

[77] C. M. Lieber, *Nano Lett.* **2002**, *2*, 81.
[78] M. S. Gudiksen, L. J. Lauhon, J. Wang, D. C. Smith, C. M. Lieber, *Nature* **2002**, *415*, 617.
[79] T. Rueckes, K. Kim, E. Joselevich, G. Y. Tseng, C. L. Cheung, C. M. Lieber, *Science* **2000**, *289*, 94.
[80] Y. K. Kwon, D. Tomanek, S. Iijima, *Phys. Rev. Lett.* **1999**, *82*, 1470.
[81] G. Binnig, M. Despont, U. Drechsler, W. Häberle, M. Lutwyche, P. Vettiger, H. J. Mamin, B. W. Chui, T. W. Kenny, *Appl. Phys. Lett.* **1999**, *74*, 1329.
[82] M. I. Lutwyche, M. Despont, U. Drechsler, U. Dürig, W. Häberle, H. Rothuizen, R. Stutz, R. Widmer, G. K. Binnig, P. Vettiger, *Appl. Phys. Lett.* **2000**, *77*, 3299.
[83] P. Vettiger, M. Despont, U. Drechsler, U. Dürig, W. Häberle, M. I. Lutwyche, H. E. Rothuizen, R. Stutz, R. Widmer, G. K. Binnig, *IBM J. Res. Dev.* **2000**, *44*, 323.
[84] K. M. Roth, N. Dontha, R. B. Dabke, D. T. Gryko, C. Clausen, J. S. Lindsey, D. F. Bocian, W. G. Kuhr, *J. Vac. Sci. Technol. B* **2000**, *18*, 2359.
[85] B. L. Feringa, *Molecular Switches*, Wiley-VCH, Weinheim, **2001**.
[86] S. J. Tans, A. R. M. Verschueren, C. Dekker, *Nature* **1998**, *393*, 49.
[87] T. Sato, H. Ahmed, D. Brown, B. F. G. Johnson, *J. Appl. Phys.* **1997**, *82*, 696.
[88] R. P. Andres, T. Bein, M. Dorogi, S. Feng, J. I. Henderson, C. P. Kubiak, W. Mahoney, R. G. Osifchin, R. Reifenberger, *Science* **1996**, *272*, 1323.
[89] R. P. Andres, S. Datta, M. Dorogi, J. Gomez, J. I. Henderson, D. B. Janes, V. R. Kolagunta, C. P. Kubiak, W. Mahoney, R. F. Osifchin, R. Reifenberger, M. P. Samanta, W. Tian, *J. Vac. Sci. Technol. A* **1996**, *14*, 1178.
[90] Y. Wada, *Pure Appl. Chem.* **1999**, *71*, 2055.
[91] Y. Wada, *J. Vac. Sci. Technol. A* **1999**, *17*, 1399.
[92] C. Joachim, J. K. Gimzewski, *Chem. Phys. Lett.* **1997**, *265*, 353.
[93] C. Joachim, J. K. Gimzewski, R. R. Schlittler, C. Chavy, *Phys. Rev. Lett.* **1995**, *74*, 2102.
[94] F. Moresco, G. Meyer, K. H. Rieder, H. Tang, A. Gourdon, C. Joachim, *Phys. Rev. Lett.* **2001**, *86*, 672.
[95] Y. Wada, T. Uda, M. Lutwyche, S. Kondo, S. Heike, *J. Appl. Phys.* **1993**, *74*, 7321.
[96] D. M. Eigler, C. P. Lutz, W. E. Rudge, *Nature* **1991**, *352*, 600.
[97] R. A. Bissell, E. Cordova, A. E. Kaifer, J. F. Stoddart, *Nature* **1994**, *369*, 133.
[98] A. Credi, V. Balzani, S. J. Langford, J. F. Stoddart, *J. Am. Chem. Soc.* **1997**, *119*, 2679.
[99] C. P. Collier, G. Mattersteig, E. W. Wong, Y. Luo, K. Beverly, J. Sampaio, F. M. Raymo, J. F. Stoddart, J. R. Heath, *Science* **2000**, *289*, 1172.
[100] S. M. Sze, *Physics of Semiconductor Devices*, 2nd Ed., Wiley, New York, **1981**.
[101] R. H. Mathews, J. P. Sage, T. C. L. G. Sollner, S. D. Calawa, C.-L. Chen, L. J. Mahoney, P. A. Maki, K. M. Molvar, *Proc. IEEE* **1999**, *87*, 596.
[102] J. Chen, M. A. Reed, A. M. Rawlett, J. M. Tour, *Science* **1999**, *286*, 1550.
[103] J. Chen, W. Wang, M. A. Reed, A. M. Rawlett, D. W. Price, J. M. Tour, *Appl. Phys. Lett.* **2000**, *77*, 1224.
[104] J. M. Seminario, A. G. Zacarias, J. M. Tour, *J. Am. Chem. Soc.* **2000**, *122*, 3015.
[105] A. W. Ghosh, F. Zahid, S. Datta, R. R. Birge, *Chem. Phys.* **2002**, *281*, 225.
[106] Y. Q. Xue, S. Datta, S. Hong, R. Reifenberger, J. I. Henderson, C. P. Kubiak, *Phys. Rev. B* **1999**, *59*, R7852.
[107] Y. Karzazi, J. Cornil, J. L. Brédas, *J. Am. Chem. Soc.* **2001**, *123*, 10076.
[108] C. B. Gorman, R. L. Carroll, R. R. Fuierer, *Langmuir* **2001**, *17*, 6923.
[109] J. Berg, S. Bengtsson, P. Lundgren, *Solid-State Electron.* **2000**, *44*, 2247.
[110] S. Creager, C. J. Yu, C. Bamdad, S. O'Connor, T. MacLean, E. Lam, Y. Chong, G. T. Olsen, J. Y. Luo, M. Gozin, J. F. Kayyem, *J. Am. Chem. Soc.* **1999**, *121*, 1059.
[111] J. R. Reimers, T. X. Lu, M. J. Crossley, N. S. Hush, *Nanotechnology* **1996**, *7*, 424.
[112] C. Joachim, J. P. Launay, S. Woitellier, *Chem. Phys.* **1990**, *147*, 131.
[113] K. Weber, L. Hockett, S. Creager, *J. Phys. Chem. B* **1997**, *101*, 8286.
[114] P. G.. Collins, M. S. Arnold, P. Avouris, *Science* **2001**, *292*, 706.
[115] Since the submission of this review, two significant papers that address this issue have appeared. a) J. Park, A. N. Pasupathy, J. I. Goldsmith, C. Chang, Y. Aish, J. R. Petta, M. Rinkoski, J. P. Sethna, H. D. Abruña, P. L. McEuen, D. C. Ralph, *Nature* **2002**, *417*, 722; b) W. Liang, M. P. Shores, M. Bockrath, J. R. Long, H. Park, *Nature* **2002**, *417*, 725.

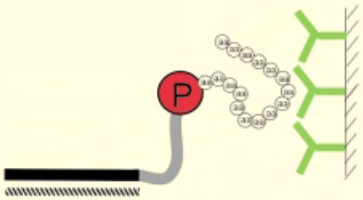




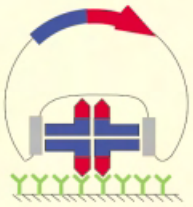
phage display



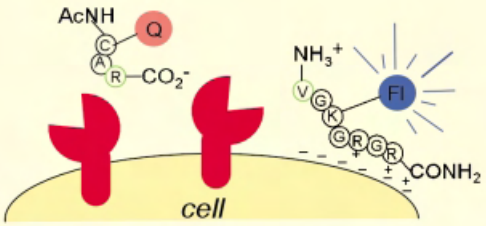
ribosome display



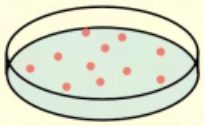
mRNA–peptide fusion



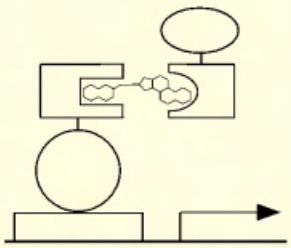
plasmid display



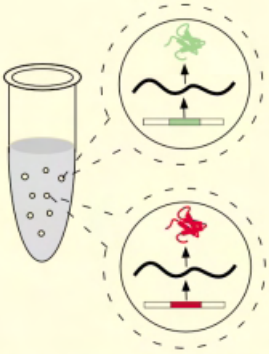
cell-surface display



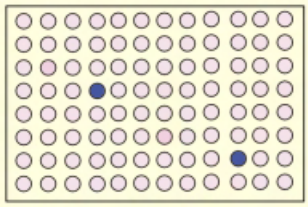
genetics



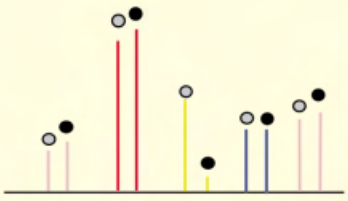
n-hybrid systems



in vitro compartmentalization



spatial address



mass spectrometry

ANGEWANDTE CHEMIE
© WILEY-VCH

Screening and Selection Methods for Large-Scale Analysis of Protein Function

Hening Lin and Virginia W. Cornish*

High-throughput assays hold tremendous promise for protein engineering and proteomics. With powerful assays it should be possible to evolve, for example, a stereoselective esterase for the chemical synthesis or a site-specific endonuclease for biomedical research. Entire cDNA libraries, which encode all of the proteins expressed in a given organism or cell line, should simply be passed through a battery of biochemical assays to determine the function of each individual protein. Herein we look at the types of assays that have been developed and how close we are to our goals of engineering proteins with new activities as well as rapidly assigning function to the thousands of proteins that make up each genome.

Keywords: directed evolution · high-throughput screening · protein engineering · proteomics · selection

1. Introduction

High-throughput assays are beginning to show promise for the evolution of proteins with new properties. Because of the complexity of protein function, it has proven difficult to engineer proteins with new specificities, let alone new functions, simply by introducing directed mutations in the active site of the proteins. Thus, attention has turned to generating millions of mutants simultaneously and then testing these mutants for the desired activity. Advances in molecular biology have made it fairly straightforward to generate the protein variants at the DNA level. Because the manipulations are at the DNA level, the same methods can be used to generate the proteins, no matter what the protein fold or desired function is. This is in contrast to small molecule libraries in which new chemistry has to be developed for each new scaffold. It has proven more difficult, however, to design high-throughput assays that allow millions of proteins to be tested at once. Thus, in this Review we have chosen to focus on advances made during the last two decades in high-throughput assays for protein function.

In addition to applications in protein engineering, high-throughput assays for protein function have long been used for enzymology and drug discovery. More recently, high-throughput assays have proved critical to proteomics. The ability to generate and compare the activity of millions of protein variants not only allows us to engineer proteins with new properties, but also provides a powerful new tool for understanding protein structure and function. The pharmaceutical industry, of course, has relied on high-throughput assays for decades to identify small molecules that inhibit protein function. More recently, with the completion of several genome sequencing projects, we are left with the challenge of figuring out what these proteins do. The genome sequencing project is of limited use if we still have to determine protein function one at a time. Whereas some classes of proteins can be identified based on sequence homology, high-throughput assays still are needed to deconvolute the substrate specificities of these proteins. High-throughput assays are essential for determining the activity of the large percentage of all proteins whose functions are not known.

To develop high-throughput assays for protein function, there are two challenges. First, because DNA is much easier to amplify and sequence than proteins, methods are needed for tagging each protein with its unique DNA sequence (Figure 1). Just like a tag is used to encode each member of a small

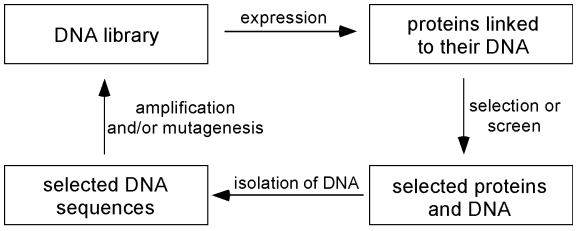


Figure 1. General strategy for large-scale analysis of protein function.

[*] Prof. Dr. V. W. Cornish, H. Lin
Department of Chemistry, Columbia University
New York, NY 10027 (USA)
Fax: (+1) 212-932-1289
E-mail: vc114@columbia.edu

 © 2002 WILEY-VCH Verlag GmbH & Co. KGaA, Weinheim 1433-7851/02/4123-4403 $ 20.00+.50/0

Table 1. The link between genotype and phenotype in different assay methods

Entry	Method	Genotype–phenotype link	Assay (selection or screening) method
1	Phage display	Phage particle	Binding to affinity matrix
2	Ribosome display	Ribosome complex	Binding to affinity matrix
3	mRNA peptide fusion	Peptide–mRNA fusion	Binding to affinity matrix
4	Peptide on plasmid	Peptide–plasmid complex	Binding to affinity matrix
5	Cell surface display	Cell	Fluorescence-activated cell sorting (FACS)
6	In vitro compartmentalization	Water-in-oil droplet	Polymerase chain reaction (PCR)
7	Genetic assay	Cell	Complementation, colormetric assay
8	Microtiter plates and protein chips	Spatial address	Radiometric, UV/Vis absorption, or fluorescence assay

molecule library, the DNA will serve as a tag for the protein sequence. DNA is an ideal tag for protein libraries because DNA naturally serves as the code for protein synthesis in vivo. Second, a high-throughput assay is needed that is compatible with this connection between the protein and the DNA (Figure 1).

Most of the advances in high-throughput assays in the last two decades have been in the first area—designing methods for tagging each protein with its unique DNA sequence. Several refined formats are now well developed. In approaches such as phage display, it is literally a physical linkage between the protein and the DNA. For cell-based assays the linkage is cellular compartmentalization because the protein is only made if a piece of DNA that encodes the protein is present in the cell. For microtiter plate assays, the protein and DNA are given a common "spatial address". Put more simply, the protein in column F, row 11 is encoded by the DNA on a second plate in column F, row 11. Although several methods for tagging protein libraries with their DNA sequence are now available, there may be advantages to completely new approaches. For example, it is interesting to think about the possibilities with methods such as mass spectrometry that might eliminate the need for a DNA tag.

A method to tag a protein with its DNA sequence, however, is only the first step. The actual assays still have to be developed (Table 1). Throughout this paper, "selection" is used to refer to methods in which only proteins with the desired function are carried through, "screening" refers to methods in which all the proteins must be examined, and "assay" is a general term that encompasses both selections and screens. Several methods, such as ribosome display, lend themselves naturally to binding assays. The protein–DNA complex is passed over an affinity matrix, and proteins that bind to the matrix are then eluted with a concentrated salt



V. W. Cornish



H. Lin

Virginia W. Cornish was born in Louisville, KY in 1969. She completed her undergraduate studies at Columbia University. As an undergraduate, Virginia carried out research in Professor Ronald Breslow's laboratory aimed at identifying the receptor for a new class of anticancer compounds being developed in the laboratory. She graduated from Columbia summa cum laude with a B.A. in Biochemistry in 1991. She then moved west to do research with Professor Peter Schultz in the Chemistry Department at the University of California, Berkeley. In Professor Schultz's laboratory she helped develop a new method for incorporating synthetic amino acids into proteins by using the protein biosynthetic machinery. At Berkeley she was a National Science Foundation Predoctoral Fellow and a recipient of fellowships from the American Chemical Society Division of Organic Chemistry and the Howard Hughes Medical Institute. In 1996, she became an NSF Postdoctoral Fellow in the Biology Department at M.I.T. under the guidance of Professor Bob Sauer. At M.I.T. she initiated an independent project which is the basis of her research at Columbia. Virginia joined the Columbia faculty in 1999. Her group uses a combination of chemistry and molecular genetics to develop a cell-based assay for screening large collections of molecules simultaneously based on function. She is the recipient of a Beckman Young Investigator Award, a Burroughs-Wellcome Fund New Investigator Award in the Toxological Sciences, a Camille and Henry Dreyfus New Faculty Award, and a National Science Foundation Career Award.

Hening Lin was born in Tsingdao, China in 1975. He completed his undergraduate study at Tsinghua University in Beijing, China and received his B.A. in Chemistry in 1998. He then went to Columbia University and joined the research group of Virginia W. Cornish. He is one of V.W.C.'s first students and is now a fifth-year graduate student, working on the development of a cell-based assay for screening large collections of molecules simultaneously based on function. He is the Arun Guthikonda Memorial Fellow of 2001.

solution or a solution of the ligand. The same assay can be used, regardless of the particular protein–molecule interaction. Enzymatic turnover is more of a challenge. For the most part, researchers have focused on reactions in which the chemistry provides an intrinsic read-out—when the product is fluorescent, the substrate is a peptide or the product is an essential metabolite. With recent success in this area, attention has turned to the design of assays that are reaction-independent and compatible with a broad range of chemical reactions.

In this Review, rather than focus on a particular method, we have tried to compare and contrast these different methods and to ask which methods are best suited to which problems. For high-throughput assays, the key question, of course, is one of numbers. For studies of protein function or to test all the proteins in a given cell line, we know what these numbers are and the problem is clear. For example, *Sacchromyces cerevisiae* encodes approximately 6000 different proteins, and the human genome compromises about 30000 proteins. It is more difficult to evaluate the number of tests required for the evolution of proteins with new properties, because the question is tied to the answer. We do not know how many variants need to be tested to change enzyme specificity or to create an enzyme that catalyzes new reactions. It is worth reemphasizing that even for a small, monomeric protein, the potential diversity is staggering. Given that 32 DNA codons, half of the genetic code, are sufficient to encode all 20 amino acids found in proteins, to test all possible combinations of all 20 amino acids at every position in a 200-residue protein represents a library of 32^{200} variants. If we consider the necessity of insertions and deletions, the complexity of the problem increases. Although, interestingly, if all 20 amino acids at each position in a 200-residue protein are tested independently of one another, the library size is only 32×200. As a point of reference, 1 mg of plasmid DNA, a tractable amount of DNA to prepare routinely on a large scale, represents about 10^{14} plasmid DNA molecules. Thus, if the DNA is the limiting reagent, approximately 10^{12} positions can be randomized independently of one another, but only nine positions can be randomized if the positions are all varied simultaneously. A few methods are beginning to approach the limit at which the DNA is the limiting reagent, but for the most part other steps in the process limit the numbers. For each method for tagging a protein with its DNA sequence, we look at the steps that limit the numbers, what the numbers are, and what the possibilities are for improving the limiting steps. We are only now beginning to have a sense of how many residues must be varied and whether or not these variations can be made independently of one another to change protein specificity; we do not yet have a feel for this problem when the function of the protein is changed. The examples in this Review are presented with the aim of addressing the question of what numbers have been needed to answer different questions.

In addition to the numbers, we focus on the generality of these methods and the technical ease with which they can be carried out. There are two issues with respect to generality: First, is the method compatible with a broad range of proteins with different structures? Small, monomeric, cytosolic proteins tend to be easy to handle and can be displayed readily in a variety of formats. Oligomeric, membrane-bound, and more complex proteins are often difficult to express outside the cell. For protein engineering this is less of an issue because one can just work with a protein that is easy to handle. To test all the proteins expressed in a given cell line, however, one must be able to display a variety of different types of proteins. The other issue of generality is in the chemistry and the assay. Ideally one wants methods that are compatible with a broad range of molecular interactions and reactions. By considering the applications carried out with different methods, we hope to show which methods are better suited to binding assays and which to assays for enzyme catalysis, and for which methods one can develop assays that are reaction-independent. Finally, as with any chemical technique, the technical ease with which a method can be used often will dictate its utility. Ideally, methods should be accessible to laboratories that do not specialize in the methods themselves. By presenting selected examples in detail we hope to draw out issues such as whether or not specialized equipment is needed to display the proteins or carry out the assay, what the frequency of false positive results is and how easy they are to eliminate with a secondary assay, and finally how straightforward it is to amplify the DNA at the end of the assay for further rounds of mutagenesis or for sequencing.

This Review is organized around the method used to tag the protein with its DNA sequence. We have divided these methods into those based on a physical linkage, compartmentalization, or spatial separation. A brief overview of new approaches is presented at the end of each section. For each method, we describe how the method works, key technical improvements, and selected applications. The applications have been chosen to address the questions of the numbers, generality, and technical ease. There have been impressive technical improvements and achievements in each of these areas, which we cannot even begin to do justice in this Review, and so references are given at the beginning of each section for more detailed reviews in each area.

2. Physical Linkage Method

Perhaps the most straightforward way to tag a protein with its DNA sequence is simply to create a physical link between each protein and the DNA that encodes it. This link can be direct (as in the case of mRNA display or peptide on plasmid) or indirect (phage and cell-surface display). A variety of approaches have been developed to create this physical link. These strategies lend themselves naturally to assays based on binding, and there have been several impressive applications in the engineering of proteins with new specificities. Recently, several groups have reported variations that allow them to measure catalytic activities. The library sizes obtained by using these methods are closest to the DNA limit of 10^{14} different molecules. The technical issues to be considered in these methods are the stability of the physical linkage and whether it is compatible with a wide range of proteins.

2.1. Phage Display

Phage display is one of the first methods introduced for physically linking a protein with its DNA sequence. Not surprisingly, some of the most exciting advances have been made with this technique, which has been reviewed extensively.[1–4] The phage particle provides the physical connection between each protein and its unique DNA sequence. The M13 phage particles commonly used in phage display consist of a single-stranded DNA molecule (the phage genome), which is surrounded by thousands of copies of the phage coat proteins (Figure 2A). These coat proteins are encoded by the

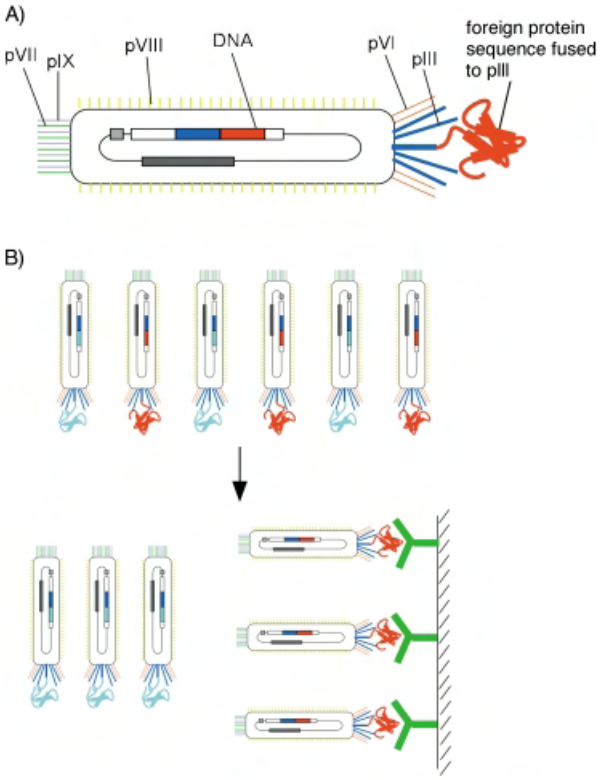


Figure 2. A) The structure of the M13 filamentous phage used in phage display. A phage particle consists of a single stranded DNA molecule surrounded by several coat proteins—pVIII, the major coat protein, pVII and pIX on one end, and pIII and pVI on the other end. A foreign protein sequence can be fused to any of the coat proteins. Shown here is a protein (in red) fused to the N-terminus of pIII (in blue). B) Enrichment of phage by affinity purification (panning).

single-stranded DNA genome that they encapsulate. In phage display, the DNA that encodes the protein of interest is fused to one of the coat protein genes such that the DNA sequence is part of the phage genome and the protein is expressed on the phage surface as a fusion with the coat protein. The coat proteins include thousands of copies of pVIII (the major coat protein), five copies of pIII and pVI at one end of the phage particle, and five copies of pVII and pIX at the other end (Figure 2A). In 1985, Smith introduced the idea of using phage particles to enrich protein libraries by using affinity chromatography to purify the phage particles that express foreign peptide sequences, EcoRI endonuclease fragments in this example, on their surface.[5] EcoRI endonuclease fragments were inserted into coat protein pIII by cloning the EcoRI endonuclease gene fragments in frame with the pIII gene in the phage genome. These modified phage were shown to retain their viability and infectivity. Further, preincubation with anti-EcoRI antibodies significantly reduced infectivity. As a whole, this work showed that foreign protein sequences can be displayed on the phage surface in an immunologically accessible form. Finally, anti-EcoRI antibodies were adsorbed on a polystyrene petri dish and were used to purify selectively phage that display the EcoRI endonuclease fragments from a background of wild-type phage.

2.1.1. Technical Considerations

Phage display libraries are limited in size by the transformation efficiency of bacteria. In a typical phage display experiment, a phagemid DNA library is first constructed in vitro, and then transformed into competent *Escherichia coli* (*E. coli*) cells. Assuming that 10 μg of DNA (10^{12} DNA molecules) is transferred into 200 μL of competent cells (10^{11} cells), by using electroporation, 10^{10} cells can be obtained, each of which contains a unique DNA molecule. In practice, libraries with approximately 10^8 elements are usually prepared. Recently, Sblattero and Bradbury used recombination in bacteria to produce a phage scFv library of 3×10^{11}.[6] In theory, the electroporation can be optimized with 1 mg of DNA and 20 mL of competent cells to give a library of 10^{12} members.[7] In the transformants, proteins will be expressed from the phagemid, and phage particles will assemble if the fusion protein has no effect on this process. Phage particles are then harvested from the transfected bacteria and selected for proteins with specific binding properties by passing them through an affinity matrix in a process called "panning". Non-binding phage will be washed away, and binding phage can then be eluted with a high salt or low pH solution or a solution of the ligand (Figure 2B). The selected phage can be used to infect bacteria, amplified and subjected to further rounds of panning with more stringent selection conditions. Finally, the selected clones will be analyzed by sequencing and in vitro binding assays.

Since the initial report by Smith, there have been several important technical improvements to phage display. Co-infection with helper phage has been used to control the valency of display.[8] Besides pIII, other coat proteins, including pVIII,[9] pVII, and pIX,[10] have also been used to control the valency, orientation, or allow multiple components to be displayed on the phage surface. A particularly clever derivation, selectively infective phage (SIP)[11, 12] takes advantage of the modular structure of coat protein pIII, which consists of three domains: N1 (68 amino acids), N2 (132 amino acids), and CT (149 amino acids) (Figure 3A). N1 is required for *E. coli* infection. N2 specifically recognizes the F-pilus and helps to improve infectivity but is not essential. The CT domain forms part of the coat and is required for phage morphogenesis. Duenas and Borrebaeck were the first to demonstrate this approach:[11] In their initial report, anti-hen-egg white lysozyme (HEL) antibody fragments were displayed on the phage surface as a fusion to pIII proteins that lack N1. These phage were not infective since they lacked the

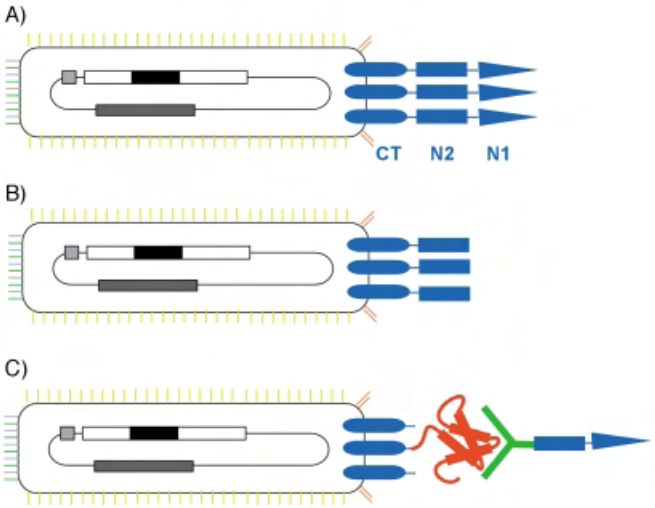


Figure 3. Selectively infective phage. A) In wild-type phage, coat protein pIII consist of three domains: the N-terminal domains N1 and N2 and the C-terminal domain CT. B) Phage particles that lack N1 are not infective; phage particles that lack N1 and N2 (not shown) are also not infective. C) The infectivity can be restored if a protein fused to CT can interact with a protein fused to N1 – N2.

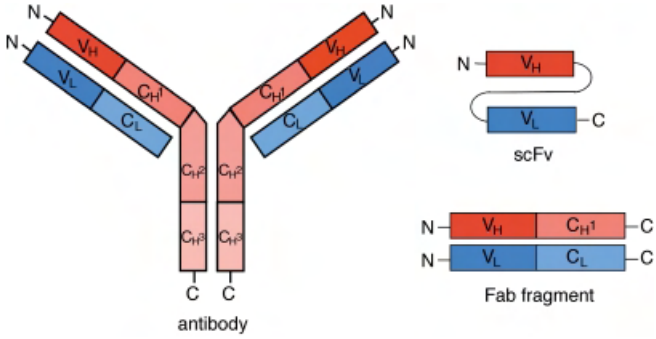


Figure 4. Antibody fragments displayed on phage. An antibody consists of two polypeptide chains, a light (L) chain and a heavy (H) chain. The subunit composition is L_2H_2. Each chain has a variable region (V_L, V_H) and a constant region (C_L, C_{H1}, C_{H2}, C_{H3}). The light chain and the heavy chain are connected to each other by disulfide bonds, and the two heavy chains are also connected by disulfide bonds. Antibodies can be displayed on phage as an scFv (single chain Fv fragment) where the heavy chain variable domain (V_H) is fused to the light chain variable domain (V_L), or as a Fab fragment where the light chain ($V_L - C_L$) and the N-terminal half of the heavy chain ($V_H - C_{H1}$) are displayed as a heterodimer.

N1 domain (Figure 3B). But when these phage were assembled in *E. coli* cells that express an HEL – N1 fusion protein, the binding interaction between the anti-HEL antibody fragment and HEL restored pIII function and phage infectivity (Figure 3C). Thus, phage that display the anti-HEL antibody were enriched 10^5-fold when used to infect bacteria. SIP has two significant advantages over traditional phage display. First, because it circumvents the affinity-panning step, it can be carried out more rapidly than conventional phage display. Second, in theory, it overcomes a significant technical limitation of phage display—the inability of many proteins to be expressed as fusions with pIII on the phage surface.

2.1.2. Protein – Protein Interactions

Short peptide sequences were among the first "proteins" to be displayed on phage. Phage-displayed peptide libraries have been used to search for optimal epitope sequences,[13] peptide ligands,[14] enzyme inhibitors,[15] and even to create peptides that can discriminate semiconductor monolayers with subtle differences in structure.[16] Phage peptide libraries are now commercially available. Phage display has been used most extensively in the field of antibody engineering in the hope that it could replace time-consuming hybridoma technology.[17, 18] A major hurdle was the successful display of antibodies on the phage surface (the different antibody fragments employed are shown in Figure 4). It was first shown in 1990 that the heavy and light chain variable domains of an antibody can be displayed as a single chain Fv fragment on the surface of fd phage.[19] Soon after, phage display of Fab fragments was also reported.[20, 21] Once this hurdle was overcome, many successful applications were reported. Different phage antibody libraries, including immunized, nonimmunized, and synthetic libraries, have been used to isolate new antibodies and improve the affinity of existing antibodies for a given antigen. Catalytic antibodies have even been selected by using phage display.[22–24]

Phage display is clearly well suited to applications built around a common protein fold, such as antibodies and peptides. It is less clear, however, how well the technique will work with problems such as assigning function to proteins expressed in a cDNA library with thousands of different proteins. Shanmugavelu et al. recently reported the isolation of a novel protein that binds to juvenile hormone esterase (JHE) from an insect tissue cDNA library by using phage display.[25] Juvenile hormone (JH) acts in conjunction with ecdysteroids to control gene expression in insects. JHE is critical to insect development since it degrades JH. The authors were interested in identifying proteins that interact with JHE and might regulate its activity. In this application, the library size was not an issue since the cDNA library only includes approximately 10^4 proteins. The challenge instead was to express the thousands of different proteins included in the insect tissue cDNA library. Because of the presence of a high percentage of stop codons in the cDNA library, the cDNA library could not be expressed as an N-terminal fusion to pIII or pVIII. Instead, the cDNAs were expressed as C-terminal fusions to the Fos leucine zipper domain, whereas the Jun leucine zipper domain was fused to the N-terminus of pIII. The heterodimerization of Fos and Jun effectively displayed proteins on the phage surface. Four rounds of panning were used to enrich proteins that bound to JHE immobilized on one well of a polystyrene 24-well microtiter plate. In the first three rounds of the selection, acidic buffer was used to elute bound phage. In the fourth round, purified JHE was used. The eluted phage was then used to infect *E. coli*. Phage particles isolated from individual colonies were assayed for JHE-binding activity in a 96-well plate format by using an enzyme-linked immunosorbent assay. Notably, multiple rounds of panning were required, not to test more proteins, but because the signal-to-noise in the panning step is quite low. Nine positive clones were sequenced, and one of

them was found to encode a protein, P29, which had not been characterized previously.

2.1.3. Protein – DNA Interactions

After the antibodies, DNA-binding proteins were one of the first classes of proteins whose binding specificity was engineered by using phage display.[26, 27] Pioneering work in this field was carried out by Rebar and Pabo.[28] They displayed the three zinc fingers of the Zif268 protein on the surface of filamentous phage as a pIII fusion. The four amino acids in the first zinc finger were chosen for randomization because they had been shown to be most important for DNA recognition, which resulted in a 10^6-membered library that was readily covered by a pool of 10^{10} phage particles. These phage fingers were then selected against three biotinylated duplex DNA sequences immobilized on streptavidin-coated microtiter wells. The DNA sequences (GACC, GCAC, or CCTG) were different from the wild-type DNA sequence (GCGC) in the region recognized by the first finger. Zinc fingers that could bind to the modified DNA sequences with K_D values in the low picomolar range and with 10- to 100-fold preference for the modified over the wild-type DNA sequence were identified for the GACC and GCAC, but not the CCTG, sequences. Again, five rounds of selection were required because of the high background of nonspecific phage particles carried through in the panning step (Figure 13B). Interestingly, the authors note that during the course of panning with the Zif library, retention efficiencies began at 0.01% and rose to ca. 1% in cases where the selection was successful. These and other similar results show that for a natural protein, whose mode of recognition is well understood, targeted mutations to produce libraries on the order of 10^6 are sufficient to modify protein specificity.

2.1.4. Protein-Small Molecule Interactions

The next question, then, is how many more variants need to be tested to go beyond changes in specificity to the de novo evolution of recognition. While antibodies, of course, have been routinely engineered to bind different molecules, it is generally assumed that the antibody scaffold is uniquely malleable. There have been several successes with protein-protein interactions,[29] but a major breakthrough recently was proof that a lipocalin protein, the bilin-binding protein (BBP) from the butterfly *Pieris brassicae*, could be evolved to bind small molecules de novo.[30, 31] The lipocalins have an eight-stranded antiparallel β-barrel structure, and the four loops on one end of the barrel form the entrance to the binding pocket. The sixteen residues that directly contact bilin, which lie along these four loops, were completely randomized. Since only 10^8 individual transformants were obtained, only a very small portion of all possible 10^{24} lipocalin variants was tested. The mutant BBPs were fused to pIII and monovalently displayed on phage. Selection was achieved by panning the phage fusion library against BSA or RNase conjugated fluorescein. After six rounds of panning to increase the percentage of specific phage eluted from the fluorescein conjugate, mutant BBPs with 10^{-7} M affinity and high specificity for fluorescein were isolated.[30] Similarly, mutant BBPs with high affinity and specificity for the steroid digoxigenin were obtained.[31] Further experiments are needed to test whether the lipocalin fold, like the IgG fold, is a privileged scaffold, or in fact libraries on the order of 10^8 are sufficient to engineer molecular recognition de novo.

2.1.5. Enzyme Catalysis

While phage display seems naturally suited to selections based on binding, a more difficult challenge is to adapt this powerful technique to catalysis. Catalytic antibodies that catalyze a broad range of transformations have been generated by evolving catalytic antibodies that bind to transition state analogues. In theory, it should not be difficult to adapt this method to phage display since phage display selection is naturally based on binding. For example, catalytic antibody 17E8, obtained by immunization with a norleucine phosphate transition state analogue, catalyzes the hydrolysis of amino acid phenyl esters.[32] Baca et al.[23] grafted the antigen binding loop of 17E8 onto a human antibody framework to improve its recombinant expression efficiency and displayed it on pIII as a Fab fragment. Site directed mutagenesis was used to generate humanized 17E8 (hu17E8) libraries. Five to six rounds of panning were used to select for mutants that bind to the norleucine phosphate transition state analogue. A mutant with two-fold increased catalytic activity was identified. However, this mutant bound the transition state analogue less tightly than the original hu17E8, while all the mutants isolated with increased binding affinity gave lower catalytic efficiency. This example illustrates that binding to a transition state analogue and catalytic activity are not the same. Surprisingly, despite widespread use in the catalytic antibody field, there are few reports of using transition state analogues to generate catalysts with phage display. Attention seems to have turned to direct selections for catalytic activity.

Suicide substrates have also been used in the affinity panning step to select for enzymes based on catalytic activity. Soumillion[33] and coworkers synthesized a β-lactamase suicide inhibitor linked to biotin through a disulfide bond linker. β-Lactamase was fused to pIII with a proteolytic cleavage site in between them. Phage particles displaying active and inactive β-lactamases were incubated with the suicide inhibitor, after which the active enzymes were labeled with biotin. Panning through streptavidin beads then selectively enriched phage particles displaying active enzymes. A similar approach that selects enzymes by linking phage infectivity to catalytic activity was also reported.[34] While suicide substrates have been used to isolate the wild type enzyme, it is not clear that they can be used to discriminate enzymes with different catalytic efficiencies.

What is really wanted is a direct assay for catalytic activity, ideally one that is reaction independent. Recently several related methods,[35–39] where the basis for selection is the formation or cleavage of a bond from solid support or differential recognition of substrate and product, have been reported. In one such example, a non-specific nuclease, staphylococcal nuclease (SNase), was enriched from a phage library that contained unrelated proteins.[35] As shown in

Figure 5, both SNase and the DNA substrate were displayed simultaneously on the phage surface. SNase, an enzyme that hydrolyzes RNA and DNA, was displayed as a pIII fusion using a phage vector. A Fos–Jun leusine zipper heterodimer

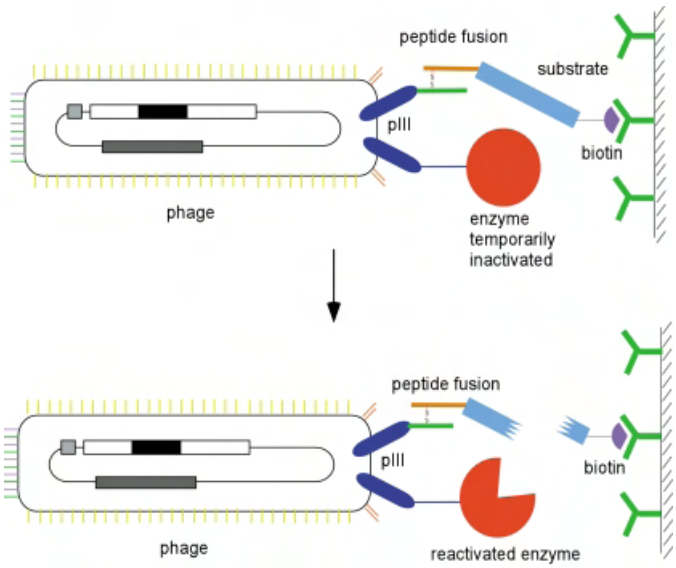


Figure 5. A selection for enzymatic activity by using phage display.[35] The substrate, an oligonucleotide, was attached to the phage particle using a peptide heterodimer. The pIII–peptide fusion was provided by a helper phage. The enzyme, staphylococcal nuclease (SNase), was displayed as a pIII fusion by using a phagemid vector. SNase was first displayed in an inactive form by leaving out Ca^{2+} (top). Then the phage were incubated with the complex of peptide substrate and biotin and absorbed to streptavidin beads. After the unbound phage were washed away, the SNase was reactivated by adding back Ca^{2+}. Phage that displayed active SNase enzymes cleaved the DNA substrate, thus releasing the phage from the solid support (bottom).

was used to display the DNA substrate. Helper phage provide the pIII–Fos fusion, and the biotin–DNA substrate–Jun fusion was prepared using synthetic chemistry. Phage displayed SNase was first displayed in an inactive form by leaving out Ca^{2+} from the buffer, incubated with Jun–substrate–biotin, then absorbed to the strepavidin beads. After the unbound phage were washed away, SNase was activated by adding Ca^{2+} to the buffer. Phage displaying active SNase cleaved the substrate, releasing the phage particle from the solid support. It was shown that phage displaying SNase could be enriched 100-fold after one round of panning from a 1:100 mixture of phage displaying SNase and control phage displaying a Fab fragment. Very recently, this approach was used to convert *Thermus aquaticus* DNA polymerase into an RNA polymerase.[88] The use of the leucine zipper peptides to incorporate the substrate should allow the chemistry to be varied readily. As currently designed, this assay is limited to metal-dependent enzymes in which enzymatic activity can be turned on and off during different steps in the selection procedure. It is not clear that this switch is fast enough to distinguish between enzymes with different levels of catalytic activity.

2.2. Ribosome display and mRNA-peptide fusion

In this method, the linkage between phenotype and genotype is provided by the non-covalent or covalent complex formed between the translated peptide and the mRNA that encodes it, as shown in Figure 6.[40] This method was first

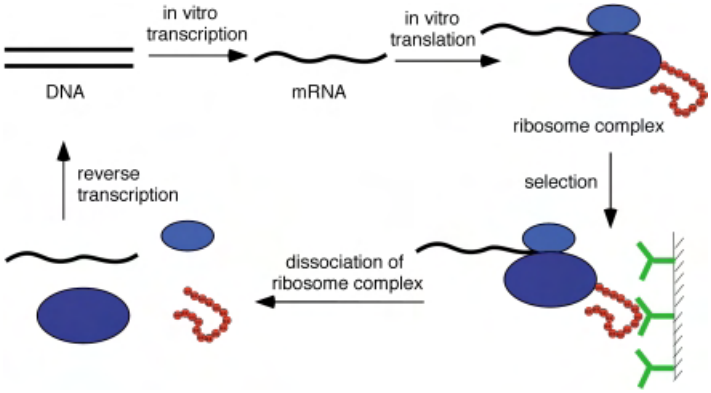


Figure 6. Ribosome display.[41, 42]

demonstrated by Mattheakis et al.[41] in 1994 and then optimized by Hanes and Plückthun.[42] Using an *E. coli* S30 coupled transcription/translation system, Mattheakis et al. in vitro transcribed and translated a library of DNA sequences that encode short peptides. When the translation reaction was stopped by the addition of chloramphenicol, the translated peptide and mRNA were found to remain associated with the ribosome complex. The ribosome complexes were selected based on binding of the peptides to an immobilized antibody. The mRNA was then dissociated from the complex, reverse transcribed to cDNA and amplified, enriching genes encoding peptides that recognized the antibody target. These selected DNA sequences can be subjected to further rounds of transcription/translation and selection (Figure 6).

2.2.1. Technical Considerations

In Mattheakis's experiment,[41] 400 ng DNA (10^{12} molecules) was transcribed to 3×10^{12} mRNA molecules in a 50 μL transcription/translation reaction containing about 3×10^{12} ribosomes (the ribosome concentration is ca. 0.1 μM). At the end of the transcription/translation reaction, about 27% of the mRNA molecules were found to be complexed with the ribosomes. However, the yield of ribosome complex formation is dependent on the length of the transcribed peptide. For whole proteins, even under optimized conditions, the yield is only 0.2%.[42] Thus for short peptides, 1 mg of DNA would give a library size of 10^{15}, but for large proteins only 10^{12}.

A problem with ribosome display is the instability of the ribosome–mRNA–peptide ternary complex. It is difficult to keep the complex intact during the selection steps. A major technical advance was the introduction of a covalent linkage between the peptide and the mRNA.[43, 44] The covalent linkage between the peptide and the mRNA was introduced using puromycin, an antibiotic that mimics the aminoacyl end of tRNA (Figure 7A). As shown in Figure 7B, puromycin was

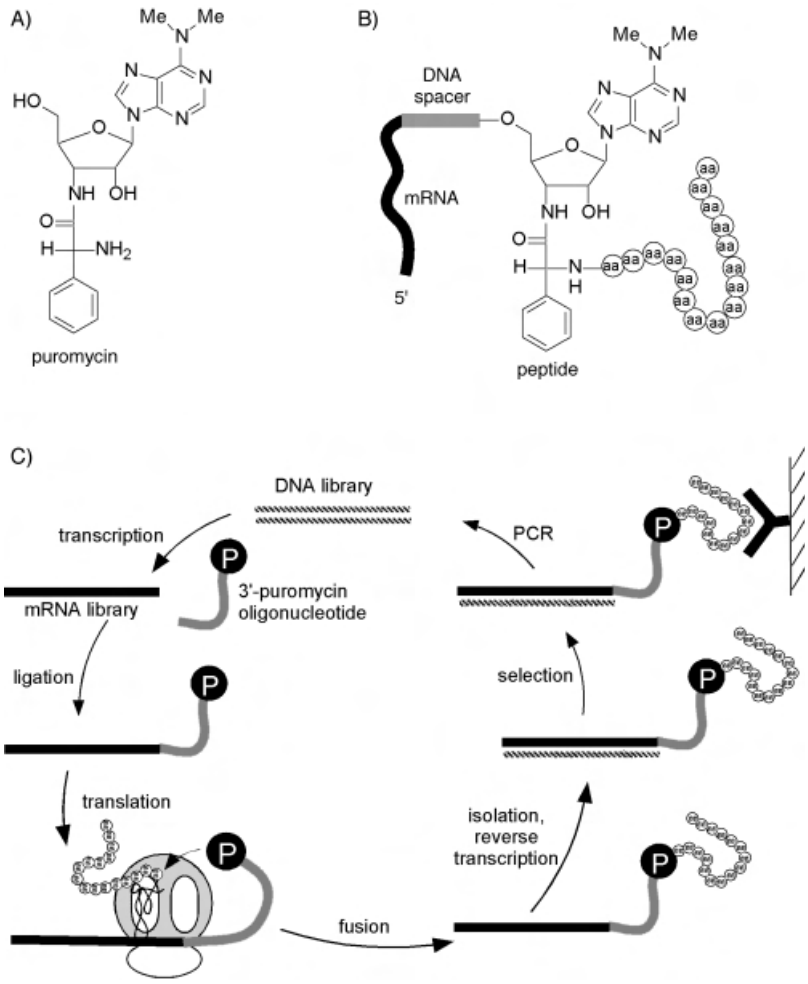


Figure 7. A) Structure of the amino acyl–tRNA analogue puromycin. B) The covalent complex formed between the mRNA and the peptide through puromycin. C) Typical mRNA–peptide fusion experiment procedure. Figure 7C reproduced from reference [46], Copyright (2000), with permission from Elsevier Science.

attached to the 3′ end of mRNA lacking a stop codon via a DNA spacer. When the mRNA was translated in vitro, the ribosome paused at the DNA spacer, allowing the puromycin molecule at the end of the message to enter the ribosome A site and react with the nascent polypeptide. This method is also called mRNA display. Optimized conditions for the puromycin coupling reaction that increase the efficiency with which puromycin adds to the stalled polypeptide recently have been reported.[45, 46]

A typical mRNA display experiment is shown in Figure 7C. A DNA library is first in vitro transcribed to give the mRNA library. Then the total mRNA is ligated to a chemically synthesized 30-bp DNA sequence with puromycin at the 3′ end. An in vitro translation reaction is then carried out for these mRNA-DNA-puromycin hybrid molecules. Covalent complexes between the mRNA and the peptides are formed via puromycin. The complexes are isolated from the reaction mixture, reverse transcribed, and selected against an immobilized antigen or ligand. Selected complexes can then be PCR amplified for sequencing or further rounds of mutation and selection.

The mRNA-peptide fusion method also increases the library size. In the initial paper by Roberts and Szostak[43], 5 picomoles of mRNA molecules were used in a 25 μL translation reaction, and 0.7% of the mRNA were incorporated into mRNA-peptide fusions. Thus the library size was only 2.1×10^{10}. Since this initial paper, the coupling conditions have been optimized and coupling yields as high as 40% for short peptides have been reported.[46] The potential disadvantage to this method is that all steps are carried out in vitro, making it difficult to express membrane proteins or proteins that require post-translational modifications.

2.2.2. Protein-Protein Interactions

As with phage display, the first applications of ribosome display have been in the field of antibody engineering. For example, Hanes et al. evolved picomolar affinity scFvs against insulin from a synthetic antibody library.[47] While there are few reports of using ribosome display for evolving proteins with new specificities or activities, presumably this is simply because this method is relatively new and these types of applications are just yet to be undertaken. In theory, ribosome display should be well suited to the same types of problems as phage display.

Szostak and co-workers recently took advantage of the diversity of mRNA display to isolate high-affinity binding proteins from completely random peptide libraries.[48] They constructed a random peptide library 88 amino acids in length using the optimized puromycin-coupling method.[45, 46] With an estimated library size of 7×10^{12}, only a small percentage of all possible 88-mers were examined. After seven rounds of affinity panning against immobilized streptavidin, peptides with K_Ds for streptavidin as low as 5 nM were isolated. Similarly, nanomolar ATP-binding polypeptides were selected from a random peptide library.[49] As in phage display, multiple rounds of panning are being used not to test more variants, but to enrich the RNA-peptide fusions for true hits because a high percentage of false positives are carried through at each round of panning. These results are surprising and raise the interesting possibility that the evolution of protein structure and function may be a much easier problem than one would assume. Based on the panning percentages in the ATP-binding selection, the authors argue that the frequency of occurrence of functional polypeptides was on the order of 10^{-11} and that these peptides could only have been isolated with ribosome display, which allows libraries on the order of 10^{12} to be tested.

2.3. Peptide on plasmid

In this method, the noncovalent interaction between a DNA-binding protein and the plasmid DNA is used to link the protein to its DNA sequence. The first DNA-binding

protein used for this approach was lac repressor.[50] Lac repressor is encoded by the *lacI* gene and binds very tightly to the specific DNA sequence *lacO*. As shown in Figure 8, a library of 10^8 dodecapeptides was fused to the C-terminus of lac repressor by cloning synthetic oligonucleotides downstream of the *lacI* gene in plasmid pMC5, which also contained tandem *lacO* sequences. Inside a cell, the plasmid directed the synthesis of the lac repressor-dodecapeptide fusions, which subsequently formed tetramers and bound to the lacO sites on the plasmid. After lysing the cells, the peptide-plasmid complexes were selected based on the binding interaction between the peptides and an immobilized antibody.

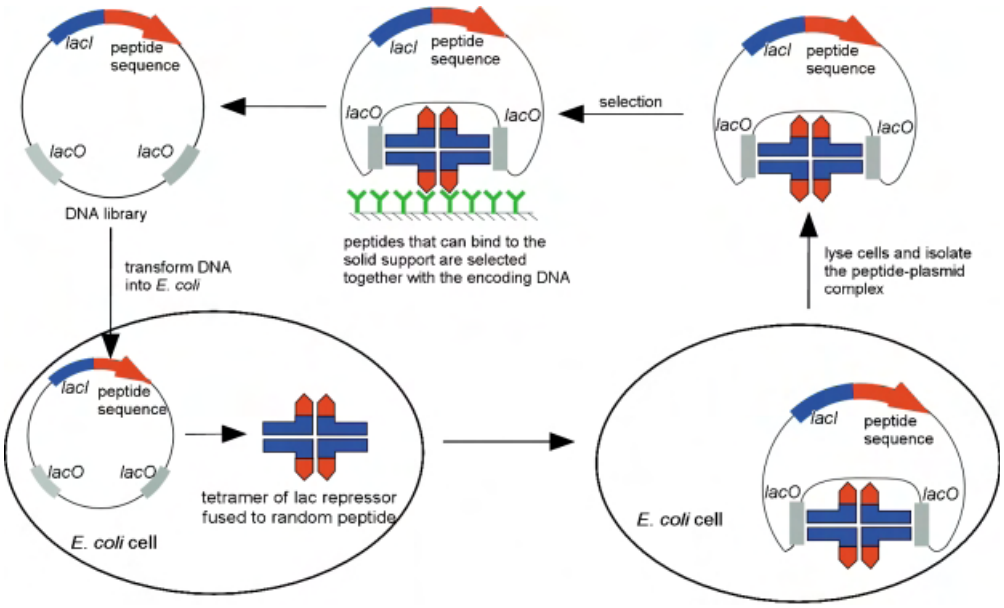


Figure 8. Peptide on plasmid.[50] Random DNA sequences are fused to the *lacI* gene in a plasmid that also contains *lacO* sites. This DNA library is then transformed into *E. coli*. Random peptides (red) fused to lac repressor (blue) are then synthesized and bind to the *lacO* sites on the plasmid as tetramers.

2.3.1 Technical Considerations

In this method, the peptides were displayed in a multivalent format since the lac repressor binds DNA as a tetramer, and each plasmid can bind up to two tetramers. Therefore this method is good for selecting low to moderate affinity binders. In order to make this method suitable to select for high affinity binders, Gates et al.[51] developed a lac repressor "headpiece dimer" as the DNA-binding domain. The headpiece dimer, which presented fewer copies of the peptide library, was shown to be suitable for selecting higher affinity binders, although the DNA binding mechanism of the headpiece dimer was not clear. The library size of this method is similar to phage display because it is also limited by the DNA transformation efficiency of bacteria.

2.3.2. Protein – Protein Interactions

While in theory this method could be used for the same variety of applications as with phage display, to date this method has been used primarily for screening peptide libraries. In 1997 Cwirla et al. reported the successful isolation of a nanomolar peptide agonist for the thrombopoietin receptor.[52] Of interest as a point of comparison, the authors not only used the peptide-on-plasmid method, but also phage display and ribosome display. They first used pVIII phage display and lac repressor, both multivalent display formats, to select for peptides with IC_{50}s ranging from 20 mM to 60 nM. Then they used headpiece dimer and ribosome display, which allow monovalent display, to further enrich for mutant peptides with IC_{50}s ranging from 20 to 60 nM. Finally, the headpiece dimer method was employed to select a high affinity peptide, AF12505, which had an IC_{50} of 2 nM. The dimer of AF12505 showed an IC_{50} of 0.5 nM and was as potent as recombinant human thrombopoietin. Although not clear why to this reviewer, the authors conclude that the peptide-on-plasmid selection is the most effective of all three methods for generating high affinity peptide binders. This application illustrates the importance of being able to control the valency of display. High valency is needed early on to detect low affinity binders, while low valency is needed in the final rounds to discriminate the highest affinity binders.

2.4. Cell Surface Display

Methods for displaying proteins on the surface of living cells have long been available, although these methods were not initially introduced as a means to screen protein libraries.[53] For example, the most common application of bacteria display is the development of live-bacteria-vaccine delivery systems. The principle of this method is relatively simple. A protein, or protein library, is fused to a membrane protein, which serves as an anchor to present the proteins on the cell surface. Selection or screening, normally fluorescence-activated cell sorting (FACS), can then be carried out using the cells displaying the proteins. In bacteria, the most frequently used anchor protein is an Lpp-OmpA hybrid, lipoprotein fused to amino acids 46 – 159 of the outer membrane protein A.[54] More recently, a yeast system has been designed that uses the yeast cell-surface receptor a-agglutinin, which is involved in the yeast mating pathway, as an anchor.[55] Mammalian systems have also been developed.[56]

2.4.1. Protein-Protein Interactions

To date, cell surface display has primarily been used for the display of peptide,[57] antibody,[58] and T cell receptor libraries,[59] although again this method should be compatible with

the same variety of applications as phage display. One of the most impressive examples is a recent report by Boder and coworkers in which they evolved scFvs that bind to fluorescein with femtomolar affinity.[60] The fluorescein binding antibody scFv 4-4-20 was mutagenized using error-prone DNA shuffling and displayed on the yeast surface via a-agglutinin. Cells were incubated with fluorescein-biotin, washed, and then incubated with 5-aminofluorescein competitor. Cells that remained bound to fluorescein-biotin were then labeled with streptavidin-*R*-phycoerythrin and isolated by fluorescence-activated cell sorting (FACS). After three additional rounds of mutagenesis and screening, an scFv with a K_D of 48 fM, a dissociation constant even lower that that for the interaction between biotin and streptavidin, was isolated. Presumably because FACS has a low background, the library can be further mutagenized and screened with FACS, allowing antibodies with increased affinity to be generated.

2.4.2. *Enzyme Catalysis*

Recently, bacterial cell surface display has been used to screen for enzymatic activity. Olsen et al. displayed a mutagenized *E. coli* OmpT protein library on the surface of *E. coli* cells.[61] In this case, no anchor protein was necessary since OmpT itself is a membrane-associated protein. OmpT is a serine protease implicated in microbial pathogenicity and has a strong preference for the basic residues Arg and Lys in the P1 and P1′ subsites. The OmpT library was screened for proteases with modified substrate specificity that would hydrolyze substrates with Arg and Val in the P1 and P1′ subsites. The substrate used, shown in Figure 9, was a peptide derivatized with a fluorophore (Fl) and quenching fluorophore (Q), which acted as an intramolecular fluorescence resonance energy transfer (FRET) partner. The substrate was designed to bear a +3 charge on the Fl side, so that when the peptide was incubated with *E. coli* cells, whose surface is negatively charged, it would bind to the cell surface. Cells displaying mutants of OmpT that were active toward the Arg-Val substrate would cleave the peptide, releasing the quenching fluorophore Q and changing the fluorescence profile of the cells. Thus, cells displaying active enzyme could be isolated by FACS. Using this method, the authors screened 1.9×10^6 cells and isolated 352 successful clones. The 352 hits were further analyzed for protease activity in a 96-well plate assay. The most active OmpT mutant was shown to have a 60-fold improvement in catalytic efficiency for the Arg-Val substrate. This approach is similar to that reported with phage display, except the assay is based on FRET rather than cleavage/formation of a bond to solid support. This approach is general and should be compatible with a broad range of bond formation and cleavage reactions. Presumably the chemistry will be somewhat limited by the reliance on FRET. FRET has a marked distance dependence and is influenced by the orientation of the donor and acceptor molecules. Additionally, to use this method to detect a range of catalytic activities, the ratio of the enzyme molecules to the substrate molecules on the cell surface as well as their diffusion rates must be further characterized.

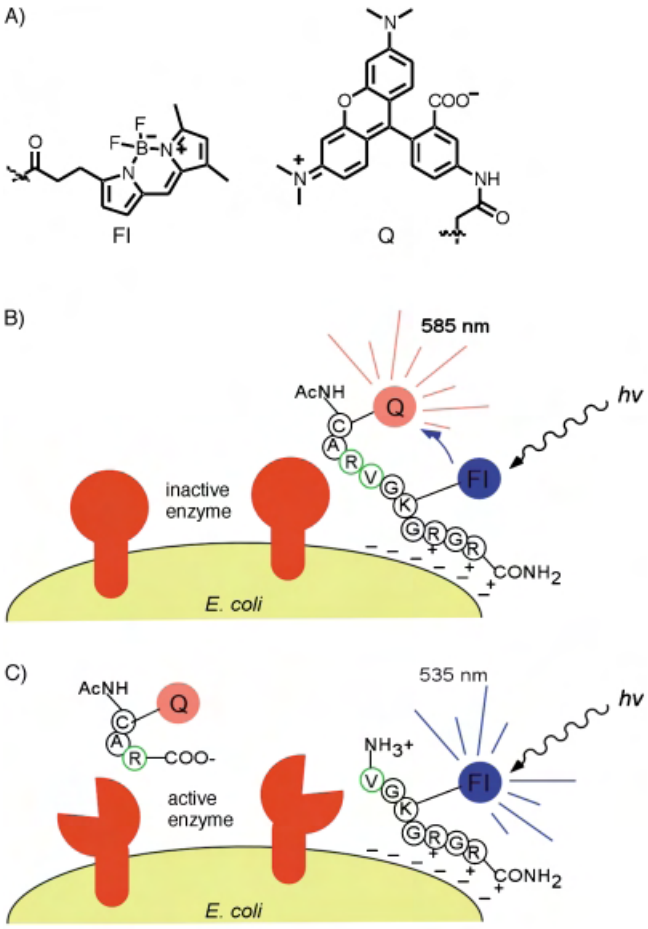


Figure 9. Screening for protease activity by bacteria display.[61] A) Structures of the fluorophore (Fl) and quenching fluorophore (Q) attached to the peptide substrate. B) and C) The enzyme library is displayed on the surface of *E. coli* cells, while the substrate with Fl and Q is attracted to the cell surface through the ionic interactions between the negatively charged cell surface and the positively charged substrate. When an inactive enzyme is displayed, the quenching fluorophore Q efficiently quenches the fluorescence of Fl, which results in fluorescence at 585 nm (B). When an active enzyme is displayed, the enzyme cleaves the substrate, releasing Q from the substrate and resulting in fluorescence at 535 nm (C). By detecting fluorescence of the cells, active enzymes can be isolated.

2.5. Summary

Phage display, as well as newer methods for physically linking a protein to its DNA sequence, provides a robust method for re-engineering the binding specificity of an existing protein scaffold. While the DNA itself limits the number of protein variants that can be tested to ca. 10^{14}, phage display, peptide on plasmid, and cell surface display are all further limited by transformation efficiency. While in theory libraries on the order of 10^{10} can be achieved if the transformations are done with *E. coli*, in practice libraries on the order of 10^8 usually are reported. Ribosome display shows the most promise for reaching the limit where DNA itself is the limiting reagent, and the puromycin coupling method can already easily produce libraries of 10^{12}. Surprisingly these library sizes seem sufficient to modify protein function. Starting with proteins whose mode of action is well under-

stood, libraries on the order of $10^6 - 10^8$ have proven sufficient to generate proteins with new DNA or small molecule specificities. Further work is needed to ensure that these results are general and that engineering proteins with new specificities is in fact a tractable problem. It still remains unclear, however, how many protein variants need to be tested to evolve new function. All of these methods place constraints on the protein being displayed, and these limitations are best documented in the case of phage display. While not a problem for protein engineering, where presumably one would just begin with a well behaved scaffold, more work is needed to establish what percentage of proteins expressed in a given cDNA library are in fact displayed in an active form with these different methods. These methods are naturally inclined toward assays based on molecular recognition, and the same panning procedure can be used no matter what the protein-molecule interaction is. With the exception of peptide on plasmid, the linkage between protein and DNA is quite robust and places few constraints on the panning conditions. It will be a challenge, however, to adapt these methods to detect catalysis. Some clever approaches based on breaking or forming a bond to solid support or FRET recently have been reported. The difficulty will be to use these on/off assays to discriminate enzymes with a range of catalytic efficiencies. While effort must go into the preparation of these libraries, whether it be the phage particles or the in vitro transcription/translation system, the methods seem to be robust and are carried out by many laboratories. There clearly is poor signal to noise in the panning step, and multiple rounds of library amplification and panning are needed to identify true interactions. The fact that multiple panning steps are required makes it impractical to carry out multiple rounds of mutagenesis, limiting the number of protein variants ultimately tested. For most of these methods, the DNA can be amplified for sequencing or further rounds of mutagenesis easily, whether it be infecting bacteria with the phage particle, retransforming plasmid, or growing the cells. The only exception is ribosome display, where the RNA must be reverse transcribed before it can be amplified.

3. Compartmentalization Methods

A related approach to physically linking a protein to its DNA sequence is to restrict each protein and its DNA sequence to a distinct compartment. This compartmentalization is achieved naturally by introducing plasmid DNA encoding the protein into a cell. More recently, water-in-oil emulsions have been introduced as an artificial compartment that in a way is a stripped-down cell. With cell-based assays, the advantage is the ease of molecular biology and genetic techniques, although the library size is limited to the transformation efficiency of the cell. As with mRNA display, water-in-oil emulsions have the potential to reach the limit where DNA is the limiting reagent for library size. Both approaches seem well suited to assays based on enzyme catalysis. Arguably the most advances in evolving enzymes with new properties have been with cell-based assays.

3.1. Cell-Based Assays

Geneticists, essentially, have always been doing high-throughput screening, and much can be learned from the approaches taken in this field. With cell-based assays, the protein is linked to the DNA that encodes it because the DNA directs the synthesis of the protein inside the cell. The cell then provides a compartment that links each protein to its DNA sequence. These assays are powerful because millions of plasmid DNA molecules, each encoding a different protein or protein variant, can be transferred into cells en masse. The statistics of DNA transfer and the use of selectable markers ensure that each cell ends up with a single plasmid encoding a single protein variant. The cells can be physically isolated from one another simply by growing them at an appropriate dilution on solid media. At the end of the experiment, the DNA encoding the protein variant can be readily extracted from the cell for sequencing or further rounds of mutagenesis using standard molecular biology techniques. In a now classic experiment, Beadle and Tatum used genetic analysis in the early 1940s to identify enzymes responsible for the biosynthesis of essential metabolites (Figure 10).[62] They introduced random mutations throughout the chromosomal DNA of the ascomycete *Neuospora crassa* by treating the *Neurospora* with X-rays. Approximately 2000 individual mutated strains were then screened for growth in both rich and minimal medium, where the minimal medium contained only nutrients such as

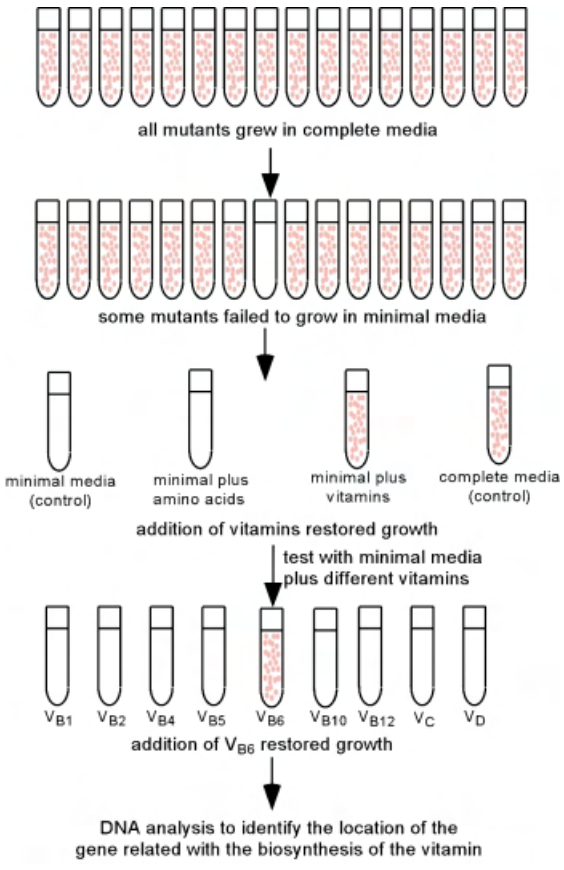


Figure 10. A genetic method to identify genes responsible for the biosynthesis of essential metabolites.[62]

biotin that *Neurospora* cannot make themselves. Three mutant strains were identified that had growth rates indistinguishable from the wild-type strain in rich media, but grew poorly or not at all in minimal medium. By adding back individual metabolites to the minimal media and then measuring the cell growth rates, the three strains were shown to be unable to synthesize vitamin B_6, vitamin B_1, and *p*-aminobenzoic acid, respectively. This basic approach of mutating the DNA encoding the proteins and then assaying for some detectable phenotype such as cell growth is the basis for genetic analysis. Most of the genes whose function is known have been identified through this type of method, and the functions of thousands of proteins have been determined in this manner. The contribution of Beadle and Tatum was to point out that the mutant strains could be screened based on enzymatic activity, as opposed to just cell death. As we discuss in this section, the challenge in fact continues to be developing clever assays that target the activity of interest.

3.1.1. Technical Considerations

Based on advances in molecular biology, a number of original genetic tricks have been developed that increase the ease with which cell-based assays can be carried out. One of the biggest hurdles in genetic analysis is "backing-out" which gene has the mutation of interest. For example, in the experiment by Beadle and Tatum described above, several additional years of experiments were required to determine which genes in the *Neurospora* genome had the mutations that affected cofactor biosynthesis and hence encoded the biosynthetic enzymes. A refined twist, introduced by Holden and co-workers in 1995,[63] is to replace every open reading frame in an organism with a unique 20 bp tag rather than simply mutating the chromosomal DNA. This way the gene responsible for a given mutant phenotype can be assigned rapidly based on its unique 20 bp tag. In the 1950s, Benzer introduced the strategy of complementation, which provided a general solution to this problem.[64] In genetic complementation, a pool of plasmid DNA encoding fragments of wild type chromosomal DNA is introduced into the mutant cell line and then the DNA fragment that complements the mutation is identified based on the recovery of the wild-type phenotype. In the *Neurospora* example above, plasmid DNA that encoded fragments of the wild-type *Neurospora* genome would be introduced into the mutant *Neurospora* deficient in vitamin B_6 biosynthesis. Only mutant *Neurospora* with a copy of the wild type vitamin B_6 biosynthetic gene would be able to grow in the absence of vitamin B_6, allowing the plasmid DNA encoding the vitamin B_6 biosynthetic gene to be distinguished readily. The recent availability of several complete genome sequences further simplifies genetic complementation because the plasmid DNA sequence can be compared to the complete genome sequence. In addition, it has allowed several labs to construct libraries of plasmid DNA not just encoding random fragments of chromosomal DNA, but instead explicitly encoding every open-reading frame (ORF) expressed in a given organism or cell line.[65]

A major limitation to genetic analysis is that it is limited to activities naturally found in the cell that are screenable or selectable. "Two-hybrid" assays provide a way to open these powerful genetic assays up to a wide variety of chemistry. The two-hybrid assay, which was first introduced as a method for testing potential protein-protein interactions in vivo, has now been adapted to detect protein-DNA, protein-RNA and protein-small molecule interactions, and, most recently, even catalytic activity.[66–72] The two-hybrid assay is based on reconstitution of eukaryotic transcriptional activators from dimerization of the DNA-binding (DBD) and transcription activation (AD) domains. As outlined in Figure 11 A, if the two proteins of interest interact, they effectively dimerize the DBD and the AD, recruiting the transcription machinery and activating transcription of a downstream reporter gene. The assay was demonstrated initially using two yeast proteins, the serine-threonine protein kinase SNF1 and the SNF1 activator protein SNF4, known to be physically associated in vivo.[73] SNF1 was fused to the GAL4 DNA-binding domain (DBD), and SNF4 was fused to the GAL4 activation domain (AD). A GAL4 binding sequence was placed upstream of a β-galactosidase reporter gene. Plasmids encoding the protein fusions and the reporter gene were introduced into yeast, and β-galactosidase synthesis levels were quantified using standard biochemical assays. Control experiments established that neither the DBD nor the AD domain on their own nor the individual protein chimeras induced β-galactosidase synthesis above background levels. β-Galactosidase synthesis levels were increased 200-fold when the DBD-SNF1 and SNF4-AD fusion proteins were introduced together. By comparison, the direct DBD-AD fusion protein activated β-galactosidase synthesis levels 4000-fold.

3.1.2. Protein-Protein Interactions

Traditional genetic assays and the yeast two-hybrid assay have primarily been used to identify natural protein-protein interactions. A particularly impressive recent application is the use of automation techniques to identify all possible protein-protein interactions in *S. cerevisiae*.[65] Every open-reading frame encoding a protein—there are ca. 6000 in *S. cerevisiae*—was fused both to the Gal4 DBD and to the Gal4 AD, and the two fusion libraries were screened against one another. The major challenge here is how to transform all combinations of the 6000 DBD and 6000 AD fusions into yeast and then how to assay so many cells. A library of 10^7 is at the limit of the transformation efficiency of yeast and so in theory is achievable. Uetz and Glot and co-workers compared two approaches. One, they explicitly mated haploid MATa cells containing 192 DBD fusions with haploid MATα cells containing the 6000 AD fusions in a spatially addressable format and assayed each well using a *HIS3* growth selection. Two, MATa cells containing the 6000 DBD fusions were mated with MATα cells containing the 6000 AD fusions, and only diploids that survived in a *LEU2* growth selection were arrayed and analyzed individually. Interestingly, there were significantly more "hits" in the spatially addressable format, underscoring the importance of parameterizing new methods for high-throughput screening and the problem of distinguishing false positives and negatives in genetic assays.

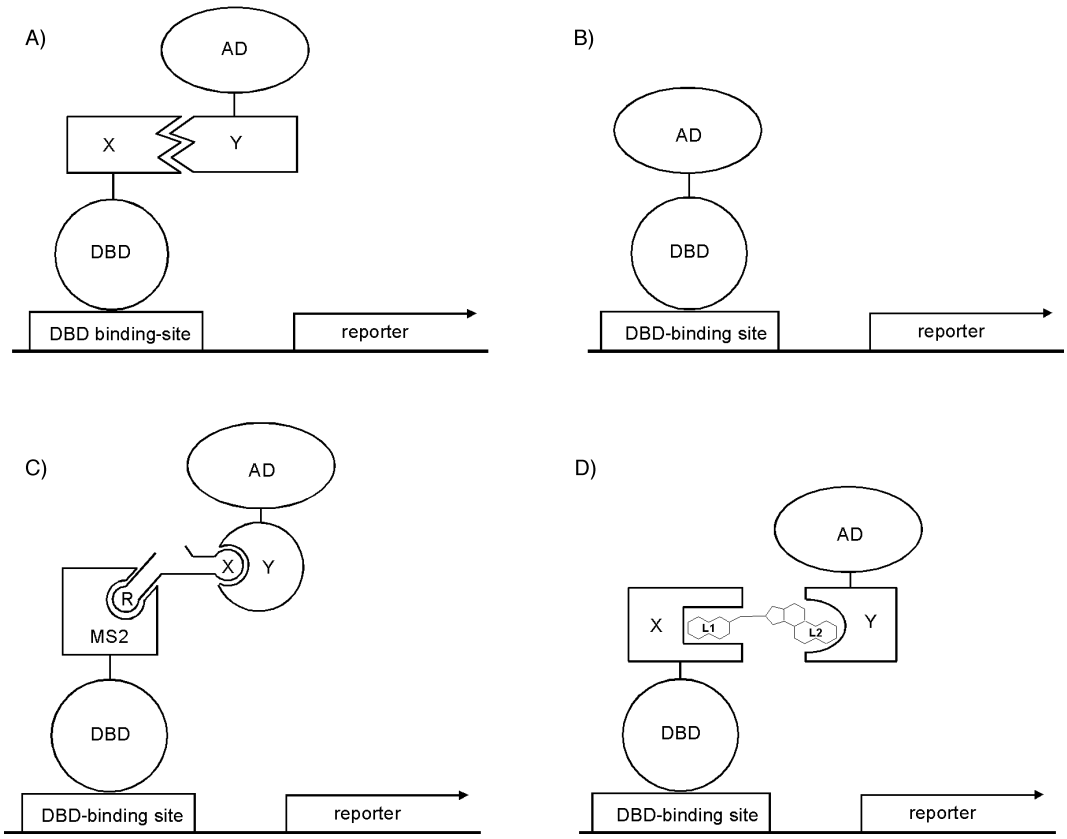


Figure 11. Different yeast *n*-hybrid systems that have been developed to study protein–protein, protein–DNA, protein—RNA, and protein–small molecule interactions. A) In the original version of the yeast two-hybrid system, transcriptional activation of the reporter gene is reconstituted by recruitment of the activation domain (AD) to the promoter region through direct interaction of protein X and Y, since protein X is fused to a DNA-binding domain (DBD) and protein Y is fused to the AD. B) In the one-hybrid assay, the AD is fused directly to the DBD. This assay can be used to assay either DBDs that can bind to a specific DNA sequence or the in vivo binding site for a given DBD. C) The three-hybrid system used to detect RNA-protein interactions has one more component than the yeast two-hybrid system: a hybrid RNA molecule. One half of the hybrid RNA is a known RNA (R) that binds to the MS2 coat protein (MS2) with high affinity and serves as an anchor. The other half is RNA X, whose interaction with protein Y is being tested. D) Another version of the yeast three-hybrid system can be used to detect small molecule–protein interactions. Ligand L1 which interacts with protein X is covalently linked to ligand L2. Thus if L2 interacts with Y, transcriptional activation of the reporter gene will be reconstituted.

While the two-hybrid method has been used primarily to detect natural protein-protein interactions, it should also be well suited to protein evolution. Brent and co-workers[74] demonstrated that the two-hybrid assay could be used to identify peptide aptamers that inhibit cyclin-dependent kinase 2 (Cdk2) from a library of random peptide sequences (Figure 12). The 20 residue peptide library was displayed, not as a simple extension to the AD, but rather in the active site of *E. coli* thioredoxin (TrxA). The TrxA loop library was fused to the B42 AD, and Cdk2 was fused to the LexA DBD. In a single round of assay, 6×10^6 B42-TrxA transformants, a very small percentage of the 10^{27} 20mers possible, were tested for binding to LexA-Cdk2. From this assay, they isolated 66 colonies that activated transcription of both a *LEU2* and a *lacZ* reporter gene. Impressively, these colonies converged on 14 different peptide sequences that bound Cdk2 with high affinity. Using surface plasmon resonance, the peptide aptamers were shown to bind Cdk2 with K_Ds of 30–120 nM (Table 2). In kinase inhibition assays, the peptide aptamers had IC_{50}s for the Cdk2/cyclin E kinase complex of 1–100 nM.

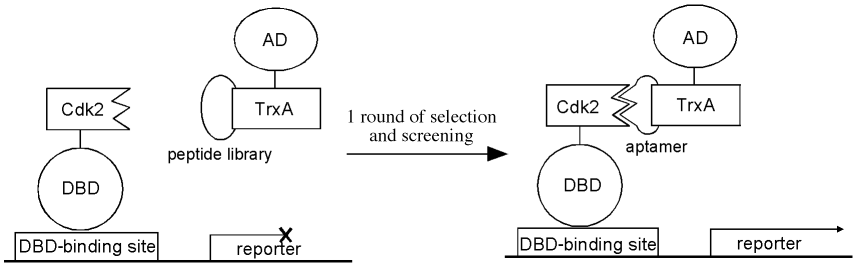


Figure 12. The yeast two-hybrid system can be used to evolve peptides that bind target proteins with high affinities.

What is particularly impressive about this experiment is that nanomolar affinity ligands are being isolated in a single round of selection. As in the phage display applications presented earlier in this Review, this example suggests that libraries on the order of 10^6–10^8 may be sufficient to modify protein specificity. In contrast to phage display, however, only one round of selection is needed to distinguish true high affinity binders. Similar results have been obtained using peptide aptamers in a traditional genetic selection.[75]

Table 2. The sequences and binding affinities of the 14 different aptamers isolated in a yeast two-hybrid assay.[74]

Aptamer	K_D [nM]	Amino Acid Sequence
pep1	ND[a]	ELRHRLGRAL SEDMVRGLAW GPTSHCATVP GRSDLWRVIR FL
pep2	64 ± 16	LVCKSYRLDW EAGALFRSLF
pep3	112 ± 1	YRWQQGVVPS NMASCSFRCQ
pep4	ND	SSFSLWLLMV KSIKRAAWEL GPSSAWNTSG WASLSDFY
pep5	52 ± 3	SVRMRYGIDA FFDLGGLLHG
pep6	ND	RVKLGYSFWA QSLLRCISVG
pep7	ND	QLYAGCYLGV VIASSLSIRV
pep8	38 ± 5	YSFVHHGFFN FRVSWREMLA
pep9	ND	QQRFVFSPSW FTCAGTSDFW GPEPLFDWTR D
pep10	105 ± 10	QVWSLWALGW RWLRRYGWNM
pep11	87 ± 7	WRRMELDAEI RWVKPISPLE
pep12	ND	RPLTGRWVVW GRRHEECGLT
pep13	ND	PVCCMMYGHR TAPHSVFNVD
pep14	ND	WSPELLRAMV AFRWLLERRP

[a] ND: not determined.

3.1.3. Protein-DNA Interactions

Early on, it was realized that, just as the yeast two-hybrid assay could be used to detect protein-protein interactions, transcriptional activators could be used directly, in a "one-hybrid" assay, to detect DNA-protein interactions (Figure 11B). In truth, this type of experiment was done before the one-hybrid assay was conceptualized as such. For example, as early as 1983 a His6 $\rightarrow$Pro Mnt variant was generated that preferentially binds a mutant Mnt operator using a transcription-based selection[76]. More recently, Pabo and coworkers adapted a bacterial two-hybrid assay[77] to evolve zinc finger variants with defined DNA-binding specificities (Figure 13).[78] In this assay, protein-protein interactions are detected based on dimerization of a DNA-binding protein and the α-domain of RNA Polymerase (RNAP) and activation of RNAP-dependent transcription. To create a read-out for protein-DNA interactions, three tandem zinc-fingers were fused to Gal11, and Gal4 (which binds with high affinity to Gal11), was fused to the α-domain of RNAP. In addition, a reporter system was engineered, such that if the zinc fingers bound with high affinity to the desired DNA sequence, they would activate transcription of a *HIS3* reporter gene. As with the peptide aptamers, zinc fingers with new DNA-binding specificities could be isolated from a library of circa 2×10^8 zinc finger variants in a single round of selection. The authors, who have used phage display routinely in the past,[28, 79] note that the ease of selection is in contrast to phage display, where multiple rounds of selection and amplification were required in their lab for the identical evolution experiment (Figure 13, Table 3).

3.1.4. Protein-Small Molecule Interactions

The two-hybrid assay has been extended to protein-small molecule and protein-RNA interactions by adding a bridging small-molecule or RNA to provide a yeast "three-hybrid" system (Figure 11C,D).[80–82] One half of the bridging molecule is used as an anchor and the other half is the molecule of interest. Licitra and Liu built a small-molecule yeast "three-

Table 3. Comparison of the zinc finger sequences (which bind to the target DNA sequence AAA), isolated by using a bacteria two-hybrid method and a phage-display method.[78, 79]

	Bacteria two-hybrid system (1 round of selection)						Phage display (5–8 Rounds of selection)					
	-1	**1**	**2**	**3**	**5**	**6**	**-1**	**1**	**2**	**3**	**5**	**6**
	Q	R	G	N	L	V	Q	R	T	N	I	T
	Q	K	T	N	M	V	Q	Q	H	N	K	L
	Q	K	Y	N	I	L	Q	R	N	N	L	L
	Q	R	Y	N	V	V	Q	A	N	N	R	T
	Q	K	G	N	M	V	Q	K	T	N	L	N
	Q	K	G	N	H	V	Q	H	G	N	V	A
	Q	K	G	N	M	V	Q	K	T	N	L	T
	Q	R	G	N	K	V	Q	K	T	N	D	T
	Q	R	G	N	K	T	Q	K	H	N	Q	V
	Q	L	G	N	M	V	Q	P	G	N	Q	T
	Q	K	G	N	K	V	Q	K	T	N	E	H
	Q	L	G	N	K	V						
Consensus:[a]	**Q**	+	**g**	**N**	_	**v**	**Q**	_	_	**N**	_	_
	N	S	G	A	Y	N	N	S	G	N	H	T
	N	S	G	A	W	N	N	S	G	A	S	N
	N	S	G	A	F	N	N	S	G	A	A	N
	N	S	G	T	H	N	N	S	G	A	T	N
	N	T	G	A	Y	N	N	S	G	A	T	N
Consensus:[a]	**N**	**s**	**G**	**a**	_	**N**	**N**	**S**	**G**	**a**	_	**n**
	G	S	G	A	Y	N	A	T	G	A	H	N

[a] Capital letters indicate that all sequences showed this amino acid; lower case letters indicate a strong preference for this amino acid; "+" represents a preference for a positively charged amino acid; while "_" indicates that no preference could be determined.

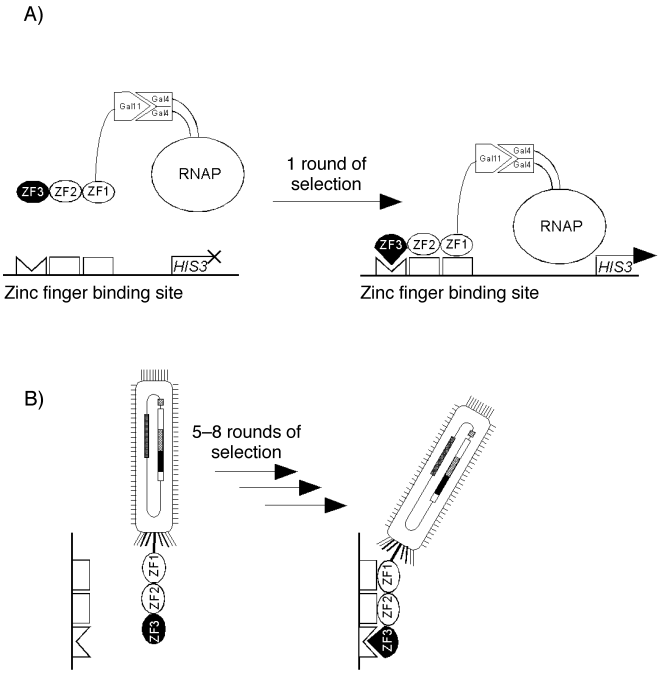


Figure 13. Development of zinc fingers specific for the DNA sequence AAA using a two-hybrid assay[78] and a phage display selection[26, 79]. A) The bacterial RNA Polymerase (RNAP) system was used for the two-hybrid assay. Zinc fingers (ZF) 1, 2, and 3 from the Zif268 protein were fused to the Gal11 protein. The Gal4 protein, which binds Gal11 with high affinity, was fused to the N-terminal domain of the α-subunit of RNAP. A subsite sequence AAA was engineered at the binding site for ZF3, and six residues in ZF3 were randomized. Thus, if ZF3 bound to the AAA site with high affinity, the RNAP complex would be recruited, activating transcription of a *HIS3* reporter gene. Significantly, in just one round of assay, several proteins were identified that bound specifically to the target DNA sequence. These sequences, which fall into two distinct sequence categories, are shown in Table 3. B) A similar experiment was carried out by phage display, in which ZF 1, 2, and 3 from the Zif268 were displayed on the phage surface as a fusion to coat protein pIII.

hybrid" assay that uses the steroid dexamethasone as an anchor and demonstrated that it could be used to find the in vivo target of a drug. As a proof of principle, they showed that FKBP12 could be pulled out from a Jurkat cDNA library using Dex-FK506 as the bridging small molecule. Specifically, Dex-FK506 dimerized a LexA-Glucocorticoid Receptor (GR) fusion protein and a cDNA-B42 AD library. First a *LEU2* growth selection was used to select for proteins that bound to FK506. Then hits were confirmed by comparing the levels of transcription of a *lacZ* reporter gene with and without the Dex-FK506 small molecule. In the three-hybrid assays, the bridging molecule provides a convenient tool for ruling out false positives. The authors noted that while several FKBPs were present in the Jurkat cDNA library, only FKBP12 was identified. FKBP12 is the highest affinity FK506 binding protein and binds FK506 with a K_D of 0.4 nM. Presumably the key to the success of the three-hybrid assays is the anchor. Anchors with high affinity to the DBD-receptor fusion are needed if small molecule and RNA-protein interactions with a range of affinities are to be detected. For example, our lab recently developed methotrexate (Mtx), which binds to dihydrofolate reductase (DHFR) with picomolar affinity, for use in this system.[83]

3.1.5. Enzyme Catalysis

Genetic methods seem to provide particularly powerful screens and selections for enzymatic activity. The trick here is finding an activity that is screenable or selectable. One approach is to choose a reaction where the product is fluorescent. For example, Arnold and co-workers generated P450 variants that use hydrogen peroxide, rather than dioxygen and NADH, as a cofactor using a genetic screen (Figure 14).[84] Briefly, random mutations were introduced throughout the gene encoding cytochrome P450 using error-prone PCR. Naphthalene was used as the substrate in an *E. coli* strain that had been engineered such that any hydroxylated naphthalene products would be oxidatively coupled to produce fluorescent dimers. Cells containing P450 variants with the desired activity could then be identified by fluorescence digital imaging of cells grown on a petri plate containing the naphthalene substrate. Because a screen rather than a selection was used, the experiment was limited to a smaller number of protein variants, about 20000 per plate, than would be the case in a growth selection. In the first round, where 200000 colonies were screened, a large number of clones showed enhanced fluorescence. Three mutants from the group showing the highest fluorescence were character-

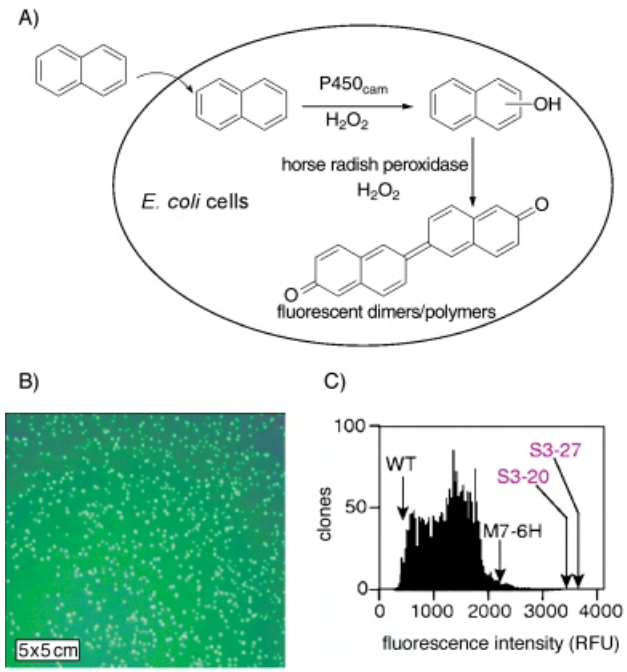


Figure 14. A genetic screen for evolving cytochrome P450 variants that use hydrogen peroxide as a cofactor.[84] A) The screening strategy: The screen is based on the detection of fluorescent products, produced by first hydroxylation of naphthalene catalyzed by $P450_{cam}$ variants and then oxidative coupling catalyzed by horseradish peroxidase. B) Fluorescence digital imaging of *E. coli* cells harboring $P450_{cam}$ variants. Cells with $P450_{cam}$ mutants were grown on plates that contained naphthalene and hydrogen peroxide. Fluorescence digital imaging was then carried out. The cells that contained an active $P450_{cam}$ mutant and therefore displayed higher fluorescence intensities were subsequently analyzed. C) The histogram showing the fluorescence values of ~70000 clones from the second generation of mutants. The fluorescence intensity of the wild-type $P450_{cam}$, the first generation mutant M7–6H, and the second generation mutants S3–20 and S3–27 are indicated. Reproduced from reference [84] with permission from Nature, Copyright (1999), Macmillan Magazines Limited.

ized and found to be about 10-fold more active than wt P450. In a second round, five active mutants were recombined using Staggered extension process (StEP), and the progeny were screened. Several variants were isolated from this step that showed about a 20-fold improvement in activity compared to the wild type enzyme. It is interesting to speculate if the activity might have been improved further if a larger number of mutants could have been tested. Here the problem may have been distinguishing proteins with a small increase in activity from those with a more significant change.

In addition to its utility in genetic analysis, complementation seems a natural choice for evolving proteins with new functions. The idea here is that, rather than testing fragments of the chromosome for complementation of a mutant phenotype, a protein is mutated and "evolved" to complement a given phenotype.[85, 86] A recent example by Yano and co-workers, in which they used this strategy to evolve an aspartate aminotransferase into a branched-chain amino transferase, illustrates the power of this approach.[87] First, they engineered an *E. coli* strain with a knock-out in the wild type branched-chain aminotransferase gene and showed that this strain was not viable unless the growth media was supplemented with Val, Ile, and Leu. The wild type aspartate aminotransferase gene was mutated and recombined using DNA shuffling and then introduced into the *E. coli* selection strain. The authors point out that DNA shuffling, a PCR-based method, could be used both to introduce point mutations and to generate recombined gene products. Five rounds of mutagenesis and selection were carried out. At each round, $10^6 - 10^7$ mutants were examined, and the stringency of the selection could be readily increased by changing the concentration of 2-oxovaline in the growth media, the expression level of the enzyme, or the incubation time. After the final round, a mutant enzyme with 13 point mutations was isolated that had a 10^5-fold increase in k_{cat}/K_M for β-branched amino acids and a 30-fold decrease in k_{cat}/K_M for aspartate. The improvement in k_{cat}/K_M here is impressive and likely reflects the importance of being able to modulate the stringency of a selection—first to detect poor catalysts and finally to demand high catalytic efficiency. The authors also address the question of how hard it is to alter specificity. By testing each of the 13 mutations individually, they showed that in fact only 6 point mutations are required for a 10^5-fold increase in activity toward a new substrate. Interestingly, their results also showed that all 6 mutations are beneficial on their own—raising the possibility that each position in a protein can be randomized independently.

3.2. Liposome-Based Assays

Natural selection, the driving force of Darwinian evolution, happens within the compartmentalization of cells. Tawfik and Griffiths[91] sought to mimic cellular compartmentalization in a simpler in vitro system of water-in-oil emulsions. By adding an in vitro transcription/translation reaction mixture to a stirred suspension of mineral oil that contained surfactants, an emulsion with mean droplet diameter similar to that of bacterial cells was obtained. DNA could then be transcribed and translated within the aqueous compartments of these emulsions. The conditions were controlled so that each water-in-oil droplet contained only a single gene on average. A mixture of two genes, the *M. HaeIII* gene (which encodes DNA methyltransferase HaeIII) and the *folA* gene (which encodes DHFR), were transcribed and translated in the aqueous compartments. Then the emulsion was broken, and the DNA in the aqueous phase was subjected to cleavage by HaeIII endonulease followed by amplification by PCR. Because the DNA methyltransferase methylated HaeIII-cleavage sites in droplets that contained the *M. HaeIII* gene, only the *M. HaeIII* gene would survive the cleavage by HaeIII and be amplified by PCR. After one round of selection, a mixture of *M. HaeIII* to *folA* gene with a ratio of 1:1000 was enriched to a ratio of 1:1 (Figure 15).[91] A similar approach to select Ni-binding proteins was also reported.[92]

Since all of the steps in in vitro compartmentalization are, indeed, carried out in vitro, this method has the potential to reach the limit at which the DNA is the limiting reagent in library size. In the initial paper by Tawfik and Griffiths, 50 μL of an in vitro transcription/translation reaction mixture was added to 950 μL of mineral oil that contained surfactants. The mean diameter of the droplets formed was 2.6 μm. Therefore, there were approximately 10^{10} droplets per mL of emulsion, which means that 10^{10} unique proteins could be tested on this scale. In vitro compartmentalization, as opposed to methods like RNA display, provides a suitable format for the detection

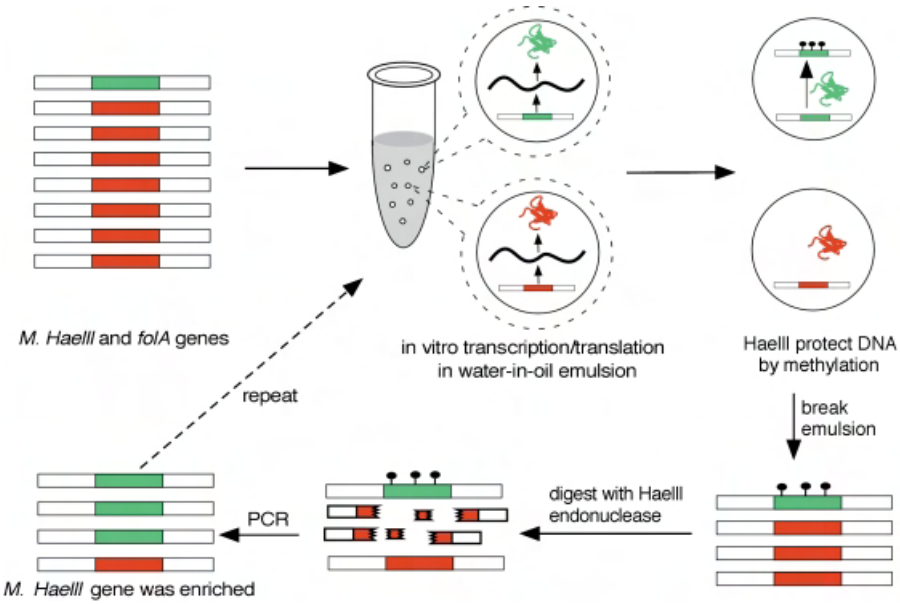


Figure 15. In vitro compartmentalization.[91] A mixture of two genes, *M. HaeIII* and *folA* was transcribed and translated in the aqueous compartments of water-in-oil emulsions. The *M. HaeIII* gene product, the DNA methyltransferase HaeIII, methylated the DNA and prevented cleavage by HaeIII endonulease. After disrupting the emulsion and cleavage by HaeIII endonulease, only M. HaeIII survived and was amplified by PCR. Therefore, the M. HaeIII gene was selectively enriched.

of catalytic reactions with multiple turnovers. Thus far, the assays have been limited to DNA modification or amplification enzymes.[93] The challenge will be to extend this method to chemical reactions that don't involve DNA.

3.3. Summary

Genetic complementation and in vitro compartmentalization seem to provide the most powerful assays for enzyme catalysis. The number of protein variants that can be tested with genetic assays, as with phage display, are limited by DNA transformation efficiencies, whereas in vitro compartmentalization, like RNA display, is limited only by the DNA. Again, 10^6 – 10^8-membered libraries seem to be sufficient to engineer enzymes with new specificities. There are several impressive applications for the modification of enzyme specificities with in vivo complementation. The advantage of carrying out the assays in vivo, particularly for cDNA libraries, is that the protein is expressed in its native environment. While initially applied to the complementation of natural enzyme function, one-, two-, and three-hybrid assays have extended these powerful assays to protein – DNA, protein – protein, protein – RNA, and protein – small molecule interactions. The next challenge is to modify these assays to detect reactions that are not natural to the cell. A recent twist is in vitro compartmentalization. To be general, this method will have to be adapted to detect functions other than DNA chemistry. Genetic assays are technically straightforward because they build from advances in molecular biology. The DNA from positive cells can simply be extracted and carried on to further rounds of mutagenesis or sequencing. The major challenge with genetic assays is discriminating false positive and negative hits. Here the key seems to be a powerful secondary screen. In vitro compartmentalization is similar technically to RNA display. The question is how robust the emulsion technology will prove.

4. Spatially Addressable Methods

Spatially addressable methods link the identity of a peptide or protein to a unique address in space such as a well in a microtiter plate or a patch on a solid support, so that any protein hits can be traced back to their DNA sequence.[94–97] Microtiter or "96-well" plates have long been used for this purpose. More recently, progress has been made in derivatizing a solid support with proteins to give a "protein chip".

4.1. Microtiter-Plate Assay

The use of 96-well plates in biochemical research dates back to the 1950s.[98] Microtiter plates have been routinely used in the enzyme-linked immunosorbent assay (ELISA) since this assay was first introduced in the 1970s.[99] ELISA is a sensitive method that detects antibody binding of an antigen, the substance used to immunize mice, by detecting the catalytic activity of an enzyme fused to the antibody. The antigen is adsorbed to the wells of a 96-well plate and then incubated with the enzyme-linked antibody. After washing away the unbound antibody, bound antibody is detected by monitoring the chromogenic reaction catalyzed by the enzyme. The screening of peptide or protein libraries based on a biochemical function in a microtiter plate is very similar to carrying out an ELISA. Peptide or protein solutions can be dispensed into the wells of a microtiter plate, and suitable biochemical assays can then be carried out in each well of the plate.

4.1.1. Technical Considerations

In microtiter-plate assays, thousands of protein samples, either cell cultures, crude cell extracts or purified proteins, must first be prepared and then transferred to the thousands of wells of the microtiter plates. Then biochemical assays can be carried out in each well of the plate to identify proteins with the desired function. Therefore one of the major challenges is the rapid and cost-effective purification of thousands of proteins. If the desired activity can be assayed using crude cell extracts, this collapses to an engineering problem. The range of activities that could be tested, however, would be greatly increased if methods could be developed for purifying proteins en masse. Martzen et al. solved this problem by purifying the proteins as GST-fusion proteins. Specifically, they purified all 6000 yeast open-reading frames (ORFs) expressed in *S. cerevisiae* by using a GST tag and screened these ORF libraries for several enzymatic activities.[100] The trick was how to construct the GST fusion library. The ORFs were amplified by a two-step PCR procedure so that all the ORFs could be amplified by a universal primer in the second PCR step. This approach allows the ORF library to be cloned readily into a new expression format in the future. In this example, the ORFs were placed under control of an inducible copper promoter. The resulting 6144 yeast strains, each of which contains a yeast ORF fused to GST, were arrayed into 64 96-well plates. First, these yeast strains were grown in 64 pools with each 96-well plate as a pool, and the GST – ORF fusion proteins were purified and assayed in these 64 pools. Then the positive pool was deconvoluted by doing the same assay with each row in the 96-well plate as a pool and each column in the 96-well plate as a pool to identify the GST – ORF that was responsible for the enzyme activity. The proteins were assayed for tRNA ligase, 2′-phosphotransferase, and cyclic phosphodiesterase activity by using thin-layer-chromatography assays with radioactive substrates. In this way, five enzymes were cloned, three of which were not previously known.

It is important to remember that while microtiter plates provide a tool to link the protein to its DNA sequence, they do not provide the screen or selection. The advantage, however, is that many traditional biochemical assays can be readily adapted to this format and automated.[101–103] Popular assays include scintillation proximity assays,[104] UV/Vis absorbance assays, chemiluminescent assays, and fluorescence assays.[105] Fluorescence assays are particularly powerful, and variations such as FRET and fluorescence polarization are quite general. The trend in microtiter plate assays is assay miniaturization, and high-density microtiter plates with 384 or 1536 wells are now standard. Fluorescence assay methods, because of their high sensitivity and analysis speed, are gaining more and more

attention in miniaturized high-throughput assays. For example, Eigen and co-workers[106] applied dual-color fluorescence cross-correlation spectroscopy (FCS) to detect catalytic turnovers by restriction endonucleases. They termed the method RAPID FCS (rapid assay processing by integration of dual-color FCS). A 66-bp oligonucleotide with endonuclease cleavage sites was labeled with the fluorescent dye Cy5 on one end and Rhodamine Green on the other end. Cross-correlation analysis was carried out to give distinguishable cleaved and uncleaved oligonucleotide samples. Analysis time of approximately 1 second was sufficient to give distinguishable cross-correlation values. The sample volume required for the measurement was only a few microliters. The short analysis time and small assay volume make RAPID FCS well suited for high-throughput screening.

4.1.2. Enzyme Catalysis

Microtiter plate assays are particularly well suited to assays for enzyme catalysis because each reaction is kept spatially isolated. Hilvert and co-workers used a 96-well plate assay as a secondary screen in their efforts to engineer a catalytic antibody that catalyzes a rearrangement reaction. They screened thousands of monoclonal antibodies generated against a transition-state analogue and were able to isolate an antibody that catalyzed the decomposition of substituted benzisoxazoles into 2-cyanophenols with a rate acceleration of 10^8.[107] First, monoclonal antibodies were generated against a transition-state analogue by using standard hybridoma technology. Then, about 1000 antibodies were transferred to 96-well plates and screened for the desired activity based on an increase in the absorption at 340 nm upon formation of the 2-cyanophenol product (Figure 16). Two of these antibodies

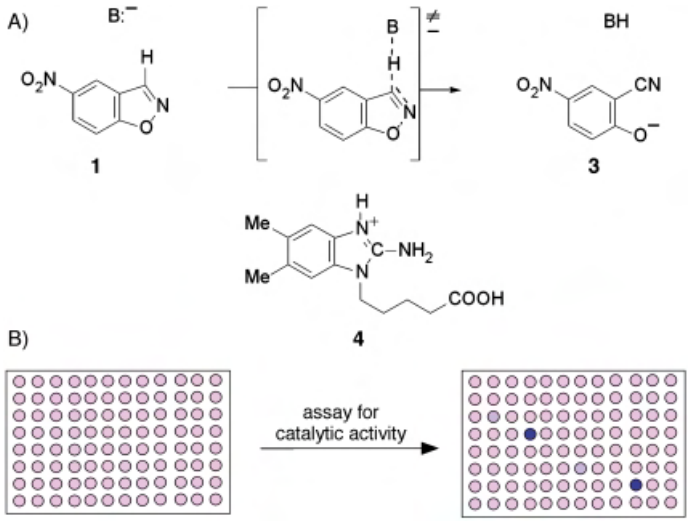


Figure 16. High efficiency catalytic antibodies generated by using transition state analogue and microtiter plate screening.[107] A) The structure of the transition state analogue **4** used to generate the catalytic antibodies that catalyze the transformation from **1** to **3**. B) The antibodies generated were transferred to 96-well plates and screened for catalytic activity by monitoring the absorption change at 340 nm upon conversion of **1** into **3**. Two highly active antibodies were isolated. Figure 16A and Table 4 reprinted from reference [107] with permission from Nature, Copyright (1995), Macmillan Magazines Limited.

were chosen for further analysis and showed rate accelerations of 3.4×10^8 and 3.5×10^7 compared with the non-catalyzed reaction (Table 4). Typically, only 10–100 monoclonal antibodies are screened for the desired activity, and each antibody is analyzed in a separate kinetic assay. The 10^8-fold rate acceleration obtained in this example is much greater than that normally achieved for catalytic antibodies and demonstrates the benefit of such a large-scale secondary screen and of assaying directly for catalytic activity.

Table 4. Kinetic parameters of the catalytic antibodies obtained by Hilvert and co-workers.[107]

Catalyst	k_{cat} [s^{-1}]	K_m [μM]	k_{cat}/K_m [$s^{-1}M^{-1}$]	$\frac{k_{cat}/K_m}{k_{AcO^-}}$	p*K*a	k_{cat}/k_{AcO^-} [M]
34E4	0.66	120	5.5×10^3	3.4×10^8	6.0	41000
35F10	0.35	630	5.6×10^2	3.5×10^7	5.5	22000

Microtiter plate assays have been used, not only for antibody engineering, but also for protein engineering generally. For example, Giver et al. screened a mutagenized *Bacillus subtilis* *p*-nitrobenzyl esterase (pNBE) library to evolve thermostable pNBEs and to elucidate the relationship between thermostability and catalytic activity.[108] The protein library shown in Figure 17 was generated by mutagenic PCR and DNA shuffling and then expressed in *E. coli*. Between

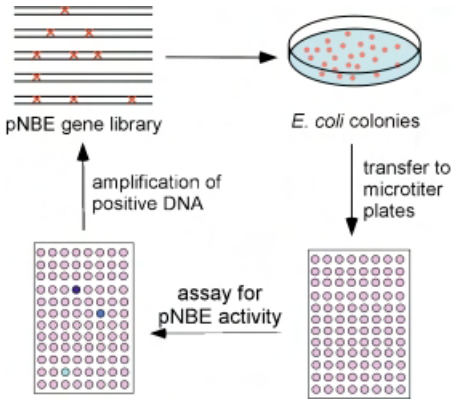


Figure 17. The evolution of thermostable pNBE.[108] The protein library, generated from the wild-type pNBE gene by mutagenic PCR and DNA shuffling, was expressed in *E. coli*. Single colonies were picked and transferred to 96-well plates in which the activities and thermostabilities of the proteins were assayed by using a standard *p*-nitrobenzyl acetate assay. The DNA from the clones that showed increased thermostability were isolated and subjected to further rounds of mutagenesis and screening. After six rounds, the T_m of the enzyme was increased by 14 °C, whereas its activity was unchanged at room temperature.

500 and 2000 colonies in each generation were picked and transferred to 96-well plates. The pNBE activities and thermostabilities of the proteins were measured in a standard *p*-nitrobenzyl acetate assay, which monitors enzymatic turnover based on the formation of a chromogenic product by using crude cell extracts. Six rounds of mutagenesis and screening stabilized pNBE significantly, with a T_m increase of 14 °C. Interestingly, the activity of the mutant enzyme was unchanged at room temperature. This application was successful, probably because a tractable problem—increasing the

thermostability of a known enzyme—that could be addressed with a 10^4-membered library was chosen and because a convenient cell assay was available for the esterase activity.

Spatially addressable libraries seem particularly well suited to screening cDNA libraries in which fewer proteins need to be tested than when evolving a protein with new activity. Haushalter et al. used in vitro expression cloning to identify new DNA glycosylases from a *Xenopus* embryo cDNA library.[109] The cDNA library was divided into 120 pools, each containing roughly 100 cDNAs. These cDNA pools were transcribed and translated in vitro in the wells of microtiter plates. The translated proteins were incubated with ^{32}P-labeled mechanism-based glycosylase inhibitors and then subjected to native polyacrylamide gel electrophoresis. The pool that showed distinct inhibitor binding was progressively subdivided and retested until a single active clone was identified. This clone was characterized and shown to be a new single-strand-selective monofunctional uracil-DNA glycosylase.

4.2. Protein Chips

Recently, inspired by successes with DNA microchips, effort has turned to developing protein microchips; in this case proteins are immobilized on a solid support with a high density to study protein function on a genomic scale. For example, proteins have been immobilized on a polyvinylidene difluoride membrane,[110] a nitrocellulose membrane,[111] glass slides,[112, 113] and in a polyacrylamide gel.[114] Macbeath and Schreiber[112] covalently attached several proteins to a glass slide in a high density format by using a high-precision contact-printing robot. The glass slides were first derivatized with an aldehyde-containing silane reagent. Then nanoliter volumes of protein samples were printed to the slides. The aldehyde groups on the glass slides reacted with primary amines on the proteins to form a Schiff base link, thus attaching the proteins covalently to the slides. The density of the protein chips thus made is about 1600 spots per square centimeter. The utility of these protein chips was also demonstrated by screening for known protein–protein and protein–small molecule interactions and identifying protein substrates of protein kinases.

4.2.1. Technical Considerations

In contrast to microtiter plate assays in which crude cell lysates can be used, in protein microchip assays the proteins must be purified and then printed onto the chips. Therefore, the purification of thousands of proteins is a key limiting step for this method. A higher throughput is found with protein chips than with microtiter plate assays, and only nanoliters of purified protein solution are needed for each spot on the chip. Another advantage of protein chips over microtiter plates is that wash steps do not disrupt the protein location. On the other hand, as shown in these proof of principle studies,[111, 114, 115] immobilized protein libraries are more suitable to binding assays than catalytic assays. A clever solution that combines the advantages of the two methods is to immobilize proteins in nanowells.[116] A particularly interesting recent approach taken by Ziauddin and Sabatini is to immobilize cDNAs on a solid support and then transfect cells en masse.[117]

4.2.2. Applications

Most reports to date have focused on establishing the methodology for attaching a few proteins to solid supports. An impressive recent advance is the printing and application of a chip displaying the complete yeast proteome. Zhu et al.[118] cloned 5800 ORFs of yeast into a yeast high-copy expression vector as GST–His6 fusion proteins under control of the *GAL1* promoter. The proteins were purified by using glutathione–agarose beads in a 96-well plate format. These purified proteins were then printed to glass slides coated with either aldehydes or nickel. The aldehyde groups react with the primary amines on the proteins, or the nickel forms complexes with the His6 tag on the protein termini, therefore linking the proteins to the glass slide. Detection of the GST tag on the protein chip showed that more than 90% of the proteins were expressed, purified, and printed. Calmodulin-binding proteins were identified by incubating the protein chip with biotinylated calmodulin, followed by detection of bound biotinylated calmodulin with Cy3-conjugated streptavidin after washing away unbound biotinylated calmodulin (Figure 18). This experiment identified six known calmodulin-binding proteins and 33 unknown potential calmodulin-binding proteins. There were six known calmodulin-binding proteins that were not detected. Similarly, phospholipid-binding proteins were also detected. Importantly, by probing for the GST tag and camodulin-binding proteins, the authors establish that the chip successfully presents a high percentage of the cDNA library.

4.3. Summary

The advantage of spatially addressable methods seems to be the ease with which they can be adapted to traditional biochemical assays for protein function. Particularly in applications in which the proteins must be purified, spatially addressable libraries realistically are limited to approximately 10^4 protein variants. Although there are applications in protein engineering, spatially addressable methods seem best suited to testing cDNA libraries to determine protein function. As with any in vitro method, these assays are limited to proteins that are stable outside the cell. In addition, it is not yet clear how the solid support may influence protein function. A wide variety of chemical reactions can be detected with these methods since many traditional assays can be used. Proteins printed in microwells are compatible with both assays for binding and for enzyme catalysis. The drawback of spatially addressable methods is that they are technically demanding. Purifying and printing proteins is labor-intensive. It is reasonable to assume that protein chips will not be as robust for multiple assays as DNA chips. Also at the end of the assay each protein must be traced back to its unique DNA tag.

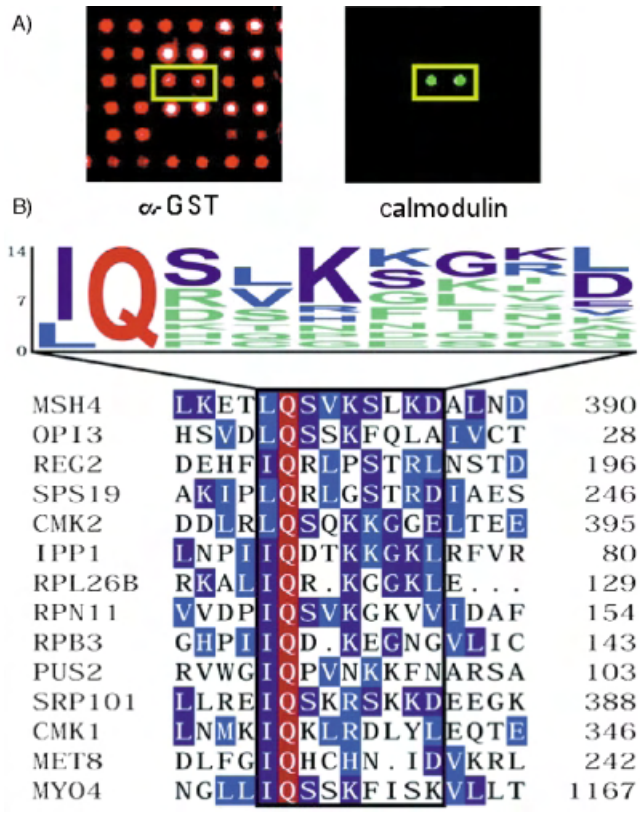


Figure 18. Assay for camodulin-binding proteins on proteome chips.[118] A) On the left, a control proteome chip probed with anti-GST (red) is shown. This control experiment demonstrated that more than 90% of the proteins were successfully expressed, purified, and spotted on the glass slides. The second panel shows positive signals in duplicate (green) detected by a biotinylated calmodulin probe. B) Positive proteins (39) were identified and 14 of them share a motif whose consensus is (I/L)QXK(K/X)GB,. X is any residue and B is a basic residue. The size of the letter indicates the relative frequency of the amino acid indicated. Reprinted with permission from reference [118]. Copyright (2001), American Association for the Advancement of Science.

5. Direct Protein-Sequencing Methods

Another possibility is that methods for sequencing proteins will advance to the point where a tag is unnecessary. In this section we look at recent advances in mass spectrometry that begin to achieve this goal.

5.1. Technical Considerations

Mass spectrometry (MS) is emerging as a powerful tool for proteomics. The driving force comes from advances in both MS and genome sequencing. Advances in MS include development of novel ionization techniques such ESI and MALDI.[119–121] MS can be used to determine protein sequence because the protein can be fragmented into small peptides whose masses or sequences can be obtained by MS, and then the protein sequence can be deduced from the masses or sequences of the fragmented peptides with the aid of the genome sequence. Therefore, a known genome sequence is a prerequisite for these MS methods. Henzel et al. first introduced this approach in the late 1980s.[122] They purified *E. coli* protein extracts by 2D gel electrophoresis. The proteins were then electroblotted onto poly(vinylidene difluoride) (PVDF) membrane and stained with Coomassie Blue. Individual protein spots were excised, reduced in situ with dithiothreitol, alkylated with iodoacetic acid, and digested with trypsin. Peptide fragments thus generated were then subjected to MALDI analysis. The masses of the peptide fragments were analyzed by using the computer program FRAGFIT, which searched for peptide sequences that matched the obtained masses from a protein sequence database. In this way, the identity of the proteins separated by 2D gel electrophoresis can be inferred. Of the 10 protein spots chosen for analysis, the identity of 9 spots was confirmed by N-terminal sequence analysis. Methods that improve the sensitivity and certainty of identification have been reported.[123]

5.2. Applications

MS methods can be used to identify the proteins that make up a protein complex, that is, proteins that associate with each other. An advantage to this approach is that the entire complex rather than one protein–protein interaction at a time, can be assigned in a single step. Link et al. identified 75 of 78 predicted yeast ribosomal proteins in the 80S ribosome complex by using MS.[124] The protein complex was purified, denatured, reduced, and digested to peptide fragments. These peptide fragments were then separated by 2D column chromatography and eluted into a mass spectrometer. Peptide sequences were obtained by using tandem mass spectrometry (MS/MS) and used to search translated genomic databases. By using 120 μg of the purified protein complex, 95 polypeptides were identified, 90 of which were from distinct ribosomal genes and represent 75 of the 78 proteins (some proteins are encoded by two separate genes with >98% amino acid sequence identity). A protein that had not been previously identified as part of the yeast ribosome complex, YMR116C (BEL1), was also identified.

Quantitative MS methods can be used to measure protein expression levels at different cellular states. This approach is similar to DNA microarrays, except that the actual protein levels, as opposed to mRNA levels, can be monitored. Global profiling of gene expression levels at different cellular states can help to identify proteins and genes involved in a given biological pathway. Gygi et al. developed a method that used isotope-coded affinity tags (ICAT) to measure relative protein expression levels at different cellular states.[125] As shown in Figure 19, the ICAT consists of a biotin molecule, a linker that can incorporate isotopes, and a thiol-specific reactive group. Soluble proteins from yeast cells grown in either 2% galactose or 2% ethanol as the carbon source were isolated and reduced. Two ICAT reagents, one with a heavy isotope and one with a light isotope, were used to label the two protein samples, respectively. Then the two protein samples were mixed and digested. Cysteine-containing peptides were isolated by avidin-affinity chromatography and analyzed by using microcapillary liquid chromatography–MS/MS. Protein sequences were obtained by searching the sequence database using the identified peptide sequences, and

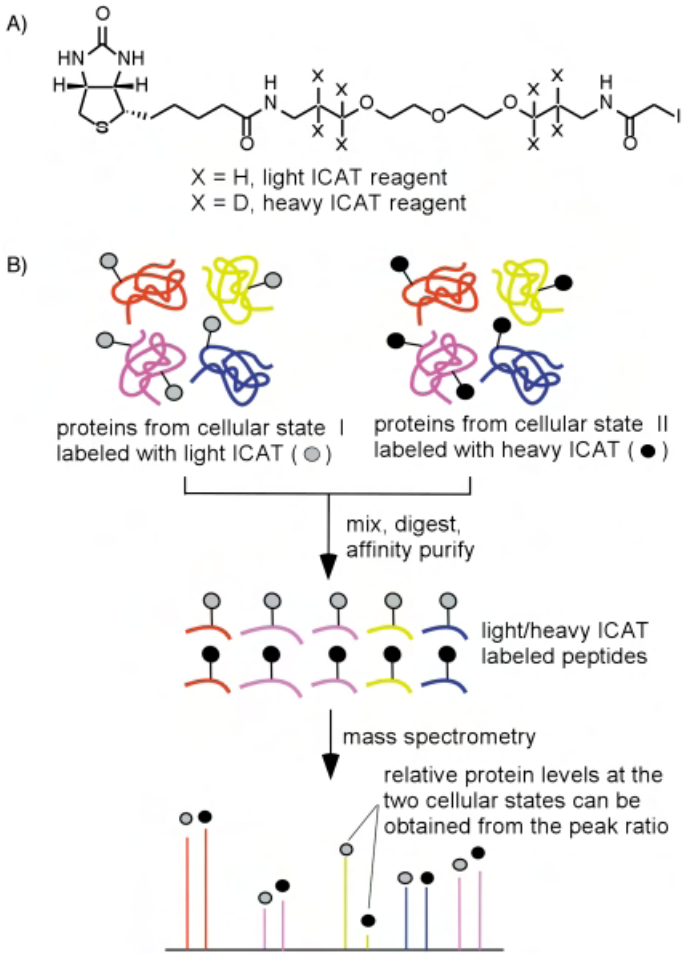


Figure 19. A mass spectrometry method to measure relative protein expression levels in different cellular states.[125] A) The structure of the isotope-coded affinity tags (ICAT), which consist of a biotin molecule, a linker that can incorporate isotopes, and a thiol-specific reactive group. B) Soluble proteins from two different cellular states are isolated and reduced. Two ICAT reagents, one with heavy isotope, one with light isotope are used to label the two protein samples respectively. Then the two protein samples are mixed and digested. Cysteine-containing peptides, which are labeled with the ICAT reagents, are isolated by avidin affinity chromatography. After separation by microcapillary liquid chromatography, these labeled peptides are analyzed by MS. The relative protein expression levels at the two cellular states can be obtained by measuring the ratio of the two peaks for the same peptide sequence from the two different cellular states. The identity of the protein can be obtained by first obtaining the peptide sequence via tandem MS and then searching the peptide sequence in the database.

the relative protein expression levels of the two different cellular states were obtained by comparing the intensity of the pairs of peptide ions of identical sequences that were labeled with isotopically differentiated ICAT reagents. The expression levels of 34 genes for yeast grown in either 2% galactose or 2% ethanol as the carbon source were compared and the results correlate well with what is known about yeast metabolism.

As with phage display and ribosome display, the challenge with MS methods is how to assay enzyme catalysis as well as binding. Cravatt and co-workers recently used an inhibitor of serine hydrolases in a method they termed "activity-based protein profiling" to detect serine hydrolyases from crude tissue extracts.[89] In their specific case, they used a biotinylated fluorophosphonate (FP–biotin). Fluorophosphonate derivatives are selective and irreversible inhibitors for serine hydrolases, and they only react with enzymes that are in a catalytically active state. Crude rat brain extracts were incubated with FP–biotin, after which the proteins were subjected to standard SDS/PAGE-Western blotting procedures and detected by using an avidin–horseradish peroxidase conjugate. More than ten proteins were detected, two of them, a 75-kDa protein and an 85-kDa protein, were subjected to MS analysis. Genome database searching identified the 75-kDa protein as the rat orthologue of a human protein sequence KIAA0436 and the 85-kDa protein as acylpeptide hydrolase. Chemical probes for cysteine proteases have also been described.[90]

5.3. Summary

MS methods are more recent and much may change technically in the next several years. In theory, MS assays are limited only by the mass of the proteins, thus allowing libraries even larger than those obtainable with RNA display. However, only relatively small libraries have been tested to date. MS methods place no inherent limits on the type of proteins that can be tested and are compatible with both in vitro and in vivo assays. It is not yet clear what type of assays will be applied to MS methods, and there is much opportunity here. Likewise, many technical issues are yet to be resolved, such as how to detect proteins with very low cellular concentrations or how to regenerate the DNA that encodes a protein hit for further rounds of mutagenesis. In addition to MS, there may be other methods for the direct sequencing of proteins that are being overlooked.

6. Summary and Outlook

The development of robust methods for assaying proteins based on function over the past two decades seems to promise a breakthrough in protein engineering and proteomics in the near term. Several methods for tying a protein to its DNA sequence are now well developed, ranging from methods such as phage display (in which a physical link is created between the protein and its DNA sequence) to microtiter plate assays (in which each protein is simply assayed independently) to cell-based assays (in which each cell contains a single plasmid that encodes a unique protein variant). While these methods are already impressive, recent advances in protein chips and MS emphasize that new methods can still be advantageous. Researchers are building on these methods and are beginning to modify the specificity of existing proteins successfully. It should be noted that these successes are partly a result of the correct choice of reactions that provide a convenient selection or screen, for example, a reaction in which the product is fluorescent or an essential cellular metabolite. The next challenge is to develop general assays for enzymatic activity that allow us to engineer new chemistry and to apply these methods not only to protein engineering, but also to proteomics.

We would like to thank S. Licht, C. Noren, T. Yano, and the members of our lab for their helpful comments as we were preparing this manuscript. V.W.C. is a recipient of a Beckman Young Investigator Award, a Burroughs-Wellcome Fund New Investigator Award in the Toxological Sciences, a Camille and Henry Dreyfus New Faculty Award, and a National Science Foundation Career Award. H.L. is a Arun Guthikonda Memorial Fellow.

Received: June 6, 2001 [A 478]

[1] G. P. Smith, V. A. Petrenko, *Chem. Rev.* **1997**, *97*, 391.
[2] S. S. Sidhu, *Curr. Opin. Biotechnol.* **2000**, *11*, 610.
[3] D. J. Rodi, L. Makowski, *Curr. Opin. Biotechnol.* **1999**, *10*, 87.
[4] P. Forrer, S. Jung, A. Plückthun, *Curr. Opin. Struct. Biol.* **1999**, *9*, 514.
[5] G. P. Smith, *Science* **1985**, *228*, 1315.
[6] D. Sblattero, A. Bradbury, *Nat. Biotechnol.* **2000**, *18*, 75.
[7] S. S. Sidhu, H. B. Lowman, B. C. Cunningham, J. A. Wells, *Methods Enzymol.* **2000**, *328*, 333.
[8] S. Bass, R. Green, J. A. Wells, *Proteins: Struct. Funct. Genet.* **1990**, *8*, 309.
[9] J. Greenwood, A. E. Willis, R. N. Perham, *J. Mol. Biol.* **1991**, *220*, 821.
[10] C. Gao, S. Mao, C. L. Lo, P. Wirsching, R. A. Lerner, K. D. Janda, *Proc. Natl. Acad. Sci. USA* **1999**, *96*, 6025.
[11] M. Duenas, C. A. Borrebaeck, *Bio/Technology* **1994**, *12*, 999.
[12] K. Gramatikoff, O. Georgiev, W. Schaffner, *Nucleic Acids Res.* **1994**, *22*, 5761.
[13] J. K. Scott, G. P. Smith, *Science* **1990**, *249*, 386.
[14] N. C. Wrighton, F. X. Farrell, R. Chang, A. K. Kashyap, F. P. Barbone, L. S. Mulcahy, D. L. Johnson, R. W. Barrett, L. K. Jolliffe, W. J. Dower, *Science* **1996**, *273*, 458.
[15] R. Hyde-DeRuyscher, L. A. Paige, D. J. Christensen, N. Hyde-DeRuyscher, A. Lim, Z. L. Fredericks, J. Kranz, P. Gallant, J. Zhang, S. M. Rocklage, D. M. Fowlkes, P. A. Wendler, P. T. Hamilton, *Chem. Biol.* **2000**, *7*, 17.
[16] S. R. Whaley, D. S. English, E. Hu, P. F. Barbara, A. M. Belcher, *Nature* **2000**, *405*, 665.
[17] W. Dall′Acqua, P. Carter, *Curr. Opin. Struct. Biol.* **1998**, *8*, 443.
[18] H. R. Hoogenboom, P. Chames, *Immunol. Today* **2000**, *21*, 371.
[19] J. McCafferty, A. D. Griffiths, G. Winter, D. J. Chiswell, *Nature* **1990**, *348*, 552.
[20] A. S. Kang, C. F. Barbas III, K. D. Janda, S. J. Benkovic, R. A. Lerner, *Proc. Natl. Acad. Sci. USA* **1991**, *88*, 4363.
[21] C. F. Barbas, III, A. S. Kang, R. A. Lerner, S. J. Benkovic, *Proc. Natl. Acad. Sci. USA* **1991**, *88*, 7978.
[22] J. Yu, S. Y. Choi, K.-D. Moon, H.-H. Chung, H. J. Youn, S. Jeong, H. Park, P. G. Schultz, *Proc. Natl. Acad. Sci. USA* **1998**, *95*, 2880.
[23] M. Baca, T. S. Scanlan, R. C. Stephenson, J. A. Wells, *Proc. Natl. Acad. Sci. USA* **1997**, *94*, 10063.
[24] K. D. Janda, L.-C. Lo, C.-H. L. Lo, M.-M. Sim, R. Wang, C.-H. Wong, R. A. Lerner, *Science* **1997**, *275*, 945.
[25] M. Shanmugavelu, A. R. Baytan, J. D. Chesnut, B. C. Bonning, *J. Biol. Chem.* **2000**, *275*, 1802.
[26] Y. Choo, A. Klug, *Proc. Natl. Acad. Sci. USA* **1994**, *91*, 11163.
[27] A. C. Jamieson, S.-H. Kim, J. A. Wells, *Biochemistry* **1994**, *33*, 5689.
[28] E. J. Rebar, C. O. Pabo, *Science* **1994**, *263*, 671.
[29] G. A. Weiss, H. B. Lowman, *Chem. Biol.* **2000**, *7*, 547.
[30] G. Beste, F. S. Schmidt, T. Stibora, A. Skerra, *Proc. Natl. Acad. Sci. USA* **1999**, *96*, 1898.
[31] S. Schlehuber, G. Beste, A. Skerra, *J. Mol. Biol.* **2000**, *297*, 1105.
[32] J. C. Guo, W. Huang, T. S. Scanlan, *J. Am. Chem. Soc.* **1994**, *116*, 6062.
[33] P. Soumillion, L. Jespers, M. Bouchet, J. Marchand-Brynaert, G. Winter, J. Fastrez, *J. Mol. Biol.* **1994**, *237*, 415.
[34] C. Gao, C.-H. Lin, C.-H. L. Lo, S. Mao, P. Wirsching, R. A. Lerner, K. D. Janda, *Proc. Natl. Acad. Sci. USA* **1997**, *94*, 11777.
[35] H. Pedersen, S. Holder, D. P. Sutherlin, U. Schwitter, D. S. King, P. G. Schultz, *Proc. Natl. Acad. Sci. USA* **1998**, *95*, 10523.
[36] S. Demartis, A. Huber, F. Viti, L. Lozzi, L. Giovannoni, P. Neri, G. Winter, D. Neri, *J. Mol. Biol.* **1999**, *286*, 617.
[37] J.-L. Jestin, P. Kristensen, G. Winter, *Angew. Chem.* **1999**, 111, 1196; Angew. *Chem. Int. Ed.* **1999**, *38*, 1124.
[38] S. Atwell, J. A. Wells, *Proc. Natl. Acad. Sci. USA* **1999**, *96*, 9497.
[39] I. Ponsard, M. Galleni, P. Soumillion, J. Fastrez, *ChemBioChem* **2001**, *2*, 253.
[40] R. W. Roberts, *Curr. Opin. Chem. Biol.* **1999**, *3*, 268.
[41] L. C. Mattheakis, R. R. Bhatt, W. J. Dower, *Proc. Natl. Acad. Sci. USA* **1994**, *91*, 9022.
[42] J. Hanes, A. Plückthun, *Proc. Natl. Acad. Sci. USA* **1997**, *94*, 4937.
[43] R. W. Roberts, J. W. Szostak, *Proc. Natl. Acad. Sci. USA* **1997**, *94*, 12297.
[44] N. Nemoto, E. Miyamoto-Sato, Y. Husimi, H. Yanagawa, *FEBS Lett.* **1997**, *414*, 405.
[45] G. Cho, A. D. Keefe, R. Liu, D. S. Wilson, J. W. Szostak, *J. Mol. Biol.* **2000**, *297*, 309.
[46] R. Liu, J. E. Barrick, J. W. Szostak, R. W. Roberts, *Methods Enzymol.* **2000**, *318*, 268.
[47] J. Hanes, C. Schaffitzel, A. Knappik, A. Plükthun, *Nat. Biotechnol.* **2000**, *18*, 1287.
[48] D. S. Wilson, A. D. Keefe, J. W. Szostak, *Proc. Natl. Acad. Sci. USA* **2001**, *98*, 3750.
[49] A. D. Keefe, J. W. Szostak, *Nature* **2001**, *410*, 715.
[50] M. G. Cull, J. F. Miller, P. J. Schatz, *Proc. Natl. Acad. Sci. USA* **1992**, *89*, 1865.
[51] C. M. Gates, W. P. C. Stemmer, R. Kaptein, P. J. Schatz, *J. Mol. Biol.* **1996**, *255*, 373.
[52] S. E. Cwirla, P. Balasubramanian, D. J. Duffin, C. R. Wagstrom, C. M. Gates, S. C. Singer, A. M. Davis, R. L. Tansik, L. C. Mattheakis, C. M. Boytos, P. J. Schatz, D. P. Baccanari, N. C. Wrighton, R. W. Barrett, W. J. Dower, *Science* **1997**, *276*, 1696.
[53] S. Ståhl, M. Uhlén, *Trends Biotechnol.* **1997**, *15*, 185.
[54] J. A. Francisco, C. F. Earhart, G. Georgiou, *Proc. Natl. Acad. Sci. USA* **1992**, *89*, 2713.
[55] E. T. Boder, K. D. Wittrup, *Nat. Biotechnol.* **1997**, *15*, 553.
[56] W. Ernst, R. Grabherr, D. Wegner, N. Borth, A. Grassauer, H. Katinger, *Nucleic Acids Res.* **1998**, *26*, 1718.
[57] A. Christmann, K. Walter, A. Wentzel, R. Kratzner, H. Kolmar, *Protein Eng.* **1999**, *12*, 797.
[58] P. S. Daugherty, G. Chen, M. J. Olsen, B. L. Iverson, G. Georgiou, *Protein Eng.* **1998**, *11*, 825.
[59] M. C. Kieke, E. V. Shusta, E. T. Boder, L. Teyton, K. D. Wittrup, D. M. Kranz, *Proc. Natl. Acad. Sci. USA* **1999**, *96*, 5651.
[60] E. T. Boder, K. S. Midelfort, K. D. Wittrup, *Proc. Natl. Acad. Sci. USA* **2000**, *97*, 10701.
[61] M. J. Olsen, D. Stephens, D. Griffiths, P. Daugherty, G. Georgiou, B. L. Iverson, *Nat. Biotechnol.* **2000**, *18*, 1071.
[62] G. W. Beadle, E. L. Tatum, *Proc. Natl. Acad. Sci. USA* **1941**, *27*, 499.
[63] M. Hensel, J. E. Shea, C. Gleeson, M. D. Jones, E. Dalton, D. W. Holden, *Science* **1995**, *269*, 400.
[64] S. Benzer, *Sci. Am.* **1962**, 72.
[65] P. Uetz, L. Giot, G. Cagney, T. A. Mansfield, R. S. Judson, J. R. Knight, D. Lockshon, V. Narayan, M. Srinivasan, P. Pochart, A. Qureshi-Emili, Y. Li, B. Godwin, D. Conover, T. Kalbfleisch, G. Vijayadamodar, M. Yang, M. Johnston, S. Fields, J. M. Rothberg, *Nature* **2000**, *403*, 623.
[66] B. L. Drees, *Curr. Opin. Chem. Biol.* **1999**, *3*, 64.
[67] D. S. McNabb, L. Guarente, *Curr. Opin. Biotechnol.* **1996**, *7*, 554.
[68] E. Warbrick, *Structure* **1997**, *5*, 13.
[69] H. Lin, V. W. Cornish, *Angew. Chem.* **2001**, *113*, 895; *Angew. Chem. Int. Ed.* **2001**, *40*, 871.
[70] R. K. Brachmann, J. D. Boeke, *Curr. Opin. Biotechnol.* **1997**, *8*, 561.
[71] M. Vidal, P. Legrain, *Nucleic Acids Res.* **1999**, *27*, 919.
[72] P. Colas, R. Brent, *Trends Biotechnol.* **1998**, *16*, 355.
[73] S. Fields, O. Song, *Nature* **1989**, *340*, 245.
[74] P. Colas, B. Cohen, T. Jessen, I. Grishina, J. McCoy, R. Brent, *Nature* **1996**, *380*, 548.
[75] T. C. Norman, D. L. Smith, P. K. Sorger, B. L. Drees, S. M. O′Rourke, T. R. Hughes, C. J. Roberts, S. H. Friend, S. Fields, A. W. Murray, *Science* **1999**, *285*, 591.
[76] P. Youderian, A. Vershon, S. Bouvier, R. T. Sauer, M. M. Susskind, *Cell* **1983**, *35*, 777.
[77] S. L. Dove, J. K. Joung, A. Hochschild, *Nature* **1997**, *386*, 627.

[78] J. K. Joung, E. I. Ramm, C. O. Pabo, *Proc. Natl. Acad. Sci. USA* **2000**, *97*, 7382.
[79] H. A. Greisman, C. O. Pabo, *Science* **1997**, *275*, 657.
[80] D. M. Spencer, T. J. Wandless, S. L. Schreiber, G. R. Crabtree, *Science* **1993**, *262*, 1019.
[81] E. J. Licitra, J. O. Liu, *Proc. Natl. Acad. Sci. USA* **1996**, *93*, 12817.
[82] E. C. Griffith, E. J. Licitra, J. O. Liu, *Methods Enzymol.* **2000**, *328*, 89.
[83] H. Lin, W. M. Abida, R. T. Sauer, V. W. Cornish, *J. Am. Chem. Soc.* **2000**, *122*, 4247.
[84] H. Joo, Z. Lin, F. H. Arnold, *Nature* **1999**, *399*, 670.
[85] B. Hall in *Evolutionary Biology*, *Vol. 15* (Eds.: M. Hecht, B. Wallace, G. Pierce), Plenum Press, New York, **1982**, p. 85.
[86] J. D. Hermes, S. C. Blacklow, J. R. Knowles, *Proc. Natl. Acad. Sci. USA* **1990**, *87*, 696.
[87] T. Yano, S. Oue, H. Kagamiyama, *Proc. Natl. Acad. Sci. USA* **1998**, *95*, 5511.
[88] G. Xia, L. Chen, T. Sera, M. Fa, P. G. Schultz, F. E. Romesberg, *Proc. Natl. Acad. Sci. USA* **2002**, *99*, 6597.
[89] Y. Liu, M. P. Patricelli, B. F. Cravatt, *Proc. Natl. Acad. Sci. USA* **1999**, *96*, 14694.
[90] D. Greenbaum, K. F. Medzihradszky, A. Burlingame, M. Bogyo, *Chem. Biol.* **2000**, *7*, 569.
[91] D. S. Tawfik, A. D. Griffiths, *Nat. Biotechnol.* **1998**, *16*, 652.
[92] N. Doi, H. Yanagawa, *FEBS Lett.* **1999**, *457*, 227.
[93] F. J. Ghadessy, J. L. Ong, P. Holliger, *Proc. Natl. Acad. Sci. USA* **2001**, *98*, 4552.
[94] A. Q. Emili, G. Cagney, *Nat. Biotechnol.* **2000**, *18*, 393.
[95] G. Walter, K. Büssow, D. Cahill, A. Lueking, H. Lehrach, *Curr. Opin. Microbiol.* **2000**, *3*, 298.
[96] E. J. Grayhack, E. M. Phizicky, *Curr. Opin. Chem. Biol.* **2001**, *5*, 34.
[97] H. Zhu, M. Snyder, *Curr. Opin. Chem. Biol.* **2001**, *5*, 40.
[98] R. Manns, http://www.messebasel.ch/miptec/mission-history.htm, **1999**.
[99] A. Voller, D. Bidwell, G. Huldt, E. Engvall, *Bull. WHO* **1974**, *51*, 209.
[100] M. R. Martzen, S. M. McCraith, S. L. Spinelli, F. M. Torres, S. Fields, E. J. Grayhack, E. M. Phizicky, *Science* **1999**, *286*, 1153.
[101] S. A. Sundberg, *Curr. Opin. Biotechnol.* **2000**, *11*, 47.
[102] R. P. Hertzberg, A. J. Pope, *Curr. Opin. Chem. Biol.* **2000**, *4*, 445.
[103] J. E. González, P. A. Negulescu, *Curr. Opin. Biotechnol.* **1998**, *9*, 624.
[104] N. Bosworth, P. Towers, *Nature* **1989**, *341*, 167.
[105] A. J. Pope, U. Haupts, K. J. Moore, *Drug Discovery Today* **1999**, *4*, 350.
[106] A. Koltermann, U. Kettling, J. Bieschke, T. Winkler, M. Eigen, *Proc. Natl. Acad. Sci. USA* **1998**, *95*, 1421.
[107] S. N. Thorn, R. G. Daniels, M. M. Auditor, D. Hilvert, *Nature* **1995**, *373*, 228.
[108] L. Giver, A. Gershenson, P.-O. Freskgard, F. H. Arnold, *Proc. Natl. Acad. Sci. USA* **1998**, *95*, 12809.
[109] K. A. Haushalter, P. T. Stukenberg, M. W. Kirschner, G. L. Verdine, *Curr. Biol.* **1999**, *9*, 174.
[110] A. Lueking, M. Horn, H. Eickhoff, K. Büssow, H. Lehrach, G. Walter, *Anal. Biochem.* **1999**, *270*, 103.
[111] H. Ge, *Nucleic Acids Res.* **2000**, *28*, e3.
[112] G. MacBeath, S. L. Schreiber, *Science* **2000**, *289*, 1760.
[113] C. A. Rowe, L. M. Tender, M. J. Feldstein, J. P. Golden, S. B. Scruggs, B. D. MacCraith, J. J. Cras, F. S. Ligler, *Anal. Chem.* **1999**, *71*, 3846.
[114] P. Arenkov, A. Kukhtin, A. Gemmell, S. Voloshchuk, V. Chupeeva, A. Mirzabekov, *Anal. Biochem.* **2000**, *278*, 123.
[115] B. Schweitzer, S. Wiltshire, J. Lambert, S. O'Malley, K. Kukanskis, Z. Zhu, S. F. Kingsmore, P. M. Lizardi, D. C. Ward, *Proc. Natl. Acad. Sci. USA* **2000**, *97*, 10113.
[116] H. Zhu, J. F. Klemic, S. Chang, P. Bertone, A. Casamayor, K. G. Klemic, D. Smith, M. Gerstein, M. Reed, M. Snyder, *Nat. Genet.* **2000**, *26*, 283.
[117] J. Ziauddin, D. M. Sabatini, *Nature* **2001**, *411*, 107.
[118] H. Zhu, M. Bilgin, R. Bangham, D. Hall, A. Casamayor, P. Bertone, N. Lan, R. Jansen, S. Bidlingmaier, T. Houfek, T. Mitchell, P. Miller, R. A. Dean, M. Gerstein, M. Snyder, *Science* **2001**, *293*, 2101.
[119] J. S. Andersen, M. Mann, *FEBS Lett.* **2000**, *480*, 25.
[120] M. J. Chalmers, S. J. Gaskell, *Curr. Opin. Biotechnol.* **2000**, *11*, 384.
[121] J. Godovac-Zimmermann, L. R. Brown, *Mass Spectrom. Rev.* **2001**, *20*, 1.
[122] W. J. Henzel, T. M. Billeci, J. T. Stults, S. C. Wong, C. Grimley, C. Watanabe, *Proc. Natl. Acad. Sci. USA* **1993**, *90*, 5011.
[123] A. Shevchenko, O. N. Jensen, A. V. Podtelejnikov, F. Sagliocco, M. Wilm, O. Vorm, P. Mortensen, A. Shevchenko, H. Boucherie, M. Mann, *Proc. Natl. Acad. Sci. USA* **1996**, *93*, 14440.
[124] A. J. Link, J. Eng, D. M. Schieltz, E. Carmack, G. J. Mize, D. R. Morris, B. M. Garvik, I. J R Yates, *Nat. Biotechnol.* **1999**, *17*, 676.
[125] S. P. Gygi, B. Rist, S. A. Gerber, F. Turecek, M. H. Gelb, R. Aebersold, *Nat. Biotechnol.* **1999**, *17*, 994.

The Chemistry of the Antibody Molecule

Peter G. Schultz,* Jun Yin, and Richard A. Lerner*

Immunochemistry has traditionally focused on understanding the molecular basis of antibody binding affinity and specificity. In the last 20 years a major shift has occurred in the field. We are now asking how we can exploit the remarkable properties of the antibody molecule and the immune response in chemistry—from testing basic theories of enzymatic catalysis to the synthesis of new catalysts. Moreover, the concept of molecular diversity, which underlies these experiments, is now being applied to a large number of other problems—from libraries of biopolymers to libraries of solid-state materials. Importantly, theses studies are providing fundamental molecular insights into many biological, chemical, and physical phenomena, as well as changing the way we approach the synthesis of new molecular function.

1. Introduction

1.1. Synthesis at the Interface of Chemistry and Biology

Synthesis has been and will continue to remain a cornerstone of chemistry. It provides access to new molecular structures with novel chemical, biological, and physical properties, ranging from antibiotics and genes to conducting polymers and superconductors. Synthesis also provides a unique opportunity to test fundamental principles of chemistry and gain new insights into chemical phenomena. For example, our understanding of reactive intermediates has come in large part from iterative synthetic and mechanistic studies.

As the field of synthesis continues to evolve there will be an increasing shift in focus from the synthesis of structure to the synthesis of molecular function. Unfortunately, we as chemists are not nearly as sophisticated in our ability to rationally design and synthesize molecules with defined chemical, biological, or materials properties, as we are in our ability to synthesize complex molecular structures. How then do we develop synthetic strategies that enable us to create molecules with novel functions efficiently? One answer is to look to biology for guidance. After all, living organisms are unparalleled in their ability to generate molecular function—from molecular recognition by antibodies to energy conversion by the photosynthetic complex. Unfortunately, the synthetic machinery of the cell is not as easily adapted to new targets as are traditional synthetic methods. However, if we combine the "synthetic strategies" and processes of nature with the methods and principles of classical synthetic chemistry, it should be possible to generate new molecular function that is not accessible by either approach alone.

[*] Prof. Dr. P. G. Schultz, Prof. Dr. R. A. Lerner, J. Yin
Department of Chemistry and
The Skaggs Institute for Chemical Biology
The Scripps Research Institute
10550 North Torrey Pines Road, La Jolla, CA 92037 (USA)
Fax: (+1) 858-784-9440 (PGS), (+1) 858-784-9899 (RAL)
E-mail: schultz@scripps.edu, rlerner@scripps.edu

1.2. The Synthesis of Biological Catalysts

To illustrate this chemical–biological approach to synthesis, consider the generation of enzymatic catalysts. Enzymes catalyze biological transformations with exquisite specificity and efficiency using a limited number of functional groups—they do not have organolithium reagents or metal hydrides available. Given their remarkable catalytic function, considerable effort has gone into understanding the molecular basis of enzymatic catalysis using an array of spectroscopic and mechanistic tools. Nevertheless, the best test of our understanding of the principles of biological catalysis is in the synthesis of new enzymes. But how does one synthesize something as complex as an enzyme when we do not even yet understand the rules that govern the folding of amino acid sequences?

The answer comes from our understanding of the evolutionary process Nature uses to create enzymes. This process, at its most fundamental level, involves genetic recombination and mutation to generate a large diverse library of molecular scaffolds. This library is then subjected to natural selection in order to identify those molecules with the requisite catalytic function. Further rounds of mutation and selection lead to improved function.[1] This approach is very different from that of traditional synthetic chemistry, in which molecules are designed and synthesized one at a time, and optimized in an iterative fashion by structural refinement. Unfortunately, in contrast to laboratory synthesis, natural evolution occurs on

 © 2002 WILEY-VCH Verlag GmbH & Co. KGaA, Weinheim 1433-7851/02/4123-4427 $ 20.00+.50/0

an evolutionary timescale of up to billions of years. The challenge then in the synthesis of new biological catalysts is to recreate the basic features of enzyme evolution on the laboratory timescale.

If one accepts the basic principle that catalytic function results from the selective use of binding energy to stabilize transition states or to destabilize ground states preferentially, then the problem is simplified to one of synthesizing highly selective molecular receptors.[2] While this remains a major challenge for synthetic chemistry, there does exist a biological solution to the problem of molecular recognition. It is a well-known fact in immunochemistry that the immune response can generate an antibody that is complementary to virtually any foreign molecular structure presented to it. The process whereby these selective, high-affinity receptors are generated resembles in many ways the natural evolution of enzymes[3–5] (Table 1).

Table 1. A comparison of the evolution of enzymes and antibodies.

Enzymes	Antibodies
exon shuffling	V-D-J rearrangement
gene duplication	batteries of V, D, and J gene elements
accumulation of point mutations	somatic hypermutation
natural selection	clonal selection
timescale: $10^1 - 10^8$ years	timescale: weeks

The immune system "synthesizes" on the order of 10^8 different germline antibodies as initial solutions to the recognition problem by assembling the full-length antibody gene from the different V, D, J, and C gene segments (V = variable, J = joining, D = diversity, and C = constant segments). If each gene segment can be derived from any one of multiple genes, and insertion or deletion can occur during recombination of the segments, large numbers of antibody sequences can be generated (Figure 1). This particular "synthetic" strategy focuses molecular diversity in six hypervariable loops that make up the ligand-combining site on a core eight-stranded antiparallel β-sheet scaffold.[6] Once a germline antibody is selected from the pool based on its affinity for an antigen, additional structural diversity is generated by a process of affinity maturation in which somatic mutations are introduced throughout the variable region. Iteration of this process leads to a high-affinity antibody.

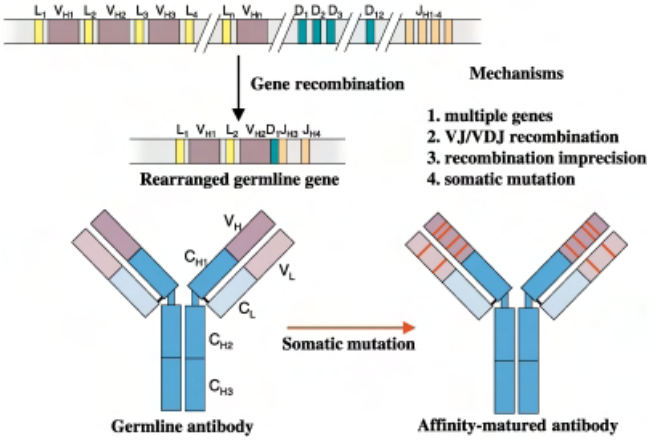


Figure 1. The generation of immunological diversity by genetic recombination and somatic mutation.

The key "synthetic" strategy used by the immune response, the generation of molecular diversity, is the same as that used in natural selection. The fundamental difference is in the timescales, the latter process occurs over millions of years; in contrast, the immune response occurs over a period of weeks. Consequently, if one can direct the immunological evolution of an antibody down the same path as the natural evolution of an enzyme, one should, in principle, generate enzyme-like catalysts from antibodies. This can be done by programming the immune response with mechanistic information about the chemical transformation of interest, in much the same way that mechanistic insight drives the development of classical synthesis and synthetic methodologies. But in the former approach, the principles and tools of chemistry are used *together* with the powerful biological notion of molecular diversity to synthesize new function. Herein we describe a number of experiments in antibody catalysis that illustrate this new synthetic paradigm.

2. Strategies for the Synthesis of Catalytic Antibodies

2.1. Transition-State Stabilization

One of the earliest theories put forth to explain enzymatic catalysis was Pauling's notion of transition-state stabilization: "The assumption that the enzyme has a configuration complementary to the activated complex, and accordingly has the strongest power of attraction for the activated complex, means that the activation energy for the reaction is less in the presence of the enzyme than in its absence, and accordingly that the reaction would be speeded up by the enzyme."[7, 8] One should be able to test this notion experimentally by chemically programming the immune response with a stable molecule which mimics the presumed structural and electronic features of the rate-limiting transition state for a particular reaction. The result should be the evolution of an antibody binding site with maximum complementarity to the transition state versus substrate or product. This antibody should catalyze the reaction by selectively stabilizing the bound transition state and thereby lowering the free energy of activation of the reaction.

To test whether one can synthesize enzymatic function using this approach, we attempted to generate antibodies that catalyze acyl transfer reactions. The transesterification reaction illustrated in Figure 2a is thought to proceed through a tetrahedral transition state generated by addition of alcohol **1** to ester **2** to produce a tetrahedral intermediate **3**, which breaks down to give product **4**. Antibody 13D6.1 generated to the phosphonate diester **5**, which mimics the charge distribution and geometry in the transition state, was found to catalyze the reaction with an effective molarity (EM; the concentration of substrate required in the absence of catalyst to achieve the same rate) of $\approx 10^4 - 10^5$ M.[9] This value begins to approach the theoretical maximum of 10^8 M calculated by

 © 2002 WILEY-VCH Verlag GmbH & Co. KGaA, Weinheim 1433-7851/02/4123-4428 $ 20.00+.50/0 *Angew. Chem. Int. Ed.* **2002**, *41*, No. 23

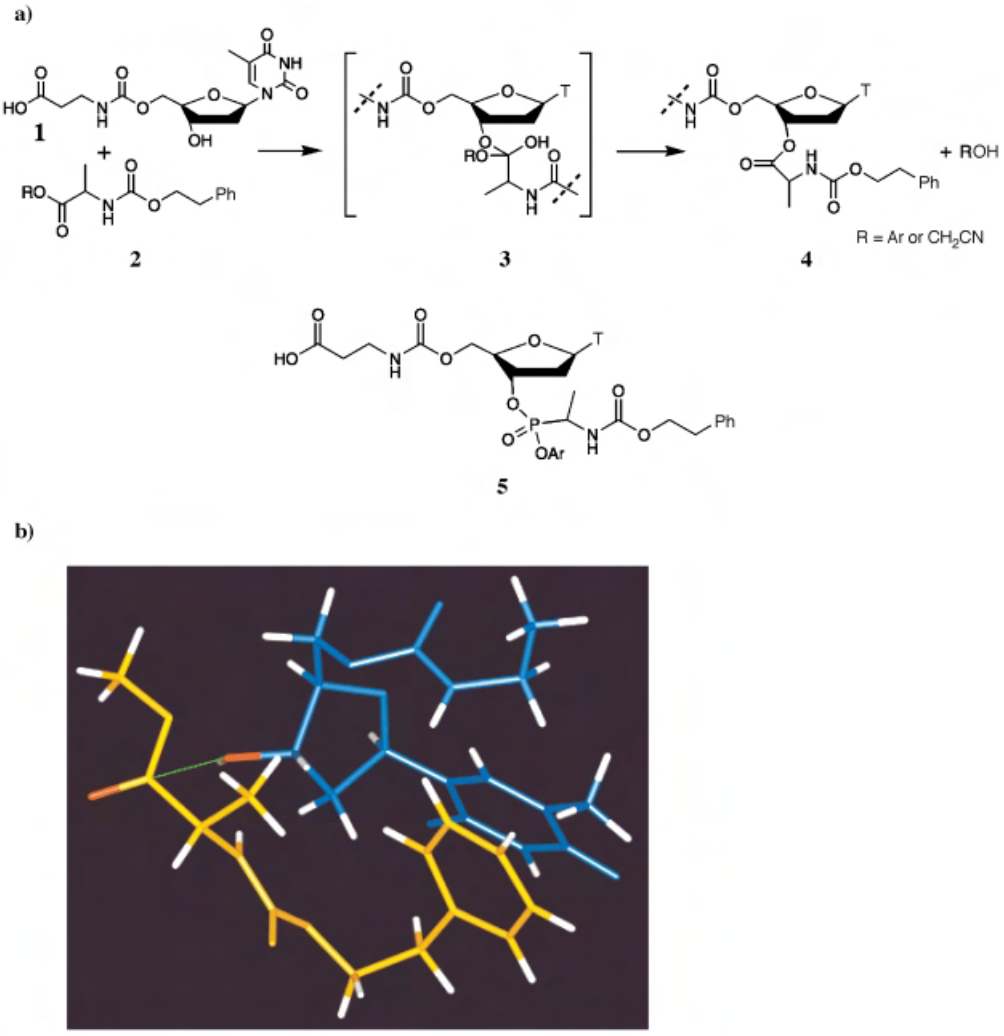


Figure 2. a) Acyl transfer from the ester **2** to the alcohol **1** catalyzed by antibody 13D6.1, which was generated against the phosphonate diester **5**; b) NMR structure of the Michaelis complex, with **1** shown in blue and **2** in orange.

Page and Jencks for a bimolecular reaction in which all translational and rotational modes along the reaction coordinate are frozen out in an enzyme active site.[10] NMR spectroscopic studies of the Michaelis complex (Figure 2b) confirmed that the antibody binds the substrate **1** in an optimal geometry for attack on the ester carbonyl group of **2**.[11] This antibody-catalyzed reaction is also characterized by remarkable selectivity—the antibody does not catalyze acyl transfer to water despite its presence at 55 M. Such selectivity is similar to that seen in enzymes such as triosephosphate isomerase, which is able to sequester bound intermediates from water.

Not only is it possible to create an enzyme-like catalyst by this approach, one can also recreate other mechanisms by which enzymes have evolved to catalyze similar acyl-group transfer reactions. For example, an antibody which was generated against the phosphonate monoester **9** (Figure 3a) is also a highly selective and efficient acyl transfer catalyst (EM = 10^5 – 10^6 M).[12] However, in this case the reaction was found to proceed through the formation of an acyl-antibody intermediate. Based on X-ray crystallographic and mutagenesis studies, the mechanism likely involves attack of the active site Ser 98^H residue on the bound ester[12, 13] (Figure 3b). In this example, immunological evolution has converged on a mechanism similar to that used by serine proteases and esterases to catalyze acyl-transfer reactions.

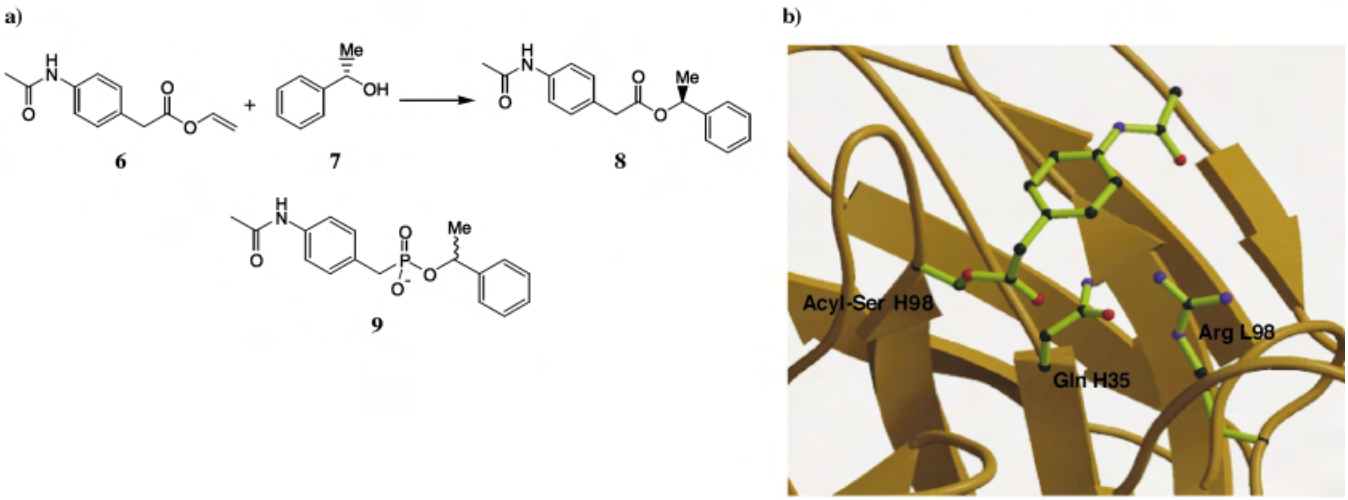


Figure 3. a) Acyl transfer from the ester **6** to the alcohol **7**, catalyzed by antibody 21H3, which was generated against the hapten **9**; b) modeled structure of the acyl–antibody intermediate based on the X-ray crystal structure of the antibody–hapten **9** complex.

 © 2002 WILEY-VCH Verlag GmbH & Co. KGaA, Weinheim 1433-7851/02/4123-4429 $ 20.00+.50/0

One interpretation of this phenomenon is that because of the limited "reagent pool" available to proteins, there are only a limited number of ways to accomplish particular chemical transformations.

2.2. Strain

Another classical theory of enzymatic catalysis is the notion of substrate strain put forth by Haldane in the 1930s.[14] Rather than selectively stabilize a transition state, Haldane argued that enzymes (with β-glucosidase as an example) use binding energy to strain or distort the bound substrate: "The enzyme would thus tend to pull the salicin molecule apart…(or) push the molecules of glucose and saligenin together. The same hypothesis might clearly be applied to other hydrolytic enzymes. Using Fisher's lock and key simile, the key does not fit the lock quite perfectly but exercises a certain strain on it" (Figure 4). This theory has been quite difficult to prove, despite considerable mechanistic effort. Once again synthesis offers an opportunity to test this notion by using it as the basis for the immunological evolution of a catalytic antibody.

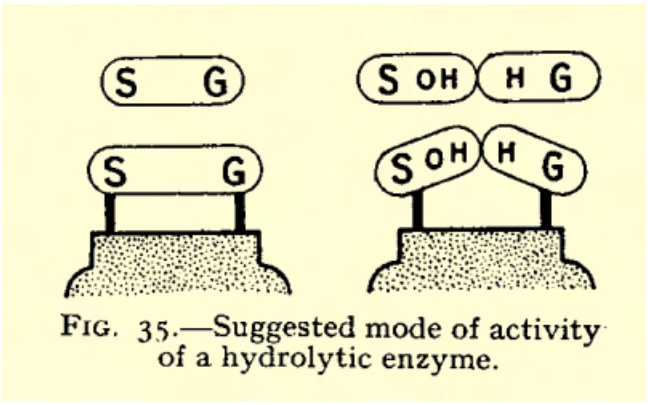


Figure 4. Haldane's strain theory of enzyme catalysis with β-glucosidase as an example (from reference[14]).

The enzyme ferrochelatase catalyzes the last step in heme biosynthesis—metal-cation insertion into the porphyrin ring. The enzyme is thought to catalyze the reaction by distorting the porphyrin ring out of planarity, which facilitates the chelation of the metal ion by the lone pairs of the pyrrole nitrogen atom.[15] If this is indeed the case, then one should be able to synthesize a ferrochelatase by generating antibodies against a distorted porphyrin. To test this concept, antibodies were generated against *N*-methylmesoporphyrin (**12**), a mimic of the strained substrate **10**, synthesized by alkylating an internal nitrogen atom of the mesoporphyrin (Figure 5a). The antibody 7G12 was able to catalyze the metalation of mesoporphyrin (**10**) with Zn^{2+} ions, with rates comparable to the natural biosynthetic enzyme.[16] Resonance Raman studies have shown that the porphyrin ring is distorted out of planarity in an alternating up–down mode.[17] The X-ray crystal structures of both the antibody–*N*-methylmesoporphyrin and antibody–mesoporphyrin complexes provide direct structural evidence for the strain hypothesis—in both

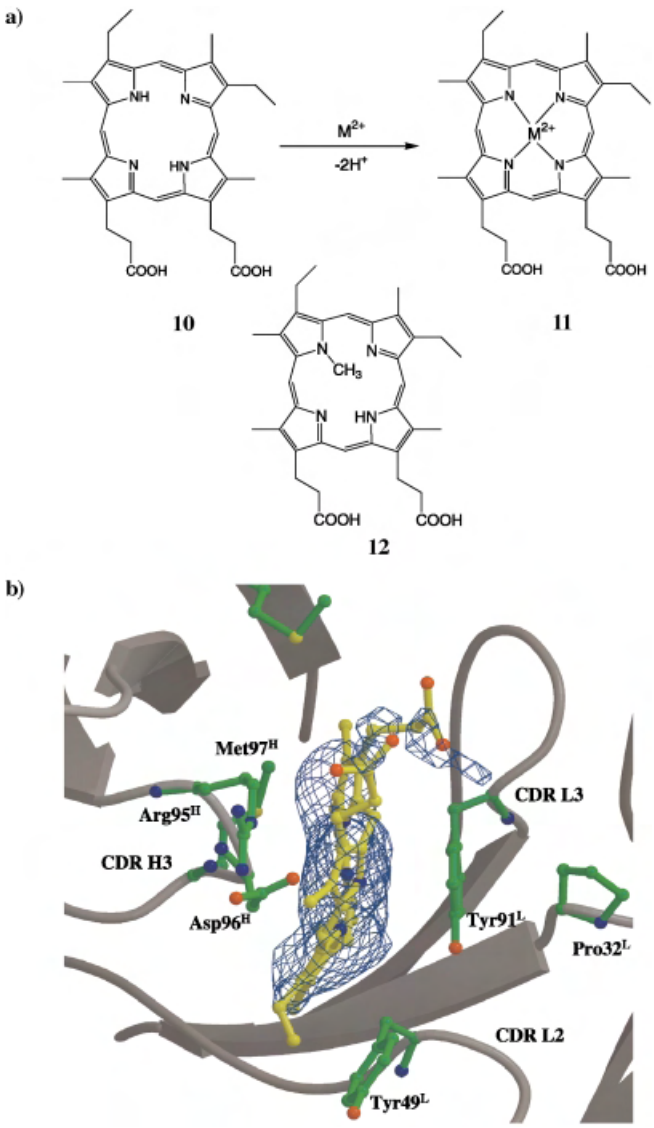


Figure 5. a) Metalation reaction of mesoporphyrin (**10**) catalyzed by antibody 7G12, which was generated against *N*-methylmesoporphyrin (**12**); b) the X-ray crystal structure of the antibody 7G12–**10** Michaelis complex with the *Fo*–*Fc* electron density contoured at 2.0σ. The structure of **10** is shown in yellow, residues of 7G12 that make critical packing interactions with **10** are shown in green.

cases the ring system is clearly distorted (Figure 5b).[18, 19] This distortion is mediated by packing interactions between the pyrrole rings and the Tyr49^{L} and Tyr91^{L} residues in the active site. Thus the synthesis of catalytic antibodies not only yields new biological catalysts, but also tests and validates fundamental principles of enzyme catalysis.

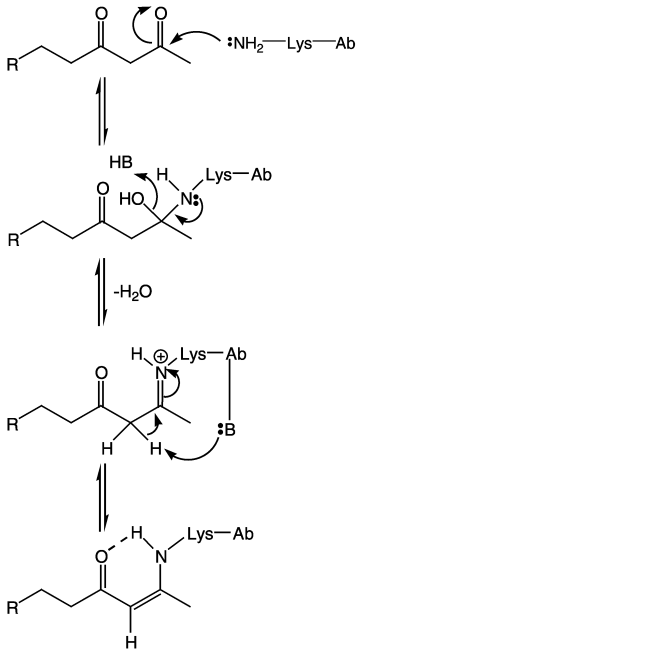
This antibody also catalyzes the H_2O_2-dependent oxidation of organic substrates. We have shown that one can further evolve the catalytic efficiency of this antibody in vitro. A library of active-site mutants was displayed on phage and selected based on the ability to oxidize the substrate tyramine linked to biotin. Oxidation of the tyramine moiety results in covalent attachment of biotin to the peroxidase antibody displayed on phage, which can then be captured by streptavidin beads. A single Tyr49^{L}Trp mutant selected by this method led to a 20-fold increase in rate.[19] Active mutants are

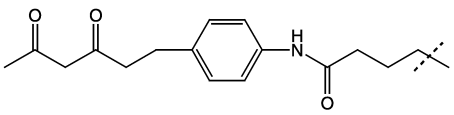
 © 2002 WILEY-VCH Verlag GmbH & Co. KGaA, Weinheim 1433-7851/02/4123-4430 $ 20.00+.50/0

currently being subjected to DNA shuffling to enhance catalytic efficiency further.

2.3. Covalent Catalysis

Another important principle of enzymatic catalysis is covalent catalysis—the use of covalent intermediates to lower the free energy of activation for a reaction.[20–22] How much can the formation of these intermediates contribute to the catalytic efficiency of enzymes? To answer this question, an effort was made to generate an antibody that catalyzes the aldol reaction—the key carbon–carbon bond-forming reaction in organic synthesis. This reaction is catalyzed in glycolysis by an aldolase through the initial formation of a Schiff base intermediate with an active-site lysine.[23] By using the β-diketone **13** as an immunogen[24, 25] (Scheme 1), the evolution of an antibody with a reactive lysine in the active site was chemically programmed. Antibodies containing an





13

Scheme 1. Generation of an aldolase antibody by reactive immunization with the 2-diketone hapten **13**.

appropriately positioned lysine residue were selected based on their ability to form a stable Schiff base (a process termed reactive immunization) with β-diketone protein conjugate.

The result of this experiment was an antibody (38C2) that catalyzes aldol reactions with exquisite specificity and rates close to the natural biosynthetic enzyme. In fact, this catalytic antibody has a broad substrate scope and can catalyze a wide array of aldol reactions with very high enantioselectivities (Figure 6a; >98% *ee*).[26–28] Antibody 38C2 has also been used to carry out the chiral resolution of β-hydroxyketones on gram scale,[29] as well as the selective activation of prodrugs. Moreover, catalytic antibodies (93F3 and 84G3) have been generated that catalyze aldol reactions with the opposite enantioselectivities, again with high *ee* values.[30]

Solution of the X-ray crystal structures of these antibodies reveals a deep hydrophobic pocket containing a buried lysine residue[26] (Figure 6b). This structure is quite similar in many respects to the corresponding enzyme despite the very different frameworks used by these proteins—another example of convergent evolution. These experiments again show that, through a combination of immunological diversity and basic chemical principles, efficient catalysts that rival enzymes can be created.

2.4. Selective Transition-State Stabilization in Disfavored Reactions

Not only can one "synthesize" antibodies that stabilize a rate-limiting transition state, one can generate antibodies that differentially stabilize two competing transition states to afford the kinetically disfavored reaction product which corresponds to the higher energy transition state. Once such example is an antibody-catalyzed elimination reaction in which the antibody 1D4 preferentially stabilizes the disfavored transition that leads to the *syn* elimination of HF from the β-fluoroketone **14** (Scheme 2)[31]. This transition state is calculated to be roughly 5 kcal mol^{-1} higher in energy than that for the favored *anti* elimination reaction. In fact, the antibody catalyzes exclusive formation of the disfavored product. The X-ray crystal structure of the hapten **15**–antibody complex reveals the structural basis for the *syn* binding mode of the substrate and periplanar base-catalyzed elimination.[32] A number of other disfavored reactions have also been catalyzed by antibodies, including epoxide ring opening,[33] Diels-Alder[34, 35] and cationic rearrangement reactions.[36–38] Thus, with the help of antibody binding energy, one can control transition-state energies in ways that might be difficult with classical synthesis.

2.5. Antibody Binding Energy and the Excited-State Reaction Manifold

The previous examples have focused on the use of antibody binding energy to affect the relative energies of various species along a thermally populated reaction coordinate. However, there have also been experiments carried out in which antibody binding energy has been used to control the photophysics and photochemistry of excited-state energy surfaces.[39] For example, the *trans*-stilbene hapten **16** was used to elicit a panel of monoclonal antibodies that display a range of fluorescent spectral behavior when bound to **16** (Figure 7a). The antibody 19G2 afforded a blue fluorescence indicative of an excited-state complex or "exciplex" between *trans*-stilbene and antibody with a fluorescence quantum yield (ϕ_f) of $\approx$0.80 and a radiative lifetime of >30 ns. The behavior of the blue antibody is reminiscent of what occurs as solutions

 © 2002 WILEY-VCH Verlag GmbH & Co. KGaA, Weinheim 1433-7851/02/4123-4431 $ 20.00+.50/0

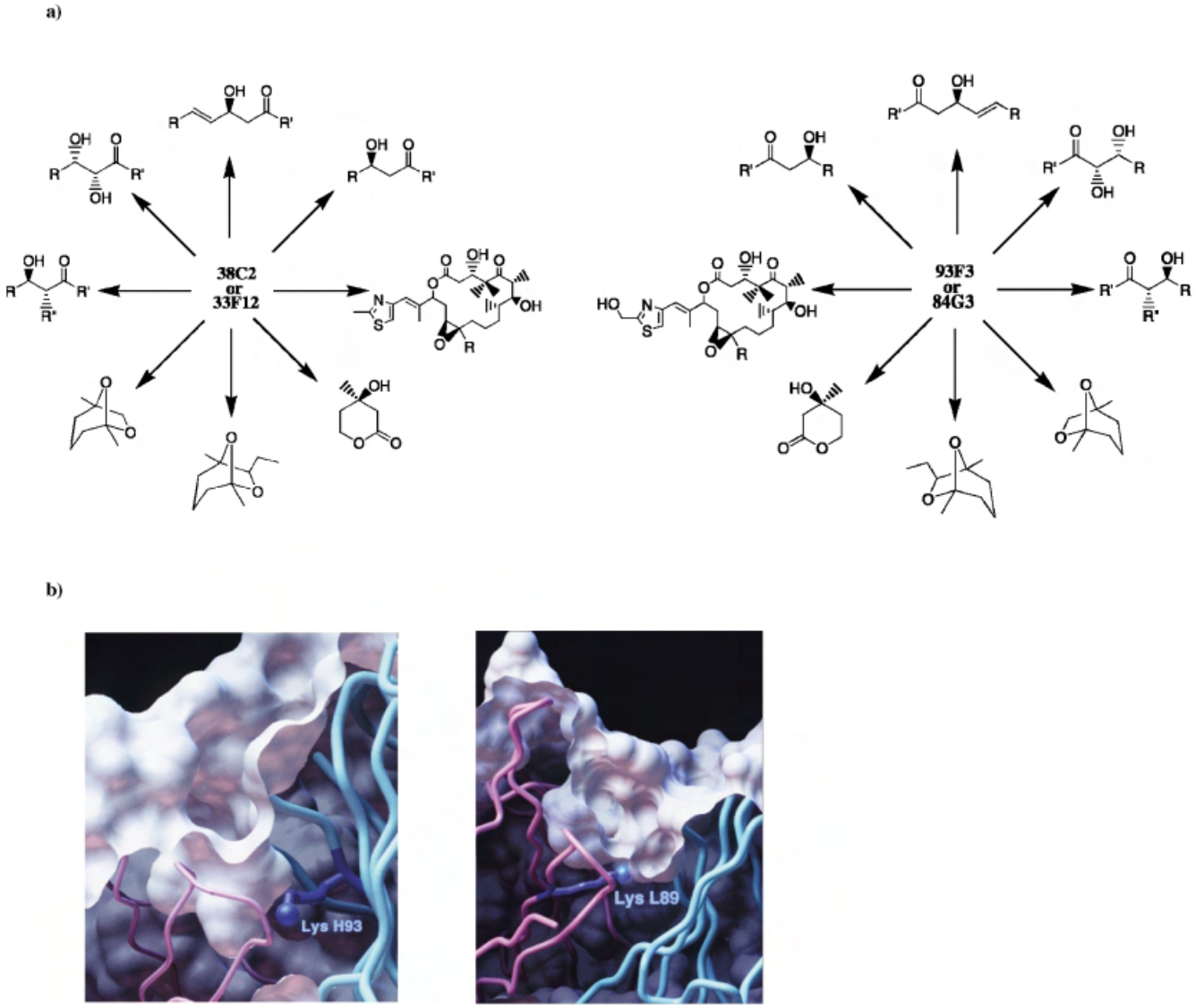
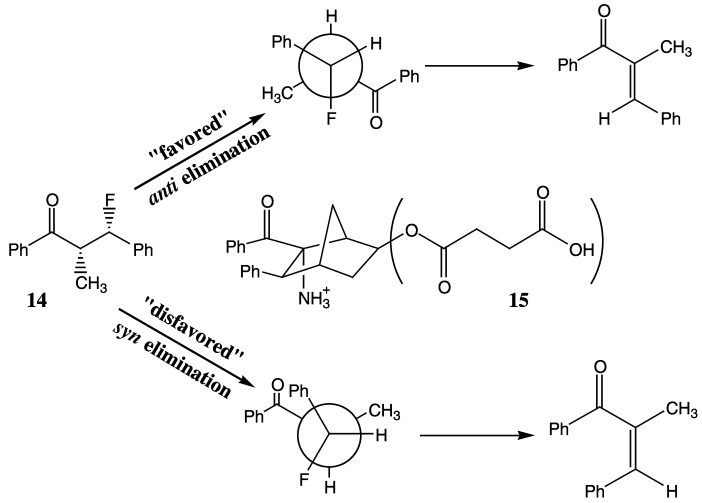


Figure 6. a) Broad substrate scope of antibody-catalyzed aldol reactions. The two antibodies have antipodal activities; b) substrate binding pockets for the antibodies 33F12 (left) and 93F3 (right). The light chain is shown in pink and the heavy chain in blue. The active-site lysine residue is also shown.



Scheme 2. Disfavored *syn*-elimination reaction catalyzed by the antibody 1D4, which was generated against hapten **15**.

of *trans*-stilbene are cooled to very low temperatures, which restricts the isomerization pathway in the excited state and therefore increases the fluorescence quantum yield. Yet, unexpectedly, cooling of a blue-fluorescent antibody complex below a critical temperature (250 K) caused disappearance of the blue emission and produces a purple complex. Thus, antibody 19G2 not only controls the isomerization coordinate of *trans*-stilbene, but also dynamically couples this manifold with active-site residues (Figure 7b). These experiments, and others involving excited-state photocleavage reactions,[40] provide a unique experimental approach for controlling the energetics and interconversion of short-lived excited-state species.

2.6. Endogenous Antibody Catalysis

Given the demonstrated catalytic potential of the antibody molecule, is it possible that endogenous catalytic antibodies

 © 2002 WILEY-VCH Verlag GmbH & Co. KGaA, Weinheim 1433-7851/02/4123-4432 $ 20.00+.50/0

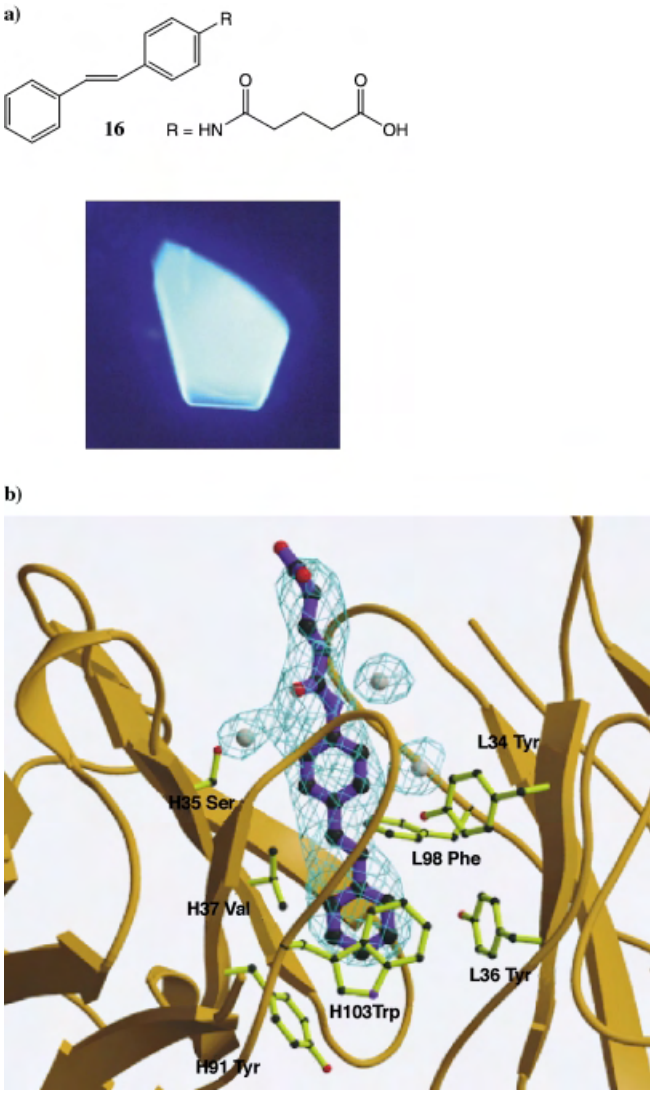


Figure 7. a) Structure of the *trans*-stilbene **16** and a crystal of the Fab 19G2–**16** complex under UV irradiation; b) X-ray crystal structure of Fab 19G2–**16** complex with hapten **16** in blue. The *Fo*–*Fc* electron-density map was contoured at 2.0σ.

may exist in humans? Paul and co-workers have reported that antigen-specific autocatalytic antibodies can be found in the serum of patients with autoimmune disease.[41] In particular, antibodies have been found that efficiently hydrolyze vasoactive intestinal peptide (VIP). The mechanism for the formation of these endogenous catalytic antibodies is to date unknown. It may involve the formation of antiidiotypic antibodies, an approach that has been used in the laboratory to generate antibody esterases and phosphodiesterases.[42] Alternatively, it may be that a selection based solely on binding affinity can in some cases lead to catalysis. Indeed, monoclonal antibodies independently generated to a VIP-protein carrier conjugate were shown to hydrolyze VIP with a catalytic efficiency (k_{cat}/K_m) of $6 \times 10^5\,M^{-1}\,min^{-1}$.[41] Molecular modeling and mutagenesis studies suggest that these antibodies have a catalytic dyad (Ser–His) in the active site. A similar catalytic dyad has been identified crystallographically in a phosphonate-specific esterolytic antibody.[43]

3. The Evolution of Binding Energy and Catalysis

Not only does antibody catalysis give us an opportunity to test fundamental notions of enzymatic catalysis by "synthesis", it also gives us a unique opportunity to characterize the evolution of binding energy and catalytic function in proteins. As we have seen, the combinatorial and mutational processes of the immune system are similar in many respects to those that occur during the natural evolution of enzymes (Table 1 and Figure 1). However, because the immune response occurs in real time, one has the opportunity to analyze the entire immunological evolution of a catalytic antibody—from the germline precursor to the affinity-matured catalyst, as well as putative intermediates along the pathway. Such an analysis has been carried out for five catalytic antibodies to date, and a number of fundamental insights have emerged.

Consider, for example, the evolution of the ferrochelatase catalytic antibody 7G12. As described above, this antibody adopts a similar catalytic mechanism to the naturally occurring enzyme. The germline antibody accumulates five somatic mutations (two in the light chain and three in the heavy chain) as it undergoes affinity maturation.[18] These mutations lead to a 100-fold increase in binding affinity with a concomitant increase in catalytic efficiency. The X-ray crystal structures of the germline (hapten bound and free) and affinity-matured (hapten bound and free) antibodies have been determined[18, 19] (Figure 8). The affinity-matured antibody binds the *N*-methylmesoporphyrin in a Fischer "lock and key" fit binding mode[44] as expected for a high-affinity binding site in which the active site conformation is preorganized. In

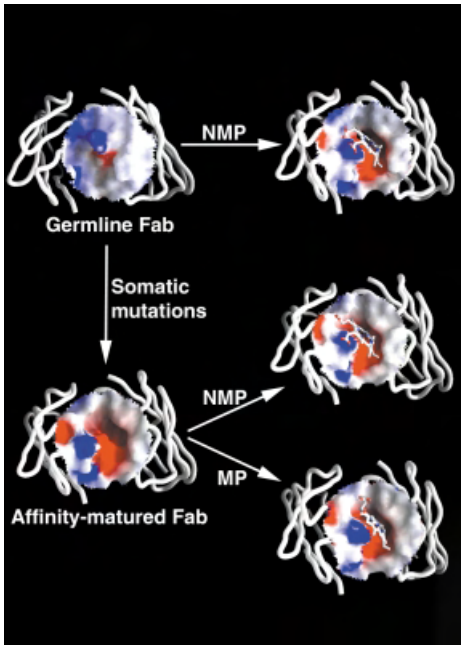


Figure 8. The difference in electrostatic surface potential of the antibody-combining site in the germline Fab and the affinity-matured Fab of antibody 7G12 and their different responses to the binding of hapten *N*-methylmesoporphyrin (NMP) **12** and substrate mesoporphyrin (MP) **10**. The red and blue colors correspond to negative and positive surface potential, respectively.

 © 2002 WILEY-VCH Verlag GmbH & Co. KGaA, Weinheim 1433-7851/02/4123-4433 $ 20.00+.50/0

contrast, the germline antibody undergoes a significant conformational change upon binding of the hapten, especially in the CDR H3 loop. This induced-fit binding conformation is locked by somatic mutation, in particular through a $Ser\,97^{H}$-Met mutation, which introduces a kink into the backbone of the CDR H3 loop. In addition, there is an $Ala\,32^{L}$Pro somatic mutation, which reinforces the packing interaction with $Tyr\,91^{L}$ that appears to distort the bound porphyrin ring.[18]

The conformational flexibility seen in the ferrochelatase germline ligand-free and -bound structures is also evident in three of the other four germline antibodies that have been structurally characterized: a hydrolytic antibody (48G7),[45, 46] an oxy-Cope catalyst (AZ28),[47, 48] and a redox-active antibody (28B4).[49, 50] In each case significant side-chain reorganization of the germline active site occurs upon ligand binding, whereas there are no significant structural differences in the ligand-bound and -free forms of the affinity-matured antibody. Somatic mutations play a key role in fixing the optimal active site conformation.[18, 46, 48, 50, 51] Only the germline antibody for a Diels–Alder catalyst does not show this behavior; in this case the germline light chain was shown to be polyspecific.[52]

Over half a century ago there was considerable debate over the mechanisms by which the immune system is able to evolve selective, high-affinity receptors for a multitude of ligands. Once it was established that the immune system can produce a large number of antibodies with different sequences through recombination and somatic mutation, this sequence diversity was widely accepted as the basis for the tremendous binding potential of antibody repertoire.[3–5] However, Haurowitz, Breitl, and Pauling argued that conformational diversity could also account for the virtually infinite binding potential of the antibody molecule.[53, 54] Just as a human hand can bind and adapt its shape to a large number of structures, so could an antibody active site change its shape to complement a virtually infinite number of ligands. This theory was termed the chemical-instruction theory (Figure 9).

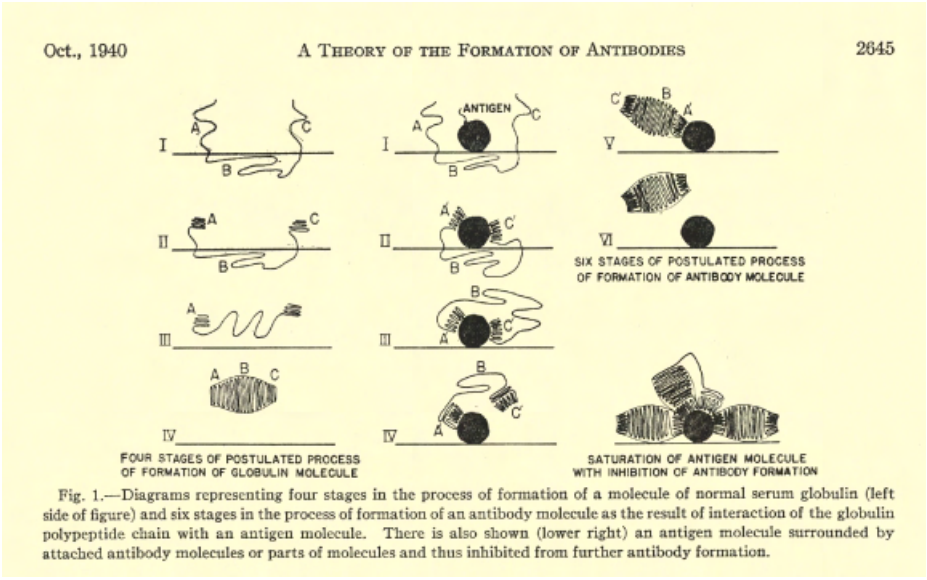


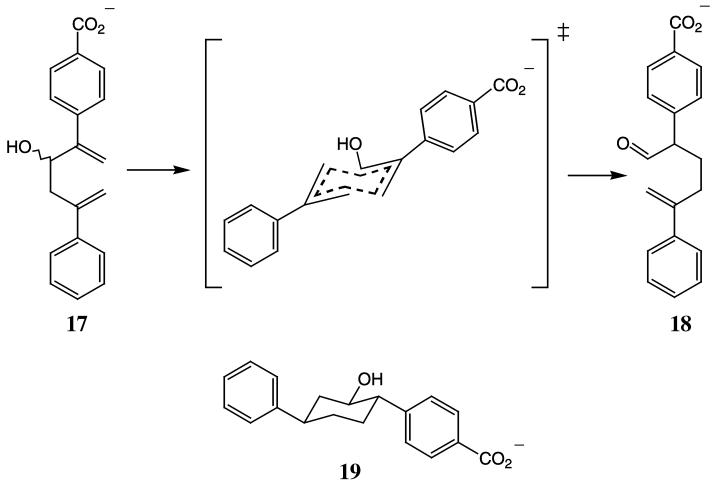
Figure 9. The "chemical-instruction theory" of Pauling (from reference [54]).

We now see with these first structural studies of germline antibodies that conformational diversity does indeed play a key role in germline-binding potential, and allows the germline antibody to adapt many different structures (and ligand-binding modes).[18, 46, 48, 50] This conformational diversity dramatically increases the number of possible germline-combining-site structures. The active-site conformation of the affinity-matured antibody (which has optimal complementarity to the bound ligand) is locked not by folding of the rest of the antibody molecule (as proposed by Pauling), but rather by somatic mutations. Importantly, these studies have also shown that somatic mutation can be either in the active site, or significantly removed in distance, and affect ligand binding through coupled secondary-sphere interactions.

Not only do these experiments provide fundamental new insights into the molecular basis of the immune response, they are relevant to the evolution of the binding and/or catalytic function of other proteins as well. For example, recently it has been shown that many receptor surfaces for protein ligands are also conformationally amorphous, which allows them to bind a large number of different protein and small molecule ligands using the same molecular surface.[55] Moreover, mutational studies of enzymes are beginning to show that one can significantly affect the binding and catalytic properties of enzymes through mutations outside the active site, in much the same way that somatic mutations throughout the antibody variable region affect the maturation of binding affinity.[56] This realization is significantly changing current mutagenesis strategies for the in vitro evolution of enzymes to reflect those used by the immune system.[57]

Similar studies of the immunological evolution of the antibody AZ28, which catalyzes an oxy-Cope rearrangement, suggest that the conformational diversity of the germline repertoire can also play a dynamic role in catalysis. It was thought that an antibody generated to the chairlike hapten **19** might catalyze the related oxy-Cope rearrangement (Scheme 3) by binding the acyclic substrate **17** in a cyclic conformation with favorable π-orbital alignment.[58] Such stereoelectronic effects are thought to play a key role in enzymatic catalysis.[59, 60] Surprisingly, the germline antibody accelerated the reaction by 3×10^{5} fold (within a factor of three of the corresponding enzyme chorismate mutase), while the affinity-matured antibody of AZ28 was roughly 100 fold less active. Structural studies of the affinity-matured antibody again showed that the hapten is bound in a lock and key conformation with packing interactions between the antibody and 2,5-aryl substituents locking the substrate into the desired cyclic conformation (consistent with NMR spectroscopic studies of the Michaelis complex).[47] An anionic substituent effect also appears to

 © 2002 WILEY-VCH Verlag GmbH & Co. KGaA, Weinheim 1433-7851/02/4123-4434 $ 20.00+.50/0 *Angew. Chem. Int. Ed.* **2002**, *41*, No. 23



Scheme 3. Transition-state analogue **19** and the oxy-Cope rearrangement catalyzed by antibody AZ28.

contribute to the rate enhancement. However, the 2-aryl ring of bound **19** is orthogonal to the six electron π system, which results in poor orbital overlap in the transition state.[47] The structures of the ligand-bound and -free forms of the germline antibody provide an explanation for the increased rate of this antibody despite its lower affinity for the hapten **19** (Figure 10). Again, there appears to be conformational flexibility in the germline antibody, which in this case allows the 2-aryl ring to rotate into planarity, which increases π overlap and as a result lowers the activation energy.[47, 48, 61] This is of course a static picture and must be confirmed by NMR spectroscopy, but it strongly suggests that the conformational diversity of the germline repertoire can also play a dynamic role in catalysis, much as it is now being realized that side-chain dynamics play a key role in enzymatic catalysis. It may also be possible that the induced-fit mechanisms of enzymes may be vestiges of earlier conformational flexibility that was retained through evolution based on a catalytic, selective advantage.

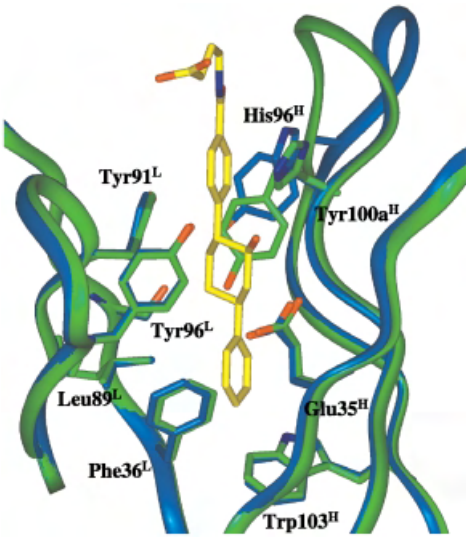


Figure 10. Overlay of the active sites for the germline antibody structures of AZ28 with the hapten **19** (blue) and without hapten (green). The hapten is shown in yellow.

4. Expanding Upon the Concept of Biological Diversity

The combinatorial strategies embodied by the immune response, and well-known to immunochemists, are now being applied by chemists to a huge number of synthetic challenges.[62] This approach is applicable to any molecular structure that can be assembled either in a stepwise or concerted fashion from a set of molecular precursors, and where a screen or selection for a desired function exists. For example, synthetic libraries of protein and nucleic acids are being screened for novel catalytic and binding properties. Synthetic small molecules can also be assembled in a combinatorial fashion from building blocks to create chemical diversity that can be screened for selective binding to biological receptors (the inverse of the immune response). Combinatorial methods have even been used to screen the entire periodic table successfully for combinations of elements that lead to new materials with novel electronic, catalytic, structural, magnetic, and optical properties (Figure 11).[63, 64] Characterization of

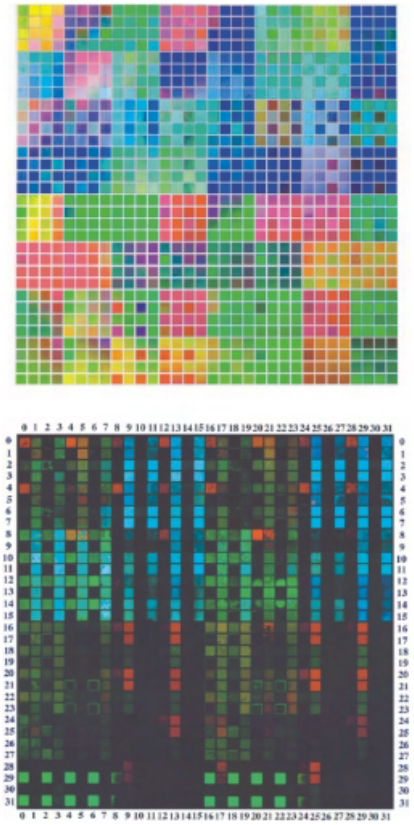


Figure 11. A library of metal oxides that contains novel fluorescent materials under ambient light (above) and UV irradiation (below).

the properties of these new molecules affords new physical, chemical, and biological insights that lead to an improved theoretical understanding of the relationship between molecular structure and function. This mechanistic insight leads in turn to an improved ability to synthesize molecular function.

 © 2002 WILEY-VCH Verlag GmbH & Co. KGaA, Weinheim 1433-7851/02/4123-4435 $ 20.00+.50/0

5. All Antibodies Are Catalytic—A New Paradigm

The above examples of antibody catalysis underscore the tremendous chemical potential of natural molecular diversity to produce selective catalysts, when programmed by chemists with the appropriate chemical instructions. Over one hundred reactions have been catalyzed to date, including carbon–carbon bond-forming reactions (e.g. Diels–Alder and aldol reactions), redox reactions (e.g. heteroatom, carbon atom, and H_2O oxidation), rearrangement reactions (e.g. sigmatropic rearrangements and cationic cyclization reactions) and hydrolytic reactions (e.g. ester, amide, phosphodiester, and glycosidic-bond hydrolysis). The broad scope of antibody catalysis raises the inevitable question of whether natural antibody catalysis is an intrinsic component of the immune response, which either converts toxic products into harmless materials, or actually generates toxic materials to kill infectious agents. The demonstration of such activity would represent a major shift in the general belief that antibodies simply use their binding to target antigens, which then initiate destruction by using effector systems which are not part of the antibody molecule.

Remarkably, it now appears that all antibodies, regardless of their source or antigenic specificity, are themselves catalysts that have the potential to generate a remarkable array of highly toxic oxidants with the capacity to destroy antigens.[65–68] Some of these oxidants are similar to those known to be generated by phagocytes, whereas others have not been encountered in biology. These findings may demonstrate a shift in the way the humoral component of the immune system is thought to function.

Work carried out over the last century has led to a consensus on how the humoral component of the immune system is organized (Figure 12). The central idea is that, unlike enzymes, antibodies do not have sophisticated chemical functions—they simply function as signaling molecules which activate effector systems upon binding with an antigen. These effector systems, which include the complement cascade and phagocytic cells, are in contrast to antibodies considered to be highly sophisticated chemical cascades that generate reactive proteins and chemical oxidants, respectively, that may be capable of killing infectious agents. But if the antibody itself is a catalyst for the generation of oxidants, then recognition and killing become linked within the antibody molecule itself and the role of the antibody in defense goes far beyond simple signaling. In addition to changing our concepts about the role of antibodies in immune defense, we may gain new insights into the role of antibodies in disease, in that oxidants generated by them may play a previously unrecognized role in the pathology that occurs when this defense system is not perfectly controlled.

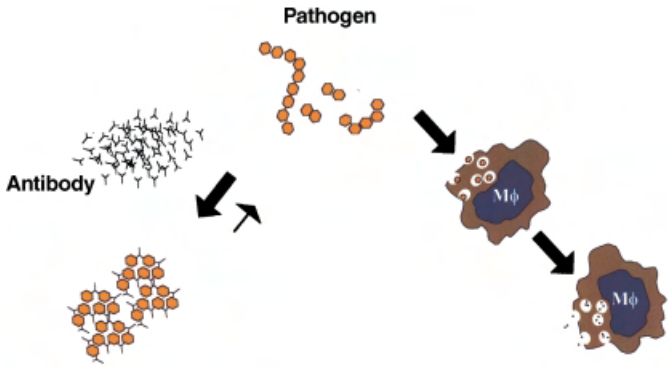


Figure 12. The conventional view of the roles of antibodies in the humoral system: antibodies bind whereas phagocytes destroy pathogens.

Studies of the blue fluorescent antibody[39] mentioned above led to the observation that this antibody and all others characterized to date can produce H_2O_2 from $^1O_2$ without damage to the protein catalyst. Metals or Cl^- ions have been excluded as the source of electrons. On the basis of isotope-incorporation experiments and kinetic data, it has been proposed that antibodies use H_2O as an electron source, which facilitates its addition to $^1O_2$ to form H_2O_3 as an intermediate: [Eq. (1)]

$$^1O_2 + H_2O \rightleftarrows [H_2O_3] \rightarrow H_2O_2 + O_2 \quad (1)$$

X-ray crystallographic studies with xenon indicate putative conserved oxygen-binding sites within the antibody fold, where this chemistry could be initiated. The exact nature of the oxidants produced by the antibody-catalyzed water-oxidation cascade is still under study, but Goddard and coworkers have calculated a number of energetically reasonable pathways by which H_2O_3 can collapse to form H_2O_2.[67, 68] Many of these pathways can be expected to produce highly reactive oxidants not previously observed in biology.

One question often asked concerns the source of the substrate singlet oxygen that antibodies need to initiate the oxidative cascade. Interestingly, when antibody that is bound to the infectious agent signals activation of the cellular effector systems in white blood cells, they generate $^1O_2$ from the reaction of H_2O_2 with HOCl to produce HO_2Cl, which subsequently reacts to afford $^1O_2$. Thus, signaling by the antibody causes its own substrate to be generated such that the very molecule that started the process and is still attached to the infectious agent can generate its own oxidants. While this cascade might seem complicated, it should be remembered that the function of the system is to generate highly toxic substances and their production must be tightly controlled to avoid collateral damage to the host. Because the antibody molecule is the most proximal to the infectious agent, one might expect the oxidant that it generates to be the most effective, while at the same time minimizing collateral damage. This is especially important when the oxidants are short-lived. What is perhaps most surprising is that the field of antibody catalysis, of which the aim was to exploit the selective binding energy of antibody molecules for catalysis, ultimately led to the discovery that these proteins were enzymes all along.

The authors gratefully acknowledge the valuable assistance of Tanya Gresham, Coran Watanabe, and Andrew Martin, whose efforts have made this review possible. This is manuscript 14904-CH of the Scripps Research Institute.

Received: April 2, 2002 [M1561]

 © 2002 WILEY-VCH Verlag GmbH & Co. KGaA, Weinheim 1433-7851/02/4123-4436 $ 20.00+.50/0

[1] M. Eigen, *Steps Towards Life, a Perspective on Evolution*, Oxford University, Oxford, **1992**.
[2] W. P. Jencks, *Catalysis in Chemistry and Enzymology*, McGraw-Hill, New York, **1969**.
[3] F. M. Burnet, *The Clonal Selection Theory of Acquired Immunity*, Cambridge University, Cambridge, **1959**.
[4] D. W. Talmage, *Science* **1959**, *129*, 1643.
[5] S. Tonegawa, *Nature* **1983**, *302*, 575.
[6] D. R. Davies, S. Chacko, *Acc. Chem. Res.* **1993**, *26*, 421.
[7] L. Pauling, *Chem. Eng. News* **1946**, *24*, 1375.
[8] L. Pauling, *Am. Scient.* **1948**, *36*, 51.
[9] J. R. Jacobsen, J. R. Prudent, L. Kochersperger, S. Yonkovich, P. G. Schultz, *Science* **1992**, *256*, 365.
[10] M. I. Page, W. P. Jencks, *Proc. Natl. Acad. Sci. USA* **1971**, *68*, 1678.
[11] E. M. Driggers, C. W. Liu, D. E. Wemmer, P. G. Schultz, *J. Am. Chem. Soc.* **1998**, *120*, 7395.
[12] P. Wirsching, J. A. Ashley, S. J. Benkovic, K. D. Janda, R. A. Lerner, *Science* **1991**, *252*, 680.
[13] R. C. Stevens, personal communication.
[14] J. B. S. Haldane, *Enzymes*, Longmans Green, London, **1930**.
[15] M. J. Bain-Ackerman, D. K. Lavallee, *Inorg. Chem.* **1979**, *18*, 3358.
[16] A. G. Cochran, P. G. Schultz, *Science* **1990**, *249*, 781.
[17] M. E. Blackwood, Jr., T. S. Rush III, F. Romesberg, P. G. Schultz, T. G. Spiro, *Biochemistry* **1998**, *37*, 779.
[18] F. E. Romesberg, B. D. Santarsiero, B. Spiller, J. Yin, D. Barnes, P. G. Schultz, R. C. Stevens, *Biochemistry* **1998**, *37*, 14404.
[19] J. Yin, A. E. Beuscher III, S. Andryski, R. C. Stevens, P. G. Schultz, unpublished work.
[20] E. E. Snell, S. J. Di Mari in *The Enzymes*, *Vol. 2* (Ed.: P. D. Boyer), Academic Press, New York, **1970**, p. 335.
[21] G. A. Hamilton, F. H. Westheimer, *J. Am. Chem. Soc.* **1959**, *81*, 6332.
[22] O. Tsolas, B. L. Horecker in *The Enzymes*, *Vol. 7* (Ed.: P. D. Boyer), Academic Press, New York, **1972**, p. 259.
[23] A. Heine, G. DeSantis, J. G. Luz, M. Mitchell, C. H. Wong, I. A. Wilson, *Science* **2001**, *294*, 369.
[24] J. Wagner, R. A. Lerner, C. F. Barbas III, *Science* **1995**, *270*, 1797.
[25] P. Wirsching, J. A. Ashley, C. H. Lo, K. D. Janda, R. A. Lerner, *Science* **1995**, *270*, 1775.
[26] C. F. Barbas III, A. Heine, G. Zhong, T. Hoffmann, S. Gramatikova, R. Bjornestedt, B. List, J. Anderson, E. A. Stura, I. A. Wilson, R. A. Lerner, *Science* **1997**, *278*, 2085.
[27] T. Hoffmann, G. Zhong, B. List, D. Shabat, J. Anderson, S. Gramatikova, R. A. Lerner, C. F. Barbas III, *J. Am. Chem. Soc.* **1998**, *120*, 2768.
[28] S. C. Sinha, C. F. Barbas III, R. A. Lerner, *Proc. Natl. Acad. Sci. USA* **1998**, *95*, 14603.
[29] G. Zhong, D. Shabat, B. List, J. Anderson, S. C. Sinha, R. A. Lerner, C. F. Barbas III, *Angew. Chem.* **1998**, *110*, 2609; *Angew. Chem. Int. Ed.* **1998**, *37*, 2481.
[30] G. Zhong, R. A. Lerner, *Angew. Chem.* **1999**, *111*, 3957; *Angew. Chem. Int. Ed.* **1999**, *38*, 3738.
[31] B. F. Cravatt, J. A. Ashley, K. D. Janda, D. L. Boger, R. A. Lerner, *J. Am. Chem. Soc.* **1994**, *116*, 6013.
[32] N. A. Larsen, A. Heine, L. Crane, B. F. Cravatt, R. A. Lerner, I. A. Wilson, *J. Mol. Biol.* **2001**, *314*, 93.
[33] K. D. Janda, C. G. Shevlin, R. A. Lerner, *Science* **1993**, *259*, 490.
[34] A. C. Braisted, P. G. Schultz, *J. Am. Chem. Soc.* **1990**, *112*, 7430.
[35] V. E. Gouverneur, K. N. Houk, B. de Pascual-Teresa, B. Beno, K. D. Janda, R. A. Lerner, *Science* **1993**, *262*, 204.
[36] K. D. Janda, C. G. Shevlin, R. A. Lerner, *J. Am. Chem. Soc.* **1995**, *117*, 2659.
[37] L. Ma, E. H. Sweet, P. G. Schultz, *J. Am. Chem. Soc.* **1999**, *121*, 10227.
[38] P. G. Schultz, R. A. Lerner, *Acc. Chem. Res.* **1993**, *26*, 391.
[39] A. Simeonov, M. Matsushita, E. A. Juban, E. H. Thompson, T. Z. Hoffman, A. E. Beuscher IV, M. J. Taylor, P. Wirsching, W. Rettig, J. K. McCusker, R. C. Stevens, D. P. Millar, P. G. Schultz, R. A. Lerner, K. D. Janda, *Science* **2000**, *290*, 307.
[40] J. R. Jacobsen, A. G. Cochran, J. C. Stephans, D. S. King, P. G. Schultz, *J. Am. Chem. Soc.* **1995**, *117*, 5453.
[41] M. Sun, Q. S. Gao, L. Kirnarskiy, A. Rees, S. Paul, *J. Mol. Biol.* **1997**, *271*, 374.
[42] A. V. Kolesnikov, A. V. Kozyr, E. S. Alexandrova, F. Koralewski, A. V. Demin, M. I. Titov, B. Avalle, A. Tramontano, S. Paul, D. Thomas, A. G. Gabibov, A. Friboulet, *Proc. Natl. Acad. Sci. USA* **2000**, *97*, 13526.
[43] G. W. Zhou, J. Guo, W. Huang, R. J. Fletterick, T. S. Scanlan, *Science* **1994**, *265*, 1059.
[44] E. Fischer, *Ber. Dtsch. Chem. Ges.* **1894**, *27*, 3189.
[45] P. A. Patten, N. S. Gray, P. L. Yang, C. B. Marks, G. J. Wedemayer, J. J. Boniface, R. C. Stevens, P. G. Schultz, *Science* **1996**, *271*, 1086.
[46] G. J. Wedemayer, P. A. Patten, L. H. Wang, P. G. Schultz, R. C. Stevens, *Science* **1997**, *276*, 1665.
[47] H. D. Ulrich, E. Mundorff, B. D. Santarsiero, E. M. Driggers, R. C. Stevens, P. G. Schultz, *Nature* **1997**, *389*, 271.
[48] E. C. Mundorff, M. A. Hanson, A. Varvak, H. Ulrich, P. G. Schultz, R. C. Stevens, *Biochemistry* **2000**, *39*, 627.
[49] L. C. Hsieh-Wilson, P. G. Schultz, R. C. Stevens, *Proc. Natl. Acad. Sci. USA* **1996**, *93*, 5363.
[50] J. Yin, E. C. Mundorff, P. L. Yang, K. U. Wendt, D. Hanway, R. C. Stevens, P. G. Schultz, *Biochemistry* **2001**, *40*, 10764.
[51] P. L. Yang, P. G. Schultz, *J. Mol. Biol.* **1999**, *294*, 1191.
[52] F. E. Romesberg, B. Spiller, P. G. Schultz, R. C. Stevens, *Science* **1998**, *279*, 1929.
[53] F. Breinl, F. Haurowitz, *Z. Physiol. Chem.* **1930**, *192*, 45.
[54] L. Pauling, *J. Am. Chem. Soc.* **1940**, *62*, 2643.
[55] W. L. DeLano, M. H. Ultsch, A. M. de Vos, J. A. Wells, *Science* **2000**, *287*, 1279.
[56] M. C. Orencia, J. S. Yoon, J. E. Ness, W. P. Stemmer, R. C. Stevens, *Nat. Struct. Biol.* **2001**, *8*, 238.
[57] W. P. Stemmer, *Nature* **1994**, *370*, 389.
[58] A. C. Braisted, P. G. Schultz, *J. Am. Chem. Soc.* **1994**, *116*, 2211.
[59] D. R. Storm, D. E. Koshland, *J. Am. Chem. Soc.* **1972**, *94*, 5805.
[60] A. J. Kirby, *Crit. Rev. Biochem.* **1987**, *22*, 283.
[61] E. M. Driggers, H. S. Cho, C. W. Liu, C. P. Katzka, A. C. Braisted, H. D. Ulrich, D. E. Wemmer, P. G. Schultz, *J. Am. Chem. Soc.* **1998**, *120*, 1945.
[62] D. R. Liu, P. G. Schultz, *Angew. Chem.* **1999**, *111*, 36; *Angew. Chem. Int. Ed.* **1999**, *38*, 36.
[63] X.-D. Xiang, X. Sun, G. Briceno, Y. Lou, K.-A. Wang, H. Chang, W. G. Wallace-Freedman, S.-W. Chen, P. G. Schultz, *Science* **1995**, *268*, 1738.
[64] J. Wang, Y. Yoo, C. Gao, I. I. Takeuchi, X. Sun, H. Chang, X. Xiang, P. G. Schultz, *Science* **1998**, *279*, 1712.
[65] A. D. Wentworth, L. H. Jones, P. Wentworth, Jr., K. D. Janda, R. A. Lerner, *Proc. Natl. Acad. Sci. USA* **2000**, *97*, 10930.
[66] P. Wentworth, Jr., L. H. Jones, A. D. Wentworth, X. Zhu, N. A. Larsen, I. A. Wilson, X. Xu, W. A. Goddard III, K. D. Janda, A. Eschenmoser, R. A. Lerner, *Science* **2001**, *293*, 1806.
[67] D. Datta, N. Vaidehi, X. Xu, W. A. Goddard III, *Proc. Natl. Acad. Sci. USA* **2002**, *99*, 2636.
[68] X. Xu, R. P. Muller, W. A. Goddard III, *Proc. Natl. Acad. Sci. USA* **2002**, *99*, 3376.

 © 2002 WILEY-VCH Verlag GmbH & Co. KGaA, Weinheim 1433-7851/02/4123-4437 $ 20.00+.50/0

Emil Fischer—Unequalled Classicist, Master of Organic Chemistry Research, and Inspired Trailblazer of Biological Chemistry

Horst Kunz*

Even if in life one has the good fortune to meet many important scientists and chemists, much reverence descends whenever the name of Emil Fischer is mentioned (Figure 1). This reverence and admiration increases still further the closer one looks into the scientific life work of this ingenious natural-science researcher. This year, 2002, there are numerous reasons to commemorate the pioneering achievements of Emil Fischer. His 150th birthday falls on October 9, and this year it is 100 years since Emil Fischer was awarded the Nobel Prize for Chemistry by the Royal Academy of Sciences in Stockholm.

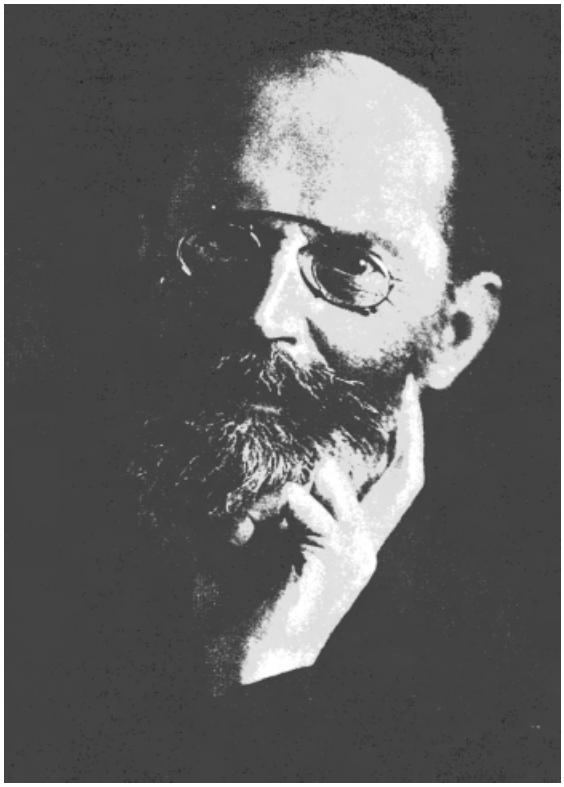


Figure 1. Portrait of Emil Fischer (reproduced, with permission from Springer Verlag, from reference [2]).

[*] Prof. Dr. H. Kunz
Institut für Organische Chemie der Universität Mainz
Duesbergweg 10–14, 55128 Mainz (Germany)
Fax: (+49) 6131-3924786
E-mail: hokunz@mail.uni-mainz.de

The scientific achievements of Emil Fischer has left a lasting impression in many areas of chemistry, and even today they are of fundamental importance and influence. His student and professional career in the 1870s began with the then fascinating chemistry of organic dyes. With his first major discovery, phenylhydrazine, he opened up new pathways in heterocyclic chemistry with the synthesis of indoles. With his investigations into caffeine, uric acids, and other purines he moved into the area of natural product chemistry, which he led to its first great peak of achievement with his fundamental work on carbohydrates (based on their reactions with phenylhydrazine), peptides, and proteins, the results of which are still pertinent today. If one considers further that Emil Fischer performed pioneering work in the synthesis of tanning agents and fats, that he was able to provide a concept of the structure of nucleic acids, that with Heinrich Kiliani he became the founder of stereoselective synthesis, that he introduced stereochemical nomenclature and structural assignment, and that with his work on enzymes from beer yeast and bitter almonds he became the founder of biochemistry, it is quite obvious that Emil Fischer "is to the present day the greatest genius of organic chemistry".[1]

Amazed, one must ask oneself how a single scientist could achieve such a tremendous life's work? The main reasons are of course to be sought in Emil Fischer's talents. On the other hand, for such talents to come to full development and fruition the family and professional environment and the social factors in Germany during the second half of the 19th century and the beginning of the 20th century must have exercised a distinctly beneficial influence. Fortunately, Emil Fischer himself has provided some insight in this respect.[2] It is not at all a matter of course that in this point the present, overburdened with proclamations and predictions, bears comparison with the Wilhelminic reign, generally regarded as reactionary.

Emil Fischer[2] was born on October 9, 1852 in Euskirchen, about 30 km west of Bonn, as the youngest of eight children of Laurenz Fischer and his wife Julie, née Poensgen. Two of the siblings had died previously; thus Emil Fischer grew up with five older sisters. In order to escape their upbringing wiles occasionally, he frequently withdrew for a few days, with the permission of his parents, to the neighboring house occupied

 © 2002 WILEY-VCH Verlag GmbH & Co. KGaA, Weinheim 1433-7851/02/4123-4439 $ 20.00+.50/0

by the family of his uncle August Fischer, where there were five sons and a daughter. One of the cousins, Otto Fischer, was later also to become a chemist and with him demonstrated the structure of the rosaniline dyes to be triphenylmethane derivatives.[3] It transpires from his memoirs[2] that Emil Fischer grew up in a lively, extended Rheinland protestant family and had a "totally happy youth". The harmonious relationships in the extended Fischer family gave the boy much stimulation for his later professional life. Particularly striking was the influence of his parents, whose personality Emil Fischer described with affection. Although quite different "in character, opinion, and inclination", they led a "very happy marriage". One has the impression that their considerable but different talents complemented each other in the best possible way in the exceptional gifts of the son.

The father, Laurenz Fischer, ran a flourishing business with two of his brothers, first in Flamersheim, then in Euskirchen, where his brothers managed the office and warehouse "with the greatest care" whilst he ran the external relationships of the company Gebrüder Fischer (Fischer Brothers) with enterprise, vigor, and considerable success. From his enterprise arose the purchase of a small wool spinner in the neighboring community of Wisskirchen. Aniline dyes were then almost unknown, and dying with the natural colors indigo, fustic, and logwood proved to be a poorly reproducible art. The father, Laurenz, "who at all times had regarded self-reliance highly" set up a small experimental dye-works in Euskirchen. Not only did his regard for chemistry grow from this experience, but at the same time it inspired Emil Fischer and his cousin Otto in their later choice of career. This was reinforced still further when father Laurenz became involved in a cement works near Bonn which was managed by the chemist Dr. Bleibtreu (a student of A. W. von Hofmann), who repeatedly encouraged the young Emil Fischer to become a chemist.

When in the 1860s the enterprising father became decisively involved in the establishment of a brewery in Dortmund further motivation arose for Emil Fischer, at least in his later professional life as a chemist. Thus during his years in Munich he heard of the Linde refrigerating machines, the installation of which he supervised for cellar cooling in his father's brewery. Some time later, when he stayed at Strasbourg University for a second time to perfect his analytical experience, he learnt of Louis Pasteur's book "Ètudes sur la bière". During his reading he learnt that contamination of beer yeast by other microorganisms had a deleterious effect on the condition of the beer. When he informed his father of this fact, he was asked to study the matter immediately in greater detail for the brewery. Thus, using a microscope and with the help of the Strasbourg biologists Fitz and de Bary, Emil Fischer carried out studies on schizomycetes, mould fungus, and *Blastomyces* fungi, which resulted in the introduction of microscopic purity control of brewing yeast in the Dortmund brewery. This came in very useful for him later in his work on sugars and their converting enzymes.

The bold enterprise of the father, who at the same time displayed "a great clarity of mind" was not only a model for the young Emil, but it was also reflected in his own character, which was important for his development as a scientist. Emil Fischer described his mother as a very clever woman, thirsty for knowledge, who came from a family of iron manufacturers in an Eifel valley.[2] Her forefathers had worked there for centuries as producers of iron and iron products. Emil Fischer himself assumed that he had inherited his joy of chemical and technical processes from them. His mother's deeply religious nature stems from her upbringing, in part in the evangelical Moravian community in Neuwied. She was more serious than the father, but could laugh heartily at his jokes. "Only when she encountered crude or common expression did she express her indignation so clearly that in her presence everyone was forced to behave with decency." She was clearly very independent in her political opinions: In the 1863/64 dispute between the Prussian government and the parliament, the father belonged to the opposition party, like most Rhinelanders, while she supported Bismarck. In her political judgments she opposed the father so vigorously that he jokingly called her "Frau Bismarck". She always supported her son's leanings towards scientific studies, and it can be assumed that it was from her side that Emil Fischer inherited his interest in natural science processes and experimentation, and also thoughtfulness, ability for analytical rigor, and courage for independent assessment. Together with the vigor, the energy, and the resolve of the father, the young Emil Fischer was so clearly equipped with the aptitude to open up critical pathways of clarity in the then still hugely unknown primeval forest of chemical sciences.

These abilities became evident even during his school years, which for Emil Fischer began after his fifth birthday. Until his ninth year he was taught by an excellent teacher, Mr. Vierkoetter, in a private school founded by his father for the children of the few protestant families in his home town. Although children aged 5 to 14 years were taught in one room, this teacher not only understood how to treat the elementary subjects thoroughly, but he also introduced, for example, Euclidian mathematics to the more talented students. Thus the transfer to the secondary schools in Euskirchen and later to the high school was easy for the young Emil.

The first two years of his high-school period were spent with his cousin Ernst Fischer in the Hessian town of Wetzlar, where he again experienced excellent tuition in mathematics. The time in Wetzlar had for the young Fischers the traits of an anticipated student life, filled with music and conviviality. Emil Fischer considered that the reason for his "later gastric illness lay in his immoderation in smoking and drinking". He spent the last two years of his schooling at the high school in Bonn. He was "always an exceptionally gifted and good student, even in subjects that he did not like, supported by an excellent memory that remained true to him into his old age".[4] In the Spring of 1869 he graduated "primus omnium".

Emil Fischer's particular interest lay in physics and mathematics. However, he complied with his father's wish and commenced a commercial apprenticeship in the timber business of his brother-in-law in Rheydt in preparation for a later entry into the family business. However, the activity did not constrain him so that in addition he undertook private tuition in chemistry and set up a tiny laboratory in an empty room in the company building. The experiments undertaken by him there "ended in a smell or dirty, burnt fingers, and

 © 2002 WILEY-VCH Verlag GmbH & Co. KGaA, Weinheim 1433-7851/02/4123-4440 $ 20.00+.50/0 *Angew. Chem. Int. Ed.* **2002**, *41*, No. 23

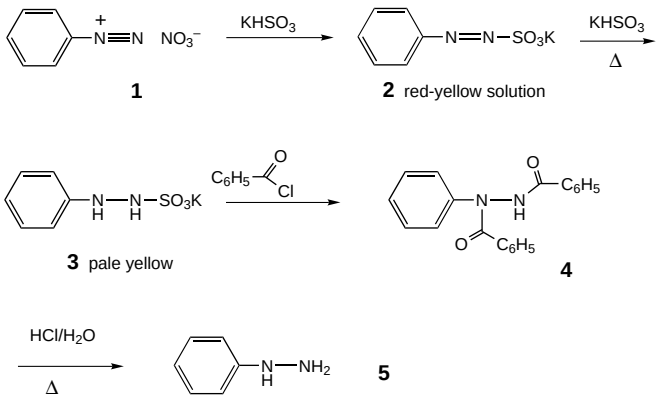
because of the risk of fire became uncomfortable for the owner of the business".[2] Thus the attempt to make a businessman out of Emil Fischer was abandoned, and the father agreed, possibly also because of his own experiences at the dye-works of the wool spinners, that the son should study not physics and mathematics, but chemistry.

From the summer semester of 1871 Emil Fischer spent the first three semesters at Bonn University, where he attended botany, physics, and chemistry lectures. The latter, held by Kekulé, particularly impressed him. However, the analytical practical course was old-fashioned in both equipment and procedure. The use of water pumps, which had long before been introduced by Bunsen, was unknown. When a precipitate of iron and aluminum hydroxides could not be filtered and washed, Emil Fischer would have switched from chemistry to physics, his old preference, had it not been for his cousin Ernst Fischer, now a medical student in Bonn. He suggested that he change institute. The other cousin, Otto Fischer, who had also begun to study chemistry, joined in the move.

More by chance the choice fell on Strasbourg in the Alsace, which Emil Fischer regarded as complete luck, for in this way the two cousins entered the laboratory of Adolf von Baeyer in the fall of 1872. The two Fischers followed a modern analytical practical course under the guidance of Adolf von Baeyer and Friederich Rose, in which they experienced a fascinating introduction into the art of experimental chemistry and what was then known of the underlying theoretical principles. Emil Fischer underlined frequently and with great respect the striking influence which Adolf von Baeyer had on him and the young chemists.[2] The open and relaxed atmosphere of this university, founded just after the war of 1871/1872, also proved attractive, as did the social life in Strasbourg, where Emil Fischer had reserved for himself an imposing barrel of excellent burgundy by the "understanding landlord" of the Badischer Hof.

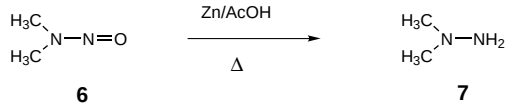
In this well-organized institute, in which Adolf von Baeyer had established an effective course and where he himself took care of the students during the initial semester, Friedrich Rose was responsible for the students learning the methods of quantitative analysis in depth. Emil Fischer was a brilliant analyst, and he was finally won over for chemical science. After less than one year he joined the organic chemistry department where he commenced his doctoral studies on the reduction of mellitic acid from honeystone (mellite). However this intention was rudely interrupted when a board of the rotten floor broke under the experimentalist who at that moment was carrying a large stoppered flask of reduction product and approximately 25 kg of mercury, and the valuable treasure disappeared into the cracks in the jagged wooden floor.[5] Adolf von Baeyer changed the topic and allowed Emil Fischer to work on the structural elucidation of fluorescein and other phthaleins, which, apart from the assignment of a few substituent positions, was successful. Emil Fischer received his doctorate in Strasbourg in 1874.

Adolf von Baeyer, who had recognized the exceptional talents of his student, appointed him as an assistant in the organic chemistry practical laboratory. When advising a student in the diazotization of benzidine Emil Fischer made his first great discovery. The student had always obtained an impure product during the reaction of benzidine with nitric acid, and Emil Fischer was also not able to improve upon the reaction when he repeated the experiment himself. As a result he added sodium sulfite to the reaction mixture to suppress the oxidizing effect of the nitric acid, which resulted in the formation of a precipitate.[6] When repeating this reaction with aniline, which was converted into the phenyldiazonium salt **1**, Emil Fischer succeeded in the first synthesis of phenylhydrazine by reaction with potassium hydrogen sulfite (Scheme 1).[7]



Scheme 1. Synthesis of phenylhydrazine (**5**).

It was this, the first compound of its class ("for which I [Emil Fischer] suggested the name hydrazine compounds"), which was to bring forth magnificent research results for its inventor. It has to be noted that in the same year Emil Fischer described the 1,1-disubstituted hydrazines.[8] Thus he obtained 1,1-dimethylhydrazine from dimethylnitrosamine (**6**) by boiling with zinc in acetic acid ("until the intense smell of the nitroso compound has disappeared") (Scheme 2).



Scheme 2. Synthesis of 1,1-dimethylhydrazine (**7**).

In 1875 Adolf von Baeyer succeeded Justus von Liebig at Munich University. After instructive visits to Tübingen and Stuttgart Emil Fischer (Figure 2) decided to follow his teacher; a tour of a few "amusing inns" which von Baeyer bestowed upon Emil and his cousin Ernst Fischer, the medical doctor, may have contributed to this decision. Emil Fischer continued his investigations on hydrazines in Baeyer's laboratories in Munich. The results formed the basis of his Habilitation in 1876, and in the fall of the same year he was able to present this chemistry at the Conference of German Natural Scientists and Doctors in Hamburg under the chairmanship of Ladenburg (known for his synthesis of racemic coniine).

After a training semester in analytical chemistry with Friederich Rose in Strasbourg, where he undertook the

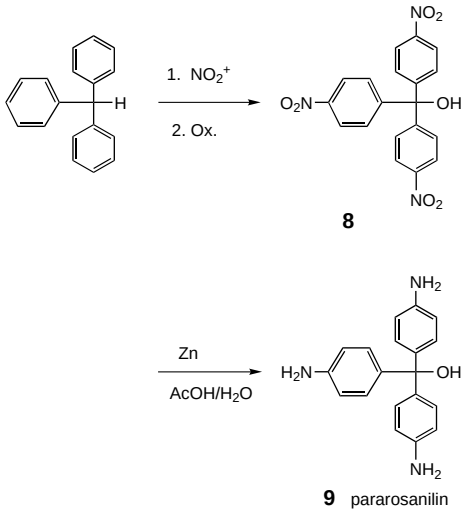
 © 2002 WILEY-VCH Verlag GmbH & Co. KGaA, Weinheim 1433-7851/02/4123-4441 $ 20.00+.50/0



Figure 2. Emil Fischer during his time in Munich (reproduced, with permission from Springer Verlag, from reference [2]).

previously mentioned microscopic studies on beer yeast, he was appointed professor and head of the analytical chemistry department in Munich in 1879. Amongst his comrades-in-arms with Baeyer were Wilhelm Koenigs (who was later to publish the Koenig–Knorr glycoside synthesis[9]) and Siegmund Gabriel (after whom the Gabriel synthesis of amines was named), who knew how to garnish an evening of beer with a barrage of jokes. Finally, cousin Otto Fischer also came to Munich, with whom Emil Fischer started a new line of work: the elucidation of the structure of the rosaniline dyes, which the old master A. W. von Hofmann had obtained by the oxidation of a mixture of *p*-toluidine, *o*-toluidine, and aniline with nitrobenzene[10] and for which he had postulated a structure similar to that of the azo compounds. The two Fischers were able to demonstrate unambiguously that this postulate was incorrect and that the rosaniline dyes are triphenylmethane derivatives. For example, they prepared pararosaniline (**9**) by the nitration of triphenylmethane, oxidation of the product to tris(*p*-nitrophenyl)methanol (**8**), and its reduction with zinc in acetic acid (Scheme 3).[3]

In the end, they stood correct against the authority of A. W. von Hofmann, which further promoted their reputations. Because of the work on hydrazines and on the rosaniline dyes, Emil Fischer was already in a position in 1880 to be able to decline an invitation from the Aachen Polytechnic to become Landolt's successor. In Munich he now switched to the chemistry of urea derivatives and the structural elucidation of uric acid, an area which had already been advanced by his mentor Adolf von Baeyer and by Adolph Strecker (known for the Strecker amino acid synthesis). Nevertheless, the structure of uric acid was still unknown. Its synthesis was as elusive as that of caffein, theobromine, and other purine derivatives. Uric acid was at that time mainly obtained from guano.



Scheme 3. Based on the synthesis of pararosaniline (**9**), Emil Fischer showed that the rosaniline dyes are triphenylmethane derivatives.

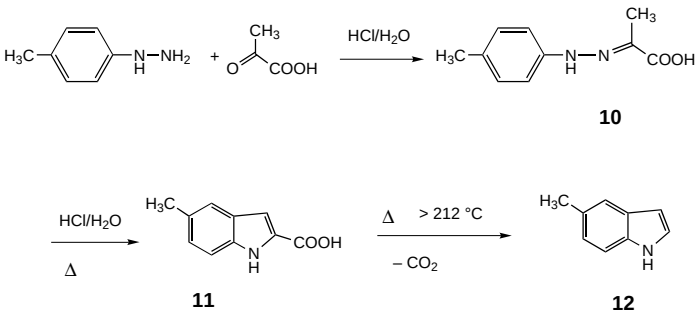
When Emil Fischer was appointed Professor of Chemistry at Erlangen University in 1882 as successor to J. Volhard, Wilhelm Koenigs contributed to a merry farewell party for Fischer with a humorous guano song, undoubtedly a reference to the above-mentioned activity. At the time Koenigs and Fischer lived with the same host and enjoyed many a glass of wine together in the evenings. Emil Fischer wrote in his memoirs:[2] "My wine stocks were at that time not small and amongst them were a few very good sorts. At the time of my move to Erlangen in Easter 1882, I gave my host the job of sending them on to me. The wine failed to arrive, and an inquiry elicited that Koenigs had drunk it all with his friends. Instead I received a large barrel of Münchner Hofbräu beer as a replacement for the lost wine. He knew that I would laugh at the joke, as he would have done in the same situation."

Erlangen was an important station in Emil Fischer's life, although he was to remain there for only three years. By chance he met his later wife Agnes Gerlach, the daughter of the Erlangen anatomist Joseph von Gerlach, on a train journey. Although only 30 years old, as professor in Erlangen he was responsible for the whole institute. The large experimental lecture course was also his duty. It was characteristic of Emil Fischer that through clever organization he sought to raise education and research at the institute in his care to a high degree of effectiveness. Thus he collated a collection of methods for the preparation of organic compounds which in 1887 became his "Anleitung zur Darstellung organische Präparate", one of the first books of practical chemistry.

Research in Erlangen was soon operating at full intensity, to which Lorenz Knorr (after whom the pyrrole synthesis was named) contributed; Knorr counted amongst Fischer's students in Munich and had followed him to Erlangen. The reactions of phenylhydrazine were studied in depth, which led to the discovery of the Fischer indole synthesis. In the reaction of (*p*-methylphenyl)hydrazine with pyruvic acid, Fischer and Jourdan observed a multistage process (Scheme 4).[11]

Of compound **10** the authors wrote: "Its behavior towards acids is quite remarkable. If the same is warmed in 10%

 © 2002 WILEY-VCH Verlag GmbH & Co. KGaA, Weinheim 1433-7851/02/4123-4442 $ 20.00+.50/0 *Angew. Chem. Int. Ed.* **2002**, *41*, No. 23



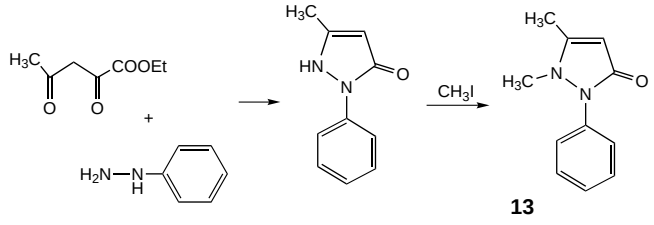
Scheme 4. The Fischer indole synthesis.

hydrochloric acid it turns reddish-yellow and goes into solution. On stronger heating the coloration disappears and fine, colorless needles separate… A noticeable amount of ammonia is present in the acid liquid… This process is so remarkable that for the time being we dare not venture an explanation for the reaction." Only a year later they identified the new compound as the indole carboxylic acid **11**,[12] which on heating above its melting point undergoes decarboxylation to give 5-methylindole (**12**, Scheme 4).

By oxidation to the isatins, the relationship with the heterocyclic pseudoisatins previously found by von Baeyer was established. A broad pathway into the new territory of heterocyclic chemistry had been opened, even though the mechanism of the Fischer indole synthesis as a [3s,3s] sigmatropic rearrangement first became clear after formulation of the Woodward – Hoffmann Rules.[13]

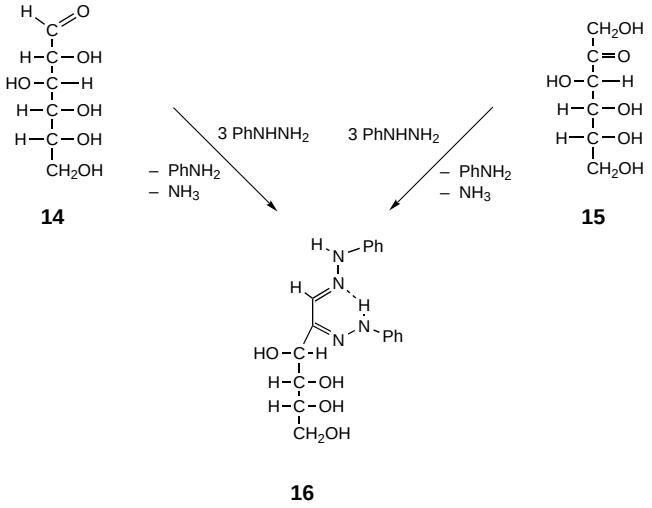
In these syntheses Emil Fischer (together with "Mr. Knoevenagel") also used aldehydes, including propionaldehyde. The latter ended with the formation of skatole,[14] which naturally correspondingly contaminated the clothing of the experimentalist. As a consequence a similarly impregnated loden jacket hindered the control of Emil Fischer's baggage through French customs during a journey to Ajaccio.[2]

The synthesis of antipyrine (**13**), starting from ethyl acetoacetate and phenyl hydrazine was successfully carried out by Lorenz Knorr, Fischer's Habilitation student, during this fruitful period at Erlangen (Scheme 5).[15] One of the first



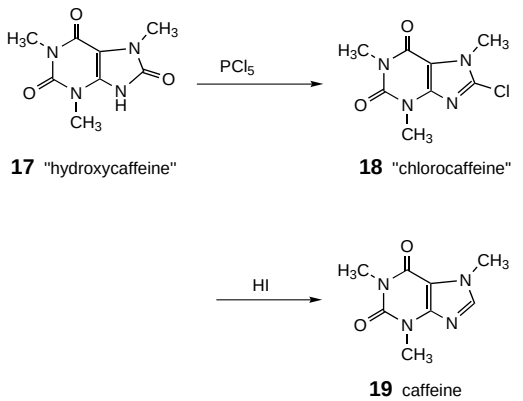
Scheme 5. Synthesis of antipyrine (**13**).

synthetic drugs was born. Phenylhydrazine as a reagent for ketones and aldehydes was extensively studied by Emil Fischer.[16] During these studies the reagent was also treated with sugars such as dextrose (glucose, **14**) and levulose (fructose, **15**).[17] With this reaction Emil Fischer discovered the formation of the crystalline and characterizable osazones, which were to become the overture to one of his Olympic achievements in organic chemistry. In this initial work Fischer described not only the osazones of galactose, maltose, and sorbose (which he obtained from Victor Meyer), but he also recognized that glucose and fructose gave the identical osazone **16** (Scheme 6). This finding was to bring him to his brilliant elucidation of the stereochemistry of sugars and to the breakthrough assignment of spatial configuration during his subsequent period in Würzburg.



Scheme 6. Glucose and fructose give rise to the same osazone **16**.

In 1883 in Erlangen an invitation from the Badische Anilin- und Soda Fabrik (BASF) reached Emil Fischer to succeed Heinrich Caro as head of research, who had, amongst other ventures, worked on the rosolic acid dyes related to the rosanilines. However, he preferred "academic activity with total freedom of scientific work", but accepted the invitation to visit BASF for a number of weeks. With this opportunity he was able to carry out on a larger scale the methylation of uric acid, which had been worked out in Erlangen,[18] as several kilograms of snake excrement, from which uric acid was preferably isolated, was made available to him. The work in Erlangen was concentrated on the reactions of *N*-methylated uric acids **17** with phosphorus pentachloride and pentabromide; purine compounds, including caffeine (**19**), were obtained by the reduction of the chloropurines **18** with fuming hydroiodic acid (Scheme 7).



Scheme 7. Studies on *N*-methylated uric acids led to the synthesis of caffeine (**19**).

 © 2002 WILEY-VCH Verlag GmbH & Co. KGaA, Weinheim 1433-7851/02/4123-4443 $ 20.00+.50/0

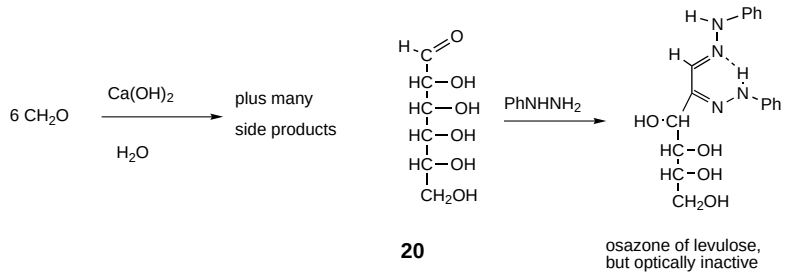
During the numerous reactions with the phosphorus chlorides, Emil Fischer contracted such a severe nose, throat, and bronchial infection that he had to interrupt his work in the institute and recover at a health resort. The leadership of the institute was in the meantime transferred to his cousin Otto Fischer by the Bavarian Ministry. During one of the journeys to Switzerland, Emil Fischer became acquainted with the president of the Swiss Board of Education in a mountain resort in Graubünden,[2] on whose prompting he was evidently invited to take over as Professor of Chemistry at the Zurich Polytechnic Institute as the position had fallen vacant following the appointment of Victor Meyer in Göttingen. On account of his state of health Emil Fischer did not accept this offer.

Later, after periods in Corsica and in the Black Forest, he received an invitation to succeed Johannes Wislicenus in Würzburg, who had received an appointment from Leipzig. There were concerns about the state of Emil Fischer's health and to investigate it the zoologist Semper, from the family of the famous Gottfried Semper (architect of the Semper Opera in Dresden), went to Heidelberg for a meeting with Fischer. Emil Fischer described this meeting as follows:[2] "Semper suggested that we take a walk to the castle. Although he was much older than I, he intentionally set off at a brisk pace so that he arrived at the top quite breathless, whereas I, then used to mountaineering, found the tempo quite comfortable. Then came the second test: Semper suggested that we drink a bottle of sparkling wine. That was not unsympathetic to me as the enjoyment of wine was one of my habits. The success of this breakfast was what one would expect: mild drunkenness on the part of the older gentleman while the younger colleague was not affected. The examination was passed."

Thus, in 1885 Emil Fischer went to Würzburg University where he was to spend seven fruitful and also personally happy years. His work at the large institute of this university, to which he was followed by Lorenz Knorr as lecturer, concentrated at first on the chemistry of purines. During this time, Emil Fischer elucidated the structure of numerous members of this class of compounds. The synthesis of uric acid, purine itself, and caffeine was achieved during his time in Berlin and will be outlined later.

In Würzburg Emil Fischer, who for a long time had intended as a bachelor to focus his attention on science, decided to marry. Without doubt the main reasons for this change of mind are to be found in the personal virtues of Miss Agnes Gerlach from Erlangen, who was to become his wife. Briefly he admitted that she "was through her physical beauty, purity of soul, and gentle nature a perfect being".[2] The happiness of this marriage, which produced three sons, unfortunately only lasted seven years. In November 1895, Frau Agnes Fischer died of meningitis in Berlin, and of the three sons only the eldest, Hermann O. L. Fischer, who was later to make significant contributions to the development of biochemistry, in particular at Berkeley, survived the First World War. The great researcher was afflicted in his lifetime by heavy reversals of fortune.

During his time in Würzburg Emil Fischer carried out his pioneering work on the chemistry and stereochemistry of sugars. The already discussed key was the reaction with phenylhydrazine to form the crystalline and characterizable osazones. He found that not only did glucose and fructose form the same osazone **16**, but so did mannose (which he had also discovered). With the help of this reaction he was also able to identify components of the sweet-tasting syrup (formose) obtained by Butlerow[19] and Loew[20] by reaction of formaldehyde (trioxan) with lime water as sugarlike substances. He proposed the molecular formula $C_6H_{12}O_6$ for one of the main components **20**[21] (Scheme 8).



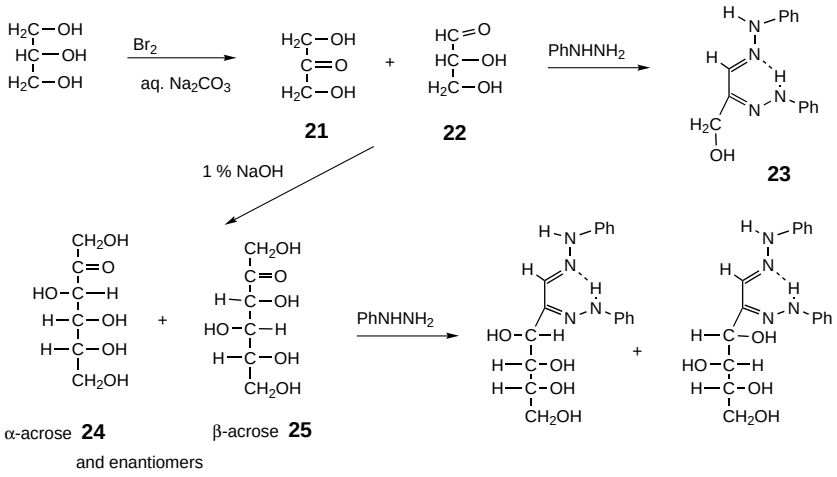
Scheme 8. Emil Fischer identified **20** as the main component of formose.

His own syntheses of sugars were carried out mainly with Julius Tafel, who had come with him to Würzburg from Erlangen. They started out from "2,3-dibromoacrolein" and later glycerol, which was oxidized to glyceraldehyde.[22] During work-up of the osazones of the products formed from 2,3-dibromoacrolein with barium sulfate, osazones of C_6 compounds were found, the formation of which was clarified in the same year. By oxidation of glycerol with bromine in soda solution, a mixture of dihydroxyacetone (**21**) and glyceraldehyde (**22**) was obtained. After reduction of the excess bromine with sulfurous acid, the osazone **23** of "glycerose" was formed with phenylhydrazine. However, when the mixture of **21** and **22** was allowed to stand in 1% NaOH for five days the osazones of two (racemic) hexoses **24**/**25** were isolated, which Emil Fischer called α- and β-acrose (from acrolein) (Scheme 9).[23, 24]

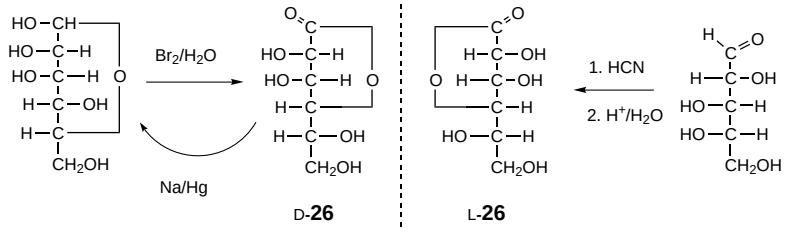
Emil Fischer soon realized that α-acrose was identical to levulose (i.e. fructose) but was optically inactive. β-Acrose thus corresponded to D,L-sorbose. From previous work (see, for example, ref. [17] the relationship between fructose and glucose was already clear. Soon that with D-mannose, which could be isolated from vegetable ivory, was established.[25] Oxidation of mannose with bromine water gave after acidification D-mannonic acid lactone (D-**26**; $[\alpha]_D = +53.8^\circ$). Fischer recognized that apart from the direction of the optical rotation, this compound was identical to L-mannonic acid lactone (L-**26**; $[\alpha]_D = -54.8^\circ$), which had already been obtained by Heinrich Kiliani[26] from L-arabinose (isolated from cherry gum) by cyanhydrin synthesis (Scheme 10).

The reduction of mannonic acid lactone to mannose with sodium amalgam, as well as that of glucosaccharic acid via the dilactone to glucuronic acid, had already been discovered by Emil Fischer.[27] With these tools—phenylosazone formation,

 © 2002 WILEY-VCH Verlag GmbH & Co. KGaA, Weinheim 1433-7851/02/4123-4444 $ 20.00+.50/0 *Angew. Chem. Int. Ed.* **2002**, *41*, No. 23



Scheme 9. Discovery of the "acroses".



Scheme 10. Synthesis of the mannonic acid lactones D-**26** and L-**26** by Fischer and Kiliani, respectively.

the total synthesis of optically inactive hexoses from acrolein, glyceraldehyde, or formaldehyde, chain extension by cyanhydrin synthesis (the Kiliani–Fischer synthesis can be regarded as the entry into asymmetric synthesis), hydrolysis of osazones to osones, oxidation of hexoses to aldonic acids, and the reduction of aldonic acid lactones to the hexoses—Emil Fischer was now able successfully to cast light on the subject of sugar configuration, then considered tremendously complex, which not only required unerring analytical rigor, but also the characteristic ability of Emil Fischer[4] to order experimental results systematically. In impressive work[28] he brought clarity to the structural relationships of D- and L-mannose, mannite, glucose, and fructose when he introduced new methods with the separation of the enantiomers of mannonic acid in the form of their strychnine or morphine salts and with the enantioselective fermentation of α-mannose from the racemic mixture with beer yeast (reminiscent of the brewing activities of his father). (Figure 3 was taken from the original work[28] and illustrates this breakthrough.)

In addition to fermentation with yeasts Emil Fischer also applied selective microbiological methods, for example, the use of *Penicillium glaucum* and later *Saccharomyces* species[29] for the selective cleavage of polysaccharides. He may justly be regarded as the pioneer of enantioselective enzymatic catalysis.

Based on the syntheses in the mannose/fructose series, Emil Fischer succeeded in the same year[30] with the total synthesis of grape sugar (i.e. D-glucose). The starting point was the D-mannonic acid lactone (D-**26**). On heating to 150–155 °C in quinoline/water, D-**26** partly epimerized to gluconolactone (**27**). The phenylhydrazides of the two aldonic acids were separated. Gluconolactone (**27**) was isolated via calcium gluconate from the hydrazide of gluconic acid with lime water and was then reduced to D-glucose (**28**) with sodium amalgam (Scheme 11).

Thus it was proven that glucose and mannose differ only in the configuration at C2. Emil Fischer wrote of the two hexoses:[30] "On the basis of the Le Bel–van't Hoff conception their difference rests on the asymmetry of the carbon atom labeled as1 in the following formula".

$$\mathrm{CHO \cdot CHOH \cdot CHOH \cdot CHOH \cdot CH_2OH}$$
as1

With this work[28, 30] the brilliant breakthrough of the van't Hoff interpretation[31] of the spatial structure of aliphatic carbon compounds was implemented.

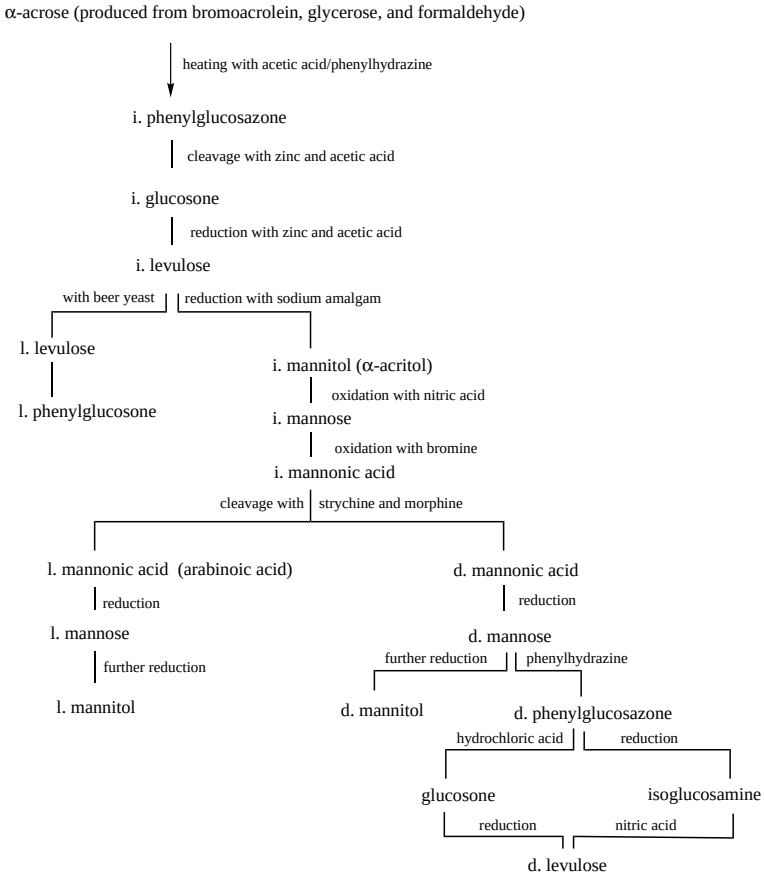
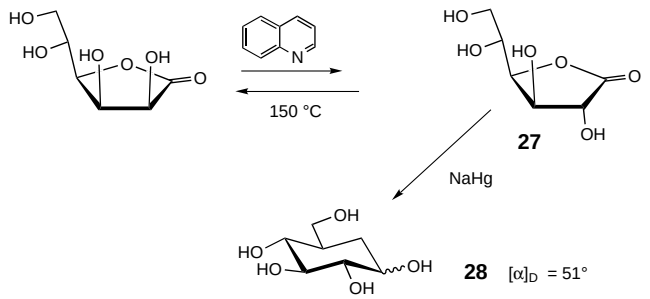


Figure 3. Structural relationships and enantiomers of fructose and mannose and their derivatives.

 © 2002 WILEY-VCH Verlag GmbH & Co. KGaA, Weinheim 1433-7851/02/4123-4445 $ 20.00+.50/0



Scheme 11. The first total synthesis of glucose (**28**). The intermediate **27** was isolated via the phenylhydrazide from which the calcium gluconate derivative was obtained.

On June 23, 1890, Emil Fischer summarized the state of carbohydrate research at a special meeting of the Deutsche Chemische Gesellschaft (German Chemical Society) in Berlin. In 1952, Burckhardt Helferich wrote:[4] "It must have been an unusually fascinating and comprehensive lecture. Even Harries, an exceptionally critical observer, wrote of it: 'I have never heard a better lecture in form and content, full of passion and noble restraint, when the greater researcher stood out'. Emil Fischer became for us the measure of all personalities!" The original lecture can be read in the "Chemische Berichte".[32]

In this work Emil Fischer established configurational assignment, systematics, and nomenclature of sugars and also that of all centrochiral compounds.[33] He put forward that the symbols "d." and "l." should be used only according to the spatial orientation of the substituents, independent of the direction of rotation. The carbohydrates were named after the number of carbon atoms, for example, as pentoses, hexoses, etc., and finally Emil Fischer ventured the assumption of the absolute configuration of glucose, galactose, mannose, fructose, arabinose, and xylose according to the Fischer projection still used today.[34] Fortunately, as was to be demonstrated much later by Bijvoet et al.[35] by the X-ray structural analysis of sodium rubidium tartrate, he was correct in his assignment.

With few exceptions he was able within a few years to assign the stereoisomeric forms to the whole spectrum of known sugars,[36] when he astutely established the number of isomers by oxidation of the hexoses to the sugar acids and oxidative degradation to lower dicarboxylic acids such as tartaric acid and mesotartaric acid.[37]

With this monumental work on sugars, about which previously only little was known from the studies of Kiliani and Tollens, Emil Fischer entered the topmost ranks of chemists. When A. W. von Hofmann[38] died in the spring of 1892 the list of the faculty of the Berlin University (today the Humboldt University) for successors to this chemist, likewise distinguished by his scientific achievements and worldly personality, contained the names August Kekulé, Adolf von Baeyer, and Emil Fischer. From what has just been described it is understandable today that the decision fell on Emil Fischer, the youngest of the candidates. Emil Fischer, who with his family was very happy in Würzburg, hesitated at first to go to the large city, then undergoing acrimonious development. His wife and his father (who was proud of the professional success of his son, and "had heard of the Berlin offer and immediately set out to persuade me not to reject such a good deal lightly"[2]) persuaded him to follow the calling. After eight days of hesitation he accepted, as "the active scientific life in the capital city of the Reich, the considerable prospects, the possibilities to gather around me a large circle of students was very appealing to a man of my age (I was not yet 40 years old)".

Amongst other things, the Ministry in Berlin had promised Emil Fischer to build a new institute. The Hofmann Institute in Georgenstrasse was clearly an imposing building externally, but unsuitably organized inside. Light and ventilation were inadequate. The major deficiencies had to be removed at considerable cost. But eight years were to pass until the completion of the new building in Hessische Strasse in Berlin (Figure 4), where two years ago the institute celebrated its

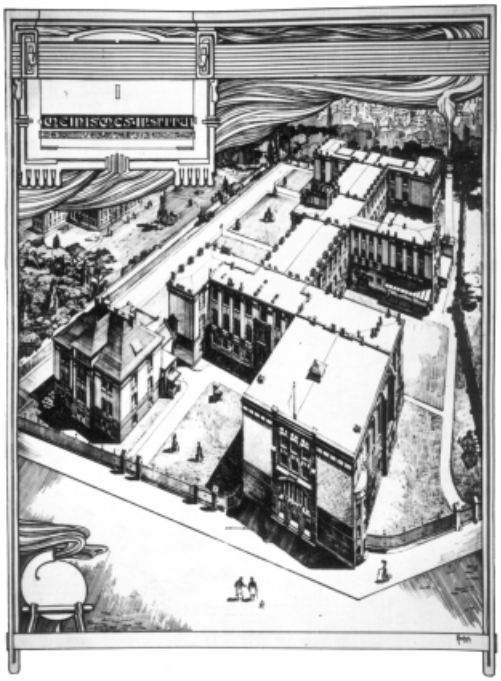


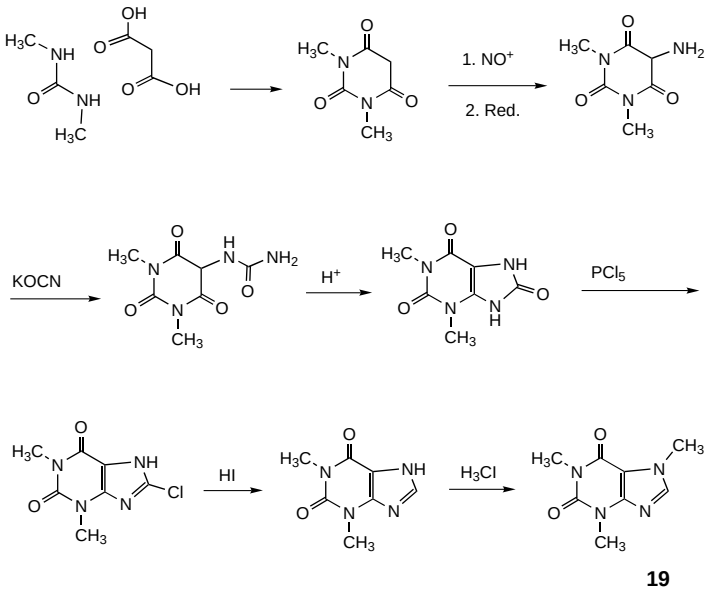
Figure 4. The new building of the chemical institute. (We thank the Humboldt-Universität zu Berlin for providing us with the original picture.)

100th anniversary.[39] In 1952 Burckhardt Helferich wrote of this institute:[4] "In accordance with the conceptions of Emil Fischer, everything in this institute is subordinate to the purpose of work. The means available were used to this end only, no value was laid on external appearances. Light, good ventilation, and especially clear layout were the decisive factors according to which building work was carried out… In the purposefulness of design it has also to this day not been superceded by any other German institute."

In Berlin it was not to Emil Fischer's liking that the Philosophy Faculty was not split into natural science and liberal arts departments. Meetings lasted many hours, as "in general the natural scientists in the Berlin faculty did not play the role they could claim. The representatives of the liberal arts are more numerous and undoubtedly more adept at speaking, perhaps also more expressive in manner. Since they also have more time and attend the meetings more regularly and for longer periods of time, they have most to say,…".[2]

 © 2002 WILEY-VCH Verlag GmbH & Co. KGaA, Weinheim 1433-7851/02/4123-4446 $ 20.00+.50/0 *Angew. Chem. Int. Ed.* **2002**, *41*, No. 23

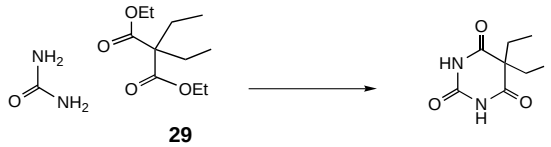
But the Berlin faculty welcomed Emil Fischer with open arms, "above all Helmholtz, who gave a dinner in his honor to which the most important representatives of the University and leading men in industry were invited".[4] In Berlin Emil Fischer continued his work on purines and carbohydrates. With Lorenz Ach, who followed him from Würzburg to the capital as his personal assistant, he completed the total synthesis of uric acid (Fischer–Ach synthesis[40]) and following this principle, the first total synthesis of caffeine (**19**; Scheme 12).



19

Scheme 12. Total synthesis of caffeine (**19**).

The fundamental substance purine itself was also prepared for the first time during this period and, of particular worldwide interest, the first synthetic narcotic veronal (**30**) (Scheme 13).[41]

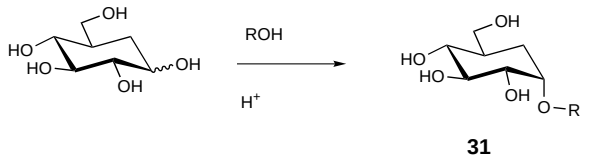


29 **30**

Scheme 13. Synthesis of the barbiturate veronal (**30**) from urea and 2,2-diethylmalonic acid diethyl ester (**29**).

In addition to further constitution and configuration elucidation, amongst the most important results in carbohydrate chemistry of his period in Berlin was the first synthesis of glucosides **31** (Scheme 14) and other glycosides.[42] Much earlier, still in Würzburg, the formation of a disaccharide, isomaltose, from glucose by the action of hydrochloric acid had been observed.

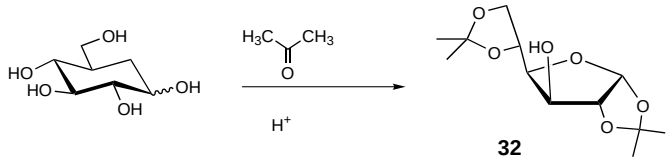
Emil Fischer was also presumably the first to have undertaken protective group chemistry when he introduced the



31

Scheme 14. Acid-catalyzed synthesis of glucosides **31**.

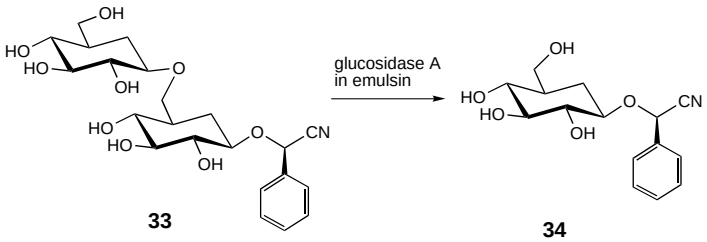
isopropylidene group into different carbohydrates (including glycerol) (Scheme 15).[42]



32

Scheme 15. The first use of protecting groups probably dates back to Emil Fischer.

Finally, the considerable amount of work in which Emil Fischer investigated the action of enzymes in relation to substrate structure must be mentioned at this point,[43] for example, the cleavage of β-glucosides or amygdalin (**33**) to mandelonitrile glucoside **34** by emulsin from bitter almonds (Scheme 16), and of saccharose by invertase, maltose by maltase, and lactose by emulsin. From the experience thus gained he formulated the now famous lock-and-key principle for the selectivity of enzyme action as the fundamental principle of biological-selection processes. Until today, this description of molecular recognition by Emil Fischer has lost none of its impact.[44, 45]



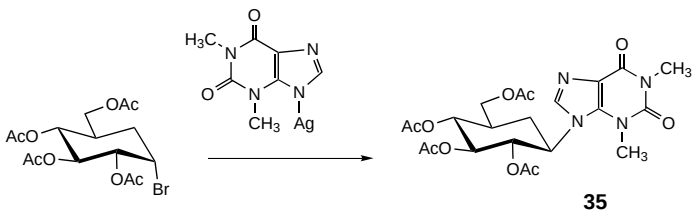
33 **34**

Scheme 16. Enzymatic catalysis and the lock-and-key principle.

His magnificent and enduring scientific achievements, which were a quantum leap in the quality of natural-product research, were recognized in 1902 by the award of the Nobel Prize for Chemistry by the Royal Academy in Stockholm.

Emil Fischer was thus strengthened in his exceptionally creative work. He entered new, unexplored fields. In one he brought together purine and carbohydrate chemistry into the first synthesis of nucleosides. Thus amongst others adenine and uracil were glycosylated,[46] as well as theophyllin, presumably to the isomer **35** (Scheme 17). Phosphorylation of the nucleosides to a "nucleotide" did not lead to a well-defined product, but already provided some insight into later nucleotide chemistry. Based on knowledge of the building blocks, Emil Fischer was in the position to develop ideas on the structure and function of nucleic acids that were

 © 2002 WILEY-VCH Verlag GmbH & Co. KGaA, Weinheim 1433-7851/02/4123-4447 $ 20.00+.50/0



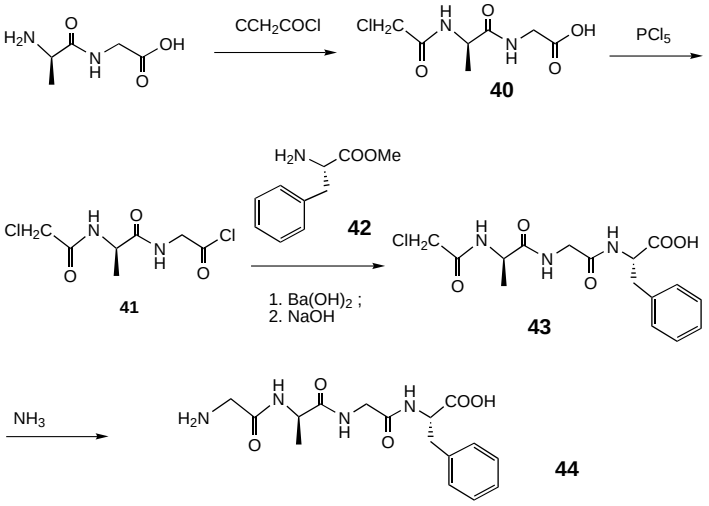
Scheme 17. One of the first nucleoside syntheses.

remarkable for that time. During the early years in Berlin a new oxazole synthesis was developed by the acid-catalyzed reaction of cyanohydrins with aldehydes[47] as well as optimization of the acid-catalyzed formation of esters.[48]

In Berlin Emil Fischer entered a totally new, extensive field with his investigations on peptides and proteins. Some work on glycine and diketopiperazine had previously been described by Curtius. Emil Fischer's interest was directed initially at the separation of *N*-protected amino acids, for example *N*-benzoylalanine, *N*-benzoylaspartic acid, and *N*-benzoylglutamic acid into their enantiomers with the help of their brucine or strychnine salts.[49] He also pursued the total synthesis of amino acids, for example 2,4-diaminobutyric acid. With a general method for the formation of amino acid esters[50] he discovered a key reaction for the synthesis of peptides. However, this was first achieved by opening of the simple diketopiperazine with concentrated hydrochloric acid to give glycylglycine (**36**), the N-terminus of which was then protected with ethyl chloroformate to form (→**37**; Scheme 18).[51]

The conversion of **37** into its ethyl ester **38** was accomplished, either directly or by acid alcoholysis of diketopiperazine, and subsequent introduction of the ethoxycarbonyl group. Warming **38** with the ethyl ester of leucine resulted in the first synthesis of an optically active peptide **39** 100 years ago.[52] The formation of esters of amino acids was used frequently by Emil Fischer for the analysis of natural proteins: the amino acids formed by hydrolysis were converted into their esters and these were separated by fractional distillation. Proteins, such as silk fibroin, were also hydrolyzed to obtain oligopeptides.[53]

Fischer and co-workers introduced the use of α-haloacylamino acids such as **40** and their conversion into an acid chloride such as **41** as a general method for the construction of peptides. Upon reaction with an amino acid ester such as **42**, the extended peptide ester was formed; careful alkaline hydrolysis led to the haloacylpeptide **43**, which was finally converted into the target peptide **44** with ammonia (Scheme 19).[54] During this work Emil Fischer showed that the product **44** was attacked rather quickly by "fresh pancreatic extract from dogs".



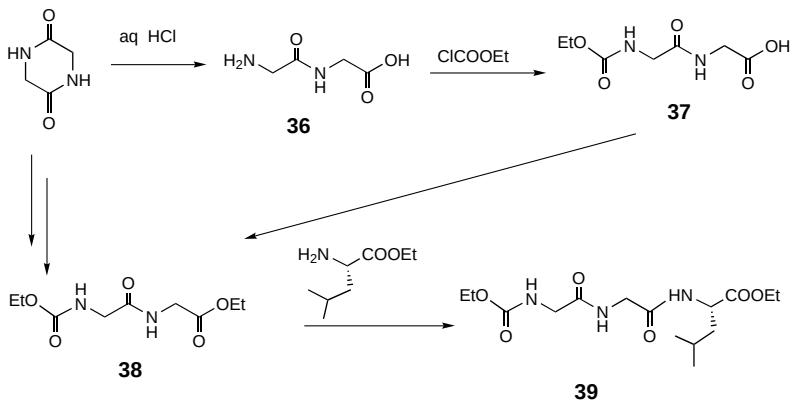
Scheme 19. General procedure for the synthesis of peptides.

As well as ethoxycarbonyl and α-haloacyl groups Emil Fischer was already using arylsulfonyl[55] and formyl protective groups.[56] He was able to increase the efficiency of his methods to achieve the synthesis of an octadecapeptide consisting of three L-leucine and 15 glycine units,[57] which for that time was an impressive achievement. Of course, syntheses which reliably avoided racemization were to require protective groups that were removable under mild conditions. The first of this type was introduced by his student Max Bergmann[58] with the benzyloxycarbonyl (Z) group.

A detailed discussion of all the fundamental contributions of Emil Fischer to peptide and protein chemistry are beyond the scope of this tribute. It has to be noted, however, that he involved himself with the stereochemical mechanisms and in particular he investigated nucleophilic substitution and the Walden inversion.[59] However, special relationships are present in the reactions of amino acids with nitrosyl bromide which will not be described in more detail here.

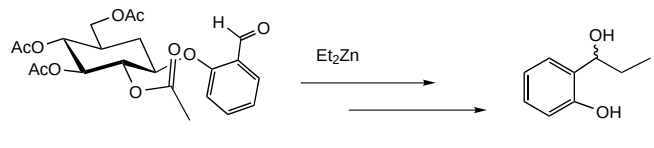
A further stereochemical topic could be asymmetric synthesis controlled by auxiliaries. Emil Fischer already had this idea during the course of his investigations on phenylglycosides, tanning agents, and lichens when he treated protected *O*-glycosyl salicylaldehyde **45** with diethyl zinc (Scheme 20). The optical activity initially observed in the isolated product **46** proved later to be mainly due to impurities in the glucose. But the idea sounds as if it were from recent times.

Lichens and tanning materials had interested Emil Fischer since his youth, certainly from the



Scheme 18. An early example of an asymmetric peptide synthesis.

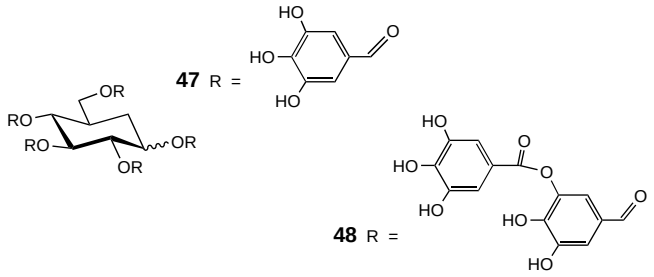
 © 2002 WILEY-VCH Verlag GmbH & Co. KGaA, Weinheim 1433-7851/02/4123-4448 $ 20.00+.50/0 *Angew. Chem. Int. Ed.* **2002**, *41*, No. 23



45 **46**

Scheme 20. Attempted enantioselective synthesis with control by a chiral auxiliary.

time of his doctoral work. On the basis of his mastery of carbohydrate chemistry he approached this topic once more on the path to synthesis. Thus he was successful in the synthesis of galloyl glycosides **47**,[60] depsides, and tanninlike compounds,[61] and the pentakis(digalloyl) glucose derivative **48** (Scheme 21) and even higher-molecular-weight structures.



Scheme 21. Experiments on tannin chemistry.

Fatty compounds[62] obtained by acylation of isopropylidene-protected multivalent alcohols were also part of his work. The World War, the personal tragedies, and the increasingly troublesome diseases of the intestinal canal, possibly caused by his favorite tool, phenylhydrazine, undermined his energies so that further developments in his later research area remained unfulfilled.

Under Emil Fischer's leadership the Berlin Chemical Institute became one of the leading research institutes in the world. In addition to the Nobel Prize he was awarded numerous honors for his exceptional research. He was made "Ritter der Friedenklasse des Ordens Pour le Mérite" (for information on this distinction, see: http://www.orden-pour-lemerite.de) and active privy councilor with the title of Excellency. He received the Award of the French Legion of Honor, and high scientific honors and medals which carry the names of Cothenius, Lavoisier, Helmholtz, Davy, and Tiedemann. "They did not in any decisive way have a modifying effect on his personality, on his social behavior", wrote Burckhardt Helferich.[4]

From the facts described by himself[2] and others[37] Emil Fischer no longer appeared to be the gregarious, enterprising contemporary he was during his youth in Strasbourg and in Munich. He felt the weight of his responsibilities and in particular too his mission to clarify biologically selective processes, whose main components he investigated with peptide, nucleoside, and carbohydrate chemistry as well as with his studies on enzymes. He foresaw the complexity of this biological material which he tried to master with increased passion. This effort, certainly reinforced by the personal tragedy inflicted upon him by the fate of his family, left him increasingly lonely.

Nevertheless, he served science and its organizations with considerable dedication. He took part in the meetings of the Prussian Academy of Sciences, during which he took interest in many areas of natural science outside of chemistry. His influence characterized by deed and decisiveness through which he sought to generate a particularly fruitful atmosphere in scientific research must be particularly emphasized.

He actively pursued the setting up of institutes devoted solely to research. Thus he contributed decisively to the founding of the "Kaiser Wilhelm Gesellschaft zur Förderung der Wissenschaften" in 1911, today the Max Planck Gesellschaft (Max Planck Institute). In October 1912, in the presence of the then German Kaiser, the "Kaiser Wilhelm-Institut für Chemie" was dedicated in Berlin-Dahlem as the first establishment of this research organization (Figure 5).[63] Soon thereafter came the formation of the Institut für Physikalische Chemie und Elektrochemie, also in Berlin, and the Institut für Kohlenforschung in Mülheim, led by Franz Fischer, a former colleague of Emil Fischer (the connection between the two Fischers lives on in the term Fischer–Tropsch synthesis). The latter circumstance illustrates the farsightedness with which Emil Fischer influenced the research landscape in Germany and beyond. He had recognized quite early the importance of radioactivity and had welcomed the young researchers Otto Hahn and Liese Meitner into his Berlin Institute. He aided inorganic chemistry with enthusiasm in that he recommended research and teaching in the area of inorganic chemistry to his talented assistants Alfred



Figure 5. Opening ceremony of the Kaiser-Wilhelm-Institute für Chemie und für Physikalische Chemie und Elektrochemie by Kaiser Wilhelm II. Behind Kaiser Wilhelm: Adolf Harnack and Emil Fischer (from right to left; reproduced, with permission, from the archives of the history of the Max-Planck-Gesellschaft, Berlin-Dahlem.

 © 2002 WILEY-VCH Verlag GmbH & Co. KGaA, Weinheim 1433-7851/02/4123-4449 $ 20.00+.50/0

Stock and Otto Ruff (after whom the Ruff degradation was named).[39]

Many distinguished chemists came from his Institute as doctors, postdoctoral fellows, and lecturers, including amongst many Hans Fischer (Nobel Prize 1930, porphyrin synthesis), Otto Warburg (Nobel Prize 1931, respiratory enzymes), Adolf Windaus (Nobel Prize 1928, vitamin D), Otto Diels (Nobel Prize 1950, Diels–Alder reaction), Karl Landsteiner (Nobel Prize for medicine 1930, blood group compounds) Geza Zemplén (transesterification), Wilhelm Traube (Traube synthesis of purines), Emil Abderhalden, Hermann Leuchs, and Max Bergmann (peptide chemistry), Karl Freudenberg, Burckhardt Helferich, and many others, including those already mentioned (e.g. Ludwig Knorr or Julius Tafel). To this day we still profit from the outstanding research results that Emil Fischer and his colleagues and school achieved for humanity.

If one considers that at that time this chemical elucidation and synthetic work on complex, polyfunctional compounds was accomplished without chromatography, HPLC, NMR spectroscopy, or mass spectrometry, and that the only means available were distillation, crystallization, careful elemental analysis, unerring analytical acumen, and bold hypotheses based on sound knowledge, one can have only the deepest respect (Figure 6).

Emil Fischer was blessed with excellent gifts for a natural-science researcher. He had an outstanding memory[4] and the ability for mathematical conclusions. He was stimulated and fostered by an outstanding academic teacher, Aldof von Baeyer, and was able gather about him many excellent co-workers and students. Through his pioneering work he came into the position to make far-reaching assumptions on the structure and function of biologically important molecules, proteins, and nucleic acids. One has to refrain therefore from calling him a visionary, as today this term is unfortunately reserved for addressing people, predominantly from political and economic spheres, many of whom base their "grand design" without shame on a small reservoir of knowledge according to the motto: knowledge imposes limitations, but ignorance leads to independence. With Emil Fischer it is quite the opposite: On a foundation of extensive knowledge, gained by his own experimental work constantly scrutinized for consistency and by evaluation of the results of other and new experiments, he was able to enter new areas boldly and with foresight and to make predictions still valid today. That bestowed on him in his time a status described by the words of Richard Willstätter reiterated, somewhat modified and abbreviated, in the title.[64]



Figure 6. Emil Fischer in the laboratory (reproduced, with permission from Springer Verlag, from reference [2]).

In future, chemists will have need of his guidance and his methodical resolution when, after the magnificent analytical work in biochemistry and molecular biology on the elucidation of the genome and its translation into the proteome, they want to address the recognizable biological functional space with active synthetic ligands which, like molecular microchips, control hydrophilic, hydrophobic, and hydrogen-binding sites, are not rapidly digested but yet remain degradable. At the same time the impact of Emil Fischer is a shining example of what fruitful work a chemist can achieve in the elucidation of molecular biological processes. In today's world he and his life's work encourage and stimulate the concentration of research efforts on the wonderful processes of biological control, not only to describe the sequences, but also to understand them mechanistically at a molecular level.

My special thanks go to my colleagues Professor Johann Mulzer, University of Vienna, Professor Ulrich Koert, University of Marburg, and Professor Jürgen Liebscher, Humboldt Universität, Berlin who generously provided me with literature for this article.

[1] J. Mulzer in *Berlinische Lebensbilder*, *Vol. 1* (Eds.: W. Treue, G. Hildebrand), Colloquium, Berlin, **1987**, p. 34.
[2] E. Fischer, *Aus meinem Leben*, Springer, Berlin, **1922** and **1987** (With a Prologue and an Epilogue by Bernhard Witkop; Reprint from Emil Fischer, Gesammelte Werke, Edited by M. Bergmann).
[3] E. Fischer, O. Fischer, *Liebigs Ann. Chem.* **1878**, *194*, 242.
[4] "Emil Fischer zum 100. Geburtstag": B. Helferich, *Angew. Chem.* **1953**, *65*, 45.
[5] "Emil Fischer. Sein Leben und sein Werk.": K. Hoesch, *Ber. Dtsch. Chem. Ges.* **1921**, *54*, 50 (Sonderheft).
[6] "Emil Fischer. Sein Leben und sein Werk.": K. Hoesch, *Ber. Dtsch. Chem. Ges.* **1921**, *54*, 206. (Special issue.)
[7] E. Fischer, *Ber. Dtsch. Chem. Ges.* **1875**, *8*, 589.
[8] E. Fischer, *Ber. Dtsch. Chem. Ges.* **1875**, *8*, 1587.
[9] W. Koenigs, E. Knorr, *Ber. Dtsch. Chem. Ges.* **1901**, *34*, 957.
[10] A. W. Hofmann, A. Geyger, *Ber. Dtsch. Chem. Ges.* **1872**, *5*, 472.
[11] E. Fischer, F. Jourdan, *Ber. Dtsch. Chem. Ges.* **1883**, *16*, 2242.
[12] E. Fischer, O. Hess, *Ber. Dtsch. Chem. Ges.* **1884**, *17*, 559.

 © 2002 WILEY-VCH Verlag GmbH & Co. KGaA, Weinheim 1433-7851/02/4123-4450 $ 20.00+.50/0

[13] R. Hoffmann, R. B. Woodward, *J. Am. Chem. Soc.* **1965**, *87*, 4388; R. Hoffmann, R. B. Woodward, *J. Am. Chem. Soc.* **1965**, *87*, 4389
[14] E. Fischer, *Ber. Dtsch. Chem. Ges.* **1886**, *19*, 1563.
[15] L. Knorr, *Ber. Dtsch. Chem. Ges.* **1883**, *16*, 2597, DRP 26429 (1883).
[16] E. Fischer, *Ber. Dtsch. Chem. Ges.* **1884**, *17*, 572.
[17] E. Fischer, *Ber. Dtsch. Chem. Ges.* **1884**, *17*, 579.
[18] E. Fischer, *Justus Liebigs Ann. Chem.* **1882**, *215*, 253.
[19] A. Butlrow, *Justus Liebigs Ann. Chem.* **1861**, *120*, 295.
[20] O. Loew, *J. Prakt. Chem.* **1886**, *33*, 321.
[21] E. Fischer, F. Passmore, *Ber. Dtsch. Chem. Ges.* **1889**, *22*, 360.
[22] E. Fischer, J. Tafel, *Ber. Dtsch. Chem. Ges.* **1887**, *20*, 1088.
[23] E. Fischer, J. Tafel, *Ber. Dtsch. Chem. Ges.* **1887**, *20*, 2384.
[24] E. Fischer, J. Tafel, *Ber. Dtsch. Chem. Ges.* **1887**, *20*, 2566.
[25] E. Fischer, J. Hirschberger, *Ber. Dtsch. Chem. Ges.* **1889**, *22*, 3218.
[26] H. Kiliani, *Ber. Dtsch. Chem. Ges.* **1886**, *19*, 3029.
[27] E. Fischer, *Ber. Dtsch. Chem. Ges.* **1889** , *22*, 220.
[28] E. Fischer, *Ber. Dtsch. Chem. Ges.* **1890**, *23*, 370.
[29] E. Fischer, P. Lindner, *Ber. Dtsch. Chem. Ges.* **1895**, *28*, 3034.
[30] E. Fischer, *Ber. Dtsch. Chem. Ges.* **1890**, *23*, 799.
[31] For the pioneering discoveries of J. H. van't Hoff on the stereochemistry of tetravalent carbon atoms, see: E. W. Meijer, *Angew. Chem*. **2001**, *113*, 3899; *Angew. Chem*. *Int. Ed.* **2001**, *40*, 3783.
[32] E. Fischer, *Ber. Dtsch. Chem. Ges.* **1890**, *23*, 2114.
[33] An excellent tribute to this achievement of Emil Fischer is found in: F. W. Lichtenthaler, *Angew. Chem*. **1992**, *104*, 1577; *Angew. Chem*. *Int. Ed. Engl.* **1992**, *31*, 1541.
[34] E. Fischer, *Ber. Dtsch. Chem. Ges.* **1891**, *24*, 1836; E. Fischer, *Ber. Dtsch. Chem. Ges.* **1891**, *24*, 2683.
[35] J. M. Bijvoet, A. F. Peerdeman, A. J. van Bommel, *Nature* **1951**, *168*, 271.
[36] E. Fischer, *Ber. Dtsch. Chem. Ges.* **1894**, *27*, 3208.
[37] A summary is found in: C. Harries, *Naturwissenschaften* **1919**, *9*, 843 In this case, however, the old nomenclature is used, for example, for gulose and idose.
[38] J. Mulzer in ref. [1], p. 27.
[39] M. Meisel, *100 Jahre Chemie in der Hessischen Straße*, Festschrift der Humboldt-Universität zu Berlin, **2000**.
[40] E. Fischer, L. Ach, *Ber. Dtsch. Chem. Ges.* **1895**, *28*, 3135.
[41] E. Fischer, J. von Mering, *Ther. Monatsh.* **1903**, *17*, 208; E. Fischer, A. Dilthey, *Justus Liebigs Ann. Chem.* **1904**, *335*, 334.
[42] E. Fischer, *Ber. Dtsch. Chem. Ges.* **1895**, *28*, 1145; E. Fischer, *Ber. Dtsch. Chem. Ges.* **1895**, *28*, 1167.
[43] E. Fischer, *Ber. Dtsch. Chem. Ges.* **1895**, *28*, 1429; E. Fischer, *Ber. Dtsch. Chem. Ges.* **1895**, *28*, 1508.
[44] A. Eschenmoser, *Angew. Chem*. **1994**, *106*, 2455; *Angew. Chem*. *Int. Ed. Engl.* **1994**, *33*, 2363.
[45] F. W. Lichtenthaler, *Angew. Chem*. **1994**, *106*, 2456; *Angew. Chem*. *Int. Ed. Engl.* **1994**, *33*, 2364.
[46] E. Fischer, B. Helferich, *Ber. Dtsch. Chem. Ges.* **1914**, *47*, 210.
[47] E. Fischer, *Ber. Dtsch. Chem. Ges.* **1896**, *29*, 205.
[48] E. Fischer, A. Speier, *Ber. Dtsch. Chem. Ges.* **1895**, *28*, 3252.
[49] E. Fischer, *Ber. Dtsch. Chem. Ges.* **1899**, *32*, 2451.
[50] E. Fischer, *Ber. Dtsch. Chem. Ges.* **1901**, *34*, 433.
[51] E. Fischer, E. Forneau, *Ber. Dtsch. Chem. Ges.* **1901**, *34*, 2868.
[52] E. Fischer, *Ber. Dtsch. Chem. Ges.* **1902**, *35*, 1095.
[53] E. Fischer, *Ber. Dtsch. Chem. Ges.* **1906**, *39*, 2315.
[54] E. Fischer, *Ber. Dtsch. Chem. Ges.* **1908**, *41*, 850.
[55] E. Fischer, P. Pergell, *Ber. Dtsch. Chem. Ges.* **1903**, *36*, 2592.
[56] E. Fischer, *Ber. Dtsch. Chem. Ges.* **1906**, *39*, 2893.
[57] E. Fischer, *Ber. Dtsch. Chem. Ges.* **1907**, *40*, 1754.
[58] M. Bergmann, L. Zervas, *Ber. Dtsch. Chem. Ges.* **1932**, *65*, 1192.
[59] E. Fischer, L. von Mechel, *Ber. Dtsch. Chem. Ges.* **1916**, *49*, 1355.
[60] E. Fischer, K. Freudenberg, *Ber. Dtsch. Chem. Ges.* **1912**, *45*, 915.
[61] E. Fischer, M. Bergmann, *Ber. Dtsch. Chem. Ges.* **1918**, *51*, 1760.
[62] E. Fischer, C. Rund, *Ber. Dtsch. Chem. Ges.* **1916**, *49*, 88.
[63] H. Remane, *Biographien hervorragender Naturwissenschaftler*, *Techniker und Mediziner*, *Vol. 74*, B. G. Teubner, Leipzig, **1984**, p. 53.
[64] R. Willstätter, A*us meinem Leben. Von Arbeit*, *Muse und Freuden*, *2nd ed.*, Verlag Chemie, Weinheim, **1958**, p. 212.

 © 2002 WILEY-VCH Verlag GmbH & Co. KGaA, Weinheim 1433-7851/02/4123-4451 $ 20.00+.50/0

Chain Compounds Based on Transition Metal Backbones: New Life for an Old Topic

Jitendra K. Bera and Kim R. Dunbar*

1. Interest in One-Dimensional Materials

One-dimensional and "pseudo" one-dimensional materials have long fascinated physicists and chemists because of their unusual properties but, over the last two decades, research activity in this area had been steadily declining. One possible explanation for this trend is that researchers have been preoccupied with the search for materials that exhibit high-temperature superconductivity and magnetic ordering, properties that are not typically associated with one-dimensional (1D) materials. As with many trends in science, however, this situation has now come full circle. Research in the preparation and characterization of materials with high anisotropy and restricted dimensionality is currently paving the way for a new era of nanoscale science and technology. The reason for this is very simple: tiny pieces of matter exhibit very unusual optical, magnetic, and conducting properties due to their size. Much of the current attention in nanoscience is being directed at the study of small domains in the form of quantum dots, nanotubes, and electrically or magnetically bistable molecules.

Decades before the term "molecular wire" came into common usage, physicists and chemists recognized that mixed-valence stacks of organic as well as inorganic molecules exhibit unusual electrical properties. The general goal of this area was to prepare "synthetic metals", but the possibility of stabilizing the superconducting state in low-dimensional materials was also contemplated. This interest was largely fueled by the exciton theory of superconductivity proposed by W. A. Little in 1964,[1] and by the report of superconducting fluctuations in the 1D metal [(TTF)(TCNQ)] by Heeger and co-workers in 1973.[2] Little's theory, which is based on an electron-polarization (exciton) coupling mechanism, predicts that a superconducting material with a T_c value as high as room temperature is possible in 1D systems composed of a conducting backbone and photochemically active side-chains (dye molecules). The theory was never actually tested, however, because of the lack of an appropriate chemical system, and it gradually faded into obscurity.[3] A recent report has led to renewed speculation about Little's exciton theory of superconductivity and about the properties of 1D polymeric materials in general.[4]

During the decades spanning the period 1960–80, a considerable body of literature was published on the synthesis and properties of materials composed of interacting metal ions along the backbone of a chain.[5] One of the largest classes of these materials is the family of partially oxidized tetracyanoplatinate salts, commonly referred to as Krogmann salts.[6] The square-planar $[Pt(CN)_4]^{n-}$ anions in these materials form infinite stacks in the solid state based on the overlap of the d_{z^2} orbitals normal to the plane of the molecule. The short Pt···Pt contacts lead to band formation (Figure 1), and oxidative doping of the Pt^{II} compounds produces nonstoichiometric conducting phases. For example, salts of the type

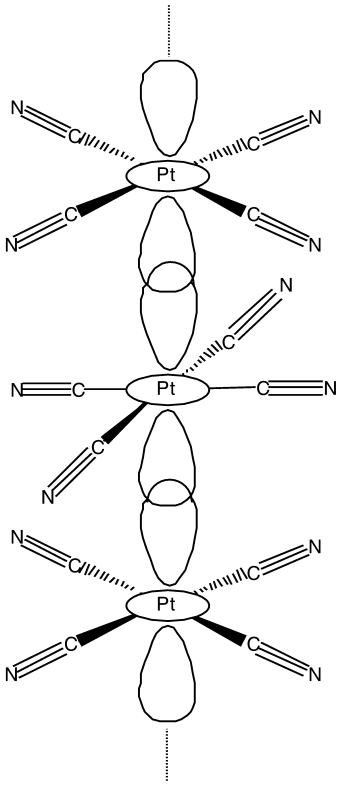


Figure 1. A schematic representation of a square planar $[Pt(CN)_4]^{n-}$ stack, to emphasize the overlapping d_{z^2} orbitals.

[*] Prof. Dr. K. R. Dunbar, Dr. J. K. Bera
Department of Chemistry
Texas A&M University
P.O. Box 30012, College Station, TX 77842-3012 (USA)
Fax: (+1) 979-845-7177
E-mail: dunbar@mail.chem.tamu.edu

 © 2002 WILEY-VCH Verlag GmbH & Co. KGaA, Weinheim 1433-7851/02/4123-4453 $ 20.00+.50/0

$K_2[Pt(CN)_4]X_{0.3}\cdot(H_2O)_n$ (X = Cl, Br) in which platinum has an average oxidation state of approximately +2.3, exhibit metallic luster and high conductivity. These materials represent the first synthetically designed "wires" based on inorganic molecules. It is worth noting that, in recent years, a new family of Pt chains based on alternating cations and anions of the types $[Pt(CNR)_4]^{2+}$ (R = *i*Pr, *c*-$C_{12}H_{23}$, *p*-$(C_2H_5)C_6H_4$) and $[Pt(CN)_4]^{2-}$ has been reported. These are being explored as novel vapochromic sensor materials.[7]

2. Renaissance of 1D Metal–Metal Chain Compounds

The subject of this Highlight article is the recent renaissance of research in the area of 1D oligomers and polymers with metal-containing backbones. There is a systematic effort currently underway in a number of laboratories to design and understand the properties of compounds based on linear chains of transition-metal atoms. The new research is divided into two distinct types of activities. In one approach, the metal atoms are positioned in a linear array by the use of carefully designed ligands. In this manner, researchers have demonstrated that they can prepare oligomers composed of a predetermined number of metal ions. In a completely different approach, it has been shown that it is possible to use stable, dinuclear metal–metal bonded precursors as building blocks for polymeric chains.

3. Oligomers based on M–M Interactions Engendered by Polydentate Ligands

3.1. Polypyridylamine Ligands

One method for stabilizing M_n^{m+} chains is to bring the metal ions into close proximity by the use of specifically designed polydentate ligands whose number and orientation of donor atoms determines the nuclearity of the product. The use of polypyridylamine ligands with flexible backbones is a particularly attractive choice that has led to the isolation of metal chains with 3–9 metal atoms. By employing this approach, the independent research groups of Cotton and Peng have prepared a family of trinuclear compounds of the type $[M_3(\mu_3\text{-dpa})_4X_2]$ (M = Cu,[8a] Ni,[8b] Cr,[8c] Ru,[8d] Rh,[8d] Co;[8e–g] dpa = *syn-syn* bis(α-pyridyl)amido; Figure 2). Interestingly, the tricobalt analogues exhibit fascinating subtleties in their molecular structures in that both the symmetrical (s; Co–Co distance 2.3178(9) Å)[8g] and unsymmetrical (u; Co–Co distances 2.294(1) and 2.466(1) Å) analogues can be isolated.[9] These observations have led to renewed speculation of the possibility of the existence of "bond stretch isomers". As discussed in detail in the recent literature,[10] all previous claims of bond stretch isomerism can be attributed to crystallographic artifacts. In the case of the s- and u-$[Co_3(dpa)_4Cl_2]$ compounds, however, there is no question about the chemical formula and there are no problems

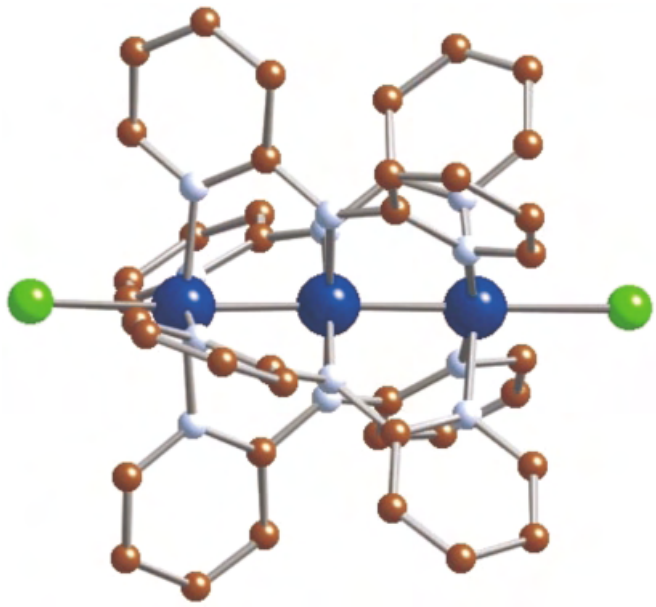


Figure 2. Molecular structure of the tricobalt molecule, $[Co_3(\mu_3\text{-dpa})_4Cl_2]$ (dpa = *syn-syn* bis(α-pyridyl)amido).

resulting from disorder. Whether this molecule represents a true case of bond stretch isomerism or not is unclear, however, the fact that both a symmetrical trinuclear chain and a dinuclear Co–Co unit with an independent Co^{II} "appendage" can be stabilized in the solid state, represents an intriguing example of how crystallization conditions can have a profound effect on the structural parameters of a simple molecule.[9] Apart from this intriguing issue, the magnetic properties of the tricobalt compounds are also quite interesting, as they show spin-crossover behavior that varies with the nature of the solid-state structure.[11]

The success of the aforementioned approach has progressed well beyond the preparation of trinuclear compounds. Indeed, by sequentially adding binding sites to the ligands, it is possible to prepare higher nuclearity analogues, for example, M_5 linear chains (M = Ni,[12a,b] Cr;[12c,d] ligand: *N*,*N*′-bis(α-pyridyl)-2,6-diaminopyridine or tripyridyldiamine (H_2tpda)), M_7 chains (M = Ni,[13a] Cr;[13b] ligand: tetrapyridyltriamine (H_3teptra); Figure 3) and M_9 chains (M = Ni;[13c] ligand: pentapyridyltetramine (H_4peptea).

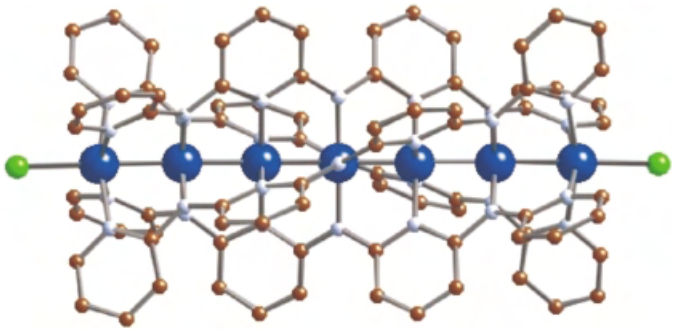


Figure 3. Molecular structure of the heptanickel molecule, $[Ni_7(\mu_7\text{-teptra})_4Cl_2]$ (teptra = tetrapyridyltriamino).

 © 2002 WILEY-VCH Verlag GmbH & Co. KGaA, Weinheim 1433-7851/02/4123-4454 $ 20.00+.50/0

3.2. Olefin Ligands

One recent finding that is particularly interesting in the context of 1D metal "wires" is the report that unsaturated hyrdocarbons can be used as to construct Pd chains surrounded by a "π-electron sheath".[14] The groups of Murahashi and Kurosawa reported that mononuclear Pd^0 and Pd^{II} precursors react with conjugated polyenes to form linear Pd–Pd bonded chains stabilized solely by the olefin ligands. The authors have isolated "sandwich chains" with three, four, and five Pd atoms by this approach. A single-crystal X-ray diffraction study of the tetrapalladium molecule confirmed the formulation as a Pd–olefin chain compound whose molecular structure is depicted in Figure 4.[14c]

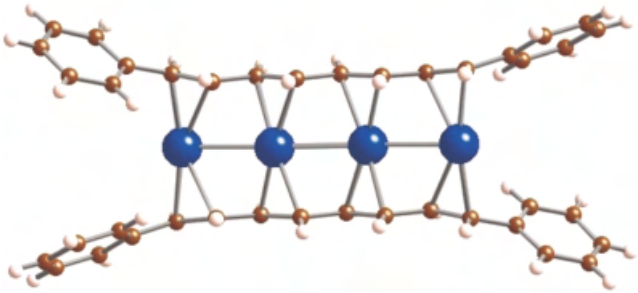


Figure 4. Molecular structure of the tetrapalladium cation, $[Pd_4(DPOT)_2]^{2+}$ (DPOT = *all-trans*-1,8-diphenyl-1,3,5,7-octatetraene).

The Pd–olefin "wires" are of interest for several reasons. They constitute the first examples of metal–metal bonded arrays stabilized entirely by metal–carbon bonds, which constitutes a significant contribution to organometallic chemistry.[15] Most importantly, however, the supporting ligand is a conducting molecule in its own right. The prospect of making more elaborate 1D chains in which a conducting organic and inorganic backbone are embedded in the same architecture is attractive with respect to enhancing conducting behavior, and certainly presents intriguing possibilities for additional work in this area.

3.3. Future Prospects for Ligand-Supported Metal Arrays

One obvious question in the field of ligand-supported metal arrays is how far can one extend the chain length? The main limitation is the maximum number of binding units that can be fused together into one ligand, which is an issue of organic synthesis. In addition to the general challenge of progressively adding binding units to the ligand is the problem of eventual insolubility. If these synthetic barriers can be overcome in the next generation of chains, it may be possible to prepare molecules whose chain lengths approach a size regime that allows for measurements to be made on individual molecules.

4. Oligomers and Polymers Based on Unsupported M–M Interactions

4.1. Oligomeric Mixed-Valence Chains

The $[Rh_4(1,3\text{-diisocyanopropane})_8Cl]^{5+}$ ion, reported by Gray[16a, b] and Mann,[16c] was the first structurally characterized chain based on the Rh^I-Rh^{II}-Rh^{II}-Rh^I unit (Figure 5). Subsequently, numerous examples of oligomeric mixed-valence rhodium complexes have been prepared.[17] In order to favor the formation of these complexes, it is necessary to use

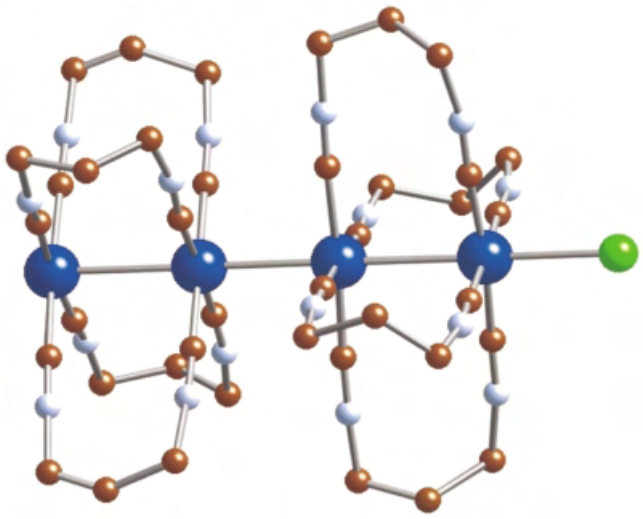


Figure 5. Molecular structure depicting the Rh^I-Rh^{II}-Rh^{II}-Rh^{II}-Cl unit in the $[Rh_4(1,3\text{-diisocyanopropane})_8Cl]^{5+}$ cation.

sterically undemanding ligands that do not restrict intermolecular interactions along the axial direction, for example, planar chelating ligands such as 9,10-phenanthroquinonediimine.[18] One particular category of these mixed-valence oligomers is the "Platinum Blue" family.[19] The first X-ray structural characterization of the platinum blues was carried out by Lippard and co-workers[20] who established the existence of the mixed-valence tetranuclear platinum compounds based on $[Pt_4(NH_3)_8(C_5H_6NO)_4]^{5+}$ ions. The tetraplatinum chemistry has been extended to even longer chains of metal atoms, for example, the octanuclear chains $[\{Pt_2(NH_3)_4(CH_3CONH)_2\}_4]^{10+}$ and $[\{Pt_2(NH_3)_4(CH_2FCONH)_2\}_4]^{8.66+}$ in which four sets of amidate-bridged Pt_2 "dimers" are held together by Pt···Pt interactions.[19]

New developments in this area include the work of Oro and co-workers, who have prepared analogous tetranuclear rhodium and iridium blues.[21] The researchers present two general ways of preparing mixed-valence species of Rh and Ir. The tetrarhodium cation $[Rh(\mu\text{-pz})(CN\textit{t}Bu_2)_4]^{2+}$ (pz = pyrazolato) was obtained by mixing $[\{Rh^I(\mu\text{-pz})(CN\textit{t}Bu)_2\}_2]$ and $[\{Rh^{II}(\mu\text{-pz})(CN\textit{t}Bu)_2(NCCH_3)\}_2][PF_6]_2$ in a 1:1 ratio, and the neutral tetrairidium compound $[\{(NC\textit{t}Bu)_2(I)[Ir^I(\mu\text{-pz})_2\text{-}Ir^{II}(CN\textit{t}Bu)_2]\}_2]$ was prepared by oxidation of $[\{Ir^I(\mu\text{-pz})(CN\textit{t}Bu)_2\}_2]$ with iodine (Figure 6). Both methods appear to be quite general for the preparation of tetranuclear compounds of rhodium and iridium.

4.2. Infinite Mixed-Valence Chains

Discrete dinuclear complexes with metal–metal bonds occupy a central role in modern transition-metal chemistry,[22]

 © 2002 WILEY-VCH Verlag GmbH & Co. KGaA, Weinheim 1433-7851/02/4123-4455 $ 20.00+.50/0

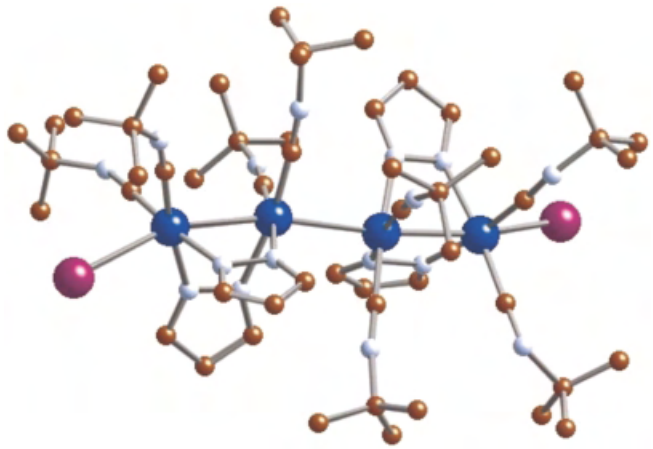


Figure 6. Molecular structure of the tetrairidium molecule, $[\{(CNtBu)_2(I)Ir(\mu\text{-}pz)_2Ir(CNtBu)_2\}_2]$.

but it has only been recently demonstrated that these complexes can be used as precursors for 1D metal chains. Infinite metal-based chains are expected to be much more promising as conducting inorganic "molecular wires" than short-chain oligomers. Work in our laboratories in this area has led to the isolation of the novel solvated 1D rhodium chain, $[\{Rh(CH_3CN)_4\}(BF_4)_{1.5}]_\infty$, obtained by slow reduction of $[Rh_2(CH_3CN)_{10}][BF_4]_4$ at a Pt electrode (Figure 7).[23] The

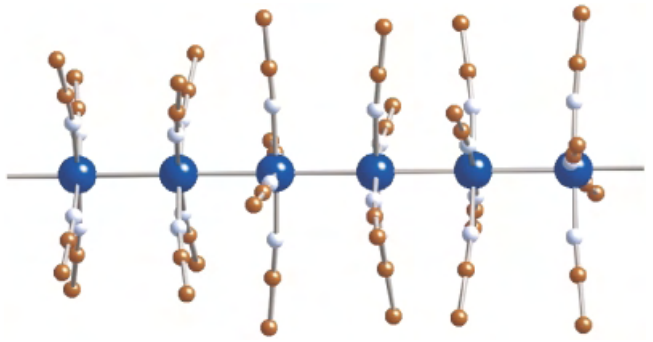


Figure 7. A section of the infinite cationic chain in $[\{Rh(CH_3CN)_4\}(BF_4)_{1.5}]_\infty$.

infinite chain results from radical polymerization of the unstable mixed-valence $Rh_2^{I,II}$ species and consists of alternating Rh–Rh interactions of 2.8442(8) and 2.9277(8) Å. This compound is the first example of an infinite metal-containing chain synthesized from a dimetal precursor, and it provides a rare opportunity to probe 1D behavior in a metal chain that differs considerably from the mixed-valence $[Pt(CN)_4]^{n-}$ systems. Although the charge transport experiments indicate that $[\{Rh(CH_3CN)_4\}(BF_4)_{1.5}]_\infty$ is a semiconductor, theoretical calculations predict that the d_{z^2} orbitals interact quite strongly along the chain. It is feasible to expect that a metallic state could be stabilized with subtle chemical modifications.

It is interesting to note that the prospect for isolating linear chains of interacting dirhodium metal ions is not limited to acetonitrile chemistry. One recent example of such a system is a 1D chain compound composed of the repeat units $[\{Rh_2^{II,II}(O_2CCF_3)_4\}\{Rh_2^{I,I}(O_2CCF_3)_2(CO)_4\}_2]$.[24] In addition, dirhodium-containing metal chains of the type $[\{Rh_2(O_2CCH_3)_2(bpy)_2\}(BF_4)\cdot H_2O]_n$ have been prepared by one-electron reduction reactions of $[Rh_2(O_2CCH_3)_2(bpy)_2(H_2O)_2]^{2+}$ in alcohols.[25, 26] The X-ray structures of one of these products revealed that intermolecular Rh···Rh separations are much longer (2.833(2) Å) than the intramolecular interactions (2.666(2) Å), which is an indication of the stabilizing influence of the bridging acetate ligands in the parent complex.

4.3. Future Prospects for Unsupported Metal Chains

The successful isolation of infinite mixed-valence rhodium chains from dinuclear precursors leads to an obvious question, namely, will it be possible to prepare metal chains with other 4d and even 5d metal ions? Possible candidates for this chemistry are $Os^{II,III}$ and $Ir^{I,II}$ species. The choice of suitable precursors and the optimization of crystal growth conditions are the key issues that need to be explored. The recent explosion of interest in nanoscale electronic devices is expected to fuel the growth of this chemistry and related topics in the coming years.

[1] W. A. Little, *Phys. Rev. A* **1964**, *134*, 1416.
[2] L. B. Coleman, M. J. Cohen, D. J. Sandman, F. G. Yamagishi, A. F. Garito, A. J. Heeger, *Solid State Commun.* **1973**, *12*, 1125.
[3] S. Roth, *One-Dimensional Metals*, VCH, New York, **1995**.
[4] D. Jerome, K. Bechgaard, *Nature* **2001**, *410*, 162.
[5] a) *Extended Linear Chain Compounds*, *Vol. 1–3* (Ed.: J. S. Miller), Plenum, New York, **1982**; b) J. S. Miller, A. J. Epstein, *Prog. Inorg. Chem.* **1976**, *20*, 1.
[6] a) J. M. Williams, *Adv. Inorg. Chem. Radiochem.* **1983**, *26*, 235; b) K. Krogmann, *Angew. Chem.* **1969**, *81*, 10; *Angew. Chem. Int. Ed. Engl.* **1969**, *8*, 35; c) J. R. Ferraro, J. M. Williams, *Introduction to Synthetic Electrical Conductors*, Academic Press, San Diego, **1987**, chap. 4.
[7] a) J. W. Grate, L. K. Moore, D. E. Janzen, D. J. Veltkamp, S. Kaganove, S. M. Drew, K. R. Mann, *Chem. Mater.* **2002**, *14*, 1058; b) C. E. Buss, K. R. Mann, *J. Am. Chem. Soc.* **2002**, *124*, 1031; c) C. E. Buss, C. E. Anderson, M. K. Pomije, C. M. Lutz, D. Britton, K. R. Mann, *J. Am. Chem. Soc.* **1998**, *120*, 7783.
[8] a) G. J. Pyrka, M. El-Mekki, A. A. Pinkerton, *J. Chem. Soc. Chem. Commun.* **1991**, 84; b) S. Aduldecha, B. Hathaway, *J. Chem. Soc. Dalton Trans.* **1991**, 993; c) F. A. Cotton, L. M. Daniels, C. A. Murillo, I. Pascual, *J. Am. Chem. Soc.* **1997**, *119*, 10223; d) J.-T. Sheu, C.-C. Lin, I. Chao, C.-C. Wang, S.-M. Peng, *Chem. Commun.* **1996**, 315; e) E.-C. Yang, M.-C. Cheng, M.-S. Tsai, S.-M. Peng, *J. Chem. Soc. Chem. Commun.* **1994**, 2377; f) F. A. Cotton, L. M. Daniels, G. T. Jordan IV, *Chem. Commun.* **1997**, 421; g) F. A. Cotton, L. M. Daniels, G. T. Jordan IV, C. A. Murillo, *J. Am. Chem. Soc.* **1997**, *119*, 10377.
[9] F. A. Cotton, C. A. Murillo, X. Wang, *J. Chem. Soc. Dalton Trans.* **1999**, 3327.
[10] a) M.-M. Rohmer, M. Bénard, *Chem. Soc. Rev.* **2001**, *30*, 340; b) M.-M. Rohmer, A. Strich, M. Bénard, J.-P. Malrieu, *J. Am. Chem. Soc.* **2001**, *123*, 9126; c) M.-M. Rohmer, M. Bénard, *J. Am. Chem. Soc.* **1998**, *120*, 9372.
[11] a) R. Clérac, F. A. Cotton, L. M. Daniels, K. R. Dunbar, C. A. Murillo, X. Wang, *Inorg. Chem.* **2001**, *40*, 1256; b) R. Clérac, F. A. Cotton, K. R. Dunbar, T. Lu, C. A. Murillo, X. Wang, *J. Am. Chem. Soc.* **2000**, *122*, 2272.
[12] a) C.-C. Wang, W.-C. Lo, C.-C. Chou, G.-H. Lee, J.-M. Chen, S.-M. Peng, *Inorg. Chem.* **1998**, *37*, 4059; b) S.-J. Shieh, C.-C. Chou, G.-H. Lee, C.-C. Wang, S.-M. Peng, *Angew. Chem.* **1997**, *109*, 57; *Angew. Chem. Int. Ed. Engl.* **1997**, *36*, 56; c) H.-C. Chang, J.-T. Li, C.-C. Wang, T.-W. Lin, H.-C. Lee, G.-H. Lee, S.-M. Peng, *Eur. J. Inorg. Chem.* **1999**,

 © 2002 WILEY-VCH Verlag GmbH & Co. KGaA, Weinheim 1433-7851/02/4123-4456 $ 20.00+.50/0

1243; d) F. A. Cotton, L. M. Daniels, T. Lu, C. A. Murillo, X. Wang, *J. Chem. Soc. Dalton Trans.* **1999**, 517.

[13] a) S.-Y. Lai, T.-W. Lin, Y.-H. Chen, C.-C. Wang, G.-H. Lee, M. Yang, M. Leung, S.-M. Peng, *J. Am. Chem. Soc.* **1999**, *121*, 250; b) Y.-H. Chen, C.-C. Lee, C.-C. Wang, G.-H. Lee, S.-Y. Lai, F.-Y. Li, C.-Y. Mou, S.-M. Peng, *Chem. Commun.* **1999**, 1667; c) S.-M. Peng, C.-C. Wang, Y.-L. Jang, Y.-H. Chen, F.-Y. Li, C.-Y. Mou, M.-K. Leung, *J. Magn. Magn. Mater.* **2000**, *209*, 80.

[14] a) T. Murahashi, T. Nagai, Y. Mino, E. Mochizuki, Y. Kai, H. Kurosawa, *J. Am. Chem. Soc.* **2001**, *123*, 6927; b) T. Murahashi, T. Nagai, T. Okuno, T. Matsutani, H. Kurosawa, *Chem. Commun.* **2000**, 1689; c) T. Murahashi, E. Mochizuki, Y. Kai, H. Kurosawa, *J. Am. Chem. Soc.* **1999**, *121*, 10660.

[15] Cyanoplatinates are not considered to be in the category of organometallic 1D chains.

[16] a) V. M. Miskowski, I. S. Sigal, K. R. Mann, H. B. Gray, S. J. Milder, G. S. Hammond, P. R. Ryason, *J. Am. Chem. Soc.* **1979**, *101*, 4384; b) I. S. Sigal, K. R. Mann, H. B. Gray, *J. Am. Chem. Soc.* **1980**, *102*, 7252; c) K. R. Mann, M. J. DiPierro, T. P. Gill, *J. Am. Chem. Soc.* **1980**, *102*, 3965.

[17] a) M. O. Albers, D. J. Robinson, N. J. Coville, *Coord. Chem. Rev.* **1986**, *69*, 127; b) T. R. Felthouse, *Prog. Inorg. Chem.* **1982**, *29*, 73.

[18] S.-S. Chern, G.-H. Lee, S.-M. Peng, *J. Chem. Soc. Chem. Commun.* **1994**, 1645.

[19] K. Matsumoto, K. Sakai, K. Nishio, Y. Tokisue, R. Ito, T. Nishide, Y. Shichi, *J. Am. Chem. Soc.* **1992**, *114*, 8110, and references therein.

[20] a) J. K. Barton, H. N. Rabinowitz, D. J. Szalda, S. J. Lippard, *J. Am. Chem. Soc.* **1977**, *99*, 2827; b) J. K. Barton, D. J. Szalda, H. N. Rabinowitz, J. V. Waszczak, S. J. Lippard, *J. Am. Chem. Soc.* **1979**, *101*, 1434.

[21] a) M. A. Ciriano, S. Sebastián, L. A. Oro, A. Tiripicchio, M. T. Camellini, F. J. Lahoz, *Angew. Chem.* **1988**, *100*, 406; *Angew. Chem. Int. Ed. Engl.* **1988**, *27*, 402; b) C. Tejel, M. A. Ciriano, L. A. Oro, *Chem. Eur. J.* **1999**, *5*, 1131; c) C. Tejel, M. A. Ciriano, J. A. López, F. J. Lahoz, L. A. Oro, *Angew. Chem.* **1998**, *110*, 1647; *Angew. Chem. Int. Ed.* **1998**, *37*, 1542; d) C. Tejel, M. A. Ciriano, B. E. Villarroya, R. Gelpi, J. A. Lopez, F. J. Lahoz, L. A. Oro, *Angew. Chem.* **2001**, *113*, 4208; *Angew. Chem. Int. Ed.* **2001**, *40*, 4084.

[22] F. A. Cotton, R. A. Walton, *Multiple Bonds Between Metal Atoms*, 2nd ed., Clarendon, Oxford, **1993**.

[23] a) G. M. Finniss, E. Candell, C. Campana, K. R. Dunbar, *Angew. Chem.* **1996**, *108*, 2946; *Angew. Chem. Int. Ed. Engl.* **1996**, *35*, 2772; b) M. E. Prater, L. E. Pence, R. Clérac, G. M. Finniss, C. Campana, P. Auban-Senzier, D. Jérome, E. Candell, K. R. Dunbar, *J. Am. Chem. Soc.* **1999**, *121*, 8005.

[24] a) F. A. Cotton, E. V. Dikarev, M. A. Petrukhina, *J. Organomet. Chem.* **2000**, *596*, 130; b) F. A. Cotton, E. V. Dikarev, M. A. Petrukhina, *J. Chem. Soc. Dalton Trans.* **2000**, 4241.

[25] a) F. P. Pruchnik, P. Jakimowicz, Z. Ciunik, *Inorg. Chem. Commun.* **2001**, *4*, 726; b) F. P. Pruchnik, P. Jakimowicz, Z. Ciunik, K. Stanislawek, L. A. Oro, C. Tejel, M. A. Ciriano, *Inorg. Chem. Commun.* **2001**, *4*, 19.

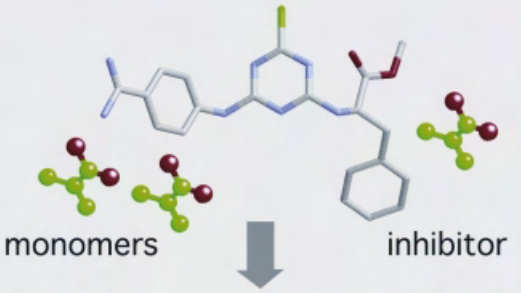
[26] We have recently obtained structural characterization of the analogous chloride complex $[\{Rh_2(O_2CCH_3)_2(bpy)_2\}Cl \cdot 3\,CH_3OH]$. K. Sorasaenee, K. R. Dunbar, unpublished results. The presence of the chloride anion in the crystal leads to three sets of Rh–Rh distances, 2.6755(6) (intramolecular), 2.7858(7) and 2.9034(7) Å (both intermolecular).

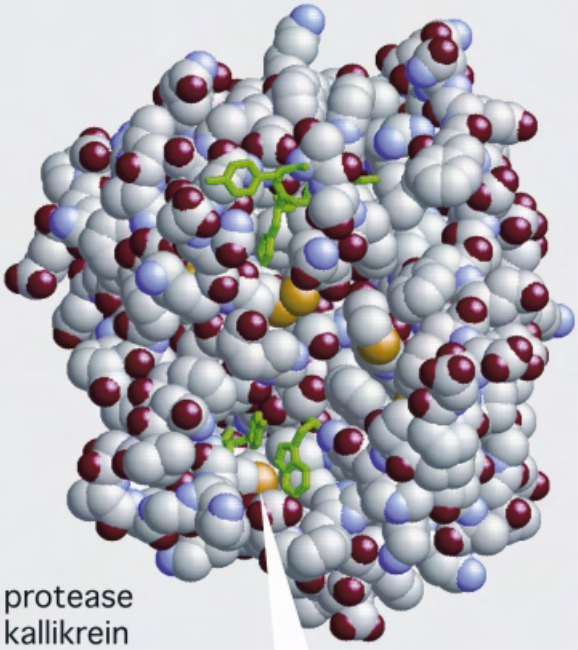
 © 2002 WILEY-VCH Verlag GmbH & Co. KGaA, Weinheim 1433-7851/02/4123-4457 $ 20.00+.50/0

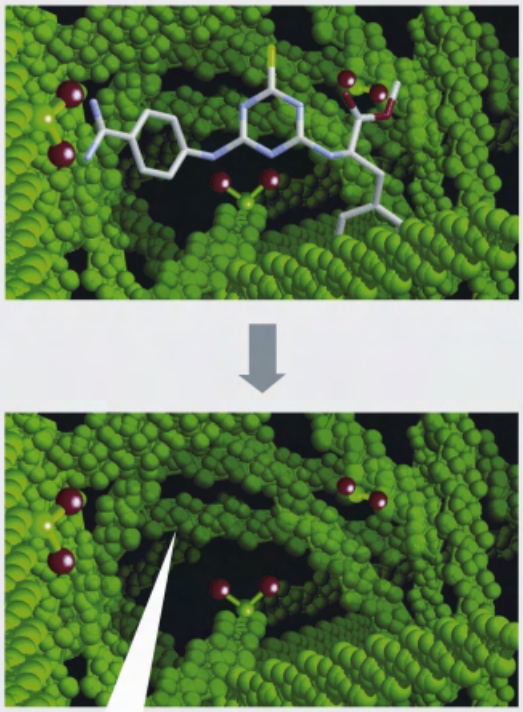
A library of new enzyme inhibitors

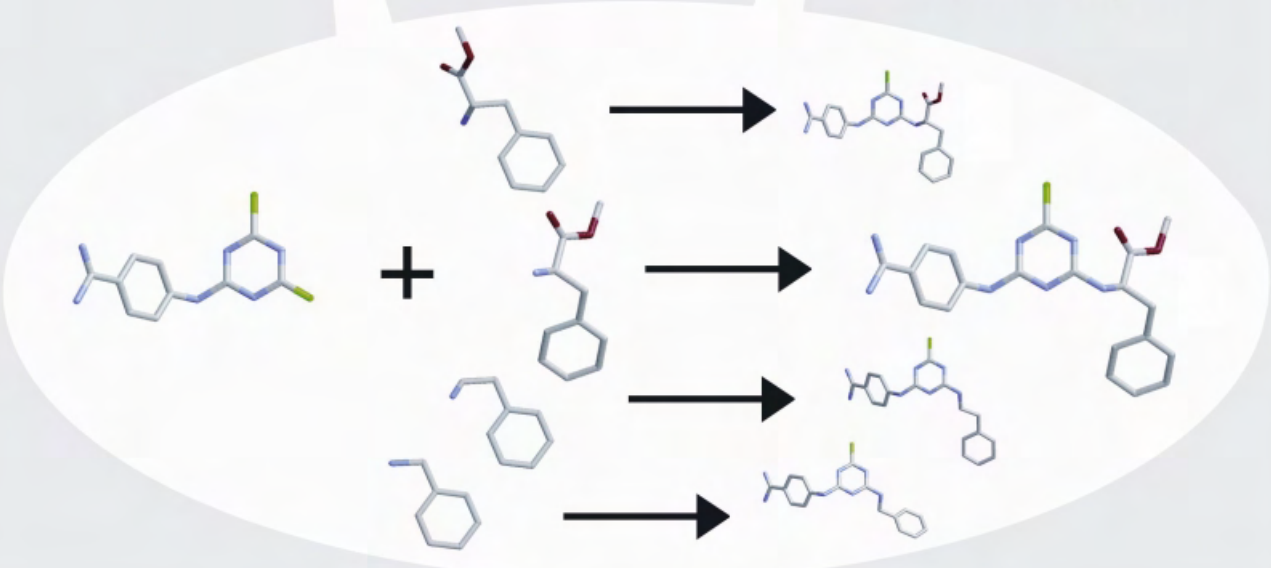
is obtained by connecting building blocks in molecular-scale reaction vessels :

- active site of the enzyme (left)
  direct molding
- moleculary imprinted cavity (right)
  anti-idiotypic imprinting









- For more information, see the Communication by Ye, Mosbach et al. on the following pages.

 © 2002 WILEY-VCH Verlag GmbH & Co. KGaA, Weinheim 1433-7851/02/4123-4459 $ 20.00+.50/0

Formation of a Class of Enzyme Inhibitors (Drugs), Including a Chiral Compound, by Using Imprinted Polymers or Biomolecules as Molecular-Scale Reaction Vessels**

Yihua Yu, Lei Ye,* Karsten Haupt, and Klaus Mosbach*

The design of novel materials with cavities that can behave as specific hosts to virtually any target molecules has become a topic of extreme scientific and technological interest in recent years. Within this broad area, the class of materials referred to as molecularly imprinted polymers (MIPs) has gained increasing interest.[1] Synthesis of MIPs is a process in which functional and cross-linking monomers are copolymerized in the presence of a target species that acts as a molecular template. The functional monomers initially form a complex with the template, and following polymerization, their functional groups are held in position by the highly cross-linked polymer structure. Subsequent removal of the template results in artificial receptors that are complementary in size, shape, and chemical functionality to the template. MIP materials are frequently used for solid-phase extraction, chromatography, and biomimetic sensor applications. One aspect that also deserves mention in the context of this article are studies carried out by several research groups towards the formation of enantiospecific imprints with potentially useful properties, for example, in the resolution of racemic drugs or for "enantiomeric polishing".[2]

For several years our research group has explored what we consider to be the next generation of molecular imprinting, which may improve synthesis and/or lead to new drugs and better affinity materials. Herein we describe two new approaches towards realizing this goal, in which we use kallikrein as a model system. Kallikrein was chosen because of its medicinal interest as well as its well-characterized structure and properties. In addition a number of inhibitors have been isolated or prepared against this proteinase enzyme.[3]

In the first approach we imprinted a known kallikrein inhibitor. After extracting the template inhibitor, we performed condensation reactions within the cavities of the MIP. The products of these condensations were evaluated for their ability to inhibit kallikrein. Thus, the products synthesized within the MIP cavities can be considered as "double imprints". We call this method the "anti-idiotypic" approach, as it relates to the known biological phenomenon of the formation of anti-antibodies to existing immunoglobulins.[4] In the second approach we target the enzyme itself by allowing it to direct the assembly of small building blocks within the biologically active site. New inhibitors for the enzyme are obtained by extraction following the condensation of these building blocks. We call this approach "direct molding". The theme that unites these two approaches is the use of cavities, either within a synthetic polymer (anti-idiotypic imprinting) or within the active site of an enzyme (direct molding), as molecular-scale reaction vessels (Figure 1).

The latter studies have been influenced by our interest over the years in immobilization and affinity chromatography of biomolecules. These studies have involved, for example, the coupling of a preformed inhibitor–enzyme complex directly to supports through the active group of the inhibitor, and affinity precipitation of, for example, bis-NAD dehydrogenase complexes.[5] In addition, bio-imprinting within the active sites of enzymes leading to induced alteration of stereo- and substrate selectivities has been studied.[6] In these examples the active sites of enzymes have been utilized, either to direct the

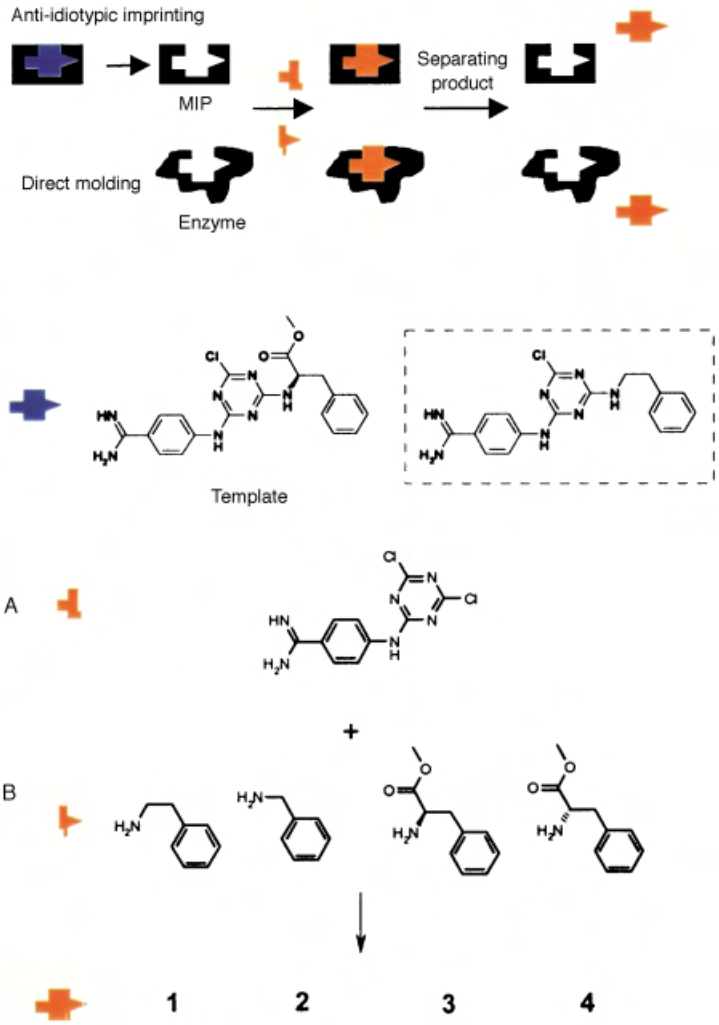


Figure 1. Schematic representation of the anti-idiotypic and direct molding approaches used, and subsequent synthetic reactions investigated in this study. The inserted structure in the middle (boxed) shows the template used in our previous study.

[*] Dr. L. Ye, Prof. Dr. K. Mosbach, Dr. Y. Yu, Dr. K. Haupt
Center for Molecular Imprinting, Pure and Applied Biochemistry
Chemical Center, Lund University
Box 124, 22100 Lund (Sweden)
Fax: (+46) 46-222-4611
E-mail: lei.ye@tbiokem.lth.se
klausmosbach@compuserve.com

[**] This work was supported in part by the Swedish Foundation for Strategic Research program "Biomimetic Materials Science" and the Swedish Research Council program "Immunoanalytical Applications of Imprinted Polymers". We thank Dr. R. Schmidt for linguistic advice and Dr. E. Yilmaz for valuable scientific discussions. Klaus Mosbach is presently a visiting professor at the Institute of Biotechnology, ETH, Zürich.

 © 2002 WILEY-VCH Verlag GmbH & Co. KGaA, Weinheim 0044-8249/02/4123-4460 $ 20.00+.50/0

assembly of properly oriented enzyme complexes or to provide binding pockets for non-native substrates or inhibitors.

We extended our earlier anti-idiotypic imprinting by using a chiral template, namely a L-phenylalanine methyl ester derivative (Figure 1).[7] This template permitted us to investigate enantiospecific synthesis inside the MIP binding cavities. (2-Trifluoromethyl)acrylic acid (TFMAA) and divinylbenzene (DVB) were used as the functional monomer and cross-linker, respectively. After preparing the MIP and removing the template, we allowed the nucleophilic reaction to take place between the positively charged triazine derivative and various hydrophobic amines inside the cavities to give either the same or related inhibitors, depending on the added amine. Condensation in the polymer cavities allowed formation of the larger product (**3**), which was not possible with an imprinted polymer prepared for the smaller template (**1**) in a previous study—presumably because of steric hindrance.[7]

Apart from the formation of the original template, the smaller compounds (**1** and **2**) could also be formed in the cavity (Figure 2). In contrast, the blank polymer (BP), which was prepared in the absence of the template, exhibited very little affect in facilitating the syntheses. This result can be explained by the fact that the BP is most unlikely to contain any specific binding site.

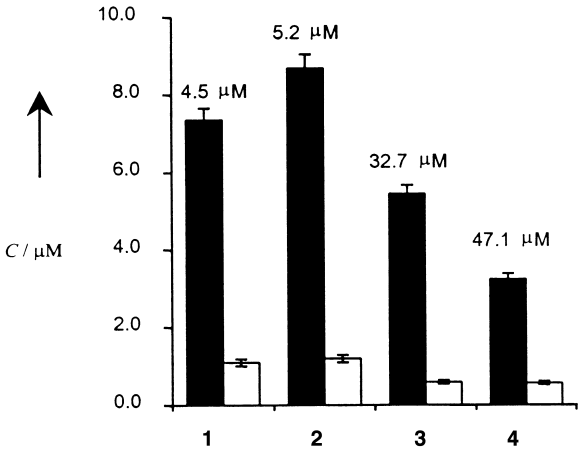


Figure 2. MIP-directed generation of inhibitors (anti-idiotypic imprinting). *C*: Concentration of the inhibitor extracted after its synthesis from the imprinted polymer (solid column) and the blank polymer (open column). The imprinted polymer was prepared using a molar ratio of template/TFMAA/DVB = 1/4/40. The inhibition constants for kallikrein are as indicated.

We observed that the MIP could produce more L enantiomer (67% more) than the D enantiomer, while the blank polymer yielded virtually equal amounts of the two enantiomers. Thus, we can conclude that the MIP cavities are themselves chiral, since they tend to direct the synthesis of products with the same stereochemistry as the initial template. This result is somewhat surprising in light of the relatively weak binding strength of the amine component that contains the asymmetric carbon atom. All products of the condensation reactions were tested for their ability to inhibit kallikrein. The lower yield of **3** and **4** are likely caused by some steric hindrance within the MIP cavities.

In the direct molding approach[8] kallikrein was chosen as a model enzyme to direct the formation of its own inhibitors. Previous studies along these lines also involved the enzyme trypsin.[9] It should be mentioned that related studies based on the self-assembly of small building blocks have been reported by other research groups utilizing either the dynamic combinatorial chemistry technique[10] or "click chemistry".[11]

To test the feasibility of using the active site of the enzyme directly to generate its inhibitors, kallikrein was first incubated with 2-(4-amidinophenylamino)-4,6-dichlorotriazine (building block A, Figure 1), followed by exposure to various amines (building blocks B, Figure 1).

As seen from Figure 3, several inhibitors could be synthesized in the presence of kallikrein. As a control, we used the strong protein inhibitor aprotinin to block the active site of

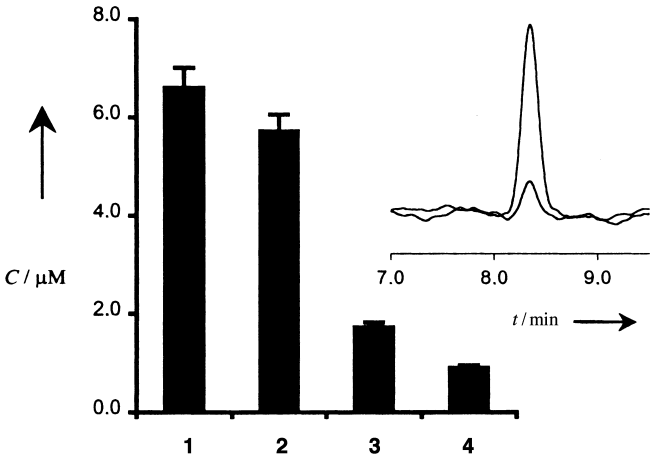


Figure 3. Enzyme-directed generation of inhibitors (direct molding). *C*: Concentration of the inhibitor obtained using kallikrein as a biotemplate. Insert: Chromatograms of **1** obtained using kallikrein as the biotemplate, in which the bottom trace represents the result of blocking the active site of the enzyme with one equivalent of aprotinin.

kallikrein, and we then proceeded to attempt the synthesis of **1**. HPLC chromatograms illustrating the formation of **1** in the presence and absence of aprotinin are also shown in Figure 3. As seen, the yield of **1** was dramatically reduced in the presence of aprotinin ($K_i = 1.0 \times 10^{-9}$ M). This result demonstrates the key role of the enzyme's active site in facilitating the synthesis of the inhibitor. This conclusion was further confirmed by substituting a nonrelated protein, bovine serum albumin (BSA), for kallikrein. The amount of **1** obtained was reduced by more than 90% when BSA was used.[12] It is interesting to note that kallikrein also showed some chiral selectivity in generating the inhibitors (**3** (L form) and **4** (D form)) in that twice the amount of **3** was formed compared to **4**. The K_i value of the D enantiomer is larger than that of the L enantiomer (47 and 33 μM, respectively), which supports the above finding of a higher yield of the L form and is consistent with a higher affinity of the L enantiomer with the enzyme compared to the D enantiomer.

In summary, we have described two novel techniques that may be useful for the discovery of new inhibitors and drugs. In

 © 2002 WILEY-VCH Verlag GmbH & Co. KGaA, Weinheim 0044-8249/02/4123-4461 $ 20.00+.50/0

the anti-idiotypic approach the MIP behaves as an enzyme or receptor binding site mimic and allows the screening of building blocks for the production of new compounds that mimic the biological activity of the original bioactive template. Three distinct advantages of this approach are: 1) there is virtually no need for detailed structural information or isolation of the real biological target; 2) it does not involve costly synthesis of a large amount of products; and 3) other functional monomers such as, for example, silanes might be used, the latter with possibly higher in vivo stability. It should also be emphasized that the MIPs prepared can be used repeatedly. In general, one can regard a MIP cavity as a single molecular reactor that guides, through its complementary size, shape, and chemical functionality, the condensation of small building blocks into a structure similar or identical to that of the initial template. With the "direct molding" approach, one would not have to rely on known bioactive molecules. However, the number of utilizable reactions is limited, because the side-chain functionalities of many amino acid residues of an enzyme/receptor may react with the building blocks. Clearly other additional applications, such as for the preparation of specific affinity ligands for separation, can be envisaged for both approaches.

Experimental Section

3: 2-(4-Amidinophenylamino)-4,6-dichlorotriazine (473 mg, 1.5 mmol) was dissolved in DMF (15 mL) and a solution of L-phenylalanine methyl ester (269 mg, 1.5 mmol) in DMF (7.5 mL) added. The mixture was stirred at 20–30 °C for 48 h, during which time the reaction was monitored by HPLC. After the reaction was completed, the solvent was completely removed by rotary evaporation (50 °C). The residue was then dissolved in chloroform/methanol (3/1, v/v), and purified by column chromatography on silica gel. Yield: 76 %. ^{1}H NMR (400 MHz, [D$_6$]DMSO): $\delta = 10.56$ (s, 1H; NH), 9.25 (s, 1H; NH), 8.95 (br s, 2H; NH), 8.02 (m, 1H), 7.80 (m, 3H), 7.4–7.15 (m, 5H; Ph), 4.78 (br d, 1H; NH), 3.71 (m, 4H; OCH_3, CH), 3.25 (dd, 1H, J = 13.5, 4.9 Hz; CH_A), 3.09 ppm (m, 1H; CH_B). Optical activity ($[\alpha]_{589}^{20}$) in methanol: +4.6.

Preparation of imprinted polymer: **3** (0.1 mmol), (2-trifluoromethyl)acrylic acid (TFMAA, 0.4 mmol), divinylbenzene (4.0 mmol), and recrystallized 2,2′-azobis(2-isobutyronitrile) (10 mg) were dissolved in anhydrous acetonitrile (0.5 mL) in a borosilicate glass tube equipped with a screw cap. The template could be dissolved in acetonitrile after addition of TFMAA, which indicated favorable molecular association between the template and TFMAA. The solution was purged with dry nitrogen for 5 min and sealed immediately. Polymerization was induced thermally at 60 °C and continued for 16 h. The resulting polymer monolith was ground manually and suspended in acetone. The slurry was forced through a 25-μm test sieve (Retsch, Germany). A second grinding was performed, if necessary, until all the particles passed through the test sieve. The particles with diameters of 10–25 μm were collected by repeated sedimentation in acetone. To remove the template, the MIP particles were extensively washed with methanol/acetic acid (9/1, v/v) until no UV adsorption at 300 nm was detected in the supernatant. The polymer particles were washed with acetone for several times and dried in a desiccator under vacuum. A nonimprinted blank polymer was prepared in the same way as that used for preparing the MIP, except that no template was used during the whole process.

MIP-directed generation of inhibitors (anti-idiotypic imprinting): Imprinted polymer (20 mg) or blank polymer (20 mg) was incubated with 40 μg of 2-(4-amidinophenylamino)-4,6-dichlorotriazine (building block A) in acetonitrile (1.0 mL) at 20 °C for 4 h. Polymers with bound 2-(4-amidinophenylamino)-4,6-dichlorotriazine (building block A) were separated by centrifugation (NANOSEP centrifugal concentrator, Gelman Laboratory, Michigan, USA, molecular weight cut-off 300 K) at 14000 rpm for 5 min. The polymers were resuspended in acetonitrile (1.0 mL), followed by adding the individual amine reactant (2-phenylethylamine: 152 μg, benzylamine: 134 μg, L-phenylalanine methyl ester: 224 μg, D-phenylalanine methyl ester: 224 μg). The mixture was gently stirred at 20 °C for 16 h. Centrifugal filtration was performed using the NANOSEP concentrator. To extract the product, the polymer particles were resuspended in 10 % acetic acid in MeOH (1.0 mL) and mixed at 20 °C for 2 h. After centrifugation (14000 rpm, 10 min), the concentration of the product in the supernatant (0.8 mL) was measured by HPLC analysis.

Enzyme-directed generation of inhibitors (direct molding): Kallikrein solution (0.4 mL at 1.0 mg mL^{-1} in tris(hydroxymethyl)aminomethane-hydrochloric acid (Tris-HCl) buffer, 50 mM, pH 7.0) was mixed with 2-(4-amidinophenylamino)-4,6-dichlorostriazine (0.6 mL at 1.0 mg mL^{-1} in Tris-HCl buffer, 50 mM, pH 7.0) in a 1.5-mL eppendorf tube and incubated at 20 °C for 4 h. Centrifugation was performed using a NANOSEP centrifugal concentrator (molecular weight cut-off 3 K) to remove excess of building block A. The kallikrein with bound building block A was transferred into Na_2CO_3/$NaHCO_3$ buffer (1.0 mL, 50 mM, pH 10.0), to which excess of amine (building block B, 10 mg mL^{-1}) was added separately (phenylethylamine: 30 μL, benzylamine: 34 μL, L-phenylalanine methyl ester: 44 μL, D-phenylalanine methyl ester 44 μL). After incubation at 20 °C for 48 h, a NANOSEP centrifugal concentrator (molecular weight cut-off 3 K) was used to remove the excess of free amine, and the kallikrein–inhibitor complex was transferred into 6.0 M guanidine hydrochloride (1.0 mL) and incubated at 20 °C for 2 h to disassociate the inhibitor from kallikrein. After centrifugation (NANOSEP, molecular weight cut-off 3 K), the filtrate was analyzed by HPLC for product quantification. When aprotinin was used to block the active site of kallikrein, it was added to the enzyme solution and incubated for 2 h prior to the addition of the building blocks.

HPLC analysis: Reverse-phase HPLC analysis was carried out by using a LaChrom L-7100 solvent delivery system, a L-7455 diode array detector, and a software package D-7000 HPLC System Manager (Merck KgaA, Darmstadt, Germany). A chromolith performance column (RP-18 e) from Merck (Darmstadt, Germany) was used with a gradient elution (0–10 min, 20–50 % acetonitrile in water, both containing 0.1 % trifluoroacetic acid) at a flow rate of 1.0 mL min^{-1}. For each analysis 20 μL of sample was injected.

Enzyme assays: The inhibitory activities of the compounds against porcine pancreatic kallikrein were determined from their effect on the enzyme-catalyzed hydrolysis of the chromogenic substrate D-Val-Leu-Arg-4-nitroanilide. Each assay (total volume of 1 mL) contained: *N*-tris(hydroxymethyl)methylglycine (tricine)/NaOH buffer (100 mM, pH 8.2, 940 μL); D-Val-Leu-Arg-4-nitroanilide (20–60 nmol in 20 μL of water); the inhibitor (2.5–20 nmol in a mixture of 10 μL of DMSO and 10 μL of water); and porcine pancreatic kallikrein (4 μg in 20 μL of water). The change in absorbance at 410 nm was monitored at 20 °C to determine the initial rates (ρ) of hydrolysis. Assays were carried out at a minimum of five inhibitor concentrations ($[I]$) and three substrate concentrations. The inhibition constant (K_i) was determined from the Dixon plot ($1/\rho$ versus $[I]$), where K_i was taken as the absolute value of $[I]$ that corresponded to the intersection point of a series of curves at different substrate concentrations.[13]

Received: August 19, 2002 [Z19994]

[1] a) K. Mosbach, *Trends Biochem. Sci.* **1994**, *19*, 9–14; b) K. Shea, *Trends Polym. Sci.* **1994**, *2*, 166–173; c) G. Wuff, *Angew. Chem.* **1995**, *107*, 1958–1979; *Angew. Chem. Int. Ed.* **1995**, *34*, 1812–1832; d) A. Friggeri, H. Kobayashi, S. Shinkai, D. N. Reinhoudt, *Angew. Chem.* **2001**, *113*, 4865–4867; *Angew. Chem. Int. Ed.* **2001**, *40*, 4729–4731; e) K. Haupt, K. Mosbach, *Chem. Rev.* **2000**, *100*, 2495–2504.

[2] R. J. Ansell, K. Mosbach, *Pharm. News* **1995**, *3*, 16–20.

[3] W. Bode, Z. Chen, K. Bartels, *J. Mol. Biol.* **1983**, *164*, 237–282.

[4] a) N. K. Jerne, *Ann. Immunol.* **1974**, *125C*, 373–389; b) L. Izadyar, A. Friboulet, M. H. Remy, A. Roseto, D. Thomas, *Proc. Natl. Acad. Sci.* **1993**, *90*, 8876–8880; c) B. Avalle, A. Friboulet, D. Thomas, *Ann. New York Acad. Sci.* **1998**, *864*, 118–130.

[5] a) S. Flygare, T. Griffin, P.-O. Larsson, K. Mosbach, *Anal. Biochem.* **1983**, *133*, 409–416; b) M.-O. Månsson, N. Siegbahn, K. Mosbach, *Proc. Natl. Acad. Sci. USA* **1983**, *80*, 1487–1491.

[6] M. Stahl, U. Jeppson-Wistrand, M.-O. Månsson, K. Mosbach, *J. Am. Chem. Soc.* **1991**, *113*, 9366–9368.

[7] K. Mosbach, Y. Yu, J. Andersch, L. Ye, *J. Am. Chem. Soc.* **2001**, *123*, 12420–12421.

 © 2002 WILEY-VCH Verlag GmbH & Co. KGaA, Weinheim 0044-8249/02/4123-4462 $ 20.00+.50/0

[8] a) K. Mosbach, P. A. G. Cormack, O. Ramström, K. Haupt, US patent 6127154 [*Chem. Abstr.* **1999**, *132*, 423]; b) K. Mosbach, *Anal. Chim. Acta* **2001**, *435*, 3–8.
[9] K. Mosbach, European Patent 0743870 [*Chem. Abstr.* **1995**, *123*, 250956].
[10] R. Nguyen, I. Huc, *Angew. Chem.* **2001**, *113*, 1824–1826; *Angew. Chem. Int. Ed.* **2001**, *40*, 1774–1776.
[11] W. G. Lewis, L. G. Green, F. Grynszpan, Z. Radi, P. R. Carller, P. Taylor, M. G. Finn, K. B. Sharpless, *Angew. Chem.* **2002**, *114*, 1095–1099; *Angew. Chem. Int. Ed.* **2002**, *41*, 1053–1057.
[12] In the absence of any protein, there was a small amount of inhibitor **1** formed in solution from the nucleophilic reaction between the two building blocks.
[13] M. Dixon, *Biochem. J.* **1953**, *55*, 170–171.

Facile Assembly of Cell Surface Oligosaccharide Mimics by Copolymerization of Carbohydrate Modules**

Kenji Sasaki, Yoshihiro Nishida,* Tomoaki Tsurumi, Hirotaka Uzawa, Hirosato Kondo, and Kazukiyo Kobayashi*

Artificial glycoconjugate polymers (glycopolymers) and other multivalent carbohydrate ligands constitute a new class of biomimetic supramolecules.[1] They have shown many biological applications in, for example, cultivation, tumor diagnosis and detection, and the trapping of viruses and bacterial toxins.[2] Their utility is ascribed mainly to their strong and species-specific interactions with the receptor proteins as a result of multivalent binding and/or carbohydrate cluster effects. Although most of the glycopolymers so far prepared and applied were made up of simple mono- and disaccharides, more intense interest has been directed to glycopolymers carrying cell-surface oligosaccharides such as sialyl Lewis^X (sLe^X)[3] and globosyl oligosaccharides[4] that have potentially greater biological significance. From a practical viewpoint, however, the synthesis and application of these glycoconjugates are seriously restricted by the difficulty in preparing target oligosaccharides in sufficient amounts prior to their incorporation into the multivalent models.

In the course of our synthetic study of glycopolymers carrying the mimics of cell-surface oligosaccharides,[5] we found recently that an acrylamide copolymer carrying α-L-fucopyranoside and 3-sulfo-β-D-galactopyranoside as a side chain shows strong activity in blocking L-selectin/sLe^X tetrasaccharide adhesion.[6] As judged from the observation that none of the acrylamide copolymers carrying only one of the two glycosides showed a notable activity, the observed activity was ascribed to the cooperative binding of the α-L-fucoside and 3-sulfo-β-D-galactoside to L-selectin. This finding indicated the potential utility of the module approach and prompted us to generalize it as a "carbohydrate module method".

For the facile understanding of our "carbohydrate module method", let us assume a model consisting of the binding of a branching pentasaccharide with the receptor protein (Figure 1). In this model the two glycoside residues (A1 and A2) at the nonreducing terminal provide key binding interactions with the receptor protein at the *r*(A1) and *r*(A2) binding sites. Conventional mimic syntheses may target a branching trisaccharide carrying A1, A2, and B residues, thus developing the multivalent model (polymer-(A1 + A2 + B)) in Figure 1b. Our approach targets a copolymer-(A1/A2) species carrying the key interactive sugars (Figure 1c) to circumvent the difficulty in preparing the branching saccharide. The copolymer-(A1/A2) species is assumed to have a certain probability of occupying both of the binding sites and, thus, is expected to show a higher binding activity than the polymers carrying only one of the key sugars (poly-(A1) and poly-(A2)). This situation means that copolymerization of two key interactive sugars (A1 and A2 in the present case) provides a facile way to mimic the biologically active structures of oligosaccharides. The glycopolymers thus derived may show potent biological activity in blocking the binding of the oligosaccharide to receptor proteins.

The present approach involves the following three steps: segmentation of a targeted oligosaccharide into smaller sugars, synthesis of the corresponding glycosylated monomers (defined as "carbohydrate modules" in this study), and the reassembly of oligosaccharide mimics by copolymerization of the modules. Previously, we employed this process for sLe^X tetrasaccharide **1a**, which was segmented into modules of allyl α-L-fucoside and *p*-acrylamidophenyl 3-sulfo-β-D-galactopyranoside to afford the copolymer (**2**) with potent activity in blocking L-selectin/sLe^X binding.[6] In the present study, we took the module approach to 6-sulfo-sialyl Lewis^X (6-sulfo-sLe^X) tetrasaccharide **1b** which has a 6-sulfo-GlcNAc at the reducing residue. The biological significance of **1b** is evident from recent studies[7] in which it was substantiated that the 6-sulfo analogue **1b** is a better ligand than sLe^X (**1a**) for L-selectin. We aimed to not only prepare multivalent 6-sulfo-Le^X mimics but also to investigate the possible role of the 6-sulfo-GlcNAc residue in binding to L-selectin.

The oligosaccharide sequence was divided into Lewis^X (Le^X), sLe^X, and 6-sulfo-GlcNAc to investigate key epitopes for L-selectin. To construct the library of Le^X, sLe^X, and 6-

[*] Dr. Y. Nishida, Prof. Dr. K. Kobayashi, K. Sasaki, T. Tsurumi
Department of Molecular Design and Engineering
Graduate School of Engineering
Nagoya University
Chikusa-ku, Nagoya 464–8603 (Japan)
Fax: (+81) 52–789–2528
E-mail: nishida@mol.nagoya-u.ac.jp
kobayash@mol.nagoya-u.ac.jp
Dr. H. Uzawa
National Institute of Advanced Industrial Science and Technology (AIST) (Japan)
Dr. H. Kondo
Research & Development Division
Nippon Organon K. K. (Japan)

[**] Part of this research is supported by grants from the Japanese Ministry of Education and Science (K.K. and Y.N). We thank the Japan Society for the Promotion of Science Research for a research fellowship for young scientists (K.S.).

Supporting information for this article is available on the WWW under http://www.angewandte.org or from the author.

 © 2002 WILEY-VCH Verlag GmbH & Co. KGaA, Weinheim 0044-8249/02/4123-4463 $ 20.00+.50/0

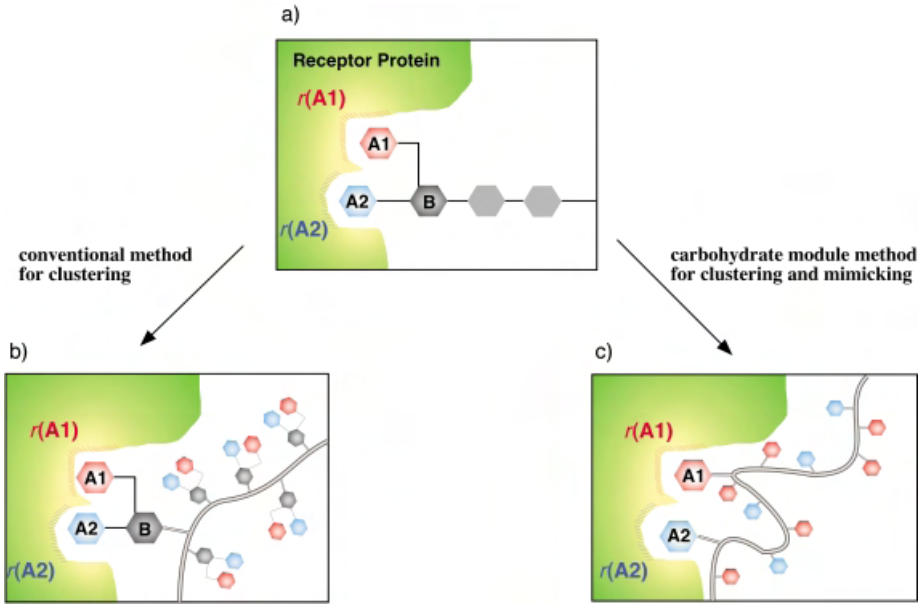
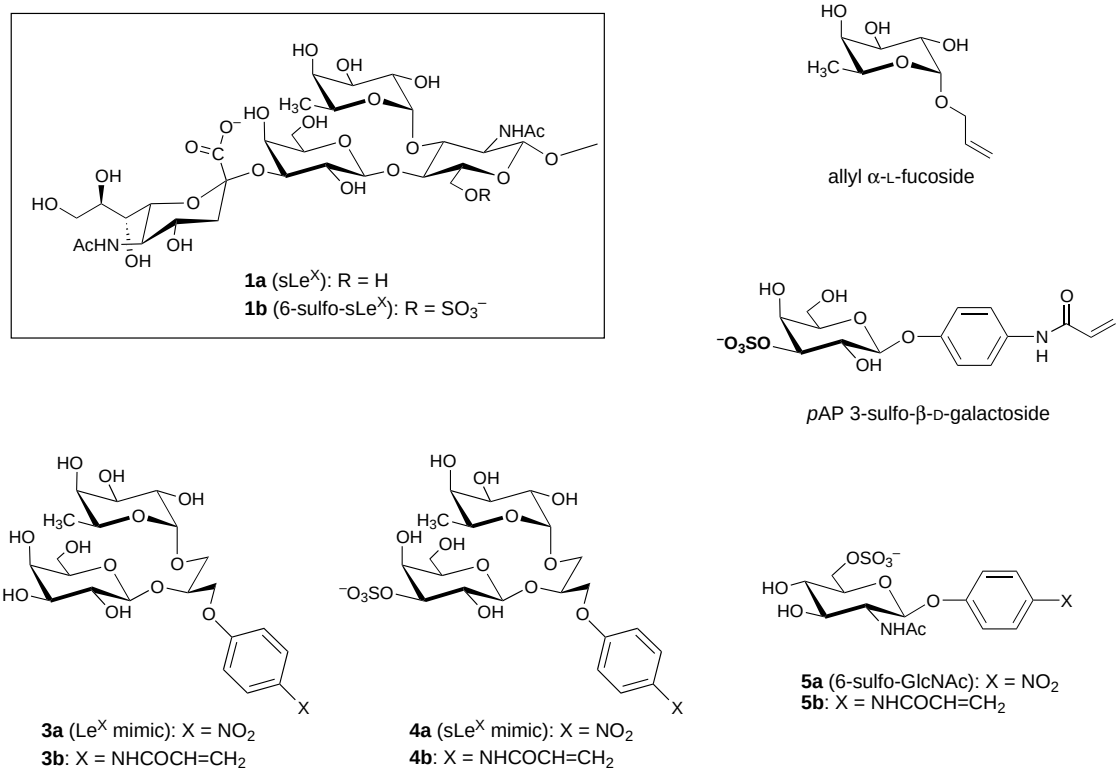


Figure 1. Concept of the carbohydrate module approach for the mimic synthesis of oligosaccharides. a) A targeting branching trisaccharide carrying A1, A2, and B residues to bind to the receptor protein. b) The conventional multivalent model. c) The copolymer-(A1/A2) species carrying the key interactive sugars prepared on the basis of our concept of "carbohydrate module method".

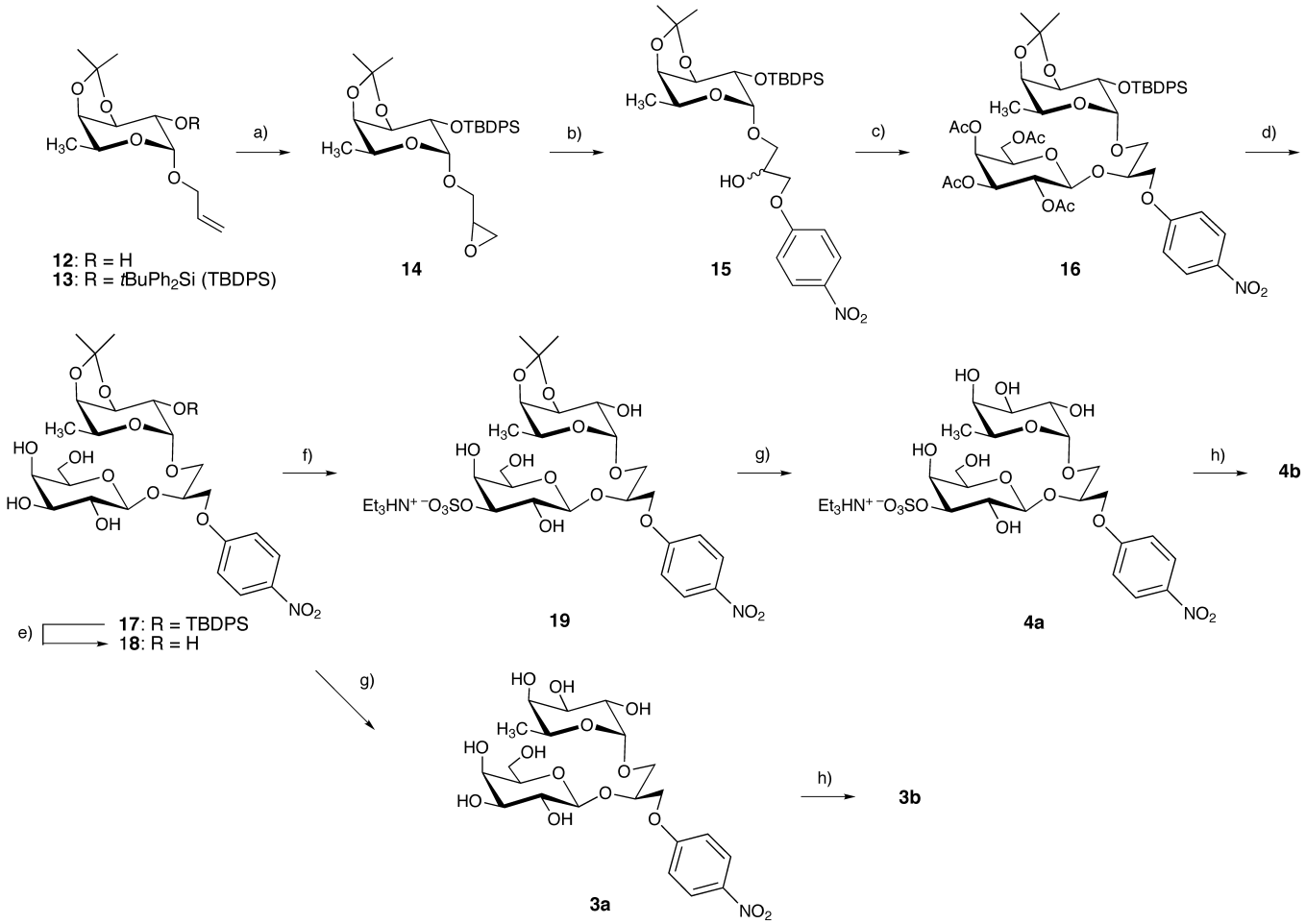
sulfo-Le^X mimics, *p*-*N*-acrylamidophenyl (*p*AP) glycosides **3b** and **4b** were designed as simple Le^X and sLe^X modules, respectively (Scheme 1). They were prepared from allyl α-L-fucopyranoside as depicted in Scheme 2. The diastereomeric mixture **15** (50% *de*) could be resolved by either fractional crystallization or reversed-phase HPLC column chromatography to afford single isomers **3b** and **4b** (>95% *de* by ^{1}H NMR analysis). The *R* configuration of the acyclic moiety corresponds to the absolute stereochemistry along the C-3, C-4, and C-5 bonds of the GlcNAc residue in sLe^X **1a**. Another key module **5b** (*p*AP 6-sulfo-β-D-GlcNAc) was prepared from *p*-nitrophenyl (*p*NP) β-D-GlcNAc with a sulfur trioxide/trimethylamine complex.[8] Each of these 6-sulfo-sLe^X modules **3b**–**5b** was copolymerized with acrylamide to give a series of acrylamide copolymers **6**–**8**. Moreover, copolymerization of **4b** and **5b** in the presence of acrylamide gave a terpolymer **9** (Scheme 3).[9]

An enzyme-linked immunosorbent assay (ELISA) was performed in microtiter plates (96 wells, PROBIND) coated with sLe^X pentaceramides as reported previously.[10] Both the polymeric **6**–**9** and monomeric ligands **3a**–**5a** were assayed in the same way to evaluate the effect of multivalent binding on their ability to block L-selectin. The results summarized in Table 1 indicate that none of the monomeric glycosides possesses notable activity (IC_{50} > 50 μM), while most of the polymers, except for Le^X mimic **6**, possess potent activity. The strong multivalent binding effect thus observed suggests the



Scheme 1. Segmentation of sialyl Le^X **1a** and 6-sulfo-sLe^X tetrasaccharides **1b** into key carbohydrate modules.

 © 2002 WILEY-VCH Verlag GmbH & Co. KGaA, Weinheim 0044-8249/02/4123-4464 $ 20.00+.50/0



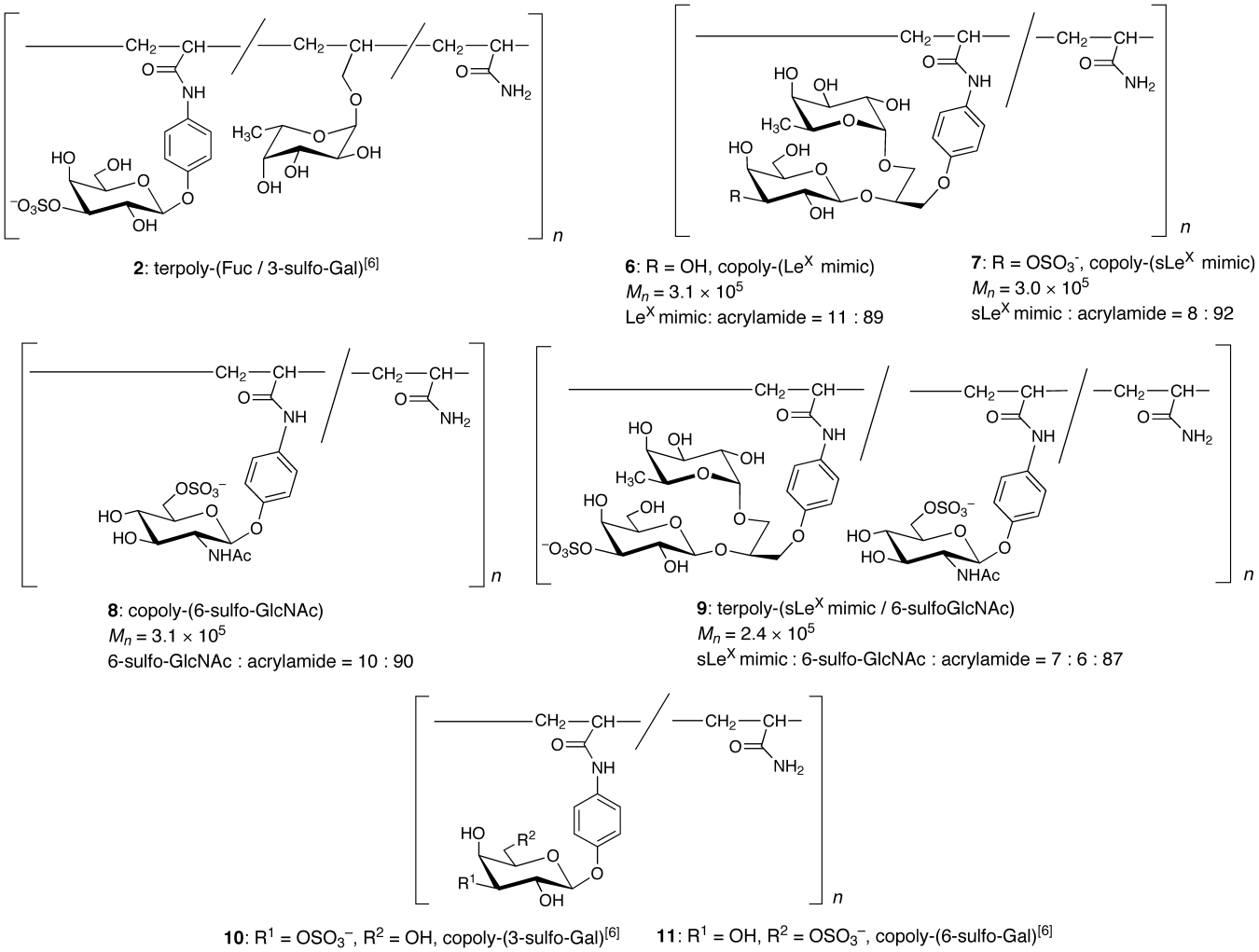
Scheme 2. Synthesis of Le^X module **3b** and sLe^X module **4a**. a) mCPBA, CH_2Cl_2, −40 °C→RT, 17 h (89 %); b) sodium *p*-nitrophenoxide, DMF, 70 °C, 13 h (50 % yield, 80 % *de* crystallized); c) *O*-(2,3,4,6-tetra-*O*-acetyl-α-D-galactopyranosyl)trichloroacetimidate,[16] TMSOTf, 4Å-MS, CH_2Cl_2, −40 °C→RT, 1 h; d) NaOMe, MeOH, 2 h (40 % over two steps from **15**); e) TBAF, THF, 24 h (90 %); f) Bu_2SnO, benzene, reflux, 5 h, then $Me_3N{\cdot}SO_3$, Et_3N, DMF, 40 °C, 2 h (76 %); g) TFA, MeOH, H_2O, 1 h (99 %); h) 1. H_2, $Pd(OH)_2$/C, MeOH, 1 h; 2. acryloyl chloride, Et_3N, THF, CH_2Cl_2, 2 h, then Dowex (Na^+ form) (63 % for **4b**, 75 % for **3b** over two steps, 95 % *de* for **4b**, 99.5 % *de* for **3b**). mCPBA = *meta*-chloroperoxybenzoic acid, TMSOTf = trimethylsilyl trifluoromethanesulfonate, MS = molecular sieves, TBAF = terabutylammonium fluoride, TFA = trifluoroacetic acid.

presence of multiple carbohydrate binding sites in L-selectin. The poor activity of **6** indicates that the nonspecific binding of the polyacrylamide backbone is negligibly small. Moreover, it is also clear that the 3′-sulfate group in the sLe^X mimic **7**, which serves as a substitute for 3′-silalic acid, plays a major role in the binding to L-selectin.

Roy et al. had previously prepared an acrylamide copolymer carrying the 3′-sulfo-Le^X trisaccharide to prove its ability to block L- and E-selectins at micromolar concentrations.[3a] Our polyvalent 3′-sulfo-Le^X **7** could also show comparable binding to L-selectin (6 μM), even though the mimic has a much simpler and acyclic skeleton that allows facile preparation. Moreover, comparison of the blocking activity of **7** and **2** provides a useful measure to assess the efficiency of our previous copolymerization approach since the activity of **7** (which serves as a typical model of polymer-(A1 + A2 + B) in Figure 1b) could represent the maximal activity of **2** (which serves as a model of copolymer-(A1/A2) in Figure 1c) if L-selectin possesses binding sites specific for the sLe^X structure. The blocking activity of **7** was approximately 2.5 fold stronger than **2**. The enhanced activity could support the presence of sLe^X binding site in L-selectin, and the level of incorporation could substantiate the efficiency of our module approach. Moreover, the terpolymer **9** carrying both the sLe^X and 6-sulfo-GlcNAc modules showed much higher activity than **7**. This observation indicates the major role of the 6-sulfo-GlcNAc residue in the adhesion to L-selectin and suggests the presence of another binding site for 6-sulfo-Glc residue. The potent activity, which seems to be the strongest of the L-selectin blockers so far reported,[11] supports the utility of the carbohydrate module method as a tool to assemble oligosaccharide mimics of high biological significance.

To our surprise 6-sulfo-GlcNAc copolymer **8** was found to show potent activity that was comparable to that of the terpolymer **9**. The possibility of there being nonsepecific interactions observed between P-selectin and polyanions such as fucoidin[12] and ion-exchange resins[13] is ruled out in the case of E- and L-selectins.[6] Moreover, as judged from our preceding results which showed that neither of the copolymers **10** and **11** carrying respective 3- and 6-sulfo-β-D-galactopyranoside showed such potent activity (Table 1),[6] it is clear that the 6-sulfo-GlcNAc residue provides a key and

 © 2002 WILEY-VCH Verlag GmbH & Co. KGaA, Weinheim 0044-8249/02/4123-4465 $ 20.00+.50/0



2: terpoly-(Fuc / 3-sulfo-Gal)[6]

6: R = OH, copoly-(Le^X mimic)
$M_n = 3.1 \times 10^5$
Le^X mimic: acrylamide = 11 : 89

7: R = OSO_3^-, copoly-(sLe^X mimic)
$M_n = 3.0 \times 10^5$
sLe^X mimic : acrylamide = 8 : 92

8: copoly-(6-sulfo-GlcNAc)
$M_n = 3.1 \times 10^5$
6-sulfo-GlcNAc : acrylamide = 10 : 90

9: terpoly-(sLe^X mimic / 6-sulfoGlcNAc)
$M_n = 2.4 \times 10^5$
sLe^X mimic : 6-sulfo-GlcNAc : acrylamide = 7 : 6 : 87

10: $R^1 = OSO_3^-$, R^2 = OH, copoly-(3-sulfo-Gal)[6]

11: R^1 = OH, $R^2 = OSO_3^-$, copoly-(6-sulfo-Gal)[6]

Scheme 3. Structures of polyvalent Le^X **6**, 3′-sulfo-Le^X **7**, 6-sulfo-GlcNAc **8**, 3′,6-disulfo sLe^X mimics **9**.

Table 1. Activity of monomeric and polymeric ligands to block L-selectin/sLe^X binding.

Ligands	Carbohydrate modules	Activity (IC_{50}) [μM][a]
Monomeric		
3a	Le^X (α-L-Fuc + Gal)	> 50
4a	3′-sulfo-Le^X (α-L-Fuc + 3-sulfo-Gal)	> 50
5a	6-sulfo-GlcNAc	> 50
Polymeric		
2	α-L-Fuc/3-sulfo-Gal (1/2)	15[6]
6	Le^X (α-L-Fuc + Gal)	> 50
7	3′-sulfo-Le^X (α-L-Fuc + 3-sulfo-Gal)	6
8	6-sulfo-GlcNAc	3
9	3′-sulfo-Le^X/6-sulfo-GlcNAc (1/1)	3
10	3-sulfo-Gal	> 50[6]
11	6-sulfo-Gal	> 50[6]

[a] IC_{50} values are given per glycoside unit.

species-specific interaction with L-selectin. This finding, which suggests the high biological significance of polyvalent 6-sulfo-GlcNAc **8**, may lead to the mass production of sugar-based medicinal agents through the abundant resources of chitin/chitosans. Moreover, the strong activity of **8** provides a significant insight into the carbohydrate recognition of L-selectin, although the precise mechanism awaits further synthetic and biological studies.

In conclusion, we have proposed a carbohydrate module method as a facile approach to assemble the biologically active structure of cell-surface oligosaccharides. This approach has enabled us to prepare glycopolymers that show potent activity in blocking L-selectin/sLe^X binding, in which a glycopolymer carrying a 6-sulfo-GlcNAc cluster was found to serve as one of the most promising agents. This finding supports recent studies[7,14] on the biological role of 6-sulfo-sLe^X tetrasaccharides and GlcNAc-6-*O*-sulfotransferases. Just recently, Patel and Lindhorst reported their module approach for the synthesis of oligosaccharide mimics.[15] Although their approach is based on the assembly of different sugar epitopes on dendric glycoconjugates and may be discriminated in principle from ours, these approaches will provide a promising pathway to construct artificial glycoconjugates with high biological potential.

Received: May 16, 2002
Revised: September 9, 2002 [Z19315]

 © 2002 WILEY-VCH Verlag GmbH & Co. KGaA, Weinheim 0044-8249/02/4123-4466 $ 20.00+.50/0

[1] Y. C. Lee, R. T. Lee in *Neoglycoconjugates: Preparation and Applications*, Academic Press, San Diego, **1994**.
[2] a) N. V. Bovin, H. J. Gabius, *Chem. Soc. Rev.* **1995**, *24*, 413 – 422; b) R. Roy, *Curr. Opin. Struct. Biol.* **1996**, *6*, 692 – 702; c) P. D. Rye, *Biotechnology* **1997**, *14*, 155 – 157.
[3] a) R. Roy, W. K. C. Park, O. P. Srivastava, C. Foxall, *Bioorg. Med. Chem. Lett.* **1996**, *6*, 1399 – 1402; b) H. Miyauchi, M. Tanaka, H. Koike, N. Kawamura, M. Hayashi, *Bioorg. Med. Chem. Lett.* **1997**, *7*, 985 – 988; c) E. J. Gordon, W. J. Sanders, L. L. Kiessling, *Nature* **1998**, *392*, 30 – 31; d) G. Thoma, J. T. Patton, J. L. Magnani, B. Ernst, R. Öhrlein, R. O. Duthaler, *J. Am. Chem. Soc.* **1999**, *121*, 5919 – 5929.
[4] a) H. Dohi, Y. Nishida, M. Mizuno, M. Shinkai, T. Kobayashi, T. Takeda, H. Uzawa, K. Kobayashi, *Bioorg. Med. Chem.* **1999**, *7*, 2053 – 2062; b) P. I. Kitov, J. M. Sadowska, G. Mulvey, G. D. Armstrong, H. Ling, N. S. Pannu, R. J. Read, D. R. Bundle, *Nature* **2000**, *403*, 669 – 672.
[5] For a recent paper, see H. Dohi, Y. Nishida, Y. Furuta, H. Uzawa, S-I. Yokoyama, S. Ito, H. Mori, K. Kobayashi, *Org. Lett.* **2002**, *4*, 355 – 357.
[6] Y. Nishida, H. Uzawa, T. Toba, K. Sasaki, H. Kondo, K. Kobayashi, *Biomacromolecules* **2000**, *1*, 68 – 74.
[7] C. Mistuoka, M. Sawada-Kasugai, K. Ando-Furui, M. Izawa, H. Nakanishi, S. Nakamura, H. Ishia, M. Kiso, R. Kannagi, *J. Biol. Chem.* **1998**, *273*, 11225 – 11233.
[8] H. Uzawa, T. Toba, Y. Nishida, K. Kobayashi, N. Minoura, K. Hiratani, *Chem. Commun.* **1998**, 2311 – 2312, and references therein.
[9] For the synthetic procedure for the preparation of these glycopolymers, see ref. [6]. Selected data for copolymer **6**, **7**, **8**, and terpolymer **9** are as follows: **6**: $M_n = 3.1 \times 10^5$, $M_w/M_n = 1.86$ (size-exclusion chromatography (SEC) in phosphate buffer saline (pH 7.4), calibrated with pullulans); ^{1}H NMR (500 MHz, D_2O, 60 °C): $\delta = 7.36$ (brs, 2H, aromatic-H), 7.06 (brs, 2H; aromatic-H), 4.91 (brs, 1H; Fuc H-1), 4.61 (brd, 1H, $J = 8.5$ Hz; Gal H-1), 4.40–3.53 (brm, 15H), 2.40–2.17 (brm, C*H*CH$_2$), 1.79–1.45 (brm, CHC*H*$_2$), 1.11 ppm (brs, 1H; Fuc H-6); (Le^x:acrylamide = 11:89). **7**: $M_n = 3.0 \times 10^5$, $M_w/M_n = 1.87$ (SEC in phosphate buffer saline (pH 7.4), calibrated with pullulans); ^{1}H NMR (500 MHz, D_2O, 60 °C): $\delta = 7.56$ (brs, 2H, aromatic-H), 7.25 (brs, 2H, aromatic-H), 5.11 (brs, 1H, Fuc H-1), 4.91 (brd, 1H, $J = 7.0$ Hz, Gal H-1), 4.50–3.84 (brm, 15H), 2.60–2.30 (brm, C*H*CH$_2$), 2.00–1.75 (brm, CHC*H*$_2$), 1.32 ppm (brd, 1H, $J = 6.5$ Hz, Fuc H-6); (3′-sulfo-Le^x:acrylamide = 8:92). **8**: $M_n = 3.1 \times 10^5$, $M_w/M_n = 1.74$ (SEC in phosphate buffer saline (pH 7.4), calibrated with pullulans); ^{1}H NMR (500 MHz, D_2O, 60 °C): $\delta = 7.60$ (brs, 2H, aromatic-H), 7.27 (brs, 2H, aromatic-H), 5.32 (brs, 1H, GlcNAc H-1), 4.57 (brs, 1H), 4.42 (brs, 1H), 4.19 (brs, 1H), 4.00 (brs, 1H), 3.85 (brm, 1H), 3.78 (brm, 1H), 2.52–2.22 (brm, C*H*CH$_2$), 2.10 (brs, 3H, COCH$_3$), 2.00–1.75 (brm, CHC*H*$_2$); (6-sulfo-GlcNAc:acrylamide = 10:90). **9**: $M_n = 2.4 \times 10^5$, $M_w/M_n = 1.77$ (SEC analysis in phosphate buffer saline (pH 7.4), calibrated with pullulans); ^{1}H NMR (500 MHz, D_2O, 60 °C): $\delta = 7.58$ (brm, 4H, aromatic-H), 7.23 (brm, 4H, aromatic-H), 5.32 (brs, 1H, GlcNAc H-1), 5.11 (brs, 1H, Fuc H-1), 4.90 (brs, 1H, Gal H-1), 4.60–3.78 (brm, 22H), 2.60–2.30 (brm, C*H*CH$_2$), 2.20 (brs, 3H COCH$_3$), 2.12–1.75 (brm, CH-C*H*$_2$-), 1.29 ppm (brs, 1H, Fuc H-6); (3′-sulfo-Le^x: 6-sulfo-GlcNAc:acrylamide = 7:6:87).
[10] H. Ohmoto, K. Nakamura, T. Inoue, N. Kondo, Y. Inoue, K. Yoshino, H. Kondo, *J. Med. Chem.* **1996**, *39*, 1339 – 1343.
[11] For a recent review, see E. E. Simanek, G. J. McGarvey, J. A. Jablonowski, C.-H. Wong, *Chem. Rev.* **1998**, *98*, 833 – 862.
[12] L. M. Stoolman, S. D. Rosen, *J. Cell. Biol.* **1983**, *96*, 722 – 729.
[13] G. Kretzschmar, A. Toepfer, C. Hüls, M. Kause, *Tetrahedron* **1997**, *53*, 2485 – 2494.
[14] a) K. G. Bowman, B. N. Cook, C. L. Graffenried, C. R. Bertozzi, *Biochemistry* **2001**, *40*, 5382 – 5391; b) R. E. Bruehl, C. R. Bertozzi, S. D. Rosen, *J. Biol. Chem.* **2000**, *275*, 32642 – 32648; c) B. N. Cook, S. Bhakta, T. Biegel, K. G. Bowman, J. I. Armstrong, S. Hemmerich, C. R. Bertozzi, *J. Am. Chem. Soc.* **2000**, *122*, 8612 – 8622.
[15] A. Patel, T. K. Lindhorst, *J. Org. Chem.* **2001**, *66*, 2674 – 2680.
[16] P.-H. Amvam-Zollo, P. Sinaÿ, *Carbohydr. Res.* **1986**, *150*, 199 – 212.

Attachment of Molecules at a Molecular Printboard by Multiple Host–Guest Interactions**

Jurriaan Huskens,* Menno A. Deij, and David N. Reinhoudt*

Dedicated to Professor Manfred T. Reetz on the occasion of his 60th birthday

The exact positioning of molecules on surfaces has become essential for the development of molecular electronics[1] and biochip applications,[2] as well as for conducting single molecule experiments. Commonly, one of two possible routes is followed, either by chemically reacting molecules to surfaces or to anchoring molecules present at a surface, or by physisorption, that is, the use of nonspecific physical interactions between molecule and surface, and between molecules themselves. Covalent chemical modification usually requires synthetic effort, is hard to control at surfaces, and does not allow either self-correction or (intentional) desorption. Physisorption does allow self-correction, which is common for all self-assembly processes, but the thermodynamic and kinetic parameters governing adsorption and desorption are difficult to control. Moreover, neighboring molecule–molecule interactions are usually needed for obtaining stable and ordered layers, thus the formation of densely packed layers is a prerequisite.[3]

Supramolecular interactions serve as an intermediate case with the possibility of employing advantages from both routes. Supramolecular interactions, such as those observed in host–guest complexes, are specific and directional, and a wealth of information is usually available on their binding strengths and kinetics. The application of molecules that allow the formation of multiple supramolecular interactions provides a tool to tune adsorption and desorption process parameters because thermodynamics and kinetics are, in principle, straightforwardly related to the number of interactions, and the strength and kinetics of an individual interaction.

It is therefore our goal to apply host surfaces as "molecular printboards" at which multivalent guest molecules can be positioned. Prerequisites will need to be identified to reach thermodynamically and/or kinetically stable assemblies that can be employed in nanotechnology. It is envisaged that one can control adsorption and desorption by environmental stimuli, for example, by competition with another host in solution. Herein we address the thermodynamic and kinetic

[*] Dr. ir. J. Huskens, Prof. dr. ir. D. N. Reinhoudt, Ir. M. A. Deij
University of Twente, MESA$^+$ Research Institute
Laboratory of Supramolecular Chemistry and Technology
P.O. Box 217, 7500 AE Enschede (The Netherlands)
Fax: (+31) 53-489-4645
E-mail: smct@ct.utwente.nl

[**] Dr. Maurice Baars and Prof. Dr. Bert Meijer (TUE) are gratefully acknowledged for supplying the adamantyl-terminated dendrimers. Frank Geurts (Akzo Nobel, Arnhem) is acknowledged for performing the XPS measurements, and Paul Koster for assistance with the grazing-angle FTIR measurements. Szczepan Zapotoczny is acknowledged for performing the AFM measurements. The Dutch Technology Foundation STW is gratefully acknowledged for funding the Simon Stevin Award project on Nanolithography.

 © 2002 WILEY-VCH Verlag GmbH & Co. KGaA, Weinheim 0044-8249/02/4123-4467 $ 20.00+.50/0

issues relating to the use of multiple interactions for stable surface attachment. In the future, this will be extended to real positioning, for example, by the use of dip-pen nanolithography[4] for the delivery of molecules to a molecular printboard.

Here, we describe the interaction between adamantyl- (Ad-) functionalized poly(propylene imine) (PPI) dendrimers[5] ranging from 4–64 Ad groups per molecule, and self-assembled monolayers (SAMs) of β-cyclodextrin (CD) adsorbates[6,7] (a host suitable for the complexation of Ad derivatives[8] and capable of forming well-ordered, densely packed monolayers) on gold substrates. The delivery of such dendrimers from solution-phase CD complexes to CD SAMs is described, which makes use of the competition between the solution and the surface host sites, as well as the cooperativity of the surface sites. Furthermore, we will show the possibility of switching between states of slow and fast desorption kinetics by changing the CD concentration in solution, and describe the use of densely packed dendrimer layers and individually imaged and addressed dendrimer molecules.

We prepared SAMs of a β-cyclodextrin heptathioether adsorbate (Figure 1) on gold substrates, as described previously.[6,8] We have shown that such adsorbates form densely packed, well-ordered SAMs, the hexagonal packing of which can be visualized by using atomic force microscopy (AFM).[6] The binding of small univalent guest molecules to these SAMs has been studied by electrochemical impedance spectroscopy (EIS)[7] and surface plasmon resonance (SPR) spectroscopy.[8]

The Ad-functionalized PPI dendrimers employed in the present study (generations G2–G4, with 8–32 adamantyl endgroups, Figure 1) were solubilized in water using an excess of CD in water at pH 2, which ensures the full complexation of all adamantyl groups by CD and protonation of the core amines.[5a] Such dendrimer assemblies have been employed as nanocontainers for dye molecules[5a] and as nanoreactors for the formation of gold nanoparticles.[5b]

By comparison of the molecular sizes of these dendrimers (G2–G4) with the lattice constant (1.7 nm) of the hexagonally ordered CD SAMs, it can be shown that G2 (with 8 Ad endgroups) can interact with only two CD sites simultaneously at a SAM. Analogously, G3 (16 Ad groups) may interact with three CD sites, whereas G4 (32 Ad groups) can access at least four sites. Furthermore, the concentration of the Ad endgroups of G4 matches the CD SAM lattice constant, which makes this dendrimer an especially interesting case for studying cooperativity of surface host sites in binding multivalent guests.

The (intrinsic) binding constant K_i of an individual Ad–CD interaction is known to be about $6 \times 10^4\,\mathrm{M}^{-1}$ (25 °C), both in solution and at CD SAMs, as determined previously[8] for an Ad guest which closely resembles the Ad endgroups of the dendrimers employed here. The kinetics of such CD complexes commonly follow diffusion-controlled association (k_f is approximately $10^9\,\mathrm{M}^{-1}\mathrm{s}^{-1}$), and thus dissociation rates follow directly from this association rate and from thermodynamics.

A mathematical model has been developed in which all Ad–CD interactions are judged to be equal and independent, both in solution and at a SAM, in which cooperativity on the surface is only viewed as an increase of the effective molarity of the CD host upon binding of the first guest site of a

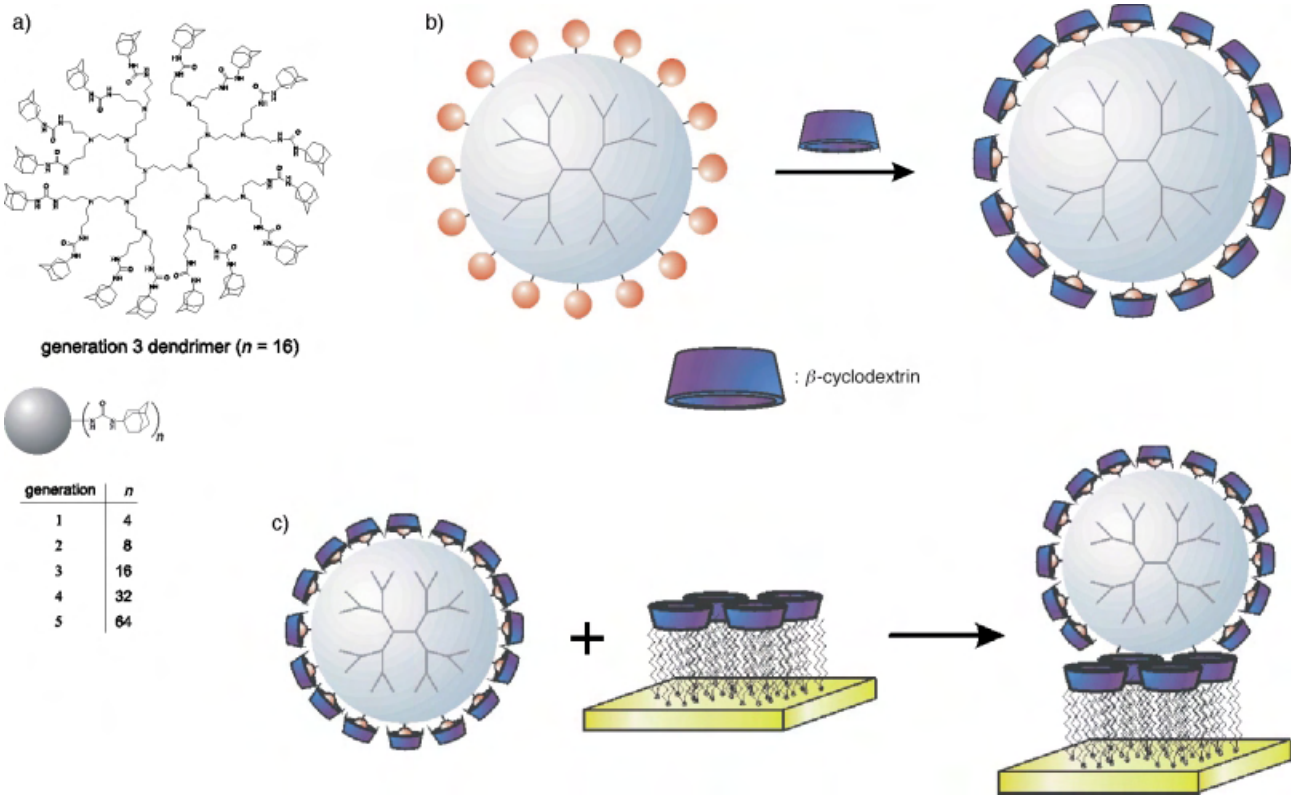


Figure 1. Adamantyl-functionalized poly(propylene imine) dendrimers (a), their formation of water-soluble assemblies by CD (b; see ref. [5a]), and the adsorption of these assemblies onto a CD SAM on gold (c).

 © 2002 WILEY-VCH Verlag GmbH & Co. KGaA, Weinheim 0044-8249/02/4123-4468 $ 20.00+.50/0

multivalent guest.[9] This model implies that: a) simultaneous use of at least four CD sites is needed to obtain kinetically slow assemblies under certain conditions, and b) the desorption rate is (positively, but not linearly) dependent on the CD concentration in solution. The results given below are discussed partly as a validation of these model implications.

A CD SAM was immersed in a solution of the G4 dendrimer–CD assemblies, and the adsorption (Figure 1) was studied by SPR spectroscopy. Figure 2a shows a typical SPR time trace in which the adsorption rate and level were studied as a function of dendrimer concentration and of

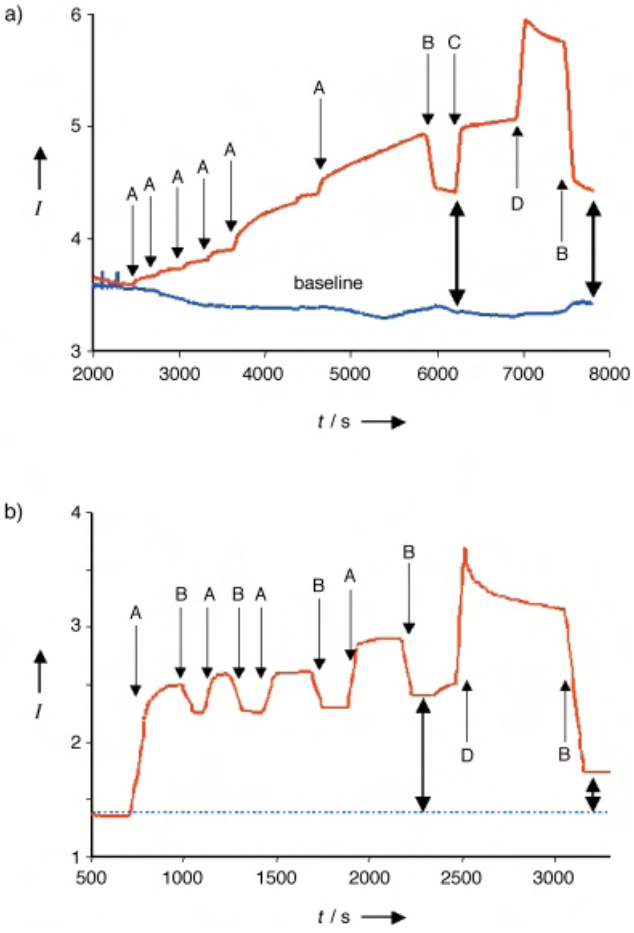


Figure 2. Surface plasmon resonance (SPR) spectroscopy time traces of the adsorption and (attempted) desorption of G4 a) and G3 b) dendrimer–cyclodextrin assemblies onto a CD SAM on a gold substrate; solutions (all in 0.01M aqueous HCl): A) dendrimer–CD, B) 0.01M HCl, C) 1 mM CD, D) 8 mM CD.

washing conditions with 0.01M HCl and 8 mM aqueous CD in 0.01M HCl. These results clearly show the adsorption of dendrimer assemblies at the SAM. Water did not remove the assemblies from the surface, and even 8 mM CD did not lead to detectable desorption under the SPR conditions.

The presence of the dendrimer assemblies after adsorption was verified by FTIR[10] and X-ray photoelectron spectroscopy (XPS).[11] Water contact angle goniometry shows increased wetting upon adsorption,[12] which implies that CD molecules remain to cover the hydrophobic Ad endgroups of the adsorbed dendrimers at the outer surface. EIS showed an increase of the charge-transfer resistance upon adsorption of G4–CD_{32} from 45 to 500 kΩ when the positively charged redox couple $[Ru^{II}(NH_3)_6]^{2+}/[Ru^{III}(NH_3)_6]^{3+}$ was used. This increase results from charge repulsion with the protonated, and thus positively charged, inner core of the dendrimers.[13] In principle, the thermodynamics and/or kinetics of adsorption can be studied by using EIS,[6] but this was not attempted for practical reasons (relatively slow adsorption, response dependent on charge and thus on protonation degree).

Immersion of a hydroxyundecanethiol SAM in a solution of the G4 assemblies led to nonspecific physisorption as shown by SPR. These assemblies were washed away rapidly, however, using 8 mM CD. As indicated before, the CD SAMs are much less prone to nonspecific adsorption. Combined with the stability of the surface assemblies to water and 8 mM CD, and the different adsorption behavior of individual dendrimers at hydroxy- or CD SAMs (see below), we conclude that the adsorption of the G4 dendrimers at the CD SAMs stems from specific host–guest interactions. As a result of the equal interaction strength of individual Ad–CD interactions in solution and at SAMs, the adsorption solely stems from cooperativity between the surface host sites.

The SPR traces (Figure 2a) do not allow any conclusions regarding the adsorption[14] or desorption kinetics. No appreciable desorption occurs in either pure water, or in a relatively concentrated (8 mM) CD solution. In principle, this could be because of thermodynamic stability in the SPR setup and/or the kinetic stability of the surface assemblies. The mathematical model sketched above is indicative of thermodynamic stability in 8 mM CD, rather than kinetic stability, because of the relatively small volume of the CD solution in the SPR setup. In pure water, both thermodynamic and kinetic stability may play a role.

The influence of the number of host–guest interactions on the thermodynamic and kinetic stabilities of the surface assemblies was assessed in the SPR experiments of the G2 and G3 dendrimers. Both showed adsorption from solution (data for G3 shown in Figure 2b). Changing the solution to pure water did not result in loss of material, which indicates thermodynamic and/or kinetic stability of the assemblies. Application of 8 mM CD, however, led to rapid and considerable desorption. The residual signal (20%) in Figure 2b probably reflects a thermodynamic equilibrium in the SPR setup at this CD concentration, which is indicated from both the mathematical model and the relatively high desorption rate.

AFM was used to image and study individual G4 dendrimer assemblies at SAMs. Figure 3a shows an AFM image of a CD SAM immersed for a short time in a dilute solution of G4 assemblies in water. The fact that such assemblies can be imaged at all proves their relative robustness at the CD SAM surface. In contrast, Figure 3c shows islands of G4 dendrimers physisorbed onto a hydroxyundecanethiol SAM. No individual dendrimers can be visualized, which emphasizes the different interaction mechanism of the G4 dendrimer assemblies binding to the CD and the hydroxyundecanethiol SAMs (see above).

 © 2002 WILEY-VCH Verlag GmbH & Co. KGaA, Weinheim 0044-8249/02/4123-4469 $ 20.00+.50/0

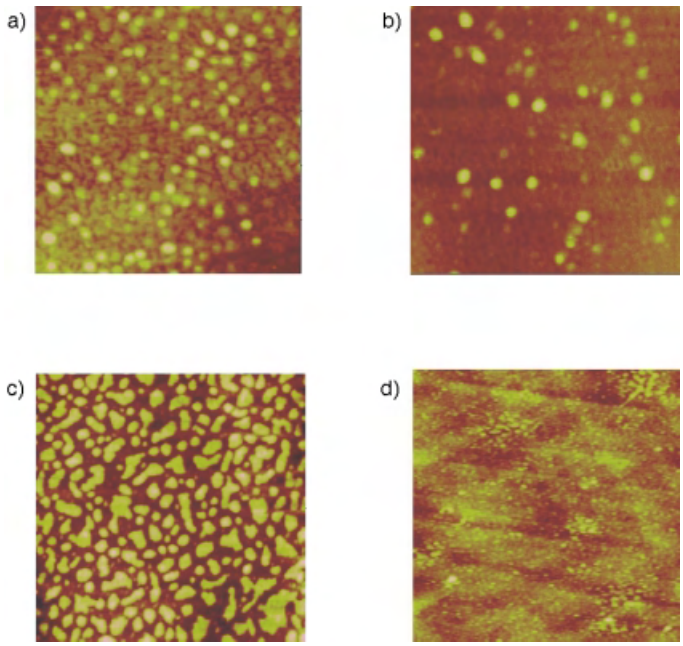


Figure 3. Tapping-mode AFM images (500 × 500 nm): after the adsorption of G4 dendrimer–cyclodextrin assemblies onto a CD SAM on gold a), and the washing of these surface assemblies with 8 mM CD b); after the adsorption of G4 dendrimer–cyclodextrin assemblies onto a hydroxyundecanethiol SAM on gold c), the washing of these surface assemblies with 8 mM CD d).

Water did not appreciably remove the adsorbed material from either SAM. However, an 8 mM CD solution did completely remove the dendrimer islands from the hydroxyundecanethiol SAM (Figure 3d). In contrast, a considerable number of the individual dendrimers on the CD SAM remained on the surface after treatment with 8 mM CD (Figure 3b). Nevertheless, the diminished surface concentration is obvious. It implies a relatively high desorption rate under these conditions, and thus confirms a thermodynamic, rather than kinetic, stability.

In conclusion, these experiments show that stable assemblies on surfaces can be prepared by employing multiple, intrinsically weak supramolecular interactions. Thermodynamically stable complexes can be achieved when employing two or three host–guest interactions of the strength found in the Ad–CD system. Data on the G4 dendrimer, which probably employs at least four such interactions, indicate that the kinetics can be tuned from very slow desorption in pure water to relatively fast (in the order of minutes) at high CD concentrations. The removal of material in the AFM experiment and the absence of desorption during SPR may be attributed to different thermodynamic equilibrium concentrations, or maybe to different desorption rates for individual dendrimers, compared to dendrimers packed in a full layer. More detailed kinetic experiments, possibly in flow setups, may validate the model in a more quantitative way.

This work may open new ways of preparing structured surfaces, essential for nanotechnological, electronic, or biochip applications. It shows that host surfaces can be employed as molecular printboards on which molecules can be placed in a firm manner, based solely on specific host–guest interactions, and addressed individually.

Experimental Section

CD SAMs on gold were prepared by the immersion of a clean gold substrate (200 nm thick gold film on 2.54 cm glass wafers, coated with 2 nm Ti) in a solution of the CD heptathioether adsorbate (100 mg L^{-1}) in ethanol/chloroform (2:3) for 16 h at 60 °C.

A typical SPR experiment consisted of increasing the concentration of G4–CD_{32} in solution from 1 to 10 μM in several steps. At 10 μM, full surface coverage was reached rapidly. When a stable signal was obtained, the solution was replaced with 0.01 M HCl. This led to a decrease of the signal through both desorption of CD molecules from the surface assemblies and to a change in the bulk refractive index. No subsequent slow desorption, which might indicate desorption of the dendrimers, was observed. To probe desorption, the cell was flushed with 8 mM CD in 0.01 M HCl. As a result of a change of the bulk refractive index, the signal increased. After a stable signal was obtained, the cell was flushed with water and the signal was recorded again, which then became comparable to the signal obtained before attempted desorption.

For AFM measurements, SAMs of the CD heptathioether adsorbate and of hydroxyundecanethiol were briefly exposed (20–30 s) to a drop of a 0.5 μM solution of G4 and rinsed with water. The samples were dried under a stream of N_2 and imaged by using tapping-mode AFM (TM-AFM).

Received: June 28, 2002
Revised: August 22, 2002 [Z19631]

[1] a) C. Joachim, J. K. Gimzewski, A. Aviram, *Nature* **2000**, *408*, 541; b) M. A. Reed, *MRS Bull.* **2001**, 113; c) J. M. Tour, *Acc. Chem. Res.* **2000**, *33*, 791; d) *Molecular Electronics: Science and Technology* (Ed.: A. Aviram), American Institute of Physics, New York, **1992**.

[2] a) A. D. Mehta, M. Rief, J. A. Spudich, D. A. Smith, R. M. Simmons, *Science* **1999**, *283*, 1689; b) S. Weiss, *Science* **1999**, *283*, 1676; c) *Molecular and Biomolecular Electronics* (Ed.: R. R. Birge) American Chemical Society, Washington, **1991**.

[3] a) A. Ulman, *An Introduction to Ultrathin Organic Films*, Academic Press, San Diego **1991**; b) H. O. Finklea in *Electroanalytical Chemistry, Vol. 19* (Eds.: A. J. Bard, I. Rubinstein), Marcel Dekker, New York, **1996**, pp. 109–335.

[4] a) R. D. Piner, J. Zhu, F. Xu, S. Hong, C. A. Mirkin, *Science* **1999**, *283*, 661; b) S. Hong, J. Zhu, C. A. Mirkin, *Science* **1999**, *286*, 523; c) L. M. Demers, C. A. Mirkin, *Angew. Chem.* **2001**, *113*, 3159; *Angew. Chem. Int. Ed.* **2001**, *40*, 3069; d) A. Ivanisevic, C. A. Mirkin, *J. Am. Chem. Soc.* **2001**, *123*, 7887; e) K.-B. Lee, S.-J. Park, C. A. Mirkin, J. C. Smith, M. Mrksich, *Science* **2002**, *295*, 1702; f) L. M. Demers, D. S. Ginger, S.-J. Park, Z. Li, S.-W. Chung, C. A. Mirkin, *Science* **2002**, *296*, 1836.

[5] a) J. J. Michels, M. W. P. L. Baars, E. W. Meijer, J. Huskens, D. N. Reinhoudt, *J. Chem. Soc. Perkin Trans. 2* **2000**, 1914; b) J. J. Michels, J. Huskens, D. N. Reinhoudt, *J. Chem. Soc. Perkin Trans. 2* **2002**, 102.

[6] M. W. J. Beulen, J. Bügler, B. Lammerink, F. A. J. Geurts, E. M. E. F. Biemond, K. G. C. van Leerdam, F. C. J. M. van Veggel, J. F. J. Engbersen, D. N. Reinhoudt, *Langmuir* **1998**, *14*, 6424.

[7] a) H. Schönherr, M. W. J. Beulen, J. Bügler, J. Huskens, F. C. J. M. van Veggel, D. N. Reinhoudt, G. J. Vancso, *J. Am. Chem. Soc.* **2000**, *122*, 4963; b) M. W. J. Beulen, J. Bügler, M. R. de Jong, B. Lammerink, J. Huskens, H. Schönherr, G. J. Vancso, B. A. Boukamp, H. Wieder, A. Offenhäuser, W. Knoll, F. C. J. M. van Veggel, D. N. Reinhoudt, *Chem. Eur. J.* **2000**, *6*, 1176.

[8] M. R. de Jong, J. Huskens, D. N. Reinhoudt, *Chem. Eur. J.* **2001**, *7*, 4164.

[9] In this model, a guest with n interaction sites for cyclodextrin is assumed to have equal intrinsic binding strengths, K_i, with CD in solution as well as at the surface. The sequential binding events occur thus with binding strength K_1 to K_n, where $K_j = (n+1-j) \times K_i/j$. The free CD concentration at the surface, $[CD]_{surf}$, used in the equilibrium for the interaction of the first binding site to the surface, is equal to the number of moles of surface CDs divided by the sample volume. For successive surface interactions, the free CD concentration is equal to the effective molarity, estimated from molecular mechanics to be about 1 M, multiplied by the fraction of free CD surface sites ($= [CD]_{surf}/[CD]_{surf,total}$). The model will be described in full detail in a future publication.

 © 2002 WILEY-VCH Verlag GmbH & Co. KGaA, Weinheim 0044-8249/02/4123-4470 $ 20.00+.50/0

[10] FTIR difference spectroscopy showed asymmetric and symmetric methylene stretching vibrations characteristic for the G4–CD assemblies at 2852 and 2916 cm^{-1}, respectively, as well as a broad band centered around 3250 cm^{-1} for the vibrations of ammonium, urea, and hydroxyl protons of the dendrimer and CD.
[11] XPS analysis confirmed the adsorption of the G4–CD_{32} assemblies by an increase in N_{1s} and a decrease in S_{2p} signals, which are most indicative of adsorption. Moreover, the C_{1s} and O_{1s} signals increased and decreased, respectively.
[12] Advancing contact angles are $68 \pm 2°$ and approximately 20° before and after adsorption of G4 assemblies onto the CD SAMs, respectively.
[13] EIS was performed with an external redox couple at the open cell potential. From the Nyquist plot, the charge-transfer resistance was determined by using an equivalent Randles circuit. When the negatively charged $[Fe^{III}(CN)_6]^{3-}/[Fe^{II}(CN)_6]^{4-}$ couple was used, the charge-transfer resistance decreased from 38 to 3 kΩ, because the electrostatic attraction by the dendritic core facilitates the oxidation/reduction at the electrode surface.
[14] The apparently slow adsorption as shown in the first parts of Figure 2a upon increase of the G4 concentration can be attributed to diffusion of G4 in solution, since the adsorption in the SPR setup leads to a depletion of the liquid above the surface of > 100 μm, while diffusion in solution over such distances probably takes more than 1 s.

QMOF-1 and QMOF-2: Three-Dimensional Metal–Organic Open Frameworks with a Quartzlike Topology**

Jinyu Sun, Linhong Weng, Yaming Zhou, Jinxi Chen, Zhenxia Chen, Zhicheng Liu, and Dongyuan Zhao*

The construction of metal–organic framework (MOF) coordination polymers is currently receiving considerable attention owing to their potential properties as functional solid materials, as well as their fascinating framework structures.[1–3] Particularly widely explored have been MOFs with porous chiral structures in which chiral ligands, chiral templates, or chiral functionalization of achiral zeolites are used to perform enantioselective separations and syntheses.[4–7] It is challenging to prepare chiral MOF materials with known chiral topology from an achiral building unit.

[*] Prof. Dr. D. Zhao, Dr. L. Weng, Dr. Y. Zhou, Dr. J. Chen, Z. Chen, Z. Liu
Department of Chemistry
Fudan University
Shanghai, 200433 (P.R. China)
Fax: (+86) 21-6564-1740
E-mail: dyzhao@fudan.edu.cn
J. Sun
Department of Chemistry
Liaoning University, Shenyang,
110036 (P.R. China)

[**] This work was supported by the NSF of China (Grants No. 29925309), the Chinese Ministry of Education, the Shanghai Science Foundation (C00JC14014) and the State Key Basic Research Program of PRC (G200048001). We thank Dr. Y. Yan, Dr. L. Huang, and Dr. H. Wang of U.C.-Riverside for helpful discussions.

Supporting information for this article is available on the WWW under http://www.angewandte.org or from the author.

Learning from nature's minerals, and utilizing the well-defined coordination geometries of metal centers, some structures of minerals with specific functionality, such as perovsktie,[8] rutile,[9] PtS,[10] and feldspar[11] have been artificially produced by replacing monoatomic anions (O^{2-}, S^{2-}) with polyatomic organic μ ligands. The quartz phase, which is chiral, has unique piezoelectricity and thermally sensitive properties and is widely used in resonators and sensors.[12] Although the SiO_2 phase with quartz topology is thermodynamically more stable than cristobalite which has diamond topology, in nature or in artificial materials, known phases which have quartz topology are rare with only one example, a cyano-bridged coordination polymer, reported by Robson and co-workers.[13] Generally, most materials comprising four-connected tetrahedral (T) units, including MOFs, exist in the diamond topology,[1c,d,14] rather than the quartz topology, while SiO_2 and GeO_2 are minerals that have both a quartz polymorph and cristobalite with diamond topology. Interestingly, when cristobalite is quenched to room temperature,[15] it is transformed reconstructively to the quartz polymorph.

Herein we report the preparation of two quartzlike, chiral, open MOFs, $Zn(ISN)_2 \cdot 2H_2O$ (ISN = isonicotinate), assigned QMOF-1, with the low symmetry of α-quartz and $InH(BDC)_2$ (BDC = terephthalate), QMOF-2, with the high symmetry of β-quartz. QMOF-1 with a large (~8.6 Å) left-handed channel was successfully synthesized with an asymmetric ISN ligand by using a low-temperature diffusion method (room temperature) similar to the preparation of metal carboxylate[17]. On using a highly distorted complex anion $[In(O_2CR)_4]^-$ as the T block,[16] and terephthalate as a linear rod, we could assemble the anion-type β-quartzlike network QMOF-2 with a right-handed channel (~7.8 Å).

The preparation of QMOF-1 was carried out in a wide range of conditions: $Zn(NO_3)_2 \cdot 6H_2O$: 1.5–3.0 ISN: 1–10 triethylamine (TEA): 5–10000 dimethylsulfoxide (DMSO): 0–20000 ethanol. After one week, large colorless needlelike single crystals with dimensions up to $0.200 \times 0.200 \times 3$ mm were obtained quantitatively (relative to Zn). QMOF-2 was solvothermally obtained from $InCl_3$:terephthalate (1:2) at 160 °C for 3 days, yield 60 % (relative to In). The IR spectra showed that the carboxylate group in QMOF-1 has monodentate coordination to the metal center, while that in QMOF-2 is bidentate.[18]

The single-crystal X-ray diffraction studies reveal that all the zinc ions in QMOF-1 are four-coordinate (Figure 1a).[19] Each Zn atom is coordinated by two nitrogen atoms of two ISN ligands and two oxygen atoms of two carboxylate groups from two other ISN ligands. All of the T units are slightly distorted, the Zn–O and Zn–N bonds are 1.95 and 2.02 Å, respectively, and the angles of N(1)-Zn(1)-N(2), N(1)-Zn(1)-O(2), N(1)-Zn(1)-O(1), O(1)-Zn(1)-O(2) are 113.5, 117.5, 104.9, 100.4°, respectively. The 3D twofold interpenetrated network with T blocks is characteristic of a 6^48^2-b net, similar to that of α-quartz (Figure 2, Figure S1 in the supporting information).[1c] In the QMOF-1 structure, large Zn cations replace the Si atoms in quartz structure, and the long ISN anions replace the O atoms, so that the separation between two T units can be expanded to 8.813 Å, only slightly different from the Zn–Zn separations in the diamondoid network

 © 2002 WILEY-VCH Verlag GmbH & Co. KGaA, Weinheim 0044-8249/02/4123-4471 $ 20.00+.50/0

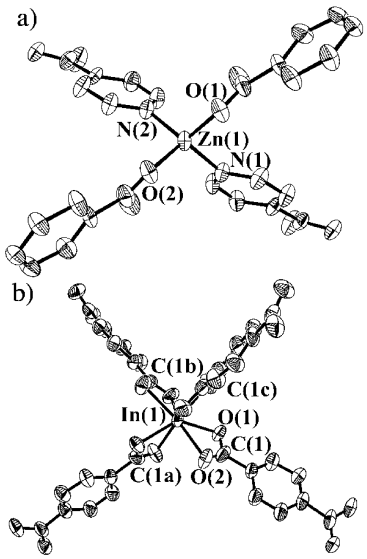


Figure 1. ORTEP drawings (thermal ellipsoids set at 50% probability, all H atoms omitted for clarity) showing the. a) coordination of zinc ion in QMOF-1, b) coordination of the indium ion in QMOF-2.

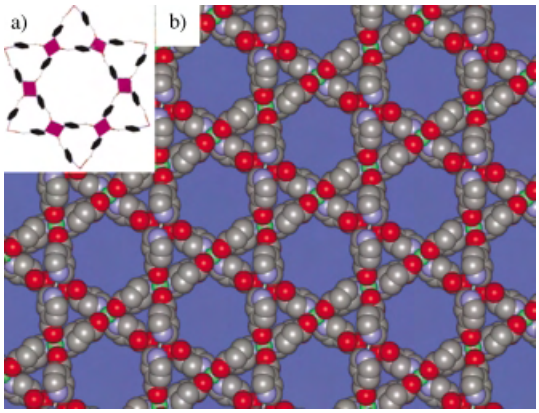


Figure 2. The crystal structure projection of QMOF-1 in the *c* direction, a) a single quartzlike net, ◆ = Zn atom, ⬬ = pyridine ring, b) CPK diagram of extended structure. The atoms are: ● = oxygen, ● = nitrogen, ● = zinc, ● = carbon.

recently reported (8.74 and 8.81 Å).[14] In contrast to the silica prototype, the $Zn(ISN)_2{\cdot}2H_2O$ open framework of QMOF-1 also contains a 3-fold screw axis in the *c* direction (Figure S2), and Zn tetrahedra along the 3-fold axis produce a left-handed channel (Figure 2b), which when the van der vaals radii are considered, is about 8.6 Å in diameter. Two disordered water molecules are observed in the pseudo-hexagonal channels, which are composed of 8-membered rings (eight Zn tetrahedrons). The asymmetry of the ISN anion results in a lower symmetry (from D_3 to C_3) than that of silica α-quartz. In contrast to the preparation of the diamondoid $Zn(ISN)_2$ which is produced by the solvothermal method at 130 °C,[14] the lower temperature used in the preparation of QMOF-1 might play a key role in the formation of the quartz structure, similar to the reconstructive transformation of cristobalite into quartz in silica polymorphs.[15]

In contrast to the tetrahedral zinc centers in QMOF-1, all the indium centers in QMOF-2 adopt triangulated dodecahedral geometries by the chelation of four carboxylate groups from four terephthalate anions (Figure 1b, 3a). The molecular structure shows that QMOF-2 is a complex anion with a proton to balance the charge.[16] If the carboxylate groups are considered as connecting points,[20] T blocks comprising

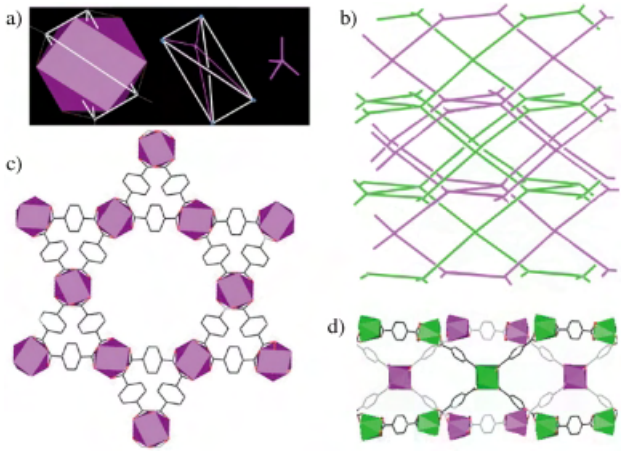


Figure 3. a) the T blocks model, showing that an 8-coordinated indium center acts as a 4-connected node b) the extended twofold interpenetrated networks with the simplified tetrahedron knot, c) the single quartz net in the *c* direction; d) showing the interpenetrated catenane structure.

carbon atoms around the indium centers in QMOF-2 show a highly distorted pseudo-tetrahedral geometry (Figure 3a), the angles of C-In-C are 91.5, 143.1, 100.0°. Each indium center in QMOF-2 connects to the other indium centers by linear terephthalate bridges to produce a quartz network (Figure 3b,c), the linear organic rods result in the high symmetry of β-quartz, $P6_422$. QMOF-2 is characteristic of twofold interpenetrated 6^48^2-b nets (Figure 3b) in which the pseudo-tetrahedron centers in one net occupy on the center of the 6-ring in another network, and the four "arms" of tetrahedron are interpenetrated through 6-ring each other in the up-down-up-down form (Figure 3b,d). Similar to β-quartz silica, the structure of QMOF-2 has not only a six-fold screw axis, but also a right-handed channel along this axis which runs in the *c* direction (Figure S3). The diameter of channel calculated from the distance between diagonally opposite In atoms is 15.0 Å. If van der waals radii are considered, the diameter of the channel is about 7.8 Å.

Thermal analysis for QMOF-1 shows a shoulder peak at 100–140 °C with the weight loss of approximately 13 wt%, and an intense peak at 350–430 °C with the weight loss of approximately 58 wt%. The former is attributed to the desorption of two water molecules (calcd, 10.4 wt%); and the later corresponds to the collapse of the framework. Variable temperature XRD experiments reveal that the $Zn(ISN)_2{\cdot}2H_2O$ product is thermally stable up to 200 °C in air.

The results of thermal analysis of QMOF-2 in air show two endothermal peaks at around 100 and 270 °C, with about 25 wt% and 27.5 wt% weight loss respectively. The former is attributed to the desorption of the solvents adsorbed, which include 1.5 equivalents of dimethylformide and 4 equivalents of water (calcd, 27.5 wt%), the latter is related to the complete decarboxylization process (calcd, 27.5 wt%), so the frame-

 © 2002 WILEY-VCH Verlag GmbH & Co. KGaA, Weinheim 0044-8249/02/4123-4472 $ 20.00+.50/0

work of QMOF-2 collapses at 270 °C. These results suggest that two structures are thermally stable. N_2-adsorption/desorption measurements performed according to the normal method for microporous zeolite materials show that QMOF-1 and QMOF-2 products (Figure S9, S10) have type I isotherms, which suggests that the products have uniformed microporsity with large surface areas ($150\ m^2 g^{-1}$ for QMOF-1 and $190\ m^2 g^{-1}$ for OMOF-2).

In summary, two novel chiral open MOFs with rare α and β-quartz structures have been successfully synthesized. QMOF-1, prepared by using a simple diffusion method at room temperature has a neutral open framework with the low symmetry of α-quartz and a large (~ 8.6 Å) left-handed channel. QMOF-2, prepared by solvothermal method at 160 °C is the first anion β-quartz-like network with uniform T units.

Experimental Section

QMOF-1 was synthesized by liquid–liquid diffusion at room temperature. Typical procedure: A colorless solution of $Zn(NO_3)_2{\cdot}6H_2O$ (0.301 g, 1 mmol) in DMSO (10 mL) was mixed with isonicotinic acid (0.224 g, 2 mmol) in DMSO (5 mL) and stirred for 30 min. A solution of triethylamine (1–10 mmol) in ethanol was slowly diffused into the colorless solution, and large single needles were obtained quantitatively. A suitable crystal was selected for single crystal X-ray diffraction studies. Elemental analysis calcd (%) for QMOF-1 ($Zn(ISN)_2{\cdot}2H_2O$): C 41.74, H 3.48, N 8.12, Zn 18.84; found: C 42.78, H 2.71, N 8.54, Zn 18.90; IR spectra (KBr): $\tilde{\nu}$ = 3437 cm^{-1} (br, OH of water), ν_{as} and ν_s, 1633, 1365 cm^{-1} (C=O, mondentate carboxylate group).

QMOF-2 was solvothermally prepared. Typical procedure: $InCl_3$ (0.301 g, 1 mmol) and terephthalic acid (0.332 g, 2 mmol) were dissolved in DMF (8 mL) with stirring to form a gel solution. The solution was left for 8 h at room temperature, then sealed in a 25-mL teflon-lined bomb and placed in an oven at 160 °C for 3 days. The resulting large colorless needles (ca. $0.100 \times 0.100 \times 1.00$ mm) were collected and washed with DMF, yield 60%. Elemental analysis calcd (%) for QMOF-2 ($[InH(BDC)_2]$): C 43.26, H 2.03, In 25.87, found after vacuum desiccation: C 42.78, H 2.71, In 26.01; IR spectra (KBr): $\tilde{\nu} = \nu_{as}$ and ν_s, 1575, 1401 cm^{-1} (C=O for chelated carboxylate group).

Received: June 28, 2002 [Z19634]

[1] a) M. Eddaoudi, D. B. Moler, H. Li, B. Chen, T. M. Reineke, M. O'Keeffe, O. M. Yaghi, *Acc. Chem. Res.* **2001**, *34*, 319–330; b) M. J. Zaworotko, *Chem. Soc. Rev.* **1994**, *24*, 283–288; c) S. R. Batten, R. Robson, *Angew. Chem.* **1998**, *110*, 1558–1595; *Angew. Chem. Int. Ed.* **1998**, *37*, 1460–1494; d) O. R. Evans, W. Lin, *Acc. Chem. Res.* **2002**, *35*, 511–522; e) J. C. Noveron, M. S. Lah, R. E. Del Sesto, A. M. Arif, J. S. Miller, P. J. Stang, *J. Am. Chem. Soc.* **2002**, *124*, 6613–6625; f) M. Fujita, K. Umemoto, M. Yoshizawa, N. Fujita, T. Kusukawa, K. Biradha, *Chem. Commun.* **2001**, 509–518.

[2] a) J. Lu, A. Mondal, B. Moulton, M. J. Zaworotko, *Angew. Chem.* **2001**, *113*, 2171–2174; *Angew. Chem. Int. Ed.* **2001**, *40*, 2113–2116; b) L. Pan, X. Huang, J. Li, Y. Wu, N. Zheng, *Angew. Chem.* **2000**, *112*, 537–540; *Angew. Chem. Int. Ed.* **2000**, *39*, 527–530; c) M. J. Zaworotko, *Angew. Chem.* **2000**, *112*, 3180–3182; *Agnew. Chem. Int. Ed.* **2000**, *39*, 3052–3054; d) K. Barthelet, J. Marrot, D. Riou, G. Férey, *Angew. Chem.* **2002**, *114*, 291–294; *Angew. Chem. Int. Ed.* **2002**, *41*, 281–284.

[3] H. Li, M. Eddaoudi, M. O'Keeffe, O. M. Yaghi, *Nature* **1999**, *402*, 276–279.

[4] a) C. Kepert, J. T. J. Prior, M. J. Rossensky, *J. Am. Chem. Soc.* **2000**, *122*, 5158–5168; b) J. S. Seo, D. Whang, H. Lee, S. I. Jun, J. Oh, Y. J. Jean, K. Kim, *Nature* **2000**, *404*, 982–986; c) R. Xiong, X. You, B. F. Abrahams, Z. Xue, C. Che, *Angew. Chem.* **2001**, *113*, 4554–4557; *Angew. Chem. Int. Ed.* **2001**, *40*, 4422–4425.

[5] Y. H. Kiang, G. B. Gardner, S. Lee, Z. Xu, E. B. Lobkovsky, *J. Am. Chem. Soc.* **1999**, *121*, 8204–8215.

[6] a) S. Neeraj, S. Natarajan, C. N. R. Rao, *Chem. Commun.* **1999**, 165–166; b) D. A. Ruce, A. P. Wilkinson, M. G. White, J. A. Bertrand, *J. Chem. Soc. Chem. Commun.* **1995**, 2059–2060.

[7] S. B. Ogunwumi, T. Bein, *Chem. Commun.* **1997**, 901–902.

[8] L. Carlucci, G. Ciani, D. M. Proserpio, A. Sirni, *Angew. Chem.* **1995**, *107*, 2037–2041; *Angew. Chem. Int. Ed. Engl.* **1995**, *34*, 1895–1898.

[9] S. R. Batten, B. F. Houskins. R. Robson, *J. Chem. Soc. Chem. Commun.* **1991**, 445–446.

[10] a) R. W. Gable, B. F. Houskins. R. Robson, *J. Chem. Soc. Chem. Commun.* **1990**, 762–763; b) B. Chen, M. Eddaoudi, T. M. Reineke, J. W. Kampf, M. O'Keeffe, O. M. Yaghi, *J. Am. Chem. Soc.* **2000**, *122*, 11559–11560.

[11] S. W. Keller, *Angew. Chem.* **1997**, *109*, 295–297; *Angew. Chem. Int. Ed. Engl.* **1997**, *36*, 247–248.

[12] S. Defregger, G. F. Engel, P. W. Krempl, *Phys. Rev. B* **1991**, *43*, 6733–6738.

[13] B. F. Hoskins, R. Robson, N. V. Y. Scarlett, *Angew. Chem.* **1995**, *107*, 1317–1318; *Angew. Chem. Int. Ed.* **1995**, *34*, 1203–1204, and references therein.

[14] O. R. Evens, R. Xiong, Z. Wang, G. K. Wong, W. Lin, *Angew. Chem.* **1999**, *111*, 557–559; *Angew. Chem. Int. Ed.* **1999**, *38*, 536–538.

[15] B. G. Hyde, S. Andersson, *Inorganic Crystal Structures*, Wiley, New York, **1988**, p. 393–397.

[16] K. Wade, A. J. Banster in *Comprehensive Inorganic Chemistry, Vol. 1* (Eds.: J. C. Bailer, H. J. Emeleus, R. Nyholm, A. F. Trotman), Dickenson, New York, **1973**, p. 1105–1107.

[17] T. M. Reineke, M. Eddaoudi, M. Fehr, D. Kelley, O. M. Yaghi, *J. Am. Chem. Soc.* **1999**, *121*, 1651–1657.

[18] R. C. Mehrotra, R. Bohra, *Metal Carboxylates*, Academic Press, New York, **1983**.

[19] The full hemisphere of data was collected on a Brucker SMART Apex CCD diffractometer with $Mo_{K\alpha}$ radiation ($\lambda = 0.71073$ Å). The frames were integrated with the Saint Software Package. The structure was solved by direct method and the subsequent difference Fourier synthesis and refined with the SHELXTL (Version 5.10) software package. X-ray data for QMOF-1 ($Zn(ISN)_2{\cdot}2H_2O$), crystal size, $0.080 \times 0.080 \times 1.000$ mm, hexagonal, space group, $P3_1$ (No. 144), a = 15.526(5), c = 6.258(3) Å, $\gamma = 120°$, $Z = 3$, V = 1306.4(8) Å^3, ρ_{calcd} = 1.250 mg m^{-3}, μ = 1.424 mm^{-1}, $1.57 < \theta < 27.08°$, T = 293 K, R_1 = 0.0636, wR_2 = 0.1707 for 3663 ($I > 2\sigma(I)$) of 3664 [R_{int} = 0.0364] unique reflections and 180 parameters. GOF = 1.142, refinement method was full-matrix least-squares on F^2; X-ray data for QMOF-2 ($H[In(BDC)_2]$), crystal size, $0.100 \times 0.100 \times 1.000$ mm, hexagonal, space group $P6_422$ (No. 181), a = 15.087(4), c = 12.032(5) Å, γ = 120°; $Z = 3$, V = 2371.7(13) Å^3, ρ_{calcd} = 1.827 mg m^{-3}, μ = 1.537 mm^{-1}, $1.56 < \theta < 25.0°$, T = 293 K, R_1 = 0.0669, wR_2 = 0.2182 ($I > 2\sigma(I)$) of 1400 [R_{int} = 0.0697] unique reflections and 58 parameters. GOF = 1.339, Refinement method was full-matrix least-squares on F^2. CCDC-188415 (QMOF-1), CCDC-187976 (QMOF-2) contains the supplementary crystallographic data for this paper. These data can be obtained free of charge via www.ccdc.cam.ac.uk/conts/retrieving.html (or from the Cambridge Crystallographic Data Centre, 12, Union Road, Cambridge CB2 1EZ, UK; fax: (+44) 1223-336-033; or deposit @ccdc.cam.ac.uk).

[20] A. F. Wells in *Structure Inorganic Chemistry*, 5th ed, Oxford University Press, Oxford, **1983**.

 © 2002 WILEY-VCH Verlag GmbH & Co. KGaA, Weinheim 0044-8249/02/4123-4473 $ 20.00+.50/0

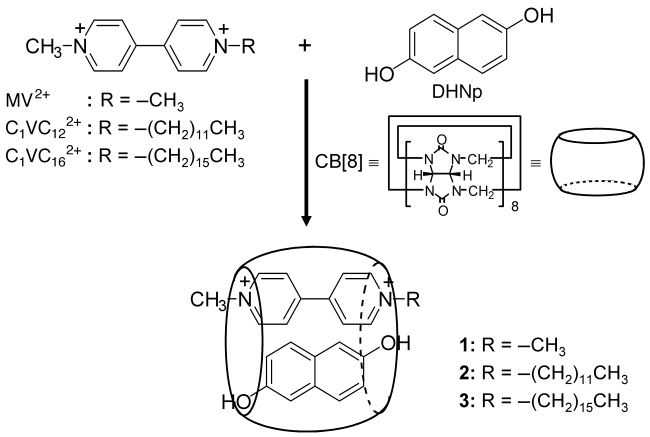
Supramolecular Amphiphiles: Spontaneous Formation of Vesicles Triggered by Formation of a Charge-Transfer Complex in a Host**

Young Jin Jeon, Parimal K. Bharadwaj, SooWhan Choi, Jae Wook Lee, and Kimoon Kim*

Studies on vesicles have received much attention in recent years as they are important building blocks of all living systems and are potentially useful in many areas of chemistry, biology, and material science: for example, in the development of light-harvesting systems, artificial ion channels, drug/gene delivery systems, and new smart materials.[1–3] Over the last decade a wide variety of synthetic amphiphiles with different polar head groups and hydrophobic tails have been reported.[2,3] With only a few exceptions,[4] however, these amphiphiles are single molecules prepared by conventional covalent synthesis. Herein we report, for the first time, the spontaneous formation of giant vesicles triggered by the formation of a stable ternary inclusion complex that behaves as a large supramolecular amphiphile. Furthermore, the disruption of the vesicles can be easily triggered by a redox process.

Cucurbit[6]uril (CB[6]), a macrocyclic cavitand comprising six glycoluril units, has a hydrophobic cavity that is accessible through two identical carbonyl-fringed portals. It has been widely used as a synthetic receptor[5,6] and as a building block for supramolecular architectures.[7] Our recent synthesis of new cucurbituril homologues,[8] cucurbit[*n*]uril (CB[*n*], $n = 5$, 7, and 8) containing five, seven, and eight glycoluril units, respectively, has opened up new opportunities in supramolecular chemistry.[9,10] For example, CB[8], which has a cavity comparable to that of γ-cyclodextrin, can form a stable 1:1:1 complex (**1**) with methyl viologen (MV^{2+}) and 2,6-dihydroxynaphthalene (DHNp) (Scheme 1).[9a] The formation of the ternary complex is driven by charge-transfer interaction between the electron-deficient and electron-rich guest molecules inside the hydrophobic cavity of CB[8]. This discovery prompted us to explore supramolecular assemblies of higher hierarchy based on formation of a ternary complex.

Sonication of an equimolar mixture of CB[8], a viologen with a C_{12} or C_{16} alkyl chain ($C_1VC_{12}^{2+}$ or $C_1VC_{16}^{2+}$, respectively),[11] and DHNp in water results in a transparent or turbid solution with a violet color corresponding to **2** and **3**, respectively.[12] A broad absorption band centered at about 550 nm in their UV/Vis spectra,[13] as in **1**, indicates the formation of charge-transfer complexes inside CB[8] (Scheme 1). Without CB[8], binary mixtures of $C_1VC_{12}^{2+}$ (or $C_1VC_{16}^{2+}$) and DHNp do not produce any color change, which supports the theory that these charge-transfer complexes are indeed formed inside the CB[8] cavity. Conclusive evidence for the formation of stable 1:1:1 ternary complexes were further obtained from ^{1}H NMR and ESI mass measurements.[12] For example, in the ^{1}H NMR spectrum of **2**, the signals for the bipyridinium unit of $C_1VC_{12}^{2+}$ and DHNp shift up-field, whereas those for the alkyl tail of $C_1VC_{12}^{2+}$ (particularly those for the methylene units close to the bipyridinium unit) shift down-field relative to those in their free forms. This observation is consistent with the formation of a charge-transfer complex between the bipyridinium unit of $C_1VC_{12}^{2+}$ and DHNp inside CB[8], and the presence of a signal at m/z 914.30 [M^{2+}] in the ESI mass spectrum exactly matching the formula mass of **2** (m/z 942.86 for **3**) further confirms the formation of a ternary complex.



Scheme 1. Formation of stable ternary complexes **1**, **2**, and **3**.

Most interestingly, the ternary complexes **2** and **3** form large vesicles, which has been confirmed by light microscopy, TEM, and SEM measurements.[13] The TEM images (Figure 1a) of **2**, which has a C_{12} hydrophobic tail, reveal nearly monodispersed vesicles with an average diameter of 20 nm. On the other hand, **3**, which has a C_{16} hydrophobic tail, forms relatively large vesicles with a diameter ranging from 20 nm to 1.2 μm (TEM images, Figure 1b). A high-resolution TEM image of the vesicles[13] shows their hollow structures. Dynamic light scattering data of **3** in water indicate the presence of supramolecular aggregates with an average diameter of 870 nm. The SEM images (Figure 1c) of **3** also show large spheres with a diameter ranging from 20 nm to 1.2 μm; the typical vesicle size lies between 400 and 950 nm. The SEM images also demonstrate that the vesicles are robust as they maintain the spherical shape even when they are dried on a solid surface. This observation is in sharp contrast to most vesicle systems made of natural or synthetic amphiphiles, which are flattened on a surface under similar conditions.[2a] The origin of the extraordinary stability of the present vesicles is, however, not yet clear. We must point out that $C_1VC_{12}^{2+}$

[*] Prof. Dr. K. Kim, Y. J. Jeon, Prof. Dr. P. K. Bharadwaj, Dr. S. Choi, Dr. J. W. Lee
National Creative Research Initiative Center for Smart Supramolecules and
Department of Chemistry, Division of Molecular and Life Sciences
Pohang University of Science and Technology
San 31 Hyojadong, Pohang 790–784 (Republic of Korea)
Fax: (+82) 54–279–8129
E-mail: kkim@postech.ac.kr

[**] We gratefully acknowledge the Creative Research Initiative Program of the Korean Ministry of Science and Technology for support of this work and the Brain Korea 21 Program of the Korean Ministry of Education for a graduate studentship (Y.J.J.). We thank Drs. Hee-Joon Kim and Young Ho Ko for helpful suggestions and help, respectively, in the NMR study. We also thank Prof. Hee-Tae Jung of KAIST for helpful discussions on the TEM experiments.

Supporting information for this article is available on the WWW under http://www.angewandte.org or from the author.

 © 2002 WILEY-VCH Verlag GmbH & Co. KGaA, Weinheim 0044-8249/02/4123-4474 $ 20.00+.50/0

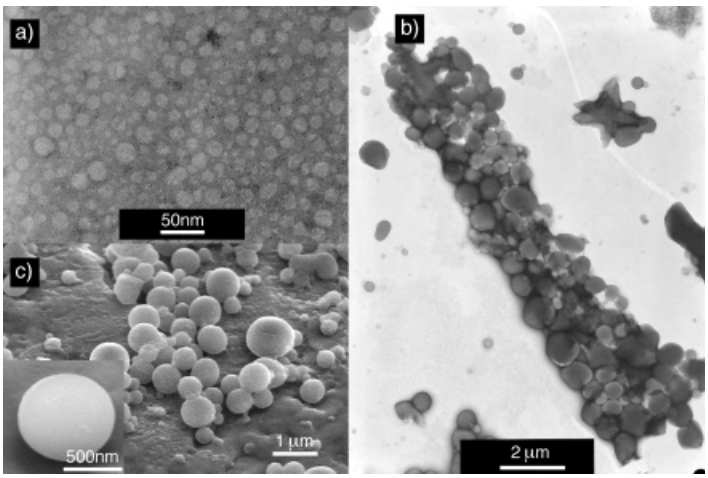


Figure 1. a) TEM image of ternary complex **2**. b) TEM image of ternary complex **3**. c) SEM image of ternary complex **3**. Samples (concentration = 6.9×10^{-4} M) were negatively stained with uranyl acetate (2 wt % in water) for observation by TEM.

and $C_1VC_{16}^{2+}$ itself form only micellar aggregates at the same concentration (6.9×10^{-4} M, critical micelle concentration (cmc) = ca. 1×10^{-4} M).[14] Therefore, the formation of vesicles is triggered by the formation of the ternary complexes CB[8]-DHNp-$C_1VC_{12}^{2+}$ (or $C_1VC_{16}^{2+}$), which behave as supramolecular amphiphiles with a large polar head group and a hydrophobic tail. Such spontaneous formation of vesicles triggered by the formation of a ternary complexes is unprecedented.

Further evidence for the formation of vesicles of **2** and **3** is provided by encapsulation of the fluorescent dye sulforhodamine G (**S**) within the interior of the vesicles. Figure 2 (inset) is a representative fluorescence microscopy image of **3**, which has been prepared in the presence of **S** and purified by dialysis, and shows the entrapment of **S** in the vesicle **3**. The stability of the vesicles is also demonstrated by very slow release of the fluorescent dye trapped inside the vesicles (Figure 2). Addition of Triton X-100, which is known to solublize vesicles, triggers a quick release of the dye. The dye-entrapment experiment, which is known to provide a clue to the lamellarity of vesicles,[15] suggests that the vesicle **3** is unilamellar rather than multilamellar.[13]

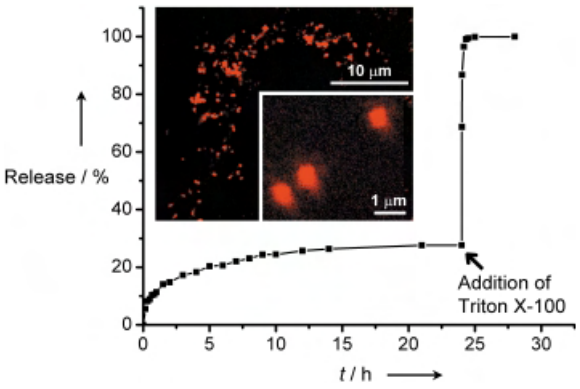


Figure 2. Confocal fluorescence microscope images of vesicle **3** containing entrapped sulforhodamine G (inset) and release profile of the dye from the vesicle.

The two components, DHNp and $C_1VC_{12}^{2+}$ (or $C_1VC_{16}^{2+}$), which reside inside the cavity of CB[8] in **2** (or **3**) are redox active. Therefore, we anticipated that oxidation of DHNp or reduction of $C_1VC_{12}^{2+}$ (or $C_1VC_{16}^{2+}$) would result in destruction of the ternary complex as a result of the loss of charge-transfer interaction between the two guests, which may in turn cause collapse of the vesicles. With this idea in mind, we treated **2** and **3** with cerium(IV) ammonium nitrate (CAN) which can oxidize DHNp to naphthoquinone. The charge-transfer band at 550 nm disappears in the UV/Vis spectrum of **2** or **3** upon treatment with CAN which indicates destruction of the charge-transfer complex inside CB[8].[13] The collapse of vesicles of **3** has been confirmed by SEM; the previously observed spherical objects no longer exist in the SEM images of the CAN-treated sample.[16] We are currently exploring other methods to disrupt the vesicles under mild conditions.

In conclusion, we have demonstrated the spontaneous formation of giant vesicles triggered by formation of a stable ternary inclusion complex that behaves as a large supramolecular amphiphile. Since the ternary complex is stabilized by charge-transfer interaction of an electron donor–acceptor pair inside a host, redox chemistry can be used to trigger the collapse of the vesicles. These novel vesicles may find useful applications in many areas including development of smart materials. We are currently exploring these possibilities.

Received: August 6, 2002 [Z19898]

[1] a) J. H. Fendler, *Membrane Mimetic Chemistry*, Wiley, New York, **1982**; b) T. Kunitake, *Angew. Chem.* **1992**, *104*, 692; *Angew. Chem. Int. Ed. Engl.* **1992**, *31*, 709.

[2] a) Y. Tanaka, M. Miyachi, Y. Kokube, *Angew. Chem.* **1999**, *111*, 565; *Angew. Chem. Int. Ed.* **1999**, *38*, 504; b) Y. Einaga, O. Sato, T. Iyoda, A. Fujishima, K. Hashimoto, *J. Am. Chem. Soc.* **1999**, *121*, 3745; c) Q. Cheng, T. Peng, R. C. Stevens, *J. Am. Chem. Soc.* **1999**, *121*, 6767; d) Y. R. Vandenberg, B. D. Smith, M. N. Pérez-Payán, A. P. Davis, *J. Am. Chem. Soc.* **2000**, *122*, 3252; e) S. Kolusheva, T. Shahal, R. Jelinek, *J. Am. Chem. Soc.* **2000**, *122*, 776; f) A. Veronese, P. L. Luisi, *J. Am. Chem. Soc.* **1998**, *120*, 2662; g) T. Renkes, H. J. Schäfer, P. M. Siemens, E. Neumann, *Angew. Chem.* **2000**, *112*, 2566; *Angew. Chem. Int. Ed.* **2000**, *39*, 2515; h) P. Ghosh, S. Sengupta, P. K. Bharadwaj, *Langmuir* **1998**, *14*, 5712; i) P. Bandyopadhyay, P. K. Bharadwaj, *Langmuir* **1998**, *14*, 7537.

[3] a) B. J. Ravoo, R. Darcy, *Angew. Chem.* **2000**, *112*, 4494; *Angew. Chem. Int. Ed.* **2000**, *39*, 4324; b) M. Brettreich, S. Burghardt, C. Böttler, T. Bayerl, S. Bayerl, A. Hirsch, *Angew. Chem.* **2000**, *112*, 1915; *Angew. Chem. Int. Ed.* **2000**, *39*, 1845; c) A. M. Cassell, C. C. Asplund, J. M. Tour, *Angew. Chem.* **1999**, *111*, 2565; *Angew. Chem. Int. Ed.* **1999**, *38*, 2403; d) M. Hetzer, H. Clausen-Schaumann, S. Bayerl, T. M. Bayerl, X. Camps, O. Vostrowsky, A. Hirsch, *Angew. Chem.* **1999**, *111*, 2103; *Angew. Chem. Int. Ed.* **1999**, *38*, 1962; e) S. Zhou, C. Burger, B. Chu, M. Sawamura, N. Nagahama, M. Toganoh, U. E. Hackler, H. Isobe, E. Nakamura, *Science* **2001**, *291*, 1944.

[4] a) V. Marchi-Artzner, L. Jullien, T. Gulik-Krzywicki, J.-M. Lehn, *Chem. Commun.* **1997**, 117; b) F. Ilhan, T. H. Galow, M. Gray, G. Clavier, V. M. Rotello, *J. Am. Chem. Soc.* **2000**, *122*, 5895.

[5] For reviews of cucurbituril, see a) W. L. Mock, *Comprehensive Supramolecular Chemistry, Vol. 2*, (Ed.: F. Vögtle) Pergamon, Oxford, **1996**, p477; b) P. Cintas, *J. Inclusion Phenom. Mol. Recognit. Chem.* **1994**, *17*, 205.

[6] a) Y.-M. Jeon, J. Kim, D. Whang, K. Kim, *J. Am. Chem. Soc.* **1996**, *118*, 9790; b) D. Whang, J. Heo, J. H. Park, K. Kim, *Angew. Chem.* **1998**, *110*, 83; *Angew. Chem. Int. Ed.* **1998**, *37*, 78; c) H.-J. Kim, J. Heo, W. S. Jeon, E. Lee, J. Kim, S. Sakamoto, K. Yamaguchi, K. Kim, *Angew. Chem.* **2001**, *113*, 1574; *Angew. Chem. Int. Ed.* **2001**, *40*, 1526.

 © 2002 WILEY-VCH Verlag GmbH & Co. KGaA, Weinheim 0044-8249/02/4123-4475 $ 20.00+.50/0

[7] a) D. Whang, Y.-M. Jeon, J. Heo, K. Kim, *J. Am. Chem. Soc.* **1996**, *118*, 11333; b) D. Whang, K. Kim, *J. Am. Chem. Soc.* **1997**, *119*, 451; c) D. Whang, K.-M. Park, J. Heo, K. Kim, *J. Am. Chem. Soc.* **1998**, *120*, 4899; d) S.-G. Roh, K.-M. Park, G.-J. Park, S. Sakamoto, K. Yamaguchi, K. Kim, *Angew. Chem.* **1999**, *111*, 672; *Angew. Chem. Int. Ed.* **1999**, *38*, 638; e) E. Lee, J. Heo, K. Kim, *Angew. Chem.* **2000**, *112*, 2811; *Angew. Chem. Int. Ed.* **2000**, *39*, 2699; f) E. Lee, J. Kim, J. Heo, D. Whang, K. Kim, *Angew. Chem.* **2001**, *113*, 413; *Angew. Chem. Int. Ed.* **2001**, *40*, 399; g) J. W. Lee, Y. H. Ko, S.-H. Park, K. Yamaguchi, K. Kim, *Angew. Chem.* **2001**, *113*, 768; *Angew. Chem. Int. Ed.* **2001**, *40*, 746; h) K.-M. Park, D. Whang, E. Lee, J. Heo, K. Kim, *Chem. Eur. J.* **2002**, *8*, 498; i) K.-M. Park, S.-Y. Kim, J. Heo, D. Whang, S. Sakamoto, K. Yamaguchi, K. Kim, *J. Am. Chem. Soc.* **2002**, *124*, 2140; j) K. Kim, *Chem. Soc. Rev.* **2002**, *31*, 96.

[8] J. Kim, I.-S. Jung, S.-Y. Kim, E. Lee, J.-K. Kang, S. Sakamoto, K. Yamaguchi, K. Kim, *J. Am. Chem. Soc.* **2000**, *122*, 540.

[9] a) H.-J. Kim, J. Heo, W. S. Jeon, E. Lee, J. Kim, S. Sakamoto, K. Yamaguchi, K. Kim, *Angew. Chem.* **2001**, *113*, 1574; *Angew. Chem. Int. Ed.* **2001**, *40*, 1526; b) S.-Y. Kim, I.-S. Jung, E. Lee, J. Kim, S. Sakamoto, K. Yamaguchi, K. Kim, *Angew. Chem.* **2001**, *113*, 2177; *Angew. Chem. Int. Ed.* **2001**, *40*, 2119; c) S. Y. Jon, Y. H. Ko, S. H. Park, H.-J. Kim, K. Kim, *Chem. Commun.* **2001**, *19*, 1938; d) H.-J. Kim, W. S. Jeon, Y. H. Ko, K. Kim, *Proc. Natl. Acad. Sci. USA*, **2002**, 99, 5007.

[10] a) A. Day, A. P. Arnold, R. J. Blanch, B. Snushall, *J. Org. Chem.* **2001**, *66*, 8094; b) R. J. Blanch, A. J. Sleeman, T. J. White, A. P. Arnold, A. I. Day, *Nano Lett.* **2002**, *2*, 147; c) A. I. Day, R. J. Blanch, A. P. Arnold, S. Lorenzo, G. R. Lewis, I. Dance, *Angew. Chem.* **2002**, *114*, 285; *Angew. Chem. Int. Ed.* **2002**, *41*, 275; d) C. Marqiez, W. M. Nau, *Angew. Chem.* **2001**, *113*, 4515; *Angew. Chem. Int. Ed.* **2001**, *40*, 4387.

[11] a) Y. Lei, J. K. Hurst, *J. Phys. Chem.* **1991**, *95*, 7918; b) K. L. Kovacs, A. Der, *Biochimie* **1986**, *68*, 211.

[12] The vesicles were prepared as follows: A small amount of THF (0.3–0.5 mL) and distilled water (10 mL) were added to a vial containing an equimolar ratio (6.9 μmol) of three components: CB[8], viologen with a long alkyl chain ($C_1VC_{12}^{2+}$ or $C_1VC_{16}^{2+}$), and 2,6-dihydroxynaphthalene. The resulting suspension was sonicated at 60 °C for 1 h to remove the initially added THF and then kept overnight at room temperature to give a transparent (**2**) or turbid (**3**) solution. The formation of 1:1:1 ternary complexes in **2** and **3** has been confirmed by UV/Vis and ^{1}H NMR spectroscopy as well as ESI mass spectrometry. **2**: ^{1}H NMR (500 MHz, D_2O, 25 °C, TMS) $\delta = 8.81$ (2H, brs), 8.54 (2H, brs), 7.73 (2H, brs), 7.25 (2H, brs), 6.87 (3H, brs), 6.64 (3H, brs), 6.45 (2H, brs), 5.89 (2H, brs), 5.75 (16H, d), 5.47 (16H, s), 4.54 (3H, s), 4.17 (16H, d), 2.26 (2H, brs), 1.75–1.15 (18H, brs), 0.86 (3H, brs); UV/Vis (H_2O): $\lambda_{CT} = 552$ nm; ESI-MS: *m/z* (%): 914.30 (100) [M^{2+}]. **3**: ^{1}H NMR (500 MHz, D_2O, 25 °C, TMS) $\delta = 9.02$ (2H, brs), 8.49 (2H, brs), 7.56 (2H, brs), 7.21 (2H, brs), 7.10–6.04 (6H, brs), 5.74 (16H, d), 5.46 (16H, s), 4.16 (16H, d), 2.42–0.65 (34H, brs); UV/Vis (H_2O): $\lambda_{CT} = 548$ nm; ESI-MS: *m/z* (%): 942.86 (70) [M^{2+}].

[13] See Supporting Information.

[14] a) A. Diaz, P. A. Quintela, J. M. Schuette, A. E. Kaifer, *J. Phy. Chem.* **1988**, *92*, 3537; b) Y. Lee, C. Lee, *Bull. Korean Chem. Soc.* **1999**, *20*, 1.

[15] Preparation of the dye-entrapped vesicles and calculation of the dye-entrapped volume were carried out by conventional experimental procedures used for liposomes: R. C. C. New, *Liposomes: A practical approach*, Oxford University, Oxford, **1990**.

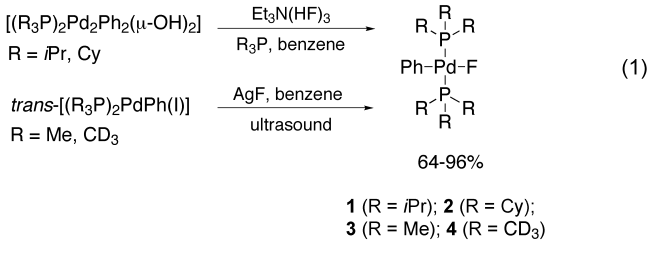
[16] Addition of CAN to an aqueous solution of sulforhodamine G results in immediate quenching of its fluorescence as a consequence of the rapid oxidation of the dye; therefore, the release of the dye from the dye-entrapped vesicle triggered by CAN could not be monitored.

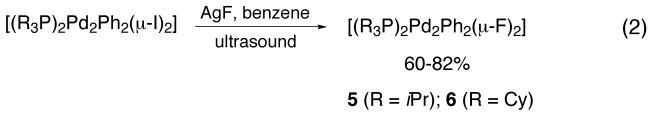
Is Fluoride Bonded to Two Pd Acceptors Still Basic? Three CH_2Cl_2 Molecules Encapsulating a $Pd_2(\mu\text{-}F)_2$ Square and New Implications for Catalysis**

Vladimir V. Grushin* and William J. Marshall

Organotransition-metal fluoro complexes have recently received much attention due to their useful, uncommon properties,[1] and potential use in the synthesis of highly desired, selectively fluorinated organic molecules,[2–4] in catalysis,[5,6] and in C–H activation.[7] Further progress in this new, promising area will depend on firm knowledge of the nature and reactivity of the metal–fluorine bond. As a ligand for the catalytically important platinum group metals, fluoride still remains scantily explored. Thus, being ubiquitous in catalysis, palladium has been shown[6,8] to form isolable fluoro complexes only recently. Here we report on the synthesis, unexpectedly strong basicity, and peculiar reactivity of the first dinuclear organopalladium μ-fluorides and their mononuclear analogues stabilized by $(alkyl)_3P$ ligands.

Using our previously developed methods[6,8] we prepared a series of new Pd fluorides **1**–**6** [Eq. (1) and (2)], which were characterized by analytical, spectroscopic, and X-ray diffraction data (see Supporting Information for details).[9]





Considering the particularly strong π basicity of coordinated terminal fluoride[1,6,10–12] and the enhanced donating properties of iPr_3P (compared to Ph_3P), Pd–F d_π–p_π filled/filled repulsions in **1** and **3** were expected to be stronger than in their Ph_3P analogue $[(Ph_3P)_2PdPh(F)]$,[8] resulting in elongation rather than shortening of the Pd–F bond. Surprisingly, the Pd–F bond lengths in both **1** (Figure 1; 2.050(2) and 2.057(2) Å for two structurally similar molecules in the asymmetric unit), and **3** (Figure 2; 2.057(2) Å) are shorter

[*] Dr. V. V. Grushin, W. J. Marshall
Central Research and Development
E. I. DuPont de Nemours & Co., Inc.
Experimental Station
Wilmington, Delaware 19880–0328 (USA)
Fax: (+1) 302-695-8281
E-mail: vlad.grushin-1@usa.dupont.com

[**] Contribution No. 8331. We thank Dr. D. Christopher Roe for variable-temperature NMR experiments.

Supporting information for this article is available on the WWW under http://www.angewandte.org or from the author.

 © 2002 WILEY-VCH Verlag GmbH & Co. KGaA, Weinheim 0044-8249/02/4123-4476 $ 20.00+.50/0

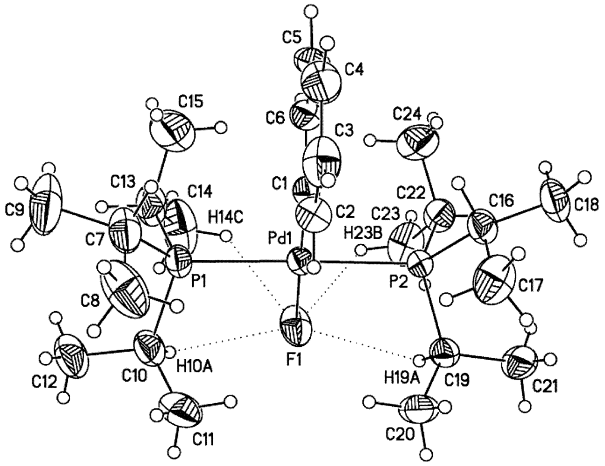


Figure 1. Structure of **1** (ORTEP view; 50% probability ellipsoids), showing C–H···F interactions (2.434–2.575 < 2.67 Å = sum of the van der Waals radii).

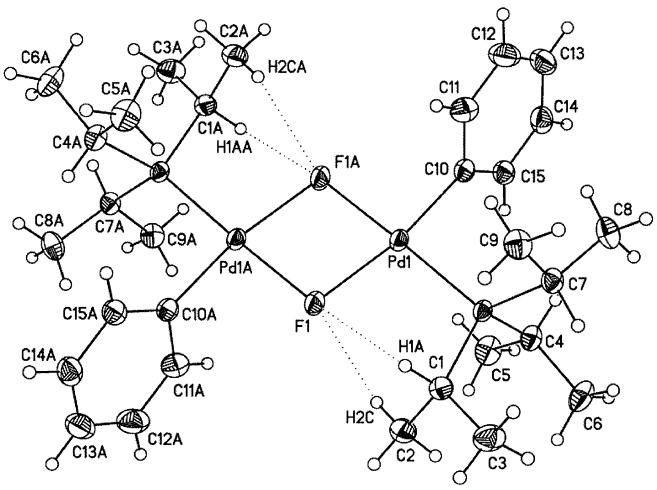


Figure 3. Structure of **5** (ORTEP view; 50% probability ellipsoids), showing PCH···F (2.593 Å) and CCH···F (2.399 Å) contacts.

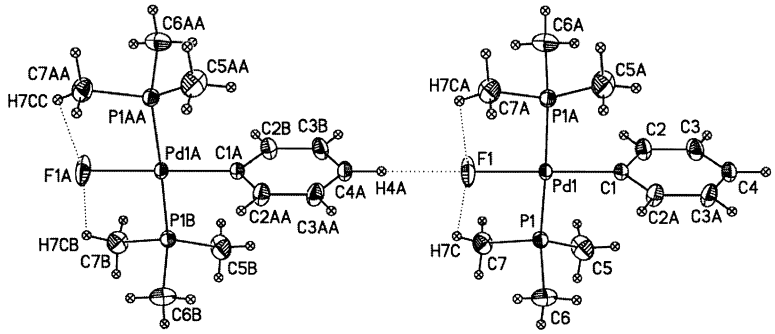


Figure 2. Structure of **3** (ORTEP view; 50% probability ellipsoids), showing intramolecular and intermolecular C–H···F contacts.

than in $[(Ph_3P)_2PdPh(F)]$ (2.085(3) Å).[8a] The opposite effect observed could be accounted for only[13] by stronger C–H···F–M interactions[1,6,14] (Figure 1 and 2) efficiently alleviating the Pd–F filled/filled repulsions in **1** and **3**. A previously unobserved combination of both intramolecular[14b–d] and intermolecular[14a] C–H···F–M interactions was found in **3** (Figure 2); the intermolecular CH···F contact to the para-H(sp^2C) was surprisingly shorter (2.370 Å) than the intramolecular F···H(sp^3C) distance of 2.496 Å.

Homobimetallic μ^2-F complexes of the platinum group metals are extremely rare, especially for Pd and Pt.[11h,15] As a result, little is known about the basicity of μ^2-F bridging two platinum metal Lewis acid centers. It was logical to propose that the binding to two Pd^{II} acceptors would eliminate π-basic properties of the F atoms in **5** and **6**, much like in metal bifluorides.[12] Nonetheless, C–H···F interactions were found in **5** (Figure 3), the first dinuclear organopalladium complex with a fluoride bridge. Therefore, even when coordinated to two Pd centers fluoride retains considerable excessive basicity that requires additional interactions with an electron acceptor for stabilization.[15b,c]

Further manifestation of the striking basicity of fluoride bound to two Pd atoms came from the ability of **6** to form a stable hydrogen-bond adduct with CH_2Cl_2. In pure form, **6** was isolated as a white powder of limited solubility in benzene and toluene. Recrystallization of **6** from CH_2Cl_2/hexane produced clear crystals which, to our surprise, were readily soluble in aromatic solvents. A singlet at $\delta = 4.3$ ppm was observed in the ^{1}H NMR spectrum ([D_6]benzene) of the recrystallized **6**. The difference in the behavior of **6** before (the signal at $\delta = 4.3$ ppm was absent) and after the recrystallization prompted us to analyze the recrystallized material by X-ray diffraction (Figure 4).

As seen from Figure 4, *three* CH_2Cl_2 molecules are hydrogen-bonded to the Pd_2F_2 core of **6**. One of the three CH_2Cl_2 molecules is coordinated to both F ligands through the two hydrogen atoms in a bridging fashion (H···F 2.492 Å). The other two CH_2Cl_2 molecules are "terminal", forming much shorter H···F contacts of 2.083 Å.[16] Owing to the CH_2Cl_2 interactions, the Pd_2F_2 fragment is distorted[15a] from the planar geometry (found in **5**); the fluorides tilt toward the central dichloromethane molecule. The Pd–F bond lengths in **6**·3 CH_2Cl_2 are slightly longer than in **5**, that is, 2.119(1) versus 2.098(1) Å *trans* to P and 2.134(1) versus 2.118(1) Å *trans* to Ph.

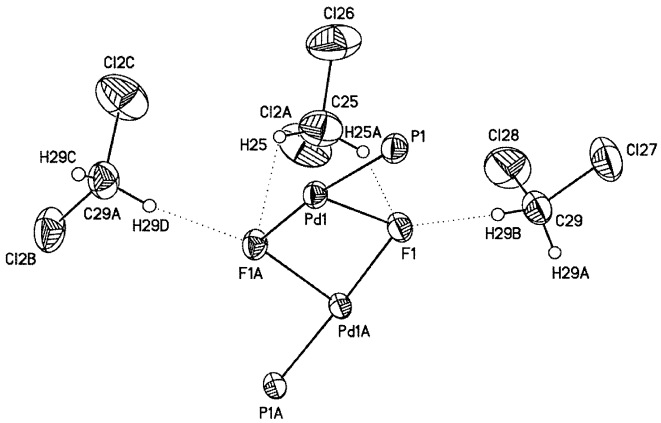


Figure 4. Structure of the Pd_2F_2 core of **6** (ORTEP view; 50% probability ellipsoids) with three CH_2Cl_2 molecules hydrogen-bonded to the fluorine atoms.

 © 2002 WILEY-VCH Verlag GmbH & Co. KGaA, Weinheim 0044-8249/02/4123-4477 $ 20.00+.50/0

Under anhydrous conditions, the F ligand is inert on the NMR time scale for all **1**–**6** (see Supporting Information). The dimers **5** and **6** exist in PhH or PhMe solution as 2–3:1 mixtures of *anti* and *syn* isomers, for which no fast (NMR) interconversion was observed at 20 °C. Thus, well-resolved multiplets were observed in the ^{19}F NMR spectrum of **6** in [D_8]toluene, a doublet at $\delta = -302.3$ ppm with *trans* J(P,F) = 142 Hz (*anti* isomer) and two 1:1 signals (*syn* isomer) at $\delta = -280.0$ ppm (*trans* to P; doublet of triplets, J(P,F) = 157, J(F,F) = 60 Hz), and $\delta = -324.9$ ppm (doublet, J(F,F) = 60 Hz). The ^{31}P NMR spectrum exhibited two doublets at $\delta = 42.2$ (*syn*) and 44.7 ppm (*anti*) with the same *trans* J(P,F) of 157 and 142 Hz, respectively. In contrast, only broad unresolved resonance signals with similar chemical shifts were observed in the NMR spectrum of **6**·3 CH_2Cl_2, suggesting exchange. The latter did not influence substantially the thermodynamics of the *syn–anti* isomerization as the same *anti* to *syn* ratio of 3 was observed for **6** and **6**·3CH_2Cl_2 in toluene or benzene. ^{1}H NMR studies of **6**·3CH_2Cl_2 in [D_8]toluene, in the absence or presence of two extra equivalents of CH_2Cl_2, led to the observation of only one singlet ($\delta =$ 4.3 ppm) for *all* the dichloromethane in the sample at 20 °C, indicating fast inter- and intramolecular exchange processes. On cooling the sample to −80 °C the singlet from CH_2Cl_2 in exchange did not resolve but shifted upfield to $\delta = 3.9$ ppm. Therefore, the exchange processes could not be frozen out at −80 °C. The $\Delta\delta$ value of 0.4 ppm resulting from the cooling of the sample from 20 °C ($\delta = 4.3$ ppm) to −80 °C ($\delta = 3.9$ ppm) is less significant than the $\Delta\delta$ value of 1.05 ppm (5.35 (free CH_2Cl_2) − 4.3 (**6**·n CH_2Cl_2) ppm) at 20 °C. This points to efficient hydrogen bonding of the CH_2Cl_2 molecules to the Pd_2F_2 square in solution even at ambient temperature.

The high π basicity of the F ligand and C−H···FM interactions in **1**–**6** may bear implications for some catalytic reactions involving platinum metal fluoride complexes.[3,5,6] The thermal decomposition of **3** in toluene under rigorously anhydrous conditions (N_2) at 115 °C (> 95 % conversion after 72 h; monitored by ^{19}F and ^{31}P NMR) produced Pd metal, Me_3PF_2, $Me_2(Ph)PF_2$, and $[Me_3PPh]^+FHF^-$. Both difluorophosphoranes (unambiguously identified by their characteristic ^{19}F and ^{31}P NMR spectra[17]) and the phosphonium cation emerged from C−P and P−F reductive elimination reactions similar to those described for [$(Ph_3P)_2PdPh(F)$].[6] In contrast, the formation of bifluoride (^{19}F NMR spectroscopy: broadened doublet, $\delta = -142.6$ ppm, J(H,F) = 121 Hz)[18] was unexpected. Apparently, the source of hydrogen in the FHF^- was the Me groups of the Me_3P ligands, as was demonstrated by repeating the experiment with **4**, the $(CD_3)_3P$ analogue of **3**. Owing to broadening ($\Delta\nu_{1/2}$ = ca. 50 Hz) the bifluoride ^{19}F resonance signal appeared as an unresolved singlet (J(D,F) = 18.8 Hz)[18] but no H,F coupling of about 120 Hz was observed. While the basic fluoride[3k] might deprotonate the phosphonium salt product, it is also conceivable that the intramolecular C−H···F−Pd interactions (see above) mediate proton abstraction at elevated temperatures.[19,20] This reaction path is worth taking into consideration when using $(alkyl)_3P$ late transition metal fluorides in synthesis and catalysis.

Received: August 6, 2002 [Z19896]

[1] a) N. M. Doherty, N. W. Hoffman, *Chem. Rev.* **1991**, *91*, 553; b) E. F. Murphy, R. Murugavel, H. W. Roesky, *Chem. Rev.* **1997**, *97*, 3425.

[2] a) *Organofluorine Chemistry: Principles and Commercial Applications*, (Eds.: R. E. Banks, B. E. Smart, J. C. Tatlow), Plenum, New York, **1994**; b) T. Hiyama, *Organofluorine Compounds*, Springer, Berlin, **2000**.

[3] For examples of metal complex promoted/catalyzed fluorination reactions and transition metal fluorides in synthesis, see: a) T. Sakakura, M. Claisupakitsin, T. Hayashi, M. Tanaka, *J. Organomet. Chem.* **1987**, *334*, 205; b) T. Okano, N. Harada, J. Kiji, *Bull. Chem. Soc. Jpn.* **1992**, *65*, 1741; c) W. W. Dukat, J. H. Holloway, E. G. Hope, M. R. Rieland, P. J. Townson, R. L. Powell, *J. Chem. Soc. Chem. Commun.*, **1993**, 1429; d) B. K. Bennett, R. G. Harrison, T. G. Richmond, *J. Am. Chem. Soc.* **1994**, *116*, 11165; e) J. H. Holloway, E. G. Hope, P. J. Townson, R. L. Powell, *J. Fluorine Chem.* **1996**, *76*, 105; f) J. H. Holloway, E. G. Hope, *J. Fluorine Chem.*, **1996**, *76*, 209; g) A. C. Cooper, K. G. Caulton, *Inorg. Chim. Acta* **1996**, *251*, 41; h) D. R. Gauthier, Jr., E. M. Carreira, *Angew. Chem.* **1996**, *108*, 2521; *Angew. Chem. Int. Ed. Engl.* **1996**, *35*, 2363; i) R. Dorta, P. Egli, F. Zuercher, A. Togni, *J. Am. Chem. Soc.* **1997**, *119*, 10857; j) J. Krueger, E. M. Carreira, *J. Am. Chem. Soc.* **1998**, *120*, 837; k) V. V. Grushin, *Angew. Chem.* **1998**, *110*, 1042; *Angew. Chem. Int. Ed.* **1998**, *37*, 994; l) B. L. Pagenkopf, E. M. Carreira, *Tetrahedron Lett.* **1998**, *39*, 9593; B. L. Pagenkopf, E. M. Carreira, *Chem. Eur. J.* **1999**, *5*, 3437; m) P. Barthazy, L. Hintermann, R. M. Stoop, M. Worle, A. Mezzetti, A. Togni, *Helv. Chim. Acta* **1999**, *82*, 2448; n) L. Hintermann, A. Togni, *Angew. Chem.* **2000**, *112*, 4530; *Angew. Chem. Int. Ed.* **2000**, *39*, 4359; o) P. Barthazy, A. Togni, A. Mezzetti, *Organometallics* **2001**, *20*, 3472; p) J. W. Bode, D. R. Gauthier, Jr., E. M. Carreira, *Chem. Commun.* **2001**, 2560.

[4] For most recent reports on perfluoroalkyl metal complexes, see: a) R. P. Hughes, S. Willemsen, A. Williamson, D. Zhang, *Organometallics* **2002**, *21*, 3085; b) R. P. Hughes, J. M. Smith, C. D. Incarvito, K.-C. Lam, B. Rhatigan, A. L. Rheingold, *Organometallics* **2002**, *21*, 2136; c) A. A. Bowden, R. P. Hughes, D. C. Lindner, C. D. Incarvito, L. M. Liable-Sands, A. L. Rheingold, *J. Chem. Soc. Dalton Trans.* **2002**, 3245.

[5] A. Togni, A. Mezzetti, P. Barthazy, C. Becker, I. Devillers, R. Frantz, L. Hintermann, M. Perseghini, M. Sanna, *Chimia* **2001**, *55*, 801.

[6] V. V. Grushin, *Chem. Eur. J.* **2002**, *8*, 1006.

[7] A. C. Cooper, K. Folting, J. C. Huffmann, K. G. Caulton, *Organometallics* **1997**, *16*, 505.

[8] a) S. L. Fraser, M. Yu. Antipin, V. N. Khroustalyov, V. V. Grushin, *J. Am. Chem. Soc.* **1997**, *119*, 4769; b) M. C. Pilon, V. V. Grushin, *Organometallics* **1998**, *17*, 1774.

[9] CCDC-191228 (**1**), CCDC-191231 (**3**), CCDC-191232 (**4**), CCDC-191229 (**5**), and CCDC-191230 (**6**·3 CH_2Cl_2) contain the supplementary crystallographic data for this paper. These data can be obtained free of charge via www.ccdc.cam.ac.uk/conts/retrieving.html (or from the Cambridge Crystallographic Data Centre, 12, Union Road, Cambridge CB2 1EZ, UK; fax: (+44) 1223-336-033; or deposit @ccdc.cam.ac.uk).

[10] K. G. Caulton, *New J. Chem.* **1994**, *18*, 25.

[11] a) For a review of early reports on X···H···F−M interactions, see: T. G. Richmond, *Coord. Chem. Rev.* **1990**, *105*, 221; b) E. Peris, J. C. Lee, Jr., R. H. Crabtree, *J. Chem. Soc. Chem. Commun.* **1994**, *22*, 2573; c) E. Peris, J. C. Lee, Jr., J. R. Rambo, O. Eisenstein, R. H. Crabtree, *J. Am. Chem. Soc.* **1995**, *117*, 3485; d) G. P. A. Yap, A. L. Rheingold, P. Das, R. H. Crabtree, *Inorg. Chem.* **1995**, *34*, 3474; e) J. E. Veltheer, P. Burger, R. G. Bergman, *J. Am. Chem. Soc.* **1995**, *117*, 12478; f) B. P. Patel, R. H. Crabtree, *J. Am. Chem. Soc.* **1996**, *118*, 13105; g) O. Lopez, M. Crespo, M. Font-Bardia, X. Solans, *Organometallics* **1997**, *16*, 1233; h) J. Gil-Rubio, B. Weberndörfer, H. Werner, *J. Chem. Soc. Dalton Trans.* **1999**, 1437; i) D.-H. Lee, H. J. Kwon, B. P. Patel, L. M. Liable-Sands, A. L. Rheingold, R. H. Crabtree, *Organometallics* **1999**, *18*, 1615; j) L. Brammer, E. A. Bruton, P. Sherwood, *New J. Chem.* **1999**, *23*, 965; k) M. A. Esteruelas, M. Olivan, E. Onate, N. Ruiz, M. Tajada, *Organometallics* **1999**, *18*, 2953; l) E. Clot, O. Eisenstein, R. H. Crabtree, *New J. Chem.* **2001**, *25*, 66.

[12] For recent reports on bifluoride complexes, see: a) N. A. Jasim, R. N. Perutz, *J. Am. Chem. Soc.* **2000**, *122*, 8685, and references therein; b) D. C. Roe, W. J. Marshall, F. Davidson, P. D. Soper, V. V. Grushin, *Organometallics*, **2000**, *19*, 4575, and references therein; c) U. Bentrup,

 © 2002 WILEY-VCH Verlag GmbH & Co. KGaA, Weinheim 0044-8249/02/4123-4478 $ 20.00+.50/0

K. Harms, W. Massa, J. Pebler, *Solid State Sci.* **2000**, *2*, 373; d) N. A. Jasim, R. N. Perutz, S. P. Foxon, P. H. Walton, *J. Chem. Soc. Dalton Trans.* **2001**, 1676; e) M. S. Kirkham, M. F. Mahon, M. K. Whittlesey, *Chem. Commun.* **2001**, 813.

[13] Other mechanisms for diminishing filled/filled repulsions[10] cannot be operative in **1** and **3**. Both F→Pd π donation and push–pull interactions of p_π(F) with π*(Ph) through d_π(Pd) are symmetry-forbidden due to zero overlap[10] of p_π(F) and empty d(x^2-y^2) on Pd, and the Ph ring being orthogonal (Figure 1) to the Pd coordination plane.[6]

[14] a) C. E. Osterberg, M. A. King, A. M. Arif, T. G. Richmond, *Angew. Chem.* **1990**, *102*, 960; *Angew. Chem. Int. Ed. Engl.* **1990**, *29*, 888; b) K. S. Coleman, J. Fawcett, J. H. Holloway, E. Hope, D. R. Russell, *J. Chem. Soc. Dalton Trans.* **1997**, 3557; c) W. J. Marshall, D. L. Thorn, V. V. Grushin, *Organometallics*, **1998**, *17*, 5427; d) P. Barthazy, R. M. Stoop, M. Woerle, A. Togni, A. Mezzetti, *Organometallics* **2000**, *19*, 2844.

[15] a) G. Aullon, G. Ujaque, A. Lledos, S. Alvarez, P. Alemany, *Inorg. Chem.* **1998**, *37*, 804. b) Only one such structurally characterized complex (Ru; no CH···F interactions reported) has been described: J. N. Coalter III, J. C. Huffman, W. E. Streib, K. G. Caulton, *Inorg. Chem.* **2000**, *39*, 3757; c) CH···F interactions have been found in a Ru(μ-F)Tl^I complex,[3o] possibly due to electron-enriched Tl^I.

[16] A weak hydrogen-bonding interaction between CH_2Cl_2 and terminal chloride on Pt has been detected in the solid state (H···Cl 2.60 Å): P. Suman, P. W. Dyer, P. J. Dyson, S. L. James, J. W. Steed, *New J. Chem.* **1998**, 1311.

[17] G. S. Reddy, R. Schmutzler, *Z. Naturforsch B.* **1970**, *25*, 1199.

[18] K. O. Christe, W. W. Wilson, *J. Fluorine Chem.* **1990**, *47*, 117.

[19] Deprotonation of Me_3P coordinated to Ni with BuLi has been reported: M. Wada, *J. Chem. Soc. Chem. Commun.* **1981**, 680.

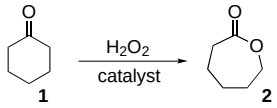
[20] Thermal decomposition of **1**, **2**, **5**, and **6** under similar conditions did not produce observable free FHF^- but rather led to the formation of PdFHF species, as can be judged by the appearance of ^{19}F resonance signals at about $\delta = -280$ and -180 ppm from the proximal and distal F, respectively.[12]

 © 2002 WILEY-VCH Verlag GmbH & Co. KGaA, Weinheim 0044-8249/02/4123-4479 $ 20.00+.50/0

Baeyer–Villiger Oxidations with Hydrogen Peroxide in Fluorinated Alcohols: Lactone Formation by a Nonclassical Mechanism**

Albrecht Berkessel,* Marc R. M. Andreae, Hans Schmickler, and Johann Lex

The Baeyer–Villiger oxidation of ketones to esters or lactones is of high synthetic utility.[1,2] In the vast majority of cases, peracids such as 3-chloroperbenzoic acid have been employed as the source of oxygen. Hydrogen peroxide as oxidant clearly offers a number of advantages, in particular the lack of a by-product (except for water). Strained ketones such as cyclobutanones have long been known to afford γ-butyrolactones rapidly and in high yield when treated with alkaline hydrogen peroxide.[3] On the other hand, the Baeyer–Villiger oxidation of nonstrained ketones such as cyclohexanone (**1**) to ε-caprolactone (**2**) with H_2O_2 is much more difficult to achieve [Eq. (1)]. Until recently, highly



(1)

concentrated hydrogen peroxide, long reaction times and/or heterogeneous[4] or homogeneous catalysts such as transition metal complexes,[5,6] arsonic[7] and seleninic acids[8,9] were required for satisfactory conversions. In contrast, we recently reported that in 1,1,1,3,3,3-hexafluoro-2-propanol (HFIP) as solvent, the Baeyer–Villiger oxidation of **1** to **2** proceeds smoothly and efficiently in the presence of Brønsted acid catalysts such as *para*-toluenesulfonic acid.[10,11] With the aim of developing a generally applicable method for the Baeyer–-Villiger oxidation of nonstrained ketones with hydrogen peroxide, we investigated the mechanism of this remarkably simple process. As it turned out, the formation of **2** from **1** proceeds in a two-step fashion, via a distinct, isolable intermediate, formed initially from the ketone and H_2O_2. This intermediate was unambiguously identified as the bisperoxide 7,8,15,16-tetraoxadispiro[5.2.5.2]hexadecane. In the second step, the cation-stabilizing solvent HFIP allows the hitherto unknown acid-catalyzed rearrangement of this tetroxane to give two equivalents of the product lactone.

A first hint to the formation/decay of a reaction intermediate came from the observation that at temperatures of about 30 °C, ketones such as **1**, 2-methylcyclohexanone, or cyclopentanone were consumed rapidly, but the formation of the product lactones lagged behind. Furthermore, it was surprising to see that camphor—a well-known substrate of the Baeyer–Villiger oxidation with peracids—was not significantly consumed.[1,2,13] These results clearly indicated that a mechanism different from the classical peracid-induced Baeyer–Villiger oxidation may be operative. To gain further insight, we performed the oxidation of **1** in [D_2]HFIP and monitored the reaction by ^{13}C NMR spectroscopy (Figure 1).

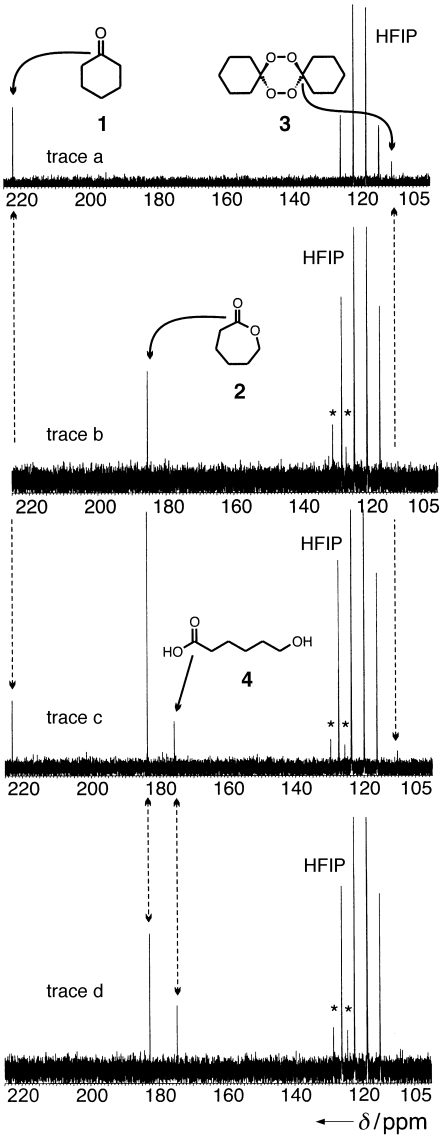


Figure 1. In situ NMR-monitoring of the Baeyer–Villiger oxidation of **1** with hydrogen peroxide in [D_2]HFIP (*:signals of *p*-TsOH). See text for details.

At 55 °C, treatment of **1** with 1.3 equivalents of 50 % aqueous hydrogen peroxide and one crystal of *p*-toluenesulfonic acid resulted in smooth conversion, and **2** was formed in 71 % yield. ε-Hydroxycaproic acid (**4**) was formed as a side product (29 %, Figure 1, trace d). However, when **1** was treated with H_2O_2 in the absence of acid at room temperature, it was cleanly converted within minutes to a single product which was *not* **2**. Instead, this material showed a characteristic ^{13}C NMR peak at $\delta = 110$ ppm, indicative of an acetal-like structure (Figure 1, trace a). When the reaction was repeated in nondeuterated HFIP on larger scale, this primary product

[*] Prof. A. Berkessel, M. R. M. Andreae, Dr. H. Schmickler, Dr. J. Lex
Institut für Organische Chemie der Universität zu Köln
Greinstrasse 4, 50939 Köln (Germany)
Fax: (+49) 221-470-5102
E-mail: berkessel@uni-koeln.de

[**] This work was supported by the Fonds der Chemischen Industrie and by the BASF AG, Ludwigshafen. The authors thank Dr. Matthias Schäfer for assistance in the interpretation of the MS experiments.

Supporting information for this article is available on the WWW under http://www.angewandte.org or from the author.

 © 2002 WILEY-VCH Verlag GmbH & Co. KGaA, Weinheim 0044-8249/02/4123-4481 $ 20.00+.50/0

could be isolated in significant quantities: Upon application of mild vacuum (0.2 Torr), the compound deposited on a condenser in the form of colorless crystals. The X-ray analysis of this material enabled us to unambiguously assign the spiro-bisperoxide structure **3** (Figure 2, Eq. (2)).[14,15] Clearly, the

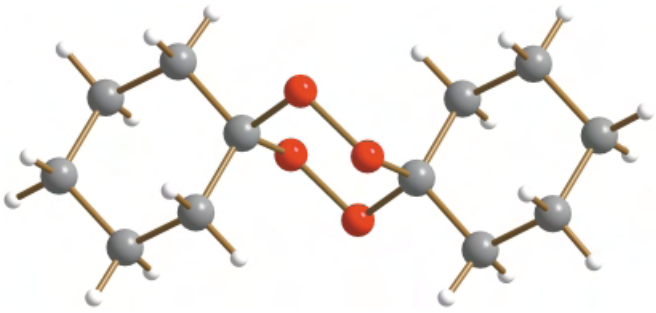
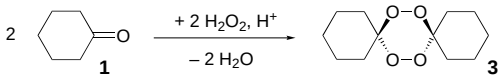


Figure 2. X-ray crystal structure of **3**.

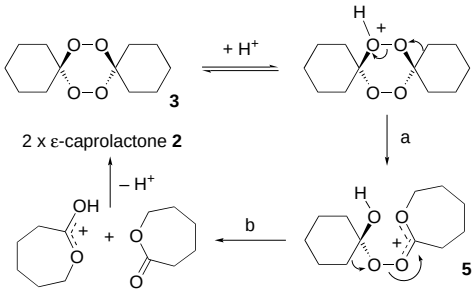
NMR spectroscopic data of isolated **3** were identical to those obtained by combining **1** with hydrogen peroxide in HFIP in situ (see above).



(2)

Treatment of isolated **3** in HFIP with catalytic amounts of strong acids (such as *p*-TsOH) resulted in rapid and quantitative rearrangement to **2**. For example, monitoring of a solution of isolated **3** in dry [D_2]HFIP by ^{13}C NMR spectroscopy showed complete conversion within seconds (with evolution of heat; Figure 1, trace b). Upon addition of water to the HFIP solvent, the rearrangement becomes increasingly slow, and **4** becomes more and more prominent as a side product (Figure 1, trace c). The time course of the reaction (not shown) indicated that **4** is *not* formed by subsequent hydrolysis of **2**, but that these two compounds are formed *in parallel*. In line with the above results, anhydrous urea-hydrogen peroxide clathrate as oxidant cleanly afforded **2** and only traces of **4** (monitoring by NMR spectroscopy, not shown). When cyclopentanone was treated with hydrogen peroxide in HFIP, the formation of the analogous spiro-bisperoxide was indicated by the appearance of a new resonance signal at $\delta = 124.58$ ppm. Camphor did *not* afford a detectable adduct with H_2O_2. Thus, the overall activity pattern of ketones in the Baeyer–Villiger oxidation with hydrogen peroxide in HFIP is determined by the reactivity/unreactivity in the initial step, that is peroxide formation [Eq. (2)].

We interpret our experimental observations based on the mechanism shown in Scheme 1. Upon protonation, **3** rearranges to the lactonium cation **5** (step a, Scheme 1). Fragmentation of cation **5** with concomitant rearrangement of the second six-membered ring affords two equivalents of **2** (step b, Scheme 1). Interestingly, the cyclohexyl spiro-bisperoxide **3** was isolated and characterized as early as 1940, in the course of a first attempt to perform the Baeyer–Villiger oxidation of **1** with hydrogen peroxide.[16] However, the



Scheme 1. Postulated mechanism for the rearrangement of **3** to **2**.

authors were unable to transform the peroxide **3** to **2**, and they concluded correctly that **3** cannot be an intermediate in the Baeyer–Villiger oxidation with peracids, but represents a "dead end".[16] Various other peroxidic adducts of **1** with hydrogen peroxide have been reported,[17–20] and a number of further attempts have been made to isomerize them to **2**. However, in standard organic solvents, acid or Lewis acid catalysis never afforded reasonable yields of lactone,[21–23] and thermolysis invariably gave rise to decomposition initiated by homolytic fission of the peroxide bond(s).[24–26]

What is the peculiar effect of HFIP that allows the long-sought rearrangement of the bisperoxide **3** to the lactone **2**? HFIP is well known to form strong hydrogen bonds to anions, thus stabilizing "naked" cations and radical cations.[27–29] Hence we conclude that HFIP 1) not only allows the formation of the protonated spiro-bisperoxide (Scheme 1), but also 2) enables this cation to rearrange by preventing competing intermolecular interception by nucleophiles. The vigor of the peroxide rearrangement in HFIP as compared to other solvents is impressively demonstrated by IR thermography (Figure 3): At identical peroxide and acid loadings, the reaction in dry HFIP gives rise to an immediate temperature increase of more than 20 °C, whereas the evolution of heat is much less pronounced in all other solvents. The reaction retarding effect of water is also clearly visible (wells nos. 1 and 2 from the top; Figure 3).

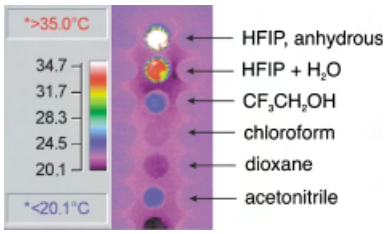
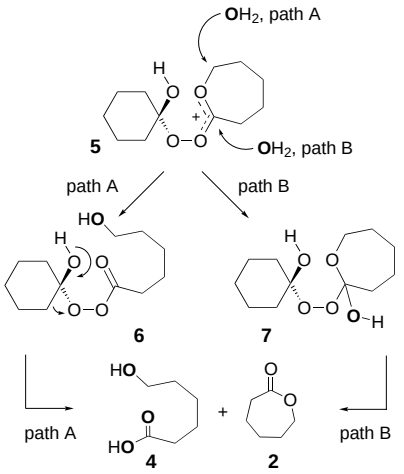


Figure 3. IR-thermographic solvent screening of the acid-catalyzed rearrangement of **3**.

Finally, the mechanism shall be addressed by which **4** is formed from **3**. In principle, addition of a water molecule to the seven-membered ring of the lactonium cation **5** may occur in two ways (Scheme 2): nucleophilic attack at the ε-carbon atom (path A, Scheme 2) gives rise to the ring-opened product **6** which in fact represents the Criegee-intermediate of a "normal" Baeyer–Villiger oxidation. The decay of this intermediate gives rise to **4** and one equivalent of **2**. Attack of

 © 2002 WILEY-VCH Verlag GmbH & Co. KGaA, Weinheim 0044-8249/02/4123-4482 $ 20.00+.50/0



Scheme 2. Postulated reaction paths to **4** and **2**.

water at the acyl carbon atom of **5** (path B, Scheme 2) gives rise to the bishemiperhydrate **7** which may undergo cleavage to **4** and **2** in an analogous fashion. We reasoned that the use of ^{18}O-labeled water should allow a distinction between paths A and B: In the former case, the ^{18}O label should end up in the hydroxy function of **4**, whereas the latter mechanism should integrate the water-derived oxygen atom into the carboxyl group of **4** (Scheme 2). In fact, when the acid-catalyzed rearrangement of **3** was carried out in the presence of $^{18}OH_2$, GC-MS analysis revealed that 1) *one* oxygen atom of the product **4** was derived from $^{18}OH_2$, and that 2) this oxygen atom was part of the *carboxy* function. Consequently, path B (Scheme 2) appears to be the most reasonable mechanism for the formation of the by-product **4**. The latter result is in agreement with earlier studies on the mechanism of hydrolysis of orthoesters, structurally related to the intermediates **5** and **7** (Scheme 2).[30]

In summary, we have shown that the Baeyer–Villiger oxidation of ketones with hydrogen peroxide in HFIP proceeds by a novel mechanism, via spiro-bisperoxides as intermediates. Most importantly, the use of cation-stabilizing HFIP as the solvent opens a new reaction channel for 2,3,5,6-tetroxanes, that is a smooth protonation-induced rearrangement to lactones. In other solvents, this type of peroxide rearrangement does not occur to a significant extent. We could furthermore demonstrate that in the case of **1**, the by-product **4** is produced in parallel and not by subsequent hydrolysis of the main product **2**. Isotopic labeling experiments support the idea of an intermediate lactonium ion (**5**) as the branching point between rearrangement (leading to the lactone **2**) and interception by water (leading to **4**). Further work in this area will address the question of whether the use of fluorinated alcohols as solvent may allow other novel reaction modes of high-energy compounds such as peroxides.

Received: May 17, 2002 [Z19329]

[1] G. R. Krow, *Org. React.* **1993**, *43*, 251 – 798.

[2] M. Renz, B. Meunier, *Eur. J. Org. Chem.* **1999**, 737 – 750.

[3] a) M. J. Bogdanowicz, T. Ambelang, B. M. Trost, *Tetrahedron Lett.* **1973**, 923 – 926; b) B. M. Trost, J. M. Balkovec, M. K. T. Mao, *J. Am. Chem. Soc.* **1986**, *108*, 4974 – 4983.

[4] a) A. Corma, L. T. Nemeth, M. Renz, S. Valencia, *Nature* **2001**, *412*, 423 – 425; b) A. Corma, M. T. Navarro, L. Nemeth, M. Renz, *Chem. Commun.* **2001**, 2190 – 2191.

[5] A. Gusso, C. Baccin, F. Pinna, G. Strukul, *Organometallics* **1994**, *13*, 3442 – 3451.

[6] G. Strukul, *Angew. Chem.* **1998**, *110*, 1256 – 1267; *Angew. Chem. Int. Ed.* **1998**, *37*, 1198 – 1209.

[7] S. E. Jacobson, F. Mares, P. M. Zambri, *J. Am. Chem. Soc.* **1979**, *101*, 6938 – 6946.

[8] G.-J. ten Brink, J.-M. Vis, I. W. C. E. Arends, R. A. Sheldon, *J. Org. Chem.* **2001**, *66*, 2429 – 2433.

[9] P. A. Grieco, Y. Yokoyama, S. Gilman, Y. Ohfune, *J. Chem. Soc. Chem. Commun.* **1977**, 870 – 871.

[10] A. Berkessel, M. R. M. Andreae, *Tetrahedron Lett.* **2001**, *42*, 2293 – 2295.

[11] See ref. [12] for the report of an uncatalyzed Baeyer–Villiger oxidation of **1** and other nonstrained ketones in HFIP. As decribed in ref. [10], Brønsted acid catalysis of this process was discovered in our laboratory.

[12] K. Neimann, R. Neumann, *Org. Lett.* **2000**, *2*, 2861 – 2863.

[13] J. L. Mateos, H. Menchaca, *J. Org. Chem.* **1964**, *29*, 2026 – 2028.

[14] Crystals suitable for X-ray structural analysis were obtained by recrystallization of **3** from methanol. Crystal data for **3**: $C_{12}H_{20}O_4$, $M_r = 228.28$, colorless platelet, $0.20 \times 0.20 \times 0.10$ mm, triclinic, $a = 5.7373(6)$, $b = 5.9759(7)$, $c = 9.3955(11)$ Å, $\alpha = 85.143(6)$, $\beta = 87.743(7)$, $\gamma = 62.874(5)°$, $V = 285.67(6)$ Å^3, space group $P\bar{1}$, $Z = 1$, $\rho_{calcd} = 1.327$ g cm^{-3}, $\mu = 0.098$ mm^{-1}, $T = 100$ K. A total of 3049 reflections were measured, 1593 unique, 114 parameters, final residuals were $R1 = 0.045$ and $\omega R2 = 0.095$ for 1037 observed reflections with $I > 2\sigma(I)$. Data were collected on a Nonius KappaCCD diffractometer ($2\theta_{max} = 60°$, $Mo_{K\alpha}$ radiation ($\lambda = 0.71073$ Å), graphite monochromator, φ/ω scans. The structure was solved by using direct methods (G. M. Sheldrick, SHELXS-97, Program for the Solution of Crystal Structures, University of Göttingen, Göttingen (Germany), **1997**), followed by full-matrix least-squares refinement (using all unique reflections) with anisotropic thermal parameters for C and O and isotropic parameters for H (G. M. Sheldrick, SHELXS-97, Program for the Refinement of Crystal Structures, University of Göttingen, Göttingen (Germany), **1997**). CCDC-185714 contains the supplementary crystallographic data for this paper. These data can be obtained free of charge via www.ccdc.cam.ac.uk/conts/retrieving.html (or from the Cambridge Crystallographic Data Centre, 12, Union Road, Cambridge CB2 1EZ, UK; fax: (+44) 1223-336-033; or deposit @ccdc.cam.ac.uk).

[15] a) P. Groth, *Acta Chem. Scand.* **1964**, *18*, 1301 – 1302; b) P. Groth, *Acta Chem. Scand.* **1967**, *21*, 2608 – 2630.

[16] W. Dilthey, M. Inckel, H. Stephan, *J. Prakt. Chem.* **1940**, *154*, 219 – 237.

[17] R. Criegee, W. Schnorrenberg, J. Becke, *Justus Liebigs Ann. Chem.* **1949**, *565*, 7 – 21.

[18] C. W. Jefford, A. J. J. Boukouvalas, *Synthesis* **1988**, 391 – 393.

[19] a) A. J. R. Sanderson, K. Paul, P. R. Story, D. D. Denson, J. A. Alford, *Synthesis* **1975**, 159 – 161; b) J. R. Sanderson, R. J. Wilterdink, A. G. Zeiler, *Synthesis* **1976**, 479 – 481.

[20] K. J. McCullogh, A. R. Morgan, D. C. Nonhebel, P. L. Pauson, G. J. White, *J. Chem. Res. (S)* **1980**, 34; K. J. McCullogh, A. R. Morgan, D. C. Nonhebel, P. L. Pauson, G. J. White, *J. Chem. Res. Miniprint* **1980**, 601 – 628.

[21] S. Matsugo, I. Saito in *Organic Peroxides* (Ed.: W. Ando), Wiley, Chichester, **1992**, pp. 157 – 194.

[22] M. Miura, M. Nojima, S. Kusabayashi, *J. Chem. Soc. Perkin 1* **1980**, 1950 – 1954.

[23] A. Isard, F. Weiss, Fr. 1,533,936 **1968** [*Chem. Abstr.* **1969**, *71* 112434s].

[24] L. F. R. Cafferata, G. N. Eyler, E. L. Svartman, A. I. Canizo, E. Alvarez, *J. Org. Chem.* **1991**, *56*, 411 – 414.

[25] L. F. R. Cafferata, G. N. Eyler, E. L. Svartman, A. I. Canizo, E. J. Borkowski, *J. Org. Chem.* **1990**, *55*, 1058 – 1061.

[26] a) K. J. McCullogh, A. R. Morgan, D. C. Nonhebel, P. L. Pauson, *J. Chem. Res. (S)* **1980**, 35;b) K. J. McCullogh, A. R. Morgan, D. C. Nonhebel, P. L. Pauson, *J. Chem. Res. (M)* **1980**, 629 – 650; c) K. J. McCullogh, A. R. Morgan, D. C. Nonhebel, P. L. Pauson, *J. Chem.*

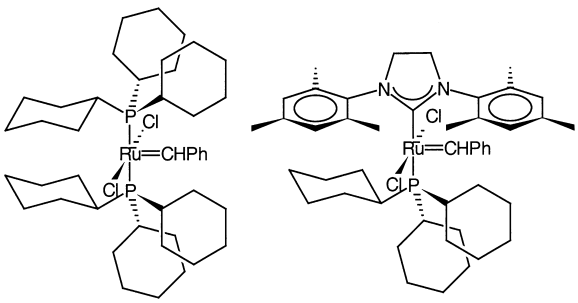
 © 2002 WILEY-VCH Verlag GmbH & Co. KGaA, Weinheim 0044-8249/02/4123-4483 $ 20.00+.50/0

Res. (S) **1980**, 36–37; d) K. J. McCullogh, A. R. Morgan, D. C. Nonhebel, P. L. Pauson, *J. Chem. Res. (M)* **1980**, 651–676.
[27] F. L. Schadt, P. von R. Schleyer, T. W. Bentley, *Tetrahedron Lett.* **1974**, 2335–2338.
[28] L. Eberson, M. P. Hartshorn, J. J. McCullough, O. Persson, F. Radner, *Acta Chem. Scand.* **1998**, *52*, 1024–1028.
[29] L. Eberson, M. P. Hartshorn, O. Persson, F. Radner, *Chem. Commun.* **1996**, 2105–2112.
[30] P. Deslongchamps, *Stereoelectronic Effects in Organic Chemistry*, Pergamon, Oxford, **1986**, pp. 72–84.

Ligand Rotation Distinguishes First- and Second-Generation Ruthenium Metathesis Catalysts**

Christian Adlhart and Peter Chen*

We report herein a combined quantum mechanical/molecular mechanics (QM/MM) study of the olefin-metathesis reaction catalyzed by ruthenium carbene complexes. The discovery and progressive improvement of Ru-based metathesis catalysts[1] makes an understanding of the mechanistic basis for the high activity and broad substrate tolerance of considerable theoretical as well as practical interest. The discovery of the "first-generation" metathesis catalysts $[(Cy_3P)_2(Cl)_2Ru{=}CHPh]$ (**1**, Cy = cyclohexyl) by Grubbs and co-workers,[2] of which **1** is representative, and the subsequent discovery of the "second-generation" catalysts **2** by the groups of Grubbs,[3] Nolan,[4] and Herrmann,[5] in which an *N*-heterocyclic carbene (NHC) ligand replaces one phosphane group in the first-generation systems, has spurred the synthesis of even more varied structural variants as well as extensive mechanistic work. Recently, Grubbs and co-workers presented an extensive in situ kinetic study[6] in which it was concluded that the origin of the greatly increased activity in the second-generation catalysts derived from a more favorable branching ratio for the partitioning of the active carbene complex, ($[(L)(Cl)_2Ru{=}CHR]$, L = Cy_3P or NHC), between entry into the catalytic cycle and rebinding of a phosphane. We have reported gas-phase mechanistic studies[7,8] with substituent and isotope effects aimed at identifying the rate-determining step as well as the role of preequilibria in determining catalyst activity.



1 **2**

This growing body of experimental work on metathesis catalysts makes a computational study timely, particularly given the recent successes of mixed quantum-mechanical/classical methods (QM/MM) that allow a reasonable treatment of large organometallic complexes with explicit inclusion of the full ligand set[9] with conformational flexibility. Our calculations show that the first-generation catalysts **1** have a high barrier in the middle of the reaction coordinate imposed by the necessity of rotation of the threefold symmetric phosphane ligand; a comparable barrier is absent in second-generation catalysts **2** because of the twofold symmetry of the NHC ligand. Depending on whether the metathesis reaction is exothermic, thermoneutral, or endothermic, the rate-determining step should therefore change.

Calculations were carried out on the metathesis reaction of both **1** and **2** using the IMOMM approach[10] implemented in the ADF2000.02 (ADF = Amsterdam Density Functional) package[11] on Quant-X Alpha (Compaq Unix Tru64 Unix 5.3) and AMD Athlon (Red Hat Linux 7.1) machines. The QM model was the $[(Me_3P)_2(Cl)_2Ru{=}CHPh]$ unit with hydrogen atoms as dummies for the carbon atoms of the actual complexes. The α values[12] were obtained by full DFT calculations on the QM model units and the full complexes. A triple-ζ basis set was used on ruthenium;[13] a polarized double-ζ basis set was used for all other elements. The $1s^2 2s^2 2p^6 3s^2 3p^6 3d^{10}$ electrons of the ruthenium atoms, the $1s^2 2s^2 2p^6$ electrons of the chlorine and phosphorus atoms, and the $1s^2$ electrons of the carbon atoms were treated within a frozen-core approximation. A set of auxiliary s, p, d, f, and g STO functions (STO = Slater orbital) centered on all nuclei was used to fit the molecular density and present Coulomb and exchange potentials accurately in each SCF cycle (SCF = self-consistent field).[13] The local density approximation by Vosko, Wilk, and Nusair,[14] and generalized gradient approximation were used with the BP86 functional.[15] Scalar relativistic corrections were added to the total energy.[16] Because all systems investigated showed a large HOMO–LUMO gap, a spin-restricted formalism could be employed throughout. For the MM part of the calculation, a modified sybyl/tripos 5.2 force field[17] was implemented.[18] In the course of comparing QM/MM to full DFT energies, we noticed that there was a systematic error that could be traced back to a double counting of MM interactions. Therefore the MM contribution to the hybrid DFT/MM energy has been removed, as most of this interaction is already taken into account by the imposed strain of the MM system on the DFT system. Validation against full DFT energies at full DFT-optimized structures show that the QM/MM energies simulate full DFT values to within 3–4 kcal mol^{-1} in the worst case; the agreement is often much better. The conformational space,

[*] Prof. Dr. P. Chen, C. Adlhart
Laboratorium für Organische Chemie, ETH Hönggerberg
8093 Zürich (Switzerland)
Fax: (+41) 1-632-1280
E-mail: chen@org.chem.ethz.ch

[**] We acknowledge helpful discussions with Professor U. Röthlisberger and Dr. A. Magistrato in implementing QM/MM calculations in our group. This project was supported by the Swiss National Science Foundation and the Research Commission of the ETH Zürich.

Supporting information for this article is available on the WWW under http://www.angewandte.org or from the author.

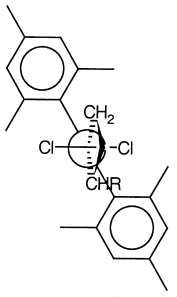
 © 2002 WILEY-VCH Verlag GmbH & Co. KGaA, Weinheim 0044-8249/02/4123-4484 $ 20.00+.50/0

especially with regard to the cyclohexyl rings, was systematically searched. When X-ray structures were available, the optimized QM/MM structures were found to be in excellent agreement.[19]

Transition states were approached by a linear transit from the reactant to the product and from the product to the reactant by calculation of a series of structures constrained to a particular value of the geometric parameter corresponding to the reaction coordinate (the C–C distances in the metallacyclobutane or the Cl-Ru-P-C torsional angle for PCy_3 rotation) with unconstrained optimization of all other geometric parameters. As a further check for each transition state, the geometries were then relaxed in both forward and reverse directions to confirm that they converge to the reactants and products (or intermediates in the case of PCy_3 rotation, which shows several transition states).[20] With full DFT validation at the important critical points, the potential surfaces for the metathesis reactions with **1** and **2** were explored widely with QM/MM. In contrast to previous studies,[8,21] the steric effects of the very large ligands (Tolman cone angles[22] for PCy_3, PMe3, and PH_3 are 170°, 118° and 87°, respectively) can be explicitly treated; these steric effects are, in fact, critical to the conclusion of this study (see below).

The results for the degenerate metathesis of styrene with **1** are shown in Figure 1. Alternative reaction pathways involving *cis* dichloro complexes, as well as an associative ligand exchange of an olefin for phosphane were calculated and found to be less favorable.[20] Similar surfaces for the metathesis of simple olefins with **2**, and the metathesis of ethyl vinyl ether with **1** and **2**, were also calculated.[20] Grubbs and co-workers reported enthalpies of activation for phosphane exchange of 23.6 ± 0.5 kcal mol (with **1**) and 27 ± 2 kcal mol^{-1} (with **2**).[6] These values agree gratifyingly well with the calculated full DFT values of 20.8 and 28.0 kcal mol^{-1}, as well as with the QM/MM results. The reaction coordinate in Figure 1 is representative of a thermoneutral metathesis reaction with a first-generation catalyst. Rotation of the tricyclohexylphosphane in any of the structures is primarily hindered by the unfavorable steric interaction with the large chlorine atoms. The barrier of rotation for PH_3 was calculated to be only 0.16 kcal mol^{-1}, illustrating the very large difference between PH_3 and PCy_3 (6.0 kcal mol^{-1}). In other studies, rotation barriers between 7 and 18 kcal mol^{-1} were found for bulky phosphanes.[23] The potential surface for the metathesis of ethyl vinyl ether, calculated to be exothermic by 9.45 kcal mol^{-1}, is very similar to that in Figure 1 for structures **I**–**IV**′. The exothermicity appears only upon cleavage of the metallacyclobutane, meaning that transition states from **IV** to **VI** or from **IV**′ to **III**′, are the first structures to be substantially lowered in energy—all subsequent structures are also lowered.

For second-generation catalysts **2**, the potential surface is much simpler; a cursory examination of the structure analogous to **IV** shows that no rotation is needed because the NHC ligand has only twofold symmetry, as opposed to the threefold symmetry of the phosphane ligand in **1**. As mentioned above, the calculated barrier for phosphane dissociation from **2** agrees well with the experimental value. The structures **II**–**IV** (analogous to **2**) for the metathesis of ethylene have calculated energies (full DFT) of 28.0, 14.6, and 12.9 kcal mol^{-1}, respectively; the rest of the surface would be the mirror image of **IV**–**I** in the case of a thermoneutral metathesis reaction.



analogue of **IV**

Our calculations, which establish the gross topology of the potential surfaces, should substantially facilitate the interpretation of experimental mechanistic studies. Given that the QM/MM method reproduces QM energies to within 3–4 kcal mol^{-1}, and given the (previously unknown) accuracy of even a full DFT calculation, good agreement with experimental data is found,[8] if one presumes that the transition state for **IV**→**VI** lies, in reality, slightly higher in energy that that for **IV**→**IV**′; the two transition states differ by less than 1 kcal mol^{-1} in the QM/MM calculation. For near-thermoneutral metathesis reactions with first-generation catalysts, the rate-determining step would then be ligand rotation at the metallacyclobutane structure. For strongly exothermic metathesis reactions, for example, vinyl ethers, lowering of the energy of the transition state for **IV**→**VI**, but not that for **IV**→**IV**′, by strain release would allow rotation to occur at a later stage.

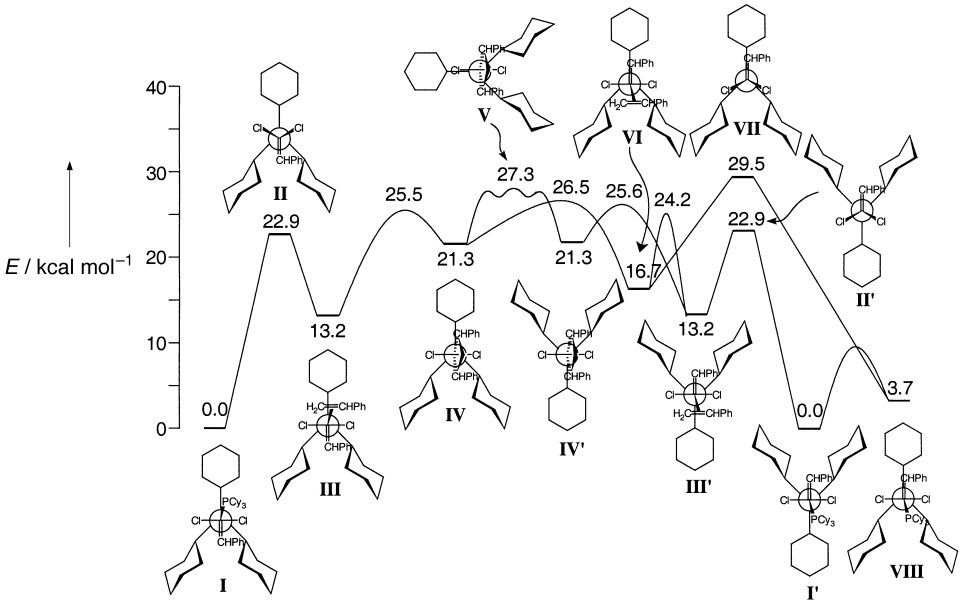


Figure 1. Reaction coordinate for the degenerate metathesis of styrene with **1** as catalyst; the values are QM/MM energies in kcal mol^{-1}. Free ligands needed for mass balance are not shown but were included in the calculation. Complex **1** is depicted in a Newman-like projection viewed along the P–Ru bond to emphasize conformational differences.

 © 2002 WILEY-VCH Verlag GmbH & Co. KGaA, Weinheim 0044-8249/02/4123-4485 $ 20.00+.50/0

Metallacyclobutane formation becomes rate-limiting in the exothermic case.

Nevertheless, the transition state for **III**→**IV** remains higher than that for phosphane dissociation in the first-generation catalysts. In metathesis reactions with second-generation, a higher barrier is found for phosphane dissociation, whereas the barrier for metallacyclobutane formation is comparable to that in the first-generation systems. Phosphane dissociation is always rate-limiting for second-generation catalysts. These conclusions are completely consistent with the experimental findings of Grubbs and co-workers in the metathesis of ethyl vinyl ether,[6] although the nature of the barriers after phosphane dissociation was not identified in that work. Moreover, the gas-phase results from our group[8] are also consistent with the calculated surfaces. In that work, we interpreted substituent and isotope effects as indicating that the metallacyclobutane structure must be the rate-determining transition state. A more appropriate formulation would be to say that the rate-determining transition state in first-generation catalysts has a metallacyclobutane structure, which is not exactly the same statement, but is now fully supported by experiment and theory.

It is clear that electronic effects[6,21] have a significant effect on the precise height of the barrier for phosphane dissociation. The major topological differences between the potential surfaces for first- and second-generation metathesis catalysts can be traced to the different symmetries of the phosphane and the NHC ligands. We propose that high barriers on the potential surface after the phosphane dissociation can be eliminated by choosing ligands with twofold as opposed to threefold symmetry. A concrete test of the proposal will be provided by a next-generation ruthenium metathesis catalyst in which the tricyclohexylphosphane ligands in **1** are replaced by 2,5-diarylphosphabenzene ligands similar to those prepared by Breit et al.[24] for rhodium hydroformylation catalysts. The complex combines the advantages of the first- and second-generation catalysts: the complex should show both a reduced barrier for dissociation of the remaining phosphane *and* a favorable partitioning of the olefin π-complex towards the product. The synthesis and characterization of the new catalyst is underway.

Received: May 16, 2002 [Z19321]

[1] K. J. Ivin, J. C. Mol, *Olefin Metathesis and Metathesis Polymerization*, Academic Press, San Diego, **1997**; T. M. Trnka, R. H. Grubbs, *Acc. Chem. Res.* **2001**, *34*, 18; A. Fürstner, *Angew. Chem.* **2000**, *112*, 3140; *Angew. Chem. Int. Ed.* **2000**, *39*, 3012; R. H. Grubbs, S. Chang, *Tetrahedron* **1998**, *54*, 4413.

[2] S. T. Nguyen, L. K. Johnson, R. H. Grubbs, J. W. Ziller, *J. Am. Chem. Soc.* **1992**, *114*, 3974.

[3] J. P. Morgan, R. H. Grubbs, *Org. Lett.* **2000**, *2*, 3153; M. Scholl, S. Ding, C. W. Lee, R. H. Grubbs, *Org. Lett.* **1999**, *1*, 953; M. Scholl, T. M. Trnka, J. P. Morgan, R. H. Grubbs, *Tetrahedron Lett.* **1999**, *40*, 2247.

[4] J. Huang, E. D. Stevens, S. P. Nolan, J. L. Peterson, *J. Am. Chem. Soc.* **1999**, *121*, 2674.

[5] T. Weskamp, F. J. Kohl, W. Hieringer, D. Gleich, W. A. Herrmann, *Angew. Chem.* **1999**, *111*, 2573; *Angew. Chem. Int. Ed.* **1999**, *38*, 2416.

[6] M. S. Sanford, M. Ulman, R. H. Grubbs, *J. Am. Chem. Soc.* **2001**, *123*, 749; M. S. Sanford, J. A. Love, R. H. Grubbs, *J. Am. Chem. Soc.* **2001**, *123*, 6543.

[7] C. Adlhart, M. A. O. Volland, P. Hofmann, P. Chen, *Helv. Chim. Acta* **2000**, *83*, 3306; C. Adlhart, P. Chen, *Helv. Chim. Acta* **2000**, *83*, 2192; C. Hinderling, C. Adlhart, P. Chen, *Angew. Chem.* **1998**, *110*, 2831; *Angew. Chem. Int. Ed.* **1998**, *37*, 2685.

[8] C. Adlhart, C. Hinderling, H. Baumann, P. Chen, *J. Am. Chem. Soc.* **2000**, *122*, 8204.

[9] J. Vasquez, B. Goldfuss, G. Helmchen, *J. Organomet. Chem.* **2002**, *641*, 67; L. Cavallo, M. Sola, *J. Am. Chem. Soc.* **2001**, *123*, 12294; M. A. Esteruelas, A. Lledos, M. Martin, F. Maseras, R. Oses, N. Ruiz, J. Tomas, *Organometallics* **2001**, *20*, 5297; S. A. Decker, T. R. Cundari, *J. Organomet. Chem.* **2001**, *635*, 132; J. J. Carbo, F. Maseras, C. Bo, P. W. N. M. van Leeuwen, *J. Am. Chem. Soc.* **2001**, *123*, 7630; A. Macchioni, C. Zuccaccia, E. Clot, K. Gruet, R. H. Crabtree, *Organometallics* **2001**, *20*, 2367; S. Feldgus, C. R. Landis, *Organometallics* **2001**, *20*, 2374; E. Jacobsen, L. Cavallo, *Chem. Eur. J.* **2001**, *7*, 800; P. Longo, F. Grisi, G. Guerra, L. Cavallo, *Macromolecules* **2000**, *33*, 4647; T. K. Woo, G. Pioda, U. Röthlisberger, A. Togni, *Organometallics* **2000**, *19*, 2144; B. Goldfuss, M. Steigelmann, F. Rominger, *Eur. J. Org. Chem.* **2000**, 1785; T. K. Woo, P. E. Blochl, T. Ziegler, *J. Phys. Chem. A* **2000**, *104*, 121; B. Goldfuss, M. Steigelmann, S. I. Khan, K. N. Houk, *J. Org. Chem.* **2000**, *65*, 77; D. Gleich, W. A. Herrmann, *Organometallics* **1999**, *18*, 4354; G. Ujaque, F. Maseras, A. Lledos, *J. Am. Chem. Soc.* **1999**, *121*, 1317; A. C. Cooper, E. Clot, J. C. Huffman, W. E. Streib, F. Maseras, O. Eisenstein, K. G. Caulton, *J. Am. Chem. Soc.* **1999**, *121*, 97; L. Cavallo, T. K. Woo, T. Ziegler, *Can. J. Chem.* **1998**, *76*, 1457; D. Gleich, R. Schmid, W. A. Herrmann, *Organometallics* **1998**, *17*, 4828; J. Jaffart, R. Mathieu, M. Etienne, J. E. McGrady, O. Eisenstein, F. Maseras, *Chem. Commun.* **1998**, 2011; L. Q. Deng, T. Ziegler, T. K. Woo, P. Margl, L. Y. Fan, *Organometallics* **1998**, *17*, 3240; L. Q. Deng, T. K. Woo, L. Cavallo, P. M. Margl, T. Ziegler, *J. Am. Chem. Soc.* **1997**, *119*, 6177.

[10] F. Maseras, K. Morokuma, *J. Comput. Chem.* **1995**, *16*, 1170.

[11] G. T. Velde, F. M. Bickelhaupt, E. J. Baerends, C. F. Guerra, S. J. A. van Gisbergen, J. G. Snijders, T. Ziegler, *J. Comput. Chem.* **2001**, *22*, 931.

[12] For each covalent bond that crosses the QM/MM boundary, there is one atom that lies on the MM side of the partition and one atom that lies on the QM side. For each of these link bonds, a dummy hydrogen atom is used to cap the electronic system. The link bond is constrained to lie along the dummy bond vector such that the ratio, $\alpha = |R_{\mathrm{link}}|/|R_{\mathrm{dummy}}|$ (R = bond length) is constant. The ratio α used in the calculations was determined by comparing the bond lengths in the full QM calculation of **1** with the equivalent bond lengths of the dummy bonds in the model and then taken as the average. We find $\alpha = 1.3971 \pm 0.0013$.

[13] J. G. Snijders, E. J. Baerends, P. Vernoijs, *At. Data Nucl. Data Tables* **1981**, *26*, 483; P. Vernoijs, J. G. Snijders, E. J. Baerends, *Slater Type Basis Functions for the Whole Periodic System*, Department of Theoretical Chemistry, Free University of Amsterdam, **1981**; J. Krijn, E. J. Baerends, *Fit Functions in the HFS Method*, Department of Theoretical Chemistry, Free University of Amsterdam, **1984**.

[14] S. Vosko, M. Wilk, M. Nusair, *Can. J. Phys.* **1980**, *58*, 1200.

[15] A. D. Becke, *Phys. Rev. A* **1988**, *38*, 3098; J. P. Perdew, *Phys. Rev. B* **1986**, *33*, 8822.

[16] J. G. Snijders, E. J. Baerends, *Mol. Phys.* **1979**, *36*, 1789; J. G. Snijders, E. J. Baerends, P. Ros, *Mol. Phys.* **1978**, *38*, 1909.

[17] M. Clark, R. Cramer III, N. van Opdenbosch, *J. Comp. Chem.* **1989**, *10*, 982.

[18] Modifications for Ru: $E_{\mathrm{bond}} = 0.5\,K(r-r_0)^2$; $K = 600$; r(Ru-P3) = 2.436; r(Ru-Cl) = 2.400; (Ru-C2) = 1.839; $E_{\mathrm{bend}} = 0.5\,K(\theta-\theta_0)^2$; $K = 200$; θ(Ru-P3-C3) = 119.2; θ(Cl-Ru-P3) = 87.2; θ(C2-Ru-Cl) = 88.7; θ(C2-Ru-P3) = 101.1; θ(Cl-Ru-Cl) = 167.6; $E_{\mathrm{torsion}} = 0.5\,K(1 + \mathrm{per}\cos(\mathrm{per}\,\phi))$; for C2-Ru-P3-C3, Cl-Ru-P3-C3, and P3-Ru-P3-C3, $K = 0.2740$ and per = 3.0; van der Waals parameters for Ru: $E_{\mathrm{min}} = 0.56$; $r_{\mathrm{min}} = 2.963$; $\alpha = 12.0$.

[19] Root-mean-square deviation of bond distances [Å], bond angles [deg], and torsional angles [deg]: crystal QM/MM: 0.028 ± 0.0032, 1.2 ± 0.32, 4.2 ± 2.0; crystal, DFT: 0.017 ± 0.0042, 0.8 ± 0.22, 1.6 ± 0.53; QM/MM, DFT: 0.016 ± 0.0027, 0.8 ± 0.25, 3.9 ± 1.75. Reference for crystal of $[(Cy_3P)_2(Cl)Ru{=}CH(p\text{-}C_6H_4Cl)]$: P. Schwab, M. B. France, J. W. Ziller, R. H. Grubbs, *Angew. Chem.* **1995**, *107*, 2179; *Angew. Chem. Int. Ed. Engl.* **1995**, *34*, 2039.

 © 2002 WILEY-VCH Verlag GmbH & Co. KGaA, Weinheim 0044-8249/02/4123-4486 $ 20.00+.50/0

[20] A full account of the calculations with structures and energies for all of the examined cases, that is, the search of conformational space, is in preparation. Cartesian coordinates and energies for validation for all structures reported herein are given in the Supporting Information.
[21] O. M. Aagaard, R. J. Meier, F. Buda, *J. Am. Chem. Soc.* **1998**, *120*, 7174; R. J. Meier, O. M. Aagaard, F. Buda, *J. Mol. Catal. A* **2000**, *160*, 189; S. F. Vyboishchikov, M. Bühl, W. Thiel, *Chem. Eur. J.* **2002**, *8*, 3962..
[22] C. A. Tolman, *Chem. Rev.* **1977**, *77*, 313.
[23] J. W. Faller, B. V. Johnson, *J. Organomet. Chem.* **1975**, *96*, 99; W. D. Jones, F. J. Feher, *Inorg. Chem.* **1984**, *23*, 2376; J. Polowin, M. C. Baird, *J. Organomet. Chem.* **1994**, *478*, 45; F. P. Fanizzi, M. Lanfranchi, G. Natile, A. Tiripicchio, *Inorg. Chem.* **1994**, *33*, 3331; J. Albert, R. Bosque, J. M. Cadena, S. Delgado, J. Granell, *J. Organomet. Chem.* **2001**, *634*, 83.
[24] B. Breit, R. Winde, T. Mackewitz, R. Paciello, K. Harms, *Chem. Eur. J.* **2001**, *7*, 3106; B. Breit, *J. Mol. Catal. A* **1999**, *143*, 143; B. Breit, R. Winde, K. Harms, *J. Chem. Soc. Perkin Trans. 1* **1997**, 2681.

Solvothermal Synthesis, Crystal Structure, Thermal Stability, and Mössbauer Spectroscopic Investigation of the Mixed-Valent Thioantimonate(III,V) $[Ni(dien)_2]_2Sb_4S_9$**

Ralph Stähler, Bernd-Dieter Mosel, Hellmut Eckert, and Wolfgang Bensch*

During the last decade it was impressively demonstrated by several groups that the solvothermal technique is not only a promising route for the preparation of new and exciting open framework oxidic compounds but also for the syntheses of fascinating thio- and selenometalates.[1–7] Since the pioneering work of Schäfer and co-workers,[8] about 50 new thioantimonates have been prepared and characterized. In most compounds antimony occurs as Sb^{III} and, because of the variable coordination behavior caused by the stereochemically active lone pair),[9] the dimensionalities of the anionic Sb_xS_y frameworks range over 1D chains, 2D layers, and 3D interconnection of the SbS_x primary building units. Thioantimonates(v) always contain tetrahedral $[Sb^VS_4]^{3-}$ ions that are not further interconnected or condensed. To date the coexistence of Sb^{III} and Sb^V within a polymeric thioantimonate anion was never observed.

Normally solvothermal syntheses are performed using organic molecules as structure-directors. Recently, we demonstrated that transition-metal complexes can also be used as "template" molecules[11–13,15–18]. During our systematic experiments with the in situ formed $[Ni(dien)_2]^{2+}$ ion (dien = diethylenetriamine) as the structure-directing molecule, we synthesized and fully characterized the first mixed-valent thioantimonate anion $^1_\infty[Sb_4S_9]^{4-}$ which contains Sb^{III} and Sb^V. The title compound was obtained under solvothermal conditions as yellow polyhedra that are stable to air, in water, and in acetone. The results of a large number of syntheses performed at different temperatures and for different reaction times suggest that the $[Ni(dien)_2]_2Sb_4S_9$ is formed at higher temperatures and in short reaction times. The compound crystallizes in the monoclinic space group $P2_1/c$.[10]

The $^1_\infty[Sb_4S_9]^{4-}$ ion is composed of three $Sb^{III}S_3$ pyramids (Sb2, Sb3, and Sb4), which share common corners leading to the formation of an Sb_3S_7 moiety (Figure 1). The Sb1 atom is in a tetrahedral coordination environment of four S atoms to form a Sb^VS_4 tetrahedron. The interconnection of the Sb_3S_7 unit and the Sb^VS_4 tetrahedron through the S4 atom yields the $[Sb_4S_9]^{4-}$ ionic chain. The bond lengths in the $Sb^{III}S_3$ units are between 2.331(1) and 2.637(1) Å, with S-Sb^{III}-S angles ranging from 88.33(3) to 102.21(4)°. The longest Sb–S bond is between Sb2 and S4 joining the Sb_3S_7 and SbS_4 units.

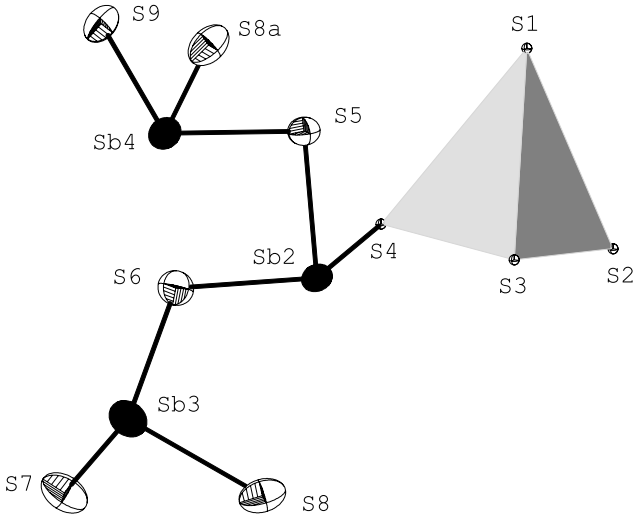


Figure 1. The $^1_\infty[Sb_4S_9]^{2-}$ ion with labelling. The Sb^VS_4 unit is shown as a tetrahedron. The displacement ellipsoids are drawn at the 50 % probability level. Selected bonds angles [°]: S1-Sb1-S2 113.64(4), S1-Sb1-S3 110.33(4), S1-Sb1-S4 110.36(4), S2-Sb1-S3 109.86(4), S2-Sb1-S4 106.02(4), S3-Sb1-S4 106.30(4). Symmetry code for S8a: $-x$, $-0.5+y$, $0.5-z$.

The Sb^{III}–S interatomic distances, as well as the angles, are in the range reported in the literature.[2,5,7,11–15] The Sb^V1–S interatomic distances are significantly shorter than Sb^{III}–S bonds and vary between 2.294(1) and 2.390(1) Å, with S-Sb1-S angles ranging from 106.02(4) to 113.64(4)°, which indicate only a slight deviation from the ideal tetrahedral geometry. Sb^V1–S interatomic distances and S-Sb^V-S angles are in the range found in the literature.[12,16,17] The anionic chains have a sinusoidal shape and run along [010] (Figure 2). The Sb^VS_4 tetrahedra are located at the exterior of the central Sb_3S_7 backbone of the anion. The compound decomposes in two steps starting at about $T_{onset} = 257$ °C, as evidenced by differential thermal analysis–thermogravimetric analysis–

[*] Prof. Dr. W. Bensch, Dipl.-Chem. R. Stähler
Institut für Anorganische Chemie
Universität Kiel
Olshausenstrasse 40, 24098 Kiel (Germany)
Fax: (+49) 431–880–1520
E-mail: wbensch@ac.uni-kiel.de
Dr. B.-D. Mosel, Prof. Dr. H. Eckert
Institut für Physikalische Chemie
Westfälische Wilhelms-Universität Münster
Schlossplatz 7, 48149 Münster (Germany)

[**] This work was supported by the States of Schleswig-Holstein and Nordrhein-Westfalen, and the Fonds der Chemischen Industrie. dien = diethylenetriamine.

 © 2002 WILEY-VCH Verlag GmbH & Co. KGaA, Weinheim 0044-8249/02/4123-4487 $ 20.00+.50/0

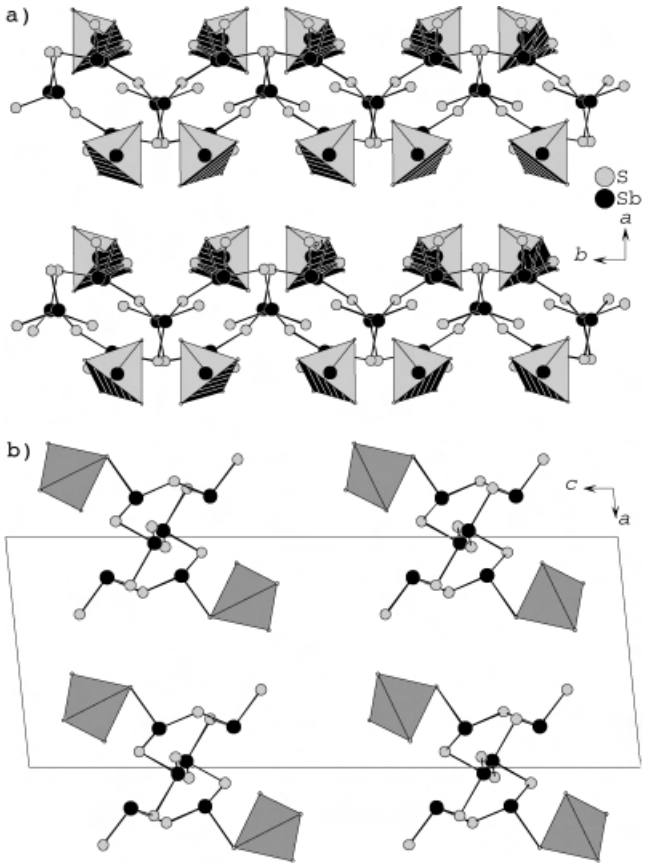


Figure 2. Arrangement of the anion in $[Ni(dien)_2]_2Sb_4S_9$ with a view along [001] (a) and [010] (b).

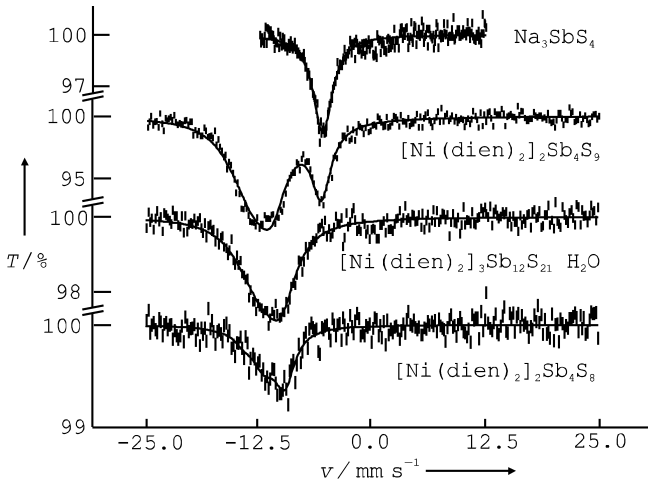


Figure 3. ^{121}Sb Mössbauer spectra of thioantimonates. From top to bottom: $Na_3Sb^VS_4$ (4.2 K), $[Ni(dien)_2]_2Sb_4S_9$ (4.2 K), $[Ni(dien)_2]_3Sb_{12}S_{21}{\cdot}H_2O$[18] (78 K), and $[Ni(dien)_2]_2Sb_4S_8$[11] (78 K).

Table 1. ^{121}Sb Mössbauer isomer shifts (IS), quadrupolar splittings (QS), and linewidths (Γ) of the thioantimonate compounds of the present study. All values are given in mm s^{-1}.

Compound	IS ($\pm$0.2)	QS ($\pm$0.4)	Γ ($\pm$0.2)	Oxidation state
Na_3SbS_4	−5.5	0.0	2.6	Sb^V
$[Ni(dien)_2]_2Sb_4S_9$	−5.7	0.0	2.6	Sb^V
	−12.5	−14.3	3.8	Sb^{III}
$[Ni(dien)_2]_2Sb_4S_8$	−11.0	−15.9	2.7	Sb^{III}
$[Ni(dien)_2]_3Sb_{12}S_{21}{\cdot}H_2O$	−11.4	−14.8	4.0	Sb^{III}

mass spectrometry (DTA–TG–MS) experiments. The degradation is accompanied by two weight losses ($-\Delta m_{exp1} = 30.5\,\%$ and $-\Delta m_{exp2} = 3.5\,\%$) and by one strong endothermic peak in the curve at $T_p = 270.8\,°C$ with a shoulder at $T_p = 277\,°C$, and one small broad endothermic signal at $T_p = 328\,°C$. The experimental mass change corresponds roughly with the loss of the dien ligands in the first step ($-\Delta m_{theo_4(dien)} = 31.6\,\%$) and the emission of H_2S in the second step ($-\Delta m_{theo(H_2S)} = 2.6\,\%$, $m/z_{H_2S} = 34$). The shoulder in the spectrum at $T_p = 277\,°C$ was often observed during the thermal decomposition of compounds containing $[M(dien)_2]^{2+}$ (M = Fe, Ni) complexes.[11,12,15] In the gray decomposition product Sb_2S_3, NiS, and NiSbS were identified by X-ray powder diffraction.

The mixed-valence character of $[Ni(dien)_2]_2Sb_4S_9$ is unambiguously demonstrated by the ^{121}Sb Mössbauer spectrum shown in Figure 3, which also includes the spectra of some suitable reference compounds. The lineshape parameters obtained by least-squares fitting are listed in Table 1. Clearly, the spectrum of $[Ni(dien)_2]_2Sb_4S_9$ is a superposition of two lineshape contributions. The contribution centered near −12.5 mm s^{-1} reflects all the typical lineshape parameters of Sb^{III} compounds.[19] The lineshape is asymmetrically broadened by the effect of strong nuclear electric quadrupolar interactions. These interactions reflect a large electric field gradient, created at the ^{121}Sb site by the local ligand distribution and the partially hybridized electron pair. The contribution near −5.7 mm s^{-1} is attributable to the Sb^V site. For this species, no quadrupolar interactions are detectable, which suggests a highly symmetric local environment, as is typically observed for pentavalent antimony in solids. The area ratio determined from the transmission integral fit is 76.8:23.2, which is in close agreement with the value (3:1) expected from the crystallographically determined structure. This result also confirms that at 4.2 K the Lamb–Mössbauer factors for both antimony species are very similar.

Experimental Section

Yellow polyhedra of $[Ni(dien)_2]_2Sb_4S_9$ were obtained by treating a mixture of elemental Ni (0.058 g, 1 mmol), Sb (0.121 g, 1 mmol), and S (0.096 g, 3 mmol) in a 50% water solution of dien (2 mL) under solvothermal conditions. The slurry was heated in an autoclave to 140 °C, held at this temperature for ten days and cooled to room temperature within 3 h. The products were filtered off, washed with water and acetone, and dried under vacuum. The yield was 10% based on Ni. The main product (55%) was identified as $[Ni(dien)_2]_3(SbS_4)_2$,[12] and is stable to air, in water, and in acetone. Stirring the reaction mixture during the synthesis, increasing the temperature to 180–200 °C, and reducing the reaction time to about 1.5 h resulted in a phase-pure product (45% based on Ni). Elemental analysis (%) calcd: C 14.72, H 4.01, N 12.87, S 22.10; found: C 13.43, H 3.61, N 10.97, S 21.39.

DTA-TG-MS measurements were performed on a STA-409CD device from Netzsch. All measurements were corrected for buoyancy and current effects, and were made with a heating rate of 4 K min^{-1} in Al_2O_3 crucibles under a dynamic helium atmosphere (flow rate: 75 mL min^{-1}, purity: 5.0). 37.2 keV Mössbauer spectra were obtained in transmission geometry using a $Ba^{121m}SnO_3$ source (activity 18 MBq) from New England Nuclear. The samples were investigated within polyacrylate containers of 3 cm^2 area; typically 100–200 mg of sample was used. Sample thicknesses were adjusted to 10 mg Sb cm^{-2}. To maximize the Lamb–Mössbauer factors the samples

 © 2002 WILEY-VCH Verlag GmbH & Co. KGaA, Weinheim 0044-8249/02/4123-4488 $ 20.00+.50/0

were measured at low temperatures (4.2 K or 78 K). The source was kept at room temperature. Spectra were recorded over a velocity range of $\pm$ 25 mm s^{-1} using an NaI(Tl) scintillation counter. Fitting of the spectra was carried out on the basis of the theoretically expected lineshape arising from the allowed transitions between the quadrupolar-split energy levels of the ground state ($I = 5/2$) and the excited state ($I = 7/2$).

Received: June 27, 2002 [Z19623]

[1] W. S. Sheldrick, M. Wachhold, *Coord. Chem. Rev.* **1998**, *176*, 211 – 322.
[2] A. V. Powell, R. Paniagua, P. Vaqueiro, A. M. Chippindale, *Chem. Mater.* **2002**, *14*, 1220 – 1224.
[3] W. S. Sheldrick, M. Wachhold, *Angew. Chem.* **1997**, *109*, 214 – 234; *Angew. Chem. Int. Ed.* **1997**, *36*, 206 – 224.
[4] X. Wang, F. Liebau, *Acta Crystallogr. Sect. B.* **1996**, *52*, 7 – 15.
[5] W. S. Sheldrick, H.-J. Häusler, *Z. Anorg. Allg. Chem.* **1988**, *557*, 105 – 111.
[6] X. Wang, F. Liebau, *Z. Kristallogr.* **1996**, *211*, 437 – 439.
[7] A. V. Powell, S. Boissiere, A. M. Chippindale, *J. Chem. Soc. Dalton Trans.* **2000**, *22*, 4192 – 4195.
[8] a) G. Dittmar, H. Schäfer, *Z. Anorg. Allg. Chem.* **1977**, *437*, 183 – 187; b) G. Dittmar, H. Schäfer, *Z. Anorg. Allg. Chem.* **1975**, *414*, 211 – 219; c) G. Dittmar, H. Schäfer, *Z. Anorg. Allg. Chem.* **1978**, *441*, 93 – 97; d) G. Dittmar, H. Schäfer, *Z. Anorg. Allg. Chem.* **1978**, *441*, 98 – 102; e) B. Eisenmann, H. Schäfer, *Z. Naturforsch. B* **1979**, *34*, 383 – 385; f) G. Cordier, H. Schäfer, C. Schwidetzky, *Z. Naturforsch. B* **1984**, *39*, 131 – 134; g) K. Volk, P. Bickert, R. Kolmer, H. Schäfer, *Z. Naturforsch. B* **1979**, *34*, 380 – 382; h) G. Cordier, H. Schäfer, *Rev. Chim. Miner.* **1981**, *18*, 218 – 223; i) G. Cordier, H. Schäfer, C. Schwidetzky, *Rev. Chim. Miner.* **1985**, *22*, 722 – 727; j) H. A. Graf, H. Schäfer, *Z. Naturforsch. B* **1972**, *27*, 735 – 739.
[9] X. Wang, F. Liebau, *Acta Crystallogr. Sect. B.* **1996**, *52*, 7 – 15.
[10] a) The compound crystallizes in the monoclinic space group $P2_1/c$, $a =$ 11.743(2), $b = 11.358(2)$, $c = 30.878(6)$ Å, $\beta = 95.78(3)°$, $V =$ 4097.5(14) Å^3, $Z = 4$, $\rho = 2.117$ mg m^{-1}, $\mu(Mo_{K\alpha}) = 3.99$ mm^{-1}, $F(000) = 2544$. STOE AED-II diffractometer, monochromated $Mo_{K\alpha}$ radiation ($\lambda = 0.71073$ Å). Lorentz, polarization, and absorption corrections; 17068 reflections; range $1.74 \le \theta \le 27.53$; 9436 unique data; 8164 with $I \ge 2\sigma(I)$. Structure solution was performed with SHELXS-97 using direct methods.[10b] Refinement was done against F^2 using SHELXL-97.[10c] All heavy atoms were refined anisotropically. Several C atoms are disordered with occupancies given in parentheses: C6(50%), C6′(50%), C9(60%), C9′(40%), C11(50%), C11′(50%), C13(70%), C13′(30%). The hydrogen atoms were positioned with idealized geometry and refined with fixed isotropic displacement parameters using a riding model. Final reliability values: $R1 = 0.0344$ for all reflections, $wR2 = 0.0682$ for all reflections, goodness-of-fit = 1.058. CCDC-188070 contains the supplementary crystallographic data for this paper. These data can be obtained free of charge via www.ccdc.cam.ac.uk/conts/retrieving.html (or from the Cambridge Crystallographic Data Centre, 12 Union Road, Cambridge CB2 1EZ, UK; fax: (+44) 1223-336-033; or deposit@ccdc.cam.ac.uk); b) G. M. Sheldrick, SHELXS-97, Program for the Solution of Crystal Structures, Universität of Göttingen, Göttingen (Germany), **1997**; c) G. M. Sheldrick, SHELXL-97, Program for the Refinement of Crystal Structures, University of Göttingen, Göttingen (Germany), **1997**.
[11] W. Bensch, C. Näther, R. Stähler, *Chem. Commun.* **2001**, *5*, 477 – 478.
[12] R. Stähler, C. Näther, W. Bensch, *Acta Crystallogr. Sect. C* **2001**, *57*, 26 – 27.
[13] R. Stähler, W. Bensch, *Z. Anorg. Allg. Chem.* **2002**, *628*, 1657 – 1662.
[14] J. Ellermeier, W. Bensch, *Monatsh. Chem.* **2001**, *132*, 565 – 573.
[15] R. Stähler, C. Näther, W. Bensch, *Eur. J. Inorg. Chem.* **2001**, 1835 – 1840.
[16] M. Schur, W. Bensch, *Acta Crystallogr. Sect. C* **2000**, *56*, 1107 – 1108.
[17] M. Schur, H. Rijnberk, C. Näther, W. Bensch, *Polyhedron* **1998**, *18*, 101 – 107.
[18] R. Stähler, C. Näther, W. Bensch, unpublished work.
[19] J. G. Stevens in *"Chemical Mössbauer Spectroscopy"*, (Ed.: R. H. Herber) Plenum Press, New York, **1984**, p. 319.

Efficient Solid-Phase Synthesis of a Complex, Branched *N*-Glycan Hexasaccharide: Use of a Novel Linker and Temporary-Protecting-Group Pattern**

Xiangyang Wu, Matthias Grathwohl, and Richard R. Schmidt*

Oligosaccharides are known to be important molecules in various biological processes; therefore, they have gained increasing interest in recent years.[1] However, in contrast to oligopeptides[2] and oligonucleotides[3] which are routinely constructed on automated synthesizers employing standardized building blocks and polymer supports, no generally applied synthetic methodology has yet appeared for the solid-phase synthesis of complex oligosaccharides.[4] Success in this challenging task would provide several advantages over solution-phase techniques: 1) the required standardized building blocks could become commercially available, 2) an excess of building blocks and/or reagents could be used to drive reactions to completion, 3) the synthesis could become much faster, and 4) purification procedures could become simpler.

Another fundamental key issue for solid-phase oligosaccharide synthesis is the availability of a high-yielding and stereoselective glycosylation strategy. Of the various glycosyl donors employed for this purpose,[5–11] *O*-glycosyl trichloroacetimidates[12] are suitable because of their high glycosyl-donor properties in the presence of just catalytic amounts of a (Lewis) acid. In combination with solvent and temperature effects, type of catalyst, protecting-group pattern, and anchimeric assistance these donors also permit the desired control of the stereoselectivity at the anomeric center.[13]

An additional requirement for solid-phase oligosaccharide synthesis is access to branching which is found in many oligosaccharides and glycoconjugates but not in peptides and oligonucleotides. Thus, for chain extension and branching, besides permanently protected functional groups, to be liberated only after completion of the solid-phase oligosaccharide synthesis, a suitable temporary-protecting-group pattern is required. This temporary-protecting-group pattern provides the orthogonality required for branching and should also accommodate the demands of the linker which necessitates an additional temporary functional group.

Based on our recent studies on new temporary protecting groups,[12,14] new linker types,[14] and the synthesis of branched oligosaccharides,[12e,15] we report herein a novel strategy which

[*] R. R. Schmidt, Dipl.-chem. X. Wu, Dr. M. Grathwohl
Department of Chemistry
University of Konstanz
78457 Konstanz (Germany)
Fax: (+49) 7531-88-3135
E-mail: richard.schmidt@uni-konstanz.de

[**] This work was supported by the Deutsche Forschungsgemeinschaft, the Fonds der Chemischen Industrie, and the European Community (Grant No. HRPN-CT-2000-00001/GLYCOTRAIN).

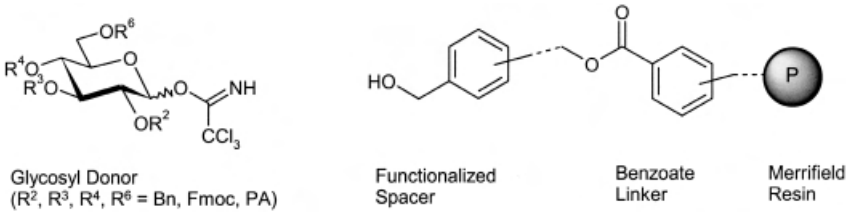
 © 2002 WILEY-VCH Verlag GmbH & Co. KGaA, Weinheim 0044-8249/02/4123-4489 $ 20.00+.50/0

should fulfil the demands of a generally applicable methodology. As shown in Scheme 1, the system comprises:

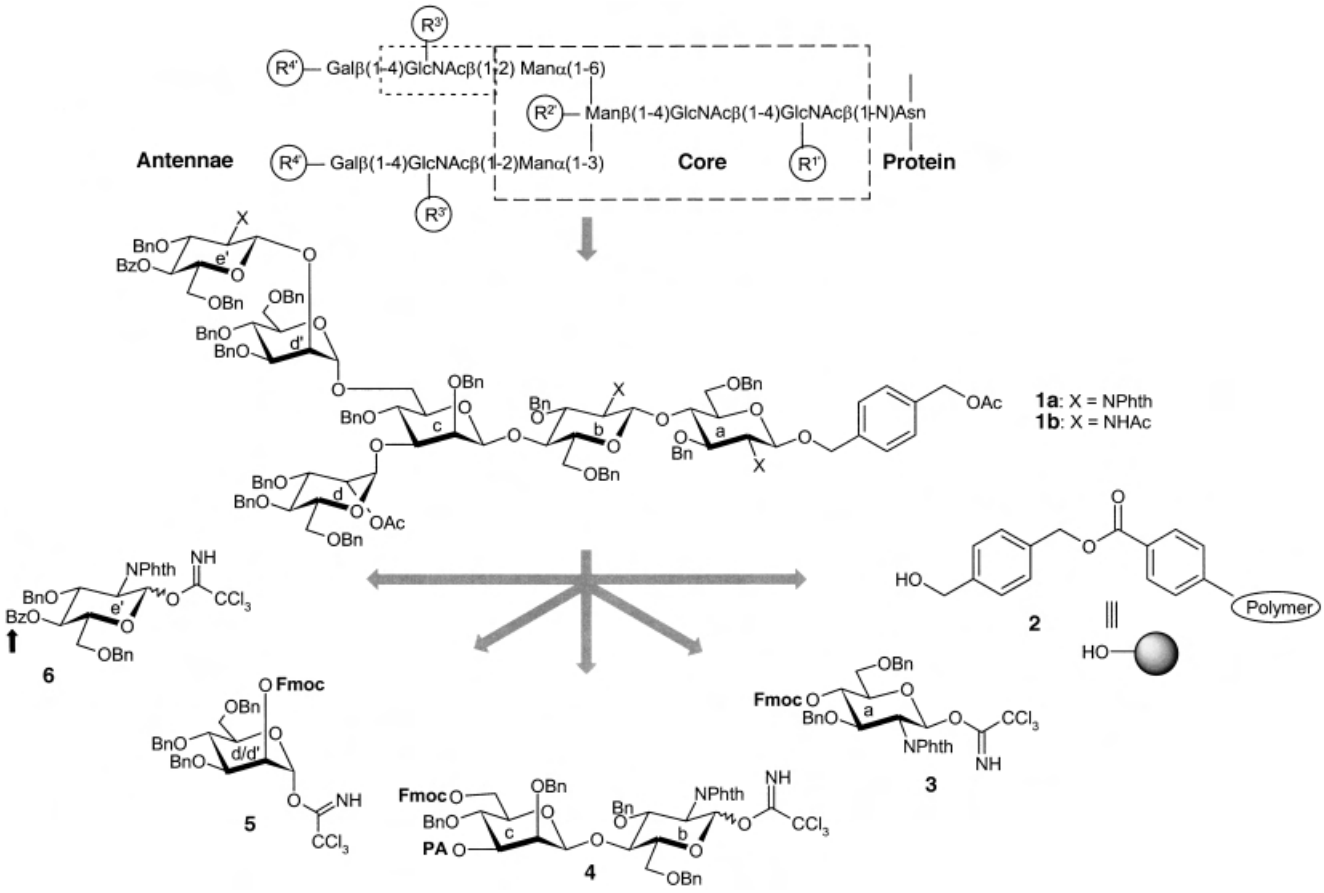
1) a Merrifield-type resin
2) a enzoate ester as the linker because this offers the desired stability towards acid and base and it permits the cleavage of more reactive esters under very mild alcoholysis conditions
3) a benzyl spacer linked to the anomeric center of the sugar residue at the reducing end, thus leading, after final cleavage, to a structurally defined target molecule which can be deprotected under standard hydrogenolysis conditions
4) *O*-glycosyl trichloroacetimidates as glycosyl donors, with the advantages discussed above
5) essentially benzyl for permanent protection of hydroxy groups and phthaloyl, dimethylmaleoyl, or azido for the masking of amino groups
6) 9-fluorenylmethyloxycarbonyl (Fmoc) and/or phenoxyacetyl (PA) groups for temporary protection because these groups permit selective cleavage (with NEt_3 for Fmoc, release of 9-methylenefluorene; with NaOMe (0.5 equiv) or $MeNH_2$ in CH_2Cl_2/MeOH for PA, release of phenoxyacetate) in the presence of the benzoate linker and UV monitoring of the cleavage product
7) NaOMe (four equivalents) in CH_2Cl_2/MeOH for final cleavage of the target molecule from the resin. This simple ester based methodology is very efficient as will be shown below.

One of the most difficult tasks constitutes the synthesis of complex type N-glycans[16] which consist of a branched core pentasaccharide having different antennae-like sugar side chains (Scheme 2, R^1–R^4 = H or sugar residues).

Therefore, the efficiency of our strategy was investigated with the synthesis of hexasaccharide **1a** comprising the core pentasaccharide and one GlcNAc residue. Retrosynthetic analysis considering the strategy discussed above leads to the spacer-linker-polymer support **2** containing the previously employed benzene-1,4-dimethanol unit[17] as the spacer and to glycosyl donors **3**–**6**. Hence, for the selective attachment of different antennae at the 2-*O* position of Man residues d and d′, orthogonal protection of Man residue c is required,



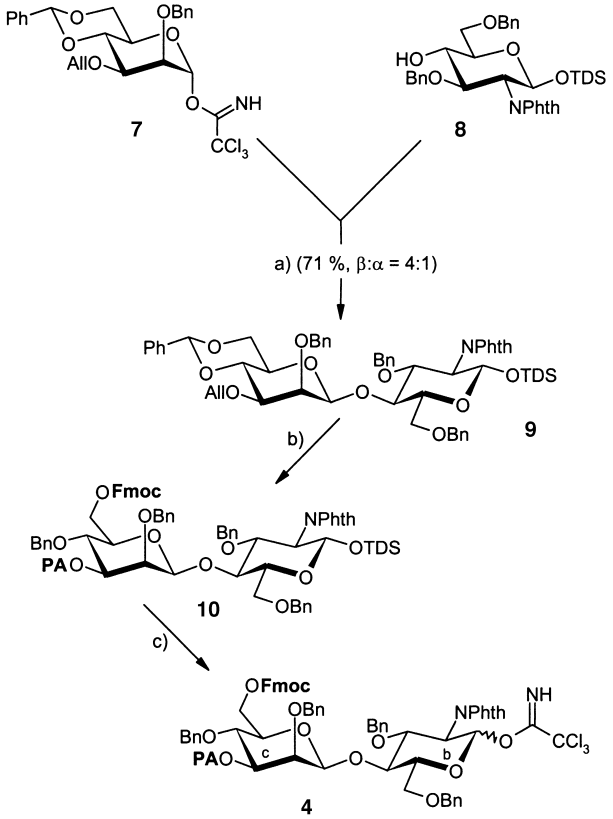
Scheme 1. Solid-phase synthesis based on different esters (Fmoc and PA) for both temporary protection and linkage to the solid support, benzyl groups for permanent protection and as spacer to the anomeric center (see text for full details).



Scheme 2. General structure of complex type N-glycans and retrosynthetic analysis of core hexasaccharide **1** for the synthesis on solid phase; Phth = phthaloyl

 © 2002 WILEY-VCH Verlag GmbH & Co. KGaA, Weinheim 0044-8249/02/4123-4490 $ 20.00+.50/0 *Angew. Chem. Int. Ed.* **2002**, *41*, No. 23

as exhibited by building block **4**. Because of the lack of a highly β-selective mannosyl donor,[18,19] the required Manβ(1-4)GlcN disaccharide donor **4** had to be prepared independently (Scheme 3).



Scheme 3. Synthesis of the required Manβ(1-4)GlcN building block **4** having orthogonal temporary protecting groups. a) TMSOTf, CH_2Cl_2, −50 °C; b) 1. *trans*-[$Pd(NH_3)_2Cl_2$], *t*BuOH (68 %); 2. PACl, py (88 %); 3. BH_3·THF, Bu_2BOTf (79 %); 4. FmocCl, py (68 %); c) 1. HF·py, THF (65 %); 2. CCl_3-CN, NaH (78 %); py = pyridine, TDS = thexyldimethylsily; All = allyl.

The synthesis is based on a recently reported direct β-selective mannosylation procedure with **7**[18] as donor and **8**[20] as acceptor furnishing the desired β-disaccharide **9** in good yield (β:α = 4:1, 71 %). For the introduction of the temporary protecting groups first the allyl protecting group was removed under Pd catalysis with *tert*-butanol as the nucleophile[21] and phenoxyacetylation was performed; then, reductive opening of the 4c,6c-*O*-benzylidene group with borane in the presence of dibutylborane triflate[22] afforded the desired 6c-O-unprotected intermediate which on treatment with Fmoc-Cl in pyridine gave disaccharide **10** with the two orthogonal temporary protecting groups. Removal of the *O*-silyl group with HF·pyridine and then reaction with trichloroacetonitrile in the presence of sodium hydride as base furnished the desired glycosyl donor **4** without affecting the temporary protecting groups; even the base-sensitive Fmoc group was retained. Building blocks **3**, **5**, and **6** are readily available following previously reported procedures.[12a,23]

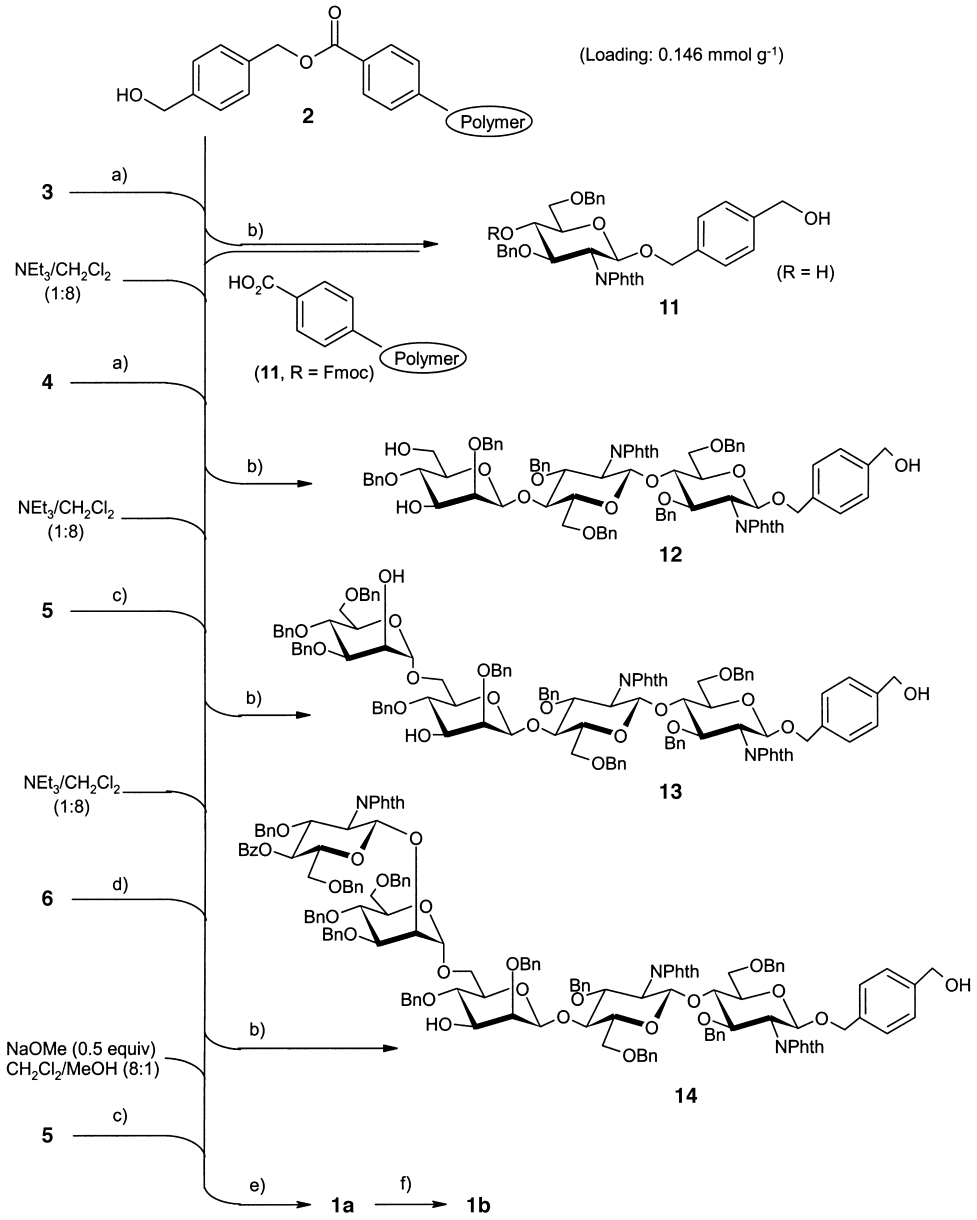
For the solid-phase oligosaccharide synthesis commercially available Merrifield resin containing benzoic acid groups was selected. As spacer and linker to the benzoyl group 1,4-bis(hydroxymethyl)benzene[17] was chosen; after monotritylation, reaction with the acid chloride of the solid support in pyridine in the presence of 4-dimethylaminopyridine (DMAP), then capping of excess acid chloride with methanol in pyridine, and finally detritylation with trifluoroacetic acid in CH_2Cl_2 afforded polymer **2** (Scheme 4). The loading could be easily determined by the amount of trityl cation released; 0.146 mmol g^{-1} of dry resin led to good results; higher loadings diminished the overall yields of the oligosaccharide synthesis.

Reaction of polymer **2** as acceptor with glycosyl donor **3** in CH_2Cl_2 at −40 °C in the presence of trimethylsilyl trifluoromethanesulfonate (TMSOTf) as catalyst (0.2 equivalents) afforded cleanly the desired glycosylated polymer. This reaction was monitored by analytical cleavage with NaOMe (4 equivalents) in CH_2Cl_2:MeOH (8:1) furnishing 4-hydroxymethylbenzyl glycoside **11** (R = H; see Experimental Section). Alternatively, reaction of **11** (R = Fmoc)[23] with the Merrifield resin in the presence of diisopropyl carbodiimide and DMAP in CH_2Cl_2 afforded the same polymer.

Chain extension on the solid-phase followed a convenient, standardized procedure. Treatment of the polymer, to which the Fmoc containing glucosamine residue was linked, with NEt_3 in CH_2Cl_2 (1:8) to remove the Fmoc group, then, after washing with CH_2Cl_2:THF (1:1), glycosylation with donor **4** in CH_2Cl_2 at −20 °C in the presence of TMSOTf (0.35 equivalents) as catalyst led to the desired trisaccharide as shown by monitoring the reaction by the cleavage of glycoside **12** from small resin samples (see Experimental Section). After washing with CH_2Cl_2/THF and repetition of the same procedure with donors **5** and **6**, tetrasaccharide **13** and pentasaccharide **14** were obtained. Because the antenna was to be terminated with building block **6**, a benzoyl group was selected as protecting group for the 4-hydroxy group. Thus, the selective removal of the PA protecting group at 3c-O with NaOMe (0.5 equivalents) in CH_2Cl_2:MeOH (8:1) could be performed without release of other groups. Then washing with CH_2Cl_2/MeOH and CH_2Cl_2/THF and glycosylation with donor **5** furnished the desired hexasaccharide on the polymer which was ready for further chain extension. Preparative cleavage under the conditions of analytical cleavage and then O-acetylation with acetic anhydride furnished after chromatography pure target molecule **1a** as ascertained by the NMR spectroscopy data (see Experimental Section). The total yield was 19 % over eleven steps which is an average yield of 86 % per step. Cleavage of the *N*-phthaloyl groups under standard conditions[24] and then N,O-acetylation afforded **1b**; the physical data of **1b**[23] are also in accordance with the assigned structure.

In conclusion, a highly efficient solid-phase synthesis of a branched N-glycan oligosaccharide containing the core structure could be performed, which in terms of time and yield is superior to a solution-phase approach. The novel linker and temporary-protecting-group pattern containing different types of ester linkages offers the advantage of releasing (after cleavage) from the polymer support a benzyl aglycon moiety, which can be removed by hydrogenolysis. The simplicity and efficiency of the chain-extension procedure and of the final removal of the target molecule from the solid support should

 © 2002 WILEY-VCH Verlag GmbH & Co. KGaA, Weinheim 0044-8249/02/4123-4491 $ 20.00+.50/0



Scheme 4. Synthesis of target molecule **1** on a functionalized solid support **2** with **3**–**6** as glycosyl donors. a) TMSOTf, CH_2Cl_2; b) NaOMe (4 equiv), CH_2Cl_2:MeOH (8:1); c) TMSOTf, CH_2Cl_2:Et_2O (4:1), −20 °C; d) TMSOTf, CH_2Cl_2:MeCN (4:1), −40 °C; e) 1. NaOMe, MeOH (4 equiv); 2. Ac_2O; py; f) 1. $H_2NCH_2CH_2NH_2$, BuOH; 2. Ac_2O, py.

provide also a basis for the development of a generally applicable automated synthesis of oligosaccharides having different glycosidic linkages.

Experimental Section

General procedure for glycosylation: Dry acceptor-loaded resin was directly swollen in a CH_2Cl_2 solution (15 mL g^{-1} resin) containing donor (3 equiv). The resulting suspension was cooled under argon to −20 °C and shaken for 10 min. A solution of a freshly prepared 0.5 M TMSOTf solution in CH_2Cl_2 (0.3 equiv) was added, and shaking was continued for 1 h. The resin was collected by filtration, washed alternately with THF (3 × 15 mL g^{-1} resin) and CH_2Cl_2 (3 × 15 mL g^{-1}) and dried under high vacuum.

General deprotection procedure: Fmoc-cleavage was performed on solid phase according to the procedure previously described.[12b] For PA deprotection dry resin was swollen in CH_2Cl_2 (10 mL g^{-1} resin) and the resulting suspension was shaken under argon for 10 min. A solution of MeONa in MeOH (0.5 equiv; 10 % of the total volume) was added and the resulting mixture was shaken for 10 min, then the resin was collected by filtration and the procedure repeated until the UV spot of the washing solution completely disappeared. Finally, the resin was washed alternately with THF (3 × 15 mL g^{-1} resin) and CH_2Cl_2 (3 × 15 mL g^{-1} resin) and dried under high vacuum.

Cleavage of the products was performed according to the procedure previously described.[12b]

MALDI MS: **11** *m/z* 632.2 [*M*+Na$^+$]; $C_{36}H_{35}NO_8$ (609.67); **12** *m/z* 1446.8 [*M*+Na$^+$]; $C_{84}H_{82}N_2O_{19}$ (1423.55); **13** *m/z* 1880.6 [*M*+Na$^+$]; $C_{111}H_{110}N_2O_{24}$ (1856.06); **14** *m/z* 2454.7 [*M*+Na$^+$]; $C_{146}H_{139}N_3O_{31}$ (2431.67).

1a: MALDI MS: *m/z* 2970.6 [*M*+Na$^+$]; $C_{177}H_{171}N_3O_{38}$ (2948.25); ^{1}H NMR (600 MHz, $CDCl_3$): sugar residue a: $\delta = 4.91$ (d, $^3J_{1,2} = 8.5$ Hz, 1 H, 1-H), 4.15 (2-H) 4.07 (3-H), 4.17 (4-H), 3.24 (5-H), 3.37 (6-H), 3.37 ppm (6-H); sugar residue b: $\delta = 5.20$ (d, $^3J_{1,2} = 8.2$ Hz, 1 H, 1-H), 4.15 (2-H), 4.19 (3-H), 4.00 (4-H), 3.18 (5-H), 3.37 ppm (2 6-H); sugar residue c: $\delta = 4.61$ Hz (dd, $^3J_{1,2} < 1.0$ Hz, 1 H, 1-H), 3.86 (2-H), 3.6 (3-H), 3.84 (4-H), 3.1 (5-H), 3.68, 3.60 ppm (2 6-H); sugar residue d: $\delta = 5.12$ (dd, $^3J_{1,2} <$ 1.0 Hz, 1 H, 1-H) 5.48 (2-H), 3.96 (3-H), 3.82 (4-H), 3.92 (5-H), 3.69 ppm (2 6-H); sugar residue d′: $\delta = 4.49$ (dd, $^3J_{1,2} < 1.0$ Hz, 1 H, 1-H), 4.01 (2-H), 3.69 (3-H), 3.42 (4-H), 3.31 (5-H), 3.17, 2.81 ppm (2 6-H); sugar residue e′: $\delta =$ 4.98 (1-H), 4.34 (2-H), 4.28 (3-H), 5.35 (t, $^3J = 9.4$ Hz, 1 H, 4-H), 3.04 (5-H), 3.42 ppm (2 6-H); ^{13}C NMR (150.9 MHz, $CDCl_3$): sugar residue a: $\delta = 97.1$ (C-1), 56.7 (C-2), 76.3 (C-3), 75.5 (C-4), 74.5 ppm (C-5); sugar residue b: $\delta = 96.7$ (C-1), 55.6 (C-2), 76.8 (C-3), 90.3 (C-4), 74.8 ppm (C-5); sugar residue c: $\delta = 102.4$ (C-1), 77.9 (C-2), 80.9 (C-3), 74.1 (C-4, C-5), 68.9 ppm (C-6); sugar residue d: $\delta =$ 99.5 (C-1), 68.5 (C-2), 78.1 (C-3), 72.4 (C-4), 67 ppm (C-5); sugar residue d′: $\delta = 97.0$ (C-1), 73 (C-2), 76.8 (C-3), 74 (C-4), 72.2 (C-5), 69.6 ppm (C-6); sugar residue e′: $\delta = 97.0$ (C-1), 55.1 (C-2), 76.6 (C-3), 72.7 (C-4), 72.8 (C-5), 69.7 ppm (C-6).

1b: MALDI MS: *m/z* 2706.3 [*M*+Na$^+$]; $C_{159}H_{171}N_3O_{35}$ (2684.1); ^{1}H NMR (600 MHz, $CDCl_3$): $\delta = 4.62$ (1a-H), 4.36 (1b-H), 4.56 (1c-H), 5.16 (1d-H), 4.80 (1d′-H), 5.00 ppm (1e′-H); ^{13}C NMR (150.9 MHz, $CDCl_3$): $\delta = 99.8$ (C-1a), 100.3 (C-1b), 101.7 (C-1c), 99.7 (C-1d), 98.7 (C-1d′), 97.8 ppm (C-1e′).

Received: April 11, 2002
Revised: August 21, 2002 [Z19076]

[1] A. Varki, *Glycobiology* **1993**, *3*, 97 – 130; B. Hart, G. W. Hart, P. Sinaÿ, *Carbohydrates in Chemistry and Biology, Part II: Biology of Saccharides*, Wiley-VCH, Weinheim, **2000**.

[2] M. Bodzansky, *Peptide Chemistry: A Practical Textbook*, 2nd Ed., Springer-Verlag, Berlin, **1993**.

 © 2002 WILEY-VCH Verlag GmbH & Co. KGaA, Weinheim 0044-8249/02/4123-4492 $ 20.00+.50/0

[3] G. Jung, A. G. Beck-Sickinger, *Angew. Chem.* **1992**, *104*, 375 – 391; *Angew. Chem. Int. Ed. Engl.* **1992**, *31*, 367 – 383.
[4] For a recent review on solid-phase oligosaccharide synthesis see: P. H. Seeberger, W.-C. Haase, *Chem. Rev.* **2000**, *100*, 4349 – 4393. a) For a first investigation of solid-phase oligosaccharide synthesis with an automated synthesizer see: O. J. Plante, E. R. Palmacci, P. H. Seeberger, *Science* **2001**, *291*, 1523 – 1527; b) E. R. Palmacci, O. J. Plante, P. H. Seeberger, *Eur. J. Org. Chem.* **2002**, 595 – 606.
[5] a) T. Zhu, G.-J. Boons, *Chem. Eur. J.* **2001**, *7*, 2382 – 2389; b) T. Zhu, G.-J. Boons, *J. Am. Chem. Soc.* **2000**, *122*, 10222 – 10223; c) K. C. Nicolaou, N. Watanabe, J. Li, J. Pastor, N. Winssinger, *Angew. Chem.* **1998**, *110*, 1636 – 1638; *Angew. Chem. Int. Ed.* **1998**, *37*, 1559 – 1561; d) K. C. Nicolaou, N. Winssinger, J. Pastor, F. DeRoose, *J. Am. Chem. Soc.* **1997**, *119*, 449 – 452.
[6] R. Liang, L. Yan, J. Loebach, M. Ge, Y. Uozumi, K. Sekanina, N. Horan, J. Gildersleeve, A. Smith, K. Biswas, D. E. Kahne, *Science* **1996**, *274*, 1520 – 1522.
[7] Y. Ito, T. Ogawa, *J. Am. Chem. Soc.* **1997**, *119*, 5562 – 5566.
[8] S. J. Danishefsky, K. F. McClure, J. T. Randolph, R. B. Ruggeri, *Science* **1993**, *260*, 1307 – 1309.
[9] a) M. C. Hewitt, P. H. Seeberger, *J. Org. Chem.* **2001**, *66*, 4233 – 4243; b) R. B. Andrade, O. J. Plante, L. G. Melean, P. H. Seeberger, *Org. Lett.* **1999**, 1811 – 1814.
[10] R. Rodebaugh, S. Joahi, B. Fraser-Reid, M. H. Geysen, *J. Org. Chem.* **1997**, *62*, 5660 – 5663.
[11] O. Seitz, C. -H, Wong, *J. Am. Chem. Soc.* **1997**, *119*, 8766 – 8776.
[12] a) M. Grathwohl, R. R. Schmidt, *Synthesis* **2001**, 2263 – 2272; b) X. Wu, M. Grathwohl, R. R. Schmidt, *Org. Lett.* **2001**, *3*, 747 – 750; c) F. Roussel, L. Knerr, R. R. Schmidt, *Eur. J. Org. Chem.* **2001**, 2066 – 2073; d) L. Knerr, R. R. Schmidt, *Eur. J. Org. Chem.* **2000**, 2803 – 2808; e) L. Knerr, R. R. Schmidt, *Synlett* **1999**, 1802 – 1804; f) J. Rademann, A. Geyer, R. R. Schmidt, *Angew. Chem.* **1998**, *110*, 1309 – 1313; *Angew. Chem. Int. Ed.* **1998**, *37*, 1241 – 1245; g) J. Rademann, R. R. Schmidt, *J. Org. Chem.* **1997**, *62*, 3650 – 3653; h) A. Heckel, E. Mross, K.-J. Jung, J. Rademann, R. R. Schmidt, *Synlett* **1998**, 171 – 173.
[13] a) R. R. Schmidt, *Angew. Chem.* **1986**, *98*, 213 – 236; *Angew. Chem. Int. Ed. Engl.* **1986**, *25*, 212 – 235; b) R. R. Schmidt, W. Kinzy, *Adv. Carbohydr. Chem. Biochem.* **1994**, *50*, 21 – 123.
[14] F. Roussel, L. Knerr, M. Grathwohl, R. R. Schmidt, *Org. Lett.* **2000**, *2*, 3043 – 3046.
[15] F. Roussel, M. Takhi, R. R. Schmidt, *J. Org. Chem.* **2001**, *66*, 8540 – 8548.
[16] For recent examples of N-glycan synthesis in solution see: M. V. Chiesa, R. R. Schmidt, *Eur. J. Org. Chem.* **2000**, 3541 – 3554 and references [5–15] therein.
[17] S. P. Douglas, D. M. Whitfield, J. J. Krepinsky, *J. Am. Chem. Soc.* **1995**, *117*, 2116 – 2117.
[18] For leading references on β-mannopyranoside synthesis see: R. Weingart, R. R. Schmidt, *Tetrahedron Lett.* **2000**, *41*, 8753 – 8758.
[19] For a highly selective β-mannopyranoside synthesis see: A. A.-H. Abdel-Rahman, S. Jonke, E. S. H. El Ashry, R. R. Schmidt, *Angew. Chem.* **2002**, *114*, 3100 – 3103; *Angew. Chem. Int. Ed.* **2002**, *41*, 2710 – 2716.
[20] M. Grathwohl, Diplomarbeit, University of Konstanz, **1997**.
[21] T. Bieg, W. Szeja, *J. Carbohydr. Chem.* **1985**, *4*, 441 – 446.
[22] L. Liang, T.-H. Chan, *Tetrahedron Lett.* **1998**, *39*, 355 – 358.
[23] R. R. Schmidt, X. Wu, unpublished results.
[24] O. Kanie, S. C. Crawley, M. M. Palcic, O. Hindsgaul, *Carbohydr. Res.* **1993**, *243*, 139 – 164.

First Direct Observation of the Two Distinct Steps in an S_N1 Reaction**

Herbert Mayr* and Shinya Minegishi

The differentiation of bimolecular (S_N2) and unimolecular nucleophilic substitutions (S_N1) by Ingold and co-workers marks the beginning of the mechanistic period of organic chemistry.[1] Since then, countless investigations on the rates and products of S_N1 reactions have been performed. A considerable part of our knowledge of the relationships between structure and reactivity of carbocations (R^+), the intermediates of these reactions, has been derived from solvolysis studies[2–5] [Eq. (1)].

$$R{-}Cl \overset{\text{slow}}{\rightleftharpoons} R^+ + Cl^- \xrightarrow[\text{fast}]{\text{SolvOH}} R{-}OSolv + HCl \qquad (1)$$

The discovery by Olah and co-workers that many types of carbocations exist as long-lived species in superacidic solutions, media of low nucleophilicity, allowed the direct observation of carbocations by spectroscopic methods.[6,7]

In recent years, much information on the rates of the reactions of carbocations with nucleophiles,[8,9] including solvents (SolvOH) of S_N1 reactions,[10,11] became available. In agreement with earlier conclusions from solvolysis studies,[12,13] the rates of decay of laser-flash photolytically generated carbocations in 2,2,2-trifluoroethanol (TFE) revealed this alcohol as a weakly nucleophilic solvent.[10] Accordingly, we have now found a first-order rate constant of $12.7 \pm 0.4\ s^{-1}$ for the decay of bis(4-methoxyphenyl)carbenium tetrafluoroborate (**1**-BF_4) in TFE/acetonitrile (91:9 (v/v)) at 20 °C, corresponding to a half-life of 55 ms (Table 1, entry 1). This rate constant is only slightly reduced in the presence of tetra-*n*-butylammonium chloride (nBu_4NCl) (Table 1, entry 2) and remains almost constant as the TFE/CH_3CN ratio is reduced from 91:9 to 20:80 (Table 1, entries 3–5). Entries 6 and 7 in Table 1 indicate that the presence of 0.5 M $NaClO_4$ or $LiClO_4$ does not affect the rate of the reaction of $\mathbf{1}^+$ with TFE.[14]

The ethanolysis rate constant of chlorobis(4-methoxyphenyl)methane (**1**-Cl), that is the rate of the S_N1 reaction in ethanol, has previously been determined as $k = 57\ s^{-1}$ at 25 °C, a million times higher than the ethanolysis rate constant of the parent chlorodiphenylmethane ($5.34 \times 10^{-5}\ s^{-1}$).[15] Since chlorodiphenylmethane, on the other hand, was reported to undergo solvolysis in TFE/water (97:3 (w/w)) with $k = 1.05\ s^{-1}$,[16] we extrapolated an S_N1 reactivity of **1**-Cl in TFE/water (97:3 (w/w)) of $57\ s^{-1} \times (1.05/5.34 \times 10^{-5}) = 1.1 \times 10^6\ s^{-1}$.

The ionization of **1**-Cl in TFE was thus expected to be 10^5 times faster than the reaction of $\mathbf{1}^+$ with this solvent. Since

[*] Prof. Dr. H. Mayr, S. Minegishi
Department Chemie
Ludwig-Maximilians-Universität München
Butenandtstrasse 5–13 (Haus F), 81377 München (Germany)
Fax: (+49) 89-2180-7717
E-mail: herbert.mayr@cup.uni-muenchen.de

[**] We thank Prof. D. N. Kevill and Dr. J. Crooks for comments and helpful suggestions. Financial support by the Deutsche Forschungsgemeinschaft and the Fonds der Chemischen Industrie is gratefully acknowledged.

 © 2002 WILEY-VCH Verlag GmbH & Co. KGaA, Weinheim 0044-8249/02/4123-4493 $ 20.00+.50/0

Table 1. Kinetics of the reaction of **1**-BF_4 in TFE/CH_3CN solutions at 20 °C.

Entry	TFE/CH_3CN[a]	Additive	k_{TFE} [s^{-1}][b]
1	91:9		12.7[c]
2	91:9	nBu_4NCl (0.01 M)	10.3
3	80:20		13.5
4	60:40		13.1
5	20:80		10.0
6	20:80	$NaClO_4$ (0.5 M)	10.0
7	20:80	$LiClO_4$ (0.5 M)	10.4

[a] Solvent ratio in (v/v). [b] Reactions were monitored at $\lambda = 500$ nm. [c] Four independent experiments gave a standard deviation for k_{TFE} of ± 0.4.

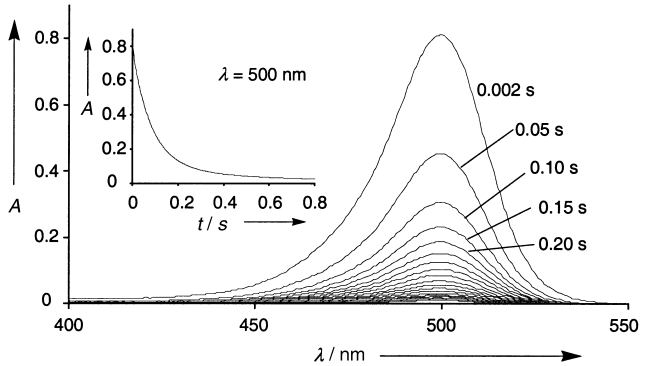
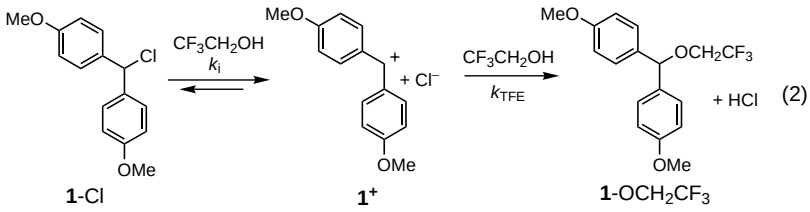


Figure 1. Decay of the absorbance of the carbenium ion $\mathbf{1}^+$ generated from **1**-Cl in TFE/CH_3CN (91:9 (v/v)) at 20 °C.

intermediates, which are produced faster than they are consumed, enrich during a reaction sequence, we were prompted by these considerations to search for the intermediate bis(4-methoxyphenyl)carbenium ion $\mathbf{1}^+$ during the trifluoroethanolysis of **1**-Cl [Eq. (2)].



(2)

Immediately after mixing the colorless solution of **1**-Cl in CH_3CN with the tenfold volume of TFE (dried by distillation over $CaSO_4$) in a stopped-flow apparatus, the well-known UV/Vis spectrum of the cation $\mathbf{1}^+$ with an absorption maximum at $\lambda = 500$ nm was observable (Figure 1). This spectrum is identical to that obtained for $\mathbf{1}^+$ in pure CH_3CN ($\lambda_{max} = 500$ nm).[17]

From the molar absorption coefficient ($\lg \varepsilon = 5.10$),[17] one can derive that immediately after mixing, the concentration of $\mathbf{1}^+$ equals 80 % of that of the initial concentration of **1**-Cl ($c_0 = 8.5 \times 10^{-6}$ M). This band disappeared with a first-order rate constant of 11.4 s^{-1} (Figure 1), that is, a similar rate as previously observed (Table 1) for the reaction of **1**-BF_4 with TFE under the same conditions.

Only small changes of the rate of the first-order decay were observable when the TFE/CH_3CN ratio was reduced from 91:9 to 50:50 (Table 2, entries 1 and 6–9). Addition of tetra-*n*-butylammonium chloride caused a slight decrease of the rate of the carbocation decay (Table 2, entries 1–5). In the presence of 10^{-2} M nBu_4NCl, a hypsochromic shift of $\Delta\lambda = 1$ nm and a decrease of the intensity of the absorption band by 35 % was observed. In all cases, the maximum of the carbocation absorption (A_{max}) was detected immediately after mixing, in accord with the high ionization rate constant of **1**-Cl estimated above.

Attempts to slow down the ionization reaction to measurable rates by employing TFE/CH_3CN mixtures with a smaller solvent ionizing power than pure TFE[12] were not successful. While the maximal absorbance was still observed immediately after mixing, even in TFE/CH_3CN in the ratio 30:70 (v/v) (Table 2, entry 11), the absorption coefficients were considerably smaller than in solutions with a high TFE/CH_3CN ratio, indicating that under these conditions the ionization equilibrium (first step in Equation (2)) was shifted towards the covalent diarylchloromethane **1**-Cl. Because of incomplete ionization, the carbocation consumption did not show an exponential decay in the cases with small initial absorbance, and the rate constants of entries 10, 11, and 13 in Table 2 have to be considered as approximations.

Formation as well as decay of the carbocation $\mathbf{1}^+$ was observable, however, in a TFE/CH_3CN mixture (20:80 (v/v)) which contained 1.0 M of $LiClO_4$[14] (Figure 2).

At the maximum of the carbocation concentration, that is, 7 ms after mixing, 40 % of the initial **1**-Cl was observable as

Table 2. Kinetics of the solvolysis of **1**-Cl in TFE/CH_3CN solutions at 20 °C.

Entry	[**1**-Cl]$_0$ [M]	TFE/CH_3CN[a]	Additive	A_{max}[b]	k_i [s^{-1}]	k_{TFE} [s^{-1}]
1	8.51×10^{-6}	91:9		0.81	fast	11.4
2	8.51×10^{-6}	91:9	nBu_4NCl (5×10^{-4} M)	0.83	fast	11.1
3	8.51×10^{-6}	91:9	nBu_4NCl (1×10^{-3} M)	0.81	fast	11.0
4	8.51×10^{-6}	91:9	nBu_4NCl (5×10^{-3} M)	0.68	fast	10.6
5	8.51×10^{-6}	91:9	nBu_4NCl (1×10^{-2} M)	0.54[c]	fast	10.6
6	7.44×10^{-6}	80:20		0.67	fast	14.1
7	7.44×10^{-6}	70:30		0.61	fast	14.8
8	7.44×10^{-6}	60:40		0.55	fast	13.2
9	7.44×10^{-6}	50:50		0.50	fast	12.4
10	7.44×10^{-6}	40:60		0.37	fast	(6.47)[d]
11	7.44×10^{-6}	30:70		0.20	–[e]	(3.80)[d]
12	1.10×10^{-5}	30:70	$LiClO_4$ (1.0 M)	0.64	7×10^2	12.7
13	7.44×10^{-6}	20:80		0.10	–[e]	(2.66)[d]
14	7.44×10^{-6}	20:80	$NaClO_4$ (1.0 M)	0.26	3×10^2	10.1
15	1.10×10^{-5}	20:80	$LiClO_4$ (1.0 M)	0.52	5×10^2	10.4

[a] Solvent ratio in (v/v). [b] Maximum absorbance at $\lambda = 500$ nm during the course of the reaction. [c] Maximum absorbance at $\lambda = 499$ nm during the course of the reaction. [d] The rate constant (k_{TFE}) has to be considered as an approximation. The initial carbocation absorbance was small and did not show an exponential decay because of incomplete ionization. [e] The rate constant of ionization (k_i) was not determined because of a too small increase of absorbance in the cation formation step.

 © 2002 WILEY-VCH Verlag GmbH & Co. KGaA, Weinheim 0044-8249/02/4123-4494 $ 20.00+.50/0 *Angew. Chem. Int. Ed.* **2002**, *41*, No. 23

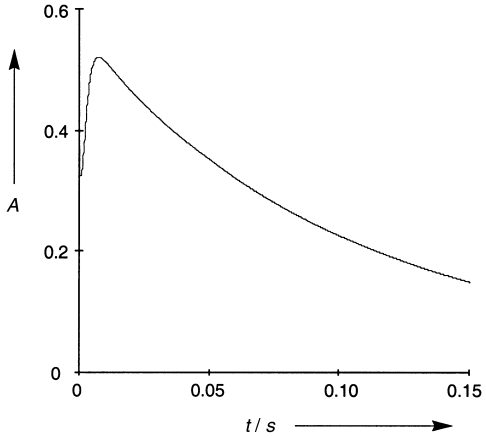


Figure 2. Generation and decay of $\mathbf{1}^+$ observed after dissolving **1**-Cl in TFE/CH_3CN (20:80 (v/v)) containing 1.0 M of $LiClO_4$.

the diarylmethyl cation $\mathbf{1}^+$. The carbocation, which was formed with a rate constant (k_i) of $5 \times 10^2\ s^{-1}$ was consumed with a rate constant (k_{TFE}) of 10.4 s^{-1} under these conditions (Table 2, entry 15). Analogously, formation and consumption of $\mathbf{1}^+$ was observable in other TFE/CH_3CN mixtures containing alkali metal perchlorates[14] (Table 2, entries 12 and 14).

The direct observation of the carbocationic intermediate demonstrated in this experiment is certainly not a singular case. Increasing stabilization of the carbocation and decreasing solvent nucleophilicity transform the generally accepted energy profiles of S_N1 reactions with carbocations as short-lived intermediates (Figure 3, upper graph) into energy profiles which imply the buildup of significant concentrations of the intermediate carbocations (Figure 3, lower graph).

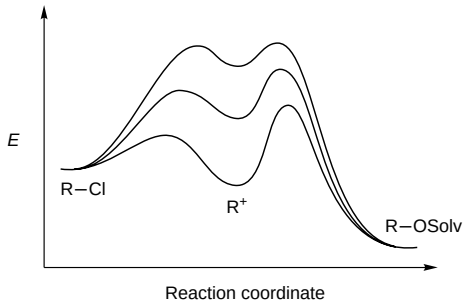


Figure 3. Schematic energy profiles for solvolytic displacement reactions in TFE. Upper graph: Slow ionization (conventional S_N1). Lower graph: Rate-determining carbocation–nucleophile combination with directly observable intermediate. Ion-pairing and proton transfer steps are neglected.

The occurrence of such scenarios can easily be predicted from available ionization and combination rate constants as demonstrated herein. Since ionization and nucleophile addition must be uncoupled when the intermediate is observable, the investigation of such reaction cascades may open a new era in the study of solvolytic displacement reactions. As salt and solvent effects on the two steps of the reaction can now be studied separately, many ambiguities in the earlier interpretations of the mechanisms of solvolytic displacement reactions can be resolved.

Received: July 5, 2002 [Z19671]

[1] a) C. K. Ingold, E. Rothstein, *J. Chem. Soc.* **1928**, 1217 – 1221; b) C. K. Ingold, *Structure and Mechanism in Organic Chemistry*, 2nd ed., Cornell University, New York, **1969**.
[2] *Carbonium Ions, Vol. 1–5* (Eds.: G. A. Olah, P. von R. Schleyer), Interscience, New York, **1968–1976**.
[3] P. Vogel, *Carbocation Chemistry*, Elsevier, Amsterdam, **1985**.
[4] a) X. Creary, *Advances in Carbocation Chemistry, Vol. 1*, JAI, Greenwich, CT, **1989**; b) J. M. Coxon, *Advances in Carbocation Chemistry, Vol. 2*, JAI, Greenwich, CT, **1995**.
[5] a) "Carbocations": R. A. Cox in *Organic Reaction Mechanisms* (Eds.: A. C. Knipe, W. E. Watts), Wiley, Chichester, **1985–2001**; b) A. Streitwieser, Jr., *Solvolytic Displacement Reactions*, McGraw-Hill, New York, **1962**.
[6] G. A. Olah, W. S. Tolgyesi, S. J. Kuhn, M. E. Moffatt, I. J. Bastien, E. B. Baker, *J. Am. Chem. Soc.* **1963**, *85*, 1328 – 1334.
[7] G. A. Olah, *Angew. Chem.* **1995**, *107*, 1519 – 1532; *Angew. Chem. Int. Ed. Engl.* **1995**, *34*, 1393 – 1405.
[8] H. Mayr, M. Patz, *Angew. Chem.* **1994**, *106*, 990 – 1010; *Angew. Chem. Int. Ed. Engl.* **1994**, *33*, 938 – 957.
[9] H. Mayr, T. Bug, M. F. Gotta, N. Hering, B. Irrgang, B. Janker, B. Kempf, R. Loos, A. R. Ofial, G. Remennikov, H. Schimmel, *J. Am. Chem. Soc.* **2001**, *123*, 9500 – 9512.
[10] R. A. McClelland, *Tetrahedron* **1996**, *52*, 6823 – 6858.
[11] J. P. Richard, T. L. Amyes, M. M. Toteva, *Acc. Chem. Res.* **2001**, *34*, 981 – 988.
[12] T. W. Bentley, G. Llewellyn, *Prog. Phys. Org. Chem.* **1990**, *17*, 121 – 158.
[13] D. N. Kevill in *Advances in Quantitative Structure-Property Relationships, Vol. 1* (Ed.: M. Charton), JAI, Greenwich, CT, **1996**, pp. 81 – 115.
[14] For salt effects in solvolysis reactions, see: D. J. Raber, J. M. Harris, P. von R. Schleyer in *Ions and Ion Pairs in Organic Reactions, Vol. 2* (Ed.: M. Szwarc), Wiley, New York, **1974**, pp. 247 – 374.
[15] C. Schade, H. Mayr, *Tetrahedron* **1988**, *44*, 5761 – 5770.
[16] C. A. Bunton, M. M. Mhala, J. R. Moffatt, *J. Org. Chem.* **1984**, *49*, 3639 – 3641.
[17] J. Bartl, S. Steenken, H. Mayr, R. A. McClelland, *J. Am. Chem. Soc.* **1990**, *112*, 6918 – 6928.

A Europium-Ion-Based Luminescent Sensing Probe for Hydrogen Peroxide**

Otto S. Wolfbeis,* Axel Dürkop, Meng Wu, and Zhihong Lin

Molecular probes and molecular sensors for hydrogen peroxide (H_2O_2) are important in the environmental and bioanalytical sciences for a number of reasons. H_2O_2 is present in small but significant concentrations in the atmosphere[1] and the marine environment.[2] It is widely used in industry for bleaching, cleaning, and disinfection,[3] and released to the environment in large quantities.[4] H_2O_2 is one of the products of the activity of almost all oxidases,[5] and this enables a quantitative assay of a) the activity of the respective enzyme, b) numerous substrates including glucose,[6] and c) a so-called

[*] Prof. O. S. Wolfbeis, Dr. A. Dürkop, M. Wu, Z. Lin
Institute of Analytical Chemistry, Chemo- and Biosensors
University of Regensburg
93040 Regensburg (Germany)
Fax: (+ 49) 941–943–4064
E-mail: otto.wolfbeis@chemie.uni-regensburg.de

[**] We thank Dr. Jörg Enderlein (FZ Jülich) for the determination of some of the fluorescence decay times.

 © 2002 WILEY-VCH Verlag GmbH & Co. KGaA, Weinheim 0044-8249/02/4123-4495 $ 20.00+.50/0

enzyme-linked immunoassay (ELISA) to be carried out, if an oxidase is used as a label.[7] Finally, H_2O_2 is known to be the cause of various kinds of DNA damage in mammalian[8] and plant[9] cells; an area of particular current research activity. Obviously, molecular probes for H_2O_2 are of broad interest in environmental and biochemistry research, in clinical assay and screening.

H_2O_2 can be optically detected with extreme sensitivity by chemiluminescence[10] (CL) or electroluminescence,[11] however usually at pH values above 8.0 only. A sensitivity similar to that of CL assays is achieved by using (laser-induced) fluorescence. The reaction of H_2O_2 with certain phenols in the presence of peroxidase yields fluorescent dimers (excitation at around 320 nm; emission maximum at 415 nm), which can be used to visualize and detect H_2O_2,[12] ideally through the long-decaying fluorescence of the respective europium complexes.[13] This method requires, however, the use of several reagents including a) a fluorogenic precursor; b) a peroxidase, c) a lanthanide ion such as Eu^{3+}, and d) in some instances a fluorescence-enhancing solution.

We present a new fluorescent probe for hydrogen peroxide and its use for sensitive but simple detection of H_2O_2. The procedure is based on the rather surprising finding that the Eu^{3+}–tetracycline complex[14] referred to herein as [Eu(tc)], when used as an aqueous solution in a 4-morpholine propanesulfonic acid (MOPS) buffer,[15] binds H_2O_2 to form a strongly fluorescent complex ([Eu(hp)(tc)]) that can be excited at 390 to 405 nm, for example, by using a 405-nm diode laser. On addition of H_2O_2 to [Eu(tc)], a 15-fold increase in luminescence intensity at 616 nm occurs (Figure 1). Simultaneously,

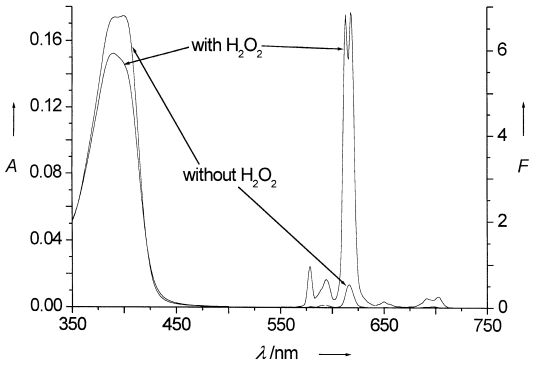


Figure 1. Absorption and emission spectra of the Eu^{3+}–tetracycline complex ([Eu(tc)][15]) in pH 6.9 buffer, in the presence and absence of 0.8 mmol·L^{-1} of hydrogen peroxide. Fluorescence excitation at λ_{exc} 405 nm.

large changes are observed in the luminescence decay time of [Eu(tc)], which was reported to be in the 10–20 μs range and highly pH-dependent.[14,16] The increase is most pronounced at physiological pH values and does not require the presence of an enzyme. The effects observed are constant over time which implies that a) they are not caused by chemiluminescence, and b) that the reagent and the product of its reaction with H_2O_2 do not measurably photobleach.

Eu^{3+}–ligand complexes of the type of [Eu(tc)] have coordination numbers of eight or nine.[17,18] Both [Eu(tc)] and [Eu(hp)(tc)] display the typical absorption and emission spectra of a lanthanide–ligand complex. The absorption band (with peaks at 398 and 405 nm) is caused by the presence of the tetracycline ligand which—in its uncomplexed form—has a very similar absorption spectrum. As in other complexes of this type, the photonic energy absorbed by the ligand is transferred from the triplet state of the ligand to the central Eu^{3+} ion with its typical emission spectrum[18] of a main band which peaks at 616 nm ($^5D_0 \rightarrow {}^7F_2$) and several side bands centered at 579, 597, 654, and 688 nm, respectively (Figure 1). In the case of [Eu(hp)(tc)], the main emission band is split into two bands when the concentration of [Eu(tc)] exceeds 1 μmol L^{-1}, provided a spectrometer is used with a resolution of < 1 nm.

The probe [Eu(tc)] is highly specific for H_2O_2. Its luminescence is not affected by alkali and ammonium ions, nor by chloride, sulfate, or nitrate anions in concentrations of up to 100 mmol L^{-1}. However, citrate and phosphate interfere, leading to an increase in fluorescence. The emission intensities of [Eu(tc)] and [Eu(hp)(tc)] are strongest at pH 6.6–7.2 and rapidly drop outside this range. In fact, the fluorescence is only 15% of the maximum intensity at pH 8.0, and 8% at pH 6.0. The quantum yield of [Eu(tc)] in MOPS buffer solution of pH 6.9 is 0.003 ± 0.002 at 22 °C, which increases to 0.040 ± 0.001 on addition of excess H_2O_2.

In contrast to Hirschy et al.[14] we find the decay characteristics of [Eu(tc)] to be rather complex. The decay profile of in pH 6.9 buffer solution has two main components, one having a decay time of 8.7 μs (weighting 58%), the other of 30.4 μs (40%). We also found a third component (2%) which, with a decay time as long as 174 μs, indicates a quite different deactivation channel. The decay of the [Eu(hp)(tc)] also has two main components, of which the decay times are 13.2 μs (34%) and 59.4 μs (64%), respectively. The third component (2%) is present as well and has a decay time of 158 μs. From these results it is obvious that time-resolved measurements are best performed after a lag time of > 30 μs to detect the major (59.4 μs) component of the [Eu(hp)(tc)] selectively. Fortunately, this lag time can be programmed into many fluorescence (and microplate) readers.

Complexes of Eu^{3+} with organic ligands are known to contain water as an additional ligand, usually at the ninth coordination site.[17] From the experimental findings we conclude that on exposure to H_2O_2 the water ligand is replaced by H_2O_2, without the occurrence of a redox reaction. This interpretation is based on the findings that the absorption spectrum of [Eu(hp)(tc)] is very similar in shape to that of [Eu(tc)] (Figure 1) and that the H_2O_2 in [Eu(hp)(tc)] is still available to reduction (e.g. by thiosulfate). We assume that the binding of the H_2O_2 ligand causes a structural rearrangement of the [Eu(tc)] complex in solution, such that the tc ligands come closer to the central metal ion, which would lead to a distinctly more efficient transfer of energy from the ligand to the central ion (i.e. a higher quantum yield and less quenching) and to an increase in luminescence decay time (for the two main fractions; we also assume that water molecules act as quenchers). Unfortunately, and despite many attempts, we failed to obtain crystals of the obviously weak complex formed between [Eu(tc)] and H_2O_2.

 © 2002 WILEY-VCH Verlag GmbH & Co. KGaA, Weinheim 0044-8249/02/4123-4496 $ 20.00+.50/0 *Angew. Chem. Int. Ed.* **2002**, *41*, No. 23

The potential of the above findings is demonstrated by applying the Eu complex in the detection of trace levels of H_2O_2, a kinetic enzyme-activity assay (glucose oxidase), a kinetic assay for glucose, and an optical sensor for H_2O_2. The respective procedures are rather simple. The first[19] consists of the addition of [Eu(tc)] to the buffered (pH 6.9) sample; the reaction is complete in about 10 min. In contrast to previous methods, the addition of an enzyme (or an enzyme mimetic) is not needed. The plot of intensity versus concentration of H_2O_2 in Figure 2 shows that H_2O_2 can be determined in the 2–400

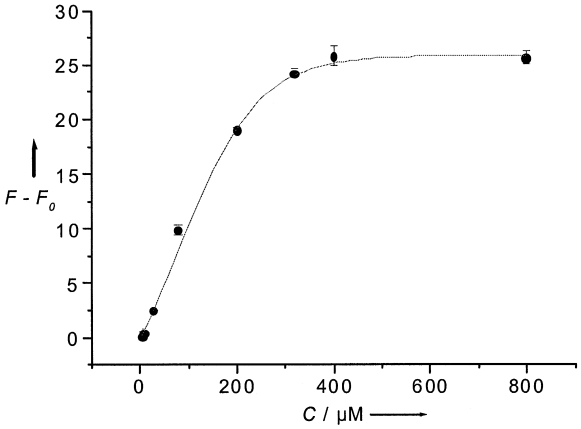


Figure 2. Plot of $(F-F_0)$ versus concentration of H_2O_2 including error bars (for n = 6) at pH 6.9, showing the dynamic range of the system. Here, F_0 is the initial fluorescence of the system (caused by [Eu(tc)]), which increases to F on addition of H_2O_2 because of the formation of the strongly fluorescent [Eu(hp)(tc)]. The linear range is from 0 to about 200 µmol·L^{-1}.

µmol L^{-1} concentration range. The limit of detection (LOD; defined as 3σ/slope) is 1.8 µmol L^{-1}. This LOD is not comparable to the extremely sensitive methods based on chemiluminescence, but better by a factor of ten than the peroxytitanyl ion method, which has the additional disadvantages that it is a nonfluorescent system and requires a pH value of <3, so that it is not applicable to probing biological systems.

The determination of the activity of the enzyme glucose oxidase (GOx) requires the addition of only glucose and the reagent [Eu(tc)].[20] This process is much simpler than any other optical assay reported to date. The determination of glucose (which is important in clinical analysis, in food chemistry, and in the monitoring of processes occurring in bioreactors) becomes possible by addition of only GOx and [Eu(tc)].[21] Figure 3 gives time plots of a typical kinetic glucose assay.

Finally, we have obtained an optical sensor by immobilizing the [Eu(tc)] complex in an optically transparent layer of a polyurethane hydrogel. The sensor enables continuous monitoring of H_2O_2 in the 0.001–0.3 % concentration range. By analogy to the imaging of chemical species by using ruthenium probes with relatively long decay times,[22] we are currently performing experiments to visualize H_2O_2 by fluorescence imaging using the new [Eu(tc)] probe.

While steady-state luminescence intensity was used as the analytical information in the experiments described so far,

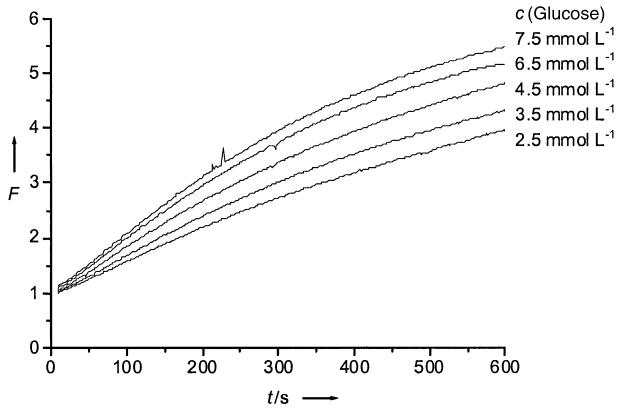


Figure 3. Time-dependent oxidation of glucose (2.5 to 7.5 mmol·L^{-1}) by glucose oxidase (15 units in 3 mL) in MOPS buffer at pH 7.0, monitored by the formation of [Eu(hp)(tc)]. Luminescence excitation was at 405 nm and measurements at 616 nm.

gated measurements may also be performed using a time-resolving fluorometer. In a typical experiment, the delay time of a time-resolving fluorometer[23] was set to 30 µs and the integration time to 100 µs. This led to an eight–ten-fold reduction in background luminescence (resulting from both the sample and the microtiterplate). However, it has to be noted that gated measurements with the [Eu(tc)] probe do not lead to complete suppression of background luminescence, because background luminescence is always predetermined by the fraction of free [Eu(tc)] present. The luminescence of [Eu(tc)] is weaker than that of the [Eu(hp)(tc)] complex by a factor of 15, but has spectral characteristics which are virtually identical to those of [Eu(hp)(tc)]. Fortunately, the main component of the three (at 59.4 µs) is well separated from that of the [Eu(tc)] complex (30.4 µs), so that the latter is largely eliminated by gating.

In conclusion, the new luminescent probe for H_2O_2 has unique properties;[24] it works at neutral pH values, has the general advantages of a fluorescent probe (e.g. sensitivity), displays a very large Stokes shift (210 nm) and a µs fluorescence decay time. The latter enables gated assays, and also provides decay-time-based information (not discussed here). Unlike other europium labels, which can only be excited by diode lasers by using two-photon excitation or second-harmonic generation, the new probe can be directly excited with the violet (405 nm) diode laser. Finally, [Eu(tc)] is the first probe for the determination of H_2O_2 that does not require the presence of an enzyme (such as peroxidase) or an enzyme mimic to form a fluorescent product.

The findings may be exploited in a) the detection of H_2O_2 in the environment and in process control, b) the determination of the activity of oxidases, either directly as shown here, or in ELISAs or gene assays, c) the determination of enzyme inhibitors, in particular heavy-metal ions, and d) the quantification of substrates for oxidases. Europium reagents that are covalently linked to appropriate biomolecules are widely used in binding assays, known for example as the DELFIA or FIAGEN immunoassays, and in gene assays,[25] some based on the use of nanobeads and lanthanide phosphors that, ideally, may be adapted to microarray formats.[26] The new europium reagent [Eu(tc)] is an attractive alternative because it need

 © 2002 WILEY-VCH Verlag GmbH & Co. KGaA, Weinheim 0044-8249/02/4123-4497 $ 20.00+.50/0

not be covalently attached to a receptor and it does not require the addition of a detergent to enhance fluorescence intensity.

Received: June 5, 2002 [Z19477]

[1] a) A. M. Thompson, *Science* **1992**, *256*, 1157 – 1165; b) J. M. Anglada, Ph. Aplincourt, J. M. Bofill, D. Cremer, *ChemPhysChem* **2002**, *3*, 215 – 221.

[2] D. Price, P. J. Worsfold, R. Mantoura, C. Fauzi, *Trends Anal. Chem.* **1992**, *11*, 379 – 384.

[3] a) S. Wilson, *Chem. Ind. (London)* **1994**, *7*, 255 – 258; b) C. Hachem, F. Bocquillon, O. Zahraa, M. Bouchy, *Dyes Pigm.* **2001**, *49*, 117 – 125; c) *Fed. Regist.* **2000**, *65*, 75 174 – 75 179.

[4] J. Chen, W. H. Rulkens, H. Bruning, *Water Sci. Technol.* **1997**, *35*, 231 – 238.

[5] *The Enzyme Handbook* (Ed.: T. E. Barman) Springer, Berlin, **1974**.

[6] *Methods of Enzymatic Analysis* (Ed.: H. G. Bergmeyer), Verlag Chemie, Weinheim, **1984**.

[7] D. B. Papkovsky, T. C. O'Riordan, G. G. Guilbault, *Anal. Chem.* **1999**, *71*, 1568 – 1573.

[8] a) P. Leanderson, K. Wennerberg, C. Tagesson, *Cancerogenesis* **1994**, *15*, 137 – 139; b) A. Barbouti, P. T. Doulias, B. Z. Zhu, B. Frei, D. Galaris, *Free Radical Biol. Med.* **2001**, *31*, 490 – 498.

[9] D. A. Stavreva, T. Gichner, *Mutat. Res.* **2002**, *514*, 147 – 152.

[10] *Bioluminescence and Chemiluminescence* (Eds.: M. A. DeLuca, W. D. McElroy), Academic Press, New York, **1981**.

[11] K. A. Fähnrich, M. Prawda, G. G. Guilbault, *Talanta* **2001**, *54*, 531 – 559.

[12] H. Perschke, E. Broda, *Nature* **1961**, *190*, 257 – 258.

[13] a) J. Meyer, U. Karst, *Nachr. Chem. Tech. Lab.* **1999**, *47*, 1116 – 1119; b) J. Weber, U. Karst, *Analyst* **2000**, *125*, 1537 – 1538 and references therein.

[14] L. M. Hirschy, T. F. van Geel, J. D. Winefordner, R. N. Kelly, S. G. Schulman, *Anal. Chim. Acta* **1984**, *166*, 207 – 219.

[15] Reagent: A solution containing $EuCl_3 \cdot 6H_2O$ (9.6 mg) and tetracycline hydrochloride (4 mg) in a MOPS buffer (200 mL, 10 mmol L^{-1}) of pH 6.9. The absorbance at 405 nm is $\approx 0.78 \pm 0.01$ cm^{-1}. The reagent is stable for at least 1 month if stored at 4 °C in the dark.

[16] M. Mathew, P. Balaram, *J. Inorg. Biochem.* **1980**, *13*, 339 – 342.

[17] a) L. C. Thompson in *Handbook on the Physics and Chemistry of Rare Earths* (Eds.: K. A. Gschneidner, L. Eyring), North-Holland Publ., Amsterdam, **1979**, pp. 210 – 290; b) F. S. Richardson, *Chem. Rev.* **1982**, *82*, 541 – 552; b) S. I. Klink, H. Keizer, F. C. J. M. van Veggel, *Angew. Chem* **2000**, *112*, 4489 – 4491; *Angew. Chem. Int. Ed.* **2000**, *39*, 4319 – 4321.

[18] a) B. Alpha, J. M. Lehn, G. Mathis, *Angew. Chem.* **1987**, *99*, 259 – 261; *Angew. Chem. Int. Ed. Engl.* **1987**, *26*, 266 – 267; b) M. Xiao, P. Selvin, *J. Am. Chem. Soc.* **2001**, *123*, 7067 – 7073.

[19] Assay protocol for H_2O_2: The aqueous sample (1 mL; containing 1 to 2 $\mu g \cdot mL^{-1}$ of H_2O_2) was added to the [Eu(tc)][15] (1 mL) in a cuvette, and the increase in luminescence intensity at > 616 nm was measured after 10 min (excitation at 405 nm). If a time-resolving reader was available, the lag time was adjusted to > 30 μs and the integration time to 100 μs.

[20] GOx assay procedure: The following solutions were placed in the wells of a microtiterplate: a) A [Eu(tc)] solution (in the ten-fold concentration of that given in [15], except for the buffer concentration); b) a solution of GOx (of unknown activity) in the same buffer; c) enough buffer to fill up to a volume of 200 μL; d) β-D-glucose (50 μL, 28 mmol L^{-1}) in buffer, to start the reaction. The increase in fluorescence intensity between 610 and 630 nm was measured over 10 min (ΔI_{10min}). The activity of GOx was calculated by use of a calibration graph, established by plotting ΔI_{10min} versus known activities of GOx. Note: citrate and phosphate interfere.

[21] Procedure for glucose assay: The [Eu(tc)] reagent solution[15] (1 mL) was placed in a cuvette, to which a solution of GOx (2 mL, 15 units, from Sigma, product no. G 2133) in MOPS buffer (10 mL) was added. The reaction was initiated by adding 2 mL of a sample containing between 2 and 10 mmol L^{-1} of glucose. The increase in luminescence intensity after 10 min (ΔI_{10min}) at 616 nm (excitation at 400–440 nm) was measured, and ΔI_{10min} used to read off the glucose concentration using a calibration graph established with β-D-glucose. Note: citrate and phosphate interfere.

[22] G. Liebsch, I. Klimant, B. Frank, G. Holst, O. S. Wolfbeis, *Appl. Spectrosc.* **2000**, *54*, 548 – 559.

[23] We used a Genios Plus microplate fluorometer from Tecan AG, Grödig, Austria.

[24] German Patent Application , No. 101 11 392.7 (9 March 2001).

[25] a) R. A. Evangelista, A. Pollak, E. F. G. Gudgin Templeton, *Anal. Biochem.* **1991**, *197*, 213 – 221; b) M. H. V. Werts, J. W. Hoofstraat, F. A. J. Geurts, J. W. Verhoven, *Chem. Phys. Lett.* **1997**, *276*, 196 – 201; c) B. Alpha-Bazin, G. Mathis, *Nucleosides Nucleotides* **1999**, *18*, 1277 – 1278.

[26] F. van de Rijke, H. Zijlmans, S. Li, T. Vail, A. K. Raap, K. Anton, R. S. Niebala, H. J. Tanke, *Nature Biotechnol.* **2001**, *19*, 273 – 275.

Conversion of *arachno*-Nonaborane into Azanonaborane: Unexpected Loss of a Firmly Integrated Boron Atom**

Mohamed E. El-Zaria,* Udo Dörfler, Matthias Hofmann, and Detlef Gabel

The polyhedral azanonaborane $(RH_2N)B_8H_{11}NHR$ (R = *i*Pr, **1**) is easily prepared by treating dimethylsulfido *arachno*-nonaborane 4-$(Me_2S)B_9H_{13}$ with three equivalents of a primary amine.[1] The reaction has been shown to proceed stepwise, by an initial ligand exchange to give 4-$(RH_2N)B_9H_{13}$, which reacts with an additional amine NH_2R^1 to give the mixed species $R^1H_2NB_8H_{11}NHR$.[1b] These compounds have been shown to constitute a good entry into azacarbaborane[2] and azametallaborane chemistry[3] and may also be useful in neutron capture therapy.[4] The transformation of $(Me_2S)B_9H_{13}$ to $(RH_2N)B_8H_{11}NHR$ involves the loss of one boron atom and cluster rearrangement. Herein we report the conversion of boron-substituted nonaboranes into azanonaboranes. These experiments make it possible to determine which boron atom is eliminated, and to speculate on the mechanism of the cluster rearrangement.

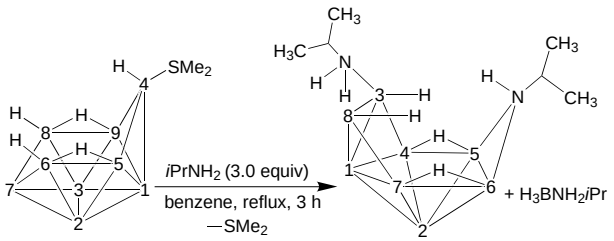
A variety of B-substituted $B_{10}H_{14}$ derivatives are known.[5] These can be converted readily by a two-step process via 6,9-$(Me_2S)_2B_{10}H_{12}$ derivatives into the corresponding *arachno*-nonaborane system.[6] We prepared some ethyl, bromine, and deutero derivatives of decaborane(14), which are stable under the reaction conditions (neither the bromine atom nor the ethyl group can be removed by Et_3N,[6a] and no deuterium exchange has been noted on heating the tetradeuterated $(Me_2S)B_9H_{13}$ with diethylamine under reflux in benzene[6c]).

[*] M. E. El-Zaria, Dr. U. Dörfler, Prof. Dr. D. Gabel
Department of Chemistry
University of Bremen
P.O. Box 330440, 28334 Bremen (Germany)
Fax: (+ 49) 421-218-2871
E-mail: marzok@uni-bremen.de
Dr. M. Hofmann
Anorganisch-Chemisches Institut
Ruprecht-Karls Universität Heidelberg
69120 Heidelberg (Germany)

[**] We thank the Deutsche Forschungsgemeinschaft for support.

 © 2002 WILEY-VCH Verlag GmbH & Co. KGaA, Weinheim 0044-8249/02/4123-4498 $ 20.00+.50/0

The following $(Me_2S)B_9H_{13}$ compounds with labeled B-atoms were prepared (Scheme 1, Table 1): Et at B^2 (**2**) or B^7 (**3**), Br at B^2 (**4**) or B^6 (**5**) or B^1 (**6**), D at B^1, B^2, B^3, and B^7 (**7**). The presence and the positions of the substituents were confirmed by NMR and IR spectroscopy and mass spectrometry.



Scheme 1. Conversion of the B_9 clusters **2**–**7** into the B_8N clusters **1**, **8**—**12**. The numbering of the clusters is given in Table 1, (*exo*-H atoms are omitted for clarity.

Table 1. Position of the substituents on the B_9 and B_8N clusters (see Scheme 1).

B_9	Substituent	Position on B_9 cluster	Position on B_8N cluster	B_8N
2	Et	2	2	**8**
3	Et	7	6	**9**
4	Br	2	2	**10**
5	Br	6	7	**11**
6	Br	1	–	**1**
7	D	1, 2, 3, 7	2, 5, 7 or 2, 4, 6	**12**

The labels of the B_9 cluster appeared in the following positions of the B_8N cluster after reaction with isopropylamine (Scheme 1, Table 1): Et at B^2 of **2** ⇒ B^2 in **8**; Et at B^7 of **3** ⇒ B^6 in **9**; Br of B^2 in **4** ⇒ B^2 in **10**, and the Br of B^6 in **5** ⇒ B^7 **11**, the Br of B^1 in **6** ⇒ bromine free B_8N cluster **1**. The 1,2,3,7-tetradeuterated nonaborane **7** was transformed to either the 2,4,6- or the 2,5,7- trideuterated B_8N cluster **12**. The NMR spectroscopy results show clearly the loss of one deuterium atom (Table 2) while it was not possible to determine whether the remaining three deuterium atoms were at B^2, B^5, and B^7, or at B^2, B^4, and B^6.

Thus, the boron atoms B^2, B^3, B^6, and B^7 in the B_9 cluster end up at the positions B^2, B^4, B^7, and B^6 in B_8N, respectively, while B^1 of the B_9 cluster is lost during the conversion (Scheme 1).

According to these results we suggest the following stepwise mechanism for the conversion starting with the amino-substituted B_9 cluster (Scheme 2):

a) Initially, an R^1NH_2 molecule attacks the 4-$(RH_2N)B_9H_{13}$ cluster at B^9 or B^5. This proposal is supported by two observations: 1) A 5-$(RH_2N)B_9H_{13}$ intermediate can be isolated from the reaction of 4-$(Me_2S)B_9H_{13}$ with RNH_2.[7] 2) No reaction is observed when 5-OMe-4-(iPrH$_2$N)B_9H_{12} is heated under refluxed with excess iPrNH$_2$ in benzene.
b) The RNH_2 moiety of B^4 exchanges its position from *exo* to *endo* as described in the literature[8] possibly aided by a weakened bond between B^9 and B^4.
c) The RNH_2 moiety migrates from B^4 to form a bridge between B^7 and B^8. This assumption is supported by the reaction rate of **3** (with Et on B^7) which is slower than that of **2** (with Et on B^2). In addition, the R^1NH_2 moiety migrates from B^9 to the *exo* position of B^4.[7] (See also ref. [6b] for an analogous migration.)
d) A third amine, R^2NH_2, attacks at B^9.
e) The B^8–B^9 and B^7–B^3 bonds opens and a diamond-square-diamond (DSD) rearrangement[9] which involves the atoms B^2, B^3, B^7, and B^8 yields a bond between B^2 and B^8.
f) Migration of R^1NH_2 from B^4 to B^1 leads to loss of the B^1-NH_2R^1 unit together with two additional H atoms. Specific elimination of B^1 was shown by reactions of the deuterium substituted **7** and the bromine substituted compound **6**. Closing the B^5–B^3, B^5–B^9, and B^6–B^4 connections completes the formation of the azanonaborane cluster.

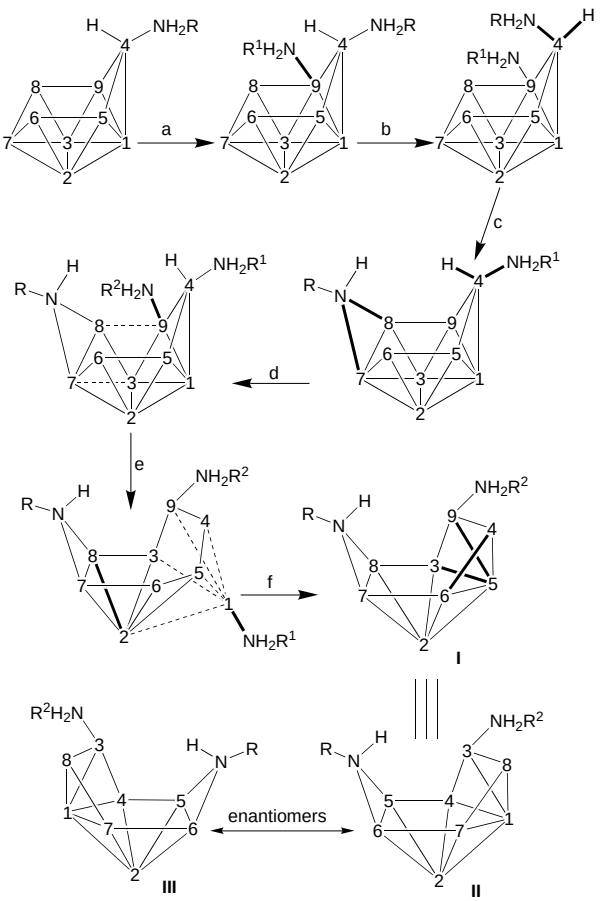
The experimental basis for the proposed mechanism is the fate of the boron atoms B^1, B^2, B^6, and B^7 (on the basis of the

Table 2. ^{11}B and ^1H NMR spectroscopic data ($CDCl_3$ at 20 °C, 200 MHz) for B_8N clusters **1**, **8**–**12**.[a]

B_8N	B^1	B^2	B^3	B^4	B^5	B^6	B^7	B^8	μ-H(4,5) μ-H(6,7)	NH
1	1.82	−55.61	−21.46	−31.76	−11.11	−11.11	−33.41	−30.76		
	[2.57]	[−0.65]	[1.29]	[0.86]	[2.51]	[2.51]	[0.86]	[0.55]	[−2.04]	[−1.56]
								[−0.64]	[−1.99]	
8	2.94	−43.91	−20.06	−32.3	−9.88	−10.6	−31.65	−30.62		
	[2.58]	[−]	[1.28]	[0.84]	[2.34]	[2.49]	[0.84]	[0.56]	[−1.9]	[−1.55]
								[−0.48]	[−1.75]	
9	0.76	−53.79	−21.73	−31.67	−10.6	0.76	−32.91	−30.68		
	[2.48]	[−0.55]	[1.26]	[0.77]	[2.21]	[−]	[0.77]	[0.52]	[−2.24]	[−1.36]
								[−0.55]	[−1.89]	
10	3.46	−41.77	−20.58	−28.8	−10.08	−10.08	−28.8	−28.8		
	[3.06]	[−]	[1.21]	[1.25]	[2.75]	[2.86]	[1.25]	[0.73]	[−1.34]	[−1.34]
								[−0.41]	[−1.34]	
11	12.06	−47.28	−18.09	−28.77	−7.41	−4.72	−38.92	−23.25		
	[3.59]	[−0.29]	[1.18]	[0.82]	[2.70]	[2.93]	[−]	[0.77]	[−2.47]	[−0.95]
								[−0.51]	[−1.72]	
12	1.64	−55.64	−21.46	−32.53	−10.65	−11.14	−31.82	−30.65		
	[2.49]	[−]	[1.36]	[0.74][b]	[−][c]	[2.55][c]	[−][b]	[0.46]	[−2.21]	[−1.64]
								[−0.61]	[−2.09]	

[a] All entries in ppm, δ(1H) in square parentheses All spectra measured on a Bruker DP 200 spectrometer. [b], [c] A clear assignment of the deuterium substitutes to either B^5 or B^6 or to B^4 or B^7 is not possible.

 © 2002 WILEY-VCH Verlag GmbH & Co. KGaA, Weinheim 0044-8249/02/4123-4499 $ 20.00+.50/0



Scheme 2. Mechanistic pathway of the conversion of the nonaborane cluster into the azanonaborane cluster (**I** IUPAC numbering of the B_9 cluster, **II** and **III** IUPAC numbering of the B_8N cluster).[10] Bold lines: new bonds; dashed lines: bonds to be broken.

experiments with the Et- and Br-substituted clusters) and B^3 (concluded from the experiments with a tetradeuterated cluster). Computed ^{11}B NMR chemical shifts, supported by 2D–^{11}B COSY and ^1H CW ^{11}B NMR spectra showed the Et group to be connected to B^6, opposite to the *exo*-amino ligand at B^3 in the B_8N cluster **9**; the data further indicated that the Br atom at B^6 in the B_9 cluster **5** is located at B^7 and not at B^4 in the B_8N cluster **11**. The fate of the boron atoms B^5, B^8, and B^9 has not been clarified, but the proposed mechanism would require only a minimal rearrangement of the bonds (one DSD rearrangement and the closing of the cluster after the loss of B^1). The loss of B^1, which is *not* part of the open face, is surprising. Quantum-mechanical computations might give indications about the feasibility of the proposed pathway, the relative stability of the proposed intermediates, the origin of the H atoms which leave together with B^1, and the rearrangement of the other H atoms.

Experimental Section

1, **8**–**12**: Isopropylamine (0.1 g, 1.74 mmol) was added to a solution of $(Me_2S)B_9H_{13}$ in dry benzene (10 mL, 0.1 g) at room temperature. The mixture was heated to reflux for 3 h. All volatile components were removed under vacuum and the resulting substance was recrystallized from ethanol:water (1:1). Compounds **8** and **9** were purified by TLC by using CH_2Cl_2 as eluent ($R_f = 0.31$). For further purification the substance was dissolved in $CHCl_3$:hexane (1:3) at −20 °C. The solution was filtered and the resulting filtrate was evaporated to dryness to yield the purified product. **1** (DCI): *m*/*z* (%) 214 (95) [M^+]; **8**, **9** MS (EI, 750 eV, 200 °C): *m*/*z* (%) 242 (24) [M^+]; **10**, **11**, (EI, 750 eV, 200 °C): *m*/*z* (%) 293 (18) [M^+]; **12** (FAB$^+$): *m*/*z* (%) 217 (100) [M^+].

Received: April 30, 2002
Revised: September 2, 2002 [Z19208]

[1] B. M. Graybill, A. R. Pitochelli, M. F. Hawthorne, *Inorg. Chem.* **1962**, 1, 626–631;b) U. Dörfler, M. Thornton-Pett, J. D. Kennedy, *J. Chem. Soc. Dalton Trans.* **1997**, 2547–2550.
[2] U. Dörfler, D. L. Ormsby, R. Greatrex, J. D. Kennedy, *Inorg. Chim. Acta.* **2000**, 304, *268–273.*
[3] a) U. Dörfler, J. D. Kennedy, L. Barton, C. M. Collins, N. P. Rath, *J. Chem. Soc. Dalton Trans.* **1997**, 707–708; b) U. Dörfler, P. A. Salter, X. L. R. Fontaine, N. N. Greenwood, J. D. Kennedy, M. Thornton-Pett, *Collect. Czech. Chem. Commun.* **1999**, *64*, 947–958.
[4] a) M. E. El-Zaria, U. Dörfler, D. Gabel, *J. Med. Chem.*, in press; b) C. Bauer, U. Dörfler, D. Gabel, *Eur. J. Med. Chem.*, in press.
[5] a) N. J. Blay, I. Dunstan, R. L. Williams, *J. Chem. Soc.* **1960**, 430–433; b) J. A. Dopke, D. F. Gaines, *Inorg. Chem.* **1999**, *38*, 4896–4897; c) R. F. Sprecher, B. E. Aufderheide, G. W. Luther III, J. C. Carles, *J. Chem. Soc.* **1974**, *96*, 4404–4410.
[6] a) T. L. Heying, C. Naar-Colin, *Inorg. Chem.* **1964**, *3*, 282–285; b) H. Beall, D. F. Gaines, *Inorg. Chem.* **1998**, *37*, 1420–1422; c) G. M. Bodner, F. R. Scholer, L. J. Todd, L. E. Senor, J. C. Carter, *Inorg. Chem.* **1971**, *10*, 942–945.
[7] L. F. K. Callaghan, U. Dörfler, D. T. McGrath, M. Thornton-Pett, D. J. Kennedy, *J. Organomet. Chem.* **1998**, *550*, 441–444.
[8] a) X. L. R. Fontaine, J. D. Kennedy, *J. Chem. Soc. Dalton Trans.* **1987**, 1573–1575; b) J. Müller, P. Paetzold, U. Englert, J. Runsink, *Chem. Ber.* **1992**, 125, 97–102.
[9] R. Hoffmann, W. N. Lipscomb, *Inorg. Chem.* **1963**, *2*, 231–232.
[10] G. J. Leigh in *Nomenclature of Inorganic Chemistry*, Blackwell, Oxford, **1990**, pp. 217–225.

Fluorous Biphasic Catalysis without Perfluorinated Solvents: Application to Pd-Mediated Suzuki and Sonogashira Couplings**

Carl Christoph Tzschucke, Christian Markert, Heiko Glatz, and Willi Bannwarth*

In catalytic reactions easy handling of the catalyst together with its straightforward recovery and possible reuse remain an important topic. A widespread solution to reach these goals is the application of immobilized catalysts. Immobilization can be achieved by covalent attachment to organic polymers or inorganic support materials.[1] Alternatively, catalysts can be adsorbed on silica gel[2–4] or on reversed-phase silica gel.[5] In some cases the immobilization has a beneficial effect on the catalyst's stability.[6,7] One profound advantage of such supported catalysts is the easy separation from the reaction

[*] Prof. Dr. W. Bannwarth, Dipl.-Chem. C. C. Tzschucke, Dipl.-Chem. C. Markert, Dipl.-Chem. H. Glatz
Institut für Organische Chemie und Biochemie
Albert-Ludwigs-Universität Freiburg
Albertstrasse 21, 79104 Freiburg (Germany)
Fax: (+49) 761-203-8705
E-mail: willi.bannwarth@organik.chemie.uni-freiburg.de

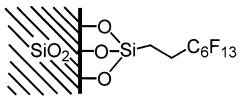
[**] This work was supported by Fluka (Buchs, Switzerland).

 © 2002 WILEY-VCH Verlag GmbH & Co. KGaA, Weinheim 0044-8249/02/4123-4500 $ 20.00+.50/0

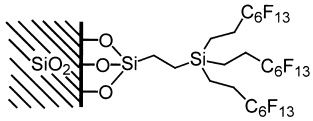
product by filtration or decantation. Ideally, without further purification, there should be little or no contamination of the product with transition metals, which is important when the substances are to be tested in biological assays. A further aspect is the straightforward recovery and reuse of the catalyst. Generally, simplification of workup protocols and handling of small amounts of catalysts is especially important in multiparallel and automated synthesis in combinatorial chemistry.[8,9]

Biphasic systems comprising perfluoro-tagged catalysts, which can be extracted out of organic products with fluorous solvents, have emerged as alternative tools for the separation, recovery, and reuse of catalysts as well as for simplified product isolation.[10–15] This method, known as fluorous biphasic catalysis (FBC), has been applied to numerous catalytic reactions.[8,10,16–31] Although perfluorinated solvents have certain advantages, they are expensive and environmentally persistent.[32] Thus, it would be beneficial to perform separation and recovery of perfluoro-tagged catalysts without recourse to a perfluorinated solvent as a second liquid phase. Recently, the thermomorphic solution behavior of a fluorous phosphane was utilized in this context.[33] While fluorous reversed-phase silica gel (FRPSG) has found application as the stationary phase for chromatographic separation of perfluoro-tagged compounds,[34,35] it has not been used to support catalysts.

Our rational was to substitute fluorous solvents by FRPSG, thus gaining easy separation and at the same time retaining the advantages of soluble perfluoro-tagged catalysts. As a first example for this strategy, we report on the immobilization of perfluoro-tagged bis(triphenylphosphane)palladium complexes on FRPSG and their successful application to the Suzuki and Sonogashira C–C coupling reactions without need for a fluorous solvent.



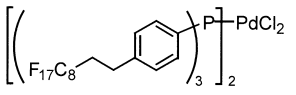
1



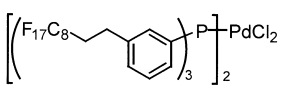
2

The fluorous solid supports **1** and **2** were prepared by adapted standard procedures.[36,37] Palladium complexes **3a–c**were synthesized by our established procedures.[30]

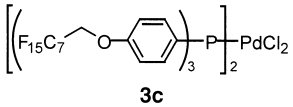
To immobilize the complexes, FRPSG was added to a solution of the respective complex in diethyl ether and hexafluorobenzene and the solvent was evaporated. The immobilized precatalyst is an air-stable, free-flowing powder. For ease of handling, especially in separations, FRPSG with a coarse grain (100–300 μm particle size) was used. Silica gels **1** containing 0.1, 1.0, 10, and 100 mg complex per g FRPSG, respectively, were evaluated in the Suzuki cross-coupling of phenylboronic acid and *para*-nitrobromobenzene and in the Sonogashira coupling of phenylacetylene and *para*-nitrobromobenzene (Table 1).



3a



3b



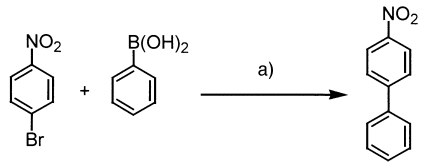
3c

Table 1. Suzuki and Sonogashira reactions with different amounts of complex **3a**.

Entry	Catalyst loading of FRPSG [mg g^{-1}]	Catalyst loading [mol%]	Yield [%][a]
Suzuki			
1	100	1.5	> 98 (> 98, 92)
2	10	0.1	> 98 (> 98)
3	1	0.01	> 98 (> 98)
4	0.1	0.001	86 (45)
Sonogashira			
5	100	2	> 98 (97, 71)
6	10	0.2	> 98 (30, 0)
7	1	0.02	22 (0)
8	0.1	0.002	11 (0)

[a] The yields in parentheses are for the second (and third) runs with the same catalyst.

In the Suzuki reaction (Scheme 1) complete conversions were obtained with catalyst loadings down to 0.01 mol% and the catalyst could be recycled (Table 1, entries 1–3). With 0.001 mol% of catalyst, the yield in the first run was 86% and dropped to 45% in the second run (Table 1, entry 4). This corresponds to a cumulated turnover number (TON) of 131 000.



Scheme 1. Suzuki reactions performed with **3a–c** immobilized on support **1** as catalysts. a) 0.001–1.5 mol% catalyst, DME, 2 M aq. Na_2CO_3, 80 °C.

Further experiments were performed by using 10 mg Pd complex per g FRPSG, and a catalyst loading of 0.1 mol%. The three different complexes **3a–c** were used in the coupling of *para*-nitrobromobenzene and phenylboronic acid. Complexes **3a** and **3b** both have an ethylene spacer separating the perfluoroalkyl chain and the phenyl ring, the perfluoro tag is attached to the *para* or *meta* position, respectively. In complex **3c** an OCH_2 spacer is used. Earlier experiments had shown that spacers between the perfluoroalkyl chain and the aromatic ring are advantageous for the stability of the catalysts.[38]

All three catalysts gave complete conversions and could be recycled without significant decrease of activity (Table 2). Catalyst leaching was assessed for the coupling of *para*-nitrobromobenzene and phenylboronic acid with 0.1 mol% of complex **3a**. Using support **1**, a Pd content of 5.4 ppm in the crude organic product was determined by inductively coupled

 © 2002 WILEY-VCH Verlag GmbH & Co. KGaA, Weinheim 0044-8249/02/4123-4501 $ 20.00+.50/0

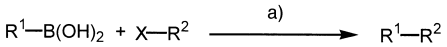
Table 2. Suzuki reactions with complexes **3a–c** immobilized on **1** (see Scheme 1).

Entry	Pd complex	Yield [%][a]
1	**3a**	> 98 (93, 93, 93)
2	**3b**	96 (98, 93, 91)
3	**3c**	> 98 (96, 95, 95)

[a] The yields in parentheses are for the second (third, and fourth) runs with the same catalyst.

plasma mass spectrometry (ICP-MS),[39] which corresponds to 1.8% of the total Pd. In the inorganic residue, which consists mainly of Na_2CO_3, 0.2 ppm of Pd was found, which corresponds to less than 0.1% of the Pd. Thus, less than 1.9% of the catalyst was washed off from FRPSG **1**. In an identical experiment using support **2** a Pd leaching of less than 1.6% was determined. Accordingly, the nature of the fluorous solid support seems to influence the leaching only marginally.

The catalyst **3a** on support **1** was tested with a number of different substrates (Scheme 2, Table 3). Yields were generally high for electron-deficient aryl bromides (Table 3,



Scheme 2. Suzuki reactions with different substrates performed with **3a** immobilized on support **1** as catalyst. X = Br, I. a) 0.1 mol% catalyst, DME, 2 M aq. Na_2CO_3, 80 °C, 15 h.

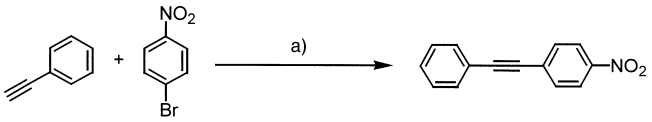
Table 3. Suzuki reactions with different substrates, using 0.1 mol% **3a** on support **1** (see Scheme 2).

Entry	R^1	R^2	Yield [%][a]
1	Ph	4-NO_2-C_6H_4	95 (97, 97)
2	Ph	4-CH_3CO-C_6H_4	> 98 (85, 14)
3	Ph	4-EtOOC-C_6H_4	93 (69, 4)
4	Ph	2-naphthyl	82 (17)
5	Ph	3,4-$F_2C_6H_3$	78 (6, 0)
6	Ph	3,4,5-$F_3C_6H_2$	83 (34, 2)
7	Ph	4-MeO-C_6H_4	48 (2)
8[b]	Ph	4-MeO-C_6H_4	76, (75, 52)
9[c]	Ph	4-MeO-C_6H_4	70, (10, 0)
10[d]	Ph	4-MeO-C_6H_4	73 (4, 0)
11	4-MeO-C_6H_4	4-NO_2-C_6H_4	94 (97, 94)
12	4-MeO-C_6H_4	4-CN-C_6H_4	94 (97, > 98)
13	4-MeO-C_6H_4	4-CH_3CO-C_6H_4	85 (> 98, 29)
14	4-MeO-C_6H_4	4-EtOOC-C_6H_4	72 (56, 19)
15	3-thienyl	4-NO_2-C_6H_4	89 (0)
16	3-thienyl	4-CH_3CO-C_6H_4	61 (0)
17	Cy	4-NO_2-C_6H_4	0 (0)
18	Cy	4-CH_3CO-C_6H_4	0 (0)

[a] The yields in parentheses are for the second (and third) runs with the same catalyst. [b] 4-Iodoanisole was used instead of 4-bromoanisole. [c] 0.3 mol% **3a** was used. [d] 0.2 mol% of the corresponding phosphane was added.

entries 1–6, and 11–15) and for aryl iodides (Table 3, entry 8). For electron-rich *para*-bromoanisole only 48% conversion was achieved (Table 3, entry 7), but higher conversions were obtained with either higher catalyst loading (Table 3, entry 9) or additional phosphane ligand (Table 3, entry 10). Recycling was successful for very reactive substrates (Table 3, entries 1, 11, and 12). For all other substrates a significant decrease of catalyst activity was observed, the decrease being the greater, the less reactive the halide was. With 3-thienylboronic acid high conversions were obtained in the first run, but no conversion was found with recycled catalyst and only the aryl bromide was recovered (Table 3, entries 15 and 16). This complete loss of activity might be due to catalyst poisening by the thiophene. With cyclohexylboronic acid no conversion was observed (Table 3, entries 17 and 18).

In the Sonogashira reaction (Scheme 3) with 2 mol% catalyst high yields were obtained for three successive experiments (Table 1, entry 5). With 0.2 mol% catalyst conversion was still complete, but the yield dropped significantly when the catalyst was reused (Table 1, entry 6). With lower catalyst loadings, conversions were not complete within 14 h and the recovered FRPSG showed no catalytic activity (Table 1, entries 7 and 8).



Scheme 3. Sonogashira reactions performed with complex **3a** immobilized on support **1** as catalyst. a) 0.002–2 mol% catalyst, CuI, DME, nBu$_2$NH, 100 °C, 14 h.

In summary, we could demonstrate the immobilization of perfluoro-tagged palladium catalysts on FRPSG, and their use for Suzuki and Sonogashira cross-coupling reactions. The catalysts showed activities comparable to those found in liquid–liquid FBC. The catalysts were separated from the product by simple decantation. Leaching was as low as 1.9% and 1.6% for **1** and **2**, respectively, and the recovered catalyst could be reused in several instances. Because of the dilution of the catalyst with FRPSG, very small amounts of catalysts could be easily and precisely handled. In contrast to conventional FBC approaches, no fluorous solvent was needed for the reaction and the isolation and recovery of the catalyst. An advantage of our strategy compared to conventional covalent catalyst immobilization is that the same support can be used for different catalysts, without the need for a separate linker unit. Before attachment, the catalyst can be characterized by usual methods. It is also conceivable to adjust the reaction conditions in such a way that the catalyst is detached from the FRPSG during the reaction and re-attached during workup. Further investigations to extend this immobilization strategy to other catalytic systems are currently underway.

Experimental Section

General procedure for Suzuki cross-coupling reactions: A 50 mL Schlenk tube was charged with FRPSG supported catalyst (100 mg), evacuated, and refilled with argon (3×). Stock solutions of the aryl halide (0.3 M in dimethoxyethane (DME), 1.0 mL, 0.3 mmol), the boronic acid (0.33 M in DME (with 4-methoxyphenylboronic acid methanol was used instead), 1.0 mL, 0.33 mmol) and Na_2CO_3 (2 M in water, 1.0 mL, 2.0 mmol) were added. The tube was sealed with a screw cap and shaken at 80 °C for 15 h. The reaction mixture was cooled to 0 °C and the liquid phase was removed under argon with a pipette. The FRPSG was washed with DME (2 × 2 mL), water (2 × 2 mL), and DME (2 × 2 mL). The combined liquid phases were diluted with water (40 mL) and brine (20 mL) and were extracted with *tert*-butyl methyl ether (3 × 20 mL). The combined extracts were concentrated in vacuo, the residue was take up in diethyl ether (2 mL), put on a plug of

 © 2002 WILEY-VCH Verlag GmbH & Co. KGaA, Weinheim 0044-8249/02/4123-4502 $ 20.00+.50/0

neutral alumina (3 mL, activity 2–3) and eluted with diethyl ether (~14 mL). Evaporation of the solvent gave the product. Yields were determined by ^{1}H NMR integration against a known amount of 1,2-dibromoethane. The immobilized catalyst was reused as such in further experiments.

Determination of catalyst leaching: A 100 mL Schlenk flask was charged with FRPSG supported catalyst (500 mg, 10 mg Pd complex per g FRPSG, 1.48 μmol), 4-bromonitrobenzene (303 mg, 1.50 mmol), and phenylboronic acid (205 mg, 1.68 mmol), evacuated and refilled with argon (3×). DME (10 mL) and Na_2CO_3 (2 M in water, 5.0 mL, 10.0 mmol) were added. The flask was shaken under argon at 80 °C for 15 h, and then the reaction mixture was cooled to room temperature and filtered. The residue was washed with DME (2×10 mL), water (2×10 mL), and again with DME (2×10 mL), and the organic and aqueous filtrates were collected separately. The solvents were removed in vacuo, the resulting solids were powdered, and the Pd content determined by ICP-MS.

Received: June 24, 2002 [Z19606]

[1] B. Clapham, T. S. Reger, K. D. Janda, *Tetrahedron* **2001**, *57*, 4637–4662.
[2] C. Bianchini, D. G. Burnaby, J. Evans, P. Frediani, A. Meli, W. Oberhauser, R. Psaro, F. Vizza, *J. Am. Chem. Soc.* **1999**, *121*, 5961–5971.
[3] J. P. Arhancet, M. E. Davis, J. S. Merola, B. E. Hanson, *Nature* **1989**, *339*, 454–455.
[4] M. E. Davis, *Chemtech.* **1992**, 498–502.
[5] M. S. Anson, A. R. Mirza, L. Tonks, J. M. J. Williams, *Tetrahedron Lett.* **1999**, *40*, 7147–7150.
[6] I. Fenger, C. Le Drian, *Tetrahedron Lett.* **1998**, *39*, 4287–4290.
[7] D. Seebach, A. Heckel, *Helv. Chim. Acta* **2002**, *85*, 913–926.
[8] C. C. Tzschucke, C. Markert, W. Bannwarth, S. Roller, A. Hebel, R. Haag, *Angew. Chem.* **2002**, *114*, 4136–4173; *Angew. Chem. Int. Ed.* **2002**, *41*, 3964–4001.
[9] W. Bannwarth, E. Felder, *Combinatorial Chemistry : A practical approach*, Wiley-VCH, Weinheim, **2000**.
[10] I. T. Horváth, J. Rábai, *Science* **1994**, *266*, 72–75.
[11] E. de Wolf, G. van Koten, B.-J. Deelman, *Chem. Soc. Rev.* **1999**, *28*, 37–41.
[12] B. Cornils, *Angew. Chem.* **1997**, *109*, 2147–2149; *Angew. Chem. Int. Ed. Engl.* **1997**, *36*, 2057–2059.
[13] A. Endres, G. Maas, *Chem. Unserer Zeit* **2000**, *34*, 382–393.
[14] R. H. Fish, *Chem. Eur. J.* **1999**, *5*, 1677–1680.
[15] I. T. Horváth, *Acc. Chem. Res.* **1998**, *31*, 641–650.
[16] I. T. Horváth, G. Kiss, R. A. Cook, J. E. Bond, P. A. Stevens, J. Rábai, E. J. Mozeleski, *J. Am. Chem. Soc.* **1998**, *120*, 3133–3143.
[17] J. J. J. Juliette, I. T. Horváth, J. A. Gladysz, *Angew. Chem.* **1997**, *109*, 1682–1684; *Angew. Chem. Int. Ed. Engl.* **1997**, *36*, 1610–1612.
[18] J. J. J. Juliette, D. Rutherford, I. T. Horváth, J. A. Gladysz, *J. Am. Chem. Soc.* **1999**, *121*, 2696–2704.
[19] I. Klement, H. Lütjens, P. Knochel, *Angew. Chem.* **1997**, *109*, 1605–1607; *Angew. Chem. Int. Ed. Engl.* **1997**, *36*, 1454–1456.
[20] J.-M. Vincent, A. Rabion, V. K. Yachandra, R. H. Fish, *Angew. Chem.* **1997**, *109*, 2438–2440; *Angew. Chem. Int. Ed. Engl.* **1997**, *36*, 2346–2349.
[21] G. Pozzi, M. Cavazzini, F. Cinato, F. Montanari, S. Quici, *Eur. J. Org. Chem.* **1999**, 1947–1955.
[22] G. Pozzi, F. Cinato, F. Montanari, S. Quici, *Chem. Commun.* **1998**, 877–878.
[23] B. Betzemeier, F. Lhermitte, P. Knochel, *Tetrahedron Lett.* **1998**, *39*, 6667–6670.
[24] B. Betzemeier, F. Lhermitte, P. Knochel, *Synlett* **1999**, 489–491.
[25] A. Endres, G. Maas, *Tetrahedron Lett.* **1999**, *40*, 6365–6368.
[26] R. King, D. Sinou, G. Pozzi, A. Choplin, F. Quignard, S. Busch, S. Kainz, D. Koch, W. Leitner, *Tetrahedron Lett.* **1998**, *39*, 9439–9442.
[27] B. Betzemeier, P. Knochel, *Angew. Chem.* **1997**, *109*, 2736–2738; *Angew. Chem. Int. Ed. Engl.* **1997**, *36*, 2623–2624.
[28] J. Moineau, G. Pozzi, S. Quici, D. Sinou, *Tetrahedron Lett.* **1999**, *40*, 7583–7686.
[29] C. Markert, W. Bannwarth, *Helv. Chim. Acta* **2002**, *85*, 1877–1882.
[30] S. Schneider, W. Bannwarth, *Angew. Chem.* **2000**, *112*, 4293–4296; *Angew. Chem. Int. Ed.* **2000**, *39*, 4142–4145.
[31] S. Schneider, W. Bannwarth, *Helv. Chim. Acta* **2001**, *84*, 735–742.
[32] A. R. Ravishankara, S. Solomon, A. A. Turnipseed, R. F. Warren, *Science* **1993**, *259*, 194–199.
[33] M. Wende, R. Meier, J. A. Gladysz, *J. Am. Chem. Soc.* **2001**, *123*, 11490–11491.
[34] D. P. Curran, Y. Oderaotoshi, *Tetrahedron* **2001**, *57*, 5243–8253.
[35] D. P. Curran, *Synlett* **2001**, 1488–1496.
[36] M. D. Matteucci, M. H. Caruthers, *J. Am. Chem. Soc.* **1981**, *103*, 3185–3191.
[37] H. Engelhardt, P. Orth, *J. Liq. Chromatogr.* **1987**, *10*, 1999–2022.
[38] S. Schneider, Dissertation, Albert-Ludwigs-Universität, Freiburg, **2000**.
[39] Pd analysis was performed by Solvias AG, Basel, Switzerland.

9,9-Dilithiofluorene: The First Crystal-Structure Analysis of an α,α-Dilithiated Hydrocarbon**

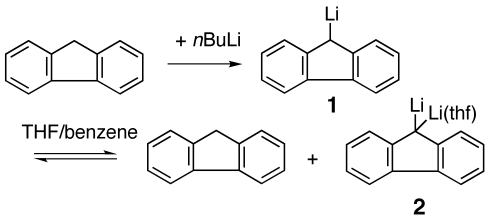
Gerald Linti,* Alexander Rodig, and Hans Pritzkow

Lithiated hydrocarbons are one of the most important classes of compounds in organoelement chemistry. Many of these compounds have been structurally investigated in solution and the crystalline state, as well;[1–3] di- and oligometallated species earned special interest.[4,5] Dilithiomethane is mentioned as one example here, it is available from the thermolysis of lithium methanide[6,7] and used in many synthetic procedures. A series of oligomeric structures of lithium methanide was investigated with quantum-chemical methods, in which carbon atoms take the coordination number six.[8] In monomeric dilithiomethane the planar coordination of the carbon atom is only less stable than the tetrahedral coordination of the carbon atom by 71 kJ mol^{-1}.[9,10] However, the final structure in solution and of the solid state has not been determined.[11,12] Several substituted derivatives, such as Me_3CCHLi_2, $Me_3SiCHLi_2$,[13] and the title compound 9,9-Dilithiofluorene,[14] have been synthesized, but their structures are not known. It was possible to solve the crystal structures of heteroatom substituted derivatives, such as $PhS(O)(NMe)CLi_2Ph$,[15] $(Me_3SiNPPh_2)_2CLi_2$,[16,17] $(MeO)_2P(O)CLi_2SiMe_3$ (as aggregate with dimethylamide),[18] and $PhSO_2CLi_2(SiMe_3)$,[19] where Li–O and Li–N bonds dominate the structures. The anion $(CHPMe_2NSiMe_3)^{2-}$ together with $BuMe_2SiO^-$ forms the backbone of a Li_{14} cluster.[20] $[\{(Me_3Si)_2CH\}_6Al_2CH_2Li_2]$ was considered as a R_3Al-adduct to CH_2Li_2.[21] Herein, we describe the crystal structure of the 9,9-dilithiofluorene complex **2** [Eq. (1)].

[*] Prof. Dr. G. Linti, Dr. A. Rodig, Dr. H. Pritzkow
Anorganisch-Chemisches Institut
Universität Heidelberg
Im Neuenheimer Feld 270, 69120 Heidelberg (Germany)
Fax: (+49) 6221-54-6617
E-mail: gerald.linti@urz.uni-heidelberg.de

[**] This work was supported by the Deutsche Forschungsgemeinschaft and the Fonds der Chemischen Industrie.

If lithiofluorene **1** is dissolved in a solvent mixture of benzene:THF (10:1) at 0 °C pale orange cubes of **2** crystallize [Eq. (1)]. On redissolving of crystallized **2** in THF or benzene, in the ^{1}H and ^{13}C NMR spectra only the resonance signals of **1** can be observed. Therefore, it was not possible to investigate **2** in solution. Donor-free $Li_2C_{13}H_8$ has already been prepared by the thermolysis of lithiofluorene and its constitution demonstrated by deuterolysis experiments.[14]



(1)

Compound **2** crystallizes together with one molecule of benzene in the orthorhombic crystal system (space group *Pnma*).[22] In the crystal structure the fluorenylidene units are each linked together by two lithium atoms to form polymeric chains (Figure 1). These can be considered as a double ribbon

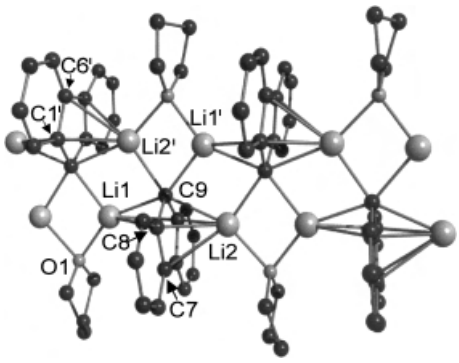


Figure 1. Section of the polymeric structure of **2** (hydrogen atoms are omitted for clarity). Selected bond lengths [pm] and angles [°]: C9-Li1 222.9(3), C9-Li1′ 216.1(13), C9-Li2′ 218.6(3), C9-Li2 234.3(3), C1-Li1 242(1), C1-Li2, 237(1), C6-Li2 257(2), C7-Li2 253(1), C8-Li1 245(2), C10-Li2 241(2), Li1-O1 197.8(3), Li2-O1 205.4(3), C1-C9 147.4(7), C8-C9 141.0(8), C1-C6 145.2(9), C6-C7 141.7(6), C7-C8 144.5(9) Li1-Li2′ 267.5(4), Li1-Li2′ 265.3(4); Li1-C9-Li2 75.9(1), C1-C9-C8 102.3(3). C1 and C6 are not labeled, however, they are symmetry equivalents of C1′ and C6′.

of lithium atoms, which are bridged alternately by fluorenylidene groups and THF molecules, that is, a planar band of edge-connected Li_2C_2 and Li_2CO rings results. The Li–Li separations within the rings (d_{Li-Li} = 264.9(4)–268.0(4) pm) are similar to those in aggregated lithium alkanides $(LiR)_n$ (R = Me, Et, Bu).[23–25] Markedly longer (d_{Li-Li} = 427 pm) are the fluorene-bridged Li–Li separations. The lithium cations coordinate to both sides of the five-membered ring of the fluorene groups. Here, the coordination of Li1 (d_{Li-C} = 222.9, 242.3, 245.3, 279.5, and 285.6 pm) may be considered as η^3, that of Li2 (d_{Li-C} = 234.3–256.7 pm) as η^5. Both of the lithium atoms are shifted from the center of the ring towards C9. In the $[Cp_2Li]^-$ ion (Cp = C_5H_5) the lithium atom is positioned almost between the centers of the rings and the Li–C separations are in a narrower range (d_{Li-C} = 229.8(4)–236.2(3) pm).[26] In addition, every lithium atom has an interaction with the carbon atom C9 of a second fluorenylidene ring on the other side of the ribbon (d_{Li-C} = 216.1, 218.6 pm) and a Li–O bond. The THF molecules coordinate in a bridging mode between two lithium atoms. The distances between the oxygen atom and the lithium centers are in the normal range (d_{Li-O} = 198.3(3)–205.7(3) pm).[1]

The atom C9 is coordinated by four lithium ions; the corresponding lithium–carbon separations are the shortest found in **2** (d_{Li-C} = 215.9(13), 219.1(3), 222.4(3), and 234.2(3) pm). On the whole, C9 is sixfold coordinate. Usually, this coordination number is only found for carbon in clusters such as $[\{C(AuPPh_3)_6\}]^{2+}$.[27,28] In quantum-chemically calculated structures of $(CH_2Li_2)_2$ as well as in $[(Me_3Si)_2CH]_6Al_2$-CH_2Li_2,[29], short Li–C bonds lead to a coordination number of six for the carbon atoms. A comparison of the lithium–carbon bonds of the six coordinated carbon atoms in $(CH_2Li_2)_2$ (d_{Li-C} = 195.5 pm and 239.7 pm; Figure 2) and **2** reveals, at least regarding these distances, good agreement of the calculated model with the experimental data for **2**.

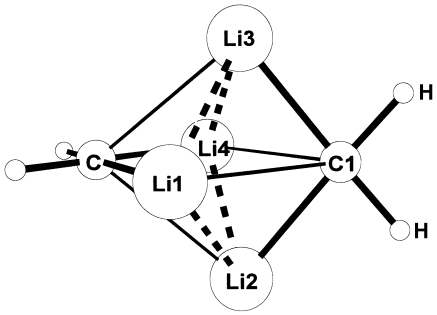


Figure 2. Calculated structure of $(CH_2Li_2)_2$ from ref. [29]. Selected bond lengths [pm] and angles [°]: Li1-Li2 223.4, Li1-Li4 303.4, Li1-C1 239.7, Li2-C1 195.5; H-C1-H 97.76, Li4-C1-Li1 101.79.

To get a better insight into the bonding and structural situation of this class of compounds, density functional calculations on a model compound by using an uniform SV(P) base set for all atoms were performed (B-P86 functional).[30–35] As a model system, which is treatable by quantum-chemical methods, **3**, which exhibits only a section of the polymeric structure of **2** was used. This section consists of two fluorenylidene fragments, six lithium atoms, and six water molecules (which replace THF). Thus, **3** is a doubly positive charged $[Li_6(C_{13}H_8)_2(H_2O)_6]^{2+}$ ion. The basic structural motif of **2** remains nearly unchanged (Figure 3). This conformity is also found with the corresponding bond lengths and angles. Deviations in the structure of **2** compared to **3** can be derived from the enormous shortening of the original polymeric molecule chain in **2** to the "molecule chain" in **3**, which contains only two fluorenylidene units.

In addition, the shared electron numbers (SEN), obtained by Ahlrichs–Heinzmann population analyses,[36] confirm, that there are no significant lithium–lithium interactions in **3** ($SEN_{Li-Li} < 0.1$). It is found, too, that in **3** the negative partial charges are located mainly at the carbon centers C9 and C22 ($\delta_{C9,C22}$ = -0.5, δ_{Li} = + 0.5).

The structures of **2** and **3** differ markedly from that of **1**, which forms a sandwich-type dimer, where the lithium ions

 © 2002 WILEY-VCH Verlag GmbH & Co. KGaA, Weinheim 0044-8249/02/4123-4504 $ 20.00+.50/0

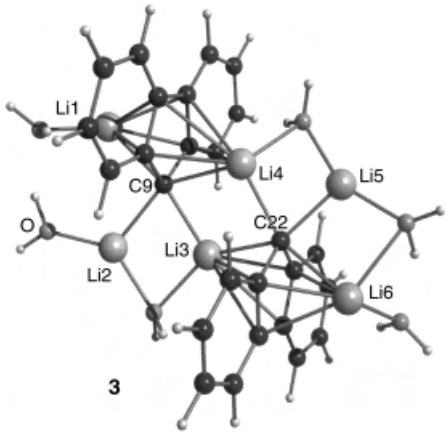


Figure 3. View of the calculated structure of **3**. Selected lithium–carbon bond lengths and the lithium–lithium separations [pm] of **3**: Li1-C9 228.8, Li2-C9 219.4, Li3-C9 220.3, Li4-C9 234.3, Li3-C22 222.3, Li4-C22 220.0, Li5-C22 214.7, Li6-C22 228.7, Li1-$C_{fluorene}$ 227.6–239.5, Li3-$C_{fluorene}$ 220.3–276.5, Li4-$C_{fluorene}$ 234.3–273.7, Li6-$C_{fluorene}$ 228.7–249.7, Li2-Li3 260.4, Li3-Li4 271.5, Li4-Li5 269.7, Li5-Li6 292.6.

are coordinated by the six-membered rings.[37] For **1**, a polymeric array with coordination of the five-membered rings is calculated to be less stable by 112 kJ mol^{-1}. Such a structure would correspond to the structures of CpLi,[38] $[Cp_2Li]^-$,[26] and $[Cp^B_2]^-$[39] ($Cp^B = (C_6H_5CH_2)_5C_5$). In fluorenyl lithium bis(quinuclidin) the lithium atom is bonded to C1, C2, and C9 in a η^3-mode.[40] Comparing two monomeric dilithiofluorene molecules **4** and **5**, which have a lithium atom bonded terminal to C9 as well as a second one, bonded to the five- or six-membered ring respectively, the structure of **5** is calculated to be more stable by 30 kJ mol^{-1} (Figure 4). In **4** the negative charge is located mainly at C9, as is the case in **3**. In contrast, in **5**, C9 and C8 ($\delta = -0.32$) as well as C1 and C12 ($\delta = -0.13$, -0.19) have high negative partial charges.

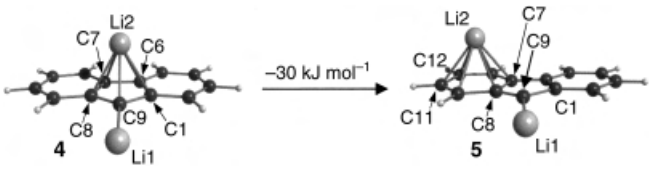


Figure 4. View of the calculated structures of **4** and **5**. Lithium–carbon bond lengths [pm]: **4**: Li1-C9 198.6, Li2-C9 214.9, Li2-C1 216.7, Li2-C8 216.7, Li2-C6 224.6, Li2-C7 224.5; **5**: Li1-C9 198.6, Li2-C 223.9–226.3.

The observed structure of **2** is remarkable for several reasons. In this X-ray structurally characterized dilithiated hydrocarbon an unsymmetrical η^5 coordination of the fluorene group is present. Therefore, **2** contains a carbon atom, which is six-coordinate, being bound to four lithium and two carbon atoms. Thus, Li_2C_5-sandwich-columns are formed (the inverse of Cp_2Li-type sandwich compounds), which are linked by additional σ-Li–C interactions to form ribbons.

Experimental Section

Freshly prepared **1** (0.9 g, 4.9 mmol) was dissolved in a mixture of benzene (50 mL) and THF (5 mL). The solution was filtered and reduced to a volume of 15 mL. On cooling to 0 °C; **2** (0.26 g, 18 % based on **1**) crystallized as orange crystal cubes.

^{1}H NMR (250 MHz, C_6D_6, 25 °C, TMS): $\delta = 1.16$ (cm, thf), 3.17 (cm, thf), 5.78 (s, $LiC_{13}H_9$), 6.86–7.16 (m, $LiC_{13}H_9$), 7.34 (t, $LiC_{13}H_9$), 7.70 (d, $LiC_{13}H_9$), 8.20 ppm (d, $LiC_{13}H_9$); ^{13}C NMR (C_6D_6, 25 °C, TMS): $\delta = 25.1$ (thf), 68.3 (thf), 74.8 ($LiC_{13}H_9$), 113.1 ($LiC_{13}H_9$), 118.2 ($LiC_{13}H_9$), 120.2 ($LiC_{13}H_9$), 121.6 ($LiC_{13}H_9$), 122.5 ($LiC_{13}H_9$), 134.8 ppm ($LiC_{13}H_9$).

Received: July 10, 2002 [Z19711]

[1] *Lithium Chemistry* (Eds.: A.-M. Sapse, P. von R. Schleyer), Wiley, New York, **1995**.
[2] G. Boche, *Angew. Chem.* **1989**, *101*, 286–303; *Angew. Chem. Int. Ed. Engl.* **1989**, *28*, 277–292.
[3] W. Setzer, P. von R. Schleyer, *Adv. Organomet. Chem.* **1985**, *24*, 353–451.
[4] A. Maercker, M. Theis, *Top. Curr. Chem.* **1987**, *138*, 1–61.
[5] A. Maercker in *Lithium Chemistry* (Eds.: A. M. Sapse, P. von R. Schleyer), Wiley, New York, **1995**, p 477.
[6] K. Ziegler, K. Nagel, M. Patheiger, *Z. Anorg. Allg. Chem.* **1955**, *282*, 345–351.
[7] J. R. Baran, Jr., R. J. Lagow, *J. Organomet. Chem.* **1992**, *427*, 1–7.
[8] E. D. Jemmis, P. von R. Schleyer, J. A. Pople, *J. Organomet. Chem.* **1978**, *154*, 327–335.
[9] J. B. Collins, J. D. Dill, E. D. Jemmis, Y. Apeloig, P. von R. Schleyer, R. Seeger, J. A. Pople, *J. Am. Chem. Soc.* **1976**, *98*, 5419–5427.
[10] W. D. Laidig, H. F. Schäfer, *J. Am. Chem. Soc.* **1978**, *100*, 5972–5973.
[11] G. D. Stucky, M. M. Eddy, W. H. Harrison, R. Lagow, H. Kawa, D. E. Cox, *J. Am. Chem. Soc.* **1990**, *112*, 2425–2427.
[12] J. A. Gurak, J. W. Chinn, R. J. Lagow, H. Steinfink, S. C. Yannoni, *Inorg. Chem.* **1984**, *23*, 3717–3720.
[13] H. Kawa, B. C. Manley, R. J. Lagow, *Polyhedron* **1988**, *7*, 2023–2025.
[14] H. P. S. Chauhan, H. Kawa, R. J. Lagow, *J. Org. Chem.* **1986**, *51*, 1632–1633.
[15] J. F. K. Müller, M. Neuburger, B. Spingler, *Angew. Chem.* **1999**, *111*, 3766–3769; *Angew. Chem. Int. Ed.* **1999**, *38*, 3549–3552.
[16] C. M. Ong, D. W. Stephan, *J. Am. Chem. Soc.* **1999**, *121*, 2939–2940.
[17] A. Kasani, R. K. Babu, R. McDonald, R. G. Cavell, *Angew. Chem.* **1999**, *111*, 1580–1582; *Angew. Chem. Int. Ed.* **1999**, *38*, 1483–1484.
[18] J. F. K. Müller, M. Neuburger, B. Spingler, *Angew. Chem.* **1999**, *111*, 97–99; *Angew. Chem. Int. Ed.* **1999**, *38*, 92–94.
[19] H. J. Gais, J. Vollhardt, H. Günther, D. Moskau, H. J. Lindner, S. Braun, *J. Am. Chem. Soc.* **1988**, *110*, 978–980.
[20] A. Müller, B. Neumüller, K. Dehnicke, J. Magull, D. Fenske, *Z. Allg. Anorg. Chem.* **1997**, *623*, 1306–1310.
[21] W. Uhl, M. Layh, W. Massa, *Chem. Ber.* **1991**, *124*, 1511–1516.
[22] Data on the crystal structure analysis of **2**: Bruker AXS SMART CCD, $Mo_{K\alpha}$ adiation, $T = 173$ K, drect methods, fll-atrix refinement against F^2, hydrogen atoms as riding model (Bruker AXS SHELXTL 5.1). Data: $C_{13}H_8Li_2{\cdot}OC_4H_8{\cdot}C_6H_6$, $M_r = 328.3$, crystal measurements $0.44 \times 0.29 \times 0.27$ mm, orthorhombic, space group *Pnma*, $a =$ 694.20(9), $b = 1347.1(2)$, $c = 2010.4(3)$ pm, $V = 1.8800(4)$ nm^3, $Z = 4$, $\rho_{calcd} = 1.160$ g cm^{-3}, $\mu_{Mo} = 0.067$ mm^{-1}, 2θmax = 53°, 2000 independent reflections, 1325 reflections with $F_0 > 4\sigma(F_0)$, $R1 = 0.043$, $wR2 = 0.124$, residual electron density 188/−125 e nm^{-3}. Finally, note that the fluorenyldianions as well as the thf molecules in the crystal structure are disordered with respect to a mirror plane in such a way, that two independent orientations of the single molecules result. Further crystals of **2** showed the same disorder. CCDC-188077 (**2**) contains the supplementary crystallographic data for this paper. These data can be obtained free of charge via www.ccdc.cam.ac.uk/conts/retrieving.html (or from the Cambridge Crystallographic Data Centre, 12, Union Road, Cambridge CB2 1EZ, UK; fax: (+44) 1223-336-033; or deposit @ccdc.cam.ac.uk).
[23] H. Dietrich, *J. Organomet. Chem.* **1981**, *205*, 291–299.
[24] E. Weiss, T. Lambertsen, B. Schubert, J. K. Cockcroft, A. Wiedenmann, *Chem. Ber.* **1990**, *123*, 79–81.
[25] T. Kottke, D. Stalke, *Angew. Chem.* **1993**, *105*, 619; *Angew. Chem. Int. Ed. Engl.* **1993**, *32*, 580.
[26] S. Harder, M. H. Prosenc, *Angew. Chem.* **1994**, *106*, 1830–1832; *Angew. Chem. Int. Ed. Engl.* **1994**, *33*, 1744–1745.

 © 2002 WILEY-VCH Verlag GmbH & Co. KGaA, Weinheim 0044-8249/02/4123-4505 $ 20.00+.50/0

[27] F. Scherbaum, A. Grohmann, B. Huber, C. Krüger, H. Schmidbaur, *Angew. Chem.* **1988**, *100*, 1602; *Angew. Chem. Int. Ed. Engl.* **1988**, *27*, 1544.
[28] F. P. Gabbai, A. Schier, J. Riede, H. Schmidbaur, *Chem. Ber.* **1997**, *130*, 113.
[29] A. Streitwieser, S. M. Bachrach, A. Dorigo, P. von R. Schleyer in *Lithium Chemstry* (Eds.: A. M. Sapse P. von R. Schleyer), Wiley, New York, **1995**, p. 19.
[30] *Quantum chemical calculations*: The quantum chemical calculations were performed with the program TURBOMOLE. A SV(P) base set was used for all atoms [B-P86 functional; exchange: LDA + Becke (B88), correlation: LDA(VWN) + Perdew (P86); Basis def-SV(P), RI-approximation).
[31] O. Treutler, R. Ahlrichs, *J. Chem. Phys.* **1995**, *102*, 346 – 354.
[32] A. D. Becke, *Phys. Rev. A* **1998**, *38*, 3098 – 3100.
[33] J. P. Perdew, *Phys. Rev. B* **1996**, *33*, 8822 – 8824.
[34] K. Eichkorn, O. Treutler, H. Ohm, M. Häser, R. Ahlrichs, *Chem. Phys. Lett.* **1995**, *242*, 652 – 660.
[35] K. Eichkorn, F. Weigend, O. Treutler, R. Ahlrichs, *Theor. Chem. Acc.* **1997**, *97*, 119 – 124.
[36] R. Heinzmann, R. Ahlrichs, *Theoret. Chim. Acta* **1976**, *42*, 33 – 45.
[37] C. Üffing, R. Köppe, H. Schnöckel, *Organometallics* **1998**, *17*, 3512 – 3515.
[38] R. E. Dinnebier, U. Behrens, F. Olbrich, *Organometallics* **1997**, *16*, 3855 – 3858.
[39] C. Dohmeier, E. Baum, A. Ecker, R. Köppe, H. Schnöckel, *Organometallics* **1996**, *15*, 4702 – 4706.
[40] J. J. Brooks, W. Rhine, G. D. Stucky, *J. Am. Chem. Soc.* **1972**, *94*, 7339 – 7346.

 © 2002 WILEY-VCH Verlag GmbH & Co. KGaA, Weinheim 0044-8249/02/4123-4506 $ 20.00+.50/0

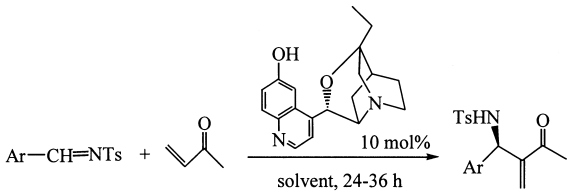
Catalytic, Asymmetric Baylis–Hillman Reaction of Imines with Methyl Vinyl Ketone and Methyl Acrylate**

Min Shi* and Yong-Mei Xu

The Baylis–Hillman reaction has made great progress,[1] including development of a catalytic, asymmetric version,[2] since Baylis and Hillman first reported the reaction of acetaldehyde with ethyl acrylate or acrylonitrile in the presence of catalytic amounts of a strong Lewis base such as 1,4-diazabicyclo[2.2.2]octane (DABCO) in 1972.[3] However, the catalytic, asymmetric Baylis–Hillman reaction is still not fruitful, because it is limited to the specialized α,β-unsaturated ketones or acrylates such as ethyl vinyl ketone (71% *ee*) or 1,1,1,3,3,3-hexafluoroisopropyl acrylate (99% *ee*).[2] High enantioselectivity has so far not been reported in Baylis–Hillman reactions involving simple acceptors such as methyl vinyl ketone (MVK) or methyl acrylate. Here we report unprecedented catalytic, asymmetric Baylis–Hillman reactions of imines with MVK or methyl acrylate, in which high enantioselectivities (up to 99% *ee*) were achieved with MVK, the simplest Baylis–Hillman acceptor.

During our investigations on the Baylis–Hillman reaction,[4] we found that the reactions of aryl aldehydes bearing electron-donating groups such as Et or MeO on the phenyl ring with MVK or methyl acrylate were sluggish or did not occur at all under the traditional Baylis–Hillman reaction conditions. Hence, we used *N*-arylidene-4-methylbenzenesulfonamides ArCH=NTs instead of aryl aldehydes in the traditional Baylis–Hillman reaction with MVK, because we expected the tosylated imino group to have high reactivity toward nucleophilic attack, even when the phenyl ring bears electron-donating groups. Indeed, such reactions, promoted by a catalytic amount of a Lewis base such as DABCO or 4-(dimethylamino)pyridine (DMAP), exclusively give the normal Baylis–Hillman adducts in good yields for many *N*-arylidene-4-methylbenzenesulfonamides.[4g,5] We then sought a suitable chiral Lewis base for a catalytic, asymmetric version of this reaction. We chose 4-(3-ethyl-4-oxa-1-azatricyclo[4,4,0,$0^{3,8}$]dec-5-yl)quinolin-6-ol[2d] (TQO, 10 mol%), because it is easily prepared from (+)-quinidine[2a,d] and high enantioselectivities were achieved in the reactions of 1,1,1,3,3,3-hexafluoroisopropyl acrylate with aryl aldehydes.[2] We first used *N*-(4-ethylbenzylidene)-4-methylbenzenesulfonamide and *N*-(4-chlorobenzylidene)-4-methylbenzenesulfonamide as substrates for the Baylis–Hillman reaction with MVK (Table 1). At 0–20 °C, moderate enantioselectivity (42–78% *ee*) for adducts **1c** and **1e** were achieved in THF or MeCN (Table 1, entries 1, 3, and 7). Moreover, at lower temperatures (−20 to −30 °C), the *ee* values of **1c** and **1e** can reach 81 and 86%, with 64 and 80% yield, respectively (entries 4 and 9). The highest *ee* values (96 and 95%) for **1c** and **1e** were achieved in DMF at −30 to −40 °C with 50 and 51% yield (entries 6 and 10). Thus, the highest *ee* value is attained at −30 °C in DMF, but the best chemical yield at −30 °C in MeCN. To obtain the Baylis–Hillman adducts **1** with high *ee* values and yields, we next investigated the reaction of *N*-(4-ethylbenzylidene)-4-methylbenzenesulfonamide with MVK in MeCN/DMF at −30 °C (Table 2). The best conditions were MeCN/DMF (1:1) at −30 °C, which gave **1e** in 68% yield with 93% *ee* (entry 3). The absolute configuration of **1e** was determined by X-ray crystallography to be *R* (Figure 1).[6]

Table 1. Baylis–Hillman reactions of *N*-(benzylidene)-4-methylbenzenesulfonamide or *N*-(benzylidene)-4-chlorobenzenesulfonamide (1.0 equiv) with MVK in the presence of a chiral Lewis base (10 mol%).



1

Entry	Ar	**1**	Solvent	*t* [h]	*T* [°C]	Yield of **1** [%][a]	*ee* value [%]
1	*p*-EtC_6H_4	**c**	THF	36	20	30	62
2	*p*-EtC_6H_4	**c**	THF	24	−25	33	76
3	*p*-EtC_6H_4	**c**	MeCN	24	0	50	78
4	*p*-EtC_6H_4	**c**	MeCN	24	−20	64	86
5	*p*-EtC_6H_4	**c**	DMF	24	−20	55	93
6	*p*-EtC_6H_4	**c**	DMF	24	−40	50	96
7	*p*-ClC_6H_4	**e**	THF	24	0	71	42
8	*p*-ClC_6H_4	**e**	THF	24	−20	65	63
9	*p*-ClC_6H_4	**e**	MeCN	24	−30	80	81
10	*p*-ClC_6H_4	**e**	DMF	24	−30	51	95

[a] Yields of isolated products.

In the reaction of other *N*-(arylidene)-4-methylbenzenesulfonamides with MVK in the presence of TQO as Lewis base, similar results were obtained under the optimized reaction conditions (Table 3). For various *N*-(arylidene)-4-methylbenzenesulfonamides, Baylis–Hillman adducts **1** were obtained with high *ee* values(90–99%) and moderate to good yields (55–80%; Table 3, entries 1–5). The reaction of *N*-(*p*-nitrobenzylidene)-4-methylbenzenesulfonamide, *N*-furan-2-ylmethylene-4-methylbenzenesulfonamide, and 4-methyl-*N*-

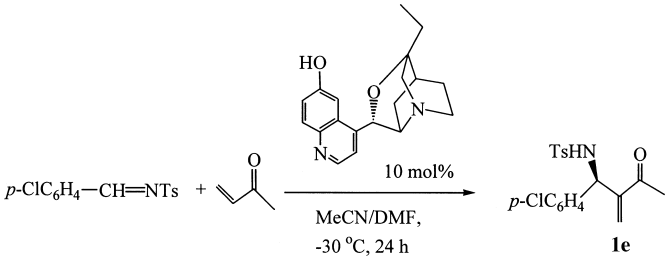
[*] M. Shi, Y.-M. Xu
State Key Laboratory of Organometallic Chemistry
Shanghai Institute of Organic Chemistry
Chinese Academy of Sciences
354 Fenglin Lu, Shanghai 200032 (China)
Fax: (+86) 21-6416-6128
E-mail: mshi@pub.sioc.ac.cn

[**] We thank the State Key Project of Basic Research (Project 973; No. G2000048007) and the National Natural Science Foundation of China (20025206) for financial support.

Supporting information for this article is available on the WWW under http://www.angewandte.org or from the author.

 © 2002 WILEY-VCH Verlag GmbH & Co. KGaA, Weinheim 0044-8249/02/4123-4507 $ 20.00+.50/0

Table 2. Baylis–Hillman reactions of *N*-(*p*-chlorobenzylidene)-4-methylbenzenesulfonamide (1.0 equiv) with MVK in the presence of a chiral Lewis base (10 mol%).



Entry	MeCN/DMF	Yield of **1e** [%][a]	*ee* value [%]	Absolute configuration
1	5:1	76	78	*R*
2	4:1	78	90	*R*
3	1:1	68	93	*R*
4	1:2	66	93	*R*

[a] Yields of isolated products.

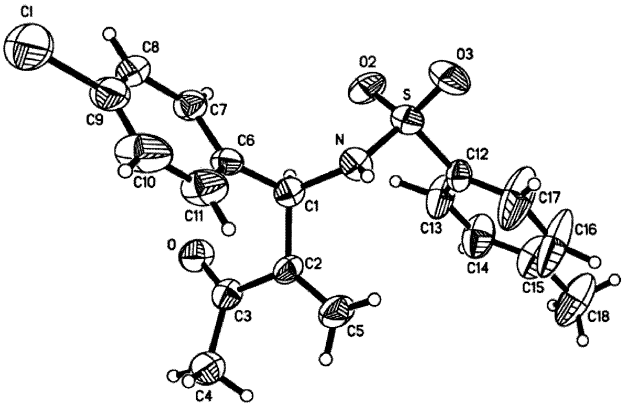
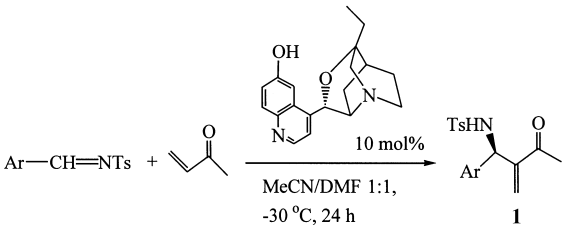


Figure 1. Crystal structure of **1e**.

Table 3. Baylis–Hillman reactions of *N*-(benzylidene)-4-methylbenzenesulfonamide (1.0 equiv) with MVK in the presence of a chiral Lewis base (10 mol%).

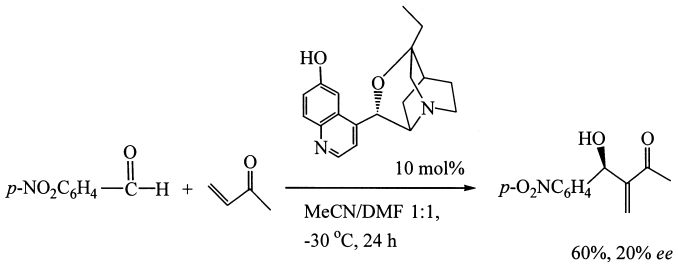


Entry	Ar	**1**	Yield of **1** [%][a]	*ee* value [%]	Absolute configuration
1	C_6H_5	**a**	80	97[b]	*R*
2	*p*-MeC_6H_4	**b**	76	96	*R*
3	*p*-EtC_6H_4	**c**	74	96	*R*
4	*p*-$MeOC_6H_4$	**d**	64	99[c,d]	*R*
5	*m*-FC_6H_4	**f**	55	90	*R*
6	*p*-$NO_2C_6H_4$	**g**	60	74[e]	*R*
7	2-furyl	**h**	58	73[d]	*R*
8	C_6H_5–CH=CH	**i**	54	46[d]	*R*

[a] Yields of isolated products. [b] In DMF, 57% yield, 96% *ee*. [c] In DMF, 59% yield, 99% *ee*. [d] The reaction mixture was stirred for 36 h. [e] In DMF, no imine Baylis–Hillman adduct was formed because the imine decomposed rapidly.

(3-phenylallylidene)benzenesulfonamide with MVK under the same reaction conditions gave **1g–i** with moderate *ee* values (entries 6–8). No formation of adduct **1g** was observed in DMF at −40 °C, because *N*-(4-nitrobenzylidene)-4-methylbenzenesulfonamide decomposes rapidly in DMF under these conditions.

The reaction of *p*-nitrobenzaldehyde with MVK under the same conditions gave the Baylis–Hillman adduct in only 20% *ee* with 60% yield of isolated product (Scheme 1). Thus, the use of sulfone-protected imines as substrates is important for achieving high enantioselectivity in Baylis–Hillman reactions with MVK as acceptor, although high enantioselectivities have been achieved in the reactions of 1,1,1,3,3,3-hexafluoroisopropyl acrylate with aldehydes.[2a]



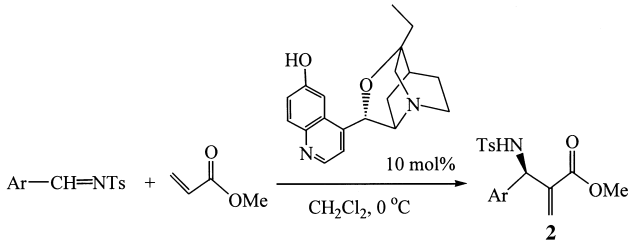
Scheme 1. Baylis–Hillman reaction of *p*-nitrobenzaldehyde with MVK in the presence of TQO (10 mol%).

On the other hand, the reactions of *N*-tosylated imines with methyl acrylate under the same conditions were sluggish, and most *N*-tosylated imines decomposed during the reaction in DMF or MeCN. However, with DABCO as Lewis base in dichloromethane at 0 °C, the reaction proceeded smoothly to give the Baylis–Hillman adducts **2** in good yields. Moreover, in the presence of the chiral Lewis base TQO, products **2** were obtained in 58–87% yield with 70–83% *ee* (Table 4). Similar enantioselectivities were obtained when the reactions were carried out at −20 °C. The results are summarized in Table 4. In addition, the Baylis–Hillman reaction of an *N*-tosylated imine with acrylonitrile afforded adduct **3** in 35% yield with 55% *ee* in CH_2Cl_2, and in 34% yield with 68% *ee* in THF, under the same conditions as for methyl acrylate (Scheme 2).

To expand the scope and explore the limitations of this novel catalytic, asymmetric aza-Baylis–Hillman reaction, we tried to synthesize aliphatic *N*-tosylated imines as starting materials. However, we found that many of these are very labile, even when stored below −20 °C. We used literature procedures[7] to prepare the aliphatic *N*-tosylated imines **4** and **5**, which must be used immediately for the reaction. The attempted catalytic

 © 2002 WILEY-VCH Verlag GmbH & Co. KGaA, Weinheim 0044-8249/02/4123-4508 $ 20.00+.50/0 *Angew. Chem. Int. Ed.* **2002**, *41*, No. 23

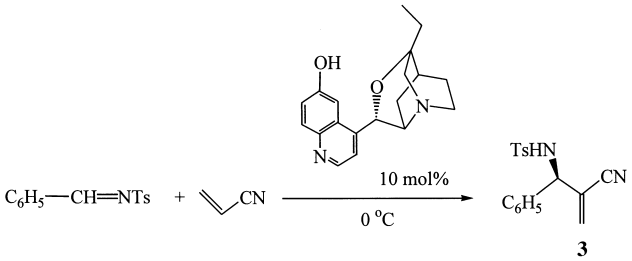
Table 4. Baylis–Hillman reactions of *N*-(benzylidene)-4-methylbenzenesulfonamide (1.0 equiv) with methyl acrylate in the presence of a chiral Lewis base (10 mol %).



2

Entry	Ar	**2**	Yield of **2** [%][a]	*t* [h]	*ee* [%]	Absolute configuration
1	C_6H_5	**a**	62	72	83	*R*
2	*p*-MeC_6H_4	**b**	67	72	80	*R*
3	*p*-EtC_6H_4	**c**	62	72	82	*R*
4	*p*-$MeOC_6H_4$	**d**	64	72	70	*R*
5	*p*-ClC_6H_4	**e**	60	36	77	*R*
6	*m*-FC_6H_4	**f**	87	32	83	*R*
7	*p*-$NO_2C_6H_4$	**g**	58	35	72	*R*
8	2,3-$Cl_2C_6H_3$	**h**	58	38	71	*R*

[a] Yields of isolated products.



3

Scheme 2. Baylis–Hillman reaction of *N*-(benzylidene)-4-methylbenzenesulfonamide with acrylonitrile in CH_2Cl_2 (55 % *ee*, 35 % yield) and THF (68 % *ee*, 34 % yield).

asymmetric Baylis–Hillman reaction of **4** or **5** with MVK in the presence of TQO gave many unidentified products, and the Baylis–Hillman adduct was not formed (Scheme 3).

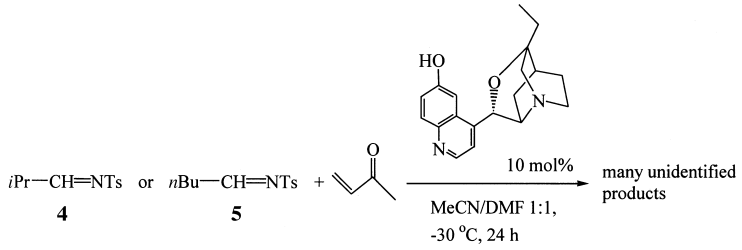
Note that (+)-quinidine and (−)-quinine showed no catalytic activity for this reaction. The hydroxy group on the quinolyl ring is also crucial, because the reaction became sluggish and gave the product with only about 10 % *ee* in very low yield when O-methylated TQO was used as chiral Lewis base. Thus, the structure of the Lewis base plays an important role in this reaction. Scheme 4 shows a possible mechanism, based on that proposed by Hatakeyama et al.[2a] We believe that the key factor is intramolecular hydrogen bonding between the phenolic OH group and the nitrogen-centered anion, stabilized by a sulfonyl group to give a relatively rigid transition state. The steric interaction of the C(O)Me group with the aromatic group in this stabilized transition state causes the formation of the Baylis–Hillman adduct with *R* configuration.

In conclusion, we have achieved the thus far highest *ee* values for Baylis–Hillman reactions involving MVK or methyl acrylate as acceptor. Moreover, this is the first case of highly enantioselective Baylis–Hillman reactions of imines with α,β-unsaturated ketones. Efforts are underway to elucidate the mechanistic details of this reaction and to disclose its scope and limitations.

Experimental Section

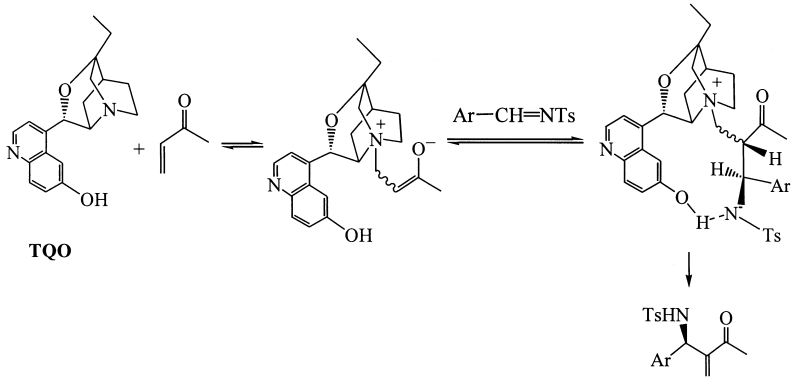
Melting points were obtained with a Yanagimoto micro melting point apparatus and are uncorrected. ^{1}H NMR spectra were recorded on a Bruker AM-300 spectrometer. Mass spectra were recorded on an HP-5989 instrument. *N*-Tosylimines were prepared according to literature procedures.[8] All solid compounds reported here gave satisfactory C,H,N microanalyses (Carlo-Erba 1106 analyzer). Commercially obtained reagents were used without further purification. All reactions were monitored by TLC on Huanghai plates coated with GF_{254} silica gel. Flash column chromatography was carried out on 200–300 mesh silica gel under pressure. The optical purities of the Baylis–Hillman adducts were determined by HPLC analysis on a chiral stationary phase (Daicel Co. Chiralcel OD, AS, and OJ; eluent, 95:5 hexane/2-propanol; flow rate, 1.0 mL min^{-1}; detection, 254 nm light). The absolute configuration of the major enantiomer of **1e** was determined by X-ray crystallography, and the others were subsequently assigned according to the sign of the specific rotation.

Typical TQO-catalyzed Baylis–Hillman reaction of methyl vinyl ketone (MVK) with *N*-(*p*-ethylbenzenesulfonyl)benzaldimine: MVK (41 μL, 0.5 mmol) was added to a solution of *N*-(*p*-ethylbenzenesulfonyl)benzaldimine (72 mg, 0.25 mmol) and TQO (8.0 mg, 0.025 mmol) in CH_3CN/DMF (1:1, 1.0 mL) at −30 °C. The reaction mixture was stirred at −30 °C for 24 h. After the reaction was completed, the solvent was removed under reduced pressure, and the residue purified by flash column chromatography (SiO_2, EtOAc/petroleum ether 1:5) to yield **1c** (69 mg, 74 %) as a colorless



4 **5**

Scheme 3. Baylis–Hillman reaction of aliphatic imines with MVK in the presence of TQO (10 mol %).



TQO

Scheme 4. A plausible reaction mechanism for the catalytic asymmetric Baylis–Hillman reaction of imines with MVK.

 © 2002 WILEY-VCH Verlag GmbH & Co. KGaA, Weinheim 0044-8249/02/4123-4509 $ 20.00+.50/0

solid (96% *ee*). M.p. 114 °C; $[\alpha]_D^{25} = -46.9°$ ($c = 1.00$, $CHCl_3$); IR ($CHCl_3$): $\tilde{\nu} = 1674\ cm^{-1}$ (C=O); ^1H NMR ($CDCl_3$, TMS, 300 MHz): $\delta = 1.23$ (3H, t, $J = 7.6$ Hz, Me), 2.15 (3H, s, Me), 2.39 (3H, s, Me), 2.54 (2H, q, $J = 7.6$ Hz, CH_2), 5.20 (1H, d, $J = 6.1$ Hz, NH), 5.51 (1H, d, $J = 8.4$ Hz, CH), 6.09 (2H, s), 6.97 (2H, d, $J = 6.1$ Hz, Ar), 6.98 (2H, $J = 6.1$ Hz, Ar), 7.21 (2H, d, $J = 8.4$ Hz, Ar), 7.63 ppm (2H, d, $J = 8.4$ Hz); MS (EI): *m/z* (%): 358 [$M^+ - 1$] (0.5), 288 [$M^+ - 69$] (5.6), 202 [$M^+ - 155$] (100); Elemental analysis (%) calcd for $C_{20}H_{23}NO_3S$: C 67.20, H 6.49, N 3.92; found: C 67.04, H 6.42, N 3.74.

Received: June 12, 2002 [Z19146]

[1] a) E. Ciganek, *Org. React. (N.Y.)* **1997**, *51*, 201 – 350; b) D. Basavaiah, P. D. Rao, R. S. Hyma, *Tetrahedron* **1996**, *52*, 8001 – 8062; c) S. E. Drewes, G. H. P. Roos, *Tetrahedron* **1988**, *44*, 4653 – 4670; d) L. J. Brzezinski, S. Rafel, J. W. Leahy, *J. Am. Chem. Soc.* **1997**, *119*, 4317 – 4318; e) T. Miyakoshi, S. Saito, *Nippon Kagaku Kaishi* **1983**, 1623 – 1628; *Chem. Abstr.* **1984**, *100*, 156191g; f) I. E. Marko, P. G. Giles, N. J. Hindley, *Tetrahedron* **1997**, *53*, 1015 – 1024; g) H. Richter, G. Jung, *Tetrahedron Lett.* **1998**, *39*, 2729 – 2730; h) E. P. Kündig, L. H. Xu, P. Romanens, G. Bernardinelli, *Tetrahedron Lett.* **1993**, *34*, 7049 – 7052; i) V. K. Aggarwal, A. Mereu, G. J. Tarver, R. McCague, *J. Org. Chem.* **1998**, *63*, 7183 – 7189; j) M. Kawamura, S. Kobayashi, *Tetrahedron Lett.* **1999**, *40*, 1539 – 1542; k) M. Ono, K. Nishimura, Y. Nagaoka, K. Tomioka, *Tetrahedron Lett.* **1999**, *40*, 1509 – 1512; l) G.-G. Li, H.-X. Wei, J.-J. Gao, T. D. Caputo, *Tetrahedron Lett.* **2000**, *41*, 1 – 5; m) G.-G. Li, J. Gao, H.-X. Wei, M. Enright, *Org. Lett.* **2000**, *2*, 617 – 620.

[2] a) Y. Iwabuchi, M. Nakatani, N. Yokoyama, S. Hatakeyama, *J. Am. Chem. Soc.* **1999**, *121*, 10219 – 10220; b) A. G. M. Barrett, A. S. Cook, A. Kamimura, *Chem. Commun.* **1998**, 2533 – 2534; c) P. Langer, *Angew. Chem.* **2000**, *112*, 3177 – 3180; *Angew. Chem. Int. Ed.* **2000**, *39*, 3049 – 3052; d) for the first preparation of the catalyst TQO, see: C. von Riesen, H. M. R. Hoffmann, *Chem. Eur. J.* **1996**, *2*, 680 – 684.

[3] a) A. B. Baylis, M. E. D. Hillman, DE-B 2155113 **1972**; M. E. D. Hillman, A. B. Baylis, US Patent, 3743669 **1973**; *Chem. Abstr.* **1972**, *77*, 34174q; b) K. Morita, Z. Suzuki, H. Hirose, *Bull. Chem. Soc. Jpn.* **1968**, *41*, 2815 – 2816.

[4] a) M. Shi, J.-K. Jiang, Y.-S. Feng, *Org. Lett.* **2000**, *2*, 2397 – 2400; b) M. Shi, Y.-S. Feng, *J. Org. Chem.* **2001**, *66*, 406 – 411; c) M. Shi, J.-K. Jiang, S.-C. Cui, Y.-S. Feng, *J. Chem. Soc. Perkin Trans. 1.* **2001**, 390 – 393; d) M. Shi, J.-K. Jiang, *Tetrahedron* **2000**, *56*, 4793 – 4797; e) M. Shi, C.-Q. Li, J.-K. Jiang, *Chem. Commun.* **2001**, 833 – 834; f) M. Shi, Y.-M. Xu, *Chem. Commun.* **2001**, 1876 – 1877; g) M. Shi, Y.-M. Xu, *Eur. J. Org. Chem.* **2002**, 696 – 701.

[5] For previous reports on the Baylis–Hillman reaction of methyl acrylate with imines, see a) P. Perlmutter, C. C. Teo, *Tetrahedron Lett.* **1984**, *25*, 5951 – 5952; b) M. Takagi, K. Yamamoto, *Tetrahedron* **1991**, *47*, 8869 – 8882. For Baylis–Hillman reactions of MVK with imines generated in situ, see c) S. Bertenshow, M. Kahn, *Tetrahedron Lett.* **1989**, *30*, 2731 – 2732.

[6] CCDC-167239 contains the supplementary crystallographic data for this paper. These data can be obtained free of charge via www.ccdc.cam.ac.uk/conts/retrieving.html (or from the Cambridge Crystallographic Data Centre, 12, Union Road, Cambridge CB21EZ, UK; fax: (+44) 1223-336-033; or deposit@ccdc.cam.ac.uk). Crystal data of **1e**: $C_{18}H_{18}ClNO_3S$; $M_r = 363.84$; $T = 293(2)$ K; monoclinic, space group $P2(1)$; $a = 8.513(3)$, $b = 12.076(4)$, $c = 9.767(3)$ Å, $\beta = 112.259(6)°$, $V = 929.3(5)$ Å^3; $Z = 2$; $\rho_{calcd} = 1.300\ Mg\,m^{-3}$; $F_{000} = 380$; final R indices [$I > 2\sigma(I)$]: $R_1 = 0.0475$l, $R_2 = 0.0833$.

[7] F. Chemla, V. Hebbe, J. F. Normant, *Synthesis* **2000**, *1*, 75 – 77.

[8] B. E. Love, P. S. Raje, T. C. Williams, *Synlett* **1994**, 493 – 494.

[(salen)Al]-Mediated, Controlled and Stereoselective Ring-Opening Polymerization of Lactide in Solution and without Solvent: Synthesis of Highly Isotactic Polylactide Stereocopolymers from Racemic D,L-Lactide

Zhiyuan Zhong, Pieter J. Dijkstra, and Jan Feijen*

Polylactides (PLAs) are among the most important synthetic biodegradable polymers investigated for biomedical and pharmaceutical applications such as controlled drug delivery, resorbable sutures, medical implants, and scaffolds for tissue engineering.[1] On the basis of annually renewable resources such as corn and sugar beets, PLAs are also promising degradable substitutes for petrochemical-based polyolefins.[2] The physical, mechanical, and degradation properties of PLAs are intimately dependent on the chain stereochemistry. For instance, isotactic poly(L-LA) (LA = lactide), a highly crystalline material with a $T_m \approx 170\,°C$, has excellent mechanical properties and degrades rather slowly, whereas atactic poly(D,L-LA) is amorphous and subject to a relatively fast degradation. Stereocontrol, therefore, is crucial in the synthesis of polylactides. Most catalysts, including stannous octoate, zinc lactate, and aluminum alkoxides, do not bias towards different enantiomers in the ring-opening polymerization of D,L-lactide, thereby furnishing PLAs with randomly distributed stereocenters.[3] Recently it was reported that a few single-site lactide-polymerization catalysts did show stereoselectivity. For example, [(bdi)ZnO*i*Pr] (bdi = β-diiminate) polymerized D,L-LA in such a way as to afford a heterotactic PLA, and chiral tris(pyrazolyl)borate magnesium complexes preferentially polymerized *meso*-LA in the presence of a mixture of *meso*-LA and D,L-LA (diastereoselectivity).[4]

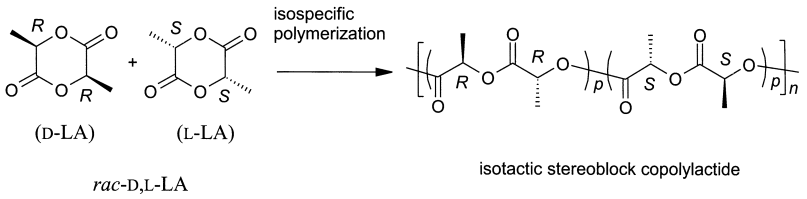
It has long been a challenge to prepare PLAs with long isotactic sequences out of D,L-LA through isospecific polymerization (Scheme 1), since these stereoblock copolylactides are expected to be hard and strong as highly crystalline poly(L-LA)s but with varying degrees of crystallinity and degradation rates, depending on the average length of the isotactic blocks. So far, examples of isospecific lactide polymerization are limited to Schiff base aluminum alkoxide catalysts in CH_2Cl_2 or in toluene,[5] in which the binaphthyl Schiff base ligands impose the best stereochemical as well as molecular-weight control. However, the synthesis of the binaphthyl Schiff base ligand is time-consuming. Besides, solution polymerization with these catalysts is not a practically viable process. The following requirements must be satisfied for a catalyst to be industrially attractive:

1) The starting organic ligands should be commercially available and inexpensive.

[*] Prof. Dr. J. Feijen, Z. Zhong, Dr. P. J. Dijkstra
Department of Chemical Technology
Institute for Biomedical Technology, University of Twente
P.O.Box 217, 7500 AE Enschede (Netherlands)
Fax: (+31) 53-489-3823
E-mail: j.feijen@ct.utwente.nl

Supporting information for this article is available on the WWW under http://www.angewandte.org or from the author.

 © 2002 WILEY-VCH Verlag GmbH & Co. KGaA, Weinheim 0044-8249/02/4123-4510 $ 20.00+.50/0



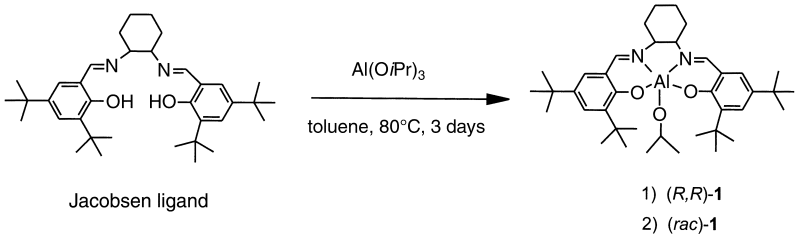
Scheme 1. Isospecific polymerization of D,L-LA to isotactic stereoblock copolylactides.

2) The synthesis of the catalyst must be straightforward and high-yielding.
3) The polymerization should preferably be conducted in the absence of solvents, which implies that a high temperature of at least 130 °C is required for the solvent-free polymerization of D,L-LA. Therefore the catalyst has to be sufficiently stable at the polymerization temperature.
4) Polymers with a controlled M_n and low polydispersity should be obtained in high yield.
5) Ideally, new polymers with distinct microstructures as well as useful properties should be prepared from inexpensive substrates.

Herein, we report the synthesis of new salen aluminum alkoxides (both enantiopure and racemic) by employing the Jacobsen ligand, an inexpensive commercial starting material with demonstrated usefulness in various asymmetric reactions, for example, asymmetric olefin epoxidation, asymmetric epoxide-ring-opening reactions, hydrolytic kinetic resolution of terminal epoxides.[6] Most notably, these catalysts provide high isospecificity and excellent control in both solution and solvent-free polymerization of lactide at elevated temperatures. To the best of our knowledge, this is the first example of solvent-free stereoselective lactide polymerization.

Both (*R,R*)-**1** and *rac*-**1** were obtained in high yields by the reaction of *R,R* or *rac* Jacobsen ligand with aluminum triisopropoxide in toluene (Scheme 2). The ^{27}Al NMR spectrum of (*R,R*)-**1** in [D_8]toluene/toluene (*v*/*v* 1:2) solvent had only a single resonance at $\delta = 35.45$ ppm ($w_{1/2} = 954$ Hz), which supports a five-coordinate state for Al.[7]

Initial experiments conducted in toluene at 70 °C ($[M]_0/[I]_0 = 62{:}1$, $[M]_0 = 0.8$ mol L^{-1}) revealed that both (*R,R*)-**1** and (*rac*)-**1** yielded PLAs with a well-controlled M_n and a very low polydispersity index (M_w/M_n) (Table 1, entries 1–3, 6–7). End-group analysis by NMR spectroscopy and MALDI-TOF mass spectroscopy showed that the polymer chains were systematically end-capped with an isopropyl ester and a hydroxy group, respectively. A steady evolution of M_n, while retaining a low M_w/M_n over the course of polymerization, was evidenced by gel-permeation chromatography (GPC) (Figure 1). Transesterification was practically absent, even after a long polymerization time, as revealed by



Scheme 2. Preparation of (*R,R*)-**1** and (*rac*)-**1** from the Jacobsen ligand.

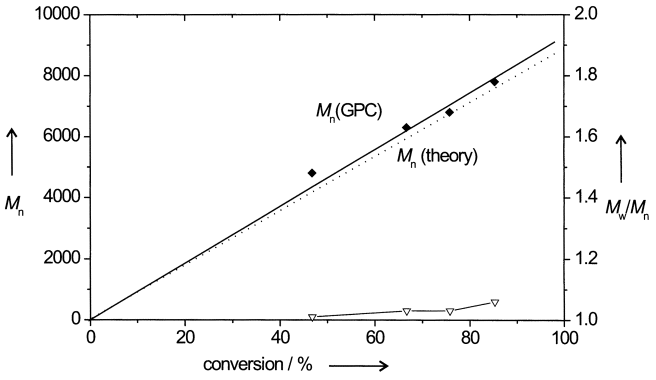


Figure 1. Dependence of M_n and polydispersity index (M_w/M_n) of polylactide on monomer conversion using (*rac*)-**1** for D,L-LA polymerization in toluene at 70 °C. $[M]_0/[I]_0 = 62/1$. ◆: M_n (GPC), ▽ : M_w/M_n, ····: M_n (theory).

Table 1. Ring-opening polymerization of lactide mediated by (*R,R*)-**1** or (*rac*)-**1**.

Entry	Catalyst	Monomer	M/I	*T* [°C]	*t* [d]	Conversion [%]	$M_n \times 10^{-3}$ NMR[a]	$M_n \times 10^{-3}$ GPC[b]	$M_n \times 10^{-3}$ Theo.[c]	M_w/M_n GPC[b]	P_i[d]
1		L-LA	62	70	4	97.0	9.6	9.9	8.7	1.05	–
2a		D,L-LA	62	70	2	21.1	2.5	2.4[f]	1.9	1.04[f]	0.92
2b	(*R,R*)-**1**	D,L-LA	62	70	4	36.3	3.5	3.3[f]	3.2	1.04[f]	–
3		D,L-LA	62	70	24	87.8	8.4	8.5	7.8	1.08	–
4		D,L-LA	100	110	6	94.0	13.9	13.7	13.5	1.31	–
5[e]		D,L-LA	200	130	2	86.4	23.7	21.6	24.7	1.18	–
6		L-LA	62	70	5.1	93.1	7.4	8.6	8.1	1.09	–
7	(*rac*)-**1**	D,L-LA	62	70	12	85.3	8.5	7.7	7.6	1.06	0.93
8[e]		D,L-LA	200	130	2	94.8	20.3	24.9	27.3	1.37	0.88

[a] Obtained by ^{1}H NMR spectroscopic end-group analysis. [b] Determined by gel-permeation chromatography (GPC) in $CHCl_3$, universal calibration relative to polystyrene standard. [c] Calculated based on monomer/initiator ratio and conversion. [d] The parameter P_i is the probability of forming a new *i*-dyad. On the basis of enantiomorphic site control statistics, the tetrad proportions of PLAs obtained from D,L-LA polymerization in terms of P_i can be expressed as follows: $[iii] = [P_i^2 + (1-P_i)^2 + P_i^3 + (1-P_i)^3]/2$, $[isi] = [P_i(1-P_i) + P_i(1-P_i)^2]/2$, $[iis] = [sii] = [sis] = [P_i^2(1-P_i) + P_i(1-P_i)^2]/2$, where *i* denotes isotactic and *s* syndiotactic.[5g] [e] Solvent-free polymerization conducted at 130 °C. [f] Determined by MALDI-TOF mass spectrometry.

 © 2002 WILEY-VCH Verlag GmbH & Co. KGaA, Weinheim 0044-8249/02/4123-4511 $ 20.00+.50/0

the MALDI-TOF mass spectrum (see Supporting Information). This is in sharp contrast with the results reported for achiral [2,2′-{ethylenebis(nitrilomethylidine)}diphenolate]aluminum methoxides, which promoted significant ester-exchange reactions under similar conditions.[8] Therefore, it is clear that the polymerization is a perfectly living process, and the polymerization involves acyl-oxygen cleavage of lactide monomer and insertion into aluminum–alkoxide bonds.

Most remarkably, in all cases a crystalline PLA was isolated, suggesting that long isotactic sequences are generated during D,L-LA polymerization. Detailed microstructural analysis by using ^{13}C NMR spectroscopy corroborated the high isotacticity of the PLAs. The carbonyl as well as the methine carbon regions of the ^{13}C NMR spectrum of the PLA obtained by polymerizing D,L-LA with (*rac*)-**1** are shown in Figure 2. Resonances in terms of tetrad or hexad sensitivity were

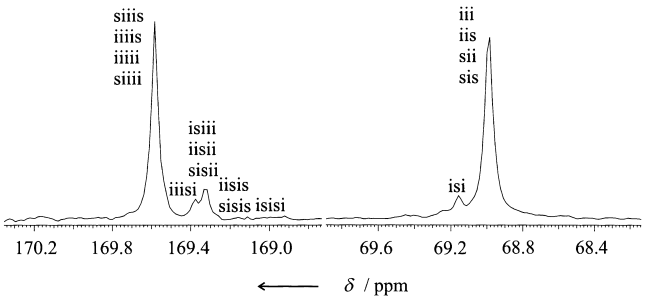


Figure 2. ^{13}C NMR spectrum (75.26 MHz, $CDCl_3$) showing hexad and tetrad probabilities of PLA prepared by polymerizing D,L-LA using (*rac*)-**1** ($[M]_0/[I]_0 = 62/1$, $[M]_0 = 0.8$ mol L^{-1}, toluene, 70 °C, 12 days, 85.3 % conversion).

assigned according to Kasperczyk and Vert and co-workers.[9] The degree of stereoselectivity, which may be defined by the parameter P_i (the probability of forming a new *i*-dyad), can be determined from the relative tetrad intensities.[5g] According to enantiomorphic-site-control statistics, a P_i value of 0.93 is obtained for (*rac*)-**1**-initiated D,L-LA polymerization (Table 1, entry 7). The high isotacticity was further confirmed by the high intensity of the *iii*-resonance in the methine region of the homonuclear decoupled ^1H NMR spectrum (see Supporting Information).[10] In addition, differential scanning calorimetry (DSC) revealed that this polymer had a high T_m of 183.5 °C ($\Delta H_{fus} = 41.3$ J g^{-1}), which is significantly higher than that of the optically pure poly(L-LA) ($T_m = 168.4$ °C, see Supporting Information).[11] These results are very close to those reported for the PLAs prepared by the polymerization of D,L-LA using racemic binaphthyl Schiff base aluminum catalysts.[5e–g] Based on the microstructural data and thermal characteristics, we conclude that isotactic stereoblock copolylactides are the most likely structures.

Under identical polymerization conditions, the polymerization of D,L-LA with enantiopure catalyst (*R,R*)-**1** afforded polymers with high isotacticity at low conversion, but decreased isotacticity at higher conversion. The P_i based on a PLA sample acquired at 21.1 % conversion is 0.92 (Table 1, entry 2a), which is close to the stereoselectivity observed for D,L-LA polymerization with (*rac*)-**1** at high conversion. Kinetic studies revealed that (*R,R*)-**1** polymerized L-LA significantly faster than did the D-enantiomer, with a relative polymerization rate $k_{rel} = k_{L\text{-}LA}/k_{D\text{-}LA} = \sim 14$. The gradually increasing relative concentration of the D-LA isomer in the monomer pool as the "selected" L-LA is converted into PLA during the polymerization process is responsible for the decreasing isotacticity at high conversion. The PLA thus obtained has a gradient stereosequence changing from long isotactic L-lactyl units to long isotactic D-lactyl units. Similar results were reported for D,L-LA polymerization with a (*R,R*)-binaphthyl Schiff base complex of aluminum, but it should be emphasized that contrary to (*R,R*)-**1**, (*R*)-binaphthyl Schiff base aluminum methoxide preferentially polymerizes D-LA.[5d] All these observations indicate that the Jacobsen ligand imposes stereochemical control that is comparable with binaphthyl Schiff base in toluene at 70 °C and that a site-control mechanism is operative in the stereoselection process.

Polymerization at higher temperatures was carried out to investigate the influence of reaction temperature on the polymerization rate and stereoselectivity. D,L-LA polymerization in toluene at 110 °C with (*R,R*)-**1** proceeded much faster than polymerization at 70 °C, and, most importantly, a crystalline polymer with a controlled M_n resulted (Table 1, entry 4). The high level of stereoselectivity maintained at elevated temperatures encouraged us to carry out solvent-free polymerization. Interestingly, excellent molar-mass control as well as stereochemical control was observed, even when D,L-LA was polymerized in the absence of solvent at 130 °C (Table 1, entries 5 and 8). At a monomer/initiator molar ratio of 200, high conversions were obtained within 2 days, providing polymers of rather low polydispersity ($M_w/M_n = 1.18$ for (*R,R*)-**1**, 1.37 for (*rac*)-**1**). Microstructural analysis showed that both polymers contain long isotactic sequences. (*R,R*)-**1** furnished an amorphous polylactide, whereas (*rac*)-**1** afforded a hard crystalline polymer. A P_i value of 0.88 was determined for D,L-LA polymerization in the presence of (*rac*)-**1** (Table 1, entry 8). These results are extraordinary, since no other catalyst reported thus far is able to effect such a high stereoselectivity in lactide polymerization under these polymerization conditions (110 °C in toluene or in the absence of solvent at 130 °C).

In summary, we have demonstrated that new [(salen)Al] catalysts, either in solution or in the absence of solvent, exert excellent molecular-weight control as well as stereochemical control in lactide polymerization. Polylactides with varying isotactic lengths, which affords either a crystalline or amorphous polymer, can be prepared directly from racemic D,L-lactide. Additionally, selective polymerization of L-LA in the presence of D,L-lactide imposed by (*R,R*)-**1** might provide a novel and efficient pathway to optically pure D-lactide monomer. Kinetic and mechanistic studies as well as new polymer syntheses are underway.

Experimental Section

General: All experiments were carried out under argon using Schlenk techniques or under nitrogen in a glovebox. Solvents were thoroughly dried prior to use.

(*R,R*)-**1**: Aluminum isopropoxide (0.583 g, 2.85 mmol), *R,R* Jacobsen ligand (1.56 g, 2.85 mmol), and toluene (15 mL) were added to a dried

 © 2002 WILEY-VCH Verlag GmbH & Co. KGaA, Weinheim 0044-8249/02/4123-4512 $ 20.00+.50/0

reaction vessel equipped with a magnetic stirrer bar. After the mixture was stirred for 3 days at 80 °C, the solvent and volatile components were removed in vacuo. The yellow solid was then washed with hexane, filtered, and dried in vacuo. Yield: 95.6 %. Elemental analysis: calcd: C 74.25, H 9.43, N 4.44, Al 4.27; found: C 73.94, H 9.53, N 4.52, Al 4.24; ^{1}H NMR (300 MHz, $CDCl_3$): $\delta = 8.36$ (s, 1H), 8.15 (s, 1H), 7.47–7.50 (dd, $J = 2.7$, 8.0 Hz, 2H), 6.98–7.05 (dd, $J = 2.7$, 17.0 Hz, 2H), 3.92 (t, $J = 9.6$ Hz, 1H), 3.71 (sept, $J = 5.7$ Hz, 1H), 3.04 (t, J 9.6 Hz, 1H), 2.60 (br s, 1H), 2.40 (br s, 1H), 2.06 (b, 2H), 1.55 (s, 9H), 1.52 (s, 9H), 1.47 (m, 4H), 1.30 (s, 9H), 1.29 (s, 9H), 0.86 ppm (dd, $J = 5.7$, 7.5 Hz, 6H); ^{27}Al NMR (104 MHz, toluene/[D_8]toluene (v/v: 2/1), $Al_2(SO_4)_3$ in D_2O): $\delta = 35.45$ ppm ($w_{1/2} = 954$ Hz). (*rac*)-**1**: Elemental analysis: calcd: C 74.25, H 9.43, N 4.44, Al 4.27; found: C 74.28, H 9.42, N 4.50, Al 4.13; ^{1}H NMR (300 MHz, $CDCl_3$): $\delta = 8.36$ (s, 1H), 8.15 (s, 1H), 7.47–7.50 (dd, $J = 2.4$, 7.5 Hz, 2H), 6.98–7.05 (dd, $J = 3.0$, 17.1 Hz, 2H), 3.92 (t, $J = 10.5$ Hz, 1H), 3.71 (sept, $J = 5.7$ Hz, 1H), 3.04 (t, $J = 10.5$ Hz, 1H), 2.60 (br s, 1H), 2.40 (br s, 1H), 2.06 (br s, 2H), 1.55 (s, 9H), 1.52 (s, 9H), 1.47 (m, 4H), 1.30 (s, 9H), 1.29 (s, 9H), 0.86 ppm (dd, $J =$ 5.7, 7.5 Hz, 6H).

Solution polymerization (typical experiment): The catalyst (*rac*)-**1** (0.102 g, 0.162 mmol), D,L-LA (1.44 g, 10 mmol), and toluene (12 mL) were added to a dried reaction vessel equipped with a magnetic stirrer bar. The vessel was placed in an oil bath at 70 °C (thermostat control) and stirred for 12 days. Acetic acid was added to terminate the polymerization. A sample was taken for the determination of the conversion by ^{1}H NMR spectroscopy. The solvent was removed by rotary evaporation, the remaining residues were redissolved in CH_2Cl_2, and the polymer was precipitated from excess cold methanol. Filtration, followed by drying at 40 °C in vacuo yielded a white crystalline polymer. Conversion = 85.3 %, M_n (GPC) = 7.7×10^3, $M_w/M_n = 1.06$.

Solvent-free polymerization (typical experiment): The catalyst (*rac*)-**1** (0.065 g, 0.103 mmol) and D,L-LA (3.0 g, 20.8 mmol) were stirred at 130 °C for 2 days. A sample was taken for determination of the conversion by ^{1}H NMR spectroscopy. The polymer was isolated by dissolution in CH_2Cl_2, precipitation from excess ethanol, filtration, and drying at 40 °C in vacuo. Conversion = 94.8 %, M_n (GPC) = 24.9×10^3, $M_w/M_n = 1.37$.

Received: June 28, 2002 [Z19632]

[1] a) E. Chiellini, R. Solaro, *Adv. Mater.* **1996**, *8*, 305; b) K. E. Uhrich, S. M. Cannizzaro, R. S. Langer, K. M. Shakesheff, *Chem. Rev.* **1999**, *99*, 3181.

[2] a) R. E. Drumright, P. R. Gruber, D. E. Henton, *Adv. Mater.* **2000**, *12*, 1841; b) Y. Ikada, H. Tsuji, *Macromol. Rapid Commun.* **2000**, *21*, 117.

[3] a) H. R. Kricheldorf, C. Boettcher, K. U. Tonnes, *Polymer* **1992**, *33*, 2817; b) H. R. Kricheldorf, C. Boettcher, *Makromol. Chem.* **1993**, *194*, 1653; c) G. Schwach, J. Coudane, R. Engel, M. Vert, *Polym. Bull.* **1994**, *32*, 617.

[4] a) B. M. Chamberlain, M. Cheng, D. R. Moore, T. M. Ovitt, E. B. Lobkovsky, G. W. Coates, *J. Am. Chem. Soc.* **2001**, *123*, 3229; b) M. Cheng, A. B. Attygalle, E. B. Lobkovsky, G. W. Coates, *J. Am. Chem. Soc.* **1999**, *121*, 11 583; c) M. H. Chisholm, N. W. Eilerts, J. C. Huffman, S. S. Iyer, M. Pacold, K. Phomphrai, *J. Am. Chem. Soc.* **2000**, *122*, 11 845.

[5] There are two different stereocontrol mechanisms: chain-end control versus catalyst-site control; chain-end control is operative when achiral Schiff base aluminum alkoxides were used: a) M. Wisniewski, A. LeBorgne, N. Spassky, *Macromol. Chem. Phys.* **1997**, *198*, 1227; b) D. Jhurry, A. Bhaw-Luximon, N. Spassky, *Macromol. Symp.* **2001**, *175*, 67; c) N. Nomura, R. Ishii, M. Akakura, K. Aoi, *J. Am. Chem. Soc.* **2002**, *124*, 5938; site-control mechanism is operative when chiral binaphthyl Schiff base aluminum alkoxides were used: d) N. Spassky, M. Wisniewski, C. Pluta, A. LeBorgne, *Macromol.Chem.Phys.* **1996**, *197*, 2627; e) T. M. Ovitt, G. W. Coates, *J. Polym. Sci. Polym. Chem. Ed.* **2000**, *38*, 4686; f) C. P. Radano, G. L. Baker, M. R. Smith, *J. Am. Chem. Soc.* **2000**, *122*, 1552; g) T. M. Ovitt, G. W. Coates, *J. Am. Chem. Soc.* **2002**, *124*, 1316.

[6] a) E. N. Jacobsen, *Acc. Chem. Res.* **2000**, *33*, 421; b) S. E. Schaus, J. Branalt, E. N. Jacobsen, *J. Org. Chem.* **1998**, *63*, 403; c) N. S. Finney, P. J. Pospisil, S. Chang, M. Palucki, R. G. Konsler, K. B. Hansen, E. N. Jacobsen, *Angew. Chem.* **1997**, *109*, 1798; *Angew. Chem. Int. Edit. Engl.* **1997**, *36*, 1720; d) M. Tokunaga, J. F. Larrow, F. Kakiuchi, E. N. Jacobsen, *Science* **1997**, *277*, 936.

[7] a) R. Benn, A. Rufinska, H. Lemkuhl, E. Janssen, C. Kruger, *Angew. Chem.* **1983**, *95*, 808; *Angew. Chem. Int. Edit. Engl.* **1983**, *22*, 779; b) R. Benn, A. Rufinska, *Angew. Chem.* **1986**, *98*, 851; *Angew. Chem. Int. Edit. Engl.* **1986**, *25*, 861; c) D. A. Atwood, M. J. Harvey, *Chem. Rev.* **2001**, *101*, 37.

[8] G. Montaudo, M. S. Montaudo, C. Puglisi, F. Samperi, N. Spassky, A. LeBorgne, M. Wisniewski, *Macromolecules* **1996**, *29*, 6461.

[9] a) J. E. Kasperczyk, *Macromolecules* **1995**, *28*, 3937; b) J. Coudane, C. UstarizPeyret, G. Schwach, M. Vert, *J. Polym. Sci. Polym. Chem. Ed.* **1997**, *35*, 1651.

[10] a) K. A. M. Thakur, R. T. Kean, E. S. Hall, J. J. Kolstad, T. A. Lindgren, M. A. Doscotch, J. I. Siepmann, E. J. Munson, *Macromolecules* **1997**, *30*, 2422; b) K. A. M. Thakur, R. T. Kean, E. S. Hall, M. A. Doscotch, E. J. Munson, *Anal. Chem.* **1997**, *69*, 4303.

[11] PLA stereocomplexes formed from enantiomerically pure poly(L-LA) and poly(D-LA) have a $T_m = 230$ °C, whereas stereo diblock copolymers of L-LA and D-LA prepared by sequential polymerization show a $T_m = 205$ °C. The PLA obtained in this study gave a $T_m = 183.5$ °C, which suggests an isotactic stereoblock microstructure and the formation of stereocomplexes between blocks of opposite configurations: a) S. Brochu, R. E. Prudhomme, I. Barakat, R. Jerome, *Macromolecules* **1995**, *28*, 5230; b) N. Yui, P. J. Dijkstra, J. Feijen, *Macromol. Chem. Phys.* **1990**, *191*, 481.

Unprecedented Coupling of Allenylidene and Diynyl Metal Complexes: A Bimetallic Ruthenium System with a C_7 Conjugated Bridge**

Stéphane Rigaut, Julien Massue, Daniel Touchard,* Jean-Luc Fillaut, Stéphane Golhen, and Pierre H. Dixneuf

Organometallic complexes with π-conjugated bridges have gained importance in view of potential applications in the emerging field of molecular-scale electronic devices.[1,2] An attractive pursuit in this area is the design of molecular wire precursors that allow exchange of electrons through bridges between remote terminal groups.[2–6] A variety of different approaches have been applied to construct such entities, the majority of which have contained an even number of carbon atoms in the bridge.[2,3] By contrast, only a few complexes with

[*] Prof. D. Touchard, Dr. S. Rigaut, J. Massue, Dr. J.-L. Fillaut, Prof. P. H. Dixneuf
Institut de Chimie de Rennes
UMR 6509 CNRS-Université de Rennes 1
Organométalliques et Catalyse
Campus de Beaulieu, 35042 Rennes Cedex (France)
Fax: (+ 33) 2-2323-5200
E-mail: daniel.touchard@univ-rennes1.fr

Dr. S. Golhen
Institut de Chimie de Rennes
UMR 6511 CNRS - Université de Rennes 1
LCSIM
Campus de Beaulieu, 35042 Rennes Cedex (France)

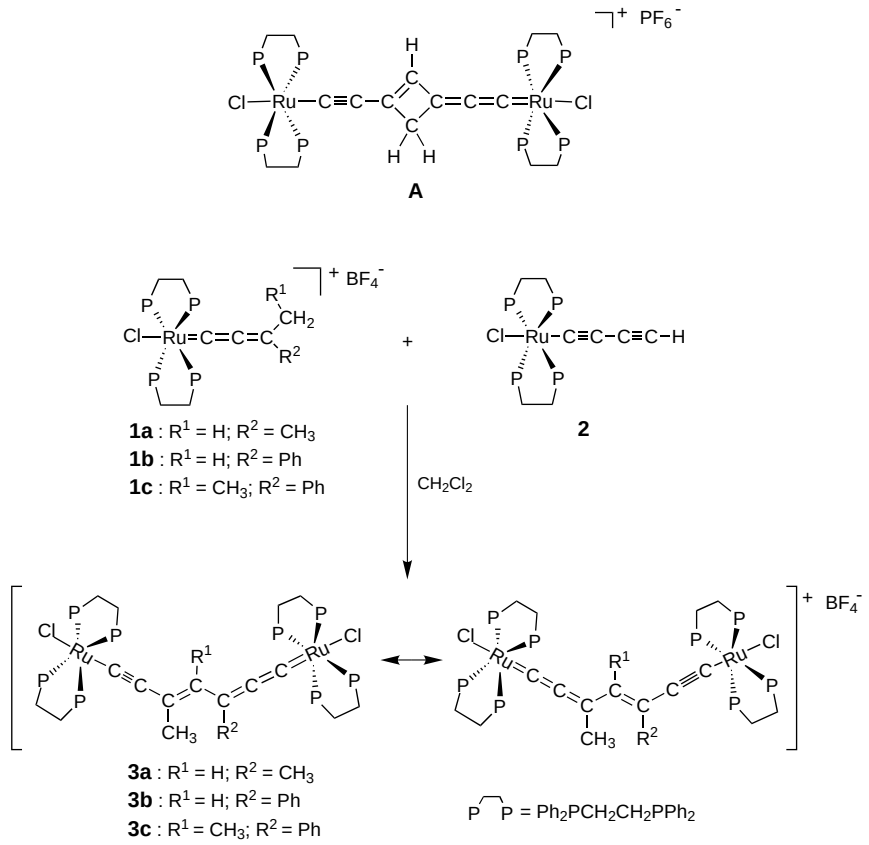
[**] We thank the CNRS, the Université de Rennes 1, and the Région Bretagne for support, and Dr. P. Guenot, J. P. Hurvois, and J. Perruchon for help.

Supporting information for this article is available on the WWW under http://www.angewandte.org or from the author.

 © 2002 WILEY-VCH Verlag GmbH & Co. KGaA, Weinheim 0044-8249/02/4123-4513 $ 20.00+.50/0

odd-numbered carbon chains or cyclic bridges have been described.[4–7] The most general process involves [2+2] cycloadditions between vinylidene [M]=C=CHR or allenylidene [M]=C=C=CR^{1}R^2 species and the $C_\alpha \equiv C_\beta$ bond of acetylides [M]−C≡C−R or diynyl complexes [M]−C≡C−C≡C−R. These reactions lead to the formation of rigid four-membered cyclic bridges with a delocalized C_3 path between the metal centers.[6] Thus, the limited number of well-defined synthetic processes limits the construction of systems with odd-numbered carbon chains from small to nanoscale devices. Recently, we reported the first complex with an annelated C_7 bridge **A** (Scheme 1); complex **A** resulted from an unprecedented electron-promoted [2+2] cycloaddition exclusively at the $C_\gamma \equiv C_\delta$ bond of a diynyl metal complex, and involved a transient radical cumulenic species.[7] These results provided impetus to investigate reactions between cationic cumulenic species and a diynyl metal complex in which steric protection at the $C_\alpha \equiv C_\beta$ bond controls the regioselective addition at the $C_\gamma \equiv C_\delta$ bond. Based on the use of the [Cl(dppe)$_2$Ru]$^+$ moiety[8] (dppe = 1,2-diphenyphosphanylethane), we now report a novel simple method for coupling metal allenylidenes with a metal diyne to obtain a new class of C_7 carbon-rich bimetallic systems *trans*-[Cl(dppe)$_2$Ru−C≡C−C(CH$_3$)=C(R^1)−C(R^2)=C=C=Ru(dppe)$_2$Cl]BF$_4$ with pendant groups on the linear conjugated bridging ligand.

The synthetic route to the new ruthenium bimetallic complexes is outlined in Scheme 1. The allenylidene complexes **1a–c** were synthesized by reaction of the 16-electron species [Cl(dppe)$_2$Ru]BF$_4$ with the appropriate propargylic alcohol. These cationic complexes **1a–c** were allowed to react overnight, at room temperature, with one equivalent of the neutral diyne compound **2.** Consequently, a metal-assisted C−C bond-forming reaction took place and stable dark green crystals of **3a–c** were isolated in good yields (69–75 %) after several crystallizations. The complexes **3a–c** were also obtained in similar yields when the reaction was performed with the protected diyne *trans*-[Cl(dppe)$_2$Ru−C≡C−C≡C−SiMe$_3$][7] as starting material instead of **2**. Thus, spontaneous deprotection occurs in the reaction medium in the presence of the ruthenium allenylidene salt, and prior desilylation is not necessary. Compounds **3a–c** were fully characterized on the basis of their NMR, IR, UV/Vis, and HR-MS (FAB) data. The FTIR spectra for all compounds display an intense absorption around 1900 cm^{-1}, characteristic of the cumulenic character of the chain. The ^{31}P NMR spectrum of **3a** shows one singlet at $\delta = 47.1$ ppm typical for a symmetrical structure, indicating that the two metal sites are equivalent with a *trans* disposition of the chlorine atom to the chain on each metal center. The ^{1}H NMR spectrum of **3a** displays a singlet at $\delta = 5.50$ ppm for the proton (R^1 = H) on the C_δ atom of the chain, and a single signal for two methyl groups at $\delta = 1.35$ ppm. Conversely, NMR analyses indicate an unsymmetrical structure for the systems **3b** and **3c**. Indeed, the ^{31}P NMR spectrum of **3c** displays two singlets at $\delta = 43.8$ and 49.6 ppm, and the ^{1}H NMR spectrum shows two signals for the two methyl groups at $\delta = 1.27$ and 1.06 ppm. Furthermore the ^{13}C NMR spectrum displays seven different signals for the delocalized carbon chain.[9] It is noteworthy that the resonance signals for the carbon atoms C_α and C_α' of these compounds (**3a**: $\delta = 224$ ppm) are found upfield to that of an allenylidene complex (**1a**: $\delta = 320$ ppm) and downfield to that of an acetylide complex (**2**: $\delta = 123$ ppm), indicating a highly delocalized structure (Scheme 1).



Scheme 1. Synthesis of **3a–3c**.

The structure of complex **3a** was confirmed by X-ray structure analysis (Figure 1).[10] Owing to the inversion center, the structure can be described as two identical bulky ruthenium fragments [RuCl(dppe)$_2$]$^+$ that are connected by a planar "W"-shaped C_9H_7 bridge to minimize steric repulsions. The Cl-Ru1-C53-C54-C55 arrangement is almost linear. As observed for the annelated compound **A**,[7] the Ru1−C53 (1.923(9) Å) and C54−C55 (1.390(13) Å) bonds are significantly shorter than the related single bonds in a ruthenium alkyne system and longer than the corresponding double bonds in a metal allenylidene.[11] On the other hand, the C53−C54 bond length (1.218(12) Å) is intermediate between the values found in these mononuclear systems. The different angles about C55 and C56 are close to 120° showing the high sp^2 nature of these carbon atoms. Along with the C55−C56 bond length (1.401(11) Å),

 © 2002 WILEY-VCH Verlag GmbH & Co. KGaA, Weinheim 0044-8249/02/4123-4514 $ 20.00+.50/0 *Angew. Chem. Int. Ed.* **2002**, *41*, No. 23

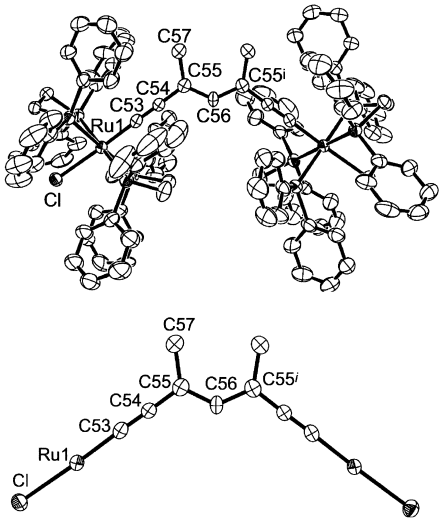


Figure 1. Molecular structure of **3a**. Selected bond lengths [Å] and angles [°]: Ru1-C53 1.923(9), C53-C54 1.218(12), C54-C55 1.390(13), C55-C56 1.401(11), C55-C57 1.528(12); C53-Ru1-Cl 177.3(2), C54-C53-Ru1 178.0(8), C53-C54-C55 178.1(11), C54-C55-C56 118.0(9), C54-C55-C57 118.5(8), C56-C55-C57 123.6(9), C55-C56-C55^{i} 129.8(13).

these data reveal extended π conjugation along this bridge which bears two identical methyl groups (C55−C57 1.528(12) Å) as indicated by the NMR data.

Cyclic voltammetry was performed on complexes **3a–c**, and the results are reported in Table 1. The three compounds undergo a well-defined one-electron reversible oxidation wave followed by an almost reversible or irreversible second oxidation wave consistent with the doubly oxidized species undergoing subsequent chemical reactions. To a first approximation, these two oxidation steps could be viewed as essentially involving the two Ru^{II}/Ru^{III} couples.[5b,8d,12] The large separation of the processes ($\Delta E° = 650$ mV, $K_c = \exp(\Delta E° F/RT) = 1.27 \times 10^{11}$ for **3b**[2a]) is attributable to a combination of phenomena such as strong electronic coupling, columbic repulsion, and/or structural distortion through the oxidations. The singly oxidized compounds (mixed valence) should be stable and isolatable for further studies. These complexes also undergo a well-defined one-electron reduction wave attributable to the reduction of the unsaturated carbon chain,[7,8c] the rather negative values show that the new compounds are electron-rich. This assignment is also supported by the fact that the reduction potential is highly influenced by the introduction of the phenyl group (compare **3b** and **3c** with **3a**). UV/Vis spectra of **3a–c**, which were recorded from the deep green solutions in CH_2Cl_2, show a strong charge transfer band with a significant absorption coefficient (Table 1), and the λ_{max} values are clearly influenced by the nature of the pendant groups on the bridge. These results are consistent with those on the C_5 "V"-shaped compound $[CpRu(PPh_3)_2{=}C{=}C{=}CH{-}C{\equiv}C{-}Ru(PPh_3)_2Cp]BF_4$, which shows an intense band at lower wavelength ($\lambda_{max} = 600$ nm, $\varepsilon = 72000\ mol^{-1}\,L\,cm^{-1}$), in accord with its shorter conjugated path.[5a] The optical band gaps roughly correlate with the electrochemical band gaps and are indicative of the metal-to-ligand charge transfer (MLCT) nature of the transitions. For example, for **3a** the optical band gap is 1.70 eV and $\Delta E° = 1.69$ V. It is worth noting that for complex **A** a band was observed at $\lambda_{max} = 633$ nm (1.95 eV, $\varepsilon = 141000\ mol^{-1}\,L\,cm^{-1}$) and that this red shift (100 nm, 0.25 eV) matches the observed difference in the electrochemical band gap of 0.21 eV ($\Delta E° = 1.90$ V for **A**). Thus, these preliminary results show that a slight structural variation in the C_7 bridges, that is, the "bridging CH_2" in **A** is replaced by two methyl groups in **3a**, induces a significant difference in their optical and redox properties. The new linear systems display the highest conjugation and this could be related to the absence of a cycle constraint in the delocalized path by contrast with **A**. These observations support the necessity to tune a general system to find the best physical properties.

Table 1. Cyclic voltammetry[a] and UV/Vis data for complexes **3a–c**.

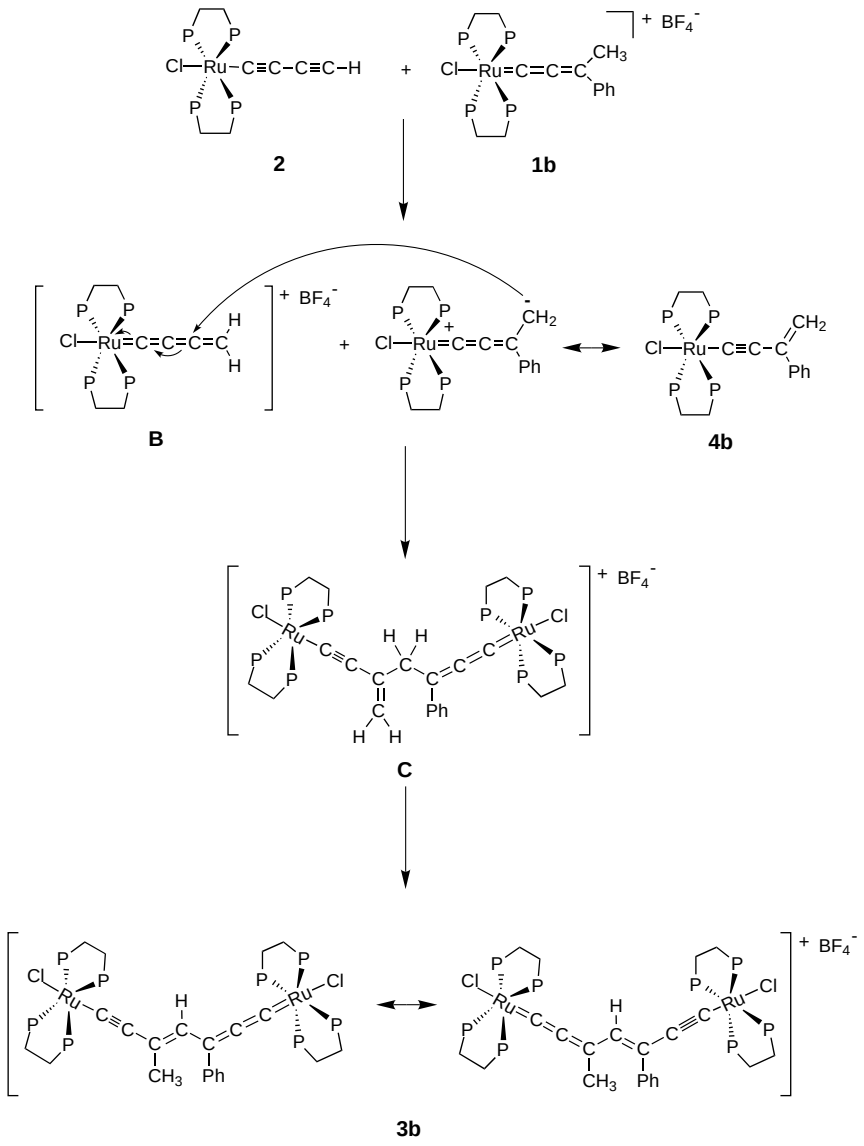
	$E°_{red}$ [V][b]	$E°_{ox1}$ [V][b]	$E°_{ox2}$ [V]	λ_{max} [nm]	ε [$mol^{-1}\,L\,cm^{-1}$][e]
3a	−1.38	0.31	0.99[d]	730	122000
3b	−1.24	0.32	0.97[e]	746	98000
3c	−1.25	0.23	1.06[d]	764	109000

[a] Sample, 1 mM; Bu_4NPF_6 (0.1M) in CH_2Cl_2; $\upsilon = 100\ mV\,s^{-1}$; potentials are reported in Volt versus ferrocene as an internal standard. [b] Reversible redox processes $\Delta E_p \approx 60$ mV, $I_{pc}/I_{pa} \approx 1$. [c] In CH_2Cl_2. [d] Peak potential of an irreversible process. [e] Partially reversible peak $\Delta E_p \approx 95$ mV, $I_{pc}/I_{pa} < 1$.

A possible mechanism for the reaction was established by monitoring the formation of **3b** by ^{31}P NMR spectroscopy. Two features were observed: 1) at the beginning of the reaction, the appearance of two signals of similar intensity at $\delta = 53.6$ and 43.2 ppm and a signal of weak intensity at $\delta = 51.2$ ppm; 2) the gradual disappearance of these peaks and the emergence of two new signals corresponding to the final complex **3b**. The signal at $\delta = 51.2$ ppm can be attributed to the transient formation of the acetylide **4b** as the initial step of the reaction (Scheme 2). Indeed, ruthenium allenylidenes with a -CHRR′ group at the C_γ atom are easily deprotonated into stable ruthenium acetylides by the action of weak bases.[13] As **4** can be easily protonated at the C_δ atom,[8a] the transfer of this proton from **3b** could transform **4** into the unstable butatrienylidene complex **B**. A fast addition of the nucleophilic C_δ atom of **4b** at the electrophilic C_γ atom[12b] of **B** could lead to the intermediate **C**, which formally bears an enyne moiety ($\delta = 53.6$ ppm) and an allenylidene moiety ($\delta = 43.2$ ppm). ^1H NMR spectroscopy revealed two broad signals at $\delta = 4.20$ and 5.05 ppm, which were attributable to the ethylenic protons of **C**. They progressively disappeared and were replaced by a unique signal at $\delta = 5.79$ ppm for complex **3b**. The formation of **3b** would result from an allylic hygrogen transfer in the intermediate **C**. This mechanism can be applied to **3a** and **3c**, and is supported by the fact that the reaction does not work with allenylidene complexes such as *trans*-$[(dppe)_2(Cl)Ru{=}C{=}C{=}CR^3Ph]BF_4$ with $R^3 = H$, Ph, or $CH(CH_3)_2$. Hence, two hydrogen atoms on one group at the C_γ atom of the allenylidene are required: one for the proton exchange between **1** and **2** and another one for the final transfer in **C**.

In conclusion, a novel rational synthesis has been developed to obtain the first bimetallic complexes containing a "W"-shaped C_7 bridge that display remarkable stabilities, and

 © 2002 WILEY-VCH Verlag GmbH & Co. KGaA, Weinheim 0044-8249/02/4123-4515 $ 20.00+.50/0



Scheme 2. Proposed mechanism for the formation of **3a**–**3c**.

interesting spectroscopic and structural properties. To gain a better understanding of the properties of these complexes, theoretical calculations and isolation of mixed-valence species are in progress. The reaction also shows the potential of allenylidene systems as pronucleophiles for further syntheses. In addition, these systems could serve as valuable models for new functionalized one-dimensional wirelike arrangements with the introduction of functional pendant groups on the chain through exhange of R^1 and R^2.

Experimental Section

General procedure for the synthesis of **3a:** CH_2Cl_2 (30 mL) was added to a Schlenk tube containing **1a** (163 mg, 0.15 mmol), and in another tube, **2** (158 mg, 0.15 mmol) was dissolved in CH_2Cl_2 (100 mL). The latter solution was slowly added to the first one over 6 h, using a dropping funnel. This mixture was stirred for an additional 18 h at room temperature. After filtration, the solution was evaporated and the residue was washed with diethyl ether (3×25 mL). Crystallization in a CH_2Cl_2/pentane mixture yielded dark green crystals of **3a** (233 mg; 75%), which were characterized by spectroscopic analysis (see Supporting Information).

Received: July 2, 2002 [Z19650]

[1] J.-M. Lehn, *Supramolecular Chemistry: Concepts and Perspectives*, VCH, Weinheim, **1995**, chap. 8; I. R. Whittall, A. M. McDonagh, M. G. Humphrey, M. Samoc, *Adv. Organomet. Chem.* **1998**, *43*, 349–405; M. Mayor, C. von Hänisch, H. B. Weber, J. Reichert, D. Beckmann, *Angew. Chem.* **2002**, *114*, 1228–1231; *Angew. Chem. Int. Ed.* **2002**, *41*, 1183–1186.

[2] a) F. Paul, C. Lapinte, *Coord. Chem. Rev.* **1998**, *178–180*, 431–509; b) R. E. Martin, F. Diederich, *Angew. Chem.* **1999**, *111*, 1440–1469; *Angew. Chem. Int. Ed.* **1999**, *38*, 1350–1377.

[3] For selected examples see: R. Dembinski, T. Bartik, B. Bartik, M. Jaeger, J. A. Glagysz, *J. Am. Chem. Soc.* **2000**, *122*, 810–822; F. Paul, W. E. Meyer, L. Toupet, H. Jiao, J. A. Gladysz, C. Lapinte, *J. Am. Chem. Soc.* **2000**, *122*, 9405–9414; J. G. Rubio, M. Laubender, H. Werner, *Organometallics* **2000**, *19*, 1365–1372; F. J. Fernandez, O. Blacque, M. Alfonso, H. Berke, *Chem. Commun.* **2000**, 1266–1267; M. I. Bruce, P. J. Low, K. Costuas, J.-F. Halet, S. P. Best, G. A. Heath, *J. Am. Chem. Soc.* **2000**, *122*, 1949–1962.

[4] T. Bartik, W. Weng, J. A. Ramsden, S. Szafert, S. B. Falloon, A. M. Arif, J. A. Gladysz, *J. Am. Chem. Soc.* **1998**, *120*, 11071–11081; R. Dembinski, S. Szafert, P. Haquette, T. Lis, J. A. Gladysz, *Organometallics* **1999**, *18*, 5438–5440.

[5] a) G. Jia, H. P. Xia, W. F. Wu, W. S. Ng, *Organometallics* **1997**, *16*, 2940–2947; b) H. P. Xia, W. S. Ng, J. S. Ye, X. Y. Li, W. T. Wong, Z. Lin, C. Yang, G. Jia, *Organometallics* **1999**, *18*, 4552–4557.

[6] T. Bartik, M. T. Johnson, A. M. Arif, J. A. Gladysz, *Organometallics* **1995**, *14*, 889–897; H. Fischer, F. Leroux, R. Stumpf, G. Roth, *Chem. Ber.* **1996**, *129*, 1475–1482; F. Leroux, R. Stumph, H. Fischer, *Eur. J. Inorg. Chem.* **1998**, 1225–1234; N. Y. Kolokova, V. V. Skripkin, G. G. Alexandrov, Y. T. Struchkov, *J. Organomet. Chem.* **1979**, *169*, 293–300; W. Weng; J. R. Berenguer, J. Fornies, E. Lalind, F. Martinez, L. Sanchez, B. Serrano, *Organometallics* **1998**, *17*, 1640–1642; R. M. Bullock, *J. Am. Chem. Soc.* **1987**, *109*, 8087–8091; C. Hartbaum, H. Fischer, *J. Organomet. Chem.* **1999**, *578*, 186–192.

[7] S. Rigaut, L. Le Pichon, J.-C. Daran, D. Touchard, P. H. Dixneuf, *Chem. Commun.* **2001**, 1206–1207.

[8] a) D. Touchard, P. H. Dixneuf, *Coord. Chem. Rev.* **1998**, *178–180*, 409–429; b) D. Touchard, P. Haquette, A. Daridor, A. Romero, P. H. Dixneuf, *Organometallics* **1998**, *17*, 3844–3852; c) S. Rigaut, O. Maury, D. Touchard, P. H. Dixneuf, *Chem. Commun.* **2001**, 373–374; d) S. Rigaut, F. Monnier, F. Mousset, D. Touchard, P. H. Dixneuf, *Organometallics* **2002**, *21*, 2657–2661.

[9] Selected data for **3c**: $^{13}C\{^1H\}$ NMR (75 MHz, CD_2Cl_2, TMS): $\delta =$ 245.26 and 220.37 (quint., $^2J(P,C) = 14$ Hz; C_α and $C_{\alpha'}$), 170.47 and 158.22 (s; C_β and $C_{\beta'}$), 157.99 and 146.64 (s; C_γ and $C_{\gamma'}$), 152.11 (s; C_δ-CH_3), 31.01 and 28.97 (m, $|{}^1J(P,C) + {}^3J(P,C)| = 23$ Hz; CH_2), 30.70 (s; C_γ-CH_3), 22.47 ppm (s; C_δ-CH_3).

[10] Data for X-ray structure analysis of **3a**: $C_{113}H_{103}BCl_2F_{3.5}OP_8Ru_2$: ($M_r = 2075.06$); crystal size $0.20 \times 0.15 \times 0.10$ mm^3, orthorhombic, space group *Pbna*, $a = 13.5145(1)$, $b = 23.8041(3)$, $c = 33.4320(4)$ Å, $V = 10755.1(2)$ Å^3, $Z = 4$, $\rho_{calcd} = 1.282$ g cm^{-3}, $2\theta_{max} = 25.35°$, $T =$

 © 2002 WILEY-VCH Verlag GmbH & Co. KGaA, Weinheim 0044-8249/02/4123-4516 $ 20.00+.50/0

293(2) K; 18793 reflections measured, 9847 unique (R(int) = 0.0612) and 5293 $I > 2\sigma(I)$; Nonius Kappa CCD, $Mo_{K\alpha}$ radiation (λ = 0.71073 Å), graphite monochromator, Lp correction. The structure was solved by direct methods and refined against F^2 with the full-matrix, least-squares method (G. M. Sheldrick, SHELXS-98, Program for Crystal Structure Analysis, University of Göttingen, Göttingen (Germany), **1998**), 583 parameters, $R1 = 0.1578$, $wR2 = 0.2990$ for all data and $R1 = 0.0892$, $wR2 = 0.2574$ for $I > 2\sigma(I)$; residual electron density 2.104/−0.579 e Å^{-3}. Owing to disorder in the BF_4^- ion, restrain distances were introduced and an occupation factor of 0.5 was applied to all B and F atoms in general positions; the highest residual electron density peaks are localized near this anion. CCDC-188436 (**3a**) contains the supplementary crystallographic data for this paper. These data can be obtained free of charge via www.ccdc.cam.ac.uk/conts/retrieving.html (or from the Cambridge Crystallographic Data Centre, 12, Union Road, Cambridge CB2 1EZ, UK; fax: (+44) 1223-336-033; or deposit@ccdc.cam.ac.uk).

[11] M. Younus, N. J. Long, P. R. Raithby, J. Lewis, N. A. Page, A. J. P. White, D. J. Williams, M. C. B. Colbert, A. J. Hodge, M. S. Khan, D. G. Parker, *J. Organomet. Chem.* **1999**, 578, 198–209; J. P. Selegue, *Organometallics* **1982**, *1*, 217–218.

[12] a) O. F. Koentjoro, R. Rousseau, P. J. Low, *Organometallics* **2001**, *20*, 4502–4509; b) R. F. Winter, K.-W. Klinkhammer, S. Zalis, *Organometallics* **2001**, *20*, 1317–1333.

[13] Complex **4b** has been separately obtained and characterized by the deprotonation of **1b**, see: P. Haquette, D. Touchard, L. Toupet, P. H. Dixneuf, *J. Organomet. Chem.* **1998**, *565*, 63–73.

Towards Stepwise Cluster Assembly: A Decacopper(II) Complex Obtained by Controlled Expansion of a Metallasiloxane Cage**

Gian Luca Abbati,* Andrea Caneschi, Andrea Cornia,* Antonio C. Fabretti, Yulia A. Pozdniakova, and Olga I. Shchegolikhina

The synthesis of new magnetic clusters with unprecedented spin topologies is a central topic in the field of molecular magnetism. Among different strategies that have been developed, serendipitous assembly[1] and rational design[2] represent opposite limiting approaches. The rational construction of heptanuclear clusters with high-spin ground states has been reported starting from hexacyanometalates $[M(CN)_6]^{3-}$ (M = Cr, Fe) and mononuclear complexes bearing a capping ligand.[2] The use of robust, preformed clusters as central cores represents an even more appealing approach, which we are currently pursuing. In particular, we are focusing on metallasiloxane cages such as $[Cu_6\{(PhSiO_2)_6\}_2L_6]$[3] (where L = monodentate ligand). The $[Cu_6\{(PhSiO_2)_6\}_2]$ skeleton features a layer of six coplanar metal ions, sandwiched between two $[(PhSiO_2)_6]^{6-}$ ligands. Similar architectures containing other first-row divalent metal ions and encapsulating a chloride ion are known.[3a,4] The twelve six-membered chelate rings in the $[Cu_6\{(PhSiO_2)_6\}_2]$ structure convey a remarkable inertness and thermodynamic stability to the cluster core. In contrast, the monodentate ligands which surround the Cu_6 cage are labile and can be easily replaced in solution by open-shell units bearing suitable bridging groups. In principle, this allows a fully controlled organization of a second shell of magnetic centers around the Cu_6 unit, Figure 1.

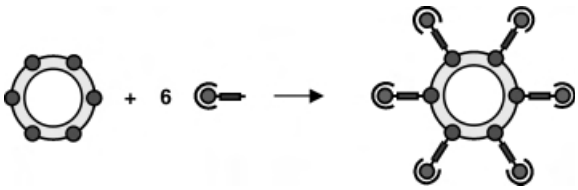


Figure 1. Addition of a second shell of magnetic centers to a central Cu_6 core.

Herein we report the successful expansion of the hexacopper(II) cage **1** through the addition of four $[Cu(tmpa)CN]^+$ (tmpa = tris(2-pyridylmethyl)amine)[5,6] units from **3** to give a decacopper(II) cluster **2**.

$[Cu_6\{(PhSiO_2)_6\}_2(n\text{BuOH})_{6-x}(H_2O)_x]$ **1**

$[Cu(tmpa)CN]PF_6$ **3**

$[Cu_6\{(PhSiO_2)_6\}_2\{NCCu(tmpa)\}_4](PF_6)_4$ **2**

Compound **2** was synthesized by reaction of **1**[3b] with the copper cyanide complex **3**[5a] in a methanol–chloroform solvent mixture (see Experimental Section).

The composition of the crystalline compound, $\mathbf{2}\cdot 2\,CHCl_3\cdot 2.75\,MeOH\cdot 0.25\,H_2O$, was established by elemental analysis and a low-temperature single-crystal X-ray diffraction investigation. The molecular structure of the cation of **2** has idealized D_2 point-group symmetry (Figures 2 and 3). The metal topology comprises an hexagonal, almost planar Cu_6 array (within ±0.0108(6) Å), plus four peripheral Cu(tmpa) units linked to the central core through cyanide bridges. Formation of the cyanide bridge induces only minor structural changes in the $[Cu(tmpa)CN]^+$ unit, the bond lengths of which are equal to within 3σ of those in **3**. On the other hand, the trigonal-bipyramidal (TB) coordination geometry of the copper(II) ion of **2** is slightly more distorted, with τ values[7] in the range 0.843(7)–0.902(7), compared with 0.943(3) in **3**.[5a] The arrangement of the bulky Cu(tmpa) units around the Cu_6 core of **2** results in significant departures from linearity in the Cu-N-C-Cu(tmpa) moieties, which have a *cisoid* conformation with N-C-Cu(tmpa) and Cu-N-C angles in the range 168.8(7)–

[*] Dr. G. L. Abbati, Dr. A. Cornia, Prof. Dr. A. C. Fabretti
Dipartimento di Chimica
INSTM and Università degli Studi di Modena e Reggio Emilia
Via G. Campi 183, 41100 Modena (Italy)
Fax: (+39) 059-373-543
E-mail: abbati@unimore.it
acornia@unimore.it

Dr. A. Caneschi
Dipartimento di Chimica
INSTM and Università degli Studi di Firenze
50019, Sesto Fiorentino (Italy)

Dr. Y. A. Pozdniakova, Dr. O. I. Shchegolikhina
A. N. Nesmeyanov Institute of Organoelement Compounds
119991 Moscow (Russian Federation)

[**] This work was supported by Italian MIUR and CNR and by the network MOLNANOMAG. We thank Prof. Dr. M. Monari and Prof. Dr. V. Albano, Università di Bologna (Italy) for assistance in X-ray data collection.

 © 2002 WILEY-VCH Verlag GmbH & Co. KGaA, Weinheim 0044-8249/02/4123-4517 $ 20.00+.50/0

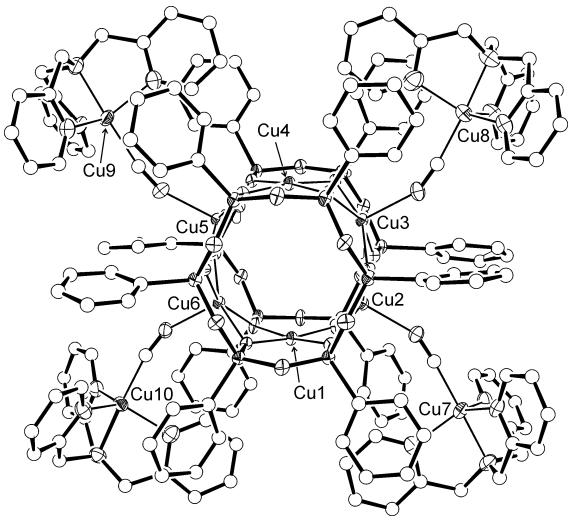


Figure 2. Molecular structure of the cation of **2** (thermal ellipsoids for the Cu, Si, O and N atoms are set at 50 %-probability). C atoms are represented as spheres of arbitrary radius. Hydrogen atoms are omitted for clarity (see Figure 3 for the atom labeling scheme).

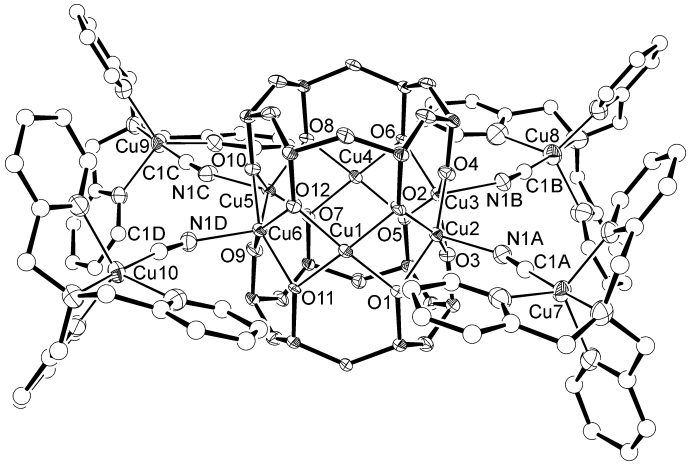


Figure 3. ORTEP[11d] plot of the cation of **2** (thermal ellipsoids for Cu, Si, O and N atoms are set at 50 %-probability). C atoms are represented as spheres with arbitrary radius. The phenyl rings of the siloxanolate ligand, as well as hydrogen atoms, have been omitted for clarity. Selected interatomic distances [Å] and interbond angles [°]: Cu1···Cu2 2.7614(12), Cu2···Cu3 2.9083(12), Cu3···Cu4 2.7598(12), Cu4···Cu5 2.7769(12), Cu5···Cu6 2.9129(11), Cu1···Cu6 2.7742(11), Cu1···Cu4 5.4164(11), Cu2···Cu5 5.7408(11), Cu3···Cu6 5.7205(11), Cu2···Cu1···Cu6 126.19(4), Cu1···Cu2···Cu3 116.77(4), Cu4···Cu3···Cu2 117.26(4), Cu3···Cu4···Cu5 126.15(4), Cu4···Cu5···Cu6 116.57(4), Cu1···Cu6···Cu5 117.05(4), Cu1-O1-Cu2 90.63(19), Cu1-O2-Cu2 90.91(19), Cu2-O3-Cu3 97.4(2), Cu2-O4-Cu3 97.9(2), Cu3-O5-Cu4 91.13(19), Cu3-O6-Cu4 90.57(18), Cu4-O7-Cu5 91.31(19), Cu4-O8-Cu5 91.84(18), Cu5-O9-Cu6 97.3(2), Cu5-O10-Cu6 96.5(2), Cu6-O11-Cu1 91.25(18), Cu6-O12-Cu1 91.04(19), Cu2-N1A-C1A 153.0(7), Cu3-N1B-C1B 153.2(7), Cu5-N1C-C1C 159.9(7), Cu6-N1D-C1D 156.3(7), N1A-C1A-Cu7 173.5(8), N1B-C1B-Cu8 171.9(8), N1C-C1C-Cu9 170.1(7), N1D-C1D-Cu10 168.8(7).

173.5(8)° and 153.0(7)–159.9(7)°, respectively. Interestingly, a pyridine group of each tmpa ligand is sandwiched between two siloxanolate phenyl rings, with dihedral angles between the pyridine and phenyl mean planes ranging from 11.3(7) to 51.5(3)°.

The geometry of the cyanide bridge in **2** is fully consistent with the blue shift observed in the C–N stretching frequency (2172 cm^{-1} vs. 2147 cm^{-1} in **3**[5a]). This behavior strongly points to a quite rigid cyanide bridge acting mainly as a σ–donor toward the metal centers.[8]

The docking of the complex ligands has a dramatic impact on the geometry of the intrinsically symmetric copper–siloxanolate framework. The cyanide-nitrogen-bound copper(II) ions have a slightly distorted square-pyramidal (SP) coordination environment, with Cu–O bond lengths in the range 1.909(5)–2.005(4) Å (av. 1.96 Å) and an average shift of the copper ions of 0.41 Å from the basal planes towards the cyanide donors. In contrast, Cu1 and Cu4 have a square-planar (S) coordination environment, with Cu–O separations in the range 1.876(5)–1.922(5) Å (av. 1.90 Å) and considerably smaller deviations from the basal planes ($\leq$ 0.13 Å). The coordination number of Cu1 and Cu4 results from the steric hindrance of the tmpa ligands which precludes coordination of a fifth axial ligand to Cu1 and Cu4. Consequently, the hexacopper(II) moiety is compressed approximately along the Cu1–Cu4 vector, the distances between opposite copper ions range from 5.4164(11) to 5.7408(11) Å. The angles at the bridging siloxanolate oxygen atoms also vary considerably around the ring, with average values of 91.1(4) and 97.3(5)° for Cu_S-O-Cu_{SP} and Cu_{SP}-O-Cu_{SP}, respectively.

The magnetic properties of a microcrystalline sample of **2** were investigated as a function of temperature (T) and applied magnetic field (B). The temperature dependence of the molar magnetic susceptibility at 1 T is shown in Figure 4 (top) as a χT versus T plot. The value of χT is 4.9 emu K mol^{-1} at 300 K and increases smoothly upon lowering the temperature, which reaches a maximum (6.2 emu K mol^{-1}) at approximately 10 K, and then decreases rapidly to 4.6 emu K mol^{-1} at 2.0 K. The molar magnetization (M) measured at 2.0 and 4.5 K as a function of B is plotted versus

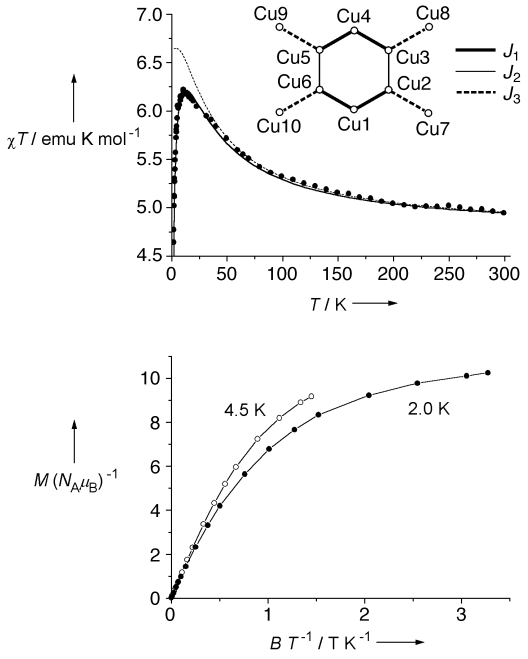


Figure 4. χT versus T (top) and M versus B/T (bottom) data for **2.** Calculated χT versus T data are also shown as solid —— ($g = 2.25$, $J_1 = -47$ cm^{-1}, $J_2 = 0$, $J_3 = 1.7$ cm^{-1}) and dashed - - - - ($g = 2.25$, $J_1 = -47$ cm^{-1}, $J_2 = 0$, $J_3 = 0$) curves.

 © 2002 WILEY-VCH Verlag GmbH & Co. KGaA, Weinheim 0044-8249/02/4123-4518 $ 20.00+.50/0 *Angew. Chem. Int. Ed.* **2002**, *41*, No. 23

B/T in Figure 4 (bottom). At the highest B/T ratio, the magnetization is close to $10N_A\mu_B$, which indicates the presence of a low-lying $S=5$ state. However, the highest measured χT value in Figure 4 (top) is far below that expected for a $S=5$ state (15 emu K mol^{-1} with $g=2$), which indicates that low-lying states with a lower spin multiplicity must be present.

The molar magnetic susceptibility data (χT vs T) were quantitatively analyzed using a Heisenberg hamiltonian [Eq. (1)] with three independent exchange-coupling constants, which was suggested by the different Cu_S-O-Cu_{SP} and Cu_{SP}-O-Cu_{SP} angles (see Figure 3).

$$\mathscr{H} = J_1[\mathbf{S_1}(\mathbf{S_2}+\mathbf{S_6})+\mathbf{S_4}(\mathbf{S_3}+\mathbf{S_5})]+J_2(\mathbf{S_2}\,\mathbf{S_3}+\mathbf{S_5}\,\mathbf{S_6})+J_3(\mathbf{S_2}\,\mathbf{S_7}+\mathbf{S_3}\,\mathbf{S_8}+\mathbf{S_5}\,\mathbf{S_9}+\mathbf{S_6}\,\mathbf{S_{10}}) \quad (1)$$

The observed magnetic behavior is accurately reproduced by setting $J_1 \sim -47$ cm^{-1} with J_2 and J_3 very weakly antiferromagnetic in nature (1–2 cm^{-1}) to account for the decrease of χT at $T<10$ K. A precise, independent evaluation of J_2 and J_3 is impracticable, and is further precluded by the occurrence of magnetic anisotropy and saturation effects at low temperature. The J_1 value is close to that found in $[Cu_6\{(PhSiO_2)_6\}_2(EtOH)_6]$ ($J=-42$ cm^{-1} for Cu-O-Cu = 92.8°).[3c] The small value of J_2 is consistent with a larger Cu_{SP}-O-Cu_{SP} angle (av. 97.3(5)°) compared with Cu_S-O-Cu_{SP} (av. 91.1(4)°). Finally, a small antiferromagnetic J_3 constant is expected considering: a) the poor overlap between the d orbitals that carry the unpaired electron on Cu_{SP} ($d_{x^2-y^2}$) and on Cu_{TB} (d_{z^2}), the lobes of which are directed toward the siloxanolate and the cyanide bridges, respectively; and b) the δ-type symmetry of the $d_{x^2-y^2}$ orbitals on Cu_{SP} with respect to the C–N vector.[9]

These results show that the metallasiloxane cages can be conveniently exploited as building blocks for constructing higher-nuclearity metal clusters in a controlled fashion. Furthermore, the size and properties of the resulting complexes can be manipulated through careful choice of the complex ligands employed.

The possibility of controlling the number of Cu(tmpa) units in the cluster by varying the reaction ratio between the Cu_6 cage and the complex ligand is now under investigation.

Experimental Section

n-Butanol was distilled over CaO shortly before use, while all the other solvents were used as received. Compound **3** was prepared by a literature method[5a] and characterized by elemental analysis.

1: The compound was obtained by a variation on the synthesis reported by Lindeman and co-workers:[3b] solid polyphenylsiloxane[10] (3.226 g, 0.0250 mol) and KOH 85 % (1.710 g, 0.0259 mol) were stirred together in *n*-butanol (60.0 mL) and heated to reflux on a water bath for 1 h after complete dissolution. A solution of $CuCl_2$ (1.683 g, 0.0125 mol) in *n*-butanol (30.0 mL) was added dropwise to the continuously stirred and heated reaction mixture. The solution immediately turned to green-blue, and as the addition progressed the solution darkened and a green precipitate was formed. After the addition was complete, the suspension was heated at reflux for 10 min, then left undisturbed for 15 min. The green solid was removed by filtration and the blue filtrate was stored in a closed vessel at room temperature, which afforded a crop of green-blue prisms after a few days. Elemental analysis calcd. (%) for $C_{92}H_{120}Cu_6O_{34}Si_{12}$: C 45.73, H 4.67; found (on a vacuum dried sample 0.2 mm Hg, ca. 1 h): C 45.73, H 4.81.

2: Compound **3** (0.0314 g, 0.0592 mmol) was dissolved in chloroform (10.0 mL) and slowly added dropwise to a vigorously stirred solution of **1** (0.0251 g, 0.0103 mmol) in chloroform (1.0 mL). During the addition, a few drops of methanol were immediately added whenever the solution became cloudy. After filtration, rapid diffusion of methanol vapors into the blue filtrate afforded air-stable small blue blocks of **2**·2 $CHCl_3$·2.75 MeOH·0.25 H_2O after two days (yield ca. 25 %). Prismatic crystals suitable for an X-ray diffraction study were obtained by slow diffusion of methanol vapors into the reaction mixture. Elemental analysis calcd (%) for $C_{152.75}H_{145.5}Cl_6Cu_{10}F_{24}N_{20}O_{27}P_4Si_{12}$: C 41.15, H 3.39, N 6.28; found (on a vacuum dried sample 0.1–0.2 mmHg, 90 min.): C 41.09, H 3.44, N 6.37. IR (NaBr): $\tilde{\nu}=2172$ cm^{-1} (w, CN^-).

Crystal structure data for **2**·2 $CHCl_3$·2.75 MeOH·0.25 H_2O: $C_{152.75}H_{145.5}Cl_6Cu_{10}F_{24}N_{20}O_{27}P_4Si_{12}$, $M_r=4458.51$, crystal dimensions $0.60\times0.40\times0.40$ mm, orthorhombic, space group $Pc2_1n$, $a=21.0176(2)$, $b=25.2589(2)$, $c=33.5011(3)$ Å, $V=17785.1(3)$ Å^3, $Z=4$, $\rho_{calcd}=1.660$ g cm^{-3}, $\rho=1.64(2)$ g cm^{-3}, $2\theta_{max}=57.38°$, $Mo_{K\alpha}$ radiation, $\lambda=0.71073$ Å, $T=223(2)$ K. Of the 208363 reflections collected on a SMART-CCD system, 44176 were independent and were used in the structure refinement (Lorentz, polarization and absorption corrections applied, $\mu=1.48$ mm^{-1}, min./max. transmission = 0.4715/0.5900). The structure was solved by direct methods (SIR-92)[11a] and refined on F_o^2 using SHELXL-97 program[11b] implemented in the WINGX suite.[11c] The asymmetric unit comprises one cluster and four hexafluorophosphate ions along with two chloroform and disordered lattice methanol and water molecules. All non-hydrogen atoms were refined anisotropically, except for those of methanol and water molecules and for some fluorine atoms of a disordered hexafluorophosphate ion. The hydrogen atoms of the cluster were added in idealized positions and treated isotropically. The values of $R1$ and $wR2$ are 0.0648 [$I>2\sigma(I)$] and 0.1814 (all data) for 2280 parameters and 22 restraints. The maximum and minimum residual electron density are 1.15 and -1.32 e Å^{-3}, respectively. CCDC-186933 (**2**) contains the supplementary crystallographic data for this paper. These data can be obtained free of charge via www.ccdc.cam.ac.uk/conts/retrieving.html (or from the Cambridge Crystallographic Data Centre, 12, Union Road, Cambridge CB2 1EZ, UK; fax: (+44) 1223-336-033; or deposit@ccdc.cam.ac.uk).

Received: June 6, 2002 [Z19482]

[1] R. E. P. Winpenny, *J. Chem. Soc. Dalton Trans.* **2002**, 1.

[2] a) T. Mallah, C. Auberger, M. Verdaguer, P. Veillet, *J. Chem. Soc. Chem. Commun.* **1995**, 61; b) A. Sculler, T. Mallah, M. Verdaguer, A. Nivorozkhin, J.-L. Tholence, P. Veillet, *New J. Chem.* **1996**, *20*, 1; c) G. Rogez, A. Marvilliers, E. Rivière, J.-P. Audière, F. Lloret, F. Varret, A. Goujon, N. Mendenez, J.-J. Girerd, T. Mallah, *Angew. Chem.* **2000**, *112*, 3007; *Angew. Chem. Int. Ed.* **2000**, *39*, 2885.

[3] a) V. A. Igonin, O. I. Shchegolikhina, S. V. Lindeman, M. M. Levitsky, Yu. T. Strutchkov, A. A. Zhdanov, *J. Organomet. Chem.* **1992**, *423*, 351; b) S. V. Lindeman, O. I. Shchegolikhina, Yu. A. Molodtsova, A. A. Zhdanov, *Acta Crystallogr. Sect. C* **1997**, *53*, 305; c) E. Rentschler, D. Gatteschi, A. Cornia, A. C. Fabretti, A.-L. Barra, O. I. Shchegolikhina, A. A. Zhdanov, *Inorg. Chem.* **1996**, *35*, 4427.

[4] C. Zucchi, M. Mattioli, A. Cornia, A. C. Fabretti, G. Gavioli, M. Pizzotti, R. Ugo, Yu. A. Pozdniakova, O. I. Shchegolikhina, A. A. Zhdanov, G. Pályi, *Inorg. Chim. Acta* **1998**, *280*, 282, and references therein.

[5] a) D. M. Corsi, N. N. Murthy, V. G. Young, Jr., K. D. Karlin, *Inorg. Chem.* **1999**, *38*, 848; b) B. S. Lim, R. H. Holm, *Inorg. Chem.* **1998**, *37*, 4898.

[6] a) G. Anderegg, F. Wenk, *Helv. Chem. Acta* **1967**, *50*, 2330; b) Z. Tyeklàr, R. R. Jacobson, N. Wei, N. N. Murthy, J. Zubieta, K. D. Karlin, *J. Am. Chem. Soc.* **1993**, *115*, 2677.

[7] A. W. Addison, T. N. Rao, J. Reedijk, J. van Rijn, G. C. Vershoor, *J. Chem. Soc. Dalton Trans.* **1984**, 1349.

[8] a) M. J. Scott, S. C. Lee, R. H. Holm *Inorg. Chem.* **1994**, *33*, 4651; b) K. Nakamoto, *Infrared and Raman Spectra of Inorganic and Coordination Compounds*, 4th ed., Wiley InterScience, New-York, **1986**, p. 272.

[9] A. Rodrìguez-Fortea, P. Alemany, S. Alvarez, E. Ruiz, A. Sculler, C. Decroix, V. Marvaud, J. Vaissermann, M. Verdaguer, I. Rosenmann, M. Julve, *Inorg. Chem.* **2001**, *40*, 5868.

[10] a) C. Zucchi, O. I. Shchegolikhina, M. Borsari, A. Cornia, G, Gavioli, A. C. Fabretti, E. Rentschler, D. Gatteschi, R. Ugo, R. Psaro, Yu. A.

 © 2002 WILEY-VCH Verlag GmbH & Co. KGaA, Weinheim 0044-8249/02/4123-4519 $ 20.00+.50/0

Pozdniakova, S. V. Lindeman, A. A. Zhdanov, G. Pályi, *J. Mol. Catal. A* **1996**, *107*, 313; b) K. A. Andrianov, A. A. Zhdanov, *Dokl. Akad. Nauk SSSR* **1957**, *114*, 1005.

[11] a) A. Altomare, G. Cascarano, C. Giacovazzo and A. Guagliardi, *J. Appl. Crystallogr.* **1993**, *26*, 343; b) G. M. Sheldrick, SHELXL-97 (release 9F-2), Program for Crystal Structure Refinement, University of Göttingen, Göttingen (Germany), **1998**; c) L. J. Farrugia, *J. Appl. Crystallogr.* **1999**, *32*, 837; d) L. J. Farrugia, *J. Appl. Crystallogr.* **1997**, *30*, 565.

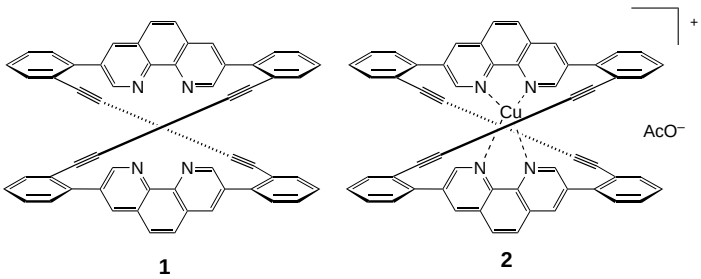


Figure 1. Phenanthrolenophane **1** and its copper(I) complex, **2**.

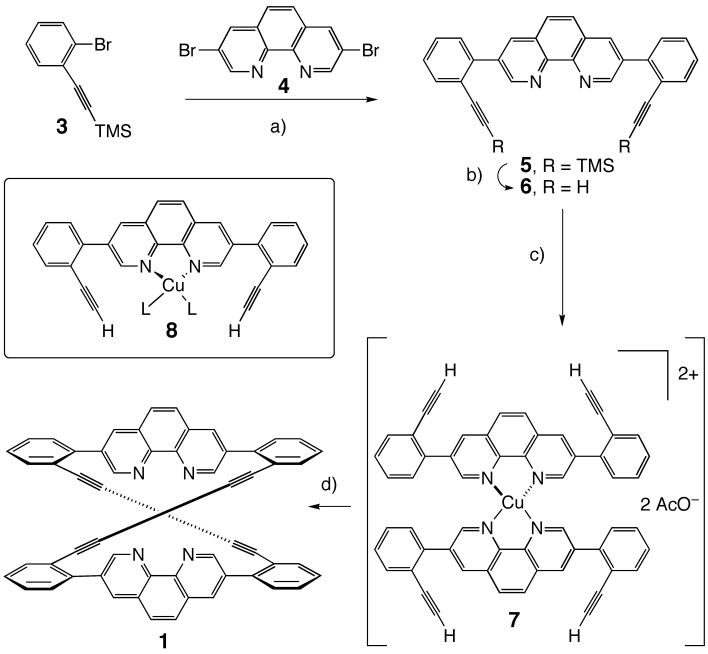
Template-Directed Synthesis of Helical Phenanthroline Cyclophanes**

Matthew A. Heuft and Alex G. Fallis*

Recently the synthesis and study of assorted carbocyclic cyclophanes and cage compounds[1] has been augmented by novel heterocyclic arrays. Representative examples include bis-2,2′-bipyridine units in twisted diyne dehydroannulenes for spectroscopic detection of metal ions,[2] butadiyne-bridged [4_4](2,6)pyridinophanes,[3] rigid cross-conjugated acetylenic macrocycles as a cyclic alternative for 4,4′-bipyridine functionalities for metal complexation,[4] and related thiophene-bridged macrocycles.[5]

Phenanthroline-based investigations involve studies of copper complex induced DNA cleavage,[6] the mechanism of strand scission,[7] enhancement of Diels–Alder reactions,[8] and applications of a cationic platinum–phenanthroline complex.[9] Substituted 1,10-phenanthrolines are highly fluorescent and the spectra are modulated by protonation or metal-ion complexation.[10] [2]Catenanes have been assembled by employing copper(I)–phenanthroline units,[11] and copper(I)–biphenanthrolines have provided scaffolds for molecular grids.[12]

We report here the synthesis of the helical 1,10-phenanthroline-capped cyclophanes **1** (Figure 1) and **11** (Scheme 2), which possess the potential for complexation with various metals, as illustrated by the insertion of copper(I) ions in **2** and **12**. Bromosilylacetylene **3** was converted into its organozincate[1e–g,13] by in situ halogen metal exchange with *n*BuLi, followed by transmetalation with $ZnBr_2$ (Scheme 1). Addition of [$Pd(PPh_3)_4$] and 3,8-dibromophenanthroline (**4**)[14] afforded **5** in 87% yield when DMF was used as a co-solvent.[15] Suzuki couplings also provide 3,8-diaryl-1,10-phenanthrolines.[14c,16] Deprotection of **5** with K_2CO_3 in MeOH/THF provided **6** in 85% yield.



Scheme 1. Synthesis of phenanthrolenophanes **1** and **2**. a) 1) *n*BuLi, THF, −78 °C; 2) $ZnBr_2$, 0 °C, 15 min; 3) **4**, [$Pd(PPh_3)_4$], THF/DMF (1/1), Δ, 72 h, 87%; b) K_2CO_3, CH_2Cl_2, MeOH, H_2O, 72 h, 85%; c) $Cu(OAc)_2$ (0.5 equiv), diethyl ether/py, 2 h; d) 1. $Cu(OAc)_2$ (5.5 equiv), diethyl ether/py, 18 h; 2. KCN (aq), CH_2Cl_2, 5 min, 70%.

We anticipated that controlled addition of copper(II) acetate to **6** (diethyl ether/pyridine) would initially generate the intermediate complex **7**. This "copper template" would then facilitate the desired coupling reaction and circumvent the competing formation of acetate **8** from direct coordination with $Cu(OAc)_2$.[17] The geometric environment of intermediate **8** will inhibit the desired reaction relative to that of **7** in which the terminal acetylene groups are suitably disposed for intermolecular coupling. In addition, polymerization pathways often observed in similar dimerizations should be diminished.[18]

Experimentally, addition of copper(II) acetate (initially 0.5 equiv) in a mixture of pyridine/diethyl ether initiated the reaction and allowed for the formation of **7**. Subsequent addition of excess reagent (5.5 equiv) completed the coupling and afforded the copper(I)-complexed cyclophane **2** in 84% yield (Scheme 1). Supporting evidence for this mechanism was provided by the observed color changes from yellow (**6**) to red (**7**) to green after an excess of $Cu(OAc)_2$ was added. Further confirmation of the importance of the copper

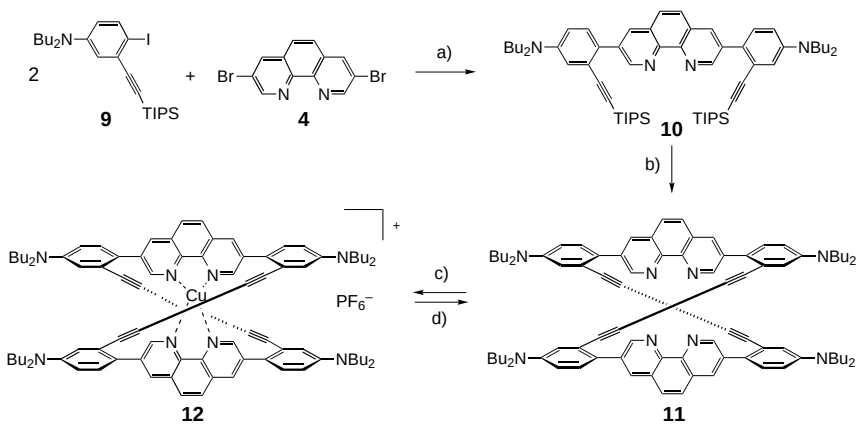
[*] Prof. Dr. A. G. Fallis, M. A. Heuft
Department of Chemistry
University of Ottawa
10 Marie Curie, Ottawa, Ontario, K1N 6N5 (Canada)
Fax: (+1) 613-562-5170
E-mail: afallis@science.uottawa.ca

[**] We are grateful to the Natural Sciences and Engineering Research Council of Canada (NSERC) for financial support. We thank R. Mainville-Dale and D. Fogg (University of Ottawa) for molecular modeling studies. We also thank A. Côté and G. Shimizu (University of Calgary) for providing metal salts. M.A.H. thanks the NSERC for a Graduate Scholarship.

 © 2002 WILEY-VCH Verlag GmbH & Co. KGaA, Weinheim 0044-8249/02/4123-4520 $ 20.00+.50/0

template in these oxidative couplings was revealed by the diminished yield of **2** (15%) when the reaction was conducted with direct exposure of **6** to $Cu(OAc)_2$ (6 equiv, pyridine/diethyl ether).[19]

The parent cyclophane **1**, was liberated from the copper(I)-coordinated phenanthroline cyclophane **2** upon treatment with aqueous potassium cyanide. Unfortunately, cyclophane **1** was only sparingly soluble in a range of organic solvents. The synthesis of the *N*,*N*-dibutylamine-substituted analogue **11** was investigated in an attempt to circumvent this difficulty and provide a substituted member of this series for comparison of the electronic properties. In addition, the butyl groups are diastereotopic in helical (chiral) cyclophane conformations and this should be reflected in the ^{13}C NMR spectrum, thus allowing the conformational behavior of the cyclophane to be probed.[20]



Scheme 2. Synthesis of phenanthrolenophanes **11** and **12**. a) 1. **9**, *n*BuLi, THF, −78°C; 2. $ZnBr_2$, 0°C, 15 min; 3. **4**, $[Pd(PPh_3)_4]$, THF/DMF (1/1), Δ, 72 h, 70%; b) 1. TBAF, diethyl ether/py, 15 min; 2. $Cu(OAc)_2$ (0.5 equiv), diethyl ether/py, 2 h; 3. $Cu(OAc)_2$ (5.5 equiv), diethyl ether/py, 2 h; 4. KCN (aq), 39%; c) $[Cu(MeCN)_4PF_6]$, CH_2Cl_2, 15 min, 97%; d) KCN (aq), CH_2Cl_2, 5 min, 97%. py = pyridine.

A very direct synthesis of **11** has been developed to improve the preparation of these compounds. Dibromide **4** was treated with known iodide **9**[18] through a parallel palladium coupling sequence to generate diacetylene **10** (Scheme 2). Compound **10** was transformed into the metal-free cyclophane **11** in a single reaction vessel by a sequential in situ desilylation/dimerization/decomplexation protocol related to the experiments we have developed recently.[21] These steps culminated in an aqueous potassium cyanide work-up to give **11** in 39% yield. Cyclophane **11** was soluble in a variety of chlorinated solvents.

Copper(I) complexes **2** and **12** were prepared independently as above, but crystals suitable for X-ray analysis were not obtained. However, molecular modeling studies (Figure 2) revealed the twisted nature and key features of the phenanthrolenophane copper complex **2** (Figure 1).[22] The heterocyclic rings displayed an orthogonal disposition with respect to each other and created a pseudotetrahedral coordination site for copper(I) or other electronically related metal ions. The helical nature of cyclophane **12** resulted from our synthetic protocol and the bridges selected.[1d–f]

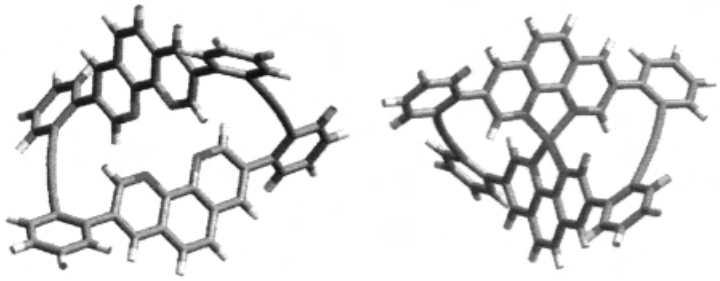


Figure 2. Molecular models of cyclophanes **1** and **2**.

Variable temperature ^{13}C NMR analysis of **12** indicated the helical isomerization barrier was 13.6 kcal mol^{-1}, an increase of approximately 4 kcal mol^{-1} relative to the uncomplexed cyclophane **11** (Figure 3). Different metals and substituent combinations may increase this barrier sufficiently to inhibit isomerization and facilitate resolution of the individual enantiomers.

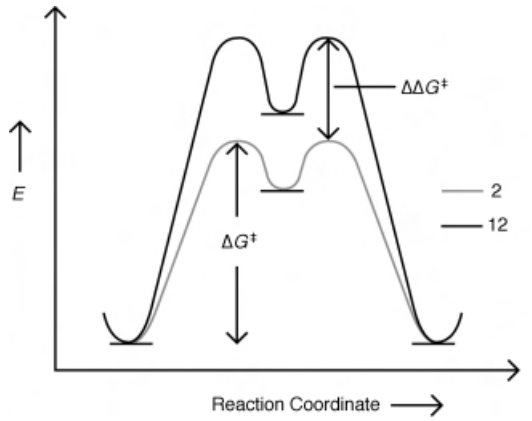


Figure 3. Potential energy diagram for the enantiomerization of cyclophanes **2** and **12**. $\Delta G_2^{\ddagger} < 9.4$ kcal mol^{-1}, $\Delta G_{12}^{\ddagger} = 13.6$ kcal mol^{-1}, $\Delta\Delta G^{\ddagger} > 4.2$ kcal mol^{-1}.

Electronic absorption (Figure 4) were obtained for cyclophanes **1**, **2**, **11**, and **12** and compared to related compounds (Table 1). Copper template **7** absorbed in the 600 to 700 nm range, which is indicative of copper(II) complexes. Emission spectra (Figure 5) of **1** and **11** were recorded but the metallocyclophanes (**2** and **12**) did not fluoresce.

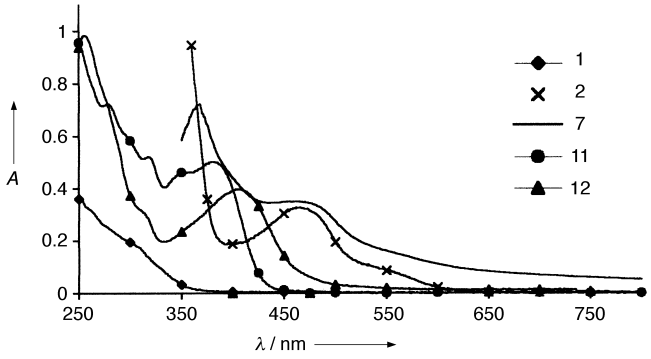


Figure 4. UV/Vis absorption spectra of **1**, **11**, and **12**.[23]

In summary, we have developed a short, efficient syntheses of a series of functionalized acetylenic phenanthroline cyclophanes by Pd- and Cu-mediated coupling reactions. Molecular modeling studies have established the nature of the

 © 2002 WILEY-VCH Verlag GmbH & Co. KGaA, Weinheim 0044-8249/02/4123-4521 $ 20.00+.50/0

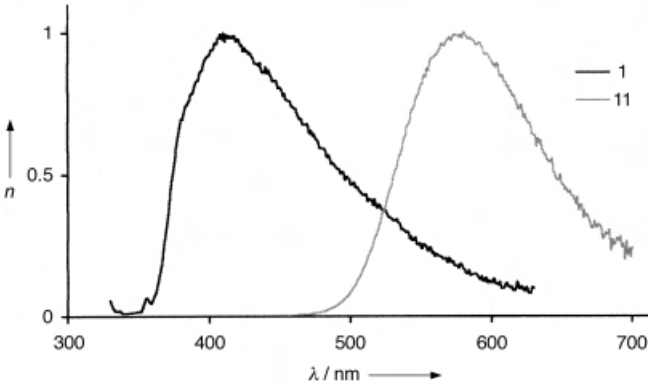
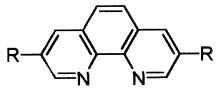


Figure 5. Normalized fluorescence spectra of **1** and **11** (*n*: counts).[24]

Table 1. UV/Vis absorption maxima of phenanthroline compounds and copper–phenanthrolic complexes.



13

Compound	λ_{max}(abs) [nm]	λ_{max}(em) [nm]
13 (R = H)[25]	440	
$[Cu(\mathbf{13})_2]^+$ (R = H)[26]	458	
13 (R = C≡C-Ph)[10]	346	376, 395
13 (R = C≡C-(*p*-PhNMe$_2$))[10]	410	523
1	307 (sh)	416
2 $[Cu(\mathbf{1})_2]^+$	473, 553 (sh)	
7 $[Cu(\mathbf{6})_2]^{2+}$	462	
11	383	584
12 $[Cu(\mathbf{11})_2]^+$	407	

copper-complexed core. In addition, resolution of the helical isomers may be feasible with additional ring substituents and metal complexation. The synthetic protocol above will facilitate the preparation of new derivatives that may possess unusual optical properties, while modification of the acetylene spacers offers some control of the helical conformation.

Experimental Section

Sequential in situ desilylation/dimerization/decomplexation procedure (**11**): A solution of tetrabutylammonium fluoride (TBAF) (1M in THF, 1.32 mL, 1.32 mmol, 2.5 equiv) was added in one portion to a stirred solution of **10** (500 mg, 0.53 mmol, 1 equiv) in pyridine/diethyl ether (3/1, 20 mL). After stirring the solution for 15 min, a solution of $Cu(OAc)_2$ (48 mg, 0.26 mmol, 0.5 equiv) in pyridine/diethyl ether (3/1, 20 mL) was added over 2.5 h by syringe pump. Once the addition was complete, additional $Cu(OAc)_2$ (530 mg, 2.92 mmol, 5.5 equiv) was added to the reaction and the solution turned green immediately. The reaction was stirred for 18 h at room temperature and partitioned between CH_2Cl_2 and water. The aqueous phase was extracted with CH_2Cl_2 (×3) and the combined extracts were washed with KCN (10%, aq) and water, filtered through celite, and concentrated. Following chromatography on silica gel (CH_2Cl_2/MeOH, 30/1), **11** was isolated as an orange solid (130 mg, 39%).

1: m.p. 150 °C slow decomp.; ^{1}H NMR (500 MHz, [D$_6$]DMSO, 25 °C, TMS): δ = 9.33 (brs, 4H), 8.87 (brs, 4H), 7.82–7.77 (m, 12H), 7.63 (brs, 4H), 7.40 ppm (brs, 4H); ^{13}C NMR (125 MHz, [D$_6$]DMSO, 25 °C, TMS): δ = 150.4 (d), 144.3 (s), 140.0 (s), 135.9 (d), 133.7 (s), 133.1 (d), 132.3 (d), 131.4 (d), 130.8 (d), 127.7 (s), 126.9 (d), 118.9 (s), 81.4 (s), 76.3 ppm (s); MS (ES) *m*/*z* (%): 757.0 (1), 579.1 (2), 279.0 (4), 141.9 (53).

2: m.p. > 260 °C; IR (CH_2Cl_2): $\tilde{\nu}$ = 3049.9, 1604.0, 1436.7, 1266.8, 1119.7 cm^{-1}; ^{1}H NMR (500 MHz, [D$_6$]DMSO, 25 °C, TMS): δ = 9.25 (brs, 4H), 8.84 (brs, 4H), 8.37 (brs, 4H), 7.65 (brs, 4H), 7.41 ppm (brs, 12H); ^{13}C NMR (125 MHz, [D$_6$]DMSO, 25 °C, TMS): δ = 149.2 (d), 141.6 (s), 139.8 (s), 136.7 (d), 136.4 (s), 133.5 (d), 130.8 (d), 129.8 (d), 129.0 (d), 128.7 (s), 127.7 (d), 118.9 (s), 81.3 (s), 76.0 ppm (s); MS (70 eV): *m*/*z* (%): 819.3 (100) [M^+], 136.0 (55).

11: m.p. 138–140 °C; IR (CH_2Cl_2): $\tilde{\nu}$ = 2960.9, 1596.2, 1369.8, 847.2 cm^{-1}; ^{1}H NMR (500 MHz, $CDCl_3$, 25 °C, TMS): δ = 9.27 (s, 4H), 8.46 (s, 4H), 7.40 (d, *J* = 8.6 Hz, 4H), 7.03 (s, 4H), 6.91 (s, 4H), 6.75 (d, *J* = 6.9 Hz, 4H), 3.29 (t, *J* = 7.1 Hz, 16H), 1.62–1.53 (m, 16H), 1.41–1.32 (m, 16H), 0.96 ppm (t, *J* = 7.2 Hz, 24 Hz); ^{13}C NMR (125 MHz, $CDCl_3$, 25 °C, TMS): δ = 150.6 (d), 147.5 (s), 144.3 (s), 134.9 (d), 134.3 (s), 130.6 (d), 127.8 (s), 127.7 (s), 126.5 (d), 120.8 (s), 116.5 (d), 113.5 (d), 81.9 (s), 75.6 (s), 50.7 (t), 29.3 (t), 20.3 (t), 13.9 ppm (q); MS (ES) 1266.5 (1) [M^+], 579 (1.2), 279.0 (48), 186.1 (100).

12: m.p. > 250 °C (decomp); IR (CH_2Cl_2): $\tilde{\nu}$ = 2960.9, 1596.2, 1369.8, 847.2, 769.8 cm^{-1}; ^{1}H NMR (500 MHz, $CDCl_3$, 25 °C, TMS): δ = 9.18 (brs, 4H), 8.30 (brs, 4H), 8.08 (brs, 4H), 7.19 (brs, 4H), 6.71 (s, 4H), 6.62 (brs, 4H), 3.21 (brs, 16H), 1.51 (brs, 16H), 1.32 (brs, 16H), 0.92 ppm (brs, 24 Hz); ^{13}C NMR (125 MHz, $CDCl_3$, 25 °C, TMS): δ = 150.0 (d), 148.1 (s), 141.6 (s), 137.8 (s), 134.8 (d), 130.5 (d), 128.9 (s), 127.3 (d), 126.6 (s), 120.5 (s), 115.4 (d), 113.7 (d), 81.9 (s), 75.4 (s), 50.6 (t), 29.6 (t), 20.2 (t), 13.9 ppm (q); MS (ES) 1328.5 (6) [M^+–PF_6], 342.1 (10), 186.2 (24).

Received: July 9, 2002 [Z19694]

[1] a) G. J. Bodwell, *Angew. Chem.* **1996**, *108*, 2221–2224; *Angew. Chem. Int. Ed. Engl.* **1996**, *35*, 2085–2088; b) A. de Meijere, B. Koenig, *Synlett* **1997**, 1221–1232; c) B. König, *Top. Curr. Chem.* **1998**, *196*, 92–136; d) S. K. Collins, G. P. A. Yap, A. G. Fallis, *Angew. Chem.* **2000**, *112*, 393–396; *Angew. Chem. Int. Ed.* **2000**, *39*, 385–388; e) S. K. Collins, G. P. A. Yap, A. G. Fallis, *Org. Lett.* **2000**, *2*, 3189–3192; f) S. K. Collins, G. P. A. Yap, A. G. Fallis, *Org. Lett.* **2002**, *4*, 11–14, and references therein.

[2] P. N. W. Baxter, *J. Org. Chem.* **2001**, *66*, 4170–4179.

[3] Y. Tobe, A. Nagano, K. Kawabata, M. Sonoda, K. Naemura, *Org. Lett.* **2000**, *2*, 3265–3268.

[4] K. Campbell, R. McDonald, N. R. Branda, R. R. Tykwinski, *Org. Lett.* **2001**, *3*, 1045–1048.

[5] M. J. Marsella, Z.-Q. Wang, R. J. Reid, K. Yoon, *Org. Lett.* **2001**, *3*, 885–887.

[6] D. R. McMillin, K. M. McNett, *Chem. Rev.* **1998**, *98*, 1201–1219.

[7] T. Oyoshi, H. Sugiyama, *J. Am. Chem. Soc.* **2000**, *122*, 6313–6314.

[8] S. Otto, J. B. F. N. Engberts, *J. Am. Chem. Soc.* **1999**, *121*, 6798–6806.

[9] a) J. W. Madine, X. Wang, R. A. Widenhoefer, *Org. Lett.* **2001**, *3*, 385–388; b) L. A. Goj, R. A. Widenhoefer, *J. Am. Chem. Soc.* **2001**, *123*, 11133–11147.

[10] H. S. Joshi, R. Jamshidi, Y. Tor, *Angew. Chem.* **1999**, *111*, 2888–2891; *Angew. Chem. Int. Ed.* **1999**, *38*, 2722–2725.

[11] F. Ibukuro, M. Fujita, K. Yamaguchi, J.-P. Sauvage, *J. Am. Chem. Soc.* **1999**, *121*, 11014–11015.

[12] a) S. Toyota, C. R. Woods, M. Benaglia, R. Haldimann, K. Warnmark, K. Hardcastle, J. S. Siegel, *Angew. Chem.* **2001**, *113*, 773–776; *Angew. Chem. Int. Ed.* **2001**, *40*, 751–754; b) J. C. Loren, J. S. Siegel, *Angew. Chem.* **2001**, *113*, 776–779; *Angew. Chem. Int. Ed.* **2001**, *40*, 754–757.

[13] a) S. Sengupta, V. Snieckus, *J. Org. Chem.* **1990**, *55*, 5680–5683; b) P. Knochel, D. Seebach, *Tetrahedron Lett.* **1982**, *23*, 3897–3900.

[14] a) D. Tzalis, Y. Tor, S. Failla, J. S. Siegel, *Tetrahedron Lett.* **1995**, *36*, 3489–3490; b) Y. Saitoh, T.-A. Koizumi, K. Osakada, T. Yamamoto, *Can. J. Chem.* **1997**, *75*, 1336–1339; c) C. Dietrich-Buchecker, M. C. Jimenez, J.-P. Sauvage, *Tetrahedron Lett.* **1999**, *40*, 3395–3396.

[15] M. Sjoegren, S. Hansson, P. O. Norrby, B. Aakermark, M. E. Cucciolito, A. Vitagliano, *Organometallics* **1992**, *11*, 3954–3964.

[16] M. Kimura, T. Shiba, T. Muto, K. Hanabusa, H. Shirai, *Tetrahedron Lett.* **2000**, *41*, 6809–6813.

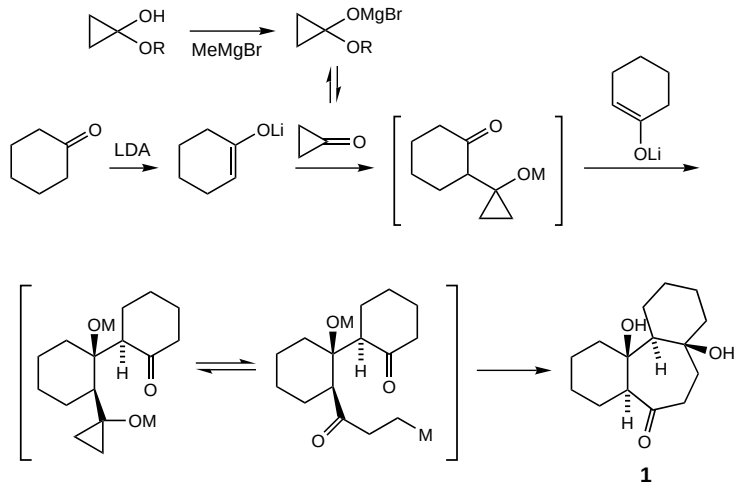
[17] a) *Templated Organic Synthesis* (Eds.: F. Diederich, P. J. Stang), Wiley-VCH, Weinheim, **2000**; b) C. Dietrich-Buchecker, J.-P. Sauvage, N. Geum, A. Hori, M. Fujita, S. Sakamoto, K. Yamaguchi, *Chem. Commun.* **2001**, 1182–1183.

[18] J. J. Pak, T. J. R. Weakley, M. M. Haley, *J. Am. Chem. Soc.* **1999**, *121*, 8182–8192.

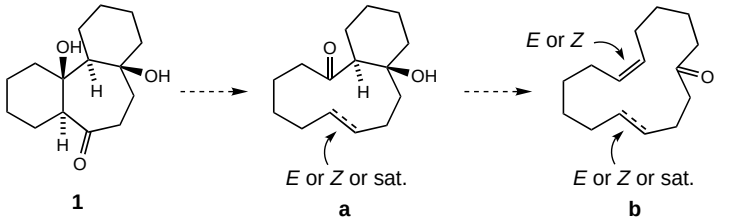
[19] a) R. Berscheid, F. Vögtle, *Synthesis* **1992**, 58–62; b) M. Brake, V. Enkelmann, U. H. F. Bunz, *J. Org. Chem.* **1996**, *61*, 1190–1191; c) P.

 © 2002 WILEY-VCH Verlag GmbH & Co. KGaA, Weinheim 0044-8249/02/4123-4522 $ 20.00+.50/0

Siemsen, R. C. Livingston, F. Diederich, *Angew. Chem.* **2000**, *112*, 2740 – 2767; *Angew. Chem. Int. Ed.* **2000**, *39*, 2632 – 2657; d) M. M. Haley, M. L. Bell, S. C. Brand, D. B. Kimball, J. J. Pak, W. B. Wan, *Tetrahedron Lett.* **1997**, *38*, 7483 – 7486.
[20] a) R. Boese, A. J. Matzger, K. P. C. Vollhardt, *J. Am. Chem. Soc.* **1997**, *119*, 2052 – 2053; b) A. R. Lim, B. M. Novak, *Solid State Commun.* **1999**, *112*, 459 – 464.
[21] M. A. Heuft, S. K. Collins, G. P. A. Yap, A. G. Fallis, *Org. Lett.* **2001**, *3*, 2883 – 2886.
[22] Density functional theory (DFT) calculations were obtained using a DN basis set with the Cerius^2-Dmol^3 molecular modeling suite from Molecular Simulations Inc. San Diego, 1999 (counterion in **2** not shown for clarity).
[23] Electronic absorption spectra λ_{max} nm^{-1} (CH_2Cl_2): **1**, 307 (sh); **11**, 383; **12**, 407.
[24] Emission spectra (CH_2Cl_2): **1**: $\lambda_{ex} = 320$ nm, $\lambda_{max} = 416$ nm; **11**: $\lambda_{ex} = 437$ nm, $\lambda_{max} = 584$ nm.
[25] C. T. Cunningham, K. L. H. Cunningham, J. F. Michalec, D. R. McMillin, *Inorg. Chem.* **1996**, *35*, 6406 – 6412.
[26] M. Ruthkosky, F. N. Castellano, G. J. Meyer, *Inorg. Chem.* **1996**, *35*, 6406 – 6412.



Scheme 1. Synthesis of ketone **1**.[5]



Scheme 2. Projected route to unsaturated C-15 macrocyclic ketones.

Access to C-15 Macrocyclic Ketones by Iterative Fragmentations of a Tricyclic System

Charles Fehr,* José Galindo, Olivier Etter, and Walter Thommen

In recent years, macrocyclic musks[1,2] have gained renewed interest for their excellent odor qualities (warm, sensual, animal, natural), and for their better biodegradability than benzenoid musks.[2,3]

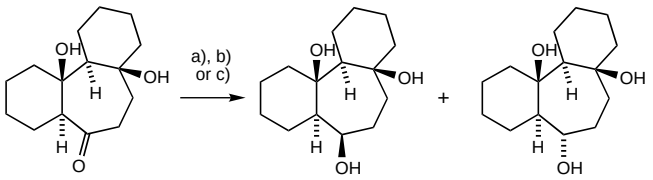
In particular, there is still a great need to find efficient syntheses for the construction of C-15 macrocyclic ketones possessing specific unsaturation. We herein report the first application of a new synthetic strategy in which the target compounds are obtained from an appropriately functionalized tricyclic system by two consecutive fragmentations. This approach is complementary to the metathesis-based annulations, which are often more direct but require high dilution and generally afford *E*/*Z* mixtures.[4]

Access to the targeted tricyclic fragmentation precursor was provided by the ready availability of the known dihydroxy ketone **1**, which was prepared in one pot from cyclohexanone and cyclopropanone (Scheme 1).[5] Despite a reported yield of 67%, it was only after modification of the experimental procedure that we were able to attain a reproducible yield of 44% (see Experimental Section).

The 1,3,5-functionalization of **1**, in which one oxygen atom is adjacent to a bridgehead and the two other oxygen atoms are situated at bridgehead positions, is ideally suited for cascade Grob fragmentations[6] and should allow, via intermediates **a**, ready access to new unsaturated C-15 macrocyclic ketones of type **b** (Scheme 2).

Reduction of **1** with $LiAlH_4$ afforded a 74:26 mixture of triols **2** and **3** (Scheme 3), whereas by using Red-Al® in THF at low temperature the all-*cis* triol **2** was obtained almost quantitatively in a highly diastereoselective manner (99:1). On the other hand, reduction with $BH_3{\cdot}SMe_2$ followed the opposite facial selectivity with an equally high diastereoselectivity (98:2), affording triol **3** in 81% yield (Scheme 3).[7]

For the conversion of alcohol **2** into tosylate **4**, whereas the application of classical conditions (TsCl, pyridine) gave rise to partial epimerization (by successive substitutions) and chloride formation, deprotonation of **2** with *n*BuLi followed by rapid treatment with TsCl gave the best results (Scheme 4).

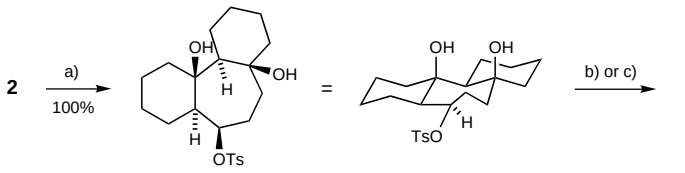


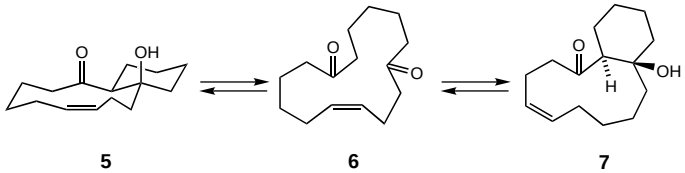
a)	74	:	26	
b)	99	:	1	(98%)
c)	2	:	98	(81%)

Scheme 3. Diastereoselective reductions of ketone **1**. a) $LiAlH_4$ (1.15 equiv), THF, −70°C to −50°C; b) Red-Al® (3.0 equiv), THF, −70°C to room temperature; c) $BH_3{\cdot}SMe_2$ (0.71 equiv), THF, room temperature.

[*] Dr. C. Fehr, J. Galindo, O. Etter, W. Thommen
Firmenich SA
Corporate R&D Division
P. O. Box 239, 1211 Geneva 8 (Switzerland)
Fax: (+41) 22-780-3334
E-mail: charles.fehr@firmenich.com

 © 2002 WILEY-VCH Verlag GmbH & Co. KGaA, Weinheim 0044-8249/02/4123-4523 $ 20.00+.50/0

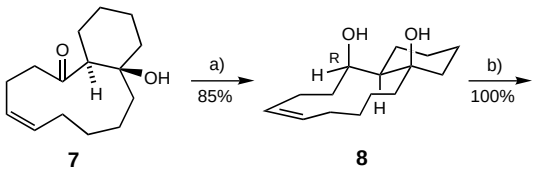


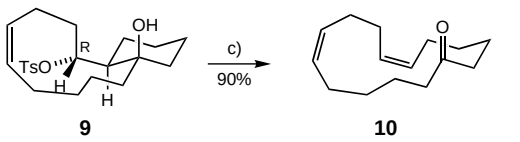


5 **6** **7**

b)	3%	15%	59%
c)	34%	15%	17%

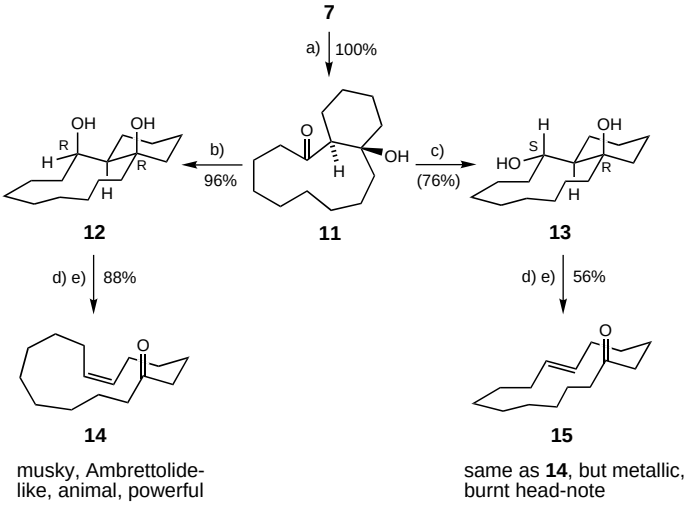
Scheme 4. Grob fragmentation of tosylate **4**: a) *n*BuLi (1.5 equiv), TsCl (1.15 equiv), THF, −15 °C, 20 min; b) KO*t*Bu (3 equiv), *t*BuOH, THF, −6 to 0 °C, 25 min; c) KO*t*Bu (3 equiv), DMF/THF (3:2), 0 to 15 °C, 15 min.





musky, greasy, waxy

Scheme 5. Conversion of **7** to the tosylate **9** and the subsequent Grob fragmentation to give (*Z*,*Z*)-6,10-cyclopentadecadienone **10**: a) $LiAlH_4$ (1.05 equiv), Et_2O; b) *n*BuLi (1.5 equiv), TsCl (1.15 equiv), THF, −15 °C, 20 min; c) KO*t*Bu (3 equiv), *t*BuOH, 25–29 °C, 10 min.



musky, Ambrettolide-like, animal, powerful

same as **14**, but metallic, burnt head-note

Scheme 6. Syntheses of (*Z*)-6- and (*E*)-6-cyclopentadecenones **14** and **15**: a) H_2, Pd (10 %)/C, cyclohexane; b) $LiAlH_4$ (1.2 equiv), Et_2O, RT; c) Red-Al® (4.0 equiv), THF, −78 °C to room temperature; d) *n*BuLi (1.5 equiv), TsCl (1.15 equiv), THF, −15 °C, 20 min; e) KO*t*Bu (3 equiv), *t*BuOH, 25–31 °C, 10 min.

Fragmentation of **4** was effected with KO*t*Bu in *t*BuOH/THF. To our surprise, only trace amounts (3 %) of the expected hydroxy ketone **5** were detected, the main product (59 % yield from **2**) being the isomeric hydroxy ketone **7**, in which the position of the C–C double bond is shifted by two carbon atoms. The concomitant formation of macrocyclic diketone **6**, isolated in 15 % yield, provided a clue for the explanation of the reaction course. This retroaldol product of **5** (and of **7**!) undergoes diastereoselective re-aldolization between two other centers to afford **7**. Indeed, reaction of **6** with KO*t*Bu in *t*BuOH also selectively furnished the more stable aldol **7**; assignment of the *trans* configuration for the ring junction is based on the similarity of the multiplicities of the ^{1}H NMR signals of the α-keto-methine group in **1**, **5**, and **7** (dd, J(H,H) = 4 and 12–13 Hz), and also on the fact that hydrogenation of a mixture of **5** and **7** gives **11** (see below) exclusively. This *trans* configuration of **6** was subsequently confirmed at a later stage of the synthesis (see acetonides **16** and **17**; Scheme 7). The *Z* configuration of the C–C double bond in **7** is in accord with the stereoelectronically imposed *trans*-antiperiplanar arrangement of the bridge C–C bond and the C–OTs bond in **4**. Incidentally, this is further proof for the all-*cis* relationship of the OH groups in **2**.

Interestingly, when the fragmentation was performed in DMF/THF,[6c] the initially formed **5** could be isolated as the major product (**5** + **7**: 51 %; **5**:**7** = 2:1), due to a slower re-aldolization.

A second sequence of reduction/tosylation/fragmentation was then applied to **7** (Scheme 5). Reduction with $LiAlH_4$ produced exclusively diol **8** in 85 % yield.[8] Subsequent tosylation followed by fragmentation afforded (*Z*,*Z*)-6,10-cyclopentadecadienone **10** in 90 % yield (two steps).

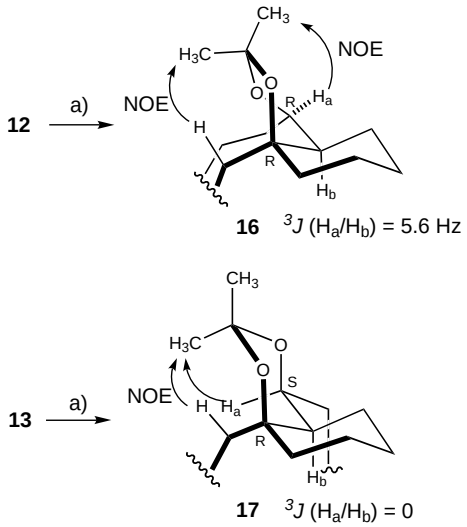
The attractiveness of our synthetic plan lies in its flexibility: any 3-hydroxy ketone can in principle be converted into either a *Z*- or an *E*-unsaturated ketone, depending on the stereochemical outcome of the reduction (*syn* or *anti*). This is illustrated by the synthesis of (*Z*)-6- and (*E*)-6-cyclopentadecenone **14** and **15**. Our common starting point was hydroxy ketone **11**, which was readily prepared by hydrogenation of **7** (Scheme 6). Reduction of **11** using $LiAlH_4$ afforded **12** with excellent diastereoselectivity (97:3) and 96 % yield. $BH_3{\cdot}SMe_2$ (0.7 equiv) in THF at room temperature was also highly selective (> 99:1), but showed low reactivity (34 % conversion).[9]

An opposite mode of reduction was observed by using Red-Al®. Whereas reduction at room temperature only moderately favored the (*S*,*R*)-diol **13** (**13**:**12** = 70:30), reduction at −70 °C produced **13** selectively (**13**:**12** = 92:8 to 95:5).[7] Unfortunately, the reaction did not go to completion (76 % yield based on conversion (74 %)), and 16 % of 1,7-cyclopentadecadione was also formed by retro-aldol condensation (perhaps during workup).

Tosylation of **12** and fragmentation afforded (*Z*)-6-cyclopentadecenone **14** in high yield (88 %; 52 % from **1**) with complete stereocontrol. Unexpectedly, the synthesis of **15** from **13** proved more difficult, due to the instability of the intermediate tosylate, which, in competition with the stereocontrolled fragmentation (56 % yield), also undergoes elimination reactions.

 © 2002 WILEY-VCH Verlag GmbH & Co. KGaA, Weinheim 0044-8249/02/4123-4524 $ 20.00+.50/0 *Angew. Chem. Int. Ed.* **2002**, *41*, No. 23

The stereospecific course of the fragmentation reactions (**12** to **14** and **13** to **15**) lends additional support to the configurations attributed to **12** and **13**, although inversion of *both* stereogenic centers which ultimately become sp^2-carbon atoms, would lead to *the same* fragmentation product. Therefore, for further corroboration of the attributed structures, **12** and **13** were converted into their acetonides **16** and **17**. The measured ^{1}H NMR coupling constants and NOE effects are perfectly in agreement with the postulated structures, as drawn in their most stable conformations (MM2 calculations) (Scheme 7).



Scheme 7. Structure determination of acetonides **16** and **17**: a) 2-methoxypropene, cat. TFA, DMF, 25 °C, 3 h.

All three unsaturated macrocyclic ketones **10**, **14**, and **15** are new[10] and possess the typical musk odor; in particular, **14** represents an excellent, powerful musk odorant.

Experimental Section

Tricyclic ketone **1**: Modified version of the procedure published in reference [5]. Under mechanical stirring, a solution of MeMgBr in *Et_2O* (!) (Aldrich, 3 N; 44.7 mL, 134.0 mmol) was added dropwise at 25–28 °C (water-bath cooling) to a solution of cyclopropanone ethyl hemiacetal[11] (containing variable amounts of cyclopropanone methyl hemiacetal) (11.07 g, ca. 111.7 mmol) (methyl/ethyl ca. 3:1; 92 % pure) in Et_2O (305 mL). Gas evolution (methane) and the formation of a white precipitate were observed. After 10 min, the suspension was treated (by using a cannula; introduction time: ca. 2 min) with a solution of deprotonated cyclohexanone (from cyclohexanone (10.95 g, 111.7 mmol) in THF (74 mL) and LDA (117.3 mmol; from HN*i*Pr$_2$ (12.44 g, 17.14 mL, 123.2 mmol), *n*BuLi (1.48 N in hexane, 79.3 mL, 117.3 mmol) in THF (187 mL); −78 °C to RT). The temperature was maintained below 30 °C. After 2 h, the almost clear reaction mixture was treated at 18–20 °C with saturated NH_4Cl solution (180 mL). The phases were separated and the aqueous phase was extracted with CH_2Cl_2. Washing of the organic layers (H_2O, then sat. aq. NaCl), drying (Na_2SO_4) and concentration afforded 15.5 g of a partly crystallized oil. Upon addition of Et_2O (75 mL), ketone **1** precipitated. The suspension was stored at 0 °C for 15 h and filtered. Yield of **1**: 6.22 g (44 %) of a white solid, whose analytical data were identical with those reported. ^{1}H NMR (360 MHz, $CDCl_3$): $\delta = 2.89$ (dd, J(H,H) = 13 and 4 Hz, 1 H; CH−CO), 2.71 (ddd, J(H,H) = 16, 12 and 6 Hz, 1 H; CH_2−CO), 2.36 ppm (ddd, J(H,H) = 16, 6 and 3 Hz, 1 H; CH_2−CO).

Triol **2**: A solution of Red-Al® (= Vitride® = $NaAlH_2(OCH_2CH_2OCH_3)_2$; ca. 70 % in toluene) (40.56 g, 140.5 mmol)) in THF (70 mL) was added in 40 min to a solution of **2** (11.81 g, 46.9 mmol) in THF (330 mL) at −70 °C. The reaction mixture was allowed to reach room temperature (2 h) and was then quenched at 15–20 °C with 5 % aqueous NaOH (280 mL), and **2** was extracted twice with EtOAc. Washing (H_2O, $NaHCO_3$, then sat. aq. NaCl), drying (Na_2SO_4), and concentration of the filtrate afforded a white solid (11.73 g, yield 98 %) consisting of **2** (**2**:**3** = 99:1). ^{1}H NMR (360 MHz, $CDCl_3$): $\delta = 3.86$ ppm (m, J(H,H) = 4 Hz + smaller couplings, 1 H; CH−O).

Triol **3**: $BH_3{\cdot}SMe_2$ (136 mg, 0.170 mL, 1.70 mmol) was added at room temperature to a stirred solution of **1** (600 mg, 2.40 mmol) in THF (20 mL). After 15 h, MeOH (10 mL) and 5 % aqueous NaOH (10 mL) were added. The reaction mixture was stirred for 3 h and concentrated at the rotavapor (60 °C/50 Torr). The remaining aqueous phase was treated with saturated aqueous NaCl (40 mL) and the product was extracted twice with AcOEt. Washing (H_2O, then sat. aq. NaCl), drying (Na_2SO_4), and concentration of the filtrate afforded a white solid (0.495 mg, yield 81 %) consisting of **3** (**3**:**2** = 98:2). ^{1}H NMR (360 MHz, $CDCl_3$): $\delta = 3.41$ ppm (m, J(H,H) = 9 Hz, 4 Hz + smaller couplings, 1 H; CH−O).

Tosylate **4**: A solution of *n*BuLi in hexane (1.48 M, 59.7 mL, 88.4 mmol) was added at 25 °C to a solution of **2** (11.23 g, max. 44.2 mmol) in THF (678 mL). The solution was stirred at 40 °C for 15 min, cooled at −18 °C, and treated at once with TsCl (9.68 g, 50.8 mmol). After 20 min at −15 °C, the mixture was poured into 5 % aqueous HCl, and **4** was extracted with AcOEt in the usual manner. Yield: 18.36 g of a white-ocher powder (100 %).

Preparation of **7** by fragmentation: KO*t*Bu (14.29 g, 127.7 mmol) was added in one portion to a solution of **4** (17.36 g, max. 42.5 mmol) in *t*BuOH (340 mL) and THF (170 mL). The temperature was maintained between −6 and 0 °C by means of a NaCl/ice–water bath (−9 °C). After 25 min, the mixture was poured into 5 % aqueous HCl and the products were extracted with Et_2O in the usual manner to afford an oil, consisting of **7** and **6** (11.15 g; ca. 4:1). Flash chromatography (SiO_2 (250 g); cyclohexane/AcOEt = 95:5) afforded **7** (6.20 g; containing 4–5 % of an unknown isomer and 3 % of **5**; 62 % yield) and **6** (1.49 g; 15 %). ^{1}H NMR (360 MHz, $CDCl_3$) of **7**: $\delta = 5.48$ (m, 1 H; CH=), 5.27 (m, 1 H; CH=), 2.62 (dd, J(H,H) = 13 and 4 Hz, 1 H; CH−CO), 2.60 (dist. t, J(H,H) = 11 Hz, 1 H; from CH_2−CO), 2.35–2.53 (m, 2 H; CH_2C=), 2.15–2.28 (m, 2 H; 1 H from CH_2−CO + 1 H from CH_2C=), 1.90–2.03 ppm (m, 1 H; from CH_2C=); ^{13}C NMR (360 MHz, $CDCl_3$): $\delta = 131.5$ (d), 128.7 (d), 24.7 and 24.3 ppm (t of allylic C).

Preparation of **5** (containing **7**) by fragmentation: Repetition of the above conditions in DMF/THF (3:2) at 0 to 15 °C for 15 min afforded a mixture enriched in **5** (**5**:**7** ca. 66:34), together with about 20 % of diketone **6**. Chromatographic purification (SiO_2; cyclohexane/AcOEt = 95:5) afforded a 65:35 mixture of **5** and **7**. ^{1}H NMR (360 MHz, $CDCl_3$) of **5**: δ = ca. 5.37–5.50 (m, 2 H; CH=CH)), 2.93 (dd, J(H,H) = 12 and 4 Hz, 1 H; CH−CO), 2.84 (ddd, J(H,H) = 13, 8, and 4 Hz, 1 H; from CH_2−CO), 2.33–2.42 ppm (m, 1 H; from CH_2−CO); ^{13}C NMR (360 MHz, $CDCl_3$): $\delta = 130.6$ (d), 129.8 ppm (d).

Characteristic data of **10**: GC: ca. 90 % pure; contains two other isomers (*E,Z* isomer of **10** + unknown isomer). ^{1}H NMR (360 MHz, $CDCl_3$): δ = 5.32–5.48 (m, 4 H; CH=), 2.42 ppm (t, J(H,H) = 7 Hz, 4 H; CH_2CO)); ^{13}C NMR (360 MHz, $CDCl_3$): $\delta = 129.9$ (d), 129.3 (d), 28.2 and 26.1 ppm (t of allylic C); coalescent signals due to the symmetry of **10**.

Characteristic data of **11**: GC: ca. 98 % pure; ^{1}H NMR (360 MHz, $CDCl_3$): $\delta = 2.88$ (d, J(H,H) = 12 and 4 Hz, 1 H; CH−CO), 2.48 (m, 1 H; CH_2−CO), 2.25 ppm (m, 1 H; CH_2−CO).

Characteristic data of **12**: GC: ca. 96 % pure; ^{1}H NMR (360 MHz, $CDCl_3$): $\delta = 3.56$ ppm (dt, J(H,H) = 12 and 4 Hz, 1 H; CH−O).

Characteristic data of **13**: GC: ca. 96 % pure; ^{1}H NMR (360 MHz, $CDCl_3$): $\delta = 4.25$ ppm (br s, 1 H; CH−O).

Characteristic data of **14**: M.p. 35–36 °C; GC: ca. 96 % pure; ^{1}H NMR (360 MHz, $CDCl_3$): $\delta = 5.35$ (m, 2 H; CH=), 2.35–2.45 ppm (m, 4 H; CH_2COCH_2); ^{13}C NMR (360 MHz, $CDCl_3$): $\delta = 130.7$ (d), 129.5 (d), 26.6 and 26.2 ppm (t of allylic C).

Characteristic data of **15**: GC: ca. 96 % pure; ^{1}H NMR (360 MHz, $CDCl_3$): $\delta = 5.32$ (m, 2 H; CH=), 2.30–2.42 ppm (m, 4 H; CH_2COCH_2); ^{13}C NMR (360 MHz, $CDCl_3$): $\delta = 131.9$ (d), 130.6 (d), 31.8 and 31.7 ppm (t of allylic C).

Acetonide **16**: A solution of diol **12** (50 mg, 0.21 mmol) and 2-methoxypropene (0.1 mL; ca. 5 equiv) in DMF (1.3 mL) was treated at 25 °C with

 © 2002 WILEY-VCH Verlag GmbH & Co. KGaA, Weinheim 0044-8249/02/4123-4525 $ 20.00+.50/0

trifluoroacetic acid (0.012 mL). After stirring for 3 h, NEt_3 (three drops) and AcOEt (20 mL) were added. The solution was poured into saturated aqueous $NaHCO_3$, the phases were separated, and the organic phase was washed (sat. aq. NaCl), dried (Na_2SO_4), and concentrated. Yield: 50 mg (85%).^{1}H NMR (360 MHz, $CDCl_3$): $\delta = 3.67$ ppm (dd, J(H,H) = 6.2 and 5.65 Hz (coupling with 1 H of CH_2 and with CH), 1 H; CH–O).

Characteristic data of **17**: ^{1}H NMR (360 MHz, $CDCl_3$): $\delta = 4.29$ ppm (dd, J(H,H) = 9.5 and 4 Hz (coupling with CH_2), 1 H; CH–O).

Received: July 9, 2002 [Z19697]

[1] A. S. Williams, *Synthesis* **1999**, 1707.

[2] a) G. Fráter, J. A. Bajgrowicz, P. Kraft, *Tetrahedron* **1998**, *54*, 7633; b) P. Kraft, J. A. Bajgrowicz, C. Denis, G. Fráter, *Angew. Chem.* **2000**, *112*, 3106; *Angew. Chem. Int. Ed.* **2000**, *39*, 2980.

[3] a) C. Fehr, N. Chaptal-Gradoz, J. Galindo, *Chem. Eur. J.* **2002**, *8*, 853; b) C. Fehr, N. Chaptal-Gradoz, *Helv. Chim. Acta* **2002**, *85*, 533.

[4] Recent example: R. Hamasaki, S. Funakoshi, T. Misaki, Y. Tanabe, *Tetrahedron* **2000**, *56*, 7423. As mentioned by a referee, the selectivity problem could be solved by metathesis of an appropriate non-terminal diacetylene. See: A. Fürstner, G. Seidel, *Angew. Chem.* **1998**, 110, 1758; *Angew. Chem. Int. Ed.* **1998**, *37*, 1734.

[5] J. T. Carey, C. Knors, P. Helquist, *J. Am. Chem. Soc.* **1986**, *108*, 8313.

[6] a) P. S. Wharton, G. A. Hiegel, *J. Org. Chem.* **1965**, *30*, 3254; R. Zurfluh, E. N. Wall, J. B. Siddall, J. A. Edwards, *J. Am. Chem. Soc.* **1968**, *90*, 6224; b) Review: D. Caine, *Org. Prep. Proced. Int.* **1988**, *20*, 3; c) K. C. Nicolaou, S. A. Snyder, A. Bigot, J. A. Pfefferkorn, *Angew. Chem.* **2000**, *112*, 1135; *Angew. Chem. Int. Ed.* **2000**, *39*, 1093, and references therein.

[7] The factors that govern "internal" versus "external" hydride attacks are not yet fully understood.

[8] Here, Red-Al® reduction at room temperature led to a 43:57 diastereomeric mixture of alcohol **8** and its diastereomer (85%). At −70 °C no reduction was observed.

[9] This reaction was not tested with larger amounts of reagent.

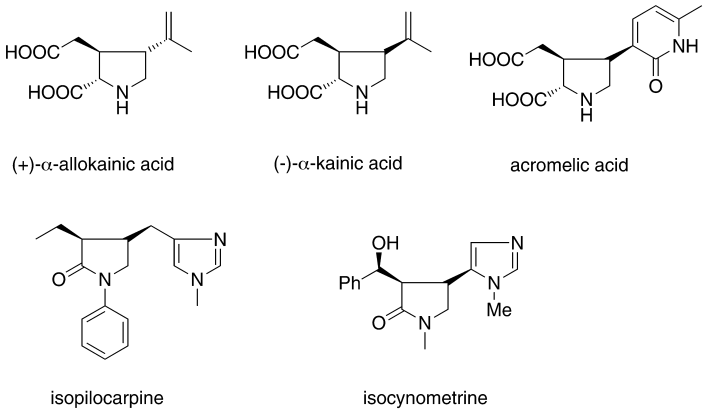
[10] However, the *E*,*E* and *E*,*Z* isomers of **10** have been synthesized: G. Büchi, H. Wüest, *Helv. Chim. Acta* **1979**, *62*, 2661.

[11] a) J. Salaün, J. Marguerite, *Org. Synth.* **1985**, *63*, 147; b) *Org. Synth. Coll. Vol. VII*, Wiley, New York, **1990**, pp. 131.

Highly Enantioselective Cycloisomerization of Enynes Catalyzed by Rhodium for the Preparation of Functionalized Lactams**

Aiwen Lei, Jason P. Waldkirch, Minsheng He, and Xumu Zhang*

The rising demand for chiral raw materials, intermediates, and active ingredients in pharmaceuticals, agrochemicals, food additives, and fragrances provides the impetus for rapid developments in chiral technology.[1] It remains a huge challenge for organic chemists to develop highly enantioselective reactions for the preparation of enantiomerically pure compounds in a cost-effective manner. Lactams are a versatile motif in organic chemistry and when functionalized, lactams often either show biological activity themselves, or are important building blocks for biologically active molecules such as (+)-α-allokainic acid, (+)-α-kainic acid,[2] acromelic



acid,[3] isopilocarpine,[4] and isocynometrine.[5] Generally, lactams are synthesized by intramolecular C–N bond formation. However, this method for the synthesis of enantiomerically pure and functionalized lactams requires that the chiral centers and functional groups must be assembled in advance. Therefore, methodology that allows enantioselective carbon–carbon bond formation for the generation of functionalized lactams without presetting the chiral centers will be a significant advance in synthetic organic chemistry.

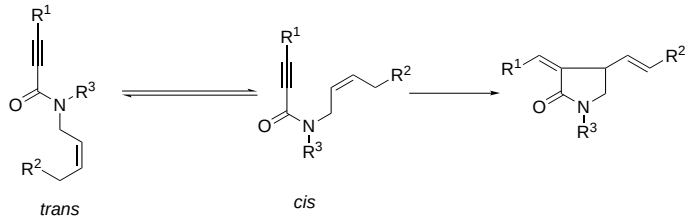
The transition-metal-catalyzed intramolecular Alder-ene-type reactions of enynes are well-developed[6] and provide efficient entries to a variety of useful functionalized carbocyclic[7] and heterocyclic compounds.[8] However, the number of lactam preparations reported involving the transition-metal-catalyzed cycloisomerization of enynes is limited. In fact, the literature contains only a single example describing a palladium-catalyzed cycloisomerization of alkynyl *N*-acyl enamines.[9] Very recently, a mechanistically different palladium(II)-catalyzed synthesis of α-alkylidene-γ-butyrolactams was reported.[10] Previously, we have discovered a Rh-catalyzed cycloisomerization of enynes and developed its asymmetric version.[11] Although this was a substrate- and ligand-dependent reaction, up to 96% *ee* was achieved.[11b] This led us to consider strategies for expanding the scope of the reaction as well as improving the enantioselectivity. We report herein the results of this effort: in an efficient, mild, and general route to synthesize a variety of lactams in high enantioselectivity using a catalyst derived from a commercially available metal precursor [{Rh(cod)Cl}$_2$] and the ligand binap.[12]

Initially, the reaction was studied with unprotected enyne amides (Scheme 1, $R^3 = H$) as the cycloisomerization substrates. However, none of the desired cyclization products were detected and the starting materials were recovered. The negative results may be because the *trans*-isomer of this type of unprotected enyne amide is dominant, which would be unfavorable for the cycloisomerization (Scheme 1).[13] There-

[*] Prof. Dr. X. Zhang, Dr. A. Lei, J. P. Waldkirch, M. He
Department of Chemistry
The Pennsylvania State University
University Park, PA 16802 (USA)
Fax: (+1) 814–863–8403
E-mail: xumu@chem.psu.edu

[**] This work was supported by NSF and NIH grants. We acknowledge a generous loan of precious metals from Johnson Matthey Inc. We thank Dr. Daniel A. Jones for his help in obtaining the mass spectral data. The Perseptive Mariner mass spectrometer was purhased in part with funds from NIH grant RR11318.

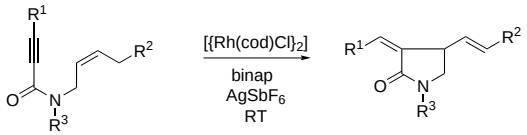
 © 2002 WILEY-VCH Verlag GmbH & Co. KGaA, Weinheim 0044-8249/02/4123-4526 $ 20.00+.50/0



Scheme 1. Effect of *trans*/*cis*-isomers in the Rh-catalyzed Alder-ene reaction.

fore, we turned our efforts to making the protected enyne amides (Scheme 1, $R^3 \neq H$). The reaction of **1a** in the presence of [{Rh(cod)Cl}$_2$], (*rac*)-binap, and $AgSbF_6$ provided the desired γ-lactam **2a** in 95% yield at RT. Further experimentation indicated that high enantioselectivity (> 99% *ee*) was obtained using (*S*)-binap while the other enantiomer was obtained in high enantioselectivity using (*R*)-binap as the ligand (Table 1, entries 1 and 2).

Table 1. Rh^I-catalyzed intramolecular Alder-ene reaction.[a]



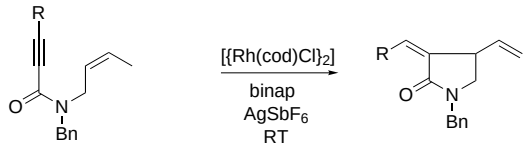
1 **2**

Entry	Substrate					Product		
	1	R^1	R^2	R^3	binap	**2**	Yield [%][b]	*ee* [%][c]
1	**1a**	Ph	Et	Bn	(*S*)	(+)-**2a**	95	> 99
2	**1a**	Ph	Et	Bn	(*R*)	(−)-**2a**	96	> 99
3	**1b**	Ph	H	Bn	(*S*)	(+)-**2b**	90	> 99
4	**1c**	Ph	Me	Bn	(*S*)	(+)-**2c**	91	> 99
5	**1d**	Me	H	Bn	(*R*)	(−)-**2d**	91	> 99
6	**1d**	Me	H	Bn	(*S*)	(+)-**2d**	92	> 99
7	**1e**	Me	H	Me	(*S*)	(+)-**2e**	91	> 99
8	**1f**	Me	Me	Bn	(*S*)	(+)-**2f**	96	> 99
9	**1g**	n-C_5H_{11}	H	Bn	(*S*)	(+)-**2g**	93	> 99
10	**1h**	n-C_5H_{11}	Me	Bn	(*S*)	(+)-**2h**	91	> 99
11	**1i**	n-C_5H_{11}	Et	Bn	(*S*)	(+)-**2i**	92	> 99
12	**1j**	n-C_5H_{11}	Et	Bn	(*S*)	(+)-**2j**	90	> 99

[a] All the reactions were carried out in 1 mL $ClCH_2CH_2Cl$ on a 0.1 mmol scale. The ratio of substrate/[{Rh(cod)Cl}$_2$]/binap/$AgSbF_6$ was 1:0.05:0.12:0.20. [b] Yield of product isolated. [c] The *ee* value was measured by HPLC.

Encouraged by the above results, a range of substrates were examined and the results are summarized in Table 1. A variety of γ-lactams were formed in high yields (90–96%) by the Rh-catalyzed cycloisomerization of a broad range of the enyne amides **1**. Significantly, all substrates listed in Table 1 gave the corresponding lactams with high enantioselectivity (> 99% *ee*) using binap as the ligand.[14] These results demonstrate the great potential of this reaction in organic synthesis.

To examine the functional-group tolerance of this Rh-catalyzed cycloisomerization, the reactions of the enyne substrates **3a–c** functionalized at the alkynyl terminus were investigated under the above-described conditions. The results listed in Scheme 2 showed that a number of functionalized γ-lactams were isolated in high yields (82–92%) and excellent enantioselectivities (> 99% *ee*).



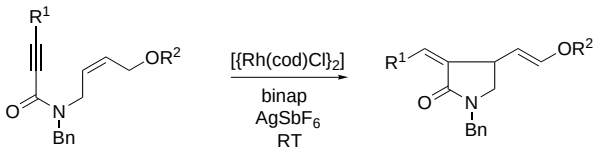
3 **4**

R = CH_2OMOM	**3a**	(*S*)-binap	(+)-**4a**	87%	>99% *ee*
	3a	(*R*)-binap	(–)-**4a**	88%	>99% *ee*
R = $CH_2OTBDMS$	**3b**	(*S*)-binap	(+)-**4b**	82%	>99% *ee*
	3b	(*R*)-binap	(–)-**4b**	84%	>99% *ee*
R = CH_2OBn	**3c**	(*S*)-binap	(+)-**4c**	92%	>99% *ee*

Scheme 2. High functional tolerance of the Rh-catalyzed Alder-ene reaction. MOM = methoxymethyl, TBDMS = *tert*-butyldimethylsilyl, Bn = benzyl.

Vinyl ethers and vinyl acetates are versatile building blocks.[15] Developing efficient routes toward these types of compounds would be valuable. On the basis of the mechanism of the Rh-catalyzed cycloisomerization reaction, we envisioned that functional vinyl derivatives would form by regioselective β-H elimination. Therefore, we investigated the behavior of the enynes **5** as potential substrates in the cycloisomerization process. This path would provide efficient entries to a variety of useful vinyl ethers and vinyl esters from readily available allylic ether or allylic acetate compounds. The vinyl methyl ether, vinyl benzyl ether, and vinyl acetate containing lactams were synthesized in high yields and over 99% *ee* (Scheme 3). Further experiments revealed that this reaction can tolerate terminal olefins. The vinyl allylic ether[16] substituted lactam **8**, which is an excellent substrate for the Claisen rearrangement, was obtained in 84% yield and over 99% *ee* [Eq. (1)].

To expand the scope of the functionalized vinyl derivatives, we investigated the method for the preparation of versatile enamides,[17] which are important organic synthetic intermediates. Although the reactions list-

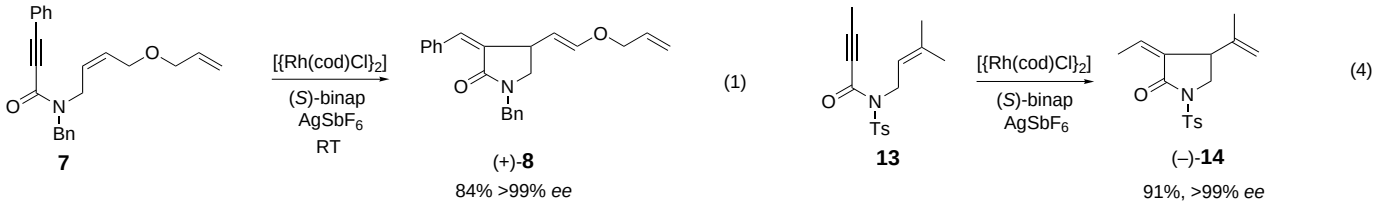


5 **6**

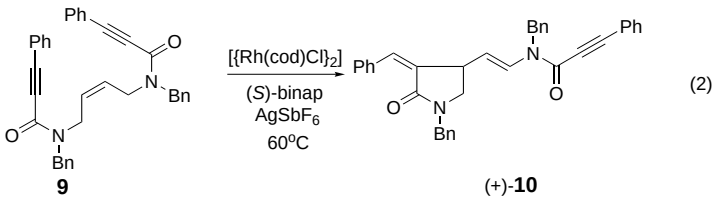
R^1 = Ph, R^2 = Me	**5a**	(*S*)-binap	(+)-**6a**	87%	>99% *ee*
	5a	(*R*)-binap	(–)-**6a**	88%	>99% *ee*
R^1 = Ph, R^2 = Bn	**5b**	(*S*)-binap	(+)-**6b**	89%	>99% *ee*
R^1 = n-C_5H_{11}, R^2 = Me	**5c**	(*S*)-binap	(+)-**6c**	92%	>99% *ee*
R^1 = Ph, R^2 = Ac	**5d**	(*S*)-binap	(+)-**6d**	89%	>99% *ee*

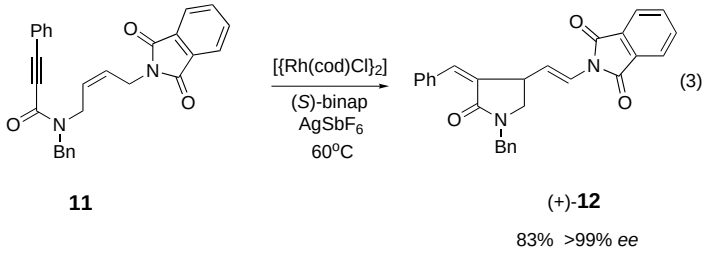
Scheme 3. Functionalized lactams prepared from the highly regioselective Alder-ene reaction.

 © 2002 WILEY-VCH Verlag GmbH & Co. KGaA, Weinheim 0044-8249/02/4123-4527 $ 20.00+.50/0



ed in Equation (2) and Equation (3) are very slow at RT, at 60 °C the cycloisomerization proceeded smoothly and yielded the desired enamides in high yields and over 99 % *ee*.





The use of an enyne substrate containing a trisubstituted olefin was investigated in the Rh-catalyzed cycloisomerization reaction. The cyclization of the *N*-tosylate-protected amide **13** produced the desired lactam in high yield and high enantioselectivity within 24 h at RT [Equation (4)]. The presence of the tosylate group was important to the success of this cyclization.[18]

A catalytic cycle has been proposed for the Rh-catalyzed intramolecular Alder-ene reaction (Scheme 4).[6c,7a,19] We believe that the reaction, by the coordination of enynes with a Rh^{I} species, forms the coordinated intermediate **II**. Oxidative cyclization of enynes affords the metallacyclopentane **III**. Subsequently, β-H elimination of the metallacyclopentane **III-A** yields the Rh-H species **IV**. Finally, the reductive elimination of this Rh-H species **IV** produces the desired product.

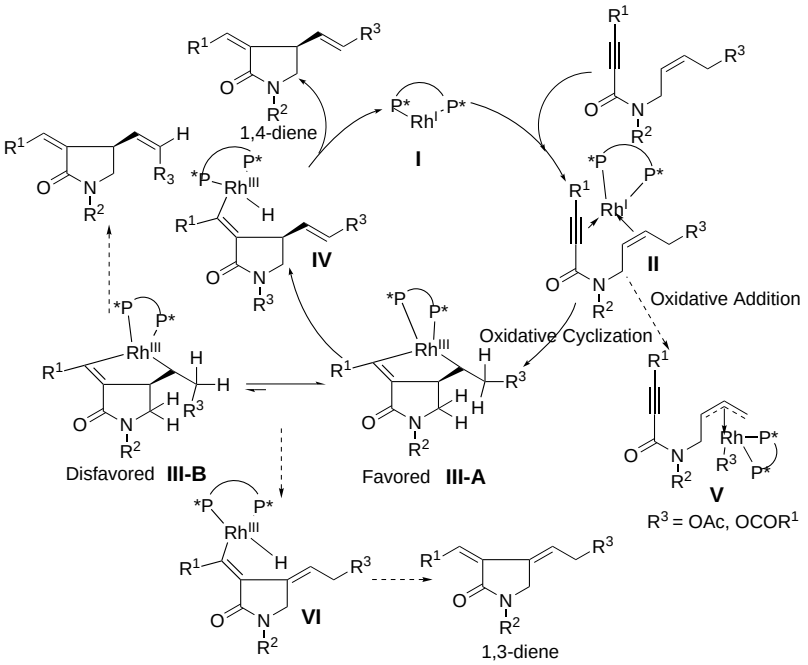
The high regioselectivity of the formation of 1,4-diene products can be explained by the *cis*-relationship between the C–Rh and C–H bonds for the β-H elimination in Scheme 4.[6a] Based on the proposed mechanistic rationale, the *E* geometry of the double bond formed by the β-H elimination can be expected because of the less !sterically hindered metallacyclopentanes **III-A**, and the *Z* geometry of the exocyclic double bond should form from the reductive elimination of the Rh-H intermediate **IV**. The NOE investigation of **6a** does confirm the expected geometry of the double bonds.

The information gained from the reaction of **5d** was important. It showed that the cycloisomerization can tolerate the allylic acetate group, which has high reactivity towards low-valent transition metals, such as Pd^{0}, Ni^{0}, etc. in oxidative addition. The clean and high-yielding reaction reveals that, at least in this system, oxidative cyclization is strongly favored over any other competitive reaction pathways.

In summary, we successfully explored a highly enantioselective cycloisomerization of enynes for the preparation of functionalized lactams. The high *ee* value (> 99 %) obtained in these reactions was especially remarkable. The potential of this new reaction lies not only its broad functional tolerance, but in the functionalized vinyl derivatives such as vinyl ether, vinyl acetate, vinyl allylic ether, and enamides containing lactams that were formed. Further efforts towards the syntheses of biologically active compounds are in process and will be reported in due course.

Experimental Section

Procedure for the rhodium-catalyzed reaction of **3a** to form (+)-**4a**: In a flame-dried Schlenk tube, the $[\{Rh(cod)Cl\}_2]$ (2.5 mg, 0.005 mmol) and (*S*)-binap (6.9 mg, 0.012 mmol) were dissolved in freshly distilled 1,2-dichloroethane (1 mL), then freshly prepared **3a** (28.7 mg, 0.1 mmol) was added to



Scheme 4. The proposed mechanism and competitive routes.

 © 2002 WILEY-VCH Verlag GmbH & Co. KGaA, Weinheim 0044-8249/02/4123-4528 $ 20.00+.50/0 *Angew. Chem. Int. Ed.* **2002**, *41*, No. 23

the solution at RT under nitrogen. After stirring for 1 min, $AgSbF_6$ (0.02 mmol in $ClCH_2CH_2Cl$) was added to the mixture. The reaction was completed within 5 min. The reaction mixture was directly subjected to column chromatography, from which (+)-**4a** (24.9 mg, 87%, over 99% *ee*)[20] was obtained. The *ee* value was determined by HPLC with an OJ-H column (hexane:isopropanol = 95:5, 1 mL min^{-1}, 254 nm). $[\alpha]_D^{25} = +3.52$ ($c = 1.0$, $CHCl_3$); ^{1}H NMR (400 MHz, $CDCl_3$) $\delta = 7.28$–7.16 (m, 5H), 5.85 (dt, $J = 2.2$, 5.9 Hz, 1H), 5.58–5.53 (m, 1H), 5.08–5.02 (m, 2H), 4.80–4.77 (m, 2H), 4.61 (s, 2H), 4.48 (d, $J = 14.6$ Hz, 1H), 4.35 (d, $J = 14.6$ Hz, 1H), 3.32 ppm (s, 3H); ^{13}C NMR (90 MHz, $CDCl_3$) $\delta = 167.72$, 137.76, 136.57, 134.50, 129.13, 128.65, 128.07, 118.00, 96.84, 95.57, 64.04, 54.54, 50.22, 47.15, 42.17 ppm; MS *m/z*: 288.1 [M^++1]; HRMS (APCI) calcd for $C_{17}H_{22}NO_3$ [M^++1)]: 288.1600; found: 288.1603.

Received: July 11, 2002
Revised: September 19, 2002 [Z19714]

[1] A. M. Rouhi, *C&E News* **2002**, *80(23)*, 43–50.
[2] a) S. Marukami, T. Takemoto, Z. Shimizu, *J. Pharm. Soc. Jpn.* **1953**, *73*, 1026–1028; b) A. F. Parsons, *Tetrahedron* **1996**, *52*, 4149–4174.
[3] a) K. Konno, H. Shirahama, T. Matsumoto, *Tetrahedron Lett.* **1983**, *24*, 939; b) K. Konno, K. Hashimoto, Y. Ohfune, H. Shirahama, T. Matsumoto, *J. Am. Chem. Soc.* **1988**, *110*, 4807.
[4] M. E. Garst, L. J. Dolby, S. Esfandiari, N. A. Fedoruk, N. C. Chamberlain, A. A. Avey, *J. Org. Chem.* **2000**, *65*, 7098, and references therein.
[5] F. Khuong-Huu, X. Monseur, G. Ratle, G. Lukacs, R. Goutarel, *Tetrahedron Lett.* **1973**, 14, 1757.
[6] Reviews: a) C. Aubert, O. Buisine, M. Malacria, *Chem. Rev.* **2002**, *102*, 813–834; b) I. Ojima, M. Tzamarioudaki, Z. Li, R. J. Donovan, *Chem. Rev.* **1996**, *96*, 635–662; c) B. M. Trost, *Acc. Chem. Res.* **1990**, *23*, 34; d) B. M. Trost, M. J. Krische, *Synlett* **1998**, 1; e) B. M. Trost, *Chem. Eur. J.* **1998**, *4*, 2405.
[7] a) B. M. Trost, M. Lautens, C. Chan, D. J. Jebaratnam, T. Mueller, *J. Am. Chem. Soc.* **1991**, *113*, 636–644, and references therein; b) B. M. Trost, Y. Li, *J. Am. Chem. Soc.* **1996**, *118*, 6625–6633; c) B. M. Trost, M. J. Krische, *J. Am. Chem. Soc.* **1999**, *121*, 6131–6141; d) B. M. Trost, J. R. Corte, M. S. Gudiksen, *Angew. Chem.* **1999**, *111*, 3945–3947; *Angew. Chem. Int. Ed.* **1999**, *38*, 3662–3664; e) B. M. Trost, J. R. Corte *Angew. Chem.* **1999**, *111*, 3947–3949; *Angew. Chem. Int. Ed.* **1999**, *38*, 3664–3666; f) C. Fernandez-Rivas, M. Mendez, A. M. Echavarren, *J. Am. Chem. Soc.* **2000**, *122*, 1221–1222; g) S. J. Sturla, N. M. Kablaoui, S. L. Buchwald, *J. Am. Chem. Soc.* **1999**, *121*, 1976–1977; h) Y. Takayama, S. Okamoto, F. Sato, *J. Am. Chem. Soc.* **1999**, *121*, 3559–3560; i) B. M. Trost, C. D. Haffner, D. J. Jebaratnam, M. J. Krische, A. P. Thomas, *J. Am. Chem. Soc.* **1999**, *121*, 6183–6192.
[8] Tetrahydrofuran: a) M. Hatano, M. Terada, K. Mikami, *Angew. Chem.* **2001**, *113*, 255–259; *Angew. Chem. Int. Ed.* **2001**, *40*, 249–253; pyrrolidine: b) A. Goeke, M. Sawamura, R. Kuwano, Y. Ito, *Angew. Chem.* **1996**, *108*, 686; *Angew. Chem. Int. Ed. Engl.* **1996**, *35*, 662.
[9] B. M. Trost, C. Pedregal, *J. Am. Chem. Soc.* **1992**, *114*, 7292–7294.
[10] X. Xie, X. Lu, Y. Liu, W. Xu, *J. Org. Chem.* **2001**, *66*, 6545–6550.
[11] a) P. Cao, B. Wang, X. Zhang, *J. Am. Chem. Soc.* **2000**, *122*, 6490–6491; b) P. Cao, X. Zhang, *Angew. Chem.* **2000**, *112*, 4270–4272; *Angew. Chem. Int. Ed.* **2000**, *39*, 4104–4106.
[12] Some other preliminary results for preparing lactones, and tetrahydrofurans will be published.
[13] a) From the NMR spectra, there is clear evidence that all of these protected enyne amides are *trans*/*cis*-mixtures while the unprotected enyne amides are single isomers: b) W. E. Stewart III, T. H. Siddall, *Chem. Rev.* **1970**, *70*, 517; c) L. A. LaPlanche, M. T. Rogers, *J. Am. Chem. Soc.* **1963**, *85*, 3728.
[14] a) The reactions of the substrates that contained *E* olefins were totally different. The reaction of (*E*)-**1c** was examined; 20% conversion and 6% *ee* were obtained under the same conditions; b) the different reactivity of *Z* and *E* substrates may be explained by the stronger coordination of *Z* substrates to Rh^I. F. R. Hartley, *The Chemistry of Platinum and Palladium: with Particular Reference to Complexes of the Elements*, Applied Science Publication Ltd, London, **1973**, p. 377; c) a terminal alkynyl-ene substrate was also examined in this reaction; high reactivity (100% conversion within 5 min) but poor enantioselectivity (6.5% *ee*) was observed.
[15] a) M. Blouin, R. Frenette, *J. Org. Chem.* **2001**, *66*, 9043–9045, and references therein; b) M. C. Croudace, N. E. Schore, *J. Org. Chem.* **1981**, *46*, 5357–5363.
[16] L. Abraham, R. Czerwonka, M. Hiersemann, *Angew. Chem.* **2001**, *113*, 4835–4837; *Angew. Chem. Int. Ed.* **2001**, *40*, 4700–4703, and references therein.
[17] B. M. Trost, J.-P. Surivet, *Angew. Chem.* **2001**, *113*, 1516–1519; *Angew. Chem. Int. Ed.* **2001**, *40*, 1468–1471, and references therein.
[18] Bn-substituted substrates failed to yield the desired 1,4-diene products, while the starting materials were completely consumed.
[19] J. Tsuji, *Transition Metal Reagents and Catalysts: Innovations in Organic Synthesis*, Wiley, Chichester, **2000**, pp. 10–14 and pp. 238–280.
[20] Using freshly prepared **3a** and freshly distilled solvent was important to achieve 99% *ee*.

Mechanistic Studies of HPP Epoxidase: Configuration of the Substrate Governs Its Enzymatic Fate**

Zongbao Zhao, Pinghua Liu, Kazuo Murakami, Tomohisa Kuzuyama, Haruo Seto, and Hung-wen Liu*

Non-heme iron-dependent enzymes are an important class of catalysts involved in many biological transformations of medical, pharmaceutical, and environmental significance. Although considerable progress has been made in our understanding of their catalyses, characterization of the metal centers and the modes of dioxygen activation remain a challenge because of the great structural and mechanistic diversity found among these enzymes.[1] Recently, HPP epoxidase,[2] an enzyme in the biosynthetic pathway of the antibiotic fosfomycin, was recognized as a new member of this enzyme family.[3] This epoxidase performs the final transformation in the fosfomycin biosynthesis by converting (*S*)-2-hydroxypropylphosphonic acid (HPP, (*S*)-**1**) to (1*R*,2*S*)-epoxypropylphosphonic acid (**2**), also known as fosfomycin

[*] Prof. Dr. H.-w. Liu, Dr. Z. Zhao,[+] Dr. P. Liu,[+] Dr. K. Murakami
Division of Medicinal Chemistry
College of Pharmacy and
Department of Chemistry and Biochemistry
University of Texas
Austin, TX 78712 (USA)
Fax: (+1) 512-471-2746
E-mail: h.w.liu@mail.utexas.edu
Prof. Dr. T. Kuzuyama
Institute of Molecular and Cellular Biosciences
University of Tokyo
Bunkyo-ku, Tokyo 113-0032 (Japan)
Prof. Dr. H. Seto
Faculty of Applied Bio-Science
Tokyo University of Agriculture
Setagaya-ku, Tokyo 156-8502 (Japan)
[+] Contributed equally to the work.
[**] We thank Ms. Bettina Høj for her assistance on the chemical synthesis of **12**, and Amano Pharmaceutical Co. Ltd. for a gift of lipase PS from *Pseudomonas cepacia*. This work was supported in part by a National Institutes of Health Grant (GM40541).

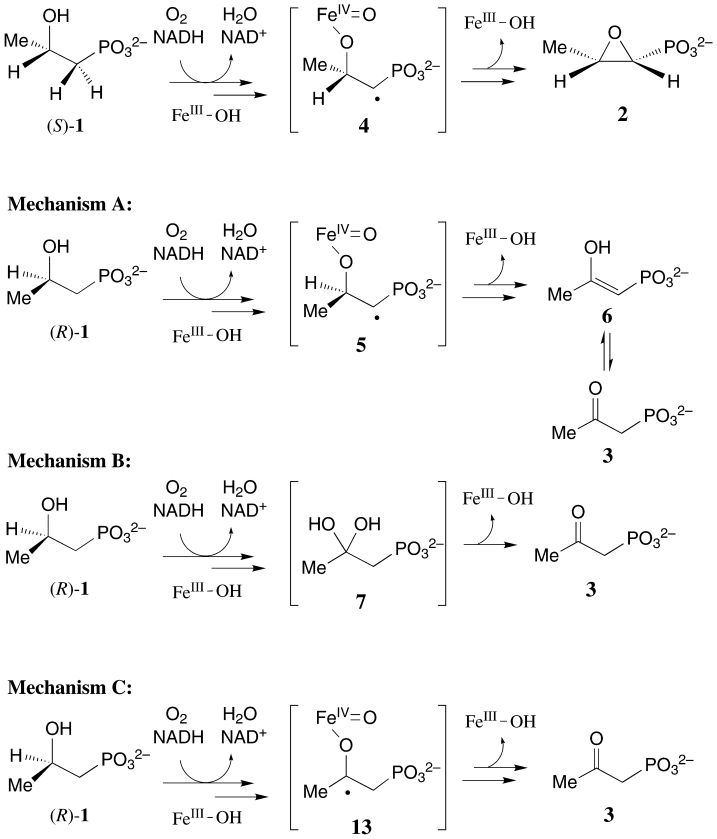
 © 2002 WILEY-VCH Verlag GmbH & Co. KGaA, Weinheim 0044-8249/02/4123-4529 $ 20.00+.50/0

(Scheme 1). The epoxidation catalyzed by HPP epoxidase is unusual since it is effectively a dehydrogenation of a secondary alcohol ((*S*)-**1**→**2**).[3–5]

Recent studies of HPP epoxidase from *Streptomyces wedmorensis* revealed that this enzyme is a mononuclear non-heme iron-containing catalyst, and unlike most other enzymes in the same class, its activity is α-ketoglutarate-independent.[3] The conversion of (*S*)-**1** into **2** consumes NADH wherein the ultimate oxidant is dioxygen. While a reductase is required to mediate the transfer of the reducing equivalents, alternative electron carriers, such as FMN and FAD, have been shown to be competent substitutes for NADH.[3] Several mechanisms are conceivable for this intriguing transformation in which an iron–oxo intermediate has been proposed to be the reactive species that triggers the reaction, and the catalysis probably involves radical intermediates.[3] To gain more insight into the functioning of HPP epoxidase, a study of the stereospecificity of this enzyme was carried out. Reported herein are the results and the mechanistic implications of our investigation.

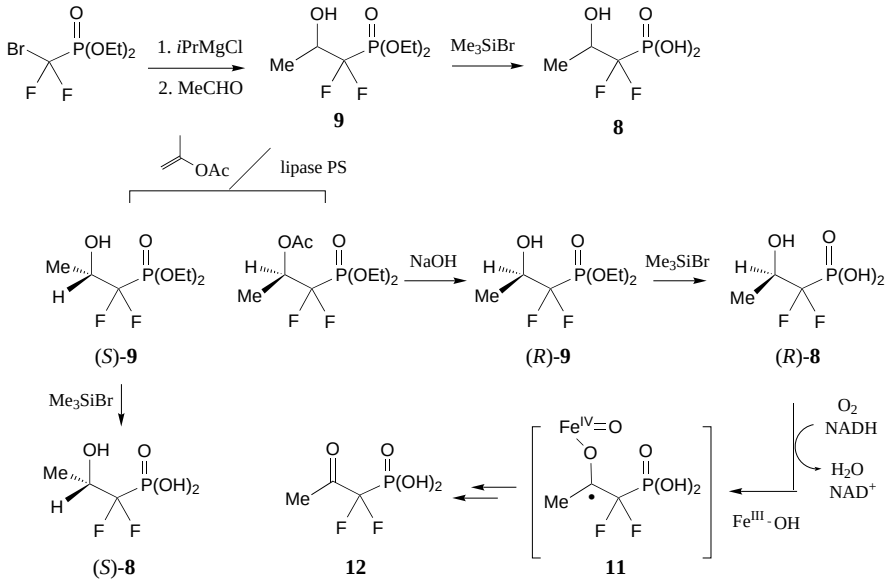
Our interest in this subject was inspired by the observation that incubation of racemic HPP with HPP epoxidase in high concentration resulted in the total consumption of all substrate to generate fosfomycin and a new product in 1:1 ratio. Since it has been established that (*S*)-HPP ((*S*)-**1**) is the immediate precursor of fosfomycin (**2**), the new product is probably derived from the oxidation of (*R*)-HPP ((*R*)-**1**) by HPP epoxidase. Subsequently, enantiomerically pure (*R*)-**1** was chemically prepared (> 97 % *ee*),[6] which, upon incubation with the epoxidase, led to 2-oxopropylphosphonic acid (**3**) as the sole product (Scheme 1).[7] The turnover rates for (*R*)-**1** and (*S*)-**1** were determined to be (162 ± 7) and (149 ± 2) nmol mg^{-1} min^{-1}, respectively, under our assay conditions.[8] Clearly, HPP epoxidase is not selective with regard to substrate recognition, but can stereospecifically convert each enantiomer into a unique product with similar efficiency.

As depicted in Scheme 1, the key step in the formation of fosfomycin from (*S*)-HPP may involve the abstraction of an α-H atom from (*S*)-**1** by a reactive iron–oxo species (formation of **4**), followed by a radical-induced homolytic cleavage of the Fe–O bond in **4** to produce **2**. Thus, an analogous route initiated by the generation of the α radical **5**, followed by the abstraction of a β-H atom and tautomerization of the resulting enol **6** can be envisioned for the conversion of (*R*)-**1** into **3** (Scheme 1, mechanism A). Alternatively, a direct hydroxylation–dehydration at β-C of (*R*)-**1** via a *gem*-diol intermediate (**7**) could also explain the formation of **3** (Scheme 1, mechanism B).[9] To probe these possibilities, an HPP sample ^{13}C-labeled at β-C ([2-^{13}C]HPP)[10] and an HPP analogue carrying two fluorine atoms at α-C (1,1-difluoro-HPP, **8**)[11] were prepared (Scheme 2). The ^{13}C-labeled HPP was designed to facilitate the detection of hydroxy incorporation at C-2, and the difluoro derivative **8** was expected to be an inhibitor if α radical formation is a prerequisite for the catalysis.



Scheme 1. The oxidation of (*S*)-**1** by HPP epoxidase and three possible mechanisms for the oxidation of (*R*)-**1** by the same enzyme. The phosphonic acids are shown as dianions although strictly speaking the formula numbers refer to the protonated forms.

Upon treatment with HPP epoxidase under an $^{18}O_2$ atmosphere, the racemic [2-^{13}C]HPP was converted into **3** the ^{13}C NMR spectrum of which is superimposable on that of



Scheme 2. Synthesis and reactions of a difluoro analogue of HPP.

 © 2002 WILEY-VCH Verlag GmbH & Co. KGaA, Weinheim 0044-8249/02/4123-4530 $ 20.00+.50/0 *Angew. Chem. Int. Ed.* **2002**, *41*, No. 23

3 produced under an $^{16}O_2$ atmosphere (air). Since no additional keto signal arising from the ^{18}O isotope shift[12] is discernible and no ^{18}O washout from **3** to solvent is expected under the incubation conditions (pH 7.5, 60 min), these results do not support a hydroxylation–dehydration mechanism as predicted in mechanism B.[13] It should be noted that fosfomycin formation via α hydroxylation of HPP (**1**) followed by the attack of β-OH at α-C to displace the newly introduced hydroxyl group had already been ruled out by early feeding experiments.[4b] Thus, the current observation is consistent with the fact that HPP epoxidase lacks hydroxylation ability.

To our surprise, when **8** was incubated with HPP epoxidase, partial turnover occurred with concomitant loss of enzyme activity. Further experiments were conducted using (*R*)- and (*S*)-1,1-difluoro-HPP ((*R*)-**8** and (*S*)-**8**) the syntheses of which involved a lipase-catalyzed stereoselective acylation to resolve the diethyl ester intermediate **9** (Scheme 2).[14] The absolute configurations of the resolved phosphonic acid esters were assigned based on NMR analysis of their Mosher ester derivatives,[15] and the enantiomeric purity of (*R*)-**9** and (*S*)-**9** was determined by NMR to be greater than 99 and 95%, respectively. When these pure enantiomers were incubated with HPP epoxidase, (*S*)-**8** was found to be a tight-binding inhibitor, while (*R*)-**8** was converted into 1,1-difluoro-2-oxopropylphosphonic acid (**12**).[16] The identity of this product was unambiguously confirmed by comparison to a synthetic standard. Expectedly, this product exists in aqueous solution as a mixture of its keto (major) and hydrate form, and the turnover rate for (*R*)-**8** (76 nmol mg^{-1} min^{-1}) is comparable to the rates for the nonfluorinated substrates (*R*)-**1** and (*S*)-**1**.

The fact that (*R*)-**8** can be processed by HPP epoxidase is mechanistically revealing. On the basis of this result, an enol–keto tautomerization mechanism initiated by an α-H atom abstraction as outlined in mechanism A (Scheme 1) can be excluded. Since the turnover rates of (*R*)-**1** and (*R*)-**8** under our assay conditions are similar, the involvement of a β carbocation intermediate in the reaction may be ruled out because of the insensitivity of the catalysis to the electronic effect imposed by the α-difluoromethylene group. Pathways involving C-2 deprotonation are also unlikely as β carbanion formation in (*R*)-**8** may prompt fluorine anion release.[17] Thus, oxidation of the *R* isomers of HPP ((*R*)-**1**) and 1,1-difluoro-HPP ((*R*)-**8**) by HPP epoxidase most probably involves the formation of a carbon-centered ketyl radical, such as **13**/**11** (Scheme 1, mechanism C/Scheme 2),[18] which is distinct from the α radical intermediate **4** proposed for the oxidation of (*S*)-HPP ((*S*)-**1**).

In summary, this study provides strong evidence for the radical nature of reactions catalyzed by HPP epoxidase. The fact that each enantiomer is stereospecifically converted into a single product suggests that a unique and specific enzyme–substrate binding mode must take place for (*S*)-**1** and (*R*)-**1** turnover. While the hydroxyl and the phosphonate group from both isomers are expected to be similarly anchored in the active site, the chirality at C-2 may allow only α-H in (*S*)-**1** or β-H in (*R*)-**1** to be productively poised for abstraction by the yet-elusive, reactive iron–oxo species, leading to the corresponding products. Thus, the regiospecificity of the initial hydrogen atom abstraction appears to be determined not by the chemical reactivity but by the relative orientation of the C–H bond to be cleaved in each enzyme–substrate complex. Such a distinct outcome from a pair of enantiomers catalyzed by a single enzyme is rare.[19] In addition, it is noteworthy that the conversion of (*S*)-**1** and (*R*)-**1** by HPP epoxidase into their respective products, **2** and **3**, is exclusive.[20] Our results also imply that oxidation of (*S*)-**1** and (*R*)-**1** involves different substrate-based radical intermediates (**4** and **13**). Such findings lend further credence to the participation of a highly reactive species, such as an iron–oxo intermediate, capable of abstracting a hydrogen atom from HPP in the catalytic mechanism. A variety of biochemical and biophysical techniques are currently employed to further elucidate this unique enzyme transformation.

Received: July 11, 2002 [Z19717]

[1] a) L. Que, Jr., R. N. Y. Ho, *Chem. Rev.* **1996**, *96*, 2607–2624; b) E. I. Solomon, T. C. Brunold, M. I. Davis, J. N. Kemsley, S.-K. Lee, N. Lehnert, F. Neese, A. J. Skulan, Y.-S. Yang, J. Zhou, *Chem. Rev.* **2000**, *100*, 235–349.

[2] a) T. Hidaka, M. Goda, T. Kuzuyama, N. Takei, M. Hidaka, H. Seto, *Mol. Gen. Genet.* **1995**, *249*, 274–280; b) T. Kuzuyama, T. Seki, S. Kobayashi, T. Hidaka, H. Seto, *Biosci. Biotechnol. Biochem.* **1999**, *63*, 2222–2224.

[3] a) P. Liu, K. Murakami, T. Seki, X. He, S.-M. Yeung, T. Kuzuyama, H. Seto, H.-w. Liu, *J. Am. Chem. Soc.* **2001**, *123*, 4619–4620; b) a full account of the biochemical and spectroscopic characterization of the iron center of HPP epoxidase will be published elsewhere.

[4] a) F. Hammerschmidt, G. Bovermann, K. Bayer, *Liebigs Ann. Chem.* **1990**, 1055–1061; b) F. Hammerschmidt, *J. Chem. Soc. Perkin Trans. 1* **1991**, 1993–1996.

[5] Two closely related examples are the epoxide ring formation catalyzed by hyoscyamine 6β-hydroxylase involved in the biosynthesis of scopolamine (T. Hashimoto, J. Matsuda, Y. Yamada, *FEBS Lett.* **1993**, *329*, 35–39) and the ring closure of proclavaminic acid catalyzed by clavaminate synthase (K. H. Baggaley, A. G. Brown, C. J. Schofield, *Nat. Prod. Rep.* **1997**, 14, 309–333; D. Iwata-Reuyl, A. Basak, C. A. Townsend, *J. Am. Chem. Soc.* **1999**, *121*, 11356–11368). Both enzymes belong to the family of α-ketoglutarate-dependent non-heme iron oxygenases.

[6] F. Hammerschmidt, *Monatsh. Chem.* **1991**, *122*, 389–393.

[7] Spectral data of **3**: ^1H NMR (D_2O): $\delta = 3.11$ (d, $J = 21.0$ Hz, 2H), 2.46 ppm (3H, s); ^{13}C NMR (D_2O): $\delta = 211.5$, 47.9 (d, $J = 106$ Hz), 31.0 ppm; ^{31}P NMR (D_2O): $\delta = 11.1$ ppm (s).

[8] The reaction mixture contained 22.5 mM NADH, 12.0 mM substrate, 62.5 μM FMN, and 24.7 μM reconstituted enzyme in 200 μL of 25 mM Tris·HCl buffer (pH 7.5). The reaction was incubated with shaking at 250 rpm for 30 min at 30 °C, quenched by adding EDTA to a final concentration of 100 mM. D_2O was added to a final volume of 600 μL, and the mixture analyzed by ^1H NMR spectroscopy. Reaction rates were estimated based on the integrals of the well-resolved methyl signals associated with substrate and product.

[9] Oxidation of an alcohol to the corresponding ketone via a *gem*-diol intermediate is well documented for P450-catalyzed reactions (for a recent example see: L. C. Bell-Parikh, F. P. Guengerich, *J. Biol. Chem.* **1999**, *274*, 23833–23840).

[10] The synthesis of [2-^{13}C]HPP was achieved by reacting *n*BuLi-treated diethylmethylphosphonate with [1-^{13}C]acetyl chloride in the presence of copper(I) iodide, followed by reduction with $NaBH_4$ and then bromotrimethylsilane-mediated hydrolysis.

[11] Spectral data for 1,1-difluoro-HPP (**8**): ^1H NMR (D_2O): $\delta = 3.98$ (m, 1H), 1.15 ppm (d, $J = 6.6$ Hz, 3H); ^{19}F NMR (D_2O): $\delta = -119.8$ (ddd, $J = 281.1$, 83.7, 9.9 Hz, 1F), −128.8 ppm (ddd, $J = 283.4$, 81.8, 18.0 Hz, 1F,); ^{31}P NMR (D_2O): $\delta = 5.44$ ppm (t, $J = 82.4$ Hz).

[12] J. M. Risley, R. L. van Etten, *J. Am. Chem. Soc.* **1979**, *101*, 252–253.

[13] While the dehydration is expected to be a nonstereoselective event, precedence does exist for a stereoselective enzymatic event, as shown

 © 2002 WILEY-VCH Verlag GmbH & Co. KGaA, Weinheim 0044-8249/02/4123-4531 $ 20.00+.50/0

by Arigoni et al. in the dehydration by dioldehydrase (J. Rétey, A, Umani-Ronchi, J. Seibl, D. Arigoni, *Experientia* **1966**, *22*, 502). It should also be noted that the possibility of dehydration occurring prior to a complete conformational equilibration of the formed *gem*-diol and leading to the release of the newly incorporated ^{18}O atom cannot be ruled out based on our current data.

[14] Attempts to derivatize the diethyl ester **9** with various chiral acids to resolve the racemic mixture were futile.

[15] I. Ohtani, T. Kusumi, Y. Kashman, H. Kakisawa, *J. Am. Chem. Soc.* **1991**, *113*, 4092 – 4096.

[16] The incubation conditions were similar to those in ref. [8]. Spectral data of **12** in the keto form (74 %): ^1H NMR (D_2O): $\delta = 2.29$ ppm (s, 3H); ^{19}F NMR (D_2O): $\delta = -118.59$ ppm (d, $J = 77.8$ Hz); ^{31}P NMR (D_2O): $\delta = 2.90$ (t, $J = 76.0$ Hz); high resolution MS (CI) calcd for $C_3H_6F_2PO_4$ [M^++H]: m/z: 174.9972, found 174.9979. Spectral data of **12** in the hydrate form (26 %): ^1H NMR (D_2O): $\delta = 1.32$ ppm (s, 3H); ^{19}F NMR (D_2O): $\delta = -124.17$ ppm (d, $J = 79.8$ Hz); ^{31}P NMR (D_2O): $\delta = 5.69$ ppm (t, $J = 79.0$ Hz); high resolution MS (CI) calcd for $C_3H_8F_2PO_5$ [M^++H]: m/z: 193.0077, found 193.0072.

[17] Recent examples of adjacent carbanion formation triggering fluoride release: a) J. W. Gross, A. D. Hegeman, B. Gerratana, P. A. Frey, *Biochemistry* **2001**, *40*, 12497 – 12504; b) C. W. Koo, A. Sutherland, J. C. Vederas, J. S. Blanchard, *J. Am. Chem. Soc.* **2000**, *122*, 6122 – 6123.

[18] The possible involvement of a ketyl radical in the turnover of (*R*)-**1** and (*R*)-**8** is reminiscent of the mechanism of the oxidation of primary alcohols catalyzed by galactose oxidase (M. M. Whittaker, D. P. Ballou, J. W. Whittaker, *Biochemistry* **1998**, *37*, 8426 – 8436; B. E. Turner, B. P. Branchaud, *Bioorg. Med. Chem. Lett.* **1999**, *9*, 3341 – 3346).

[19] Two recent examples include the conversion of (1*S*,2*R*)- and (1*R*,2*S*)-*trans*-1-methyl-2-phenylcyclopropane into a primary alcohol and a phenol, respectively, by methane monooxygenase from *Methylococcus capsulatus* (A. M. Valentine, M.-H. LeTadic-Biadatti, P. H. Toy, M. Newcomb, S. J. Lippard, *J. Biol. Chem.* **1999**, *274*, 10771 – 10776), and the oxidation of 2-ethylhexanol by cytochrome $P450_{cam}$ in which 2-ethylhexanoic acid and 2-ethyl-1,2-hexanediol, respectively, are derived from the *R* and *S* isomer as the major product (K. J. French, D. A. Rock, D. A. Rock, J. I. Manchester, B. M. Goldstein, J. P. Jones, *Arch. Biochem. Biophys.* **2002**, *398*, 188 – 197).

[20] A recent report has shown that the (1*S*,2*S*)-epoxypropylphosphonic acid exists as a co-metabolite of fosfomycin ((1*R*,2*S*)-epoxypropylphosphonic acid, **2**) in the culture broth of *Streptomyces fradiae*. Formation of this 1*S* epimer has been speculated as a result of racemization of the radical intermediate (such as **4** or its equivalent) generated during turnover catalyzed by HPP epoxidase (B. P. Simov, F. Wuggenig, M. Lämmerhofer, W. Lindner, E. Zarbl, F. Hammerschmidt, *Eur. J. Org. Chem.* **2002**, 1139 – 1142).

Novel Achiral Biphenol-Derived Diastereomeric Oxovanadium(IV) Complexes for Highly Enantioselective Oxidative Coupling of 2-Naphthols**

Zhibin Luo, Quanzhong Liu, Liuzhu Gong,* Xin Cui, Aiqiao Mi, and Yaozhong Jiang

Optically pure 1,1′-binaphthol and its derivatives have been evaluated as versatile chiral auxiliaries and ligands in asymmetric transformations. Research in this area has provided many efficient and useful methods for the preparation of key chiral building blocks, some of which have been used for the construction of complex natural products.[1] They have also been extensively applied to the preparation of chiral organic materials.[2] The wide-ranging and important applications of such compounds in organic synthesis have stimulated great interest in developing efficient methods for their preparation.[3] Compared to the well-established resolution of racemic binaphthol for the preparation of optically pure BINOL,[3a–f] catalytic asymmetric preparation of chiral binaphthols has developed much more slowly. The discovery of efficient catalysts for the highly enantioselective formation of optically active binaphthol and its derivatives is an attractive target. The oxidative coupling of 2-naphthols in the presence of a catalytic amount of a copper complex of a chiral amine has provided several promising results, but high enantioselectivity has been achieved only for the coupling of 3-carboalkoxyl-2-naphthols (93 % *ee*).[4] A photo-activated chiral [Ru^{II}(salen)(NO)] complex catalyzes the aerobic oxidative coupling of 2-naphthols with 33–71 % *ee*.[5] Chen et al. and Uang et al. independently designed similar oxovanadium(IV) complexes of chiral Schiff bases for the asymmetric oxidative coupling of 2-naphthols with moderate enantioselectivities of up to 62 % *ee*.[6]

We developed the catalyst (*R*,*S*)-**1c** for the oxidative coupling of 2-naphthol with high enantioselectivity, and found that the chiral centers on the amino acid part and the axially chiral binaphthyl unit are both crucial to stereocontrol by the catalyst.[7] However, a drawback is that the chiral oxovanadium complex must be prepared from an optically pure 3,3′-diformyl-2,2′-dihydroxy-1,1′-binaphthol and (*S*)-amino acid. The catalyst is only highly enantioselective when the two

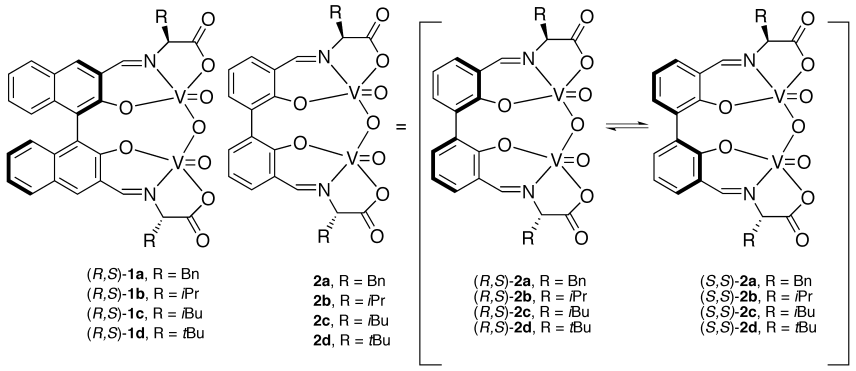
[*] Prof. L. Gong, Z. Luo, Q. Liu, X. Cui, Prof. A. Mi, Y. Jiang
Union Laboratory of Asymmetric Synthesis
Chengdu Institute of Organic Chemistry
Chinese Academy of Sciences
Chengdu, 610041 (P.R. China)
Fax: (+86) 28-8522-3978
E-mail: gonglz@cioc.ac.cn

[**] We are grateful for financial support from the National Science Foundation of China (20102005). We thank Prof. Lin Pu at the University of Virginia for helpful discussions and English revision. We also thank Prof. Nengyu Chen at Lanzhou University for HRMS measurements.

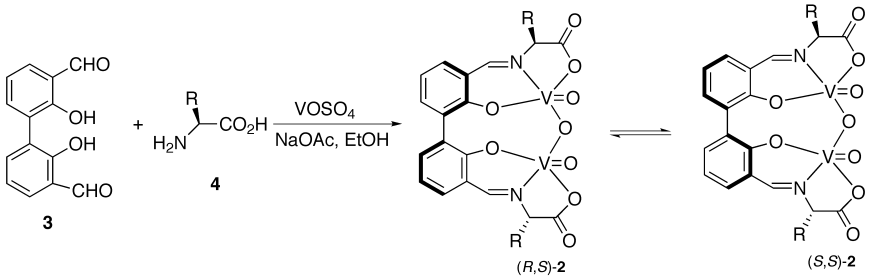
Supporting information for this article (general procedures for the preparation of chiral oxovanadium catalysts and asymmetric couplings of 2-naphthols; HRMS spectra of **2a–d**; HPLC spectra of **6a–c**, **6e**, and **6g–k**) is available on the WWW under http://www.angewandte.org or from the author.

 © 2002 WILEY-VCH Verlag GmbH & Co. KGaA, Weinheim 0044-8249/02/4123-4532 $ 20.00+.50/0

chiral strucutres match; for example, both (*R*,*S*)-**1a** and (*S*,*S*)-**1a** show similar reactivity, but (*R*,*S*)-**1a** gives much higher enantioselectivity than (*S*,*S*)-**1a**.[7] Oxovanadium(IV) complexes **2** are structurally similar to **1**, except that the binaphthyl unit of **1** is replaced with a conformationally flexible biphenyl unit (Scheme 1). In principle, diastereomeric complexes will be generated when 3,3′-diformyl-2,2′-dihydroxy-1,1′-phenol (**3**)[8] is condensed with (*S*)-amino acids **4** and vanadyl sulfate because of the higher rotation barrier in **2** (Scheme 2).[9] We anticipated that the diastereomers with



Scheme 1. Catalysts evaluated in this study.



Scheme 2. Preparation of catalysts **2**.

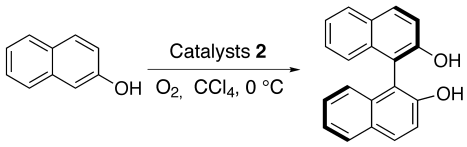
matching chirality between the chiral centers of the amino acid unit and the induced axially chiral biphenyl unit should provide high enantioselectivity for oxidative coupling. This system, which dispenses with the use of optically pure 1,1′-binaphthyls, should have significant practical advantages over the chiral binaphthyl-based catalysts (*R*,*S*)-**1**. Here we present our work on this new type of catalysts for the asymmetric synthesis of 1,1′-binaphthols.

Oxovanadium complexes **2** were prepared by condensation of **3** with (*S*)-amino acids **4** and vanadyl sulfate (Scheme 2) according to the previously reported procedure.[7,10] Preliminary characterization of complexes **2** by HRMS, IR spectroscopy, and elemental analysis supported the structures. These complexes possibly exist as mixtures of diastereomers. Although it is difficult to separate these and determine their absolute structures at this stage, the mixtures of diastereomers were found to be efficient for the asymmetric oxidative coupling of 2-naphthols.

The oxidative coupling of 2-naphthol was employed as a model reaction to investigate the effects of the substituents of the amino acids and the catalyst loading on reactivity and enantioselectivity (Table 1). The reactions to examine substituent effects were carried out in the presence of 10 mol % of **2** in CCl_4 at 0 °C with molecular oxygen as oxidant. Both the reactivity and enantioselectivity are dependent on the substituent R of the amino acids. Complex **2a**, derived from (*S*)-phenylalanine, gives a yield of 77 % and a moderate enantioselectivity of 80 % *ee* (entry 1). Replacement of the phenyl group in **2a** with an isopropyl substituent (**2b**) results in a much lower yield of 42 % and an *ee* value of 79 % (entry 2). Catalyst **2d** bearing bulky *tert*-butyl groups leads to 79 % *ee* and 56 % yield (entry 4). The highest yield of 89 % and an *ee* value of 89 % were observed for catalyst **2c** (R = 2-butyl, entry 3). Lowering the catalyst loading of **2c** does not affect the enantioselectivity, but lowers the reaction rate and yield (entries 6–8). Even in the presence of 1 mol % **2c**, good enantioselectivity is still obtained (entry 8). To our knowledge, these results represent the most enantioselective catalytic coupling of 2-naphthol. More importantly, most of these newly designed catalysts **2**, even though employed as mixtures of diastereomers, still give higher or comparable enantioselectivities in comparison with their 1,1′-binaphthyl analogues (*R*,*S*)-**1**.[7] These results imply that the major diastereomers in **2** might have an axial chirality similar to that of the 1,1′-binaphthyl unit of *(R,S)*-**1**, which matches the chirality of the (*S*)-amino acid unit and controls the stereodiscrimination.

We also prepared the C_1-symmetric complex **2e**, and characterized its structure preliminarily by HRMS and IR specroscopy. Under optimal reaction conditions, only 40 % yield and 57 % *ee* were obtained in the oxidative coupling of 2-

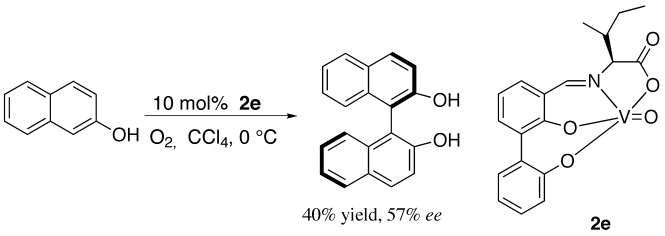
Table 1. Oxidative coupling of 2-naphthol in the presence of oxovanadium complexes **2**.[a]



Entry	Catalyst	R	Cat. load [mol %]	*t* [c]	Yield [%][b]	*ee* [%][c]
1	**2a**	Bn	10	7	77	80
2	**2b**	*i*Pr	10	7	42	79
3	**2c**	*i*Bu	10	7	89	89
4	**2d**	*t*Bu	10	7	56	79
5	(*R*,*S*)-**1c**	*i*Bu	10	8	93	83[d]
6	**2c**	*i*Bu	5	7	62	90
7	**2c**	*i*Bu	2	7	60[e]	91
8	**2c**	*i*Bu	1	7	20[e]	89

[a] Reactions were performed in CCl_4 at 0 °C. [b] Yields of isolated products. [c] The *ee* values were determined by HPLC on a Kromasil CHI-TBB column, and the absolute configuration is *R*. [d] See ref. [7]. [e] Conversion was determined by HPLC.

 © 2002 WILEY-VCH Verlag GmbH & Co. KGaA, Weinheim 0044-8249/02/4123-4533 $ 20.00+.50/0



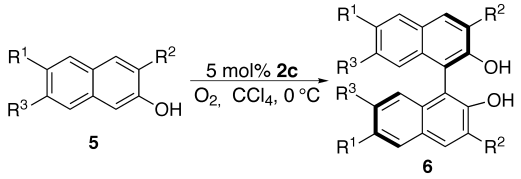
Scheme 3. Oxidative coupling of 2-naphthol in the presence of **2e**.

naphthol (Scheme 3). This demonstrates that the C_2 symmetry of complexes **2a–d** is important for asymmetric induction, and also indicates that the axial chirality induced by the (*S*)-amino acid exists in complexes **2a–d** and is crucial for the enantioselectivity.[9]

The optimized protocol was subsequently extended to a range of substrates (Table 2). For substrates bearing substituents in the 6- or 7-position, coupling takes place smoothly to give the corresponding binaphthols in high yields and 90–97% *ee*. Catalyst **2c** gave higher enantioselectivities for 7-substituted 2-naphthols (entries 3, 6, 8–12) than for 6-bromo-2-naphthol (entry 4) and 2-naphthol itself (entry 1). The enantioselectivity does not depend on the size of the substituents. Variation of the substituent at C7 from methoxy to other alkoxy groups hardly changed the enantioselectivity. Substitution at C3 of 2-naphthol suppresses the coupling reactivity for this catalyst system (entries 5 and 7), and this is similar to the results obtained with (*R*,*S*)-**1c**.[7]

We have further extended our study on the previously reported catalyst **1c**.[7] Table 3 summarizes the results of **1c**-catalyzed oxidative coupling of 2-naphthol derivatives.

Table 2. Oxidative coupling of 2-naphthols in the presence of 5 mol% oxovanadium(IV) complex **2c**.[a]



Entry	Products	Substituentes in **6**	*t* [days]	Yield [%][b]	*ee* [%][c]
1	**6a**	$R^1=R^2=R^3=H$	8	62	90
2	**6a**	$R^1=R^2=R^3=H$	7	89	89[d]
3	**6b**	$R^1=R^2=H$, $R^3=OMe$	7	95	95
4	**6c**	$R^1=Br$, $R^2=R^3=H$	4	98	90
5	**6d**	$R^1=H$, $R^2=OMe$, $R^3=H$	6	trace	–
6	**6e**	$R^1=R^2=H$, $R^3=OEt$	4	99	96
7	**6f**	$R^1=H$, $R^2=OBn$, $R^3=H$	6	trace	–
8	**6g**	$R^1=R^2=H$, $R^3=OBn$	6	80	95
9	**6h**	$R^1=R^2=H$, $R^3=O$*n*Bu	4	99	94
10	**6i**	$R^1=R^2=H$, $R^3=OCH_2CH{=}CH_2$	4	99	95
11	**6j**	$R^1=R^2=H$, $R^3=OC_8H_{17}$	4	99	94
12	**6k**	$R^1=R^2=H$, $R^3=OC_{12}H_{25}$	4	94	97

[a] The reactions were carried out at 0°C in the presence of 5 mol% catalyst **2c** in CCl_4. [b] Yields of isolated products. [c] The *ee* values were determined by HPLC on a Kromasil CHI-TBB or chiralpak AD column, the configuration of **6a–c** is *R*. [d] In the presence of 10 mol% **2c**.

Table 3. Oxidative coupling of 2-naphthols in the presence of 10 mol% oxovanadium(IV) complex **1c**.[a]

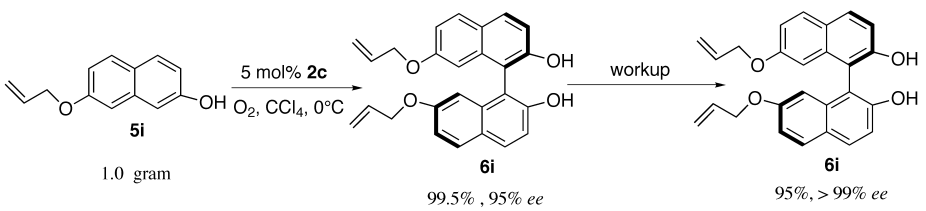
Entry	Products	*t* [days]	Yield [%][b]	*ee* [%][c]
1	**6a**	8	95	83[d]
2	**6b**	7	88	98[d]
3	**6c**	7	99	88[d]
4	**6e**	7	99	93
5	**6h**	7	95	96
6	**6i**	7	98	95
7	**6j**	7	93	94
8	**6k**	7	91	92

[a] The reactions were carried out at 0°C in the presence of 10 mol% catalyst **1c** in CCl_4. [b] Yields of isolated products. [c] The *ee* values are determined by HPLC on a Kromasil CHI-TBB or chiralpak AD column, the configuration of **6a–c** is *R*. [d] From ref. [7].

This complex exhibits almost the same enantioselectvity as **2c** for most of the 7-alkoxynaphthols, with 92–98% *ee* (Table 3, entries 2 and 4–8), while **2c** provides 94–97% *ee* (Table 2, entries 3, 6, and 8–12). Generally, **2c** gives a slightly higher enantioselectivity with 2-naphthol (90% *ee*, Table 2, entry 1) and 6-bromo-2-naphthol (90% *ee*, Table 2, entry 4) than (*R*,*S*)-**1c** (Table 3, entries 1 and 3).[7] Remarkably, when the optically pure binaphthyl catalysts are replaced with the achiral biphenol-derived mixtures of diastereomers, oxidative coupling still occurs with high enantioselectvity. Complexes **2c** and (*R*,*S*)-**1c** represent the most enantioselective catalysts for the catalytic oxidative coupling of 2-naphthols, and, together with the results of Kozlowski et al.,[4b] will provide a practical way to prepare optically active binaphthols catalytically.

As a test of the practicality, oxidative coupling of **5i** in the presence of 5 mol% of catalyst **2c** was scaled up to 1.0 g, and gave **6i** with 95% *ee* and nearly quantitive yield, similar to the result obtained on a small scale (Scheme 4). After purification, **6i** was obtained as a sticky oil with over 99% *ee* and 95% yield. It can be transformed into many useful chiral ligands by modification through several known reaction sequences.

In summary, we have presented the most enantioselective catalytic oxidative coupling of 2-naphthols by a series of novel achiral biphenol-derived diastereomeric oxovanadium(IV)



Scheme 4. Asymmetric, catalytic preparation of optically pure **6i** on a large scale.

 © 2002 WILEY-VCH Verlag GmbH & Co. KGaA, Weinheim 0044-8249/02/4123-4534 $ 20.00+.50/0 *Angew. Chem. Int. Ed.* **2002**, *41*, No. 23

complexes **2**. In the presence of 5 mol % of the best catalyst **2c**, excellent enantioselectivities of 90–97 % *ee* and high yields were obtained for nine 2-naphthols. Compared with its structural analogue (*R*,*S*)-**1c**, which contains an optically pure 1,1′-binaphthyl unit, **2c**, despite its conformationally flexible biphenyl unit, still exhibits comparable or higher enantioselectivities. This discovery not only provides practical catalysts for the asymmetric synthesis of 1,1′-binaphthols but is also of significant fundamental interest.

Received: July 12, 2002 [Z19726]

[1] For reviews, see a) R. Noyori, *Asymmetric Catalysis in the Organic Synthesis*; Wiley, New York, **1994**; b) R. Noyori, H. Takaya, *Acc. Chem. Res.* **1990**, *23*, 345; c) *Comprehensive Asymmetric Catalysis* (Eds.: E. N. Jacobsen, A. Pfaltz, H. Yamamoto), Springer, Berlin, **1999**; d) K. A. Jørgensen, *Angew. Chem.* **2000**, *112*, 3702; *Angew. Chem. Int. Ed.* **2000**, *39*, 3558; e) C. Bolm, J. P. Hildebrand, K. Muniz, N. Hermanns, *Angew. Chem.* **2001**, *113*, 3382; *Angew. Chem. Int. Ed.* **2001**, *40*, 3284.

[2] For reviews, see a) L. Pu, *Chem. Rev.* **1998**, *98*, 2405; for leading representative research, see b) M. Irie, T. Yorozu, K. Hayashi, *J. Am. Chem. Soc.* **1978**, *100*, 2236; c) T. D. James, K. R. A. S. Sandanayke, S. Shinkai, *Nature* **1995**, *374*, 345; d) K. Akagi, G. Piao, S. Kaneko, K. Sakamaki, H. Shirakawa, M. Kyotani, *Sciences* **1998**, *282*, 1683; e) L. Zheng, R. C. Urian, Y. Liu, A. K. Y. Jen, L. Pu, *Chem. Mater.* **2000**, *12*, 13; f) V. Pugh, Q. S. Hu, L. Pu, *Angew. Chem.* **2000**, *112*, 3784; *Angew. Chem. Int. Ed.* **2000**, *39*, 3638; g) L. Z. Gong, Q. S. Hu, L. Pu, *J. Org. Chem.* **2001**, *66*, 2358; h) J. Lin, Q. S. Hu, M. H. Xu, L. Pu, *J. Am. Chem. Soc.* **2002**, *124*, 2088; i) Y. Cui, O. R. Evans, H. L. Ngo, P. S. White, W. B. Lin, *Angew. Chem.* **2002**, *114*, 1207; *Angew. Chem. Int. Ed.* **2002**, *41*, 1159.

[3] For resolution of binaphthols, see a) B. Feringa, H. Wynberg, *Bioorg. Chem.* **1978**, *7*, 397; b) F. Toda, K. Tanaka, *J. Org. Chem.* **1988**, *53*, 3607; c) S. Miyano, K. Kawahara, Y. Inoue, H. Hashimoto, *Tetrahedron Lett.* **1987**, *28*, 355; d) W. H. Pirkle, J. L. Schreiner, *J. Org. Chem.* **1981**, *46*, 4988; e) Q. S. Hu, D. Vitharana, L. Pu, *Tetrahedron: Aymmetry* **1995**, *6*, 2123; f) D. Cai, D. L. Hughes, T. R. Verhoeven, P. J. Reider, *Tetrahedron Lett.* **1995**, *36*, 7991; for nonoxidative syntheses of chiral binaphthyl, see g) T. Hayashi, K. Hayashizaki, T. Kiyoi, Y. Ito, *J. Am. Chem. Soc.* **1988**, *110*, 8153; h) M. Shindo, K. Koga, K. Tomioka, *J. Am. Chem. Soc.* **1992**, *114*, 8732; i) A. N. Cammidge, K. V. L. Crepy, *Chem. Commun.* **2000**, 1723; k) J. Yin, S. L. Buchwald, *J. Am. Chem. Soc.* **2000**, *122*, 12051.

[4] a) M. Nakajima, I. Miyoshi, K. Kanayama, S.-I. Hashimoto, *J. Org. Chem.* **1999**, *64*, 2264; b) X. Lin, J. Yang, M. C. Kozlowski, *Org. Lett.* **2001**, *3*, 1137, and references therein.

[5] R. Irie, K. Masutani, T. Katsuki, *Synlett* **2000**, 1433.

[6] a) C. Y. Chu, D. R. Hwang, S. K. Wang, B. J. Uang, *Chem. Commun.* **2001**, 980; b) S. W. Hon, C. H. Li, J. H. Kuo, N. B. Barhate, Y. H. Liu, Y. Wang, C. T. Chen, *Org. Lett.* **2001**, *3*, 869.

[7] Z. Luo, Q. Liu, L. Gong, X. Cui, A. Mi, Y. Jiang, *Chem. Commun.* **2002**, 914.

[8] H. C. Zhang, W. S. Huang, L. Pu, *J. Org. Chem.* **2001**, *66*, 481.

[9] For applications of a similar strategy in other reactions, see a) K. Mikami, T. Korenaga, M. Terada, T. Ohkuma, T. Pham, R. Noyori, *Angew. Chem.* **1999**, *111*, 517; *Angew. Chem. Int. Ed.* **1999**, *38*, 495; b) T. Ooi, Y. Uemastu, M. Kameda, K. Maruoka, *Angew. Chem.* **2002**, *114*, 1621; *Angew. Chem. Int. Ed.* **2002**, *41*, 1551; c) K. Mikami, K. Aikawa, Y. Yusa, *Org. Lett.* **2002**, *4*, 95.

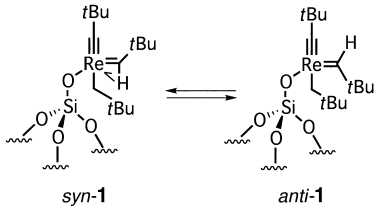
[10] a) L. J. Theriot, G. O. Carlisle, H. J. Hu, *J. Inorg. Nucl. Chem.* **1969**, *31*, 2841; b) J. J. R. Frausto da Silva, R. Wootton, R. D. Gillard, *J. Chem. Soc. A* **1970**, 3369.

Observation of a H-Agostic Bond in a Highly Active Rhenium–Alkylidene Olefin Metathesis Heterogeneous Catalyst by Two-Dimensional Solid-State NMR Spectroscopy**

Anne Lesage, Lyndon Emsley,* Mathieu Chabanas, Christophe Copéret,* and Jean-Marie Basset*

Heterogeneous catalysis is still the industrial cornerstone in the production of basic chemicals, polymers, and in some instances fine chemicals. One of the key problems in developing new heterogeneous catalysts has been the low content of active sites coupled with their diversity, which makes their characterization very difficult and which often does not allow a rational understanding of their reactivity and selectivity. Even in cases where, using approaches such as surface organometallic chemistry (SOMC), well-defined complexes are prepared, a detailed structural characterization of the geometry of such surface species is extremely difficult.

In molecular chemistry the local geometries can be probed by NMR spectroscopy, for example, by measuring scalar coupling constants. So far coupling constants on surfaces could not be determined. Herein we demonstrate how $J_{C,H}$ coupling constants can be measured in solids by using two-dimensional (2D) *J*-resolved spectroscopic methods, and how they are related to the local structure of the well-defined silica-supported rhenium complex **1**. This complex was shown



to be a highly active heterogeneous catalyst for the metathesis of a variety of olefins at room temperature.[1] In addition, two isomers can be obtained upon thermal or photochemical treatment (referred to as *syn* and *anti*, depending on the position of the *t*Bu fragment on the carbene ligand relative to the metallocarbyne), which were both characterized by solid-

[*] Prof. L. Emsley, Dr. A. Lesage
Laboratoire de Stéréochimie et des Interactions Moléculaires (UMR-5532 CNRS/ENS), Laboratoire de Recherche Conventionné du CEA (23 V)
Ecole Normale Supérieure de Lyon
46 Allée d'Italie, 69364 Lyon (France)
Fax: (+33) 4-7272-8384
E-mail: lyndon.emsley@ens-lyon.fr
Dr. C. Copéret, Prof. J.-M. Basset, Dr. M. Chabanas
Laboratoire de Chimie Organométallique de Surface (UMR-9986 CNRS/CPE Lyon)
Ecole Supérieure de Chimie Physique Electronique de Lyon
43, Bd du 11 Novembre 1918, 69616 Villeurbanne Cedex (France)
Fax: (+33) 4-7243-1795
E-mail: coperet@cpe.fr
basset@cpe.fr

[**] We thank the C.N.R.S., the ESCPE-Lyon, and ENS-Lyon for financial support. M.C. is grateful to the French Ministry for Education and Research for a fellowship (MENRT).

 © 2002 WILEY-VCH Verlag GmbH & Co. KGaA, Weinheim 0044-8249/02/4123-4535 $ 20.00+.50/0

state NMR spectroscopy using short- and long-range two-dimensional carbon–proton through-space correlation experiments.[2] Access to the precise molecular structure of these two metallocarbenes would help in better understanding the high activity of the rhenium complex.

In solution-state NMR studies, heteronuclear *J*-resolved 2D NMR spectroscopy is one of the most basic techniques available to investigate heteronuclear multiplet structures and can be used to measure $J_{C,H}$ couplings with high accuracy.[3] For solid materials, in contrast, the measurement of $J_{C,H}$ couplings is a challenging problem since the size of the scalar interactions is usually much smaller than that of the anisotropic interactions, that is, the dipolar couplings or the chemical shift anisotropies. Thus, in solid-state NMR spectroscopy, heteronuclear *J*-resolved experiments have been limited so far to compounds with fast molecular reorientation,[4] or to mobile organic products intercalated in zeolite channels[5] or kaolinite.[6] As a result of remarkable improvements in the efficiency of homonuclear dipolar decoupling pulse sequences, we have shown that the anisotropic interactions can be suppressed efficiently enough to resolve the heteronuclear $J_{C,H}$ couplings on much more strongly coupled systems under conditions of relatively fast magic angle spinning (MAS).[7,8] Thus a *J*-resolved technique should be applicable to rigid solids, and could be used to measure heteronuclear scalar couplings in strongly coupled systems.

The pulse sequence for the solid-state *J*-resolved experiment that we used in this study is indicated in Figure 1. A cross polarization step first transfers the proton magnetization to the carbon nuclei. During the evolution period t_1, the proton–proton dipolar couplings are removed by the homonuclear decoupling sequence, whereas the remaining inhomogenous interactions, that is, the chemical shift and the heteronuclear couplings, are averaged out by magic angle spinning to their isotropic part, leaving only the isotropic chemical shift and the heteronuclear scalar couplings. As the 180° carbon pulse applied in the middle of t_1 refocuses the chemical shift, the carbon magnetization will be only modulated during t_1 by the heteronuclear $J_{C,H}$ couplings. A *z*-filter is then applied to allow phase sensitive detection in t_1 before direct signal detection in t_2. A two-dimensional Fourier transform yields correlations between heteronuclear *J* multiplet structures (in ω_1) and carbon chemical shifts (in ω_2). Due to the homonuclear decoupling sequence, the heteronuclear couplings extracted in the ω_1 dimension are scaled by a factor λ which can be determined experimentally (see Experimental Section). It is important to underline the fact that the carbon π pulse applied in the middle of the t_1 evolution period refocuses the carbon chemical shift distribution which is often one of the main sources of carbon line broadening in solid species.[9]

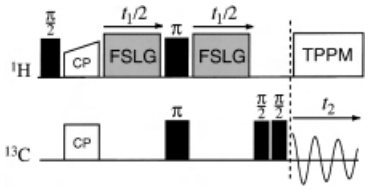


Figure 1. Pulse sequence for the solid-state *J*-resolved experiment (the pulse program and the phase cycle are available from our website[14]). Quadrature detection in ω_1 was achieved by using the TPPI method[15] by incrementing the phase of the first 90° carbon pulse. Proton–proton homonuclear decoupling was performed by using the frequency-switched Lee–Goldburg (FSLG) decoupling sequence,[16] but other homonuclear decoupling schemes can be employed.[8,17] During the acquisition period, TPPM heteronuclear decoupling[18] is applied.

Figure 2 shows the *J*-resolved spectrum recorded on the surface complex (**1**) prepared with ^{13}C labeling at the α positions. The traces extracted along the ω_1 dimension are shown in Figure 3 for various carbon resonance signals. As expected, the CH_3 groups yield a quartet, while the CH_2 and CH groups are correlated in the ω_1 dimension with triplet and doublet structures, respectively. The carbyne resonance of the *syn* rotamer is not split, as this carbon atom is not directly bonded to any proton. $^1J_{C,H}$ coupling constants of 126 Hz are measured for both the CH_3 and CH_2 groups. This is a typical value for H-bearing sp^3 hydridized carbon atoms.

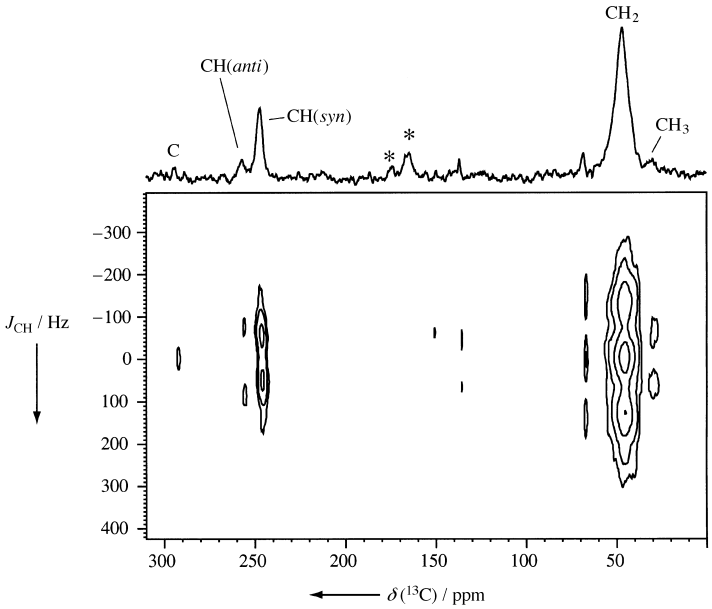


Figure 2. Contour plot of a two-dimensional *J*-resolved spectrum of the surface complex **1**, isotopically enriched in ^{13}C at the α positions, and, at the top, the one-dimensional CP-MAS carbon spectrum (256 scans). The CH_3 resonance signal is weak because the CH_3 groups are unlabeled. The stars indicate spinning sidebands. The other unlabeled peaks correspond to impurities (4% integration by ^{13}C NMR spectroscopy) that arise during the isomerization step carried out at 120 °C under argon. The carbyne resonance signal of the *anti* conformer does not appear in this spectrum and in the 2D map because of its low intensity. For further details see the Experimental Section.

The scalar couplings of the metallocarbene CH groups are significantly different for the *syn* and *anti* rotamers (109 and 159 Hz, respectively). This is in agreement with several observations for homogeneous molecular organometallic complexes where *syn* rotamers of alkylidene complexes always have smaller $^1J_{C,H}$ values than the *anti* rotamers.[10] The difference in scalar coupling suggests a difference in bond order of the carbenic C–H bond, stemming from the formation of a three-center, two-electron C-H-Re bond in the *syn* rotamer, which is also referred to as an agostic

 © 2002 WILEY-VCH Verlag GmbH & Co. KGaA, Weinheim 0044-8249/02/4123-4536 $ 20.00+.50/0

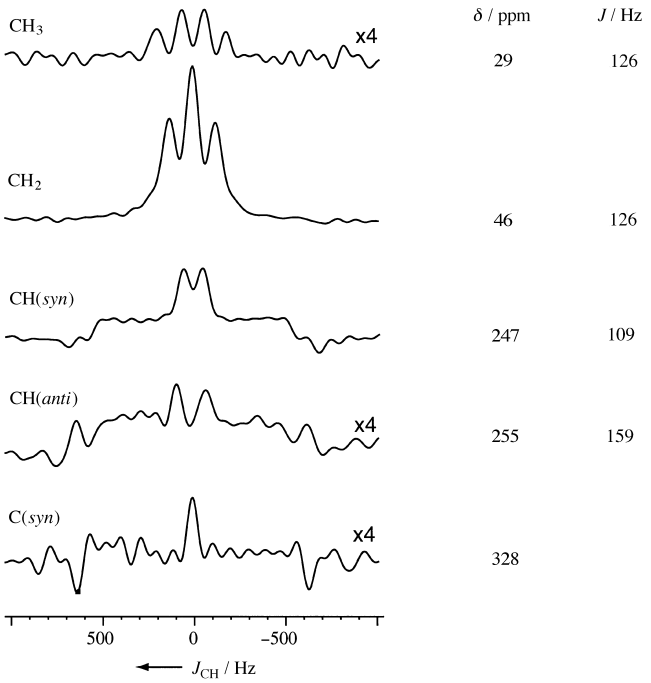


Figure 3. Traces extracted along the ω_1 dimension of the 2D *J*-resolved spectrum of Figure 2 at different carbon chemical shift frequencies. No signal apodization was applied. The values for the one-bond $J_{C,H}$ couplings were determined by peak deconvolution using Gaussian lineshapes. Errors in the measurement of the scalar couplings are about ± 4 Hz.

interaction.[11] The $^1J_{C,H}$ couplings have indeed been shown to be directly correlated to the degree of agosticity as the coupling varies from its unperturbed value of about 150 Hz to as low as 70 Hz in the most strongly agostic complexes.[12] This variation is logical since an increasing agostic interaction of the proton with the metal center will consequently weaken the C–H bond, which leads to a smaller $^1J_{C,H}$ coupling constant. A relation was established by using the observed change of the M-C-C bond angle from its normal value (120° for a sp^2 carbon) to around 170° for strongly agostic complexes in a range of model alkylidene complexes in solution.[12] The $^1J_{C,H}$ coupling constant can therefore be used to determine the local structure of the alkylidene ligand in the surface complexes. Using this relationship, values of 155 and 120° were obtained for the M-C-C bond angles of the *syn* and *anti* rotamer, respectively. The large value for the M-C-C bond angle for the *syn* rotamer indicates a small M-C-H bond angle of around 100° as a result of the interaction of the C–H bond and the Re center. Formally, complex **1** is a d^0 14-electron complex, assuming that the siloxy ligand is a poor π-donor ligand.[13] The lack of electron density on the metal center is therefore compensated by the participation of the two electrons from the C–H bond in a C–H agostic interaction to the metal. As a result, the formally empty orbital is not available to coordinate an incoming olefin. This is probably the reason for the lower activity of *syn* isomers in the metathesis reaction in solution, and the same situation is likely on the surface, on which it is also possible to control the alkylidene stereochemistry through thermal or photochemical treatment.[2]

Moreover, our data clearly show that the Re center is highly electron deficient, which probably explains the unprecedentedly high activity in olefin metathesis for silica-supported catalysts. They also indicate that the absence of activity of the silica-supported catalysts in classical heterogeneous catalysis is not due to the support per se, but suggest that the rate-determining step is the formation of the propagating center, an alkylidene.

In conclusion, 2D *J*-resolved solid-state NMR spectrsocopy has allowed us to determine the local structure of a heterogeneous catalyst, and to provide direct experimental evidence for the presence of a H-agostic bond. Note that the only obvious alternative to this method would be to precisely locate the position of the hydrogen atom by X-ray diffraction techniques. The determination of proton positions by this technique is notoriously difficult in the best of cases, and it currently seems unrealistic for surface species using EXAFS-based methods. The method proposed herein provides a unique structural probe of surface species that will yield valuable new insights into the molecular understanding of the active sites in heterogeneous catalysts.

Experimental Section

The NMR experiments were performed on a Bruker DSX 500 spectrometer with a conventional double-resonance 4 mm CP-MAS probe. The sample volume was restricted to the center of the rotor. A total of 48 t_1 increments of 465.5 μs with 4096 scans each were collected. A spectral width of 1073 Hz (uncorrected value) was used in the ω_1 dimension. The rotor spinning frequency was 12 kHz. The proton radio frequency (RF) field strength was set to 83 kHz during t_1 (FSLG decoupling) and during acquisition (TPPM decoupling). The lengths of carbon and proton 180° pulses were 6.5 and 6 μs, respectively. For the cross-polarization (CP) step, the RF field was set to 62 kHz for carbon, while a ramped RF field was applied on protons and matched to obtain optimal signals. The contact time for CP was 1 ms and the recycle delay was 2 s. The sample temperature was set to 20 °C. The overall experimental time was 110 h.

Details to Figure 2: Approximately 20 mg of sample was used. The surface area in these samples was around 200 $m^2 g^{-1}$. The one-dimensional CP-MAS spectrum was assigned by one- and two-dimensional heteronuclear correlation spectroscopy as reported in reference [2]. The experimental scaling factor λ of the FSLG decoupling sequence was obtained by comparing the proton spectra of L-alanine recorded under fast MAS conditions (30 kHz) and under FSLG decoupling, as described in reference [19]. At a RF field of 83 kHz, a scaling factor of 0.52 was found, which gave a corrected spectral width of 2065 Hz in the ω_1 dimension. Note that the pulse sequence used in this study differs from those proposed so far for solid-state studies: the *J*-resolved experiments used previously to obtain 2D *J* spectra in highly mobile solids were based on the gated decoupler method, which reduces the scaling factor of the homonuclear decoupling sequence by an additional factor of one half. Notably, the gated decoupler technique is not suitable for strongly coupled systems, and in our case it would not have allowed a clear identification of the agostic bond. Note that although the surface complex is not entirely rigid, since motion is allowed around the Si–O bond, homonuclear decoupling during t_1 is necessary for the $J_{C,H}$ couplings to be resolved.

Received: July 18, 2002 [Z19761]

[1] a) M. Chabanas, A. Baudouin, C. Copéret, J.-M. Basset, *J. Am. Chem. Soc.* **2001**, *123*, 2062; M. Chabanas, C. Copéret, J.-M. Basset, unpublished.

[2] M. Chabanas, A. Baudouin, C. Copéret, J.-M. Basset, A. Lesage, S. Hediger, L. Emsley, W. Lukens, *J. Am. Chem. Soc.* **2002**, in press.

[3] R. R. Ernst, G. Bodenhausen, A. Wokaun, *Principles of Nuclear Magnetic Resonance in One and Two Dimensions*, Clarendon Press, Oxford, **1987**.

[4] T. Terao, H. Miura, A. Saika, *J. Am. Chem. Soc.* **1982**, *104*, 5228; W. K. Zilm, D. M. Grant, *J. Magn. Reson.* **1982**, *48*, 524; C. L. Mayne, R. J.

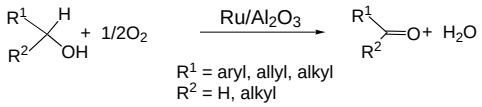
 © 2002 WILEY-VCH Verlag GmbH & Co. KGaA, Weinheim 0044-8249/02/4123-4537 $ 20.00+.50/0

Pugmire, D. M. Grant, *J. Magn. Reson.* **1984**, *56*, 151; H. Miura, T. Terao, A. Saika, *J. Magn. Reson.* **1986**, *68*, 593.
[5] M. W. Anderson, J. Klinowski, *Chem. Phys. Lett.* **1991**, *172*, 275; A. G. Stepanov, V. N. Zudin, K. I. Zamaraev, *Solid State NMR* **1993**, *2*, 89.
[6] J. Rocha, W. Kolodziejski, J. Klinowski, *Chem. Phys. Lett.* **1991**, *176*, 395.
[7] A. Lesage, S. Steuernagel, L. Emsley, *J. Am. Chem. Soc.* **1998**, *120*, 7095.
[8] D. Sakellariou, A. Lesage, P. Hodgkinson, L. Emsley, *Chem. Phys. Lett.* **2000**, *319*, 253.
[9] D. L. VanderHart, W. L. Earl, A. N. Garroway, *J. Magn. Reson.* **1981**, *44*, 361; A. Lesage, M. Bardet, L. Emsley, *J. Am. Chem. Soc.* **1999**, *121*, 10987.
[10] R. Toreki, R. R. Schrock, W. M. Davis, *J. Am. Chem. Soc.* **1992**, *114*, 3367.
[11] N. A. Bailey, J. M. Jenkins, R. Mason, B. L. Shaw, *J. Chem. Soc. Chem. Commun.* **1965**, 237; S. J. LaPlaca, J. A. Ibers, *Inorg. Chem.* **1965**, *4*, 778; J. A. Ibers, *Abst. Am. Crystallogr. Assoc.* **1965**, B10; F. A. Cotton, T. LaCour, A. G. Stanislowski, *J. Am. Chem. Soc.* **1974**, *96*, 754; F. A. Cotton, A. G. Stanislowski, *J. Am. Chem. Soc.* **1974**, *96*, 5074; M. Brookhart, M. L. H. Green, *J. Organomet. Chem.* **1983**, *250*, 395.
[12] W. A. Nugent, J. M. Mayer, *Metal–Ligand Multiple Bond*, Wiley, New York, **1988**, p. 134; R. R. Schrock, *Acc. Chem. Res.* **1979**, *12*, 98.
[13] D. G. H. Ballard, *Adv. Catal.* **1973**, *23*, 263; T. E. Lapointe, P. T. Wolczanski, G. D. VanDuyne, *Organometallics* **1985**, *4*, 1810.
[14] http://www.ens-lyon.fr/STIM/NMR.
[15] D. Marion, K. Wüthrich, *Bioch. Biophys. Res. Commun.* **1983**, *113*, 967.
[16] A. Bielecki, A. C. Kolbert, M. H. Levitt, *Chem. Phys. Lett.* **1989**, *155*, 341; A. Bielecki, A. C. Kolbert, H. J. M. deGroot, M. H. Levitt, *Adv. Magn. Reson.* **1989**, *14*, 111; M. H. Levitt, A. C. Kolbert, A. Bielecki, D. J. Ruben, *Solid State NMR* **1993**, *2*, 151.
[17] E. Vinogradov, P. H. Madhu, S. Vega, *Chem. Phys. Lett.* **1999**, *314*, 443; P. K. Madhu, X. Zhao, M. H. Levitt, *Chem. Phys. Lett.* **2001**, *346*, 142.
[18] A. E. Bennett, C. M. Rienstra, M. Auger, K. V. Lakshmi, R. G. Griffin, *J. Chem. Phys.* **1995**, *103*, 6951.
[19] A. Lesage, L. Duma, D. Sakellariou, L. Emsley, *J. Am. Chem. Soc.* **2001**, *123*, 5747.

Supported Ruthenium Catalyst for the Heterogeneous Oxidation of Alcohols with Molecular Oxygen**

Kazuya Yamaguchi and Noritaka Mizuno*

Although catalytic oxidation of alcohols to carbonyl compounds has attracted much attention both in industrial processes and in organic syntheses,[1–3] alcohols are traditionally oxidized by non-catalytic methods with stoichiometric oxidants such as dichromate and permanganate.[1–3] These methods produce enormous amounts of metal salts as wastes. Much effort has been made to develop homogeneous catalytic systems to solve these problems.[4–6] However, most systems are applicable only for the oxidation of activated benzylic and allylic alcohols, or large quantities of additives such as NaOAc, NaOH, and K_2CO_3 are needed.[7–10] There is little known about the oxidation of alcohols with molecular oxygen, which could be applied to a wide range of alcohols. If these oxidation reactions could be performed by using solid-supported catalysts (heterogeneous catalysis), they would be considerably cheaper and environmentally more friendly because of the ease with which the catalysts could be separated from products and recycled.[11–14] Examples of solid-supported catalysts that have been tested include tetrapropylammonium perruthenate (TPAP)/MCM-41,[15] Ru/CeO_2,[16] Ru-hydrotalcite,[17] Ru-hydroxyapatite,[18] $[RuCl_2(p\text{-cymene})]_2$/activated carbon,[19] Pd-hydrotalcite,[20] and Pd or Pt on activated carbon.[21] However, heterogeneous oxidation reactions are limited to activated alcohols and/or have turn over numbers (TONs) which are very low (less than 20).[15–21] If oxidation reactions could be carried out without solvents, then the system would facilitate the separation of catalyst from products. Despite the advantage of using solid catalysts without solvents or additives for oxidation of both activated and non-activated alcohols, nothing has been reported on the use of highly active solvent-free heterogeneous catalysts with only molecular oxygen. Herein we report an effective aerobic heterogeneous oxidation reaction of both activated and non-activated alcohols, which may have a sulfur atom, a nitrogen atom, or a carbon-carbon double bond, by using molecular oxygen or air catalyzed by Ru supported on alumina (Ru/Al_2O_3) and demonstrate the use of solvent-free oxidation reactions [Eq. (1)]. The results we present offer a strategy for the design of heterogeneous alcohol-oxidation catalysts for use in conjunction with molecular oxygen.



(1)

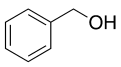
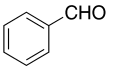
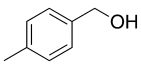
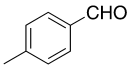
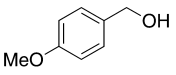
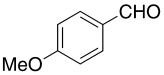
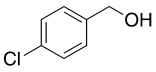
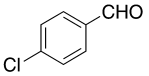
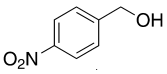
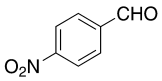
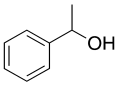
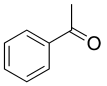
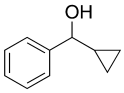
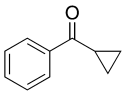
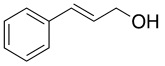
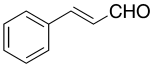
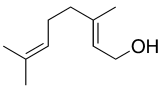
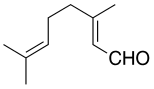
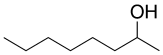
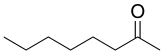
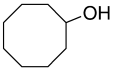
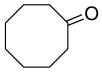
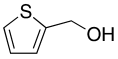
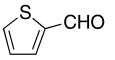
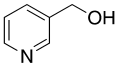
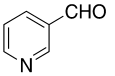
The Ru/Al_2O_3 system had high catalytic activities for the oxidation of activated and non-activated alcohols with only 1 atm of O_2 as shown in Table 1. Reaction selectivity was over 97% in all cases and all primary and secondary benzylic alcohols were converted quantitatively into the corresponding benzaldehydes and ketones, respectively. Primary and secondary allylic alcohols afforded the corresponding enals or enones without intramolecular hydrogen transfer or geometrical isomerization of the double bonds. Additionally, the catalytic system efficiently oxidized non-activated alcohols to the corresponding carbonyl compounds: for the oxidation of 2-octanol, 2-octanone was produced in a 91% yield (entry 14). Similarly, alicyclic alcohols such as cyclopentanol and cyclooctanol were selectively oxidized to the corresponding cyclic ketones (entries 15 and 16). Less reactive aliphatic primary alcohols, 1-octanol and 1-decanol, were also oxidized. However, increasing the reaction time did not improve the yields of the aldehydes because of successive oxidation to the corresponding carboxylic acids. The addition of a small amount of hydroquinone (1 equiv based on Ru) completely

[*] Prof. Dr. N. Mizuno, Dr. K. Yamaguchi
Department of Applied Chemistry,
School of Engineering
The University of Tokyo
7-3-1 Hongo, Bunkyo-ku, Tokyo 113-8656 (Japan)
Fax: (+81) 3-5841-7220
E-mail: tmizuno@mail.ecc.u-tokyo.ac.jp

[**] This work was supported in part by a Grant-in-Aid for Scientific Research from the Ministry of Education, Culture, Sports, Science, and Technology of Japan.

 © 2002 WILEY-VCH Verlag GmbH & Co. KGaA, Weinheim 0044-8249/02/4123-4538 $ 20.00+.50/0

Table 1. Results of oxidations of various alcohols catalyzed by Ru/Al_2O_3 with molecular oxygen.[a]

Entry	Substrate	Product	t [h]	Conv. [%]	Selectivity [%]
1			1	> 99	> 99
2			1	> 99	> 99
3			1	> 99	> 99
4			1	> 99	> 99
5			3	97	> 99
6			1	> 99	> 99
7			1	> 99	> 99
8			1.5	> 99	98
9[b]			6	84	> 99
10			6	89	97
11[b,c]	$C_7H_{15}CH_2OH$	$C_7H_{15}CHO$	4	87	98
12[b,c]	$C_9H_{19}CH_2OH$	$C_9H_{19}CHO$	4	71	99
13			5	90	> 99
14			2	91	> 99
15[b]			8	92	> 99
16[b]			6	81	> 99
17			1.5	> 99	> 99
18[b]			2	93	> 99

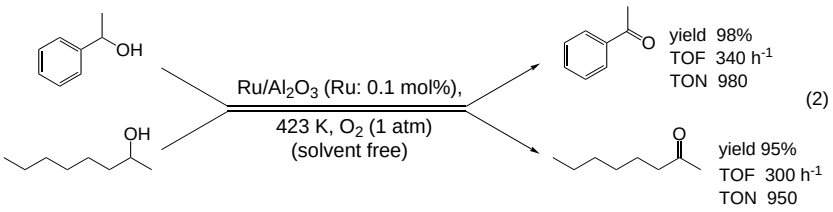
[a] Reaction conditions were as follows: alcohol (1 mmol), Ru/Al_2O_3 (Ru: 2.5 mol %),$PhCF_3$ (1.5 mL), 356 K, under 1 atm of O_2: conversion and selectivity were determined by gas chromatography with an internal standard. [b] Ru/Al_2O_3 (Ru: 5 mol %). [c] Hydroquinone (1 equiv based on Ru) was added.

suppressed the over-oxidation, which afforded only aliphatic aldehydes in fairly good yields. Ru/Al_2O_3 catalyzed the oxidation of alcohols also containing nitrogen or sulfur atoms to the corresponding aldehydes in high yields (entries 17 and 18), while monomeric Ru complexes cannot affect catalytic oxidation of these alcohols because of the strong coordination to the metal center.[10]

Among various Ru catalysts tested, Ru/Al_2O_3 showed the highest catalytic activity for the oxidation of benzyl alcohol at 356 K. $Ru(OH)_3{\cdot}n\,H_2O$ gave benzaldehyde in a 29 % yield (TON = 12) after 20 h and other Ru compounds of $RuCl_3{\cdot}n$-H_2O, $[RuCl_2(PPh_3)_3]_2$, $[RuCl_2(p\text{-cymene})]$, and RuO_2 showed no catalytic activity.

The heterogeneous oxidation of alcohols without solvents would be more feasible for industrialized processes. The Ru/Al_2O_3 catalyst system efficiently facilitated the oxidation of non-activated 2-octanol and activated 1-phenylethanol without the use of solvents. The solvent-free oxidation of 2-octanol, and 1-phenylethanol at 423 K had turn over frequencies (TOFs) of 300 h^{-1} and 340 h^{-1}, and TONs of 950 and 980, respectively [Eq. (2)]. These TOFs and TONs are higher than those reported for the aerobic oxidation of 2-octanol by other Ru catalysts: ($[RuCl_2(PPh_3)_3]$/TEMPO (TON and TOF, 466 and 104 h^{-1}),[10] Ru/quinone/Co–salen (194, 97 h^{-1}),[8] TPAP (20, 6 h^{-1}),[15] Ru/CeO_2 (30, 5 h^{-1}),[16] Ru–Co–hydrotalcite (9, 5 h^{-1}),[17] and Ru–hydroxyapatite (6, 1 h^{-1})[18]). Furthermore,

 © 2002 WILEY-VCH Verlag GmbH & Co. KGaA, Weinheim 0044-8249/02/4123-4539 $ 20.00+.50/0



(2)

air can be used instead of molecular oxygen in the present system without changes in conversion and selectivity values.

It was confirmed by induced coupled plasma techniques (ICP) that the Ru content of the used Ru/Al_2O_3 catalyst was the same as that of the fresh catalyst and that no Ru was in the filtrate. In addition, the oxidation of benzyl alcohol was completely stopped by the removal of Ru/Al_2O_3 from the reaction solution. These results indicate that any Ru species that leached into the reaction solution is not an active homogeneous catalyst and that the observed catalysis is truly heterogeneous in nature.[22] The Ru/Al_2O_3 catalyst system is reusable (Figure 1). When the oxidation of benzyl alcohol was repeated seven times with the same sample of catalyst, benzaldehyde was quantitatively produced at the same rate as that of the first run.

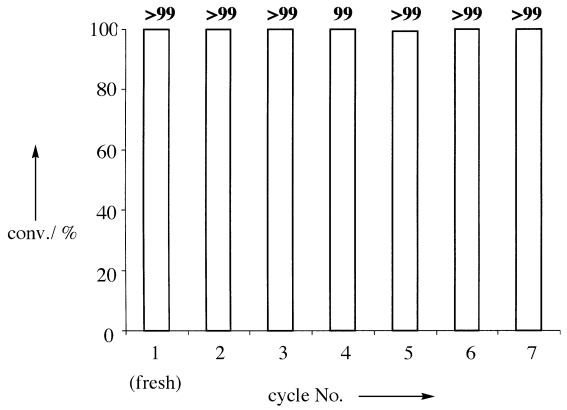


Figure 1. Recycling of Ru/Al_2O_3 catalyst for the oxidation of benzyl alcohol. Reaction conditions were as follows: benzyl alcohol (1 mmol), Ru/Al_2O_3 (Ru: 2.5 mol%), $PhCF_3$ (1.5 mL), 356 K, under 1 atm of O_2, 1 h.

The conversion and selectivity were not changed by the addition of a free-radical trap, for example, 2,6-di-*tert*-butyl-4-methylphenol, and hydroquinone. The skeletal isomerization of a cyclopropyl ring used as a radical clock did not proceed at all. This evidence shows that a radical is not involved in the oxidation reaction. Primary alcohols were selectively oxidized even in the presence of secondary ones, an equimolar mixture of benzyl alcohol and 1-phenylethanol gave a mixture of benzaldehyde and acetophenone in 90% and 24% yields, respectively. Similarly, competitive oxidations of 1-octanol and 4-octanol showed 84 and 8% conversions, respectively. These faster oxidations of primary alcohols show that Ru–alcoholate **II** (see scheme 1) is formed as an intermediate, since the formation of metal–alcoholate species is well known for such selective oxidation of primary hydroxy groups.[23,24] Competitive oxidations of *para*-substituted benzyl alcohols gave a Hammett ρ value of -0.461 ($r^2 = 0.99$; Figure 2), which suggests that hydride abstraction from **II** to form the carbocation-type intermediate is involved in the oxidation path.

The number of moles of water produced was equivalent to that of acetone produced for the oxidation of 2-propanol (19.6 mmol, at 343 K) by using Ru/Al_2O_3 and molecular oxygen. This 1:1 stoichiometry suggests that the simple dehydrogenation does not proceed. Under anaerobic conditions, the number of moles of acetone produced was approximately the same as those of Ru loaded on Al_2O_3,

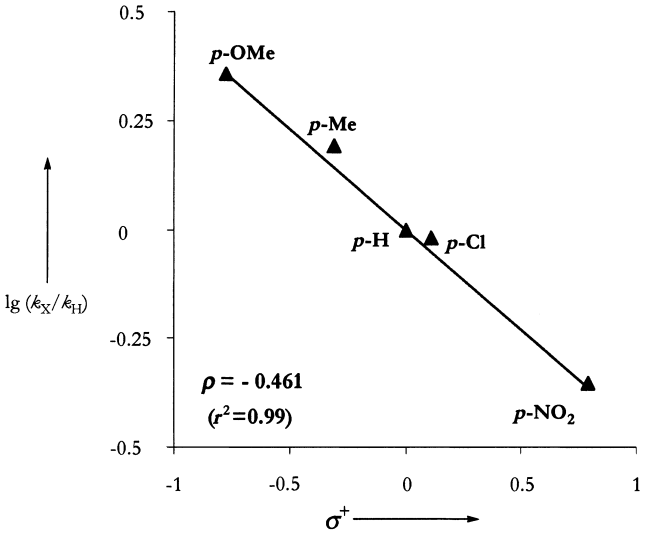
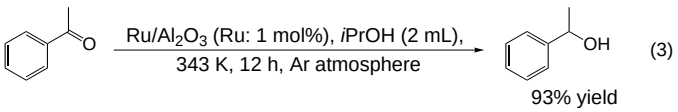


Figure 2. Hammett plots for the aerobic oxidation of *p*-substituted benzyl alcohols by using Ru/Al_2O_3 catalyst. Reaction conditions were as follows: alcohol (1 mmol), Ru/Al_2O_3 (1 mol%), $PhCF_3$ (1.5 mL), 333K, under 1 atm O_2..

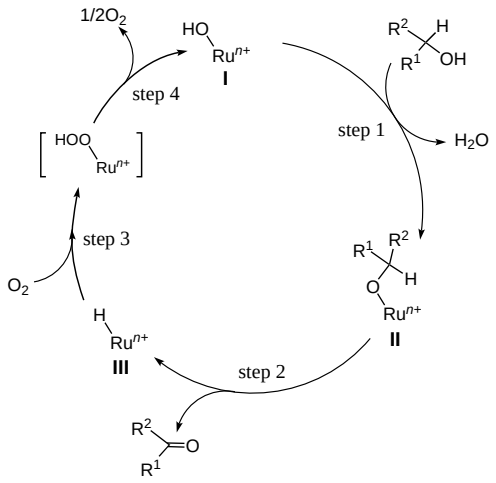
and water produced. When acetophenone (1M) was treated in 2-propanol under Ar, almost equimolar amounts of acetone and 1-phenylethanol were produced, which shows that transfer hydrogenation takes place [Eq. (3)].[25] These facts suggest that a Ru-H species **III** is formed. On the basis of all the results, Scheme 1 is proposed: Ru–alcoholate species **II** is formed by ligand exchange between Ru–hydroxide **I** then, an alcohol undergoes typical β elimination to afford the corresponding carbonyl compound and **III**. The hydride species is then reoxidized by molecular oxygen.[26]



(3)

The rate did not change with a decrease in oxygen partial pressure (P_{O_2}) from 1.0 to 0.2 atm (air). Kinetic data could well be expressed by the Michaelis-Menten type equation.[27] The kinetic isotope effects (k_H/k_D) were 5.0 and 2.4 for the intramolecular competitive oxidation of α-deuterio-*p*-methylbenzyl alcohol and for the intermolecular competitive

 © 2002 WILEY-VCH Verlag GmbH & Co. KGaA, Weinheim 0044-8249/02/4123-4540 $ 20.00+.50/0 *Angew. Chem. Int. Ed.* **2002**, *41*, No. 23



Scheme 1.

oxidation of benzyl alcohol and benzyl [D_7]alcohol ($C_6D_5CD_2OH$) at 333K, respectively. The apparent activation energies for steps 1 (alcoholate formation) and 2 (β elimination) were 40.0 and 54.9 kJ mol^{-1}, respectively. On the basis of these facts, step 2 is rate-determining.

In summary, Ru/Al_2O_3 can act as an efficient heterogeneous catalyst for the oxidation of alcohols with 1 atm of molecular oxygen or air, without additives. The high activity of, and ease with which, the catalyst can be recovered and reused raise the prospect of using this type of simple supported catalyst for organic syntheses and the industrial oxidation of alcohols. The catalyst would be considerably cheaper than organometallic and inorganic compounds.

Experimental Section

The Ru/Al_2O_3 catalyst was prepared by the modification of a literature preparation of $Ru(OH)_3{\cdot}nH_2O$:[28] γ-Al_2O_3 (2.0 g, JRC-ALO-4, BET surface area: 174 m^2 g^{-1}) was vigorously stirred with an aqueous solution of $RuCl_3$ (60 mL, 8.3×10^{-3} M) for 15 min at room temperature. The initially brown aqueous phase became lighter, and the alumina powder turned dark gray. The solid was separated by filtration and washed with a large amount of water, then dried in vacuo. This solid was added to deionized water (30 mL), the pH of the solution was adjusted to 13.2 by the addition of an aqueous solution of NaOH (1.0 M) and the resulting slurry was stirred for 24 h. During this period, the powder changed from dark gray to dark green. The solid was separated by filtration and copiously washed with water, then dried in vacuo to afford 2.1 g of Ru/Al_2O_3 as a dark green powder. The contents of ruthenium and chloride was 1.4 and 0 wt%, respectively, and the BET surface area was 182 m^2 g^{-1}. The ESR spectrum had a signal at $g=2.11$, which is assigned to Ru^{3+} with low-spin d^5 electron configuration.[29] The XRD pattern was the same as that of the γ-Al_2O_3 support and no signals arising from ruthenium metal or dioxide were observed. Particles of ruthenium metal or dioxide were not detected by TEM. The IR spectrum showed a very broad ν(OH) band in the range of 2900–3700 cm^{-1}. These facts suggest that ruthenium(III) hydroxide is highly dispersed on γ-Al_2O_3. Thus, the Ru/Al_2O_3 catalyst can be easily prepared in a quantitative yield and the content of Ru can be controlled.

Oxidations of alcohols were typically carried out as follows. A suspension of Ru/Al_2O_3 (0.11 g, Ru: 2.5 mol%) in trifluorotoluene (1.5 mL) was stirred for 5 min. Benzyl alcohol (0.108 g, 1 mmol) was added to the reaction mixture and the suspension was purged with molecular oxygen. The resulting mixture was heated at 356 K for 1 h, and benzaldehyde was produced in >99% yield determined by GC. After the reaction, the catalyst was separated by filtration (or centrifugation) and was further washed with acetone. The filtrate was evaporated in vacuo, and the crude product was purified by column chlomatography on silica gel, which gave 0.101 g of pure benzaldehyde (95% yield). The separated Ru/Al_2O_3 was washed with an aqueous solution of NaOH (1.0 M) and water (30 mL), and dried in vacuo before recycling.

Received: July 16, 2002 [Z19744]

[1] R. A. Sheldon, J. K. Kochi, *Metal Catalyzed Oxidations of Organic Compound*, Academic Press, New York, **1981**.

[2] C. L. Hill in *Advances in Oxygenated Processes, Vol. 1* (Eds.: A. L. Baumstark), JAI, London, **1988**, p. 1.

[3] M. Hudlucky, *Oxidations in Organic Chemistry*, ACS Monograph Series, American Chemical Society, Washington, **1990**.

[4] CuCl/Phen/K_2CO_3[5] and $Pd(OAc)_2$/bathophenanthroline disulfonate/NaOAc[6] systems are reported to be efficient examples. In the former system, the turnover number (TON, moles of product per mol of catalyst) and turnover frequency (TOF, TON hr^{-1}) for the oxidation of 2-undecanol are 9 and 5 h^{-1}, respectively. In the latter system, the TON and TOF for the oxidation of 2-pentanol are 400 and 100 h^{-1}, respectively. Even in these systems, large quantities of additives such as NaOAc, NaOH, or K_2CO_3 (0.05–2 equivalents based on alcohol) are needed to acheive high yields of carbonyl conpounds. In addition, the $Pd(OAc)_2$/PhenS*/NaOAc system can not oxidize sulfur, nitrogen, carbon–carbon double-bond-containing alcohols because of the strong coordination to the metal center.

[5] I. E. Markó, P. R. Giles, M. Tsukazaki, S. M. Brown, C. J. Urch, *Science* **1996**, *274*, 2044.

[6] G.-J. ten Brink, I. W. C. E. Arends, R. A. Sheldon, *Science* **2000**, *287*, 1636.

[7] Some Ru compounds have high catalytic activity for the oxidation of alcohols with molecular oxygen by use of hydrogen/electron transfer agents: hydroquinone and 2,2′,6,6′-tetramethylpyperidine *N*-oxyl (TEMPO).[8–10]

[8] G. Csjernyik, A. H. Ell, L. Fadini, B. Pugin, J.-E. Bäckvall, *J. Org. Chem.* **2002**, *67*, 1657.

[9] A. Hanyu, E. Takezawa, S. Sakaguchi, Y. Ishii, *Tetrahedron Lett.* **1998**, *39*, 5557.

[10] A. Dijksman, A. Marino-González, A. M. i Payeras, I. W. C. E. Arends, R. A. Sheldon, *J. Am. Chem. Soc.* **2001**, *123*, 6826.

[11] R. A. Sheldon, I. W. C. E. Arends, A. Dijksman, *Catal. Today* **2000**, *57*, 157.

[12] J. M. Thomas, R. Raja, G. Sankar, *Nature* **1999**, *398*, 227.

[13] A. Corma, L. T. Nemeth, M. Renz, S. Valencia, *Nature* **2001**, *412*, 423.

[14] J. T. Rhule, W. A. Neiwert, K. I. Hardcastle, B. T. Do, C. L. Hill, *J. Am. Chem. Soc.* **2001**, *123*, 12101.

[15] A. Bleloch, B. F. G. Johnson, S. V. Ley, A. J. Price, D. S. Shephard, A. W. Thomas, *Chem. Commun.* **1999**, 907.

[16] F. Vocanson, Y. P. Guo, J. L. Namy, H. B. Kagan, *Synth. Commun.* **1998**, *28*, 2577.

[17] T. Matsushita, K. Ebitani, K. Kaneda, *Chem. Commun.* **1999**, 265.

[18] K. Yamaguchi, K. Mori, T. Mizugaki, K. Ebitani, K. Kaneda, *J. Am. Chem. Soc.* **2000**, *122*, 7144.

[19] E. Choi, C. Lee, Y. Na, S. Chang, *Org. Lett.* **2002**, *4*, 2369.

[20] N. Kakiuchi, Y. Maeda, T. Nishimura, S. Uemura, *J. Org. Chem.* **2001**, *66*, 6620.

[21] T. Mallat, A. Baiker, *Catal. Today* **1994**, *19*, 247.

[22] R. A. Sheldon, M. Wallau, I. W. C. E. Arends, U. Schuchardt, *Acc. Chem. Res.* **1998**, *31*, 485.

[23] K. B. Sharpless, K. Akashi, K. Oshima, *Tetrahedron Lett.* **1976**, *17*, 2503.

[24] S. Kanemoto, S. Matsubara, K. Takai, K. Oshima, K. Utimoto, H. Nozaki, *Bull. Chem. Soc. Jpn.* **1988**, *61*, 3607.

[25] R. Noyori, M. Yamakawa, S. Hashiguchi, *J. Org. Chem.* **2001**, *66*, 7932.

[26] While step 3 may proceed via the formation of hydrogen peroxide, the filtrate for the oxidation of benzyl alcohol with molecular oxygen showed a negative peroxide test (Quantofix test stick, detection limit 1 mg L^{-1} hydrogen peroxide). The catalytic oxidation of benzyl alcohol with hydrogen peroxide hardly proceeded because of the rapid decomposition of hydrogen peroxide, in agreement with the rapid decomposition of Ru^{n+}-OOH without contributing to the oxidation of alcohols in Scheme 1.

 © 2002 WILEY-VCH Verlag GmbH & Co. KGaA, Weinheim 0044-8249/02/4123-4541 $ 20.00+.50/0

[27] The catalytic rate (R) of the oxidation of benzyl alcohol was expressed by $R = k_2[C]/\{1 + k_2/(k_1[A])\}$, where [C] and [A] are the amount of Ru/Al_2O_3 and the concentration of benzyl alcohol, respectively, and k_1 and k_2 are the rate constants for step 1 and step 2, respectively, and at 356 K these were 38 $h^{-1}g^{-1}$ and 42 M $h^{-1}g^{-1}$, respectively.

[28] J. W. Mellor, *A Comprehensive Treatise on Inorganic and Theoretical Chemistry, Vol. XV*, Longmans & Green, London, **1936**, pp. 498–544.

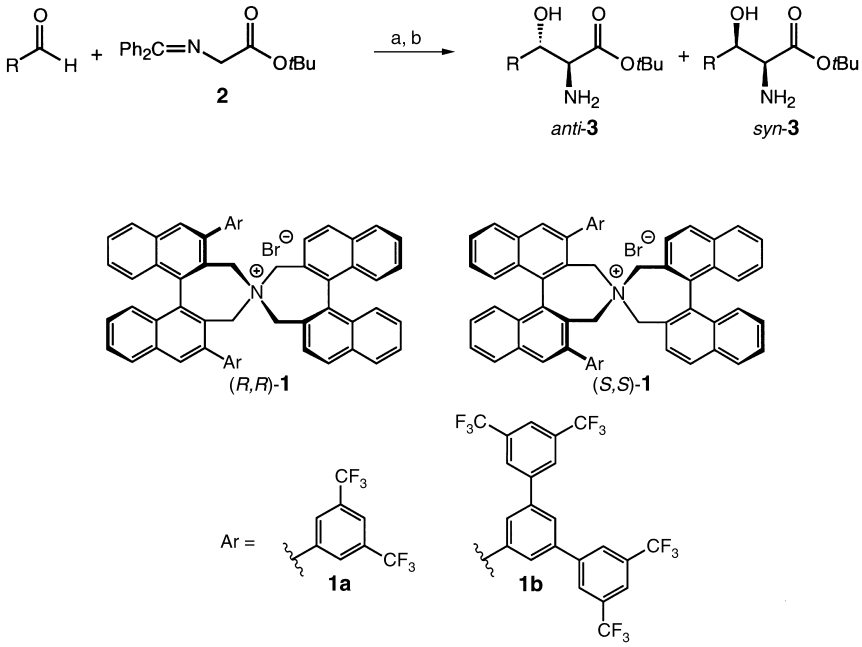
[29] B.-Z Wan, J. H Lunsford, *Inorg. Chim. Acta* **1982**, *65*, 29; M. G. Cattania, A. Gervasini, F. Morazzoni, P. Scotti, D. Strumolo, *J. Chem. Soc. Faraday Trans. 1* **1987**, *83*, 3619.

Direct Asymmetric Aldol Reactions of Glycine Schiff Base with Aldehydes Catalyzed by Chiral Quaternary Ammonium Salts**

Takashi Ooi, Mika Taniguchi, Minoru Kameda, and Keiji Maruoka*

As naturally occurring α-amino acids as well as components of many complex biologically active cyclic peptides and enzyme inhibitors, optically active β-hydroxy-α-amino acids are extremely important chiral units, especially from the pharmaceutical viewpoint.[1] Furthermore, they are useful chiral building blocks in organic synthesis[2] as exemplified by their transformation into β-lactams,[3] β-halo-α-amino acids,[4] and aziridines.[5] Accordingly, numerous methods for the asymmetric synthesis of β-hydroxy-α-amino acids have been elaborated, most of which unfortunately involve multistep procedures and/or the inevitable use of a stoichiometric amount of chiral auxiliaries.[6–8] In this regard, the construction of their primary structure with the correct stereochemistry by the direct catalytic asymmetric aldol reaction of a glycine donor with aldehyde acceptors has been considered to be an ideal protocol.[9] However, there have been few successful examples to date,[10,11] except for the chemoenzymatic process with glycine-dependent aldolases.[9b,12] We report herein an efficient and direct asymmetric aldol reaction of glycine Schiff base **2**[13] with aldehydes under organic/aqueous biphasic conditions by using enantiomerically pure, C_2-symmetric chiral quaternary ammonium salt **1**[14] as a phase-transfer catalyst (Scheme 1). This approach provides a practical and environmentally benign chemical process for the synthesis of optically active β-hydroxy-α-amino acids.

Initially, we examined the direct asymmetric aldol reaction of prochiral glycine Schiff base **2** and 3-phenylpropanal as a representative acceptor under phase-transfer conditions. Thorough optimization of the catalyst structure and reaction conditions revealed that treatment of **2** with 3-phenylpropanal (2 equiv) in toluene/aqueous NaOH (1%) (*v*/*v* 1.25:1; 2 equiv of base for **2**) in the presence of chiral quaternary ammonium salt (*R*,*R*)-**1a** (2 mol%)[14d] at 0°C for 2 h and subsequent hydrolysis with HCl (1N) in THF resulted in the formation of the corresponding β-hydroxy-α-amino ester **3** (R = $PhCH_2CH_2$) in 76% yield with the *anti*/*syn* ratio of 3.3:1. The enantiomeric excess of the major *anti* isomer was determined to be 91% by chiral HPLC analysis (Table 1, entry 1). Significantly, use of (*R*,*R*)-**1b** (which contains a 3,5-bis(3,5-bis(trifluoromethyl)phenyl)phenyl substituent) as a catalyst enhanced both diastereo- and enantioselectivities in this system (*anti*/*syn* 12:1; 96% *ee* for *anti* isomer) (Table 1, entry 2).[15]



Scheme 1. Direct catalytic asymmetric aldol reaction of glycine Schiff base **2** with aldehydes in the presence of **1** under phase-transfer conditions. a) (*R*,*R*)-**1** (2 mol%), toluene/aqueous NaOH (1%), 0°C, 2 h; b) HCl (1N)/THF.

A variety of aldehydes were examined for this direct asymmetric aldol reaction with (*R*,*R*)-**1** and the results are listed in Table 1. Generally, the reaction proceeded smoothly at 0°C for 2 h to afford the *anti* isomer predominantly, with excellent enantioselectivity. Heptanal, an aliphatic aldehyde with a long hydrocarbon chain, was found to be a good candidate (Table 1, entry 3), thus indicating the feasibility of direct asymmetric synthesis of a variety of lipo β-hydroxy-α-amino acids, a useful component for the preparation of lipophilic peptides and glycopeptides with characteristic high

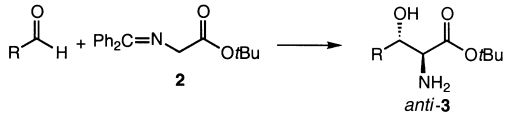
[*] Prof. K. Maruoka, Dr. T. Ooi, M. Taniguchi, M. Kameda
Department of Chemistry
Graduate School of Science, Kyoto University
Sakyo, Kyoto, 606-8502 (Japan)
Fax: (+81) 75-753-4041
E-mail: maruoka@kuchem.kyoto-u.ac.jp

[**] This work was partially supported by a Grant-in-Aid for Scientific Research from the Ministry of Education, Culture, Sports, Science, and Technology, Japan. M.K. is grateful to the Japan Society for the Promotion of Science for Young Scientists for a Research Fellowship.

Supporting information for this article is available on the WWW under http://www.angewandte.org or from the author.

 © 2002 WILEY-VCH Verlag GmbH & Co. KGaA, Weinheim 0044-8249/02/4123-4542 $ 20.00+.50/0

Table 1. Direct asymmetric aldol reactions of **2** with aldehydes by chiral phase-transfer catalysis of **1**.[a]



Entry	R	Catalyst	Yield [%][b]	*anti*/*syn*[c]	*ee* [%][d]
1	$PhCH_2CH_2$	**1a**	76	3.3:1	91
2	$PhCH_2CH_2$	**1b**	71	12:1	96
3	$CH_3(CH_2)_4CH_2$	**1b**	65	10:1	91
4	iPr_3SiOCH_2	**1b**	72	20:1	98
5	CH_2=$CHCH_2CH_2$	**1b**	62	6.3:1	80
6	CH_2=$CHCH_2CH_2$	**1a**	71	2.4:1	90
7	CH_3	**1a**	58	2.3:1	92[e]
8	*c*-C_6H_{11}	**1a**	40	2.8:1	95
9	*c*-C_6H_{11}	**1a**	78	1.2:1	93[f]

[a] Unless otherwise specified, the reaction was carried out with 2 equiv of aldehyde in the presence of (*R*,*R*)-**1** (2 mol %) in toluene/aqueous NaOH (1 %) at 0 °C for 2 h. [b] Yield of isolated product. [c] Determined by ^{1}H NMR analysis. [d] Enantiomeric excess of *anti*-**3**, which was determined by HPLC analysis of its *N*-benzoate by using a chiral column (DAICEL Chiralcel OD-H) with hexane/2-propanol or hexane/ethanol as solvent. [e] The reaction with (*S*,*S*)-**1a** as catalyst displayed similar reactivity and selectivity. [f] Use of dibutyl ether as solvent.

enzymatic stability and enhanced drug transport activity.[16] The reaction with α-triisopropylsiloxyacetaldehyde cleanly produced the desired β-hydroxy-α-amino ester **3** (R = iPr_3SiOCH_2) in 72 % yield with virtually complete stereochemical control (*anti*/*syn* 20:1; 98 % *ee*) (Table 1, entry 4), which parallels the L-threonine aldolase catalyzed aldol reaction used for the synthesis of the monobactam antibiotic carunoman and its analogues.[12b] Moreover, a key building block for the synthesis of the carbacephem antibiotic loracarbef, previously prepared by a chemoenzymatic process with serine hydroxymethyltransferase (SHMT),[12f] was readily assembled with 4-pentenal as acceptor; (*R*,*R*)-**1a** resulted in a higher enantioselectivity than did (*R*,*R*)-**1b** (Table 1, entries 5 and 6). We also found that L-*allo*-threonine *tert*-butyl ester can be obtained by the reaction of **2** with acetaldehyde in the presence of (*R*,*R*)-**1a**, which confirmed that the absolute configuration of the newly created α stereocenter is *S* (Table 1, entry 7).[17] This method allows a facile preparation of non-natural D-*allo*-threonine because of the ready availability of the enantiomerically pure catalyst (*S*,*S*)-**1a**. Interestingly, (*R*,*R*)-**1a** was also a suitable catalyst for the reaction with α-substituted aldehydes such as cyclohexanecarbaldehyde as acceptor; to attain sufficient reactivity, dibutyl ether was used as solvent (Table 1, entries 8 and 9).

In summary, the direct asymmetric aldol reaction of glycine Schiff base **2** with aldehyde acceptors proceeds under mild organic/aqueous biphasic conditions with excellent stereochemical control by using chiral quaternary ammonium salts as catalysts. This reaction offers a powerful chemical method for the synthesis of optically active β-hydroxy-α-amino acids, and complements the aldolase-based chemoenzymatic processes. Therefore, the present system can be regarded as an artificial glycine-dependent aldolase; its operational simplicity, environmentally friendly conditions, and suitability for large-scale reaction represent distinct advantages for practical industrial applications.

Experimental Section

Aqueous NaOH (1 %; 2.4 mL) was added at 0 °C under an argon atmosphere to a solution of *tert*-butyl glycinate benzophenone Schiff base **2** (88.6 mg, 0.3 mmol) and (*R*,*R*)-**1b** (9.9 mg, 2 mol %) in toluene (3.0 mL), and 3-phenylpropanal (79.0 μL, 0.6 mmol) was introduced dropwise. The whole mixture was stirred for 2 h at 0 °C, and water and diethyl ether were then added. The ether phase was separated and washed with brine. The organic phase was dried over Na_2SO_4 and concentrated. The crude product was dissolved in THF (8.0 mL) and treated with HCl (1.0 N, 1.0 mL) at 0 °C for 1 h. After removal of THF in vacuo, the aqueous solution was washed with diethyl ether three times and neutralized with $NaHCO_3$. The mixture was then extracted with CH_2Cl_2 three times. The combined extracts were dried over $MgSO_4$ and concentrated. Purification of the residue by column chromatography on silica gel with MeOH/CH_2Cl_2 (1:15) as eluent afforded the corresponding β-hydroxy-α-amino ester **3** (R = $PhCH_2CH_2$) (56.8 mg, 0.214 mmol, 71 %, *anti*/*syn* 12:1). *anti*-**3** (R = $PhCH_2CH_2$): ^{1}H NMR (400 MHz, $CDCl_3$): δ = 7.30–7.26 (m, 2H; Ph), 7.22–7.16 (m, 3H; Ph), 3.77 (ddd, *J* = 3.2, 4.4, 10.0 Hz, 1H; C*H*OH), 3.47 (d, *J* = 4.4 Hz, 1H; C*H*NH_2), 2.91–2.84 (ddd, *J* = 4.8, 9.2, 13.6 Hz, 1H; PhCH), 2.73–2.65 (ddd, *J* = 8.0, 8.0, 13.6 Hz, 1H; PhCH), 1.85 (br s, 3H; OH and NH_2), 1.75–1.65 (m, 1H; $PhCH_2CH$), 1.62–1.53 (m, 1H; $PhCH_2CH$), 1.41 ppm (s, 9H; *t*Bu). *syn*-**3** (R = $PhCH_2CH_2$): δ = 7.29–7.25 (m, 2H; Ph), 7.22–7.16 (m, 3H; Ph), 3.70 (ddd, *J* = 4.8, 5.2, 7.6 Hz, 1H; C*H*OH), 3.24 (d, *J* = 5.2 Hz, 1H; C*H*NH_2), 2.90–2.82 (ddd, *J* = 6.2, 9.0, 13.6 Hz, 1H; PhCH), 2.74–2.67 (ddd, *J* = 7.2, 8.8, 13.6 Hz, 1H; PhCH), 2.17 (br s, 3H; OH and NH_2), 1.85–1.78 (m, 2H; $PhCH_2CH_2$), 1.46 ppm (s, 9H; *t*Bu). The enantiomeric excess of the major *anti* isomer was determined to be 96 % by HPLC analysis of its *N*-benzoate: chiral column, DAICEL Chiralcel OD-H, hexane/2-propanol (20:1), flow rate = 0.5 mL min^{-1}, retention times 23.06 min (minor) and 39.79 min (major).

Received: July 16, 2002 [Z19746]

[1] a) *Glycopeptide Antibiotics* (Ed.: R. Nagarajan), Marcel-Dekker, New York, **1994**; b) *Amino Acids, Peptides and Proteins; Special Periodical Reports; Vols. 1–28*, Chemistry Society, London, **1968–1995**; c) M. A. Blaskovich, G. Evindar, N. G. W. Rose, S. Wilkinson, Y. Luo, G. A. Lajoie, *J. Org. Chem.* **1998**, *63*, 3631, and references therein.

[2] a) G. M. Coppola, H. F. Schuster, *Asymmetric Synthesis: Construction of Chiral Molecules Using Amino Acids*, Wiley, Toronto, **1987**; b) A. Goleciowski, J. Jurczak, *Synlett* **1993**, 241; c) J.-P. Genet, *Pure Appl. Chem.* **1996**, *68*, 593.

[3] M. J. Miller, *Acc. Chem. Res.* **1986**, *19*, 49.

[4] a) S. V. Pansare, J. C. Vederas, *J. Org. Chem.* **1987**, *52*, 4804; b) R. Badorrey, C. Cativiela, M. D. Diaz-de-Villegas, J. A. Galvez, *Tetrahedron: Asymmetry* **2000**, *11*, 1015.

[5] D. Tanner, *Angew. Chem.* **1994**, *106*, 625; *Angew. Chem. Int. Ed. Engl.* **1994**, *33*, 599.

[6] For recent examples, see: a) A. M. P. Koskinen, H. Hasilla, V. T. Myllymaki, K. Rissanen, *Tetrahedron Lett.* **1995**, *36*, 5619; b) H. Shao, M. Goodman, *J. Org. Chem.* **1996**, *61*, 2582; c) T. Nagamitsu, T. Sunazuka, H. Tanaka, S. Omura, P. A. Sprengeler, A. B. Smith III. , *J. Am. Chem. Soc.* **1996**, *118*, 3584; d) C. Cativiela, M. D. Diaz-de-Villegas, J. A. Galvez, J. I. Garcia, *Tetrahedron* **1996**, *52*, 9563; e) M. Horikawa, Y. Shigeri, N. Yumoto, S. Yoshikawa, T. Nakajima, Y. Ohfune, *Bioorg. Med. Chem. Lett.* **1998**, *8*, 2027; f) C. A. Hutton, *Org. Lett.* **1999**, *1*, 295; g) P. D. Felice, G. Porzi, S. Sandri, *Tetrahedron: Asymmetry* **1999**, *10*, 2191.

[7] With enolates of glycine derivatives: a) S. Kanemasa, T. Mori, A. Tatsukawa, *Tetrahedron Lett.* **1993**, *34*, 8293; b) Y. N. Belokon, K. A. Kochetkov, N. S. Ikonnikov, T. V. Strelkova, S. R. Harutyunyan, A. S. Saghiyan, *Tetrahedron: Asymmetry* **2001**, *12*, 481; c) J. B. MacMillan, T. F. Molinski, *Org. Lett.* **2002**, *4*, 1883.

[8] For a few examples in which a catalytic amount of chiral sources is employed, see: a) Y. Ito, M. Sawamura, E. Shirakawa, K. Hayashizaki, T. Hayashi, *Tetrahedron* **1988**, *44*, 5253; b) H. Suga, K. Ikai, T. Ibata, *Tetrahedron Lett.* **1998**, *39*, 869; c) D. A. Evans, J. M. Janey, N. Magomedov, J. S. Tedrow, *Angew. Chem.* **2001**, *113*, 1936; *Angew. Chem. Int. Ed.* **2001**, *40*, 1884.

[9] For a recent review on the direct catalytic asymmetric aldol reaction, see: a) B. Alcaide, P. Almendros, *Eur. J. Org. Chem.* **2002**, 1595; see

 © 2002 WILEY-VCH Verlag GmbH & Co. KGaA, Weinheim 0044-8249/02/4123-4543 $ 20.00+.50/0

also: b) R. Mahrwald, *Chem. Rev.* **1999**, 1095; c) T. D. Machajewski, C.-H. Wong, *Angew. Chem.* **2000**, *112*, 1406; *Angew. Chem. Int. Ed.* **2000**, *39*, 1352.

[10] For a synthesis that leads to products with low *ee* values, see: C. M. Gasparski, M. J. Miller, *Tetrahedron* **1991**, *47*, 5367.

[11] For a Mukaiyama-type reaction with ketene silyl acetal of glycine Schiff base, see: M. Horikawa, J. Busch-Petersen, E. J. Corey, *Tetrahedron Lett.* **1999**, *40*, 3843.

[12] a) A. Saeed, D. W. Young, *Tetrahedron* **1992**, *48*, 2507; b) V. P. Vassilev, T. Uchiyama, T. Kajimoto, C.-H. Wong, *Tetrahedron Lett.* **1995**, *36*, 5063; c) T. Kimura, V. P. Vassilev, G.-J. Shen, C.-H. Wong, *J. Am. Chem. Soc.* **1997**, *119*, 11734; d) T. Miura, M. Fujii, K. Shingu, I. Koshimizu, J. Naganoma, T. Kajimoto, Y. Ida, *Tetrahedron Lett.* **1998**, *39*, 7313; e) N. Wymer, E. J. Toone, *Curr. Opin. Chem. Biol.* **2000**, *4*, 110; f) B. G. Jackson, S. W. Pedersen, J. W. Fisher, J. W. Misner, J. P. Gardner, M. A. Staszak, C. Doecke, J. Rizzo, J. Aikins, E. Farkas, K. L. Trinkle, J. Vicenzi, M. Reinhard, E. P. Kroeff, C. A. Higginbotham, R. J. Gazak, T. Y. Zhang, *Tetrahedron* **2000**, *56*, 5667.

[13] For reviews on the use of glycine Schiff base for the preparation of enantiomerically pure α-amino acids, see: a) T. Abellan, R. Chinchilla, N. Galindo, G. Guillena, C. Najera, J. M. Sansano, *Eur. J. Org. Chem.* **2000**, 2689; b) M. J. O'Donnell, *Aldrichimica Acta* **2001**, *34*, 3.

[14] a) T. Ooi, M. Kameda, K. Maruoka, *J. Am. Chem. Soc.* **1999**, *121*, 6519; b) T. Ooi, M. Takeuchi, M. Kameda, K. Maruoka, *J. Am. Chem. Soc.* **2000**, *122*, 5228; c) T. Ooi, M. Kameda, H. Tannai, K. Maruoka, *Tetrahedron Lett.* **2000**, *41*, 8339; d) T. Ooi, K. Doda, K. Maruoka, *Org. Lett.* **2001**, *3*, 1273; e) T. Ooi, M. Takeuchi, K. Maruoka, *Synthesis* **2001**, 1716.

[15] Attempted reaction of **2** with 3-phenylpropanal using *O*-allyl-*N*-(9-anthracenylmethyl)cinchonidinium bromide as catalyst under otherwise similar conditions gave rise to **3** ($R = PhCH_2CH_2$) in 60% yield with an *anti*/*syn* ratio of 1:5.3; the enantiomeric excess of the major *syn* isomer was 25%. Similar *syn* selectivity was observed in the Mukaiyama-type reaction catalyzed by the cinchonidine-derived bifluoride salt.[11]

[16] M. M. Palian, R. Polt, *J. Org. Chem.* **2001**, *66*, 7178.

[17] Treatment of the aldol product *anti*-**3** ($R = CH_3$) with HCl (6N) in MeOH gave rise to the corresponding β-hydroxy-α-amino acid hydrochloride; its absolute configuration was determined to be 2*S*,3*S* by comparison of the optical rotation value with that of the hydrochloride salt of commercially available L-*allo*-threonine.

The Absolute Configuration of Bromochlorofluoromethane**

Prasad L. Polavarapu*

Bromochlorofluoromethane is the simplest chiral molecule that is used as an example to illustrate chirality or asymmetric carbon atoms, yet its absolute configuration remains uncertain. The synthesis of bromochlorofluoromethane in a pure form was achieved by Berry and Sturtevant in 1942.[1] They determined its boiling point, melting point, and refractive dispersion, but the individual enantiomers were not resolved. Despite the unavailability of enantiomers and their optical rotation values, Brewster hypothesized that (*S*)-bromochlorofluoromethane would have positive optical rotation, assuming that the polarizabilities decrease in the order Br > Cl > H > F.[2] Hargreaves and Modarai were able to resolve the enantiomers of 1-bromo-1-chloro-1-fluoroacetone and convert them into the corresponding bromochlorofluoromethane enantiomers.[3] They reported the specific rotations to be +0.20 and −0.13. In 1973 Applequist predicted, using an atom–dipole interaction model and assuming the polarizabilities to be in the order, Br > Cl > F > H, that (*S*)-bromochlorofluoromethane would have positive optical rotation.[4] However, the different polarizability orders chosen by Brewster and Applequist would yield opposite conclusions.[5] Collet and co-workers achieved optical resolution of bromochlorofluoromethane by enantioselective inclusion in cryptophan C.[6] Using the NMR resonance signals of (+) and (−) enantiomers encapsulated in cryptophan, they estimated the enantiomeric excess and maximum rotation values at five different wavelengths. In a different approach, Wilen et al. also resolved the enantiomers of bromochlorofluoromethane using brucine[5] and addressed the ambiguity remaining in the absolute configuration of bromochlorofluoromethane; Brewster and Applequist had arrived at the same assignment but using mutually conflicting polarizability trends. Wilen et al. concluded that "experimental determination of the absolute configuration of bromochlorofluoromethane is a challenge".[5] Using a quantum-mechanical static method, the specific rotation of (*R*)-bromochlorofluoromethane at the sodium D line was predicted (without the Lorentz factor) to be −6.[7,8] Comparison of this value with the experimental value of −1.78 reported by Collet et al. for enantiopure (−)-bromochlorofluoromethane, and based on the comparison of experimental and ab initio predicted Raman optical-activity (ROA) spectra, it was concluded that the absolute configuration of bromochlorofluoromethane is (*S*)-(+) and (*R*)-(−).[7]

Previous conclusions[7] on the absolute configuration were based on quantum-mechanical calculations of both ROA and specific rotation, carried out at the Hartree–Fock (HF) level using smaller basis sets. Since then, evidence has been collected[9] to indicate that the HF level calculations, because of lack of electron correlation, are not quantitatively accurate. DFT,[10] which includes electron correlation using density functionals, has now been widely accepted as the preferred approach for predicting molecular properties accurately. For reliable quantum mechanical predictions of specific rotations, those predicted at the HF level using small basis sets are not considered to be adequate and predictions with DFT and larger basis sets are necessary. Electron correlation and larger basis sets are also important for molecular polarizability derivatives, and hence Raman properties. Because the absolute configuration of bromochlorofluoromethane was suggested[7] based on HF calculations, the previously predicted specific rotation and ROA parameters of bromochlorofluoromethane must be verified using DFT and larger basis sets. The DFT method has been implemented recently for the prediction of specific rotation[11a] and of ROA[11b] in the quantum-mechanical program DALTON.[12] Thus it is important to reinvestigate the specific rotation and ROA of bromochlorofluoromethane. Recently Grimme[13] has reported DFT predictions of $[\alpha]_D$ for bromochlorofluoromethane. Because

[*] Prof. Dr. P. L. Polavarapu
Department of Chemistry
Vanderbilt University
Nashville, TN 37235 (USA)
Fax: (+1) 615–322–4936
E-mail: prasad.l.polavarapu@vanderbilt.edu

[**] I thank NSF (CHE0092922) for research grants and Dr. K. Ruud for the developmental version of DALTON program which was used for the calculations reported here.

 © 2002 WILEY-VCH Verlag GmbH & Co. KGaA, Weinheim 0044-8249/02/4123-4544 $ 20.00+.50/0

those calculations were origin-dependent, the predicted rotations with a larger aug-SV(d) basis set for the *S* enantiomer varied from 1.0–5.3, depending on the choice of origin. More recently, Autschbach et al. reported $[\alpha]_D$ predictions for (*S*)-bromochlorofluoromethane using various nonhybrid density functionals.[14] Their predictions for $[\alpha]_D$ varied from 1.3–4.0 depending on the functional used. These two calculations, although they supported the previous assignment of absolute configuration,[7] did not investigate the optical rotatory dispersion in bromochlorofluoromethane, which has been experimentally measured.[6,7]

Herein we report a) the origin-independent DFT predictions of specific rotation as well as its wavelength dependence and b) DFT predictions of ROA parameters for (*S*)-bromochlorofluoromethane, both using very large basis sets. A comparison between these predictions with the corresponding experimental values provides state-of-the-art conclusions on the absolute configuration of bromochlorofluoromethane.

Specific rotation was computed using the DALTON program.[12] A linear response method and gauge including atomic orbitals were used. The Lorentz factor, $(n^2+2)/3$ where n is the refractive index, which was included in earlier calculations[7,8] was not included in the present calculations. Specific rotations were calculated at five different wavelengths. For comparison, calculations were also carried out at both HF and B3LYP levels of theory. Five different sets of specific rotations calculations were undertaken using the geometry optimizations and levels of theory described in Table 1. Unlike in the previous studies,[7,13,14] it is possible here to verify the trend in dispersion of specific rotation with wavelength, in addition to verifying the sign and magnitude of specific rotation.

A number of observations can be made from the specific rotation values compiled in Table 1: a) The HF/DZP values represent the lowest level predictions of all those reported in Table 1, yet they give the same sign and similar dispersion trend as those obtained in the highest level calculation. The magnitudes of HF/DZP-predicted specific rotations however differ significantly from those observed; b) the rotatory dispersion predicted in B3LYP/6–311++G(2d,2p) calculations at MP2/DZP geometry does not have the same trend as that observed in the experimental values, but that predicted at B3LYP/6–311++G(2d,2p) geometry has the same trend as that of the experimental values. As the differences in these two geometries are minor (see Table 1), these differences in the dispersion trend probably arise because contributions from either Rydberg orbitals or valence orbitals (or both) are not properly accounted for in the B3LYP/6–311++G(2d,2p) calculation at the MP2/DZP geometry. These observations suggest that it is preferable, at least for bromochlorofluoromethane, to calculate both the optimum geometry and the specific rotation using the same basis set. For this reason, large basis-set calculations were performed at B3LYP/6–311++G(2d,2p), B3LYP/aug-cc-pVDZ, and B3LYP/aug-cc-pVTZ level (see Table 1) at their respective optimum geometries; c) among these values, those obtained in the B3LYP/aug-cc-pVTZ calculation at B3LYP/aug-cc-pVTZ geometry are the highest level predictions and the results obtained therein are expected to be the most reliable ones. The predicted values in this calculation suggest that (+)-bromochlorofluoromethane is in the *S* configuration, not only because the predicted values are in close agreement (both in sign and magnitude) with experimental values, but also the predicted rotatory dispersion trend matches that observed in the experimental values. The same conclusion can be reached from the predictions at the B3LYP/6–311++G(2d,2p) and B3LYP/aug-cc-pVDZ levels.

Some additional factors should however be noted. The experimental specific rotations were reported for the neat liquid and for cyclohexane solutions.[5–7] In liquid bromochlorofluoromethane, one can anticipate the presence of dipole–dipole and dispersion interactions, but it is not obvious how these interactions would influence the specific rotation. Inclusion of the Lorentz factor, which represents bulk-phase effects, would increase the predicted values by a factor of $(n^2+2)/3$, while the Cavity Field model of Applequist[15] would increase the predicted values by $(5n^2+1)/(4n^2+2)$. In either case the predicted sign of specific rotation would not be affected. First, because experimental rotations obtained for the neat liquid[6] and the cyclohexane solution[7] are the same within experimental error, it is probable that the solvent effect on specific rotations is insignificant and that bulk-phase effects would not have influenced the experimentally measured sign of specific rotation. Second, zero-point vibrational effects,[16] which are not included in the present calculations, are known to contribute to specific rotation. However they

Table 1. Experimental and predicted specific rotations for (*S*)-(+)-CHFClBr.

	DZP[a]		6-311++G(2d,2p)[a]		6-311++G(2d,2p)[b]		aug-cc-pVDZ[c]		aug-cc-pVTZ[d]		Experimental	
Wavelength [nm]	HF[e]	B3LYP[f]	HF[e]	B3LYP[f]	HF[e]	B3LYP[f]	HF[e]	B3LYP[f]	HF[e]	B3LYP[f]	Neat liquid[g]	(c = 6.5, cyclohexane)[h]
589	4.6	5.5	0.06	1.39	0.88	2.54	1.32	1.28	1.05	1.09	1.6	1.8
578	4.8	5.7	0.05	1.42	0.91	2.63	1.38	1.34	1.09	1.13	1.6	1.8
546	5.5	6.6	0.01	1.52	1.00	2.92	1.57	1.51	1.22	1.26	1.8	2.1
436	9.6	11.7	−0.39	1.6	1.39	4.28	2.68	2.51	1.89	1.85	2.7	3.2
365	15.6	19.6	−1.47	0.47	1.55	5.41	4.30	3.97	2.65	2.40	3.2	3.7

[a] The geometry used was optimized at the MP2 level with the DZP basis set. The lengths of the C−H, C−F, C−Cl, and C−Br bonds are respectively, 1.09, 1.3427, 1.758, and 1.9397 Å; the H-C-F, H-C-Cl, and H-C-Br angles are, respectively, 109.83, 108.86, and 107.06°. [b] The geometry used was optimized at the B3LYP level with the 6–311++G(2d,2p) basis set. The lengths of the C-H, C-F, C-Cl, and C-Br bonds are respectively, 1.0815, 1.3486, 1.7766, and 1.9611 Å; the H-C-F, H-C-Cl, and H-C-Br angles are, 109.96, 108.81, and 107.13°, respectively. [c] The geometry used was optimized at the B3LYP level with aug-cc-pVDZ basis set. The lengths of the C-H, C-F, C-Cl, and C-Br bonds are 1.0927, 1.3582, 1.7826, and 1.9571 Å, respectively; the H-C-F, H-C-Cl, and H-C-Br angles are 109.69, 108.76, and 107.78°, respectively.[d] The geometry used was optimized at the B3LYP level with the aug-cc-pVTZ basis set. The lengths of the C-H, C-F, C-Cl, and C-Br bonds are 1.0827, 1.3478, 1.7758, and 1.9559 Å, respectively; the H-C-F, H-C-Cl, and H-C-Br angles are 109.95, 108.66, and 107.28, respectively. [e] HF method. [f] Density-functional method with the B3LYP functional. [g] From reference [6].[h] The values given in reference [7] for the (−)-enantiomer were multiplied by −1 and scaled up to the pure enantiomer. c = concentration of solution.

 © 2002 WILEY-VCH Verlag GmbH & Co. KGaA, Weinheim 0044-8249/02/4123-4545 $ 20.00+.50/0

Table 2. Experimental and predicted ROA properties of (*S*)-(+)-CHFClBr.

DZP		6-311++G(2d,2p)			aug-cc-pVDZ			aug-cc-pVTZ			Experimental[d]		Assignment[a]
HF[a]		B3LYP[b]		HF[c]	B3LYP[b]		HF[c]	B3LYP[b]		HF[c]			
Freq[e]	$\Delta_z \times 10^4$	Freq[e]	$\Delta_z \times 10^4$	$\Delta_z \times 10^4$	Freq[e]	$\Delta_z \times 10^4$	$\Delta_z \times 10^4$	Freq[e]	$\Delta_z \times 10^4$	$\Delta_z \times 10^4$	Freq[e]	$\Delta_z \times 10^4$	
3209	−0.2	3173	−0.3	−0.3	3162	−0.2	−0.2	3156	−0.2	−0.3	3022	−0.7	C−H stretch
1372	−0.5	1321	0.5	0.4	1293	1.0	1.1	1322	1.0	1.1	1305	−2.4	C−H bend
1266	0.0	1212	−1	0.03	1199	−3.0	−1.5	1215	−2.9	−1.6	1206	−2.8	C−H bend
1151	−0.3	1065	−0.2	−0.1	1057	0.3	0.1	1076	0.01	−0.01	1062	−4.5	C−F stretch
822	−3.9	744	−4.9	−2.0	750	−4.0	−1.6	743	−4.4	−1.8	774	−5.1	C−Cl stretch
678	3.8	634	3.2	1.7	641	2.4	1.3	639	2.4	1.3	662	5.9	C−Br stretch
439	0.6	417	1.1	1.2	415	1.6	1.5	418	1.2	1.3	427	10.2	inversion bend
321	0.3	305	0.01	−0.5	305	0.1	−0.4	306	0.2	−0.3	315	−2.1	C−halogen bend
233	−0.5	218	−0.3	−0.2	219	−0.3	−0.3	218	−0.4	−0.3	228	−1.9	C−halogen bend

[a] HF method with the DZP basis set. The geometry and force constants used were obtained at the MP2 level with the DZP basis set. These values are from reference [7]. [b] Density-functional method with the B3LYP functional. The geometry and force constants used were obtained at the same level using the basis set indicated. [c] HF method. The geometry and force constants used were obtained at the B3LYP level using the basis set indicated. [d] The experimental values given for the (−)-enantiomer in reference [7] are multiplied by −1. [e] Frequencies in cm^{-1}.

are not anticipated to be significant in bromochlorofluoromethane because the vibrations (except the C−H modes) involve heavy atoms and are of low frequency.

The same three large basis sets (6–311++G(2d,2p), aug-cc-pVDZ, and aug-cc-pVTZ) were used for ROA calculations. The optimum geometry and force constants were obtained at the DFT level with the B3LYP functional using the Gaussian 98 program.[17] These force constants were transferred to the ROA calculation and numerical differentiation of polarizability tensors was used, as implemented in the DALTON program. The density converged to 10^{-7} and the iterative solution of the linear-response equations to 5×10^{-5}. For comparison purposes, ROA calculations were also carried out at the HF level, using the same geometry and force constants obtained in the B3LYP calculation with each of three large basis sets. The depolarized circular-intensity differences (CIDs), Δ_z, predicted for (*S*)-bromochlorofluoromethane are summarized in Table 2 along with the experimental values for (+)-bromochlorofluoromethane and the values obtained in the previous study.[7] The following can be noted from these values: a) The ROA signs observed for six bands in the experimental spectrum at 3022 (C−H stretch), 1206 (C−H bend), 774 (C−Cl stretch), 662 (C−Br stretch), 427 (inversion bend at C atom), and 228 cm^{-1} (a C−halogen bend) have been reproduced (ignoring the cases in which the predicted magnitude is zero) in all of the calculations; b) the ROA sign of the band in the observed spectrum at 1305 cm^{-1} (another C−H bend) has not been reproduced in the calculations except for the HF calculation[7] with the DZP basis set; c) the ROA sign of the band observed at 1062 cm^{-1} (C−F stretch) has been reproduced in only four of the seven calculations, while that at 315 cm^{-1} (a halogen bend) has been reproduced in only three of the seven calculations; d) of the seven different calculations in Table 2, the experimentally observed ROA signs are reproduced for a minimum of six to a maximum of eight bands. This observation supports the conclusion reached earlier from specific rotations that (+)-bromochlorofluoromethane has the *S* configuration.

In summary, the highest theoretical level predictions of specific rotations and ROA parameters using 6–311++G(2d,2p), aug-cc-pVDZ, and aug-cc-PVTZ basis sets, in conjunction with the corresponding experimental data, reaffirm the assignment[7] of the absolute configuration of bromochlorofluoromethane to be (*S*)-(+) and (*R*)-(−).

Received: July 31, 2002 [Z19862]

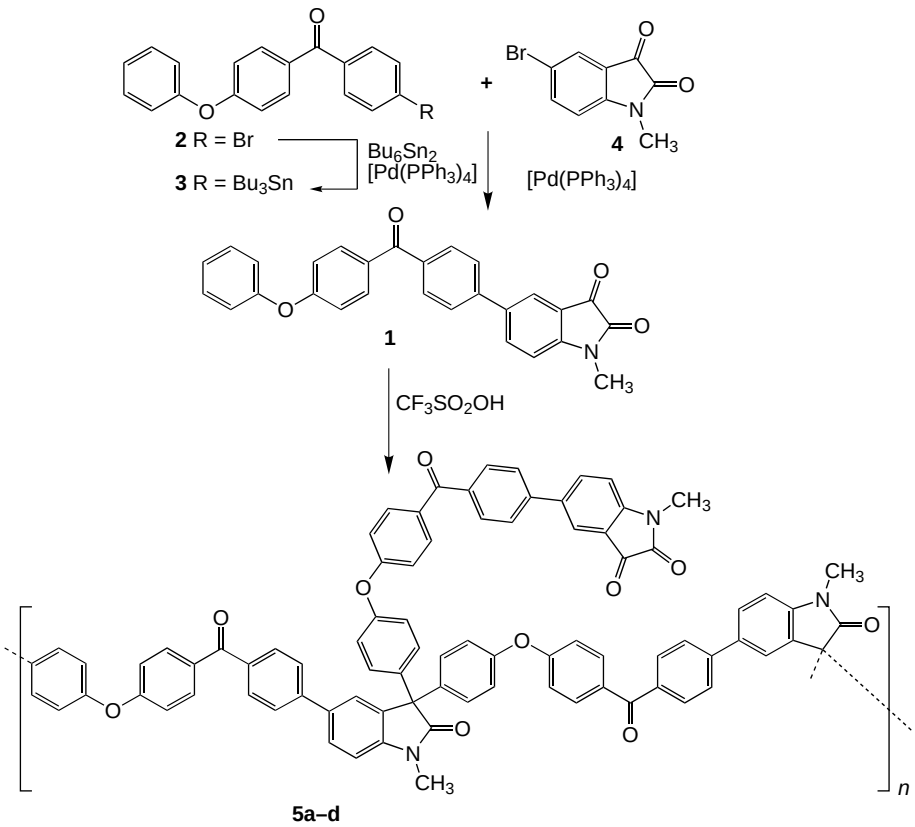
[1] K. L. Berry, J. M. Sturtevant, *J. Am. Chem. Soc.* **1942**, *64*, 1599–1600.
[2] J. H. Brewster, *J. Am. Chem. Soc.* **1959**, 81, 5475–5483.
[3] M. K. Hargreaves, B. Modarai, *J. Chem. Soc. C*, **1971**, 1013–1025.
[4] J. Applequist, *J. Chem. Phys.* **1973**, *58*, 4251–4259.
[5] S. H. Wilen, K. A. Bunding, C. M. Kascheres, M. J. Weider, *J. Am. Chem. Soc.* **1985**, *107*, 6997–6998.
[6] J. Canceill, L. Lacombe, A. Collet, *J. Am. Chem. Soc.* **1985**, *107*, 6993–6996.
[7] J. Costante, L. Hecht, P. L. Polavarapu, A. Collet, L. D. Barron, *Angew. Chem.* **1997**, *109*, 917–919; *Angew. Chem. Int. Ed.* **1997**, *36*, 885–887.
[8] P. L. Polavarapu, *Mol. Phys.* **1997**, *91*, 551–554.
[9] J. R. Cheeseman, M. J. Frisch, F. J. Devlin, P. J. Stephens, *J. Phys. Chem.* A. **2000**, *104*, 1039–1046.
[10] R. G. Parr, W. Yang, *Density functional theory of atoms and molecules*, Oxford University, Oxford, **1989**.
[11] a) K. Ruud, T. Helgaker, *Chem. Phys. Lett.* **2002**, *352*, 533–539; b) K. Ruud, T. Helgaker, P. Bour, *J. Phys. Chem. A.* 2002, 106, 7448–7455.
[12] T. Helgaker, H. J. Aa. Jensen, P. Jørgensen, J. Olsen, K. Ruud, H. Ågren, A. A. Auer, K. L. Bak, V. Bakken, O. Christiansen, S. Coriani, P. Dahle, E. K. Dalskov, T. Enevoldsen, B. Fernandez, C. Hättig, K. Hald, A. Halkier, H. Heiberg, H. Hettema, D. Jonsson, S. Kirpekar, R. Kobayashi, H. Koch, K. V. Mikkelsen, P. Norman, M. J. Packer, T. B. Pedersen, T. A. Ruden, A. Sanchez, T. Saue, S. P. A. Sauer, B. Schimmelpfennig, K. O. Sylvester-Hvid, P. R. Taylor, O. Vahtras, *Dalton*, *a molecular electronic structure program*, Release 1.2 (**2001**). See dhttp://www.kjemi.uio.no/software/dalton/dalton.html.
[13] S. Grimme, *Chem. Phys. Lett.* **2001**, *339*, 380–388.
[14] J. Autschbach, S. Patchkovskii, T. Ziegler, S. J. A. van Gisbergen, E. J. Baerends, *J. Chem. Phys.* **2002**, *117*, 581–592.
[15] J. Applequist, *J. Phys. Chem.* **1990**, *94*, 6564–6573.
[16] K. Ruud, P. R. Taylor, P. Astrand, *Chem. Phys. Lett.* **2001**, *337*, 217–223.
[17] *Gaussian 98 Revision A.3*, M. J. Frisch, G. W. Trucks, H. B. Schlegel, G. E. Scuseria, M. A. Robb, J. R. Cheeseman, V. G. Zakrzewski, J. A. Montgomery, Jr., R. Stratmann, J. C. Burant, S. Dapprich, J. M. Millam, A. D. Daniels, K. N. Kudin, M. C. Strain, O. Farkas, J. Tomasi, V. Barone, M. Cossi, R. Cammi, B. Mennucci, C. Pomelli, C. Adamo, S. Clifford, J. Ochterski, G. A. Petersson, P. Y. Ayala, Q. Cui, K. Morokuma, D. K. Malick, A. D. Rabuck, K. Raghavachari, J. B. Foresman, J. Cioslowski, J. V. Ortiz, B. B. Stefanov, G. Liu, A. Liashenko, P. Piskorz, I. Komaromi, R. Gomperts, R. L. Martin, D. J. Fox, T. Keith, M. A. Al-Laham, C. Y. Peng, A. Nanayakkara, C. Gonzalez, M. Challacombe, P. M. W. Gill, B. Johnson, W. Chen, M. W. Wong, J. L. Andres, C. Gonzalez, M. Head-Gordon, E. S. Replogle, J. A. Pople, Gaussian, Inc., Pittsburgh PA, **1998**.

 © 2002 WILEY-VCH Verlag GmbH & Co. KGaA, Weinheim 0044-8249/02/4123-4546 $ 20.00+.50/0

Synthesis, Characterization, and Modification of Hyperbranched Poly(arylene oxindoles) with a Degree of Branching of 100 %**

Mario Smet,* Etienne Schacht, and Wim Dehaen

Hyperbranched polymers are of high importance as readily available substitutes for dendrimers. Whereas the preparation of the latter requires a multistep synthesis, hyperbranched polymers can be obtained in a single step.[1] However, a degree of branching of 100 %, which is a characteristic property of dendrimers, can be achieved only by postsynthetic modification[2] or when certain requirements for the monomer are met.[3] To date, the only example of a hyperbranched polymer (which necessarily consists exclusively of dendritic and terminal units) was based on an AB_2 monomer possessing an azine and a maleimide functional group, which react in a "criss-cross" cycloaddition.[4] However, to improve features such as accessibility, convenience of functionalization, and attractive physical properties, it is highly desirable to devise new strategies towards hyperbranched polymers with a degree of branching of 100 %.



Scheme 1. Synthesis of the polymers **5a–d**.

We applied the acid-catalyzed condensation of isatins[5] with aromatic compounds for the synthesis of hyperbranched poly(arylene oxindoles). The linear analogues have been shown to display a high glass-transition temperature (T_g) and excellent thermal stability.[6] The use of *para*-phenoxybenzophenones as the aromatic reaction partner results exclusively in *para*-substitution and hence in structural homogeneity of the polymer.[6] Therefore, the AB_2 monomer **1** was designed and synthesized by Stille coupling of the tin derivative **3** and 5-bromo-1-methylisatin (**4**)[7] (Scheme 1). The methyl group was introduced to enhance the solubility of both the monomer and the polymers and to facilitate the characterization of the latter by NMR spectroscopy. As it is known that this type of condensation of isatin and aromatic compounds exclusively yields 3,3-diaryl oxindoles,[5] we can exclude the possibility of the presence of linear units in the hyperbranched polymers obtained from **1**. The tin derivative **3** was obtained by palladium-catalyzed transmetalation of the bromide **2** and hexakis-*n*-butylditin. The bromide **2** was formed by Friedel–Crafts acylation of diphenyl ether (five-fold excess) with 4-bromobenzoyl chloride.

Monomer **1** was polymerized over 24 h using trifluoromethanesulfonic acid, to yield the polymers **5a–d**, which possess 3,3-diaryl oxindole groups as dendritic units and isatin residues at the periphery. These polymers were soluble in chloroform, dichloromethane, and toluene. They were poorly soluble in THF and insoluble in acetone. These solubility properties are in sharp contrast to the linear analogues which were only soluble in highly polar solvents such as *N*,*N*-dimethylacetamide and *N*-methylpyrrolidinone, or in the presence of strong acids.[6] As can be seen from Table 1, the obtained molecular weights are strongly dependent upon the reaction temperature and the concentration. At room temperature, only oligomers were obtained although, according to the literature,[6] the linear polymerization occurred readily at 25 °C. Higher temperatures and higher concentrations favor the formation of higher molecular-mass species. Higher molecular masses result in higher polydispersities. It should be emphasized that the molecular weights obtained by size-exclusion chromatography (SEC) are likely to be underestimated because of the compact structure of our macro-

[*] Dr. M. Smet, Prof. W. Dehaen
Department of Chemistry
University of Leuven
Celestijnenlaan 200F, 3001 Heverlee, Leuven (Belgium)
Fax: (+32) 16–327–990
E-mail: mario.smet@chem.kuleuven.ac.be
Prof. E. Schacht
Department of Chemistry
University of Ghent
Krijgslaan 281 (S4), 9000 Ghent (Belgium)

[**] This work was supported by the University of Leuven, the Ministerie voor Wetenschapsbeleid and the FWO-Vlaanderen. M.S. thanks the FWO Vlaanderen for a postdoctoral fellowship.

Supporting information for this article is available on the WWW under http://www.angewandte.org or from the author.

 © 2002 WILEY-VCH Verlag GmbH & Co. KGaA, Weinheim 0044-8249/02/4123-4547 $ 20.00+.50/0

Table 1. Overview of the synthesized hyperbranched polymers.

Polymer	Temperature [°C]	Concentration [mg mL^{-1}]	Yield [%]	M_n[a] [g mol^{-1}]	M_w[a] [g mol^{-1}]	D[a]
5a	25	10	58	–[b]	–[b]	–[b]
5b	40	10	63	3900	4900	1.27
5c	60	10	68	4200	5700	1.37
5d	60	20	76	7100	20000	2.9

[a] GPC with chloroform as the eluent. [b] Only oligomers were obtained.

molecules. In the future, absolute molecular weights will be determined, to provide evidence for this assumption.

In the FTIR spectrum of the monomer, a strong absorption band at 1731 cm^{-1} is observed which can be attributed to both the carbonyl groups of the five-membered ring. Another absorption band of medium intensity at 1650 cm^{-1} is characteristic for the carbonyl group of the benzophenone unit. In the polymers, the latter absorption remains unaffected, yet two signals are observed for the carbonyl groups of the indole residues at 1742 and 1718 cm^{-1}, respectively. The first one can be assigned to both the carbonyl groups of the terminal isatin units, whereas the lactam carbonyl group of the dendritic diphenyloxindole residues gives rise to the latter. It is also possible to monitor the polymerization by UV spectroscopy. The monomer has an extinction coefficient of 789 L mol^{-1} cm^{-1} at 437 nm. However, for the polymers, an apparent extinction coefficient of 427 L mol^{-1} cm^{-1} was found at this wavelength. This is in agreement with the theoretical expectations that the ratio of terminal units (which can reasonably be expected to have an extinction coefficient close to that of the monomer) and the dendritic units (showing no absorbance in the visible region) should be close to (or over) 1,[8] which should give rise to an extinction coefficient of about half the value of the monomer.

In the ^{1}H NMR spectrum, extensive line broadening is observed (Figure 1). Two main clusters of signals for the CH_3 groups can be distinguished. The resonance signals at 3.37 ppm can be assigned to the internal (dendritic) groups, whereas the cluster at 3.31 ppm can be assigned to peripheral isatin residues. This assignment is supported by comparison of the chemical shifts of the latter peak and that arising from the methyl protons of the monomer. The observation that the ratio of the integral of the latter peak to the first is near 0.9 reflects again the expected ratio of terminal and dendritic units. The intensity of the peak at 7.80 ppm is lowered to the expected intensity for one proton with respect to the intensity of the signals of the monomer in this region. Indeed, the signals arising from the two protons which are *ortho* and *para* to the reactive isatin carbonyl group shift to $\approx$7.5 and $\approx$7.6 ppm, respectively, for the dendritic residues, but hardly move for the terminal units. Hence, the signal for the equivalent of only one proton per repeat unit will shift to the ensemble of signals between 7.49 and 7.6 ppm. Finally, it is clear that the protons which are *ortho* to the spiro center account for the resonance observed at 7.33 ppm.

In the ^{13}C NMR spectrum (see Supporting Information), analogous observations can be made. Multiple splitting is observed. Two clusters of almost equal intensity at 26.4 and 26.9 ppm account for the methyl groups. The signal at 61.6 ppm corresponds to the newly formed spiro carbon

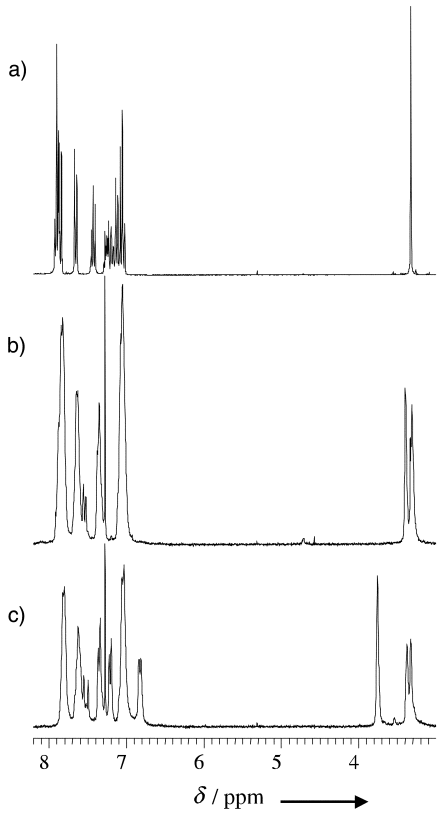


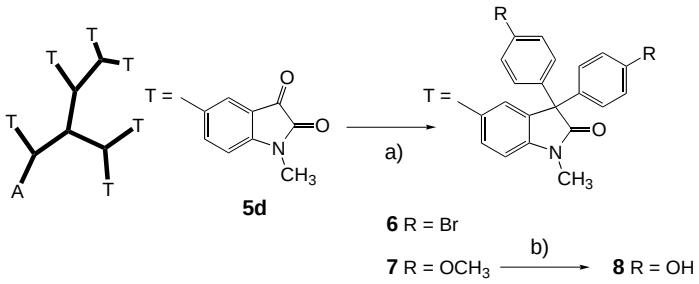
Figure 1. ^{1}H NMR spectrum in $CDCl_3$ of a) the monomer **1** and the hyperbranched polymers b) **5d** and c) **7** (see Scheme 2).

center. The cluster of signals at 177.3 ppm arises from the amide carbonyl group of the dendritic units. All NMR spectroscopic data are consistent with our assumption of a degree of branching of 100 % as no traces of linear units could be observed.

The glass-transition temperature of the polymer **5d** is 190 °C, which is significantly lower than that of the linear analogues in the literature.[6] The thermal stability was very good; no decomposition could be observed by heating at 420 °C under a nitrogen atmosphere (heating rate in both cases = 10 K min^{-1}).

The isatin periphery of the hyperbranched polymers can easily be functionalized with differently substituted arenes in the presence of trifluoromethanesulfonic acid (Scheme 2). In this way, bromophenyl and methoxyphenyl substituents could readily be introduced, with complete conversion reached within 1 h, to yield the derivatives **6** and **7** (see Scheme 2). This conversion was confirmed by NMR spectroscopy. For instance, in the ^{1}H NMR spectrum of the methoxy derivative **7**, apart from the new signals from the methoxyphenyl

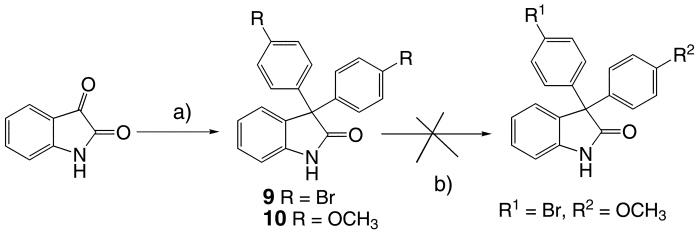
 © 2002 WILEY-VCH Verlag GmbH & Co. KGaA, Weinheim 0044-8249/02/4123-4548 $ 20.00+.50/0



Scheme 2. a) Trifluoromethanesulfonic acid, bromobenzene (for the preparation of **6**) or anisole (for the preparation of **7**); b) BBr_3, $CHCl_3$. A = focal phenoxy residue.

substituents, another intensity shift of the equivalent of one proton in intensity from the signal at 7.80 ppm to the ensemble of signals between 7.50 and 7.65 ppm is observed, which indicates the disappearance of all the isatin residues. The functional groups introduced in this way allow further functionalization. As an example, the methoxyphenyl derivative was deprotected using BBr_3, which resulted in the polyhydroxy derivative **8**. These observations show that a large variety of functional groups can be introduced at the periphery of these hyperbranched macromolecules, which allows a convenient modification of their physical properties.

As exchange between the phenoxy residues of the incorporated monomers and the added aromatic compound, which is supposed only to react with the peripheral isatin moieties, could reduce the molecular weight of the hyperbranched poly(arylene oxindoles), we ran a control experiment to provide evidence for the absence of such an exchange. Therefore, compounds **9** and **10** were prepared by treatment of isatin and bromobenzene or anisole with trifluoromethanesulfonic acid (Scheme 3). These compounds were then left



Scheme 3. a) Trifluoromethanesulfonic acid and bromobenzene (for the preparation of **9**) or anisole (for the preparation of **10**); b) Trifluoromethanesulfonic acid, anisole (in combination with **9**) or bromobenzene (in combination with **10**).

overnight in the presence of anisole (for **9**) or bromobenzene (for **10**), respectively, in the same acid. In neither case was evidence for exchange found. However, in the case of compound **10**, some decomposition occurred after long reaction times (> 24 h). As the hyperbranched polymers condensed within a short time (< 1 h) with the large excess of aromatic compound added, and as the electron-withdrawing benzophenone unit can be expected to stabilize the phenoxyphenyloxindole unit, we did not anticipate any problems arising from decomposition upon functionalization of the isatin periphery. By SEC, the molecular mass of the polymer **7** was found to be slightly higher (≈10 %) than that of the starting material **5d**. This clearly indicates that modification of the periphery of the polymers in the described way does not degrade the substrate.

In conclusion, we have shown that hyperbranched poly(arylene oxindoles) with a degree of branching of 100 % can be prepared in a convenient way. Moreover, these compounds show a high glass-transition temperature and excellent thermal stability. These polymers allow easy and extensive functionalization at the periphery which opens up a number of possibilities to modify their mechanical and physical properties. Further research towards the latter goal, as well as towards modification of the internal skeleton, is currently ongoing.

Experimental Section

Synthesis of 4-bromo-4′-phenoxybenzophenone (**2**): Thionyl chloride (20 mL) and one drop of DMF was added to 4-bromobenzoic acid (2 g, 10 mmol) and the mixture was heated under reflux for 2 h. The solvent was evaporated in vacuum, the residue dissolved in $(CH_2Cl)_2$ (10 mL) and added dropwise to a suspension of diphenyl ether (8.5 g, 50 mmol) and $AlCl_3$ (3.2 g, 24 mmol) in $(CH_2Cl)_2$ (150 mL) at room temperature. The mixture was heated under reflux for 10 min, cooled to room temperature, and poured onto crushed ice (ca. 200 g). The organic phase was separated and the solvent evaporated in vacuum. The bromide **2** was obtained as a white solid (3.2 g, 91 %) by crystallization from petroleum ether. ^{1}H NMR (300 MHz, $CDCl_3$, 25 °C, TMS): $\delta = 7.03$ (d, ^3J (H-H) = 9 Hz, 2H), 7.10 (d, ^3J(H-H) = 7 Hz, 2H), 7.21 (t, ^3J(H-H) = 7 Hz, 1H), 7.41 (d, ^3J(H-H) = 7 Hz, 2H), 7.63 (AB system, 4H), 7.79 ppm (d, ^3J (H-H) = 9 Hz, 2H); ^{13}C NMR (75 MHz, $CDCl_3$, 25 °C, TMS): $\delta = 117.2$, 120.2, 124.7, 127.1, 130.1, 131.3, 131.4, 131.5, 132.3, 136.7, 155.4, 161.9, 194.3 ppm; MS (EI, 70 eV): *m/z* 352 [M^+].

Synthesis of 4-(tris-*n*-butyltin)-4′-phenoxybenzophenone (**3**): $[Pd(PPh_3)_4]$ (3 mol %) was added to a solution of **2** (0.20 g, 0.57 mmol) and hexabutylditin (0.66 g, 1.14 mmol) in toluene under argon. The mixture was heated at 80 °C for 15 h, cooled to room temperature, and the solvent evaporated in vacuum. The tin derivative **3** was obtained as a clear oil (0.13 g, 40 %) after column chromatography (SiO_2, CH_2Cl_2). ^{1}H NMR (300 MHz, $CDCl_3$, 25 °C, TMS): $\delta = 0.89$ (t, ^3J(H-H) = 8 Hz, 9H), 1.10 (m, 6H), 1.35 (m, 6H), 1.56 (m, 6H), 7.04 (d, ^3J(H-H) = 8 Hz, 2H), 7.09 (d, ^3J(H-H) = 7 Hz, 2H), 7.19 (t, ^3J(H-H) = 7 Hz, 1H), 7.22 (t, ^3J(H-H) = 7 Hz, 2H), 7.37 (d, ^3J(H-H) = 7 Hz, 2H), 7.42 (d, ^3J(H-H) = 7 Hz, 2H), 7.61 ppm (d, ^3J(H-H) = 8 Hz, 2H); ^{13}C NMR (75 MHz, $CDCl_3$, 25 °C, TMS): $\delta = 9.7$, 13.7, 27.3, 29.0, 117.1, 120.1, 124.5, 128.7, 130.0, 132.1, 132.5, 136.2, 137.3, 148.8, 155.6, 161.5, 195.8 ppm; MS (ES): *m/z* 564.3 [M^+].

Synthesis of the monomer **1**: 1-Methyl-5-bromoisatin (**4**; 97 mg, 0.40 mmol) and the tin derivative **3** (0.19 g, 0.34 mmol) were dissolved in toluene (4 mL). The solution was placed under argon and $[Pd(PPh_3)_4]$ (3 mol %) was added. The mixture was heated under reflux for 16 h. After cooling to room temperature, the solvent was evaporated in vacuum and **1** was obtained as an orange solid (106 mg, 72 %) after column chromatography (silica, CH_2Cl_2). ^{1}H NMR (300 MHz, $CDCl_3$, 25 °C, TMS): $\delta = 3.31$ (s, 3H; CH_3), 7.02 (d, ^3J(H-H) = 9 Hz, 1H; 7-H isatin), 7.05 (d, ^3J(H-H) = 9 Hz, 2H; *o*-H to OPh), 7.11 (d, ^3J(H-H) = 7 Hz, 2H; *o*-H to COPhO), 7.18 (d, ^3J(H-H) = 7 Hz, 1H; *p*-H to COPhO), 7.42 (t, ^3J(H-H) = 7 Hz, 2H; *m*-H to COPhO), 7.64 (d, ^3J(H-H) = 8 Hz, 2H; *o*-H to isatin), 7.84 (d, ^3J(H-H) = 9 Hz, 2H; *m*-H to OPh), 7.87 (d, ^3J(H-H) = 8 Hz, 2H; *m*-H to isatin), 7.89 (d, ^4J(H-H) = 2 Hz, 1H; 4-H isatin), 7.90 ppm (dd, ^3J(H-H) = 9 Hz, ^4J(H-H) = 2 Hz, 1H; 5-H isatin); ^{13}C NMR (100 MHz, $CDCl_3$, 25 °C, TMS): $\delta =$ 26.4, 194.6, 183.1, 161.7, 158.2, 155.4, 151.0, 142.5, 137.1, 136.9, 136.0, 132.3, 131.7, 130.6, 130.0, 126.3, 124.6, 123.7, 120.1, 117.9, 117.1, 110.5 ppm; MS (EI, 70 eV): *m/z* 433 [M^+].

Preparation of polymer **5d**: The monomer (20 mg) was dissolved in trifluoromethanesulfonic acid (1 mL) and placed under argon. The mixture was stirred at 60 °C for 24 h. After cooling to room temperature, the solution was added dropwise to vigorously stirred water (50 mL). After stirring for 30 min, the suspension was centrifuged (3600 r min^{-1}; 5 min)

 © 2002 WILEY-VCH Verlag GmbH & Co. KGaA, Weinheim 0044-8249/02/4123-4549 $ 20.00+.50/0

and the supernatant decanted. Water (10 mL) was added to resuspend the precipitate, which was shaken vigorously and again centrifuged. After decanting, acetone was added to the precipitate which was again shaken vigorously and centrifuged. This was repeated once more, after which the precipitate was dried in vacuum. The polymer was obtained as an orange-brown solid (15 mg, 76%).

Received: August 20, 2002 [Z50010]

[1] a) Y. H. Kim, *J. Polym. Sci. Polym. Chem. Ed.* **1998**, *36*, 1685–1698; b) B. I. Voit, *J. Polym. Sci. Part A: Polym. Chem.* **2000**, *38*, 2505; M. Jikei, M. Kakimoto, *Progr. Polym. Sci.* **2001**, 26, 1233–1285.

[2] a) K. Yamanaka, M. Jikei, M. Kakimoto, *Macromolecules* **2001**, *34*, 3910–3915; b) R. Haag, A. Sunder, J. F. Stumbé, *J. Am. Chem. Soc.* **2000**, *122*, 2954–2955; c) C. Lach, H. Frey, *Macromolecules* **1998**, *31*, 2381–2383.

[3] J. L. Hobson, W. J. Feast, *Polymer* **1999**, *40*, 1279–1297.

[4] a) G. Maier, C. Zech, B. Voit, H. Komber, *Macromol. Chem. Phys.* **1998**, *199*, 2655–2664; b) G. Maier, C. Zech, B. Voit, H. Komber, *Macromol. Symp.* **2001**, *163*, 75–86.

[5] D. A. Klumpp, K. Y. Yeung, G. K. Surya Prakash, G. A. Olah, *J. Org. Chem.* **1998**, *63*, 4481–4484.

[6] H. M. Colquhoun, M. G. Zolotukhin, *Macromolecules* **2001**, *34*, 1122–1124.

[7] a) W. Borsche, W. Jacobs, *Chem. Ber.* **1914**, *47*, 354–363; b) A. Stankevicius, L. Mazilis, V. Garaliene, S. Riselis, M. Sapragoniene, L. Dzekciorius, *Khim.-Farm. Zh.* **1981**, *15*, 31–34.

[8] $\frac{T}{D}=\frac{n+1}{n-1}$ where T is the number of terminal units, D the number of dendritic units, and n the degree of polymerization. This equation is readily derived by observing the obvious facts that $T=D+1$ and $n=T+D$.

[(arene)Rh(cod)]$^+$ Complexes as Catalysts for [5+2] Cycloaddition Reactions**

Paul A. Wender* and Travis J. Williams

As part of our studies on the design and development of new metal-catalyzed [*m*+*n*] cycloaddition reactions, we previously reported the first examples of metal-catalyzed [5+2] cycloadditions of vinylcyclopropanes and tethered π systems.[1] In our initial and ongoing screening of catalysts for these reactions, rhodium(I) complexes have proven to be the most general. These complexes are active in both inter- and intramolecular cycloadditions. The latter reactions involve alkynes, alkenes, and allenes as the 2-π component and provide cycloadducts in high yields often at 25–40°C.[2] This finding is consistent with earlier observations by our group[3] and others[4] on the utility of rhodium(I) in metal-catalyzed [4+2] cycloadditions of dienes and π systems. More recently, the groups of Gilbertson,[4e] Trost,[5] and Zhang[6] have reported other catalysts that are also effective in certain types of [5+2] cycloadditions.

Recently, Chung and co-workers have reported a readily prepared, air-stable naphthalene complex of rhodium ($[(C_{10}H_8)Rh(cod)]^+BF_4^-$) which is an efficient catalyst for [4+2] cycloaddition reactions of dienes and alkynes.[7] We have now examined the effectiveness of this and several related complexes in [5+2] cycloaddition reactions and have found them to be exceptionally effective in all cases studied, often providing cycloadducts in excellent yields in minutes at room temperature. The details of this study and X-ray crystallographic data on selected complexes are described herein.

Complex $[(C_{10}H_8)Rh(cod)]^+SbF_6^-$ (**1**) is prepared in a single step from commercially available $[\{RhCl(cod)\}_2]$[8] by treatment with $AgSbF_6$, followed by introduction of the naphthalene ligand.[9] The complex is air-stable at room temperature and retains its catalytic activity even after several months of storage.

Although complexes differing from **1** in only the counter ion have been reported,[7,9] characterization data available for these complexes do not directly establish the hapticity of the naphthalene ligand. Fortunately, with some effort, we were able to crystallize complex **1** from a concentrated dichloromethane solution under an anhydrous atmosphere. X-ray crystallographic analysis of these crystals led to the ORTEP representation of this complex given in Figure 1. This is apparently the first X-ray structure of a simple η^6 naphthalene–rhodium complex,[10] and is comparable to crystal structures that have been recorded for some similar ruthenium– and rhodium–naphthalene complexes.[11]

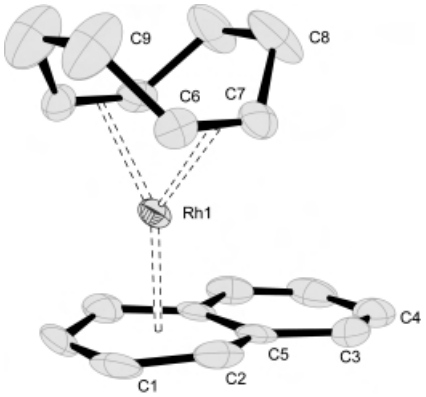


Figure 1. ORTEP diagram of $[(C_{10}H_8)Rh(cod)]^+SbF_6^-$ (**1**). Ellipsoids drawn at 50% probability level.

Complex **1** was tested in a variety of [5+2] cycloaddition reactions and compared, where relevant, with some other effective catalysts (Table 1). The initial series was selected to explore the utility of the catalyst with a diverse variety of substitution patterns. Excellent results were obtained with vinylcyclopropanes tethered to terminal and internal alkynes, alkynoates, and alkenes. Substitution of the vinylcyclopropane is tolerated both on and adjacent to the cyclopropane

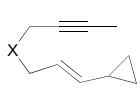
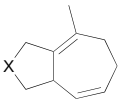
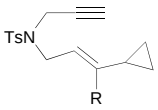
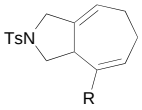
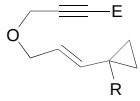
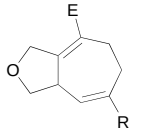
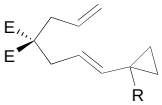
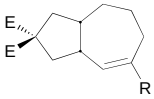
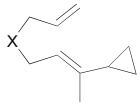
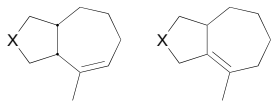
[*] Prof. P. A. Wender, T. J. Williams
Department of Chemistry, Stanford University
Stanford, CA 94305-5080 (USA)
Fax: (+1) 650-725-0259
E-mail: wenderp@leland.stanford.edu

[**] This research was supported from the National Science Foundation (CHE-0131944). Mass spectra were provided by the Mass Spectrometry Facility, University of California, San Francisco. Elemental analysis was conducted by the Desert Analytics Laboratory of Tucson, Arizona. The authors extend utmost gratitude to Mr. Adam Cole for analysis of crystallographic data and Dr. Fred Hollander (University of California, Berkeley) for X-ray data collection. (cod = cycloocta-1,5-diene.)

Supporting information for this article is available on the WWW under http://www.angewandte.org or from the author.

 © 2002 WILEY-VCH Verlag GmbH & Co. KGaA, Weinheim

Table 1. Performance of complex **1** with a variety of alkyne vinylcyclopropanes and alkene vinylcyclopropanes.

Entry	Substrate, Catalyst	Cycloadduct, Yield	Conditions[a]
			
	2 X = $C(CO_2Me)_2$	**3**	
1	2 mol % **1**	> 99 %[b]	15 min, RT, 0.15 M
2	1 mol % [{RhCl(CO)$_2$}$_2$]	89 %	PhMe, 3 h, 110 °C, 2.0 M
3	10 mol % [RhCl(PPh$_3$)$_3$]	90–95 %	TFE,[c] 19 h, 55 °C, 0.01 M
	4 X = NTs	**5**	
4	5 mol % **1**[d]	90 %	65 min, RT, 0.20 M
			
	6 R = H	**7**	
5	5 mol % **1**[d]	90 %[e]	65 min, RT, 0.20 M
	8 R = Me	**9**	
6	5 mol % **1**	93 %	60 min, 60 °C, 0.03 M
			
	10 R = H	**11**	
7	2 mol % **1**	96 %	16 min, RT, 0.15 M
8	10 mol % [RhCl(PPh$_3$)$_3$], AgOTf	81 %	PhMe, 1 h, 110 °C, 5.0 M
	12 R = Me	**13**	
9	2 mol % **1**	98 %	10 min, RT, 0.11 M
10	10 mol % [RhCl(PPh$_3$)$_3$], AgOTf	83 %	PhMe, 1 h, 110 °C, 5.0 M
			
	14 R = H	**15**	
11	5 mol % **1**	96 %	6 h, 60 °C, 0.05 M
12	0.1 mol % [RhCl(PPh$_3$)$_3$], AgOTf	90 %	PhMe, 15 h, 110 °C, 0.01 M
	16 R = Me	**17**	
13	5 mol % **1**	90 %	6.5 h, 60 °C, 0.01 M
14	1 mol % [RhCl(PPh$_3$)$_3$], AgOTf	90 %	PhMe, 10 h, 110 °C, 0.01 M
			
	18 X = NTs	**19**	
15	5 mol % **1**	76 %	19 h, 60 °C, 0.03 M
	20 X = $C(CO_2Me)_2$	**21a**, **21b**	
16	10 mol % **1**	75 % (**a**)	10 h, 70 °C, 0.03 M
17	5 mol % [RhCl(PPh$_3$)$_3$], AgOTf	78 % (**b**)	PhMe, 15 h, 110 °C, 0.01 M
18	5 mol % [RhCl(PPh$_3$)$_3$], AgOTf	67 %, 2.3:1 (**a**:**b**)	PhMe, 66 h, 85 °C, 0.01 M

[a] Unless otherwise indicated, each reaction was run in a tightly capped vial at the indicated temperature, catalyst load, and concentration in 1,2-dichloroethane. [b] Found 85 % with BF_4^- anion. [c] TFE = 2,2,2-trifluoroethanol. [d] Catalyst added in four aliquots. [e] 1-g scale, found 96 % with BF_4^- anion.

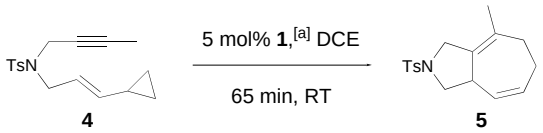
ring. Diester-substituted and heteroatom (O, NTs) tethers are well tolerated. Reactions were conducted with 2 to 10 mol % catalyst at up to 0.20 M. It is noteworthy that the yields obtained with this catalyst exceed those recorded with other previously explored catalysts of the [5+2] reaction.[1,2] Furthermore, the reactions with the naphthalene catalyst (**1**) were found to be more rapid than those with other catalysts. For example, substrate **2** is readily converted in > 99 % yield to cycloadduct **3** in only 15 min at room temperature (entry 1). By contrast, this same transformation requires 3 h in refluxing toluene when [RhCl(PPh$_3$)$_3$] (Wilkinson's catalyst) is used (89 %, entry 2) and 19 h at 55 °C in 2,2,2-trifluoroethanol when [{RhCl(CO)$_2$}$_2$] is employed (90–95 %, entry 3). Importantly, in a test preparative experiment, the yield for the conversion of **6** to **7** was found to change by < 1 % as the scale was increased over two orders of magnitude (from milligrams to grams).

Complex **1** efficiently catalyzes the reactions of both alkynes and alkenes with vinylcyclopropanes (Table 1, entries 11, 13, 15, and 16) and offers greater generality than non-rhodium catalysts reported thus far.[5] This is particularly advantageous in the case of substrate **18**, for which a complex mixture of side products is observed with Wilkinson's catalyst. In the case of substrate **20**, product alkene isomerization is observed with Wilkinson's catalyst, but not with complex **1**. Isomerization is also not seen in unconjugated cycloheptadiene products of the reactions of tethered alkyne vinylcyclopropanes,[12] as is sometimes encountered when such compounds are treated with Wilkinson's catalyst.[2] Diester- and ether-tethered substrates afforded optimum performance with 2 mol % catalyst at 0.20 M substrate concentration. Sulfonamide-tethered substrates were found to be less reactive at lower catalyst loading, yet **4** was found to react efficiently at high concentrations (Table 2) when catalyst was added in portions.

Given the excellent performance of complex **1** in the above study, we next examined several related complexes that differ in the arene ligand. Three additional complexes based on 1,4-dimethylnaphthalene, benzene, and hexamethylbenzene were prepared (Table 3). X-ray crystallographic data (obtained for **1**, **22**, and **24**) and solution NMR data suggest that these complexes have a similar η^6-arene-coordination state.[13] The complexes were compared with each other and with the catalyst generated in situ by the treatment of [{RhCl(cod)}$_2$] with $AgSbF_6$ (Table 3, entry 1) by using the conditions found to be optimal for conversion of substrate **2** with catalyst **1**.

 © 2002 WILEY-VCH Verlag GmbH & Co. KGaA, Weinheim 0044-8249/02/4123-4551 $ 20.00+.50/0

Table 2. Effect of concentration on the conversion of **4**.

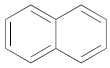
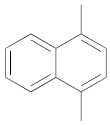
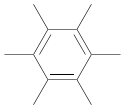


4 **5**

Initial Conc.	Yield
0.20 M	90 %
0.80 M	88 %
1.60 M	84 %

[a] Catalyst added as four aliquots delivered every 15 min from a suspension in 1,2-dichloroethane (DCE).

Table 3. Synthesis and reaction of some $[(\text{arene})\text{Rh(cod)}]^+\text{SbF}_6^-$ complexes.

Entry[a]	Rhodium complex (yield)	Yield[b] of **3**
1	$[\{\text{RhCl(cod)}\}_2]$ + 2 AgSbF_6	90 %
	Arene Complexes ($[(\text{arene})\text{Rh(cod)}]^+\text{SbF}_6^-$)	
2	**1** (70 %) arene = 	> 99 %
3	**22** (67 %) arene = 	88 %
4	**23** (65 %) arene = 	91 %
5	**24** (87 %) arene = 	Trace

[a] Arene complexes prepared as with **1**, see Supporting Information for preparative details. [b] Yield of the conversion of **2** to **3** with 2 mol % Rh catalyst, each run in 1,2-dichloroethane (0.15 M) at room temperature in 15 min.

The trend is noticed that increasing arene substitution with methyl groups results in lower yields.[14] For example, benzene-ligated complex **23** was found to be quite effective in mediating the intramolecular [5+2] reaction, while the hexamethylbenzene-ligated complex **24** was not. These findings are consistent with the results of Chung et al. according to which $[(C_6Me_6)\text{Rh(cod)}]^+\text{BF}_4^-$ has no catalytic activity in the [4+2] cycloaddition. We observed similar results when complexes **1**, **23**, and **24** were examined in the intermolecular [4+2] cycloaddition of 2,3-dimethyl-1,3-butadiene and propargyl methyl ether; [4+2] cycloadduct yields of > 99 %, 88 %, and ≈ 0 % were obtained, respectively.[15]

In conclusion, we have shown that complex **1** is an exceptionally effective and, in cases where comparisons have been made, preferred catalyst for the [5+2] cycloaddition reaction of tethered alkyne vinylcyclopropanes and alkene vinylcyclopropanes. The alkyne substrates are converted to cycloadducts in high yield (> 90 %) and in only minutes at room temperature. Alkene vinylcyclopropanes, which do not undergo cycloaddition with ruthenium catalysts, are readily converted to cycloadducts with the new catalysts, often in higher yields and under milder conditions than are found with other rhodium(I) catalysts reported thus far. Tether variations as well as substitution of the C_5 and C_2 components are well tolerated. Further studies on these and new catalysts for this reaction are continuing.

Experimental Section

Full procedures and characterization data are given in the Supporting Information.

Sample procedure: Freshly prepared and crystallized substrate **6** (1.00 g, 3.46 mmol) was weighed out in an oven-dried 25 mL flask equipped with a stir bar. 1,2-Dichloroethane (DCE) (17.3 mL, 0.20 M) and catalyst complex **1** (99.3 mg, 173 μmol, added in four aliquots dispersed in 1.25 mL DCE and spaced 15 min apart) were then added as the reaction was stirred at room temperature for a total 55 minutes. The crude product was concentrated and purified by flash column chromatography (elution with 10 % diethyl ether in pentane). Product-containing fractions were concentrated and recrystallized to yield product **7**, 900.3 mg (90 %) as a white solid.

Received: August 9, 2002 [Z19933]

[1] Alkynes: a) P. A. Wender, H. Takahashi, B. Witulski, *J. Am. Chem. Soc.* **1995**, *117*, 4720 – 4721; b) P. A. Wender, A. J. Dyckman, C. O. Husfeld, D. Kadereit, J. A. Love, H. Rieck, *J. Am. Chem. Soc.* **1999**, *121*, 10442 – 10443; c) P. A. Wender, A. J. Dyckman, *Org. Lett.* **1999**, *1*, 2089 – 2092; d) P. A. Wender, F. C. Bi, M. A. Brodney, F. Gosselin, *Org. Lett.* **2001**, *3*, 2105 – 2108; e) P. A. Wender, H. Rieck, M. Fuji, *J. Am. Chem. Soc.* **1998**, *120*, 10976 – 10977; alkenes: f) P. A. Wender, C. O. Husfeld, E. Langkopf, J. A. Love, *J. Am. Chem. Soc.* **1998**, *120*, 1940 – 1941; g) P. A. Wender, C. O. Husfeld, E. Langkopf, J. A. Love, N. Pleuss, *Tetrahedron* **1998**, *54*, 7203 – 7220; allenes: h) P. A. Wender, F. Glorius, C. O. Husfeld, E. Langkopf, J. A. Love, *J. Am. Chem. Soc.* **1999**, *121*, 5348 – 5349; i) P. A. Wender, L. Zhang, *Org. Lett.* **2000**, *2*, 2323 – 2326.

[2] P. A. Wender, D. Sperandio, *J. Org. Chem.* **1998**, *63*, 4164 – 4165. Other metals screened include Fe, Co, Ni, Ru, Pd, Ir, and Pt.

[3] For examples see: a) P. A. Wender, T. E. Jenkins, *J. Am. Chem. Soc.* **1989**, *111*, 6432 – 6434; b) P. A. Wender, T. E. Jenkins, S. Suzuki, *J. Am. Chem. Soc.* **1995**, *117*, 1843 – 1844.

[4] For examples see: a) R. S. Jolly, G. Luedtke, D. Sheehan, T. Livinghouse, *J. Am. Chem. Soc.* **1990**, *112*, 4965 – 4966; b) L. McKinstry, T. Livinghouse, *Tetrahedron* **1994**, *50*, 6145 – 6154; c) K. Kumar, R. S. Jolly, *Tetrahedron Lett.* **1998**, *39*, 3047 – 3048; d) S. R. Gilbertson, G. S. Hoge, D. G. Genov, *J. Org. Chem.* **1998**, *63*, 10077 – 10080; e) S. R. Gilbertson, G. S. Hoge, *Tetrahedron Lett.* **1998**, *39*, 2075 – 2078, and references to the intermolecular process therein; f) M. Murakami, K. Ubukata, K. Itami, Y. Ito, *Angew. Chem.* **1998**, *110*, 2362 – 2364; *Angew. Chem. Int. Ed.* **1998**, *37*, 2248 – 2250; g) D. J. R. O'Mahony, D. B. Belanger, T. Livinghouse, *Synlett* **1998**, 443 – 445; h) H. Heath, B. Wolfe, T. Livinghouse, S. K. Bae, *Synthesis* **2001**, 2341 – 2347.

[5] a) B. M. Trost, F. D. Toste, H. Shen, *J. Am. Chem. Soc.* **2000**, *122*, 2379 – 2380; b) B. M. Trost, H. C. Shen, *Org. Lett.* **2000**, *2*, 2523 – 2525; c) B. M. Trost, H. C. Shen, *Angew. Chem.* **2001**, *113*, 2375 – 2378; *Angew. Chem. Int. Ed.* **2001**, *40*, 2313 – 2315; d) B. M. Trost, F. D. Toste, *Angew. Chem.* **2001**, *113*, 1148 – 1150; *Angew. Chem. Int. Ed.* **2001**, *40*, 1114 – 1116.

[6] B. Wang, P. Cao, X. Zhang, *Tetrahedron Lett.* **2000**, *41*, 8041 – 8044.

[7] S.-J. Paik, S. U. Son, Y. K. Chung, *Org. Lett.* **1999**, *1*, 2045 – 2047. For more information on metal-catalyzed [4+2] cycloadditions, see reference [4].

[8] Available from Strem Chemicals, catalog no. 45–0380, 105 $ g^{-1}.

[9] M. Scotti, M. Valderrama, R. Ganz, H. Werner, *J. Organomet. Chem.* **1985**, *286*, 399. Other silver salts are known to be effective.

[10] Crystal structure analysis of complex **1** (also see Supporting Information): Crystal dimensions are $0.06 \times 0.11 \times 0.18$ mm^3, orthorhombic, spacegroup *Pnma*, $a = 13.199(1)$ Å, $b = 9.605(1)$ Å, $c = 15.007(1)$ Å, $V = 1902.4(0)$ Å^3, $Z = 4$, $\rho_{calcd} = 2.01$ g cm^{-3}, $Mo_{K\alpha}$ radiation, $\lambda = 0.71069$ Å, $\mu(Mo_{K\alpha}) = 23.38$ cm^{-1}, $T = -133$ °C. Data were collected on a Bruker-Siemens SMART CCD diffractometer, 8469 measured

 © 2002 WILEY-VCH Verlag GmbH & Co. KGaA, Weinheim 0044-8249/02/4123-4552 $ 20.00+.50/0

reflections, 2495 unique reflections, 1700 used ($4° < 2\Theta < 49.36°$), $R_1 = 0.030$ (3344 reflections, $I > 10\sigma(I)$), $wR_2 = 7.4\%$ (all data), GOF = 0.97. Minimum and maximum peaks in the final difference map are −1.25 and 1.47 e Å^{-3}. CCDC-191383 (**1**), CCDC-191384 (**7**), CCDC-191385 (**22**), and CCDC-191386 (**24**) contain the supplementary crystallographic data for this paper. These data can be obtained free of charge via www.ccdc.cam.ac.uk/conts/retrieving.html (or from the Cambridge Crystallographic Data Centre, 12, Union Road, Cambridge CB2 1EZ, UK; fax: (+44) 1223-336-033; or deposit@ccdc.cam.ac.uk)

[11] The nearest examples are [(η^6-$C_{10}H_8$)Ru(cod)], M. Crocker, M. Green, J. A. K. Howard, N. C. Norman, D. M. Thomas, *J. Chem. Soc. Dalton Trans.* **1990**, 2299; and [(η^4-$C_{10}H_8$)Rh(Cp)], G. Müller, P. E. Gaede, C. Hirsch, K. Qaio, *J. Organomet. Chem.* **1994**, *472*, 329–335.

[12] As determined by X-ray crystallography (**7**) and NMR, see Supporting Information.

[13] No other hapticity was noticed for the naphthalene ligand. For more structural and NMR information on related ruthenium–naphthalene complexes, see a) M. A. Bennett, H. Neumann, M. Thomas, X.-Q. Wang, P. Pertici, P. Salvadori, G. Vituilli, *Organometallics* **1991**, *10*, 3237–3245; b) M. A. Bennett, Z. Lu, X. Wang, M. Brown, D. C. R. Hockless, *J. Am. Chem. Soc.* **1998**, *120*, 10409–10415.

[14] For more information on the effect of arene methylation in {(η^6-arene)Rh^I} complexes, see: E. T. Singewald, C. S. Slone, C. L. Stern, C. A. Mirkin, G. P. A. Yap, L. M. Liable-Sands, A. L. Rheingold, *J. Am. Chem. Soc.* **1997**, *119*, 3048–3056.

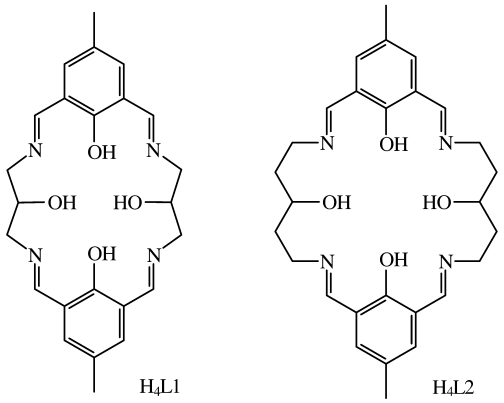
[15] See supporting information for details; yields given for the conversion of 2,3-dimethylbutadiene and propargyl methyl ether to the corresponding cyclohexadiene.

Di-, Tri-, and Tetracopper(II) Complexes of a Pseudocalixarene Macrocycle**

Julia Barreira Fontecha, Sandrine Goetz, and Vickie McKee*

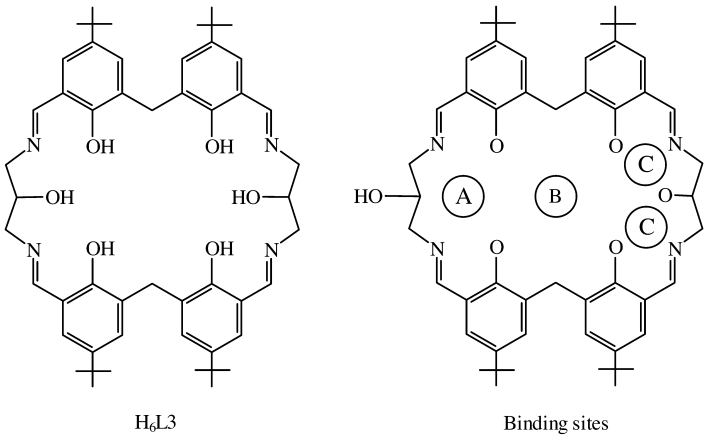
Schiff base Robson-type macrocycles containing two bridging phenol groups have been widely used to synthesize homo- and heterodinuclear complexes for many years. Detailed investigation of the chemistry of these systems has enabled insights in a number of areas, such as magnetochemistry, site selection, and bioinorganic model chemistry.[1] Expansion to larger macrocycles accommodating polynuclear assemblies has been achieved in the last ten years.[2,3] Interest in such complexes is centered on their ability to hold a number of metal ions in a fixed geometric relationship and has potential relevance in bioinorganic and catalytic chemistry as well as nanotechnological applications.

The macrocycle H_4L1 can form mono- and dinuclear complexes, but is unable to use the pendant alcohol groups to bind more than two metal ions within the macrocycle because of geometric constraints imposed by the overall



cavity size.[4] The longer saturated chain in H_4L2 permits formation of homo- and heterotetranuclear complexes, as well as complexes in which some sites are vacant.[3]

We have now synthesized the new dialdehyde dihydroxy-5,5′-di-*tert*-butyl-3,3′-methanediyldibenzaldehyde (dhtmb)[5] and used this group to expand the H_4L1 macrocycle. Schiff base condensation of dhtmb with 1,3-diaminopropan-2-ol in the presence of metal template ions yields complexes of the new macrocycle H_6L3 (Scheme 1). This ligand can be



Scheme 1. Pseudocalixarene ligand and binding sites.

considered as an expanded calix[4]arene containing two =$NCH_2CH(OH)CH_2N$= inserts. Unlike most aza- or oxocalixarenes (where inserts are placed between each pair of phenol rings),[6] H_6L3 preserves two methylene linkages while introducing imine and pendant alcohol donors.

Approximately planar conformations are sterically prohibited in genuine calix[*n*]arenes (where $n = 4$–6) and metal ions cannot take advantage of the bridging potential of the phenol groups, which generally leads to mononuclear complexes.[6,7] In contrast, H_6L3 can use some or all of the phenolic oxygen donors in the bridging mode and can be di- or polynucleating. The presence of relatively soft imine donors in addition to the phenolic oxygen atoms also widens the range of metal ions that might be expected to bind with high stability constants.

Three types of metal binding site are potentially available within H_6L3 (Scheme 1): site A is analogous to the conventional "Robson" site and is similar to that observed for complexes of H_4L1;[4] there are two of these in the macrocycle.

[*] Prof. V. McKee, J. Barreira Fontecha, S. Goetz
Chemistry Department
Loughborough University
Loughborough, Leics LE11 3TU (UK)
Fax: (+44) 1509-222-566
E-mail: v.mckee@lboro.ac.uk

[**] We are grateful to the EPSRC Mass Spectrometry Service Centre, Swansea for FAB (LSIMS) spectra and to Loughborough University for support.

 © 2002 WILEY-VCH Verlag GmbH & Co. KGaA, Weinheim 0044-8249/02/4123-4553 $ 20.00+.50/0

The unique central calixarene-type site B involves the four phenol (or phenolate) donors. Finally, there are four equivalent sites of type C; occupation of similar sites has been reported for open-chain complexes based on 1,3-diaminopropan-2-ol[8] as well as in macrocyclic complexes of H_4L2.[3]

The macrocycle is formed by Schiff base condensation of dhtmb with 1,3-diaminopropan-2-ol in the presence of a metal template ion. When Cu^{II} is used as the template ion di-, tri-, and tetranuclear complexes can be isolated depending on the reaction conditions. Reaction of 1,3-diaminopropan-2-ol and dhtmb with equimolar amounts of $CuCl_2$ yields a green dicopper complex (**1**), while reaction with two equivalents of $Cu(NO_3)_2{\cdot}6H_2O$ yields a green tetracopper product (**3**) on short reflux. The tetranuclear complex converts into the brown tricopper species (**2**) on recrystallization from *N*,*N*-dimethylformamide (DMF). The structure of each complex has been investigated by X-ray crystallography.

The dicopper(II) cation of $[Cu_2Cl(H_4L3)]Cl{\cdot}1.6\,Et_2O{\cdot}EtOH$ (**1**$\cdot 1.6\,Et_2O{\cdot}EtOH$) is shown in Figure 1. The copper ions occupy the A sites, with each coordinated to two imine groups, two phenol oxygen atoms, and a bridging chloride ion. The geometry at each metal ion is square pyramidal, with the chloride ligand apical. The macrocycle adopts a saddle conformation with adjacent phenol rings inclined at 68.5(1) and 68.7(1)° to each other. This shape is maintained by three interactions: the Cu-Cl-Cu bridge (104.55(5)°) and two hydrogen bonds linking adjacent phenol oxygen atoms (O1···O2 2.414(4) and O4···O5 2.402(4) Å). The stoichiometry of the reaction suggests that the macrocycle is doubly deprotonated and the presence of the hydrogen bonds suggest that one proton is lost from each pair of phenols. The alcohol groups are not involved in bonding to the copper ions.

The tricopper(II) complex $[Cu_3(H_2L3)(NO_3)](NO_3)(dmf)_3$ (**2**) is dark brown, presumably because of charge transfer between the fully deprotonated phenolate groups and the Cu^{II} ions. The cations occupy the two A sites and the central C site (Figure 2), with each ion bound to four macrocyclic donors in its basal plane; the planes about Cu2 and Cu3 are inclined to that at Cu1 by 41.7(1) and 34.2(1)°, respectively. A coordinated nitrate counterion lies within the concave curve

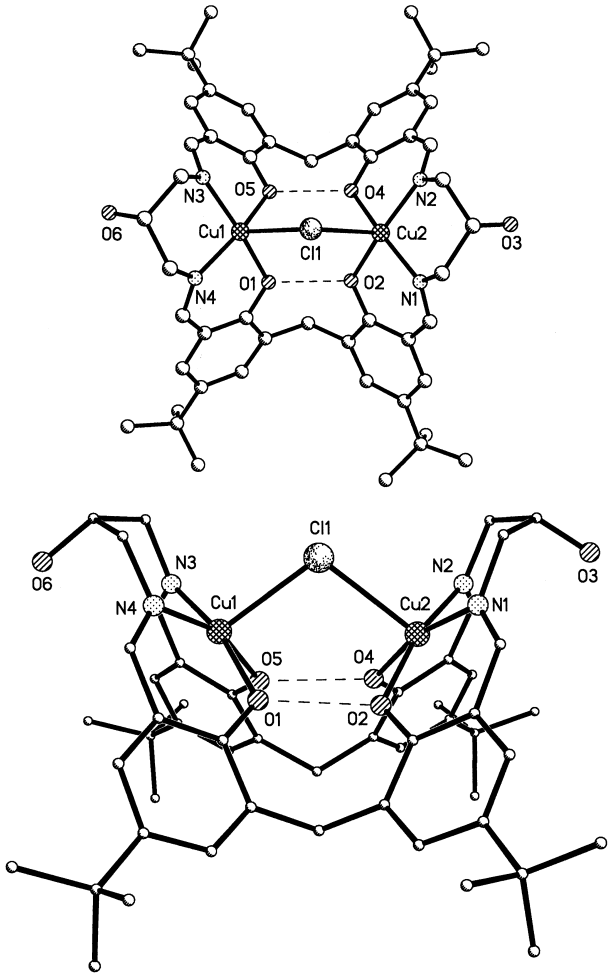


Figure 1. Two views of the $[Cu_2Cl(H_4L3)]^+$ ion of **1**, dotted lines represent hydrogen bonds. Selected bond lengths [Å] and angles [°]: Cu1-N3 1.952(4), Cu1-O1 1.958(3), Cu1-N4 1.978(4), Cu1-O5 1.989(3), Cu1-Cl1 2.5145(13), Cu2-O2 1.962(3), Cu2-N1 1.967(4), Cu2-O4 1.970(3), Cu2-N2 1.983(4), Cu2-Cl1 2.5423(14), O1-O2 2.414(4), O4-O5 2.402(4); Cu1-Cl1-Cu2 104.55(5).

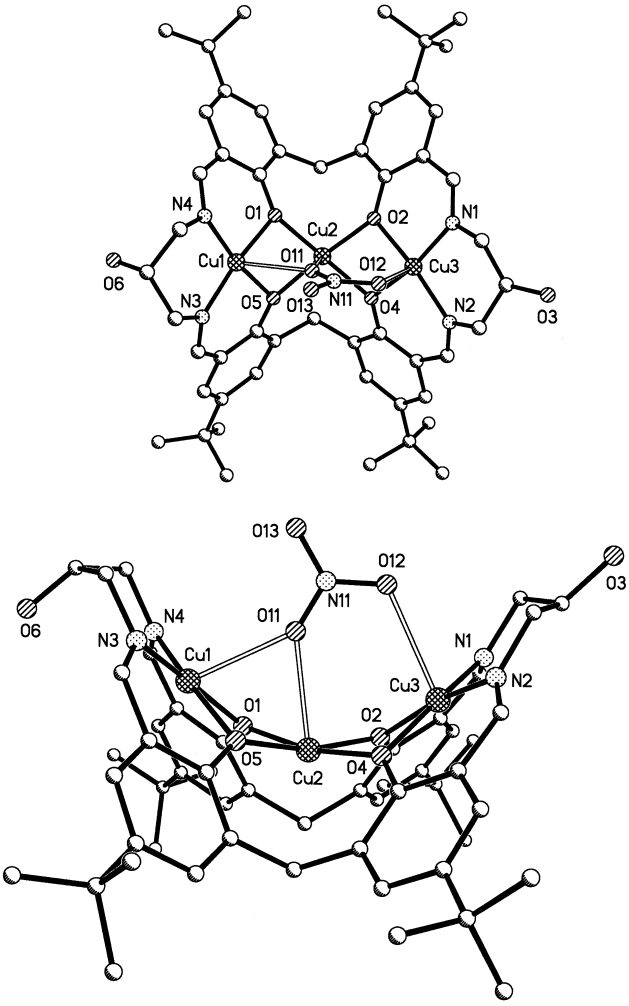


Figure 2. Two views of the $[Cu_3(H_2L3)(NO_3)]^+$ ion of **2**. Selected bond lengths [Å] and angles [°]: Cu1-O1 1.957(3), Cu1-O5 1.956(4), Cu1-N3 1.935(4), Cu1-N4 1.935(5), Cu1-O11 2.432(5), Cu1-Cu2 2.8428(8), Cu2-O1 1.918(3), Cu2-O5 1.925(3), Cu2-O2 1.928(3), Cu2-O4 1.929(3), Cu2-O11 2.490(5), Cu2-Cu3 2.8616(9), Cu3-O2 1.945(3), Cu3-O4 1.952(3), Cu3-N2 1.936(4), Cu3-N1 1.942(5), Cu3-O12 2.613(9); Cu2-O1-Cu1 94.38(14), Cu2-O2-Cu3 95.28(14), Cu2-O4-Cu3 95.02(14), Cu2-O5-Cu1 94.18(15).

 © 2002 WILEY-VCH Verlag GmbH & Co. KGaA, Weinheim 0044-8249/02/4123-4554 $ 20.00+.50/0 *Angew. Chem. Int. Ed.* **2002**, *41*, No. 23

of the three copper sites. The nitrate is disordered (7:3) between two related positions; one site involves a single atom bridge between Cu1 and Cu2 and a three atom bridge between Cu2 and Cu3, while the minor site provides a single atom bridge between Cu3 and Cu2 with a three atom bridge linking Cu2 and Cu1. The conformation of the macrocycle is very similar to that in **1**.

The cation of $[Cu_4(H_2L3)(OH)_2(H_2O)(EtOH)](NO_3)_2$ (**3**) is shown in Figure 3; the Cu^{II} ions occupy the four equivalent B sites. As observed in complex **1**, each adjacent pair of phenols is monodeprotonated and linked by a hydrogen bond (O1···O2, 2.395(7); O4···O5, 2.417(6) Å). The overall conformation of the tetranuclear complex is, however, very different from that of **1** and **2**.

The saturated portions of the ring are fully extended to allow each alkoxo group to bridge two Cu^{II} ions and the macrocycle is sharply folded down its long axis, with each half approximately planar; the angles between adjacent phenol groups are 65.6(2) and 66.3(2)°. Each Cu^{II} ion has approximate square pyramidal geometry: the base comprises macrocyclic phenoxo, alkoxo, and imine donors as well as an exogenous μ_2-hydroxo group. The axial ligands are disordered and have been modeled as having 50% occupancy of water and ethanol at each site.

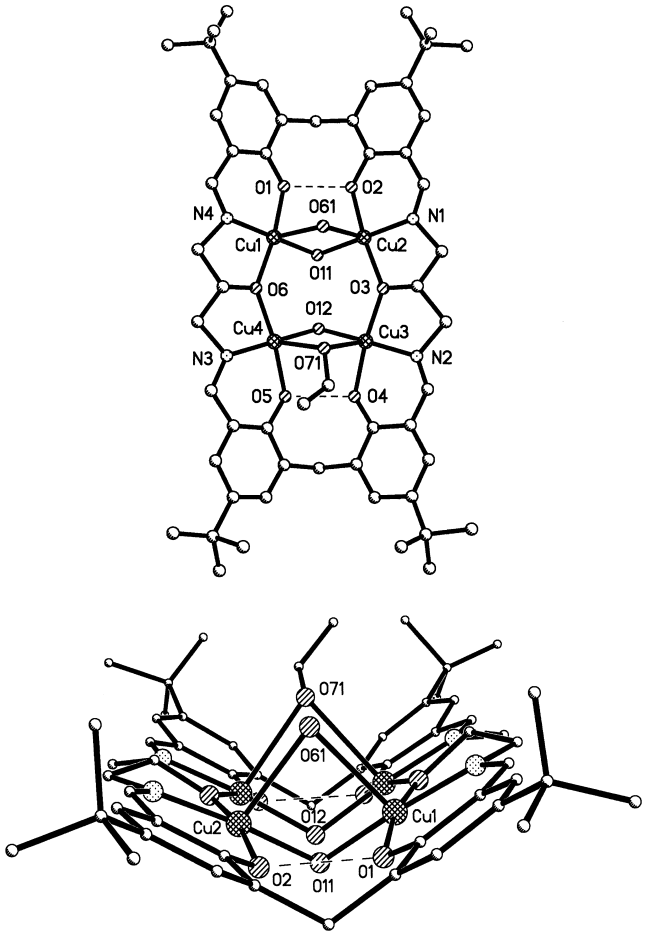


Figure 3. Two views of the $[Cu_4(H_2L3)(OH)_2(H_2O)(EtOH)]^{2+}$ ion of **3**, hydrogen bonds are shown as dotted lines. Selected bond lengths [Å] and angles [°]: Cu1-O11 1.927(5), Cu1-N4 1.932(8), Cu1-O6 1.961(5), Cu1-O1 1.995(5), Cu1-O61 2.420(6), Cu2-N1 1.904(6), Cu2-O11 1.928(5), Cu2-O3 1.963(5), Cu2-O2 1.977(5), Cu2-O61 2.402(6), Cu1-Cu2 3.143(1), Cu2-Cu3 3.681(1), Cu3-O12 1.889(5), Cu3-N2 1.935(7), Cu3-O3 1.963(5), Cu3-O4 2.007(5), Cu3-O71 2.520(7), Cu4-N3 1.898(7), Cu4-O12 1.909(5), Cu4-O6 1.979(5), Cu4-O5 1.997(5), Cu4-O71 2.527(7), Cu3-Cu4 3.160(1), Cu4-Cu1 3.677(1); Cu3-O3-Cu2 139.4(3), Cu1-O6-Cu4 137.9(3), Cu1-O11-Cu2 109.2(2), Cu3-O12-Cu4 112.6(2), Cu2-O61-Cu1 81.36(16), Cu3-O71-Cu4 77.54(18).

The most striking feature of this series of complexes is the variation in nuclearity within the same ligand system. This effect is linked to the variation in the extent of deprotonation of the ligand, the orientation of the phenol groups, and the overall shape of the macrocyclic host. Preliminary investigations suggest that the dicopper complex is only isolated in the presence of a good coordinating anion which is also large enough to fit the cavity defined by the hydrogen-bonding interactions of the ligand. When NO_3^-, ClO_4^-, or BF_4^- were used, the initial product of the template reaction was the tetracopper complex, irrespective of the stoichiometry of the template reaction.

Formally, the tricopper complex can be generated from the dinuclear analogue by displacement of the two central, hydrogen-bonding protons by a Cu^{II} ion. Comparison of Figures 1 and 2 shows that the two structures are closely related except that the saddle shape in **2** is maintained by the Cu^{II} ion in the central site and by two hydrogen bonds in **1**. Surprisingly, however, it seems that the tricopper complex is actually formed by rearrangement of the tetracopper complex. Extended reflux of the template mixture causes the green color to darken to brown and mixtures of **2** and **3** are formed, as indicated by FAB mass spectrometry. The same color change occurs within minutes if the tetracopper complex is dissolved in DMF and clean tricopper complex is obtained. Consequently, it seems that the tetranuclear complex (**3**) is the kinetic product of the template reaction and that **2** is the thermodynamic product. In view of the extensive structural rearrangement required, it is not unexpected that the rearrangement is slow in alcohol but faster in a solvent with better donor properties.

Experimental Section

2,2′-dihydroxy-5,5′-di-*tert*-butyl-3,3′-methanediyldibenzyl alcohol was synthesized from 4-*tert*-butylphenol following the literature procedure.[9] The alcohol groups were oxidized to aldehydes by MnO_2 after the phenol groups had been protected using allylbromide. The allyl groups were removed with 10% Pd on charcoal to yield 2,2′-dihydroxy-5,5′-di-*tert*-butyl-3,3′-methanediyl dibenzaldehyde (dhtmb) in 40% yield for the three-step process.[5] Elemental analysis calcd (%) for $C_{23}H_{28}O_4$: C 74.97, H 7.66; found: C 74.51, H 7.86. ^{1}H NMR ($CDCl_3$, 250 MHz): $\delta = 9.86$ (s, 2H), 7.64 (d, 2H), 7.37 (d, 2H), 4.03 (s, 2H), 1.26 ppm (s, 18H).

$[Cu_2Cl(H_4L3)]Cl\cdot 2MeOH$ (**1**·2MeOH). Anhydrous $CuCl_2$ (0.073 g 0.543 mmol) was dissolved in hot dry ethanol (40 ml) and added to a solution of dhtmb (0.20 g 0.543 mmol) in hot dry ethanol (35 mL). After 10 min reflux a solution of 1,3-diaminopropan-2-ol (0.52 g, 0.543 mmol) in dry methanol (20 mL) was added. The green solution was heated at reflux for 2 h, then cooled, filtered, and the volume reduced to give the product in 36% yield. Elemental analysis calcd (%) for **1**·2MeOH: C 58.7, H 6.7, N 5.1; found: C 58.4, H 6.6, N 5.1. Emerald green crystals of the solvate **1**·1.6Et_2O·EtOH were obtained by diffusion of diethyl ether into the filtrate. Crystal dimensions: $0.35 \times 0.14 \times 0.07$ mm^3, triclinic, space group $P\bar{1}$ $a = 13.707(3)$, $b = 14.568(3)$, $c = 16.827(4)$ Å, $\alpha = 103.472(3)$, $\beta = 95.935(3)$, $\gamma = 93.429(3)$°, $V = 3238(1)$ Å^3, $\rho_{calcd} = 1.237$ Mg m^{-3}. 22822 reflections, 11279 independent ($R_{int} = 0.0455$), $\mu = 0.792$ mm^{-1}, $T_{max} = 1.000$, $T_{min} = 0.880$, 830 least-squares parameters $R1 = 0.0579$ $wR2 = 0.1384$ (2σ data).

 © 2002 WILEY-VCH Verlag GmbH & Co. KGaA, Weinheim 0044-8249/02/4123-4555 $ 20.00+.50/0

$[Cu_3(H_2L3)(NO_3)](NO_3)(dmf)_4{\cdot}H_2O$ (**2**·4 dmf·H_2O). A mixture of $Cu(NO_3)_2{\cdot}6H_2O$ (0.321 g, 1.08 mmol) and dhtmb (0.20 g, 0.543 mmol) in dry ethanol (80 mL) were heated to reflux for 10 min and a solution of 1,3-diaminopropan-2-ol (0.052 g, 0.543 mmol) in dry methanol (20 mL) added dropwise. The emerald green solution darkened as reflux was continued for 2 h. the mixture was filtered, cooled, and concentrated under vacuum where upon a green solid precipitated (analyzed as $[Cu_4(H_4L)(NO_3)(OH)_2(H_2O)_4]$). This complex was dissolved in DMF and the color changed to brown; crystals of the trinuclear complex **2**·3 dmf were obtained in 40% yield by diffusion of diethyl ether into the solution. Elemental analysis calcd (%) for **2**·4 dmf·H_2O: C 51.8, H 6.4, N 9.4; found: C 52.1, H 6.5, N 9.4. Crystal dimensions: $0.45 \times 0.24 \times 0.04$ mm^3, monoclinic, space group $P2_1/c$, $a = 17.234(1)$, $b = 22.130(2)$, $c = 17.658(1)$ Å, $\beta = 103.488(1)°$, $V = 6549.0(8)$ Å^3, $\rho_{calcd} = 1.395$ Mg m^{-3}. 46 309 reflections, 11 521 independent ($R_{int} = 0.0424$), $\mu = 1.036$ mm^{-1}, $T_{max} = 1.000$, $T_{min} = 0.885$; 859 least-squares parameters $R1 = 0.0646$ $wR2 = 0.1638$ (2σ data).

$[Cu_4(H_2L3)(OH)_2(sol)_2](NO_3)_2$ (**3**·2 H_2O where sol = water or ethanol). A mixture of $Cu(NO_3)_2{\cdot}6H_2O$ (0.16 g, 0.543 mmol) and dhtmb (0.20 g, 0.543 mmol) in dry ethanol (70 mL) was heated to reflux for 10 min and a solution of 1,3-diaminopropan-2-ol (0.052 g, 0.543 mmol) in dry methanol (20 mL) added dropwise. The solution changed to emerald green and darkened as reflux was continued for 1 h. The solution was cooled, filtered, and evaporated to dryness. The residue was then dissolved in dichloromethane, filtered, and evaporated again before being dissolved in ethanol. Green $[Cu_4(H_2L3)(OH)_2(H_2O)_2](NO_3)_2{\cdot}2H_2O$ was obtained from this solution in 79% yield. Elemental analysis calcd (%) for **3**·2 H_2O: C 47.1, H 5.6, N 6.3; found: C 47.1, H 5.5, N 6.3. Crystals of $[Cu_4(H_2L3)(OH)_2(H_2O)(EtOH)](NO_3)_2{\cdot}2EtOH{\cdot}H_2O$ (**3**·2 EtOH·H_2O) were obtained by slow evaporation of a solution of **3**·2 H_2O in an ethanol/benzene/petroleum ether mixture. Crystal dimensions: $0.31 \times 0.13 \times 0.04$ mm^3, monoclinic, space group $P2_1/c$, $a = 11.867(2)$, $b = 14.125(3)$, $c = 41.220(7)$ Å, $\beta = 93.406(3)°$, $V = 6897(2)$ Å^3, $\rho_{calcd} = 0.352$ Mg m^{-3}. 47 670 reflections, 12 095 independent ($R_{int} = 0.0902$), $\mu = 1.285$ mm^{-1}, $T_{max} = 1.000$, $T_{min} = 0.766$; 696 least-squares parameters $R1 = 0.0763$ $wR2 = 0.21.19$ (2σ data). The uncoordinated solvate molecules and nitrate ions were highly disordered and were treated using the SQUEEZE program[10] (see the Supporting Information).

X-ray data were collected at 150(2) K on a Bruker SMART 1000 diffractometer using $Mo_{K\alpha}$ radiation ($\lambda = 0.71073$ Å) to $2\theta_{max}$ of 25°. The structures were solved by direct methods and refined on F^2 using all the data.[11] Non-hydrogen atoms were refined with anisotropic ADPs and hydrogen atoms attached to full-occupancy carbon atoms were inserted at calculated positions. Details concerning treatment of disorders and of hydrogen atoms not bonded to carbon atoms are described in the Supporting Information. CCDC 190246.(**1**·1.6 Et_2O·EtOH) CCDC 190247 (**2**·3 dmf), and CCDC 190248 (**1**·2 H_2O) contain the supplementary crystallographic data for this paper. These data can be obtained free of charge via www.ccdc.cam.ac.uk/conts/retrieving.html (or from the Cambridge Crystallographic Data Centre, 12 Union Road, Cambridge CB21EZ, UK; fax: (+44) 1223-336-033; or deposit@ccdc.cam.ac.uk).

Received: August 6, 2002 [Z19906]

[1] a) R. C. Long, D. N. Hendrickson, *J. Am. Chem. Soc.* **1983**, *105*, 1513; b) H. Okawa, J. Nishio, M. Ohba, M. Tadokoro, N. Matsumoto, M. Koikawa, S. Kida, D. E. Fenton, *Inorg. Chem.* **1993**, *32*, 2949; c) M. Yonemura, N. Usuki, Y. Nakamura, M. Ohba, H. Okawa, *J. Chem. Soc. Dalton Trans.* **2000**, 3624; d) A. Atkins, D. Black, A. J. Blake, A. Marin-Becerra, S. Parsons, L. Ruiz-Ramirez, M. Schröder, *Chem. Commun.* **1996**, 457.

[2] a) A. Hori, M. Yonemura, M. Ohba, H. Okawa, *Bull. Chem. Soc. Jpn.* **2001**, *74*, 495; b) M. J. Grannas, B. F. Hoskins, R. Robson, *Inorg. Chem.* **1994**, *33*, 1071; c) K. K. Nanda, S. Mohanta, U. Florke, S. K. Dutta, K. Nag, *J. Chem. Soc. Dalton Trans.* **1995**,3831; d) J. McCrea, V. McKee, T. Metcalfe, S. S. Tandon, J. Wikaira, *Inorg. Chim. Acta* **2000**, *297*, 220.

[3] a) V. McKee, S. S. Tandon, *J. Chem. Soc. Dalton Trans.* **1991** 221; b) P. E. Kruger, V. McKee, *Chem. Commun.* **1997** 1341; c) S. Cromie, F. Launay, V. McKee, *Chem. Commun.* **2001**, 1918.

[4] a) S. S. Tandon, V. McKee, *J. Chem. Soc. Dalton Trans.* **1989** 19; b) A. J. Downard, V. McKee, S. S. Tandon, *Inorg. Chim. Acta* **1990**, *173*, 181; c) S. S. Tandon, L. K. Thompson, J. N. Bridson, V. McKee, A. J. Downard, *Inorg. Chem.* **1992**, *31*, 4635.

[5] S. Goetz, Ph.D Thesis, Loughborough University (UK), **2002**.

[6] a) V. Böhmer, *Angew. Chem.* **1995**, *107*, 785; *Angew. Chem. Int. Ed. Engl.* **1995**, *34*, 713; b) D. C. Gutsche, *Calixarenes revisited*, The Royal Society of Chemistry, Cambridge, **1998**.

[7] a) F. Hamada, K. D. Robinson, G. W. Orr, J. L. Atwood, *Supramol. Chem.* **1993**, *2*, 19; b) S. E. J. Bell, J.K. Browne, V. McKee, M. A. McKervey, J. F. Malone, M. O'Leary, A. Walker, F. Arnaud Neu, O. Boulangeot, O. Mauprivez, M.-J. Schwing-Weill, *J. Org. Chem.* **1998**, *63*, 489; c) G. Guillemot, E. Solari, C. Floriani, N. Re, C. Rizzoli, *Organometallics* **2000**, *19*, 5218.

[8] a) A. Gelasco, M. L. Kirk, J. W. Kampf, V. L. Pecoraro, *Inorg.Chem.* **1997**, *36*, 1829; b) P. E. Kruger, B. Moubaraki, G. D. Fallon, K. S. Murray, *J. Chem. Soc. Dalton Trans.* **2000**, 713; c) Y. Nishida, M. Takeuchi, K. Takahashi, S. Kida, *Chem. Lett.* **1985**, *631*, 631.

[9] B. Dhawan, C. D. Gutsche, *J. Org. Chem.* **1983**, *48*, 1536.

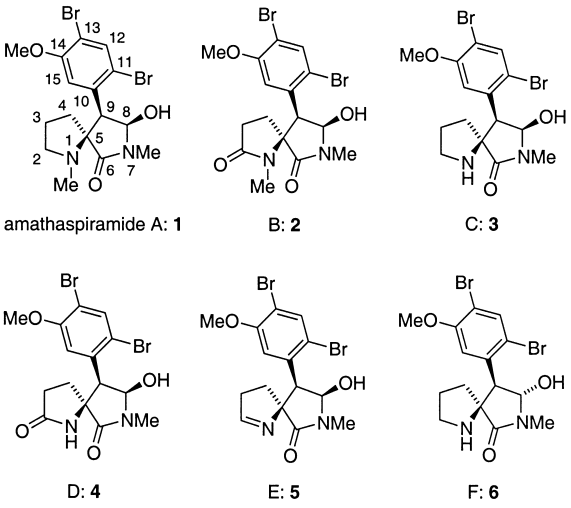
[10] P. v. d. Sluis, A. L. Spek, *Acta Cryst.* **1990**, *A46*, 194.

[11] G. M. Sheldrick, *SHELXTL version 5.1*, Bruker-AXS, Madison WI, **1998**.

The Total Synthesis of (−)-Amathaspiramide F**

Chambers C. Hughes and Dirk Trauner*

The amathaspiramides A–F (**1**–**6**) are a family of marine alkaloids recently isolated from a New Zealand collection of the bryozoan *Amathia wilsoni*.[1,2] Marked by a dense array of polar functionality, the natural products feature a novel



[*] Prof. D. Trauner, C. C. Hughes
Center for New Directions in Organic Synthesis
Department of Chemistry
University of California, Berkeley
Berkeley, CA 94720-1460 (USA)
Fax: (+1) 510-643-9480
E-mail: trauner@cchem.berkeley.edu

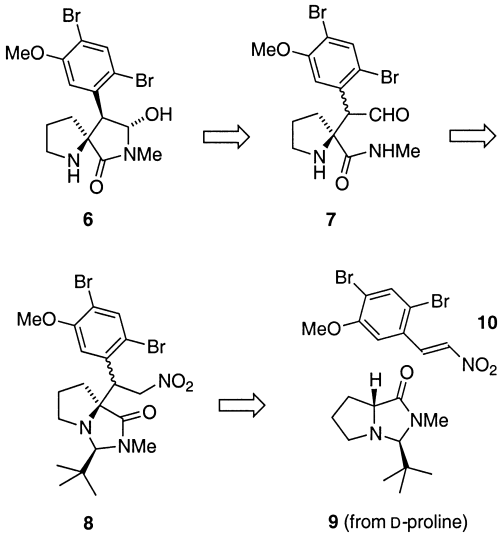
[**] The Center for New Directions in Organic Synthesis is supported by Bristol-Myers Squibb as a Sponsoring Member and Novartis as a Supporting Member. We also thank Eli Lilly for a pre-doctoral fellowship (C.C.H.) and Dr. Frederick J. Hollander and Dr. Allen G. Oliver (Berkeley) for crystal structure determinations.

 © 2002 WILEY-VCH Verlag GmbH & Co. KGaA, Weinheim 0044-8249/02/4123-4556 $ 20.00+.50/0

spirobicyclic core consisting of pyrrolidine and pyrrolidinone rings and an unusual dibromomethoxyphenyl ring. Their structures and absolute configurations were established by anomalous X-ray diffraction of amathaspiramide F and extensive NMR studies. Though several of the amathaspiramides are moderately cytotoxic or show antiviral and antibiotic properties, they attracted our attention mostly due to their intriguing molecular architecture. We now report the first total synthesis of a member of this family, amathaspiramide F (**6**).

Our synthetic program provided an opportunity to showcase Seebach's concept of "self-regeneration of stereochemistry (SRS)",[3] a method for the asymmetric α alkylation of amino acids that has been widely exploited in the preparation of novel amino acids and peptidomimetics and in the total synthesis of several natural products.[4]

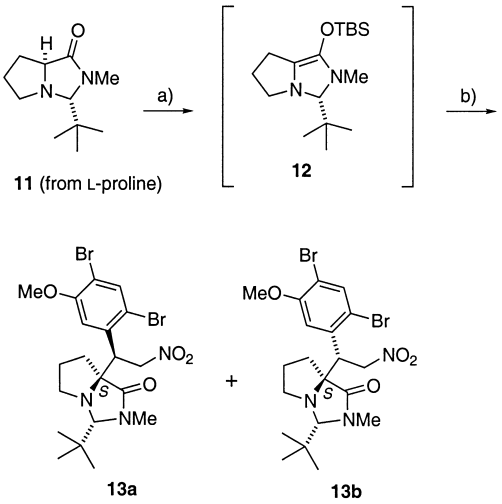
Retrosynthetically, disconnection of the *N*-acyl hemiaminal function in amathaspiramide F (**6**) leads to the amino aldehyde **7**, which can be traced back to the nitroalkyl compound **8** via Nef reaction and engagement of the aldehyde and amide function in a cyclic acetal (Scheme 1). We reasoned that this key intermediate could be derived from *N*,*N*-acetal **9**



Scheme 1. Retrosynthetic analysis of amathaspiramide F.

by conjugate addition of its lithium enolate to the nitrostyrene derivative **10**.[5] The *N*-methyl moiety of the final product would thus be introduced at an early stage of the synthesis. Following ample precedence given by Seebach and others, the alkylation of **9** should proceed under retention of configuration. In other words, the substituent replacing the bridgehead hydrogen atom would reside *cis* with respect to the *tert*-butyl group ("*cis* rule"). We were not particularly concerned about the stereochemical outcome of the conjugate addition with respect to the benzylic stereocenter at C9. Given its position next to a masked carbonyl group, the aryl ring would probably adopt the thermodynamically most stable configuration in the final product.

According to this retrosynthetic analysis, the synthesis of natural 5*S*-configured amathaspiramide F (or C) would require an acetal derived from D-proline as starting material. Because of the relatively high cost of D-proline, however, we decided to first use its cheaper enantiomer, aiming at a synthesis of nonnatural (+)-amathaspiramide F. Our synthesis therefore started with the known *N*,*N*-acetal **11**,[6] the alkylation of which has not been previously reported (Scheme 2). Initial attempts to alkylate **11** were unsuccessful since the α position proved difficult to deprotonate. Fortu-



Scheme 2. Reagents and conditions: a) 1. *t*BuLi, HMPA, THF, −78 °C→RT; 2. TBSCl, 0 °C; b) 1. **10**, −78 °C; 2. $MgBr_2 \cdot OEt_2$, −78 °C→RT, 72 %, 10:1 (**13a**:**13b**) mixture of diastereomers. HMPA = hexamethylphosphoramide, TBSCl = *tert*-butyldimethysilyl chloride.

nately, in the presence of HMPA, the desired enolate could be cleanly generated using *tert*-butyllithium. Simple addition of nitro olefin **10**[7] to this enolate, however, resulted in the formation of a complex mixture with no detectable trace of the desired product. This difficult conjugate addition was finally realized when the silyl ketene acetal **12** was generated in situ and reacted with the nitro olefin in the presence of $MgBr_2 \cdot OEt_2$.[8] A 10:1 mixture of diastereomers **13a** and **13b** was thus obtained (see *Experimental Section*).

To our surprise, however, the two diastereomers **13a** and **13b** turned out to be both *S*-configured at the newly formed quaternary center. This fortuitous violation of the *cis* rule was confirmed by an X-ray analysis of the major diastereomer **13a** (Figure 1).[9,10] Remarkably, both the quaternary and the benzylic stereocenter in **13a** correspond to the natural amathaspiramide series.

According to literature precedence[3b] and our own calculations, the bicyclic silyl ketene acetal **12** adopts a cup-shaped conformation wherein the two nitrogen atoms are pyramidalized and the *tert*-butyl group resides on the convex side of the bicycle (Scheme 3). Conventionally, the alkylation would proceed from this side as well. However, in **12** the bulky TBS substituent is also oriented towards the convex side of the diazabicyclo[3.3.0]octene framework, considerably crowding the corresponding diastereoface of the nucleophilic double bond. Apart from this ground state argument, unfavorable torsional interactions between the *N*-methyl group and the OTBS substituent may occur in a transition state leading to the *cis* product (**14b**). Hence the alkylation takes place from

 © 2002 WILEY-VCH Verlag GmbH & Co. KGaA, Weinheim 0044-8249/02/4123-4557 $ 20.00+.50/0

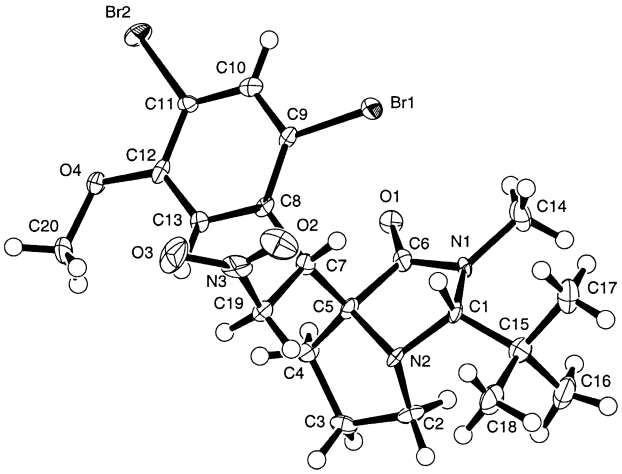
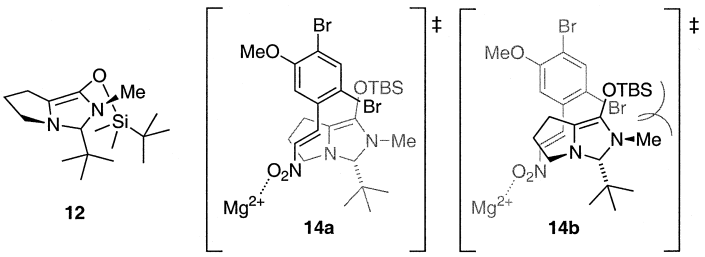


Figure 1. Molecular structure of **13a**.

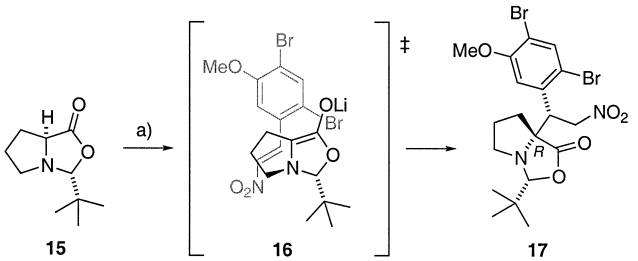


Scheme 3. Stereochemical rationale for the preferred formation of diastereomer **13a**.

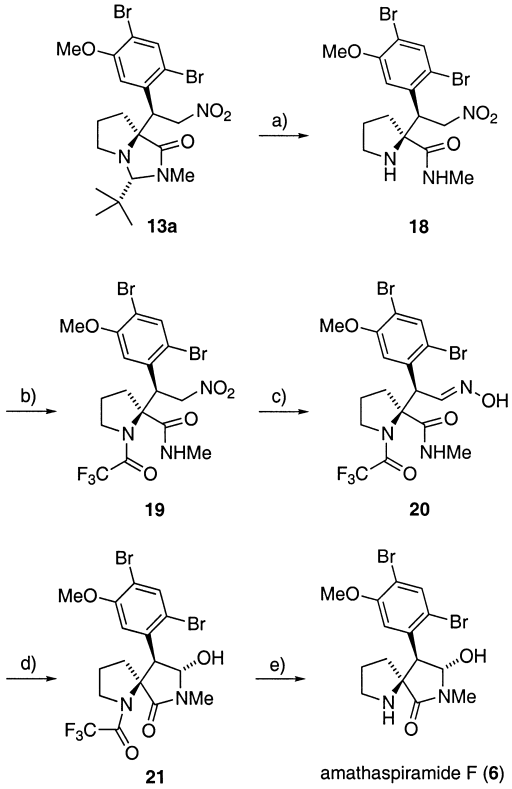
the opposite side, via **14a**, resulting in *trans* substitution with inversion of the stereocenter (Scheme 3). The high simple diastereoselection (10:1 in favor of **13a**) can be explained by invoking an open transition state with the dibrominated phenyl ring oriented away from the bicyclic component.

Supporting this stereochemical rationale, the well-precedented alkylation of *N,O*-acetal **15**[3a] afforded the expected 5*R-cis* product **17**[10] as the only isolated diastereomer (Scheme 4). In this case, the reaction presumably proceeds through the open transition state **16**.

Having quickly assembled the carbon skeleton of the amathaspiramides, we turned our attention toward the formation of the missing heterocyclic ring. The completion of the synthesis required cleavage of the acetal, conversion of the primary nitro group to an aldehyde via a Nef reaction[11] (or its equivalent), and subsequent cyclization to yield amathaspiramide F. Though the hydrolysis of the *N,N*-acetal was achieved without difficulties (Scheme 5), direct implementation of the Nef reaction proved problematic. Starting from either acetal **13a** or its hydrolysis product **18**, no aldehyde or cyclized product could be obtained under a variety of hydrolytic or oxidative conditions.[12]



Scheme 4. Reagents and conditions: a) 1. LDA, THF, −78 °C; 2. **10**, −78 °C→−30 °C, 18 %. LDA = lithium diisopropylamide.



Scheme 5. Reagents and conditions: a) 4 M H_2SO_4, THF, RT, 86 %; b) 1. TFAA, py, CH_2Cl_2, 0 °C; 2. MeOH, 0 °C→RT, 98 %; c) $SnCl_2$, PhSH, Et_3N, MeCN, RT, 85 %; d) IBX, THF, DMSO, RT, 65 %; e) $LiBH_4$, THF, 0 °C→RT, 80 %. TFAA = trifluoroacetic anhydride, IBX = 1-hydroxy-1,2-benziodoxol-3(*1H*)-one-1-oxide.

Since all attempts to convert the nitro group into the aldehyde in the presence of a free secondary amine failed, we reluctantly resorted to protecting group manipulations. Recently, the trifluoroacetyl function has emerged as a useful protecting group for sterically hindered amines,[13] for example, those attached to a quaternary center. Accordingly, **18** was treated with trifluoroacetic anhydride to afford **19** (Scheme 5). With the basic nitrogen thus protected, **19** could be efficiently converted to oxime **20** following a protocol described by Bartra et al.[14] Hydrolysis of the oxime with concomitant cyclization was then achieved with a hypervalent iodine reagent (IBX)[15] to afford *N*-trifluoroacetyl amathaspiramide F (**21**).[16] Notably, no formation of the diastereomer corresponding to amathaspiramide C was observed under these conditions. Finally, amathaspiramide F (**6**) was obtained upon treatment of **21** with lithium tetrahydroborate in THF.[17] The spectra of our synthetic material (NMR, IR, MS) closely match the ones published for the natural product,[1] and the optical rotation of our sample ($[\alpha]_D^{25} = -41.0$, $c = 0.50$, MeOH; ref. [1]: $[\alpha]_D = -10$, $c = 0.0023$, MeOH) confirmed the absolute configuration of our synthetic amathaspiramide F.[18]

In summary, a highly stereocontrolled total synthesis of (−)-amathaspiramide F was achieved in six steps starting

 © 2002 WILEY-VCH Verlag GmbH & Co. KGaA, Weinheim 0044-8249/02/4123-4558 $ 20.00+.50/0 *Angew. Chem. Int. Ed.* **2002**, *41*, No. 23

from the known acetal **11**. The synthesis features a remarkable exception to the well-established *cis* rule governing SRS chemistry, reaffirming that subtle changes in the substrate can lead to dramatically different stereochemical outcomes. It also presents an efficient method for circumventing a problematic Nef reaction in the presence of densely spaced polar functionality. Studies toward the synthesis of other members of the amathaspiramide family, particularly amathaspiramides C and E, are underway and will be reported in due course.

Experimental Section

To amide **11** (235 mg, 1.19 mmol) in THF (4.0 mL) at −78 °C a solution of *t*BuLi in pentane (0.88 mL, 1.5 M, 1.3 mmol) was added dropwise using a syringe. After 10 min HMPA (250 μL, 1.44 mmol) was added by syringe, and after additional 10 min the solution was allowed to warm to room temperature over 1 h. The solution was then cooled to 0 °C, and TBSCl (218 mg, 1.44 mmol) in THF (1.0 mL) was added dropwise using a cannula. After 1 h at 0 °C the solution was cooled to −78 °C, and nitroalkene **10** (485 mg, 1.44 mmol) in THF (7.0 mL) was added dropwise by cannula. Immediately, $MgBr_2{\cdot}OEt_2$ (372 mg, 1.44 mmol) was added in one portion. The reaction mixture was maintained at −78 °C for 2 h then allowed to warm to room temperature over 10 h. The solution was poured into saturated $NaHCO_3$ solution (200 mL) and extracted five times with CH_2Cl_2 (100 mL). The combined organic layers were washed once with brine (100 mL), dried, filtered, and concentrated. The product was purified by column chromatography (40 % EtOAc in hexanes) to afford 459 mg (72 %) of **13a/b** as a white solid. The major diastereomer **13a** could be purified by recrystallization from CH_2Cl_2/hexanes. The crystals obtained had a clear, columnar appearance distinct from the yellow, blocky appearance of the minor diastereomer **13b**.

13a: $[\alpha]_D^{25} = -21.7$ ($c = 1.00$, $CHCl_3$); mp: 198–200 °C; IR (KBr): $\tilde{\nu} = 2966$, 1694, 1549, 1476, 1368, 1251, 1058 cm^{-1}; ^1H NMR (500 MHz, $CDCl_3$, 25 °C): $\delta = 7.73$ (s, 1H), 6.78 (s, 1H), 4.97 (dd, $J = 13.5$, 5.5 Hz, 1H), 4.82 (dd, $J = 13.5$, 9.5 Hz, 1H), 4.53 (dd, $J = 9.5$, 5.5 Hz, 1H), 3.88 (s, 3H), 3.78 (s, 1H), 3.07 (m, 1H), 2.88 (s, 3H), 2.78 (m, 1H), 2.01–2.11 (m, 2H), 1.67–1.82 (m, 2H), 1.12 ppm (s, 9H); ^{13}C NMR (125 MHz, $CDCl_3$, 25 °C): $\delta = 177.5$, 155.6, 136.9, 135.8, 117.7, 112.4, 111.0, 83.6, 76.7, 75.4, 56.7, 49.5, 44.6, 33.4, 30.8, 30.6, 25.3 ppm; HRMS (FAB$^+$): $m/z(M-H^+)$: calcd for $C_{20}H_{28}{}^{79}Br^{81}BrN_3O_4$: 534.0426; found: 534.0417.

Received: July 22, 2002 [Z19801]

[1] B. D. Morris, M. R. Prinsep, *J. Nat. Prod.* **1999**, *62*, 688 – 693.

[2] A series of related but distinct brominated alkaloids, amathamides A–G, were isolated from a Tasmanian collection of *A. wilsoni* Kirkpatrick. See a) A. J. Blackman, D. J. Matthews, *Heterocycles* **1985**, *23*, 2829 – 2833; b) A. J. Blackman, R. D. Green, *Aust. J. Chem.* **1987**, *40*, 1655 – 1662; c) A. J. Blackman, T. P. D. Eldershaw, S. M. Garland, *Aust. J. Chem.* **1993**, *46*, 401 – 405.

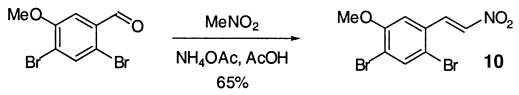
[3] a) D. Seebach, M. Boes, R. Naef, W. B. Schweizer, *J. Am. Chem. Soc.* **1983**, *105*, 5390 – 5398; b) for an extensive review, see: D. Seebach, A. R. Sting, M. Hoffmann, *Angew. Chem.* **1996**, *108*, 2880 – 2921; *Angew. Chem. Int. Ed. Engl.* **1996**, *35*, 2708 – 2748.

[4] For the use of proline-derived acetals in natural product synthesis, see: a) R. M. Williams, T. Glinka, E. Kwast, *J. Am. Chem. Soc.* **1988**, *110*, 5927 – 5929; b) N. Isono, M. Mori, *J. Org. Chem.* **1995**, *60*, 115 – 119.

[5] For an extensive review of asymmetric Michael additions to nitroalkenes, see: O. M. Berner, L. Tedeschi, D. Enders, *Eur. J. Org. Chem.* **2002**, 1877 – 1894.

[6] W. O. Moss, A. C. Jones, R. Wisedale, M. F. Mahon, K. C. Molloy, R. H. Bradbury, N. J. Hales, T. Gallagher, *J. Chem. Soc. Perkin Trans. 1* **1992**, *20*, 2615 – 2624.

[7] The nitro olefin was obtained from a Henry reaction involving the known aldehyde (H. H. Hodgson, H. G. Beard, *J. Chem. Soc.* **1925**, 875 – 881) and nitromethane:



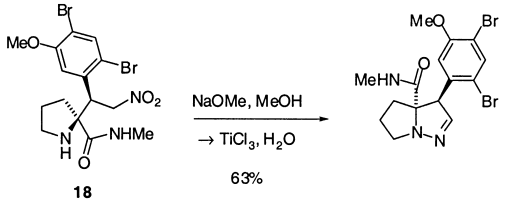
[8] J. A. Tucker, T. L. Clayton, D. M. Mordas, *J. Org. Chem.* **1997**, *62*, 4370 – 4375.

[9] The stereochemistry of **13a** and **13b** was further substantiated by NOE's observed between the acetalic proton and benzylic protons in both isomers.

[10] All X-ray measurements were made on a SMART CCD area detector with graphite monochromated $Mo_{K\alpha}$ radiation ($\lambda = 0.71069$ Å). **13a** ($C_{20}H_{27}Br_2N_3O_4$): crystal dimensions $0.32 \times 0.21 \times 0.13$ mm, monoclinic, space group $P2_1$, $a = 14.5715(4)$, $b = 7.7135(1)$, $c = 20.3642(5)$ Å, $\beta = 108.981(1)^o$, $V = 2164.43(9)$ Å^3, $Z = 4$, $\rho_{calcd} = 1.633$ g cm^{-3}, $2\theta_{max} = 49.4^o$, $T = 138$ K, 9660 measured reflections, 4007 independent reflections ($R_{int} = 0.061$), data were corrected for Lorentz and polarization effects, $\mu = 37.88$ cm^{-1}, $[\delta/\sigma]_{max} = 0.00$, 522 parameters refined, $R = 0.037$ (for 4982 reflections with $I > 3.00\sigma(I)$), $R_w = 0.043$, max./min. residual peaks in the final difference map 0.35/−0.53 e Å^{-3}. **17** ($C_{19}H_{24}Br_2N_2O_5{\cdot}0.5\,CH_2Cl_2$): crystal dimensions $0.22 \times 0.20 \times 0.07$ mm, orthorhombic, space group $P2_12_12_1$, $a = 9.1876(8)$, $b = 16.632(2)$, $c = 30.276(3)$ Å, $V = 4626.3(7)$ Å^3, $Z = 8$, $\rho_{calcd} = 1.619$ g cm^{-3}, $2\theta_{max} = 46.5^o$, $T = 138$ K, 18751 measured reflections, 3963 independent reflections ($R_{int} = 0.108$), data were corrected for Lorentz and polarization effects, $\mu = 36.62$ cm^{-1}, $[\delta/\sigma]_{max} = 0.01$, 532 parameters refined, $R = 0.040$ (for 4202 reflections with $I > 3.00\sigma(I)$), $R_w = 0.044$, max./min. residual peaks in the final difference map 0.32/−0.43 e Å^{-3}. CCDC-188930 (**13a**) and CCDC-192396 (**17**) contain the supplementary crystallographic data for this paper. These data can be obtained free of charge via www.ccdc.cam.ac.uk/conts/retrieving.html (or from the Cambridge Crystallographic Data Centre, 12, Union Road, Cambridge CB2 1EZ, UK; fax: (+44) 1223-336-033; or deposit@ccdc.cam.ac.uk).

[11] H. W. Pinnick in *Organic Reactions, Vol. 38* (Eds.: P. Beak, R. Bittman, E. Ciganek, S. Hanessian, L. Hegedus, R. C. Kelly, S. V. Ley, L. E. Overman, H. J. Reich, C. J. Sih, A. B. Smith III, M. Uskokovic), Wiley, New York, **1990**, p. 655, and references therein.

[12] Nevertheless, some remarkable reactivity was noticed. For instance, when nitro compound **18** was deprotonated to form the corresponding nitronate and then treated with $TiCl_3$, an unexpected cyclization occurred that (to our knowledge) represents a conceptually novel method for synthesizing hydrazones:



[13] For recent applications of the TFA protecting group, see: a) K. C. Nicolaou, B. S. Safina, C. Funke, M. Zak, F. J. Zécri, *Angew. Chem.* **2002**, *114*, 2017 – 2020; *Angew. Chem. Int. Ed.* **2002**, *41*, 1937 – 1940; b) M. W. Carson, G. Kim, M. F. Henteman, D. Trauner, S. J. Danishefsky, *Angew. Chem.* **2001**, *113*, 4582 – 4584; *Angew. Chem. Int. Ed.* **2001**, *40*, 4450 – 4452; c) M. W. Carson, G. Kim, S. J. Danishefsky, *Angew. Chem.* **2001**, *113*, 4585 – 4588; *Angew. Chem. Int. Ed.* **2001**, *40*, 4453 – 4456.

[14] M. Bartra, P. Romea, F. Urpi, J. Vilarrasa, *Tetrahedron* **1990**, *46*, 587 – 594.

[15] D. S. Bose, P. Srinivas, *Synlett* **1998**, 977 – 978.

[16] All attempts to perform a one-pot Nef reaction on **19** to afford **21** directly were unsuccessful.

[17] Deprotection with sodium tetrahydroborate in ethanol resulted in significant reduction of the hemiaminal function.

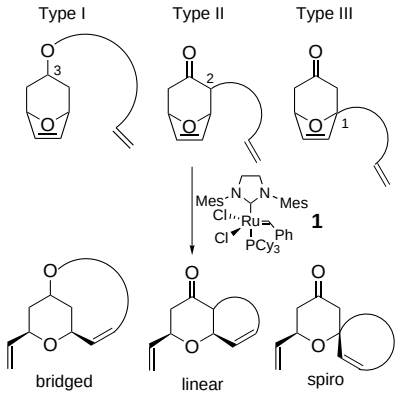
[18] The large discrepancy in value of the optical rotation is perhaps due to the low concentration of the natural sample.

 © 2002 WILEY-VCH Verlag GmbH & Co. KGaA, Weinheim 0044-8249/02/4123-4559 $ 20.00+.50/0

Synthesis of Functionalized Pyrans by Domino Metathesis Reaction of Oxabicyclo Derivatives: Dramatic Effect of Remote Substituents on Reactivity and Selectivity**

Lynn C. Usher, Maria Estrella-Jimenez, Ion Ghiviriga, and Dennis L. Wright*

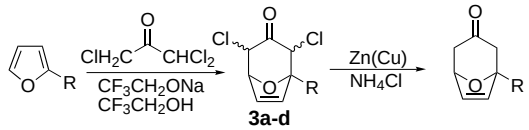
Highly substituted pyrans are a common structural feature found in natural products and have been the focus of many synthesis studies.[1] They are often present as an integral part of macrocyclic structures of marine origin. We previously reported[2] a general method for the preparation of *cis*-2,6-disubstitued-4-pyrones through the intermolecular ring-opening cross-metathesis reaction of 8-oxabicyclo[3.2.1]octene derivatives, which are conveniently prepared by the [4+3] cycloaddition between furan and an oxyallyl cation equivalent.[3] A more advanced variation occurs when the donor olefin is tethered to the bicyclic ring system. The second metathesis process would effect a ring closure, thereby resulting in the synthesis of annulated pyran systems. In principle, there are three manifolds for this bond-reorganization process, determined by placement of the tether (Scheme 1).[4]



Scheme 1. Synthesis of fused pyrans by metathesis-promoted bond reorganization.

A type I bond-reorganization process would arise if the tether was attached at C3, leading to the synthesis of bridged fused pyrans. Placement of the tether at C2 leads to a linear fused system, whereas a type III cyclization from the C1 position would lead to spiro-fused pyrans. Herein, we wish to report our studies on the type III cyclization and the dramatic influence of remote substituents on the domino process. These compounds are of interest as building blocks for natural product syntheses[5] and as novel scaffolds for combinatorial libraries.[6]

To examine the facility of this process, a series of oxabicyclo[3.2.1]octan-3-one derivatives with an olefinic tether at the bridgehead were prepared by oxyallyl cation cycloaddition of 2-substituted furans (Scheme 2). Reaction

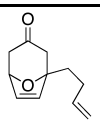
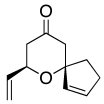
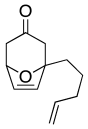
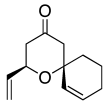
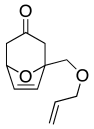
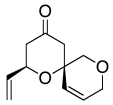
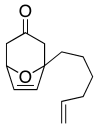
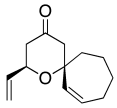


2a: R = $(CH_2)_2CH{=}CH_2$ — **4a**, 69% for two steps
2b: R = $(CH_2)_3CH{=}CH_2$ — **4b**, 72% for two steps
2c: R = $CH_2OCH_2CH{=}CH_2$ — **4c**, 65% for two steps
2d: R = $(CH_2)_4CH{=}CH_2$ — **4d**, 68% for two steps

Scheme 2. Synthesis of substituted bicyclic ethers.

of the furans under the conditions of Föhlisch et al.[7] led to a smooth conversion into the oxabicyclo[3.2.1]octenes **3a–d**. Direct dechlorination upon exposure to zinc–copper couple gave the metathesis precursors **4a–d** in good yields. With a series of dienes in hand, we were able to study the domino metathesis process (Table 1).

Table 1. Synthesis of spirocyclic pyrans.

Alkene	Product[a]	Yield [%][b]
4a 	**5a** 	56 (16)
4b 	**5b** 	82 (10)
4c 	**5c** 	80
4d 	**5d** 	< 15 (44)[c]

[a] Reaction conditions: substrate in CH_2Cl_2 (0.01M), **1** (2 mol%). [b] Yield of recovered starting material in parentheses. [c] The dimer was also isolated (38%).

Exposure of a dilute solution of the dienes **4a–c** to the Grubbs catalyst **1**[8] led to rearrangement to the corresponding five- and six-membered spirocycles **5a–c** in good yield. Cyclization to form the seven-membered homologue **5d** was extremely poor, the major product arising from dimerization of the terminal vinyl groups. Furthermore, much of the starting alkene was recovered unchanged. Increased catalyst or elevated temperatures did little to improve the yield of the reaction.

This method is also compatible with the analogous oxabicyclo[2.2.1]heptene derivatives leading to perhydro-spirofur-

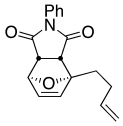
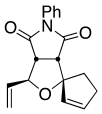
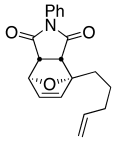
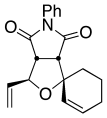
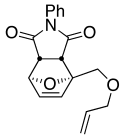
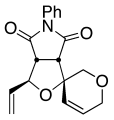
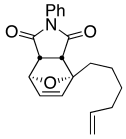
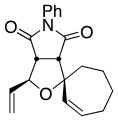
[*] Prof. Dr. D. L. Wright, L. C. Usher, M. Estrella-Jimenez, Dr. I. Ghiviriga
Department of Chemistry, University of Florida
Gainesville, FL 32611-7200 (USA)
Fax: (+1) 352-846-0296
E-mail: dwright@chem.ufl.edu

[**] We thank the National Science Foundation for support of this work. MEJ thanks the University of Florida for a graduate minority fellowship. We thank Professor Merle A. Battiste and Professor William R. Dolbier for helpful discussions.

 © 2002 WILEY-VCH Verlag GmbH & Co. KGaA, Weinheim 0044-8249/02/4123-4560 $ 20.00+.50/0

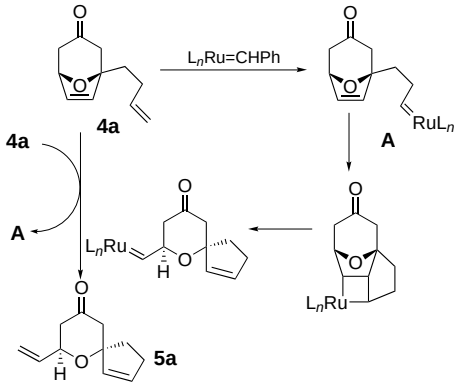
ans. The substrates were easily prepared from furans **2a–d** by Diels–Alder reaction with *N*-phenylmaleimide. The major *exo* adducts were treated with the Grubbs catalyst to trigger rearrangement (Table 2). The reactions of these derivatives delivered the rearranged furans **7a–d** in moderate to excellent yields. Again, five- and six-membered cyclizations were the most efficient. Interestingly, the formation of the seven-membered ring **7d** was significantly better in this series. This could be related to the enhanced reactivity of the more strained oxabicyclo[2.2.1]heptene nucleus.

Table 2. Synthesis of spirocyclic perhydrofurans.

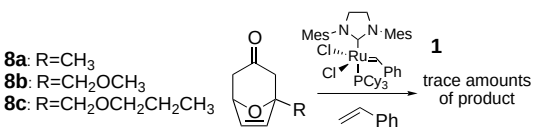
	Alkene		Product[a]	Yield [%][b]
6a		**7a**		84
6b		**7b**		78
6c		**7c**		95
6d		**7d**		54 (19)

[a] Conditions: substrate in CH_2Cl_2 (0.01 M), **1** (2 mol%). [b] Yield of recovered starting material in parentheses.

One possible mechanism[9] involves initial reaction with the vinyl group followed by cyclization to close the carbocyclic ring and open the bicyclic olefin simultaneously (Scheme 3). An alternative path would require a regioselective opening of the bridged olefin followed by cyclization onto the pendant olefin. Since the reactions had proceeded cleanly and in high yield, we favored the former mechanism. However, there is little information regarding the influence of bridgehead substituents,[10] and we felt that the intermolecular variant



Scheme 3. Proposed mechanism for the domino metathesis reaction.



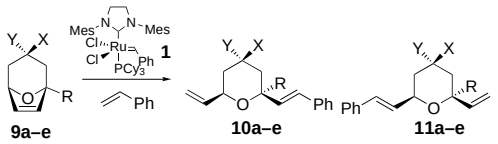
Scheme 4. Attempted ring-opening of substituted systems.

offered an opportunity to probe these regiochemical issues (Scheme 4).

Surprisingly, exposure of the substituted compounds **8a–c** to catalyst and styrene gave only trace amounts of product, even after prolonged reaction times and elevated temperatures. In fact, the compounds could not even be forced to undergo ROMP in refluxing toluene. The inability to effect ring-opening of these systems may be related to shielding of the *exo* face of the olefin by the bridgehead group. This suggests that the intramolecular reaction proceeded by initial reaction with the terminal olefin. Since ensuing attack at the bridge alkene would be intramolecular, it would be less sensitive to these steric effects.

In previous studies,[2] an unusual influence of the group at C3 was observed: reduction/silylation of the ketone greatly increased the reactivity of the bicyclic alkene towards ring opening. It seemed possible that this remote effect may be used to induce reactivity in the unreactive olefins. To examine this possibility, a series of reduced derivatives was prepared[11] and subjected to metathesis conditions (Table 3).

Table 3. Intermolecular cross-metathesis of reduced derivatives.



Alkene[a]	R	X	Y	Yield [%]	**10**/**11**[b]
9a	Me	OTBS	H	83	6:1
9b	CH_2OMe	OTBS	H	65	1:1
9c	Me	OH	H	85	20:1
9d	CH_2OMe	OH	H	66	20:1
9e	Me	H	OH	15	6:1

[a] Conditions: substrate in CH_2Cl_2 (0.3 M), styrene (3–4 equiv), **1** (1.5 mol%). [b] Ratios approximated by NMR spectroscopy and GC analysis.

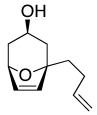
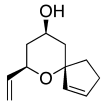
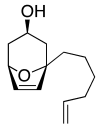
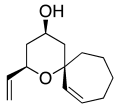
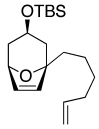
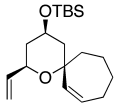
Reduction/silylation of ketones **8a** and **8b** gave adducts **9a**/**9b**. As previously observed, this structural change resulted in a dramatic change in reactivity. Both compounds opened readily with styrene to give the cross-metathesis products **10**/**11**. The methyl-substituted compound **9a** showed good regioselectivity, giving the more substituted isomer **10a** as the major product (6:1). The methoxymethyl derivative **9b** was not selective, thus giving an almost equal mixture of the two regioisomers. In a very surprising result, opening of the *endo* alcohols **9c**/**9d** with styrene, although a much slower reaction, showed a dramatic increase in regioselectivity, producing the more substituted derivatives **10c**/**10d** in an approximately 20:1 predominance. This high selectivity was lost when the reactions were run at higher temperatures or in

 © 2002 WILEY-VCH Verlag GmbH & Co. KGaA, Weinheim 0044-8249/02/4123-4561 $ 20.00+.50/0

the presence of a larger excess of catalyst. The origin of this enhanced reactivity and selectivity appears to be an exclusive *endo* effect. Opening of the *exo* alcohol **9e** was extremely sluggish, only proceeding to about 15%. Moreover, the regioselectivity of the product had decreased to a ratio of about 6:1. These effects could be a result of the steric interaction of the axial group with the bridged alkene or an electronic effect similar to those seen in norbornyl systems.[12]

Although the nature of the effect is unclear, we proposed that this rate acceleration could be used to improve some of the previous spirocyclizations. If the reaction proceeds as in Scheme 3, then the second ring-closing step should be accelerated by similar structural changes. Therefore, we examined the spirocyclization with reduced forms of dienes **4a** and **4d** (Table 4). We examined the five- and seven-membered ring closures, since these were less efficient than

Table 4. Spirocyclizations with reduced derivatives.

Alkene		Product[a]		Yield[b]
12		**13**		83%
14		**15**		48%
15		**17**		80%

cyclizations to form cyclohexyl rings. In the case of cyclopentyl rings it may be somewhat difficult for the shorter tether to reach the bridged alkene, whereas the seven-membered ring may be slowed by nonbonded interactions in the tether. Diene **4a** was reduced to the *endo* alcohol **12**, and rearrangement gave **13** in an improved yield of 83%. The more difficult cyclization to form the seven-membered ring systems was also better with *endo* alcohol **14**, tripling the yield to 48%. Since the silyl ethers were more reactive in the intermolecular case, it seemed possible that an even better rate enhancement could be produced. Treatment of **16** with the ruthenium catalyst resulted in a rapid reaction, delivering the spiro product **17** in 80% yield. This study nicely illustrates the potential of tuning alkene reactivity in these types of reactions.

Olefin-metathesis reactions have become important bond-forming reactions in contemporary synthetic chemistry. Domino ring-opening/ring-closing reactions are a convenient way to construct polycyclic systems from readily available bridged bicyclic alkenes. We have been able to develop a method to prepare spiro-annulated pyrans from furan. An important aspect of this study is the finding that the reactivity and selectivity of the metathesis reactions can be tuned by manipulation of functional groups on the substrate. Although the origins of these effects are still under investigation, it is clear that they can play an extremely important part in metathesis reactions. Further studies on these effects and the synthesis of other types of annulated pyrans are currently under investigation.

Received: July 8, 2002 [Z19679]

[1] M. C. Elliot, *J. Chem. Soc. Perkin Trans. 1* **1998**, 4175–4200, and references therein.

[2] D. L. Wright, L. C. Usher, M. Estrella-Jimenez, *Org. Lett.* **2001**, *3*, 4275–4277;a) for other approaches to pyrans by RCM, see: M. E. Maier, M. Bugl, *Synlett* **1998**, 1390–1392; b) B. Schmidt, H. Wildemann, *J. Org. Chem.* **2000**, *65*, 5817–5822; c) B. Schmidt, H. Wildemann, *J. Chem. Soc. Perkin Trans. 1* **2000**, 2916–2925.

[3] For excellent reviews, see: a) H. M. R. Hoffmann, *Angew. Chem.* **1984**, *96*, 29–48; *Angew. Chem. Int. Ed. Engl.* **1984**, *23*, 1–19; b) J. H. Rigby, F. C. Pigge in *Organic Reactions, Vol. 51* (Ed.: L. A. Paquette), Wiley, New York, **1997**, p. 351.

[4] For examples of domino metathesis reactions, see: a) N. Buschmann, A. Rückert, S. Blechert, *J. Org. Chem.* **2002**, *67*, 4325–4329; b) O. Arjona, A. G. Csaky, R. Medel, J. Plumet, *J. Org. Chem.* **2002**, *67*, 1380–1383; c) R. Stragies, S. Blechert, *J. Am. Chem. Soc.* **2000**, *122*, 9584–9591; d) O. Arjona, A. G. Csaky, M. C. Murcia, J. Plumet, *Tetrahedron Lett.* **2000**, *41*, 9777–9779; e) R. Stragies, S. Blechert, *Tetrahedron*, **1999**, *55*, 8179–8188; f) R. Stragies, S. Blechert, *Synlett* **1998**, 169–170.

[5] a) S. W. Pelletier, N. V. Mody, Z. Djarmati, S. D. Lajsic, *J. Org. Chem.* **1976**, *41*, 3042–3044; b) D. J. Aberhart, K. H. Oberton, S. Huneck, *J. Chem. Soc. C.* **1970**, *11*, 1612–1614.

[6] M. A. Walters, F. La, P. Desmukh, D. O. Omencinsky, *J. Comb. Chem.* **2002**, *4*, 125–130.

[7] B. Föhlisch, E. Gehrlach, B. Geywitz, *Chem. Ber.* **1987**, *120*, 1815–1824.

[8] M. Scholl, S. Ding, C. W. Lee, R. H. Grubbs, *Org. Lett.* **1999**, *1*, 953–956.

[9] M. F. Schneider, N. Lucas, J. Velder, S. Blechert, *Angew. Chem.* **1997**, *109*, 257–259; *Angew. Chem. Int. Ed. Engl.* **1997**, *36*, 257–259; for a review, see: A. Fürstner, *Angew. Chem.* **2000**, *112*, 3140–3172; *Angew. Chem. Int. Ed.* **2000**, *39*, 3012–3043.

[10] a) J. Plumet, O. Arjona, A. G. Csaky, *Synthesis* **2000**, *6*, 857–861; b) M. L. Randall, J. A. Tallarico, M. L. Snapper, *Tetrahedron*, **1997**, *48*, 16511–16520; c) M. L. Randall, J. A. Tallarico, M. L. Snapper, *J. Am. Chem. Soc.* **1995**, *117*, 9610–9611; d) O. Arjona, A. G. Csaky, M. C. Murcia, J. Plumet, *J. Org. Chem.* **1999**, *64*, 9739–9741; e) J. G. Hamilton, K. J. Ivin, M. McCann, J. J. Rooney, *J. Chem. Soc. Chem. Commun.* **1984**, 1379–1381.

[11] Reduction with L-selectride at −78 °C gave exclusively the *endo* alcohols in 80–90% yield. The *exo* alcohol was prepared by reduction with SmI_2 (60% yield, one isomer).

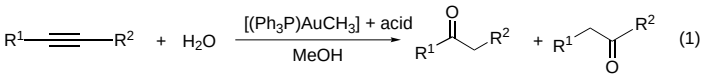
[12] For some examples, see: a) G. Mehta, G. Gunasekaran, S. R. Gadre, R. N. Shirsat, B. Ganguly, J. Chandrasekhar, *J. Org. Chem.* **1994**, *59*, 1953–1955; b) G. Mehta, F. A. Khan, *J. Am. Chem. Soc.* **1990**, *112*, 6140–6142.

 © 2002 WILEY-VCH Verlag GmbH & Co. KGaA, Weinheim 0044-8249/02/4123-4562 $ 20.00+.50/0

Highly Efficient Au^I-Catalyzed Hydration of Alkynes**

Eiichiro Mizushima, Kazuhiko Sato, Teruyuki Hayashi,* and Masato Tanaka*

Hydration of unsaturated carbon compounds is one of the most straightforward and environmentally benign methods to form the carbon–oxygen bond. Synthesis of carbonyl compounds by the hydration of alkynes is an important variation in this category, which has been extensively studied.[1] Acid-catalyzed hydration of alkynes is long known.[2,3] However, only electron-rich acetylene compounds, such as alkynyl ethers, alkynyl thioethers and ynamines react satisfactorily.[1d,4] The reaction of simple alkynes is usually sluggish and needs cocatalysts, typically toxic mercury(II) salts, to enhance the reactivity.[5] More recent interest lies in the use of transition-metal-complex catalysts containing Ru^{II},[6] Ru^{III},[7] Rh,[8] Pt,[9] Au^{III},[10] and other metal centers.[11] However, the process catalyzed by these complexes is not efficient either. The highest turnover frequency (TOF) is 550 h^{-1} claimed as the initial TOF for the hydration of 3-pentyn-1-ol catalyzed by [*cis*-$PtCl_2$(tppts)$_2$] (tppts = P(*m*-$C_6H_4SO_3Na)_3$), but its overall TOF is no more than approximately 100 h^{-1}.[9c] Recently Teles and co-workers reported the addition of methanol to alkynes catalyzed by Au^I species in conjunction with acidic cocatalysts.[12] Hydration of propargyl alcohol was also briefly mentioned in their patent application,[13] although the yield was quite low.[14] Herein we report that the Au^I–acid systems in aqueous methanol serve as powerful catalysts,[15] which promote the hydration of alkynes [Eq. (1)] and have turnover frequencies of at least two orders of magnitude higher than [*cis*-$PtCl_2$(tppts)$_2$].



(1)

In a preliminary experiment, a mixture of 1-octyne (1 mmol), [$(Ph_3P)AuCH_3$] (0.01 mmol, 1 mol %) and concentrated sulfuric acid (0.5 mmol, 50 mol %) in aqueous methanol (1.5 mL, methanol:H_2O = 2:1 v/v) was heated for 1 h at 70 °C affording the corresponding Markovnikov hydration product, 2-octanone, in 95 % yield without anti-Markovnikov hydration, or possible methanol addition.[12] The reaction did not proceed in the absence of either the Au catalyst or sulfuric acid.

[*] Dr. T. Hayashi, Prof. Dr. M. Tanaka, Dr. E. Mizushima, Dr. K. Sato
National Institute of Advanced Industrial Science and Technology
Tsukuba Central 5, Tsukuba, Ibaraki 305-8565 (Japan)
Fax: (+81) 298-61-4511
E-mail: t.hayashi@aist.go.jp
m.tanaka@res.titech.ac.jp
Prof. Dr. M. Tanaka
Chemical Resources Laboratory
Tokyo Institute of Technology
4259 Nagatsuta, Midori-ku, Yokohama 226-8503 (Japan)
Fax: (+81) 45-924-5244

[**] E.M. thanks the NEDO for a postdoctoral fellowship.

The following aspects about the catalytic system are worth noting. First, the nature of the reaction medium significantly affects the reaction. The reaction run without using solvent (in otherwise the same conditions as the preliminary experiment) did not furnish 2-octanone. On the other hand, the use of 2-propanol (71 %), dioxane (56 %), acetonitrile (53 %), or THF (11 %) resulted in a low yield, and the yield obtained with dichloromethane, DMF, or toluene was even lower. Thus methanol was the solvent of choice for this particular transformation.[16]

Second, the efficiency of the catalyst was significantly enhanced by addition of appropriate ligands, which enabled the quantity of the precious catalyst used to be minimized. For instance, the control experiment run without ligand addition under the conditions shown in Table 1 (only 0.01 mol % catalyst) gave 2-octanone in only 35 % yield (TOF = 3500 h^{-1}, entry 1), while the yield dramatically increased to 99 % when the reaction was carried out under an atmosphere of carbon monoxide (TOF = 9900 h^{-1}, entry 2). Addition of triphenyl phosphite (2 equiv relative to Au) also boosted the yield, to 90 % (TOF = 9000 h^{-1}, entry 3). The reaction of phenylacetylene under the standard conditions of Table 1 gave a 14 % yield of acetophenone (TOF = 1400 h^{-1}), while the same reaction carried out under an atmosphere of carbon monoxide resulted in a 33 % yield (TOF = 3300 h^{-1}). Although the provenance of the ligand effect is ambiguous at this time, it is envisaged to be associated with the stability of the catalyst. The reactions without the addition of ligand occasionally proceeded with catalyst deterioration, which could be observed as metallic particle precipitation. However, when these reactions were run in the presence of CO, phosphites, or ethyl diphenylphosphinite, particle formation was not evident. On the other hand, addition of triphenylphosphane resulted in a total loss of catalytic activity.

Table 1. Hydration of 1-octyne in methanol.[a]

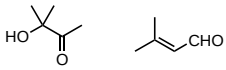
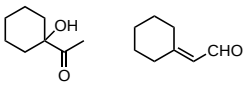
Entry	Acid	Additive	Yield[b]
1	H_2SO_4	–	35 %
2	H_2SO_4	CO (1 atm)	99 %
3	H_2SO_4	$(PhO)_3P$ (0.004 mmol)	90 %
4	CF_3SO_3H	–	99 %
5	CH_3SO_3H	–	77 %
6	$H_3PW_{12}O_{40}$	–	80 %

[a] Reaction conditions: [$(Ph_3P)AuCH_3$] 0.002 mmol, acid 0.5 mmol, 1-octyne 20 mmol, water 1 mL, methanol 10 mL, 70 °C, 1 h. [b] GC yield of 2-octanone.

Third, other acid catalysts, such as CF_3SO_3H, CH_3SO_3H, and $H_3PW_{12}O_{40}$ (entries 4–6) also gave extremely high yields even in the absence of the coordinative additives. The reaction of 1-octyne in the presence of CF_3SO_3H using only 0.005 mol % of the gold catalyst under otherwise the same conditions as those in entry 4 gave a 70 % yield (TOF = 14000 h^{-1}). Since the activity was already high, the effect of carbon monoxide was only marginal, but a distinct increase in the yield to 78 % (TOF = 15600 h^{-1}) was obtained when the reaction was run under an atmospheric pressure of carbon monoxide. The turnover frequency reported herein is the highest recorded.

 © 2002 WILEY-VCH Verlag GmbH & Co. KGaA, Weinheim 0044-8249/02/4123-4563 $ 20.00+.50/0

Table 2. Gold(I)-catalyzed hydration of alkynes, see Equation (1).[a]

Entry	Alkynes		Adducts	Cat. mol%	Time	Yield[b]	
	R^1	R^2					
1[c]	n-C_6H_{13}	H	n-$C_6H_{13}C(O)CH_3$	0.1	1 h	80%	
2[d]	n-C_4H_9	H	n-$C_4H_9C(O)CH_3$	0.2	2 h	99%	
3		H		1.0	1 h	90%	
4	$NC(CH_2)_3$	H	$NC(CH_2)_3C(O)CH_3$	0.2	1 h	83%	
5[e]	$Cl(CH_2)_3$	H	$Cl(CH_2)_3C(O)CH_3$	1.0	4 h	72%	
6		H		1.0	2 h	44%[f]	20%[g]
7[h]		H		1.0	2 h	45%[f]	17%[g]
8[i]	C_6H_5	H	$C_6H_5C(O)CH_3$	0.2	1 h	98%	
9	o-$CH_3OC_6H_4$	H	o-$CH_3OC_6H_4C(O)CH_3$	0.2	1 h	95%	
10	m-$CH_3OC_6H_4$	H	m-$CH_3OC_6H_4C(O)CH_3$	1.0	1 h	77%	
11	p-$CH_3OC_6H_4$	H	p-$CH_3OC_6H_4C(O)CH_3$	0.2	1 h	93%	
12[i]	p-$CH_3C_6H_4$	H	p-$CH_3C_6H_4C(O)CH_3$	0.2	1 h	96%	
13	o-ClC_6H_4	H	o-$ClC_6H_4C(O)CH_3$	0.2	1 h	66%	
14	p-ClC_6H_4	H	p-$ClC_6H_4C(O)CH_3$	1.0	1 h	54%	
15	n-C_3H_7	n-C_3H_7	n-$C_4H_9C(O)(n$-$C_3H_7)$	0.2	5 h	92%	
16	C_6H_5	C_6H_5	$C_6H_5CH_2C(O)C_6H_5$	1.0	5 h	53%	
17[d]	n-C_3H_7	CH_3	n-$C_4H_9C(O)CH_3$ n-$C_3H_7C(O)C_2H_5$	0.2	5 h	42%	34%

[a] Reaction conditions: $[(Ph_3P)AuCH_3]$, H_2SO_4 50 mol%, alkyne 1 mmol, water 0.5 mL, methanol 1–3 mL, 70°C. [b] GC yield. [c] H_2SO_4 25 mol%, alkyne 2 mmol. [d] 60°C. [e] Run under CO (1 atm). [f] Yield of ketone. [g] Yield of aldehyde. [h] $H_3PW_{12}O_{40}$ was used as acid in place of H_2SO_4. [i] CF_3SO_3H was used as acid in place of H_2SO_4.

The new procedure was applied to various alkynes as summarized in Table 2. Besides 1-octynes, other terminal alkynes, both aliphatic and aromatic, including those bearing functional groups such as alkoxy, cyano, chloro, and olefinic groups were all able to undergo hydration under similar reaction conditions. However, the reactivity significantly depended on the nature of the substituent, and ligand addition was occasionally required to obtain acceptable yields.

Ethynylcyclohexene and hexynonitrile reacted smoothly (entries 3 and 4) leading to the formation of the corresponding methyl ketones in good yields. Interestingly, the olefinic and cyano functional groups remained intact although these functional groups could be potentially hydrated or hydrolyzed. Conversely, the reactions of 5-chloropentyne and 5-hexyn-1-ol did not give satisfactory yields (11 and ~1% yields in 1 h, respectively) even when 1 mol% catalyst was used (otherwise identical conditions).[17] Since metallic particle precipitation was evident in these reactions, the low activity was a result of the deterioration of the catalyst. When the reaction with 5-chloropentyne was carried out under an atmospheric pressure of carbon monoxide for 4 h, the corresponding methyl ketone was obtained with a 72% yield (entry 5). The yield of the 5-hexyn-1-ol reaction was also improved in the presence of carbon monoxide or triphenyl phosphite, resulting in 33 and 31% yields, respectively, over 3 h.

Propargylic alcohols, which are totally inert in the Au^{III}-catalyzed hydration,[10a] also reacted smoothly in the new procedure (entries 6 and 7). However, they afforded mixtures of methyl ketones (Markovnikov addition) and α,β-unsaturated aldehydes (anti-Markovnikov addition[6] followed by dehydration[18]), although all the other terminal alkynes examined formed only Markovnikov adducts.

Phenylacetylene derivatives having electron-donating groups (entries 8, 9, 11, and 12), reacted smoothly. However, as the results of *o*- and *p*-chlorophenylacetylenes and *m*-methoxyphenylacetylene show, electronegative groups bound to the aromatic ring appear to weaken the reactivity towards hydration, which suggest that the hydration (entries 10, 13, and 14) mechanism has an electrophilic nature.

Finally, internal alkynes displayed a low reactivity, presumably because of steric hindrance. Diphenylacetylene being less reactive (entry 16) than more electron-rich 4-octyne (entry 15) is in agreement with the forgoing statement on the nature of the hydration.

In summary, the $[(Ph_3P)AuCH_3]$ and acid catalyst systems are highly efficient in the hydration of a wide range of alkynes in aqueous methanol. The new procedure offers a valuable alternative to the Wacker oxidation, especially in the field of total synthesis.

Experimental Section

Typical procedure (entry 4, Table 1): A mixture of $[(PPh_3)AuMe]$ (1.0 mg, 0.002 mmol), CF_3SO_3H (75 mg, 0.5 mmol), water (1 mL), 1-octyne (2.2 g, 20 mmol) dissolved in methanol (10 mL) was stirred at 70°C for 1 h. Analysis of the resulting mixture by gas chromatography showed the formation of 2-octanone in 99% yield.

Received: July 3, 2002 [Z19655]

[1] a) P. F. Hudrlik, A. M. Hudrlik in *The Chemistry of the Carbon-Carbon Triple Bond, Part 1* (Ed.: S. Patai), Wiley, New York, **1978**, p. 199; b) G. H. Schmid in *The Chemistry of the Carbon-Carbon Triple Bond, Part 1* (Ed.: S. Patai), Wiley, New York, **1978**, p. 275; c) R. C. Larock, W. W. Leong in *Comprehensive Organic Synthesis, Vol. 4* (Eds.: B. M. Trost, I. Fleming, M. F. Semmelhack), Pergamon, Oxford,

 © 2002 WILEY-VCH Verlag GmbH & Co. KGaA, Weinheim 0044-8249/02/4123-4564 $ 20.00+.50/0

1991, p. 269; d) J. March, *Advanced Organic Chemistry*, Wiley, New York, **1992**, p. 762.
[2] a) A. Schrohe, *Chem. Ber.* **1875**, *8*, 367; b) A. Baeyer, *Ber.* **1882**, *15*, 2705; c) W. H. Perkin, Jr., *J. Chem. Soc.* **1884**, *45*, 170.
[3] a) T. Tsuchimoto, T. Joya, E. Shirakawa, Y. Kawakami, *Synlett* **2000**, *12*, 1777; b) Y. Izumi, *Catal. Today* **1997**, *33*, 371; c) I. V. Kozhevnikov, *Chem. Rev.* **1998**, *98*, 171.
[4] a) W. Drenth, H. Hogeveen, *Recl. Trav. Chim. Pays-Bas* **1960**, *79*, 1002; b) A. D. Allen, Y. Chiang, A. J. Kresge, T. T. Tidwell, *J. Org. Chem.* **1982**, *47*, 775, and references therein.
[5] a) V. Jäger, H. G. Viehe in *Methoden Org. Chem. (Houben-Weyl) 4th ed. 1952–, Vol. 5/2a* **1977**, p. 726; b) M. Kutscheroff, *Chem. Ber.* **1884**, *17*, 13; c) R. J. Thomas, K. N. Campbell, G. F. Hennion, *J. Am. Chem. Soc.* **1938**, *60*, 718; d) G. W. Stacy, R. A. Mikulec in *Organic Syntheses, Coll. Vol. 4* (Ed.: N. Rabjohn), Wiley, New York, **1963**, p. 13; e) G. A. Olah, D. Meider, *Synthesis* **1978**, 671.
[6] a) M. Tokunaga, Y. Wakatsuki, *Angew. Chem.* **1998**, *110*, 3024; *Angew. Chem. Int. Ed.* **1998**, *37*, 2867; b) T. Suzuki, M. Tokunaga, Y. Wakatsuki, *Org. Lett.* **2001**, *3*, 735; c) M. Tokunaga, T. Suzuki, N. Koga, T. Fukushima, A. Horiuchi, Y. Wakatsuki, *J. Am. Chem. Soc.* **2001**, *123*, 11917; d) D. B. Grotjahn, C. D. Incarvito, A. L. Rheingold, *Angew. Chem.* **2001**, *113*, 4002; *Angew. Chem. Int. Ed.* **2001**, *40*, 3884.
[7] a) J. Harpern, B. R. James, A. L. W. Kemp, *J. Am. Chem. Soc.* **1961**, *83*, 4097; b) J. Harpern, B. R. James, A. L. W. Kemp, *J. Am. Chem. Soc.* **1966**, *88*, 5142; c) T. Khan, S. B. Halligudi, S. Shukla, *J. Mol. Catal.* **1990**, *58*, 299.
[8] a) B. R. James, G. L. Rempel, *J. Am. Chem. Soc.* **1969**, *91*, 863; b) J. Blum, H. Huminer, H. Alper, *J. Mol. Catal.* **1992**, *75*, 153.
[9] a) W. Hiscox, P. W. Jennings, *Organometallics* **1990**, *9*, 1997; b) W. Baidossi, M. Lahav, J. Blum, *J. Org. Chem.* **1997**, *62*, 669; c) L. W. Francisco, D. A. Moreno, J. D. Atwood, *Organometallics* **2001**, *20*, 4237.
[10] a) Y. Fukuda, K. Utimoto, *J. Org. Chem.* **1991**, *56*, 3729; b) Y. Fukuda, K. Utimoto, *Bull. Chem. Soc. Jpn.* **1991**, *64*, 2013.
[11] a) K. Imi, K. Imai, K. Utimoto, *Tetrahedron Lett.* **1987**, *28*, 3127; b) I. K. Meier, J. A. Marsella, *J. Mol. Catal.* **1993**, *78*, 31.
[12] J. H. Teles, S. Brode, M. Chabanas, *Angew. Chem.* **1998**, *110*, 1475; *Angew. Chem. Int. Ed.* **1998**, *37*, 1415.
[13] J. H. Teles, M. Schulz BASF AG, WO-A1 9721648 **1997** [*Chem. Abstr.* **1997**, *127*, 121499].
[14] The authors reported 200–400 turnovers for propynol and but-1-yn-3-ol, however, the product yield was no more than approximately 2 and 6%, respectively.
[15] a) For catalysis by gold species, see: G. Dyker, *Angew. Chem.* **2000**, *112*, 4407; *Angew. Chem. Int. Ed.* **2000**, *39*, 4237; b) A special issue on gold catalysis has appeared: *Catal. Today* **2002**, *72*, whole issue.
[16] One reviewer pointed out a possible mechanism that involves methanol addition forming a dimethyl acetal as a transient intermediate, which is rapidly hydrolyzed under the acidic conditions to give the final ketone product. Although we are unable to rigorously exclude this possibility when the reaction is run in methanol, the following points strongly support the theory that the reaction involves the direct attack of water. First, the hydration reaction reported herein proceeds in non-alcoholic solvents. Second, the regiochemistry of the hydration reaction is not in full agreement with the methanol addition reaction. In addition, the [*cis*-$PtCl_2(tppts)_2$]-catalyzed reaction of alkynes in aqueous methanol showed that hydration proceeds preferentially, without forming the methanol adduct.[9a] Note that this platinum-catalyzed hydration was run in the absence of acid promoters.
[17] The reaction of 5-hexyn-1-ol did not form any other product and the substrate could be recovered nearly quantitatively.
[18] Acid-catalyzed Rupe-type rearrangement of the starting propargylic alcohols appeared to be another possibility leading to the formation of the α,β-unasturated aldehydes. However, the following control experiments exclude this possibility. A reaction similar to entry 7, Table 2 run using only $H_3PW_{12}O_{40}$ in the absence of the gold complex did not furnish the α,β-unsaturated aldehyde and the 1-ethynyl-1-cyclohexanol was recovered quantitatively. Another control experiment using $H_3PW_{12}O_{40}$ and PPh_3 (1 mol% relative to 1-ethynyl-1-cyclohexanol) in the absence of the gold complex did not form the α,β-unsaturated aldehyde either. In general, Rupe rearrangement of tertiary α-acetylenic alcohols gives α,β-unsaturated ketones as the major product, which is not consistent with our observation. See: S. Swaminathan, K. V. Narayanan, *Chem. Rev.* **1971**, *71*, 429.

 © 2002 WILEY-VCH Verlag GmbH & Co. KGaA, Weinheim 0044-8249/02/4123-4565 $ 20.00+.50/0

Polymerization on Solid Supports**

Xiaoyu Li and David G. Lynn*

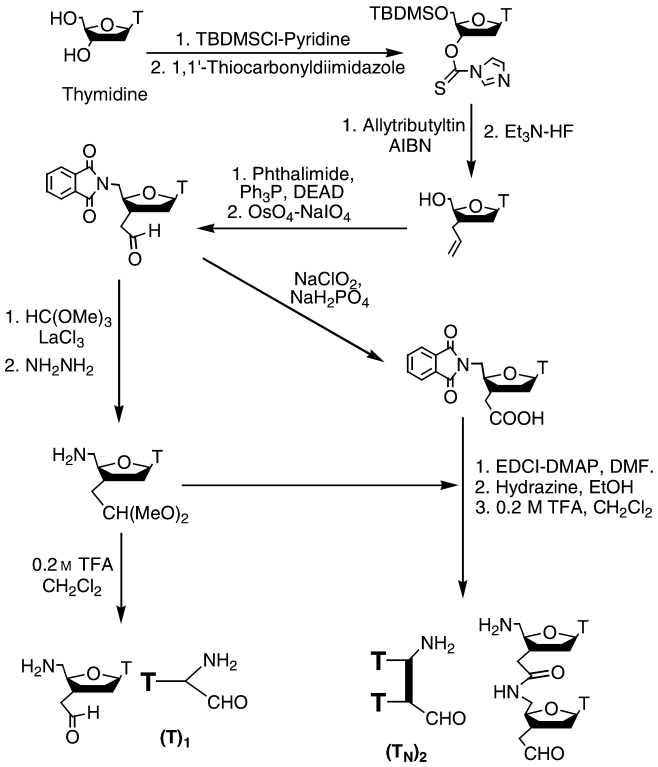
Dedicated to Fredric M. Menger and Albert Padwa on the occasion of their 65th birthdays

Solid-phase synthesis methods have made possible the construction of chain-length- and sequence-specific polymers, which have revolutionized biopolymer research.[1–8] Likewise, incorporating catalysts on solid supports has dramatically improved catalyst lifetimes and enabled facile catalyst recycling.[9–17] Here we combine these strategies, by using solid-supported DNA for both catalysis and product capture, to enable multiple rounds of chain-length-specific polymerizations along a DNA template.

With oligonucleotide or peptide solid-phase synthesis, one "monomer" is added with each reaction cycle. Such a linear, iterative process ensures sequence specificity, but with longer polymers the lengthy reaction time and the overall yield often limit synthetic success. Moreover, the density of sites/solid-support area limits the synthetic scale with supports that typically cannot be recycled. To overcome these limitations, a DNA homopolymer, 5′-dApApApApApApApA-3′, was prepared by solid-phase methods on oligoaffinity-supports–polystyrene/polyethyleneglycol copolymer support (OAS-PS) beads and deprotected in such a way as to retain the polymer on the support, giving S(dAp)$_8$. A small number of beads were cleaved from the polymer and the purity of the resulting DNA polymer was confirmed by analysis, and the remaining beads were used as catalysts for the polymerization of the amino aldehydes 5′-H_2N-T-3′-CH_2CHO ((T)$_1$, T = thymine) and 5′-H_2N-T_NT-3′-CH_2CHO ((T$_N$)$_2$).

As outlined in Scheme 1, (T)$_1$ and (T$_N$)$_2$ can both be constructed efficiently from 5′ and 3′ functionalization of thymidine.[18,19] The differentially protected amine and carboxylic acid products can be condensed and deprotected to give (T$_N$)$_2$, where the subscripted N signifies an amide-backbone linkage replacing the native phosphate of this thymidine dinucleotide analogue.

The product (T$_N$)$_2$ showed no reaction under aqueous reductive amination conditions in the absence of the supported DNA template S(dAp)$_8$. However, when allowed to react at a 4:1 molar excess relative to the template (Figure 1, R2), classic step-growth polymerization ensued. MALDI-TOF mass spectroscopy analyses and HPLC comparisons confirmed the accumulation of an intermediate tetramer product prior to conversion into the octamer, similar to the kinetics seen with soluble catalysts.[18] When the reaction was complete, the beads were washed to remove excess reagent, and the polymer product was recovered with a hot MeOH elution. Two pure products were present in the methanol eluent as



Scheme 1. Syntheses of the substrates (T)$_1$ and (T$_N$)$_2$. TBDMS = *tert*-butyldimethylsilyl; AIBN = azobisisobutyronitrile; DEAD = diethylazodicarboxylate; EDCI = 3-(3-dimethylaminopropyl)-1-ethylcarbodiimide; DMAP = 4′-aminopyridine; TFA = trifluoroacetic acid.

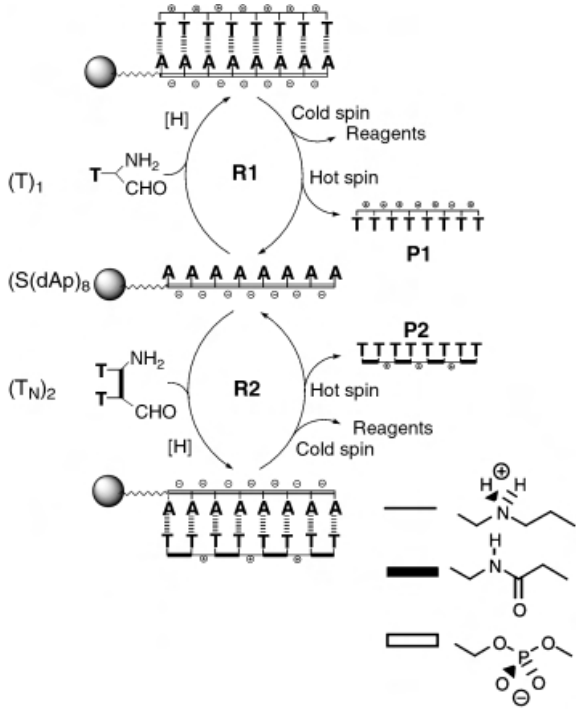


Figure 1. DNA-templated polymerization of (T)$_1$ and (T$_N$)$_2$ on solid-supports.

[*] Dr. D. G. Lynn, X. Li
Center for the Analysis of Supramolecular Self-Assemblies
Departments of Chemistry and Biology
Emerson Hall, Emory University
Atlanta, GA 30322 (USA)
Fax: (+1) 404-727-6586
E-mail: dlynn2@emory.edu

[**] This work is partial fulfillment of the Doctor of Philosophy requirements (X.L.) in the Department of Chemistry, University of Chicago, Chicago IL, 60637. We gratefully acknowledge the NIH RR12723 and Emory University for financial support.

 © 2002 WILEY-VCH Verlag GmbH & Co. KGaA, Weinheim 0044-8249/02/4123-4567 $ 20.00+.50/0

seen in the HPLC chromatogram (Figure 2). The MALDI-TOF molecular ion analyses and induced fragmentation patterns were consistent with the $(T_N)_2$ octamer, 5′-H_2N-$(T_N)_2$-[NH-$(T_N)_2$]$_3$-3′-CHO, as the major product and the

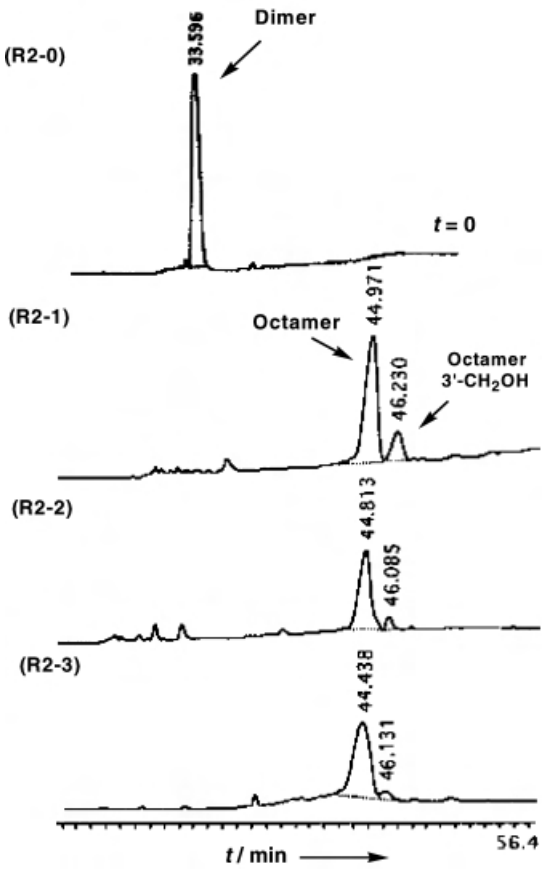


Figure 2. HPLC analysis of S(dA$_p$)$_8$-directed polymerization of $(T_N)_2$. Profiles of (R2-0) at $t = 0$, $(T_N)_2$ only, and the first to third reaction cycle, (R2-1) to (R2-3).

octamer alcohol, 5′-H_2N-$(T_N)_2$-[NH-$(T_N)_2$]$_3$-3′-CH_2OH as the minor product. The beads were reused for additional rounds of synthesis as shown in Figure 2 and the yields of each cycle are given in Table 1, R2. Each subsequent reaction gave a similar product distribution; a total yield of $\approx 90\,\%$ for each cycle. While each individual reaction occurs on a small scale, the efficient sequential reactions and facile purification suggests that scale-up syntheses could be automated.

The S(dAp)$_8$-catalyzed polymerization of $(T)_1$, in this case at an 8:1 monomer molar excess under the same reductive amination conditions (Figure 1, R1), again showed clear

Table 1. Yield of octomer and octomer-3′-ethanol from each indicated reaction cycle of Figure 1. All yields [%] are calculated by HPLC peak integration following template purification.

Reaction Cycles	Octamer	Octamer 3′-CH_2OH
R2-1	78.9	11.0
R2-2	83.2	4.6
R2-3	87.7	5.8
R1-1	85.1	None
R1-2	88.6	None
R1-3	89.4	None

evidence for step-growth polymerization in the early stages. Again the yields of the octamer product approached 90 % at the end of the reaction (Figure 3, Table 1, R1). In each cycle, seven new bonds were formed and at the end of the reaction no octamer alcohol could be detected, which suggests that the octamer product still had reactive ends. Therefore, S(dAp)$_8$ functions as a general catalyst for efficiently templating chain-length-specific polymerization, and offers efficient cycle-dependent amplification of specific DNA templates.

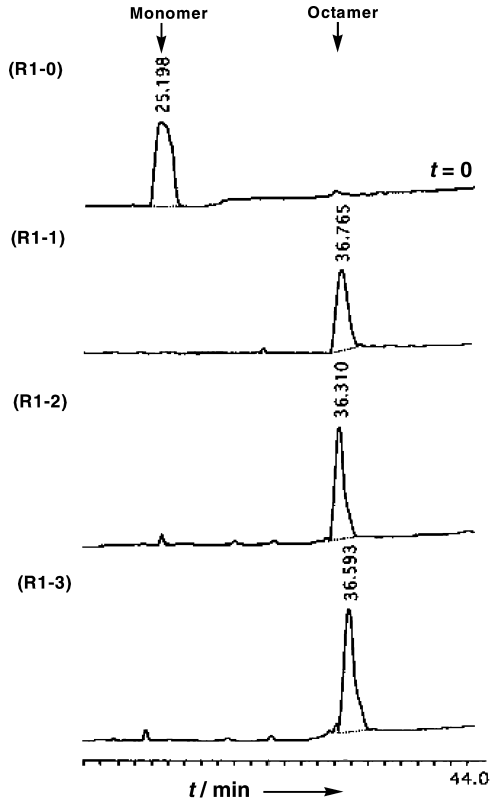


Figure 3. HPLC analysis of S(dA$_p$)$_8$-directed polymerization of $(T)_1$. Profiles of (R1-0) at $t = 0$, $(T)_1$ only, and the first to third reaction cycle, (R1-1) to (R1-3).

In conventional solid-phase synthesis, the formed products are covalently bound to solid supports. In contrast, S(dAp)$_8$ associates with the product through hydrogen bonds, which enables convenient removal of reactants and byproducts, as well as temperature-controlled recovery of the chain-length-specific product. This noncovalent association with the solid support avoids the additional reagents traditionally required for cleavage of the product from the support.

The reaction appears to follow step-growth-polymerization kinetics exclusively, consistent with those seen for soluble oligonucleotide catalysts.[18] For the $(T_N)_2$ reaction, only the tetramer intermediate is observed, for $(T)_1$, only dimer and tetramer intermediates. Polymerization does not proceed past the length of the template, S(dAp)$_8$ in this case, which is consistent with a mechanism in which the template becomes saturated with the thermodynamically most stable duplex and no intermediate ternary complexes (for example, S(dAp)$_8$/P1/P2 see Figure 1) accumulate to a sufficient concentration to be reduced. This observation is significant because the reactive

 © 2002 WILEY-VCH Verlag GmbH & Co. KGaA, Weinheim 0044-8249/02/4123-4568 $ 20.00+.50/0

5′-amino and 3′-acetaldehyde groups remain at the end of the reaction.

As in the polymerase chain reaction (PCR),[20–22] $S(dAp)_8$ templates the ligation of multiple monomers in a single reaction cycle. Unlike PCR, where both strands of the DNA duplex are amplified to give exponential growth, the DNA-templated polymerization reactions employ only a single strand as the template and growth is presumably linear with each reaction cycle. In addition, the requirement for primers compatible with the double-strand-binding polymerase is avoided, and short sequences of DNA are amplified efficiently.

Finally, the reaction does not synthesize native DNA, but a backbone analogue. Therefore, solid-supported oligomeric DNA can be used to catalyze the rapid synthesis of polymers containing different backbones simply by changing the structure of the reactant, in this case $(T)_1$ and $(T_N)_2$, Quite unlike other solid-supported syntheses, $S(dAp)_n$ can be used repeatedly both to catalyze the polymerization as well as purify the product, which greatly reduces the time and effort for the synthesis of modified DNA-analogues. The extension of this chemistry to mixed-sequence templates should enable the rapid amplification of DNA sequence information into specific backbone-modified analogues. Moreover, this general strategy for solid-phase synthesis can now be extended more broadly, through other molecular recognition elements, to accomplish chain-length-specific polymerizations.

Experimental Section

DNA Synthesis: All native DNA oligomers were prepared by the Emory University Microchemical Facility on a PE-Biosystems 394 DNA Synthesizer. The DNA $S(dAp)_8$ template was synthesized on OAS-PS (Glen Research, Batch No. G008062, Cat. No. 26-4001) solid supports by standard cyanoethyl phosphoramidite chemistry. The linker of OAS-PS is stable to the last step of ammonium hydroxide deprotection treatment in the automated synthesis. To confirm purity, the DNA oligomers were removed from the resin and analyzed by Rainin HPXL RP-HPLC: Phenomenex Prodigy 5 analytical ODS(2) C18; Rainin Dynamax UV detector at 260 nm, and eluted with MeOH in H_2O (0–100 % in 50 min), and the structure confirmed by MALDI-MS: $C_{80}H_{97}N_{40}O_{38}P_7$ calcd m/z: 2443.69 $[M+H^+]$; found 2444.87.

Polymerization: The substrates, 8 mM for $(T_N)_2$ and 16 mM for $(T)_1$, were mixed with $S(dAp)_8$ at the indicated stoichiometry, heated to 75 °C for 2–3 min, and cooled to 4 °C for 3 h.[23] $NaBH_3CN$ (20 equiv) was added at room temperature and the mixture stirred vigorously in a vortex mixer for 72 h, with the addition of more $NaBH_3CN$ (10 equiv) after 48 h to ensure complete reaction. The mixture was subjected to centrifugation in the Ultrafree-MC (Millipore Corp.) centrifugal filter tube at room temperature to remove the reagents, and the beads resuspended in MeOH, heated to 75 °C, and subjected to centrifugation whilst hot, with 3 × 1 mL MeOH. The MeOH washes were combined, evaporated to dryness, and analyzed by reverse-phase HPLC (same system as above), and eluted with MeOH in H_2O: 0–5 % from 0–8 min, 5–20 % from 8–9 min, 20–35 % from 9–24 min, 35–60 % from 24–25 min, 60–100 % from 25–50 min. The product assignments were justified by co-injection with standard samples and by mass spectrometry. MALDI-TOF (2′,4′,6′-trihydroxyacetophenone monohydrate (THAP)/citrate): $(T_N)_2$-[NH-$(T_N)_2]_3$-CHO, $C_{96}H_{128}N_{24}O_{29}$ calcd m/z: 2080.9279 $[M^+]$; found 2082.85 $[M+2H]^+$; $(T_N)_2$-[NH-$(T_N)_2]_3$-CH_2OH, $C_{96}H_{130}N_{24}O_{29}$ calcd m/z: 2082.9436 $[M^+]$; found 2083.84 $[M+H]^+$; $(T)_1$-[NH-$(T)_1]_7$, $C_{96}H_{136}N_{24}O_{25}$, calcd m/z: 2025.0109 $[M^+]$; found 2026.12 $[M+H]^+$.

For resin recovery, the beads were washed 3 × 1 mL with deionized H_2O and resuspended in H_2O overnight under vortex mixing before being used for the next reaction cycle.

Received: June 5, 2002 [Z19473]

[1] D. C. Neckers, *J. Chem. Educ.* **1975**, *52*, 695.
[2] E. Atherton, M. J. Gait, R. C. Sheppard, B. J. Williams, *Bioorg. Chem.* **1979**, *8*, 351.
[3] G. Barany, R. B. Merrifield, *Peptides* **1980**, *2*, 1.
[4] T. T. Nguyen, U. Asseline, *Biochimie* **1985**, *67*, 673.
[5] K. N. Ganesh, *Curr. Sci.* **1985**, *54*, 103.
[6] R. B. Merrifield, *Science* **1986**, *232*, 341.
[7] G. Barany, N. Kneib-Cordonier, D. G. Mullen, *Int. J. Pept. Protein Res.* **1987**, *30*, 705.
[8] A. R. Brown, P. H. H. Hermkens, H. C. J. Ottenheijm, D. C. Rees, *Synlett* **1998**, *8*, 817.
[9] B. Clapham, T. S. Reger, K. D. Janda, *Tetrahedron* **2001**, *57*, 4637.
[10] A. M. Harned, P. R. Hanson, *Org. Lett.* **2002**, *4*, 1007.
[11] S. Booth, P. H. H. Hermkens, H. C. J. Ottenheijm, D. C. Rees, *Tetrahedron* **1998**, *54*, 15385.
[12] B. Doerner, R. Steinauer, P. White, *Chimia* **1999**, *53*, 11.
[13] C. Saluzzo, R. ter Halle, F. Touchard, F. Fache, E. Schulz, M. Lemaire, *J. Organomet. Chem.* **2000**, *603*, 30.
[14] A. Kirschning, H. Monenschein, R. Wittenberg, *Angew. Chem.* **2001**, *113*, 670; *Angew. Chem. Int. Ed.* **2001**, *40*, 650.
[15] S. J. Shuttleworth, S. M. Allin, P. K. Sharma, *Synthesis* **1997**, *11*, 1217.
[16] K. C. Hultzsch, J. A. Jernelius, A. H. Hoveyda, R. R. Schrock, *Angew. Chem.* **2002**, *114*, 609; *Angew. Chem. Int. Ed.* **2002**, *41*, 589.
[17] J. S. Kingsbury, S. B. Garber, J. M. Giftos, B. L. Gray, M. M. Okamoto, R. A. Farrer, J. T. Fourkas, A. H. Hoveyda, *Angew. Chem.* **2001**, *113*, 4381; *Angew. Chem. Int. Ed.* **2001**, *40*, 4251.
[18] X. Li, Z.-Y. J. Zhan, R. Knipe, D. G. Lynn, *J. Am. Chem. Soc.* **2002**, *124*, 746.
[19] Z.-Y. J. Zhan, D. G. Lynn, *J. Am. Chem. Soc.* **1997**, *119*, 12420.
[20] R. K. Saiki, S. Scharf, F. Faloona, K. B. Mullis, G. T. Horn, H. A. Erlich, N. Arnheim, *Science* **1985**, *230*, 1350.
[21] H. A. Erlich, D. Gelfand, J. J. Sninsky, *Science* **1991**, *252*, 1643.
[22] T. J. White, *Trends Biotechnol.* **1996**, *14*, 478.
[23] A. Luther, R. Brandsch, G. von Kiedrowski, *Nature* **1998**, *396*, 245.

Asymmetric Syntheses of Pectenotoxins-4 and -8, Part I: Synthesis of the C1–C19 Subunit**

David A. Evans,* Hemaka A. Rajapakse, and Dirk Stenkamp

The first members of the pectenotoxin family of marine natural products were isolated off the northeastern coast of Japan in 1985. Subsequently, ten members of this group have been identified.[1] The structural diversity within the pectenotoxins stems from variations in the oxidation state at C43, as well as the differing configurations of the AB spiroketal portion of the structures. Pectenotoxin-2 (C43 = Me) is cytotoxic towards human lung, colon, and breast cancer cell lines with LC_{50} values in the nanomolar range.[1c] Pectenotox-

[*] Prof. D. A. Evans, H. A. Rajapakse, D. Stenkamp
Department of Chemistry & Chemical Biology
Harvard University
Cambridge, MA 02138 (USA)
Fax: (+1) 617-495-1460
E-mail: evans@chemistry.harvard.edu

[**] Financial support has been provided by the National Institutes of Health (GM33327-16). A BASF-Forschungsstipendum Postdoctoral Fellowship to D.S. and a Howard Hughes Medical Institute Predoctoral Fellowship to H.A.R. are gratefully acknowledged. The NIH BRS Shared Instrumentation Grant Program 1-S10RR04870 and the NSF (CHE 88-140019) are acknowledged for providing NMR facilities.

 © 2002 WILEY-VCH Verlag GmbH & Co. KGaA, Weinheim 0044-8249/02/4123-4569 $ 20.00+.50/0

ins-1, -4, and -8 (C43 = CH_2OH) are differentiated by their AB spiroketal subunits that are interconvertable by acid equilibration (Figure 1, Eq. (1)).[1b] While no total synthesis of

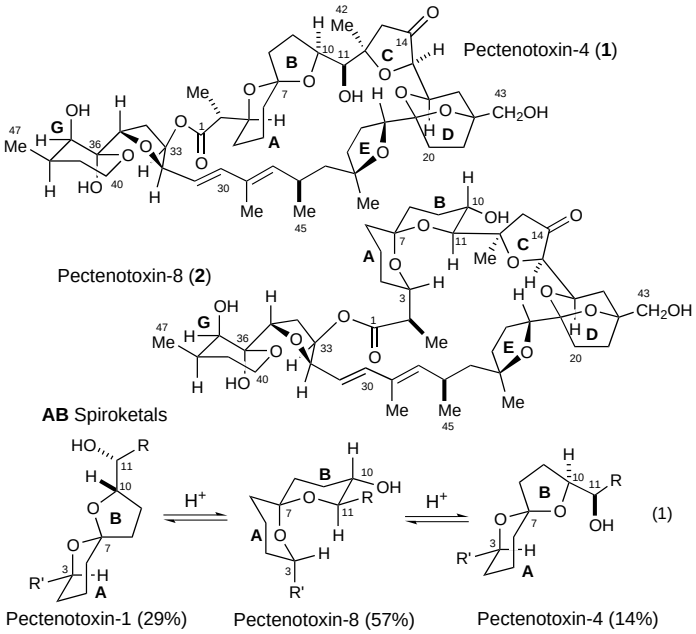
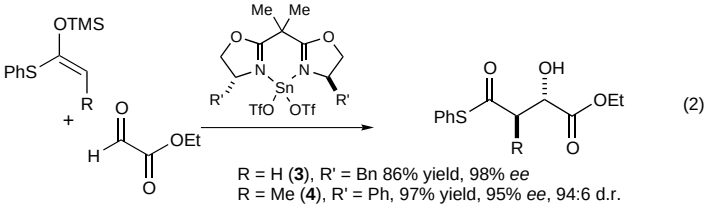


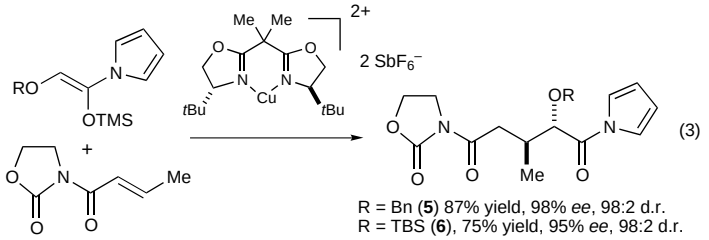
Figure 1. The pectenotoxin family of natural products, and their interconversion by acid equilibration [Eq. (1)].

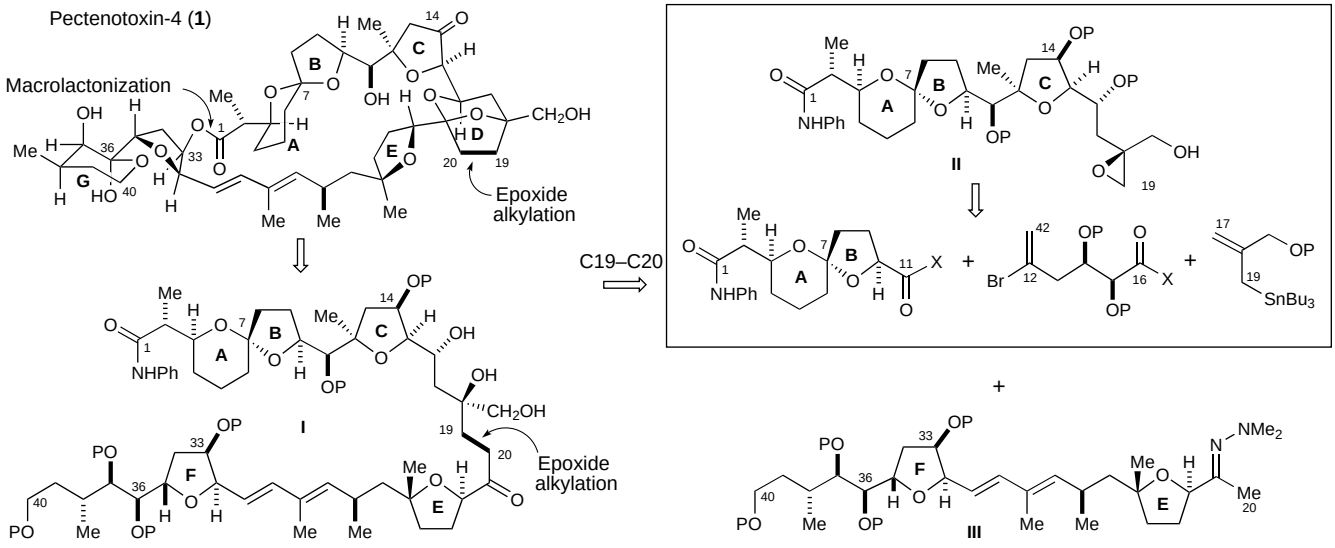
any pectenotoxin has been reported, there have been efforts directed toward the synthesis of these architecturally complex natural products.[2] In this and the following communication,[3] we describe our efforts culminating in the synthesis of pectenotoxin-4 (**1**).

Pectenotoxin-4 was chosen as our initial target. Although this spiroketal is the most stable isomer in acyclic precursors it becomes the least favored when constrained in the macrolide framework.[1b,d] Our principal disconnections are illustrated in Scheme 1. Application of the macrolactonization transform and ring opening of the D-ring bicyclic ketal reveals intermediate **I**, a synthesis subgoal that might be assembled from fragments **II** and **III** through a metalloenamine-epoxide alkylation.[4] The synthesis plan calls for masking the ketones at C14 and C36 as protected alcohols until late in the synthesis. Protection of the carboxylate terminus at C1 as its derived *N*-phenylamide would enable the preservation of the C1 carboxyl carbon atom in its correct oxidation state throughout the synthesis.[5] In the retrosynthesis of the ABC tricyclic fragment **II**, convenient disconnections could be made about the C16–C17 and C11–C12 bonds (Scheme 1). The stereocenters at C11 and C16 could be constructed by chelate-controlled reduction of the corresponding ketone, or by Felkin-controlled addition of an appropriate nucleophile to the respective aldehydes.

The integration of catalytic enantioselective processes into our synthesis projects has been an ongoing objective. In this regard, the enantioselective Sn^{2+}-catalyzed aldol reaction [Eq. (2)] provides the foundation for the synthesis of the C8–C11 acetate and C36–C39 propionate fragments.[6,7] The asymmetric Michael addition reaction reported from these laboratories provides a useful alternate route for the construction of the C36–C40 propionate fragment [Eq. (3)].[8]



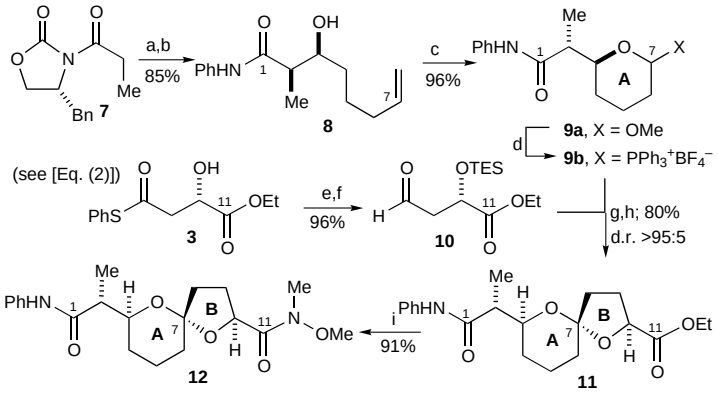




Scheme 1. Retrosynthetic analysis of pectenotoxin-4.

 © 2002 WILEY-VCH Verlag GmbH & Co. KGaA, Weinheim 0044-8249/02/4123-4570 $ 20.00+.50/0

Synthesis of the AB spiroketal began with the addition of the boron enolate derived from **7** to 5-hexenal, which afforded the desired *syn*-aldol adduct in 87% yield (d.r. > 95:5; Scheme 2).[9] Transamidation to *N*-phenylamide **8** ($AlMe_3$, aniline, CH_2Cl_2, 98%), olefin ozonolysis, followed by in situ ether formation afforded the A-ring lactol methyl ether **9a**. In preparation for a Wittig-based fragment coupling, **9a** was

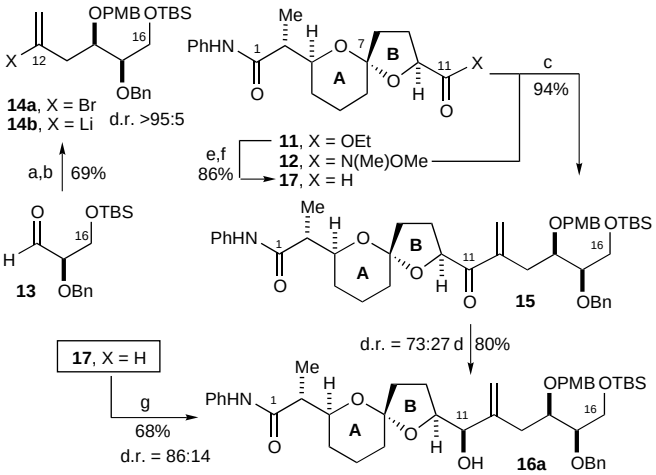


Scheme 2. Synthesis of the AB spiroketal. a) 1. nBu$_2$BOTf, Et_3N, CH_2Cl_2, −78°C; 2. 5-hexenal, CH_2Cl_2, −78°C; 87%; b) $AlMe_3$, aniline; CH_2Cl_2; 98%; c) 1. O_3, MeOH, then DMS, −78°C; 2. CSA; 96%; d) PPh_3·HBF_4, CH_3CN, 60°C; e) TESOTf, lut., CH_2Cl_2, −78°C; 99%; f) Pd/C, Et_3SiH, acetone; 97%; g) 1. 2 equiv nBuLi, THF, −78°C; 2. aldehyde **10**; h) CSA, MeOH/CH_2Cl_2 (1:1); 80% (three steps); i) MeONHMe·HCl, iPrMgCl,THF, −78°C→−20°C; 91%. See reference [7] for abbreviations.

transformed into the anomeric phosphonium salt **9b** (PPh_3·HBF_4, CH_3CN, 60°C).[10] The aldehyde partner **10** was readily accessed by protection of aldol adduct **3**, followed by chemoselective half reduction of the *S*-phenyl thioester under conditions (Pd/C, Et_3SiH, acetone, 97%) reported by Fukuyama et al.[11]

Wittig coupling of the ylide derived from **9b** and aldehyde **10** afforded the corresponding enol ether, which was immediately subjected to camphorsulfonic acid (CSA) in MeOH to provide the desired AB spiroketal **11** in 80% overall yield (d.r. > 95:5). In preparation for the next fragment coupling, the ethyl ester group at C11 of **11** was transformed to the Weinreb amide **12** by using a modified literature procedure.[12]

With the spiroketal in hand, the C11–C12 bond construction was examined. The desired C12–C16 *syn*-diol was readily accessed from the allylation of the differentially protected glyceraldehyde derivative **13** (d.r. > 95:5; Scheme 3).[13] PMB protection of the resulting C14 alcohol required the use of PMB-trichloroacetimidate.[14] Attempts to employ basic conditions resulted in the formation of alkyne by-products from the elimination of hydrogen bromide. Lithium–halogen exchange of vinyl bromide **14a** (tBuLi, Et_2O/pentane, −78°C), followed by addition of Weinreb amide **12** afforded the desired C1–C16 carbon chain. Reduction of the resulting carbonyl group at C11 in **15** afforded moderate chelate-controlled diastereoselectivity with $Zn(BH_4)_2$ (d.r. 73:27, 80% yield). The use of superior chelating reagents such as

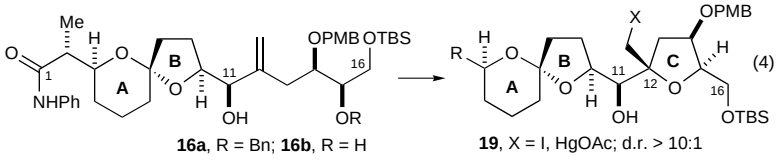


Scheme 3. Synthesis of C1–C16 Fragment **16a**. a) [Ti(OiPr)Cl_3], 2-bromoallyltrimethylsilane, CH_2Cl_2, −78°C; 87%; b) PMB-trichloroacetimidate, TfOH, Et_2O, −20°C→0°C; 79%; c) **14a**, tBuLi, Et_2O/pentane, −78°C then **12**; 94%; d) $Zn(BH_4)_2$, Et_2O/CH_2Cl_2, −40°C; 80%; e) $LiBH_4$, THF, −10°C; 93%; f) SO_3·Py, Et_3N, DMSO/CH_2Cl_2 (1:1); 91%; g) **14a**, tBuLi, Et_2O, −78°C, then $MgBr_2$, then aldehyde **17**, Et_2O, −78°C; 68%. See reference [7] for abbreviations.

$LiBHBu_3$ afforded better selectivity[15] (d.r. 81:19, 58% yield), but resulted in competitive 1,4-reduction (38%).

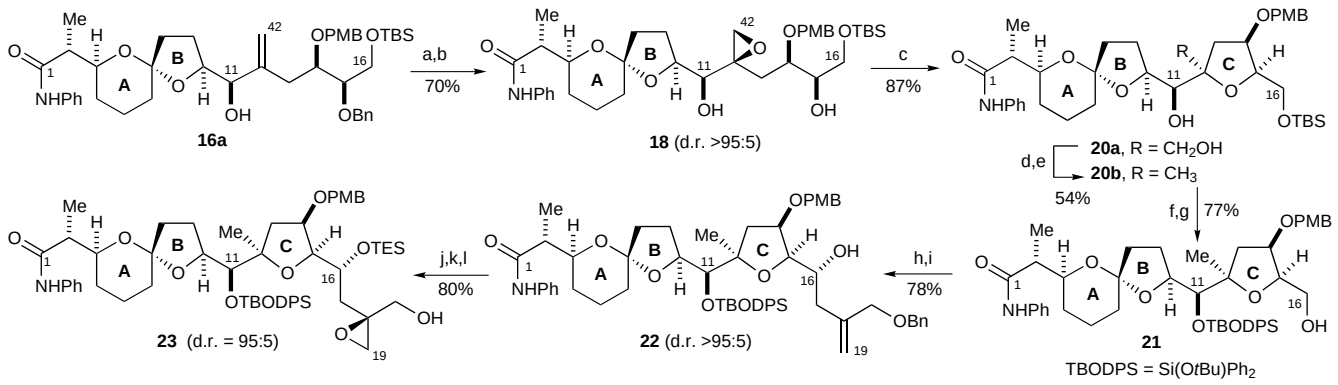
A viable alternative to the construction of **16a** was to access the stereocenter at C11 *directly* by a Felkin-controlled addition to the corresponding spiroketal aldehyde **17**.[16] The desired aldehyde **17** was accessed in two steps:[17] full reduction of the ethyl ester ($LiBH_4$, THF, −10°C, 94%) followed by Parikh–Doering oxidation (SO_3·Py, Et_3N, CH_2Cl_2/DMSO, −10°C, 91%).[18] The Grignard reagent derived from vinyl bromide **14** added to aldehyde **17** to afford **16a** with good selectivity (86:14) and yield (68%).[19]

The completion of the fragment synthesis began with an investigation into electrophile-induced heterocyclizations to form ring-C [Eq. (4)]. Unfortunately, all attempts to induce cyclization of either **16a** or **16b** with either halogenating agents or with mercuric salts afforded the undesired ring-C C12 diastereomer **19**.



The successful solution to the ring-C construction and the synthesis of the ABC epoxide fragment began with the selective deprotection of the benzyl ether group at C15 under reducing conditions[20] (LiDBB, THF, −78°C, 81%) (Scheme 4). This step was followed by C11 hydroxy-directed epoxidation[21] ([VO(acac)$_2$], TBHP, PhH, 99%, d.r. > 95:5) to afford a single epoxide diastereomer **18**, which was cyclized to **20a** under mildly acidic conditions (PPTS, CH_2Cl_2, 87%). Acylation of the primary alcohol with phenylthiono chloroformate (DMAP, CH_2Cl_2, −10°C, 75%), followed by

 © 2002 WILEY-VCH Verlag GmbH & Co. KGaA, Weinheim 0044-8249/02/4123-4571 $ 20.00+.50/0



Scheme 4. Completion of C1–C19 ABC fragment. a) LiDBB, THF, −78 °C; 81 %; b) $[VO(acac)_2]$, TBHP, PhH; 99 %; c) PPTS, CH_2Cl_2; 87 %; d) PhOC(S)Cl, DMAP, CH_2Cl_2, −10 °C; 75 %; e) Bu_3SnH, AIBN, xylenes, 160 °C; 72 %; f) TBODPSCl, DMAP, Et_3N, DMF; 90 %; g) CSA, CH_2Cl_2/MeOH (1:1), −20 °C; 85 %; h) SO_3·Py, Et_3N, CH_2Cl_2/DMSO (1:1), −10 °C; i) 2-(benzyloxymethyl) allyltributylstannane, BF_3·OEt_2, CH_2Cl_2, −78 °C; 78 % (two steps); j) TESCl, Im, CH_2Cl_2; 92 %; k) LiDBB, THF, −78 °C; 87 %; l) Ti(O*t*Bu)$_4$, (L)-(+)-DET, TBHP, 3 Å MS, CH_2Cl_2, −30 °C; 99 %. See reference [7] for abbreviations.

deoxygenation under standard Barton conditions completed the synthesis of the C-ring tetrahydrofuran **20b**.[22,23]

The hydroxy group at C11 was protected as a *tert*-butoxydiphenylsilyl (TBODPS) ether.[24] Selective deprotection of the primary TBS ether (CSA, CH_2Cl_2/MeOH), oxidation of the resulting alcohol **21** (SO_3·Py, Et_3N, CH_2Cl_2/DMSO, −10 °C)[18] to the unstable α,β-bisalkoxy aldehyde, followed by Felkin controlled allylation with 2-(benzyloxymethyl)allyltributylstannane[25] (BF_3·OEt_2, CH_2Cl_2, −78 °C, 78 % over two steps, d.r. 95:5) provided homoallyl alcohol **22**, the complete carbon chain of the C1–C19 fragment. Protection of the hydroxy group at C16 (TESCl, Im, CH_2Cl_2, 92 %), benzyl deprotection[20] (LiDBB, THF, −78 °C, 87 %), and a stoichiometric Sharpless asymmetric epoxidation[26] ([Ti(O*t*-Bu)$_4$], (L)-(+)-DET, TBHP, 3 Å MS, CH_2Cl_2, −30 °C, 99 %, d.r. 95:5) afforded the desired ABC epoxide **23** with excellent selectivity.

The preceding discussion describes the stereoselective synthesis of the C1–C19 ABC epoxide fragment of the pectenotoxin skeleton. The following communication describes the syntheses of the C20–C30 E-ring and C31–C40 FG fragments, and the fragment assemblage to pectenotoxin-4.

Received: September 18, 2002 [Z50190]

[1] a) T. Yasumoto, M. Murata, Y. Oshima, M. Sano, G. K. Matsumoto, J. Clardy, *Tetrahedron* **1985**, *41*, 1019–1025; b) K. Sasaki, J. L. C. Wright, T. Yasumoto, *J. Org. Chem.* **1998**, *63*, 2475–2480; c) J. H. Jung, C. J. Sim, C.-O. Lee, *J. Nat. Prod.* **1995**, *58*, 1722–1726; d) M. Daiguji, M. Satake, K. J. James, A. Bishop, L. Mackenzie, H. Naoki, T. Yasumoto, *Chem. Lett.* **1998**, 653–654.

[2] a) S. Amano, K. Fujiwara, A. Murai, *Synlett* **1997**, 1300–1302; b) D. Awakura, K. Fujiwara, A. Murai, *Synlett* **2000**, 1733–1736; c) G. C. Micalizio, W. R. Roush, *Org. Lett.* **2001**, *3*, 1949–1952; d) L. A. Paquette, X. Peng, D. Bondar, *Org. Lett.* **2002**, *4*, 937–940.

[3] D. A. Evans, H. A. Rajapakse, A. Chiu, D. Stenkamp, *Angew. Chem.* **2002**, *114*, 4755; *Angew. Chem. Int. Ed.* **2002**, *41*, 4573.

[4] For similar bond constructions in a complex setting see: a) D. A. Evans, S. L. Bender, J. Morris, *J. Am. Chem. Soc.* **1988**, *110*, 2506–2526; b) D. A. Evans, R. P. Polniaszek, K. M. DeVries, D. E. Guinn, D. J. Mathre, *J. Am. Chem. Soc.* **1991**, *113*, 7613–7630.

[5] For the use of *N*-phenylamides as carboxyl surrogates see: a) D. A. Evans, P. H. Carter, E. M. Carreira, J. A. Prunet, M. Lautens, *J. Am. Chem. Soc.* **1999**, *121*, 7540–7552; b) D. A. Evans, D. M. Fitch, T. E. Smith, V. J. Cee, *J. Am. Chem. Soc.* **2000**, *122*, 10033–10046.

[6] D. A. Evans, D. W. C. MacMillan, K. R. Campos, *J. Am. Chem. Soc.* **1997**, *119*, 10859–10860.

[7] Abbreviations: OTf = trifluoromethanesulfonyl; Bn = benzyl, TBS = *tert*-butyldimethylsilyl; d.r. = diastereomeric ratio; TES = triethylsilyl; lut. = 2,6-lutidine; PMB = 4-methoxybenzyl; DMSO = dimethyl sulfoxide; LiDBB = lithium di-*tert*-butyl biphenylide; DMAP = 4-(*N*,*N*-dimethylamino)pyridine; AIBN = 2,2′-azobisisobutyronitrile; TBODPS = *tert*-butoxydiphenylsilyl; Im = imidazole; PPTS = pyridinium *para*-toluenesulfonate; DMF = dimethylformamide; CSA = camphorsulfonic acid; TBHP = *tert*-butyl hydroperoxide; DET = diethyl tartrate; MS = molecular sieves.

[8] D. A. Evans, K. A. Scheidt, J. N. Johnston, M. C. Willis, *J. Am. Chem. Soc.* **2001**, *123*, 4480–4491.

[9] D. A. Evans, J. Bartroli, T. L. Shih, *J. Am. Chem. Soc.* **1981**, *103*, 2127–2129.

[10] a) J. Godoy, S. V. Ley, B. Lygo, *J. Chem. Soc. Chem. Commun.* **1984**, 1381–1382; b) D. Culshaw, P. Grice, S. V. Ley, G. A. Strange, *Tetrahedron Lett.* **1985**, *26*, 5837–5840.

[11] T. Fukuyama, S.-L. Lin, L. Li, *J. Am. Chem. Soc.* **1990**, *112*, 7050–7051; See also: D. A. Evans, B. W. Trotter, P. J. Coleman, B. Cote, L. Carlos Dias, H. A. Rajapakse, A. N. Tyler, *Tetrahedron* **1999**, *55*, 8671–8726.

[12] The typical conditions of adding *i*PrMgCl to a cooled solution of ester and MeNHOMe·HCl resulted in the formation of significant amounts of isopropyl ketone. Preforming the magnesium amide of the Weinreb salt, thus ensuring that all the Grignard reagent was consumed prior to ester addition, was critical for the success of this reaction. For the original procedure, see: J. M. Williams, R. B. Jobson, N. Yasuda, G. Marchesini, U.-H. Dolling, E. J. Grabowski, *Tetrahedron Lett.* **1995**, *36*, 5461–5464.

[13] M. T. Reetz, K. Kesseler, *J. Org. Chem.* **1985**, *50*, 5434–5436.

[14] a) H. P. Wessel, T. Iversen, D. R. Bundle, *J. Chem. Soc. Perkin Trans. 1* **1985**, 2247–2250; b) N. Nakajima, K. Horita, R. Abe, O. Yonemitsu, *Tetrahedron Lett.* **1988**, *29*, 4139–4142.

[15] A.-M. Faucher, C. Brochu, S. R. Landry, I. Duchesne, S. Hantos, A. Roy, A. Myles, C. Legault, *Tetrahedron Lett.* **1998**, *39*, 8425–8428.

[16] N. T. Ahn, O. Einstein, *Nouv. J. Chim.* **1977**, *1*, 61–70.

[17] Attempts to access aldehyde **17** directly by half reduction with electrophilic reagents such as diisobutylaluminum hydride resulted in *N*-phenylamide decomposition. This was the only reagent incompatibility observed throughout the synthesis.

[18] J. R. Parikh, W. von E. Doering, *J. Am. Chem. Soc.* **1967**, *89*, 5505–5507.

[19] The Grignard reagent was prepared by adding a Et_2O/PhH solution of $MgBr_2$ to vinyllithium **14b**. See: M. Nakatsuka, J. A. Ragan, T. Sammakia, D. B. Smith, D. E. Uehling, S. L. Schreiber, *J. Am. Chem. Soc.* **1990**, *112*, 5583–5601.

 © 2002 WILEY-VCH Verlag GmbH & Co. KGaA, Weinheim 0044-8249/02/4123-4572 $ 20.00+.50/0

[20] a) P. K. Freeman, L. L. Hutchinson, *J. Org. Chem.* **1980**, *45*, 1924–1930; b) R. E. Ireland, M. G. Smith, *J. Am. Chem. Soc.* **1988**, *110*, 854–860.
[21] B. E. Rossiter, T. R. Verhoeven, K. B. Sharpless, *Tetrahedron Lett.* **1979**, *20*, 4733–4736.
[22] D. H. Barton, W. B. Motherwell, A. Stange, *Synthesis* **1981**, 743–745.
[23] The stereochemistry of the newly formed C12 stereocenter of tetrahydrofuran **20b** was assigned by using 2D NMR spectroscopy.
[24] J. W. Gillard, R. Fortin, H. E. Morton, C. Yoakim, C. A. Quesnelle, S. Daignault, Y. Guidan, *J. Org. Chem.* **1988**, *53*, 2602–2608. This unusual protecting group offered the necessary acid stability during the synthesis, as well as the required fluoride ion lability for the final global deprotection with tris(dimethyamino)sulfur(trimethylsilyl) difluoride (See: K. A. Scheidt, H. Chen, B. C. Follows, S. R. Chemler, D. S. Coffey, W. R. Roush, *J. Org. Chem.* **1998**, *63*, 6436–6437). Under these conditions, the time required for C11-OTBS deprotection was prohibitively long. The use of a more base-labile TES ether did not afford the required acid stability during the synthesis.
[25] S. V. Ley, L. R. Cox, *J. Chem. Soc. Perkin Trans. 1* **1997**, 3315–3324.
[26] L. D.-L Lu, R. A. Johnson, M. G. Finn, K. B. Sharpless, *J. Org. Chem.* **1984**, *49*, 728–731. Sharpless has noted (See: Y. Gao, R. M. Hanson, J. M. Klunder, S. Y. Ko, H. Masamune, K. B. Sharpless, *J. Am. Chem. Soc.* **1987**, *109*, 5765–5780, and references therein) that 1,1-disubstituted olefins are problematic substrates for epoxidation under stoichiometric [Ti(O*i*Pr)$_4$] conditions due to epoxide opening by isopropyl alcohol. The use of [Ti(O*t*Bu)$_4$] conveniently avoided any such side reactions.



Asymmetric Syntheses of Pectenotoxins-4 and -8, Part II: Synthesis of the C20–C30 and C31–C40 Subunits and Fragment Assembly**

David A. Evans,* Hemaka A. Rajapakse, Anna Chiu, and Dirk Stenkamp

In the preceding communication,[1] the proposed synthesis plan identified the two principal pectenotoxin-4 subunits **II** and **III** (Figure 1). It was our intention to couple these fragments through the alkylation of the metalloenamine derived from hydrazone **III**, readily available from the coupling of advanced intermediates **IV** and **V** (transform T_2), by epoxide **II**. However, this investigation revealed that the above bond construction was not feasible due to the decomposition of metalloeneamine **III** under the reaction conditions.[2] Accordingly, the objective in the present communication is the synthesis of the subunits **IV** and **V**, and the completion of the syntheses of pectenotoxin-4 (**1**) and pectenotoxin-8 by a revised fragment coupling strategy, where epoxide alkylation (transform T_1) precedes diene formation (transform T_2).

The plan for the construction of the F-ring tetrahydrofuran **IV** was to involve a C37 hydroxy-directed epoxidation of olefin **VI** with a subsequent ring closure by the C32 hydroxy moiety (transform T_3). Finally, the stereoselective formation of the E-ring tetrahydrofuran **V** from its acyclic precursor **VII** was based on an iodoetherification precedent provided by Bartlett and Rychnovsky (transform T_4).[3]

The synthesis of the ring-E synthon **V** began with the known aldol adduct adduct **2** (Scheme 1).[4] Reduction of **2** ($LiBH_4$, THF, 0 °C), and selective protection of the primary alcohol (TBSCl, Im, CH_2Cl_2, 100 % over two steps) afforded allylic alcohol **3**.[5] Acylation of **3** with the PMB-protected lactic acid **4**[6] (DCC, DMAP, CH_2Cl_2, 52 %), followed by carbonyl olefination of **5a** with Tebbe reagent[7] afforded the 1,5-diene **5b**. Claisen rearrangement of **5b** in refluxing toluene gave the desired rearrangement product **6** in 82 % yield for the two steps. Chelate-controlled reduction of the resulting ketone ($Zn(BH_4)_2$, Et_2O, −78 °C, 86 %, d.r. 86:14) provided the precursor for the key iodoetherification reaction. In spite of the modest selectivity that was observed for the formation of the desired tetrahydrofuran **7** (NIS, CH_3CN, −40 °C, 89 %, d.r. 72:28), this outcome proved sufficient to pursue the planned route.

Successive radical dehalogenation of **7** (Bu_3SnH, AIBN, toluene, 100 %) and deprotection of the primary TBS ether (TBAF, THF, 95 %) afforded alcohol **8**. Oxidation with Dess–Martin reagent[8] (py, CH_2Cl_2, 99 %), Wittig homologation ($EtOC(O)CC(CH_3)PPh_3$, THF, 65 °C; 100 % $E:Z > 95:5$), and ester reduction ($LiAlH_4$, Et_2O, 0 °C, 92 %) completed the carbon assembly of the E-ring fragment. Benzyl protection (NaH, BnBr, TBAI, THF/DMF, 94 %) followed by PMB deprotection (DDQ, CH_2Cl_2/pH 7 buffer, 95 %) gave alcohol **10**. Oxidation to the methyl ketone[8] (Dess–Martin periodinane, py, CH_2Cl_2, 93 %), and hydrazone formation (TMSCl, CH_2Cl_2/Me_2NNH_2, 100 %) completed the synthesis of hydrazone **11**.

As summarized in Figure 1, the first stage of the synthesis of the ring-F fragment **IV** will be simplified to the construction of the C31–C35 phosphonium salt, the C36–C40 aldehyde, and their union through a Wittig coupling to afford the *Z*-olefin **VI**.

The synthesis of the C31–C35 phosphonium salt began with the known triol derivative **12** (Scheme 2).[9] Protection of the hydroxy group at C33 of **12** as a PMB ether (PMBBr, NaH, THF/DMF, 95 %) followed by reductive ozonolysis (O_3, EtOH, then DMS, then $NaBH_4$, 95 %) afforded alcohol **13**. Transformation of **13** to the corresponding iodide (I_2, Im, Ph_3P, CH_2Cl_2, 0 °C, 89 %) proceeded smoothly, but careful control of the temperature was required to access phosphonium salt **14** (Ph_3P, CH_3CN, 55 °C, 89 %).[10]

The synthesis of the aldehyde partner **17** began with protection of the hydroxy group at C37 of aldol adduct **15**[11] as a base-sensitive triphenylsilyl ether (TPSCl, Im, DMAP, DMF, 0 °C, 98 %; Scheme 2). Half reduction of the *S*-phenyl thioester[12] (Pd/C, Et_3SiH, acetone, 95 %), and olefination under modified Lombardo conditions[13] ($[Cp_2ZrCl_2]$, Zn dust, CH_2I_2, THF, 0 °C, 84 %) afforded olefin **16**. Rhodium-

[*] Prof. D. A. Evans, H. A. Rajapakse, A. Chiu, D. Stenkamp
Department of Chemistry & Chemical Biology
Harvard University
Cambridge, MA 02138 (USA)
Fax: (+1) 617-495-1460
E-mail: evans@chemistry.harvard.edu

[**] Financial support has been provided by the National Institutes of Health (GM33327-16). A BASF-Forschungsstipendum Postdoctoral Fellowship to D.S. and a Howard Hughes Medical Institute Predoctoral Fellowship to H.A.R. are gratefully acknowledged. The NIH BRS Shared Instrumentation Grant Program 1-S10RR04870 and the NSF (CHE 88-140019) are acknowledged for providing NMR facilities.

 © 2002 WILEY-VCH Verlag GmbH & Co. KGaA, Weinheim 0044-8249/02/4123-4573 $ 20.00+.50/0

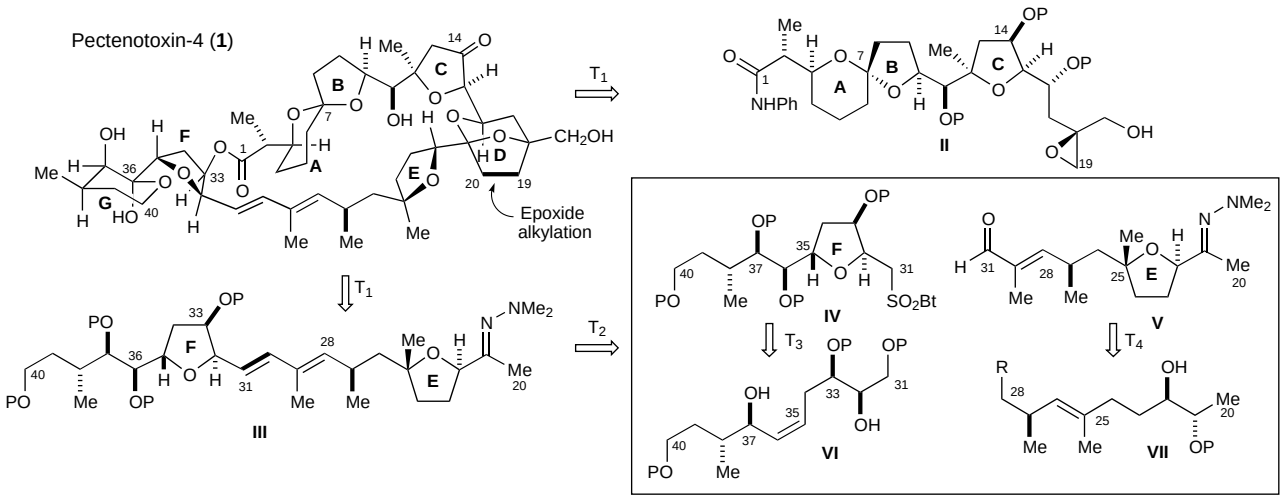
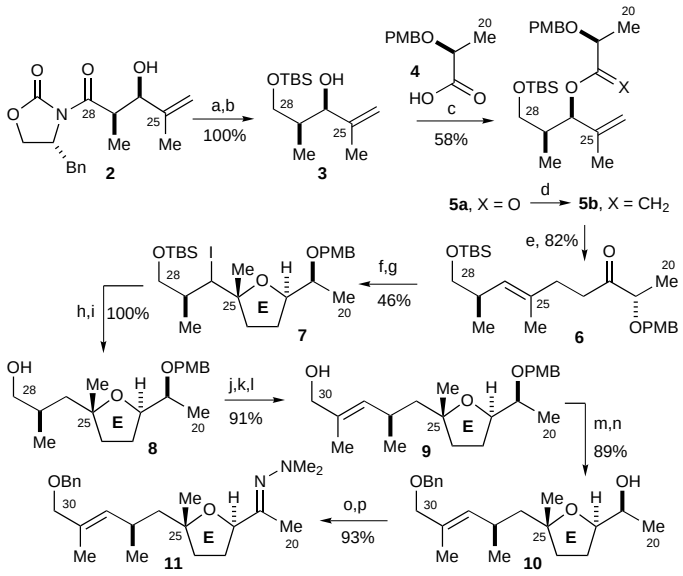


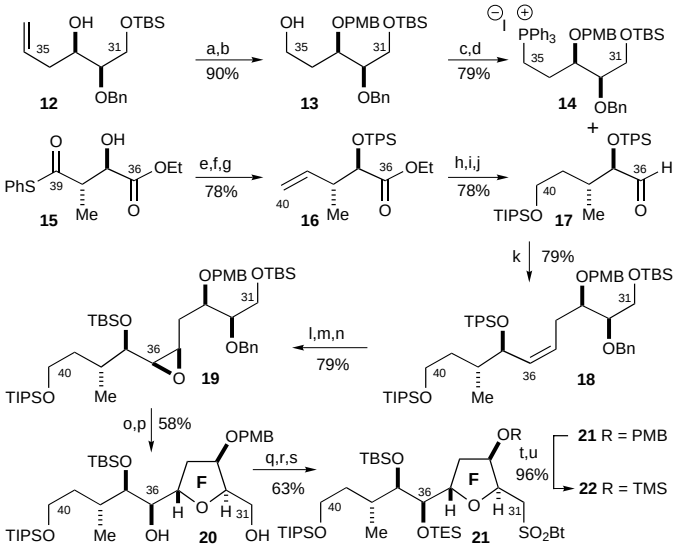
Figure 1. The major disconnections.



Scheme 1. Synthesis of C20–C30 E-ring fragment. a) $LiBH_4$, THF, 0 °C; b) TBSCl, Im, CH_2Cl_2; 100 % (two steps); c) DCC, DMAP, CH_2Cl_2; 52 %; d) $[Cp_2TiCl_2]$, $AlMe_3$, THF, then **5a**; e) toluene, 110 °C; 82 % (two steps); f) $Zn(BH_4)_2$, Et_2O, −78 °C; 74 %; g) NIS, CH_3CN, −40 °C; 64 %; h) Bu_3SnH, AIBN, toluene; 100 %; i) TBAF, THF; 95 %; j) Dess–Martin periodinane, py, CH_2Cl_2; 99 %; k) $EtOC(O)CC(CH_3)PPh_3$, THF, 65 °C; 100 %; l) $LiAlH_4$, Et_2O, 0 °C; 92 %; m) NaH, BnBr, TBAI, THF/DMF (3:1); 94 %; n) DDQ, CH_2Cl_2/pH 7 buffer (8:1); 95 %; o) Dess–Martin periodinane, py, CH_2Cl_2; 93 %; p) TMSCl, CH_2Cl_2/Me_2NNH_2 (1:1), 0 °C; 100 %. See reference [5] for abbreviations.

catalyzed hydroboration[14] ([$(Ph_3P)_3RhCl$], catecholborane, THF, 0 °C, then H_2O_2, EtOH, pH 7 buffer, 88 %), TIPS protection of the resulting primary alcohol (TIPSOTf, lut., CH_2Cl_2, −78 °C, 100 %), and half reduction of the ethyl ester (DIBAL-H, toluene, −78 °C, 89 %) completed the synthesis of aldehyde **17**.

Wittig coupling of phosphonium salt **14** and aldehyde **17** proceeded smoothly (LiHMDS, THF, −78 °C, 79 %, $Z:E$ > 95:5) to afford **18**. Selective deprotection of the TPS ether under basic conditions (K_2CO_3, MeOH/CH_2Cl_2, 87 %), directed epoxidation with *m*-CPBA[15] (CH_2Cl_2, 0 °C, 95 %, d.r. > 95:5) and reprotection of the hydroxy group at C37 as a TBS ether (TBSOTf, lut., CH_2Cl_2, −78 °C, 95 %) afforded epoxide **19** as a single diastereomer. Selective deprotection of the benzyl ether group at C32 was possible under reducing conditions.[16] When the resulting epoxy alcohol was exposed to PPTS in MeOH/CH_2Cl_2, cyclization to form the F-ring tetrahydrofuran with simultaneous deprotection of the C31-OTBS ether afforded diol **20** in 73 % yield.[17] Installation of the benzthiazole sulfide at C31 under Mitsunobo conditions (BtSH, DIAD, Ph_3P, THF, 0 °C), oxidation to the sulfone[18]

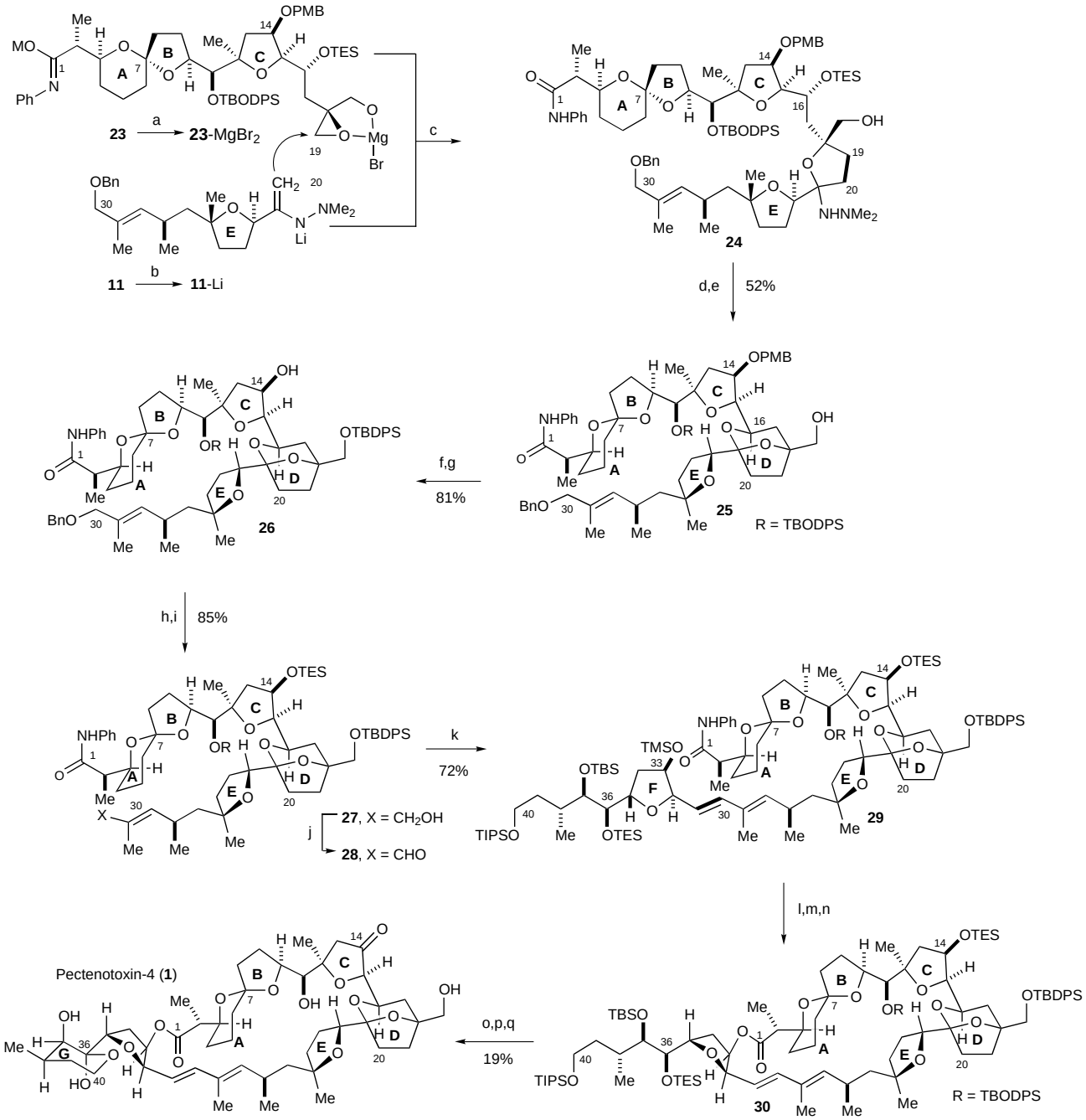


Scheme 2. C31–C40 FG fragment synthesis. a) PMBBr, NaH, THF/DMF (3:1), 0 °C; 95 %; b) O_3, EtOH, −78 °C, then DMS, then $NaBH_4$; 95 %; c) I_2, Im, Ph_3P, CH_2Cl_2, 0 °C; 89 %; d) Ph_3P, CH_3CN, 55 °C, 89 %; e) TPSCl, Im, DMAP, DMF, 0 °C; 98 %; f) Pd/C, Et_3SiH, acetone; 95 %; g) $[Cp_2ZrCl_2]$, Zn dust, CH_2I_2, THF, 0 °C; 84 %; h) $[(Ph_3P)_3RhCl]$, catecholborane, THF, then pH 7 buffer, H_2O_2; 88 %; i) TIPSOTf, lut., CH_2Cl_2, −78 °C; 100 %; j) DIBAL-H, toluene, −78 °C; 89 %; k) LiHMDS, THF, then aldehyde **17**, −78 °C→0 °C; 79 %; l) K_2CO_3, MeOH/CH_2Cl_2 (2:1); 87 %; m) *m*-CPBA, CH_2Cl_2, 0 °C; 95 %; n) TBSOTf, lut., CH_2Cl_2, −78 °C; 95 %; o) LiDBB, THF, −78 °C; 79 %; p) PPTS, MeOH/CH_2Cl_2 (1:1); 73 %; q) BtSH, Ph_3P, DIAD, THF, 0 °C; r) *m*-CPBA, CH_2Cl_2, 0 °C; 70 % (two steps); s) TESCl, Im, CH_2Cl_2; 90 %; t) DDQ, CH_2Cl_2/pH 7 buffer (10:1); 97 %; u) TMSCl, Im, CH_2Cl_2, 99 %. See reference [5] for abbreviations.

 © 2002 WILEY-VCH Verlag GmbH & Co. KGaA, Weinheim 0044-8249/02/4123-4574 $ 20.00+.50/0 *Angew. Chem. Int. Ed.* **2002**, *41*, No. 23

(*m*-CPBA, CH_2Cl_2, 0 °C, 70 % over two steps), and protection of the hydroxy group at C36 as a TES ether (TESCl, Im, CH_2Cl_2, 90 %) afforded **21**. In preparation for the diene formation step, the C33-OPMB ether of sulfone **21** was exchanged for the corresponding TMS ether (DDQ, CH_2Cl_2/pH 7 buffer, 97 %; then TMSCl, Im, CH_2Cl_2, 0 °C, 99 %) to afford **22**.[19]

Completion of the synthesis is shown in Scheme 3. The C19–C20 bond construction joining advanced intermediates **11** and **23** was accomplished by the addition of the magnesium bromide activated epoxide complex **23**-$MgBr_2$[20] to the metalloenamine derived from **11**. The resulting unstable hydrazinyl lactol **24** was treated with acid under biphasic conditions (pentane/CH_2Cl_2/10 % aq. $NaHSO_4$) to access the corresponding lactol, which underwent desilylation at C16 and spontaneous bicyclic ketal formation to afford adduct **25** upon exposure to PPTS in MeOH/CH_2Cl_2 (52 % over three steps). Protection of the hydroxymethyl moiety at C18



Scheme 3. Fragment assembly and completion of synthesis. a) **23**, EtMgBr, HMPA, THF, −67 °C→0 °C; b) **11**, LDA, THF, −67 °C→0 °C; c) add **23**-$MgBr_2$ to **11**-Li, +10 °C; d) pentane/CH_2Cl_2/10 % $NaHSO_4$ (4.5:1.5:4); e) PPTS, CH_2Cl_2/MeOH (1:1); 52 % (three steps); f) TBDPSCl, Im, DMAP, CH_2Cl_2; 90 %; g) DDQ, CH_2Cl_2/pH 7 buffer (6:1); 90 %; h) TESCl, Im, CH_2Cl_2; 100 %; i) LiDBB, THF, −78 °C; 85 %; j) SO_3·Py, Et_3N, CH_2Cl_2/DMSO (1:1); k) sulfone **22**, LiHMDS, THF, −78 °C→0 °C; 72 % (two steps); l) Boc_2O, DMAP, CH_3CN; 91 %; m) LiOH, H_2O_2, THF/H_2O (3:1); n) trichorobenzoyl chloride, *i*Pr_2NEt, then DMAP, toluene; RT; o) PPTS, CH_2Cl_2/MeOH (1:1); 35 % (three steps); p) Dess–Martin periodinane, py, CH_2Cl_2; 72 %; q) TAS-F, H_2O, DMF; 85 %. See reference [5] for abbreviations.

 © 2002 WILEY-VCH Verlag GmbH & Co. KGaA, Weinheim 0044-8249/02/4123-4575 $ 20.00+.50/0

(TBDPSCl, Im, DMAP, CH_2Cl_2, 90%), exchange of the C14 hydroxy protecting group (DDQ, CH_2Cl_2/pH 7 buffer, 90%; TESCl, Im, CH_2Cl_2, 100%), and benzyl deprotection[16] (LiDBB, THF, −78°C) afforded **27**, the fully elaborated precursor needed for the diene formation step.

On the basis of convergency considerations the C1–C30 ABCDE fragment **27** was employed as the electrophilic partner in the Julia olefination with the β-alkoxy sulfone **22**.[21] Oxidation[22] of alcohol **27** to aldehyde **28** (SO_3·Py, Et_3N, DMSO/CH_2Cl_2) was followed by the addition of LiHMDS to a pre-mixed solution of **28** and sulfone **22** in THF at −78°C to provide the desired diene **29** as a 88:12 mixture of C32 epimers (72% over two steps, $E:Z > 95:5$).[23] Pursuant to revealing the terminal carboxyl residue, *N*-phenylamide **29** was activated through its *N*-Boc imide, and hydrolysis to the acid (LiOH, H_2O_2, THF/H_2O) proceeded with with concomitant C33-OTMS deprotection to give pectenotoxin-4 *seco* acid.[24] Macrocyclization under Yamagichi conditions[25] (2,4,6-trichlorobenzoyl chloride, *i*Pr_2NEt, toluene, then DMAP, toluene) at room temperature provided adduct **30**. Selective deprotection of the C14 and C36 OTES ethers with PPTS in MeOH/CH_2Cl_2 (35% over three steps), oxidation to the diketone[8] (Dess–Martin periodinane, py, CH_2Cl_2, 72%) and global deprotection[26] (TAS-F, H_2O, DMF, 85%) afforded pectenotoxin-4 in 36 steps (longest linear sequence) and 0.3% overall yield. The synthetic material was identical by ^{1}H NMR spectroscopy and optical rotation to natural pectenotoxin-4.[27] Further proof of structure was obtained by isomerizing synthetic pectenotoxin-4 to pectenotoxin-8[28] (1% TFA in CH_3CN/H_2O, 40%), and this material was identical to natural pectenotoxin-8 as judged by ^{1}H NMR, HPLC, TLC R_f, and UV spectroscopy.

Received: September 18, 2002 [Z50191]

[1] D. A. Evans, H. A. Rajapakse, D. Stenkamp, *Angew. Chem.* **2002**, *114*, 4751; *Angew. Chem. Int. Ed.* **2002**, *41*, 4569.

[2] A full account of this work will be published in due course.

[3] P. A. Bartlett, S. D. Rychnovsky, *J. Am. Chem. Soc.* **1981**, *103*, 3964–3966.

[4] D. A. Evans, D. M. Fitch, *J. Org. Chem.* **1997**, *62*, 454–455.

[5] Abbreviations: TBS = *tert*-butyldimethylsilyl; DCC = dicyclohexyl carbodiimide; DMAP = 4-(*N*,*N*-dimethylamino)pyridine; Cp = cyclopentadienyl, d.r. = diastereomeric ratio; NIS = *N*-iodosuccinimide; AIBN = 2,2′-azobisisobutyronitrile; TBAF = tetra-(*n*-butyl)ammonium fluoride; THF = tetrahydrofuran; py = pyridine; Bn = benzyl; TBAI = tetra-(*n*-butyl)ammonium iodide; DMF = dimethylformamide; DDQ = 2,3-dichloro-5,6-dicyano-1,4-benzoquinone; TMS = trimethylsilyl; DMS = dimethyl sulfide; Im = imidazole; TPS = triphenylsilyl; TIPS = triisopropylsilyl; lut. = 2,6-lutidine; DIBAL-H = diisobutylaluminum hydride; LiHMDS = lithium hexamethyldisilazide; *m*-CPBA = *meta*-chloroperoxybenzoic acid; Bt = benzthiazole; TES = triethylsilyl; PPTS = pyridinium *para*-toluenesulfonate; TBDPS = *tert*-butyldiphenylsilyl; LiDBB = lithium di-*tert*-butylbiphenylide; Boc_2O = di-*tert*-butyl dicarbonate; LDA = lithium diisopropylamide; HMPA = hexamethylphosphoramide; TBODPS = *tert*-butoxydiphenylsilyl; RT = room temperature; TAS-F = tris(dimethyamino)sulfur(trimethylsilyl)difluoride.

[6] A. Chen, A. Nelson, N. Tanikkul, E. J. Thomas, *Tetrahedron Lett.* **2001**, *42*, 1251–1254.

[7] S. H. Pine, R. Zahler, D. A. Evans, R. H. Grubbs, *J. Am. Chem. Soc.* **1980**, *102*, 3270.

[8] D. B. Dess, J. C. Martin, *J. Am. Chem. Soc.* **1991**, *113*, 7277–7287.

[9] M. T. Reetz, K. Kesseler, *J. Org. Chem.* **1985**, *50*, 5434–5436.

[10] At temperatures above 55°C, intramolecular alkylation of the C_{32} benzyl ether to form the corresponding tetrahydrofuran was observed. For a similar side reaction, see: D. A. Evans, A. M. Ratz, B. E. Huff, G. S. Sheppard, *J. Am. Chem. Soc.* **1995**, *117*, 3448–3467.

[11] D. A. Evans, D. W. C. MacMillan, K. R. Campos, *J. Am. Chem. Soc.* **1997**, *119*, 10859–10860.

[12] T. Fukuyama, S.-L. Lin, L. Li, *J. Am. Chem. Soc.* **1990**, *112*, 7050–7051; see also: D. A. Evans, B. W. Trotter, P. J. Coleman, B. Cote, L. Carlos Dias, H. A. Rajapakse, A. N. Tyler, *Tetrahedron* **1999**, *55*, 8671–8726.

[13] Conditions adapted from: M. Hartman, E. Zibral, *Tetrahedron Lett.* **1990**, *31*, 2875–2878. Both Wittig and Petersen conditions resulted in aldehyde decomposition with no observed product.

[14] D. A. Evans, G. C. Fu, A. H. Hoveyda, *J. Am. Chem. Soc.* **1992**, *114*, 6671–6674.

[15] B. E. Rossiter, T. R. Verhoeven, K. B. Sharpless, *Tetrahedron Lett.* **1979**, *20*, 4733–4736.

[16] a) P. K. Freeman, L. L. Hutchinson, *J. Org. Chem.* **1980**, *45*, 1924–1930; b) R. E. Ireland, M. G. Smith, *J. Am. Chem. Soc.* **1988**, *110*, 854–860.

[17] No undesired tetrahydropyran byproducts were observed in this reaction.

[18] J. B. Baudin, G. Hareau, S. A. Julia, O. Ruel, *Bull. Soc. Chim. Fr.* **1993**, *130*, 856–878.

[19] PMB deprotection with DDQ was incompatible with the pectenotoxin diene, as exclusive allylic oxidation was observed. For *successful* deprotections of PMB ethers in the presence of allylic dienes see: a) N. Murakami, W. Wang, M. Aoki, Y. Tsutsui, M. Sugimoto, M. Kobayashi, *Tetrahedron Lett.* **1998**, *39*, 2349–2352; b) G. Pattenden, A. T. Plowright, J. T. Tornos, T. Ye, *Tetrahedron Lett.* **1998**, *39*, 6099–6102.

[20] a) J. A. Marshall, R. C. Andrews, *J. Org. Chem.* **1985**, *50*, 1602–1606; b) D. A. Evans, R. P. Polniaszek, K. M. DeVries, D. E. Guinn, D. J. Mathre, *J. Am. Chem. Soc.* **1991**, *113*, 7613–7630.

[21] For examples of β-alkoxy sulfone couplings see: a) ref. [19b]; b) D. A. Evans, D. M. Fitch, T. E. Smith, V. J. Cee, *J. Am. Chem. Soc.* **2000**, *122*, 10033–10046; c) A. B. Smith, B. M. Brandt, *Org. Lett.* **2001**, *3*, 1685–1688.

[22] J. R. Parikh, W. E. von Doering, *J. Am. Chem. Soc.* **1967**, *89*, 5505–5507.

[23] Initial feasibility studies on a model system revealed a dramatic counterion effect for this Julia coupling reaction. The use of KHMDS as the base resulted in a 29:71 ratio of C32 epimers favoring the undesired product. We attribute this epimerization side reaction to be due to ring-F cleavage through β-alkoxy elimination and readdition to the intermediate unsaturated sulfone.

[24] D. A. Evans, P. H. Carter, C. J. Dinsmore, J. C. Barrow, J. L. Katz, D. W. Kung, *Tetrahedron Lett.* **1997**, *38*, 4535–4538.

[25] J. Inanaga, K. Hirata, H. Saeki, T. Katsuki, M. Yamaguchi, *Bull. Chem. Soc. Jpn.* **1979**, *52*, 1989–1993.

[26] K. A. Scheidt, H. Chen, B. C. Follows, S. R. Chemler, D. S. Coffey, W. R. Roush, *J. Org. Chem.* **1998**, *63*, 6436–6437.a) For previous uses of TAS-F for silyl ether deprotection see: R. A. Holton, C. Somoza, H.-B. Kim, F. Liang, R. J. Biediger, P. D. Boatman, M. Shindo, C. C. Smith, S. Kim, H. Nadizadeh, Y. Suzuki, C. Tao, P. Vu, S. Tang, P. Zhang, K. K. Murthi, L. N. Gentile, J. H. Liu, *J. Am. Chem. Soc.* **1994**, *116*, 1597–1598; b) P. A. Wender, N. F. Badham, S. P. Conway, P. E. Floreancig, T. E. Glass, C. Gränicher, J. B. Houze, J. Jänichen, D. Lee, D. G. Marquess, P. L. McGrane, W. Meng, T. P. Mucciaro, M. Muhnlebach, M. G. Natchus, H. Paulsen, D. B. Rawlings, J. Satkofsky, A. J. Shuker, J. C. Sutton, R. E. Taylor, K. Tomooka, *J. Am. Chem. Soc.* **1997**, *119*, 2755–2756.

[27] A natural sample of pectenotoxin-4 was unavailable for comparison. Professor M. Satake of Tohoku University is thanked for kindly providing copies of ^{1}H NMR spectra of pectenotoxin-1, -4, and -8, as well as samples of pectenotoxin-1 and -8.

[28] K. Sasaki, J. L. C. Wright, T. Yasumoto, *J. Org. Chem.* **1998**, *63*, 2475–2480. We observed a 11:10:79 ratio of pectenotoxins-1:-4:-8.

 © 2002 WILEY-VCH Verlag GmbH & Co. KGaA, Weinheim 0044-8249/02/4123-4576 $ 20.00+.50/0

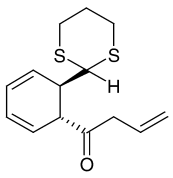
trans-Addition of Two Carbon Substituents across a Benzene Double Bond in [(η⁶-Benzene)Mo(CO)₃]**

E. Peter Kündig,* Charles-H. Fabritius, Gabriele Grossheimann, Fabrice Robvieux, Patrick Romanens, and Gérald Bernardinelli

[(Arene)$Cr(CO)_3$] complexes have found widespread application in organic synthesis as a result of the activating and stereodirecting influence of the π Lewis acid fragment $Cr(CO)_3$. The applications include nucleophilic addition to the aromatic ring, to carbonyl and imine functions in side chains, and to configurationally stable benzylic carbocations. Arene lithiation reactions and reactions via benzylic anions also are much more facile in the complex than in the free arene. Diastereoselective and enantioselective variants have been developed for many transformations and they have found application in asymmetric organic synthesis and in the synthesis of chiral ligands for asymmetric catalysis.[1] [(benzene)$Mo(CO)_3$] is readily accessible from $Mo(CO)_6$[2] but, surprisingly, analogous reactions to the ones listed above for the $Cr(CO)_3$ complex have not been reported. Intrigued by this situation, we started a research project on [(arene)Mo$(CO)_3$] complexes and here report the first results.

Thermochemical studies show the arene–Mo bond (68 kcal mol^{-1} in [(η^6-C_6H_6)$Mo(CO)_3$] (**1**)) to be stronger than the arene–Cr bond (53 kcal mol^{-1} in [(η^6-C_6H_6)$Cr(CO)_3$]) (**2**)).[3] M–H bonds are also stronger with the second-row transition metal, as shown by the values of 62 kcal mol^{-1} and 54 kcal mol^{-1} in [$CpMo(CO)_3(H)$] and [$CpCr(CO)_3(H)$], respectively.[4] Kinetically, however, the situation is reversed. The metal–arene bond in **1** is far more labile than that in **2**. This lability and the resulting difficulty in handling the Mo compounds have retarded their use in synthesis. We anticipated that there would be different selectivities in the reactions of the Cr and Mo complexes and that the higher bond strength of the Mo–C and Mo–H bonds would make possible the isolation of intermediates that have eluded characterization in the Cr-mediated reaction sequence. Both of these hypotheses have now been fulfilled.

Addition of 2-lithio-1,3-dithiane[5](**2a**; Scheme 1) to a cold (−78 °C) solution of the benzene–Mo complex **1** in THF*** afforded a yellow precipitate **3a**, which dissolved when the reaction mixture was warmed to −20 °C. The ^{1}H NMR spectrum of **3a** was consistent with that expected for the anionic cyclohexadienyl complex. Treatment of the THF solution of **3a** with allyl bromide (**4a**) produced the [(η^3-allyl)(η^5-cyclohexadienyl)$Mo(CO)_2$] complex (**5a**) which was isolated as a yellow solid. In solution, **5a** is present as a mixture of the two rapidly interconverting *exo–endo* allyl isomers. Analogous reactions with [(η^6-benzene)$Cr(CO)_3$] have been shown previously to give directly the decomplexed cyclohexadiene **6**.[6]

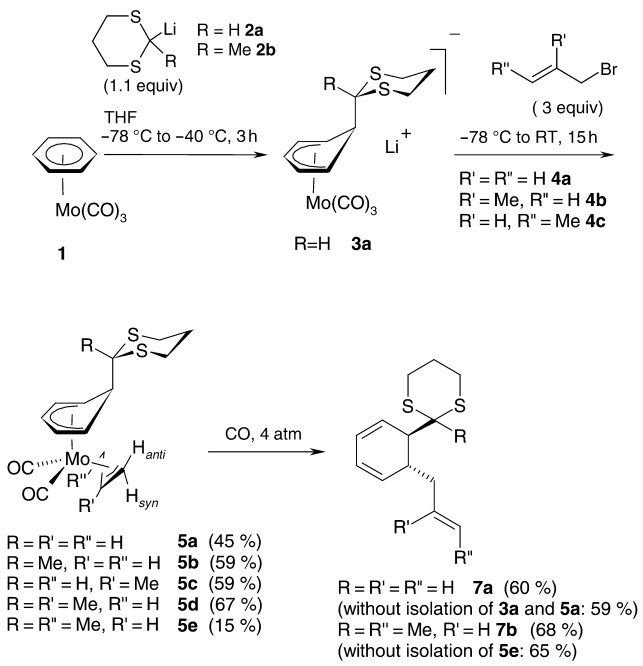


6

In the Cr-mediated reaction, metal allylation, followed by CO insertion, reductive elimination, and decomplexation occurred readily and intermediates could not be detected. In marked contrast to the above, the Mo–allyl complex **5a** is stable at room temperature. Its intermediacy on the pathway to a *trans*-disubstituted cyclohexadiene was shown by placing a solution of the complex **5a** under 4 atm of CO to give the allyl cyclohexadiene **7a** exclusively (60% yield). No ketone product was observed and this attests to the decreased tendency to carbonylation reactions of the Mo-bound allyl group when compared to Cr-bound groups. Literature precedent to resistance to carbonylation in Mo complexes is exemplified by the report by King et al. that [(η^5-C_5H_5)$MoMe(CO)_3$] does not undergo migratory carbonylation even under 300 atm of CO.[7]

The alkylation/allylation of **1** was then repeated without the isolation of intermediates and with the allylation step carried out under CO pressure. After work-up, **7a** was obtained in 59% yield in this one-pot procedure (see Scheme 1).

Analogous reactions with lithium dithiane and lithium methyldithiane as nucleophiles and allyl and crotyl bromides



Scheme 1. Reaction sequence for formation of **7a**. In situ IR spectroscopic measurements were carried out under conditions designed to optimize the spectra obtained.

[*] Prof. Dr. E. P. Kündig, C.-H. Fabritius, Dr. G. Grossheimann, F. Robvieux, P. Romanens
Department of Organic Chemistry
University of Geneva
30 Quai Ernest Ansermet, 1211 Geneva 4 (Switzerland)
Fax: (+41) 22-328-7396
E-mail: peter.kundig@chiorg.unige.ch
Dr. G. Bernardinelli
Laboratoire de Crystallographie
Université de Genève
24 Quai Ernest Ansermet, 1211 Genève 4 (Switzerland)

[**] Support of this work by the Swiss National Foundation is gratefully acknowledged (SNF grant 2000–66962.01).

[***] The benzene ligand in **1** is susceptible to substitution by THF at ambient temperature but stable solutions can be prepared by maintaining low temperatures at all times.

 © 2002 WILEY-VCH Verlag GmbH & Co. KGaA, Weinheim 0044-8249/02/4123-4577 $ 20.00+.50/0

as electrophiles are shown in Scheme 1. The structures of the complexes **5** were deduced from spectroscopic data (IR, NMR) and comparison to closely related complexes such as [CpMo(η^3-*endo*-allyl)(CO)$_2$] and [CpMo(CO)$_2$(η^3-2-methylallyl)].[8] The yield of **5e** was a low 15% because the decomplexed product **7b** was also formed under the reaction conditions and isolated from the mixture in 26% yield. The conditions for reductive elimination thus depend on the substitution pattern of the allyl moiety in the complexes **5**. The 2-methylallyl complex **5c**, exclusively present as the *endo* complex, could not be induced to give the coupled product **7** even under 60 atm pressure of CO. Treatment of **5c** with PPh_3, MeCN, or attempts at oxidation-induced coupling (I_2, air, Ce^{IV}) furnished neither **7** nor the carbonylated product. The structure of the complex **5c** was confirmed by X-ray diffraction (see Figure 1).

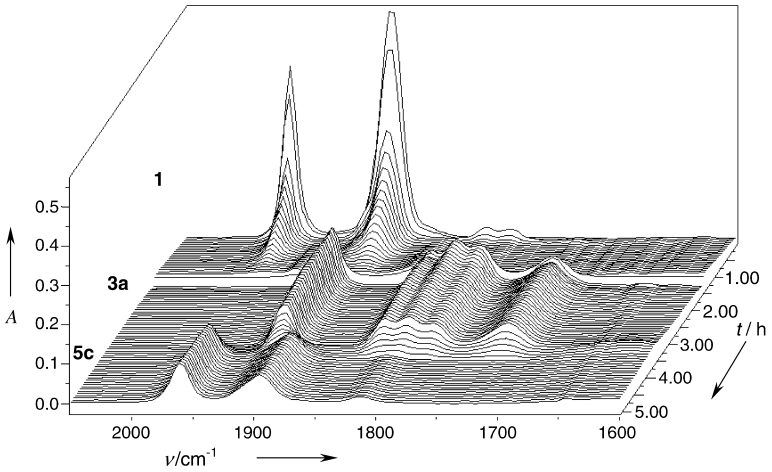


Figure 2. IR stack plot for the sequential reaction of **1** with **2a** and **4b** in THF.

In situ IR spectroscopic measurements[9] were of considerable help in delineating the reaction sequence. Figure 2 shows the sequence for the formation of the complex **5c**.

Complex **1** is characterized by its CO stretching bands at 1969 and 1884 cm^{-1} in the IR spectrum in THF. On addition of **2a** at −78°C (2 equiv), the intensity of these resonances rapidly decreased and after 1 hour at −50°C the ν_{CO} bands of the starting complex **1** had totally disappeared. No new bands were apparent apart from the fleeting appearance of a shoulder at 1899 cm^{-1} and two absorptions at 1803 cm^{-1} and 1783 cm^{-1}. This can be readily explained as the reaction mixture at this stage showed a yellow preciptate. On raising the temperature to 0°C ($t = 1.5$ h), the spectrum of the clear yellow solution now showed $\tilde{\nu}_{CO}$ bands at 1899, 1803, 1783, and 1720 cm^{-1}. These bands are similar to those of the anionic cyclohexadienyl chromium complex previously reported by Semmelhack et al.[10] The pattern of resonances at first appears too complicated for a Mo(CO)$_3$ fragment but it has to be borne in mind that the Li cation coordinates to one of the carbonyl ligands. The band at 1720 cm^{-1} is assigned to the carbonyl ligand bearing the Li cation.[10,11] Addition of allyl bromide at 0°C (at $t = 3.5$ h) brings about the final change to the spectrum with resonances at 1957 and 1891 cm^{-1} assigned to **5c**. In experiments in which methyl allyl bromide (**4b**) was added at −20°C, additional absorptions at 2011, 1965, and 1930 cm^{-1} appeared briefly after the addition of the electrophile. They are tentatively assigned to the η^1-methyl allyl intermediate by comparison with the bands reported for [CpMo(CO)$_3$(η^1-2,4-hexadien-1-yl)] (2015, 1962, 1942 cm^{-1}).[12] Figure 3 shows the decline and growth of the amount of the different species in solution. The experiment illustrates the value of in situ IR spectroscopy for monitoring reactions in real time.

This first study of a sequential nucleophile/electrophile addition sequence to an arene–Mo(CO)$_3$ complex in a nucleophilic/allyl bromide double-addition sequence demonstrates the viability of using π-arene–molybdenum complexes

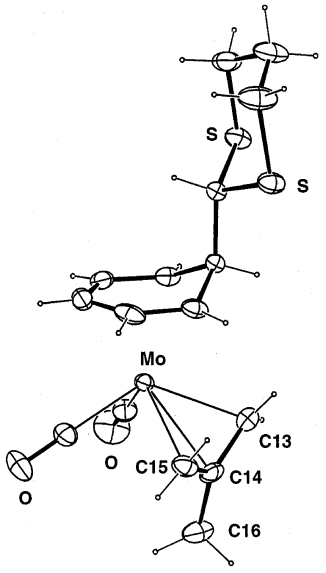


Figure 1. ORTEP view of the X-ray crystal structure of **5c**. Ellipsoids are represented at the 50% probability level. Selected bond lengths [Å] and angles [°] (in brackets for the second molecule of the asymmetric unit): Mo-C13 2.333(3) {2.321(2)}, Mo-C14 2.330(2) {2.320(2)}, Mo-C15 2.322(2) {2.328(2)} , C13-C14 1.415(4) {1.403(4)}, C14-C15 1.398(3) {1.405(4)}, C14-C16 1.514(4) {1.514(4)}; C13-C14-C15 117.4(2) {117.6(2)}, C13-C14-C16 121.3(3) {120.5(3)}, C15-C14-C16 121.1(2) {121.7(3)}.

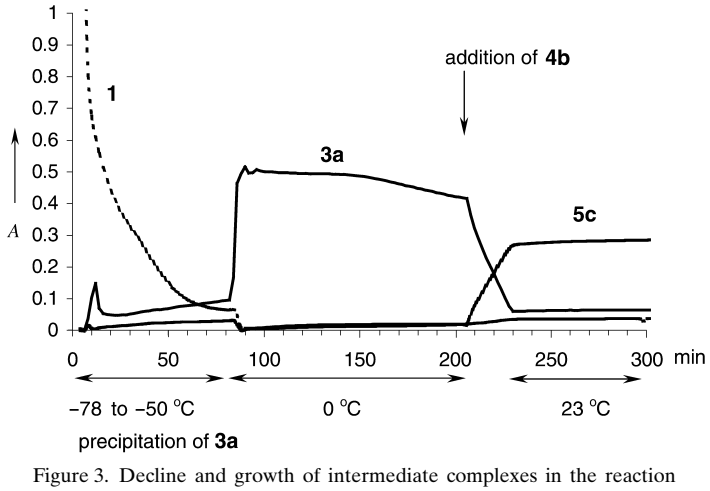


Figure 3. Decline and growth of intermediate complexes in the reaction **1**→**3a**→**5c**.

 © 2002 WILEY-VCH Verlag GmbH & Co. KGaA, Weinheim 0044-8249/02/4123-4578 $ 20.00+.50/0

in organic synthesis. The reported reactions, the isolation of intermediates, and the final products highlight analogies but also differences between the chromium and molybdenum complexes. These first results are very promising and we predict exciting developments in transition metal-mediated and ultimately catalytic arene transformations by transition-metal–π Lewis acid complexation.

Experimental Section

5c: Under an N_2 atmosphere [(η^6-benzene)Mo(CO)$_3$] (**1**) (250 mg, 0.97 mmol) was added as a solid to cold, freshly distilled, dry, and degassed THF (−78 °C, 5 mL) in a Schlenk reaction vessel. In parallel, a solution of **2a** was prepared by adding *n*BuLi (0.67 mL of a 1.6 M solution in hexanes, 1.07 mmol, 1.1 equiv) to a solution of dithiane (128 mg, 1.07 mmol, 1.1 equiv) in 10 mL of dry THF(−78 to −30 °C, 2 h).[5] After recooling to −78 °C, this solution was transferred rapidly through a Teflon cannula to the solution of the Mo complex at −78 °C. The stirred mixture was allowed to warm to −40 °C over 3 h to give a suspension of a yellow product (complex **3a**). The solution was then recooled to −78 °C and treated with 3-bromo-2-methylpropene (0.30 mL, 2.91 mmol, 3 equiv). The reaction mixture was allowed to warm up to room temperature overnight, and the yellow solution was concentrated to 1 mL. Addition of hexane (10 mL) caused precipitation of a yellow solid which was separated and washed with 3 × 10 mL of hexane to give **5c** (230 mg, 59 %); m.p.: 120–125 °C (decomp.); IR (hexane): $\tilde{\nu}$(CO) = 1970 (vs), 1910 (s); ^{1}H NMR (200 MHz, C_6D_6, 20 °C): δ = 5.27 (t, ^3J(H,H) = 5.5 Hz, 1H; CH), 4.39 (t, ^3J(H,H) = 5.5 Hz, 2H; CH), 3.34 (t, ^3J(H,H) = 5.5 Hz, 2H; CH), 3.13 (d, ^3J(H,H) = 10.0 Hz, 1H; CH), 2.98 (s, 2H; CH_{syn}), 2.52 (dt, ^3J(H,H) = 10.0, 4.6 Hz, 1H; CH), 1.98–2.30 (m, 4H; CH_2), 1.91 (s, 3H; CH_3), 1.83 ppm (s, 2H; CH_{anti}); ^{13}C NMR (75 MHz, C_6D_6, 20 °C): δ = 236.0 (2CO), 108.5 (C quaternary), 98.1 (2CH), 86.3 (CH), 61.8 (2CH), 56.8 (CH), 45.8 (2$C_{terminal}$), 37.7 (CH), 27.6 (2CH_2), 26.2 (CH_2), 24.9 ppm (CH_3); MS: *m*/*z* (%): 287 (13), 231 (16), 161 (55, $C_7H_{13}S_2$), 119 (100, $C_4H_7S_2$), 91 (28); elemental analysis (%) calcd for $C_{16}H_{20}MoO_2S_2$: C 47.52; H 4.98; found: C 47.77; H 5.26.

Crystal structure of **5c:** $(C_{10}H_{13}S_2)(CO)_2(C_4H_7)$; M_r = 404.4; μ = 1.02 mm^{-1}, d_x = 1.579 g cm^{-3}, triclinic, $P\bar{1}$, Z = 4, a = 12.0586(10), b = 12.3014(11), c = 13.1125(11) Å, α = 76.498(10), β = 89.553(10), g = 64.742(10)°, V = 1701.2(3) Å^3; yellow prism 0.14 × 0.17 × 0.31 mm mounted on a quartz fibre with protection oil. Cell dimensions and intensities were measured at 200 K on a Stoe IPDS diffractometer with graphite-monochromated $Mo_{K\alpha}$ radiation (λ = 0.71073 Å); θ_{max} = 25.8°; 25953 measured reflections, 7571 independent reflections (R_{int} = 0.034) of which 5210 with $|F_o| > 4\sigma(F_o)$; Data were corrected for Lorentz and polarization effects and for absorption ($T_{min,max}$ = 0.8296, 0.9135). The structure was solved by direct methods using SIR97,[13] all other calculations were performed with the XTAL system[14] and ORTEP[15] programs. Full-matrix least-squares refinement based on F using a weight of $1/(\sigma^2(F_o) + 0.0001\,(F_o^2))$ gave the final values R = 0.019, ωR = 0.020, and GOF(F) = 1.00(1) for 499 variables and 5379 contributing reflections. Maximum shift/error = 0.66 × 10^{-3}, max/min residual electron density 0.39/−0.69 e Å^{-3}. Both molecules of the asymmetric unit are similar. CCDC-192276 (**5c**) contains the supplementary crystallographic data for this paper. These data can be obtained free of charge via www.ccdc.cam.ac.uk/conts/retrieving.html (or from the Cambridge Crystallographic Data Centre, 12 Union Road, Cambridge CB2 1EZ, UK; fax: (+44) 1223-336-033; or deposit@ccdc.cam.ac.uk).

7a: Allyl bromide (**4a**) (0.131 mL, 1.50 mmol, 3 equiv) was added at −78 °C to a solution of **3a** in THF, prepared as described above starting with **1** (129 mg, 0.50 mmol). The mixture was warmed up to room temperature overnight and then stirred for 12 h under 4 atm of CO. The brown solution was stripped of volatiles under vacuum. The residue was dissolved in hexane and filtered through celite and silica gel. Purification by flash chromatography with cyclohexane/Et_2O (98:2) yielded the cyclohexadiene **7a** as a yellow oil (70 mg, 59 % yield) after evaporation of the solvent. IR (hexane): $\tilde{\nu}$ = 3078 (w), 3038 (m), 2979–2846 (s), 1640 (m), 1462 (s), 1275 (m), 1181 (m), 1099 (m), 1017 (m), 993 (m), 913 (s), 807 (m), 703 (s); ^{1}H NMR (400 MHz, $CDCl_3$): δ = 5.85–5.95 (m, 2H; 2CH), 5.65–5.80 (m, 3H; 3CH), 5.00–5.05 (m, 2H; CH_2), 4.13 (d, ^3J(H,H) = 6.4 Hz, 1H; CH), 2.75–2.85 (*m*, 4H; 2CH_2), 2.65–2.75 (m, 1H; CH), 2.50–2.60 (m, 1H; CH), 1.80–2.20 ppm (m, 4H; 2CH_2); ^{13}C NMR (100 MHz, $CDCl_3$, DEPT, C-H Correlation): δ = 135.9 (CH), 130.1 (CH), 124.8 (CH), 124.3 (CH), 122.6 (CH), 116.9 (CH_2), 51.8 (CH), 41.5 (CH), 37.8 (CH_2), 34.9 (CH), 30.2, 30.1 (2CH_2), 26.0 ppm (CH_2); MS: *m*/*z* (%): 238 (1.9, M^+), 196 (3, $C_{10}H_{12}S_2$), 119 (100, $C_4H_7S_2$), 91 (49), 77 (21,C_6H_5); HR-MS: calcd for $C_{13}H_{18}S_2$ 238.0821; found 238.0850.

Received: August 27, 2002 [Z50049]

[1] Reviews: a) M. F. Semmelhack in *Comprehensive Organometallic Chemistry II, Vol. 12* (Eds.: E. W. Abel, F. G. A. Stone, G. Wilkinson), Elsevier Science, Oxford, **1995**, pp. 979–1015; b) S. G. Davies, T. D. McCarthy in *Comprehensive Organometallic Chemistry II, Vol. 12* (Eds.: E. W. Abel, F. G. A. Stone, G. Wilkinson), Elsevier Science, Oxford, **1995**, pp. 1039–1070; c) H.-G. Schmalz, S. Siegel in *Transition Metals in Organic Synthesis, Vol. 1* (Eds.: M. Beller, C. Bolm), Wiley-VCH, Weinheim, **1998**, pp. 550–559; d) C. Bolm, K. Muniz, *Chem. Soc. Rev.* **1999**, *28*, 51–59; e) F. Rose-Munch, E. Rose, *Curr. Org. Chem.* **1999**, *3*, 445–467; f) K. Kamikawa, M. Uemura, *Synlett* **2000**, 938–949; g) A. Pape, K. Kaliappan, E. P. Kündig, *Chem. Rev.* **2000**, *100*, 2917–2940.

[2] a) E. O. Fischer, K. Z. Öfele, *Z. Naturforsch. B* **1958**, *13*, 458; b) W. Strohmeier, *Chem. Ber.* **1961**, *94*, 3337–3341; c) A. N. Nesmeyanov, V. V. Krivykh, V. S. Kaganovich, I. Rybinskaya, *J. Organomet. Chem.* **1975**, *102*, 185–193; d) G. K.-I. Magomedov, *J. Organomet. Chem.* **1990**, *385*, 113–130.

[3] S. L. Mukerjee, R. F. Lang, T. Ju, G. Kiss, C. D. Hoff, S. P. Nolan, *Inorg. Chem.* **1992**, *31*, 4885–4889.

[4] M. Tilset, V. D. Parker, *J. Am. Chem. Soc.* **1989**, *111*, 6711–6717.

[5] D. Seebach, E. J. Corey, *J. Org. Chem.* **1975**, *40*, 231–237.

[6] E. P. Kündig, A. F. Cunningham, Jr., P. Paglia, D. P. Simmons, G. Bernardinelli, *Helv. Chim. Acta* **1990**, *73*, 386–404.

[7] R. B. King, A. D. King, Jr., M. Z. Iqbal, C. C. Frazier, *J. Am. Chem. Soc.* **1978**, *100*, 1687–1694.

[8] a) J. W. Faller, C.-C. Chen, M. J. Mattina, A. Jakubowski, *J. Organomet. Chem.* **1973**, *52*, 361–386;b) N. W. Murall, A. J. Welch, *Acta Crystallogr. Ser. C; Cryst. Struct. Commun.* **1984**, *C40*, 401–403;c) J. W. Faller, B. C. Whitmore, *Organometallics* **1986**, *5*, 752–755.

[9] Carried out with a Mettler Toledo ReactIR 1000 instrument equipped with a SiComp window.

[10] M. F. Semmelhack, H. T. Hall, R. Farina, M. Yoshifuji, G. Clark, T. Bargar, K. Hirotsu, J. Clardy, *J. Am. Chem. Soc.* **1979**, *101*, 3535–3544.

[11] a) J. P. Djukic, F. Rose-Munch, E. Rose, Y. Dromzee, *J. Am. Chem. Soc.* **1993**, *115*, 6434–6435; b) A. Fretzen, A. Ripa, R. Liu, G. Bernardinelli, E. P. Kündig, *Chem. Eur. J.* **1998**, *4*, 251–259.

[12] T.-W. Lee, R.-S. Liu, *Organometallics* **1988**, *7*, 878–883.

[13] A. Altomare, M. C. Burla, M. Camalli, G. Cascarano, C. Giacovazzo, A. Guagliardi, A. G. G. Moliterni, G. Polidori, R. Spagna, *J. Appl. Crystallogr.* **1999**, *32*, 115–119.

[14] S. R. Hall, H. D. Flack, J. M. Stewart, XTAL3.2 User's Manual, Universities of Western Australia and Maryland, **1992**.

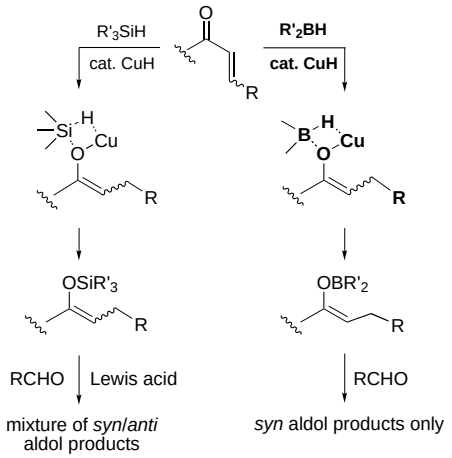
[15] C. K. Johnson, *ORTEP II*, Report ORNL-5138, Oak ridge National Laboratory, Oak Ridge, TN, **1976**.

 © 2002 WILEY-VCH Verlag GmbH & Co. KGaA, Weinheim 0044-8249/02/4123-4579 $ 20.00+.50/0

Copper-Catalyzed Reductive Alkylations of Enones: A Novel Transmetalation Protocol**

Bruce H. Lipshutz* and Patrick Papa

Previously,[1] we outlined an effective one-pot procedure for the 1,4-reduction/Mukaiyama aldol sequence which utilizes catalytic [(Ph$_3$P)CuH] (Stryker's reagent)[2] in the presence of a silane (e.g., polymethylhydrosiloxane).[3] Although the silylenol ethers derived in situ readily participated in Lewis acid mediated additions to various aldehydes at −78 °C, mixtures of diastereomers were invariably produced, in line with expectations based on literature precedents (Scheme 1).[4] The sequence leading to these intermediates



Scheme 1. Silanes versus boranes in transmetalations with copper enolates derived in situ.

presumably involves a transmetalation[5] between the initially formed copper enolate and silane.[6] It was reasoned that replacement of R$_3$SiH with a dialkyl borane (R$_2$BH) might likewise encourage the analogous ligand exchange, perhaps driven by the strength of the boron–oxygen bond, to afford the corresponding boron enolate. Although such a process is unknown, the thermodynamically favored *Z* orientation found in boron enolates derived from acyclic ketones might prevail, whereas cyclic enones would necessarily lead to the corresponding (*E*)-enolates. Should this unprecedented transmetalation occur cleanly and with good selectivity, in both situations subsequent aldol reactions in typical fashion would ultimately provide products in a regio- and stereocontrolled manner. Previous studies on 1,4-reduction[7] of enones (e.g., with Li/NH$_3$) indicate that limited control over enolate geometry and/or the derived aldol product[8] is to be expected from such an approach.[9] Alternatively, 1,4-hydroboration of acyclic conjugated enones provides a direct entry to (*Z*)-boron enolates,[10] although in practice most substitution patterns of the enone double bond are not amenable, especially in the important case of unsubstituted vinyl ketones (see below).[11] Herein we disclose new organometallic technology for site-specific boron enolate formation by using a transmetalation sequence.

The dialkyl borane selected to participate in the key transmetalation event, Et$_2$BH, could be easily generated by equilibration between commercial samples of Et$_3$B (in hexanes) and BH$_3$·THF.[12] An excess of the former is required to consume the majority of BH$_3$ present in solution, since borane appears to react over time adversely with Stryker's reagent. Once Et$_2$BH is formed, addition of an acyclic enone in toluene at 0 °C followed by a catalytic amount of [(Ph$_3$P)CuH] leads to clean conjugate reduction with concomitant (*Z*)-boron enolate formation (or the corresponding (*E*)-enolate with cyclic enones).[13] Evacuation of roughly half the solvent volume at 0 °C under vacuum and replacement with CH$_2$Cl$_2$ allows, upon cooling to −78 °C, the subsequent aldol reaction to smoothly take place, as expected.[14] Thus, introduction of an aldehyde to the intermediate (*Z*)-enolate leads to *syn*-aldol products[15a,b] in excellent overall yields. Cyclic enones, on the other hand, cleanly afford *anti*-aldol products.[15a,c] Table 1 provides a representative sampling of the enones examined to date. A number of examples are noteworthy in that they reflect cases which react nonproductively under hydroboration conditions.[10,11] For example, cyclohexenones **1** and **2**, which cannot hydroborate in a 1,4-sense,[11] readily participate to arrive at the corresponding (*E*)-boron enolates to ultimately yield the anticipated *anti* products (entries 1, 2). Vinyl ketone **3**, which is also a troublesome substrate toward 1,4-hydroboration,[11] is an ideal starting material toward a Cu^{I}-based conjugate addition in that it is sterically unencumbered at the β-site. Thus, an excellent sequence ensues and ultimately affords the *all-syn* diastereomer in high yield (entry 3). It should also be noted that unsubstituted vinyl ketones, albeit simple, are among the most synthetically valuable in that they provide an alternative inroad to the "methyl, hydroxy, methyl" array characteristic of the macrolide antibiotics.[16] On the basis of high-field NMR analyses, the limits of stereoselectivity are at least > 97:3, since neither of the diastereomeric products in each case could be detected. The coupling constant observed for the proton at C-3 in each aldol product (see Table 1) is in agreement with the expected literature values for simple aldol products unperturbed by proximate or remote stereocenters.[15]

Dihydrocarvone (**4**) is representative of a site-specific generation of a boron enolate which might be otherwise difficult to form regiospecifically from the corresponding saturated (cyclohexanone) analogue (Scheme 2).[17] Application of the three-step/one-pot sequence affords mainly *anti* product **5**[18] that bears an α-quaternary center of defined stereochemistry[19] resulting from favored axial alkylation.[20]

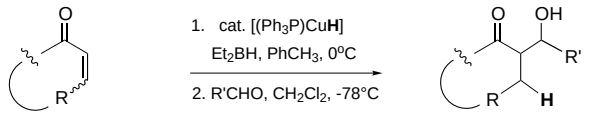
[*] Prof. B. H. Lipshutz, Dr. P. Papa
Department of Chemistry
University of California
Santa Barbara, CA 93106 (USA)
Fax: (+1) 805-893-8265
E-mail: lipshutz@chem.ucsb.edu

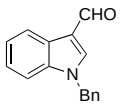
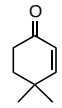
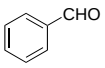
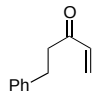
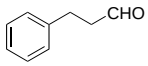
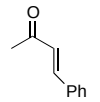
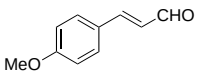
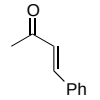
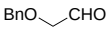
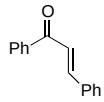
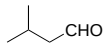
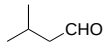
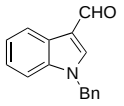
[**] We warmly thank the NSF (CHE 0213522) for supporting our programs. We are indebted to Dr. T. Saito and Mr. H. Shimizu (Takasago) for a generous sample of dtbm-segphos. We thank Mr. Mike Scott for general assistance in the early stages of this work.

Supporting information for this article is available on the WWW under http://www.angewandte.org or from the author.

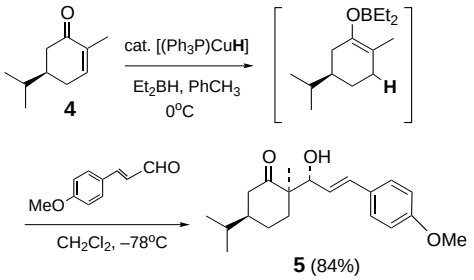
 © 2002 WILEY-VCH Verlag GmbH & Co. KGaA, Weinheim 0044-8249/02/4123-4580 $ 20.00+.50/0

Table 1. Representative conjugate reduction/transmetalation/aldol reactions.



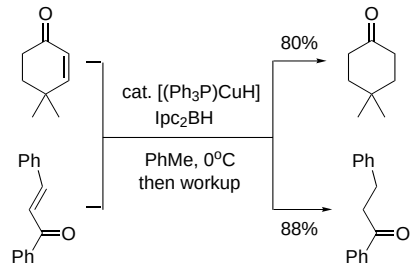
Entry	Enone	Aldehyde	Yield [%][c]
1	 **1**		85
2	 **2**		80
3	 **3**		86
4			90
5			83
6			95
7			85
8			86

[a] J_{syn}: entry 3, 4.6 Hz; entry 4, 5.4 Hz; entry 5, 6.3 Hz; entry 6, 4.0 Hz; entry 7, 3.7 Hz; entry 8, 7.0 Hz. [b] J_{anti}: entry 1, 9.2 Hz; entry 2, 8.6 Hz. [c] Yield of isolated product, that is, chromatographically purified material. All aldol products were fully characterized by IR, NMR, MS, and HRMS data.



Scheme 2. 1,4-Reduction/transmetalation/aldol reaction of dihydrocarvone.

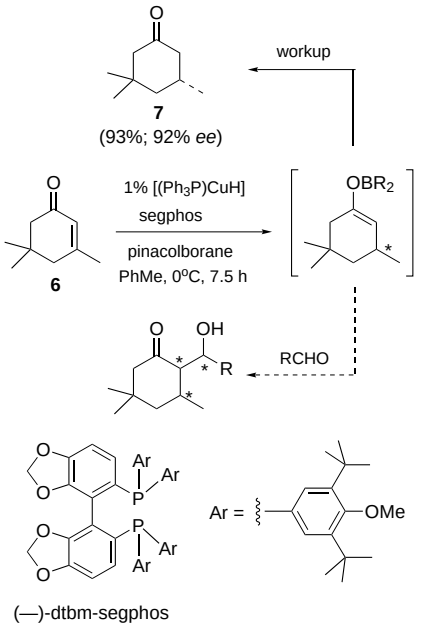
In anticipation of controlling the absolute stereochemical outcome from a related 1,4-reduction/transmetalation/aldol sequence, nonracemic Ipc_2BH[21] was investigated as the stoichiometric source of hydride in place of Et_2BH (Scheme 3). From both an acyclic and cyclic example, the products of 1,4-reduction/proton quenching were obtained in good yields which strongly implicates a nonracemic boron enolate intermediate in each reaction.



Scheme 3. CuH-catalyzed 1,4-reductions/transmetalations with nonracemic Ipc_2BH (Ipc = isopinocampheyl).

Lastly, whereas conjugate reductions of highly hindered β,β-disubstituted enones with [(Ph$_3$P)CuH] remain problematic,[2a, 22] we have found that with proper choices of ligand, such reductions can be realized. Thus, by adding 0.5 mol %[23] of the di-*tert*-butylmethoxy (DTBM) analogue of Takasago's new segphos series of biaryl ligands[24] to Stryker's reagent in the presence of a borane (e.g., pinacolborane), ligand-accelerated catalysis leading to 1,4-reduction of isophorone **6** is complete at 0 °C (Scheme 4).[25] The keto product (*R*)-**7**[22] was isolated in high yield and with an *ee* of 92 %. This finding suggests that in the presence of the appropriate dialkyl borane,[26] a subsequent aldol reaction could allow control of three contiguous asymmetric centers.

In summary, a 1,4-reduction/transmetalation protocol has been uncovered which is catalytic in transition metal and provides a novel entry to essentially isomerically pure boron enolates of unsymmetrical ketones. The methodology is of



Scheme 4. Asymmetric 1,4-reduction of isophorone by using CuH chelated by (−)-dtbm-segphos (0.5 mol %).

 © 2002 WILEY-VCH Verlag GmbH & Co. KGaA, Weinheim 0044-8249/02/4123-4581 $ 20.00+.50/0

broad scope; it relies on an efficient ligand exchange process between a dialkyl borane and an in situ generated copper enolate. Thus, a unique route to boron enolates which avoids base-induced enolization/electrophilic trapping with a sensitive and expensive dialkyl boron halide or triflate is now in hand. Ongoing studies involving nonracemic boron (and titanium) enolate formation/aldol couplings, and new 1,4- (and 1,2-) additions of nonracemic ligand-modified CuH, will be reported in due course.

Experimental Section

1,4-Reduction/transmetalation/aldol reactions; representative procedure: An oven-dried round-bottomed flask equipped with a stir bar and two septa was cooled under an argon atmosphere. The reaction flask was cooled to 0 °C, charged with Et_3B (1.0 M in hexane, 8.0 equiv), followed by slow addition of BH_3 (1.0 M in THF, 0.5 equiv) and the mixture allowed to stir for 30 min. The reaction mixture was warmed to RT, stirred for an additional 15 min, then cooled back down to 0 °C. The enone (1.0 equiv) was slowly added through a syringe or, in the case of a solid, dissolved in toluene (1.0 mL) and transferred through a cannula. [$(Ph_3P)CuH$] (0.05 equiv) was dissolved in toluene (3.0 mL) and then transferred to the reaction mixture through a cannula and allowed to stir at 0 °C until the enone had been consumed to form the intermediate boron enolate (usual times for reaction completion range from 10 min to 2 h). After the conjugate reduction was complete approximately half of the solvent was removed under vacuum and CH_2Cl_2 (6.0 mL) was added through a syringe. The reaction was cooled to −78 °C followed by addition of the aldehyde (1.5 equiv, neat or as a solution in CH_2Cl_2). Upon consumption of the boron enolate and formation of the aldol product (ca. 15 min) the reaction was warmed to 0 °C and slowly quenched with pH 7 phosphate buffer (2.0 mL), followed by 30 % H_2O_2 (2.0 mL) and allowed to stir for 2 h. The quenched reaction mixture was then subjected to an aqueous extractive workup (2×10 mL H_2O, 4×10 mL Et_2O). The combined organic layers were then washed with brine (1×20 mL), dried with anhydrous Na_2SO_4, and the solvent removed in vacuo. The residue was purified by column chromatography on silica gel with triethylamine (1–2 %) as a doping agent which prevents elimination and retro-aldol side reactions. Under these conditions, no retro-aldol side reaction was observed.

Received: August 23, 2002 [Z50033]

[1] B. H. Lipshutz, W. Chrisman, K. Noson, P. W. Papa, J. A. Sclafani, R. W. Vivian, J. Keith, *Tetrahedron* **2000**, *56*, 2779.

[2] a) W. S. Mahoney, D. M. Brestensky, J. M. Stryker, *J. Am. Chem. Soc.* **1988**, *110*, 291; b) W. S. Mahoney, J. M. Stryker, *J. Am. Chem. Soc.* **1989**, *111*, 8818; D. M. Brestensky, J. M. Stryker, *Tetrahedron Lett.* **1989**, *30*, 5677.

[3] N. J. Lawrence, M. D. D. Drew, S. M. Bushell *J. Chem. Soc. Perkin Trans.* **1999**, *1*, 3381.

[4] T. Mukaiyama, K. Banno, K. Narasaka, *J. Am. Chem. Soc.* **1974**, *96*, 7503.

[5] P. Wipf, *Synthesis* **1993**, 537.

[6] a) K. Miura, H. Sato, K. Tamaki, H. Ito, A. Hosomi, *Tetrahedron Lett.* **1997**, *38*, 8887; b) H. Ito, T. Ishizuka, K. Arimoto, K. Miura, A. Hosomi, *Tetrahedron Lett.* **1997**, *38*, 888.

[7] H. O. House, *Modern Synthetic Reactions*, 2nd ed., Benjamin/Cummings, Menlo Park, CA, **1972**, 145.

[8] a) P. Arya, H. Qin, *Tetrahedron* **2000**, *56*, 917; C. J. Cowden, I. Paterson, *Org. React.* **1997**, *51*, 1; b) I. Paterson, C. J. Cowden, D. Wallace, *Modern Carbonyl Chemistry*, Wiley-VCH, Weinheim, **2000**, 249.

[9] a) S. Masamune, T. Sato, B. M. Kim, T. A. Wollmann, *J. Am. Chem. Soc.* **1986**, *108*, 8279; b) S. Masamune, J. W. Ellingboe, W. Choy, *J. Am. Chem. Soc.* **1982**, *104*, 5526.

[10] D. A. Evans, G. C. Fu, *J. Org. Chem.* **1990**, *55*, 5678.

[11] G. P. Boldrini, M. Bortolotti, F. Mancini, E. Tagliavini, C. Trombini, A. Umani-Ronchi, *J. Org. Chem.* **1991**, *56*, 5820.

[12] P. Knochel, P. Bhanu, S. Appana, H. Eick, *J. Organomet. Chem.* **1998**, *562*, 133.

[13] Irradiation at the frequency of the resonance of the vinyl proton of the boron enolate derived from 4-hexen-3-one showed two interactions which can only exist for the *Z* geometry.

[14] a) D. A. Evans, E. Vogel, J. V. Nelson, *J. Am. Chem. Soc.* **1979**, *101*, 6120; b) D. A. Evans, V. J. Nelson, E. Vogel, *J. Am. Chem. Soc.* **1981**, *103*, 3099; c) D. A. Evans, T. R. Taber, *Tetrahedron Lett.* **1980**, *21*, 4675; d) S. Masamune, W. Choy, F. Kerdesky, *J. Am. Chem. Soc.* **1981**, *103*, 1566.

[15] a) Aldol products uncomplicated by additional stereocenters in either coupling partner can be readily assigned on the basis of coupling constants between protons at the C-2 and C-3 sites; see D. A. Evans, J. Bartoli, T. L. Shih, *J. Am. Chem. Soc.* **1981**, *103*, 2127; L. M. Jackman, S. Sternhell, *Applications of Nuclear Magnetic Resonance Spectroscopy in Organic Chemistry*, 2nd ed., Pergamon Press, Oxford, UK, **1969**; b) typically, *syn* products show $J = 3$–6 Hz; c) isomers bearing an *anti* relationship tend to show $J = 5$–9 Hz.

[16] *Recent Progress in the Chemical Synthesis of Antibiotics* (Eds.: G. Lukacs, M. Ohno), Springer, Berlin, **1990**; R. D. Norcross, I. Paterson, *Chem. Rev.* **1995**, *95*, 2041.

[17] I. Paterson, M. Goodman, M. A. Lister, R. C. Schumann, C. K. McClure, R. D. Norcross, *Tetrahedron* **1990**, *46*, 4663.

[18] Determined by NMR analysis of crude material to be a 9:1 mixture of *anti* products.

[19] Confirmed via X-ray analysis.

[20] J. D. Morrison, *Asymmetric Synthesis*, Academic Press, London, UK, **1984**.

[21] H. C. Brown, N. N. Joshi, *J. Org. Chem.* **1988**, *53*, 4059.

[22] Y. Moritani, D. H. Appella, V. Jurkauskas, S. L. Buchwald, *J. Am. Chem. Soc.* **2000**, *122*, 6797.

[23] This corresponds to a substrate:ligand (S/L) ratio of 2000:1; see ref. [22a].

[24] T. Saito, T. Yokozawa, T. Ishizaki, T. Moroi, T. Miura, N. Sayo, H. Kumobayashi, *Adv. Synth. Catal.* **2001**, *343*, 264.

[25] By contrast, use of biphemp[22a] in place of dtbm-segphos under otherwise identical conditions on isophorone afforded ca. 10–20 % (by TLC analysis) of the product of 1,4-reduction.

[26] a) R. W. Hoffmann, K. Ditrich, *Tetrahedron Lett.* **1984**, *25*, 1781; b) C. Gennari, L. Colombo, C. Scolastico, R. Todeschini, *Tetrahedron* **1984**, *40*, 4051.

 © 2002 WILEY-VCH Verlag GmbH & Co. KGaA, Weinheim 0044-8249/02/4123-4582 $ 20.00+.50/0

ANGEWANDTE CHEMIE
INTERNATIONAL EDITION

A Journal of the Gesellschaft Deutscher Chemiker

2002
41/24
Pages 4595 – 4802



Cover Picture of the Year
Cast your vote at
www.angewandte.org
and win a great book!



The editorial staff and the publishers thank all readers, authors, referees, and advertisers for their interest and support over the past year and wish them all a happy new year.



Editorial Note

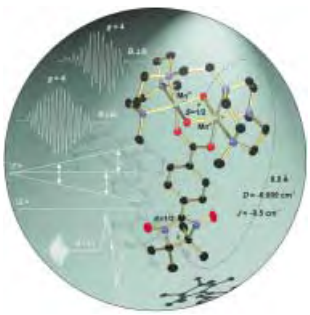


In 2002 there were 26 issues of *Angewandte Chemie International Edition*, two of which were indexes: in Spring there was an index of all the Reviews from the last 40 years; this appeared without an issue number. With this current issue (No. 24) the Annual Index for 2002 is included as a separate issue. This Annual Index should be bound with the other issues. However, for the 40-Year Index, which has its own separate page numbering, this is not necessary. **Copies of the 40-Year Index can be obtained at the special price of € 19.80 (including postage) from the Editorial Office.**



COVER PICTURE

The cover picture shows the structure of a paramagnetic dimanganese complex tethered to a distant organic radical. The long-distance magnetic interaction between the two $S = 1/2$ centers in this complex models a similar situation detected in the $S_2Y_z^{\bullet}$ state of photosystem II (PSII). In their article on page 4775, D. S. Marlin, E. Bill, and K. Wieghardt et al. shed light on the nature of this interaction through the use of SQUID magnetic measurements as well as dual-mode X-band EPR spectroscopy. One of the most remarkable features observed from such dual-mode EPR measurements is the identification of well-resolved "forbidden" half-field multiline signals at $g = 4$ that arise from the dipolar coupling. This latter feature may also be noteworthy in the context of a poorly understood signal at $g = 4.1$ that has been observed in various EPR spectra of PSII.



 © 2002 WILEY-VCH Verlag GmbH & Co. KGaA, Weinheim 1433-7851/02/4124-4597 $ 20.00+.50/0

REVIEWS

Far more important (by orders of magnitude) than previously believed: this is the answer to the question in the title according to calculations based on recently introduced methods of electroweak quantum chemistry. However, the energy differences between enantiomers of chiral molecules are still very small, on the order of pico- to femtojoules per mole. This review covers the following aspects of parity violation: How can such small energies be measured and what are the consequences for our understanding of molecular chirality, biomolecular homochirality, and perhaps fundamental physics?

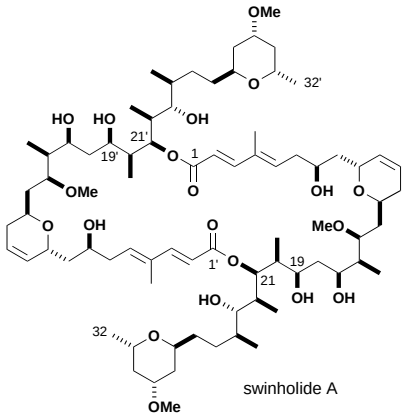
Angew. Chem. **2002**, *114*, 4812 – 4825

M. Quack* ..... 4618 – 4630

How Important is Parity Violation for Molecular and Biomolecular Chirality?

Keywords: biological homochirality · chirality · parity violation · symmetries

Marine organisms provide a rich source of highly functionalized macrolides (such as swinholide A) that interact with the actin cytoskeleton by mechanisms similar to actin-binding proteins. Total syntheses of these potent cytotoxic natural products have been accomplished recently, making use of a variety of strategies for introducing the multiple stereogenic centers and constructing the characteristic 22- to 44-membered macrocycles.



swinholide A

Angew. Chem. **2002**, *114*, 4826 – 4847

K.-S. Yeung,* I. Paterson ... 4632 – 4653

Actin-Binding Marine Macrolides: Total Synthesis and Biological Importance

Keywords: actin · antitumor agents · macrolides · natural products · total synthesis

VIPs

The following communications are "Very Important Papers" in the opinion of two referees. They will be published shortly. Short summaries of these articles can be found on the *Angewandte Chemie* homepage at the address http://www.angewandte.org

Tuning the Regioselectivity in the Palladium(II)-Catalyzed Isomerization of Alkylidenecyclopropyl Ketones: A Dramatic Salt Effect — S. Ma*, J. Zhang

Porphyrazines as Molecular Scaffolds: Periphery–Core Spin Coupling Between Metal Ions of a Schiff Base Porphyrazine — M. Zhao, C. Stern, A. G. M. Barrett,* B. M. Hoffman*

Beyond the Icosahedron: The First 13-Vertex Carborane — A. Burke, D. Ellis, B. T. Giles, B. E. Hodson, S. A. Macgregor, G. M. Rosair, A. J. Welch*

Topomerization of a Distorted-Rhomboid Tetraborane(4) and its Hydroboration to a Pentaborane(7) — C. Präsang, M. Hofmann, G. Geiseler, W. Massa, A. Berndt*

A New Diversity-Oriented Synthesis of α-Amino Acid Derivatives by a Silyltelluride-Mediated Radical Coupling Reaction of Imines and Isonitriles — S. Yamago,* H. Miyazoe, T. Nakayama, M. Miyoshi, J. Yoshida*

Facile Solid-State Synthesis of Highly Conducting Poly(ethylenedioxythiophene) — H. Meng, D. F. Perepichka, F. Wudl*

[3+2]/[4+1] Cycloaddition Reactions of Fischer Alkoxy(alkenyl)carbene Complexes with Electronically Neutral 1,3-Dienes — J. Barluenga,* S. López, J. Flórez

Salinosporamide A, a Highly Cytotoxic Proteasome Inhibitor from a Novel Microbial Source, a Marine Bacterium of the New Genus *Salinospora* — R. H. Feling, G. O. Buchanan, T. J. Mincer, C. A. Kauffman, P. R. Jensen, W. Fenical*

New Open-Network Architectures from the Self-Assembly of $AgNO_3$ and 5,10,15,20-Tetra(4-pyridyl)porphyrin Building Blocks: The Exceptional Self-Penetrating Topology of the 3D Network of $[Ag_8(Zn^{II}tpyp)_7(H_2O)_2](NO_3)_8$ — L. Carlucci, G. Ciani,* D. M. Proserpio, F. Porta

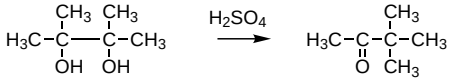
Large Parity Violation Effects in Heavy-Metal-Containing Chiral Compounds — P. Schwerdtfeger,* J. Gierlich, T. Bollwein

Cyanide-Bridged Iron(III)-Cobalt(II) Double Zigzag Ferromagnetic Chains: Two New Molecular Magnetic Nanowires — R. Lescouëzec, J. Vaissermann, C. Ruiz-Pérez, F. Lloret, R. Carrasco, M. Julve,* M. Verdaguer,* Y. Dromzee, D. Gatteschi, W. Wernsdorfer

 © 2002 WILEY-VCH Verlag GmbH & Co. KGaA, Weinheim 1433-7851/02/4124-4598 $ 20.00+.50/0

ESSAY

Radical changes in the chemical community's thinking were required in the discovery of the pinacol rearrangment [Eq. (a)]. Clarity was achieved only after the incorrect "conventional" atomic weights, which gave completely erroneous molecular formulas, were rejected and people dared to violate Kekulé's rules of reaction concerning the connectivity of the carbon skeleton in chemical reaction.



(a)

pinacol pinacolone

Angew. Chem. **2002**, *114*, 4848 – 4854

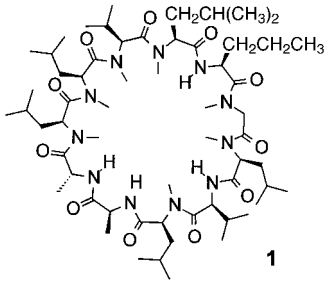
J. A. Berson* ..... 4655 – 4660

What Is a Discovery? Carbon Skeletal Rearrangements as Counter-Examples to the Rule of Minimal Structural Change

Keywords: carbon · history of chemistry · pinacol · rearrangement · structure elucidation

HIGHLIGHTS

An efficient coupling reaction in peptide chemistry is achieved through the use of Fmoc-protected amino acid chlorides generated in situ. This method permits racemization-free incorporation of *N*-methyl amino acids into peptides, as could be shown in the syntheses of cyclosporin O (**1**) and omphalotin A.



1

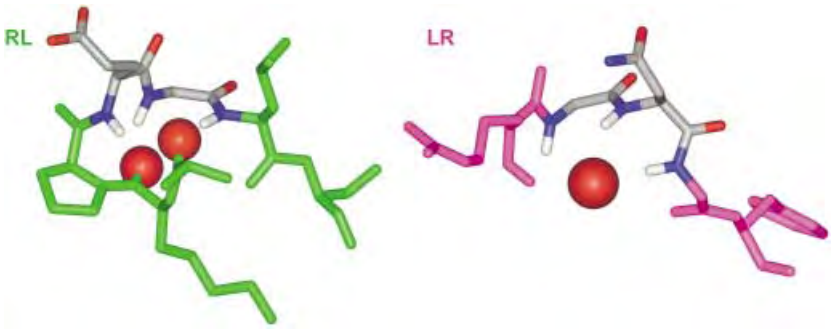
Angew. Chem. **2002**, *114*, 4855 – 4857

N. Sewald* ..... 4661 – 4663

Efficient, Racemization-Free Peptide Coupling of *N*-Alkyl Amino Acids by Using Amino Acid Chlorides Generated In Situ—Total Syntheses of the Cyclopeptides Cyclosporin O and Omphalotin A

Keywords: amino acids · bioorganic chemistry · coupling reagent · peptides · total synthesis · triphosgene

Protein structure prediction, not only description: A step in this direction is the discovery that many anion and cation binding sites (where ions can be atoms exhibiting a full or partial charge) in proteins are made up of three amino acids of which two exhibit "enantiomeric" main-chain conformations. The combination of torsion angle pairs determines whether an RL or an LR nest is formed (see picture).



Angew. Chem. **2002**, *114*, 4857 – 4860

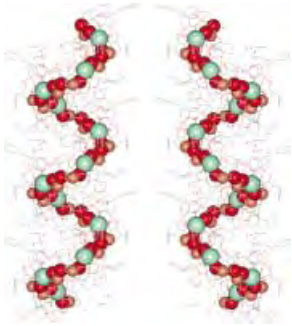
D. Pal, J. Sühnel,*
M. S. Weiss* ..... 4663 – 4665

New Principles of Protein Structure: Nests, Eggs—and What Next?

Keywords: protein structures · structural bioinformatics · structural motifs

COMMUNICATIONS

The chirality of the ligand determines the nature of the helix: Coordination of a chain of [15]metallacrown-5 complexes based on phenylalanine hydroxamic acid results in an amphiphilic metallohelix with a 4_1 screw axis. The use of the L isomer of the acid gives the right-handed helix (see left structure) while the D isomer gives the mirror image structure.



Angew. Chem. **2002**, *114*, 4862 – 4864

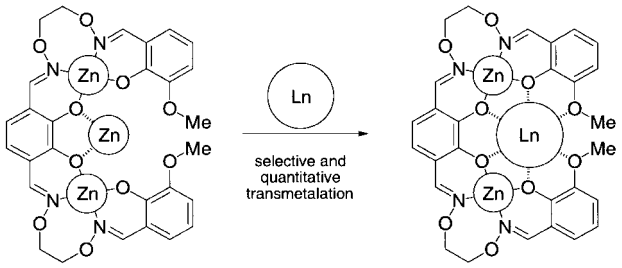
A. D. Cutland-Van Noord, J. W. Kampf, V. L. Pecoraro* ..... 4667 – 4670

Preparation of Resolved Fourfold Symmetric Amphiphilic Helices Using Chiral Metallacrown Building Blocks

Keywords: copper · crown compounds · helical structures · lanthanides · supramolecular chemistry

 © 2002 WILEY-VCH Verlag GmbH & Co. KGaA, Weinheim 1433-7851/02/4124-4599 $ 20.00+.50/0

Only the central metal atom of the homotrinuclear complex $[LZn_3]^{2+}$, prepared by cooperative complexation between a linear ligand and $Zn(OAc)_2$, is replaced with a Ln^{3+} ion by selective and quantitative transmetalation to give a helical heterotrinuclear complex $[LZn_2Ln]^{3+}$ (see scheme). Ln = lanthanide.



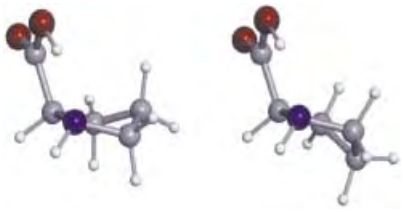
Angew. Chem. **2002**, *114*, 4864 – 4867

S. Akine, T. Taniguchi, T. Nabeshima* ..... 4670 – 4673

Novel Synthetic Approach to Trinuclear 3d-4f Complexes: Specific Exchange of the Central Metal of a Trinuclear Zinc(II) Complex of a Tetraoxime Ligand with a Lanthanide(III) Ion

Keywords: cooperative phenomena · host – guest systems · lanthanides · N,O ligands · transmetalation

An intramolecular hydrogen bond of the type OH···N is present in both conformers of proline (see picture) that were observed in the gas phase using laser-ablation molecular-beam Fourier-transform microwave spectroscopy.



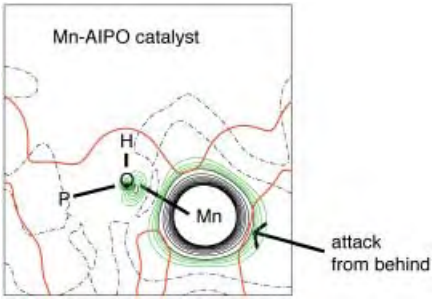
Angew. Chem. **2002**, *114*, 4867 – 4870

A. Lesarri, S. Mata, E. J. Cocinero, S. Blanco, J. C. López, J. L. Alonso* ..... 4673 – 4676

The Structure of Neutral Proline

Keywords: amino acids · conformational analysis · laser chemistry · rotational spectroscopy

Periodic quantum mechanical calculations on transition-metal-doped AlPO-34 show that the Lewis acidity is linked to the electronic distribution at the transition metal site. A "from behind" attack of 2+ dopant ions by Lewis bases is favored (see picture), and is expected to yield stronger Lewis acidity for polymorphs with single-wall framework structures or intersecting channels, rather than polymorphs with one-dimensional channels that are composed solely of double-walled structural units.



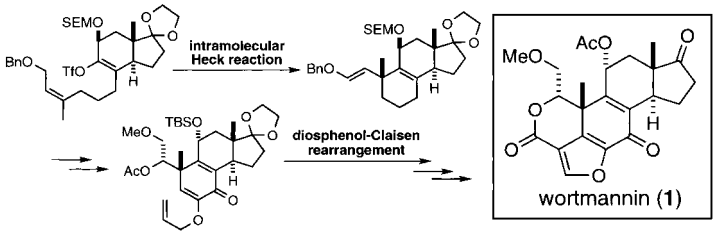
Angew. Chem. **2002**, *114*, 4871 – 4874

F. Corà,* I. Saadoune, C. R. A. Catlow ..... 4677 – 4680

Lewis Acidity in Transition-Metal-Doped Microporous Aluminophosphates

Keywords: ab initio calculations · density functional calculations · heterogeneous catalysis · Lewis acids · zeolite analogues

A potent and specific phosphoinositide 3-kinase inhibitor (±)-wortmannin has been achieved through an intramolecular Heck reaction for the construction of an allylic quaternary carbon center and a diosphenol – Claisen rearrangement (see scheme). SEM = 2-(Trimethylsilyl)ethoxymethyl.



Angew. Chem. **2002**, *114*, 4874 – 4876

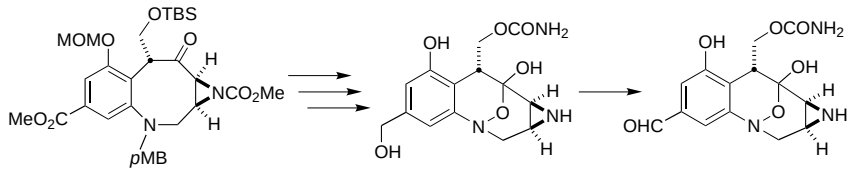
T. Mizutani, S. Honzawa, S.-y. Tosaki, M. Shibasaki* ..... 4680 – 4682

Total Synthesis of (±)-Wortmannin

Keywords: Heck reaction · natural products · phosphoinositide 3-kinase · rearrangement · total synthesis

 © 2002 WILEY-VCH Verlag GmbH & Co. KGaA, Weinheim 1433-7851/02/4124-4600 $ 20.00+.50/0

The remarkable one-step deprotection/oxidative cyclization of an eight-membered-ring aminoketone **1** in the presence of dimethyldioxirane gives rise to the unique hydroxylamine hemiketal ring system of FR66979 (**2**) and FR900482 (**3**), clinically important antitumor antibiotics. The concise 33-step enantioselective synthesis of **3** is the shortest route reported to date.



1 **2** **3**

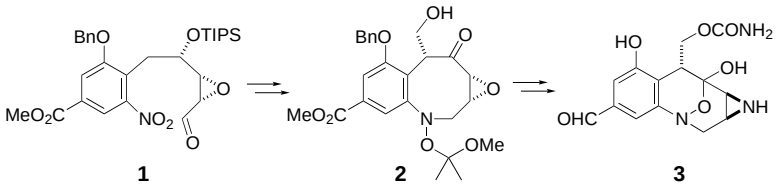
T. C. Judd, R. M. Williams* 4683 – 4685

Concise Enantioselective Synthesis of (+)-FR66979 and (+)-FR900482: Dimethyldioxirane-Mediated Construction of the Hydroxylamine Hemiketal

Angew. Chem. **2002**, *114*, 4877 – 4879

Keywords: antitumor agents · asymmetric synthesis · hydroxylamines · natural products · total synthesis

Intramolecular hydroxylamination of ω-formyl nitrobenzene **1** followed by stereoselective hydroxymethylation led to the formation of *N*-hydroxybenzazocine **2**, a key intermediate in the enantioselective total synthesis of the antitumor antibiotic FR900482 (**3**).



1 **2** **3**

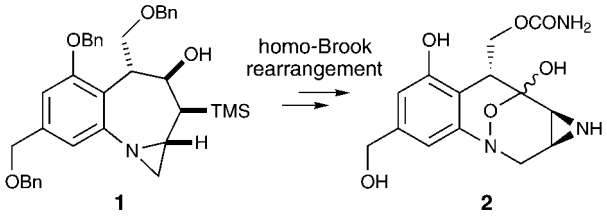
M. Suzuki, M. Kambe, H. Tokuyama, T. Fukuyama* 4686 – 4688

Facile Construction of *N*-Hydroxybenzazocine: Enantioselective Total Synthesis of (+)-FR900482

Angew. Chem. **2002**, *114*, 4880 – 4882

Keywords: aldol reaction · antitumor agents · asymmetric synthesis · hydroxylamines · natural products · total synthesis

An unusual fragmentation of aziridine 1, triggered by a preliminary homo-Brook transposition is the key step in the total synthesis of the racemate of the antitumor agent FR66979 (**2**).



1 **2**

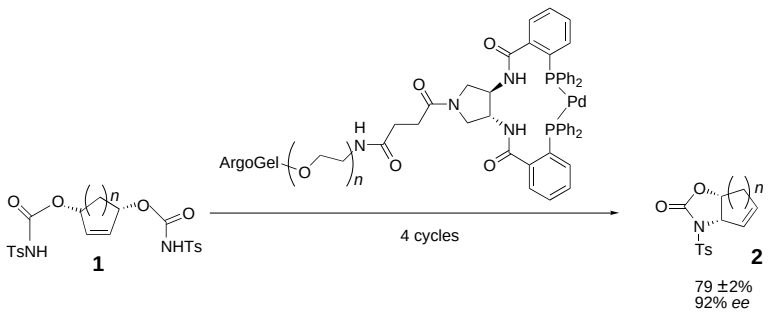
R. Ducray, M. A. Ciufolini* 4688 – 4691

Total Synthesis of (±)-FR66979

Angew. Chem. **2002**, *114*, 4882 – 4885

Keywords: antitumor agents · asymmetric synthesis · natural products · rearrangement · total synthesis

The choice of scaffold and tether has a marked influence on the enantiomeric excesses obtained in Pd-catalyzed asymmetric allylic alkylations, such as the cyclization of the bisurethane **1** to the oxazolidin-2-one **2** [Eq. (1); Ts = *p*-toluenesulfonate], performed with polymer-supported chiral catalysts. The best results were obtained by using an ArgoGel resin, an amide tether, and a pyrrolidine scaffold.



1 **2** (1)

B. M. Trost,* Z. Pan, J. Zambrano, C. Kujat 4691 – 4693

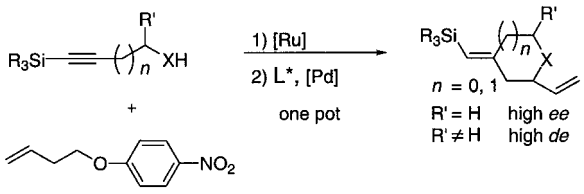
Polymer-Supported C_2-Symmetric Ligands for Palladium-Catalyzed Asymmetric Allylic Alkylation Reactions

Angew. Chem. **2002**, *114*, 4885 – 4887

Keywords: allylic alkylation · asymmetric synthesis · N ligands · palladium · polymer-supported catalysts

 © 2002 WILEY-VCH Verlag GmbH & Co. KGaA, Weinheim 1433-7851/02/4124-4601 $ 20.00+.50/0

Five- and six-membered nitrogen and oxygen heterocycles are accessible from two acyclic precursors in a one-pot reaction that comprises a Ru-catalyzed ene–yne addition followed by a Pd-catalyzed asymmetric allylic alkylation (see scheme). The stereochemistry of the products derives from the catalyst rather than from substrate control using chiral substrates.



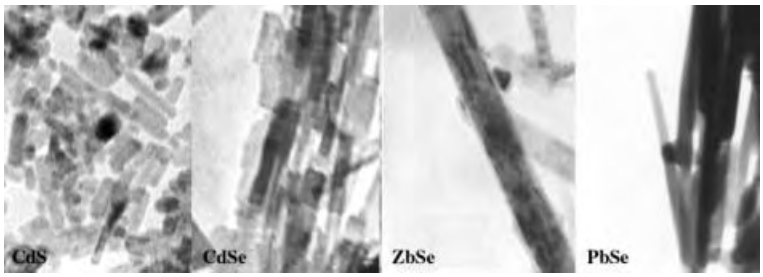
Angew. Chem. **2002**, *114*, 4887–4891

B. M. Trost,*
M. R. Machacek 4693–4697

An Efficient One-Pot Enantio- and Diastereoselective Synthesis of Heterocycles

Keywords: alkylation · asymmetric synthesis · heterocycles · homogeneous catalysis · palladium · ruthenium

Solvothermal synthesis in a monodentate ligand, namely, *n*-butylamine, is a general route for the synthesis of semiconductor chalcogenide nanorods from cheap inorganic reactants. The amine proved to be a good shape controller for producing CdS, CdSe, ZnSe, and PbSe nanorods (see picture) under relatively mild conditions.



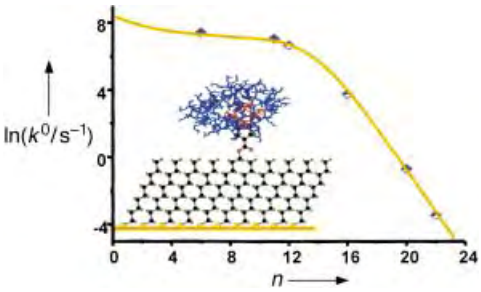
Angew. Chem. **2002**, *114*, 4891–4894

J. Yang,* C. Xue, S.-H. Yu,* J.-H. Zeng, Y.-T. Qian 4697–4700

General Synthesis of Semiconductor Chalcogenide Nanorods by Using the Monodentate Ligand *n*-Butylamine as a Shape Controller

Keywords: crystal growth · nanostructures · semiconductors · solvothermal synthesis

Directly linking a gold electrode coated with pyridine-terminated self-assembled monolayers (SAMs) to the redox-active heme unit of cytochrome c has enabled the electron-transfer mechanism to be studied as a function of distance. Comparison of the kinetic data for this system (see graph) with earlier data on COOH-terminated SAMs requires a change in the electron-transfer mechanism with distance from the electrode surface that does not involve large-amplitude conformational rearrangement.



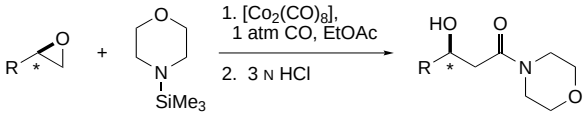
Angew. Chem. **2002**, *114*, 4894–4897

J. Wei, H. Liu, D. E. Khoshtariya, H. Yamamoto, A. Dick, D. H. Waldeck* 4700–4703

Electron-Transfer Dynamics of Cytochrome C: A Change in the Reaction Mechanism with Distance

Keywords: bioorganic chemistry · cytochromes · electron transfer · proteins · self-assembly

Keeping the CO pressure down is a crucial, practical feature of the new methodology for the carbonylation of terminal epoxides. β-Hydroxy morpholinyl amides are generated directly in optically pure form [Eq. (1)], and these building blocks can be applied in a variety of acyl transfer reactions. A useful illustration is provided in the concise synthesis of δ-hydroxy-β-ketoesters, key intermediates for the preparation of the statin class of HMG-CoA reductase inhibitors.



(1)

Angew. Chem. **2002**, *114*, 4897–4899

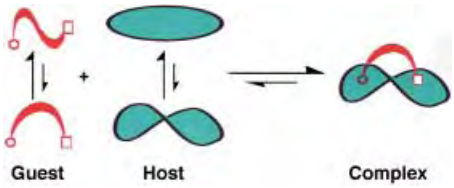
S. N. Goodman, E. N. Jacobsen* 4703–4705

Enantiopure β-Hydroxy Morpholine Amides from Terminal Epoxides by Carbonylation at 1 atm

Keywords: amides · carbonylation · cobalt · epoxides · homogeneous catalysis

 © 2002 WILEY-VCH Verlag GmbH & Co. KGaA, Weinheim 1433-7851/02/4124-4602 $ 20.00+.50/0

Adaptive systems: The conformationally flexible *p*-sulfonated calix[8]arene and photolabile cholinergic ligands adapt to each other and select the right conformers to form ditopic binding complexes (see schematic representation), thus mimicking ligand binding in biological receptors or enzymes.



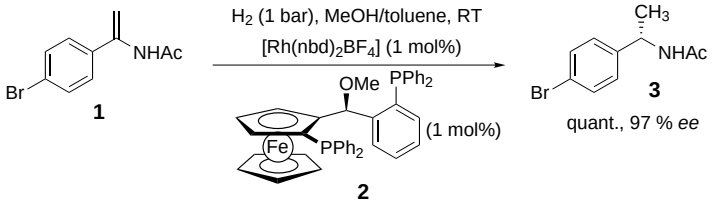
Angew. Chem. **2002**, *114*, 4900 – 4902

A. Specht, P. Bernard, M. Goeldner,* L. Peng* ..... 4706 – 4708

Mutually Induced Formation of Host – Guest Complexes between *p*-Sulfonated Calix[8]arene and Photolabile Cholinergic Ligands

Keywords: calixarenes · cholinergic ligands · host – guest systems · inclusion compounds · receptors

A new synthetic approach allows the synthesis of taniaphos-analogous ligands **2** with inverted α configuration (S_p,α*S*). This new class of ferrocenyl ligands displays excellent enantioselectivity and enhanced reactivity in several types of asymmetric hydrogenation reactions (e.g. **1** →**3**).



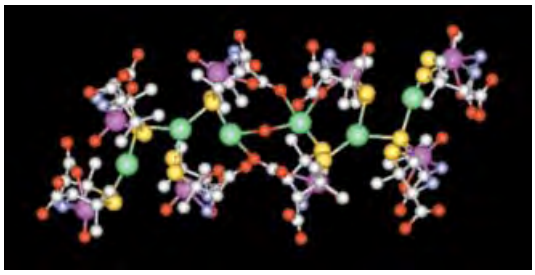
Angew. Chem. **2002**, *114*, 4902 – 4905

M. Lotz, K. Polborn, P. Knochel* ..... 4708 – 4711

New Ferrocenyl Ligands with Broad Applications in Asymmetric Catalysis

Keywords: asymmetric synthesis · ferrocenyl ligands · homogeneous catalysis · hydrogenation · P ligands

Re^V polymer/oligomer switching: The aggregation of Re^V octahedra, $[ReO(D\text{-pen-}N,O)(D\text{-pen-}N,O,S)]^-$ (D-H_2pen = D-penicillamine), assisted by Ag^I ions, leads to the formation of a 2D $(Re^V_2Ag^I_2)_n$ coordination polymer **1**, which is converted into a $Re^V_8Ag^I_6$ coordination oligomer **2** (see picture; Ag green, S yellow, Re purple, O red, N blue). While **1** results from the self-assembly of $Re^V_2Ag^I_2$ units through Ag–O coordination bonding, the self-assembly of $Re^V_8Ag^I_6$ molecules in **2** is through COOH ··· OOC hydrogen bonding.



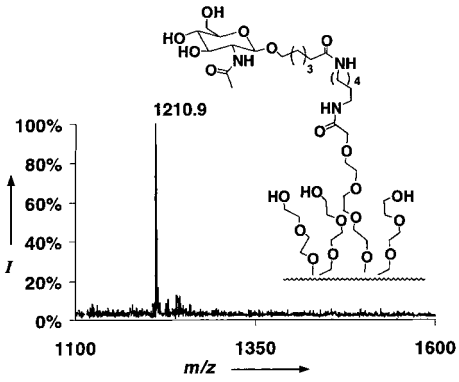
Angew. Chem. **2002**, *114*, 4905 – 4909

T. Konno,* Y. Shimazaki, T. Yamaguchi, T. Ito, M. Hirotsu ..... 4711 – 4715

A Remarkable 14-Nuclear $Re^V_8Ag^I_6$ Coordination Oligomer Derived from a 2D $(Re^V_2Ag^I_2)_n$ Coordination Polymer with D-Penicillaminate

Keywords: aggregation · rhenium · S ligands · silver · supramolecular chemistry

Peptide and carbohydrate biochips can be assayed with MALDI mass spectrometry. Self-assembled monolayers (SAMs) that are modified with ligands provide a platform for identifying selective protein – ligand and enzyme – substrate interactions. MALDI provides a rapid and sensitive method for detection and avoids the need to label protein analytes with fluorescent or radioactive tags. The picture shows the mass spectrum of a SAM presenting a carbohydrate.



Angew. Chem. **2002**, *114*, 4909 – 4912

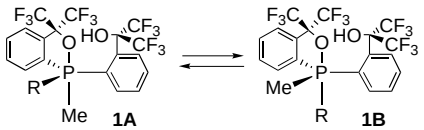
J. Su, M. Mrksich* ..... 4715 – 4718

Using Mass Spectrometry to Characterize Self-Assembled Monolayers Presenting Peptides, Proteins, and Carbohydrates

Keywords: biochips · carbohydrates · glycosylation · mass spectrometry · monolayers

 © 2002 WILEY-VCH Verlag GmbH & Co. KGaA, Weinheim 1433-7851/02/4124-4603 $ 20.00+.50/0

Position of importance: The relative apicophilicity of two substituents linked by a carbon atom to a pentacoordinate phosphorus center such as that in compounds **1** was determined based on the equilibrium ratio of pseudorotamers (**1A** and **1B**) in solution. A distinct solvent effect on the relative apicophilicity and a novel phenomenon in which two different pseudorotamers cocrystallized in the same single crystal were observed.



R: Et, *n*Pr, *n*Bu, CH_2OMe, Ph, $CH_2C_6H_4$(*p*-Me), CH_2Ph, $CH_2C_6H_4$(*p*-F)

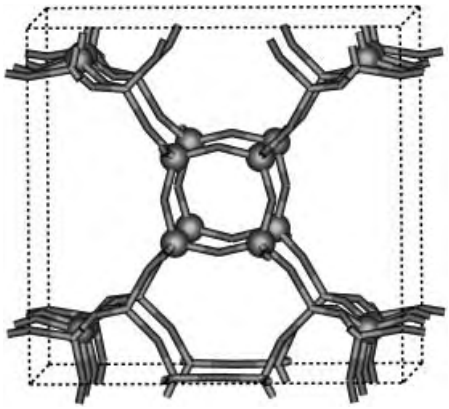
Angew. Chem. **2002**, *114*, 4912 – 4916

S. Matsukawa, K. Kajiyama, S. Kojima, S.-y. Furuta, Y. Yamamoto, K.-y. Akiba* ..... 4718 – 4722

A Method for Determining the Difference in Relative Apicophilicity of Carbon-Containing Substituents of 10-P-5 Phosphoranes

Keywords: apicophilicity · hypervalent compounds · phosphorus · solvent effects · structure elucidation

Ge-directed zeolites. Forcefield atomic simulations are used to investigate the location of the Ge atoms and the structure-directing agents (SDAs) in the Ge containing ITQ-17 zeolite (see picture). The Ge atoms are found to locate preferentially at the T1 sites which form double four-ring (D4R) units. A combined theoretical and experimental treatment has allowed us to prove the preferential location of Ge atoms in the double four-member rings of the polymorph C of Beta zeolite, and its corresponding structure-directing effect to be demonstrated.



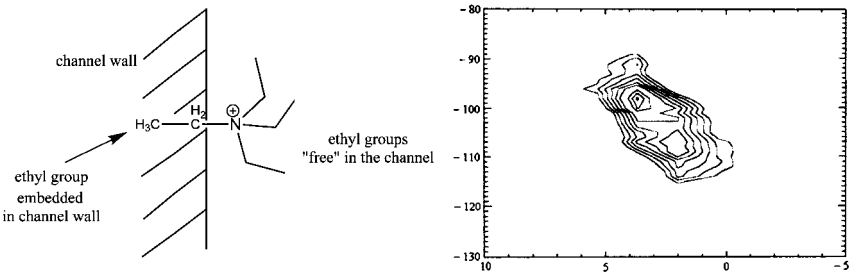
Angew. Chem. **2002**, *114*, 4916 – 4920

G. Sastre, J. A. Vidal-Moya, T. Blasco, J. Rius, J. L. Jordá, M. T. Navarro, F. Rey, A. Corma* ..... 4722 – 4726

Preferential Location of Ge Atoms in Polymorph C of Beta Zeolite (ITQ-17) and Their Structure-Directing Effect: A Computational, XRD, and NMR Spectroscopic Study

Keywords: germanium · polymorphism · silicates · structure elucidation · zeolites

New insight into the binding modes of bimetallic clusters and catalytically active nanoparticles to the mesoporous solid MCM-41 has been obtained from solid-state NMR spectroscopic data (see figure, right). From this study, a model has been proposed to explain the interactions between the pore walls and the cluster. It has been shown that the counterion plays an important role in the anchoring process (see figure, left).



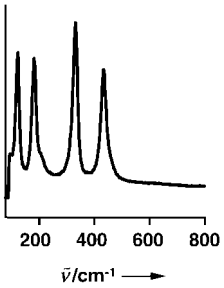
Angew. Chem. **2002**, *114*, 4920 – 4923

M. D. Jones, M. J. Duer,* S. Hermans, Y. Z. Khimyak, B. F. G. Johnson, J. M. Thomas ..... 4726 – 4729

Solid-State NMR Studies of MCM-41 Supported with a Highly Catalytically Active Cluster

Keywords: bimetallic clusters · heterogeneous catalysis · mesoporous materials · NMR spectroscopy

Getting all steamed up: The active phase formed in situ in the catalytic hydrolysis of chlorinated compounds, such as CCl_4, at relatively low temperatures consists of a lanthanide oxide chloride, as evident from vibrational frequencies at 125, 188, 215, 335, and 440 cm^{-1} in the Raman spectrum (see picture). This active phase remains stable as long as steam is provided, and produces CO_2 and HCl as the only reaction products.



Angew. Chem. **2002**, *114*, 4924 – 4926

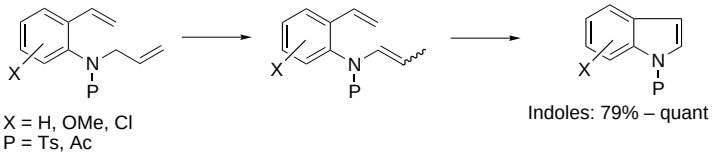
P. Van der Avert, B. M. Weckhuysen* ..... 4730 – 4732

Low-Temperature Destruction of Chlorinated Hydrocarbons over Lanthanide Oxide Based Catalysts

Keywords: chlorinated hydrocarbons · heterogeneous catalysis · lanthanides · Raman spectroscopy

 © 2002 WILEY-VCH Verlag GmbH & Co. KGaA, Weinheim 1433-7851/02/4124-4604 $ 20.00+.50/0

A ruthenium complex, generated from the Grubbs carbene catalyst with vinyloxytrimethylsilane, catalyzed the isomerization of terminal alkenes $RCH_2{-}CH{=}CH_2$ to internal alkenes $RCH{=}CH{-}CH_3$. Application of this olefin isomerization to 2-(*N*-allylamino)styrene gave the corresponding enamines, which were converted into indoles by a standard ring-closing metathesis, see scheme (Ts = tosyl).



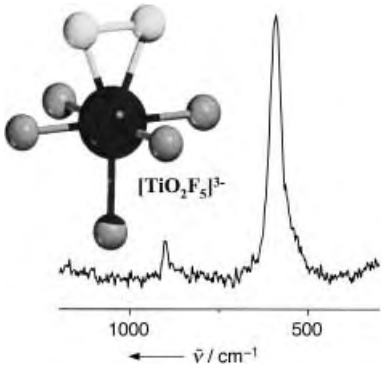
Angew. Chem. **2002**, *114*, 4926 – 4928

M. Arisawa, Y. Terada, M. Nakagawa, A. Nishida* ..... 4732 – 4734

Selective Isomerization of a Terminal Olefin Catalyzed by a Ruthenium Complex: The Synthesis of Indoles through Ring-Closing Metathesis

Keywords: heterocycles · isomerization · metathesis · ring closure · vinyls

The characteristic yellow color of the TS-1/H_2O_2/H_2O system is attributed to a "side-on" Ti – peroxo species, presumed to be the active intermediate in partial oxidation reactions. Resonance Raman spectroscopic analysis of both the zeolite system and a model salt ($(NH_4^+)_3(TiO_2F_5)^{3-}$, see picture) are combined with the analysis of a Ti-free silicalite to prove the structure of the hitherto unknown species.



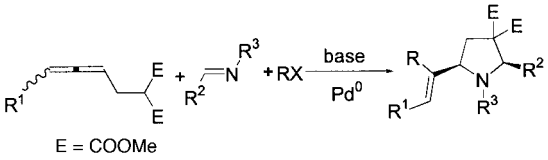
Angew. Chem. **2002**, *114*, 4928 – 4931

S. Bordiga,* A. Damin, F. Bonino, G. Ricchiardi, C. Lamberti, A. Zecchina ..... 4734 – 4737

The Structure of the Peroxo Species in the TS-1 Catalyst as Investigated by Resonant Raman Spectroscopy

Keywords: charge transfer · peroxides · Raman spectroscopy · titanium · zeolites

***cis*-2,5-Disubstituted pyrrolidine skeletons** have been constructed by the Pd^0-catalyzed three-component tandem double-addition – cyclization reaction of 2-(2,3-butadienyl)malonates, organohalides, and imines (see scheme, yields: 81 – 100 %; *cis*/*trans* > 95:5).



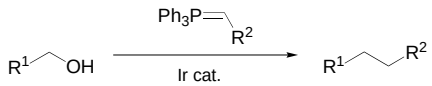
Angew. Chem. **2002**, *114*, 4931 – 4934

S. Ma,* N. Jiao ..... 4737 – 4740

Pd^0-Catalyzed Three-Component Tandem Double-Addition – Cyclization Reaction: Stereoselective Synthesis of *cis*-Pyrrolidine Derivatives

Keywords: allenes · cyclization · diastereoselectivity · palladium · solvent effects

Hydrogen atoms are borrowed during the in situ oxidation of the starting alcohol to the corresponding aldehyde and are subsequently returned in the hydrogenation of the alkene intermediate, which is formed by Wittig olefination of the aldehyde. This process permits an indirect Wittig reaction of alcohols without overall oxidation and offers an alternative to traditional methods that involve, for example, conversion of an alcohol into an alkyl halide.



Angew. Chem. **2002**, *114*, 4934 – 4937

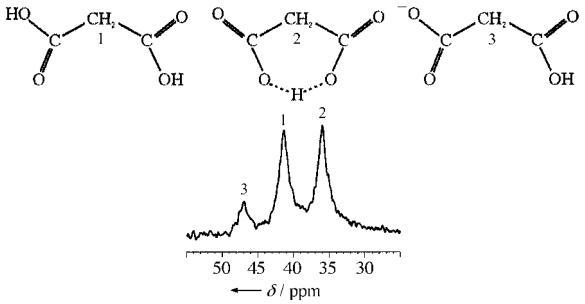
M. G. Edwards, J. M. J. Williams* ..... 4740 – 4743

Catalytic Electronic Activation: Indirect "Wittig" Reaction of Alcohols

Keywords: alcohols · homogeneous catalysis · iridium · transfer hydrogenation · wittig reactions

 © 2002 WILEY-VCH Verlag GmbH & Co. KGaA, Weinheim 1433-7851/02/4124-4605 $ 20.00+.50/0

Information about the presence and the nature of various deprotonated forms of malonic acid in lyophilizates prepared from parent solutions at different pH values can be obtained by solid-state, natural abundance ^{13}C NMR spectroscopy, particularly if a ^{13}C-enriched substrate is used (see picture). p*K* values calculated from solid-state acid:base ratios are found to be equal to those classically measured in the liquid state.



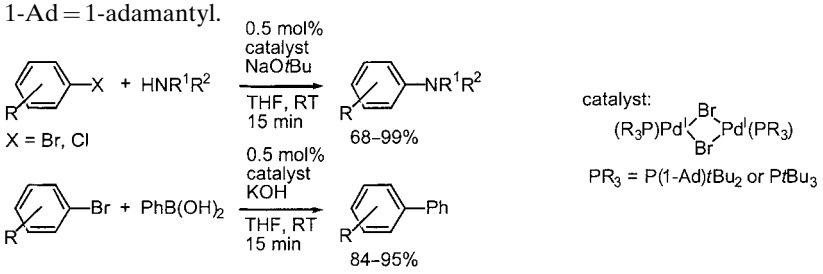
Angew. Chem. **2002**, *114*, 4937 – 4939

R. Colsenet, C. Gardiennet, B. Henry, P. Tekely* ..... 4743 – 4745

A Straightforward Detection of Deprotonated Conformers of Malonic Acid by Solid-State ^{13}C NMR Spectroscopy

Keywords: basicity · carboxylic acids · hydrogen bonds · NMR spectroscopy

Exceptionally fast oxidative addition of an aryl chloride (or a deactivated aryl bromide) to the active Pd^0 center, which is ligated by sterically demanding phosphanes, occurs during coupling reactions catalyzed by air-stable Pd^I dimers as shown in the scheme. As a result, the reactions of aryl chlorides and bromides with amines and boronic acids at room temperature are complete within a few minutes. 1-Ad = 1-adamantyl.



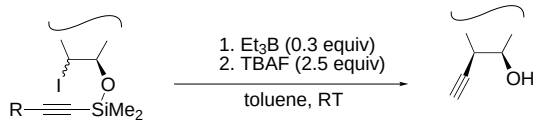
Angew. Chem. **2002**, *114*, 4940 – 4942

J. P. Stambuli, R. Kuwano, J. F. Hartwig* ..... 4746 – 4748

Unparalleled Rates for the Activation of Aryl Chlorides and Bromides: Coupling with Amines and Boronic Acids in Minutes at Room Temperature

Keywords: amination · aryl chlorides · C–C coupling · oxidative addition · palladium

Atom-transfer 5-*exo* cyclization and subsequent elimination occur when ethynyldimethylsilyl ethers of iodohydrins are treated with Et_3B followed by tetrabutylammonium fluoride (TBAF) to give the corresponding *cis*-configured α-hydroxy ethynyl compounds in high yield (see scheme). This is the first example of the use of a radical reaction to introduce an ethynyl group.



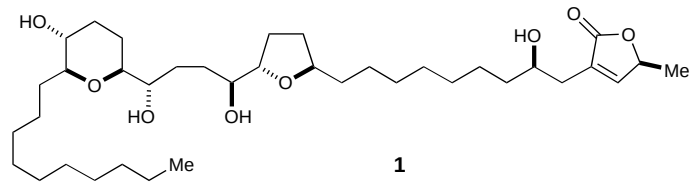
Angew. Chem. **2002**, *114*, 4942 – 4945

M. Sukeda, S. Ichikawa, A. Matsuda, S. Shuto* ..... 4748 – 4750

A New Entry to the Stereoselective Introduction of an Ethynyl Group by a Radical Reaction: Synthesis of the Potential Antimetabolite 2′-Deoxy-2′-*C*-ethynyluridine

Keywords: alkynes · C–C coupling · elimination · nucleosides · radical reactions

The THP and THF rings which are regarded as the characteristic structural features of mucocin (**1**) were constructed by a SmI_2-induced reductive cyclization of β-alkoxy acrylate and oxidative cyclization of a homoallyl alcohol, respectively. The key intermediates were synthesized through an efficient desymmetrization of a C_2-symmetric tetraol.



1

Angew. Chem. **2002**, *114*, 4945 – 4948

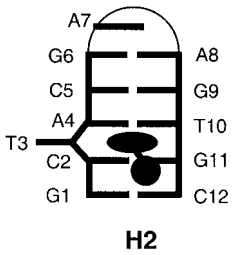
S. Takahashi,* A. Kubota, T. Nakata* ..... 4751 – 4754

Stereoselective Total Synthesis of Mucocin, an Antitumor Agent

Keywords: antitumor agents · cyclization · natural products · samarium · total synthesis

 © 2002 WILEY-VCH Verlag GmbH & Co. KGaA, Weinheim 1433-7851/02/4124-4606 $ 20.00+.50/0

A bulged conformation in which the T3 base is flipped-out of the helical stack of the novel DNA hairpin **H2** allowing complementary pairing downstream of the intercalation site (see picture) is stabilized by binding of the drug nogalamycin. This finding was readily confirmed by detailed analysis of the chemical shift and NOE data.



H2

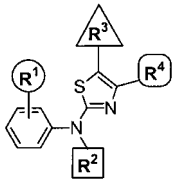
Angew. Chem. **2002**, *114*, 4948 – 4951

M. L. Colgrave, H. E. L. Williams, M. S. Searle* ..... 4754 – 4756

Structure of a Drug-Induced DNA T-Bulge: Implications for DNA Frameshift Mutations

Keywords: DNA recognition · DNA structures · molecular dynamics · NMR spectroscopy · noncovalent interactions

A 10-step (!) solid-phase synthesis employing the traceless hydrazide linker provides efficient access to a 2-aminothiazole library (see scheme) that yielded access to a new class of tyrosine kinase inhibitors with dual selectivity for the vascular endothelial growth factor receptor VEGFR-2 and the Tie-2 receptor tyrosine kinases.



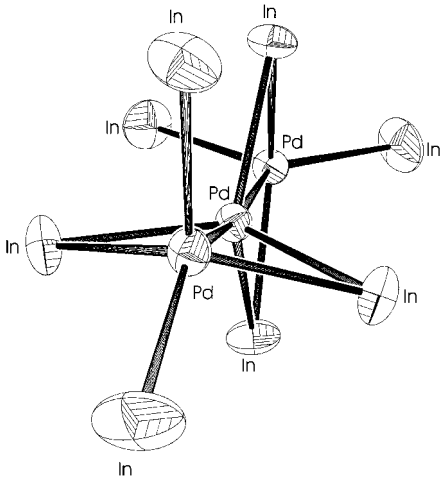
Angew. Chem. **2002**, *114*, 4951 – 4955

F. Stieber, R. Mazitschek, N. Soric, A. Giannis,* H. Waldmann* 4757 – 4761

Traceless Solid-Phase Synthesis of 2-Aminothiazoles: Receptor Tyrosine Kinase Inhibitors with Dual Selectivity for Tie-2 and VEGFR-2

Keywords: combinatorial chemistry · heterocycles · inhibitors · solid-phase synthesis

There is still much to discover: The assumption that monovalent Group 13 organometallic compounds exhibit a high potential as ligands in organometallic chemistry beyond their analogy to CO is confirmed by the synthesis of the title compound **1**. Complex **1**, the structure of which is unique and has no analogue in carbonyl cluster chemistry, is prepared by reaction of $[(tmeda)Pd(CH_3)_2]$ with [InCp*]. tmeda = *N*,*N*,*N*′,*N*′-tetramethylethylenediamine, Cp* = pentamethylcyclopentadienide.



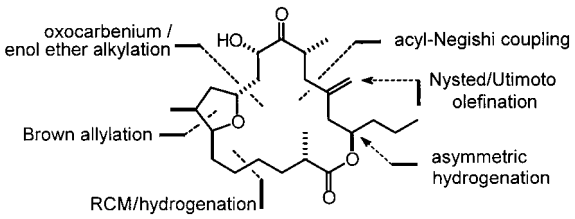
Angew. Chem. **2002**, *114*, 4955 – 4957

T. Steinke, C. Gemel, M. Winter, R. A. Fischer* ..... 4761 – 4763

$[Pd_3(InCp^*)_4(\mu_2\text{-}InCp^*)_4]$: Three Linearly Arranged Palladium Atoms Wrapped into a Fluxional Shell of Eight InCp* Ligands

Keywords: cluster compounds · cyclopentadienyl ligands · Group 13 elements · indium · palladium

Organometallic chemistry in general and catalysis in particular are used in the first total synthesis of amphidinolide T4 (see scheme); a prototype member of a series of macrolide antibiotics of marine origin with rings containing an odd number of carbon atoms.



Angew. Chem. **2002**, *114*, 4958 – 4960

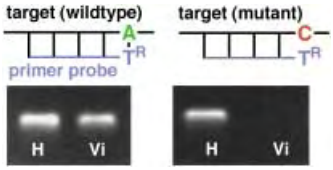
A. Fürstner,* C. Aïssa, R. Riveiros, J. Ragot ..... 4763 – 4766

Total Synthesis of Amphidinolide T4

Keywords: macrolides · metathesis · natural products · ruthenium · total synthesis · zinc

 © 2002 WILEY-VCH Verlag GmbH & Co. KGaA, Weinheim 1433-7851/02/4124-4607 $ 20.00+.50/0

Increased selectivity in PCR! Robust systems that allow the direct detection of single nucleotide variations through PCR methods will be increasingly important for rapid comparative genome analysis or mutation detection. Primer probes bearing supplemental chemical modifications (R = vinyl) significantly increase the selectivity of PCR compared to unmodified probes (R = H), even when the target sequences differ in only one nucleotide (see picture).



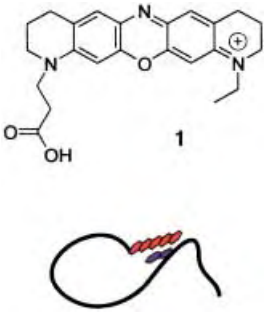
Angew. Chem. **2002**, *114*, 4961 – 4963

M. Strerath, A. Marx* ..... 4766 – 4769

Tuning PCR Specificity by Chemically Modified Primer Probes

Keywords: DNA · mutations · oligonucleotides · polymerase chain reaction · polymerases

Single-molecule spectroscopy for cancer diagnostics: Short dye-labeled peptide epitopes derived from human p53 show strong fluorescence quenching owing to efficient electron transfer from a tryptophan residue to the fluorophore (**1**, see picture). The specific recognition of the peptide epitope by the antibody induces a change in the conformation which is accompanied by a strong increase in fluorescence intensity. The fluorescing antibody – peptide complex can be detected at the single-molecule level even in slightly diluted serum samples by using confocal fluorescence microscopy.



Angew. Chem. **2002**, *114*, 4964 – 4968

H. Neuweiler, A. Schulz, A. C. Vaiana, J. C. Smith, S. Kaul, J. Wolfrum, M. Sauer* ..... 4769 – 4773

Detection of Individual p53-Autoantibodies by Using Quenched Peptide-Based Molecular Probes

Keywords: antibodies · fluorescent probes · hydrophobic effect · immunoassays · single-molecule studies

An excellent tool for gaining a better understanding of long-distance exchange interactions in complicated systems, such as the $S_2Y_Z^{\bullet}$ state of photosystem II, is provided by a relatively simple model for similar interactions between a dimanganese core and an organic radical in the complex $[(Me_4dtne)Mn^{III}\text{-}Mn^{IV}(\mu\text{-}O)_2(\mu\text{-}O_2CPhNIT)](ClO_4)_2$. Dual-mode EPR spectroscopy serves as an additional tool for determining the extent of these long-distance dipolar coupling interactions. Me_4dtne = 1,2-bis(4,7-dimethyl-1,4,7-triazacyclonon-1-yl)ethane; $HO_2CPhNIT$ = 2-(4-carboxyphenyl)-4,4,5,5-tetramethyl-3-oxyimidazolidin-1-oxide.

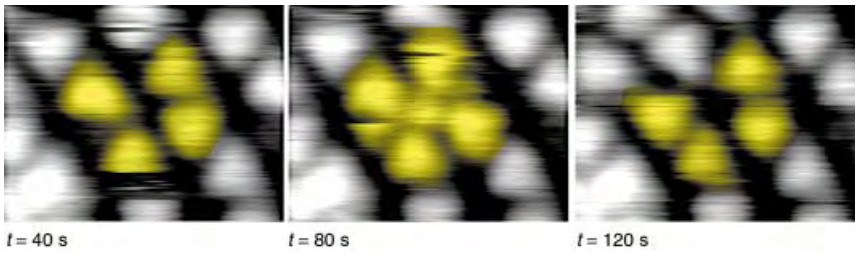
Angew. Chem. **2002**, *114*, 4969 – 4973

D. S. Marlin,* E. Bill,* T. Weyhermüller, E. Rentschler, K. Wieghardt* ..... 4775 – 4779

Long-Distance Magnetic Interaction between a $Mn^{III}Mn^{IV}$ ($S = 1/2$) Core and an Organic Radical: A Spectroscopic Model for the $S_2Y_Z^{\bullet}$ State of Photosystem II

Keywords: EPR spectroscopy · magnetic properties · manganese · photosystem II · radicals

Reaction sequences under the microscope: Scanning tunneling microscopy has been used to follow the association and dissociation of the cloverleaf-shaped complex from 1,3,5-benzenetricarboxylic acid and Cu atoms from a metal surface one molecule at a time (see images). The lifetime of the complexes depends crucially on their local chemical enviroment.



Angew. Chem. **2002**, *114*, 4973 – 4977

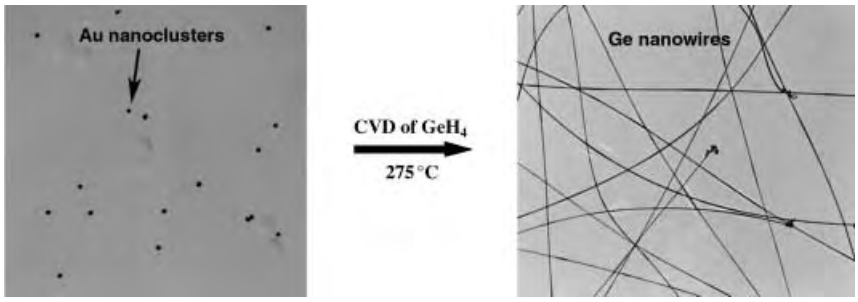
N. Lin,* A. Dmitriev, J. Weckesser, J. V. Barth,* K. Kern* ..... 4779 – 4783

Real-Time Single-Molecule Imaging of the Formation and Dynamics of Coordination Compounds

Keywords: reaction dynamics · scanning probe microscopy · self-assembly · single-molecule studies · surface chemistry

 © 2002 WILEY-VCH Verlag GmbH & Co. KGaA, Weinheim 1433-7851/02/4124-4608 $ 20.00+.50/0

Live-wire potential: Low-temperature growth of Ge nanowires has been achieved by the chemical vapor deposition of GeH_4 onto a SiO_2 substrate coated with Au nanoparticles (see picture). This technique, which represents the mildest growth conditions for single-crystal nanowire synthesis, can also be used for patterned growth processes. Under such conditions, the growth of high-quality nanowires on a variety of substrates is possible, which may yield many possibilities in nanotechnological applications.



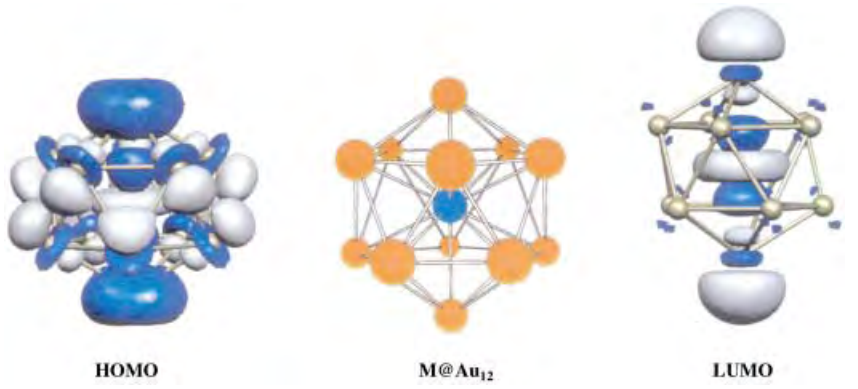
Angew. Chem. **2002**, *114*, 4977 – 4980

D. Wang, H. Dai* ..... 4783 – 4786

Low-Temperature Synthesis of Single-Crystal Germanium Nanowires by Chemical Vapor Deposition

Keywords: chemical vapor deposition · germanium · nanotechnology · nanowires · patterned growth

Yes, $W@Au_{12}$ is icosahedral! We provide experimental verification of the recently proposed new class of gold clusters. Anion photoelectron spectroscopy and relativistic density functional calculations were used to show that both $W@Au_{12}$ and $Mo@Au_{12}$ are highly stable icosahedral clusters with large HOMO – LUMO gaps. The HOMO and LUMO of the I_h $M@Au_{12}$ clusters, both of h_g symmetry, are bonding and antibonding orbitals between the W(Mo) 5d(4d) and the Au 6s – $5d_{Z^2}$ hybrids oriented along the radial directions of the icosahedron, similar to the C 2s – $2p_z$ radial hybrids in C_{60}.



Angew. Chem. **2002**, *114*, 4980 – 4983

X. Li, B. Kiran, J. Li, H.-J. Zhai, L.-S. Wang* ..... 4786 – 4789

Experimental Observation and Confirmation of Icosahedral $W@Au_{12}$ and $Mo@Au_{12}$ Molecules

Keywords: cluster compounds · density functional calculations · gold · photoelectron spectroscopy · tungsten

It's a small world! The hydrothermal synthesis of a family of lanthanide hydroxide single-crystal nanowires has been achieved (see picture), the properties and dimensions of which can be tailored by changes in chemical potential and the pH value of the reaction media. Such materials might serve as templates for biological labeling agents, as one of many potential applications.



Angew. Chem. **2002**, *114*, 4984 – 4987

X. Wang, Y. Li* ..... 4790 – 4793

Synthesis and Characterization of Lanthanide Hydroxide Single-Crystal Nanowires

Keywords: electron microscopy · hydrothermal synthesis · lanthanides · nanostructures

Supporting information on the WWW (see article for access details).

Accelerated publications

* Author to whom correspondence should be addressed

 © 2002 WILEY-VCH Verlag GmbH & Co. KGaA, Weinheim 1433-7851/02/4124-4609 $ 20.00+.50/0

BOOKS

Radicals in Organic Synthesis — Philippe Renaud, Mukund P. Sibi — *S. R. Waldvogel* 4795

Catalytic Heterofunctionalization — Antonio Togni, Hansjörg Grützmacher — *K. Muñiz* 4795

WEB SITES

http://www.itl.nist.gov/div898/handbook/ — Electronic Data Refinement — *W. Schrader* 4797

SERVICE

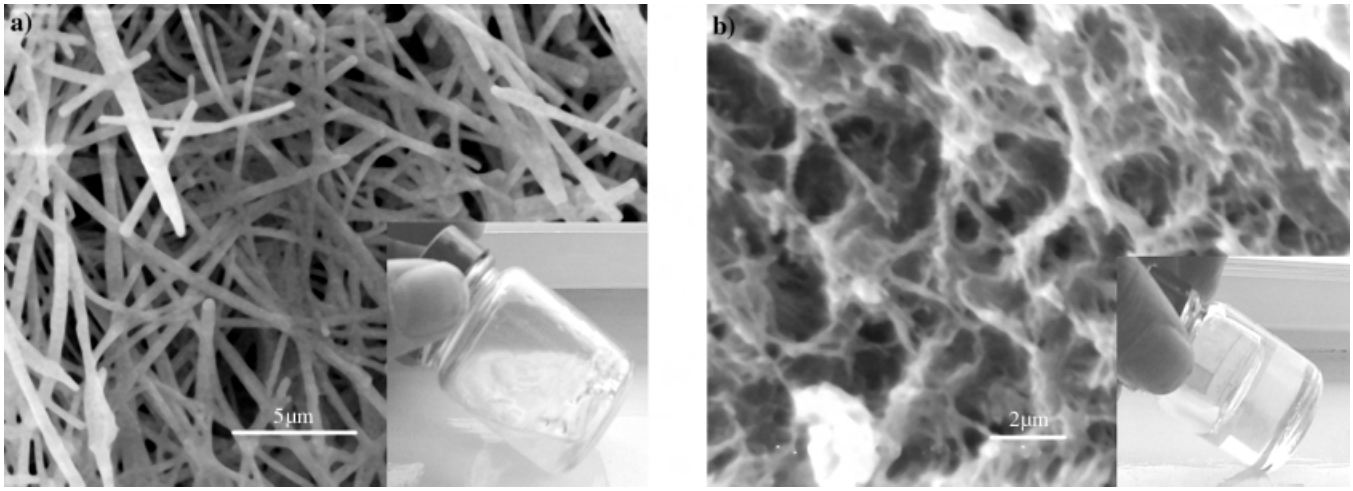
- **VIPs** 4598
- ***Angewandte's* Sister-Journals** 4614 – 4615
- **Keywords** 4798
- **Authors** 4799
- **Preview** 4802

Don't forget all the Tables of Contents from 1998 onwards may be still found on the WWW under: http://www.angewandte.org

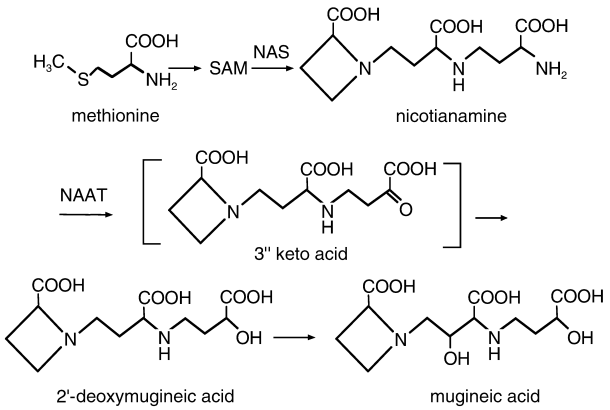
Issue 23, 2002 was published online on November 27.

CORRIGENDUM

In the Communication by **X. Y. Liu** and **P. D. Sawant** in Issue 19, **2002**, pp. 3641 – 3645, the improved pictures shown below should have been used for Figure 1. For Figures 2 and 3, EVA should read EVACP. Throughout the paper lanosterol should read L/DHL.



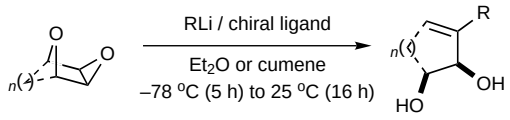
In the Minireview by **D. Staiger** in Issue 13, **2002**, pp. 2259 – 2264, Scheme 2 should be represented as follows:

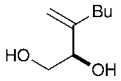
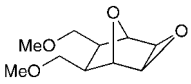
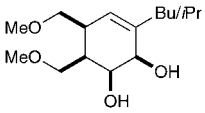
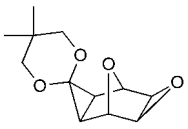
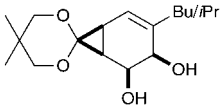
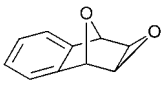
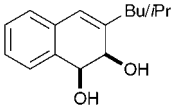
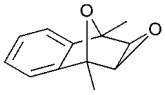
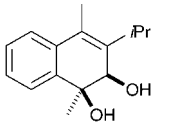


© 2002 WILEY-VCH Verlag GmbH & Co. KGaA, Weinheim

In the Communication by **D. M. Hodgson** et al. in Issue 22, **2002**, pp. 4313 – 4316 errors were inadvertently introduced into Tables 1 and 2 during the printing. The correct sections of the tables are now given below. The editorial office apologizes for these errors.

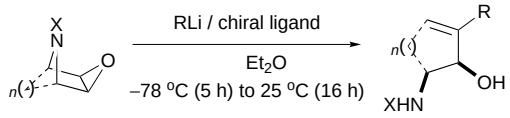
Table 1. Formation of enantioenriched diols.

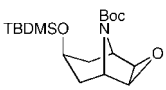
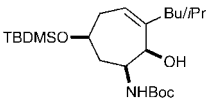
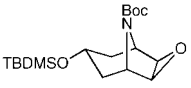
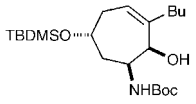
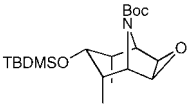
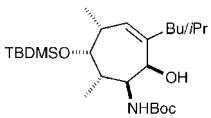
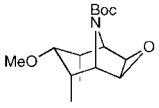
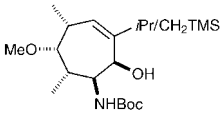


Entry[a]	Epoxide	RLi/ligand	Product[b]	Yield [%][c]	*ee* [%][d]
1		*n*BuLi/**1**		16	43
2		*n*BuLi/**2**		44	–42
3		*n*BuLi/**1**		46	34
4		*n*BuLi/**2**		34	–40
5		*i*PrLi/**1**		34	63
6		*n*BuLi/**1**		57	27
7		*i*PrLi/**1**		49	59
8		*n*BuLi/**1**		50	51
9		*i*PrLi/**1**		44	74
10		*i*PrLi/**1**		42	56

[a] Entries 1–10 carried out in Et_2O; entries 11–13 carried out in cumene. [b] Absolute configuration of predominant enantiomer obtained with (−)-sparteine (**1**) is shown (assigned by analogy with the sense of asymmetric induction in deprotonations of other *meso*-epoxides).[3] Bisoxazoline **2** preferentially produced the opposite configuration. [c] Yield of isolated product. [d] Determined by HPLC on a chiral stationary phase. TBDMS = *tert*-butyldimethylsilyl.

Table 2. Formation of enantioenriched amino alcohols.



Entry[a]	Epoxide	RLi/ligand	Product[b]	Yield [%][c]	*ee* [%][d]
9		*n*BuLi/**1**		83	41
10		*n*BuLi/**2**		60	–67
11		*i*PrLi/**1**		59	65
12		*n*BuLi/**1**		68	79
13		*n*BuLi/**1**		84	66
14		*n*BuLi/**2**		71	–67
15		*i*PrLi/**1**		85	71
16		*i*PrLi/**2**		72	–75
17		*i*PrLi/**1**		69	82
18		$TMSCH_2Li$/**1**		61	57
19		mixed[e]/**1**		66[f]	64

[a] Quenched at 25 °C, apart from entries 9–11 and 18, 19 (−5 °C), entry 12 (−78 °C), entries 13–16 (−30 °C), and entry 17 (−50 °C). [b] See Table 1 footnote [b]. [c] Yield of isolated product. [d] Determined by HPLC or GC on a chiral stationary phase. [e] *i*PrLi (1.1 equiv) and $TMSCH_2Li$ (2.5 equiv). [f] Allylsilane major product, 7% of *i*Pr incorporation additionally observed. TMS = trimethylsilyl.

 © 2002 WILEY-VCH Verlag GmbH & Co. KGaA, Weinheim 1433-7851/02/4124-4611 $ 20.00+.50/0

In the Communication of **F. E. Romesberg** and **P. G. Schultz** et al. in Issue 20, **2002**, p. 3841–3844, the authors should be given in the following order: Chengzhi Yu, Allison A. Henry, Peter G. Schultz,* and Floyd E. Romesberg*.

In the Communication by **K. Kim** et al. in Issue 23, **2002**, pp. 4474 – 4476, the permanent address for Professor Parimal K. Bharadwaj was unfortunately removed during editing. The editorial office apologizes for this error. His permanent address is:

Department of Chemistry
Indian Institute of Technology
Kanpure 208016 (India).

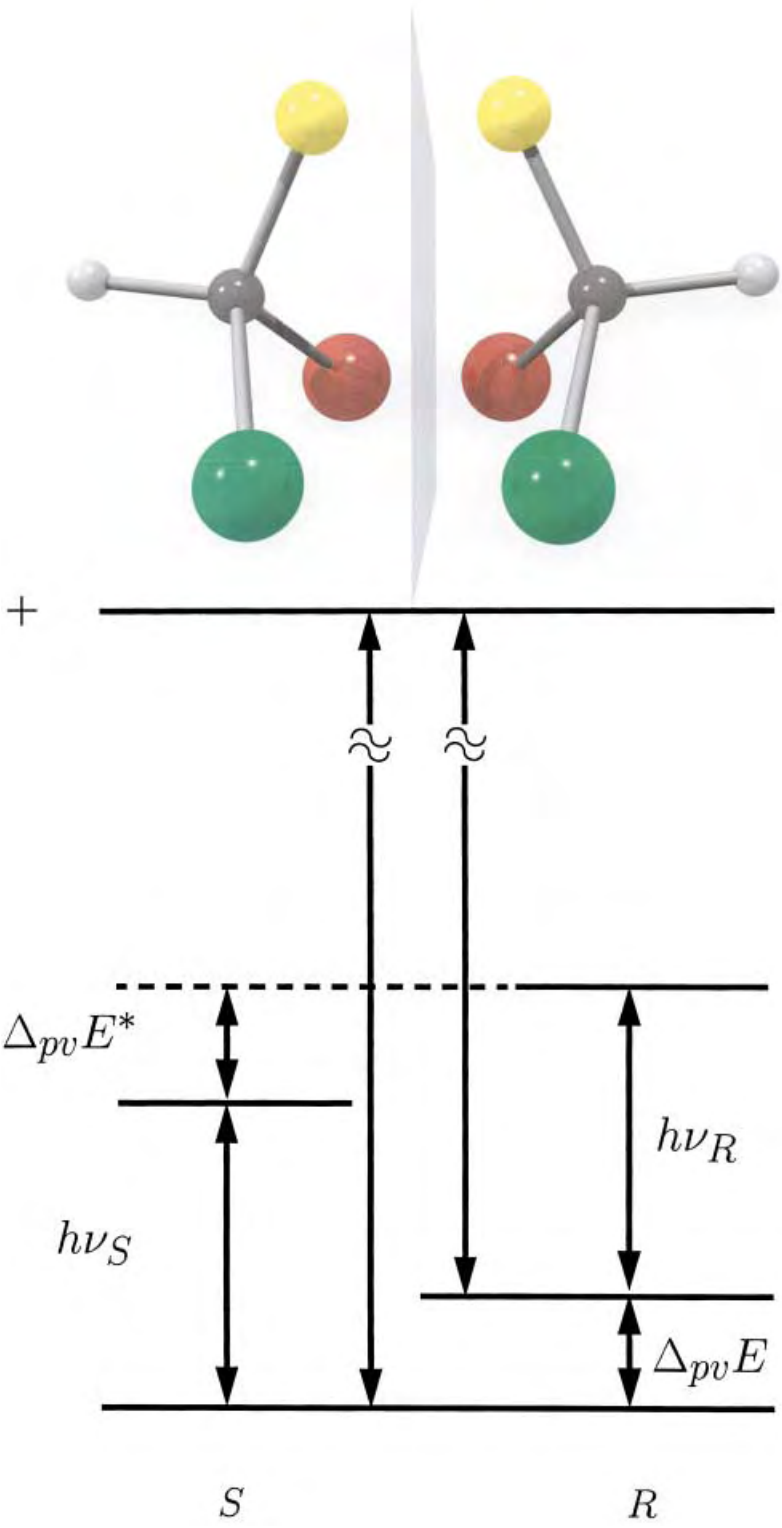
APOLOGY

In the Communication "Synthesis of Amphiphilic Conjugated Diblock Oligomers as Molecular Diodes" by **L. Yu** and **M.-K. Ng** (*Angew. Chem.* **2002**, *114*, 3750 – 3753; *Angew. Chem. Int. Ed.***2002**, *41*, 3598 – 3601) the authors missed a cross-reference to their thematically related but independent communication "Molecular Diodes Based on Conjugated Diblock Co-oligomers" (M.-K. Ng, D.-C. Lee, L. Yu, *J. Am. Chem. Soc.* **2002**, *124*(40), 11862 – 11863) and vice versa. The authors apologize for this oversight.

 © 2002 WILEY-VCH Verlag GmbH & Co. KGaA, Weinheim 1433-7851/02/4124-4612 $ 20.00+.50/0

The energies of enantiomers are different because of a symmetry violation.

ANGEWANDTE CHEMIE © WILEY-VCH



The energy difference $|N_A\Delta_{pv}E| = |\Delta_{pv}H_0^{\ominus}|$ for the reaction $S \rightleftarrows R$ might be measured following the spectroscopic scheme shown. It is predicted to be about 10^{-11} J mol^{-1}. How important would this tiny difference be for chemistry? What are the consequences for physics and biology?

How Important is Parity Violation for Molecular and Biomolecular Chirality?

Martin Quack*

Dedicated to Professor Hans H. Günthard on the occasion of his 85th birthday

Parity violation leads to energy differences $\Delta_{pv}H_0^\circ = N_A\Delta_{pv}E$ of enantiomers in the femtojoule to picojoule per mole range. Recently introduced methods of electroweak quantum chemistry predict such energy differences to be one to two orders of magnitude larger than previously accepted—but still very small. How can such small energies be measured and what are the consequences for our understanding of molecular chirality, biomolecular homochirality, and perhaps fundamental physics? The review gives some tentative answers to these questions. We discuss the current status of theory and some of the current experimental approaches.

Keywords: biological homochirality · chirality · parity violation · symmetries

1. Introduction: Chirality and Fundamental Symmetries

The short introductory answer to the question in the title of this review might be: Parity violation is much more important—even by orders of magnitude—than believed on the basis of calculations commonly accepted until recently.[1, 2] The history of this striking development will briefly be reviewed and an outlook presented on possible consequences for our understanding of the two big open questions on chirality discussed by us in a review a little more than a decade ago.[1]

1. What is the origin of chirality in molecular physics and thus the "nature" or intrinsic structural feature of a chiral molecule or a chiral structure?
2. What is the origin of (homo)chirality in molecular biology, that is, the *chiral bias* that favors some enantiomers over others (in the chemistry of life as we know it)?

   At the end of this review we shall complement this with a tentative answer to a third question:
3. Can a new experimental and theoretical understanding of molecular chirality contribute to our understanding of the fundamental laws of physics?

It should be made clear at the outset, that the purpose of this short review cannot be a complete and encyclopedic, technically detailed review of the current status of the field, which is best dealt with separately. Rather we intend here to highlight briefly the development of the main concepts (and some controversies) with an outlook also towards ongoing research. Most current efforts of chemists in the field of chirality pertain to the enantioselective syntheses of chiral compounds and their industrial applications. Such work has been repeatedly honored, recently with the Nobel prizes conferred upon W. S. Knowles, R. Noyori, and K. B. Sharpless in 2001.[3] Other important questions in chemistry concern the analysis of the structure and composition of complex chiral compounds—for instance by crystallographic or spectroscopic techniques or else simply tricky problems in the description of and the nomenclature for chiral compounds (see ref. [4, 5] for examples). Indeed, chirality-related research plays a substantial role in many chemistry departments worldwide, and the ETH-chemistry department is but one example among many (nicely summarized in ref. [6])

In addition to such classical "chemical" questions, however, molecular chirality is also important in relation to fundamental physics, in particular in relation to the underlying symmetries of physical laws. This relationship was already addressed in very general terms by the discoverer of molecular chirality, Louis Pasteur, 150 years ago.[7]

More specifically, in an early review of the stereochemical concepts introduced in parallel by J. A. Le Bel and himself[8] van't Hoff explicitly uses the "exact mechanical symmetry" between enantiomers to argue (rewritten and shown here in modern notation) that the standard Gibbs energy $\Delta_R G^\circ$, the enthalpy $\Delta_R H^\circ$ and the entropy $\Delta_R S^\circ$ of an isomerization reaction between the *R* and *S* enantiomers of a chiral

[*] Prof. M. Quack
ETH Zürich
Physical Chemistry
Wolfgang-Pauli-Strasse 10, CH-8093 Zürich (Switzerland)
E-mail: Martin@Quack.CH

 © 2002 WILEY-VCH Verlag GmbH & Co. KGaA, Weinheim 1433-7851/02/4124-4619 $ 20.00+.50/0

molecule must all be exactly zero at all temperatures [Eq. (1) and (2); including 0 K with $\Delta_R H_0^\circ$] and thus the equilibrium constant K must equal exactly 1 because of Equation (3)

$$R \rightleftharpoons S \qquad \Delta_R H_0^\circ \tag{1}$$

$$\Delta_R G^\circ = \Delta_R H^\circ - T\Delta_R S^\circ \tag{2}$$

$$K = \exp(-\Delta_R G^\circ / RT) \tag{3}$$

This is a clear reasoning that leads from a fundamental physical symmetry to a chemical result: $K = 1$. In modern words, he refers to the invariance of the mechanical laws that govern molecular motion under the space inversion operation leading from a left-handed to a right-handed coordinate system (i.e. replacement of all particle coordinates following $x \rightarrow -x$, $y \rightarrow -y$, $z \rightarrow -z$; see Figure 1). Such a symmetry (and thus in chemistry the equilibria (1) – (3)) is related in a most fundamental way to our understanding of nature, what is "observable" and "not observable". If the exact symmetry is present, then the absolute handedness is not observable (only the relative handedness of enantiomeric objects can be observed). In the words of Einstein[9] "There are thus two types of cartesian coordinate systems which are called "right-handed" or "left-handed" systems. The difference between the two is familiar to every physicist and engineer. Interestingly, an absolute geometric definition of the right or left handedness is impossible, only the relationship of opposition between the two can be defined."

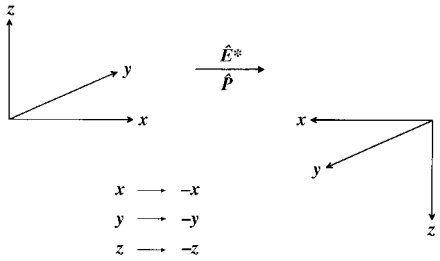


Figure 1. The symmetry operation of space inversion $\hat{E}^*$ or $\hat{P}$ transforms a right-handed coordinate system (left) into a left-handed system (right). In electroweak quantum chemistry, the symmetry with respect to space inversion is not valid. By rotating the coordinate system on the right by 180° around the x-axis, one can show the equivalent standard "mirror-image" relationship of these coordinate systems as enantiomeric structures.

Chemists could test whether that symmetry actually applies, for instance by measuring the equilibrium constant to very high precision. If K were found to be systematically different from 1 within high experimental confidence, the symmetry would be proven by experiment to be absent and thus the absolute handedness would become observable. It should perhaps be pointed out here that the determination of a conventional "absolute configuration" in the chemist's sense is not a determination of absolute handedness of space, the latter being on a more fundamental level. The symmetry reasoning is valid within both classical and quantum mechanics. However, in single measurements there will be statistical deviations from the value $K = 1$.

2. Hund's Quantum-Mechanical Treatment of the Stereomutation of Chiral Molecules by the Tunnel Effect with Parity Conservation (1927)

In 1927 F. Hund[10] noted in the framework of quantum mechanics that with the invariance of the molecular Hamiltonian operator $\hat{H}$ under space inversion $\hat{P}$, as expressed by the commutation relation (4), the energy eigenstates χ_+ and

$$\hat{P}\hat{H} = \hat{H}\hat{P} \tag{4}$$

χ_- of chiral molecules will have a well-defined positive or negative parity π (the eigenvalues of $\hat{P}$ are $\pi = \pm 1$). They will



Martin Quack studied Chemistry and Chemical Physics in Darmstadt, Grenoble, and Göttingen, where he received his chemistry diploma in 1971. He worked on his diploma thesis on high-resolution fluorescence spectroscopy with Manfred Stockburger and Albert Weller at the Max-Planck-Institutes for Spectroscopy and Biophysical Chemistry. He received his doctoral degree from the Ecole Polytechnique Fédérale de Lausanne in 1975 after work with Jürgen Troe in reaction kinetics. As Max Kade Fellow he stayed with William H. Miller at the University of California Berkeley in 1976/77 and habilitated in Göttingen in 1978 (with research on the subject of IR-multiphoton excitation and laser chemistry), where he was Privatdozent and later Professor (C2) until 1982. In this year he was appointed full professor at the University of Bonn (C4) and in 1983 he became Professor Ordinarius for Physical Chemistry at the ETH Zürich, where he has been since then. Chemistry with its sometimes striking transformations through the processes of molecular kinetics, spectroscopy, and fundamental symmetries in nature leading to conservation laws and their subtle violations have been his scientific hobbies ever since his school days. He has been honored for his work in these areas, for instance by the Nernst-Haber-Bodenstein Prize, the Otto Klung Prize, the Paracelsus Prize, and the Otto Bayer Prize. He has been Hinshelwood lecturer and Christensen fellow (Oxford 1988), was elected fellow of the American Physical Society in 1990 and later member of the Deutsche Akademie der Naturforscher Leopoldina (1998) and the Berlin Brandenburg (formerly Prussian) Academy of Sciences (1999). He is a member of the board of the Swiss Chemical Society as well as a member of several further scientific societies.

thus be delocalized over both enantiomeric structures. This quantum number parity is conserved as a constant of motion related to the fundamental symmetry (parity conservation). Hund explained the observation of stable *R* and *S* enantiomers of chiral molecules by noting that one can generate localized wavefunctions by the superposition of parity eigenstates [Eq. (5) and (6)]. These localized wavefunctions reside

$$\sigma = (\chi_+ - \chi_-)/\sqrt{2} \quad (5)$$

$$\rho = (\chi_+ + \chi_-)/\sqrt{2} \quad (6)$$

at low energies in the wells of the lowest potential, which is drawn schematically in the upper part of Figure 2. The wavefunctions move periodically from one well to the other,

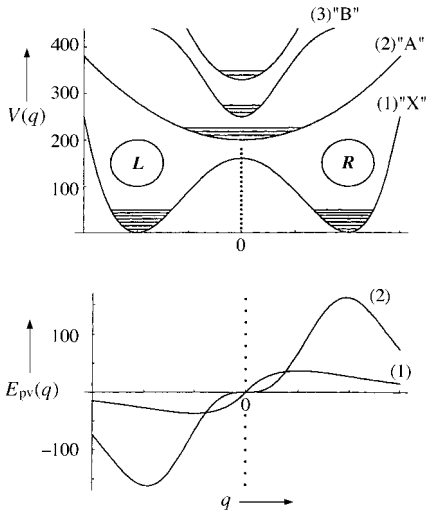


Figure 2. General illustration for parity-conserving and parity-violating molecular potentials (from ref. [2]). Upper: Born–Oppenheimer-type or possibly more general ground and excited-state effective potentials (V(q) in kJ mol^{-1}) which are exactly inversion symmetric (i.e. symmetric under $q \rightarrow -q$), and separate this space into a left-handed (L) and right-handed (R) section; in this example with a general notation (standard conventions might associate *L* with *S* and *R* with *R* enantiomers or *L* with *M* and *R* with *P* enantiomers with helical chirality here, but this is quite arbitrary). The ground-state potential has a chiral equilibrium geometry and the excited states have achiral equilibrium geometries in this example. Lower: Small parity-violating effective potentials for the two lower states (schematic; E_{pv}(q) in fJ mol^{-1}). These should not be interpreted naively as additions to a Born–Oppenheimer potential, but instead as effective potentials of a different symmetry (antisymmetric under $q \rightarrow -q$) and of a very different, very small order of magnitude. Recent work in electroweak quantum chemistry has shown that these antisymmetric potentials are orders of magnitude larger than previously accepted.[1, 2]

that is, from *R* to *S* structures and the reverse, even at a low energy that is well below the top of the barrier to stereomutation in this potential, in a time corresponding to the half period of motion [Eq. (7)], where $\Delta E_{\pm} = E_- - E_+$ is the energy difference between the energy eigenstates of well-defined parity. The possibility of such a process in quantum mechanics was figuratively said to be caused by a "tunneling process".

$$\tau_{RS} = h/(2\Delta E_{\pm}) \quad (7)$$

Hund's treatment of chiral molecules seems in fact to be the historical discovery and first application of the important tunnel effect in chemistry and physics, just one year after Schrödinger's famous papers on wave mechanics in 1926 and not even two years after Heisenberg's formulation of quantum mechanics. Thus a careful treatment of a stereochemical problem within the framework of the then new quantum mechanics led to the discovery of this important physical phenomenon. Its 75th anniversary can be dated 28 May 2002. Physics textbooks frequently attribute the discovery of the tunnel effect to a later paper by Gamow on nuclear α decay.[11]

For typical tetrahedral van't Hoff structures of chiral molecules, Hund estimated tunneling times of millions of years, which readily explains the stability of enantiomers (for a critical discussion of these quantitative estimates see ref. [12]). The qualitative conceptual understanding of chirality again appeared complete within this picture, with retention of space inversion symmetry. At that time the firm belief was expressed that the underlying physical laws for all of chemistry were known.[13] This turned out to be in error with respect to chirality. While thus, in this round, molecular chirality in chemistry was fruitful in introducing a fundamental physical concept, which was later to be used in nuclear and high energy physics and elsewhere, the next important development came about another three decades later from atomic and nuclear physics.

3. The Discovery of Parity Violation and its Relationship to Molecular Chirality

In 1956, Lee and Yang pointed out in a discussion of the experiments available at the time that there was actually no good evidence for parity conservation and thus for the underlying space inversion symmetry in nuclear β decay.[14] Subsequent experimental tests, indeed, quickly led to the confirmation of parity violation.[15] Many physicists were highly reluctant to accept the removal of this symmetry from their theories and Wolfgang Pauli is said to have bet large amounts of champagne against it when the suggestion of parity violation first appeared. Similarly, as reported in the December 2001 news of the American Physical Society, Richard Feynman considered at the time the notion of parity violation to be "unlikely, but possible, and a very exciting possibility", and he made a 50 dollar bet with a friend that parity would not be violated. However, Feynman lost that bet and experimental proof of parity violation was swift and complete.

The concept was rather quickly transferred to molecular chirality. While one can find a few early, scattered remarks about the importance of parity violation for molecular chirality (for instance by Wigner and others), it was Yamagata in 1966 who clearly formulated the possible consequences both for molecular chirality and biomolecular homochirality.[16] He pointed out that, because of parity violation, there will be a small difference in energy between enantiomers and thus in Equation (8) we have a parity-violating energy

$$\Delta_R H_0^{\circ} = \Delta_{pv} H_0^{\circ} = N_A \Delta_{pv} E \quad (8)$$

difference. He also discussed, in a simple kinetic model, the possible kinetic consequences of generating homochirality in the formation of biopolymers with monomeric units from different families of monomeric enantiomers (*R* and *S*). In the concluding sentence, he correctly points out the qualitative conceptual consequences for the hypotheses of the appearance of homochirality in the biochemistry of life with the famous phrase of "chance and necessity".[17]

Yamagata's extremely rough quantitative estimates were, however, somewhat overoptimistic, and in fact were flawed. One can cautiously interpret Yamagata's proposal with a value of $\Delta_{pv}H^{\circ} \simeq 10^{-6}\,RT$ ($\simeq 10^{-3}\,\mathrm{J\,mol^{-1}}$ below room temperature), which is many orders of magnitude too large according to present knowledge.[2] Also, his selection mechanism is problematic because in the limiting case in which the parameters of the model allow for substantial selection of one enantiomeric form, no appreciable product would ever be formed.[18] Other mechanisms are needed to explain selection of homochirality on this basis (see ref. [12] and Section 6). Nevertheless, Yamagata's contribution had great merit, in that it kept interest alive in the quantitative question of molecular parity violation and introduced the distinct issue of biological evolution into the discussion.

In the 1970s and early 1980s, several papers addressed the estimation of $\Delta_{pv}H^{\circ}$, providing more adequate estimates,[19–24] which were still qualitative and covered quite a range of values. By 1980 this corresponded to about $\Delta_{pv}H^{\circ}_0 \simeq 10^{-10}\,\mathrm{J\,mol^{-1}}$, with acknowledged uncertainties of more than five orders of magnitude that arose mostly from the nature of the molecular electronic wavefunction, which was not properly calculated in any of these estimates. It should be mentioned that some of the progress in these estimates was certainly stimulated by parallel work on atomic parity violation and optical activity, a field which we cannot cover here (see ref. [25] for reviews). These estimates of the order of magnitude of $\Delta_{pv}H^{\circ}$, although still extremely crude, were already sufficient to predict qualitatively that parity violation actually dominated over tunneling, given the extremely long tunneling times of millions of years already predicted by Hund (really even much longer[12]). These times would correspond to tunneling energies of about $10^{-25}\,\mathrm{J\,mol^{-1}}$; much smaller than any acceptable estimate for $\Delta_{pv}H^{\circ}$ at that time. This situation, in which the parity-violating energy difference in principle becomes an measurable difference between the zero-point levels of enantiomers was in fact predicted by all authors from 1966 to 1977.[16–21] It was thus clear that, in spite of its small magnitude, parity violation had a real stereochemical significance in molecules such as CHFClBr [in terms of a real, nonvanishing $\Delta_R H^{\circ}_0$ in Eq. (1)].

Another limiting case with large tunneling splitting and effective parity conservation was routinely observed in the high resolution spectroscopy of molecules such as the textbook example NH_3[26] ("chiral" NHDT has not been studied, to my knowledge) or C_6H_5-NHD,[27–29] which is chiral in its equilibrium geometry but not in its energy eigenstates (for the older available theories of tunneling in symmetrical and asymmetrical potentials see for example ref. [30]).

There were also attempts to measure infrared line shifts caused by parity violation[20] on CHFClBr[31] and camphor.[32] With a best relative uncertainty of $\Delta\tilde{\nu}/\tilde{\nu} = 10^{-8}$ in these experiments, there was no hope of seeing an effect (and none was seen); we know today that at least about 10^{-16} is needed. Another interesting point was raised by Harris and Stodolsky in 1978:[22] If the barrier to stereomutation were such that the tunneling splittings and parity-violation energies were about equal, one might experimentally observe a time-dependent oscillation of optical activity with an amplitude significantly different from Hund's prediction for a symmetrical potential. In such cases, one could indirectly derive the parity-violating coupling-matrix element, from this amplitude of optical activity, by reference to the tunneling splitting. Because optical activity is difficult to observe at the high dilutions in a molecular beam needed for such an experiment, and because the class of suitable molecules is very special, this remained only a theoretical possibility. For the usual case of stable chiral molecules with negligible tunneling, dominated by parity violation, the time dependence of optical activity is practically indistinguishable whether or not there is parity violation. This time dependence would change from millions or billions of years in Hund's traditional theory to infinite time with parity violation, a change which is not suitable for laboratory observations on isolated molecules.

In 1980 and the following years, another experimental concept that should give direct access to the measurement of $\Delta_{pv}H^{\circ}_0$ for the realistic case of dominant parity violation was proposed by the present author and reported at several meetings. It is based on generating a new form of strange, unstable superposition isomers of well-defined parity for chiral molecules and observing the time evolution caused by parity violation. Because initially the technical difficulties seemed insurmountable, the details were published only in 1986[33] and we shall return to this point below when discussing experiments that are currently pursued (Section 5). Around 1980 all experiments on molecular parity violation seemed far removed from successful realization.

From the theoretical side we may summarize the also somewhat unsatisfactory situation until about 1980 as follows: The estimates of $\Delta_{pv}H^{\circ}_0$ were uncertain by about five orders of absolute magnitude and there was no knowledge about the sign (whether *R* or *S* would be more stable for a given pair).

4. The Quantitative Theory of Molecular Parity Violation

Quantitative calculations of molecular parity violation were seriously attempted around 1980 in the work of Hegström, Rein, and Sandars, who formulated a theory based on the single determinant excitations—restricted Hartree–Fock approach (SDE–RHF).[34, 35] This theoretical approach was widely used for the following decade (refs. [36–38] and references cited therein), leading to highly publicized results for biochemically relevant molecules such as amino acids and sugars.[36–40] While alternatives were considered,[41] the results of the SDE–RHF approach were generally believed to be firm and reliable for more than a decade (see also the review in ref. [1]).

It thus came as a surprise that the calculated parity-violating energy differences increased by one to two orders of magnitude when our group introduced the new CIS–RHF (CIS = configuration interaction singles) approach to *electroweak quantum chemistry* in 1995[2, 42, 43] (this is where the latter term was coined), and later the more efficient and powerful multiconfiguration linear-response approaches (MC-LR).[44] The starting point for this discovery was by no means spectacular. When rederiving all the basic equations again from scratch (see ref. [2] for the full account) and taking a closer look at the perturbation expressions for the parity violating potentials, it appeared that the SDE–RHF wavefunctions were really not very suitable for the description of the excited states appearing in the perturbation expressions for the parity violating potentials. Thus, we tried practically the simplest possible improvement of the theory (which is CIS–RHF), which immediately yielded the very large changes mentioned above. At the same time we showed that the parity-violation potentials E_{pv} appear as the trace of a tensor, $E_{pv} = E_{pv}^{xx} + E_{pv}^{yy} + E_{pv}^{zz}$, where the individual elements may have different signs and evolve independently in the calculations. This result implies that none of the calculations of sign and magnitude of $\Delta_{pv}E$ in polyatomic molecules prior to 1995 can be relied upon with any degree of certainty. Although changes of the order of magnitude and of the sign for a calculated heat of reaction ($\Delta_R H^\circ \equiv N_A \Delta E_{pv}$) are certainly spectacular, it must be remembered that the absolute values remain exceedingly small.

Our new approaches have been applied to various problems in different molecules such as H_2O_2, H_2S_2, ethylene torsion (all these having been investigated already in the earlier work, but with very different results)[35–37] distorted CH_4 and C_2H_2, N_2O_4, CHBrClF, CDBrClF, fluorooxirane, S_2Cl_2, and alanine in both the gas phase and solution.[2, 42–51] For many of these molecules, significant coordinate-dependent parity-violating potentials such as shown in Figure 2 could be calculated, giving the magnitude, the sign, and the antisymmetry of these effective potentials. Careful convergence checks indicated that, with appropriate computational expense, convergence can be reached.[44] Some of these new results were also confirmed by independent calculations in other research groups.[52–56]

Table 1 provides a short survey of results for H_2O_2, H_2S_2, and S_2Cl_2, which indicates that, in recent work, the order of magnitude obtained increases as well as demonstrating the good convergence of recent results from different groups. In this context in particular the approach by Schwerdtfeger and co-workers is noteworthy,[54–56] because it uses quite a different quantum chemical framework within Dirac–Fock theory, but agrees nevertheless very well with the results of our group. One may thus hope that the recent theoretical approaches give quantitatively accurate results within the limits of basis sets and methodological convergence, which results in remaining uncertainties of perhaps 30% in $|\Delta_{pv}E|$, depending on the molecule. With appropriate care (and cost) even more accurate results should be accessible using our methods. Very recently a density-functional theory approach to molecular parity violation has also been published.[57]

Table 1. Parity-violating energy differences $\Delta_{pv}H_0^\circ = \Delta_f H_0^\circ(\mathrm{M}) - \Delta_f H_0^\circ(\mathrm{P})$ for H_2O_2, H_2S_2, and Cl_2S_2 at the geometries of the P and M enantiomers indicated (close to but not exactly equilibrium geometries, chosen for intercomparison of different results). The geometry parameters used were: $r_{OO} = 149$ pm, $r_{OH} = 97$ pm, $\alpha_{OOH} = 100^\circ$, $\tau_{HOOH} = 90^\circ$ for H_2O_2, $r_{SS} = 205.5$ pm, $r_{SH} = 135.2$ pm, $\alpha_{SSH} = 92^\circ$, $\tau_{HSSH} = 92^\circ$ for H_2S_2, and $r_{SS} = 194.7$ pm, $r_{SCl} = 205.2$ pm, $\alpha_{SSCl} = 107.55^\circ$, $\tau_{ClSSCl} = 85.12^\circ$ for Cl_2S_2.

Molecule	Method	References	$\Delta_{pv}H_0^\circ$ [10^{-12} J mol^{-1}]
H_2O_2	SDE-RHF 6-31G	[36]	– 0.0036
	CIS-RHF 6-31G	[2, 42, 43]	– 0.60
	TDA 6-31G	[52]	– 0.84
	DHF	[54]	– 0.44
	CASSF-LR/cc-pVTZ	[44]	– 0.41
H_2S_2	SDE-RHF 6-31G	[36]	0.24
	TDA 4.31G	[52] (scaled 75% [43])	14.4
	CIS-RHF 6-31G**	[2, 43]	22.5
	MC-LR RPA/aug-cc-pVTZ	[48]	22.4
	DHF	[54]	33.5
Cl_2S_2	MC-LR RPA/aug-cc-pVTZ-A	[47]	– 15.4

A more complete critical review of the "technical" question of which theoretical approaches are most suitable for the calculation of molecular parity violation in a given instance is best dealt with separately.[18] From a formal point of view, a relativistic theory of molecular parity violation is the most logical starting point (see ref. [2, 41, 54]). However, this does not imply that direct relativistic approaches at a given computational expense (for instance the maximum possible expense with current resources) will also provide the most accurate description of molecular parity violation. Indeed, physically, molecular parity violation arises as a contactlike interaction between electron and nucleons (in practice the nucleus) because of the short range of the weak nuclear interaction mediated by the massive Z boson as a field particle. This can be related to the gradient of the wavefunction of the electron at the position of the nucleus,[46] which is somewhat comparable (but not identical!) to the Fermi contact interaction which is responsible for the hyperfine structure in ESR spectra or the *J*-coupling constants in NMR spectra. It is thus important that the theory provides an accurate electronic wavefunction at the position of all the nuclei. For very accurate calculations on small molecules with light nuclei, the best strategy may well be to use as a starting point a very high-level standard nonrelativistic quantum-chemical approach and introduce relativistic corrections by perturbation theory, as necessary.[2] Because of the very high computational expense, the direct relativistic (Dirac–Fock-type) approaches[54] may not allow for a sufficiently high-level treatment at the same (maximum) computational expense. On the other hand, for large polyatomic molecules the most efficient, and thus relatively most accurate, approach may be the application of density-functional theory,[57] although it suffers from the notorious lack of systematic improvement to convergence. Finally, for molecules involving heavy, highly charged (high Z) nuclei, direct relativistic approaches may provide the most efficient starting point. However, it would be misleading to state that the direct relativistic approaches are always numerically the most accurate.[53] All approaches should give similar and approximately correct results at the

appropriate level of theory. We exclude here the ever-present possibility of some fundamental omission that might be common to all current theories. This possibility could be tested by experiment.[33]

5. Experimental Approaches towards Detecting Molecular Parity Violation

Experimental approaches towards molecular parity violation have been suggested repeatedly, but to date no experiment has been successful in confirming the effect. Very broadly one may distinguish here between spectroscopic measurements on isolated molecules in the gas phase and experiments on macroscopic condensed-phase samples. The latter have led to a number of claims of success, but not to adequate proof, in our opinion. Recent crystallization experiments[58] may be mentioned here, among several examples. The main problem of all macroscopic approaches can be summarized as follows: Even if reproducible effects are found, how can one guarantee that their origin is intrinsically from parity violation and not from some parasitic effects arising from intermolecular interactions in the macroscopic experiments? Minor impurities could play major roles because we are talking about energetic effects of the order of 1 in $10^{12}-10^{15}$ (at ordinary temperatures) and thus interactions with impurities (and differences in impurities) of that order might become important. How can one guarantee the absence of effects of this type and of other parasitic effects in a macroscopic experiment? The other difficulty is to relate quantitatively the macroscopic observations to the theory of parity violation. This seems to be extremely difficult at present.

We think that definitive and useful experiments will come from the spectroscopy of isolated molecules in the gas phase. Figure 3 summarizes the type of experiments which have been proposed and are under current study in our laboratory, as well as in a few others worldwide.[1, 20, 31–33, 46, 59–67] The energy-level diagram for the enantiomers of a chiral molecule is shown here—not to scale at all, with the parity-violating value $\Delta_{pv}E$ greatly overemphasized (by ten orders of magnitude or more). Different concepts for spectroscopic experiments on parity violation can be distinguished by the nature of the transitions observed in Figure 3 (see also the review in ref. [59]).

Historically, the first concept relies on the measurement of separate spectroscopic transitions in R and S enantiomers (originally in the IR region).[20, 31, 32] Because of parity violation, the corresponding transition energies $h\nu_S$ and $h\nu_R$ will be slightly different. The realization of such experiments has been discussed for the radiofrequency range in NMR spectroscopy[60, 61] and the microwave range, where for CHFClBr a modest Doppler-restricted limit with $\Delta\nu_D/\nu \simeq 7\times10^{-7}\sqrt{(T/\mathrm{K})/(m/\mathrm{u})}$ was reported in supersonic-jet spectra at low effective temperatures T for the absence of parity-violating splittings.[62]

At the same time a first, full rotational analysis was given for an infrared band accessible to CO_2 laser line coincidences and thus ultrahigh-resolution sub-Doppler spectroscopy was suggested.[62, 63] Such experiments were subsequently reported

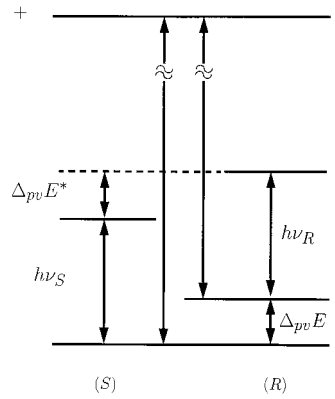


Figure 3. Energy level diagram for R and S enantiomers of a chiral molecule (from ref. [46]). Experimental (spectroscopic) schemes to observe effects from parity violation can measure differences in spectral transitions $h\nu_S$ and $h\nu_R$ in the separate enantiomers. These yield *differences* $|\Delta_{pv}E^* - \Delta_{pv}E|$ in parity-violating energy differences (ν_S and ν_R can correspond to NMR, microwave, IR, UV/Vis, or γ ray spectroscopy). Alternatively one can observe transitions to an achiral excited (vibrational or electronic) state with well-defined parity (here positive, +). Such a state can combine allowed transitions to both enantiomers and thus the differences of the two spectral lines in the middle provide $\Delta_{pv}E = \Delta_{pv}H_0^\circ/N_A$ directly. This approach can be realized with time-independent and time-dependent spectroscopic approaches.[1, 33] Vertical lines between full horizontal lines correspond to allowed spectroscopic transitions, whereas connections to the dashed horizontal line or transitions labeled by $\Delta_{pv}E$ are forbidden and illustrate only energy differences.

by the Paris group of Bordé and Chardonnet, and show a null effect with an very small estimated relative experimental uncertainty of $\Delta\nu/\nu \simeq 4\times10^{-13}$.[64, 65] Calculations in our group both prior to and after those experiments predicted that the actual effect would be three to four orders of magnitude smaller[45, 46] as confirmed in further calculations[55] (for a more complete history of the CHFClBr experiments and theory see ref. [59]). We had, however, anticipated that, for chiral molecules with two or more heavier atoms, the parity-violating frequency shift might become observable in infrared spectra in the relatively near future, although the quantitative theoretical analysis of the effect is difficult for such heavy molecules.

The highest frequency range considered for this experimental concept is Mössbauer (γ ray) spectroscopy.[66] NMR and Mössbauer spectra of condensed phases may have extra problems of interpretation because of intermolecular interactions, even if the nuclei at the origin of those spectra may be considered to be relatively well-shielded. In any case, this whole experimental concept is unable to provide direct access to the parity-violating energy difference $\Delta_{pv}E = \Delta_{pv}H_0^\circ/N_A$, as can be seen from Figure 3. Rather, *differences* $|\Delta_{pv}E^* - \Delta_{pv}E|$ of parity-violating energy differences are measured (this point has been misrepresented in several of the relevant publications).

The second proposal, historically, for experiments in which parity violation in molecules could be detected concerned the measurement of time-dependent optical activity in chiral molecules, in which the parity-violating potentials and stereomutation tunneling splittings are of about the same magnitude.[22] This experiment can be discussed in relation to Figure 3, if we reinterpret and rename some quantities in the level scheme. In the case of tunneling without parity violation,

the splitting between the two lowest levels is caused only by pure tunneling and corresponds to two delocalized energy states [$\Delta E_{\pm}$ in Eq. (7)]. This difference is unrelated to parity violation and no information on parity violation can be drawn from observation of the time-dependent oscillation expressed by Eq. (7), for instance as a time-dependent optical activity of period $2\tau_{RS}$. Indeed, this observation of time-dependent optical activity would be the tunneling variant of the first quantitative kinetic experiment carried out by Wilhelmy in 1850 on the "inversion" of sucrose, which is, however, not an elementary reaction (see the short review in ref. [71] for a discussion and citation of the original literature).

If parity violation becomes important compared to hypothetical tunneling $\Delta E_{\pm}$ in the symmetric case, then the amplitude of the oscillation of optical activity will decrease and from this decrease one can derive the parity-violating coupling V_{pv} as compared to the tunneling splitting, as pointed out by Harris and Stodolsky.[22] A significant observation in the ground level is possible only for a very special class of molecules, in which the tunneling splitting $\Delta E_{\pm}$ and V_{pv} are fairly similar, a rare exception. The generalization of this concept to excited states is discussed in ref. [1]. In the limiting case, in which parity violation becomes dominant, and the splitting between the lowest levels is $\Delta_{pv}E$ (see Figure 3) the time dependence of the optical activity vanishes and thus $\Delta_{pv}E$ cannot be directly measured by this technique. Indeed, this experimental approach is best adapted to a direct measurement of tunneling stereomutation τ_{RS} without parity violation, while parity violation appears as a perturbation of this process, whenever it becomes important. We note in concluding the discussion of this experimental concept that with the identification of an "intermediate tunneling" molecule,[48] the proposal of measuring the rate and amplitude of time-dependent optical activity[22–24] for such a rather special case has also gained some practical, experimental credibility, although such experiments will surely be very difficult. The use of excited (vibrational or electronic) states with proper tunneling splittings has also been suggested in connection with this idea.[1] This would also solve the problem of state preparation (by optical transition from a chiral ground state) not addressed in ref. [22], but it might introduce other problems.

It has also been discussed[1] that for such intermediate tunneling molecules, as well as for ordinary achiral molecules such as "achiral" methane or methane derivatives, one might measure the time-independent optical activity, because with the inclusion of parity violation even "achiral" molecules become chiral and optically active. This could be considered to be a separate experimental concept similar to the optical activity of atoms.[1, 25]

The first experimental concept that allows a direct measurement of $\Delta_{pv}E$ in the effective absence of tunneling relies on the key idea of using an intermediate spectroscopic level of well-defined parity (denoted by "+" for the example of positive parity in Figure 3).[33] Such intermediate levels can arise from excited electronic states with achiral equilibrium geometry, as schematically shown in Figure 2 for the excited electronic potentials (as predicted for amines,[27] methane derivatives,[67] and allenes[1, 33, 119]), or else they can arise from excited vibrational states with large tunneling splittings. These intermediate levels possess allowed spectroscopic transitions to both the *R* and *S* enantiomers. As seen in Figure 3, the measurement of the difference of frequencies, either directly or by a beat frequency of two stabilized lasers,[1] would provide us with the desired value $\Delta_{pv}E$. We note that theoretically $\Delta_{pv}E$ shown in Figure 3 and $\Delta_{pv}H_0^{\circ}$ has important anharmonic vibrational zeropoint corrections as recently shown[59, 121]

A particularly interesting variant of this approach utilizes the "synthesis" of the strange, unstable achiral "parity isomers" which are superpositions of normally stable *R* and *S* enantiomers. These strange achiral isomers have different line spectra at rotational resolution, which combine together to give the ordinary rotational–vibrational spectrum of the enantiomers or racemates. The situation is somewhat similar to nuclear-spin isomers such as *ortho* and *para*-hydrogen or the more interesting case of H_3^+,[68, 69] in which the nuclear-spin isomers also have complementary spectra, although the analogy should not be overemphasized. Indeed, such unstable parity isomers have to date not yet been prepared, but if this were to succeed, for instance by the method of ref. [33] they would be unstable with respect to collisions and parity violation. In the absence of collisions and other external perturbations, the time evolution would initially be quadratic in time. If at $t=0$ the π isomer (positive parity isomer) is populated, we find the relationships (9) and (10),[33] where c_{μ} is the concentration of the negative parity isomer (μ). We previously suggested calling these P (plus) and M (minus) isomers, but because of the quite different use of the P and M nomenclature for axially (helically) chiral molecules, the Greek letters π and μ are now preferred. Such exotic isomers will not be harmed by an exotic, that is Greek, nomenclature.[70]

$$\pi \rightarrow \mu \tag{9}$$

$$c_{\mu} \propto (\pi \Delta_{pv} E\, t/h)^2 \qquad (\text{for } c_{\mu} \ll c_{\pi}) \tag{10}$$

The preparation of such exotic isomers following ref. [33] could, in a sense, introduce a new kind of chemistry into molecular chirality, an important application of which would be to measure $\Delta_{pv}E$ by c_{μ}, following Equation (10). However, as discussed in ref. [1] the experiment in ref. [33] would also be able to also test other hypotheses of molecular chirality such as the superselection-rule hypothesis of Pfeiffer and Primas[72] or the collision hypothesis of Harris and Stodolsky,[24] as well as other fundamental concepts.

The same fundamental scheme as described in ref. [33] can also be used to measure excited-state parity violation by exchanging the role of lower and upper states (also in the Figures 2 and 3). This was pointed out at an early stage and the idea has been revived recently.[73] There have also been proposals of numerous further variations on the different schemes to measure parity violation including level-crossing experiments[67] and other possibilities, but it is not the aim here to provide a complete listing.

To summarize our discussion of the main experimental (spectroscopic) concepts, these comprise three fundamentally different approaches:

1. Measurement of small differences of spectral line frequencies between enantiomers of ordinary, stable chiral mole-

cules (in spectra ranging from the radiofrequency over infrared to the γ range).[20, 31, 32]
2. Measurement of time-dependent optical activity in a very special class of molecules, in which tunneling splittings and parity-violating potentials are of similar magnitude.[22–24]
3. Direct spectroscopic measurement of the parity-violating energy difference $\Delta_{pv}E$ between enantiomers by means of a spectroscopic combination difference or by means of the time dependence of the quantum number "parity", which corresponds to an isomerization between the unusual "parity isomers" of chiral molecules.[33]

Only the third of these three approaches is able directly to provide the reaction enthalpy $\Delta_R H_0^\circ(1) = \Delta_{pv} H_0^\circ = N_A \Delta_{pv} E$. A nonzero value of $\Delta_R H_0^\circ(1)$ also introduces a new viewpoint for this isomerization process: It becomes more similar to a simple isomerization of, for example, *cis* and *trans* isomers in achiral molecules, as the exact symmetry relationship between *R* and *S* isomers is removed: These isomers are now predicted to differ slightly in their scalar properties such as ground-state energies, in NMR, microwave, or infrared spectra, structures, and other properties. There is also a new concept here concerning the predicted existence of unstable[11] "achiral" parity isomers[33] with lifetimes of the order of seconds in addition to the ordinary, stable "chiral" enantiomers. To our knowledge, currently active experimental programs exist only along the lines of concepts 1.[62, 64–66] and 3.[33, 47, 49, 59]

The advantage of all spectroscopic experiments on isolated molecules resides in the possibility of a quantitative theoretical analysis by electroweak quantum chemistry.[42–49] We shall return to this point in the concluding remarks.

6. Parity Violation and Biomolecular Homochirality

The origin of biomolecular homochirality has certainly been the most extensively discussed and most controversial issue in relation to molecular parity violation. It concerns the nearly exclusive selection of L amino acids and D monosaccharides exhibited by terrestrial biopolymers and indicates the central role chirality plays in life as we know it. In contrast to the other topics discussed in this essay, this particular topic has received extensive and even excessive attention in numerous papers and reviews. With apologies to many other authors not cited we may cite here refs. [1, 12, 16, 38, 42, 50, 51, 56, 58, 74–90]. This subject has been the specific theme of a recent review[91] and Highlights.[92] We thus will be brief here, and follow essentially the line of thinking expressed in ref. [93] The whole field related to this question is characterized by the existence of "communities of belief" on how biomolecular homochirality has arisen on earth rather than any safe empirical or theoretical knowledge. The beliefs can be broadly classified according to the old phrases of selection by "chance" or by "necessity",[16, 17] or in more technical terms caused by symmetry breaking de facto (factlike) or de lege (lawlike)[1] in the selection process. Each of these fundamental hypotheses can be further subdivided into further subsections as follows:

1. One may have a stochastic "all or nothing" selection in a biochemical selection mechanism[74–76] or an abiotic mechanism, for instance by crystallization.[77, 78] According to this hypothesis, each selection will lead uniquely to either "D" or "L" life evolution, but on average over many independent evolutionary processes to equally frequent D and L (referring to amino acids, for example).
2. One may have an accidental external chiral influence in evolution, such as a locally existing chiral quartz crystal,[79, 80] a local existence of circularly polarized light,[81] or the local influence of external magnetic fields.[83–85] This local influence could be reversed in another environment with equal probability; this is then also a "chance" (de facto) mechanism. The influence of circularly polarized γ rays or polarized β radioactivity might appear under the de facto or—in view of parity violation—the de lege mechanisms.[82]
3. It has been suggested that a low-temperature phase transition under the influence of parity violation might provide a prebiotic mechanism for enantiomer enrichment, [86–88] and if so, this would be a de lege ("necessity") selection.
4. Finally, in a nonlinear kinetic scheme, even the very small selection advantage arising from parity violation might be sufficient to provide selection of one and always the same kind of enantiomer—for example, L amino acids.[38, 89, 90]

These four basic hypotheses may appear as numerous variants. Indeed, each time some new effect for some perhaps possible mechanism in chiral selection comes up in the literature, this is quickly praised as the "solution to the problem" (sometimes with cautious remarks in very small print) in the popular science press. There was a considerable amount of speculation in relation to the early findings of the stabilization of L amino acids and D sugars by parity violation.[36–40] These results were, however, refuted by recent theory[2, 42, 50, 51, 56] and it was argued that, in any case, the calculation of transition states, precursors, or intermediates in biochemical mechanisms would be more relevant.[50, 51, 120] We think that no clear answer to the question of the origin of biochemical homochirality exists at present or is to be expected in the near future.[93] Minimal conditions for such an answer would be that 1) in each possible mechanism for a desired selection all possible control experiments for proving the opposite outcome must be carried out and 2) the precise mechanism by which the effect leads to a selection of homochirality must be theoretically understood. To our knowledge none of the numerous suggestions existing today come even close to satisfying these minimal requirements. Even the observed data are frequently suspect, as is, for instance, the case for the alleged extraterrestrial enantiomeric enrichments.[94, 95] The alleged excess of L amino acids found in meteorites is a fairly typical case with "proof" and "refutation" being repeated more than once.

The question is not definitely settled for this and related examples. With these skeptical remarks we do not imply that the fundamental question is only "philosophical" or pure speculation. On the contrary, the problem of either de lege ("necessity") or de facto ("chance") selection of homochirality is a clear scientific question with a clear answer, in principle. For instance, if some day we were able to repeat

evolution of life in the test tube, the de lege mechanism would always generate (or predominantly) one form (e.g. L amino acid life) in repeated experiments, whereas the de facto ("chance") hypothesis would predict equal probability for both forms (averaged over many separate experiments, even if each single experiment gave only one form). Also there might be observational evidence. If we were to find some day remnants of D amino acid life on Mars, this would clearly contradict the strong forms of the de lege hypotheses (the reverse would not be true, though). We even have some very limited observational evidence already. The mere fact that we observe L amino acid life today on earth excludes at least the strong form of the de lege hypothesis in favor of the D amino acid life forms. By means of a game analogy (the "world game")[96] it can be argued that if an appropriate bias of principle caused by parity violation can be proven, then *the best guess* (in a statistical sense) could be in favor of the de lege hypothesis. It would be a very weak guess, though, which might be easily overthrown by contrary observed evidence. The only thing that can be said at present is that, given the recent prediction of substantially increased energetic effects from parity violation in molecules, the chances of the de lege hypothesis being correct have improved, but they are still very close to 50%.

A remark on common misunderstandings that can be found in either camp ("chance" or "necessity") might be appropriate. The de lege (parity violation) community often expresses the belief that, because we know for certain that there is *some* preference at the molecular level that is caused by parity violation, there must "somehow" be a connection to the evolution of biomolecular homochirality at the next higher level of organization. Such an argument can be easily refuted because, at the still higher level of organization, human biosystems may choose left or right-handed traffic rules, or screws, or left or right-side partings of the hair. Both choices are in fact made clearly unrelated to the fact that all human beings are made up preferentially of L amino acids. On the other hand—and this opposes a common belief of the "de facto" camp—this kind of argument does not rule out that at the lower levels of molecular and biomolecular organization a fundamental connection to parity violation might exist. We just do not know at present.

7. Conclusion

In the conclusion of this review, we return to the three questions raised at its beginning. Clearly, these questions have been around for a while, but our recent discovery of the order of magnitude increases of parity-violating energies in chiral molecules[42] has triggered substantial recent work—both theoretical and experimental—with the objective of demonstrating the importance of parity violation. Thus, of the five existing basic hypotheses on molecular chirality identified in ref. [1] (see also ref. [93]), the fundamental hypothesis number 5 has received a special status from the recent theoretical findings.[97] Except for a still possible (but less likely) fundamental omission, quantitative theory shows that parity violation is as a rule quantitatively important, or even essential in answering the first question about the physical–chemical nature of chirality, certainly in relation to the traditional hypotheses (numbers 1 and 2[1,97]). While this result was qualitatively anticipated as early as 1966,[16] current theoretical results are distinguished by their quantitative nature. Experimental confirmation (or rejection) of this quantitative theory can be expected in the near future. It should be pointed out that one proposed type of experiment[33] would also allow for testing the remaining alternative superselection rule hypothesis[72] (no. 3[1,97]) or collisional and related "environmental" hypotheses[24, 97, 98] (no. 4 in ref. [1, 97]).

The second question on the origin of biomolecular homochirality in evolution is both subtle and complex, and a definitive answer is hardly impending.[93] Current quantitative theories of molecular parity violation[42–56] can be combined with kinetic models of evolution[12, 74, 75, 89] to provide a *starting point* for a theoretical understanding of the possible role of de lege symmetry breaking in evolution. A conclusive *answer*, which implies the exclusion (or confirmation) of alternative explanations by experiment and theory, is in our opinion only expected in the more distant future, and one should refrain from the premature claims that are all too abundant. A substantial research effort is still needed in this area. Systematic biochemical efforts on enantioselective enzymes[99] or other types of chiral amplification in polymers[115] in relation to theoretical calculation of parity violation and later—why not?—investigation by resynthesis of bacteria with opposing chirality could provide experimental routes.[100]

The third question on the role of molecular parity violation for fundamental physics leads us to further motivation for a sustained experimental and theoretical research effort in this field. A combination of accurate experiments with accurate calculations of the expected effects can be used as a testing ground for the "standard model",[102] which is really a theory which comprises the current understanding of the fundamental microscopic physics of all known matter. This has been pointed out in accounts of experiments and theories of atomic parity violation[25, 101, 116] as well as molecular parity violation.[2, 42, 43] It is a particular feature of the standard model that, while providing a complete theoretical framework, it contains parameters that can only be determined by experiment. Each time such parameters are newly determined with higher accuracy (or by providing tighter bounds on parameter ranges), some new fundamental insights arise. The determination of the mass and lifetime (2.6×10^{-25} s = 0.26 ys) of the Z boson (which led to a determination of the allowed number of fundamental-particle families) in 1983 is a "historic" example.[103] The current search for the Higgs particle and its mass in billion dollar (or euro) projects in huge accelerators is a current example.

It may be that the investigations of much lower cost on molecular parity violation may provide crucial information in the future.[33, 42, 43] For this to happen, first accurate theory and second accurate measurement are needed, for instance of $\Delta_{pv}H_0^\circ$. We think that our recent theoretical advances have essentially provided the first part of the necessary input, or at least provided a neatly paved route towards this. With the first

analyses of rotational-vibrationally resolved spectra of chiral molecules[49, 62–65] the second, experimental part for the answer will also approach its completion. In this context is should be pointed out that, for *chiral molecules*, experiments should be feasible that involve only light elements, and thus exclude the uncertainties that necessarily arise from relativistic theory and complex, poorly known nuclear structure when heavy elements are involved. Heavy elements are unfortunately a requirement in all currently feasible experiments on *atomic* parity violation.[25, 101, 117] While the statistical uncertainty in the atomic approaches has been sometimes quoted to be smaller than 1 %, the systematic experimental and theoretical uncertainties are presumably larger. A high precision in atomic experiments and calculations does not necessarily imply high accuracy.

Finally, chiral molecules could be important in even more fundamental tests of the symmetries of physics. If pairs of chiral molecules and their counterparts made of antimatter are considered,[104–108] then an experiment similar to the one proposed in ref. [33] can be devised[109, 110] that would lead to a fundamental test of CPT (charge, parity, and time reversal) symmetry[118] at a relative resolution $\Delta m/m$ or $\Delta E/E$ of about 10^{-30}, about 20 orders of magnitude better than achieved today in proton–antiproton experiments and about 10 orders of magnitude better than what is currently available (K meson or electron–positron pair experiments) or even proposed in still-hypothetical experiments on antihydrogen.[111] This would render not only the handedness of space "observable", but even the absolute direction of time and, in combination with this, the definition of what is matter versus antimatter (see ref. [93] for a review). It should be clear, however, that such an experiment is at present entirely hypothetical, although it could become a reality in the more distant future. It would relate to fundamental aspects of our understanding of the world beyond elementary particle physics and molecular physics and biology.[93, 112–114]

I am most grateful to my students and co-workers for their continuous help, insight, and stimulus. While their important contributions can be seen from the list of references, particular mention should be made of the theoretical work of Ayaz Bakasov, Robert Berger, Tae-Kyu Ha and Jürgen Stohner, the spectroscopic work of Andreas Beil, Benjamin Fehrensen, Heike Gross, Michael Hippler, Hans Hollenstein, David Luckhaus, Roberto Marquardt, Jörg Pochert, and Georg Seyfang, and finally the recent, essential, and in part still unpublished progress made by Sieghard Albert, Michael Gottselig, Achim Sieben, and Martin Willeke. Continuous technical support in our experiments came from Guido Grassi, Eduard Peyer, and Hansjörg Schmutz and secretarial help from Ruth Schüpbach. Karen Kepler-Albert carefully read and criticized the English manuscript, while Michael Gottselig worked on the German translation. I also enjoyed discussions and correspondence with numerous colleagues worldwide on the topics discussed here. Our work is financially supported by ETH Zürich (including CSCS and C4) and by the SNF.

Received: January 31, 2002 [A 517]

[1] M. Quack, *Angew. Chem.* **1989**, *101*, 588–604; *Angew. Chem. Int. Ed. Engl.* **1989**, *28*, 571–586. The second line of the abstract there is misprinted. It should read "chiral molecule". Further corrections include ref. [42] therein which is to be complemented by ref. [16] (Yamagata) of the present paper, in ref. [45] it should read correctly "Sandars" and in ref. [64] it should read "totaliter aliter" (instead of taliter aliter).

[2] A. Bakasov, T. K. Ha, M. Quack, *J. Chem. Phys.* **1998**, *109*, 7263–7285; A. Bakasov, T. K. Ha, M. Quack, *J. Chem. Phys.* **1999**, *110*, 6081.

[3] W. S. Knowles, *Angew. Chem.* **2002**, *114*, 2096–2107; *Angew. Chem. Int. Ed.* **2002**, *41*, 1998–2007; R. Noyori, *Angew. Chem.* **2002**, *114*, 2108–2123; *Angew. Chem. Int. Ed.* **2002**, *41*, 2008–2022; K. B. Sharpless, *Angew. Chem.* **2002**, *114*, 2126–2135; *Angew. Chem. Int. Ed.* **2002**, *41*, 2024–2032.

[4] K. Mislow, *Introduction to Stereochemistry*, Benjamin, New York, **1965**; V. Prelog, G. Helmchen, *Angew. Chem.* **1982**, *94*, 614–631; *Angew. Chem. Int. Ed. Engl.* **1982**, *21*, 567–583, and references therein.

[5] K. C. Nicolaou, C. N. C. Boddy, J. S. Siegel, *Angew. Chem.* **2001**, *113*, 723–726; *Angew. Chem. Int. Ed.* **2001**, *40*, 701–704.

[6] A. Togni, *Chimia* **2001**, *55*, 752–852, where the contributions from the groups of Baiker, Togni, Pregosin, Grützmacher, Carreira, Diederich, Seebach, Vasella, Meier, Jaun, Hilvert, and Morbidelli have an essential "chirality" component (as do some other contributions to some extent).

[7] L. Pasteur, *Leçons de chimie professées en 1860 par MM. Pasteur, Cahours, Wurtz, Berthelot, Sainte-Claire Devile, Barral et Dumas*, Hachette, Paris, **1861**; reprinted in *Sur la dissymétrie moléculaire* (Ed.: C. Bourgeois), Collection Epistème, Paris, **1986** (see also L. Pasteur, *Bull. Soc. Chim. Fr.* **1884**, *42*, 215). Pasteur wrote: "*Si les principes immédiats de la vie immédiate sont dissymétriques, c'est que, à leur élaboration, président des forces cosmiques dissymétriques, c'est là, suivant moi, un des liens entre la vie à la surface de la terre et le cosmos, c'est-à-dire l'ensemble des forces répandues dans l'univers.*" (English translation: "If the principles of life are chiral, then because of chiral cosmic forces at their origin; this I think, is one of the links between life on earth and the cosmos, or the totality of forces in the universe". In ref. [1] this was used as a motto for the article.

[8] J. H. van't Hoff, *La chimie dans l'espace*, Rotterdam, **1887**; reprinted in *Sur la dissymétrie moléculaire* (Ed.: C. Bourgeois), Collection Epistème, Paris, **1986**.

[9] The German original reads: "*Es gibt also zweierlei kartesische Koordinatensysteme, welche man als "Rechtssysteme" und "Linkssysteme" bezeichnet. Der Unterschied zwischen beiden ist jedem Physiker und Ingenieur geläufig. Interessant ist, dass man Rechtssysteme bzw. Linkssysteme an sich nicht geometrisch definieren kann, wohl aber die Gegensätzlichkeit beider Typen.*" A. Einstein, *Grundzüge der Relativitätstheorie*, Vieweg, Wiesbaden, **1922**, (Reprint 1984).

[10] F. Hund, *Z. Phys.* **1927**, *43*, 788–804; F. Hund, *Z. Phys.* **1927**, *43*, 805–826.

[11] G. Gamow, *Z. Phys.* **1928**, *51*, 204.

[12] R. Janoschek, *Chirality*, Springer, Berlin, **1991**, p. 18.

[13] P. Dirac, *Proc. R. Soc. London Ser. A* **1929**, *123*, 714–733.

[14] T. Lee, C. Yang, *Phys. Rev.* **1956**, *104*, 254–258.

[15] C. Wu, E. Ambler, R. Hayward, D. Hoppes, R. Hudson, *Phys. Rev.* **1957**, *105*, 1413–1415.

[16] Y. Yamagata, *J. Theor. Biol.* **1966**, 495–498.

[17] J. Monod, *Le Hasard et la Necessité – Essai sur la philosophie naturelle de la biologie moderne*, Editions du Seuil, Paris, **1970**.

[18] M. Quack, unpublished results, also an examination problem for the ETH class of 2000.

[19] D. Rein, *J. Mol. Evol.* **1974**, *4*, 15–22.

[20] V. Letokhov, *Phys. Lett. A* **1975**, *53*, 275–276.

[21] B. Y. Zel'dovich, D. Saakyan, I. Sobel'man, *JETP Lett.* **1977**, *25*, 94.

[22] R. Harris, L. Stodolsky, *Phys. Lett.* **1978**, *78*B, 313–317.

[23] R. Harris, L. Stodolsky, *J. Chem. Phys.* **1980**, *73*, 3862.

[24] R. Harris, L. Stodolsky, *J. Chem. Phys.* **1981**, *74*, 2145.

[25] M. A. Bouchiat, C. Bouchiat, *J. Phys.* **1974**, *35*, 899–927; M. A. Bouchiat, C. Bouchiat, *Rep. Prog. Phys.* **1997**, *60*, 1351–1396.

[26] G. Herzberg, *Molecular Spectra and Molecular Structure*, *Vol. II*, Van Nostrand, Princeton, NJ, **1945**.

[27] M. Quack, M. Stockburger, *J. Mol. Spectrosc.* **1972**, *43*, 87 – 116.
[28] B. Fehrensen, M. Hippler, M. Quack, *Chem. Phys. Lett.* **1998**, *298*, 320 – 328.
[29] B. Fehrensen, D. Luckhaus, M. Quack, *Z. Phys. Chem.* **1999**, *209*, 1 – 19.
[30] E. Heilbronner, H. H. Günthard, R. Gerdil, *Helv. Chim. Acta* **1956**, *39*, 1171 – 1181; H. Zimmermann, *Angew. Chem.* **1964**, *76*, 1 – 9; *Angew. Chem. Int. Ed. Engl.* **1964**, *3*, 157 – 164; J. Brickmann, H. Zimmermann, *Z. Naturforsch. A* **1968**, *23*, 11 – 18; see also the recent general review: V. A. Benderskii, D. E. Makarov, C. A. Wight, *Adv. Chem. Phys.* **1994**, *87*, 1 – 385.
[31] O. Kompanets, A. Kukudzhanov, V. Letokhov, L. Gervits, *Opt. Commun.* **1976**, *19*, 414 – 416.
[32] E. Arimondo, S. Glorieux, T. Oka, *Opt. Commun.* **1977**, *23*, 369.
[33] M. Quack, *Chem. Phys. Lett.* **1986**, *132*, 147 – 153.
[34] D. Rein, R. Hegström, P. Sandars, *Phys. Lett. A* **1979**, *71*, 499.
[35] R. Hegström, D. Rein, P. Sandars, *J. Chem. Phys.* **1980**, *73*, 2329 – 2341.
[36] S. F. Mason, G. E. Tranter, *Mol. Phys.* **1984**, *53*, 1091 – 1111, and references therein.
[37] G. Tranter, A. McDermott, *Chem. Phys. Lett.* **1986**, *130*, 120, and references therein.
[38] S. F. Mason, *Chemical Evolution: Origins of the Elements, Molecules and Living Systems*, Clarendon, Oxford, **1991**, and references therein.
[39] S. F. Mason, *Nature* **1984**, *311*, 19 – 23.
[40] G. Tranter, *Nachr. Chem. Tech. Lab.* **1986**, *34*, 866.
[41] L. Wiesenfeld, *Mol. Phys.* **1988**, *64*, 739.
[42] A. Bakasov, T. K. Ha, M. Quack in *Proceedings of the 4th Trieste Conference (1995), Chemical Evolution: Physics of the Origin and Evolution of Life* (Eds.: J. Chela-Flores, F. Raulin), Kluwer, Dordrecht, **1996**, pp. 287 – 296.
[43] A. Bakasov, M. Quack, *Chem. Phys. Lett.* **1999**, *303*, 547 – 557 (see also A. Bakasov, T. K. Ha, M. Quack, *Chimia* **1997**, *51*, 559).
[44] R. Berger, M. Quack, *J. Chem. Phys.* **2000**, *112*, 3148 – 3158.
[45] M. Quack, J. Stohner, *Phys. Rev. Lett.* **2000**, *84*, 3807 – 3810.
[46] M. Quack, J. Stohner, *Z. Phys. Chem.* **2000**, *214*, 675 – 703; M. Quack, J. Stohner, unpublished results; J. Stohner, A. Beil, H. Hollenstein, O. Monti, M. Quack, *Proc. 37th IUPAC congress*, Berlin **1999**, p. 525 (the history of the calculations is told in ref. [59]).
[47] R. Berger, M. Gottselig, M. Quack, M. Willeke, *Angew. Chem.* **2001**, *113*, 4342 – 4345; *Angew. Chem. Int. Ed.* **2001**, *40*, 4195 – 4198.
[48] M. Gottselig, D. Luckhaus, M. Quack, J. Stohner, M. Willeke, *Helv. Chim. Acta* **2001**, *84*, 1846 – 1861.
[49] R. Berger, M. Quack, J. Stohner, *Angew. Chem.* **2001**, *113*, 1716 – 1719; *Angew. Chem. Int. Ed.* **2001**, *40*, 1667 – 1670; H. Hollenstein, D. Luckhaus, J. Pochert, M. Quack, G. Seyfang, *Angew. Chem.* **1997**, *109*, 136 – 140; *Angew. Chem. Int. Ed.* **1997**, *36*, 140 – 143.
[50] R. Berger, M. Quack, *ChemPhysChem* **2000**, *1*, 57 – 60.
[51] R. Berger, M. Quack, G. S. Tschumper, *Helv. Chim. Acta* **2000**, *83*, 1919 – 1950.
[52] P. Lazzeretti, R. Zanasi, *Chem. Phys. Lett.* **1997**, *279*, 349 – 354; R. Zanasi, P. Lazzeretti, *Chem. Phys. Lett.* **1998**, *286*, 240 – 242.
[53] F. Faglioni, P. Lazzeretti, *Phys. Rev. E* **2002**, *65*, 011904-1 – 011904-11.
[54] J. K. Laerdahl, P. Schwerdtfeger, *Phys. Rev. A* **1999**, *60*, 4439 – 4453.
[55] J. K. Laerdahl, P. Schwerdtfeger, H. M. Quiney, *Phys. Rev. Lett.* **2000**, *84*, 3811 – 3814.
[56] J. K. Laerdahl, R. Wesendrup, P. Schwerdtfeger, *ChemPhysChem* **2000**, *1*, 60 – 62.
[57] A. C. Hennum, T. Helgaker, W. Klopper, *Chem. Phys. Lett.* **2002**, *354*, 274 – 282.
[58] A. Szabo-Nagy, L. Keszthelyi, *Proc. Natl. Acad. Sci. USA* **1999**, *96*, 4252 – 4255; L. Keszthelyi, *J. Biol. Phys.* **1994**, *20*, 241 – 245.
[59] M. Quack, J. Stohner, *Chirality* **2001**, *13*, 745 – 753, and references therein.
[60] A. L. Barra, J. B. Robert, L. Wiesenfeld, *Phys. Lett. A* **1986**, *115*, 443 – 447.
[61] J. B. Robert, A. L. Barra, *Chirality* **2001**, *13*, 699 – 702.
[62] A. Bauder, A. Beil, D. Luckhaus, F. Müller, M. Quack, *J. Chem. Phys.* **1997**, *106*, 7558 – 7570.
[63] A. Beil, D. Luckhaus, R. Marquardt, M. Quack, *Faraday Discuss.* **1994**, 49 – 76.
[64] C. Daussy, Dissertation, Université Paris 13, **1999**.
[65] C. Daussy, T. Marrel, A. Amy-Klein, C. T. Nguyen, C. J. Bordé, C. Chardonnet, *Phys. Rev. Lett.* **1999**, *83*, 1554 – 1557. This approach requires separation of enantiomers; see J. Crassons, A. Collet, Enantiomer **2000**, *5*, 429.
[66] A. S. Lahamer, S. M. Mahurin, R. N. Compton, D. House, J. K. Laerdahl, M. Lein, P. Schwerdtfeger, *Phys. Rev. Lett.* **2000**, *85*, 4470 – 4473.
[67] M. J. M. Pepper, I. Shavitt, P. von R. Schleyer, M. N. Glukhovtsev, R. Janoschek, M. Quack, *J. Comput. Chem.* **1995**, *16*, 207 – 225.
[68] M. Quack, *Mol. Phys.* **1977**, *34*, 477 – 504; M. Quack, *Faraday Discuss.* **1995**, *102*, 90 – 93.
[69] D. Uy, M. Cordonnier, T. Oka, *Phys. Rev. Lett.* **1997**, *78*, 3844 – 3847.
[70] M. Quack, *Faraday Discuss.* **1994**, *99*, 98 – 99.
[71] M. Quack, *Chimia* **2001**, *55*, 753 – 758.
[72] P. Pfeiffer in *Proceedings of Two Workshops, Bielefeld, June 1980* (Ed.: J. Hinze), Plenum, New York, NY, **1983**, pp. 315 – 326; H. Primas, *Chemistry, Quantum Mechanics and Reductionism*, Springer, Berlin, **1981**; see also A. Ammann, *J. Math. Chem.* **1991**, *6*, 1 – 15.
[73] M. Quack, *Faraday Discuss.* **1994**, 389 – 395; R. Berger, *PCCP* **2002**, in press.
[74] M. Eigen, *Naturwissenschaften* **1971**, *58*, 465 – 523.
[75] F. C. Frank, *Biochim. Biophys. Acta* **1953**, *11*, 459 – 463.
[76] M. Bolli, R. Micura, A. Eschenmoser, *Chem. Biol.* **1997**, *4*, 309 – 320.
[77] M. Calvin, *Chemical Evolution*, Oxford University Press, Oxford, **1969**.
[78] G. Nicolis, I. Prigogine, *Proc. Natl. Acad. Sci. USA* **1981**, *78*, 659 – 663.
[79] W. A. Bonner, *Origins Life Evol. Biosphere* **1991**, *21*, 59 – 111; P. R. Kavasmaneck, W. A. Bonner, *J. Am. Chem. Soc.* **1977**, *99*, 44 – 50.
[80] H. Kuhn, J. Waser in *Biophysics* (Eds.: W. Hoppe, W. Lohmann, H. Markl, H. Ziegler), Springer, Berlin, **1983**.
[81] W. Bonner, *Top. Stereochem.* **1988**, *18*, 1 – 96.
[82] F. Vester, T. L. V. Ulbricht, H. Krauch, *Naturwissenschaften* **1959**, *46*, 68, see also O. Merwitz, *Radiat. Environ. Biophys.* **1976**, *13*, 63 – 69.
[83] P. Kleindienst, G. H. Wagnière, *Chem. Phys. Lett.* **1998**, *288*, 89 – 97.
[84] G. Rikken, E. Raupach, *Nature* **2000**, *405*, 932 – 935; L. D. Barron, *Nature* **2000**, *405*, 895 – 896.
[85] V. A. Avetisov, V. I. Goldanskii, V. V. Kuz'min, *Phys. Today* **1991**, *44*, 33 – 45.
[86] A. Salam, *J. Mol. Evol.* **1991**, *33*, 105 – 113.
[87] A. Salam in *Conceptual Tools for Understanding Nature. Proc. 2nd Intl. Symp. of Science and Epistemology Seminar*, Trieste 1993 (Eds.: G. Costa, G. Calucci, M. Giorgi), World Scientific, Singapore, **1995**.
[88] J. Chela-Flores, *Chirality* **1991**, *3*, 389.
[89] D. K. Kondepudi, G. W. Nelson, *Phys. Lett. A* **1984**, *106*, 203 – 206, D. K. Kondepudi, G. W. Nelson, *Phys. A* **1984**, *125*, 465 – 496; D. K. Kondepudi, G. W. Nelson, *Nature* **1985**, *314*, 438 – 441.
[90] A. J. MacDermott, G. E. Tranter, *Chem. Phys. Lett.* **1989**, *163*, 1 – 4.
[91] R. N. Zare, W. Bonner, P. Frank in *Chemistry for the 21st century* (Eds.: E. Keinan, I. Schechter), Wiley-VCH, Weinheim, **2000**, chap. 11, pp. 175 – 208.
[92] H. Buschmann, R. Thede, D. Heller, *Angew. Chem.* **2000**, *112*, 4197 – 4200; *Angew. Chem. Int. Ed.* **2000**, *39*, 4033 – 4036; see also P. Cintas, *Angew. Chem.* **2002**, *114*, 1187 – 1193; *Angew. Chem. Int. Ed.* **2002**, *41*, 1139 – 1145.
[93] M. Quack, *Nova Acta Leopold.* **1999**, *81*, 137 – 173.
[94] S. F. Mason, *Origins Life Evol. Biosphere* **2000**, *30*, 435 – 437.
[95] M. H. Engel, S. A. Macko, *Nature* **1997**, *389*, 265 – 268.
[96] M. Quack, *J. Mol. Struct.* **1995**, *347*, 245 – 266. The "world game" consists of a game leader who draws tetrahedral dice arbitrarily from two boxes, a) the "de facto" box, where each die has four different faces (denoted *S*, *R*, *S**, *R**) and b) the "de lege" box (four types of die, each one having only one letter on all four faces, say *S*, or else *R*, *S**, *R**). The players are allowed to make just one throw with the selected tetrahedral die and observe the one face of the tetrahedron showing towards them. Then the players, who may be called also the "scientists", must guess from which box the die has been drawn, that is, what are the "rules of the game" (de facto or de lege, there will be a reward for the right guess of the rules of the game, as there might be in science). Now, if the "de lege" box has equal numbers of each die ("*S*", "*R*", "*S**" and "*R**") and if the game leader is a statistically honest person, the statistics are fairly simple and the player does not

have much of a winning strategy against other players. If one player knows, however, that the de lege box contains a bias towards one type of die (say 40% *S* and 20% each of the others), he will win with the strategy of guessing "de lege" if he sees an "*S*" in the single throw and "de facto" if he sees any of the other faces. In fact, however small the known bias is, in the long run he will always win over those who don't know the bias and that is, why it is important to know the bias, also in the analogous physical situation. In our world we observe living matter to be made of *S* amino acids, and of ordinary matter, not of antimatter, where in the general notation *S* and *R* indicate the type of enantiomer and the star indicates antimatter as opposed to ordinary matter (without star). One obvious conclusion concerning the physical situation in biochemical evolution can be drawn from the single observation of an *S* amino acid world: The bias cannot be 100% in favor of any combination of *R**, *R*, *S**.

[97] The five competing fundamental hypotheses of chirality that were identified by the time of writing the review[1] are: 1. the classical hypothesis of macroscopic molecular models (basically van't Hoff's description of spontaneous symmetry breaking); 2. the quantum-mechanical hypothesis of de facto symmetry breaking with parity conservation, originally from Hund; 3. the superselection-role hypothesis of Pfeiffer and Primas with spontaneous symmetry breaking caused by the influence of the radiation field; 4. the "environmental" or collison hypothesis of Simonius, Harris, and Stodolsky that induces de facto symmetry breaking in chiral molecules because of interactions with an external medium; 5. the hypothesis of de lege symmetry breaking in chiral molecules because of parity violation. A detailed discussion of these hypotheses can be found in sections 2.1 to 2.5 of ref. [1], where it is also shown how one might distinguish experimentally which hypothesis might be applicable, mostly by using the scheme in Lit. [33].

[98] M. Simonius, *Phys. Rev. Lett.* **1978**, *40*, 980 – 983.

[99] M. T. Reetz, K. E. Jaeger, *Chem. Eur. J.* **2000**, *6*, 407 – 412.

[100] M. Quack, *Philos. Trans. R. Soc. London Ser. A* **1990**, *332*, 203 – 220.

[101] S. C. Bennett, C. E. Wieman, *Phys. Rev. Lett.* **1999**, *82*, 2484 – 2487.

[102] L. Hoddeson, L. Brown, M. Riordan, M. Dresden, *The Rise of the Standard Model*, Cambridge University Press, Cambridge, **1999**.

[103] H. Schopper, *Nova Acta Leopold.* **1999**, *81*, 109 – 134.

[104] L. D. Barron, *Chem. Phys. Lett.* **1981**, *79*, 392 – 394.

[105] L. D. Barron in *New Developments in Molecular Chirality* (Ed.: P. G. Mezey), Kluwer, Dordrecht, **1991**, p. 1.

[106] P. Jungwirth, L. Skala, R. Zahradnik, *Chem. Phys. Lett.* **1989**, *161*, 502 – 506.

[107] M. Quack, *J. Mol. Struct.* **1993**, *292*, 171 – 195.

[108] L. D. Barron, *Chem. Phys. Lett.* **1994**, *221*, 311 – 316.

[109] M. Quack, *Chem. Phys. Lett.* **1994**, *231*, 421 – 428.

[110] M. Quack in *Femtosecond chemistry, Proc. Berlin Conf. Femtosecond Chemistry, Berlin (March 1993)* (Eds.: J. Manz, L. Woeste), VCH, Weinheim, **1994**, chap. 27, pp. 781 – 818.

[111] C. Zimmermann, T. W. Hänsch, *Phys. Bl.* **1993**, *49*, 193 – 196.

[112] I. Kant in *Prolegomena zu einer jeden künftigen Metaphysik die als Wissenschaft wird auftreten können*, (Ed. K. Pollock), Felix Meiner Verlag, Hamburg, **2001**, pp. 44 – 46.

[113] E. Noether, Invariante Variationsprobleme, *Nachr. Akad. Wiss. Goettingen Math.-Phys. Kl. 2* **1918**, 235 – 257.

[114] K. Mainzer, *Symmetrien der Natur, ein Handbuch zur Natur- und Wissenschaftsphilosophie*, de Gruyter, Berlin, **1988**.

[115] M. M. Green, J. W. Park, T. Sato, A. Teramoto, S. Lifson, R. L. B. Selinger, J. V. Selinger, *Angew. Chem.* **1999**, *111*, 3328 – 3345; *Angew. Chem. Int. Ed.* **1999**, *38*, 3138 – 3154.

[116] J. L. Rosner, *Phys. Rev. D* **2002**, *65*, 073026 – 1 – 073026 – 5.

[117] M. G. Kozlov, G. S. Porsev, I. I.Tupitsyu, *Phys. Rev. Lett.* **2002**, *86*, 3260 – 3263.

[118] CPT symmetry concerns the symmetry under the simultaneous change $x(-x)\,y(-y)\,z(-z)$ (P = parity), $t_z(-t)$ (T = time) and change from particle to antiparticle (C for charge conjugation). This CPT symmetry was discussed as a general symmetry about 50 years ago by Schwinger, Lueders, and Pauli and since that time has been a fundamental feature of theories in physics(the standard model, but also other fundamental approaches). Violation of CPT symmetry would result in fundamental revisions of our current theories in physics. Simple consequences of CPT symmetry are the exactly equal masses of electron and positron or proton and antiproton or of *S* enantiomers and *R** enantiomers of antimatter (see ref. [93] for further discussion).

[119] M. Gottselig, M. Quack, *Chimia* **2002**, *56*, 378 and unpublished results.

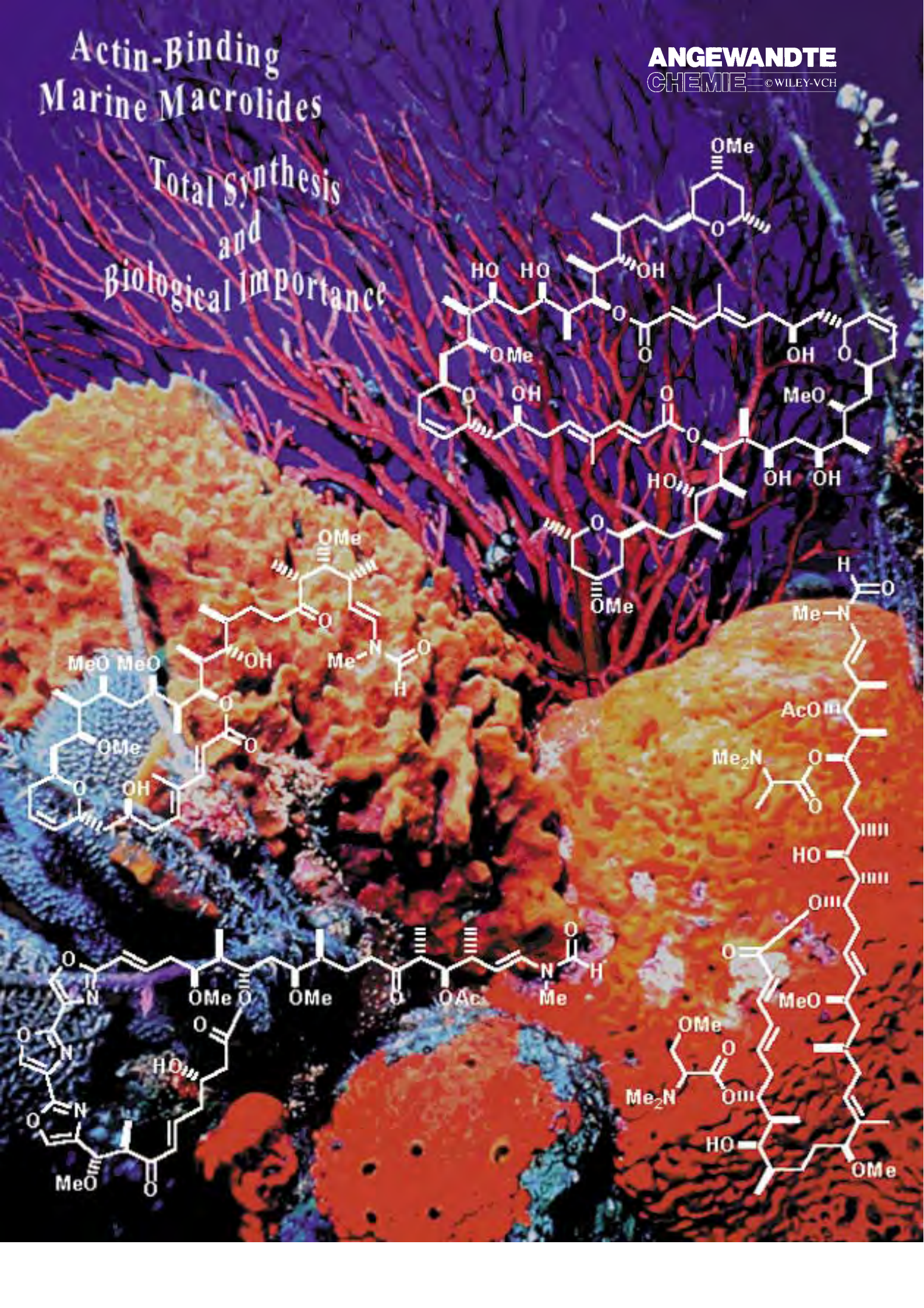
[120] T. Kitayama, T. Watanabe, O. Takahashi, K. Morihashi, O. Kikuchi, *J. Mol. Struct. (Theochem)* **2002**, *584*, 89 – 94.

[121] M. Quack, J. Stohner, *Chimia* **2002**, *56*, 381, and unpublished results.

ANGEWANDTE
CHEMIE
©WILEY-VCH

Actin-Binding Marine Macrolides

Total Synthesis and Biological Importance



Actin-Binding Marine Macrolides: Total Synthesis and Biological Importance

Kap-Sun Yeung* and Ian Paterson

Marine organisms produce a fascinating range of structurally diverse secondary metabolites, which often possess unusual and sometimes unexpected biological activities. This structural diversity makes these marine natural products excellent molecular probes for the investigation of biochemical pathways. Recently, a number of novel and stereochemically complex macrolides, having a large macrolactone (22- to 44-membered) ring, that interact with the actin cycloskeleton have been isolated from different marine sources. Actin, like tubulin, is a major component of the cytoskeleton and has important cellular functions. Although the details of these interactions are still under investigation, these marine macrolides are becoming increasingly important as novel molecular probes to help elucidate the cellular functions of actin. Owing to their potent antitumor activities, these compounds, for example the aplyronines, also have potential for preclinical development in cancer chemotherapy. Their appealing molecular structures, with an abundance of stereochemistry, and biological significance, coupled with the extremely limited availability from the marine sources, have stimulated enormous interest in the synthesis of these compounds. This review summarizes the biological properties of these unusual marine natural products and features the recently completed total syntheses of swinholide A, scytophycin C, aplyronine A, mycalolide A—all of these being potent cytotoxic agents that target actin—and a diastereoisomer of ulapualide A. Rather than detailing each individual step of these multistep total syntheses, the different synthetic strategies, key reactions, and methods adopted for controlling the stereochemistry are compared.

Keywords: actin · antitumor agents · macrolides · natural products · total synthesis

1. Introduction

1.1. The Actin Cytoskeleton

Actin is one of the two major components of the cytoskeleton in eukaryotic cells.[1] The other major component, tubulin, is more familiar to the chemistry community, primarily due to the success of paclitaxel in the treatment of cancer[2] and the subsequent discovery of a number of other natural products (the epothilones, discodermolide, laulimalide, the eleutherobins, and sarcodictyins) that share paclitaxel's microtubule-stabilizing properties.[3] The actin cytoskeleton plays a critical role in the determination of cell shape, and in a variety of cellular processes, including cell motility, division, adhesion, and intracellular transportation. Actin also interacts with tubulin, although the two cytoskeleton systems more often operate independently. Very recently, an actin-dependent cell cycle checkpoint that ensures the proper orientation of microtubule spindles during metaphase has been uncovered by Gachet and Hyams et al.[4] Furthermore, certain bacterial and viral (e.g. HIV) pathogens have been found to exploit the actin cytoskeleton during their lifecycle of infection.[5] As a consequence, the implications of the actin cytoskeleton and the release of actin filaments into extracellular space in numerous disease states are now being recognized.[6]

In cells, actin structures are assembled and disassembled constantly in a reversible process. The dynamic polymerization/depolymerization equilibrium between monomeric soluble globular actin (G-actin; about 43 kDa) and helical filamentous actin (F-actin), and the organization of the three-dimensional architecture of actin filaments in response to intracellular and extracellular stimulations is regulated and performed by a panoply of actin-binding proteins[7] (e.g. profilin, cofilin, gelsolin, filamin, actinin and Arp2/3 complex) (Figure 1). These proteins act through a number of mecha-

[*] Dr. K.-S. Yeung,[+] Prof. I. Paterson
University Chemical Laboratory
Lensfield Road, Cambridge, CB2 1EW (UK)
[+] Current address:
Bristol-Myers Squibb
Pharmaceutical Research Institute
5 Research Parkway, P.O. Box 5100
Wallingford, CT 06492 (USA)
Fax: (+1) 203-677-7072
E-mail: kapsun.yeung@bms.com

 © 2002 WILEY-VCH Verlag GmbH & Co. KGaA, Weinheim 1433-7851/02/4124-4633 $ 20.00+.50/0

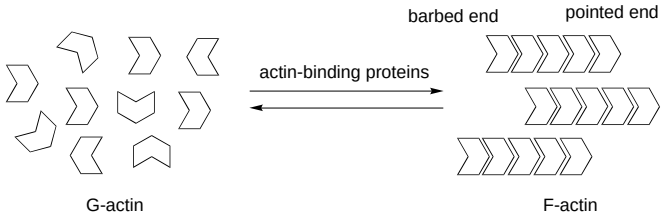


Figure 1. A simplified schematic representation of the dynamic equilibrium between G-actin and F-actin controlled by actin-binding proteins or protein complexes through a number of mechanisms. Novel actin-binding marine macrolides interfere with the equilibrium using similar mechanisms.

nisms, including the sequestering of G-actin, severing of F-actin, control of nucleation, and capping of the barbed or pointed ends of F-actin.[8] G-actin itself is an ATPase and this activity affects the polymerization kinetics. The ATP- and ADP-bound actin monomers dissociate from actin filaments at different rates, and are recognized by different sets of actin-binding proteins. Genetic approaches are often used to study the highly complex and dynamic actin cytoskeleton and its associated cellular functions. However, new and versatile molecular probe agents[9] are becoming increasingly valuable in advancing the understanding of actin organization and by unveiling important cellular functions of actin.

The fungal secondary metabolites, cytochalasins (e.g. cytochalasin B (**1**) and cytochalasin D (**2**); Figure 2), are the earliest agents that were widely adopted as molecular probes to study the actin cytoskeleton.[10] However, these agents exhibit nonspecific modes of actions, often complicating experiments performed with them. Latrunculin A (**3**) and

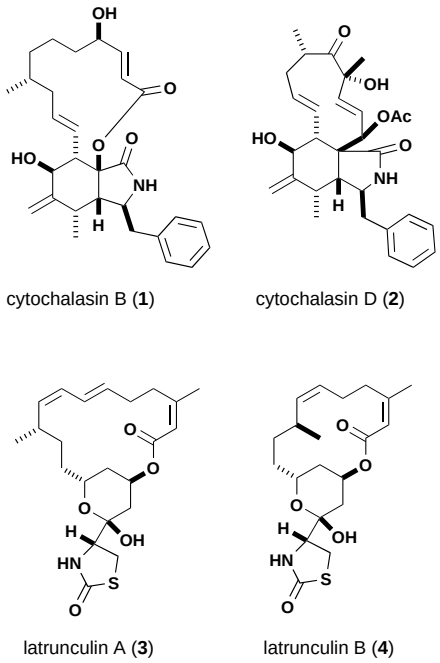


Figure 2. Structures of cytochalasin B (**1**), cytochalasin D (**2**), latrunculin A (**3**), and latrunculin B (**4**).

Dr. Kap-Sun Yeung was born in Fujian, China. His fascination with organic synthesis grew out of research conducted with Professor Henry N. C. Wong at The Chinese University of Hong Kong, from which he received his B.Sc. degree in Chemistry in 1990 and then worked as a research assistant with Professor Chi-Ming Che at The University of Hong Kong. In 1991, he was awarded a Croucher Scholarship to study at Cambridge University, where he worked on the total synthesis of swinholide A and scytophycin C under the guidance of Professor Ian Paterson. Following a rewarding and enjoyable three-year period, he obtained his PhD. and then spent a postdoctoral period with Professor Chi-Huey Wong at The Scripps Research Institute. In 1996, he started research in drug discovery at Bristol-Myers Squibb in the United States. Dr. Yeung has broad research interests in synthetic organic chemistry and drug design.


K.-S. Yeung


I. Paterson

Professor Ian Paterson was born in Dundee, Scotland. He received his B.Sc. degree in Chemistry from St. Andrews University. In 1979, he obtained his PhD from Cambridge University, working with Professor Ian Fleming on the development of new synthetic methods using allylsilanes and silyl enol ethers. After spending a postdoctoral year with Professor Gilbert Stork at Columbia University, working on the total synthesis of erythromycin A, he joined the faculty at University College London. In 1983, he moved back to Cambridge University, where he is now Professor of Organic Chemistry and a Professorial Fellow of Jesus College. His research interests are centered on the design and development of new synthetic methods for the control of stereochemistry and their application to the total synthesis of a range of biologically active compounds. He has developed novel strategies and general methods for the asymmetric synthesis of polyol building blocks, particularly by using substrate- and reagent-controlled aldol reactions, which facilitate the practical synthesis of structurally complex, polyketide natural products. Within his group, this has enabled the total synthesis of rare anticancer agents, including spongistatin 1 (altohyrtin A), swinholide A, and discodermolide, as well as antibiotics, such as concanamycin F and oleandolide.

latrunculin B (**4**) were the first marine macrolides identified to have well-defined actin-binding properties.[11] These 2-thiazolidinone-containing macrocycles form a 1:1 complex with G-actin, inhibiting its polymerization. They also induce F-actin depolymerization. Latrunculin B (**4**) was used in the seminal work of Gachet and Hyams et al.[4] that established the very important and previously unknown role of the actin cytoskeleton in spindle orientation.

1.2. Actin-Binding Marine Macrolides

From the mid-1990s, a number of structurally complex and closely related macrolides have been identified as novel actin-binding molecules (Figure 3–5). These include the swinholides (isolated from the marine sponge *Theonella swinhoei*),[12] scytophycins (isolated from blue-green alga (cyanobacteria) *Scytonema pseudohofmanni*),[13] aplyronines (isolated from the sea hare *Aplysia kurodai*),[14] sphinxolides/reidispongiolides (first isolated from an unidentified Pacific nudibranch, then from the marine sponges *Neosiphonia superstes* and *Reidispongia coreulea*);[15] and a series of trisoxazole-containing macrolides that include the mycalolides (isolated from marine sponges of the genus *Mycale* and the hard coral *Tubastrea faulkneri*),[16] and the ulapualides/kabiramides/halichondramides (isolated from egg masses of the marine nudibranch *Hexabranchus sanguineas* and the sponge *Halichondria sp.*).[17]

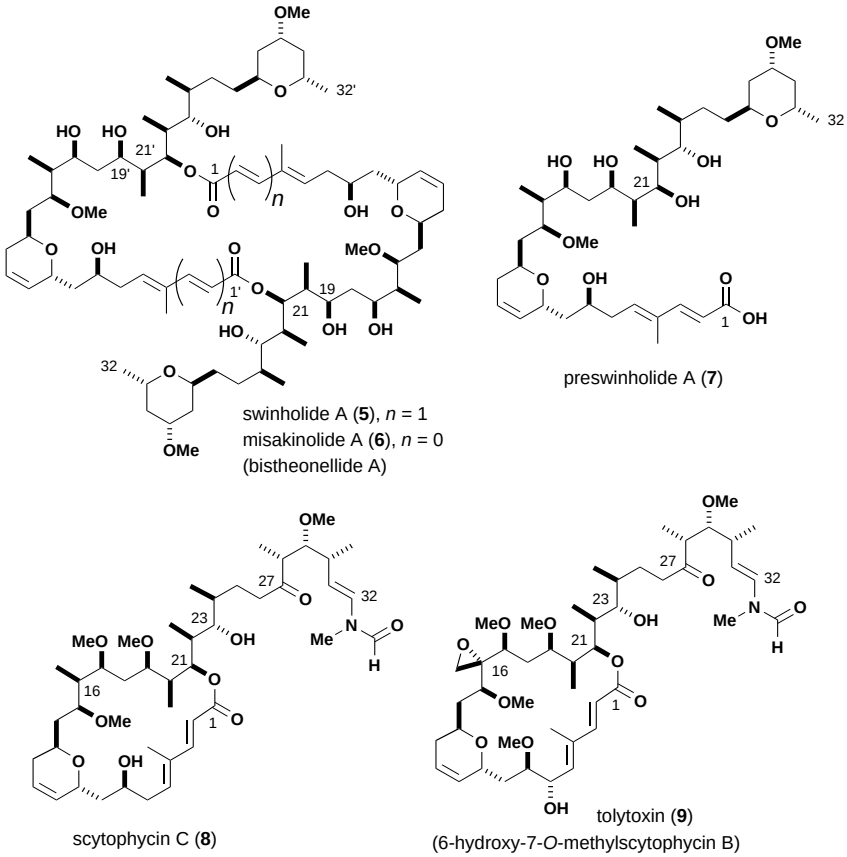


Figure 3. Structures of swinholide A (**5**), misakinolide A (**6**), preswinholide A (**7**), scytophycin C (**8**), and tolytoxin (**9**).

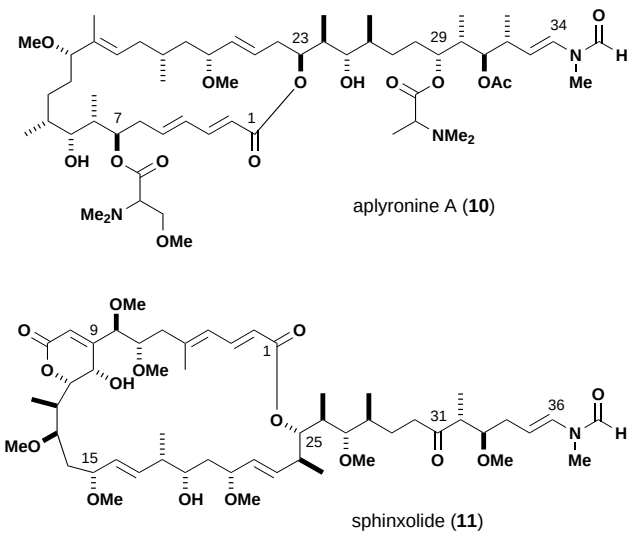


Figure 4. Structures of aplyronine A (**10**) and sphinxolide (**11**). The configurational assignment has not been rigorously established for the sphinxolides.

The structural similarity among these macrolides obtained from different marine organisms is striking (the scytophycins are the only members of this class of macrolides that were isolated from a terrestrial cyanobacteria source), and suggests a genetic link indicative of associated microorganisms as the true origin of these compounds, as demonstrated by swinholide A (**5**, Figure 3) being produced by symbiotic unicellular heterotrophic bacteria.[18] In particular, the full stereostructure of scytophycin C (**8**) spanning from C_1 to C_{26} is identical to that of swinholide A (**5**). The side chain structures of scytophycin C (**8**), aplyronine A (**10**, Figure 4), sphinxolide (**11**), mycalolide A (**12**, Figure 5), and ulapualide A (**13**) are remarkably similar, and all have an *N*-methylvinylformamide group at the terminus. Notably, the stereostructures of the C21–C32 side chain of scytophycin C (**8**) and the C23–C34 side chain of aplyronine A (**10**) are identical.

These macrolides exhibit impressive cytotoxic activities against a range of human cancer cell lines. Swinholide A (**5**),[12g] the scytophycins,[13b,c] sphinxolide (**11**),[15a] and the ulapualides[17a] have all been reported to show potent cytotoxicity against L1210 and/or KB cells with IC_{50} values ranging from $ng\,mL^{-1}$ to $pg\,mL^{-1}$. The mycalolides are cytotoxic against B-16 melanoma cells with IC_{50} values of 0.5–1.0 $ng\,mL^{-1}$.[16a] Aplyronine A (**10**) has been reported to show exceedingly potent antitumor activities in vivo against P388 leukemia, colon 26 carcinoma, Lewis lung carcinoma, and B16 melanoma with a treatment to control (T/C) ratio in the range of 200–550%, and hence has potential as a clinical candidate.[14a] Importantly, the scytophycins and sphinxolides have been shown to circumvent multidrug resistance

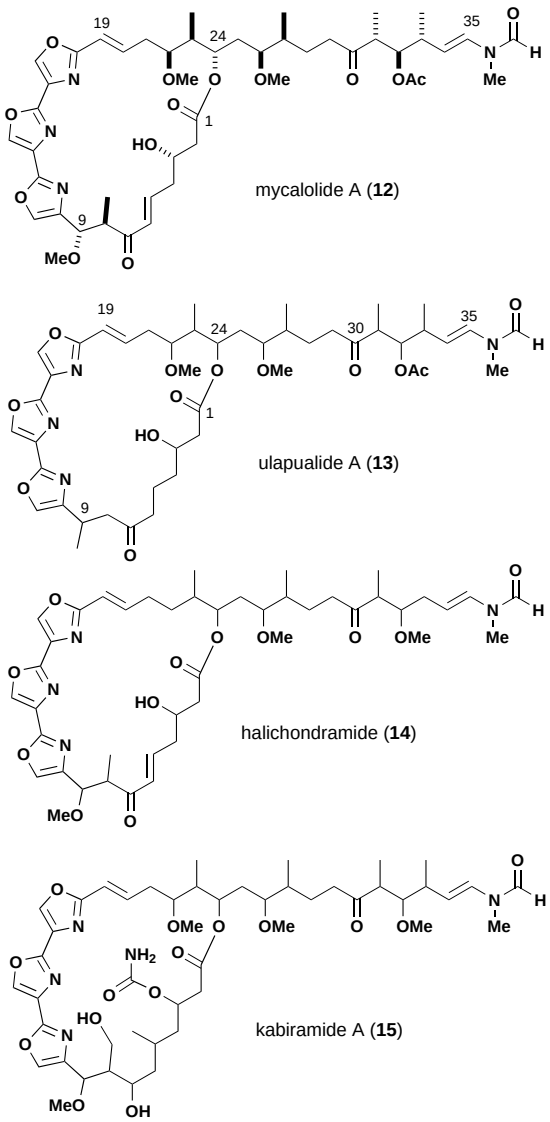


Figure 5. Structures of mycalolide A (**12**), ulapualide A (**13**), halichondramide (**14**), and kabiramide A (**15**).

mediated by the overexpression of either P-glycoprotein or multidrug resistance associated protein.[19]

The actin-binding activities of these macrolides and related natural products have been summarized recently by Spector et al.[9a] The scytophycins were the first of these macrolides to be identified as having effects on the actin cytoskeleton.[19a, 20] They inhibited G-actin polymerization and induced the depolymerization of F-actins, and were 100- to 1000-fold more potent than cytochalasin B (**1**).

Swinholide A (**5**) and misakinolide A (**6**; bistheonellide A, Figure 3) are readily cell permeable and exhibit effects on the actin cytoskeleton at concentrations of 10 to 50 nM in cell cultures.[21] In vitro, swinholide A inhibits the polymerization by sequestering G-actin with one macrolide molecule binding to two actin monomers (1:2 complex). It also catalyzes actin filament depolymerization by a severing mechanism. The two macrolide-bound G-actin monomers are then prevented from participating in actin filament elongation or nucleation. Misakinolide A has similar effects on G-actin and also binds in a 1:2 ratio. However, it does not sever F-actin. Instead, the misakinolide–actin dimer complex caps the barbed ends of the actin filaments and inhibits filament elongation.[22] These distinctly different effects on actin are especially intriguing as misakinolide A (**6**) is structurally very similar to swinholide A (**5**), lacking only the C2–C3 and C2′-C3′ double bonds and thus having a somewhat smaller 40-membered ring. This might conceivably induce a change in the orientation of the side chains relative to each other.

Aplyronine A (**10**) and the mycalolides also inhibit polymerization by sequestering G-actin and forming a 1:1 complex. They also depolymerize F-actin by a severing mechanism.[23, 24] Furthermore, the mycalolides inhibit actin-activated myosin Mg^{2+}-ATPase activity. However, the mycalolides are not specific actin binders, and it has been demonstrated that the C7 α,β-unsaturated ketone acts as a Michael acceptor, enabling the formation of covalent adducts with other cellular proteins. Recently, a C5 glutathione adduct of mycalolide B has been isolated from *Mycale sp.*[24c] In contrast to some of the actin-binding proteins, these macrolides do not promote nucleation nor accelerate the rate of polymerizaton. Preliminary studies also suggest that the kabiramides (e.g. **15**, Figure 5) have similar G-actin sequestering properties, but unlike the mycalolides, their binding to actin is highly specific.[24c] The sphinxolides (e.g. **11**, Figure 4) were reported to inhibit actin polymerization and actin-activated myosin Mg^{2+}-ATPase activity.[19b] However, to deconvolute their mechanism of action, further studies are needed.

As indicated in Figure 3–5, these macrolides all share similar or even identical side chains, but exhibit significant structural diversity in their macrocyclic rings, including ring size. Furthermore, the C_2-symmetric macrodiolides swinholide A and misakinolide A bind to actin in a 1:2 ratio, while aplyronine A and the mycalolides bind to actin in a 1:1 ratio, suggesting that these molecules bind to actin through their side chains.

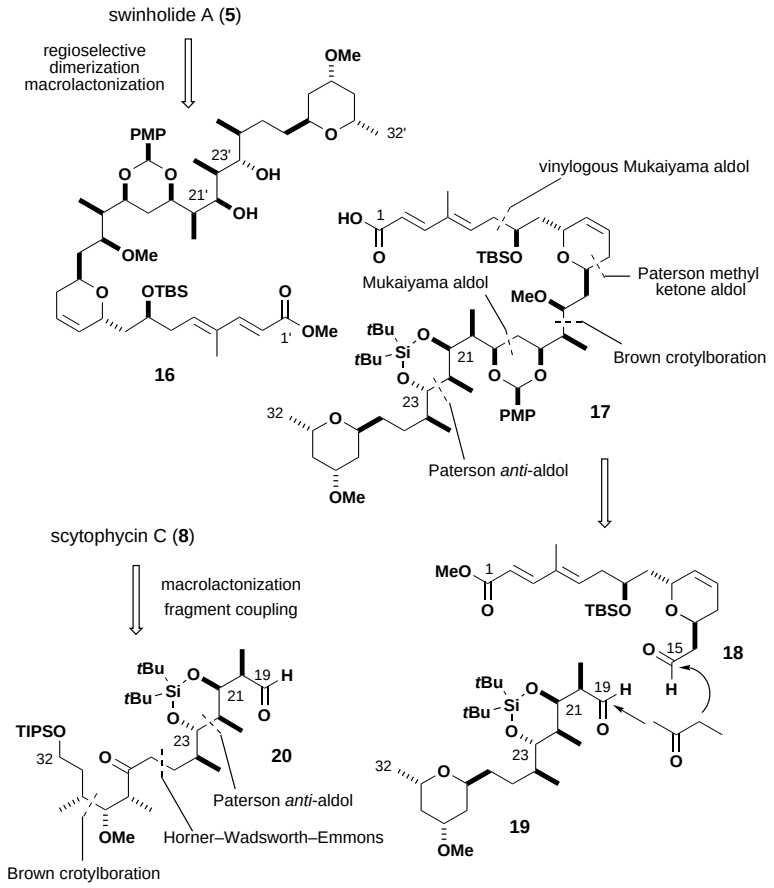
Recent studies using various G-actin mutants suggest that tolytoxin (**9**, Figure 3) binds to actin in a region comprising subdomains 2 and 4 and in the vicinity of the nucleotide binding site.[25] Very recent findings indicate that the control of actin polymerization and depolymerization depends on a conformational shift in the subdomain 2 between the ADP-P_i and ADP-bound actin.[26] Moreover, a crystal structure of ADP–actin[27] revealed that its subdomain 2 adopts an α-helical conformation that is significantly different to the β strand conformation of subdomain 2 in the crystal structures of ATP–actin. In light of this information, it would be particularly interesting to obtain structural information showing how the aforementioned macrolides bind to actin and how the conformation of actin is subsequently changed. Such information might explain how the small structural differences between swinholide A (**5**) and misakinolide A (**6**) impart such distinctly different actions on actin.

2. Total Synthesis

In view of their fascinating and complex molecular architectures, and their important biological activities, these

marine macrolides have been the subject of intensive efforts directed towards their total synthesis.[28] As an attractive alternative to isolation from marine organisms, which usually provides only minuscule quantities of the compounds, total synthesis aims to provide sizeable quantities of the natural product, along with enabling access to novel structural analogues, for further biological evaluation. Total synthesis is also used to establish configurational assignments, as in the case of aplyronine A (**10**)[14b] and mycalolide A (**12**).[16d]

In the following sections, the recently completed total syntheses of some previously mentioned actin-binding macrolides (swinholide A (**5**), scytophycin C (**8**), aplyronine A (**10**), mycalolide A (**12**), and a diastereoisomer of ulapualide A (isomer-**13**)) are featured, with the focus on comparing the different synthetic strategies, key reactions, and methods adopted for controlling the stereochemistry.

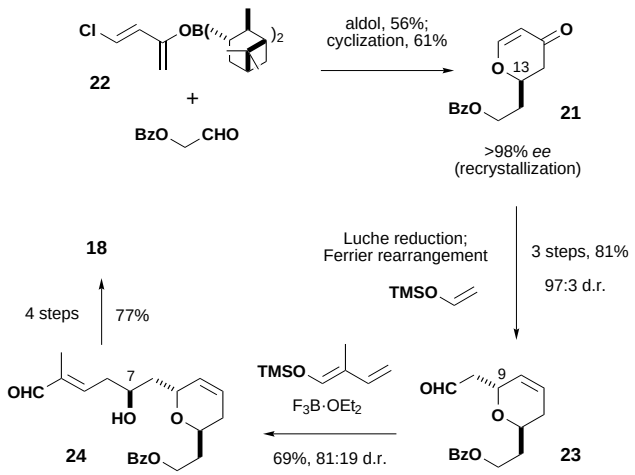


Scheme 1. The unified strategy for the total synthesis of swinholide A (**5**)[29] and scytophycin C (**8**)[33] developed by Paterson et al. The abbreviations are explained at the end of the review.

2.1. Swinholide A (Paterson)

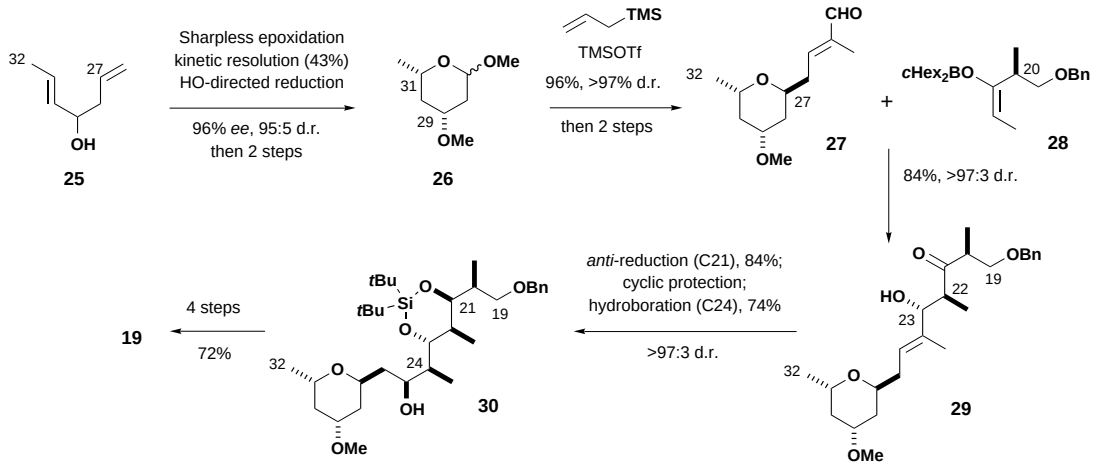
The strategy developed by Paterson and coworkers[29] for the synthesis of swinholide A (**5**) is based on the application of versatile asymmetric aldol methodology in combination with the optimal use of substrate-controlled reactions (Scheme 1). The strategic bond disconnections are indicated on intermediate **17**, corresponding to a protected version of preswinholide A (**7**, Figure 3). The C_2-symmetrical, 44-membered, macrolactone ring of swinholide A was constructed by regioselective esterification of 1,3-diol **16** with acid **17** and subsequent macrolactonization onto the C21 hydroxy group in the presence of the free C23 hydroxy group, both of which are presumably in a similar steric environment. Such a bold strategy proved to be rewarding, as it was later evident that reactions on the free C21 hydroxy group in the presence of a protected C23 hydroxy group were impeded by the increased steric hindrance around the C21 position. A butanone linking unit was used to stitch the C1 – C15 aldehyde **18** and C19 – C32 aldehyde **19** together. This strategy offered flexibility in determining the most efficient coupling sequence. The resulting synthesis was highly convergent and could be applied to the synthesis of novel swinholide analogues. In addition, it was successfully adapted to the total synthesis of scytophycin C (**8**) by using the corresponding aldehyde **20**, in place of **19** (see Section 2.3).

The synthesis of the dihydropyran-containing C1 – C15 segment **18** (Scheme 2) began with the preparation of the dihydropyranone **21** by an asymmetric methyl ketone aldol reaction using bis(isopinocampheyl) enol borinate **22**, followed by cyclization of the aldol product. This gave **21** in > 98 % *ee* after recrystallization and set the C13 stereogenic center. Luche reduction followed by a $[Cl_2Ti(OiPr)_2]$-mediated Ferrier-type rearrangement provided the aldehyde **23** in high diastereoselectivity. The C1 – C7 side chain was introduced by a vinylogous Mukaiyama aldol reaction using a silyl dienol ether, favoring the required configuration at C7 in **24**.



Scheme 2. Synthesis of the common C1 – C15 segment **18** of swinholide A (**5**) and scytophycin C (**8**) according to Paterson et al.[29] *ee* = enantiomeric excess, d.r. = diastereomeric ratio.

The synthesis of the C19 – C32 aldehyde **19** (Scheme 3) was characterized by the use of a series of substrate-controlled reactions to set up five of the seven stereogenic centers. Starting from the racemic allylic alcohol **25** and using

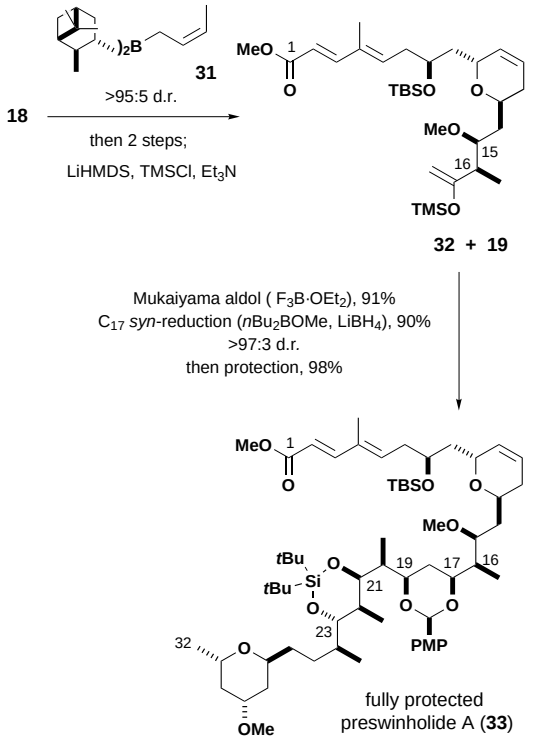


Scheme 3. Synthesis of the C19–C32 segment **19** of swinholide A (**5**) according to Paterson et al.[29]

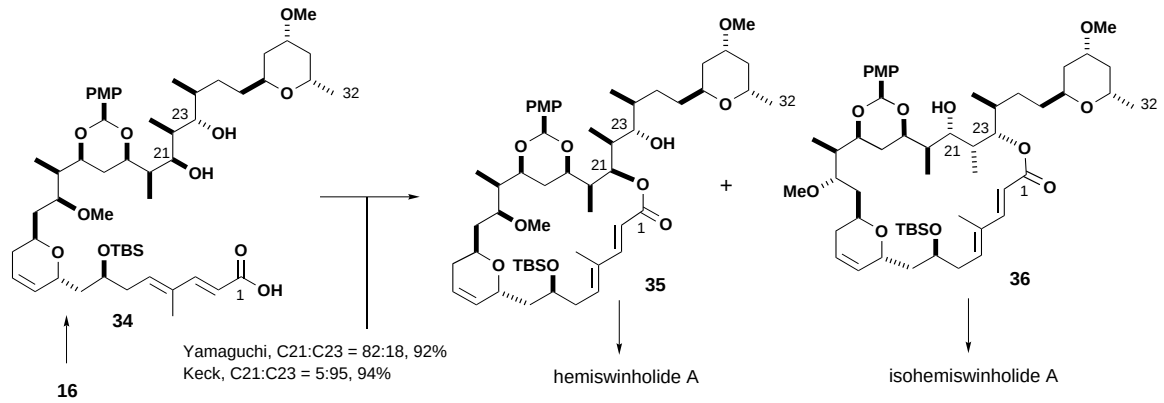
Sharpless epoxidation with attendant kinetic resolution, tetrahydropyran **26** was obtained with the desired configurations at C31 and C29. Sequential use of a TMSOTf-promoted allylsilane addition and an *anti* aldol reaction between the aldehyde **27** and (*E*)-dicyclohexyl enol borinate **28** generated **29**, which was followed by an Evans *anti*-reduction and Still hydroboration (thexylborane) to set up the remaining stereogenic centers in **30** with high diastereoselectivity (>97:3 d.r.).

During the coupling of key segments **18** and **19** (Scheme 4), the most efficient order of bond constructions proved to be to first set up the C15–C16 stereogenic centers by Brown crotylboration using the reagent **31** (>95:5 d.r.) followed by Wacker oxidation to provide the methyl ketone. A Mukaiyama aldol reaction ($F_3B \cdot OEt_2$) between the derived silyl enol ether **32** and aldehyde **19** then provided the desired Felkin–Anh product in high diastereoselectivity (>97:3 d.r.). Introduction of the final stereogenic center in preswinholide A (**7**) then relied on a modified Narasaka *syn*-reduction (nBu$_2$BOMe/LiBH$_4$; >97:3 d.r.) to give the fully protected seco acid **33**.

The final stages of Paterson's total synthesis focused on the controlled elaboration of fully protected preswinholide A (**33**). Selective macrolactonization onto the C21 hydroxy group and the C23 hydroxy group was performed on the derived seco acid **34** (Scheme 5) to form hemiswinholide A



Scheme 4. Synthesis of a fully protected preswinholide A (**33**) according to Paterson et al.[29]



Scheme 5. Macrolactonization of preswinholide A seco acid **34** according to Paterson et al.[29]

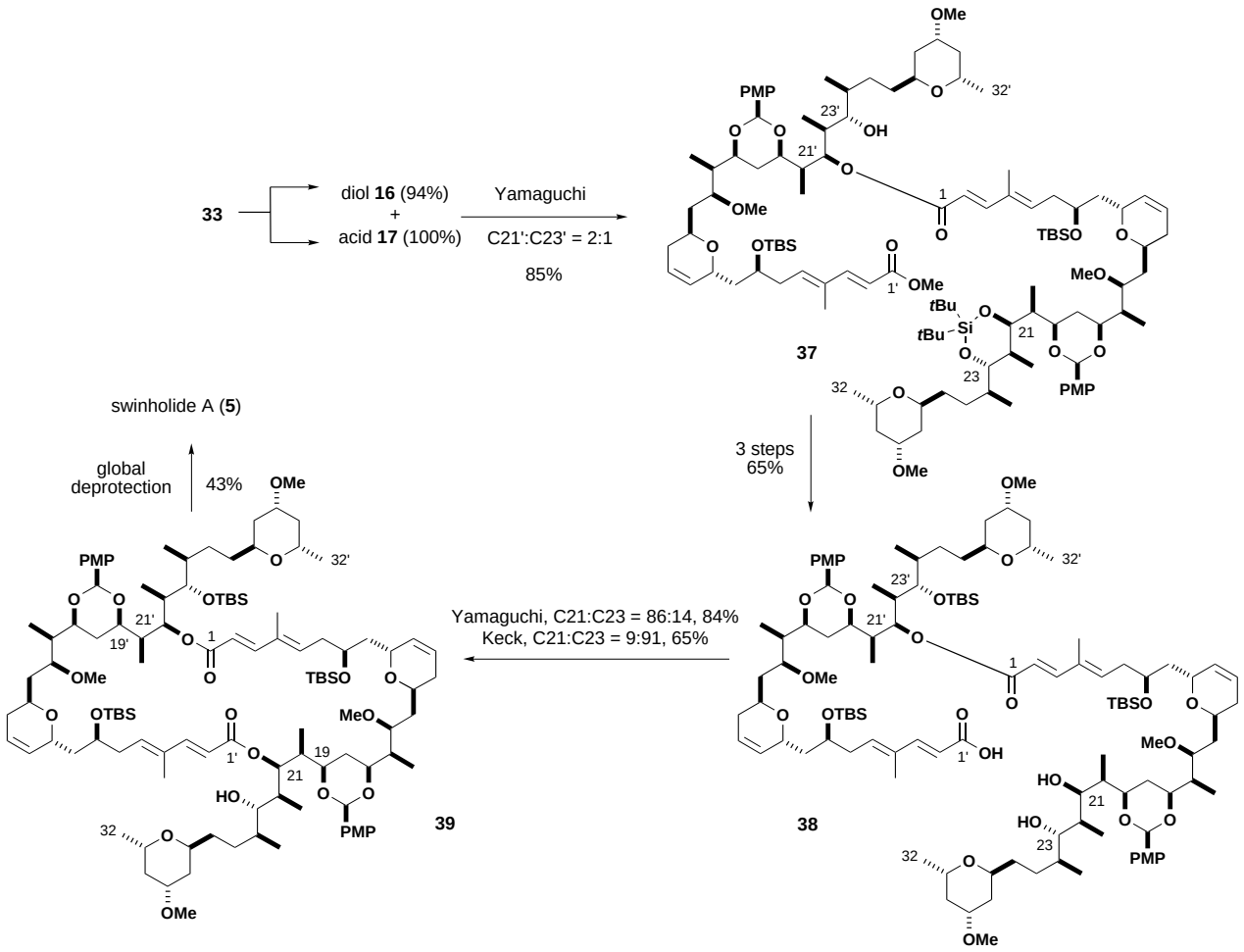
(from **35**) and isohemiswinholide A (from **36**), respectively, as monomeric analogues.[29a] Similarly, Yamaguchi's conditions (2,4,6-$Cl_3(C_6H_2)$COCl, Et_3N, PhMe; 4-(dimethylamino)pyridine (DMAP)) also favored acylation onto the C21 hydroxy group during the challenging dimerization (**16** + **17** → **37**) and macrolactonization (**38** → **39**) steps, to form the required 44-membered ring of swinholide A in good yield (Scheme 6). Remarkably, the regioselectivity was reversed using Keck's protocol (dicyclohexylcarbodiimide (DCC), DMAP, DMAP · HCl, $CHCl_3$) to give preferentially the 46-membered ring of isoswinholide A.[30] Global deprotection of **39** (HF, MeCN) then completed the first total synthesis of swinholide A (**5**) in 0.4 % yield over the 25-step longest linear sequence (43 total steps).

2.2. Swinholide A (Nicolaou)

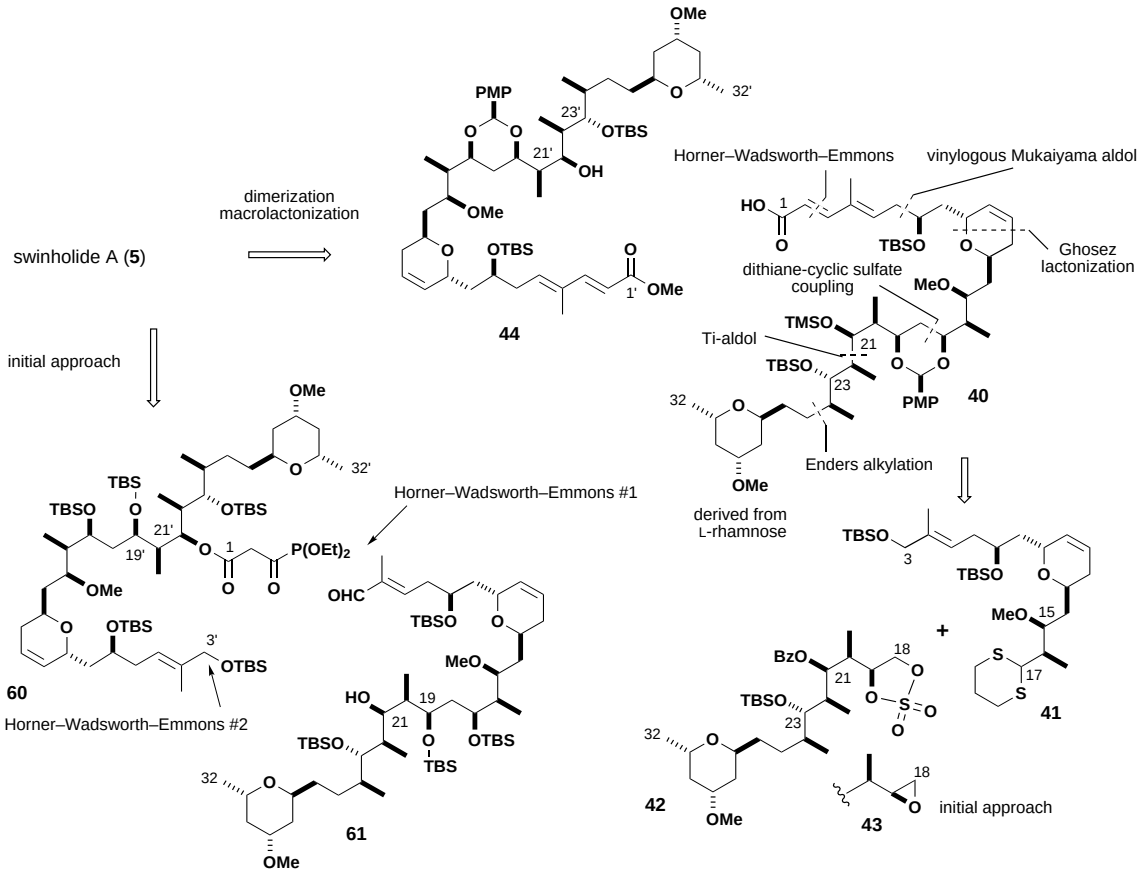
Scheme 7 shows the strategy employed by Nicolaou and co-workers[31] for the total synthesis of swinholide A where the strategic bond disconnections are indicated on intermediate **40**, corresponding to a protected version of preswinholide A. The main coupling partners selected were the C3 – C17 dithiane **41** and the C18 – C32 cyclic sulfate **42** as a surrogate for the epoxide **43**. In contrast to the synthesis by Paterson and co-workers, the C21 – C23 diol was differentially protected (C21-OTMS and C23-OTBS) to allow for site-specific esterification of **44** and macrolactonization onto the C21 hydroxy group to form the required C_2-symmetric macrodiolide ring.

The dihydropyran ring of the C3 – C17 segment **41** was constructed using Ghosez's method (Scheme 8), where epoxide **45** was combined with the lithiated derivative of sulfone **46** to provide the α,β-unsaturated lactol **47** following reduction. The required epoxide **45** was synthesized from methyl (*S*)-3-hydroxy-2-methylpropionate (**48**) by Brown allylboration, setting the C15 stereogenic center in **49**, followed by iodocarbonation of the alkene to give the desired C13 stereocenter in iodide **50**. The intermediate lactol **47** was then converted into the aldehyde **51** with the correct configuration at C9 by allylsilane addition ($F_3B \cdot OEt_2$). In a similar manner to a transformation used in Paterson's synthesis of a C1 – C15 segment (Scheme 2, **23** → **24**), a vinylogous Mukaiyama aldol reaction on **51** with silyl ketene acetal **52** set up the configuration at C7.

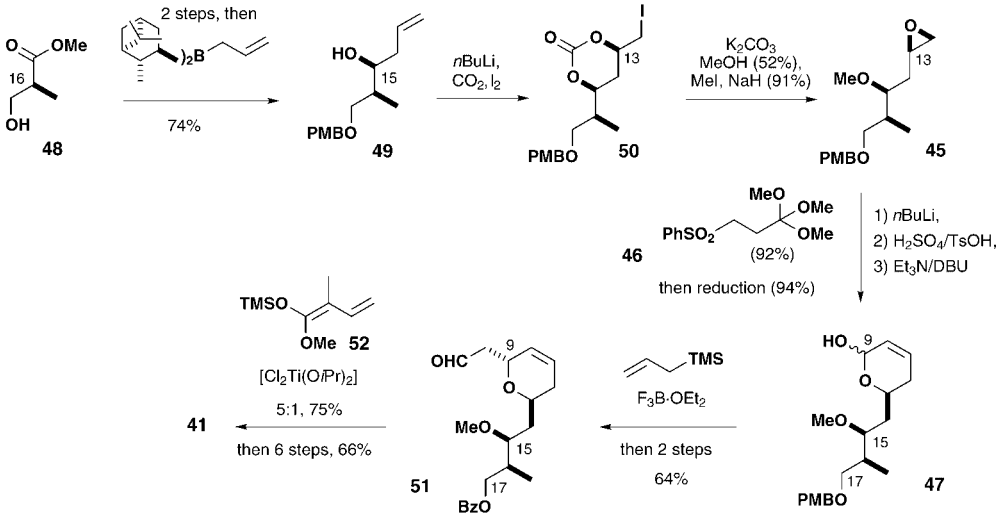
For the synthesis of the C18 – C32 segment **42**, Nicolaou and co-workers started from the readily available L-rhamnose (**53**) (Scheme 9). An eight-step sequence, including a diastereoselective allylsilane addition at C27 ($F_3B \cdot OEt_2$/TMSOTf) and regioselective methylation at C29, converted **53** into the



Scheme 6. Total synthesis of swinholide A (**5**) according to Paterson et al.[29]



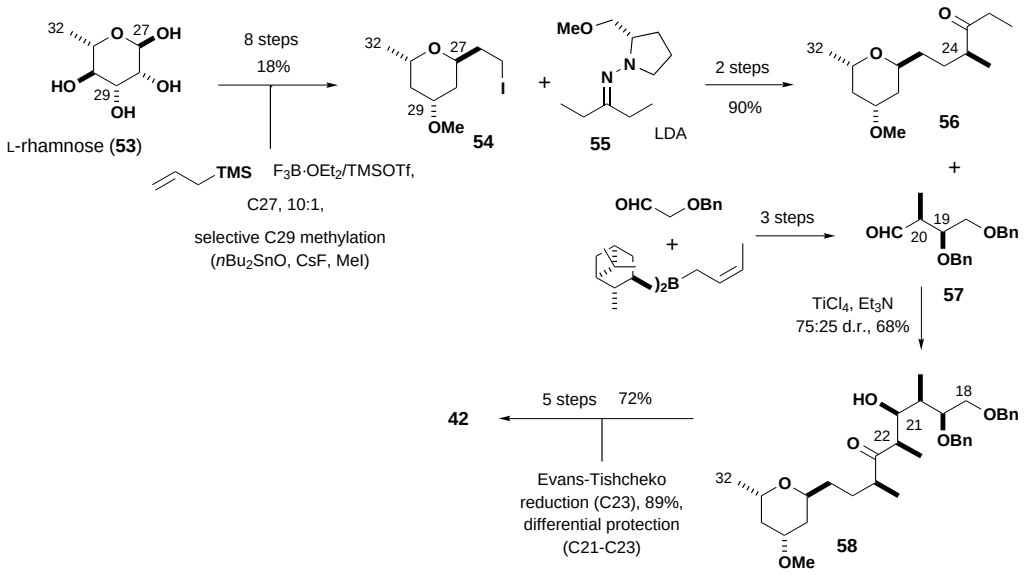
Scheme 7. Strategy for the total synthesis of swinholide A (**5**) developed by Nicolaou et al.[31]



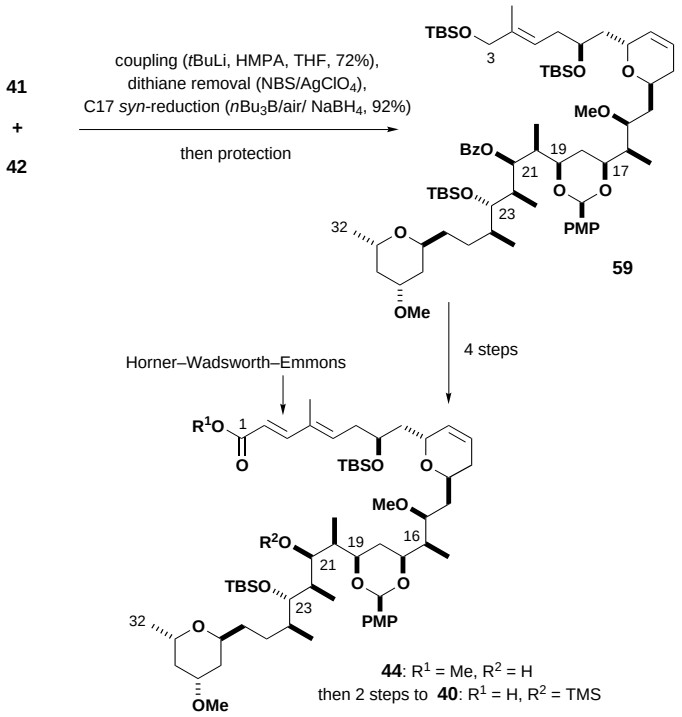
Scheme 8. Synthesis of the C3 – C17 segment **41** of swinholide A (**5**) according to Nicolaou et al.[31]

iodide **54**. Alkylation of Enders' SAMP hydrazone **55** with **54** gave the ketone **56**, with the correct configuration at C24, after ozonolytic cleavage. This set the stage for the titanium-mediated *syn*-aldol addition of ethyl ketone **56** to aldehyde **57**, which was obtained by a Brown *syn*-crotylboration. Under the Evans protocol ($TiCl_4$, Et_3N), the aldol coupling step favored the desired C21 – C22 configuration in **58** (75:25 d.r.). An Evans – Tishchenko reduction then established the remaining stereogenic center at C23 with differentiation of the hydroxy groups at C21 and C23.

The key segment coupling for the synthesis of protected preswinholide A used the van der Klein reaction between the dithiane **41** and the cyclic sulfate **42**, providing the intermediate 19-β-hydroxydithiane (Scheme 10). In contrast, the more conventional use of the corresponding epoxide **43** (Scheme 7) gave only trace amounts of the desired product. Deprotection



Scheme 9. Synthesis of the C18 – C32 segment **42** of swinholide A (**5**) according to Nicolaou et al.[31]



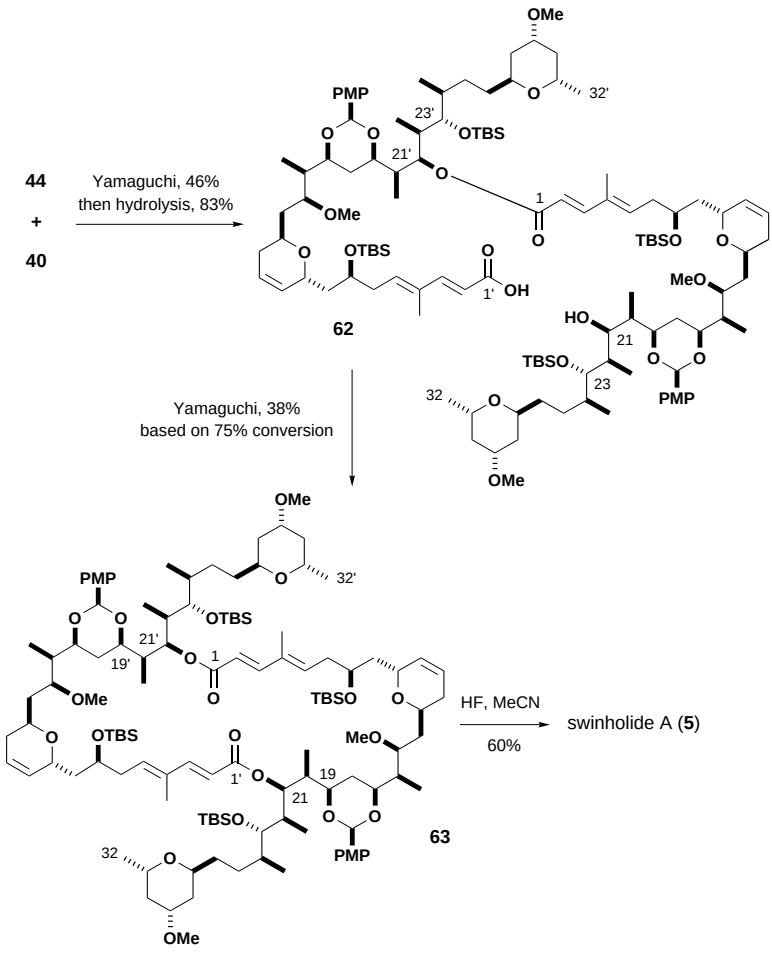
Scheme 10. Synthesis of C1 – C32 segments **40** and **44** of swinholide A (**5**) according to Nicolaou et al.[31]

of the dithiane revealed the β-hydroxy ketone, which was reduced by using Narasaka conditions (nBu$_3$B/air/NaBH$_4$) to set the desired configuration at C17 in **59** (Scheme 10). The resulting C3 – C32 segment **59** was then elaborated into **44** and **40**, corresponding to protected derivatives of preswinholide A.

Initially,[31c] the formation of the macrocyclic ring was planned via an ambitious HWE reaction (**60** + **61**, Scheme 7) but this did not prove viable in practice due to steric problems. Consequently, Yamaguchi's protocol was used to acylate the C21′ hydroxy group of **44** with the corresponding acid derivative **40** to provide **62** (Scheme 11), followed by its application to the formation of the symmetrical 42-membered macrodilactone **63**. Final deprotection then gave swinholide A (**5**) in about 0.3 % yield over a 32-step longest linear sequence (53 total steps).[32]

2.3. Scytophycin C (Paterson)

The synthetic strategy developed by Paterson and coworkers for swinholide A (**5**; Section 2.1) proved flexible enough to be adapted successfully to enable the first total synthesis of scytophycin C (**8**).[33] This employed the C19 – C32 aldehyde **20**, which was obtained by a HWE reaction between the sterically hindered aldehyde **64** and the phosphonate **65** (Scheme 12). A Brown asymmetric crotylboration was first used on aldehyde **66** to introduce the C29 – C30 *anti*-stereochemistry of the homoallylic alcohol **67**, which was then converted in seven steps to the β-ketophosphonate **65**. An *anti*-aldol reaction between (*E*)-dicyclohexyl enol borinate **28** and methacrolein provided the adduct **68** with high diastereoselectivity (> 97:3 d.r.) and provided a platform for an *anti*-reduction, followed by a hydroboration (9-BBN), to complete the synthesis of the stereopentad sequence in C19 – C25 aldehyde **64**. The testing HWE coupling was best achieved by using barium hydroxide[34] to provide the enone **69**. As in the total synthesis of swinholide A (**5**; Section 2.1), the Mukaiyama aldol coupling of the C1 – C18 silyl enol ether **32** and the C19 – C32 aldehyde **20** was equally effective (Scheme 13), giving the β-hydroxy ketone **70** with the desired Felkin – Anh stereoinduction at C19 (> 97:3 d.r.). However, in contrast to the situation with swinholide A, the *syn*-reduction of the C17-ketone group in the aldol product **70** was complicated by the presence of the ketone group at C27. Instead of using nBu$_2$BOMe/LiBH$_4$, catecholborane proved to be the most effective reducing agent in realizing this chemo- and stereo-



Scheme 11. Total synthesis of swinholide A (**5**) according to Nicolaou et al.[31]

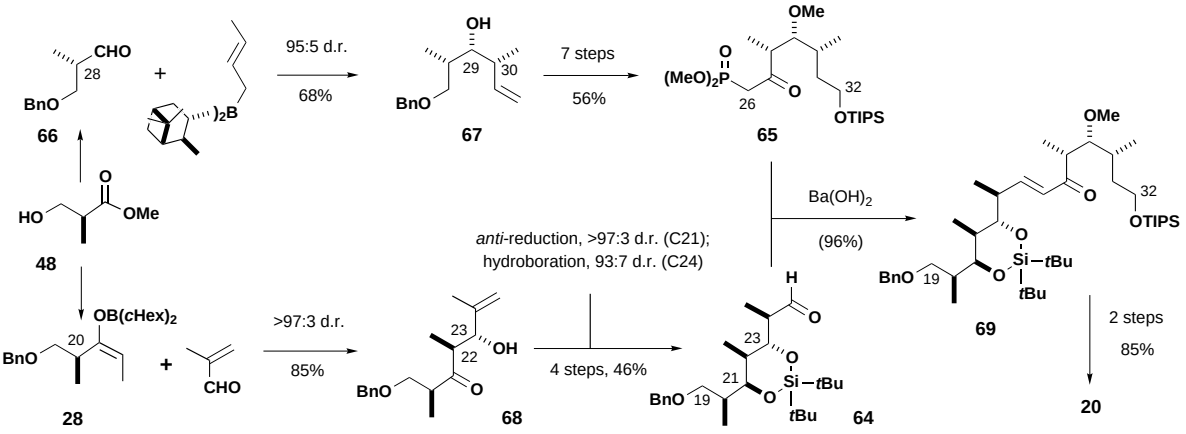
selective transformation to provide **71** (92:8 d.r.). In this way, the synthesis of the fully protected C1 – C32 seco acid **71**, which incorporates all the 15 stereocenters of scytophycin C (**8**), was achieved in a direct and efficient manner.

The elaboration of the advanced intermediate **71** to scytophycin C (**8**) proved to be a challenging task. The crucial ring-closure step and final functional group adjustments imposed greater difficulties than encountered in the synthesis of swinholide A and hemiswinholide A. The C27-ketone group related problems of β-elimination or hemiacetal formation on exposure of **71** to silylene deprotection conditions necessitated its temporary reduction (Scheme 14). Macrolactonization of the derived triol acid **72** under the Yonemitsu modification of the standard Yamaguchi conditions gave a roughly equimolar mixture of the C21- and C23-acylated products **73** and **74**, without the formation of any of the C27-acylated product. These results are in sharp contrast to the highly selective macrolactonization onto the C21 or C23 hydroxy group realized with the monomeric seco acid **34** (see Scheme 5, Section 2.1). By taking advantage of the thermodynamic preference for the required 22-membered macrolactone **73**, the 24-membered macrolactone **74** was isomerized efficiently to give predominantly **73**.

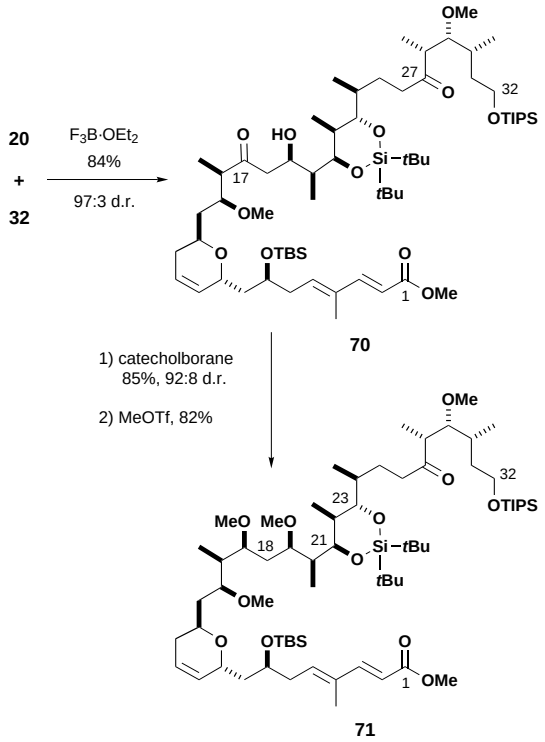
The oxidation state adjustments that followed (Scheme 15) provided an interesting example of selective hydroxy oxidation using tetrapropylammonium perruthenate (TPAP) in demanding situations, as in **73** → **75** and **76** → **77**. The final introduction of the *N*-methylvinylformamide group into the aldehyde **77** was far from straightforward due to the known acid sensitivity of scytophycin C (**8**).[13a] After considerable experimentation, it was found that brief treatment of aldehyde **77** with P_2O_5[35] in neat HNMeCHO gave scytophycin C (**8**) in 0.7 % overall yield over 22 linear steps (41 total steps).[36]

2.4. Aplyronine A (Yamada)

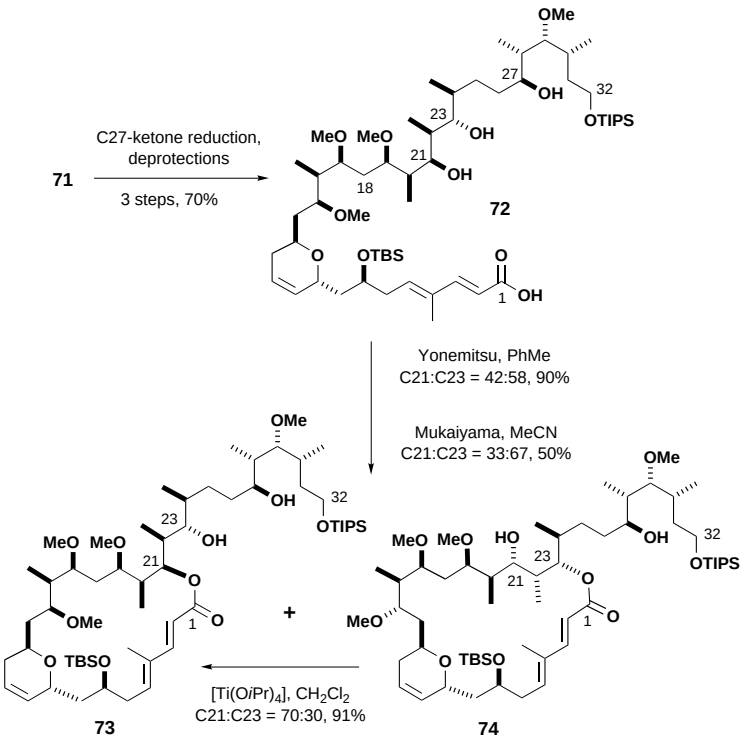
The strategy developed by Yamada and co-workers[37] for the synthesis of the aplyronines was dictated by the need to maintain stereochemical flexibility, while the full configuration was elucidated through chemical correlation of synthetic



Scheme 12. Synthesis of the C19 – C32 segment **20** of scytophycin C (**8**) according to Paterson et al.[33]



Scheme 13. Synthesis of the C1 – C32 segment **71** of scytophycin C (**8**) according to Paterson et al.[33]

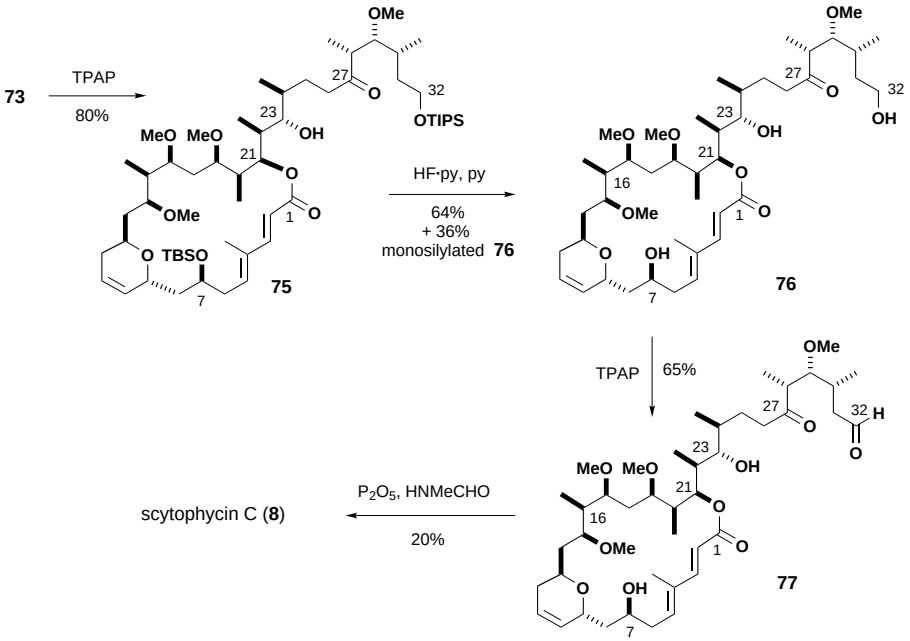


Scheme 14. Synthesis of the 22-membered macrolactone intermediate **73** for scytophycin C (**8**) according to Paterson et al.[33]

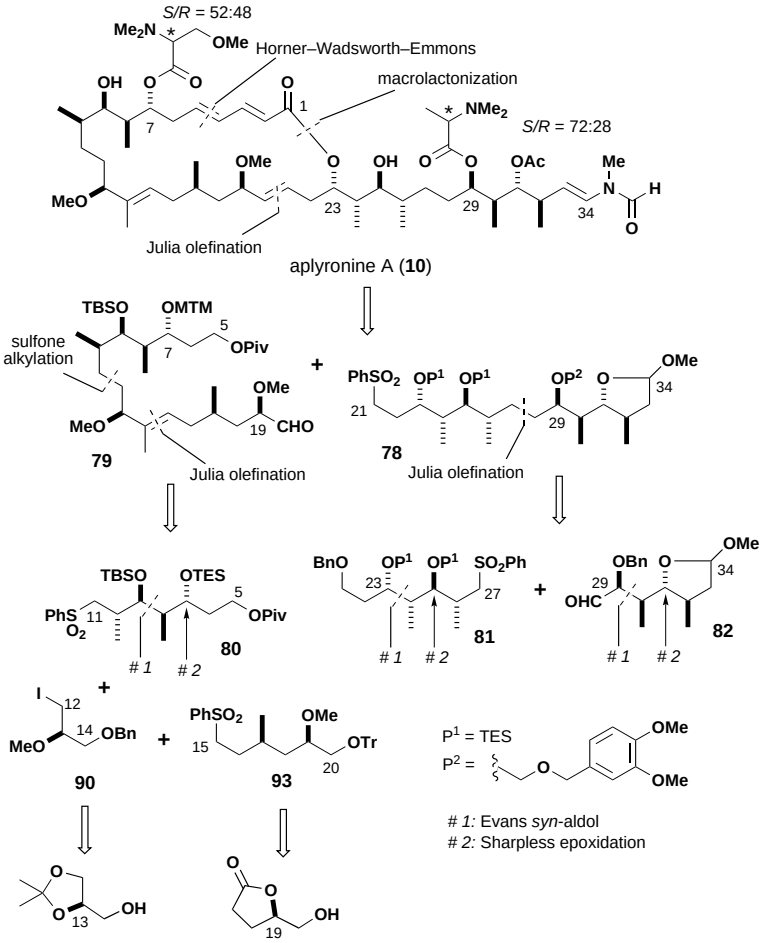
segments with degraded fragments of the natural product. For aplyronine A (**10**), the final route selected (Scheme 16) was based on the coupling of the C21 – C34 sulfone **78** with the C5 – C20 aldehyde **79**. The appropriate stereotetrad sequences, as featured in the three segments **80**, **81**, and **82**, were set up by sequential use of the Evans aldol reaction and Sharpless epoxidation, followed by epoxide ring opening.

As the *syn-anti-anti* sequences of the C21 – C27 segment **81** and C28 – C34 segment **82** are enantiomeric, it proved convenient to make use of antipodal Evans chiral auxiliaries. As an illustration (Scheme 17), an Evans aldol reaction of the *Z*-boron enolate derived from propionimide **83** with 3-benzyloxypropanal provided **84** with the desired configurations at C23 and C24. A Sharpless epoxidation on the derived allylic alcohol **85** then introduced the required stereogenic center at C25 in **86**. Stereo- and regioselective (81:19) epoxide ring opening at C26 using methyl cuprate gave diol **87**, which was then converted into the C21 – C27 sulfone **81**. Similarly, the C5 – C11 segment **80** was prepared by methyl cuprate addition to epoxide **88**, while the C28 – C34 segment **82** was prepared starting from the chiral aldehyde **89**.

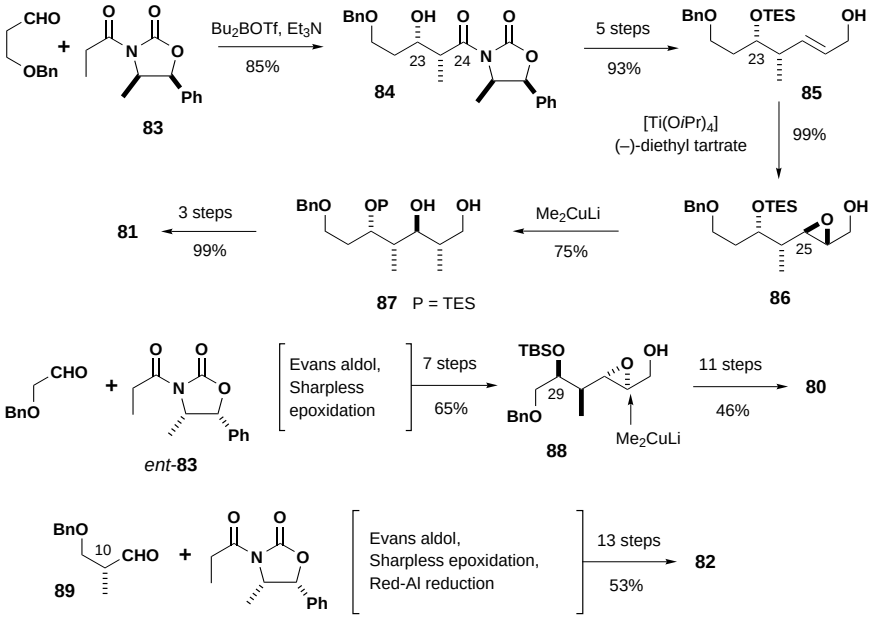
As outlined in Scheme 18, the Yamada synthesis of aplyronine A was characterized by the extensive use of sulfone chemistry for sequentially coupling advanced intermediates (as in **80** + **90** → **91**; **92** + **93** → **94**; **81** + **82** → **95**; **78** + **79** → **96**) to build up the C1 – C34 skeleton containing all the 15 stereogenic centers. However, the formation of the desired C5 – C20 (*E*)-trisubstituted alkene **94** by Julia olefination between the sulfone **93** and methyl ketone **92** proved less efficient, being accompanied by



Scheme 15. Total synthesis of scytophycin C (**8**) according to Paterson et al.[33]



Scheme 16. Strategy for the total synthesis of aplyronine A (**10**) developed by Yamada et al.[37]



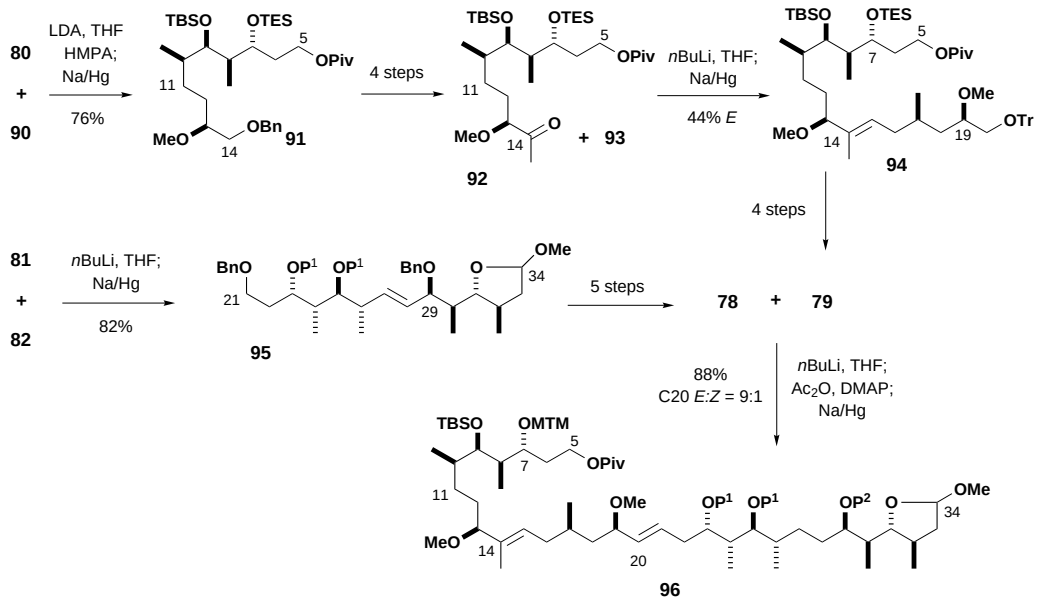
Scheme 17. Synthesis of segments **80** to **82** of aplyronine A (**10**) according to Yamada et al.[37]

the (*Z*)-alkene and corresponding C14 tertiary alcohol. During these manoeuvres, the benzyl protecting group at C29 was exchanged with a [(3,4-dimethoxybenzyl)oxy]methyl ether group. This latter protecting group enabled a smooth deprotection by treatment with DDQ, thus avoiding decomposition of the conjugated lactone in the late stages of the synthesis. The TES protecting group at C7 was also exchanged with a MTM group to allow for the differential deprotection of both C23 and C25 TES groups before the macrolactonization step.

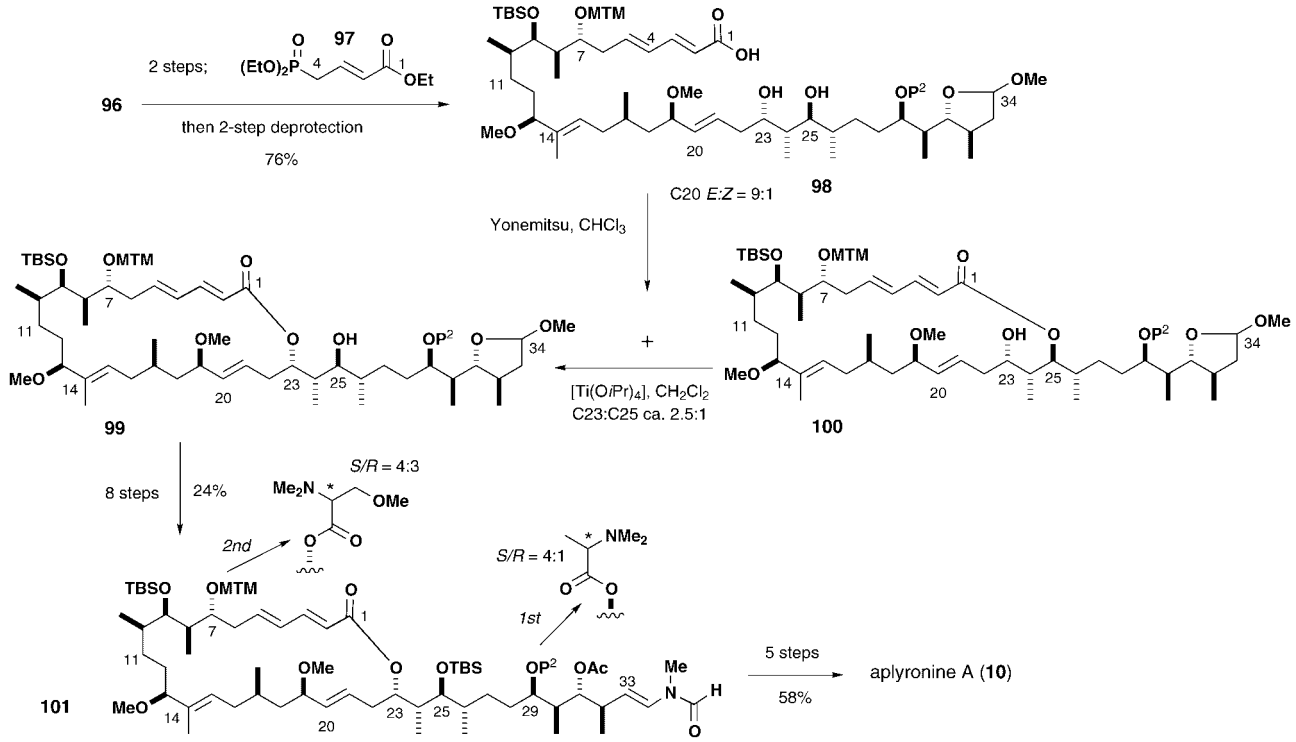
The advanced intermediate **96** was chain-extended by a HWE reaction with phosphonate **97** and then deprotected to give the seco acid **98** (Scheme 19). Macrolactonization of **98** selectively onto the hydroxy group at C23 in the presence of the hydroxy group at C25 was a challenging step. Under Yonemitsu–Yamaguchi conditions, a 59:41 mixture in favor of the required 24-membered macrolactone **99** was obtained; where the accompanying 26-membered macrolactone **100** was isomerized to generate more of **99** on treatment with [Ti(O*i*Pr)$_4$]. Following an eight-step elaboration into **101**, where the terminal vinyl formamide was introduced by a condensation of HNMeCHO with the aldehyde at C34 in **99**, esterification with *N*,*N*-dimethylalanine ($S/R = 3/2$) at C29 produced a diastereomeric ester mixture, while attachment of *N*,*N*,*O*-trimethylserine ($S/R = 5/2$) at C7 produced another epimeric mixture. Note that in natural samples of aplyronine A, the amino acid residues exist respectively as 6:1–3:1 and 2:1–1.1:1 mixtures of the *S* and *R* configurations, and these ratios were found to vary with the animal samples collected, indicating that partial epimerization may be occurring during isolation. After final deprotection, this led to the first total synthesis of aplyronine A (**10**) in about 0.5% overall yield over 47 linear steps (99 total steps). This route was adapted by Yamada and co-workers to provide the congeners, aplyronine B (**102**) and aplyronine C (**103**), along with various structural analogues (e.g. **104**–**106**) for biological evaluation to establish structure–activity relationships (Figure 6).[38]

2.5. Aplyronine A (Paterson Approach)

Paterson and co-workers[39] have proposed an entirely different strategy for aplyronine A (**10**) and have completed a synthesis of an advanced 24-membered macrocyclic intermediate **107** (Scheme 20), selecting a potential HWE-type disconnection at C27–C28 to reveal the β-ketophosphonate **108**. In contrast



Scheme 18. Synthesis of the C5 – C34 segment **96** of aplyronine A (**10**; P^1 and P^2 as shown in Scheme 16) according to Yamada et al.[37]



Scheme 19. Total synthesis of aplyronine A (**10**; P^2 as shown in Scheme 16) according to Yamada et al.[37]

to the total synthesis of aplyronine A (**10**) by Yamada and co-workers (Section 2.4), Paterson and co-workers planned to introduce the *N*-methylvinylformamide group into the phosphonate **108** at an early stage. The macrolactone **107** was constructed by a three-component coupling of the C1 – C11 iodide **109**, the C15 – C27 aldehyde **110**, and a four-carbon linker **111**. The strategy also relied on asymmetric aldol methodology using boron and tin(II) enolates developed in the Paterson group to generate the stereotetrad sequences contained in the intermediates **109** and **110**. The application of the HWE reaction for the coupling of key segments is also noteworthy, where the controlled installation of an enone is followed by reagent-controlled 1,2-reduction to set up the C13 and C19 stereogenic centers.

In the synthesis of the C1 – C11 iodide **109**, the (*E*,*E*)-diene ester was masked as an alkyne ester, as in aldehyde **112** (Scheme 21). An *anti*-aldol reaction between the (*E*)-enol borinate derived from chiral ketone **113** and aldehyde **112** then gave the adduct **114** (> 97:3 d.r.). An Evans – Tishchenko reduction was then used to set up the desired configuration at

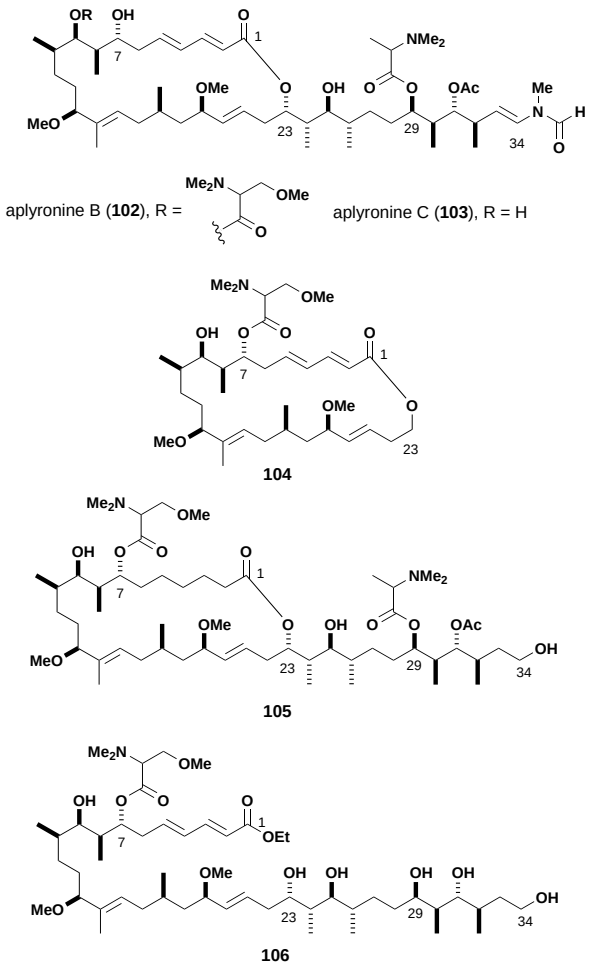


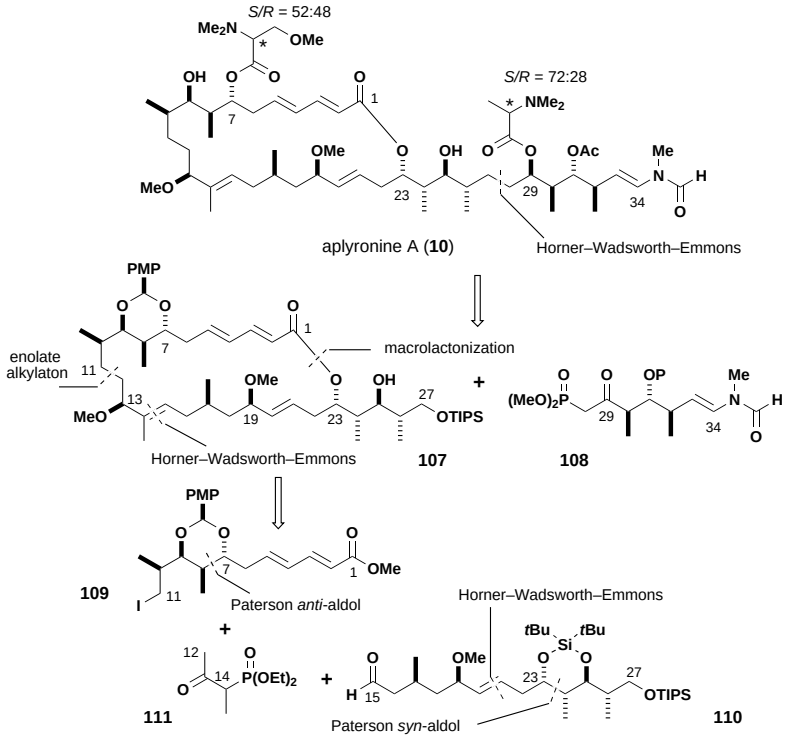
Figure 6. Aplyronine B (**102**), aplyronine C (**103**), and structural analogues (**104** to **106**) synthesized by Yamada et al.[38]

C9 in **115** (>97:3 d.r.). At this stage, the alkyne ester was isomerized efficiently to the required (*E*,*E*)-diene **116** using Ph_3P/PhOH.

The C23–C26 stereotetrad in aldehyde **117**, which was required for the synthesis of segment **110**, was generated through a $Sn(OTf)_2$-mediated *syn*-aldol reaction (90:10 d.r.) between chiral ketone **118** and 3-benzyloxypropanal, followed by an *anti*-reduction of ketone **119** (93:7 d.r.) (Scheme 22). The HWE reaction between the derived C21–C27 aldehyde **117** and the C15–C20 β-ketophosphonate **120**, prepared from the acid **121**, was effected by $Ba(OH)_2$ to give the *E*-configured enone **122** efficiently. The remaining C19 stereogenic center was configured by CBS reduction of the enone using oxazaborolidine (*S*)-**123** to give the allylic alcohol **124** (90:10 d.r.), which was converted into aldehyde **110**.

The C1–C11 iodide **125** and the phosphonate **111** were first coupled to generate the β-ketophosphonate **126** (Scheme 23), followed by a $Ba(OH)_2$-promoted HWE reaction with the aldehyde **110** to cleanly install the *E*-configured trisubstituted double bond in the C1–C27 segment **127**. The ketone group was then reduced using oxazaborolidine reagent (*R*)-**123** to introduce the isolated C13 stereogenic center in **128** (>95:5 d.r.).

DDQ-mediated oxidative desilylation of **128** to give aldehyde **129** was followed by conversion into the seco acid **130** (Scheme 24). Macrolactonization under modified Yamaguchi conditions gave exclusively the 26-membered ring **131**, where the cyclic acetal protection across C7–C9 strongly influences the conformation for cyclization. Following the Yamada precedent, isomerization with $[Ti(OiPr)_4]$ led to predominantly (3:1) the more stable, 24-membered macrolactone **107**, which now requires introduction of the full side chain to access aplyronine A (**10**).[40]

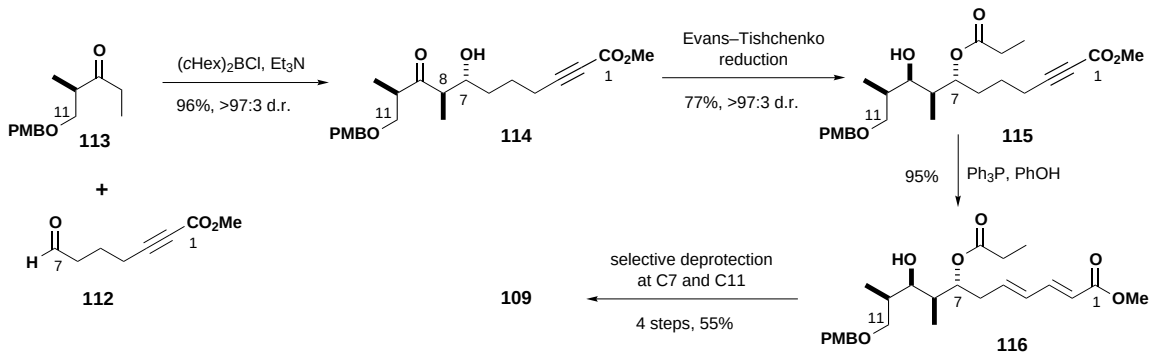


Scheme 20. Strategy proposed by Paterson et al. for the synthesis of aplyronine A (**10**).[39]

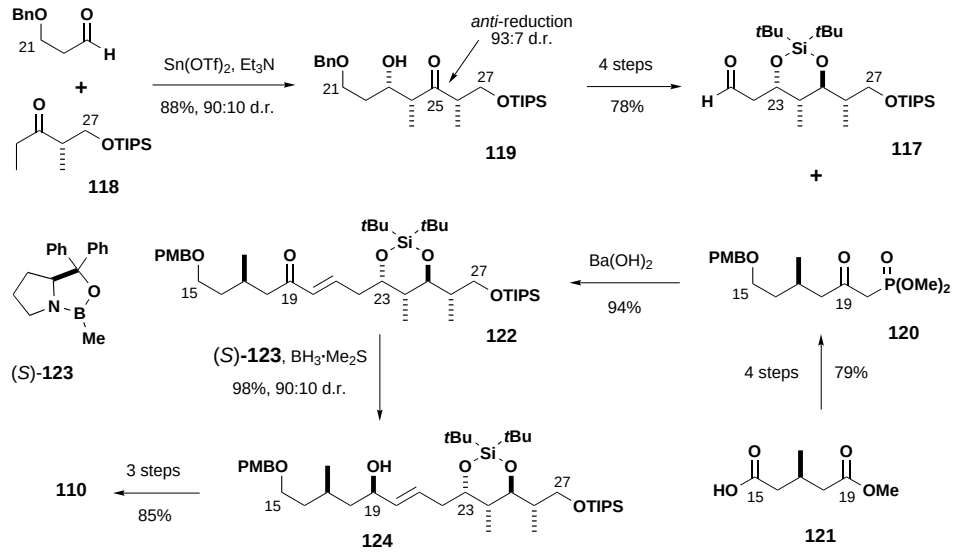
2.6. A Diastereoisomer of Ulapualide A (Pattenden)

To date, the full absolute configuration of the ulapualides has not been determined unequivocally. Based on a molecular mechanics modeling study performed on a Co^{III}–ulapualide A chelate and comparison with the scytophycins, Pattenden et al. proposed the configurational assignment shown in Scheme 25 (isomer-**13**). [41, 42] However, recent chemical degradation and synthetic studies by Fusetani and Panek on the mycalolides have shown that the C20–C35 segment of ulapualide B has the same configuration as the corresponding C20–C35 segment of the mycalolides.[16d] The full stereostructure of mycalolide A (**12**) has been unambiguously confirmed by Panek et al. by total synthesis (Section 2.7), whereas the Pattenden group have synthesized isomer-**13**, which proved to be a diastereoisomer of ulapualide A.

Pattenden's approach to the synthesis of isomer-**13** (Scheme 25), involves its assembly from the trisoxazole-containing phosphonium salt **132**,



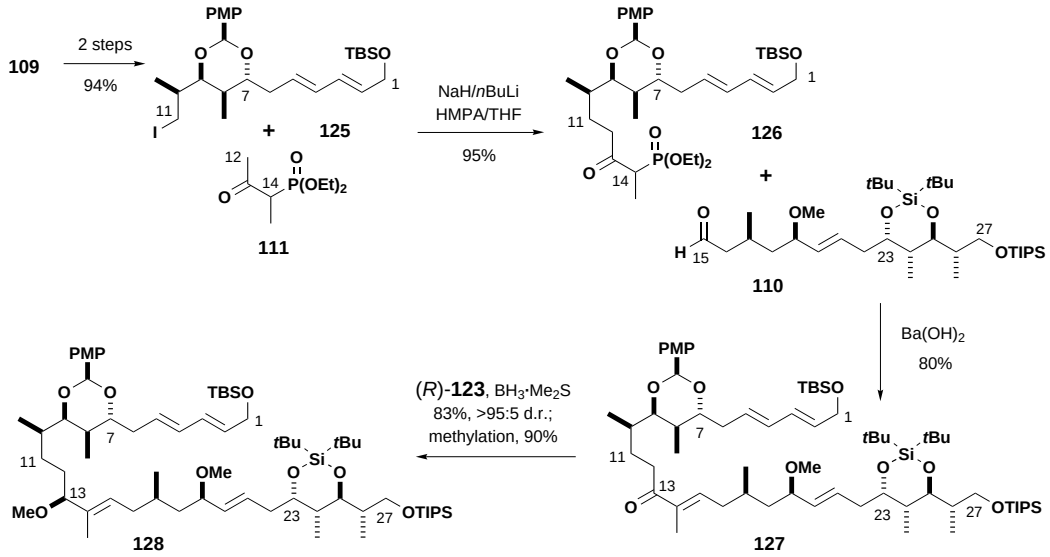
Scheme 21. Synthesis of the C1 – C11 segment **109** of aplyronine A (**10**) according to Paterson et al.[39]



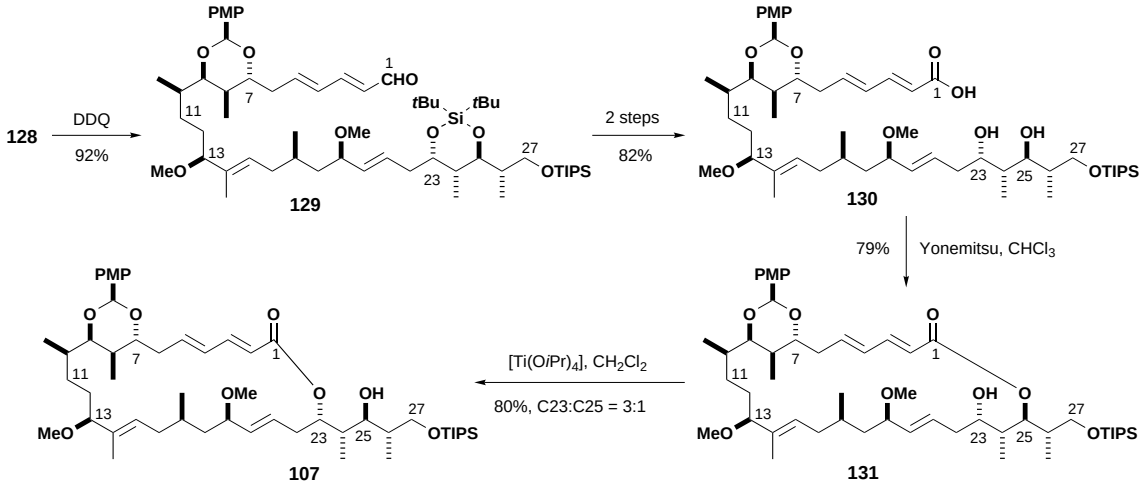
Scheme 22. Synthesis of the C15 – C27 segment **110** of aplyronine A (**10**) according to Paterson et al.[39]

the aldehyde **133** incorporating the C22 – C33 stereogenic centers, and the C1 – C8 β-ketophosphonate **134**. The isolated C3 stereogenic center was installed by baker's yeast reduction of the β-keto acid of **135**. The aldehyde **133** was produced by a Ba(OH)$_2$-promoted HWE coupling between the C29 – C35 β-ketophosphonate **136** and the C20 – C28 aldehyde **137**, both of which were obtained from Sharpless epoxidation and epoxide opening as the stereodetermining steps.

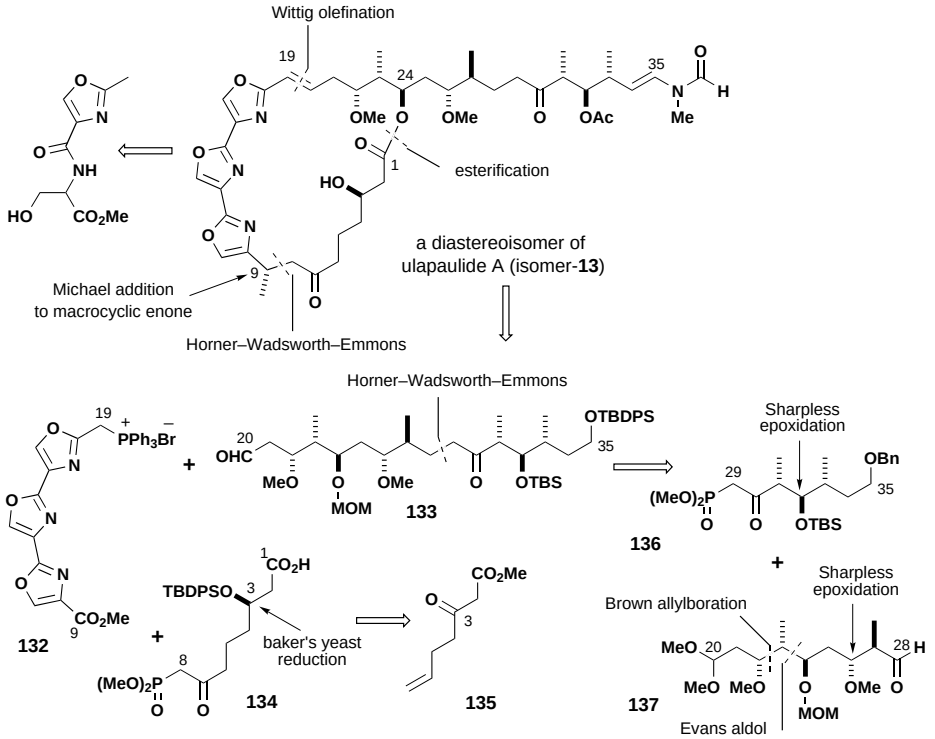
The three key subunits were coupled sequentially by first performing a Wittig olefination between **132** and **133**, producing the (*E*)-alkene **138** (Scheme 26) without any epimerization at C31. The C1 – C8 segment **134** was then connected to the derived alcohol **139** by a Yamaguchi-type esterification, followed by a HWE cyclization under Nicolaou conditions to form the 25-membered macrocyclic (*E*)-enone **140**. Next, methyl cuprate 1,4-addition to **140** gave a 3:2 mixture of α- and β-adducts, where **141** has the configuration at C9 indicated in isomer-**13**. Finally, PPTS-promoted condensation between HNMeCHO and the derived aldehyde



Scheme 23. Synthesis of the C1 – C27 segment **128** of aplyronine A (**10**) according to Paterson et al.[39]



Scheme 24. Synthesis of the advanced C1 – C27 macrolactone intermediate **107** for aplyronine A (**10**) according to Paterson et al.[39]



Scheme 25. Strategy for the synthesis of ulapualide A (isomer-**13**) developed by Pattenden et al.[41]

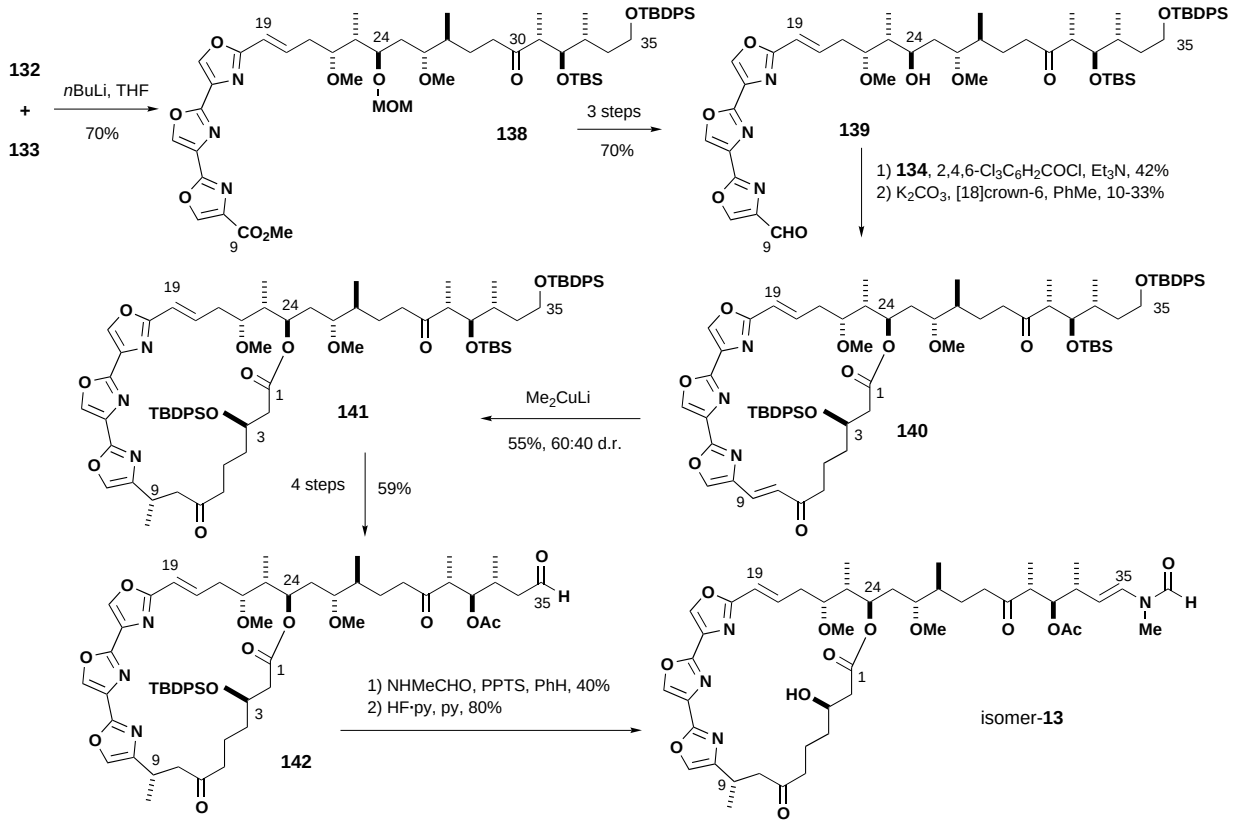
142 served to install the terminal *N*-methylvinylformamide, which provided isomer-**13** on deprotection in about 0.4% yield over 37 steps for the longest linear sequence (ca. 63 total steps). While the ^{1}H NMR data were essentially identical to that recorded for natural ulapualide A, there were distinct differences apparent in the ^{13}C NMR resonance signals at C26, C27-Me, and C28, suggesting at the time that the configuration at one or more centers was incorrect.

2.7. Mycalolide A (Panek)

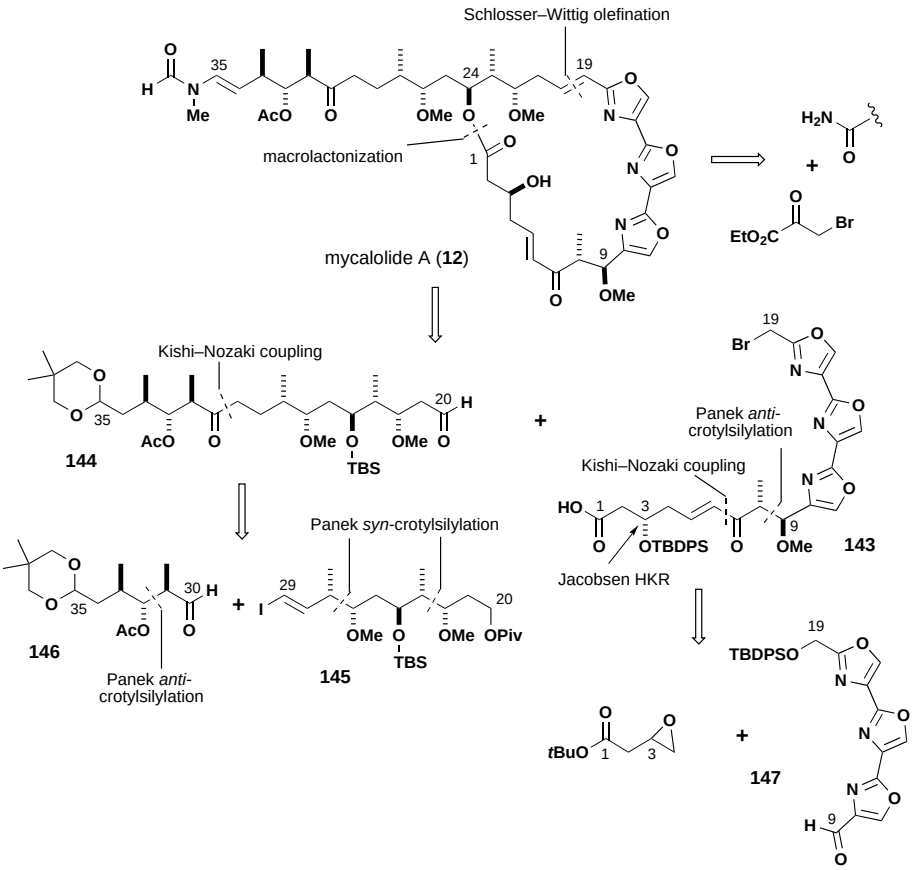
The strategy used by Panek and co-workers[43] for the total synthesis of mycalolide A (**12**) is shown in Scheme 27. A Schlosser – Wittig olefination was employed to couple the C1 – C19 trisoxazole **143** and the C20 – C35 aldehyde **144**. This was followed by a macrolactonization to close the 25-membered ring. The Kishi – Nozaki coupling reaction was used effectively in the formation of these two key segments. The synthesis also demonstrated the use of asymmetric *syn*- and *anti*- crotylsilylation reactions, as developed in Panek's laboratories, to construct the required stereochemical relationships in the C20 – C29 vinyl iodide **145**, the C30 – C35 aldehyde **146**, and the C8 – C9 stereogenic centers in segment **143**. The remote C3 stereocenter was controlled by using a Jacobsen hydrolytic kinetic resolution (HKR) of racemic *tert*-butyl-3,4-epoxybutanoate. The trisoxazole-containing C9 – C19 segment **147** was obtained by the use of three consecutive Hantzsch condensations using ethyl bromopyruvate.

The synthesis of **144** was characterized by the use of chiral allylsilane reagents to install the stereogenic centers (Scheme 28). A $TiCl_4$-promoted addition of silane (*S*)-**148** to the aldehyde **89** gave the homoallylic alcohol **149**, which was elaborated into **146**. Similarly, a $TiCl_4$-promoted addition of (*S*)-**150** to aldehyde **151** provided alcohol **152** with a *syn* relationship at C26 – C27. This alcohol **152** was then converted into vinyl iodide **145** ready for the Kishi – Nozaki coupling with aldehyde **146**, providing the allylic alcohol **153** which was converted into **144**.

Reaction of the trisoxazole aldehyde **147** with the crotylsilane reagent (*S*)-**154**, mediated by $TiCl_4$, gave the tetrahydrofuran **155** having the desired configuration at C8 – C9 (Scheme 29). Repeated treatment of **155** with $F_3B \cdot OEt_2$ induced ring opening to provide the *anti*-isomer **156**, which

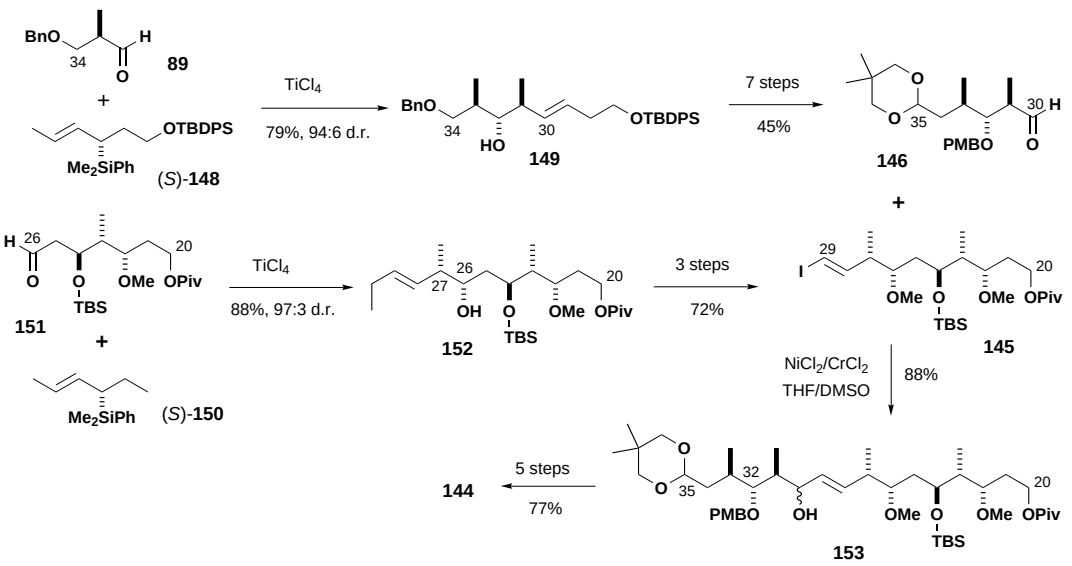


Scheme 26. Total synthesis of a diastereoisomer of ulapualide A (isomer-**13**) according to Pattenden et al.[41]

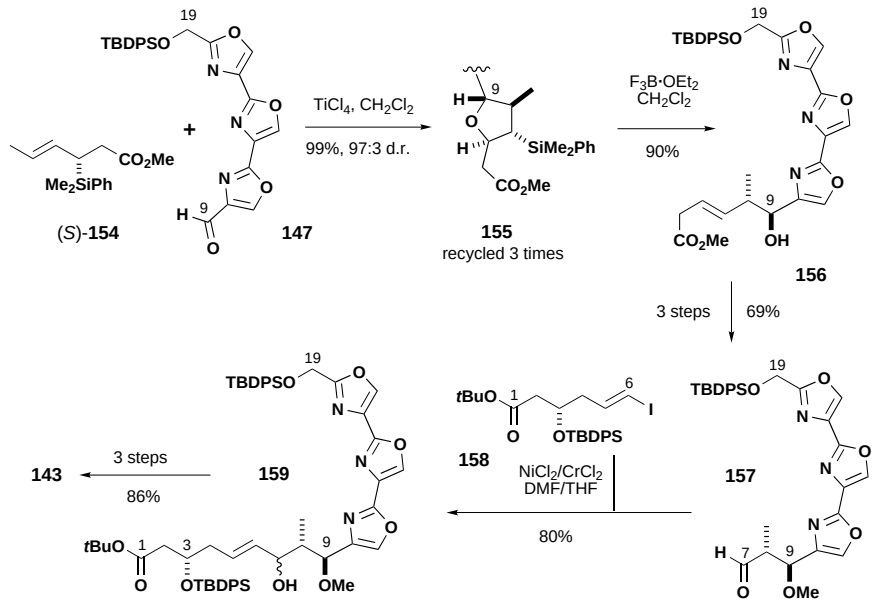


Scheme 27. Strategy for the total synthesis of mycalolide A (**12**) developed by Panek et al.[43]

was converted into aldehyde **157**. The vinyl iodide **158** was then coupled with **157** using the Kishi–Nozaki, $NiCl_2/CrCl_2$-mediated, protocol to generate the C1–C19 segment **159** and this was transformed into **143**. Notably, the crucial Wittig olefination step between the C1–C19 bromide **143** (having an unprotected carboxylic acid) and the C20–C35 aldehyde **144** was performed under mild conditions, using Et_3P/DMF and then DBU as the base, to give the (*E*)-alkene **160** (Scheme 30). Following TBS ether deprotection, macrolactonization onto the C24 hydroxyl group using Yonemitsu–Yamaguchi conditions gave the 25-membered macrolactone **161**. Treatment of **161** with moist PPTS liberated the C35 aldehyde, which was followed by introduction of the *N*-methylvinylformamide by condensation with HNMeCHO to give **162**. Finally, liberation of the C3 hydroxy group completed the first total synthesis of mycalolide A (**12**) in about 1% overall yield over 26 steps for the longest linear sequence (55 total steps).



Scheme 28. Synthesis of the C20 – C35 segment **144** of mycalolide A (**12**) according to Panek et al.[43]

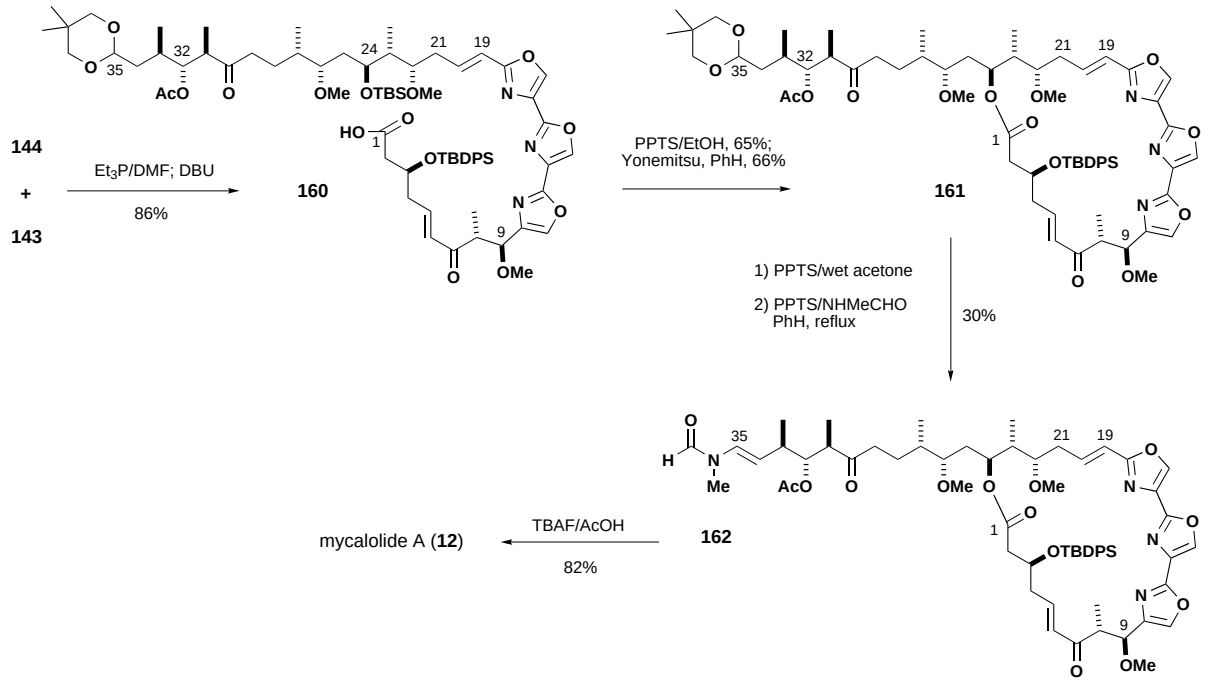


Scheme 29. Synthesis of the C1 – C19 segment **143** of mycalolide A (**12**) according to Panek et al.[43]

3. Conclusions and Outlook

As described above, different synthetic strategies and methodologies have been applied to the total synthesis of these structurally complex, actin-binding, marine macrolides. The successful total syntheses of swinholide A (**5**), scytophycin C (**8**), aplyronine A (**10**), and mycalolide A (**12**) highlight the level of progress and the state of the art in contemporary organic synthesis. However, it also demonstrates the pressing demand for realizing even more efficient and scaleable synthetic pathways to provide cost-effective routes to these rare compounds, and their analogues, for biological studies and preclinical evaluation. This is particularly important where the isolation of the natural material from the marine organism is severely limited and ecologically unacceptable. Significant synthetic challenges still remain in the areas of 1) developing more efficient asymmetric reactions for setting up multiple stereogenic centers in acyclic situations and for the construction of ring systems (e.g. dihydropyrans); 2) devising general strategies and methodologies for the efficient coupling of highly functionalized, advanced segments; 3) minimizing the use of functional group protection and deprotection steps, as well as oxidation state adjustments; 4) achieving high yielding macrocyclization reactions to provide the large ring sizes (22- to 44-membered) commonly associated with this class of compounds. A compelling (and hopefully achievable) synthetic goal is to be able to design highly convergent routes to these rare marine macrolides that require an average of one step per stereogenic center (e.g. ca. 15 linear steps for scytophycin C) and are efficient enough in practice to be able to deliver useful quantities for extensive biological studies. In the future, the full configurational assignments of some other actin-binding macrolides (e.g. the ulapualides, kabiramides, sphinxolide, reidispongiolides, etc.) are likely to be determined by stereocontrolled total synthesis.

Finally, the total synthesis of these bioactive marine macrolides sets the foundation for the design and preparation of novel structural analogues that may have distinct actin-binding properties, enabling more wide-ranging biological studies of the actin cytoskeleton. Notably, a small structural difference in swinholide A (**5**) relative to misakinolide A (**6**) imparts a wholly different mode of interaction with actin, similar to those of different classes of actin-binding proteins. These novel molecular probes, based on these structurally



Scheme 30. Total synthesis of mycalolide A (**12**) according to Panek et al.[43]

unique marine natural products, are expected to be increasingly valuable in further advancing our understanding of actin organization, as well as unveiling hitherto unknown cellular functions of actin.

The background picture used in the frontspiece is provided by courtesy of the National Oceanic and Atmospheric Administration and Florida Keys National Marine Sanctuary.

Abbreviations

9-BBN	9-borabicyclo[3.3.1]nonane
CSA	camphorsulfonic acid
DBU	1,8-diazabicyclo[5.4.0]undec-7-ene
DCC	*N*,*N*-dicyclohexylcarbodiimide
DDQ	2,3-dichloro-5,6-dicyano-1,4-benzoquinone
DMAP	4-(dimethylamino)pyridine
HKR	hydrolytic kinetic resolution
HMPA	hexamethylphosphoramide
HWE	Horner – Wadsworth – Emmons
LDA	lithium diisopropylamide
LiHMDS	lithium hexamethyldisilylamide
MOM	methoxymethyl
MTM	(methylthio)methyl
NBS	*N*-bromosuccinimide
OTf	trifluoromethanesulfonate
Piv	pivaloyl
PMB	*para*-methoxybenzyl
PMP	*para*-methoxyphenyl
PPTS	pyridinium *para*-toluenesulfonate
Py	pyridine
SAMP	(*S*)-(−)-1-amino-2-methoxymethyl pyrrolidine
TBAF	tetrabutylammonium fluoride
TBDPS	*tert*-butyldiphenylsilyl
TBS	*tert*-butyldimethylsilyl
TES	triethylsilyl
TFA	trifluoroacetic acid
TFAA	trifluroacetic anhydride
TIPS	triisopropylsilyl
TMS	trimethylsilyl
TPAP	tetrapropylammonium perruthenate
Tr	triphenylmethyl
TsOH	*p*-toluenesulfonic acid

Received: April 2, 2002 [A549]

[1] P. Sheterline, J. Clayton, J. C. Sparrow, *Actin*, 4th ed., Oxford University Press, New York, **1999**.
[2] For a recent review see: D. G. I. Kingston, *Chem. Commun.* **2001**, *10*, 867 – 880.
[3] L. He, G. A. Orr, S. B. Horwitz, *Drug Discovery Today* **2001**, *6*, 1153 – 1164.
[4] Y. Gachet, S. Tournier, J. B. A. Millar, J. S. Hyams, *Nature* **2001**, *412*, 352 – 355.
[5] a) L. A. Cameron, P. A. Giardini, F. S. Soo, J. A. Theriot, *Nat. Rev. Mol. Cell Biol.* **2000**, *1*, 110 – 119; b) A. Ploubidou, M. Way, *Curr. Opin. Cell Biol.* **2001**, *13*, 97 – 105.
[6] a) M. A. Jordan, L. Wilson, *Curr. Opin. Cell Biol.* **1998**, *10*, 123 – 130; b) P. A. Janmey, C. Chaponnier, *Curr. Opin. Cell Biol.* **1995**, *7*, 111 – 117.
[7] a) T. P. Stossel, J. Hartwig, D. Kwiatkowski, P. Allen, The Cell Biology and Cytoskeleton Group Home Page, http://zk.bwh.harvard.edu; b) T. P. Stossel, *J. Biol. Chem.* **1989**, *264*, 18261 – 18264.
[8] T. D. Pollard, L. Blanchoin, R. D. Mullins, *Annu. Rev. Biophys. Biomol. Struct.* **2000**, *29*, 545 – 576.
[9] a) I. Spector, F. Braet, N. R. Shochet, M. Bubb, *Microsc. Res. Tech.* **1999**, *47*, 18 – 37; b) S-y. Saito, H. Karaki, *Clin. Exp. Pharmacol. Physiol.* **1996**, *23*, 743 – 746.
[10] J. A. Cooper, *J. Cell Biol.* **1987**, *105*, 1473 – 1478.
[11] I. Spector, N. R. Shochet, Y. Kashman, A. Groweiss, *Science* **1983**, *219*, 493 – 495.

[12] a) S. Carmely, Y. Kashman, *Tetrahedron Lett.* **1985**, *26*, 511 – 514; b) Y. Kato, N. Fusetani, S. Matsunaga, K. Hashimoto, R. Sakai, T. Higa, Y. Kashman, *Tetrahedron Lett.* **1987**, *28*, 6225 – 6228; c) M. Kobayashi, J. Tanaka, T. Katori, M. Matsuura, M. Yamashita, I. Kitagawa, *Chem. Pharm. Bull.* **1990**, *38*, 2409 – 2418; d) M. Doi, T. Ishida, M. Kobayashi, I. Kitagawa, *J. Org. Chem.* **1991**, *56*, 3629 – 3632, and references therein; e) S. Tsukamoto, M. Ishibashi, T. Sasaki, J. Kobayashi, *J. Chem. Soc. Perkin Trans. 1* **1991**, 3185 – 3188; f) J. S. Todd, K. A. Alvi, P. Crews, *Tetrahedron Lett.* **1992**, *33*, 441 – 442; g) M. Kobayashi, K. Kawazoe, T. Okamoto, T. Sasaki, I. Kitagawa, *Chem. Pharm. Bull.* **1994**, *42*, 19 – 26.

[13] a) M. Ishibashi, R. E. Moore, G. M. L. Patterson, C. Xu, J. Clardy, *J. Org. Chem.* **1986**, *51*, 5300 – 5306; b) R. E. Moore, G. M. L. Patterson, J. S. Mynderse, J. Barchi, Jr., T. R. Norton, E. Furusawa, S. Furusawa, *Pure Appl. Chem.* **1986**, *58*, 263 – 271; c) S. Carmeli, R. E. Moore, G. M. L. Patterson, *J. Nat. Prod.* **1990**, *53*, 1533 – 1542.

[14] a) K. Yamada, M. Ojika, T. Ishigaki, Y. Yoshida, H. Ekimoto, M. Arakawa, *J. Am. Chem. Soc.* **1993**, *115*, 11 020 – 11 021; b) M. Ojika, H. Kigoshi, T. Ishigaki, T. Tsuboi, T. Ogawa, K. Yamada, *J. Am. Chem. Soc.* **1994**, *116*, 7441 – 7442.

[15] a) G. Guella, I. Mancini, G. Chiasera, F. Pietra, *Helv. Chim. Acta* **1989**, *72*, 237 – 246; b) M. V. D'Auria, L. Gomez-Paloma, L. Minale, A. Zampella, J. F. Verbist, C. Roussakis, C. Debitus, *Tetrahedron* **1993**, *49*, 8657 – 8664; c) M. V. D'Auria, L. Gomez-Paloma, L. Minale, A. Zampella, J. F. Verbist, C. Roussakis, C. Debitus, J. Patissou, *Tetrahedron* **1994**, *50*, 4829 – 4834; d) C. Bassarello, G. Bifulco, A. Zampella, M. V. D'Auria, R. Riccio, L. Gomez-Paloma, *Eur. J. Org. Chem.* **2001**, 39 – 44.

[16] a) N. Fusetani, K. Yasumuro, S. Matsunaga, K. Hashimoto, *Tetrahedron Lett.* **1989**, *30*, 2809 – 2812; b) M. A. Rashid, K. R. Gustafson, J. H. Cardellina II, M. R. Boyd, *J. Nat. Prod.* **1995**, *58*, 1120 – 1125; c) S. Matsunaga, T. Sugawara, N. Fusetani, *J. Nat. Prod.* **1998**, *61*, 1164 – 1167; d) S. Matsunaga, P. Liu, C. A. Celatka, J. S. Panek, N. Fusetani, *J. Am. Chem. Soc.* **1999**, *121*, 5605 – 5606.

[17] a) J. A. Rosener, P. J. Scheuer, *J. Am. Chem. Soc.* **1986**, *108*, 846 – 847; b) S. Matsunaga, N. Fusetani, K. Hashimoto, *J. Am. Chem. Soc.* **1986**, *108*, 847 – 849; c) M. R. Kerman, T. F. Molinski, D. J. Faulkner, *J. Org. Chem.* **1988**, *53*, 5014 – 5020; d) S. Matsunaga, N. Fusetani, K. Hashimoto, K. Koseki, M. Noma, H. Noguchi, U. Sankawa, *J. Org. Chem.* **1989**, *54*, 1360 – 1363.

[18] a) J. Kobayashi, M. Ishibashi, *Chem. Rev.* **1993**, *93*, 1753 – 1769; b) C. A. Bewley, N. D. Holland, D. J. Faulkner, *Experientia* **1996**, *52*, 716 – 722.

[19] a) C. D. Smith, S. Carmeli, R. E. Moore, G. M. L. Patterson, *Cancer Res.* **1993**, *53*, 1343 – 1347; b) X. Zhang, L. Minale, A. Zampella, C. D. Smith, *Cancer Res.* **1997**, *57*, 3751 – 3758.

[20] G. M. L. Patterson, C. D. Smith, L. H. Kimura, B. A. Britton, S. Carmeli, *Cell Motil. Cytoskeleton* **1993**, *24*, 39 – 48.

[21] a) M. R. Bubb, I. Spector, A. D. Bershadsky, E. D. Korn, *J. Biol. Chem.* **1995**, *270*, 3463 – 3466; b) M. R. Bubb, I. Spector, *Methods Enzymol.* **1998**, *298*, 26 – 32.

[22] a) D. R. Terry, I. Spector, T. Higa, M. R. Bubb, *J. Biol. Chem.* **1997**, *272*, 7841 – 7845; b) S-y. Saito, S. Watabe, H. Ozaki, M. Kobayashi, T. Suzuki, H. Kobayashi, N. Fusetani, H. Karaki, *J. Biochem.* **1998**, *123*, 571 – 578.

[23] S. Saito, S. Watabe, H. Ozaki, H. Kigoshi, K. Yamada, N. Fusetani, H. Karaki, *J. Biochem.* **1996**, *120*, 552 – 555.

[24] a) M. Hori, S. Saito, Y. Z. Shin, H. Ozaki, N. Fusetani, H. Karaki, *FEBS Lett.* **1993**, *322*, 151 – 154; b) S. Saito, S. Watabe, H. Ozaki, N. Fusetani, H. Karaki, *J. Biol. Chem.* **1994**, *269*, 29 710 – 29 714; c) S. Wada, S. Matsunaga, S-y. Saito, N. Fusetani, S. Watabe, *J. Biochem.* **1998**, *123*, 946 – 952.

[25] L. D. Belmont, G. M. L. Patterson, D. G. Drubin, *J. Cell Sci.* **1999**, *112*, 1325 – 1336.

[26] L. D. Belmont, A. Orlova, D. G. Drubin, E. H. Egelman, *Proc. Natl. Acad. Sci. USA* **1999**, *96*, 29 – 34.

[27] L. R. Otterbein, P. Graceffa, R. Dominguez, *Science* **2001**, *293*, 708 – 711.

[28] For a review on the total synthesis of bioactive marine macrolides, see: R. D. Norcross, I. Paterson, *Chem. Rev.* **1995**, *95*, 2041 – 2114.

[29] a) I. Paterson, K.-S. Yeung, R. A. Ward, J. D. Smith, J. G. Cumming, S. Lamboley, *Tetrahedron* **1995**, *51*, 9467 – 9486; b) I. Paterson, R. A. Ward, J. D. Smith, J. G. Cumming, K.-S. Yeung, *Tetrahedron* **1995**, *51*, 9437 – 9466; c) I. Paterson, J. D. Smith, R. A. Ward, *Tetrahedron* **1995**, *51*, 9413 – 9436; d) I. Paterson, J. G. Cumming, R. A. Ward, S. Lamboley, *Tetrahedron* **1995**, *51*, 9393 – 9412; e) I. Paterson, K.-S. Yeung, R. A. Ward, J. G. Cumming, J. D. Smith, *J. Am. Chem. Soc.* **1994**, *116*, 9391 – 9392; f) I. Paterson, J. D. Smith, R. A. Ward, J. G. Cumming, *J. Am. Chem. Soc.* **1994**, *116*, 2615 – 2616.

[30] The regioselective macrolactonization of unprotected 1,2-diols in sterically demanding environments has been demonstrated in the construction of the 42-membered macrolactone of the altohyrtins/spongistatins: a) D. A. Evans, B. W. Trotter, B. Côté, P. J. Coleman, L. C. Dias, A. N. Tyler, *Angew. Chem.* **1997**, *109*, 2957 – 2961; *Angew. Chem. Int. Ed. Engl.* **1997**, *36*, 2744 – 2747; b) D. A. Evans, B. W. Trotter, P. J. Coleman, B. Côté, L. C. Dias, H. A. Rajapakse, A. N. Tyler, *Tetrahedron* **1999**, *55*, 8671 – 8726; c) J. Guo, K. J. Duffy, K. L. Stevens, P. I. Dalko, R. M. Roth, M. M. Hayward, Y. Kishi, *Angew. Chem.* **1998**, *110*, 198 – 202; *Angew. Chem. Int. Ed.* **1998**, *37*, 187 – 192; d) M. M. Hayward, R. M. Roth, K. J. Duffy, P. I. Dalko, K. L. Stevens, J. Guo, Y. Kishi, *Angew. Chem.* **1998**, *110*, 202 – 206; *Angew. Chem. Int. Ed.* **1998**, *37*, 192 – 196; e) A. B. Smith III, Q. Lin, V. A. Doughty, L. Zhuang, M. D. McBriar, J. K. Kerns, C. S. Brook, N. Murase, K. Nakayama, *Angew. Chem.* **2001**, *113*, 202 – 205; *Angew. Chem. Int. Ed.* **2001**, *40*, 196 – 199; f) I. Paterson, D. Y.-K. Chen, M. J. Coster, J. L. Aceña, J. Bach, K. R. Gibson, L. E. Keown, R. M. Oballa, T. Trieselmann, D. J. Wallace, A. P. Hodgson, R. D. Norcross, *Angew. Chem.* **2001**, *113*, 4179 – 4184; *Angew. Chem. Int. Ed.* **2001**, *40*, 4055 – 4060; g) M. T. Crimmins, J. D. Katz, D. G. Washburn, S. P. Allwein, L. F. McAtee, *J. Am. Chem. Soc.* **2002**, *124*, 5661 – 5663. For an early example of this strategy, as used in the total synthesis of bryostatin, see: M. Kageyama, T. Tamura, M. H. Nantz, J. C. Roberts, P. Somfai, D. C. Whritenour, S. Masamune, *J. Am. Chem. Soc.* **1990**, *112*, 7407 – 7408.

[31] a) K. C. Nicolaou, A. P. Patron, K. Ajito, P. K. Richter, H. Khatuya, P. Bertinato, R. A. Miller, M. J. Tomaszewski, *Chem. Eur. J.* **1996**, *2*, 847 – 868; b) K. C. Nicolaou, K. Ajito, A. P. Patron, H. Khatuya, P. K. Richter, P. Bertinato, *J. Am. Chem. Soc.* **1996**, *118*, 3059 – 3060; c) A. P. Patron, P. K. Richter, M. J. Tomaszewski, R. A. Miller, K. C. Nicolaou, *J. Chem. Soc. Chem. Commun.* **1994**, 1147 – 1150; d) P. K. Richter, M. J. Tomaszewski, R. A. Miller, A. P. Patron, K. C. Nicolaou, *J. Chem. Soc. Chem. Commun.* **1994**, 1151 – 1152.

[32] a) For another total synthesis of preswinholide A, see: K. Nagasawa, I. Shimizu, T. Nakata, *Tetrahedron Lett.* **1996**, *37*, 6885 – 6888; K. Nagasawa, I. Shimizu, T. Nakata, *Tetrahedron Lett.* **1996**, *37*, 6881 – 6884; b) for some other synthetic studies on swinholide A, see: G. E. Keck, G. D. Lundquist, *J. Org. Chem.* **1999**, *64*, 4482 – 4491; H. Hayakawa, M. Miyashita, *J. Chem. Soc. Perkin Trans. 1* **1999**, 3399 – 3401.

[33] a) I. Paterson, K.-S. Yeung, C. Watson, R. A. Ward, P. A. Wallace, *Tetrahedron* **1998**, *54*, 11 935 – 11 954; b) I. Paterson, C. Watson, K.-S. Yeung, R. A. Ward, P. A. Wallace, *Tetrahedron* **1998**, *54*, 11 955 – 11 970; c) I. Paterson, C. Watson, K.-S. Yeung, P. A. Wallace, R. A. Ward, *J. Org. Chem.* **1997**, *62*, 452 – 453.

[34] a) I. Paterson, K.-S. Yeung, J. B. Smaill, *Synlett* **1993**, 774 – 776; b) C. Alvarez-Ibarra, S. Arias, G. Bañón, M. J. Fernández, M. Rodríguez, V. Sinisterra, *J. Chem. Soc. Chem. Commun.* **1987**, 1509 – 1511.

[35] I. Paterson, C. Cowden, C. Watson, *Synlett* **1996**, 209 – 211.

[36] For other synthetic studies on scytophycin C, see: a) K. W. Hunt, P. A. Grieco, *Org. Lett.* **2002**, *4*, 245 – 248; b) W. R. Roush, G. J. Dilley, *Tetrahedron Lett.* **1999**, *40*, 4955 – 4959; c) P. A. Grieco, J. D. Speake, *Tetrahedron Lett.* **1998**, *39*, 1275 – 1278.

[37] a) H. Kigoshi, K. Suenaga, T. Mutou, T. Ishigaki, T. Atsumi, H. Ishiwata, A. Sakakura, T. Ogawa, M. Ojika, K. Yamada, *J. Org. Chem.* **1996**, *61*, 5326 – 5351; b) H. Kigoshi, M. Ojika, T. Ishigaki, K. Suenaga, T. Mutou, T. A. Sakakura, T. Ogawa, K. Yamada, *J. Am. Chem. Soc.* **1994**, *116*, 7443 – 7444.

[38] a) H. Kigoshi, K. Suenaga, M. Takagi, A. Akao, K. Kanematsu, N. Kamei, Y. Okugawa, K. Yamada, *Tetrahedron* **2002**, *58*, 1075 – 1102; b) K. Suenaga, N. Kamei, Y. Okugawa, M. Takagi, A. Akao, H. Kigoshi, K. Yamada, *Bioorg. Med. Chem. Lett.* **1997**, *7*, 269.

[39] a) I. Paterson, C. J. Cowden, M. D. Woodrow, *Tetrahedron Lett.* **1998**, *39*, 6037 – 6040; b) I. Paterson, M. D. Woodrow, C. J. Cowden,

Tetrahedron Lett. **1998**, *39*, 6041 – 6041; c) I. Paterson, C. J. Cowden, V. S. Rahn, M. D. Woodrow, *Synlett* **1998**, 915 – 917.

[40] Marshall has reported the synthesis of C5 – C20 and C21 – C34 segments of the aplyronines using chiral allenylindium reagents: J. A. Marshall, B. A. Johns, *J. Org. Chem.* **2000**, *65*, 1501 – 1510.

[41] a) S. K. Chattopadhyay, J. Kempson, A. McNeil, G. Pattenden, M. Reader, D. E. Rippon, D. Waite, *J. Chem. Soc. Perkin Trans. 1* **2000**, 2415 – 2428; b) S. K. Chattopadhyay, G. Pattenden, *J. Chem. Soc. Perkin Trans. 1* **2000**, 2429 – 2454; c) S. K. Chattopadhyay, G. Pattenden, *Tetrahedron Lett.* **1998**, *39*, 6095 – 6098.

[42] J. Maddock, G. Pattenden, P. G. Wight, *J. Comput. Aided Mol. Des.* **1993**, *7*, 573.

[43] a) J. S. Panek, P. Liu, *J. Am. Chem. Soc.* **2000**, *122*, 11 090 – 11 097; b) P. Liu, J. S. Panek, *J. Am. Chem. Soc.* **2000**, *122*, 1235 – 1236; c) P. Liu, C. A. Celatka, J. S. Panek, *Tetrahedron Lett.* **1997**, *38*, 5445 – 5448; d) J. S. Panek, R. T. Beresis, C. A. Celatka, *J. Org. Chem.* **1996**, *61*, 6494 – 6495.

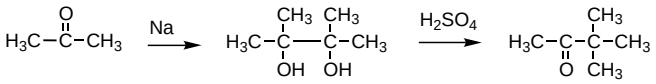
What Is a Discovery? Carbon Skeletal Rearrangements as Counter-Examples to the Rule of Minimal Structural Change

Jerome A. Berson*

Dedicated to Professor Waldemar Adam on the occasion of his 65th birthday

The Pinacol Rearrangement

Today we know that the pinacol rearrangement is the reaction **2** →**3** shown in Scheme 1. Its emergence presaged the enormous wealth and variety of carbocationic transformations so central to modern organic chemistry. The history of how this reaction came to light records a major upheaval in chemical thought. It also raises again the vexatious question of just what we mean by the word "discovery".



acetone (**1**) pinacol (**2**) pinacolone (**3**)

Scheme 1. From acetone to pinacolone.

Structure and Reactions

Chemists will be familiar with Kekulé's seminal paper of 1858[1] in which he not only lays down the basis for representing the *structures* of organic compounds, but also puts forward two rules for *chemical transformations*. The first rule describes simple reactions, in which the reactant gives a product containing the same number of carbon atoms. Kekulé assumes that this will change peripheral atoms or groups but leave the structure of the carbon skeleton unchanged.

The second rule proposes that in other reactions which disrupt the carbon skeleton itself and give products with fewer numbers of carbon atoms than the reactant, the carbon atoms of the fragments have the same mutual attachments as they had in the intact reactant. Then the chemist mentally can recombine the fragments and thereby deduce the structure of the original molecule.

Both of the rules derive from the same more general idea, which came to be called the principle of minimal structural change. We recognize in the rules the foundations of two great branches of organic chemistry. The first rule really provides the source of our confidence that we can undertake a multistep synthesis of an organic compound with a strong expectation of eventually arriving at the correct structure. The second is the basis of the determination of molecular structure by degradative analysis.

Of course, Kekulé was making a bold extrapolation from his examination of the small number of organic molecules then available. Chemists today accept the possibility of violations of the rule of minimal structural change, but I think we may not be aware of how fiercely many chemists clung to it and thus delayed the recognition of a new chemical principle.

A rearrangement of the carbon skeleton is itself the definitive violation of the rule. The first such violations to be recognized were the transformations of pinacol to pinacolone, described here, and of benzil to benzilic acid.

That the pinacol rearrangement does not bear the name of a discoverer is especially puzzling, although, as we shall see, not unjust. During much of the 20th century and continuing now, most reviews that attempt to trace the development of this reaction (I have found no less than eight in this category) come to the quite definite conclusion that the discoverer was Rudolf Fittig. I quote from only one of these, written in 1938[2] where two papers of Fittig are mentioned: ref. [3] and ref. [4]. The reactions mentioned are those shown in Scheme 1, which started with acetone (**1**).

> *"In 1859 Fittig published the results of a series of experiments which he had made in a study of the reducing action of sodium on acetone. The compound pinacol was obtained. In the following year he published a paper which showed that if this substance be heated with sulfuric acid a ketone, pinacolone, is produced. Numerous examples of this reaction, now known as the pinacol rearrangement, have been found since the time of Fittig's discovery…"*

It will become clear that the form of these statements is misleading. The literature of the time shows that Fittig's experiments had entirely different objectives and were not

[*] Prof. J. A. Berson
Department of Chemistry
Yale University
New Haven, CT 06520-8107 (USA)
Fax: (+1) 203-432-6144
E-mail: jerome.berson@yale.edu

 © 2002 WILEY-VCH Verlag GmbH & Co. KGaA, Weinheim 1433-7851/02/4124-4655 $ 20.00+.50/0

knowingly directed toward "a study of the reducing action of sodium on acetone". First of all, he did not know the structure of acetone, he did not even know its atomic composition or those of pinacol or pinacolone. Therefore, he could not have known that pinacol had been formed by a reduction. Further, he did not know that the substance pinacolone, to which pinacol was transformed by acid, was a ketone, and he certainly did not know it was formed by a rearrangement. Consequently, we must question whether the terminology "Fittig's discovery" is appropriate. Later in this paper, I argue that Fittig's work was a necessary part of the eventual full discovery but by itself fell well short of meriting that term. I propose to show that not only did Fittig not really discover the pinacol rearrangement, but in fact, he could not have done so at the time he worked on the problem.

The Early History

The discovery of the pinacol rearrangement was not a sudden event. It was a process which actually took about fifteen years, from 1859 – 1874. That was a crucial period in the history of organic chemistry, one which embodied what Alan Rocke has called a "quiet revolution"[5, 6] in the whole conceptualization of the science.

The Atomic Weight Controversy and the Rise of Structural Theory

Before the advent of the structural theory in 1858, the basic principles of organic chemistry were a turmoil of conflicting ideas expressed in several different notations. Not only were the protagonists constantly in battle over their theories, but they sometimes abandoned their positions to join the opponents on one point or another. By the middle of the 19th century, the chemical community faced a crisis over the issue of atomic weights. After several decades of dispute, many chemists had reached a consensus on the values of the atomic weights of the most common elements found in organic chemistry. These were the "conventional" weights[7] $H = 1$, $C = 6$, $O = 8$, and so on. Also in use at that time was the less popular set of weights proposed by Berzelius, and adopted with little change by a "reform" group. These are close to the modern values.

Note that the conventional atomic weights lead to molecular formulas that look strange to the present-day chemist: Methane would be CH_2 or a higher multiple instead of $(CH_4)_n$, ethanol C_2H_3O or $(C_2H_3O)_n$ instead of C_2H_6O, to name two examples. One way to think about the differences is to recognize that the modern atomic weights would require that for a given number of hydrogen atoms, the number of carbon and oxygen atoms would each have to be half the number in the conventional formulas.

Prominent among the reform group were the "structuralists," notably Kekulé, Couper, and Butlerov.[5, 8] Their analysis of structure, as given, for example, in Kekulé's textbook,[9] depended on the assumption of the "reformed" atomic weights. How the atomic weight controversy ultimately was resolved makes a fascinating story which historians have treated extensively.[5, 6, 8] Although we cannot review all of that history here, one important theme must be stressed. In the late 1850s it became increasingly clear that no internally consistent set of structures for the known organic compounds could be devised using the conventional atomic weights. As Kekulé and his co-structuralists realized, to solve the problem of structure, it is essential to have both a set of correct weights and a set of correct valences. The "reformed" atomic weights, together with a set of valences with $C = 4$, $O = 2$, $Cl = 1$, $H = 1$, etc., led in a straightforward manner to satisfactory structural formulas for known compounds and to verifiable predictions of new structures. Thus, self-consistency now required that the reformed atomic weights be accepted.

In fact, many chemists were now quietly[10] converted to the new atomic weights perforce: If one wanted to apply the powerful new structural theory, one could hardly argue at the same time that the conventional atomic weights were correct. The early events of the pinacol rearrangement story took place in 1858 – 1860 and thus coincided with this major discontinuity in the development of organic chemistry.

The structuralists did not hesitate to point out that those chemists (and there were many) who adhered to the conventional atomic weights suffered a disabling handicap in their attempts to determine molecular structure. The first requirement of that process must be to count the number and kind of atoms. The conventional atomic weights gave a completely erroneous measure of those properties, and chemists who used those weights thus had no chance to determine the structure of any compound. It is important to know that Fittig, the putative discoverer of the pinacol rearrangement, was one of those who at that time adhered to the conventional atomic weights system. This fact prevented him from completing that problem. But who was Fittig, and how did he come to be on the wrong side of the atomic weight controversy?

Rudolf Fittig (1835 – 1910)

Fittig was born in Hamburg, Germany in 1835. He was one of many children of a private school principal and was to prove himself a brilliant student. In 1856 Fittig entered the University of Göttingen, where Friedrich Wöhler led the institute of chemistry. Fittig became associated there with Professor Heinrich Limpricht, who held the rank of extraordinary professor (roughly associate professor) and was the leader of a section of organic chemistry. Fittig carried out his early research on the sulfonation of benzamide and toluamide under Limpricht's supervision. The resulting paper appeared in the "Annalen" in 1858 with Fittig as the sole author.[11] It is significant that Limpricht was similarly generous with other students.[12] This relationship with Limpricht will become important in our subsequent discussion.

Fittig went on to a noteworthy career as a professor of organic chemistry, becoming associate professor at Göttingen, moving then to Tübingen and later to Strasbourg. He and his students published almost 400 scientific papers, among which some of the best known are those reporting a modification of the Wurtz synthesis of alkanes to permit the synthesis of alkylarenes (now called the Wurtz – Fittig reaction). There is no doubt that during his time, he was one of the major figures in German organic chemistry.

 © 2002 WILEY-VCH Verlag GmbH & Co. KGaA, Weinheim 1433-7851/02/4124-4656 $ 20.00+.50/0 *Angew. Chem. Int. Ed.* **2002**, *41*, No. 24

The Structure of Acetone; Uncertainty Piled on Obscurity

Fittig's work on the pinacol rearrangement was his first independent research. It grew out of an interest in a readily available substance, acetone. The first real scientific evidence on the nature of acetone had already come in 1832 from the work of Liebig,[13] who determined its elemental percentage composition by combustion analysis. These percentage composition values, derived from the Berzelius (or reformed) atomic weights, of course fit the modern empirical formula of acetone $(C_3H_6O)_n$, where n is an integer. However, with the conventional atomic weights of the mid-19th century, Liebig's results would lead to the formula $(C_3H_3O)_n$.

Pinacol and Pinacolone

During the years before and after the Liebig analysis, several chemists made attempts to determine the chemical nature of acetone. For our purposes, it will be sufficient to focus on one of them, reported in a paper by Löwig and Weidmann in 1840.[14] They were investigating the then-popular idea that acetone was an alcohol and decided to test this by treatment of it with metallic potassium, hoping to obtain a salt. Instead, they found that the main products were mesityl oxide and phorone (resulting from what we now would call an aldol condensation). These are the same products that had previously been observed from the action of potassium hydroxide on acetone.

Fittig started out with the modest objective of repeating the Löwig – Weidmann experiment with sodium instead of potassium. Superficially, one might have expected the two experiments to give similar results, but that was not to be the case.

As we have mentioned, to bring Liebig's determination of the atomic composition of acetone into harmony with the conventional system of atomic weights, Fittig had to convert Liebig's formula C_3H_6O into the incorrect conventional formula C_3H_3O. So his project was in immediate trouble.

Fittig's intention to make and alkylate a sodium salt from acetone might have been considered dubious in view of the failure of Löwig and Weidmann with the *potassium* enolate. Nevertheless, Fittig apparently was encouraged by the work of Ebersbach[15] only a year before his own. Ebersbach had reported an analogous reaction with valeraldehyde and had carried out a successful alkylation of the sodium salt with ethyl iodide. The result of Fittig's similar experiment with acetone was negative, in that he was unable to find the expected alkylation product. However, he did find an unexpected and most interesting substance, which he isolated as large, tablet-shaped crystals and which he called "paraceton." This was the substance that later would be called "pinacol". Fittig's name for this product, paraceton, came from his belief that it was a hydrate of a *dimer* of acetone. Thus, he started out trying to do an alkylation and, in his view, succeeded instead in causing a dimerization.

A rancorous and essentially inconclusive dispute then flared up between Fittig and another chemist, Städeler.[16] The argument centered around the elemental composition of pinacol, but we need not spend much time on it. It was doomed to eventual inconsequentiality, because both chemists used the incorrect conventional atomic weights. Städeler did get one thing right though: He proposed that pinacol was not a dimer of acetone, as Fittig thought, but rather a reduction product of a dimer. Eventually, others showed that Städeler's conclusion was correct. A fair historical treatment thus would be obliged to credit Städeler, not Fittig, with recognizing this.

The Transformation of Pinacol to Pinacolone

Fittig's second paper[4] on this subject, published in 1860, continued the dispute with Städeler but, more significantly, reported an observation that baffled the chemical community for years afterward. Fittig found that heating pinacol with aqueous sulfuric acid or hydrochloric acid gave rise to a new substance now known as pinacolone. The reasoning in his discussion of what the nature of this product might be was quite confusing, but in summary, he believed that pinacolone is an isomer or polymer of the anhydrous form of pinacol.

The problem of representing the *structures* of pinacol and pinacolone remained. No matter how strenuously the two investigators contested the validity of each other's conclusions, their efforts could not bring further progress as long as they adhered to their custom of using the conventional atomic weights. Apparently, they gradually recognized that they had reached an impasse. As far as I have been able to determine, neither Fittig (after 1860) nor Städeler (after 1859) ever published another word about pinacol or pinacolone.

Fittig's Atomic Weight Problem

Before we go on to later developments in this story, we must make clear Fittig's own attitude to the atomic weight issue. It is significant, and puzzling, that by 1859 Fittig had put himself into a self-contradictory position by joining the large number of chemists who were climbing onto the Kekulé bandwagon. Indeed, Rocke[17] already has called attention to a passage from Fittig's diary dated September 17, 1859, in which Fittig describes his profoundly epiphanic reaction to the appearance of the first fasicle of Kekulé's textbook:

> *" … in my opinion, all of the books on organic chemistry known to me cannot bear comparison with it. I read it page by page and with truly intense interest, and in the words said of St. Louis, 'we are all in the true sense students of Kekulé. The field that has been sown with his ideas will be cultivated everywhere and will bear unceasingly the richest harvest."'*

As we have seen, Kekulé made a major point, both in his paper on the structural theory and in his textbook, that the conventional atomic weights must now be abandoned in favor of the reformed weights. Fittig's reaction to the book in September 1859 was an emotional experience almost as intense as a religious conversion. Why then did he continue to adhere to the by then discredited conventional atomic weights in his second paper on pinacol,[4] which was submitted to the "Annalen" several months later, in December 1859?

The answer to this question must be speculative. It does not seem probable that Fittig, despite all his enthusiasm for Kekulé's book, had failed to absorb its central lesson. Fittig, after all, was a highly motivated, conscientious, thorough

 © 2002 WILEY-VCH Verlag GmbH & Co. KGaA, Weinheim 1433-7851/02/4124-4657 $ 20.00+.50/0

chemist. It seems to me unlikely that he would absentmindedly overlook the contradiction between his own line of thinking on constitutional questions and that of Kekulé, which had made such a deep impression on him. I believe a more plausible conjecture is that there were forces external to the chemistry itself that kept him temporarily in thrall to the conventional atomic weights. What might these have been?

Consider that in 1859–1860, the 24-year old Fittig was still dependent on his mentor Limpricht for laboratory space. Moreover, Fittig was sensitive about his personal relationship to Limpricht. From Fittig's diary[18] we learn that he was apprehensive that Limpricht's plans for him to join a project on the sulfonation of benzoic acid derivatives would hamper Fittig's own progress. He even considered leaving Limpricht's laboratory and asking Wöhler for a place. Although the matter was smoothed over when Limpricht eventually allowed Fittig to publish his results from his thesis problem independently, one gets the impression that Fittig was wary about putting himself at cross-purposes with his mentor. We might wonder whether Fittig was being overcautious here, since Limpricht had been quite generous in granting independent publication to Fittig and to other students.[11, 12] Nevertheless, there can be no doubt that Limpricht's name and laboratory would be closely associated with these studies. Limpricht had been engaged in them for some time, and they were a centerpiece of his research program. His (necessarily incorrect) interpretation of the results employed the conventional atomic weights, as was usual for him.

Now as it happened, Kekulé had published the first part of his structural theory in 1857,[19] and in developing his arguments on the quadrivalency of carbon, he used Limpricht's immediately preceding work[12,20] on the sulfonated arenecarboxylic acids to exemplify the erroneous nature of the conventional atomic weights. In fact, in Rocke's words,[21]

> *"These two papers [of Limpricht] gave Kekulé the opportunity he had been looking for to publish his structural ideas, for Limpricht had opened himself to criticism in several ways, and such a critique provided the rhetorical launching platform for more general considerations."*

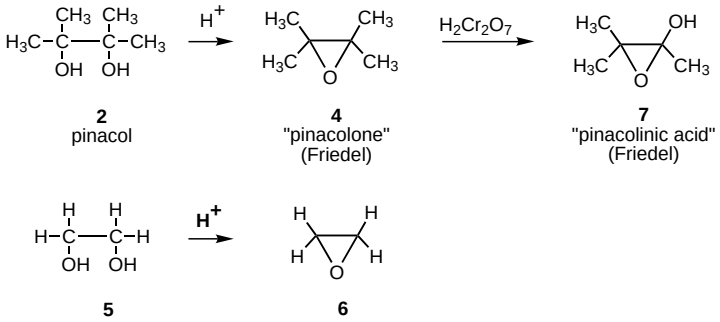
Although Limpricht published a rebuttal,[22] Kekulé soon followed with an expanded counter-rebuttal in the climactic 1858 paper[1] of his structural theory. Limpricht thus found himself battling Kekulé, in a very public arena, over the most significant question in organic chemistry.

Fittig now could not have been unaware of his own vulnerability. Although, by his own words, we know that he was strongly attracted to Kekulé's ideas, he could hardly have ignored the fact that adopting them publicly at that moment would signify a break with his mentor, one which might have been considered an act of disloyalty. For someone in his dependent position, this would have been a risky step indeed. Moreover, as an ambitious and perspicacious young chemist, he would have been wary of an association with what could well turn out to be a prominent defeat for Limpricht. One can only sympathize with his dilemma.

So is it possible that Fittig somehow rationalized and suppressed his own doubts about the conventional atomic weights when he published his 1860 paper[4] on pinacol? Did loyalty and dependency win out over science? I have no evidence on this point, but it is noteworthy that within the following year, Fittig had won laboratory space of his own. He published a paper[23] on another subject in which he once and for all abandoned the conventional atomic weights and adopted the reformed values without dissent and without even mentioning that this step represented a complete turnover in his chemical thinking. In this, he joined many other organic chemists of the time. I think we cannot ignore the possibility that Fittig's awkward personal circumstances at a crucial time may have prevented him from thinking the pinacol problem through to a satisfactory answer.

The Structures of Pinacol and Pinacolone

On the other hand, the advocates of the reformed atomic weights, including Kekulé himself, did not immediately solve the problem either. Foremost among the "pinacolists" in that group was Charles Friedel, who, like Fittig, had been a student of Wurtz. We need not outline here the various inconclusive results and the eventual insight by Friedel that pinacol was tetramethylethylene glycol (**2**, Scheme 1), the structure we recognize today. Perhaps the most important contribution of Friedel's work, summarized in an 1869 paper,[24] was the demonstration that the acid-induced transformation of pinacol to pinacolone is an overall dehydration. This became immediately apparent from the empirical molecular compositions. Friedel proposed that the two compounds are related as **2** and **4**, in the same way that ethylene glycol (**5**) is related to its dehydration product, ethylene oxide (**6**, Scheme 2).



Scheme 2. Structures postulated by Friedel in analogy to ethylene glycol and ethylene oxide.

There followed a stretch of fruitless experimentation and misguided interpretation by Friedel reported in a flurry of papers. However, these contained one important result, again misinterpreted, namely, the finding that pinacolone can be oxidized by dichromate to CO_2 and an acid isomeric with valeric acid. Friedel and Silva at first proposed[25] that this acid, "pinacolinic acid," in contrast to other known organic acids, did not have the usual carboxyl group but instead contained a hydroxyoxirane group, as in **7** (Scheme 2).

The fog surrounding all this chemistry was finally dispelled by two brilliant papers of Alexander Butlerov of St. Petersburg. In the first of these, in 1873,[26a] Butlerov accepted the pinacol structure **2** (Scheme 2) favored by Friedel, but he

 © 2002 WILEY-VCH Verlag GmbH & Co. KGaA, Weinheim 1433-7851/02/4124-4658 $ 20.00+.50/0 *Angew. Chem. Int. Ed.* **2002**, *41*, No. 24

questioned the necessity of the special hypothesis of a unique new kind of acid structure (**7**, Scheme 2) for the oxidation product obtained from pinacolone. He proposed instead that Friedel and Silva's "pinacolinic acid" was in fact trimethylacetic acid, an assignment which he supported by direct synthesis of that compound by formation of trimethylacetonitrile from *t*-butyl iodide and mercuric cyanide followed by hydrolysis. Butlerov noted that his synthetic acid showed properties very similar to those of the pinacolinic acid obtained by Friedel and Silva from pinacolone. Later, Friedel agreed that his acid is "probably identical with trimethylacetic acid."

After having established to his own satisfaction the identity of the acid, Butlerov[26b] forged ahead boldly to suggest that the reaction of pinacol in acidic solution involves a *molecular rearrangement of the carbon skeleton* and dehydration. The product, pinacolone, is simply *t*-butyl methyl ketone (**3**, Scheme 1). He pointed out that such a reaction finds analogy in the already known transformation of ethylene glycol to acetaldehyde.

Friedel and Silva,[27] by some muddled reasoning, criticized Butlerov's analysis. However, Butlerov soon answered with a plan[26b] to confirm his proposal by the synthesis of pinacolone **3** itself from trimethylacetic acid, a task he completed the following year, 1874,[28] by the reaction of trimethylacetyl chloride with dimethylzinc. He considered the proof of the structure of pinacolone then to be complete.

One might argue that in 1874, at a time when chemists did not have reliable means for predicting when molecular rearrangements might occur, Friedel's apparent capitulation on the structure of pinacolone might have been premature. Logically, for example, it was not clear then that Butlerov's synthesis did not itself involve a rearrangement. However, the passage of time rendered such doubts less and less likely. Despite its refutation in the case of the pinacol rearrangement, Kekulé's rule that the connectivity of the carbon skeleton tends to persist throughout a chemical reaction still claimed the adherence of most chemists. For many of them, the acceptance of carbon skeletal rearrangements came only grudgingly and slowly.

Butlerov thus recognized one of the first rearrangements of the carbon skeleton and, in my opinion, deserves credit at least equal to that later assigned largely to Fittig as the discoverer of the pinacol rearrangement. Although Roscoe and Schorlemmer's textbook[29, 30] of 1881 gives a clear account of the importance of Butlerov's work, I have been unable to determine the reasons why 20th century authors slight it or overlook it entirely.

What Is a Discovery?

We now have to face the question: What is a discovery? In the context of science, there is a perception (or misperception) that a discovery takes place in a sharply defined moment of time. I believe that this idea underlies many of the frequent disputes in the scientific literature over priority. Historians of science are well acquainted with this problem and tend to take a more nuanced view. For example, Thomas Kuhn[31] wrote that it is misleading to suggest that discovering something is a simple act, directly cognizable by the senses:

> *"… That is why we so readily assume that discovering, like seeing or touching, should be unequivocally attributable to an individual and to a moment in time. But the latter attribution is always impossible, and the former often is as well … discovering a new sort of phenomenon is necessarily a complex event, one which involves recognizing both* that *something is and* what *it is."*

In the discovery of the pinacol rearrangement, fourteen years elapsed before Butlerov explained Fittig's transformation of pinacol to pinacolone. Applying Kuhn's formula, we can say Fittig found *that* a reaction of pinacol occurred in acidic medium, and it was Butlerov who recognized *what* that reaction was.

Why Worry about Proper Attribution of Credit?

If praise for a discovery is inaccurately assigned, the error has a high probability of being propagated in the literature. But why is it important to assign credit accurately? After all, there are critics of science who ascribe the scientists' obsession with this subject to our enslavement to the false gods of competition and self-promotion. A candid response would be that it is good to be first for some easily listed reasons: our grant proposals, our patent applications, our tenure resumés, and, above all, our egos. Also, simple justice and fair play demand that we try to make the right attribution. I think all of these motivations are real, although perhaps not all are admirable.

However, there is another purpose. That is the need to understand the dynamics and temporal course of the process of discovery itself. Only by this kind of analysis is it possible to apprehend the mutual influences of scientific theories and experiments. Only in this way can the effects of the scientific and cultural milieu of the time on the act of discovery be evaluated. Wrongly assigned credit for a discovery may not only offend against justice, it may distort the historical picture of the event and result in an ignorant, blunted, or superficial description. At the end of the day, we must get the assignment of credit right if we wish to understand how science works.

[1] A. Kekulé, *Justus Liebigs Ann. Chem.* **1858**, *106,* 129.
[2] E. S. Wallis in *Organic Chemistry An Advanced Treatise, Vol. I* (Ed.: H. Gilman), Wiley, New York, **1938**, p. 965.
[3] R. Fittig, *Justus Liebigs Ann. Chem.* **1859**, *110*, 23.
[4] R. Fittig, *Justus Liebigs Ann. Chem.* **1860**, *114*, 54.
[5] A. J. Rocke, *Brit. J. Hist. Sci.* **1981**, *14*, 27.
[6] A. J. Rocke, *The Quiet Revolution: Hermann Kolbe and the Science of Organic Chemistry*, University of California Press, Berkeley, **1993**.
[7] See ref. [6], pp. 71.
[8] A. Ihde, *The Development of Modern Chemistry*, Dover reprint of the original Harper and Row edition, New York, **1964**, chapt. 6.
[9] A. Kekulé, *Lehrbuch der Organischen Chemie, Vol. 1*, Ferdinand Enke, Erlangen, **1861**, p. 1. Kekulé's textbook was published first as a series of fascicles, of which the first fascicle of Volume 1 appeared in 1859.
[10] See ref. [6], pp. 134.
[11] R. Fittig, *Justus Liebigs Ann. Chem.* **1858**, *106,* 277.
[12] O. Mendius, *Justus Liebigs Ann. Chem.* **1857**, *103,* 39.

 © 2002 WILEY-VCH Verlag GmbH & Co. KGaA, Weinheim 1433-7851/02/4124-4659 $ 20.00+.50/0

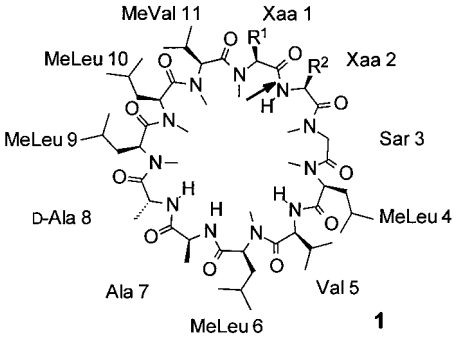
[13] J. Liebig, *Ann. Pharm.* **1832**, *1*, 225.
[14] C. Löwig, S. Weidmann, *J. Prakt. Chem.* **1840**, *21*, 64.
[15] C. Ebersbach, *Justus Liebigs Ann. Chem.* **1858**, *106*, 262.
[16] G. Städeler, *Justus Liebigs Ann. Chem.* **1859**, *111*, 277.
[17] See ref. [6], pp. 172.
[18] F. Fichter, *Ber. Dtsch. Chem. Ges.* **1911**, *44*, 1348. This biographical sketch of Fittig contains several excerpts from his diary.
[19] A. Kekulé, *Justus Liebigs Ann. Chem.* **1857**, *104*, 129.
[20] H. Limpricht, L. von Uslar, *Justus Liebigs Ann. Chem.* **1857**, *102*, 259.
[21] See ref. [6], pp. 168.
[22] H. Limpricht, *Justus Liebigs Ann. Chem.* **1858**, *105,* 177.
[23] R. Fittig, *Justus Liebigs Ann. Chem.* **1861**, *117,* 68.
[24] C. Friedel, *Ann. Chim. Phys. Ser. 4* **1869**, *16*, 310.
[25] C. Friedel, R. Silva, *Ber. Dtsch. Chem. Ges.* **1873**, *6,* 145.
[26] a) A. Butlerov, *Justus Liebigs Ann. Chem.* **1873**, *170,* 151; b) A. Butlerov, *Justus Liebigs Ann. Chem.* **1873**, *170,* 162.
[27] C. Friedel, R. Silva, *Ber. Dtsch. Chem. Ges.* **1873**, *6*, 826.
[28] A. Butlerov, *Justus Liebigs Ann. Chem.* **1874**, *174*, 125.
[29] H. E. Roscoe, C. Schorlemmer, *A Treatise on Organic Chemistry*, *Vol. III, part 1*, Macmillan, London, **1881**, p. 632.
[30] H. E. Roscoe, C. Schorlemmer, *A Treatise on Organic Chemistry, Vol. III, part 2*, Macmillan, London, **1881**, p. 259, 632.
[31] T. S. Kuhn, *The Structure of Scientific Revolutions*, University of Chicago Press, Chicago, **1962**, p. 55.

 © 2002 WILEY-VCH Verlag GmbH & Co. KGaA, Weinheim 1433-7851/02/4124-4660 $ 20.00+.50/0

Efficient, Racemization-Free Peptide Coupling of *N*-Alkyl Amino Acids by Using Amino Acid Chlorides Generated In Situ—Total Syntheses of the Cyclopeptides Cyclosporin O and Omphalotin A**

Norbert Sewald*

Linear or cyclic peptides that contain *N*-alkyl amino acids (e.g. *N*-methyl amino acids, MeXaa), frequently occur in nature and display interesting biological activities. The cyclosporins, a family of about 25 cyclic peptides, are produced by the fungus *Beauveria nivea* (previously designated *Tolypocladium inflatum*). Cyclosporin O (**1b**, Scheme 1)[1] and the well-known relative cyclosporin A (**1a**) are sequence-homologous



1

Scheme 1. Structures of cyclosporin A (**1a**, Xaa 1: MeBmt, $R^1 = CH(OH)$-$CH(CH_3)$-CH_2-(*E*)-CH=CH-CH_3; Xaa 2: Abu, $R^2 = CH_2CH_3$) and cyclosporin O (**1b**, Xaa 1: MeLeu, $R^1 = CH_2$-$CH(CH_3)$; Xaa 2: Nva, $R^2 = CH_2CH_2CH_3$). The arrow marks the macrocylization site in the synthesis of cyclosporin O.

cyclic undecapeptides with antifungal, anti-inflammatory, and immunosuppressive activity. Omphalotin A (**2**), which is structurally related to the cyclosporins, belongs to a family of cyclic dodecapeptides formed by *Omphalotus olearius*. It outweighs known nematicides in vitro with respect to activity and selectivity. This has been interpreted as a hint towards a novel biological mode of action.[2] Cyclosporins and omphalotin A contain several *N*-methyl amino acids (cyclosporin A, O: seven MeXaa; omphalotin A: nine MeXaa). *N*-Alkylation results in a decreased number of possible hydrogen bonds and, consequently, in increased conformational flexibility.

Biosynthesis of the cyclosporins occurs non-ribosomally at the multienzyme complex cyclosporin synthetase (~1600 kDa) according to the thiotemplate mechanism.[3] More than 40 single chemical steps are catalyzed by this enzyme complex en route to the cyclosporins.

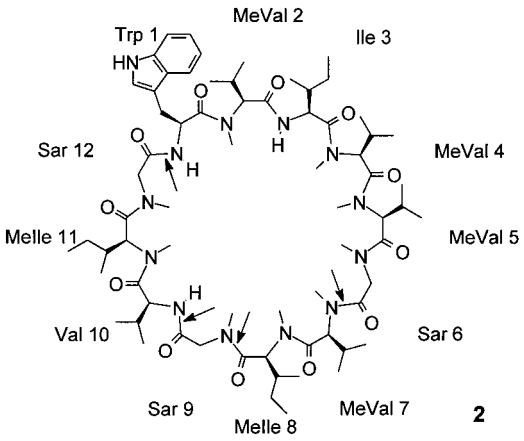
The chemical synthesis of peptides that are rich in *N*-alkyl amino acids faces severe difficulties because of the steric hindrance exerted by the secondary amino groups. Despite the fact that several hundred analogues of cyclosporin A have been obtained chemically after it was synthesized for the first time, there is no generally applicable method for peptide couplings involving *N*-alkyl amino acids. Practically quantitative coupling yields are an indispensable precondition especially in solid-phase peptide synthesis (SPPS), as the separation of the target peptide from core sequences (truncation of the peptide because of unattainable further acylation) or mismatch sequences (omission of amino acids in the sequence because of incomplete peptide coupling) after cleavage from the polymeric support often is impossible even by preparative HPLC.[3] The reactivity of resin-bound secondary amines sometimes is even lower compared to reactions in solution. Slow coupling reactions may be accompanied by undesired side reactions like racemization or diketopiperazine formation. Moreover, peptides containing *N*-alkyl amino acids are acid-labile.

Jung et al. recently reported in two publications on the total syntheses of cyclosporin O[1] (**1b**, Scheme 1) and omphalotin A[2] (**2**, Scheme 2) on solid support in which triphosgene (bis(trichloromethyl)carbonate, BTC) was used as the coupling reagent in accord with a method originally introduced by Gilon et al.[4] Carboxy group activation of N^{α}-protected amino acids by using BTC is likely to succeed through in situ generation of the corresponding acid chloride.[4] Alternatively, mixed anhydrides may be formed. Triphosgene (m.p. 81–83 °C) is a safe replacement of phosgene and diphosgene.[5] Gilon et al. used BTC in combination with collidine as the base in THF at 50 °C to obtain in situ N^{α}-Fmoc-protected amino acid chlorides both from proteinogenic and *N*-alkyl amino acids.[4] The resin-bound peptide is allowed to react with these pre-activated derivatives. These authors also proved that this method is devoid of racemization even for

[*] Prof. Dr. N. Sewald
Organische und Bioorganische Chemie
Universität Bielefeld
Postfach 100131, 33501 Bielefeld (Germany)
Fax: (+49) 521-106-8094
E-mail: norbert.sewald@uni-bielefeld.de

[**] A list of the abbreviations used in this article is located directly before the references.

 © 2002 WILEY-VCH Verlag GmbH & Co. KGaA, Weinheim 1433-7851/02/4124-4661 $ 20.00+.50/0



Scheme 2. Structure of omphalotin A (**2**). The arrows mark the different variants of the macrocyclization.

a sequence containing three consecutive *N*-methyl amino acids.

Amino acid chlorides were used already by Emil Fischer for peptide couplings. However, amino acid halides were reputed for a long time in peptide chemistry to be inappropriate "over-activated" derivatives. During the past decade *N*-urethane-protected amino acid fluorides and chlorides experienced a renaissance as stable and highly efficient building blocks for peptide synthesis due to pioneering contributions by Carpino et al.[6] While the former display a somewhat broader tolerance towards acid-labile functionalities, amino acid chlorides are applied nearly exclusively as N^{α}-Fmoc-protected derivatives.[6] N^{α}-Fmoc-protected amino acid chlorides that require side chain protection by acid-labile groups (Boc, *t*Bu, Trt) for tactical reasons, however, are not sufficiently stable and not accessible in all cases.

The in situ generation of N^{α}-Fmoc amino acid chlorides avoids this problem by the addition of collidine.[4] Jung et al. confirmed that BTC activation is significantly superior to a series of other methods (DCC, DIC/HOAt, in situ generation of amino acid fluorides with TFFH[6]).[2] The formation of diastereomeric peptides by racemization of activated amino acids was not detected. According to these investigations, however, the original protocol by Gilon et al.[4] turned out to be inappropriate for the synthesis of longer peptides. The highly acid-labile TCP resin (trityl anchor on polystyrene, cleavage with hexafluoroisopropyl alcohol) is required because of the pronounced lability of the products towards treatment with stronger acids. It can only be applied if coupling of the in situ generated N^{α}-Fmoc-protected amino acid chloride to the resin-bound peptide is performed in the presence of several equivalents of diisopropylethylamine.[2] Interestingly, elevated reaction temperatures as required according to Gilon et al.[4] are not necessary under these conditions. A similar increase in coupling efficiency by combined application of a weak base for carboxy group activation and a stronger base in the coupling reaction has been described for the system DIC/HOAt.[7]

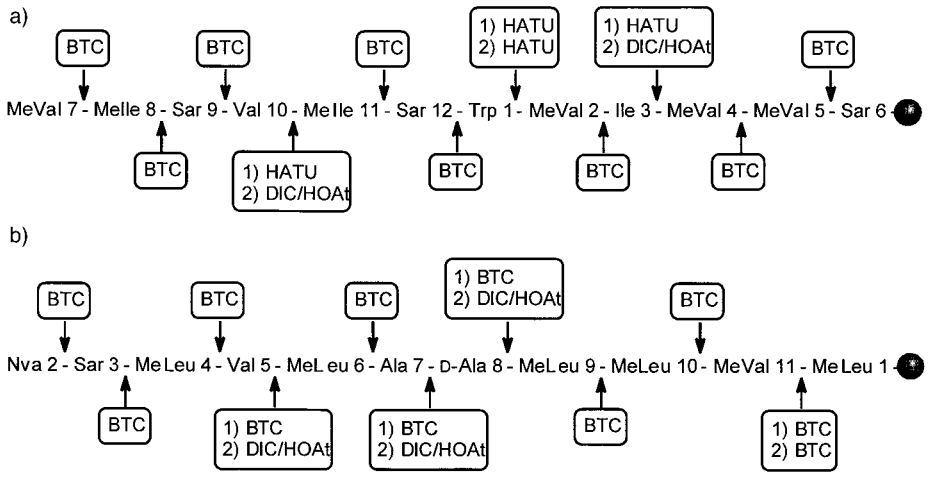
Jung et al. also found that the BTC protocol may be inferior to activation by DIC/HOAt or HATU in coupling of amino acids that are not *N*-alkylated. In such cases double couplings, first with BTC and then with DIC/HOAt or HATU were found to be the method of choice (Scheme 3). The final cyclization of the linear precursors succeeded in all cases with EDC/HOAt.

The coupling steps in the syntheses of **1b** and **2** are displayed in Scheme 3. In the synthesis of omphalotin A (OmA), assembly and cyclization of different linear peptides was examined, starting from resin-bound Sar 12 (OmA(1–12)), Sar 9 (OmA(10–9)), and Sar 6 (OmA(7–6), Scheme 3a), as well as from resin-bound MeIle 8 (OmA(9–8)). Peptide macrocycle formation by activation of a C-terminal sarcosine residue (Sar) has to be preferred, as otherwise considerable epimerization of the C-terminal residue occurs. This was, for instance, observed upon activation of MeIle 8 in the linear peptide OmA(9–8).

In all cases investigated by the authors the BTC method reliably led to quantitative formation of peptide bonds upon activation of N^{α}-Fmoc-protected *N*-methyl amino acids. Thus, Jung et al. have succeeded in establishing a reproducible and generally applicable method for incorporation of these sterically hindered derivatives by modification and optimization of the BTC protocol.[4] This paves the way for a broader application in the synthesis of naturally occurring peptides that contain *N*-methyl amino acids and are characterized by interesting biological properties. Automated parallel syntheses or large-scale syntheses of such peptides and analogues thereof can now be performed reliably.

Abbreviations

Abu: 2-aminobutyric acid; Boc: *tert*-butoxycarbonyl; BTC: bis(trichloromethyl)carbonate; DCC: *N*,*N*′-dicyclohexylcarbodiimide; DIC: *N*,*N*′-diisopropylcarbodiimide; EDC: *N*-



Scheme 3. a) Solid-phase synthesis of the linear precursor of omphalotin A (**2**) suited best for cyclization. b) Solid-phase synthesis of the linear precursor of cyclosporin O (**1b**).

 © 2002 WILEY-VCH Verlag GmbH & Co. KGaA, Weinheim 1433-7851/02/4124-4662 $ 20.00+.50/0

ethyl-*N*′-(3-dimethylaminopropyl)carbodiimide hydrochloride; Fmoc: 9-fluorenylmethoxycarbonyl; HATU: O-(7-azabenzotriazol-1-yl)-1,1,3,3-tetramethyluronium hexafluorophosphate (IUPAC: 1-[bis-(dimethylamino)methyliumyl]-1*H*-1,2,3-triazolo[4,5-*b*]pyridin-3-oxide hexafluorophosphate); HOAt: 1-hydroxy-7-azabenzotriazole; MeBmt: (4*R*)-4[(*E*)-2-butenyl-4,*N*-dimethyl-L-threonine; Nva: norvaline; tBu: *tert*-butyl; TFFH: tetramethylfluoroformamidinium hexafluorophosphate; Trt: triphenylmethyl (trityl).

[1] B. Thern, J. Rudolph, G. Jung, *Tetrahedron Lett.* **2002**, *43*, 5013 – 5016.
[2] B. Thern, J. Rudolph, G. Jung, *Angew. Chem.* **2002**, *114*, 2401 – 2403; *Angew. Chem. Int. Ed.* **2002**, *41*, 2307 – 2309.
[3] N. Sewald, H.-D. Jakubke, *Peptides: Chemistry and Biology*, Wiley-VCH, Weinheim, **2002**.
[4] E. Falb, Y. Yechezkel, Y. Salitra, C. Gilon, *J. Pept. Res.* **1999**, *53*, 507 – 517.
[5] H. Eckert, B. Forster, *Angew. Chem.* **1987**, *99*, 922 – 923; *Angew. Chem. Int. Ed. Engl.* **1987**, *26*, 894 – 895.
[6] L. A. Carpino, M. Beyermann, H. Wenschuh, M. Bienert, *Acc. Chem. Res.* **1996**, *29*, 268 – 274.
[7] L. A. Carpino, A. El-Faham, *Tetrahedron* **1999**, *55*, 6813 – 6830.

New Principles of Protein Structure: Nests, Eggs—and What Next?**

Debnath Pal, Jürgen Sühnel,* and Manfred S. Weiss*

Based on results from refolding experiments on urea-denatured ribonuclease conducted more than 40 years ago, the chemistry nobel laureate Anfinsen formulated the still to a large extent valid paradigm of protein folding: "… *it may be concluded that the information … for the assumption of the native secondary and tertiary structures* (of proteins) *is contained in the amino acid sequence itself.*"[1] As a direct consequence of this, one has to postulate that it should be possible to predict the native structure of a protein from the protein's amino acid sequence alone. However, despite much work of many excellent scientists and a database of experimentally determined protein structures that is increasing frighteningly fast on a daily basis,[2] successes in protein structure prediction are scarce, and the current situation is rather disappointing. The reasons for this are not entirely clear. A large body of experimental information has become available with the boost structural biology has experienced in the last decade and much effort has been put into the thorough analysis of these data over the years,[3–5] but, with the predictive power largely lacking, current knowledge of the basic principles of protein structure is still mainly descriptive. One explanation may be that currently known structural principles do not disclose the complete picture and that new concepts and new ideas are necessary to propel the field from the mainly descriptive into a more predictive mode.

[*] Dr. J. Sühnel, Dr. D. Pal
Institut für Molekulare Biotechnologie
Beutenbergstrasse 11, 07745 Jena (Germany)
Fax: (+49) 3641-656210
E-mail: jsuehnel@imb-jena.de
Dr. M. S. Weiss
EMBL Hamburg Outstation
c/o DESY, Notkestrasse 85, 22603 Hamburg (Germany)
Fax: (+49) 40-89902-149
E-mail: msweiss@embl-hamburg.de

[**] The authors are grateful to E. James Milner-White for introducing them to his nest concept and for stimulating discussions.

In this respect, two interesting papers have been published recently in the *Journal of Molecular Biology*.[6, 7] Based on the analysis of main-chain torsion angles of adjacent amino acid residues, Watson and Milner-White discovered that many anion and cation binding sites (where anions and cations can be any atoms exhibiting a full or a partial negative and positive charge, respectively) in proteins are made up by a sequence of three amino acids of which two exhibit "enantiomeric" main-chain conformations. The term "enantiomeric" refers to the fact that the main-chain torsion angles (ϕ,ψ) of the two adjacent amino acids are approximately inverted about the center of the Ramachandran plot.[3] Whereas successive residues with identical or nearly identical main-chain conformations form α helices, β strands, or polyproline type II helices, adjacent residues with enantiomeric main-chain conformations form so-called "nests" when their (ϕ,ψ)-values are close to ($-90°$,$0°$) and ($+90°$,$0°$) or the other way round.

The term "nest" is derived from the fact that the NH groups of three successive residues obeying this torsion angle criterion form a concave depression which can serve as a binding site for an atom or a group of atoms with a full or partial negative charge. Depending on which combination of the two torsion angle pairs is observed, the nests can be divided into RL nests ($\phi_1,\psi_1 = -90°,0°$; $\phi_2,\psi_2 = +90°,0°$) and LR nests ($\phi_1,\psi_1 = +90°,0°$; $\phi_2,\psi_2 = -90°,0°$). Two or more of these nests can also constitute a compound nest, a tandem nest, or a combination of both with up to eight successive residues involved. In the majority of cases the nests bind to an atom or a group of atoms, which we suggest may, as a binding partner of a "nest", be descriptively and conveniently called an "egg". It is intriguing that many structural motifs described previously, such as Schellman loops, the oxyanion holes of serine proteases, and P loops in ATP- or GTP-binding proteins can be subsumed under this nest/egg concept. If dipeptides with different enantiomeric main-chain torsion angle combinations are considered, the nest/egg concept can

 © 2002 WILEY-VCH Verlag GmbH & Co. KGaA, Weinheim 1433-7851/02/4124-4663 $ 20.00+.50/0

even be extended to cation binding sites,[7] although the experimental evidence for this is not as ample as for the anion-binding nests.[6]

Watson and Milner-White[6, 7] conducted their analysis on a limited data base of 67 protein structures. An extended analysis of their concept in a database about 20 times larger, which had been assembled previously for a different purpose,[8] confirms most of their conclusions and also adds new aspects. As introduced above, nests can be described by the main-chain torsion angles of the two successive amino acids. However, a more convenient description utilizes the two torsion angles involving the NH groups of two successive amino acids and the angle formed by the three nitrogen atoms (Figure 1). Unlike in the Ramachandran plot, where the R and L regions of the RL and LR nests naturally overlap, the two nest classes (RL and LR) form islands clearly separated from each other in the three-dimensional plot shown in Figure 1. The average values of the geometrical parameters are given in Table 1. Two representative structural models of an RL and an LR nest are drawn in Figure 1 and clearly show the concave arrangement of the three NH groups in both cases. Two actual cases are shown in Figure 2.

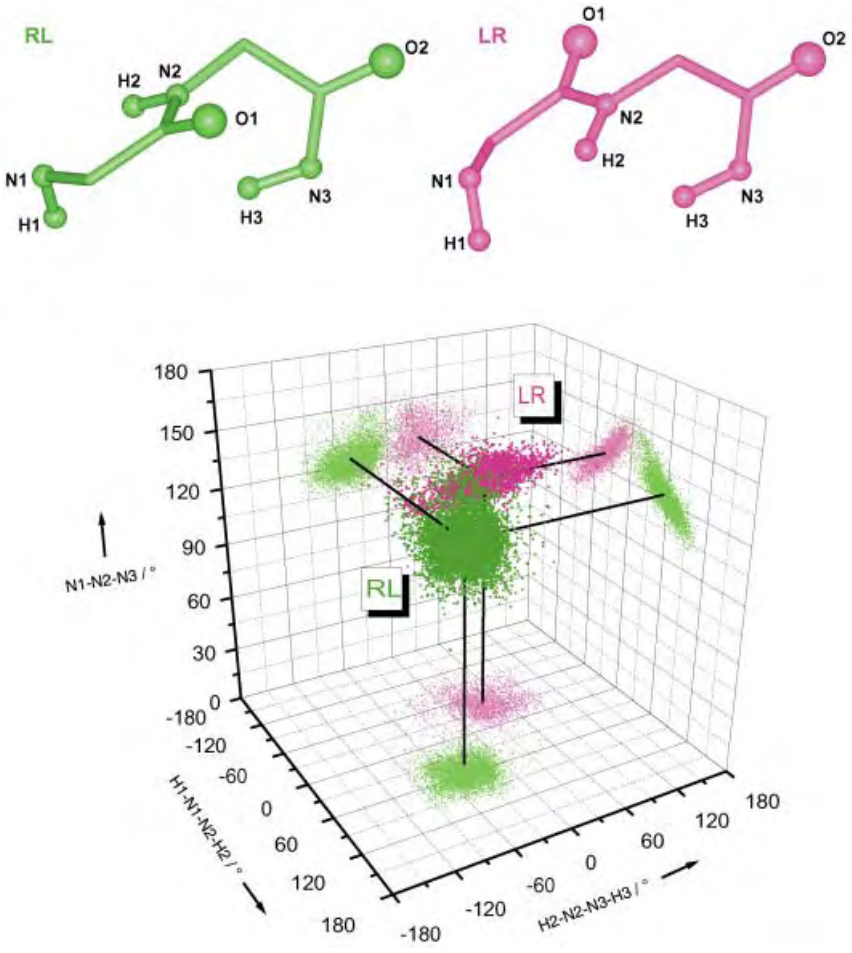


Figure 1. Three-dimensional plot of all amino acid pairs obeying the nest criterion. The three axes are: a) the torsion angle between the four atoms H1-N1-N2-H2; b) the torsion angle between the four atoms H2-N2-N3-H3; and c) the angle between the three nitrogen atoms N1-N2-N3. The RL nests are shown in green and the LR nests in pink. The respective projections are drawn in lighter colors. The mean values of the distributions of the respective parameters above are indicated by solid black lines originating from the islands and projecting onto the three walls of the coordinate system. Two representative structures corresponding approximately to the centers of the distributions of the geometric parameters for the RL and LR motifs are also shown.

Frequencies of nest occurrence in protein structures are given in Table 1 together with the average geometric parameters. Overall, 2.1% of all dipeptides in the database constitute RL nests and about 1.0% LR nests. This brings the total involvement of amino acid residues in nests up to about 5.4%. The next striking observation is the fact that the number of RL nests observed is about double that of LR nests. This effect has already been noted by Watson and Milner-White,[6] although in their case the observed ratio of 4:1 was almost certainly a consequence of the database being too small. At this point, we do not have a good explanation for this prevalence of RL over LR, but the observation seems to imply that the main-chain conformation of amino acids in a polypeptide chain is to some extent determined by the identity of the neighboring residues as well as by their location with respect to chain direction.

Since the L conformation is energetically unfavorable for all amino acids except glycine, it is clear that the majority of the RL nests have to be, and indeed are, of the type Xaa-Gly (61%) and the majority of the LR nests of the type Gly-Xaa (55%). In total, 21% of all glycine residues in proteins are involved in either an RL or an LR nest. This may provide an explanation for the fact that glycine residues are often better conserved than other amino acids.

Nests occur preferentially at the ends of α helices and reverse turns. It is clear from the torsion angle criterion that RL nests are more frequently found at the C-terminal ends of

Table 1. Occurrences and average geometric parameters of the observed nests.

	Total[a]	ϕ_1	ψ_1	ϕ_2	ψ_2	$\sphericalangle H_1N_1N_2H_2$	$\sphericalangle H_2N_2N_3H_3$	$\sphericalangle N_1N_2N_3$
RL[b]	5773	-91°	-5°	$+74^\circ$	$+23^\circ$	$+56^\circ$	-41°	123°
LR[b]	2492	$+72^\circ$	$+21^\circ$	-85°	-22°	-44°	$+38^\circ$	128°

[a] The data base used contained 1154 protein chains, 285 794 amino acids, and 280 563 dipeptides (terminal residues were excluded from the list of dipeptides, because only one main-chain torsion angle can be defined for a terminal amino acid residue).[8] [b] R: $-140^\circ < \phi < -20^\circ$; $-90^\circ < \psi < +40^\circ$; L: $+20^\circ < \phi < +140^\circ$; $-40^\circ < \psi < +90^\circ$; the peptide bond in between the two amino acids is always in the *trans* conformation in both the RL and LR nests. The average values for ϕ and ψ angles of the R and the L region are very similar to the values determined by Watson and Milner-White[6] from their smaller data base.

 © 2002 WILEY-VCH Verlag GmbH & Co. KGaA, Weinheim 1433-7851/02/4124-4664 $ 20.00+.50/0 *Angew. Chem. Int. Ed.* **2002**, *41*, No. 24

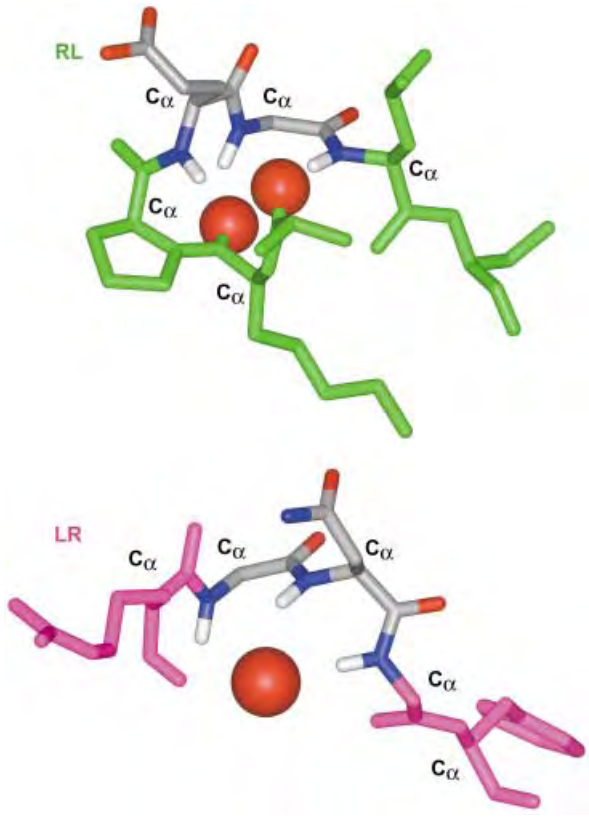


Figure 2. An example of an RL and an LR nest/egg motif as observed in the structure of lysozyme (PDB code: 153L).[10] The two nest amino acids and the NH group of the third amino acid in atom-specific coloring are depicted as well as the flanking amino acids in green (RL) or pink (LR). The oxygen atoms of the egg are shown as red balls. The RL nest is comprised of the amino acids Glu 24, Gly 25, and Leu 27 and the respective egg(s) are the carbonyl oxygen atoms of Ala 21 and Lys 22. The LR nest consists of Gly 88, Asn 89, and Gly 90 and the respective egg is a water molecule (water 216).

α helices, whereas LR nests are more often located at the N-terminal ends. No such preference is observed for typical turns. Also, we have found no occasion where a nest is actually coincident with either a type II or a type II′ turn.[9]

Another important issue is raised by the question: how many nests contain an egg, that is, serve as binding sites, or according to Watson and Milner-White[6] are functional? The answer to this is that 77% of all RL nests and 52% of all LR nests contain a ligand atom bound at hydrogen-bonding distance (Table 2). In most cases, main-chain carbonyl oxygen atoms of amino acids from different parts of the chain constitute the egg. This situation is different when the eggs are formed from side-chain atoms. In the case of Ser-OG and Thr-OG1 atoms as eggs, more than half of them belong to the nest amino acids themselves. Apart from amino acid atoms serving as eggs, many water molecules and ions are also observed. In this respect it is interesting to note that only about 3% of all RL nests bind water, whereas 18% of all LR nests do (Table 2). These observations suggest a general role of nests as binding sites. Also, it may be that the nests together with their respective eggs and not just the nests alone have to be considered as structural motifs.

Table 2. Categories of observed nest/egg structures.

	RL	LR
nests:		
total	5773 (100%)	2492 (100%)
occupied	4419 (76.5%)	1290 (51.8%)
empty	1354 (23.5%)	1202 (48.2%)
eggs:[a]		
total[b]	4838 (100%)	1386 (100%)
main-chain carbonyl O atom	3009 (62.2%)	560 (40.4%)
side-chain carboxylate O atom	630 (13.0%)	234 (16.9%)
side-chain amide O atom	200 (4.1%)	44 (3.2%)
side-chain hydroxy O atom	795 (16.4%)	49 (3.5%)
ions[c]	48 (1.0%)	55 (4.0%)
water molecules	156 (3.2%)	444 (32.0%)

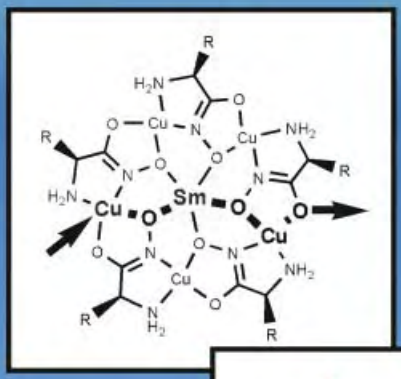
[a] In accordance with Watson and Milner-White,[6] all ligands at a distance of less than 3.8 Å to both N1 and N3 were considered. [b] The total number of eggs is larger than the number of occupied nests, because some nests contain more than one egg. [c] Possible ions were: phosphate, sulfate, chloride, iron-sulfur clusters, phosphate-containing cofactors. For examples, see Table 5 and Figure 5 of ref. [6].

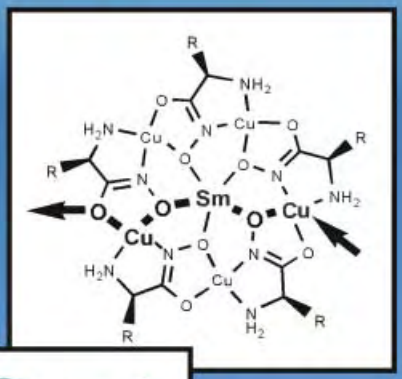
In summary, the intriguingly simple concept presented by Watson and Milner-White appears to be a valuable contribution to the principles of protein structure, since it not only unifies a variety of observed motifs but also unveils a few novel motifs. The concept is not limited to just the protein itself, but also takes ligands, cofactors, water molecules, etc. into account, and therefore sets the stage for a general approach to binding sites in proteins. One may also speculate whether nests within the protein context may constitute stable structures very early along the pathway of folding since they are inherently local structures and thus would not result in a large reduction in entropy upon formation. It is to be hoped that concepts such as this one, and possibly others still to come, will further our knowledge about protein structures in general and help move the field from structure description to structure prediction.

[1] C. B. Anfinsen, E. Haber, M. Sela, F. H. White, Jr., *Proc. Natl. Acad. Sci. USA* **1961**, *47*, 1309–1314.
[2] H. M. Berman, J. Westbrook, Z. Feng, G. Gilliland, T. N. Bhat, H. Weissig, I. N. Shindyalov, P. E. Bourne, *Nucleic Acids Res.* **2000**, *28*, 235–242.
[3] G. N. Ramachandran, V. Sasisekharan, *Adv. Protein Chem.* **1968**, *23*, 293–437.
[4] G. E. Schulz, R. H. Schirmer, *Principles of Protein Structure*, Springer, New York, **1979**.
[5] P. Chakrabarti, D. Pal, *Prog. Biophys. Mol. Biol.* **2001**, *76*, 1–102.
[6] J. D. Watson, E. J. Milner-White, *J. Mol. Biol.* **2002**, *315*, 187–198.
[7] J. D. Watson, E. J. Milner-White, *J. Mol. Biol.* **2002**, *315*, 199–207.
[8] M. Brandl, M. S. Weiss, A. Jabs, J. Sühnel, R. Hilgenfeld, *J. Mol. Biol.* **2001**, *307*, 357–377.
[9] T. E. Creighton, *Proteins: Structure and Molecular Properties*, W. H. Freeman, New York, **1993**.
[10] L. H. Weaver, M. G. Grütter, B. W. Matthews, *J. Mol. Biol.* **1995**, *245*, 54–68.

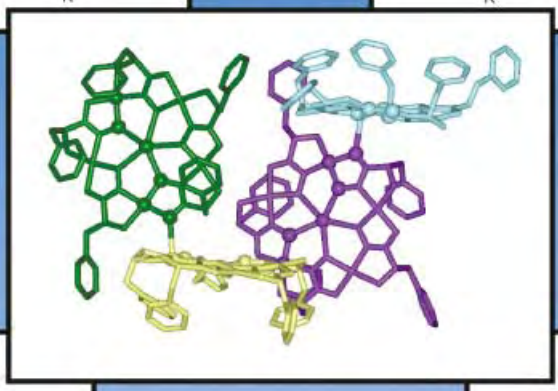
 © 2002 WILEY-VCH Verlag GmbH & Co. KGaA, Weinheim 1433-7851/02/4124-4665 $ 20.00+.50/0

$[(Sm^{III})\{[15]\text{-}MC_{Cu^{II}N(PheHA)}\text{-}5\}]^{3+}$ complexes are chiral building blocks for making metallahelices

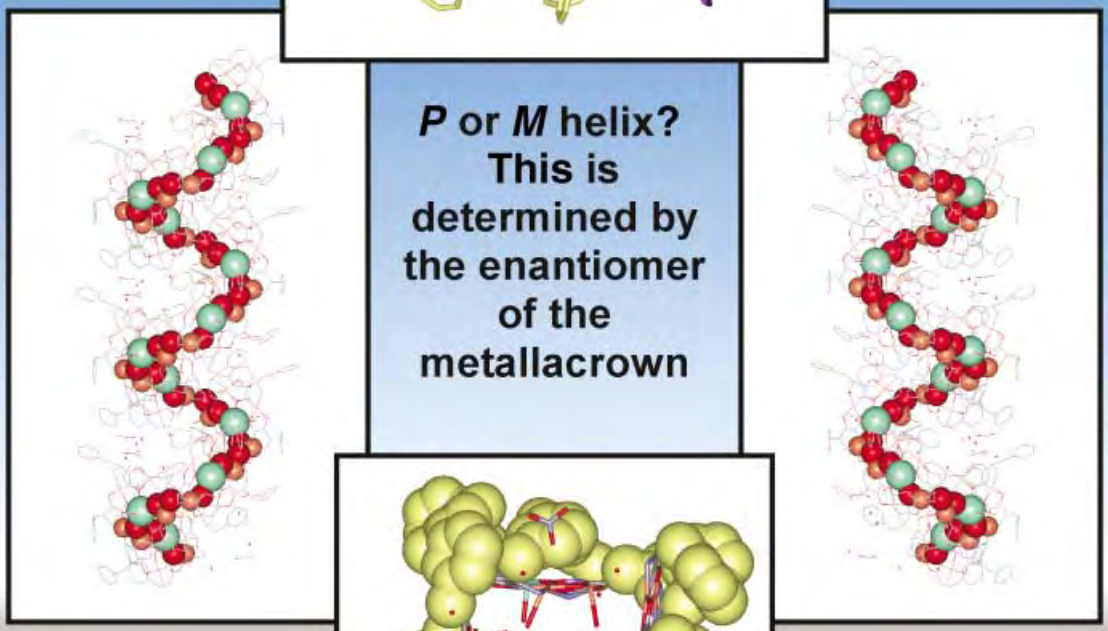




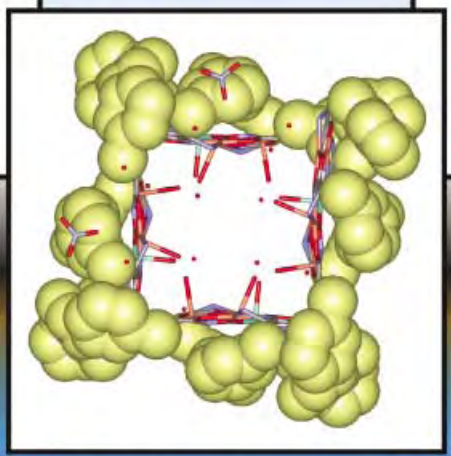
Amphiphilic metallacrowns coordinate in a chain...



...to make a helix based on a $P4_1$ axis



P or ***M*** helix? This is determined by the enantiomer of the metallacrown



The helix is amphiphilic with a hydrophobic exterior

A hydrophilic pore is formed in the interior of the helix

For more information see the following pages

 © 2002 WILEY-VCH Verlag GmbH & Co. KGaA, Weinheim 1433-7851/02/4124-4667 $ 20.00+.50/0

Preparation of Resolved Fourfold Symmetric Amphiphilic Helices Using Chiral Metallacrown Building Blocks

Annabel D. Cutland-Van Noord, Jeff W. Kampf, and Vincent L. Pecoraro*

Helical structures are critical motifs in molecular biology and biochemistry, and are also generating interest in the field of materials science. The field of metallahelicates and metal-containing helical chains has attracted attention as a result of interest in building macromolecular structures with chiral and nonlinear optical properties and for the development of molecules with host–guest interactions.[1] An important goal is to form resolved *P* or *M* helices in noncentrosymmetric solids. Unresolved helicates or infinite helices existing as racemates are usually recovered.[2]

Current development of metallahelicates involves the use of polydentate ligands such as oligopyridines and oligocatechols that "wrap around" and coordinate to transition-metal ions.[2] These systems typically yield double- and triple-stranded molecular helicates rather than extended/infinite coordination polymers. Strategies that have been used to obtain a single enantiomer of a helix include the use of ligands that incorporate bulky chiral side chains[3] and the use of chiral anions that are cocrystallized with the helicate.[4] Infinite helical chains have also been made, frequently through the use of a "twisted" ligand that bridges metal ions. Infinite helices prepared with achiral starting materials form a mixture of both enantiomers.[5] Single enantiomers of helical chains are realized through the use of resolved chiral "bridging" ligands.[6] Chiral metal complexes can make twofold symmetric helical chains through the coordination of a peripheral group of one molecule to a central Cu^{II} ion of the next molecule.[7]

An attractive strategy for obtaining resolved, helical solids is by assembling chiral metallacrowns into extended structures. Metallacrowns were first recognized in 1989, when we reported a metallamacrocyclic complex analogous to a crown ether.[8a] Different ligands and transition metals may be used to form metallacrowns in a variety of structure types, including [9]metallacrown-3 (9-MC-3), 12-MC-4, 15-MC-5, and larger rings up to 30-MC-10.[8b–d] Metallacrowns have been made with ligands derived from α-amino acids that provide side chains at the periphery of the disk-shaped complex.[8e,f] The use of such chiral ligands results in face-differentiated molecules that include resolved chiral centers and which may be amphiphilic. Cationic [15]metallacrown-5 complexes made from α-aminohydroximates can form chiral cavities showing selective anion recognition.[8g] Such planar [15]metallcrown-5 complexes are prepared in high yield from simple precursors in a one-step reaction, and are stable to ligand exchange in solution. We now show that metallacrowns can be easily linked to form resolved fourfold symmetric, amphiphilic metallahelices by using chiral [15]metallacrown-5 building blocks.

The metallacrown $[\{Sm(NO_3)\}\{15\text{-}MC_{Cu^{II}N(L\text{-}pheHA)}\text{-}5\}](NO_3)_2$ (**1**, Figure 1) is prepared using L-phenylalanine hydroxamic acid (L-H_2pheHA).[9] The complex is planar, with five

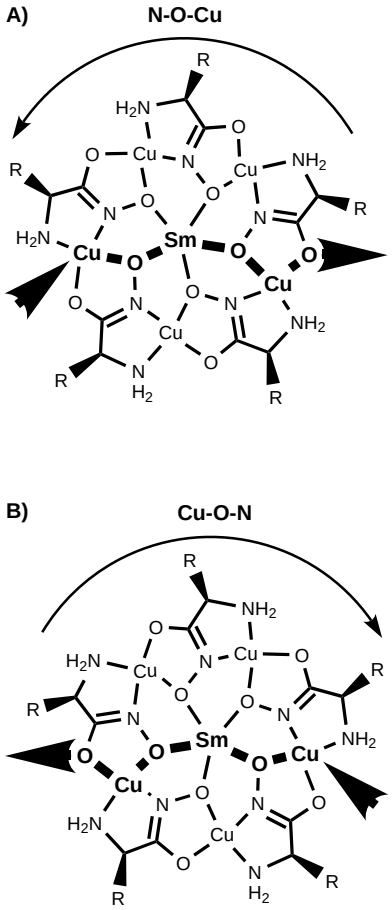


Figure 1. Schematic representation of the metallacrowns **1** and **1a**. The Cu-O-Sm-O-Cu-O path through the metallacrown between the coordination points to and from adjacent metallacrowns is highlighted. A) Metallacrown **1** has an anticlockwise Cu-O-N rotational sense. B) **1a** has a clockwise Cu-O-N rotational sense. Benzyl side chains are indicated by "R" for clarity.

peripheral benzyl groups that are oriented to the same "hydrophobic" face. These side chains come from five pheHA ligands that coordinate in a cyclic fashion to five Cu^{II} ions. A Sm^{III} ion is encapsulated in the center of the complex through ligation of the oxime oxygen atoms, which gives a formula of $[C_{45}H_{50}N_{10}O_{10}Cu_5Sm]^{3+}$. The metallacrown is pseudo-fivefold symmetric as a consequence of the $\{Cu^{II}$pheHA$\}$ repeat unit that rotates around the central Sm^{III} ion.

A *P*-type helical chain is generated by the linkage of adjacent metallacrowns. There is one unique metallacrown in the crystal structure[10] (space group $P4_1$), which is related to its nearest neighbors by an S_4 screw axis that runs parallel to the face of the complex. Each metallacrown interacts with a neighboring molecule through their edges, by providing a peripheral carbonyl oxygen atom as an axial ligand to a

[*] Prof. V. L. Pecoraro, A. D. Cutland-Van Noord, Dr. J. W. Kampf
Department of Chemistry
Willard H. Dow Laboratories
The University of Michigan
Ann Arbor, MI 48109-1055 (USA)
Fax: (+1) 734-647-4865
E-mail: vlpec@umich.edu

 © 2002 WILEY-VCH Verlag GmbH & Co. KGaA, Weinheim 0044-8249/02/4124-4668 $ 20.00+.50/0

Cu^{II} ion in the next complex (Cu–O = 2.791 Å). This arrangement places the metallacrowns at 90° to each other, with the hydrophilic faces forming the interior of this angle. The second metallacrown provides an oxygen donor, in the same way, to a Cu^{II} ion in a third complex, and so forth. The result is a chain of metallacrowns as shown in Figure 2.

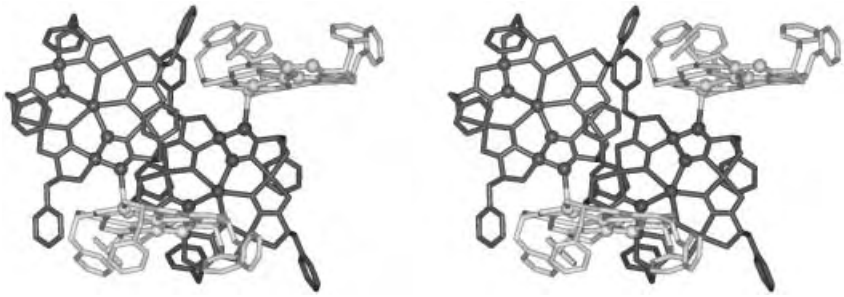


Figure 2. Stereoview of **1** from the X-ray crystal structure. A chain of four linked metallacrowns is shown. Solvents and anions have been removed for clarity.

The pseudo-fivefold symmetry displayed by the planar [15]metallacrown-5 complex $[Sm\{15\text{-}MC_{Cu^{II}N(L\text{-}pheHA)}\text{-}5\}]^{3+}$ is integrally related to the formation of the helix. The positioning of the Cu ions in each complex forces the metallacrowns to be staggered to allow the $O_{(carbonyl)}$–Cu interaction. The noncommensurate nature of this interaction prevents the formation of a "molecular box" and an infinite helical chain of metallacrowns is formed instead. The bulky benzyl side chains, directed to the same face of the metallacrown by the chiral α-carbon atom, are also critical as they prevent a "zigzag" chain orientation of metallacrowns. Even more importantly, they induce the right-handed (*P*) form of the helix. Combining these factors yields a resolved fourfold-symmetric metallohelix using self-associating chiral building blocks.

The helix of metallacrowns form the walls of a hydrophilic "square pore", which contains water solvent molecules, with a face-to-face distance of approximately 11 Å (including the van der Waal radii). As shown in Figure 3, a solvent water is coordinated to the samarium ion on the hydrophilic face and points into the channel. There are also two water molecules that axially ligate copper(II) ions on the hydrophilic face.

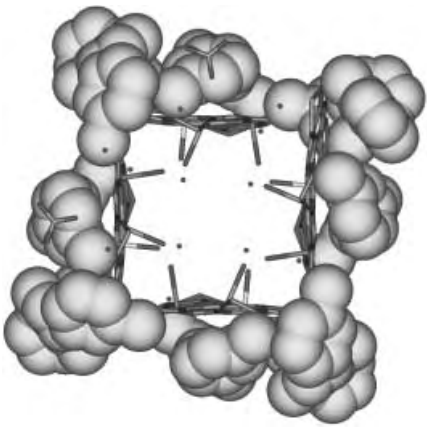


Figure 3. View of **1** down the *z*-axis. The ligand benzyl groups are shown as a CPK representation.

Additional hydrogen-bonded solvents fill the channel. The hydrophobic faces of the metallacrowns are oriented toward the outside of the helix, with the benzyl groups of adjacent helices being well-packed. The resulting structure is an amphiphilic helix with a hydrophilic interior and hydrophobic exterior.

We predicted that a metallacrown made with D-pheHA would form a helix that was the mirror image of **1** (**1** uses L-pheHA which yields the opposite enantiomer of the metallacrown). The metallacrown $[\{Sm(NO_3)\}\{15\text{-}MC_{Cu^{II}N(D\text{-}pheHA)}\text{-}5\}](NO_3)_2$ (**1a**) crystallized in the space group $P4_3$.[11,12] As shown in Figure 4, the helices in **1** and **1a** are indeed mirror images. The Cu-O-N linkage of the metallacrown defines the rotational symmetry of the molecule.[8b] The metallacrown, when oriented with the side chains directed out of the page, forms the clockwise (C) isomer or the anticlockwise (A) isomer depending on the rotational sense of the Cu-O-N linkage (Figure 1). The thick lines illustrate the Cu-O-Sm-O-Cu-O pathway that links adjacent metallacrowns of the helix. This pathway has a positive (*P*) rotational sense for the A isomer and a minus (*M*) sense for the C isomer. Thus, the ligand chirality defines the *P* or *M* helix because the benzyl groups must be oriented toward the helix exterior.

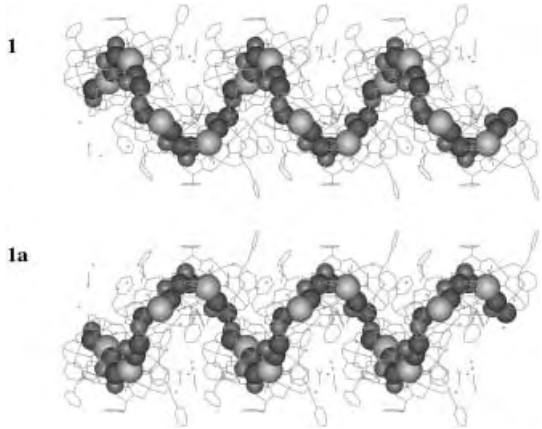


Figure 4. Comparison of the structures of **1** and **1a**. The continuous chain of Cu-O-Sm-O-Cu-O through the metallacrowns is highlighted as CPK models.

In conclusion, we have prepared enantiomerically pure helical solids (either *P* or *M*) through the use of an appropriate chiral metallacrown building block. To the best of our knowledge this is a novel technique for the formation of helical chains based on a 4_1 screw axis that provides a channel through the amphiphilic helix.

Experimental Section

1: L-phenylalanine hydroxamic acid (L-H_2pheHA, 0.180 g, 1.00 mmol) was treated with $Cu(OAc)_2 \cdot H_2O$ (0.200 g, 1 mmol) and $Sm(NO_3)_3 \cdot 6H_2O$ (0.090 g, 0.20 mmol) in methanol (20 mL) and water (2 mL). The reaction mixture was filtered after 2 h. Blue-violet crystals were obtained by slow

 © 2002 WILEY-VCH Verlag GmbH & Co. KGaA, Weinheim 0044-8249/02/4124-4669 $ 20.00+.50/0

evaporation of the solvent. A similar procedure was used to prepare X-ray quality crystals of **1a** that contain D-H_2pheHA.

Received: September 2, 2002 [Z50082]

[1] C. Piguet, G. Bernardinelli, G. Hopfgertner, *Chem. Rev.* **1997**, *97*, 2005 – 2067.

[2] a) M. Albrecht, *Chem. Soc. Rev.* **1998**, *27*, 281 – 288; b) M. Albrecht, *Chem. Rev.* **2001**, *101*, 3457 – 3497.

[3] a) U. Knof, A. von Zelewsky, *Angew. Chem.* **1999**, *111*, 312 – 333; *Angew. Chem. Int. Ed.* **1999**, *38*, 302 – 322; b) C. J. Carrano, K. N. Raymond, *J. Am. Chem. Soc.* 1978, *100*, 5371 – 5374; c) E. C. Constable, T. Kulke, G. Baum, D. Fenske, *Inorg. Chem. Commun.* **1998**, *1*, 80 – 82.

[4] a) J. J. Jodry, J. Lacour, *Chem. Eur. J.* **2000**, *6*, 23, 4297 – 4304; b) J. Lacour, J. J. Jodry, D. Monchaud, *Chem. Commun.* **2001**, 2302 – 2303; c) R. M. Yeh, M. Ziegler, D. W. Johnson, A. J. Terpin, K. N. Raymond, *Inorg. Chem.* **2001**, *40*, 2216 – 2217.

[5] a) R. W. Saalfrank, H. Maid, F. Hampel, K. Peters, *Eur. J. Inorg. Chem.* **1999**, 1859 – 1867; b) D. Gaynor, Z. A. Starikova, W. Haase, K. B. Nolan, *J. Chem. Soc. Dalton Trans.* **2001**, 1578 – 1581; c) R. W. Saalfrank, H. Maid, N. Mooren, F. Hampel, *Angew. Chem.* **2002**, *41*, 323 – 326; *Angew. Chem. Int. Ed.* **2002**, *41*, 304 – 307.

[6] a) P. K. Powyer, K. A. Porter, A. D. Rae, A. C. Willis, S. B. Wild, *Chem. Commun.* **1998**, 1153 – 1154; b) B. Wu, W.-J. Zhang, S.-Y. Yu, X.-T. Wu, *J. Chem. Soc. Dalton Trans.* **1997**, *11*, 1795 – 1796; c) M. Kimura, M. Sano, T. Muto, K. Hanabusa, H. Shirai, *Macromolecules* **1999**, *32*, 7951 – 7953; d) J. F. Modder, G. van Koten, K. Vrieze, A. L. Spek, *Angew. Chem.* **1989**, *101*, 1723 – 1725; *Angew. Chem. Int. Ed. Engl.* **1989**, *28*, 1698 – 1700.

[7] R. W. Saalfrank, M. Decker, F. Hampel, K. Peters, H. G. von Schnering, *Chem. Ber.* **1997**, *130*, 1309 – 1313.

[8] a) M. S. Lah, V. L. Pecoraro, *J. Am. Chem. Soc.* **1989**, *111*, 7258; b) V. L. Pecoraro, A. J. Stemmler, B. R. Gibney, J. J. Bodwin, H. Wang, J. W. Kampf, A. Barwinski in *Progress in Inorganic Chemistry, Vol. 45* (Ed.: K. D. Karlin), Wiley, New York, **1997**, pp. 83 – 177; c) R. W. Saalfrank, N. Löw, F. Hampel, H.-D. Stachel, *Angew. Chem.* **1996**, *108*, 2353; *Angew. Chem. Int. Ed. Engl.* **1996**, *35*, 2209; d) S.-X. Liu, S. Lin, B.-Z. Lin, C.-C. Lin, J.-Q. Huang, *Angew. Chem.* **2001**, *113*, 1118 – 1121; *Angew. Chem. Int. Ed.* **2001**, *40*, 1084 – 1087; e) A. J. Stemmler, A. Barwinski, M. J. Baldwin, V. Young, V. L. Pecoraro, *J. Am. Chem. Soc.* **1996**, *118*, 11962; f) A. J. Stemmler, J. W. Kampf, M. L. Kirk, B. H. Atasi, V. L. Pecoraro, *Inorg. Chem.* **1999**, *38*, 2807; g) A. D. Cutland, J. A. Halfen, J. W. Kampf, V. L. Pecoraro, *J. Am. Chem. Soc.* **2001**, *123*, 6211 – 6212.

[9] Elemental analysis calcd for $[C_{45}H_{50}N_{10}O_{10}Cu_5Sm](NO_3)_3(H_2O)_{2.5}$ (**1**): C 33.99, H 3.49, N 11.45, Cu 19.98; found: C 33.97, H 3.53, N 11.30, Cu 18.9. ESMS (methanol): m/z: 1482.8 $[M{\cdot}2NO_3]^+$.

[10] Crystal data for **1**: $[C_{45}H_{50}N_{10}O_{10}Cu_5Sm](NO_3)_3(H_2O)_8$, $M_r = 1689.18$, tetragonal, space group $P4_1$ (no. 76), $a = 19.310(2)$, $b = 19.310(2)$, $c = 18.330(3)$, $\alpha = 90.000$, $\beta = 90.000$, $\gamma = 90.000°$, $V = 6835.0(15)$ Å^3, $Z = 4$; $\rho_{calcd} = 1.641$ g cm^{-1}; $2.98 < \theta < 26.50°$; crystal dimensions, $0.24 \times 0.34 \times 0.40$ mm; $\mu = 24.52$ cm^{-1}; $T = 133(2)$ K; 14015 unique of 60540 reflections collected. 14015 reflections and 784 parameters were used for the full-matrix, least-squares refinement on F^2, $R1 = 0.0560$, and $wR2 = 0.1543$. A PLATON/SQUEEZE subroutine (Spek, A. L. Platon, *Acta Crystallogr. Sect. A* **1990**, *46*, C-34) was used to handle solvent and anion disorder. Further details are given in the Supporting Information.

[11] Elemental analysis calcd for **1a** $[C_{45}H_{50}N_{10}O_{10}Cu_5Sm](NO_3)_3(H_2O)_{4.5}$: C 33.24, H 3.66, N 11.20, Cu 19.54; found: C 33.19, H 3.69, N 11.04, Cu 19.2. ESMS (methanol): m/z: 1482.8 $[M{\cdot}2NO_3]^+$.

[12] Crystal data for **1a**: $[C_{45}H_{50}N_{10}O_{10}Cu_5Sm](NO_3)_3(H_2O)_{12}$, $M_r = 1761.22$, tetragonal, space group $P4_3$ (no. 78), $a = 19.253(3)$, $b = 19.253(3)$, $c = 18.313(4)$, $\alpha = 90.000$, $\beta = 90.000$, $\gamma = 90.000°$, $V = 6788(2)$ Å^3, $Z = 4$; $\rho_{calcd} = 1.723$ g cm^{-1}; $2.99 < \theta < 28.35°$; crystal dimensions(mm), $0.20 \times 0.24 \times 0.42$; $\mu = 24.82$ cm^{-1}; $T = 133(2)$ K; 16835 unique of 77985 reflections collected. 16835 reflections and 784 parameters were used for the full-matrix, least-squares refinement on F^2, $R1 = 0.0387$, $wR2 = 0.1025$. A PLATON/SQUEEZE subroutine (Spek) was used to handle solvent and anion disorder. Further details are given in the Supporting Information. CCDC-192390 (**1**) and CCDC-192391 (**1a**) contain the supplementary crystallographic data for this paper. These data can be obtained free of charge via www.ccdc.cam.ac.uk/conts/retrieving.html (or from the Cambridge Crystallographic Data Centre, 12 Union Road, Cambridge CB21EZ, UK; fax: (+44) 1223-336-033; or deposit@ccdc.cam.ac.uk).

Novel Synthetic Approach to Trinuclear 3d-4f Complexes: Specific Exchange of the Central Metal of a Trinuclear Zinc(II) Complex of a Tetraoxime Ligand with a Lanthanide(III) Ion**

Shigehisa Akine, Takanori Taniguchi, and Tatsuya Nabeshima*

Salen (*N*,*N*′-disalicylideneethylenediamine) and its analogues are fascinating and versatile ligands because their metal complexes are known to serve as catalysts of organic reactions,[1] models of catalytic centers of metalloenzymes,[2] and nonlinear optical materials.[3] The negatively charged oxygen atoms of the transition-metal complexes of the salen-type ligands can coordinate to a different cation such as an alkali metal,[4] an alkaline-earth metal,[5] a d-block transition metal,[6] or an f-block transition metal[7] to provide a number of attractive heteronuclear complexes. In particular, synthesis and characterization of heterodinuclear complexes bearing 3d and 4f transition metals are interesting and important because magnetic superexchange interactions between the bridged metal atoms may exist in the complexes.[8,9]

A variety of acyclic and cyclic "compartmental ligands" bearing two different sites have also been designed to synthesize such a heteronuclear complex.[10] However, preparation of the complexes is limited mostly to stepwise reactions using a readily available mononuclear complex. The method of the strategy can be regarded as an "addition reaction". In recent years, advanced synthetic methodology for these types of heteronuclear complexes has been developed. For example, the metal initially bound to one site of some ligands migrates to another site during the second metalation step.[11] Metal exchange between two "coordination-position isomers" of a heterodinuclear complex has also been reported.[12] Here we describe a new method—a "substitution reaction"—to synthesize a $(3d)_2(4f)$ trinuclear complex. A $(3d)_3$ homotrinuclear complex generated in a cooperative manner from three zinc(II) ions and acyclic tetraoxime ligand **1** bearing two salen-type chelating moieties[13] under-

[*] Prof. Dr. T. Nabeshima, Dr. S. Akine, T. Taniguchi
Department of Chemistry, University of Tsukuba
Tsukuba, Ibaraki 305-8571 (Japan)
Fax: (+81) 298-53-6503
E-mail: nabesima@chem.tsukuba.ac.jp

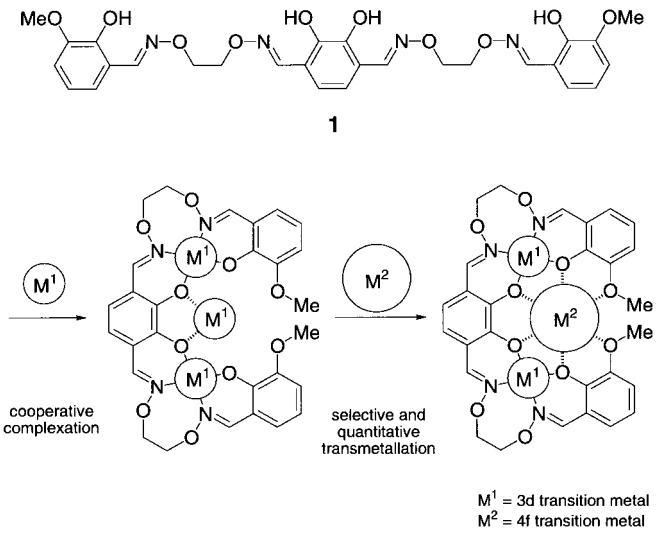
[**] This work was supported by a Grant-in-Aid for Scientific Research from the Ministry of Education, Culture, Sports, Science, and Technology, Japan.

Supporting information for this article is available on the WWW under http://www.angewandte.org or from the author.

 © 2002 WILEY-VCH Verlag GmbH & Co. KGaA, Weinheim 0044-8249/02/4124-4670 $ 20.00+.50/0

goes exclusive and quantitative transmetalation of the central 3d metal ion with a 4f metal ion.

When **1** reacts with two equivalents of 3d transition metal ions the linear form of **1** changes into a C-shaped one to give a cavity surrounded by the six oxygen atoms (Scheme 1). The complex is expected to have a high affinity toward metal cations, since the donor atoms are arranged in a cyclic fashion and negatively charged.



Scheme 1. A novel synthetic approach to a $(3d)_2(4f)$ heterotrinuclear complex via a $(3d)_3$ homonuclear complex.

Addition of a solution of zinc(II) acetate to a solution of **1**[14] (H_4L) resulted in the solution changing from colorless to yellow and the appearance of a new band (332 nm) in the UV/Vis spectrum (Figure 1). Although **1** has two chelating moieties, spectroscopic titration of **1** and zinc(II) acetate clearly indicated the exclusive formation of the 1:3 complex $[LZn_3]^{2+}$ (inset of Figure 1). Formation of other complexes with a different stoichiometry is ruled out because of the observed spectroscopic changes having three isosbestic points (256, 286, and 322 nm). This interesting and high cooperativity was also observed in the ^{1}H NMR spectroscopic titration.[14]

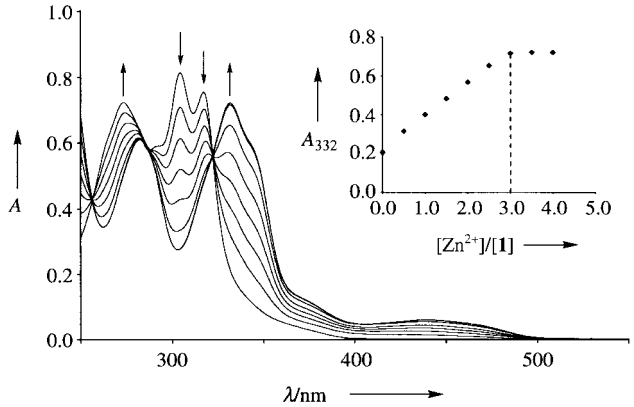


Figure 1. UV/Vis spectral changes of **1** on addition of zinc(II) acetate ($CHCl_3/CH_3OH$ (1/1), $[\mathbf{1}] = 2.0 \times 10^{-4}$ M). The inset shows the plot of absorbance at 332 nm against the molar ratio of $[Zn^{2+}]/[\mathbf{1}]$.

The structure of the 1:3 complex $[LZn_3]^{2+}$ in the crystalline state was determined by X-ray crystallography using a single crystal of $[LZn_3(OAc)_2(EtOH)]$ (Figure 2).[15] The complex

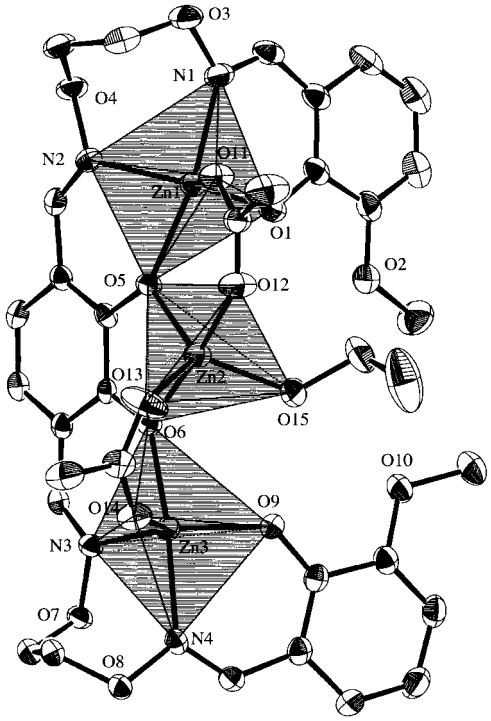


Figure 2. Crystal structure of the trinuclear zinc(II) complex $[LZn_3(OAc)_2(EtOH)]$. Hydrogen atoms and solvent molecules have been omitted for clarity. Selected bond lengths [Å]: Zn1-O1 1.922(3), Zn1-O5 2.077(3), Zn1-O11 1.982(3), Zn1-N1 2.137(3), Zn1-N2 2.151(3), Zn2-O5 2.023(3), Zn2-O6 2.059(3), Zn2-O12 1.995(3), Zn2-O13 2.009(3), Zn2-O15 2.001(3), Zn3-O6 2.041(3), Zn3-O9 1.964(3), Zn3-O14 1.999(3), Zn3-N3 2.072(3), Zn3-N4 2.149(3).

$[LZn_3]^{2+}$ has three zinc atoms arranged in a trigonal bipyramidal geometry. The two salamo (H_2salamo: 1,2-bis(salicylideneaminooxy)ethane) moieties provide the N_2O_2 donor set to the two outer zinc atoms (Zn1 and Zn3), while the oxygen atoms (O5 and O6) of the central catechol moiety coordinate to all three zinc atoms. In addition, the two μ-acetato ligands link Zn1 to Zn2 and Zn2 to Zn3. Although the central metal (Zn2) was located in the cavity, four of the six oxygen atoms (O1, O2, O9, and O10) arranged along the rim of the cavity do not coordinate to Zn2. Deprotonated ligand **1** is expected to bind to Zn2 more weakly than Zn1 and Zn3, because only two donor atoms of **1** coordinate to Zn2. Namely, it would be expected that the central Zn2 ion would be replaced more easily with another metal ion possessing a larger radius and coordination number suitable for the O_6 cavity than Zn1 and Zn3. Thus, we utilized $[LZn_3]^{2+}$ to synthesize novel heteronuclear $(3d)_2(4f)$ complexes.

Treatment of a solution of $[LZn_3]^{2+}$ with lanthanide(III) ions resulted in a hypsochromic shift in the absorption spectra. A typical example of the titration of $[LZn_3]^{2+}$ with $Ln(NO_3)_3$ is shown in Figure 3 (Ln = Eu). The absorption band at 370 nm (shoulder) arising from the formation of a new species increased while a concomitant decrease in the absorption band at 440 nm of $[LZn_3]^{2+}$ was observed. Isosbestic points

 © 2002 WILEY-VCH Verlag GmbH & Co. KGaA, Weinheim 0044-8249/02/4124-4671 $ 20.00+.50/0

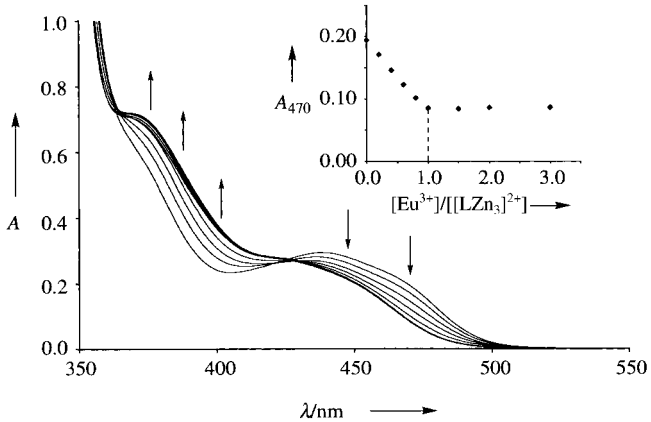


Figure 3. UV/Vis spectral changes of $[LZn_3]^{2+}$ on addition of europium(III) nitrate ($CHCl_3/CH_3OH$ (1/1), $[[LZn_3]^{2+}] = 1.0 \times 10^{-4}$ M). The inset shows the plot of absorbance at 470 nm against the molar ratio of $[Eu^{3+}]/[[LZn_3]^{2+}]$.

were evident at 426 and 364 nm. The spectral changes are completed by the addition of just one equivalent of Ln^{3+} ions (inset of Figure 3), which indicates the formation of the expected species $[LZn_2Ln]^{3+}$. The stoichiometry was also supported by ^1H NMR spectroscopic measurements.[14]

The formation of the heterotrinuclear complex was further confirmed by ESI mass spectroscopic analysis of $[LZn_3(OAc)_2]$ in the presence of one equivalent of $Eu(NO_3)_3$. Intense peaks at m/z 977.0 and 460.0 and the isotope distribution in the spectrum indicate the existence of $[LZn_2Eu(OAc)_2]^+$ and $[LZn_2Eu(OAc)]^{2+}$, respectively. One equivalent of Zn^{2+} ions was apparently liberated from the complex to give $[LZn_2Eu(OAc)_2]^+$, since no peak attributed to the homonuclear species $[LZn_3]^{2+}$ was observed.

Yellow single crystals were obtained from a solution of $[LZn_3]^{2+}$ containing one equivalent of $Eu(NO_3)_3$. X-ray crystallographic analysis[16] reveals that the crystals correspond to a heterotrinuclear complex containing a trinuclear Zn-Eu-Zn core bridged by the phenolate oxygen atoms of the ligand and μ-acetato ligands (Figure 4). The two zinc atoms (Zn1 and Zn2) have an octahedral and a square-pyramidal environment, respectively, in which the four equatorial positions are occupied by the N_2O_2 donor sets of the salamo moieties. The europium atom, with a nonacoordinate geometry, is located in the pseudo cavity consisting of the six oxygen atoms of the ligand. The distances between the europium atom (Eu1) and the six donor atoms (O1, O2, O5, O6, O9, and O10) range from 2.380 to 2.614 Å, which suggests there is effective incorporation of the europium(III) ion (Figure 5). Consequently, the ligand wraps around the europium atom and results in a helical complex in which the terminal benzene rings lie close to each other.

Very interestingly, a mixture of **1** with excess zinc(II) and europium(III) ions (four and three equivalents, respectively) gave spectra identical to that of $[Zn_2Eu(OAc)_2]^+$. The zinc(II) ions, thus, bind selectively to the two salamo moieties and the europium(III) ion in the central cavity. This selective uptake of two zinc(II) ions and one europium(III) ion can be attributed to the fact that the cavity size and shape of the two different sites fit more suitably to the ionic radius, the coordination geometry, and the coordination number of these ions. Hence,

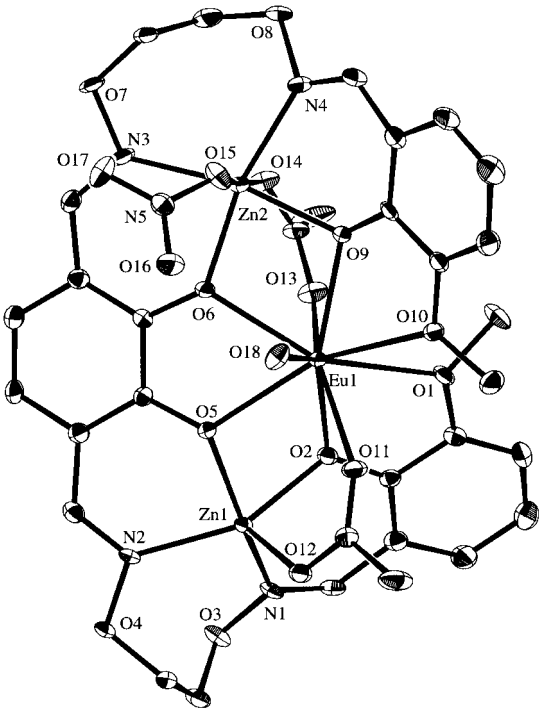


Figure 4. ORTEP drawing (30% probability level) of the trinuclear complex $[LZn_2Eu(OAc)_2(NO_3)(H_2O)]$. Hydrogen atoms and solvent molecules have been omitted for clarity. Selected bond lengths [Å]: Eu1-O1 2.594(3), Eu1-O2 2.435(2), Eu1-O5 2.380(2), Eu1-O6 2.385(2), Eu1-O9 2.384(2), Eu1-O10 2.614(3), Eu1-O11 2.372(3), Eu1-O13 2.457(3), Eu1-O18 2.412(3), Zn1-O2 2.045(2), Zn1-O5 1.995(2), Zn1-O12 1.991(3), Zn1-N1 2.071(3), Zn1-N2 2.109(3), Zn2-O6 2.017(2), Zn2-O9 2.090(2), Zn2-O14 2.088(3), Zn2-O15 2.201(3), Zn2-N3 2.179(3), Zn2-N4 2.136(3).

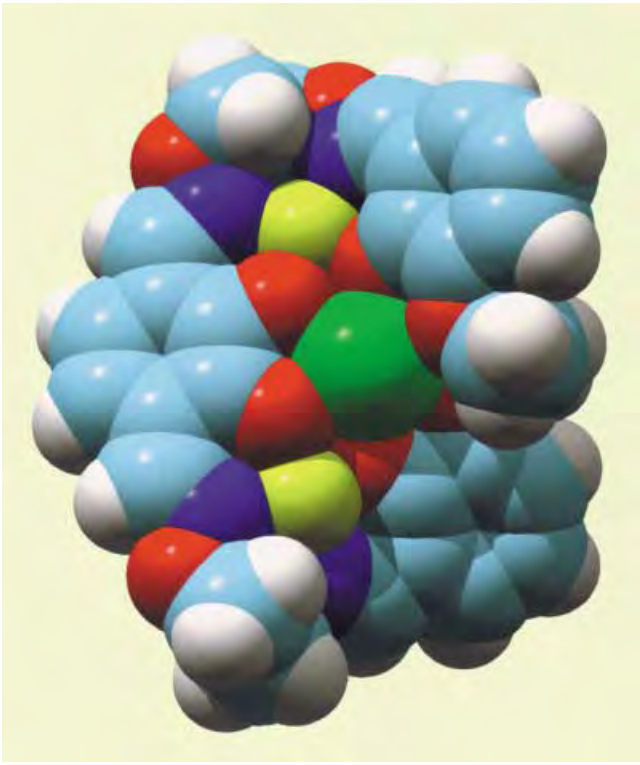


Figure 5. Space-filling representation of $[LZn_2Eu]^{3+}$. Anions and the water molecule coordinating to the metal atoms have been omitted for clarity.

 © 2002 WILEY-VCH Verlag GmbH & Co. KGaA, Weinheim 0044-8249/02/4124-4672 $ 20.00+.50/0

the heteronuclear complex containing the lanthanide atom is stabilized to a greater extent than the homotrinulcear zinc(II) complex. As a result, only the central zinc ion of the homo complex formed initially is replaced quantitatively by the lanthanide(III) ion.

We believe that this facile and effective strategy to synthesize helical or cyclic heteronuclear complexes will open a new way to construct various functionalized coordination systems

Received: June 13, 2002 [Z19528]

[1] a) E. N. Jacobsen in *Catalytic Asymmetric Synthesis* (Ed.: I. Ojima) VCH, New York, **1993**; b) T. Katsuki, *Coord. Chem. Rev.* **1995**, *140*, 189 – 214.

[2] a) T.-T. Tsou, M. Loots, J. Halpern, *J. Am. Chem. Soc.* **1982**, *104*, 623 – 624; b) M. F. Summers, L. G. Marzilli, N. Bresciani-Pahor, L. Randaccio, *J. Am. Chem. Soc.* **1984**, *106*, 4478 – 4485.

[3] a) S. di Bella, I. Fragalà, *Synth. Met.* **2000**, *115*, 191 – 196; b) P. G. Lacroix, *Eur. J. Inorg. Chem.* **2001**, 339 – 348.

[4] D. Cunningham, P. McArdle, M. Mitchell, N. Ní Chonchubhair, M. O'Gara, F. Franceschi, C. Floriani, *Inorg. Chem.* **2000**, *39*, 1639 – 1649, and references therein.

[5] L. Carbonaro, M. Isola, P. la Pegna, L. Senatore, F. Marchetti, *Inorg. Chem.* **1999**, *38*, 5519 – 5525, and references therein.

[6] S. J. Gruber, C. M. Harris, E. Sinn, *J. Inorg. Nucl. Chem.* **1968**, *30*, 1805 – 1830.

[7] a) G. Condorelli, I. Fragalà, S. Giuffrida, A. Cassol, *Z. Anorg. Allg. Chem.* **1975**, *412*, 251 – 257; b) U. Casellato, P. Guerriero, S. Tamburini, P. A. Vigato, C. Benelli, *Inorg. Chim. Acta* **1993**, *207*, 39 – 58.

[8] a) A. Bencini, C. Benelli, A. Caneschi, R. L. Carlin, A. Dei, D. Gatteschi, *J. Am. Chem. Soc.* **1985**, *107*, 8128 – 8136; b) J.-P. Costes, F. Dahan, A. Dupuis, *Inorg. Chem.* **2000**, *39*, 165 – 168; c) M. Sasaki, K. Manseki, H. Horiuchi, M. Kumagai, M. Sakamoto, H. Sakiyama, Y. Nishida, M. Sakai, Y. Sadaoka, M. Ohba, H. Okawa, *J. Chem. Soc. Dalton Trans.* **2000**, 259 – 263.

[9] a) C. Edder, C. Piguet, J.-C. G. Bünzli, G. Hopfgartner, *Chem. Eur. J.* **2001**, *7*, 3014 – 3024; b) J.-C. G. Bünzli, C. Piguet, *Chem. Rev.* **2002**, *102*, 1897 – 1928.

[10] P. Guerriero, S. Tamburini, P. A. Vigato, *Coord. Chem. Rev.* **1995**, *139*, 17 – 243.

[11] Y. Nakamura, M. Yonemura, K. Arimura, N. Usuki, M. Ohba, H. Okawa, *Inorg. Chem.* **2001**, *40*, 3739 – 3744.

[12] M. Yonemura, K. Arimura, K. Inoue, N. Usuki, M. Ohba, H. Okawa, *Inorg. Chem.* **2002**, *41*, 582 – 589.

[13] S. Akine, T. Taniguchi, T. Nabeshima, *Chem. Lett.* **2001**, 682 – 683.

[14] For the synthesis of **1** as well as ^{1}H NMR titration experiments, see the Supporting Information.

[15] Crystallographic data for $[LZn_3(OAc)_2(EtOH)]\cdot 0.5\,EtOH\cdot 0.5\,CHCl_3$ ($C_{35.5}H_{41.5}Cl_{1.5}N_4O_{15.5}Zn_3$, $M_r = 1021.51$): monoclinic, space group $P2_1/n$ (no. 14), $a = 10.6324(15)$, $b = 23.665(2)$, $c = 16.371(2)$ Å, $\beta = 103.8170(5)°$, $V = 4000.2(9)$ Å^3, $Z = 4$, $\rho_{calcd} = 1.696$ g cm^{-3}, $T = 120$ K, Rigaku Mercury CCD diffractometer, $Mo_{K\alpha}$ ($\lambda = 0.71069$ Å), $\mu = 1.961$ mm^{-1}, collected reflections 23 896, of which 6981 were unique ($R_{int} = 0.0596$), $2\theta_{max} = 50.00°$, $R1 = 0.0425$ ($I > 2\sigma(I)$), $wR2 = 0.1143$ (all data).[17,18]

[16] Crystallographic data for $[LZn_2Eu(OAc)_2(NO_3)]\cdot 3.5\,Me_2CO$ ($C_{42.5}H_{55}EuN_5O_{21.5}Zn_2$, $M_r = 1262.61$): triclinic, space group $P\bar{1}$ (no. 2), $a = 12.987(5)$, $b = 13.475(4)$, $c = 14.808(5)$ Å, $\alpha = 73.201(9)$, $\beta = 87.921(11)$, $\gamma = 84.247(10)°$, $V = 2468.3(14)$ Å^3, $Z = 2$, $\rho_{calcd} = 1.699$ g cm^{-3}, $T = 120$ K, Rigaku Mercury CCD diffractometer, $Mo_{K\alpha}$ ($\lambda = 0.71069$ Å), $\mu = 2.304$ mm^{-1}, collected reflections 17 507, of which 9389 were unique ($R_{int} = 0.0254$), $2\theta_{max} = 52.00°$, $R1 = 0.0342$ ($I > 2\sigma(I)$), $wR2 = 0.0818$ (all data).[17,18]

[17] G. M. Sheldrick, SHELXL 97. Program for crystal structure refinement, University of Göttingen, Göttingen (Germany), **1997**.

[18] CCDC-187146 and CCDC-187147 contain the supplementary crystallographic data for this paper. These data can be obtained free of charge via www.ccdc.cam.ac.uk/conts/retrieving.html (or from the Cambridge Crystallographic Data Centre, 12 Union Road, Cambridge CB2 1EZ, UK; fax: (+44) 1223-336-033; or deposit@ccdc.cam.ac.uk).

The Structure of Neutral Proline**

Alberto Lesarri, Santiago Mata, Emilio J. Cocinero, Susana Blanco, Juan C. López, and José L. Alonso*

The conformational behavior of amino acids is of critical importance to understand the dynamic role of these molecules in protein or polypeptide formation.[1] Consequently, extensive structural research has been conducted on amino acids in their natural solid-state phase. This point is worth noting because solid amino acids present a zwitterionic structure in the solid state (i.e. a bipolar, ionized form of the type $^+H_3N{-}CH(R){-}COO^-$), which does not occur in the polypeptide chain.[2] To obtain the structure of the neutral form of amino acids, research should be conducted in the gas phase, in an atmosphere that is essentially free of intermolecular interactions with other partners. In particular, the collisionless environment of a supersonic jet[3] seems particularly well adapted for such studies. The obvious difficulties of experimental studies in the gas phase are caused by the high melting points and associated low vapor pressures of amino acids. Classical heating methods were employed for the analysis of the only two amino acids that have been studied to date in the gas phase, glycine[4] and alanine[5]. As an alternative, laser ablation offers an advantageous way of vaporizing solid organic compounds,[6] in which the fast desorption produced by the energy of a laser pulse prevents the thermal decomposition caused by the heating methods. Despite the extensive use of laser ablation with mass-spectrometry techniques,[7] few groups have explored the possibility of combining laser ablation with the high resolution of rotational spectroscopy. Suenram et al.[8] and Walker and Gerry[9] independently developed two laser-ablation devices, mostly devoted to investigate the rotational spectra of metal oxides and halides. The first was also applied in the structural study of glycine in the gas phase, but it was reported that the classical heating method was more reliable.[10]

In this context we have configured a new experiment in which a laser-ablation system especially constructed for solid organic compounds is combined with Fourier-transform (FT) microwave spectroscopy in a supersonic jet, to allow the structural characterization of the vaporized species in the gas phase. The ablation nozzle is accommodated at the back side of one mirror of the Fabry–Pérot resonator, close to the resonator axis (Figure 1). An oil diffusion pump, backed by a roots blower, evacuates the chamber. Laser ablation is produced by the second harmonic ($\lambda = 532$ nm) of a pulsed

[*] Prof. Dr. J. L. Alonso, Prof. Dr. A. Lesarri, S. Mata, E. J. Cocinero, Prof. Dr. S. Blanco, Prof. Dr. J. C. López
Grupo de Espectroscopía Molecular
Departamento de Química Física
Facultad de Ciencias, Universidad de Valladolid
Prado de la Magdalena s/n, 47005 Valladolid (Spain)
Fax: (+34) 983-423204
E-mail: jlalonso@qf.uva.es

[**] The authors would like to thank the Fundación Ramón Areces and the Dirección General de Investigación – Ministerio de Ciencia y Tecnología for financial support.

Supporting information for this article is available on the WWW under http://www.angewandte.org or from the author.

 © 2002 WILEY-VCH Verlag GmbH & Co. KGaA, Weinheim 0044-8249/02/4124-4673 $ 20.00+.50/0

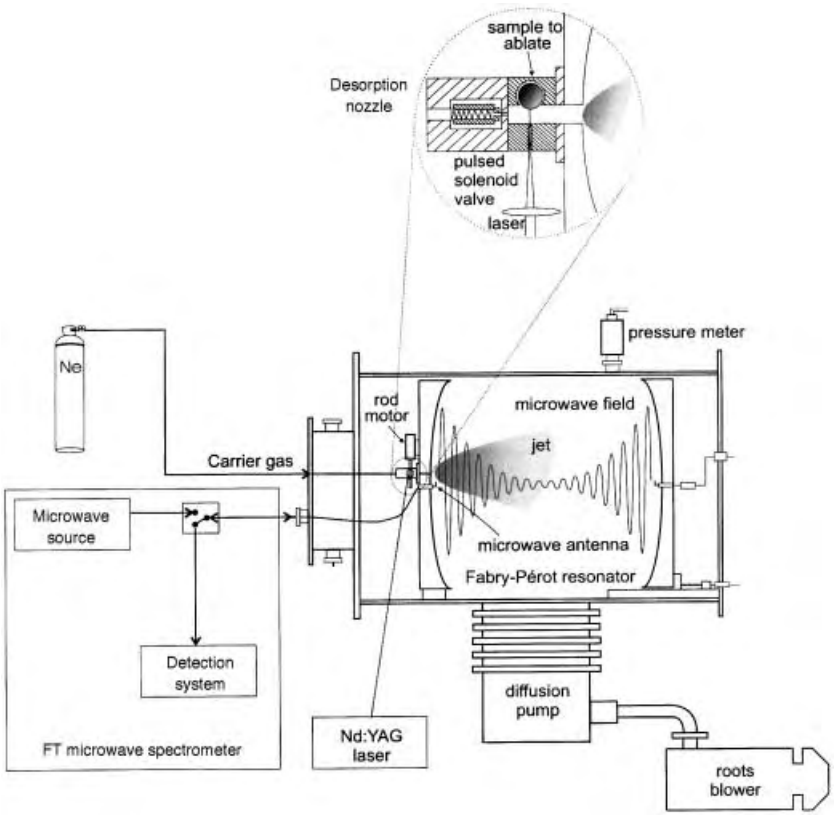


Figure 1. A general block diagram of the experimental setup.

Q-switching Nd:YAG laser, focused on the target rod trough a small lateral orifice of the desorption nozzle. The sample rod is held vertically at the nozzle exit channel and is rotated and translated, so the laser beam reaches a different fresh surface position for each pulse. The experimental sequence starts with a gas pulse of a light inert gas, followed by a laser hit on the solid sample, which generates the ablation products. These desorbed species are seeded in the carrier gas and expanded supersonically between the mirrors of the evacuated Fabry–Pérot microwave resonator, to create a supersonic expansion. A very short microwave pulse from the FT microwave spectrometer follows, which induces a polarization in the vaporized molecules. Once the microwave excitation ceases, the molecular emission signal containing the resonance frequencies that correspond to the rotational transitions is captured in the time domain by the detection system of the spectrometer. Finally, the usual frequency-domain spectrum is obtained from the Fourier transformation of the time-domain signal. Several thousand cycles can be phase-coherently coadded to detect very weak transitions. The species present in the supersonic expansion are thus probed by their rotational spectrum. Initial tests carried out with the known rotational spectrum of glycine[4,10] and alanine[5] confirmed the excellent performance of the experiment.

Proline (m.p. 228 °C) is unique among natural amino acids because of its special role in the formation of polypeptides.[11] This amino acid is the only natural amino acid which contains a secondary amino group as part of a flexible five-membered ring. Structural studies conducted in the condensed phase,[12–17] which include an X-ray crystal-diffraction analysis of the zwitterion,[12] yield different interpretations concerning the ring conformation. A recent infrared spectroscopic study of matrix-isolated neutral proline[18] has been interpreted with the help of ab initio calculations in terms of the existence of two bent conformers. However, to date no experimental structure of neutral proline has been reported.

The conformational behavior of isolated proline will be conditioned by the potential formation of three different types of intramolecular hydrogen bonds. Type **1** involves hydrogen bonding between the lone pair of the nitrogen atom and the hydroxy group hydrogen atom (N···H–O). Types **2** and **3** have an interaction that links the hydrogen atom on the imino group to the the oxygen atom of the carbonyl (N–H···O=C) and hydroxy (N–H···O–H) groups, respectively. Furthermore, and assuming a bent configuration of the pyrrolidine ring, *endo*-like (a) and *exo*-like (b) conformations with respect to the carboxy moiety can also be expected. Hence, a total of six plausible conformers, shown in Figure 2, can be initially considered. All of them can be independently detected in the supersonic expansion by their rotational spectra, just as in the case of a mixture of stable species, their individual structures can be determined.

The analysis of the rotational spectrum was started with the aid of the estimated values of rotational constants for each of the conformers in Figure 2. After completing a wide frequency scan, it was possible to assign a set of transitions to an asymmetrical, nearly prolate rotor. All measured lines exhibit ^{14}N nuclear quadrupole hyperfine structure,[19] which helped

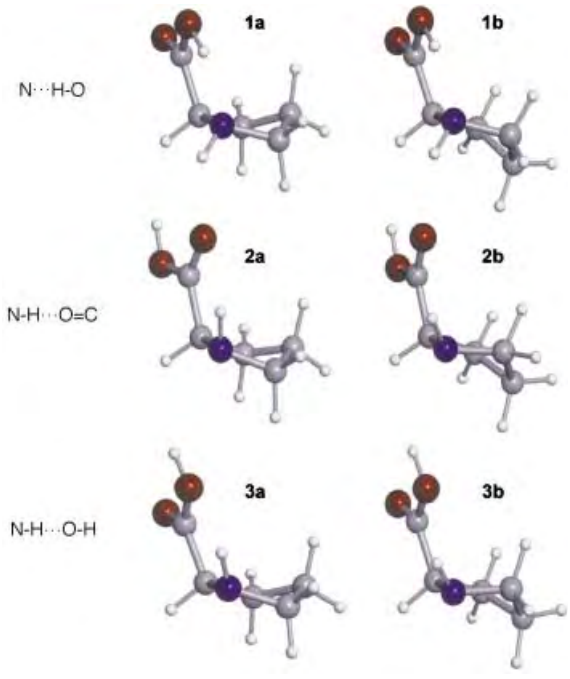


Figure 2. Plausible conformers of proline.

 © 2002 WILEY-VCH Verlag GmbH & Co. KGaA, Weinheim 0044-8249/02/4124-4674 $ 20.00+.50/0

us to confirm that they belonged to one of the proline conformers. By comparison of preliminary rotational constants with those predicted for all the plausible conformers of Figure 2, the good agreement with the *endo*-like conformer **1a** soon became apparent. To confirm unambiguously the presence of this conformer, the rotational assignment was extended to the minor ^{13}C-monosubstituted species, which are present in a natural abundance of 1.1%. After a careful search, the very weak spectra of all these species were observed. This clearly shows the high sensitivity reached in our experiment. The analysis was completed with the assignment of the spectrum of the *N*-deuterated and *O*-deuterated proline species (ND-proline and OD-proline, respectively) and a commercially enriched ^{15}N-proline sample. The final values of the spectroscopic parameters for all species were derived from an iterative least-squares analysis of the transition frequencies (110 were fitted for the parent) to a semirigid A-reduced Watson Hamiltonian ($\mathscr{H}_R^{(A)}$) supplemented with a nuclear quadrupole coupling interaction term [Eq. (1) $\mathscr{H}_Q$]:

$$\mathscr{H} = \mathscr{H}_R^{(A)} + \mathscr{H}_Q \quad (1)$$

The semirigid Watson Hamiltonian[20] is given by Equation (2)

$$\begin{aligned}\mathscr{H}_R^{(A)} = {} & A\,\mathbf{P}_a^2 + B\,\mathbf{P}_b^2 + C\,\mathbf{P}_c^2 \\ & -\Delta_J\,\mathbf{P}^4 - \Delta_{JK}\,\mathbf{P}^2\,\mathbf{P}_a^2 - \Delta_K\,\mathbf{P}_a^4 - 2\,\delta_J\,\mathbf{P}^2\,(\mathbf{P}_b^2 - \mathbf{P}_c^2) - \delta_K\,[\mathbf{P}_a^2(\mathbf{P}_b^2 - \mathbf{P}_c^2) \\ & + (\mathbf{P}_b^2 - \mathbf{P}_c^2)\,\mathbf{P}_a^2]\end{aligned} \quad (2)$$

where A, B, and C represent the rotational constants and Δ_J, Δ_{JK}, Δ_K, δ_J, and δ_K are the quartic centrifugal distortion constants. The nuclear-quadrupole coupling term $\mathscr{H}_Q$[19] accounts for the interaction of the ^{14}N nuclear electric quadrupole moment with the molecular electric field gradient at the ^{14}N nucleus. The associated determinable spectroscopic parameters are the elements of the nuclear quadrupole coupling tensor $\chi_{\alpha\beta}$ ($\alpha, \beta = a, b,$ and c). The final rotational parameters are presented in Table 1.

In the hope of observing the spectrum of the other conformers, a further search was performed. Once the lines belonging to the conformer **1a** were discarded, it was possible to identify the weak transitions of a second conformer. The values of the rotational constants given in Table 2 were very similar to those predicted for the *exo*-like conformer **1b**. However, the definitive identification was done once the ^{15}N isotopic species was analyzed from a commercially enriched sample. Rough calculations of the dipole moment gave similar values for both conformers, so the large differences observed in the intensities of the rotational transitions between conformers are conclusive evidence that the *endo*-like form is the most stable in the gas phase. No lines which could be attributed to other conformers with N–H···O=C or N–H···O–H intramolecular hydrogen bonds remained in the rotational spectrum of the jet-cooled laser-ablated proline. All the observed transitions of the conformers **1a** and **1b** are available as Supporting Information.

Table 2. Rotational parameters for the proline conformer **1b**.

	Parent[a]	^{15}N-Proline
A [MHz]	3923.5648(53)	3880.3957(236)
B [MHz]	1605.87630(62)	1602.37833(163)
C [MHz]	1279.79761(46)	1274.91634(119)
Δ_J [kHz]	1.0198(105)	1.0128(136)
Δ_{JK} [kHz]	−4.645(85)	−4.621(89)
Δ_K [kHz]	−0.0119(49)	[−0.0119]
δ_J [kHz]	0.2512(63)	0.2552(133)
δ_K [kHz]	[0.0]	[0.0]
χ_{aa} [MHz]	0.0427(89)	–
χ_{bb}-χ_{cc} [MHz]	−2.1216(144)	–
σ [kHz]	2.1	1.0
N	51	14

[a] Parameter definition as in Table 1.

The 27 rotational constants of the conformer **1a** were used in an iterative fit procedure[19,21] to determine the effective structure shown in Figure 3 and Table 3. The only assumed constrains of the fit were the planarity of the carboxy group and a local C_{2v} symmetry for the hydrogen atoms of the three methylene groups. The derived structure reproduces the observed rotational constants of all isotopomers to within 1 MHz. The pyrrolidine ring in the conformer **1a** is bent, with atoms C_3-C_2-N-C_5 in a plane and an *endo*-like puckering of 138(2)°. The atoms involved in the intramolecular N···H–O hydrogen bond complete a five-membered planar ring, with an hydrogen-bond length of r(N···H) = 1.915(6) Å calculated

Table 1. Rotational parameters for the proline conformer **1a**.

	Parent	$^{13}C_2$-Proline	$^{13}C_3$-Proline	$^{13}C_4$-Proline	$^{13}C_5$-Proline	$^{13}C_6$-Proline	^{15}N-Proline	ND-Proline	OD-Proline
A [MHz][a]	3673.90038(148)[d]	3656.9342(271)	3624.1035(273)	3643.635(33)	3664.5317(278)	3674.0579(294)	3638.06914(265)	3562.988(108)	3598.566(99)
B [MHz]	1688.42056(56)	1685.16963(312)	1685.18403(316)	1669.39682(268)	1664.63186(252)	1678.16956(261)	1682.55372(85)	1670.7719(32)	1685.02037(275)
C [MHz]	1407.37716(55)	1407.38153(102)	1398.09116(104)	1395.07345 (103)	1389.55374(89)	1400.26855(90)	1400.75783(74)	1394.2992(33)	1394.70467(302)
Δ_J [kHz]	0.6341(89)	[0.6341][e]	[0.6341]	[0.6341]	[0.6341]	[0.6341]	0.6204(152)	0.594(64)	0.601(50)
Δ_{JK} [kHz]	−2.402(47)	[−2.402]	[−2.402]	[−2.402]	[−2.402]	[−2.402]	−2.342(58)	−2.24(72)	2.05(69)
Δ_K [kHz]	5.118(311)	[5.118]	[5.118]	[5.118]	[5.118]	[5.118]	5.14(54)	[5.118]	[5.118]
δ_J [kHz]	0.1210(48)	[0.1210]	[0.1210]	[0.1210]	[0.1210]	[0.1210]	0.1129(109)	[0.1210]	[0.1210]
δ_K [kHz]	0.581(214)	[0.581]	[0.581]	[0.581]	[0.581]	[0.581]	[0.581]	[0.581]	[0.581]
χ_{aa} [MHz]	0.8820(30)	[0.8820]	[0.8820]	[0.8820]	[0.8820]	[0.8820]	–	0.844(153)	0.863(139)
χ_{bb}-χ_{cc} [MHz]	-0.2166(58)	[−0.2166]	[−0.2166]	[−0.2166]	[−0.2166]	[−0.2166]	–	[−0.2166]	[−0.2166]
σ [kHz][b]	1.9	2.6	2.3	2.4	2.3	2.0	1.3	4.7	3.6
N[c]	110	11	10	9	12	11	24	30	32

[a] A, B, and C represent the rotational constants; Δ_J, Δ_{JK}, Δ_K, δ_J, δ_K are the quartic centrifugal distortion constants and χ_{aa}, χ_{bb} and χ_{cc} are elements of the ^{14}N nuclear quadrupole coupling tensor. [b] rms deviation of the fit. [c] Number of transitions. [d] Standard error in parenthesis in the units of the last digit. [e] Parameters in square brackets were fixed in the fit.

 © 2002 WILEY-VCH Verlag GmbH & Co. KGaA, Weinheim 0044-8249/02/4124-4675 $ 20.00+.50/0

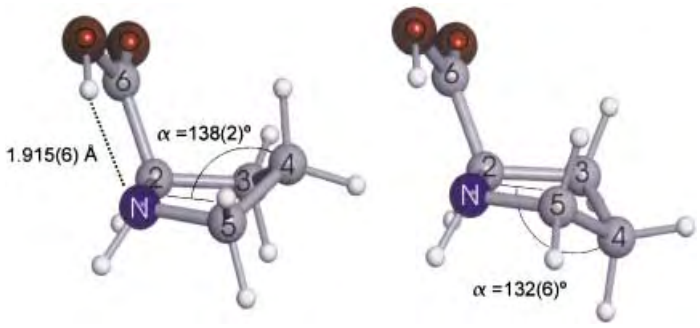


Figure 3. Calculated structure for the observed conformers of proline.

Table 3. Structure of proline.

	1a-*endo*-like	**1b**-*exo*-like[a]
$r(C_5\text{-}N)$ [Å]	1.451(6)	
r(C-C) [Å]	1.544(16)	
$r(C_6\text{-}O)$ [Å]	1.340(10)	
$r(C_6{=}O)$ [Å]	1.210(10)	
$\measuredangle(O{=}C_6\text{-}O)$ [°]	124.9(9)	
$\measuredangle(C_2\text{-}C_6\text{-}O)$ [°]	116.2(8)	
$\measuredangle(N\text{-}C_2\text{-}C_6)$ [°]	111.0(9)	
$\measuredangle(C_5\text{-}N\text{-}C_2)$ [°]	108.3(9)	
$\measuredangle(C_4\text{-}C_5\text{-}N)$ [°]	103.7(1)	
$\measuredangle(C_3\text{-}C_4\text{-}C_5)$ [°]	101.9(9)	
τ $(C_5\text{-}N\text{-}C_2\text{-}C_6)$ [°]	121(1)	
τ $(N\text{-}C_2\text{-}C_6\text{-}O)$ [°]	0(2)	
τ $(C_3\text{-}C_2\text{-}N\text{-}C_5)$ [°]	2(2)	
α [°]	138(2)	132(6)

[a] Structural parameters constrained to those of the **1a** conformer, except for the angle α, (see text).

from the Kraitchman equations.[22] With the two isotopic species available for the conformer **1b**, it was only possible to determine the ring-puckering angle α (see Figure 3 and Table 3), constraining the other structural parameters to those of **1a**.

Unlike the lowest energy conformers in glycine[4,10] and alanine[5] (stabilized by an intramolecular hydrogen bond NH···O=C), the observed conformers of proline exhibit an hydrogen bond between the hydroxy group and the nitrogen atom of the imino group (N···H–O). This result could be regarded as a consequence of the torsional restrictions imposed by the five-membered ring. The bent ring configuration observed in neutral proline contrasts with the twistlike configuration proposed by some authors[14–16] in peptide chains.

This study confirms that laser ablation combined with rotational spectroscopy in a supersonic jet may constitute a new technique (namely, laser-ablation molecular-beam Fourier-transform microwave spectroscopy or LA–MB–FTMW) which can be broadly applied to low volatility organic compounds. It makes possible the structural determination of solids in gas phase, which is particularly valuable for the neutral forms of amino acids. The results on proline and other amino acids which are presently being investigated are opening up new horizons in structural research.

Experimental Section

A new laser-ablation molecular-beam Fourier-transform microwave spectrometer working in the frequency region 8–18 GHz was used in this study. Commercial samples of proline (Aldrich) and ^{15}N-proline (Cambridge Isotope Laboratories) were used without further purification. ND- and OD-proline species were obtained by treating normal proline with D_2O. Laser pulses with energies of about 50 mJ pulse^{-1} (8 ns) were satisfactory to vaporize the samples. Argon or neon at stagnation pressures of 3–6 bar were used as carrier gases (gas pulses of 0.5–0.7 ms), with polarization pulses of 0.2–0.4 μs (0–10 dBm). Delays between the gas, laser-ablation, and microwave pulses were adjusted for maximum signal-to-noise ratio. The time-domain signal was recorded with 40-ns sampling intervals, up to 8 k data points. Frequency accuracy is better than 5 kHz.

Received: August 1, 2002 [Z19866]

[1] a) T. E. Creighton, *Protein Structure and Molecular Properties*, Freeman, New-York, **1993**; b) C. Branden, J. Tooze, *Introduction to Protein Structure*, Garland, New York, **1991**.
[2] M. F. Jarrold, *Annu. Rev. Phys. Chem.* **2000**, *51*, 179.
[3] *Jet Spectroscopy and Molecular Dynamics* (Eds.: J. M. Hollas, D. Phillips), Chapman and Hall, Glasgow, **1995**.
[4] P. D. Godfrey, R. D. Brown, *J. Am. Chem. Soc.* **1995**, *117*, 2019.
[5] P. D. Godfrey, S. Firth, L. D. Hatherley, R. D. Brown, A. P. Pierlot, *J. Am. Chem. Soc.* **1993**, *115*, 9687.
[6] R. J. Levis, *Annu. Rev. Phys. Chem.* **1994**, *45*, 483.
[7] a) *Lasers and Mass Spectrometry* (Ed.: D. M. Lubman), Oxford University Press, New York, **1990**; b) U. Bahr, M. Karas, F. Hillenkamp, *Fresenius J. Anal. Chem.* **1994**, *348*, 783.
[8] R. D. Suenram, F. J. Lovas, G. Fraser, K. Matsumura, *J. Chem. Phys.* **1990**, *92*, 4724.
[9] K. A. Walker, M. C. L. Gerry, *J. Mol. Spectrosc.* **1997**, *182*, 178.
[10] F. J. Lovas, Y. Kawashima, J.-U. Grabow, R. D. Suenram, G. T. Fraser, E. Hirota, *Astrophys. J.* **1995**, *455*, L201.
[11] a) A. Yaron, F. Naider, *Crit. Rev. Biochem. Mol. Biol.* **1993**, *28*, 31; b) M. McArthur, J. Thornton, *J. Mol. Biol.* **1991**, *218*, 397; c) D. N. Woolfson, D. H. Williams, *FEBS Lett.* **1990**, *277*, 185.
[12] R. L. Kayushina, B. K. Vainshtein, *Sov. Phys. Crystallogr. (Engl. Trans.)* **1966**, *10*, 698.
[13] R. Balasubramanian, A. V. Lakshminarayanan, M. N. Sabesan, G. Tegoni, K. Venkatesan, G. N. Ramachandran, *Int. J. Protein Res.* **1971**, *3*, 25.
[14] D. F. DeTar, N. P. Luthra, *J. Am. Chem. Soc.* **1977**, *99*, 1232.
[15] D. F. DeTar, N. P. Luthra, *J. Org. Chem.* **1979**, *44*, 3299.
[16] C. A. G. Haasnoot, F. A. A. M. De Leeuw, H. P. M. De Leew, C. Altona, *Biopolymers* **1991**, *20*, 1211.
[17] E. J. Milner-White, L. H. Bell, P. H. Maccallum, *J. Mol. Biol.* **1992**, *228*, 725.
[18] S. G. Stepanian, I. D. Reva, E. D. Radchenko, L. Adamowicz, *J. Phys. Chem. A* **2001**, *105*, 10664.
[19] W. Gordy, R. L. Cook, *Microwave Molecular Spectra*, Wiley, New York **1984**.
[20] J. K. G. Watson in *Vibrational Spectra and Structure, Vol. 6* (Ed.: J. R. Durig), Elsevier, Amsterdan, **1977**, pp. 1–89.
[21] H. D. Rudolph, *Struct. Chem.* **1991**, *2*, 581.
[22] J. Kraitchman, *Am. J. Phys.* **1953**, *21*, 17.

 © 2002 WILEY-VCH Verlag GmbH & Co. KGaA, Weinheim 0044-8249/02/4124-4676 $ 20.00+.50/0

Lewis Acidity in Transition-Metal-Doped Microporous Aluminophosphates**

Furio Corà,* Iman Saadoune, and C. Richard A. Catlow

The origin of Lewis acidity in microporous framework oxides, such as zeolites and aluminophosphates (AlPOs) has been extensively debated.[1,2] Experimental temperature-programmed desorption (TPD) and calorimetric data probing the interaction of Lewis basic molecules, such as ammonia or acetonitrile, with doped AlPOs, show the presence of two distinct adsorption sites, attributed in one case to the Brønsted and in the other to the Lewis acid sites within the framework.[3,4] When transition metal ions are incorporated into the framework of AlPOs during synthesis, the Lewis acidity is likely to be associated with the transition metal centers. Not all the dopant ions, however, interact in the same way with Lewis bases in metal–AlPO compounds; for instance, AlPOs containing Ni^{2+} ions have been shown to possess much less pronounced Lewis acidity than their Co and Mn analogues.[3] The cause of the different behavior is still unclear. Given the interest in doped AlPOs for their applications in heterogeneous catalysis,[5,6] the desire to understand the mechanism by which the Lewis acidity operates and influences the interaction of reactants with the active sites within the framework is a topic of primary importance.

In this communication we investigate, with periodic ab initio quantum mechanical (QM) calculations, the electronic distribution of a set of $2+$ and $3+$ transition metal ions, isomorphously substituted for Al in the framework of AlPO-34. We use the results of our calculations to examine the possible origin of the Lewis acidity in the doped aluminophosphates. The factors controlling the Lewis acidity will be discussed by examining the calculated electronic distribution of the transition metal dopants; in particular, we shall consider the orientation of the empty d atomic orbitals (AOs) on the metal site.

The doped AlPO-34 framework employed in these calculations is a supercell model in which one dopant ion is included in each unit cell of the host framework (composed of 36 atoms, or $6\,AlPO_4$ formula units). Even at this high concentration, compared to the level of doping achievable experimentally, the dopant ions are separated approximately 10 Å from each other, and thus represent non-interacting defect centers. The supercell model describes correctly the extended nature of the solid catalyst; the crystal field and the structural strain caused by the crystalline matrix on the substitutional ion are therefore included in the computational model.

[*] Dr. F. Corà, I. Saadoune, Prof. C. R. A. Catlow
Davy Faraday Research Laboratory
The Royal Institution of Great Britain
21 Albemarle Street, London W1S 4BS (UK)
Fax: (+44) 20-7629-3569
E-mail: furio@ri.ac.uk

[**] We would like to thank the EPSRC for funding this research project; F.C. acknowledges a grant from the Royal Society for the purchase of computer equipment.

The dopant ions investigated are Cr^{2+}, Mn^{2+}, Fe^{2+}, Co^{2+}, Ni^{2+}; Cr^{3+}, Mn^{3+}, Fe^{3+}, and Co^{3+}, each replacing one Al^{3+} ion of the host framework. The low-valent $(2+)$ ions are charge-compensated by protonating one of the framework oxygen ions that is a nearest neighbor to the dopant, as shown in Figure 1.

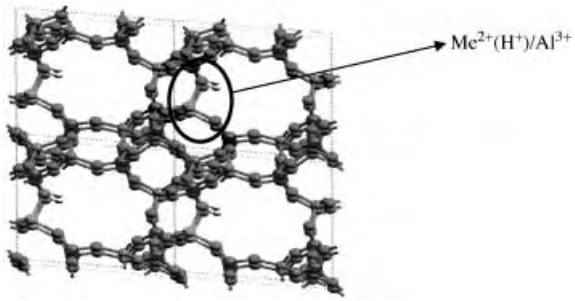


Figure 1. Structure of a $2+$ dopant ion, charge-compensated by an acid proton, that replaces a framework Al^{3+} ion in ALPO-34, described using periodic boundary conditions.

Since the dopants examined are open-shell transition metal ions, we performed our calculations at the Unrestricted Hartree–Fock (UHF) level; this Hamiltonian employs the exact expression of exchange forces, which are important for a correct representation of the unpaired electrons. Calculations for the Ni^{2+} dopant have also been repeated with a B3LYP density functional Hamiltonian, employing the hybrid exchange functional proposed by Becke.[7] This functional has been shown both in molecular[7] and in solid-state calculations[8] to provide a very accurate description of the electronic density and energetics of the systems investigated. The calculations have been performed with the latest version of the CRYSTAL code,[9] which includes the analytical evaluation of forces.[10,11] The transition metal ions are described with an 8-64111d41G basis set, available from the online database of the CRYSTAL code.[12] For each dopant ion investigated, we have determined the equilibrium structure by performing a geometry optimization of all the internal coordinates within the unit cell using P1 symmetry. The Lewis acidity properties are calculated for the equilibrium structure of each ion.

In transition-metal-doped AlPOs, the unpopulated and/or partially filled d AOs of the transition metal site are obvious candidates to explain the presence or absence of Lewis acidity in the framework. To investigate this feature we have calculated the total and spin electronic density of each metal dopant in its equilibrium structure; the result is plotted in Figure 2 for the isovalent $3+$ ions, and in Figure 3 for the low-valent $2+$ ions. The plane of the figures is chosen to contain the transition metal dopant, one of its nearest-neighbor oxygen ions (for the $2+$ ions we chose the oxygen ion bonded to the charge-compensating proton), and the next-nearest phosphorus ion bonded to the oxygen ion previously described. In each plot, the continuous and dashed black and green lines are the isodensity levels calculated from the spin density.

Not all of the interstitial space within the microporous framework is accessible to adsorbed molecules: the Pauli

 © 2002 WILEY-VCH Verlag GmbH & Co. KGaA, Weinheim 0044-8249/02/4124-4677 $ 20.00+.50/0

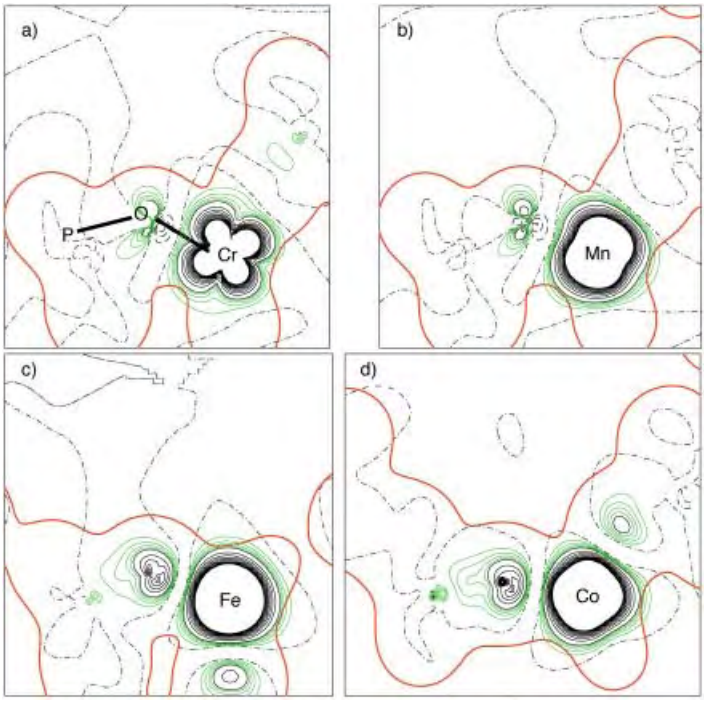


Figure 2. Electron and spin density maps for the isovalent 3+ transition metal ions in AlPO-34. The black and green lines represent the spin density, plotted between −0.05 and +0.05 a.u. at linear steps of 0.005 a.u. (black), and between 0.001 and 0.005 a.u. at linear steps of 0.001 a.u. (green). Continuous and dashed lines refer to positive and negative spin density, respectively. The continuous red line is the isodensity level of 0.01 a.u. calculated from the total electronic density, and represents the effective size of the framework. The substitutional ions are Cr^{3+} (a), Mn^{3+} (b), Fe^{3+} (c), and Co^{3+} (d).

repulsion caused by the overlap between the electronic density of the molecule and of the framework atoms makes the adsorption process energetically unfavorable when the molecule is too close to the framework atoms. How close the adsorbed molecules can approach the framework and its active sites depends therefore on the radial extent of the electronic density of the framework itself. To have an indication of this feature, we have calculated the total electronic density of the doped materials; in Figure 2 and Figure 3 we plot in red the isodensity level of 0.01 a.u., which represents an "effective" framework size beyond which the adsorbed molecules cannot approach the framework ions.

The transition metal ions investigated have a partially filled d shell, with electronic configurations ranging between the d^3 of Cr^{3+} to the d^8 of Ni^{2+}. When they are isomorphously substituted for Al in the AlPO-34 framework, our calculations show that all the transition metal ions investigated are stable in the spin state with highest multiplicity compatible with their count of d electrons. A high-spin state would indeed be expected, because of the low crystal-field splitting caused by the tetrahedral coordination of the transition metal ions; the partially covalent character of the oxygen ligands with the phosphorus ions[13,14] decreases their net charge, and makes the crystal field they create insufficient to stabilize low-spin states on the transition metals.

The spin density of Figure 2 and Figure 3 represents the distribution of the half filled d AOs of the metal dopant. When considering the Lewis acidity of open-shell transition metal ions in the high-spin state, we have to distinguish between ions with less than half filled d AOs (that is, with electronic configuration d^3–d^4), and ions with d AOs that are at least half filled (with electronic configuration d^5–d^8). In the former case the spin density represents the orbitals which are least active towards Lewis acidity: they are half filled, while the other d orbitals are empty and therefore stronger Lewis acids, whereas in the latter case, the spin density represents the d orbitals responsible for the Lewis acidity: they are half filled, while the remaining levels are all occupied by two electrons, and hence inactive for Lewis acidity.

We clearly see in Figure 2 and Figure 3 that the orientation and radial extent of the spin density differs according to the electronic configuration of the dopant ion. As a result, the extent of spin density that spills outside the Pauli repulsion area (red line) varies considerably among the dopants. In particular, we notice that the Lewis-active orbitals of the Ni^{2+} ion are oriented along the framework; a molecule inside the microporous cages of a Ni-doped AlPO will therefore be subject to Pauli repulsion from the framework before having

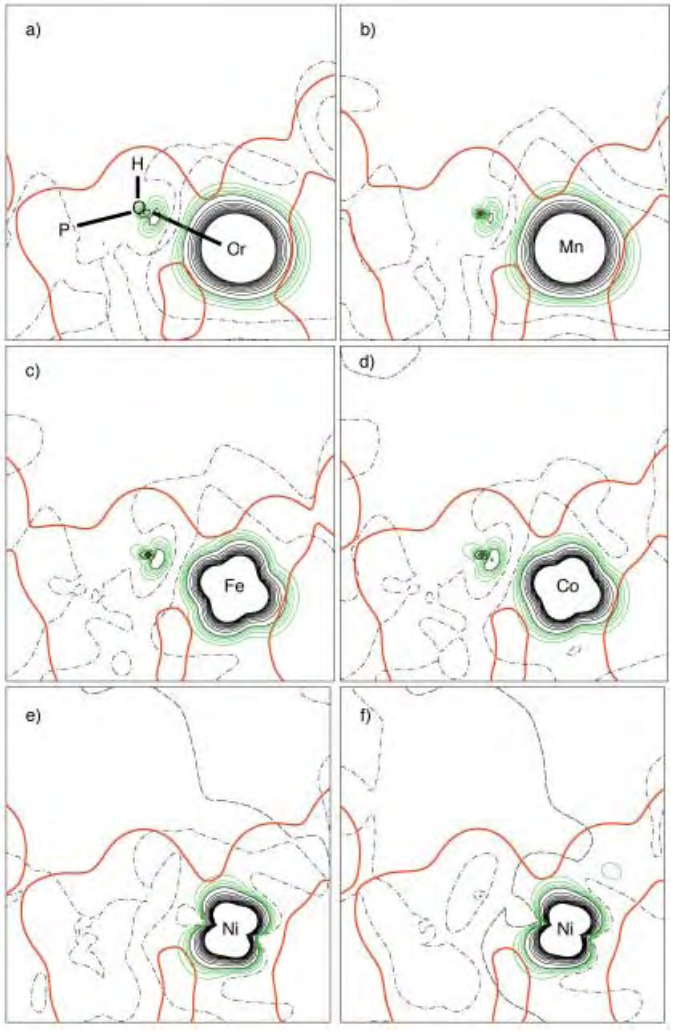


Figure 3. Electron and spin density maps for the low-valent 2+ transition metal ions in AlPO-34. Symbols and units as in Figure 2. The substitutional ions are Cr^{2+} (a), Mn^{2+} (b), Fe^{2+} (c), Co^{2+} (d), and Ni^{2+} (e). The plot (f) refers to the solution for Ni^{2+}, calculated with the B3LYP Hamiltonian.

 © 2002 WILEY-VCH Verlag GmbH & Co. KGaA, Weinheim 0044-8249/02/4124-4678 $ 20.00+.50/0

an effective interaction with the Lewis-active orbitals of the Ni ion. This is not the case, however, for Mn, Fe, and Co dopant ions; molecules in Mn, Fe, and Co-doped materials can undergo an appreciable chemical interaction with the Lewis-active orbitals before being repelled by the framework. We consider that this result explains effectively the origin of the Lewis acidity in the latter frameworks, and its absence in the Ni-doped materials, in agreement with the experimental results of reference[3]. The presence of empty d states on the transition metal site, oriented in a perpendicular direction to the framework structure, is necessary to initiate a Lewis acid–base interaction with adsorbed molecules.

To investigate whether this result depends on the Hamiltonian employed in the calculations, we have repeated the study of Ni-AlPO-34 with the B3LYP density functional. We find no significant qualitative changes, suggesting that our results have general validity.

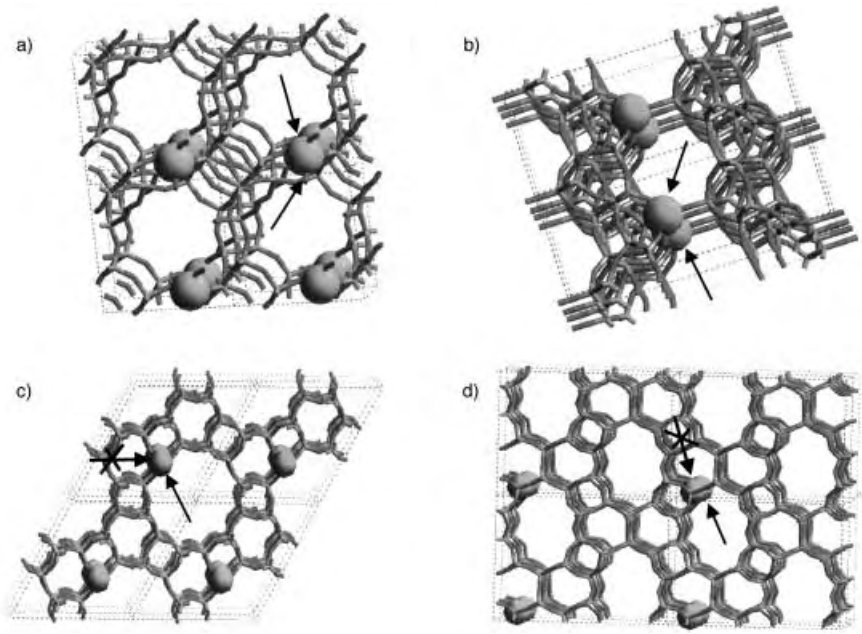


Figure 4. Structural environment of the cationic framework sites in different zeotypic framework topologies: a) chabasite (AlPO-34), b) ferrierite, c) AlPO-5, and d) AlPO-11. The two-dimensional open space in chabasite and ferrierite is visible, which allows "attack from behind" of the framework ions, along with the one-dimensional character of AlPO-5 and AlPO-11, which prevents such a form of attack.

It is also important to notice in Figure 3 that for the 2+ dopant ions, the spilling of the spin density outside the Pauli repulsion area is most effective on the side of the framework opposite to the proton. This feature suggests that the interaction of Lewis bases with the 2+ transition metal ions is most effective when the molecule can approach the framework from the side opposite to the protonated oxygen ion, while interaction of the adsorbed molecule with the Brønsted acid proton prevents a Lewis-type acid–base interaction with the transition metal ion. We refer to this structural requirement as an "attack from behind" of the Lewis-basic molecule to the transition metal dopant. This suggestion of our computational work is indirectly supported by experimental work on Co^{2+}-doped AlPOs,[15,16] in which the authors found that to achieve complexation (Lewis interaction) of the framework Co^{2+} ions by acetonitrile, the Co–OH bond between the Co^{2+} ion and the Brønsted acid OH group must be broken, that is, that Lewis and Brønsted acid interactions are mutually exclusive. Such a structural property of Lewis-type interactions is able to differentiate the Lewis acidity of different AlPO frameworks. We expect, in fact, that the transition metal ions will be more Lewis active when they are located in open regions of a framework, where the space behind the dopant and the protonated oxygen ion is not protected by other ions of the framework. Instead, the structures are expected to be less Lewis-active when the dopant and the protonated oxygen ion cannot be approached from behind by adsorbed molecules, as is the case when the transition metal dopant is located in a double-walled structural unit. As a general rule, we predict therefore that the microporous polymorphs of zeolites and AlPOs with intersecting channels, or with single walls between large cages, such as the Chabasite (AlPO-34 and its closely related AlPO-18) and Ferrierite framework topologies (Figure 4a,b), will have more active Lewis acid sites than those framework structures with one-dimensional channels made of "double-wall" building units, such as those found in the AlPO-5 and AlPO-11 structures (Figure 4c,d). This result may explain why, experimentally, the Lewis-acidic behaviour of Co-AlPO-5 towards the adsorption of acetonitrile was found to be similar to that of Co-AlPO-11,[17] but different from that of Co-AlPO-18.[15,16] We leave open for further experimental verifications this prediction of the computational work.

In conclusion, results of our QM calculations on transition-metal-doped AlPO-34 suggest an electronic explanation for the Lewis acidity of these materials. This feature requires the presence of empty d states on the transition metal site, oriented in a perpendicular direction to the framework structure, which is necessary to initiate a Lewis acid–base interaction with adsorbed molecules. Attack "from behind" of Lewis basic molecules to 2+ dopant ions is favored, and is expected to yield stronger Lewis acidity for polymorphs with single-wall framework structure, rather than polymorphs with one-dimensional channels and composed only of double-walled structural units.

Received: August 13, 2002
Revised: September 30, 2002 [Z19959]

[1] H. G. Karge, V. Dondur, *J. Phys. Chem.* **1990**, *94*, 765.
[2] H. G. Karge, V. Dondur, J. Weitkamp, *J. Phys. Chem.* **1991**, *95*, 283.
[3] G. Lischke, B. Parlitz, U. Lohse, E. Schreier, R. Fricke, *Appl. Catal. A* **1998**, *166*, 351.
[4] "Zeolites and Related Microporous Materials: State of the Art 1994": J. Jänchen, M. J. Haanepen, M. P. J. Peeters, J. H. M. C. van Wolput, J. P. Wolthuizen, J. H. C. van Hooff, *Stud. Surf. Sci. Catal.* **1994**, 84.
[5] A. Corma, H. García, *Catal. Today* **1997**, *38*, 257.

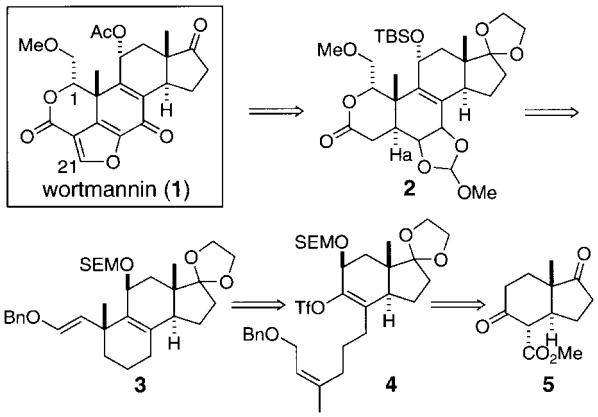
 © 2002 WILEY-VCH Verlag GmbH & Co. KGaA, Weinheim 0044-8249/02/4124-4679 $ 20.00+.50/0

[6] J. M. Thomas, *Angew. Chem.* **1999**, *111*, 3800; *Angew. Chem. Int. Ed.* **1999**, *38*, 3588.
[7] A. D. Becke, *J. Chem. Phys.* **1993**, *98*, 5648.
[8] J. Muscat, A. Wander, N. M. Harrison, *Chem. Phys. Lett.* **2001**, *342*, 397.
[9] V. R. Saunders, R. Dovesi, C. Roetti, M. Causà, N. M. Harrison, R. Orlando, C. M. Zicovich-Wilson, K. Doll, B. Civalleri, CRYSTAL User's Manual, Univ. of Torino, Torino, **1998** and **2001**.
[10] K. Doll, V. R. Saunders, N. M. Harrison, *Int. J. Quantum Chem.* **2001**, *82*, 1.
[11] B. Civalleri, Ph. D'Arco, R. Orlando, V. R. Saunders, R. Dovesi, *Chem. Phys. Lett.* **2001**, *348*, 131.
[12] http://www.chimifm.unito.it/teorica/crystal/Basis_Sets/mendel.html.
[13] F. Corà, C. R. A. Catlow, *J. Phys. Chem. B* **2001**, *105*, 10278.
[14] F. Corà, C. R. A. Catlow, A. D'Ercole, *J. Mol. Catal. A* **2001**, *166*, 87.
[15] J. Chen, J. M. Thomas, G. Sankar, *J. Chem. Soc. Faraday Trans.* **1994**, *90*, 3455.
[16] P. A. Barrett, G. Sankar, R. H. Jones, C. R. A. Catlow, J. M. Thomas, *J. Phys. Chem. B* **1997**, *101*, 9555.
[17] J. Jänchen, M. P. J. Peeters, J. H. M. C. van Wolput, J. P. Wolthulzen, J. H. C. van Hooff, *J. Chem. Soc. Faraday Trans.* **1994**, *90*, 1033.

Total Synthesis of (±)-Wortmannin**

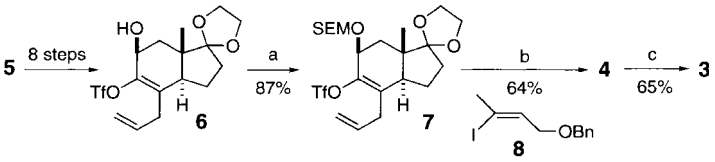
Takashi Mizutani, Shinobu Honzawa, Shin-ya Tosaki, and Masakatsu Shibasaki*

Wortmannin (**1**) is a potent and specific phosphoinositide 3-kinase (PI3K) inhibitor with a low nanomolar IC_{50} value[1] that was originally isolated from *Penicillium Wortmannii* as an anti-inflammatory and antibiotic agent.[2] Wortmannin (**1**) acts by covalently binding Lys802 in the ATP binding pocket of PI3K through nucleophilic attack of the Lys amino group at the C21 position of **1**.[3] PI3K is an important enzyme that functions in signal transduction pathways, and is a potential target for preventing proliferation of cancer cells.[4] Unfortunately, **1** has not yet been applied to medical use because of its high toxicity. Thus, wortmannin derivatives, which possess more potent inhibitory activity against PI3K and have less general toxicity, are necessary for the development of new antitumor drugs. In addition to the medicinal aspect, the challenging structural features of **1**, namely an allylic quaternary carbon center and a furanocyclohexadienone lactone unit, are very attractive from a synthetic point of view. In 1996, we reported the first chemical synthesis of **1** from hydrocortisone.[5] Following this primary achievement, we planned to develop a direct total synthesis of **1**, which would hopefully lead to many more derivatives. Here, we report the first direct total synthesis of (±)-**1** using an intramolecular Heck reaction for stereoselective construction of an allylic quaternary carbon center (Scheme 1)[6] and a diosphenol–Claisen rearrangement (Scheme 3)[7] as key steps.



Scheme 1. Retrosynthesis of (±)-wortmannin. SEM = 2-(trimethylsilyl)-ethoxymethyl; TBS = *tert*-butyldimethylsilyl; Tf = trifluoromethanesulfonyl; Bn = benzyl.

Our synthesis began with alkenyl triflate **6**, which was synthesized from compound **5**, and obtained as a racemate[8] in eight steps and in 27% overall yield (Scheme 2).[6c] After conversion of **6** into the SEM-protected ether **7** (87%), it was chemoselectively coupled with **8** by the Suzuki method to give **4** (64%).[9] An intramolecular Heck reaction of **4** afforded



Scheme 2. Synthesis of enol ether **3**. a) SEMCl, 2,6-lutidine, nBu$_4$NI, CH_2Cl_2, 40°C; b) 9-BBN, THF, RT then **8**, [$PdCl_2$(dppf)], K_3PO_4, THF/DMF, 60°C; c) 10 mol% of $Pd(OAc)_2$, 22 mol% of 1,3-bis(diphenylphosphanyl)propane, 1.0 equiv of nBu$_4$NBr, 2.5 mol equiv of K_2CO_3, toluene, 100°C, 17 h. SEMCl = 2-(trimethylsilyl)ethoxymethyl chloride, 9-BBN = 9-borabicyclo[3.3.1]nonane, dppf = 1,1′-bis(diphenylphosphanyl)ferrocene.

enol ether **3** in 65% yield and in excellent diastereoselectivity (β-Me:α-Me = 18:1). It is noteworthy that the stereochemistry of the β-SEM ether in **4** plays a crucial role in the excellent stereoselectivity achieved by the Heck reaction.[6] Unfortunately, the use of the epimer, the α-SEM ether, afforded the undesired (α-Me) isomer as the major product.

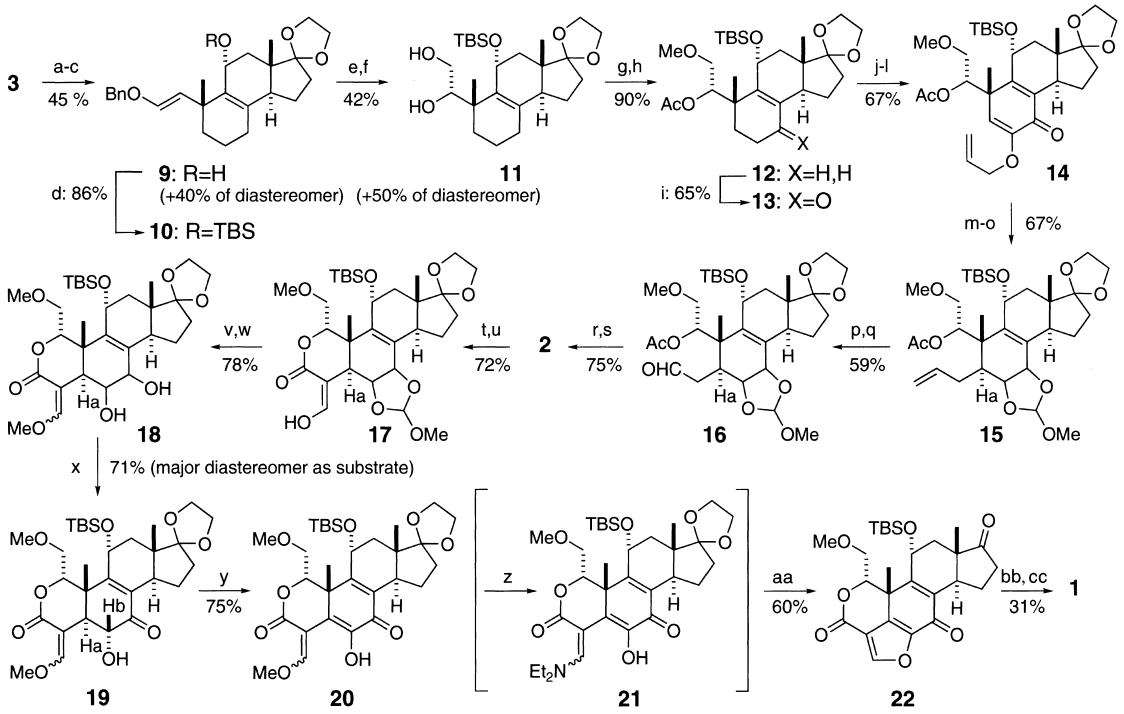
Removal of the SEM group, followed by oxidation and reduction, produced α-allylic alcohol **9** (3 steps) together with the β alcohol (Scheme 3). The β-alcohol can be recycled by conventional methods. After protection of **9** as the TBS ether to give **10**, oxidation of the enol ether with 2.5 mol% of OsO_4 and 1.5 equivalents of NMO gave the hydroxyaldehyde, which was then reduced with $LiAlH_4$ to give the desired diol **11**

[*] Prof. Dr. M. Shibasaki
Graduate School of Pharmaceutical Sciences
The University of Tokyo
Hongo, Bunkyo-ku, Tokyo 113-0033 (Japan)
Fax: (+81) 3-5684-5206
E-mail: mshibasa@mol.f.u-tokyo.ac.jp
T. Mizutani, S. Honzawa, S.-y. Tosaki
Graduate School of Pharmaceutical Sciences
The University of Tokyo (Japan)

[**] We thank Dr. Yuzuru Matsuda (Kyowa Hakko Co., Ltd) for kindly supplying a sample of wortmannin. This work was financially supported by CREST, JST, and RFTF. T.M. thanks the Japan Society for the Promotion of Science (JSPS) for a research fellowship.

Supporting information for this article is available on the WWW under http://www.angewandte.org or from the author.

 © 2002 WILEY-VCH Verlag GmbH & Co. KGaA, Weinheim 0044-8249/02/4124-4680 $ 20.00+.50/0



Scheme 3. Total synthesis of **1**. a) CsF, DMF, 130 °C; b) PDC, NaOAc, CH_2Cl_2, RT; c) DIBAL-H, toluene, −78 °C; d) TBSCl, imidazole, DMF, RT; e) OsO_4, NMO, acetone/H_2O, RT; f) $LiAlH_4$, THF, −40 °C; g) MeI, Ag_2O, RT; h) Ac_2O, DMAP, pyridine, CH_2Cl_2, RT; i) CrO_3, 3,5-dimethylpyrazole, CH_2Cl_2, −20 °C; j) 1. TMSOTf, Hünig base, CH_2Cl_2, −78 °C; 2. dimethyldioxirane, acetone, RT; 3. PPTS, MeOH, RT; k) $(COCl)_2$, DMSO, CH_2Cl_2, −40 °C; Et_3N, −40 °C; l) allyl bromide, K_2CO_3, acetone, 40 °C; m) xylene, 200 °C, 50 min; n) $NaBH_4$, $CeCl_3 \cdot 7H_2O$, MeOH, 0 °C; o) $HC(OMe)_3$, PPTS, RT; p) OsO_4, NMO, CH_3CN/H_2O, RT; q) nBu_4NIO_4, $CHCl_3$, 40 °C; r) K_2CO_3, MeOH, RT; s) TPAP, NMO, 4Å MS, CH_2Cl_2, RT; t) $HC(NMe_2)_3$, DMF, 100 °C; u) phosphate buffer (pH 4–5), THF, RT; v) Me_2SO_4, K_2CO_3, acetone, RT; w) 1N NaOH, THF, RT; x) PDC, NaOAc, CH_2Cl_2, RT; y) $(COCl)_2$, DMSO, CH_2Cl_2, −20 °C; Et_3N, −20 °C; z) Et_2NH, CH_2Cl_2, RT; aa) 1N HCl, THF, RT; bb) 3 HF·Et_3N, THF, 40 °C; cc) Ac_2O, pyridine, RT. PDC = pyridinium dichromate; DIBAL-H = diisobutylaluminum hydride; TBSCl = *tert*-butyldimethylsilyl chloride; DMAP = 4-(dimethylamino)pyridine; TMSOTf = trimethylsilyl trifluoromethanesulfonate; PPTS = pyridinium *p*-toluenesulfonate; NMO = 4-methylmorpholine *N*-oxide; TPAP = tetrapropylammonium perruthenate.

(2 steps, 42 %) together with the undesired diol (50 %).[10,11] Selective methylation of the primary alcohol of diol **11** and successive protection of the remaining secondary alcohol as an acetyl group gave **12** (2 steps, 90 %). Allylic oxidation of **12** proceeded well with 15 equivalents of CrO_3 and 3,5-dimethylpyrazole at −20 °C to give enone **13**. In the next transformation, we faced a difficult task, that is, introduction of a carbon unit at the sterically crowded neopentyl position for lactone formation. After numerous attempts, a diosphenol–Claisen rearrangement[7] of **14** was found to be effective for introducing a C–C bond at the neopentyl position.[12,13] Thus, enone **13** was converted into **14**, by five successive transformations: enol silyl ether formation, oxidation of enol ether with dimethyldioxirane, removal of the TMS group, oxidation of α-hydroxyketone to a mixture of diosphenol and α-diketone, and allylation with allyl bromide. The Claisen rearrangement of **14** proceeded very well under thermal conditions to give the α-diketone as a single diastereomer.[14,15] The obtained α-diketone was subsequently reduced to the diol, followed by protection to give cyclic orthoester **15** (3 steps) as an inseparable mixture of several diastereomers. The formation of several diastereomers is not a serious problem, because in principle all the isomers can be transformed into **1**. The terminal olefin of cyclic orthoester **15** was oxidatively cleaved (cat. OsO_4 then nBu_4NIO_4[16] in $CHCl_3$ at 40 °C) to give aldehyde **16** (2 steps). Removal of the acetyl group of **16** led to the formation of hemiacetal, which was oxidized by tetrapropylammonium perruthenate (TPAP) to give lactone **2** (2 steps).

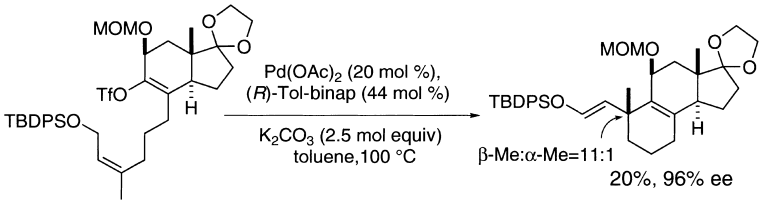
After production of **2**, the introduction of a C1 unit at the α position of the lactone and formation of the furan ring remained. Similar to previous reports on synthetic studies[17] and chemical synthesis of **1**,[5] aminomethylenation was effective for the introduction of the C1 unit. As expected, treatment of lactone **2** with $HC(NMe_2)_3$ at 100 °C gave the desired compound in good yield, and the rather unstable product was successively treated with aqueous acid to furnish enol **17** (2 steps). Protection of the enol and conversion of the cyclic orthoester into a formate group occurred simultaneously following treatment of **17** with Me_2SO_4 and K_2CO_3 in acetone, and further treatment with aquous NaOH gave diol **18** (2 steps, ca. 3:1 mixture of diastereomers). Oxidation of the major diastereomer of diol **18** with PDC gave **19**,[14] and then Swern oxidation of **19** afforded diosphenol **20**.[18] Direct construction of the furan ring from **20** was first investigated under acidic conditions. Unexpectedly, however, only decomposition occurred. Several subsequent trials revealed that diosphenol **20** was very reactive toward nucleophiles. Thus, there was clean consumption of **20** to give **21** when it was treated with Et_2NH, and successive treatment of **21** with 1N HCl promoted the desired cyclization and simultaneous deprotection of acetal to afford furan **22** (2 steps). Finally,

 © 2002 WILEY-VCH Verlag GmbH & Co. KGaA, Weinheim 0044-8249/02/4124-4681 $ 20.00+.50/0

removal of the TBS group proceeded smoothly with excess $3\,HF{\cdot}Et_3N$, and subsequent acetylation of the generated alcohol gave (±)-**1** (2 steps).

In conclusion, we have achieved the first total synthesis of **1**. Although several issues remain to be addressed, such as the low stereoselectivities in several steps, much useful information about the synthesis of wortmannin derivatives has been accumulated. Further optimization of the current scheme and continuing efforts to realize an efficient catalytic asymmetric synthesis are now under intense investigation and the results will be reported in due course.

Received: August 21, 2002 [Z50016]



Scheme 4. MOM = methoxymethyl; TBDPS = *tert*-butyldiphenylsilyl; binap = 2,2′-bis(diphenylphosphanyl)-1,1′-binaphthyl.

because of the problem of deprotection. Optimization using **4** is currently under investigation, see c) S. Honzawa, T. Mizutani, M. Shibasaki, *Tetrahedron Lett.* **1999**, *40*, 311 – 314.

[7] a) W. G. Dauben, A. A. Ponaras, A. Chollet, *J. Org. Chem.* **1980**, *45*, 4413 – 4417; b) A. A. Ponaras, *Tetrahedron Lett.* **1980**, *21*, 4803 – 4806.

[8] A. S. Caselli, D. J. Collins, G. M. Stone, *Aust. J. Chem.* **1982**, *35*, 799 – 808.

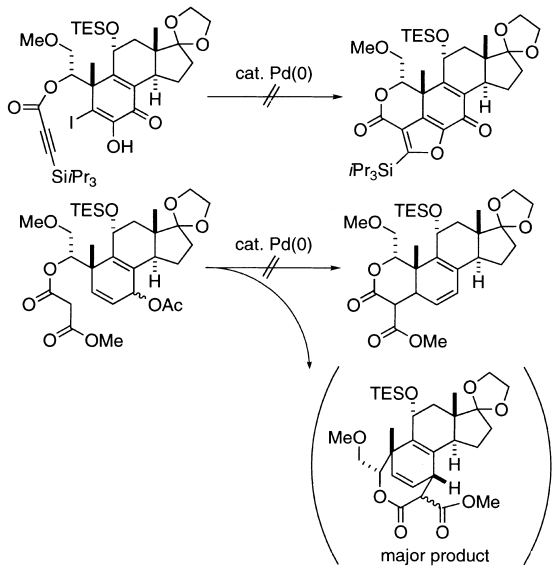
[9] For B-alkyl Suzuki coupling, see S. R. Chemler, D. Trauner, S. J. Danishefsky, *Angew. Chem.* **2001**, *113*, 4676 – 4701; *Angew. Chem. Int. Ed.* **2001**, *40*, 4544 – 4568.

[10] At this stage, the undesired diastereomer of **11** was recrystallized from acetone and an X-ray crystallographic analysis succeeded in confirming the stereochemistry. CCDC-191844 contains the supplementary crystallographic data for this paper. These data can be obtained free of charge via www.ccdc.cam.ac.uk/conts/retrieving.html (or from the Cambridge Crystallographic Data Centre, 12 Union Road, Cambridge CB2 1EZ, UK; fax: (+44) 1223-336-033; or deposit@ccdc.cam.ac.uk).

[11] The undesired diastereomer could be readily recycled to the desired diastereomer in several ways.

[12] Intermolecular Michael addition of various reagents to the corresponding enone failed.

[13] We tried other several strategies for the construction of wortmannin skeleton from **3** (Scheme 5). These strategies, however, were unsuccessful.



Scheme 5. TES = triethylsilyl.

[14] The stereochemistry of Ha was clearly determined by NOE measurements on **19**, and that of Hb was also determined by the same method.

[15] Longer reaction times (e.g. 3 h) produced the corresponding diosphenol, which could not be converted into **15**.

[16] E. Santaniello, A. Manzocchi, C. Farachi, *Synthesis* **1980**, 563 – 564.

[17] C. A. Broka, B. Ruhland, *J. Org. Chem.* **1992**, *57*, 4888 – 4894.

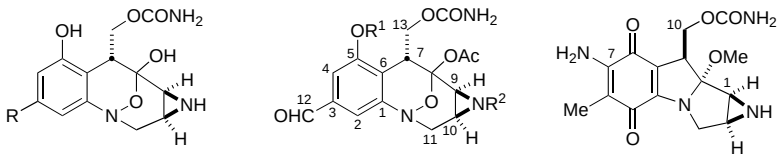
[18] When a minor diastereomer was used as a substrate for successive oxidations, only a low yield of **20** was obtained (ca. 10%).

 © 2002 WILEY-VCH Verlag GmbH & Co. KGaA, Weinheim 0044-8249/02/4124-4682 $ 20.00+.50/0

Concise Enantioselective Synthesis of (+)-FR66979 and (+)-FR900482: Dimethyldioxirane-Mediated Construction of the Hydroxylamine Hemiketal**

Ted C. Judd and Robert M. Williams*

Dedicated to Professor Albert I. Meyers on the occasion of his 70th birthday.

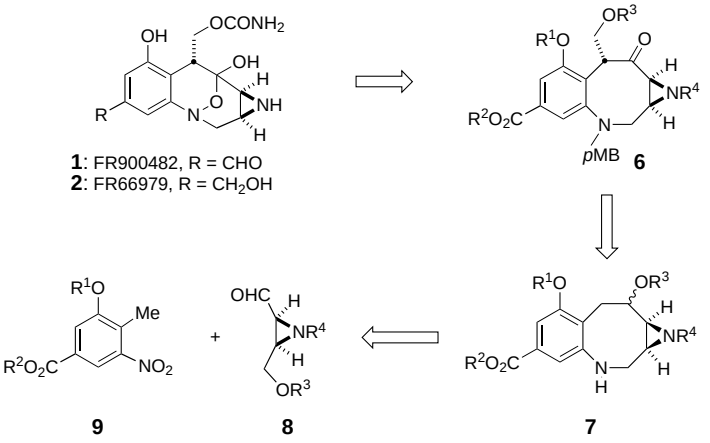


Scheme 1. Structures of FR900482 (**1**) and congeners.

The antitumor antibiotic natural products FR900482 (**1**) and FR66979 (**2**) were isolated from *Streptomyces sandaensis* No. 6897 by the Fujisawa Pharmaceutical Co. in 1987.[1] Both compounds have been shown to crosslink DNA preferentially at $^{5'}$CpG$^{3'}$ steps in the minor groove following reductive activation.[2–4] Additionally, recent studies from our laboratory have demonstrated that FR900482 (**1**) and FK317 (**4**) crosslink the minor groove-binding HMGA1 oncoprotein to DNA in vivo, which has very significant implications for the mode of action of these agents.[5] Both FK973 (**3**)[6] and FK317 (**4**),[7] semisynthetic derivatives of FR900482 (**1**), have shown highly promising antitumor activity in human clinical trials in Japan[6] and hold significant promise to replace the structurally related and widely used antitumor drug mitomycin C (**5**).[8] Notably, FK317 (**4**) has been shown not to induce vascular leak syndrome (VLS), a highly detrimental side effect observed in human clinical trials with the natural products FR900482 (**1**), FR66979 (**2**), and the semisynthetic derivative FK973 (**3**). The mechanistic basis for the anomalous difference between **1** and **4** in causing VLS has been revealed at a biochemical level, but the structural and chemical basis for these very important phenomena remains unclear (Scheme 1).[5b]

In conjunction with these studies, research from our laboratories has focused on a concise enantioselective total synthesis of the natural products **1** and **2** that would be amenable to the preparation of biologically useful analogues. To date, there have been three total syntheses of FR900492 (**1**) reported;[9] of these, only one was asymmetric, but required a 57-step sequence.[9c–e] Additionally, a formal total synthesis was disclosed recently, applicable to an enantioselective variation.[10] In addition to the above-mentioned syntheses, several other synthetic approaches have been reported since the isolation of **1**.[11] Herein, we describe a concise, enantioselective total synthesis of **1** and **2**. This sequence is the shortest total synthesis of **1** and **2** reported to date and features a new method to construct the hydroxylamine hemiketal ring system unique to this family of natural substances.

Our approach to the construction of **1** and **2** was predicated on two bold strategies: 1) the labile aziridine would be installed in the very beginning and carried intact to the end, and 2) a simultaneous oxidative deprotection of an eight-membered-ring aminoketone **6** was envisioned to form the hydroxylamine hemiketal functionality in a single operation (Scheme 2). Ketone **6** could in turn be obtained from the eight-membered-ring amine **7**, which would ultimately be derived from the coupling of the optically active aziridine **8** and the trisubstituted nitrobenzene **9**.



Scheme 2. Retrosynthesis of FR900482 (**1**) and FR66979 (**2**). *p*MB = *p*-methoxybenzyl.

Aziridine **14** was prepared according to a recent report from this laboratory in 21 steps from the commercially available reagents **10** and **12** (Scheme 3).[12,13]

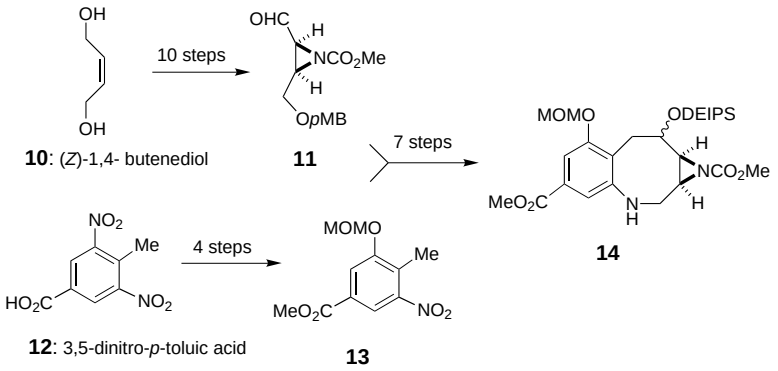
Reaction of **14** with *p*-methoxybenzyl bromide, followed by removal of the DEIPS group with TASF in DMF/H_2O[14] and subsequent oxidation with Dess–Martin periodinane[15] afforded ketone **15**, which corresponds to **6**. Treatment of **15** with LDA in dry DMF at −45 °C followed by the addition of an anhydrous formaldehyde solution in THF[16] furnished the aldol adducts **16** and **17** as a ~1:1 mixture of diastereomers in 50% yield (45% recovery of unreacted starting material). Separation of **16** and **17** by preparative thin-layer chromatography (PTLC) followed by treatment of the undesired adduct **17** with DBU in toluene afforded a 2.5:1 mixture of epimers favoring **16**, which has the desired configuration at C7. Treatment of the primary alcohol of **16** with TBSOTf and

[*] Prof. Dr. R. M. Williams, T. C. Judd
Department of Chemistry, Colorado State University
Fort Collins, CO 80523 (USA)
Fax: (+1) 970-491-3944
E-mail: rmw@chem.colostate.edu

[**] This work was supported by the National Institutes of Health (Grant CA51875). We are grateful to Boehringer-Ingelheim for fellowship support to T.C.J. Mass spectra were obtained on instruments supported by the National Institutes of Health Shared Instrumentation Grant GM49631. We are grateful to Fujisawa Pharmaceutical Co., Japan, for the generous gift of natural FR900482.

Supporting information for this article is available on the WWW under http://www.angewandte.org or from the author. Spectroscopic data for all new compounds is included.

 © 2002 WILEY-VCH Verlag GmbH & Co. KGaA, Weinheim 0044-8249/02/4124-4683 $ 20.00+.50/0



Scheme 3. Synthesis of aziridine precursor **14**.[12]

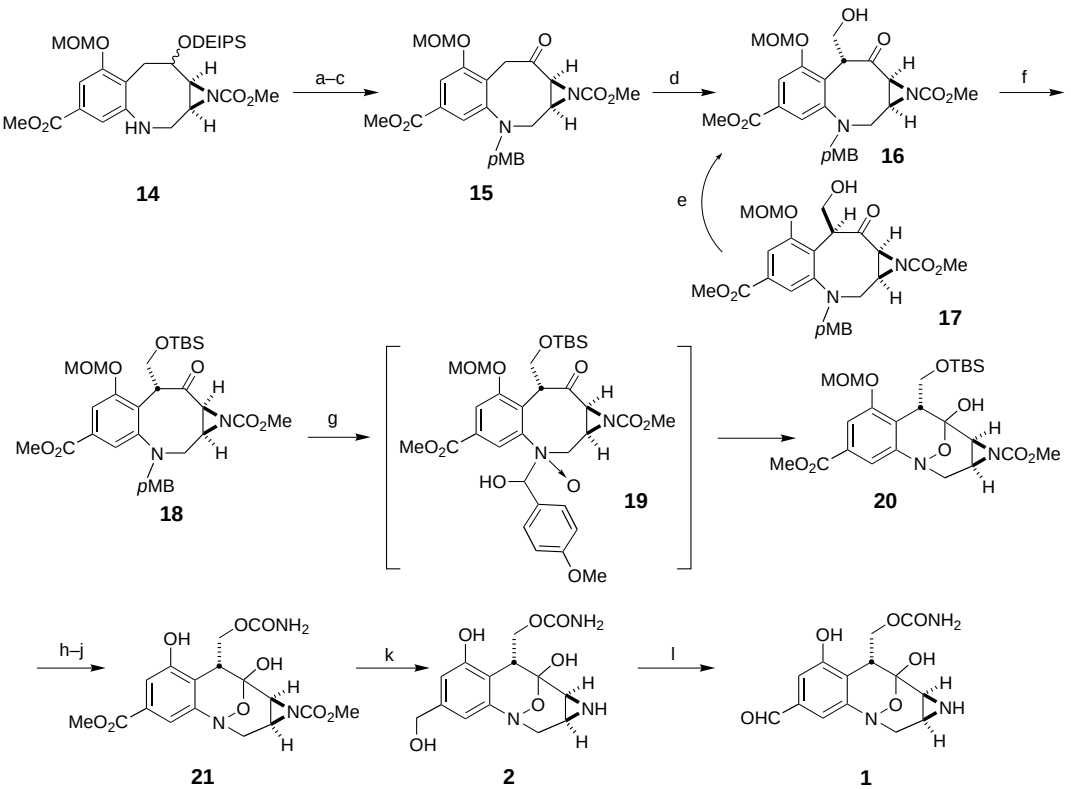
2,6-lutidine gave the silyl ether **18** in essentially quantitative yield (Scheme 4).

For the construction of **20**, a one-step protocol was employed that both cleaved the *N*-*p*-methoxybenzyl residue and oxidized the amine to the corresponding hydroxylamine, thus forming the desired hydroxylamine hemiketal. Reaction of **18** with excess dimethyldioxirane (DMDO)[17] in a 1:1 mixture of CH_2Cl_2 and saturated aqueous K_2CO_3 furnished **20** as the only isolated product in 30–50 % yield, along with recovered starting material (40–50 %). Attempts to drive this reaction to completion by varying the stoichiometry of DMDO, time, temperature, etc., proved unsuccessful. The very clean nature of this reaction allowed the practical recycling of recovered **18**.[18]

The mechanism for the formation of **20** from **18** is presumed to involve initial insertion of the dioxirane into the C–H bond of the *N*-*p*-methoxybenzyl methylene residue to form a methanolamine species.[19] The hydroxy group of the methanolamine is invoked to direct the DMDO oxidation of the amine to the corresponding *N*-oxide species **19**.[20] Subsequent collapse of the methanolamine with concomitant loss of *p*-anisaldehyde and transannular closure of the incipient hydroxylamine on the ketone furnishes **20**.[21]

Removal of the TBS protecting group followed by reaction of the primary hydroxy group with trichloroacetyl isocyanate (methanol/silica gel workup)[22] installed the urethane moiety at C13. TMSBr effected removal of the methoxymethyl ether (MOM) in the presence of the acid-sensitive aziridine functionality at −45 °C over 3 h to afford **21** in 60 % yield.[23]

Final reduction of both carbomethoxy groups with $LiBH_4$/MeOH in THF[24] followed by Pd-catalyzed cleavage of the resulting borane amine complex,[25] furnished the natural product FR66979 (**2**) in 78 % yield. Synthetic **2** was identical to the natural substance (^{1}H NMR spectra, mobility on TLC, mass spectra (ES^+), optical rotation, and IR spectra). Finally, the natural product FR900482 (**1**) can obtained by Swern oxidation of **2** in 33 % yield.[26,27]



Scheme 4. Synthesis of **1** and **2**. Reagents and conditions: a) *p*-methoxybenzyl bromide, *i*Pr_2NEt, CH_2Cl_2 (86 %); b) TASF, DMF/H_2O, room temperature; c) Dess–Martin oxidation (75 %, 2 steps); d) LDA, DMF, −45 °C; CH_2O/THF, −45 °C, (50 %; **16**/**17** 1:1); e) DBU, toluene (70 % + 30 % starting material); f) TBSOTf, 2,6-lutidine, CH_2Cl_2, −78→0 °C (96 %); g) DMDO, aqueous K_2CO_3/CH_2Cl_2, 0 °C→RT (30–50 %); h) TBAF, THF, 0 °C (92 %); i) $Cl_3CCONCO$, CH_2Cl_2, 0 °C; then MeOH, silica gel, room temperature (86 %); j) TMSBr, CH_2Cl_2, −45 °C (60 %); k) $LiBH_4$/MeOH, THF, room temperature (78 %); l) $(COCl)_2$, Me_2SO, THF, −78→−40 °C; then Et_3N (33 %). DEIPS = diethylisopropylsilyl, TASF = tris(dimethylamino)sulfonium difluorotrimethylsilicate, DMF = *N*,*N*-dimethylformamide, LDA = lithium diisopropylamide, DBU = 1,8-diazabicyclo[5.4.0]undec-7-ene, TBSOTf = *tert*-butyldimethylsilyl triflate, DMDO = dimethyldioxirane, TBAF = tetrabutylammonium fluoride, TMS = trimethylsilyl.

 © 2002 WILEY-VCH Verlag GmbH & Co. KGaA, Weinheim 0044-8249/02/4124-4684 $ 20.00+.50/0 *Angew. Chem. Int. Ed.* **2002**, *41*, No. 24

The chemistry described herein represents the most concise total synthesis of either (+)-FR66979 (**2**) or (+)-FR900482 (**1**) reported to date.[28] Future efforts in the preparation and biological evaluation of synthetic analogues are currently underway and will be reported in due course.

Received: July 22, 2002 [Z19786]

[1] a) M. Iwami, S. Kiyoto, H. Terano, M. Kohsaka, H. Aoki, H. Imanaka, *J. Antibiot.* **1987**, *40*, 589; b) S. Kiyoto,, T. Shibata, M. Yamashita, T. Komori, M. Okuhara, H. Terano, M. Kohsaka, H. Aoki, H. Imanaka, *J. Antibiot.* **1987**, *40*, 594; c) I. Uchida, S. Takase, H. Kayakiri, S. Kiyoto, M. Hashimoto, T. Tada, S. Koda, Y. Morimoto, *J. Am. Chem. Soc.* **1987**, *109*, 4108; d) K. Shimomura, O. Hirai, T. Mizota, S. Matsumoto, J. Mori, F. Shibayama, H. Kikuchi, *J. Antibiot.* **1987**, *40*, 600; e) O. Hirai, K. Shimomura, T. Mizota, S. Matsumoto, J. Mori, H. Kikuchi, *J. Antibiot.* **1987**, *40*, 607; f) H. Terano, S. Takase, J. Hosoda, M. Kohsaka, *J. Antibiot.* **1989**, *42*, 145.

[2] T. Fukuyama, S. Goto, *Tetrahedron Lett.* **1989**, *30*, 6491.

[3] a) R. M. Williams, S. R. Rajski, *Tetrahedron Lett.* **1992**, *33*, 2929; b) R. M. Williams, S. R. Rajski, *Tetrahedron Lett.* **1993**, *34*, 7023; c) H. Huang, S. R. Rajski, R. M. Williams, P. B. Hopkins, *Tetrahedron Lett.* **1994**, *35*, 9669; d) J. Woo, S. T. Sigurdsson, P. B. Hopkins, *J. Am. Chem. Soc.* **1993**, *115*, 1199; e) H. Huang, T. K. Pratum, P. B. Hopkins, *J. Am. Chem. Soc.* **1994**, *116*, 2703; f) M. M. Paz, P. B. Hopkins, *Tetrahedron Lett.* **1997**, *38*, 343; g) M. M. Paz, P. B. Hopkins, *J. Am. Chem. Soc.* **1997**, *119*, 5999.

[4] R. M. Williams, S. R. Rajski, *Chem. Biol.* **1997**, *4*, 127.

[5] a) L. Beckerbauer, J. J. Tepe, R. A. Eastman, P. F. Mixter, R. M. Williams, R. Reeves, *Chem. Biol.* **2002**, *9*, 427; b) L. Beckerbauer, J. J. Tepe, J. Cullison, R. Reeves, R. M. Williams, *Chem. Biol.* **2000**, *7*, 805; for a biochemical model study, see: c) S. R. Rajski, S. B. Rollins, R. M. Williams, *J. Am. Chem. Soc.* **1998**, *120*, 2192.

[6] a) K. Shimomura, T. Manda, S. Mukumoto, K. Masuda, T. Nakamura, T. Mizota, S. Matsumoto, F. Nishigaki, T. Oku, J. Mori, F. Shibayama, *Cancer Res.* **1988**, *48*, 1166; b) T. Nakamura, K. Masuda, S. Matsumoto, T. Oku, T. Manda, J. Mori, K. Shimomura, *Jpn. J. Pharmacol.* **1989**, *49*, 317; K. Masuda, T. Nakamura, T. Mizota, J. Mori, K. Shimomura, *Cancer Res.* **1988**, *48*, 5172; b) K. Masuda, T. Nakamura, K. Shimomura, *J. Antibiot.* **1988**, *41*, 1497.

[7] a) Y. Naoe, M. Inami, S. Matsumoto, F. Nishigaki, S. Tsujimoto, I. Kawamura, K. Miyayasu, T. Manda, K. Shimomura, *Cancer Chemother. Pharmacol.* **1998**, *42*, 31; b) Y. Naoe, M. Inami, I. Kawamura, F. Nishigaki, S. Tsujimoto, S. Matsumoto, T. Manda, K. Shimomura, *Jpn. J. Cancer Res.* **1998**, *89*, 666; c) Y. Naoe, M. Inami, S. Takagaki, S. Matsumoto, I. Kawamura, F. Nishigaki, S. Tsujimoto, T. Manda, K. Shimomura, *Jpn. J. Cancer Res.* **1998**, *89*, 1047; d) Y. Naoe, M. Inami, S. Matsumoto, S. Takagaki, T. Fujiwara, S. Yamazaki, I. Kawamura, F. Nishigaki, S. Tsujimoto, T. Manda, K. Shimomura, *Jpn. J. Cancer Res.* **1998**, *89*, 1306; e) Y. Naoe, I. Kawamura, M. Inami, S. Matsumoto, F. Nishigaki, S. Tsujimoto, T. Manda, K. Shimomura, *Jpn. J. Cancer Res.* **1998**, *89*, 1318; f) M. Inami, I. Kawamura, S. Tsujimoto, F. Nishigaki, S. Matsumoto, Y. Naoe, Y. Sasakawa, M. Matsuo, T. Manda, T. Goto, *Cancer Lett.* **2002**, *181*, 39.

[8] a) M. Tomasz, R. Lipman, D. Chowdary, J. Pawlak, G. Verdine, K. Nakanishi, *Science* **1987**, *235*, 1204; b) M. Tomasz, *Chem. Biol.* **1995**, *2*, 575, and references therein.

[9] a) T. Fukuyama, L. Xu, S. Goto, *J. Am. Chem. Soc.* **1992**, *114*, 383; b) J. M. Schkeryantz, S. J. Danishefsky, *J. Am. Chem. Soc.* **1995**, *117*, 4722; c) T. Katoh, E. Itoh, T. Yoshino, S. Terashima, *Tetrahedron Lett.* **1996**, *37*, 3471; d) T. Yoshino, Y. Nagata, E. Itoh, M. Hashimoto, T. Katoh, S. Terashima, *Tetrahedron Lett.* **1996**, *37*, 3475; e) T. Katoh, T. Yoshino, Y. Nagata, S. Nakatani, S. Terashima, *Tetrahedron Lett.* **1996**, *37*, 3479.

[10] I. M. Fellows, D. E. Kaelin, Jr., S. F. Martin, *J. Am. Chem. Soc.* **2000**, *122*, 10781.

[11] a) N. Yasuda, R. M. Williams, *Tetrahedron Lett.* **1989**, *30*, 3397; b) R. J. Jones, H. Rapoport, *J. Org. Chem.* **1990**, *55*, 1144; c) S. J. Miller, S.-H. Kim, Z.-R. Chen, R. H. Grubbs, *J. Am. Chem. Soc.* **1995**, *117*, 2108; d) H.-J. Lim, G. A. Sulikowski, *Tetrahedron Lett.* **1996**, *37*, 5243; e) F. E. Ziegler, M. Belema, *J. Org. Chem.* **1997**, *62*, 1083; f) S. Mithani, D. M. Drew, E. H. Rydberg, N. J. Taylor, S. Mooibroek, G. I. Dmitrienko, *J. Am. Chem. Soc.* **1997**, *119*, 1159; g) W. Zhang, C. Wang, L. S. Jimenez, *Synth. Commun.* **2000**, *30*, 351; h) M. Kambe, E. Arai, M. Suzuki, H. Tokuyama, T. Fukuyama, *Org. Lett.* **2001**, *3*, 2575.

[12] a) S. B. Rollins, R. M. Williams, *Tetrahedron Lett.* **1997**, *38*, 4033; b) S. B. Rollins, T. C. Judd, R. M. Williams, *Tetrahedron* **2000**, *56*, 521; c) T. C. Judd, R. M. Williams, *Org. Lett.* **2002**, *4*, 3711.

[13] M. R. Spada, M. Ubukata, K. Isono, *Heterocycles* **1992**, *34*, 1147.

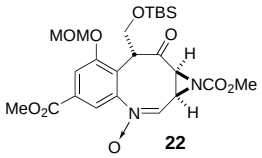
[14] a) K. A. Scheidt, H. Chen, B. C. Follows, S. R. Chemler, D. S. Coffey, W. R. Roush, *J. Org. Chem.* **1998**, *63*, 6436; b) M. Kurosu, L. R. Marcin, T. J. Grinsteiner, Y. Kishi, *J. Am. Chem. Soc.* **1998**, *120*, 6627; c) R. Noyori, I. Nishida, J. Sakata, *J. Am. Chem. Soc.* **1983**, *105*, 1598.

[15] a) D. B. Dess, J. C. Martin, *J. Org. Chem.* **1983**, *48*, 4155; b) D. B. Dess, J. C. Martin, *J. Am. Chem. Soc.* **1991**, *113*, 7277; c) R. E. Ireland, L. Liu, *J. Org. Chem.* **1993**, *58*, 2899.

[16] L. Rodriguez, N. Lu, N.-L. Yang, *Synlett* **1990**, 227.

[17] R. W. Murray, M. Singh, *Organic Syntheses*, Wiley, New York, **1998**, Collect. Vol. IX, p. 288.

[18] In the absence of the saturated aqueous base, exclusive formation of nitrone **22** was the only product observed. Alternative oxidation systems resulted in no reaction (*m*-chloroperoxybenzoic acid, Davis' reagent) or direct oxidative cleavage of the *p*-methoxybenzyl group to a mitosene ([$VO(acac)_2$] or [$Mo(CO)_6$] and *t*BuOOH; [$MeReO_3$] and H_2O_2).



22

[19] For related DMDO-mediated oxidative benzylic C–H insertions, see: a) R. W. Murray, R. Jeryaraman, L. Mohan, *J. Am. Chem. Soc.* **1986**, *108*, 1598; b) B. A. Marples, J. P. Muxworthy, K. H. Baggaley, *Synlett* **1992**, *8*, 646; c) R. Csuk, P. Dörr, *Tetrahedron Lett.* **1994**, *50*, 9983.

[20] R. Curci, L. D'Accolti, A. Detomaso, C. Fusco, K. Takeuchi, Y. Ohga, P. E. Eaton, Y. C. Yip, *Tetrahedron Lett.* **1993**, *34*, 4559.

[21] The exact mechanism of the oxidative rearrangement is unknown at this time and alternative mechanisms are certainly possible. An interesting alternative mechanism suggested by a reviewer included a Meisenheimer-type rearrangement of an *N*-oxide to the *O*-*p*-methoxybenzyl hydroxylamine, *N*-oxidation, and Cope elimination to afford the free hydroxylamine.

[22] P. Kocóvsky, *Tetrahedron Lett.* **1986**, *27*, 5521.

[23] S. Hanessian, D. Delorme, Y. Dufresne, *Tetrahedron Lett.* **1984**, *25*, 2515.

[24] We were also able to reduce **21** to **2** with DIBAL-H; however, the workup and isolation proved more difficult. A similar reduction of both functionalities with DIBAL-H on a fully protected intermediate was employed in a previous total synthesis reported by Danishefsky and co-workers (see reference [9b]).

[25] M. Couturier, J. L. Tucker, B. M. Andresen, P. Dubé, J. T. Negri, *Org. Lett.* **2001**, *3*, 465.

[26] a) K. Omura, D. Swern, *Tetrahedron* **1978**, *34*, 1651; b) R. E. Ireland, D. W. Norbeck, *J. Org. Chem.* **1985**, *50*, 2198.

[27] A previous report (see reference [9c]) demonstrated the successful oxidation of monoacetylated FR66979 by Swern oxidation.

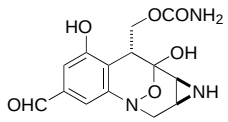
[28] After submission of our manuscript, we recently learned that Professor Tohru Fukuyama and co-workers (Tokyo University) and Prof. Marco Ciufolini and co-workers (Université Claude Bernard Lyon 1) have independently completed syntheses of FR900482 and FR66979, respectively. We appreciate receiving preprints of their manuscripts. See the following communications: M. Suzuki, M. Kambe, H. Tokuyama, T. Fukuyama, *Angew. Chem.* **2002**, *114*, 4880; *Angew. Chem. Int. Ed.* **2002**, *41*, 4686; R. Ducray, M. A. Ciufolini, *Angew. Chem.* **2002**, *114*, 4882; *Angew. Chem. Int. Ed.* **2002**, *41*, 4688.

 © 2002 WILEY-VCH Verlag GmbH & Co. KGaA, Weinheim 0044-8249/02/4124-4685 $ 20.00+.50/0

Facile Construction of *N*-Hydroxybenzazocine: Enantioselective Total Synthesis of (+)-FR900482**

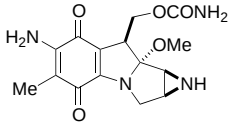
Masashi Suzuki, Mika Kambe, Hidetoshi Tokuyama, and Tohru Fukuyama*

The antitumor antibiotic FR900482 (**1**) was isolated from *Streptomyces sandaensis* No. 6897 by Imanaka et al. at the Fujisawa Pharmaceutical Co.[1] Biological studies have revealed that this and the related compounds exhibit the same level of antitumor activities as mitomycin C (**2**).[2] Extensive



FR900482

1

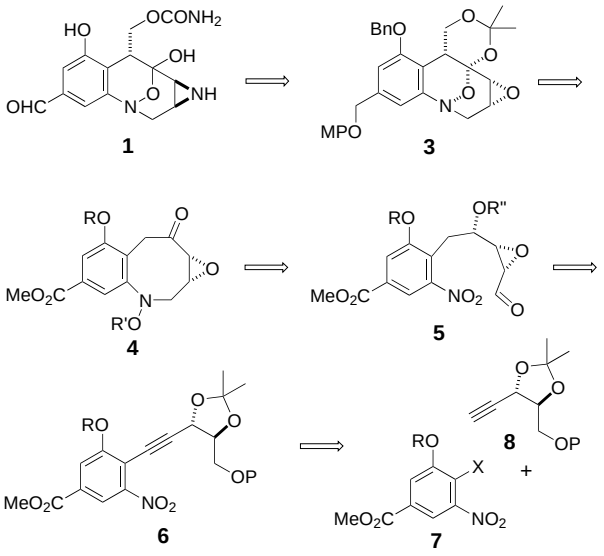


mitomycin C **2**

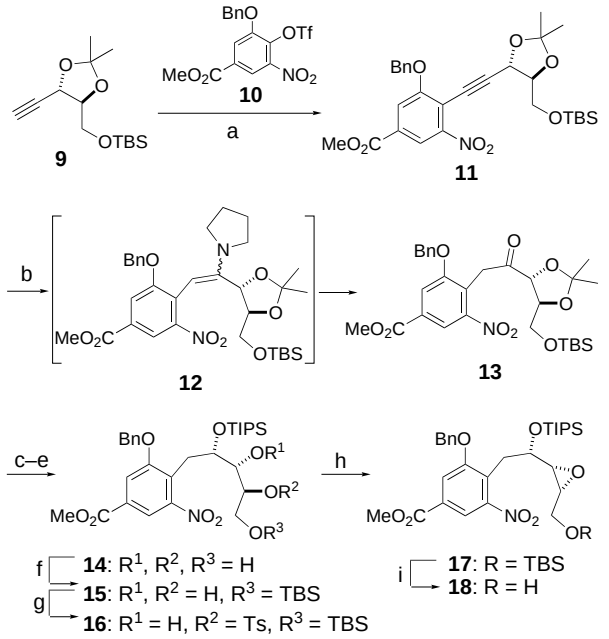
investigations of the structure–activity relationships and its mode of action have revealed that this class of compounds crosslink DNA in a fashion analogous to mitomycin C.[3] In addition to these promising biological activities, the structure of **1** featuring the unique hydroxylamine hemiacetal has made it an attractive target for synthetic chemists. Although numerous approaches[4] have been explored to construct this densely functionalized structure, only three total syntheses[5,6] and a formal total synthesis[7] have been reported to date.[8] After the completion of our first total synthesis of racemic **1**,[5a] we have devoted continuous efforts to establish a more efficient route to prepare the optically active FR900482 (**1**).[9] We report herein a stereocontrolled, enantioselective total synthesis of **1** through a facile construction of the *N*-hydroxybenzazocine intermediate.

Our synthetic plan is outlined in Scheme 1. For the construction of the key intermediate *N*-hydroxybenzazocine **4**, we planned to exploit intramolecular reductive hydroxylamination of a fully functionalized ω-formyl nitrobenzene derivative **5**. Hydroxymethylation and subsequent hydroxylamine hemiacetal formation would lead to the pentacyclic intermediate **3** in our racemic total synthesis. Cyclization precursor **5** would be accessible from aryl acetylene **6**, which in turn would be obtained by coupling of the aromatic fragment **7** and the terminal acetylene **8**.

Preparation of the epoxy alcohol precursor **18** commenced with Sonogashira-coupling of acetylene **9**[10] and aryl triflate **10**[5b] to provide aryl acetylene **11** (Scheme 2).[11,12] At this juncture, it was necessary to devise a regioselective trans-



Scheme 1. Retrosynthesis of FR900482 (**1**). Bn = benzyl, MP = *p*-methoxyphenyl.



Scheme 2. Synthesis of epoxy alcohol **18**. a) $[Pd(OAc)_2]$ (0.1 equiv), PPh_3 (0.2 equiv), THF/NEt_3 (2:1 v/v), 65 °C, 1 h, then room temperature, 12 h, 75%; b) pyrrolidine (2 equiv), benzene, room temperature, 1 h, then aqueous AcOH (50%), room temperature, 2 h; c) $Zn(BH_4)_2$ (1.2 equiv), Et_2O, −30 °C, 3 h, 94% (2 steps), 9:1 diastereoselectivity; d) TIPSOTf (3 equiv), 2,6-lutidine (6 equiv), CH_2Cl_2, room temperature, 7 h; e) AcOH/H_2O (5:1 v/v), 100 °C, 4 h, 61% (2 steps); f) TBSCl (1.2 equiv), NEt_3 (2.4 equiv), DMAP (0.1 equiv), CH_2Cl_2, room temperature, 13 h; g) TsCl (1.2 equiv), DABCO (2 equiv), CH_2Cl_2, room temperature, 1.5 h; h) NaH (1.5 equiv), DMF, 0 °C→RT, 0.5 h, 76% (3 steps); i) CSA (0.1 equiv), MeOH, room temperature, 1 h. TIPS = triisopropylsilyl, OTf = trifluoromethanesulfonate, TBS = *tert*-butyldimethylsilyl; DMAP = 4-dimethylaminopyridine, Ts = *p*-toluenesulfonyl, DABCO = 1,4-diazabicyclo[2.2.2]octane, DMF = *N*,*N*-dimethylformamide, CSA = 10-camphorsulfonic acid.

formation of the acetylene into the required ketone under mild conditions. To this end, we developed a novel conjugate addition of secondary amines to *ortho*-nitroaryl acetylenes.

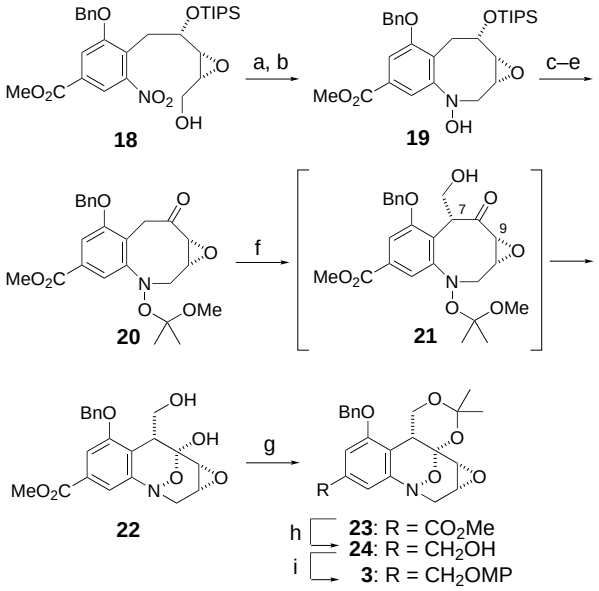
[*] Prof. Dr. T. Fukuyama, M. Suzuki, M. Kambe, Dr. H. Tokuyama
Graduate School of Pharmaceutical Sciences, The University of Tokyo
7-3-1 Hongo, Bunkyo-ku, Tokyo 113-0033 (Japan)
Fax: (+81) 3-5802-8694
E-mail: fukuyama@mol.f.u-tokyo.ac.jp

[**] This work was supported by CREST, the Japan Science and Technology Corporation (JST), and by the Grant-in-Aid for Scientific Research on Priority Areas (A) "Exploitation of Multi-Element Cyclic Molecules" from the Ministry of Education, Culture, Sports, Science and Technology, Japan.

 © 2002 WILEY-VCH Verlag GmbH & Co. KGaA, Weinheim 0044-8249/02/4124-4686 $ 20.00+.50/0

Thus, addition of pyrrolidine proceeded smoothly at room temperature to furnish intermediate enamine **12**, which upon treatment with AcOH/H_2O (50%) in a one-pot procedure gave the desired ketone **13** in excellent yield. After stereoselective reduction of the ketone[13] and protection of the resultant alcohol, both the acetonide and the TBS group were removed by heating in aqueous acetic acid to give triol **14**. The desired epoxide was then obtained by a three-step sequence: TBS protection of the primary alcohol, tosylation of the sterically less-hindered secondary alcohol,[14] and treatment with NaH. Finally, selective deprotection of the TBS group afforded epoxy alcohol **18**.

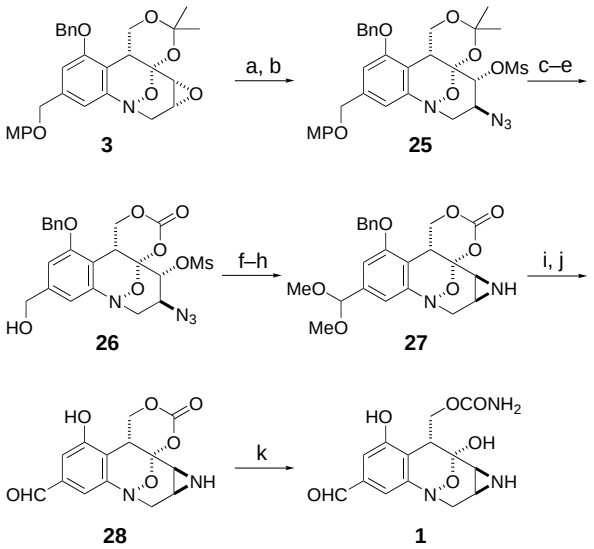
Having synthesized epoxy alcohol **18** in a straightforward manner, we then focused on the facile construction of the *N*-hydroxybenzazocine **19**. Alcohol **18** was oxidized with Dess–Martin periodinane to the corresponding aldehyde, which was then subjected to a variety of reductive conditions for construction of the desired *N*-hydroxybenzazocine. After numerous attempts, we found that catalytic hydrogenation over Pt/C (5%) in MeOH cleanly afforded *N*-hydroxybenzazocine **19** as the sole product (89% overall yield from **17**). No product of further reduction was observed during the hydrogenation. Protection of the hydroxylamine of **19** as the 1-methoxy-1-methylethyl ether followed by deprotection of the TIPS group, and Swern oxidation furnished ketone **20** (Scheme 3).



Scheme 3. Construction of the pentacyclic compound **3**. a) Dess–Martin periodinane (1.4 equiv), CH_2Cl_2, 0°C→RT, 0.5 h; b) H_2 (1 atm), Pt/C (5%; 15 wt%), MeOH, room temperature, 2 h, 89% (from **17**); c) 2-methoxypropene (22 equiv), TsOH·H_2O (0.1 equiv), CH_2Cl_2, room temperature, 10 min; d) TBAF (3.5 equiv), THF, room temperature, 12 h, 85% (2 steps); e) $(COCl)_2$ (2 equiv), DMSO (4 equiv), CH_2Cl_2, −78°C, 0.5 h, then NEt_3 (6 equiv), −78°C→RT, 0.5 h, 82%; f) aqueous HCHO (37%; 115 equiv), LiOH (0.4 equiv), THF/H_2O (20:3 v/v), 0°C, 5 h, then HCl (1N; 2 equiv), 0°C→RT, 14 h; g) 2-methoxypropene (5 equiv), PPTS (0.1 equiv), 2,2-dimethoxypropane/acetone (1:1 v/v), room temperature, 3 h; separation of the isomers, 56% (from **20**); h) DIBAL (3 equiv), CH_2Cl_2, −78°C, 1 h, 99%; i) 4-methoxyphenol (2 equiv), PPh_3 (2 equiv), DEAD (2 equiv), benzene, room temperature, 15 min, 96%. TBAF = tetrabutylammonium fluoride, DMSO = dimethyl sulfoxide, PPTS = pyridinium *p*-toluenesulfonate, DIBAL = diisobutylaluminum hydride, DEAD = diethyl azodicarboxylate.

For the ensuing hydroxymethylation and hemiacetal formation, we developed a sequential one-pot procedure. Hydroxymethylation was best effected by treatment of ketone **20** with formalin in the presence of a catalytic amount of LiOH to furnish the desired **21** with high diastereoselectivity (94:6).[15] Acidification of the reaction mixture with HCl (1N) afforded hemiacetal **22**,[16] which was subjected to acetonide-formation conditions to give the pentacyclic compound **23** in 56% yield from ketone **20**.[17] Acetonide **23** was then reduced with DIBAL, and the resultant benzyl alcohol **24** was protected as the *p*-methoxyphenyl ether to give the pentacyclic compound **3**.

With the key intermediate **3** in hand, we completed the total synthesis of optically active FR900482 (**1**) by modifying the protocol established during our racemic synthesis.[5a] Thus, regioselective opening of the epoxide **3** with LiN_3 and mesylation of the resultant alcohol gave acetonide **25** (Scheme 4). Conversion of **25** into hydroxy carbonate **26** was effected by a three-step sequence involving acidic hydrolysis of the acetonide, treatment with triphosgene, and deprotection of the *p*-methoxyphenyl group with ceric ammonium nitrate.[18] The resultant alcohol **26** was oxidized to the aldehyde, which was protected as the dimethyl acetal.[19] After formation of the aziridine by heating with PPh_3 in the presence of *i*Pr_2NEt, hydrogenolysis of the benzyl ether followed by treatment with $HClO_4$ in THF/H_2O afforded aldehyde **28**. Finally, ammonolysis of the cyclic carbonate provided exclusively the desired FR900482 (**1**), whose spec-



Scheme 4. Completion of the total synthesis of **1**. a) LiN_3 (27 equiv), DMF/H_2O (10:1 v/v), 120°C, 3.5 h, 83%; b) MsCl (2 equiv), NEt_3 (3 equiv), CH_2Cl_2, room temperature, 2.5 h, 80%; c) TFA (8 equiv), CH_2Cl_2, room temperature, 3 h; d) $(Cl_3CO)_2C=O$ (5 equiv), pyridine (6 equiv), CH_2Cl_2, 0°C, 30 min, 92% (2 steps); e) $(NH_4)_2Ce(NO_3)_6$ (2.5 equiv), MeCN/H_2O (4:1 v/v), room temperature, 10 min, 84%; f) PCC (2 equiv), $MgSO_4$ (4 equiv), CH_2Cl_2, room temperature, 1.5 h; g) CSA (0.08 equiv), $CH(OMe)_3$/MeOH (1:4 v/v), room temperature, 1 h, 81% (2 steps); h) PPh_3 (2 equiv), *i*Pr_2NEt (1.2 equiv), THF/H_2O (10:1 v/v), 60°C, 1.5 h, 85%; i) H_2 (1 atm), Pd/C (10%; 15 wt%), EtOH, room temperature, 2.5 h; j) $HClO_4$ (1%; 0.2 equiv), THF/H_2O (10:1 v/v), room temperature, 5 h; k) NH_3 (gas), THF, room temperature, 3 h, 89% (3 steps). Ms = methanesulfonyl, TFA = trifluoroacetic acid, PCC = pyridinium chlorochromate.

 © 2002 WILEY-VCH Verlag GmbH & Co. KGaA, Weinheim 0044-8249/02/4124-4687 $ 20.00+.50/0

tral data were completely identical with those reported in literature.[1b]

In conclusion, we have completed a highly efficient total synthesis of FR900482 (**1**). The present synthesis features a facile formation of *N*-hydroxybenzazocine by intramolecular reductive hydroxylamination and an ensuing facile construction of the hydroxylamine hemiacetal. The synthetic strategy described above should be applicable to the synthesis of analogues of FR900482 as well as of other benzazocine derivatives. Application of this approach to the synthesis of mitomycin C is currently under investigation in our laboratories.

Received: August 6, 2002 [Z19901]

[1] a) M. Iwami, S. Kiyoto, H. Terano, M. Kohsaka, H. Aoki, H. Imanaka, *J. Antibiot.* **1987**, *40*, 589; b) S. Kiyoto, T. Shibata, M. Yamashita, T. Komori, M. Okuhara, H. Terano, M. Kohsaka, H. Aoki, H. Imanaka, *J. Antibiot.* **1987**, *40*, 594; c) I. Uchida, S. Takase, H. Kayakiri, S. Kiyoto, M. Hashimoto, *J. Am. Chem. Soc.* **1987**, *109*, 4108.

[2] K. Shimomura, O. Hirai, T. Mizota, S. Matsumoto, J. Mori, F. Shibayama, H. Kikuchi, *J. Antibiot.* **1987**, *40*, 600.

[3] a) R. M. Williams, S. R. Rajski, S. B. Rollins, *Chem. Biol.* **1997**, *4*, 127; b) M. M. Paz, P. B. Hopkins, *J. Am. Chem. Soc.* **1997**, *119*, 5999; c) R. M. Williams, S. B. Rollins, S. R. Rajski, *J. Am. Chem. Soc.* **1998**, *120*, 2192.

[4] For representative examples, see: a) N. Yasuda, R. M. Williams, *Tetrahedron Lett.* **1989**, *30*, 3397; b) R. J. Jones, H. Rapoport, *J. Org. Chem.* **1990**, *55*, 1144; c) S. J. Miller, S. H. Kim, Z. R. Chen, R. H. Grubbs, *J. Am. Chem. Soc.* **1995**, *117*, 2108; d) H. J. Lim, G. A. Sulikowski, *Tetrahedron Lett.* **1996**, *37*, 5243; e) S. Mithani, D. M. Drew, E. H. Rydberg, N. J. Taylor, S. Mooibroek, G. I. Dmitrienko, *J. Am. Chem. Soc.* **1997**, *119*, 1159.

[5] a) T. Fukuyama, L. Xu, S. Goto, *J. Am. Chem. Soc.* **1992**, *114*, 383; b) J. M. Schkeryantz, S. J. Danishefsky, *J. Am. Chem. Soc.* **1995**, *117*, 4722.

[6] a) T. Katoh, E. Itoh, T. Yoshino, S. Terashima, *Tetrahedron* **1997**, *53*, 10229; b) T. Yoshino, Y. Nagata, E. Itoh, M. Hashimoto, T. Katoh, S. Terashima, *Tetrahedron* **1997**, *53*, 10239; c) T. Katoh, Y. Nagata, T. Yoshino, S. Nakatani, S. Terashima, *Tetrahedron* **1997**, *53*, 10253.

[7] I. M. Fellows, D. E. Kaelin, Jr., S. F. Martin, *J. Am. Chem. Soc.* **2000**, *122*, 10781.

[8] After submission of this manuscript, we learned that two groups have independently completed enantioselective total syntheses; see the previous communication: a) T. C. Jude, R. M. Williams, *Angew. Chem.* **2002**, *114*, 4877; *Angew. Chem. Int. Ed.* **2002**, *41*, 4683; and the following communication: b) R. Ducray, M. A. Ciufolini, *Angew. Chem.* **2002**, *114*, 4882; *Angew. Chem. Int. Ed.* **2002**, *41*, 4688.

[9] For an approach utilizing intramolecular [3+2] cycloaddition of nitrile oxide, see: M. Kambe, E. Arai, M. Suzuki, H. Tokuyama, T. Fukuyama, *Org. Lett.* **2001**, *3*, 2575.

[10] G. Pandey, M. Kapur, *Tetrahedron Lett.* **2000**, 41, 8821. Alternatively, we prepared **9** by a modified procedure: 2,3-di-*O*-isopropylidene-L-threitol, NaH, TBSCl, THF; cat. TEMPO (2,2,6,6-tetramethyl-1-piperidinyloxy, free radical), $PhI(OAc)_2$, CH_2Cl_2; dimethyl-1-diazo-2-oxopropylphosphonate, K_2CO_3, MeOH (S. Müller, B. Liepold, G. J. Roth, H. J. Bestmann, *Synlett* **1996**, 521).

[11] K. Sonogashira, Y. Tohda, N. Hagihara, *Tetrahedron Lett.* **1975**, *16*, 4467.

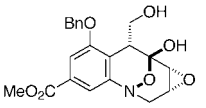
[12] The coupling reaction under typical conditions ($[PdCl_2(PPh_3)_2]$ and CuI in Et_3N) gave a considerable amount of the homocoupling by-product of the acetylene.

[13] T. Nakata, Y. Tani, M. Hatozaki, T. Oishi, *Chem. Pharm. Bull.* **1984**, 32, 1411.

[14] J. Hartung, S. Hünig, R. Kneuer, M. Schwarz, H. Wenner, *Synthesis* **1997**, 1433.

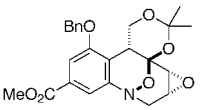
[15] Ketone **21** could be isolated when the reaction was quenched with NH_4Cl (1N) instead of HCl (1N), and its diastereomeric ratio was estimated by means of ^1H NMR spectroscopy. The structure of **21** was unambiguously confirmed by observation of NOE interactions between 7-H and 9-H.

[16] In addition to **22**, formation of a side product, which was tentatively assigned as hydroxylamine hemiacetal diastereomer **22′**, was observed. This mixture was subjected to the next acetonide formation without separation.



22'

[17] The ratio of **22**/**22′** was almost the same as that of **23** and a side product, which was tentatively assigned as **23′**. Furthermore, deprotection of the acetonide of **23** and **23′** under acidic conditions (HCl (1N) in THF, room temperature) gave only **22** and **22′**, respectively. These observations would indicate that neither epimerization of C7 nor interconversion of the hemiacetal diastereomers via the eight-membered ring ketone occurred during the acetonide formation.



23'

[18] T. Fukuyama, A. A. Laird, L. M. Hotchkiss, *Tetrahedron Lett.* **1985**, *26*, 6291.

[19] The aldehyde was protected as the dimethyl acetal to prevent reduction during hydrogenolysis of the phenolic benzyl ether.

Total Synthesis of (±)-FR66979**

Richard Ducray and Marco A. Ciufolini*

In the late 1980s, scientists at the Fujisawa Co. (Japan) unveiled a new class of antitumor agents with general structure **1** (Scheme 1).[1] These substances, denoted FR-66979 (**1a**) and FR-900482 (**1b**), are structurally related to the mitomycins (see mitomycin C (**2**)).[2] Indeed, the two families of anticancer agents possess comparable bioactivity[3] and are believed to act by a similar mechanism, yet FR-type compounds are less toxic than mitomycins, probably as a result of the absence of a quinoid nucleus.[4] Derivatives of **1b** are currently undergoing clinical trials.[5]

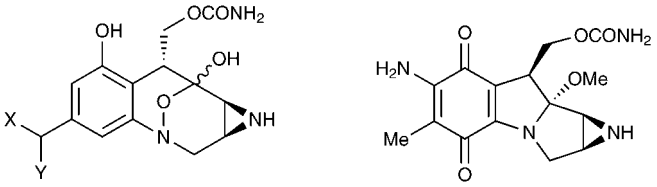
The biomedical potential and unusual architecture of compounds **1** have stimulated substantial interest at a

[*] Prof. Dr. M. A. Ciufolini, R. Ducray
Laboratoire de Synthèse et Méthodologie Organiques
CNRS UMR 5078
Université Claude Bernard Lyon 1
and
Écôle Supérieure de Chimie, Physique, Electronique de Lyon
43, Bd. du 11 Novembre 1918, 69622 Villeurbanne cedex (France)
Fax: (+33) 4-7243-2963
E-mail: ciufi@cpe.fr

[**] We thank the MENRT (doctoral fellowship to R.D.), the CNRS, and the Région Rhône-Alpes for support of our research. We are grateful to Ms. Laurence Rousset and Dr. Denis Bouchu for the mass spectral data, to Dr. Bernard Fenet for the NMR spectroscopic data. Finally, we thank the Fujisawa Co. for a gift of natural FR-66979. M.A.C. is the recipient of a Merck & Co. Academic Development Award.

Supporting information for this article is available on the WWW under http://www.angewandte.org or from the author.

 © 2002 WILEY-VCH Verlag GmbH & Co. KGaA, Weinheim 0044-8249/02/4124-4688 $ 20.00+.50/0

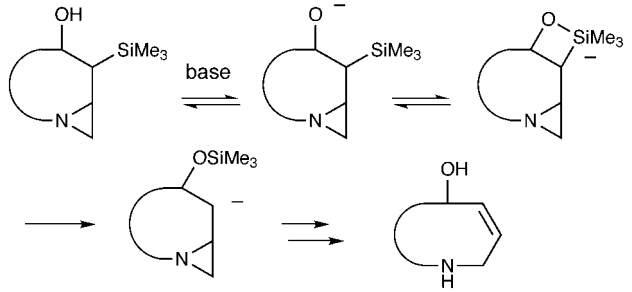


FR66979 **1a**: X = H; Y = OH
FR900482 **1b**: X, Y = O

mitomycin C **2**

Scheme 1. Structure of FR66979 (**1a**), FR900482 (**1b**), and mitomycin C (**2**).

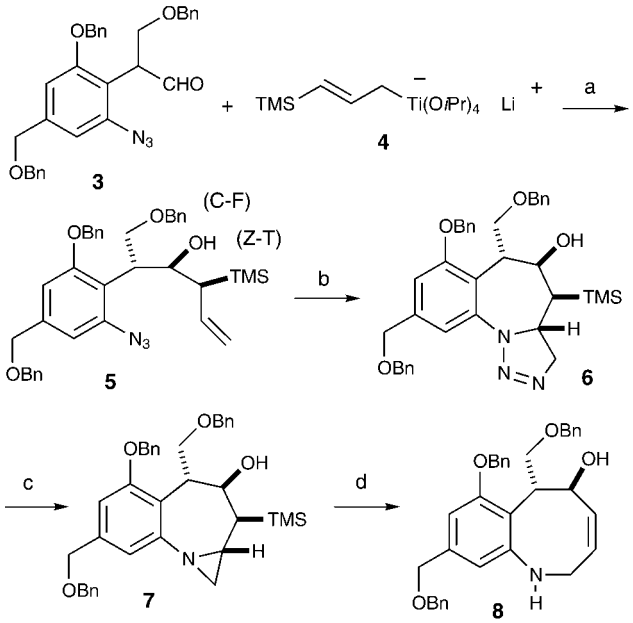
chemical level. In that respect, the fragile nature of these molecules and their problematic structural features have inspired the development of much innovative synthetic chemistry.[6,7] Our own involvement in this area[8] has recently produced a new method for benzazocene assembly through an unusual fragmentation of a silylated aziridine[9] orchestrated by a preliminary homo-Brook[10] transposition (Scheme 2). We describe herein a total synthesis of (±)-FR-66979 (**1a**), which showcases this new reaction as a key step.



Scheme 2. Presumed mechanism for the homo-Brook aziridine fragmentation.

Aldehyde (±)-**3**[11] reacted with the organometallic species arising through the interaction of lithiated allyltrimethylsilane and $[Ti(iPrO)_4]$,[12] and represented simply in Scheme 3 as **4**, to furnish adduct **5** as a diastereomerically homogeneous product (by ^{1}H NMR spectroscopy). The relative configuration of this intermediate[13] suggests that the addition process occurred with essentially complete Cram–Felkin selectivity (see **5**, descriptor "C-F") within the manifold of a Zimmerman–Traxler-type cyclic transition state (descriptor "Z-T"). The simultaneous presence of an activated double bond (the allylsilane) and of a 1,3-dipole (the azido group) in **5** engendered a smooth intramolecular cycloaddition upon heating in toluene. Triazoline **6** thus emerged as a single diastereomer (by ^{1}H NMR spectroscopy). Brief photolysis of **6**[14] provided aziridine **7**,[13] which underwent a homo-Brook-triggered fragmentation to form benzazocenol **8**. This crucial eight-membered N-heterocycle was thus assembled in just four steps in a fully diastereocontrolled manner from readily available **3**.

Substances of the type **8** are known intermediates for the synthesis of FR900482 and of mitomycinoids,[6] except that their construction normally requires considerably longer sequences; hence, the interest of the new methodology. To



Scheme 3. Reagents and conditions: a) THF, −78 °C; b) toluene, 100 °C, 80 % over two steps; c) *hν*, THF, 77 %; d) nBu_4NOH, DMF, −20 °C, 49 %. DMF = *N*,*N*-dimethylformamide.

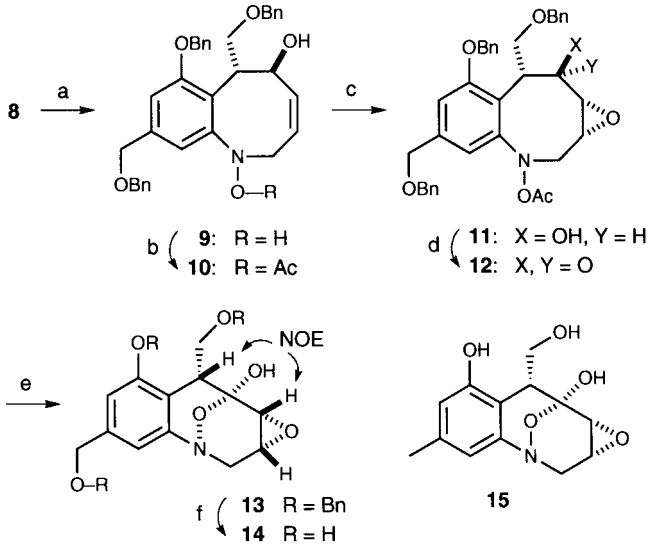
the best of our knowledge, only approaches that rely on olefin metathesis[7k] appear to be competitive with our aziridine fragmentation methodology for the creation of such medium-ring N-heterocycles.

Straightforward operations patterned after reported syntheses of **1b**[6a] advanced **8** to **11**, oxidation of which to ketone **12** was best carried out with TPAP–NMO.[15] Release of the hydroxylamine O-acetyl group precipitated transannular cyclization to **13**, which upon hydrogenolytic cleavage of all benzyl groups furnished **14**. The progress of the debenzylation step was carefully monitored to minimize formation of by-product **15** (Scheme 4). The latter is an interesting intermediate in its own right,[6h] but, of course, it is not useful for the pursuit of the total synthesis. The relative configuration of **13** and **14** was assigned as shown in Scheme 4 on the basis of an observed NOE interaction between the indicated protons (2D-NOESY).

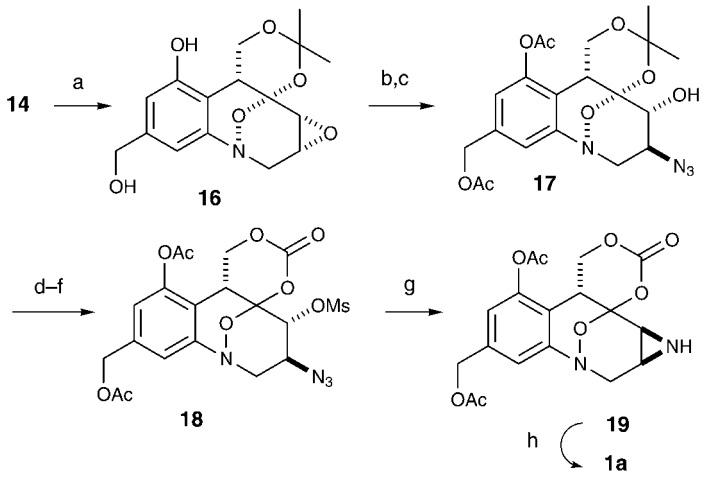
Tetraol **14** was elaborated to (±)-**1a** by a modification of known procedures,[6a,h] as detailed in Scheme 5. Selective acetonide formation led to **16**, which underwent regioselective azidolysis of the oxirane, followed by selective acetylation of primary and phenolic OH groups, to give **17**. Mesylation of the hindered, electronically deactivated secondary alcohol and exchange of the acetonide with a cyclic carbonate provided **18**.[16] Finally, sequential Staudinger-type aziridine formation and ammonolysis of both cyclic carbonate and acetate units in **19** produced the target (±)-**1a**, which was spectrally and chromatographically identical to authentic material.

In summary, the homo-Brook-mediated aziridine fragmentation avenue to medium-sized N-heterocycles can be used to prepare molecules of at least moderate complexity (e.g. **1a**). The applicability of the new method to the construction of other mitomycinoids, as well as further simplifications of the

 © 2002 WILEY-VCH Verlag GmbH & Co. KGaA, Weinheim 0044-8249/02/4124-4689 $ 20.00+.50/0



Scheme 4. Reagents and conditions: a) MCPBA, CH_2Cl_2, 0 °C; b) neat Ac_2O, room temperature, 87% over two steps; c) MCPBA, CH_2Cl_2, $NaHCO_3$, room temperature, 70%; d) cat. TPAP, NMO, CH_2Cl_2, molecular sieves (4 Å), room temperature, 83%; e) $N_2H_4{\cdot}H_2O$, MeOH, CH_2Cl_2, 100%; f) H_2 (1 atm), Pd/C, EtOAc, 97% crude. MCPBA = *m*-chloroperoxybenzoic acid, TPAP = tetrapropylammonium perruthenate, NMO = 4-methylmorpholine *N*-oxide.



Scheme 5. Reagents and conditions: a) 2-Methoxypropene, PPTS, DMF, room temperature, 83%; b) LiN_3, DMF, 100 °C, 67%; c) Ac_2O, K_2CO_3, THF, room temperature, 81%; d) MsCl, Et_3N, CH_2Cl_2, room temperature, 71%; e) TFA, CH_2Cl_2, room temperature; f) $COCl_2$, CH_2Cl_2, Et_3N, 0 °C, 28%; g) Ph_3P, iPr_2NEt, aqueous THF (90%), 60 °C, 78%; h) NH_3, MeOH, room temperature, 40%. PPTS = pyridinium *p*-toluenesulfonate, Ms = methanesulfonyl, TFA = trifluoroacetic acid.

synthetic pathway, are currently under study and will be reported in due course.

Received: September 18, 2002 [Z50186]

[1] a) I. Uchida, S. Takase, H. Kayakiri, S. Kiyoto, M. Hashimoto, T. Tada, S. Koda, Y. Morimoto, *J. Am. Chem. Soc.* **1987**, *109*, 4108; b) H. Terano, S. Takase, J. Hosoda, M. Kohsaka, *J. Antibiot.* **1989**, *42*, 145.

[2] For a review, see: W. T. Bradner, *Cancer Treat. Rev.* **2001**, *27*, 35.

[3] K. Shimomura, O. Hirai, T. Mizota, S. Matsumoto, J. Mori, F. Shibayama, H. Kikuchi, *J. Antibiot.* **1987**, *40*, 600.

[4] a) T. Fukuyama, S. Goto, *Tetrahedron Lett.* **1989**, *30*, 6491; b) R. M. Williams, S. R. Rajski, *Tetrahedron Lett.* **1992**, *33*, 2929; c) R. M. Williams, S. R. Rajski, *Tetrahedron Lett.* **1993**, *34*, 7023; d) H. Huang, S. R. Rajski, R. M. Williams, P. B. Hopkins, *Tetrahedron Lett.* **1994**, *35*, 9669; e) J. Woo, S. T. Sigurdsson, P. B. Hopkins, *J. Am. Chem. Soc.* **1993**, *115*, 1199; f) H. Huang, T. K. Pratum, P. B. Hopkins, *J. Am. Chem. Soc.* **1994**, *116*, 2703; g) M. M. Paz, P. B. Hopkins, *Tetrahedron Lett.* **1997**, *38*, 343; h) M. M. Paz, P. B. Hopkins, *J. Am. Chem. Soc.* **1997**, *119*, 5999; i) R. M. Williams, S. R. Rajski, *Chem. Biol.* **1997**, *4*, 127; j) L. Beckerbauer, J. J. Tepe, R. A. Eastman, P. Mixter, R. M. Williams, R. Reeves, *Chem. Biol.* **2002**, *9*, 427; k) L. Beckerbauer, J. Tepe, J. Cullison, R. Reeves, R. M. Williams, *Chem. Biol.* **2000**, *7*, 805; l) R. M. Williams, S. R. Rajski, *J. Am. Chem. Soc.* **1998**, *120*, 2192; m) T. C. Judd, R. M. Williams, *Org. Lett.* **2002**, *4*, 3711.

[5] a) K. Shimomura, T. Manda, S. Mukumoto, K. Masuda, T. Nakamura, T. Mizota, S. Matsumoto, F. Nishigaki, T. Oku, J. Mori, F. Shibayama, *Cancer Res.* **1988**, *48*, 1166; b) T. Nakamura, K. Masuda, S. Matsumoto, T. Oku, T. Manda, J. Mori, K. Shimomura, *Jpn. J. Pharmacol.* **1989**, *49*, 317; c) K. Masuda, T. Nakamura, T. Mizota, J. Mori, K. Shimomura, *Cancer Res.* **1988**, *48*, 5172; d) K. Masuda, T. Nakamura, K. Shimomura, *J. Antibiot.* **1988**, *41*, 1497; e) Y. Naoe, M. Inami, S. Matsumoto, F. Nishigaki, S. Tsujimoto, I. Kawamura, K. Miyayasu, T. Manda, K. Shimomura, *Cancer Chemother. Pharmacol.* **1998**, *42*, 31; f) Y. Naoe, M. Inami, I. Kawamura, F. Nishigaki, S. Tsujimoto, S. Matsumoto, T. Manda, K. Shimomura, *Jpn. J. Cancer Res.* **1998**, *89*, 666; g) Y. Naoe, M. Inami, S. Takagaki, S. Matsumoto, I. Kawamura, F. Nishigaki, S. Tsujimoto, T. Manda, K. Shimomura, *Jpn. J. Cancer Res.* **1998**, *89*, 1047; h) Y. Naoe, M. Inami, S. Matsumoto, S. Takagaki, T. Fujiwara, S. Yamazaki, I. Kawamura, F. Nishigaki, S. Tsujimoto, T. Manda, K. Shimomura, *Jpn. J. Cancer Res.* **1998**, *89*, 1306; i) Y. Naoe, I. Kawamura, M. Inami, S. Matsumoto, F. Nishigaki, S. Tsujimoto, T. Manda, K. Shimomura, *Jpn. J. Cancer Res.* **1998**, *89*, 1318; j) M. Inami, I. Kawamura, S. Tsujimoto, F. Nishigaki, S. Matsumoto, Y. Naoe, Y. Sasakawa, M. Matsuo, T. Manda, T. Goto, *Cancer Lett.* **2002**, *181*, 39; k) M. Tomasz, R. Lipman, D. Chowdary, J. Pawlak, G. Verdine, K. Nakanishi, *Science* **1987**, *235*, 1204; l) M. Tomasz, *Chem. Biol.* **1995**, *2*, 575, and references therein.

[6] For total syntheses of **1b**, see: a) T. Fukuyama, L. Xu, S. Goto, *J. Am. Chem. Soc.* **1992**, *114*, 383; b) J. M. Schkeryantz, S. J. Danishefsky, *J. Am. Chem. Soc.* **1995**, *117*, 4722; c) T. Katoh, E. Itoh, T. Yoshino, S. Terashima, *Tetrahedron* **1997**, *53*, 10229; d) T. Yoshino, Y. Nagata, E. Itoh, M. Hashimoto, T. Katoh, S. Terashima, *Tetrahedron* **1997**, *53*, 10239; e) T. Katoh, Y. Nagata, T. Yoshino, S. Nakatani, S. Terashima, *Tetrahedron* **1997**, *53*, 10253; see also two previous communications: f) T. C. Judd, R. M. Williams, *Angew. Chem.* **2002**, *114*, 4877; *Angew. Chem. Int. Ed.* **2002**, *41*, 4683; g) M. Suzuki, M. Kambe, H. Tokuyama, T. Fukuyama, *Angew. Chem.* **2002**, *114*, 4882; *Angew. Chem. Int. Ed.* **2002**, *41*, 4688. We are grateful to Profs. Robert M. Williams and Tohru Fukuyama for informing us of their independent syntheses of FR-900482 and FR-66979 prior to submission of our work, and for agreeing to have our three papers appear consecutively in this issue of *Angewandte Chemie*.

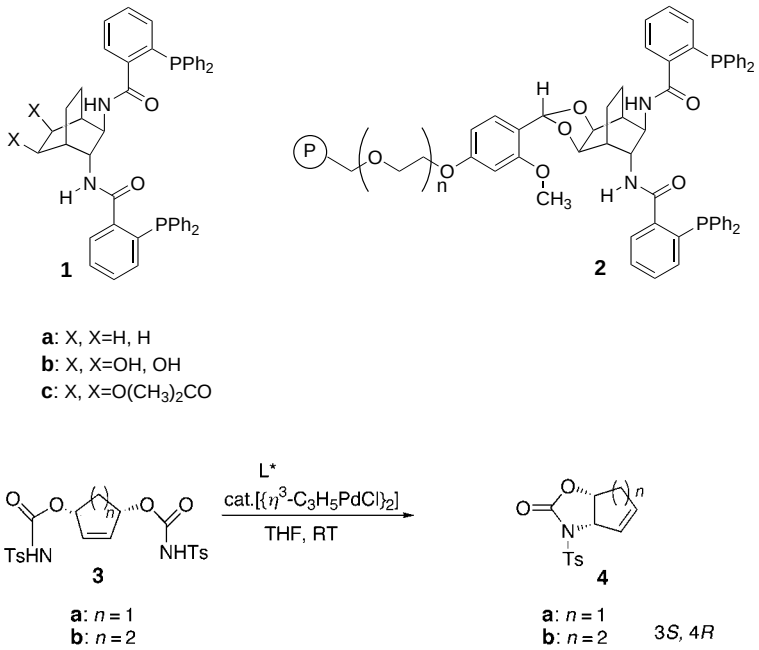
[7] For synthetic studies, see: a) N. Yasuda, R. M. Williams, *Tetrahedron Lett.* **1989**, *30*, 3397; b) R. J. Jones, H. Rapoport, *J. Org. Chem.* **1990**, *55*, 1144; c) S. J. Miller, S. H. Kim, Z. R. Chen, R. H. Grubbs, *J. Am. Chem. Soc.* **1995**, *117*, 2108; d) T. Katoh, E. Itoh, T. Yoshino, S. Terashima, *Tetrahedron Lett.* **1996**, *37*, 3471; e) T. Yoshino, Y. Nagata, E. Itoh, M. Hashimoto, T. Katoh, S. Terashima, *Tetrahedron Lett.* **1996**, *37*, 3475; f) T. Katoh, T. Yoshino, Y. Nagata, S. Nakatani, S. Terashima, *Tetrahedron Lett.* **1996**, *37*, 3479; g) H. J. Lim, G. A. Sulikowski, *Tetrahedron Lett.* **1996**, *37*, 5243; h) F. E. Ziegler, M. Belema, *J. Org. Chem.* **1997**, *62*, 1083; i) S. Mithani, D. M. Drew, E. H. Rydberg, N. J. Taylor, S. Mooibroek, G. I. Dmitrienko, *J. Am. Chem. Soc.* **1997**, *119*, 1159; j) W. Zhang, C. Wang, L. S. Jimenez, *Synth. Commun.* **2000**, *30*, 351; k) I. M. Fellows, D. E. Kaelin, Jr., S. F. Martin, *J. Am. Chem. Soc.* **2000**, *122*, 10781; l) M. Kambe, E. Arai, M. Suzuki, H. Tokuyama, T. Fukuyama, *Org. Lett.* **2001**, *3*, 2575.

[8] cf. a) M. A. Ciufolini, M. Chen. , D. P. Lovett, M. V. Deaton, *Tetrahedron Lett.* **1997**, *38*, 4355; b) M. A. Ciufolini, M. V. Deaton, S. Zhu, M. Chen, *Tetrahedron* **1997**, *53*, 16299.

[9] R. Ducray, N. Cramer, M. A. Ciufolini, *Tetrahedron Lett.* **2001**, *42*, 9175.

 © 2002 WILEY-VCH Verlag GmbH & Co. KGaA, Weinheim 0044-8249/02/4124-4690 $ 20.00+.50/0

[10] a) P. F. Hudrlik, A. M. Hudrlik, A. K. Kulkarni, *J. Am. Chem. Soc.* **1982**, *104*, 6809; b) P. F. Hudrlik, P. E. Holmes, A. M. Hudrlik, *Tetrahedron Lett.* **1988**, *29*, 6395.
[11] Prepared from the corresponding, known 2-(2-nitroaryl)-propanediol (see compound **24** in reference [7k]), readily available in > 10-g batches, by: a) H_2, Raney Ni; b) HONO/NaN_3; c) BnBr, NaH (facile monobenzylation); d) IBX, DMSO, 53% overall yield; Bn = benzyl, IBX = *o*-iodoxylbenzoic acid, DMSO = dimethyl sulfoxide.
[12] M. T. Reetz, R. Steinbach, J. Westermann, R. Peter, B. Wenderoth, *Chem. Ber.* **1985**, *118*, 1441.
[13] The relative configuration of this intermediate was inferred from the X-ray crystal structure of compound **7**.
[14] This photolysis reaction occurred most efficiently when a Sylvania 250-W suntanning lamp was used as the light source (water-cooled pyrex reactor). A standard Hanovia lamp produced less satisfactory results.
[15] S. V. Ley, J. Norman, W. P. Griffith, S. P. Marsden, *Synthesis* **1994**, 639.
[16] The relative configuration of the bridged system of this substance was not determined.



Polymer-Supported C_2-Symmetric Ligands for Palladium-Catalyzed Asymmetric Allylic Alkylation Reactions**

Barry M. Trost,* Zhengying Pan, Jorge Zambrano, and Christof Kujat

Development of immobilized ligands/catalysts for asymmetric synthesis is a rapidly growing field.[1] Because of palladium's broad applications in organic synthesis,[2] many types of supported ligands have been reported for allylic,[3] alkylation,[4] amination, and cross-coupling reactions.[5] However, there are surprisingly few successful polymer-bound ligands for palladium-catalyzed asymmetric allylic alkylations.[6,7] In the late 1970s, we demonstrated the use of polymer-bound phosphane ligands in Pd-catalyzed transformations.[8] We here report a competent, easily prepared, recyclable chiral ligand for asymmetric allylic alkylation (AAA) reactions.

Initially, we examined the supported ligand **2**, which was derived from the rigid bicyclic templates **1**[9] to minimize any perturbation of the chiral pocket. The supported ligand **2** formed readily by reacting the diol **1b** with ArgoGel-CHO catalyzed by *p*-toluenesulfonic acid (TsOH) in dichloromethane. Cyclization of the bisurethane **3a** to the oxazolidin-2-one **4a**[10,11] was examined as the test reaction [Eq. (1)]. As a baseline, the reaction was performed in normal solution phase with the simple ligands **1a** and **1b**. Table 1, entries 1 and 2, reveals the effectiveness of this class of ligands. It is somewhat surprising that a small dip in enantiomeric excess (*ee*) occurs on introducing electronegative oxygen atoms into the remote bridge (91 to 87% *ee*). The supported ligand **2** was effective in performing the reaction but there was a more significant drop in enantiomeric excess (Table 1, entry 3) although it was still reasonable. Simply decanting the reaction mixture from the solid support and washing the beads with fresh THF prepared the beads for the next cycle. No additional palladium was loaded after the initial charge. The yield dipped in the second cycle but subsequently stabilized at 60 ± 5%. Thus, the supported catalyst was quite robust remaining highly active even after seven cycles (Table 1, entries 3–9). The enantiomeric excess also remained quite constant through most of the cycles at 70 ± 1%. In earlier experiments with normal solution ligands, addition of triethylamine led to a significant enhance-

Table 1. First-generation bicyclic ligands.[a]

Entry	Ligand	Run	Yield of **4a** [%]	*ee*[b] [%]
1[c]	**1a**	–[d]	69	91
2[c]	**1c**	–[d]	79	87
3	**2**	1	81	73
4	**2**	2	74	71
5	**2**	3	70	70
6	**2**	4	63	71
7	**2**	5	63	69
8	**2**	6	60	70
9	**2**	7	66	69
10	**2**	–[d]	78	68

[a] All reactions were performed with 10 mol% [{η³-C_3H_5PdCl}$_2$] and 25 mol% ligand in THF at room temperature; the vessel was shaken for mixing unless otherwise indicated. [b] Determined by chiral HPLC in an AD chiralpak column. [c] Performed with 2.5 mol% [{η³-C_3H_5PdCl}$_2$], 7.5 mol% ligand in THF at room temperature with normal magnetic stirring for mixing. [d] Not applicable. [e] Triethylamine added.

[*] Prof. B. M. Trost, Z. Pan, J. Zambrano, C. Kujat
Department of Chemistry
Stanford University
Stanford, CA 94305-5080 (USA)
Fax: (+1) 650-725-0259
E-mail: bmtrost@stanford.edu

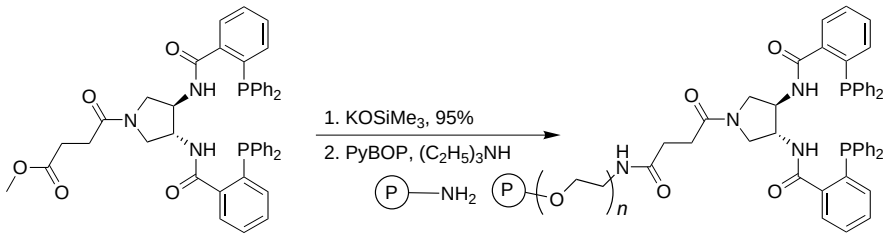
[**] We thank the National Science Foundation and the National Institute of Health, General Medical Sciences (GM13598), for their generous support of our programs. We thank Argonaut Technologies for a generous gift of ArgoGel resins.

Supporting information for this article is available on the WWW under http://www.angewandte.org or from the author.

 © 2002 WILEY-VCH Verlag GmbH & Co. KGaA, Weinheim 0044-8249/02/4124-4691 $ 20.00+.50/0

ment of the enantiomeric excesss. That effect was not observed with this supported ligand (Table 1, entry 10). In related experiments, ArgoPore or Merrifield resins proved less efficacious; immobilizing the ligand in the solid support had no effect on the absolute configuration of the major enantiomer produced.

While the reactivity of the supported catalyst was satisfactory, less loss of enantiomeric excess was desired. Speculation that the polar amide linkages may be interacting with the polyether polymer led us to envision an amide tether. Consequently, we examined ligand **5**, which was generated from the known corresponding diamide bis(Boc-pyrrolidine) compound (Boc = *tert*-butyloxycarbonyl),[12] and its supported version **6** derived from ArgoGel-NH_2 and **5** (Scheme 1).



5 **6**

Scheme 1. Synthesis of the supported compound **6** from the ligand **5**. PyBOP = (benzotriazol-1-yloxy)tripyrrolidinophosphonium hexafluorophosphate.

Hydrolysis of the ester **5** with $KOSiMe_3$ (95% yield) followed by coupling of the resulting acid with ArgoGel-NH_2 using PyBOP and triethylamine (quantitative yield; the disappearance of free NH_2 groups was monitored by Kaiser and chloranil tests)[13] gave the desired supported ligand (0.37 mmol g^{-1}). Once again, cyclization of the bisurethane **3b** to the oxazolidin-2-one **4b** [Eq. (1)] was examined as the test reaction. As entry 1 in Table 2 indicates, the pyrrolidine ligand **5** performs superbly.

Loading the polymer with $[(dba)_3Pd_2]\cdot CHCl_3$ as the palladium source proved problematic and required the presence of substrate to be successful. On the other hand, using $[\{\eta^3\text{-}C_3H_5PdCl\}_2]$ was straightforward. Furthermore, comparison of entries 2 and 3 to those of entries 4 and 5 in Table 2 suggests that the π-allylpalladium chloride precatalyst generates a somewhat better catalyst and therefore this was adopted as the standard palladium source. In this case, addition of one equivalent of triethylamine has a noticeable effect (Table 2, entry 2 versus 3 and 4 versus 5) of improving the enantiomeric excess but slowing the reaction somewhat as observed in the solution phase with the standard ligand.[10a] Further addition of the triethylamine was not beneficial (Table 2, entry 6), and switching to dichloromethane (Table 2, entry 7) or toluene (Table 2, entry 8) proved quite deleterious. On the other hand, increasing the concentration of the substrate to 1M had little effect (Table 2, entries 9 and 10). The reaction in Equation (1) was equally effective in the case of the five-membered-ring substrate **4a**, whereby the oxazolidin-2-one **4b** was formed in 63% yield with 93% *ee*. The absolute configuration of the product was the same for the same chiral scaffold generated by using the soluble and supported catalysts. The key question was the ability to recycle the catalyst. Table 3 summarizes the results. In each recycle step, no additional loading of palladium after the initial charge was performed. After 1 h, the reaction mixture was decanted off by using a cannula, and the solution of the reactants for the next cycle was then added to the beads. Over four cycles, no significant differences in either yield or enantiomeric excess were observed.

Table 2. Second-generation pyrrolidine-based ligands.[a]

Entry	Ligand	$(C_2H_5)_3N$ [equiv]	Conc. [M]	Solvent	Yield **4b** [%]	*ee* **4b** [%]
1[b]	**5**	1	0.2	THF	97	> 99
2[b]	**6**	1	0.2	THF	70	87
3[b]	**6**	none	0.2	THF	54	71
4	**6**	none	0.2	THF	93	80
5	**6**	1	0.2	THF	78	90
6	**6**	2	0.2	THF	64	89
7	**6**	1	0.2	CH_2Cl_2	35	50
8	**6**	1	0.2	$PhCH_3$	–[c]	–
9	**6**	1	0.5	THF	72	86
10	**6**	1	1.0	THF	77	85

[a] All reactions were performed with 5 mol% catalyst at room temperature overnight using $[\{\eta^3\text{-}C_3H_5PdCl\}_2]$ as the palladium precatalyst (ratio of bound ligand to palladium 1.5:1) unless otherwise noted. [b] For this run, $[(dba)_3Pd_2]\cdot CHCl_3$ used as precatalyst (dba = *trans,trans*-dibenzylideneacetone. [c] No reaction.

Table 3. Recycling experiments with catalyst **6**.[a]

Entry	Reaction time [h]	Yield [%]	*ee* [%]
1	1	81	92
2	1	81	92
3	1	77	91
4	1	77	92

[a] All reactions were run with 20 mol% catalyst and one equivalent of $(C_2H_5)_3N$ at 0.2M in THF at room temperature.

The results herein demonstrate that polymer-supported chiral catalysts can function for palladium-catalyzed asymmetric allylic alkylations. The more solution-like environment of the ArgoGel resins make them more efficacious than the other polymeric supports such as the Merrifield or ArgoPore resins. Nevertheless, the choice of the scaffold and the bond type for tethering is critical. While reactivities were normally not an issue, the impact of the solid support on enantiomeric excess was significant. The degree of loss of enantiomeric excess was dependent upon both parameters. The use of an amide tether and a pyrrolidine scaffold gave a solution and a supported catalyst that closely resembled each other and kept the *ee* value $\geq$ 90%. In all the cases examined, good recyclability of the catalyst (up to seven recycles were examined) was observed as long as the reaction mixtures were thoroughly degassed to ensure that the oxygen content was as low as possible. The readily available supported catalyst generated from ligand **6** should prove to be generally useful for palladium reactions.[14] The ability to produce

 © 2002 WILEY-VCH Verlag GmbH & Co. KGaA, Weinheim 0044-8249/02/4124-4692 $ 20.00+.50/0 *Angew. Chem. Int. Ed.* **2002**, *41*, No. 24

oxazolidin-2-ones with high enantiomeric excesses has already proved to be useful in generating a number of biologically significant targets such as mannostatin A,[15a] allosamizoline,[15a] and swainsonine.[15b]

Received: August 26, 2002 [Z50043]

[1] For recent reviews, see: B. Clapham, T. S. Reger, K. D. Janda, *Tetrahedron* **2001**, *57*, 4637 – 4662; Y. R. de Miguel, E. Brule, R. G. Margue, *J. Chem. Soc. Perkin Trans. 1* **2001**, 3085 – 3094; S. J. Shuttleworth, S. M. Allin, R. D. Wilson, D. Nasturica, *Synthesis* **2000**, 1035 – 1074; S. J. Shuttleworth, S. M. Allin, P. K. Sharma, *Synthesis* **1997**, 1217 – 1239; K. Fodor, S. G. A. Kolmschot, R. A. Sheldon, *Enantiomer* **1999**, *4*, 497 – 511.

[2] J. Tsuji, *Palladium Reagents and Catalysts-innovations in Organic Synthesis*, Wiley, New York, **1995**.

[3] Y. Uozumi, H. Danjo, T. Hiyashi, *Tetrahedron Lett.* **1998**, *39*, 8303; Y. Uozumi, H. Danjo, T. Hiyashi, *J. Org. Chem.* **1999**, *64*, 3884.

[4] C. A. Parrish, S. L. Buchwald, *J. Org. Chem.* **2001**, *66*, 3820.

[5] Heck reaction: P. W. Wang, M. A. Fox, *J. Org. Chem.* **1994**, *59*, 5358; M. R. Buchmeiser, K. Wurst, *J. Am. Chem. Soc.* **1999**, *121*, 11101; J. Schwarz, V. P. W. Bohm, M. G. Gardiner, M. Grosche, W. A. Herrmann, W. Hieringer, G. Raudashl-Sieber, *Chem. Eur. J.* **2000**, *6*, 1773; Stille reaction: J. K. Stille, H. Su, D. H. Hill, P. Schneider, M. Tanaka, D. L. Morrison, L. S. Hegedus, *Organometallics* **1991**, *10*, 1993; Suzuki reaction: S.-B. Jang, *Tetrahedron Lett.* **1997**, *38*, 1793; I. Finger, C. Le Drian, *Tetrahedron Lett.* **1998**, *39*, 4287; T. Y. Zhang, M. J. Allen, *Tetrahedron Lett.* **1999**, *40*, 5813; ref. [4].

[6] K. Hallman, E. Macedo, K. Nordstrom, C. Moberg, *Tetrahedron: Asymmetry* **1999**, *10*, 4037; K. Hallman, C. Moberg, *Tetrahedron: Asymmetry* **2001**, *12*, 1475.

[7] Y. Uozumi, K. Shibatomi, *J. Am. Chem. Soc.* **2001**, *123*, 2919; see also: H.-J. Park, J. W. Han, H. Seo, H. -Y, Jang, Y. K. Chung, J. Suh, *J. Mol. Catal. A* **2001**, *174*, 151.

[8] B. M. Trost, E. Kainan, *J. Am. Chem. Soc.* **1978**, *100*, 7779.

[9] B. M. Trost, J. Zambrano, W. Reichter, *Synlett* **2001**, 907.

[10] a) B. M. Trost, D. E. Patterson, *J. Org. Chem.* **1998**, *63*, 1339; b) B. M. Trost, D. L. VanVranken, C. Bingel, *J. Am. Chem. Soc.* **1992**, *114*, 9327.

[11] B. M. Trost, *Chem. Pharm. Bull.* **2002**, *50*, 1; B. M. Trost, C.-B. Lee in *Catalytic Asymmetric Synthesis*, (Ed.: I. Ojima), Wiley-VCH, New York, **2000**, pp. 593 – 650; B. M. Trost, *Acc. Chem. Res.* **1996**, *29*, 355.

[12] A. J. Brouner, R. van der Linden, M. J. Liskamp, *J. Org. Chem.* **2000**, *65*, 1750; J. Skarzewski, A. Gupta, *Tetrahedron: Asymmetry* **1997**, *8*, 1861.

[13] J. M. Stewart, J. D. Young, *Solid Phase Reptide Synthesis*, 2nd ed., Pierce Chemical Co., Rockford, IL, **1984**, p. 105 and 108.

[14] For an overview of applications of solid supported reagents and catalyst see: S. V. Ley, I. R. Baxendale, R. N. Bream, P. S. Jackson, A. G. Leach, D. A. Longbottom, M. Nesi, J. S. Scott, R. I. Storer, S. J. Taylor, *J. Chem. Soc. Perkin Trans. 1* **2000**, 3815.

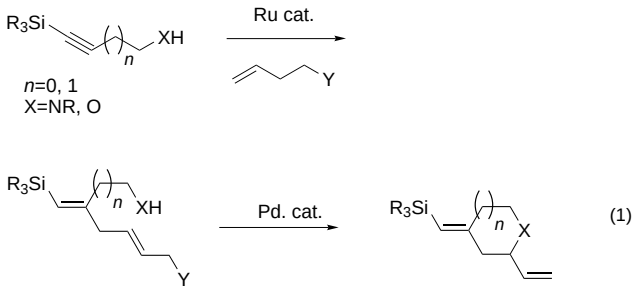
[15] a) B. M. Trost, D. L. Vranken, *J. Am. Chem. Soc.* **1993**, *115*, 444; b) B. M. Trost, D. E. Patterson, *Chem. Eur. J.* **1999**, *5*, 3279.

An Efficient One-Pot Enantio- and Diastereoselective Synthesis of Heterocycles**

Barry M. Trost* and Michelle R. Machacek

Heterocycles comprise the core of many complex natural products. The most common method for their formation is based on intramolecular ring closure. However, in most intramolecular closure strategies it is necessary to synthesize and then isolate the open-chain precursor. On an industrial scale the environmental and economic costs of the isolation step are considerable. In contrast, a more efficient strategy utilizes a domino alkylation–cyclization[1] to form the ring without isolation of the acyclic intermediate. For the development of ideal syntheses, processes are sought that generate multiple bonds in one pot.[2]

We aimed to design a one-pot heterocyclization process that was both efficient and permitted control of the stereochemistry of our products. We therefore focused on the Pd-catalyzed asymmetric allylic alkylation (AAA)[3,4] for the critical stereochemical determining step. This was combined with the Ru-catalyzed ene–yne coupling[5] to create the proper juxtaposition of functionality for the second step. Recently we have shown that in the presence of $[CpRu(CH_3CN)_3PF_6]$,[6] silyl-substituted alkynes form 1,4-dienes with complete regio- and stereoselectivity.[7] If the ene partner is a homoallylic group, the resulting 1,4-diene will contain a *newly formed allylic* group as illustrated in Equation (1). This intermediate



(1)

may then *without isolation* be subjected to Pd-catalyzed asymmetric allylic alkylation. An additional feature of this strategy is that the resulting vinylsilanes offer a pathway for further structural elaboration[8] and permit differentiation of the two resulting double bonds.

[*] Prof. B. M. Trost, M. R. Machacek
Department of Chemistry
Stanford University
Stanford, CA 94305-5080 (USA)
Fax: (+1) 650-725-0002
E-mail: bmtrost@stanford.edu

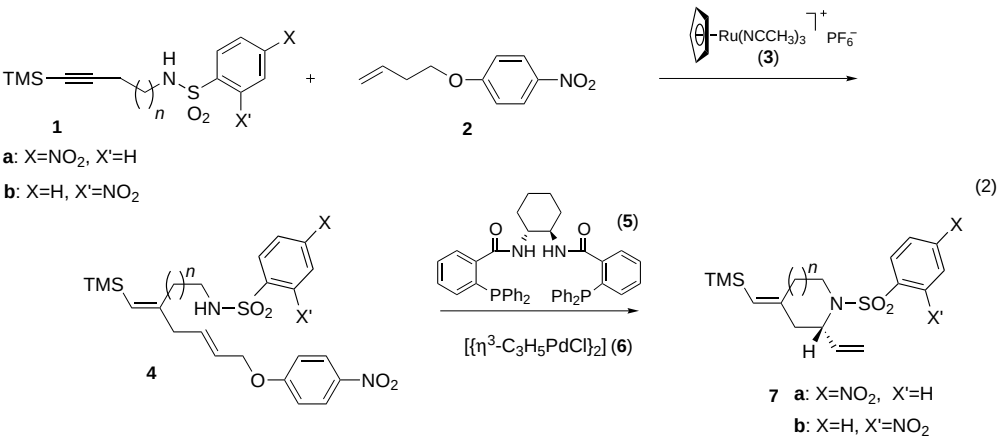
[**] We thank the National Science Foundation and the National Institutes of Health, General Medical Science (GM-13598) for their generous support of our programs. GMS has been supported in part by a fellowship from Bristol Myers Squibb Pharmaceutical Company. Mass spectra were provided by the Mass Spectrometry Regional Center of the University of California, San Francisco, supported by the NIH Division of Research Resources.

Supporting information for this article is available on the WWW under http://www.angewandte.org or from the author.

 © 2002 WILEY-VCH Verlag GmbH & Co. KGaA, Weinheim 0044-8249/02/4124-4693 $ 20.00+.50/0

Incorporating asymmetric transition-metal catalysis into a tandem process is a formidable goal.[9] The key issue is the compatibility of the two catalyst systems. The reagents or catalysts may interfere with each other by distorting the chiral pocket that is crucial for enantioselectivity, or by acting as nondissociating ligands that shut down the catalytic cycle. For our dual catalytic reaction, we required a substituent Y that was compatible with both asymmetric allylic alkylation and the ene–yne coupling. We previously demonstrated that allylic esters serve as excellent substrates for Ru-catalyzed allylic alkylations.[10] However, to obtain high asymmetric induction, the group Y must allow the ene–yne coupling to proceed to completion *without* appreciable ionization of the resulting allylic group. This group Y must then still participate effectively in the Pd-catalyzed allylic alkylation.

In our initial work using an ester for Y, the desired ene–yne coupling was always accompanied by varying amounts of Ru-catalyzed ionization. While phenol has been reported as a leaving group in simple Pd-catalyzed allylic alkylations,[11] our early efforts revealed that such reactions were not general and failed with many routine nucleophiles. We therefore examined a *p*-nitrophenyl ether to enhance the reactivity for the Pd-catalyzed step without disturbing the Ru-catalyzed step. Indeed, reaction of **1a** ($n=1$) with 1-butenyl-4-*p*-nitrophenyl ether (**2**) in the presence of a catalytic amount of ruthenium complex **3**[6] in acetone at room temperature gave the desired adduct **4** in 91 % yield as a single regio- and geometric isomer within 2 h [Eq. (2)]. Further treatment with the Pd complex



(2)

generated by mixing the precatalyst (2 mol % **6** with 6 mol % ligand **5**) in acetone in the presence of 1,8-diazabicyclo[5.4.0]undec-7-ene (DBU) gave the piperidine **7a** ($n=1$)[12] in 72 % yield and 74 % *ee*. The choice of the *p*-nitrobenzenesulfonamide as the nucleophile derived from the compatibility of this functionality with the Ru-catalyzed ene–yne addition and its ease of removal.[13] Optimization studies of the AAA reaction revealed that solvent had the biggest impact on enantioselectivity. The best results were obtained by using chloroform (99 % yield, 90 % *ee*) or dichloromethane (100 % yield, 89 % *ee*). Because the Ru-catalyzed reaction is best run in acetone, mixed solvents were also examined. A 75:25 (v:v) mixture of dichloromethane and acetone gave 84 % *ee* which increased to 88 % *ee* by using a 90:10 (v:v) mixture. A one-pot protocol then evolved by allowing **1a** ($n=1$) and **2** in a 1:1.7 ratio to react in the presence of **3** (2 mol %) at room temperature in acetone. Addition of DBU (1 equiv) along with the precatalyst in dichloromethane and stirring for 1 h, followed by evaporation and flash chromatography, resulted in an 83 % yield of **7a** ($n=1$) with 88 % *ee* (see Table 1, entry 3). The use of the *o*-nitrobenzesulfonamide (**2b**, $n=1$) gave a somewhat higher enantiomeric excess. Under conditions where the *p*-nitro analogue **2a** ($n=1$) gave 84 % *ee*, the *o*-nitro substrate resulted in 88 % *ee*. Therefore, it is apparent that the ruthenium catalyst affects neither the chiral pocket nor the turnover of the palladium catalyst. Furthermore, the yield for the overall process is much higher than when each step is individually isolated.

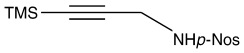
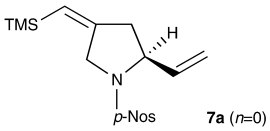
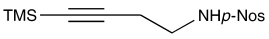
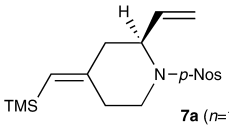
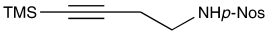
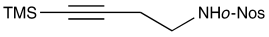
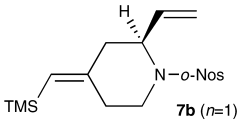
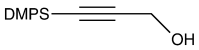
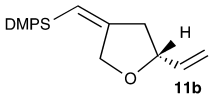
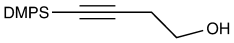
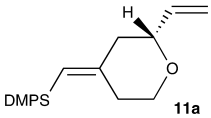
The absolute configuration of this product was assigned based upon our mnemonic wherein the initial ionization constitutes the enantiodiscriminating event.[14] Support for this assignment derives from the effect of chloride salts on the enantiomeric excess. Addition of tetra-*n*-butylammonium chloride to increase the rate of π-σ-π equilibration of intermediates[15] decreases the enantiomeric excess dramatically. Entries 1–4, Table 1, summarize the results for forming the pyrrolidine and piperidine systems.

The formation of the corresponding oxygen heterocycles was examined as shown in Equation (3). To abate product volatility, a dimethylphenylsilyl(DMPS)-substituted alkyne was employed. The presence of a free alcohol on alkyne **8** led to a rate retardation that was overcome by using excess alkene partner and higher Ru catalyst loadings (10 mol %). Again, the ene–yne adduct **9** that formed as a single isomer in 75 % yield showed no propensity to cyclize. Simple alkyl alcohols are not known to participate well in enantioselective Pd π-allyl alkylations.[16,17] However, in an intramolecular sense we found that AAA reactions with simple alkyl alcohols were very successful. The alcohol nucleophiles showed a similar solvent effect wherein dichoromethane was strongly preferred. Consequently, these reactions were performed by evaporating the acetone from the first stage followed by adding a solution of Pd catalyst and base in dichloromethane. For oxygen nucleophiles, $[Pd_2(dba)_3]\cdot CHCl_3$ and triethylamine were the preferred Pd^0 source and base, respectively. Addition of tetra-*n*-butylammonium chloride had no significant effect on the enantiomeric excess. This observation is consistent with the nucleophilic addition step being the enantiodiscriminating event leading to the assigments depicted in Table 1. Entries 5 and 6, Table 1, summarize the results.

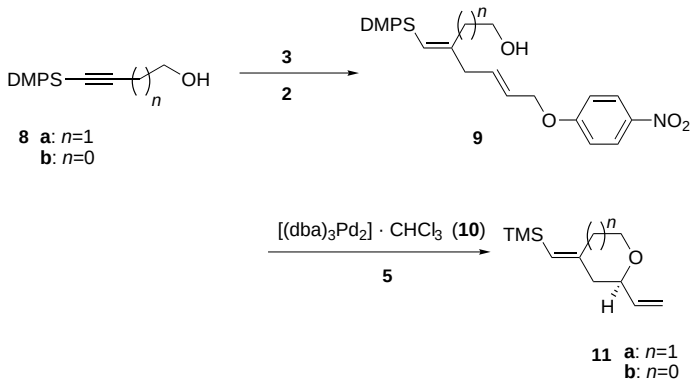
Palladium catalysis offers an opportunity for diastereo- as well as enantiocontrol in reactions. Table 2 summarizes the extent to which the chiral ligands overcame the intrinsic diastereoselectivity of the substrates. Enantiomerically pure

 © 2002 WILEY-VCH Verlag GmbH & Co. KGaA, Weinheim 0044-8249/02/4124-4694 $ 20.00+.50/0 *Angew. Chem. Int. Ed.* **2002**, *41*, No. 24

Table 1. Examples of enantioselective formation of heterocycles.

Entry	Alkyne	Product	Conditions[a]	Yield	*ee* [%][b]
1		 **7a** (*n*=0)	A	90	91
2		 **7a** (*n*=1)	A	90	84
3		**7a** ($n=1$)	B	83	88
4		 **7b** (*n*=1)	A	90	88
5		 **11b**	C	84	76
6		 **11a**	C	80	94

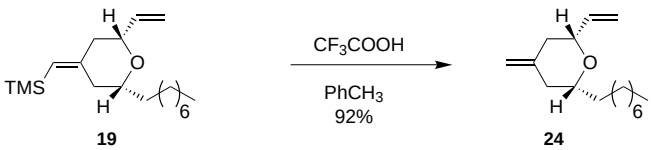
[a] Conditions: A: a) 5 mol% **3**, CH_3COCH_3, RT, 3–4 h; b) 2 mol% **6**, 6 mol% **5**, DBU, RT, CH_2Cl_2:CH_3COCH_3 (75:25) 1 h. B: a) 2 mol% **3**, CH_3COCH_3, RT, 3–4 h; b) 2 mol% **6**, 6 mol% **5**, DBU, CH_2Cl_2:CH_3COCH_3 (90:10). C: a) 10 mol% **3**, CH_3COCH_3, RT, 3–4 h; b) 2 mol% **6**, 6 mol% **5**, $(C_2H_5)_3N$, 0 °C, CH_2Cl_2. [b] Enantiomeric excess (*ee*) determined by HPLC.



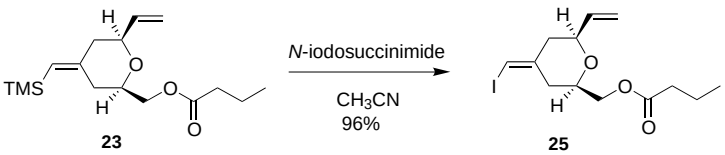
(3)

substrates of known absolute configuration were employed in all cases. As expected, a matched and mismatched pair[15] was formed. In piperidine formation, the *cis* isomer predominates 2:1 with the achiral 1,3-bis(diphenylphosphanyl)propane (dppp) ligand. Under matched conditions, the *cis* isomer is formed nearly exclusively (Table 2, entry 2), while when the mismatched ligand system is used, the *trans* isomer is favored 2:1 (Table 2, entry 1). In the case of oxygen heterocyles, the level of control exercised by the ligands increased. For the furan system (Table 2, entries 3 and 4), the *cis*:*trans* ratio switched from 10:1 in the matched case to 1:3.5 in the mismatched. These selectivities compare to a 4:1 *cis*:*trans* ratio with the achiral ligand dppp. Dramatically, in pyran formation (Table 2, entries 5–8) the selectivity was complete—the *cis* isomer was formed exclusively in the matched cases (Table 2, entries 5 and 8) and the *trans* isomer was formed exclusively in the mismatched cases (Table 2,entries 6 and 7). Cyclization methods for forming *cis* 2,6-disubstituted tetrahydropyrans are prevalent. However, very few methods offer direct access to the thermodynamically unfavorable *trans*-pyran in isomerically pure form.[18] For this class of substrates, the ability of the chiral ligands to control relative stereochemistry[19] is indeed impressive and indicates the potential of this catalytic system.

In addition to providing access to a very important class of compounds, this methodology also introduces several functional groups into the heterocycle that readily allow further elaboration. For example, the resulting vinylsilane moiety offers access to a variety of stereochemically defined trisubstitued alkenes by *ipso*-substitution reactions. We were also able to smoothly convert the vinylsilane to a vinyl iodide [Eq. (4b)], allowing access to many cross-coupling reactions. The resulting vinyl-



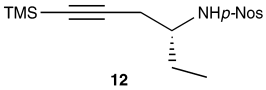
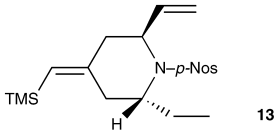
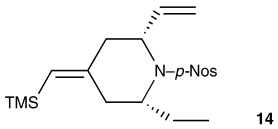
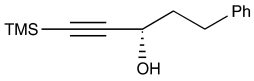
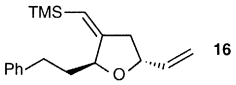
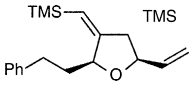
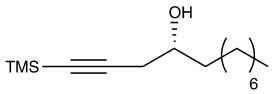
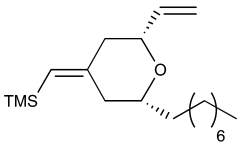
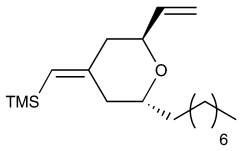
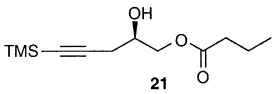
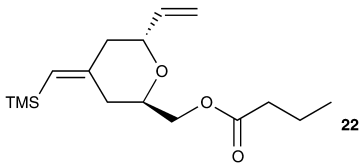
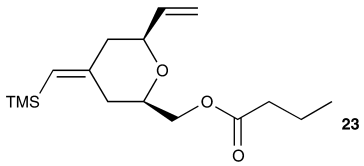
(4a)



(4b)

 © 2002 WILEY-VCH Verlag GmbH & Co. KGaA, Weinheim 0044-8249/02/4124-4695 $ 20.00+.50/0

Table 2. Examples of diastereoselective formation of heterocycles.

Entry	Alkyne	Ligand	Major Product	Conditions[a]	Yield	d.r.[b]
1	 **12**	**5**	 **13**	A	73	2:1
2	**12**	*ent*-**5**	 **14**	A	68	99:1
3	 **15**	**5**	 **16**	C	87	3.5:1
4	**15**	*ent*-**5**	 **17**	C	80	10:1
5	 **18**	**5**	 **19**	C	80	> 97:3
6	**18**	*ent*-**5**	 **20**	C	80	> 97:3
7	 **21**	**5**	 **22**	C	60	> 97:3
8	**21**	*ent*-**5**	 **23**	C	58	> 97:3

[a] See footnote [a] of Table 1 for conditions. [b] Ratios determined by ^{1}H NMR spectroscopy.

silane also acts to differentiate the two resulting double bonds and can ultimately be converted to the parent methylene by protodesilation without altering the regiochemistry by isomerization of the double bond [Eq. (4a)].

Received: September 16, 2002 [Z50173]

[1] P. J. Parsons, C. S. Penkett, A. J. Shell, *Chem. Rev.* **1996**, *96*, 195 – 206; See also: H. Hopf, J. Wolff, *Eur. J. Org. Chem.* **2001**, 4009 – 4030; B. M. Trost, A. J. Frontier, *J. Am. Chem. Soc.* **2000**, *122*, 11727 – 11728; K. Neuschuetz, J. Velker, R. Neier, *Synthesis* **1998**, 227 – 255; J. Markandu, H. A. Dondas, M. Frederickson, R. Grigg, *Tetrahedron* **1997**, *53*, 13165 – 13176.

[2] P. A. Wender, B. L. Miller, *Organic Synthesis: Theory and Applications, Vol. 2* (Ed.: T. Hudlicky), JAI, Greenwich, **1993**, p. 70.

[3] B. M. Trost, *Chem. Pharm. Bull.* **2002**, *50*, 1 – 14; B. M. Trost, C. Lee, *Catalytic Asymmetric Synthesis II*, (Ed.: I. Ojima), Wiley-VCH, New York, **2000**, pp. 593 – 650; B. M. Trost, D. C. Van Vranken, *Chem. Rev.* **1995**, *95*, 395 – 422.

[4] See also: B. M. Trost, M. J. Krische, R. Radinov, G. Zanoni, *J. Am. Chem. Soc.* **1996**, *118*, 6297 – 6298.

[5] B. M. Trost, *Acc. Chem. Res.* **2002**, *35*, in press; B. M. Trost, F. D. Toste, A. B. Pinkerton, *Chem. Rev.* **2001**, *101*, 2067 – 2096.

[6] T. P. Gill, K. R. Mann, *Organometallics* **1982**, *1*, 485 – 488. For an improved procedure, see: B. M. Trost, C. M. Older, *Organometallics* **2002**, *8*, 2455 – 2546.

[7] B. M. Trost, M. Machacek, M. J. Schnaderbeck, *Org. Lett.* **2000**, *2*, 1761 – 1764.

[8] W. P. Weber, *Silicon Reagents for Organic Synthesis*, Springer, Berlin, **1983**.

[9] Other dual transition metal sequences: N. Jeong, S. Deok, J. Y. Shin, *J. Am. Chem. Soc.* **2000**, *122*, 10220 – 10221; T. Doi, M. Kobuko, K. Yamamoto, T. Takahashi, *Org. Syn.* **1998**, *63*, 428 – 429; a recent example of catalytic sequences with Ru-catalyzed ene–yne coupling: F. Lopez, L. Castedo, J. L. Mascarenas, *J. Am. Chem. Soc.* **2002**, *124*, 4218 – 4219.

[10] B. M. Trost, P. Fraisse, Z. T. Ball, *Angew. Chem.* **2002**, *114*, 1101 – 1103; *Angew. Chem. Int. Ed.* **2002**, *41*, 1059 – 1061.

[11] K. Takahashi, A. Miyake, G. Hata, *Bull. Chem. Soc. Jpn.* **1972**, *45*, 230 – 236; K. Takahashi, A. Miyake, G. Hata, *Bull. Chem. Soc. Jpn.* **1973**, *46*, 1012 – 1013; D. G. Brady, *Chem. Commun.* **1970**, 434 – 435; I. Onoue Moritani, S. I. Murahashi, *Tetrahedron Lett.* **1977**, 121 – 124; J. C. Fiaud, A. Hibon de Gournay, M. Larchevegere, H. B. Kagan, *J.*

 © 2002 WILEY-VCH Verlag GmbH & Co. KGaA, Weinheim 0044-8249/02/4124-4696 $ 20.00+.50/0

Organomet. Chem. **1978**, *154*, 175–185; J. Tsuji, Y. Kobayashi, T. Takahashi, *Tetrahedron Lett.* **1980**, *21*, 3393–3394; for a review see: B. M. Trost, T. R. Verhoeven in *Comprehansive Organometalic Chemistry, Vol. 8*, 1st ed. (Eds.: G. Wilkinson, F. G. A. Stone, E. Abel), Pergamon, Oxford, **1982**, p. 799–938.

[12] This compound has been fully characterized by spectroscopic methods and the elemental composition has been established by high-resolution mass spectrometry and/or combustion analysis.

[13] T. Fukayama, C. K. Jow, M. Cheung, *Tetrahedron Lett.* **1995**, *36*, 6373–6374; T. Fukuyama, M. Cheung, C. K. Jow, ; Y. Hidai, T. Kan, *Tetrahedron Lett.* **1997**, *38*, 5831–5834.

[14] B. M. Trost, *Acc. Chem. Res.* **1996**, *29*, 355–364.

[15] B. M. Trost, F. D. Toste, *J. Am. Chem. Soc.* **1999**, *121*, 4545–4554.

[16] Simple alkyl alcohol nucleophiles can be used if the boron cocatalyst turns the intermolecular delivery into an intramolecular one: B. M. Trost, E. MacEachern, F. D. Toste, *J. Am. Chem. Soc.* **1998**, *120*, 815–816.

[17] B. M. Trost, F. D. Toste, *J. Am. Chem. Soc.* **1998**, *120*, 12702–12703.

[18] For a notable exception see: F. E. McDonald, A. D. Singhi, *Tetrahedron Lett.* **1997**, *38*, 7683–7686.

[19] The assignment of relative configuration was straightforward by NMR spectroscopy. Since the absolute stereochemistry of the starting substrate is known, the absolute configuration of the newly created allylic stereogenic center is also known. These stereochemical assignments are furthermore consistent with our mnemonic and with those made in Table 1.

General Synthesis of Semiconductor Chalcogenide Nanorods by Using the Monodentate Ligand *n*-Butylamine as a Shape Controller**

Jian Yang,* Can Xue, Shu-Hong Yu,* Jing-Hui Zeng, and Yi-Tai Qian

Currently, research on fundamental properties and practical applications of nanomaterials are attracting much attention.[1] However, most studies have focused on the size effect of nanocrystals. In fact, the shape of semiconductor nanomaterials has considerable influence on physical properties and is also important in many potential applications, such as solar cells, light-emitting diodes, and scanning-microscopy probes.[2] In spite of this, since little is known about the mechanism of crystal growth of anisotropic nanocrystals, shape control of nanocrystals remains a challenge to synthetic chemists.[1c,3]

Over the past few years, remarkable progress has been made in the shape control of nanomaterials. Alivisatos et al. controlled the size and shape of CdSe nanocrystals in the presence of strong ligands.[4] This approach was extended to control the size and shape of magnetic cobalt nanocrystals.[5] Lieber et al. developed a laser-assisted catalytic growth (LCG) technique to synthesize a broad range of binary and ternary semiconductor nanowires by a vapor–liquid–solid (VLS) mechanism.[6] Highly crystalline III–V semiconductor nanowires were synthesized by a solution–liquid–solid (SLS) method introduced by Buhro et al.[7] Recently, Weller et al. grew ZnO nanorods by oriented attachment of small quasi-spherical particles by concentrating and refluxing a solution.[8] Very thin one- (1D) and two-dimensional (2D) $CdWO_4$ nanocrystals with controlled aspect ratios were conveniently fabricated at ambient temperature or by hydrothermal ripening.[9] However, to the best of our knowledge, a general route for the synthesis of various semiconductor chalcogenide nanorods under mild solution conditions has still not been realized.

We have successfully controlled the size and shape of semiconductor nanocrystals by means of solvothermal reactions.[10–12] In-depth studies on the formation processes of these nanorods provided useful guidelines for the preparation of 1D nanocrystals.[10,11] We found that the anisotropic nature of the building blocks in the crystal structure, which are infinite linear chains in the case of M_2S_3 (M = Sb, Bi), plays a crucial role in the formation of nanorods.[11,12] In other words, this 1D growth of nanocrystals is actually the outward embodiment of the internal crystal structure.

The temporal evolution of CdS nanocrystals in solvothermal reactions demonstrated that ethylenediamine (en) molecules adsorbed on the surface of CdS play a critical role in the formation of nanorods.[10] FTIR spectra of these en molecules show that they are not in chelating (*cis*) configuration but in *trans* configuration. Reetz et al. reported that a nonchelating coordination mode of α-hydroxycarboxylates on a metal surface is likely to be the morphology-determining factor in shape-selective preparation.[13] However, on the basis of IR data alone, it is difficult to judge whether the mode of coordination between Cd^{2+} on the surface and en molecules is monodentate (Scheme 1a) or bridging (Scheme 1b), although it is possible that the en molecules in both cases are in the *trans* configuration.

Because *n*-butylamine has only one anchor atom, its coordination mode with metal ions must be monodentate (Scheme 1c), and hence we employed it as solvent to clarify this point. First, CdS nanocrystals were chosen as the target to examine whether the same reaction in a monodentate ligand can produce nanorods. In the IR spectrum of the as-prepared CdS nanocrystals, the characteristic absorption peak at 1573.0 cm^{-1} can be unambiguously assigned to the NH_2 bending vibration, which is shifted to lower frequency relative to that of pure *n*-butylamine[14] (see Supporting Information). A red shift of the C–N bending vibration resulting from

[*] Dr. J. Yang,[+ ++] Dr. S.-H. Yu,[++] Mr. C. Xue, Dr. J.-H. Zeng, Prof. Y.-T. Qian
Department of Chemistry and Structure Research Laboratory
University of Science and Technology of China
Hefei, Anhui 230026 (P. R. China)
Fax: (+86) 551-360-7402
E-mail: jyang2000@ustc.edu.cn
shyu@ustc.edu.cn

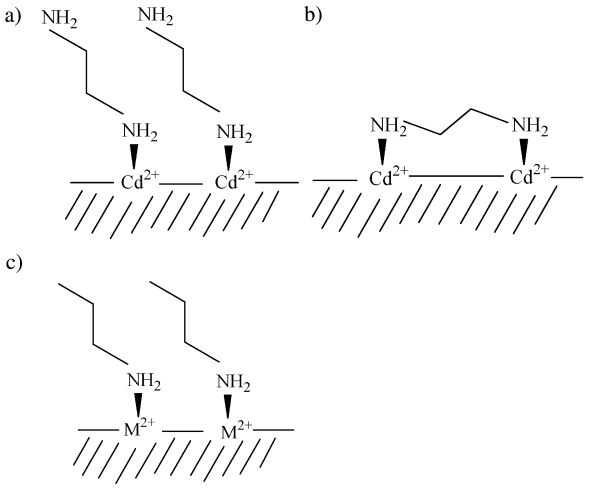
[+] Present address: Department of Chemistry
National Taiwan Normal University
Tingchow Road, Sec. 4, 88, Taipei 116 (R. O. C.)

[++] Present address: Max Planck Institute of Colloids and Interfaces
Department of Colloid Chemistry
MPI Research Campus Golm
14424, Potsdam (Germany)

[**] We gratefully acknowledge the Chinese Natural Science Foundation for financial support. Beneficial discussion with Miss Xin-Yuan Liu and Dr. L. Song at USTC is appreciated.

Supporting information for this article is available on the WWW under http://www.angewandte.org or from the author.

 © 2002 WILEY-VCH Verlag GmbH & Co. KGaA, Weinheim 0044-8249/02/4124-4697 $ 20.00+.50/0



Scheme 1. Possible surface coordination modes: a) monodentate mode of en molecules; b) polydentate mode of en molecules; c) monodentate mode of *n*-butylamine.

coordination was also observed.[14] These results indicate that the N atom of *n*-butylamine is coordinated to metal ions on the surface of CdS nanocrystals.

The XRD pattern (Figure 1 a) of CdS obtained at 220 °C for 12 h can be identified as that of a hexagonal phase (JCPDS Card, No. 41-1049). The lattice constants calculated from this pattern ($a = 4.12$ Å, $c = 6.68$ Å) are in good agreement with the reported values. The crystal dimensions, which can be roughly estimated by using the Scherrer equation, are 50 and 9 nm based on (002) and (110) reflections, respectively. The large difference between the coherence lengths in the [002] and [110] directions implies an unusual shape of the products.[14] This result agrees well with that observed by TEM (Figure 1 b). Short nanorods, 7–10 nm in width and 30–55 nm in length can be readily observed. We believe that the abundance of (002) planes in and the anisotropic shape of the nanorods result in the remarkable increase in intensity and sharpening of the (002) reflection.[15]

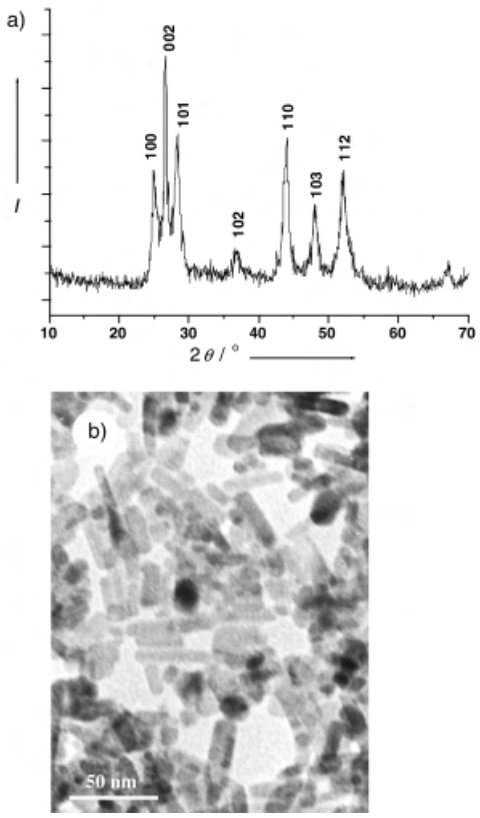


Figure 1. a) XRD pattern and b) TEM image of CdS nanocrystals obtained at 220 °C for 12 h.

Because the mode of coordination between *n*-butylamine and Cd^{2+} on the surface of CdS is monodentate (Scheme 1 c), the existence of rodlike nanoparticles in the products indicates that one anchor atom in a ligand is necessary and sufficient for the formation of nanorods, even though more anchor atoms may be present in a ligand. The close interaction between anchor atoms in ligands (Lewis base) and metal ions on the surface (Lewis acid) is another prerequisite for the formation of nanorods, because this weak interaction means that ligand molecules will not impose effective influence on the nucleation and growth of nanoparticles.[16] Altering the strength of interaction between ligands and metal ions could control the shape and size of various chalcogenides nanocrystals, as demonstrated previously in the synthesis of CdS nanocrystals.[16]

According to the above two conclusions, nanorods can be synthesized by choosing an appropriate monodentate ligand as solvent. If this is correct, it should be extendible to many other chalcogenides. *n*-Butylamine should be a suitable solvent because its NH_2 group can interact with many metal ions. PbSe and ZnSe are important semiconductors with extensive practical applications, but few strategies for the preparation and characterization of 1D nanocrystals thereof have been reported up to now.[6,17] Hence, we chose PbSe, ZnSe, and CdSe as targets for examining this deduction.

Figure 2 a presents the XRD pattern of CdSe nanocrystals obtained at 160 °C for 12 h. According to this pattern, the product consists of a mixture of hexagonal-phase CdSe (JCPDS Card, No. 8-459) and cubic-phase CdSe (JCPDS Card, No. 19-191). As shown in Figure 3 a, the as-prepared CdSe consists of nanorods 12–16 nm in width and 200–300 nm in length. A bundle of typical nanorods is shown in Figure 3 b. A selected-area electron diffraction (SAED) pattern (inset in Figure 3 b) on this sample revealed that the nanorods grew along the close-packing direction.

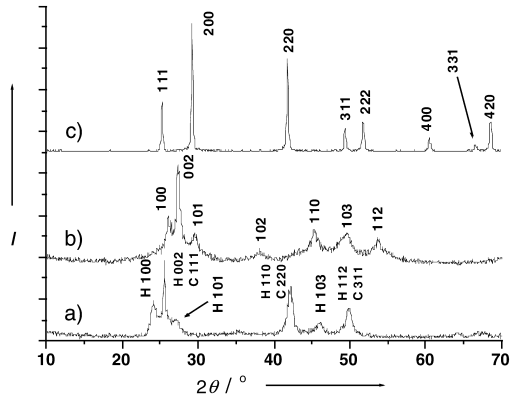


Figure 2. XRD pattern of a) CdSe nanocrystals (160 °C, 12 h, H: hexagonal, C: cubic), b) ZnSe nanocrystals (220 °C, 12 h), c) PbSe nanocrystals (80 °C, 12 h).

 © 2002 WILEY-VCH Verlag GmbH & Co. KGaA, Weinheim 0044-8249/02/4124-4698 $ 20.00+.50/0

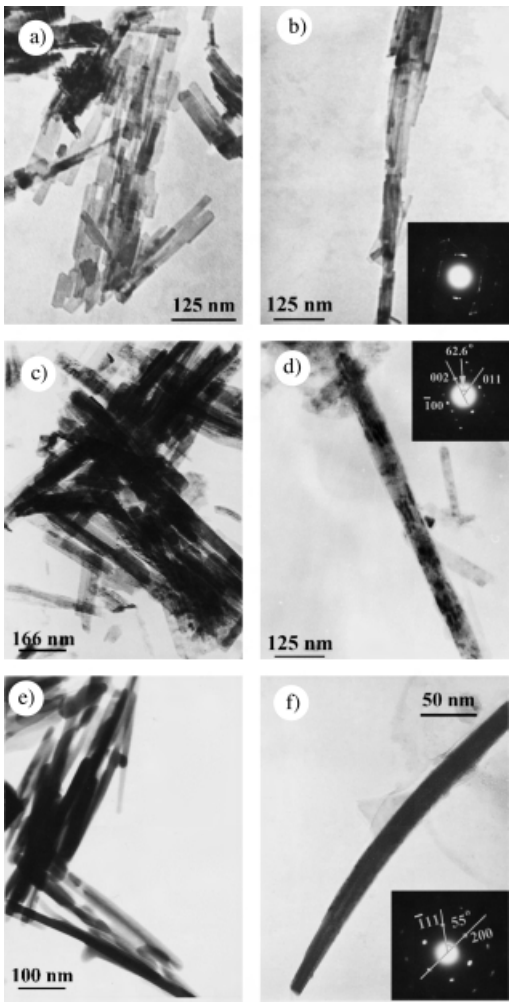


Figure 3. TEM images of a), b) CdSe nanocrystals (160 °C, 12 h); c), d) ZnSe nanocrystals, (220 °C, 12 h); e), f) PbSe nanocrystals (80 °C, 12 h).

The XRD pattern of ZnSe obtained at 220 °C for 12 h (Figure 2b) can be indexed as a hexagonal-phase ZnSe (JCPDS Card, No. 15-105). The lattice constants calculated from this pattern ($a = 3.98$ Å, $c = 6.53$ Å) are in accordance with the reported values. However, the unusually high intensity of the (002) reflection indicates preferential growth of nanocrystals.[10]

The TEM image in Figure 3c shows that the as-prepared ZnSe nanocrystals are nanorods with diameters in the range of 25–50 nm and lengths of up to 1 μm. A well-crystallized single ZnSe nanorod with the growth direction along the *c* axis is presented in Figure 3d. To the best of our knowledge, it is the first reported synthesis of wurtzite ZnSe nanorods. Elemental analysis by energy-dispersive spectroscopy (EDS) gave a molar Zn:Se ratio of 51.5:48.5, which coincides with the formula ZnSe. The Zn 2p and Se 3d lines in the XPS spectrum are at 1022.45 and 54.80 eV, respectively, consistent with the reported values of ZnSe[18] (see Supporting Information). Quantitative analysis of the peak areas gave a molar Zn:Se ratio of 1.04:1, which agrees well with the result from EDS.

The XRD pattern of PbSe obtained at 80 °C for 12 h (Figure 2c) can be indexed as a cubic-phase PbSe (JCPDS Card, No. 6-354). The lattice constant calculated from this pattern ($a = 6.12$ Å) is in good agreement with the reported value. The TEM image of the PbSe nanocrystals (Figure 3e) shows many nanorods 12–20 nm in width and 200–450 nm in length. Figure 3f shows a typical nanorod with the growth direction along ⟨200⟩, as revealed by the SAED pattern (inset in Figure 3f). Elemental analysis by EDS on this sample gave a molar ratio of Pb and Se close to the formula PbSe. The Pb 4f and Se 3d lines at 137.95 and 53.15 eV, respectively, in the XPS spectrum of this sample are consistent with the reported values of PbSe[18] (see Supporting Information).

The above-mentioned chalcogenide nanorods were synthesized under optimized experimental conditions. Any change in these conditions leads to a change in the size and shape of the product. The influence of reaction temperature on the product is larger than that of reaction time, which is illustrated here for CdS. As shown in Figure 4a, CdS powders prepared at 160 °C consist of irregular nanoparticles. At 220 °C, short nanorods with an aspect ratio of about 4–5 are obtained (Figure 4b). These results indicate that selecting the proper experimental conditions is also important for the formation of nanorods.

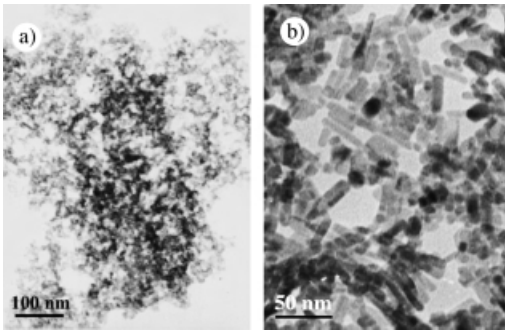


Figure 4. CdS nanocrystals prepared at different temperatures for 12 h: a) 160 °C; b) 220 °C.

In summary, the successful preparation of CdS nanorods in *n*-butylamine demonstrates that chalcogenide nanorods can be prepared by using a monodentate ligand as solvent. This result implies that one anchor atom in a ligand is necessary and sufficient for the formation of 1D nanocrystals, even though more anchor atoms may be present in a ligand. Close interaction between anchor atoms in ligands and metal ions on the surface is another prerequisite for nanorod formation, and *n*-butylamine is suitable for the syntheses of other chalcogenide nanorods, because its NH_2 group can interact with many different metal ions. The notion that solvothermal synthesis of nanorods can only be carried out in the presence of polydentate ligands must now be revised. Furthermore, this route not only provides a possible general route to other chalcogenide nanorods on a large scale, but also a guide for further rational design of 1D chalcogenides.

Experimental Section

All chemicals were of analytical grade and were used without further purification. 1.5 mmol of a metal salt ($Cd(NO_3)_2 \cdot 4H_2O$ for CdS, CdSe; $Zn(NO_3)_2 \cdot 6H_2O$ for ZnSe; $Pb(CH_3COO)_2 \cdot 3H_2O$ for PbSe) and 1.5 mmol

 © 2002 WILEY-VCH Verlag GmbH & Co. KGaA, Weinheim 0044-8249/02/4124-4699 $ 20.00+.50/0

of thiourea (or Se) were added to 20 mL of *n*-butylamine. The resulting solution was stirred for several minutes and then sealed in a stainless steel autoclave with a Teflon liner. This autoclave was maintained at the appropriate temperature (80–220 °C) for 12 h. Subsequently, the autoclave was allowed to cool to room temperature. The solution from the autoclave (except for CdS) was filtered and the obtained powders were washed with distilled water and absolute ethanol and dried in vacuum at 70 °C for 1 h. CdS powders were separated from the solution by centrifugation and washed with absolute ethanol.

X-ray powder diffraction patterns were obtained on a Japan Rigaku DMax-γA rotating-anode X-ray diffractometer with graphite-monochromatized $Cu_{K\alpha}$ radiation ($\lambda = 1.54178$ Å). TEM photographs and SAED patterns were recorded on a Hitachi Model H-800 transmission electron microscope at an accelerating voltage of 200 kV. The samples were dispersed in absolute ethanol in an ultrasonic bath. Then the suspensions were dropped onto Cu grids coated with amorphous carbon films. XPS spectra were recorded on a VEGSCALAB MKII X-ray photoelectron spectrometer with nonmonochromatized $Mg_{K\alpha}$ radiation as the excitation source. IR spectra were recorded on a Bruker Vector-22 FT-IR spectrometer from 4000 to 400 cm^{-1} at room temperature on KBr mulls.

Received: April 17, 2002
Revised: September 11, 2002 [Z19104]

[1] a) J. R. Heath, *Acc. Chem. Res.* **1999**, *32*, 388 (special issue on nanostructures); b) J. Hu, T. W. Odom, C. M. Lieber, *Acc. Chem. Res.* **1999**, *32*, 435; c) P. D. Yang, Y. Y. Wu, R. Fan, *Int. J. Nanoscience* **2002**, *1*, 1.
[2] a) W. U. Huynh, J. J. Dittmer, A. P. Alivisatos, *Science* **2002**, *295*, 2425; b) T. S. Ahmadi, Z. L. Wang, T. C. Green, A. Henglein, M. A. Elsayed, *Science* **1996**, *272*, 1924; c) H. Mattoussi, L. H. Radzilowski, B. O. Dabbousi, E. L. Thomas, M. G. Bawendi, M. F. Rubner, *J. Appl. Phys.* **1998**, *83*, 7965.
[3] Z. A. Peng, X. G. Peng, *J. Am. Chem. Soc.* **2001**, *123*, 1389.
[4] X. G. Peng, L. Manna, W. D. Yang, J. Wickham, E. Scher, A. Kadavanich, A. P. Alivisatos, *Nature* **2000**, *404*, 59.
[5] V. F. Puntes, K. M. Krishnan, A. P. Alivosatos, *Science* **2001**, *291*, 2115.
[6] X. F. Duan, C. M. Lieber, *Adv. Mater.* **2000**, *12*, 298.
[7] T. J. Trentler, K. M. Hickman, S. C. Goel, A. M. Viano, P. C. Gibbons, W. E. Buhro, *Science*, **1995**, *270*, 1791.
[8] C. Pacholski, A. Kornowski, H. Weller, *Angew. Chem.* **2002**, *114*, 1234; *Angew. Chem. Int. Ed.* **2002**, *41*, 1188.
[9] S. H. Yu, M. Antonietti, H. Cölfen, M. Giersig, *Angew. Chem.* **2002**, *114*, 2462; *Angew. Chem. Int. Ed.* **2002**, *41*, 2356.
[10] J. Yang, J. H. Zeng, S. H. Yu, L. Yang, G. E. Zhou, Y. T. Qian, *Chem. Mater.* **2000**, *12*, 3259.
[11] J. Yang, J. H. Zeng, S. H. Yu, L. Yang, Y. H. Zhang, Y. T. Qian, *Chem. Mater.* **2000**, *12*, 2924.
[12] S. H. Yu, L. Shu, J. Yang, Z. H. Han, Y. T. Qian, Y. H. Zhang, *J. Mater. Res.* **1999**, *14*, 4157.
[13] J. S. Bradley, B. Tesche, W. Busser, M. Maase, M. T. Reetz, *J. Am. Chem. Soc.* **2000**, *122*, 4631.
[14] X. Y. Jing, S. L. Chen, S. Y. Yao, *Practical Guide to Infrared Spectrum*, Tianjin Science and Technology Press, Tianjin, **1992**, Chap. 6.
[15] C. B. Murray, D. J. Norris, M. G. Bawendi, *J. Am. Chem. Soc.* **1993**, *115*, 8706.
[16] S. H. Yu, J. Yang, Z. H. Han, Y. Zhou, R. Y. Yang, Y. Xie, Y. T. Qian, Y. H. Zhang, *J. Mater. Chem.*, **1999**, *9*, 1283.
[17] W. Z. Wang, Y. Geng, Y. T. Qian, M. R. Ji, X. M. Liu, *Adv. Mater.*, **1998**, *10*, 1479.
[18] C. D. Wagner, W. W. Riggs, L. E. Davis, J. F. Moulder, G. E. Muilenberg, *Handbook of X-ray Photoelectron Spectroscopy*, Perkin-Elmer, Eden Prairie, MN, **1978**.

Electron-Transfer Dynamics of Cytochrome C: A Change in the Reaction Mechanism with Distance**

Jianjun Wei, Haiying Liu, Dimitri E. Khoshtariya, Hiromichi Yamamoto, Allison Dick, and David H. Waldeck*

Redox processes are ubiquitous in nature, and the understanding of electron transfer in complex systems, for example, biological structures such as proteins, membranes, and the photosynthetic reaction center, is an outstanding challenge. Here we provide new results on the electron-transfer dynamics of the protein cytochrome c as a function of distance from a metal electrode. Comparison of this distance-dependence with previous studies indicates that a conformationally gated mechanism involving a large amplitude protein motion is not operative, but a change in the electron-transfer mechanism occurs and is linked to the protein environment.

The redox protein cytochrome c is very well characterized and numerous studies of its electron transfer have been performed, both under homogeneous and heterogeneous conditions.[1] A number of research groups have immobilized cytochrome c on gold electrodes that are coated with a self-assembled monolayer (SAM) of -S-$(CH_2)_{n-1}$-COOH, presumably by binding to the protein's lysine groups.[2] The electronic coupling strength between the electrode and the protein can be varied by changing the length of the alkane chain. At large SAM thicknesses the electron-transfer rate constant declines exponentially with distance (electron tunneling mechanism), but it is distance-independent at lower thicknesses, hence there is a change in the rate-limiting step and the mechanism of reaction. More recently, mixed monolayer films of pyridine-terminated alkanethiols embedded in an alkanethiol diluent have been used to directly tether the heme to the surface.[3] This strategy for immobilization (Figure 1) should eliminate large-amplitude conformational motion of the protein on the surface of the SAM as a gating mechanism for the electron transfer, because the heme is directly linked to the alkanethiol tunneling barrier.

The immobilization of the cytochrome on the film has been demonstrated through electrochemical control experiments and by direct imaging by STM.[3b] The primary evidence for binding near the heme is the negative shift of the redox potential, relative to that in solution, and the differential adsorption strength of different functional end groups

[*] Prof. Dr. D. H. Waldeck, J. Wei, H. Liu, H. Yamamoto, A. Dick
Department of Chemistry
University of Pittsburgh
Pittsburgh, PA 15260 (USA)
Fax: (+1) 412–624–8611
E-mail: dave@pitt.edu

D. E. Khoshtariya
Institute of Molecular Biology and Biophysics
Georgian Academy of Sciences
Gotua 14, Tbilisi 380060 (Georgian Republic)

[**] We acknowledge partial support from the US-Israel BSF and the NSF-REU program at the University of Pittsburgh.

Supporting information for this article is available on the WWW under http://www.angewandte.org or from the author.

 © 2002 WILEY-VCH Verlag GmbH & Co. KGaA, Weinheim 0044-8249/02/4124-4700 $ 20.00+.50/0

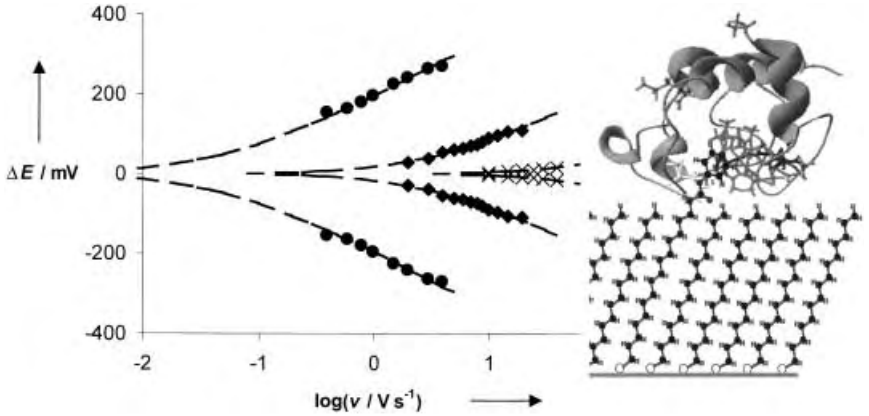


Figure 1. The dependence of the peak separation ΔE on the voltage scan rate ρ is shown for pyridine-terminated chains having lengths of 20 methylene groups (circles), 16 methylene groups (diamonds), and 6 methylene groups (×). In each case the data is fit to the Marcus model with a reorganization energy of 0.8 eV. A schematic diagram of the cytochrome immobilization strategy is shown on the right.

(nitriles, imidazole, and pyridine).[3b] The rate constants for electron-transfer between the Au electrode and the cytochrome c were determined by cyclic voltammetry.[3b] The composition of the mixed films (Table 1) consists of 3–4 % pyridine-terminated chains in a diluent of alkane-terminated chains,

Table 1. Rate-constant data for cytochrome c immobilized on pyridinylalkanethiols.[8]

System	k^0 [Hz]	No. trials
C6py/C5	1670 ± 60	2
C11py/C10	1150 ± 80	5
C12py/C11	783 ± 36	3
C16py/C15	43 ± 10	7
C20py/C19	0.50 ± 0.06	3
C22py/C21	0.032 ± 0.026	2

and the coverage of cytochrome corresponds to about 10 % of the pyridine sites, which is less than 1 % overall. The nearly ideal quality of the voltammograms stands in strong contrast to that reported with pure layers of pyridine-terminated alkanes,[3a] for which the voltammetry studies showed there to be severe asymmetry in the redox rates and significant inhomogeneity. The homogeneous behavior of the voltammetry that is observed for the mixed films indicates that the protein does not denature.[4] Spectroscopic studies are underway to characterize the adsorbed cytochrome and will be reported elsewhere.

Figure 1 shows the dependence of the voltammetric peak positions on the voltage scan rate for three different systems. The shift of the peak position with voltage scan rate is used to quantify the standard rate constant k^0 for electron transfer.[5] The eicosanethiol (C20) chain has the slowest k^0 value: its peaks move apart at lower scan rates than the peaks for shorter methylene chain lengths (C16 and C6). The dashed curves in this figure show the best fit to the Marcus theory model with a reorganization energy λ_o of 0.8 eV for each of the systems. The fits are not very sensitive to the value of the reorganization energy because the data do not extend to high overpotentials, for example, a λ_o value of 0.5 eV gives similar quality fits and a k^0 value that only differs by a few percent from those in Table 1.[5]

The thickness dependence of the k^0 value is summarized in Table 1 and plotted in Figure 2, together with earlier data for cytochrome c adsorbed on COOH-terminated SAMs. Both data sets obtained at large thicknesses display an exponential dependence on distance. The value of k^0 is proportional to the electronic coupling squared for nonadiabatic electron transfer [Eq. (1)]. $|V^0|^2$ is the electronic coupling

$$k^0_{NA} \propto |V|^2 = |V^0|^2 \exp(-\beta R) \quad (1)$$

matrix element at the minimum donor–acceptor separation distance and β is a characteristic decay factor.[6,7] The two

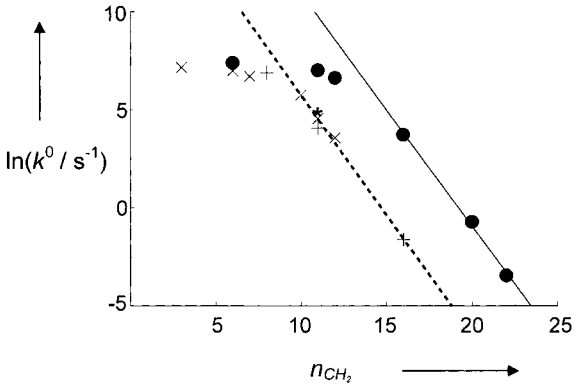


Figure 2. Plot of k^0 versus number of methylene groups for cytochrome c on SAM-coated gold electrodes (× from ref. [2c,d], + from ref. [2a,b], and ● from this work for COOH and · for pyridine-terminated layers). The lines are fits to Equation (1).

data sets (COOH and pyridinyl SAMs) should have the same distance dependence in the nonadiabatic ("tunneling") regime since the distance in both cases is being changed by the number of methylene units in the tether. A best fit to the rate data at long distance gives a β value of 1.22 per CH_2 group for the COOH-terminated SAMs and 1.19 per CH_2 group for the pyridine-terminated SAMs. Although the slopes are similar, the absolute value of the rate constant is significantly larger (at a given methylene number) for the pyridine-terminated tethers, which indicates a larger tunneling probability (electronic coupling).

Both data sets show a plateau region at short donor–acceptor separations, however, the plateau region for the pyridine-terminated SAMs extends to larger film thicknesses (about 12 methylene groups). The maximum rate constants for both film types are similar (the hexyl chains have a rate constant of about 1100 Hz for the COOH-terminated SAMs and about 1700 Hz for the pyridine-terminated SAMs) and display plateau behavior. Previous research groups[2] explained the plateau behavior as resulting from a change in the rate-determining step from electron tunneling at large distances to conformational rearrangement of the protein–

 © 2002 WILEY-VCH Verlag GmbH & Co. KGaA, Weinheim 0044-8249/02/4124-4701 $ 20.00+.50/0

SAM system to a redox-active state at short thickness; this situation is analogous to the conformationally gated mechanism used to describe protein–protein electron transfer. Since the pyridine ring binds near the heme, the conformationally gated mechanism would need to involve local changes near the redox center, rather than large-amplitude motion of the protein. In addition, the alternating current impedance and cyclic voltammetry data indicate a typical charge-transfer step[2,5] and do not support a more complex mechanism involving a conformational rearrangement step. Direct spectroscopic detection of redox species immobilized on the SAMs terminated with carboxylic acids[9] support the view that the conformational changes are small. In summary, the mode of binding restricts the type of conformational change that can be linked to the electron-transfer process at short distances, which implies that large-amplitude motion of the protein is not involved.

Murgida and Hildebrandt[9] observed a significant deuterium isotope effect for the electron-transfer rate constant on thin (C2 and C3) films and suggested that proton transfer may be coupled to the electron transfer or that rearrangement of the hydrogen-bonded network in the protein may constitute a rate-limiting step. In addition, they observed a thickness dependence for the isotope effect and postulated that the change in mechanism is modulated by the applied electric field. Thus, the influence of a D_2O buffer on the electron-transfer rate constant was evaluated for the C16 and C11 pyridinyl systems. The rate constant for the C16-pyridinal tether was 50 Hz, which is very similar to that observed in the H_2O buffer. The rate constant for the C11-pyridinyl tether was 900 Hz, which is a factor of 0.78 smaller than that found in the H_2O buffer. These findings are consistent with those of Murgida and Hildebrandt.

The large difference in the extent of the plateau region and the higher electron-transfer rates for the pyridine system (see Figure 2) is consistent with a larger electronic coupling for the pyridine-immobilized cytochrome c than for the carboxylate-immobilized cytochrome c. The enhanced electronic coupling suggests that the change in the electron-transfer mechanism may be linked to the change in electronic coupling with distance from the electrode. In the adiabatic, or strong coupling, regime the rate constant $k_A{}^0$ does not display an exponential distance dependence, but does depend on the polarization relaxation in the medium.[10] The simple limit is given by Equation (2), where the activation free energy is

$$k_A^0 = \frac{1}{\tau_{eff}}\sqrt{\frac{\lambda_o}{\pi^3 RT}}\exp\left(-\frac{\Delta G_a^*}{RT}\right) \quad (2)$$

given by Equation (3) when the free energy of the reaction is zero. The reorganization energy λ_o is difficult to calculate

$$\Delta G_a^* = \frac{\lambda_o}{4} - |V| \quad (3)$$

since it depends in a detailed manner on the protein structure,[11a] the SAM-coated electrode,[11b] and the solvent. The characteristic polarization relaxation time τ_{eff} gives a measure of the time-scale for the response of the surrounding medium (the solvent molecules, protein interior, etc.[10]) to the change in the charge distribution associated with the electron transfer, and will depend on detailed properties of the SAM-associated protein. A simple approximation treats this relaxation time as the longitudinal dielectric relaxation, which in a Debye dielectric continuum model is given by Equation (4). τ_L is the longitudinal relaxation time of the solvent

$$\tau_{eff} \approx \tau_L = \left(\frac{\varepsilon_\infty}{\varepsilon_s}\right)\frac{3\eta V_m}{RT} \quad (4)$$

polarization, η is the solvent shear viscosity, V_m is the molar volume, ε_s is the static dielectric constant, and ε_∞ is the high-frequency dielectric constant. Hence, the experimental characteristic of electron transfer in the adiabatic limit is a friction-dependent rate constant,[12] and the rate constant for the cytochrome c in the plateau region displays a viscosity dependence.[2d,13] This model is also consistent with the results obtained in D_2O, since the D_2O-"hydrated" protein would have a different relaxation time than the H_2O-hydrated protein and D_2O has a slower dielectric relaxation time than H_2O. Although the pyridinyl system has a larger rate constant in the plateau region than that of the COOH system, their similarity suggests that the free energies of activation in the two cases are similar, despite the different manner of protein immobilization. This observation requires that any significant changes in the reorganization energy between the two systems must be compensated for by changes in the polarization relaxation time and the electronic coupling magnitude, which also modifies the relaxation time.[10,12] A more detailed study of this correspondence is being pursued since the current method does not provide a precise measurement of λ_o.

This work demonstrates how a new strategy for immobilizing cytochrome c on electrode surfaces which directly tethers the redox-active site to the metal electrode can be used to explore the change in the mechanism of electron transfer with distance between the protein and the electrode. The distance was changed through the variation in the number of methylene groups in the tether, but differs from earlier studies by the nature of the SAM–cytochrome interaction. The difference in binding modes provides a stronger electronic coupling for the pyridinyl systems than for the COOH system and changes the SAM thickness at which the onset of a plateau (nonexponential dependence on distance) is observed. This circumstance also causes different rate constants in the tunneling regime for the two different binding modes (but same number of methylene groups in the chain). These findings indicate that electron transfer at short distances need not be linked to a large-amplitude conformational change of the protein with respect to the electrode surface. A change in the electron-transfer mechanism that arises from the enhanced electronic coupling at short distance is also consistent with the observations.

Received: May 6, 2002
Revised: September 11, 2002 [Z19233]

[1] a) M. Fedurco, *Coord. Chem. Rev.* **2000**, *209*, 263; b) R. A. Scott, *Cytochrome C: A Multidisciplinary Approach* (Eds.: R. A. Scott, A. G. Mauk), University Science Books, Sausalito, **1996**, p. 515.

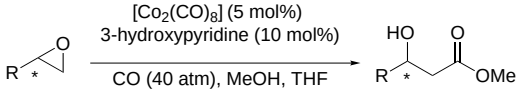
 © 2002 WILEY-VCH Verlag GmbH & Co. KGaA, Weinheim 0044-8249/02/4124-4702 $ 20.00+.50/0

[2] a) M. J. Tarlow, F. F. Bowden, *J. Am. Chem. Soc.* **1991**, *113*, 1847; b) S. Song, R. A. Clark, F. F. Bowden, M. J. Tarlow, *J. Phys. Chem.* **1993**, *97*, 6564; c) Z. Q. Feng, S. Imabayashi, T. Kakuichi, K. Niki, *J. Chem. Soc. Faraday Trans.* **1997**, *93*, 1367; d) A. Avila, B. W. Gregory, K. Niki, T. M. Cotton, *J. Phys. Chem. B* **2000**, *104*, 2759.
[3] a) H. Yamamoto, H. Liu, D. H. Waldeck, *Chem. Commun.* **2001**, 1032; b) J. Wei, H. Liu, A. Dick, H. Yamamoto, Y. He, D. H. Waldeck, *J. Am. Chem. Soc.* **2002**, *124*, 9591.
[4] a) F. A. Armstrong, *J. Chem. Soc. Dalton Trans.* **2002**, 661; b) earlier work that immobilized cytochrome c onto pure films of pyridine-terminated alkanes showed asymmetric redox kinetics and inhomogeneity in the redox potential; see ref. [3a].
[5] a) A. M. Napper, H. Liu, D. H. Waldeck, *J. Phys. Chem. B* **2001**, *105*, 7699; b) L. Tender, M. T. Carter, R. W. Murray, *Anal. Chem.* **1994**, *66*, 3173; c) K. Weber, S. E. Creager, *Anal. Chem.* **1994**, *66*, 3166; d) M. J. Honeychurch, *Langmuir* **1999**, *15*, 5158.
[6] H. O. Finklea, *Electroanal. Chem.* **1996**, *19*, 109.
[7] W. B. Curry, M. D. Grabe, I. V. Kurnikov, S. S. Skourtis, D. N. Beratan, J. J. Regan, A. J. A. Aquino, P. Beroza, and J. N. Onuchic, *J. Bioenerg. Biomembr.* **1995**, *27*, 285.
[8] The reported error is two standard deviations. In each case the SAM is a pyridine-terminated alkanethiol (for example, C6py has six CH_2 groups) immersed in an alkanethiol diluent. See ref. [3b] for details of film composition and characterization.
[9] D. H. Murgida, P. Hildebrandt, *J. Am. Chem. Soc.* **2001**, *123*, 4062.
[10] a) L. D Zusman. , *Z. Phys. Chem.* **1994**, *186*, 1; b) J. N. Onuchic, D. N. Beratan, J. J. Hopfield, *J. Phys Chem.* **1986**, *90*, 3707.
[11] a) I. Muegge, P. X. Qi, A. J. Wand, Z. T. Chu, A. Warshel, *J. Phys. Chem. B.* **1997**, *101*, 825; b) Y. P. Liu, M. D. Newton, *J. Phys. Chem.* **1994**, *98*, 7162.
[12] a) D. E. Khoshtariya, T. D. Dolidze, L. D. Zusman, D. H. Waldeck *J. Phys. Chem. A* **2001**, *105*, 1818; b) M. J. Weaver, *Chem. Rev.* **1992**, *92*, 463.
[13] J. J. Wei, H. Liu, D. H. Waldeck, unpublished results.

Enantiopure β-Hydroxy Morpholine Amides from Terminal Epoxides by Carbonylation at 1 atm**

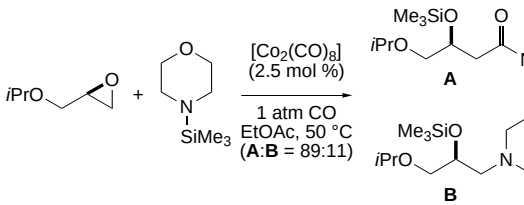
Steven N. Goodman and Eric N. Jacobsen*

As a consequence of the recently developed hydrolytic kinetic resolution (HKR) reaction,[1] a wide variety of terminal epoxides are now readily accessible in enantiopure form. The synthetic utility of this family of chiral building blocks is certainly well established, yet it is likely that new and valuable reactivity remains to be uncovered. In that context, we have sought to develop practical methodology to effect elaboration of these compounds to more highly functionalized chiral intermediates. In 1999, we reported the $[Co_2(CO)_8]$-catalyzed carbonylation of enantiomerically enriched epoxides under 40 atm of CO, to afford β-hydroxy methyl esters in good yield [Eq. (1)].[2] However, the relatively high CO pressure precludes its widespread application in laboratory and industrial settings, and the scope of nucleophiles that could be employed to trap the acylcobalt intermediate was in fact quite limited.[3] As a result, we became interested in devising complementary methodology that would afford general access to broadly useful β-hydroxy carbonyl derivatives under mild conditions.



(1)

The accelerating effect of silyl groups on cobalt-catalyzed carbonylation reactions has been documented.[4] Most relevant to the present study, Tsuji and co-workers described the carbonylative opening of racemic epoxides by *N*-silylamines at low pressures of CO.[5] We sought to extend this methodology to the direct generation of morpholine amides, which, like Weinreb amides, are intermediates with widespread utility in synthesis because of their ability to effect clean acyl transfer to a variety of nucleophiles without product overreduction.[6,7] The reaction of isopropyl glycidyl ether with 4-(trimethylsilyl)morpholine in the presence of 2.5 mol% $[Co_2(CO)_8]$ provided the anticipated β-silyloxy morpholine amide derivative in 58% yield under 1 atm of CO. However, approximately 30% of the crude product mixture was identified as the corresponding amine-opened product.[8] Variation of solvent and reaction conditions provided slight improvement in selectivity, with the use of ethyl acetate and a reaction temperature of 50°C affording best results (80:20 amide:amine ratio). Selectivity for the carbonylation pathway was improved further by carrying out the reaction under scrupulously anhydrous conditions, leading to product formation in an 89:11 amide:amine ratio [Eq. (2)].



(2)

Despite substantial effort to optimize the reaction conditions further, it was not possible to suppress formation of the amine by-product completely. Fortunately, a workup procedure involving simple treatment of the crude product mixture with aqueous acid effectively removed both the amine and the cobalt catalyst. This practical protocol was applied successfully to a variety of epoxides to afford synthetically useful yields of β-hydroxy morpholine amides isolated in >95% purity without chromatography (Table 1).

The transformation is compatible with a variety of functional groups, including ethers, olefins, halides, and esters. Reactions proceeded with no compromise of the optical purity of the starting epoxides, and carbonylations were completely regioselective for the terminal position. However, epoxides bearing sp^2-hybridized α-carbon substituents fared

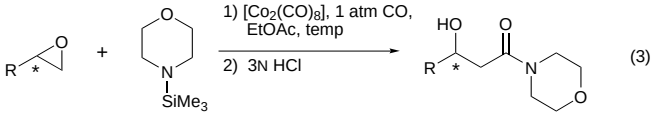
[*] Prof. E. N. Jacobsen, Dr. S. N. Goodman
Department of Chemistry and Chemical Biology
Harvard University
Cambridge, MA 02138 (USA)
Fax: (+1) 617-496-1880
E-mail: jacobsen@chemistry.harvard.edu

[**] We gratefully acknowledge the NIH (GM-59316) for support of this research.

Supporting information for this article is available on the WWW under http://www.angewandte.org or from the author.

 © 2002 WILEY-VCH Verlag GmbH & Co. KGaA, Weinheim 0044-8249/02/4124-4703 $ 20.00+.50/0

Table 1. Carbonylation of enantioenriched terminal epoxides to generate morpholinoamides [Eq. (3)].[a]

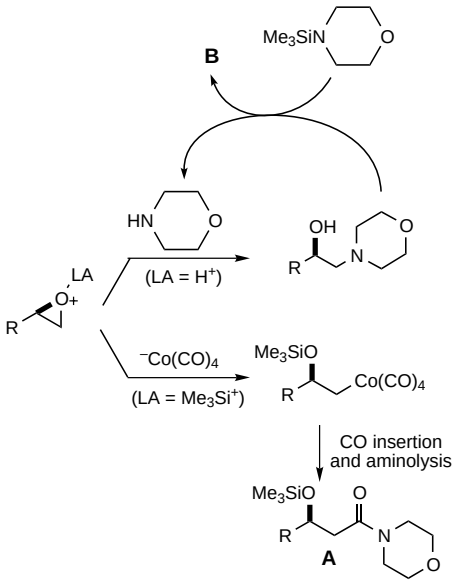


Entry	R	T [°C]	t [h]	Crude ratio [amide:amine]	Yield[b] [%]
1	CH_3	25	12	87:13	67
2	CH_3	25	12	86:14	72[c]
3	CH_2CH_3	25	12	89:11	82
4	$(CH_2)_3CH_3$	50	5	92:8	85
5[d]	$CH_2{=}CHCH_2CH_2$	25	24	88:12	80
6	iPrOCH_2	50	4	89:11	85
7[d]	BnOCH_2	50	8	83:17	79
8[d]	ClCH_2	25	12	80:20	75
9[d]	nPrCO_2CH_2	50	12	80:20	56[e]

[a] All reactions were performed with enantioenriched epoxide (1 mmol; > 99% *ee*) and 4-(trimethylsilyl)morpholine (1.3 mmol) in EtOAc (1.5 mL), using 2.5 mol% [$Co_2(CO)_8$], unless noted otherwise. [b] Yield of pure product after aqueous workup. [c] Reaction performed on 5 mmol of epoxide; product isolated as the trimethylsilyl ether by distillation of the crude mixture. [d] 5 mol% [$Co_2(CO)_8$] was used. [e] Product isolated by column chromatography.

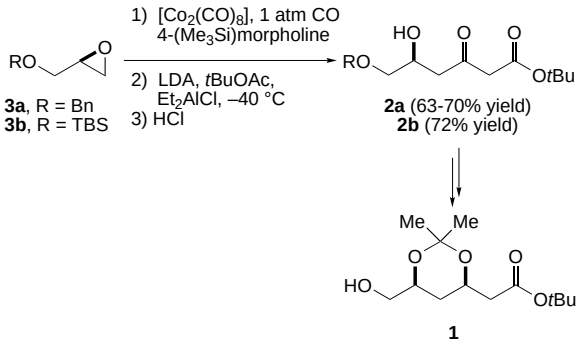
poorly as substrates: methyl glycidate and 3,4-epoxybutanone reacted slowly, affording significant amounts of amine by-product; styrene oxide underwent ring-opening with poor regioselectivity; and butadiene monoepoxide was unreactive.

We propose that amide and amine products are generated by distinct catalytic mechanisms (Scheme 1).[9] The amide pathway is most likely promoted by the catalyst $[R_2N(SiMe_3)_2]^+[Co(CO)_4]^-$, as proposed initially by Tsuji and co-workers (Scheme 1, LA = $SiMe_3$ or possibly $R_2N(SiMe_3)_2$).[5] This complex bears both Lewis acidic and strongly nucleophilic components well-suited for epoxide activation and ring-opening. In contrast, amine formation is attributable to the presence of trace unsilylated morpholine. Thus, addition of catalytic amounts of morpholine or water (to hydrolyze 4-(trimethylsilyl)morpholine in situ) led to large increases in the amount of amine by-product formation (up to 31:69 ratio of amide:amine with 20 mol% water). It is likely that catalysis by a Brønsted acid such as $[R_2NH_2]^+[Co(CO)_4]^-$ gives rise to the amine product.[10] As expected, treatment of epoxides such as isopropyl glycidyl ether with morpholine and a catalytic amount of morpholinium hydrochloride led to exclusive formation of the amine adduct at room temperature.



Scheme 1. Pathway to amide and amine products.

The utility of the morpholine amide products in acyl transfer reactions was illustrated in a concise synthesis of β-ketoester **2,** a known intermediate in the synthesis of **1** (Scheme 2). Acetonide **1** is the standard building block for



Scheme 2. Synthesis of β-ketoester **2**, an intermediate in the synthesis of acetonide **1**.

HMG-CoA reductase inhibitors such as compactin, mevinolin, and synthetic analogues such as Lipitor and Crestor. We envisioned that β-ketoester **2** could be obtained from the morpholine amide prepared from glycidyl ether derivatives by a simple acetate enolate homologation.

Unfortunately, no general method for adding enolates to amides was available.[11] Although the addition of lithium enolates to Weinreb amides is well-precedented,[12] morpholine amides are less electrophilic and were found to be unreactive toward these nucleophiles. In contrast, use of more reactive aluminum enolates afforded the corresponding δ-hydroxy-β-ketoesters cleanly. In a one-pot procedure, benzyl glycidyl ether **3a** was transformed to the corresponding morpholine amide, then treated with the aluminum enolate of *t*BuOAc to afford **2a** in 63–70% overall yield (Scheme 2). This reaction sequence was performed with resolved epoxide

 © 2002 WILEY-VCH Verlag GmbH & Co. KGaA, Weinheim 0044-8249/02/4124-4704 $ 20.00+.50/0

on multigram scale to provide enantiopure **2a**. Similar results were obtained for *tert*-butyldimethylsilyl (TBS) glycidyl ether **2b** (72% yield of isolated product over two steps). Given the ready availability of enantiopure terminal epoxides[1] and the relative simplicity and efficiency of the overall sequence, this route appears to provide an attractive alternative to existing routes to **2**.[13]

In summary, we have developed a mild and efficient carbonylation protocol for the conversion of optically active epoxides to β-hydroxy morpholine amides. The methodology is effective with a variety of epoxides obtained readily by the HKR, and pure products can easily be isolated simply by treatment of the crude product mixture with aqueous acid. In addition, the discovery that aluminum enolate derivatives add cleanly to morpholine amides provides a valuable new approach for the preparation of synthetically valuable δ-hydroxy-β-ketoesters.

Experimental Section

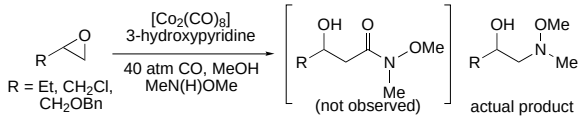
General carbonylation procedure**:** $[Co_2(CO)_8]$ (8.5 mg, 0.025 mmol) under a nitrogen atmosphere was added to an oven-dried 10-mL Schlenk flask equipped with a stirbar and septum. The atmosphere was exchanged for CO (vacuum/fill 3×) from a double balloon affixed to the stopcock sidearm. Ethyl acetate (1.5 mL) was added, and the solution stirred for ten minutes. 4-(Trimethylsilyl)morpholine (0.23 mL, 1.3 mmol) and epoxide (1.0 mmol) were added sequentially, and the septum was replaced with a greased glass stopper. The reaction mixture was stirred at the desired temperature for the specified length of time, at which point 3N HCl (aq) (1.5 mL) was added to the reaction mixture at room temperature. After the mixture had been stirred for ten minutes, the layers were separated, the aqueous layer was extracted with EtOAc (15 mL), and the combined organic layers were washed with brine (2 mL). The aqueous layers were further extracted with EtOAc (2×15 mL each). The combined organic layers were dried over Na_2SO_4 and the solvent was removed under reduced pressure to provide the β-hydroxy morpholine amide as a clear to yellow oil.

Received: September 2, 2002 [Z50084]

[1] a) M. Tokunaga, J. F. Larrow, F. Kakiuchi, E. N. Jacobsen, *Science* **1997**, *277*, 936–938; b) S. E. Schaus, B. D. Brandes, J. F. Larrow, M. Tokunaga, K. B. Hansen, A. E. Gould, M. E. Furrow, E. N. Jacobsen, *J. Am. Chem. Soc.* **2002**, *124*, 1307–1315.

[2] a) K. Hinterding, E. N. Jacobsen, *J. Org. Chem.* **1999**, *64*, 2164–2165; For earlier, related work, see: b) E. Drent, E. Kragtwijk, Eur. Pat. Appl. 577206 **1994**; [*Chem. Abstr.* **1994**, *120*, 191517c]; c) J. L. Eisenmann, R. L. Yamartino, J. F. Howard, Jr., *J. Org. Chem.* **1961**, *26*, 2102–2104.

[3] In the original report,[2] we noted in a footnote preliminary results indicating that Weinreb amides could be generated directly from terminal epoxides by carrying out the carbonylation in the presence of MeN(H)OMe. Upon closer examination, we have found that the products obtained under those conditions were misassigned and are in fact the corresponding amino alcohols..



[4] For examples of epoxide ring-opening reactions mediated by $[Co_2(CO)_8]$ in the presence of silanes, see: a) T. Murai, E. Yasui, S. Kato, Y. Hatayama, S. Suzuki, Y. Yamasaki, N. Sonoda, H. Kurosawa, Y. Kawasaki, S. Murai, *J. Am. Chem. Soc.* **1989**, *111*, 7938–7946; b) T. Murai, S. Kato, S. Murai, T. Toki, S. Suzuki, N. Sonoda, *J. Am. Chem. Soc.* **1984**, *106*, 6093–6095.

[5] a) Y. Watanabe, K. Nishiyama, K. Zhang, F. Okuda, T. Kondo, Y. Tsuji, *Bull. Chem. Soc. Jpn.* **1994**, *67*, 879–882; b) Y. Tsuji, M. Kobayashi, F. Okuda, Y. Watanabe, *J. Chem. Soc. Chem. Commun.* **1989**, 1253–1254.

[6] Numerous examples of the utility of morpholine amides have been reported. Organolithium/Grignard additions: a) R. Martín, P. Romea, C. Tey, F. Urpí, J. Vilarrasa, *Synlett* **1997**, 1414–1416; b) S. Sengupta, S. Mondal, D. Das, *Tetrahedron Lett.* **1999**, *40*, 4107–4110. Methylcerium addition: c) M. Kurosu, Y. Kishi, *Tetrahedron Lett.* **1998**, *39*, 4793–4796. $LiAlH_4$ reductions: d) C. Douat, A. Heitz, J. Martinez, J.-A. Fehrentz, *Tetrahedron Lett.* **2000**, *41*, 37–40. For a recent comparison of Weinreb and morpholine amides, see: e) M. M. Jackson, C. Leverett, J. F. Toczko, J. C. Roberts, *J. Org. Chem.* **2002**, *67*, 5032–5035.

[7] Generally, morpholine is easier to handle and significantly less expensive than MeN(H)OMe·HCl, and 4-(trimethylsilyl)morpholine is available commercially (Aldrich) or can be prepared readily from morpholine and Me_3SiCl (see Supporting Information).

[8] Application of the conditions documented by Tsuji and co-workers led, in our hands, to formation of significant levels of amine by-products. This reactivity pathway was not noted in the original report.

[9] For recent mechanistic discussions of epoxide carbonylations directed toward the preparation of β-lactones, see: a) V. Mahadevan, Y. D. Y. L. Getzler, G. W. Coates, *Angew. Chem.* **2002**, *114*, 2905–2908; *Angew. Chem. Int. Ed.* **2002**, *41*, 2781–2784; b) Y. D. Y. L. Getzler, V. Mahadevan, E. B. Lobkovsky, G. W. Coates, *J. Am. Chem. Soc.* **2002**, *124*, 1174–1175.

[10] The nucleophilicity of $^-Co(CO)_4$ should be attenuated in this complex due to strong association with the ammonium counterion. This is not expected with $[R_2N(SiMe_3)_2]^+[Co(CO)_4]^-$.

[11] M. Yamaguchi, I. Hirao, *J. Org. Chem.* **1985**, *50*, 1975–1977.

[12] J. A. Turner, W. S. Jacks, *J. Org. Chem.* **1989**, *54*, 4229–4231.

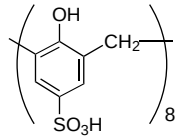
[13] For a review of synthetic approaches to the HMG-CoA reductase inhibitors up to 1986, see: a) T. Rosen, C. H. Heathcock, *Tetrahedron* **1986**, *42*, 4909–4951; for selected, more recent examples of routes to these intermediates, see: b) G. Beck, H. Jendralla, K. Kesseler, *Synthesis* **1995**, 1014–1018; c) R. A. Singer, E. M. Carreira, *J. Am. Chem. Soc.* **1995**, *117*, 12360–12361; d) J. Krüger, E. M. Carreira, *J. Am. Chem. Soc.* **1998**, *120*, 837–838; e) D. A. Evans, M. C. Kozlowski, J. A. Murry, C. S. Burgey, K. R. Campos, B. T. Connell, R. J. Staples, *J. Am. Chem. Soc.* **1999**, *121*, 669–685; f) "Synthesis of the Common Lactone Moiety of HMG-CoA Reductase Inhibitors": I. M. McFarlane, C. G. Newton, P. Pitchen in *Process Chemistry in the Pharmaceutical Industry* (Ed.: K. G. Gadamasetti), Dekker, New York, **1999**, pp. 243–259.

 © 2002 WILEY-VCH Verlag GmbH & Co. KGaA, Weinheim 0044-8249/02/4124-4705 $ 20.00+.50/0

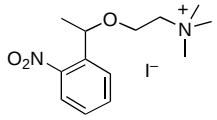
Mutually Induced Formation of Host–Guest Complexes between *p*-Sulfonated Calix[8]arene and Photolabile Cholinergic Ligands**

Alexandre Specht, Philippe Bernard, Maurice Goeldner,* and Ling Peng*

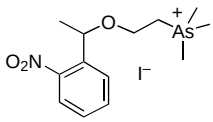
Molecular recognition is a fundamental phenomenon in biology that has inspired many chemists to design artificial receptors and enzymes.[1] These biomimetic systems are mostly preorganized and are relatively rigid receptors capable of forming host–guest complexes with small molecules. A few flexible receptors were exploited for their biomimetic properties.[2] Here we report an original example of adaptive host–guest systems which employs the mutually induced fit between conformationally flexible molecules, namely *p*-sulfonated calix[8]arene (**A**) and photolabile cholinergic ligands (**1**–**3**) as host and guests, respectively (Figure 1).



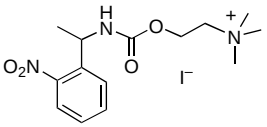
A



1



2



3

The calixarene family plays an important role in host–guest chemistry. While calix[4]arenes and calix[6]arenes have been widely studied, calix[8]arenes were exploited much less because of their more challenging chemistry and higher conformational flexibility.[3] Water-soluble *p*-sulfonated calix[4]arene and calix[6]arene, which bind cholinergic ligands such as choline and acetylcholine, can be considered as simple prototypes for an artificial cholinergic receptor.[4] While bridged calix[8]arenes have been involved in alkali-cation-induced "conformational templatation",[5] we reasoned that the large annular cavity of *p*-sulfonated calix[8]arene **A** with nonrestricted conformational flexibility would be suitable for displaying a mutually induced fit (Figure 1) with flexible guests such as photolabile cholinergic ligands **1**–**3**.[6,7]

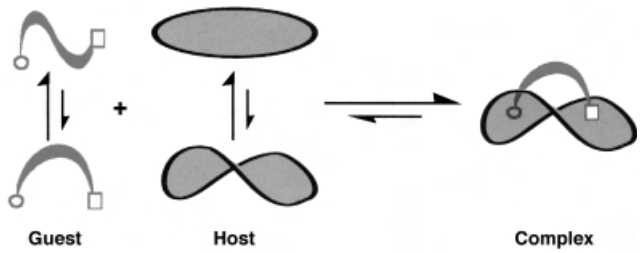


Figure 1. Mutually induced fit in a host–guest complex.

Compounds **1**–**3** are inhibitors of cholinesterases (ChEs) such as acetylcholinesterase (AChE) and butyrylcholinesterase (BuChE). Upon photolysis, these ligands release choline,[6a] arsenocholine,[6b] and carbamylcholine, respectively.[6c–d] They are thus ideal probes for time-resolved crystallographic studies on cholinesterases. Our previous studies showed that *p*-sulfonated calix[4]arene formed host–guest complexes with **1** or **3** at neutral pH by specific inclusion of their ammonium group to give monotopic binding complexes.[8] Here we show that *p*-sulfonated calix[8]arene **A** forms host–guest systems with **1**–**3** by ditopic binding of both the aromatic ring and the cationic ammonium moiety of the guest. Interestingly, these complexes are formed through mutually induced fit, thus mimicking more closely the binding occurring in the active site of ChEs.

The complexes between **A** and **1**–**3** were formed in 0.1M phosphate buffer at pD = 7.3, as indicated by ^{1}H NMR analysis (Figure 2). Progressive addition of **A** to a solution containing the guest molecule led to increasing upfield chemical shifts ($\Delta\delta$) of both the aromatic protons and the ammonium group of **1**–**3** (Figure 2a). These shifts suggest an inclusion of both the aromatic ring and the ammonium group

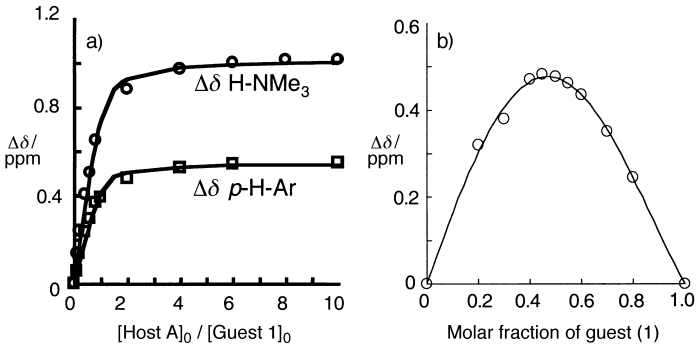


Figure 2. NMR analysis of the complex [**A**-**1**]. a) The observed (symbols) and calculated (curves) upfield shifts $\Delta\delta$ (ppm) of the N-CH_3 (○) and *p*-H-Ar (□) signals of **1** obtained by progressive addition of **A** to 3.10^{-4}M **1** in 0.1M phosphate buffer pD 7.3, 20°C. b) Job plot.

[*] Prof. Dr. M. Goeldner, A. Specht
CNRS UMR 7514, Laboratoire de Chimie Bio-organique
Université Louis Pasteur Strasbourg
BP 24, 67401 Illkirch cedex (France)
Fax: (+33) 3-9024-4306
E-mail: goeldner@bioorga.u-strasbg.fr
Dr. L. Peng
Chemistry Department
Wuhan University (P.R. China)
and
AFMB CNRS UMR 6098
13009 Marseille (France)
Fax: (+33) 4-9182-9491
E-mail: ling@afmb.cnrs-mrs.fr
Dr. P. Bernard
CNRS UMR 7081
Laboratoire de Pharmacochimie de la Communication Cellulaire
Faculté de Pharmacie
Université Louis Pasteur Strasbourg
BP 24, 67401 Illkirch cedex (France)

[**] This work was supported by the CNRS, the COST program D11, the Région Alsace, and the EC Biotechnology Program No. 960081. L.P. is a Cheung Kong Scholar at Wuhan University.

Supporting information for this article is available on the WWW under http://www.angewandte.org or from the author.

 © 2002 WILEY-VCH Verlag GmbH & Co. KGaA, Weinheim 0044-8249/02/4124-4706 $ 20.00+.50/0

of **1**–**3** into the cavity of **A**. Moreover, the curves $\Delta\delta = f$[host]/[guest] (Figure 2a) indicate the formation of 1:1 complexes, which was confirmed by a Job plot (Figure 2b). The association constants of **A** for **1**–**3** were determined by ^{1}H NMR spectroscopy,[9] and similar values for both the aromatic ring and the ammonium group were obtained (Figure 2a). These association constants are in the same range for all three ligands (Table 1) and approach their binding affinities for AChE and BuChE.

Table 1. Binding affinities ($10^3\,\text{M}^{-1}$) of **1**–**3** for **A**, AChE, and BuChE.

	1	**2**	**3**
$K_{A,}$ **A** ($10^3\,\text{M}^{-1}$)	34.4	21.7	21.3
$1/K_{I,}$ AChE ($10^3\,\text{M}^{-1}$)	77.0	59.0	22.7
$1/K_{I,}$ BuChE ($10^3\,\text{M}^{-1}$)	91.0	55.5	12.8

To analyze the supramolecular nature of the complex more accurately, we studied the complex [**A-1**] at lower pH values (pD = 0.4) where all the phenol groups in **A** are protonated, and thus favor inclusion of the aromatic group.[10] However, no pronounced pH preference was observed for the upfield chemical shifts and the binding affinities of either the aromatic protons or the ammonium group of **1** in the complex [**A-1**] in going from pD 7.3 to 0.4 (data not show). Considering the large annular cavity of **A** and the previous findings, we propose that a ditopic binding occurs in the complex [**A-1**] with concomitant inclusion of both aromatic and ammonium groups of the guest into the cavity of **A**, rather than monotopic binding with a fast equilibrium between two complexes hosting either the ammonium or the aromatic group of **1**. The latter case is observed when **1** is complexed by *p*-sulfonated calix[4]arene at pD 0.4, which demonstrates that complexation shows a clear pH dependence (data not show).

To gain more insight into the formation of these complexes, we studied separately the binding features of **A** with the two essential parts of guest **1**, namely 2-nitrobenzyl alcohol and choline, respectively. While 2-nitrobenzyl alcohol showed a very poor binding affinity with **A** ($K_A < 10^3\,\text{M}^{-1}$), choline formed a stable complex. However, we could not establish a defined stoichiometry for this latter complex, which might be a mixture of 1:1 and 1:2 complexes, as suggested by the Job plot (data not shown). Even though a precise binding constant for choline could not be determined from these experiments, it forms a much weaker complex with **A** than does the bifunctional guest **1**, thus emphasizing the ditopic binding feature of [**A-1**].

Complex [**A-1**] could exist as a bimolecular 1:1 host:guest complex or higher order aggregation. No dependency of the chemical shifts of [**A-1**] on concentration was observed upon dilution,[11] which suggests that [**A-1**] has no propensity to aggregate. Moreover, a series of NMR titration experiments with different concentrations of guest were undertaken for [**A-1**]. The experimental data matched perfectly with the curves fitted for a 1:1 bimolecular complex, and led to the same binding constants and the same maximal chemical shifts.[11] All these results are in agreement with [**A-1**] being a bimolecular complex with ditopic binding of both the aromatic and ammonium groups of **1** into the cavity of **A**.

The ditopic binding mode of [**A-1**] was further confirmed by NOESY experiments. A specific NOE signal was observed between the methyl protons of the ammonium group and the aromatic proton in the position *para* to the side chain of **1** in [**A-1**] (Figure 3a). A distance of 4.0 Å between these two groups could be deduced within this complex (Figure 3b) at both pD 7.3 and pD 0.4. However, this particular NOE signal

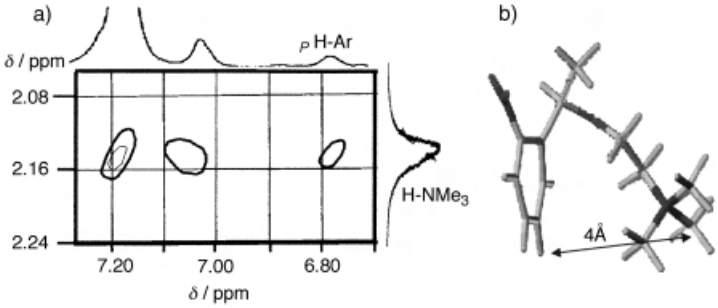


Figure 3. a) Specific NOE signal between the ammonium moiety and and aromatic proton of **1** in [**A-1**]. b) Intramolecular distance constraint deduced from the NOE data.

was not observed when **1** was either free or complexed with *p*-sulfonated calix[4]arene. Thus, when **1** was complexed by **A**, it adopted a constrained conformation by bringing the ammonium moiety and the aromatic ring closer (to a distance of 4.0 Å) so that it could to be accommodated concomitantly in the cavity of **A**. When **1** was either free or complexed with *p*-sulfonated calix[4]arene, it was in more relaxed conformations, with the ammonium moiety and the aromatic ring further apart. These results suggest that the cavity of **A** directs the flexible guest **1** to adopt a bent conformation for a favorable fit in the complex.

Conversely, guest **1** is able to select a suitable conformation of **A** for an optimal fitting, as supported by molecular modeling studies.[12] Both the pleated loop conformation[13] and the pinched conformation[14] of calix[8]arene were used as starting points to minimize the energy of **A**. Without the guest, the pleated loop conformation of **A** is 10 kcal mol^{-1} lower in energy than the pinched one. However, when **A** was docked with **1**, a stable complex was obtained only with the pinched conformer of **A**. In this complex the aromatic part and the ammonium moiety of **1** were 3.7 Å apart and inserted simultaneously into the two aromatic pockets of **A** (Figure 4). This is in excellent agreement with the results obtained from NOE experiments. Moreover, the aromatic ring of **1** stacked with one of the phenol units of **A**, and the ammonium moiety of **1** formed a π–cation interaction with another phenol unit of

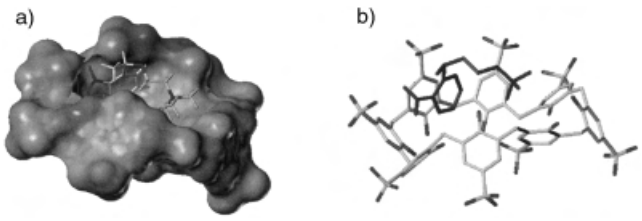


Figure 4. Molecular modeling studies of [**A-1**]. **1** is shown in stick presentation and **A** is shown in space-filling a) and stick presentation b).

 © 2002 WILEY-VCH Verlag GmbH & Co. KGaA, Weinheim 0044-8249/02/4124-4707 $ 20.00+.50/0

A (Figure 4). Thus, [**A**-**1**] is stabilized by both π–π and π–cation interactions. Furthermore, the binding of the guest would displace the water molecules in the cavity of **A**, thus providing a favorable entropic gain in [**A**-**1**].

In conclusion, we report an original example of adaptive host–guest systems which employs mutually induced fit between the conformationally flexible host **A** and guests **1**–**3**. Both the host and the guests adapted to each other and selected the higher energy but correct geometric conformers so that the guest could fit favorably into the cavity of the host to give ditopic binding. While mutually induced fit has been demonstrated mostly in biological macromolecules interactions, that is, in protein/DNA,[15] protein/RNA,[16] protein/tRNA complexes,[17] it has been recently depicted within a neocarzinostatin–chromophore/DNA complex.[18] Recent development in drug design has considered mutual adaptability between a ligand and a receptor as a key element in molecular recognition[19] and has prompted the outlining of the "relaxed-complex" method as a novel dynamic computational model to take into account the flexibility of receptors.[20] Therefore, our system represents an original example of adaptive supramolecular biomimetic chemistry.

Experimental Section

General: NMR spectra were recorded on a Bruker VPC 300 spectrophotometer unless otherwise mentioned. Solutions of complexes for NMR analysis were prepared in 0.1M deuterated phosphate buffer at pD 7.3 and 0.4. The molecular modeling study was performed by using Sybyl 6.8 on a Silicon Graphics Octane 2XR10000 station.

NMR titration: Experiments were carried out by keeping the concentration of guest (**1**–**3**) constant while varying that of the host (**A**) from 0.1 equiv to 10 equiv. Association constants K_A of the complexes were calculated with a nonlinear least-squares method.[9]

2D NMR analysis: Solutions for 2D NMR analysis were prepared with 20 mM of **1** and 40 mM of the host, which ensured over 99% complex formation between the guest and the host. 2D NMR spectra were recorded by using a NOESY sequence from Bruker (Noesyprtp) and a mixing time of 400 ms. Experiments were performed on **1**, [**A**-**1**], and the complex of *p*-sulfonated calix[4]arene with **1**.

Molecular modeling studies: The starting structure **1** was constructed from the coordinates of the crystal structure of an analogue.[6b] For **A**, two crystal structures of calix[8]arene (Dovhif[13] and Foztix[14]) were used as starting points to construct the structure and led to the pleated loop conformation and the pinched conformation, respectively. For the complex [**A**-**1**], **1** was manually docked with each conformer of **A**. All the starting structures of **1**, **A**, and [**A**-**1**] were optimized by a molecular mechanics algorithm using the Tripos force field with a convergence criterion of 0.01 kcal mol^{-1}. The electrostatic component was applied by means of the Gasteiger–Hückel charges and a dielectric function equal to 1.

Received: April 26, 2002
Revised: September 23, 2002 [Z19198]

[1] J. M. Lehn, *Supramolecular Chemistry: Concepts and Perspectives*, VCH, Weinheim, **1995**.
[2] a) Guest editor: S. H. Gellman "Molecular Recognition": *Chem. Rev.* **1997**, *97*, 1231–1734; b) J. Halpern in "Supramolecular Chemistry And Self-Assembly Special Feature": *Proc. Natl. Acad. Sci. USA* **2002**, *99*, 4762–5206.
[3] a) C. D. Gutsche, *Calixarenes*, Royal Society of Chemistry, Cambridge, **1989**; b) *Calixarenes: A Versatile Class of Macrocyclic Compounds* (Eds.: J. Vicens, V. Böhmer), Kluwer, Dordrecht, **1991**; c) V. Böhmer, *Angew. Chem.* **1995**, *107*, 785–818; *Angew. Chem. Int. Ed. Engl.* **1995**, *34*, 713–745; d) A. Ikeda, S. Shinkai, *Chem. Rev.* **1997**, *97*, 1713–1734; e) C. D. Gutsche, *Calixarenes Revisited*, Royal Society of Chemistry, Cambridge, **1998**.
[4] a) J.-M. Lehn, R. Meric, J.-P. Vigneron, M. Cesario, J. Guilhem, C. Pascard, Z. Asfari, J. Vicens, *Supramol. Chem.* **1995**, *5*, 97–103; b) K. N. Koh, K. Araki, A. Ikeda, H. Otsuka, S. Shinkai, *J. Am. Chem. Soc.* **1996**, *118*, 755–758.
[5] a) G. M. L. Consoli, F. Cunsolo, C. Geraci, P. Neri, *Org. Lett.* **2001**, *3*, 1605–1608; b) G. M. L. Consoli, F. Cunsolo, C. Geraci, E. Gavuzzo, P. Neri, *Tetrahedron Lett.* **2002**, *43*, 1209–1211.
[6] a) L. Peng, M. Goeldner, *J. Org. Chem.* **1996**, *61*, 185–191; b) L. Peng, F. Nachon, J. Wirz, M. Goeldner, *Angew. Chem.* **1998**, *110*, 2838–2840; *Angew. Chem. Int. Ed.* **1998**, *37*, 2691–2693; c) L. Peng, I. Silman, J. Sussman, M. Goeldner, *Biochemistry* **1996**, *35*, 10854–10861; d) J. W. Walker, J. A. McCray, G. P. Hess, *Biochemistry* **1986**, *25*, 1799–1805.
[7] L. Peng, M. Goeldner, *Methods Enzymol.* **1998**, *291*, 265–278.
[8] A. Specht, M. Goeldner, J. Wirz, L. Peng, *Synlett* **1999**, *S1*, 981–983.
[9] *Frontiers in Supramolecular Organic Chemistry and Photochemistry* (Eds.: H.-J. Schneider, H. Dürr), VCH, Weinheim, **1991**, pp. 123–143.
[10] S. Shinkai, K. Araki, T. Mutsuda, N. Nishiyama, H. Ikeda, I. Takasu, M. Iwamoto, *J. Am. Chem. Soc.* **1990**, *112*, 9053–9058.
[11] For details see the Supporting Information.
[12] SYBYL 6.8 Tripos Inc., 1699 South Hanley Rd., St. Louis, Missouri, 63144, USA, **2002**.
[13] C. D. Gutsche, A. E. Gutsche, A. I. Karoulov, *J. Inclusion Phenom.* **1985**, *3*, 447–451.
[14] A. W. Coleman, S. G. Bott, J. L. Atwood, *J. Inclusion Phenom.* **1987**, *5*, 581–590.
[15] A. Pingoud, A. Jeltsch, *Eur. J. Biochem.* **1997**, *246*, 1–22.
[16] a) H. Mao, S. A. White, J. R. Williamson, *Nat. Struct. Biol.* **1999**, *6*, 1139–1147; b) A. D. Frankel, *Nat. Struct. Biol.* **1999**, *6*, 1081–1083.
[17] B. Delagoutte, D. Moras, J. Cavarelli, *EMBO J.* **2000**, *19*, 5599–5610.
[18] L. S. Kappen, Z. Xi, I. H. Goldberg, *Biochemistry* **2001**, *40*, 15378–15383.
[19] B. Testa, A. J. Bojarski, *Eur. J. Pharm. Sci.* **2000**, *11*, S3-S14 (*Suppl. 2*).
[20] J.-H. Lin, A. L. Perryman, J. R. Schames, J. A. McCammon, *J. Am. Chem. Soc.* **2002**, *124*, 5632–5633.

New Ferrocenyl Ligands with Broad Applications in Asymmetric Catalysis**

Matthias Lotz, Kurt Polborn, and Paul Knochel*

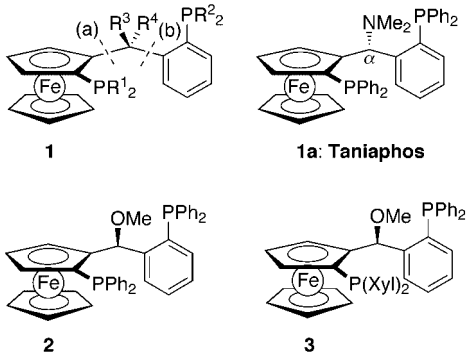
The development of new ligands for asymmetric catalysis is an highly active field of research.[1] Although many chiral ligands have been prepared, only a few, such as binaphthyl-,[2] salen-,[3] pybox-,[4] and DuPHOS-type[5] ligands have found broad applications in various asymmetric reactions. The ferrocenyl unit has proven to allow excellent spatial recognition,[6] and we recently reported new ferrocenyl diphosphanes of type **1** (taniaphos),[7] which gave excellent results in

[*] Prof. Dr. P. Knochel, Dipl.-Chem. M. Lotz, Dr. K. Polborn
Department Chemie, Ludwig-Maximilians-Universität
Butenandtstrasse 5–13, Haus F, 81377 München (Germany)
Fax: (+49) 89-2180-7680
E-mail: paul.knochel@cup.uni-muenchen.de

[**] We thank Degussa AG for generous support. We also thank Chemetall GmbH (Frankfurt) and BASF AG (Ludwigshafen) for the generous gift of chemicals.

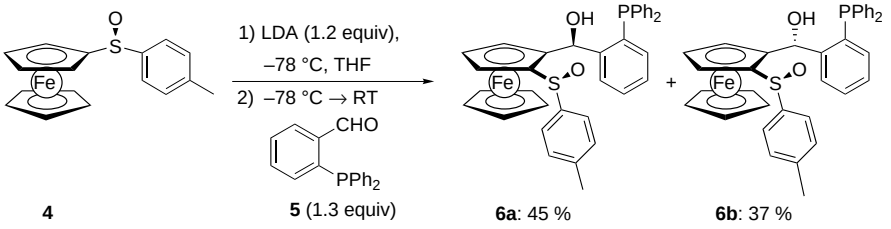
Supporting information for this article is available on the WWW under http://www.angewandte.org or from the author.

 © 2002 WILEY-VCH Verlag GmbH & Co. KGaA, Weinheim 0044-8249/02/4124-4708 $ 20.00+.50/0



Ru-catalyzed asymmetric hydrogenations of 1,3-dicarbonyl compounds.[8,9]

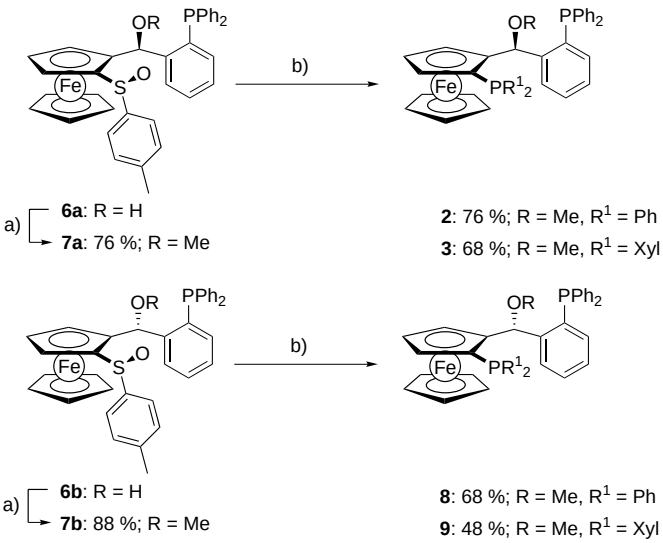
Although the original synthesis (retrosynthetic cleavage (a)) was concise, high-yielding, and stereoselective, it suffered from two major drawbacks: 1) it did not allow independent variation of the phosphane substituents R^1 and R^2, 2) it was not possible to prepare ligands with $R^3 \neq H$—only the nature of R^4 could be altered. This hampered the full exploitation of the modular character of ligands **1**. Herein we report a new preparation of ligands **2** and **3** (involving the retrosynthetic bond cleavage (b)) which solves these two previous synthetic limitations. The new ligands **2** and **3**, which bear a methoxy substituent instead of a hydrogen atom at the α position, provided high enantioselectivities in many asymmetric transformations.[10] Thus, the reaction of lithiated ferrocenyl sulfoxide (*S*)-**4** (first used by Kagan and co-workers[11]) with 2-diphenylphosphanylbenzaldehyde (**5**) furnished the two diastereomeric alcohols (S_p,α*S*)-**6a** and (S_p,α*R*)-**6b** (55:45) in 82% yield (Scheme 1). The diastereomers were readily separated by column chromatography.



Scheme 1. Preparation of the diastereomeric ferrocenyl alcohols **6a** and **6b**. LDA = lithium diisopropylamide.

X-ray crystallographic analysis[12] proved that the major diastereomer (S_p,α*S*)-**6a** has the opposite configuration at the α-position compared to taniaphos (**1a**), whereas the second diastereomer (S_p,α*R*)-**6b** has the same configuration as ligand **1a**. Both intermediate ferrocenyl alcohols **6a**,**b** can be converted readily into the corresponding methyl ethers **7a**–**b** in 76–88% yield by deprotonation and methylation (Scheme 2). Treatment of **7a**–**b** with *t*BuLi (2.0 equiv) in THF at −78 °C (10 min), followed by the addition of chlorodiphenylphosphane or chloro[bis(3,5-dimethylphenyl)]phosphane, provides the desired diphosphanes **2**, **3**, **8**, and **9** in 48–76% yield.[13]

As mentioned above, the new diphosphanes **2** and **3**, which are epimeric to taniaphos (**1a**) at the α position, lead to high



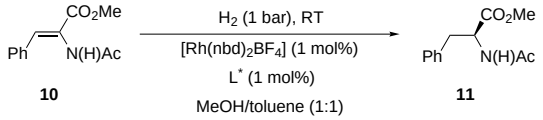
Scheme 2. Reagents and conditions: a) KH (1.3 equiv), THF, 0 °C; then MeI (1.1 equiv), 0 °C→RT; b) *t*BuLi (2.0 equiv), THF, −78 °C, 10 min; then $ClPPh_2$ or $ClP(Xyl)_2$ (3.5 equiv), −78 °C→RT.

enantioselectivities in a wide range of asymmetric reactions. First, we compared all the new ligands in the Rh-catalyzed hydrogenation of (*Z*)-α-methylacetamidocinnamate (**10**).[8,14]

Thus, treatment of **10** with hydrogen (1 bar, room temperature, 0.5–1.5 h) in the presence of $[Rh(nbd)_2BF_4]$ (nbd = norbornadiene) (1 mol%) and the ligand (1 mol%) in methanol/toluene (1:1) leads to (*S*)-*N*-acetyl phenylalanine methyl ester (**11**) in quantitative yield and with high enantioselectivity. Whereas taniaphos (**1a**) gives the (*R*)-*N*-acetyl phenylalanine methyl ester (**11**) in 95% *ee*, all the new catalysts **2**, **3**, **8**, and **9** furnish the (*S*)-*N*-acetyl phenylalanine methyl ester. This behavior is general and was observed in all hydrogenation reactions. Ligands **2** and **3** give the highest enantioselectivities (99% *ee*), thus showing the importance of the configuration at the α position (Table 1).

Similarly, the Rh-catalyzed hydrogenation of dimethyl itaconate[8,14,15] (**13**) to (*R*)-methyl succinic acid dimethyl ester (**14**) proceeds with excellent enantioselec-

Table 1. Rh-catalyzed asymmetric hydrogenation of **10** to (*S*)-*N*-acetyl phenylalanine methyl ester (**11**).



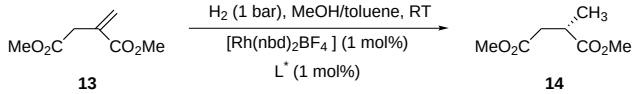
Entry	Ligand	*t* [h]	Conversion [%]	*ee* [%][a]
1	**2**	1.5	100	99 (*S*)
2	**3**	1.5	100	99 (*S*)
3	**8**	2	100	94 (*S*)
4	**9**	1.5	100	92 (*S*)
5	**1a**	0.5	100	95 (*R*)

[a] Determined by means of chiral GC (Chirasil-*L*-Val column). The absolute stereochemistry was established by comparison with literature data.[5b]

 © 2002 WILEY-VCH Verlag GmbH & Co. KGaA, Weinheim 0044-8249/02/4124-4709 $ 20.00+.50/0

tivity in the presence of ligand **2** (98% *ee*), which again gives superior results than do the ligands **8** and **1a** (Table 2).

Table 2. Rh-catalyzed asymmetric hydrogenation of dimethyl itaconate (**13**) to (*R*)-methyl succinic acid dimethyl ester (**14**).



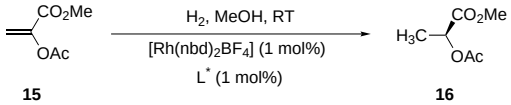
13 **14**

Entry	Ligand	*p* [bar]	*t* [h]	Conversion [%]	*ee* [%][a]
1	**2**	1	0.5	100	98 (*R*)
2	**3**	1	1	100	90 (*R*)
3	**8**	1	2.5	100	95 (*R*)
4[b]	**1a**	1	14	100	91 (*S*)

[a] Determined by chiral HPLC (Daicel Chiracel OD column). The absolute stereochemistry was established by comparison with literature data.[14] [b] Reaction was performed in MeOH.

Whereas the taniaphos ligands with S_p,α*R* configuration display a low reactivity and moderate enantioselectivity in the asymmetric hydrogenation of α-acetoxy acrylic acid esters such as **15**[5a,15] (Table 3; see ligands **1a**, **8**, **9**), the new epimeric diphosphanes **2** and **3** (S_p,α*S*) have a significantly higher catalytic activity (the reaction proceeds at 1 bar compared to 5–10 bar with ligands **1a**, **8**, **9**) and lead to excellent enantioselectivities (99% *ee*).

Table 3. Asymmetric hydrogenation of α-acetoxy acrylic acid methyl ester (**15**).



15 **16**

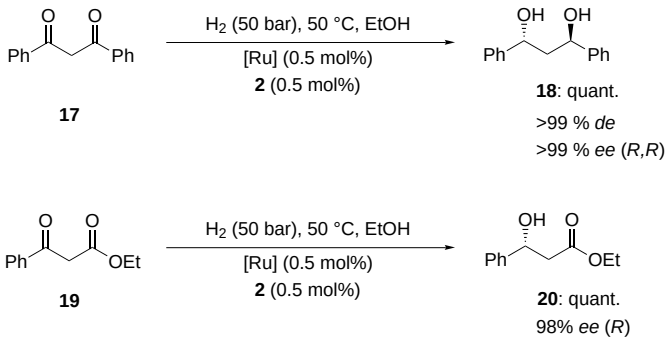
Entry	Ligand	*p* [bar]	*t* [h]	Conversion [%]	*ee* [%][a]
1	**2**	1	20	100	98 (*S*)
2	**3**	1	20	100	99 (*S*)
3	**8**	1	20	40	–[b]
4	**8**	10	20	100	80 (*S*)
5	**9**	10	20	100	78 (*S*)
6	**1a**	5	22	95	72 (*R*)

[a] Determined by chiral HPLC (Daicel Chiracel OD-H column). The absolute stereochemistry was established by comparison with literature data.[16] [b] The *ee* value was not determined.

Remarkable enantioselectivity is also observed in the Ru-catalyzed hydrogenation of dibenzoylmethane (**17**), which furnishes only the *anti*-(1*R*,3*R*)-diol **18** in >99% *ee* and >99% *de* (Scheme 3).

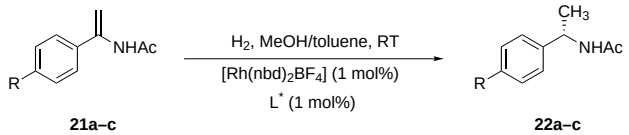
Similarly, the Ru-catalyzed hydrogenation of ethyl 3-phenyl-3-oxopropionate (**19**) provides the aldol product **20** with 98% *ee*. These hydrogenation reactions were performed under the standard conditions: $[Ru(cod)(C_4H_7)_2]/HBr$[17] (cod = cycloocta-1,5-diene) (0.5 mol%), ligand **2** (0.5 mol%) in ethanol at 50°C and under 50 bar H_2.

Finally, we examined the Rh-catalyzed hydrogenation of aryl-substituted enamides[18] of type **21**. The ligands **2** and **3** turned out to be very active in this reaction and provided excellent enantioselectivities of up to 97% *ee* (Table 4). Remarkably, these hydrogenations occur at 1 bar H_2 with complete conversion within 1.5–15 h at 25°C.



Scheme 3. Enantioselective hydrogenation of dibenzoylmethane (**17**) and ethyl 3-phenyl-3-oxopropionate (**19**).

Table 4. Rh-catalyzed asymmetric hydrogenation of enamides **21** to amides **22**.



21a–c **22a–c**

Entry	Substrate	Ligand	R	*p* [bar]	*t* [h]	Product	*ee* [%][a,b]
1	**21a**	**2**	H	1	15	**22a**	96 (*S*)
2	**21b**	**2**	Br	1	6	**22b**	97 (*S*)
3	**21a**	**3**	H	1	1.5	**22a**	92 (*S*)
4	**21b**	**3**	Br	1	1.5	**22b**	93 (*S*)
5	**21c**	**3**	Me	1	1.5	**22c**	95 (*S*)

[a] Determined by chiral HPLC (Daicel Chiracel OD column). [b] Determined by chiral GC (columns: Chirasil-L-Val, Chirasil-Dex CD, Chirasil-Dex CB). The absolute stereochemistry was established by comparison with literature data.[18]

We assume that the high activity and excellent enantioselectivity of ligands **2** and **3** in asymmetric catalysis is a result of the *S* configuration at the carbon atom that bears the methoxy group. This configuration may lead to a shielding of the upper half of the diphosphane–metal complex, thus forcing the asymmetric reaction to occur from the bottom face.

Although a rational explanation of the observed enantioselectivities is difficult at this point in time, the short, modular synthesis of the new ligands (S_p,α*S* configuration) and the remarkably high enantioselectivities obtained in asymmetric catalysis, combine to provide a new family of powerful and broadly applicable chiral ligands. Extension of the field of application of these ligands in asymmetric catalysis is currently underway.

Experimental Section

Enantioselective hydrogenation of **21a**: $[Rh(nbd)_2BF_4]$ (2.8 mg, 1 mol%) and ligand **2** (5.0 mg, 1 mol%) were dissolved in MeOH/toluene (2 mL) in a 25-mL Schlenk tube under argon. After 20 min, a solution of **21a** (120 mg, 0.74 mmol) in MeOH (5 mL) was added. The Schlenk tube was connected to a hydrogen balloon and the inert atmosphere was replaced by hydrogen. After complete conversion (monitored by TLC) the solvent was removed, and the crude reaction mixture was filtered through a short silica-gel column with Et_2O as eluent. After evaporation of the solvent (*S*)-**22a** was obtained in quantitative yield (122 mg, 0.74 mmol) as a yellowish solid (96% *ee*).

Received: July 19, 2002 [Z19783]

 © 2002 WILEY-VCH Verlag GmbH & Co. KGaA, Weinheim 0044-8249/02/4124-4710 $ 20.00+.50/0

[1] a) R. Noyori, *Asymmetric Catalysis in Organic Synthesis*, Wiley, New York, **1994**; b) T. Ohkuma, M. Kitamura, R. Noyori in *Catalytic Asymmetric Synthesis* (Ed.: I. Ojima), Wiley-VCH, Weinheim, **2000**, p. 1; c) J. M. Brown in *Comprehensive Asymmetric Catalysis* (Eds.: E. N. Jacobsen, A. Pfaltz, H. Yamamoto), Springer, Berlin, **1999**, p. 121; d) G. Helmchen, A. Pfaltz, *Acc. Chem. Res.* **2000**, *33*, 336; e) A. Börner, *Eur. J. Inorg. Chem.* **2001**, 327.

[2] a) A. Miyashita, A. Yasuda, H. Takaya, K. Toriumi, T. Ito, T. Souchi, R. Noyori, *J. Am. Chem. Soc.* **1980**, *102*, 7932; b) H. Takaya, K. Mashima, K. Koyano, M. Yagi, H. Kumobayashi, T. Taketomi, S. Akutagawa, R. Noyori, *J. Org. Chem.* **1986**, *51*, 629; c) H. Takaya, S. Akutagawa, R. Noyori, *Org. Synth.* **1988**, *67*, 20; d) K. Mashima, K. Kusano, N. Sato, Y. Matsumura, K. Nozaki, H. Kumobayashi, N. Sayo, Y. Hori, T. Ishizaki, S. Akutagawa, H. Takaya, *J. Org. Chem.* **1994**, *59*, 3064.

[3] a) M. H. Wu, K. B. Hansen, E. N. Jacobsen, *Angew. Chem.* **1999**, *111*, 2167; *Angew. Chem. Int. Ed.* **1999**, *38*, 2012; b) A. G. Dossetter, P. F. Jamison, E. N. Jacobsen, *Angew. Chem.* **1999**, *111*, 2549; *Angew. Chem. Int. Ed.* **1999**, *38*, 2398; c) M. S. Sigman, E. N. Jacobsen, *J. Am. Chem. Soc.* **1998**, *120*, 5315; d) W. Zhang, J. L. Loebach, S. R. Wilson, E. N. Jacobsen, *J. Am. Chem. Soc.* **1990**, *112*, 2801.

[4] H. Nishiyama, *Enantiomer* **1999**, *4*, 569.

[5] a) M. J. Burk, *J. Am. Chem. Soc.* **1991**, *113*, 8518; b) M. J. Burk, J. E. Feaster, W. A. Nugent, R. L. Harlow, *J. Am. Chem. Soc.* **1993**, *115*, 10125.

[6] a) A. Togni, R. L. Halterman, *Metallocenes, Vol. 2*, Wiley-VCH, Weinheim, **1998**, pp. 685–721; b) C. J. Richards, A. Locke, *Tetrahedron: Asymmetry* **1998**, *9*, 2377; c) A. Togni, N. Bieler, U. Burckhardt, C. Kollner, G. Pioda, R. Schneider, A. Schnyder, *Pure Appl. Chem.* **1999**, *71*, 1531; d) C. Bolm, K. Muniz, J. P. Hildebrand, *Org. Lett.* **1999**, *1*, 491.

[7] a) T. Ireland, G. Grossheimann, C. Wieser-Jeunesse, P. Knochel, *Angew. Chem.* **1999**, *111*, 3397; *Angew. Chem. Int. Ed.* **1999**, *38*, 3212; b) T. Ireland, K. Tappe, G. Grossheimann, P. Knochel, *Chem. Eur. J.* **2002**, *8*, 843.

[8] For reviews see: a) K. E. Koenig, *Asymmetric Synthesis, Vol 5* (Ed.: J. D. Morrison), Academic Press, Orlando, FL, **1985**, p. 71–101; b) H. Takaya, T. Ohta, R. Noyori, *Catalytic Asymmetric Synthesis* (Ed.: I. Ojima), VCH, New York, **1993**, pp. 1–39.

[9] M.J. Burk, M. F. Gross, T. G. Harper, C. S. Kalberg, J. R. Lee, J. P. Martinez, *Pure Appl. Chem.* **1996**, *68*, 37.

[10] The new ligands were patented in collaboration with Degussa AG: M. Lotz, P. Knochel, A. Monsees, T. Riermeier, R. Kadyrov, J. J. Almena Perea, Ger. Pat. No. DE 10219490.

[11] a) D. Guillaneux, H. B. Kagan, *J. Org. Chem.* **1995**, *60*, 2502; b) O. Riant, G. Argouarch, D. Guillaneux, O. Samuel, H. B. Kagan, *J. Org. Chem.* **1998**, *63*, 3511.

[12] CCDC 189275 contains the supplementary crystallographic data for this paper. These data can be obtained free of charge via www.ccdc.cam.ac.uk/conts/retrieving.html (or from the Cambridge Crystallographic Data Centre, 12, Union Road, Cambridge CB21EZ, UK; fax: (+44) 1223-336-033; or deposit@ccdc.cam.ac.uk).

[13] A typical procedure for the synthesis of diphosphane **2** is described in the Supporting Information.

[14] a) A. Togni, C. Breutel, A. Schnyder, F. Spindler, H. Landert, A. Tijani, *J. Am. Chem. Soc.* **1994**, *116*, 4062; b) M. J. Burk, J. R. Lee, J. P. Martinez, *J. Am. Chem. Soc.* **1994**, *116*, 10847; c) K. Junge, G. Oehme, A. Monsees, T. Riermeier, U. Dingerdissen, M. Beller, *Tetrahedron Lett.* **2002**, *43*, 4977.

[15] a) M. J. Burk, F. Bienewald, M. Harris, A. Zanotti-Gerosa, *Angew. Chem.* **1998**, *110*, 2034; *Angew. Chem. Int. Ed.* **1998**, *37*, 1931; b) J. Holz, M. Quirmbach, U. Schmidt, D. Heller, R. Stürmer, A. Börner, *J. Org. Chem.* **1998**, *63*, 8031.

[16] a) M. D. Fryzuk, B. Bosnich, *J. Am. Chem. Soc.* **1978**, *100*, 5491; b) M. J. Burk, C. S. Kalberg, A. Pizzano, *J. Am. Chem. Soc.* **1998**, *120*, 4345; c) M. Lotz, T. Ireland, J. J. Almena Perea, P. Knochel, *Tetrahedron: Asymmetry* **1999**, *10*, 1839.

[17] a) J. P. Genêt, C. Pinel, S. Mallart, S. Jugé, S. Thorimbert, J. A. Laffitte, *Tetrahedron: Asymmetry* **1991**, *2*, 555; b) J. P. Genêt, C. Pinel, V. Ratovelomanana-Vidal, S. Mallart, X. Pfister, L. Bischoff, S. Darses, C. Galopin, J. A. Laffitte, *Tetrahedron: Asymmetry* **1994**, *5*, 675.

[18] a) M. J. Burk, Y. M. Wang, J. R. Lee, *J. Am. Chem. Soc.* **1996**, *118*, 5142; b) M. J. Burk, G. Casy, N. B. Johnson, *J. Org. Chem.* **1998**, *63*, 6084; c) G. Zhu, X. Zhang, *J. Org. Chem.* **1998**, *63*, 9590; d) I. D. Gridnev, M. Yasutake, N. Higashi, T. Imamoto, *J. Am. Chem. Soc.* **2001**, *123*, 5268; e) W. Tang, X. Zhang, *Angew. Chem.* **2002**, *114*, 1682; *Angew. Chem. Int. Ed.* **2002**, *41*, 1612.

A Remarkable 14-Nuclear $Re^{V}_{8}Ag^{I}_{6}$ Coordination Oligomer Derived from a 2D $(Re^{V}_{2}Ag^{I}_{2})_n$ Coordination Polymer with D-Penicillaminate

Takumi Konno,* Yuichi Shimazaki, Tadashi Yamaguchi, Tasuku Ito, and Masakazu Hirotsu

There has been considerable interest in the design and creation of metallo-supramolecular systems that exhibit unique structural and chemical properties.[1] In many cases, metallo-supramolecular structures have been constructed from organic multidentate ligands and metal ions through self-assembly processes. Our synthetic strategy involves the use of octahedral metal complexes containing relatively simple thiolate ligands, such as 2-aminoethanethiolate (aet), L-cysteinate (L-cys), and D-penicillaminate (D-pen; D-H_2pen = D-penicillamine), as building blocks that are aggregated by forming S-bridged structures with metal ions.[2–5] This method allows the construction of well-organized heterometallic aggregates which have several chiral centers by a systematic variation and combination of metal ions with different coordination geometries. For example, a number of chiral S-bridged aggregates, which include $Co^{III}_4Pd^{II}_2M^{I}_2$ octanuclear metallacycles $[M^{I}_2\{Pd^{II}[Co^{III}(aet)_3]_2\}_2]^{6+}$ (M = Ag, Au),[2e] have been prepared just from $[Co^{III}(aet)_3]$ and appropriate metal ions.[2]

While it has been established that thiolato groups coordinated to an M^{II} or M^{III} metal center have the ability to bind to a second metal ion to form S-bridged structures,[2–6] the coordinating ability of thiolato groups bound to a metal center with a higher oxidation state has not been widely investigated.[7] In fact, S-bridged heterometallic aggregates based on

[*] Prof. T. Konno, Y. Shimazaki
Department of Chemistry
Graduate School of Science
Osaka University
Toyonaka, Osaka 560-0043 (Japan)
Fax: (+81) 6-6850-5765
E-mail: konno@ch.wani.osaka-u.ac.jp
Dr. T. Yamaguchi, Prof. T. Ito
Department of Chemistry
Graduate School of Science
Tohoku University
Sendai, Miyagi 980-8578 (Japan)
Dr. M. Hirotsu
Department of Chemistry
Faculty of Engineering
Gunma University
Kiryu, Gunma 376-8515 (Japan)

 © 2002 WILEY-VCH Verlag GmbH & Co. KGaA, Weinheim 0044-8249/02/4124-4711 $ 20.00+.50/0

thiolato metal complexes with an oxidation state higher than +5 have never been reported. The higher oxidation state of the metal center may cause the reduction of electron density on the thiolato donor atoms, which prevents the formation of stable S-bridged heterometallic structures with other metal ions. Thus, as part of our recent study on oxorhenium(v) complexes with aminothiolate ligands,[8c] we investigated the ability of thiolato groups coordinated to a $[Re^{V}O]^{3+}$ core to ligate to other metal ions, with the aim of expanding the range of chiral supramolecular architectures based on octahedral metal complexes with thiolate ligands. We found that $[Re^{V}O(D\text{-pen-}N,S)(D\text{-pen-}N,O,S)]^{-}$ ions which have two coordinated thiolato groups and one free carboxylate group can aggregate with the use of Ag^{I} centers as the bridging metal ions, which leads to the creation of a novel 2D $(Re^{V}_{2}Ag^{I}_{2})_{n}$ polymeric structure **1**. Furthermore, the $(Re^{V}_{2}Ag^{I}_{2})_{n}$ structure can be converted into an unprecedented 14-nuclear $Re^{V}_{8}Ag^{I}_{6}$ oligomeric structure **2** that exhibits a fascinating metallo-supramolecular stereochemistry (Scheme 1).

Treatment of a purple aqueous solution of $[Re^{V}O(D\text{-Hpen-}N,S)(D\text{-pen-}N,O,S)]$[8a] with $AgNO_3$ in a ratio approximately 1:1 gave a dark purple solution, from which dark purple plate crystals of **1** were isolated. The FT-IR spectrum of **1** shows relatively sharp $\tilde{\nu}(C=O)$ bands at 1675 and 1626 cm^{-1}, which are distinct from a broad $\tilde{\nu}(C=O)$ band at 1669 cm^{-1} with a shoulder at approximately 1695 cm^{-1} for $[Re^{V}O(D\text{-Hpen-}N,S)(D\text{-pen-}N,O,S)]$. This spectral behavior suggests the absence of COOH groups in **1**.[9] Moreover, the plasma emission spectral and elemental analyses of **1** are in agreement with the formula for the 1:1 adduct of $[Re^{V}O(D\text{-pen})_{2}]^{-}$ and Ag^{+} ions.

Single-crystal X-ray analysis of **1** revealed the presence of an asymmetric unit consisting of one $[Re^{V}O(D\text{-pen-}N,S)(D\text{-pen-}N,O,S)]^{-}$ ion and one Ag^{I} atom, and lattice water molecules.[10] The overall structure of the $[Re^{V}O(D\text{-pen-}N,S)(D\text{-pen-}N,O,S)]^{-}$ unit in **1** is very similar to that of the starting mononuclear $[Re^{V}O(D\text{-Hpen-}N,S)(D\text{-pen-}N,O,S)]$,[8b] and have a distorted octahedral geometry with a *cis*(N)·*cis*-(S)·*trans*(O) configuration. As shown in Figure 1, the two Re^{V}

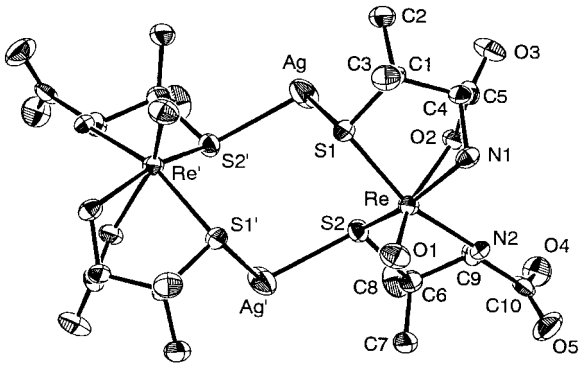
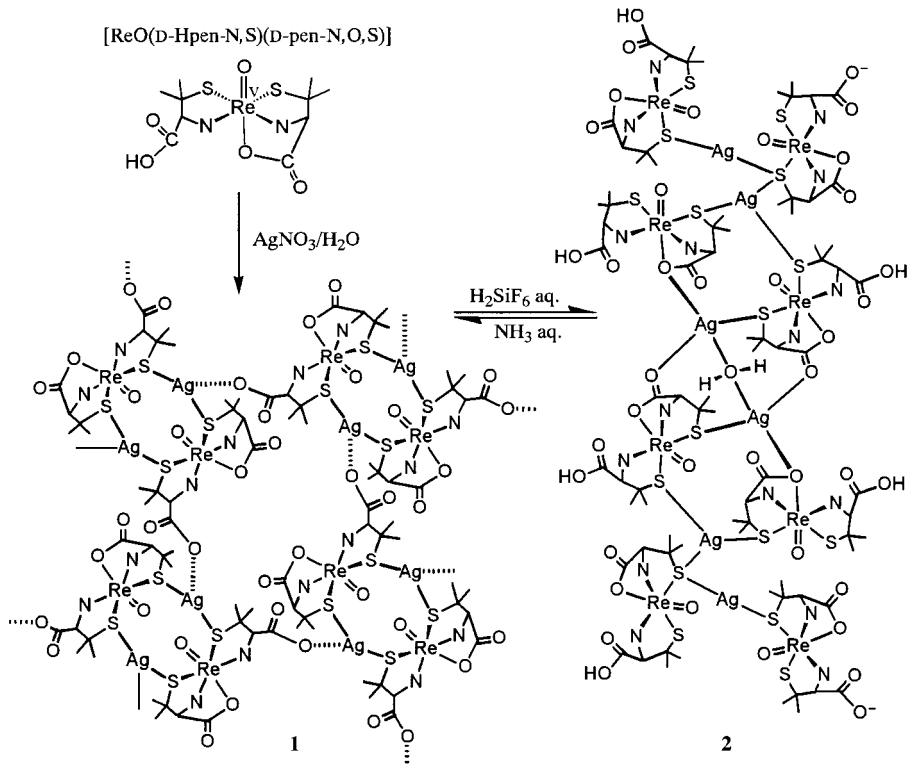


Figure 1. An ORTEP drawing of the $Re^{V}_{2}Ag^{I}_{2}$ unit of **1**, (thermal ellipsoids set to 50% probability).

octahedra are linked by two Ag^{I} atoms through sulfur bridges to form a $Re^{V}_{2}Ag^{I}_{2}$ tetranuclear structure $[Ag_{2}\{Re^{V}O(D\text{-pen-}N,S)(D\text{-pen-}N,O,S)\}_{2}]$ (average Re–S 2.324(3) Å, Ag–S 2.477(3) Å). This S-bridged tetranuclear structure is to be expected, however, the S-Ag-S angle (109.29(9)°) deviates significantly from linearity. An inspection of the extended structure of **1** (Figure 2) reveals that each Ag^{I} atom in the $Re^{V}_{2}Ag^{I}_{2}$ tetranuclear unit is bound by a D-pen-N,S COO^{-} group from a neighboring tetranuclear unit (Ag-O4′ 2.351(10) Å), so as to adopt a trigonal-planar geometry. Thus, in **1** the S-bridged $Re^{V}_{2}Ag^{I}_{2}$ tetranuclear units are connected with one another through Ag–O bonds, which completes a 2D sheetlike structure made up by the cyclic $Re^{V}_{4}Ag^{I}_{4}$ network unit.



Scheme 1. Synthesis of **1** and **2**.

Compound **1** is sparingly soluble in water, consistent with its polymeric structure. However, treatment of an aqueous suspension of **1** with H_2SiF_6 gave a clear purple solution (pH < 1), from which a brown-purple compound **2** was isolated. It was anticipated that a discrete $Re^{V}_{2}Ag^{I}_{2}$ tetranuclear complex, $[Ag_{2}\{Re^{V}O(D\text{-Hpen-}N,S)(D\text{-pen-}N,O,S)\}_{2}]^{2+}$, was produced by the protonation at D-pen-N,S COO^{-} groups, which results in the cleavage of Ag–O bonds in **1**. Indeed, the IR spectrum of **2** exhibits a $\tilde{\nu}(C{=}O)$ band at 1722 cm^{-1} indicative of the presence of a COOH

 © 2002 WILEY-VCH Verlag GmbH & Co. KGaA, Weinheim 0044-8249/02/4124-4712 $ 20.00+.50/0 *Angew. Chem. Int. Ed.* **2002**, *41*, No. 24

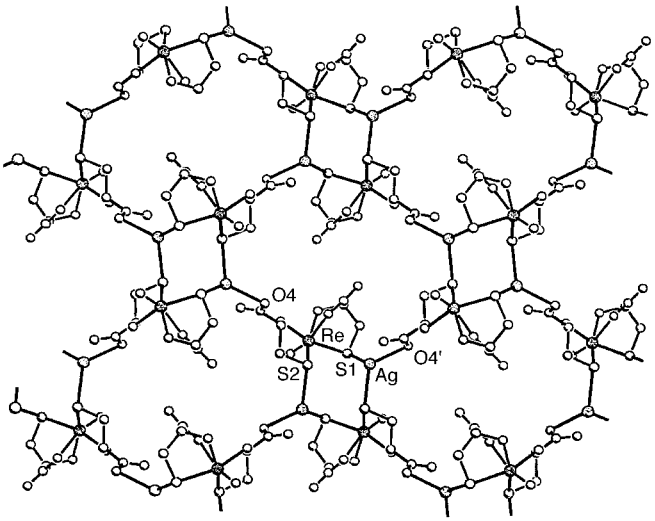


Figure 2. The 2D sheetlike structure of **1**. Methyl groups of each D-pen ligand and hydrogen atoms, as well as the lattice water molecules, are omitted for clarity.

group,[9] in addition to $\tilde{\nu}$(C=O) bands at 1655 and 1602 cm^{-1} arising from COO^- groups. However, the plasma emission spectral analysis indicates a 3:4 ratio of Ag:Re atoms in **2**, and the elemental analysis agrees with the 3:4 stoichiometry $[Ag_3\{ReO(D\text{-}Hpen)(D\text{-}pen)\}_3\{ReO(D\text{-}pen)_2\}](SiF_6)\cdot n H_2O$, rather than the expected 2:2 stoichiometry.

The molecular structure of **2** was established by a single-crystal X-ray analysis.[10] The complex cation of **2** is an unprecedented 14-nuclear coordination oligomer consisting of eight *cis*(N)·*cis*(S)·*trans*(O) configuration Re^V octahedral units and six Ag^I atoms. The presence of two SiF_6^{2-} ions implies that the entire complex cation of **2** has an overall charge of 4+. Six of the eight Re^V units adopt a protonated form [ReO(D-Hpen-N,S)(D-pen-N,O,S)], while the remaining two units have a deprotonated form [ReO(D-pen-N,S)(D-pen-N,O,S)]$^-$. In the complex cation of **2**, the eight Re^V units are zigzag linked by three types of Ag^I atoms with different coordination geometries (Figure 3): a) Ag^I atoms coordinated by two S atoms from two Re^V units (Ag1 and Ag6; average Ag–S 2.473(4) Å), b) a trigonal-planar environment for Ag^I atoms coordinated by three S atoms from three Re^V units (Ag2 and Ag5; average Ag–S 2.513(4) Å), and c) Ag^I atoms in a tetrahedral geometry coordinated by one S and two O atoms from three Re^V units, as well as a water O atom (O41) located at the center of the 14-nuclear structure (Ag3 and Ag4; average Ag–S 2.500(4) Å, Ag–O 2.438(12) Å). Although the entire complex cation has no crystallographically imposed symmetry, a quasi C_2 axis passes through the central water oxygen atom. Interestingly, three types of thiolato S atoms are found in the complex cation of **2**: a) non-bridging S atoms (S2, S4, S6, S12, S14, and S16; average Re–S 2.282(4) Å), b) μ_2-S atoms bridging Ag^I and Re^V centers (S1, S5, S7, S8, S9, S10, S11, and S15; average Re–S 2.331(4) Å, Ag–S 2.489(4) Å), and c) μ_3-S atoms bridging two Ag^I and a Re^V centers (S3 and S13; average Re–S 2.373(4) Å, Ag–S 2.514(4) Å). In addition, there exist four types of Re^V units with different coordination modes: a) a monodentate S coordination with a μ_2-S bridge (Re1 and Re8), b) a monodentate S coordination with a μ_3-S bridge (Re2 and Re7), c) a bidenate O,S coordination with μ_2-O and μ_2-S bridges (Re3 and Re6), and d) a tridenate O,S,S coordination with a terminal O atom and two μ_2-S bridges (Re4 and Re5). Thus, the 14-nuclear $Re^V_8Ag^I_6$ oligomeric structure in **2** is constructed by the ingenious organization of three types of coordination geometries around the Ag^I atoms and four types of coordination modes of Re^V octahedral units, as well as three types of bridging modes of thiolato S atoms (Scheme 2). This situation is in contrast with the 2D extended structure of **1** (compare Figure 2 with Figure 4), in which the Ag^I atoms have only one kind of coordination environment and the Re^V units have only one type of coordination mode. It is noteworthy that each $Re^V_8Ag^I_6$ molecule of **2** is bound to four neighboring $Re^V_8Ag^I_6$ molecules through COOH···OOC

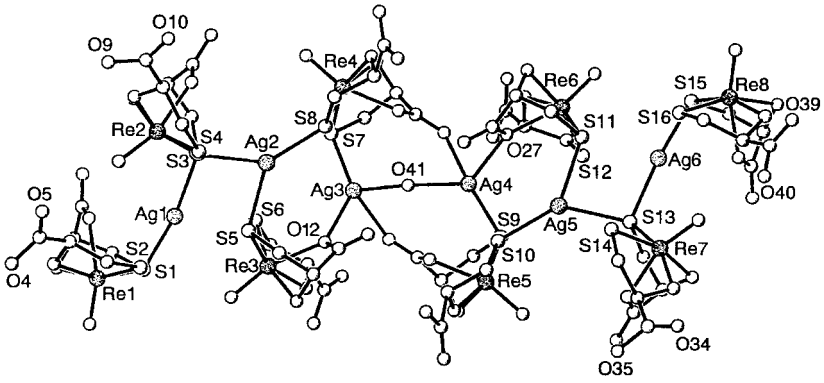
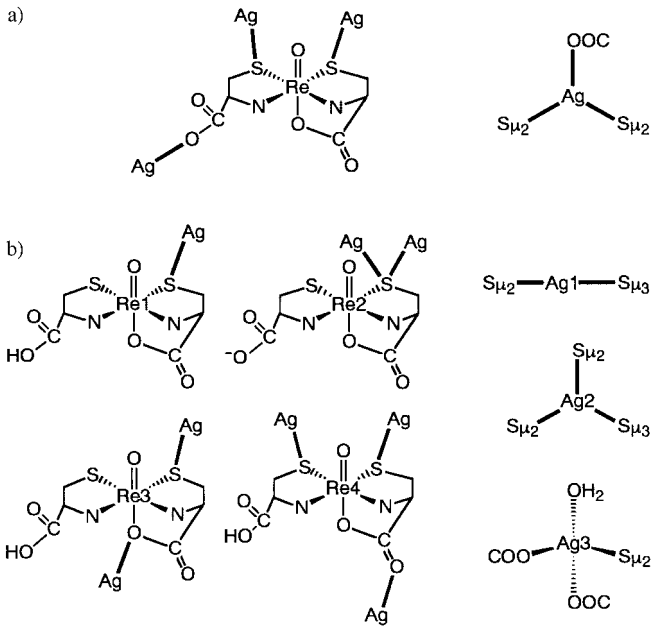


Figure 3. A perspective view of the $Re^V_8Ag^I_6$ olygomeric cation of **2**. Methyl groups of each D-pen ligand and hydrogen atoms are omitted for clarity.



Scheme 2. Coordination modes of Re^V units and coordination geometries of Ag^I atoms in **1** (a) and **2** (b).

 © 2002 WILEY-VCH Verlag

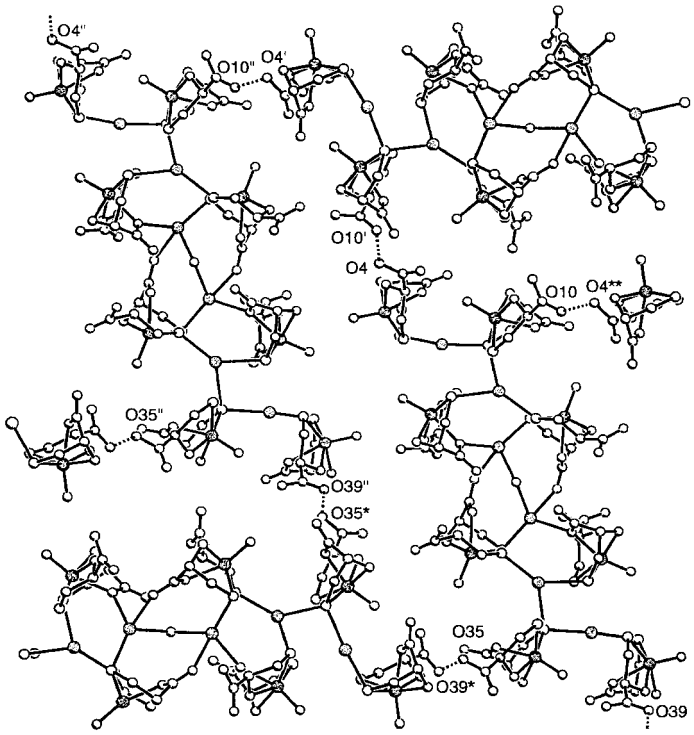


Figure 4. The 2D sheetlike structure of **2**. Methyl groups of each D-pen ligand and hydrogen atoms, as well as SiF_6^{2-} ions and lattice water molecules, are omitted for clarity.

hydrogen bonds (O4···O10′ 2.64(2) Å, O35···O39* 2.48(2) Å), which creates a 2D sheetlike structure made up of huge cyclic-$Re^{V}_{14}Ag^{I}_{10}$-network units. The existence of two deprotonated [ReO(D-pen-N,S)(D-pen-N,O,S)]$^-$ units,[11] together with the protonated [ReO(D-Hpen-N,S)(D-pen-N,O,S)] units, is essential for this hydrogen bonding, which would in turn contribute significantly to the stabilization of the 14-nuclear oligomeric structure of **2**. Thermogravimetric (TGA) analysis showed that the structure of **2** collapses above approximately 210 °C, while the collapsing temperature for **1** was approximately 240 °C. These results show that **2** is thermally less stable than **1**, partly because the COOH···OOC hydrogen bonds in **2** are expected to be weaker than the Ag–O coordination bonds in **1**.[12]

When an aqueous solution of **2** was treated with aqueous ammonia to adjust the pH to approximately 5, purple microcrystals of **1** were formed. This result implies that **2** reverts back to the polymeric structure of **1** on changing the pH of the solution, despite the different stoichiometries found in **1** (Ag:Re = 1:1) and **2** (Ag:Re = 3:4; Scheme 1). The electronic absorption and circular dichroism (CD) spectra of **1** and **2** in water, which were only qualitatively measured because of the poor solubility of the compounds, are essentially the same as the spectra of the starting material [Re^{V}O(D-Hpen-N,S)(D-pen-N,O,S)],[8] which shows a characteristic near-UV absorption band at approximately 340 nm with a shoulder at the shorter wavelength side and a major positive CD band also in this region. Furthermore, in the ^{1}H NMR spectrum in D_2O, **1** and **2** give only a single set of resonance signals arising from four methyl and two methine groups at nearly the same positions as the resonance signals observed for [Re^{V}O(D-Hpen-N,S)(D-pen-N,O,S)]. Thus, the rapid exchange of the Re^{V} octahedral units occurs in solution with retention of the *cis*(N)·*cis*(S)·*trans*(O) geometry, which is responsible for the pH dependent interconversion between **1** and **2**.[13]

In summary, the chiral mononuclear compound [Re^{V}O(D-Hpen-N,S)(D-pen-N,O,S)] readily reacts with Ag^+ ions to afford the 2D sheetlike coordination polymer **1**. This result shows that thiolato groups coordinated to a $[Re^{V}O]^{3+}$ core have an ability to bind with metal ions to form an S-bridged heterometallic polynuclear structure. In addition, the polymeric structure in **1** was successfully converted into **2** by treatment with aqueous H_2SiF_6 while retaining the coordination environment around the Re^{V} center. To our surprise, **2** was found to be a remarkable coordination oligomer composed of eight Re^{V} octahedra and six Ag^{I} ions. Although a large number of coordination polymers have been prepared from organic ligands and Ag^{I} ions, coordination oligomers containing Ag^{I} ions are quite rare.[14] Furthermore, **2** is the first example of a highly organized chiral molecular architecture involving three different coordination geometries of Ag^{I}, four different coordination modes of Re^{V} units, and three different bridging modes of thiolato donors, all existing in one quasi C_2 symmetrical molecule. Note that **2** constructs a 2D sheetlike structure, which results from the self-assembly of the 14-nuclear $Re^{V}_8Ag^{I}_6$ molecules through COOH···OOC hydrogen bonds, while the structure of **1** is the result of the self-assembly of tetranuclear $Re^{V}_2Ag^{I}_2$ molecules through Ag–O coordination bonds. Accordingly, the present results should provide an insight into the design and construction of second-generation metallo-supramolecular systems,[14b] which are generated by self-assembly processes of discrete metallo-supramolecules consisting of metal polyhedra, and should also contribute to the development of thiolatooxorhenium(V) chemistry which is currently drawing much attention for potential therapeutic applications in nuclear medicine.

Experimental Section

1: A solution of $AgNO_3$ (0.07 g, 0.41 mmol) in water (15 mL) was added to a stirred solution of [ReO(D-Hpen-N,S)(D-pen-N,O,S)][8a] (0.20 g, 0.40 mmol) in water (120 mL). The mixture was allowed to stand at RT for 3 days, and the resulting purple microcrystals were collected by filtration. Yield: 0.22 g (73 %); elemental analysis calcd (%) for [Ag{ReO(D-pen)$_2$}]·8H_2O; $C_{10}H_{34}AgN_2O_{13}ReS_2$: C 16.04, H 4.58, N 3.73; found: C 16.08, H 4.51, N 3.67; ^{1}H NMR (D_2O): δ = 1.29, 1.65, 1.82, 2.06 (CH_3), 3.14, 4.08 (CH). Dark purple plate crystals suitable for X-ray analysis were obtained as follows: a solution of $AgNO_3$ (0.07 g) in water (2 mL) was added to a stirred solution of [ReO(D-Hpen-N,S)(D-pen-N,O,S)] (0.20 g) in water (400 mL). The mixture was allowed to stand at RT for 3 days.

2: A 40 % solution of H_2SiF_6 (0.3 mL) was added dropwise to a stirred suspension of **1** (0.075 g, 0.05 mmol) in water (30 mL) , which gave a clear purple solution. The solution was allowed to stand at RT for 3 days, and the resulting brown-purple crystalline solid was collected by filtration. Yield: 0.044 g (69 %); elemental analysis calcd (%) for [Ag_6{ReO(D-Hpen)(D-pen)}$_6${ReO(D-pen)$_2$}$_2$(H_2O)](SiF_6)$_2$·10H_2O; $C_{80}H_{172}Ag_6F_{12}N_{16}O_{51}Re_8S_{16}Si_2$: C 18.81, H 3.39, N 4.39; found: C 18.47, H 3.35, N 4.34; ^{1}H NMR (D_2O): δ = 1.34, 1.66, 1.84, 2.08 (CH_3) 3.27, 4.13 (CH). Brown-purple plate crystals suitable for X-ray analysis were obtained as follows: several drops of 5 % aqueous H_2SiF_6 were added to a purple solution of **1** (0.03 g) dissolved in 0.4 % aqueous HBF_4 (10 mL), and the resulting solution was allowed to stand at RT for 2 weeks.

Received: July 15, 2002 [Z19739]

 © 2002 WILEY-VCH Verlag GmbH & Co. KGaA, Weinheim 0044-8249/02/4124-4714 $ 20.00+.50/0

[1] a) J. M. Lehn, *Supramolecular Chemistry: Concepts and Perspectives*, VCH, Weinheim, **1995**; b) P. J. Stang, B. Olenyuk, *Acc. Chem. Res.* **1997**, *30*, 502; c) C. Piguet, G. Bernardinelli, G. Hopfgartner, *Chem. Rev.* **1997**, *97*, 2005; d) M. Fujita, *Chem. Soc. Rev.* **1998**, *27*, 417; e) C. J. Jones, *Chem. Soc. Rev.* **1998**, *27*, 289; f) B. Olenyuk, A. Fechtenkötter, P. J. Stang, *J. Chem. Soc. Dalton Trans.* **1998**, 1707; g) D. L. Caulder, K. N. Raymond, *J. Chem. Soc. Dalton Trans.* **1999**, 1185; h) A. J. Blake, N. R. Champness, P. Hubberstey, W.-S. Li, M. A. Withersby, M. Schröder, *Coord. Chem. Rev.* **1999**, *183*, 117; i) J. A. R. Navarro, B. Lippert, *Coord. Chem. Rev.* **1999**, *185–186*, 653; j) S. Leininger, B. Olenyuk, P. J. Stang, *Chem. Rev.* **2000**, *100*, 853; k) G. F. Swiegers, T. J. Malefetse, *Chem. Rev.* **2000**, *100*, 3483; l) J. M. Lehn, *Science* **2002**, 295, 2400.

[2] a) T. Konno, T. Nagashio, K. Okamoto, J. Hidaka, *Inorg. Chem.* **1992**; b) Y. Kageyama, T. Konno, K. Okamoto, J. Hidaka, *Inorg. Chim. Acta* **1995**, 239, 19; c) T. Konno, K. Tokuda, T. Suzuki, K. Okamoto, *Bull. Chem. Soc. Jpn.* **1998**, *71*, 1049; d) K. Okamoto, C. Sasaki, Y. Yamada, T. Konno, *Bull. Chem. Soc. Jpn.* **1999**, *72*, 1685; e) T. Konno, Y. Chikamoto, K. Okamoto, T. Yamaguchi, T. Ito, M. Hirotsu, *Angew. Chem.* **2000**, *112*, 4264; *Angew. Chem. Int. Ed.* **2000**, *39*, 4098.

[3] a) T. Konno, K. Okamoto, J. Hidaka, *Inorg. Chem.* **1992**, *31*, 3875; b) T. Konno, K. Okamoto, J. Hidaka, *Inorg. Chem.* **1994**, *33*, 538; c) T. Konno, K. Okamoto, *Inorg. Chem.* **1997**, *36*, 1403.

[4] a) T. Konno, K. Tokuda, J. Sakurai, K. Okamoto, *Bull. Chem. Soc. Jpn.* **2000**, *73*, 2767; b) T. Konno, M. Hattori, T. Yoshimura, M. Hirotsu, *Chem. Lett.* **2000**, 852; c) T. Konno, M. Hattori, T. Yoshimura, M. Hirotsu, *Chem. Lett.* **2002**, 230.

[5] a) T. Konno, K. Tokuda, K. Okamoto, M. Hirotsu, *Chem. Lett.* **2000**, 1258; b) T. Konno, T. Yoshimura, K. Aoki, K. Okamoto, M. Hirotsu, *Angew. Chem.* **2001**, *113*, 1815; *Angew. Chem. Int. Ed.* **2001**, *40*, 1765; c) T. Konno, T. Kawamoto, R. Kuwabara, T. Yoshimura, M. Hirotsu, *Chem. Lett.* **2002**, 304.

[6] a) D. C. Jicha, D. H. Busch, *Inorg. Chem.* **1962**, *1*, 878; b) D. H. Busch, D. C. Jicha, *Inorg. Chem.* **1962**, *1*, 884; c) M. J. Heeg, R. C. Elder, E. Deutsch, *Inorg. Chem.* **1979**, *18*, 2036; d) M. J. Heeg, R. C. Elder, E. Deutsch, *Inorg. Chem.* **1980**, *19*, 554; e) T. Konno, K. Yonenobu, J. Hidaka, K. Okamoto, *Inorg. Chem.* **1994**, *33*, 861; f) T. Beissel, F. Birkelbach, E. Bill, T. Glaser, F. Kesting, C. Krebs, T. Weyhermüller, K. Wieghardt, C. Butzlaff, A. X. Trautwein, *J. Am. Chem. Soc.* **1996**, *118*, 12376; g) T. Glaser, T. Beissel, E. Bill, T. Weyhermuller, V. Schunemann, W. M. Klaucke , A. X. Trautwein, K. Wieghardt, *J. Am. Chem. Soc.* **1999**, *121*, 2193; h) S. Fox, R. T. Stibrany, J. A. Potenza, H. J. Schugar, *Inorg. Chim. Acta* **2001**, *316*, 122; i) A. C. Marr, D. J. E. Spencer, M. Schröder, *Coord. Chem. Rev.* **2001**, *219–221*, 1055.

[7] Only one report has appeared on the Mo^{IV} complex with four thiolato and two thioether donor groups, $[Mo^{IV}(SCH_2CH_2SCH_2CH_2S)_2]$, which binds with a single Ag^I ion in which the Ag^I center has a tetrahedral environment to form an S-briged $Mo^{IV}Ag^IMo^{IV}$ trinuclear structure. J. Hyde, J. Zubieta, *Inorg. Chim. Acta* **1981**, *54*, L137.

[8] a) L. Hansen, X. Xu, K. T. Yue, Z. Kuklenyik, A. Taylor, Jr., L. G. Marzilli; b) S. Kirsch, B. Noll, H. Spies, P. Leibnitz, D. Scheller, T. Krueger, B. Johannsen, *J. Chem. Soc. Dalton Trans.* **1998**, 455; c) T. Konno, Y. Shimazaki, M. Kawai, M. Hirotsu, *Inorg. Chem.* **2001**, *40*, 4250.

[9] K. Nakamoto, *Infrared and Raman Spectra of Inorganic and Coordination Compounds*, Wiley, New York, **1997**.

[10] Crystal structure analysis for **1**: Rigaku AFC7S diffractometer, $T = 23\,^\circ C$, $Mo_{K\alpha}$ radiation ($\lambda = 0.71069$ Å). The structure was solved by direct method (SIR92) and refined with full-matrix least-squares analysis on F^2 using SHELXL-93. Hydrogen atoms except those of water molecules were placed at calculated positions but were not refined. $C_{10}H_{34}AgN_2O_{13}ReS_2$, crystal size $0.07 \times 0.20 \times 0.22$ mm, orthorhombic, space group $C222_1$, $a = 13.636(3)$, $b = 22.586(4)$, $c = 15.486(3)$ Å, $V = 4769(1)$ Å^3, $Z = 8$, $\rho_{calcd} = 2.085$ g cm^{-3}, $\mu = 61.26$ cm^{-1}, ω–2θ scan mode, $2\theta_{max} = 55.0$, 3039 reflections collected, 3030 independent reflections, 2614 observed reflections ($F > 4\sigma(F)$), 264 parameters, empirical absorption corrections based on ψ scans, max/min transmission 0.999/0.550, R ($F > 4\sigma(F)$) = 0.034, wR_2 (all data) = 0.107, Flack parameter −0.01(1), residual electron density 1.19/−1.27 e Å^{-3}. Crystal structure analysis for **2**: Bruker CCD area detector, $T = -70\,^\circ C$, $Mo_{K\alpha}$ radiation ($\lambda = 0.71069$ Å). The structure was solved by direct methods (SHELXS-97) and refined with full-matrix least-squares analysis on F^2 using SHELXL-97. Hydrogen atoms were not included in the calculations. $C_{80}H_{172}Ag_6F_{12}N_{16}O_{51}Re_8S_{16}Si_2$, crystal size $0.11 \times 0.11 \times 0.45$ mm, monoclinic, space group $P2_1$, $a = 11.816(2)$, $b = 20.295(3)$, $c = 31.156(5)$ Å, $\beta = 90.049(3)^\circ$, $V = 7472(2)$ Å^3, $Z = 2$, $\rho_{calcd} = 2.271$ g cm^{-3}, $\mu = 75.51$ cm^{-1}, ω scan mode, $2\theta_{max} = 55.1$, 52277 reflections collected, 28443 independent reflections, 26902 observed reflections ($F > 4\sigma(F)$), 1721 parameters, empirical absorption corrections with SADABS, max/min transmission 0.549/0.186, $R_1(F > 4\sigma(F)) = 0.038$, wR_2(all data) = 0.083, Flack parameter −0.006(5), residual electron density 1.84/−1.61 e Å^{-3} (the peaks larger than 1.0 e Å^{-3} were found in the vicinity of heavy atoms). CCDC-189338 (**1**) and CCDC-189339 (**2**) contain the supplementary crystallographic data for this paper. These data can be obtained free of charge via www.ccdc.cam.ac.uk/conts/retrieving.html (or from the Cambridge Crystallographic Data Centre, 12 Union Road, Cambridge CB2 1EZ, UK; fax: (+44) 1223-336-033; or deposit@ccdc.cam.ac.uk).

[11] Based on the comparison of the C–O bond lengths (C6–O4 1.34(2), C16–O10 1.24(2), C66–O35 1.33(3), C76–O39 1.23(2) Å), the Re2 unit containing O10 and the Re8 unit containing O39 are assigned to have a deprotonated form (see Figure 3).

[12] a) M. Meot-Ner (Mautner), L. W. Sieck, *J. Am. Chem. Soc.* **1986**, *108*, 7525; b) T. Shoeib, K. W. M. Siu, A. C. Hopkinson, *J. Phys. Chem. A* **2002**, *106*, 6121.

[13] As indicated by the referees, the solid-state structures of **1** and **2** would not be retained in solution. The electrospray-ionization (ESI) mass spectrum of **2** in water mainly showed four clusters of peaks centered at m/z 605.1 (relative intensity: 100%), 623.2 (19%), 1103.1 (83%), and 1209.0 (21%). The calculated molecular mass and the isotopic distribution of these clusters of peaks match very well with those for $[Ag\{ReO(D\text{-}Hpen)(D\text{-}pen)\}]^+$, $[Ag\{ReO(D\text{-}Hpen)(D\text{-}pen)\}(H_2O)]^+$, $[Ag\{ReO(D\text{-}Hpen)(D\text{-}pen)\}_2]^+$, and $[Ag_2\{ReO(D\text{-}Hpen)(D\text{-}pen)\}\{ReO(D\text{-}pen)_2\}]^+$ ions, respectively. This result suggests that in water the $Re^V_8Ag^I_6$ 14-nuclear structure in **2** breaks down to $Re^V_2Ag^I$ trinuclear and $Re^V_2Ag^I_2$ tetranuclear species, followed by the dissociation of $Re^V_2Ag^I_2$ tetranuclear species into Re^VAg^I dinuclear species. Attempts to measure the ESI mass spectrum of **1** were unsuccessful, because of its extremely poor solubility in water.

[14] a) S.-P. Yang, X.-M. Chen, L.-N. Ji, *J. Chem. Soc. Dalton Trans.* **2000**, 2337; b) M. J. Hannon, C. L. Painting, E. A. Plummer, L. J. Childs, N. W. Alcock, *Chem. Eur. J.* **2002**, *8*, 2226.

Using Mass Spectrometry to Characterize Self-Assembled Monolayers Presenting Peptides, Proteins, and Carbohydrates**

Jing Su and Milan Mrksich*

Mass spectrometry (MS) is an important technique for characterizing the structures of surfaces and has several characteristics that are especially valuable in bioanalytical applications. In biochip applications, for example, MS offers the significant advantage that it does not require analytes to be labeled—either by direct attachment of fluorescent and radioactive labels or by binding of antibodies—and therefore offers greater flexibility in experiments.[1–4] Further, the use of immobilized ligands to isolate active proteins from the

[*] Prof. M. Mrksich, J. Su
Department of Chemistry
Institute for Biophysical Dynamics
The University of Chicago
5735 S. Ellis Avenue, Chicago, IL 60637 (USA)
Fax: (+1) 773-702-0805
E-mail: mmrksich@midway.uchicago.edu

[**] This work was supported by DARPA (N00173-01-1-G010).

background in a complex sample greatly simplifies the analysis of MS spectra.[5–7] Yet MS remains a secondary option to the use of fluorescence and radioactivity for characterizing biochips, in part because many programs still use home-built instrumentation and often require sophisticated protocols for analyzing mass data.[8–10] Here we demonstrate that matrix-assisted laser desorption/ionization and time-of-flight mass spectrometry (MALDI-TOF MS), when combined with self-assembled monolayers (SAMs) that are engineered to give specific interactions with biomolecules, is well suited for characterizing biological activities. We describe examples that use MS to characterize the immobilization of ligands, the selective binding of proteins, and the enzymatic modification of immobilized molecules.

Our approach relies on SAMs that present oligo(ethylene glycol) groups and peptide or carbohydrate ligands in low densities. The glycol groups are critical to this design, because they are highly effective at preventing nonspecific interactions with proteins and thereby ensure that the interactions of soluble proteins occur only by way of the immobilized ligands.[11–14] First, we used MALDI to characterize the immobilization of a peptide on a monolayer. Figure 1 a shows the mass spectrum of a SAM presenting maleimide and pentakis(ethylene glycol) groups in the ratio 1:4.[15–18] The spectrum shows the peaks for the sodium adducts of the symmetric glycol-substituted disulfide ($C_{42}H_{86}O_{12}S_2Na$, m/z 870) and for the mixed disulfide containing one maleimide group ($C_{52}H_{98}N_2O_{16}S_2Na$, m/z 1094).[19] The monolayer was treated with an aqueous solution containing the cysteine-terminated peptide Ac-IYAAPKKKC-NH_2 (2 mM) for 2 h, rinsed, and then analyzed by MS. The absence of the peak at m/z 1094 showed that the maleimide group had reacted under these conditions and gave rise to two new peaks (Figure 1 b), which represent the peptide-terminated alkanethiol ($C_{80}H_{139}N_{15}O_{21}S_2Na$, m/z 1733) and the mixed disulfide resulting from Michael addition of the cysteine-terminated peptide with the maleimide group ($C_{101}H_{181}N_{15}O_{27}S_3Na$, m/z 2155). We found that MALDI-TOF MS can identify substituted alkanethiolates with excellent sensitivity, with an adequate signal for the maleimide group even when presented at a density of 1 %.[20]

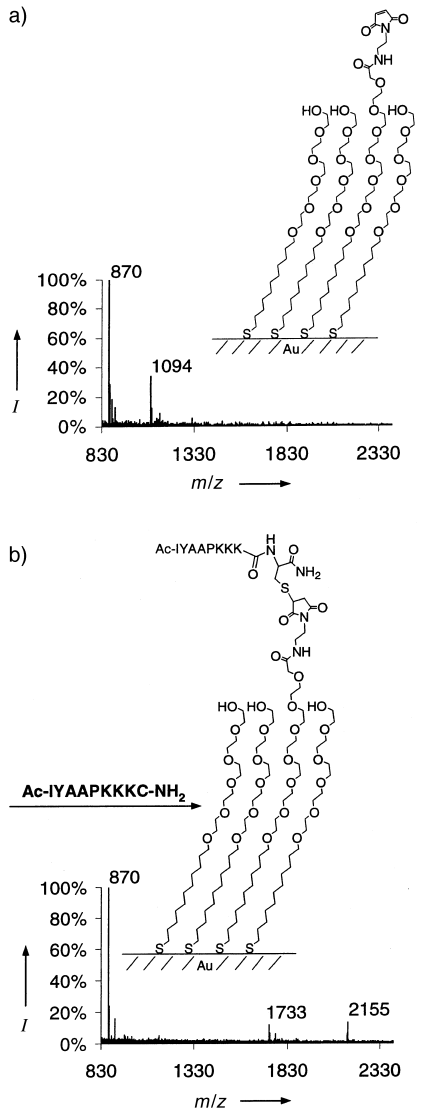


Figure 1. a) The MALDI spectrum of a mixed monolayer presenting pentakis(ethylene glycol) groups and maleimide groups shows a peak for the mixed disulfide (m/z 1094). b) The MALDI spectrum of the monolayer after treatment with the cysteine-terminated peptide Ac-IYAAPKKKC-NH_2 shows mass peaks resulting from immobilization of the peptide. The structure of each monolayer is shown above the spectra.

In an example relevant to biochips, a monolayer presenting the carbohydrate α-mannose and tris(ethylene glycol) groups in the ratio 1:4 was treated with a solution of Concanavalin A ($M \approx 102$ kD, 1 mg mL^{-1} in phosphate buffer, pH 7.4, containing 1 mM Ca^{2+} and 1 mM Mn^{2+}) for 30 min and then rinsed with distilled water (Figure 2 a). 3,5-Dimethoxy-4-hydroxycinnamic acid in 50 % aqueous acetonitrile solution containing 0.1 % trifluoroacetic acid (10 mg mL^{-1}) was applied to the monolayer and allowed to evaporate prior to MALDI analysis. The spectrum in Figure 2 b reveals peaks corresponding to the doubly ionized tetramer, trimer, and monomer of Concanavalin A, and to the singly charged dimer and monomer; this demonstrates that MALDI can directly observe proteins bound to ligands immobilized on monolayers.[21] Identical experiments with monolayers presenting only glycol groups gave no peaks in this mass range, and incubation of the mannose-presenting SAMs with lectin from *E. Cristagalli* ($M = 56$ kD), which does not bind to mannose, also gave no protein ion peaks. This example demonstrates that MALDI can identify proteins that are bound to SAMs presenting ligands.

In a third example, we used MALDI to characterize the enzymatic modification of an immobilized ligand (Figure 3 a). The MALDI spectrum of a monolayer presenting the carbohydrate *N*-acetylglucosamine (β-GlcNAc) and tris(ethylene glycol) groups in the ratio 1:4 showed a single intense peak at m/z 1211 that corresponds to the mixed disulfide with a single GlcNAc group ($C_{58}H_{113}N_3O_{17}S_2Na$, m/z 1211; Figure 3 b).[13] This monolayer was then treated with a HEPES buffer (50 mM, pH 7.5) containing β-1,4-galactosyltransferase (GalTase, 250 mU mL^{-1}), $MnCl_2$ (10 mM), and uridine diphosphogalactose (UDP-Gal, 20 μM) for 1 h at 20 °C and then rinsed. Analysis by MALDI showed a single intense peak at m/z 1373 that corresponds to the mixed disulfide containing *N*-acetyllactosamine (LacNAc, $C_{64}H_{123}N_3O_{22}S_2Na$, m/z 1373),

 © 2002 WILEY-VCH Verlag GmbH & Co. KGaA, Weinheim 0044-8249/02/4124-4716 $ 20.00+.50/0 *Angew. Chem. Int. Ed.* **2002**, *41*, No. 24

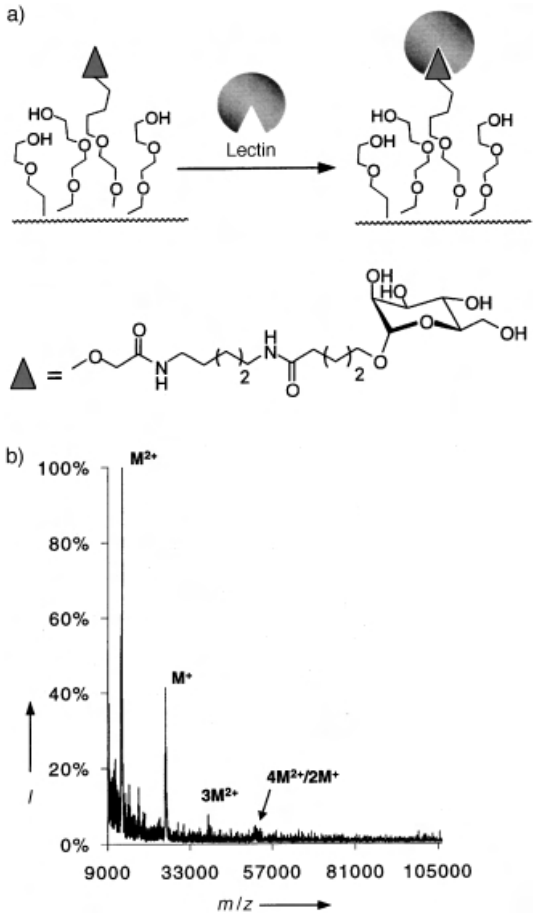


Figure 2. MALDI was used to characterize the selective binding of protein to ligands immobilized on a monolayer. a) A monolayer presenting the carbohydrate α-mannose was treated with an aqueous solution containing the lectin Concanavalin A (1 mg mL^{-1} in phosphate buffer, pH 7.4, 1 mM Ca^{2+} and 1 mM Mn^{2+}), rinsed, and then analyzed by MALDI. b) The peaks at *m*/*z* 25.6 kD and 12.8 kD correspond to the singly and doubly ionized monomer of Concanavalin A, respectively, and the small peaks at *m*/*z* 51 kD and 38 kD correspond to doubly ionized tetramer and trimer, respectively. This demonstrates that MALDI can be used to identify selective protein-binding interactions.

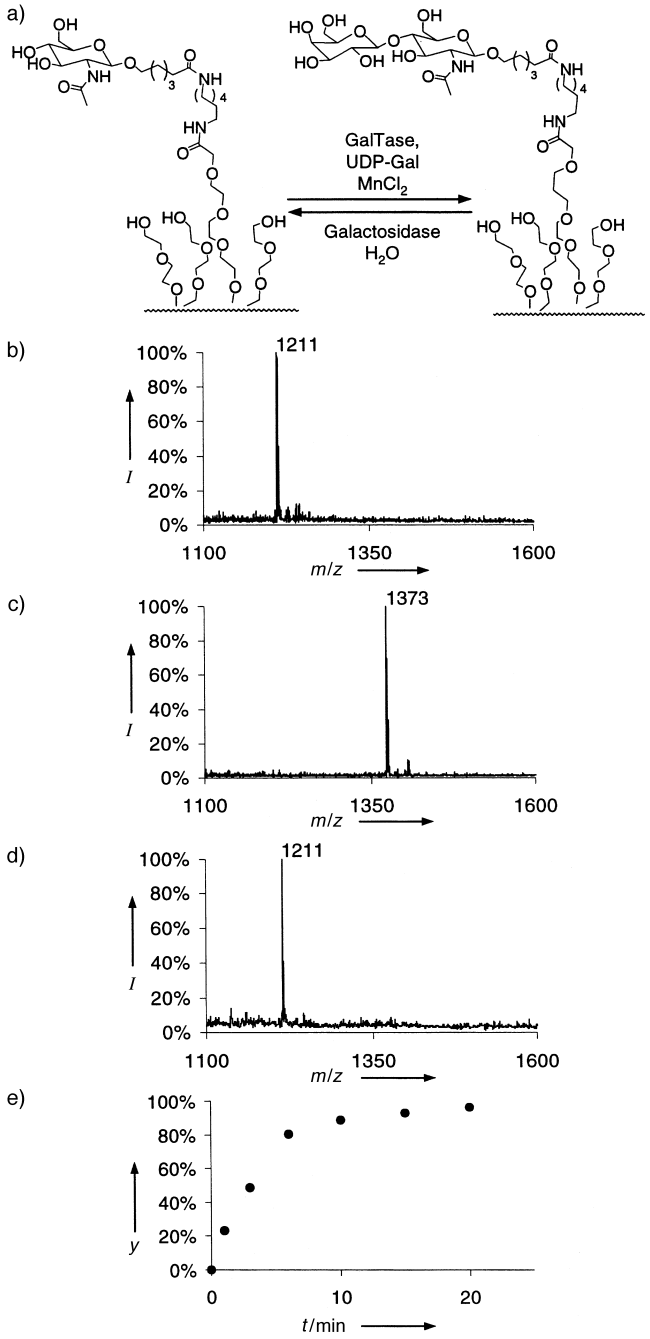


Figure 3. MALDI was used to characterize the enzymatic modification of an immobilized substrate. A monolayer presenting the carbohydrate β-GlcNAc (a) was analyzed by MALDI to reveal a peak at *m*/*z* 1211 for the mixed disulfide (b). c) After the monolayer was treated with the enzyme GalTase to introduce a terminal galactose residue, analysis by MALDI revealed a new peak at *m*/*z* 1373 corresponding to the disaccharide product. d) Treatment of this monolayer with the enzyme galactosidase removed the terminal galactose residue and regenerated the GlcNAc group. e) MALDI was used to determine the time-dependence of the enzymatic galactosylation which demonstrates that this technique can provide kinetic information on biological activities.

the disaccharide product that results from enzymatic galactosylation of GlcNAc (Figure 3c). The absence of a peak at *m*/*z* 1211 demonstrates that the enzymatic reaction was essentially complete. We next treated this chip with a solution containing the enzyme galactosidase (25 U mL^{-1}), $MgCl_2$ (1 mM), KCl (10 mM), and β-mercaptoethanol (50 mM) in phosphate buffer (pH 7.0) for 8 h at 37 °C. MALDI revealed that the LacNAc was enzymatically converted to GlcNAc in quantitative yield (Figure 3d). Control experiments showed that treatment of monolayers presenting α-mannose with either GalTase or galactosidase had no effect which again demonstrates the specificity intrinsic to this class of SAMs.

In a final example, we show that the combination of MALDI-TOF MS and SAMs can provide kinetic data for biological interactions on chips. We investigated the time-dependence of the GalTase-mediated galactosylation by treating identical SAMs presenting β-GlcNAc with the enzyme as described above for periods of time ranging from 0 to 20 min. The monolayers were each rinsed, dried, and analyzed by MALDI. We calculated the yield of the enzymatic conversion on each chip by taking a ratio of the peak integration area for LacNAc relative to the sum of the peak areas for LacNAc and GlcNAc (percentage yield $= A_L/[A_L + A_G] \times 100$).[22] Figure 3e demonstrates that the yield

 © 2002 WILEY-VCH Verlag GmbH & Co. KGaA, Weinheim 0044-8249/02/4124-4717 $ 20.00+.50/0

increased smoothly with time and reached a maximum at complete conversion. The same experiment was repeated several times, and the variability for each time point was less than 5%. This result indicates that MALDI, when combined with SAMs, may find wider use for kinetic analysis of interfacial reactions.

The most significant result of this work is that a commercial instrument for MALDI-TOF MS, when combined with self-assembled monolayers engineered for bioanalytical applications, is a very effective technique for characterizing biological activities at interfaces. We believe that this finding will be exploited for a range of purposes, but in particular for examining biochips. The recent development of strategies that use self-assembled monolayers for the preparation of peptide, protein, and carbohydrate arrays makes this technique immediately applicable.[14,23,24] The use of MALDI in these applications is significant because it can identify unexpected biological activities, while current methods for characterizing biochips require preliminary knowledge of the activity to be identified. Fluorescence detection of antibodies that bind to arrays, for example, will only identify activities that introduce or delete an antigen. Mass spectrometry, by contrast, will identify any change in mass at the interface—whether resulting from binding of a protein or modification by an enzyme—and hence can discover unanticipated activities. We believe that these properties, together with the widespread availability of commercial instruments, will make MALDI a popular and effective technique for applications in bioanalytical and surface chemistry.

Received: May 22, 2002
Revised: September 27, 2002 [Z19349]

[1] H. Zhu, J. F. Klemic, S. Chang, P. Bertone, A. Casmayor, K. G. Klemic, D. Smith, M. Gerstein, M. A. Reed, M. Snyder, *Nat. Genet.* **2000**, *26*, 283 – 289.
[2] R. M. T. de Wildt, C. R. Mundy, B. D. Gorick, I. M. Tomlinson, *Nat. Biotechnol.* **2000**, *18*, 989 – 994.
[3] U. Reineke, R. Volkmer-Engert, J. Schneider-Mergener, *Curr. Opin. Biotechnol.* **2001**, *12*, 59 – 64.
[4] P. J. Hergenrother, K. M. Depew, S. L. Schreiber, *J. Am. Chem. Soc.* **2000**, *122*, 7849 – 7850.
[5] M. Merchant, S. R. Weinberger, *Electrophoresis* **2000**, *21*, 1164 – 1177.
[6] T. Natsume, H. Nakayama, T. Isobe, *Trends Biotechnol.* **2001**, *19*, S28-S33.
[7] H. Zou, Q. Zhang, Z. Guo, B. Guo, Q. Zhang, X. Chen, *Angew. Chem.* **2002**, *114*, 668 – 670; *Angew. Chem. Int. Ed.* **2002**, *41*, 646 – 648.
[8] R. L. McCarley, T. D. McCarley, *Anal. Chem.* **1997**, *69*, 130 – 136.
[9] J. L. Trevor, K. R. Lykke, M. J. Pellin, L. Hanley, *Langmuir* **1998**, *14*, 1664 – 1673.
[10] L. Hanley, O. Kornieko, E. T. Ada, E. Fuoco, J. L. Trevor, *J. Mass Spectrom.* **1999**, *34*, 705 – 723.
[11] K. L. Prime, G. M. Whitesides, *J. Am. Chem. Soc.* **1993**, *115*, 10714 – 10721.
[12] M. Mrksich, G. B. Sigal, G. M. Whitesides, *Langmuir* **1995**, *11*, 4383 – 4385.
[13] B. T. Houseman, M. Mrksich, *Angew. Chem.* **1999**, *111*, 876 – 880; *Angew. Chem. Int. Ed.* **1999**, *38*, 782 – 785.
[14] B. T. Houseman, J. H. Huh, S. J. Kron, M. Mrksich, *Nat. Biotechnol.* **2002**, *20*, 270 – 274.
[15] G. Pale-Grosdemange, E. S. Simon, K. L. Prime, G. M. Whitesides, *J. Am. Chem. Soc.* **1991**, *113*, 12 – 20.
[16] B. T. Houseman, E. S. Gawalt, M. Mrksich, *Langmuir*, in press.
[17] Monolayers were prepared as described previously.[13] Substrates were cut into 1 cm^2 chips and treated with acetonitrile containing 2,5-dihydroxybenzoic acid (10 $mg\,mL^{-1}$, 1 μL). The substrates were allowed to dry and then analyzed on a Voyager-DE Biospectrometry mass spectrometer operating in the delayed extraction mode with a 3-ns pulse nitrogen laser (337 nm) for desorption and ionization with an accelerating voltage of 20 kV. Ions were detected as positive ions on a time-of-flight mass detector in the reflector mode, and external standards were used for mass calibration.
[18] When reporting the ratio of alkanethiolates present in a mixed SAM, we give the ratio of alkanethiols in the solutions used for the formation of the monolayer.
[19] The majority of the SAMs in this work gave mainly sodium adducts of the molecular ions. Throughout the text we provide empirical formulas and the expected monoisotopic masses for each observed disulfide.
[20] We found that application of a matrix was necessary for the observation of molecular ions from the monolayers, but we have not optimized the formulation of the matrix for these applications.
[21] Concanavalin A is a tetramer with four identical subunits. Under acidic conditions, this noncovalent protein polymer dissociates easily. For a reference spectrum, see: M. Monatte, C. Lesieur, B. Vécsey-Semjén, J. T. Buckley, F. Pattus, F. G. van der Goot, A. Van Dorsselaer, *Int. J. Mass Spectrom. Ion Processes* **1997**, *169*/170, 179 – 199.
[22] *A*: integration area of peaks, L: peak for LacNAc, G: peak for GlcNAc.
[23] B. T. Houseman, M. Mrksich, *Chem. Biol.* **2002**, *9*, 443 – 454.
[24] C. D. Hodneland, Y. S. Lee, D. H. Min, M. Mrksich, *Proc. Natl. Acad. Sci. USA* **2002**, *99*, 5084 – 5052.

A Method for Determining the Difference in Relative Apicophilicity of Carbon-Containing Substituents of 10-P-5 Phosphoranes**

Shiro Matsukawa, Kazumasa Kajiyama, Satoshi Kojima, Shin-ya Furuta, Yohsuke Yamamoto, and Kin-ya Akiba*

Apicophilicity is the relative preference of substituents to occupy the apical positions as opposed to the equatorial positions in trigonal bipyramidal (TBP) structures and is one of the fundamental properties of pentacoordinate compounds.

[*] Prof. Dr. K.-y. Akiba
Advanced Research Center for Science and Engineering
Waseda University
3-4-1 Ohkubo, Shinjuku-ku, Tokyo 169-8555 (Japan)
Fax: (+81) 3-5286-3165
E-mail: akibaky@waseda.jp
S. Matsukawa, Dr. S. Kojima, S.-y. Furuta, Prof. Dr. Y. Yamamoto
Department of Chemistry, Graduate School of Science
Hiroshima University
1-3-1 Kagamiyama, Higashi-Hiroshima 739-8526 (Japan)
Dr. K. Kajiyama
Department of Chemistry, School of Science
Kitasato University
1-15-1 Kitasato, Sagamihara 228-8555, Japan

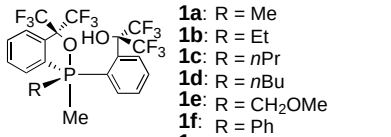
[**] The authors are grateful to Central Glass Co. Ltd. for a generous gift of hexafluorocumyl alcohol. Partial support of this work through Grant-in-Aid for Scientific Research (Nos. 09239103, 09440218, 11166248, 11304044, 12304044) provided by the Ministry of Education, Culture, Sports, Science, and Technology of the Japanese Government is acknowledged.

Supporting information for this article is available on the WWW under http://www.angewandte.org or from the author.

 © 2002 WILEY-VCH Verlag GmbH & Co. KGaA, Weinheim

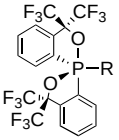
Especially, the implication that pentacoordinate intermediates play important roles in the reaction of phosphoryl groups in biological systems has given rise to theoretical and experimental investigations, which culminated in several apicophilicity scales for a variety of heteroatom substituents.[1,2] Experimental scales have mostly been built upon the relative activation energy of pseudorotation (a kinetic feature) of a series of phosphoranes that differ only in the substituent in question, by using techniques such as dynamic NMR spectroscopy in solution. According to the definition, however, the ideal apicophilicity scale should be based on the relative thermodynamic stability of two configurationally isomeric phosphoranes that differ only by interchange of one apical and one equatorial substituent, which are directly attached to the phosphorus center. Comparisons of stability between such isomers should especially be effective for the determination of relative apicophilicity among substituents of similar electronegativities, which would otherwise be extremely difficult to establish. Although some publications have appeared on the coexistence of such positional isomers in equilibrated mixtures,[3,4] no experimental investigation on relative apicophilicity in a thermodynamic sense has been reported except for that on CF_3 and F, which are of very similar apicophilicities.[4] In addition, although reactions of biological systems occur in aqueous media and it is thus essential to examine the effect of solvents on apicophilicity, no such effects have been observed to date, probably because of a lack of suitable systems to examine.

We recently prepared a novel family of phosphoranes **2** with an "anti-apicophilic" *O-cis* array of substituents containing carbon and oxygen atoms directly attached to the phosphorus center (equatorial oxygen–apical carbon atoms).[5] In an investigation of the reactivity of these unique phosphoranes, **1a** was a reaction product with MeLi.[6] This compound shows two distinct signals for the two methyl groups in the ^{1}H NMR spectrum, which suggested the possibility to freeze pseudorotation on the NMR spectroscopic timescale for phosphoranes bearing two different monodentate substituents directly connected to the phosphorus center through carbon atoms, and thus simultaneously show the presence of two isomeric phosphoranes which differ only in the position of these two substituents. To this end, several such compounds were prepared; these did show the coexistence of pairs of pseudorotamers. Here we report on a new method for determining the relative apicophilicity of several substituents on the phosphorus center that are directly attached by a carbon atom, based on the equilibrium ratio of these pairs of pseudorotamers in solution, that is, based on relative thermodynamic stability. In the process, we also found a distinct solvent effect on relative apicophilicity, and a novel phenomenon in which two different pseudorotamers (**1hA** and **1hB**) cocrystallize in the same single crystal by adjustment of the two substituents, which are carbon-containing groups (benzyl, Me), and of the recrystallization solvent (CH_3CN).



1a-i

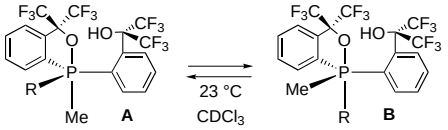
1a: R = Me
1b: R = Et
1c: R = *n*Pr
1d: R = *n*Bu
1e: R = CH_2OMe
1f: R = Ph
1g: R = $CH_2C_6H_4$(*p*-Me)
1h: R = CH_2Ph
1i: R = $CH_2C_6H_4$(*p*-F)



2

The ^{31}P NMR spectrum of **1a** in $CDCl_3$ showed a singlet ($\delta = -34.8$ ppm), and two resonance signals arising from methyl groups ($\delta = 2.57$ (d, $^2J_{PCH} = 13.7$ Hz, 3H), 1.46 ppm (d, $^2J_{PCH} = 5.9$ Hz, 3H)) were observed in the ^{1}H NMR spectrum at 23 °C. These observations suggested that the two-step Berry pseudorotation process,[7] which interchanges an apical and an equatorial substituent, was slowed down and the stereochemistry was fixed on the NMR spectroscopic timescale (Table 1). There have been ample demonstrations that pseudorotation is too fast to enable the determination of such equilibrium ratios in ordinary monocyclic compounds.[1a,b,2,8] However, the present system shows a unique and successful example, in which an intramolecular hydrogen bond between the hydroxy group of the monodentate aryl group and the apical oxygen atom of the five-membered ring could stabilize the stereochemistry of the 10-P-5 phosphoranes **1**.

Table 1. Substituent effect on the equilibrium ratios ($CDCl_3$) in **1b–1i**, and chemical shifts ($CDCl_3$, δ), and coupling constants ($^2J_{PCH}$) of the resonance signals for the methyl groups in the ^{1}H NMR spectra of **1a–1i**.



	R	Equilibrium ratio **A**:**B**[a]	$\Delta G°_{A\text{-}B}$ [kcal mol^{-1}]	σ_I	E_S	Chemical shifts δ [ppm] **A**	**B**	Coupling constants $^2J_{PCH}$ [Hz] **A**	**B**
1a	Me			−0.01	0.00	1.46	2.57	5.9	13.7
1b	Et	3.8:1	−0.79	−0.01	−0.07	1.47	2.59	5.9	13.3
1c	*n*Pr	5.0:1	−0.95	−0.01	−0.36	1.48	2.60	6.0	13.3
1d	*n*Bu	5.0:1	−0.95	−0.01	−0.39	1.48	2.60	5.9	13.7
1e	CH_2OMe	1:10	1.35	0.11	−0.19	1.60	2.64	7.0	14.5
1f	Ph	< 2: > 98	> 2.7	0.12		–	2.75	–	13.7
1g	$CH_2C_6H_4$(*p*-Me)	3.7:1	−0.77			1.17	2.63	6.3	13.4
1h	CH_2Ph	3.0:1	−0.65	0.03	−0.38	1.17	2.64	6.4	13.7
1i	$CH_2C_6H_4$(*p*-F)	2.4:1	−0.52			1.18	2.63	8.3	13.4

[a] **A**:**B** was determined by the integral values taken from the ^{1}H or ^{19}F NMR spectra.

 © 2002 WILEY-VCH Verlag GmbH & Co. KGaA, Weinheim 0044-8249/02/4124-4719 $ 20.00+.50/0

The phosphorane **1b** was prepared by a similar method.[9] The ^{31}P NMR spectrum of **1b** showed two singlets ($\delta = -21.9$ (major) and -25.3 ppm (minor); ratio: 3.8:1 in $CDCl_3$ at 23 °C) and two sets of signals arising from methyl and ethyl groups were observed in the ^1H and ^{13}C NMR spectra. For the major component, the coupling constants for the coupling of the methyl group protons and carbon atom to the phophorus center ($\delta = 1.47$ ($^2J_{PCH} = 5.8$ Hz), and 21.3 ppm ($^1J_{PC} = 27.1$ Hz)) were much smaller than the corresponding coupling constants of the minor component ($\delta = 2.59$ ($^2J_{PCH} = 13.3$ Hz) and 24.5 ppm ($^1J_{PC} = 97.9$ Hz)). Because coupling constants between an atom of an equatorial group and the central atom are generally larger than those between an atom of an apical group and the central atom,[1,10] the major component was assigned the structure **1bA** (apical methyl and equatorial ethyl groups), which coincides with its X-ray crystal structure (Figure 1). Likewise, the minor component was assigned to be

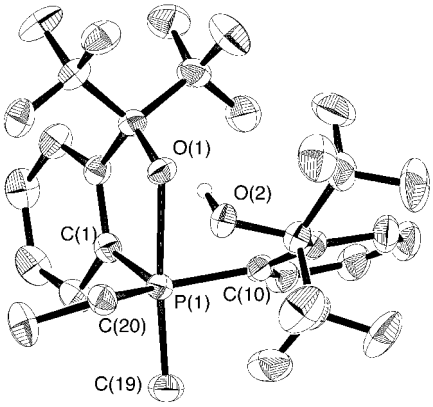


Figure 1. ORTEP drawing of **1bA** (thermal ellipsoids set at 30 %).

the pseudorotamer **1bB** (apical ethyl and equatorial methyl groups; Table 1). The X-ray analysis showed that the geometry about the phosphorus atom in **1bA** is a slightly distorted TBP with three carbon atoms (two *ipso* carbon atoms of the two Martin ligands,[1i] and the α carbon atom of the ethyl group in **1bA**) are at the equatorial sites of the TBP. As expected, the hydroxy proton on the oxygen atom O(2) of the monodentate ligand is hydrogen-bonded with the apical oxygen atom O(1) of the Martin ligand, which holds the relatively electronegative aryl group in the equatorial position.

Apicophilicity is governed by electronic and steric effects. Electronically, the more electronegative substituent usually prefers the apical position, whereas the more bulky substituent usually prefers the equatorial position. In the major component **1bA** the methyl group occupies the apical position, which supports the expectation that the apicophilicity of a methyl group is higher than that of an ethyl group, based on steric grounds, because the electronic effect is the same for both methyl and ethyl groups ($\sigma_I = -0.01$ for both, see Table 1).[1] To confirm that the assignments of stereochemistry are correct and that the observed ratio is based on thermodynamics, the crystal used for X-ray analysis was dissolved in toluene at −40 °C. At this temperature, only one set of signals (consistent with the major isomer **1bA**) was observed in the ^{31}P, ^1H, and ^{13}C NMR spectra. After the solution was warmed to −20 °C, another set of signals (corresponding to **1bB**) appeared gradually; equilibration was complete after 2 h at −20 °C. The rates of equilibration were calculated to be $3.22 \pm 0.12 \times 10^{-5}\ s^{-1}$ (**1bA**→**1bB**) and $1.40 \pm 0.05 \times 10^{-4}\ s^{-1}$ (**1bA**←**1bB**). Based on these values, the equilibration should be complete at 23 °C within 0.1 s.

Other derivatives (**1c**–**1i**) were also prepared, the ^1H, ^{13}C, and ^{31}P NMR spectroscopic data of which were very similar to those of **1b** (Table 1; see Supporting Information for ^{13}C and ^{31}P NMR spectroscopic data).[9] Therefore, the structures of the pseudorotamers in **1c**–**1i** were assigned similarly. The equilibrium ratios of **1c**–**1i** in $CDCl_3$ are summarized in Table 1 together with the values of their Hammett inductive constants (σ_I),[11] and the steric substituent constants (E_s).[12] A comparison among the series of phosphoranes bearing two different alkyl substituents (**1b**–**1d**) shows that steric factors play important roles in apicophilicity, because the σ_I constants are the same for the methyl, ethyl, *n*-propyl, and *n*-butyl groups. For **1f**, which has a phenyl group, only one singlet was observed ($\delta = -22.5$ ppm) in the ^{31}P NMR spectrum ($CDCl_3$) and one resonance signal of a methyl group ($\delta = 2.75$ ppm (d, $^2J_{PCH} = 13.7$ Hz, 3H)) was observed in the ^1H NMR spectrum, which indicate that the isomer **1fB** (apical phenyl and equatorial methyl groups) is exclusive in solution. The assignment was consistent with the X-ray analysis of **1f**, which does have the proposed structure **1fB** (see Supporting Information). This result shows that the apicophilicity of a phenyl group is considerably higher than that of a methyl group. The reason is probably because the phenyl group ($\sigma_I = 0.12$ in Table 1) is more electronegative than the methyl group ($\sigma_I = -0.01$).[1] Previous examinations of the relative apicophilicity between methyl and phenyl groups have produced conflicting results as, for example, Trippett and co-workers concluded that the methyl group was more apicophilic than the phenyl group,[13] whereas Holmes reported the opposite.[1b] Our results are consistent with those of Holmes.

The examination of intermediary cases would be interesting, that is, compounds in which one of the hydrogen atoms in the methyl group of **1a** is replaced with an electronegative group. Here, steric hindrance and electronegativity of the group are expected to work in opposite directions. Thus, for the highly electronegative and relatively small methoxymethyl group, a higher composition of the isomer of type **B** is expected than that in **1b** or **1c**. For the pair of isomers bearing the methoxymethyl group **1e**, the major isomer in the equilibrium is **1eB**, which shows that the inductive electronic effect overrides the steric effect. For **1h**, the major component was assigned the structure **1hA** (apical methyl and equatorial benzyl) and the minor component **1hB** (apical benzyl and equatorial methyl). The effect of the *para*-CH_3 and F substituents (**1g** and **1i**) on the equilibrium ratio resulted in a shift of the equilibrium ratio towards isomer **B** with the more electronegative substituent (**1g** < **1h** < **1i**), which indicates that the remote electronic effect through a benzene ring can also play a significant role. Therefore, in these cases, there is a counterbalance between the two factors, with the steric factor slightly dominating the electronic factor. Thus, the apicophilicity order of ligands that are directly attached to the

 © 2002 WILEY-VCH Verlag GmbH & Co. KGaA, Weinheim 0044-8249/02/4124-4720 $ 20.00+.50/0

Table 2. Solvent effect on the equilibrium ratios in **1b–1i** together with solvent parameters.

		$CDCl_3$	C_6D_6	[d_8]THF	[d_6]Acetone	CD_3CN
	ε[a]	4.89	2.40	7.47	21.36	36.00
	μ [$\times 10^{-30}$ Cm][a]	3.8	0	5.8	9.0	11.8
	E_T^N[a]	0.259	0.111	0.207	0.355	0.460
	R	**A**:**B**[b]	**A**:**B**[b]	**A**:**B**[b]	**A**:**B**[b]	**A**:**B**[b]
1b	Et	3.8:1	3.8:1	3.3:1	2.8:1	2.8:1
1c	*n*Pr	5.0:1	4.5:1	3.7:1	3.2:1	3.8:1
1d	*n*Bu	5.0:1	4.6:1	3.5:1	3.2:1	4.0:1
1e	CH_2OMe	1:10	1:9.8	1:15	1:11	1:9.7
1f	Ph	<2:>98	<2:>98	<2:>98	<2:>98	<2:>98
1g	$CH_2C_6H_4$(*p*-Me)	3.7:1	3.1:1	2.0:1	1.6:1	1.1:1
1h	CH_2Ph	3.0:1	2.3:1	1.3:1	1:1	1:1.2
1i	$CH_2C_6H_4$(*p*-F)	2.4:1	2.2:1	1.1:1	1:1.5	1:1.7

[a] Values of undeuterated solvents. [b] **A**:**B** was determined by the integral values in the ^1H or ^{19}F NMR spectra.

phosphorus by a carbon atom in $CDCl_3$ is as follows: Ph ≫ CH_2OMe ≫ Me > $CH_2C_6H_4$(*p*-F) > CH_2Ph > $CH_2C_6H_4$(*p*-Me) ≈ Et > *n*Pr ≈ *n*Bu.

When the solvent was changed from $CDCl_3$ to other solvents a distinct difference was observed, especially for the benzyl-substituted compounds (**1g–1i**). The equilibrium ratios in these solvents are shown in Table 2 together with solvent parameters (ε,[14] μ,[14] and E_T^N[14]). As a general trend, pseudorotamer **A** (**1gA–1iA**) was preferred in less polar solvents, and the ratios depended on the polarity of solvents. It should be noted that in CD_3CN the order of apicophilicity of the benzyl and methyl groups is reversed to 1:1.2 for **1h** and 1:1.7 for **1i**. This phenomenon suggests that the contribution of the electronic factor overcomes that of the steric factor in more polar solvents, especially in CD_3CN. Thus, in CD_3CN the apicophilicity order of ligands with carbon atoms directly attached to the carbon center is changed to Ph ≫ CH_2OMe ≫ $CH_2C_6H_4$(*p*-F) > CH_2Ph > Me > $CH_2C_6H_4$(*p*-Me) > Et > *n*Pr > *n*Bu.

Interestingly, the X-ray structures of **1g** and **1i**, which were crystallized from CH_3CN, coincided with the major pseudorotamer in CD_3CN, that is, **1gA** and **1iB**, respectively, although the isomer compositions were not far from 1:1. Similar precedence was recently seen in the study of spirophosphoranes bearing an eight-membered ring.[3e] The X-ray analysis of **1h** was more surprising, as it showed the presence of two pseudorotamers in the same crystal, that is, **1hA** and **1hB**. The ORTEP drawings of the two independent molecules are shown in Figure 2.[15] To our knowledge, this is the first example of the cocrystallization of two different pentacoordinate pseudorotamers in the same single crystal. Further investigations on analogous pseudorotamers with two carbon-atom-linked substituents of similar apicophilicity are in progress.

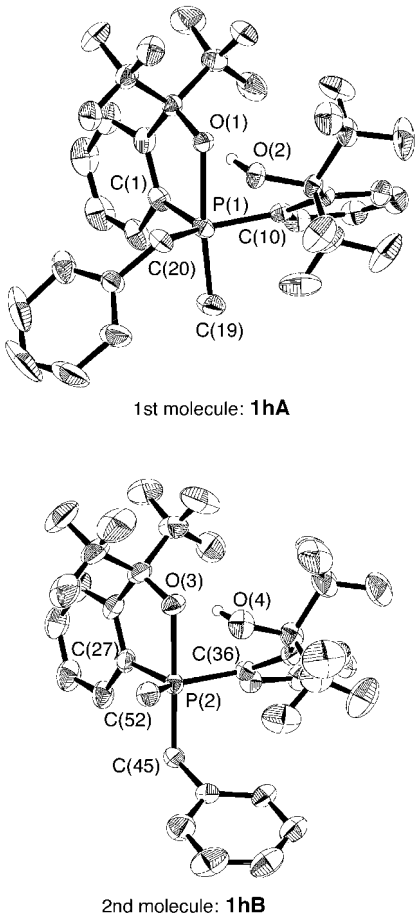


Figure 2. ORTEP drawing of **1h** (thermal ellipsoids set at 30%).

Received: May 10, 2002
Revised: September 11, 2002 [Z19280]

[1] a) K.-y. Akiba, *Chemistry of Hypervalent Compounds*, Wiley-VCH, Weinheim, **1999**; b) R. R. Holmes, *Pentacoordinated Phosphorus—Structure and Spectroscopy; ACS Monograph 175, 176, Vols. I, II*, American Chemical Society, Washington, DC, **1980**; c) S. Trippett, *Phosphorus Sulfur* **1976**, *1*, 89–98; d) R. Burgada, R. Setton in *The Chemistry of Organophosphorus Compounds* (Ed.: F. R. Hartley), Wiley-Interscience, Chichester, **1994**, pp. 185–272; e) R. S. McDowell, A. Streitwieser, Jr., *J. Am. Chem. Soc.* **1985**, *107*, 5849–5855; f) P. Wang, Y. Zhang, R. Glaser, A. E. Reed, P. v. R. Schleyer, A. Streitwieser, *J. Am. Chem. Soc.* **1991**, *113*, 55–64; g) G. R. J. Thatcher, A. S. Campbell, *J. Org. Chem.* **1993**, *58*, 2272–2281; h) B. D. Wladkowski, M. Krauss, W. J. Stevens, *J. Phys. Chem.* **1995**, *99*, 4490–4500; i) J. C. Martin, *Science* **1983**, *221*, 509–514; j) E. L. Muetterties, W. Mahler, R. Schmutzler, *Inorg. Chem.* **1963**, *2*, 613–618.

[2] a) M. Nakamoto, S. Kojima, S. Matsukawa, Y. Yamamoto, K.-y. Akiba, *J. Organomet. Chem.* **2002**, *643–644*, 441–452; b) S. Kojima, M. Nakamoto, K. Kajiyama, K.-y. Akiba, *Tetrahedron Lett.* **1995**, *36*, 2261–2264; c) S. Kojima, M. Nakamoto, K. Yamazaki, K.-y. Akiba, *Tetrahedron Lett.* **1997**, *38*, 4107–4110.

 © 2002 WILEY-VCH Verlag GmbH & Co. KGaA, Weinheim 0044-8249/02/4124-4721 $ 20.00+.50/0

[3] a) T. Kawashima, T. Soda, K. Kato, R. Okazaki, *Phosphorus Sulfur Silicon* **1996**, *109–110*, 489–492; b) T. Kawashima, T. Soda, R. Okazaki, *Angew. Chem.* **1996**, *108*, 1206–1208; *Angew. Chem. Int. Ed. Engl.* **1996**, *35*, 1096–1098; c) N. V. Timosheva, T. K. Prakasha, A. Chandrasekaran, R. O. Day, R. R. Holmes, *Inorg. Chem.* **1995**, *34*, 4525–4526; d) N. V. Timosheva, A. Chandrasekaran, T. K. Prakasha, R. O. Day, R. R. Holmes, *Inorg. Chem.* **1996**, *35*, 6552–6560; e) S. Kumaraswamy, C. Muthiah, K. C. Kumara Swamy, *J. Am. Chem. Soc.* **2000**, *122*, 964–965.

[4] O. Lösking, H. Willner, H. Oberhammer, J. Grobe, D. L. Van, *Inorg. Chem.* **1992**, *31*, 3423–3427.

[5] a) K. Kajiyama, M. Yoshimune, M. Nakamoto, S. Matsukawa, S. Kojima, K.-y. Akiba, *Org. Lett.* **2001**, *3*, 1873–1875; b) S. Kojima, K. Kajiyama, M. Nakamoto, K.-y. Akiba, *J. Am. Chem. Soc.* **1996**, *118*, 12866–12867; c) K. Kajiyama, S. Kojima, K.-y. Akiba, *Tetrahedron Lett.* **1996**, *37*, 8409–8412.

[6] S. Matsukawa, S. Kojima, K. Kajiyama, Y. Yamamoto, K.-y. Akiba, S. Re, S. Nagase, *J. Am. Chem. Soc.* **2002**, *124*, in press.

[7] R. S. Berry, *J. Chem. Phys.* **1960**, *32*, 933–938.

$$\mathbf{1bA} \xrightarrow{\Psi_{Et}} \xrightarrow{\Psi_{Me}} \mathbf{1bB}$$

[8] R. M. Moriarty, J. Hiratake, K. Liu, A. Wendler, A. K. Awasthi, R. Gilardi, *J. Am. Chem. Soc.* **1991**, *113*, 9374–9375.

[9] Spectroscopic data and ORTEP drawings are in the Supporting Information. Synthesis and complete characterization of the compounds will be reported in due course.

[10] S. Berger, S. Braun, H.-O. Kalinowski, *NMR Spectroscopy of the Non-Metallic Elements*, Wiley, Chichester, **1997**, p. 900.

[11] M. Charton, *Prog. Phys. Org. Chem.* **1981**, *13*, 119–251.

[12] R. W. Taft, Jr., *Steric Effects in Organic Chemistry* (Ed.: M. S. Newman), Wiley, New York, **1956**, p. 598.

[13] S. A. Bone, S. Trippett, P. J. Whittle, *J. Chem. Soc. Perkin Trans. 1* **1977**, 437–438.

[14] C. Reichardt, *Solvents and Solvent Effects in Organic Chemistry*, VCH, Weinheim, **1988**, pp. 407–411.

[15] CCDC-192716 (**1b**) and CCDC-153789 (**1h**) contain the supplementary crystallographic data for this paper. These data can be obtained free of charge via www.ccdc.cam.ac.uk/conts/retrieving.html (or from the Cambridge Crystallographic Data Centre, 12 Union Road, Cambridge CB2 1EZ, UK; fax: (+44) 1223-336-033; or deposit @ccdc.cam.ac.uk). Crystals suitable for X-ray structure determination were mounted on a Mac Science DIP2030 imaging plate equipped with graphite-monochromated $Mo_{K\alpha}$ radiation ($\lambda = 0.71073$ Å). Unit cell parameters were determined by autoindexing several images in each data set separately with program DENZO.[16] For each data set, rotation images were collected in 3° increments with a total rotation of 180° about ϕ. Data were processed by using SCALEPACK.[16] The structure was solved using the teXsan (Rigaku) system and refined by the full-matrix least-squares method. Crystal data for **1b**: monoclinic system, space group $P2_1/n$ (no. 14), $a = 10.4300(2)$, $b = 18.0140(4)$, $c = 12.4740(3)$ Å, $\beta = 102.795(1)°$, $V = 2285.49(9)$ Å^3, $Z = 4$, $\rho_{calc} = 1.628$ g cm^{-3}. $R = 0.0650$ ($Rw = 0.1453$) for 4749 observed reflections (325 parameters) with $I > 3\sigma(I)$. Goodness of fit = 1.362. Selected bond lengths [Å]: P(1)-O(1) 2.120(2), P(1)-C(1) 1.824(3), P(1)-C(10) 1.849(3), P(1)-C(19) 1.855(3), P(1)-C(20) 1.838(3). **1h**: triclinic system, space group $P\bar{1}$ (no. 2), $a = 11.7550(4)$, $b = 12.5610(8)$, $c = 18.904(1)$ Å, $\alpha = 93.532(2)$, $\beta = 102.047(3)$, $\gamma = 100.279(4)°$, $V = 2671.8(2)$ Å^3, $Z = 4$, $\rho_{calc} = 1.547$ g cm^{-3}. $R = 0.0658$ ($Rw = 0.1320$) for 7190 observed reflections (740 parameters) with $I > 3\sigma(I)$. Goodness of fit = 1.767. Selected bond lengths [Å], **1hA**: P(1)-O(1) 2.078(3), P(1)-C(1) 1.809(5), P(1)-C(10) 1.850(4), P(1)-C(19) 1.853(5), P(1)-C(20) 1.865(4); **1hB**: P(2)-O(3) 2.043(3), P(2)-C(27) 1.844(5), P(2)-C(36) 1.858(4), P(2)-C(45) 1.892(5), P(2)-C(52) 1.819(5).

[16] Z. Otwinowski, University of Texas, Southwestern Medical Center.

Preferential Location of Ge Atoms in Polymorph C of Beta Zeolite (ITQ-17) and Their Structure-Directing Effect: A Computational, XRD, and NMR Spectroscopic Study**

German Sastre, Jose A. Vidal-Moya, Teresa Blasco, Jordi Rius, Jose L. Jordá, Maria T. Navarro, Fernando Rey, and Avelino Corma*

Zeolites are crystalline aluminosilicates with a regular array of microporous systems which are responsible for the outstanding properties of these materials in adsorption, ion exchange, and catalysis.[1–3] Since most of these properties strongly depend on pore dimensions and topology, there is an incentive to develop tailor-made syntheses of zeolites. Although improvements in the understanding of zeolite synthesis have been made through the rational design of organic structure-directing agents (SDAs),[4] the predictable synthesis of the desired structures is far from being achieved, this is because of the large number of parameters that influence the reactions.

We recently showed that the rate of nucleation of zeolite ITQ-7, a zeolite containing double four-member rings (D4Rs), is strongly accelerated when Ge atoms are introduced into the framework.[5] Furthermore, by means of ^{19}F and ^{29}Si MAS NMR (MAS = magic-angle spinning) spectroscopy we indirectly postulated that the Ge atoms were preferentially occupying framework positions at the D4R units.[6] These observations made us think that the introduction of Ge atoms could direct the synthesis of zeolites towards structures containing D4Rs as secondary building units (SBUs), which are rare.[7] Our first attempt was directed to the synthesis of the previously elusive pure polymorph C of Beta zeolite, which contains D4Rs (with the International Zeolite Associ-

[*] Prof. A. Corma, Dr. G. Sastre, J. A. Vidal-Moya, Dr. T. Blasco, Dr. M. T. Navarro, Dr. F. Rey
Instituto de Tecnologia Química, (UPV-CSIC)
Universidad Politecnica de Valencia
Avenida Los Naranjos s/n, 46022 Valencia (Spain)
Fax: (+34) 96-387-7809
E-mail: acorma@itq.upv.es
Dr. J. Rius, Dr. J. L. Jordá
Institut de Ciencia de Materials de Barcelona (CSIC)
Campus de la UAB, 08193 Bellaterra, Catalunya (Spain)

[**] We thank Generalitat Valenciana (project GV01-492) and Spanish CICYT (projects MAT 2000-1392, MAT 2000-1167-C02-01, and PB98-0483) for financial support, and C^4 (Centre de Computacio i Comunicacions de Catalunya) and Centro de Cálculo de la Universidad Politécnica de Valencia for the use of their computational facilities. The High Performance Computational Chemistry Group from Pacific Northwest National Laboratory (Richland, Washington 993520999), is acknowledged for making available NWChem version 4.0, a computational chemistry package for parallel computers. The authors also acknowledge financial support from EEC ARI contract HPRI-CT-1999-00042 to access the HRSHTLNMR facility. We also thank Dr. L. Delevoye from Bruker Biospin for recording some NMR spectra. J.L.J. thanks UPV for a postdoctoral grant. J.A.V.M. acknowledges Bruker (Program I3P) for a predoctoral grant.

Supporting information for this article is available on the WWW under http://www.angewandte.org or from the author.

 © 2002 WILEY-VCH Verlag GmbH & Co. KGaA, Weinheim 0044-8249/02/4124-4722 $ 20.00+.50/0

ation code BEC[7a]). The silicon-free Ge material with BEC structure (named FOS-5[7b]) was first isolated from a ASU-9 and FOS-5 mixture. Later, a pure phase was obtained as a silicogermanate (ITQ-17[8]). We showed that pure polymorph C of Beta zeolite could be synthesized with a large variety of organic SDAs when Si atoms were partially substituted by Ge atoms,[8] regardless of whether F^- or OH^- ions were used as mineralizing agents.[8b] The synthesis of pure polymorph C of Beta zeolite represents a unique opportunity to prove the preferential occupation of Ge atoms in the D4Rs. Indeed, as ITQ-17 is a pure structure, XRD techniques can be used to unequivocally ascertain whether Ge tends to locate in the positions of the D4Rs.

Herein we report a complete study of ITQ-17 zeolite with different Si:Ge ratios by means of: a) computational chemistry techniques based on force-field methods and lattice-energy minimization, b) XRD and electron density studies, and c) ^{19}F MAS NMR spectroscopy. All these techniques point to the preferential siting of Ge at the D4R until four Ge atoms are present in these SBUs. As the Ge content increases, other sites start to become occupied preferentially to avoid the formation of Ge–O–Ge bonds in D4Rs, which would decrease the stability of the system.

The syntheses of Ge-containing ITQ-17 samples were performed by using a modified literature method (see Supporting Information).[8a]

The chemical composition and the main properties of the samples studied are summarized in Table 1. Pure polymorph C of the Beta intergrowth (BEC structure) is the only phase obtained in the whole range of Si:Ge ratios used. In contrast, when Ge is not present, ITQ-4 or Beta zeolites are produced. The directing effect of the Ge atoms is also reflected by the increasing crystallization time needed to obtain completely crystalline ITQ-17 zeolite when the Ge content in the synthesis gel is decreased.

Since the Ge atoms enter the BEC framework during the synthesis, the calculation of the stability of the different sites (Figure 1) must take into consideration the interaction of the SDA and fluoride species with the framework (the general unit cell composition is $Ge_xSi_{32-x}O_{64}F_2BD_2$; BD = the 1-benzyl-4-aza-1-azoniacyclo[2,2,2]octane cation).

The positions of the two fluoride anions can be safely placed at the two existing D4R cages per unit cell of the BEC structure by means of NMR spectroscopic techniques.

The orientation of the two BD^+ molecules was optimized by searching for the minimum energy configuration on the pure silica structure. Computational details are provided as Supporting Information.

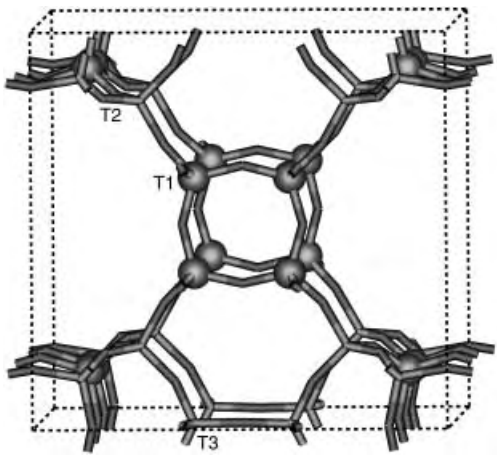


Figure 1. Crystallographic structure of ITQ-17 showing the three different T sites. T1 positions are at the D4Rs. T2 positions are connecting D4Rs, and T3 positions are part of single four-rings. Three interconnected straight 12 membered ring channels are present, the dimensions of which are: 5.9 × 6.5 Å (parallel to [100] and [010]) and 6.3 × 6.3 Å (parallel to [001]).

One Ge atom was alternatively placed at different T sites of the unit cell and the resultant systems were optimized again. The stability of the Ge-substituted frameworks was then calculated (Table 2). The Ge-atom incorporation in site T1 is the most favorable in the presence of SDA and F species. The Ge1 position appears more favored with respect to Ge2 and Ge3 by 44.3 and 58.0 kJ mol^{-1}, respectively. This points to a preferential location of the Ge atoms in the T1 sites, and to similar occupations of Ge at the T2 and T3 sites.

Table 2. Excerpt of the geometry analysis[20] of the calculated Ge-ITQ-17 with one Ge per unit formula, and including the template ($Ge_1Si_{31}O_{64}F_2BD_2$). The Ge atom is alternatively introduced in sites T1, T2, and T3.

	Ge in T1		Ge in T2		Ge in T3	
T-label	T-O-T [°]	T–O [Å]	T-O-T [°]	T–O [Å]	T-O-T [°]	T–O [Å]
Si1	138.1	1.623	138.1	1.625	138.2	1.625
Ge1	132.6	1.745	–	–	–	–
Si2	146.9	1.606	147.1	1.606	146.9	1.606
Ge2	–	–	142.5	1.715	–	–
Si3	154.7	1.598	154.4	1.597	155.2	1.597
Ge3	–	–	–	–	150.6	1.707

It is interesting to calculate the possible distributions of Ge for a composition within the samples of ITQ-17 synthesized in this work. The selected unit-cell composition was $Ge_{12}Si_{20}O_{64}F_2BD_2$. Again, all the atoms of the system, as well as

Table 1. Chemical compositions and main characterization results of Ge containing ITQ-17 samples.

Sample	Chemical composition [mol/unit cell]				Si:Ge ratio	Unit cell volume	Micropore volume	Crystallinity [%][b]
	Si	Ge	SDA	F	[Å^3/unit cell]		[cm^3 mol$_{TO2}^{-1}$][a]	
17 Ge[c]	14.80	17.20	2.96	1.74	0.9:1	2215	14.8	100
11 Ge[d]	20.57	11.43	2.68	1.95	1.8:1	2194	15.6	106
7 Ge[d]	24.87	7.13	2.32	1.58	3.5:1	2167	13.4	90
6 Ge[d]	26.05	5.95	2.53	1.19	4.4:1	2144	14.2	96
4 Ge[d]	28.08	3.92	2.00	n.d.	7.2:1	2145	12.0	81

[a] Calculated from the micropore volume determined by applying the t-plot method to the adsorption branch of the N_2 isotherm. [b] With respect to sample 17 Ge. [c] Synthesized using tetramethylammonium cations as SDA. [d] Synthesized using 1-benzyl-4-aza-1-azoniacyclo [2,2,2,] octane cations as SDA.

 © 2002 WILEY-VCH Verlag GmbH & Co. KGaA, Weinheim 0044-8249/02/4124-4723 $ 20.00+.50/0

the cell parameters, were allowed to relax during the optimizations. Although the most stable distribution of the twelve Ge atoms in the unit cell is unknown, it may be assumed that a) site T1 will be the most populated and b) the Ge occupations at T2 and T3 are similar. Therefore, the starting Ge occupations of eight Ge1, two Ge2, two Ge3 were proposed, so that eight T1, two T2, and two T3 positions were occupied by Ge atoms. Since the total number of sites is sixteen T1, eight T2, eight T3, there are many possible distributions. We checked a sampling of 100 random configurations with eight Ge1, two Ge2, two Ge3 and the final optimized energies are shown in Figure 2. From the analysis of these data it is difficult to extract trends which explain what makes one configuration more stable than another in terms of a single variable.

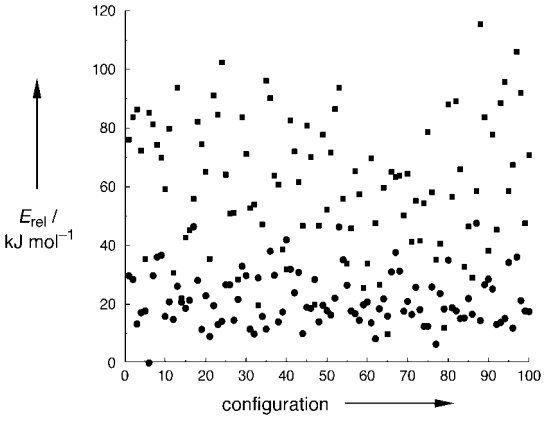


Figure 2. Plot of the energetic stability of 100 random configurations generated in the $Ge_{12}Si_{20}O_{64}F_2BD_2$ unit cell with eight Ge in T1 sites, two Ge in T2 sites, and two Ge in T3 sites (■); and with eight Ge in opposite corners of D4Rs, two Ge in T2 sites and two Ge in T3 sites (●).

The next step was to place eight Ge1 atoms in opposite corners of the two D4Rs since, because of their higher symmetry, this may induce low energy configurations. As in the previous case, the two Ge2 and two Ge3 atoms were distributed randomly among the corresponding eight T2 and eight T3 sites, respectively. 100 Random configurations were generated and the final minimized energies are plotted in Figure 2. It can be seen that most of these new 100 configurations are more stable than the previous 100 configurations. These computational calculations allow us to conclude that, in the presence of SDAs, the substitution of Si atoms by Ge atoms at the T1 site is energetically favored, and that at Si:Ge≅1.67:1, configurations with Ge at the opposite sites of a D4R are preferred to avoid formation of Ge–O–Ge bonds.

Calculations with five Ge1, one Ge2, and one Ge3 in the unit cell have also been performed ($Ge_7Si_{25}O_{64}F_2BD_2$ that is, Si:Ge≅3.5:1). Several distributions of a total of five Ge atoms among the two D4Rs (T1 sites) have been tested: a) three and two Ge atoms; b) four and one Ge atom(s), and finally, c) five and no Ge atoms. 100 Random configurations were generated and optimized for each starting distribution (Figure 3). It can be seen that the configurations with five Ge atoms in one D4R are clearly higher in energy, and consequently less probable

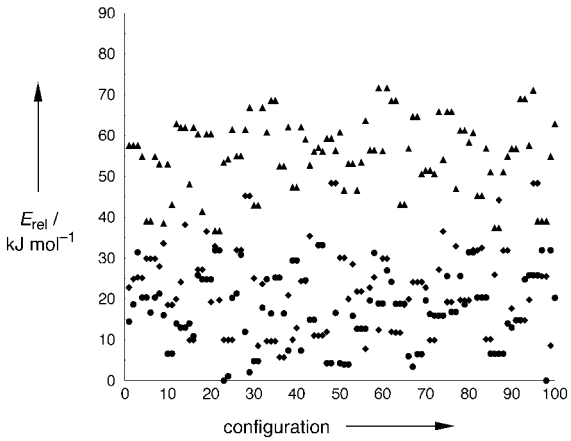


Figure 3. Plot of the energetic stability of 100 random configurations generated in the $Ge_7Si_{25}O_{64}F_2BD_2$ unit cell with: five Ge in T1 sites, one Ge in T2 sites, and one Ge in T3 sites. The five Ge in the two D4R (T1 sites) present in the unit cell have been distributed: three Ge in a D4R and two Ge in the other D4R (●), four Ge and one Ge (◆), and five Ge and zero Ge (▲).

than the configurations with three or four Ge atoms in each D4R.

The indexing of the XRD patterns of the calcined Ge-ITQ-17 samples and the subsequent analysis of the systematic absences confirm that all the samples belong to space group $P4_2/mmc$ (no. 131), that is, the space group is independent from the isomorphic replacement of Si atoms by Ge atoms. The corresponding Rietveld refinements were carried out starting from the previously reported structure of polymorph C[8] in which Si atoms had been partially substituted with Ge atoms.

As expected from its larger ionic radii, an increase in the Ge content produces a lengthening of the cell parameters and consequently an increase in the cell volume (Table 1), indicating that the Ge atoms replace the Si atoms isomorphically in the BEC stucture.

Additionally, the Ge distribution among the three different T sites of the BEC structure can be derived from the refinement of the respective scattering powers.

However, prior to any further discussion it is worth studying the stability of Ge atoms placed in framework positions upon calcination by comparing the Ge-atom distribution among the different crystallographic sites of a particular ITQ-17 sample (11 Ge) before and after calcination (see Supporting Information). No important differences in the Ge distribution are observed between the untreated ITQ-17 sample and the corresponding calcined ITQ-17 material, which indicates that the Ge atoms essentially remain in the framework, and at the same crystallographic sites upon calcination. Consequently, XRD analyses on the calcined materials can be safely performed.

The relative distribution of Ge atoms in these sites as a function of the total Ge content in the calcined ITQ-17 sample is given in Figure 4. The graphic shows that for a Ge content of less than approximately eight Ge atoms per unit cell (that is, Ge:(Si + Ge) ≈ 1:4), the Ge population grows more steeply at site T1 than at sites T2 and T3 which indicates the preferential incorporation of the Ge atoms in the D4R units. However, the

 © 2002 WILEY-VCH Verlag GmbH & Co. KGaA, Weinheim 0044-8249/02/4124-4724 $ 20.00+.50/0

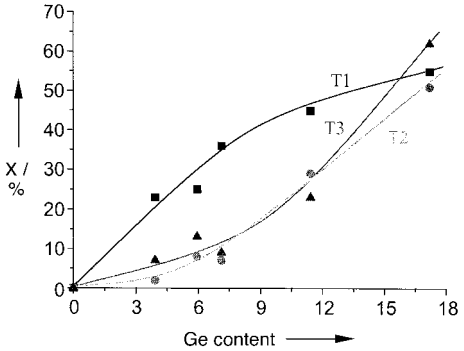


Figure 4. Relative Ge occupation in the different T sites of the polymorph C of the Beta zeolite as a function of the Ge content (number of Ge atoms per unit cell) of the ITQ-17.

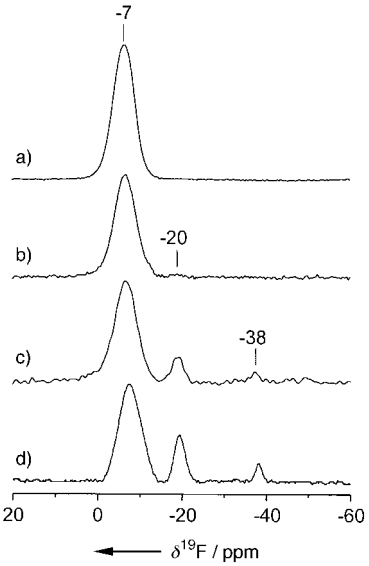


Figure 5. ^{19}F MAS NMR spectra of ITQ-17 at different Ge contents: a) 17 Ge, Si:Ge = 0.8:1; b) 11 Ge, Si:Ge = 1.8:1; c) 7 Ge, Si:Ge = 3.5:1; d) 4 Ge, Si:Ge = 7.2:1.

populations at T2 and T3 sites rise faster than for T1 when the Ge content is further increased.

Finally, it is interesting to calculate the evolution of the mean T1–O bond length in a D4R unit, for the sample Si:Ge = 0.9:1 it is 1.70(1) Å. For the rest of studied samples, the average oscillates between 1.67 and 1.68(1) Å. This small variation indicates a fast and selective filling of this site.

On the other hand, T2–O and T3–O bond lengths for the low-Ge-content samples correspond to that obtained for a typical Si–O bond that is, 1.62(1) Å, as expected from their low Ge occupancy at these positions. However, for the sample with a Si:Ge ratio of 0.9:1 (17 Ge), where a high replacement of Si atoms with Ge atoms takes place, these T–O bond lengths increase up to a value of 1.70(1) Å, as found for the T1 site.

The analysis of the XRD data clearly shows that, for low Ge contents, the incorporation of Ge atoms occurs preferentially at the T1 sites in the D4R units, with up to a 50% replacement. However, as soon as this value is reached, the two remaining T sites (T2 and T3) start to be preferentially occupied by Ge atoms. The XRD data gives information on the overall substitution of Ge atoms at T1 sites, but not about the distribution of the hetero atoms among the D4R cages. ^{19}F MAS NMR spectroscopy is very sensitive to the F^--ion environment and provides evidence for the heterogeneous nature of the D4R composition of Ge-ITQ-7.[6] Figure 5 shows the ^{19}F MAS NMR spectra of four Ge-ITQ-17 samples with different Ge contents. For sample 4 Ge (Si:Ge = 7.1:1), the spectrum consists of a relatively weak signal at $\delta = -38$ ppm typical of F^- ions located in pure siliceous D4R cages,[9,10] and two more resonance signals at $\delta = -20$ and -7 ppm. According to previous results for Ge-ITQ-7, the incorporation of Ge into the D4R sites can be estimated from the relative intensity of the ^{19}F resonance signals.[6] Assuming that the signal at $\delta = -20$ ppm is produced by F[7Si 1Ge] sites,[6] the assignment of the signal at $\delta = -7$ ppm to F[5Si 3Ge] or to F[4Si 4Ge] leads to site occupancies of 30% or 40%, respectively, the former having a better agreement with the XRD results (23% Ge at site T1).

For the samples with higher Ge content, 11 Ge and 17 Ge (Si:Ge = 1.8:1 and 0.9:1), the corresponding ^{19}F spectra only contain one resonance signal at $\delta = -7$ ppm, although some residual intensity at $\delta = -20$ ppm remains for the former. For these two samples, the Rietveld refinements yield around 50% Ge occupancy at site T1, so that the signal at $\delta = -7$ ppm in the ^{19}F NMR spectrum should be assigned to a fluoride ion in a D4R formed by four SiO_4 and four GeO_4 tetrahedra; that is, F[4Si, 4Ge].

Although the complete interpretation of the ^{19}F NMR spectra is not definitive, the results are consistent with those derived from the analysis of the XRD data. The downfield resonance signals in the ^{19}F NMR spectrum increase with the Ge content, and for Ge-rich samples 11 Ge and 17 Ge (Figure 5) almost the only spectral feature is the downfield signal.

In conclusion, these results suggest that in the ITQ-17 zeolite, Ge is being progressively incorporated into a D4R to reach four (or three) Ge atoms per cage, and then a further increase of the Ge content favors the substitution of Si atoms at crystallographic sites other than T1 at the D4R. In light of our previous results[5] and those presented here, it is possible to predict the formation of new zeolite structures containing D4R SBUs by introducing the directing effect of the Ge atoms.[11]

Experimental Section

XRD: The XRD measurements were carried out in an X'Pert diffractometer provided with a secondary graphite monochromator. In situ calcination of the prepared samples and the subsequent XRD measurements were performed as described in the Supporting Information. Inspection of the diffraction patterns indicates no significant amorphous material except for the sample prepared with the highest Si:Ge ratio.

Rietveld Refinement: The space-group symmetry of the calcined samples was first checked with the whole-profile fitting program AJUST.[12] The subsequent Rietveld refinements with the program FULLPROF 98[13] were performed using the 2Θ range from 5 to 70° with two excluded regions, 38.76°–40.76° and 45.24°–47.24°, because of the presence of the (111) and (200) diffraction peaks of the Pt sample holder. Eight profile parameters (including cell parameters and zero shift) and 25 structural parameters were refined using a pseudo-Voigt function with a visually estimated background. The Ge distribution among the different T sites was derived

 © 2002 WILEY-VCH Verlag GmbH & Co. KGaA, Weinheim 0044-8249/02/4124-4725 $ 20.00+.50/0

from the refined effective number of electrons at each T site by taking advantage of the high contrast between the scattering powers of Si and Ge.

Solid state NMR spectroscopy: The spectra were recorded under magic angle spinning (MAS) at room temperature. ^{19}F spectra were was measured in a Bruker Av-400 spectrometer at 376.8 MHz in 2.5 mm diameter zirconia rotors at spinning rate of 30 kHz. The ^{19}F spectra were collected using pulses of 3 μs corresponding to a magnetization flip angle of π/2 rad and a recycle delay of 100 s to ensure the complete recovery of the magnetization. The ^{19}F spectra were referred to $CFCl_3$.

Computational chemistry: methodology and model. All calculations were performed using lattice-energy minimization techniques and the GULP code,[14] employing the Ewald method for summation of the long-range Coulombic interactions, and direct summation of the short-range interactions with a cutoff distance of 12 Å. The RFO (rational function optimiser) technique was used as the cell minimization scheme with a convergence criterion of a gradient norm below 0.001 eV Å^{-1}. The empirical shell model forcefield for zeolites[15] was used throughout, with the inclusion of the forcefields for Ge[16] and F[17] atoms. The force-fields by Kiselev et al.,[18] and by Oie et al.[19] were used for the SDA–zeolite and SDA–SDA interactions, respectively. In the organic SDA, the charge distribution has been obtained by means of the quantum chemistry Hartree–Fock method by using a 6-31G** basis set and the calculations have been performed by means of the NWCHEM package.

Received: May 22, 2002
Revised: September 24, 2002 [Z19356]

[1] J. A. Rabo, P. H. Kasai, *Prog. Solid State Chem.* **1975**, *9*, 1.
[2] D. Barthomeuf, *J. Phys. Chem.* **1979**, *83*, 249.
[3] P. A. Jacobs, *Catal. Rev. Sci. Eng.* **1982**, *24*, 415.
[4] R. F. Lobo, S. I. Zones, M. E. Davis, *J. Inclusion Phenom. Mol. Recognit. Chem.* **1995**, *21*, 47.
[5] A. Corma, M. J. Díaz-Cabañas, V. Fornés, *Angew. Chem.* **2000**, *112*, 2436; *Angew. Chem. Int. Ed.* **2000**, *39*, 2346.
[6] T. Blasco, A. Corma, M. J. Diaz-Cabañas, F. Rey, J. A. Vidal-Moya, C. M. Zicovich-Wilson, *J. Phys. Chem. B* **2002**, *106*, 2634.
[7] a) C. Baerlocher, W. M. Meier, D. H. Olson, *Atlas of Zeolite Framework Types*. 5th revised edition, Elsevier, Amsterdam, **2001**. Also in http://www.iza-structure.org/; b) T. Conradsson, M. S. Dadachov, X. D. Zou, *Microporous Mesoporous Mater.* **2000**, *41*, 183.
[8] a) A. Corma, M. T. Navarro, F. Rey, J. Rius, S. Valencia, *Angew. Chem.* **2001**, *113*, 2337; *Angew. Chem. Int. Ed.* **2001**, *40*, 2277; b) A. Corma, M. T. Navarro, F. Rey, S. Valencia, *Chem. Commun.* **2001**, 1486.
[9] P. Caullet, J. L. Guth, J. Hazm, J. M. Lamblin, *Eur. J. Solid State Inorg. Chem.* **1991**, *28*, 359.
[10] L. A. Villaescusa, P. A. Barrett, M. A. Camblor, *Angew. Chem.* **1999**, *111*, 2164; *Angew. Chem. Int. Ed.* **1999**, *38*, 1997.
[11] A. Corma, M. J. Díaz-Cabañas, J. Martínez-Triguero, F. Rey, J. Rius, *Nature* **2002**, *418*, 514.
[12] J. Rius, J. L. Jordá, AJUST/01, Institut de Ciència de Materials de Barcelona (CSIC).
[13] J. Rodríguez-Carvajal, T. Roisnel, FULLPROF 98 and WinPLOTR: New Windows 95/NT Applications for Diffraction Commission For Powder Diffraction, International Union for Crystallography, Newletter No. 20 (May-August) **1998**.
[14] J. D. Gale, *J. Chem. Soc. Faraday Trans.* **1997**, *93*, 629.
[15] R. A. Jackson, C. R. A. Catlow, *Mol. Simul.* **1988**, *1*, 207.
[16] G. Sastre, J. D. Gale, *Chem. Mater.*, submitted.
[17] A. R. George, C. R. A. Catlow, *Zeolites* **1997**, *18*, 67.
[18] A. V. Kiselev, A. A. Lopatkin, A. A. Shulga, *Zeolites* **1985**, *5*, 261.
[19] T. Oie, T. M. Maggiora, R. E. Christoffersen, D. J. Duchamp, *Int. J. Quantum Chem. Quantum Biol. Symp.* **1981**, *8*, 1.
[20] G. Sastre, J. D. Gale, *Microporous Mesoporous Mater.* **2001**, *43*, 27.

Solid-State NMR Studies of MCM-41 Supported with a Highly Catalytically Active Cluster**

Matthew D. Jones, Melinda J. Duer,*
Sophie Hermans, Yaroslav Z. Khimyak,
Brian F. G. Johnson, and John Meurig Thomas

In 1992, Beck et al.[1] reported the first synthesis of a new classification of silicate/aluminosilicate materials. The topic of this work, MCM-41, is one such member of this extensive family of mesoporous materials.[1] The high surface area, typically up to 1000 $m^2 g^{-1}$, and the high concentration of silanol groups has led to the exploitation of this material as a support for anchored catalysts, in particular the highly promising catalysts derived from bimetallic clusters.[2,3] Bimetallic nanoparticles are becoming increasingly important in modern heterogeneous catalysis,[4] because of enhanced catalytic activity arising from the synergetic effects between the two metallic moieties. Further enhancement of activity is brought about by the small size of the particles. Recently, highly effective hydrogenation catalysts based on bimetallic clusters encapsulated in the channels of MCM-41 have been developed.[3,5–7] For example, the nanocatalyst derived from the cluster $[Pd_6Ru_6(CO)_{24}][NEt_4]_2$ is highly effective in the conversion of naphthalene to *cis*-decalin under mild conditions.[7] The formation of these nanocatalysts involves first the deposition of the anionic cluster within the pores of MCM-41 followed by removal of CO ligands, which produces the supported "naked" nanoparticles. Significantly, we have been able to establish, by FT-IR and EXAFS spectroscopy, that the structural motif of the cluster is maintained in the mesopore.[7,8] The further development of these very important catalytic systems depends crucially on understanding how the clusters are supported in the mesopore. We have recently completed a study which demonstrates the importance of the counterion in the binding process. We show that the counterion is intrinsically linked to the walls of the mesopore, acting like a molecular "glue" binding the cluster.

In particular we have studied the interactions between the surface of MCM-41 and the highly effective catalyst derived from the $[Pd_6Ru_6(CO)_{24}][NEt_4]_2$ cluster, by solid-state NMR spectroscopy. We have used $^{29}Si\{^1H\}$ cross polarization (CP)

[*] Dr. M. J. Duer, M. D. Jones, Dr. S. Hermans, Dr. Y. Z. Khimyak, Prof. B. F. G. Johnson
Department of Chemistry
University of Cambridge
Lensfield Road, Cambridge CB2 1EW (UK)
Fax: (+44) 1223-336017
E-mail: mjd13@cam.ac.uk
Prof. Sir J. M. Thomas
The Royal Institution of Great Britain
Davy Faraday Research Laboratory
21 Albermarle Street, London W1X 4BS (UK)

[**] We thank the EPSRC for a studentship to M.D.J. and for their general financial support, ICI for financial support, Newnham College Cambridge for a research fellowship to S.H., and an Oppenheimer Research Fellowship for Y.K.

Supporting information for this article is available on the WWW under http://www.angewandte.org or from the author.

 © 2002 WILEY-VCH Verlag GmbH & Co. KGaA, Weinheim 0044-8249/02/4124-4726 $ 20.00+.50/0

magic angle spinning (MAS) for the main characterization. This selects the ^{29}Si sites that are close to the silanol groups, that is, predominantly ^{29}Si sites on the MCM-41 channel surfaces. A ^{1}H–^{29}Si two-dimensional heteronuclear correlation (HETCOR) experiment and $^{13}C\{^{1}H\}$ CP/MAS gives a compelling picture of the nature of the counterion binding. The combined results of these experiments leads to unusually detailed conclusions about the location and structure of the deposited cluster in MCM-41, which raises new questions about the possible catalytic activity of a catalyst formed in this way.

Initial $^{29}Si\{^{1}H\}$ CP/MAS NMR studies on freshly prepared dehydrated MCM-41 yielded three distinct Gaussian peaks (Figure 1) with centers at $\delta = -91$ ppm, $Si(OSi)_2(OH)_2$, (Q^2), $\delta = -100$ ppm, $Si(OSi)_3OH$, (Q^3), and $\delta = -109$ ppm $Si(OSi)_4$, (Q^4), wholly consistent with literature data.[9,10]

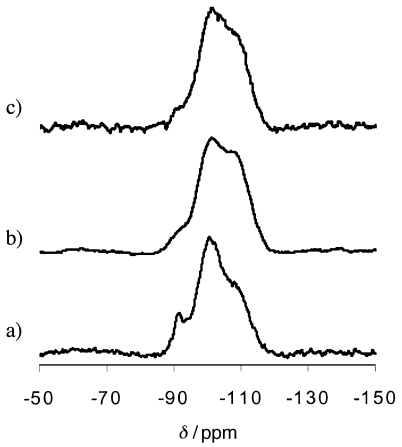


Figure 1. $^{29}Si\{^{1}H\}$ CP/MAS spectra: a) calcined dehydrated MCM-41 (6000), b) fuctionalized with $[Pd_6Ru_6(CO)_{24}]NEt_4]_2$ (6708), and c) activated cluster on MCM-41 (6116). Contact time = 8 ms and a recycle delay of 8 s. Spinning rate = 4 kHz. Numbers in brackets represent the number of scans taken per spectrum.

Deposition of $[Pd_6Ru_6(CO)_{24}][NEt_4]_2$ within the channels reduces the relative intensity of the signals from the Q^2 and Q^3 sites compared with the Q^4, as indicated by the ^{29}Si CP/MAS NMR spectra recorded under the same experimental conditions (Figure 1). We have also studied the catalytically active species, generated by removing the protective CO ligand sheath by gentle thermolysis in a vacuum.[6] This process is known from previous studies to form discrete bimetallic particles highly dispersed on the internal surface of MCM-41.[3,8] Comparison of the spectra in Figure 1 shows that the change in the relative intensity of the Q^2/Q^3/Q^4 peaks upon forming the "naked" metallic particle is not substantial. The elemental analysis of the activated and nonactivated forms are given in the Experimental Section. They show that a significant amount of the counterion is still present after the thermal treatment; this might explain why there is no significant change once activated.

The peak intensity of a cross polarization (CP) spectrum depends not only on the occupancy of ^{29}Si sites but on cross polarization dynamics. The CP dynamics are affected by changes in the structure and number of ^{1}H sites in close proximity to the ^{29}Si site as well as by any molecular motion in the system. CP/MAS ^{29}Si spectra were recorded for contact times in the range 0.5–15.0 ms for both pure MCM-41 and MCM-41 deposited with $[Pd_6Ru_6(CO)_{24}][NEt_4]_2$. The CP dynamic curves for the two systems (Figure 2) were fitted according to Equation (1).[11,12]

The curves show a significant change in the $^{29}Si\{^{1}H\}$ CP/MAS dynamics once the MCM-41 is impregnated with the cluster. In particular, the rate of cross polarization transfer increases dramatically for the Q^4 site, and both Q^2 and Q^3 curves show pronounced ^{1}H $T_{1\rho}$ relaxation effects, which are not observed for the pure MCM-41. For the Q^3 sites the parameter T_{cp} changes from 1.2 ms for MCM-41 to 1.4 ms for that of the supported species (within experimental error bounds of the experiment), whilst for the Q^4 site T_{cp} decreases significantly from 27 ms to 5.3 ms for the supported species. The Supporting Information contains a full analysis of the CP dynamics. This parameter, T_{cp}, is a measure of polarization transfer rate, and effectively the closer the source of ^{1}H is to the ^{29}Si site the shorter the T_{cp}. The much stronger $T_{1\rho}$ relaxation effect in the MCM-41 impregnated with the cluster suggests that in this system there is a much more extensive ^{1}H network contributing to the cross polarization to ^{29}Si than in the pure MCM-41. Very slow $T_{1\rho}$ relaxation for pure MCM-41 suggests that the ^{1}H source is very mobile or that there is a weakly coupled ^{1}H network. For MCM-41 the cross polarization proceeds from the SiOH groups within the mesopore. It is clear that upon deposition of the cluster, a new polarization source occurs. The most obvious explanation of this phenomenon is that the counterion of the cluster is in close proximity to the surface of MCM-41 and participates in

$$M(t_m) = M_0\left(1 - T_{CP}/T_{1\rho H}\right)^{-1}\left[\exp\left(-t_m/T_{1\rho H}\right) - \exp\left(-t_m/T_{CP}\right)\right] \qquad (1)$$

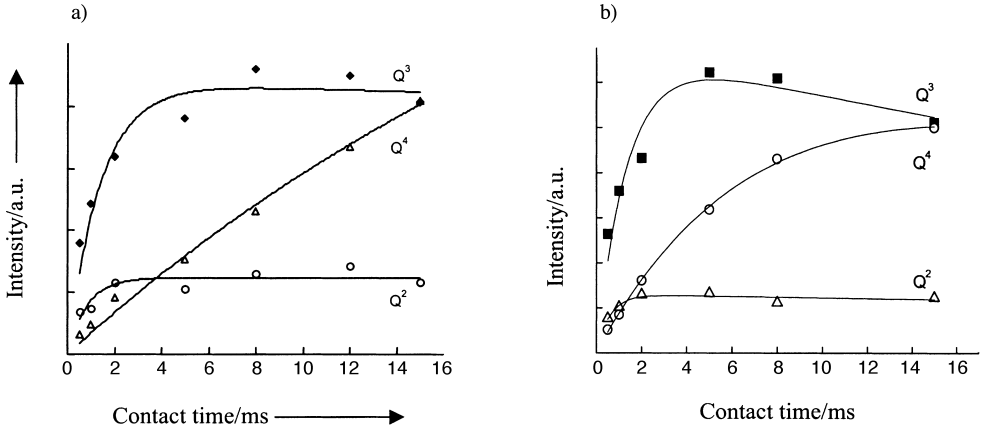
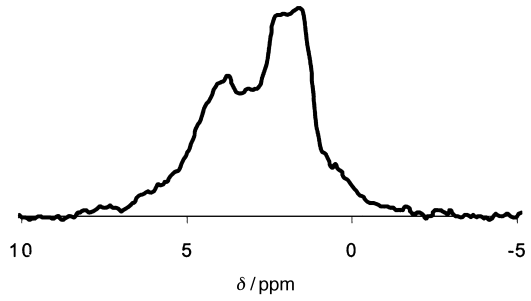


Figure 2. CP dynamic curves for a) MCM-41 and b) MCM-41 impregnated with $[Pd_6Ru_6(CO)_{24}][NEt_4]_2$.

 © 2002 WILEY-VCH Verlag GmbH & Co. KGaA, Weinheim 0044-8249/02/4124-4727 $ 20.00+.50/0

the polarization transfer to the ^{29}Si sites at the surface from the counterions' ^{1}H moieties.To further probe the interaction between the cluster and the surface a two-dimensional ^{1}H–^{29}Si HETCOR experiment was performed on the supported $[Pd_6Ru_6(CO)_{24}][NEt_4]_2$ system (Figure 3). It is clear from the HETCOR spectrum (Figure 3) that the ^{29}Si groups of MCM-



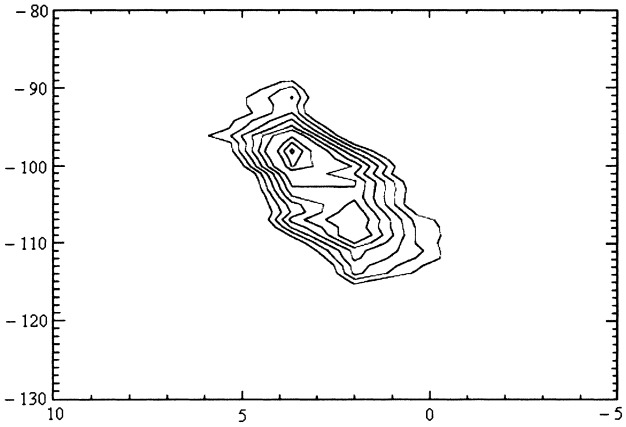


Figure 3. Top: ^{1}H NMR spectrum of MCM-41 impregnated with $[Pd_6Ru_6(CO)_{24}][NEt_4]_2$, showing two ^{1}H resonance signals for the counterion, corresponding to CH_2 and CH_3 groups. Spinning rate = 4 kHz. Bottom: Two-dimensional correlation spectrum between ^{29}Si (vertical axis) and ^{1}H (horizontal axis) sites for MCM-41 impregnated with $[Pd_6Ru_6(CO)_{24}][NEt_4]_2$.

41 with the cluster derive a considerable proportion of their intensity from the counterion, NEt_4^+. This infers, as we surmized from analysis of the cross polarization dynamic curves, that the counterion must be located at or very near the channel surfaces in the mesoporous material. This is the first direct evidence for this phenomenon. It is also noteworthy that the signal generated from the Q^4 site obtains a greater degree of enhancement from the $-CH_3$ moieties of the counterion, as opposed to the Q^2 and Q^3 sites, which obtain most of their intensity from the $-CH_2-$ groups within an ethyl group of the counterion. None of the ^{29}Si resonance signals derive significant cross polarization intensity from the surface silanol groups. The only structure of the impregnated mesopore, which is consistent with these observations, is one in which the ethyl group of the NEt_4^+ ion is embedded within the channel wall. We therefore conclude that an ethyl group is inserted into the channel wall of MCM-41. This structure brings a methyl group in close proximity with the Q^4 sites of the bulk MCM-41, whilst the CH_2 group of the embedded

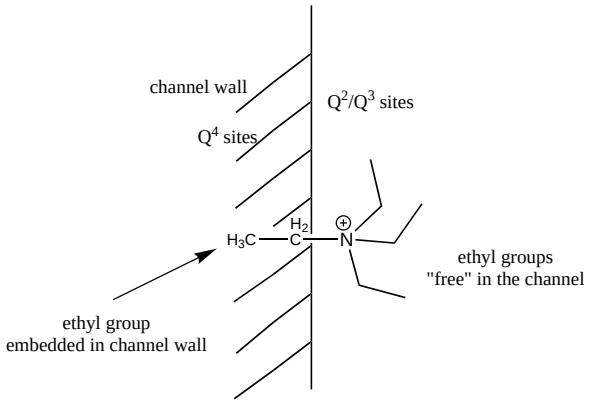


Figure 4. Schematic diagram illustrating the interaction between the NEt_4^+ ion and the channel wall of MCM-41.

ethyl group is brought in close proximity to the surface Q^2/Q^3 sites (Figure 4).

There is precedent for such an interaction: in the kaolinite/DMSO (dimethyl sulfoxide) intercalation compound where the methyl group of the DMSO molecule is inserted into the six-membered $-(SiO)_3-$ rings of the silicate layer in the kaolinite structure.[13]

To verify this conclusion, we have examined the $^{13}C\{^{1}H\}$ CP/MAS NMR spectrum of MCM-41 impregnated with $[Pd_6Ru_6(CO)_{24}][NEt_4]_2$, (Figure 5a). The spectrum for the unsupported cluster (Figure 5b) affords two distinct reso-

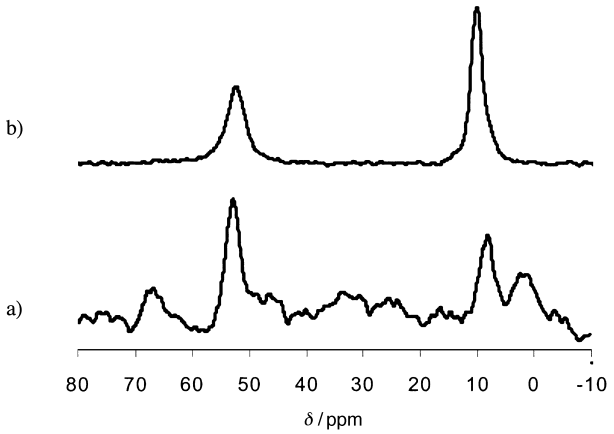


Figure 5. $^{13}C\{^{1}H\}$ CP/MAS spectra: a) MCM-41 impregnated with $[Pd_6Ru_6(CO)_{24}][NEt_4]_2$ (9668), and b) pure unsupported $[Pd_6Ru_6(CO)_{24}]$-$[NEt_4]_2$ cluster (1000). Contact time = 5 ms, and a recycle delay of 8 s. Spinning rate = 4.0 kHz.

nance signals at $\delta = 52$ and 10 ppm, respectively, originating from the methylene and methyl carbon atoms of the counterion, respectively. When the cross-polarization pulse sequence was used, signals for the CO ligands were not detected. Upon impregnation of the bimetallic cluster into MCM-41, both the methyl and methylene ^{13}C resonance signals split into two components; we thus infer a loss in the symmetry of the counterion. The principal methyl resonance signal shifts to $\delta = 6$ ppm, and a new lower intensity signal appears at $\delta = 3$ ppm. The methylene resonance signal shifts slightly to

 © 2002 WILEY-VCH Verlag GmbH & Co. KGaA, Weinheim 0044-8249/02/4124-4728 $ 20.00+.50/0 *Angew. Chem. Int. Ed.* **2002**, *41*, No. 24

$\delta = 54$ ppm and a new, lower intensity component appears at $\delta = 65$ ppm. The very low shift (to $\delta = 3$ ppm) of a component of the methyl signal is consistent for a methyl group close to Si moieties. The shift to higher frequency ($\delta = 65$ ppm) of a component of the CH_2 signal is consistent with this component being close to a more electron-withdrawing group that is, an oxygen moiety of MCM-41. This is consistent with the CH_2 being close to surface Q^2/Q^3 groups, which can (albeit weakly) interact with the CH_2 groups. It is worth noting that the two methyl and two methylene signals occur in approximately a 3:1 ratio. These relative intensities of course depend upon cross polarization dynamics of the groups concerned as well as on the relative number of sites of each. However, the cross polarization dynamics are not expected to be very different between the two different CH_3/CH_2 groups and so the 3:1 intensity ratio is entirely consistent with the proposed structure, in which one ethyl group of the NEt_4^+ ion is in a different environment to the other three.[1]

We have demonstrated that the counterion, often ignored in previous studies, plays a pivotal role in the adsorption of the mixed-metal clusters to the walls of MCM-41. We have shown, by means of a ^1H–^{29}Si HETCOR experiment that when the cluster $[Pd_6Ru_6(CO)_{24}][NEt_4]_2$ is deposited in MCM-41 the cation becomes embedded in the MCM-41 channel walls through one ethyl group. There is a substantial change in the ^{13}C chemical shifts of the ethyl group compared with those which remain "free" in the channel space. This implies a significant rearrangement of the electron density in this ethyl group and would suggest a significant interaction with the channel wall. Further work will be published in due course to fully investigate this complex paradigm and to probe the vital role the counterion plays and to examine how general these findings are in related systems.

Experimental Section

$[Pd_6Ru_6(CO)_{24}][NEt_4]_2$ was prepared by using a standard literature preparation.[14] The MCM-41 was synthesized by using a previously reported methodology, and was characterized by powder X-ray diffraction.[15] Patterns were recorded on a Philips 1710 powder diffractometer with $Cu_{K\alpha}$ radiation (40 kV, 40 mA), 0.02° step size, and 1 s step time. The d_{100} spacing for MCM-41 was found to be 32.5 Å. The BET surface area, as determined by N_2 adsorption measurements, of the MCM-41, was found to be 880 $m^2 g^{-1}$, which is entirely consistent with the literature precedent.[15] The cluster was anchored to MCM-41 using a previously proven method:[7] MCM-41 (200 mg) was initially dried by heating at 190 °C for 24 h in a dynamic vacuum to remove any surface water. ^1H MAS NMR spectroscopy of the resulting MCM-41 showed no signs of any water being present. The anionic cluster (100 mg) was mixed with the MCM-41, to which a small amount of solvent (0.1 mL) in which the cluster is soluble (CH_2Cl_2) and a large volume of solvent (15 mL) in which the cluster is insoluble (Et_2O) were added. The mixture was stirred for 72 h, in the absence of light, after which time the solid was filtered off, washed with diethyl ether until the washings became clear, and then dried at 30 °C in a dynamic vacuum for 24 h. The presence of the carbonyl cluster was verified by using Nujol mull IR spectroscopy, on a Perkin Elmer Paragon 1000 FT-IR spectrometer. Elemental analysis (%): C 10.41, H 1.30, N 0.67. The removal of CO was achieved by heating the sample at 190 °C in vacuum for 2 h, the absence of CO stretching frequencies being verified by solid-state IR spectroscopy. Elemental analysis (%): C 4.67, H 0.62, N 0.31.

[1] A ^{13}C CP/MAS spectrum is available as Supporting Information for $[NEt_4]Br$ adsorbed onto MCM-41. This greatly improves the signal-to-noise ratio.

$^{29}Si\{^1H\}$ CP/MAS solid-state NMR spectra were recorded on a Chemagnetics CMX 400 MHz and a 500 MHz Varian Infinity Plus spectrometer. The 400 MHz spectrometer operated at 399.875 MHz for ^1H and 79.437 MHz for ^{29}Si and the 500 MHz spectrometer at 499.871 MHz and 99.303 MHz, respectively. Samples were placed in zirconia rotors 4 mm/7.5 mm in diameter and spun in nitrogen at 4 kHz. The ^1H–^{29}Si Hartmann–Hahn match was optimized by using kaolinite. All ^{29}Si spectra were externally referenced to liquid tetramethylsilane (TMS) at 0 ppm. A pulse delay of 8 s between scans and a contact time of 8 ms were used for the majority of ^{29}Si NMR experiments with a 90° pulse of 4.0 μs. For the ^1H–^{29}Si variable contact time experiments, the contact time was varied in the range 0.5–15.0 ms. The ^1H–^{29}Si HETCOR NMR experiment was performed on the 400 MHz NMR instrument, using the experimental conditions detailed above. The $^{13}C\{^1H\}$ CP/MAS spectra were recorded on the CMX-400 MHz NMR spectrometer operating at 100.561 MHz for ^{13}C. The ^1H–^{13}C Hartmann–Hahn match was optimized by using hexamethylbenzene (HMB). All ^{13}C spectra were referenced to external TMS at 0 ppm. A delay of 8 s between scans and a contact time of 5.0 ms was employed, with a 90° pulse of 4.2 μs.

Received: June 3, 2002
Revised: September 30, 2002 [Z19428]

[1] J. S. Beck, J. C. Vartuli, W. J. Roth, M. E. Leonowicz, C. T. Kresge, K. D. Schmitt, C. T.-W. Chu, D. H. Olson, E. W. Sheppard, S. B. McCullen, J. B. Higgins, J. L. Schlenker, *J. Am. Chem. Soc.* **1992**, *114*, 10834.
[2] S. A. Raynor, J. M. Thomas, R. Raja, B. F. G. Johnson, R. G. Bell. M. D. Mantle, *Chem. Commun.* **2000**, 1925.
[3] S. Hermans, R. Raja, J. M. Thomas, B. F. G. Johnson, G. Sankar, D. Gleeson, *Angew. Chem.* **2001**, *113*, 1251; *Angew. Chem. Int. Ed.* **2001**, *40*, 1211.
[4] J. M. Thomas, W. J. Thomas, *Principles and Practice of Heterogeneous Catalysts*, Wiley-VCH, Weinheim, **1997**.
[5] D. S. Shephard, T. Maschmeyer, B. F. G. Johnson, J. M. Thomas, G. Sankar, D. Ozkaya, W. Zhou, R. D. Oldroyd, R. G. Bell, *Angew. Chem.* **1997**, *109*, 2337; *Angew. Chem. Int. Ed. Engl.* **1997**, *36*, 2242.
[6] D. S. Shephard, T. Maschmeyer, G. Sankar, J. M. Thomas, D. Ozkaya, B. F. G. Johnson, R. Raja, R. D. Oldroyd, R. G. Bell, *Chem. Eur. J.* **1998**, *4*, 1214.
[7] R. Raja, G. Sankar, S. Hermans, D. S. Shephard, S. Bromley, J. M. Thomas, B. F. G. Johnson, *Chem. Commun.* **1999**, 1571.
[8] W. Zhou, J. M. Thomas, D. S. Shephard, B. F. G. Johnson, D. Ozkaya, T. Maschmeyer, R. G. Bell, Q. Ge, *Science* **1998**, *280*, 1998.
[9] C.-F. Cheng, W. Zhou, J. Klinowski, *Chem. Phys. Lett.* **1996**, *263*, 247.
[10] X. S. Zhao, G. Q. Lu, A. K. Whittaker, G. J. Millar, H. Y. Zhu, *J. Phys. Chem. B* **1997**, *101*, 6525.
[11] R. Voelkel, *Angew. Chem.* **1988**, *100*, 1525; *Angew. Chem. Int. Ed. Engl.* **1988**, *27*, 1468.
[12] W. Kolodziejski, J. Klinowski, *Chem. Rev.* **2002**, *102*, 613.
[13] M. J. Duer, J. Rocha, J. Klinowski, *J. Am. Chem. Soc.* **1992**, *114*, 6867.
[14] E. Brivio, A. Ceriotti, R. D. Pergola, L. Garaschelli, F. Demartin, M. Manassero, M. Sansoni, P. Zanello, F. Lushi, B. T. Heaton, *J. Chem. Soc. Dalton Trans.* **1994**, 3247.
[15] C. Cheng, W. Zhou, D. Park, J. Klinowski, M. Hargreaves, L. F. Gladden, *J. Chem. Soc. Faraday Trans.* **1997**, *93*, 359.

 © 2002 WILEY-VCH Verlag GmbH & Co. KGaA, Weinheim 0044-8249/02/4124-4729 $ 20.00+.50/0

Low-Temperature Destruction of Chlorinated Hydrocarbons over Lanthanide Oxide Based Catalysts**

Pieter Van der Avert and Bert M. Weckhuysen*

Chlorinated hydrocarbons (CHCs) have widespread industrial applications as, for example, lubricants, cleaning solvents, heat-transfer fluids, and intermediates of pharmaceuticals, herbicides, and fungicides.[1] The increasing volume of CHCs released into the environment, together with the suspected toxicity and carcinogenic properties, have prompted researchers world-wide to find clean and effective routes for destroying CHCs. The method currently used most frequently is thermal incineration at temperatures higher than 1300 °C, so as to avoid formation of dioxins and polychlorinated biphenyls (PCBs).[2] The high incineration temperatures and related costs forced researchers to look for other solutions. As a result, a number of methods have been developed for the degradation of CHCs. These include for example, sonolysis,[3] electrochemical dehalogenation,[4] microbial systems,[5] destructive adsorption,[6] and catalytic transformation over supported metals, noble metals, and transition metal oxides.[7–10]

Two main catalytic routes are reported in the literature. The first one is the (total) oxidation of CHCs at temperatures between 300 and 550 °C over supported noble metal catalysts (for example, Pt, Pd, and Au).[7] The essential drawback of this method is the deactivation of the catalyst by the decomposition products, such as Cl_2 and HCl. This problem can be (partially) solved by using supported transition metal oxide catalysts (for example, V_2O_5 and Cr_2O_3),[8] although the formation of volatile metal oxychlorides can still be a problem. Another possibility to avoid catalyst deactivation is the use of steam.[9] A second catalytic route is hydrodechlorination, in which CHCs are transformed in the presence of hydrogen into alkanes and HCl. Commonly used catalysts are supported Ni, Pd, and Pt.[8,10] Although this method has clear economic and environmental advantages, including the re-use of reaction products and the elimination of hazardous by-products (for example, Cl_2 and $COCl_2$), it is not very often used. The main reason is the very fast deactivation of the catalyst material as a result of chlorine poisoning and coke formation.

Here, we report on a new and stable catalyst material, which destroys different CHCs, such as CCl_4, in the presence of steam at temperatures between 250 and 350 °C. This destruction process can be written as $CCl_4 + 2H_2O \rightarrow 4HCl + CO_2$, and no other products than HCl and CO_2 are found in the effluent gas and condensate. The reaction is also not equilibrium limited. The catalyst itself is based on the use of lanthanide oxides, such as La_2O_3, Nd_2O_3, Pr_2O_3, and Ce_2O_3, which are supported on a high surface area support, preferably Al_2O_3. Figure 1 illustrates the catalytic performance of

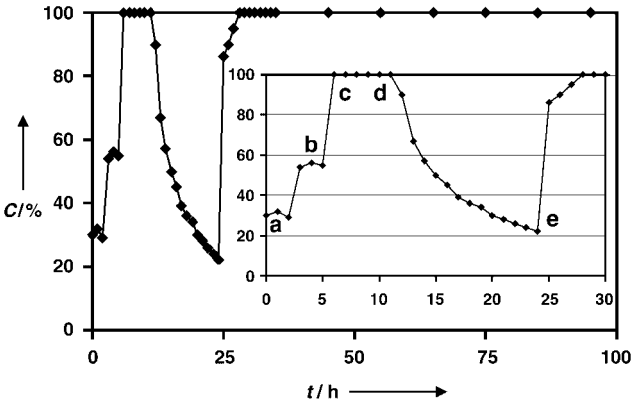


Figure 1. Catalytic conversion (C) of CCl_4 over 10 wt% La_2O_3/Al_2O_3 catalysts in the presence and absence of steam at various reaction temperatures (T) as a function of the reaction time (t; GHSV = 800 h^{-1} and inlet concentration of CCl_4 = 47000 ppm (v/v)): a) T = 250 °C; b) T = 300 °C; c) T = 350 °C; d) T = 350 °C; switching off the steam, and e) T = 350 °C and switching on the steam.

a 10 wt% La_2O_3/Al_2O_3 catalyst for the destruction of 47000 ppm (v/v) CCl_4 between 250 and 350 °C and the effects of changing the amount of steam in the CHC feed. It can be concluded that there is an increase in catalyst activity with increasing reaction temperature when steam was added to the CCl_4 feed. The catalyst material is able to convert 30% of the CCl_4 feed at 250 °C (case a in Figure 1), this conversion rises to around 55% at 300 °C (case b in Figure 1) and reaches a maximum of 100% at 350 °C (case c in Figure 1). After 3 h of operation at 350 °C (case d in Figure 1), the water source was switched off and the conversion gradually decreases with increasing time-on-stream. After 15 h of operation at 350 °C only a conversion of 22% could be observed at 350 °C. This result confirms the essential role of steam in the catalytic destruction of CCl_4, and the remaining activity must arise from the destructive adsorption of CCl_4 over supported La_2O_3.[11] The activity increased when steam was again added to the feed (case e in Figure 1), and a conversion of about 100% could be reached and maintained for more than 60 h of operation at 350 °C. Since the gas streams of commercial plants—where the removal of CHCs is required—may contain oxygen we have also studied the influence of oxygen in the CCl_4 stream on the catalytic performances of the 10 wt% La_2O_3/Al_2O_3 catalyst. This was done by mixing He and O_2 in a ratio 95:5 and keeping all the other experimental conditions the same. It was found that the catalytic conversion of CCl_4 at

[*] Prof. dr. ir. B. M. Weckhuysen, ir. P. Van der Avert
Centrum voor Oppervlaktechemie en Katalyse
Departement Interfasechemie, K.U. Leuven
Kasteelpark Arenberg 23, 3001 Leuven (Belgium)
and
Departement Anorganische Chemie en Katalyse
Debye Instituut, Universiteit Utrecht
Sorbonnelaan 16 3584 CA Utrecht (The Netherlands)
Fax: (+31) 30-251-1027
E-mail: b.m.weckhuysen@chem.uu.nl

[**] This work was supported by the Instituut voor Aanmoediging van Innnovatie door Wetenschap en Technologie in Vlaanderen (IWT-Vlaanderen; project ADV/990177). The authors acknowledge fruitful discussions with Prof. Robert Schoonheydt (K.U. Leuven), Dr. G. Mestl (Nanoscape, Germany), Dr. I. Langhans (CQ, Belgium), Dr. K. Ooms (CQ, Belgium), Dr. Dirk Van Deynse (Tessenderlo Chemie, Belgium), Dr. Yves Sergeant (Tessenderlo Chemie, Belgium), and Dr. Marc Belmans (Tessenderlo Chemie, Belgium).

 © 2002 WILEY-VCH Verlag GmbH & Co. KGaA, Weinheim 0044-8249/02/4124-4730 $ 20.00+.50/0

350 °C was lowered to a value of 60 %. Thus, a somewhat lower, but still stable and high catalytic activity could be obtained and retained with this catalyst.

Table 1 compares the destruction process of CCl_4 at 350 °C of some catalytic solids reported in the literature with our 10 wt % La_2O_3/Al_2O_3 catalyst and pure La_2O_3.[12–14] Although comparison is not easy because of the different experimental conditions used, the destruction capacity of the 10 wt % La_2O_3/Al_2O_3 is superior over the existing oxidation catalysts, and a stable destruction capacity of 0.289 g CCl_4 per hour per gram of catalyst could be reached for several days. Weiss et al. already reported the catalytic hydrolysis of CCl_4 to HCl and CO_2 in the presence of steam over unsupported MgO at 500 °C, but these authors observed a significantly lower catalytic activity than we do.[15] Actually, our own investigations indicate that alkaline and earth alkaline metal oxides (for example, MgO, CaO, SrO, and BaO) are not very active in comparison with lanthanide oxides (for example, La_2O_3, Nd_2O_3, Pr_2O_3, and Ce_2O_3) for the catalytic hydrolysis of CHCs.

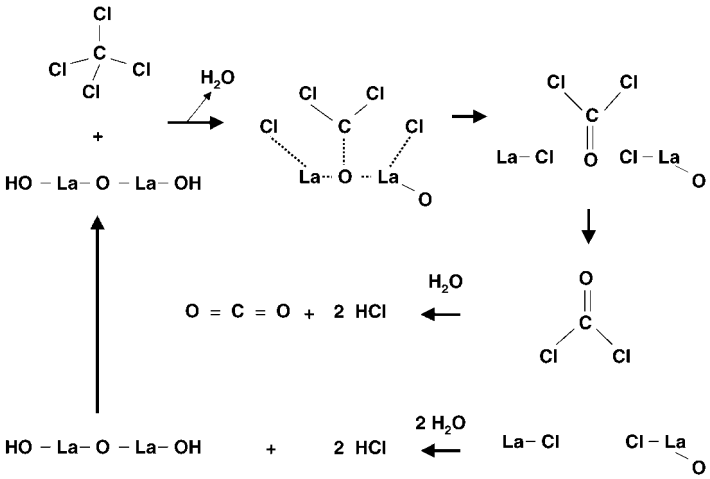
Table 1. Comparison of the destruction capacities of different catalytic solids for the destruction of CCl_4 at 350 °C, together with the experimental conditions.

Catalyst	Loading of CCl_4 [ppm]	GHSV [h^{-1}]	Destruction capacity [g $CCl_4\,h^{-1}\,g^{-1}$ catalyst]	Ref.
$LaMnO_3$	500	6000	0.004	12
$LaCoO_3$	500	6000	0.016	12
Co-Y	1000	1367	0.009	13
Cr-Y	1000	1367	0.009	13
Cr_2O_3/Al_2O_3	1000	15000	0.036	14
Pt, Pd, or Rh/TiO_2	1000	15000	0.102	14
La_2O_3	47000	800	0.145	this work
La_2O_3/Al_2O_3	47000	800	0.289	this work

To obtain more insight into the destruction mechanism of this catalyst material, several (in situ) characterization techniques were applied to study the physicochemical changes taking place in the catalytic solid, in particularly La_2O_3, as a function of the reaction time during the destruction of CCl_4 at 350 °C.[11] X-ray diffraction (XRD) studies revealed that lanthanum hydroxide was formed in the presence of steam at the reaction temperature. X-ray photoelectron spectroscopy (XPS) was then used to monitor the chlorination process of $La(OH)_3$ as a function of the reaction time. Chlorination was evident from an increase in the intensity of the Cl2p peak at around 198 eV in the spectrum, and a concomitant decrease in the intensity of the O1s peak at around 530 eV of the lanthanide hydroxide. The extent of chlorination increases with increasing reaction time, but reaches a maximum after about four hours. Thus, the subsurface of $La(OH)_3$ was partially transformed to a chlorinated lanthanide oxide during the catalytic reaction, but was not converted into $LaCl_3$. No substantial deposition of coke at the catalyst surface was evident by XPS during the destruction of CCl_4. The partial conversion of $La(OH)_3$ to LaOCl was confirmed by X-ray diffraction (XRD) studies, although additional diffraction peaks of a yet unknown compound were also detected. It was possible to confirm the formation of LaOCl in the catalytic reactor by using in situ Raman spectroscopy. This compound is characterized by vibrational frequencies at 125, 188, 215, 335, and 440 cm^{-1}. Finally, in situ infrared spectroscopy revealed the presence of CO_2 (2348 cm^{-1}), HCl (2884 cm^{-1}), and traces of $COCl_2$ (1827 cm^{-1}) evolving from the catalyst surface. No CO (2170 cm^{-1}) or products originating from dichlorocarbene (CCl_2), such as C_2Cl_4 (920 cm^{-1}), could be detected by vibrational spectroscopy during the reaction.

A plausible catalytic cycle can be proposed for this destruction process on the basis of the results (Scheme 1). In a first step, CCl_4 reacts with the partially hydrated La_2O_3 and a dichlorocarbene-like intermediate is formed at the catalyst surface. This reaction intermediate is very reactive and is therefore difficult to observe. A consequence of this first reaction step is the formation of a partially chlorinated catalyst. The adsorbed dichlorocarbene intermediate could in principle react with steam according to the equation: $CCl_2 + H_2O \rightarrow 2\,HCl + CO$. However, since no CO was observed, this reaction should be minor. Most probably CCl_2 reacts with an oxygen atom of the lanthanide oxide to make phosgene, which is then released from the catalyst surface and relatively easy hydrolyzed with steam into HCl and CO_2. In a final step, steam regenerates the partially chlorinated La_2O_3, and HCl is formed. Thus, the presence of steam is essential for the hydrolysis of the reaction intermediate phosgene as well as for the in situ regeneration of the catalyst material.

In summary, we have developed novel and stable catalyst systems based on supported lanthanide oxides for the hydrolysis of CHCs into CO_2 and HCl at relatively low temperatures in the presence of steam. The active phase consists of a lanthanide oxide chloride, and $COCl_2$ is a reaction intermediate involved in this catalytic hydrolysis process. Further studies will be directed towards the destruction of chlorinated aromatic compounds and mixtures of aliphatic and aromatic CHCs under relevant industrial conditions.



Scheme 1. Reaction cycle for the conversion of CCl_4 in the presence of steam over La_2O_3/Al_2O_3 catalysts.

 © 2002 WILEY-VCH Verlag GmbH & Co. KGaA, Weinheim 0044-8249/02/4124-4731 $ 20.00+.50/0

Experimental Section

The lanthanide oxide based catalysts were prepared by the incipient wetness impregnation technique with aqueous solutions of, for example, lanthanum acetate (Aldrich, $>99.9\,\%$) with Al_2O_3 (Condea, surface area of 220 $m\,g^{-1}$) as support. La_2O_3 (99.99 %) was purchased from Alfa Aesar. The catalyst material was dried at 100 °C for 1 h, followed by granulation. The size fraction of 0.25–0.50 mm was loaded into the catalytic reactor. Catalytic tests were performed in a fixed-bed reactor at atmospheric pressure. The reactor consisted of a quartz tube, which was loaded successively with quartz wool, quartz pearls, quartz wool, catalyst (1 g), quartz wool, quartz pearls, and quartz wool. Before the reaction started, the catalyst was calcined for 8 h in O_2 at 450 °C. During reaction, the feed consisted of a He flow, which was led through a saturator filled with CCl_4 (VEL, p.a.) and maintained at 0 °C in an icebath to preserve the same vapor pressure of CCl_4. All the tubes were made of Vitton, and the total He flow was set at 0.480 $L\,h^{-1}$. This resulted in a CCl_4 loading of 47 000 ppm (v/v). The gaseous hourly space velocity (GHSV) was 800 h^{-1} (contact time of 4.5 s). The gas flows were controlled with Bronkhorst mass flow controllers, while H_2O was added to the reactor at a rate of 1.2 $mL\,h^{-1}$ by a Methrom dosimeter and evaporated at the inlet of the reactor. The reaction temperature was controlled using a K-type thermocouple placed in the reactor. The condensate was trapped after the reactor in an impinger at room temperature and analyzed by GC-MS. The remaining gases were guided to a gas chromatograph (HP 4890D with a FID detector and methanator) and analyzed on a packed Hayesep Q CP column (80–100 mesh, 3 m length). X-ray diffraction patterns of the solids were measured with a Siemens D5000 Matic instrument, while Raman spectra were recorded with a Holoprobe Kaiser Optical spectrometer equipped with a holographic notch filter and CCD camera. XPS measurements were done with a VG MT 500 spectrometer. FTIR spectra were measured using a Nicolet 730 spectrometer.

Received: June 24, 2002
Revised: September 23, 2002 [Z19595]

[1] *Chlorine, principles and industrial practice* (Ed.: P. Schmittinger), Wiley-VCH, Weinheim, **2000**; W. Gerhartz, *Ulmann's Encyclopedia of Industrial Chemistry*, VCH Verlagsgesellschaft, Weinheim, **1986**.
[2] D. Bose, S. M. Senkan, *Combust. Sci. Technol.* **1983**, *35*, 187; H. Valeirs, A. K. Gupta, S. M. Senkan, *Combust. Sci. Technol.* **1984**, *36*, 123.
[3] I. Hua, M. R. Hoffmann, *Environ. Sci. Technol.* **1996**, *30*, 864.
[4] C. S. Criddle, P. L. McCarthy, *Environ. Sci. Technol.* **1991**, *25*, 973.
[5] R. Galli, P. L. McCarthy, *Appl. Environ. Microbiol.* **1989**, *55*, 837.
[6] P. D. Hooker, K.J. Klabunde, *Environ. Sci. Technol.* **1994**, *28*, 1243.
[7] M. Bonarowska, A. Malinowski, W. Juszczyk, Z. Karpinski, *Appl. Catal. B* **2001**, *30*, 187; G. C. Bond, N. Sadeghi, *J. Appl. Chem. Biotechnol.* **1975**, *25*, 241; M. M. R. Feijen-Jeurissen, J. J. Jorna, B. E. Nieuwenhuys, G. Sinquin, C. Petit, J. P. Hindermann, *Catal. Today* **1999**, *54*, 65.
[8] K. A. Frankel, B. W. Jang, J. J. Spivey, G. W. Roberts, *Appl. Catal. A* **2001**, *205*, 263; W. Juszczyk, A. Malinowski, Z. Karpinski, *Appl. Catal. A* **1998**, *166*, 311; S. Krishnamoorthy, J. A. Rivas, M. D. Amiridis, *J. Catal.* **2000**, *193*, 264.
[9] J. D. Ortego, J. T. Richardson, M. V. Twigg, *Appl. Catal. B* **1997**, *12*, 339; N. Coute, J. D. Ortego, J. T. Richardson, M. V. Twigg, *Appl. Catal. B* **1998**, *19*, 175; K. Intarajang, J. T. Richardson, *Appl. Catal. B* **1999**, *22*, 27.
[10] M. Wilde, K. Anders, *Chem. Tech.* **1994**, *6*, 316.
[11] B. M. Weckhuysen, M. P. Rosynek, J. H. Lunsford, *Phys. Chem. Chem. Phys.* **1999**, *1*, 3157; B. M. Weckhuysen, G. Mestl, M. P. Rosynek, T. R. Krawietz, J. F. Haw, J. H. Lunsford, *J. Phys. Chem. B* **1998**, *102*, 3773.
[12] G. Sinquin, C. Petit, J. P. Hindermann, A. Kiennemann, *Catal. Today* **2001**, *70*, 183; G. Sinquin, C. Petit, S. Libs, J. P. Hindermann, A. Kiennemann, *Appl. Catal. B* **2000**, *27*, 105; G. Sinquin, J. P. Hindermann, C. Petit, A. Kiennemann, *Catal. Today* **1999**, *54*, 107.
[13] S. Chatterjee, H. L. Greene, Y. Joon Park, *J. Catal.* **1992**, *138*, 179.
[14] G. R. Lester, *Catal. Today* **1999**, *53*, 407.
[15] U. Weiss, M. P. Rosynek, J. H. Lunsford, *Chem. Commun.* **2000**, 405.

Selective Isomerization of a Terminal Olefin Catalyzed by a Ruthenium Complex: The Synthesis of Indoles through Ring-Closing Metathesis**

Mitsuhiro Arisawa, Yukiyoshi Terada, Masako Nakagawa, and Atsushi Nishida*

Isomerization of olefins may proceed under acidic, basic, or photochemical conditions to give a mixture of olefins that depends on their thermodynamic stability. Recent advances in transition-metal chemistry (Fe, Pd, Rh, Pt, Ni, Ir, Ru, Co, and Cr) have enabled milder conditions for olefin isomerization to be used to realize selective and synthetically useful transformations, such as the deprotection of an allyl group on nitrogen and oxygen functionalities.[1] Recently, a few reports have appeared concerning this olefin isomerization using ruthenium–carbene catalysts, such as the Grubbs catalyst.[1m–o] This isomerization reaction is limited to substrates which contain an oxygen or a nitrogen substituent in the olefinic side chain. In addition, the reaction competes with metathesis.[2]

During the course of our investigation of the synthesis of nitrogen-containing heterocycles by using ring-closing metathesis (RCM),[3] we found a novel method for synthesizing substituted quinolines by RCM, which included a metathesis reaction of a silyl-protected enol ether with an alkene.[3f] These results prompted us to investigate cross metathesis to prepare a silyl enol ether. However, unexpectedly, we found selective isomerization of the terminal olefin to the corresponding internal olefin, which made a novel indole-ring synthesis possible by RCM. Herein, we report a novel and selective isomerization of a terminal olefin by combining a ruthenium–carbene catalyst with vinyloxytrimethylsilane, and its application to the synthesis of an indole ring from 2-(*N*-allyl-*N*-tosylamino)styrene by RCM.

When **1** was heated in CH_2Cl_2 at 50 °C with 2 molar equivalents of silyl enol ether (**2a**) in the presence of the Grubbs catalyst (**A**, 5 mol %),[4] we unexpectedly found that the terminal double bond of **1** isomerized to the internal double bond to give **3** in 60 % yield, 40 % of **1** was recovered (Table 1, entry 1, full experimental details are given in the supporting information). The exclusive formation of **3** was

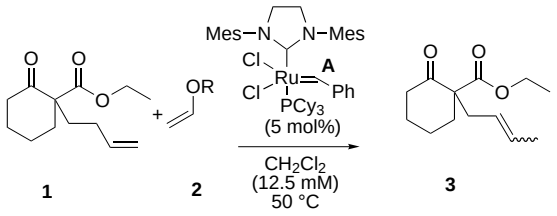
[*] Prof. A. Nishida, Dr. M. Arisawa, Y. Terada
Graduate School of Pharmaceutical Sciences
Chiba University
1-33 Yayoi-cho, Inage-ku, Chiba 263–8522 (Japan)
Fax: (+81) 43-290-2909
E-mail: nishida@p.chiba-u.ac.jp
Prof. M. Nakagawa
Present Address: Faculty of Science
Kanagawa University

[**] We thank Prof. Amir H. Hoveyda at Boston College for his helpful discussions and for the generous gift of his catalyst. This research was supported by a Grant-in-Aid for Scientific Research on Priority Areas (A) "Exploitation of Multi-Element Cyclic Molecules" and a Grant-in-Aid for Exploratory Research from the Ministry of Education, Culture, Sports, Science and Technology, Japan. M.A. is also grateful for a Takeda Chemical Industries, Ltd. Award in Synthetic Organic Chemistry, Japan for financial support.

Supporting information for this article is available on the WWW under http://www.angewandte.org or from the author.

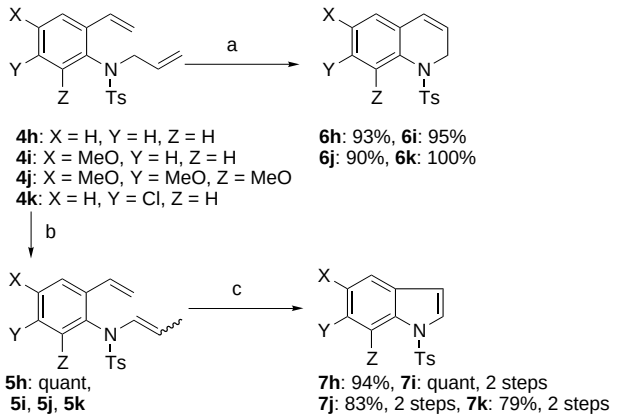
 © 2002 WILEY-VCH Verlag GmbH & Co. KGaA, Weinheim 0044-8249/02/4124-4732 $ 20.00+.50/0

Table 1. Reaction of **1** with various silyl enol ethers and vinyl ethers in the presence of a ruthenium–carbene catalyst.



Entry		R	Equiv	*t* [h]	Product [%]	*E*/*Z* Ratio of **3**[a]
1	**2a**	TMS	2	20	60	3.2/1
2	**2a**	TMS	10	3	quantitative	3.5/1
3	**2b**	Ac	10	23	no reaction	
4	**2c**	Et	10	3	12	–[b]
5	**2c**	Et	10	24	quantitative	3.2/1

[a] The ratios were determined by ^{1}H NMR spectroscopy. [b] Not determined.



Scheme 1. Selective isomerization of terminal olefins, a) **A** (5 mol%), CH_2Cl_2, 50 °C, 1 h; b) **A** (5 mol%), vinyloxytrimethylsilane (1 eq.), CH_2Cl_2, 50 °C, 1.5 h; c) for **5h**: **A** (5 mol%), benzene, 80 °C, 1 h, for **5i**: **A** (5 mol%), benzene, 80 °C, 3 h, for **5j**: **A** (5 mol%), toluene, 110 °C, 17 h for **5k**: **A** (5 mol%), toluene, 110 °C, 13 h.

observed in the reaction with 10 equivalents of **2a**, again as a mixture of *E* and *Z* isomers (entry 2). However, neither isomerization nor dimerization of **1** occurred when vinyl acetate **2b** was subjected to similar reaction conditions (entry 3). On the other hand, the combination of ethylvinyl ether **2c** with catalyst **A** under optimized conditions promoted the quantative isomerization of **1** (entry 5).[5] Clearly, **2a** is the most favorable enol ether for isomerization.

Several terminal olefins were subjected to the same reaction conditions (Table 2). All of the monosubstituted olefins (**4a**–**4g**) were isomerized in moderate to excellent yields, even when the substrate did not have an oxygen substituent. Therefore, this reaction is quite general and selective for terminal olefins.

We carried out the isomerization of **4h** (Scheme 1) in competition with RCM. While the reaction of **4h** with ruthenium-catalyst **A** gave 1,2-dihydroquinoline (**6h**) in excellent yield,[3f] the reaction of **4h** with catalyst **A** in the presence of vinyloxytrimethylsilane (1 equiv is sufficient for this substrate) gave enamine (**5h**; Scheme 1) in quantitative yield, which is inaccessible by conventional methods. Although the use of a ruthenium–carbene catalyst in the isomerization of olefin has been reported,[1m–o], to our knowledge, this is the first example of a highly selective isomerization using a ruthenium–carbene complex that proceeds faster than RCM.

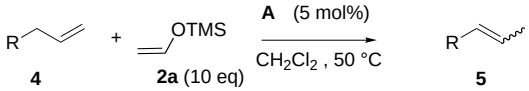
Since this method is quite effective for generating enamines, we applied this reaction to the synthesis of indoles.[6] Enamine **5h** was obtained by the evaporation of volatile material after the isomerization of **4h** and was subjected to normal RCM conditions using catalyst **A** at 80 °C in benzene. The expected indole (**7h**) was isolated in 94 % yield. Similarly, **4i**, **4j**, and **4k** gave **7i**, **7j**, and **7k** via isomerized enamines **5i**, **5j**, and **5k**, respectively.

The protective group on a nitrogen atom is not limited to the *p*-toluenesulfonyl group. 2-(*N*-Acetyl-*N*-allylamino)styrene gave *N*-acetylindole in 96 % yield under the same conditions.

While a detailed mechanism of this isomerization is not clear, we considered that the new catalyst was formed by the reaction of **A** and vinyloxytrimethylsilane. The results of monitoring the reaction of the Grubbs catalyst **A** with **2a** in $CDCl_3$ at 50 °C by ^{1}H and ^{31}P NMR spectroscopy showed that: 1) in the ^{1}H NMR spectrum, the signal arising from the methyne proton of the Grubbs catalyst (19.1 ppm) disappeared and signals associated with styrene appeared; and 2) in the ^{31}P NMR spectrum, the signal arising from the tricyclohexylphosphane group of the Grubbs catalyst (29.6 ppm) completely disappeared and a new signal appeared at 33.1 ppm. Furthermore, the IR spectrum of the crude product showed a new signal at 1935 cm^{-1}.

These results offer an extremely facile and selective isomerization of terminal olefins by combining a ruthenium–carbene catalyst and vinyloxytrimethylsilane. The utility of this reaction was demonstrated in a novel and efficient synthesis of an indole ring from 2-(*N*-allylamino)-styrene using RCM. As a consequence of its simplicity, chemo-selectivity, and the mild reaction conditions, this procedure should lead to new aspects of olefin metathesis.

Table 2. Novel isomerization of various terminal olefins.



Entry	Substrate	*t* [h]	Product	Yield [%][a]	*E*/*Z*[b]
1	$PhCH_2CH{=}CH_2$ (**4a**)	1.5	$PhCH{=}CHCH_3$ (**5a**)	34 (quantitative)	12.8/1
2	$Ph(CH_2)_2CH{=}CH_2$ (**4b**)	3.0	$PhCH_2CH{=}CHCH_3$ (**5b**)	58	2.8/1
3	p-$MeOC_6H_4CH_2CH{=}CH_2$ (**4c**)	3.0	p-$MeOC_6H_4CH{=}CHCH_3$ (**5c**)	78	8.5/1
4	$HO(CH_2)_4CH{=}CH_2$ (**4d**)	3.0	$HO(CH_2)_3CH{=}CHCH_3$ (**5d**)	34 (quantitative)	6.1/1
5	$BnO(CH_2)_4CH{=}CH_2$ (**4e**)	3.0	$BnO(CH_2)_3CH{=}CHCH_3$ (**5e**)	96 (quantitative)	8.2/1
6	$BnOCH_2CH{=}CH_2$ (**4f**)	3.0	$BnOCH{=}CHCH_3$ (**5f**)	73	1/1.25
7	$BnO(CH_2)_2C(Me){=}CH_2$ (**4g**)	3.0	$BnOCH_2CH{=}CMe_2$ (**5g**)	no reaction	–

[a] Isolated yield. Yields in parenthesis were estimated by ^{1}H NMR spectroscopy. [b] Determined by ^{1}H NMR spectroscopy.

Received: July 9, 2002 [Z19690]

 © 2002 WILEY-VCH Verlag GmbH & Co. KGaA, Weinheim 0044-8249/02/4124-4733 $ 20.00+.50/0

[1] For example: a) C. F. Lochow, R. G. Miller, *J. Org. Chem.* **1976**, *41*, 3020 – 3022; b) H. Suzuki, H. Yashima, T. Hirose, M. Takahashi, Y. Moro-oka, T. Ikawa, *Tetrahedron Lett.* **1980**, *21*, 4927 – 4930; c) I. Matsuda, T. Kato, S. Sato, Y. Izumi, *Tetrahedron Lett.* **1986**, *27*, 5747 – 5750; d) A. Zoran, Y. Sasson, J. Blun, *J. Org. Chem.* **1981**, *46*, 255 – 260; e) M. Sodeoka, H. Yamada, M. Shibasaki, *J. Am. Chem. Soc.* **1990**, *112*, 4906 – 4911; f) F. Guibé, *Tetrahedron* **1997**, *53*, 13509 – 13556; g) D. Joe, L. E. Overmann, *Tetrahedron Lett.* **1997**, *38*, 8635 – 8638; h) F. Guibé, *Tetrahedron* **1998**, *54*, 2967 – 3042; i) T. Taniguchi, K. Ogasawara, *Angew. Chem.* **1998**, *110*, 1137 – 1139; *Angew. Chem. Int. Ed.* **1998**, *37*, 1136 – 1137; j) T. Taniguchi, K. Ogasawara, *Tetrahedron Lett.* **1998**, *39*, 4679 – 4682; k) T. Ohmura, Y. Shirai, Y. Yamamoto, N. Miyaura, *Chem. Commun.* **1998**, 1337 – 1338; l) H. Wakamatsu, M. Nishida, N. Adachi, M. Mori, *J. Org. Chem.* **2000**, *65*, 3966 – 3970; m) A. Fürstner, O. R. Thiel, L. Ackermann, H.-J. Schanz, S. P. Nolan, *J. Org. Chem.* **2000**, *65*, 2204 – 2207; n) B. Alcaide, P. Almendros, J. M. Alonso, M. F. Aly, *Org. Lett.* **2001**, *3*, 3781 – 3784; o) C. Cadot, P. I. Dalko, J. Cossy, *Tetrahedron Lett.* **2002**, *43*, 1839 – 1841, and references therein.

[2] Recent reviews: a) T. M. Trnka, R. H. Grubbs, *Acc. Chem. Res.* **2001**, *34*, 18 – 29; b) A. Fürstner, *Angew. Chem.* **2000**, *112*, 3140 – 3172; *Angew. Chem. Int. Ed.* **2000**, *39*, 3012 – 3043; c) R. H. Grubbs, S. Chang, *Tetrahedron* **1998**, *54*, 4413 – 4450; d) S. K. Armstrong, *J. Chem. Soc. Perkin Trans. 1* **1998**, 371 – 388; e) M. Schuster, S. Blechert, *Angew. Chem.* **1997**, *109*, 2124 – 2145; *Angew. Chem. Int. Ed. Engl.* **1997**, *36*, 2036 – 2056.

[3] a) M. Arisawa, E. Takezawa, A. Nishida, M. Mori, M. Nakagawa, *Synlett* **1997**, 1179 – 1180; b) H. Uchida, Y. Torisawa, A. Nishida, M. Nakagawa, *J. Synth. Org. Chem. Jpn.* **1999**, *57*, 1004 – 1015; c) M. Arisawa, C. Kato, H. Kaneko, A. Nishida, M. Nakagawa, *J. Chem. Soc. Perkin Trans. 1* **2000**, 1873 – 1876; d) M. Arisawa, H. Kaneko, A. Nishida, K. Yamaguchi, M. Nakagawa, *Synlett* **2000**, 841 – 843; e) M. Arisawa, M. Takahashi, E. Takezawa, T. Yamaguchi, Y. Torisawa, A. Nishida, M. Nakagawa, *Chem. Pharm. Bull.* **2000**, *48*, 1593 – 1596; f) M. Arisawa, C. Theeraladanon, A. Nishida, M. Nakagawa, *Tetrahedron Lett.* **2001**, *42*, 8029 – 8033; g) M. Arisawa, H. Kaneko, A. Nishida, M. Nakagawa, *J. Chem. Soc. Perkin Trans. 1* **2002**, 959 – 964.

[4] The tricyclohexylphosphane dihydroimidazolidene ruthenium catalyst (a) M. Scholl, T. M. Trnka, J. P. Morgan, R. H. Grubbs, *Tetrahedron Lett.* **1999**, *40*, 2247 – 2250; b) M. Scholl, S. Ding, C. W. Lee, R. H. Grubbs, *Org. Lett.* **1999**, *1*, 953 – 956; c) A. K. Chatterjee, R. H. Grubbs, *Org. Lett.* **1999**, *1*, 1751 – 1753) is an effective catalyst; A phosphane-free N-heterocyclic carbene complex (d) S. B. Garber, J. S. Kingsbury, B. L. Gray, A. H. Hoveyda, *J. Am. Chem. Soc.* **2000**, *122*, 8168 – 8179; e) S. Gessler, S. Randl, S. Blechert, *Tetrahedron Lett.* **2000**, *41*, 9973 – 9976) is also effective. The catalysts, $[Cl_2Ru(PCy_3)_2{=}CHCH{=}Ph]$ and $[Cl_2Ru(PCy_3)_2{=}CHPh]$, were ineffective for this isomerization.

[5] Grubbs and co-workers found that vinylic ethers were not reactive in cross-metathesis. He also reported the formation of a new Fischer carbene species prepared by the reaction of a ruthenium–alkylidene complex with ethyl vinyl ether. (a) A. K. Chatterjee, J. P. Morgan, M. Scholl, R. H. Grubbs, *J. Am. Chem. Soc.* **2000**, *122*, 3783 – 3784; b) J. Louie, R. H. Grubbs, Organometallics **2002**, *21*, 2153 – 2164).

[6] a) *The Chemistry of Heterocyclic Compounds, Indoles* (Ed.: W. J. Houlihan), Wiley-International, Toronto, **1972**; b) G. W. Gribble, *J. Chem. Soc. Perkin Trans. 1* **2000**, 1045 – 1075.

The Structure of the Peroxo Species in the TS-1 Catalyst as Investigated by Resonant Raman Spectroscopy**

Silvia Bordiga,* Alessandro Damin, Francesca Bonino, Gabriele Ricchiardi, Carlo Lamberti, and Adriano Zecchina

Ti-silicalite-1 (TS-1)[1] has exhibited a remarkably high efficiency and molecular selectivity in oxidation reactions with H_2O_2 under mild conditions, such as for olefin epoxidation, phenol hydroxylation, cyclohexanone ammoximation, and conversions of ammonia to hydroxylamine, secondary alcohols to ketones, and secondary amines to dialkylhydroxylamines[2] (Figure 1). Because of its relevance in industrial applications, it has been one of the most studied materials in heterogeneous catalysis in recent years.[3–13]

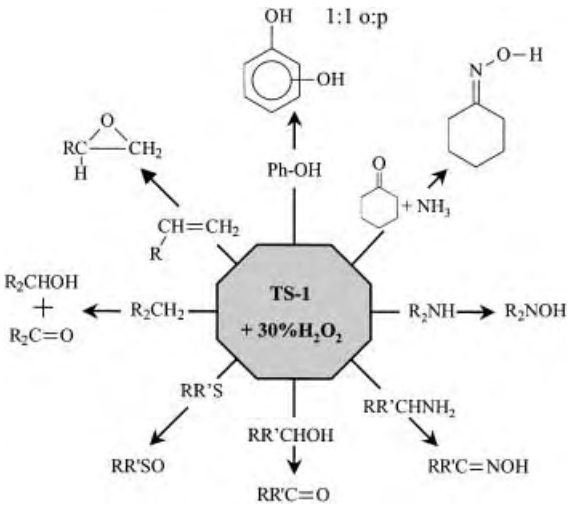


Figure 1. Schematic representation of the most relevant oxidation reactions catalyzed by TS-1.

It has been shown that the active species is a Ti^{IV} atom isomorphically inserted into the MFI-type framework.[1] TS-1 is characterized by an increase of the unit cell volume proportional to the Ti content[1,5,7,14] and by the presence of a "fingerprint" IR absorption component[1,6b,8–10,13] centered at 960 cm^{-1}, the intensity of which grows proportionally with increased Ti content. This band is clearly visible in IR spectra appearing on the low-energy tail of the very strong absorption resulting from the ν_{asym}(Si-O-Si) modes that appear in the broad 1250–1030 cm^{-1} region. In addition to the component at

[*] Prof. Dr. S. Bordiga,[+] A. Damin, F. Bonino, Dr. G. Ricchiardi, Dr. C. Lamberti,[+] Prof. Dr. A. Zecchina
Dipartimento di Chimica IFM and
INSTM Research Unit, Turin University
Via P. Giuria 7, 10125 Torino (Italy)
Fax: (+39) 011-670-7855
E-mail: silvia.bordiga@unito.it

[+] also with INFM UdR di Torino Università (Italy)

[**] This project has been supported by MURST (Cofin 2000, Area 03): "*Structure and reactivity of catalytic centers in zeolitic materials*". We are indebted to R. Tagliapietra, M. Ricci, F. Rivetti, and G. Spanò for fruitful discussions.

 © 2002 WILEY-VCH Verlag GmbH & Co. KGaA, Weinheim 0044-8249/02/4124-4734 $ 20.00+.50/0

960 cm^{-1}, Raman experiments[9] have also revealed the presence of a second fingerprint band at 1125 cm^{-1} which is not obscured by the ν_{asym}(Si-O-Si) modes (very weak in Raman spectra). Conventional Raman spectroscopy is, however, a critical technique when applied to these systems because of both the high dilution of Ti centers in the MFI framework (less than 3 wt % in TiO_2[4]) and the presence of a strong fluorescence background.

In this regard, a remarkable improvement has been achieved recently by Li et al.[12] who have collected Raman spectra of TS-1 using an excitation laser at $\lambda = 244$ nm (40 984 cm^{-1}), that is, in the low-energy tail of the ligand (O) to metal (Ti) charge-transfer transition (LMCT) centered around 48 000 cm^{-1} (208 nm,[8,10,13] Figure 2a). The transition

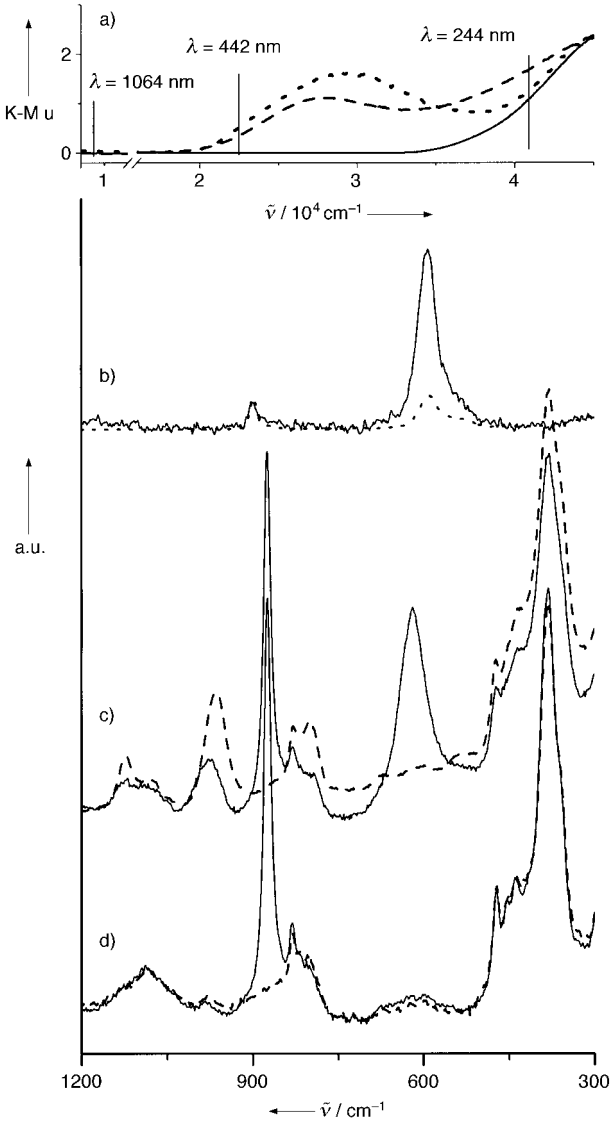


Figure 2. a) Diffuse reflectance UV/Vis spectra of a TS-1 sample in vacuo (——), in contact with a H_2O_2/H_2O solution (– – –), and of $[NH_4^+]_3[TiF_5O_2]^{3-}$ (••••); K-M u = Kubelka–Munk units. Vertical lines indicate the positions of the exciting Raman sources used in this work ($\lambda = 1064$ and 442 nm) and in two previous studies exploiting the resonant condition on TS-1 ($\lambda = 244$ nm);[12,13] b) Raman spectra of $[NH_4^+]_3[TiF_5O_2]^{3-}$ ($\lambda = 1064$ (••••) and 442 nm (——), respectively); c) Raman spectra ($\lambda = 442$ nm) of pure TS-1 (– – –) and in contact with a H_2O_2/H_2O solution (——); d) Raman spectra ($\lambda = 442$ nm) of pure silicalite (– – –) and contacted with a H_2O_2/H_2O solution (——).

occurs from the four nearly equivalent oxygen atoms coordinated to the Ti^{IV} center in the quasitetrahedral TiO_4 unit, and leads to the symmetric expansion of the tetrahedral unit.[13] Li et al. have demonstrated, for the first time, that the band at 1125 cm^{-1} undergoes a remarkable resonant enhancement, while the intensity of the 960 cm^{-1} component is almost unchanged. The reason for this behavior has been successfully explained in a combined ab initio and spectroscopic study,[13] in terms of the symmetry of the vibrational and electronic transitions that are involved.[15]

In this work, we wish to extend the vibrational study of the TiO_4 groups in TS-1 through an investigation of the material in an H_2O_2/H_2O solution, which is the key reactant in partial oxidation reactions.[1–3] As a result of the presence of H_2O (which precludes an extended use of IR spectroscopy) and the high lability of complexes formed by H_2O_2 at the Ti^{IV} centers in TS-1, very few characterization papers have been reported on the TS-1/H_2O_2 system to date. The most commonly used technique is UV/Vis diffuse reflectance spectroscopy (DRS), which is not affected by the presence of H_2O. This technique has revealed the formation, upon contact with the H_2O_2/H_2O solution, of a new LMCT from the peroxidic moiety to the Ti center that appears at around 26 000 cm^{-1} (385 nm, see Figure 2a).[16–18] Some other papers have appeared that use EPR,[16] IR,[19] Raman,[19] EXAFS,[18,20] and computational[19–21] approaches to investigate the complexes formed upon dosing H_2O_2 (or more complex species such as *tert*-butyl hydroperoxide) on titanosilicates. However, more than twenty years after the discovery of the material, the detailed structure of the peroxidic species formed at the catalytic center, which is thought to be the active intermediate in partial oxidation reactions, is still unknown. The two most frequently proposed structures are a "side-on" Ti–peroxo species or an "end-on" Ti–hydroperoxo species.

A previous Raman study[19] (exploiting a conventional 1064 nm exciting source) was only able to measure the O–O stretching frequency of peroxo complexes formed at the Ti sites in TS-1 upon contact with $H_2O_2/NH_3/H_2O$ (840 cm^{-1}) and $H_2O_2/NaOH/H_2O$ (843 cm^{-1}) basic solutions.[22] The reason for this partial success is probably because in basic solutions the peroxo species are more stable and hence they are not readily destroyed by the laser beam. The same experiment with an H_2O_2/H_2O solution was not successful because of the labile nature of the complex. On this basis it is apparent that the only route that can be followed to improve the quality of the Raman spectra in this field is that reported by Li et al.[12] As the peroxo species absorb in the visible region, an exciting source in the same spectral region must be used, because in this way the vibration associated with the Ti–peroxo species can undergo a Raman enhancement phenomenon, if the selection rules are fulfilled.[15] We have used a 442 nm (22 625 cm^{-1}) laser source, which lies on the low-energy tail of the LMCT band at around 26 000 cm^{-1} that is typical of the TS-1/H_2O_2/H_2O system (see Figure 2a), and should stimulate the resonant enhanced response. Figure 2c shows the Raman spectra of TS-1 both before and after interaction with the H_2O_2/H_2O solution. Interaction with H_2O_2 causes: a) the reduction and blue shift of the 960 cm^{-1} mode, shifted to 976 cm^{-1}, b) the quenching of the 1125 cm^{-1}

 © 2002 WILEY-VCH Verlag GmbH & Co. KGaA, Weinheim 0044-8249/02/4124-4735 $ 20.00+.50/0

mode, which results from a breakdown of the T_d-like symmetry,[13] c) the appearance of the strong and sharp O–O stretching mode at 875 cm^{-1}, resulting from the H_2O_2/H_2O solution being physisorbed into the zeolite channels, and d) the appearance of a strong and complex new feature centered at 618 cm^{-1}. Features a–c are also observed when the same experiment is performed with a 1064 nm laser source (spectra not reported, see Ref. [19]). Conversely, the 618 cm^{-1} vibration is only found in Raman spectra obtained with a 442 nm exciting source, and is therefore ascribed to a Raman-enhanced vibration mode of the Ti–peroxo complex. To assign this new feature, two control experiments have been performed, with the model compound $[NH_4^+]_3[TiF_5O_2]^{3-}$ [23] (Figure 2b), and with the Ti-free silicalite-1 molecular sieve, (Figure 2d) respectively. Interaction of the H_2O_2/H_2O solution with the Ti-free silicalite results only in the appearance of the 875 cm^{-1} mode, already assigned to H_2O_2 that is physisorbed into the zeolite channels. The Raman spectrum of $[NH_4^+]_3[TiF_5O_2]^{3-}$ exhibits a band at 898 cm^{-1} and a composite absorption with a maximum at 595 cm^{-1} which undergoes a distinct enhancement when the 442 nm excitation source is used. To assign this spectrum, it is useful to consider that the crystalline structure of $[NH_4^+]_3[TiF_5O_2]^{3-}$ (see Figure 3) consists of TiF_5O_2 units intercalated with NH_4^+ counterions. For this reason the discussion of the vibrational spectrum can be based on the TiF_5O_2 molecular unit and in particular the $Ti(O)_2$ fragment. The $Ti(O)_2$ unit has C_{2v} symmetry and Γ_{vib} for this moiety is $2A_1 + B_1$. The three normal modes, labeled ν_1, ν_2, and ν_3 following literature data on peroxo–metal complexes in argon matrices,[24] are assigned to: an O–O stretching vibration with A_1 symmetry (ν_1); a symmetric breathing mode of the $Ti(O)_2$ cycle with A_1 symmetry (ν_2); an asymmetric breathing mode of the $Ti(O)_2$ cycle with B_1 symmetry (ν_3). Literature data for the cyclic structures $Fe(O)_2$, $Co(O)_2$, $Ni(O)_2$, and $Ca(O)_2$ show that the ν_1 mode lies in the 990–742 cm^{-1} spectral range.[24] This suggests that the band at 898 cm^{-1} can be associated with the O–O stretching vibration. It is of note that even if this mode is totally symmetric (A_1 symmetry), its intensity is not substantially enhanced in the spectrum obtained with the 442 nm source. By analogy with the data obtained on the previously cited structures, this behavior can be explained by considering that among the two A_1 modes which meet the symmetry requirements, the ν(O–O) mode (where the Ti center is not directly involved) is not affected by the resonant Raman effect. Literature data[24] on $Fe(O)_2$, $Co(O)_2$, $Ni(O)_2$, and $Ca(O)_2$ show that ν_2 and ν_3 are usually only about 30 cm^{-1} apart and are located in the range 600–500 cm^{-1}. Because of the proximity of the two contributions, and with only the ν_2 mode being Raman enhanced, we associate the absorption centered at 595 cm^{-1} to the symmetric breathing mode of the $Ti(O)_2$ cycle, the asymmetric mode giving a minor contribution. The similarity between the spectroscopic features in both the UV/Vis (Figure 2a) and Raman (Figure 2b,c) spectra of the $[NH_4^+]_3[TiF_5O_2]^{3-}$ and TS-1/H_2O_2/H_2O systems allows us to conclude definitively that the species responsible for the band at 26000 cm^{-1} of the TS-1/H_2O_2/H_2O system is a "side-on" Ti–peroxo species, characterized by a Raman mode at 618 cm^{-1} which is resonance-enhanced upon laser excitation at a wavelength falling within the LMCT region.

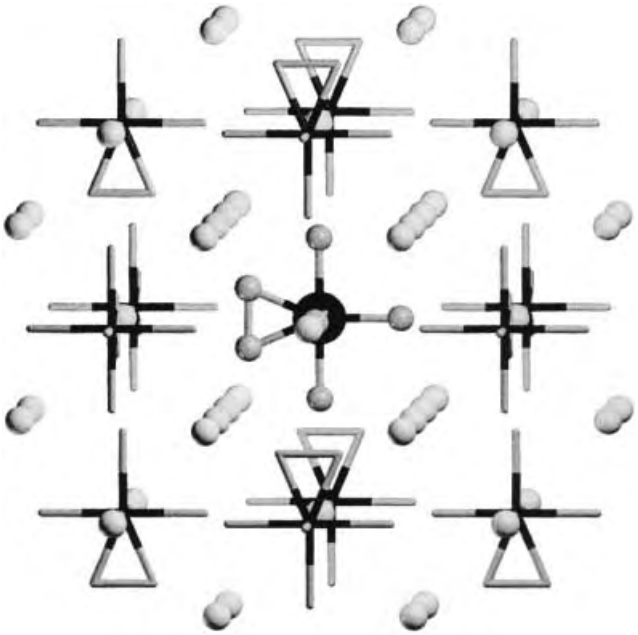


Figure 3. Graphical representation of the crystalline structure of $[NH_4^+]_3[TiF_5O_2]^{3-}$. The TiF_5O_2 unit is represented by balls and sticks: Ti^{IV} (black), O and F (gray). NH_4^+ counterions are represented by white spheres.

Experimental Section

TS-1 (3.0 TiO_2 wt%) and silicalite-1 samples have been synthesized in EniChem laboratories (now PolimeriEuropa) following a procedure described in the original patent.[1] The complete insertion of Ti atoms within the MFI framework has been proved by comparison of the amount of Ti, as determined by chemical analysis, with the cell volumes obtained by Rietveld refinement of powder X-ray diffraction data, according to Ref. [7]. TiO_2 extra-framework particles are below the detection limit (about 0.03 wt%) of the UV/Vis technique (Figure 2a).[25] X-ray absorption near-edge spectroscopy (XANES; from the width and intensity of the 4967 eV pre-edge peak[13]) and Raman[25] (from the absence of the 144 cm^{-1} band) analysis confirm the complete insertion of Ti into the framework. A sample of TS-1 was analyzed when in contact with a 30% H_2O_2 aqueous solution, which represents the working conditions of the catalyst.[2] The experiment is carried out in an excess of H_2O_2 molecules, with respect to Ti–peroxo complexes. Note that the presence of water is necessary, since it has been shown that the TS-1/H_2O_2/H_2O system loses its yellow color upon water desorption.[18] $[NH_4^+]_3[TiF_5O_2]^{3-}$ has been synthesized in the PolimeriEuropa laboratories and characterized by XRD (Figure 3), UV/Vis, (Figure 2a) and Raman spectroscopy (Figure 2b).

Raman spectra were obtained on a Perkin Elmer 2000 NIR-FT Raman spectrometer equipped with an InGaAs detector. The lasing medium was an Nd-YAG crystal pumped with a high-pressure krypton lamp, which results in an excitation wavelength of 1064 nm (9398 cm^{-1}). The power output was approximately 1 W. Resonance Raman spectra were obtained using a Renishaw Micro-Raman System 1000 by excitation with a He/Cd laser operating at 442 nm (22624 cm^{-1}). The photons scattered by the sample were dispersed by a 2400 lines mm^{-1} grating monochromator and simultaneously collected on a CCD camera; the collection optic was set at x20 objectivity. A laser output of 8.3 mW and an exposure time of 500 s per spectrum were used in case of zeolite samples. Care was taken with the measurements on $[NH_4^+]_3[TiF_5O_2]^{3-}$ in order to avoid decomposition, where a laser output of 0.3 mW and an exposure time of 200 s per spectrum were employed.[26] The diffuse reflectance UV/Vis spectra were obtained on a Varian Cary 5 spectrometer.

Received: July 1, 2002 [Z19643]

 © 2002 WILEY-VCH Verlag GmbH & Co. KGaA, Weinheim 0044-8249/02/4124-4736 $ 20.00+.50/0

[1] M. Taramasso, G. Perego, B. Notari, US Patent 4410501 **1983**. TS-1 is a microporous titanosilicate with a three-dimensional pore system consisting of two intersecting sets of tubular channels (approximately 5.5 Å in diameter) defined by 10-membered rings of TO_4 tetrahedra (T = Si or Ti). TS-1 is the Ti-analogue of ZSM-5 aluminosilicate (zeolite), which exhibits the MFI structure (IUPAC nomenclature).
[2] B. Notari, *Adv. Catal.* **1996**, *41*, 253 – 334, and references therein.
[3] W. Hölderich, M. Hesse, F. Naümann, *Angew. Chem.* **1988**, *100*, 232; *Angew. Chem. Int. Ed. Engl.* **1988**, *27*, 226 – 246.
[4] R. Millini, E. Previdi Massara, G. Perego, G. Bellussi, *J. Catal.* **1992**, *137*, 497 – 503.
[5] C. Lamberti, S. Bordiga, A. Zecchina, A. Carati, A. N. Fitch, G. Artioli, G. Petrini, M. Salvalaggio, G. L. Marra, *J. Catal.* **1999**, *183*, 222 – 231.
[6] a) G. Ricchiardi, A. J. M. de Man, J. Sauer, *Phys. Chem. Chem. Phys.* **2000**, *2*, 2195 – 2204; b) A. Damin, S. Bordiga, A. Zecchina, C. Lamberti, *J. Chem. Phys.* **2002**, *117*, 226 – 237; c) A. Damin, F. Bonino, G. Ricchiardi, S. Bordiga, A. Zecchina, C. Lamberti, *J. Phys. Chem. B* **2002**, *106*, 7524 – 7526; d) S. Bordiga, A. Damin, F. Bonino, A. Zecchina, G. Spanò, F. Rivetti, V. Bolis, C. Lamberti, *J. Phys. Chem B* **2002**, *106*, 9892 – 9905.
[7] C. Lamberti, S. Bordiga, A. Zecchina, G. Artioli, G. L. Marra, G. Spanò, *J. Am. Chem. Soc.* **2001**, *123*, 2204 – 2212.
[8] M. R. Boccuti, K. M. Rao, A. Zecchina, G. Leofanti, G. Petrini, *Stud. Surf. Sci. Catal.* **1989**, *48*, 133 – 144.
[9] a) D. Scarano, A. Zecchina, S. Bordiga, F. Geobaldo, G. Spoto, G. Petrini, G. Leofanti, M. Padovan, G. Tozzola, *J. Chem. Soc. Faraday Trans.* **1993**, *89*, 4123 – 4130; b) G. Deo, A. M. Turek, I. E. Wachs, D. R. C. Huybrechts, P. A. Jacobs, *Zeolites* **1993**, *13*, 365 – 373.
[10] a) S. Bordiga, S. Coluccia, C. Lamberti, L. Marchese, A. Zecchina, F. Boscherini, F. Buffa, F. Genoni, G. Petrini, G. Vlaic, *J. Phys. Chem.* **1994**, *98*, 4125 – 4132; b) T. Blasco, M. Camblor, A. Corma, J. Pérez-Parriente, *J. Am. Chem. Soc.* **1993**, *115*, 11806 – 11813.
[11] D. Gleeson, G. Sankar, C. R. A. Catlow, J. M. Thomas, G. Spanò, S. Bordiga, A. Zecchina, C. Lamberti, *Phys. Chem. Chem. Phys.* **2000**, *2*, 4812 – 4817.
[12] C. Li, G. Xiong, Q. Xin, J. Liu, P. Ying, Z. Feng, J. Li, W. Yang, Y. Wang, G. Wang, X. Liu, M. Lin, X. Wang, E. Min, *Angew. Chem.* **1999**, *111*, 2358 – 2360; *Angew. Chem. Int. Ed.* **1999**, *38*, 2220 – 2222.
[13] G. Ricchiardi, A. Damin, S. Bordiga, C. Lamberti, G. Spanò, F. Rivetti, A. Zecchina, *J. Am. Chem. Soc.* **2001**, *123*, 11409 – 11419.
[14] D. Trong On, S. Kaliaguine, L Bonneviot, *J. Catal.* **1995**, *157*, 235 – 243.
[15] To help with further reading, we note briefly that resonant Raman spectroscopy is defined as a Raman experiment in which the exciting wavelength coincides with, or is near to, the wavelength of an electronic absorption of the sample. This condition guarantees a high transfer of energy to the sample. Moreover, the use of a UV exciting source also guarantees a significant reduction of the fluorescence background signal. If the electronic absorption involves a localized center, such as a transition-metal atom and its ligands in the nearest coordination shells, excitation is also partially localized and the vibrational features of the grouping of atoms constituted by the central ions and the surrounding ligands can be enhanced by several orders of magnitude, if they meet the appropriate enhancement selection rules. Two kinds of vibrations are enhanced: a) the vibrations which are totally symmetric with respect to the absorbing center, and b) the vibrational modes directly involving atoms that undergo the same molecular deformation induced by the electronic excitation. a) Y. Nishimura, A. Y. Hirakawa, M. Tsuboi in *Advances in Infrared and Raman Spectroscopy* (Eds.: R. J. H. Clark, R. E. Hester), Heyden & Son, London, **1978**; b) P. R. Carey, *Biochemical Applications of Raman and Resonance Raman Spectroscopies*, Academic Press, New York, **1982**, and references therein.
[16] F. Geobaldo, S. Bordiga, A. Zecchina, E. Giamello, G. Leofanti, G. Petrini, *Catal. Lett.* **1992**, *16*, 109 – 115.
[17] C. Zecchina, S. Bordiga, C. Lamberti, G. Ricchiardi, D. Scarano, G. Petrini, G. Leofanti, M. Mantegazza, *Catal. Today* **1996**, *32*, 97 – 106.
[18] A. Zecchina, S. Bordiga, G. Spoto, A. Damin, G. Berlier, F. Bonino, C. Prestipino, C. Lamberti, *Top. Catal.* **2002**, *21*, 67 – 78.
[19] G. Tozzola, M. A. Mantegazza, G. Ranghino, G. Petrini, S. Bordiga, G. Ricchiardi, C. Lamberti, R. Zulian, A. Zecchina, *J. Catal.* **1998**, *179*, 64 – 71.
[20] C. M. Barker, D. Gleeson, N. Katsoyannis, R. C. A. Catlow, G. Sankar, J. M. Thomas, *Phys. Chem. Chem. Phys.* **2002**, *4*, 1128 – 1240.
[21] P. E. Sinclair, R. C. A. Catlow, *J. Phys. Chem. B* **1999**, *103*, 1084 – 1095.
[22] Note that the O–O stretching frequency of the H_2O_2 molecules in aqueous solution occurs at 875 cm^{-1}.
[23] Z. Ruzic-Toros, B. Kojic-Prodic, M. Sljukic, *Inorg. Chimica Acta* **1984**, 86, 205 – 208.
[24] a) L. Andrews, G. V. Cherthin, A. Ricca, C. W. Bauschlicher, Jr., *J. Am. Chem. Soc.* **1996**, 118, 467 – 470; b) G. V. Cherthin, A. Citra, L. Andrews, C. W. Bauschlicher, Jr., *J. Phys. Chem. A* **1997**, *101*, 8793 – 8802; c) A. Citra, G. V. Cherthin, L. Andrews, M. Neurock, *J. Phys. Chem. A* **1997**, *101*, 3109 – 3118; d) L. Andrews, G. V. Cherthin, C. A. Thompson, J. Dillon, S. Byrne, R. D. Davy, C. W. Bauschlicher, Jr., *J. Phys. Chem.* **1996**, *100*, 10088 – 10100.
[25] A. Zecchina, G. Spoto, S. Bordiga, A. Ferrero, G. Petrini, G. Leofanti, M. Padovan, *Stud. Surf. Sci. Catal.* **1991**, *69*, 251 – 258.
[26] When longer time exposure or higher laser power were adopted, a component at 875 cm^{-1} has been observed, suggesting H_2O_2 evolution.

Pd^0-Catalyzed Three-Component Tandem Double-Addition–Cyclization Reaction: Stereoselective Synthesis of *cis*-Pyrrolidine Derivatives**

Shengming Ma* and Ning Jiao

Pd^0-catalyzed cyclization reactions of functionalized allenes[1] leading to carbo- and heterocyclic compounds[2–4] has been studied extensively. In some of these reactions, the π-allyl palladium intermediate formed in situ[5] was trapped by an intramolecular nucleophile (path A, Scheme 1). Recently, development of multicomponent reactions to preserve atom economy[6] and stereoselectively construct an array of several stereogenic centers in one pot is attracting the attention of many chemists.[7] Therefore, if there is another potential electrophilic receptor such as an imine group in the reaction system, the Pd^0-catalyzed reaction of organohalides and allenes with a nucleophilic center would allow the formation of pyrrolidine derivatives (path B, Nu = C, Scheme 1). To make this concept synthetically attractive, we must address the issues of matched relay, regioselectivity (by excluding the formation of seven-membered product **6**), and diastereoselectivity (Scheme 1).

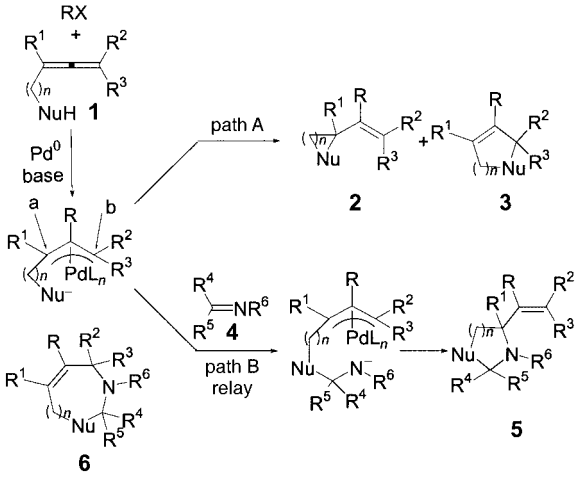
The construction of pyrrolidine skeletons, a frequently observed structural unit in various natural products, ligands, etc., is of current interest.[8,9] Although the transition-metal-catalyzed cyclization of γ-allenic amides to yield 2-substituted

[*] Prof. S. Ma, N. Jiao
State Key Laboratory of Organometallic Chemistry
Shanghai Institute of Organic Chemistry, Chinese Academy of Sciences
354 Fenglin Lu, Shanghai 200032 (P.R. China)
Fax: (+86) 21-6416-6128
E-mail: masm@pub.sioc.ac.cn

[**] Financial support from the Major State Basic Research Development Program (Grant No. G2000077500), the National Natural Science Foundation of China, and the Shanghai Municipal Committee of Science and Technology are greatly appreciated.

Supporting information for this article is available on the WWW under http://www.angewandte.org or from the author.

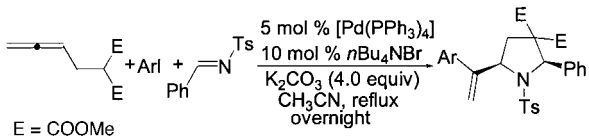
 © 2002 WILEY-VCH Verlag GmbH & Co. KGaA, Weinheim 0044-8249/02/4124-4737 $ 20.00+.50/0



Scheme 1. Protocol for the selective synthesis of pyrrolidine derivatives through a three-component reaction.

pyrrolidine has been well-documented,[10,11] the transition-metal-catalyzed multicomponent reaction of functionalized allenes to form polysubstituted heterocyclic compounds with high stereoselectivity has not been reported. Herein we disclose our recent results on the three-component tandem double-addition–cyclization of 2-(2,3-allenyl)malonates, organohalides, and imines. By tuning the reaction conditions, we have addressed the issues of smooth relay, regio-, and diastereoselectivity.

We recently developed four sets of reaction conditions under which the coupling–cyclization of 2-(2,3-allenyl)malonates with organohalides afforded cyclopropane derivative **2** or cyclopentene derivatives **3** with high regioselectivity (Nu = C, Scheme 1).[12–14] Fortunately, under the same conditions for path A[14d] ([$Pd(PPh_3)_4$] (5 mol %), K_2CO_3 (4 equiv), nBu_4NBr (10 mol %), CH_3CN, reflux), the reaction of 2-(2,3-allenyl)-malonates with PhI and *N*-benzylidene *p*-toluenesulfonamide (**4a**) afforded pyrrolidine derivative **5a** in 89 % yield (*cis*/*trans* 9:1; Scheme 2). Premature products **2a** and **3a** and seven-membered product **6a** ($n = 1$; Nu = C; R^1, R^2, R^3, R^4 = H; R, R^5 = Ph; R^6 = Ts) were not observed. The structure of *cis*-**5a** was determined by X-ray diffraction studies (Figure 1).[15] On the other hand, the corresponding reaction of **1a** and **4a** with



ArI (1.2 equiv)	**4a** (equiv)	yield of **5**	*cis*/*trans*
C_6H_5I	1.2	82% (**5a**)	90:10
p-$CH_3C_6H_4I$	1.2	92% (**5b**)	86:14
o-$CH_3C_6H_4I$	3.0	36% (**5c**)	94:6
o-$CH_3C_6H_4I$[a]	3.0	57% (**5c**)	>99:1

[a] Na_2CO_3 was used as the base.

Scheme 2. Control of stereoselectivity by the steric effect and base.

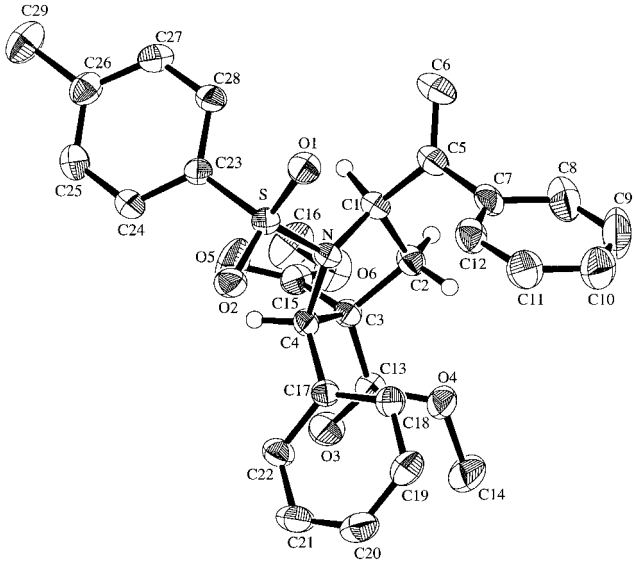


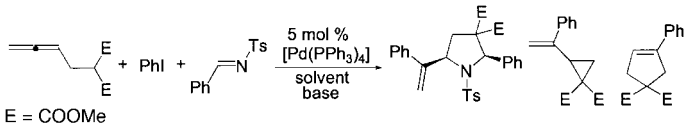
Figure 1. ORTEP representation of *cis*-**5a**.

o-methylphenyl iodide afforded pyrrolidine derivative **5c** in 36 % yield (*cis*/*trans* 94:6; Scheme 2). The use of Na_2CO_3 as base gives higher yield and stereoselectivity. Based on the results shown in Scheme 2, it can be concluded that the base and the steric hindrance of the aryl iodide are two of the major factors that control the stereoselectivity of this tandem coupling–cyclization reaction. Thus, control of the stereoselectivity of the two carbon centers in a general manner would be a new challenge.

The effects of different bases, solvents, and additives for the reaction of Pd^0-catalyzed reaction of **1a**, iodobenzene, and imine **4a** are shown in Table 1. Of several bases tested, K_2CO_3 and Na_2CO_3 gave higher yields of **5a**, but the *cis*/*trans* ratio is still not excellent (Table 1, entries 2 and 4). The use of a stronger base (e.g. Cs_2CO_3, nBu_4NBr (10 mol %), or NaH) in the reaction favors the formation of the premature three-membered cycle **2a** or cyclopentene derivative **3a** (Table 1, entries 3 and 5), indicating a lower relay ability. The use of a phase-transfer catalyst (nBu_4NBr, 10 mol %) has no dramatic effect on the stereoselectivity (compare Table 1, entries 1 with 2). Fortunately, the use of THF as the solvent led to the isolation of **5a** in 72 % yield with excellent stereoselectivity (*cis*/*trans* > 99:1), albeit that **2a** was also formed in 26 % yield (Table 1, entry 8). Even with 3.0 equivalents of imine, the relay is still not satisfactorily smooth (Table 1, entries 10 and 11). The addition of a Lewis acid did not produce better relaying results; on the contrary, the *cis*/*trans* ratio decreased (Table 1, entries 12). Furthermore, the effect of the temperature on the reaction is clear: in THF as solvent, the reaction in a sealed screw tube at 85 °C overnight afforded pyrrolidine derivative **5a** in 90 % yield exclusively, and the ratio is still excellent (Table 1, entry 13; compare entries 10, 11, and 13). A decrease in the amount of imine **4a** from 3.0 to 1.2 equivalents also gave a similar result (Table 1, entry 14). The reaction at 100 °C afforded **5a** with a slightly lower stereoselectivity (98:2; Table 1, entry 15). Similar results are also observed in 1,4-dioxane (Table 1, entries 16 and 17). Thus, the solvent (THF or 1,4-dioxane) and reaction temperature

 © 2002 WILEY-VCH Verlag GmbH & Co. KGaA, Weinheim 0044-8249/02/4124-4738 $ 20.00+.50/0

Table 1. $[Pd(PPh_3)_4]$-catalyzed tandem double-addition–cyclization of **1a** with PhI and imine **4a** under different reaction conditions.[a]



1a **4a** **5a** **2a** **3a**

Entry	Base	Additive[b]	Imine [equiv]	Solvent	T [°C]	Time [h]	**5a** Yield [%]	*cis*/*trans*	Yield **2a** [%]
1	K_2CO_3	–	1.2	CH_3CN	reflux	11	71	86:14	0
2	K_2CO_3	A	1.2	CH_3CN	reflux	10	82	90:10	0
3	Cs_2CO_3	A	1.2	CH_3CN	reflux	11	trace	-	43[c]
4	Na_2CO_3	A	1.2	CH_3CN	reflux	11	89	95:5	0
5	NaH	–	1.2	DMF	85	11	31	86:14	0[d]
6	K_2CO_3	–	1.2	DMF	85	12	73	75:25	0[e]
7	K_2CO_3	A	1.2	toluene	85	12	63	80:20	8
8	K_2CO_3	–	1.2	THF	reflux	11	72	>99:1	26
9	Na_2CO_3	–	1.2	THF	reflux	36	65	>99:1	11
10	K_2CO_3	–	3.0	THF	40	58	82	>99:1	10
11	K_2CO_3	–	3.0	THF	reflux	12	88	>99:1	8
12	K_2CO_3	B	3.0	THF	reflux	11	89	96:4	5
13	K_2CO_3	–	3.0	THF	85[f]	11	90	>99:1	0
14	K_2CO_3	–	1.2	THF	85[f]	10	86	>99:1	0
15	K_2CO_3	–	1.2	THF	100[f]	10	87	98:2	0
16	K_2CO_3	–	1.2	C[g]	85	7	86	>99:1	0
17	K_2CO_3	–	1.2	C[g]	reflux	6	75	>99:1	0

[a] PhI (1.2 equiv), base (4.0 equiv), and NaH (1.1 equiv) were used. [b] A = nBu$_4$NBr (10 mol %), B = $Cu(OTf)_2$ (10 mol %); [c] 4 % of **3a** was produced. [d] 57 % of **3a** was produced. [e] 5 % of **3a** was produced. [f] The reaction was carried out in a tube with a screw cap. [g] C = 1,4-Dioxane.

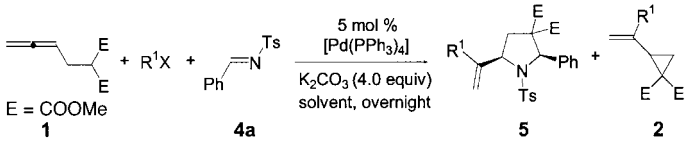
(85 °C) are key to a smooth relay and high stereoselectivity of **5a**.

The results of the $[Pd(PPh_3)_4]$-catalyzed tandem coupling–cyclization reaction of **1a** with different organohalides and imines in THF or 1,4-dioxane are summarized in Tables 2 and 3. In all other cases, except in the reactions of aryl halides with strongly electron-withdrawing substituents (Table 2, entries 7–9) the *cis*-pyrrolidine derivatives **5** are formed exclusively with high stereoselectivities by a subtle adjustment of the solvent or the amount of the corresponding imine. From Tables 2 and 3, it is clear that the current reaction can be successfully extended to a variety of organoiodides (Table 2, entries 1–14), phenyl bromide (Table 2, entry 15), phenyl triflate (Table 2, entry 16) and imines (Table 3) leading to the formation of the corresponding *cis*-pyrrolidine derivatives in 81–100 % yield with excellent stereoselectivities. The electron-withdrawing tosyl group of imine **4** is important for this reaction since the corresponding reaction of **1a** with PhI and *N*-(4-chlorobenzylidene)aniline afforded **2a** as the only product in 92 % yield, probably as a result of the lower reactivity of this imine.

The corresponding reaction of dimethyl 2-(2,3-decadienyl)malonate with PhI and **4a** afforded *cis*-**5l** in 85 % yield (Scheme 3). The configuration of the C=C bond in **5l** was determined from the ^{1}H,^{1}H NOESY spectra.

In conclusion, we have developed a three-component tandem double-addition–cyclization reaction that provides an efficient route to polysubstituted *cis*-pyrrolidine derivatives with matched relay and excellent regio- and stereoselectivity. As all three building blocks are readily available, this study will open a new area for the transition-metal-catalyzed chemistry of allenes. Further studies on the scope and synthetic applications of this reaction are being pursued in our laboratory.

Table 2. $[Pd(PPh_3)_4]$-catalyzed tandem double-addition–cyclization of **1a** with imine **4a** and different organohalides and triflates in THF or 1,4-dioxane.[a]



1 **4a** **5** **2**

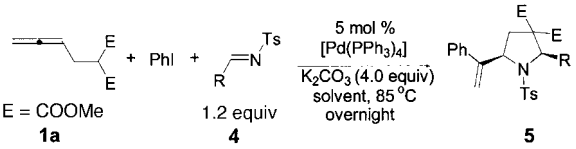
Entry	R^1X	Imine [equiv]	Solvent[b]	T [°C]	**5** Yield	*cis*/*trans*	Yield of **2** [%]
1	*p*-$CH_3C_6H_5I$	3.0	A	reflux	92 (**5b**)	>99:1	6 (**2b**)
2	*p*-$CH_3C_6H_5I$	1.2	A	85	92 (**5b**)	97:3	0
3	*p*-$MeOC_6H_5I$	1.2	A	85	85 (**5d**)	95:5	3 (**2d**)
4	*p*-$MeOC_6H_5I$	3.0	A	85	84 (**5d**)	95:5	0
5	*p*-$MeOC_6H_5I$	1.2	B	85	90 (**5d**)	>98:2	0
6	*p*-$MeOC_6H_5I$	1.2	B	reflux	81 (**5d**)	>98:2	0
7	*p*-$MeO_2CC_6H_5I$	3.0	A	85	92 (**5e**)	>99:1	6 (**2e**)
8	*p*-$MeO_2CC_6H_5I$	3.0	B	reflux	92 (**5e**)	>99:1	7 (**2e**)
9	*p*-$MeO_2CC_6H_5I$	1.2	B	reflux	64 (**5e**)	>99:1	35 (**2e**)
10	thienyl-I	3.0	A	85	100 (**5f**)	>99:1	0
11	(*E*)-PhC=C–I	3.0	A	85	96 (**5g**)	97:3	0
12	(*E*)-PhC=C–I	1.2	B	85	83 (**5g**)	95:5	0
13	(*E*)-*n*BuC=C–I	1.2	A	85	84 (**5h**)	96:4	0
14	(*E*)-*n*BuC=C–I	1.2	B	85	84 (**5h**)	97:3	0
15	C_5H_5Br	3.0	A	85	82 (**5a**)	>98:2	0
16	C_5H_5OTf	3.0	A	85	86 (**5a**)	96:4	0

[a] R^1I (1.2 equiv) was used. [b] A = THF, B = 1,4-dioxane.

Experimental Section

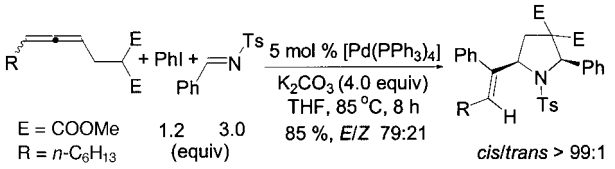
Typical procedure: Malonate **1a** (46 mg, 0.25 mmol) and iodobenzene (61 mg, 0.3 mmol, 1.2 equiv) were added consecutively to a sealed tube charged with a mixture of potassium carbonate (138 mg, 1.0 mmol, 4.0 equiv), $[Pd(PPh_3)_4]$ (14.5 mg, 0.0125 mmol, 5 mol %), and **4a** (78 mg, 0.3 mmol, 1.2 equiv) in THF (3 mL) under nitrogen. The resulting mixture was heated at 85 °C overnight and monitored by TLC. After evaporation, the residue was purified by flash column chromatography on silica gel (eluent: petroleum ether/ether 3:1) to afford pure **5a** (111 mg, 86 %; *cis*/*trans* >99:1). *cis*-**5a**: white solid, m.p. 146–147 °C (ethyl acetate/hexane); ^{1}H NMR (300 MHz, $CDCl_3$): δ = 7.53 (d, J = 8.29 Hz, 2H), 7.41–7.30 (m, 5H), 7.28–7.11 (m, 7H), 5.86 (s, 1H), 5.36 (s, 1H), 5.25 (s, 1H), 4.50 (dd, J = 11.68, 5.98 Hz, 1H), 3.65 (s, 3H), 3.15 (s, 3H), 2.84 (dd, J = 13.70, 11.68 Hz,

Table 3. [Pd(PPh$_3$)$_4$]-catalyzed tandem double-addition–cyclization of **1a** with PhI and different imines **4** in THF or 1,4-dioxane.[a]



Entry	R	Solvent[b]	5 Yield[%]	*cis*/*trans*	Yield of **2a** [%]
1	*p*-$O_2NC_6H_4$ (**4b**)	THF	89 (**5i**)	95:5	0
2	*p*-$O_2NC_6H_4$ (**4b**)	A	95 (**5i**)	97:3	0
3	*p*-$MeOC_6H_4$ (**4c**)	THF	52 (**5j**)	>99:1	42
4[c]	*p*-$MeOC_6H_4$ (**4c**)	THF	99 (**5j**)	>99:1	0
5	*p*-$MeOC_6H_4$ (**4c**)	A	52 (**5j**)	97:3	29
6	*p*-ClC_6H_4 (**4d**)	THF	95 (**5k**)	>98:2	0

[a] PhI (1.2 equiv) was used. [b] A = 1,4-dioxane; [c] Imine **4c** (3.0 equiv) was used.



Scheme 3. Synthesis of **5l** from **1b** and imine **4a**.

1H), 2.60 (dd, J = 13.70, 5.98 Hz, 1H), 2.39 ppm (s, 3H); ^{13}C NMR (75.4 MHz, $CDCl_3$): δ = 170.04, 167.18, 147.84, 143.71, 139.88, 139.05, 139.04, 135.69, 129.34, 128.55, 128.51, 128.46, 128.38, 128.25, 128.08, 116.63, 68.14, 64.03, 63.83, 53.73, 52.62, 39.28, 21.79 ppm; MS (70 eV): *m*/*z* (%): 520 (14.32) $[M+H]^+$, 364 (100); IR (KBr): $\tilde{\nu}$ = 1749, 1729, 1635, 1597, 1493, 1350, 1165 cm^{-1}; elemental analysis: calcd for $C_{29}H_{29}NO_6S$ (%): C 67.03, H 5.63, N 2.70; found C 67.04, H 5.48, N 2.63.

Received: July 9, 2002
Revised: September 10, 2002 [Z19689]

[1] a) H. F. Schuster, G. M. Coppola, *Allenes in Organic Synthesis*, John Wiley, New York, **1984**; *The Chemistry of Ketenes, Allenes, and Related Compounds, Part 1* (Ed.: S. Patai), Wiley, New York, **1980**.
[2] For a review on the palladium-catalyzed chemistry of allenes, see: R. Zimmer, C. U. Dinesh, E. Nandanan, F. A. Khan, *Chem. Rev.* **2000**, *100*, 3067; for a recent highlight, see: A. S. K. Hashmi, *Angew. Chem.* **2000**, *112*, 3737; *Angew. Chem. Int. Ed.* **2000**, *39*, 3590.
[3] For some of the most recent publications, see: a) J. Löfstedt, J. Franzén, J.-E. Bäckvall, *J. Org. Chem.* **2001**, *66*, 8015; b) W. F. J. Karstens, D. Klomp, F. P. J. T. Rutjes, H. Hiemstra, *Tetrahedron* **2001**, *57*, 5123; c) G. Liu, X. Lu, *Org. Lett.* **2001**, *3*, 3879; d) P. K. Dieter, H. Yu, *Org. Lett.* **2001**, *3*, 3855; e) Y.-H. Ha, S.-K. Kang, *Org. Lett.* **2002**, *4*, 1143; f) S.-K. Kang, Y.-H. Ha, B.-S. Ko, Y. Lim, J. Jung, *Angew. Chem.* **2002**, *114*, 353; *Angew. Chem. Int. Ed.* **2002**, *41*, 343.
[4] For some of the most recent results from our group, see: a) S. Ma, S. Zhao, *J. Am. Chem. Soc.* **2001**, *123*, 5578; b) S. Ma, Z. Shi, *Chem. Commun.* **2002**, 540; c) S. Ma, W. Gao, *Synlett* **2002**, 65; d) S. Ma, D. Duan, Y. Wang, *J. Comb. Chem.* **2002**, *4*, 239; e) S. Ma, Z. Yu, *Angew. Chem.* **2002**, *114*, 1853; *Angew. Chem. Int. Ed.* **2002**, *41*, 1775.
[5] a) I. Shimizu, J. Tsuji, *Chem. Lett.* **1984**, 233; b) M. Ahmar, B. Cazes, J. Gore, *Tetrahedron Lett.* **1984**, *25*, 4505.
[6] a) B. M. Trost, *Science* **1991**, *254*, 1471; b) B. M. Trost, *Angew. Chem.* **1995**, *107*, 285; *Angew. Chem. Int. Ed. Engl.* **1995**, *34*, 259.
[7] a) L. F. Tietze, *Chem. Rev.* **1996**, *96*, 115; b) P. J. Parsons, C. S. Penkett, A. J. Shell, *Chem. Rev.* **1996**, *96*, 195; c) R. A. Bunce, *Tetrahedron* **1995**, *51*, 13103.
[8] For some reviews, see: a) D. Enders, C. Thiebes, *Pure. Appl. Chem.* **2001**, *73*, 573; b) D. O'hagan, *Nat. Prod. Rep.* **2000**, *17*, 435; c) A. R. Pinder, *Nat. Prod. Rep.* **1992**, *9*, 17; d) G. Massiot, C. Ddelaude in *Alkaloids* (Ed.: A. Brossi), Academic Press, New York, **1996**, *27*, 269.
[9] a) J.-E. Bäckvall, H. E. Schink, Z. D. Renko, *J. Org. Chem.* **1990**, *55*, 826; b) E. Lee, E. J. Jeong, S. J. Min, S. Hong, J. Lim, S. K. Kim, H. J. Kim, B. G. Chio, K. C. Koo, *Org. Lett.* **2000**, *2*, 2169; c) A. Boto, R. Hernández, Y. de León, E. Suárez, *J. Org. Chem.* **2001**, *66*, 7796; d) B. Schlummer, J. F. Hartwig, *Org. Lett.* **2002**, *4*, 1471.
[10] For the Pd(0)-catalyzed coupling–cyclization reaction of γ-allenic amides with aryl or vinyl halides, see: a) S.-K. Kang, K.-J. Kim, *Org. Lett.* **2001**, *3*, 511; b) I. W. Davies, D. I. C. Scopes, T. Gallagher, *Synlett* **1993**, 85.
[11] For the Ag^+-catalyzed cycloisomerization of γ-allenic amides, see: a) I. W. Davies, T. Gallagher, R. B. Lamont, D. I. C. Scopes, *J. Chem. Soc. Chem. Commun.* **1992**, 335; b) D. N. A. Fox, D. Lathbury, M. F. Mahon, K. C. Molloy, T. Gallagher, *J. Chem. Soc. Chem. Commun.* **1989**, 1073; c) R. Kinsman, D. Lathbury, P. Vernon, T. Gallagher, *J. Chem. Soc. Chem. Commun.* **1987**, 243; for lanthanide-catalyzed cycloisomerization of γ-allenic amides, see: V. M. Arredondo, S. Tian, F. E. McDonald, T. J. Marks, *J. Am. Chem. Soc.* **1999**, *121*, 3633.
[12] For the Pd-catalyzed two-component reaction of 2-(2,3-allenyl)malonates with electron-deficient alkenes leading to five-membered carbocycles, see: M. Meguro, Y. Yamamoto, *J. Org. Chem.* **1999**, *64*, 694.
[13] For the Pd-catalyzed cycloisomerization of allenes with a nucleophilic center, see: a) S. Kamijo, Y. Yamamoto, *Tetrahedron Lett.* **1999**, *40*, 1747; b) M. Meguro, S. Kamijo, Y. Yamamoto, *Tetrahedron Lett.* **1996**, *37*, 7453; c) B. M. Trost, P.-Y. Michellys, V. J. Gerusz, *Angew. Chem.* **1997**, *109*, 1837; *Angew. Chem. Int. Ed.* **1997**, *36*, 1750.
[14] For the Pd-catalyzed coupling cyclization of 2-(2,3-allenyl)malonates with organohalides, see: a) L. Besson, J. Bazin, J. Gore, B. Cazes, *Tetrahedron Lett.* **1994**, *35*, 2881; b) M. Ahmar, B. Cazes, J. Gore, *Tetrahedron Lett.* **1985**, *26*, 3795; c) S. Ma, S. Zhao, *Org. Lett.* **2000**, *2*, 2495; d) S. Ma, N. Jiao, S. Zhao, H. Hou, *J. Org. Chem.* **2002**, *67*, 2837.
[15] X-ray data for compound **5a**: $C_{29}H_{29}NSO_6$, M_r = 519.61, triclinic, space group $P\bar{1}$ (#2), a = 10.228(2), b = 13.310(4), c = 9.980(2) Å, V = 1328.9(5) Å^3, α = 97.57(2)°, β = 96.13(2)°, γ = 96.17(2)°, T = 20.0 °C, Z = 2, $\mu(Mo_{K\alpha})$ 1.65 cm^{-1}, reflections collected 4926 (unique 4642), number of data with $I > 3.00\sigma(I)$ 3978, parameters 335, R_1 = 0.043, R_w = 0.057, R_{int} = 0.022. CCDC-189277 contains the supplementary crystallographic data for this paper. These data can be obtained free of charge via www.ccdc.cam.ac.uk/conts/retrieving.html (or from the Cambridge Crystallographic Data Centre, 12, Union Road, Cambridge CB2 1EZ, UK; fax: (+44) 1223-336-033; or deposit@ccdc.cam.ac.uk).

Catalytic Electronic Activation: Indirect "Wittig" Reaction of Alcohols**

Michael G. Edwards and Jonathan M. J. Williams*

Tandem, domino, and cascade reactions have become increasingly popular in recent years, driven by the opportunity to simplify linear sequences and achieve otherwise unfeasible reactions.[1] Contributions from this group have involved the idea of "catalytic electronic activation", which temporarily enhances the electronic nature of a functional group to a given reaction. We have recently reported the indirect addition of

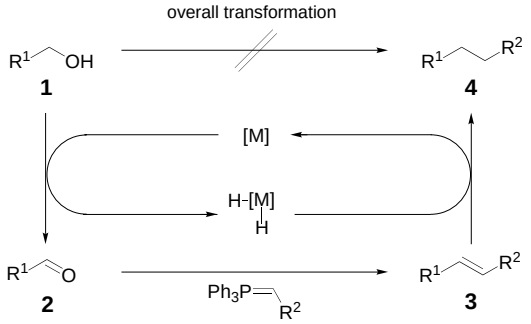
[*] Prof. Dr. J. M. J. Williams, M. G. Edwards
Department of Chemistry
University of Bath
Claverton Down, Bath BA2 7AY (UK)
Fax: (+44) 1225-826-231
E-mail: j.m.j.williams@bath.ac.uk

[**] This work was supported by the EPSRC (M.G.E.).

Supporting information for this article is available on the WWW under http://www.angewandte.org or from the author.

 © 2002 WILEY-VCH Verlag GmbH & Co. KGaA, Weinheim 0044-8249/02/4124-4740 $ 20.00+.50/0

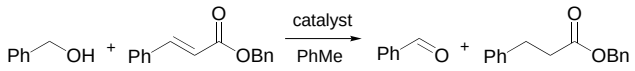
nucleophiles to allylic alcohols[2] and the directed asymmetric epoxidation of enals.[3] Here we report an extension of catalytic electronic activation to the indirect "Wittig" reaction of alcohols (Scheme 1).



Scheme 1. Indirect Wittig reaction of alcohols by catalytic electronic activation.

A substrate alcohol **1** can be activated by dehydrogenation to afford an intermediate carbonyl compound **2**, which will then readily undergo olefination. The sequence is completed by hydrogenation of intermediate alkene **3** to provide the alkane **4**. This domino reaction sequence affords alkane derivatives directly from the alcohol. An important feature of this method is that only one equivalent of alcohol is required where the hydrogen atoms "borrowed" during the oxidation step are subsequently returned in the hydrogenation of the alkene intermediate. Several research groups have reported in situ oxidation of alcohols coupled with Wittig olefination to afford alkene derivatives.[4] However, our system is unusual in that there is no net oxidation transformation. The one-pot sequence illustrated in Scheme 1 potentially offers an alternative to the traditional route involving conversion of alcohol into alkyl halides, malonate substitution and decarboxylation.

The starting point for our studies was to establish that the necessary oxidation and reduction steps were feasible. The crossover transfer hydrogenation reaction between benzyl alcohol and benzyl cinnamate was chosen to demonstrate this (Scheme 2, Table 1). These data indicated that judicious choice of catalyst enabled virtually complete conversion into benzaldehyde and benzyl dihydrocinnamate, respectively. The iridium-based catalyst system reported by Ishii and co-workers[5] (Table 1, entry 7) provided the optimal results, and was the system chosen for examination in the complete cycle.



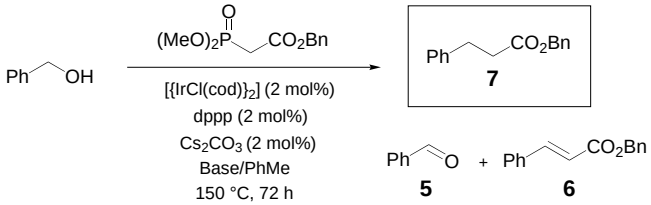
Scheme 2. Crossover transfer hydrogenation (CTH) of benzyl cinnamate with benzyl alcohol.

Table 1. Crossover transfer hydrogenation (CTH) studies.[a]

Entry	Catalyst (mol %)	T [°C]	t [h]	Conv. [%][b]
1	Raney-Ni (25)	110	24	33
2	Pd/C (25)	110	48	65[c]
3	$Al(OtBu)_3$ (100)	110	48	< 5
4	[Ru(η^6-*p*-cymene)(TsDPEN)][d] (5)	110	48	25
5	[Ir(cod)(Py)(PCy_3)]PF_6[e] (4)	150	72	58
6	[{IrCl(cod)}$_2$]/dppp/Cs_2CO_3[f] (2)	80	24	35
7	[{IrCl(cod)}$_2$]/dppp/Cs_2CO_3 (2)	150	72	92

[a] The reactions were carried out on a 0.5 mmol scale in toluene (1.5 mL). [b] Measured by ^{1}H NMR spectroscopy. [c] Reaction run in THF. [d] TsDPEN = (1*S*,2*S*)1,2-diphenyl-*N*-(*p*-tolylsulfonyl)ethylenediamine. [e] Py = pyridine, Cy = cyclohexyl, cod = cycloocta-1,5-diene. [f] dppp = 1,2-bis(diphenylphosphanyl)propane.

An extensive selection of methods exists for the olefination of aldehydes, including several elegant methods reported recently.[6] The method of olefination investigated initially was the Horner–Wadsworth–Emmons (HWE) reaction; the water-soluble phosphate by-product is easily removed and the necessary phosphonates are readily available. Initial results were promising although conversion into the desired product was sluggish despite attempts to optimize the reaction conditions (Scheme 3, Table 2). The best result was obtained with the organic base MTBD (Table 2, entry 3). However, the



Scheme 3. Indirect Horner–Wadsworth–Emmons (HWE) reactions of alcohols.

Table 2. Indirect HWE reactions with benzyl alcohol.[a]

Entry	Phosphonate (equiv)	Base (equiv)	Conv. [%][b]	**5** [%]	**6** [%]	**7** [%]
1	1.0	Cs_2CO_3 (1.0)	59	11	25	23
2[c]	5.0	NaH (5.0)	67	8	11	48
3	1.0	MTBD[d] (1.0)	90	18	14	58
4[e]	1.0	Cs_2CO_3 (1.0)	30	5	3	22

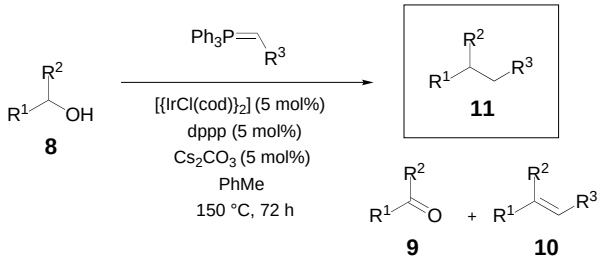
[a] The reactions were carried out on a 0.5 mmol scale in toluene (1.5 mL) at 150 °C. [b] Total conversion of benzyl alcohol into compounds **5**, **6**, and **7** measured by ^{1}H NMR spectroscopy. [c] Na salt of HWE Phosphonate was preformed. [d] MTBD = 1-Methyl-1,3,4,6,7,8-hexahydro-2*H*-pyrimido[1,2-*a*]pyrimidine. [e] With Crabtree's catalyst (2 mol %).

significant amount of intermediates **5** and **6** remaining is consistent with the presence of an alternative path for the loss of hydrogen. The coordination of β-carbonyl phosphonates (and derivatives) to metal centers is well known. In particular, they have been used for the extraction of radioactive metal cations.[7] In this respect the slow progression of the cycle is perhaps unsurprising.

We next focused upon the Wittig reaction[8] to achieve the necessary olefination step. It was anticipated that the use of stabilized Wittig ylides would prove to be more successful,

 © 2002 WILEY-VCH Verlag GmbH & Co. KGaA, Weinheim 0044-8249/02/4124-4741 $ 20.00+.50/0

since the problem of chelation to the metal center should be removed (Scheme 4). We were therefore delighted to discover that these reactions proceeded to give the expected alkane products. Optimization of the reaction conditions (5 mol% catalyst, 1.1 equiv ylide) provided a system that was applicable to various benzylic alcohols (Table 3).



Scheme 4. Typical procedure for the domino crossover transfer hydrogenation–Wittig olefination process.

Table 3. Indirect Wittig reaction of alcohol substrates **8**.[a]

Entry	R^1	R^2	R^3	Conv. [%][b]	**9** [%]	**10** [%]	**11** [%][c]
1	Ph	H	CO_2Bn	100	5	12	79(71)[d]
2	Ph	H	CO_2Me	100	21	3	68(51)[d]
3	Ph	H	$CO_2(CH_2tBu)$	96	4	20	68(54)[d]
4	Ph	H	CONMe(OMe)	99	11	11	75(47)[d]
5	Ph	H	CN	84	7	7	70(56)
6	4-ClC_6H_4	H	CN	97	10	8	79(66)
7	2-naphthyl	H	CN	90	16	2	72(46)
8	1-pyrenyl	H	CN	98	25	6	67(52)
9	Ph	Me	CN	77	30	6	41(14)

[a] The reactions were carried out on a 2 mmol scale in toluene (6 mL) at 150 °C. [b] Total conversion of alcohol **8** into compounds **9**, **10**, and **11** measured by ^1H NMR spectroscopy. [c] Figures in brackets refer to the yield of isolated products after column chromatography. [d] Following oxidative removal of the alkene by-product.[11]

The results shown in Table 3 indicate that acceptable yields of the alkane products could be obtained (entries 1–4). Dihydrocinnamate derivatives were synthesized in 46–71% yield, although a small amount of transesterification (< 10%) occurred when the alternative ester ylides were employed. In this regard, the reaction with the cyano ylide was attractive. The reaction afforded only one reduced Wittig adduct, dihydrocinnamonitrile, in 56% yield (Table 3, entry 5). The use of the same nitrile ylide with alternative benzylic alcohols was probed (entries 6–8). Successful reactions with these alcohols yielded the products in 46–66%. Attempts to extend the scope of the reaction to both unactivated alcohols and secondary alcohols were only partly successful. Reaction with *n*-butanol produced less than 5% of the capronitrile product. Reaction with 2-phenylethanol (entry 9) resulted in a low yield of the desired product, 3-phenylbutanenitrile. This is entirely consistent with the lower reactivity of ketones towards Wittig olefination.[9]

In summary, we have developed new methodology for the one-pot conversion of alcohols to alkanes by catalytic electronic activation. We anticipate that application of a more active crossover transfer hydrogenation catalyst will enable the use of more amenable reaction conditions and allow extension of this methodology to a wider range of alcohols.

Experimental Section

Sample procedure:[10] To an argon-purged pressure tube containing [{IrCl(cod)}$_2$] (0.067 g, 0.1 mmol), dppp (0.041 g, 0.1 mmol), Cs_2CO_3 (0.033 g, 0.1 mmol) and benzyl (triphenylphosphoranylidene)acetate (0.782 g, 2.2 mmol) was added benzyl alcohol (0.212 g, 2.0 mmol, 197 μL), followed by anhydrous toluene (6 mL). The tube was sealed and then heated at 150 °C for 72 h. The resulting brown mixture was poured into water (50 mL) and extracted with diethyl ether (4 × 50 mL). The combined organic extracts were washed with saturated brine (100 mL), dried ($MgSO_4$) and concentrated in vacuo. Purification by flash column chromatography (SiO_2, 40:1 petroleum ether (b.p. 40–60 °C)/diethyl ether) afforded an inseparable 5.8:1 mixture of benzyl dihydrocinnamate and benzyl cinnamate. The cinnamate by-product was removed oxidatively by using the procedure of Von Rudloff.[11] The mixture was dissolved in 50 mL of a 0.005 M potassium permanganate/0.25 M sodium metaperiodate/0.1 M potassium carbonate solution in 3:2 water/*tert*-butyl alcohol and stirred for 2 h. The mixture was extracted with diethyl ether (3 × 25 mL) and the combined organic extracts washed with 1 M sodium hydroxide (2 × 50 mL) and saturated brine (50 mL), dried ($MgSO_4$), filtered and concentrated in vacuo to afford benzyl dihydrocinnamate,[12] a colorless liquid (0.341 g, 71% yield).

Received: August 2, 2002 [Z19879]

[1] a) L. F. Tietze in *Selectivity, A Goal for Synthetic Efficiency* (Eds.: W. Bartmann, B. M. Trost), VCH, Weinheim, **1984**, p. 299; b) G. H. Posner, *Chem. Rev.* **1986**, *86*, 831; c) F. Ziegler, *Chem. Rev.* **1988**, *88*, 1423; d) L. F. Tietze, *J. Heterocycl. Chem.* **1990**, *27*, 47; e) L. F. Tietze, *Chem. Rev.* **1996**, *96*, 115.

[2] P. J. Black, W. Harris, J. M. J. Williams, *Angew. Chem.* **2001**, *113*, 4607; *Angew. Chem. Int. Ed.* **2001**, *40*, 4475.

[3] P. J. Black, K. Jenkins, J. M. J. Williams, *Tetrahedron: Asymmetry* **2002**, *13*, 317.

[4] a) R. E. Ireland, D. W. Norbeck, *J. Org. Chem.* **1985**, *50*, 2198; b) A. G. M. Barrett, D. Hamprecht, M. Ohkuba, *J. Org. Chem.* **1997**, *62*, 9376; c) S. Shuto, S. Niizuma, A. Matsuda, *J. Org. Chem.* **1998**, *63*, 4489; d) X. Wei, R. J. K. Taylor, *Tetrahedron Lett.* **1998**, *39*, 3815; e) D. Crich, X. Mo, *Synlett* **1999**, 67; f) L. Blackburn, X. Wei, R. J. K. Taylor, *Chem. Commun.* **1999**, *1337*; g) G. Kim, D. G. Lee, S. Chang, *Bull. Korean Chem. Soc.* **2001**, *22*, 943; h) L. Blackburn, R. J. K. Taylor, *Synlett* **2002**, 215.

[5] S. Sakaguchi, T. Yamaga, Y. Ishii, *J. Org. Chem.* **2001**, *66*, 4710.

[6] a) W. A. Herrmann, P. W. Roesky, M. Wang, W. Scherer, *Organometallics* **1994**, *13*, 4531; b) B. E. Ledford, E. M. Carreira, *Tetrahedron Lett.* **1997**, *38*, 8125; c) O. Fujimura, T. Honma, *Tetrahedron Lett.* **1998**, *39*, 625; d) H. Lebel, V. Paquet, C. Proulx, *Angew. Chem.* **2001**, *113*, 2971; *Angew. Chem. Int. Ed.* **2001**, *40*, 2887; f) G. A. Mirafzal, G. Cheng, L. K. Woo, *J. Am. Chem. Soc.* **2002**, *124*, 176.

[7] See for example: a) M. Gahagan, R. K. Mackie, D. J. Cole-Hamilton, D. C. Cupertino, M. Harman, M. B. Hursthouse, *J. Chem. Soc. Dalton Trans.* **1990**, 2195; b) S. M. Bowen, E. N. Duesler, D. J. McCabe, R. T. Paine, *Inorg. Chem.* **1985**, *24*, 1191, and references therein.

[8] For reviews of the Wittig reaction see: a) W. S. Wadsworth, Jr., *Org. React. (N.Y.)* **1977**, *25*, 73; b) J. I. G. Cadogan, *Organophosphorus Reagents in Organic Synthesis*, Academic Press, New York, **1979**; c) B. E. Maryanoff, A. B. Reitz, *Chem. Rev.* **1989**, *89*, 863; d) S. E. Kelly in *Comprehensive Organic Synthesis, Vol. 1* (Eds.: B. M. Trost, I. Fleming, S. L. Schreiber), Pergamon Press, Oxford, **1991**, pp. 730–817; e) A. W. Johnson, *Ylides and Imines of Phosphorus*, Wiley-Interscience, New York, **1993**; f) E. Vedejs, M. J. Peterson, *Top.*

 © 2002 WILEY-VCH Verlag GmbH & Co. KGaA, Weinheim 0044-8249/02/4124-4742 $ 20.00+.50/0

Stereochem. **1994**, *21*, 1; g) E. Vedejs, M. J. Peterson, *Adv. Carbanion Chem.* **1996**, *2*, 1.
[9] S. Trippett, D. M. Walker, *J. Chem. Soc.* **1961**, 1266.
[10] General procedures for the reaction with ester ylides and the cyano ylide together with preparations and characterization for neopentyl (triphenylphosphoranylidene) acetate, neopentyl dihydrocinnamate and pyrene-1-ylpropionitrile are contained in the Supporting Information.
[11] E. von Rudloff, *Can. J. Chem.* **1956**, *34*, 1413.
[12] P. C. Bulman Page, M. J. McKenzie, S. M. Allin, D. R. Buckle, *Tetrahedron* **2000**, *56*, 9683.

A Straightforward Detection of Deprotonated Conformers of Malonic Acid by Solid-State ^{13}C NMR Spectroscopy

Roxane Colsenet, Carole Gardiennet, Bernard Henry, and Piotr Tekely*

There is wide interest in the study of dicarboxylic acids, which are known to be substrates of a large number of enzymes.[1] Very recently, it has also been reported that malonic acid based inhibitors of matrix metalloproteinases involved in tissue remodeling, and thus in various disease processes such as tumor development and joint destruction, reveal a unique mode of binding to the enzymes.[2] In view of the role of malonic acid in biological metabolism, and of the resulting chemistry, the detection of its deprotonated forms during various processes is of prime importance.

Herein we demonstrate, for the first time, that solid-state ^{13}C NMR spectroscopy permits information to be obtained in a straightforward manner about the presence and the nature of various deprotonated forms of malonic acid in lyophilizates prepared from parent solutions at different pH values. The clear advantage of solid-state over liquid-state NMR spectroscopy arises from the existence of well-separated, isotropic ^{13}C signals for protonated and deprotonated species in the lyophilizate as a result of a dramatic slowing down of inter- and intramolecular proton exchanges on the NMR time scale.[3–4] Another benefit of solid-state measurements results from easy access to the principal values of carbon chemical shift anisotropy (CSA) tensors, which, by virtue of their nature, are much more sensitive to the changes in the ionization state and the hydrogen-bonding interactions than the isotropic chemical shift.[5]

[*] Dr. P. Tekely, R. Colsenet, C. Gardiennet
Laboratoire de Méthodologie RMN
FRE CNRS 2415
Université H. Poincaré
Nancy 1, 54500 Vandoeuvre lès Nancy (France)
Fax: (+33) 3-8368-4347
E-mail: piotr.tekely@rmn.uhp-nancy.fr
Dr. B. Henry
Laboratoire de Chimie Physique Organique et Colloïdale
UMR CNRS 7565
Université H. Poincaré
Nancy 1, 54500 Vandoeuvre lès Nancy (France)

Figure 1 shows the changes in the isotropic positions in high-resolution ^{13}C cross polarization magic-angle-spinning (CP/MAS) NMR spectra of malonic acid lyophilizates prepared from solutions at different pH values. The principal elements δ_{ii} of protonated and deprotonated carboxy CSA

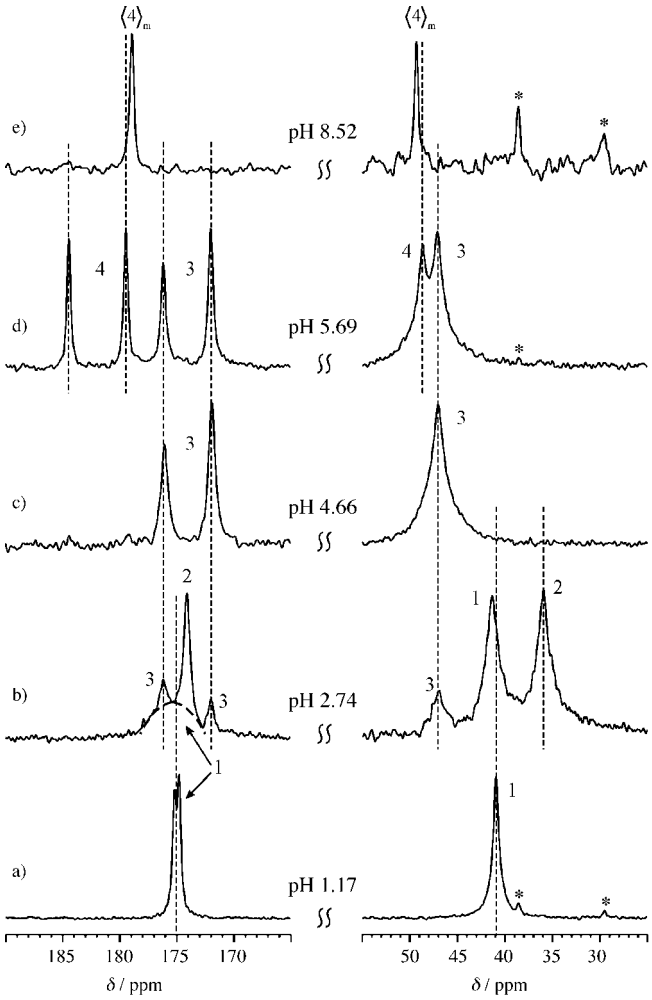


Figure 1. Evolution of isotropic positions in low-speed MAS ($\nu_r = 2.0$ kHz) ^{13}C NMR spectra of malonic acid lyophilized from solutions at pH 1.17 (a), 2.74 (b), 4.66 (c), 5.69 (d), and 8.52 (e). The numbered isotropic peaks refer to malonic acid (1), monoanion conformers (2) and (3), and double deprotonated rigid (4) as well as the motionally averaged ($\langle 4 \rangle_m$) form. For better visualization, the signals in (c) and (e) have been presented with equal height. The signals labeled as * are the isotropic positions of adamantane placed at the bottom of the rotor for the purpose of chemical shift calibration.

tensors were derived from spinning sideband manifolds (Figure 2). The isotropic chemical shifts δ_{iso} and the principal CSA elements δ_{ii} are reported in Table 1. The isotropic chemical shifts of hydroxy protons involved in hydrogen bonding, as revealed from high-speed ^{1}H MAS spectra (not shown), are also included.

The high-resolution ^{13}C spectra show that the successive steps of deprotonation are manifested by sharp changes in the δ_{iso}, δ_{11}, and δ_{22} values, which are significantly different for each species and for individual carboxy groups. We ascribe the two closely placed isotropic resonance peaks at pH 1.17 to

 © 2002 WILEY-VCH Verlag GmbH & Co. KGaA, Weinheim 0044-8249/02/4124-4743 $ 20.00+.50/0

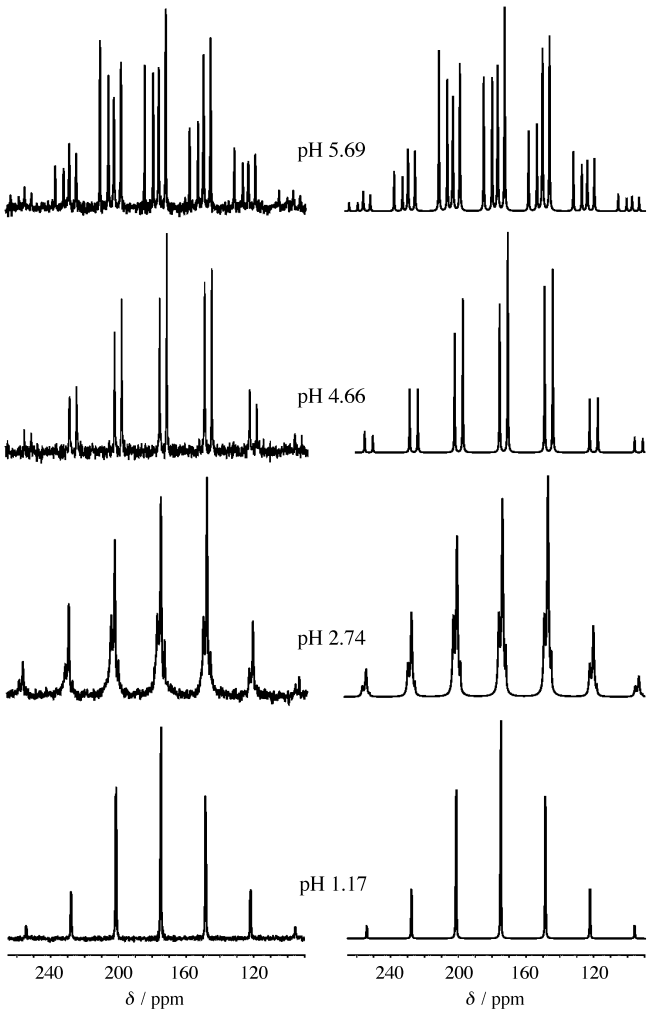


Figure 2. Experimental (left) and calculated (right) low spinning speed ($\nu_r = 2.0$ kHz) chemical shift anisotropy sideband manifolds of carboxy groups of malonic acid lyophilized from solutions at pH 1.17 (a), 2.74 (b), 4.66 (c), and 5.69 (d).

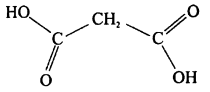
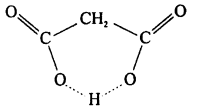
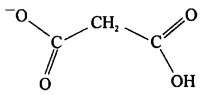
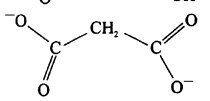
slightly magnetically inequivalent carboxy carbon atoms in the lowest energy conformer of malonic acid in which two carboxylic groups are in a nearly orthogonal arrangement, with one of them being coplanar with the carbon atom backbone.[6] The δ_{ii} values for this fully protonated malonic acid are close to those reported in alkanedicarboxylic acids.[7]

New isotropic signals are visible at pH 2.74. This clearly indicates that two different hydrogen malonate acid species are present in addition to the fully protonated form. Both types of deprotonated species show a more shielded δ_{22} value compared to the fully protonated form. We attribute these two deprotonated forms to different conformers of the hydrogen malonate ion, namely its planar and nonplanar form. A symmetrical C_{2v}, intramolecularly hydrogen-bonded planar structure was indeed found to be the most stable conformer in the case of the monoanion by ab initio calculations.[8] This conformer has to be responsible for the high-field resonance signal of the CH_2 group at $\delta = 35.9$ ppm and a single resonance signal of the carboxy groups at 174.1 ppm with δ_{11} and δ_{22} values equal to $\delta = 252$ and 165 ppm, respectively. The existence of this strongly intramolecularly hydrogen-bonded conformer at such a pH value corroborates with the appearance of a new isotropic peak corresponding to hydroxy groups at $\delta = 15.6$ ppm in the ^{1}H MAS spectrum.

The second, singly deprotonated form, is responsible for the resonance signal of the CH_2 group at $\delta = 47.1$ ppm and two signals at $\delta = 172$ and 176.8 ppm. We ascribe the higher and lower field peaks to the carboxy and carboxylate carbon atoms, respectively on the basis of different values of the δ_{11} element. We attribute this form to the most stable nonplanar conformer with carboxylate and carboxylic groups in a nearly orthogonal arrangement.[9] Somewhat surprisingly, this is a unique conformational form of the hydrogen malonate acid present in the lyophilizate at pH 4.66 in which a single isotropic chemical shift of hydroxy protons is seen at $\delta = 14.4$ ppm.

Very recently we have shown that solid-state, natural-abundance ^{13}C NMR determinations of acid:base ratios of lyophilized L-histidine can be used to measure its three pK values in parent solutions, without recourse to full titration curves and subsequent curve-fitting procedures.[4] In the

Table 1. ^{13}C and ^{1}H NMR data of malonic acid and its deprotonated species.

Entry	pH range	^{13}C CSA [ppm][a]				^{13}C [ppm]	^{1}H [ppm][b]	Form/conformer	pK[c]
		δ_{11}[d]	δ_{22}[d]	δ_{33}[d]	δ_{iso}	$\delta_{iso}^{CH_2}$	$\delta_{iso}^{hydroxyl}$		
1	1–3	235	180	109	174.8	40.3	13.2		
		242	175	109	175.2				
2	2–3	252	165	105	174.1	35.9	15.6		2.57
3	2.5–5.7	242	166	107	172	47.1	14.4		
		254	167	108	176.8				
4	5.7–8.5	242	191	105	179.4	48.6			5.52
		244	204	104	184.4				

[a] Carboxy and carboxylate groups. [b] Hydrogen-bonded hydroxy protons. [c] Calculated from solid-state acid:base ratios. [d] Average standard deviations of ± 2 ppm.

 © 2002 WILEY-VCH Verlag GmbH & Co. KGaA, Weinheim 0044-8249/02/4124-4744 $ 20.00+.50/0 *Angew. Chem. Int. Ed.* **2002**, *41*, No. 24

present case, a pK_1 value of 2.57, relative to the first ionization of malonic acid, can be obtained from the ratio of the integrated intensities of the deconvoluted, well-separated signals of CH_2 groups at pH 2.74. This pK_1 value is indeed remarkably close to the average pK_1 value of 2.66 ± 0.05 calculated from a set of 22 values measured in aqueous solutions and reported in the IUPAC Stability Constants Database.[8]

A second step of the deprotonation of the carboxylic end is clearly visible in the ^{13}C spectra of lyophilizates prepared at pH values above 5.0. Compared to the spectrum recorded at pH 4.66, a second resonance signal of CH_2 and two new resonance signals of carboxylate groups appear at pH 5.69. These two carboxylate groups, as also revealed by different NMR relaxation techniques, do not become more involved in hydrogen bonding with remaining monoanions. We ascribe the presence of two isotropic peaks (instead of a single one), both with large deshielded δ_{22} values, to two different conformations of the carboxylate groups, and is reminiscent of the orthogonal orientation of these groups in the nonplanar conformer of the monoanion. This result indicates that the variation in the middle tensor element δ_{22} of the carboxy groups not only arises because of the change in the ionization state and the presence of hydrogen bonding,[5] but may also depend strongly (as in the present case) on the conformation of the relevant molecular fragment. Somewhat unexpectedly, the second deprotonation step leads to a backward shift of the δ_{11} value for the previously deprotonated site, while the newly deprotonated site maintains its δ_{11} value. We explain the observed backward shift in the value corresponding to the carboxylate end by the disappearance of hydrogen-bonding interactions in the doubly deprotonated form, and the unchanged δ_{11} value of the newly deprotonated end by the opposite, and consequently, canceling effects of deprotonation and disappearance of hydrogen-bonding interactions. Finally, as expected, the most shielded δ_{33} element, which is orthogonal to the plane of carboxy groups,[10] is rather insensitive to any changes, whatever their origin.

From the ratio of the integrated intensity of the resonance peaks of both forms, and taking into account the $T_{1\rho}(^1H)$ relaxation decay of the deprotonated, somewhat more mobile form on the kHz frequency scale, the calculated pK_2 value is 5.52, which is only slightly higher in value than the average pK_2 value of 5.30 ± 0.06 calculated from a set of 22 values measured in aqueous solutions.[8] As in the case of L-histidine,[4] we can assign such a difference to temperature effects, since the freezing out of aqueous parent solutions begins at temperatures close to 0 °C, whereas most of the liquid-state titrations were performed at 25 °C.

Only a single resonance signal is observed for both carboxylate groups in a lyophilizate prepared from a parent solution at pH 8.52. This is a consequence of the final disappearance of the three-dimensional network of hydrogen-bonded monoanions and consequently to a substantial molecular mobility of the doubly deprotonated form. This situation leads in turn to a greatly averaged CSA tensor of carboxylate groups with a single isotropic resonance position at 178.9 ppm, which is identical to that observed in the liquid state. Table 1 summarizes the presence of different ionic forms/conformers of malonic acid together with the calculated pK values.

In conclusion, we have shown that the solid-state ^{13}C NMR study of malonic acid lyophilizates allows a straightforward detection of its deprotonated conformers present in the parent solution at different pH values. Calculated pK values from solid-state acid:base ratios r are found to be equal to those classically measured in the liquid state. Numerous applications of such an approach using readily available ^{13}C-enriched dicarboxylic acid substrates can be envisaged in order to obtain a deeper insight into the chemistry of many enzymatic processes. We believe this study also to be the first experimental observation of the planar intramolecularly hydrogen-bonded monoanion present at pH values close to the pK_1 value of the parent solution. Futher investigations will be necessary to check if the equilibrium between the two conformers of the monoanionic species can be affected by the nature of the counterions.

Experimental Section

Lyophilization: A sample of malonic acid (104 mg, Aldrich, 99 %) was dissolved in bidistilled water, and the volume adjusted to 10 mL (0.1M solution). The pH value was adjusted with NaOH at 25 °C using an Orion 901 pH meter equipped with an Orion 91-03 electrode which was previously standardized with appropriate buffer solutions. Samples were frozen out in a 50-mL rotating flask immersed in liquid nitrogen to obtain a thin solid layer with a large surface area. The flask was then detached from the rotating system (Büchi Rotavapor) and fitted to a lyophilizator (CHRIS Alpha 1–4) for 6 h at −80 °C and 300 Pa.

NMR spectroscopy: ^{13}C spectra of lyophilizates were recorded on a Bruker DSX 300 spectrometer at 75.47 MHz equipped with a 4-mm CP/MAS[11] probe and using a cross-polarization contact time of 2 ms. Chemical shifts were referenced to TMS using the CH_2 signal of adamantane ($\delta_{iso} =$ 38.56 ppm) as an internal reference. Generally, 200 transients with a 30 s recycle delay were accumulated.

Received: July 22, 2002
Revised: September 27, 2002 [Z19796]

[1] C. Walsh, *Enzymatic Reaction Mechanisms*, Freeman, San Francisco, **1979**.
[2] E. Graf von Roedern, F. Grams, H. Brandstetter, L. Moroder, *J. Med. Chem.* **1998**, *41*, 339 – 345.
[3] M. H. Frey, S. J. Opella, *J. Magn. Reson.* **1986**, *66*, 144 – 147.
[4] B. Henry, P. Tekely, J. J. Delpuech, *J. Am. Chem. Soc.* **2002**, *124*, 2025 – 2034.
[5] Z. Gu, A. J. McDermott, *J. Am. Chem. Soc.* **1993**, *115*, 4282 – 4285; Z. Gu, R. Zambrano, A. J. McDermott, *J. Am. Chem. Soc.* **1994**, *116*, 6368 – 6372; Y. Wei, A. C. de Dios, A. J. McDermott, *J. Am. Chem. Soc.* **1999**, *121*, 10389 – 10394.
[6] E. M. S Maçôas, R. Fausto, J. Lundell, M. Pettersson, L. Khriachtchev, M. Räsänen, *J. Phys. Chem.* A **2000**, *104*, 11725 – 11732.
[7] N. R. Jagannathan, *Magn. Reson. Chem.* **1989**, *27*, 941 – 946.
[8] J. F. Powell, The IUPAC Stability Constants Database, Academic Software and IUPAC, **1992**–**2000**.
[9] M. Merchán, F. Tomás, I. Nebot-Gil, *J. Mol. Struct.* **1984**, *109*, 51 – 60.
[10] F. Separovic, R. Smith, C. S. Yannoni, B. A. Cornell, *J. Am. Chem. Soc.* **1990**, *112*, 8324 – 8328.
[11] C. A. Fyfe, *Solid State NMR for Chemists*, C.F.C. Press, Guelph, ON, Canada, **1983**.

 © 2002 WILEY-VCH Verlag GmbH & Co. KGaA, Weinheim 0044-8249/02/4124-4745 $ 20.00+.50/0

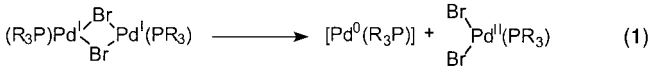
Unparalleled Rates for the Activation of Aryl Chlorides and Bromides: Coupling with Amines and Boronic Acids in Minutes at Room Temperature**

James P. Stambuli, Ryoichi Kuwano, and John F. Hartwig*

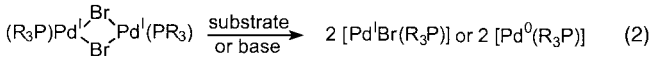
Oxidative addition initiates most palladium-catalyzed cross-couplings[1] and is often rate-limiting for reactions of aryl chlorides[2] and deactivated aryl bromides.[3] This addition usually occurs to an unsaturated complex formed from ligand dissociation or after transformation of a precatalyst to the true catalyst.[4] Although the elementary oxidative addition step could occur to the same Pd^0 intermediate and at the same rate when different catalyst precursors are used, the efficiency with which this Pd^0 intermediate is generated can differ widely. For example, reactions of aryl halides with amines, boronic acids, and olefins occur at elevated temperatures when catalyzed by isolated $[Pd(PtBu_3)_2]$[5–7] but occur at room temperature in some cases when catalyzed by a combination of $[Pd(dba)_2]$ and one equivalent of $PtBu_3$ (dba = (*E*,*E*)-dibenzylideneacetone).[7–10]

Here we describe the catalytic activity of air-stable, readily accessible, alkyl di-*tert*-butylphosphane ligated palladium(I) dimers toward selected couplings of amines with aryl chlorides on the time scale of minutes at room temperature. Furthermore, these dimers catalyze a range of aminations and Suzuki–Miyaura couplings of aryl bromides even more readily. In addition to providing a convenient catalyst for synthetic chemistry, these results indicate that the elementary step of oxidative addition of an aryl chloride to the reactive Pd^0 intermediate ligated by $PtBu_3$ or $P(1\text{-Ad})tBu_2$ (1-Ad = 1-adamantyl) occurs with rates that are unparalleled for this step.[11–14]

We and others have reported several times that the rates for cross-couplings catalyzed by palladium complexes of $PtBu_3$ are faster when a 1:1 ratio of phosphane to palladium is used.[7–10,15] Dimeric $[\{PdBrL\}_2]$ (L = $P(1\text{-Ad})tBu_2$, **1a**; L = $PtBu_3$, **1b**)[16] are formally Pd^I complexes that contain a 1:1 ratio of metal to ligand. They are readily prepared from $[Pd_2(dba)_3]\cdot C_6H_6$, $[PdBr_2(cod)]$, and the corresponding ligand in good yield (cod = (*Z*,*Z*)-cycloocta-1,5-diene). Complex **1a** is air-stable indefinitely as a solid, and **1b** is stable enough to be weighed in air. These dimers could cleave into two different monomeric units, such as a highly reactive monoligated palladium(0) complex and a palladium(II) dibromide [Eq. (1)] or could be reduced to $[Pd^0(PR_3)]$ or $[Pd^0Br(PR_3)]^-$[6,17] [Eq. (2)] by the combination of substrate and base.



1a: $PR_3 = P(1\text{-Ad})tBu_2$
1b: $PR_3 = PtBu_3$

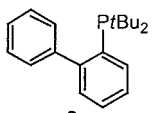


1a: $PR_3 = P(1\text{-Ad})tBu_2$
1b: $PR_3 = PtBu_3$

To evaluate the potential of **1a** and **1b** as catalysts for the aminations of aryl halides, we studied the prototype reaction of *p*-chlorotoluene with dibutylamine in the presence of sodium *tert*-butoxide as base and 0.5 mol% of **1b** in toluene at room temperature. This reaction was complete within 15 min and formed *N*,*N*-dibutyl-*p*-toluidine in 86% yield of isolated product. The reaction occurred at a similar rate and in a higher 95% yield when conducted in THF, most likely because of the greater solubility of **1b** in THF. Although the combination of $[Pd(dba)_2]$ with carbene **2**[18] and the combination of $Pd(OAc)_2$ with biphenylyl phosphane **3**[19] have been used for amination of aryl chlorides at room temperature, reactions catalyzed by these species required longer times at higher catalyst loadings.[20]



2



3

Table 1 summarizes results on the room-temperature amination of aryl chlorides and bromides catalyzed by palladium(I) dimers **1a** and **1b**. All of these reactions, except that in entry 11, were quenched after 15 min. In some cases, reactions catalyzed by **1a** gave higher conversions with 1 mol% catalyst. For example, the reaction of cyclic secondary amines with *p*-chlorotoluene occurred to only 88% completion after 15 min when catalyzed by **1b**, but to full completion when catalyzed by the **1a** (entry 2). Higher activity of **1a** was also observed for the amination of *o*-substituted aryl chlorides. The reaction of *o*-chlorotoluene with morpholine gave the desired product in 84% yield in the presence of **1a**, but only 68% yield in the presence of **1b** (entries 3 and 4). Most often, additional reaction time at room temperature did not increase conversion when the reactions were incomplete after 15 min. This result implies that high activity of these catalysts is obtained at the expense of stability.

Aryl chlorides with varied electronic properties reacted with dialkyl amines to give the coupled product within 15 min. Deactivated (entry 5) and electron-deficient (entries 6–8) chloroarenes were converted to the desired amine in high yield within 15 min. Because of the short reaction time, the process tolerated functional groups, such as nitro groups, that

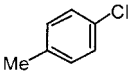
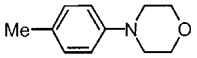
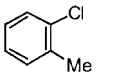
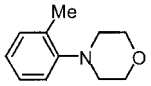
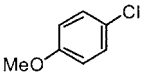
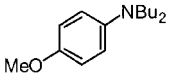
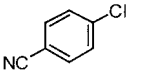
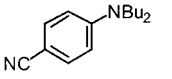
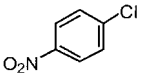
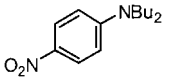
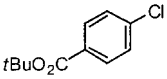
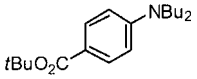
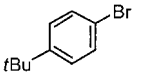
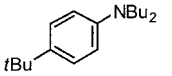
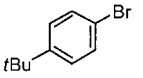
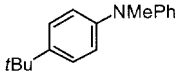
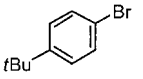
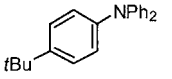
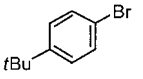
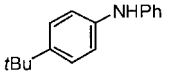
[*] Prof. J. F. Hartwig, J. P. Stambuli, Dr. R. Kuwano
Department of Chemistry
Yale University
P.O. Box 208107, New Haven, CT 06520-8107 (USA)
Fax: (+1) 203-432-6144
E-mail: john.hartwig@yale.edu

[**] We thank the NIH (GM-55382) for support of this work. R.K. was supported by Overseas Research Scholar in the Fellowship Program for Japanese Scholars and Researchers to study abroad, of the Ministry of Education, Culture, Sports, Science and Technology, Japan. We thank Johnson-Matthey for a gift of palladium salts.

Supporting information for this article is available on the WWW under http://www.angewandte.org or from the author.

 © 2002 WILEY-VCH Verlag GmbH & Co. KGaA, Weinheim 0044-8249/02/4124-4746 $ 20.00+.50/0

Table 1. Rapid amination of aryl halides with $[\{PdBr(PR_3)\}_2]$ as catalyst.[a]

Entry	Catalyst	Aryl halide	Amine	Product	Yield [%][b]
1	**1b**				88
2	**1a**				92
3	**1a**				84
4	**1b**				68
5	**1b**		$HNBu_2$		87
6	**1a**		$HNBu_2$		93
7	**1b**		$HNBu_2$		97
8	**1b**		$HNBu_2$		> 99
9	**1b**		$HNBu_2$		96
10	**1a**		HNMePh		98
11[c]	**1b**		$HNPh_2$		96
12	**1a**		H_2NPh		89
13	**1b**				82

[a] Reactions were conducted on 1 mmol scale in THF (1 mL) at room temperature for 15 min unless otherwise noted. The relative amounts of aryl halide, amine, NaO*t*Bu, and $[\{PdBr(PR_3)\}_2]$ were 200:210:300:1. [b] Yields of isolated products are an average of two runs. [c] The reaction was conducted for 1 h.

are typically unstable when the aminations are conducted with NaO*t*Bu as base.

Although **1a** and **1b** displayed high activity for the amination of aryl chlorides at room temperature with dialkylamines, the scope of this fast room-temperature chemistry is narrower than the slower room-temperature chemistry with some other catalysts.[11,21] For example, no reaction of *p*-chlorotoluene with diphenylamine or primary amines occurred at room temperature with these dimers as catalyst.

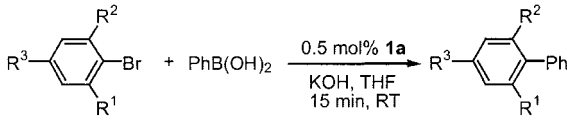
These palladium dimers, **1a** and **1b**, also catalyzed aminations of unactivated aryl bromides (entries 9–13) with remarkable rates. Each reaction that occurred with an aryl chloride substrate also occurred with the corresponding aryl bromide. In addition, reactions of aryl bromides with diarylamines occurred in high yield (entry 11), though these reactions were faster when catalyzed by the combination of $[Pd(dba)_2]$ and P*t*Bu_3.

To explore the versatility of catalysts **1a** and **1b**, we examined their activity toward Suzuki–Miyaura reactions. Catalyst **1a** induced couplings of various aryl bromides, such as *p*-bromotoluene, *o*-cyano-, *o*-trifluoromethyl-, and *o*-methoxybromobenzene, with phenylboronic acid at similarly fast rates at room temperature (Table 2). *o*-Substituted aryl bromides (entries 2–4) were as reactive as *p*-bromotoluene (entry 1) in the presence of dimer **1a**. Even the more hindered 2-bromo-*m*-xylene coupled with phenylboronic acid within minutes in 84% yield (entry 5). Reactions of phenyl boronic acids with deactivated aryl chlorides at room temperature occurred rapidly, but did not exceed 70% conversion.

Preliminary mechanistic studies of amination reactions catalyzed by **1a** suggest that oxidative addition is rate limiting, even with these short reaction times. The rates for reaction of aryl bromides and chlorides were measured at −20 °C and 0 °C, respectively. Loadings of 20 mol% were required to obtain full conversion of aryl chlorides at 0 °C. Catalyst decomposition and the observation of several ^{31}P NMR signals corresponding to palladium complexes we have not been able to identify made detailed kinetic studies unwarranted. However, reactions conducted with varying concentrations of aryl chloride clearly showed the reaction to be first order in this reagent. In contrast to reactions catalyzed by the disphosphane complex $[Pd(PtBu_3)_2]$,[6] the concentration of base did not influence the reaction rate.

In conclusion, air-stable palladium dimers $[\{PdBr(PRtBu_2)\}_2]$ are active as catalysts for reactions of various aryl chlorides or bromides and amines that proceed within minutes at room temperature. The fast rates of these reactions show that the proper choice of catalyst precursor can allow the overall rate to approach that for the elementary step of oxidative addition and that the elementary oxidative addition of an aryl chloride can be remarkably fast, even at room temperature. This fast rate for P*t*Bu_3-ligated Pd^0 creates the highest turnover frequencies for cross-couplings of aryl chlorides.

Table 2. Room-temperature Suzuki–Miyaura coupling of hindered aryl bromides catalyzed by **1a**.[a]



Entry	R^1	R^2	R^3	Yield [%][b]
1	H	H	CH_3	95
2	CN	H	H	92
3	CF_3	H	H	90
4	OCH_3	H	H	96
5	CH_3	CH_3	H	84

[a] Reactions were conducted on 1 mmol scale in THF (3 mL) at room temperature for 15 min. The relative amounts of aryl halide, phenylboronic acid, KOH, and **1a** were 200:216:600:1. [b] Yields of isolated products are an average of two runs.

 © 2002 WILEY-VCH Verlag GmbH & Co. KGaA, Weinheim 0044-8249/02/4124-4747 $ 20.00+.50/0

Experimental Section

1a: $[Pd(dba)_2]$ (288 mg, 0.50 mmol) and P(1-Ad)P*t*Bu_2[22] (560 mg, 2.00 mmol) were stirred in toluene (15 mL) in a vial for 3 h. After this time, $[PdBr_2(cod)]$[23] (378 mg, 1.01 mmol) was added, and the mixture was stirred for an additional 4 h. The reaction volume was concentrated by half, and the contents were filtered through a glass-fritted funnel. The dark-green solid was washed three times with acetone (10 mL) and dried under vacuum. Yield: 498 mg (0.533 mmol, 53.4 %); ^{1}H NMR (400 MHz, C_6D_6): $\delta = 1.39$ (t, 36 H, 6 Hz, *t*Bu), 1.47–1.61 (br m, 12 H, CH_2), 1.77 (br s, 6 H, CH), 2.32 ppm (br s, 12 H, CH_2); ^{13}C NMR (100 MHz, C_6D_6, 40 °C): $\delta = 29.4$ (t, 4.0 Hz, CH_2), 33.0 (br s, CH_2), 36.8 (t, 1.8 Hz, C Ad), 36.9 (s, CH_3), 41.7 (br s, CH), 42.0 ppm (br s, *C*Me_3); ^{31}P NMR (202 MHz, C_6D_6): $\delta = 88.0$ ppm (s); Anal. calcd. for $C_{36}H_{66}Br_2P_2Pd_2$: C 46.32, H 7.13, Br 17.12; found: C 45.94, H 7.03, Br 17.02.

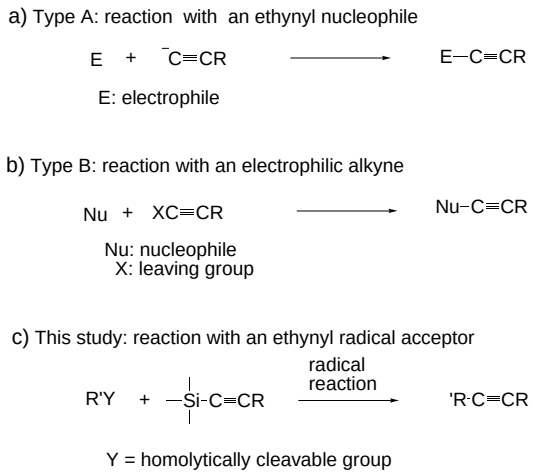
Received: September 2, 2002 [Z50085]

[1] R. H. Crabtree *The Organometallic Chemistry of the Transition Metals*, 3rd ed, Wiley, New York, **2001**.
[2] M. Portnoy, D. Milstein, *Organometallics* **1993**, *12*, 1665 – 1673.
[3] L. M. Alcazar-Roman, J. F. Hartwig, A. L. Rheingold, L. M. Liable-Sands, I. A. Guzei, *J. Am. Chem. Soc.* **2000**, *122*, 4618 – 4630.
[4] J. K. Stille in *The Chemistry of the Metal–Carbon Bond* (Ed.: F. R. Hartley, S. Patai), Wiley, New York, **1985**.
[5] R. Kuwano, M. Utsunomiya, J. F. Hartwig, *J. Org. Chem.* **2002**, 67, 6479 – 6486.
[6] L. M. Alcazar-Roman, J. F. Hartwig, *J. Am. Chem. Soc.* **2001**, *123*, 12 905 – 12 906.
[7] A. F. Littke, C. Dai, G. C. Fu, *J. Am. Chem. Soc.* **2000**, *122*, 4020 – 4028.
[8] J. F. Hartwig, M. Kawatsura, S. I. Hauck, K. H. Shaughnessy, L. M. Alcazar-Roman, *J. Org. Chem.* **1999**, *64*, 5575 – 5580.
[9] M. Kawatsura, J. F. Hartwig, *J. Am. Chem. Soc.* **1999**, *121*, 1473 – 1478.
[10] A. F. Littke, G. C. Fu, *J. Am. Chem. Soc.* **2001**, *123*, 6989 – 7000.
[11] N. Kataoka, Q. Shelby, J. P. Stambuli, J. F. Hartwig, *J. Org. Chem.* **2002**, *67*, 5553 – 5566.
[12] M. S. Viciu, R. M. Kissling, E. D. Stevens, S. P. Nolan, *Org. Lett.* **2002**, *4*, 2229 – 2231.
[13] C. W. K. Gstöttmayr, V. P. W. Böhm, E. Herdtweck, M. Grosche, W. A. Herrmann, *Angew. Chem.* **2002**, *114*, 1421 – 1423; *Angew. Chem. Int. Ed.* **2002**, *41*, 1363 – 1365.
[14] J. P. Wolfe, S. L. Buchwald, *Angew. Chem.* **1999**, *111*, 2570 – 2573; *Angew. Chem. Int. Ed.* **1999**, *38*, 2413 – 2416.
[15] G. A. Grasa, M. S. Viciu, J. Huang, S. P. Nolan, *J. Org. Chem.* **2001**, *66*, 7729 – 7737.
[16] V. Dura-Vila, D. M. P. Mingos, R. Vilar, A. J. P. White, D. J. Williams, *J. Organomet. Chem.* **2000**, *600*, 198 – 205.
[17] C. Amatore, A. Jutand, *Acc. Chem. Res.* **2000**, *33*, 314 – 321.
[18] S. R. Stauffer, S. Lee, J. P. Stambuli, S. I. Hauck, J. F. Hartwig, *Org. Lett.* **2000**, *2*, 1423 – 1426.
[19] J. P. Wolfe, H. Tomori, J. P. Sadighi, J. Yin, S. L. Buchwald, *J. Org. Chem.* **2000**, *65*, 1158 – 1174.
[20] The reaction of *p*-chlorotoluene with dibutylamine under the conditions described in ref. [18] and [19] showed approximately 75 % conversion by GC after 12 h.
[21] A. R. Muci, S. L. Buchwald, *Top. Curr. Chem.* **2002**, *219*, 131 – 209.
[22] J. P. Stambuli, S. R. Stauffer, K. H. Shaughnessy, J. F. Hartwig, *J. Am. Chem. Soc.* **2001**, *123*, 2677 – 2678.
[23] D. Drew, J. R. Doyle, *Inorg. Synth.* **1972**, *13*, 47 – 55.

A New Entry to the Stereoselective Introduction of an Ethynyl Group by a Radical Reaction: Synthesis of the Potential Antimetabolite 2′-Deoxy-2′-*C*-ethynyluridine**

Makoto Sukeda, Satoshi Ichikawa, Akira Matsuda, and Satoshi Shuto*

Ethynyl groups are present in many biologically active compounds, including clinically useful drugs,[1] and are also valuable in organic synthesis because the triple bond can be converted into a variety of functional groups.[2] Accordingly, much effort has been expended to develop methods for introducing ethynyl and/or substituted ethynyl groups into compounds to produce alkynes by C–C bond formation.[2] These methods can be generally classified as Type A, reactions of ethynyl nucleophiles such as acetylides or their congeners (Scheme 1 a), and Type B, reactions of electrophilic alkynes bearing a leaving group (Scheme 1 b). Type A includes reactions of alkynyl metals with carbon electrophiles[3] and transition metal catalyzed cross-coupling reactions with alkyne derivatives.[4] Type B is typified by reactions between an alkynyl halide and a carbon nucleophile, which appear to proceed by an addition–elimination mechanism.[5] Although these are very effective, regio- and stereoselective introduction of an ethynyl group at aliphatic carbon centers is sometimes troublesome.



Scheme 1. Methods for introducing ethynyl and substituted ethynyl groups.

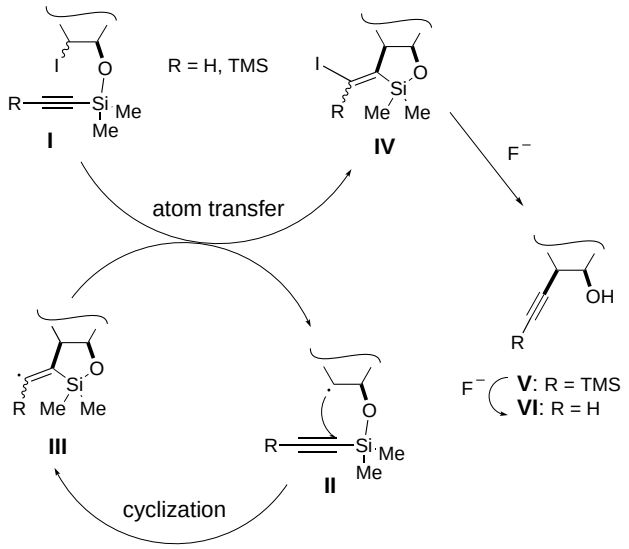
[*] Prof. S. Shuto, M. Sukeda, Dr. S. Ichikawa, Prof. A. Matsuda
Graduate School of Pharmaceutical Sciences, Hokkaido University
Kita-12, Nishi-6, Kita-ku, Sapporo 060–0812 (Japan)
Fax: (+81) 11–706–4980
E-mail: shu@pharm.hokudai.ac.jp

[**] Nucleosides and Nucleotides, Part 216. This work was supported by a Grant-in-Aid for Creative Scientific Research (13NP0401) and a Grant-in-Aid for Scientific Research (S.S.) from the Japan Society for Promotion of Science. For Part 215, see: N. Minakawa, D. Kaga, Y. Kato, K. Endo, M. Tanaka, T. Sasaki, A. Matsuda, *J. Chem. Soc. Perkin Trans. 1*, 2002, 2182–2189.

 © 2002 WILEY-VCH Verlag GmbH & Co. KGaA, Weinheim 0044-8249/02/4124-4748 $ 20.00+.50/0

In the course of our synthetic study on antitumor branched-sugar nucleosides,[6] a new method for the stereoselective introduction of an ethynyl group was needed. Here we describe a new method for introducing ethynyl groups by adaption of an atom-transfer radical cyclization reaction[7] with an ethynylsilyl group (Scheme 1c), which was devised on the basis of our recent studies on radical reactions with a silicon tether,[8,9] and is clearly different from the previous ionic reaction method.

Our strategy that uses ethynyldimethylsilyl (EDMS) or [2-(trimethylsilyl)ethynyl]dimethylsilyl (TEDMS)[10] ethers of iodohydrins **I** as reaction substrates is shown in Scheme 2. The



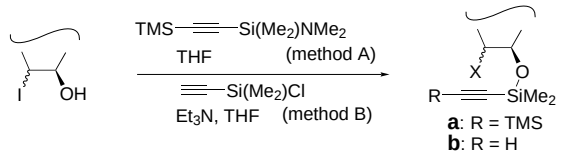
Scheme 2. Ethynyl group introduction by atom-transfer radical cyclization and subsequent elimination. TMS = trimethylsilyl.

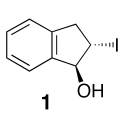
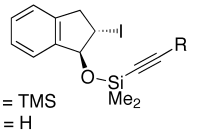
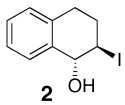
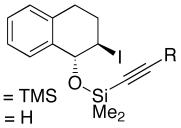
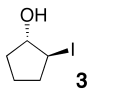
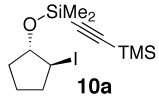
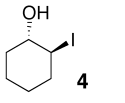
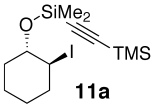
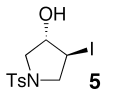
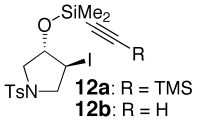
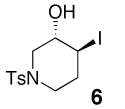
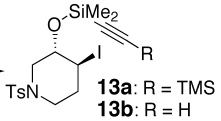
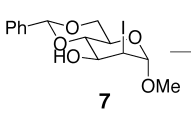
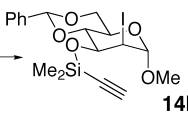
radical **II** generated from **I** preferentially undergoes 5-*exo* cyclization to produce the radical **III**. In the absence of a hydrogen source, **III** would abstract the iodine atom of another substrate **I** to regenerate the radical **II** along with the atom-transfer radical cyclization product **IV**.[11] Turnover of this scheme would accumulate the desired product **IV**, subsequent treatment of which with fluoride ion would promote elimination[12] to give the desired ethynyl product **V** or **VI**.

The reaction was carried out with EDMS and TEDMS ethers of a variety of iodohydrins as substrates, which were prepared with EDMS-Cl[13] or TEDMS-NMe_2[14] (Table 1). We first examined the radical atom-transfer reaction with the TEDMS and EDMS ethers of 2-iodoindanol (**8a** and **8b**) under various conditions, and found that when the substrate was treated with Et_3B (0.3 equiv) at room temperature in toluene under argon, the expected atom-transfer cyclization proceeded effectively, and immediate treatment of the product, without purification, with tetrabutylammonium fluoride (TBAF) gave the desired ethynyl product **15**[15] in high yield (Table 2, entries 1 and 2).

By using the same procedure, the reactions with various TEDMS and EDMS ethers were examined, and the results are summarized in Table 2. The reactions with the EDMS and

Table 1. Preparation of the ethynylsilyl ethers.

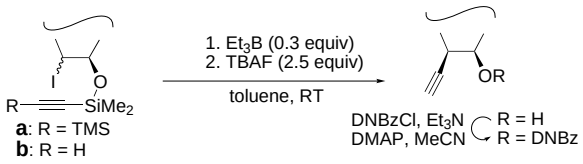


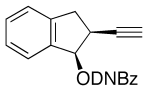
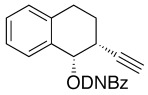
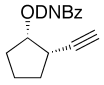
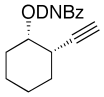
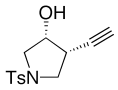
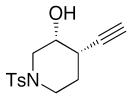
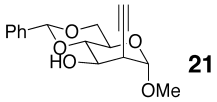
Iodohydrin	Method	Ethynylsilyl ether	Yield [%]
	A or B	 **8a**: R = TMS **8b**: R = H	83
	A or B	 **9a**: R = TMS **9b**: R = H	71 67
	A	 **10a**	70 78
	A	 **11a**	90
	A or B	 **12a**: R = TMS **12b**: R = H	63 quant.
	A or B	 **13a**: R = TMS **13b**: R = H	77 quant.
	B	 **14b**	90

TEDMS ethers of *trans*-2-iodotetrahydronaphthol (**9a** and **9b**) as well as pyrrolidine and piperidine derivatives (**12a**, **12b**, **13a**, and **13b**) effectively produced the products of atom-transfer cyclization and subsequent elimination **16**, **19**, and **20**, respectively, in good yields (entries 3, 4, and 7–10). On the other hand, the reactions with TEDMS ethers of 2-iodocyclopentanol (**10a**) and 2-iodocyclohexanol (**11a**) gave the corresponding 2-ethynyl products **17** and **18** in only moderate yields (entries 5 and 6). In these reactions, the comparatively low yields of isolated products might be explained by their volatility, since TLC analysis suggested that both of the reactions seemed to proceed effectively. The reaction was used to synthesize a branched sugar; treatment of the EDMS ether of the 2-deoxy-2-iodo-D-mannoside **14b** by the above procedure furnished the expected 2-ethynyl product **21** in 85% yield. Thus, it appears that the atom-transfer radical cyclization and subsequent elimination effectively occurs in iodohydrin substrates with five- or six-membered rings.

 © 2002 WILEY-VCH Verlag GmbH & Co. KGaA, Weinheim 0044-8249/02/4124-4749 $ 20.00+.50/0

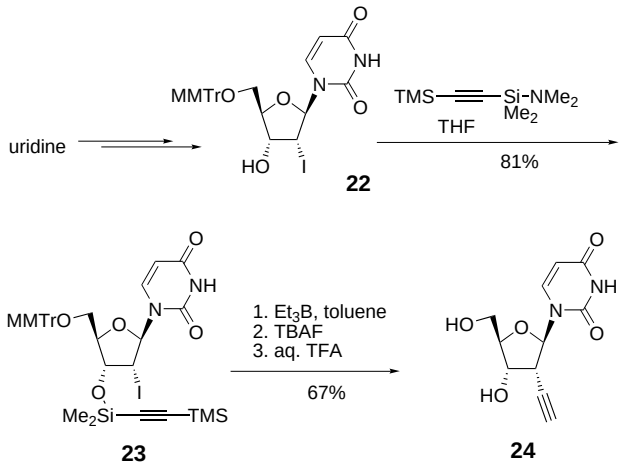
Table 2. Atom-transfer radical cyclization and subsequent elimination reaction of the ethynylsilyl ethers.[a]



Entry	Substrate	Product[b]	Yield [%]
1	**8a**	 **15**	87
2	**8b**		88
3	**9a**	 **16**	83
4	**9b**		86
5	**10a**	 **17**	33
6	**11a**	 **18**	36
7	**12a**	 **19**	80
8	**12b**		80
9	**13a**	 **20**	55
10	**13b**		68
11	**14b**	 **21**	85

[a] DMAP = 4-dimethylaminopyridine, DNBz = 3,5-dinitrobenzoyl. [b] In entries 1–4, the atom-transfer radical cyclization product was isolated after conversion to the corresponding 3,5-dinitrobenzoate (R = DNBz).

Finally, we applied the reaction to the synthesis of 2′-deoxy-2′-*C*-ethynyluridine (**24**), designed as a potential antimetabolite (Scheme 3). When the 2′-deoxy-2′-iodo-3′-*O*-TEDMS-uridine derivative **23**, prepared from known **22**,[6] was subjected to the above procedure, the desired **24** was obtained in 67% yield.



Scheme 3. Synthesis of 2′-deoxy-2′-*C*-ethynyluridine (**24**). TFA = trifluoroacetic acid, MMTr = monomethoxytrityl.

In summary, we have developed an efficient method for introducing an ethynyl group by means of an atom-transfer radical cyclization reaction. This is the first example in which a radical reaction was used for introducing an ethynyl group.

Experimental Section

General procedure for the atom-transfer radical cyclization and subsequent elimination reaction with Et_3B: Et_3B (1.0 M in hexane, 30 μL, 0.030 mmol) was added dropwise to a solution of a substrate (0.10 mmol) in toluene (1 mL) under argon, and the mixture was stirred at room temperature for 2 h. After addition of TBAF (1.0 M in THF, 250 μL, 0.25 mmol), the mixture was stirred at room temperature for 2 h, evaporated, and purified by column chromatography on silica gel.

Received: August 1, 2002 [Z19870]

[1] For examples, see a) J. W. Goldzieher, S. A. Brody, *Am. J. Obstet. Gynecol.* **1990**, *163*, 2114–2119; b) S. Takeo, *Cardiovasc. Drug Rev.* **1992**, *10*, 392–403; c) S. Anton, *Ann. N.Y. Acad. Sci.* **1988**, *544*, 46–62.

[2] a) L. Brandsma, *Preparative Acetylene Chemistry*, 2nd ed., Elsevier, Amsterdam, **1988**; b) M. Furber, in *Comprehensive Organic Functional Group Transformations* (Ed.: S. M. Roberts), Cambridge University Press, Cambridge, **1995**, pp. 998–1085.

[3] For examples of reactions of acetylides, see A. I. Meyers, S. Bienz, *J. Org. Chem.* **1990**, *55*, 791–798, and references therein.

[4] For examples of cross-coupling reactions to introduce ethynyl groups, see W. Tao, S. Nesbitt, R. F. Heck, *J. Org. Chem.* **1990**, *55*, 63–69, and references therein.

[5] For examples of reactions of alkynylhalides, see A. S. Kende, P. Fludzinski, J. H. Hill, W. Swenson, J. Clardy, *J. Am. Chem. Soc.* **1984**, *106*, 3551–3562, and references therein.

[6] M. Sukeda, S. Shuto, I. Sugimoto, S. Ichikawa, A. Matsuda, *J. Org. Chem.* **2000**, *65*, 8988–8996, and references therein.

[7] First report of atom-transfer radical cyclization: D. P. Curran, M. H. Cheng, D. Kim, *J. Am. Chem. Soc.* **1986**, *108*, 2489–2490;a) other examples: B. Giese, B. Kopping, T. Gobel, J. Dickhaut, G. Thoma, K. J. Kulicke, F. Trach, *Org. React.* **1996**, *48*, 301–856; b) *Radicals in Organic Synthesis* (Eds.: P. Renaud, M. P. Sibi), Wiley-VCH, Weinheim, **2001**; c) J. Robertson, J. Pillai, R. K. Lush, *Chem. Soc. Rev.* **2001**, *30*, 94–103, and references therein.

[8] Introduction of a vinyl group with a silicon tether by radical atom-transfer cyclization and subsequent elimination: a) I. Sugimoto, S. Shuto, A. Matsuda, *J. Org. Chem.* **1999**, *64*, 7153–7157; b) T. Kodama, S. Shuto, M. Nomura, A. Matsuda, *Chem. Eur. J.* **2001**, *7*, 2332–2340.

[9] For examples, see a) S. Shuto, M. Kanazaki, S. Ichikawa, A. Matsuda, *J. Org. Chem.* **1997**, *62*, 5676–5677; b) S. Shuto, M. Kanazaki, S. Ichikawa, N. Minakawa, A. Matsuda, *J. Org. Chem.* **1998**, *63*, 746–754; c) S. Shuto, I. Sugimoto, A. Matsuda, *J. Am. Chem. Soc.* **2000**, *122*, 1343–1351; d) S. Shuto, Y. Yahiro, S. Ichikawa, A. Matsuda, *J. Org. Chem.* **2000**, *65*, 5547–5557, and references therein.

[10] Radical cyclization reactions with a (2-phenyethynyl)silyl group as tether: a) G. Stork, H. S. Suh, G. Kim, *J. Am. Chem. Soc.* **1991**, *113*, 7054–7055; With a TEDMS group as tether: b) Z. Xi, J. Rong, J. Chattopadhyaya, *Tetrahedron* **1994**, *50*, 5255–5272.

[11] Atom-transfer radical cyclization reactions to a C≡C bond: a) D. P. Curran, M. H. Chen, D. Kim, *J. Am. Chem. Soc.* **1986**, *108*, 2489–2490; b) Y. Ichinose, S. Matsunaga, K. Fugami, K. Oshima, K. Utimoto, *Tetrahedron Lett.* **1989**, *30*, 3155–3158.

[12] Fluoride-promoted elimination to produce alkynes: R. Yamaguchi, H. Kawasaki, T. Yoshitome, H. Kawanishi, *Chem. Lett.* **1982**, 1485–1486.

[13] Preparation of EDMS-Cl: N. Shinohara, M. Arai. S. Ichinohe, JP-52065226 **1977** [*Chem. Abstr.* **1977**, *87*, 135905r].

[14] Preparation of TEDMS-NMe_2: G. Stork, P. F. Keitz, *Tetrahedron Lett.* **1989**, *30*, 6981–6984.

[15] The *cis* configuration was determined by NOE experiments.

 © 2002 WILEY-VCH Verlag GmbH & Co. KGaA, Weinheim 0044-8249/02/4124-4750 $ 20.00+.50/0

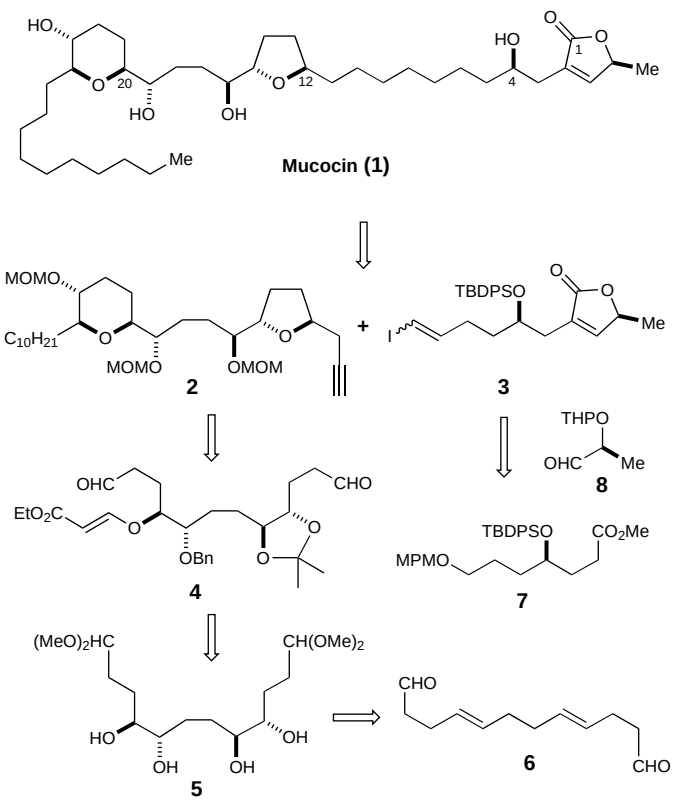
Stereoselective Total Synthesis of Mucocin, an Antitumor Agent**

Shunya Takahashi,* Akemi Kubota, and Tadashi Nakata*

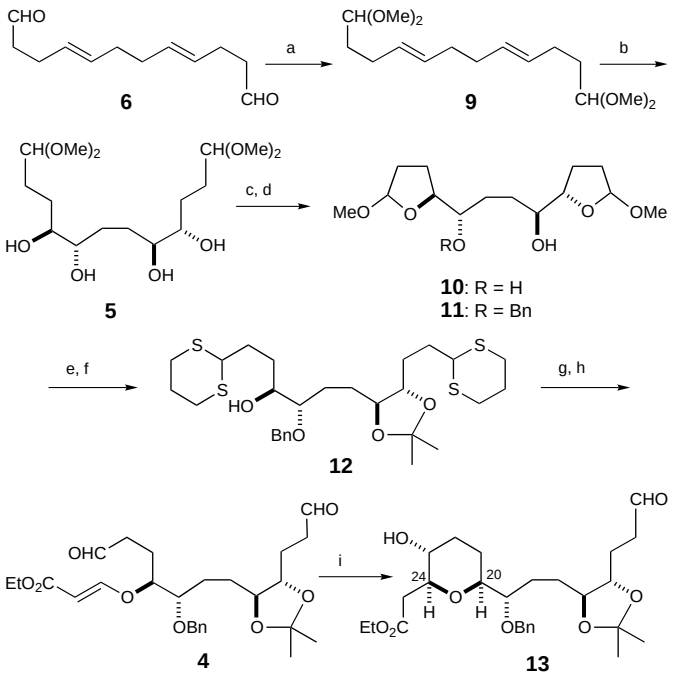
Mucocin (**1**) is a representative annonaceous acetogenin[1] having a tetrahydropyran (THP) and a tetrahydrofuran (THF) ring.[2] This novel type of acetogenin is known to show remarkable inhibitory activities against A-549 (lung cancer) and PACA-2 (pancreatic cancer) solid tumor lines with a potency of more than 10000 times that of adriamycin. The powerful antitumor activity and the unique structure of **1** have consequently stimulated synthetic efforts,[3] and quite recently three research groups (including ours) have succeeded in its total synthesis.[4] Recently, we developed a highly efficient method for the synthesis of tetrahydropyrans and oxepanes based on a SmI_2-induced[5] reductive cyclization of β-alkoxy acrylate containing a formyl group.[6] We thus planned the total synthesis of **1** to demonstrate the utility of the method and now describe here an efficient total synthesis of **1** based on the SmI_2-induced reductive cyclization as a key step.

Our synthetic strategy directed toward **1** was based on a convergent process which involves a Pd-catalyzed cross-coupling reaction of the THP/THF segment **2** and a vinyl iodide **3** as illustrated in Scheme 1. The THP ring in the central core **2** could be constructed by the SmI_2-induced reductive cyclization, whereas the *trans*-THF ring should be synthesized by oxidative cyclization[7] of a homoallyl alcohol. This retrosynthetic approach can revert **2** back to the β-alkoxy acrylate **4** having two formyl groups, and then to a tetraol **5**. Therefore, dialdehyde **6** with the requisite carbon backbone was selected as the starting material. In this scenario, whether the C-12 formyl group in the reductive cyclization of **4** could be retained or not and the development of an efficient method for desymmetrization of C_2-symmetric **5** were problems to be solved. On the other hand, the γ-lactone **3** should be synthesized by aldol condensation of chiral ester **7** and aldehyde **8**.[8]

Synthesis began with acetalization of the dialdehyde **6**[4a] to afford the bis(dimethyl acetal) **9** in 99% yield (Scheme 2). The Sharpless asymmetric dihydroxylation[9] of **9** gave the C_2-symmetric tetraol **5**[10] in almost quantitative yield. To achieve efficient desymmetrization **5** was transformed into a bisTHF derivative **10** by treatment with CSA in methanol at −5 °C. Formation of THP derivatives was observed when the acetalization was conducted at RT. Benzylidenation of **10** followed by reduction with DIBAH gave a monobenzyl ether



Scheme 1. Structure of mucocin (**1**) and its retrosynthetic analysis.



Scheme 2. Synthesis of the THP derivative **13**: a) $HC(OMe)_3$ (6.0 equiv), CSA (0.02 equiv), MeOH, RT, 1 h, 99%; b) AD-mix α, $MeSO_2NH_2$, H_2O/*t*BuOH (1/1), 0 °C, 24 h; c) CSA (0.83 equiv), MeOH, −5 °C, 3 h, 89% (2 steps); d) BnBr (1.1 equiv), NaH (1.1 equiv), THF, −15 °C→RT, 16 h, 93%; e) 1,3-propanedithiol (6.0 equiv), $Zn(OTf)_2$ (1.5 equiv), $(CH_2Cl)_2$, 50 °C, 2 h; f) $Me_2C(OMe)_2$ (3.0 equiv), CSA (0.03 equiv), CH_2Cl_2, RT, 1 h, 86% (2 steps); g) ethyl propiolate (10 equiv), *N*-methylmorpholine (5.0 equiv), CH_2Cl_2, RT, 5 h; h) CH_3I (8.0 equiv), $NaHCO_3$ (12 equiv), $MeCN/H_2O$ (10/1), RT, 35 h, 73% (2 steps); i) SmI_2 (3.0 equiv), MeOH (4.4 equiv), THF, −5 °C, 15 min, 87%. CSA = 10-camphorsulfonic acid, Bn = benzyl, Tf = trifluoromethanesulfonyl.

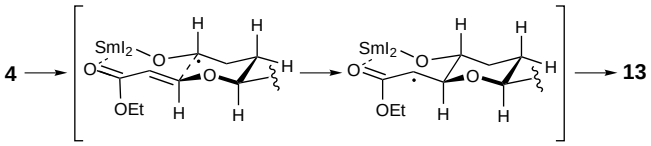
[*] Dr. S. Takahashi, Prof. Dr. T. Nakata
RIKEN (The Institute of Physical and Chemical Research)
Wako-shi, Saitama 351-0198 (Japan)
Fax: (+81) 48-462-4666
E-mail: shunyat@riken.go.jp
nakata@riken.go.jp

A. Kubota
Graduate School of Science and Engineering
Saitama University, Saitama, Saitama 338-8570 (Japan)

[**] We are grateful to Dr. J. L. Mclaughlin (Purdue University) for providing us with copies of the NMR spectra of mucocin. We also thank Ms. K. Harata (RIKEN) for mass spectral measurements.

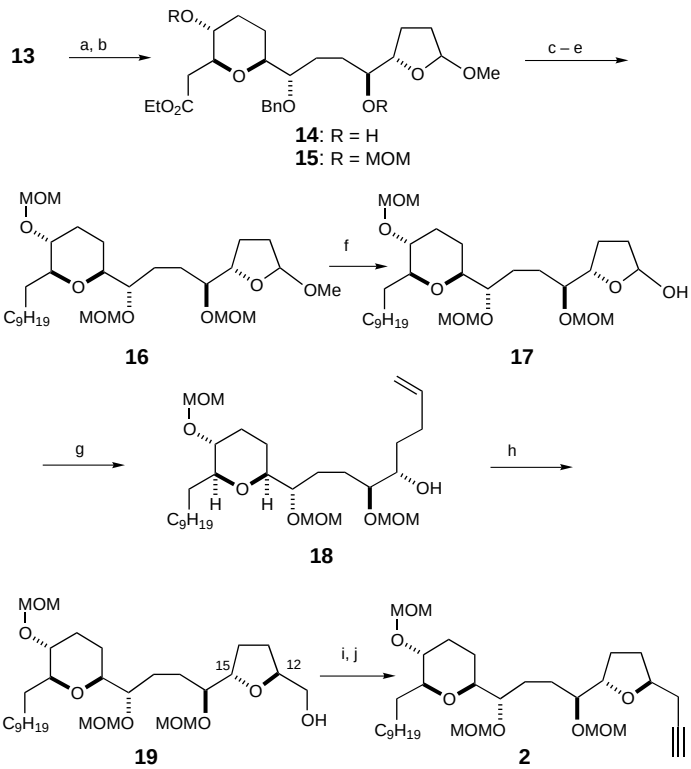
 © 2002 WILEY-VCH Verlag GmbH & Co. KGaA, Weinheim 0044-8249/02/4124-4751 $ 20.00+.50/0

11 in 61% yield. After several attempts, a more efficient method for preparing **11** was found. Direct benzylation of **10** with BnBr (1.1 equiv) and NaH (1.1 equiv) in THF at −15°C afforded **11** in 93% yield. At this stage, exchange of the dimethylacetal into the corresponding dithioacetal was necessary for the latter step. Transacetalization[11] of **11** was achieved by using 6.0 equivalents of ethanedithiol in the presence of 1.5 equivalents of $Zn(OTf)_2$[12] in 1,2-dichloroethane at 50°C to give the desired bis(thioacetal) **12** in 86% yield after isopropylidenation. Hetero-Michael addition of **12** to ethyl propiolate followed by dethioacetalization (CH_3I, $NaHCO_3$, aq CH_3CN) afforded the key intermediate **4** in 73% yield. SmI_2-induced reductive cyclization of **4** was effected by treatment with 3.0 equivalents of SmI_2 in the presence of methanol (4.4 equiv) in THF at −5°C to give a 20,24-*syn*-23,24-*trans*-THP derivative **13**[13,14] in 87% yield. The stereochemistry of the THP ring system was established by NMR analysis: $J_{23,24} = 9.9$ Hz and an NOE effect was observed between H_{20} and H_{24}. The high stereoselectivity could be explained by the transition state involving a cyclic chelate as shown in Scheme 3. Very interestingly, the formyl group was retained during this reaction. However, a prolonged reaction time or the use of a large amount of SmI_2 caused destruction of this functional group and afforded higher polar substances such as reduction or pinacol-type coupling products.



Scheme 3. SmI_2-induced reductive cyclization of **4**.

As several attempts for the construction of the THF ring prior to completion of the C_{10} side chain gave unsatisfactory results, the formyl group was protected as an internal acetal with trimethyl orthoformate/CSA to give **14** in 93% yield (Scheme 4). To enable subsequent chain elongation, the two hydroxy groups were protected as methoxymethyl (MOM) ethers to afford **15** (91% yield). Installation of the C_{10} unit on **15** was conducted in three steps: 1) DIBAH reduction of the ester carbonyl group, 2) Wittig reaction ($Ph_3P^+C_8H_{17}Br^-$, *n*BuLi), and 3) hydrogenation. After methoxymethylation, exposure of the thus obtained **16** to mild acidic conditions led to selective hydrolysis of the methyl acetal to give **17**. The resulting hemiacetal **17** was subjected to olefination with $Ph_3P{=}CH_2$ to furnish **18** in 85% yield. The homoallyl alcohol **18** was oxidized with *t*BuO_2H in the presence of $[Co(modp)_2]$ in an oxygen atmosphere to give rise to 5-*exo* cyclization[7a] and afford alcohol **19** with a 12,15-*trans* THF ring system. The structure of **19** was established by comparison with an authentic sample, which had been previously synthesized by us.[4b,f] Transformation of **19** into the "left-half" segment **2**[15] proceeded in high overall yield (90%) as follows: 1) triflation of the primary hydroxy group, 2) a coupling reaction with lithium trimethylsilylacetylide, and 3) desilylation with potassium carbonate.

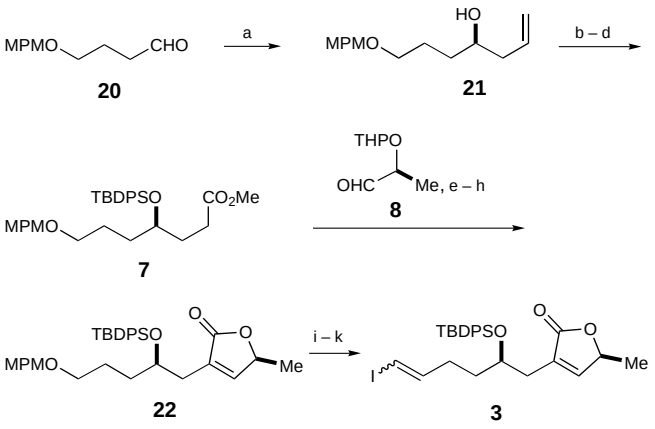


Scheme 4. Synthesis of the THP/THF segment **2**: a) $HC(OMe)_3$ (2.0 equiv), CSA (0.2 equiv), MeOH, 0°C, 30 h, 93%; b) MOMBr (4.0 equiv), *i*Pr_2NEt (8.0 equiv), $(CH_2Cl)_2$, 0°C, 0.5 h; →40°C, 7.5 h, 91%; c) DIBAH (1.0 equiv), CH_2Cl_2, −78°C, 1 h and then $C_8H_{17}PPh_3Br$ (2.7 equiv), *n*BuLi (2.5 equiv), THF, −15°C, 1 h, 91%; d) 10% Pd/C, H_2 (1 bar), MeOH, RT, 24 h; e) MOMBr (4.0 equiv), *i*Pr_2NEt (8.0 equiv), $(CH_2Cl)_2$, 0°C, 0.5 h; →60°C, 1 h, 95% (2 steps); f) AcOH/H_2O (4/1), RT, 2 h; →40°C, 1 h, 77%; g) CH_3PPh_3I (6.0 equiv), NaHMDS (5.0 equiv), THF, −15°C, 1 h; →RT, 1 h, 85%; h) $[Co(modp)_2]$ (0.04 equiv), O_2, *t*BuO_2H (2.0 equiv), 4Å-MS, *i*PrOH, 50°C, 5 h, 78%; i) Tf_2O (1.1 equiv), 2,6-lutidine (2.3 equiv), CH_2Cl_2, −78°C, 30 min; j) TMSC≡C−Li (8.0 equiv), HMPA (15 equiv), THF, −78°C, 40 min, and then K_2CO_3 (1.1 equiv) MeOH, RT, 17 h, 90% (2 steps). MOM = methoxymethyl, DIBAH = diisobutylaluminium hydride, NaHMDS = sodium hexamethyldisilazide, $[Co(modp)_2]$ = bis(1-morpholinocarbamoyl-4,4-dimethyl-1,3-pentanedionato)cobalt(II), Tf_2O = trifluoromethanesulfonic anhydride, HMPA = hexamethylphosphoric triamide, TMS = trimthylsilyl.

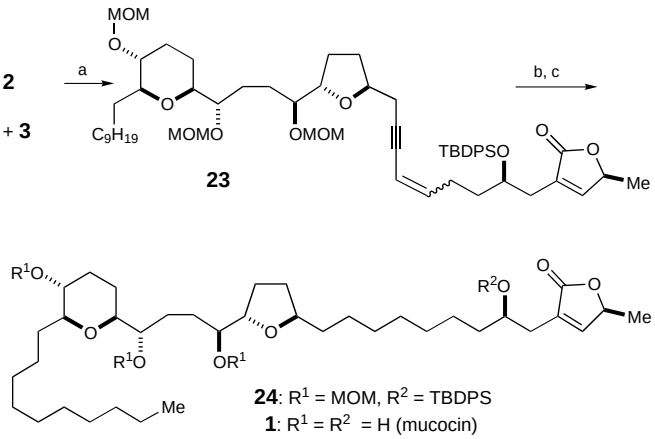
Synthesis of terminal butenolide unit **3** began with asymmetric allylation[16] of **20** to give **21** (> 98% *ee*) in 76% yield (Scheme 5). After silylation of **21**, hydroboration followed by Jones oxidation and methylation gave methyl ester **7** in 58% yield. Aldol reaction of the lithium enolate prepared from **7** with the chiral aldehyde **8**[8a] gave a mixture of coupled products, which was, without purification, submitted sequentially to lactonization, mesylation, and β-elimination reaction, giving butenolide **22** in 67% overall yield. After deprotection of the MPM group, the resulting alcohol was oxidized to an aldehyde, which was then transformed into the corresponding vinyl iodide **3** according to the method of Takai et al.[17]

The complete carbon skeleton of **1** was assembled by joining **2** and **3** under Hoye's conditions[18] to give **23** in 84% yield (Scheme 6). Finally, regioselective reduction of **23** using Wilkinson's catalyst gave **24** in which all the protecting groups were removed to afford mucocin (**1**). The spectral data of **1** were indistinguishable from those of the natural product.

 © 2002 WILEY-VCH Verlag GmbH & Co. KGaA, Weinheim 0044-8249/02/4124-4752 $ 20.00+.50/0 *Angew. Chem. Int. Ed.* **2002**, *41*, No. 24



Scheme 5. Synthesis of the lactone **3**: a) (*S*)-binol (0.2 equiv), $Ti(OiPr)_4$, (0.2 equiv), allyltributyltin (1.1 equiv), −78 °C, 1 h; →−25 °C, 5 d, 76 %; b) TBDPSCl (1.1 equiv), imidazole (2.5 equiv), DMF, RT, 6 h; c) BH_3·THF (1.5 equiv), THF, 0 °C→RT, 24 h and then NaOH, 30 % H_2O_2, 0 °C→RT, 1 h; d) Jones reagent, acetone, 0 °C, 30 min and then CH_2N_2, diethyl ether, 0 °C, 30 min, 58 % (3 steps); e) LDA (1.6 equiv), **8** (2.0 equiv), THF, −78 °C, 1 h; f) CSA (1.1 equiv), MeOH/H_2O (9/1), RT, 4 h; g) MsCl (3.0 equiv), Et_3N (5.0 equiv), CH_2Cl_2, −10 °C, 1.5 h; h) DBU (2.0 equiv), CH_2Cl_2, −10 °C, 30 min, 67 % (4 steps); i) DDQ (2.0 equiv), CH_2Cl_2/phosphate buffer (pH 7.4, 10/1), 0 °C, 2 h; j) $(COCl)_2$ (3.0 equiv), DMSO (6.0 equiv), CH_2Cl_2, −78 °C, 30 min, and then Et_3N (12 equiv), −78 °C→RT, 2 h; k) $CrCl_2$ (6.8 equiv), CHI_3 (2.3 equiv), THF, 0 °C→RT, 4 h, 83 % (3 steps). binol = bi-2-naphthol, TBDPS = *tert*-butyldiphenylsilyl, LDA = lithium diisopropylamide, DBU = 1,8-diazabicyclo[5.4.0]undec-7-ene, DDQ = 2,3-dichloro-5,6-dicyano-1,4-benzoquinone, Ms = methanesulfonyl, DMSO = dimethylsulfoxide.



Scheme 6. Total synthesis of mucocin (**1**): a) $[PdCl_2(Ph_3P)_2]$ (0.1 equiv), CuI (0.3 equiv), Et_3N, 0 °C→RT, 1 h, 84 %; b) $(Ph_3P)_3RhCl$, H_2, C_6H_6/EtOH (1/1), RT, 48 h, 85 %; c) 10 % HCl/MeOH, CH_2Cl_2, 0 °C→RT, 95 %.

In summary, we have succeeded in an efficient synthesis of **1** through desymmetrization of **5**, an SmI_2-induced radical cyclization reaction of **4**, and oxidative cyclization of **18** as the key steps. This procedure would also be useful for the preparation of a variety of analogues of **1**.

Received: September 11, 2002 [Z50140]

[1] For reviews, see a) J. K. Rupprecht, Y.-H. Hui, J. L. McLaughlin, *J. Nat. Prod.* **1990**, *53*, 237 – 278; b) X.-P. Fang, M. J. Rieser, Z.-M. Gu, G.-X. Zhao, J. L. McLaughlin, *Phytochem. Anal.* **1993**, *4*, 27 – 67; c) Z.-M. Gu, G.-X. Zhao, N. H. Oberlies, L. Zeng, J. L. McLaughlin, *Recent Advances in Phytochemistry, Vol. 29*, Plenum, New York, **1995**, pp. 249 – 310; d) U. Koert, *Synthesis* **1995**, 115 – 132; e) R. Hoppe, H.-D. Scharf, *Synthesis* **1995**, 1447 – 1464; f) B. Figadere, *Acc. Chem. Res.* **1995**, *28*, 359 – 365; g) M. C. Zafra-Polo, M. C. Gonzalez, E. Estornell, S. Sahpaz, D. Cortes, *Phytochemistry* **1996**, *42*, 253 – 271; h) L. Zeng, Q. Ye, N. H. Oberlies, G. Shi, Z.-M. Gu, K. He, J. L. McLaughlin, *Nat. Prod. Rep.* **1996**, *13*, 275 – 306; i) M. C. Zafra-Polo, B. Figadere, T. Gallardo, J. R. Tormo, D. Cortes, D. *Phytochemistry* **1998**, *48*, 1087 – 1117; j) F. Q. Alali, X.-X. Liu, J. L. McLaughlin, *J. Nat. Prod.* **1999**, *62*, 504 – 540, and references therein.

[2] G. Shi, D. Alfonso, M. O. Fatope, L. Zeng, Z-m. Gu, G-x. Zhao, K. He, J. M. MacDougal, J. L. McLaughlin, *J. Am. Chem. Soc.* **1995**, *117*, 10409 – 10410.

[3] a) M. T. Crimmins, S. W. Rafferty, *Tetrahedron Lett.* **1996**, *37*, 5649 – 5652; b) P. A. Evans, J. D. Roseman, *Tetrahedron Lett.* **1997**, *38*, 5249 – 5252; c) P. A. Evans, V. S. Murthy, *Tetrahedron Lett.* **1998**, *39*, 9627 – 9628; d) P. A. Evans, V. S. Murthy, *Tetrahedron Lett.* **1999**, *40*, 1253 – 1256; e) S. Takahashi, K. Fujisawa, N. Sakairi, T. Nakata, *Heterocycles* **2000**, *53*, 1361 – 1370; f) S. Hoppen, U. Emde, T. Friedrich, L. Grubert, U. Koert, *Angew. Chem.* **2000**, *112*, 2181 – 2184; *Angew. Chem. Int. Ed.* **2000**, *39*, 2099 – 2102.

[4] a) P. Neogi, T. Doundoulakis, A. Yazbak, S. C. Sinha, S. C. Sinha, E. Keinan, *J. Am. Chem. Soc.* **1998**, *120*, 11279 – 11284; b) S. Takahashi, T. Nakata, *Tetrahedron Lett.* **1999**, *40*, 723 – 726; c) S. Takahashi, T. Nakata, *Tetrahedron Lett.* **1999**, *40*, 727 – 730; d) S. Bäurle, S. Hoppen, U. Koert, *Angew. Chem.* **1999**, *111*, 1341 – 1344; *Angew. Chem. Int. Ed.* **1999**, *38*, 1263 – 1266; e) S. Hoppen, S. Baurle, U. Koert, U. *Chem. Eur. J.* **2000**, *6*, 2382 – 2396; f) S. Takahashi, T. Nakata, *J. Org. Chem.* **2002**, *67*, 5739 – 5752.

[5] For reviews, see a) H. B. Kagan, *New J. Chem.* **1990**, *14*, 453 – 460; b) G. A. Molander, *Chem. Rev.* **1992**, *92*, 29 – 68; c) G. A. Molander, C. R. Harris, *Chem. Rev.* **1996**, *96*, 307 – 338.

[6] a) N. Hori, H. Matsukura, G. Matsuo, T. Nakata, *Tetrahedron Lett.* **1999**, *40*, 2811 – 2814; b) G. Matsuo, N. Hori, T. Nakata, *Tetrahedron Lett.* **1999**, *40*, 8859 – 8863; c) N. Hori, H. Matsukura, T. Nakata, *Org. Lett.* **1999**, *1*, 1099 – 1101; d) N. Hori, H. Matsukura, G. Matsuo, T. Nakata, *Tetrahedron* **2002**, *58*, 1853 – 1864; e) G. Matsuo, H. Kadohama, T. Nakata, *Chem. Lett.* **2002**, 148 – 149.

[7] a) S. Inoki, T. Mukaiyama, *Chem. Lett.* **1990**, 67 – 70; b) R. M. Kennedy, S. Tang, *Tetrahedron Lett.* **1992**, *33*, 3729 – 3732; c) S. Tang, R. M. Kennedy, *Tetrahedron Lett.* **1992**, *33*, 5299 – 5302; d) S. Tang, R. M. Kennedy, *Tetrahedron Lett.* **1992**, *33*, 5303 – 5306; e) R. S. Boyce, R. M. Kennedy, *Tetrahedron Lett.* **1994**, *35*, 5133 – 5136.

[8] a) H. Naito, E. Kawahara, K. Maruta, M. Maeda, S. Sasaki, *J. Org. Chem.* **1995**, *60*, 4419 – 4427; b) T.-L. Wang, X. E. Hu, J. M. Cassady, *Tetrahedron Lett.* **1995**, *36*, 9301 – 9304.

[9] H. C. Kolb, M. S. VanNieuwenhze, K. B. Sharpless, *Chem. Rev.* **1994**, *94*, 2483 – 2547.

[10] The enantiopurity (> 97 % *ee*) was determined by the ^1H NMR analyses of the corresponding MTPA esters of **12**. Furthermore, the optical purity could be improved by recrystallization of **5** from hexane/ethyl acetate to give an optically pure **5**, m.p. 82–82.5 °C (*n*-hexane/ethyl acetate), $[\alpha]_D^{26} = -27.9°$ ($c = 0.84$, $CHCl_3$).

[11] The thioacetalization of **11** with ethanedithiol and other Lewis acids such as BF_3·Et_2O and $TiCl_4$ furnished the corresponding bis(thioacetal) in a low yield because of the unstability of the benzyl ether moiety under the conditions employed.

[12] E. J. Corey, K. Shimoji, *Tetrahedron Lett.* **1983**, *24*, 1289 – 1292.

[13] Data for **13**: $[\alpha]_D^{26} = -41.1°$ ($c = 1.09$ in $CHCl_3$); ^1H NMR (400 MHz, C_6D_6): $\delta = 9.33$ (t, $J = 1.5$ Hz, 1H), 7.40–7.07 (m, 5H), 4.55 (dd, $J = 11.7$, 11.7 Hz, 2H), 4.00 (m, 2H), 3.70 (ddd, $J = 8.8$, 8.8, 4.3 Hz, 1H), 3.49, (m, 2H), 3.44 (ddd, $J = 8.3$, 5.4, 2.5 Hz, 1H), 3.36 (m, 1H), 3.10 (ddd, $J = 9.8$, 8.8, 4.3 Hz, 1H), 2.94 (dd, $J = 15.1$, 3.4 Hz, 1H), 2.53 (dd, $J = 15.1$, 8.8 Hz, 1H), 2.20–2.02 (m, 2H), 1.85–1.37 (m, 2H), 1.70–1.59 (m, 8H), 1.35 (s, 3H), 1.34 (s, 3H), 0.95 ppm (t, $J = 7.3$ Hz, 3H); ^{13}C NMR (100 MHz, C_6D_6): $\delta = 200.4$, 171.9, 139.8, 128.5, 128.2, 128.0, 127.9, 127.8, 108.2, 80.9, 80.7, 80.3, 79.7, 73.1, 72.8, 70.0, 60.4, 40.5, 38.6, 33.1, 29.0, 27.6, 27.4, 27.2, 26.4, 25.3, 14.2 ppm; IR (neat): $\tilde{\nu} = 3447$, 2984, 2936, 2868, 1732, 1456, 1379, 1371, 1348, 1302, 1248, 1221, 1180, 1159, 1092, 1029, 950, 921, 887, 748, 700, 683 cm^{-1}; HRMS calcd for $C_{27}H_{40}O_8Na$ $[M+Na]^+$: m/z 515.2621, found: 515.2621.

[14] The numbering of mucocin was adopted.

 © 2002 WILEY-VCH Verlag GmbH & Co. KGaA, Weinheim 0044-8249/02/4124-4753 $ 20.00+.50/0

[15] Data for **2**: $[\alpha]_D^{26} = -61.4°$ ($c = 1.04$ in $CHCl_3$); ^1H NMR (400 MHz, $CDCl_3$): $\delta = 4.81–4.59$ (m, 6H), 4.10, (m, 2H), 3.47 (m, 2H), 3.39 (s, 3H), 3.38 (s, 3H), 3.36 (s, 3H), 3.33 (m, 1H), 3.21 (m, 1H), 3.10 (m, 1H), 2.47 (ddd, $J = 4.9, 2.9, 1.7$ Hz, 1H), 2.35 (ddd, $J = 7.3, 2.4, 1.7$ Hz, 1H), 2.24–1.22 (m, 12H), 1.25 (br s, 18H), 0.88 ppm (t, $J = 6.8$ Hz, 3H); ^{13}C NMR (75 MHz, $CDCl_3$): $\delta = 96.9, 96.8, 95.3, 81.6, 81.0, 80.9, 79.7, 79.5, 79.1, 77.1, 75.8, 69.6, 55.7, 55.5, 32.1, 31.9, 31.3, 30.1, 29.7, 29.6, 29.3, 28.2, 26.9, 26.6, 26.3, 25.5, 25.3, 22.7, 14.1$ ppm; IR (neat): $\tilde{\nu} =$ 3312, 3273, 2926, 2855, 2823, 1465, 1457, 1396, 1375, 1363, 1340, 1293, 1214, 1150, 1103, 1075, 1036, 918 cm^{-1}; HRMS calcd for $C_{32}H_{58}O_8Na$ $[M+Na]^+$: m/z 593.4029, found: m/z 593.4037.

[16] G. E. Keck, D. Krishnamurthy, M. C. Grier, *J. Org. Chem.* **1993**, *58*, 6543–6544.

[17] K. Takai, K. Nitta, K. Utimoto, *J. Am. Chem. Soc.* **1986**, *108*, 7408–7410.

[18] T. R. Hoye, Z. Ye, *J. Am. Chem. Soc.* **1996**, *118*, 1801–1802.

Structure of a Drug-Induced DNA T-Bulge: Implications for DNA Frameshift Mutations**

Michelle L. Colgrave, Huw E. L. Williams, and Mark S. Searle*

The biological function of nucleic acids is recognized to embrace a wide variety of structural topologies whose stability, conformation, and dynamics may be strongly influenced by the interaction of drug molecules. Single-base bulges, arising from slippage of DNA strands, particularly in homopolymeric tracts of DNA, can result in mutation "hotspots" due to DNA strand misalignment during replication.[1] Addition or deletion mutations at these sites can arise according to whether the extra base stacks within the DNA helix or is displaced into solution. Unpaired pyrimidines have been shown to adopt either an intrahelical or extrahelical conformation depending on flanking sequence, while purines preferentially stack within the helix.[2] The interaction of drug molecules at bulge sites has been of considerable interest since binding close to these sites has the potential to stabilize and increase the lifetime of the bulge state and its susceptibility to frameshift mutations. It has already been demonstrated that ethidium bromide and 9-aminoacridine have increased affinity for sites on duplex DNA carrying an extrahelical cytosine,[3] while neocarzinostatin induces highly efficient site-specific strand cleavage at bulge sites in folded single-stranded DNA.[4] In other cases, chemical modification (base alkylation) of DNA and RNA by drugs appears to occur primarily near bulge sites because of better binding site access,[5] while selective drug binding to RNA bulges has been shown to inhibit protein–RNA recognition.[6] In general, detailed structural information is lacking, although a number of low-resolution NMR studies of bulge recognition by simple DNA intercalators have been described.[3]

The anthracycline antibiotic nogalamycin (Figure 1) has a high sequence specificity for 5′-CG or 5′-TG sites with its bound orientation dictated by the requirement for a guanine (G) base on the 3′-side of the intercalation site.[7] Nogalamycin

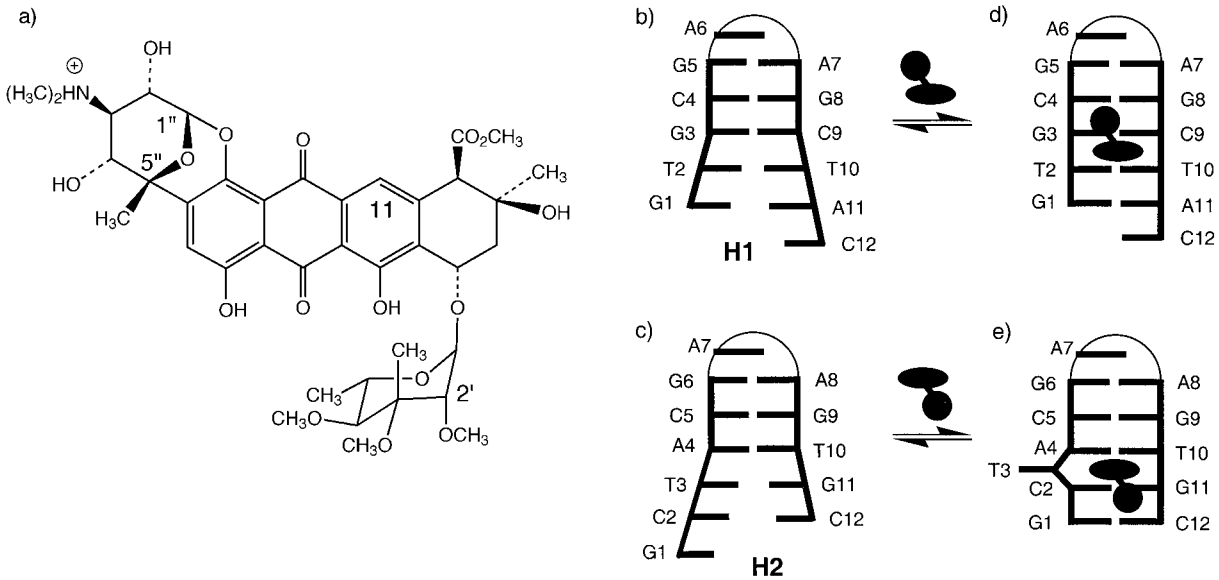


Figure 1. a) Structure of nogalamycin, and oligonucleotide sequences **H1** (b) and **H2** (c) in their proposed folded conformation with frayed ends. Conformations and base-pair alignment adopted in the bound stated with nogalamycin intercalated at the 5′-TpG step ((d) and (e)).

threads its aglycon chromophore through the DNA helix and positions bulky sugar residues in both grooves simultaneously. Interactions in the major groove involving the two hydroxy groups on the bicycloaminoglucose sugar appear to account for the drugs orientational specificity through hydrogen bonding to guanine. Thus, binding to the 5′-TG site results in a unique binding orientation dictated by the G base. With

[*] Dr. M. S. Searle, Dr. M. L. Colgrave, Dr. H. E. L. Williams
School of Chemistry
University Park, Nottingham NG7 2RD (UK)
Fax: (+44) 115-951-3564
E-mail: mark.searle@nottingham.ac.uk.

[**] We thank the EPSRC of the UK, the Australian Research Council, and Boehringer Ingelheim Fonds for supporting this work.

 © 2002 WILEY-VCH Verlag GmbH & Co. KGaA, Weinheim 0044-8249/02/4124-4754 $ 20.00+.50/0

this requirement in mind, we report NMR studies of two hairpin sequences each containing a single 5′-TG binding site incorporating an extra bulged thymine (T) base on the complementary strand (5′-C^{T}A; see Figure 1). We examine how G–C base pair specificity dictates the conformation of the extra T which could be accommodated through a drug-induced frameshift with base mispairing occurring downstream of the drug binding site, or through local stabilization of a T-bulge at the 5′-C^{T}A step preserving Watson–Crick base pairing downstream.

We have designed two novel DNA hairpins (**H1** and **H2**) containing a 5′-GAA loop sequence that has previously been reported to show remarkable thermal stability.[8] Both **H1** and **H2** contain the 5′-TG nogalamycin intercalation site but in different orientations with respect to the stabilizing loop sequence (Figure 1b and c). We have investigated the conformation of the two hairpins in the absence of drug using 1D and 2D NMR spectroscopy in H_2O and D_2O solutions.[9] The hairpins show characteristic NMR parameters that demonstrate that the 5′-GAA loop is formed in both cases.[8] Examination of the imino-proton region of the spectrum at 278 K reveals only two stabilized Watson–Crick pairs in each case. For **H1**, we see signals for G3 and G8 (Figure 2a); in spectra of **H2** signals are evident only for G9 and T10, with the latter showing exchange broadening (Figure 2b). Detailed NMR analysis shows that while the stem region close to the loop is well formed in both structures, the ends of the two hairpins are destabilized and poorly structured (Figure 1b and c).

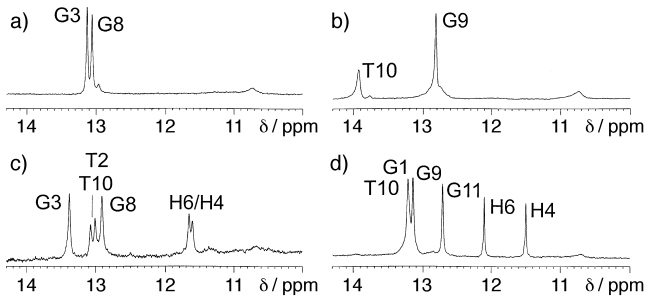


Figure 2. Imino-proton region of the 500 MHz 1D NMR spectra (278 K) of a) free **H1** and b) free **H2**, and in the presence of bound drug **Nog-H1** (c) and **Nog-H2** (d); labeling scheme in accord with Figure 1.

Complex formation with nogalamycin (**Nog**) was monitored by 1D ^{1}H NMR spectroscopy and showed that drug binds cleanly to each sequence in a 1:1 stoichiometry with the free and bound species in slow exchange on the chemical shift time scale. The imino-proton region of the **Nog-H1** complex reveals two sharp signals corresponding to G3 and G8, as evident for uncomplexed **H1,** plus two additional weaker signals of similar intensity at $\delta \approx 13.0$ ppm (Figure 2c), which simultaneously broaden and disappear above 298 K. The site of intercalation and the bound orientation of the drug is established from drug–DNA NOEs; for example, Nog-H11 shows clear interactions with the deoxyribose H1′ of T2 and G3 indicating that the drug is intercalating at the 5′-TG step. Numerous NOEs from methyl and methoxy groups on the nogalose sugar identify hydrophobic interactions within the minor groove consistent with previous studies.[7] NOEs from Nog-H1″ and Nog-5″-CH_3 on the bicycloamino glucose sugar to T2 CH_3 confirm its orientation in the major groove with the drug hydroxy groups positioned to interact with the G3–C9 base pair. The signals for T10 show evidence for exchange broadening, however, weak NOEs from Nog-2′-OCH_3 to T10 H2″/H4′, together with the observation of the two broadened imino-proton signals in Figure 2c, suggest that the drug stacks with a weakly stabilized T2–T10 mismatched pair with the 3′- and 5′-termini poorly structured (Figure 1d).

In contrast, drug binding to hairpin **H2** produces a highly stabilized 1:1 complex. Four imino-proton signals are identified (G1 and T10 overlapped in Figure 2d) indicating that G1, G9, T10, and G11 are involved in stable Watson–Crick base pairs with only the terminal G1 base showing evidence for exchange broadening at 308 K. The chemical shift and NOE data readily confirmed that drug binding stabilizes a bulged conformation in which the T3 base is flipped-out of the helical stack allowing complementary pairing downstream of the intercalation site (Figure 1e). We see that both the base and sugar proton signals of T3 are significantly downfield of those of the uncomplexed DNA ($\Delta\delta$(H1′) = 0.75 ppm; $\Delta\delta(CH_3)$ = 0.48 ppm) suggesting an absence of ring current effects from neighboring stacked bases. In addition, we see only a very weak sequential NOE (base H6/H8 to sugar H2′/2″) from T3 to C2, and none from A4 to T3 (Figure 3) providing strong evidence that T3 is not accommodated within the helical stack. Weak NOEs from T3 CH_3 to C2 H6 and C2 H3′, but very weak or an absence of NOEs to C2 H1′ and C2 H2′/2″, indicate that the extrahelical T base is located in the major groove. A detailed analysis of the NOE data substantiates this conclusion as well as identifying many drug–DNA interactions in both grooves that are analogous to those described above; Nog-H11 unambiguously pins down the bound ori-

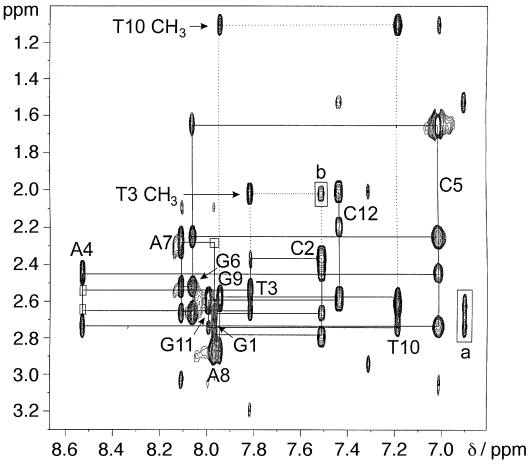


Figure 3. Portion of the 600 MHz NOESY spectrum (300 ms mixing time) of the **Nog-H2** complex showing NOEs between base H6/H8 and sugar H2′/2″. Vertical lines identify the positions of the base H6/H8 signals, while horizontal lines show sequential connectivities. Intranucleotide H6/H8–H2′/H2″ are labeled G1 through to C12. Boxes mark the positions of sequential NOEs that are too weak to observe (A4 H8–T3 H2′/H2″ and A8 H8–A7 H2′/H2″, the latter in the GAA loop). Dotted lines show NOEs from T10 CH_3 and T3 CH_3. Additional cross-peaks are labeled a) Nog-H11–T10 H2′/H2″ and b) T3 CH_3–C2 H6.

 © 2002 WILEY-VCH Verlag GmbH & Co. KGaA, Weinheim 0044-8249/02/4124-4755 $ 20.00+.50/0

entation giving strong NOEs to T10 H1′ and G11 H1′. 340 NOE distance restraints (including some 39 drug–DNA interactions) have enabled us to calculate a family of structures of the **Nog-H2** complex using a combination of distance geometry simulated annealing and restrained molecular dynamics to model this unusual structure (Figure 4).[10]

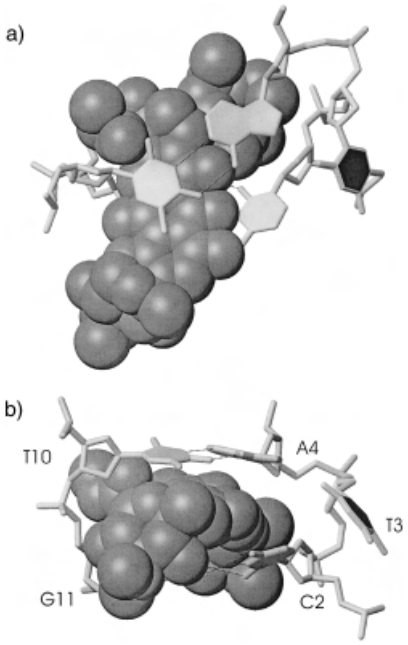


Figure 4. NOE-refined structure of the **Nog-H2** complex showing base-pair alignment and orientation of the extrahelical T-bulge at the drug intercalation site: a) view of the complex down the helix axis illustrating the orientation of the extrahelical T base located in the major groove and drug stacking with A4–T10 (top) and C2–G11 (below), b) view into the major groove showing close van der Waals contacts with the drug at the A4–C2 step with the T3 base flipped out of the helical stack.

Earlier structural studies have rationalized nogalamycin binding specificity for the 5′-TG site in the context of specific interactions in the major groove between the polar bicycloaminoglucose sugar and an intact G–C base pair.[7] These interactions appear to be primary determinants in stablizing an extrahelical base in the **Nog-H2** complex where forcing the bulged-T out of the stack facilitates formation of the required binding site G–C base pair. In contrast, for **H1** the required G–C pairing is already present in the free hairpin such that the nogalamycin–DNA recognition criteria are already partially satisfied. However, the drug appears to be noninstructional downstream of the binding site in the sense that a weakly stabilized T2–T10 mispaired conformation prevails mimicking a "frameshift" (Figure 1 d). Earlier studies of nogalamycin binding to 5′-CG terminal bulge sites in two DNA heptamers, C^{T}GTACG and CGTAC^{T}G,[11] have reported a strand misalignment with T–G and C–T mispairs formed at the terminal sites, leaving 5′-C and 3′-G dangling nucleotides, respectively. However, we demonstrate that the structural distortion observed is context-dependent as a consequence of base-specific recognition, leading to either a highly localized T-bulge, or a frameshift that can potentially propagate along the DNA sequence.

DNA intercalators have already been shown to have a significant impact in inducing mutations during replication by perturbing the recognition of DNA defects by proofreading and repair enzymes.[12] The ability of some intercalators to act as mutagens has already been reported.[3b,13] Here we describe one of the first detailed NMR structural analyses of a drug-stabilized DNA bulge.

Received: August 14, 2002 [Z19970]

[1] a) G. Streisinger, J. Owen, *Genetics* **1985**, 633–659; b) S. A. Woodson, D. M. Crothers, *Biochemistry* **1987**, *26*, 904–912; c) S. A. Woodson, D. M. Crothers, *Biochemistry* **1988**, *27*, 436–445.

[2] a) D. J. Patel, S. A. Kozlowski, L. A. Marky, J. A. Rice, C. Broka, K. Itakura, K. Breslauer, *Biochemistry* **1982**, *21*, 445–451; b) K. M. Morden, Y. G. Chu, F. H. Martin, I. Tinoco, *Biochemistry* **1983**, *22*, 5557–5563; c) S. A. Woodson, D. M. Crothers, *Biochemistry* **1988**, *27*, 3130–3141; d) M. W. Kalnik, D. G. Norman, M. G. Zagorski, P. F. Swann, D. J. Patel, *Biochemistry* **1989**, *28*, 294–303; e) J. Zhu, R. M. Wartell, *Biochemistry* **1999**, *38*, 15986–15993.

[3] a) J. W. Nelson, I. Tinoco, *Biochemistry* **1985**, *24*, 6416–6421; b) S. A. Woodson, D. M. Crothers, *Biochemistry* **1988**, *27*, 8904–8914; c) K. Nakatani, S. Sando, I. Saito, *J. Am. Chem. Soc.* **2000**, *122*, 2172–2177.

[4] a) L. S. Kappen, I. H. Goldberg, *Biochemistry* **1997**, *36*, 14861–14867; b) Z. Xi, Q. K. Mao, I. H. Goldberg, *Biochemistry* **1999**, *38*, 4342–4354.

[5] a) L. D. Williams, I. H. Goldberg, *Biochemistry* **1988**, *27*, 3004–3011; b) A. Stassinopoulous, J. Ji, X. Gao, I. H. Goldberg, *Science* **1996**, *272*, 1943–1946; c) K. Nakatani, A. Okamoto, I. Saito, *Angew. Chem.* **1999**, *111*, 3581–3584; *Angew. Chem. Int. Ed.* **1999**, *38*, 3378–3381.

[6] F. Hamy, E. R. Felder, G. Heizmann, J. Lazdins, F. Aboul-ela, G. Varani, J. Karn, T. Klimkait, *Proc. Natl. Acad. Sci. USA* **1997**, *94*, 3548–3553.

[7] a) X. L. Zhang, D. J. Patel, *Biochemistry* **1990**, *29*, 9451–9466; b) C. K. Smith, J. A. Brannigan, M. H. Moore, *J. Mol. Biol.* **1996**, *263*, 237–258; c) H. E. Williams, M. S. Searle, *J. Mol. Biol.* **1999**, *290*, 699–716.

[8] a) I. Hirao, G. Kawai, S. Yoshizawa, Y. Nishimura, Y. Ishido, K. A. Watanabe, K.-I. Miura, *Nucleic Acids Res.* **1994**, *22*, 576–582; b) S. Yoshizawa, G. Kawai, K. A. Watanabe, K.-I. Miura, I. Hirao, *Biochemistry* **1997**, *36*, 4761–4767.

[9] Oligonucleotides were synthesized by using standard solid-phase methods and purified by reverse-phase HPLC "trityl-on". NMR data were collected at oligonucleotide sample concentrations of 3 mM in 100 mM NaCl and 10 mM Na_2HPO_4 pH 7.0 at the temperatures indicated by using Bruker DRX500 and Avance600 spectrometers and standard phase-sensitive pulse sequences.

[10] Distance restraints (232 DNA–DNA, 39 drug–DNA and 69 drug–drug NOEs) were derived from NOESY data collected at mixing times of 75, 100, and 125 ms by extrapolating to zero mixing time (J. Baleja, J. Moult, B. D. Sykes, *J. Magn. Reson.* **1990**, *87*, 375–384). Candidate structures were obtained from a set of 100 randomly generated starting structures using NMR-derived distance restraints and a simulated annealing/torsion angle dynamics protocol using DYANA (P. Guntert, C. Mumenthaler, K. Wüthrich, *J. Mol. Biol.* **1997**, *273*, 283–292). Subsequently, NOE-restrained MD simulations were carried out for a total of 700 ps, using an explicit solvent model, with the structures minimized by cooling from 300 K to 0 K over the final 100 ps resulting in well-defined structures with a low NOE restraint violation energy; previously reported procedures were used throughout (E. Gavathiotis, G. J. Sharman, M. S. Searle, *Nucleic Acids Res.* **2000**, *28*, 728–735). Structures were displayed and analyzed using MOLMOL (R. Koradi, M. Billeter, K. Wüthrich, *J. Mol. Graphics* **1996**, *14*, 51–55).

[11] J. Caceres-Cortes, A. H.-J. Wang, *Biochemistry* **1996**, *35*, 616–625.

[12] a) W.-C. Lam, E. J. C. Van der Schans, L. C. Sowers, D. P. Millar, *Biochemistry* **1999**, *38*, 2661–2668; b) V. A. Malkov, I. Biswas, R. D. Camerini-Otero, P. Hsieh, *J. Biol. Chem.* **1997**, *272*, 23811–23817.

[13] B. Ames, F. D. Lee, W. E. Durston, *Proc. Natl. Acad. Sci. USA* **1973**, *70*, 782–786.

 © 2002 WILEY-VCH Verlag GmbH & Co. KGaA, Weinheim 0044-8249/02/4124-4756 $ 20.00+.50/0

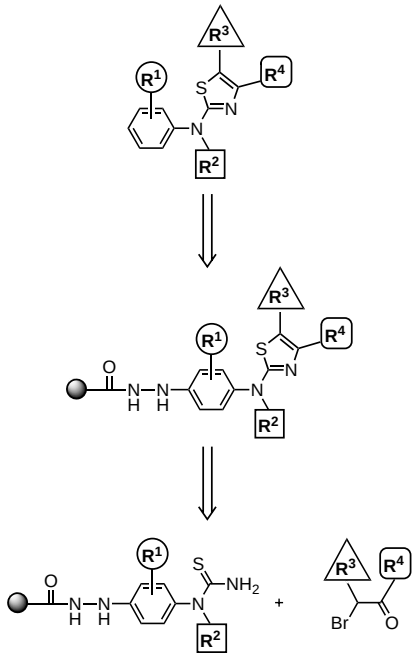
Traceless Solid-Phase Synthesis of 2-Aminothiazoles: Receptor Tyrosine Kinase Inhibitors with Dual Selectivity for Tie-2 and VEGFR-2**

Frank Stieber, Ralph Mazitschek, Natascha Soric, Athanassios Giannis,* and Herbert Waldmann*

Paramount to success in the combinatorial and parallel synthesis of compound libraries on polymeric supports is the proper choice of the molecular scaffolds onto which different functional groups are grafted, the development of reliable multistep sequences on the polymeric support including widely differing types of transformations, and the use of linker groups that guarantee release of the target compounds from the solid support under the mildest conditions. Ideally, a linker should release the products while forming a C–H bond in place of the resin attachment, thus leaving behind no trace of a solid-phase synthesis ("traceless linker").[1,2]

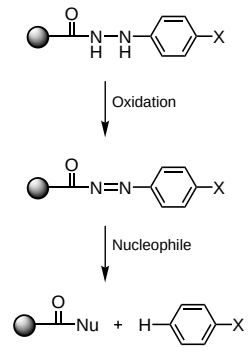
2-Aminothiazoles have recently found application in drug development for the treatment of allergies,[3] hypertension,[4] inflammation,[5] schizophrenia,[6] bacterial[7] and HIV infections,[8] and very recently for the treatment of pain,[9] as fibrinogen receptor antagonists with anti-thrombotic activity,[10] as new inhibitors of bacterial DNA gyrase B,[11] and in the development of cyclin-dependent kinase (CDK) inhibitors.[12]

Here we describe a new and efficient method for the solid-phase synthesis[13] of 2-aminothiazoles that employs the traceless hydrazide linker[14] and report the biological investigation of the library. The Hantzsch synthesis was employed as the key step (Scheme 1) for the solid-phase synthesis of the 2-aminothiazole core. We intended to generate the intermediary thioureas from polymer-bound anilines by treatment with an N-protected isothiocyanate. The *para*-position to the aniline amino group was chosen as the attachment point for the traceless hydrazide linker. Traceless cleavage of the linker is achieved by oxidation of the phenylhydrazide to the acyldiazene and subsequent nucleophilic attack on the carbonyl group (Scheme 2).



Scheme 1. Plan for the traceless solid-phase synthesis of the 2-aminothiazoles.

Amino-functionalized polystyrene **1** (1.3 mmol g^{-1}) was coupled with monomethyl adipicate (**2**) to yield the corresponding polymer-bound amide, and the methyl ester was saponified by treatment with LiOH (Scheme 3). This two-step sequence proceeds with an overall yield of 93–98%.[15] The resulting acid-functionalized resin **3** was then converted into the *p*-nitrophenylhydrazides **5** by activation with *N*,*N*-diisopropylcarbodiimide (DIC) and *N*-hydroxybenzotriazole (HOBt) and treatment with differently substituted 4-nitrophenylhydrazines **4**. Prior to the planned reduction of the nitrobenzene groups to the anilines the two hydrazide nitrogen atoms were acylated with Fmoc-Cl (Fmoc = fluorenylmethoxycarbonyl) to avoid problems in a subsequent step employing Fmoc-isothiocyanate **9** (see below). Reduction of the nitro group to the amino function proceeded quantitatively if $SnCl_2$[16a] was employed in DMF as solvent[16b,c] (determined by GC-MS).



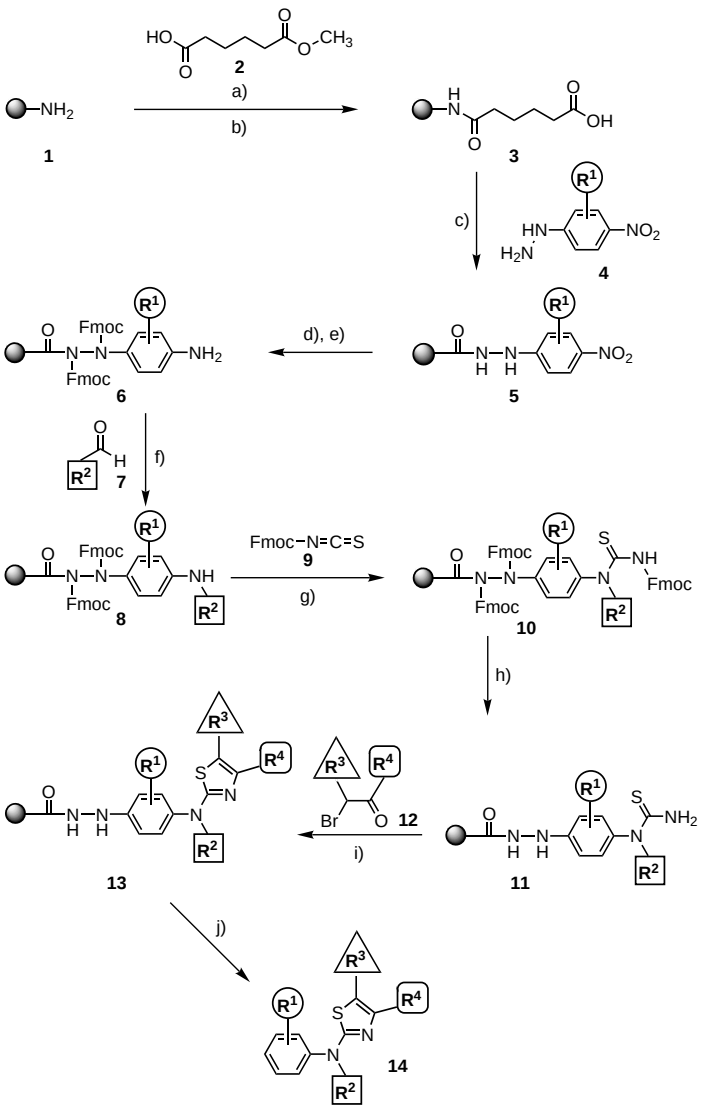
Scheme 2. Principle of the oxidative cleavage of the hydrazide linker.

The use of polymer-bound anilines **6** in the subsequent synthesis sequence leads to the formation of N-monosubstituted 2-aminothiazoles. To also get access to the N,N-disubstituted heterocycles N-functionalization of the amines

[*] Prof. Dr. A. Giannis
Institut für Organische Chemie
Universität Leipzig
Johannisallee 29, 04103 Leipzig (Germany)
Fax: (+49) 341-9736-599
E-mail: giannis@chemie.uni-leipzig.de
Prof. Dr. H. Waldmann, Dr. F. Stieber
Max-Planck-Institut für molekulare Physiologie
Abteilung Chemische Biologie
Otto-Hahn-Strasse 11, 44227 Dortmund (Germany)
Fax: (+49) 231-133-2499
E-mail: herbert.waldmann@mpi-dortmund.mpg.de
and
Universität Dortmund
Fachbereich 3, Organische Chemie
44221 Dortmund (Germany)
Dr. F. Stieber
Semaia Pharmaceuticals GmbH&Co.KG
Emil-Figge-Strasse 76a, 44227 Dortmund (Germany)
Dr. R. Mazitschek, Dipl.-Chem. N. Soric
Institut für Organische Chemie
Universität Karlsruhe
Richard-Willstätter-Allee 2, 76128 Karlsruhe (Germany)

[**] This research was supported by the Bundesministerium für Bildung und Forschung (BMBF), the BASF AG, and the Fonds der Chemischen Industrie (Kekulé-fellowship for F.S.). R.M. and F.S. are grateful to the State of Baden-Württemberg for a scholarship from the Landesgraduiertenförderung. VEGFR = vascular endothelial growth factor receptor.

 © 2002 WILEY-VCH Verlag GmbH & Co. KGaA, Weinheim 0044-8249/02/4124-4757 $ 20.00+.50/0



Scheme 3. Traceless solid-phase synthesis of 2-aminothiazoles **14**. a) 3 equiv **2**, 3 equiv DIC, 3 equiv HOBt, 3 equiv NEt_3, CH_2Cl_2, room temperature, 18 h; b) THF/1 % LiOH in H_2O (1:1), room temperature, 24 h; c) 3 equiv **4**, 3 equiv DIC, 3 equiv HOBt, 3 equiv NEt_3, CH_2Cl_2, room temperature, 18 h; d) 10 equiv Fmoc-Cl, pyridine, CH_2Cl_2, 15 h; e) 2 M $SnCl_2 \cdot 2H_2O$, DMF, room temperature, 18 h; f) 10 equiv aldehyde **7**, THF, HOAc, room temperature, 1 h, wash, then 10 equiv $NaCNBH_3$, THF/HOAc, room temperature, 15 h; g) 3 equiv Fmoc-NCS **9**, CH_2Cl_2, pyridine, room temperature, 15 h; h) DMF/piperidine 4:1, room temperature, 2 × 5 min; i) 0.1 M solution of **12** in dioxane, room temperature, 2 × 3 h; j) 0.5 equiv $Cu(OAc)_2$, *n*-propylamine, O_2, room temperature, 2 h, then solid-phase extraction.

6 by means of reductive amination was investigated. Although this type of transformation is well-established in solid-phase synthesis, its application to anilines **6** turned out to be unexpectedly difficult. After substantial experimentation it was found that quantitative conversion was achieved if 10 equivalents of aldehyde and $NaCNBH_3$ were employed in THF/AcOH (100:1).[17] However, under these conditions formation of the tertiary amine due to double reductive alkylation was also observed. This problem was overcome by separating imine formation and reduction into two individual steps.

Anilines **8** were converted efficiently to the corresponding thioureas **11** by treatment with Fmoc-NCS (**9**)[13b] and subsequent removal of all three Fmoc groups present in intermediates **10** with piperidine in DMF. With polymer-bound thioureas **11** in hand we investigated the Hantzsch thiazole synthesis on the polymeric support. Gratifyingly, the desired 2-aminothiazoles were formed smoothly upon two successive treatments with 0.1 M solutions of different α-bromocarbonyl compounds **12** in dioxane (Scheme 3). Finally, the target compounds **14** were released from the solid support by treatment with a catalytic amount of $Cu(OAc)_2$ in *n*-propylamine and purging with O_2 for reoxidation of the Cu^+ formed in the oxidation of the linker group. The copper salt was readily and efficiently separated from the products by treatment of the reaction mixture with 10 equivalents of a copper-chelating polyamine resin (Advanced Chemtech) or by simple filtration through a silica gel column for solid-phase extraction. In both cases examination of the crude reaction products by atomic absorption spectroscopy indicated that more than 99.9 % of the copper had been removed.

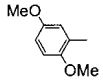
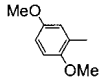
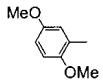
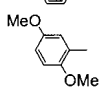
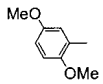
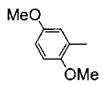
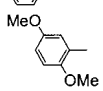
A total of 23 differently substituted 2-aminothiazoles were synthesized by using this procedure, and the results are summarized in Table 1. The data demonstrate that the 2-aminothiazoles are obtained in 9-step (*N*-monosubstituted) and 10-step (N,N-disubstituted) sequences in very high overall yield (19–69 %, average yield per step 84–96 %). The synthesis tolerates substantial variation in the structure of the substituents, that is different aromatic, heteroaromatic, and aliphatic groups can be introduced efficiently. The synthesis sequence proceeds so cleanly that the compounds are obtained after cleavage of the traceless linkers in excellent purity (81–99 %) without any further separation and purification steps. In any case they are pure enough to be employed directly for further purposes, for example biological testing. Of particular interest is the mildness of the conditions required for the completely selective cleavage of the traceless hydrazide linker. In the presence of catalytic amounts of the copper salt employed, even oxidation-sensitive functional groups like furans, thiophenes, and sulfides are not attacked at all.

From the different biological and pharmacological activities of compounds with the 2-aminothiazole scaffold we were particularly intrigued by the ability of certain 2-aminothiazole derivatives to inhibit cyclin-dependent kinases (CDKs, see above).[12] These serine/threonine kinases drive and control cell cycle progression and have essential roles in cell proliferation[18a,19a] and at least two CDK inhibitors are undergoing human clinical trials to suppress tumor growth.[18,19] Given the relevance of these proteins we investigated the 2-aminothiazoles as possible inhibitors of CDK-2 and CDK-4. However, none of the compounds showed appreciable inhibitory activity, which indicates that the individual decoration of the 2-aminothiazole core is paramount to achieving biological activity in the compound class.

In the light of the high similarity among the structure of the ATP-binding domains of protein kinases[18,19] and the notion that this evolutionary conservatism of Nature can be employed as the guiding principle for the development of compound libraries,[20] the library was screened for possible

 © 2002 WILEY-VCH Verlag GmbH & Co. KGaA, Weinheim 0044-8249/02/4124-4758 $ 20.00+.50/0 *Angew. Chem. Int. Ed.* **2002**, *41*, No. 24

Table 1. Results of the traceless solid-phase synthesis of 2-aminothiazoles **14**.

Entry	R^1	R^2	R^3	R^4	Overall yield [%][a]	Purity [%][a]
14/1		H	H		69	96
14/2		H	H		49	99
14/3		H			34	86
14/4		H			19	99
14/5		H	H		29	89
14/6			H		28	99
14/7					31	92
14/8			H		38	99
14/9			H		25	92
14/10			H		42	99
14/11			H		20	86
14/12					30	87
14/13			H		47	81
14/14			H		35	84
14/15					19	98
14/16			H		24	99
14/17					35	86
14/18			H		20	82
14/19			H		33	85
14/20					35	81
14/21					28	93
14/22			H		42	82
14/23			H		31	84

[a] Yield and purity were determined for the crude products after release from the solid support and SPE without further purification. Purity was determined by means of HPLC and GC-MS. The structures of all compounds were confirmed by NMR.

inhibitors against receptor tyrosine kinases (RTKs), selected to cover a wide spectrum of biological activities. To this end, epidermal growth factor receptor (EGFR; ErbB-1),[21] ErbB-2 (Her-2/Neu), insulin-like growth factor 1 receptor (IGF1R),[22] fibroblast growth factor receptor 1 (FGFR1),[23] vascular endothelial growth factor receptors 2 and 3 (VEGFR-2 and -3), and Tie-2[24–26] were chosen as test systems.

The library of the 2-aminothiazoles did not contain any inhibitor of EGFR, ErbB-2, and IGF1R which warranted further investigation. Remarkably, however, six compounds turned out to be inhibitors of Tie-2 and five compounds inhibited VEGFR-2 from a library of only 23 aminothiazoles (Table 2). In addition, a potent inhibitor of the FGFR-1 and two inhibitors of VEGFR-3 were identified. This means that three of the most important regulators of angiogenesis (the development of new blood vessels from pre-existing ones) and lymphoangiogenesis can be inhibited by the prepared 2-aminothiazoles..

Angiogenesis is central to wound repair, inflammation, and embryonic development. Futhermore, aberrant angiogenesis is considered to be a key step in tumor growth, spread, and metastasis.[24,25] Vascular development depends on the endothelium-specific vascular endothelial growth factor receptors 1–3 (VEGFR1–3) and the Tie-2 receptor.[26] All these receptors have been implicated in tumor angiogenesis,[27–31] and antagonization of Tie-2, VEGFR-2, or VEGF-D (a ligand of VEGFR-3) inhibits tumor growth and tumor metastasis in vivo.[30,32,33] The development of low-molecular-weight inhibitors of these receptor tyrosine kinases is among the most promising approaches for the development of new, alternative antitumor drugs, and several inhibitors of VEGFR-2 are in clinical trials.[34,35] The combination of VEGFR-2 inhibitors with Tie-2 antagonists should potentiate their antiangiogenic effects.[29] Furthermore, inhibitors of VEGFR-3 would suppress the lymphogenic metastasis of tumors. To date however, only a few cases of small-molecule inhibitors of Tie-2 and VEGFR-3 have been reported.[36]

Several of the already known VEGFR-2 and Tie-2 inhibitors display nanomolar affinities towards the isolated kinases and are significantly more potent than the inhibitors identified in this study. However, the 2-aminothiazole inhibitors described above represent a new structural class of VEGFR-2/3 and Tie-2 inhibitors and, in particular, they are clearly differentiated from the other known inhibitors by their dual specificity for VEGFR-2 and Tie-2.

In conclusion we have developed an efficient method for the traceless synthesis of 2-aminothiazoles that display dual specifity against the receptor tyrosine kinases VEGFR-2 and Tie-2. This finding opens possibilities for the suppression of angiogenesis and for the development of new antitumor agents. The synthesis method should rapidly give access to a

 © 2002 WILEY-VCH Verlag GmbH & Co. KGaA, Weinheim 0044-8249/02/4124-4759 $ 20.00+.50/0

Table 2. Inhibition of different receptor tyrosine kinases by 2-aminothiazoles **14** (IC_{50} [μM]).[a, b].

Entry	Compound	VEGFR-2	VEGFR-3	Tie-2	FGFR 1
1	**14/1**	–	–	21	–
2	**14/2**	–	–	13	–
3	**14/7**	7.4	44	9.8	8.6
4	**14/8**	31	–	4.8	–
5	**14/14**	12	41	–	–
6	**14/20**	86	–	28	–
7	**14/23**	63	–	31	–

[a] None of the introduced compounds inhibited IGF1R, EGFR, or ErbB-2. [b] To assay the inhibitory activity, the kinase-catalyzed phosphorylation of poly(Glu-Tyr) in the presence of varying concentrations of inhibitor was determined. The kinases were employed as fusion proteins of glutathione-S-transferase (GST) and the respective kinase domain. The relative amount of phosphorylated substrate was quantified by means of an anti-phosphotyrosine enzyme-linked immunosorbent assay (ELISA), which employed an anti-phosphotyrosine antibody conjugated to horseradish peroxidase (POD). The bound antibody was detected by the light emission after addition of a chemiluminescence substrate for POD.

much larger library of 2-aminothiazoles from which dual-selective VEGFR-2 and Tie-2 inhibitors with enhanced biological potency may be identified that could be developed into a new class of anti-angiogenesis drugs.

Received: May 21, 2002
Revised: August 26, 2002 [Z19344]

[1] F. Guillier, D. Orain, M. Bradley, *Chem. Rev.* **2000**, *100*, 2091 – 2157.
[2] *Handbook of Combinatorial Chemistry* (Eds.: K. C. Nicolaou, R. Hanko, W. Hartwig), Wiley-VCH, Weinheim, **2002**.
[3] K. D. Hargrave, F. K. Hess, J. T. Oliver, *J. Med. Chem.* **1983**, *26*, 1158 – 1163.
[4] W. C. Patt, H. W. Hamilton, M. D. Taylor, M. J. Ryan, D. G. Taylor, Jr., C. J. C. Connolly, A. M. Doherty, S. R. Klutchko, I. Sircar, B. A. Steinbaugh, B. L. Batley, C. A. Painchaud, S. T. Rapundalo, B. M. Michniewicz, S. C. J. Olson, *J. Med. Chem.* **1992**, *35*, 2562 – 2572.
[5] a) F. Haviv, J. D. Ratajczyk, R. W. DeNet, F. A. Kerdesky, R. L. Walters, S. P. Schmidt, J. H. Holms, P. R. Young, G. W. Carter, *J. Med. Chem.* **1988**, *31*, 1719 – 1728; b) F. Clemence, O. L. Martret, F. Delevallee, J. Benzoni, A. Jouanen, S. Jouquey, M. Mouren, R. Deraedt, *J. Med. Chem.* **1988**, *31*, 1453 – 1462.
[6] J. C. Jaen, L. D. Wise, B. W. Caprathe, H. Tecle, S. Bergmeier, C. C. Humblet, T. G. Heffner, L. T. Meltzner, T. A. Pugsley, *J. Med. Chem.* **1990**, *33*, 311 – 317.
[7] K. Tsuji, H. Ishikawa, *Bioorg. Med. Chem. Lett.* **1994**, *4*, 1601 – 1606.
[8] F. W. Bell, A. S. Cantrell, M. Hogberg, S. R. Jaskunas, N. G. Johansson, C. L. Jordon, M. D. Kinnick, P. Lind, J. M. Morin Jr. , R. Noréen, B. Öberg, J. A. Palkowitz, C. A. Parrish, P. Pranc, C. Sahlberg, R. J. Ternansky, R. T. Vasileff, L. Vrang, S. J. West, H. Zhang, X. X. Zhou, *J. Med. Chem.* **1995**, *38*, 4929 – 4936.
[9] J. S. Carter, S. Kramer, J. J. Talley, T. Penning, P. Collins, M. J. Graneto, K. Seibert, C. M. Koboldt, J. Masferrer, B. Zweifel, *Bioorg. Med. Chem. Lett.* **1999**, *9*, 1171 – 1174.
[10] A. Badorc, M.-F. Bordes, P. de Cointet, P. Savi, A. Bernat, A. Lalé, M. Petitou, J.-P. Maffrand, J.-M. Herbert, *J. Med. Chem.* **1997**, *40*, 3393 – 3401.
[11] J. Rudolph, H. Theis, R. Hanke, R. Endermann, L. Johannsen, F.-U. Geschke, *J. Med. Chem.* **2001**, *44*, 619 – 626.
[12] a) W. K. M. Chong, S. S. Chu, R. R. Duvadie, L. Li, W. Xiao, Y. Yang Agouran Pharmaceuticals Inc., WO 99/21845 **1999**; b) "Aminothiazole Inhibitors of Cyclin Dependent Kinases": K. S. Kim, S. D. Kimball, M. A. Poss, R. N. Misra, Z.-W. Cai, D. B. Rawlins, K. Webster, J. T. Hunt, W.-C. Han, PCT, Int. Appl. WO9924416A1-990520.
[13] a) J. Stadtwieser, E. P. Ellmerer-Müller, A. Takó, N. Maslouh, W. Bannwarth, *Angew. Chem.* **1998**, *110*, 1487 – 1489; *Angew. Chem. Int. Ed.* **1998**, *37*, 1402 – 1404; b) P. C. Kearney, M. Fernandez, J. A. Flygare, *J. Org. Chem.* **1998**, *63*, 196 – 200; c) K. H. Bleicher, C. Lutz, Y. Wüthrich, *Tetrahedron Lett.* **2000**, *41*, 9037 – 9042.
[14] a) F. Stieber, U. Grether, H. Waldmann, *Angew. Chem.* **1999**, *111*, 1142 – 1145; *Angew. Chem. Int. Ed.* **1999**, *38*, 1073 – 1077; for previous use of the hydrazide linker for peptide synthesis in solution and on solid support, see: b) H. B. Milne, C. F. Most, Jr., *J. Org. Chem.* **1968**, *33*, 169 – 175; b) A. N. Semenov, K. Y. Gordeev, *Int. J. Pept. Protein Res.* **1995**, *45*, 303 – 304; c) C. R. Millington, R. Quarrell, G. Lowe, *Tetrahedron Lett.* **1998**, *39*, 7201 – 7204; d) C. Rosenbaum, H. Waldmann, *Tetrahedron Lett.* **2001**, *42*, 5677 – 5680.
[15] The loading of resin **3** was determined by nucleophilic esterification with 2-methoxy-5-nitrobenzyl bromide, basic saponification of the resulting ester groups and UV-spectroscopic quantification of the released 2-methoxy-5-nitrobenzyl alcohol.
[16] a) D. Tumelty, M. K. Schwarz, K. Cao, M. C. Needels, *Tetrahedron Lett.* **1999**, *40*, 6185 – 6188; b) J. P. Mayer, Z. Jingwen, K. Bjergarde, D. M. Lenz, J. J. Gaudino, *Tetrahedron Lett.* **1996**, *37*, 8081 – 8084; c) A. S. Kiselyov, R. W. Armstrong, *Tetrahedron Lett.* **1997**, *38*, 6163 – 6166.
[17] E. G. Brown, J. M. Nuss, *Tetrahedron Lett.* **1997**, *38*, 8457 – 8460.
[18] a) T. M. Sielecki, J. F. Boylan, P. A. Benfield, G. L. Trainor, *J. Med. Chem.* **2000**, *43*, 1 – 18; b) N. Gray, L. Détivaud, C. Doernig, L. Meijer, *Curr. Med. Chem.* **1999**, *6*, 859 – 875.
[19] a) P. Cohen, *Nat. Rev. Drug Discovery* **2002**, *1*, 309 – 315; b) A. J. Bridges, *Chem. Rev.* **2001**, *101*, 2541 – 2571.
[20] R. Breinbauer, I. Vetter, H. Waldmann, *Angew. Chem.* **2002**, *114*, 3002 – 3015; *Angew. Chem. Int. Ed.* **2002**, *41*, 2878 – 2890.
[21] C. Heldin, L. Rönnstrand, *Oncogenes and Tumor Suppressors* (Eds.: G. Peters, K. Vousden), Oxford University Press, Oxford, **1997**, p. 62.
[22] M. J. Ellis, S. Jenkins, J. Hanfeldt, M. E. Redington, M. Taylor, R. Leek, K. Siddle, A. Harris, *Breast Cancer Res. Treat.* **1998**, *52*, 175 – 184.
[23] a) Y. Wang, D. Becker, *Nat. Med.* **1997**, *3*, 887 – 893; b) A. Compagni, P. Wilgenbus, M. A. Impagnatiello, M. Cotten, G. Christofori, *Cancer Res.* **2000**, *60*, 7163 – 7169.
[24] a) J. Folkman, *Nat. Med.* **1995**, *1*, 27 – 31; b) A. Giannis, F. Rübsam, *Angew. Chem.* **1997**, *109*, 606 – 609; *Angew. Chem. Int. Ed. Engl.* **1997**, *36*, 588 – 590.
[25] a) J. Folkman, *N. Engl. J. Med.* **1971**, *285*, 1182 – 1186; b) P. Carmeliet, R. K. Jain, *Nature* **2000**, *407*, 249 – 257.
[26] G. D. Yancopoulos, S. Davis, N. W. Gale, J. S. Rudge, S. J. Wiegand, J. Holash, *Nature* **2000**, *407*, 242 – 248; P. C. Maisonpierre, C. Suri, P. F. Jones, S. Bartunkova, S. J. Wiegand, C. Radziejewiski, D. Compton, J. McClain, T. H. Aldrich, N. Papadopoulos, T. J. Daly, S. Davis, T. N. Sato, G. D. Yancopoulos, *Science* **1997**, *277*, 55 – 60.
[27] S. Hiratsuka, Y. Maru, A. Okada, M. Seiki, T. Noda, M. Shibuya, *Cancer Res.* **2001**, *61*, 1207 – 1213.
[28] H. Kubo, T. Fujiwara, L. Jussila, H. Hashi, M. Ogawa, K. Shimizu, M. Awane, Y. Sakai, A. Takabayashi, K. Alitalo, Y. Yamaoka, S. I. Nishikawa, *Blood* **2000**, *96*, 546 – 553.
[29] A. Stratmann, T. Acker, A. M. Burger, K. Amann, W. Risau, K. H. Plate, *Int. J. Cancer* **2001**, *91*, 273 – 282.
[30] S. A. Stacker, C. Caesar, M. E. Baldwin, G. E. Thornton, R. A. Williams, R. Prevo, D. G. Jackson, S. Nishikawa, H. Kubo, M. G. Achen, *Nat. Med.* **2001**, *7*, 186 – 191.
[31] M. Skobe, T. Hawighorst, D. G. Jackson, R. Prevo, L. Janes, P. Velasco, L. Riccardi, K. Alitalo, K. Claffey, M. Detmar, *Nat. Med.* **2001**, *7*, 192 – 198.
[32] P. Lin, J. A. Buxton, A. Acheson, C. Radziejewski, P. C. Maisonpierre, G. D. Yancopoulos, K. M. Channon, L. P. Hale, M. W. Dewhirst, S. E. George, K. G. Peters, *Proc. Natl. Acad. Sci. USA* **1998**, *95*, 8829 – 8834.
[33] J. Drevs, I. Hofmann, H. Hugenschmidt, C. Wittig, H. Madjar, M. Muller, J. Wood, G. Martiny-Baron, C. Unger, D. Marmé, *Cancer Res.* **2000**, *60*, 4819 – 4824.
[34] D. H. Boschelli, *Drugs Future* **1999**, *24*, 515 – 537.
[35] See, for example: G. Bold, K.-H. Altmann, J. Frei, M. Lang, P. W. Manley, P. Traxler, B. Wietfeld, J. Brüggen, E. Buchdunger, R. Cozens, S. Ferrari, P. Furet, F. Hofmann, G. Martiny-Baron, J. Mestan, J. Rösel, M. Sills, D. Stover, F. Acemoglu, E. Boss, R. Emmenegger, L. Lässer, E. Masso, R. Roth, C. Schlachter, W. Vetterli, D. Wyss, J. M. Wood, *J. Med. Chem.* **2000**, *43*, 2310 – 2323, and references therein.

 © 2002 WILEY-VCH Verlag GmbH & Co. KGaA, Weinheim 0044-8249/02/4124-4760 $ 20.00+.50/0

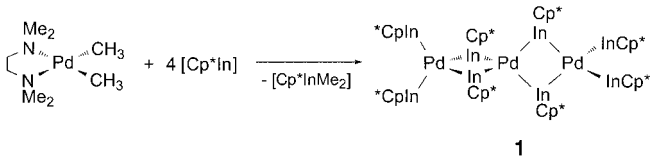
[36] Tie-2: a) P. Stahl, L. Kissau, R. Mazitschek, A. Giannis, H. Waldmann, *Angew. Chem.* **2002**, *114*, 1222 – 1226; *Angew. Chem. Int. Ed.* **2002**, *41*, 1174 – 1178; b) L. D. Arnold, D. J. Calderwood, R. W. Dixon, D. N. Johnston, J. S. Kamens, R. Munschauer, P. Rafferty, S. E. Ratnofsky, *Bioorg. Med. Chem. Lett.* **2000**, *10*, 2167 – 2170; c) A. F. Burchat, D. J. Calderwood, G. C. Hirst, N. J. Holman, D. N. Johnston, R. Munschauer, P. Rafferty, G. B. Tometzki, *Bioorg. Med. Chem. Lett.* **2000**, *10*, 2171 – 2174; VEGFR-3: d) V. Kirkin, R. Mazitschek, J. Krishnan, A. Steffen, J. Waltenberger, M. S. Pepper, A. Giannis, J. P. Sleeman, *Eur. J. Biochem.* **2001**, *268*, 5530 – 5540.

$[Pd_3(InCp^*)_4(\mu_2\text{-}InCp^*)_4]$: Three Linearly Arranged Palladium Atoms Wrapped into a Fluxional Shell of Eight InCp* Ligands**

Tobias Steinke, Christian Gemel, Manuela Winter, and Roland A. Fischer*

In 1999 Murugavel and Chandrasekhar stated in a Highlight article in this journal on monovalent Group 13 organometallic compounds that "the use of these compounds … in transition metal chemistry is likely to have a huge impact on the way new metal–metal bonds are made in the future … and there is no doubt that we will be witnessing the synthesis of a whole range of new cluster types in the future."[1] The monovalent homoleptic complexes $[M\{EC(SiMe_3)\}_4]$ (M = Ni, E = Ga; M = Pt, E = In) synthesized by Uhl et al. in 1998[2] and $[Ni(GaCp^*)_4]$ (Cp^* = pentamethylcyclopentadienide) synthesized by Jutzi et al. in 1999[3] confirmed this statement. Hitherto, most of the studies concerning complexes of these new ligands ER (E = Al, Ga, In, R = Alkyl, Aryl), which are isolobal to CO, were focused on the coordination to transition metal carbonyl fragments $[(CO)_nM_a]$,[4,5] a chemistry that has also been stimulated by our work on $[(CO)_4Fe(AlCp^*)]$.[6] Constitution and structural characteristics of new [GaCp*]-substituted Ni_4 and Rh_6 carbonyl clusters or $[\{(CpNi)(\mu\text{-}AlCp^*)\}_2]$, which were synthesized by Jutzi et al.[7] and Schnöckel et al.,[8] respectively, are directly related to classical transition metal carbonyl cluster structures. Another heuristically valuable analogy of ER ligands to phosphanes is observed for the compounds $[(dcpe)Pt(ER)_2]$ (dcpe = bis(dicyclohexyl)phosphanylethane),[9] a series related to $[Pt(PR_3)_4]$. We recently synthesized the Pt_2Ga_5 complex $[Pt_2(GaCp^*)_2(\mu_2\text{-}GaCp^*)_3]$ selectively by reaction of $[Pt(\eta^2\text{-}C_2H_4)_3]$ and an excess of [GaCp*], and this complex represents the first example of a homoleptic complex of the new series $[M_a(ER)_b]$ $(b > a > 1)$.[10] No structural analogue is known in carbonyl or phosphane cluster chemistry for this complex. Further investigations of this chemistry led us to the title compound $[Pd_3(InCp^*)_4(\mu_2\text{-}InCp^*)_4]$ (**1**).

When $[(tmeda)Pd(CH_3)_2]$ (tmeda = *N*,*N*,*N*′,*N*′-tetramethylethylenediamine) is treated with an excess of [InCp*] in solution in hexane (Scheme 1), and the reaction mixture is warmed to 60 °C, the trinuclear complex $[Pd_3(InCp^*)_4(\mu_2\text{-}InCp^*)_4]$ (**1**) is quantitavely formed, instead of the expected monomeric complex $[Pd(InCp^*)_4]$ (**2**). Complex **1** can be crystallized from benzene as large deep red single crystals in reproducible yields of 90%. The molecular structure of **1** (Figure 1) exhibits three edge-bridging $PdIn_4$



1

Scheme 1. Preparation of **1** from $[Pd(tmeda)(CH_3)_2]$ and [Cp*In].

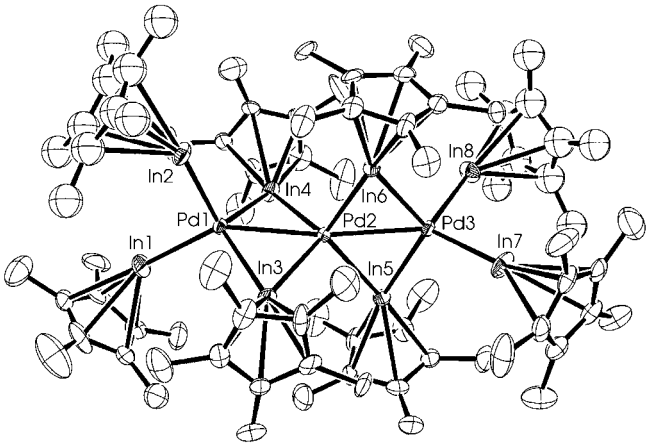


Figure 1. Structure of **1** (ORTEP plot; ellipsoids for 30% probability). Hydrogen atoms are omitted for clarity. Selected distances [Å] and angles [°]: $Cp^*_{centroid}$-In1 2.247, $Cp^*_{centroid}$-In2 2.343, $Cp^*_{centroid}$-In3 2.239, $Cp^*_{centroid}$-In4 2.236, $Cp^*_{centroid}$-In5 2.231, $Cp^*_{centroid}$-In6 2.246, $Cp^*_{centroid}$-In7 2.276, $Cp^*_{centroid}$-In8 2.315, $Cp^*_{centroid}$-In1- Pd1 153.8, $Cp^*_{centroid}$-In2- Pd1 147.3, $Cp^*_{centroid}$-In7-Pd3 174.3, $Cp^*_{centroid}$-In8- Pd3 157.0.

tetrahedrons. The three central palladium atoms are arranged with only a small deviation from linearity of 10° (Figure 2). The distortion of the $PdIn_4$ tetrahedrons is expressed in the In-Pd-In angles, which are smaller than 109° for the terminal In atoms (101.3° and 104.0°) and larger than 109° for the bridging In atoms (114.0° to 116.6°). Correspondingly the dihedral angles In3-Pd1-Pd2-In4 and In6-Pd2-Pd3-In5 deviate from planarity (22.34° and 6.67°). The two bridging In atoms that exihibit the higher deviation (In3, In4) are bent towards the site slightly opened by the Pd-Pd-Pd angle, resulting in a butterfly-shaped structure. The terminal Pd–In distances (2.54–2.57 Å) are somewhat shorter than the bridging ones (2.58–2.61 Å); the Pd–In distances around the central Pd2 atom are the longest (about 2.63 Å). In comparison, the Pd–In distances in the intermetallic phase Pd_3In_7, which contains

[*] Prof. Dr. R. A. Fischer, T. Steinke, Dr. C. Gemel, M. Winter
Lehrstuhl für Anorganische Chemie II - Organometallics & Materials
Ruhr-Universität Bochum
44780 Bochum (Germany)
Fax: (+49) 234-321-4174
E-mail: roland.fischer@ruhr-uni-bochum.de

[**] Organoearth Metal Complexes of d-Block Elements, Part XXVII. Part XXVI see ref. [9b]. The authors thank Degussa AG for generous donations of chemicals.

Supporting information for this article is available on the WWW under http://www.angewandte.org or from the author.

 © 2002 WILEY-VCH Verlag GmbH & Co. KGaA, Weinheim 0044-8249/02/4124-4761 $ 20.00+.50/0

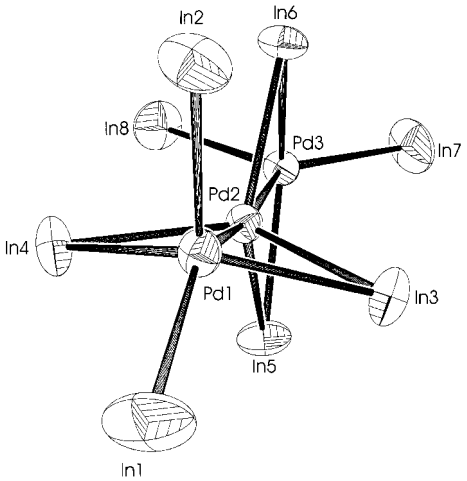
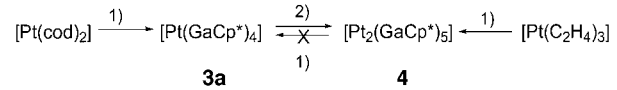


Figure 2. Arangement of the Pd and In atoms in **1** (ORTEP plot; ellipsoids for 50% probability). Selected distances [Å] and angles [°]: Pd1-Pd2 2.7762(14), Pd2-Pd3 2.7747(14), Pd1-In1 2.5397(15), Pd1-In3 2.5831(14), Pd2-In3 2.6319(14), Pd2-In5 2.6258(14), Pd3-In5 2.5962(14), Pd3-In7 2.5520(15); Pd1-Pd2-Pd3 169.52(5), In1-Pd1-In2 101.24(5), In3-Pd1-In4 113.96(5), In3-Pd2-In4 110.70(5), In5-Pd2-In6 114.76(5), In5-Pd3-In6 16.60(5), In7-Pd3-In8 104.00(6), In3-Pd1-Pd2-In4 157.66(6), In6-Pd2-Pd3-In5 173.33(5).

an eight-coordinate palladium center, are 2.76 to 2.79 Å.[12] These Pd–Pd distances of 2.78(1) and 2.77(1) Å do not exclude a bonding Pd^0–Pd^0 interaction. In comparison, the tetranuclear cluster $[Pd_4(CO)_5(PPh_3)_4]$ exhibits a bonding Pd–Pd distance of 2.75–2.77 Å, whereas the nonbonding Pd–Pd distance in the same molecule is 3.21 Å.[13] The In–$Cp^*_{centroid}$ distances are somewhat longer for the terminal (2.28–2.34 Å) than for the bridging ligands (2.23–2.25 Å), and are similar to the distance found in the free ligand (gas phase: 2.29 Å;[14] solid state: 2.30 Å[15]). This is indicative of weakly polar Pd–In bonds, as was also reported for $[(dcpe)Pt(InCp^*)_2]$ (2.28 Å).[9b] In contrast, in $[(CO)_5Cr(InCp^*)]$ the In–$Cp^*_{centroid}$ distance is shorter (2.17 Å).[7a] The Pd-In-$Cp^*_{centroid}$ angles deviate from 180° (144.7–174.3°), but a systematic difference between terminal and bridging ligands is not apparent. These and the other deviations mentioned are probably attributed to steric congestion. A similar situation was found for $[Ni(GaCp^*)_4]$.[3]

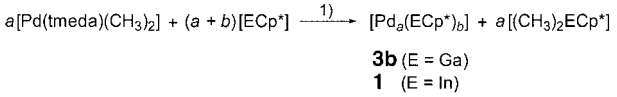
The ^1H and the ^{13}C NMR spectrum of **1** at ambient temperature in C_6D_6 exhibits only one signal or one set of signals for the C_5Me_5 ligands, respectively. No decoalescence or broadening of the signals was observed down to −30 °C ($[D_8]$toluene). Evidently, a fast process takes place, in which the terminal and bridging [InCp*] units are exchanged. At −80 °C a decoalescence of the signal into two signals at $\delta =$ 2.26 and 2.16 ppm with an integral ratio of 1:3 is observed. Whether the structure of **1** in solution corresponds to that in the solid state remains to be clarified. In contrast, the related Pt_2Ga_5 complex $[Pt_2(GaCp^*)_2(\mu_2\text{-}GaCp^*)_3]$ (**4**) exhibits nonfluxional behavior in solution.[10] Experiments to prepare mononuclear $[Pd(InCp^*)_4]$ (**2**) from **1** and excess of [InCp*] failed. Instead, the ^1H NMR spectrum of a mixture of **1** and [InCp*] (1:4) shows coalescence of the signals of **1** ($\delta =$ 2.12 ppm) and [InCp*] ($\delta = 2.04$ ppm) at $\delta = 2.07$ ppm (calcd at $\delta = 2.09$ ppm). The product that crystallizes from this solution is pure **1**. In contrast, the monomeric M–Ga Complexes $[Pt(GaCp^*)_4]$ (**3a**) and $[Pd(GaCp^*)_4]$ (**3b**) (which are analogous to **2**) are readily available from $[Pt(cod)_2]$ (cod = *cis*,*cis*-1,5-cyclooctaiene) or $[(tmeda)Pd(CH_3)_2]$ and [GaCp*], respectively,[16] and thus complete the homologous series $[M(GaCp^*)_4]$ (M = Ni,[7a] Pd, Pt). Additionally, the dinuclear Pt complex $[Pt_2(GaCp^*)_2(\mu_2\text{-}GaCp^*)_3]$ (**4**), which is related to the title complex **1**, is also formed in the reaction of $[Pt(GaCp^*)_4]$ (**3a**) with $[Pt(cod)_2]$ and [GaCp*] in an exact molar ratio of 1:1:1 (Scheme 2). Treatment of **4** with [GaCp*]



Scheme 2. General scheme for the preparation of homoleptic Pt^0-[GaCp*] complexes. 1) Excess of [Cp*Ga], 2) $[Pt(cod)_2]$ and one equivalent of [Cp*Ga] in toluene.

at 25 °C leads in a very slow, nonquantitative reaction back to **3a**. Likewise, **3a** is not available from $[Pt(\eta^2\text{-}C_2H_4)_3]$ and excess of [GaCp*]: In this case **4** is exclusively formed. Clearly, complex mechanisms occur in which kinetic factors and association–dissociation equilibria play a key role. At least for the fluxional Pd/In system very similar lattice energies of the molecular crystals could be responsible for the preferred formation of **1** over **2** or alternative products even in presence of excess of [InCp*].[11]

Closer inspection of the synthesis of the title compound **1** (Scheme 1) reveals that the formation of $[Pd(PR_3)_4]$ from $[(tmeda)Pd(CH_3)_2]$ and phosphanes occurs by reductive elimination of ethane induced by precoordination of PR_3 and subsequent replacement of the tmeda ligand by PR_3.[17] Thus, the reaction of [InCp*] with $[(tmeda)Pd(CH_3)_2]$ in a ratio of 4:1 to give $[Pd(InCp^*)_4]$ (**2**) can be considered to have proceeded as expected. Similarly, the related syntheses of the PtE_2 complexes $[(dcpe)Pt(ER)_2]$[9] (E = Al, Ga, In; R = $C(SiMe_3)_3$, Cp*) from $[(dcpe)Pt(H)(CH_2tBu)]$ and exactly two molar equivalents of ER in methylcyclohexane show a remarkable increase of the reaction rate (100% yield in 20–30 min at 70 °C)[18] in comparison to the unimolecular elimination of neopentane from $[(dcpe)Pt(H)(CH_2tBu)]$ in the same solvent ($t_{1/2} = 2$ h at 70 °C).[19] In contrast, another pathway becomes more important in the reaction of $[(tmeda)Pd(CH_3)_2]$ with [GaCp*] and [InCp*]: The reduction of Pd^{II} to Pd^0 is accompanied by the transfer of a methyl group to the Ga or In centers, that is, an oxidation giving a Ga^{III} or In^{III} side product, respectively (Scheme 1 and Scheme 3).[20] Monitoring of our reactions by NMR spectroscopy showed only traces of ethane. The classical reaction mechanisms of CO-containing complexes, that is, "insertion" into M–C(alkyl) bonds and "reductive elimination", can evidently be transferred to [GaCp*] and [InCp*] ligands. Experiments that used



Scheme 3. General scheme for the preparation of homoleptic Pd^0-[GaCp*] and Pd^0–[InCp*] complexes. For E = Ga, $a = 1$ and $b = 4$ (**3b**); for E = In, $a = 3$, and $b = 8$ (**1**).

 © 2002 WILEY-VCH Verlag GmbH & Co. KGaA, Weinheim 0044-8249/02/4124-4762 $ 20.00+.50/0 *Angew. Chem. Int. Ed.* **2002**, *41*, No. 24

[(tmeda)$PdCl_2$] as the precursor showed that a reduction of palladium(II) chlorides by [InCp*] and [GaCp*] leading to formation of [Cp*ECl_2] is in principle possible, but these reactions are less selective and yields are lower.

In summary, our results confirm the opening quotation that [InCp*] and [GaCp*] exhibit interesting potential as novel ligands for transition metals which exceeds the analogy to CO ligands and phosphanes. In this context, it is worth mentioning that photolysis of a solution of **1** in C_6D_6 (25 °C, 2 h, 150 W) results in selective cleavage of the Cp* shell of the Pd_3In_8 in the form of decamethylfulvalene, and we are currently investigating the metallic precipitate formed. The results are indicative of a link to the current field of mixed-metal nanoparticles and colloids.

Experimental Section

1: A solution of [(tmeda)$Pd(CH_3)_2$] (0.100 g, 0.396 mmol) in hexane (4 mL) was treated with four equivalents of [InCp*] (0.396 g, 1.584 mmol) in hexane (10 mL). The reaction mixture was warmed to 60 °C for 1 h, whereupon a red crystalline precipitate was formed. After recrystallization from benzene, the crystals were isolated by removal of the mother liquor by using a cannula, washed twice with a small amount of cold hexane, and dried in vacuo. Yield: 0.275 g, 90 %. M.p. 81 °C (decomp); ^{1}H NMR (C_6D_6, 250 MHz, 25 °C): $\delta = 2.12$ ppm (s, 120 H); ^{13}C NMR (C_6D_6, 250 MHz, 25 °C): $\delta = 113.7$, 11.2 ppm; elemental analysis: calcd for $C_{80}H_{120}In_8Pd_3 \cdot C_6D_6$: C 42.97; H 5.53, found: 42.79, 5.64.

Received: June 27, 2002 [Z19628]

[1] R. Murugavel, V. Chandrasekhar, *Angew. Chem.* **1999**, *111*, 1289 – 1293; *Angew. Chem. Int. Ed.* **1999**, *38*, 1211 – 1215.

[2] a) W. Uhl, M. Pohlmann, R. Wartchow, *Angew. Chem.* **1998**, *110*, 1007 – 1009; *Angew. Chem. Int. Ed.* **1998**, *37*, 961 – 963; b) W. Uhl, S. Melle, *Z. Anorg. Allg. Chem.* **2000**, *626*, 2043 – 2045; c) W. Uhl, M. Benter, S. Melle, W. Saak, G. Frenking, J. Uddin, *Organometallics* **1999**, *18*, 3778 – 3780.

[3] P. Jutzi, B. Neumann, L. O. Schebaum, A. Stammler, H. G. Stammler, *Organometallics* **1999**, *18*, 4462 – 4464.

[4] J. Weiss, D. Stetzkamp, B. Nuber, R. A. Fischer, C. Boehme, G. Frenking, *Angew. Chem.* **1997**, *109*, 95 – 97; *Angew. Chem. Int. Ed. Engl.* **1997**, *36*, 70 – 72.

[5] a) P. Jutzi, B. Neumann, G. Reumann, H.-G. Stammler, *Organometallics* **1998**, *17*, 1305 – 1314; b) W. Uhl, M. Pohlmann, *Organometallics* **1997**, *16*, 2478 – 2480, and references therein.

[6] J. Uddin, G. Frenking, *J. Am. Chem. Soc.* **2001**, *123*, 1683 – 1693.

[7] a) P. Jutzi, B. Neumann, L. O. Schebaum, A. Stammler, H. G. Stammler, *Organometallics* **1999**, *18*, 4462 – 4464; b) E. V. Grachova, P. Jutzi, B. Neumann, L. O. Schebaum, H. G. Stammler, S. P. Tunik, *J. Chem. Soc. Dalton Trans.* **2002**, 302 – 304.

[8] C. Dohmeier, H. Krautscheid, H.-G. Schnöckel, *Angew. Chem.* **1994**, *106*, 2570 – 2571; *Angew. Chem. Int. Ed. Engl.* **1994**, *33*, 2482 – 2483.

[9] a) D. Weiss, T. Steinke, M. Winter, R. A. Fischer, *Organometallics* **2000**, *19*, 4583 – 4588; b) D. Weiss, M. Winter, K. Merz, A. Knüfer, R. A. Fischer, *Polyhedron* **2002**, *21*, 535 – 542.

[10] D. Weiss, M. Winter, R. A. Fischer, C. Yu, K. Wichmann, G. Frenking, *Chem. Commun.* **2000**, 2495 – 2496.

[11] Crystal structure analysis of **1**·C_6D_6: crystal size: $0.35 \times 0.28 \times 0.20$ mm, triclinic, $P\bar{1}$, $a = 12.826(3)$, $b = 16.146(4)$, $c = 25.215(6)$ Å, $\alpha = 97.595(4)$, $\beta = 101.316(4)$, $\gamma = 111.313(4)°$, $V = 4650.0(18)$ Å^3, $Z = 2$, $\rho_{calcd} = 1.657$ mg m^{-3}, $2\Theta_{max.} = 50.160$, $\lambda(Mo_{K\alpha}) = 0.71073$ Å, $T = 213(3)$ K. A total of 23 924 reflections (16 005 unique) were collected on a Bruker-axs SMART diffractometer (R(int) = 0.0322). The structure solution and refinement was performed by using the programs SHELXS-86 and SHELXL-97. The final values for $R1$ and $wR2(F^2)$ were 0.0705 and 0.2253, respectively. The reason for the unusually high value for $wR2(F^2)$ is not yet clear and is currently under investigation. The Cp* rings at In2 and In8 were isotropically refined and the interatomic distances and angles in all of the Cp* rings were fixed. The Cp* rings are disordered. The unit cell contains other atoms, which probably belong to benzene molecules, but cannot be accurately assigned and refined. As the molecular structure of **1** clearly shows, the high steric demand of the Cp* units excludes the formation of higher [Pd(InCp*)$_2$] oligomers. The key for the synthesis of [Pd(InCp*)$_2$]$_n$ ($n > 3$) is the design of new, sterically less hindered, yet soluble ligands of the type In(CpR) (R = alkyl). CCDC-187560 contains the supplementary crystallographic data for this paper. These data can be obtained free of charge via www.ccdc.cam.ac.uk/conts/retrieving.html (or from the Cambridge Crystallographic Data Centre, 12, Union Road, Cambridge CB2 1EZ, UK; fax: (+44) 1223-336-033; or deposit@ccdc.cam.ac.uk).

[12] U. Häussermann, M. Elding-Pontén, C. Svensson, S. Lidin, *Chem. Eur. J.* **1998**, *4*, 1007 – 1015.

[13] R. D. Feltham, G. Elbaze, R. Ortega, C. Eck, J. Dubrawski, *Inorg. Chem.* **1985**, *24*, 1503 – 1510.

[14] O. T. Beachley, Jr., A. Blom, M. R. Churchill, K. Faegri, Jr., J. C. Fettinger, J. C. Pazik, L. Victoriano, *Organometallics* **1989**, *8*, 346 – 356.

[15] O. T. Beachley, Jr., M. R. Churchill, J. C. Fettinger, J. C. Pazik, L. Victoriano, *J. Am. Chem. Soc.* **1986**, *108*, 4666 – 4668.

[16] T. Steinke, C. Gemel, M. Cokoja, M. Winter, R. A. Fischer, unpublished results, **2002**.

[17] a) W. de Graaf, J. Boersma, W. J. J. Smeets, A. L. Spek, G. van Koten, *Organometallics* **1989**, *8*, 2907 – 2917; b) J. Krause, G. Cestaric, K.-J. Haack, K. Seevogel, W. Storm, K.-R. Pörschke, *J. Am. Chem. Soc.* **1999**, *121*, 9807 – 9823.

[18] D. Weiss, Ph.D. thesis, Ruhr-Universität Bochum, **2001**.

[19] a) M. Hackett, G. M. Whitesides, *J. Am. Chem. Soc.* **1988**, *110*, 1436 – 1448; b) M. Hackett, G. M. Whitesides, *J. Am. Chem. Soc.* **1988**, *110*, 1449 – 1462.

[20] Identification of the Ga^{III} and In^{III} side products by ^{1}H and ^{13}C NMR spectroscopy (C_6D_6, 250 MHz, 25 °C). [Cp*$Ga(CH_3)_2$]: ^{1}H NMR: $\delta = -0.15$ ppm; ^{13}C NMR: $\delta = -7.8$ ppm. [Cp*$In(CH_3)_2$]: ^{1}H NMR: $\delta = -0.11$ ppm; ^{13}C NMR: $\delta = -6.9$ ppm.

Total Synthesis of Amphidinolide T4**

Alois Fürstner,* Christophe Aïssa, Ricardo Riveiros, and Jacques Ragot

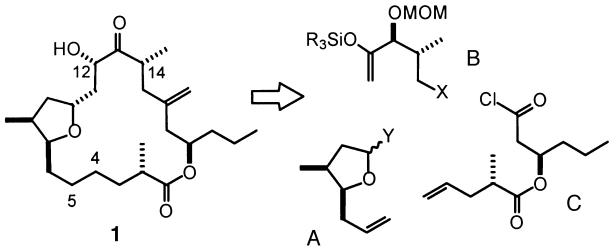
Marine dinoflagellates of the genus *Amphidinium* sp. living in symbiosis with the Okinawan (Japanese) flatworm *Amphiscolops* sp. are exceedingly rich sources of bioactive macrolides.[1] Though structurally quite diverse, all "amphidinolides" known to date exhibit pronounced cytotoxicity against various cancer cell lines, with some members reaching potencies which rank them amongst the most cytotoxic compounds that are presently known.[2] In contrast to macrolide antibiotics derived from terrestrial microorganisms, the majority of amphidinolides feature an odd-numbered macrolide ring, which raises questions concerning the biosynthesis of these structurally unique secondary metabolites.

[*] Prof. A. Fürstner, Dr. C. Aïssa, Dr. R. Riveiros, Dr. J. Ragot
Max-Planck-Institut für Kohlenforschung
45470 Mülheim an der Ruhr (Germany)
Fax: (+49) 208-306-2994
E-mail: fuerstner@mpi-muelheim.mpg.de

[**] Generous financial support by the Deutsche Forschungsgemeinschaft (Leibniz award to A.F.) and the Fonds der Chemischen Industrie is gratefully acknowledged.

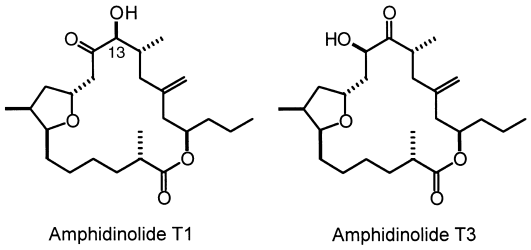
 © 2002 WILEY-VCH Verlag GmbH & Co. KGaA, Weinheim 0044-8249/02/4124-4763 $ 20.00+.50/0

Described below is the first total synthesis of amphidinolide T4 (**1**; Scheme 1), a prototype member of this series containing a 19-membered lactone core.[3,4] Because its



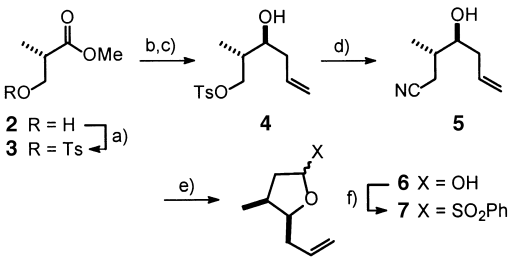
Scheme 1. Structure and retrosynthetic analysis of amphidinolide T4 (**1**).

congeners T1 and T3 differ from **1** only in the oxygenation pattern of the C-12/C-14 region,[3,5] the synthesis is planned such that it can later be adapted to the preparation of these compounds as well.



For the sake of convergency, it was envisaged to assemble this target from three building blocks of similar size and complexity (**A**–**C**) by means of a stereoselective Lewis acid mediated alkylation of a silyl enol ether with a lactol-derived oxocarbenium cation,[6] a palladium-catalyzed acylation of an organozinc reagent with an enantiomerically pure acid chloride,[7] as well as a ring-closing metathesis (RCM) reaction for the formation of the macrocyclic ring (Scheme 1).[8] In this maneuver, the C-4/C-5 bond is targeted for efficiency reasons as the required precursors seem to be particularly easily accessible.

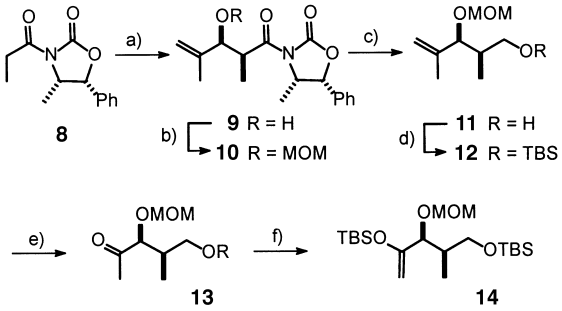
This aspect is evident from Scheme 2, which shows the preparation of compound **7** as the synthetic equivalent of **A**. Compound **7** is readily available from the commercial hydroxyester **2** which is tosylated prior to reduction with



Scheme 2. Synthesis of segment **A**: a) TsCl, Et_3N, DMAP, CH_2Cl_2, 94%; b) Dibal-H, toluene, −95°C; c) (−)-Ipc_2B-allyl, Et_2O, −100°C, 70% (over both steps); d) KCN, DMSO, 99%; e) Dibal-H, CH_2Cl_2, −78°C, 91%; f) $PhSO_2H$, $CaCl_2$, CH_2Cl_2, 0°C, 87%. DMAP = 4-dimethylaminopyridine, Ts = tosyl, Dibal-H = diisobutylaluminum hydride, Ipc_2B-allyl = allyldiisopinocamphanylborane.

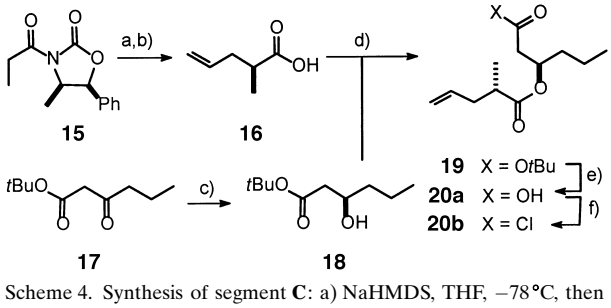
Dibal-H. Treatment of the resulting aldehyde with (−)-Ipc_2B-allyl[9] at a low temperature affords the alcohol **4** in a diastereomerically pure form on a multigram scale. While the tosylate is sufficiently stable to act as a protecting group for the primary alcohol during the hydride reduction and the allylation steps, it serves as an appropriate leaving group in the subsequent reaction with KCN. The resulting nitrile **5** is again reduced with Dibal-H to afford hemiacetal **6** after acidic work-up, which is converted into the sulfone **7** upon treatment with an excess of $PhSO_2H$ in the presence of $CaCl_2$ as the dehydrating agent.[6a]

The coupling partner needed for further elaboration is obtained from *N*-propionyl oxazolidinone **8**[10] by a sequence of high yielding steps (Scheme 3). Specifically, a boron aldol reaction with methacrolein provides the *syn*-aldol **9** on a multigram scale which is protected by a MOM group prior to reduction with $LiBH_4$. The resulting primary alcohol **11** is converted into the TBS ether **12** which is subjected to ozonolysis to provide the methyl ketone **13** in excellent overall yield.[11]



Scheme 3. Synthesis of segment **B**: a) 1. Bu_2BOTf, Et_3N; 2. methacrolein, 90%; b) MOMCl, $(iPr)_2NEt$, CH_2Cl_2, 93%; c) $LiBH_4$, Et_2O, 92%; d) TBSCl, imidazole, DMF, 90%; e) O_3, CH_2Cl_2, 86%; f) TBSOTf, Et_3N, Et_2O, 0°C→RT, 91%. MOMCl = methoxymethylchloride, TBSCl = *tert*-butyldimethylsilylchloride

The last segment is easily prepared on a large scale as shown in Scheme 4. Thus, the β-keto ester **17** is hydrogenated in the presence of $[\{(R)\text{-binap})RuCl_2\}_2]\cdot(NEt_3)$ as the catalyst to give **18** in excellent enantiomeric purity (*ee* = 98%).[12] This alcohol is then esterified with the acid **16** which is readily available from the *N*-acyl oxazolidinone **15** by a standard

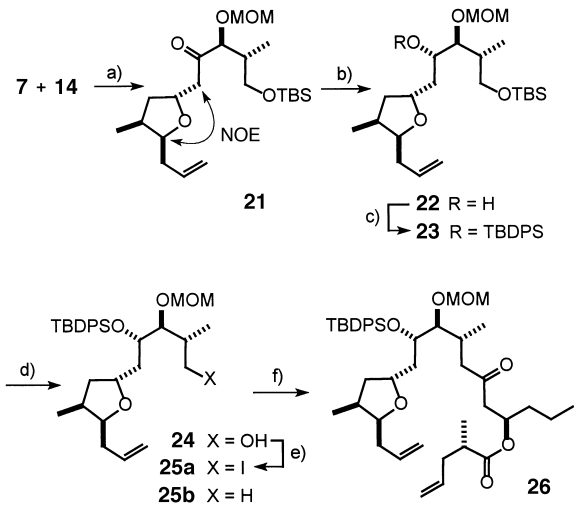


Scheme 4. Synthesis of segment **C**: a) NaHMDS, THF, −78°C, then allyl bromide, 60%; b) LiOH, H_2O_2, THF/H_2O, 93%; c) cat. $[\{(R)\text{-binap})RuCl_2\}_2]\cdot NEt_3$, H_2 (10 atm), MeOH, 95°C, 84%; d) EDCI, DMAP, CH_2Cl_2, 93%; e) F_3CCOOH, Et_3SiH, CH_2Cl_2, quantitative; f) $(COCl)_2$, CH_2Cl_2/DMF cat., quantitative. NaHMDS = sodium hexamethyldisilazide, binap = 2,2′-bis(diphenylphosphanyl)-1,1′-binaphthyl, EDCI = 1-(3-dimethylaminopropyl)-3-ethylcarbodiimide hydrochloride.

 © 2002 WILEY-VCH Verlag GmbH & Co. KGaA, Weinheim 0044-8249/02/4124-4764 $ 20.00+.50/0 *Angew. Chem. Int. Ed.* **2002**, *41*, No. 24

allylation reaction[13] followed by hydrolytic cleavage of the auxiliary. Deprotection of the *tert*-butyl ester in **19** with F_3CCOOH in the presence of Et_3SiH and subsequent conversion of the resulting acid **20a** into the corresponding acid chloride **20b** furnishes the missing building block **C** needed for the envisaged synthesis of amphidinolide T4.

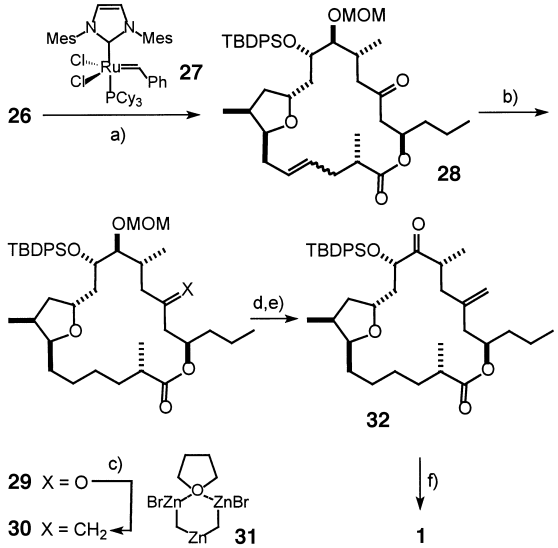
With all building blocks in hand, the assembly of the metathesis precursor was investigated. For this purpose, the ketone **13** is transformed into the *tert*-butyldimethylsilyl enol ether **14** which is stable in air and can be rigorously purified by flash chromatography.[14] While the reaction of enol ethers with tetrahydropyranyl sulfones mediated by Lewis acids has an excellent record, the corresponding tetrahydrofuranyl sulfones have the reputation of poor stereoselectivity.[6a] Gratifyingly, however, the reaction of the anomeric sulfone **7** gave very satisfactory results. After careful optimization of the individual parameters, treatment of a solution of **7** and **14** in CH_2Cl_2 at −78 °C with $SnCl_4$ afforded the desired ketone **21** in 86% yield after standard work-up. The product **21** is obtained as the desired *trans* isomer (*trans*:*cis* ≈ 26:1) as can be deduced from the strong NOE effect indicated in Scheme 5. This outcome probably reflects the shielding of the α side of the intermediate oxocarbenium cation by the methyl- and the allyl units.[6b,15] The reason why $SnCl_4$ is far superior to all other Lewis acids tested, however, is far from obvious.



Scheme 5. Fragment coupling: a) $SnCl_4$, CH_2Cl_2, −78 °C, 86%; b) L-Selectride, THF, −78 °C, 72%; c) KHMDS, TBDPSCl, THF, 77%; d) TsOH, aq. MeOH, 75%; e) I_2, PPh_3, imidazole, toluene, 80%; f) 1. Zn/Cu couple, THF; 2. **20b**, cat. $Pd_2(dba)_3$, cat. P(2-furyl)$_3$, 40–50% (**26**) + 28% (**25b**). TBDPSCl = *tert*-butyldiphenylsilylchloride, dba = dibenzylidene acetone.

Reduction of this compound with L-Selectride affords the desired *S*-configured alcohol **22** in 72% yield,[16] which was protected as the silyl ether **23** by treatment with KHMDS and TBDPSCl. Cleavage of the orthogonal TBS group at the terminal position of **23** under acidic conditions, followed by conversion of the resulting primary alcohol **24** into the corresponding iodide **25** sets the stage for the last segment coupling. Thus, exposure of **25** to Zn/Cu couple activated with TMSCl immediately prior to use gives the corresponding organozinc reagent which reacts with the enantiomerically pure acid chloride **20b** in the presence of $[Pd_2(dba)_3]$ catalyst and tris(2-furyl)phosphane as the ligand to give the desired ketone **26** together with small amounts of the reduced product **25b**.[7] To date, attempts to improve on this result by using nucleophiles other than the organozinc reagent and/or different catalysts and ligands have been in vain. Notably, however, this reaction is one of the most advanced examples of an acyl-Negishi coupling reaction reported to date.[17]

In line with our expectations,[8,18] the subsequent formation of the macrocyclic ring by RCM of the diene **26** worked exquisitely well when carried out in the presence of the "second-generation" ruthenium carbene complex **27** as the catalyst bearing an imidazol-2-ylidene ligand (Scheme 6).[19] Hydrogenation of the resulting cycloalkene **28** (*E*:*Z* = 6:1)



Scheme 6. Completion of the total synthesis: a) catalyst **27**, CH_2Cl_2, reflux, 86%; b) H_2 (1 atm), Pd/C, EtOAc, 86%; c) Nysted's reagent **31** (excess), THF, reflux, 64%; d) TMSCl, nBu_4NBr, CH_2Cl_2, 0 °C, 85%; e) Dess–Martin periodinane, CH_2Cl_2, 83%; f) HF·pyridine, MeCN, 87%.

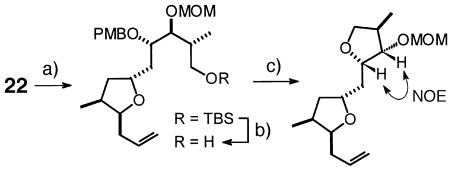
delivers **29** in high yield and sets the stage for the conversion of the keto group into the *exo*-methylene branch of the target. This reaction, however, turned out to be quite delicate. While $Ph_3P{=}CH_2$ was far too basic and led only to a β elimination of the aldol with concomitant opening of the macrocycle, the use of CH_2Br_2 in the presence of TiX_4/Zn (X = Cl, O*i*Pr) gave the desired olefin in somewhat variable yields.[20] The best results were obtained by applying Nysted's reagent **31**,[21] which delivers **30** in up to 64% yield.

Having secured good access to the intact carbon skeleton of **1**, removal of the MOM group in **30** by using TMSBr generated in situ followed by oxidation of the resulting alcohol on treatment with Dess–Martin periodinane[22] cleanly led to the ketone **32**. The final deprotection step was readily achieved by using HF·pyridine to give amphidinolide T4 (**1**). The analytical and spectroscopic data of the synthetic material are in excellent agreement with those published for the natural product, thus rigorously confirming the assignments previously made.[3]

 © 2002 WILEY-VCH Verlag GmbH & Co. KGaA, Weinheim 0044-8249/02/4124-4765 $ 20.00+.50/0

As mentioned above, the other members of the amphidinolide T family, that is, amphidinolide T1-T3, differ from T4 (**1**) mainly or exclusively in the C-12 to C-14 region of the macrocycle;[3] because the stereocenter at C-13 in **30** is appropriately set, however, the synthesis of these compounds is just a matter of a different timing of the final deprotection steps and/or simple inversion reactions. Therefore it is expected that the synthesis summarized above will give access to these valuable marine natural products as well. This and related aspects are subject to ongoing studies in our laboratory.

Received: August 16, 2002 [Z19984]



(1)

This assignment was ultimately confirmed by the conversion of **22** into **1** and comparison of the data of the synthetic sample with those of the natural product.

[1] a) M. Ishibashi, J. Kobayashi, *Heterocycles* **1997**, *44*, 543 – 572; b) T. K. Chakraborty, S. Das, *Curr. Med. Chem. Anti Cancer Agents* **2001**, *1*, 131 – 149.

[2] Specifically, amphidinolides H and N exhibit antitumor potency similar to that of the spongistatins, see ref. [1] and references therein.

[3] J. Kobayashi, T. Kubota, T. Endo, M. Tsuda, *J. Org. Chem.* **2001**, *66*, 134 – 142.

[4] For total syntheses of other amphidinolides see: a) D. R. Williams, W. S. Kissel, *J. Am. Chem. Soc.* **1998**, *120*, 11198 – 11199; b) D. R. Williams, B. J. Myers, L. Mi, *Org. Lett.* **2000**, *2*, 945 – 948; c) D. R. Williams, K. G. Meyer, *J. Am. Chem. Soc.* **2001**, *123*, 765 – 766; d) H. W. Lam, G. Pattenden, *Angew. Chem.* **2002**, *114*, 526 – 529; *Angew. Chem. Int. Ed.* **2002**, *41*, 508 – 511; e) T. K. Chakraborty, S. Das, *Tetrahedron Lett.* **2001**, *42*, 3387 – 3390; f) R. E. Maleczka, L. R. Terrell, F. Geng, J. S. Ward, *Org. Lett.* **2002**, *4*, 2841 – 2844; g) B. M. Trost, J. D. Chisholm, S. T. Wrobleski, M. Jung, *J. Am. Chem. Soc.* **2002**, *124*, 12420–12421.

[5] a) M. Tsuda, T. Endo, J. Kobayashi, *J. Org. Chem.* **2000**, *65*, 1349 – 1352; b) T. Kubota, T. Endo, M. Tsuda, M. Shiro, J. Kobayashi, *Tetrahedron* **2001**, *57*, 6175 – 6179.

[6] a) D. S. Brown, M. Bruno, R. J. Davenport, S. V. Ley, *Tetrahedron* **1989**, *45*, 4293 – 4308; b) A. Schmitt, H.-U. Reißig, *Eur. J. Org. Chem.* **2001**, 1169 – 1174.

[7] a) E. Negishi, V. Bagheri, S. Chatterjee, F.-T. Luo, J. A. Miller, A. T. Stoll, *Tetrahedron Lett.* **1983**, *24*, 5181 – 5184; b) E. Negishi, F. Liu, in *Metal-catalyzed Cross-coupling Reactions* (Eds.: F. Diederich, P. J. Stang), Wiley-VCH, Weinheim, **1998**, pp. 1 – 47; c) Y. Tamaru, H. Ochiai, F. Sanda, Z.-I. Yoshida, *Tetrahedron Lett.* **1985**, *26*, 5529 – 5532; d) P. Knochel, R. D. Singer, *Chem. Rev.* **1993**, *93*, 2117 – 2188.

[8] a) T. M. Trnka, R. H. Grubbs, *Acc. Chem. Res.* **2001**, *34*, 18 – 29; b) A. Fürstner, *Angew. Chem.* **2000**, *112*, 3140 – 3172; *Angew. Chem. Int. Ed.* **2000**, *39*, 3012 – 3043; c) M. Schuster, S. Blechert, *Angew. Chem.* **1997**, *109*, 2124 – 2144; *Angew. Chem. Int. Ed. Engl.* **1997**, *36*, 2037 – 2056.

[9] U. S. Racherla, Y. Liao, H. C. Brown, *J. Org. Chem.* **1992**, *57*, 6614 – 6617.

[10] J. R. Gage, D. A. Evans, *Org. Synth.* **1990**, *68*, 83 – 91.

[11] For a similar sequence see: K. Makino, K. Kimura, N. Nakajima, S. Hashimoto, O. Yonemitsu, *Tetrahedron Lett.* **1996**, *37*, 9073 – 9076.

[12] a) R. Noyori, *Asymmetric Catalysis in Organic Synthesis*, Wiley, New York, **1994**; b) T. Ohkuma, R. Noyori in *Comprehensive Asymmetric Catalysis, Vol. 1* (Eds.: E. N. Jacobsen, A. Pfaltz, H. Yamamoto), Springer, Berlin, **1999**, pp. 199 – 246.

[13] D. A. Evans, M. D. Ennis, D. J. Mathre, *J. Am. Chem. Soc.* **1982**, *104*, 1737 – 1739.

[14] The corresponding TMS enol ether is labile and leads to erratic results.

[15] For a review on the stereoselective synthesis of natural products with polysubstituted THF units see: U. Koert, *Synthesis* **1995**, 115 – 132.

[16] Protection of the alcohol **22** as a PMB ether [PMB = *para*-methoxybenzyl; a) PMBBr, KHMDS], cleavage of the terminal TBS group [b) TBAF, THF] and treatment of the resulting alcohol with c) I_2, PPh_3, and imidazole delivers the tetrahydrofuran shown in Equation (1) rather than the expected primary iodide, compare O. R. Martin, F. Yang, F. Xie, *Tetrahedron Lett.* **1995**, *36*, 47 – 50. Its relative stereochemistry was elucidated by NOE measurements, from which the stereochemistry of **22** formed with L-Selectride can be deduced.

[17] For another advanced example see: A. Fürstner, H. Weintritt, *J. Am. Chem. Soc.* **1998**, *120*, 2817 – 2825.

[18] These expectations stem from results in the following projects: a) A. Fürstner, K. Radkowski, C. Wirtz, R. Goddard, C. W. Lehmann, R. Mynott, *J. Am. Chem. Soc.* **2002**, *124*, 7061 – 7069; b) A. Fürstner, F. Jeanjean, P. Razon, *Angew. Chem.* **2002**, *114*, 2203 – 2206; *Angew. Chem. Int. Ed.* **2002**, *41*, 2097 – 2101; c) A. Fürstner, T. Dierkes, O. R. Thiel, G. Blanda, *Chem. Eur. J.* **2001**, *7*, 5284 – 5296; d) A. Fürstner, O. R. Thiel, N. Kindler, B. Bartkowska, *J. Org. Chem.* **2000**, *65*, 7990 – 7995; e) A. Fürstner, T. Müller, *J. Am. Chem. Soc.* **1999**, *121*, 7814 – 7821; f) A. Fürstner, K. Langemann, *J. Am. Chem. Soc.* **1997**, *119*, 9130 – 9136; g) A. Fürstner, K. Langemann, *J. Org. Chem.* **1996**, *61*, 3942 – 3943.

[19] a) M. Scholl, T. M. Trnka, J. P. Morgan, R. H. Grubbs, *Tetrahedron Lett.* **1999**, *40*, 2247 – 2250; b) J. Huang, E. D. Stevens, S. P. Nolan, J. L. Pedersen, *J. Am. Chem. Soc.* **1999**, *121*, 2674 – 2678; c) L. Ackermann, A. Fürstner, T. Weskamp, F. J. Kohl, W. A. Herrmann, *Tetrahedron Lett.* **1999**, *40*, 4787 – 4790; d) A. Fürstner, L. Ackermann, B. Gabor, R. Goddard, C. W. Lehmann, R. Mynott, F. Stelzer, O. R. Thiel, *Chem. Eur. J.* **2001**, *7*, 3236 – 3253.

[20] K. Takai, Y. Hotta, K. Oshima, H. Nozaki, *Tetrahedron Lett.* **1978**, 2417 – 2420;b) T. Okazoe, J. Hibino, K. Takai, H. Nozaki, *Tetrahedron Lett.* **1985**, *26*, 5581 – 5584; c) for a highly successful application in a case where the Wittig reaction had also failed see: A. Fürstner, O. Guth, A. Düffels, G. Seidel, M. Liebl, B. Gabor, R. Mynott, *Chem. Eur. J.* **2001**, *7*, 4811 – 4820.

[21] S. Matsubara, M. Sugihara, K. Utimoto, *Synlett* **1998**, 313 – 315.

[22] R. K. Boeckman, Jr., P. Shao, J. J. Mullins, *Org. Synth.* **2000**, *77*, 141 – 152.

Tuning PCR Specificity by Chemically Modified Primer Probes**

Michael Strerath and Andreas Marx*

Dedicated to Professor Peter Welzel on the occasion of his 65th birthday

Since the publication of the first draft of the human genome sequence in 2001, the discovery of genomic dissimilarities such as single nucleotide polymorphisms (SNPs) between different individuals has been a main focus of many research

[*] Dr. A. Marx, Dipl.-Chem. M. Strerath
Kekulé-Institut für Organische Chemie und Biochemie
Universität Bonn
Gerhard-Domagk-Strasse 1, 53121 Bonn (Germany)
Fax: (+ 49) 228-73-5388
E-mail: a.marx@uni-bonn.de

[**] This work was supported by the DFG, the Volkswagenstiftung, and the Fonds der Chemischen Industrie. We thank Prof. Dr. M. Famulok for his continuing support and Prof. Dr. A. Pingoud and his co-workers for many stimulating discussions. PCR = polymerase chain reaction.

Supporting information for this article is available on the WWW under http://www.angewandte.org or from the author.

 © 2002 WILEY-VCH Verlag GmbH & Co. KGaA, Weinheim 0044-8249/02/4124-4766 $ 20.00+.50/0

efforts.[1] This is an specially intriguing issue since it is becoming increasingly apparent that variable effects of drugs on different patients or predisposition for various diseases can often be linked to variations in the genome sequence.[1] In the future, the exact knowledge of medicinally relevant nucleotide variations may allow any therapy to be adapted to the genetic equipment of the individual and would abolish treatment with drugs that are ineffective or cause severe side effects.[1] Methods that allow time- and cost-efficient verification of nucleotide variations should lead to further advances in pharmacogenetics.[1,2]

Many methods for the detection of nucleotide variations in genes have been described to date.[2] Each method exhibits advantages and disadvantages, and thus no methodology has prevailed so far. Most known methods are applied after amplification of the target genome sequence through the polymerase chain reaction (PCR). Thus, after isolation of the genetic material, the sequence of interest has to be amplified by PCR prior to the analytical step determining nucleotide variation.[2] Methods for the direct detection of nucleotide variations through PCR are rare. Allele-specific amplification (ASA) determines nucleotide variations through either the presence or absence of a DNA product obtained through PCR amplification.[3] The principle of ASA is based on the formation of matched or mismatched primer template complexes through allele-specific primer probes. From matched 3′-primer termini PCR amplification by a DNA polymerase proceeds, while a mismatch should obviate amplification. Nevertheless, there have been many reports indicating the low selectivity of this approach, thus necessitating further tedious time- and cost-intensive optimizations.[4] Therefore, any means of increasing the selectivity of allele-specific PCR amplification should have significant impact on the reliability and robustness of direct SNP analysis by PCR.

Recently, we reported that nucleotide insertion selectivity of a DNA polymerase can be increased by chemical means by using 4′-alkylated nucleotides.[5] The supplemental small modifications are believed to cause less flexibility within the DNA polymerase substrate complex and thus decrease the tolerance for formation of geometrically altered nascent nucleotide pairs.[5,6] Based on this model, we speculated that the flexibility at the 3′-primer end can be decreased as well through these modifications, resulting in lower DNA polymerase propensity for extension of geometrically altered mismatched primer template complexes. Such a system could in turn be the basis for the development of a novel highly allele-specific PCR approach. Here we show that this concept is indeed applicable and report on a significant increase of the specificity of PCR by the use of chemically modified primer probes. Our results represent a major advancement in the development of robust methods for the detection of nucleotide variation through PCR.

We first synthesized DNA strands bearing 4′-modified thymidine residues at the 3′-terminal position and subsequently used these DNA strands as primers in primer extension assays.[5b,7] First, we screened several thermostable DNA polymerases in their ability to extend from 4′-modified primer ends, which are either bound to the template according to the Watson–Crick rule or which cause a single mismatch through a mutated template nucleotide (Figure 1).[8] To mimic a cycle in PCR we employed reaction conditions commonly used in standard PCR protocols and used reaction buffers as recommended by the supplier.[7] Screening several commercially available thermostable DNA polymerases we identified Vent DNA polymerase (exonuclease-deficient mutant, Vent$^-$) as the best mismatch discriminating enzyme in primer extensions employing 4′-modified oligonucleotides. The data obtained for Vent$^-$ employing unmodified probes reveal that the enzyme significantly promotes primer extension even from mismatched primers under the applied conditions (Figure 1, lanes 2–5).

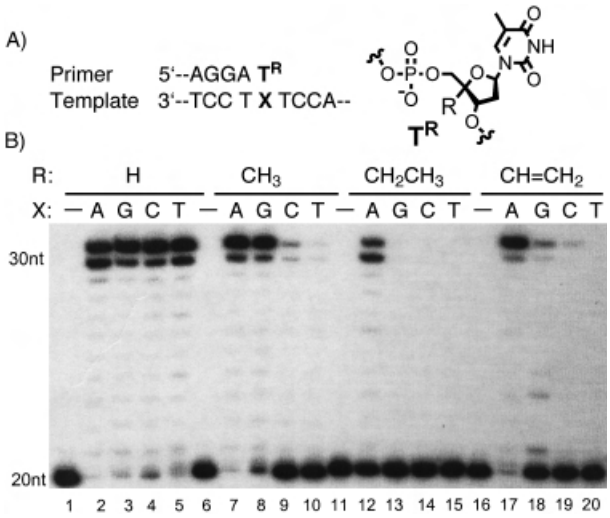


Figure 1. Effects of 4′-modifications on the primer extension catalyzed by Vent$^-$. A) Section of the primer template sequences employed. B) Results of primer extension reactions obtained when canonical (X = A) or noncanonical (X = G, C, or T) primer ends were employed. The respective template nucleobases and 4′-substituents are depicted in the figure. Lanes 1, 6, 11, 16: primer only.[7]

However, 4′-modifications at the primer termini cause in most incidences significantly increased discrimination between matched and mismatched primer template complexes (Figure 1, lanes 6–20). Discriminative primer extension turns out to be dependent on the bulk of the 4′-modification. Thus, 4′-methylated primer strands are extended efficiently by the DNA polymerase in the case of primer template T^{Me}/A as well as T^{Me}/G, while extension from T^{Me}/C and T^{Me}/T is significantly hampered (Figure 1, lanes 6–10). Increasing the bulk of the 4′-modification by employment of ethyl modifications led to significantly increased apparent mismatch discrimination but nevertheless, at the cost of efficiency for extension of matched complexes (Figure 1, lanes 11–15). Interestingly, 4′-vinyl-modified primers exhibit good discrimination under the conditions applied, combined with a significantly increased extension propensity in the matched case compared to the 4′-ethylated probes (Figure 1, lanes 16–20). These combined features render the 4′-vinyl modification the most interesting for further investigations.

For genotyping needs we next envisaged the synthesis of the corresponding probes bearing 4′-vinylated 2′-deoxycytidine moieties. Furthermore, subsequent investigations of their interplay with DNA polymerases should reveal whether the

 © 2002 WILEY-VCH Verlag GmbH & Co. KGaA, Weinheim 0044-8249/02/4124-4767 $ 20.00+.50/0

observed effects on mismatch discrimination are exclusively linked to thymidine residues. Following a published procedure for the synthesis of **1**,[9] we synthesized the modified solid support **2** bearing adequately protected 4′-vinylated 2′-deoxycytidine (Figure 2A).[10]

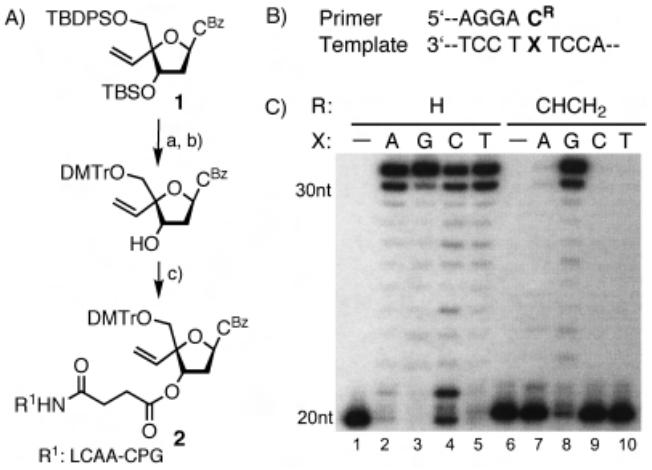


Figure 2. Synthesis of probes containing 4′-vinylated 2′-deoxycytidine and their effects on primer extension. A) Synthesis of solid supports bearing 4′-modified 2′-deoxycytidines. Reagents and conditions: a) TBAF, THF, 25 °C, 4 h; b) DMTrCl, cat. DMAP, pyridine, 25 °C, 7 h, 55 % (two steps); c) succinylated LCAA-CPG, DMAP, EDC, NEt_3, pyridine, 25 °C, 16 h; then 4-nitrophenol, 25 °C, 14 h, then piperidine, 25 °C, 5 min, then acetic anhydride, DMAP, pyridine, 25 °C, 14 h. C^{Bz} = benzoyl-protected cytosine, TBS = tert-butyldimethylsilyl; TBDPS = tert-butyldiphenylsilyl, DMTr = 4,4′-dimethoxytrityl; DMAP = 4-dimethylaminopyridine; LCAA-CPG = long-chain alkyl amine modified controlled pore glass; EDC = 1-(3-dimethylaminopropyl)-3-ethylcarbodiimide hydrochloride. B) Section of the primer template sequences employed. C) Results of primer extension reactions obtained when canonical (X = G) or noncanonical (X = A, C, or T, respectively) primer ends were employed. The respective template nucleobases and 4′-substituents are depicted in the figure. Lanes 1 and 6: primer only.[7]

The required 4′-modified primer probes were synthesized by means of automated DNA synthesis by employing the modified solid supports. Subsequent primer extension studies with 4′-vinylated primer and Vent$^-$ conducted under identical conditions as above led to results similar to those obtained with 4′-modified thymidines. The 4′-vinylated 2′-deoxycytidine residues likewise show significant beneficial effects on the apparent mismatch discrimination by enzymatic primer extension.

Encouraged by these promising findings we next explored whether the results of the primer extension can be further developed to a highly allele-specific PCR. First, we studied PCR amplification by Vent$^-$ of a 63nt gene fragment of the human acid ceramidase, which contains nucleotide variations at a single position opposite the 3′-terminus of the respective primer probe.[8] To explore the impact of 4′-vinyl modifications in primer probes on the discrimination of ASA we studied every possible single nucleotide variation in the template strand. As shown in Figure 3, usage of unmodified primer probes resulted in little discrimination between matched and single mismatched primer template complexes. Strikingly, employment of primer probes bearing 4′-vinylated thymidine residues resulted in a markedly diminished amplification of DNA when the primer probes were mismatched. These effects are significant in the presence of primer pyrimidine/template purine mismatches (T^{vi}/G; C^{vi}/A), but nevertheless even more pronounced when pyrimidine/pyrimidine mismatched probes were present. In the latter cases the extent of product amplification was beyond the detection limit under the employed conditions (Figure 3). Noteworthy, it has been shown that discrimination through PCR of pyrimidine/purine mismatches at the 3′-primer end (e.g. T/G) is difficult to achieve; thus, our findings of significantly increased selectivity due to 4′-modified primer probes are a significant advancement in this respect.[4]

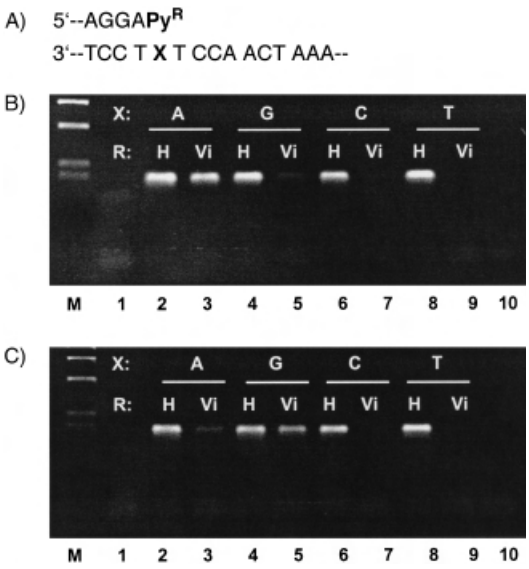


Figure 3. Effects of modified primer probes on the selectivity of PCR amplification. A) Section of sequences employed. Py^R = pyrimidine residues bearing 4′-hydrogen atom or 4′-vinyl modifications; X = respective template nucleobase as depicted in B) and C). B) Results obtained with primer probes bearing 4′-vinylated thymidine residues. C) Results obtained with primer probes bearing 4′-vinylated 2′-deoxycytidine residues. M = size marker; Lanes 1, 10: Experiments conducted in the absence of template and in each case with unmodified primers or 4′-modified primers.[7]

To gain detailed quantitative insight into this process we employed radioactively labeled primer probes and analyzed the ratio of product amplification after every cycle.[7] The obtained results clearly show the highly beneficial effects of our modified primer probes on PCR amplification selectivity (Figure 4). For instance, 4′-vinylated primer termini are proficiently elongated in matched cases with somewhat lower efficiency than the unmodified probes. Nevertheless, single mismatches at the primer ends prevent efficient amplification significantly more pronounced in the 4′-modified cases resulting in a more selective PCR amplification with respect to a single nucleotide variation at the primer end.

In summary, we report on effects of 4′-modified primer probes on single mismatch discrimination in allele-specific PCR amplification. We found that in all investigated single mismatches, significantly higher amplification selectivity is observed by use of 4′-vinylated primer probes and Vent$^-$ DNA polymerase compared to cases were unmodified primers were used. This study reveals that small chemical modifications of DNA can trigger distinct enzymatic respons-

 © 2002 WILEY-VCH Verlag GmbH & Co. KGaA, Weinheim 0044-8249/02/4124-4768 $ 20.00+.50/0

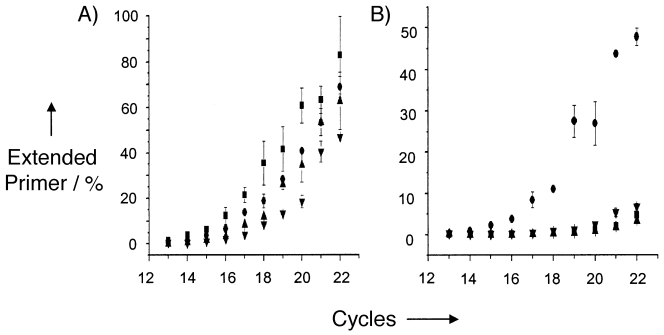


Figure 4. Quantification of PCR products. Results were obtained by employing the same conditions as shown in Figure 3 using 5′-^{32}P-labeled primer probes. Aliquots were removed after every cycle and subsequently analyzed by denaturating PAGE using phosphorimaging technology. The percentage of product relative to the overall radioactivity in one lane was plotted against the number of cycles. Error bars derive from repeated experiments. A) Results obtained with probes bearing unmodified thymidine residues at the 3′-primer end. B) Results obtained with primer probes bearing 4′-vinylated thymidine residues at the 3′-primer end. The respective primer/template duplexes were indicated by the following symbols: ● T^R/A, ▼ T^R/G, ▲ T^R/C, ■ T^R/T.[7]

es that are not easily accessible with unmodified substrates. Considering recent developments in the use of real-time quantitative PCR as an analytical tool for detecting variations in nucleotides,[11] these findings should have significant impact on the development of reliable and robust methods.

Received: July 15, 2002 [Z19731]

[1] For example: a) A. D. Ross, *Nature* **2000**, *405*, 857–865; b) J. J. McCarthy, R. Hilfiker, *Nat. Biotechnol.* **2000**, *18*, 505–508; c) W. E. Evans, M. V. Relling, *Science* **1999**, *286*, 487–491; d) P. W. Kleyn, E. S. Vesell, *Science* **1998**, *281*, 1820–1821.

[2] For example: a) M. M. Shi, *Clin. Chem.* **2001**, *47*, 164–172; b) I. G. Gut, *Hum. Mutat.* **2001**, *17*, 475–492; c) M. Chicurel, *Nature* **2001**, *412*, 580–582; d) P. Y. Kwok, *Annu. Rev. Genomics Hum. Genet.* **2001**, *2*, 235–258.

[3] D. Y. Wu, L. Ugozzoli, B. K. Pal, R. B. Wallace, *Proc. Natl. Acad. Sci. USA* **1989**, *86*, 2757–2760.

[4] For example: a) Z. Guo, Q. Liu, L. M. Smith, *Nat. Biotechnol.* **1997**, *15*, 331–335; b) Y. Ishikawa, K. Tokunaga, K. Kashiwase, T. Akaza, K. Tadokoro, T. Juji, *Hum. Immunol.* **1995**, *42*, 315–318; c) P. R. Wenham, C. R. Newton, W. H. Price, *Clin. Chem.* **1991**, *37*, 241–244; d) C. R. Newton, A. Graham, L. E. Heptinstall, S. J. Powell, C. Summers, N. Kalsheker, J. C. Smith, A. F. Markham, *Nucleic Acids Res.* **1989**, *17*, 2503–2516.

[5] a) D. Summerer, A. Marx, *Angew. Chem.* **2001**, *113*, 3806–3808; *Angew. Chem. Int. Ed.* **2001**, *40*, 3693–3695; b) D. Summerer, A. Marx, *J. Am. Chem. Soc.* **2002**, *124*, 910–911; c) M. Strerath, D. Summerer, A. Marx, *ChemBioChem* **2002**, *3*, 578–580.

[6] E. T. Kool, *Annu. Rev. Biochem.* **2002**, *71*, 191–219.

[7] Detailed experimental procedures as well as DNA sequences applied are provided in the Supporting Information.

[8] All DNA polymerases experiments conducted were done in the sequence context of human acid ceramidase comprising the recently discovered mutation at A107. See: J. Bär, T. Linke, K. Ferlinz, U. Neumann, E. H. Schuchman, K. Sandhoff, *Hum. Mutat.* **2001**, *17*, 199–209.

[9] N. Nomura, S, Shuto, M. Tanaka, T. Sasaki, S. Mori, S. Shigata, A. Matsuda, *J. Med. Chem.* **1999**, *42*, 2901–2908.

[10] R. T. Pon in *Current Protocols in Nucleic Acids Chemistry* (Eds.: S. L. Beaucage, D. E. Bergstrom, G. D. Glick, R. A. Jones), Wiley, **2000**, chapters 3.2.1–3.2.23.

[11] *Rapid Cycle Real-Real Time PCR* (Eds.: S. Meuer, C. Wittwer, K. Nakagawara), Springer, Berlin, **2001**.

Detection of Individual p53-Autoantibodies by Using Quenched Peptide-Based Molecular Probes**

Hannes Neuweiler, Andreas Schulz, Andrea C. Vaiana, Jeremy C. Smith, Sepp Kaul, Jürgen Wolfrum, and Markus Sauer*

The development of new fast and sensitive assay formats for cancer diagnosis is one of the most challenging tasks in biomedical analysis. Since p53-autoantibodies are independent and highly specific tumor markers with a substantial potential for early-stage diagnosis they have become a focus of modern cancer diagnosis.[1] Here we report on the development of a sensitive and fast assay for p53-autoantibodies using a novel single-molecule fluorescence spectroscopic method. The method involves detection of reversible fluorescence quenching of dyes by tryptophan residues in labeled short peptides derived from the antibody recognition sequence of the p53 protein. The effectiveness of these peptide-based molecular probes for early-stage diagnosis and follow-up of malignant diseases is demonstrated by the detection of individual p53-autoantibodies directly in sera of cancer patients in the concentration range relevant for clinical tests.Gene mutation in p53—the guardian of the genome[2]—is the most frequently found abnormality in human cancer[3] and often triggers the immune system to produce antibodies directed against the nuclear tumor suppressor protein p53—the DNA transcript of the p53 gene. The presence of p53-autoantibodies in human serum validates a malignant disease with a specificity of 100% if autoimmune diseases are neglected.[1] Commonly, the enzyme-linked immunosorbant assay (ELISA) technique is used as heterogeneous assay format to detect p53-autoantibodies, whose detection limit lies in the range of 10^{-9}–10^{-11}M. The major disadvantages of this method are that it is slow (several hours) and, due to the requirement of recombinant p53, expensive.

Lubin and co-workers have shown that the immune response of cancer patients is not directed against the mutated central segment of the p53 sequence, but rather is directed against a small subset of linear peptide epitopes localized mainly in the N-terminal region (the transactivation domain)

[*] Priv.-Doz. Dr. M. Sauer, H. Neuweiler, Dr. A. Schulz, Prof. Dr. J. Wolfrum
Physikalisch-Chemisches Institut
Universität Heidelberg
Im Neuenheimer Feld 253, 69120 Heidelberg (Germany)
Fax: (+49) 6221-54-4225
E-mail: sauer@urz.uni-heidelberg.de
A. C. Vaiana, Prof. Dr. J. C. Smith
IWR
Universität Heidelberg
Im Neuenheimer Feld 368, 69120 Heidelberg (Germany)
Dr. S. Kaul
Universitätsfrauenklinik Heidelberg
Voßstrasse 7, 69115 Heidelberg (Germany)

[**] The authors thank K.H. Drexhage for the oxazine derivative MR121, and the Volkswagen-Stiftung, the Forschungsschwerpunktprogramm of the Land Baden-Wuerttemberg, and the Bundesministerium für Bildung, Wissenschaft, Forschung und Technologie for financial support.

 © 2002 WILEY-VCH Verlag GmbH & Co. KGaA, Weinheim 0044-8249/02/4124-4769 $ 20.00+.50/0

of the protein chain.[4] Hence, these peptides may be promising systems on which to base the development of a homogeneous fluorescence immunoassay.

The sequences of both peptide epitopes each contain a tryptophan residue. The indole derivative tryptophan is an efficient fluorescence quencher of several environment-sensitive fluorescent dyes, which absorb and emit in the red spectral region. Here we demonstrate that hydrophobic interactions of inherent tryptophan residues in peptide epitopes with fluorescent dyes and protein binding sites enable the design of efficiently quenched peptide-based molecular probes which indicate specific binding to antibodies by a strong increase in fluorescence.

We labeled both immunodominant epitopes of human p53 with a red-absorbing oxazine derivative MR121 (Figure 1 a) at the N-terminal ends of the peptides. Hydrophobic interactions lead to a peptide conformation in which the fluorescence of the oxazine dye is efficiently quenched by the nearby tryptophan residue; the relative fluorescence quantum yields $\Phi_{f,rel}$ are 0.38 (epitope I) and 0.21 (epitope II, Table 1). Shifts in absorption and emission spectra indicate ground- and excited-state interactions between tryptophan and the dye. In combination with time-resolved fluorescence measurements, which show nearly unchanged average decay times (Table 1), these data strongly support the expected static interaction of the dye with tryptophan residues, that is, the formation of non- or only weakly fluorescent charge-transfer complexes. The remaining fluorescence intensity can be explained by a dynamic equilibrium between a folded (quenched) and an open (unquenched) state of the conjugate. Measurements of the tryptophan fluorescence in the labeled peptides provide evidence for the suggested mechanism. The tryptophan residues in both peptides show a strongly reduced fluorescence quantum yield and a considerable blue shift in emission maximum (from 349 to 337 nm) upon dye conjugation (Figure 1 c).

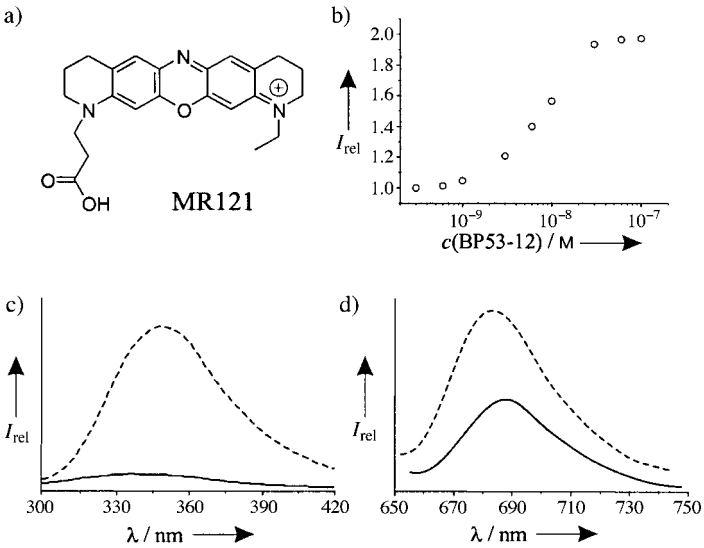


Figure 1. a) Molecular structure of the oxazine dye MR121 labeled to the N-terminal end of both epitopes (epitope I: amino acid residues 15 to 29, MR121-SQETFSDL**W**KLLPEN; epitope II: amino acid residues 46 to 65, MR121-SPDDIEQ**W**FTEDPGPDEAPR). b) Relative fluorescence intensity (I_{rel}) of a 10^{-8} M solution of labeled epitope I in the presence of varying concentrations of the model antibody BP53-12. Measurements were performed in assay buffer. c) I_{rel} of tryptophan in labeled (——) and unlabeled (- - - -) epitope I ($\lambda_{exc} = 290$ nm). d) I_{rel} of the dye in the labeled epitope I in the absence (——) and presence (- - - -) of an 100-fold excess of model antibody BP53-12 ($\lambda_{exc} = 640$ nm). Abbreviations for the amino acid residues are: A: alanine; D: aspartic acid; E: glutamic acid; F: phenylalanine; G: glycine; I: isoleucine; K: lysine; L: leucine; N: asparagine; P: proline; Q: glutamine; R: arginine; S: serine; T: threonine; W: tryptophan.

Table 1. Spectroscopic characteristics of the oxazine derivative MR121 and labeled peptide epitopes.[a]

	λ_{abs} [nm]	λ_{em} [nm]	$\Phi_{f,rel}$	τ_1 [ns]	a_1	τ_2 [ns]	a_2	χ^2
MR121	661	673	1.00	1.85	1.00	–		1.066
MR121-epitope I	666	683	0.38	0.56	0.06	2.11	0.94	1.107
MR121-epitope I + BP53-12	666	680	0.76	1.06	0.06	2.16	0.94	1.105
MR121-epitope II	667	683	0.21	0.51	0.09	2.00	0.91	1.138
MR121-epitope II + PAb 1801	666	679	0.56	0.61	0.09	1.89	0.91	1.085

[a] Measurements were performed in assay buffer (100 mM sodium phosphate, pH 7.7, 0.3 mg mL^{-1} albumin, 0.05 % Tween 20) at room temperature. λ_{abs} and λ_{em} are the absorption and the emission maxima of the measured probes, $\Phi_{f,rel}$ denotes the relative fluorescence quantum yield, and τ_i the fluorescence lifetimes with corresponding amplitudes a_i.

The in vitro binding of the fluorescently labeled epitopes to antibodies was studied by using monoclonal mouse antibodies directed against the N-terminus of human p53. The mouse clones BP53–12,[5] and Pab 1801[6] recognize specifically the residues 20 to 25 of epitope I, and residues 46 to 55 of epitope II, respectively, in the human p53 sequence. As exemplified in Figure 1 d, the addition of an excess of antibody to the labeled epitopes leads to a strong increase in fluorescence intensity (Table 1). The specific recognition process of the antibody induces a conformational change in the peptide-probe and diminishes the tryptophan–dye contact. The suggested mechanism is depicted in Figure 2.

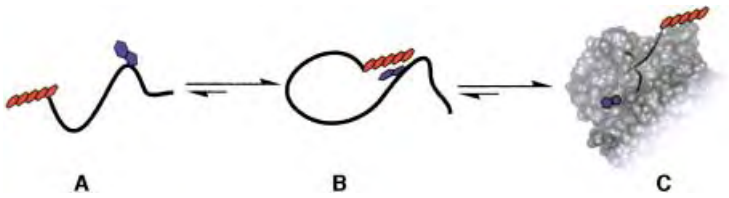


Figure 2. Principle of operation of the peptide-based molecular probes. Driven by the hydrophobic effect the peptide adopts a conformation (**B**) in which the dye interacts with the tryptophan residue. The quenched conformation coexists in an equilibrium with an open, less quenched conformation (**A**). Upon specific binding to the antibody binding site, the peptide adopts a new conformation (**C**), and charge-transfer interactions between tryptophan and the dye are diminished. As a consequence, the fluorescence intensity increases.

Upon addition of the antibody the emission maximum of the dye slightly shifts into the blue, which indicates, in contrast to the tryptophan fluorescence, a more hydrophilic environment of the dye (Table 1). To test the applicability of these peptide-based molecular probes for the quantification of antibodies in homogeneous solution we monitored the fluorescence intensity of 10^{-8} M solutions of the two labeled epitopes in the presence of different antibody concentrations. As depicted for epitope I in Figure 1 b, antibodies can be

 © 2002 WILEY-VCH Verlag GmbH & Co. KGaA, Weinheim 0044-8249/02/4124-4770 $ 20.00+.50/0 *Angew. Chem. Int. Ed.* **2002**, *41*, No. 24

easily detected by the increased fluorescence intensity, down to concentrations as low as a few nanomolar. These data suggest that the epitopes rearrange their conformation upon binding to the model antibody: the tryptophan residue shows strong interactions with the antibody binding pocket accompanied by reduced fluorescence quenching (Figure 2).

To increase detection sensitivity, we implemented confocal fluorescence microscopy. The application of a small excitation/detection volume reduces considerably elastic and inelastic scattering as well as background fluorescence. The use of a detection volume of about 1 fL enables the observation of single molecules in 10^{-9} to 10^{-12} M solutions. Hence, single molecules diffusing through the detection volume can be observed as fluorescence bursts with high signal-to-background ratios.[7] In combination with red, pulsed diode lasers as excitation sources and fluorescent dyes emitting in the far red spectral region, this technique represents a valuable method for measurements in human serum samples.[8] Furthermore, since single-molecule spectroscopy allows one to detect subpopulations even with only slightly changed spectroscopic characteristics it represents the technique of choice for discriminating between bound and free labeled eptitopes through their different fluorescence intensities, that is, burst sizes.[9] Details of the experimental set-up and data analysis are described in reference [10]. Figure 3 shows fluorescence intensity time traces of 5×10^{-11} M solutions of the two labeled epitopes in absence and presence of different concentrations of model antibodies. The quenched epitopes exhibit only small burst sizes with count rates (photon counts s^{-1}) of up to ~20–30 kHz under the applied laser excitation energy of 250 μW (Figure 3a, d). Binding to the antibody induces a conformational change in the peptide chain leading to reduced charge-transfer interactions. Therefore, higher fluorescence burst rates (bursts per time) and burst sizes with count rates of up to 100 kHz are observed (Figure 3b, c, e, f). The slightly smaller number of fluorescence bursts detected from eptiope II (Figure 3e, f) indicates a lower binding affinity to the antibody. To count the number of bursts above a certain threshold we used an automated burst recognition procedure. To suppress bursts of quenched (unbound) epitopes efficiently, only bursts with a count rate of higher than 30 kHz and 20 kHz for epitope I and II, respectively, were used. The starting and end point of a burst were defined by a count rate of 5 kHz. This procedure results in a background burst rate of 0.04 Hz for the two labeled epitopes. Counting of all fluorescence bursts above these threshold levels provides an easy and rapid way to increase the assay sensitivity. Figure 3g shows the binding isotherm obtained from a 5×10^{-11} M solution of epitope I in the presence of different concentrations of the mouse antibody BP53-12. At a background burst rate of 0.04 Hz, an acquisition time of 3 min is sufficient to detect 10^{-11} M model antibody on the basis of a sixfold increased burst rate (0.24 bursts s^{-1}). Under saturation conditions, that is, 10^{-8} M model antibody, the burst rate increases 62.5-fold (2.50 Hz, Figure 3g). The error of the determined burst rates is mainly controlled by the acquisition time. The relative error in the measured burst rates, ν_b, is proportional to $N^{-1/2}$ for N bursts recorded over an infinite time window, that is, for a burst rate of 2.5 Hz calculated from 450 detected bursts in 3 min, the error is negligible. For smaller burst rates, for example, 0.24 Hz, the error is in the range of 15%. Unlike in the single-molecule measurements, the fluorescence intensity increased only approximately twofold in ensemble measurements. The substantially enhanced discrimination between quenched and unquenched peptide epitopes demonstrates the advantage of single-molecule spectroscopy for diagnostic applications.

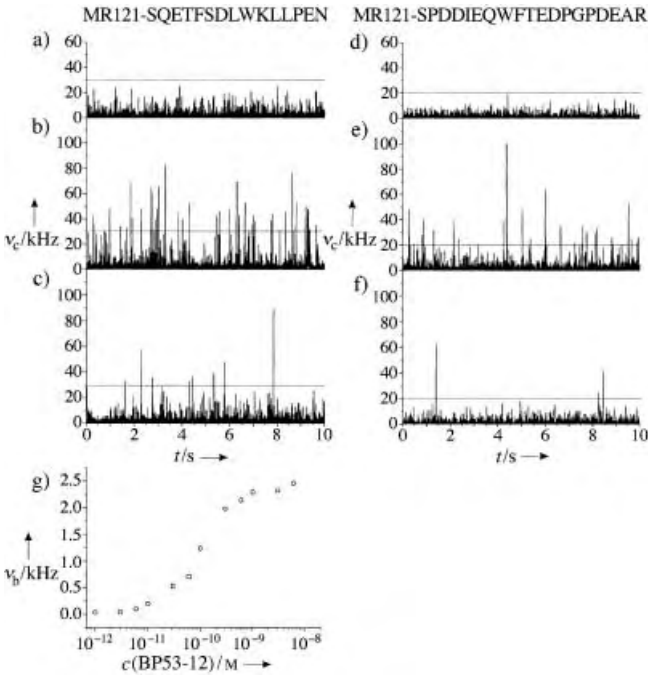


Figure 3. Fluorescence signals (count rate ν_c versus time t) observed from 5×10^{-11} M solutions of epitope I (left side) and epitope II (right side) in assay buffer in the absence (a, d) and presence of 10^{-9} M (b, e) and 10^{-10} M (c, f) concentrations of the model antibodies BP53-12 and PAb 1801. In addition, the threshold levels for burst collection are given. The data were grouped into 1 ms time intervals. Excitation energy at the sample: 250 μW. g) Binding isotherm, that is, number of fluorescence bursts above a threshold of 30 kHz (burst rate, ν_b) obtained from a 5×10^{-11} M solution of epitope I in the presence of different antibody concentrations (BP53-12).

To answer the question whether the developed peptide-based molecular probes can be utilized for early-stage detection and follow-up of malignant diseases directly in human sera, that is, whether the epitopes are recognized by human p53-autoantibodies, we undertook a study with serum samples from tumor patients and healthy donors. As potentially positive probes we tested sera of 40 breast tumor patients. All samples were allowed to equilibrate for one hour at room temperature with a 10^{-11} M solution of both epitopes.

Figure 4a and 4b show the time-dependent fluorescence intensities obtained from a 1:10 and 1:100, respectively, diluted serum sample from a healthy donor; Figures 4c, 4d, and 4e represent the fluorescence traces obtained from one of the positive tested serum samples. While the sera of healthy persons exhibit burst sizes of < 60 kHz for 1:10 dilutions, and < 30 kHz for 1:100 dilutions, the sera of 8 of the 40 breast tumor patients showed considerably higher fluorescence bursts, which can be easily identified among the signals of the free epitopes and the autofluorescence (Figure 4c–e). For serum measurements the threshold level for efficient discrim-

 © 2002 WILEY-VCH Verlag GmbH & Co. KGaA, Weinheim 0044-8249/02/4124-4771 $ 20.00+.50/0

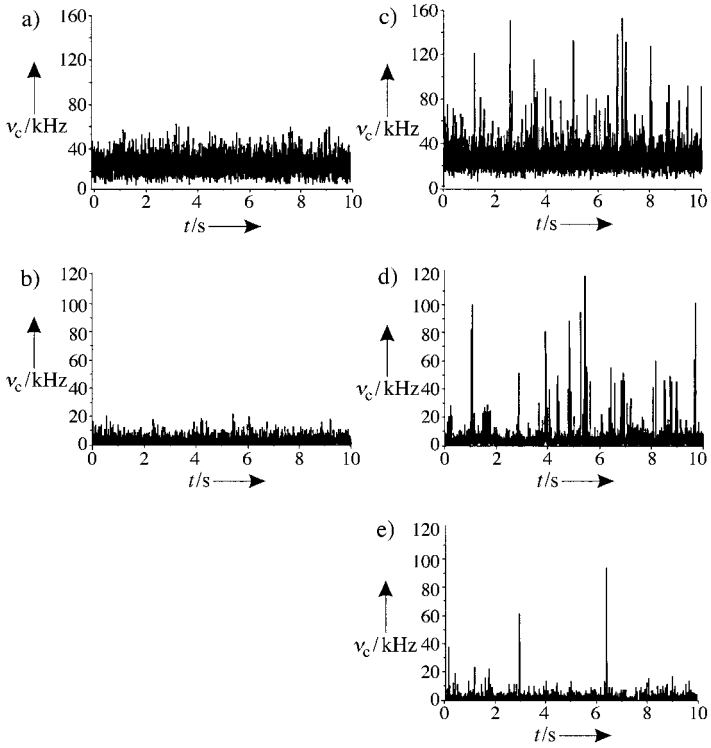


Figure 4. Time-resolved fluorescence intensities observed from a 1:1 mixture of both labeled epitopes (5×10^{-11} M) in diluted human serum samples. a) 1:10 and b) 1:100 dilutions of a serum sample from a healthy donor. c)–e) 1:10, 1:100, and 1:1000 dilutions, respectively, of a serum sample from a breast cancer patient with proven p53 accumulation in the tumor tissue.

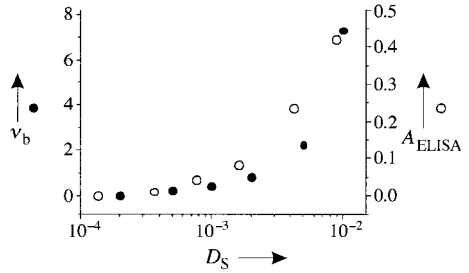


Figure 5. Direct comparison of the sensitivity and dynamic range of the new homogeneous assay (burst rate, ν_b, that is, mean number of bursts per second above a threshold of 30 kHz averaged over 400 s) and the conventional heterogeneous ELISA (relative absorption measurement at 450 nm after enzymatic amplification, A_{ELISA}) measured from the same serum sample at different serum dilutions, D_S. Nonspecific adsorption and subsequent binding of the secondary detector antibodies prevent the use of the ELISA for serum samples diluted less than 100-fold.

ination between positive and negative signals must be adjusted with respect to the autofluorescence intensity, that is, the dilution of the sera. For example, for 1:100 or 1:1000 serum dilutions a threshold level of 30 kHz was used, while 1:10 dilutions require a threshold level of about 60 kHz. Figure 4e demonstrates that, even in the 1:1000 dilution of a positive serum, p53-autoantibodies are unequivocally identified by the measured burst rate of 0.16 Hz. For negative serum samples burst rates of 0.01–0.05 Hz were obtained by using the same burst recognition procedure.

To compare the results with heterogeneous assay formats, we performed ELISA tests with the same samples using recombinant p53 as antigen at similar serum dilutions. As can be seen in Figure 5, the achievable sensitivity and the dynamic range of our new molecular probes and the conventional ELISA test are comparable. Unspecific adsorption of serum proteins at the microtiter plate surface and subsequent binding of secondary detector antibodies complicates the use of the ELISA at serum dilutions lower than 1:100. By contrast, the new homogeneous assay permits measurements also in only slightly diluted serum samples (Figure 4c). As the homogeneous assay requires an incubation time of only one hour it is also considerably faster than the heterogeneous ELISA test which requires several additional time-consuming washing and incubation steps. Furthermore, the synthesis of large quantities of peptide-based molecular probes is uncomplicated and inexpensive compared to the use of recombinant p53. Since more than 90% of p53-autoantibody positive sera of patients with various cancer types react with at least one of the two investigated immunodominant N-terminal epitopes,[4] the presented homogeneous assay might be useful for high-throughput screening of p53-autoantibodies within several minutes. Moreover, by monitoring the time-dependent burst rate, the presented technique permits the direct determination of binding kinetics. Finally, the use of single-molecule spectroscopy offers an elegant method for efficient discrimination between species, which emit different fluorescence intensities. In the experiments described here, we did not focus on the clinical value of the developed assay. Rather the results demonstrate that the use of rationally designed labeled peptide-based molecular probes in homogeneous fluorescence assays and single-molecule detection in the red spectral region can open new avenues for early-stage detection and follow-up of malignant diseases directly in human serum samples.

A study of the specificity of the assay for real clinical p53-autoantibody tests is currently in progress. Unfortunately, a simple comparison of the results obtained with our new assay and conventional ELISA assays is not straightforward. It has been shown that different ELISAs do not always give consistent results for the same serum sample.[11] This problem is probably due to the utilization of different antigens, different cut-off levels, and different surface immobilization and passivation techniques. Our new homogeneous assay raises hope that these problems can be circumvented.

Experimental Section

The N-terminal labeling of the peptides with the fluorescent dye was performed by classical *N*-hydroxysuccinimidyl ester (NHS-ester) chemistry using standard solvents purchased from Merck (Darmstadt, Germany). The oxazine dye MR121 (1 μmol mL^{-1}) and the synthetic peptides (1 μmol mL^{-1}) were dissolved in dimethylformamide (DMF). The dye solution (10 μL, 10 nmol) was added to the peptide (100 μL, 100 nmol; tenfold excess) and diisopropylethylamine (DIPEA; 2 μL). The solution was incubated for 3 h at room temperature in the dark. The N-terminal conjugate was purified by reversed-phase HPLC (Hypersil-ODS column, Knauer, Berlin; HPLC: Agilent Technologies, Waldbronn, Germany) using a linear gradient of 0–75% acetonitrile in 0.1 M aqueous triethylammonium acetate. Reaction yields of the N-terminal products of about 55% were achieved. Purity of the probes was checked by capillary gel electrophoresis. For antibody binding studies and serum measurements, the premixed solutions (assay buffer: 0.1 M sodium phosphate pH 7.7, 0.3 mg mL^{-1} hen

 © 2002 WILEY-VCH Verlag GmbH & Co. KGaA, Weinheim 0044-8249/02/4124-4772 $ 20.00+.50/0 *Angew. Chem. Int. Ed.* **2002**, *41*, No. 24

eggwhite albumin, 0.05 % Tween 20) of antibody or serum and probe were allowed to equilibrate for 1 h at room temperature in the dark. The p53-autoantibody ELISA kit was purchased from Dianova (Hamburg, Germany). Assays of the serum dilutions were performed following exactly the experimental protocol purchased with the kit. Relative fluorescence quantum yields, $\Phi_{f,rel}$, were measured with respect to the fluorescence intensity of the free dye. Ensemble fluorescence lifetimes τ were measured with a standard spectrometer from IBH (model 5000 mC; Glasgow, UK) for time-correlated single-photon counting (TCSPC) using a pulsed diode laser (635 nm) as excitation source (4096 channels à 12.5 ps, 5000 photons in the maximum channel). To exclude polarization effects, fluorescence was observed under the magic angle (54.7°). The decay parameters were determined by least-square deconvolution, and their quality was judged by the reduced χ^2 values, and the randomness of the weighted residuals. In the case that a monoexponential model was not adequate to describe the measured decay, a multiexponential model was used to fit the decay [Eq. (1)]. Here a_i are the pre-exponential factors that describe the ratio of

$$I(t) = I(0) \sum a_i \tau_i \quad (1)$$

the excited species, and τ_i denote their lifetimes. Owing to the limited time resolution strongly quenched populations with decay times shorter than about 50 ps are not revealed.

The set-up for the single-molecule experiments consists essentially of a standard inverse fluorescence microscope equipped with a pulsed diode laser emitting laser pulses at 635 nm (100 ps FWHM) with a repetition rate of 64 MHz, (Picoquant, Berlin, Germany). The collimated laser beam was coupled into an oil-immersion objective (100×, NA 1.4; Nikon, Japan) by a dichroic beam splitter (645DLRP; Omega Optics; Brattleboro, VT, USA). The average laser power was adjusted to be 250 μW at the sample. The fluorescence signal was collected by the same objective, filtered by a band-pass filter (675RDF50; Omega Optics; Brattleboro, VT, USA), and imaged onto a 100-μm pinhole oriented directly in front of an avalanche photodiode (AQR-14; EG&G, Canada). The detector signal was registered by a PC plug-in card (SPC-630; Becker&Hickl, Berlin, Germany). The premixed samples were transferred onto a microscope slide with a small depression and covered by a cover slip.

Received: June 18, 2002
Revised: October 15, 2002 [Z19549]

[1] T. Soussi, *Immunol. Today* **1996**, *17*, 354 – 356.
[2] D. P. Lane, *Nature* **1992**, *358*, 15 – 16.
[3] a) J. M. Nigro, S. J. Baker, A. C. Preisinger, J. M. Jessup, R. Hostetter, K. Cleary, S. H. Bigner, N. Davidson, S. Baylin, P. Devilee, *Nature* **1989**, *342*, 705 – 708; b) M. Hollstein, D. Sidransky, B. Vogelstein, C. C. Harris, *Science* **1991**, *253*, 49 – 53.
[4] R. Lubin, B. Schlichtholz, D. Bengoufa, G. Zalcman, J. Trédaniel, A. Hirsch, C. Caron de Fromentel, C. Preudhomme, P. Fenaux, G. Fournier, P. Mangnin, P. Laurent-Puig, G. Pelletier, M. Schlumberger, F. Desgrandchamps, A. Le Duc, J. P. Peyrat, N. Janin, B. Bressac, T. Soussi, *Cancer Res.* **1993**, *53*, 5872 – 5876.
[5] J. Bartek, J. Bartkova, J. Lukas, Z. Staskova, B. Vojtesek, D. P. Lane, *J. Pathol.* **1993**, *169*, 27 – 34.
[6] L. Banks, G. Matlashewski, L. Crawford, *Eur. J. Biochem.* **1986**, *159*, 529 – 534.
[7] S. Nie, D. T. Chiu, R. N. Zare, *Science* **1994**, *266*, 1018 – 1021.
[8] M. Sauer, C. Zander, R. Mueller, B. Ullrich, K. H. Drexhage, S. Kaul, J. Wolfrum, *Appl. Phys. B* **1997**, *65*, 427 – 431.
[9] S. Weiss, *Science* **1999**, *283*, 1676 – 1683.
[10] M. Sauer, B. Angerer, W. Ankenbauer, Z. Foldes-Papp, F. Goebel, K. T. Han, R. Rigler, A. Schulz, J. Wolfrum, C. Zander, *J. Biotechnol.* **2001**, *86*, 181 – 201.
[11] M. Montenarh, *Dtsch. Med. Wochenschr.* **2000**, 125, 141 – 143.

 © 2002 WILEY-VCH Verlag GmbH & Co. KGaA, Weinheim 0044-8249/02/4124-4773 $ 20.00+.50/0

Long-Distance Magnetic Interaction between a $Mn^{III}Mn^{IV}$ ($S = 1/2$) Core and an Organic Radical: A Spectroscopic Model for the $S_2Y_z^{\bullet}$ State of Photosystem II**

Dana S. Marlin,* Eckhard Bill,*
Thomas Weyhermüller, Eva Rentschler, and
Karl Wieghardt*

The nature of the magnetic interaction between the tyrosine radical $Y_z^{\bullet}$ and the paramagnetic manganese cluster at the reaction center of photosystem II (PSII) has generated a long-standing controversy within the bioinorganic community.[1–3] In PSII, the oxidation of water to molecular oxygen occurs in five discrete steps which have been labeled S_0 through S_4.[4] In the S_2 state, the tetranuclear manganese cluster has an effective spin $S = 1/2$ and exhibits a multiline EPR spectrum that bears resemblance to that from an antiferromagnetic interaction in a $Mn^{III}Mn^{IV}$ dimer.[5–7a] In addition, EPR spectra of the S_2 state feature a second signal at $g = 4.1$ which, under certain conditions, also has an underlying multiline pattern.[7a,b] However, despite extensive studies, the origin of this signal and the induced hyperfine splitting remain unclear.

In PSII samples depleted of Ca^{2+} or Cl^-, the S_2 to S_3 transition is blocked and water oxidation is inhibited.[8] Illumination of these depleted preparations at 273 K results in a state wherein a magnetic interaction between $Y_z^{\bullet}$ and the paramagnetic manganese cluster ($S = 1/2$) is detected. This state is often referred to as $S_2Y_z^{\bullet}$. At the heart of the controversy is the proximity of $Y_z^{\bullet}$ to the manganese cluster in $S_2Y_z^{\bullet}$ as well as the strength and type of coupling between the two spins.[9–14] The significance of the distance is manifested in several proposals for the mechanism of water oxidation that are based on the interplay between these two paramagnets and the possibility of electron transfer between them.[9–15] However, even with the use of powerful magnetic resonance techniques there remains much uncertainty regarding the distance and nature of the interaction between the two $S = 1/2$ centers.[9–14] Proposals for the distance that range from 4.5 Å[16] to 30 Å,[17] and more recently centered around 8 Å,[13,14] attest to the complexity of such an interaction and the difficulties associated with interpretation of spectroscopic data in the absence of concrete model systems.

Indeed, not until the recent monumental crystallographic feat by Zouni et al. and solution of the X-ray structure of PSII (in the S_1 state) at a resolution of 3.8 Å was the location of Y_z verified, and a distance of 7.5 Å measured between Y_z and the Mn cluster.[18] The crystallographic data of the S_1 state, however, only serve to put constraints on the metric parameters between these centers in $S_2Y_z^{\bullet}$, and are not a direct solution to the problem.

Synthetic complexes that model such long-distance Mn_n/organic radical ($n \geq 2$) interactions are lacking in the literature. Such model complexes would not only be useful for detailed analysis of the effect that distance has on the strength of the magnetic coupling, but would also allow a thorough physical description of such interactions wherein dipole coupling may be distinguished from exchange coupling, and subtle rhombicity and Euler angle dependent effects may be observed. Therefore, we have endeavored to synthesize and thoroughly characterize such manganese model complexes wherein weak, long-distance coupling interactions exist, and to provide a detailed description of the electronic structure of these models. Herein we report one such complex, namely $\mathbf{1}(ClO_4)_2$, that possesses a weak interaction between an organic radical ($S = 1/2$) and an antiferromagnetic exchange coupled $Mn^{III}Mn^{IV}$ dimer ($S = 1/2$). A spin-triplet ground state for this complex has been clearly identified, and in addition, the multiline half-field signal (at $g = 4$) that arises from such an interaction, to our knowledge, is shown here for the first time in a dimanganese/organic radical coupled system.

$[(Me_4dtne)Mn^{III}Mn^{IV}(\mu\text{-}O)_2(\mu\text{-}O_2CPhNIT)](ClO_4)_2$ $\mathbf{1}(ClO_4)_2$

Compound $\mathbf{1}(ClO_4)_2$ was synthesized by reacting two equivalents of $Mn(ClO_4)_2$ with Me_4dtne[19] and $HO_2CPhNIT$[20] in acetonitrile. Oxidation of $2\,Mn^{II}$ to $Mn^{III}Mn^{IV}$ was accomplished in air following addition of aqueous NaOH (3 equiv). Addition of excess $NaClO_4$ resulted in separation of microcrystalline $\mathbf{1}(ClO_4)_2$[21] from the reaction mixture. X-ray quality crystals of $\mathbf{1}(ClO_4)_2$[22] were obtained by recrystallization from acetonitrile. A drawing of the structure of dication **1** is displayed in Figure 1a, while selected bond lengths and angles are presented in an expanded view shown in Figure 1b.

Three especially noteworthy characteristics derived from the metric parameters of **1** are as follows: The first is a clear identification of separated Mn^{III} and Mn^{IV} centers illustrated

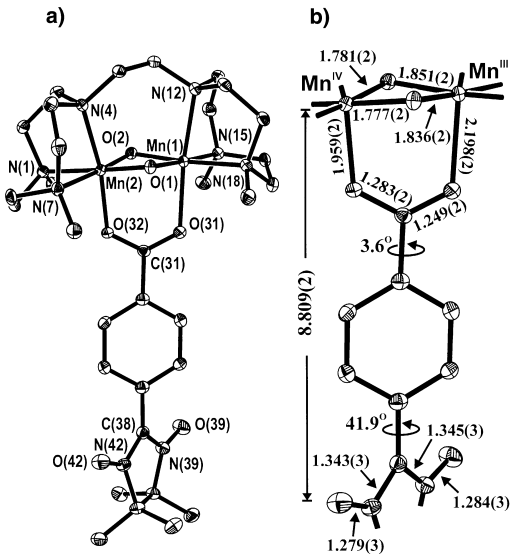


Figure 1. a) X-ray crystal structure of cation **1** (50% thermal ellipsoids). b) Expanded view of a portion of **1** showing selected bond lengths and angles.

[*] Dr. D. S. Marlin, Dr. E. Bill, Prof. Dr. K. Wieghardt,
Dr. T. Weyhermüller, Dr. E. Rentschler
Max-Planck-Institut für Strahlenchemie
Stiftstraße 34-36, 45470 Mülheim an der Ruhr (Germany)
Fax: (+49) 208-306-3952
E-mail: marlin@mpi-muelheim.mpg.de
bill@mpi-muelheim.mpg.de
wieghardt@mpi-muelheim.mpg.de

[**] This work was supported by the Fonds der Chemischen Industrie.

 © 2002 WILEY-VCH Verlag GmbH & Co. KGaA, Weinheim 0044-8249/02/4124-4775 $ 20.00+.50/0

by the difference in bond lengths of the Mn centers to the bridging ligands that form the $Mn^{III}Mn^{IV}$(μ-carboxylato)di(μ-oxo) core. For the Mn^{III} ion these distances are 2.198(2), 1.851(2), and 1.836(2) Å, while for the Mn^{IV} center these bonds contract by approximately 0.1 Å (Figure 1b). The second important characteristic is the equivalence of the two N–O and of the two N–C bond lengths as well as the similar thermal displacement parameters of the nitronyl nitroxide moiety (NIT), indicating that a) the unpaired electron is equivalently present on both O(39) and O(42) atoms of this O-N-C-N-O fragment, and b) no noticeable decomposition of the NIT fragment results from the synthesis.[23] The third characteristic is the asymmetry between the individual Mn centers and the oxygen atoms of the NIT ligand. This results from the different bond lengths in the $Mn^{III}Mn^{IV}$(μ-carboxylato)di(μ-oxo) core noted above, and also the twist of the N(42)-C(38)-N(39) plane of the NIT ligand relative to the O(32)-C(31)-O(31) plane (Figure 1b). Although this latter characteristic is probably a solid-state phenomenon, the asymmetry of the radical relative to the $Mn^{III}Mn^{IV}$ core is also evidenced in solution from EPR spectra of **1** (see below).

The magnetic properties[24] of the three-spin system **1** were explored by multiple-field variable-temperature magnetization measurements on powdered $\mathbf{1}(ClO_4)_2$ (Figure 2). The

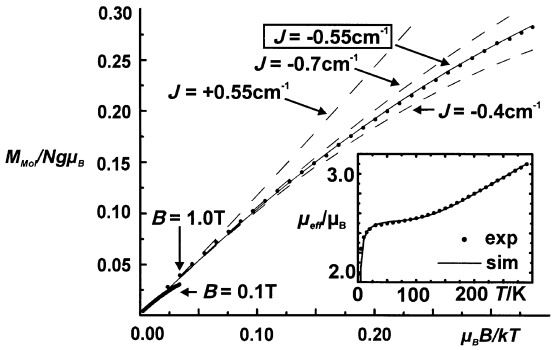


Figure 2. Multiple-field and variable-temperature SQUID magnetic measurements and magnetic moment (inset) measurements on $\mathbf{1}(ClO_4)_2$. Measurement (···) and simulation (——).

overall variation of the magnetic moment of $\mathbf{1}(ClO_4)_2$ with temperature was satisfactorily simulated by using the symmetric spin Hamiltonian [Eq. (1)] with $S_{NIT}=1/2$, $S_{Mn^{III}}=2$, $S_{Mn^{IV}}=3/2$ (Figure 2 inset). Strong antiferromagnetic coupling was found for the manganese ions, $J_{Mn}=-127\ cm^{-1}$, and weak antiferromagnetic coupling for the manganese(III)/organic radical and manganese(IV)/organic radical exchange interaction, $J'=-1(\pm 1)\ cm^{-1}$.

$$H = -2J'\,\mathbf{S}_{NIT}\,(\mathbf{S}_{Mn^{III}}+\mathbf{S}_{Mn^{IV}}) - 2J_{Mn}\,\mathbf{S}_{Mn^{III}}\,\mathbf{S}_{Mn^{IV}} + \sum \mu_B\,\mathbf{S}_i\,\mathbf{g}_i\,\mathbf{B} \qquad (1)$$

Since J_{Mn} is much larger than J' (and $J_{Mn} \gg kT$ at liquid helium temperatures) the spin ground state of **1** can be regarded as a subsystem of two interacting $S=1/2$ species, that is, the radical and the manganese cluster ground state. Correspondingly, the low-temperature behavior ($T<100$ K) of the effective magnetic moment μ_{eff}, closely resembles that of two weakly coupled $S=1/2$ species for which a spin-only value of 2.45 μ_B is expected. Data for **1** level off at about 2.5 μ_B for T between 10–100 K (Figure 2, inset). The rise of μ_{eff} with $T>120$ K indicates increasing population of excited states as shown for similar antiferromagnetic coupled $Mn^{III}Mn^{IV}$ cores.[6] The isoelectronic dimanganese cluster **2** without a NIT pendant arm exhibits strong antiferromagnetic coupling and has an excited spin quartet at $\Delta E = 3J_{Mn} = -360\ cm^{-1}$ above the ground doublet.[6] The radical/cluster interaction renders the ground state of **1** a subsystem of close-lying singlet–triplet states, $|S\rangle$ and $|T\rangle$, with exchange and zero-field splittings (zfs) arising from dipolar and exchange interaction of the NIT radical ($S_{NIT}=1/2$) and the manganese cluster ($S^*=1/2$). The subsystem is properly described by the interaction Hamiltonian [Eq. (2)], where $\boldsymbol{J}_d$ is the matrix of dipolar coupling and J_0 is the exchange coupling constant ($\boldsymbol{I}$ is a unity matrix). The latter leads to a singlet–triplet splitting, $\Delta_{S-T}=2J_0$ (equivalent to J' from Equation (1)). The cluster spin $S^*=1/2$ is a good quantum number for X-band EPR ($h\nu=0.3\ cm^{-1}$) or low-temperature magnetic experiments since the energy gap to other excited total spin manifolds is more than 300 cm^{-1}. The strength of the cluster/NIT exchange interaction was accurately determined from multiple-field magnetization data that were sampled in the range 2–30 K on a $1/T$ scale as shown in Figure 2. A value for J_0 of $-0.55\pm 0.1\ cm^{-1}$ was determined from this model. From single crystal analysis, we presume that this weak exchange coupling arises from *intra-* rather than *intermolecular* coupling. The crystal packing of $\mathbf{1}(ClO_4)_2$ shows that the individual cations of **1** stack in a head-to-tail fashion with the Mn ions sheltered by the Me_4dtne ligands such that there is no close or direct contact between Mn and the NIT oxygen atoms of neighboring molecules. Additionally, the closest intermolecular through-space NIT–NIT distance is approximately 6 Å. Unfortunately, EPR-intensity and Boltzmann depopulation measurements ($1.7\ K<T<15\ K$) designed to probe the singlet–triplet splitting for **1** in frozen solution were obscured by saturation effects even at a low microwave power of 200 nW.

$[(Me_4dtne)Mn^{III}Mn^{IV}(\mu\text{-}O)_2(\mu\text{-}O_2CMe)]^{2+}$ **2**

$$H_{pair} = \mathbf{S}_{NIT}\,(\mathbf{J_d} - 2J_0\,\mathbf{1})\,\mathbf{S}^* \qquad (2)$$

X-band EPR measurements[25] performed on **1** in perpendicular and parallel mode, and also for related complexes **3** and **4** in perpendicular mode are displayed in Figure 3c, d, a and b, respectively.[26] The latter two represent the "parent" species of the spin-pair complex **1**, namely the mixed-valence $Mn^{III}Mn^{IV}$ dimer with its characteristic 16-line pattern (Figure 3a),[6] and the unperturbed NIT signal ($S_{NIT}=1/2$) also with characteristic organic radical hyperfine splittings (Figure 3b).[27] In the latter spectrum the homovalent manganese cluster of **4** is EPR-silent due to strong antiferromagnetic exchange of the Mn^{IV} ions and an effective electron spin $S_{eff}=0$ ground state.[6] The EPR spectrum of **1** in perpendicular mode (Figure 3c) is very different from that of the "parents" due to significant intramolecular interaction described by Equation (2). The dominant feature in the spectrum in Figure 3c is a broad derivative signal at $g=2$

 © 2002 WILEY-VCH Verlag GmbH & Co. KGaA, Weinheim 0044-8249/02/4124-4776 $ 20.00+.50/0 *Angew. Chem. Int. Ed.* **2002**, *41*, No. 24

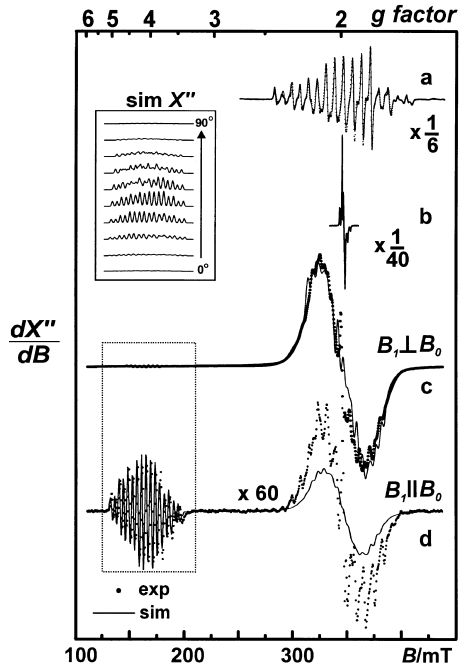


Figure 3. X-band EPR measurements (···) and simulations (——) of **1** (perpendicular (c) and parallel modes (d)), **3** (a) and **4** (d) showing reduction factor of **3** and **4** and magnification of **1** (parallel mode) relative to **1** (perpendicular mode). Experimental conditions for complex: **1**: 1.0 mM CH_3CN glass with 10 mM $tBu_4N{\cdot}PF_6$ at $T = 20$ K and MW power = 636 μW; **3**: 1.0 mM, CH_3CN glass at $T = 30$ K and 200 μW MW power; **4**: 0.1 mM, CH_3CN glass with 10 mM $tBu_4N{\cdot}PF_6$ at $T = 50$ K and 50 μW MW power. Inset shows single-crystal type simulations of the signal at $g = 4$ as a function of θ.

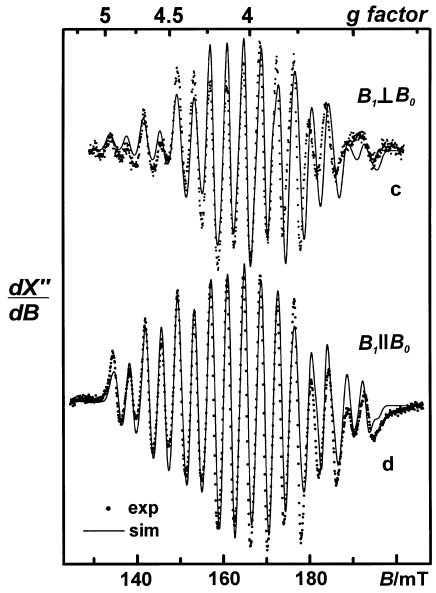


Figure 4. Dual-mode X-band EPR spectra of the $g = 4$ regions for the spectra of **1** shown in Figure 3c (perpendicular mode) and 3d (parallel mode) (boxed area in Figure 3).

featuring less overall splitting than seen for **3** (Figure 3a). However, the most striking aspect of the spectrum of **1** is the presence of a well resolved, multiline signal at $g = 4$ which resembles somewhat the 16-line pattern seen for **3** at $g = 2$. In the parallel mode X-band EPR spectrum of **1** (Figure 3d) the intensity of the "allowed" transitions are greatly attenuated relative to the "forbidden" transitions as a result of the different selection rule $\Delta m = 0$ for $\boldsymbol{B_1} \,||\, \boldsymbol{B_0}$. Figure 4 shows amplified views of the half-field spectra at $g = 4$ of **1** for both perpendicular (Figure 4c) and parallel modes (Figure 4d), wherein the intensity of the transitions clearly indicate significant intramolecular dipolar interaction of the cluster/NIT spin pair.

$[(Me_4dtne)Mn^{III}Mn^{IV}(\mu\text{-}O)_2(\mu\text{-}O_2CPh)]^{2+}$ **3**

$[(Me_4dtne)Mn^{IV}Mn^{IV}(\mu\text{-}O)_2(\mu\text{-}O_2CPhNIT)]^{3+}$ **4**

In our preliminary simulations of the pair spectra of **1** we use an effective spin Hamiltonian for a spin-triplet state [Eq. (3)], where D and E/D parameterize the zfs of the triplet that arise from the anisotropic dipolar part $\boldsymbol{J_d}$ of the J interaction matrix used in Equation (2), and $\boldsymbol{I}$ is the nuclear spin (for Mn^{55}, $I = 5/2$).

$$H = D[S_z^2 - 2/3 + E/D(S_x^2 - S_y^2)] + \mu_B \mathbf{S\,g\,B} + \mathbf{S\,A\,I} \qquad (3)$$

In this approach, singlet–triplet transitions are completely neglected. This approximation is justified by the observation of significant exchange splitting, $\Delta_{S-T} \approx 1\ cm^{-1}$, in solid $\mathbf{1}(ClO_4)_2$. In addition, given that mixing of singlet $|S,0\rangle$ and triplet $|T,0\rangle$ levels by Zeeman and hyperfine interaction may be determined by using terms of the order $\mu_B \Delta g B/(4J_0 + D)$ and $AM_I/2J_0$,[28] we estimate (with $J_0 \approx 0.5\ cm^{-1}$, a maximum $\Delta g = \max(g_{Mn,i} - g_{NIT,j}) \approx 0.01$, and typical A values for **1** of $-100 \times 10^{-4}\ cm^{-1}$) that the singlet–triplet contribution is less than 4%. Therefore, the reasonably good fit of X-band spectra ($\boldsymbol{B}_1 \perp \boldsymbol{B}_0$) substantiate this approach. We emphasize that, in particular, the characteristic "forbidden" transitions at $g = 4$ are not affected by the approximation since they owe their origin to "$\Delta m = 2$" transitions between pure $|T,+1\rangle$ and $|T,-1\rangle$ levels.

A thorough description of the electronic structure of the antiferomagnetically coupled $Mn^{III}Mn^{IV}$ core of the related complex **2** by Schäfer et al. provides an ideal foundation for the present study.[6] In this work, an in-depth magnetic resonance investigation for such complexes is presented, and precise $\boldsymbol{g}$ and ^{55}Mn hyperfine coupling tensors as well as tensor axes related to the molecular structure of the complexes have been deduced. The assigned tensor axes place the z direction perpendicular to the $Mn_2(\mu\text{-}O)_2$ plane, while the x and y axes lay in the direction of the two Mn ions and the two μ-O groups, respectively. Virtually the same parameters are found for **3** from an optimization of the simulation shown in Figure 3a. The simulation parameters found for the NIT radical (Figure 3b) are likewise very close to those of the free organic radical.[27] In our preliminary simulations of the X-band spectra of **1** we chose to neglect Euler rotational effects of the principal axes of local $\boldsymbol{g}$ matrices and $\boldsymbol{J_d}$ for the sake of simplicity.

The actual g values and the components of the ^{55}Mn hyperfine coupling tensors are accurately determined by the pattern of the well-resolved $g = 4$ transitions since these are effectively isolated from the zfs parameters. The inset in Figure 3 shows single-crystal type simulations of those tran-

 © 2002 WILEY-VCH Verlag GmbH & Co. KGaA, Weinheim 0044-8249/02/4124-4777 $ 20.00+.50/0

Table 1. The principal values of the g and Mn^{III} and Mn^{IV} hyperfine tensors (A^{III} and A^{IV} respectively) for complexes **1** and **2**.

Complex	g	A^{III} [$\times 10^{-4}$ cm^{-1}]	A^{IV} [$\times 10^{-4}$ cm^{-1}]	g_{iso}	A^{III}_{iso} [$\times 10^{-4}$ cm^{-1}]	A^{IV}_{iso} [$\times 10^{-4}$ cm^{-1}]	Ref.
	x 2.012	−148.1	62.3				
1	y 2.004	−146.8	80.4	2.001	−130.2	71.9	this
	z 1.986	−95.8	73.1				work
	x 1.996	−159.9	64.0				
2	y 2.001	−142.4	74.3	1.993	−135.1	69.9	6
	z 1.983	−103.0	71.5				

sitions (in absorption mode) as a function of the polar angle θ of the magnetic field with the z axis. Their major intensities arise from orientations intermediate between the principal axes. This demonstrates the sensitivity of the simulations for the different spatial components of the g and A matrices. On the other hand, the shape of the allowed transitions at $g = 2$ depend largely on D and E/D, which contribute to the overall width of the spectrum and its intensity distribution, respectively.

The relative intensity of the *half-field transitions*, however, also depends critically on the zfs of the triplet and hence heavily constrains these parameters, particularly the value of D. Accurate values of g and A^{III} and A^{IV} tensors for **1** are obtained from the simulation of the $g = 4$ transitions (Figure 4). The $g = 2$ region in the parallel mode is more complicated due to 1) the attenuation of the $\Delta m = 1$ transitions, and 2) the influence of $|S\rangle$ and $|T\rangle$ mixing. Therefore, a more accurate measure of zfs was obtained from simulation of the $g = 2$ region in perpendicular mode (Figure 3c). The g and A^{III} and A^{IV} tensors for **1** and **2** are listed in Table 1. Deviations between g values obtained here and those reported for **2** are small.[6] Values of $D = -90 \times 10^{-4}$ cm^{-1} and $E/D = 0.30$ were obtained for the zfs of **1**.

Since D owes its origin to the dipole interaction between the radical and manganese cluster, its value is a measure of the "mean" separation of the two spin density distributions given by $D = -3/2\, g^2 \mu_B^2 r^{-3}$ for $E/D = 1/3$ (where $\mu_B^2 = 0.433$ for D in cm^{-1} and r in Å).[29a–c] The value for D of -90×10^{-4} cm^{-1} obtained by simulation yields a corresponding distance between the radical and the cluster of 6.6 Å. The deviation of this value from the shortest molecular distance between the NIT radical and Mn center (8.809(2) Å) is astonishing, especially in the view of application of EPR spectroscopy to gauge distances in other unknown molecules.[12–14,16,17] We attribute the difference to delocalization of spin density and the r^{-3} dependence of the interaction which weight the edges of the respective magnetic orbitals rather than their centers. The average distance from the N–O groups of the NIT moiety to the O atoms of the carboxylate bridge is 7.0 Å and thus noteworthy in this context as it approximates the calculated coupling distance better.

It is important to consider the significance of a large rhombicity parameter, $E/D \approx 0.3$, as simulations with small E/D values for the triplet spectra do not show the appropriate central intensity maxima at $g = 2$.[28] Point-dipoles are unable to induce rhombic zfs of the triplet state due to the intrinsic symmetry between two points. From preliminary dipole-dipole simulations based on Equation (2) with axial ($J_d - 2J_0 \mathbf{1}$) matrix (not shown) we discard Euler rotations of the dipolar arrangement as an alternative explanation of the experimental feature, as it is not equivalent to a rhombic J matrix. Therefore, we attribute the observed rhombicity to the extended nonaxial spatial distribution of the respective spin density on the radical as well as on the manganese cluster moiety.

In conclusion, we have shown that in a relatively simple model for long-distance dimanganese/organic radical exchange interactions, an excellent tool for understanding similar interactions in more complicated systems is found. We demonstrate the efficacy of dual-mode EPR spectroscopy as an additional tool for determining the extent of these long-distance dipolar coupling interactions. We also note that our "simple" system has several complicating features such as asymmetry in the coupling interaction as well as possible contributions to the EPR spectra from singlet–triplet transitions, which have not been addressed here. These more rigorous studies are currently underway in our laboratory with this and related molecular model systems. We also seek to uncover whether there exists a relationship or parallel between our half-field signal at $g = 4$ (with its multiline pattern) and that observed in the S_2 state of PSII.[7a,b]

Received: September 19, 2002 [Z50202]

[1] A.-F. Miller, G. W. Brudwig, *Biochim. Biophys. Acta* **1991**, *1056*, 1.
[2] J. Stubbe, W. A. van der Donk, *Chem. Rev.* **1998**, *98*, 705.
[3] V. K. Yachandra, K. Sauer, M. P. Klein, *Chem. Rev.* **1996**, *96*, 2927.
[4] B. Kok, B. Forbush, M. McGloin, *Photochem. Photobiol.* **1970**, *11*, 457.
[5] G. C. Dismukes, Y. Siderer, *Proc. Natl. Acad. Sci. USA* **1981**, *78*, 274.
[6] K.-O. Schäfer, R. Bittl, W. Zweygart, F. Lendzian, G. Haselhorst, T. Weyhermüller, K. Wieghardt, W. Lubitz, *J. Am. Chem. Soc.***1998**, *120*, 13104.
[7] a) J. M. Peloquin, K. A. Campbell, D. W. Randall, M. A. Evanchik, V. L. Pecoraro, W. H. Armstrong, R. D. Britt, *J. Am. Chem. Soc.* **2000**, *122*, 10926; b) D. H. Kim, R. D. Britt, M. P. Klein, K. Sauer, *J. Am. Chem. Soc.* **1990**, *112*, 9389.
[8] R. J. Debus, *Biochim. Biophys. Acta* **1992**, *1102*, 269.
[9] P. Dorlet, A. Bossac, W. Rutherford, S. Un, *J. Phys. Chem. B* **1998**, *102*, 10945.
[10] V. A. Szalai, H. Kühne, K. V. Lakshmi, G. W. Brudvig, *Biochemistry* **1998**, *37*, 13594.
[11] W. Lubitz, F. Lendzian, R. Bittl, *Acc. Chem. Res.* **2002**, *35*, 313.
[12] M. L. Gilchrist, Jr., J. A. Ball, D. W. Randall, R. D. Britt, *Proc. Natl. Acad. Sci. USA* **1995**, *92*, 9545.
[13] P. Dorlet, M. Di Valentin, G. T. Babcock, J. L. McCracken, *J. Phys. Chem. B* **1998**, *102*, 8239.
[14] K. V. Lakshmi, S. S. Eaton, G. R. Eaton, G. W. Brudvig, *Biochemistry* **1999**, *38*, 12758.
[15] C. W. Hoganson, G. T. Babcock, *Science* **1997**, *277*, 1953.
[16] X.-S. Tang, D. W. Randall, D. A. Force, B. A. Diner, R. D. Britt, *J. Am. Chem. Soc.* **1996**, *118*, 7638.
[17] Y. Kodera, S. A. Dzuba, H. Hara, A. Kawamori, *Biochim. Biophys. Acta* **1994**, *1186*, 91.

 © 2002 WILEY-VCH Verlag GmbH & Co. KGaA, Weinheim 0044-8249/02/4124-4778 $ 20.00+.50/0

[18] A. Zouni, H.-T. Witt, J. Kern, P. Fromme, N. Krauß, W. Saenger, P. Orth, *Nature* **2001**, *409*, 739.
[19] Me_4dtne = 1,2-bis(4,7-dimethyl-1,4,7-triazacyclonon-1-yl)ethane was synthesized according to reference [6].
[20] HO_2CPhNIT = 2-(4-carboxyphenyl)-4,4,5,5-tetramethyl-3-oxyimidazolidin-1-oxide was prepared according to: C. Bätz, P. Amann, H.-J. Deiseroth, L. Dulog, *Liebigs Ann. Chem.* **1994**, 739.
[21] Selected IR stretching frequencies: $\tilde{\nu} = 1584$(m), 1543(m), 1455(m), 1375(s), 1105(s, ClO_4^-), 780(m), 689(m), 624 cm^{-1} (m). EI mass spectra show two molecular ion peaks at m/z 379 for $[\mathbf{1}]^{2+}$ and 857 for $[\mathbf{1}(ClO_4)]^+$. Elemental analyses (%) calcd for $C_{32}H_{56}Cl_2Mn_2N_8O_{14}$: C 40.13, H 5.86, N 11.71; found: C 38.80, H 5.77, N 11.71.
[22] Crystal structure analysis data for $\mathbf{1}(ClO_4)_2$: $C_{32}H_{56}Cl_2Mn_2N_8O_{14}$, $M_r = 957.63$, monoclinic, $P2_1/c$, $a = 11.6313(4)$, $b = 21.4815(10)$, $c = 16.9454(6)$ Å, $\beta = 108.17(1)°$, $V = 4022.8(3)$ Å^3, $Z = 4$, $\rho_{calcd} = 1.581$ Mg m^{-3}, $\mu(Mo_{K\alpha}) = 0.836$ mm^{-1}, $F(000) = 2000$; 56074 reflections collected at 100(2) K; 9213 independent reflections; GOF = 1.079; $R = 0.0448$, $wR2 = 0.0827$. CCDC-192780 contains the supplementary crystallographic data for this paper. These data can be obtained free of charge via www.ccdc.cam.ac.uk/conts/retrieving.html (or from the Cambridge Crystallographic Data Centre, 12, Union Road, Cambridge CB2 1EZ, UK; fax: (+44) 1223-336-033; or deposit @ccdc.cam.ac.uk).
[23] Early synthetic attempts at **1** and variants under less mild conditions resulted in complexes wherein decomposition of the NIT moiety took place yielding the imidazolidin-1-oxide radical product, which was evident from inequivalent thermal parameters of O(42) and O(39).
[24] Magnetization of solid $\mathbf{1}(ClO_4)_2$ was measured by using a SQUID magnetometer (MPMS-7, Quantum Design). The molar susceptibilities were corrected for underlying diamagnetism by using tabulated Pascal constants ($X_{dia} = -400 \times 10^{-6}$ cm^3 mol^{-1}). The routine JULIUS was used for spin Hamiltonian simulations of the data (C. Krebs, E. Bill, F. Birkelbach, V. Staemmler, unpublished results).
[25] EPR spectra were measured for solutions of **1**–**3** in acetonitrile with a Bruker ELEXSYS E300 spectrometer with standard or dual-mode cavity and Oxford Instruments ESR910 flow cryostat. Spin-Hamiltonian simulations were performed with the XSOPHE program by G. Hanson et al. that is distributed by Bruker Biospin GmbH.
[26] The latter two complexes are components of an extended and detailed investigation that will be reported in the future. We include only their X-band EPR spectra here for clarity. For **1** in acetonitrile a small degree of dissociation of the bridging carboxylato ligand O_2CPhNIT$^-$ from the mother complex $[(Me_4dtne)Mn_2(\mu\text{-}O)_2]^{3+}$ is observed. The "impurity" spectra are similar to those in Figure 3a and b and may be easily subtracted from that of intact **1** (shown in Figure 3c). The amount subtracted, integrated to less than 1% by area.
[27] E. Ullman, J. H. Osiecki, D. G. B. Boocock, R. Darcy, *J. Am. Chem. Soc.* **1972**, *94*, 7049.
[28] a) J. E. Wertz, J. R. Bolton, *Electron Spin Resonance*, McGraw-Hill, New York, **1972**; b) P. J. Hore in *Advanced EPR: Applications in Biology and Biochemistry* (Ed.: A. J. Hoff), Elsevier, Amsterdam, **1977**, pp. 405–440.
[29] a) N. M. Atherton, C. J. Winscom, *Inorg. Chem.* **1973**, *12*, 383; b) T. D. Smith, J. R. Pilbrow, *Coord. Chem. Rev.* **1974**, *13*, 173; c) A. Bencini, D. Gatteschi, *EPR of Exchange Coupled Systems*, Springer, Berlin, **1990**.

Real-Time Single-Molecule Imaging of the Formation and Dynamics of Coordination Compounds

Nian Lin,* Alexandre Dmitriev, Jens Weckesser, Johannes V. Barth,* and Klaus Kern*

A current challenge in the field of self-assembled supramolecular nanostructures is the development of strategies for the deliberate positioning of functional molecular species on suitable substrates; this is a crucial aspect in the search for molecular devices.[1] Recent studies revealed that design principles from supramolecular chemistry can be adapted to fabricate unique supramolecular aggregates at surfaces.[2,3] However, to date, mainly hydrogen bonding and electrostatic intermolecular coupling have been successfully exploited to control the ordering of molecular building blocks at low temperatures. These interactions bear the disadvantage of low thermal and mechanical stability. Thus, there is a demand to explore the construction of more rigid supramolecular architectures[4,5] on surfaces. Metal–ligand interactions, which were introduced by Werner at the turn of the 20th century,[6] are recognized as being decisive in molecular recognition and an excellent means for the fabrication of three-dimensional supramolecular arrangements.[7–9] However, the current understanding of the evolution and dynamics of such interactions on surfaces is limited, although their energetics are in a range which lets us expect reaction rates that would permit their direct elucidation at ambient temperature by imaging methods.

For the present investigation conducted on an atomically clean surface we took advantage of ligand systems based on carboxylic acids and transition metals whose characteristics are well understood.[10] Specifically, we addressed metal–ligand bonding of trimesic acid (tma) and Cu atoms. Trimesic acid is a polyfunctional carboxylic acid with threefold symmetry comprised of a phenyl ring and three identical carboxy end groups in the same plane.[11] Its complexation was observed on Cu(100) in ultrahigh vacuum at temperatures in the range 250–300 K following deposition at room temperature. Under these conditions, the carboxylic acid groups are completely deprotonated such that three reactive COO^- ligands per tma molecule exist.[12,13] The deprotonation is presumably related to the availability of Cu adatoms at the surface, which are known to exist on Cu(100) in the employed temperature range. The reason behind the presence of Cu adatoms is their continuous evaporation from atomic step

[*] N. Lin, K. Kern, A. Dmitriev, J. Weckesser
Max-Planck-Institut für Festkörperforschung
Heisenbergstrasse 1, 70569 Stuttgart (Germany)
Fax: (+49) 711–689–1662
E-mail: n.lin@fkf.mpg.de
k.kern@fkf.mpg.de
J. V. Barth, K. Kern
Institut de Physique des Nanostructures
Ecole Polytechnique Fédérale de Lausanne
1015 Lausanne (Switzerland)
E-mail: Johannes.Barth@epfl.ch

Supporting information for this article is available on the WWW under http://www.angewandte.org or from the author.

 © 2002 WILEY-VCH Verlag GmbH & Co. KGaA, Weinheim 0044-8249/02/4124-4779 $ 20.00+.50/0

edges, which accounts for the presence of a two-dimensional lattice gas at the surface. This process can be understood by analogy to the coexistence of gas and condensed phases in bulk systems described by the vapor pressure of a substance. Individual Cu adatoms cannot be resolved in STM images because of their high surface mobility at room temperature.

At appreciable coverages individual molecules appear as equilateral triangles in STM images (Figure 1 a), which reflects a flat-lying geometry where the molecule is bound

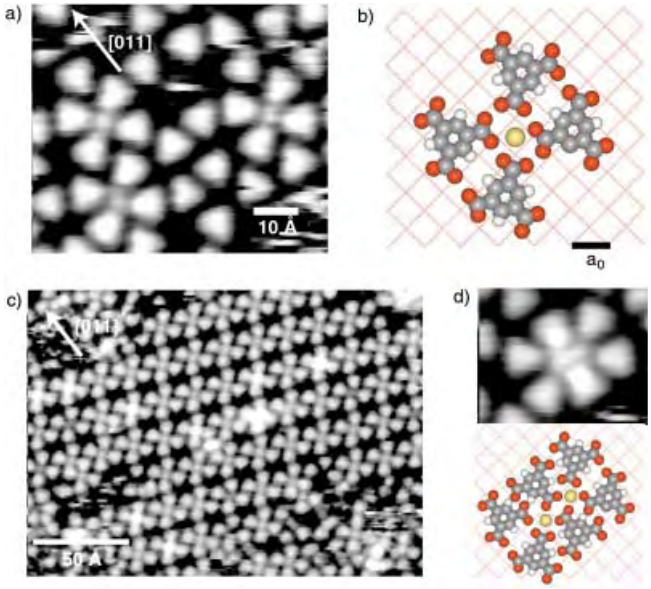


Figure 1. a) STM topograph of trimesic acid adsorbed on a Cu(100) surface at 300 K. The triangular shape reflects a flat-lying adsorption geometry. Cloverleaf-shaped arrangements of four tma molecules with a central protrusion represent $[Cu(tma)_4]^{n-}$ coordination compunds. b) Model for the $[Cu(tma)_4]^{n-}$ configuration with a central Cu atom coordinated by four carboxylate ligands, where carbon atoms are in gray, oxygen atoms in red, hydrogen atoms in white, and Cu adatoms in yellow; the Cu substrate is depicted by the orange lattice, where $a_0 = 3.61$ Å. In agreement with the tunneling data the tma triangles do not point straight to the central site, which indicates a unidentate coordination of the Cu adatom. c) Regular array of $[Cu(tma)_4]^{n-}$ complexes. d) STM image and model of the $[Cu_2(tma)_6]^{n-}$ coordination compound with four unidentate and two *syn*,*syn* coordination bonds.

with its phenyl ring parallel to the substrate. The symmetry and characteristic side length of approximately 8 Å agrees well with the shape and dimensions of tma.[12] Four distinct orientations with respect to the substrate lattice were found with one of the triangle's corners always pointing along a high-symmetry direction, [011] or [$\bar{0}$11], of the Cu(100) surface. This situation is understood to be a consequence of the occupation of high-symmetry hollow sites at the atomic lattice of the substrate. The data reveal, moreover, that the molecules tend to be arranged in a complementary manner, that is, neighboring tma molecules are oriented antiparallel, and, as such, the close packing at the surface can be explained as a consequence of the space-filling principle. However, this rule is not generally obeyed and arrangements occur where four tma molecules form a cloverleaf structure with a bright protrusion at the center. The formation of the cloverleaf structure is directly related to the density of the Cu adatom lattice gas.[14] This configuration is associated with a central Cu adatom which is coordinated by the carboxylate ligands from the four surrounding molecules and is hence designated $[Cu(tma)_4]^{n-}$.

A close inspection of the STM image in Figure 1 a reveals that the carboxylate ligands of tma do not point straight towards the central protrusion in the compound. This observation demonstrates that the oxygen atoms in the respective COO^- moieties are not equivalent, which indicates a unidentate coordination of the Cu atom as illustrated by the model in Figure 1 b. If it is assumed that the tma molecule is in an unrelaxed geometry, the Cu···O distance is estimated to be 3 Å, which is substantially larger than the characteristic Cu···O distance of approximately 2 Å encountered in three-dimensional copper carboxylates.[10] This Cu···O relaxation distance is attributed to the role of the atomic lattice of the substrate, which energetically favors high-symmetry adsorption sites. Moreover, the nature of the coordination bond itself is expected to be modified in the presence of the electrons from the Cu conduction band. Similar effects were encountered in hydrogen-bonded assemblies.[3,15] Finally, the STM topograph shown in Figure 1 c demonstrates that a regular array of $[Cu(tma)_4]^{n-}$ cloverleafs can be obtained.

The square shape of the $[Cu(tma)_4]^{n-}$ configuration with its fourfold coordination is characteristic of Cu^{II} complexes.[16,17] Thus, the cloverleaf arrangement should be considered formally as a $[Cu^{II}(tma)_4]^{10-}$ ion. However, it is important to note that the charge on both the Cu adatoms and the adsorbed tma molecules is strongly affected by the presence of the electrons of the metal surface, which effectively screen any charged adsorbate. A deprotonated tma molecule at the surface should thus not be considered as a $(tma_{ad})^{3-}$ ion, but rather as a neutral tma/Cu(001) complex. As an important consequence, the oxidation state of the central Cu atoms in the $[Cu(tma)_4]^{n-}$ configuration cannot be determined unambiguously. This contrasts the situation encountered with isolated compounds in three dimensions, where the charge is usually balanced by counterions.

Extended one-dimensional or two-dimensional networks, where more than one carboxylate ligand per tma molecule participates in the formation of coordination bonds, were not formed. This is again associated with the influence of the atomic lattice of the substrate, which pins the reactive species in a certain position and orientation to the surface. However, a second compound could be identified close to saturation of the tma monolayer, where two Cu atoms are bound by six tma molecules. An analysis of the corresponding STM data (Figure 1 d) reveals that with this $[Cu_2(tma)_6]^{m-}$ configuration four unidentate and two *syn*,*syn* coordination bonds are present.

The mechanism for the formation of the $[Cu(tma)_4]^{n-}$ compounds could be directly followed by STM measurements at room temperature.[18] The formation of single chemical bonds has been shown before; however, in these studies the bonding was typically induced by manipulating the reactants with the tip of a scanning tunneling microscope at very low temperatures.[19,20] In striking contrast, the reaction proceeds under equilibrium conditions in the present observations. As a consequence, the natural path of a multicomponent chemical

 © 2002 WILEY-VCH Verlag GmbH & Co. KGaA, Weinheim 0044-8249/02/4124-4780 $ 20.00+.50/0

reaction could be characterized: The thermal rotations of single tma molecules at appreciable coverages can be monitored, since surface diffusion is restricted by space limitations. This situation is illustrated by the sequence of images shown in Figure 2, which were taken over a time

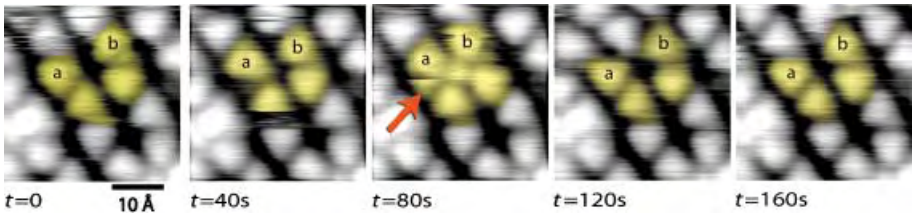


Figure 2. Molecular rotors working as dynamical atom trap: Sequence of STM images revealing the molecular mobility during the association and dissociation of a $[Cu(tma)_4]^{n-}$ cloverleaf over a 160-second time interval. The four tma molecules invloved in the complex formation are artificially highlighted by color. After rotational motions and displacements of tma molecules ($t = 40$ s), a Cu adatom is captured and the coordination compound is formed ($t = 80$ s). A tma molecule which rotated while the image was recorded is marked by an arrow. The coordination bond is subsequently disrupted and the Cu atom disappears again ($t = 120$ s).

interval of 160 s. In the initial frame, the tma molecules marked **a** and **b** change their orientation and position, thus revealing rotation and hopping of single molecules. The characteristic spikes along the scanning direction are caused by motions of the tma molecules occuring while the data were recorded; for example, molecule **a** has switched its orientation from pointing upwards to pointing downwards in the image taken after 80 s (marked by the arrow). Both **a** and **b** are aligned antiparallel with respect to their neighbors at $t = 0$ so as to achieve close packing. Neither of them was in a correct position or orientation for formation of the cloverleaf arrangement. In the second (40 s) and third frames (80 s), **a** and **b** switched orientations, respectively, and the cloverleaf configuration with a central protrusion evolved. This effect is understood to be a result of the capturing of a copper atom diffusing on the surface and the formation of coordinative bonds with the carboxylate ligands of the tma molecules, that is, an association reaction leading to a $[Cu(tma)_4]^{n-}$ complex took place. The Cu atom can exclusively be resolved when it is held by four carboxylate ligands, otherwise its high surface mobility makes STM imaging impossible. The subsequent frame ($t = 120$ s) reveals that the dissociation reaction readily takes place under the same conditions, which indicates that thermal motions or collisions with other molecules are sufficent to disrupt the metal–ligand bond. These observations reveal that molecular rotors (namely, the spinning tma molecules) with functional end groups can operate as a dynamical trap for diffusing Cu adatoms. The formation of the complex is only feasible when four tma molecules switch to the appropriate mutual orientation and snatch a Cu atom passing by at the crucial moment. In marked contrast to $[Cu(tma)_4]^{n-}$, the $[Cu_2(tma)_6]^{n-}$ species was found to be stable under the employed conditions.

Quantitative information on the lifetime and formation of the compounds was obtained from measurements made at low concentrations, where both Cu adatoms and individual tma molecules are highly mobile on the surface. Accordingly, no isolated species can be observed. However, as demonstrated by the STM image in Figure 3, single or small groups of compounds can be readily resolved. That is, the $[Cu(tma)_4]^{n-}$ configuration is stationary and can be imaged until it eventually dissociates.[21] The lifetime of the cloverleaf arrangements depends strongly on the local environment. For example, the average lifetime with two neighboring compounds (ellipse in Figure 3) is typically more than three times longer than that of an isolated species (circle in Figure 3). This observation suggests the two species have different reactivity, that is, two neighboring species are more stable than isolated ones. Since both measurements were made simultaneously at the same temperature this must be associated with steric effects. As indicated in Figure 3 (tma molecules are marked by arrows), the movement of adjacent molecules in neighboring complexes is impeded so that they experience

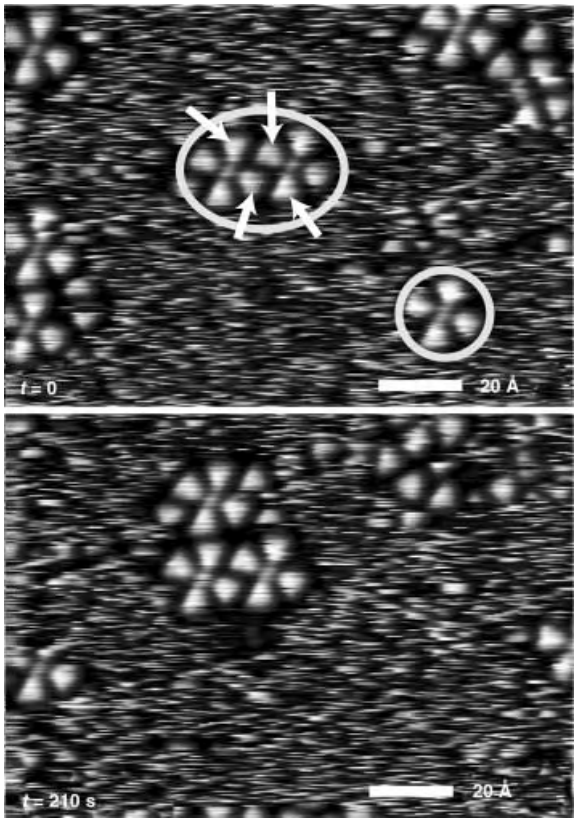


Figure 3. Observation of both isolated and small aggregates of $[Cu(tma)_4]^{n-}$ complexes for low coverages at room temperature. Freely transporting and spinning tma molecules coexist on the surface with copper adatoms, which were not imaged by STM. The characteristic spikes along the scanning direction were caused by those moving tma molecules, while the dark shadows surrounding the stationary $[Cu(tma)_4]$ compounds are areas where free molecules are not present. The lifetime of the isolated compounds (marked by a circle) was determined by sequential imaging of the same area. Aggregates of several compounds such as that marked by the ellipse have increased lifetime because of the hindered motion of neighboring molecules (marked by arrows).

 © 2002 WILEY-VCH Verlag GmbH & Co. KGaA, Weinheim 0044-8249/02/4124-4781 $ 20.00+.50/0

higher energy barriers for rotation or migration. This hindering effect thus indirectly reduces the probability of dissociation. Similarly increased lifetimes were observed for compounds at step edges, where the steps act as the hinderance. In the extreme case a $[Cu(tma)_4]^{n-}$ compound in a regular array (as shown in Figure 1 c) has never been observed to dissociate during our measurements, that is, over 5 h. Lifetimes of the $[Cu(tma)_4]^{n-}$ complexes at room temperature in different environments are compiled in Table 1.

Table 1. Average lifetime of $[Cu(tma)_4]^{n-}$ complexes in different local chemical environments at 300 K.

	Isolated on terrace	At step edge	Two neighboring	Saturated layer
lifetime [s]	34 ± 5	87 ± 5	120 ± 5	> 18000

The average lifetime of an isolated cloverleaf was determined from an analysis of STM sequences with 100 frames recorded at room temperature with high scanning velocities (9 s per frame) to be 34 ± 5 s. The inverse of this value corresponds to the mean dissociation rate. In a similar way, dissociation rates at reduced temperatures have been determined; the entire result is plotted in the Arrhenius representation in Figure 4. The data points fall on a straight line whose

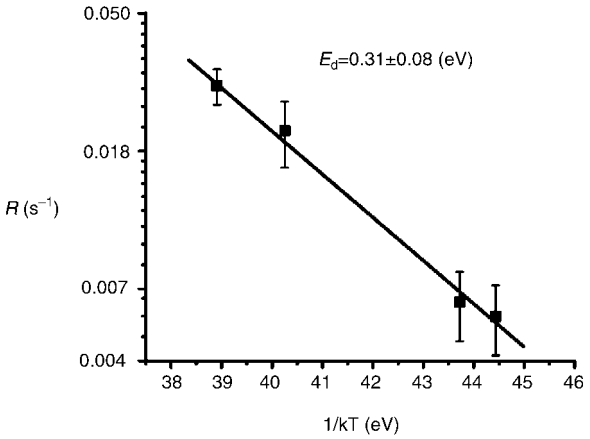


Figure 4. Arrhenius representation of the dissociation rate (R) for isolated $[Cu(tma)_4]^{n-}$ compounds derived from analysis of STM data for low coverages at temperatures in the range 260–300 K. The corresponding energy barrier is determined to be $E_d = 0.31 \pm 0.08$ eV.

slope corresponds to the energy barrier for dissociation of the coordination compound (E_d). The linear fit of the data yields $E_d = 0.31 \pm 0.08$ eV. With the present system, the determined energy value is a combination of the contributions associated with the formation of coordination bonds and the repositioning of the involved elements (note that the value of the present energy barrier is smaller than the binding energy of related coordination compounds in the gas phase. The higher stability of the $[Cu_2(tma)_6]^{n-}$ configuration is understood to be a consequence of the increased number of coordination bonds involved and possibly an increased barrier for molecular rotations in this more densely packed arrangement (steric hinderance).

Our results show that single-molecule investigations can provide comprehensive insight into the evolution of coordination compounds, where several reacting species are involved. In view of the rich potential and wide application of metal–ligand interactions, it is suggested that such insight will be valuable in the future search for nanoscale elements on templates. More generally speaking, the observations reveal that the natural path of a multicomponent chemical reaction can be directly characterized and the corresponding energetics can be quantified.

Experimental Section

The sample preparation and characterization have been conducted in an ultrahigh vacuum (UHV) environment that provides well-defined conditions for the experiment. The UHV system (base pressure about 3×10^{-10} mbar) is equipped with a home-built variable-temperature UHV-STM described elsewhere (operational in the range of 40–800 K), as well as standard facilities for sample preparation and a quadrupole mass spectrometry analysis (QMS). The Cu(100) surface was cleaned by repeated cycles of Ar^+ sputtering and subsequent annealing (500 eV, 6 μA, 800 K), which allowed atomically flat terraces of up to 200 nm width separated by monatomic steps to be obtained. The STM experiments were performed in the constant current mode, with maximum bias voltages up to 2 V. Data were obtained starting in the temperature range 180–300 K. Commercially available tma (Fluka Chemie AG) in powder form was deposited by organic molecular beam epitaxy from a Knudsen-cell-type evaporator. The temperature of the cell was held constant at 460 K during the evaporation.

Received: September 9, 2002 [Z50127]

[1] a) J. K. Gimzewski, C. Joachim, *Science* **1999**, *283*, 1683 – 1688; b) C. Joachim, J. K. Gimzewski, A. Aviram, *Nature* **2000**, *408*, 541 – 548.
[2] a) M. Böhringer, K. Morgenstern, W. D. Schneider, R. Berndt, F. Mauri, A. De Vita, R. Car, *Phys. Rev. Lett.* **1999**, *83*, 324 – 327; b) M. Furukawa, H. Tanaka, K. Sugiara, Y. Sakata, T. Kawai, *Surf. Sci.* **2000**, *445*, L58 – L63; c) T. Yokoyama, S. Yokoyama, T. Kamikado, Y. Okuno, S. Mashiko, *Nature* **2001**, *413*, 619 – 621.
[3] J. V. Barth, J. Weckesser, C. Cai, P. Gunter, L. Burgi, O. Jeandupeux, K. Kern, *Angew. Chem.* **2000**, *112*, 1285 – 1288; *Angew. Chem. Int. Ed.* **2000**, *39*, 1230 – 1234.
[4] A. Semenov, J. P. Spatz, M. Möller, J.-M. Lehn, B. Sell, D. Schubert, C. H. Weidl, U. S. Schubert, *Angew. Chem.* **1999**, *111*, 2701 – 2705; *Angew. Chem. Int. Ed.* **1999**, *38*, 2547 – 2550.
[5] D. G. Kurth, N. Severin, J. P. Rabe, *Angew. Chem.* **2002**, *114*, 3833 – 3835; *Angew. Chem. Int. Ed.* **2002**, *41*, 3681 – 3683.
[6] A. Werner, *Z. Anorg. Chem.* **1893**, *3*, 267 – 330.
[7] J.-M. Lehn, *Supramolecular Chemistry, Concepts and Perspectives*, VCH, Weinheim, **1995**.
[8] D. Philp, J. F. Stoddart, *Angew. Chem.* **1996**, *108*, 1242 – 1286; *Angew. Chem. Int. Ed.* **1996**, *35*, 1155 – 1196.
[9] B. J. Holliday, C. A. Mirkin, *Angew. Chem.* **2001**, *113*, 2076 – 2097; *Angew. Chem. Int. Ed.* **2001**, *40*, 2022 – 2043.
[10] R. C. Mehrotra, R. Bohra, *Metal Carboxylates*, Academic Press, London, **1983**.
[11] S. V. Kolotuchin, P. A. Thiessen, E. E. Fenlon, S. R. Wilson, C. J. Loweth, S. C. Zimmerman, *Chem. Eur. J.* **1999**, *5*, 2537 – 2547.
[12] A. Dmitriev, N. Lin, J. Weckesser, J. V. Barth, K. Kern, *J. Phys. Chem. B* **2002**, *106*(27), 6907 – 6912.
[13] C. C. Perry, S. Haq, B. G. Frederick, N. V. Richardson, *Surf. Sci.* **1998**, *409*, 512 – 520.
[14] The decisive role of atom evaporation from steps could be proven in the present case by the following experiments. In the first case, the step mobility was limited by step decoration with carbon monoxide which significantly delayed compound formation. In the second case, compound formation could be triggered by co-deposition of Cu or by raising the temperature.

 © 2002 WILEY-VCH Verlag GmbH & Co. KGaA, Weinheim 0044-8249/02/4124-4782 $ 20.00+.50/0

[15] J. V. Barth, J. Weckesser, G. Trimarchi, M. Vladimirova, A. De Vita, C. Cai, H. Brune, P. Günter, K. Kern, *J. Am. Chem. Soc.* **2002**, *124*, 7991 – 8000.
[16] A. Doyle, J. Felcman, M. T. Gambardella, C. N. Verani, M. L. B. Tristão, *Polyhedron* **2000**, *19*, 2621 – 2627.
[17] P. R. Raithby, G. P. Shields, F. H. Allen W. D. S. Motherwell, *Acta Cryst. B* **2000**, *56*, 444 – 454.
[18] Movies showing the formation and decay of the coordination compounds in real space are shown at http://www.mpi-stuttgart.mpg.de/kern/Res act/supmat 2.html.
[19] J. Lee, W. Ho, *Science* **1999**, *286*, 1719 – 1722.
[20] S.-W. Hla, L. Bartels, G. Meyer, K.-H. Rieder, *Phys. Rev. Lett.* **2000**, *85*, 2777 – 2780.
[21] Note, however, that single complexes are perfectly stable below 180 K, where molecular motion is frozen. No dissociation/association events are detected in the corresponding STM images, which demonstrates that the room-temperature dynamics of the complexes is not influenced by tip effects.



Low-Temperature Synthesis of Single-Crystal Germanium Nanowires by Chemical Vapor Deposition**

Dunwei Wang and Hongjie Dai*

Chemically derived nanowire materials have attracted much attention because of their interesting geometries, properties, and potential applications.[1–3] Various methods have been developed for synthesizing semiconducting nanowires including laser ablation,[2,3] physical vapor deposition under high temperatures,[3–7] and solvothermal growth under high pressures and moderate temperatures.[3,8–10] Chemical vapor deposition (CVD) has been extensively used for carbon nanotube growth,[11–13] but is much less explored for the synthesis of semiconductor nanowires, with the exception for silicon.[14,15]

Herein, we present the first synthesis of single-crystal germanium nanowires, prepared by the CVD of germane (GeH_4) at 275 °C with Au nanocrystals as seed particles. Germanium is an important semiconducting electronic material with high carrier mobility and a band gap of approximately 0.6 eV. Nanowires of germanium were first reported by the group of Heath about ten years ago, synthesized by using a solvothermal approach.[8] Recently, laser ablation (820 °C),[2] vapor transport (900–1100 °C),[4,7,16] and solvothermal methods (300–400 °C, 100 atm)[9] were used for growth. We show here that high-quality Ge nanowires are synthesized by a simple CVD process at 275 °C under atmospheric pressure. This represents the mildest growth conditions for single-crystal nanowire synthesis. An efficient Ge feedstock from GeH_4 and the low eutectic temperature of Ge–Au nanoclusters are the key factors that afford vapor-liquid-solid (VLS) growth of Ge nanowires at low temperatures. Further, we show that the CVD approach allows for patterned growth of Ge nanowires, which yields nanowires from well-defined patterned sites on surfaces.

We carried out CVD growth at 275 °C under a 10 sccm (standard cubic centimeter) flow of GeH_4 (10 % in He) in tandem with a 100 sccm flow of H_2 in a 2.5 cm furnace reactor (total gas pressure 1 atm) for 15 min. The SiO_2 substrate used in this work contained preformed Au nanocrystals (approximately 20 nm in diameter) deposited uniformly on the surface from a colloidal solution. The inset of Figure 1a shows an atomic force microscopy (AFM) image of the Au particles on a substrate, recorded before CVD. After the

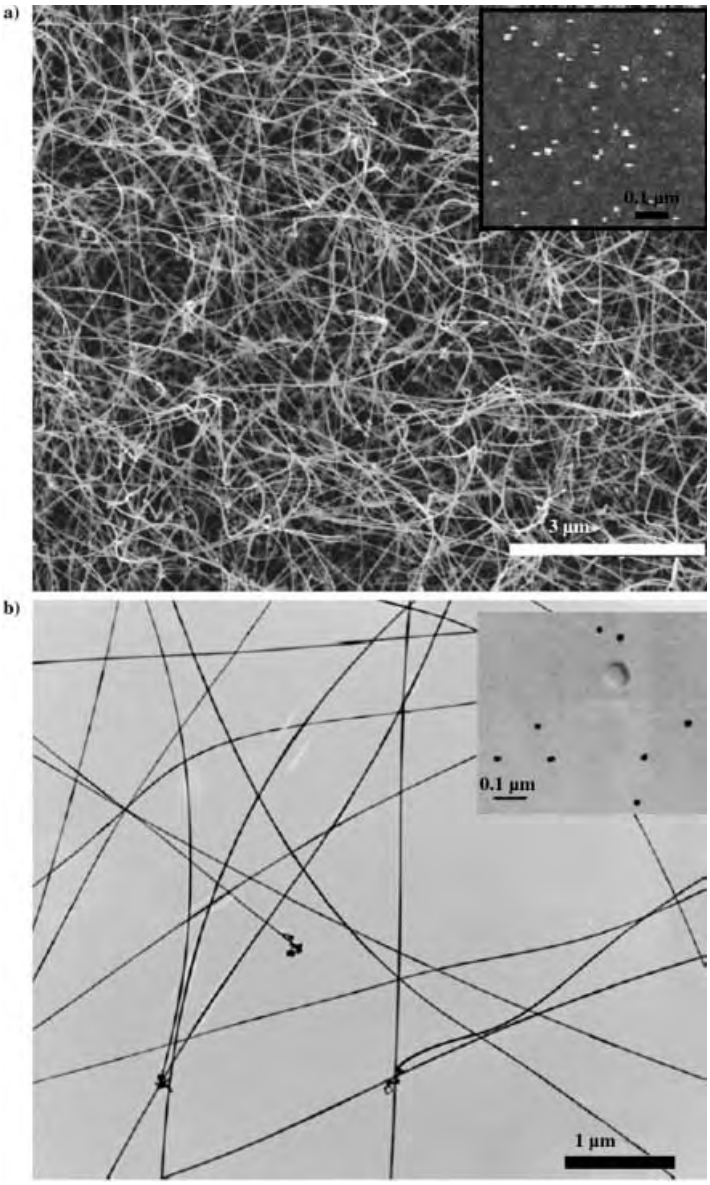


Figure 1. a) An SEM image of Ge nanowires synthesized by CVD at 275 °C on a SiO_2/Si substrate. The inset shows an AFM image of Au nanoclusters on the substrate recorded prior to CVD; b) A TEM image of Ge nanowires synthesized by CVD on a SiO_2 film (approximately 10 nm thick; light background) supported on a TEM grid. The inset shows a TEM image of Au clusters (black dots) on SiO_2 recorded prior to CVD.

[*] Prof. Dr. H. Dai, D. Wang
Department of Chemistry
Stanford University
Stanford, CA 94305 (USA)
Fax: (+1) 650-725-0259
E-mail: hdai@stanford.edu

[**] This work was supported by the MARCO MSD Focus Center, the Packard Foundation, Sloan Foundation, a Dreyfus Teacher–Scholar Award and a Terman Fellowship. We thank Prof. C. Chidsey for his insight.

 © 2002 WILEY-VCH Verlag GmbH & Co. KGaA, Weinheim 0044-8249/02/4124-4783 $ 20.00+.50/0

CVD process, characterization by scanning electron microscopy (SEM) revealed high-yield growth of nanowire materials on the substrate (Figure 1a). The nanowires were up to tens of microns in length, and exhibited high abundance and purity without any appreciable amount of particulate by-products.

Transmission electron microscopy (TEM) was used to characterize the high-order structures of our CVD-grown nanowires. In order to investigate nanowires in their as-grown form, we carried out nanowire synthesis directly on TEM grids containing thin (approximately 10 nm) SiO_2 films[17,18] that are transparent to electron beams. Au nanoparticles were first deposited onto a SiO_2 film (Figure 1b inset), followed by CVD synthesis and TEM imaging without any further processing of the sample (for example, the sonication of nanowires off of substrates in a solution). Figure 1b shows a typical low-magnification TEM image in which nanowires with lengths greater than 10 μm are clearly observed on the SiO_2 film. The clean SiO_2 background and absence of large particulates suggest that our CVD growth conditions produce pure nanowire materials with few impurities.

High-resolution TEM reveals high-quality single-crystalline Ge nanowires grown by CVD. Figure 2a is a high-magnification image that shows the crystal structure of a Ge nanowire. The convergent electron-beam diffraction pattern (Figure 2a, inset) for the nanowire is identified to be along the [011] diffraction zone-axis. The lattice fringes parallel to the viewing direction in the TEM image correspond to the {111} planes (at 54° to the wire axis) of Ge. The spacing between adjacent planes is 3.27 Å, which yields a lattice constant of $a = \sqrt{3}(3.27)$ Å $= 5.66$ Å, a figure which is in excellent agreement with the known diamond crystal structure of Ge. The same lattice constant is derived from the diffraction pattern by using the Bragg formula. The wire axis is identified to be $[01\bar{1}]$ based on the [011] zone-axis and analysis of the lattice structure (Figure 2a). The Ge nanowires are single-crystalline over most of their lengths (greater than 10 μm). When following a wire in the TEM, we sometimes observe imaging contrast variations along its length (Figure 1b). This is attributed to slight rotations of the crystal planes resulting from the van der Waals fixation forces of the substrate (that is, slight mechanical twisting of the wire). Careful examinations reveal that many of the as-grown wires do not show such variation along the wire axis for more than 5 μm. Thus far, for approximately 10 wires investigated by high-resolution TEM, all of them have exhibited a $[01\bar{1}]$ growth direction (see Figure 2b for a second example). We tentatively conclude that the majority of our Ge nanowires grown by CVD have growth axes along the ⟨110⟩ crystal direction. In terms of the size of the nanowires, statistical analysis over 40 wires reveals an average diameter of 23 nm, close to the average diameter of the Au colloidal particles.

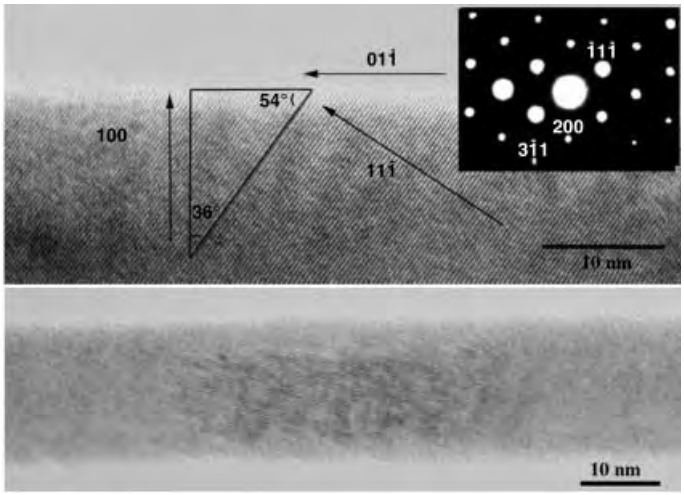


Figure 2. a) A high-resolution TEM image of a Ge nanowire. The inset shows a convergent-beam diffraction pattern; b) TEM image of another Ge nanowire.

The synthesis of nanowires directly onto TEM grids allows an examination of the ends of the nanowires in their as-grown states. Figures 3a and b display TEM images recorded for the two ends of a typical nanowire. We observe that one end of the nanowire is tipped with a Au nanoparticle (Figure 3b) and the other end is connected to the SiO_2 substrate (Figure 3a). This result suggests that the growth of Ge nanowires in our CVD process is through the Au particle-seeded VLS mechanism,[19] similar to that which is observed for Ge wires synthesized by laser ablation[2] and vapor transport[3,4,16] methods. The general VLS mechanism involves Ge vapor dissolving into a Au cluster to form an alloy at the initial stage, then under

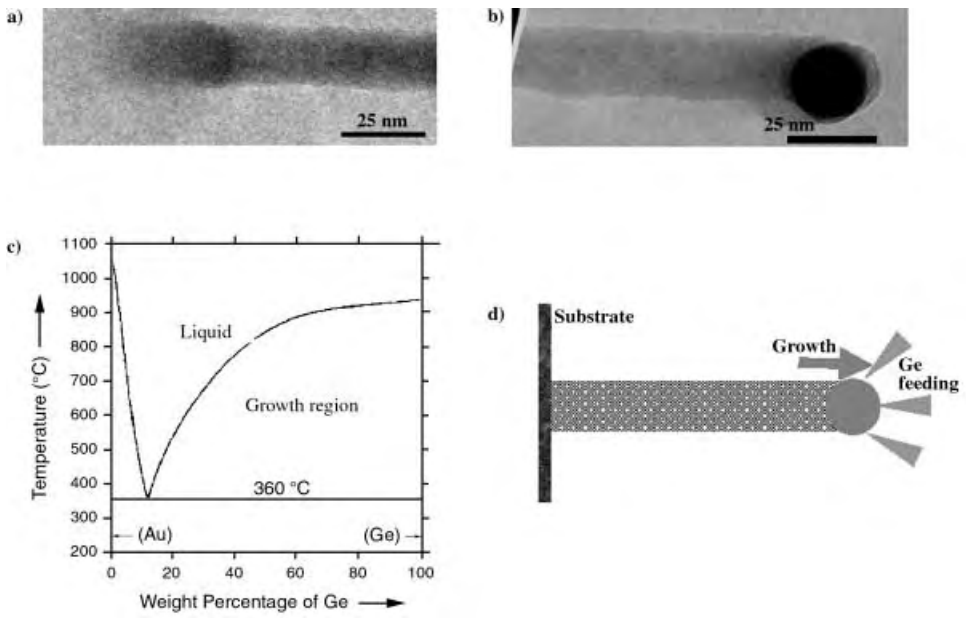


Figure 3. a) A TEM image showing the end of a Ge nanowire connected to a SiO_2 substrate; b) A TEM image of the other end of the same wire shown in (a); c) The binary phase diagram for Ge–Au, adapted from Ref. [20]; d) A schematic drawing depicting the VLS growth process.

 © 2002 WILEY-VCH Verlag GmbH & Co. KGaA, Weinheim 0044-8249/02/4124-4784 $ 20.00+.50/0

continuous Ge feeding the alloy evolves into a liquid state, at which point a further increase in the Ge concentration leads to supersaturation, precipitation, and axial growth of a nanowire.[2–4,16] The Au cluster is lifted off from its original position on the substrate and extends as the wire lengthens, while the other end of the wire remains connected to the substrate (Figure 3d). This growth process has been clearly observed by Yang et al. using TEM to illustrate an in situ growth experiment where solid Ge is vaporized to feed Au nanoparticles.[3,16]

There are several important factors that allow for the synthesis of Ge nanowires by our low-temperature CVD process, utilizing the VLS mechanism. The first is related to the conventional Au–Ge binary phase diagram[20] (Figure 3c). The phase diagram suggests that over a wide range of temperatures above 360 °C (the eutectic temperature), a VLS-type process can take place if the concentration of Ge is increased within the Au particle. When varying the growth temperatures, we find that Ge nanowires can indeed be synthesized up to 600 °C; wires can not be grown below approximately 250 °C. Since the lower limit of our growth temperature (approximately 275 °C) is lower than the eutectic temperature by about 80 °C, we suggest that the melting temperature of the Ge–Au alloy is significantly suppressed for Au nanoparticles from macroscopic Au, for which the conventional phase diagram is derived. This is not surprising considering the well-known phenomenon that nanoclusters often exhibit lower melting temperatures than bulk materials.[21] The 80 °C reduction in melting temperature for the Ge–Au cluster is an important factor for the growth of Ge nanowires below 300 °C. Nevertheless, further experimental and theoretical work is required to establish phase diagrams for materials with nanoscalar dimensions. This shall significantly facilitate the synthesis of a wide range of quasi-one-dimensional materials.

According to the Au–Ge phase diagram, the growth of Ge nanowires, seeded by Au nanoclusters, could occur at low temperatures by the VLS process. An important factor to enable such growth, however, is a suitable Ge feedstock that can provide sufficient Ge species at these temperatures. Laser ablation and physical vapor deposition techniques vaporize solid Ge to feed Au clusters, and the temperatures required to produce sufficient Ge vapor are high.[2,4,16] Solvothermal methods afford Ge by decomposing precursors in solvents at approximately 300 °C, but at rather high pressures (approximately 100 atm).[8–9] The choice of GeH_4 as the Ge feedstock in our CVD system is a natural one, but desired nanowire growth results are only obtainable by controlling the GeH_4 decomposition through H_2 addition. Germane can undergo thermal decomposition by the following routes:[22]

$$GeH_4 \rightarrow GeH_2 + H_2 \quad (1)$$

$$GeH_2 \rightarrow Ge + H_2 \quad (2)$$

The activation energies for these processes are approximately 50, and less than 35 kcal mol^{-1} for (1) and (2), respectively. When varying the flow of H_2 during CVD under a constant GeH_4 flow (10 sccm, 10 % in He) at 275 °C, we observed excessive GeH_4 pyrolysis with a H_2 flow rate below approximately 50 sccm, signaled by significant amorphous coatings on the substrate and reactor wall. In strong contrast, for H_2 flow rates greater than 200 sccm, the substrate and CVD were clean and free of appreciable amorphous deposits. However, the growth of Ge nanowires was not observed. This suggests that the increase of H_2 concentration suppresses GeH_4 decomposition (as H_2 is a product in reactions (1) and (2)), leading to an insufficient Ge feedstock for nanowire growth. Active nanowire growth is achieved with a H_2 flow of approximately 100 sccm. Under these conditions, the GeH_4 decomposition is well balanced to provide a sufficient Ge feedstock and avoid excessive pyrolytic Ge deposition. We note that similar H_2 balancing effects have been reported previously in the CVD synthesis of carbon nanotubes from the decomposition of CH_4.[23]

The synthesis of Ge nanowires by our low-temperature CVD approach, with both high purity and quality, may find many interesting applications. As an example, Figure 4 shows the patterned growth of Ge nanowires. Previously, the patterned growth of carbon nanotubes and other types of wires has been achieved,[11–13,24] but this is not the case for germanium. We patterned Au nanoparticles in arrays of microsized squares on SiO_2/Si substrates (see Experimental Section) and carried out CVD growth. SEM revealed that Ge nanowires were readily grown from the squares (Figure 4d). The remaining substrate remained clean with negligible particulate deposits. Nanowires emanating from well-defined locations on substrates will facilitate their integration for electrical characterizations and devices. A second direction that we are currently pursuing is to exploit the conditions of soft synthesis. The 275 °C synthesis temperature will allow for the growth of high-quality nanowires on a variety of substrates, including organic materials. Thus far, we have grown Ge nanowires on glass substrates with ease.

In conclusion, we have developed a simple chemical vapor deposition method to synthesize high-purity single-crystalline Ge nanowires at low temperatures. The growth conditions are the mildest for single-crystal nanowire synthesis, and are possible owing to the efficient GeH_4 feedstock and low eutectic temperature for Ge and Au nanocluster seeds.

Experimental Section

Substrate preparation and CVD growth: A Si substrate with a thermally grown oxide layer (500 nm thickness) was cleaned with acetone, methanol, and isopropanol. It was then dipped into a solution of 3-aminopropyltriethoxysilane (APTES, 12 μL in 20 mL H_2O) for 30 minutes, rinsed with deionized water and blow-dried. The substrate was soaked in an aqueous Au colloid solution (20 nm diameter, Alfa Aesar) for 1 h. The APTES monolayer renders the SiO_2 surface positively charged and allows for the deposition of Au colloids (negatively charged) with high efficiency. AFM was carried out with a Digital Instrument Nanoscope III operated in the tapping mode. For CVD, the substrate was placed at the center of a 2.5 cm quartz-tube reactor within a furnace. The reactor was heated to 275 °C under a H_2 flow of 110 sccm. The gas flow was then switched to 10 sccm of GeH_4 (10 % in He, Voltaix, NJ) and 100 sccm of H_2 (99.99 %, Praxair, CA) for 15 min before switching the gas back to H_2 only, and cooling the system to room temperature.

Electron microscopy: After CVD growth, the substrate was characterized by a field-emission SEM (Hitachi S-800) operated at an accelerating voltage of 25 kV. For TEM, we carried out the growth of Ge nanowires

 © 2002 WILEY-VCH Verlag GmbH & Co. KGaA, Weinheim 0044-8249/02/4124-4785 $ 20.00+.50/0

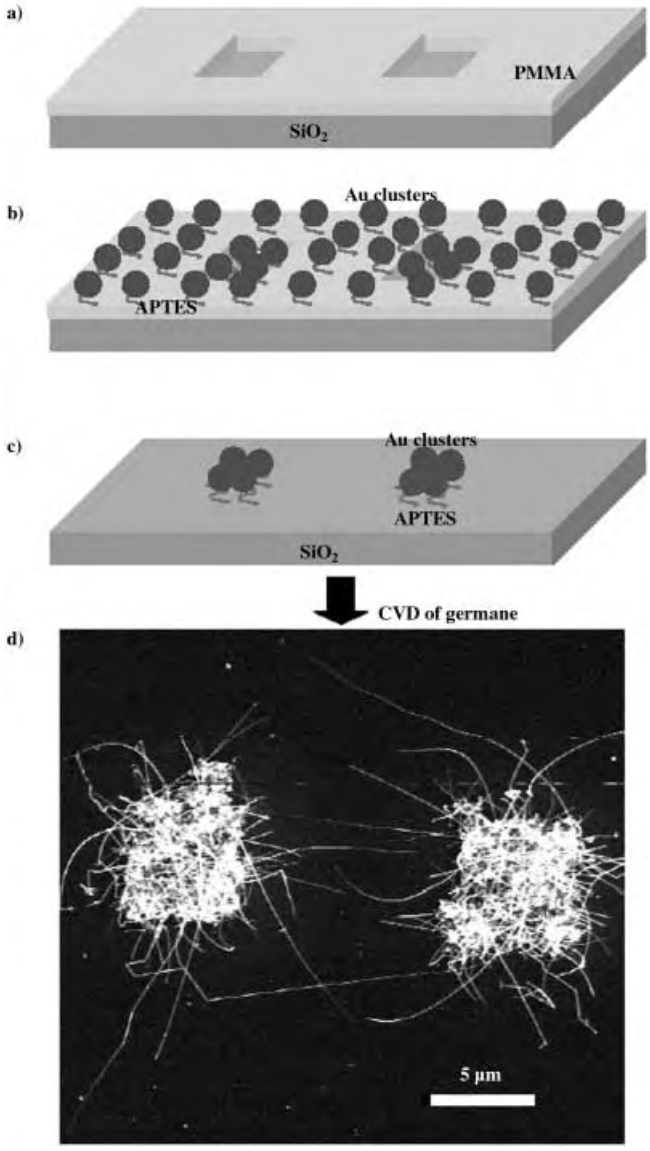


Figure 4. Patterned growth of Ge nanowires on SiO_2/Si. (a)–(c) A schematic describing the process of patterning Au particles into squared regions (see experimental section); d) An SEM image showing Ge nanowires grown from two square islands containing Au particles.

directly onto TEM grids. Ni grids supporting SiO_2 films (approximately 10 nm thick, Ted Pella) were treated by APTES in the same manner as the SiO_2/Si substrates, followed by Au particle deposition. The grids were imaged by TEM (Philips CM20, operating voltage 200 keV) before the CVD process to characterize the Au particles, and after the CVD process to characterize the grown nanowires and the particle–wire relationship.

Patterned growth: Polymethylmethacrylate (PMMA) was first patterned by electron beam lithography (or photolithography) on a SiO_2/Si substrate to form 5×5 μm wells (Figure 4a).[11] The substrate was treated with APTES and soaked in a Au colloid solution so that Au particles were deposited into the wells (Figure 4b). Removal of the PMMA in acetone affords Au particles that are confined in square islands (Figure 4c). The substrate was then subjected to CVD growth.

Received: September 10, 2002 [Z50134]

[1] H. Dai, E. W. Wong, Y. Z. Lu, F. Shoushan, C. M. Lieber, *Nature* **1995**, *375*, 769.
[2] A. Morales, C. M. Lieber, *Science* **1998**, *279*, 208.
[3] P. Yang, Y. Wu, R. Fan, *Int. J. Nanosci.* **2002**, *1*, 1.
[4] Y. Wu, P. Yang, *Chem. Mater.* **2000**, *12*, 605.
[5] M. H. Huang, S. Mao, H. Feick, Q. H. Yan, Y. Y. Wu, H. Kind, E. Weber, R. Russo, P. D. Yang, *Science* **2001**, *292*, 1897.
[6] Z. W. Pan, Z. R. Dai, Z. L. Wang, *Science* **2001**, *291*, 1947.
[7] G. Gu, M. Burghard, G. T. Kim, S. Dusberg, P. W. Chiu, V. Krstic, S. Roth, W. Q. Han, *J. Appl. Phys.* **2001**, *90*, 5747.
[8] J. R. Heath, F. K. LeGoues, *Chem. Phys. Lett.* **1993**, *208*, 263.
[9] T. Hanrath, B. K. Korgel, *J. Am. Chem. Soc.* **2001**, *123*, 1424.
[10] Y. D. Li, H. W. Liao, Y. Ding, Y. Fan, Y. Zhang, Y. T. Qian, *Inorg. Chem.* **1999**, *38*, 1382.
[11] J. Kong, H. Soh, A. Cassell, C. F. Quate, H. Dai, *Nature* **1998**, *395*, 878.
[12] H. Dai, in *Carbon Nanotubes, Vol. 80* (Eds.: M. S. Dresselhaus, G. Dresselhaus, P. Avouris), Springer, Berlin, **2001**, p. 29.
[13] H. Dai, *Surf. Sci.* **2002**, *500*, 218.
[14] J.-Y. Yu, S.-W. Chung, J. R. Heath, *J. Phys. Chem. B* **2000**, *104*, 11 864.
[15] Y. Cui, L. J. Lauhon, M. S. Gudiksen, J. F. Wang, C. M. Lieber, *Appl. Phys. Lett.* **2001**, *78*, 2214.
[16] Y. Wu, P. Yang, *J. Am. Chem. Soc.* **2001**, *123*, 3165.
[17] Y. Li, W. Kim, Y. Zhang, M. Rolandi, D. Wang, H. Dai, *J. Phys. Chem. B* **2001**, *105*, 11 424.
[18] Y. Zhang, Y. Li, W. Kim, D. Wang, H. Dai, *Appl. Phys. A* **2002**, *74*, 325.
[19] A. P. Levitt, *Whisker Technology*, Wiley-Interscience, New York, **1970**.
[20] *ASM Handbook, Alloy Phase Diagram, Vol. 3*, **1990**.
[21] F. Ercolessi, W. Andreoni, E. Tosatti, *Phys. Rev. Lett.* **1991**, *66*, 911.
[22] S. D. Chambreau, J. Zhang, *Chem. Phys. Lett.* **2002**, *351*, 171.
[23] N. R. Franklin, Y. Li, R. J. Chen, A. Javey, H. Dai, *Appl. Phys. Lett.* **2001**, *79*, 4571.
[24] S. Fan, M. Chapline, N. Franklin, T. Tombler, A. Cassell, H. Dai, *Science* **1999**, *283*, 512.

Experimental Observation and Confirmation of Icosahedral $W@Au_{12}$ and $Mo@Au_{12}$ Molecules**

Xi Li, Boggavarapu Kiran, Jun Li, Hua-Jin Zhai, and Lai-Sheng Wang*

One of the major goals of cluster science is to discover highly stable clusters which may be used as building blocks for novel nanomaterials, such as the celebrated C_{60}. Recently, Pyykkö and Runeberg predicted theoretically a series of highly symmetric and stable clusters containing 12 Au atoms

[*] Prof. Dr. L.-S. Wang, X. Li, Dr. B. Kiran, Dr. H.-J. Zhai
Department of Physics
Washington State University
2710 University Dr., Richland, WA 99352 (USA)
and
W. R. Wiley Environmental Molecular Sciences Laboratory
Pacific Northwest National Laboratory, MS K8-88
PO Box 999, Richland, WA 99352 (USA)
Fax: (+1) 509-376-6066
E-mail: ls.wang@pnl.gov
Dr. J. Li
W. R. Wiley Environmental Molecular Sciences Laboratory
Pacific Northwest National Laboratory, MS K1-96
PO Box 999, Richland, WA 99352 (USA)

[**] This work was supported by the US National Science Foundation (DMR-0095828) and performed at the W. R. Wiley Environmental Molecular Sciences Laboratory, a national scientific user facility sponsored by DOE's Office of Biological and Environmental Research and located at Pacific Northwest National Laboratory, which is operated for DOE by Battelle.

 © 2002 WILEY-VCH Verlag GmbH & Co. KGaA, Weinheim 0044-8249/02/4124-4786 $ 20.00+.50/0

with an encapsulated central impurity atom of the 5d elements, $M@Au_{12}$ ($M = W$, Ta^-, Re^+).[1] These clusters were shown to have icosahedral symmetry and a closed-shell electron configuration, stabilized by aurophilic attractions and relativistic effects in accordance with the 18-electron rule. The prototypical $W@Au_{12}$ cluster was suggested to have a HOMO–LUMO gap around 3 eV, which indicates that it should be highly inert chemically. Here we report the first experimental observation and characterization of the icosahedral $W@Au_{12}$ cluster using anion photoelectron spectroscopy (PES) and relativistic density functional theory (DFT) calculations. In addition, we have also observed and characterized $Mo@Au_{12}$, which is shown to have a nearly identical structure and electronic spectrum as $W@Au_{12}$, and suggests that a series of highly stable and symmetric $M@Au_{12}$ clusters with M = 4d elements might also exist.

The WAu_{12}^- ($MoAu_{12}^-$) cluster was produced using laser vaporization of a mixed Au/W (or Mo) target (approximately 10:1 atomic ratio) and a helium carrier gas. Details of the apparatus have been published elsewhere.[2,3] The resulting clusters were analyzed using time-of-flight mass spectrometry. Clusters with a variety of M/Au ratios were produced. The MAu_{12}^- clusters of interest were mass-selected and analyzed by PES at several photon energies. The magnetic-bottle PES spectrometer was calibrated using the known spectrum of the Rh^- ion, and has an energy resolution ($\Delta E/E$) of approximately 2.5%, that is, approximately 25 meV for 1 eV electrons. Figure 1 shows the PES spectra of the $MoAu_{12}^-$ and WAu_{12}^- ions at two photon energies (193 and 532 nm). The spectra of the two species are nearly identical, each with a sharp and weak peak (X) around 2 eV followed by a large energy gap and a high density of electronic transitions at higher binding energies. The threshold peak (X) was very sharp, as observed in the 532 nm spectra, which has a width (full width at half-maximum) of approximately 36 meV, very close to the instrumental resolution. The sharp threshold peak suggests that there is little geometry change between the MAu_{12}^- ion and its corresponding neutral ground state. The threshold peak defined an electron affinity (EA) of 2.17 ± 0.02 eV for $MoAu_{12}$ and 2.08 ± 0.02 eV for WAu_{12}. Within our experimental uncertainty, the adiabatic and vertical detachment energies for the threshold feature are the same.

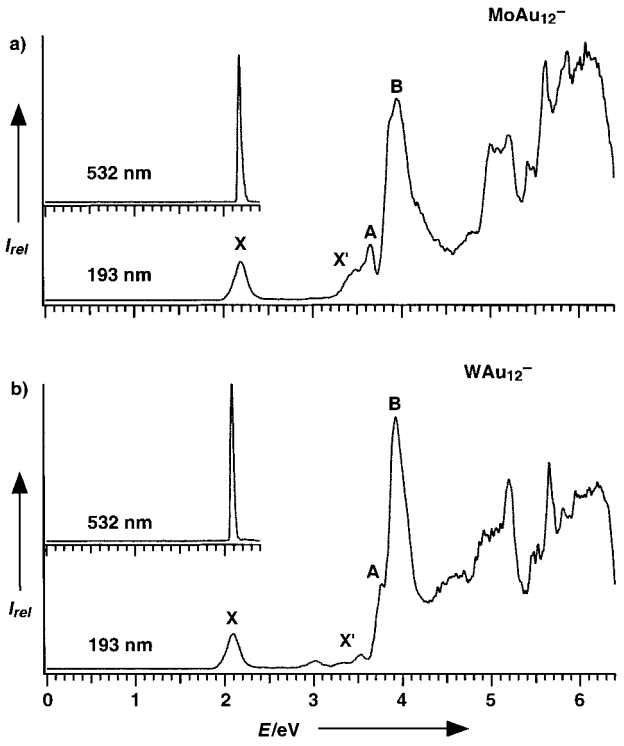


Figure 1. Photoelectron spectra of a) $Mo@Au_{12}^-$ and b) $W@Au_{12}^-$ at 532 nm (2.331 eV) and 193 nm (6.424 eV).

The weak signals labeled X′ in each spectrum are attributed to impurities or isomers as their relative intensities are dependent on the source conditions. The energy difference between the X and A features yielded an energy gap of 1.48 eV for $MoAu_{12}^-$ and 1.68 eV for WAu_{12}^-. This large energy gap is consistent with the previous prediction of a large HOMO–LUMO gap for $W@Au_{12}$. If the neutral species is closed-shell, the extra electron enters the LUMO to form the anion. Thus, the X band corresponds to removal of the LUMO electron, whereas the A band should correspond to the removal of a HOMO electron, to produce a triplet excited state. The measured X–A energy separation thus corresponds to the excitation energy of the first excited state (triplet) of the neutral $M@Au_{12}$ clusters. The features beyond the A band are attributed to electron detachment from the more deeply bound molecular orbitals. The similarity of the spectra of the $MoAu_{12}^-$ and WAu_{12}^- species indicates that they have the same electronic and geometrical structures.

To confirm the above assignment and further characterize the structure and bonding of the MAu_{12} clusters and their anions, we carried out relativistic DFT calculations. Figure 2 displays the structures of the I_h cluster and two low-lying isomers that we found for $MoAu_{12}$ and WAu_{12}, and Table 1 lists their relative energies, EAs, and structural parameters. Indeed, even though the calculations for the I_h cluster were performed in its D_{5d} subgroup, the geometry optimizations still led to the I_h structure for the neutral species, which confirms the findings of Pyykkö and Runeberg.[1] Our optimized W–Au and Au–Au bond lengths are slightly longer than those derived at the second-order Møller–Plesset (MP2) level reported by Pyykkö and Runeberg, presumably through overlooking dispersion and van der Waals interactions in the DFT methods. Additionally, we found two low-lying isomers with O_h and D_{5h} symmetries. The O_h isomer is very close in energy with the I_h ground state whereas the D_{5h} isomer is considerably higher in energy for both $MoAu_{12}$ and WAu_{12}. Our computed EAs are 2.25 and 2.02 eV for the I_h isomeric forms of $Mo@Au_{12}$ and $W@Au_{12}$, respectively, in excellent agreement with the experimental values. The calculated EAs for the O_h isomer of $MoAu_{12}$ is 2.32 eV, 0.15 eV higher than the experimental value. However, the calculated EA for the O_h isomer of WAu_{12} (2.11 eV) is too close to the experimental value to be distinguished from the I_h isomer. As will be shown below, the computed PES spectra clearly indicate that the observed species were the I_h clusters.

As pointed out by Pyykkö and Runeberg, the HOMO and LUMO of the I_h form of $W@Au_{12}$ are both of h_g symmetry, as shown in Figure 3. Thus, the I_h $W@Au_{12}^-$ ion would not be stable either at the scalar relativistic level or at the spin-orbit-

 © 2002 WILEY-VCH Verlag GmbH & Co. KGaA, Weinheim 0044-8249/02/4124-4787 $ 20.00+.50/0

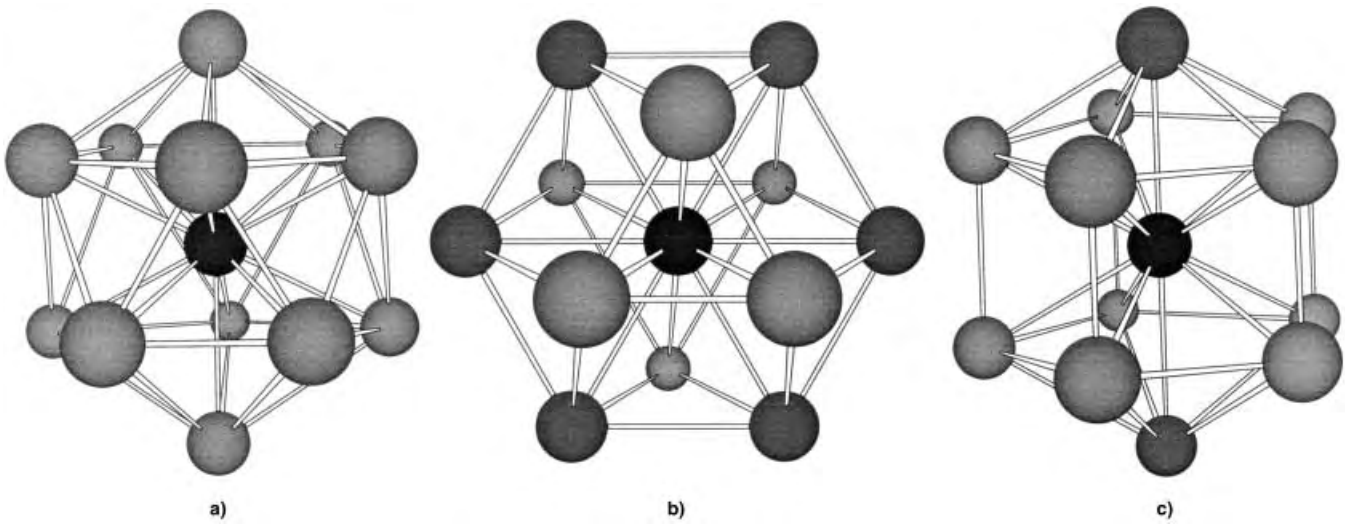


Figure 2. Optimized structures of $Mo@Au_{12}$ and $W@Au_{12}$ isomers: a) I_h symmetry, b) O_h symmetry, and c) D_{5h} symmetry (see Table 1).

Table 1. Relative energies [kJ mol^{-1}], EAs [eV], and bond lengths [pm] of $MoAu_{12}$ and WAu_{12}.

Symmetry	State	Energy	EA	R(M−Au)	R(Au−Au)
				$Mo@Au_{12}$	
I_h	$^1A_{1g}$	0.0	2.25	275.7×12	289.8×30
O_h	$^1A_{1g}$	0.3	2.32	280.6×12	280.6×24
D_{5h}	$^1A_1'$	18.4	2.48	279.5×10, 283.2×2	286.3×10, 283.9×10, 274.3×5
				$W@Au_{12}$	
I_h	$^1A_{1g}$	0.0	2.02	275.5×12	289.7×30
O_h	$^1A_{1g}$	9.8	2.11	280.6×12	280.6×24
D_{5h}	$^1A_1'$	20.4	2.26	279.4×10, 283.0×2	286.4×10, 284.2×10, 273.3×5

coupled level because of the Jahn–Teller effect.[4] Indeed, we found that the anion has a slight distortion along the fivefold axis, to yield a D_{5d} anion. However, the distortion is very small, with the Au−Au bonds increased by only 3 pm and the two axial W–Au bonds by 10 pm, consistent with the sharp ground-state transition observed in the PES spectra (Figure 1). Figure 3 displays an energy-level correlation diagram for the atomic orbitals of W and Au and the MOs of I_h $W@Au_{12}$ and its Au_{12} fragment. Even though the calculations for these levels used D_{5d} symmetry, the MOs are labeled using I_h point group symmetry for simplicity. Since the Au 6s orbitals span $a_g + t_{1u} + h_g + t_{2u}$ ligand group orbitals, the major orbital interactions in $W@Au_{12}$ occur between the W 5d and Au_{12} ligand group orbitals, to give the bonding h_g HOMO and antibonding h_g* LUMO, which is consistent with the slight expansion of the Au_{12} cage upon electron addition in the anion. As a result, the HOMO is composed mainly of Au 6s and 5d (77% Au and 23% W), whereas the LUMO is composed primarily of W 5d orbitals.

To provide a semiquantitative assignment of the observed spectra and to distinguish between the I_h and O_h isomers, we also computed the detachment transitions from the anion ground state to the ground and excited states of the neutral species at excitation energies up to 5.8 eV for both isomers, as shown in Figure 4. The simulated spectra for the I_h isomers are in excellent agreement with the experimental spectra, which confirms unequivocally that the observed species were the I_h isomers in both the WAu_{12}^- and $MoAu_{12}^-$ ions. Our calculations confirm that the X band results from detachment from the "h_g" LUMO, while the A and B bands both result from electron removal from the Jahn—Teller-distorted "h_g" HOMO. The other high-energy bands correspond to detachments from MOs of Au $5d_{5/2}$, $6s_{1/2}$, and $5d_{3/2}$. While we cannot completely rule out the possibility of impurities, the X′ features observed in the PES spectra (Figure 1) may contain contributions from the O_h isomers on the basis of the simulated spectra.

Relativistic effects are particularly important for Au.[5] As shown in Figure 3, because of the direct and indirect relativistic effects, the Au 6s and 5d orbitals are stabilized and destabilized by 1.60 and 1.17 eV, respectively, which results in strong 6s–5d hybridization in the $M@Au_{12}$ molecules. Spin-orbit coupling splits the Au 5d orbitals into $5d_{3/2}$ and $5d_{5/2}$ spinors by 1.24 eV, which causes the split of the 5d bands into two separated $5d_{3/2}$ and $5d_{5/2}$ bands in the $M@Au_{12}$ clusters. Moreover, the $6s_{1/2}$–$5d_{5/2}$ energy gap (0.75 eV) is much smaller than the scalar-relativistic 6s–5d gap (1.22 eV), again favoring strong 6s–5d hybridization. The spin-orbit splitting of the h_g HOMO is only 0.04 eV, while that of the LUMO is as large as 0.43 eV, in agreement with the atomic spin-orbit splitting of the W 5d orbital (0.56 eV).

In conclusion, the present work represents the first experimental identification of the theoretically predicted $W@Au_{12}$ cluster. The anion photoelectron spectra and theoretically calculated electron-detachment energies indicate that the $W@Au_{12}$ cluster indeed has a highly symmetric icosahedral structure with significant stability. The experimental results of the $Mo@Au_{12}$ cluster suggest that $M@Au_{12}$

 © 2002 WILEY-VCH Verlag GmbH & Co. KGaA, Weinheim 0044-8249/02/4124-4788 $ 20.00+.50/0

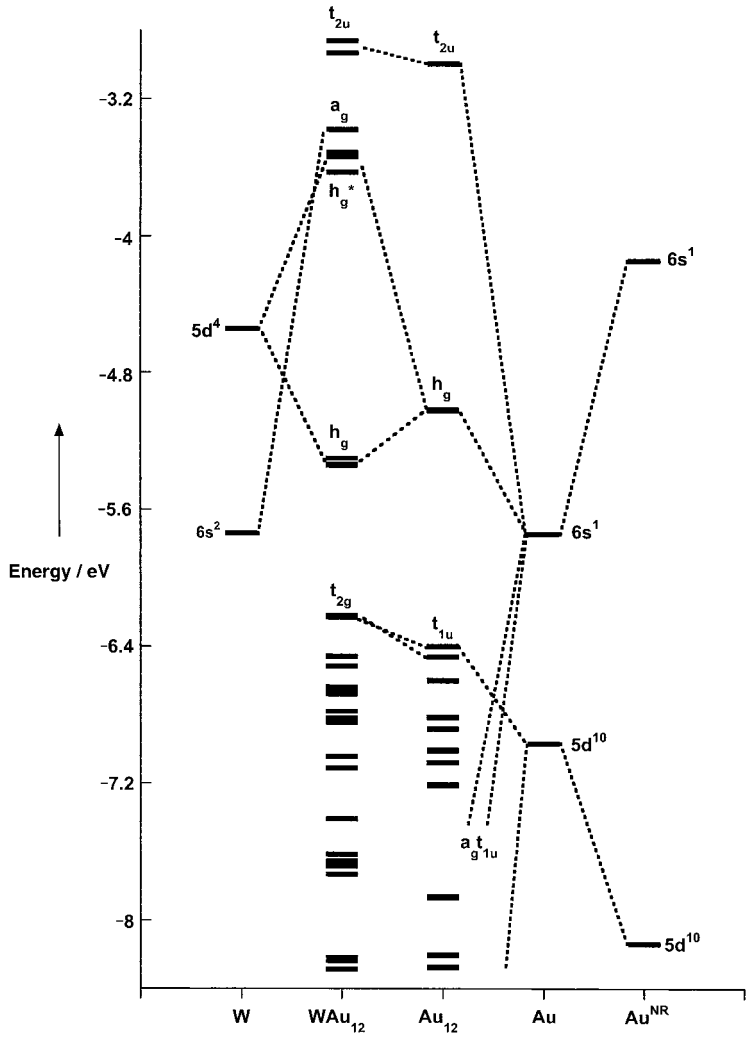


Figure 3. The energy-level correlation diagrams of W, Au, Au_{12}, and I_h W@Au_{12}. All of the energies are calculated at the scalar-relativistic level, except for Au^{NR} which is calculated at the non-relativistic level. The HOMO (h_g) and LUMO (h_g*) of the I_h W@Au_{12} are indicated.

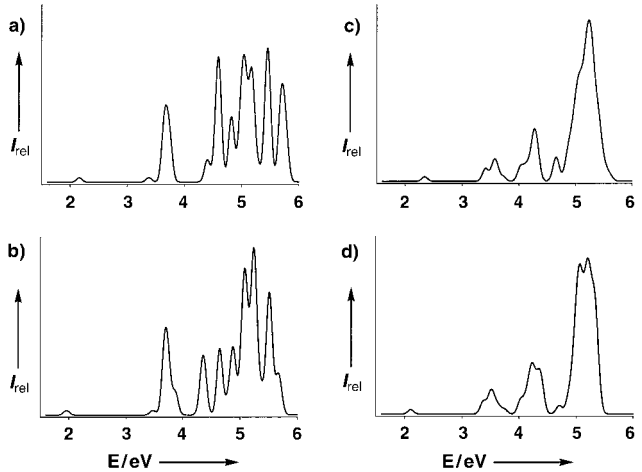


Figure 4. The simulated photoelectron spectra of $MoAu_{12}^-$ and WAu_{12}^-. a) I_h $MoAu_{12}^-$, b) I_h WAu_{12}^-, c) O_h $MoAu_{12}^-$, and d) O_h WAu_{12}^-.

clusters containing a 4d central atom are also stable. We are exploring the possibility of extending the current work to other second- and third-row as well as first-row transition-metal gold clusters. Given the significant stability of these M@Au_{12} clusters, nanomaterials with these clusters as building blocks are viable systems to explore.

Computational Methods

Relativistic density functional calculations of M@Au_{12} (M = Mo, W) and their anions were performed at the level of generalized gradient approach using the Perdew–Wang exchange-correlation functional.[6] The scalar relativistic zero-order-regular-approximation (ZORA) ansatz has been used.[7] The standard Slater-type-orbital (STO) basis sets with quality of triple-zeta plus polarization functions (TZP) were used for the valence orbitals of all the atoms, with frozen core approximation to the [$1s^2$–$3d^{10}$] core of Mo, the [$1s^2$–$4f^{14}$] core of W, and the [$1s^2$-$4d^{10}$] core of Au. The geometries of all the molecules were fully optimized with an energy gradient converging to 10^{-4} Hartree $Å^{-1}$. Frequency analyses were carried out to confirm the obtained structures. The vertical detachment energies of the anions were calculated from the ΔSCF energy difference between the neutral and anion ground states and the excitation energies of the neutral (triplet excited states only) calculated by time-dependent DFT method.[8,9] The density-of-states spectra were constructed by fitting the distribution of the detachment transition energies with unit-area Gaussian functions of 0.05 eV, full width at half-maximum. All the calculations were accomplished using the Amsterdam Density Functional (ADF 2002) program.[10]

Received: September 19, 2002 [Z50197]

[1] P. Pyykkö, N. Runeberg, *Angew. Chem.* **2002**, *114*, 2278; *Angew. Chem. Int. Ed.* **2002**, *41*, 2174.

[2] L. S. Wang, H. S. Cheng, J. Fan, *J. Chem. Phys.* **1995**, *102*, 9480.

[3] L. S. Wang, X. Li in *Cluster and Nanostructure Interfaces* (Eds.: P. Jena, S. N. Khana, B. K. Rao), World Scientific, New Jersey, **2000**, p. 293.

[4] With inclusion of spin-orbit coupling effects, the singly occupied h_g MO will split into sixfold and fourfold degenerate $g_{3/2g}$ and $i_{5/2g}$ spinors; both are subject to Jahn–Teller distortion.

[5] P. Pyykkö, *Chem. Rev.* **1988**, *88*, 563.

[6] a) J. P. Perdew, Y. Wang, *Phys. Rev. B* **1992**, *45*, 13244; b) J. P. Perdew, J. A. Chevary, S. H. Vosko, K. A. Jackson, M. R. Pederson, D. J. Singh, C. Foilhais, *Phys. Rev. B* **1992**, *46*, 6671.

[7] E. van Lenthe, E. J. Baerends, J. G. Snijders, *J. Chem. Phys.* **1993**, *99*, 4597.

[8] S. J. A. van Gisbergen, J. G. Snijders, E. J. Baerends, *Comput. Phys. Commun.* **1999**, *118*, 119.

[9] For details of the methodology for calculating anion electron detachment energies by TDDFT, see: J. Li, *Chem. Phys. Lett.*, submitted.

[10] ADF 2002, SCM, Theoretical Chemistry, Vrije Universiteit, Amsterdam, The Netherlands (http://www.scm.com).a) G. te Velde, F. M. Bickelhaupt, S. J. A. van Gisbergen, C. F. Guerra, E. J. Baerends, J. G. Snijders, T. Ziegler, *J. Comput. Chem.* **2001**, *22*, 931; b) C. F. Guerra, J. G. Snijders, G. te Velde, E. J. Baerends, *Theor. Chem. Acc.* **1998**, *99*, 391.

 © 2002 WILEY-VCH Verlag GmbH & Co. KGaA, Weinheim 0044-8249/02/4124-4789 $ 20.00+.50/0

Synthesis and Characterization of Lanthanide Hydroxide Single-Crystal Nanowires**

Xun Wang and Yadong Li*

Nanowires represent a class of quasi-one-dimensional materials, in which carrier motion is restricted in two directions so that they usually exhibit significant photochemical, photophysical, and electron-transport properties which differ from that of bulk or nanoparticle materials.[1–11] In the last decade, many important materials have been prepared in the form of nanorods or nanowires to generate some unexpected properties[2–5] based on which, many new potential applications have been explored. For example, well-controlled and monodisperse CdSe nanorods can be used in solar cells,[2] and can form liquid-crystal phases with orientational order and positional disorder in organic solvents;[3] single-crystalline, well-defined ZnO nanowires can serve as natural resonance cavities, and well-aligned ZnO nanowire arrays may serve as room-temperature ultraviolet nanolasers.[4] Along with chemical composition and crystal structure, shape and dimensionality are now regarded as particularly important factors that influence the chemical and/or physical properties of materials.

As a consequence of their unique electronic structures and the numerous transition modes involving the 4f shell of their ions, lanthanide compounds usually have outstanding optical, electrical, and magnetic properties,[12–22] and have been widely used as high-quality phosphors,[12] up-conversion materials,[13] catalysts,[14] and time-resolved fluorescence (TRF) labels for biological detection.[15] There have been extensive studies regarding lanthanide chemistry at bulk or atomic levels,[16–19] and the synthesis of lanthanide monothiooxides,[20] lanthanide-doped oxides or sulfides, organolanthanide compounds, the complexation behavior of lanthanide ions or atoms,[16,17] and the emission phenomena from lanthanides when bound to biomolecules (including calcium-binding proteins and nucleic acids).[18,19] Very recently, the synthesis of lanthanide oxide[21] and fluoride[22] nanoparticles with enhanced luminescence and photomagnetic properties has also been reported. However, to the best of our knowledge, few studies have focused on the synthesis of nanowires or nanorods of lanthanide-related compounds. Such materials would be of great significance because of the possible novel properties induced by their reduced dimensionality. Herein, we report the synthesis of lanthanide hydroxide nanowires ($La(OH)_3$, $Pr(OH)_3$, $Nd(OH)_3$, $Sm(OH)_3$, $Eu(OH)_3$, $Gd(OH)_3$, $Dy(OH)_3$, $Tb(OH)_3$, $Ho(OH)_3$, $Tm(OH)_3$, and YbOOH) through a facile solution-based hydrothermal synthetic pathway.

The synthesis of $Ln(OH)_3$ nanowires was based on the preparation of colloidal $Ln(OH)_3$ at room temperature, with subsequent hydrothermal treatment at 180 °C for about 12 h.

Figure 1 A shows typical XRD patterns for $La(OH)_3$ nanowires. All of the reflections could be readily indexed to the hexagonal phase (space group $P63/m$ (no. 176)) of $La(OH)_3$ with lattice constants $a = 6.5470$ and $c = 3.8540$ Å (JCPDS 83-2034). Colloidal $La(OH)_3$ nanoparticles have also been characterized as the corresponding hexagonal phase of $La(OH)_3$ with broadened peaks that indicate reduced particle sizes (Figure 1 B). Similar XRD patterns to those obtained for $La(OH)_3$ nanowires and colloidal nanoparticles have also been obtained from their $Pr(OH)_3$, $Nd(OH)_3$, $Sm(OH)_3$, $Eu(OH)_3$, $Gd(OH)_3$, $Dy(OH)_3$, $Tb(OH)_3$, $Ho(OH)_3$, and $Tm(OH)_3$ counterparts, all of which exhibited hexagonal crystal structures. However, under the same conditions, the hexagonal phase of $Yb(OH)_3$ could not been obtained. The final product was found to be the monoclinic phase (space group $P21/m$ (no. 11)) of YbOOH, with lattice constants $a = 5.8700$, $b = 3.5800$, and $c = 4.2700$ Å (Figure 2).

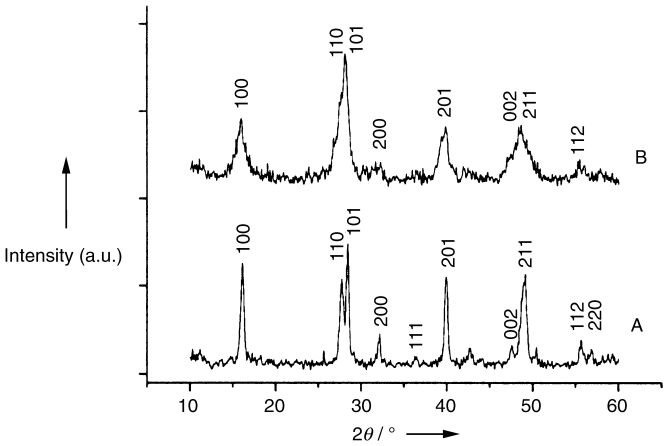


Figure 1. XRD patterns of $La(OH)_3$. A) $La(OH)_3$ nanowires; B) colloidal $La(OH)_3$.

The size and morphology of the products were further examined by transmission electron microscopy (TEM). As

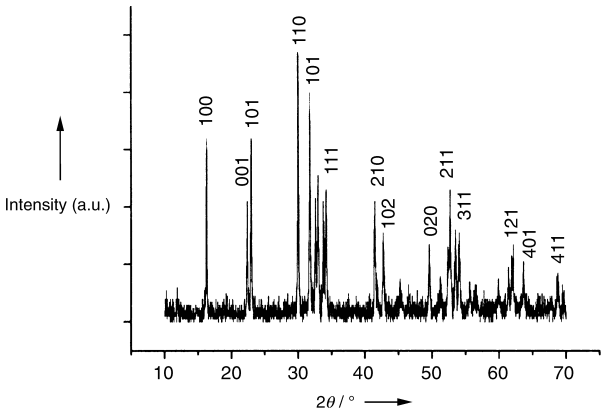


Figure 2. XRD patterns of monoclinic YbOOH.

[*] Prof. Y. Li, X. Wang
Department of Chemistry
Tsinghua University
Beijing, 100084 (P.R. China)
Fax: (+86) 10-62788765
E-mail: ydli@tsinghua.edu.cn

[**] This work was supported by the NSFC (20025102, 50028201, 20151001), the Foundation for the Author of National Excellent Doctoral Dissertation of P.R. China, and the State Key Project of Fundamental Research for nanomaterials and nanostructures.

 © 2002 WILEY-VCH Verlag GmbH & Co. KGaA, Weinheim 0044-8249/02/4124-4790 $ 20.00+.50/0

shown in Figure 3A, typical TEM images of $La(OH)_3$ nanowires display uniform morphologies with diameters of 15–20 nm and lengths up to 5 μm. Electron diffraction patterns (Figure 3B) taken form a single $La(OH)_3$ nanorod reveal the single-crystalline nature of the sample, and can be indexed as the [010] zone axis of hexagonal $La(OH)_3$, which is consistent with the XRD results presented above. High-resolution (HR)TEM images (Figure 3C) show that the nanorod is structurally uniform with an interplanar spacing is about 0.316 nm, which corresponds to the (101) plane of hexagonal $La(OH)_3$. It is interesting to observe that under controlled experimental conditions, the lighter $Ln(OH)_3$ ($La(OH)_3$, $Pr(OH)_3$, $Nd(OH)_3$, $Sm(OH)_3$, $Eu(OH)_3$, and $Gd(OH)_3$) nanowires could be prepared with high aspect ratios and uniform morphologies, whereas heavier lanthanide hydroxides ($Dy(OH)_3$, $Tb(OH)_3$, $Ho(OH)_3$, $Tm(OH)_3$ and YbOOH) usually have lower aspect ratios or less uniform morphologies when prepared under the same conditions (Table 1). Figure 3H shows a typical TEM image of $Ho(OH)_3$ nanorods with diameters of approximately 10 nm and lengths of 100–500 nm.

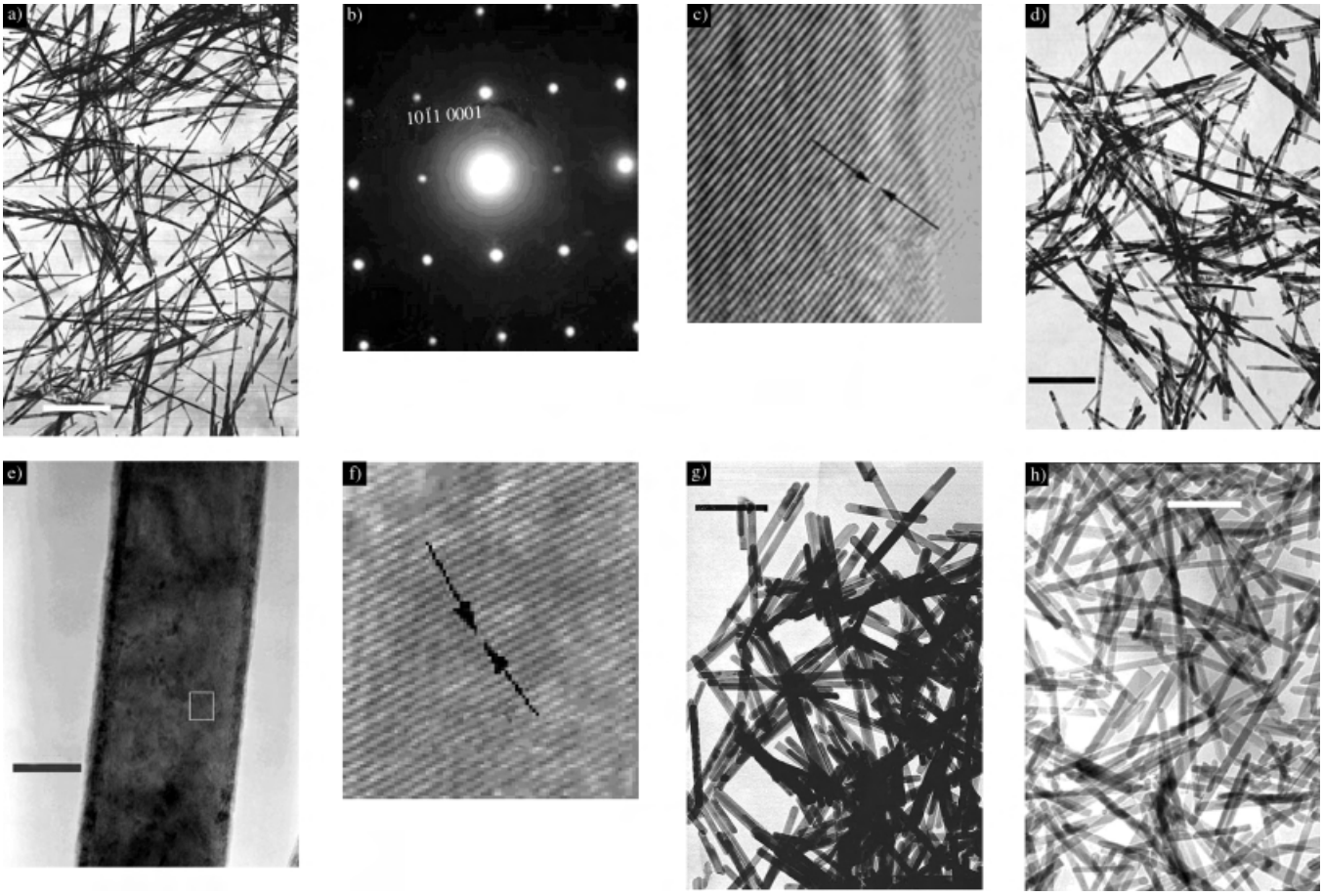


Figure 3. a) TEM image of $La(OH)_3$ nanowires (KOH, 5 mol L^{-1}, bar = 1 μm); b) Electron diffraction pattern of a single $La(OH)_3$ nanowire; c) HRTEM image of a single $La(OH)_3$ nanowire (spacing = 0.316 nm; d) TEM image of $Pr(OH)_3$ nanowires (KOH, 5 mol L^{-1}, bar = 500 nm); e) TEM image of a uniform 20 nm diameter $Pr(OH)_3$ nanowire (bar = 10 nm); f) HRTEM image of a $Pr(OH)_3$ nanowire taken from the highlighted section of (e), (spacing = 0.310 nm (101)); g) TEM image of $Eu(OH)_3$ nanowires (KOH, 5 mol L^{-1}, bar = 250 nm); h) TEM image of $Ho(OH)_3$ nanorods (at approximately pH 14, bar = 100 nm).

Table 1. Optimal experimental conditions and morphologies of lanthanide hydroxide nanowires.

Products	pH	XRD	Morphology	
			Diameter [nm]	Length [μm]
$La(OH)_3$	KOH 5 mol L^{-1}	hexagonal	15–20	2–5
$Pr(OH)_3$	KOH 5 mol L^{-1}	hexagonal	20–30	2–5
$Nd(OH)_3$	KOH 5 mol L^{-1}	hexagonal	20–30	2–5
$Sm(OH)_3$	pH 9	hexagonal	20–30	2–5
$Eu(OH)_3$	KOH 5 mol L^{-1}	hexagonal	20–30	2–5
$Gd(OH)_3$	pH 7	hexagonal	20–50	2–3
$Dy(OH)_3$	pH 14	hexagonal	40–60	0.5–1
$Tb(OH)_3$	pH 14	hexagonal	40–60	1–5
$Ho(OH)_3$	pH 14	hexagonal	~10	0.1–0.5
$Tm(OH)_3$	pH 14	hexagonal	10–20	0.5–1
YbOOH	pH 14	monoclinic	nanorods, microrods, and irregular particles coexist	

 © 2002 WILEY-VCH Verlag GmbH & Co. KGaA, Weinheim 0044-8249/02/4124-4791 $ 20.00+.50/0

Hydrothermal methods have been shown to be effective in the synthesis of nanowires, nanorods, and nanotubes.[10,11] In contrast to synthetic strategies, such as the vapor-liquid-solid (VLS) or template-confined methods, the adopted synthetic method has no catalyst to serve as the energetically favorable site for the absorption of reactant molecules (VLS), and has no template to guide the directional growth of nanowires (template-confined). Thus, it is reasonable to imagine that the driving force for the anisotropic growth of $Ln(OH)_3$ nanowires derives from the inherent crystal structure of $Ln(OH)_3$ materials and their chemical potential in solution.

The majority of the lanthanide hydroxide nanowires that were prepared possessed a hexagonal crystal structure, similar to that of ZnO, which is well-known to exhibit anisotropic growth.[4] However, under the adopted experimental conditions, those hydroxides with the smallest metal-ion centers, that is, YbOOH (which is formed here instead of the hexagonal $Yb(OH)_3$) and $Lu(OH)_3$ (which does not form nanowires) are obtained with monoclinic crystal structures. In addition to this change, the tendency to grow along a certain direction has been weakened to some extent, so that the heavier lanthanide hydroxides usually have lower aspect ratios and less uniform morphologies (Table 1).

The influence of chemical potential on the shape evolution of nanocrystals have been elucidated by Peng et al., and in the case of one-dimensional nanostructure growth it would be advantageous to have a higher chemical potential,[6,7] which is mainly determined by the pH value and monomer concentration of the solutions in our adopted reaction system. Meanwhile, faster ionic motion usually ensures a reversible pathway between the fluid phase (solution, melt, or vapor) and the solid phase, which allows atoms, ions, or molecules to adopt correct positions in developing crystal lattices.[23] Control experiments have been carried out to investigate the influence of monomer concentration and pH value on the growth of $Ln(OH)_3$ nanowires.

The synthesis of colloidal solutions of $Ln(OH)_3$ should be critical in the synthesis of lanthanide hydroxide nanowires. A rapid adjustment of the pH value of the solution leads to the formation of a white precipitate (shown to be aggregates of nanoparticles) which immediately appears in solution. This feeding mode can be regarded as a similar process to the "injection" technique adopted by Peng et al., which will ensure a higher monomer concentration so that the obtained precipitates will have many anisotropic seeds[9] for the following hydrothermal process.

Control experiments have been carried out to investigate the influence of pH value on the morphology of the final products. In the synthesis of $Sm(OH)_3$ nanomaterials, nanosheets are obtained when the pH value of the solution is maintained between 6 and 7 (Figure 4A). These nanosheets are apparently the product of a mixed-shape evolution of 1D and 2D ripening.[6] When the pH value is increased to 9, the obtained $Sm(OH)_3$ material is found to be in the form of uniform nanowires with an aspect ratio of 200–300 (Figure 4B). When the pH value is further increased to 14, or a higher concentration of KOH is employed (to 5 mol L^{-1}), the aspect ratio decreases dramatically to be about 10 (Figure 4C). From the experimental results, it seems that there exists an optimal pH value for the growth of high-aspect-ratio nanowires. This phenomenon can be explained by the complex interaction and balance between the chemical potential and the rate of ionic motion. A higher pH value implies a higher OH^- ion concentration and a higher chemical potential in solution. A high chemical potential is preferable for the growth of nanowires, however, higher OH^- ion concentrations may greatly reduce the Sm^{3+} ion concentration in solution, which is restricted by the value of K_{sp} for $Sm(OH)_3$, and thus reduce the rate of ionic motion. Thus, as the pH value is gradually changed, there must exist a value which is optimal for the preparation of nanowires. The growth behavior must also be closely related to the intrinsic properties of corresponding samples; for example, in the case of $Gd(OH)_3$, nanosheets have not been

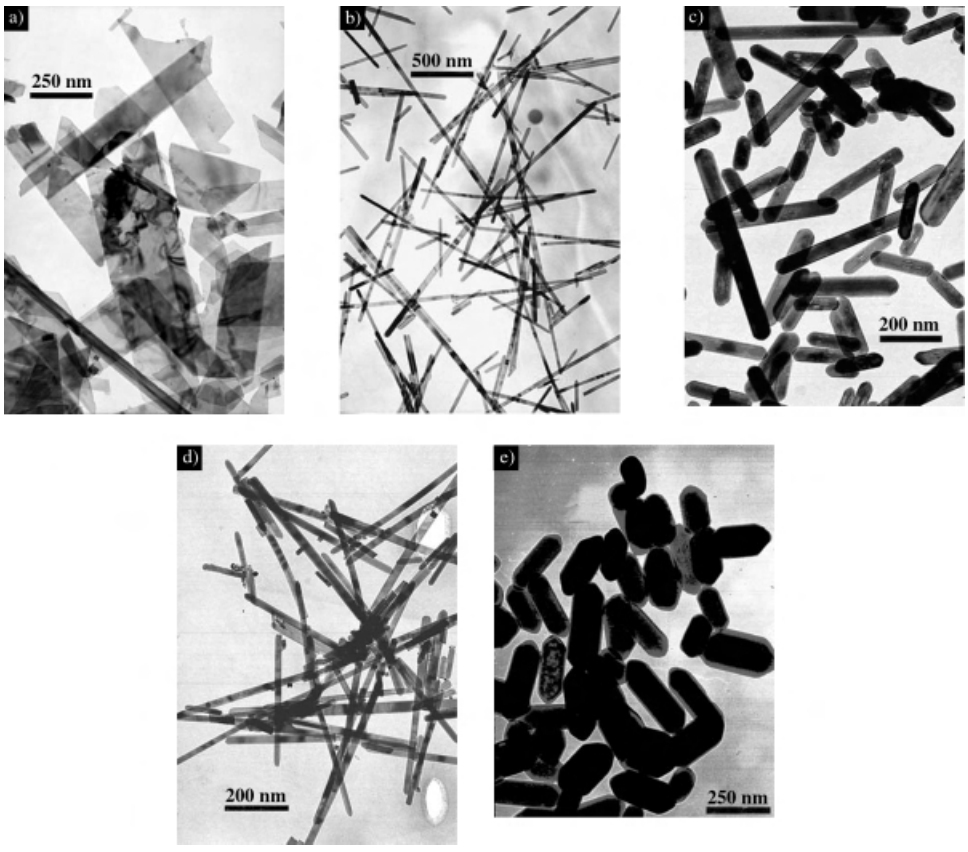


Figure 4. TEM images of: a) $Sm(OH)_3$ nanosheets (pH 6–7); b) $Sm(OH)_3$ nanowires (pH 9–10); c) $Sm(OH)_3$ nanorods (KOH, 5 mol L^{-1}); d) $Gd(OH)_3$ nanowrires, (pH 7); e) $Gd(OH)_3$ nanorods (KOH, 5 mol L^{-1}).

 © 2002 WILEY-VCH Verlag GmbH & Co. KGaA, Weinheim 0044-8249/02/4124-4792 $ 20.00+.50/0

obtained at lower pH values, although the aspect ratio of the products has been reduced, while at higher pH values, the $Gd(OH)_3$ nanocrystals have a much lower aspect ratio (Figure 4F) than that of the $Sm(OH)_3$ nanorods.

Further investigations can be carried out on the growth dynamics of the family of $Ln(OH)_3$ nanowires, which might serve as a perfect model to study crystallization on the nanoscale, as a trend in their crystal structures can be determined.

As a new material for the synthesis of nanowires, lanthanide hydroxides have many potential applications. The surface hydroxyl groups of $Ln(OH)_3$ may act as active sites for possible surface modification treatment through condensation reactions with amino acids or biologically active molecules, and thus, $Ln(OH)_3$ nanowires may have potential in the field of biological labeling. In addition, the similarity of their crystal structures and lattice constants[24] suggests that doped $Ln(OH)_3$ nanowires could be prepared by a similar growth process, as lattice mismatching would not be a serious concern. Meanwhile, since $Ln(OH)_3$ can be used to prepare oxides or sulfides through dehydration or sulfuration,[24] the $Ln(OH)_3$ or co-doped $Ln(OH)_3$ nanowires may act as important precursors to lanthanide oxide or sulfide nanowires.

In summary, we have developed a facile hydrothermal synthetic method to prepare $Ln(OH)_3$ nanowires that are expected to exhibit some novel properties, and we have displayed the successful synthesis of 1D lanthanide nanostructures, which may lead to new and important opportunities in lanthanide chemistry.

Experimental Section

To prepare lanthanide nanowires, Ln_2O_3 (0.4 g) was dissolved in concentrated nitric acid, and then the solution was rapidly adjusted to a designated pH value using 10% KOH solution. A white precipitate of amorphous $Ln(OH)_3$ appeared immediately. After stirring for about 10 min, the precipitate was then transferred into a 50-ml autoclave, which was filled with deionized water up to 80% of the total volume, sealed, and heated at 180°C for about 12 h. The system was then allowed to cool to room temperature. The final product was collected by filtration, and washed with deionized water to remove any possible ionic remnants, and then dried at 60°C.

The obtained sample was characterized on a Bruker D8-advance X-ray powder diffractometer with $Cu_{K\alpha}$ radiation ($\lambda = 1.5418$ Å). The size and morphology of the $Ln(OH)_3$ nanowires was determined at 200 kV by a Hitachi H-800 transmission electron microscope (TEM) and a JEOL JEM-2010F high-resolution transmission electron microscope.

Received: August 28, 2002 [Z50057]

[1] X. F. Duan, Y. Huang, Y. Cui, J. F. Wang, C. M. Lieber, *Nature* **2001**, *409*, 66 – 69.
[2] W. U. Huynh, J. J. Dittmer, A. P. Alivisatos, *Science* **2002**, *295*, 2425 – 2427.
[3] L. S. Li, J. Walda, L. Manna, A. P. Alivisatos, *Nano Lett.* **2002**, *2*, 557 – 560.
[4] M. H. Huang, S. Mao, H. Feick, H. Q. Yan, Y. Y. Wu, H. Kind, E. Weber, R. Russo, P. D. Yang, *Science* **2001**, *292*, 1897 – 1899.
[5] M. Law, H. Kind, B. Messer, F. Kim, P. D. Yang, *Angew. Chem.* **2002**, *114*, 2511 – 2514; *Angew. Chem. Int. Ed.* **2002**, *41*, 2405 – 2408.
[6] Z. A. Peng, X. G. Peng, *J. Am. Chem. Soc.* **2001**, *123*, 1389 – 1395.
[7] Z. A. Peng, X. G. Peng, *J. Am. Chem. Soc.* **2002**, *124*, 3343 – 3353.
[8] W. W. Yu, X. G. Peng, *Angew. Chem.* **2002**, *114*, 2474 – 2477; *Angew. Chem. Int. Ed.* **2002**, *41*, 2368 – 2371.
[9] Y. G. Sun, B. Gates, B. Mayers, Y. N. Xia, *Nano Lett.* **2002**, *2*, 165 – 168.
[10] X. Wang, Y. D. Li, *J. Am. Chem. Soc.* **2002**, *124*, 2880 – 2881.
[11] Y. D. Li, J. W. Wang, Z. X. Deng, Y. Y. Wu, X. M. Sun, D. P. Yu, P. D. Yang, *J. Am. Chem. Soc.* **2001**, *123*, 9904 – 9905.
[12] J. P. Cotter, J. C. Fitzmaurice, I. P. Parkin, *J. Mater. Chem.* **1994**, *4*, 1603 – 1609.
[13] J. A. Capobianco, F. Vetrone, J. C. Boyer, A. Speghini, M. Bettinelli, *Opt. Mater.* **2002**, *19*, 259 – 268.
[14] M. S. Palmer, M. Neurock, M. M. Olken, *J. Am. Chem. Soc.* **2002**, *124*, 8452 – 8461.
[15] A. H. Peruski, L. H. Johnson, L. F. Peruski, *J. Immunol. Methods* **2002**, *263*, 35 – 41.
[16] M. C. Cassani, Y. K. Gun'ko, P. B. Hitchcock, A. G. Hulkes, A. V. Khvostov, M. F. Lappert, A. V. Protchenko, *J. Organomet. Chem.* **2002**, *647*, 71 – 83.
[17] R. Kempe, H. Noss, T. Irrgang, *J. Organomet. Chem.* **2002**, *647*, 12 – 20.
[18] J. de Jersey, R. B. Martin, *Biochemistry* **1980**, *19*, 1127 – 1132.
[19] J. R. Lakowicz, G. Piszczek, B. P. Maliwal, I. Gryczynski, *ChemPhysChem* **2001**, *4*, 247 – 252.
[20] Y. D. Li, Y. Huang, T. Bai, L. Q. Li, *Inorg. Chem.* **2000**, *39*, 3418 – 3420.
[21] Y. Hasegawa, S. Thongchant, Y. Wada, H. Tanaka, T. Kawai, T. Sakata, H. Mori, S. Yanagida, *Angew. Chem.* **2002**, *114*, 2177 – 2179; *Angew. Chem. Int. Ed.* **2002**, *41*, 2073.
[22] J. W. Stouwdam, F. C. J. M. van Veggel, *Nano Lett.* **2002**, *2*, 733 – 737.
[23] T. J. Trentler, K. M. Hickman, S. C. Goel, A. M. Viano, P. C. Gibbons, W. E. Buhro, *Science* **1995**, *270*, 1791 – 1794.
[24] C. H. Huang, *Rare Earth Coordination Chemistry*, Science Press, Beijing, **1997**, p. 25.

 © 2002 WILEY-VCH Verlag GmbH & Co. KGaA, Weinheim 0044-8249/02/4124-4793 $ 20.00+.50/0